Cover Picture



Alois Fürstner*

Raphael's "Mass of Bolsena" depicts the "miracle" that occurred in the small Italian village of Bolsena north of Rome in 1263. The cover picture shows part of the fresco, in which a "bleeding" host is the center of attention. Today we know that such phenomena, which could only be explained as a miracle in the Middle Ages, are caused by prodigiosin-producing bacteria. With an emphasis on the total synthesis, A. Fürstner summarizes the chemistry and biology of these "prodigious" compounds in his Review on page 3582 ff.

Contents

Angewandte EarlyView

The following articles are available online (in Wiley Interscience). You can find them at www.angewandte.org, under Full Text, Forthcoming Articles.

E. F. Connor, L. K. Sundberg, H.-C. Kim, J. J. Cornelissen, T. Magbitang, P. M. Rice, V. Y. Lee, C. J. Hawker, W. Volksen, J. L. Hedrick, R. D. Miller*:*
Templating of Silsesquioxane Cross-Linking Using Unimolecular Self-Organizing Polymers
DOI: 10.1002/anie.200350930
Published online: July 28, 2003

V. Niel, A. L. Thompson, M. C. Muñoz, A. Galet, A. E. Goeta, J. A. Real:*
Crystalline-State Reaction with Allosteric Effect in Spin-Crossover, Interpenetrated Networks with Magnetic and Optical Bistability
DOI: 10.1002/anie.200351853
Published online: July 28, 2003

D. Chernyshov, M. Hostettler, K. W. Törnroos, H.-B. Bürgi:*
Ordering Phenomena and Phase Transitions in a Spin-Crossover Compound—Uncovering the Nature of the Intermediate Phase of $[Fe(2\text{-pic})_3]Cl_2 \cdot EtOH$
DOI: 10.1002/anie.200351834
Published online: July 28, 2003

V. Percec, M. Glodde, G. Johansson, V. S. K. Balagurusamy, P. A. Heiney:*
Transformation of a Spherical Supramolecular Dendrimer into a Pyramidic Columnar Supramolecular Dendrimer Mediated by the Fluorophobic Effect
DOI: 10.1002/anie.200351804
Published online: July 28, 2003

D. M. Guldi, M. Marcaccio, D. Paolucci, F. Paolucci,* N. Tagmatarchis, D. Tasis, E. Vázquez, M. Prato*:*
Single-Wall Carbon Nanotube–Ferrocene Nanohybrids: Observing Intramolecular Electron Transfer in Functionalized SWNTs
DOI: 10.1002/anie.200351289
Published online: July 28, 2003

D. R. Jensen, M. J. Schultz, J. A. Mueller, M. S. Sigman:*
A Well-Defined Complex for Palladium-Catalyzed Aerobic Oxidation of Alcohols: Design, Synthesis, and Mechanistic Considerations
DOI: 10.1002/anie.200351997
Published online: July 28, 2003

Articles judged by the referees or the editior as being either very important or very urgent are immediately edited, proof-read, and electronically published once the manuscript has arrived in the editiorial office in final form. As long as there is no page number available these articles should be cited in the following manner:

Author(s) *Angew. Chem. Int. Ed.*, online publication date, DOI.

Meeting Review

Crystal Design and Crystal Engineering — **3572 – 3574** — *Nico A. J. M. Sommerdijk*

Books

Handbook of Drug Screening — **3575** — Ramakrishna Seethala, Prabhavathi B. Fernandes. — *reviewed by Reinhold Müller*

BioNMR in Drug Research — **3576** — Oliver Zerbe — *reviewed by Thomas Peters*

Catalysis by Polyoxometalates — **3577** — Ivan V. Kozhevnikov — *reviewed by Ronny Neumann*

Highlights

Five-Vertex Clusters

Y. Canac, G. Bertrand* — **3578 – 3580**

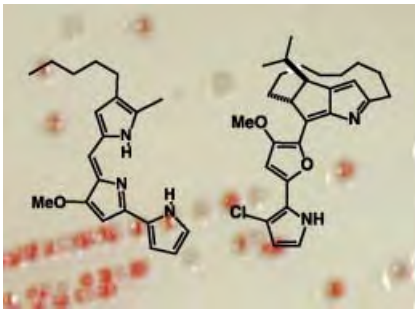
nido-Five-Vertex Clusters: In and Out of Boron Chemistry



During the early days of borane chemistry B_5H_9 was considered to be the stable pentaborane and although a BH vertex is isolobal with a naked P vertex, it is only recently that the first *nido*-five-vertex compounds with a naked phosphorus atom at the apical position were discovered. The most recent example is a valence isomer of the hitherto unknown triphosphacyclopentadienyl cation. These results shed light on the relative stability of planar and three-dimensional Cp^+ derivatives (see picture).

© 2003 Wiley-VCH Verlag GmbH & Co. KGaA, Weinheim

Reviews



Miraculous drugs: One of the most unusual chapters of natural product chemistry deals with the pyrrole alkaloids of the prodigiosin family (left), which can be traced back in history to ancient times. Together with the closely related roseophilin (right), they have attracted considerable attention owing to their promising biological activities and as challenging synthetic targets.

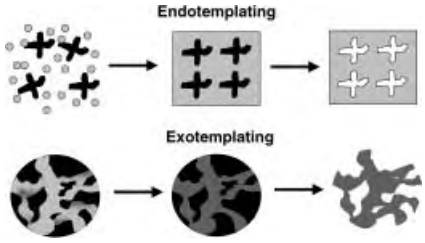
Total Synthesis of the Prodigiosins

A. Fürstner* ——— **3582 – 3603**

Chemistry and Biology of Roseophilin and the Prodigiosin Alkaloids: A Survey of the Last 2500 Years

---

Holey appropriate templates: Two different templating approaches for the creation of porous and high-surface-area solids are discussed. These methods are endotemplating, where template species are incorporated in the growing solid (see scheme, top), and exotemplating, where a rigid porous solid provides a scaffold for the formation of another solid (see scheme, bottom). Removal of both kinds of templates results in high-surface-area solids.



Inorganic Template Synthesis

F. Schüth* ——— **3604 – 3622**

Endo- and Exotemplating to Create High-Surface-Area Inorganic Materials

---

Communications



Cracking mechanisms in the zeolite literature have traditionally assumed full adsorption. Simulations indicate abnormally low adsorption in ERI-, AFX-, CHA-, RHO-, and KFI-type zeolites for chain lengths close to or longer than the cage size. Very long molecules adsorb partially into a cage near the outer surface. After scission the nonadsorbed part can end up in the product or re-adsorb and undergo another scission. This mechanism is characteristic for cage/window-type zeolites with small windows close to the diameter of the adsorbate (see picture).

Cracking Mechanisms in Zeolites

D. Dubbeldam,* S. Calero, T. L. M. Maesen, B. Smit ——— **3624 – 3626**

Understanding the Window Effect in Zeolite Catalysis

For the USA and Canada:
ANGEWANDTE CHEMIE International Edition (ISSN 1433-7851) is published weekly by Wiley-VCH PO Box 191161, D 69451 Weinheim, Germany. Air freight and mailing in the USA by Publications Expediting Inc. 200 Meacham Ave., Elmont, NY 11003. Periodicals postage paid at Jamaica NY 11431. US POSTMASTER: send address changes to *Angewandte Chemie*, Wiley-VCH, 111 River Street, Hoboken, NJ 07030. Annual institutional subscription price for institutions: Europe € 2998.00/3148.00. Outside Europe US$ 3718.00/3904.00 (valid for print or electronic/print and electronic delivery); for individuals who are personal members of a national chemical society, or whose institution already subscribes, or who are retired or self-employed consultants, print only (including postage and handling charges): Europe € 248.00/Outside Europe US$ 348.00.

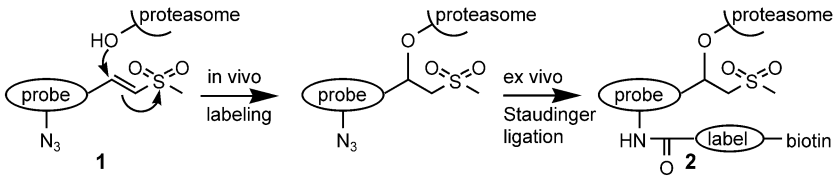
 © 2003 Wiley-VCH Verlag GmbH & Co. KGaA, Weinheim

Contents

Active-Site-Directed Probe

H. Ovaa, P. F. van Swieten, B. M. Kessler, M. A. Leeuwenburgh, E. Fiebiger, A. M. C. H. van den Nieuwendijk, P. J. Galardy, G. A. van der Marel, H. L. Ploegh, H. S. Overkleeft* _____ **3626 – 3629**

Chemistry in Living Cells: Detection of Active Proteasomes by a Two-Step Labeling Strategy

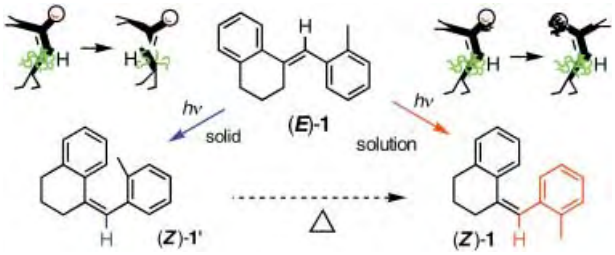


In vivo targeting of the proteasome: Probe **1** is a cell-permeable irreversible inhibitor that alkylates the active-site residues of the proteasome in a Michael fashion. After cell lysis, a biotin moiety is introduced by Staudinger ligation to yield construct **2**. This strategy allows activity profiling of the catalytic activities of the proteasome in vivo.

Photoisomerization

Y. Imamoto, T. Kuroda, M. Kataoka, S. Shevyakov, G. Krishnamoorthy, R. S. H. Liu* _____ **3630 – 3633**

Photoisomerization by Hula Twist: 2,2′-Dimethylstilbene and a Ring-Fused Analogue

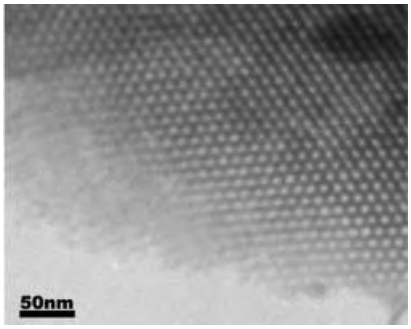


Let's twist again: While the photoisomerization of stilbene analogues in fluid solution occurs by a one-bond-flip mechanism and involves only configurational changes, in a solid solution (glass) a Hula-twist mechanism operates and results in conformational as well as configurational changes (see scheme).

Highly Stable Mesoporous Materials

Y. Han, D. Li, L. Zhao, J. Song, X. Yang, N. Li, Y. Di, C. Li, S. Wu, X. Xu, X. Meng, K. Lin, F.-S. Xiao* _____ **3633 – 3637**

High-Temperature Generalized Synthesis of Stable Ordered Mesoporous Silica-Based Materials by Using Fluorocarbon–Hydrocarbon Surfactant Mixtures

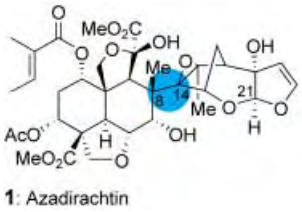


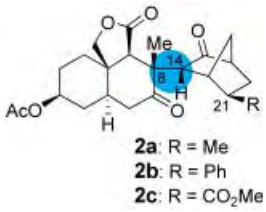
Highly ordered mesoporous silica materials are hydrothermally synthesized at high temperature by using fluorocarbon–hydrocarbon surfactant mixtures as templates. Because of the high temperature of the synthesis, the obtained materials show complete silica condensation, which give rise to ultra-stabile structures. JLU-20 for example (see TEM image of calcined JLU-20) has a fully condensed mesopore wall with a very high Q^4/Q^3 ratio of 6.5.

Azadirachtin Precursors

K. C. Nicolaou,* A. J. Roecker, H. Monenschein, P. Guntupalli, M. Follmann _____ **3637 – 3642**

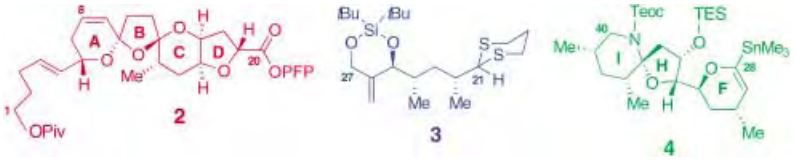
Studies Towards the Synthesis of Azadirachtin: Enantioselective Entry into the Azadirachtin Framework through Cascade Reactions





The carbon framework of azadirachtin (**1**) has been prepared enantioselectively: The synthesis of compounds **2a–c** follows two novel cascade sequences based on intramolecular radical reactions and acid-mediated redox chemistry. Such advanced intermediates should allow access to **1** through appropriate functional-group manipulations.

 © 2003 Wiley-VCH Verlag GmbH & Co. KGaA, Weinheim

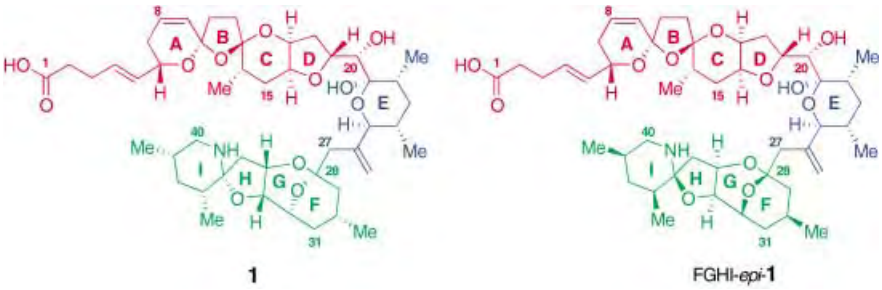


As a build-up to the synthesis of the proposed structure of azaspiracid, both enantiomers of fragments **2**, **3**, and **4** were synthesized stereoselectively. Piv = pivaloyl, PFP = pentafluorophenyl, Teoc = 2-(trimethylsilyl)ethoxycarbonyl, TES = triethylsilyl.

Natural Product Synthesis

K. C. Nicolaou,* Y. Li, N. Uesaka, T. V. Koftis, S. Vyskocil, T. Ling, M. Govindasamy, W. Qian, F. Bernal, D. Y.-K. Chen _____ **3643 – 3648**

Total Synthesis of the Proposed Azaspiracid-1 Structure, Part 1: Construction of the Enantiomerically Pure C1–C20, C21–C27, and C28–C40 Fragments



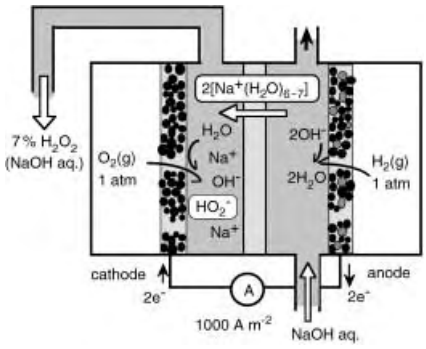
An illusive target: The two proposed structures of azaspiracid-1 (**1** and FGHI-*epi*-**1**), were synthesized and shown to be different from the natural substance, thereby invalidating the presently accepted structures for these important marine neurotoxins.

Natural Product Synthesis

K. C. Nicolaou,* D. Y.-K. Chen, Y. Li, W. Qian, T. Ling, S. Vyskocil, T. V. Koftis, M. Govindasamy, N. Uesaka _____ **3649 – 3653**

Total Synthesis of the Proposed Azaspiracid-1 Structure, Part 2: Coupling of the C1–C20, C21–C27, and C28–C40 Fragments and Completion of the Synthesis

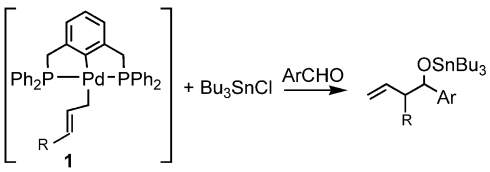
Avoiding a bang! Electrochemical reduction of O_2 in an H_2/O_2 fuel cell with a three-phase boundary (gaseous O_2, aqueous electrolyte, solid cathode) produces concentrated aqueous solutions of H_2O_2. Even air can serve as the oxygen source.



H_2O_2 Production

I. Yamanaka,* T. Onizawa, S. Takenaka, K. Otsuka _____ **3653 – 3655**

Direct and Continuous Production of Hydrogen Peroxide with 93% Selectivity Using a Fuel-Cell System



Nucleophilic rather than electrophilic reactivity is ascribed to the allyl moiety in (η^1-allyl)palladium complexes such as **1**, which are generated catalytically from allylstannanes and a palladium pincer complex and react smoothly with aldehydes.

Pd-Catalyzed Allylation

N. Solin, J. Kjellgren, K. J. Szabó* _____ **3656 – 3658**

Palladium-Catalyzed Electrophilic Substitution via Monoallylpalladium Intermediates

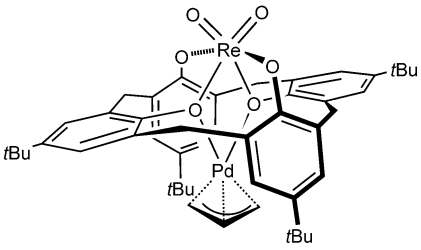
 © 2003 Wiley-VCH Verlag GmbH & Co. KGaA, Weinheim

Contents

Re–Pd Calixarene Complexes

K. Iwasa, T. Kochi, Y. Ishii* ... **3658 – 3660**

Stepwise Construction of a Re–Pd Heterodinuclear Core Inside the Cavity of *p*-*t*Bu-Calix[4]arene

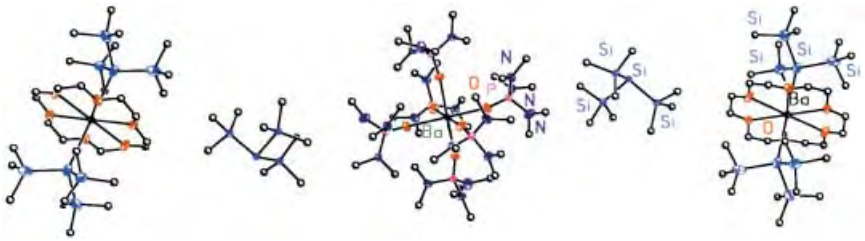


A Re–Pd heterometallic core has been constructed inside the cavity of a calixarene ligand. An unprecedented calix[4]arene–rhenium complex can incorporate a $\{Pd(\eta^3\text{-}C_3H_5)^+\}$ fragment to afford the phenoxo-bridged heterodinuclear complex $[ReO_2\{p\text{-}t\text{Bu-calix[4]arene-}(O)_4\}Pd(\eta^3\text{-}C_3H_5)]$ (see picture).

Barium Hypersilanides

W. Teng, U. Englich, K. Ruhlandt-Senge* ... **3661 – 3664**

Syntheses and Structures of Barium Silanides: Contact and Separated Ions

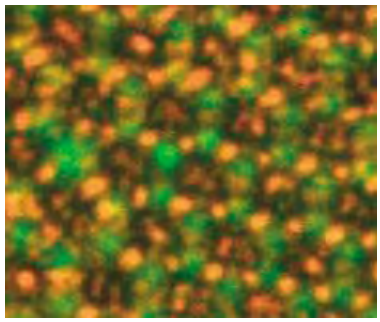


The addition of specific donor molecules affects the formation of either contact molecules or separated ions in a series of barium hypersilanides (see picture). Dissociation through the formation of separated ions is observed in aromatic solvents. The silanides are potent initiators in polymerization chemistry and are important as model compounds for the emerging organometallic complexes of the heavy alkaline-earth metals.

Blue-Light Emitting Polymer Films

C. Barner-Kowollik,* H. Dalton, T. P. Davis,* M. H. Stenzel* **3664 – 3668**

Nano- and Micro-Engineering of Ordered Porous Blue-Light-Emitting Films by Templating Well-Defined Organic Polymers Around Condensing Water Droplets



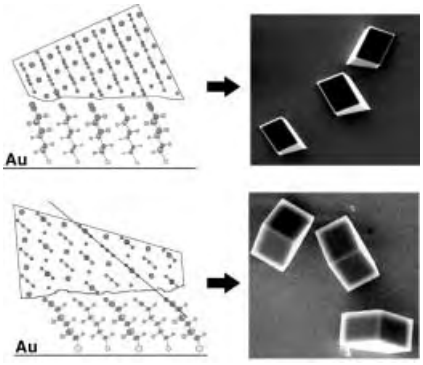
It's all in the casting: The pore sizes of nano-structured light-emitting films cast from linear and star-shaped macromolecular architectures can be engineered from the nano- to microrange by simply manipulating the casting conditions. The confocal microscopy image shows highly fluorescent organized porous materials with additional ordering within the polymer phase of the films.

Nucleation of Calcite Crystals

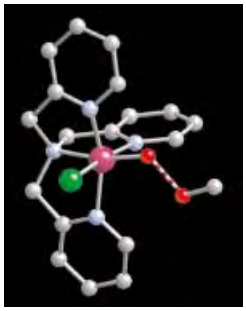
Y.-J. Han, J. Aizenberg* ... **3668 – 3670**

Face-Selective Nucleation of Calcite on Self-Assembled Monolayers of Alkanethiols: Effect of the Parity of the Alkyl Chain

In-line for promotion: A study of self-assembled monolayers of sulfanylalkanoic acids containing odd and even numbers of methylene groups supported on gold and silver has demonstrated that the crystallographic direction of nucleated calcite crystals is controlled by the orientation of the functional groups in the templating surface (see picture).



© 2003 Wiley-VCH Verlag GmbH & Co. KGaA, Weinheim

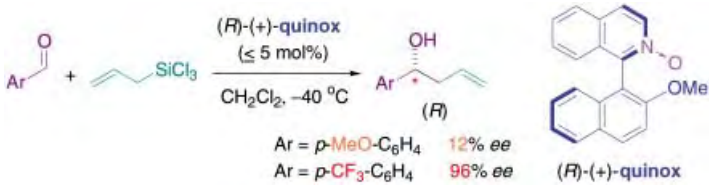


A pushy Lewis base: Previously unobserved non-heme Fe^{IV}=O intermediates can be trapped in the decay of Fe^{III}OOR species by the addition of Lewis bases (represented by the green sphere) that promote O–O bond homolysis (see picture; Fe purple, O red).

High-Valent Non-Heme Complexes

J. Kaizer, M. Costas, L. Que, Jr.* ——— 3671 – 3673

A Dramatic Push Effect on the Homolysis of Fe^{III}(OOR) Intermediates To Form Non-Heme Fe^{IV}=O Complexes

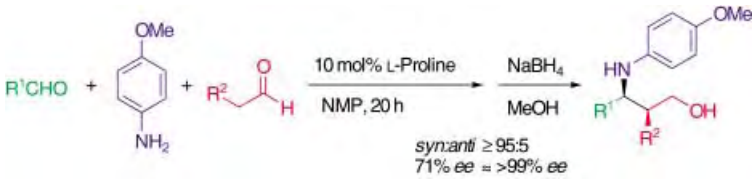


The allylation of aromatic aldehydes with allyltrichlorosilanes can be catalyzed by the new Lewis basic organocatalyst quinox with high enantioselectivity for electron-poor aldehydes and low for their electron-rich congeners (see scheme). This behavior suggests an arene–arene interaction of the electron-rich catalyst with the incoming aldehyde as the main factor determining the enantiofacial selectivity.

Asymmetric Allylation

A. V. Malkov,* L. Dufková, L. Farrugia, P. Kočovský* ——— 3674 – 3677

Quinox, a Quinoline-Type *N*-Oxide, as Organocatalyst in the Asymmetric Allylation of Aromatic Aldehydes with Allyltrichlorosilanes: The Role of Arene–Arene Interactions



A double-crossed reaction: The use of proline as an organocatalyst enables a one-pot, direct, cross-Mannich reaction to be performed between two different aldehydes and 4-methoxyaniline in a highly *syn*-diastereo- and enantioselective manner (see scheme).

Cross-Mannich Reaction of Aldehydes

Y. Hayashi,* W. Tsuboi, I. Ashimine, T. Urushima, M. Shoji, K. Sakai ——— 3677 – 3680

The Direct and Enantioselective, One-Pot, Three-Component, Cross-Mannich Reaction of Aldehydes



Hybrid core–corona nanoassemblies (shown schematically in the picture, middle) can be used as supramolecular precursors for metal hydroxide colloids (right) with long-term stability. Anionic–neutral hydrophilic diblock copolymers allow metal hydrolysis and condensation reactions to occur in suspension. Particle size and morphology can be varied by adjusting the degree of metal complexation.

Controlled Nanoparticle Growth

C. Gérardin,* N. Sanson, F. Bouyer, F. Fajula, J.-L. Putaux, M. Joanicot, T. Chopin ——— 3681 – 3685

Highly Stable Metal Hydrous Oxide Colloids by Inorganic Polycondensation in Suspension

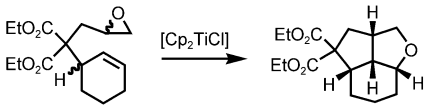
 © 2003 Wiley-VCH Verlag GmbH & Co. KGaA, Weinheim

Contents

Ti-Catalyzed Tandem Reactions

A. Gansäuer,* B. Rinker, M. Pierobon, S. Grimme,* M. Gerenkamp, C. Mück-Lichtenfeld _____ **3687 – 3690**

A Radical Tandem Reaction with Homolytic Cleavage of a Ti–O Bond

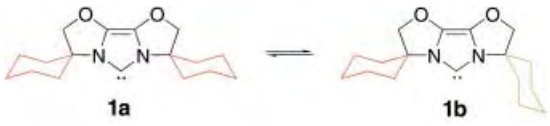


A radical merry-go-round. An electron is transferred from a titanocene(III) complex to the substrate and finally back to the catalyst in a novel atom-economical tandem reaction. Complex structures can be readily accessed (see scheme). The unprecedented mechanism involving a homolytic cleavage of a Ti–O bond is supported by DFT calculations.

Sterically Flexible Carbene Ligands

G. Altenhoff, R. Goddard, C. W. Lehmann, F. Glorius* _____ **3690 – 3693**

An N-Heterocyclic Carbene Ligand with Flexible Steric Bulk Allows Suzuki Cross-Coupling of Sterically Hindered Aryl Chlorides at Room Temperature

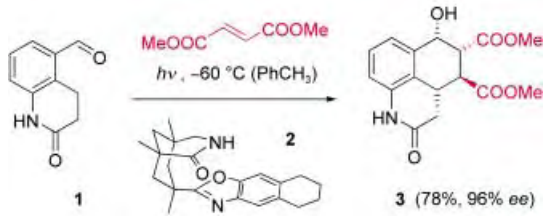


A juggling act: The steric bulk of the ligand enhances reductive elimination in the Pd-catalyzed Suzuki cross-coupling. However, it impedes the oxidative addition and transmetallation of sterically hindered substrates. This dilemma is solved with the carbene ligand **1**, which exhibits flexible steric bulk.

Asymmetric Photochemistry

B. Grosch, C. N. Orlebar, E. Herdtweck, W. Massa, T. Bach* _____ **3693 – 3696**

Highly Enantioselective Diels–Alder Reaction of a Photochemically Generated *o*-Quinodimethane with Olefins



Four stereogenic centers in one step are established with almost perfect control of the absolute and relative configuration in a photochemically induced Diels–Alder reaction of substrate **1** and dimethyl fumarate. The carrier of the chiral information, lactam **2**, fixes the substrate by hydrogen bonds in a chiral environment and in this way controls the configuration of the stereogenic centers of product **3**.

VIP Communications labeled with this symbol have been judged by two referees as being "very important papers".

The publication of Communications labeled with this symbol has been accelerated because of their topical or highly competitive nature.

Looking for outstanding employees?

Do you need another expert for your excellent team?
... Chemists, PhD Students, Managers, Professors, Sales Representatives...

Place an advert in the printed version and have it made available online for 1 month, free of charge!

Angewandte Chemie International Edition
Advertising Sales Department: Marion Schulz
Phone: 0 62 01 - 60 65 65
Fax: 0 62 01 - 60 65 50
E-Mail: MSchulz@wiley-vch.de

Service

Keywords _____ *3698*

Authors _____ *3699*

Vacancies _____ *3571*

Preview _____ *3701*



Crystal Design and Crystal Engineering**

Nico A. J. M.Sommerdijk*

For many the interest in molecular-crystal engineering is no doubt fueled by esthetic aspects; if not by the beauty of crystal morphologies, then certainly by the symmetry and complexity of the crystal structures. In addition, crystal engineering paves the road for many potential applications of organic and inorganic as well as hybrid organic–inorganic crystals. These applications range from lenses, nonlinear optics, sensors, and semiconductors, to catalysts and storage materials for small molecules. Many examples of new crystalline materials and compounds with interesting structures and properties were presented at the recent Euroconference on Molecular Crystal Engineering, which focused on the "Design and Preparation of Molecular Materials".

A great variety of approaches are already available for the synthesis of molecular crystals. K. Rissanen (University of Jyväskylä, Finnland) presented examples of self-assembly and selective recognition for the formation of supermolecules, cavitants, and capsules, as well as self-assembly through metal-ion coordination to yield coordination polymers. The combination of hydrogen bonding and coordination chemistry is also under investigation by many researchers. G. Orpen (University of Bristol, UK) showed a modular approach in which relatively simple building blocks comprising different metal complexes and bipyridinium compounds are used. A large number of crystals were conveniently produced from these building blocks in a systematic approach intended to improve understanding of the mechanisms underlying their assembly. The interest in constructing increasingly complex structures was impressively demonstrated by M. Schröder (University of Nottingham, UK), who showed how crystal structures with high connectivities at the metal centers could be obtained through the complexation of lanthanides with bipyridine *N*-oxides. By using this methodology an 8-connected net with an unprecedented structure was prepared. In this complex structure the two 4-4 nets do not lie directly above one another, as is the case for cesium chloride, but are rotated with respect to one another by an angle of 67°.

Although a great variety of assembly methods and an impressive diversity of resulting structures have been established, it is important to realize that few approaches allow one to predict the structure or properties of the resulting crystals. As the term "crystal engineering" implies the construction of predesigned structures and shapes, rather than the rationalization of molecular interactions based on resolved crystal structures, it is important to highlight some approaches that (at least to some extent) allow the synthesis of new crystal structures by design.

M. Fujita (University of Tokyo, Japan) demonstrated that through the careful choice of components true molecular architectures can be created, that is, complex, predesigned constructions. In his lecture he showed how defined square molecules can be designed and synthesized by modular assembly of the square planar building blocks $Pd(en)_2(NO_3)_2$ and 4,4'-bipyridine (en: ethylene diamine). The size of these squares can be increased by using larger rigid ligands in which the pyridine groups are separated by one or more 1,4-linked phenyl groups, whereas the replacement of the $[Pd(en)_2(NO_3)_2]$ by $Ni(NO_3)_4 \cdot 6H_2O$ leads to the formation of infinite frameworks of square grids. In this way squares with sides as long as 20 Å can be obtained, which occlude as many as four *o*-xylene molecules. The largest square that has been made so far has sides of length 25 Å and forms part of a ladderlike framework (Figure 1).

These guest molecules can be removed by heating under reduced pressure, which makes it possible to exchange them for others. Thus, a mixture of *o*,*m*-xylene was replaced by mesitylene, which was in turn replaced by *o*-xylene. In the latter exchange a change in the crystal structure was observed. It was found that the layers of square nets shift with respect to one another to accommodate for the change in the volume occupied by the guest molecules. Surprisingly, the shift in the lattice could be observed with in situ X-

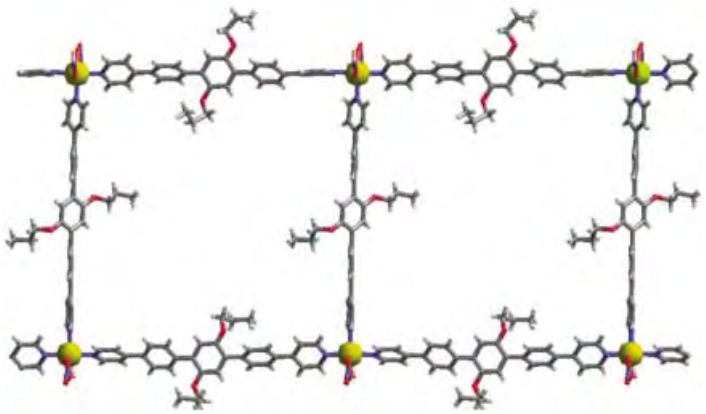


Figure 1. Fujita et al. presented a ladderlike framework with cavities of 25 × 25 Å.

[*] N. A. J. M. Sommerdijk
Laboratory of Macromolecular and Organic Chemistry
Eindhoven University of Technology
PO Box 513, 5600 MB Eindhoven
(The Netherlands)
E-mail: N.Sommerdijk@tue.nl

[**] Euroconference on Molecular Crystal Engineering, Acquafredda di Maratea (Italy), May 31 – June 5, 2003. The Conference was organized by D. Braga, University of Bologna.

 © 2003 Wiley-VCH Verlag GmbH & Co. KGaA, Weinheim

ray crystallographic experiments, which showed that the removal of the guest indeed takes place before the grids can shift.

Fujita took the design of his crystal one step further and changed the ligand geometry from linear to slightly bent (120°). Reaction of this ligand with transition metals led to exclusive formation of the cuboctahedral compound with the general formula $M_{12}L_{24}$. This molecular sphere, which has a molecular weight of approximately 14 kDa and a diameter of approximately 3.5 nm, can be functionalized on its periphery, for example, with porphyrins. Thus, not only is this molecule a protein mimetic in more than one respect, but it also serves as an illustration of how this modular approach can be used to design complex functional materials.

M. W. Hosseini (University Louis Pasteur, Strasbourg, France) also stressed that the complexation of simple building blocks can be used to generate molecular materials with a designed structure. The starting point in his strategy is the use of dicationic tectons that form a second coordination sphere to complexes of the type $[M(CN)_4]^{2-}$. In these systems it could be demonstrated that the introduction of chirality in the cationic tecton is expressed at the supramolecular level, that is, it results in hierarchically structured architectures in which five parallel strands pack to form a superhelical cable. This gives rise to chiral crystals in which the cables are arranged in a hexagonal packing environment.

To prepare polar crystals, a strategy was developed in which six coordinated metal complexes with two stable and four labile metal ions were used. When these were complexed with ligands that had one tridentate binding site (such as terpyridine) and one monodentate binding site (such as pyridine), directionality was introduced in the resulting chain. Antiparallel packing of these chains could be prevented through the complexation of cobalt with a chiral ligand: a pyridine group connected at the 4-position to a pyridine group with two optically active oxazoline moieties at the 2- and 6-positions.[1] The consequent formation of polar crystals emphasizes how careful ligand design is one of keys to the preparation of materials with predesigned structure. It is evident that this strategy may be beneficial in several advanced applications such as nonlinear optics and magnetics.

The induction of chirality in crystals is eminently present in nature, as was elegantly exemplified by L. Addadi (Weizmann Institute of Science, Rehovot, Israel), who discussed the different crystal morphologies of calcium oxalate formed in vivo and in vitro.[2] Calcium oxalate crystals grown in the laboratory have a centrosymmetric structure that displays a symmetric morphology. However, in tobacco or tomato-plant leaves tetrahedral crystals are formed that have only one of the two possible enantiomorphous forms; the other form is never encountered. Three of the four faces belong to the family of faces that are most stable and also expressed in the crystals grown in vitro; the fourth face is unique. This morphological chirality is explained by the enantiospecific interaction of biomolecules with the unique crystal face, after which growth can proceed in only one direction. This phenomenon can only lead to the growth of chiral morphologies if the protein can distinguish between the front (hkl) and back ($\bar{h}\bar{k}\bar{l}$) sides of the unique crystal plane, as the molecules on the crystal surfaces are not related by any symmetry element. Thus, chiral recognition of the crystal face is possible, even though neither the molecule nor the crystal structure is chiral.

The chiral recognition of crystal surfaces was also found in the interaction of epithelial cells with crystals of calcium tartrate. Although calcium tartrate is chiral, the crystals of the *S,S* and the *R,R* enantiomers have the same crystal morphology. Nevertheless, epithelial cells show attachment exclusively to the crystals of the *R,R* enantiomer, and more specifically only to the {011} and not to the {101} faces. It was found that this "Pasteur" type of recognition originates from the selective interaction that exists between the crystals of calcium (*R,R*)-tartrate and hyaluronan, a polysaccharide abundantly present on the surface of cells.

Addadi also discussed the selective recognition of crystal surfaces by antibodies that are able to selectively recognize the surfaces of crystals and monolayers of organic compounds. It is easy to conceive that the use of such recognition processes may lead to the selection of antibodies with a specific affinity for preselected surfaces and their use in crystal design for the specific nucleation and/or controlled growth of synthetic crystals.

Synthetic polymers can also be used for this purpose, as has been exemplified by the use of poly(isocyanopeptide)s that regulate both the nucleation and the expression of specific crystal faces of calcite.[3] These synthetic peptide-derived polymers may be regarded as protein mimetics in the sense that they contain a precisely defined helical arrangement of peptide groups that persists in aqueous media. In the crystallization medium these polymers form aggregates that specifically induce the nucleation of the {011} face of calcite, whereas the interaction of the polymer with the surface of the growing crystals results in the formation of crystals with a remarkably uniform size and shape.

The most advanced contribution with respect to the engineering of crystal morphologies was presented by J. Aizenberg (Bell Labs, Murray Hill, USA). Inspired by the sophisticated arrays of calcium carbonate microlenses found in brittlestars, in her lecture she presented a synthetic system that allows the predetermination of not only the shape but also the crystallographic orientation of inorganic crystals.[4] She used a carefully designed crystallization template consisting of patterned self-assembled monolayers. The remainder of each patterned monolayer was composed of a mixture of alkane thiols of different lengths and with different end groups, which inhibited the formation of calcite and induced the formation of amorphous calcium carbonate (ACC). After the formation of a patterned ACC film, a defined nanoregion also present induced the transformation into calcite. The crystallographic orientation of the resulting patterns can be directed by the

Meeting Reviews in *Angewandte Chemie* are meant to offer a view of the current state of a field rather than a comprehensive list of lectures. Authors are invited to describe what they feel were the most interesting contributions.

 © 2003 Wiley-VCH Verlag GmbH & Co. KGaA, Weinheim

composition of the nanoregion and the choice of the substrate.

One can easily envisage how a similar degree of design for the structure of molecular crystals would provide access to many new materials for a variety of applications.[5] The necessity to develop methods for the design of molecular crystals and the prediction of their structure and properties was recognized throughout the conference. Indeed, the theme of the next conference on Molecular Crystal Engineering will be "Evaluations and Predictions of Solid State Materials Properties" and will be organized in June 2005 in Helsinki by Kari Risanen.

[1] A. Jouatiti, M. W. Hosseini, N. Kyritsakas, *Chem. Commun.* **2002**, 1898.
[2] L. Addadi, M. Geva, *CrystEngComm* **2003**, *5*, 140.
[3] J. J. J. M. Donners, R. J. M. Nolte, N. A. J. M. Sommerdijk, *J. Am. Chem. Soc.* **2002**, *124*, 9700.
[4] J. Aizenberg, D. A. Muller, J. L. Grazul, D. R. Haman, *Science* **2003**, *299*, 1205.
[5] D. Braga, *Angew. Chem./Angew. Chem. Int. Ed.* **2003**, in press.

 © 2003 Wiley-VCH Verlag GmbH & Co. KGaA, Weinheim

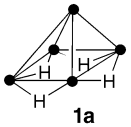
Five-Vertex Clusters

nido-Five-Vertex Clusters: In and Out of Boron Chemistry**

*Yves Canac and Guy Bertrand**

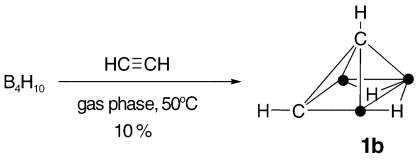
Keywords:
boron · carboranes · cations · phosphorus · valence isomerization

In the early days of borane chemistry the *nido*-pentaborane B_5H_9 (**1a**) was called the "stable pentaborane" whereas *arachno*-B_5H_{11} was called the "unstable pentaborane".[1,2] Since a BH vertex is isolobal with a CH unit as well as a naked P fragment, one could have expected that a variety of carba-, phospha-, phosphacarba-*nido*-pentaboranes or even all-carbon or all-phosphorus analogues would be readily obtained.[3]



1a

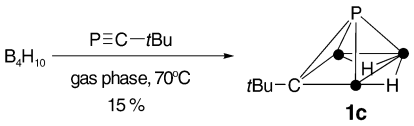
Indeed, the first carborane cage, the 1,2-$C_2B_3H_7$ (**1b**), isoelectronic and isostructural with B_5H_9 was discovered by Grimes and co-workers as early as 1970.[4] This compound was prepared in low yield (10%) from the reaction of B_4H_{10} with acetylene (Scheme 1). Compound **1b** was stable in the gas phase up to 50°C, but irreversibly polymerizes within minutes in the liquid phase at room temperature. The 1,2-dicarba-*nido*-pentaborane structure of **1b** was originally assigned from IR, ^{11}B and ^1H NMR spectroscopy, and mass spectrometry data. The results of a microwave study of **1b**, although announced as a private communication in 1972,[5] were finally published in 1988[6a] and in 1998 a combined analysis of gas-phase electron-diffraction data and rotation constants restrained by ab initio calculations was reported.[6b]



1b

Scheme 1. Synthesis of the first five-vertex *nido*-carborane in the gas phase. ● = BH.

It was only in 2002 that the second and only other known heteroborane with a *nido*-five-vertex geometry was reported, namely the phosphacarba-*nido*-pentaborane **1c** (Scheme 2).[7] Of note is that the synthesis of **1c**, in 15% yield, was by a route very similar to that which affords **1b** (Scheme 1). Instead of an alkyne, Greatrex et al. used a phosphaalkyne, and they also performed the reaction in the gas phase at 70°C. Like dicarbaborane **1b**, the phosphacarbaborane **1c** is only stable in the gas phase and decomposes in the liquid state at room temperature. The *nido*-structure has been assigned from multinuclear NMR spectroscopy and mass spectrometry. The optimized geometry has been calculated at the MP2/6-31G* level.

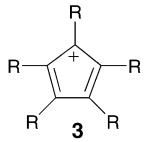


1c

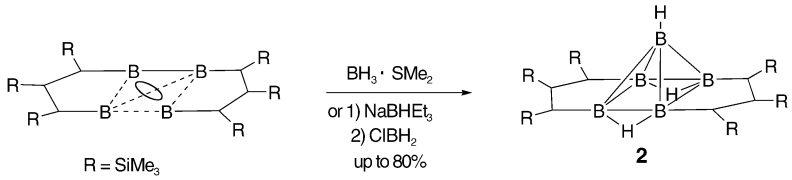
Scheme 2. Synthesis of the first five-vertex *nido*-heterocarborane in the gas phase. ● = BH.

Before leaving boron chemistry, it is worth mentioning that the first neutral *closo*-borane featuring a square-pyramidal structure, compound **2**, has recently been prepared by hydroboration of a distorted diamond-shaped tetraborane (Scheme 3).[8] This compound appears to be thermally quite stable (m.p. 113°C, decomposition) and has been fully characterized including a single-crystal X-ray diffraction study.

As mentioned above, there is, in principle, no reason to restrict the *nido*-five-vertex structure to boron-containing compounds. Indeed in 1972 Stohrer and Hoffmann[9] suggested that the antiaromatic $[C_5H_5]^+$ ion **3** (R = H) does not maintain the planar cyclopentadienyl structure, but rearranges to a square-pyramidal geometry as in **1d** (Scheme 4), which would be the unique stable structure. Although recent calculations have shown that this statement was not correct,[10] one should admit that to date, with the exception of derivatives with several strongly electron-donating substituents,[11] $[C_5R_5]^+$



3



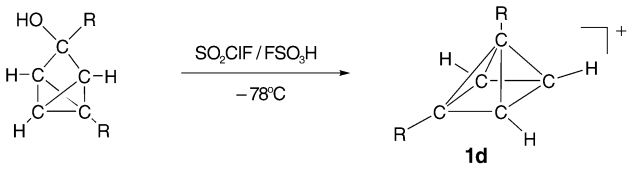
2

Scheme 3. Synthesis of the first neutral *closo*-borane with a square-pyramidal structure. ● = BH.

[*] Prof. G. Bertrand, Dr. Y. Canac
UCR-CNRS Joint Research Chemistry Laboratory, UMR 2282
Department of Chemistry
University of California, Riverside, CA 92521-0403 (USA)
Fax: (+1) 909-787-2725
E-mail: gbertran@mail.ucr.edu

[**] Financial support by the NSF (CHE0213510) and ACS PRF (38192-AC4) is gratefully acknowledged.

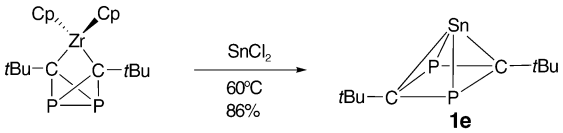
 © 2003 Wiley-VCH Verlag GmbH & Co. KGaA, Weinheim DOI: 10.1002/anie.200301648



Scheme 4. Formation of *nido*-cyclopentadienyl cations in superacid solutions.

cyclopentadienyl cations of structure **3**[12–14] have only been detected in matrices at −195 °C by ESR spectroscopy.[15] In contrast, *nido* structures of type **1d** have been reported to be stable for several hours at −73 °C even for simple $[C_5R_5]^+$ derivatives (R = Me; Scheme 4).[16] These cations have been prepared from 3-hydroxyhomotetrahedrane derivatives in superacid media. Note that species **1d** have also been postulated as intermediates to explain the carbon skeletal rearrangements and loss of alkyne in the gas-phase pyrolysis of substituted cyclopentadienyl cations **3**.[17]

As far as Group 14 elements are concerned, the recent synthesis of the first "non-transition-metal 1,3-diphosphacyclobutadienyl compound" **1e** is noteworthy (Scheme 5).[18] This fascinating species has been obtained in 86% yield from the reaction between $SnCl_2$ and a 1,3-diphosphabicyclo[1.1.0]butane zirconium complex. Compound **1e** is unusually stable, it melts without decomposition at 154–156 °C and, according to NMR spectroscopy, does not decompose in solution even when exposed to the air for 24 h.



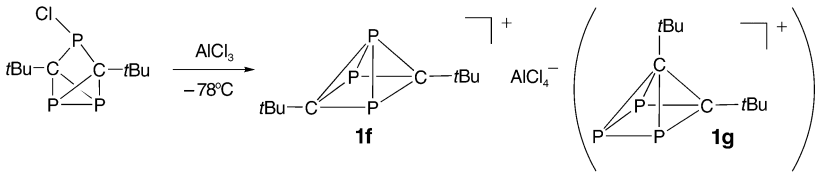
Scheme 5. A five-vertex *nido* complex with tin in the apical position.

The first example of a *nido*-five-vertex structure featuring phosphorus and carbon was recently reported.[19] The salt $[3,5\text{-}t\text{Bu}_2\text{-}1,2,4\text{-}C_2P_3]^+[AlCl_4]^-$ (**1f**) was prepared by abstraction of a chloride anion from the P–Cl bond of a tricyclic derivative (Scheme 6), a synthetic route reminiscent of that used for the all-carbon analogues **1d**. This compound seems to be stable in solution, at least up to 30 °C, and in the solid state, which allowed a single-crystal X-ray diffraction study to be carried out.

Interestingly, regardless of the elements constituting the backbone, all the compounds **1a–f** described here have in common a very distinctive spectroscopic property: in the NMR spectrum the resonance signal corresponding to the apical nucleus appears at extremely high field (**1a**: $\delta(^{11}B) = -52$ ppm; **1b**: $\delta(^{13}C) = -21$ ppm; **1c**: $\delta(^{31}P) = -501$ ppm; **1d**: $\delta(^{13}C) = -23$ ppm (R = Me); **1e**: $\delta(^{119}Sn) = -2129$ ppm; **1f**: $\delta(^{31}P) = -532$ ppm (calcd)). To emphasize this statement, white phosphorus (P_4) is usually taken to be the high-field limit in ^{31}P NMR spectroscopy, and has a resonance signal at only δ −488 ppm. In agreement with Masamune's explanation,[16a] these very unusual chemical shift values can be attributed to the especially constrained geometry of the apical position. Not surprisingly, for all of these compounds, the apical–basal bond lengths are substantially longer than the basal–basal bond lengths (**1d** (R = H): 156 and 146 ppm;[20] **1e**: 200 and 180 pm, respectively).

The characteristics of the *closo*-pentaborane **2** with the square-pyramidal structure[8] are very different from those of **1** and especially of *nido*-B_5H_9 (**1a**). The apical boron atom in **2** is strongly deshielded ($\delta = -13.6$ ppm) and the B_{apical}–B_{basal} bonds (169 pm) are even shorter than one of the B_{basal}–B_{basal} bond lengths (168 and 187 pm).

Despite their similarities, compounds **1a–f** behave very differently, especially **1f**. As demonstrated by labeling experiments, no exchange between the basal and apical carbon atoms was observed for dicarbaborane **1b** and the all-carbon analogues **1d**. In contrast, and in agreement with the prediction of Hoffmann[9] for the $[C_5H_5]^+$, an exchange is observed between the apical and basal phosphorus atoms of **1f**. This process, which is calculated to occur via a C_{2v} transition state is so fast that it prevents the observation of resonance signals in the ^{31}P NMR spectrum.

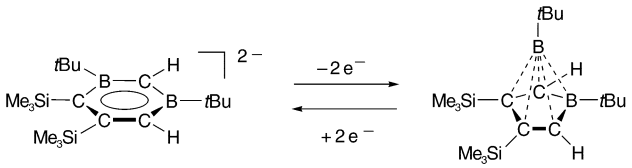


Scheme 6. Chloride abstraction with formation of the *nido* cation **1f**. The structure in parenthesis is the energetically less favored isomer **1g**.

Based on the results of calculations concerning the various isomers of **1f** (with H instead of *t*Bu), there is an interesting observation concerning the P/C diagonal relationship. In contrast to the thesis that "phosphorus is a carbon copy",[21] the authors demonstrate that replacement of three CR groups by three isolobal P atoms induces significant changes in the potential-energy surface. In marked contrast to the all-carbon analogues **1d**, the planar triphosphacyclopentadienyl, methylenecyclobutenyl, and even vinylcyclopropenyl isomers are at least 80 kJ mol^{-1} higher in energy than the square-pyramidal structure **1f**. This occurrence is readily explained by the inefficient π–π overlap in double bonds between atoms of the third period, but also to the aptitude of these elements to form small-ring structures. The latter point is nicely illustrated by the relative energies of **1f** and **1g** (Scheme 6), which has a carbon fragment in an apical position: **1f** is calculated to be more than 75 kJ mol^{-1} lower in energy than **1g**.[22,23]

These results open interesting perspectives and challenges. The aptitude of boron, phosphorus, but also carbon

 © 2003 Wiley-VCH Verlag GmbH & Co. KGaA, Weinheim



Scheme 7. An example for an induced, reversible rearrangement of a planar structure into a *nido* structure.

and tin to occupy the apical position of *nido*-five-vertex structures leads us to imagine that in the near future many other clusters of this type will be prepared. A fascinating target would be the pentaphosphorus cation *nido*-$[P_5]^+$.[24] On the other hand, to date, all of the compounds featuring a *nido*-five-vertex structure have been prepared by a route designed to directly access the three-dimensional structure. Thus, could it be possible to prepare heteroatomic analogues of planar cyclopendanienyl cations that rearrange into the *nido* structure or vice versa? An example of a related process is known (see Scheme 7).[25]

[1] A. Stock, *Hydrides of Boron and Silicon*, Cornell University Press, Ithaca, NY, **1933**.

[2] For a review on polyhedral boranes and related molecules:R. B. King, *Chem. Rev.* **2001**, *101*, 1119.

[3] From molecular orbital arguments Lipscomb predicted the existence of square-pyramidal carboranes isoelectronic with B_5H_9:W. N. Lipscomb, *Boron Hydrides*, W. A. Benjamin, New York, NY, **1963**.

[4] a) D. A. Franz, R. N. Grimes, *J. Am. Chem. Soc.* **1970**, *92*, 1438; b) D. A. Franz, V. R. Miller, R. N. Grimes, *J. Am. Chem. Soc.* **1972**, *94*, 412.

[5] In ref. [4b], it is mentioned that for **1b** a square-pyramidal structure analogous to B_5H_9 has been postulated from spectroscopic evidence and the preliminary results of a microwave study performed by R. A. Beaudet.

[6] a) R. A. Beaudet, *Advances in Boron and the Boranes* (Eds.: J. F. Liebman, A. Greenberg, R. E. Williams), VCH, New York, **1988**, Chap 20; b) M. A. Fox, R. Greatrex, A. Nikrahi, P. T. Brain, M. J. Picton, D. W. H. Rankin, H. E. Robertson, M. Buhl, L. Li, R. A. Beaudet, *Inorg. Chem.* **1998**, *37*, 2166.

[7] P. N. Condick, M. A. Fox, R. Greatrex, C. Jones, D. L. Ormsby, *Chem. Commun.* **2002**, 1448.

[8] C. Prasang, M. Hofmann, G. Geiseler, W. Massa, A. Berndt, *Angew. Chem.* **2003**, *115*, 1079; *Angew. Chem. Int. Ed.* **2003**, *42*, 1049.

[9] W. D. Stohrer, R. Hoffmann, *J. Am. Chem. Soc.* **1972**, *94*, 1661.

[10] For reviews on cyclopentadienyl cations: a) K. B. Wiberg, *Chem. Rev.* **2001**, *101*, 1317; b) A. D. Allen, T. T. Tidwell, *Chem. Rev.* **2001**, *101*, 1333.

[11] R. Gompper, H. Glockner, *Angew. Chem.* **1984**, *96*, 48; *Angew. Chem. Int. Ed. Engl.* **1984**, *23*, 53.

[12] The recently reported pentamethylcyclopentadienyl cation[13] was in fact a pentamethylcyclopentenyl cation.[14]

[13] a) J. B. Lambert, L. Lin, V. Rassolov, *Angew. Chem.* **2002**, *114*, 1487; *Angew. Chem. Int. Ed.* **2002**, *41*, 1429; b) J. B. Lambert, *Angew. Chem.* **2002**, *114*, 2383; *Angew. Chem. Int. Ed.* **2002**, *41*, 2278.

[14] a) M. Otto, D. Scheschkewitz, T. Kato, M. M. Midland, J. B. Lambert, G. Bertrand, *Angew. Chem.* **2002**, *114*, 2379; *Angew. Chem. Int. Ed.* **2002**, *41*, 2275; b) T. Müller, *Angew. Chem.* **2002**, *114*, 2380; *Angew. Chem. Int. Ed.* **2002**, *41*, 2276; c) J. N. Jones, A. H. Cowley, C. L. B. Macdonald, *Chem. Commun.* **2002**, 1520.

[15] M. Saunders, R. Berger, A. Jaffe, J. M. McBride, J. O'Neill, R. Breslow, J. M. Hoffmann, C. Perchonock, E. Wasserman, R. S. Hutton, V. J. Kuck, *J. Am. Chem. Soc.* **1973**, *95*, 3017.

[16] a) S. Masamune, M. Sakai, H. Ona *J. Am. Chem. Soc.* **1972**, *94*, 8956; b) G. Olah, G. K. S. Prakash, R. E. Williams, L. D. Field, K. Weid, *Hydrocarbon Chemistry*, Wiley, New York, **1987**.

[17] H. Schwarz, H. Thies, W. Franke, *Ionic Processes in the Gas Phase* (Ed.: M. A. A. Ferreira), Reidel Co., Dordrecht, The Netherlands, **1984**, pp. 267–286.

[18] M. D. Francis, P. B. Hitchcock, *Chem. Commun.* **2002**, 86.

[19] J. M. Lynam, M. C. Copsey, M. Green, J. C. Jeffery, J. E. McGrady, C. A. Russell, J. M. Slattery, A. C. Swain, *Angew. Chem.* **2003**, *115*, 2884; *Angew. Chem. Int. Ed.* **2003**, *42*, 2778.

[20] For calculations of the geometrical parameters and ^{13}C NMR spectroscopic chemical shifts of the parent *nido*-$[C_5H_5]^+$ ion see:G. K. S. Prakash, G. Rasul, G. A. Olah, *J. Phys. Chem. A* **1998**, *102*, 2579.

[21] K. B. Dillon, F. Mathey, J. F. Nixon, *Phosphorus, The Carbon Copy*, Wiley, Chichester, **1998**.

[22] In view of these results, it is rather surprising that the alternative isomer of **1c** (not shown), with the carbon fragment in the apical position, has been computed to be only approximately 9.6 kJ mol^{-1} higher in energy.

[23] Another illustration is the relative energy of benzene which is calculated to be 608 kJ mol^{-1} for favorable than its still unknown valence isomer *anti*-tricyclohexylene, whereas the unknown tetraphosphabenzene is calculated to be only 33 kJ mol^{-1} more stable than its tricyclic isomer, of which one derivative has been isolated. Y. Canac, D. Bourissou, A. Baceiredo, H. Gornitzka, W. W. Schoeller, G. Bertrand, *Science* **1998**, *279*, 2080.

[24] a) M. Gonsior, I. Krossing, L. Müller, I. Raabe, M. Jansen, L. van Wullen, *Chem. Eur. J.* **2002**, *8*, 4475; b) I. Krossing, *J. Chem. Soc. Dalton Trans.* **2002**, 500.

[25] C. Balzereit, H.-J. Winkler, W. Massa, A. Berndt, *Angew. Chem.* **1994**, *106*, 2394; *Angew. Chem. Int. Ed. Engl.* **1994**, *33*, 2306.

 © 2003 Wiley-VCH Verlag GmbH & Co. KGaA, Weinheim

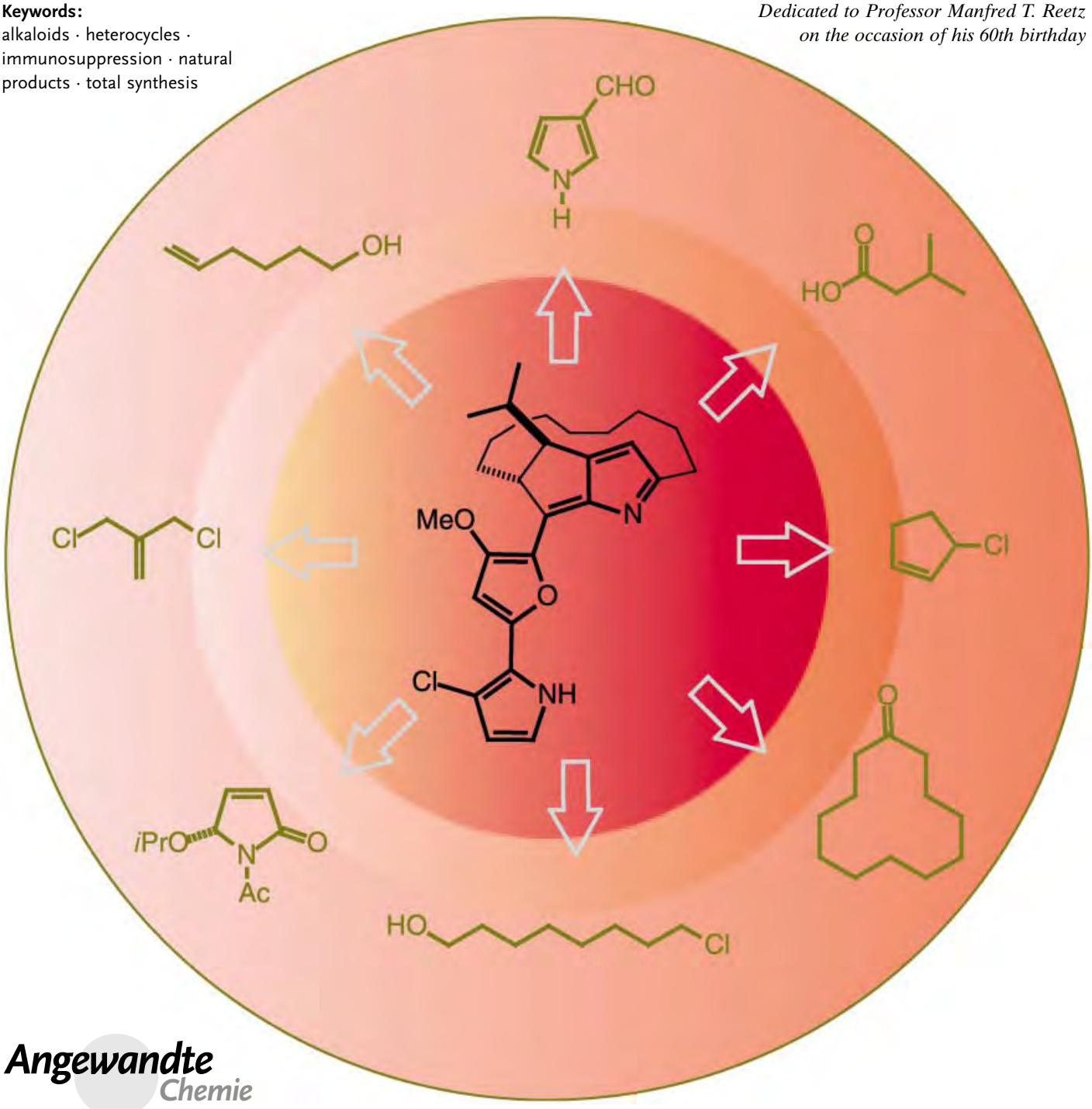
Total Synthesis of the Prodigiosins

Chemistry and Biology of Roseophilin and the Prodigiosin Alkaloids: A Survey of the Last 2500 Years

*Alois Fürstner**

Keywords:
alkaloids · heterocycles · immunosuppression · natural products · total synthesis

Dedicated to Professor Manfred T. Reetz on the occasion of his 60th birthday



 © 2003 Wiley-VCH Verlag GmbH & Co. KGaA, Weinheim DOI: 10.1002/anie.200300582

The pyrrole alkaloids of the prodigiosin family make up an unusual chapter in the chemistry of natural products. Owing to the characteristic red color of these secondary metabolites, colonies of the Gram-negative-producing bacteria may strikingly resemble droplets of blood. This phenomenon caused considerable confusion in the past and was likely responsible for many seemingly miraculous (prodigious) events. After the eventual transition from superstition to science, the prodigiosins started to attract considerable attention because of their promising physiological properties. Most interesting are the immunosuppressive activities at doses that are not cytotoxic, in particular since in vivo studies suggest that the prodigiosins act synergistically with cyclosporine A or FK506, which are presently the dominant drugs in clinical immunosuppressive regimens. Furthermore, the chemistry of the closely related and structurally rather unique alkaloid roseophilin is summarized, a cytotoxic agent that recently became the focal point of many innovative total syntheses.

From the Contents

1. A Brief Historical Excursion	3583
2. Structure and Biological Activity of the Prodigiosins	3584
3. Biosynthesis of the Prodigiosins	3587
4. Selected Total Syntheses of Prodigiosin Derivatives	3588
5. Roseophilin	3593
6. Conclusions and Outlook	3600

1. A Brief Historical Excursion

The use and abuse of alkaloids accompanies the history of mankind from the very beginning.[1] Despite this fact, it is rare that individual natural products can be linked to distinct historical events with any degree of certainty. It seems, however, that the story of the red pigments produced by a restricted group of eubacteria and actinomycetes of the *Serratia* and *Streptomyces* genera constitutes an interesting exception to this rule. Such microorganisms are fairly ubiquitous and grow on many starch-rich culture media to form distinctive red colonies. Upon reaching maturity, these colonies may eventually become fluid and suspiciously resemble droplets of blood in their color, consistency, and shape. The historical literature is full of reports of the "bleeding" of bread and other foods.[2,3] One of the oldest examples dates back to Alexander the Great's siege of Tyre in 322 B.C., when Macedonian soldiers noticed the appearance of blood inside a piece of bread. This was interpreted by the royal seers as a good omen that blood would be spilt throughout the besieged town, and was used to justify the horrible, but this time real, bloodshed that Alexander's troops subsequently inflicted on the inhabitants.[4]

Numerous reports of bloodlike coloration in food in general and of "bleeding" communion wafers in particular were documented during the European Middle Ages. It may not come as a surprise that even the intellectual authorities at that time could not help but see miracles in such incidents,[5] which seemed to provide physical evidence for the central dogma of transubstantiation occurring during the Eucharistic liturgy. The most famous case, referred to as the Miracle of Bolsena, occurred in 1263 in the Church of Saint Christina near Bolsena, a small Italian town north of Rome. A priest, fighting against his loss of faith, was celebrating mass during a pilgrimage to Rome when he noticed blood dripping from the host. Pope Urban IV rapidly approved this miracle and declared that it should be commemorated as the festival of Corpus Christi, which is now an integral part of the Christian calendar and still a public holiday in many Western European countries. Although it is difficult for us, having grown up during a scientific era, to ignore our knowledge of microbiology and chemistry, a naïve cursory look at Figure 1—assuming that its background were a communion wafer rather than an agar plate—may make us more reluctant in sentencing our predecessors. Anyway, this event in Bolsena led to the construction of the marvelous cathedral in close-by Orvieto in the then emerging Italian gothic style, where the relics of this miracle are kept as venerable religious treasures. Moreover, in 1508 Raphael chose this story as the subject of his famous fresco, the "Mass of Bolsena" decorating the papal apartments of Julius II in

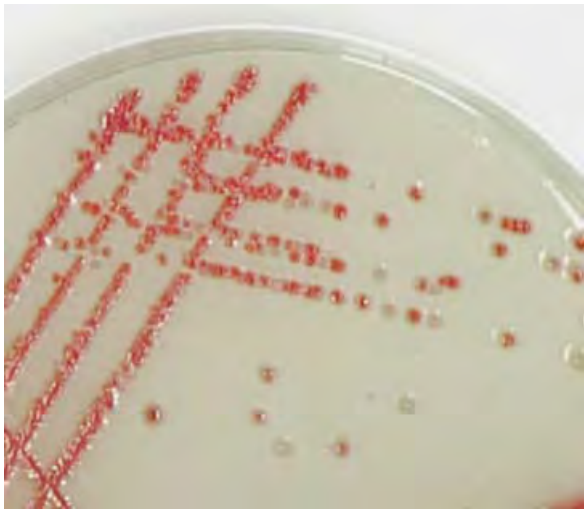


Figure 1. Agar plate with red colonies of *Serratia marcescens*.

[*] Prof. Dr. A. Fürstner
Max-Planck-Institut für Kohlenforschung
Kaiser-Wilhelm-Platz 1, 45470 Mülheim/Ruhr (Germany)
Fax: (+49) 208-306-2994
E-mail: fuerstner@mpi-muelheim.mpg.de

 DOI: 10.1002/anie.200300582 © 2003 Wiley-VCH Verlag GmbH & Co. KGaA, Weinheim



Figure 2. Raphael's "Mass of Bolsena" fresco in the Vatican.

the Vatican. Figure 2 depicts the central section of this painting, which in terms of composition and complexion, undoubtedly represents a climax in this artist's incredibly rich and fascinating career.

Many similar cases of "bleeding hosts" occurred throughout ancient Europe. Although this introduction cannot provide full historical coverage,[2] it must be mentioned that the appearance of blood on hosts did not only have religious ramifications, but was also taken as a pretext for bloodthirsty persecutions. Numerous cases are documented in which Jews were accused of having stabbed consecrated wafers, resulting in the appearance of blood. For centuries, such stories served to hide the true motives behind the bloody pogroms committed by fanatical mobs.[2]



Alois Fürstner, born 1962 in Austria, studied chemistry at the Technical University of Graz where he received his PhD in 1987 (Prof. H. Weidmann). After postdoctoral studies with Prof. Oppolzer in Geneva, he completed his Habilitation in Graz (1992) before joining the Max-Planck-Institut für Kohlenforschung, Mülheim (Germany) in 1993 as a group leader. Since 1998, he is a Director at the Institute and is also affiliated with the University of Dortmund. He has received several awards, including the prestigious Leibniz award of the Deutschen Forschungsgemeinschaft (1999), the Thieme-IUPAC prize (2000), and the Arthur C. Cope Scholar Award of the ACS (2002).

Although one must concede that no rigorous proof can be made in retrospect that all of these historical events were caused by *Serratia marcescens* and its relatives, no other microorganism seems to produce colonies that more closely resemble drops of fresh blood.[6] A series of well-documented cases in more recent times (well into the 20th century!) lend additional credence to this notion. Among them, a case that occurred in northern Italy in 1819 is particularly noteworthy for various reasons, not least because it ultimately led to a great leap forward in microbiology in general. The repeated appearance of "bleeding" food in a village near Padova was labeled as witchcraft and led to a public frenzy. Three scientists independently and almost simultaneously helped to dispel the mist of superstition: The botanist Pietro Melo, the pharmacist Bartolomeo Bizio, and the physician Vincenzo Sette all recognized that fermentation was responsible for this event (although they argued with each other for the scientific priority).[2] Although the causative germ was erroneously thought to be a fungus rather than a bacterium, these studies represent early examples of systematic microbiological investigations in the pre-Pasteur era. The investigators were able to show the transmission of the red color from one medium to another, they investigated the organism under the microscope, they demonstrated the role of humidity and temperature on its growth, and even performed some exploratory studies on the effect of certain chemicals (camphor, sulfur, tobacco smoke, etc.) on the growth of "*Serratia marcescens*". Although this name chosen by Bizio is now commonly used, many others were proposed in the following decades, some of which reflect the undisputable association of this microorganism with the historical and "prodigious" events referred to above ("*Micrococcus prodigiosus*").

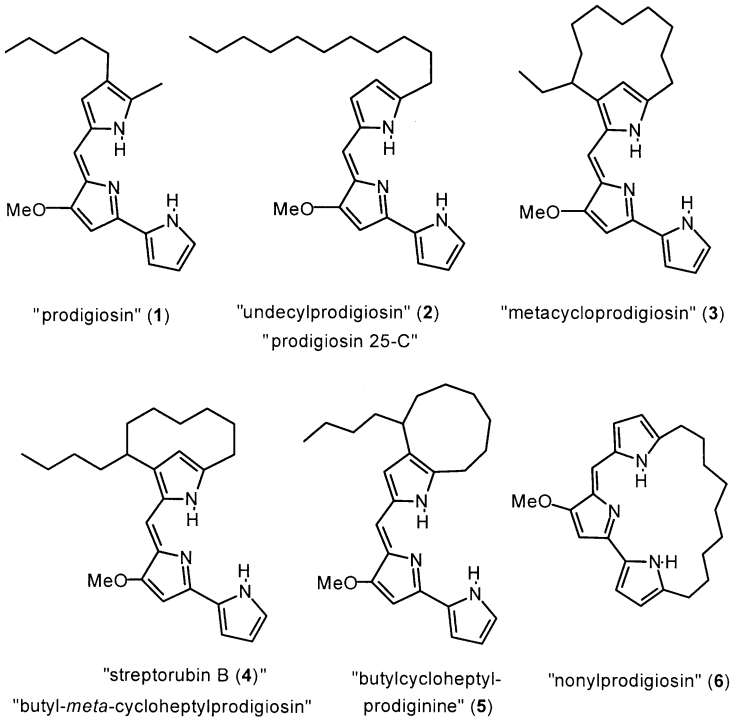
Whereas the work of Bizio and Sette later fell into oblivion, *S. marcescens* became the subject of many microbiological studies and even gained some popularity as a seemingly harmless object of classroom demonstrations. It was only in the last decades that *Serratia* strains have been recognized as potentially hazardous pathogens, which can be implicated in ailments such as meningitis, osteomyelitis, pneumonia, sinusitis, wound infection, and urinary tract infections[7] Patients with chronic debilitating disorders or in postoperative status are especially susceptible to infections by this opportunistic bacterium. The marked resistance of *Serratia* strains towards approved drugs undermines conventional therapy with standard antibiotics.[2b,7]

2. Structure and Biological Activity of the Prodigiosins

Attempts to isolate the deep red pigment produced by *Serratia* strains were already made by Bizio and Sette, who tried to use it as a dye for commercial purposes. In pure form, however, it turned out to be too sensitive to light to be of practical use.[2] It was not until the 1960s, however, that the correct chemical constitution of "prodigiosin" as the major secondary metabolite of *S. marcescens* could be established

 © 2003 Wiley-VCH Verlag GmbH & Co. KGaA, Weinheim

beyond doubt, even then only by total synthesis (see below).[8] Owing to the rapid advances in separation science and spectroscopy in the subsequent years, it became clear that "prodigiosin" (**1**) has a series of close relatives bearing the same pyrrolylpyrromethene ("prodiginine") core with different alkyl substituents.[9] These substituents are often tied back to form medium-sized rings or macrocycles, as shown in the examples in Scheme 1. The traditional nomenclature is highly inconsistent; therefore it is strongly recommended to use the expression "prodigiosin" only in a generic sense.



Scheme 1. Representative members of the prodigiosin family.

Pyrrole alkaloids of this type exhibit a broad range of activity against bacteria, protozoa, and pathogenic fungi. Despite some attempts to optimize their application profile by systematic studies of the structure–activity relationships (SAR), it appears that the therapeutic window is too narrow for clinical development as antibiotics owing to nonnegligible systemic toxicity at effective doses.[10,15] More promising is their pronounced effect on the human malaria parasite *Plasmodium falciparum* at dosages below the acute cytotoxicity threshold (IC_{50} of **3**: 5×10^{-3} μg mL^{-1}).[11,12]

The prodigiosins are able to induce apoptosis in many different human cancer cell lines with little effect on nonmalignant cells.[13,14] They show significant cytotoxicity in vitro against P388 mouse leukemia cells (IC_{50} 3.7×10^{-4} μg mL^{-1})[15] as well as against human melanoma and liver cancer cell lines.[16] A recent in vivo study on a nude mouse model concluded that the prodigiosins bear considerable promise for the treatment of hepatocellular carcinoma, for which there is no effective medication.[13] It is not entirely clear, however, to what extent their cytotoxicity derives from the potent DNA-damaging properties under oxidative conditions (see below), their bias to intercalate into DNA,[17] the ability to interfere with protein kinase C isozymes,[18] and/or their capacity to modify the pH of cell organelles through H^+/Cl^- symport.[19–21] The perturbation of vacuolar acidification caused by such pyrrole alkaloids is evident from Figure 3, in which untreated baby hamster kidney (BHK) cells (Figure 3A) stained with acridine orange are compared with BHK cells that were preexposed to prodigiosin (**1**) (Figure 3B). As can be seen, compound **1** induces neutralization of the acidic compartments of the cells, which ultimately leads to arrest of the cell cycle and eventually to apoptosis. Mechanistically speaking, this H^+/Cl^- symport capacity stems from the fact that the ion pair formed on protonation of the basic azafulvene site of the prodigiosins is sufficiently tight and lipophilic to allow proton-coupled transmembrane transport of the counteranion (in this case, chloride). However, a direct correlation could not be established between the pK_a value of the pyrrolylpyrromethene entity of different prodigiosin derivatives and their cytotoxicity against HL-60 leukaemia cells.[21]

In contrast, considerable evidence has accumulated for a possible relationship between the cytotoxicity of the prodigiosins and their DNA-damaging capacity. In the presence of metal cations, preferably Cu^{II}, these pyrrole alkaloids lead to efficient single- and even double-strand cleavage (Figure 4).[22,23] This oxidative stress is thought to derive from a cascade triggered by the formation of the π-radical cation of the electron-rich pyrrolylpyrromethene chromophore through interaction with the metal, which engenders metal-assisted activation of oxygen and results in the formation of H_2O_2 as the actual DNA-damaging agent.[23,24] SAR studies and electrochemical investigations show that any structural modification that either interferes with the cation-binding ability of these compounds and/or renders their oxidation more difficult will diminish the DNA-damaging capacity as well as the in vitro cytotoxicity of these compounds.[23,25,26] Specifically, the cytotoxicity is largely decreased upon removal of the peripheral methoxy group at C6;[15] likewise, replacement of the individual pyrrole rings by other (hetero)arenes results in

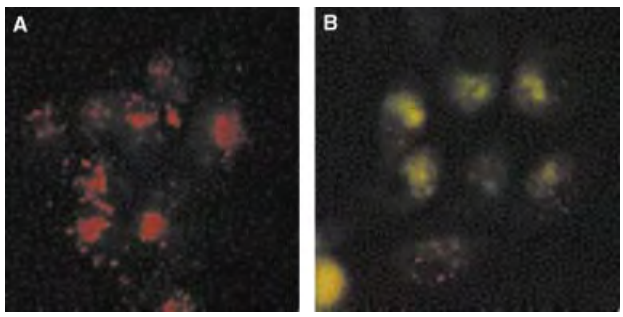


Figure 3. Fluorescence microscopy image of BHK cells stained with acridine orange: A) no pretreatment; B) cells pretreated with **1** (10 μM) for 30 min.[39]

 © 2003 Wiley-VCH Verlag GmbH & Co. KGaA, Weinheim

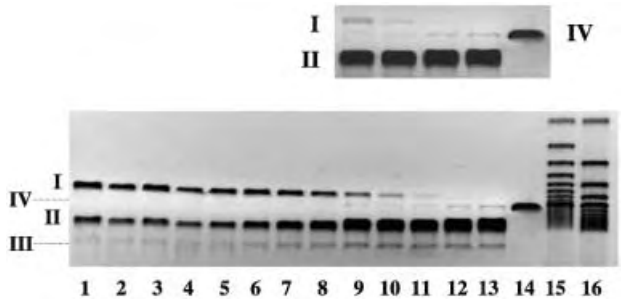
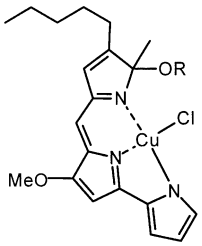


Figure 4. Agarose gel electrophoresis experiment showing the extent of DNA cleavage produced by nonylprodigiosin (**6**) in the presence of $Cu(OAc)_2$ with increasing incubation time at 37 °C. Lane 1: DNA without pretreatment; lane 2: DNA + Cu^{II} (control); lane 3: DNA + **6** (control); lanes 4–13: DNA + **6** + Cu^{II} after the following incubation times [min]: 0 (lane 4), 5 (5), 10 (6), 15 (7), 20 (8), 30 (9), 45 (10), 60 (11), 90 (12), 120 (13); lane 14: linear DNA formed from scDNA by using the restriction endonuclease Xho I; lane 15: DNA marker (500 base pairs); lane 16: DNA marker (1000 base pairs). The insert shows the relevant detail of lanes 10–14 at higher magnification.[23]

complete loss of the "copper nuclease like" activity and in a large decrease in cytotoxicity as well.[19,23]

A recent crystallographic study confirmed this scenario. Specifically, Manderville and co-workers succeeded in obtaining crystals from a 1:1 mixture of prodigiosin (**1**) and Cu^{II}, which show several remarkable features.[27] As expected, all three nitrogen atoms of the ligand in complex **7** are

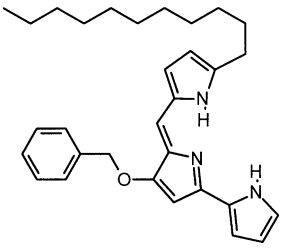


7 (R = H, Me)

coordinated to the metal cation in a distorted square-planar arrangement; remarkably, however, the pyrrole ring C has been oxidized and attacked by an external nucleophile (water or MeOH from the medium). The analogous Zn^{II} complex, in contrast, contains two molecules of **1** in the ligand sphere of the metal. Neither of the ligands has been oxidized and only two nitrogen atoms of each ligand are bound to the metal. These results shed light on the specific action of copper and corroborate the previous assumptions as to the elementary steps responsible for the nucleaselike activity of certain metal–prodigiosin combinations in the oxidative degradation of DNA.

By far the most attractive biological response of mammals to pyrrole alkaloids of this type, however, lies in their immunosuppressive activity at doses that are not cytotoxic. Their efficacy in vivo has been demonstrated by several independent studies on animal models.[28,29] Although a recent investigation indicates a rather steep dose-response curve of **1** on lymphocytes, inhibition of proliferation for such cells is reached at nanomolar concentrations (IC_{50} 3–8 ng mL^{-1}). In mice, the ED_{50} of **1** was reported to be 1.5 mg kg^{-1} for 6 days, whereas acute systemic toxicity is observed at doses $\geq$ 4 mg kg^{-1}.[30] Although this therapeutic window may be too narrow for direct clinical applications, these alkaloids constitute new leads in the search for supplementary immunosuppressive drugs.[31] Most encouraging is the fact that the mechanism of action of **1** and its congeners is distinctly different from that of the clinically used cyclosporin or FK 506, which act as calcineurine inhibitors and block the proliferation of T cells in the early G_1 stages of the cell cycle. As a consequence, a synergistic effect on the immune system is observed if, for example, **1** is administered simultaneously with either cyclosporin or FK 506,[29,32] which presently dominate clinical immunosuppressive regimens for the treatment of patients after organ transplantation.[33,34]

The immunosuppressive properties of the prodigiosins derive from their ability to inhibit the blastogenesis of T cells and to suppress the T cell-dependent antibody response in vivo without damaging the lymphoid organs.[35–37] The selectivity of action has been confirmed by many independent studies under different experimental conditions, which demonstrate that the prodigiosins interfere with concanavalin-induced T cell proliferation to a much higher degree than they do with B cell proliferation stimulated by lipopolysaccharides.[38,39] Although there is some controversy as to the origins of this selectivity, recent studies suggest that it is probably mediated through defined cellular targets. Thus, the ability of the prodigiosins to interfere with interleukin (IL-2) signal transduction by selectively inhibiting phosphorylation and hence activation of the cytoplasmic Janus tyrosine kinase JAK-3 might be the decisive trigger at the molecular level,[35,40] as this enzyme seems to be intimately coupled to the immune response in mammals. A detailed medicinal chemistry program aimed at the optimization of this effect has already led to the development of the simple prodigiosin derivative PNU-156804 (**8**) with a therapeutic index almost



8 (PNU-156804)

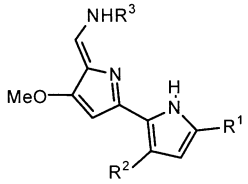
threefold that of the natural undecylprodigiosin (**2**).[31,32,36] In vivo studies have demonstrated that oral administration of PNU-156804 suppresses heart allograft rejection in rats in a dose-dependent fashion. Thereby, a promising synergistic effect was noticed when PNU-156804 was administered together with cyclosporin A. The mean survival time of heart-transplanted rats was increased to 85 $\pm$ 27.4 days upon

 © 2003 Wiley-VCH Verlag GmbH & Co. KGaA, Weinheim

treatment (oral administration) with a combination of 40 mg kg^{-1} PNU-156804 and 5 mg kg^{-1} of cyclosporin A, compared with 6.3 ± 0.5 days without treatment, 10.3 ± 1.5 days with 40 mg kg^{-1} PNU-156804 alone, or 46.6 ± 30.2 days with 5 mg kg^{-1} cyclosporin A alone.[29]

Although many aspects referred to above require further in-depth studies, the available data suggest that the immunosuppressive activities and the cytotoxic properties of the prodigiosins derive from different mechanisms of action. This, in turn, suggests that it should be possible to uncouple these physiological effects to an even larger extent in the search for clinically relevant drug candidates.

The closest relatives of the prodigiosins known to date are the tambjamines **9** (Scheme 2, Table 1), which have an enamine motif in place of one of the pyrrole rings. Whereas



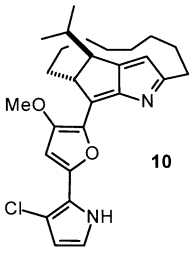
tambjamine (**9**)

Scheme 2. General structure of the tambjamines (see Table 1).

Table 1: Some representative members of the tambjamine family.

Tambjamine	R^1	R^2	R^3
A	H	H	H
B	Br	H	H
C	H	H	$CH_2CH(CH_3)_2$
D	H	Br	$CH_2CH(CH_3)_2$
E	H	H	CH_2CH_3
J	Br	H	$CH_2CH(CH_3)CH_2CH_3$

the prodigiosins are mainly derived from terrestrial microorganisms,[41] most tambjamines have been isolated from marine sources such as nudibranches, bryozoans, and ascidians,[42] although one example of a *Streptomyces* sp. is also known to produce such compounds.[43] They are thought to be involved in the defense mechanism of these marine organisms against their predators. Although they are somewhat less potent than their tripyrrole congeners, the tambjamines exhibit similar nuclease activity against DNA in the presence of Cu^{II}, they intercalate into double-stranded DNA,[17] exhibit appreciable cytotoxicity,[16,17,19] and were shown to inhibit the growth of Ehrlich ascites tumor in vivo.[43]

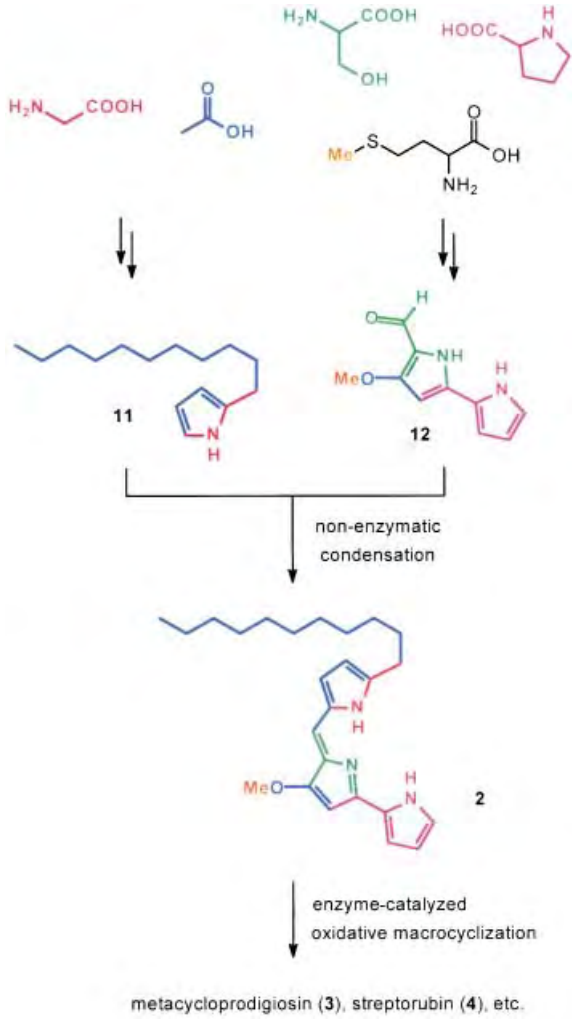


10

Another relative of the prodigiosins is the structurally rather unique alkaloid roseophilin (**10**), which was isolated from a culture broth of *Streptomyces griseoviridis*.[44] It combines a strained macrocyclic motif with an extended heterocyclic perimeter that is responsible for the deep red color of this compound. In contrast to **1**–**9**, however, roseophilin incorporates a methoxyfuran rather than a methoxypyrrole ring in its backbone, while sharing an azafulvene substructure with the prodigiosin antibiotics. Roseophilin exhibits cytotoxicity against K562 human erythroid leukemia and KB human epidermoid carcinoma cell lines in the sub-micromolar range.[16] Unlike the prodigiosins, however, roseophilin does not damage DNA under oxidative conditions.[23] Its cytotoxicity must therefore derive from a different, still-unknown mechanism of action. The interesting activity profile together with the challenging topology of its backbone has rendered this compound a rewarding target for total synthesis (see Section 5).

3. Biosynthesis of the Prodigiosins

Feeding studies showed that undecylprodigiosin (**2**) and its congeners are derived from proline, glycine, serine, and several acetate units. Methionine is the source of the methyl group of the ether substituent at C6 (Scheme 3). The biosynthetic pathway is convergent and involves a late-stage



Scheme 3. Biosynthesis of undecylprodigiosin and its macrocyclic derivatives.

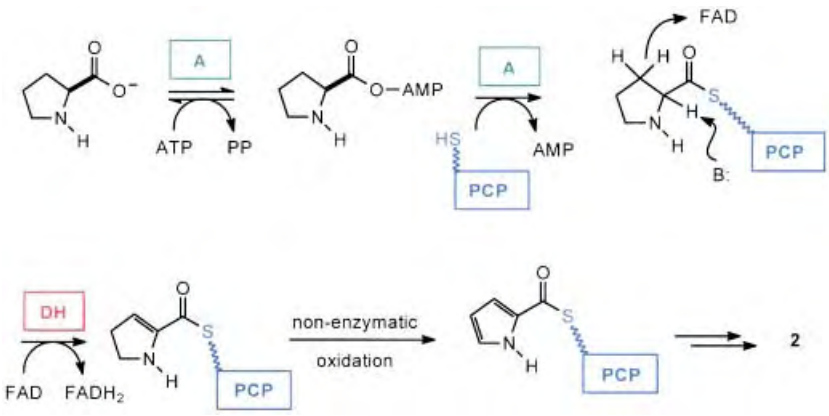
© 2003 Wiley-VCH Verlag GmbH & Co. KGaA, Weinheim

condensation of 2-undecylpyrrole (**11**) with 4-methoxy-2,2′-bipyrrole-5-carbaldehyde (**12**). Oxidative cyclization of **2** (or its homologues) then leads to the formation of the macrocyclic congeners.[45] These results suggested that the biosynthesis of the prodigiosins is totally unrelated to that of the tetrapyrrolic natural products of the porphyrin and corrin series, which derive from δ-aminolevulinate. Rather, a previously unknown mechanism for pyrrole biosynthesis based on the oxidation of proline seems to be operative.

Recent investigations have corroborated this proposition. Thus, considerable efforts led to the cloning of the entire prodigiosine biosynthesis gene cluster and its expression in a heterologous host.[46,47] These studies also provided valuable insight into the regulation of the prodigiosin production in *Streptomyces* strains, which had been known for a long time to be growth-phase dependent.[48] Recently, it was possible to sequence the entire *red* cluster, which consists of 23 genes organized into four transcription units.[49,50] The function of the individual genes could be assigned for all but five, and the complete pathway for the biosynthesis of these secondary metabolites has been deduced.[51,52]

As detailed accounts have recently been published,[50–52] it should suffice to address a few particularly interesting facets only. First, the mechanism of the assumed oxidation of the pyrrolidine ring of proline to a pyrrole unit has been elucidated in detail (Scheme 4).[52] It starts with an enzymatic activation of proline as L-prolyl-AMP followed by prolyl transfer to a thiol function of a peptidyl-carrier protein (PCP). The resulting peptidic thioester is enzymatically oxidized by a flavoprotein to the Δ^2-dehydroprolyl thioester as the primary product, which undergoes a rapid but non-enzymatic oxidation to give the aromatic heterocycle. This cascade does, in fact, present a previously unknown mechanism for the biosynthesis of pyrrole derivatives, which seems to be operative in several structurally unrelated natural products as well.[52]

As mentioned above, the last step of the bifurcated biosynthesis of the prodigiosins is the condensation of 2-undecylpyrrole (**11**) with aldehyde **12** to form the red azafulvene chromophore of the natural product (see Scheme 3). It is likely that this reaction does not require a pathway-specific enzyme in vivo but is caused by general acid catalysis.[51,53] In contrast, it was possible to identify the enzyme "RedG" encoded by one of the genes of the cluster as a non-heme iron-dependent dioxygenase capable of binding and activating molecular oxygen. This enzyme is thought to effect the formal two-electron oxidative macrocyclization that converts undecylprodigiosin (**2**) into pyrrolophane **4** by site-selective activation of the alkyl group.[51,54] The other macrocyclic prodigiosins such as **3** produced by different actinomycetes are thought to arise by the action of homologues of RedG with different regiospecificities in the oxidation step. Therefore, enzymes of this type show potential for the selective functionalization of hydrocarbons.



Scheme 4. Biosynthesis pathway for the formation of ring A of the prodigiosins from L-proline; A = L-prolyl-AMP ligase; PCP = peptidyl-carrier protein; DH = acetyl-CoA dehydrogenase homologue.

4. Selected Total Syntheses of Prodigiosin Derivatives

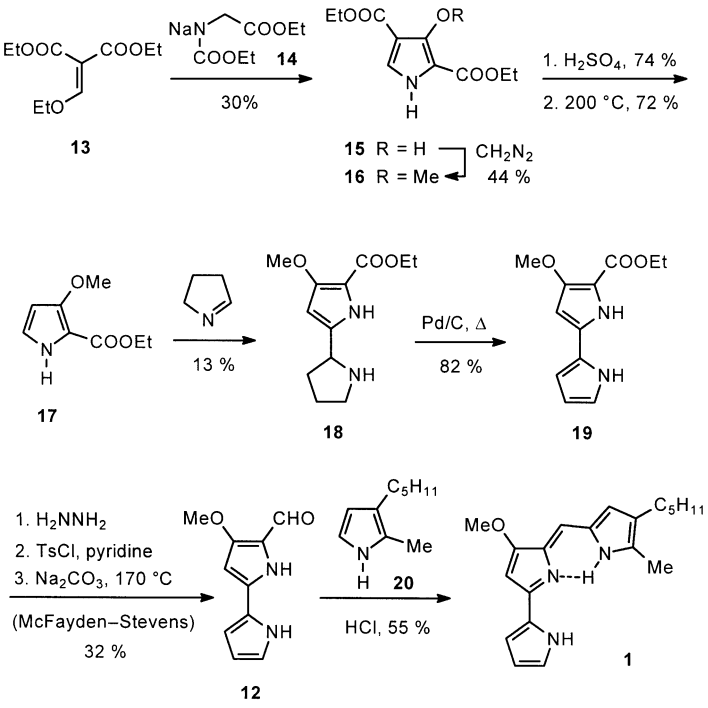
Although cloning of the gene cluster and decoding of the biosynthesis pathway might provide a framework for a rational bioengineering of novel prodigiosin derivatives with improved immunosuppressive or antitumor activities in the future, our present knowledge of the SAR of such alkaloids is solely derived from chemical synthesis. These studies illustrate the methodological advances in heterocyclic chemistry and macrocyclization reactions achieved over the last decades as evident from the selected approaches summarized below.

4.1. Syntheses with Biomimetic Condensation Steps

The first total synthesis of "prodigiosin" (**1**) was reported by Rapoport and Holden in the early 1960s.[8] It was based on the formation of the azafulvene motif by an acid-catalyzed condensation of 2-methyl-3-pentylpyrrole (**20**) with aldehyde **12**, thus mimicking the final stages of the proposed biosynthesis (Scheme 5).

The synthesis commenced with the condensation of the sodium salt of diethyl *N*-ethoxycarbonyl glycinate (**14**) with diethyl ethoxymethylenemalonate (**13**) to afford diethyl 3-hydroxypyrrole-2,4-dicarboxylate (**15**). *O*-Alkylation with diazomethane followed by selective hydrolysis of the more reactive ester group at C4 in **16** and decarboxylation of the resulting acid afforded compound **17**, which was condensed with Δ^1-pyrroline to give product **18**, albeit in very low yield. Dehydrogenation of the pyrrolidine ring in **18** was effected with Pd on charcoal, and the resulting compound **19** was converted into the corresponding aldehyde **12** by successive treatment with hydrazine, tosyl chloride in pyridine, and Na_2CO_3 at elevated temperature ("McFayden–Stevens reduction"). Finally, aldehyde **12** was subjected to an acid-catalyzed condensation with pyrrole **20** to give rise to intact prodigiosin **1**. Although in the original publication of Rapoport and Holden ring C of this compound was supposed to be the azafulvene residue,[8] recent X-ray crystallographic investigations of several prodigiosin derivatives have shown

 © 2003 Wiley-VCH Verlag GmbH & Co. KGaA, Weinheim

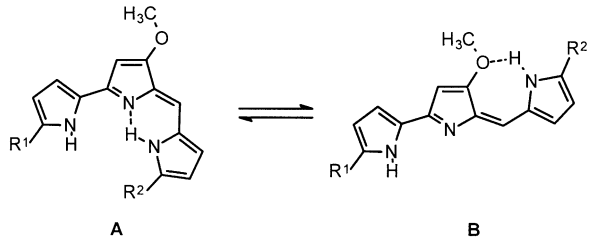


Scheme 5. The total synthesis of prodigiosin (**1**) by Rapoport and Holden.[8] Ts = *para*-toluenesulfonyl.

that the structure of these alkaloids is best described by the tautomer in which the central B-ring incorporates the basic site.[39,55,56] However, it must be kept in mind that all prodigiosins can exist in two stable isomeric forms **A** and **B** in solution, with the equilibrium distribution being determined by the pH value of the medium, that is, by the degree of protonation of the basic nitrogen atom (Scheme 6). An *E*/*Z* isomerization of the exocyclic double bond of the azafulvene is responsible for this process.

Despite the evident shortcomings of the approach of Rapoport and Holden, it constituted not only the first total synthesis of a compound of this series but also the ultimate proof of the structure of prodigiosin. Many subsequent studies relied and elaborated on this lead, especially with respect to the biomimetic condensation for the construction of the central azafulvene motif. The gradually improved access to the required components nicely highlights the progress in heterocyclic chemistry.

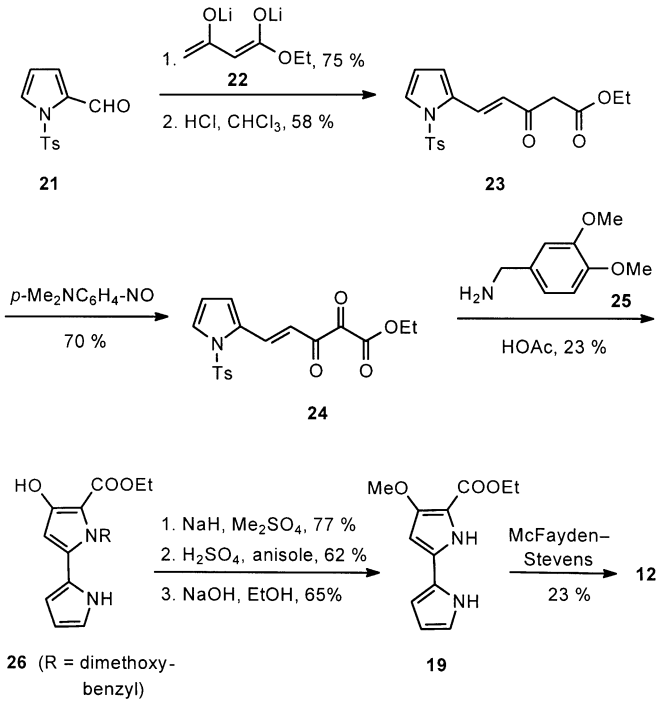
Specifically, Wasserman and co-workers developed two different approaches to the bipyrrole aldehyde **12**, one of



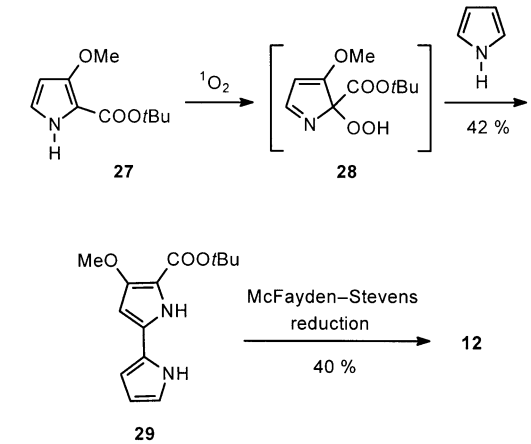
Scheme 6. Protonation-dependent equilibrium in the prodigiosin series.

which is based on the cyclization of the vicinal tricarbonyl intermediate **24** (Scheme 7),[57] while the other involves the oxidation of pyrrolecarboxylic acid ester **27** with singlet oxygen (Scheme 8).[58] The overall yield of both routes, however, remained poor, not least because of the inefficiency of the final McFayden–Stevens reduction protocol. Despite this drawback, Wasserman and co-workers successfully condensed this key building block with several differently substituted pyrroles and were thus able to complete the synthesis of prodigiosin (**1**), undecylprodigiosin (**2**), metacycloprodigiosin (**3**), and several non-natural analogues.[58–61]

An alternative route to bipyrrole aldehyde **12** was devised by Boger and Patel as part of their SAR studies



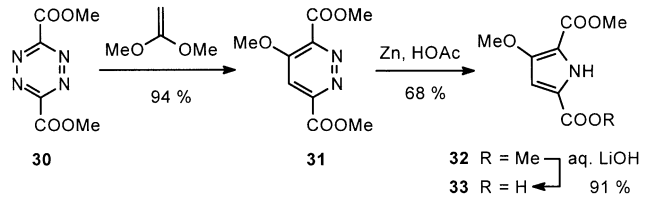
Scheme 7. The *vic*-tricarbonyl route to bipyrrole aldehyde **12**.[57]

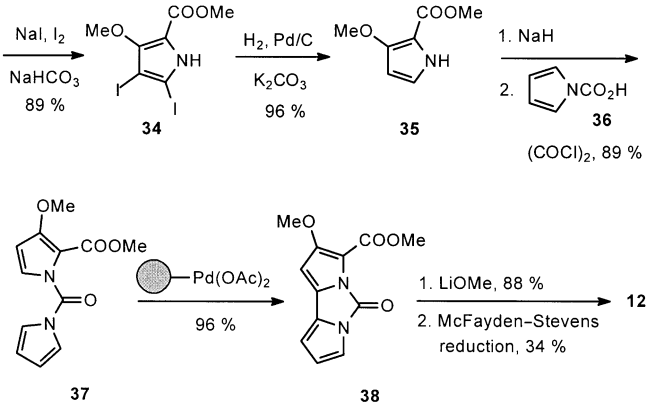


Scheme 8. Oxidative route to bipyrrole aldehyde **12**.[58]

 © 2003 Wiley-VCH Verlag GmbH & Co. KGaA, Weinheim

of the prodigiosin alkaloids (Scheme 9).[15] An inverse-electron-demand Diels–Alder reaction of 1,2,4,5-tetrazine **30** with 1,1-dimethoxyethene gave cycloadduct **31** in excellent yield, which underwent reductive ring contraction upon treatment with zinc dust in HOAc to give pyrrole dicarboxylate **32**.

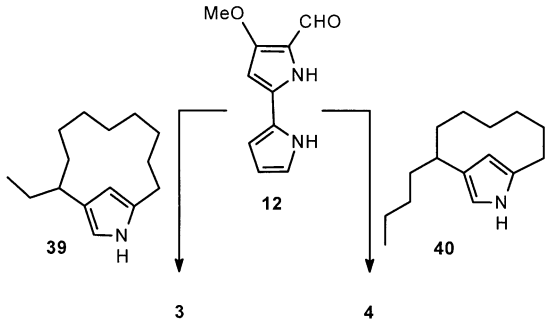




Scheme 9. Synthesis of bipyrrole aldehyde **12** by Boger and Patel.[15]

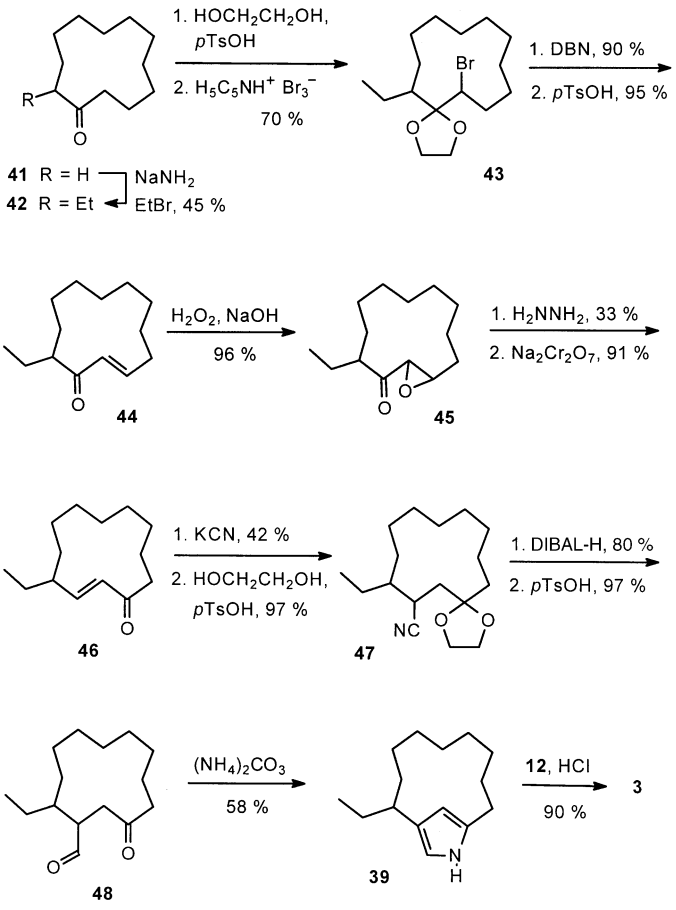
Selective hydrolysis of the sterically more accessible and more electrophilic C5 methoxycarbonyl group set the stage for the decarboxylation of acid **33** in the presence of iodine to give diiodide **34**, whereas an attempted thermal decarboxylation of **33** was unsuccessful. Subsequent hydrogenolysis of **34** provided pyrrole **35**, which was condensed with **36** to give the urea derivative **37**. The latter was subjected to an intramolecular oxidative coupling reaction to form bipyrrole **38** upon treatment with stoichiometric amounts of polymer-supported $Pd(OAc)_2$. Saponification of the cyclic urea entity followed by a conventional McFayden–Stevens reduction of the ester afforded the targeted bipyrrole aldehyde **12**. Once again, the yield of the latter process was far from optimal. Nevertheless, the material thus obtained allowed the preparation of prodigiosin (**1**) and several non-natural analogues, which were used to gain insight into the structural parameters responsible for the cytotoxic and antibacterial activity of such pigments (see above).[15]

These examples amply demonstrate the generality of the acid-catalyzed formation of the pyrrolylpyrromethene chromophore of the prodigiosins from aldehyde **12** and suitable aromatic reaction partners. Therefore, the problems associated with the synthesis of the macrocyclic natural products metacycloprodigiosin (**3**) or streptorubin B (**4**) mainly reside in the efficient formation of the corresponding building blocks **39** and **40**, respectively (Scheme 10). Wasserman and co-workers were the first to access such highly strained *meta*-pyrrolophanes by the sequence depicted in Scheme 11.[60b]



Scheme 10. Further biomimetic condensation reactions of bipyrrole aldehyde **12**.

Cyclododecanone (**41**) was elaborated into brominated compound **43** by a sequence of routine manipulations. Base-induced elimination of HBr and hydrolysis of the acetal gave enone **44** in excellent yield. This compound was subjected to a stepwise carbonyl transposition involving an epoxidation of the double bond followed by fragmentation of the hydrazone derived from the resulting epoxyketone **45**. The latter transformation, however, gave the desired allylic alcohol in only 33 % yield. After oxidation of the allylic alcohol to form **46**, conjugate addition of cyanide to the transposed enone system,



Scheme 11. Synthesis of metacycloprodigiosin (**3**) by Wasserman et al.[60b] DBN = 1,5-diazabicyclo[4.3.0]non-5-ene, DIBAL = diisobutylaluminum hydride.

 © 2003 Wiley-VCH Verlag GmbH & Co. KGaA, Weinheim

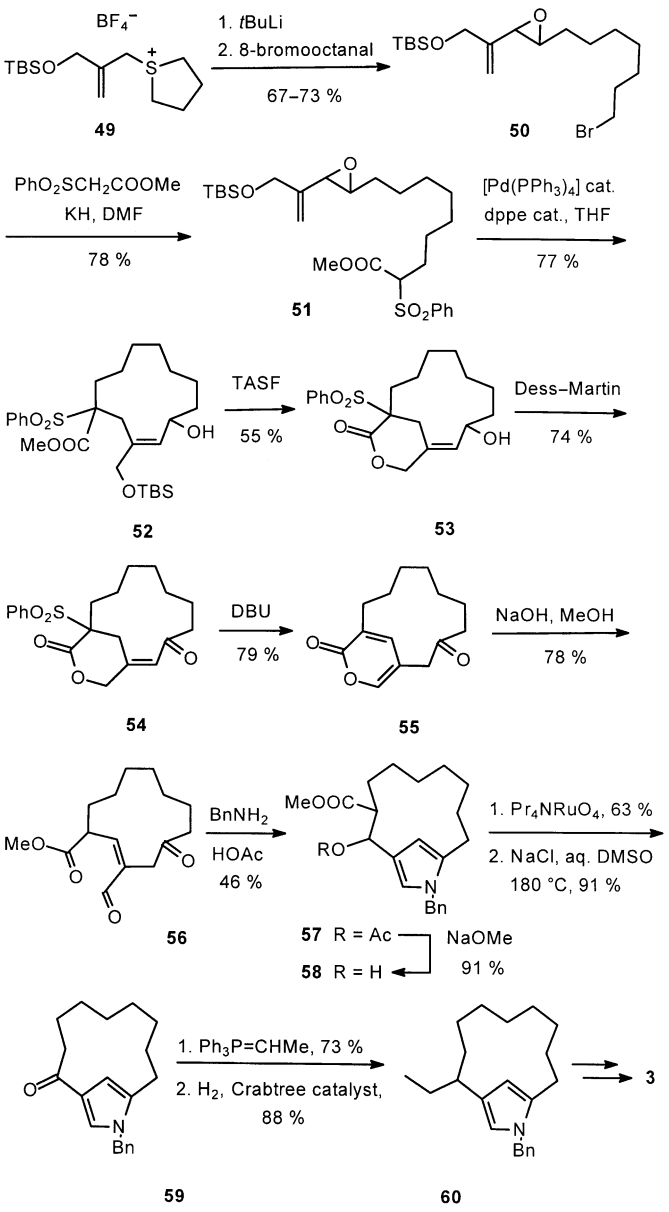
followed by a sequence of conventional protecting-group manipulations and adjustment of the oxidation state led to ketoaldehyde **48**. Paal–Knorr condensation of **48** with ammonium carbonate yielded the desired *meta*-pyrrolophane **39**. As expected, this compound could be easily condensed with bipyrrole aldehyde **12** in the presence of HCl to afford metacycloprodigiosin (**3**) as an intense red solid in excellent yield.[60b]

The difficulties encountered in several seemingly routine transformations of this sequence provoked the design of alternative routes. Specifically, our group devised two complementary entries into the *meta*-pyrrolophane cores of metacycloprodigiosin (**3**) and the closely related streptorubin B (**4**) that rely on the power of transition-metal-catalyzed C–C bond formations.[62,63] The synthesis of **3** commenced with the addition of the sulfur ylide derived from the well accessible bifunctional building block **49** to 8-bromooctanal (Scheme 12). Alkylation of the bromine substituent of the resulting product **50** with methyl (phenylsulfonyl)acetate followed by a regioselective activation of the vinyl epoxide entity in the presence of catalytic amounts of Pd^0 engendered an efficient intramolecular Tsuji–Trost reaction, resulting in the formation of the densely functionalized 12-membered ring **52**. Cleavage of the TBS group led to the spontaneous formation of lactone **53** owing to the close proximity of the resulting primary alcohol and the ester group. Oxidation of the remaining OH group (**53**→**54**) followed by base-induced elimination of the sulfone was accompanied by a shift of the double bond and formation of the *meta*-bridged α-pyrone **55**, the appropriately substituted precursor to the pyrrole ring.[62]

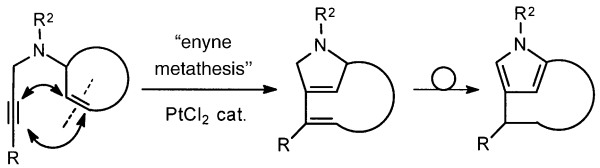
This particular heterocycle interconversion began with hydrolysis of the lactone to give the tricarbonyl compound **56**, which underwent a Paal–Knorr cyclization to give pyrrole **57** as the major product. Liberation and oxidation of the remaining OH group followed by decarboxylation of the resulting oxoester gave ketone **59** as a useful platform for the formation of metacycloprodigiosin (**3**) via **60**. Pyrrole ketone **59** also served as a convenient intermediate in the preparation of several analogues of **3** with different side chains attached to the macrocyclic core.[62]

An even more unconventional pyrrole synthesis was pursued en route to streptorubin B (**4**).[63] This route is based on a $PtCl_2$-catalyzed skeletal rearrangement, which transforms an enyne into a bicyclic diene. Shuffling of the π bonds of the diene affords the aromatic heterocycle (Scheme 13).

This approach was started by a standard allylic amination of commercially available cyclooctene **61**. *N*-Alkylation of the resulting sulfonamide **62** with propargyl bromide and acylation of the resulting terminal alkyne delivered enyne **63** as an appropriately substituted substrate for the envisaged ring expansion (Scheme 14). This compound underwent a smooth skeletal rearrangement upon heating in the presence of catalytic amounts of $PtCl_2$ in toluene to form the bicyclic product **64** in good yield on a multigram scale. Although this particular atom-economical reaction was "low-tech" from the operational point of view, it led to a significant increase in molecular complexity. Specifically, it formally involves the cleavage of the C=C bond in **63** while forming two new C–C bonds, which leads to the expansion of the preexisting ring and fashions a bridgehead alkene function incorporated into a bicyclic skeleton. Detailed mechanistic investigations

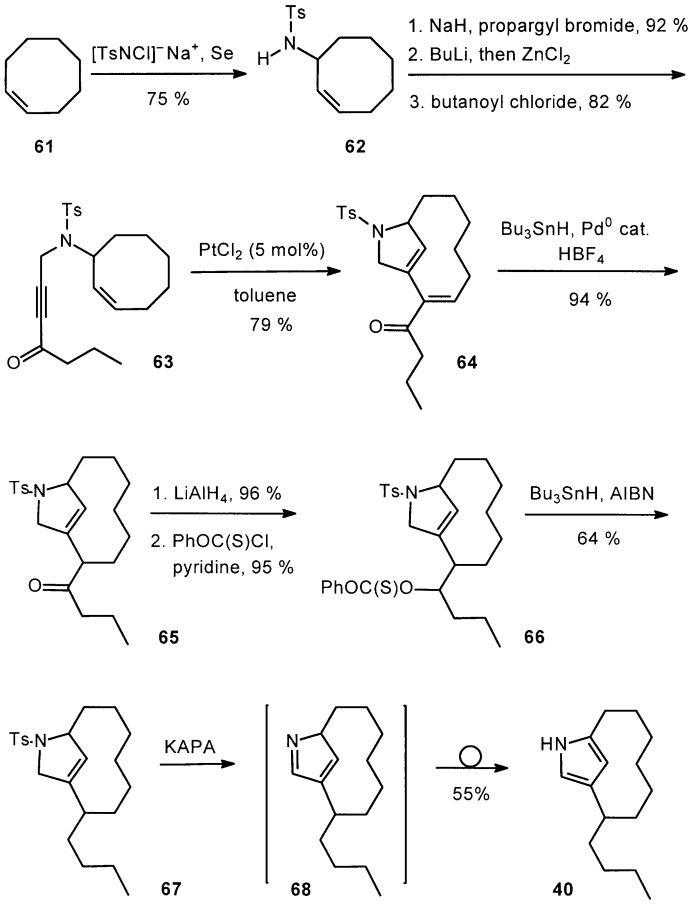


Scheme 12. Synthesis of metacycloprodigiosin (**3**) by Fürstner and Krause.[62] TBS = *tert*-butyldimethylsilyl, DMF = *N*,*N*-dimethylformamide, dppe = 1,2-bis(diphenylphosphanyl)ethane, TASF = tris(diethylamino)sulfonium difluorotrimethylsilicate, DBU = diazabicyclo[5.4.0]-undec-7-ene, DMSO = dimethyl sulfoxide.



Scheme 13. Concept of a novel pyrrole synthesis based on a Pt^{II}-catalyzed enyne metathesis.[63]

 © 2003 Wiley-VCH Verlag GmbH & Co. KGaA, Weinheim



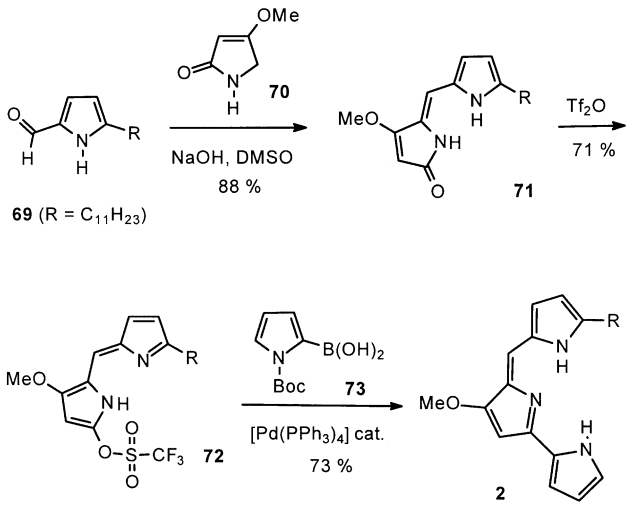
Scheme 14. Synthesis of the streptorubin B (**4**) core structure by Fürstner et al.[63] AIBN = 2,2′-azobisisobutyronitrile, KAPA = potassium salt of 1,3-diaminopropane.

revealed that this *formal* "enyne metathesis" probably involves "nonclassical" carbocations as the reactive intermediates and is therefore best described as a fascinatingly complex Wagner–Meerwein-type rearrangement.[63] This mechanistic insight allowed the concept of $PtCl_2$-catalyzed cycloisomerizations to be extended to other previously unexplored transformations.[64,65] Moreover, the same type of $PtCl_2$-catalyzed enyne metathesis was later adapted by Trost and Doherty in the formal total synthesis of roseophilin (see Section 5.5).[66]

Compound **64** was elaborated into the heterocyclic core of streptorubin B as depicted in Scheme 14. The pivotal transformations were a palladium-catalyzed reduction of the enone (**64**→**65**), a radical deoxygenation (**65**→**66**→**67**), and a base-induced elimination, which effected the deprotection of **67** with concomitant aromatization of the heterocyclic ring. This sequence delivered the streptorubin core **40** in only nine steps from cyclooctene in approximately 16 % overall yield.[63]

4.2. Syntheses of Prodigiosin Based on Cross-Coupling Reactions

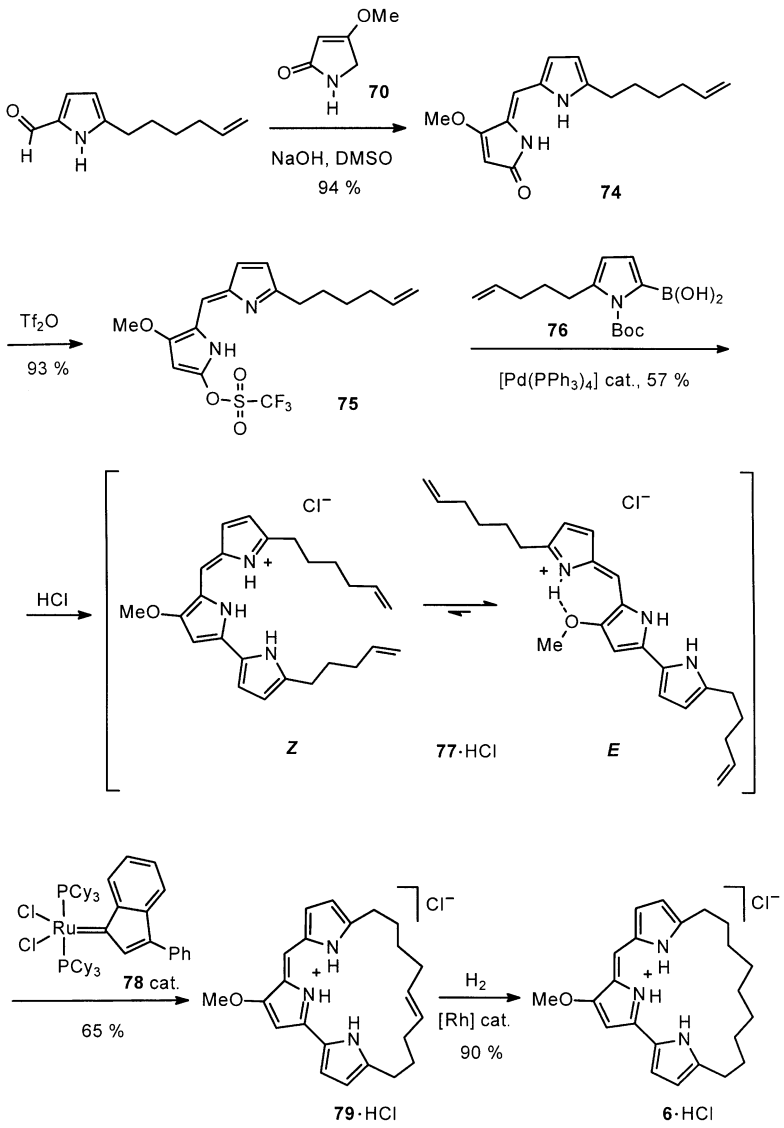
Despite the generality of the acid-catalyzed formation of the pyrrolopyrromethene chromophore from suitable pyrrole fragments and the bipyrrole aldehyde **12**, the rather poor-yielding routes to the latter detract from the appeal of this approach. A more convenient and scalable alternative to this "biomimetic" route was pioneered by D'Alessio et al. as part of their studies towards a synthesis-driven mapping of the SAR profile of the prodigiosins and the optimization of their immunosuppressive properties.[36,67] This route relies on a Suzuki reaction for the formation of the bipyrrole axis, as shown in Scheme 15 for the parent undecylprodigiosin (**2**).



Scheme 15. Synthesis of undecylprodigiosin (**2**) by D'Alessio et al.[36,67] Tf = trifluoromethanesulfonyl.

Specifically, a Vilsmeier–Haak formylation of 2-undecylpyrrole (**11**) afforded aldehyde **69**, which was condensed with commercially available pyrrolinone **70** to give enelactam **71** in high yield. Conversion of **71** into the corresponding triflate **72** upon exposure to triflic anhydride provided the electrophilic reaction partner required for the subsequent palladium-catalyzed cross-coupling reaction with *N*-Boc pyrrole-2-boronic acid (**73**), which is accessible by a standard *ortho*-metallation protocol. This Suzuki reaction delivered intact **2** in one step as a result of the cleavage of the *N*-Boc group under the basic reaction conditions. The underlying concept is highly flexible and was easily adapted to the synthesis of many different prodigiosin derivatives, among which PNU-156804 (**8**) was selected for biological investigations because of its improved immunosuppressive properties and low toxicity.[36]

In the first total synthesis of the macrocyclic nonylprodigiosin (**6**) described by our group, we adapted this sequence for the formation of diene **77** as the key intermediate (Scheme 16).[55] Although protonation of this compound strongly favors the *E* isomer, which is hardly amenable to cyclization, the metathesis catalyst **78**[68,69] can still intercept the minor isomer (*Z*)-**77**·HCl in solution and thereby constantly shift the preequilibrium to make the macrocyclization by RCM (ring-closing metathesis) productive in preparative terms. Hydrogenation of the resulting cycloalkene **79** in the presence of Wilkinson catalyst completed the first total synthesis of this demanding target.[55] The inherent flexibility of this route allowed the formation of several



Scheme 16. Synthesis of nonylprodigiosin (**6**) by Fürstner et al.[55] Boc = *tert*-butoxycarbonyl.

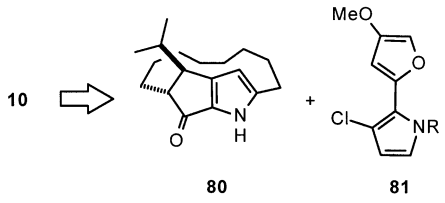
analogues, which incorporate aromatic rings other than pyrrole into their backbone and/or differ from the natural product in ring size.[23,39] These compounds helped to establish SARs concerning the DNA-cleaving and H^+/Cl^--symport properties of the prodigiosins and provided further insight into the effects of such alkaloids on the proliferation of murine spleen cells.[23,39]

5. Roseophilin

5.1. Total Synthesis by Fürstner and Co-workers

The promising cytotoxicity and the intricate topology of roseophilin (**10**), a macrocyclic pigment isolated from *Streptomyces griseoviridis*,[44] have attracted considerable attention, as witnessed by the rapidly growing number of partial and total syntheses of this alkaloid published during the last few years.[70–80] Despite the evident structural relationship between **10** and the prodigiosin family, it was recently shown that roseophilin lacks the characteristic "copper nuclease" activity of the latter.[23] Furthermore, **10** is an extremely rare case in which the non-natural enantiomer exhibits higher cytotoxicity (by a factor of 2-10) against several cancer cell lines than does the naturally occurring form.[16,72]

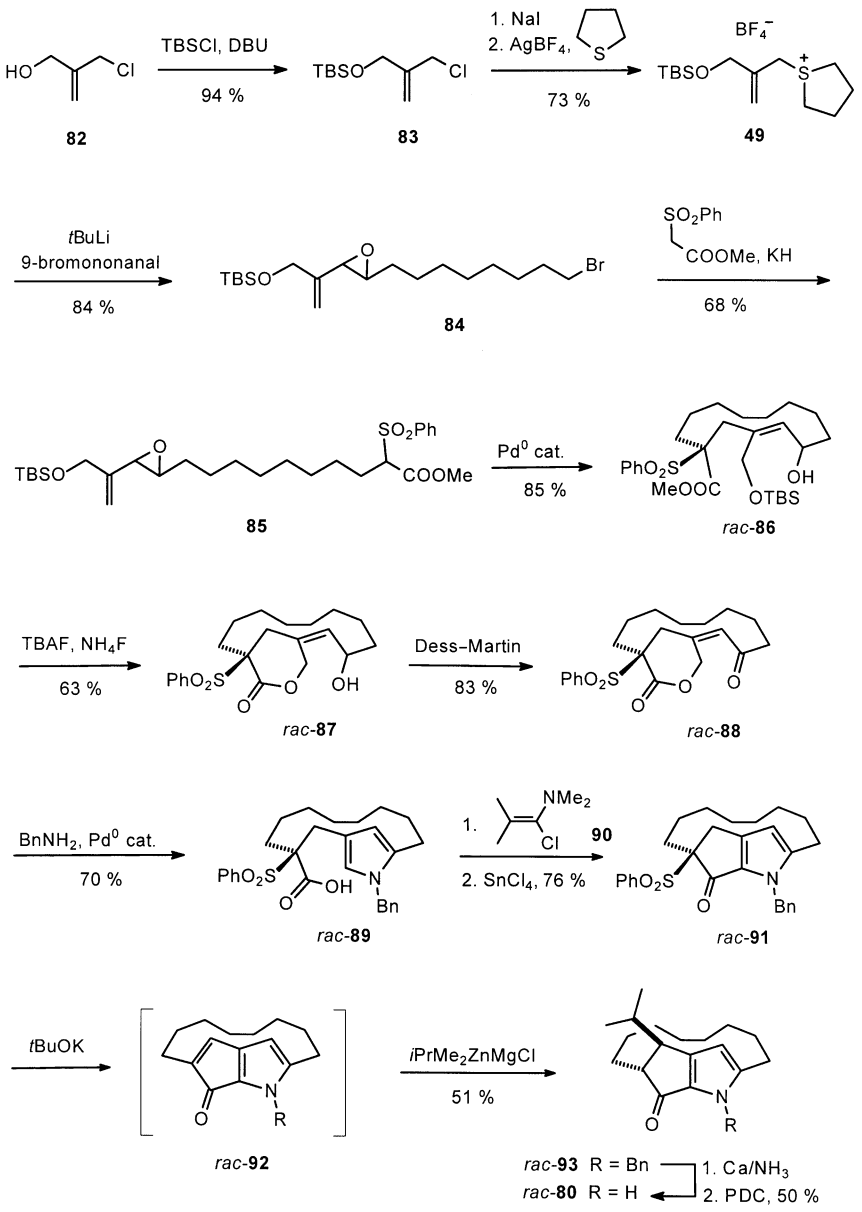
All synthetic approaches towards **10** known to date rely on the same strategic disconnection at the azafulvene site, envisaging a condensation of the macrotricyclic ketopyrrole **80** with the heterocyclic segment **81** (Scheme 17). The first to reduce this plan to practice were Fürstner and Weintritt, who proposed a highly integrated manifold based on organopalladium chemistry for the formation of the key building block **80**.[70] Strategically, it was decided to forge the macrocycle at an early stage, while trying to build up the strain inherent to this skeleton during the formation of the kinetically favored five-membered rings (Scheme 18). Alcohol **82** was chosen as a readily accessible starting material, which was converted into the sulfonium salt **49** in two routine steps. Reaction of 9-bromononanal with the sulfur ylide derived from **49** afforded the vinyl epoxide **84**, which was alkylated at the bromine terminus with methyl phenylsulfonylacetate to give product **85**. When exposed to a dilute solution of catalytic $[Pd(PPh_3)_4]$, compound **85** cyclized to the desired 13-membered ring **86** in excellent yield. This transformation likely involves the chemo- and regioselective activation of the vinyl epoxide unit of **85** by Pd^0 without affecting the adjacent allylic silyl ether; the resulting alkoxide deprotonates the terminal β-sulfonyl ester, which then serves as an internal nucleophile to attack the π-allylpalladium intermediate at the least-hindered site to give the 13-membered ring **86** as a mixture of diastereomers.



Scheme 17. Retrosynthetic analysis of roseophilin (**10**).

The functional-group pattern in **86** was ideally suited for the formation of both five-membered rings of **80**. Owing to the proximity of the ester and the silyl ether functions, treatment of **86** with TBAF/NH_4F spontaneously led to the corresponding allylic lactone **87**, which was amenable to another palladium-catalyzed bond formation. Thus, oxidation

 © 2003 Wiley-VCH Verlag GmbH & Co. KGaA, Weinheim



Scheme 18. Total synthesis of roseophilin (**10**) by Fürstner and Weintritt. Formation of the macrotricyclic core.[70] TBAF = tetrabutylammonium fluoride, PDC = pyridinium dichromate.

of the remaining OH group followed by exposure of the resulting ketone **88** to catalytic $[Pd(PPh_3)_4]$ in the presence of benzylamine as the external nucleophile delivered the *meta*-bridged pyrrole **89** in 70% yield. The subsequent use of the carboxylic acid liberated during this new palladium-catalyzed pyrrole formation for the construction of the tricyclic skeleton contributed to the atom economy of the overall synthesis. Specifically, **89** was treated with chloroenamine **90** to form the corresponding acid chloride, which was then subjected to an intramolecular Friedel–Crafts acylation at the activated 2-position of the heterocycle, thus leading to the efficient formation of **91**.

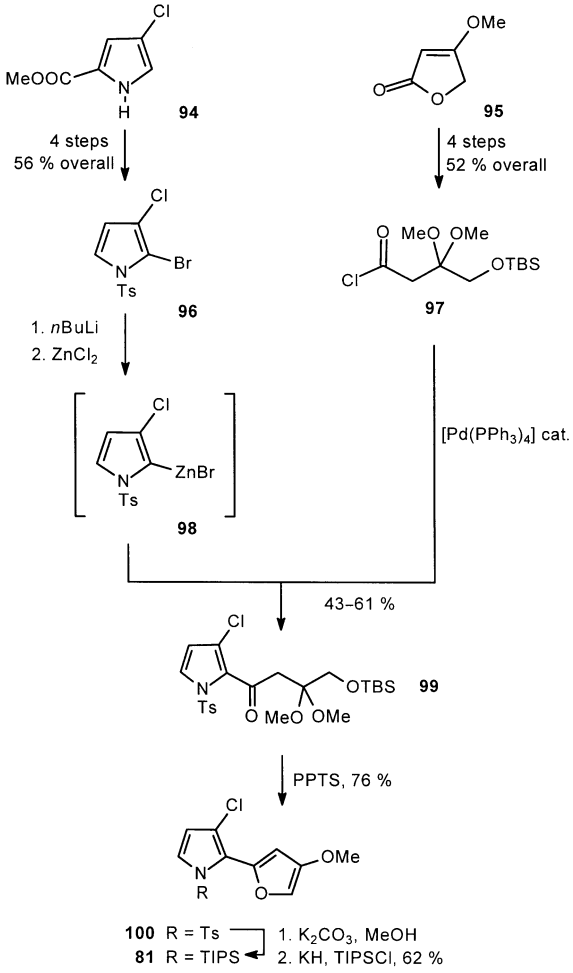
The remaining sulfone group served as a handle for the installation of the missing isopropyl side chain at the vicinal carbon atom. Treatment of **91** with excess *t*BuOK and iPrMe$_2$ZnMgCl resulted in the diastereoselective formation of the desired product **93**. This unconventional transformation likely involves the deprotonation of **91** at the benzylic position which engenders the elimination of $PhSO_2K$; the mixed zincate attacks the resulting highly strained, planar-chiral and formally antiaromatic "enone" **92** from the sterically less-hindered *exo* face. During workup, the resulting enolate is protonated again exclusively from the *exo* face as a result of the effective shielding of the other π face by the ansa chain. Subsequent debenzylation of **93** then delivered the desired target **80**.

The synthetic challenges posed by the seemingly simple heteroaromatic fragment **81** should not be underestimated. The chosen route (Scheme 19) commenced with the elaboration of substrates **94** and **95** into the polyfunctionalized building blocks **96** and **97**, respectively.[70,80] A chemoselective metal–halogen exchange in **96** followed by transmetallation of the resulting organolithium derivative with $ZnCl_2$ furnished the nucleophilic reaction partner **98** for the palladium-catalyzed cross-coupling with acid chloride **97**. Treatment of the resulting ketone **99** with PPTS triggered the formation of the methoxyfuran entity of **100** by a cascade involving the cleavage of the TBS group, formation of a hemiacetal by the reaction of the liberated hydroxy group with the ketone, and subsequent dehydration of the hemiacetal to give the aromatic system.

The final assembly (Scheme 20) started with the metallation of the heterocyclic fragment **81**. For this purpose, however, it was essential to install a TIPS group instead of the tosyl group on the pyrrole nitrogen atom of **100** to ensure selective deprotonation at the 2-position of the methoxyfuran ring. Transmetallation of the resulting organolithium derivative to the less basic organocerium reagent **101** followed by addition of the macrocyclic ketone **102** afforded the tertiary alcohol **103**. Deprotection followed by dehydration ultimately delivered the corresponding azafulvene and completed the first total synthesis of roseophilin (**10**) in racemic form.[70]

The only other total syntheses of this compound known to date closely imitated these final steps, with only minor variations.[71,72] Furthermore, it should be mentioned that sulfonium salt **49** used as a key substrate en route to **10** is a versatile building block for the syntheses of other heterocycles as well. Specifically, is served as the starting material in another approach toward roseophilin (see Section 5.2, Scheme 23)[74] as well as in the preparation of metacycloprodigiosin (**3**) described above (Scheme 12).[62] Moreover, this substrate was equally instrumental in the first total syntheses of the bioactive furanoterpenes ircinin-4 and cristatic acid.[81]

 © 2003 Wiley-VCH Verlag GmbH & Co. KGaA, Weinheim

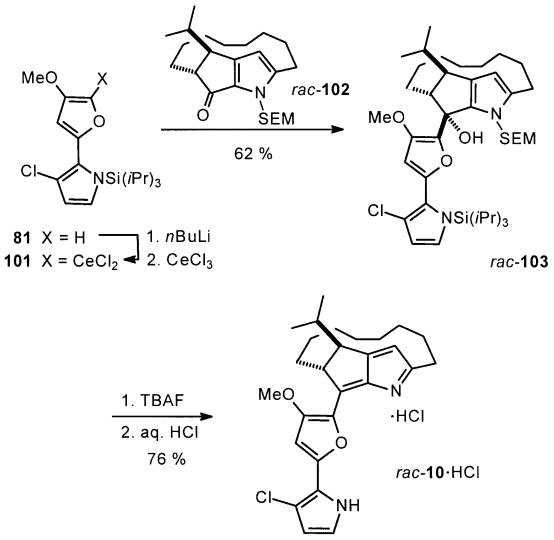


Scheme 19. Total synthesis of roseophilin (**10**) by Fürstner and Weintritt. Formation of the heterocyclic side chain.[70] PPTS = pyridinium *para*-toluenesulfonate, TIPS = triisopropylsilyl.

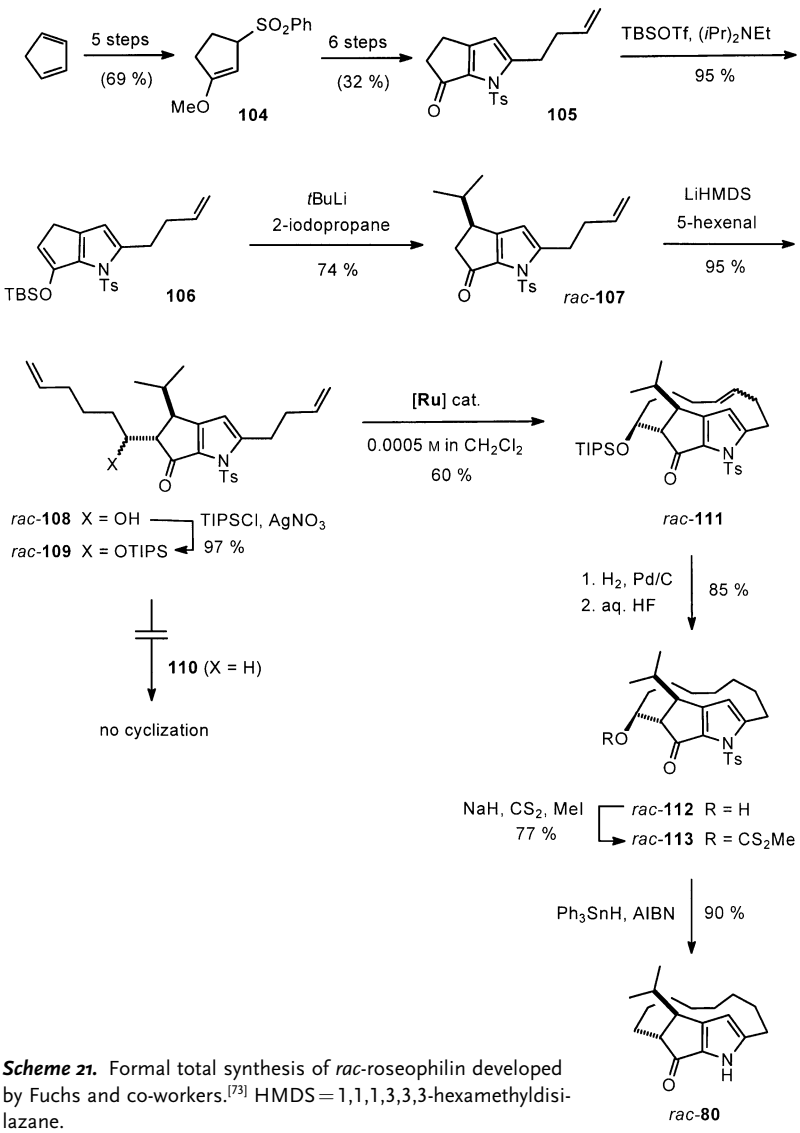
5.2. Formal Total Syntheses of Roseophilin through Ring-Closing Metathesis

The tremendous impact of RCM on organic synthesis is reflected in the different approaches to roseophilin (**10**) that employ this particular transformation.[82] RCM is generally driven by the gain in entropy that results from the release of a gaseous by-product (usually ethylene) and as such does not allow large enthalpy barriers to be overcome. Therefore, in the application of RCM to strained products, it is essential to preorganize the substrate into a conformation that favors cyclization, whereas flexible macrocycles may form without this precaution.

These aspects become evident from the approach to the macrotricyclic core pursued by Fuchs and co-workers.[73] The metathesis precursor was prepared from cyclopentadiene as depicted in Scheme 21. γ-Methoxy allylic sulfone **104** was used as a key intermediate in the annelation of the pyrrole ring system **105** by a sequence of high-yielding operations. Conversion of the resulting ketone **105** into the



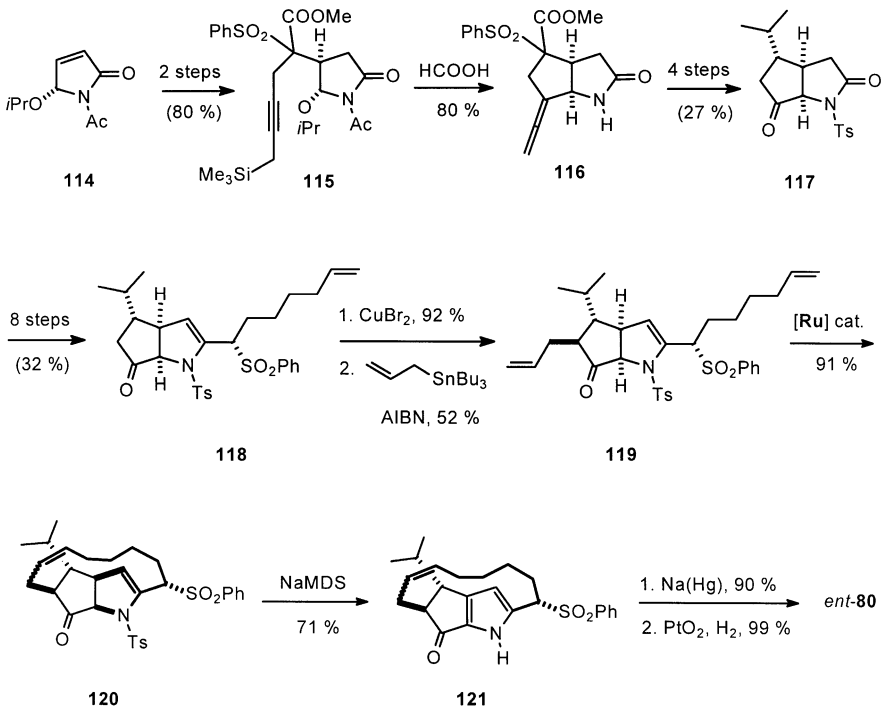
Scheme 20. Completion of the total synthesis of *rac*-**10** by Fürstner and Weintritt.[70] SEM = silylethoxymethyl.



Scheme 21. Formal total synthesis of *rac*-roseophilin developed by Fuchs and co-workers.[73] HMDS = 1,1,1,3,3,3-hexamethyldisilazane.

 © 2003 Wiley-VCH Verlag GmbH & Co. KGaA, Weinheim

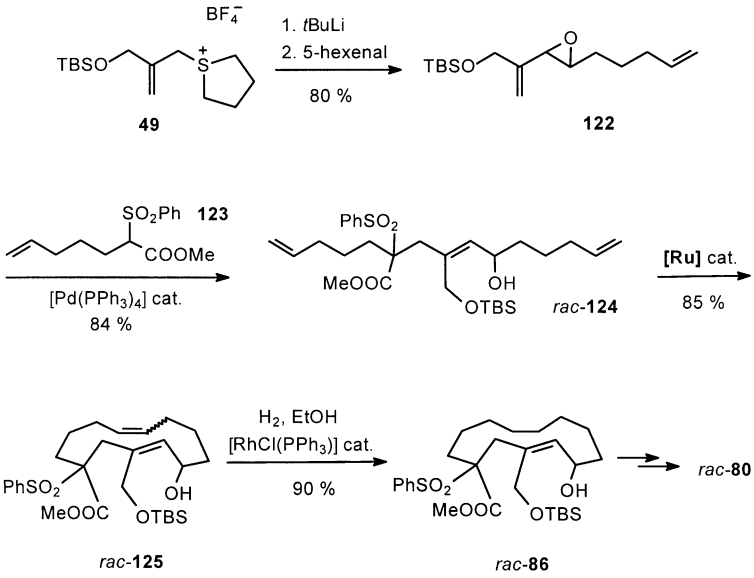
corresponding silyl enol ether **106** followed by alkylation of the allyl anion derived thereof with 2-iodopropane afforded *rac*-**107**, which was subjected to an aldol reaction with 5-hexenal to give product **108** as a mixture of diastereomers. Only after restricting the conformational space of this cyclization precursor by protection of its hydroxy function with a bulky TIPS group could productive metathesis be achieved upon exposure to the standard Grubbs catalyst [$(PCy_3)_2Cl_2Ru{=}CHPh$] ("[Ru]")[83] under high dilution conditions. Interestingly, only one diastereoisomer of **109** underwent cyclization. This fact likely reflects the directing effect of the OTIPS group, which—depending on the configuration of the stereocenter it is attached to—orients the olefinic side chains into a conformation that either favors or disfavors cyclization. In line with this interpretation, substrate **110** (X = H), which does not have the bulky OTIPS group, did not undergo cyclization. Saturation of the double bond in **111** was followed by cleavage of the silyl group, and the resulting product **112** was converted into the corresponding xanthate **113**. Subsequent treatment with triphenyltin hydride resulted in deoxygenation and concomitant cleavage of the *N*-tosyl group to deliver the desired macrotricyclic product **80** in racemic form.[73]



Scheme 22. Formal total synthesis of *ent*-roseophilin developed by Hiemstra and co-workers.[75]

The RCM approach developed by Hiemstra and coworkers was also based on the conformational preorganization of the cyclization precursor (Scheme 22).[75] This route led to the enantiomerically pure compound *ent*-**80**, which was later shown to correspond to the antipode of the natural product. Specifically, the readily available enantiomerically pure **114** was elaborated into the propargyl silane **115**, which was converted into allene **116**, via an acyliminium intermediate, upon treatment with acid. Sulfone **118** derived thereof was brominated regioselectively at the α position to the ketone group followed by the radical addition of allylstannane to give diene **119** as the substrate for the subsequent RCM event. When treated with the Grubbs catalyst [Ru][83] in CH_2Cl_2, this compound underwent ring closure to give cycloalkene **120** in 91% yield as a mixture of *E* and *Z* isomers. The efficiency of this macrocyclization was ascribed to the conformational bias induced by the sulfone and the concave shape of the bicyclic core of **119**, which cooperatively bring the reacting C=C bonds in close proximity. Subsequently, the heterocyclic ring was aromatized with concomitant deprotection upon treatment of **120** with NaMDS. Reductive cleavage of the sulfone in **121** with sodium amalgam and hydrogenation of the remaining double bond completed this formal total synthesis.[75]

Whereas all these examples illustrate the fact that the formation of strained products by RCM requires conformational assistance, the complementary approach to **80** pursued by our group shows that a fairly unstrained macrocycle can be formed in high yield without such precautions (Scheme 23).[74] Thus, sulfonium salt **49** was converted in two steps into the



Scheme 23. RCM-based formal total synthesis of roseophilin developed by Fürstner et al.[74]

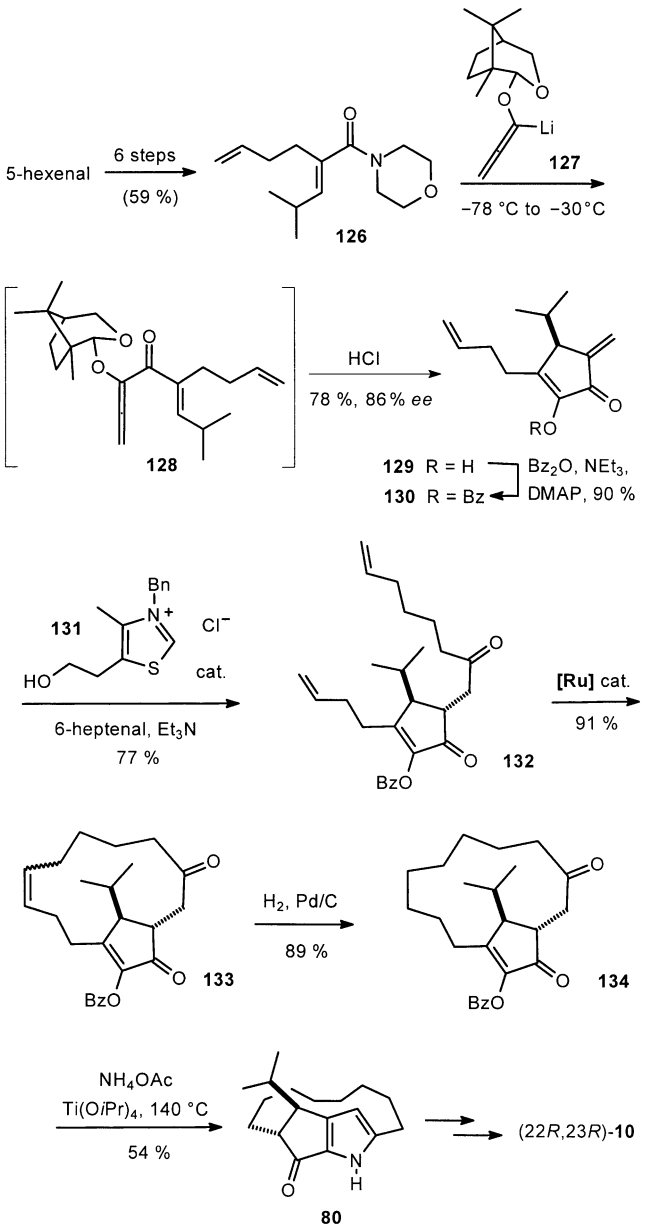
 © 2003 Wiley-VCH Verlag GmbH & Co. KGaA, Weinheim

required metathesis precursor **124**, which underwent smooth cyclization in the presence of catalytic amounts of [Ru]. This outcome also bears witness to the superb functional-group tolerance of the Grubbs catalyst, which rigorously distinguishes between the terminal and the trisubstituted alkene moieties in **124**. Selective hydrogenation of the disubstituted C=C bond in the resulting macrocycle **125** in the presence of the Wilkinson catalyst gave compound **86**, an intermediate in our previous total synthesis of roseophilin (see Section 5.1).[70]

5.3. Total Synthesis of (22R,23R)-Roseophilin by Tius and Harrington

In addition to these successful implementations of RCM into formal syntheses of **10**, metathesis also constituted a key operation in the first total synthesis of enantiomerically pure (22*R*,23*R*)-**10** published by Tius and Harrington (Scheme 24).[71] Since a direct comparison showed this material to be identical to the natural product, the previously unknown absolute configuration of roseophilin was established.

Routine elaboration of hexenal into amide **126** set the stage for the crucial asymmetric cyclization. Thus, addition of the enantiopure α-lithioallene **127** to amide **126** afforded ketone **128**, which upon activation with HCl at low temperature underwent a Nazarov-type cyclization to give the densely functionalized cyclopentenone derivative **129** in respectable yield and enantioselectivity. The camphor-based auxiliary used to control the stereochemical course of this cyclopentane formation was concomitantly cleaved under the chosen reaction conditions. After protection of the hydroxy group in **129** as an enol benzoate, the enantiomerically enriched acceptor **130** was subjected to a Stetter reaction with 6-heptenal induced by the thiazolium chloride **131**. The resulting diene **132** underwent a high-yielding macrocyclization through RCM to give the bicyclic 1,4-diketone **133**, which was transformed into the core structure of roseophilin by a regioselective hydrogenation of the less-substituted double bond followed by a Paal–Knorr pyrrole condensation reaction of diketone **134**. Enantiopure **80** thus formed was converted into the natural product upon reaction with lithiated **81** by adapting the protocol developed in our group to introduce the heterocyclic side chain (see Scheme 20).[70] A minor variation by Tius and Harrington consisted of the somewhat higher temperature chosen for the transmetallation of lithiated **81** to the required organocerium reagent **101**.[71]



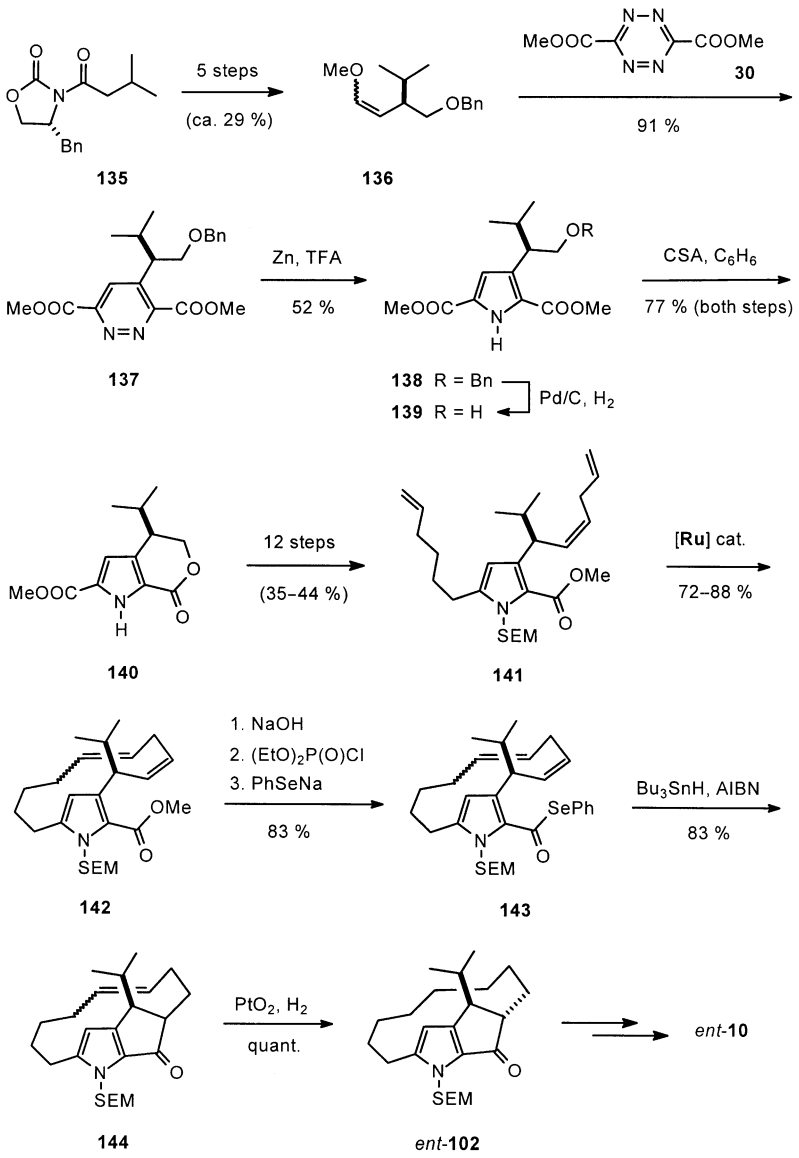
Scheme 24. Total synthesis of enantiomerically pure roseophilin by Tius and Harrington.[71] Bn = benzyl, Bz = benzoyl.

5.4. Total Synthesis of ent-10 by Boger and Hong

Another total synthesis of roseophilin based on RCM was reported by Boger and Hong.[72] As the absolute configuration of the natural product was unknown when these authors started their work, they targeted the 22*S*,23*S* enantiomer, which later turned out to be the non-natural enantiomer. Their approach (Scheme 25) re-elaborates on the hetero-Diels–Alder cycloaddition/reductive ring contraction methodology for the formation of substituted pyrrole rings that had already been applied in the prodigiosin series (see Scheme 9).

Specifically, an inverse-electron-demand cycloaddition between tetrazine **30** and the enantiopure enol ether **136** derived from the Evans oxazolidinone derivative **135** afforded 1,2-diazene **137**, which was converted into pyrrole **138** upon treatment with zinc in TFA. Debenzylation followed by acid-catalyzed lactonization of the liberated hydroxy group in **139** allowed a convenient differentiation between the two ester groups. Compound **140** thus formed was elaborated into diene **141** by a sequence of standard operations before the macrocyclization could be effected by RCM. Conversion of the methyl ester of the resulting product **142** into the correspond-

 © 2003 Wiley-VCH Verlag GmbH & Co. KGaA, Weinheim



Scheme 25. Total synthesis of *ent*-roseophilin by Boger and Hong.[72] CSA = camphorsulfonic acid.

ing acylselenide **143** preceded the formation of the last ring through 5-*exo*-trig cyclization to give product **144**. After hydrogenation of the remaining double bond, the product ketone *ent*-**102** was transformed into *ent*-**10** by following the Tius modification of our protocol.[72]

5.5. Formal Total Synthesis by Trost and Doherty

The propensity of 1,6-enynes for skeletal reorganizations in the presence of $PtCl_2$ was exploited by our group for the formation of the *meta*-bridged pyrrolophane core structure of streptorubin B (see Scheme 14).[63] Importantly, this reaction engenders the expansion of a preexisting ring by two carbon atoms (Scheme 13). As becomes evident from Scheme 26, a recent formal synthesis of roseophilin published by Trost and Doherty was based on a similar concept.[76]

Specifically, the $PtCl_2$-catalyzed reaction was elegantly used for the annelation of the carbocyclic five-membered ring and the macrocycle of the target and proceeded in virtually quantitative yield. The required substrate **149** (containing the unsaturated 11-membered ring to be expanded by this skeletal reorganization reaction) was obtained from cyclododecanone (**145**) by a Favorskii-type ring contraction, followed by adjustment of the location of the double bond, the oxidation state of the side chain, and a ligand-controlled addition of propargyl stannane to the aldehyde **146** thus obtained.

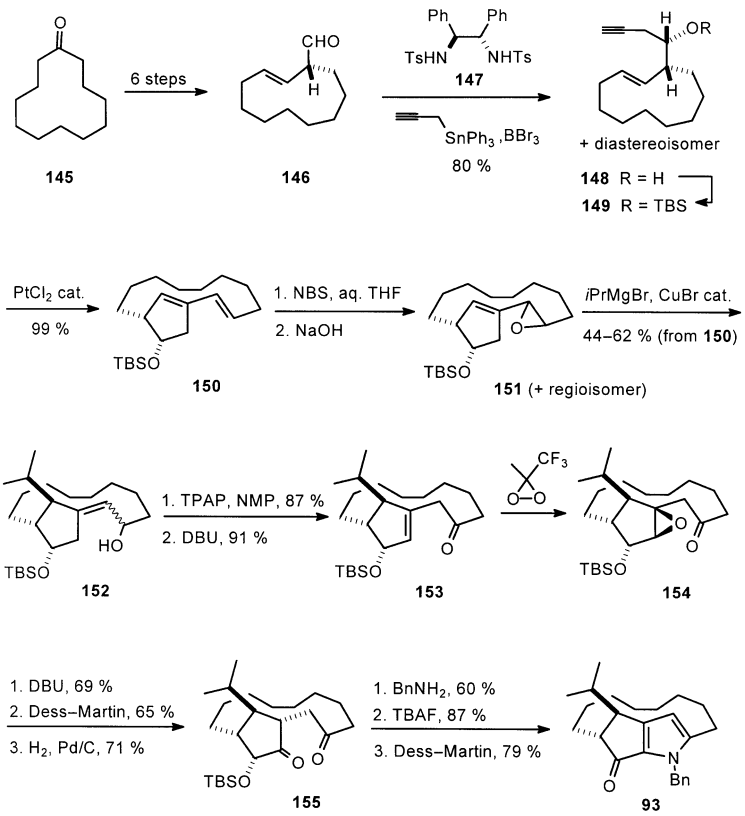
Diene **150** formed by the $PtCl_2$-catalyzed step was transformed into epoxide **151** through a moderately selective functionalization of its disubstituted double bond. Copper-catalyzed addition of isopropylmagnesium bromide to **151** introduced the lateral chain of the target in a diastereoselective fashion prior to further elaboration of the resulting compound **152** into diketone **155** by a sequence of oxidation/elimination reactions. A Paal–Knorr condensation of this intermediate followed by the conversion of the OTBS ether into ketone **93** completed this enantioselective formal total synthesis.

5.6. Formal Total Synthesis by Terashima and Coworkers

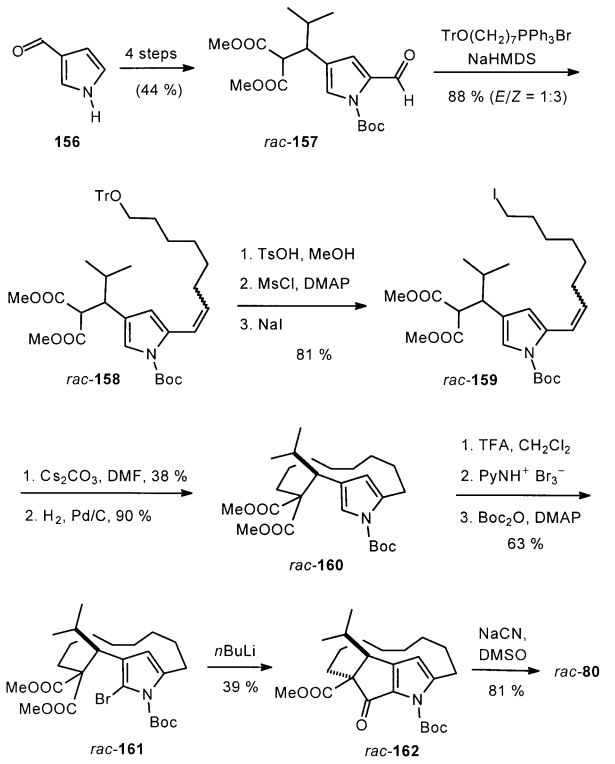
Despite the rather different blueprints of the syntheses outlined above, all approaches rely on the power of transition-metal-catalyzed C–C bond-formation reactions for the construction of the roseophilin core. This common theme distinguishes them from the only other formal total syntheses known to date described by Terashima and co-workers[77] and Robertson et al.[78]

The route by the Terashima group (Scheme 27) is the only approach that starts with an intact pyrrole ring rather than forming this moiety at a later stage of the synthesis. Thus, pyrrole-3-carbaldehyde **156** was transformed into compound **157** by a series of routine operations (Knoevenagel condensation, 1,4-addition, Vilsmeier formylation). A moderately *Z*-selective Wittig olefination then introduced the missing C atoms of the future ansa chain. Conversion of the terminal trityl ether of **158** into the corresponding iodide **159** was followed by an intramolecular malonate alkylation reaction mediated by Cs_2CO_3 to form the ansa chain in **160**. The rather low yield in this step is explained in part by the fact that the corresponding *E* isomer of **159** did not cyclize. After hydrogenation of the *meta*-pyrrolophane thus formed, the N-protecting group of **160** was temporarily removed to allow electrophilic bromination at C2 of the pyrrole as a prelude to the cyclopentanone annelation. After the *N*-Boc group was

 © 2003 Wiley-VCH Verlag GmbH & Co. KGaA, Weinheim



Scheme 26. Formal total synthesis of enantiopure roseophilin developed by Trost and Doherty.[76] NBS = *N*-bromosuccinimide, NMP = *N*-methyl-2-pyrrolidinone.

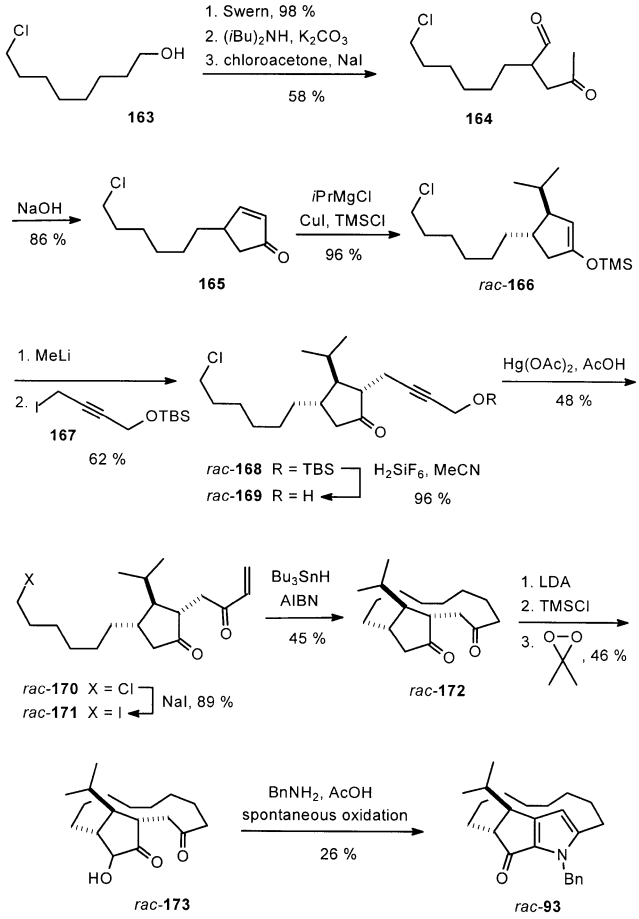


Scheme 27. Formal total synthesis of *rac*-roseophilin developed by Terashima and co-workers.[77] Tr = trityl = triphenylmethyl, Ms = mesyl = methanesulfonyl, DMAP = 4-dimethylaminopyridine, TFA = trifluoroacetic acid, Py = pyridine.

reintroduced, a selective metal–halogen exchange in **161** with *n*BuLi at low temperature gave rise to an organolithium intermediate, which intercepted one of the adjacent methyl esters to form the desired cyclic ketone **162** in racemic form. A Krapcho decarboxylation completed this formal total synthesis.

5.7. Formal Total Synthesis by Robertson et al.

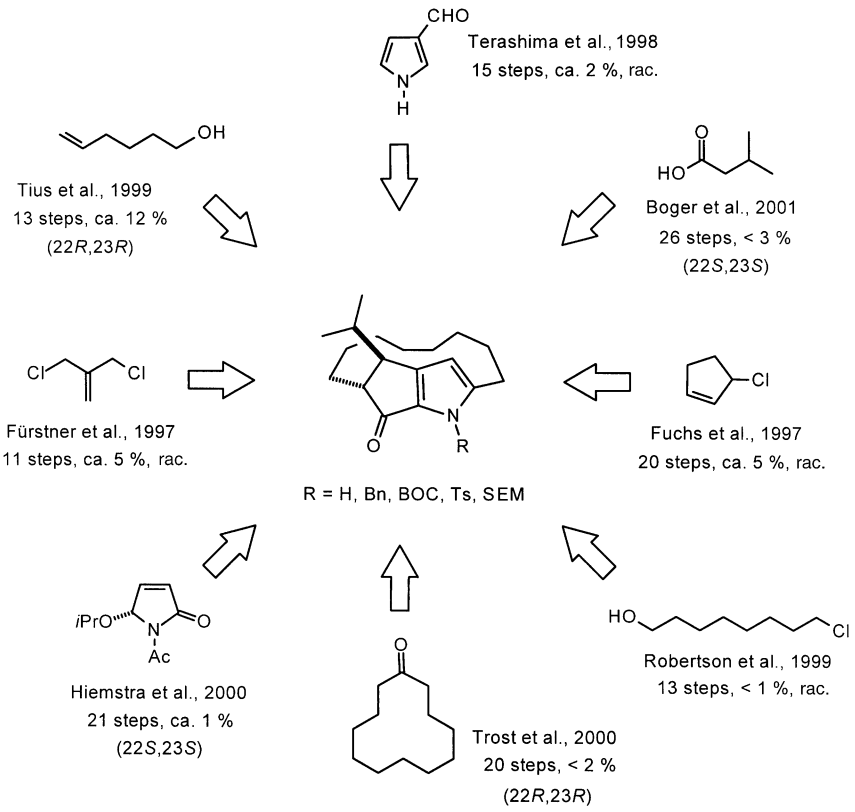
The entirely different route pursued by Robertson et al. was based on a radical macrocyclization step (Scheme 28).[78] The required precursor was obtained by elaboration of 8-chlorooctanol (**163**), which was initially oxidized to the aldehyde and converted into the corresponding enamine. The latter reacted with chloroacetone to give ketoaldehyde **164**, which cyclized to give cyclopentenone **165** upon treatment with NaOH in EtOH. This Michael acceptor was subjected to 1,4-addition of *i*PrMgCl and alkylation at the α-position with iodide **167** as shown in Scheme 28. Addition of water to the alkyne unit of **169** in the presence of Hg^{II} gave enone **170**. Its iodide



Scheme 28. Formal total synthesis of *rac*-roseophilin developed by Robertson et al.[78]

 © 2003 Wiley-VCH Verlag GmbH & Co. KGaA, Weinheim

derivative **171** underwent the envisaged macrocyclization in 45% yield upon exposure to Bu_3SnH and AIBN. A regioselective enolization of the product diketone **172** was necessary to introduce the then missing oxygen functionality. Surprisingly, product **173** not only underwent the desired Paal–Knorr reaction to form the pyrrole ring, but its residual hydroxy group was concomitantly oxidized to the target ketone **93**, although the overall yield of this transformation remained low. Investigations were carried out to determine if a reversal of the order of events might be more productive. Although the pyrrole formation with compound **172** occurred smoothly, no way was found to install the missing ketone group at C15 (roseophilin numbering).



Scheme 29. Overview over the known syntheses of the roseophilin core. Note that it may be difficult to determine the precise number of steps as well as the overall yield of a given sequence for several reasons. Most importantly, ambiguities arise where several reactions are carried out in "one pot" without isolating or rigorously purifying the intermediates. In some cases, the yields of individual steps have not been specified. Therefore the numbers compile8d in this scheme are only meant to provide a global picture.

6. Conclusions and Outlook

While the field of pyrrole natural products is largely dominated by the tetrapyrrolic "pigments of life" such as heme, chlorophyll, vitamin B_{12}, and the bile pigments,[84] a rapidly growing number of pyrrole alkaloids isolated from various marine and terrestrial sources deserves attention for their attractive biological properties and challenging molecular architectures.[85] Among them, the prodigiosin family is particularly remarkable for their diverse range of biological effects, although much deeper insight into the mode of action of these compounds is required before a fully consistent and conclusive picture can be drawn.

Alkaloids of this type together with the closely related antibiotic roseophilin also constitute a formidable testing ground for probing the efficiency and scope of existing methods. More importantly, though, they serve as inspiration for the development of novel and innovative concepts in heterocyclic chemistry (see Scheme 29). The author believes that the results summarized in this review corroborate the perception that target-oriented syntheses remains an intellectual sharpening stone and as such will continue to be one of the most powerful driving forces in chemistry and chemical biology.[86]

I sincerely thank all my co-workers engaged in the synthesis of bioactive heterocycles based on organometallic methodology for their intellectual input and skilful work in the laboratory. Their names appear in the references. The constant and generous financial support of our research programs by the Max-Planck-Gesellschaft, the Deutsche Forschungsgemeinschaft (Leibniz award program), and the Fonds der Chemischen Industrie is gratefully acknowledged, as are further financial contributions by the European Union, the Alexander-von-Humboldt Foundation, the Arthur C. Cope Funds of the ACS, and the Merck Research Council.

Received: February 10, 2003 [A582]

[1] For instructive reading, see: M. Hesse, *Alkaloide. Fluch oder Segen der Natur?*, Helvetica Chimica Acta, Zürich, **2000**.

[2] For more detailed reviews of these historical aspects, see: a) E. R. L. Gaughran, *Trans. N. Y. Acad. Sci.* **1969**, *31*, 3–24; b) J. W. Bennett, R. Bentley, *Adv. Appl. Microbiol.* **2000**, *47*, 1–32.

[3] For early reviews on prodigiosins, see: a) N. N. Gerber, *Crit. Rev. Microbiol.* **1975**, *3*, 469–485; b) R. P. Williams, W. R. Hearn, *Antibiotics* **1967**, *2*, 410–432.

[4] "Apud Macedonas quoque cum forte panem quidam militum frangerent, manantis sanguinis guttas notaverunt, territoque rege Aristander peritissimus vatum, si extrinsecus cruor fluxisset, Macedonibus id triste futurum ait: contra, cum ab interiore parte manaverat, urbi, quam obsidere destinassent, exitium portendere." (Quinti Curti Rufi, *Historiae Alexandri Magni*, Vol. 4). "Also amongst the Macedonians, when some of the soldiers happened to break bread, they noticed droplets of blood trickling out, and when the king was alerted, Aristander, the most skilled amongst the seers, declared that had the blood

flown from without, it would have been an unfavorable omen for the Macedonians; in contrast, however, since it had flown from the inside, it foretold the destruction of the city which they had determined to besiege" [Translation by the author].

[5] For a short review concerning the "chemistry of miracles", see: L. Garlaschelli, *Chem. Unserer Zeit* **1999**, *33*, 152 – 157.

[6] Although there are other microorganisms known that form red colonies, including various yeasts and fungi, none show the characteristic dripping and flowing phenomenon of mature *Serratia* strains.

[7] a) A. Hejazi, F. R. Falkiner, *J. Med. Microbiol.* **1997**, *46*, 903 – 912; b) H. M. Aucken, T. L. Pitt, *J. Med. Microbiol.* **1998**, *47*, 1105 – 1113.

[8] H. Rapoport, K. G. Holden, *J. Am. Chem. Soc.* **1962**, *84*, 635 – 642. This paper also contains a detailed discussion of the structures that were previously assigned to prodigiosin.

[9] For the isolation and structure elucidation of representative compounds of this series, see references [2,3] and the following for leading references: a) H. H. Wasserman, G. C. Rodgers, D. D. Keith, *J. Am. Chem. Soc.* **1969**, *91*, 1263 – 1264; b) N. N. Gerber, *J. Antibiot.* **1971**, *24*, 636 – 640; c) N. N. Gerber, *Tetrahedron Lett.* **1970**, *11*, 809 – 812; d) N. N. Gerber, *J. Heterocycl. Chem.* **1973**, *10*, 925 – 929; e) N. N. Gerber, *J. Antibiot.* **1975**, *28*, 194 – 199; f) H. Laatsch, M. Kellner, H. Weyland, *J. Antibiot.* **1991**, *44*, 187 – 191; g) see also: B. S. Deol, J. R. Alden, J. L. Still, A. V. Robertson, J. Winkler, *Aust. J. Chem.* **1974**, *27*, 2657 – 2662.

[10] a) A. J. Castro, G. R. Gale, G. E. Means, G. Tertzakian, *J. Med. Chem.* **1967**, *10*, 29 – 32; b) H. Berner, G. Schulz, H. Reinshagen, *Monatsh. Chem.* **1977**, *108*, 285 – 297; c) H. Berner, G. Schulz, H. Reinshagen, *Monatsh. Chem.* **1978**, *109*, 137 – 145; d) H. Berner, G. Schulz, G. Fischer, H. Reinshagen, *Monatsh. Chem.* **1978**, *109*, 557 – 566; e) H. Berner, G. Schulz, H. Reinshagen, *Monatsh. Chem.* **1977**, *108*, 233 – 242; f) D. Brown, D. Griffiths, M. E. Rider, R. C. Smith, *J. Chem. Soc. Perkin Trans. 1* **1986**, 455 – 463.

[11] A. J. Castro, *Nature* **1967**, *213*, 903 – 904.

[12] a) M. Isaka, A. Jaturapat, J. Kramyu, M. Tanticharoen, Y. Thebtaranonth, *Antimicrob. Agents Chemother.* **2002**, *46*, 1112 – 1113; b) J. E. H. Lazaro, J. Nitcheu, R. Z. Predicala, G. C. Mangalindan, F. Nesslany, D. Marzin, G. P. Concepcion, B. Diquet, *J. Nat. Toxins* **2002**, *11*, 367 – 377; c) H. S. Kim, M. Hayashi, Y. Shibata, Y. Wataya, T. Mitamura, T. Horii, K. Kawauchi, H. Hirata, S. Tsuboi, Y. Moriyama, *Biol. Pharm. Bull.* **1999**, *22*, 532 – 534.

[13] a) C. Yamamoto, H. Takemoto, H. Kuno, D. Yamamoto, A. Tsubura, K. Kamata, H. Hirata, A. Yamamoto, H. Kano, T. Seki, K. Inoue, *Hepatology* **1999**, *30*, 894 – 902; b) D. Yamamoto, Y. Kiyozuka, Y. Uemura, C. Yamamoto, H. Takemoto, H. Hirata, K. Tanaka, K. Hioki, A. Tsubura, *J. Cancer Res. Clin. Oncol.* **2000**, *126*, 191 – 197.

[14] a) C. Diaz-Ruiz, B. Montaner, R. Pérez-Tomás, *Histol. Histopathol.* **2001**, *16*, 415 – 421; b) B. Montaner, R. Pérez-Tomás, *Life Sci.* **2001**, *68*, 2025 – 2026; c) B. Montaner, S. Navarro, M. Piqué, M. Vilaseca, M. Martinell, E. Giralt, J. Gil, R. Pérez-Tomás, *Br. J. Pharmacol.* **2000**, *131*, 585 – 593.

[15] a) D. L. Boger, M. Patel, *J. Org. Chem.* **1988**, *53*, 1405 – 1415; b) D. L. Boger, M. Patel, *Tetrahedron Lett.* **1987**, *28*, 2499 – 2502.

[16] Detailed information concerning the cytotoxic properties of prodigiosins, roseophilin, and tambjamines assayed in the standard 60-cell line panel are available at the homepage of the National Cancer Institute (NCI), Bethesda, at http://www.dtp.nci.nih.gov.

[17] M. S. Melvin, D. C. Ferguson, N. Lindquist, R. A. Manderville, *J. Org. Chem.* **1999**, *64*, 6861 – 6869.

[18] a) B. M. Ramoneda, R. Pérez-Tomás, *Biochem. Pharmacol.* **2002**, *63*, 463 – 469; b) see also: B. Montaner, R. Pérez-Tomás, *Toxicol. Lett.* **2002**, *129*, 93 – 98.

[19] For a review, see: R. A. Manderville, *Curr. Med. Chem. Anti-Cancer Agents* **2001**, *1*, 195 – 218.

[20] a) T. Sato, H. Konno, Y. Tanaka, T. Kataoka, K. Nagai, H. H. Wasserman, S. Ohkuma, *J. Biol. Chem.* **1998**, *273*, 21 455 – 21 462; b) T. Kataoka, M. Muroi, S. Ohkuma, T. Waritani, J. Magae, A. Takatsuki, S. Kondo, M. Yamasaki, K. Nagai, *FEBS Lett.* **1995**, *359*, 53 – 59; c) S. Ohkuma, T. Sato, M. Okamoto, H. Matsuya, K. Arai, T. Kataoka, K. Nagai, H. H. Wasserman, *Biochem. J.* **1998**, *334*, 731 – 741; d) H. Konno, H. Matsuya, M. Okamoto, T. Sato, Y. Tanaka, K. Yokoyama, T. Kataoka, K. Nagai, H. H. Wasserman, S. Ohkuma, *J. Biochem.* **1998**, *124*, 547 – 556; e) H. Matsuya, M. Okamoto, T. Ochi, A. Nishikawa, S. Shimizu, T. Kataoka, K. Nagai, H. H. Wasserman, S. Ohkuma, *Biochem. Pharmacol.* **2000**, *60*, 1855 – 1863; f) T. Nakayasu, K. Kawauchi, H. Hirata, T. Shimmen, *Plant Cell Physiol.* **1999**, *40*, 143 – 148.

[21] M. S. Melvin, J. T. Tomlinson, G. Park, C. S. Day, G. S. Saluta, G. L. Kucera, R. A. Manderville, *Chem. Res. Toxicol.* **2002**, *15*, 734 – 741.

[22] a) M. S. Melvin, J. T. Tomlinson, G. R. Saluta, G. L. Kucera, N. Lindquist, R. A. Manderville, *J. Am. Chem. Soc.* **2000**, *122*, 6333 – 6334; b) M. S. Melvin, K. E. Wooton, C. C. Rich, G. R. Saluta, G. L. Kucera, N. Lindquist, R. A. Manderville, *J. Inorg. Biochem.* **2001**, *87*, 129 – 135.

[23] A. Fürstner, E. J. Grabowski, *ChemBioChem* **2001**, *2*, 706 – 709.

[24] Many DNA-cleaving agents use metal ions and O_2 to cause oxidative damage. Most important among them is bleomycin, an anticancer agent in clinical use. For representative reviews, see: a) W. K. Pogozelski, T. D. Tullius, *Chem. Rev.* **1998**, *98*, 1089 – 1107; b) G. Pratviel, J. Bernadou, B. Meunier, *Angew. Chem.* **1995**, *107*, 819 – 845; *Angew. Chem. Int. Ed. Engl.* **1995**, *34*, 746 – 769; c) S. M. Hecht, *J. Nat. Prod.* **2000**, *63*, 158 – 168; d) J. Stubbe, J. W. Kozarich, W. Wu, D. E. Vanderwall, *Acc. Chem. Res.* **1996**, *29*, 322 – 330; e) R. M. Burger, *Chem. Rev.* **1998**, *98*, 1153 – 1169; f) R. P. Hertzberg, P. B. Dervan, *Biochemistry* **1984**, *23*, 3934 – 3945.

[25] M. S. Melvin, M. W. Calcutt, R. E. Noftle, R. A. Manderville, *Chem. Res. Toxicol.* **2002**, *15*, 742 – 748.

[26] For a study of the cation-binding ability of tripyrrole derivatives, see: D. Eichinger, H. Falk, *Monatsh. Chem.* **1987**, *118*, 255 – 260.

[27] G. Park, J. T. Tomlinson, M. S. Melvin, M. W. Wright, C. S. Day, R. A. Manderville, *Org. Lett.* **2003**, *5*, 113 – 116.

[28] a) A. Nakamura, J. Magae, R. F. Tsuji, M. Yamasaki, K. Nagai, *Transplantation* **1989**, *47*, 1013 – 1016; b) J. Magae, M. W. Miller, K. Nagai, G. M. Shearer, *J. Antibiot.* **1996**, *49*, 86 – 90.

[29] a) S. M. Stepkowski, Z. S. Nagy, M.-E. Wang, F. Behbod, R. Erwin-Cohen, B. D. Kahan, R. A. Kirken, *Transplant. Proc.* **2001**, *33*, 3272 – 3273; b) S. M. Stepkowski, R. A. Erwin-Cohen, F. Behbod, M.-E. Wang, X. Qu, N. Tejpal, Z. S. Nagy, B. D. Kahan, R. A. Kirken, *Blood* **2002**, *99*, 680 – 689.

[30] S. Songia, A. Mortellaro, S. Taverna, C. Fornasiero, E. A. Scheiber, E. Erba, F. Colotta, A. Mantovani, A.-M. Isetta, J. Golay, *J. Immunol.* **1997**, *158*, 3987 – 3995.

[31] a) V. Rizzo, A. Morelli, V. Pinciroli, D. Sciangula, R. D'Alessio, *J. Pharm. Sci.* **1999**, *88*, 73 – 78; b) A. Mortellaro, S. Songia, P. Gnocchi, M. Ferrari, C. Fornasiero, R. D'Alessio, A. Isetta, F. Colotta, J. Golay, *J. Immunol.* **1999**, *162*, 7102 – 7109.

[32] M. Ferrari, P. Gnocchi, M. C. Fornasiero, F. Colotta, R. D'Alessio, A. M. Isetta (Pharmacia&Upjohn), WO 98/11894A1, **1998** [*Chem. Abstr.* **1998**, *128*, 275 084].

[33] R. F. Tsuji, M. Yamamoto, A. Nakamura, T. Kataoka, J. Magae, K. Nagai, M. Yamasaki, *J. Antibiot.* **1990**, *43*, 1293 – 1301.

[34] For a review on the biological response elicited by FK 506 and related immunophilins, see: M. K. Rosen, S. L. Schreiber, *Angew. Chem.* **1992**, *104*, 413 – 430; *Angew. Chem. Int. Ed. Engl.* **1992**, *31*, 384 – 400.

[35] T. Azuma, N. Watanabe, H. Yagisawa, H. Hirata, M. Iwamura, Y. Kobayashi, *Immunopharmacology* **2000**, *46*, 29 – 37.

 © 2003 Wiley-VCH Verlag GmbH & Co. KGaA, Weinheim

[36] R. D'Alessio, A. Bargiotti, O. Carlini, F. Calotta, M. Ferrari, P. Gnocchi, A. Isetta, N. Monelli, P. Motta, A. Rossi, M. Rossi, M. Tibolla, E. Vanotti, *J. Med. Chem.* **2000**, *43*, 2557 – 2565.

[37] S. B. Han, H. M. Kim, Y. H. Kim, C. W. Lee, E.-S. Jang, K. H. Son, S. U. Kim, Y. K. Kim, *Int. J. Immunopharmacol.* **1998**, *20*, 1 – 13.

[38] a) R. F. Tsuji, J. Magae, M. Yamashita, K. Nagai, M. Yamasaki, *J. Antibiot.* **1992**, *45*, 1295 – 1302; b) T. Kataoka, J. Magae, H. Nariuchi, M. Yamasaki, K. Nagai, *J. Antibiot.* **1992**, *45*, 1303 – 1312; c) A. Nakamura, K. Nagai, K. Ando, G. Tamura, *J. Antibiot.* **1986**, *39*, 1155 – 1159; d) M.-H. Lee, M. Yamashita, R. F. Tsuji, M. Yamasaki, T. Kataoka, J. Magae, K. Nagai, *J. Antibiot.* **1998**, *51*, 92 – 94; e) M.-H. Lee, T. Kataoka, J. Magae, K. Nagai, *Biosci. Biotechnol. Biochem.* **1995**, *59*, 1417 – 1421; f) T. Kataoka, K. Takaku, J. Magae, N. Shinohara, H. Takayama, S. Kondo, K. Nagai, *J. Immunol.* **1994**, *153*, 3938 – 3947; g) T. Kataoka, N. Shinohara, H. Takayama, K. Takaku, S. Kondo, S. Yonehara, K. Nagai, *J. Immunol.* **1996**, *156*, 3678 – 3686; h) T. Kataoka, M. Sato, S. Kondo, K. Nagai, *Biosci. Biotechnol. Biochem.* **1996**, *60*, 1729 – 1731; i) T. Kataoka, K. Togashi, H. Takayama, K. Takaku, K. Nagai, *Immunology* **1997**, *91*, 493 – 500; j) K. Togashi, T. Kataoka, K. Nagai, *Cytotechnology* **1997**, *25*, 127 – 135.

[39] A. Fürstner, J. Grabowski, C. W. Lehmann, T. Kataoka, K. Nagai, *ChemBioChem* **2001**, *2*, 60 – 68.

[40] See also: T. Kataoka, J. Magae, K. Kasamoo, H. Yamanishi, A. Endo, M. Yamasaki, K. Nagai, *J. Antibiot.* **1992**, *45*, 1618 – 1625.

[41] For a rare example of a marine bacterium that produces prodigiosin dervatives, see: T. Sawabe, H. Makino, M. Tatsumi, K. Nakano, K. Tajima, M. M. Iqbal, I. Yumoto, Y. Ezura, R. Christen, *Int. J. Syst. Bacteriol.* **1998**, *48*, 769 – 774.

[42] a) R. Kazlauskas, J. F. Marwood, P. T. Murphy, R. J. Wells, *Aust. J. Chem.* **1982**, *35*, 215 – 217; b) B. Carté, D. J. Faulkner, *J. Org. Chem.* **1983**, *48*, 2314 – 2318; c) N. Lindquist, W. Fenical, *Experientia* **1991**, *47*, 504 – 506; d) A. J. Blackman, C. Li, *Aust. J. Chem.* **1994**, *47*, 1625 – 1629.

[43] This compound was called BE-18591; see: K. Kojiri, S. Nakajima, H. Suzuki, A. Okura, H. Suda, *J. Antibiot.* **1993**, *46*, 1799 – 1803.

[44] Y. Hayakawa, K. Kawakami, H. Seto, K. Furihata, *Tetrahedron Lett.* **1992**, *33*, 2701 – 2704.

[45] a) H. H. Wasserman, J. E. McKeon, U. V. Santer, *Biochem. Biophys. Res. Commun.* **1960**, *3*, 146 – 149; b) M. T. M. Rizki, *Proc. Natl. Acad. Sci. USA* **1954**, *40*, 1057 – 1060; c) R. J. Cushley, D. R. Anderson, S. R. Lipsky, R. J. Sykes, H. H. Wasserman, *J. Am. Chem. Soc.* **1971**, *93*, 6284 – 6286; d) H. H. Wasserman, R. J. Sykes, P. Peverada, C. K. Shaw, R. J. Cushley, S. R. Lipsky, *J. Am. Chem. Soc.* **1973**, *95*, 6874 – 6875; e) H. H. Wasserman, C. K. Shaw, R. J. Sykes, R. J. Cushley, *Tetrahedron Lett.* **1974**, *15*, 2787 – 2790; f) R. J. Cushley, R. J. Sykes, C.-K. Shaw, H. H. Wasserman, *Can. J. Chem.* **1975**, *53*, 148 – 160; g) D. V. Lim, S. M. H. Qadri, C. Nichols, R. P. Williams, *J. Bacteriol.* **1977**, *159*, 124 – 130; h) N. N. Gerber, A. G. McInnes, D. G. Smith, J. A. Walter, J. L. C. Wright, L. C. Vining, *Can. J. Chem.* **1978**, *56*, 1155 – 1163.

[46] For early genetic studies and biochemical characterizations, see: a) B. A. M. Rudd, D. A. Hopwood, *J. Gen. Microbiol.* **1980**, *119*, 333 – 340; b) J. F. Feitelson, D. A. Hopwood, *Mol. Gen. Genet.* **1983**, *190*, 394 – 398.

[47] a) J. S. Feitelson, F. Malpartida, D. A. Hopwood, *J. Gen. Microbiol.* **1985**, *131*, 2431 – 2441; b) F. Malpartida, J. Niemi, R. Navarrete, D. A. Hopwood, *Gene* **1990**, *93*, 91 – 99.

[48] a) T. Yonekawa, Y. Ohnishi, S. Horninouchi, *Microbiology* **1999**, *145*, 2273 – 2280; b) J. White, M. J. Bibb, *J. Bacteriol.* **1997**, *179*, 627 – 633; c) E. Takano, H. C. Gramajo, E. Strauch, N. Andres, J. White, M. J. Bibb, *Mol. Microbiol.* **1992**, *6*, 2797 – 2804; d) K. E. Narva, J. S. Feitelson, *J. Bacteriol.* **1990**, *172*, 326 – 333; e) H. Ishizuka, S. Horinouchi, H. M. Kieser, D. A. Hopwood, T. Beppu, *J. Bacteriol.* **1992**, *174*, 7585 – 7594; f) E. P. Guthrie, C. S. Flaxman, J. White, D. A. Hodgson, M. J. Bibb, K. F. Chater, *Microbiology* **1998**, *144*, 727 – 738; g) R. Chakraburtty, M. Bibb, *J. Bacteriol.* **1997**, *179*, 5854 – 5861; h) J. S. Rokem, P. Weitzman, *Enzyme Microb. Technol.* **1987**, *9*, 153 – 155, and references therein.

[49] http://www.sanger.ac.uk/Projects/S coelicolor

[50] S. D. Bentley, K. F. Chater, A.-M. Cerdeño-Tárraga, G. L. Challis, N. R. Thomson, K. D. James, D. E. Harris, M. A. Quail, H. Kieser, D. Harper, A. Bateman, S. Brown, G. Chandra, C. W. Chen, M. Collins, A. Cronin, A. Fraser, A. Goble, J. Hidalgo, T. Hornsby, S. Howarth, C.-H. Huang, T. Kieser, L. Larke, L. Murphy, K. Oliver, S. O'Neil, E. Rabbinowitsch, M.-A. Rajandream, K. Rutherford, S. Rutter, K. Seeger, D. Saunders, S. Sharp, R. Squares, K. Taylor, T. Warren, A. Wietzorrek, J. Woodward, B. G. Barrell, J. Parkhill, D. A. Hopwood, *Nature* **2002**, *417*, 141 – 147.

[51] A. M. Cerdeño, M. J. Bibb, G. L. Challis, *Chem. Biol.* **2001**, *8*, 817 – 829.

[52] a) M. G. Thomas, M. D. Burkart, C. T. Walsh, *Chem. Biol.* **2002**, *9*, 171 – 184; b) see also: H. Chen, M. G. Thomas, S. E. O'Connor, B. K. Hubbard, M. D. Burkart, C. T. Walsh, *Biochemistry* **2001**, *40*, 11651 – 11659.

[53] Note, however, that there remains same ambiguity in this regard as long as the function of five genes in the *red* cluster is unknown.

[54] *Streptomyces coelicolor* produces a mixture of **2** and **4** as the main biochromes in a ratio of about 2:1; see: S.-W. Tsao, B. A. M. Rudd, X.-G. He, C.-J. Chang, H. G. Floss, *J. Antibiot.* **1985**, *38*, 128 – 131.

[55] A. Fürstner, J. Grabowski, C. W. Lehmann, *J. Org. Chem.* **1999**, *64*, 8275 – 8280.

[56] For a theoretical study, see: H. Falk, G. Streßler, N. Müller, *Monatsh. Chem.* **1988**, *119*, 505 – 508.

[57] H. H. Wasserman, L. J. Lombardo, *Tetrahedron Lett.* **1989**, *30*, 1725 – 1728.

[58] H. H. Wasserman, A. K. Petersen, M. Xia, J. Wang, *Tetrahedron Lett.* **1999**, *40*, 7587 – 7589.

[59] a) H. H. Wasserman, G. C. Rodgers, D. D. Keith, *J. Chem. Soc. Chem. Commun.* **1966**, 825 – 826; b) H. H. Wasserman, G. C. Rodgers, D. D. Keith, *Tetrahedron* **1976**, *32*, 1851 – 1854.

[60] a) H. H. Wasserman, D. D. Keith, G. C. Rodgers, *Tetrahedron* **1976**, *32*, 1855 – 1861; b) H. H. Wasserman, D. D. Keith, J. Nadelson, *Tetrahedron* **1976**, *32*, 1867 – 1871.

[61] For further syntheses of non-natural prodigiosin analogues by similar condensation reactions, see reference [9] and the following: a) W. R. Hearn, M. K. Elson, R. H. Williams, J. Medina-Castro, *J. Org. Chem.* **1970**, *35*, 142 – 146; b) A. J. Blake, G. A. Hunter, H. McNab, *J. Chem. Soc. Chem. Commun.* **1990**, 734 – 736; b) M. D'Auria, E. De Luca, G. Mauriello, R. Racioppi, *Synth. Commun.* **1999**, *29*, 35 – 42.

[62] A. Fürstner, H. Krause, *J. Org. Chem.* **1999**, *64*, 8281 – 8286.

[63] A. Fürstner, H. Szillat, B. Gabor, R. Mynott, *J. Am. Chem. Soc.* **1998**, *120*, 8305 – 8314.

[64] a) A. Fürstner, H. Szillat, F. Stelzer, *J. Am. Chem. Soc.* **2000**, *122*, 6785 – 6786; b) A. Fürstner, F. Stelzer, H. Szillat, *J. Am. Chem. Soc.* **2001**, *123*, 11863 – 11869; c) A. Fürstner, V. Mamane, *J. Org. Chem.* **2002**, *67*, 6264 – 6267.

[65] For $PtCl_2$-catalyzed skeletal reorganizations developed by other groups, see: a) N. Chatani, N. Furukawa, H. Sakurai, S. Murai, *Organometallics* **1996**, *15*, 901 – 903; b) N. Chatani, K. Kataoka, S. Murai, N. Furukawa, Y. Seki, *J. Am. Chem. Soc.* **1998**, *120*, 9104 – 9105; c) M. Méndez, M. P. Muñoz, C. Nevado, D. J. Cárdenas, A. M. Echavarren, *J. Am. Chem. Soc.* **2001**, *123*, 10511 – 10520; d) C. Fernández-Rivas, M. Méndez, A. M. Echavarren, *J. Am. Chem. Soc.* **2000**, *122*, 1221 – 1222; e) B. Martín-Matute, D. J. Cárdenas, A. M. Echavarren, *Angew. Chem.* **2001**,

113, 4890 – 4893; *Angew. Chem. Int. Ed.* **2001**, *40*, 4754 – 4757; f) S. Oi, I. Tsukamoto, S. Miyano, Y. Inoue, *Organometallics* **2001**, *20*, 3704 – 3709; g) J. Blum, H. Beer-Kraft, Y. Badrieh, *J. Org. Chem.* **1995**, *60*, 5567 – 5569; h) B. M. Trost, V. K. Chang, *Synthesis* **1993**, 824 – 832.

[66] B. M. Trost, G. A. Doherty, *J. Am. Chem. Soc.* **2000**, *122*, 3801 – 3810.

[67] R. D'Allessio, A. Rossi, *Synlett* **1996**, 513 – 514.

[68] Catalyst **78** is a readily available substitute for the classical Grubbs catalyst; for a large-scale adaptable preparation and a survey of its reactivity, see: A. Fürstner, O. Guth, A. Düffels, G. Seidel, M. Liebl, B. Gabor, R. Mynott, *Chem. Eur. J.* **2001**, *7*, 4811 – 4820.

[69] For previous applications of this catalyst in synthesis, see references [39, 55] and the following: a) A. Fürstner, A. F. Hill, M. Liebl, J. D. E. T. Wilton-Ely, *Chem. Commun.* **1999**, 601 – 602; b) A. Fürstner, O. R. Thiel, *J. Org. Chem.* **2000**, *65*, 1738 – 1742; c) A. Fürstner, K. Radkowski, *Chem. Commun.* **2001**, 671 – 672; d) A. Fürstner, F. Jeanjean, P. Razon, *Angew. Chem.* **2002**, *114*, 2203 – 2206; *Angew. Chem. Int. Ed.* **2002**, *41*, 2097 – 2101; e) A. Fürstner, K. Radkowski, C. Wirtz, R. Goddard, C. W. Lehmann, R. Mynott, *J. Am. Chem. Soc.* **2002**, *124*, 7061 – 7069; f) A. Fürstner, M. Schlede, *Adv. Synth. Catal.* **2002**, *344*, 657 – 665; g) A. Fürstner, F. Stelzer, A. Rumbo, H. Krause, *Chem. Eur. J.* **2002**, *8*, 1856 – 1871; h) A. Fürstner, F. Jeanjean, P. Razon, C. Wirtz, R. Mynott, *Chem. Eur. J.* **2003**, *9*, 320 – 326; i) A. Fürstner, A. Leitner, *Angew. Chem.* **2003**, *115*, 320 – 323; *Angew. Chem. Int. Ed.* **2003**, *42*, 308 – 311.

[70] a) A. Fürstner, H. Weintritt, *J. Am. Chem. Soc.* **1998**, *120*, 2817 – 2825; b) A. Fürstner, H. Weintritt, *J. Am. Chem. Soc.* **1997**, *119*, 2944 – 2945.

[71] a) P. E. Harrington, M. A. Tius, *J. Am. Chem. Soc.* **2001**, *123*, 8509 – 8514; b) P. E. Harrington, M. A. Tius, *Org. Lett.* **1999**, *1*, 649 – 651.

[72] D. L. Boger, J. Hong, *J. Am. Chem. Soc.* **2001**, *123*, 8515 – 8519.

[73] S. H. Kim, I. Figueroa, P. L. Fuchs, *Tetrahedron Lett.* **1997**, *38*, 2601 – 2604.

[74] A. Fürstner, T. Gastner, H. Weintritt, *J. Org. Chem.* **1999**, *64*, 2361 – 2366.

[75] a) S. J. Bamford, T. Luker, W. N. Speckamp, H. Hiemstra, *Org. Lett.* **2000**, *2*, 1157 – 1160; b) see also: S. J. Bamford, K. Goubitz, H. L. van Lingen, T. Luker, H. Schenk, H. Hiemstra, *J. Chem. Soc. Perkin Trans. 1* **2000**, 345 – 351.

[76] B. M. Trost, G. A. Doherty, *J. Am. Chem. Soc.* **2000**, *122*, 3801 – 3810.

[77] T. Mochizuki, E. Itoh, N. Shibata, S. Nakatani, T. Katoh, S. Terashima, *Tetrahedron Lett.* **1998**, *39*, 6911 – 6914.

[78] a) J. Robertson, R. J. D. Hatley, D. J. Watkin, *J. Chem. Soc. Perkin Trans. 1* **2000**, 3389 – 3396; b) J. Robertson, R. J. D. Hatley, *Chem. Commun.* **1999**, 1455 – 1456.

[79] For model studies, see: a) S. H. Kim, Z. Jin, P. L. Fuchs, *Tetrahedron Lett.* **1995**, *36*, 4537 – 4538; b) S. H. Kim, P. L. Fuchs, *Tetrahedron Lett.* **1996**, *37*, 2545 – 2548; c) M. A. Fagan, D. W. Knight, *Tetrahedron Lett.* **1999**, *40*, 6117 – 6120; d) T. Luker, W.-J. Koot, H. Hiemstra, W. N. Speckamp, *J. Org. Chem.* **1998**, *63*, 220 – 221.

[80] For further studies concerning the heteroaromatic segment **81** and its analogues, see reference [74] and the following: a) S. Nakatani, M. Kirihara, K. Yamada, S. Terashima, *Tetrahedron Lett.* **1995**, *36*, 8461 – 8464; b) J. Robertson, N. Kuhnert, Y. Zhao, *Heterocycles* **2000**, *53*, 2415 – 2420.

[81] a) A. Fürstner, T. Gastner, J. Rust, *Synlett* **1999**, 29 – 32; b) A. Fürstner, T. Gastner, *Org. Lett.* **2000**, *2*, 2467 – 2470.

[82] For selected reviews, see: a) T. M. Trnka, R. H. Grubbs, *Acc. Chem. Res.* **2001**, *34*, 18 – 29; b) A. Fürstner, *Angew. Chem.* **2000**, *112*, 3140 – 3172; *Angew. Chem. Int. Ed.* **2000**, *39*, 3012 – 3043; c) R. H. Grubbs, S. Chang, *Tetrahedron* **1998**, *54*, 4413 – 4450; d) M. Schuster, S. Blechert, *Angew. Chem.* **1997**, *109*, 2124 – 2144; *Angew. Chem. Int. Ed. Engl.* **1997**, *36*, 2037 – 2056; e) A. Fürstner, *Top. Catal.* **1997**, *4*, 285 – 299; f) S. K. Armstrong, *J. Chem. Soc. Perkin Trans. 1* **1998**, 371 – 388.

[83] a) P. Schwab, M. B. France, J. W. Ziller, R. H. Grubbs, *Angew. Chem.* **1995**, *107*, 2179 – 2181; *Angew. Chem. Int. Ed. Engl.* **1995**, *34*, 2039 – 2041; b) S. T. Nguyen, R. H. Grubbs, J. W. Ziller, *J. Am. Chem. Soc.* **1993**, *115*, 9858 – 9859.

[84] H. Falk, *The Chemistry of Linear Oligopyrroles and Bile Pigments,* Springer, Berlin, **1989**.

[85] For further studies from our laboratory and pertinent literature on other bioactive pyrrole alkaloids, see the following references and literature cited therein: a) A. Fürstner, H. Weintritt, A. Hupperts, *J. Org. Chem.* **1995**, *60*, 6637 – 6641; b) A. Fürstner, H. Krause, O. R. Thiel, *Tetrahedron* **2002**, *58*, 6373 – 6380; c) A. Fürstner, A. Hupperts, A. Ptock, E. Janssen, *J. Org. Chem.* **1994**, *59*, 5215 – 5229.

[86] For more authoritative treatises of this and related aspects, see: a) E. J. Corey, X.-M. Cheng, *The Logic of Chemical Synthesis*, Wiley, New York, **1989**; b) K. C. Nicolaou, D. Vourloumis, N. Winssinger, P. S. Baran, *Angew. Chem.* **2000**, *112*, 46 – 126; *Angew. Chem. Int. Ed.* **2000**, *39*, 44 – 122; c) K. C. Nicolaou, E. J. Sorensen, *Classics in Total Synthesis: Targets, Strategies, Methods*, Wiley-VCH, Weinheim, **1996**, and references therein.

 © 2003 Wiley-VCH Verlag GmbH & Co. KGaA, Weinheim

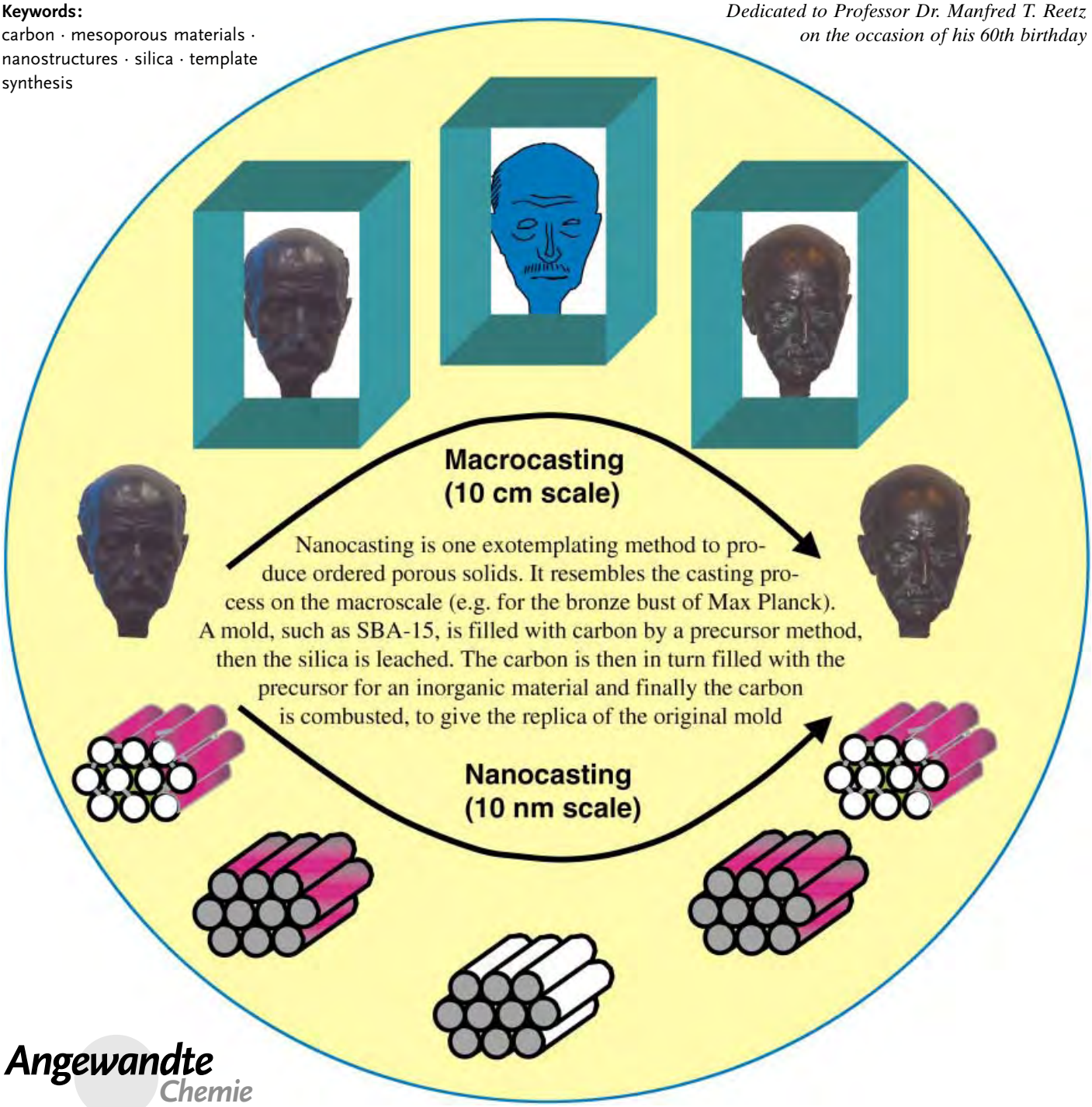
Inorganic Template Synthesis

Endo- and Exotemplating to Create High-Surface-Area Inorganic Materials

*Ferdi Schüth**

Keywords:
carbon · mesoporous materials · nanostructures · silica · template synthesis

Dedicated to Professor Dr. Manfred T. Reetz on the occasion of his 60th birthday



 © 2003 Wiley-VCH Verlag GmbH & Co. KGaA, Weinheim DOI: 10.1002/anie.200300593

Porous and high-surface-area materials are of interest to many scientific communities. Templating pathways can be used to synthesize such materials with a high degree of control over their structural and textural properties. As templates molecular or supramolecular units are added to the synthesis mixture. They are occluded in the growing solid and leave a pore system after their removal. For such templates the term "endotemplate" is introduced. Alternatively, the templates can be materials with structural pores in which another solid is created, thus providing a scaffold for the synthesis. After removal of the scaffold, a porous or finely divided solid remains, depending on the connectivity of the template. Such a template is termed an "exotemplate". By judicious choice of the templating procedure, unprecedented control of the structure and texture on length scales between nanometers and micrometers has been achieved over the last few years.

From the Contents

1. Introduction: Porous and High-Surface-Area Materials 3605

2. Endotemplating: Creating Porous Materials by Occlusion of Molecular or Supramolecular Units in the Forming Solid 3607

3. Exotemplating: Creating High-Surface-Area Materials by Synthesis within Rigid Porous Solids 3612

4. Perspectives: Novel Compositions and Novel Structures 3619

1. Introduction: Porous and High-Surface-Area Materials

The synthesis of porous and high-surface-area materials is a topic which is investigated in many laboratories all over the world, since such materials are interesting for applications as diverse as heterogeneous catalysis, adsorption, sensing, hydrogen or methane storage, and many others. Synthesis pathways to create porous solids are manifold and often depend strongly on the type of solid which is targeted. Recent surveys covering the general strategies to create porous solids are available,[1,2] numerous reviews and books covering only specific materials have also been published (zeolites,[3,4] ordered mesoporous oxides,[5–7] carbons,[8,9] sol–gel materials,[10] precipitated oxides[11]). In principle, high-surface-area materials can be created by two different means: Either the bulk material is finely divided to achieve a higher specific surface area, or the bulk material is made porous. A quick estimate shows what kind of specific surface areas can be generated using such methods. The specific surface area of a material which is present in spherical particles is given by Equation (1) where A is the surface area, r the radius, and m

$$\mathrm{A} = \frac{4\pi r^2}{m} \tag{1}$$

the mass of the particle.

Through Equation (2) (ρ being the density of the solid),

$$m = \rho \frac{4}{3}\pi r^3 \tag{2}$$

Equation (3) is obtained.

$$A = \frac{3}{\rho r} \tag{3}$$

Thus, assuming a density of $3\ \mathrm{g\,cm^{-3}}$, which is a good estimate for many oxides, a specific surface area of $1\ \mathrm{cm^2\,g^{-1}}$ is obtained for a solid composed of particles with a radius of 1 cm. Each order of magnitude decrease in particle size increases the specific surface area by one order of magnitude, that is, particles with $r = 1\ \mu\mathrm{m}$ have specific surface areas of the order of $1\ \mathrm{m^2\,g^{-1}}$, and particles of 1-nm radius have $1000\ \mathrm{m^2\,g^{-1}}$. A similar consideration holds, if one imagines that holes are drilled into a solid. If the characteristic sizes of the holes and their pitch (distance between holes) are on the micrometer scale, surface areas on the order of $1\ \mathrm{m^2\,g^{-1}}$ result, if the holes and pitches are on the nanometer scale, the surface areas are around $1000\ \mathrm{m^2\,g^{-1}}$. All strategies to create high-surface-area materials thus have to target a structuring of materials on the nanometer level, since only thus are very high surface areas accessible. The question whether the solid is ordered or disordered is of limited importance with respect to high surface areas. High-surface-area materials may be fully crystalline (such as zeolites), they may be ordered on a mesoscopic length scale, but amorphous on the atomic length scale (such as surfactant-templated materials), or they may be fully disordered (such as silica gels). Specific properties are certainly dependent on the crystalline order, but it is possible to generate high-surface-area materials with either crystalline or amorphous structures.

To structure solids on the nanometer scale one initially relied on experience and adjusted conditions in the synthesis of the materials in a manner which favored a high division of the solids. The early syntheses of porous solids can be rather considered a craft than a science.[12] Examples for this are precipitated oxides and activated carbons which are obtained, under suitable conditions, with very high surface areas and/or high porosities. The first recorded exploitation of the porosity

[*] Prof. Dr. F. Schüth
Max-Planck-Institut für Kohlenforschung
Kaiser-Wilhelm-Platz 1
45470 Mülheim (Germany)
Fax: (+49) 208-306-2995
E-mail: schueth@kofo.mpg.de

 DOI: 10.1002/anie.200300593 © 2003 Wiley-VCH Verlag GmbH & Co. KGaA, Weinheim

of porous solids traces back to ancient Egypt, where charcoal was used as adsorbent for medical applications.[13] A more scientific approach in the synthesis of porous solids began in the first half of the 20th century, when the synthesis of high-surface-area materials was more systematically studied, such as in the case of silica gels or carbons, and useful methods to investigate the properties of porous solids were developed, such as gas-adsorption techniques. The names associated with these pioneering works are, amongst others, Zsigmondy, Anderson, Patrick, Weiser, Langmuir, Brunauer, McBain, Barrer, Breck, and many others. The synthesis, however, although better understood, still relied on artful manipulation of synthesis parameters, and not so much on design principles by which an adjustment of the properties of the materials was possible.

First guiding principles for the synthesis of porous and high-surface-area materials were developed when the concept of "templating" was introduced into zeolite science. However, as much as the word "template" suggests that the pore system is a direct replica of the "template" there is little that is correct in this notion. There are cases, where indeed the shape and size of the templates seems to be correlated to the resulting pore system, but in many cases the function of the templates is still little understood if at all, at least not in the case of microporous[*] solids. This situation is different for ordered mesoporous solids or for colloidal crystals, such as inverse opals. In these cases the situation during the synthesis indeed approaches a templating, where a one-to-one replica of the template is created. This replication process can be so perfect that it is justified to use the term "nanocasting" to describe this process.[14,15]

When templates are used in the synthesis of porous solids two different modes in which the template can act can be distinguished: in analogy to the terms "endoskeleton" and "exoskeleton" in biology, it can be an "endotemplate", that is, a template species which is an isolated precursor and is included as an isolated entity into the growing solid particle, or it can be an "exotemplate", that is, a structure providing a scaffold with voids (Figure 1). If this scaffold is removed after filling of the voids, either a small-particle/high-surface-area material or a porous solid is generated, depending on the three-dimensional connectivity of the exotemplate. In contrast, the pathways occasionally labeled "scaffolding"[16,17] are most probably synthesis routes in which small particles, formed in solution, are stabilized by surfactant molecules and thus further growth is prevented. The porosity found in such materials after calcination is typically interparticle (textural) porosity, that is, the pores result from the voids created by packing of the solid particles and are not an integral part of a continuous solid structure (structural porosity).

In the following, pathways relying on endo- or exotemplating to create high-surface-area and/or porous inorganic solids are introduced and discussed. The article will be based in many cases on examples from the group of the author, but this work will be placed into context of the contributions of the many other researchers who have contributed to this vast field. Excluded from this treatment is the synthesis of organic porous or high-surface-area materials, although also the synthesis of such solids often relies on templating approaches. Those readers with interest in this field can find a recent survey by Hentze and Antonietti.[18] Also excluded are templating approaches which are more directed towards a morphosynthesis, that is, controlling the morphology of particles, such as hollow spheres, tubes, coils, on a larger scale than discussed herein. These aspects are covered thoroughly in a recent article that is more focussed on templating on length scales of several hundred nanometers.[19] Also not covered are molecularly imprinted polymers,[20,21] since the porosity or the high surface areas of such materials are not their most prominent features. The properties of such materials are more exploited in applications where molecular recognition is desired, such as in separation processes. Since complete coverage of the whole field could fill a multi-volume book, the selection is personally biased, and the author would like to apologize at this point for emphasizing some points more than others.

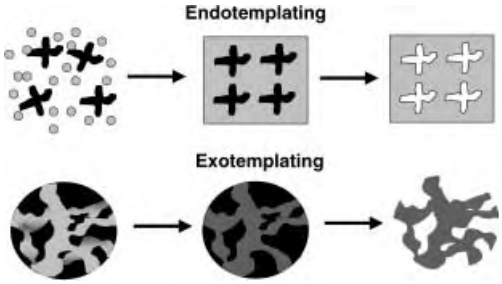


Figure 1. Schematic drawing of the endotemplating and exotemplating approach to synthesize porous and high-surface-area materials. For endotemplating, the templating species are occluded in the forming solid, for exotemplating, a rigid porous solid is infiltrated with the precursor for another solid. Endotemplates as well as exotemplates are removed from the composite to yield the porous or high-surface-area material.

[*] When referring in the following to porous materials, the IUPAC nomenclature will be used, which defines pores with sizes below 2 nm as micropores, with 2–50 nm as mesopores, and pores larger than 50 nm as macropores. The term "nanoporous" is often used. It is, however, not clearly defined and loosely refers to porous materials with pores in the nanometer size range.



Ferdi Schüth studied Chemistry and Law at the Westfälische-Wilhelms-Universität in Münster, where he received his Ph.D. in Chemistry in 1988 and the State Examination in Law in 1989. After post-doctoral work in the group of L. D. Schmidt at the University of Minnesota he joined the group of K. Unger at the University of Mainz. After Habilitation in 1995 he became Professor at the Johann-Wolfgang-Goethe Universität Frankfurt. In 1998 he was appointed Director at the Max-Planck-Institut für Kohlenforschung, Mülheim. His research interests include porous solids and high-throughput-experimentation in catalysis.

 © 2003 Wiley-VCH Verlag GmbH & Co. KGaA, Weinheim

2. Endotemplating: Creating Porous Materials by Occlusion of Molecular or Supramolecular Units in the Forming Solid

This Section covers the synthesis of porous and high-surface-area materials by molecular or supramolecular endotemplating. Specifically the following points will be addressed:

1) Synthesis of zeolitic materials, where the templating species are molecules, for which the mode of action is in many cases not very well understood.
2) The use of supramolecular aggregates, specifically those formed from surfactant molecules, to structure solids on length scales one order of magnitude larger than for zeolites.
3) Approaches selected from the multitude of endotemplating processes, which are characterized by special features of the resulting solids.

Endotemplating creates voids in a solid by inclusion of template species which occupy space around which the solid forms. If afterwards the template is removed, the space is made accessible and a pore system develops. The sizes of the voids can range from the molecular scale, where molecules are used as templates, to the macroscopic scale, where, for instance, latex particles can be the precursors of the pore system. The mechanisms by which the pore systems develop are very diverse. However, it is clear that there needs to be a favorable interaction between the templating species and the solid to be templated, since otherwise the templating species would not be incorporated and phase separation would occur. The smaller the size scale the more important this is, because the "interface" between template and solid increases with increasing dispersion. For templating on the micrometer scale, on the other hand, it is typically sufficient, that the template can be wetted by the precursor of the solid and that the density difference between templating species and the other components is not high, otherwise the templating species settle at the bottom of the vessel or float on the top of the rest of the solution.

2.1. Endotemplating with Molecules: Zeolitic Materials

The concept of "templating" and the word "template" in zeolite science (the word "zeolitic" is used here in a more general sense, that is, it does not only include crystalline microporous aluminosilicates, but also other framework compositions) started to appear on a larger scale in the early 1980s in connection with organic structure-directing agents,[22–24] although zeolite beta, the first high silica zeolite, the synthesis of which had been made possible by the help of an organic additive in the synthesis gel, had been reported already in 1968.[25] In the publication reporting the synthesis of silicalite the structure-directing role of the tetrapropylammonium ion had been discussed, however, without using the word template.[26] It is rather difficult to trace the origin of the concept of templating with organic additives, but it seems to be related to the fact that initially a rather direct specificity of one organic molecule (the first ones being tetraalkylammonium ions) for the formation of one particular zeolite structure was assumed. For those readers interested in an account of the historical development of the concepts and achievements in zeolite synthesis, a recent review by Cundy and Cox is highly recommended.[27]

A first extensive treatment of the templating concept using organic molecules in zeolite synthesis was published in 1979,[28] although Flanigen had described some of the concepts earlier also in connection with organic cations.[24] With respect to the influence of inorganic cations, such as sodium, the concept of "templating" had been used already in the 1960s to understand the influence which cations had on the zeolite structures formed,[29,30] and a discussion summarizing these early studies was published in 1973.[24]

In hindsight, the choice of the word "template" has to be considered rather unfortunate, since it is now often used indiscriminately for all organic additives in zeolite synthesis mixtures. In many such cases, however, the relationship between the templating species and the structure formed is rather indirect. Often the organic species is not even incorporated into the zeolite, such as in the case of the alumophosphate VPI-5.[31] The term "templating" creates the impression of a 1:1 correspondence between shape of the molecule used as template and shape of the void remaining after template removal. In cases, where this correspondence is not proven, it seems better to use the term "structure-directing agent" ("SDA"),[31–34] or the neutral term "organic additive".

There are at least four different modes by which an additive can operate in a zeolite synthesis:[1]

1) It can just be a space filler which occupies the voids between the framework constituents and thus contributes to the energetic stabilization of a more open structure compared to the denser structure;
2) it may control the equilibria in the synthesis mixture, such as pH value or complexation equilibria;
3) it can preorganize solution species to favor nucleation of a specific structure;
4) it may indeed act as a true template, with the framework being formed around the organic molecule which determines the shape and size of the later voids in the structure.

In specific cases this last mode of action does seem to be realized. Gies and Marler[35] have carried out an extensive study in which many different organic additives were used in the synthesis of all-silica molecular sieves. In such cases, where charge interactions are absent, the van der Waals interaction of the organic molecule and the zeolitic material seems to be the governing factor, a view which was subsequently supported by other authors.[36] Under such conditions, the shape and size of the molecule used does control the shape and the size of the cavity or channel formed in the framework. Thus molecules with spherical shape tend to favor the formation of cages or cavities, elongated molecules, such as straight chain alkyl amines, rather direct the formation of structures with unidimensional, channel-type pore systems, whereas branched additives direct the synthesis towards zeolites with interconnected pore system. Maybe the most prominent example for the latter case is the synthesis of

 © 2003 Wiley-VCH Verlag GmbH & Co. KGaA, Weinheim

MFI-type materials[*], such as ZSM-5 or silicalite I with the aid of tetrapropylammonium ions (TPA^+). The structure of the as-made material shows that the TPA^+ is located exactly in the intersections between the straight and sinusoidal channels of the structure (Figure 2). The four propyl groups

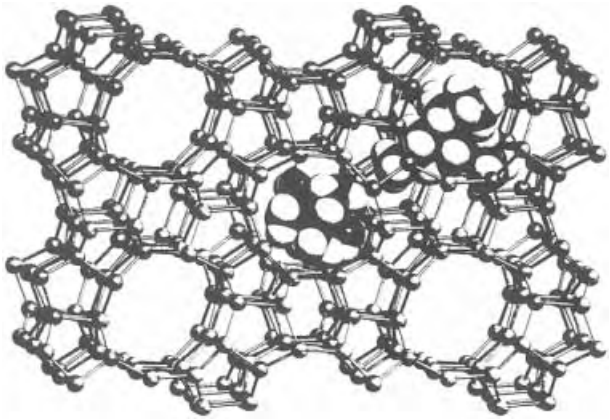


Figure 2. Structure of TPA^+-ZSM-5, showing how the tetrapropylammonium ion is located in the channel intersections. Reproduced with permission from H. van Bekkum, E. M. Flanigen, P. A. Jacobs, J. C. Jansen, *Stud. Surf. Sci. Catal.* **2001**, *137*, 207.

extend into the four channels and connect to the nitrogen atom at each intersection.[37] This structure is an indication that there is indeed a templating effect in this case, which had been proposed in the original publication describing the synthesis of ZSM-5 where a clathration of the TPA^+ ions by the silicate species was assumed.[26] In subsequent years, many experiments were directed at understanding the mode of action of TPA^+ during the formation of ZSM-5, which are summarized in refs. [38,39]. Based upon these results and their own experiments, Burkett and Davis formulated a more detailed mechanism of the templating effect of TPA^+[173] which can actually be considered to be a hybrid between cases 3) and 4) above. According to this mechanism, TPA^+ is initially clathrated by water. These water molecules are successively replaced by silicate species, which leads to a preorganization of the silicate, thus directing the formation of the MFI structure.

In recent years, substantial progress has also been made with respect to computational approaches to understand the templating of zeolitic materials.[40] The action of certain structure directing agents could be rationalized,[41] and the stabilization of silicate moieties by organic molecules in an arrangement, which would collapse in the presence of water, has been described.[40] More complex modes, by which an SDA would direct the formation of a certain zeolite structure, are at present beyond the reach of computational approaches, but the concepts developed by Gies and Marler[35] can be used to develop algorithms, which allow the de novo design of templates for a desired zeolite structure.[42–44] These algorithms essentially attempt to fit possible molecules snugly into the voids of the desired structure. The fit of many computer generated molecules is tested by these methods, and the ones with the best van der Waals interaction between molecule and framework are suggested for synthesis experiments.

Another prominent example for the successful design of a template, albeit not by computational methods, is the synthesis of EMT,[45] the hexagonal variant of faujasite, which was theoretically predicted as the so-called Breck Structure Six.[46] Crown ethers are used for its synthesis, and it has been shown that [18]crown-6 directs the formation of EMT, while [15]crown-5 directs the formation of the regular cubic faujasite. Considering both structures shows that the different templates have a perfect fit in the different structures.[47] In general, however, a true templating mechanism seems to be more often realized in the synthesis of clathrasils and to a lesser extent in the formation of the more open zeolites.

A last aspect which is important in the templating of zeolitic materials is the use of template-like functional groups to incorporate functional molecules in the channel system. This concept has been developed by the groups of Wöhrle and Schulz-Ekloff[48] and was subsequently exploited to improve the uptake of laser dyes into alumophosphates, especially into $AlPO_4$-5.[49–51] It has been found, that laser dye molecules, which bear functional groups resembling the structure-directing agents used in the synthesis, that is, amine groups, are incorporated in situ most easily with least disturbance of the growth of the molecular sieves. The uptake of other laser dyes is more difficult and proceeds only to much lower loading levels. A better understanding of templating mechanisms for zeolitic materials may thus help to facilitate the design of functional solids by incorporation of molecules with specific functions in the channel systems of porous crystals.

2.2. Endotemplating with Supramolecular Surfactant Aggregates: Ordered Mesoporous Materials

If mesoporous materials are to be created by a templating pathway, one can not rely on small single molecules as templates (as described in Section 2.1), since they would not lead to the formation of pores in the mesopore size range. Zeolite chemists had been striving to make bigger pores for many years, and the largest pore sizes gradually moved from the approximately 0.75 nm of faujasites, such as found in zeolite Y and zeolite X, to the 1.2–1.3-nm sized channels in the aluminophosphate VPI-5. It was therefore considered a major breakthrough when the scientists of Mobil Oil company disclosed the synthesis of the so-called M41S materials,[52,53] the most prominent one being MCM-41, a hexagonal arrangement of hexagonal[54] channels which have a diameter of about 4 nm, separated from each other by amorphous silica walls. These types of materials were prepared by templating with a lyotropic liquid-crystal arrangement of surfactant molecules, around which silicate ions condensed to form the

[*] The abbreviations for different zeolitic materials have developed historically and do not follow a rational nomenclature. For structure types, three letter codes derived from the name of the first reported material with a specific structure are used, such as MFI for the ZSM-5 structure. ZSM stands for Zeolite Socony Mobil, MFI stands for *M*obil *F*ive. Information on the structure-type codes can be found on the homepage of the Structure Commission of the International Zeolite Association (IZA) at http://www.iza-structure.org.

 © 2003 Wiley-VCH Verlag GmbH & Co. KGaA, Weinheim

silica framework. Using this pathway, it was possible to synthesize ordered porous materials with pore sizes in the range of 2–10 nm. At approximately the same time, a similar material was discovered independently by the group of Kuroda.[55] Here the surfactant molecules were used to intercalate a layered silica which then transformed into the ordered silica. However, it would be less appropriate to speak about a templating pathway in this case, since in its prototypic form, it resembles more a solid-state reaction in which a layered material is converted into a three-dimensional network material. Many review articles are available which cover surfactant-templated materials and related solids from different angles.[5–7,56–58]

Rather unclear in the first publications on MCM-41 and related materials was the exact mechanism by which the structure formed. In one of the first publications[52] a rather general scheme, showing the possible pathways by which the ordered silica could form (Figure 3) was given. Shortly after a

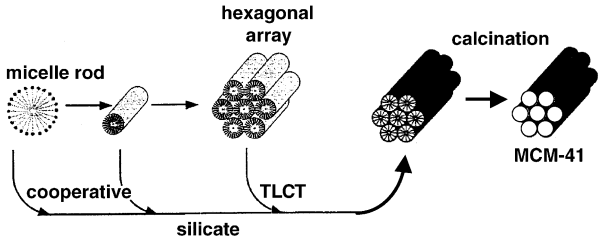


Figure 3. General pathways for the formation of surfactant-templated silica. The pathways leading from spherical and cylindrical micelles to the silica–surfactant hexagonal composite are cooperative, the direct pathway from the hexagonal pure surfactant liquid crystal to the silica–surfactant hexagonal composite has been termed "true liquid crystal templating". Adapted from ref.[52]

more detailed cooperative mechanism was formulated,[59–61] which for many synthesis conditions is still the most generally accepted one, even if small variations have been suggested.[62,63] Under most conditions for the synthesis of ordered mesoporous materials, such a cooperative mechanism, where the inorganic part and the surfactant part act together to create the final composite, is dominant. However, there are conditions, where also the first pathway proposed by the group at Mobil, the direct replication of the surfactant liquid crystal, is the driving force for the formation of a specific structure. Such a pathway prevails, when the surfactant is so concentrated that a liquid crystal is present prior to the addition of the precursor for the inorganic framework material, which was first discovered by George Attard et al.[64]

These cooperative routes are not restricted to the Coulomb interaction between the positive surfactant species and the negative silicate moieties. Also charge-reversed and counterion-mediated pathways are possible.[65] Pinnavaia et al. subsequently introduced non-charged surfactants, such as amines[66] or polyethylene oxide based surfactants,[67] which can also be used to create mesostructured materials. In these cases the interaction between the organic and inorganic part is mediated by hydrogen bonds.

Although the synthesis conditions have some influence on the structure of the resulting solid, the type of surfactant is certainly the dominating factor in directing the formation of a specific structure. The influence which a certain surfactant exerts in the synthesis of a mesoporous material could in many cases be rationalized by the packing-parameter concept originally developed by Israelachvili.[68,69] Many different structures of ordered mesoporous silicas have been synthesized by either using special surfactants or variation of the synthesis conditions. Some of these structures have analogues in surfactant chemistry, some of them, however, had not been described before.[70,71]

The assembly of the mesophase is surprisingly rapid. While typical synthesis procedures use reaction times of hours or even days, it has been shown that under the right conditions the cooperative assembly proceeds on a minute timescale or even faster.[72–74] However, after the initial formation of the mesophases, the materials still change their structures, predominantly by ongoing condensation processes in the inorganic frameworks.[74] These results obtained with conventional laboratory X-ray sources in combination with tubular reactors were subsequently corroborated by more detailed in situ synchrotron investigations which used relatively similar tubular reactor setups. This approach has been especially useful for investigating the effect of the swelling agents. Even the early papers described that the addition of organic molecules, such as mesitylene, would lead to expansion of the pore size, since the oil is incorporated in the hydrophobic part of the micelles.[52] In the time-resolved synchrotron studies it was found that incorporation of the swelling agent is possible in the first minutes, while the inorganic walls have not become rigid and expansion of the channels can proceed. After some minutes, however, the silica condensation has reduced the flexibility of the materials so much, that swelling agents can no longer lead to pore-size expansion and thus addition of swelling agent after this point has no effect.[75]

The wide variety of materials accessible by these supramolecular templating pathways is due to the discovery that this synthesis method for ordered mesoporous silica could be applied to materials other than silica, as had been predicted in the paper where the cooperative mechanism was introduced.[59] In two papers published in 1994,[65,76] the synthesis of mesostructured materials was extended to compositions beyond silica. However, from none of the mesostructured non-silica materials could the surfactant be removed by calcination without structural collapse of the framework, and thus no non-silica ordered mesoporous material was reported. Essentially three reasons can be identified for this:[6,77]

1) some of the materials reported were not fully condensed framework materials, such as the mesostructured tungsten oxide, but rather salt-like structures.[78] Removal of the organic part then inevitably leads to structural collapse.
2) The non-silica materials investigated were redox-unstable. During calcination, reduction and reoxidation of the framework takes place, which destroys the mesostructure.
3) The curvature necessary to form the mesopores in the mesostructure are best compatible with amorphous wall structures. Silica remains amorphous even up to high temperatures, while for most other framework composi-

 © 2003 Wiley-VCH Verlag GmbH & Co. KGaA, Weinheim

tions crystallization is to be expected. This change normally involves mass transfer, which will lead to structural collapse. In addition, the constraints associated with a crystalline structure can not easily be accommodated by the strong curvature of the pores.

The first mesoporous non-silica or non-silicate materials were reported in 1995 for titanium dioxide[79] and 1996 for zirconiumoxophosphate.[80] The choice of the early transition elements solves the problem of redox-instability, since titanium as well as zirconium are difficult to reduce to an oxidation state lower than +IV. It was, however, found to be more difficult to adapt the solution chemistry to the formation of mesostructured titanium or zirconium compounds, since the charges on the inorganic solution species and the surfactant headgroups have to be matched to provide a sufficiently strong interaction for the cooperative self-assembly. One way to solve this problem is the so-called ligand-assisted pathway,[81] where a surfactant group is attached to the metal center by a chemical bond, and thus the supramolecular chemistry of this metallosurfactant can be exploited to create a mesostructured non-silica material.

Alternatively, the counterion of the metal species can be used to match the properties of the inorganic and surfactant components. In the case of zirconium and titanium, sulfates and phosphates are in principle suitable. However, phosphates seem to be too strongly coordinating, and only layered compounds are obtained by the direct assembly.[82] Sulfates, however, allow the formation of hexagonal[77,80,83–85] materials and the cubic *Ia3d*-phase.[86–88] Owing to the thermal instability of sulfates, they have to be exchanged against phosphate prior to calcination. This approach leads to a stable mesoporous material with an amorphous wall structure.[77] The amorphous nature of the wall is most probably a prerequisite to maintain the ordered mesoporosity, at least if no other means to prevent collapse is used. Stabilization against collapse during crystallization is possible by using a carbon "scaffold" in the pores,[89] an approach which will be discussed in Section 3.2.

Larger pores in non-silica materials can be realized by adapting the swelling method originally developed for silica[52] by careful fine-tuning of the synthesis procedure.[90,91] More flexible, however, is the method introduced by the Stucky group. It is analogous to the pathway developed for the synthesis of SBA-15 type materials, in which triblock copolymer surfactants are used, which allow a large variability with respect to pore sizes and wall thickness.[92] The surfactant and the inorganic solution species interact through hydrogen bonds, which also allows greater flexibility in the inorganic component. The triblock-copolymer route has therefore been expanded to allow the assembly of non-silica materials, which typically relies on the use of chloride precursors in alcoholic solutions.[93] For some of the synthesis products obtained by this route (for instance titanium dioxide), it was shown that the walls are composed of crystalline oxide nanoparticles, which seem to be embedded in an amorphous matrix. The substantially thicker walls of SBA-15 as compared to the MCM-41 type materials allow the accommodation of small oxidic particles which have the bulk crystal structure. The surrounding amorphous matrix provides the flexibility necessary to realize the curvatures inherent in the nanoscale structure. There are even indications that zeolitic structural elements may be present in the walls of ordered mesoporous silica.[94,95] Such materials are accessible by adding surfactants to a pre-reacted zeolite synthesis gel. It is assumed that structural units found in zeolites are incorporated into the walls of the mesoporous material. Support for these notions does not come from structural analysis, since no periodicity can be observed in the materials on the atomic scale. However, the high acidity and thermal stability are strong indications, that a higher degree of order is realized in these materials than in conventional ordered mesoporous silica.

It should also be mentioned that the structure of the solid formed can be used to obtain information on the surfactant structures present in solution.[96] It has been shown that surfactant systems close to transition points between different surfactant phases can be „frozen" by replication in silica, thus allowing the analysis of structures which are otherwise very difficult to image owing to their fragility.[97] Figure 4 shows

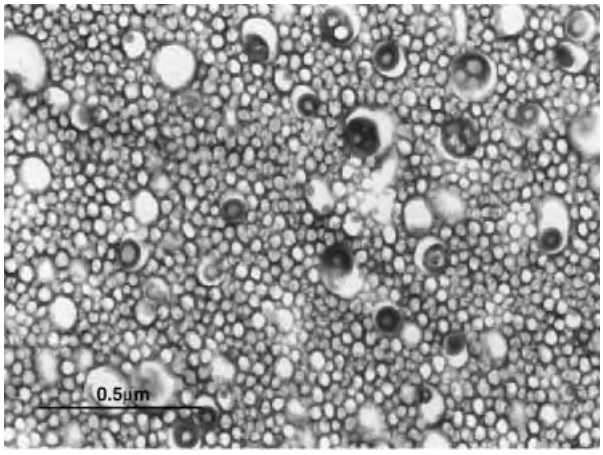


Figure 4. "Nanorattles" obtained by silica replication of a block polymer surfactant system close to the transition to the lamellar mesophase. Reproduced with permission from ref.[97]

such an image, where a block-copolymer system close to the transition to a lamellar mesophase has been obtained as a silica replica. The "rattles" are thought to be related to the presence of vesicular elements in the block copolymer which are expected close to the transition to the lamellar phase. The replication technique may thus prove to be a viable alternative to freeze fracturing and subsequent TEM analysis.

2.3. Other Approaches

Endotemplating as discussed so far was restricted to the formation of more or less ordered materials with periodic pore systems. However, any filler material which is incorporated during the formation of a solid will lead to pores after it has been removed in subsequent steps, and this holds even for macroscopic objects. Discussing these miscellaneous processes would by far exceed the scope of this article, and therefore the focus in this Section will be on processes which

create pores with a narrow size distribution and sizes substantially below 1 μm.

Rather reminiscent to the colloidal crystal templating to create ordered macroporous solids (see below) is the approach taken by Antonietti et al.[98] As in colloidal crystal templating, the templates which create the pores are polymer spheres. However, the polymer spheres are not compacted and organized into a colloidal crystal, but used as an additive in the sol–gel process to create silica. Provided that the dispersion is sufficiently stable and that the surface chemistry is adjusted in a manner to allow favorable interaction between polymer and silica, the polymer spheres are incorporated into the condensing silica gel. After removal of the polymer by calcination, silica with voids corresponding to the size of the polymer template is left. This process allows the pore size to be tuned over a wide range. If differently sized latices are used, the overall porosity and the silica-wall thickness can be adjusted by the ratio between polymer and silica source.

Imhof and Pine have developed a related approach.[99] They used monodisperse emulsion droplets to template the formation of titania, zirconia, and silica. To create a porous solid by this approach, they had to solve several problems. First, most alkoxide precursors are too reactive to be processed in a water-containing emulsion, so that a non-aqueous system had to be used. Second, the sol–gel process then had to be adapted to this system. The solution was eventually found by using stabilized oil-in-formamide emulsions which were fractionated to create emulsions with monodispersed droplets. If a partly prehydrolized alkoxide-in-formamide sol was then combined with the emulsion, and gelation induced by addition of ammonia, the emulsion droplets assembled to a rather well-ordered colloidal crystal around which the inorganic solid formed. After calcination, a structure reminiscent of the inverse opals as described below resulted.

Two other templating approaches developed recently by Kaskel et al. should also be mentioned, since they allow the synthesis of very high-surface-area silicon nitride or silicon imido nitride. The process for the creation of microporous silicon imido nitride relies on the fact that a sol–gel chemistry similar to that of silica had been developed for silicon imide by Bradley et al.[100] The idea was that it should be possible to induce the formation of ordered mesoporous materials analogous to the synthesis of MCM-41 or SBA-15, but condensing $Si(NH)_2$ instead of SiO_2. However, since silica is stable in aqueous environments and silicon imide would immediately be hydrolyzed, only a non-aqueous system could be used. In spite of numerous attempts to prepare a mesostructured material in the presence of surfactants using liquid ammonia or other non-aqueous solvents, such as acetonitrile, formamide, or dimethylformamide, no mesostructured silicon imide could be synthesized. Nevertheless, during these experiments it was possible to prepare a microporous silicon imido nitride by ammonolysis of tris(dimethylamino)silylamine in acetonitrile in the presence of long-chain alkylamines and subsequent calcination in ammonia.[101] The fact that the material is microporous does not prove a templating process, since also without alkylamines a microporous material can be synthesized.[100] However, the pore sizes of the material are clearly dependent on the alkyl chain length of the amine additive, which strongly suggests a templating effect. The pore sizes are difficult to calculate from the sorption isotherm, since the isotherms indicate that the materials are supermicroporous and no suitable algorithms are available in this pore size range. The sizes can be estimated to be below 2 nm for all the amines used, which indicates that rather the molecules themselves act as the template, and not supramolecular aggregates as in the synthesis of MCM-41 type materials. To date this pathway was found unsuitable to template ordered mesoporous silicon imido nitride. However, the materials can act as basic molecular sieves, especially after they have been modified with alkali metals, which provide very strong basicity and are thus sufficiently active for alkene isomerization reactions.[101]

A related pathway indeed allows the synthesis of mesoporous silicon imido nitride with a very sharp pore size distribution, even if the pores are not well ordered.[102,103] Figure 5 gives typical nitrogen sorption isotherms, the steep steps in the adsorption isotherms demonstrate the very high pore volumes and sharp pore size distributions. These materials are synthesized by the ammonolysis of silicon halides in different solvents without any specifically added pore builder. Depending on the type of solvent chosen and the halide used as starting material, the pore size can be tailored over a range between 5.6 nm and 9.1 nm. The template for the formation of the pores is the ammonium halide generated during the ammonolysis. Upon heating the initial gels in ammonia, the halides decompose and leave the pores in the materials. The conditions of the initial ammonolysis control the size of the ammonium halide crystallites which in turn control the pore size of the resulting pores.

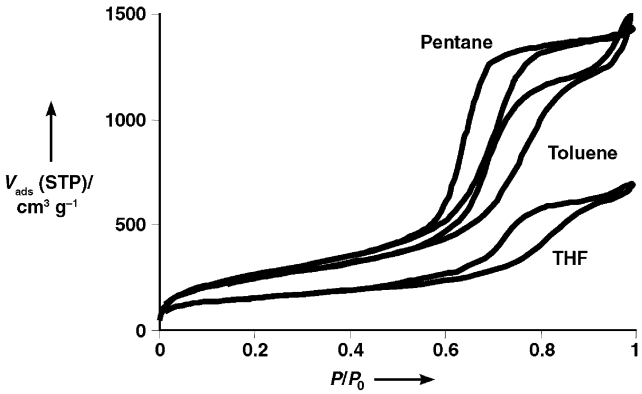


Figure 5. Sorption isotherms of mesoporous silicon imido nitrides. The silicon imido nitrides are obtained by ammonolysis of silicon halides, the ammonium halide nanoparticles formed are decomposed upon thermal treatment and create the pore system. The pore size distributions can be adjusted by the choice of the solvent (as shown in this Figure) or by the choice of the halide. Reproduced with permission from ref. [103].

An interesting templating approach has also been developed for the synthesis of zeolites with an additional mesopore system. This additional pore system is important for optimiz-

 © 2003 Wiley-VCH Verlag GmbH & Co. KGaA, Weinheim

ing mass transfer in zeolite catalysts and thus the performance of the materials in specific catalytic processes. The templating species in this case were different kinds of carbon, such as carbon blacks[104] or carbon nanotubes.[105] The general procedure consists of the impregnation of a carbon source with a zeolite precursor solution or gel, hydrothermal synthesis and subsequent calcination, which removes both the molecular template used for structure direction of the zeolite growth and the carbon template for the generation of the mesopore system. This carbon templating results in the formation of intracrystalline mesopores which facilitate mass transfer, the size of these mesopores can be adjusted by the size of the carbon template. The crystals can show the near to perfect external morphology of well-developed ZSM-5 or silicalite I zeolites. This feature indicates that the growth of the zeolite crystals is not strongly influenced by the presence of the carbon template, and the resulting zeolite particles can probably best be described as either single crystals which are penetrated by a pore system,[105] or as complex twin crystals,[106] penetrated by a pore system. The creation of a transport pore system in zeolites by using carbons as the pore builder provides an interesting alternative to previously used methods to produce mesoporous zeolitic materials, which mostly relied on post synthesis processes, such as controlled steaming and leaching.[107]

3. Exotemplating: Creating High-Surface-Area Materials by Synthesis within Rigid Porous Solids

The concept of exotemplating has been developed only over the last few years, when it was realized that it was indeed possible to obtain structure replication on a length scale of nanometers. Three approaches to create porous and high-surface-area materials by exotemplating will be discussed:

1) The use of an activated carbon matrix, which provides a pore system in which oxidic materials can be generated. The formation of unusual phases after thermal treatment has been observed. Since the activated carbons do not have a fully connected pore system, small-particle material is obtained.
2) The "nanocasting" process, in which a 3D-connected ordered mesoporous material is filled with a precursor for another solid material. The product is obtained in pure form after removal of the exotemplate as the "negative" of the exotemplate. This method allows the synthesis of different types of carbons which in turn can be used again as exotemplates.
3) The synthesis of inverse opals by filling the voids in regular sphere packings with a desired solid and subsequent removal of the original spheres. This allows the synthesis of solids with interesting photonic properties.

Exotemplates are extended structures that contain voids which provide the space in which a divided solid can form. This approach has also been termed "confined space synthesis"[108] or compartment solidification.[109] We speak of exotemplating when the structure of the template is essentially not affected by the process during which the high-surface-area solid is formed. There are certainly borderline cases, such as the route which has been labeled "nanocasting", for the synthesis of ordered mesoporous materials in which a preformed liquid-crystal phase is used as the precursor for the porous structure.[14] For specific cases there seems to be a true replication of the surfactant structures present in solution, but there are also cases where the alcohol formed during hydrolysis of the inorganic precursor disturbs the surfactant structures and has to be removed before the liquid-crystal structure reassembles, as, for instance, in the true liquid-crystal templating approach.[64] Disregarding this somewhat ill-defined boundary, the cases where a preexisting liquid-crystal structure is used to direct the formation of a metal oxide will briefly be treated in this Section. A more complete survey can be found in ref. [14]. Generally, however, in the prototypic form the exotemplating pathway is realized with solids which are rigid and belong to the "hard matter" domain.

Depending on the connectivity of the templating solid, differently dispersed solids are formed (Figure 6): A solid, which could be described as bicontinuous, that is, which consists of one fully continuous solid phase and a fully continuous pore system, will typically result in the formation of a porous solid that is a negative of the exotemplate. In contrast, a solid which does not have a continuous pore system, but rather many different, non-connected pores, will tend to lead to the formation of a high surface area, small-particle solid, in which possible pores are rather textural, that is, between the individual particles, and not structural. Examples for both types of exotemplates will be given below.

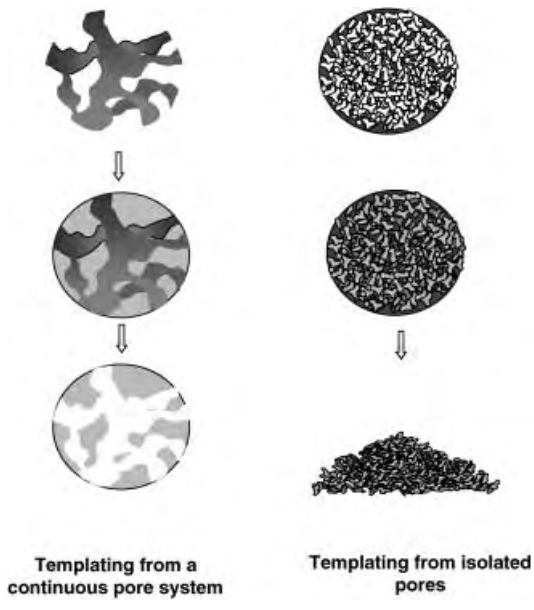


Figure 6. The two prototypes of exotemplating. Left: If the pore system of the exotemplate is continuous and high loadings are achieved, a continuous porous solid with voids corresponding to the template is obtained ("Nanocasting"). Right: If the pores of the template are not 3D connected and/or the filling of the pore system is not sufficiently high, small particles are obtained with high surface areas, but predominantly textural porosity.

 © 2003 Wiley-VCH Verlag GmbH & Co. KGaA, Weinheim

3.1. Activated-Carbon Route for the Generation of High-Surface-Area/Small-Particle Oxides

Activated carbon, that is, highly porous, high-surface-area carbon which can be obtained by an activation process from various different precursor materials, is an ideal exotemplate for the creation of high-surface-area materials. It can be removed easily by combustion, it is readily available with various different pore sizes and pore volumes, the surface polarity can be adjusted, and activated carbons are relatively cheap, so that a process based on this material would also be economically interesting. We therefore decided to start a program in which activated carbons are used as exotemplates to create high-surface-area oxides.[110,111] An isolated report on the use of activated carbon in a similar manner as explored by us had appeared earlier,[112] but there was no systematic investigation of carbons as templates for high-surface-area solids which would exploit the full potential of the material. Carbon black, which normally consists of non-porous, rather spherical carbon particles, has also been used as a matrix for the synthesis of zeolites.[108] Since carbon blacks mostly consist of spherical particles, which sometimes contain additional microporosity,[113] it is not entirely clear whether in this work the zeolites crystallized within structural pores of the carbon or within interparticle voids. Irrespective of the actual mechanism, the result were zeolite samples with remarkably small particle sizes. Another series of papers reported that, activated carbons and activated carbon fibers have been used as templates for the synthesis of nanoporous oxides. The carbons were initially impregnated with solutions of metal-oxide precursors in supercritical solvents.[114–118] It is assumed that the inner pore surface and/or interparticle pores of the template carbon are coated by the precursor, which is then converted into the oxide during a heating step. Upon removal of the carbon, the inorganic coating remains, with pores corresponding to the size of the graphene units which were present in the carbon template. The process has the advantage, that the macroscale morphology of the samples is replicated, so that shaped bodies can be obtained.

Our approach resembles this procedure, but is different in two respects. 1) we do not try to coat the pores of the template carbon but to completely fill the pores and thus to achieve a loading that is as high as possible. 2) it is much simpler, since it only involves neat alkoxides or aqueous salt solution instead of the supercritical solvents, which were assumed to be a prerequisite in the studies of Wakayama et al.[117] In short, the synthesis process consists of impregnation of an activated carbon with concentrated aqueous salt solutions or neat liquid alkoxides, drying, and subsequent combustion of the carbon. If single-metal precursors are used, the binary oxide is obtained as the final product, if mixed-metal precursors are used in correct stoichiometry, it is also possible to synthesize high-surface-area ternary oxides, such as spinels or perowskites.

There are several important factors which contribute to the surface area of the resulting oxides. The carbon precursor has to be hydrophilic so that the precursor solution penetrates the pore system. It has also been found, that the highest surface areas are typically obtained for high loadings, that is, concentrated precursor solutions or repeated impregnation. For MgO, for instance, a reduction of the specific surface area from approximately 200 $m^2 g^{-1}$ synthesized from concentrated solution (3.83 mol L^{-1}, $Mg(NO_3)_2$) to about 100 $m^2 g^{-1}$ for a solution with only a quarter of the concentration was observed. Clearly, the solids yield also decreases if less concentrated precursor solutions are used. The source of the precursor metal ion has a strong influence as well.

In cases where several highly soluble salts are available, it was consistently found that the nitrates led to the formation of the materials with the highest surface areas. Table 1 gives a survey over the types of oxides which can be formed by the activated-carbon route. Not all metals are equally suitable to be nanostructured by this route. Some metal ions, such as copper, manganese, and chromium, strongly catalyze carbon combustion and if they are used in the form of the nitrates a highly reactive mixture is obtained. If such mixtures are heated, a vigorous reaction occurs and the material essentially ignites. Therefore, great care should be taken in preparing and handling such precursors. Manganese in particular was found to be a very active catalyst for carbon combustion, and full removal of the carbon from the precursors could be achieved at temperatures as low as 180 °C, resulting in the formation of

Table 1: Selected products obtained by impregnation of activated carbon with concentrated nitrate precursor solutions. Titanium tetrabutoxide was used neat.[110]

Precursor	Activated carbon	Calcination	Product (XRD)	Surface area [$m^2 g^{-1}$][a]
$Mg(NO_3)_2$	Darco KB-B	1 h 500 °C	MgO	201
$Mg(NO_3)_2$	-	1 h 500 °C	MgO	9
$Fe(NO_3)_3$	Fluka 05120	1 h 450 °C	Fe_2O_3	123
$Fe(NO_3)_3$	Darco KB-B	1 h 450 °C	Fe_2O_3	113
$Fe(NO_3)_3$	–	1 h 450 °C	Fe_2O_3	36
$Cr(NO_3)_3$	Fluka 05120	1.5 h 450–500 °C[b]	Cr_2O_3	156
$Cr(NO_3)_3$	–	1 h 500 °C	Cr_2O_3	10
$Ti(OC_4H_9)_4$	Fluka 05120	1 h 450 °C	TiO_2	200
$Ti(OC_4H_9)_4$	–	1 h 450 °C	TiO_2	43
$Zn(NO_3)_2/Cr(NO_3)_3$	Fluka 05120	15 min. 800 °C	$ZnCr_2O_4$	72
$Zn(NO_3)_2/Cr(NO_3)_3$	–	15 min. 800 °C	$ZnCr_2O_4$	8
$Co(NO_3)_2/Cr(NO_3)_3$	Darco KB-B	1 h 500 °C	$CoCr_2O_4$	126
$Co(NO_3)_2/Cr(NO_3)_3$	Darco KB-B	45 min. 600 °C	$CoCr_2O_4$	111
$Co(NO_3)_2/Cr(NO_3)_3$	–	45 min. 600 °C	$CoCr_2O_4$[c]	27
$Ni(NO_3)_2/Al(NO_3)_3$	Darco KB-B	5 h 800 °C	$NiAl_2O_4$	165
$Ni(NO_3)_2/Al(NO_3)_3$	Darco KB-B	15 min 800 °C	$NiAl_2O_4$	220
$Ni(NO_3)_2/Al(NO_3)_3$	–	15 min. 800 °C	$NiAl_2O_4$[c]	106
$La(NO_3)_3/Fe(NO_3)_3$	Fluka 05120	20 min. 700 °C	$LaFeO_3$	49
$La(NO_3)_3/Fe(NO_3)_3$	–	20 min. 700 °C	$LaFeO_3$[c]	14

[a] From BET measurements. [b] With Ar/air in a tube furnace. [c] Multi phase.

© 2003 Wiley-VCH Verlag GmbH & Co. KGaA, Weinheim

Mn_3O_4 with a specific surface area of around 70 $m^2 g^{-1}$. Figure 7 shows a typical TEM image of the product from an activated-carbon-based synthesis. The general features are independent of the oxide produced. The oxides are always obtained in the form of small particles with sizes between somewhat below 10 nm up to several 10 nm and correspondingly high surface areas.[110,111,119]

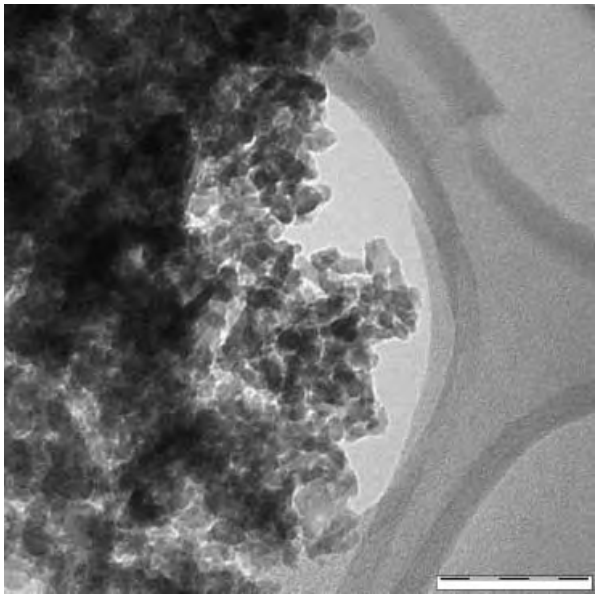


Figure 7. Activated-carbon templated Fe_2O_3 with a surface area of 125 $m^2 g^{-1}$. The TEM is typical for many other materials with different composition obtained by the activated-carbon templating route. Normally, particles in the size range around 10 nm are obtained, the scale bar represents 50 nm. (Courtesy of Manfred Schwickardi.)

Crucial parameters in the synthesis of oxides by the activated-carbon templating route are the atmosphere during heat treatment of the impregnated carbon and the temperature program used. As stated above, some of the metal ions are so active for carbon combustion that they catalyze the burn-off of the carbon template before the oxide has fully formed. Under these conditions, aggregation of the oxide precursor to larger particles is possible with corresponding loss of surface area. For example, the activated-carbon-based synthesis of Cr_2O_3 without special precautions, that is, by just placing the impregnated carbon in an oven and heating to 450 °C, led to a material with a specific surface area of around 70 $m^2 g^{-1}$. Just placing a D2 frit on top of the crucible to reduce the rate of oxygen transfer to the sample led to a surface area of 100 $m^2 g^{-1}$. Performing the carbon removal under controlled atmosphere, that is, first heating from room temperature to 450 °C over 160 min in an argon flow, then switching to an argon/oxygen (5:1) flow and heating further to 500 °C resulted in a Cr_2O_3 sample with a surface area of 155 $m^2 g^{-1}$. A similar result was obtained by performing the combustion in a fluidized bed in an argon/oxygen (5:1) mixture which was heated from room temperature to 450 °C.[110]

These observations opened the route for further development of the process.[120] Since the carbon provides an inert template matrix which keeps the particles apart, the oxide materials formed can be pretreated at high temperatures in inert gas without substantial risk of sintering. It should thus be possible to create high-temperature phases of different materials without the normally observed loss of surface area. This is not as straightforward as it might appear at first sight. We have attempted to produce α-alumina by impregnation of activated carbon, heat treatment in argon at temperatures above the temperature needed to convert the transition aluminas first formed upon heat treatment of precursors, and subsequent combustion of the carbon at lower temperature. However, if an activated-carbon impregnated with aluminum nitrate solution is heated in argon atmosphere to 1300 °C, the X-ray diffraction pattern of the resulting composite does not show the reflections of α-alumina, but those of γ-alumina, superimposed on the broad background resulting from the activated carbon (Figure 8). The highest

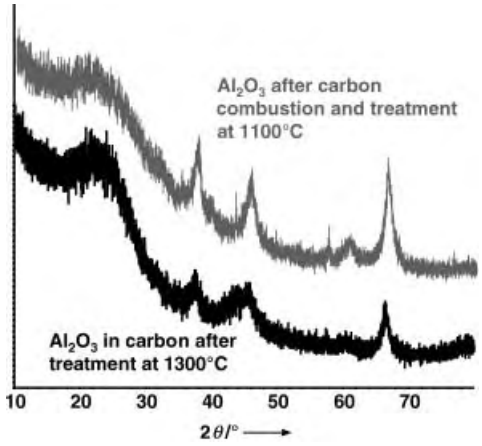


Figure 8. X-ray powder patterns of two alumina samples obtained by high-temperature treatment of activated-carbon impregnated with aluminum nitrate in inert gas. Lower pattern: Carbon/alumina composite after treatment at 1300 °C. The pattern shows only the features of the activated carbon and reflections which can be attributed to γ-alumina. Upper trace: Pattern after combustion of the carbon at 500 °C and heat treatment in air at 1100 °C for 3 h. The pattern still corresponds to γ-alumina, the broad reflections indicate small particles, the surface area of the alumina is about 90 $m^2 g^{-1}$. (Courtesy of Manfred Schwickardi.)

temperature normally observed for the transformation to α-alumina is around 1100 °C. The carbon template can now be removed at lower temperatures to obtain the oxide. After carbon combustion at 500 °C and additional heat treatment at 600 °C for 45 min a γ-alumina with a specific surface area of about 200 $m^2 g^{-1}$ is obtained. This material has a very high thermal stability even without the carbon matrix: heat treatment for 3 h at 1100 °C reduces the surface area, but it is still about 90 $m^2 g^{-1}$ even after this harsh treatment (Figure 8).

The reason for the unusual stabilization of the γ-alumina in the carbon matrix is not fully clear. It may be an effect of the impurities which are present (around 1000 ppm) even in a high-purity activated carbon. Such impurities may substitute

 © 2003 Wiley-VCH Verlag GmbH & Co. KGaA, Weinheim

the spinel-structure of γ-alumina and thus stabilize it against conversion into α-alumina.[121] Alternatively, the stabilization could be due to a particle size effect, which can manifest itself in two different ways: 1) if the surface energy of the α-alumina is higher than the surface energy of the γ-alumina, then a critical particle size exists (in the range where the surface energy is not negligible for the total energy of the system) below which the γ-phase is the more stable one. These effects have been extensively discussed for zirconia phases.[122] However, for alumina not occluded in a matrix, it has been shown that smaller particles of γ-alumina in fact transform more easily to α-alumina than bigger particles, which tends to speak against this mechanism.[123] The situation in the carbon matrix may be different, though, since the surface energies for the alumina in contact with carbon would be different. 2) Alternatively, if the particle sizes are too small, then nucleation of the more stable phase may be strongly hindered and the existence of γ-alumina in the carbon matrix at 1300 °C would be due to a kinetic barrier. Also this effect has been discussed extensively for zirconia,[124] and related arguments have been put forward for alumina as well.[125]

The pathway described above, that is, heat treatment of a material in the carbon matrix under inert atmosphere at high temperature and subsequent carbon combustion at lower temperatures has been used to create many other thermally stable high-surface-area materials, including different spinels and tetragonal zirconium–cerium oxide. Interestingly, the activated-carbon templating method can also be used to directly prepare supported noble-metal catalysts. If an activated carbon is preloaded with aluminumnitrate and dried, and then impregnated with $[Rh(acac)_3]$ in THF, heat treated in argon at 1100 °C and then in air at 500 °C, the resulting γ-alumina has a specific surface area of 320 $m^2 g^{-1}$ on which Rh_2O_3 particles of around 1–1.5 nm in size are homogeneously dispersed (Figure 9).

Considering the rather wide range of different materials which are accessible by the activated-carbon templating method, it could prove to be a scalable pathway for the preparation of many different high-surface-area materials in larger amounts. One can, for instance, consider the production of oxides by this route in a rotary kiln, in which a predried, impregnated carbon enters on one side and the counterflow brings air into contact with the material. Safety aspects are certainly important in the design of such a production process, but with suitable precautions against possible explosions, such a procedure should be manageable.

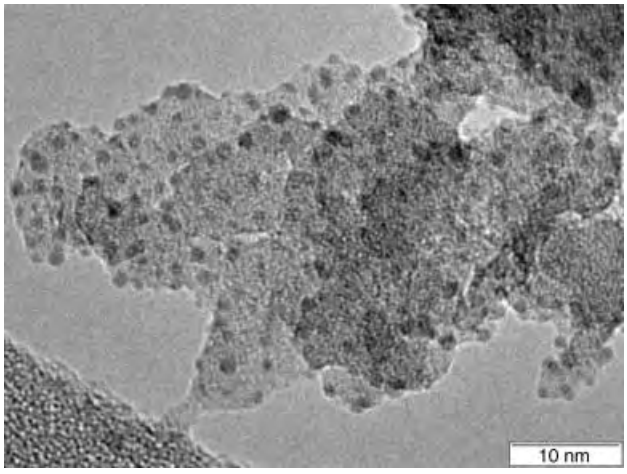


Figure 9. TEM of a supported catalyst obtained by the activated-carbon route. The sample is Rh_2O_3 on γ-alumina, the total surface area is 320 $m^2 g^{-1}$. The rhodium oxide particles have a size of approximately 1 nm. (Courtesy of Manfred Schwickardi.)

3.2. Nanocasting: Replicating Structures on the Nanometer Scale

In the activated-carbon templating described above, the pore system of the carbon template is certainly not replicated perfectly, but rather provides the voids for the solid formation and prevents growth of larger particles. The successful use of the carbon-templating route, however, induced us to extend the range of templates from activated carbons with their disordered and noncontinuous pore system to ordered carbons with a mesopore system. The aim was the exact replication of these materials which would justify the use of the term "nanocasting",[14] since the template is actually used as a true mold with characteristic dimensions in the nanometer range.

The ordered mesoporous carbons to be used as templates for an oxide nanocasting became available in 1999 as the product of a nanocasting procedure from ordered mesoporous silicas themselves. Nanocasting from ordered mesoporous silica exotemplates was pioneered by the group of Ryong Ryoo,[126] independently and somewhat later, similar approaches were published by Hyeon and co-workers (the materials were designated SNU-x).[127] Disordered porous carbons, however, had been obtained in the middle of the 1980s by using silica particles as templates to produce a polymer which was then carbonized.[128] The principal procedure is represented in Figure 10. An ordered mesoporous silica is impregnated with a precursor for carbon. Different precursors can be used, such as sucrose,[126] furfuryl alcohol,[129] resorcinol-formaldehyde,[130] which are also precursors that are often used in the preparation of carbon aerogels.[131] In the first report on this topic,[126] the cubic *Ia3d* material MCM-48 was used as the template and the pore system was filled with sucrose. Treatment of the composite at 800–1100 °C



Figure 10. Schematic description of the nanocasting pathway. An ordered mesoporous silica template (SBA-15, MCM-48, or another structure with 3D pore system) is impregnated with a carbon precursor (sucrose, furfuryl alcohol, resorcinol-formaldehyde), the precursor is carbonized by treatment at high temperature in inert atmosphere, the silica is dissolved with NaOH or HF, which creates the ordered mesoporous carbon. This material in turn can be used as a template again; for this it is filled with an oxide precursor, such as TEOS, which is hydrolyzed and condensed, then the carbon is combusted to give the ordered mesoporous oxide.

 © 2003 Wiley-VCH Verlag GmbH & Co. KGaA, Weinheim

in vacuum or inert gas led to conversion of the carbon precursor into a pure carbon material. After removal of the silica mold with NaOH or HF solution an ordered mesoporous carbon, called CMK-1, was obtained. MCM-48 is a bicontinuous structure, having two enantiomeric channel systems, separated by a silica minimal surface. After removal of the silica, the original *Ia3d* symmetry of the template silica was reduced to a space group with lower symmetry, indicated by appearance of additional reflections. In a later paper,[132] the structure of MCM-48-templated carbons was elucidated in detail. There are in fact two different carbon structures, which can be obtained by templating with MCM-48. In CMK-1, the space-group symmetry is reduced to $I4_{1/a}$. This change is attributed to the fact that first the carbon is equally formed in both channel systems, but that the filled channel systems are displaced with respect to each other after dissolution of the silica. By using a different synthesis procedure, a carbon replica which retains the *Ia3d* space group of the MCM-48 template and which is named CMK-4, is obtained. This pathway relies on carbon deposition in an alumosilicate MCM-48 from the gas phase with acetylene as the carbon source at 800 °C.

At first sight it was rather surprising that also SBA-15, an arrangement of hexagonally ordered cylindrical channels,[92] could be nanocasted as a carbon-copy, CMK-3 (Figure 10).[133] Unconnected channels should not lead to the formation of a free standing, 3D structure, but rather to disconnected carbon rods. However, there had been growing evidence since the discovery of SBA-15[92] that there were micropores connecting the hexagonally packed mesopores.[134,135] Since these micropores are also filled with the carbon precursor, they form bridges between the carbon rods, providing the 3D connectivity.[136,137]

If the mesopores of SBA-15 are not filled completely, but only covered with carbon, it is not an array of carbon rods which forms, but an array of carbon nanotubes, called CMK-5.[138] Subsequent removal of the silica then results in two different types of pores, the ones in the center of the carbon tubes and the ones which are generated by silica removal. In the initial publication the generated carbon was used as support for highly dispersed, highly loaded platinum, and not much information on textural properties and tailoring of the pore system was available.[138] Since the mode of pore formation is different for the pores within the tubes and between the tubes, it appeared possible to control the properties of two pore systems independently and we have therefore started a project to achieve this goal.[139] The wall thickness (corresponding to the intertube-pores in the carbon replica) and the pore sizes of the SBA-15 template (related to the intratube-pores) can to some extent be controlled by the choice of the template and the hydrothermal treatment.[92,140] More straightforward, however, is the control of the thickness of the carbon cladding of the SBA-15 channels. By choosing different concentrations of furfuryl alcohol dissolved in 1,3,5-trimethylbenzene for loading of the SBA-15, the thickness of the walls of the carbon nanotubes could be controlled. Figure 11 shows the sorption isotherms for templated carbons obtained for different concentrations of furfuryl alcohol. The two-step isotherm shows the existence of two pore systems,

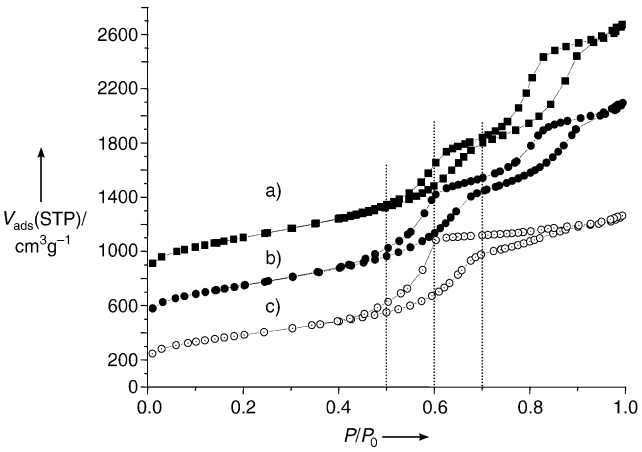


Figure 11. Nitrogen sorption isotherms of nanocasted carbons NCC-1; a) NNC-1-25, b) NCC-1-40, c) NNC-1-80. This material is a 3D arrangement of carbon nanotubes. The first step in the isotherm at low relative pressures (P/P_0) corresponds to the pores between the nanotubes (about 5 nm), the second step corresponds to the pores within the tubes (about 11 nm). The material is obtained by coating the walls of SBA-15 with a carbon precursor, subsequent carbonization, and finally leaching of the silica, similar to the synthesis of CMK-5. (Courtesy of Anhui Lu.) V_{ads}(STP) = volume adsorbed at standard temperature and pressure

with the step at lower relative pressure corresponding to the pores created by removal of the silica and the step at higher pressure to the pores in the inner part of the nanotubes. If a highly concentrated carbon-precursor solution is used, the second step is essentially lost, because the SBA-15 channels are filled to such a degree that full blocking occurs. The corresponding TEM (Figure 12) shows the projection of this structure along the channel axis. The two pore systems can clearly be identified in this image. This pathway should allow the tailoring of pore sizes over wide ranges with the possibility

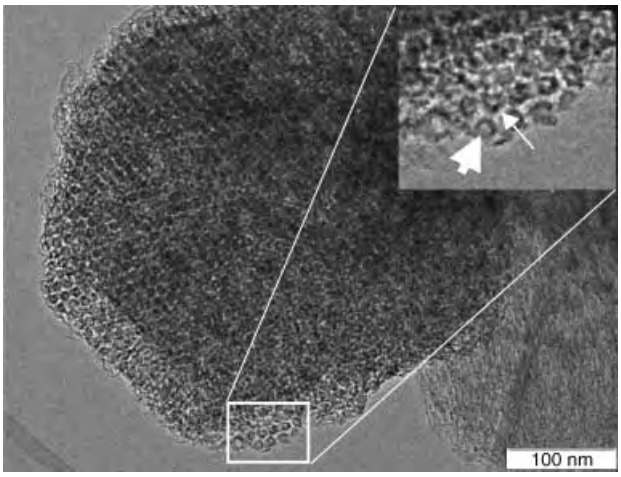


Figure 12. TEM image of NCC-1 synthesized with a low amount of carbon precursor (25 vol.% solution of furfuryl alcohol in trimethylbenzene). The arrangement of the tubes is a replica of the SBA-15 parent. The larger pores within the tubes are indicated by the bold arrow, the smaller internanotube pores are indicated by the smaller arrow in the enlarged section. (Courtesy of Anhui Lu.)

 © 2003 Wiley-VCH Verlag GmbH & Co. KGaA, Weinheim

to create independent pore systems, since the two pores are not formed at the same time, that is, the inner part of the nanotubes is created in the carbonization step, the other pore system during silica removal.

Carbon, in turn, is an ideal template to create other ordered materials, since it can be removed by simple calcination, but in principle also by other techniques, that is, reaction with sulfur, hydrogenation, or fluorination. It was indeed shown, that also repeated nanocasting is possible, whereby first SBA-15 is used as a mold for CMK-3 carbon which is then used as the new mold for silica or alumina.[141,142,91] Nanocasting of silica from CMK-3 can be considered as a feasibility study, since it essentially produces the starting material SBA-3, albeit with somewhat altered structural properties. However, if the principle is confirmed, then the route to other compositions seems open. Different silica sources can be used for replicating CMK-3. Tetraethoxysilane (TEOS) can conveniently be infiltrated into the pore system, and hydrolysis can be initiated by treatment with HCl solution. Ethanol and water are removed by heating at 80 °C, the procedure can be repeated until the desired loading is obtained.[141] Alternatively, an aqueous Na_2SiO_3 solution is used as the starting material.[142] The sample is heated to evaporate the water and then condensation is induced by exposure to HCl vapor. Both reports on the nanocasting of silica from CMK-3 type carbon give evidence for the true replication of the original SBA-15. Figure 13 shows the

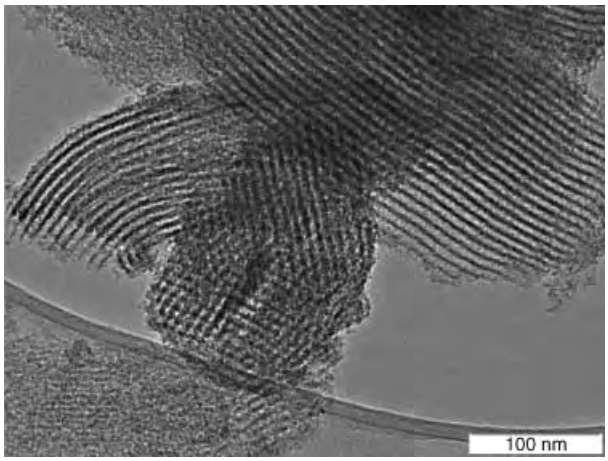


Figure 13. TEM image of nanocasted silica NCS-1 which was obtained by repeated nanocasting according to the scheme in Figure 10. The morphology is similar to the known morphologies of SBA-15. (Courtesy of Anhui Lu.)

nanocasted silica NCS-1 which was obtained by repeated nanocasting. The resemblance of the NCS-1 with the SBA-15 structure and morphology is clear. The textural parameters are changed to some extent during the nanocasting. The surface areas are normally reduced, as are the pore volumes and the pore sizes. This can probably be attributed to the repeated high-temperature-treatment steps which lead to shrinkage of the structure.

In principle, the process should be suitable for the generation of frameworks other than silica as well. In ref. [142] the authors claim that also alumina, titania, and zirconia can be structured in this way, but no evidence has been put forward to date. In ref. [90] a nanocasted alumina is reported. However, the replication is far from perfect, and the pore system is essentially disordered. An interesting, related approach, though, has been used to create single crystalline, but mesoporous niobium–tantalum oxide.[89] Thereby an amorphous niobium–tantalum oxide[143] was synthesized, the pore system of which was then filled with a carbon precursor. After pyrolysis of the carbon precursor, though, the parent template had not been removed. High-temperature treatment of the composite led to crystallization of the niobium–tantalum oxide walls, which appeared to have larger single crystalline domains which were penetrated by mesopores. Removal of the carbon template, which could rather be considered a scaffold in this case than a template, led to ordered porous niobium–tantalum oxide with crystalline walls, having single-crystalline domains and regularly arranged mesopores. This pathway may be a suitable method by which to crystallize the walls of other non-silica mesoporous materials. Although the replication of non-silica materials seems not to be as straightforward as for silica, it can be foreseen that within the next few years the nanocasting process will be extended to other structures and other framework compositions, which may even go beyond oxidic frameworks.

3.3. Colloidal-Crystal Templating

While templating with molecules, as in the synthesis of zeolites, results in porous materials with pore dimensions in the size range of molecules, and templating with supramolecular aggregates, such as liquid crystals, or the nanocasting process results in the formation of pores in the mesopore range, ordered macroporous materials are accessible by templating with colloidal crystals formed from monodisperse spherical particles with diameters of several hundred nanometers. Two excellent reviews of colloidal-crystal templating have been published recently.[144,145] Regular assemblies of such spherical particles diffract light, since the wavelength of light is on the same order as the repeat distance of the packing. The application perspectives opened up by such optical band-gap materials[146–148] in various fields have led to widespread research activities in many laboratories. Opals are a prominent class of such materials, and if opals are used as templates, the resulting structures obtained after removal of the spheres forming the opal are called "inverse opals" (Figure 14). Prerequisite for the synthesis of opals is the

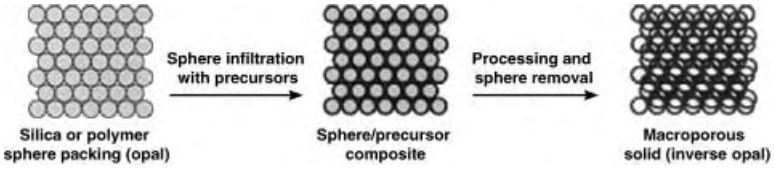


Figure 14. Schematic representation of the synthesis process for inverse opals. Reproduced with permission from ref. [144].

 © 2003 Wiley-VCH Verlag GmbH & Co. KGaA, Weinheim

availability of monodispersed spherical particles with sizes in the range of roughly 0.1–1 μm. Methods to synthesize such monodisperse particles are available for silica (the Stöber-process[149]) and for different polymers, which are most easily accessible by emulsion polymerization.[150] Natural opals consist of packings of silica spheres, while artificial opals are more frequently assembled from polymer latices owing to the wider variability which can be achieved with polymers.

If opals, formed by sphere packings (most frequently observed are space-filling packings, such as fcc or hcp), are infiltrated with precursors for inorganic solids and the spheres are subsequently removed, an ordered macroporous material is obtained. In the case of the templating with colloidal crystals, the boundary between exotemplating and endotemplating is certainly not well defined. If the spheres forming the colloidal crystal are considered as individuals, then they could be considered as endotemplates. If, however, the colloidal crystal is considered as one entity, the voids of which are filled, than exotemplating would be the more correct term according to the definition given in Section 1. For colloidal-crystal templating one could in fact argue both cases. Polymer latices typically retain their individuality and no chemical bonds are formed between different spheres, although the packing may be rather rigid because of other forces acting between the particles. In packings of monodisperse silica spheres, on the other hand, siloxane bonds may form during processing and rigidification of the colloidal template takes place.

The seminal reports on such approaches appeared in the second half of the 1990s.[151–153] The first relatively regular structure was obtained as a thin film composed of silica,[151] but subsequently also bulk material of various different compositions could be synthesized.[154] A full band-gap material which is the goal of most of the research efforts, requires a high perfection of the structure which has not been achieved to date in the bulk material. In addition, a high refractive index of the solid is mandatory. Thus the synthesis of a silicon inverse opal was considered to be a significant step in this field, although the band gap in this case is in the near infrared and not in the visible light range.[155]

Several steps in the synthesis process of an inverse opal are decisive. Firstly, the assembly of the opal template will influence the perfection of the resulting replicate. If only a transport pore system is desired, such as necessary, for instance, in catalysis, then there is no need for a high perfection of the template. If, on the other hand, a photonic band-gap material is to be produced, the perfection of the assembly is of paramount importance.[156] Defects present in the colloidal crystals are the same as those typically encountered in conventional crystals, such as point defects, line defects, or grain boundaries. Many factors influence the perfection of the opal structure, such as the dispersity of the latices, the rate of drying or filtration, the surface charges, and the solvent. To date the synthesis of colloidal crystals with a low defect concentration remains an experimental challenge.

The infiltration step is also highly influential with respect to the properties of the resulting material. Often the infiltration of the parent opal is carried out in the liquid phase, using neat metal alkoxides[154] or alkoxides dissolved in a suitable solvent,[154,157] or sols of colloidal particles with sizes well below the pore sizes of the opal template; subsequently the sol is infused into the template.[158] Wetting of the opal template is crucial to achieve a good distribution of the infiltrating solution over the mold, and therefore surface modification of the spheres forming the opal has been used to optimize the infiltration behavior. Alternatively, chemical vapor deposition (CVD) processes can also be employed to fill the voids of the opal.[155,159,160] If a CVD process is chosen, the decomposition of the precursor gases, such as silanes, typically needs temperatures which are too high for polymer latice which would be destroyed. Under such conditions it is therefore advisable to use opal templates composed of silica spheres which can be heated without damage to the structure. For a successful replication to the inverse opal, the precursors should be converted into the oxides prior to removal of the template. This step is done by hydrolysis and condensation for the alkoxide precursors (and mostly by thermal steps for the CVD-precursors). Since the hydrolysis of the alkoxides can be controlled by the dilution, the solvent, the water concentration, and other factors, this step in principle allows fine-tuning of the process, but on the other hand makes it highly susceptible to external influence. For special cases, such as the creation of metal inverse opals, other techniques have been developed, such as electroless deposition in the void space[161] or reduction of initially formed oxides.[162]

A major factor deciding the resulting structure is the filling degree of the voids of the initial opal and the condensation and template-removal conditions. Recently Marlow et al.[163] discovered a novel inverse opal structure and proposed categorizing inverse opals in three classes (a two category classification, volume-templated and surface-templated materials, had earlier been suggested by Zhakidov[159]): 1) the residual-volume structures, which is the exact inverse replica of the opal, 2) the shell structure, which is formed by coating of the spheres which form the opal mold, that is, the pores of the opal are incompletely filled, and 3) the skeleton structures, which also result from incomplete filling of the pores, but are topologically equivalent to the residual-volume structures. Figure 15 gives examples for all three categories. The exact processes by which the different structures are formed, are not yet fully understood. It is

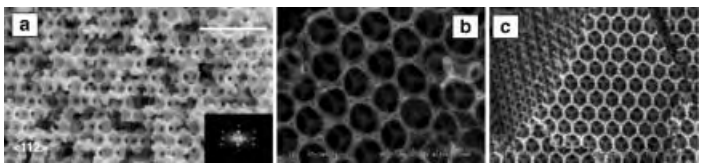


Figure 15. SEM images of the three different types of inverse opal structures. a) Residual-void structure, resulting from complete filling of the voids between the spheres of the opal template (scale bar represents 1000 nm). b) Shell structure, resulting from incomplete filling of the voids and coating of the spheres. c) Skeleton structure, also resulting from incomplete filling. However, in the formation of the network, redistribution of matter occurs, which leads to a structure different from the shell structure. Reproduced with permission from ref. [158] (a) and ref. [157] (b, c).

 © 2003 Wiley-VCH Verlag GmbH & Co. KGaA, Weinheim

clear that for the formation of a residual-volume structure filling of the mold has to be as complete as possible, which is achieved by repeated infiltration. But even in such cases, removal of the templating spheres by calcination or a leaching process does not lead to a 1:1 replica, since substantial shrinkage, on the order of around 30%, occurs.[151,154] The formation of the shell structure and the skeleton structure seems to be controlled by the processing conditions. Skeleton structures are preferred under conditions where first a gel forms in the pores of the template, which converts into the skeleton after template removal.[157] A thorough analysis of the geometric requirements for the formation of the shell structures revealed that substantial redistribution of matter must occur during removal of the opal template, since otherwise the diameters of the struts which form the skeleton could not be explained.[157]

There are a large variety of different compositions for the inverse opals. They range from simple oxides and carbon,[144] over silicon[155] and germanium[160] to more complex materials such as composites of hydroxyapatite and tricalcium phosphate phases.[164] The textural properties observed for the walls of inverse opal structures can vary widely. There are reports on nonporous materials, such as a zirconia inverse opal[154] as well as on samples exhibiting additional mesoporosity, such as silica and titania.[154] In addition, combining the synthesis of MCM-41 type materials with the colloidal-crystal templating has been described to create a bimodal pore system with both regular macropores and regular mesopores.[154]

3.4. Other Approaches

Related to the exotemplating strategies described above are two other pathways which are rather broadly used to synthesize highly divided solids, that is, reversed micelle synthesis and synthesis of small particles in one part of a phase-separated block polymer. However, these methods do not really provide a rigid exotemplate, but rather "nanoreactors", that is, confined spaces, in which the synthesis proceeds. These approaches are thus only briefly discussed.

Reversed micelle synthesis is extensively used to prepare high-surface-area nanoparticles of various different compositions. Surveys of the techniques and the materials obtained are given in reviews.[165–167] A recent compilation of oxidic materials synthesized by reversed micelle synthesis is given in the introduction of ref. [168]. In short, for a reverse micelle synthesis a water-in-oil emulsion is used which is stabilized by a surfactant. The precursor for the nanostructured material is then added and hydrolysis takes place within the water droplets. If the hydrolysis reaction is sufficiently fast and the micelles are well separated, then the coalescence of the micelles is slower than the formation of the solid, and nanoparticles with a correspondingly high surface area are formed. However, as stated above, this is rather a reaction performed in a nanoreactor, less a templating process, although the results are also highly dispersed, high-surface-area materials.

Somewhat related are the techniques to synthesize metal nanoparticles in the hydrophilic core of diblock copolymers which also function as "nanoreactors".[169,170] The block copolymers used have a hydrophilic part which contains binding sites for metal precursors, such as pyridine units. This arrangement leads to a concentration of metal centers in the hydrophilic cores which results in the formation of nanometer-sized metal particles upon reduction.

4. Perspectives: Novel Compositions and Novel Structures

The discussion above shows that templating of solids, especially the templating of highly ordered, high-surface-area materials, is a rapidly growing and developing field. Many of the ideas have been triggered by the discovery of ordered mesoporous materials templated by surfactant arrays, which was described slightly over 10 years ago, since this discovery demonstrated that it is possible to replicate structures on the scale of several nanometers. Even if in these earlier publications the formation process of the ordered solid was cooperative and not an exact replication of a preexisting structure: at the latest in 1999, with the work of Ryoo and colleagues,[126] it became clear that "casting" on a length scale of nanometers is possible. That this is a more general concept could be demonstrated by the replication of the carbon structures as silica materials.[91,141,142] These results showed that the approach is not restricted to carbon, but can be extended to other materials.

At present, it seems that there is no fundamental limit to the templating of solids. Length scales can be covered from the nanometer domain to macroporous materials essentially without major gaps. Structural diversity is still somewhat restricted, but new structures of zeolites and surfactant-templated materials are discovered every year, and these could serve in turn as exotemplates for other structures. Colloidal crystals are still predominantly restricted to space filling fcc- or hcp-types, but first results show that also in this size range a higher structural diversity may be possible.[171] Considering that the concept of "templating" to create porous and high-surface-area materials beyond the realm of zeolite synthesis is only little over 10 years old, a rapid development with respect to novel structures can be expected.

Rapid development with respect to compositions can also be expected. For about 30 years of research zeolitic materials had been confined to essentially alumosilicate compositions and materials isomorphously substituted to relatively low levels, before the work of Flanigen and her group opened up novel perspectives with the synthesis of analogous aluminophosphates,[172] and since then we have seen ever increasing compositional flexibility in crystalline microporous materials. There is every reason to believe that the same tendency will be observed in the years to come for materials with larger pores. In fact, one can even expect a more rapid development, since for zeolitic materials, the restrictions of the bond lengths and bond angles imposed by the constituent elements have to be acknowledged. Larger structural features, however, as in mesoporous or macroporous materials, allow higher flexibil-

 © 2003 Wiley-VCH Verlag GmbH & Co. KGaA, Weinheim

ity, and so we may in the future even see an ordered mesoporous NaCl crystal synthesized by the replication of an ordered carbon.

Whether such materials have any application perspective remains to be seen. With respect to catalysis, ordered pore systems are certainly not necessary, and for such applications the activated-carbon templating provides a cheaper and scalable alternative. Other possible developments, such as spatially organized nanoscopic magnetic particles or novel compositions and structures for photonic band-gap materials, may need the order achievable with the novel templating concepts. The tool box to realize a wide range of structures and compositions is certainly there and will expand further over the next years.

This article covers the research of many co-workers and colleagues with whom I have worked and cooperated over the last ten years. I am highly grateful for their contributions. They are too numerous to thank them individually here, and their names can be found in the references cited. I would like to mention, however, Dr. Anhui Lu, Dr. Wolfgang Schmidt, and Manfred Schwickardi, who have allowed me to include as yet unpublished data. I am also grateful for the financial support over the years for this work by the DFG, the EU, the FCI, BASF AG, Lurgi Metallurgy AG, and the funding provided by the institutions with which I have worked, that is, the University of Mainz, the University of Frankfurt, and the MPI für Kohlenforschung.

Received: March 17, 2003 [A593]

[1] F. Schüth in *Handbook of Porous Solids* (Eds.: F. Schüth, K. S. W. Sing, J. Weitkamp), Wiley-VCH, Weinheim, **2002**, pp. 535 – 666.
[2] T. J. Barton, L. M. Bull, W. G. Klemperer, D. A. Loy, B. McEnaney, M. Misono, P. A. Monson, G. Pez, G. W. Scherer, J. C. Vartuli, O. M. Yaghi, *Chem. Mater.* **1999**, *11*, 2633 – 2656.
[3] "Introduction to Zeolite Science and Practice": H. van Bekkum, E. M. Flanigen, J. C. Jansen, *Stud. Surf. Sci. Catal.* **1991**, *58*.
[4] *Molecular Sieves—Science and Technology, Vol. 1* (Eds.: H. G. Karge, J. Weitkamp), Springer, Berlin, **1998**.
[5] U. Ciesla, F. Schüth, *Microporous Mesoporous Mater.* **1999**, *27*, 131 – 149.
[6] F. Schüth, *Chem. Mater.* **2001**, *13*, 3184 – 3195.
[7] F. di Renzo, A. Galarneau, P. Trens, F. Fajula in ref. [1], pp. 1311–1394.
[8] a) F. Rodriguez-Reinoso in ref. [1], pp. 1766–1827; b) B. McEnaney in ref. [1], pp. 1828–1863; R. Schlögl in ref. [1], pp. 1863–1900; J. W. Patrick, S. Hanson in ref. [1], pp. 1900–1922.
[9] "Activated Carbon": K. D. Henning, H. von Kinele in *Ullman's Encyclopedia of Industrial Chemistry*, Wiley-VCH, Weinheim, **2001** available on CD, as web edition: http://www.mrw.interscience.wiley.com/ueic/articles/a05_095/sect6fs.html, or in print 2003.
[10] C. J. Brinker, G. W. Scherer, *Sol-Gel Science*, Academic Press, Boston, **1990**.
[11] M. V. Landau in ref. [1], pp. 1677–1766.
[12] B. H. Davis, K. S. W. Sing in pp. 3–23.
[13] H. Joachim, *Papyrus Ebers*, Georg Reimer, Berlin, **1890**, p. 8.
[14] For a recent review, see: S. Polarz, M. Antonietti, *Chem. Commun.* **2002**, 2593 – 2604.
[15] A. Lu, W. Schmidt, A. Taguchi, B. Spliethoff, B. Tesche, F. Schüth, *Angew. Chem.* **2002**, *114*, 3639 – 3642; *Angew. Chem. Int. Ed.* **2002**, *41*, 3489 – 3492.
[16] J. A. Knowles, M. J. Hudson, *J. Chem. Soc. Chem. Commun.* **1995**, 2083 – 2084.
[17] E. Zhao, O. Hernandez, G. Pacheco, S. Hardcastle, J. J. Fripiat, *J. Mater. Chem.* **1998**, *8*, 1635 – 1640.
[18] H. P. Hentze, M. Antonietti in ref. [1], p. 1964–2013.
[19] K. J. C. van Bommel, A. Friggeri, S. Shinkai, *Angew. Chem.* **2003**, *115*, 1010 – 1030; *Angew. Chem. Int. Ed.* **2003**, *42*, 980 – 999.
[20] G. Wulff, *Angew. Chem.* **1995**, *107*, 1958 – 1979; *Angew. Chem. Int. Ed. Engl.* **1995**, *34*, 1812 – 1832.
[21] A. Katz, M. E. Davis, *Nature* **2000**, *403*, 286 – 289.
[22] E. G. Derouane, S. Detremmerie, Z. Gabelica, N. Blom, *Appl. Catal.* **1981**, *1*, 201 – 224.
[23] F. J. van der Gaag, J. C. Jansen, H. van Bekkum, *Appl. Catal.* **1983**, *17*, 261 – 271.
[24] E. M. Flanigen, *Adv. Chem. Ser.* **1973**, *121*, 119 – 139.
[25] R. L. Wadlinger, G. T. Kerr, E. J. Rosinki (Mobil Oil Corporation), US Patent 3,375,205, **1968** [*Chem. Abstr.* **1968**, *69*, 37667.
[26] E. M. Flanigen, J. M. Bennett, R. W. Grose, J. P. Cohen, R. L. Patton, R. M. Kirchner, J. V. Smith, *Nature* **1978**, *271*, 512 – 516.
[27] C. S. Cundy, P. A. Cox, *Chem. Rev.* **2003**, *103*, 663 – 771.
[28] L. D. Rollmann, *Adv. Chem. Ser.* **1979**, *173*, 389 – 395.
[29] D. W. Breck, *J. Chem. Educ.* **1964**, *41*, 678 – 689.
[30] D. W. Breck, *Zeolite Molecular Sieves*, Wiley, New York, **1974**, pp. 340 – 341.
[31] M. E. Davis, C. Montes, P. E. Hathaway, J. P. Arhancet, D. L. Hasha, J. M. Garces, *J. Am. Chem. Soc.* **1989**, *111*, 3919 – 3924.
[32] H. Gies, B. Marler, U. Werthmann in *Molecular Sieves—Science and Technology, Vol. 1* (Eds.: H. G. Karge, J. Weitkamp), Springer, Berlin, **1998**, pp. 35 – 64.
[33] P. Behrens, C. Panz, V. Hufnagel, B. Lindlar, C. C. Freyhardt, G. van de Goor, *Solid State Ionics* **1997**, *101*, 229 – 234.
[34] A. Burton, S. Elomari, R. C. Medrud, I. Y. Chan, C. Y. Chen, L. M. Bull, E. S. Vittoratos, *J. Am. Chem. Soc.* **2003**, *125*, 1633 – 1642.
[35] H. Gies, B. Marler, *Zeolites* **1992**, *12*, 42 – 49.
[36] R. E. Boyett, A. P. Stevens, M. G. Ford, P. A. Cox, *Zeolites* **1996**, *17*, 508 – 512.
[37] K. J. Chao, J. C. Lin, Y. Wang, G. H. Lee, *Zeolites* **1986**, *6*, 35 – 38.
[38] R. Gougeon, L. Delmotte, D. Le Nouen, Z. Gabelica, *Microporous Mesoporous Mater.* **1998**, *26*, 143 – 151.
[39] K. Nishi, R. W. Thompson in ref. [1], pp. 736–814.
[40] D. W. Lewis, C. R. A. Catlow, J. M. Thomas, *Faraday Discuss.* **1997**, *106*, 451 – 471.
[41] D. W. Lewis, C. M. Freeman, C. R. A. Catlow, *J. Phys. Chem.* **1995**, *99*, 11194 – 12202.
[42] D. W. Lewis, D. J. Willock, C. R. A. Catlow, J. M. Thomas, G. J. Hutchings, *Nature* **1996**, *382*, 604 – 606.
[43] D. J. Willock, D. W. Lewis, C. R. A. Catlow, G. J. Hutchings, J. M. Thomas, *J. Mol. Catal. A* **1997**, *119*, 415 – 424.
[44] D. W. Lewis, G. Sankar, J. K. Wyles, J.M Thomas, C. R. A. Catlow, D. J. Willock, *Angew. Chem.* **1997**, *109*, 2791 – 2793; *Angew. Chem. Int. Ed. Engl.* **1997**, *36*, 2675 – 2677.
[45] F. Delprato, L. Delmotte, J. L. Guth, L. Huve, *Zeolites* **1990**, *10*, 546 – 554.
[46] D. W. Breck in *Zeolite Molecular Sieves Structure Chemistry and Use*, Wiley, New York, **1974**, p. 771.
[47] O. Terasaki, T. Ohsuna, V. Alfredsson, J.-O. Bovin, D. Watanabe, S. W. Carr, M. W. Anderson, *Chem. Mater.* **1993**, *5*, 452 – 458.
[48] G. Schulz-Ekloff, D. Wöhrle, B. van Duffel, R. A. Schoonheydt, *Microporous Mesoporous Mater.* **2002**, *51*, 91 – 138.

 © 2003 Wiley-VCH Verlag GmbH & Co. KGaA, Weinheim

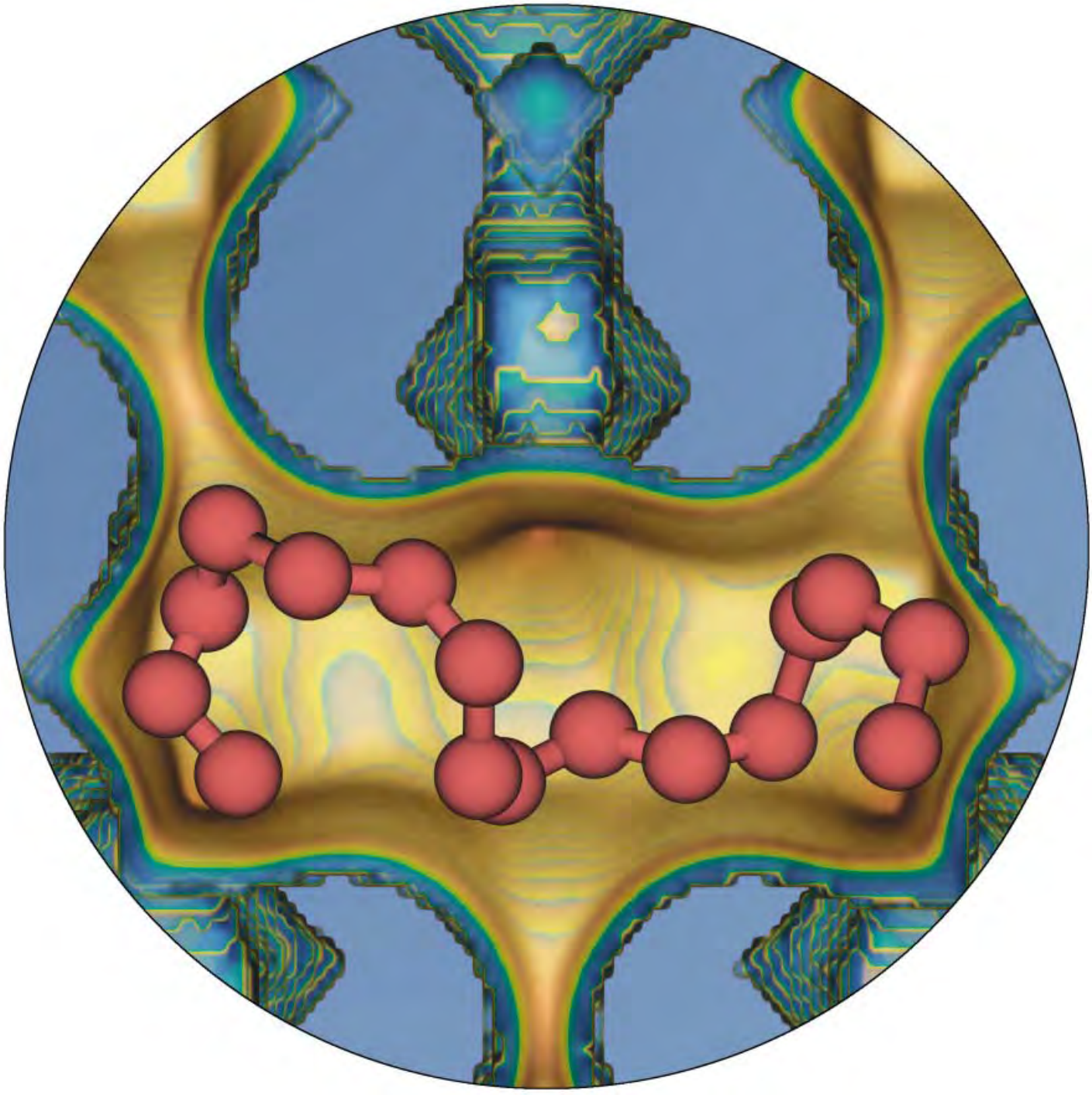
[49] G. Ihlein, F. Schüth, O. Krauss, U. Vietze, F. Laeri, *Adv. Mater.* **1998**, *10*, 1117 – 1119.
[50] I. Braun, G. Ihlein, F. Laeri, J. U. Nöckel, G. Schulz-Ekloff, F. Schüth, U. Vietze, Ö. Weiß, D. Wöhrle, *Appl. Phys. B* **2000**, *70*, 335 – 343.
[51] Ö. Weiß, J. Loerke, U. Wüstefeld, F. Marlow, F. Schüth, *J. Solid State Chem.* **2002**, *137*, 302 – 309.
[52] C. T. Kresge, M. E. Leonowicz, W. J. Roth, J. C. Vartuli, J. S. Beck, *Nature* **1992**, *359*, 710 – 712.
[53] J. S. Beck, J. C. Vartuli, W. J. Roth, M. E. Leonowicz, C. T. Kresge, K. D. Schmitt, C. T.-W. Chu, D. H. Olson, E. W. Sheppard, S. B. McCullen, J. B. Higgins, J. L. Schlenker, *J. Am. Chem. Soc.* **1992**, *114*, 10834 – 10843.
[54] V. Alfredsson, M. Keung, A. Monnier, G. Stucky, K. Unger, F. Schüth, *J. Chem. Soc. Chem. Commun.* **1994**, 921 – 922.
[55] T. Yanagisawa, T. Shimizu, K. Kuroda, C. Kato, *Bull. Chem. Soc. Jpn.* **1990**, *63*, 988 – 992.
[56] H. P. Lin, C. Y. Mou, *Acc. Chem. Res.* **2002**, *35*, 927 – 935.
[57] G. Oye, J. Sjoblom, M. Stöcker, *Adv. Colloid Interface Sci.* **2001**, *89*, 439 – 466.
[58] J. C. Ying, C. P. Mehnert, M. S. Wong, *Angew. Chem.* **1999**, *111*, 58 – 82; *Angew. Chem. Int. Ed.* **1999**, *38*, 56 – 77.
[59] A. Monnier, F. Schüth, Q. Huo, D. Kumar, D. Margolese, R. S. Maxwell, G. Stucky, M. Krishnamurty, P. Petroff, A. Firouzi, M. Janicke, B. Chmelka, *Science* **1993**, *261*, 1299 – 1303.
[60] Q. Huo, D. Margolese, U. Ciesla, D. Demuth, P. Feng, T. Gier, P. Sieger, A. Firouzi, B. Chmelka, F. Schüth, G. D. Stucky, *Chem. Mater.* **1994**, *6*, 1176 – 1191.
[61] G. Stucky, A. Monnier, F. Schüth, Q. Huo, D. Kumar, D. Margolese, M. Krishnamurty, P. Petroff, A. Firouzi , M. Jaenicke, B. Chmelka, *Mol. Cryst. Liq. Cryst.* **1994**, *240*, 187 – 200.
[62] J. Frasch, B. Lebeau, M. Soulard, J. Patarin, R. Zana, *Langmuir* **2000**, *16*, 9049 – 9057.
[63] J. Patarin, B. Lebeau, R. Zana, *Curr. Opin. Colloid Interface Sci.* **2002**, *7*, 107 – 115.
[64] G. S. Attard, J. C. Glyde, C. G. Göltner, *Nature* **1995**, *378*, 366 – 368.
[65] Q. Huo, D. Margolese, U. Ciesla, P. Feng, T. Gier, P. Sieger, R. Leon, P. M. Petroff, U. Ciesla, F. Schüth, G. Stucky, *Nature* **1994**, *368*, 317 – 321.
[66] P. T. Tanev, T. J. Pinnavaia, *Science* **1995**, *267*, 865 – 867.
[67] S. A. Bagshaw, E. Prouzet, T. J. Pinnavaia, *Science* **1995**, *269*, 1242 – 1244.
[68] J. N. Israelachvili, D. J. Mitchell, B. W. Ninham, *J. Chem. Soc. Faraday Trans. 2* **1976**, *72*, 1525 – 1568.
[69] See ref. [61].
[70] Y. Sakamoto, M. Kaneda, O. Terasaki, D. Y. Zhao, J. M. Kim, G. Stucky, H. J. Shin, R. Ryoo, *Nature* **2000**, *408*, 449 – 453.
[71] T. Kimura, T. Kamata, M. Fuziwara, Y. Takano, M. Kaneda, Y. Sakamoto, O. Terasaki, Y. Sugahara, K. Kuroda, *Angew. Chem.* **2000**, *112*, 4013 – 4017; *Angew. Chem. Int. Ed.* **2000**, *39*, 3855 – 3857.
[72] M. Lindén, S. Schunk, F. Schüth, *Angew. Chem.* **1998**, *110*, 871 – 873; *Angew. Chem. Int. Ed.* **1998**, *37*, 821 – 823.
[73] M. Linden, S. A. Schunk, F. Schüth, *Stud. Surf. Sci. Catal.* **1998**, *117*, 45 – 52.
[74] M. Linden, J. Blanchard, S. Schacht, S. A. Schunk, F. Schüth, *Chem. Mater.* **1999**, *11*, 3002 – 3008.
[75] M. Linden, P. Agren, S. Karlsson, P. Bussian, H. Amenitsch, *Langmuir* **2000**, *16*, 5831 – 5836.
[76] U. Ciesla, R. Leon, D. Demuth, P. Petroff, G. Stucky, K. Unger, F. Schüth, *J. Chem. Soc. Chem. Commun.* **1994**, 1387 – 1388.
[77] U. Ciesla, M. Fröba, G. Stucky, F. Schüth, *Chem. Mater.* **1999**, *11*, 227 – 234.
[78] A. Stein, M. Fendorf, T. P. Jarvie, K. T. Mueller, A. J. Benesi, T. E. Mallouk, *Chem. Mater.* **1995**, *7*, 304 – 313.
[79] D. M. Antonelli, J. Y. Ying, *Angew. Chem.* **1995**, *107*, 2202 – 2206; *Angew. Chem. Int. Ed. Engl.* **1995**, *34*, 2014 – 2017.
[80] U. Ciesla, S. Schacht, G. D. Stucky, K. K. Unger, F. Schüth, *Angew. Chem.* **1996**, *108*, 597 – 600; *Angew. Chem. Int. Ed. Engl.* **1996**, *35*, 541 – 543.
[81] D. Antonelli, J. Y. Ying, *Angew. Chem.* **1996**, *108*, 461 – 464; *Angew. Chem. Int. Ed. Engl.* **1996**, *35*, 426 – 430.
[82] U. Ciesla, PhD thesis, Universität Frankfurt, **1998**.
[83] J. Blanchard, F. Schüth, P. Trens, M. Hudson, *Microporous Mesoporous Mater.* **2000**, *39*, 163 – 170.
[84] V. N. Romannikov, V. B. Fenelonov, E. A. Paukshtis, A. Yu. Derevyankin, V. I. Zaikovskii, *Microporous Mesoporous Mater.* **1998**, *21*, 411 – 419.
[85] J. S. Reddy, A. Sayari, *Catal. Lett.* **1996**, *38*, 219 – 223.
[86] F. Schüth, U. Ciesla, S. Schacht, M. Thieme, Q. Huo, G. Stucky, *Mater. Res. Bull.* **1999**, *34*, 483 – 494.
[87] F. Kleitz, S. J. Thomson, Z. Liu, O. Terasaki, F. Schüth, *Chem. Mater.* **2002**, *14*, 4134 – 4144.
[88] F. Kleitz, S. J. Thomson, Z. Liu, O. Terasaki, F. Schüth, *Stud. Surf. Sci. Catal.*, in press.
[89] T. Katou, B. Lee, D. Lu, J. N. Kondo, M. Hara, K. Domen, *Angew. Chem.* **2003**, *115*, 2484 – 2487; *Angew. Chem. Int. Ed.* **2003**, *42*, 2382 – 2385.
[90] T. Czuryszkiewicz, J. Rosenholm, F. Kleitz, F. Schüth, M. Lindén, *Chem. Mater.*, accepted.
[91] F. Schüth, T. Czuryskiewicz, F. Kleitz, M. Linden, A. Lu, J. Rosenholm, W. Schmidt, A. Taguchi, *Stud. Surf. Sci. Catal.*, in press.
[92] D. Zhao, J. Feng, Q. Huo, N. W. Melosh, G. H. Frederickson, B. F. Chmelka, G. D. Stucky, *Science* **1998**, *279*, 548 – 552.
[93] P. Yang, D. Zhao, D. I. Margolese, B. F. Chmelka, G. D. Stucky, *Chem. Mater.* **1999**, *11*, 2813 – 2826.
[94] Y. Liu, W. Zhang, T. J. Pinnavaia, *Angew. Chem.* **2001**, *113*, 1295 – 1298; *Angew. Chem. Int. Ed.* **2001**, *40*, 1255 – 1258.
[95] Z. T. Zhang, Y. Han, L. Zhu, R. W. Wang, Y. Yu, S. L. Qiu, D. Y. Zhao, F. S. Xiao, *Angew. Chem.* **2001**, *113*, 1298 – 1302; *Angew. Chem. Int. Ed.* **2001**, *40*, 1258 – 1262.
[96] M. Antonietti, H. P. Hentze, B. Smarsley, M. Löffler, R. Morschhäuser, *Macromol. Mater. Eng.* **2002**, *287*, 195 – 202.
[97] E. Krämer, S. Förster, C. Göltner, M. Antonietti, *Langmuir* **1998**, *14*, 2027 – 2031.
[98] M. Antonietti, B. Berton, C. Göltner, H. P. Hentze, *Adv. Mater.* **1998**, *10*, 154 – 159.
[99] A. Imhof, D. J. Pine, *Nature* **1997**, *389*, 948 – 951.
[100] J. S. Bradley, O. Vollmer, R. Rovai, U. Specht, F. Lefebvre, *Adv. Mater.* **1998**, *10*, 938 – 942.
[101] D. Farrusseng, K. Schlichte, B. Spliethoff, A. Wingen, S. Kaskel, J. Bradley, F. Schüth, *Angew. Chem.* **2001**, *113*, 4336 – 4339; *Angew. Chem. Int. Ed.* **2001**, *40*, 4204 – 4207.
[102] S. Kaskel, D. Farrusseng, K. Schlichte, *Chem. Commun.* **2000**, 2481 – 2482.
[103] S. Kaskel, K. Schlichte, B. Zibrowius, *Phys. Chem. Chem. Phys.* **2002**, *4*, 1675 – 1681.
[104] C. J. H. Jacobsen, C. Madsen, J. Houzvicka, I. Schmidt, A. Carlsson, *J. Am. Chem. Soc.* **2000**, *122*, 7116 – 7117.
[105] I. Schmidt, A. Boisen, E. Gustavsson, K. Stahl, S. Pehrson, S. Dahl, A. Carlsson, C. J. H. Jacobsen, *Chem. Mater.* **2001**, *13*, 4416 – 4418.
[106] C. Weidenthaler, R. X. Fischer, R. D. Shannon, O. Medenbach, *J. Phys. Chem.* **1994**, *98*, 12678 – 12694.
[107] A. H. Janssen, A. J. Koster, K. P. de Jong, *Angew. Chem.* **2001**, *113*, 1136 – 1138; *Angew. Chem. Int. Ed.* **2001**, *40*, 1102 – 1104.
[108] C. Madsen, C. J. H. Jacobsen, *Chem. Commun.* **1999**, 673 – 674.
[109] M. Landau in ref. [1], pp. 1677–1765.
[110] M. Schwickardi, T. Johann, W. Schmidt, F. Schüth, *Chem. Mater.* **2002**, *14*, 3913 – 3919.

 © 2003 Wiley-VCH Verlag GmbH & Co. KGaA, Weinheim

[111] M. Schwickardi, T. Johann, W. Schmidt, O. Busch, F. Schüth, *Stud. Surf. Sci. Catal.* **2002**, *143*, 93 – 100.
[112] M. Ozawa, M. Kimura, *J. Mater. Sci. Lett.* **1990**, *9*, 446 – 448.
[113] "Carbon": M. Vol. P. Kleinschmit in *Ullman's Encyclopedia of Industrial Chemistry*, Wiley-VCH, Weinheim, **2001** available on CD, as web edition: http://www.mrw.interscience.wiley.com/ueic/articles/a05_095/sect6fs.html, or in print 2003.
[114] Y. Fukushima, H. Wakayama, *J. Phys. Chem. B* **1999**, *103*, 3062 – 3064.
[115] H. Wakayama, H. Itahara, N. Tatsuda, S. Inagaki, Y. Fukushima, *Chem. Mater.* **2001**, *13*, 2392 – 2396.
[116] H. Wakayama, Y. Fukushima, *Chem. Mater.* **2000**, *12*, 756 – 761.
[117] H. Wakayama, Y. Fukushima, *Ind. Eng. Chem. Res.* **2000**, *39*, 4641 – 4645.
[118] H. Wakayama, S. Inagaki, Y. Fukushima, *J. Am. Ceram. Soc.* **2002**, *85*, 161 – 164.
[119] T. Johann, A. Brenner, O. Busch, F. Marlow, S. Schunk, F. Schüth, *Angew. Chem.* **2002**, *114*, 3096 – 3100; *Angew. Chem. Int. Ed.* **2002**, *41*, 2966 – 2968.
[120] F. Schüth, M. Schwickardi, W. Schmidt, A. Haas, DE A-102 26 131.8, **2002**.
[121] P. Burtin, J. P. Brunelle, M. Pijolat, M. Soustelle, *Appl. Catal.* **1983**, *34*, 225 – 238.
[122] R. C. Garvie, *J. Phys. Chem.* **1978**, *82*, 218 – 224.
[123] P. Euzen, P. Raybaud, X. Krokidis, H. Toulhoat, J.-L. Le Loarer, J.-P. Jolivet, C. Froidefond in ref. [1], p. 1666, and refs. therein.
[124] A. H. Heuer, N. Claussen, W. M. Kriven, M. Rühle, *J. Am. Ceram. Soc.* **1982**, *65*, 642 – 650.
[125] I. M. Tijburg, H. de Bruin, P. A. Ellberse, J. W. Geus, *J. Mater. Sci.* **1991**, *26*, 5945 – 5949.
[126] R. Ryoo, S. H. Joo, S. Jun, *J. Phys. Chem. B* **1999**, *103*, 7743 – 7746.
[127] J. Lee, S. Yoon, T. Hyeon, S. M. Oh, K. B. Kim, *Chem. Commun.* **1999**, 2177 – 2178.
[128] J. H. Knox, B. Kaur, G. R. Millward, *J. Chromatogr.* **1986**, *352*, 3 – 25.
[129] M. Kruk, M. Jaroniec, R. Ryoo, S. H. Joo, *J. Phys. Chem. B* **2000**, *104*, 7960 – 7968.
[130] See ref. [127].
[131] A review: J. Fricke, R. Petricevic in ref. [1], pp. 2037–2062.
[132] M. Kaneda, T. Tsubakiyama, A. Carlsson, Y. Sakamoto, T. Ohsuna, O. Terasaki, S. H. Joo, R. Ryoo, *J. Phys. Chem. B* **2002**, *106*, 1256 – 1266.
[133] S. Jun, S. H. Joo, R. Ryoo, M. Kruk, M. Jaroniec, Z. Liu, T. Ohsuna, O. Terasaki, *J. Am. Chem. Soc.* **2000**, *122*, 10 712 – 10 713.
[134] M. Kruk, M. Jaroniec, C. H. Koo, R. Ryoo, *Chem. Mater.* **2000**, *12*, 1961 – 1968.
[135] C. G. Göltner, B. Smarsly, B. Berton, M. Antonietti, *Chem. Mater.* **2001**, *13*, 1617 – 1624.
[136] L. A. Solovyov, A. N. Shmakov, V. I. Zaikovskii, S. H. Joo, R. Ryoo, *Carbon* **2002**, *40*, 2477 – 2481.
[137] S. H. Joo, R. Ryoo, M. Kruk, M. Jaroniec, *J. Phys. Chem. B* **2002**, *106*, 4640 – 4646.
[138] S. H. Joo, S. J. Choi, I. Oh, J. Kwak, Z. Liu, O. Terasaki, R. Ryoo, *Nature* **2001**, *412*, 169 – 172.
[139] A. Lu, W. Schmidt, B. Spliethoff, F. Schüth, *Adv. Mater.*, accepted.
[140] J. Fan, C. Yu, L. Wang, B. Tu, D. Zhao, Y. Sakamoto, O. Terasaki, *J. Am. Chem. Soc.* **2001**, *123*, 12 113 – 12 114.
[141] A. Lu, W. Schmidt, A. Taguchi, B. Spliethoff, B. Tesche, F. Schüth, *Angew. Chem.* **2002**, *114*, 3639 – 3642; *Angew. Chem. Int. Ed.* **2002**, *41*, 3489 – 3492.
[142] M. Kang, S. H. Yi, H. I. Lee, J. E. Yie, J. M. Kim, *Chem. Commun.* **2002**, 1944 – 1945.
[143] B. Lee, T. Yamashita, D. L. Lu, J. N. Kondo, K. Domen, *Chem. Mater.* **2002**, *14*, 867 – 875.
[144] A. Stein, *Microporous Mesoporous Mater.* **2001**, *44–45*, 227 – 239.
[145] F. Marlow, W. T. Dong, *ChemPhysChem* **2003**, *5*, 549 – 554.
[146] E. Yablonovitch, *Phys. Rev. Lett.* **1987**, *58*, 2059 – 2062.
[147] S. John, *Phys. Rev. Lett.* **1987**, *58*, 2486 – 2489.
[148] J. D. Joannopoulos, R. D. Meade, N. Winn, *Photonic Crystals. Molding the Flow of Light*, Princeton University Press, Princeton, **1995**.
[149] W. Stöber, A. Fink, E. Bohn, *J. Colloid Interface Sci.* **1968**, *26*, 62.
[150] D. Kumar, G. B. Butler, *J. Macromol. Sci. Rev. Macromol. Chem. Phys.* **1997**, *C37*, 303 – 333.
[151] O. D. Velev, T. A. Jede, R. F. Lobo, A. M. Lenhoff, *Nature* **1997**, *389*, 447 – 448.
[152] B. T. Holland, C. F. Blanford, A. Stein, *Science* **1998**, *281*, 538 – 540.
[153] J. E. G. J. Wijnhofen, V. L. Vos, *Science* **1998**, *281*, 802 – 804.
[154] B. T. Holland, C. F. Blanford, T. Do, A. Stein, *Chem. Mater.* **1999**, *11*, 795 – 805.
[155] A. Blanco, E. Chomski, S. Grabtchak, M. Ibisate, S. John, S. W. Leonard, C. Lopez, F. Meseguer, H. Miguez, J. P. Mondia, G. A. Ozin, O. Toader, H. M. van Driel, *Nature* **2000**, *405*, 237 – 240.
[156] Z.-Y. Li, Z.-Q. Zhang, *Phys. Rev. B* **2000**, *62*, 1516 – 1520.
[157] W. Dong, H. Bongard, F. Marlow, *Chem. Mater.* **2003**, *15*, 568 – 574.
[158] Y. A. Vlasov, N. Gao, D. J. Norris, *Adv. Mater.* **1999**, *11*, 165 – 169.
[159] A. A. Zhakidov, R. H. Baughman, Z. Iqbal, C. Cui, I. Khayrullin, S. O. Dantas, J. Marti, V. G. Ralchenko, *Science* **1998**, *282*, 897 – 901.
[160] H. Miguez, E. Chomski, F. Garcia-Santamaria, M. Ibisate, S. John, C. Lopez, F. Meseguer, J. P. Mondia, G. A. Ozin, O. Toader, H. M. van Driel, *Adv. Mater.* **2001**, *13*, 1634 – 1636.
[161] P. Jiang, J. Cizeron, J. F. Bertone, V. L. Colvin, *J. Am. Chem. Soc.* **1999**, *121*, 7957 – 7958.
[162] H. Yan, C. F. Blanford, B. T. Holland, M. Parent, W. H. Smyrl, A. Stein, *Adv. Mater.* **1999**, *11*, 1003 – 1006.
[163] W. Dong, H. Bongard, B. Tesche, F. Marlow, *Adv. Mater.* **2002**, *14*, 1457 – 1460.
[164] B. J. Melde, A. Stein, *Chem. Mater.* **2002**, *14*, 3326 – 3331.
[165] M. Lade, H. Mays, J. Schmidt, R. Willumeit, R. Schomäcker, *Colloids Surf. A* **2000**, *163*, 3 – 15.
[166] P. Kumar, K. L. Mittal in *Handbook of Microemulsion Science and Technology*, Marcel Dekker, New York, **1999**.
[167] J. Texter in *Reactions and Synthesis in Surfactant Systems*, Marcel Dekker, New York, **2001**.
[168] H. Althues, S. Kaskel, *Langmuir* **2002**, *18*, 7428 – 7435.
[169] Y. Ng Cheong Chan, R. R. Schrock, R. E. Cohen, *J. Am. Chem. Soc.* **1992**, *114*, 7295 – 7296.
[170] J. P. Spatz, S. Mößmer, M. Möller, *Chem. Eur. J.* **1996**, *2*, 1552 – 1555.
[171] K. P. Velikov, C. G. Christova, R. P. A. Dullens, A. van Blaaderen, *Science* **2002**, *296*, 106 – 109.
[172] S. T. Wilson, B. M. Lok, C. A. Messina, T. R. Cannan, E. M. Flanigen, *J. Am. Chem. Soc.* **1982**, *104*, 1146 – 1147.
[173] a) S. I. Burkett, M. E. Davis, *J. Phys. Chem.* **1994**, *98*, 4647 – 4653; b) S. I. Burkett, M. E. Davis, *Chem. Mater.* **1995**, *7*, 1453 – 1463.

 © 2003 Wiley-VCH Verlag GmbH & Co. KGaA, Weinheim

Communications



When adsorbates are similar in size to zeolite channels then the surface pores of zeolites only adsorb part of the adsorbate molecule. The not adsorbed section can be cleaved to react further or adsorb elsewhere. This window effect can be examined with the aid of Monte Carlo simulations. For more information see the following Communication by D. Dubbeldam et al.

DOI: 10.1002/anie.200351110
© 2003 Wiley-VCH Verlag GmbH & Co. KGaA, Weinheim

Cracking Mechanisms in Zeolites

Understanding the Window Effect in Zeolite Catalysis**

David Dubbeldam, Sofía Calero, Theo L. M. Maesen, and Berend Smit*

The "window effect" is one of the most controversial and intriguing phenomena in the zeolite literature. Chen et al. discovered in 1968 that ERI-type zeolites yield a bimodal product distribution of the products for the zeolite-catalyzed hydrocracking of *n*-C_{21} and longer *n*-alkanes, with maxima for the alkanes *n*-C_{3-4} and *n*-C_{10-12} but no products in the C_{5-8} range (the window).[1] Conventional zeolite-catalyzed (hydro)cracking yields a product distribution with only a single maximum, which is consistent with the currently accepted reaction mechanisms.[2,3] A comprehensive and fundamental understanding of the product selectivity associated with these catalytic processes is of considerable practical significance, as the results of Chen would open the possibility of length-selective hydrocracking.[4] In the case in which the mandatory addition of volatile ethanol to gasoline is imminent,[5–7] the more volatile components that are currently part of gasoline would have to be removed so as to maintain gasoline volatility. This revives the interest in a process that selectively hydrocracks linear pentane and hexane so as to reduce volatility and increase the octane number. Such a process was commercialized in the 1960s, went by the name "selectoforming",[8] and used ERI-type zeolite cages. Improvements on such a process would involve a better understanding of the hydrocracking process of linear alkanes up to a certain chain length. The newly gained understanding affords a prediction of length-selective hydrocracking.

For a long time the window effect has been related almost exclusively to the diffusion rate of *n*-alkanes in ERI-type zeolites. Gorring showed that the product distribution and the diffusion coefficient as a function of *n*-alkane length correlate extremely well.[9] The low diffusion coefficients for *n*-C_7 to *n*-C_9 suggest that these molecules diffuse too slowly to leave the zeolite without cracking; the high diffusion coefficients for *n*-C_{10} to *n*-C_{12} suggest that these molecules diffuse rapidly enough to escape. However, recent diffusion measurements by Cavalcante, Jr. et al.[10] and Magalhães et al.[11] failed to reproduce the increase in diffusion coefficient for the appropriate *n*-alkane lengths. This controversy motivated us to simulate the window effect at the molecular level by using advanced molecular simulations.[12–14] In these Configurational-Bias Monte Carlo simulations molecules are grown atom by atom biasing the growth process towards energetically favorable configurations and avoiding overlap with the zeolite. During the growth we calculate the Rosenbluth factor, which is directly related to the excess chemical potential, the free energy, and the Henry coefficient.[15]

Although our simulations of the diffusion[16] confirm the experimental observations of Gorring, the results nevertheless point to an alternative mechanism based on the anomalously low adsorption of long molecules. At sufficiently low pressures the amount of adsorbed molecules is directly proportional to the pressure. The proportionality constant is known as the Henry coefficient, and shown in Figure 1 as a function of chain length for various zeolites. OFF-type sieves exhibit the usual monotonic increase of the Henry coefficient with *n*-alkane length. Longer *n*-alkanes have more attractive adsorbent–adsorbate interactions, and—therefore—a lower adsorption enthalpy. Longer *n*-alkanes also have fewer conformations in the adsorbed phase as compared to the gas phase, and—therefore—a lower adsorption entropy. The decrease in enthalpy offsets the decrease in entropy, so that the Gibbs free energy of adsorption decreases (and the Henry coefficient increases) with the lengthening of the *n*-alkane. We found that pores with constrictions (windows) that approach the diameter of the adsorbate exhibit a dramatically different behavior. Instead of attractive adsorbate–adsorbent interactions, these windows exert repulsive adsorbate–adsorbent interactions that increase the adsorption enthalpy of any *n*-alkane partially adsorbed inside such a window. Accordingly, the usual compensation between adsorption enthalpy and adsorption entropy ceases as soon as *n*-alkanes become too long to fit comfortably inside the wider part of these pores (cages). For these longer *n*-alkanes the loss of entropy with increasing length dominates their adsorption properties. For example, *n*-C_{13} in an ERI-type cage predom-

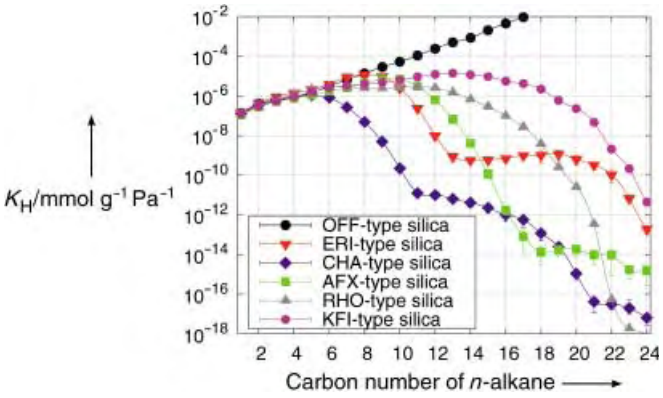


Figure 1. Henry coefficients at 600 K for various types of zeolites as a function of alkane chain length. At sufficiently low pressures the amount of adsorbed molecules is linearly related to the pressure with the Henry coefficient as the proportionality constant.

[*] Dr. D. Dubbeldam, S. Calero, B. Smit
Department of Chemical Engineering
University of Amsterdam
Nieuwe Achtergracht 166, 1018 WV Amsterdam (The Netherlands)
Fax: (+31) 20-525-5604
E-mail: dubbelda@science.uva.nl

T. L. M. Maesen
Chevron Texaco, Energy Research and Technology Company
Chevron Way 100, Richmond CA 94802-0627 (USA)

[**] We would like to thank the Netherlands Research Council for Chemical Sciences (CW), the European Commission for a Marie Curie Fellowship to S.C., ChevronTexaco for financial support, and C. Wilson, C. H. Roemkens, A. Kuperman, S. I. Zones, and R. Krishna for their comments on our manuscript.

 © 2003 Wiley-VCH Verlag GmbH & Co. KGaA, Weinheim DOI: 10.1002/anie.200351110

inantly adsorbs in a limited number of curled conformations, whereas *n*-C_{14} has to stretch through a window into two cages. For even longer *n*-alkanes this pattern is repeated, though now involving a second window. The Henry coefficients of molecular sieves with < 0.45 nm windows exhibit periodic behavior (Figure 1). The local minima correspond to alkanes that barely fit into *x* cages, so that alkanes one methylene group longer require $x+1$ cages. Our simulations indicate that all molecular sieves with a window smaller than the 0.45 nm across EUO-type window exhibit such a remarkable decrease of the Henry coefficient with *n*-alkane length. To the best of our knowledge there are no experimental data available for comparison. In fact, anomalously low adsorption has never been cited when interpreting the catalytic or diffusion data on the large number of zeolites that should exhibit this window or cage effect in adsorption. Below, we amend this situation for ERI- and AFX-type zeolites.

Our simulations for ERI-type zeolite indicate that exactly for *n*-C_9 and longer *n*-alkanes the amount adsorbed decreases. This nicely corresponds with the observed decline in activity,[17] and if we assume that the hydroconversion in ERI is similar to that of zeolites with windows nearly twice as wide (e.g. FAU-type zeolites), this decline may be seen as indirect evidence for our Henry coefficients. The selectivity as observed by Chen[1] concerns *n*-alkanes as long as *n*-C_{36}. It is important to note that the window effect has become associated only with a high *n*-C_{10-12} yield. However, a closer inspection of the raw data of Chen et al. published for *n*-C_{36} reveals additional yield maxima at *n*-C_{24-26} and at *n*-C_{15-17} in the complete chromatogram of the *n*-C_{36} cracking products. From the calculated variation of Henry coefficients with chain length it is immediately apparent that the complete *n*-C_{36} adsorption can be excluded, and yet ERI-type zeolites crack *n*-C_{36} shape selectively. The preferential yield of *n*-C_{24-26} and *n*-C_{15-17} is indicative of consecutive scissions of C_{10-12} fragments from *n*-C_{36}. The maximum at *n*-C_{10-12} indicates that the most rapidly diffusing cracking product can escape complete consumption into more refractory alkanes with six or fewer carbon atoms. This selective cracking process leaves minima at *n*-C_{18-23} and at *n*-C_{13-14}. A reasonable explanation for the persistence of shape-selective cracking of very long alkanes by ERI-type zeolites is that these long molecules adsorb partially in the surface pockets created by the ERI-type cages at the outer crystal surface. Full adsorption by more than 12 carbon atoms is unlikely. The adsorbed *n*-C_{10-12} part is chopped off, and the nonadsorbed part is released. The released parts end up in the product slate or undergo further scission reactions. This process becomes less selective with an increasing number of cracking steps because of concomitant isomerization reactions. AFX-type zeolites exhibit a hydrocracking pattern similar to ERI-type zeolites. This is not surprising, as these zeolites only differ in the size of the cages. Similar to ERI-type zeolites,[4] AFX-type zeolites preferentially hydrocrack shorter rather than longer *n*-alkanes[18] when given a choice. Thus, they consume exclusively *n*-C_6 when processing a mixture of *n*-C_6 and *n*-C_{16}, even though they hydroconvert more than 50% of either *n*-C_6 or *n*-C_{16} when processing them separately. Inspection of our Henry coefficients shows that *n*-C_6 adsorbs fully, whereas *n*-C_{16} can only adsorb partially. As partial adsorption is thermodynamically highly unfavorable,[19] fully adsorbing molecules can effectively block adsorption and hydroconversion for partially adsorbing molecules. Naturally, windows approaching the diameter of the adsorbate are a barrier to both adsorption and diffusion, and these two factors cannot be seen in isolation. Diffusion rates determine the impact of the very low adsorption on catalysis. Its impact will be higher when the diffusion is slower, because the path through consecutive windows is highly tortuous (as in ERI-, AFX-, and CHA-type zeolites). Its impact will be lower when the diffusion is faster because the path through consecutive windows is straight (as in RHO- and KFI- type zeolites) (Figure 2). This newly gained understanding of length-selective hydrocracking affords a prediction of selectivity as a function of cage size. We would predict that the larger AFX-type cage shifts the cracking selectivity by two carbon atoms towards longer *n*-alkanes as compared to the smaller ERI-type cage, and that

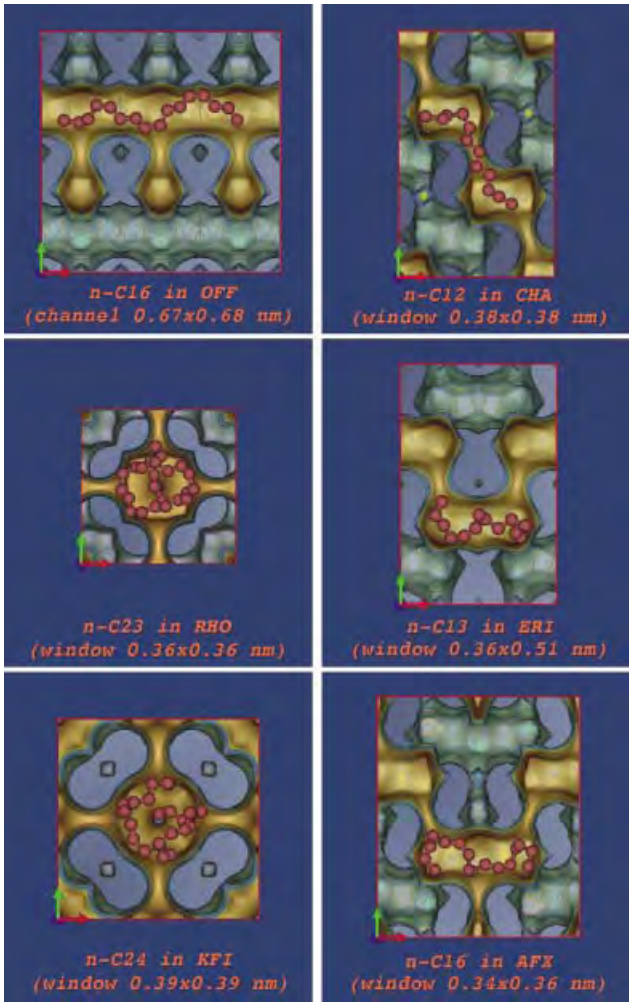


Figure 2. The crystalline structures OFF-, ERI-, RHO-, CHA-, KFI-, and AFX-type zeolites. The size of the CHA-, ERI-, and AFX-type cages limit the *n*-alkanes to 11, 13, and 16 carbon atoms, respectively. The large cages of RHO- and KFI-type zeolites accommodate molecules up to *n*-C_{24} and *n*-C_{26}, respectively, in snake-in-a-basket conformations. The red balls represent CH_3- or CH_2-groups. Arrows at the origin are 0.3 nm in length.

 © 2003 Wiley-VCH Verlag GmbH & Co. KGaA, Weinheim

the even smaller CHA-type cages shift the cracking selectivity further towards n-C_5. We further predict that RHO- and KFI-type zeolites afford length-selective hydrocracking of n-alkanes longer than those removed by AFX-type zeolites.

In summary, we refute some of the traditional cracking mechanisms found in zeolite literature based on full adsorption. The simulation results indicate abnormally low adsorption in ERI-, AFX-, CHA-, RHO-, and KFI-type zeolites for chain lengths close to or longer than the cage size. Hence, very long molecules adsorb partially into a cage near the outer surface. After scission the nonadsorbed part can end up in the product or re-adsorb and undergo another scission. This mechanism is characteristic for cage/window-type zeolites with small windows close to the diameter of the adsorbate. The newly gained understanding of length-selective hydrocracking affords prediction of selectivity as a function of cage size.

Received: February 5, 2003 [Z51110]

Keywords: alkanes · catalysis · computer chemistry · cracking · zeolites

[1] N. Y. Chen, S. J. Lucki, E. B. Mower, *J. Catal.* **1969**, *13*, 329 – 332.
[2] J. Weitkamp, S. Ernst, L. Puppe in *Catalysis and Zeolites* (Eds.: J. Weitkamp, L. Puppe), Springer, Berlin, **1999**, pp. 326 – 376.
[3] J. A. Martens, P. A. Jacobs in *Zeolite Microporous Solids: Synthesis, Structure, and Reactivity* (Eds.: E. G. Derouane, F. Lemos, C. Naccache, F. Ramão-Ribeiro), Kluwer, Amsterdam, **1992**, pp. 511 – 529.
[4] J. Wei, *Ind. Eng. Chem. Res.* **1994**, *33*, 2467 – 2472.
[5] M. Radler, *Oil Gas J.* **2002**, *100*, 5 – 9.
[6] K. Watkins, *Chem. Eng. News* **2001**, *79*(30), 21 – 21.
[7] M. Lorenzetti, *Oil Gas J.* **2003**, 101, 20 – 22.
[8] N. Y. Chen, J. Maziuk, A. B. Schwartz, P. B. Weisz, *Oil Gas J.* **1968**, *66*, 154 – 157.
[9] L. R. Gorring, *J. Catal.* **1973**, *31*, 13 – 26.
[10] C. L. Cavalcante, Jr., M. Eić, D. M. Ruthven, M. L. Occelli, *Zeolites* **1995**, *15*, 293 – 307.
[11] F. D. Magalhães, R. L. Laurence, W. C. Conner, *AIChe. J.* **1996**, *42*, 68 – 86.
[12] B. Smit, T. L. M. Maesen, *Nature* **1995**, *374*, 42 – 44.
[13] T. J. H. Vlugt, R. Krishna, B. Smit, *J. Phys. Chem. B* **1999**, *103*, 1102 – 1118.
[14] T. L. M. Maesen, M. Schenk, T. J. H. Vlugt, J. P. de Jonge, B. Smit, *J. Catal.* **1999**, *188*, 403 – 412.
[15] D. Frenkel, B. Smit in *Understanding molecular simulation*, 2nd ed., Academic Press, London, UK, **2002**.
[16] D. Dubbeldam, S. Calero, T. L. M. Maesen, B. Smit, *Phys. Rev. Lett.* **2003**, 90, 245901.
[17] N. Y. Chen, W. E. Garwood, *Adv. Chem.* **1973**, *121*, 575 – 582.
[18] D. S. Santilli, S. I. Zones, *Catal. Lett.* **1990**, *7*, 383 – 387.
[19] E. B. Webb III, G. S. Grest, *J. Chem. Phys.* **2002**, *116*, 6311 – 6321.

 © 2003 Wiley-VCH Verlag GmbH & Co. KGaA, Weinheim

Active-Site-Directed Probe

Chemistry in Living Cells: Detection of Active Proteasomes by a Two-Step Labeling Strategy**

*Huib Ovaa, Paul F. van Swieten, Benedikt M. Kessler, Michiel A. Leeuwenburgh, Edda Fiebiger, Adrianus M. C. H. van den Nieuwendijk, Paul J. Galardy, Gijsbert A. van der Marel, Hidde L. Ploegh, and Herman S. Overkleeft**

With the sequencing of the human genome and the genetic material of most relevant human pathogens nearly at an end, the focus in biomedical and biological sciences is shifting toward the global assessment of expression levels and function of the gene products. The reason for the renewed interest in protein activity is clear: It is at the protein level that biological processes are modulated in health and disease. Approaches that report on transcription levels are not informative in terms of the levels of activity of the products encoded by these transcripts. Equally importantly, the relevant activities are those in living cells and not those measured in vitro. At the same time, the global assessment of highly complex and dynamic protein mixtures as found in intact cells is a much more arduous task than that of the relatively static genome. This holds true especially when insight into the activity of proteins rather than their expression levels is desired.

Chemistry-based functional-proteomics approaches[1,2] have been developed based on the use of synthetic compounds that modify a selected subset of proteins covalently and irreversibly. These methodologies include the attractive feature that the complex proteome is simplified by selecting protein families on the basis of their function.[3] For instance, broad-spectrum, irreversible protease inhibitors have been used in the profiling of serine proteases,[4] cysteine proteases,[5] and the catalytically active subunits of the proteasome.[6,7] The inhibitors are equipped with either a radioisotope, a biotin moiety, or a fluorescent tag, to allow

[*] Prof. Dr. H. S. Overkleeft, P. F. van Swieten,[+]
Dr. M. A. Leeuwenburgh, A. M. C. H. van den Nieuwendijk,
Dr. G. A. van der Marel
Gorlaeus Laboratories, Leiden University
Einsteinweg 55, 2300 RA Leiden (The Netherlands)
Fax: (+31) 71-527-4307
E-mail: h.s.overkleeft@chem.leidenuniv.nl

Dr. H. Ovaa,[+] Dr. B. M. Kessler, Dr. E. Fiebiger, Dr. P. J. Galardy,
Prof. Dr. H. L. Ploegh
Department of Pathology, Harvard Medical School
200 Longwood Avenue, Boston MA 02115 (USA)

[+] These authors contributed equally.

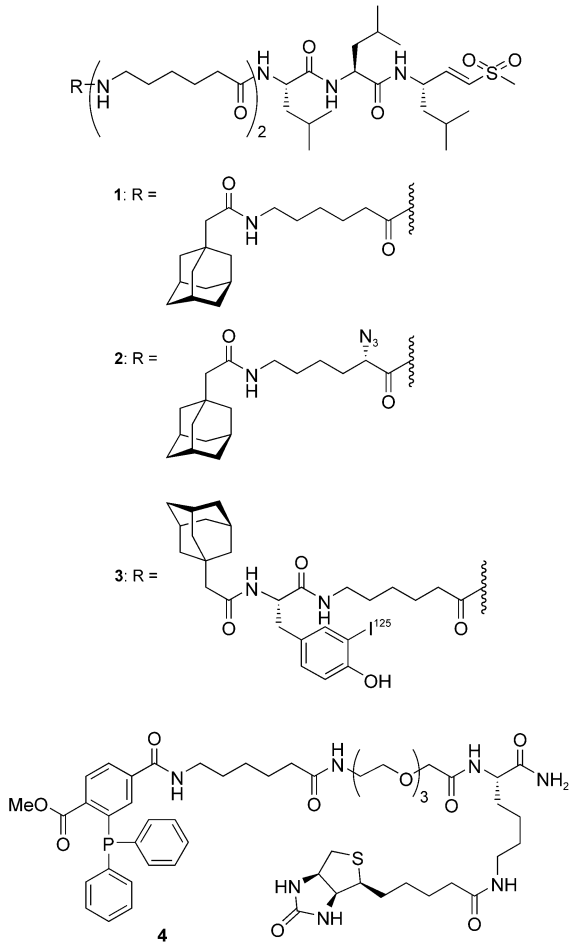
[**] This work is supported by NIH Grant GM 62502 to H.L.P and NIH Training Grant T32 HL07574 to P.J.G. E.F. is supported by the APART program of the Austrian Academy of Sciences. H.O., P.F.S., and H.S.O. are financially supported by the Netherlands Organization for Scientific Research (NWO).

Supporting information for this article is available on the WWW under http://www.angewandte.org or from the author.

 © 2003 Wiley-VCH Verlag GmbH & Co. KGaA, Weinheim DOI: 10.1002/anie.200351314

visualization, isolation, and quantification of the proteases. The cell impermeability of the compounds used in these examples[8] limits their use in living-cell systems, and this limitation is an unavoidable consequence of the use of such probes.

Herein we describe a new functional-proteomics strategy that allows two-step labeling of the catalytically active subunits of the proteasome in living cells. The proteasome is a multi-catalytic proteinase that accounts for the bulk of cytosolic and nuclear proteolysis. We have previously reported the development of a set of extended, peptide-based, irreversible proteasome inhibitors.[6] The most potent of these, $AdaAhx_3L_3VS$ **1** (Scheme 1), is unique in that it



Scheme 1. Structure of the broad-spectrum cell-permeable proteasome inhibitor **1**, the cell-impermeable radioiodinated derivative **3**, and the Staudinger ligation partners **2** and **4** described herein.

targets all catalytically active β subunits of both the constitutive- and the interferon-γ-inducible immunoproteasome with approximately equal efficiency. Although $AdaAhx_3L_3VS$ **1** proved to be cell permeable, it lacks a label that allows easy detection. We demonstrate herein that the modification of **1** with an azide group (to give **2**; Scheme 1) neither interferes with its inhibition profile nor with its cell permeability.[9] Labeling of whole cells with **2** decorates the catalytically active β subunits of the proteasome with an azide as a latent ligation handle. After cell lysis and the retrieval and denaturation of cellular protein content, the azido groups can be subjected to a modified Staudinger ligation with the biotinylated phosphane reagent **4**, in a method developed by Bertozzi and co-workers (Figure 1).[10,11]

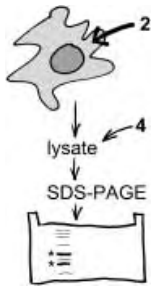
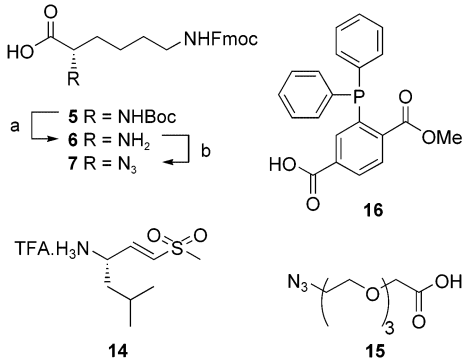


Figure 1. General strategy: irreversible proteasome inhibition and subsequent Staudinger-ligation-mediated biotinylation to enable the visualization of proteasomes in an activity-based manner. SDS-PAGE = sodium dodecylsulfate–polyacrylamide gel electrophoresis.

The synthesis of the azide-containing proteasome inhibitor **2** was carried out as follows. The treatment of *N*-α-Boc,*N*-ε-Fmoc-L-lysine (**5**) with trifluoroacetic acid and subjection of the product to diazotransfer conditions (TfN_3, $CuSO_4$)[12] readily afforded (2*S*)-2-azido-6-(fluorenylmethyloxycarbonylamino)hexanoic acid (**7**; Scheme 2). Standard Fmoc-based solid-phase peptide synthesis (SPPS) was carried out on acid-labile Wang resin



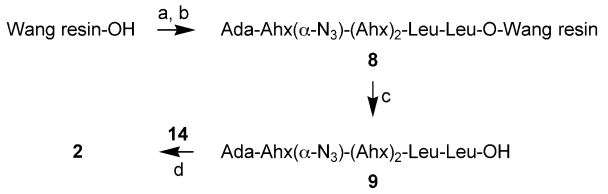
Scheme 2. Nonstandard building blocks used in the synthesis of **2** and **4**. Conditions: a) 50% TFA/CH_2Cl_2, 92%; b) TfN_3, $CuSO_4$, H_2O/MeOH, 89%. Boc = *tert*-butyloxycarbonyl, Fmoc = 9-fluorenylmethoxycarbonyl, TFA = trifluoroacetic acid, TfN_3 = trifluoromethanesulfonyl azide.

and led to immobilized peptide **8** from **7**. Cleavage from the resin and solution-phase condensation of resulting carboxylate **9** with leucine vinyl sulfone **14**[13] afforded target compound **2**, which was purified by silica-gel chromatography (58% overall yield; Scheme 3).

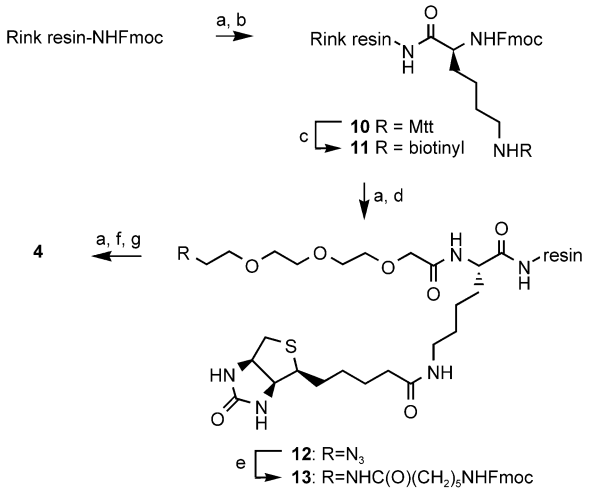
The synthesis of phosphane reagent **4** commenced with the condensation of the Rink amide linker with *N*-α-Boc,*N*-ε-Mtt-L-lysine.[14] Deprotection of the side-chain protective group in **10** was followed by condensation with biotin to afford immobilized biocytin **11**. Standard solid-phase peptide synthesis with sequential addition of azido acid **15**,[15] 6-(Fmoc-amino)hexanoic acid, and phosphane **16**, followed by acidic cleavage from the resin and HPLC purification gave the target compound **4** in 16% yield (Scheme 4).

We performed a set of competition experiments to establish the inhibition profile of **4**. We used the cell line

 © 2003 Wiley-VCH Verlag GmbH & Co. KGaA, Weinheim



Scheme 3. Synthesis of azide-containing proteasome inhibitor **2**: a) FmocLeuOH, DIC, DMAP, DMF; b) Repeated cycles of SPPS: Fmoc cleavage: 20% piperidine in DMF; amino acid condensation: Fmoc-protected amino acid, PyBOP, DiPEA, DMF; Fmoc-protected amino acid building blocks were used in the following order: FmocLeuOH, FmocAhxOH, FmocAhxOH, **7**, adamantane acetic acid; c) 10% H_2O/TFA; d) HBTU, DiPEA, DMF, 58% overall yield. Ada = adamantane acetyl, Ahx = 1-amino-6-hexanoyl, DIC = *N*,*N*′-diisopropylcarbodiimide, DiPEA = *N*,*N*-diisopropylethylamine, DMAP = 4-(dimethylamino)pyridine, DMF = *N*,*N*-dimethylformamide, HBTU = 2-(1H-benzotriazole-1-yl)-1,1,3,3-tetramethyluronium hexafluorophosphate, Leu = leucine, PyBOP = benzotriazol-1-yloxytripyrrolidinophosphonium hexafluorophosphate.



Scheme 4. Synthesis of biotinylated phosphane reagent **4**: a) 20% piperidine in DMF; b) FmocLys(Mtt)OH, PyBOP, DiPEA, DMF; c) 1% TFA/CH_2Cl_2, then biotin, PyBOP, DiPEA, DMF; d) **15**, PyBOP, DiPEA, DMF; e) Me_3P, 20% H_2O/dioxane, then FmocAhxOH, PyBOP, DiPEA, DMF; f) **16**, EDC, HOBt, CH_2Cl_2; g) 50% TFA/CH_2Cl_2, 16% overall yield. EDC = 1-(3-dimethylaminopropyl)-3-ethylcarbodiimide hydrochloride, HOBt = *N*-hydroxybenzotriazole, Mtt = 4-methyltrityl.

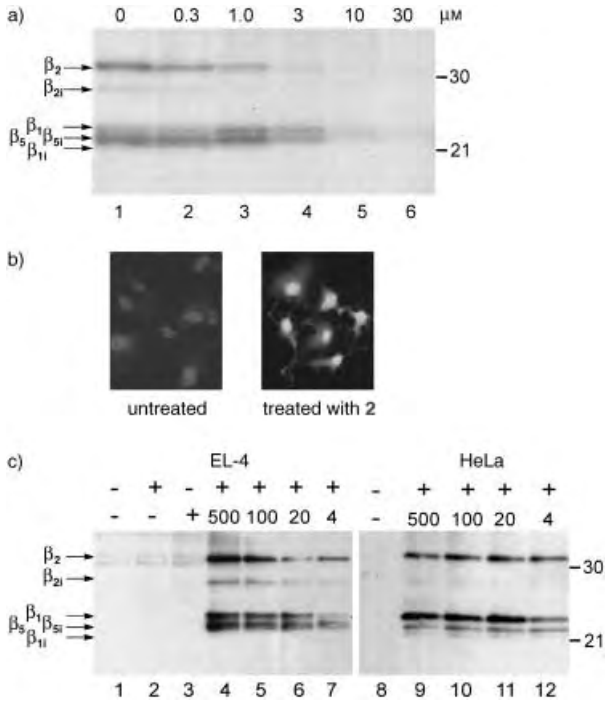


Figure 2. a) Cell lysate prepared from EL-4 cells was incubated with **2** at concentrations ranging from 0 to 30 μM. Residual unmodified subunits were labeled by subsequent incubation with radioiodinated inhibitor **3**. Labeled subunits were resolved by SDS-PAGE and visualized by autoradiography. b) Ub-R-GFP accumulates when proteasomal degradation is blocked. Cells were incubated with either a solvent control or **2** (50 μM final concentration) for 8 h and fixed, followed by blue nuclear staining of the DNA with 4,6-diamidino-2-phenylindole (DAPI blue). Confocal laser-scanning microscopy revealed **2** to be a cell-permeable proteasome inhibitor. c) Lysates from EL-4 and HeLa were treated with **2** at 37 °C for 1 h and then boiled in the presence of sodium dodecylsulfate to cause protein denaturation and exposure of the azido moieties of conjugated **2**. The azido moieties were biotinylated through a Staudinger ligation by adding an aqueous solution of reagent **4** to the reaction mixture, followed by incubation at 37 °C for 2 h. Samples were separated by SDS-PAGE and transferred to polyvinylidene difluoride membrane. Incubation with streptavidin–horseradish peroxidase (strept–HRP) conjugates allowed the visualization of active proteasomal β subunits by chemiluminescence.

EL-4, derived from a murine thymoma. This cell line is advantageous because it expresses both the constitutive proteasome and the interferon-γ-inducible immunoproteasome, which contain a total of six distinct catalytically active β subunits. We also used the cell line HeLa, derived from a human cervical carcinoma. HeLa expresses only the constitutive proteasome (three catalytically active β subunits). When lysates of EL-4 cells were incubated with azide-containing proteasome inhibitor **2** at different concentrations, prior to treatment with radioiodinated peptide vinyl sulfone **3**, we observed that labeling of the six individual subunits was abolished at final inhibitor concentrations of 10–30 μM (Figure 2a), thus demonstrating **2** to be a proteasome inhibitor of equal potency to **1**.[6] The ability of peptide vinyl sulfone **2** to disable the proteasome in living cells was determined by the following procedure: U373 cells expressing the green fluorescent protein (GFP) ubiquitin-GFP fusion protein[16] (Ub-R-GFP) were treated with compound **2** at 50 μM (final concentration) and compared with untreated cells for the presence of GFP fluorescence. Ub-R-GFP is rapidly degraded by the proteasome, which results in a steady state with hardly any green fluorescence as a result (Figure 2b). However, in cells treated with **2**, a time-dependent accumulation of fluorescence was observed, thus demonstrating the capacity of **2** to inactivate the proteasome in living cells.

Encouraged by these results, we set out to establish the suitability of a Staudinger ligation for the two-step visualization of catalytically active proteasome subunits in cell lysates, as well as in living cells. In the first experiment, cell lysates from EL-4 and HeLa cells were exposed to **2** at various

 © 2003 Wiley-VCH Verlag GmbH & Co. KGaA, Weinheim

concentrations, prior to denaturation of the cellular protein. The resulting mixtures were incubated with biotinylated Staudinger-ligation reagent **4** and separated by SDS-PAGE. Transfer of the separated protein mixture onto a polyvinylidene difluoride (PVDF) membrane, followed by chemiluminescence induced by horseradish peroxidase–streptavidin conjugate, resulted in a distinct labeling profile. Labeling intensity depended on the dose of **2**. The labeling pattern conforms to that established for radioiodinated probe **3**.[6] Importantly, proteasome-derived polypeptides were detected only when both inhibitor **2** and Staudinger reagent **4** were used (Figure 2c, lanes 4–7 and 9–12). These results establish the selectivity of **4** in complex physiological mixtures to target only those proteins modified with an azide functionality.

We then investigated the possibility of covalent proteasome inhibition in living cells, followed by postlysis Staudinger ligation and immunoblotting. EL-4 cells were incubated overnight with **2** (Figure 3). Subsequent glass-bead

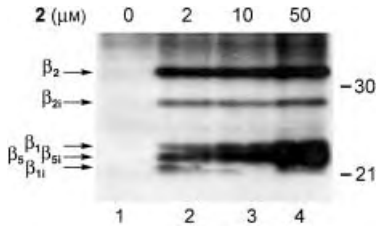


Figure 3. Proteasome labeling in living cells. Incubation of living cells (5×10^6 at 37 °C) with **2** followed by postlysis ligation and immunoblotting reveals the active proteasomal content and composition in living cells.

lysis, incubation with **4**, SDS-PAGE separation, and Western blotting afforded a labeling pattern virtually indistinguishable from that obtained for the labeling of cell lysates (Figure 2c). In vivo labeling appeared to be more effective (compare Figure 3 with the labeling patterns obtained in vitro in Figure 2c), thus indicating a more efficient targeting of all proteasomal subunits in living cells. This observation is possibly a result of partial dissociation of the proteasome particle during cell lysis and storage. We conclude that inhibitor **2** can be used in combination with biotinylation reagent **4** for the visualization of active proteasomes in living cells.

In summary, we have presented a novel strategy for the visualization of active enzymes in living cells. Compound **2** was identified as a powerful, cell-permeable inhibitor of all proteasomal activities, and **2** can subsequently undergo postlysis labeling through a chemoselective Staudinger ligation. This protocol opens the way toward the screening, in living cells, of proteasomal activity, for example, in human tissue samples. The measurement of proteasome activity in live cells remains an important goal, not only in the context of novel treatment strategies for cancer, but also in biological systems more generally. For instance, malfunction of the ubiquitin–proteasome system has been implicated in both cancer[17] and neurodegeneration.[18] Importantly, this two-step methodology (this is, covalent, irreversible enzyme modification followed by chemoselective modification) may be extended toward the development of novel chemoselective ligation partners that are compatible with desired cellular environments. We are currently pursuing the application of this strategy to the assessment of the activity of a variety of other enzyme families in living cells.[19]

Received: March 3, 2003 [Z51314]

Keywords: bioorganic chemistry · inhibitors · peptides · proteomics · solid-phase synthesis

[1] A. Borodovsky, H. Ovaa, N. Kolli, T. Gan-Erdene, K. D. Wilkinson, H. L. Ploegh, B. M. Kessler, *Chem. Biol.* **2002**, *9*, 1149–1159.
[2] D. C. Greenbaum, W. D. Arnold, F. Lu, L. Hayrapetian, A. Baruch, J. Krumrine, S. Toba, K. Chehade, D. Brömme, I. D. Kuntz, M. Bogyo, *Chem. Biol.* **2002**, *9*, 1085–1094.
[3] G. C. Adam, E. J. Sorensen, B. F. Cravatt, *Nat. Biotechnol.* **2002**, *20*, 805–809.
[4] G. C. Adam, B. F. Cravatt, E. J. Sorensen, *Chem. Biol.* **2001**, *8*, 81–95.
[5] A. M. Lennon-Duménil, A. H. Bakker, R. Maehr, E. Fiebiger, H. S. Overkleeft, M. Rosemblatt, H. L. Ploegh, C. Lagaudrière-Gesbert, *J. Exp. Med.* **2002**, *196*, 529–540.
[6] B. M. Kessler, D. Tortorella, M. Altun, A. F. Kisselev, E. Fiebiger, B. G. Hekking, H. L. Ploegh, H. S. Overkleeft, *Chem. Biol.* **2001**, *8*, 913–929.
[7] T. Nazif, M. Bogyo, *Proc. Natl. Acad. Sci. USA* **2001**, *98*, 2967–2972.
[8] K. L. Rock, A. L. Goldberg, *Annu. Rev. Immunol.* **1999**, *17*, 739–797.
[9] Large substituents, such as biotin or fluorescence tags, can also have a detrimental effect on the inhibition profile of the compound. Incorporation of ^{125}I-Tyr or biocytin abolishes cell permeability and, in case of biocytin, also partially impairs its inhibition profile.[6]
[10] E. Saxon, C. R. Bertozzi, *Science* **2000**, *287*, 2007–2010.
[11] K. L. Kiick, E. Saxon, D. A. Tirrell, C. R. Bertozzi, *Proc. Natl. Acad. Sci. USA* **2002**, *99*, 19–24.
[12] J. T. Lundquist, J. C. Pelletier, *Org. Lett.* **2001**, *3*, 781–783.
[13] M. Bogyo, J. S. McMaster, M. Gaczynska, D. Tortorella, A. L. Goldberg, H. L. Ploegh, *Proc. Natl. Acad. Sci. USA* **1997**, *94*, 6629–6634.
[14] L. Bourel, O. Carion, H. Gras-Masse, O. Melnyk, *J. Pept. Sci.* **2000**, *6*, 264–270.
[15] S. W. Yeong, D. F. O'Brien, *J. Org. Chem.* **2001**, *66*, 4799–4802.
[16] N. P. Dantuma, K. Lindsten, R. Glas, M. Jellne, M. G. Masucci, *Nat. Biotechnol.* **2000**, *18*, 538–543.
[17] T. Hideshima, K. C. Anderson, *Nat. Rev. Cancer* **2002**, *2*, 927–937.
[18] C. Soto, *Nat. Rev. Neurosci.* **2003**, *4*, 49–60.
[19] After this manuscript had been submitted, the latent in vivo labeling of serine proteases was reported: A. E. Speers, G. C. Adam, B. F. Cravatt, *J. Am. Chem. Soc.* **2003**, *125*, 4686–4687.

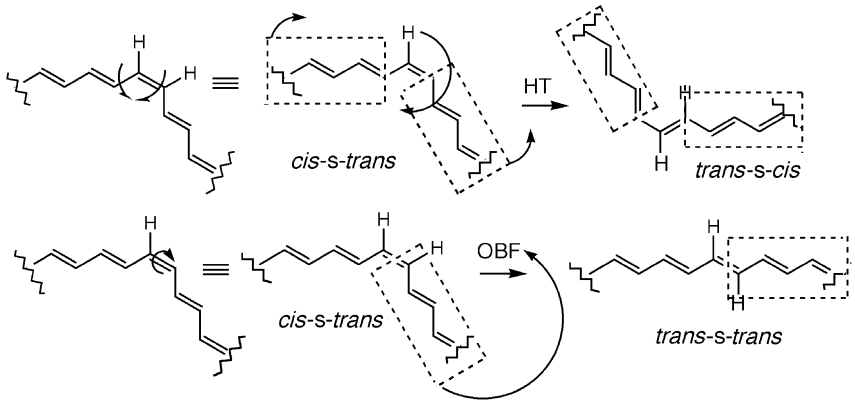
 © 2003 Wiley-VCH Verlag GmbH & Co. KGaA, Weinheim

Photoisomerization

Photoisomerization by Hula Twist: 2,2′-Dimethylstilbene and a Ring-Fused Analogue**

*Yasushi Imamoto, Takayuki Kuroda, Mikio Kataoka, Sergey Shevyakov, G. Krishnamoorthy, and Robert S. H. Liu**

Recently, the case for medium-dependent photoisomerization from the S_1 state was made;[1] it was argued that the one-bond-flip (OBF) process (or torsional relaxation)[2] dominates in solutions, but this volume-demanding process is unlikely in confined media. Instead, a volume-conserving reaction mechanism that involves the simultaneous rotation around two adjacent single and double bonds was suggested. The net result was a CH group rotating out of the plane of a polyene (which is not volume demanding; Scheme 1) and the process was termed the "Hula twist".[3,4] The concept was first introduced to account for the rapid isomerization of the confined visual chromophore in rhodopsin.[3] Interest was recently rekindled after the successful demonstration of a Hula twist in a simple organic system: pre-vitamin D in an organic glass.[5]



Scheme 1. Top: *cis* to *trans* isomerization by Hula twist (HT) with simultaneous conformational reorganization and one CH unit rotating out of the plane. Bottom: *cis* to *trans* isomerization by one-bond-flip (OBF) with half of the molecule rotating around a double bond.

[*] Prof. Dr. R. S. H. Liu, S. Shevyakov, G. Krishnamoorthy
Department of Chemistry
University of Hawaii
2545 The Mall, Honolulu, HI 96822 (USA)
Fax: (+1) 808-956-5908
E-mail: rliu@gold.chem.hawaii.edu
Dr. Y. Imamoto, T. Kuroda, Prof. Dr. M. Kataoka
Graduate School of Materials Science
Nara Institute of Science and Technology
Ikoma, Nara 630-0192 (Japan)

[**] The work was supported by a grant from the National Science Foundation (CHE-32250) and a grant from Sekisui Integrated Research Inc. We thank Dr. Alabugin for the calculated energies of the conformers of **2**. X.-S. Wang, H.-R. Li, L. U. Colmenares, and D. Chang participated in the early part of the work described here.

The specific role of the Hula twist process in a general mechanistic scheme that accounts for all the photoisomerization reactions made it possible to design specific examples to test the validity of the concept and allowed for the possibility to further broaden its scope.[2] Now we report experimental results on the first set of test systems: 2,2′-dimethylstilbene (**1**) and a related ring-fused analogue **2**[6] (which minimizes the number of possible conformers). The location of the alkyl substituent was chosen to facilitate the investigation of conformational changes occurring during photoisomerization. The results are relevant to current thoughts on the photoisomerization of organic systems,[1,2] although it does not necessarily relate to the protonated Schiff bases of the visual chromophore.[3]

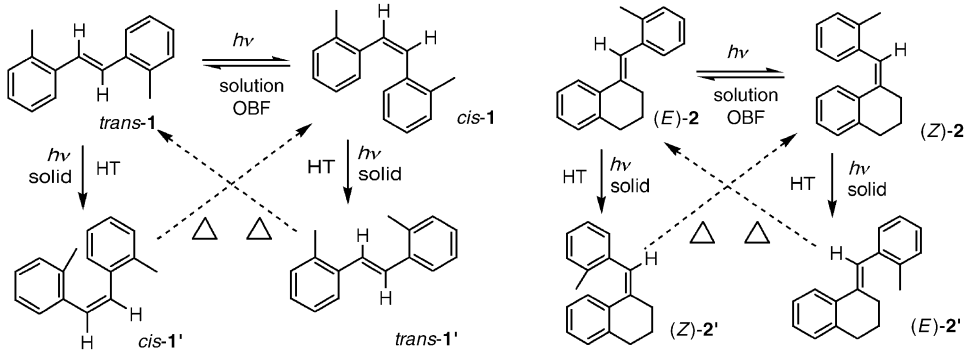
We previously predicted the photochemical reactions of 2,2′-substituted stilbenes **1** and the ring-fused stilbene **2** to be those shown in Scheme 2.[2a,b] In a fluid solution, OBF photoisomerization should lead to a stable conformer of the isomerized photoproduct, while in a frozen solid solution, HT photoisomerization should give an unstable conformer of the isomerized product. The latter should be readily converted into the stable conformer by warming.

We have now investigated the irradiation of isomers of **1** and **2** in 2-methylpentane both in a fluid solution (at 0 °C) and in the glassy state (−193 °C). The low-temperature irradiation apparatus used in this study was essentially that described in the literature.[7] The progress of the photoreactions was followed by UV/Vis spectroscopy (Figures 1–4).

These sets of data show that all these compounds indeed exhibit different photochemical behavior in solvent media of different rigidity. The difference absorption curves obtained during irradiation of *trans*-**1** and *cis*-**1** (Figure 1d and 2d), or (*E*)-**2** and (*Z*)-**2** in fluid solutions at 0 °C Figure 3d and 4d) were essentially mirror images of each other, which reflects that the same equilibrium mixture is reached from both directions. On the other hand, the absorption spectra obtained during low-temperature irradiation of (*E*)-**2** and (*Z*)-**2** (Figure 3a and 4a; less exactly for **1** because of the low conversion of the *trans* isomer making the difference spectra (Figure 1c) rather noisy) showed no mirror image relationship. At high conversion, the absorption spectrum (calculated after subtracting the residual amount of (*E*)-**2**) of the low-temperature product from (*E*)-**2** was found to be different from that of (*Z*)-**2** cooled to 80 K. At lower conversions, the difference spectra substantially deviate from that of the stable isomer. Warming the low-temperature product to 0 °C resulted in its facile conversion into the stable product (*Z*)-**2**. Such a conversion under the mild conditions of thawing and warming to 0 °C can only suggest formation of unstable conformers (namely, the hindered s-*cis* form) at low temperature. In other words, the observed photochemical events of these compounds (more clearly shown for (*E*)-**2** and (*Z*)-**2**) paralleled the reactions outlined in Scheme 2.

Not surprisingly, the efficiency of the isomerization of stilbene **1** favors reaction of the *cis* isomer over the *trans*

 © 2003 Wiley-VCH Verlag GmbH & Co. KGaA, Weinheim DOI: 10.1002/anie.200351763



Scheme 2. Predicted photoisomerization pathways. Left: 2,2′-substituted stilbenes **1**; right: ring-fused stilbene analogues **2**. Horizontal: photoisomerization in solution by OBF; vertical: isomerization in frozen solution by HT; diagonal: warming and thawing of the solid solution containing the HT product.

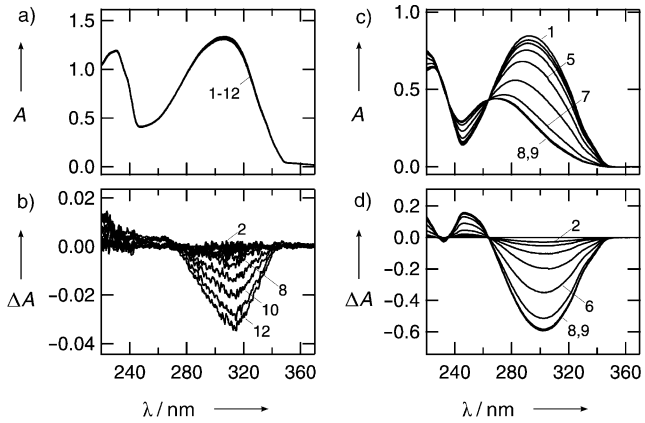


Figure 1. Progress of the photoreaction ($\lambda > 280$ nm) of *trans*-**1** at 80 K in 2-methylpentane glass (a and c) and in 2-methylpentane solvent at 273 K (b and d). Changes in the absorption spectra versus time (0, 5, 10, 20, 40, 80, 160, 320, 640, 1280, 2560, and 5120 s for a; the same intervals to 640 s for b) and difference absorption bands ($A_t - A_0$) for the 80 K (c) and 273 K (d) data are shown.

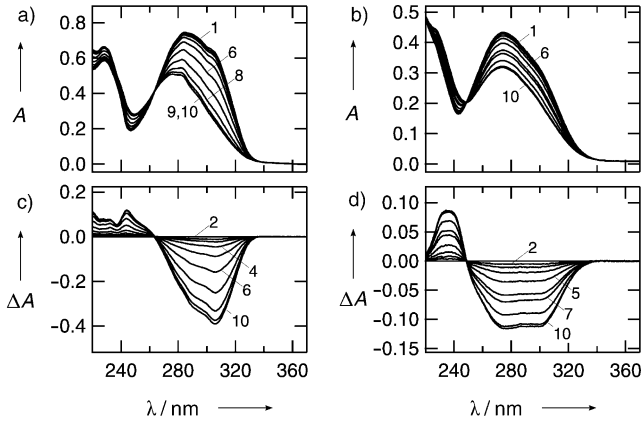


Figure 3. Progress of the photoreaction ($\lambda > 280$ nm) of (*E*)-**2** at 80 K in 2-methylpentane glass (a and c) and in 2-methylpentane solvent at 273 K (b and d). Changes in the absorption curves versus time (0, 5, 10, 20, 40, 80, 160, 320, 640, and 1280 s for a and b) and difference absorption bands ($A_t - A_0$) for the 80 K (c) and 273 K (d) data are shown.

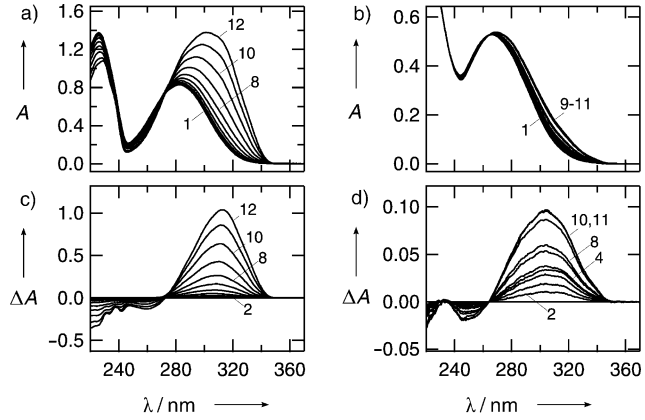


Figure 2. Progress of the photoreaction ($\lambda > 280$ nm) of *cis*-**1** at 80 K in 2-methylpentane glass (a and c) and in 2-methylpentane solvent at 273 K (b and d). Changes in the absorption curves versus time (0, 5, 10, 20, 40, 80, 160, 320, 640, 1280, 2560, and 5120 s for a; same intervals to 2560 s for b) and difference absorption bands ($A_t - A_0$) for the 80 K (c) and 273 K (d) data are shown.

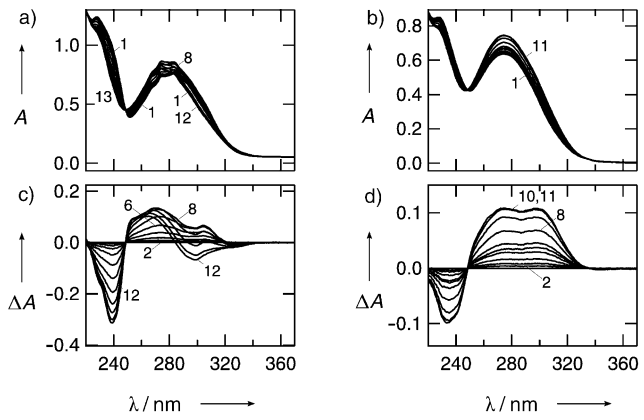


Figure 4. Progress of the photoreaction ($\lambda > 280$ nm) of (*Z*)-**2** at 80 K in 2-methylpentane glass (a and c) and in 2-methylpentane solvent at 273 K (b and d). Changes in the absorption curves versus time (0, 5, 10, 20, 40, 80, 160, 320, 640, 1280, 2560, and 5120 s for a; same intervals to 2560 s for b) and difference absorption bands ($A_t - A_0$) for the 80 K (c) and 273 K (d) data are shown.

 © 2003 Wiley-VCH Verlag GmbH & Co. KGaA, Weinheim

isomer at low temperature in organic glass. However, the *trans* isomer was not entirely photochemically inert, as claimed for many other *trans*-1,2-diarylethylenes.[8] (At 80 K, the *trans* isomer is estimated to be about 100 times less reactive than the *cis* isomer.) There are, however, distinct differences in the low-temperature photochemical behavior of the conformationally more restricted **2** relative to that of **1**. The presence of the extra ring made (*E*)-**2** sterically *cis*-stilbene-like. Therefore, the (*E*)-**2** to (*Z*)-**2** photoisomerization also proceeded efficiently. The quantum yield of the reaction was found to be 0.18 ± 0.02.[10] On the basis of the relative irradiation periods, we believe that this value is a good reflection of the ease of isomerization of *cis*-diarylethylenes in low-temperature glass.

Changes in the absorbances of isomers of **1** and **2** versus time are shown in Figure 5. It is clear that compounds *trans*-**1**, *cis*-**1**, and (*E*)-**2** all exhibit single exponential decay, which

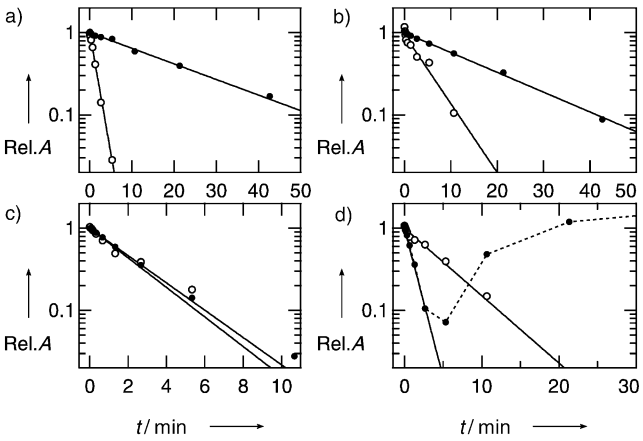
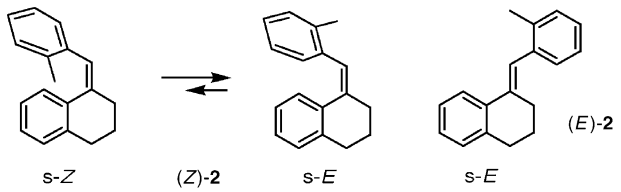


Figure 5. Changes in the absorbance maxima during irradiation of *trans*-**1** (a), *cis*-**1** (b), (*E*)-**2** (c), and (*Z*)-**2** (d) at 80 K in 2-methylpentane glass and 273 K in 2-methylpentane solution. The closed and open circles represent absorbance changes at 80 and 273 K, respectively.

indicates the reactions occur from a single species and that the reactant is conformationally homogeneous at liquid-nitrogen temperature. However, the decay of (*Z*)-**2** is clearly not a single exponential. In fact, the curve in Figure 5 d suggests the involvement of two species. Calculated results indeed support that notion: the two s-*E* and s-*Z* conformers of (*Z*)-**2** differ by 1.03 kcal mol^{-1} while for (*E*)-**2**, there was no other stable conformer within 1.5 kcal mol^{-1} of the s-*E* conformer.[9]



In conclusion, the results presented above demonstrate conclusively that photoisomerization in fluid solution involves only configurational changes, that is, by OBF. However, conformational as well as configurational changes, that is, by HT, occur in a solid solution.[1] These results reinforce the suggestion that all photoisomerizations of polyenes in rigid media (pre-vitamin D in organic glass,[5] 1,3-butadiene in argon matrix,[11] 1,3,5,7-octatetraene in an *n*-octane matrix,[12] and selected cases of diarylethylenes in organic glasses[13]) proceeded by way of HT.[1] However, at the same time, we recognize that the current results do not necessarily rule out the possibility that the isomerization at room temperature could also proceed by way of HT.[14] The fluid medium and the higher temperature would complicate detection of the unstable conformer. We consider this possibility unlikely; however, we intend to carry out similar irradiation experiments on samples in constrained and unconstrained media, but at an identical reaction temperature.

Received: April 28, 2003 [Z51763]

Keywords: alkenes · isomerization · photochemistry · reaction mechanisms

[1] a) R. S. H. Liu, G. S. Hammond, *Proc. Natl. Acad. Sci. USA* **2000**, *97*, 11153–11158; b) R. S. H. Liu, *Acc. Chem. Res.* **2001**, *34*, 555–562; c) R. S. H. Liu, G. S. Hammond, *Chem. Eur. J.* **2001**, *7*, 4536–4544.

[2] See, for example, a) J. Saltiel, D. F. Sears, Jr., D.-H. Ko, K.-M. Park in *CRC Handbook of Organic Photochemistry and Photobiology* (Eds.: W. M. Horspool, P.-L. Song), CRC, Boca Raton, **1994**, pp. 1–15; b) W. J. Leigh in *CRC Handbook of Organic Photochemistry and Photobiology* (Eds.: W. M. Horspool, P.-L. Song), CRC Press, Boca Raton, **1994**, pp. 123–142; c) H. J. C. Jacobs, W. H. Laarhoven in *CRC Handbook of Organic Photochemistry and Photobiology* (Eds.: W. M. Horspool, P.-L. Song), CRC, Boca Raton, **1994**, pp. 143–154.

[3] a) R. S. H. Liu, A. E. Asato, *Proc. Natl. Acad. Sci. USA* **1985**, *82*, 259–263; b) R. S. H. Liu, D. T. Browne *Acc. Chem. Res.* **1986**, *19*, 42–48.

[4] For selected papers on the photoisomerization pathways, torsional relaxation, and the Hula twist, see a) R. S. H. Liu, *Photochem. Photobiol.* **2002**, *76*, 580–583; b) M. Uda, T. Mizutani, J. Hayakawa, A. Momotake, M. Ikegami, R. Nagahata, T. Arai, *Photochem. Photobiol.* **2002**, *76*, 596–605; c) S. Wilsey, K. N. Houk, *Photochem. Photobiol.* **2002**, *76*, 616–621; d) M. Squillacote, T. Semple, J.-W. Chen, F. Liang, *Photochem. Photobiol.* **2002**, *76*, 634–639.

[5] A. M. Muller, S. Lochbrunner, W. E. Schmid, W. Fuss, *Angew. Chem.* **1998**, *110*, 520–522; *Angew. Chem. Int. Ed.* **1998**, *37*, 505–507.

[6] (*E*)-**2**: ^{1}H NMR (300 MHz, $CDCl_3$): $\delta = 1.82$ (dd, 2H), 2.30 (s, 3H), 2.58 (t, 2H), 2.87 (t, 2H), 7.01 (br s, 1H), 7.1–7.3 (m, 7H), 7.73 ppm (m, 1H); UV/Vis (hexane): λ_{max} 273 nm, $\varepsilon = 9500$ mol^{-1} dm^3 cm^{-1}. (*Z*)-**2**: ^{1}H NMR (300 MHz, $CDCl_3$) : $\delta = 2.02$ (q, 2H); 2.23 (s, 3H), 2.58 (q, 2H), 2.90 (dd, 2H), 6.43 (m, 1H), 6.76 (dd, 1H), 6.88 (d, 1H), 6.9–7.3 ppm (m, 6H); UV/Vis (hexane): λ_{max} 275 nm, $\varepsilon = 10700$ mol^{-1} dm^3 cm^{-1}. As expected, the *Z* isomer has a shorter retention time than the *E* isomer on silica gel.

[7] T. Yoshizawa, Y. Shichida, *Methods Enzymol.* **1982**, *81*, 333–354.

[8] U. Mazzucato, F. Momicchioli, *Chem. Rev.* **1991**, *91*, 1679–1719.

[9] Calculations were performed by Drs. Manoharan and Alabugin by using B3LYP6-31G* the density functional (DFT) method.

 © 2003 Wiley-VCH Verlag GmbH & Co. KGaA, Weinheim

[10] The actinometer system (*trans*-stilbene, $\phi = 0.49$) was run at room temperature, see J. Saltiel, A. Marinari, D. W.-L. Chang, J. C. Mitchener, E. D. Megarity, *J. Am. Chem. Soc.* **1979**, *101*, 2982 – 2996.
[11] M. E. Squillacote, R. S. Sheridan, O. L. Chapman, F. A. L. Anet, *J. Am. Chem. Soc.* **1979**, *101*, 3657 – 3659.
[12] J. R. Ackerman, S. A. Forman, M. Hussain, B. Kohler, *J. Chem. Phys.* **1984**, *80*, 39 – 44.
[13] a) M. V. Alfimov, V. F. Razumov, A. G. Rachinsky, V. N. Lisvan, Yu. B. Scheck, *Chem. Phys. Lett.* **1983**, *101*, 593 – 597; b) N. Castel, E. Fischer, *J. Mol. Struct.* **1985**, *127*, 159 – 166.
[14] D. Sempedro Ruiz, A. Cembran, M. Garavelli, M. Olivucci, W. Fuss, *Photochem. Photobiol.* **2002**, *76*, 622 – 633.

 © 2003 Wiley-VCH Verlag GmbH & Co. KGaA, Weinheim

Highly Stable Mesoporous Materials

High-Temperature Generalized Synthesis of Stable Ordered Mesoporous Silica-Based Materials by Using Fluorocarbon–Hydrocarbon Surfactant Mixtures**

*Yu Han, Defeng Li, Lan Zhao, Jiangwei Song, Xiaoyu Yang, Nan Li, Yan Di, Caijin Li, Shuo Wu, Xianzhu Xu, Xiangju Meng, Kaifeng Lin, and Feng-Shou Xiao**

The hydrothermal stability of mesoporous materials is currently of great interest because of this requirement for potential applications.[1,2] A number of successful examples of mesoporous materials with good hydrothermal stability were reported recently,[1–9] for example, an ordered hexagonal SBA-15 with thicker pore walls,[3] vesicle-like MSU-G materials with a high SiO_4 cross-linking,[4] disordered KIT-1,[5] and stable mesoporous aluminosilicates from a grafting route[6] and from a preformed solution of "zeolite seeds".[7–9] Notably, these mesostructured materials are prepared at room temperature or relatively low temperatures (80–150 °C). This is quite different from the higher temperatures (150–220 °C) used for the syntheses of many microporous zeolites or phosphates because the surfactant molecules are not able to direct the mesoporous structure formation due to the unfavorable conditions for micelle formation at the higher temperatures.[10,11] In some cases, the large-chain surfactants will even decompose at temperatures greater than 150 °C. As with silica-based materials, a critical factor in increasing hydrothermal stability is to have more silica condensation on the pore walls,[4,6] but low synthetic temperatures result in imperfectly condensed mesoporous walls with large amounts of terminal hydroxyl groups that make the mesostructure unstable, especially under hydrothermal or steam conditions.[1] It can be expected that the level of silica condensation will be enhanced by increasing the crystallization temperature. As suggested above, the strategy of using higher crystallization temperature for the synthesis of mesoporous materials may require special surfactants that can be used as template at high temperature. Fluorocarbon surfactants are a kind of stable surfactant, which are widely used at high temperatures (> 200 °C). However, due to the rigidity and strong hydrophobicity of the fluorocarbon chains,[12] fluorocarbon surfactants are not suitable as templates for the preparation of well-ordered mesoporous mateials. We demonstrate herein that when a fluorocarbon surfactant ($C_3F_7O(CFCF_3CF_2O)_2CFCF_3CONH(CH_2)_3N^+(C_2H_5)_2CH_3I^-$, FC-4) is mixed with a triblock copolymer surfactant ($EO_{20}PO_{70}EO_{20}$, Pluronic P123) to form a surfactant mixture and this mixture is used as the template, highly ordered mesoporous silica-based materials with unusual hydrothermal stability, designated JLU-20, are successfully synthesized in strong acidic media at high temperatures (160–220 °C).

The X-ray diffraction (XRD) pattern of calcined JLU-20 (Figure 1 a B) shows four clearly well-resolved peaks that can be indexed as the (100), (110), (200), (210) diffractions associated with the *p6mm* hexagonal symmetry with a lattice constant $a = 118$ Å. In contrast, ordered mesostructured silica cannot be formed by high temperature crystallization in the absence of FC-4 (Figure 1 a D). Figure 1 a A and Figure 1 a B shows that the unit cell of JLU-20 does not contract during calcination at 650 °C for 5 h and demonstrates its excellent thermal stability (Table 1). This may be attributed to the pore wall of JLU-20 being fully condensed even prior to calcination, as clarified by NMR (Figure 3). In particular, JLU-20 is much more hydrothermally stable than SBA-15.[3] Upon hydrothermal treatment in boiling water for 80 h, JLU-20 remains well-ordered with clear XRD peaks associated with the *p6mm* hexagonal symmetry (Figure 1 a C), whereas SBA-15 loses most of its mesostructure (Table 1).

Transmission electron microscopy (TEM) images (Figure 1 b, Figure 2) of calcined JLU-20 show well-ordered hexagonal arrays of mesopores with 1D channels and further confirm that JLU-20 has a 2D hexagonal (*P6mm)* mesostructure. Interestingly, JLU-20 has continuous zigzag mesoporous channels that can be as long as 6 μm (Figure 2), much longer than in conventional SBA-15.[3] Such continuous ultralong channels have not been reported before and may be related to the high crystallization temperature. Additionally, during observations by TEM, unlike most ordered mesoporous materials that are extremely vulnerable to heating and electron radiation,[14] JLU-20 was not damaged even under

[*] Prof. F.-S. Xiao, Dr. Y. Han, D. Li, L. Zhao, J. Song, X. Yang, N. Li, Y. Di, C. Li, S. Wu, X. Xu, X. Meng, K. Lin
Department of Chemistry and
State Key Laboratory of Inorganic Synthesis and Preparative Chemistry
Jilin University
Changchun 130023 (China)
Fax: (+86) 431-567-1974
E-mail: fsxiao@mail.jlu.edu.cn

[**] We thank Prof. Dezeng Wang (Department of Chemical Engineering, Tsinghua University, China) for helpful suggestions and discussions. This work is supported by NSFC, CNPC, the National High Technology Research and Development Program of China (863 Program) and State Basic Research Project (973 Program).

 DOI: 10.1002/anie.200351466 © 2003 Wiley-VCH Verlag GmbH & Co. KGaA, Weinheim

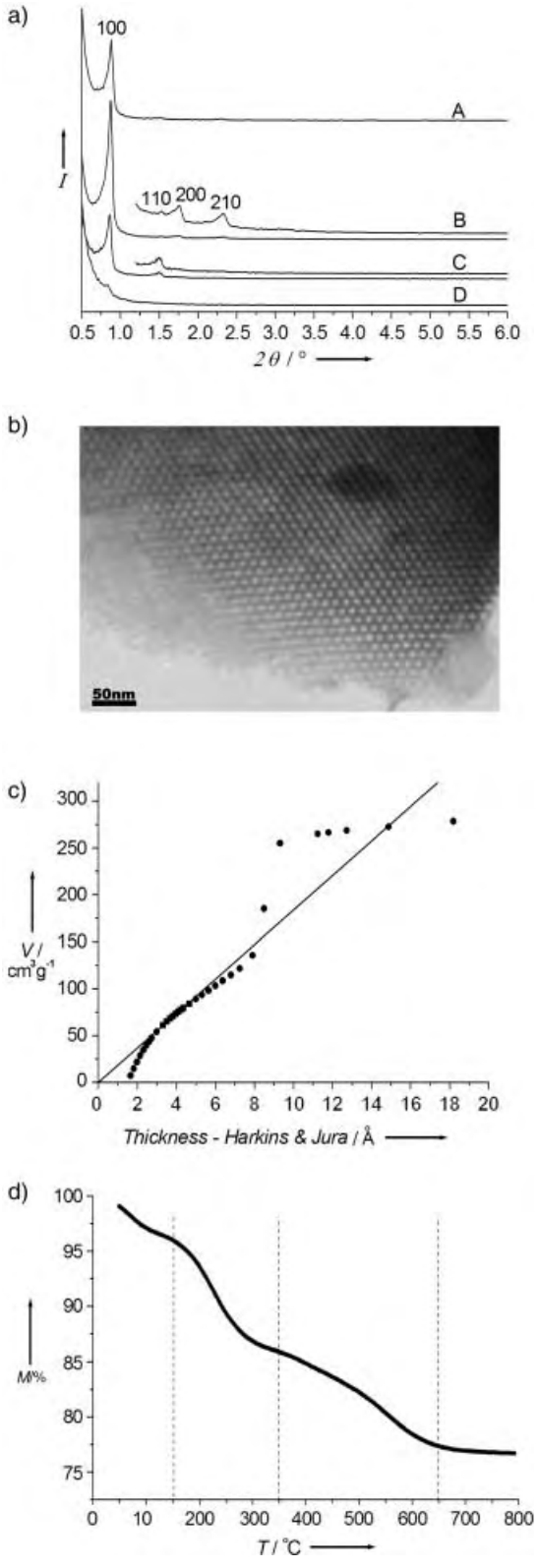


Figure 1. a) XRD patterns of as-synthesized JLU-20 (curve A), calcined JLU-20 (B), JLU-20 treated in boiling water for 80 h (C) and as-synthesized sample prepared with the same procedure as JLU-20 except for the absence of FC-4 in the initial reaction mixture (D). b) TEM image of calcined JLU-20 taken in the [100] direction. c) N_2 adsorption isotherm *t*-plots of calcined JLU-20. d) Thermogravimetry curve of JLU-20.

relatively strong current density for a long time. This is another indication that JLU-20 has unusual stability.

The ^{29}Si MAS NMR spectrum of the as-synthesized JLU-20 provides direct evidence of the extent of silica condensation. JLU-20 is primarily made up of fully condensed Q^4 silica units ($\delta = -112$ ppm) with a small contribution from incompletely cross-linked Q^3 ($\delta = -102$ ppm) as deduced from the very high Q^4/Q^3 ratio of 6.5, while no Q^2 units were observed (Figure 3 A). In contrast, SBA-15 has typical peaks correspond to Q^2, Q^3, and Q^4 silica species, and the ratio of $Q^4/Q^3 + Q^2$ is 1.9 (Figure 3 B, Table 1), thus suggesting the presence of large amounts of terminal hydroxy group in the framework. To our knowledge, JLU-20 has the highest degree of silica condensation among all kinds of mesoporous silica materials except for the vesicle-like MSU-G that has a similarly high-degree SiO_4 cross-linking.[4] In that case, however, MSU-G has a poorly ordered mesotructure (analogous to the L_α–L_3 intermediate structure) and no textural properties of the hydrothermally treated MSU-G, such as surface area and pore volume, was shown to justify its high hydrothermal stability.

The N_2 adsorption isotherms (Figure 4, Table 1) further indicate the ultra-high stability of JLU-20. For example, after hydrothermal treatment in boiling water for 80 h, there is only a decrease in BET surface area of 7 % (from 300 $m^2 g^{-1}$ to 278 $m^2 g^{-1}$) for JLU-20, whereas it is 68 % (from 1005 $m^2 g^{-1}$ to 320 $m^2 g^{-1}$) for SBA-15. Furthermore, the isotherm of the treated JLU-20 sample is still a typical IV isotherm (Figure 4 a B), which implies the good maintenance of the uniform mesopores. Its pore size distribution curve (Figure 4 b B) is as sharp as the untreated sample (Figure 4 b A). In contrast, the treated SBA-15 shows a poor isotherm (Figure 4 a D) with an indiscernible pore size distribution (Figure 4 b D). Correspondingly, the primary mesopore volume (BJH adsorption cumulative pore volume of pores between 20 and 250 Å diameter) of JLU-20 reduces by only 5 % from 0.46 $cm^3 g^{-1}$ to 0.44 $cm^3 g^{-1}$, while that of SBA-15 reduces by 30 % from 1.44 $cm^3 g^{-1}$ to 1.03 $m^2 g^{-1}$ (Table 1). Another example of the stability of JLU-20 is that when it was steamed with 100 % water vapor at 800 °C for 2 h, there was a limited effect on the structural integrity of JLU-20, whereas the mesostructure of SBA-15 is completely destroyed by the same treatment (Table 1).

From XRD and N_2 adsorption data, the wall thickness and mesopore size of JLU-20 are calculated to be 55 Å and 62 Å, respectively, and those of SBA-15 are 43 Å and 78 Å, respectively (Table 1). It is proposed that besides complete silica condensation, the thick wall and large wall thickness/pore size ratio of JLU-20 are favorable factors for its great stability, which also results from the high-temperature of the synthesis.[6c]

It is worth noting that as-synthesized JLU-20 has a relatively low surface area (300 $m^2 g^{-1}$) and pore volume (0.46 $cm^3 g^{-1}$) when compared with SBA-15. It was reported that SBA-15 has a specific surface area and pore volume that are far too large for a material with approximately uniform cylindrical (or hexagonal) pores, and there may be a large number of micropores in the wall.[13] However, JLU-20 strictly fulfills the fundamental relation between the structural

 © 2003 Wiley-VCH Verlag GmbH & Co. KGaA, Weinheim

Table 1: Properties of the samples before and after hydrothermal and steaming treatment.[a]

Sample	d(100) [Å]	Pore size [Å]	Wall thickness [Å]	Pore volume [$cm^3 g^{-1}$][d]	Surface area [$m^2 g^{-1}$]	Q^4/Q^3+Q^2	wSV^{-1}
JLU-20	101					6.5	
calcined	101	62	55	0.46	300		4.0
treated[b]	101	66	51	0.44	278		4.2
treated[c]	95	65	45	0.32	225		4.5
SBA-15	110					1.9	
calcined	105	78	43	1.44	1005		5.4
treated[b]				1.03	320		
treated[c]				0.35	214		

[a] Pore size distributions and pore volumes determined from N_2 adsorption isotherms at 77 K and the wall thickness was calculated as: thickness = a − pore size ($a = 2d_{(100)}/3^{1/2}$). Because SBA-15 was rendered amorphous after the hydrothermal or steaming treatment, there are no d(100) values, pore sizes and wall thickness for the treated SBA-15 samples given in this table. [b] Treated in boiling water for 80 h. [c] Treated with 100% water vapour at 800°C for 2 h. [d] The pore volume here is the primary mesopore volume (BJH adsorption cumulative pore volume of pores between 20 and 250 Å diameter).

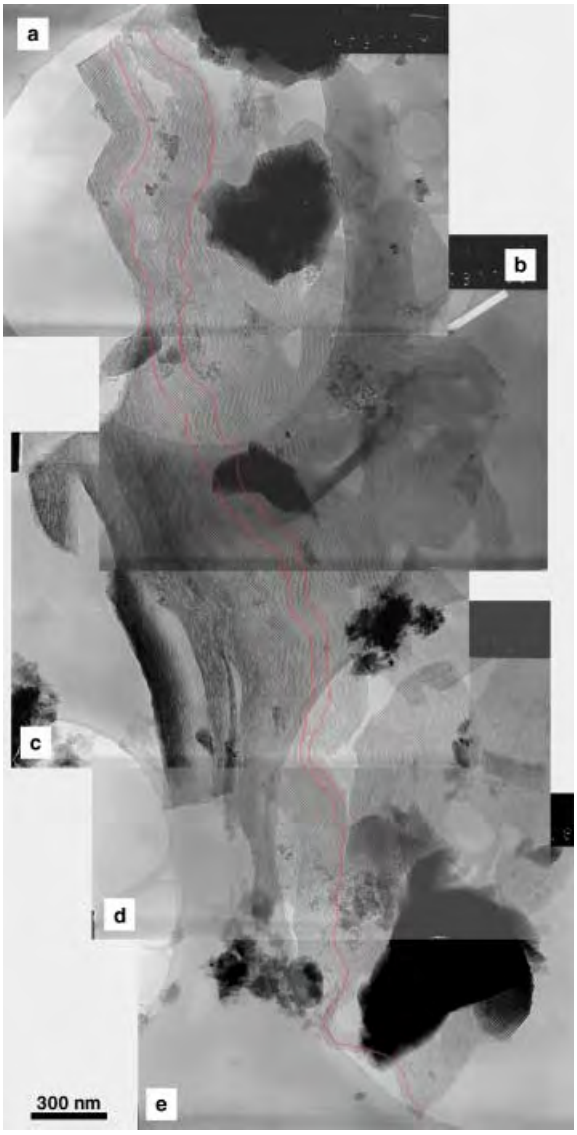


Figure 2. TEM image of calcined JLU-20 taken in the [110] direction. The ordered region is so large that fives photos (a–e) had to be taken. The five images are arranged in succession to completely show the continuous ultra-long channels, two of which are marked by red lines for clarity.

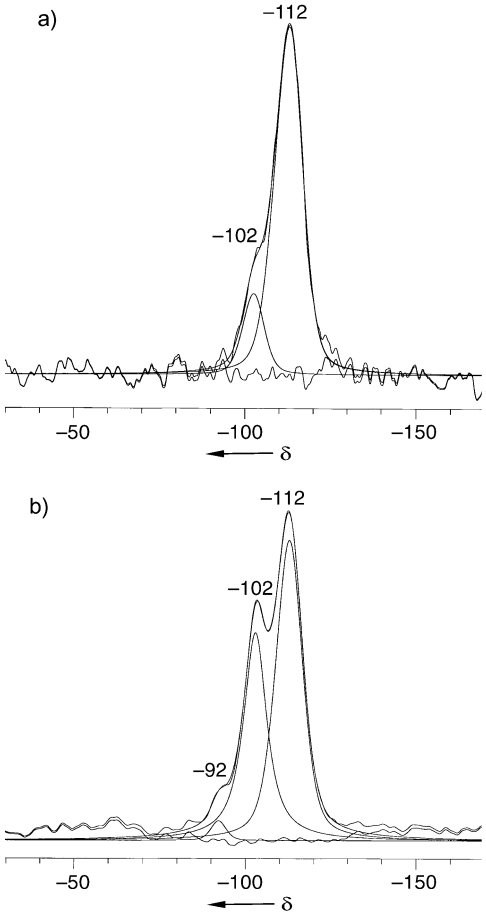


Figure 3. ^{29}Si NMR spectra of as-synthesized a) JLU-20 and b) SBA-15.

parameters for materials with uniform pores of simple cylindrical geometry: $wSV^{-1} \approx 4$ (w, S, and V denote pore size, surface area and pore volume, respectively).[13] This suggests that unlike SBA-15, JLU-20 is free of micropores in the mesoporous walls, which is confirmed by N_2 adsorption isotherm t-plots (Figure 1c). Based on reported proposals regarding the formation of micropores in SBA-15,[13] we surmise that the elimination of micropores in JLU-20 may be

 © 2003 Wiley-VCH Verlag GmbH & Co. KGaA, Weinheim

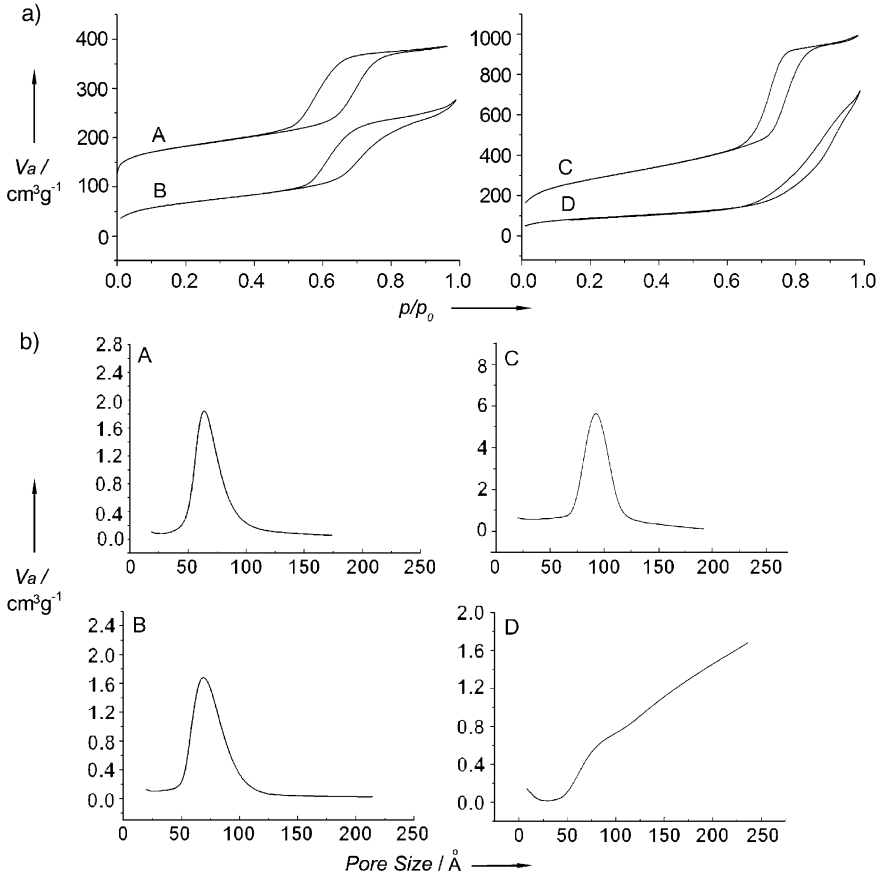


Figure 4. N_2 adsorption/desorption isotherms (a) and pore size distributions (b) of calcined samples before and after treatment in boiling water for 80 h: A) JLU-20 (before); B) JLU-20 (after); C) SBA-15 (before) and D) SBA-15 (after). Isotherms A and C have been offset by 100 $cm^3 g^{-1}$ along the vertical axis for clarity.

related to the increased hydrophobicity of the triblock copolymer surfactant in high-temperature synthesis. In the absence of micropores in the wall and the presence of a thicker wall with higher density, the relatively low values of surface area and pore volume in the case of JLU-20 is reasonable.

Due to the relatively low surface areas of JLU-20, the remaining surface area of JLU-20 is not more than that of SBA-15 after the hydrothermal treatments. However, JLU-20 has a much better ability to keep the integrity of its well-ordered mesostructure in hydrothermal conditions as shown above. Thus, in many applications where a well-ordered mesotructure (or uniform mesopores) instead of a large surface area plays the most important role (such as shape-selected catalysis, adsorption, separation, and host-guest chemistry), JLU-20 is a better candidate.

The thermogravimetric analysis curve of as-synthesized JLU-20 (Figure 1 d) shows that the total weight loss of JLU-20 is about 25 % and occurs in three steps: 5 % weight loss at 50–150 °C arising from water desorption, 10 % weight loss at 150–350 °C arising from P123 decomposition and 10 % weight loss at 350–650 °C arising from FC-4 decomposition. This result suggests that there are two kinds of surfactants in nearly equal quantities in the as-synthesized JLU-20 and is confirmed by the results of elemental analysis. It is possible that FC-4 and P123 are entangled with each other to form a mixed micella rather than forming micella in the aqueous solution separately. Evidence for this is provided by the fact that the mixture of P123 and FC-4 has a lower value of the critical micelle concentration (CMC) than either P123 or FC-4.[15–17] When a silica source is added into the synthesis system, hydrolyzed Si species can interact with P123 and FC-4 through $S^0(H^+)X^-I^+$ and $S^+X^-I^+$ routes respectively to form the mesostructure.[18–19] Although part of the P123 surfactant may decompose during high-temperature crystallization, FC-4 successfully preserves the mesostructure from collapse because of its special stability towards high temperatures. It is noted that disordered mesoporous silica with a BET surface area of 256 $m^2 g^{-1}$ is obtained if only FC-4 (without P123) is used for the synthesis. This may be because the fluorocarbon surfactant by itself tends to assemble into small-sized micella instead of periodic long-range ordered micella due to the rigidity and strong hydrophobicity of the fluorocarbon chain.[12]

The complete silica condensation and high stability of JLU-20 should be attributed directly to the high-temperature of the synthesis rather than other reasons, such as the fluorocarbon surfactant. If JLU-20 is prepared at 100 °C instead of at 190 °C, it shows no difference in both structural properties (such as surface area, pore volume, Q^4/Q^3 ratio) and stability with conventional SBA-15 although FC-4 is used. However, the use of the fluorocarbon surfactant allows full condensation by a high-temperature synthesis. This method is not limited to the combination of FC-4 with P123, and many mixtures of hydrocarbon and fluorocarbon surfactants can be used if they effectively form a regular mixed micella in solution with suitable interactions between the chosen surfactant and inorganic species. Moreover, a high-temperature synthesis can also be extended to neutral or basic media with suitable surfactants. This method may open a door for the preparation of a series of ordered mesoporous materials with various mesostructures such as 2D hexagonal *P6mm*, cubic *Ia3d*, cubic *Pm3n*, and cubic *Im3m*. For example, mesoporous silica with cubic *Im3m* symmetry has been obtained recently by using the surfactant mixture of FC-4 and triblock copolymer F127 as a template and the resulted material is more hydrothermally stable than its counterpoint prepared at low temperature, SBA-16. As catalyst supports, cubic mesoporous materials, for example, SBA-16 and MCM-48, have the

 © 2003 Wiley-VCH Verlag GmbH & Co. KGaA, Weinheim

advantage of 3D structures that lead to better transport and therefore it is of great importance to improve the hydrothermal stability of these materials.

Additionally, we have successfully introduced heteroatoms (active sites in catalysis) such as Al and Ti into the mesoporous wall of JLU-20 by a "pH-adjusting" method[20] and preformed zeolite TS-1 nanoclusters,[8c,9] respectively. Both of these exhibit much higher hydrothermal stabilities than pure silica JLU-20, which will be separately discussed in near future.

Experimental Section

In a typical synthesis, FC-4 (1.2 g) and P123 (0.4 g) were dissolved in a mixture of H_2O (20 mL) and HCl (10 M, 5 mL), followed by the addition of 2.4 mL of tetraethyl orthosilicate (TEOS). After the mixture was stirred at 40 °C for 20 h, it was transferred into an autoclave for further condensation. The crystallization temperature was slowly increased to 190 °C over 10 h and maintained there for 30 h. The product was collected by filtration, dried in air and calcined at 650 °C for 5 h to remove the surfactant template. This product is denoted as JLU-20. The SBA-15 sample was synthesized at 40 °C for 20 h and then heated at 100 °C for 2 days following the procedure reported by Zhao, Stucky and co-workers.[3]

X-ray diffraction patterns were obtained with a Siemens D5005 diffractometer by using $Cu_{K\alpha}$ radiation. Transmission electron microscopy experiments were performed on a JEM-200CX electron microscope (JEOL, Japan) with an acceleration voltage of 200 kV. The nitrogen adsorption and desorption isotherms at the temperature of liquid nitrogen were measured using a Micromeritics ASAP 2010M system. The samples were outgassed for 10 h at 300 °C before the measurements. ^{29}Si NMR spectra were recorded on a Varian Infinity plus 400 spectrometer, fitting the samples in a 7 mm ZrO_2 rotor, spinning at 8 kHz. A Perkin-Elmer TGA 7 unit was used to carry out the thermogravimetric analysis (TGA) in air at a heating rate of 20 °C min^{-1}.

Received: March 24, 2003
Revised: May 16, 2003 [Z51466]

Keywords: fluorinated ligands · high-temperature chemistry · mesoporous materials · silicates · surfactants

[1] A. Corma, *Chem. Rev.* **1997**, *97*, 2373.
[2] C. T. Kresge, M. E. Leonowicz, W. J. Roth, J. C. Vartuli, J. S. Beck, *Nature* **1992**, *352*, 710.
[3] D. Zhao, J. Feng, Q. Huo, N. Melosh, G. H. Fredrickson, B. F. Chmelka, G. D. Stucky, *Science* **1998**, *279*, 548.
[4] S. S. Kim, W. Zhang, T. J. Pinnavaia, *Science* **1998**, *282*, 1032.
[5] R. Ryoo, J. M. Kim, C. H. Shin, *J. Phys. Chem.* **1996**, *100*, 17718.
[6] a) R. Mokaya, *Chem. Commun.* **1998**, 1839; b) R. Mokaya, *Angew. Chem.* **1999**, *111*, 3079; *Angew. Chem. Int. Ed.* **1999**, *38*, 2930; c) R. Mokaya, *J. Phys. Chem. B* **1999**, *103*, 10204; d) R. Mokaya, *Chem. Commun.* **2001**, 633.
[7] a) Y. Liu, W. Zhang, T. J. Pinnavaia, *J. Am. Chem. Soc.* **2000**, *122*, 8791; b) Y. Liu, W. Zhang, T. J. Pinnavaia, *Angew. Chem.* **2001**, *113*, 1295; *Angew. Chem. Int. Ed.* **2001**, *40*, 1255.
[8] a) Z. Zhang, Y. Han, L. Zhu, R. Wang, Y. Yu, S. Qiu, D. Zhao, F.-S. Xiao, *Angew. Chem.* **2001**, *113*, 1298; *Angew. Chem. Int. Ed.* **2001**, *40*, 1258; b) Y. Han, S. Wu, Y. Sun, D. Li, F.-S. Xiao, *Chem. Mater.* **2002**, *14*, 1144; c) Y. Han, F.-S. Xiao, S. Wu, Y. Sun, X.-J. Meng, D, Li, S. Lin, *J. Phys. Chem. B* **2001**, *105*, 7963.
[9] F.-S. Xiao, Y. Han, X.-J. Meng, Y. Yu, M. Yang, S. Wu, *J. Am. Chem. Soc.* **2002**, *124*, 888.
[10] T. Sun, J. Y. Ying, *Nature* **1997**, *389*, 704.
[11] J. S. Beak, J. C. Vartuli, G. J. Kennedy, C. T. Kresge, W. J. Roth, S. E. Schramm, *Chem. Mater.* **1994**, *6*, 1816.
[12] Y. Muto, K. Esumi, K. Meguro, R. Zana, *J. Colloid Interface Sci.* **1987**, *120*, 162.
[13] R. Ryoo, C. H. Ko, M. Kruk, M. Antochshuk, M. Jaroniec, *J. Phys. Chem. B* **2000**, *104*, 11465.
[14] J. Liu, X. Zhang, Y. Han, F.-S. Xiao, *Chem. Mater.* **2002**, *14*, 2536.
[15] K. Yada, K. Tamori, K. Esumi, K. Meguno, *J. Colloid Interface Sci.* **1989**, *131*, 282.
[16] T. Suzuki, M. Ueno, K. Meguro, *J. Am. Oil Chem. Soc.* **1981**, *58*, 800.
[17] B. Y. Zhu, M. J. Rosen, *J. Colloid Interface Sci.* **1984**, *99*, 435.
[18] D. Zhao, Q. Huo, J. Feng, B. F. Chmelka, G. D. Stucky, *J. Am. Chem. Soc.* **1998**, *120*, 6024.
[19] Q. Huo, D. I. Margolcsc, G. D. Stuck, *Chem. Mater.* **1996**, *8*, 1147.
[20] S. Wu, Y. Han, F.-S. Xiao, *J. Phys. Chem. B*, submitted.

 © 2003 Wiley-VCH Verlag GmbH & Co. KGaA, Weinheim

Azadirachtin Precursors

Studies Towards the Synthesis of Azadirachtin: Enantioselective Entry into the Azadirachtin Framework through Cascade Reactions**

K. C. Nicolaou, A. J. Roecker, Holger Monenschein, Prasuna Guntupalli, and Markus Follmann*

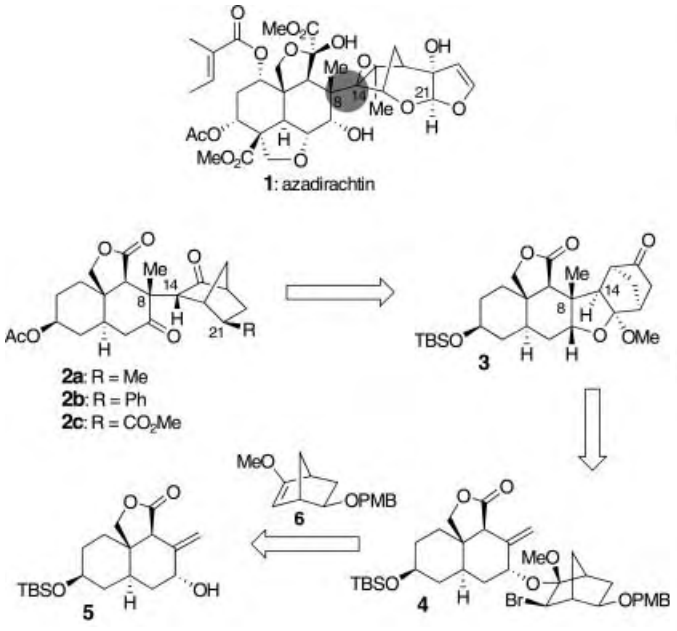
As part of a program directed towards the total synthesis of azadirachtin (**1**),[1,2] we have adopted a radical-based approach for the construction of its crowded C8–C14 bond.[3] Herein we report further advances along this path-

[*] Prof. Dr. K. C. Nicolaou, A. J. Roecker, Dr. H. Monenschein, Dr. P. Guntupalli, Dr. M. Follmann
Department of Chemistry and
The Skaggs Institute for Chemical Biology
The Scripps Research Institute
10550 North Torrey Pines Road, La Jolla, CA 92037 (USA)
Fax: (+1) 858-784-2469
E-mail: kcn@scripps.edu
and
Department of Chemistry and Biochemistry
University of California San Diego
9500 Gilman Drive, La Jolla, CA 92093 (USA)

[**] We thank Dr. D. H. Huang and Dr. G. Siuzdak for NMR spectroscopic and mass spectroscopic assistance, respectively, and Dr. Raj Chadha for X-ray crystallographic analysis. This work was financially supported by the National Institutes of Health (USA), The Skaggs Institute for Chemical Biology, predoctoral fellowships from the Division of Organic Chemistry of the ACS sponsored by Novartis and the Division of Medicinal Chemistry of the ACS sponsored by Pfizer (both to A.J.R.), a Feodor Lynen postdoctoral fellowship from the Alexander von Humboldt Foundation (to H.M.), and a postdoctoral fellowship from Bayer AG (to M.F.).

 DOI: 10.1002/anie.200351744 © 2003 Wiley-VCH Verlag GmbH & Co. KGaA, Weinheim

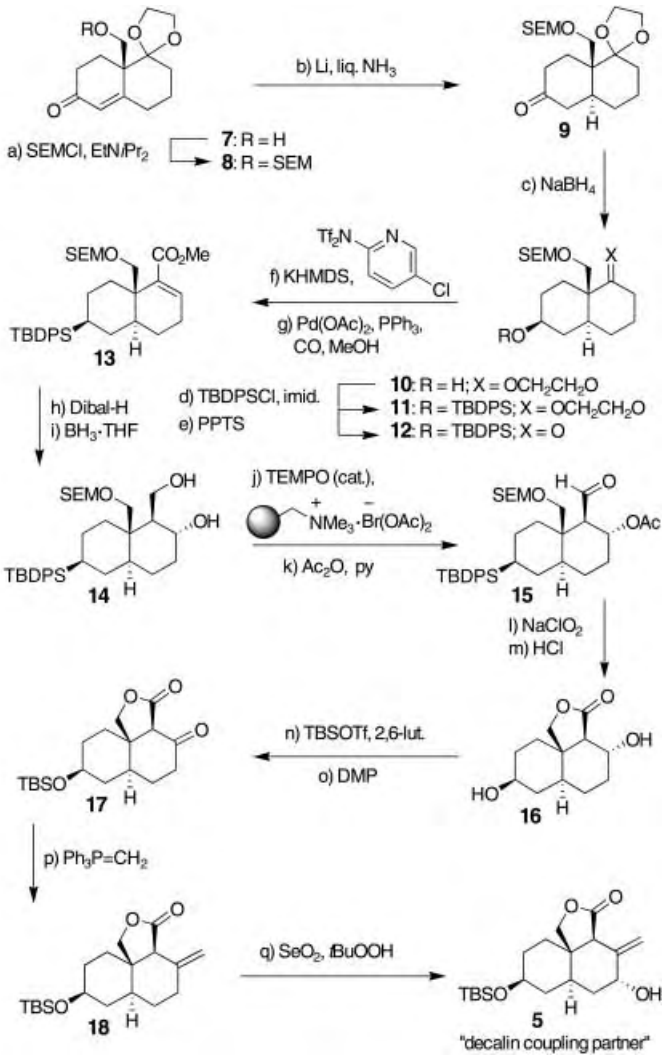
way, including a number of novel cascade reactions and the arrival at suitably functionalized advanced systems **2a–c**, which contain both domains of the target molecule (Scheme 1).



Scheme 1. Retrosynthetic analysis of advanced azadirachtin intermediate **2**.

Scheme 1 outlines the retrosynthetic plan for the enantioselective construction of azadirachtin systems such as **2a–c**, which feature both a functionalized decalin and a bicyclic framework linked together through the C8–C14 bond. It was rationalized that such a compound could be formed through an acid-induced opening of the mixed ketal moiety within the polycyclic compound **3**, followed by suitable elaboration. Lactone **3**, which contains, in principle, enough functionality for a drive towards azadirachtin, was reasoned to arise from a radical cyclization cascade sequence initiated from bromoketal **4**. As originally proposed,[3] bromoketal **4** was to be assembled from the allylic alcohol **5** and methyl enol ether **6**. Hence, enantiocontrolled sequences for the construction of both **5** and **6** were sought.

The synthesis of allylic alcohol **5** is depicted in Scheme 2. Known decalin alcohol **7** (prepared from 1,3-cyclohexanedione with approximately 70% *ee*)[4] was protected as a SEM ether (SEMCl, EtN*i*Pr$_2$, 85% yield), and the resulting enone was subjected to a Birch reduction (Li, liquid NH$_3$, 80% yield) to afford *trans*-decalin system **9**. The ketone functionality of compound **9** was then reduced stereoselectively with NaBH$_4$ (99% yield), and the obtained β-hydroxy compound was silylated (TBDPSCl, imidazole, DMAP, 80% yield), leading to protected compound **11**. The dioxolane system of compound **11** was removed upon treatment with mild acid (PPTS), and the crude ketone was transformed into the corresponding enol triflate (KHMDS, Comin reagent, 72%



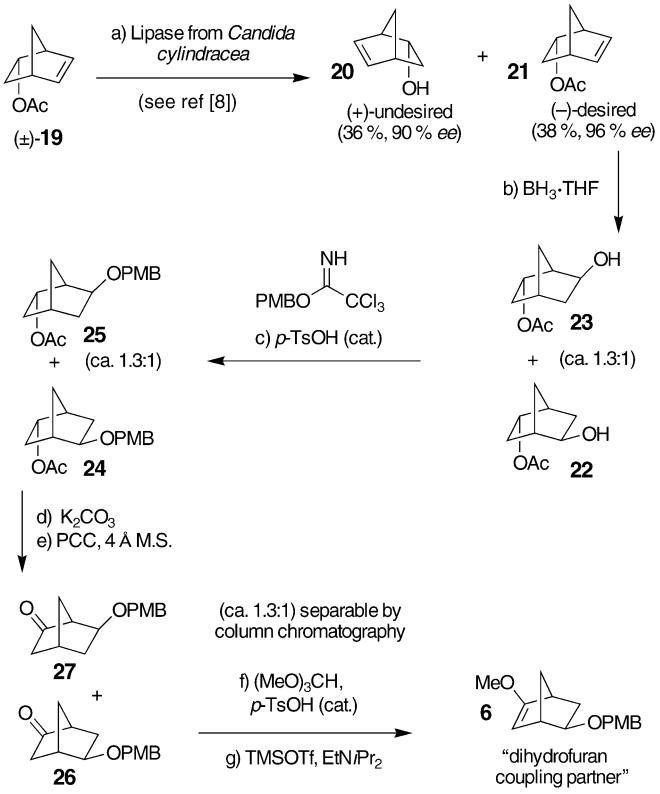
Scheme 2. Enantioselective synthesis of decalin coupling partner **5**. a) SEMCl (1.2 equiv), EtN*i*Pr$_2$ (1.5 equiv), CH_2Cl_2, 25 °C, 20 h, 85%; b) Li (7.0 equiv), liquid NH_3, −78 °C, 1 h, 80%; c) $NaBH_4$ (1.2 equiv), THF/EtOH (1:1), −78→25 °C, 3 h, 99%; d) TBDPSCl (2.0 equiv), imid. (1.5 equiv), DMAP (0.2 equiv), DMF, 25 °C, 24 h, 80%; e) PPTS (0.05 equiv), acetone, 65 °C, 24 h; f) KHMDS (3.5 equiv), Comin reagent (1.2 equiv), THF, −78 °C, 0.5 h, 72% over two steps; g) $Pd(OAc)_2$ (0.3 equiv), PPh_3 (0.6 equiv), CO (1 atm), EtN*i*Pr$_2$ (3.0 equiv), MeOH (50 equiv), DMF, 60 °C, 12 h, 89%; h) DIBAL-H (4.0 equiv), CH_2Cl_2, −78→0 °C, 2 h, 95%; i) BH_3·THF (5.0 equiv), THF, 0 °C, 12 h, 65%; j) TEMPO (0.1 equiv), resin (3.0 equiv), CH_2Cl_2, 25 °C, 2 h; k) Ac_2O (5.0 equiv), py/CH_2Cl_2 (1:4), 25 °C, 0.1 h; l) $NaClO_2$ (5.0 equiv), 2-methyl-2-butene (40 equiv), NaH_2PO_4 (3.5 equiv), *t*BuOH/H_2O (10:1), 25 °C, 2 h; m) HCl (1 N)/dioxane (1:1), 75 °C, 16 h, 83% over four steps; n) TBSOTf (1.1 equiv), 2,6-lut. (1.3 equiv), CH_2Cl_2, 25 °C, 1 h, 72%; o) DMP (1.5 equiv), $NaHCO_3$ (5.0 equiv), CH_2Cl_2, 25 °C, 3 h, 97%; p) $Ph_3P{=}CH_2$ (8.0 equiv), THF, 25 °C, 12 h, 78%; q) SeO_2 (3.0 equiv), *t*BuOOH (5.0 equiv), CH_2Cl_2, 25 °C, 6 h, 50%. SEM = 2-(trimethylsilyl)ethoxymethyl, TBDPS = *tert*-butyldiphenylsilyl, imid = imidazole, DMAP = 4-dimethylaminopyridine, DMF = *N*,*N*-dimethylformamide, PPTS = pyridinium *p*-toluenesulfonate, KHMDS = potassium bis(trimethylsilyl)amide, Comin reagent = 2-[*N*,*N*-bis(trifluoromethylsulfonyl)amino]-5-chloropyridine, TEMPO = 4-oxo-2,2,6,6-tetramethyl-1-piperidinyloxy (free radical), py = pyridine, TBS = *tert*-butyldimethylsilyl, Tf = trifluoromethanesulfonyl, DMP = Dess–Martin periodinane.

 © 2003 Wiley-VCH Verlag GmbH & Co. KGaA, Weinheim

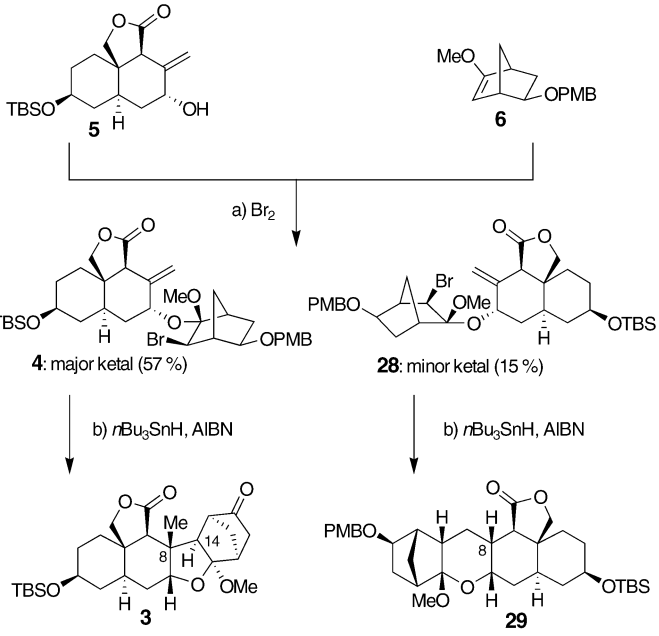
over two steps). The resulting triflate was then engaged in a palladium-catalyzed carbonylation reaction to afford α,β-unsaturated methyl ester **13** in 89% yield.[5] Reduction of **13** with DIBAL-H (95% yield), followed by regio- and stereoselective hydroboration led to diol **14** in 65% yield after basic workup. This diol was then selectively oxidized to the corresponding hydroxyaldehyde through a polymer-assisted TEMPO-catalyzed oxidation procedure[6] and subsequently acetylated (Ac_2O, Et_3N) to produce aldehyde acetate **15**. Further oxidation to the carboxylic acid, followed by treatment of the resulting compound with aqueous HCl in dioxane, gave rise to dihydroxy lactone **16** (83% yield over four steps). Diol **16** was then selectively protected as a TBS ether (72% yield), which was oxidized to the dicarbonyl system **17** with DMP (97% yield). Finally, selective olefination of the ketone functionality of **17** ($Ph_3P=CH_2$, 78% yield) followed by regio- and stereoselective allylic oxidation of the resulting **18** as effected by SeO_2 and *t*BuOOH afforded the desired allylic alcohol **5** in 50% yield.[7]

The enantioselective synthesis of the required enol ether **6** is shown in Scheme 3. A known resolution procedure was used to prepare the desired *endo* acetate **21** from racemic acetate **19** in 38% yield with high enantioselectivity (96% *ee*).[8] Hydroboration (BH_3·THF) of the C=C bond in **21** followed by basic workup with hydrogen peroxide resulted in an inseparable mixture of regioisomeric alcohols (**22**/**23** ≈ 1:1.3) in 78% combined yield. This mixture was protected with a PMB group to provide **24** and **25**, the acetate was removed (K_2CO_3, MeOH, 84% yield over two steps), and the resulting alcohols were oxidized to the corresponding ketones **26** and **27** upon treatment with PCC (88% combined yield). The desired ketone **26** was separated from its unwanted isomer **27** by flash column chromatography (silica gel), and then transformed into the targeted enol ether **6** by first constructing its dimethyl ketal ($(MeO)_3CH$, *p*-TsOH, 98% yield) and then eliminating one molecule of MeOH under the conditions reported by Gassman et al. (TMSOTf/Et*N*iPr_2, 57% yield).[9]

With both building blocks **5** and **6** in hand, the next task was the tethering of the two domains through a ketal bridge. As depicted in Scheme 4, treatment of enol ether **6** with bromine in CH_2Cl_2 in the presence of *N*,*N*-dimethylaniline at



Scheme 3. Enantioselective synthesis of bicyclic methyl enol ether **6** (dihydrofuran coupling partner). a) See reference [8]; b) BH_3·THF (1.0 equiv), THF, 0°C, 1 h; then NaOH (1 M; 5.0 equiv), aqueous H_2O_2 (30 wt%; 5.0 equiv), 30 min, 78%; c) *p*-methoxybenzyltrichloroacetimidate (2.0 equiv), *p*-TsOH (0.1 equiv), CH_2Cl_2, 25°C, 10 h; d) K_2CO_3 (0.5 equiv), MeOH, 25°C, 8 h, 84% over two steps; e) PCC (2.5 equiv), M.S. (4 Å), CH_2Cl_2, 25°C, 1 h, 88%; f) $(MeO)_3CH$ (1.5 equiv), *p*-TsOH (0.05 equiv), MeOH, 25°C, 3 h, 98%; g) TMSOTf (1.1 equiv), Et*N*iPr_2 (1.2 equiv), CH_2Cl_2, −20→25°C, 16 h, 57%. PMB = *p*-methoxybenzyl, *p*-TsOH = *p*-toluenesulfonic acid monohydrate, PCC = pyridinium chlorochromate.



Scheme 4. Radical cascade-based construction of the C8–C14 bond of azadirachtin; construction of **3** and **29**. a) Br_2 (1.0 equiv), *N*,*N*-dimethylaniline (2.0 equiv), CH_2Cl_2, **6** (1.3 equiv), **5** (1.0 equiv), −78→0°C, 12 h, 72% combined yield; b) nBu_3SnH (1.3 equiv), AIBN (0.5 equiv) in toluene (0.01 M), 110°C, 15 h, 75% (**4**), 74% (**29**). AIBN = 2,2′-azobisisobutyronitrile.

−78°C, followed by addition of allylic alcohol **5** at that temperature, afforded bromoketal **4** as the major product (57%) together with bromoketal **28** as a minor product (15%).[10] Individual treatment of these ketals with nBu_3SnH and AIBN (0.01M in toluene, 110°C) led to hexacyclic products **3** (75%, desired product for azadirachtin; see Table 1) and **29** (74%), respectively. Interestingly, loss of

 © 2003 Wiley-VCH Verlag GmbH & Co. KGaA, Weinheim

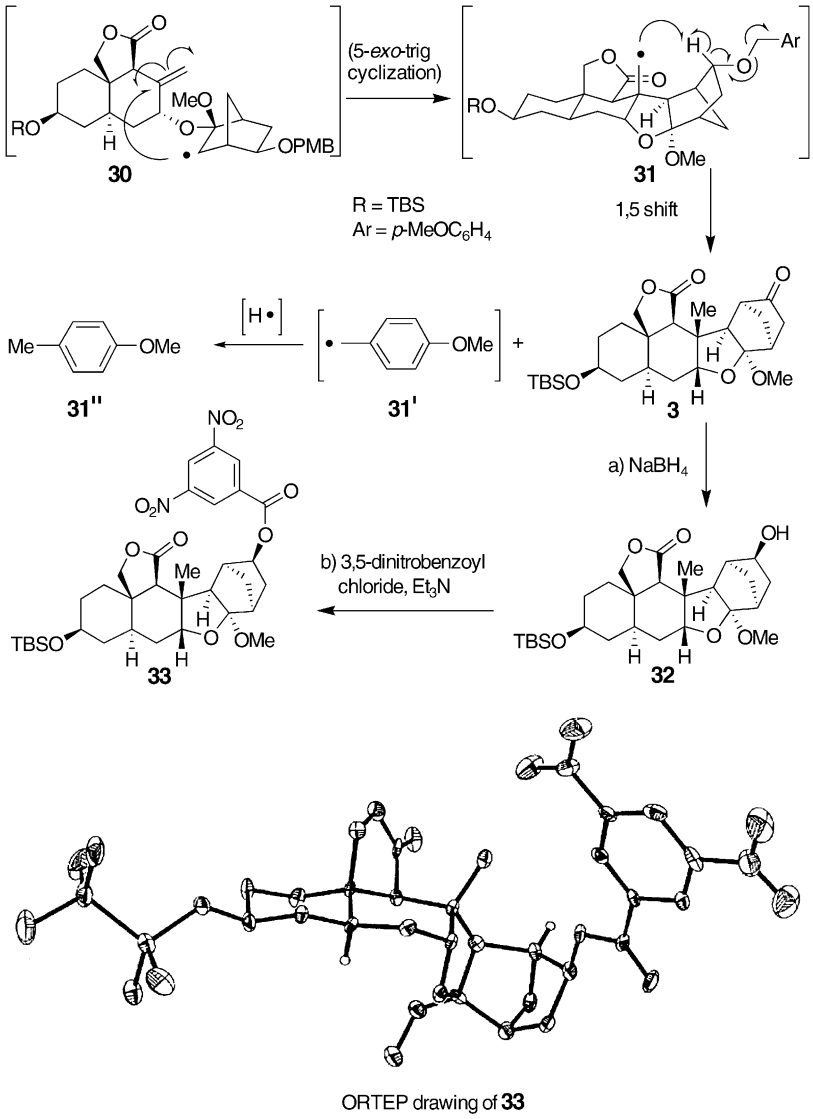
the PMB ether and concomitant conversion into a ketone accompanied the 5-*exo*-trig cyclization to give **3** from the major bromoketal **4**. Also of interest is the fact that the minor ketal underwent cyclization in a 6-*endo*-trig manner to afford **29** as opposed to the expected 5-*exo*-trig cyclization.[11]

A mechanistic explanation for the intriguing transformation of **4** into **3** is shown in Scheme 5. Thus, the secondary radical generated from **4** (i.e. **30**) undergoes the expected 5-*exo*-trig cyclization to forge the C8–C14 bond, leading to the highly reactive primary radical **31**. The proximity of the radical center within **31** to the hydrogen atom on the carbon atom that bears the PMB ether, five bonds away, coupled with the overall rigidity and reactivity of the system, apparently allows the indicated 1,5 H shift, with concomitant oxidative rupture of the benzyl bond, leading to the observed product **3** and *p*-methoxytoluene (**31″**), which presumably arises from the intermediate radical species **31′**.[12] To confirm the structure of **3**, a suitably crystalline derivative for X-ray crystallographic analysis was sought and found in the 3,5-dinitrobenzoate **33**. The latter compound was obtained by a stereoselective reduction of **3** with $NaBH_4$ (80% yield) followed by reaction with 3,5-dinitrobenzoyl chloride and Et_3N in the presence of DMAP (85% yield). Indeed, the X-ray crystallographic analysis of **33** revealed its structure (see ORTEP drawing, Scheme 5) and, by extension, that of **3**.

The radical cyclization reaction of the minor bromoketal (**28**, Scheme 4) was also intriguing in that it apparently proceeded through a 6-*endo*-trig cyclization of the initially formed radical **34** to form hexacycle **29** as shown in Scheme 6.[13] The structure of **29** was unambiguously assigned by X-ray crystallographic analysis of the 3,5-dinitrobenzoate derivative **35**, obtained by desilylation of **29** (100% yield) and ester formation (80% yield; see ORTEP structure in Scheme 6).

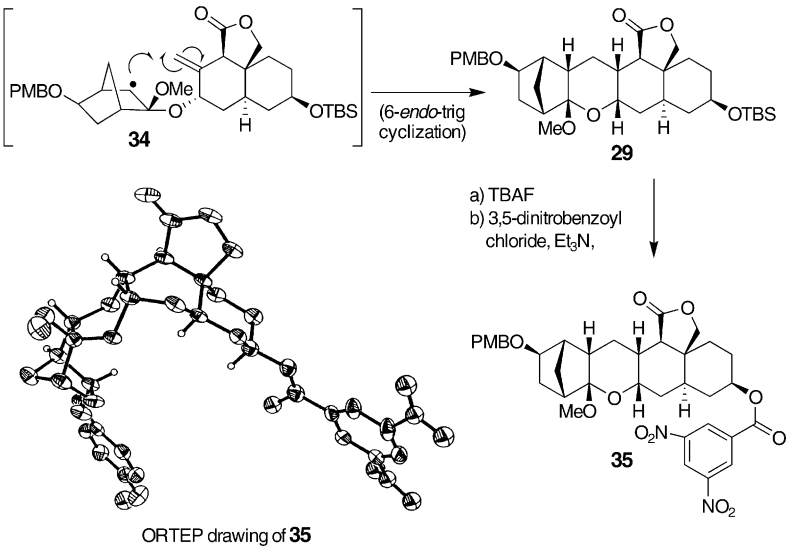
Modeling studies (ball and stick) with **28** indicate that a 5-*exo*-trig cyclization would be associated with a severe steric interaction between the methoxy group and the olefinic site in contrast to a 6-*endo*-trig mode of ring closure, which is devoid of such interactions. Similar modeling with the major bromoketal **4**, on the other hand, shows that the expected 5-*exo*-trig cyclization does not suffer from the methoxy–olefin steric interaction, explaining the difference in the behavior of the two diastereomeric bromoketals.

A significant finding in this study was the demonstration of the rupture of the mixed ketal bridge employed to facilitate C8–C14 bond formation (Scheme 7). These studies began with an attempt to hydrolyze the mixed ketal within **3**, or variants thereof, only to realize the intransigence of the resulting lactol towards opening to the desired hydroxyketone form. The sequence **3**→**36**→**37**→**38** (desilylation, *p*-bromobenzoate formation, and treatment with H_2SO_4) is illustrative of these forays. This intransigence is in contrast to previous observations with similar compounds,[3] and underscores the subtle intricacies of reactivity within the azadirachtin scaffold. In an effort to probe further these structure-based reactivity patterns, polycycle **3** was modified to its olefinic counterpart **39** through Wittig olefination (62% yield), desilylation (→**40**, 91% yield), and acetylation (→**41**, 90% yield). Gratifyingly, **41** was smoothly converted into diketone **2a** (see Table 1) in 80% yield upon exposure to H_2SO_4 in CH_2Cl_2 at 0°C.[14] To explain this unusual transformation we invoke an initial protonation of the olefinic bond leading to a

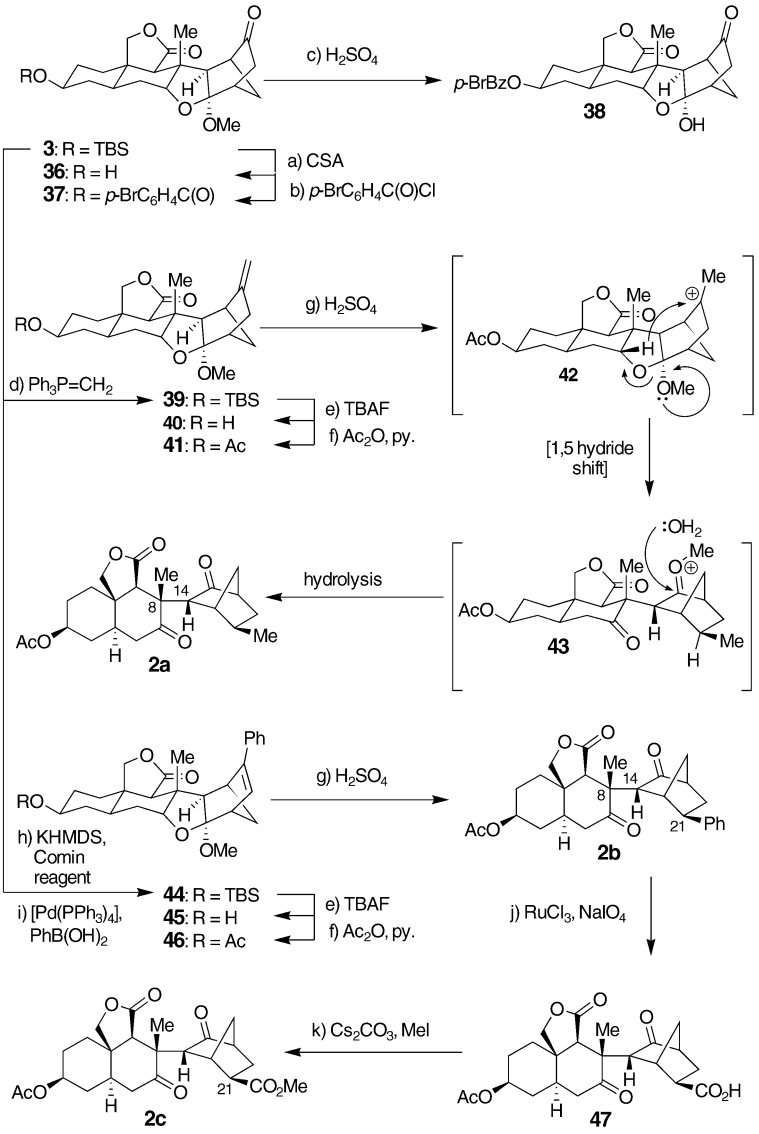


Scheme 5. Proposed cascade sequence for the formation of **3** from major ketal **4** and structural proof of product. a) $NaBH_4$ (4.0 equiv), MeOH, 0°C, 1 h, 80%; b) 3,5-dinitrobenzoyl chloride (2.0 equiv), Et_3N (4.0 equiv), DMAP (0.2 equiv), CH_2Cl_2, 25°C, 12 h, 85%.

 © 2003 Wiley-VCH Verlag GmbH & Co. KGaA, Weinheim



Scheme 6. Structural proof of polycycle **29**. a) TBAF (3.0 equiv), THF, 25 °C, 4 h, 100 %; b) 3,5-dinitrobenzoyl chloride (2.0 equiv), Et_3N (5.0 equiv), DMAP (0.2 equiv), CH_2Cl_2, 25 °C, 12 h, 80 %. TBAF = tetrabutylammonium fluoride.



Scheme 7. Hydrolysis of mixed ketal polycycles and synthesis of **2a**–**c**. a) CSA (2.0 equiv), MeOH, 25 °C, 1 h, 90 %; b) 4-bromobenzoyl chloride (2.0 equiv), Et_3N (5.0 equiv), DMAP (0.2 equiv), CH_2Cl_2, 25 °C, 12 h, 81 %; c) H_2SO_4 (5.0 equiv), CH_2Cl_2, 0 °C, 0.5 h, 85 %; d) $Ph_3P{=}CH_2$ (10.0 equiv), THF, 25 °C, 15 h, 62 %; e) TBAF (3.0 equiv), THF, 40 °C, 0.5 h, 91 %; f) Ac_2O (10.0 equiv), DMAP (1.0 equiv), py, 25 °C, 6 min, 90 %; g) H_2SO_4 (5.0 equiv), CH_2Cl_2, 0 °C, 10 min, 80 % (**2a**), 81 % (**2b**); h) KHMDS (3.0 equiv), Comin reagent (2.0 equiv), THF, −78 °C, 1 h, 65 %; i) $[Pd(PPh_3)_4]$ (0.1 equiv), $PhB(OH)_2$ (5.0 equiv), Cs_2CO_3 (10.0 equiv), DMF/MeOH (10:1), 80 °C, 1 h, 78 %; j) $RuCl_3$ (0.5 equiv), $NaIO_4$ (20.0 equiv), $CH_3CN/CCl_4/H_2O$ (1:1:1), 25 °C, 24 h; k) Cs_2CO_3 (5.0 equiv), MeI (10.0 equiv), DMF, 25 °C, 2 h, 80 % over two steps. CSA = camphorsulfonic acid.

tertiary carbocation (**42**, see Scheme 7) which then triggers an oxidative 1,5 hydride transfer with concomitant rupture of the oxygen bridge between the two domains of the molecule. Subsequent hydrolysis of the resulting intermediate **43** then leads to the observed product **2a**.

In an extension of this concept and to obtain a functional handle at what will become C21 of azadirachtin, a second foray was designed and executed. Hence, compound **3** (Scheme 7) was transformed into styrene derivative **44** via its enol triflate (KHMDS, Comin reagent, 65 % yield) and through a Suzuki reaction ($[Pd(PPh_3)_4]$, $PhB(OH)_2$, 78 % yield). The TBS group within **44** was then replaced by an acetate group to afford **46** via **45** (82 % for two steps). Exposure of **46** to H_2SO_4 as above gave **2b**, presumably through the same cascade mechanism that led to **2a**. The phenyl ring of the latter intermediate (**2b**) was then oxidatively degraded[15] by the action of $RuCl_3$ and $NaIO_4$ to reveal carboxylic acid **47**, whose methylation afforded advanced intermediate **2c** (80 % yield over two steps) equipped with a synthetically useful handle at C21.

The described chemistry represents considerable progress toward the azadirachtin structure and its congeners. Specifically, a sequence based on intramolecular radical chemistry followed by a cation-induced rupture of an initially formed bridge enabled the construction of the suitably functionalized system **2c**, setting the stage for further advances towards this formidable target. Furthermore, the observed radical- and ionic-based cascade sequences may prove

© 2003 Wiley-VCH Verlag GmbH & Co. KGaA, Weinheim

Table 1: Selected data for **3** and **2a**.

3: Colorless oil; $[\alpha]_D = -14°$ ($c = 0.10$ in $CHCl_3$); $R_f = 0.27$ (silica, 25% EtOAc in hexanes); IR (thin film): $\tilde{\nu}_{max} = 2930, 2861, 1766, 1742, 1508, 1461, 1249\ cm^{-1}$; ^1H NMR (600 MHz, C_6D_6): $\delta = 3.71$ (d, $J = 9.7$ Hz, 1H), 3.69–3.67 (m, 1H), 3.58–3.50 (m, 1H), 3.37 (d, $J = 9.7$ Hz, 1H), 3.13 (s, 3H), 2.83 (d, $J = 4.4$ Hz, 1H), 2.56 (s, 1H), 2.40 (br s, 1H), 2.32 (br s, 1H), 2.16 (dd, $J = 17.9$, 4.8 Hz, 1H), 1.88–1.80 (m, 1H), 1.61–1.42 (m, 5H), 1.39–1.22 (m, 3H), 1.14 (s, 3H), 1.03 (d, $J = 10.5$ Hz, 1H), 0.96 (s, 9H), 0.95–0.88 (m, 1H), 0.82–0.74 (m, 1H), −0.02 ppm (s, 6H); ^{13}C NMR (150 MHz, C_6D_6): $\delta = 215.1, 171.3, 115.1, 85.2, 71.1, 68.4, 67.7, 54.8, 54.1, 51.0, 42.5, 41.3, 41.1, 39.9, 38.8, 38.1, 35.6, 32.2, 30.4, 28.2, 26.0, 18.1, 16.5, -4.5, -4.6$ ppm; HRMS (MALDI, FTMS), calcd for $C_{27}H_{42}O_6Si$ [M+Na^+]: 513.2643, found: 513.2631

2a: Colorless oil; $[\alpha]_D = -34°$ ($c = 0.23$ in $CHCl_3$); $R_f = 0.52$ (silica, 50% EtOAc in hexanes); IR (thin film): $\tilde{\nu}_{max} = 2958, 2868, 1765, 1730, 1454, 1371, 1243\ cm^{-1}$; ^1H NMR (600 MHz, C_6D_6): $\delta = 4.43–4.38$ (m, 1H), 3.66 (d, $J = 9.6$ Hz, 1H), 3.48 (dd, $J = 9.6$, 2.2 Hz, 1H), 2.92 (s, 1H), 2.74 (d, $J = 4.0$ Hz, 1H), 2.62–2.58 (m, 1H), 2.52 (d, $J = 4.0$ Hz, 1H), 2.21–2.15 (m, 1H), 1.94–1.91 (m, 1H), 1.74–1.70 (m, 1H), 1.67 (s, 3H), 1.65 (d, $J = 3.5$ Hz, 1H), 1.63 (d, $J = 3.5$ Hz, 1H), 1.56–1.53 (m, 1H), 1.38–1.18 (m, 5H), 1.07–1.03 (m, 1H), 1.02–0.98 (m, 1H), 0.96 (s, 3H), 0.77 (d, $J = 7.0$ Hz, 3H), 0.58–0.52 ppm (m, 1H); ^{13}C NMR (125 MHz, C_6D_6): $\delta = 215.5, 207.1, 175.5, 169.0, 70.6, 68.6, 60.2, 58.5, 53.4, 50.4, 46.0, 43.3, 40.2, 38.6, 35.4, 34.7, 34.1, 34.0, 30.2, 27.2, 22.2, 20.7, 20.4$ ppm; HRMS (MALDI, FTMS), calcd for $C_{23}H_{30}O_6$ [M+H^+]: 403.2115, found: 403.2118

useful in other contexts within the general theme of molecular complexity and diversity construction.

Received: April 24, 2003 [Z51744]

Keywords: asymmetric synthesis · azadirachtin · domino reactions · hydride shift · natural products · radicals

[1] For the isolation, see: J. H. Butterworth, E. D. Morgan, *Chem. Commun.* **1968**, 23–24.

[2] For the structure determination, see: a) J. N. Bilton, H. B. Broughton, P. S. Jones, S. V. Ley, Z. Lidert, E. D. Morgan, H. S. Rszepa, R. N. Sheppard, A. M. Z. Slawin, D. J. Williams, *Tetrahedron* **1987**, *43*, 2805–2815; b) W. Kraus, M. Bokel, A. Bruhn, R. Cramer, I. Klaiber, A. Klenk, G. Nagl, H. Pohnl, H. Sadlo, B. Vogler, *Tetrahedron* **1987**, *43*, 2817–2830; c) C. J. Turner, M. S. Tempesta, R. B. Taylor, M. G. Zagorski, J. S. Termini, D. R. Schroeder, K. Nakanishi, *Tetrahedron* **1987**, *43*, 2789–2804; Synthetic studies: d) S. V. Ley, C. E. Gutteridge, A. R. Pape, C. D. Spilling, C. Zumbrunn, *Synlett* **1999**, 1295–1297; e) A. A. Denholm, L. Jennens, S. V. Ley, *Tetrahedron* **1995**, *51*, 6591–6604; f) S. V. Ley, A. A. Denholm, A. Wood, *Nat. Prod. Rep.* **1993**, *10*, 109–157; g) H. Kolb, S. V. Ley, *Tetrahedron Lett.* **1991**, *32*, 6187–6190; h) M. G. Brasca, H. B. Broughton, D. Craig, S. V. Ley, A. A. Somovilla, P. L. Toogood, *Tetrahedron Lett.* **1988**, *29*, 1853–1856; i) Y. Yamamoto, J. Ishihara, N. Kanoh, A. Murai, *Synthesis* **2000**, 1878–1893; j) H. Watanabe, T. Watanabe, K. Mori, T. Kitahara, *Tetrahedron Lett.* **1997**, *38*, 4429–4432; k) Y. Nishikimi, T. Iimori, M. Sodeoka, M. Shibasaki, *J. Org. Chem.* **1989**, *54*, 3354–3359; l) K. J. Henry, Jr., B. Fraser-Reid, *J. Org. Chem.* **1994**, *59*, 5128–5129; m) H. Schlesiger, E. Winterfeld, *Chirality* **1997**, *9*, 454–458; n) T. Durand-Reville, L. B. Gobbi, B. L. Gray, S. V. Ley, J. S. Scott, *Org. Lett.* **2002**, *4*, 3847–3850; o) T. Fukuzaki, S. Kobayashi, T. Hibi, T. Ikuma, J. Ishihara, N. Kanoh, A. Murai, *Org. Lett.* **2002**, *4*, 2877–2880; p) K. C. Nicolaou, A. J. Roecker, M. Follmann, R. Baati, *Angew. Chem.* **2002**, *114*, 2211–2214; *Angew. Chem. Int. Ed.* **2002**, *41*, 2107–2110.

[3] K. C. Nicolaou, M. Follmann, A. J. Roecker, K. W. Hunt, *Angew. Chem.* **2002**, *114*, 2207–2210; *Angew. Chem. Int. Ed.* **2002**, *41*, 2103–2106.

[4] R. Hanselmann, M. Benn, *Synth. Commun.* **1996**, *26*, 945–961.

[5] T. Nagamitsu, T. Sunazuka, R. Obata, H. Tomoda, H. Tanaka, Y. Harigaya, S. Omura, A. B. Smith III, *J. Org. Chem.* **1995**, *60*, 8126–8127.

[6] G. Sourkouni-Argirusi, A. Kirschning, *Org. Lett.* **2000**, *2*, 3781–3784.

[7] A. F. Barrero, S. Arseniyadis, J. F. Quilez del Moral, M. Mar Herrador, M. Valdivia, D. Jimenez, *J. Org. Chem.* **2002**, *67*, 3781–3784.

[8] G. Eichberger, G. Penn, K. Raber, H. Griengl, *Tetrahedron Lett.* **1986**, *27*, 2843–2844.

[9] P. G. Gassman, S. J. Burns, K. B. Pfister, *J. Org. Chem.* **1993**, *58*, 1449–1457.

[10] For a bromoketalization precedent, see: J. D. White, P. Theramongkol, C. Kuroda, J. R. Engegrecht, *J. Org. Chem.* **1988**, *53*, 5909–5921.

[11] For another substrate-directed 6-*endo*-trig over 5-*exo*-trig radical cyclization, see: C. Anies, L. Billot, J.-Y. Lallemand, A. Pancrazi, *Tetrahedron Lett.* **1995**, *36*, 7247–7250.

[12] For an example of a 1,5 hydrogen-transfer reaction, see: D. P. Curran, H. Yu, *Synthesis* **1992**, 123–127.

[13] For further mechanistic characterization, the cyclization of the minor bromoketal was also performed with nBu$_3$SnD. The product showed incorporation of deuterium by MALDI MS and by ^1H NMR (presumably the deuterium was incorporated at C8; the signal for the proton at C8 is obscured by other protons in the same region).

[14] For another example of an intramolecular redox reaction through a 1,5 hydride shift, see: H. Berner, G. Schultz, H. Schneider, *Tetrahedron* **1980**, *36*, 1807–1811.

[15] P. H. J. Carlsen, T. Katsuki, V. S. Martin, K. B. Sharpless, *J. Org. Chem.* **1981**, *46*, 3936–3938.

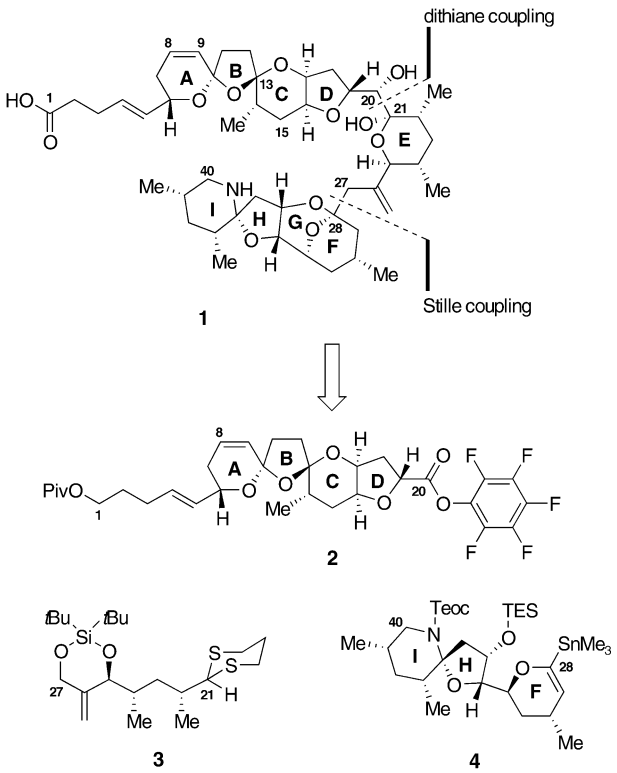
 © 2003 Wiley-VCH Verlag GmbH & Co. KGaA, Weinheim

Natural Product Synthesis

Total Synthesis of the Proposed Azaspiracid-1 Structure, Part 1: Construction of the Enantiomerically Pure C1–C20, C21–C27, and C28–C40 Fragments**

K. C. Nicolaou, Yiwei Li, Noriaki Uesaka, Theocharis V. Koftis, Stepan Vyskocil, Taotao Ling, Mugesh Govindasamy, Wenyuan Qian, Federico Bernal, and David Y.-K. Chen*

An incident of human poisoning in the Netherlands in 1995 with diarrhetic shell poisoning (DSP)-like symptoms was traced to the consumption of mussels (*Mytilus edulis*), which had been collected in Killary Harbour, Ireland.[1] Following an intense investigation, Yasumoto and co-workers reported the isolation of azaspiracid-1, the major biotoxin credited with these severe symptoms.[2] Both the structure of the substance and its pathologic effects were sufficiently different from those associated with the previously known DSP, so that a new toxic syndrome was declared and named azaspiracid poisoning (AZP). In addition to its immediate and apparent harmful effects, azaspiracid-1 has been shown to also cause lung, liver, spleen, and lymphocyte damage, as well as lung-tumor formation in mice.[3] It was on the basis of sophisticated analytical techniques that the Yasumoto group proposed the structure of azaspiracid-1 as **1**. This unprecedented structure is characterized by a trioxadispiroketal system fused to a tetrahydrofuran moiety (ABCD ring system), an azaspiro ring fused to a 2,9-dioxabicyclo[3.3.1]nonane system (FGHI ring system), a six-membered hemiketal bridge (E ring system), and a γ,δ-unsaturated terminal carboxylic acid moiety (Scheme 1). In total, there are nine rings and 20 stereogenic centers within this synthetically challenging and novel molecular architecture. Despite the heroic spectroscopic attempts to elucidate fully the structure of azaspiracid-1,[2] its daunting molecular framework yielded neither its relative stereochemistry between domains ABCDE (C1–C27) and FGHI (C28–C40) nor its absolute stereochemistry. In view of the health and environmental hazards posed by this molecule, and to clarify its molecular structure, we initiated a program directed towards its total synthesis.[4] Herein and in the following Communication[5] we report the total synthesis of the proposed structure **1** for azaspiracid-1 and its FGHI diastereoisomer, which led to the conclusion that this structure is, in fact, in error.



Scheme 1. Retrosynthetic analysis of the proposed structure **1** of azaspiracid-1, leading to key fragments **2** (C1–C20), **3** (C21–C27), and **4** (C28–C40). Relative stereochemistry between ABCDE (C1–C27) and FGHI (C28–C40) domains and absolute stereochemistry of **1** unknown. TES = triethylsilyl, Teoc = 2-(trimethylsilyl)ethoxycarbonyl.

As shown in Scheme 1, our proposed synthetic strategy was based on a twofold disconnection of the polycyclic array of azaspiracid-1 at the C20–C21 and C27–C28 junctures to provide the key synthetic precursors **2** (C1–C20 fragment), **3** (C21–C27 fragment), and **4** (C28–C40 fragment). The positions of the strategic bond scissions were carefully chosen to ensure optimum convergence and to allow the necessary flexibility to address the relative stereochemical issue between the ABCDE and FGHI domains of the molecule. The C20–C21 bond was envisaged to arise through the application of lithiated dithiane coupling technology,[6] whereas the C27–C28 bridging linkage was reserved for a palladium-mediated C(sp^2)–C(sp^3) Stille coupling.[7] We previously reported the preparation of the ABCD[8] and FGHI[9] ring systems with the desired skeletal and stereochemical arrangements, featuring the use of an auxiliary stereocontrolling group at C9 to induce the desired 13*R* stereochemistry

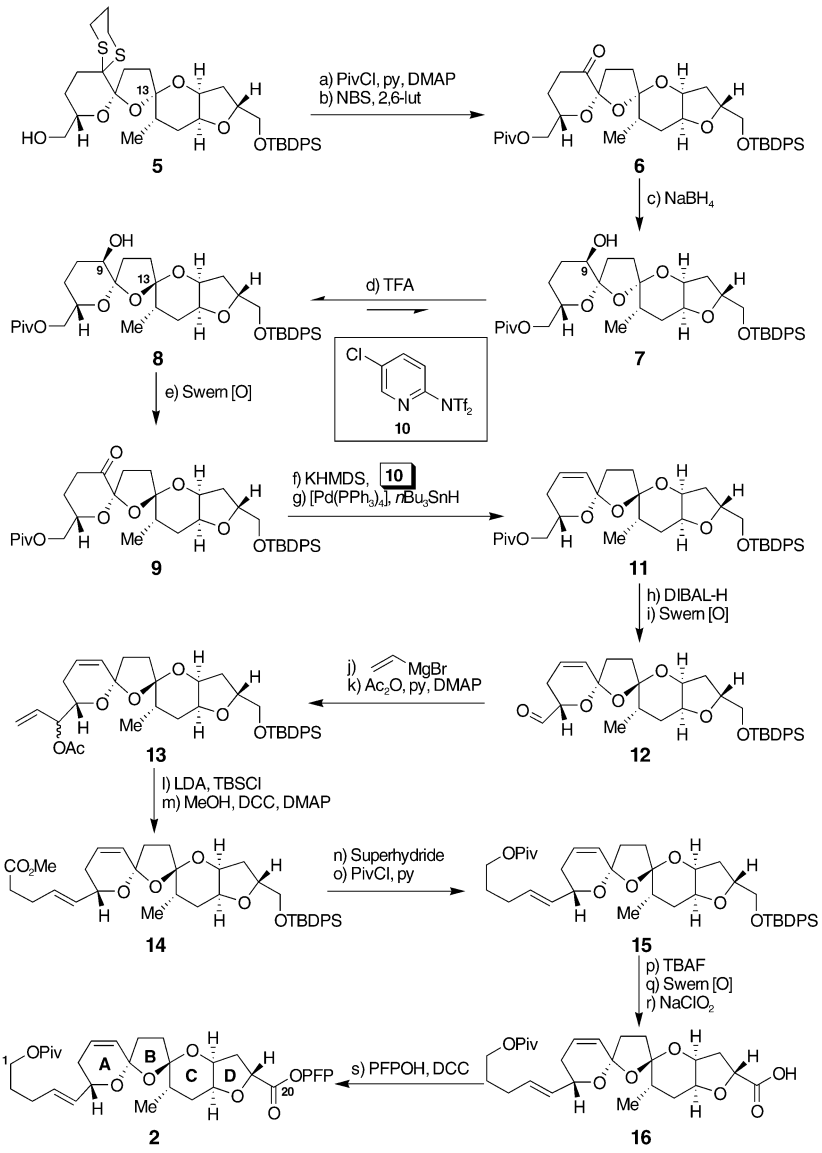
[*] Prof. Dr. K. C. Nicolaou, Y. Li, Dr. N. Uesaka, Dr. T. V. Koftis, Dr. S. Vyskocil, Dr. T. Ling, Dr. M. Govindasamy, Dr. W. Qian, F. Bernal, Dr. D. Y.-K. Chen
Department of Chemistry and
The Skaggs Institute for Chemical Biology
The Scripps Research Institute
10550 North Torrey Pines Road, La Jolla, CA 92037 (USA)
Fax: (+1) 858-784-2469
E-mail: kcn@scripps.edu
and
Department of Chemistry and Biochemistry
University of California, San Diego
9500 Gilman Drive, La Jolla, CA 92093 (USA)

[**] We thank Dr. D. H. Huang and Dr. G. Siuzdak for NMR spectroscopic and mass spectrometric assistance, respectively, and Dr. Raj Chadha for X-ray crystallographic analysis. Financial support for this work was provided by the National Institutes of Health (USA) and The Skaggs Institute for Chemical Biology, predoctoral fellowships from Bristol-Myers Squibb (to F.B.), The Skaggs Institute for Research (to Y.L. and F.B.), The Scripps Research Institute Society of Fellows (to F.B.), and Eli Lilly (to Y.L.), and a postdoctoral fellowship from The Skaggs Institute for Research (to W.Q.).

 DOI: 10.1002/anie.200351825 © 2003 Wiley-VCH Verlag GmbH & Co. KGaA, Weinheim

and the employment of a $Hg(OAc)_2$-mediated ring closure to forge the G ring of the FGHI ring system. Herein we describe the adaptation and refinement of our original sequence, and its application to the construction of appropriately functionalized fragments **2**, **3**, and **4** needed for the key carbon–carbon bond-forming reactions outlined in this retrosynthetic blueprint. To determine the relative and absolute stereochemical assignment of the nominal azaspiracid-1 (**1**) unambiguously, all three fragments **2**, **3**, and **4** were prepared in both enantiomeric forms. For conciseness, the following discussion will be limited to only one series of enantiomers (arbitrarily chosen). The synthesis of **1** and its FGHI diastereoisomer is sufficient to reveal both the relative and absolute stereochemistry of the nominal azaspiracid-1 (**1**), even though one more attempt may be needed to synthesize it.

The construction of key intermediate **2** (C1–C20 fragment) began with the protection of the previously reported alcohol **5**[8] as a pivaloate ester (with the wrong 13*S* configuration, see Scheme 2), followed by oxidative removal (NBS, 2,6-lutidine; for abbreviations of reagents and protecting groups, see legends in schemes) of the dithiane group to provide ketone **6** (75% yield over two steps). $NaBH_4$-mediated reduction of **6** afforded alcohol **7** as the major isomer (> 9:1 ratio), which was isolated in 87% yield, setting the stage for the proposed C9-OH-induced equilibration to establish the desired 13*R* spirocyclic configuration. As anticipated, upon exposure of alcohol **7** to TFA in CH_2Cl_2 at ambient temperature, an equilibrium mixture consisting of the desired tetracycle **8** and starting alcohol **7** was reached (ca. 2:1 ratio), from which **8** was isolated in pure form by flash column chromatography (66% yield). Recycling of **7** increased the supply of **8**. The auxiliary hydroxy group at C9 was then removed by a three-step sequence involving Swern oxidation, enol triflate formation[10] (KHMDS, reagent **10**, 92% yield), and $[Pd(PPh_3)_4]/nBu_3SnH$-mediated reductive elimination[11] (which generated the desired C8–C9 unsaturation, 95% yield) to afford **11**.



Scheme 2. Construction of **2**: a) PivCl (3.0 equiv), pyridine (10.0 equiv), DMAP (catalytic), CH_2Cl_2, 0→25 °C, 12 h; b) NBS (8.0 equiv), 2,6-lutidine (16 equiv), $MeCN/H_2O$ (4:1), 25 °C, 1 h, 75% over two steps; c) $NaBH_4$ (1.1 equiv), MeOH, −78→−60 °C, 3 h, 87%; d) TFA (2.0 equiv), CH_2Cl_2, 0→25 °C, 2 h, 66%; e) $(COCl)_2$ (2.0 equiv), DMSO (4.0 equiv), CH_2Cl_2, −60 °C, 2 h; then Et_3N (8.0 equiv), −60→−30 °C, 1 h, 94%; f) **10** (2.5 equiv), KHMDS (0.5 M in toluene, 2.5 equiv), THF, −78 °C, 1 h, 92%; g) LiCl (3.0 equiv), $[Pd(PPh_3)_4]$ (0.2 equiv), nBu_3SnH (3.0 equiv), THF, 25 °C, 45 min, 95%; h) DIBAL-H (1.0 M in toluene, 2.5 equiv), toluene, −78 °C, 20 min, 92%; i) $(COCl)_2$ (5.0 equiv), DMSO (11 equiv), CH_2Cl_2, −78 °C, 1 h, −60 °C, 1 h; then Et_3N (22 equiv), −78→−30 °C, 1 h, 92%; j) vinylmagnesium bromide (1.0 M in THF, 1.6 equiv), Et_2O, 0 °C, 30 min, 78%; k) Ac_2O (5.0 equiv), pyridine (10.0 equiv), DMAP (catalytic), CH_2Cl_2, 0 °C, 1 h, 94%; l) LDA (1.5 equiv), TBSCl (1.5 equiv), HMPA (1.5 equiv), THF, −78→25 °C, 72 h, 82%; m) MeOH (10.0 equiv), DCC (1.2 equiv), DMAP (0.1 equiv), CH_2Cl_2, 0→25 °C, 2 h, 86%; n) Superhydride (1.0 M in THF, 5.0 equiv), THF, −78→0 °C, 30 min, 96%; o) PivCl (3.0 equiv), pyridine (10.0 equiv), DMAP (1.0 equiv), CH_2Cl_2, 0→25 °C, 12 h, 95%; p) TBAF (1.0 M in THF, 2.0 equiv), THF, 0→25 °C, 3 h, 93%; p) $(COCl)_2$ (5.0 equiv), DMSO (11 equiv), CH_2Cl_2, −78 °C, 1 h, −60 °C, 1 h; then Et_3N (22 equiv), −78→−30 °C, 1 h, 89%; r) $NaClO_2$ (4.0 equiv), NaH_2PO_4 (4.0 equiv), 2-methyl-but-2-ene (5.0 equiv), *t*BuOH/H_2O (5:1), 25 °C, 2 h, 95%; s) PFPOH, (1.2 equiv), DCC (1.5 equiv), CH_2Cl_2, 25 °C, 2 h, 82%. TBDPS = *tert*-butyldiphenylsilyl, Piv = pivaloyl = trimethylacetyl, py = pyridine, DMAP = *N*,*N*-dimethyl-4-aminopyridine, NBS = *N*-bromosuccinimide, 2,6-lut = 2,6-lutidine, TFA = trifluoroacetic acid, KHMDS = potassium bis(trimethylsilyl)amide, DIBAL-H = diisobutylaluminum hydride, DMSO = dimethyl sulfoxide, LDA = lithium diisopropylamide, TBS = *tert*-butyldimethylsilyl, HMPA = hexamethylphosphoramide, DCC = 1,3-dicyclohexylcarbodiimide, Superhydride = lithium triethylborohydride, TBAF = tetra-*n*-butylammonium fluoride, PFPOH = pentafluorophenol.

 © 2003 Wiley-VCH Verlag GmbH & Co. KGaA, Weinheim

With tetracycle **11** in hand, we then turned our attention to the installation of the unsaturated C1–C5 carboxylic acid side chain. To this end, an Ireland modification[12] of the Claisen rearrangement was used to ensure the introduction of the desired *trans* double bond and the required four-carbon chain. Thus, the pivaloate group was cleaved from **11** by exposure to DIBAL-H (92% yield), and the resulting alcohol was treated under Swern conditions to afford aldehyde **12** in 92% yield. The latter compound, **12**, was immediately treated with vinylmagnesium bromide, and the resulting allylic alcohol (78% yield) was converted into its acetate **13** (mixture of diastereoisomers, 92% yield). Acetate **13** was exposed to LDA at −78 °C in the presence of TBSCl and HMPA, and the mixture was then warmed to room temperature to provide the corresponding γ,δ-unsaturated acid, which was subsequently esterified (MeOH, DCC, DMAP), furnishing the targeted methyl ester **14** in 71% overall yield for the two steps.

With the C1–C5 side chain in place, attention was then focused on the further elaboration of the C20 terminus in preparation for the anticipated C20–C21 bond-forming reaction. The first task was the reduction of methyl ester **14** (Superhydride, 96% yield) and protection of the resulting primary alcohol as a pivaloate ester (95% yield), a precautionary maneuver undertaken to enable the pending dithiane coupling step. The obtained intermediate **15** was then transformed into carboxylic acid **16** (Table 1) by desilylation (TBAF, 93% yield), followed by a two-step oxidation involving Swern conditions (89% yield) and $NaClO_2$ (95% yield). Finally, coupling of carboxylic acid **16** with pentafluorophenol in the presence of DCC led to pentafluoroester **2** in 82% yield, a coupling partner which proved, as we shall see, superior to its aldehyde progenitor.

The construction of the dithiane C21–C27 fragment **3** commenced from the previously synthesized lactone **17**[13] (Scheme 3). Reduction of **17** with DIBAL-H afforded the corresponding lactol in equilibrium with its open-chain hydroxy–aldehyde, which was trapped with 1,3-propanedithiol in the presence of $BF_3{\cdot}OEt_2$ to furnish hydroxy dithiane **18** in 99% overall yield. Swern oxidation then led to aldehyde **19** (94% yield), which was coupled with vinyl iodide **21** (obtained from propargyl alcohol in two steps as shown in Scheme 3) under the Nozaki–Hiyama–Kishi conditions[14] ($CrCl_2$, $NiCl_2$), leading to an epimeric mixture of allylic alcohols **22** in 95% yield. The desired stereochemistry at C25 was then set by an oxidation (IBX, 90% yield)–reduction (Red-Al, 80% yield) protocol, yielding the expected alcohol **23** (stereochemistry confirmed by NMR spectroscopic analysis), which was then desilylated by the action of TBAF to give diol **24** (99% yield). Protection of the 1,3-diol system within **24** as its silylene acetal (tBu$_2$Si(OTf)$_2$, 2,6-lut, 75% yield) then completed the synthesis of fragment **3** (Table 1).

The remaining coupling partner, C28–C40 fragment **4**, was constructed as outlined in Scheme 4. Thus, following our previous studies,[9] azide **25** was reduced (10% Pd/C, H_2) and the resulting primary amine was protected as its 2-(trimethylsilyl)ethoxy carbamate (Teoc) with reagent **26**[15] in the presence of Et_3N to afford derivative **27** (80% overall yield), setting the stage for the required spiroaminal formation. This crucial cyclization was found to proceed in good and

Table 1: Selected data for **3**, **16**, **30**, **33**, and **39**.

3: R_f = 0.25 (silica gel, Et_2O/hexanes 5:95); $[\alpha]_D$ = +76.1 ($CHCl_3$, c = 1.4); IR (film): $\tilde{\nu}_{max}$ = 2930, 2856, 1632, 1470, 1383, 1085, 1006, 826, 775, 650 cm^{-1}; ^{1}H NMR (500 MHz, $CDCl_3$): δ = 5.10 (s, 1H), 4.91 (s, 1H), 4.53 (d, J = 11.4 Hz, 1H), 4.17 (d, J = 15.0 Hz, 2H), 4.16 (d, J = 10.6 Hz, 1H), 2.97–2.91 (m, 1H), 2.86–2.80 (m, 3H), 2.18 (ddd, J = 12.2, 8.4, 4.0 Hz, 1H), 2.12–2.05 (m, 2H), 1.86–1.77 (m, 2H), 1.13 (d, J = 7.0 Hz, 3H), 1.04 (s, 9H), 0.98 (s, 9H), 0.84 ppm (d, J = 7.0 Hz, 3H); ^{13}C NMR (126 MHz, $CDCl_3$): δ = 146.0, 114.0, 81.5, 67.4, 54.5, 37.0, 36.5, 36.3, 31.4, 30.6, 27.3, 26.9, 36.4, 21.4, 20.9, 18.2, 16.3 ppm; MS (ESI): calcd for $C_{21}H_{40}NO_2S_2SiCl^-$ [M+Cl$^-$]: 451, found: 451

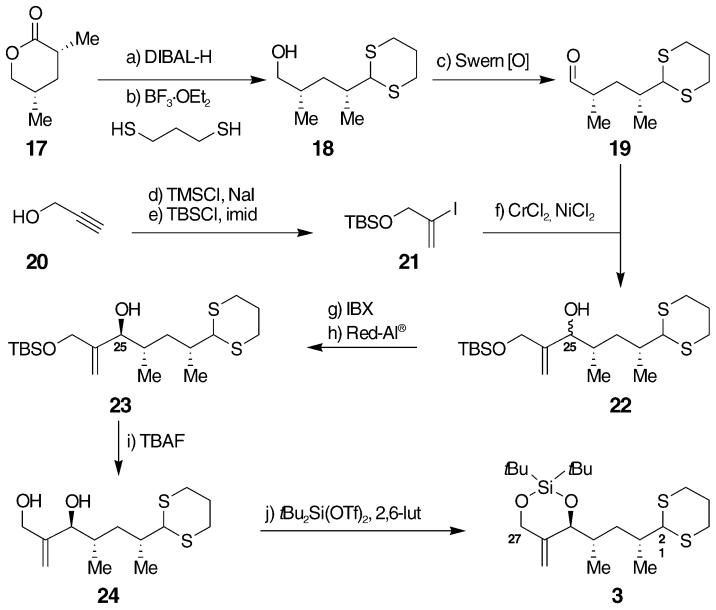
16: R_f = 0.24 (silica gel, CH_2Cl_2/MeOH 9:1); $[\alpha]_D$ = −31.5 ($CHCl_3$, c = 2.0); IR (film): $\tilde{\nu}_{max}$ = 3436, 2960, 1727, 1456, 1396, 1320, 1285, 1231, 1160, 1090, 1026, 976, 878, 802, 732, 671 cm^{-1}; ^{1}H NMR (600 MHz, $CDCl_3$): δ = 5.99 (ddd, J = 9.9, 5.7, 2.2 Hz, 1H), 5.69 (d, J = 5.7 Hz, 1H), 5.69–5.65 (m, 1H), 5.50 (dd, J = 15.4, 6.1 Hz, 1H), 4.85 (dd, J = 8.5, 7.9 Hz, 1H), 4.41 (ddd, J = 11.8, 5.1, 4.4 Hz, 1H), 4.21 (m, 1H), 4.03 (dd, J = 6.6, 6.4 Hz, 2H), 4.01 (m, 1H), 2.54 (dd, J = 13.6, 7.4 Hz, 1H), 2.24–1.95 (m, 11H), 1.72–1.68 (m, 2H), 1.50–1.46 (m, 1H), 1.19 (s, 9H), 0.91 ppm (d, J = 6.6 Hz, 3H); ^{13}C NMR (150 MHz, $CDCl_3$): δ = 178.6, 176.0, 131.2, 130.8, 128.8, 128.7, 111.4, 104.3, 77.6, 76.0, 75.4, 68.9, 63.6, 38.5, 35.6, 33.2, 30.7, 30.0, 28.7, 28.0, 27.2, 27.2, 23.5, 15.5 ppm; HRMS (MALDI): calcd for $C_{26}H_{38}O_8Na^+$ [M+Na$^+$]: 501.2459, found: 501.2467

30: R_f = 0.45 (silica gel, EtOAc/hexanes 1:4); $[\alpha]_D$ = −26.5 ($CHCl_3$, c = 0.85); IR (film): $\tilde{\nu}_{max}$ = 2955, 2914, 1745, 1697, 1460, 1392, 1350, 1253, 1170, 1067, 841, 741 cm^{-1}; ^{1}H NMR (500 MHz, $CDCl_3$): δ = 4.57 (m, 2H), 4.20 (dd, J = 7.0, 4,4 Hz, 1H), 4.18–4.08 (m, 2H), 3.69 (ddd, J = 13.2, 4.0, 1.5 Hz, 1H), 3.03 (dd, J = 13.0, 11.9 Hz, 1H), 2.79 (dd, J = 14.3, 7.3 Hz, 1H), 2.55 (m, 2H), 2.28–2.15 (m, 2H), 2.05 (ddd, J = 16.5, 10.3, 6.2 Hz, 1H), 1.89 (m, 1H), 1.68 (dt, J = 13.9, 4.6 Hz, 1H), 1.58–1.42 (m, 2H), 1.29 (q, J = 12.5 Hz, 1H), 1.09 (d, J = 6.6 Hz, 3H), 1.02–0.95 (m, 2H), 0.94 (t, J = 7.9 Hz, 9H), 0.80 (d, J = 6.6 Hz, 3H), 0.79 (d, J = 7.7 Hz, 3H), 0.59 (q, J = 7.9 Hz, 6H), 0.04 ppm (s, 9H); ^{13}C NMR (126 MHz, $CDCl_3$): δ = 172.3, 156.2, 96.6, 82.8, 76.3, 71.8, 63.1, 49.2, 43.6, 37.9, 37.8, 37.5, 31.1, 30.9, 24.0, 21.0, 18.6, 17.7, 16.7, 6.8, 4.6, −1.5 ppm; HRMS (MALDI): calcd for $C_{28}H_{53}NO_6Si_2Na^+$ [M+Na$^+$]: 578.3303, found: 578.3303

33: R_f = 0.40 (silica gel, EtOAc/hexanes 1:6); $[\alpha]_D$ = +12.1 ($CHCl_3$, c = 7.0); IR (film): $\tilde{\nu}_{max}$ = 2955, 1695, 1459, 1394, 1351, 1254, 1218, 1171, 1132, 1065, 840, 757 cm^{-1}; ^{1}H NMR (600 MHz, $CDCl_3$): δ = 5.76–5.69 (m, 1H), 5.24 (d, J = 17.1 Hz, 1H), 5.13 (d, J = 17.1 Hz, 1H), 4.74 (m, 1H), 4.24 (d, J = 5.3 Hz, 1H), 4.10–4.06 (m, 3H), 3.86 (d, J = 6.1 Hz, 1H), 3.74–3.71 (m, 2H), 3.18 (t, J = 12.9 Hz, 1H), 2.98 (dd, J = 13.8, 9.0 Hz, 1H), 2.49 (dd, J = 14.0, 5.7 Hz, 1H), 2.26 (dd, J = 14.5, 6.1 Hz, 1H), 2.03–1.97 (m, 1H), 1.87 (dt, J = 14.0, 5.7 Hz, 1H), 1.57–1.50 (m, 2H), 1.34–1.23 (m, 3H), 0.96 (d, J = 5.7 Hz, 3H), 0.97–0.93 (m, 2H), 0.79 (d, J = 6.1 Hz, 3H), 0.79 (d, J = 6.1 Hz, 3H), 0.03 ppm (s, 9H); ^{13}C NMR (150 MHz, $CDCl_3$): δ = 157.1, 132.0, 120.5, 98.1, 97.9, 79.6, 75.0, 72.9, 63.8, 50.0, 49.8, 47.4, 41.0, 39.7, 37.5, 32.2, 31.8, 29.2, 25.7, 19.6, 18.8, 17.3, −0.5 ppm; HRMS (MALDI): calcd for $C_{25}H_{42}INO_5SiNa^+$ [M+Na$^+$]: 614.1769, found: 614.1785

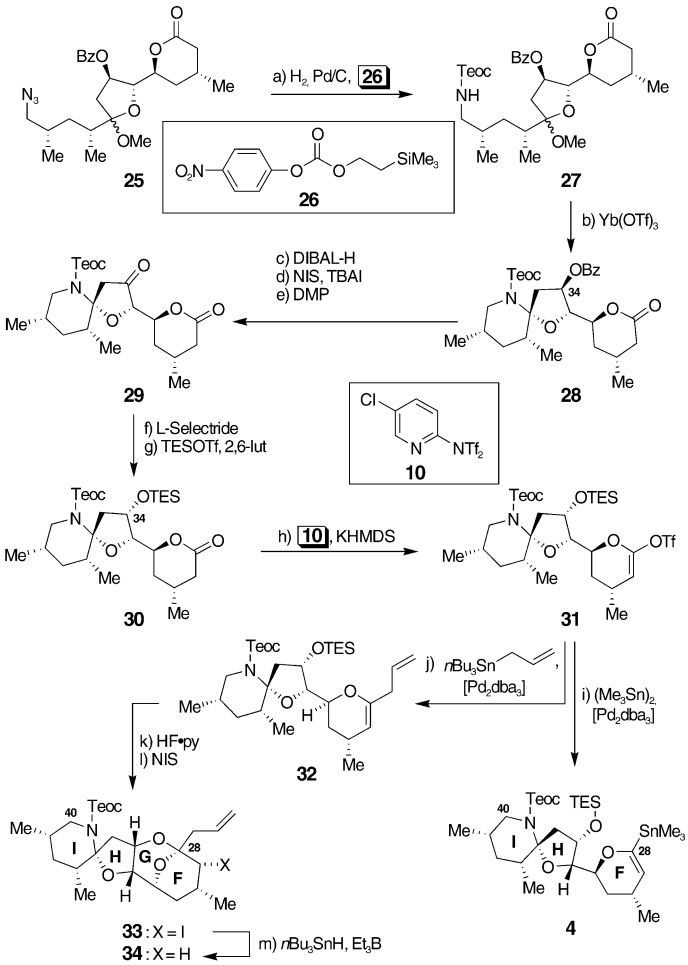
39: R_f = 0.30 (silica gel, EtOAc/hexanes 1:1); $[\alpha]_D$ = −9.8 ($CHCl_3$, c = 0.2); IR (film): $\tilde{\nu}_{max}$ = 3436, 2930, 1725, 1725, 1460, 1402, 1350, 1155, 1025, 979, 879, 585 cm^{-1}; ^{1}H NMR (600 MHz, $CDCl_3$): δ = 5.98 (ddd, J = 9.8, 5.6, 2.1 Hz, 1H), 5.70 (ddd, J = 9.8, 2.3, 1.0 Hz, 1H), 5.42 (s, 1H), 5.22 (s, 1H), 4.66 (dt, J = 10.1, 6.1 Hz, 1H), 4.31 (d, J = 6.1 Hz, 1H), 4.24–4.20 (m, 1H), 4.15 (m, 1H), 4.14–4.09 (m, 3H), 4.08–4.05 (m, 2H), 3.89 (m, 1H), 2.23–2.20 (m, 2H), 2.16–2.13 (m, 1H), 2.11–2.07 (m, 2H), 2.04–1.94 (m, 6H), 1.87–1.77 (m, 2H), 1.46–1.37 (m, 2H), 1.19 (s, 9H), 1.02 (d, J = 6.6 Hz, 3H), 0.96 (d, J = 6.6 Hz, 3H), 0.86 ppm (d, J = 6.6 Hz, 3H); ^{13}C NMR (150 MHz, $CDCl_3$): δ = 178.9, 146.4, 129.6, 128.1, 118.1, 112.0, 104.5, 100.4, 98.6, 81.5, 78.2, 75.9, 75.6, 73.7, 67.0, 66.9, 63.4, 38.7, 36.7, 36.1, 34.3, 33.7, 31.1, 27.6, 27.0, 24.6, 24.2, 23.8, 18.0, 16.5, 16.3 ppm; HRMS (MALDI): calcd for $C_{33}H_{47}ClO_{10}Na^+$ [M+Na$^+$]: 661.2750, found: 661.2749

 © 2003 Wiley-VCH Verlag GmbH & Co. KGaA, Weinheim



Scheme 3. Construction of **3**: a) DIBAL-H (1.0 M in CH_2Cl_2, 1.1 equiv), CH_2Cl_2, −78 °C, 1.5 h; b) 1,3-propanedithiol (1.1 equiv), $BF_3{\cdot}OEt_2$ (1.5 equiv), CH_2Cl_2, 0 °C, 1 h, 99% over two steps; c) $(COCl)_2$ (1.2 equiv), DMSO (2.4 equiv), CH_2Cl_2, −78 °C, 30 min; then Et_3N (5.0 equiv), −78 → −20 °C, 94%; d) TMSCl (1.2 equiv), NaI (1.2 equiv), H_2O (0.6 equiv), CH_3CN, 0 → 25 °C, 1.5 h, 51%; e) TBSCl (1.2 equiv), imidazole (2.5 equiv), DMF, 25 °C, 36 h, 96%; f) $NiCl_2$ (0.02 equiv), $CrCl_2$ (4.0 equiv), DMF, 0 °C; then **19** (1.0 equiv), **21** (2.5 equiv), 0 → 25 °C, 15 h, 95%; g) IBX (2.0 equiv), DMSO/THF (4:1), 25 °C, 2 h, 90%; h) Red-Al (2.5 equiv), toluene, −78 °C, 1 h, 80%; i) TBAF (2.2 equiv), THF, 25 °C, 1 h, 99%; j) $tBu_2Si(OTf)_2$ (1.6 equiv), 2,6-lutidine (4.0 equiv), CH_2Cl_2, −30 °C, 30 min, 75%. TMS = trimethylsilyl, imid = imidazole, DMF = *N*,*N*-dimethylformamide, IBX = *o*-iodoxybenzoic acid, Red-Al = sodium bis(2-methoxyethoxy)aluminum hydride, Tf = trifluoromethanesulfonyl.

reproducible yields in the presence of $Yb(OTf)_3$,[16] in contrast to the previously employed $BF_3{\cdot}OEt_2$[17] procedure, which proved to be unreliable. An oxidation–reduction sequence was then carried out to invert the stereochemistry at C34. Thus, exposure of benzoate lactone **28** to DIBAL-H resulted in the formation of the corresponding hydroxylactol, which was oxidized stepwise back to the hydroxylactone (NIS, TBAI,[18] 88% overall yield) and then to ketolactone **29** (DMP, 95% yield). Treatment of ketolactone **29** with L-Selectride at −78 °C furnished, exclusively, the α-hydroxy compound (85% yield), which was silylated (TESOTf, 2,6-lutidine, 86% yield) to afford the desired intermediate **30** (Table 1). In preparation for the projected Stille coupling, lactone **30** was efficiently converted into vinyl stannane **4** through the intermediacy of enol triflate **31** (KMHDS, **10**,[10] 91% yield; $(Me_3Sn)_2$, $[Pd_2dba_3]$,[19] 98% yield). Although triflate **31** itself can potentially serve as a coupling partner with an allyl stannane, model studies suggested the reverse partnership as the most efficient variant for the azaspiracid-1 framework—and thus the choice of **4** as the FHI coupling partner. At this juncture, we needed further improvements of our approach to the final steps for the casting of the FGHI ring system. Specifically, our previously developed protocol for the formation of ring G employing $Hg(OAc)_2$[20] proved problematic in the presence of the entire, highly oxygenated azaspiracid-1 skeleton, and therefore an alternative tactic was sought to achieve this objective. It was in the search of such a protocol that the model substrate **32** was synthesized from **31** by reaction with allyltri-*n*-butyltin in the presence of $[Pd_2dba_3]$, TFP,[21] and LiCl (95% yield). Upon considerable experimentation, it was found that selective removal of the TES group from **32** under the mild conditions provided by HF·py buffered with additional pyridine led to the generation of the desired hydroxy enol ether precursor, which upon



Scheme 4. Construction of **4** and model FGHI ring system **34**: a) Pd/C (10% w/w, 0.1 equiv), EtOAc, H_2, 25 °C, 5 h; then filtration through celite; then Et_3N (5.0 equiv), **26** (4.0 equiv), 25 °C, 12 h, 80%; b) $Yb(OTf)_3$ (0.1 equiv), CH_3CN, 25 °C, 3 min, 71%; c) DIBAL-H (1.0 M in THF, 4.0 equiv), toluene, −78 °C, 25 min; d) NIS (10.0 equiv), TBAI (2.0 equiv), CH_2Cl_2, 25 °C, 40 min, 88% over two steps; e) DMP (1.5 equiv), pyridine (12.5 equiv), CH_2Cl_2, 0 → 25 °C, 30 min, 95%; f) L-Selectride (1.0 M in THF, 1.8 equiv), THF, −78 °C, 20 min, 85%; g) TESOTf (1.1 equiv), 2,6-lutidine (1.5 equiv), −78 °C, 10 min, 86%; h) **10** (5.0 equiv), KHMDS (5.0 equiv), THF, −78 °C, 40 min, 91%; i) $(Me_3Sn)_2$ (10.0 equiv), TFP (0.5 equiv), LiCl (3.0 equiv), $[Pd_2dba_3]$ (0.1 equiv), THF, 25 °C, 1 h, 98%; j) allyltri-*n*-butyltin (10.0 equiv), TFP (0.5 equiv), LiCl (3.0 equiv), $[Pd_2dba_3]$ (0.1 equiv), THF, 25 °C, 1 h, 95%; k) HF·py (5.0 equiv), THF/pyridine (1:1), 0 → 25 °C, 2 h; l) NIS (10.0 equiv), $NaHCO_3$ (30.0 equiv), THF, 0 °C, 12 h, 75% over two steps; m) Et_3B (1.0 M in hexanes, catalytic), nBu_3SnH/toluene (1:2), 0 °C, 5 min, 94%. Bz = benzoyl, NIS = *N*-iodosuccinimide, TBAI = tetra-*n*-butylammonium iodide, DMP = Dess–Martin periodinane, L-Selectride = lithium tri-*sec*-butylborohydride, TFP = tri-2-furylphosphane, dba = dibenzylideneacetone.

 © 2003 Wiley-VCH Verlag GmbH & Co. KGaA, Weinheim

treatment with *N*-iodosuccinimide[22] in the presence of $NaHCO_3$ furnished the FGHI iodide **33** (Table 1) in a pleasing yield of 75% overall for the two steps. The formation of **33** as a single, crystalline product gave us the opportunity to confirm its stereochemistry by X-ray crystallographic analysis (see ORTEP drawing of *ent*-**33**, Figure 1)[23] and to test the next step, that of removing the facilitating, but now extraneous, iodine residue, without compromising the rest of the molecule. Indeed, this crucial operation (**33**→**34**) was successfully executed by the reductive rupture of the carbon–iodine bond by the mild action of nBu$_3$SnH and Et$_3$B[24] (94% yield).

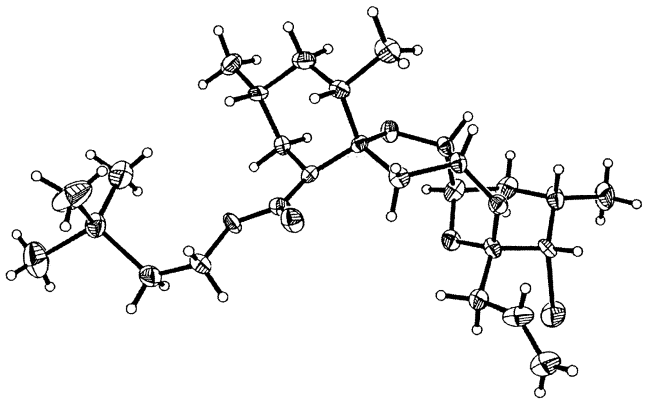
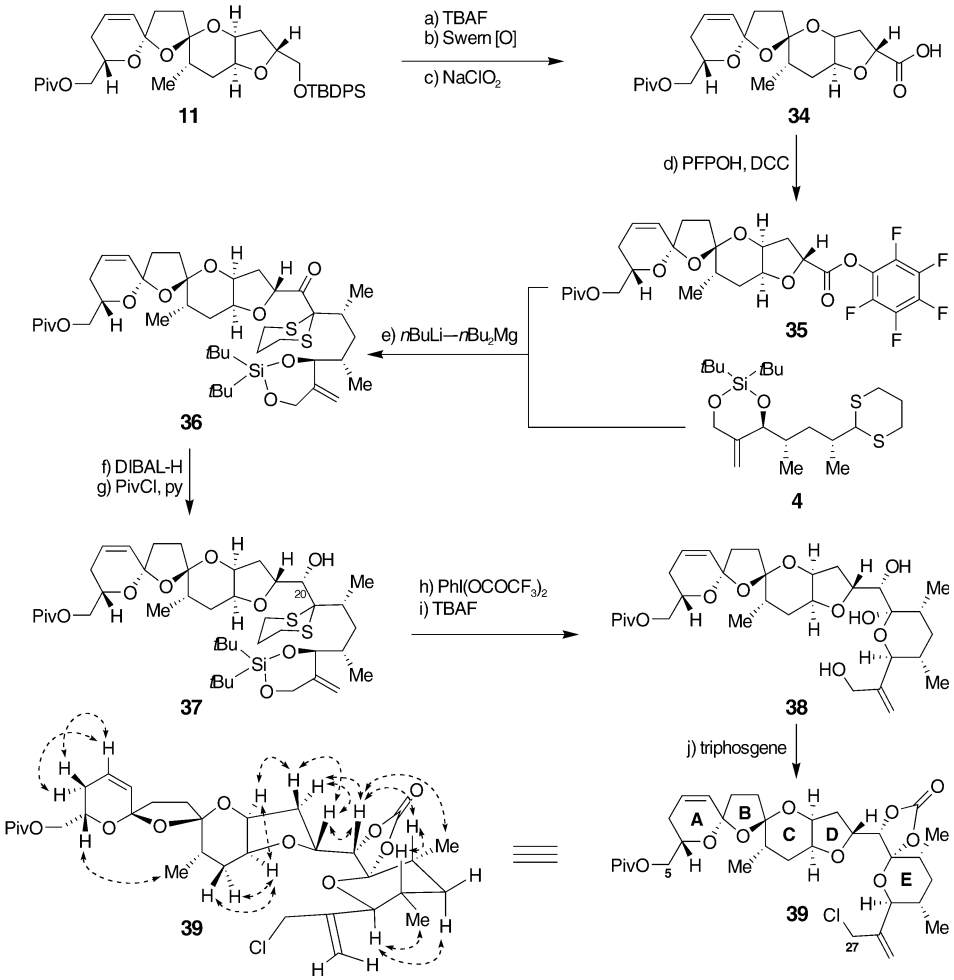


Figure 1. ORTEP drawing of compound *ent*-**33**.

Having chartered an appropriate route to access the FGHI domain of azaspiracid-1, we then turned our attention to scouting the ground for a possible means to construct the demanding C20–C21 bond and completing the requisite ABCDE domain. Thus, we targeted advanced model system **39** (Scheme 5), which contains all the rings and stereocenters embedded in the C5–C27 region of structure **1**. It was after the recognition of the reluctance of the aldehyde functionality at C20 of various ABCD-domain substrates to participate as an electrophilic partner in coupling reactions with organometal-



Scheme 5. Model dithiane coupling and structural confirmation of all stereocenters in ABCDE ring system (**39**, C5–C27 domain): a) TBAF (1.0 M in THF, 5.0 equiv), THF, 25 °C, 2 h, 88%; b) $(COCl)_2$ (5.0 equiv), DMSO (11 equiv), CH_2Cl_2, −78 °C, 30 min; then Et_3N (22 equiv), −78→0 °C, 94%; c) $NaClO_2$ (6.0 equiv), NaH_2PO_4 (6.0 equiv), 2-methyl-but-2-ene (excess), *t*BuOH/H_2O (4:1), 25 °C, 1.5 h; d) PFPOH (1.5 equiv), DCC (2.0 equiv), 25 °C, 2.5 h, 56% over two steps; e) **4** (9.0 equiv), *n*BuLi–*n*Bu_2Mg (1.1 M in hexanes, 6.0 equiv), THF, 0→25 °C, 1.5 h; then **35**, −90 °C, 15 min, 63%; f) DIBAL-H (1.0 M in CH_2Cl_2, 10.0 equiv), CH_2Cl_2, −90 °C, 1.5 h, 55%; g) PivCl (3.0 equiv), pyridine (10.0 equiv), 0→25 °C, 12 h, 75%; h) $PhI(OCOCF_3)_2$ (2.2 equiv), MeCN/pH7 buffer (4:1), 0 °C, 78%; i) TBAF (1.0 M in THF, 5.0 equiv), THF, 25 °C, 16 h, 85%; j) triphosgene (2.0 equiv), pyridine (15 equiv), CH_2Cl_2, −78→25 °C, 1 h, 54%.

 © 2003 Wiley-VCH Verlag GmbH & Co. KGaA, Weinheim

lic species (such as the lithiated derivative of dithiane **4**) that we focused on the corresponding pentafluorophenyl ester as a potential alternative for this pivotal coupling. Thus, silyl derivative **11** (obtained as described in Scheme 2) was desilylated by treatment with TBAF (88% yield), and the resulting alcohol was oxidized stepwise, first under Swern conditions (94% yield) and then with $NaClO_2$, to afford carboxylic acid, **34**, as shown in Scheme 5. Subsequent coupling of the latter compound **34** with pentafluorophenol was accomplished in the presence of DCC in 56% overall yield from the corresponding aldehyde. The rather labile pentafluorophenyl ester **35** was carefully purified by flash column chromatography and immediately employed in the coupling reaction with the lithiated form of dithiane **4** (nBuLi–nBu$_2$Mg)[25] at −90 °C to afford ketone **36** in 63% yield. The required stereoselective reduction of the C20 carbonyl group was then accomplished through the use of DIBAL-H. However, the pivaloate group at C1 was cleaved concomitantly, leading to the corresponding diol in 55% yield. This diol was reprotected selectively (PivCl, py, 75% yield) at the primary position, leading to advanced intermediate **37**. In a carefully orchestrated sequence, the dithiane moiety was cleaved from **37** through the action of PhI(O-COCF$_3$)$_2$[26] to liberate the corresponding ketone (78% yield), from which the silicon tether was removed by exposure to TBAF, furnishing the azaspiracid-1-like lactol **38** through spontaneous ring closure as a single isomer (85% yield). With the aim of imparting more structural rigidity to the ABCDE truncate of azaspiracid-1 for detailed NMR studies, the hydroxy groups at C20 and C21 were conformationally constrained within a cyclic carbonate upon exposure to triphosgene and pyridine to provide cyclic carbonate **39** (54% yield) in which the terminal position was now occupied by a chlorine residue. Despite this unexpected occurrence, however, chloride **39** proved quite useful in providing us with the required structural information (Table 1). Thus, extensive NOE studies of compound **39** (see Scheme 5) revealed the key spatial correlations for the assigned stereochemistry, particularly around the C20 stereocenter.

The described chemistry provided ample quantities of building blocks **2**, **3**, and **4**, and powerful synthetic technologies pertaining to their coupling as a prelude to further forays along the designed path to the proposed structure **1** for azaspiracid-1. In the following Communication,[5] we report the final drive to two diastereoisomers of this structure and their comparison with the natural substance.

Received: May 7, 2003 [Z51825]

Keywords: asymmetric synthesis · azaspiracid-1 · natural products · neurotoxins · structural revision · total synthesis

[1] T. MacMahon, J. Silke, *Harmful Algae News* **1996**, *14*, 2.
[2] M. Satake, K. Ofuji, H. Naoki, K. J. James, A. Fruey, T. McMahon, J. Silke, T. Yasumoto, *J. Am. Chem. Soc.* **1998**, *120*, 9967–9968; see also: Y. Román, A. Alfonso, M. C. Louzao, L. A. de la Rosa, F. Leira, J. M. Vieties, M. R. Vieytes, K. Ofuji, M. Satake, T. Yasumoto, L. M. Botana, *Cellular Signalling* **2002**, *14*, 703–716.
[3] E. Ito, M. Satake, K. Ofuji, M. Higashi, K. Harigaya, T. McMahon, T. Yasumoto, *Toxicon* **2002**, *40*, 193–203.
[4] For synthetic studies towards **1**, see: a) R. G. Carter, D. J. Weldon, *Org. Lett.* **2000**, *2*, 3913–3916; b) R. G. Carter, D. E. Graves, *Tetrahedron Lett.* **2001**, *42*, 6035–6039; c) R. G. Carter, T. C. Bourland, D. E. Graves, *Org. Lett.* **2002**, *4*, 2177–2179; d) C. J. Forsyth, J. Hao, J. Aiguade, *Angew. Chem.* **2001**, *113*, 3775–3779; *Angew. Chem. Int. Ed.* **2001**, *40*, 3663–3667; e) A. B. Dounay, C. J. Forsyth, *Org. Lett.* **2001**, *3*, 975–978; f) J. Auguade, J. Hao, C. J. Forsyth, *Tetrahedron Lett.* **2001**, *42*, 817–820; g) J. Hao, J. Aiguade, C. J. Forsyth, *Tetrahedron Lett.* **2001**, *42*, 821–824.
[5] See the following Communication in this issue: K. C. Nicolaou, D. Y.-K. Chen, Y. Li, W. Qian, T. Ling, S. Vyskocil, T. V. Koftis, M. Govindasamy, N. Uesaka, *Angew. Chem.* **2003**, *115*, 3777–3781; *Angew. Chem. Int. Ed.* **2003**, *42*, 3649–3653.
[6] E. J. Corey, D. Seebach, *Angew. Chem.* **1965**, *77*, 1134–1135; *Angew. Chem. Int. Ed. Engl.* **1965**, *4*, 1075–1077.
[7] L. Del Valle, J. K. Stille, L. S. Hegedus, *J. Org. Chem.* **1990**, *55*, 3019–3023.
[8] K. C. Nicolaou, W. Qian, F. Bernal, N. Uesaka, P. M. Pihko, J. Hinrichs, *Angew. Chem.* **2001**, *113*, 4192–4195; *Angew. Chem. Int. Ed.* **2001**, *40*, 4068–4071.
[9] K. C. Nicolaou, P. M. Pihko, N. Diedrichs, N. Zou, F. Bernal, *Angew. Chem.* **2001**, *113*, 1302–1305; *Angew. Chem. Int. Ed.* **2001**, *40*, 1262–1265.
[10] K. Tsushima, K. Araki, A. Murai, *Chem. Lett.* **1989**, 1313–1316.
[11] J. K. Stille, *Angew. Chem.* **1986**, *98*, 504–519; *Angew. Chem. Int. Ed. Engl.* **1986**, *25*, 508–524.
[12] R. E. Ireland, R. H. Mueller, A. K. Willard, *J. Am. Chem. Soc.* **1976**, *98*, 2868–2877.
[13] D. B. Collum, J. H. McDonald, W. C. Still, *J. Am. Chem. Soc.* **1980**, *102*, 2118–2120.
[14] a) K. Takai, M. Tagashira, T. Kuroda, K. Oshima, K. Utimoto, H. Nozaki, *J. Am. Chem. Soc.* **1986**, *108*, 6648–6050; b) H. Jin, J. Uenishi, W. J. Christ, Y. Kishi, *J. Am. Chem. Soc.* **1986**, *108*, 5644–5646.
[15] A. Rosowsky, J. E. Wright, *J. Org. Chem.* **1983**, *48*, 1539–1541.
[16] S. Kobayashi, M. Sugiura, M. Kitagawa, W. Lam, *Chem. Rev.* **2002**, *102*, 2227–2302.
[17] A. M. P. Koskinen, L. A. Otsomaa, *Tetrahedron* **1997**, *53*, 6473–6484.
[18] S. Hanessian, D. H. Wong, M. Therien, *Synthesis* **1981**, 394–396.
[19] C. Barker, K. Jarowicki, P. Kocienski, *Synlett* **1991**, 197–198.
[20] a) H. C. Brown, P. J. Geoghegan, *J. Org. Chem.* **1970**, *35*, 1844–1850; b) S. J. Danishefsky, W. H. Pearson, *J. Org. Chem.* **1983**, *48*, 3865–3866.
[21] V. Farina, B. Krishman, *J. Am. Chem. Soc.* **1991**, *113*, 9585–9595.
[22] a) M. Adinolfi, M. Parrilli, G. Barone, G. Laonigro, L. Mangoni, *Tetrahedron Lett.* **1976**, 3661–3662; b) G. Haaima, R. T. Weavers, *Tetrahedron Lett.* **1988**, *29*, 1085–1088.
[23] CCDC-210122 (*ent*-**33**) contains the supplementary crystallographic data for this paper. These data can be obtained free of charge via www.ccdc.cam.ac.uk/conts/retrieving.html (or from the Cambridge Crystallographic Data Centre, 12 Union Road, Cambridge CB2 1EZ, UK; fax: (+44) 1223-336-033; or deposit@ccdc.cam.ac.uk).
[24] K. Miura, Y. Ichinose, K. Nozaki, K. Fugami, K. Oshima, K. Utimoto, *Bull. Chem. Soc. Jpn.* **1989**, *62*, 143–147.
[25] M. Ide, M. Nakata, *Bull. Chem. Soc. Jpn.* **1999**, *72*, 2491–2499.
[26] G. Stork, K. Zhao, *Tetrahedron Lett.* **1989**, *30*, 287–2902.

 © 2003 Wiley-VCH Verlag GmbH & Co. KGaA, Weinheim

Natural Product Synthesis

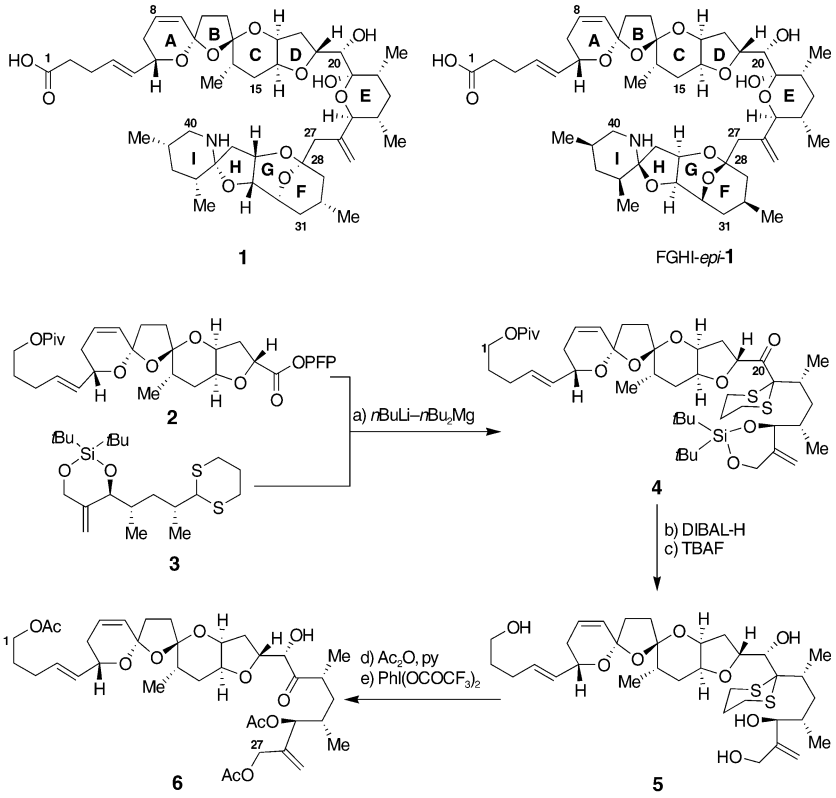
Total Synthesis of the Proposed Azaspiracid-1 Structure, Part 2: Coupling of the C1–C20, C21–C27, and C28–C40 Fragments and Completion of the Synthesis**

K. C. Nicolaou, David Y.-K. Chen, Yiwei Li, Wenyuan Qian, Taotao Ling, Stepan Vyskocil, Theocharis V. Koftis, Mugesh Govindasamy, and Noriaki Uesaka*

In the preceding paper[1] we described enantioselective constructions of the required C1–C20, C21–C27, and C28-C40 fragments for a projected total synthesis of the proposed structure of azaspiracid-1 (**1** or FGHI-*epi*-**1**),[2] and model studies for their potential fusion into the targeted entities. Herein we report the successful union of these fragments and the completion of the total synthesis of both structures **1** and its epimer FGHI-*epi*-**1**, neither of which exhibited the spectral data reported for natural azaspiracid-1.

As delineated in the preceding paper,[1] the proposed total synthesis called for two crucial couplings to forge the C20–C21 (dithiane coupling)[3] and C27–C28 (Stille coupling)[4] bonds. With the precise arrangement between the two major domains of azaspiracid-1 clouded by the uncertainty of their relative configuration,[2] the order of assembly involving dithiane coupling (C20–C21 bond) first and then Stille coupling (C27–C28 bond) was chosen as the most prudent approach to the expedient construction of both diastereoisomers **1** and FGHI-*epi*-**1**.

The first union, that between segments **2** (C1–C20) and **3** (C21–C27), was accomplished as shown in Scheme 1. Thus, we applied the conditions developed on model systems as described in the preceding paper,[1] and dithiane **3** was treated with the *n*BuLi–*n*Bu$_2$Mg[5] reagent mixture to prepare its activated organometallic species, which reacted with the freshly prepared and purified



Scheme 1. Structures of **1** and FGHI-*epi*-**1**, the coupling of key intermediates **2** and **3** and synthesis of advanced intermediate **6**: a) **3** (9.0 equiv), *n*BuLi–*n*Bu$_2$Mg (1.1 M in hexanes, 6.0 equiv), THF, 0→25 °C, 1.5 h; then **2**, −90 °C 15 min, 63%; b) DIBAL-H (1.0 M in CH_2Cl_2, 10.0 equiv), CH_2Cl_2, −90 °C, 1.5 h, 55%; c) TBAF (1.0 M in THF, 5.0 equiv), THF, 25 °C, 16 h, 78%; d) Ac_2O (50 equiv), pyridine/CH_2Cl_2 (1:1), 0→25 °C, 16 h, 84%; e) PhI(OCOCF$_3$)$_2$ (2.2 equiv), MeCN/pH7 buffer (4:1), 0 °C, 78%. PFP = pentafluorophenyl, Piv = trimethylacetyl, DIBAL-H = diisobutylaluminum hydride, TBAF = tetra-*n*-butylammonium fluoride, py = pyridine.

pentafluorophenyl ester **2** to furnish ketone **4** (Table 1) in a pleasing 63% yield (based on **2**). The reduction of the C20 carbonyl group within **4** proceeded stereoselectively under the influence of DIBAL-H (−90 °C, 55% yield), as expected from the previous model studies,[1] to afford a single dihydroxy product formed by concomitant cleavage of the pivaloate ester at C1. Although the coupling constant between 19-H and 20-H was in accord with the desired stereochemistry of C20,[6] the final proof for this assignment came later through X-ray crystallographic analysis (see below). Proceeding with the synthesis, the next desired step was the removal of the silyl protecting group from this diol, an objective that was smoothly accomplished by exposure to TBAF, unraveling tetraol **5** in 78% yield. In preparation for the pending Stille coupling, and in a rather daring maneuver, tetraol **5** was exposed to excess Ac_2O and pyridine, affording the corresponding triacetate (84% yield) with the hydroxy group at C20 remaining free, presumably as a result of the

[*] Prof. Dr. K. C. Nicolaou, Dr. D. Y.-K. Chen, Y. Li, Dr. W. Qian, Dr. T. Ling, Dr. S. Vyskocil, Dr. T. V. Koftis, Dr. M. Govindasamy, Dr. N. Uesaka
Department of Chemistry and
The Skaggs Institute for Chemical Biology
The Scripps Research Institute
10550 North Torrey Pines Road, La Jolla, CA 92037 (USA)
Fax: (+1) 858-784-2469
E-mail: kcn@scripps.edu
and
Department of Chemistry and Biochemistry
University of California, San Diego
9500 Gilman Drive, La Jolla, CA 92093 (USA)

[**] We thank Dr. D. H. Huang and Dr. G. Siuzdak for NMR spectroscopic and mass spectrometric assistance, respectively, and Dr. Raj Chadha for X-ray crystallographic analysis. Financial support for this work was provided by the National Institutes of Health (USA), The Skaggs Institute for Chemical Biology, predoctoral fellowships from Eli Lilly and The Skaggs Institute for Research (both to Y.L.), and a postdoctoral fellowship from The Skaggs Institute for Research (to W.Q.).

 DOI: 10.1002/anie.200351826 © 2003 Wiley-VCH Verlag GmbH & Co. KGaA, Weinheim

Table 1: Selected physical properties for compounds **4**, **6**, **10**, **11**, **16**, **17**, **1**, and FGHI-*epi*-**1**.

4: $R_f = 0.52$ (silica gel, EtOAc/hexanes 2:1); $[\alpha]_D = -53.2$ ($CHCl_3$, $c = 3.0$); IR (film): $\tilde{\nu}_{max} = 2933, 2860, 1728, 1707, 1531, 1515, 1467, 1383, 1320, 1284, 1234, 1157, 1084, 980, 914, 871, 826, 802, 732, 652\ cm^{-1}$; ^1H NMR (600 MHz, $CDCl_3$): $\delta = 5.97$ (ddd, $J = 10.1, 5.7, 1.7$ Hz, 1H), 5.69–5.64 (m, 2H), 5.50 (dd, $J = 15.3, 6.2$ Hz, 1H), 5.36 (dd, $J = 9.0, 6.6$ Hz, 1H), 5.10 (s, 1H), 4.95 (s, 1H), 4.55 (d, $J = 11.4$ Hz, 1H), 4.40 (ddd, $J = 10.5, 5.0, 4.9$ Hz, 1H), 4.25 (d, $J = 6.5$ Hz, 1H), 4.23 (br s, 1H), 4.17 (d, $J = 11.8$ Hz, 1H), 4.16 (br s, 1H), 4.03 (t, $J = 6.6$ Hz, 2H), 2.91 (t, $J = 13.6$ Hz, 1H), 2.85 (t, $J = 12.7$ Hz, 1H), 2.59 (tt, $J = 14.5, 4.0$ Hz, 2H), 2.29 (dd, $J = 12.7, 6.6$ Hz, 2H), 2.25–2.18 (m, 3H), 2.12–1.96 (m, 10H), 1.92–1.86 (m, 1H), 1.76–1.68 (m, 1H), 1.69 ppm (t, $J = 7.0$ Hz, 2H), 1.45 (dt, $J = 13.8, 3.1$ Hz, 1H), 1.37–1.32 (m, 1H), 1.18 (s, 9H), 1.12 (d, $J = 6.5$ Hz, 3H), 1.04 (s, 9H), 0.98 (s, 9H), 0.88 (d, $J = 6.6$ Hz, 3H), 0.87 ppm (d, $J = 7.0$ Hz, 3H); ^{13}C NMR (150 MHz, $CDCl_3$): $\delta = 204.6, 178.7, 145.8, 131.2, 130.8, 129.0, 128.5, 114.4, 111.6, 104.2, 80.7, 77.6, 76.3, 76.0, 69.4, 68.8, 67.7, 63.6, 40.5, 38.7, 38.4, 36.3, 35.7, 35.1, 33.3, 30.9, 30.7, 30.0, 28.6, 28.0, 27.3, 27.3, 27.2, 27.0, 24.6, 23.3, 21.5, 21.0, 17.2, 16.7, 15.5$ ppm; HRMS (MALDI): calcd for $C_{47}H_{76}O_9S_2SiNa^+$ [M+Na^+]: 899.4597, found: 899.4601

6: $R_f = 0.15$ (silica gel, EtOAc/hexanes 1:1); $[\alpha]_D = +1.7$ ($CHCl_3$, $c = 0.9$); IR (film): $\tilde{\nu}_{max} = 3448, 2954, 2925, 1738, 1455, 1437, 1370, 1236, 1090, 1067, 1019, 981, 867, 803\ cm^{-1}$; ^1H NMR (600 MHz, $CDCl_3$): $\delta = 5.99$ (ddd, $J = 11.7, 6.6, 3.1$ Hz, 1H), 5.72–5.64 (m, 2H), 5.51 (dd, $J = 18.4, 7.5$ Hz, 1H), 5.30 (s, 1H), 5.17 (s, 1H), 5.11 (d, $J = 8.0$ Hz, 1H), 4.84 (t, $J = 11.0$ Hz, 1H), 4.63 (d, $J = 16.3$ Hz, 1H), 4.56 (d, $J = 16.3$ Hz, 1H), 4.42–4.39 (m, 1H), 4.23 (dd, $J = 6.4, 2.2$ Hz, 1H), 4.19 (br s, 1H), 4.04 (t, $J = 7.9$ Hz, 2H), 3.83 (br s, 1H), 3.68 (d, $J = 6.2$ Hz, 1H), 2.94–2.91 (m, 1H), 2.46–2.39 (m, 1H), 2.11 (s, 3H), 2.09 (s, 3H), 2.04 (s, 3H), 2.15–1.90 (m, 14H), 1.73–1.67 (m, 1H), 1.40–1.33 (m, 1H), 1.11 (d, $J = 8.3$ Hz, 3H), 1.01–0.92 (m, 1H), 0.86 (d, $J = 7.9$ Hz, 3H), 0.85 ppm (d, $J = 8.4$ Hz, 3H); ^{13}C NMR (150 MHz, $CDCl_3$): $\delta = 212.4, 171.1, 170.5, 170.4, 141.1, 131.1, 130.8, 129.1, 128.6, 115.0, 111.3, 104.2, 78.6$ (2 x), 78.5, 76.1, 75.6, 68.8, 64.1, 63.8, 38.4, 35.8, 35.7, 33.9, 33.9, 32.3, 31.1, 30.0, 28.6, 28.0, 23.4, 21.0, 21.0, 20.9, 19.5, 16.3, 15.5 ppm; HRMS (MALDI): calcd for $C_{37}H_{54}O_{12}Na^+$ [M+Na^+]: 713.3507, found: 713.3491

10: $R_f = 0.60$ (silica gel, EtOAc/hexanes 1:1); $[\alpha]_D = +7.6$ ($CHCl_3$, $c = 2.4$); IR (film): $\tilde{\nu}_{max} = 2957, 1734, 1703, 1455, 1431, 1358, 1243, 1176, 1127, 1067, 982, 860, 727, 593\ cm^{-1}$; ^1H NMR (600 MHz, $CDCl_3$): $\delta = 5.99$ (ddd, $J = 9.8, 5.6, 1.9$ Hz, 1H), 5.71 (d, $J = 10.1$ Hz, 1H), 5.66 (m, 1H), 5.54 (s, 1H), 5.50 (dd, $J = 15.6, 6.4$ Hz, 1H), 5.33 (s, 1H), 5.06 (m, 2H), 4.95–4.92 (m, 1H), 4.59(dd, $J = 18.0, 9.2$ Hz, 1H), 4.40 (m, 1H), 4.29 (s, 1H), 4.22 (d, $J = 8.3$ Hz, 1H), 4.19 (br s, 1H), 4.16–4.12 (m, 3H), 4.04 (t, $J = 6.6$ Hz, 2H), 3.99 (d, $J = 8.8$ Hz, 1H), 3.86 (m, 1H), 3.69–3.67 (m, 1H), 3.15–3.08 (m, 4H), 2.48–2.45 (m, 2H), 2.10 (s, 3H), 2.10–2.06 (m, 5H), 2.04 (s, 3H), 1.99–1.95 (m, 5H), 1.92–1.89 (m, 2H), 1.84–1.81 (m, 2H), 1.71–1.69 (m, 2H), 1.41–1.29 (m, 4H), 1.07 (d, $J = 7.0$ Hz, 3H), 0.99–0.96 (m, 3H), 0.93 (d, $J = 6.6$ Hz, 3H), 0.88 (d, $J = 7.0$ Hz, 3H), 0.85 (d, $J = 7.0$ Hz, 3H), 0.79 (d, $J = 6.6$ Hz, 3H), 0.69 (d, $J = 6.6$ Hz, 3H), 0.02 ppm (s, 9H); ^{13}C NMR (150 MHz, $CDCl_3$): $\delta = 212.1, 172.3, 171.7, 157.2, 140.8, 132.1, 131.8, 130.1, 129.3, 118.0, 112.2, 105.2, 98.7, 97.9, 80.6, 80.4, 80.0, 77.6, 77.4, 76.9, 76.7, 73.9, 69.9, 64.8, 64.2, 50.7, 50.4, 47.3, 42.0, 38.1, 36.7, 35.7, 34.1, 33.1, 32.2, 32.0, 31.4, 31.0, 29.7, 29.2, 29.1, 29.0, 27.4, 24.6, 24.4, 22.0, 22.0, 20.3, 19.5, 18.3, 17.4, 16.6, −0.3$ ppm; HRMS (MALDI): calcd for $C_{57}H_{88}INO_{15}SiNa^+$ [M+Na^+]: 1204.4860, found: 1204.4833

Table 1 (Continued)

11: $R_f = 0.50$ (silica gel, EtOAc/hexanes 1:1); $[\alpha]_D = -2.8$ ($CHCl_3$, $c = 1.2$); IR (film): $\tilde{\nu}_{max} = 2956, 1737, 1713, 1596, 1449, 1390, 1355, 1243, 1173, 1067, 978, 855, 837, 756\ cm^{-1}$; ^1H NMR (600 MHz, $CDCl_3$): $\delta = 5.98$ (ddd, $J = 9.8, 6.2, 1.8$ Hz, 1H), 5.70 (d, $J = 9.6$ Hz, 1H), 5.66 (m, 1H), 5.50 (dd, $J = 15.4, 6.1$ Hz, 1H), 5.46 (s, 1H), 5.29 (s, 1H), 5.07 (s, 2H), 4.84–4.82 (m, 1H), 4.75 (dd, $J = 12.5, 6.4$ Hz, 1H), 4.66 (br s, 1H), 4.40 (m, 1H), 4.23 (d, $J = 5.7$ Hz, 1H), 4.19–4.17 (m, 3H), 4.04–4,02 (m, 4H), 3.92–3.91 (m, 2H), 3.76 (dd, $J = 13.4, 4.2$ Hz, 1H), 3.64 (dd, $J = 14.7, 5.0$ Hz, 1H), 3.19 (t, $J = 12.5$ Hz, 1H), 3.01–2.99 (m, 1H), 2.88 (d, $J = 14.5$ Hz, 1H), 2.69 (dd, $J = 22.4, 7.5$ Hz, 1H), 2.45–2.38 (m, 2H), 2.15–2.08 (m, 6H), 2.08 (s, 3H), 2.03 (s, 3H), 1.99–1.92 (m, 6H), 1.90–1.85 (m, 2H), 1.71–1.68 (m, 3H), 1.34–1.24 (m, 8H), 1.06 (d, $J = 7.5$ Hz, 3H), 1.06–0.96 (m, 3H), 0.97 (d, $J = 6.1$ Hz, 3H), 0.82 (d, $J = 7.5$ Hz, 3H), 0.81 (d, $J = 7.0$ Hz, 3H), 0.78 (d, $J = 6.6$ Hz, 3H), 0.02 ppm (s, 9H); ^{13}C NMR (150 MHz, $CDCl_3$): $\delta = 212.5, 172.1, 171.5, 157.4, 140.4, 132.2, 131.8, 130.1, 129.6, 116.3, 112.4, 105.1, 98.5, 98.2, 81.0, 79.9, 79.6, 78.1, 77.2, 76.4, 74.8, 74.3, 69.8, 64.8, 64.0, 52.6, 50.1, 44.8, 41.4, 39.5, 39.2, 37.7, 36.8, 36.7, 35.1, 32.9, 32.6, 32.2, 32.1, 31.9, 31.0, 30.7, 29.7, 29.0, 28.9, 25.4, 24.4, 22.0, 22.0, 20.6, 19.6, 18.5, 18.0, 17.4, 16.6, −0.5$ ppm; HRMS (MALDI): calcd for $C_{57}H_{88}INO_{15}SiNa^+$ [M+Na^+]: 1204.4860, found: 1204.4832

16: $R_f = 0.35$ (silica gel, chloroform/methanol/H_2O 20:3:1); $[\alpha]_D = +22.4$ ($CHCl_3$, $c = 0.38$); IR (film): $\tilde{\nu}_{max} = 3333, 2957, 1731, 1574, 1456, 1425, 1373, 1242, 1138, 1043, 1020, 983, 803, 755\ cm^{-1}$; ^1H NMR (600 MHz, CD_3OD): $\delta = 6.00$ (ddd, $J = 9.6, 5.5, 1.8$ Hz, 1H), 5.77–5.73 (m, 1H), 5.66 (dt, $J = 9.9, 1.9$ Hz 1H), 5.50 (dd, $J = 15.3, 6.1$ Hz, 1H), 5.39 (br s, 1H), 5.10 (s, 1H), 5.05 (s, 1H), 4.80–4.79 (m, 2H), 4.33(dd, $J = 13.8, 6.8$ Hz, 1H), 4.28 (br s, 1H), 4.24 (d, $J = 4.4$ Hz, 1H), 4.14 (d, $J = 2.2$ Hz, 1H), 3.87 (br s, 1H), 3.70 (d, $J = 3.5$ Hz, 1H), 3.19–3.16 (m, 1H), 2.66 (t, $J = 11.4$ Hz, 1H), 2.56 (dd, $J = 11.2, 4.2$ Hz, 1H), 2.40–2.28 (m, 5H), 2.24–2.18 (m, 3H), 2.09 (s, 3H), 2.10–1.98 (m, 7H), 1.98–1.87 (m, 4H), 1.81–1.71 (m, 3H), 1.70–1.62 (m, 2H), 1.55–1.45 (m, 3H), 1.05 (d, $J = 7.0$ Hz, 3H), 0.97–0.90 (m, 3H), 0.92 (d, $J = 5.7$ Hz, 3H), 0.91 (d, $J = 5.7$ Hz, 3H), 0.88 (d, $J = 6.6$ Hz, 3H), 0.86 (d, $J = 6.6$ Hz, 3H), 0.85 ppm (d, $J = 6.6$ Hz, 3H); ^{13}C NMR (150 MHz, CD_3OD): $\delta = 216.7, 182.8, 173.1, 144.1, 133.9, 131.9, 130.7, 130.7, 116.6, 113.8, 106.6, 98.6, 96.9, 82.1, 80.9, 80.2, 79.2, 79.1, 78.5, 76.5, 73.5, 71.3, 50.4, 48.3, 44.2, 43.5, 40.9, 40.4, 39.6, 38.9, 37.8, 37.6, 36.5, 35.8, 35.5, 33.9, 33.2, 32.6, 32.1, 31.4, 27.2, 25.2, 24.8, 22.0, 20.7, 20.4, 18.4, 17.1, 17.0$ ppm; HRMS (MALDI): calcd for $C_{49}H_{73}NO_{13}H^+$ [M+H^+]: 884.5154, found: 884.5119

17: $R_f = 0.30$ (silica gel, chloroform/methanol/H_2O 20:3:1); $[\alpha]_D = -9.5$ ($CHCl_3$, $c = 0.60$); IR (film): $\tilde{\nu}_{max} = 3422, 2956, 1734, 1649, 1562, 1449, 1403, 1373, 1320, 1240, 1132, 1043, 980, 755\ cm^{-1}$; ^1H NMR (600 MHz, CD_3OD): $\delta = 6.00$ (ddd, $J = 9.9, 3.7, 3.7$ Hz, 1H), 5.76–5.73 (m, 1H), 5.66 (dt, $J = 10.1, 2.0$ Hz, 1H), 5.50 (dd, $J = 15.8, 6.1$ Hz, 1H), 5.33 (d, $J = 4.8$ Hz, 1H), 5.12 (s, 1H), 5.04 (s, 1H), 4.79–4.75 (m, 2H), 4.33(dd, $J = 13.8, 7.7$ Hz, 1H), 4.27–4.19 (m, 2H), 3.87 (m, 1H), 3.72 (d, $J = 3.1$ Hz, 1H), 3.18–3.13 (m, 1H), 2.69–2.62 (m, 2H), 2.39–2.26 (m, 5H), 2.24–2.18 (m, 3H), 2.08 (s, 3H), 2.10–1.98 (m, 7H), 1.98–1.84 (m, 4H), 1.81–1.66 (m, 4H), 1.70–1.62 (m, 1H), 1.55–1.35 (m, 4H), 1.07 (d, $J = 7.0$ Hz, 3H), 1.05–0.90 (m, 3H), 0.91 (d, $J = 6.1$ Hz, 3H), 0.90 (d, $J = 6.6$ Hz, 3H), 0.87 (d, $J = 7.0$ Hz, 3H), 0.87 (d, $J = 6.6$ Hz, 3H), 0.84 ppm (d, $J = 6.6$ Hz, 3H); ^{13}C NMR (150 MHz, CD_3OD): $\delta = 215.7, 182.3, 172.7, 143.9, 133.5, 131.5, 130.4, 130.2, 116.5, 113.4, 106.1, 98.3, 96.4, 81.7, 80.4, 79.9, 78.8, 78.3, 78.0, 76.1, 73.1, 70.8, 47.6, 45.5, 43.7, 42.0, 40.5, 40.0, 39.2, 38.4, 37.3, 37.3, 35.9, 35.3, 35.2, 33.1, 32.8, 32.2, 32.1, 31.8, 31.0, 26.8, 24.8, 24.2, 21.4, 20.4, 20.0, 17.8, 16.6$ ppm ; HRMS (MALDI): calcd for $C_{49}H_{73}NO_{13}H^+$ [M+H^+]: 884.5154, found: 884.5119

severe steric hindrance associated with this site. At this stage it was decided to remove the dithiane moiety by treatment with $PhI(OCOCF_3)_2$,[7] which furnished the triacetoxy hydroxy ketone **6** (Table 1) in 78% yield. The latter was adopted as an ideal substrate for the projected Stille coupling by virtue of its delicate and carefully installed functionalities, easy accessibility from **5**, and prospects for final elaboration after the merger. Thus, it was anticipated that the primary allylic acetate at C27 within **6** would be the most suitable site for the palladium-catalyzed coupling, in contrast to the secondary

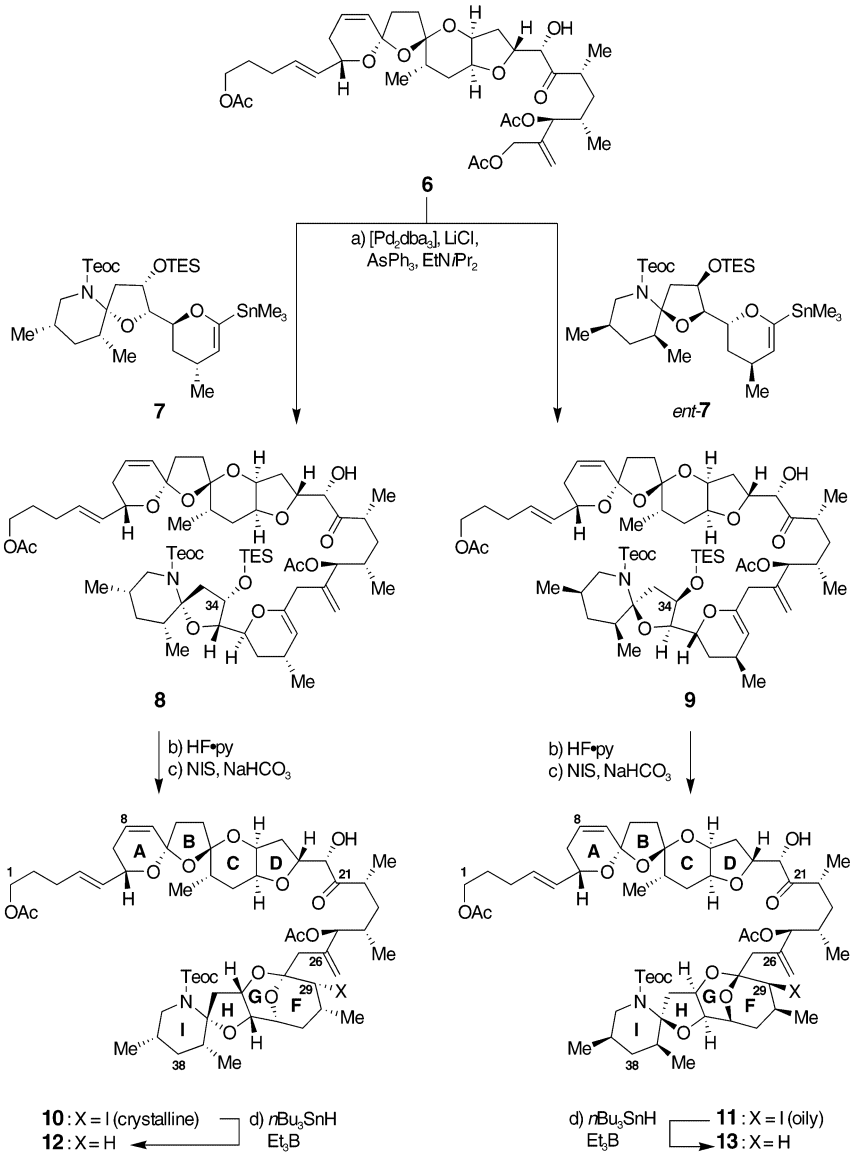
 © 2003 Wiley-VCH Verlag GmbH & Co. KGaA, Weinheim

allylic acetate (C25) whose steric hindrance should be prohibiting. Furthermore, based on model studies, the hydroxy ketone functionality at C20–C21 was expected to remain indifferent to the expected palladium reaction conditions.

Despite the careful fine-tuning of the two Stille coupling partners **6** and **7** and its enantiomer *ent*-**7** (Scheme 2), their union proved far from routine, requiring instead further attention. The challenge was mainly to find ways to prevent competitive or subsequent reaction of the secondary allylic acetate embedded within the starting component and the product, and to ensure the survival of the rather sensitive vinyl stannane functionalities within **7** and *ent*-**7**. Indeed, it was after considerable experimentation that conditions were finally found to achieve this final coupling. Thus, to modulate the effective bulkiness and electronic character of the reactive palladium species, $AsPh_3$[8] was employed together with $[Pd_2dba_3]$ (1:1 ratio), with the former ligand providing sufficient, but not prohibitive, steric hindrance to stop the secondary coupling. A slow addition of the stannane component minimized its destruction prior to its engagement in the desired process. Under these optimized conditions, compounds **8** and **9** were obtained from **6** and **7** and *ent*-**7** in 52 and 66% yields, respectively, as shown in Scheme 2.

Having assembled the complete carbon framework of the proposed azaspiracid-1 structure in advanced intermediates **8** and **9**, only the casting of two rings and the adjustment of a few functional groups remained before arrival at the targeted molecules. First to be installed from the missing cyclic motifs was ring G. Thus, the TES group was selectively removed from the hydroxy group at C34 of **8** and **9** by the action of HF·py in the presence of excess pyridine, and the resulting compound was subjected to iodoetherification with *N*-iodosuccinimide[9] and $NaHCO_3$ to afford the diastereomeric iodides **10** and **11** (Table 1) in 67 and 63% yields, respectively. Much to our delight, iodide **10** crystallized beautifully and yielded to X-ray crystallographic analysis (see ORTEP drawing, Figure 1),[10] which confirmed its molecular architecture, including all the ring and stereochemical elements of the proposed azaspiracid-1 structure, with the exception of ring E and the C21 stereocenter, whose formation was still pending. The spectral data for the oily iodide **11**, particularly when compared to those of **10**, were supportive of its structure. Initial attempts to remove the iodide residue from **10** and **11** proved problematic as the standard nBu$_3$SnH-based methods, including the mild nBu$_3$SnH–Et$_3$B protocol,[11] were plagued with complications of another product (ca. 1:1 ratio with the expected product) suspected to be formed through participation of the neighboring double bond in the radical cascade involved in the reduction. Pleasingly, it was determined that increasing the amount of nBu$_3$SnH from 5.0 equiv to a large excess solved this problem by rapidly quenching the initially formed radical at C29 before it had a chance to attack the C=C bond at C26, leading to excellent yields of 92 and 94% of **12** and **13**, respectively.

The remaining operations before arriving at **1** and FGHI-*epi*-**1** were care-



Scheme 2. Coupling of advanced intermediates **6** with **7** and *ent*-**7**, and elaboration to **12** and **13**: a) $[Pd_2dba_3]$ (0.3 equiv), $AsPh_3$ (0.3 equiv), LiCl (6.0 equiv), $EtNiPr_2$ (12 equiv); then **7** or *ent*-**7** (0.03 M in THF, syringe pump addition), NMP, 45 °C, 4 h, 52% (**8**), 66% (**9**); b) HF·py (excess), THF/pyridine (1:1), 0→25 °C, 2.5 h; c) NIS (10.0 equiv), $NaHCO_3$ (30 equiv), THF, 0 °C, 16 h, 67% (**10**), 63% (**11**) over two steps; d) Et_3B (1.0 M in hexanes, catalytic), nBu$_3$SnH/toluene (1:2), 0 °C, 5 min, 92% (**12**), 94% (**13**). TES = triethylsilyl, Teoc = 2-(trimethylsilyl)ethoxycarbonyl, dba = dibenzylideneacetone, NMP = *N*-methylpyrrolidone, NIS = *N*-iodosuccinimide.

 © 2003 Wiley-VCH Verlag GmbH & Co. KGaA, Weinheim

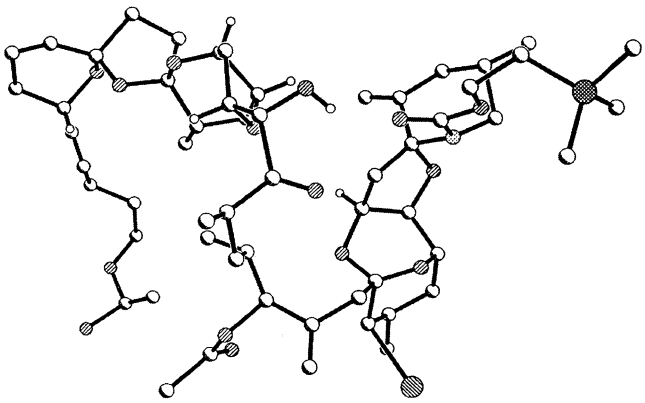


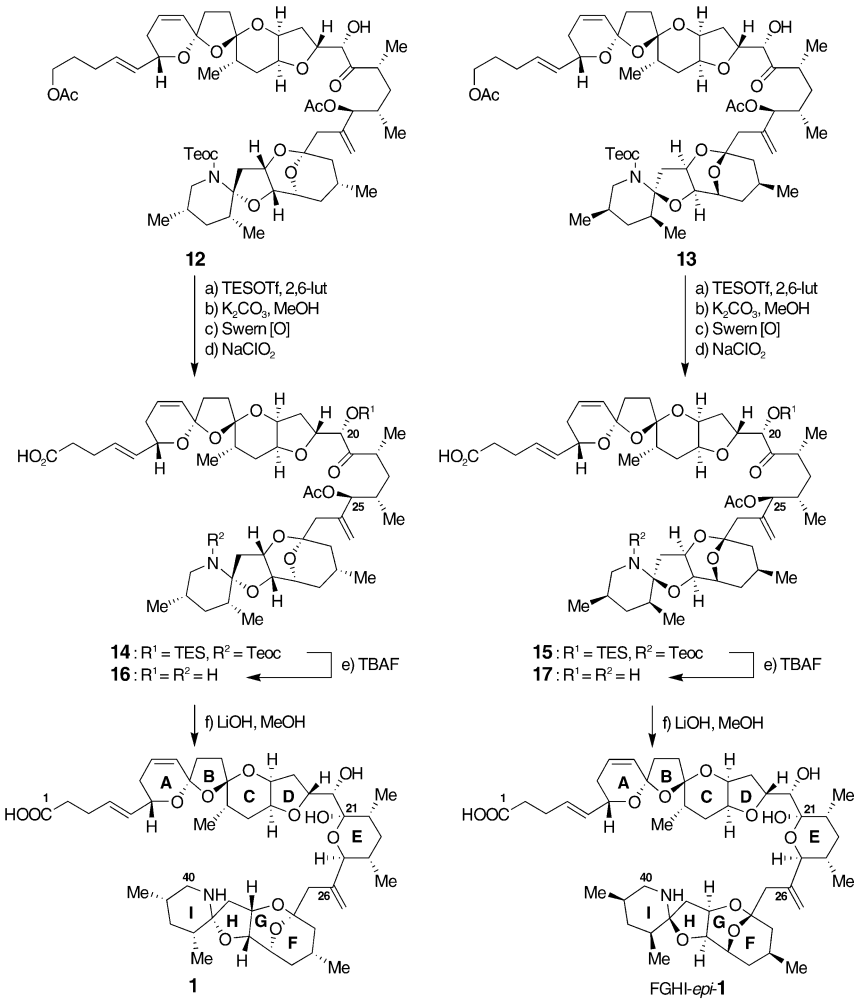
Figure 1. ORTEP drawing for compound **10**.

fully designed and navigated based on extensive experimentation and model studies (Scheme 3). Thus, in preparation for oxidation adjustment of C1, the hydroxy group at C20 was temporarily masked with a TES group, and the hydroxy group at C1 was selectively unveiled. A two-step oxidation protocol then led to carboxylic acids **14** (48% overall yield from **12**) and **15** (56% overall yield from **13**). All that now remained was the removal of the three protecting groups guarding the hydroxy groups at C20 and C25 and the secondary amine. The two fluoride-labile moieties were detached through the use of TBAF in a simple operation, leading to **16** and **17** (Table 1) in 87 and 92% yields, respectively. Finally, the acetate group of **16** and **17**, which held these molecules from folding into their resting places, was removed by the action of LiOH in MeOH, an event that led to the generation of **1** and its FGHI epimer, FGHI-*epi*-**1** (Table 1). Unlike azaspiracid-1, which was reported as a single compound, synthetic **1** and FGHI-*epi*-**1** were found to exist as mixtures of inseparable isomers. More disturbing was the realization that neither of these compounds matched, by TLC and HPLC, the naturally derived sample of azaspiracid-1, whose ^{1}H NMR data were also different from those of the synthetic samples.[12] In light of these studies, we concluded that the proposed structure **1** for azaspiracid-1 (or its epimer FGHI-*epi*-**1**) is in error, unless the error lies somewhere in the sequence after the octacyclic iodide **10** whose X-ray analysis unambiguously proved the structure of our intermediates up to that point. Pending this unlikely scenario, it seems prudent to continue the search for the true structure of azaspiracid-1, a goal which we are currently pursuing by synthetic and analytical techniques in collaboration with the Satake group in Japan.

The final outcome notwithstanding, the described chemistry herein and in the preceding Communication[1] opens new avenues to complex molecular architectures never visited before, and holds promise in the construction of further structures within this new class of potent biotoxins, including that of azaspiracid-1. Among the most powerful synthetic technologies developed in this campaign, the two C–C bond-forming reactions used to assemble the final framework and the ring closures employed to construct the delicate spiroketal moieties of the target stereoselectively stand out as both highly enabling and uniquely novel.[13]

Received: May 7, 2003 [Z51826]

Keywords: asymmetric synthesis · azaspiracid-1 · natural products · neurotoxins · structural revision · total synthesis



Scheme 3. Final stages and completion of the synthesis of the proposed azaspiracid-1 structures (**1** and FGHI-*epi*-**1**): a) TESOTf (10.0 equiv), 2,6-lutidine (20 equiv), CH_2Cl_2, −78→0 °C, 10 min; b) K_2CO_3 (catalytic), MeOH, 25 °C, 2 h; c) $(COCl)_2$ (10.0 equiv), DMSO (20 equiv), CH_2Cl_2, −78 °C, 1 h; then Et_3N (50 equiv), −78→−20 °C, 30 min; d) $NaClO_2$ (10.0 equiv), NaH_2PO_4 (10.0 equiv), 2-methyl-but-2-ene (excess), *t*BuOH/H_2O (4:1), 25 °C, 30 min, 48% (**14**) and 56% (**15**) over four steps; e) TBAF (5.0 equiv), THF, 25 °C, 2 h, 87% (**16**), 92% (**17**); f) LiOH (excess), MeOH/H_2O (5:1), 25 °C, 16 h, 45% (**1**) and 37% (FGHI-*epi*-**1**). Tf = tifluoromethanesulfonyl, DMSO = dimethyl sulfoxide.

 © 2003 Wiley-VCH Verlag GmbH & Co. KGaA, Weinheim

[1] See preceding Communication in this issue: K. C. Nicolaou, Y. Li, N. Uesaka, T. V. Koftis, S. Vyskocil, T. Ling, M. Govindasamy, W. Qian, F. Bernal, D. Y.-K. Chen, *Angew. Chem.* **2003**, *115*, 3771–3776; *Angew. Chem. Int. Ed.* **2003**, *42*, 3643–3648.

[2] M. Satake, K. Ofuji, H. Naoki, K. J. James, A. Fruey, T. McMahon, J. Silke, T. Yasumoto, *J. Am. Chem. Soc.* **1998**, *120*, 9967 – 9968; see also: Y. Román, A. Alfonso, M. C. Louzao, L. A. de la Rosa, F. Leira, J. M. Vieties, M. R. Vieytes, K. Ofuji, M. Satake, T. Yasumoto, L. M. Botana, *Cellular Signalling* **2002**, *14*, 703 – 716.

[3] E. J. Corey, D. Seebach, *Angew. Chem.* **1965**, *77*, 1134 – 1135; *Angew. Chem. Int. Ed. Engl.* **1965**, *4*, 1075 – 1077.

[4] a) J. K. Stille, *Angew. Chem.* **1986**, *98*, 504 – 519; *Angew. Chem. Int. Ed. Engl.* **1986**, *25*, 508 – 524; b) L. Del Valle, J. K. Stille, L. S. Hegedus, *J. Org. Chem.* **1990**, *55*, 3019 – 3023.

[5] M. Ide, M. Nakata, *Bull. Chem. Soc. Jpn.* **1999**, *72*, 2491 – 2499.

[6] The ^{1}H NMR (600 MHz, $CDCl_3$) signal observed for 20-H ($\delta =$ 3.62 ppm, $J = 9.6$ Hz) after reduction of compound **4** with DIBAL-H was essentially identical in terms of both chemical shift and coupling constant to that observed after the reduction of compound **36** with DIBAL-H described in the preceding Communication.[1]

[7] G. Stork, K. Zhao, *Tetrahedron Lett.* **1989**, *30*, 287 – 2902.

[8] V. Farina, B. Krishman, *J. Am. Chem. Soc.* **1991**, *113*, 9585 – 9595.

[9] a) M. Adinolfi, M. Parrilli, G. Barone, G. Laonigro, L. Mangoni, *Tetrahedron Lett.* **1976**, 3661 – 3662; b) G. Haaima, R. T. Weavers, *Tetrahedron Lett.* **1988**, *29*, 1085 – 1088.

[10] CCDC-210123 (**10**) contains the supplementary crystallographic data for this paper. These data can be obtained free of charge via www.ccdc.cam.ac.uk/conts/retrieving.html (or from the Cambridge Crystallographic Data Centre, 12, Union Road, Cambridge CB21EZ, UK; fax: (+44) 1223-336-033; or deposit@ccdc.cam.ac.uk).

[11] K. Miura, Y. Ichinose, K. Nozaki, K. Fugami, K. Oshima, K. Utimoto, *Bull. Chem. Soc. Jpn.* **1989**, *62*, 143 – 147.

[12] We thank Dr. Masayuki Satake for an authentic sample of azaspiracid-1 and for providing us with NMR spectra. Comparison of authentic azaspiracid-1 against **1** and FGHI-*epi*-**1** by TLC (chloroform/methanol/H_2O 20:3:1) showed that the authentic sample is more polar than either of the synthetic materials. In addition, the ^{1}H NMR (600 MHz, 0.5 % CD_3COOD in CD_3OD) spectra of compounds **1** and FGHI-*epi*-**1** were noticeably different from that of the natural azaspiracid-1,[2] particularly in the olefinic region; natural azaspiracid-1: $\delta = 5.74$ (4-H), 5.46 (5-H), 5.76 (8-H), 5.65 (9-H), 5.36 (44_a-H), 5.18 ppm (44_b-H); synthetic **1**: $\delta = 5.79$ (4-H), 5.57 (5-H), 6.02 (8-H), 5.76 (9-H), 5.35 (44_a-H), 5.31 ppm (44_b-H); synthetic FGHI-*epi*-**1**: $\delta = 5.79$ (4-H), 5.57 (5-H), 6.02 (8-H), 5.76 (9-H), 5.38 (44_a-H), 5.33 ppm (H-44_b). The values for the synthetic materials correspond to those of the major product in each case. It was also observed that the chemical shifts for the "upper" domain olefinic protons (4-H, 5-H, 8-H, and 9-H) remain relatively constant, whereas those of the "lower" region of the molecule (44_a-H and 44_b-H) change considerably upon addition of CD_3COOD.

[13] Note added in proof: Based on available information, we propose that the true azaspiracid-1 structure differs from that of FGHI-*epi*-**1** by the position of the double bond in ring A (7,8 instead of 8,9). Ongoing studies aim to confirm this conjecture.

 © 2003 Wiley-VCH Verlag GmbH & Co. KGaA, Weinheim

H_2O_2 Production

Direct and Continuous Production of Hydrogen Peroxide with 93% Selectivity Using a Fuel-Cell System

Ichiro Yamanaka, Takeshi Onizawa, Sakae Takenaka, and Kiyoshi Otsuka*

Hydrogen peroxide is currently one of the most essential chemicals for pulp bleaching, waste treatment, and chemical production, and it is the most promising major oxidant for green chemistry in the near future. Most H_2O_2 is manufactured by the anthraquinone process in a multistep operation with high energy consumption.[1] Some pulp-bleaching treatments rely on H_2O_2 manufactured by the electrolysis of O_2 in alkaline solutions over a carbon cathode.[2,3] The cost of the electrolysis process is high and prohibits general H_2O_2 production. Therefore, the development of a catalytic and direct method for the synthesis of H_2O_2 has been desired. It is well known that Pd/carbon catalyzes the formation of H_2O_2 from H_2 and O_2 in acidic aqueous solution. But the mixture of O_2 and H_2 explodes, and the selectivity for H_2O_2 based on H_2 is not high ($< 30\%$).[4,5] We have reported a new catalytic system for the synthesis of H_2O_2 utilizing a H_2/O_2 fuel-cell reactor under ambient conditions (Figure 1a).[6] Advantages of the fuel-cell system over the first catalytic system are, firstly, less opportunity of explosion because O_2 and H_2 are separated by the electrolyte membrane, and secondly, the generation of electric power along with H_2O_2 because of the fuel-cell setup.[7,8]

The concentration of H_2O_2 of 0.2 wt% (59 mM) in our first report was very low, and the concentrations in other industrial applications are also low.[6,9–11] The limit of the H_2O_2 concentration was due to the competitive reduction of H_2O_2 further to H_2O. The H_2O_2 concentration of 59 mM was far higher than that of O_2 (≈ 1 mM), which was limited by its solubility in the aqueous phase (Figure 1a). We have concluded that the concentrations of O_2 at the cathode must increase to produce a concentrated H_2O_2 solution. It is easy to imagine that the concentration of O_2 would be higher at higher pressures, but the probability of explosion would increase.

We propose a new concept and a new fuel-cell setup for the synthesis of H_2O_2 in order to increase the concentrations of O_2 at the cathode at atmospheric pressure. Our idea is an application of a three-phase boundary (gaseous O_2, aqueous electrolyte, and solid cathode) for the formation of H_2O_2, (Figure 1b). If a porous membrane electrode is used, a high partial pressure of O_2 (101 kPa, 45 mM) can be applied directly to the active site at the three-phase boundary.[12]

[*] Prof. I. Yamanaka, T. Onizawa, S. Takenaka, K. Otsuka
Department of Applied Chemistry
Graduate School of Science and Engineering
Tokyo Institute of Technology
Ookayama, Meguro-ku, Tokyo 152-8552 (Japan)
Fax: (+81) 3-5734-2144
E-mail: yamanaka@o.cc.titech.ac.jp

 DOI: 10.1002/anie.200351343 © 2003 Wiley-VCH Verlag GmbH & Co. KGaA, Weinheim

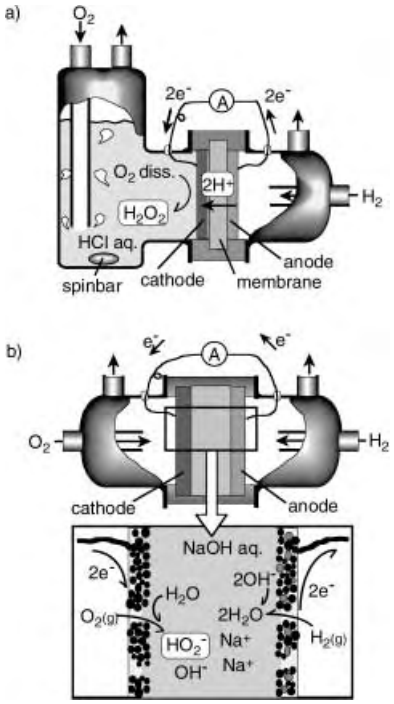


Figure 1. Schematic structure of fuel-cell reactors for H_2O_2 synthesis. a) Previous reactor, b) new reactor.

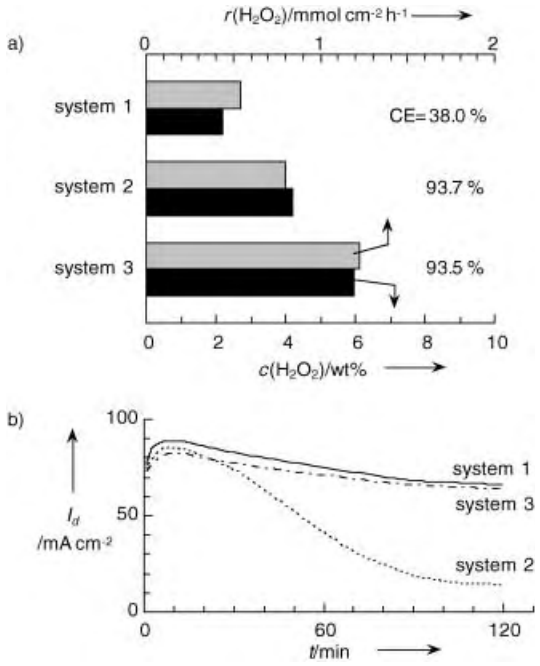


Figure 2. Synthesis of H_2O_2 by three different systems. a) Concentration of H_2O_2 in NaOH produced (2 mol L^{-1}) and rate of formation of H_2O_2. b) Time courses of the current densities of three reaction systems. CE = current efficiency.

Therefore, the reduction of O_2 to H_2O_2 should be accelerated, and the successive reduction of H_2O_2 to H_2O should be decelerated.

The porous cathode was prepared from carbon powder (vapor-grown carbon-fiber (VGCF), 13 $m^2 g^{-1}$, Showa-Denko Co.) and poly(tetrafluoroethylene) powder (PTFE, Daikin Co.) by the hot-press method.[13] The anode was also prepared from VGCF, PTFE, and Pt-black powders by the hot-press method. Pure O_2 (20 mL min^{-1}) and H_2 (20 mL min^{-1}) were supplied. The yield of H_2O_2 was determined by titration against $KMnO_4$, and the current efficiency was calculated based on the two-electron reaction. The current efficiency corresponds to H_2O_2 selectivity based on H_2.

It is well known that graphite electrodes are active for the electrolysis of O_2 to H_2O_2 in alkaline solution.[2,3] We chose VGCF as the cathode material because it has good graphitic structure and high chemical stability. First, the one-compartment cell (system 1) was used for the direct synthesis of H_2O_2 over the VGCF cathode with NaOH solutions (2 mol L^{-1}) at 298 K (Figure 2a). The concentration of H_2O_2 increased with reaction time and showed an upper limit of 2.2 wt% at 2 h. The current density gradually decreased with reaction time and was almost constant (70 mA cm^{-2}) at 2 h (Figure 2b). Therefore, current efficiency (H_2 selectivity) decreased with reaction time from 80% at 10 min to 38% at 2 h. In other words, the H_2O_2 yield decelerated with reaction time.

Although the one-compartment fuel cell described above (Figure 1b) was indeed effective for the production of more concentrated H_2O_2 solutions, the final current efficiency of 38% was not enough. We assumed that catalytic decomposition or reduction of H_2O_2 over Pt-black is occurring. Therefore, the electrolyte compartment was divided into two compartments (1.18 mL each) separated by a cation membrane (Nafion-117, DuPont) to prevent diffusion of H_2O_2 from the cathode to the anode sides (system 2). Cationic species can pass from one side to the other but anionic species cannot. In alkaline solution hydrogen peroxide is present as HO_2^-.[2,3] Therefore, we assumed that the diffusion of HO_2^- could be controlled by the Nafion membrane.

When we tested the two-compartment reactor the concentration of H_2O_2 increased with the reaction time and reached 4.2 wt% after 2 h with a high current efficiency of 93.7% (Figure 2a). The separation of the electrolyte compartment was very effective for H_2O_2 production. In contrast to system 1, however, the current density in the system 2 decreased remarkably with reaction time (Figure 2b), which is a serious problem. We have observed that the electrolyte volumes in the cathode and the anode smoothly increased and decreased, respectively, with charge passed. It could be estimated that six to seven molecules of H_2O diffused from the anode to the cathode per each electron passed. In system 2, H_2O coordinated to Na^+ should be carried from the anode to the cathode. The decrease in the amount of electrolyte in the anode should cause the decrease in the current density.

To fill up the anode, the NaOH electrolyte was injected (1.5 mL h^{-1}) with a microsyringe pump (system 3). The stability of current density was considerably improved (Figure 2b). The concentration of H_2O_2 smoothly increased and reached 6.0 wt% after 2 h with a high current efficiency of 93.5% (Figure 2a). The upper limit of the concentration of H_2O_2 was observed after 2 h, but the H_2O_2 yield increased linearly with reaction time. The upper limit of the H_2O_2

 © 2003 Wiley-VCH Verlag GmbH & Co. KGaA, Weinheim

concentration was due to the increase in the volume of the H_2O_2 solution. That is, system 3 produced H_2O_2 solution at a concentration of 6 wt% continuously with high current efficiencies $>90\%$.

To further optimize the production of H_2O_2 the rate-determining step in the system 3 was studied electrochemically. The open circuit voltage of the system 3 was 0.919 V (cathode potential: −0.102 V, anode potential: −1.021 V vs Ag | AgCl). The over potential of cathode was 0.550 V and that of anode was 0.230 V at 70 mA cm^{-2}. IR drop of the electrolyte was 0.095 V (electric resistance of NaOH electrolyte: 1.35 Ω cm) and that of the Nafion membrane was 0.044 V (resistance of Nafion in NaOH: 34.6 Ω cm). These data suggest that the cathode reaction, the reduction of O_2 to H_2O_2, limits the reaction rate of the system 3.

We have improved the electrocatalytic activity of the VGCF cathode by including several additives. We found that the addition of a small amount of carbon-black materials, Black Pearls 2000 (1475 m^2 g^{-1}, Cabot Co) and Valcan XC-72 (254 m^2 g^{-1}, Cabot Co.), to the VGCF cathode increased the current density and the formation rate of H_2O_2 by a factor of more than 1.4 with high current efficiency. We chose cathode components of VGCF (70 mg), XC72 (10 mg), and PTFE powder (7 mg) after many tests, because high activity and good reproducibility were obtained. The time course of H_2O_2 formation by the cell using the new cathode and anode (system 4) was shown in Figure 3. The concentration of H_2O_2

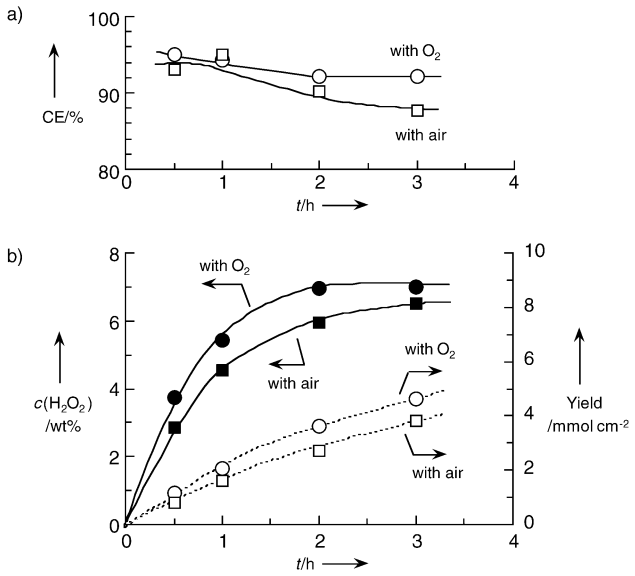


Figure 3. Time courses of the H_2O_2 synthesis by system 4. a) Concentrations and yields of H_2O_2, b) current densities.

increased rapidly, comparable to that in system 3, and reached 7.0 wt% with 94% current efficiency at 2 h. The rate of H_2O_2 formation (2.0 mmol h^{-1} cm^{-2}) in system 4 was 1.7 times greater than that in system 3 (1.2 mmol h^{-1} cm^{-2}). The current density of system 4 (100 mA cm^{-2}) was comparable to that of the electrolysis method (80–120 mA cm^{-2}).[2,3]

In all of the experiments described pure oxygen ($P(O_2) =$ 1 atm) was used for the synthesis of H_2O_2. If we could use air ($P(O_2) = 0.21$ atm), production costs could be cut tremendously. When air was used for system 4, the concentration of H_2O_2 increased smoothly with reaction time and reached 6.5 wt% with 88% current efficiency at 3 h. The formation rate of H_2O_2 (1.3 mmol h^{-1} cm^{-2}) and a current density (78 mA cm^{-2}) were slightly reduced when air was used, but performance was still very good. This result suggests that the fuel-cell method (system 4) has a great advantage for the industrial production of H_2O_2.

In conclusion, the H_2/O_2 fuel-cell method showed very good performance for the selective and continuous synthesis of H_2O_2 because gaseous O_2 could be supplied directly to the active site (the three-phase boundary) in the cathode, and the successive reduction of H_2O_2 over the anode could be avoided. If the apparent surface area of the electrodes of the system 4 could be increased to 1 m^2 with the same performance (current density: 100 mA cm^{-2} (1000 A m^{-2}) and current efficiency: 93%), aqueous alkaline solutions of 7 wt% H_2O_2 could be produced continuously at a rate of 8.3 L h^{-1} m^{-2}.

Received: March 7, 2003 [Z51343]

Keywords: electrochemistry · fuel cells · hydrogen peroxide · reduction

[1] H. Reidl, G. Pfleirender, , US Pat 2215883, **1940**.
[2] P. C. Foller, R. T. Bombard, *J. Appl. Electrochem.* **1995**, *25*, 613.
[3] N. Yamada, T. Yamaguchi, H. Otsuka, M. Sudoh, *J. Electrochem. Soc.* **1999**, *146*, 2587.
[4] Y. Izumi, , US Patent 4009252, **1978**.
[5] L. W. Gosset, , US Patent 4681751, **1988**.
[6] K. Otsuka, I. Yamanaka, *Electrochim. Acta* **1990** *35*, 319.
[7] S. H. Langer, J. A. Colucci-Rios, *CHEMTECH* **1985**, 226.
[8] K. Otsuka, I. Yamanaka, *Catal. Today* **1998**, *41*, 311.
[9] F. Alcaide, E. Brillas, P. L. Cabot, J. Casado, *J. Electrochem. Soc.* **1998**, *145*, 3444.
[10] S. P. Webb, J. A. McIntyre, *Proceedings on the Power of Electrochemistry*, 10th International Forum on Electrolysis in the Chemical Industry, Electrosynthesis, Clearwater Beach, FL, **1996**.
[11] P. Tatapudi, J. M. Fenton, *J. Electrochem. Soc.* **1993**, *140*, L55.
[12] I. Yamanaka, T. Hashimoto, K. Otsuka, *Chem. Lett.* **2002**, 852.
[13] I. Yamanaka, K. Otsuka, *J. Electrochem. Soc.* **1991**, *138*, 103.

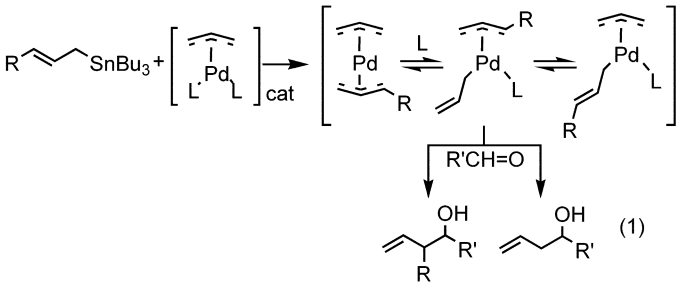
 © 2003 Wiley-VCH Verlag GmbH & Co. KGaA, Weinheim

Pd-Catalyzed Allylation

Palladium-Catalyzed Electrophilic Substitution via Monoallylpalladium Intermediates

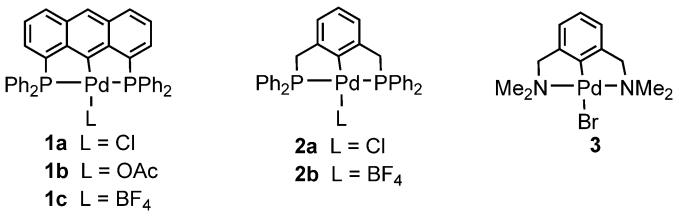
*Niclas Solin, Johan Kjellgren, and Kálmán J. Szabó**

Allylpalladium chemistry is one of the most successful areas in transition-metal catalysis. In the most common application of these complexes an allylpalladium intermediate is generated which subsequently reacts with nucleophiles.[1] The recent extension of the synthetic scope of these compounds to reactions with electrophilic substrates has attracted much attention. [2,3] It was shown that in order for the allyl moiety to have nucleophilic reactivity bisallylpalladium intermediates must be generated [Eq. (1)].[2a,3a] However, the diverse reactivity of the bisallylpalladium



(1)

intermediates imposes considerable synthetic limitations on the reaction. Controlling the regioselectivity is difficult when the two allylic moieties bear different substituents [cf. Eq. (1)].[3b,c] A further problem is that bisallylpalladium complexes may undergo allyl–allyl (Stille) coupling prior to the reaction with electrophiles.[2d] Because of these limitations it would be desirable to conduct the catalytic transformations with monoallylpalladium intermediates. This is a challenging task, since it is well known that monoallylpalladium complexes react with nucleophiles.[1] Nevertheless, our previous mechanistic studies showed that the electrophilic attack on a bisallylpalladium complex proceeds through the η^1-coordinated allyl moiety,[3a–b] while the other, η^3-coordinated allyl group acts as a strong π-donor spectator ligand [cf. Eq. (1)]. This model suggests that the catalytic generation of an (η^1-allyl)palladium intermediate coordinated to an electron-donating spectator ligand provides nucleophilic reactivity to the allyl moiety. We have now found that this type of reactivity occurs when so-called pincer complexes[4] (**1**–**3**, Scheme 1) are employed in palladium-catalyzed electrophilic substitution of allylstannanes **4a**–**c** [Eq. (2)].

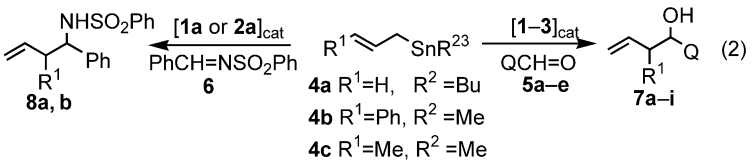


1a L = Cl
1b L = OAc
1c L = BF_4

2a L = Cl
2b L = BF_4

3

Scheme 1. Pincer complexes used as catalysts.



4a R^1=H, R^2 =Bu
4b R^1=Ph, R^2 =Me
4c R^1=Me, R^2 =Me

(2)

The reactions were performed with **4a**–**c** and various aldehydes **5** and imine **6** in the presence of catalytic amounts of **1**–**3** to obtain homoallylic alcohols **7** and amines **8**, respectively (Table 1). Complexes **1a**[4c] and **2a**[5a,c] showed high catalytic activity and very high stability under the reaction conditions. Although the reactions could be performed in many different solvents, the best results were obtained in DMF (for **1a**) and THF (for **2a**). Activated aldehydes **5b**–**e** reacted faster and usually with a higher yield than benzaldehyde (**5a**) itself (entries 1–9). The reactions proceed under neutral reaction conditions without added base or Lewis-acid catalyst, and therefore, many functionalities, such as NO_2, F, CN, and CH_3CO are tolerated (entries 3–9). Cinnamylstannane **4b** readily undergoes palladium-catalyzed allylic substitution providing exclusively the branched allylic products **7g**, **7h**, and **8b** with high diastereoselectivity (entries 13–15, 17). The corresponding reaction with crotylstannane **4c** also gives the branched allylic isomer **7i**, albeit without stereoselectivity (entry 16). The N-Pd-N type complex **3**[4a] was also tested in these reactions (entry 15); however, it showed lower catalytic activity than **1a** and **2a**. We attempted to increase the catalytic activity of **1a** and **2a** by replacing the chloride ligand with acetate (**1b**) and with tetrafluoroborate (**1c** and **2b**). These complexes displayed a very high initial catalytic activity even at room temperature; however, within a couple of hours these catalysts were completely deactivated. Nevertheless, complexes **1b** and **1c** were stable enough to achieve full conversion of **4a** with activated aldehyde **5e** (entries 7 and 8) at moderate temperature.

Transition-metal pincer complexes are widely used in organometallic chemistry and catalysis.[4] Complex **2** is known to readily undergo transmetalation with organometallic reagents.[5b,c] For example, Cotter and co-workers[5b] have shown that 2-furylstannane undergoes tin-to-palladium transmetalation with the triflate salt of **2**. It is reasonable to assume that the first step in the above reaction [Eq. (2)] is also transmetalation of the allylstannane **4** with the pincer

[*] Prof. Dr. K. J. Szabó, N. Solin, J. Kjellgren
Deparment of Organic Chemistry
Stockholm University
SE-10691 Stockholm (Sweden)
Fax: (+46) 8-154-908
E-mail: kalman@organ.su.se

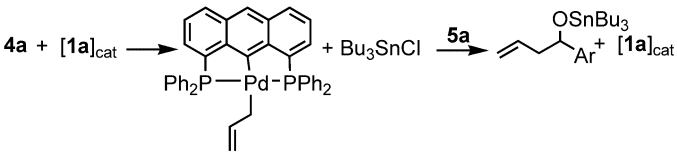
 © 2003 Wiley-VCH Verlag GmbH & Co. KGaA, Weinheim DOI: 10.1002/anie.200351477

Table 1: Palladium-catalyzed[a] electrophilic substitution reactions [Eq. (2)].

Entry	Substrates		Cat.	Prod.	Q	R^1	Solv.	Cond. [b]	Yield [%][c]
1	**4a**	**5a**	**1a**	**7a**	C_6H_5	H	DMF	60/22	81
2	**4a**	**5a**	**2a**	**7a**	C_6H_5	H	THF	60/21	88
3	**4a**	**5b**	**1a**	**7b**	4-FC_6H_5	H	DMF	60/22	77
4	**4a**	**5c**	**1a**	**7c**	4-CNC_6H_5	H	DMF	60/17	88
5	**4a**	**5d**	**1a**	**7d**	4-$CH_3COC_6H_5$	H	DMF	60/17	82
6	**4a**	**5e**	**1a**	**7e**	4-$NO_2C_6H_5$	H	DMF	60/17	82
7	**4a**	**5e**	**1b**	**7e**	4-$NO_2C_6H_5$	H	$CHCl_3$	40/2	95
8	**4a**	**5e**	**1c**	**7e**	4-$NO_2C_6H_5$	H	$CHCl_3$	20/3	95
9	**4a**	**5e**	**2a**	**7e**	4-$NO_2C_6H_5$	H	THF	40/21	95
10	**4a**	**5f**	**2a**	**7f**	cinnamyl	H	THF	60/21	80
11	**4a**	**6**	**1a**	**8a**	–	H	DMF	60/17	66
12	**4a**	**6**	**2a**	**8a**	–	H	THF	60/21	69
13	**4b**	**5a**	**2a**	**7g**	C_6H_5	Ph	THF	60/21	61[d]
14	**4b**	**5e**	**2a**	**7h**	4-$NO_2C_6H_5$	Ph	THF	60/21	95[d]
15	**4b**	**5e**	**3**	**7h**	4-$NO_2C_6H_5$	Ph	THF	20/64	85[d]
16	**4c**[e]	**5e**	**1a**	**7i**	4-$NO_2C_6H_5$	Me	DMF	60/14	77[f]
17	**4b**	**6**	**2a**	**8b**	–	Ph	THF	60/21	65 [g]

[a] Catalyst amount: 5 mol%. [b] Temperature [°C]/time [h]. [c] Yield of isolated product. [d] Diastereomer ratio *anti*/*syn*[6a] = 10:1. [e] *Z*/*E* ratio = 2:1. [f] Diasteromer ratio *syn*/*anti*[6b] = 1:1. [g] Diastereomer ratio *syn*/*anti*[6c] = 12:1.

complex (**1**, **2**). Because of the strong η^3-coordination of the pincer ligands to palladium only one coordination site is available for the allyl moiety. Accordingly, an η^1-allyl complex is formed, in which the allyl moiety is *trans* to the strongly electron-donating phenyl group [Eq. (3)]. This structure lends nucleophilic character to the allyl moiety, which is similar to



(3)

that of the η^1 moiety in the bisallylpalladium intermediates [cf. Eq. (1)]. Subsequently, the η^1-allyl complex reacts with electrophiles (**5**, **6**) providing the final product of the reaction (**7**, **8**).

An alternative mechanism may involve Lewis-acid-type activation of the aldehydes by the pincer complexes.[4a,5d] However, **1c** and **2b** undergo rapid reaction with **4a** even in the absence of aldehydes. When this reaction was carried out with **1c** and **4a** or (allyl)trimethylstannane at −10 °C in $CDCl_3$, rapid formation of propene was observed by ^{1}H NMR spectroscopy. This process indicates transmetalation of the allylstannane with palladium [cf. Eq. (3)] followed by protonation of the η^1-allyl moiety by traces of water present in the reaction mixture. The high proton affinity of the η^1-allyl moiety is a characteristic feature of bisallylpalladium complexes.[3d,5e,5f] Further evidence for the transmetalation mechanism is provided by the high reactivity of sulfonimine **6** (Table 1, entries 11, 12, and 17), which cannot be activated by Lewis-acid catalysts.

In summary, we have found a new procedure for palladium-catalyzed electrophilic substitution of allylstannanes. In this procedure pincer complexes **1**–**3** serve as catalyst sources. In contrast to previous applications proceeding via bisallylpalladium intermediates this reaction is thought to involve monoallylpalladium intermediates. Application of this procedure eliminates the side reactions that occur in bisallylpalladium-catalyzed transformations, thus extending the synthetic scope of electrophilic reagents in allylpalladium chemistry.

Experimental Section

Representative procedure for palladium-catalyzed allylation of electrophiles: To a mixture of the aldehyde (0.15 mmol) and **1a** (5 mg, 0.007 mmol) in DMF (0.5 mL) was added **4a** (59.7 mg, 0.18 mmol). This solution was then heated at the designated temperature for the allotted time (Table 1). Subsequently, the reaction mixture was quenched by addition of water and extracted with ether. The collected organic phases were dried and concentrated to dryness, and then purified by chromatography with pentane/ethyl acetate as the eluent.

Received: March 25, 2003 [Z51477]

Keywords: aldehydes · allylation · electrophilic substitution · homogenous catalysis · palladium

[1] J. Tsuji in *Palladium Reagents and Catalysis: Innovations in Organic Synthesis*, Wiley, Chichester, **1995**.

[2] a) H. Nakamura, H. Iwama, Y. Yamamoto, *J. Am. Chem. Soc.* **1996**, *118*, 6641; b) H. Nakamura, J.-G. Shim, Y. Yamamoto, *J. Am. Chem. Soc.* **1997**, *119*, 8113; c) H. Nakamura, K. Aoyagi, J.-G. Shim, Y. Yamamoto, *J. Am. Chem. Soc.* **2001**, *123*, 372; d) H. Nakamura, M. Bao, Y. Yamamoto, *Angew. Chem.* **2001**, *113*, 3308; *Angew. Chem. Int. Ed.* **2001**,*40*, 3208.

[3] a) K. J. Szabó, *Chem. Eur. J.* **2000**, *6*, 4413; b) N. Solin, S. Narayan, K. J. Szabó, *J. Org. Chem.* **2001**, *66*, 1686; c) N. Solin, S. Narayan, K. J. Szabó, *Org. Lett.* **2001**, *3*, 909; d) O. A. Wallner, K. J. Szabó, *Org. Lett.* **2002**, *4*, 1563; e) O. A. Wallner, K. J. Szabó, *J. Org. Chem.* **2003**, *68*, 2934.

[4] a) M. Albrecht, G. van Koten, *Angew. Chem.* **2001**, *113*, 3866; *Angew. Chem. Int. Ed.* **2001**,*40*, 3751; b) J. T. Singleton, *Tetrahe-*

 © 2003 Wiley-VCH Verlag GmbH & Co. KGaA, Weinheim

dron **2003**, *59*, 1837; c) M. W. Haenel, S. Oevers, J. Bruckmann, J. Kuhnigk, C. Krüger, *Synlett* **1998**, 301.
[5] a) H. Rimml, L. M. Venanzi, *J. Organomet. Chem.* **1983**, *259*, C6; b) W. D. Cotter, L. Barbour, K. L. McNamara, R. Hechter, R. J. Lachicotte, *J. Am. Chem. Soc.* **1998**, *120*, 11016; c) H. Rimml, Ph.D. Thesis, ETH Zürich, **1984**, d) Y. Motoyama, M. Okano, H. Narusawa, N. Makihara, K. Aoki, H. Nishiyama, *Organometallics* **2001**, *20*, 1580; e) P. W. Jolly, *Angew. Chem.* **1985**, *97*, 279; *Angew. Chem. Int. Ed. Engl.* **1985**, *24*, 283; f) J. Kiji, T. Okano, T. Nomura, K. Saiki, T. Sai, J. Tsuji, *Bull. Chem. Soc. Jpn.* **2001**, *74*, 1939.
[6] The diastereomer ratios were established on the basis of NMR data: a) J. P. Takahara, Y. Masuyama, Y. Kurusu, *J. Am. Chem. Soc.* **1992**, *114*, 2577; b) R. A. Batey, A. N. Thadani, D. V. Smil, A. J. Lough, *Synthesis* **2000**, 990; c) W. Lu, T. H. Chan, *J. Org. Chem.* **2000**, *65*, 8589.

 © 2003 Wiley-VCH Verlag GmbH & Co. KGaA, Weinheim

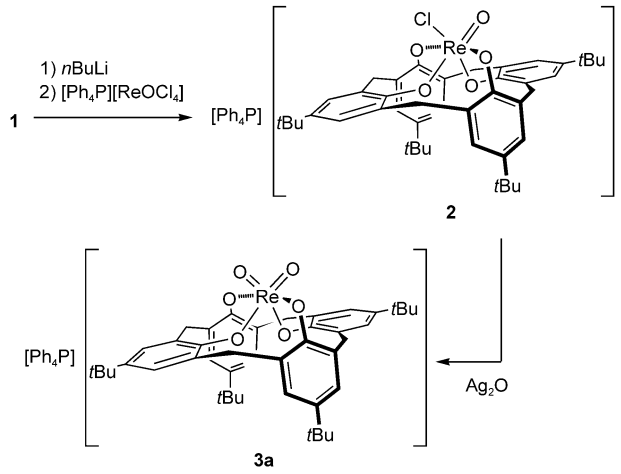
Re–Pd Calixarene Complexes

Stepwise Construction of a Re–Pd Heterodinuclear Core Inside the Cavity of *p*-*t*Bu-Calix[4]arene**

*Kentarou Iwasa, Takuya Kochi, and Youichi Ishii**

Metallocalixarenes have recently received much interest as molecular models of metal species bound on polyoxo surfaces,[1] as well as metalloreceptors with controlled structures.[2,3] The majority of the metallocalixarenes so far developed are oxophilic group 4–6 transition-metal derivatives; few examples have been reported for late-transition-metal complexes of unmodified calixarenes.[3–6] However, recent studies have revealed that late transition metals can also form stable aryloxo and alkoxo complexes that have intriguing reactivities.[7] This background prompted us to investigate the synthesis and properties of late-transition-metal derivatives of calixarenes, and we have recently found that calix[4]arenes undergo site-selective and stepwise complexation with two {M(cod)$^+$} fragments (M = Rh, Ir; cod = 1,5-cyclooctadiene), where the first metal center is coordinated to the arene ring and the second is coordinated to the phenolic oxygen atoms at the narrow rim.[4] With the intention to construct heterodinuclear late-transition-metal cores on the calixarene scaffold, we have turned our attention to the synthesis and reactivities of high-valent rhenium derivatives of calixarenes. Herein we describe the synthesis and characterization of mononuclear rhenium *p*-*t*Bu-calix[4]arene complexes and their use in the stepwise construction of a phenoxo-bridged Re–Pd heterodinuclear core inside the cavity of the calix[4]arene.

When a solution of *p*-*t*Bu-calix[4]arene-$(OH)_4$ (**1**) in THF was treated with *n*BuLi (3 equiv) and then allowed to react with $[Ph_4P][ReOCl_4]$ (1.5 equiv),[8] an anionic complex tentatively formulated as $[Ph_4P][ReCl(O)\{p\text{-}t\text{Bu-calix[4]arene-}(O)_4\}]\cdot CH_2Cl_2\cdot 0.5\,Et_2O$ (**2**·CH_2Cl_2·0.5 Et_2O) was obtained in 54% yield after repeated recrystallization (Scheme 1).[9] Although the paramagnetism of the Re^{VI} center (μ_{eff}/μ_B = 1.3 in $[D_6]$acetone solution) prevented spectroscopic full characterization of **2**, its analytical, EPR, and IR ($\tilde{\nu}$ = 929 cm^{-1}, ν(Re=O)) data are in agreement with the chloro–oxo structure. Further characterization of the rhenium complex has been achieved by oxidation to a Re^{VII} species.



Scheme 1. Synthesis of rhenium complexes **2** and **3a**.

When complex **2** was treated with excess Ag_2O in THF at room temperature, the Re^{VII} complex $[Ph_4P][ReO_2\{p\text{-}t\text{Bu-calix[4]arene-}(O)_4\}]$ (**3a**) was obtained in 89% yield (Scheme 1). The formation of Re=O bonds is confirmed by the characteristic strong IR bands at 902 and 910 cm^{-1}. The ^1H NMR spectrum of **3a** shows two aromatic and two *t*Bu signals at δ = 7.06, 6.96 ppm and δ = 1.29, 1.07 ppm, respectively, as well as one set of CH_2 signals at δ = 4.51 and 3.29 ppm (d, J = 13.7 Hz). This spectral feature is in full agreement with a formulation with an apparent C_{2v} symmetry. The structure of this anion was crystallographically determined via the PPN salt $[PPN][ReO_2\{p\text{-}t\text{Bu-calix[4]arene-}(O)_4\}]\cdot 2\,Me_2CO\cdot 0.5\,C_6H_6$ (**3b**·2 Me_2CO·0.5 C_6H_6) (Figure 1; PPN = $(Ph_3P)_2N$).[10] The rhenium atom is coordinated by the four phenolic oxygen atoms of the calix[4]arene ligand and two *cis* oxo ligands, in a distorted octahedral geometry. The Re(1)-O(5) and Re(1)-O(6) bond lengths at 1.717(5) and 1.714(5) Å, respectively, are typical for Re^{VII}=O double bonds.[11] Two of the facing aromatic rings of the calix[4]arene ligand are very open, with a dihedral angle of 168.8°, so that

[*] Prof. Dr. Y. Ishii
Department of Applied Chemistry
Faculty of Science and Engineering, Chuo University
Kasuga, Bunkyo-ku, Tokyo 112-8551 (Japan)
Fax: (+81) 3-3817-1895
E-mail: ishii@chem.chuo-u.ac.jp
K. Iwasa, T. Kochi
Institute of Industrial Science
The University of Tokyo
Komaba, Meguro-ku, Tokyo 153-8505 (Japan)

[**] This work was supported by a Grant-in-aid for Scientific Research from the Ministry of Education, Science, Sports, and Culture, Japan.

Supporting information for this article is available on the WWW under http://www.angewandte.org or from the author.

 © 2003 Wiley-VCH Verlag GmbH & Co. KGaA, Weinheim DOI: 10.1002/anie.200351530

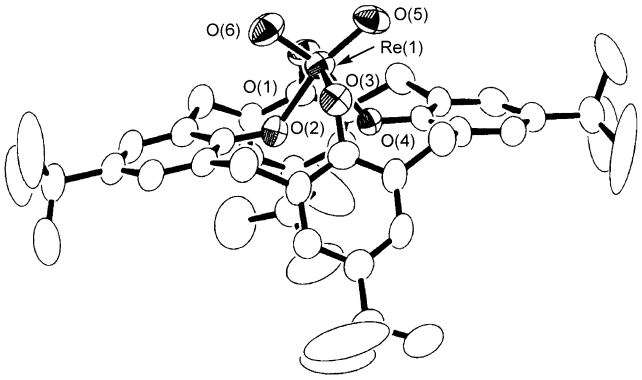
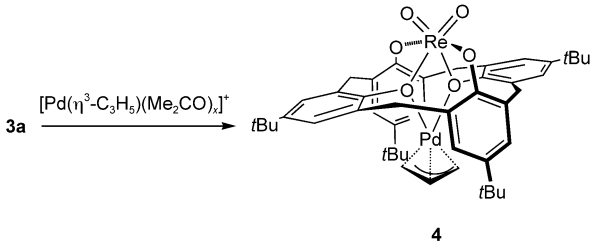


Figure 1. ORTEP diagram for the anionic part in **3b**·2 Me_2CO·0.5 C_6H_6. Thermal ellipsoids were set at 50%.

the calix[4]arene ligand adopts an elliptical cone conformation where the O(2) and O(4) atoms of the splayed phenoxo residues are mutually *cis* and occupy the *trans* positions of the oxo ligands. It should be noted that complexes **1** and **2** are the first calixarene–rhenium complexes in which the metal atom is directly bound to the body of calixarene, although several calixarene derivatives having a rhenium complex moiety as a pendant group have been synthesized.[12]

Taking advantage of the anionic nature of the dioxorhenium species, complexation of a second transition-metal fragment with **3a** was examined. When an EtOH solution of **3a** was treated with the solvated allyl–palladium complex $[Pd(\eta^3\text{-}C_3H_5)(Me_2CO)_x](OTf)$ ($OTf = OSO_2CF_3$),[13] the Re–Pd complex $[ReO_2\{p\text{-}t\text{Bu-calix[4]arene-}(O)_4\}Pd(\eta^3\text{-}C_3H_5)]$ (**4**) was obtained in 75% yield (Scheme 2). The



Scheme 2. Synthesis of heterobimetallic complex **4**.

^{1}H NMR signals for the allyl protons of **4** appear at $\delta = 4.01$ (tt, $J = 11.7$, 6.6 Hz, 1H), 2.20 (d, $J = 6.6$ Hz, 2H), and 1.20 ppm (d, $J = 11.7$ Hz, 2H), and exhibit an extraordinary high-field shift compared with those of $[\{Pd(\eta^3\text{-}C_3H_5)Cl\}_2]$ ($\Delta\delta = 1.5$–1.9 ppm). This observation strongly suggests that the $\{Pd(\eta^3\text{-}C_3H_5)^+\}$ fragment is encapsulated in the calixarene pocket and surrounded by the aromatic rings. The signals for the calix[4]arene CH_2 protons are observed as a pair of doublets at room temperature ($\delta = 4.61$, 3.53 ppm, $J =$ 14.4 Hz), indicating the dynamic behavior of the allyl group. These signals coalesce at −40 °C and split into four doublets at −80 °C ($\delta = 3.48$, 3.58, 4.32, 4.44 ppm, $J = 14.8$ Hz), which is in full agreement with the expected C_s symmetry of **4**.

The molecular structure of **4** was established by X-ray crystallography.[10] An ORTEP drawing is shown in Figure 2, which clearly confirms that the $\{Pd(\eta^3\text{-}C_3H_5)^+\}$ fragment is situated in the cavity and coordinated by the two phenoxy

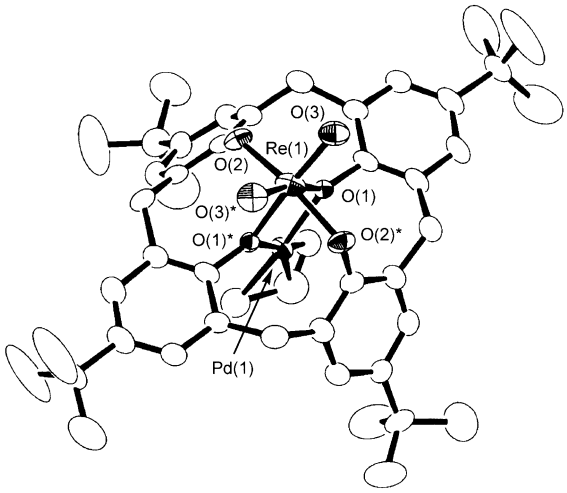


Figure 2. ORTEP diagram for complex **4**. Thermal ellipsoids were set at 50%.

oxygen atoms situated *trans* to the Re=O groups. The heterobimetallic $\{RePdO_2\}$ core is planar, and the long Re(1)···Pd(1) interatomic separation at 3.4383(8) Å excludes any metal–metal bonding interaction. The dihedral angle of the two bridging phenoxo groups at 170.7° is comparable to that of **3b**, and the conformation of the calix[4]arene moiety is deformed only slightly by the coordination of the $\{Pd(\eta^3\text{-}C_3H_5)^+\}$ fragment. Although a few alkali-metal salts of anionic calixarene complexes such as $[Ta(OPh)_2\{p\text{-}t\text{Bu-calix[4]arene-}(O)_4\}Na(thf)_2]$ have been reported to adopt a similar coordination structure,[14] complex **4** provides the first example where a heterodinuclear core composed of two different transition metals has been constructed inside the cavity of a calixarene ligand. Interestingly, complex **4** was the only bimetallic product detected in the reaction of **3a** with $[Pd(\eta^3\text{-}C_3H_5)(Me_2CO)_x]^+$, and coordination of the terminal Re=O groups in **3a** to the palladium center has not been observed.

In conclusion, we have synthesized mononuclear Re^{VI} and Re^{VII} complexes of **1** and found that the Re^{VII} dioxo complex **3** can be used to construct a Re–Pd heterodinuclear core inside the cavity of the calixarene. Although several homopolymetallic complexes of calixarenes have been described in literature,[15] a methodology to synthesize heteropolynuclear transition-metal cores on the calixarene scaffold still remains to be developed. The present study opens a potential synthetic route for such a class of complexes.

Received: March 31, 2003 [Z51530]

Keywords: bimetallic complexes · calixarenes · palladium · rhenium · transition metals

 © 2003 Wiley-VCH Verlag GmbH & Co. KGaA, Weinheim

[1] a) C. Floriani, R. Floriani-Moro in *Calixarene 2001* (Eds.: Z. Asfari, V. Böhmer, J. Harrowfield, J. Vicens), Kluwer Academic Publishers, Dordrecht, **2001**, pp. 536–560; b) C. Floriani, R. Floriani-Moro, *Adv. Organomet. Chem.* **2001**, *47*, 167–233; c) C. Floriani, *Chem. Eur. J.* **1999**, *5*, 19–23.

[2] a) P. D. Harvey, *Coord. Chem. Rev.* **2002**, *233–*234, 289–309; b) S. Steyer, C. Jeunesse, D. Armspach, D. Matt, J. Harrowfield in *Calixarene 2001* (Eds.: Z. Asfari, V. Böhmer, J. Harrowfield, J. Vicens), Kluwer Academic Publishers, Dordrecht, **2001**, pp. 513–535; c) C. Wieser, C. B. Dieleman, D. Matt, *Coord. Chem. Rev.* **1997**, *165*, 93–161.

[3] M. Staffilani, K. S. B. Hancock, J. W. Steed, K. T. Holman, J. L. Atwood, R. K. Juneja, R. S. Burkhalter, *J. Am. Chem. Soc.* **1997**, *119*, 6324–6335.

[4] Y. Ishii, K. Onaka, H. Hirakawa, K. Shiramizu, *Chem. Commun.* **2002**, 1150–1151.

[5] a) M. M. Olmstead, G. Sigel, H. Hope, X. Xu, P. P. Power, *J. Am. Chem. Soc.* **1985**, *107*, 8087–8091; b) V. Esposito, E. Solari, C. Floriani, N. Re, C. Rizzoli, A. Chiesi-Villa, *Inorg. Chem.* **2000**, *39*, 2604–2613.

[6] Late-transition-metal complexes of chemically modified calixarenes such as the phosphane derivatives have been investigated. For recent examples: a) C. J. Cobley, D. D. Ellis, A. G. Orpen, P. G. Pringle, *J. Chem. Soc. Dalton Trans.* **2000**, 1101–1107; b) C. J. Cobley, D. D. Ellis, A. G. Orpen, P. G. Pringle, *J. Chem. Soc. Dalton Trans.* **2000**, 1109–1112; c) M. Vézina, J. Gagnon, K. Villeneuve, M. Drouin, P. D. Harvey, *Organometallics* **2001**, *20*, 273–281; d) C. Jeunesse, C. Dieleman, S. Steyer, D. Matt, *J. Chem. Soc. Dalton Trans.* **2001**, 881–892; e) K. Takenaka, Y. Obora, L. H. Jiang, Y. Tsuji, *Bull. Chem. Soc. Jpn.* **2001**, *74*, 1709–1715; f) C. Dieleman, S. Steyer, C. Jeunesse, D. Matt, *J. Chem. Soc. Dalton Trans.* **2001**, 2508–2517; g) M. Lejeune, C. Jeunesse, D. Matt, N. Kyritsakas, R. Welter, J.-P. Kintzinger, *J. Chem. Soc. Dalton Trans.* **2002**, 1642–1650; h) S. Steyer, C. Jeunesse, D. Matt, R. Welter, M. Wesolek, *J. Chem. Soc. Dalton Trans.* **2002**, 4264–4274; i) K. Takenaka, Y. Obora, L. H. Jiang, Y. Tsuji, *Organometallics* **2002**, *21*, 1158–1166; j) J. Seitz, G. Mass, *Chem. Commun.* **2002**, 338–339.

[7] a) H. E. Bryndza, W. Tam, *Chem. Rev.* **1988**, *88*, 1163–1188; b) J. R. Fulton, A. W. Holland, D. J. Fox, R. G. Bergman, *Acc. Chem. Res.* **2002**, *35*, 44–56.

[8] The use of 3 equiv of *n*BuLi and 1.5 equiv of $[PPh_4][ReOCl_4]$ gave the best result (54% yield); reactions with 2 and 4 equiv of *n*BuLi resulted in a lower yield of **2** (22–53% yield).

[9] The preparative procedures and data for complexes **2**–**4** are explained in detail in the Supporting Information.

[10] a) **3b**·2 Me_2CO·0.5 C_6H_6: $C_{89}H_{97}NO_8P_2Re$: (M_r = 1556.90); crystal size 0.20 × 0.35 × 0.35 mm^3, triclinic, space group $P\bar{1}$, a = 13.044(2), b = 14.168(3), c = 22.880(5) Å, α = 80.51(2), β = 88.96(2), γ = 72.17(1)°, V = 3967(1) Å^3, Z = 2, ρ_{calcd} = 1.303 g cm^{-3}, $2\theta_{max}$ = 45.0°, T = 294(2) K; 10865 reflections measured, 10361 unique (R(int) = 0.027) and 7693 $I > 3\sigma(I)$; Rigaku AFC7R four-circle automated diffractometer, $Mo_{K\alpha}$ radiation (λ = 0.71069 Å), graphite monochromator, Lorentz-polarization and absorption corrections (μ = 16.28 cm^{-1}, range of transmission = 0.80–1.00). The structure was solved by heavy-atom Patterson methods and refined with the full-matrix, least-squares method based on F (teXsan, Crystal Structure Analysis Package, Molecular Structure Corporation, **1985** and **1999**), 838 parameters, R = 0.042, Rw = 0.043 for $I > 3\sigma(I)$; residual electron density 0.76/−0.68 e Å^{-3}. The C and O atoms in the two solvating acetone molecules were included as fixed atoms; one of these molecules was found to be disordered and the corresponding C and O atoms were treated with 60% and 40% occupancies; b) **4**: $C_{47}H_{57}O_6PdRe$ (M_r = 1010.57); crystal size 0.15 × 0.40 × 0.35 mm^3, monoclinic, space group $C2/c$, a = 24.763(3), b = 9.308(2), c = 19.239(2) Å, β = 108.154(10)°, V = 4213(1) Å^3, Z = 4, ρ_{calcd} = 1.593 g cm^{-3}, $2\theta_{max}$ = 55.0°, T = 294(2) K; 5233 reflections measured, 4856 unique (R(int) = 0.018), and 3885 $I > 2\sigma(I)$; Rigaku AFC7R four-circle automated diffractometer, $Mo_{K\alpha}$ radiation (λ = 0.71069 Å), graphite monochromator, Lorentz-polarization and absorption corrections (μ = 33.46 cm^{-1}, range of transmission = 0.61–1.00). The structure was solved by heavy-atom Patterson methods and refined with the full-matrix, least-squares method based on F^2 (teXsan), 236 parameters, $R2$ = 0.102, wR = 0.159 for all data; residual electron density 2.51/−1.80 e Å^{-3}. The allyl group was found to be disordered around the C_2 axis, and the corresponding C and H atoms were included as fixed atoms with a 50% occupancy. CCDC-205916 (**3b**·2 Me_2CO·0.5 C_6H_6) and CCDC-205917 (**4**) contain the supplementary crystallographic data for this paper. These data can be obtained free of charge via www.ccdc.cam.ac.uk/conts/retrieving.html (or from the Cambridge Crystallographic Data Centre, 12, Union Road, Cambridge CB21EZ, UK; fax: (+44) 1223-336-033; or deposit@ccdc.cam.ac.uk).

[11] a) J. R. Dilworth, S. K. Ibrahim, S. R. Khan, M. B. Hursthouse, A. A. Karaulov, *Polyhedron* **1990**, *9*, 1323–1329; b) W.-D. Wang, A. Ellern, I. A. Guzei, J. H. Espenson, *Organometallics* **2002**, *21*, 5576–5582.

[12] a) P. D. Beer, M. G. B. Drew, D. Hesek, M. Shade, F. Szemes, *Chem. Commun.* **1996**, 2161–2162; b) J. B. Cooper, M. G. B. Drew, P. D. Beer, *J. Chem. Soc. Dalton Trans.* **2000**, 2721–2728; c) K. J. C. van Bommel, W. Verboom, R. Hulst, H. Kooijman, A. L. Spek, D. N. Reinhoudt, *Inorg. Chem.* **2000**, *39*, 4099–4106; d) J. B. Cooper, M. G. B. Drew, P. D. Beer, *J. Chem. Soc. Dalton Trans.* **2001**, 392–401; e) T. Haino, H. Araki, Y. Fujiwara, Y. Tanimoto, Y. Fukazawa, *Chem. Commun.* **2002**, 2148–2149.

[13] M. A. Ciriano, J. J. Pérez-Torrente, L. A. Oro, A. Tiripicchio, M. Tiripicchio-Camellini, *J. Chem. Soc. Dalton Trans.* **1991**, 255–262.

[14] a) A. Zanotti-Gerosa, E. Solari, L. Giannini, C. Floriani, A. Chiesi-Villa, C. Rizzoli, *Chem. Commun.* **1997**, 183–184; b) V. C. Gibson, C. Redshaw, W. Clegg, M. R. J. Elsegood, *Chem. Commun.* **1997**, 1605–1606; c) L. Giannini, E. Solari, C. Floriani, N. Re, A. Chiesi-Villa, C. Rizzoli, *Inorg. Chem.* **1999**, *38*, 1438–1445; d) A. Caselli, E. Solari, R. Scopelliti, C. Floriani, *J. Am. Chem. Soc.* **1999**, *121*, 8296–8305; e) A. Caselli, E. Solari, R. Scopelliti, C. Floriani, N. Re, C. Rizzoli, A. Chiesi-Villa, *J. Am. Chem. Soc.* **2000**, *122*, 3652–3670; f) G. Guillemot, E. Solari, C. Floriani, C. Rizzoli, *Organometallics* **2001**, *20*, 607–615.

[15] For example, a) J. A. Acho, T. Ren, J. W. Yun, S. J. Lippard, *Inorg. Chem.* **1995**, *34*, 5226–5233; b) U. Radius, J. Attner, *Eur. J. Inorg. Chem.* **1998**, 299–303; c) M. H. Chisholm, K. Folting, W. E. Streib, D.-D. Wu, *Inorg. Chem.* **1999**, *38*, 5219–5229; d) C. Redshaw, M. R. J. Elsegood, *Inorg. Chem.* **2000**, *39*, 5164–5168; e) V. C. Gibson, C. Redshaw, M. R. J. Elsegood, *Chem. Commun.* **2001**, 767–769; f) V. C. Gibson, C. Redshaw, M. R. J. Elsegood, *J. Chem. Soc. Dalton Trans.* **2002**, 1200–1201.

 © 2003 Wiley-VCH Verlag GmbH & Co. KGaA, Weinheim

Barium Hypersilanides

Syntheses and Structures of Barium Silanides: Contact and Separated Ions**

*Weijie Teng, Ulrich Englich, and Karin Ruhlandt-Senge**

The chemistry of σ-bonded organometallic calcium, strontium, and barium derivatives is slowly emerging from obscurity, with a small but growing number of well-characterized target compounds published during the past decade.[1] This surge in attention may be explained by the increasing prominence of the compounds in polymer and synthetic chemistry, as well as solid-state applications. Despite the increased attention many unanswered questions remain, a prominent one being the nature of the metal–carbon bond.

Research in our group focuses on heavy-alkaline-earth-metal organometallic complexes, where the identification of viable ligand and solvent systems and the exploration of facile synthetic access routes remain critical since the high reactivity of the target compounds imposes synthetic and analytical limitations. This is specifically important for the emerging group of σ-bonded organometallic complexes, where chemistry developed for the more robust cyclopentadienide, indenyl, or fluorenyl derivatives is not applicable.[1] As such, investigation of the closely related silanides provides essential information towards the further development of the σ-bonded organometallic congeners.

To date, information on well-characterized alkaline-earth-metal silanides is limited to magnesium derivatives.[2] A small group of heavy-metal derivatives was mentioned in a patent as polymerization initiators of acrylonitrile,[3] but no synthetic, spectroscopic, or structural details are available.

Here we report a series of barium hypersilanides ($[Si(SiMe_3)_3]^-$) where the addition of various donors affects the formation of contact or separated ions in the solid state. $[Ba(thf)_4(Si(SiMe_3)_3)_2]$ (**1**) exhibits Ba–Si bonds, while $[\{Ba(hmpa)_6\}\{(Si(SiMe_3)_3)_2\}]$ (**2**) posseses separated ions (hmpa = hexamethylphosphoramide). In contrast, $[\{Ba([18]crown\text{-}6)(Si(SiMe_3)_3)_2\}\{Ba(hmpa)_6\}\{(Si(SiMe_3)_3)_2\}]$ (**3**) is a rare species containing both contact and separated ions, thus providing important information towards metal–ligand bond character and strength, and of the coordination chemistry of barium.

[*] Prof. Dr. K. Ruhlandt-Senge, W. Teng, Dr. U. Englich
Department of Chemistry
Syracuse University
1-014 Center for Science and Technology
Syracuse, NY 13244-4100 (USA)
Fax: (+1) 315-443-4070
E-mail: kruhland@syr.edu

[**] This work was supported by the National Science Foundation (CHE-9702246 and CHE-0108098). Purchase of the X-ray diffractometer was made possible with grants from NSF (CHE-95-27898), the W. M. Keck Foundation and Syracuse University. We acknowledge D. Jenkins for technical assistance.

Compounds **1**–**3** have been prepared in high yield by metathesis involving the treatment of BaI_2 with two equivalents of potassium silanide in THF [Eq. (1)]. The addition of

$$BaI_2 + 2\,K(Si(SiMe_3)_3) \xrightarrow{THF} [\{Ba(thf)_4\}\{(Si(SiMe_3)_3)_2\}] + 2\,KI \qquad (1)$$

appropriate donors dictates the formation of either contact or separated ions in the solid state.

It is critical to limit the exposure of the reaction products to THF, since extended contact results in the migration of $SiMe_3$ groups and subsequent redox chemistry through the formation of $Si(SiMe_3)_4$ and elemental silicon. In fact, if the reaction mixture is exposed to THF overnight, only $Si(SiMe_3)_4$ can be identified by NMR spectroscopy. Similarly, silyl-group migration has been identified as the major side reaction when treating R_3SiSiR_3 (R = Me, Ph) with elemental alkaline-earth metals in a THF/NH_3 mixture.[4] This chemistry is not limited to silyl derivatives, and -$SnPh_3$ migration was responsible for the concurrent formation of $[\{M([18]crown\text{-}6)(hmpa)_2\}\{Sn(SnPh_3)_3\}_2]$ and $Sn(SnPh_3)_4$ (M = Ca, Sr, Ba) from the reaction of $Ph_3SnSnPh_3$ with heavy alkaline-earth metals in a THF/NH_3 mixture.[5]

The title compounds are highly sensitive to moisture and oxygen, and most careful handling conditions are required. While compound **1** is extremely sensitive towards oxygen and moisture, compound **2** is even more reactive, decomposing violently upon exposure.

Compound **1**[6] (Figure 1) exhibits a distorted octahedral environment for the barium center, which is comprised of two silanide ligands in addition to four THF donors. The average barium–silicon and barium–oxygen separations are 3.440(9) and 2.74(1) Å, respectively. The Ba–Si bond length compares well with $[Mg(thf)_2(Si(SiMe_3)_3)_2]$ (2.682(2) Å)[2a] considering the increased ionic radius of barium[7] and higher metal coordination number. The Ba–O bond lengths are in accord with the structurally closely related $[Ba(thf)_4\{E(2,4,6\text{-}tBu_3C_6H_2)_2\}]$ (E = S, Se).[8] The distortion of **1** from octahedral geometry is significant, with a *trans* Si-Ba-Si angle of 140.62(3)°. In accord with this distortion, O-Ba-O angles are

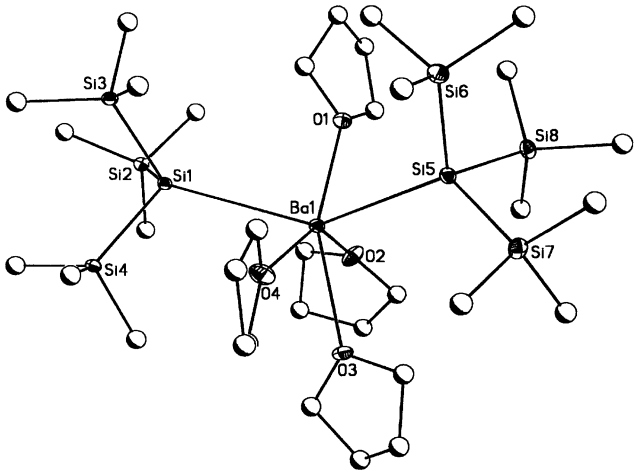


Figure 1. The crystal structure of **1**, with hydrogen atoms omitted for clarity.

 DOI: 10.1002/anie.200351610 © 2003 Wiley-VCH Verlag GmbH & Co. KGaA, Weinheim

compressed, ranging between 71.69(9) and 144.25(9)°. The Si-Si-Si angle sums of the central silicon atoms (302.63 and 306.18°) indicate significant pyramidal geometry, which is in good agreement with related alkali-metal hypersilanides.[9,10]

Compound **2** (Figure 2) exhibits separated ions in the solid state, with cation and anion separated by 10.553 Å.[11] The barium cation is coordinated in a distorted octahedral

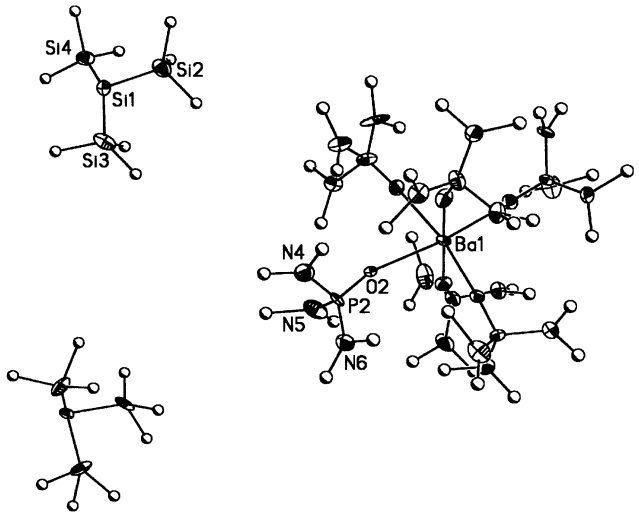


Figure 2. The crystal structure of **2**, with hydrogen atoms and disordered positions omitted for clarity.

fashion by six HMPA donors with average Ba–O separations of 2.641(6) Å. The O-Ba-O angles range from 82.4(4) to 98.2(3)°, with *trans* angles from 169.1(3) to 176.82(15)°. The two separated silanide anions display a pronounced pyramidal geometry with average angle sums at the central silicon atoms of 297.02°. These are in good agreement with the average value for the cesium hypersilanide [{Cs([18]crown-6)$_2$}{Si(SiMe$_3$)$_3$}] (298.55°).[10]

The facile formation of the [{Ba([18]crown-6)}(hmpa)$_2$] cation was shown on several occasions.[8,12] It was therefore expected that the combined addition of [18]crown-6 and HMPA would result in the quantitative formation of separated ions. Remarkably, compound **3**,[13] which contains a contact molecule, [{Ba([18]crown-6)}{(Si(SiMe$_3$)$_3$)$_2$}] and a separated HMPA adduct [{Ba(hmpa)$_6$}{Si(SiMe$_3$)$_3$}$_2$] was obtained. The separated ion in **3** shows essentially the same structural features as **2**. The cation–anion separation is 11.917 Å, and six HMPA donors coordinate to the metal center. As in **2**, the pyramidicity of the anions is pronounced with a Si-Si-Si angle sum of 301.59°. In the contact molecule, the equatorial plane on barium is occupied by the [18]crown-6 macrocycle, while two silanide ligands are located in *trans* positions. A center of symmetry at barium requires a *trans* angle of 180°. The average Ba–O(crown) bond lengths are 2.779(4) Å, while the average Ba–Si separations are 3.645(4) Å. The sum of the Si-Si-Si angles is 310.17°.

Interestingly, the Ba–Si, and to a lesser extent, Ba–O bond lengths in the contact molecule in **3** are significantly elongated as compared to **1**. Previous evidence from barium thiolates and selenolates bearing either one [18]crown-6 macrocycle or four THF donors[8] indicated only a negligible Ba–S or Ba–Se bond elongation upon replacing four THF donors by [18]crown-6. This initially surprising result was rationalized by the location of the crown in the equatorial plane and very comparable spatial requirements. In fact, the coordination sphere in the crown-ether-ligated derivatives was described as "pseudo-octahedral", an arrangement made possible by the narrow O-Ba-O(crown) angles (60.047° (av)). However, in conjunction with an extremely bulky ligand such as hypersilanide, this argument no longer holds true, and the steric repulsion between the donor and ligand results in significant bond elongation.

A comparison of Si-Ba-Si angles in **1** and the contact molecule in **3** shows a significant variation, with 140.62(3)° for **1** and linear geometry in **3**. These two vastly different values suggest the facile distortion from ideal linear geometry, enabled by the highly polar nature of the Ba–Si bond, and consequent reduction of orbital control. In fact, the variation of *trans* angles in octahedral alkaline-earth-metal derivatives is significant; with values ranging from 132° to the ideal linear geometry.[14] Theoretical studies to further investigate this phenomenon are currently in progress.

The significantly pyramidal Si-Si-Si angles in compounds **1**–**3** are in good agreement with previously published alkali-metal hypersilanides.[9,10] For his series of alkali-metal hypersilanides, Klinkhammer observed an angle compression upon descending the alkali-metal group, which was interpreted through increased metal–ligand charge transfer.[9] The extreme case of this trend, the separation of cation and anion, should result in the largest degree of angle compression. Indeed, slightly smaller angles are observed for the separated species in both the alkali-metal[10] and the alkaline-earth-metal analogues **1**–**3**, consistent with the complete transfer of electron density from the metal to the ligand. However, the small reduction in angle upon separation of ions indicates a very polar Ba–Si bond that should allow for the facile formation of separated ions in solution.

NMR experiments were conducted to obtain information about the ion association in solution. ^{29}Si NMR experiments for compounds **1**–**3** yielded a close range of chemical shifts for the SiMe$_3$ groups ($\delta = -5.80$ (**1**), -4.70 (**2**), and -4.86 ppm (**3**)). However, the signals for the quaternary silicon atoms, which would provide the most direct information on solvation and ligation, could not be obtained even after extended run times (24 hrs) on a 500 MHz spectrometer using a wide bore probe with DEPT and/or ZG techniques. This might be due to the low sensitity of the quarternary silicon atom coupled with the low solubility of the target compounds in C_6D_6 or $CD_3C_6D_5$.

While the SiMe$_3$ signals are less susceptible towards solvation effects, the close range of values, especially when compared with alkali-metal hypersilanides suggests the formation of identical ions upon dissolution. Due to the favorable formation of the [Ba(hmpa)$_6$]$^{2+}$ ion and the polar nature of the Ba–Si bond, the formation of separated ions, as proposed for the related alkali-metal hypersilanides[10] is likely. This view is further supported by the effective coordination of barium to the aromatic (C_6D_6) NMR solvent.[15]

 © 2003 Wiley-VCH Verlag GmbH & Co. KGaA, Weinheim

The puzzling coexistence of contact species and separated ions in the solid phase of **3** supports the assumption that Ba–Si bonds are weak and possess a large degree of ionic character. Selected examples of compounds containing both contact and separated ions in one crystal include a tetraphenyl butadiene disodium derivative,[16] in addition to the rubidium silanide [{(Rb([18]crown-6)$_2$)(Si(SiMe$_3$)$_3$)$_2$}{Rb([18]crown-6)(Si(SiMe$_3$)$_3$)}$_2$].[10] In both cases, weak, predominantly ionic metal–ligand bonds are observed, which enable the facile formation of separated ions.

In summary, the first examples of barium hypersilanides have been synthesized and characterized. Depending on the donors, either contact or separated ions were obtained, in addition to a compound where both contact and separated ions coexist in the solid state. Upon dissolution in C_6D_6 the compounds dissociate into separated ions. The facile formation of separated ions classifies the barium–silicon bond as weak and largely ionic.

Experimental Section

All reactions were performed under a purified nitrogen atmosphere using strict anaerobic conditions. [{K(thf)$_n$}{Si(SiMe$_3$)$_3$}] was prepared following literature procedures;[17] alkaline-earth-metal iodides (>99% purity) were obtained commercially. All reagents and solvents were purified using standard procedures.

Compounds **1**–**3** were prepared by a similar route, differing only in the addition of donor molecules: A solution containing [{K(thf)$_n$}{Si(SiMe$_3$)$_3$}] (2 mmol, 0.72 g) in THF (15 mL) was added to a solution of barium iodide (1 mmol, 0.39 g) in THF (25 mL) at room temperature. The mixture was stirred for about 45 min at room temperature, after which the solvent was removed under reduced pressure. The residue was extracted with hexane (80 ml) and filtered through a celite-layered filter frit, resulting in a clear, yellow solution that was reduced in volume to 40 ml. Crystals of **1** suitable for diffraction experiments were obtained after storing the solution for four days at −20 °C. To obtain compound **2**, HMPA (6 mmol, 1.04 mL) was added dropwise, upon which yellow crystals formed rapidly. Compound **3** was obtained after dropwise addition of a solution containing [18]crown-6 (0.5 mmol, 0.13 g) and HMPA (3 mmol, 0.52 mL) in hexane (25 ml). Upon addition, a yellow turbid solution formed immediately, that became clear after the addition of THF (10 mL). The combined solvents were removed under reduced pressure, and the resulting oily residue taken up in hexane (40 mL). After storage at −20 °C, crystals of compound **3** were obtained within 24 h.

1: Yield = 0.71 g (77%); mp 167–170 °C; ^{1}H NMR (300 MHz, 25 °C, C_6D_6): δ = 3.60 (m, 16H, THF), 1.37 (m, 16H, THF), 0.49 ppm (s, 54H, SiMe$_3$); ^{13}C NMR (75 MHz, 25 °C, C_6D_6) δ = 6.94 (SiMe$_3$), 25.34, 68.29 ppm; ^{29}Si NMR (99 MHz, 25 °C, C_6D_6): δ = −5.80 ppm (Si(*Si*Me$_3$)) (see above for missing quaternary silicon resonance); IR (Nujol): $\tilde{\nu}$ = 2923 (s), 2853 (s), 1462 (m), 1377 (w), 1232 (w), 1108 (w), 1034 (w), 828 (m), 728 (w), 670 (w), 618 cm^{-1} (m).

2: Yield = 1.17 g (68.7%); mp 160–164 °C; ^{1}H NMR (300 MHz, 25 °C, C_6D_6): δ = 2.43 (d, 108H, CH$_3$; J = 9.43 Hz), 0.71 ppm (s, 54H, SiMe$_3$); ^{13}C NMR (75 MHz, 25 °C, C_6D_6): δ = 8.58 (SiMe$_3$), 36.93 ppm (CH$_3$); ^{29}Si NMR (99 MHz, 25 °C, C_6D_6): δ = −4.70 ppm (Si(*Si*Me$_3$)); IR (Nujol): $\tilde{\nu}$ = 2922 (s), 2852 (s), 2806 (w), 1462 (m), 1377 (w), 1297 (w), 1223 (w), 1193 (w), 1163 (w), 1068 (w), 985 (w), 902 (w), 828 (w), 744 (w), 664 (w), 614 cm^{-1} (w).

3: Yield = 0.83 g (63.4%); mp 152–156 °C; ^{1}H NMR (300 MHz, 25 °C, C_6D_6): δ = 3.31 (s, 24H, CH$_2$), 2.41 (d, 108H, CH$_3$; J = 9.43 Hz), 0.62 (s, 54H, SiMe$_3$), 0.51 ppm (s, 54H, SiMe$_3$); ^{13}C NMR (75 MHz, 25 °C, C_6D_6): δ = 7.48 (SiMe$_3$), 8.53 (SiMe$_3$), 36.92, 70.12 ppm; ^{29}Si NMR (99 MHz, 25 °C, C_6D_6): δ = −4.86 ppm Si(*Si*Me$_3$); IR (Nujol): $\tilde{\nu}$ = 2918 (s), 2034 (w), 1462 (s), 1377 (s), 1350 (w), 1300 (s), 1226 (m), 1194 (s), 1165 (s), 1090 (s), 1068 (m), 989 (s), 962 (s), 900 (w), 825 (s), 745 (s), 660 (m), 615 cm^{-1} (m).

Received: April 8, 2003 [Z51610]

Keywords: barium · metathesis · model compounds · Si ligands · structure elucidation

[1] For recent reviews see: a) T. P. Hanusa, *Coord. Chem. Rev.* **2000**, *210*, 329; b) J. Alexander, K. Ruhlandt-Senge, *Eur. J. Inorg. Chem.* **2002**, *11*, 2761, and references therein.

[2] a) J. D. Farwell, M. F. Lappert, C. Marschner, C. Strissel, T. D. Tilley, *J. Organomet. Chem.* **2000**, *603*, 185; b) L. Rösch, *Angew. Chem.* **1977**, *89*, 257; *Angew. Chem. Int. Ed. Engl.* **1977**, *16*, 247; c) L. Rösch, J. Pickardt, S. Imme, U. Börner, *Z. Naturforsch. B* **1986**, *41*, 1523; d) A. R. Claggett, W. H. Ilsley, T. J. Anderson, M. D. Glick, J. P. Oliver, *J. Am. Chem. Soc.* **1977**, *99*, 1979; e) L. Rösch, U. Starke, *Z. Naturforsch. B* **1983**, *38*, 1292.

[3] O. Shizuka (H. Kunio. Jpn. Kokai Tokkyo Koho), JP 0306806, **1991**.

[4] D. Jenkins, K. Ruhlandt-Senge, unpublished results.

[5] U. Englich, K. Ruhlandt-Senge, F. Uhlig, *J. Organomet. Chem.* **2000**, *613*, 139.

[6] Crystal data for **1**: $C_{34}H_{86}BaO_4Si_8$, M_r = 921.09, orthorhombic, space group *Pbca*, a = 19.157(3), b = 17.219(3), c = 31.602(5) Å, V = 10424(3) Å^3, T = 98(2) K, Z = 8, μ = 0.975 mm^{-1} (Mo$_{K\alpha}$); yellow needles 0.70 × 0.30 × 0.20 mm^3; 12692 independent reflections, 3.34 ≤ 2θ ≤ 56.60°; $R1$ = 0.0522, $wR2$ = 0.0891 for data I > 2σ(I) and $R1$ = 0.0978, $wR2$ = 0.1011 for all data.

[7] a) R. Shannon, C. T. Previtt, *Acta Crystallogr. Sect. B* **1969**, *25*, 925; b) R. D. Shannon, *Acta Crystallogr. Sect. A* **1976**, *32*, 751.

[8] K. Ruhlandt-Senge, U. Englich, *Chem. Eur. J.* **2000**, *6*, 4063.

[9] K. W. Klinkhammer, *Chem. Eur. J.* **1997**, *3*, 1418.

[10] D. M. Jenkins, W. Teng, U. Englich, D. Stone, K. Ruhlandt-Senge, *Organometallics* **2001**, *20*, 4600.

[11] Crystal data for **2**: $C_{54}H_{162}BaN_{18}O_6P_6Si_8$, M_r = 1707.90, triclinic, space group $P\bar{1}$, a = 19.192(2), b = 19.636(2), c = 14.347(12) Å, α = 71.491(1), β = 71.232(1), γ = 81.048(2)°, V = 4845.7(6) Å^3, T = 91(2) K, Z = 2, μ = 0.655 mm^{-1} (Mo$_{K\alpha}$); yellow plate 0.60 × 0.48 × 0.10 mm^3; 39962 independent reflections, 3.26 ≤ 2θ ≤ 50.30°; $R1$ = 0.0693, $wR2$ = 0.1740 for data I > 2σ(I) and $R1$ = 0.1086, $wR2$ = 0.1991 for all data.

[12] J. Alexander, K. Ruhlandt-Senge, *Angew. Chem.* **2001**, *113*, 2732; *Angew. Chem. Int. Ed.* **2001**, *40*, 2658.

[13] Crystal data for **3**: $C_{84}H_{240}Ba_2N_{18}O_{12}P_6Si_{16}$, M_r = 2604.88, rhombohedral, space group $R\bar{3}c$, a = 17.4605(6), b = 17.4605(6), c = 84.697(5) Å, V = 22362(2) Å^3, T = 85(2) K, Z = 6, μ = 0.767 mm^{-1} (Mo$_{K\alpha}$); yellow plate 0.26 × 0.18 × 0.10 mm^3; 4313 independent reflections, 2.88 ≤ 2θ ≤ 50.48°; $R1$ = 0.0541, $wR2$ = 0.1290 for data I > 2σ(I) and $R1$ = 0.1062, $wR2$ = 0.1416 for all data. All crystals were mounted on the diffractometer as described elsewhere.[18] The data were collected using a Bruker SMART system, complete with three-circle goniometer and CCD detector as described earlier.[8] The crystal structure of **1** was solved using direct methods whereas Patterson methods were used to solve **2** and **3**. All structures were refined by full-matrix least-squares refinement on F^2.[19] An absorption correction was applied for all structures.[20] All non-hydrogen atoms in **1** and **3** were refined anisotropically. Significant disorder was detected for **2**, resulting in the isotropic refinement of some of non-hydrogen atoms and the use of bond-distance restraints.[19] CCDC 206684–206686 contain the supplementary crystallographic data for this paper. These data can be obtained free of charge via www.ccdc.cam.ac.uk/conts/retrieving.html (or from

 © 2003 Wiley-VCH Verlag GmbH & Co. KGaA, Weinheim

the Cambridge Crystallographic Data Centre, 12, Union Road, Cambridge CB21EZ, UK; fax: (+44) 1223-336-033; or deposit@ccdc.cam.ac.uk).
[14] D. C. Allis, D. Green , W. Teng, U. Englich, W. Vargas, J. Alexander, B. S. Hudson, K. Ruhlandt-Senge, unpublished results.
[15] a) G. B. Deacon, C. M. Forsyth, P. C. Junk, *J. Organomet. Chem.* **2000**, *607*, 112; b) S. Chadwick, U. Englich, K. Ruhlandt-Senge, *Organometallics* **1997**, *16*, 5792.
[16] H. Bock, C. Näther, K. Ruppert, Z. Havlas, *J. Am. Chem. Soc.* **1992**, *114*, 6907.
[17] C. Marschner, *Eur. J. Inorg. Chem.* **1998**, 221.
[18] H. Hope, *Prog. Inorg. Chem.* **1994**, *41*, 1.
[19] G. M. Sheldrick, SHELXTL-Plus, Program for crystal structure solution and refinement, University of Göttingen, Germany, **1993**.
[20] G. M. Sheldrick, SADABS, Program for Absorption Correction Using Area Detector Data, University of Göttingen, Göttingen, Germany, **1996**.

 © 2003 Wiley-VCH Verlag GmbH & Co. KGaA, Weinheim

Blue-Light Emitting Polymer Films

Nano- and Micro-Engineering of Ordered Porous Blue-Light-Emitting Films by Templating Well-Defined Organic Polymers Around Condensing Water Droplets**

Christopher Barner-Kowollik, Helen Dalton, Thomas P. Davis,* and Martina H. Stenzel**

Recent advances in the field of living free-radical polymerization techniques, such as the reversible addition fragmentation chain transfer (RAFT) process,[1–5] atom-transfer radical polymerization (ATRP),[6–8] and nitroxide-mediated polymerization (NMP),[9] have enabled the synthesis of polymers with well-defined and in some cases complex macromolecular architectures. These novel architectures include block copolymers, comb polymers, and star-shaped macromolecules.[1,10] Star, block, microgel, and comb polymers have been successfully cast into (self-assembling) porous films of regular structure and pore size.[1,11–15] Self-assembling macromolecular structures such as those reported herein may be used in a wide range of applications, such as molecular electronics, optoelectronics, and phototonics, as well as in biological applications such as microarrays and as potential substrates for studying cell growth.[12,14–20] Analogous structures based on the assembly of colloidal particles have also been reported as inverse opal substrates.[21] In a recent study Lu and Jenekhe generated blue-light-emitting polystyrene by a simple modification of polystyrene to poly(vinyldiphenylquinoline).[22] Herein we report on the application of the above-mentioned modification procedure to linear and six-arm, star-shaped polystyrene generated by the RAFT process. In addition, we utilized ATRP to synthesize poly(ethylene glycol)–styrene block copolymers, prior to chemical modification to poly(vinyldiphenylquinoline). The resulting (blue-light-emitting) modified polymers were then cast into self-assembling porous films with regular pore sizes. Confocal and scanning electron microscopy (SEM) techniques were subsequently applied as analytical tools to probe the porous structures.

The star polymers were synthesized either by copper-mediated ATRP or by RAFT polymerization.[7,23] A multifunctional initiator was employed, from which arm growth occurs. The preparation of the six-arm star-shaped polystyrene by the RAFT process utilized hexakis(thiobenzoylthiomethyl)benzene as an initiator.[23] Similar five-arm, star-shaped polymers can also be generated by ATRP using a functionlized glucose initiator.[7,8] The synthetic strategies used are given in Table 1.

An extensive discussion of these syntheses is not required as both approaches have been detailed in previous publications.[7,8,23] In addition to the star-shaped architectures, two linear architectures were prepared. Linear polystyrene with a narrow polydispersity was prepared by using the RAFT process with cumyl dithiobenzoate as the RAFT agent. A poly(ethylene glycol)–styrene block copolymer was prepared by converting the end hydroxy group of poly(ethylene glycol) methyl ether into a brominated ATRP initiator, which was subsequently chain-extended with styrene. These approaches are also detailed in Table 1.

All of the polymers generated by living radical polymerization were subsequently modified by using a two-step approach to convert the styrene groups into vinyldiphenylquinoline units.[22] The reaction was monitored by ^{1}H NMR spectroscopy and in all cases functionalization was close to 100% (see Experimental Section). A (typical) significant change in the molecular weight distribution was indicated by gel permeation chromatography analyses of the linear polystyrene (generated by RAFT; Figure 1).

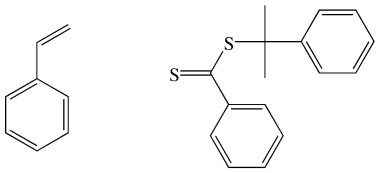
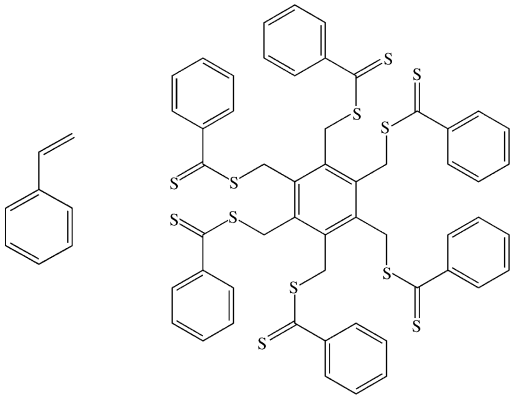
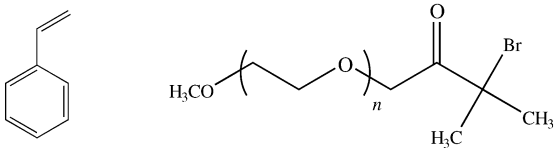
All of the above architectures (those based on polystyrene as well as those modified to poly(vinyldiphenylquinoline)) were utilized in the preparation of honeycomb films (or inverse opal substrates). The films were cast on a glass slide from a solution of the polymer in carbon disulfide under humid conditions. A typical example of the morphologies we attained from films cast from the linear poly(vinyldiphenylquinoline) and star-shaped poly(vinyldiphenylquinoline) is shown in Figure 2. Whilst pores were generated in the case of

[*] Dr. C. Barner-Kowollik, Prof. Dr. T. P. Davis, Dr. M. H. Stenzel
Centre for Advanced Macromolecular Design
School of Chemical Engineering and Industrial Chemistry
The University of New South Wales
Sydney, NSW 2052 (Australia)
Fax: (+61) 2-9385-6250
E-mail: camd@unsw.edu.au
Dr. H. Dalton
School of Biotechnology and Biomolecular Sciences
The University of New South Wales
Sydney, NSW 2052 (Australia)

[**] The authors are grateful for financial support from the Australian Research Council. T.P.D. acknowledges the award of an Australian Professorial Fellowship. The authors acknowledge the contributions of Gusni Melington, L. T. Uyen Ngyuen, and Simon Angus.

 © 2003 Wiley-VCH Verlag GmbH & Co. KGaA, Weinheim DOI: 10.1002/anie.200351612

Table 1: Synthetic strategies for the generation of light-emitting polymer material based on linear and star-shaped architectures.[a]

Synthetic approach	Reactants	Molecular architecture obtained	M_n	PDI
RAFT, 60 °C, AIBN		linear	45 000	1.15
RAFT, 60 °C, AIBN		six-arm star	72 500	1.20
ATRP, 80 °C		linear block copolymer	4600	1.22

[a] The polymers were obtained by the RAFT process and poly(ethylene glycol)-*block*-styrene polymer by ATRP. M_n: the number average molecular weights, PDI: polydispersities of the prepared architectures, AIBN: 2,2-azobisisobutyronitrile.

a the linear architectures (Figure 2b), there is clearly a lack of order, thus confirming our earlier observations[11,12] that either complex architectures or some level of amphiphilicity (sometimes supplied by the end group) are generally required to get hexagonal close packing and a narrow pore-size distribution. The ability of star-shaped polymers to generate films with a higher degree of ordering is linked to their ability to precipitate instantaneously at the solution/water interface. Experimental evidence underpins this notion by showing that linear polystyrene precipitates to a lower extent at the interface, while polystyrene stars immediately form a solid layer.[19]

Not surprisingly, some improvement in film ordering was noted with the star-shaped architecture (namely, on going from Figure 2b to 2a).[11] The cast films based on star-shaped polymer material displayed areas of hexagonal close-packed pores, however, a number of grain boundaries were observed that disrupted the overall film regularity. A significant observation is that pores were generated with diameters as low as 150 nm (Figure 2). We believe that these are the smallest pores reported to date for this simple casting process. A similar result was observed for the poly(ethylene glycol)-*block*-poly(vinyldiphenylquinoline) copolymers, with pore sizes close to 150 nm and a similar degree of ordering as in the case of the linear polystyrene. As our intention was to study the blue-light emission and porous structure using confocal microscopy, we recast the films using a very low air flow. This procedure gives the condensing water droplets time to grow prior to encapsulation with the polymer, thus forming larger pores suitable for image analysis. The resultant films, now with pores on the micron scale, displayed high levels of order. Typical confocal microscopy images of the cast star-shaped poly(vinyldiphenylquinoline) prepared by the RAFT process are shown in Figure 3.

The honeycomb structure of the film with a pore size of approximately 1 μm can clearly be observed when recording the emission between 500 and 600 nm (Figure 3a), while the emission between 640 and 740 nm seems to be generated rather irregularly throughout the film (Figure 3b). Distinct locations of the emission between 640 and 740 nm can be detected by combining both fluorescence micrographs (Figure 3c).

This emission has a maximum intensity when emitted from the polymer bridging/separating two adjacent pores, while the emission between 500 and 600 nm is most intensely emitted from the polymer bridging/separating three adjacent pores. The fluorescence spectrum recorded by confocal microscopy is given in Figure 3d. The micrographs clearly indicate that in addition to the porous patterning on the micron scale, another pattern of organization is also imposed (as revealed by the fluorescence measurements). To our knowledge this is the first time that such an observation has

 © 2003 Wiley-VCH Verlag GmbH & Co. KGaA, Weinheim

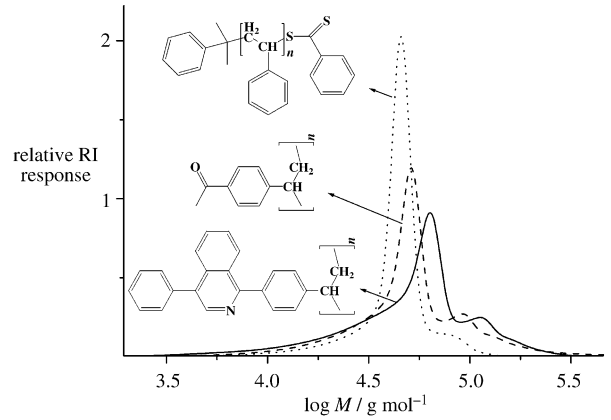


Figure 1. Sequential change in the molecular-weight distributions during the step-by-step modification of polystyryl dithiobenzoate to (light-emitting) linear poly(vinyldiphenylquinoline). RI = refractive index.

been made. The origin of the fluorescence patterning can be attributed to the enveloping of the polymer around condensing water droplets, which results in specific orientation of the polymer chains at the interface. As the water evaporates, this orientation is frozen into the final material. However, the precise molecular interactions that lead to the complex spectra remains a subject of conjecture and further analyses are currently underway.

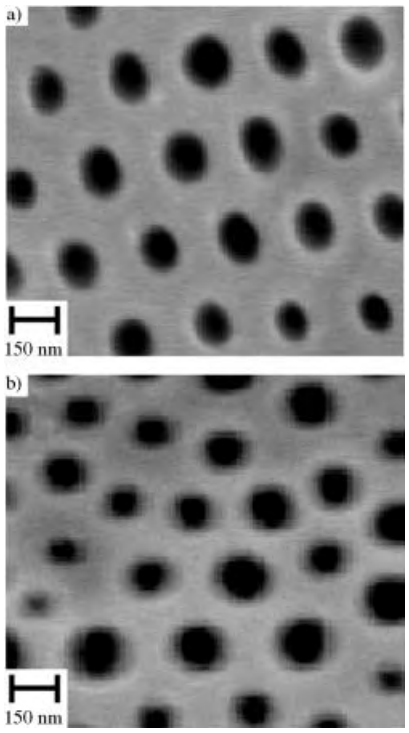


Figure 2. SEM images of porous films made from star (a) and linear (b) poly(vinyldiphenylquinoline) prepared by modification of macromolecular architectures generated by the RAFT process (see text).

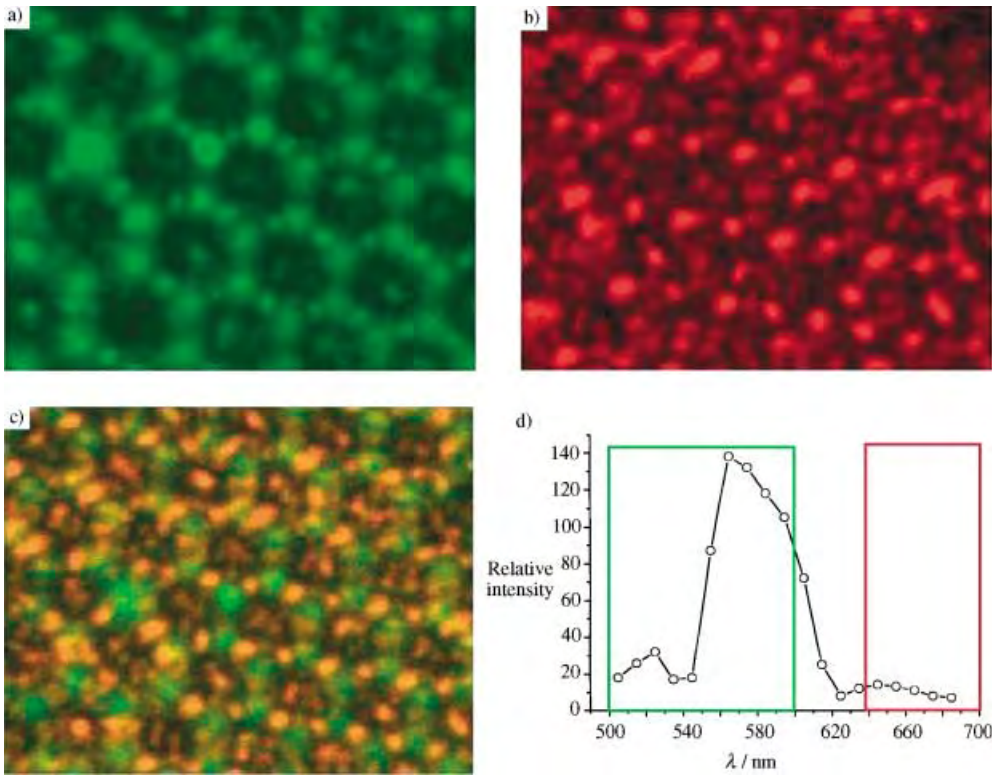


Figure 3. Confocal fluorescence microscopy images of a honeycomb-structured film prepared with poly(vinyldiphenylquinoline) star material prepared by RAFT (see Figure 1) showing the emission of the fluorescing films between 500 and 600 nm (a) and 640 and 740 nm (b). The excitation wavelength was 488 nm. Also shown is the combination of both images indicating two distinct regions for both emissions (c). Fluorescence spectrum (d) as recorded with the confocal microscope. The boxes in the red and the green regions of the spectrum indicate the emission range where the images (a, green) and (a, red) were taken, respectively. Relative intensity is given in arbitrary units.

 © 2003 Wiley-VCH Verlag GmbH & Co. KGaA, Weinheim

In conclusion, we have demonstrated the versatility of the water-droplet templating process. Blue-light-emitting films were cast and the pore sizes of the films were engineered from the nano- to the microrange by simply manipulating the casting conditions. The confocal microscopy images demonstrate highly fluorescent organized porous materials with additional ordering within the polymer phase of the films. It is envisaged that the self-assembly of macromolecular material containing light-emitting functionalities on the nano- and microscale will find potential applications in the fabrication of molecular electronic devices[24] as well as photonic and band-gap materials.[25,26]

Experimental Section

Synthesis and modification of the linear polystyrene RAFT agent: The linear polystyrene RAFT agent was synthesized by the cumyl dithiobenzoate (CDB) mediated free-radical polymerization of styrene (Aldrich, 99%, purified by passing over a column of basic alumina) at 60°C. The initial CDB concentration was close to 3.8×10^{-3} mol L^{-1}. Cumyl dithiobenzoate was prepared by a literature method, using *n*-hexane as the solvent.[27] The purity of the RAFT agent was close to 97% as verified by ^{1}H NMR analysis. The concentration of the initiator (AIBN; Aldrich, 99%, recrystallized twice from ethanol) was close to 3.5×10^{-3} mol L^{-1}. The reaction mixture was thoroughly degassed by purging with nitrogen prior to reaction. The polymeric RAFT agent ($M_w = 45000$ g mol^{-1}) was isolated from the reaction mixture after 24 h by precipitation into an excess of methanol. The polymer was subsequently dissolved in THF (Aldrich, analytical grade) and precipitated again. The resulting powdery pink polymer was dried for 2 days at 30°C under vacuum. The subsequent two-step polymer modification procedure[22] gives poly(vinyldiphenylquinoline) as an off-white powder. The polymer modification consists of a Friedel–Crafts acylation (step I) and a subsequent condensation reaction with 2-aminobenzophenone (step II). Each of the individual reaction steps were checked for completeness by ^{1}H NMR spectroscopy. Similar ^{1}H NMR data regarding the transformation of the linear polystyrene to poly(vinyldiphenylquinoline) can be found in ref. [22] In addition, the acylation product (modification step I) and the final product (poly(vinyldiphenylquinoline) were both subjected to molecular-weight analysis. The molecular-weight distributions associated with each reaction step are given in the text.

Synthesis and modification of the star-shaped polystyrene RAFT agent: The synthesis of star-shaped poly(vinyldiphenylquinoline) proceeded by the same reaction sequence as indicated above for the linear poly(vinyldiphenylquinoline). The star-shaped polystyrene RAFT agent was generated by the hexakis(thiobenzoylthiomethyl)-benzene-mediated free-radical bulk polymerization of styrene at 60°C. Hexakis(thiobenzoylthiomethyl)benzene was synthesized according to a literature method[23] and its purity (99%) was confirmed by ^{1}H NMR spectroscopy. The subsequent two-step polymer-modification procedure was identical to the procedure given above for linear polyRAFT agents.

Synthesis of PEG–STY block copolymers by ATRP: Poly(ethylene glycol) methyl ether (Aldrich, $M_n = 550$ g mol^{-1}; 20 g) and triethylamine (8.4 mL) were dissolved in anhydrous THF (500 mL). 2-Bromo-2-methylpropionyl bromide (7.2 mL) was then added dropwise under an atmosphere of dry nitrogen. After 48 h at room temperature, the reaction mixture was added to dichloromethane (200 mL) and subsequently washed repeatedly with saturated, aqueous sodium hydrogen carbonate (3×200 mL). The resulting organic phase was dried over anhydrous magnesium sulphate. The structure and purity was confirmed by ^{1}H NMR spectroscopy and elemental analysis.

Copper-mediated ATRP: An *N*-(*n*-propyl)-2-pyridylmethanimine ligand was used. The PEG chain was successfully extended with styrene and a styrene block of $M_n = 4600$ g mol^{-1} was estimated by ^{1}H NMR spectroscopy. The final polydispersity of the PEG–STY chain was 1.22 as estimated by gel-permeation chromatography using linear polystyrene standards in THF.

Molecular-weight analysis: Molecular-weight distributions were measured by SEC on a Shimadzu modular system, comprising an auto injector, a 5.0-μm bead-size guard column (50×7.5 mm, Polymer Laboratories), followed by three linear columns (10^5, 10^4, and 10^3 Å; Polymer Laboratories) and a differential refractive index detector. The eluent was THF at 40°C with a flow rate of 1 mL min^{-1}. The system was calibrated using polystyrene standards ranging from 500 to 10^6 g mol^{-1}.

Film casting: The films were prepared from carbon disulfide solutions with a concentration of 10 g L^{-1}. The films were cast on a glass support and dried with a flow of humid air at 22°C. The casting process was carried out in a custom designed box at a constant humidity level of 85%. The air flow was controlled using a flow meter to ensure reproducible conditions.

Confocal microscopy and SEM: The fluorescence micrographs were taken with a Leica confocal microscope TCS SP2 AOBS with a water lens (63.0×1.20 W CORR UV). The excitation was set at 488 nm, while the emission was measured at different wavelengths as indicated in the main text. The SEM images of chromium-coated samples were recorded on a Hitachi S900 scanning electron microscope.

Received: April 8, 2003
Revised: May 9, 2003 [Z51612]

Keywords: light-emitting polymers · materials science · nanostructures · polymerization · thin films

[1] C. Barner-Kowollik, T. P. Davis, J. P. A. Heuts, M. H. Stenzel, P. Vana, M. Whittaker, *J. Polym. Sci. Part A Polym. Chem.* **2003**, *41*, 365.
[2] J. Chiefari, E. Rizzardo, in *Handbook of Radical Polymerization,* (Eds.: K. Matyjaszewski, T. P. Davis) , Wiley, **2002**, p. 629.
[3] K. Matyjaszewski, *Controlled/Living Radical Polymerization: Progress in ATRP, NMP and RAFT*, ACS Symposium Series 2000, Vol 768.
[4] C. L. McCormick, A. B. Lowe, *Aust. J. Chem.* **2002**, *55*, 367.
[5] P. Vana, J. F. Quinn, T. P. Davis, C. Barner-Kowollik, *Aust. J. Chem.* **2002**, *55*, 425.
[6] K. Matyjaszewski, J. Xia in *Handbook of Radical Polymerization* (Eds.: K. Matyjaszewski, T. P. Davis), Wiley, p. 523.
[7] D. M. Haddleton, R. Edmonds, A. M. Heming, E. J. Kelly, D. Kukulj, *New J. Chem.* **1999**, *23*, 477.
[8] K. Ohno, D. M. Haddleton, D. Kukulj, B. Wong, *Polym. Prepr. Am. Chem. Soc. Div. Polym. Chem.* **2000**, *41*, 478.
[9] C. J. Hawker, A. W. Bosman, E. Harth, *Chem. Rev.* **2001**, *101*, 3661.
[10] Y. Gnanou, D. Taton in *Handbook of Radical Polymerization* (Eds.: K. Matyjaszewski, T. P. Davis), Wiley, **2002**, p. 775.
[11] M. H. Stenzel-Rosenbaum, T. P. Davis, A. G. Fane, V. Chen, *Angew. Chem.* **2001**, *113*, 3536; *Angew. Chem. Int. Ed.* **2001**, *40*, 3428.
[12] M. Stenzel, *Aust. J. Chem.* **2002**, *55*, 239.
[13] G. Widawski, M. Rawiso, B. Francois, *Nature* **1994**, *369*, 387.
[14] U. Stalmach, B. de Boer, C. Videlot, P. F. van Hutten, G. Hadziioannou, *J. Am. Chem. Soc.* **2000**, *122*, 5464.
[15] S. D. Angus, T. P. Davis, *Langmuir* **2002**, *18*, 9547.
[16] O. Karthaus, X. Cieren, N. Maruyama, M. Shimomura, *Mater. Sci. Eng.* **1999**, *7*, 103.

 © 2003 Wiley-VCH Verlag GmbH & Co. KGaA, Weinheim

[17] O. Karthaus, N. Maruyama, X. Cieren, M. Shimomura, H. Hasegawa, T. Hashimoto, *Langmuir* **2000**, *16*, 6071.
[18] T. Nishikawa, J. Nishida, R. Ookura, S.-I. Nishimura, S. Wada, T. Karino, M. Shimomura, *Mater. Sci. Eng.* **1999**, *7*, 495.
[19] O. Pitois, O. Francois, *Eur. Phys. J.* **1999**, *B8*, 225.
[20] M. Shimomura, T. Sawadaishi, *Curr. Opin. Colloid Interface Sci.* **2001**, *6*, 11.
[21] T. Cassagneau, F. Caruso, *Adv. Mater.* **2002**, *14*, 34.
[22] L. Lu, S. A. Jenekhe, *Macromolecules* **2001**, *34*, 6249.
[23] M. Stenzel-Rosenbaum, T. P. Davis, V. Chen, A. G. Fane, *J. Polym. Sci. Part A Polym. Chem.* **2001**, *39*, 2777.
[24] *Molecular Electronics* (Ed.: F. L. Carter), Marcel Dekker, New York, **1987**.
[25] E. Yablonovitch, *J. Opt. Soc. Am. B* **1993**, *10*, 283.
[26] J. Martorell, N. M. Lawandy, *Phys. Rev. Lett.* **1990**, *65*, 1877.
[27] S. Oae, T. Yagihara, T. Okabe, *Tetrahedron* **1972**, *28*, 3203.

 © 2003 Wiley-VCH Verlag GmbH & Co. KGaA, Weinheim

Nucleation of Calcite Crystals

Face-Selective Nucleation of Calcite on Self-Assembled Monolayers of Alkanethiols: Effect of the Parity of the Alkyl Chain**

*Yong-Jin Han and Joanna Aizenberg**

The use of self-assembled monolayers (SAMs) has provided an ideal platform to study the function of highly ordered organic surfaces for various applications, including nucleation of crystals.[1–8] In particular, SAMs of alkanethiols with a range of functionalities supported on gold and silver have been demonstrated to effectively nucleate calcium carbonate crystals, with a high degree of orientational specificity for each surface.[2,9–11] It has been shown that the face-selective nucleation of calcite cannot be explained in terms of the lattice match between the SAM and the crystal face it nucleates. It has been suggested that a match may exist between the direction of the SAM terminal groups and that of anions in the nucleated crystal.[9] This situation would imply that the mechanism of the face-selective nucleation involves the translation of the orientation of the terminal groups on the SAM into the nucleating crystals. The validity of this hypothesis could not be explicitly tested in the previously reported systems, since the SAMs used differed in multiple parameters (for example, functional groups, metal support, chain length).

[*] Dr. J. Aizenberg, Dr. Y.-J. Han
Bell Laboratories
Lucent Technologies
600 Mountain Ave, Murray Hill, NJ 07974 (USA)
Fax: (+1) 908-582-4868
E-mail: jaizenberg@lucent.com

[**] The authors would like to thank Theo Siegrist and Glen Kowach for their assistance with XRD measurements.

Herein we verify the proposed mechanism by investigating the oriented growth of calcite on SAMs in which only one parameter—the orientation of the functional group—is varied. For this purpose, we utilized the so-called "odd-even effect" in the monolayers.[8,12,13] Detailed structural studies of SAMs[14,15] have shown that the orientation of long-chain alkanethiols ($HS(CH_2)_nCH_3$) adsorbed from solution onto metal surfaces is determined by the cant (α, Figure 1a) and

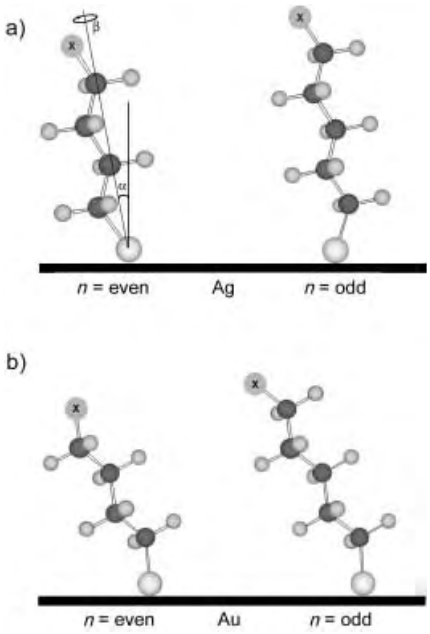


Figure 1. Schematic representation of even and odd chain length ω-terminated alkylthiols adsorbed on a) silver and b) gold. Note the differences in the orientation of the functional group X with respect to the interface as well as cant (α) and twist (β) angles.

twist (β) angles which the thiol molecules adopt in relation to the metal film during the formation of the monolayers. It has been demonstrated that when gold films are used to support SAMs, α and β have the same value and sign for all alkanethiol chains, while alkanethiol molecules assembled on silver show cant angles of opposite signs for alkyl chains of different parity. Therefore, the orientation of the terminal group X in SAMs on Ag is constant for both odd and even chains, and the terminal group X in SAMs on Au forms two different angles with the interface for odd and even chain lengths (Figure 1). SAMs with alkyl chains of different parity assembled on Au and Ag provide two ideal control systems to study the effect of terminal groups on the oriented growth of crystals. We anticipated that, if face-selective nucleation were controlled by the orientation of the functional groups in the templating surface, then all SAMs on Ag would induce the oriented crystal growth from the same crystal plane, while odd- and even-lengthed SAMs on Au should induce nucleation in two different crystallographic directions.

Several sulfanylalkanoic acids with different methylene chain lengths were assembled on gold and silver to template the nucleation of calcite. Sulfanyloctanoic acid ($HS\text{-}C_7\text{-}COOH$, denoted C_7), sulfanylundecanoic acid ($HS\text{-}C_{10}$-

 © 2003 Wiley-VCH Verlag GmbH & Co. KGaA, Weinheim DOI: 10.1002/anie.200351655

COOH, denoted C_{10}), sulfanyldodecanoic acid (HS-C_{11}-COOH, denoted C_{11}), sulfanylpentadecanoic acid (HS-C_{14}-COOH, denoted C_{14}), sulfanylhexadecanoic acid (HS-C_{15}-COOH, denoted C_{15}), and sulfanylheptadecanoic acid (HS-C_{16}-COOH, denoted C_{16}) were adsorbed from ethanol onto the surfaces of gold and silver that had been evaporated onto silicon (100) wafers.[16] The crystallization of the calcite crystals with the SAMs was performed by following the previously published methods.[9] Briefly, functionalized SAMs were submerged in a 20 mM calcium chloride solution in a desiccator containing ammonium carbonate on the side as the carbonate source. The crystallization process was performed at room temperature for two hours. The crystals were characterized by scanning electron microscopy (SEM), X-ray diffraction (XRD), and morphological computer-simulations analysis.

Indeed, both odd- (C_7, C_{11}, and C_{15}) and even-lengthed (C_{10}, C_{14}, and C_{16}) carboxylic acid terminated alkylthiols supported on silver induced the nucleation of calcite from the same crystallographic plane. The nucleated plane was indexed as (012) on the basis of computer simulations on the orientation of crystals observed by SEM (Figure 2a,b). This assignment was further confirmed by XRD data that showed

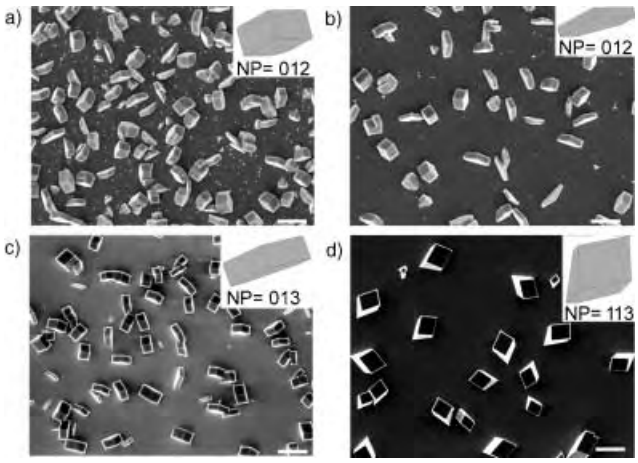


Figure 2. SEM micrographs of calcite crystals grown on carboxylate-functionalized self-assembled monolayers of a) C_{15}-Ag, b) C_{10}-Ag, c) C_{15}-Au, and d) C_{10}-Au. Scale bars: 20 μm. The micrographs were recorded on a JEOL JSM-5600 LV system operating at 10 kV. Insets: Computer simulations of similarly oriented calcite rhombohedra with the nucleating planes (NP) indicated. The simulation were performed using SHAPE V6.0 software.

only strong (012) and (024) peaks in the diffraction pattern (Figure 3a,b). SAMs on gold, on the other hand, induced the highly oriented formation calcite in two distinct crystallographic directions. As deduced from the morphological analysis (Figure 2c), odd-length alkylthiols (C_7, C_{11}, and C_{15}) templated the calcite growth from a range of (01*l*) faces (*l* = 2–5). The (012) and (024) peaks were observed in the corresponding XRD spectra (Figure 3c). Crystals observed on carboxylic acid terminated SAMs with an even chain length (C_{10}, C_{14}, and C_{16}) matched well with computer simulations of calcite crystals nucleated from the (11*l*)

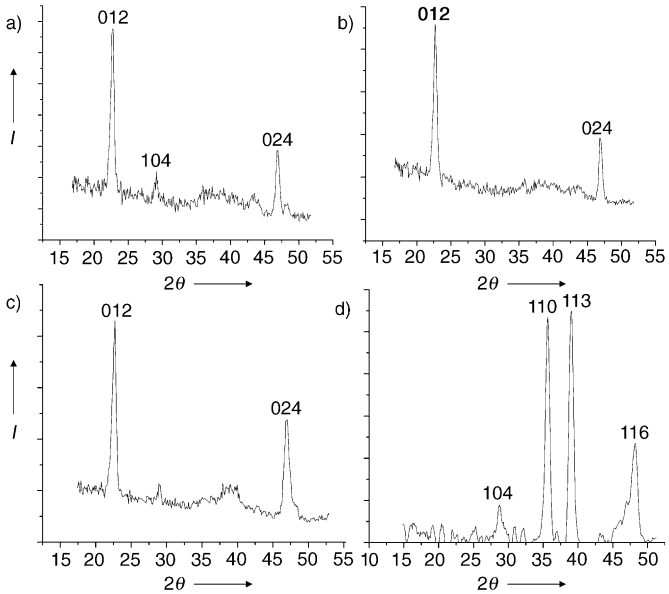


Figure 3. Representative XRD patterns of calcite crystals grown on a) C_7, C_{11}, and C_{15} on Ag, b) C_{10}, C_{12}, and C_{16} on Ag, c) C_7, C_{11}, and C_{15} on Au, and d) C_{10}, C_{12}, and C_{16} on Au. XRD measurements were made on a Bruker AXS instrument with a general area diffraction detection system (GADDS).

crystallographic planes (*l* = ca. 3; Figure 2d). The corresponding XRD spectra showed the (110), (113), and (116) calcite peaks (Figure 3d). It is important to note that SAMs supported on silver controlled the nucleating plane of calcite within about 2–4°, while the orientational specificity of calcite crystals formed on SAMs supported on gold appeared to be generally lower (within about 10–15°) and to greatly depend on the substrate preparation. This observation indicates that the carboxylate groups of adsorbed thiols may have more azimuthal freedom on the gold surfaces.[17]

Our results unequivocally confirmed the proposed mechanism of the translation of the stereochemical and orientational information at the organic/inorganic interface.[9,13,18,19] To gain a better understanding of the recognition at the nucleation stage we performed further analysis of the structure of the SAM/calcite interfaces. Previous studies[20–22] of the carboxylic acid terminated Langmuir monolayers and SAMs in the presence of Ca^{2+} and Cd^{2+} ions have shown a considerable ordering of the surface that results in the fixation of the carboxylic groups in a specific orientation. In particular, it has been shown that the overlayer of Ca^{2+} ions on a SAM of HS-C_{15}-COO^- fixes the terminal groups in a preferred orientation, in which one C–O bond is parallel to the substrate.[23] We simulated the structure of the CO_2^--terminated SAMs in the solution of Ca^{2+} ions by combining the above structural information with the reported cant and twist parameters of the SAMs on different substrates.[14] On silver ($|\alpha| = 10$–$14°$, $\beta = 42$–$45°$), the planes of the carboxylate groups for both odd and even chain lengths form an angle of about 30° with the surface normal. This orientation closely matches that of the carbonate ions in calcite crystals oriented in the [012] direction (Figure 4a). On gold ($\alpha = 26$–$28°$, $\beta =$ 50–55°), the planes of the carboxylate groups in odd chain

 © 2003 Wiley-VCH Verlag GmbH & Co. KGaA, Weinheim

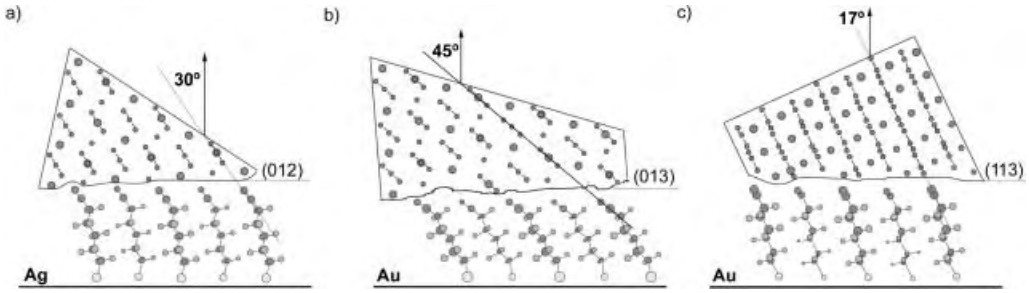


Figure 4. Schematic representations depicting the alignment of carboxylic groups on SAMs with the carbonate groups in calcite for a) odd (and even) chain length SAMs on Ag, NP = (012); b) odd chain length SAMs on Au, NP = (013); c) even chain length SAMs on Au, NP = (113). The C–O bonds in the surface carboxylate groups are parallel to the C–O bonds in the carbonates in the nucleated calcite crystals.

lengths form an angle of 40–45° with the surface normal, which is nearly parallel to the carbonate ions in calcite crystals oriented in the [01*l*] direction ($l = 2$–4; Figure 4b). For even chain lengths on Au, the plane of the carboxylate group in a symmetrical, bidentate arrangement forms an angle of about 17–22° with the surface normal, which would closely match the orientation of the carbonate ions in calcite crystals nucleated from the (11*l*) plane ($l =$ ca. 3; Figure 4c).

We propose, therefore, that when carboxylate-functionalized SAMs are introduced into the Ca^{2+} solution a counterion overlayer is formed by bonding of the Ca^{2+} ions to the carboxylate groups on the SAMs, which also fixes the position of the carboxylate functionalities on the SAMs.[23] The formation of the counterion layer starts the nucleation process by attracting free carbonate ions in solution. The ordered carboxylates may serve as surrogate oxyanions for the nucleating crystals, thus inducing the oriented bonding of the subsequent carbonates at the same angle to the carboxylate functional groups on the surface of the SAMs. This would ultimately result in a fixed, highly controlled, oriented growth of the crystals.

These observations raise a fascinating possibility that the oriented growth of crystalline materials can be regulated not only by controlling the functionality and the lattice of the templating surface, but also by varying the orientation of the terminal groups. The translation of the structural information at the organic/inorganic interface is a plausible mechanism that can explain the enormous variety of crystallographic orientations of biologically formed minerals: even slight changes in the conformation of a biological macromolecular template would result in the fine-tuning of the orientation of the nucleated crystals.

Received: April 14, 2003 [Z51655]

Keywords: biomineralization · calcite · interfaces · monolayers · nucleation

[1] J. Kuther, M. Bartz, R. Seshadri, G. B. M. Vaughan, W. Tremel, *J. Mater. Chem.* **2001**, *11*, 503.
[2] J. Aizenberg, A. J. Black, G. M. Whitesides, *Nature* **1999**, *398*, 495.
[3] K. Onuma, A. Oyane, T. Kokubo, G. Treboux, N. Kanzaki, A. Ito, *J. Phys. Chem. B* **2000**, *104*, 11950.
[4] J. F. Kang, J. Zaccaro, A. Ulman, A. Myerson, *Langmuir* **2000**, *16*, 3791.
[5] H. Bekele, J. H. Fendler, J. W. Kelly, *J. Am. Chem. Soc.* **1999**, *121*, 7266.
[6] B. R. Heywood, S. Mann, *Chem. Mater.* **1994**, *6*, 311.
[7] B. R. Heywood, S. Mann, *Adv. Mater.* **1992**, *4*, 278.
[8] V. K. Gupta, N. L. Abbott, *Science* **1997**, *276*, 1533.
[9] J. Aizenberg, A. J. Black, G. H. Whitesides, *J. Am. Chem. Soc.* **1999**, *121*, 4500.
[10] A. M. Travaille, J. Donners, J. W. Gerritsen, N. Sommerdijk, R. J. M. Nolte, H. van Kempen, *Adv. Mater.* **2002**, *14*, 492.
[11] Y.-J. Han, J. Aizenberg, *J. Am. Chem. Soc.* **2003**, *125*, 4032.
[12] R. Edgar, J. Y. Huang, R. Popovitz-Biro, K. Kjaer, W. G. Bouwman, P. B. Howes, J. Als-Nielsen, Y. R. Shen, M. Lahav, L. Leiserowitz, *J. Phys. Chem. B* **2000**, *104*, 6843.
[13] R. Popovitz-Biro, J. L. Wang, J. Majewski, E. Shavit, L. Leiserowitz, M. Lahav, *J. Am. Chem. Soc.* **1994**, *116*, 1179.
[14] P. E. Laibinis, G. M. Whitesides, D. L. Allara, Y. T. Tao, A. N. Parikh, R. G. Nuzzo, *J. Am. Chem. Soc.* **1991**, *113*, 7152.
[15] P. E. Laibinis, R. G. Nuzzo, G. M. Whitesides, *J. Phys. Chem.* **1992**, *96*, 5097.
[16] Sulfanylundecanoic acid and sulfanylhexadecanoic acid were used as purchased from Aldrich. Sulfanyloctanoic acid, sulfanyldodecanoic acid, sulfanylpentadecanoic acid, and sulfanylheptadecanoic acid were synthesized from their bromo-alkanoic acid precursors by using a previously reported method, F. Kienberger, G. Kada, H. J. Gruber, V. P. Pastushenko, C. Riener, M. Trieb, H.-G. Knaus, H. Schindler, P. Hinterdorfer *Single Mol.* **2000**, *1*, 59–65.
[17] A detailed study of the effect of the substrate preparation and texture on the oriented crystallization is in progress.
[18] E. M. Landau, M. Levanon, L. Leiserowitz, M. Lahav, J. Sagiv, *Nature* **1985**, *318*, 353.
[19] S. Mann, B. R. Heywood, S. Rajam, J. B. A. Walker, *J. Phys. D* **1991**, *24*, 154.
[20] C. Bohm, F. Leveiller, D. Jacquemain, H. Mohwald, K. Kjaer, J. Alsnielsen, I. Weissbuch, L. Leiserowitz, *Langmuir* **1994**, *10*, 830.
[21] E. L. Smith, C. A. Alves, J. W. Anderegg, M. D. Porter, L. M. Siperko, *Langmuir* **1992**, *8*, 2707.
[22] J. A. Zasadzinski, R. Viswanathan, L. Madsen, J. Garnaes, D. K. Schwartz, *Science* **1994**, *263*, 1726.
[23] J. Li, K. S. Liang, G. Scoles, A. Ulman, *Langmuir* **1995**, *11*, 4418.

 © 2003 Wiley-VCH Verlag GmbH & Co. KGaA, Weinheim

High-Valent Non-Heme Complexes

A Dramatic Push Effect on the Homolysis of Fe^{III}(OOR) Intermediates To Form Non-Heme Fe^{IV}=O Complexes**

*József Kaizer, Miquel Costas, and Lawrence Que, Jr.**

The first synthetic complexes with a mononuclear non-heme Fe^{IV}=O unit have recently been unequivocally identified, thus lending strong credence to the involvement of such species in the postulated oxygen activation mechanisms of enzymes with mononuclear non-heme iron active sites such as isopenicillin *N*-synthase, pterin-dependent phenylalanine hydroxylase, and 2-oxoglutarate-dependent clavaminate synthase.[1–4] Crystallographically characterized $[Fe^{IV}(O)(TMC)(NCCH_3)]^{2+}$[5] is obtained by oxygen-atom transfer from PhIO to $[Fe^{II}(TMC)(OTf)_2]$ in CH_3CN at −40 °C,[6] while $[Fe^{IV}(O)(TPA)]^{2+}$[5] is generated by O–O bond heterolysis in the stoichiometric reaction of $[Fe^{II}(TPA)(OTf)_2]$[5] with CH_3CO_3H in CH_3CN at −40 °C.[7] The availability of these two non-heme Fe^{IV}=O complexes allows us for the first time to identify the intrinsic spectroscopic signatures of the Fe^{IV}=O unit in the absence of a porphyrin. Besides having properties observed for oxoiron(IV) porphyrin complexes,[8] such as an Fe–O bond shorter than 1.7 Å and Mössbauer parameters characteristic of a low-spin ($S = 1$; S = spin angular momentum) iron(IV) center, the non-heme complexes are characterized by relatively weak electronic transitions in the near IR region ($\lambda_{max} \sim 700$–800 nm, $\varepsilon_M \sim 300$–400).[6,7] In the course of our efforts to synthesize functional models for non-heme iron enzymes, we have investigated the reaction of *t*BuOOH with iron(II) complexes of tris(2-pyridylmethyl)amine (TPA) and related ligands and obtained indirect evidence of the involvement of corresponding Fe^{IV}=O species in the oxidations of alkanes, dialkyl sulfides, and arenes.[9] In all cases, a transient low-spin $[Fe^{III}(L)(OO\mathit{t}Bu)]^{2+}$ intermediate could be observed, which for L = TPA (**1**) is characterized by an absorption band at 600 nm ($\varepsilon_M \sim 2000$),[10] whose intensity could have hampered observation of the pale green Fe^{IV}=O species. Herein we report direct spectroscopic evidence for the formation of $[Fe^{IV}(O)TPA]^{2+}$ (**2**) from **1**. Furthermore the addition of Lewis bases accelerates this conversion and enhances the yield of **2**, thus demonstrating a "push" effect in the O–O bond homolysis of a non-heme iron peroxo species.

Figure 1a shows the time course for the decay of $[Fe^{III}(TPA)(OO\mathit{t}Bu)]^{2+}$ (**1**) formed by the addition of ten equivalents of *t*BuOOH (in nonane) to a 1 mM $[Fe^{II}(TPA)(OTf)_2]$ in CH_3CN at −36 °C. Previously, the high conversion of iron(II) precursor to **1** obtained during the steady-state phase immediately after formation facilitated its spectroscopic characterization.[10b] Under these conditions, **1** decomposed without obvious accumulation of a new species with a long-wavelength absorption. However when only two equivalents of *t*BuOOH was used, **1** decayed in a first-order process ($k_{obs} = 2.1(1) \times 10^{-3}\ s^{-1}$) to a new species with a weak absorption at 700 nm that reached maximum intensity after 1000 s (Figure 1b). Assuming an ε_M of 300 $M^{-1}cm^{-1}$ found in the CH_3CO_3H oxidation of its iron(II) precursor,[7] then **2** was formed in about 45% yield.

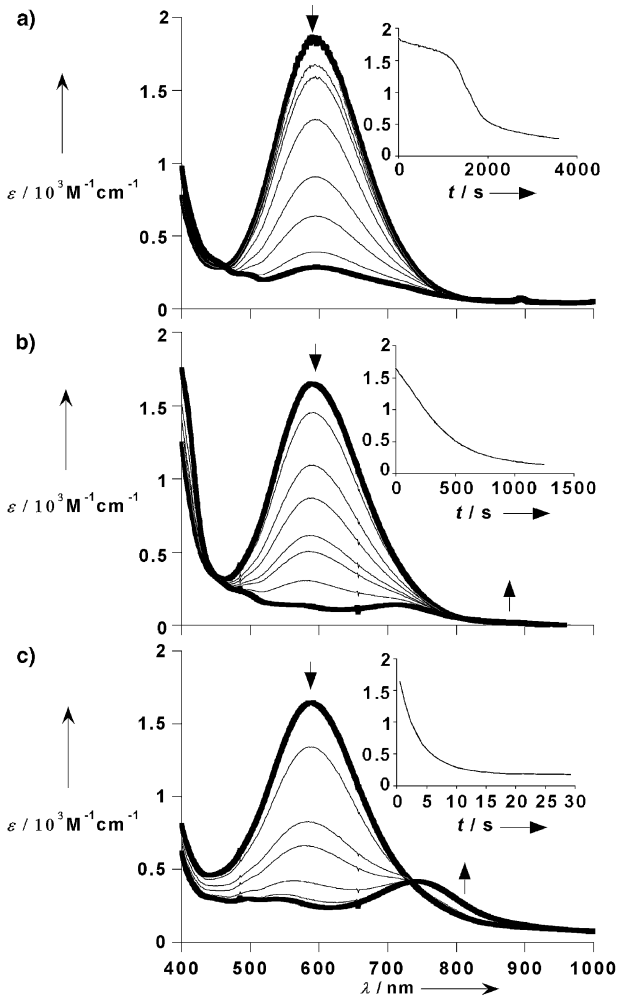


Figure 1. Visible spectral changes for the decay of **1** in acetonitrile at −36 °C formed by adding: a) 10 equiv *t*BuOOH, b) 2 equiv *t*BuOOH, and c) 2 equiv *t*BuOOH with 12 equiv of pyridine *N*-oxide. Insets: time-dependent conversions of **1** under the conditions described above monitored at 593 nm.

The addition of various Lewis bases after the formation of **1** accelerated its decay and increased the yield of **2**. For example, addition of 12 equivalents of 4-picoline to **1** increased its first order decay rate tenfold ($k_{obs} = 1.6(1) \times 10^{-2}\ s^{-1}$) and resulted in a 90% yield of **2**. However 2,6-di-*tert*-butylpyridine had no effect, thus showing that the 4-picoline was not acting simply as a Brønsted base. Even more dramatically, the addition of 12 equivalents of pyridine *N*-

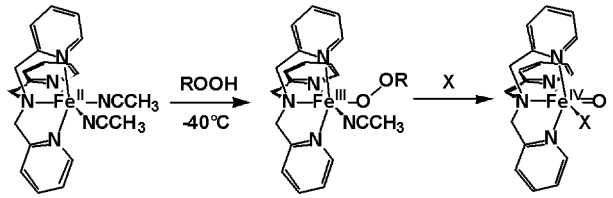
[*] Prof. L. Que, Jr., Dr. J. Kaizer, Dr. M. Costas
Department of Chemistry and Center for Metals In Biocatalysis
University of Minnesota
207 Pleasant Street SE, Minneapolis, MN 55455 (USA)
Fax: (+1) 612-624-7029
E-mail: que@chem.umn.edu

[**] We thank A. Stubna and Professor E. Münck for obtaining the Mössbauer data for complex **2**. This work was supported by a grant (GM33162) from the US National Institutes of Health.

 DOI: 10.1002/anie.200351694 © 2003 Wiley-VCH Verlag GmbH & Co. KGaA, Weinheim

oxide (PyO) to **1** accelerated its decay by another order of magnitude ($k_{obs} = 3.1(1) \times 10^{-1}\ s^{-1}$) affording **2** in >95% yield (Figure 1c)! The Mössbauer spectrum of this last species shows a quadrupole doublet ($\delta = 0.04(2)$ mm s^{-1}; $\Delta E_Q = 0.90(2)$ mm s^{-1}), very similar to that reported for $[Fe^{IV}(O)(TPA)]^{2+}$ derived from the reaction of $[Fe(TPA)(CH_3CN)_2]^{2+}$ with peracetic acid.[7]

Examination of the spectral maximum associated with **2** under these various conditions showed that it was also sensitive to the nature of the Lewis base. While this electronic transition has not yet been unequivocally assigned, its relatively low energy and intensity suggest that it is a ligand field transition. The λ_{max} of the decay product shifted from 700 nm to 718 nm or 742 nm with the respective addition of 4-picoline or PyO either before or after the decomposition of **1**. These observed shifts of the Fe^{IV}=O chromophore of **2** suggest that the added Lewis base occupies the sixth site on the Fe^{IV}=O center (Scheme 1), displacing the presumed CH_3CN ligand



Scheme 1. Formation of $[Fe^{IV}(O)(TPA)(X)]$ (**2**) complexes from $[Fe^{II}(TPA)(CH_3CN)_2]^{2+}$.

for the species with a λ_{max} of 700 nm. The fact that PyO is known to serve as an oxo transfer agent for some oxidation catalysts[11] raises the question of whether such chemistry occurs in this system. This is in fact not the case for two reasons. First, the addition of PyO to $[Fe^{II}(TPA)(OTf)_2]$ does not elicit the near IR chromophore associated with **2**. Second, the addition of even only one equivalent of PyO promoted the conversion of **1** to **2** to afford a product with the same λ_{max} of 742 nm. If PyO transferred its oxygen atom to form **2**, then the sixth ligand on **2** would have to be pyridine and a λ_{max} of 718 nm should have been observed instead.

Kinetic experiments were carried out to put a more quantitative basis on the conversion of **1** to **2** and gain insight into the dynamics of the O–O bond cleavage. The reactions, followed by measuring the absorbance decrease of the ligand-to-metal charge-transfer (LMCT) band of **1** at 593 nm (Figure 1b,c), all afforded a time profile indicating an exponential decay of [**1**]. A straight line was obtained in a plot of the reaction rate versus the initial concentration of **1** to establish a rate law of $-d[\mathbf{1}]/dt = k_{app}[\mathbf{1}]$ for all cases studied. A variation of 4-(dimethylamino)pyridine or PyO concentration revealed saturation behavior with K_{assoc} values of about 20 M^{-1} for both additives (Figure 2). These results support the likely displacement of the CH_3CN ligand in **1** prior to its conversion to **2** (Scheme 1).

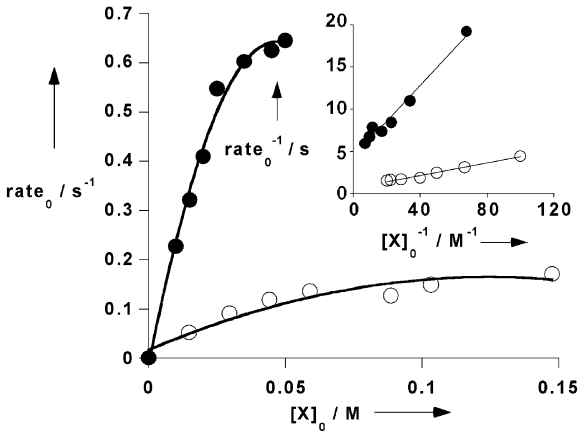


Figure 2. Initial rate of the decay of **1** as a function of [X] (X = PyO (●) or 4-$(CH_3)_2$N-C_5H_4N (○)) at −42 °C in CH_3CN. Inset: Plots of $rate_0^{-1}$ versus $[X]^{-1}$ by using the same points.

Analysis of the temperature dependence of the reaction rates (Table 1) afforded activation parameters at −40 °C of $\Delta H^{\neq} = 52(1)$ kJ mol^{-1} and $\Delta S^{\neq} = -74(3)$ J mol^{-1} K^{-1} for the decay of **1** in the absence of any additive and of $\Delta H^{\neq} = 50(2)$ kJ mol^{-1} and $\Delta S^{\neq} = -42(10)$ J mol K for its decay in the presence of 10 mM PyO. While the activation entropies differ somewhat, perhaps because of some component arising from the binding of PyO in the latter case, the activation enthalpies are nearly identical. These experimentally determined values in fact approach the enthalpy range estimated by Lehnert et al. (60–80 kJ mol^{-1}) from DFT calculations for the homolytic cleavage of the O–O bond in $[Fe^{III}(TPA)(OO\textit{t}\text{-}Bu)(OH)]^+$ along an O–O bond stretching trajectory.[12] These values are also comparable to the activation parameters for the homolysis of $[(TMP)Fe^{III}OOFe^{III}(TMP)]$[5] reported by Balch and co-workers ($\Delta H^{\neq} = 61$ kJ mol^{-1} and $\Delta S^{\neq} = -60$ J mol K) to form $[Fe^{IV}(O)TMP]$,[13] but clearly distinct from those associated with the homolysis of $[(TMP)Fe^{III}OOC(O)R]$ in toluene ($\Delta H^{\neq} = 31(2)$ kJ mol^{-1} and $\Delta S^{\neq} = -161(7)$ J mol K).[14]

Table 1: Activation parameters for homolytic O–O bond cleavage reactions of $Fe^{III}OOR$ complexes.

	$k_{-40\,°C}$ [s^{-1}]	$\Delta H^{\neq}$ [kJ mol^{-1}]	$\Delta S^{\neq}$ [J mol^{-1} K^{-1}]	
1[a]	1.25×10^{-3}	52(1)	−74(3)	This work.
1[a] + 10 equiv PyO	1.81×10^{-1}	50(2)	−42(10)	This work.
[(TMP)Fe-O-O-Fe(TMP)][b]		61	−60	[13]
[Fe(TMP)(O_3CR)][b]	2×10^{-3}	31(2)[c]	−161(7)[c]	[14]
[Fe(TMP)(O_3CR)][b] + 1-PhIm	3.3×10^{-3}	26(1)[c]	−180(5)[c]	[14]

[a] In CH_3CN. [b] In toluene. [c] Calculated from published data [14]. $\Delta H^{\neq}$ = enthalpy of activation; $\Delta S^{\neq}$ = entropy of activation.

 © 2003 Wiley-VCH Verlag GmbH & Co. KGaA, Weinheim

The significant acceleration of the decomposition of **1** upon addition of pyridine or PyO reveals a significant push effect for the sixth ligand. As shown in Figure 3, linear Hammett correlations with ρ values of −0.78 and −1.22 are obtained respectively for a series of 4-substituted pyridines

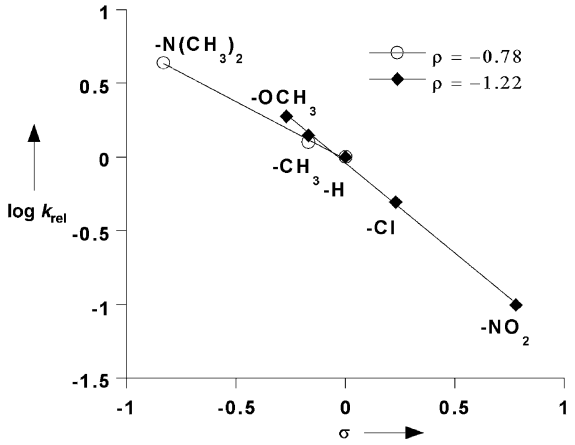


Figure 3. Substituent effects on the rate constants for homolytic O–O bond cleavage reactions of **1** in the presence of 4-substituted pyridine (○) and pyridine *N*-oxide additives (◆) in CH_3CN at −42 °C.

and pyridine *N*-oxides, demonstrating that electron-releasing groups enhance the decay of **1**. Such a push effect has been prominent in proposed mechanisms for oxygen activation by heme enzymes and emphasizes the role the proximal axial ligand can play in promoting O–O bond cleavage.[15] However in a systematic study of the decomposition of [(TMP)Fe^{III}OOC(O)R] complexes, Morishima and co-workers found homolytic O–O bond cleavage to be enhanced by a factor of at most three upon the addition of imidazoles, but, surprisingly, somewhat retarded by electron-donating groups on the porphyrins.[14] Thus, the push effect we have observed for the decomposition of **2** is quite dramatic. This accelerative effect lends credence to the proposed mechanism for O–O bond homolysis proposed by Lehnert et al.[12] that involves electron donation from the Fe d_{xy} orbital to the O–O σ* orbital. Thus donation of electron density to the low-spin iron(III) center by the ancillary sixth ligand in the plane perpendicular to the incipient Fe=O bond (designated as the z axis) promotes the cleavage of the O–O bond.

In conclusion, we have shown a significant push effect on homolysis of the FeO–OR bond in non-heme TPA complexes, unlike for heme complexes.[14] Addition of an exogenous Lewis base (Py or PyO) accelerates the decay of **2** by as much as two orders of magnitude, thus providing nucleophilic assistance to the rate-determining step. This push effect has allowed us to trap and observe [Fe^{IV}(O)(TPA)]$^{2+}$ intermediates previously proposed but unobserved in oxidation reactions of Fe(TPA) complexes with ROOH.[9]

Received: April 17, 2003 [Z51694]

Keywords: high-valent species · iron · kinetics · oxo ligands · push effect

[1] L. Que, Jr., R. Y. N. Ho, *Chem. Rev.* **1996**, *96*, 2607–2624.
[2] a) E. I. Solomon, T. C. Brunold, M. I. Davis, J. N. Kemsley, S.-K. Lee, N. Lehnert, F. Neese, A. J. Skulan, Y.-S. Yang, J. Zhou, *Chem. Rev.* **2000**, *100*, 235–349; b) E. I. Solomon, A. Decker, N. Lehnert, *Proc. Natl. Acad. Sci. USA* **2003**, *100*, 3589–3594.
[3] a) T. J. Kappock, J. P. Carradona, *Chem. Rev.* **1996**, *96*, 2659; b) P. F. Fitzpatrick, *Annu. Rev. Biochem.* **1999**, *68*, 355.
[4] C. J. Schofield, Z. H. Zhang, *Curr. Opin. Struct. Biol.* **1999**, *9*, 722–731.
[5] Abbreviations used: OTf, trifluoromethanesulfonate; 1-PhIm, 1-phenyl-imidazole; PyO, pyridine *N*-oxide; TMC, 1,4,8,11-tetramethylcyclam; TPA, tris(pyridyl-2-methyl)amine; $TMPH_2$, tetramesitylporphyrin.
[6] J.-U. Rohde, J.-H. In, M. H. Lim, W. W. Brennessel, M. R. Bukowski, A. Stubna, E. Münck, W. Nam, L. Que, Jr., *Science* **2003**, *299*, 1037–1039.
[7] M. H. Lim, J.-U. Rohde, A. Stubna, M. R. Bukowski, M. Costas, R. Y. N. Ho, E. Münck, W. Nam, L. Que, Jr., *Proc. Natl. Acad. Sci. USA* **2003**, *100*, 3665–3670.
[8] a) T. Wolter, W. Meyer-Klaucke, M. Müther, D. Mandon, H. Winkler, A. X. Trautwein, R. Weiss, *J. Inorg. Biochem.* **2000**, *78*, 117–122; b) W. Nam, S. K. Choi, M. H. Lim, J.-U. Rohde, I. Kim, J. Kim, C. Kim, L. Que, Jr., *Angew. Chem.* **2003**, *115*, 113–115; *Angew. Chem. Int. Ed.* **2003**, *42*, 109–111.
[9] a) P. A. MacFaul, K. U. Ingold, D. D. M. Wayner, L. Que, Jr., *J. Am. Chem. Soc.* **1997**, *119*, 10594–10598; b) H. Miyake, K. Chen, S. J. Lange, L. Que, Jr., *Inorg. Chem.* **2001**, *40*, 3534–3538; c) M. P. Jensen, S. J. Lange, M. P. Mehn, E. L. Que, L. Que, Jr., *J. Am. Chem. Soc.* **2003**, *125*, 2113–2128.
[10] a) J. Kim, E. Larka, E. C. Wilkinson, L. Que, Jr., *Angew. Chem.* **1995**, *107*, 2191–2194; *Angew. Chem. Int. Ed. Engl.* **1995**, *34*, 2048–2051; b) Y. Zang. J. Kim, Y. Dong, E. C. Wilkinson, E. H. Appelman, L. Que, Jr., *J. Am. Chem. Soc.* **1997**, *119*, 4197–4205.
[11] a) Y. Wang, J. H. Espenson, *Inorg. Chem.* **2002**, *41*, 2266–2274; b) D. Chatterjee, *J. Mol. Catal. A* **1999**, *150*, 49–52.
[12] a) N. Lehnert, R. Y. N. Ho, L. Que, Jr., E. I. Solomon, *J. Am. Chem. Soc.* **2001**, *123*, 8271–8290; b) N. Lehnert, R. Y. N. Ho, L. Que, Jr., E. I. Solomon, *J. Am. Chem. Soc.* **2001**, *123*, 12802–12816.
[13] A. L. Balch, *Inorg. Chim. Acta* **1992**, *198–200*, 297–307.
[14] K. Yamaguchi, Y. Watanabe, I. Morishima, *J. Am. Chem. Soc.* **1993**, *115*, 4058–4065.
[15] M. Sono, M. P. Roach, E. D. Coulter, J. H. Dawson, *Chem. Rev.* **1996**, *96*, 2841–2887.

 © 2003 Wiley-VCH Verlag GmbH & Co. KGaA, Weinheim

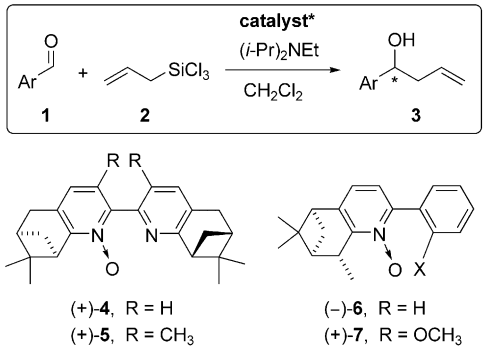
Asymmetric Allylation

Quinox, a Quinoline-Type *N*-Oxide, as Organocatalyst in the Asymmetric Allylation of Aromatic Aldehydes with Allyltrichlorosilanes: The Role of Arene–Arene Interactions**

Andrei V. Malkov, Lenka Dufková, Louis Farrugia, and Pavel Kočovský**

Dedicated to Professor Rudolf Zahradník on the occasion of his 75th birthday

Activation of allylsilane reagents **2** by a catalytic amount of a chiral Lewis base has been shown to effect asymmetric allylation of aromatic and heteroaromatic aldehydes **1** (Scheme 1).[1–4] The highest enantioselectivities were reported

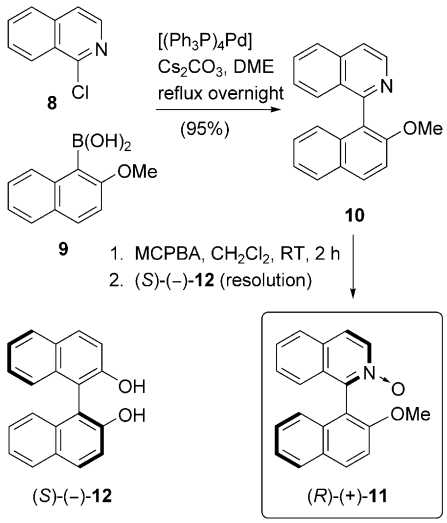


Scheme 1. Asymmetric allylation of aromatic and heteroaromatic aldehydes with a Lewis base catalyst.

by us for pindox **4** ($\leq$92% *ee*) and its dimethyl analogue **5** ($\leq$98% *ee*) as catalysts (**3**, Ar = Ph).[5] We also proposed a mechanism consistent with the available data, in which we postulated the chelation of the silicon atom by the oxygen atom of the *N*-oxide and the nitrogen atom of the second pyridine ring of **4**/**5**. However, in a subsequent study, we demonstrated that the second nitrogen is not a prerequisite for good asymmetric induction, as the simple phenyl derivative **6** and its *o*-methoxy analogue **7** (each of 87% enantiopurity) induced the formation of the allylation product **3** in 41% and 69% *ee*, respectively (**3**, Ar = Ph).[6]

The latter behavior seems to suggest that arene–arene interactions (e.g., π-stacking)[7] of the incoming benzaldehyde and the second aromatic nucleus may be involved in the reaction.[8] Furthermore, the *N*-oxide catalysts are only effective with aromatic and heteroaromatic aldehydes,[3–6] which appears to lend additional credence to this rationalization. Hence, if the catalyst contains an electron-rich aromatic system, such as the *o*-methoxy-phenyl in **7**, it should be most effective with electron-poor aromatic aldehydes (i.e., with electron-withdrawing substituent) and vice versa. In line with this hypothesis, we have endeavored to synthesize a new electron-rich catalyst and explore its activity toward electron-rich and electron-poor aromatic aldehydes. Moreover, benzaldehyde derivatives containing electron-withdrawing groups were reported to produce only modest enantioselectivities in the allylation reaction,[3–6] so that development of an effective catalyst for this class of compounds would be desirable.

We have chosen the isoquinoline *N*-oxide derivative **11** as the candidate catalyst (Scheme 2), the synthesis of which was inspired by the simplicity of the initial steps toward the well-known heterobidentate ligand quinap.[9] Thus, the Suzuki–Miyaura coupling of 1-chloro-isoquinoline (**8**)[9b] with boronic acid **9**[9b,10] afforded the biaryl derivative **10**[9] (95%), whose treatment with *m*-chloroperoxybenzoic acid provided racemic *N*-oxide (±)-**11** (99%).



Scheme 2. Synthesis of the isoquinoline *N*-oxide derivative **11**.

Racemic **11** was resolved by cocrystallization with (*S*)-(−)-binol (**12**; binol = 2,2'-dihydroxy-1,1'-biphenyl),[11] which gave the crystalline material containing binol and (+)-**11** (in a 1:1 ratio), while (−)-**11** remained in the solution. This cocrystallization, followed by a chromatographic separation of (+)-**11** from (*S*)-binol, furnished pure (+)-**11** of 98% *ee* (as revealed by chiral HPLC) in 89% yield of the isolated product.[12] The absolute configuration of **11** was found to be (*R*)-(+)-**11** by crystallographic analysis of the molecular

[*] Dr. A. V. Malkov, Prof. Dr. P. Kočovský, L. Dufková, Dr. L. Farrugia
Department of Chemistry
Joseph Black Building
University of Glasgow
Glasgow G12 8QQ (UK)
Fax: (+44) 141-33-488
E-mail: amalkov@chem.gla.ac.uk
p.kocovsky@chem.gla.ac.uk
L. Dufková
Department of Organic Chemistry
Charles University
128 40 Prague 2 (Czech Republic)

[**] We thank the University of Glasgow, the Socrates Exchange program, and Dr. Alfred Bader for financial support.

Supporting information for this article is available on the WWW under http://www.angewandte.org or from the author.

 © 2003 Wiley-VCH Verlag GmbH & Co. KGaA, Weinheim DOI: 10.1002/anie.200351737

crystal of (+)-**11** with (*S*)-(−)-**12** (Figure 1),[13] the absolute configuration of which is known. In line with the accepted acronym quinap,[9] we propose the new acronym quinox for **11**.

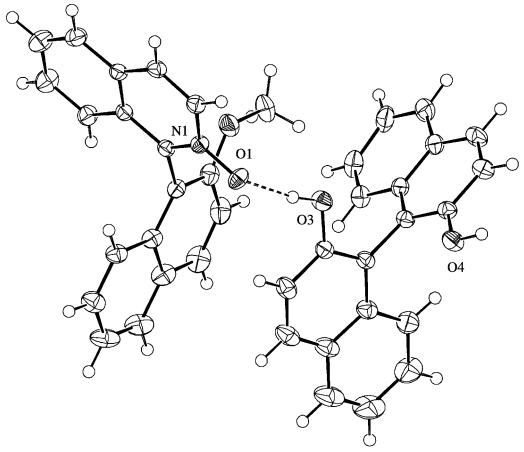


Figure 1. An ORTEP diagram illustrating the interaction of (*R*)-(+)-**11** (on the left) with (*S*)-(−)-**12** (right), in particular the hydrogen bonding N–O···H–O. Displacement parameters are shown at the 50% probability level.

The addition of allyltrichlorosilane (**2**) to benzaldehyde (**1a**) (Scheme 1), carried out in the presence of (*R*)-(+)-**11** (5 mol%) at −40°C for 2 h in CH_2Cl_2, produced (*R*)-(+)-**3a** of 87% *ee* (Table 1, entry 1). When the catalyst load was lowered to 1 mol% the reaction slowed (to ~12 h) but the enantioselectivity was not altered (entry 2).[14] In MeCN, the reaction was slower and rather less enantioselective (entry 3). A further decrease of the enantioselectivity was observed for the reaction in $CHCl_3$ (63% *ee*, entry 4) but the reaction was much faster (30 min at −40°C and ~1 h at −60°C; Table 1, entries 4 and 5). Cinnamyl derivatives **1b** and **1c** had good reactivity with modest enantioselectivity (entries 6 and 7).

Table 1: The Allylation of Aldehydes **1** with **2** Catalyzed by (*R*)-(+)-**11** (Scheme 1).[a]

entry	aldehyde	Ar	solvent	*t* [h]	yield [%][b]	*ee* [%][c,d]
1	**1a**	Ph	CH_2Cl_2	2	60	87
2	**1a**	Ph	CH_2Cl_2[e]	12	55	87
3	**1a**	Ph	MeCN	12	60	70
4	**1a**	Ph	$CHCl_3$	0.5	80	63
5	**1a**	Ph	$CHCl_3$[f]	1	79	62
6	**1b**	Cinnamyl	CH_2Cl_2	12	86	51
7	**1c**	α-Methylcinnamyl	CH_2Cl_2	12	71	55
8	**1d**	4-MeO-C_6H_4	CH_2Cl_2	12	70	12
9	**1e**	2-Furyl	CH_2Cl_2	12	68	5
10	**1f**	2-Thiophenyl	CH_2Cl_2	12	59	6
11	**1g**	2-Pyridyl	CH_2Cl_2	12	25[g]	–
12	**1h**	4-Pyridyl	CH_2Cl_2	12	trace	–
13	**1i**	4-NO_2-C_6H_4	CH_2Cl_2	2	73	89
14	**1j**	4-Cl-C_6H_4	CH_2Cl_2	2	65	93
15	**1k**	4-F-C_6H_4	CH_2Cl_2	2	79	91
16	**1l**	4-CF_3-C_6H_4	CH_2Cl_2	2	85	96

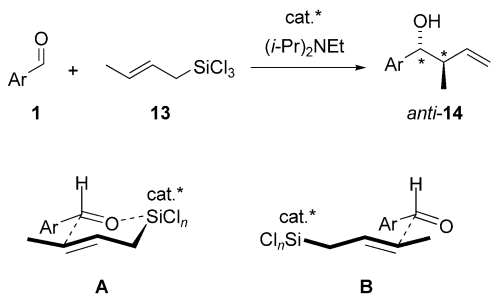
[a] The reaction was carried out at 0.4 mmol scale with 1.1 equiv of **2**, in the presence of (*R*)-(+)-**11** (5 mol%, 98% *ee*) as catalyst and (*i*-Pr)$_2$NEt (1 equiv) as base at −40°C. [b] Yield of the isolated product (note that some of the products are fairly volatile). [c] Determined by chiral HPLC or GC. [d] All products **3** were of (*R*)-(+)-configuration, as revealed by the comparison of their optical rotations (measured in $CHCl_3$) and their GC and HPLC retention times with the literature data and with the behavior of authentic samples.[3a,b,16,17] [e] With 1 mol% of the catalyst. [f] At −60°C. [g] For product identification, see reference [18, 19].

Electron-rich *p*-methoxybenzaldehyde (**1d**) and the 2-furyl and 2-thiophenyl analogues **1e** and **1f** gave almost racemic products in good yields (Table 1, entries 8–10), while pyridyl aldehydes **1g** and **1h** proved to be practically unreactive (entries 11 and 12).

By contrast, the introduction of electron-withdrawing substituents into *p*-position resulted in a dramatic increase in both reactivity and enantioselectivity. Thus, *p*-nitrobenzaldehyde **1i** afforded the corresponding product in better yield and with slightly higher *ee* than benzaldehyde (compare entries 1 and 13), and the *p*-halo derivatives **1j** and **1k** both gave >90% *ee* (Table 1, entries 14 and 15). The highest conversion and enantioselectivity (96% *ee*) was attained with the *p*-trifluoromethyl derivative **1l** (entry 16).

The observed trend in the reaction rate and enantioselectivity, with best results obtained for the electron-poor benzaldehydes **1i–l**, is fully compatible with the original hypothesis of the arene–arene interaction of the catalyst with the incoming aldehyde. The acceleration in chloroform appears to lend further support to these interactions as the driving force for the reaction.[15]

The allylation with *trans*-crotyltrichlorosilane **13** (prepared as an 87:13 *trans*/*cis* mixture by the CuCl-catalyzed reaction of crotyl chloride with $HSiCl_3$)[2b] was briefly explored to assess the scope of the reaction and to shed more light on the mechanism (Scheme 3). With pindox (**4**) as catalyst, the reaction in CH_2Cl_2 produced mainly *anti*-**14** (Table 2, entry 1), which is compatible with the generally accepted cyclic transition state **A**.[1,3] By contrast, a 2:1 *anti*/*syn* mixture (entry 2) was produced in the presence of quinox (**11**), suggesting a participation of the open-chain transition state **B**. In MeCN, the enantioselectivity was significantly reduced but the *anti*/*syn* ratio was increased (entry 3). A further drop in enantioselectivity and simultaneous increase of diastereoselectivity was observed for the electron-rich aldehyde **1d** (entry 4). By contrast, the electron-poor aldehyde **1l** (entries 5 and 6), whose arene–arene interactions with the catalyst are assumed to be stronger, exhibited high enantioselectivity and lower diastereoselectivity. This trend suggests that, in the case of quinox (**11**), the cyclic transition



Scheme 3. Proposed reaction transition states, cat.* = chiral catalyst.

 © 2003 Wiley-VCH Verlag GmbH & Co. KGaA, Weinheim

Table 2: The Allylation of Aldehydes **1** with **13** (Scheme 3).[a]

entry	aldehyde	Ar	catalyst	solvent	yield [%][b]	*anti*:*syn*	*ee* [%][c,d] *anti*, *syn*
1	**1a**	Ph	(+)-**4**[e]	CH_2Cl_2	54	93:7	87[g]
2	**1a**	Ph	(+)-**11**[f]	CH_2Cl_2	70	68:32	65, 78
3	**1a**	Ph	(+)-**11**[f]	MeCN	51	76:24	56, 60
4	**1d**	4-MeO-C_6H_4	(+)-**11**[f]	MeCN	53	82:18	50, 37
5	**1l**	4-CF_3-C_6H_4	(+)-**11**[f]	CH_2Cl_2	76	70:30	92, 95
6	**1l**	4-CF_3-C_6H_4	(+)-**11**[f]	MeCN	62	60:40	80, 84

[a] The reaction was carried out in the same way as shown in Table 1. at −40 °C. [b] Isolated yield (note that some of the products are fairly volatile). [c] Determined by chiral HPLC or GC. [d] The products **14** had the absolute configuration shown in Scheme 3, as revealed by the comparison of their optical rotations (measured in $CHCl_3$) and their GC retention times with the literature data[3a] and with the behavior of authentic samples. [e] At −60 °C for 24 h. [f] At −40 °C for 12 h. [g] Enantiomer of *anti*-**14** was formed with (+)-**4** as catalyst.

state **A** is less favored when arene–arene interactions operate (Table 2, entries 2 and 5), and more favored when the latter interactions are minimal (entry 4). Note that **1d** has the more Lewis basic carbonyl oxygen and should be more prone to coordinate to the Lewis acidic silicon, which should favor **A**. On the other hand, the less Lewis basic **1a** and **1l** are less suitable for this coordination, leaving **B** as an option, which is compatible with the experimental results.[20]

In conclusion, quinox (*R*)-(+)-**11** has been synthesized and shown to exercise an unusually high level of enantiocontrol in the Sakurai–Hosomi–Denmark-type allylation of electron-poor aromatic aldehydes ($\leq$96% *ee*, the highest value reported to date). An arene–arene interaction between the catalyst and the substrate aldehyde has been proposed as a rationale for this observation.[21] These reactions require low catalyst loading ($\leq$5 mol%) and are characterized by a substantial solvent effect upon the rate (typically 12 h in MeCN, 2 h in CH_2Cl_2, and 30 min in $CHCl_3$).

Experimental Section

(±)-1-(2-Methoxy-1-naphthyl)-isoquinoline-*N*-oxide (±)-**11**: *m*-Chloroperoxybenzoic acid (70%, 2.2 g, 9.3 mmol) was added to a solution of 1-(2-methoxy-1-naphthyl)isoquinoline **10**[9b] (1.32 g, 4.6 mmol) in dichloromethane (20 mL) at 0 °C and the mixture was stirred at room temperature for 2 h. The mixture was then extracted with saturated $NaHCO_3$ (10 mL), the organic solution was washed with brine (5 mL), dried over Na_2SO_4, and evaporated in vacuo. The crude product was purified by column chromatography on silica gel (1 × 20 cm) with an ethyl acetate/methanol mixture (4:1) to afford (±)-**11** as white solid (1.37 g, 98%): mp 107–110 °C (ethyl acetate/hexane); ^{1}H NMR (400 MHz, $CDCl_3$, 25 °C): δ = 3.75 (s, 3H), 6.96 (d, J = 8.0 Hz, 1H), 7.06 (d, J = 8.0 Hz, 1H), 7.20–7.32 (m, 3H), 7.37 (d, J = 8.8 Hz, 1H), 7.43–7.47 (m, 1H), 7.67 (d, J = 6.8 Hz, 1H), 7.76–7.82 (m, 2H), 8.10 (d, J = 8.8 Hz, 1H), 8.39 ppm (d, J = 7.2 Hz, 1H); ^{13}C NMR (100 MHz, $CDCl_3$, 25 °C): δ = 57.03 (CH_3), 113.91 (CH), 113.96 (C), 123.96 (CH), 124.23 (CH), 124.42 (CH), 125.88 (CH), 127.27 (CH), 127.90 (CH), 128.64 (CH), 128.80 (CH), 129.20 (C), 129.53 (CH), 129.57 (CH), 130.73 (C), 132.23 (CH), 132.94 (C), 138.03 (CH), 143.84 (C), 155.91 ppm (C); IR (KBr): $\tilde{\nu}$ = 3054 (w), 1319 (s), 1268 (s), 1251 cm^{-1} (s); MS (EI, 70 eV) *m*/*z* (%) 301.4 (35) [$M^{\cdot+}$], 284.4 (87), 270.3 (100), 242.3 (47), 241.3 (40), 120.7 (19); HRMS (EI) 301.1102 ($C_{20}H_{15}O_2N$ requires 301.1103).

(*R*)-(+)-1-(2-Methoxy-1-naphthyl)-isoquinoline-*N*-oxide (*R*)-(+)-**11**: Solid (*S*)-(−)-binol (*S*)-(−)-**12** (475 mg, 1.66 mmol) was added to a hot solution of racemic 1-(2-methoxy-1-naphthyl)-isoquinoline-*N*-oxide (±)-**11** (500 mg, 1.66 mmol) in dichloromethane (20 mL) and the resulting clear solution was allowed to cool to room temperature. The molecular complex (*R*)-**11**·(*S*)-**12** thus formed as a white precipitate over the period of about 30 min was collected by suction filtration and the individual components were separated by column chromatography on silica gel (1 × 20 cm) with dichloromethane, which eluted (S)-(−)-**12** (235 mg, 49%), followed by a dichloromethane/methanol mixture (93:7), which eluted (*R*)-(+)-**11** (223 mg, 45%, or 89% when calculated for a single enantiomer): mp 178–181 °C (ethyl acetate-hexane); $[\alpha]_D^{20}$ = +134 (c = 1.33 in $CHCl_3$) (lit.[3d] gives mp 180.5 °C and $[\alpha]_D$ = +132.1 (c = 0.9, $CHCl_3$); chiral HPLC (Chiralcel AD-H, hexane/2-propanol 75:25, 1 mL min^{-1}) showed 96–98% *ee*, depending on the batch (t_S = 12.36 min, t_R = 19.17 min). The filtrate from the original crystallization was evaporated and the components of the residue were separated by chromatography in the same manner as that shown for the molecular crystal to furnish (*S*)-(−)-**12** (224 mg, 47%), followed by (*S*)-(−)-**11** (215 mg, 43%, or 86% calculated for a single enantiomer), which was of 70% *ee*.

General procedure for the asymmetric allylation of aldehydes **1** with allyltrichlorosilane (**2**)**:** Allyltrichlorosilane (75 μL, 0.47 mmol) was added to a solution of catalyst (*R*)-(+)-**11** (6 mg, 0.02 mmol or 1.2 mg, 0.004 mmol), diisopropylethylamine (46 μL, 0.5 mmol), and aldehyde (0.4 mmol) in dichloromethane (2 mL) under nitrogen at −40 °C. The reaction mixture was stirred at −40 °C for 0.5–12 h (see Table 1). The reaction was quenched with saturated aqueous $NaHCO_3$ (1 mL), the layers were separated, and the aqueous layer was extracted with dichloromethane (2 × 5 mL). The combined organic extracts were washed with saturated aqueous NaCl (3 mL) and dried over Na_2SO_4. The solvent was removed in vacuo and the residue was purified by column chromatography on silica gel (1 × 20 cm) with a petroleum ether/ethyl acetate mixture (9:1). The yields and enantioselectivities are given in Table 1.

Experimental procedures, analytical and spectral data, crystallographic data, and copies of the NMR spectra for the key compounds are available in the Supporting Information.

Received: April 24, 2003 [Z51737]

Keywords: allylation · arenes · asymmetric catalysis · O ligands · organocatalysis

[1] a) S. E. Denmark, D. M. Coe, N. E. Pratt, B. D. Griedel, *J. Org. Chem.* **1994**, *59*, 6161; b) S. E. Denmark, X. Su, Y. Nishigaichi, *J. Am. Chem. Soc.* **1998**, *120*, 12990; c) S. E. Denmark, R. A. Stavenger, K.-T. Wong, X. Su, *J. Am. Chem. Soc.* **1999**, *121*, 4982; d) S. E. Denmark, R. A. Stavenger, K.-T. Wong, X. Su, *J. Am. Chem. Soc.* **1999**, *121*, 4982; e) S. E. Denmark, J. Fu, *J. Am. Chem. Soc.* **2000**, *122*, 12021; f) S. E. Denmark, S. M. Pham, *Helv. Chim. Acta* **2000**, *83*, 1846; g) S. E. Denmark, J. Fu, *J. Am. Chem. Soc.* **2001**, *123*, 9488; h) S. E. Denmark, Y. Fan, *J. Am. Chem. Soc.* **2002**, *124*, 4233; i) S. E. Denmark, J. Fu, *J. Am. Chem. Soc.* **2003**, *125*, 2208. For overviews, see: j) S. E. Denmark, R. A. Stavenger, *Acc. Chem. Res.* **2000**, *33*, 432; k) S. E. Denmark, J. Fu, *Chem. Commun.* **2003**, 167.

[2] a) K. Iseki, Y. Kuroki, M. Takahashi, Y. Kobayashi, *Tetrahedron Lett.* **1996**, *37*, 5149; b) K. Iseki, Y. Kuroki, M. Takahashi, S. Kishimoto, Y. Kobayashi, *Tetrahedron* **1997**, *53*, 3513.

[3] a) M. Nakajima, M. Saito, M. Shiro, S. Hashimoto, *J. Am. Chem. Soc.* **1998**, *120*, 6419; b) M. Nakajima, M. Saito, S. Hashimoto,

 © 2003 Wiley-VCH Verlag GmbH & Co. KGaA, Weinheim

Chem. Pharm. Bull. **2000**, *48*, 306; c) M. Nakajima, M. Saito, S. Hashimoto, *Tetrahedron: Asymmetry* **2002**, *13*, 2449; d) M. Nakajima, M. Saito, M. Uemura, S. Hashimoto, *Tetrahedron Lett.* **2002**, *43*, 8827.

[4] T. Shimada, A. Kina, S. Ikeda, T. Hayashi, *Org. Lett.* **2002**, *4*, 2799.

[5] A. V. Malkov, M. Orsini, D. Pernazza, K. W. Muir, V. Langer, P. Meghani, P. Kočovský, *Org. Lett.* **2002**, *4*, 1047.

[6] A. V. Malkov, M. Bell, M. Vassieu, V. Bugatti, P. Kočovský, *J. Mol. Catal. A* **2003**, *196*, 179.

[7] For a recent account on the face-to-face and center-to-edge interactions on aromatic systems and polar effects, see: a) F. Cozzi, R. Annunziata, M. Benaglia, M. Cinquini, L. Raimondi, K. K. Baldridge, J. S. Siegel, *Org. Biomol. Chem.* **2003**, *1*, 157; b) For a recent review on the arene–arene, π stacking, and C-H/π interactions, see: E. A. Meyer, R. K. Castellano, F. Diederich, *Angew. Chem.* **2003**, *115*, 1244; *Angew. Chem. Int. Ed.* **2003**, *42*, 1210; c) For C-H/π interactions, see: P. Hobza, Z. Havlas, *Chem. Rev.* **2000**, *100*, 4253; d) For a review on π shielding in organic synthesis, see: G. B. Jones, *Tetrahedron* **2001**, *57*, 7999.

[8] The π stacking has also been proposed by Hayashi to account for the high catalytic activity of a chiral 2,2′-bipyridine-*N,N*-bisoxide.[4]

[9] a) J. M. Brown, D. I. Hulmes, T. P. Layzell, *J. Chem. Soc. Chem. Commun.* **1993**, 1673; b) N. W. Alcock, J. M. Brown, D. I. Hulmes, *Tetrahedron: Asymmetry* **1993**, *4*, 743.

[10] Š. Vyskočil, L. Meca, I. Tišlerová, I. Císařová, M. Polášek, S. R. Harutyunyan, Y. N. Belokon, R. M. J. Stead, L. Farrugia, S. C. Lockhart, W. L. Mitchell, P. Kočovský, *Chem. Eur. J.* **2002**, *8*, 4633.

[11] For the previous use of binol to resolve bipyridine-type *N,N*-bisoxides, see refs [3,4].

[12] While this work was in progress, Nakajima published the same synthesis of (+)-**11**, including the resolution with (*S*)-(−)-binol.[3d] However, this synthesis was mentioned as a footnote without specifying the conditions and the absolute configuration of (+)-**11** was not determined.

[13] Crystal data for (*R*)-**11**·(*S*)-**12**: colorless crystals, space group $P2_12_12_1$, $a = 8.5583(1)$ Å, $b = 11.9097(1)$ Å, $c = 29.0481(4)$ Å, $V = 2960.78(6)$ Å^3, $Z = 4$, $d_{calcd} = 1.318\ g\,cm^{-3}$, $\mu = 0.085\ mm^{-1}$, $R_F(obs) = 0.0395$.

[14] Investigation of the allylation of **1a** with **2**, catalyzed by (*R*)-(+)-**11** of 29%, 50%, and 75% *ee*, respectively, has demonstrated a fully linear relationship between the enantiopurity of the catalyst and the product. In these experiments, the resulting product **3a** was of 27%, 45%, and 71% *ee*, respectively.

[15] Chloroform has been shown to be the solvent that most strongly stabilizes the arene–arene interactions: G. A. Breault, C. A. Hunter, P. C. Mayers, *J. Am. Chem. Soc.* **1998**, *120*, 3402.

[16] Y. Yamamoto, H. Yatagai, K. Maruyama, *J. Am. Chem. Soc.* **1981**, *103*, 1969.

[17] H. Doucet, M. Santelli, *Tetrahedron: Asymmetry* **2000**, *11*, 4163.

[18] U. S. Racherla, Y. Liao, H. C. Brown, *J. Org. Chem.* **1992**, *57*, 6614.

[19] J. Uenishi, T. Hiraoka, S. Hata, K. Nishiwaki, O. Yonemitsu, K. Nakamura, H. Tsukube, *J. Org. Chem.* **1998**, *63*, 2481.

[20] For a discussion on cyclic/open transition state, see: a) S. E. Denmark, N. G. Almstead, *J. Org. Chem.* **1994**, *59*, 5130; b) S. E. Denmark, S. Hosoi, *J. Org. Chem.* **1994**, *59*, 5133.

[21] Hayashi has proposed π–π stacking of **1** and the catalysts but, in his case, the variation of the enantioselectivity was less dramatic (94% *ee* for **1d** and 56% *ee* for **1l** as the extremes of the scale).[4] Furthermore, his catalyst gave the best results in MeCN, which is known not to support arene–arene interactions,[15] thus suggesting that his and our catalyst may operate through a different mode of interactions.

 © 2003 Wiley-VCH Verlag GmbH & Co. KGaA, Weinheim

The Direct and Enantioselective, One-Pot, Three-Component, Cross-Mannich Reaction of Aldehydes**

Yujiro Hayashi, Wataru Tsuboi, Itaru Ashimine, Tatsuya Urushima, Mitsuru Shoji, and Ken Sakai*

Organocatalytic enantioselective reactions[1] have received great attention in recent years since the discovery by List and Barbas et al. of aldol reactions using proline as an organocatalyst.[2] These reactions are intermolecular variants of the Hajos–Parrish–Eder–Sauer–Wiechert reaction.[3] Such catalysts have now been successfully applied to other synthetically important transformations such as the Mannich[4–6] and Michael reactions,[7] α-aminations,[8] etc.[9]

The catalytic, asymmetric Mannich reaction is one of the most powerful methods for the construction of chiral nitrogen-containing molecules. Recently several excellent results were reported, some of which are based on catalytic asymmetric additions of a preformed enolate to aldimines.[10] Unlike such Mannich reactions of preformed enolates, the research groups of Shibasaki,[11] Jørgensen,[12] Trost,[13] List,[4] and Barbas[5] have developed direct, catalytic asymmetric Mannich reactions. The former three research groups used chiral organometallic catalysts, while the latter two employed proline as an organocatalyst: List et al. developed a three-component, asymmetric Mannich reaction between an aldehyde, 4-methoxyaniline (*p*-anisidine), and a ketone,[4] while Barbas and co-workers reported a Mannich reaction of *N*-PMP-protected[14] α-imino ethyl glyoxylate and an aldehyde.[5] Although proline-mediated reactions are synthetically useful, and afford Mannich products with excellent enantioselectivity, aldehydes were not employed as the Mannich donor in the reaction performed by List et al., while *N*-PMP-protected α-imino ethyl glyoxylate was the only Mannich acceptor examined in the reaction performed by Barbas and co-workers. The development of a direct and enantioselective, one-pot, three-component cross-Mannich reaction of two different aldehydes is desirable to expand the scope of these powerful asymmetric Mannich reactions; such a system would comprise a Mannich reaction in which one aldehyde is

[*] Prof. Dr. Y. Hayashi, W. Tsuboi, I. Ashimine, T. Urushima, Dr. M. Shoji
Department of Industrial Chemistry
Faculty of Engineering
Tokyo University of Science, Kagurazaka
Shinjuku-ku, Tokyo 162-8601 (Japan)
Fax: (+81) 3-5261-4631
E-mail: hayashi@ci.kagu.tus.ac.jp

Prof. Dr. K. Sakai
Department of Applied Chemistry, Faculty of Science
Tokyo University of Science, Kagurazaka
Shinjuku-ku, Tokyo 162-8601 (Japan)

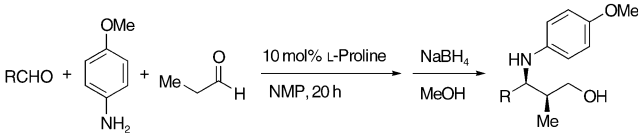
[**] This work was supported by a Grant-in-Aid for Scientific Research on Priority Areas (A; "Exploitation of Multi-Element Cyclic Molecules") from the Ministry of Education, Culture, Sports, Science, and Technology, Japan.

 DOI: 10.1002/anie.200351813 © 2003 Wiley-VCH Verlag GmbH & Co. KGaA, Weinheim

employed as the Mannich donor and the other aldehyde is utilized as a component of the Mannich acceptor to afford a synthetically versatile intermediate, a β-amino aldehyde.

Our initial attempt gave a disappointing result. We chose propanal as the Mannich donor and benzaldehyde as a component of the Mannich acceptor. Following the conditions used by List et al.[4] benzaldehyde, 4-methoxyaniline, and propanal were stirred in DMSO in the presence of a catalytic amount of L-proline at room temperature, but less than 10% yield of the cross-Mannich product was obtained, together with several unidentified products. As the formed β-amino aldehyde decomposed during purification by column chromatography on silica gel, it was isolated and characterized after reduction with $NaBH_4$ to the corresponding β-amino alcohol. As the cross-aldol condensation between benzaldehyde and propanal is a possible side reaction, propanal was added to a solution of aldimine generated in situ from benzaldehyde and 4-methoxyaniline at room temperature, but with no improvement in the yield. After several experiments, it was found that the reaction temperature is very important for this transformation. As shown in Table 1, the amino alcohol was obtained in less than 10 and 15% yield at room temperature and 0°C, respectively, together with several unidentified products (entries 1 and 2), when *N*-methyl-2-pyrrolidinone (NMP) was used as a solvent (see below). The yield increased to 50% when the reaction was performed at −10°C (entry 3), and a good yield and high enantioselectivity (90%, 98% *ee*) were obtained at −20°C (entry 4). The *syn* isomer (see below) was selectively generated, and no *anti* isomer could be detected by ^1H NMR spectroscopy (400 MHz). Possible side reactions are the self-aldol and cross-aldol condensations, which have been reported to proceed at 4°C by Northrup and MacMillan.[2j] The fact that the Mannich reaction proceeds at lower temperature (−20°C) than the aldol reaction (4°C) indicates that the aldimine is more electrophilic than the parent aldehyde. This is contrary to the generally accepted notion that an aldimine is less reactive toward nucleophilic addition than its corresponding aldehyde.[15] Recently $Yb(OTf)_3$,[16] $[PdCl_2(PPh_3)_2]$,[17] and the combination of $BF_3{\cdot}OEt_2$ and water[18] have been reported to be catalysts for the chemoselective activation of aldimines in preference to aldehydes, and the present catalyst also belongs to this rare class.

Table 1: Three-component Mannich reaction with various acceptor aldehydes.[a]



Entry	Aldehyde	*T* [°C]	Yield [%][b]	*syn*:*anti*	*ee* [%][c]
1	benzaldehyde	23	<10	n.d[d]	n.d
2	benzaldehyde	0	15	>95:5	n.d
3	benzaldehyde	−10	50	>95:5	90
4	benzaldehyde	−20	90	>95:5	98
5	benzaldehyde[e]	−20	71	>95:5	96
6	*p*-nitrobenzaldehyde	23	<10	n.d	n.d
7	*p*-nitrobenzaldehyde	0	89	>95:5	95
8	*p*-nitrobenzaldehyde	−10	93	>95:5	99
9	*p*-bromobenzaldehyde	−10	85	>95:5	95
10	*p*-bromobenzaldehyde	−20	33	>95:5	98
11	*p*-chlorobenzaldehyde	−20	91	>95:5	98
12	2-naphthaldehyde	−20	59	>95:5	96
13	*p*-tolualdehyde[e]	−20	95	>95:5	86
14	furfural	−20	87	>95:5	84
15	*p*-pyridinecarbaldehyde	−20	84[f]	>95:5	>99

[a] Reaction conditions: aldehyde:4-methoxyaniline:propanal:proline = 1.0:1.1:3.0:0.1, NMP was used as the solvent except in entries 5 and 13. Reaction time: 20 h. [b] Yield of the isolated amino alcohol. [c] The *ee* values were determined by chiral HPLC analysis (CHIRAPAK AD-H or AS-H). [d] Not determined. [e] DMF was used as the solvent. [f] Yield of the corresponding amino *tert*-butyldimethylsilyl ether, see text.

The same effect of the temperature on the yield was also observed with *p*-nitrobenzaldehyde: While at room temperature the reaction afforded several products, with the desired amino alcohol being formed in less than 10% yield, good results were obtained at 0°C and −10°C (entries 6–8).

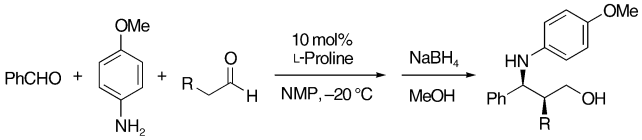
Solvent effects were examined next. Unlike the elegant enantioselective cross-aldol reaction of aldehydes by Northrup and MacMillan,[2j] in which a wide variety of solvents can be employed, the reaction scarcely proceeded in CH_3CN, CH_2Cl_2, THF, and toluene. Good yields and high enantioselectivities were obtained in DMF and NMP (entries 4 and 5).[19]

Once the best reaction conditions had been established, the generality of this one-pot, three-component cross-Mannich reaction of aldehydes was examined (Table 1). Not only benzaldehyde, but 2-naphthaldehyde and *p*-tolualdehyde are also suitable Mannich acceptor aldehydes and afford adducts in good yield with high *syn*-diastereo- and enantioselectivities (entries 12 and 13). Electron-deficient aldehydes such as *p*-nitrobenzaldehyde and *p*-chlorobenzaldehyde react smoothly, also providing Mannich products with good yields and enantioselectivities (entries 8 and 11). Although the yield of the reaction using *p*-bromobenzaldehyde at −20°C is only 33%, because of the low solubility of the aldimine, a good yield was obtained when the reaction was performed at −10°C (entries 9 and 10). In addition to aromatic aldehydes, heteroaromatic aldehydes are also good Mannich acceptor aldehydes: Furfural and *p*-pyridinecarbaldehyde react with propanal to afford the adducts in good yield with high *syn*-diastereo- and enantioselectivity (entries 14 and 15). The product from the reaction of *p*-pyridinecarbaldehyde was characterized after conversion into the corresponding *tert*-butyldimethylsilyl ether, and the yield was 84% over three steps. It is noteworthy that the basic pyridine moiety has no detrimental effect on the proline catalyst. However, under the same reaction conditions aliphatic aldehydes such as cyclohexylcarbaldehyde gave a complex mixture, while the desired product was obtained in very low yield in the reaction of electron-rich aldehydes such as *p*-anisaldehyde.

In addition to propanal, *n*-butanal can also be successfully employed as the Mannich donor and affords the Mannich products in good yield with high diastereo- and enantioselectivity (Table 2, entries 1 and 2). When *n*-pentanal was used as the Mannich donor, however, the yield and the enantioselectivity were decreased to 55% and 71% *ee*,

 © 2003 Wiley-VCH Verlag GmbH & Co. KGaA, Weinheim

Table 2: Three-component Mannich reaction with various donor aldehydes.[a]

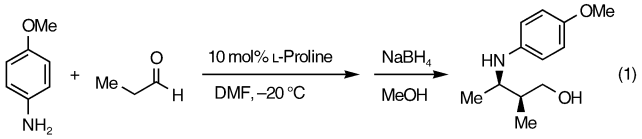


Entry	R	Yield [%][b]	*syn*:*anti*	*ee* [%][c]
1	Me	90	>95:5	98
2	Et	85	>95:5	97
3	*n*Pr	55	>95:5	71

[a] Reaction conditions: benzaldehyde:4-methoxyaniline:aldehyde:proline = 1.0:1.1:3.0:0.1 [b] Yield of the isolated amino alcohol. [c] *ee* values were determined by chiral HPLC analysis (CHIRAPAK AD-H).

respectively (entry 3). At present it is not clear why *n*-pentanal is a poor Mannich donor.

The self-Mannich reaction of propanal also proceeds effectively to afford the *syn*-3-amino-2-methylbutan-1-ol derivative in 70% yield and 96% *ee*. In this reaction, all three components (propanal, 4-methoxyaniline, and L-proline) are mixed together at −20°C without preformation of the aldimine. The success of this procedure indicates that the aldimine was formed even at −20°C, and that the reaction between the aldehyde and aldimine is faster than the self-aldol reaction. The high diastereoselectivity (*syn*:*anti* = >95:5) is in strong contrast to the self-aldol reaction of propanal, for which low diastereoselectivity (*syn*:*anti* = 4:1) is observed [Equation (1)].[2j]



A good-quality single crystal of the reduction product of the Mannich adduct of *p*-chlorobenzaldehyde, propanal, and 4-methoxyaniline was obtained and the relative and absolute configurations have been determined by X-ray crystallographic analysis.[20] The 2*S*,3*S* configuration of the 3-amino-2-methylpropan-1-ol unit (Figure 1) was determined by refinement of the Flack parameter, which converged at −0.2(4) for the configuration shown, and at 1.2(4) for the centrosymmetrically inverted structure. This result indicates that L-proline catalyzes a *si*-facial attack on the aldimine generated in situ (Figure 2), which is in good agreement with the transition-state model[21] for proline-catalyzed Mannich reactions with ketones proposed by List et al.[4] and Barbas and co-workers.[5] The present reaction gave the *syn*-β-amino-α-alkyl aldehyde with high diastereoselectivity, which is complementary to the asymmetric catalytic Mannich reactions of Kobayashi et al.[10e] and Lectka and co-workers,[10i,k] in which *anti*-β-amino-α-alkyl esters and ketones are selectively formed.

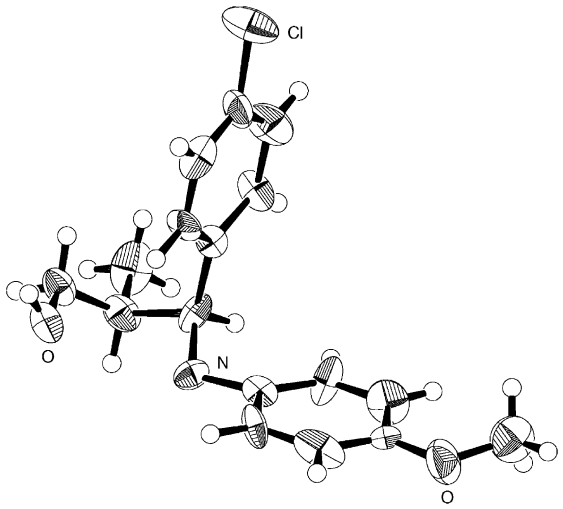


Figure 1. ORTEP diagram of the amino alcohol derived from *p*-chlorobenzaldehyde.

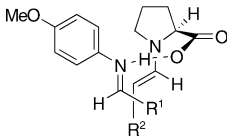


Figure 2. Transition-state model.

In summary, the one-pot, direct cross-Mannich reaction of two different aldehydes has been realized for the first time with high *syn*-diastereo- and enantioselectivities by the catalytic use of L-proline as an organocatalyst. The success of this process lies in the low reaction temperature (−20°C), at which side reactions, such as the aldol condensation, can be suppressed. There are several noteworthy features of this reaction: Proline is found to be one of the rare catalysts that activate aldimines preferentially to aldehydes. The present method for the selective formation of *syn*-β-amino-α-alkyl aldehydes is complementary to the organometal-mediated asymmetric catalytic Mannich reactions, in which the *anti*-β-amino-α-alkyl ester or ketone is selectively produced. The β-amino-α-alkyl aldehydes generated are versatile intermediates, the aldehyde portion of which can be further transformed into other functional groups.[5] The present method will be useful for the synthesis of nitrogen-containing chiral molecules.

Experimental Section

Typical experimental procedure (Table 1, entry 4): After stirring a solution of benzaldehyde (1.0 mmol), 4-methoxyaniline (1.1 mmol), and L-proline (0.1 mmol) in NMP (1.0 mL) for 2 h at RT, propanal (3.0 mmol) was added to the reaction mixture at −20°C, and stirring was continued for 20 h at this temperature. The reaction was quenched with phosphate buffer (pH 7.0), and the organic materials were extracted with ethyl acetate (×3), and the organic phases were combined and washed with brine, and dried over Na_2SO_4. After removal of the volatile materials under reduced pressure, the residue was dissolved in MeOH (3.0 mL), and then $NaBH_4$ (3.0 mmol) was added at 0°C. After stirring the mixture for 30 minutes, the reaction was quenched with phosphate buffer (pH 7.0), and the organic materials were extracted with ethyl acetate (×3). The organic phases were then combined and dried over Na_2SO_4. After removal of the volatile materials under reduced pressure, the residue was purified by thin-layer chromatography and afforded the β-amino alcohol in a

 © 2003 Wiley-VCH Verlag GmbH & Co. KGaA, Weinheim

yield of 244 mg (90%) with 98% *ee*, as determined by HPLC analysis on a chiral stationary phase.[22]

Received: May 6, 2003 [Z51813]

Keywords: aldehydes · asymmetric synthesis · enantioselectivity · organocatalysts · three-component reaction

[1] Reviews, a) B. List, *Synlett* **2001**, 1675; b) B. List, *Tetrahedron* **2002**, *58*, 5573; c) R. O. Duthaler, *Angew. Chem.* **2003**, *115*, 1005; *Angew. Chem. Int. Ed.* **2003**, *42*, 975; for an excellent review of enantioselective organocatalysis, see d) P. I. Dalko, L. Moisan, *Angew. Chem.* **2001**, *113*, 3840; *Angew. Chem. Int. Ed.* **2001**, *40*, 3726.

[2] a) B. List, R. A. Lerner, C. F. Barbas III, *J. Am. Chem. Soc.* **2000**, *122*, 2395; b) K. Sakthivel, W. Notz, T. Bui, C. F. Barbas III, *J. Am. Chem. Soc.* **2001**, *123*, 5260; c) B. List, P. Pojarliev, C. Castello, *Org. Lett.* **2001**, *3*, 573; d) W. Notz, B. List, *J. Am. Chem. Soc.* **2000**, *122*, 7386; e) A. Cordova, W. Notz, C. F. Barbas III, *J. Org. Chem.* **2002**, *67*, 301; f) L. Hoang, S. Bahmanyar, K. N. Houk, B. List, *J. Am. Chem. Soc.* **2003**, *125*, 16; g) S. Bahmanyar, K. N. Houk, H. J. Martin, B. List, *J. Am. Chem. Soc.* **2003**, *125*, 2475; see also h) Z. Tang, F. Jiang, L. Yu, X. Cui, L. Gong, A. Mi, Y. Jiang, Y. Wu, *J. Am. Chem. Soc.* **2003**, *125*, 5262; i) A. Bøgevig, N. Kumaragurubaran, K. A. Jørgensen, *Chem. Commun.* **2002**, 620; j) A. B. Northrup, D. W. C. MacMillan, *J. Am. Chem. Soc.* **2002**, *124*, 6798.

[3] a) Z. G. Hajos, D. R. Parrish, , German Patent DE 2102623, **1971** [*Chem. Abstr.* **1972**, *76*, 59072x]; b) U. Eder, R. Wiechert, G. Sauer, , German Patent DE 2014757, **1971** [*Chem. Abstr.* **1972**, *76*, 14180q]; c) U. Eder, G. Sauer, R. Wiechert, *Angew. Chem.* **1971**, *83*, 492; *Angew. Chem. Int. Ed. Engl.* **1971**, *10*, 496; d) Z. G. Hajos, D. R. Parrish, *J. Org. Chem.* **1974**, *39*, 1612.

[4] a) B. List, *J. Am. Chem. Soc.* **2000**, *122*, 9336; b) B. List, P. Pojarliev, W. T. Biller, H. J. Martin, *J. Am. Chem. Soc.* **2002**, *124*, 827.

[5] a) A. Cordova, W. Notz, G. Zhong, J. M. Betancort, C. F. Barbas III, *J. Am. Chem. Soc.* **2002**, *124*, 1842; b) A. Cordova, S. Watanabe, F. Tanaka, W. Notz, C. F. Barbas III, *J. Am. Chem. Soc.* **2002**, *124*, 1866; c) A. Cordova, C. F. Barbas III, *Tetrahedron Lett.* **2003**, *44*, 1923; d) A. Cordova, C. F. Barbas III, *Tetrahedron Lett.* **2002**, *43*, 7749; e) S. Watanabe, A. Cordova, F. Tanaka, C. F. Barbas III, *Org. Lett.* **2002**, *4*, 4519; f) W. Notz, K. Sakthivel, T. Bui, G. Zhong, C. F. Barbas III, *Tetrahedron Lett.* **2001**, *42*, 199.

[6] A. G. Wenzel, E. N. Jacobsen, *J. Am. Chem. Soc.* **2002**, *124*, 12964.

[7] a) S. P. Brown, N. C. Goodwin, D. W. C. MacMillan, *J. Am. Chem. Soc.* **2003**, *125*, 1192; b) D. Enders, A. Seki, *Synlett* **2002**, 26; c) J. M. Betancort, K. Sakthivel, R. Thayumanavan, C. F. Barbas III, *Tetrahedron Lett.* **2001**, *42*, 4441; d) J. M. Betancort, C. F. Barbas III, *Org. Lett.* **2001**, *3*, 3737; e) B. List, P. Pojarliev, H. J. Martin, *Org. Lett.* **2001**, *3*, 2423; f) S. Hanessian, V. Pham, *Org. Lett.* **2000**, *2*, 2975; g) A. Alexakis, O. Andrey, *Org. Lett.* **2002**, *4*, 3611.

[8] a) B. List, *J. Am. Chem. Soc.* **2002**, *124*, 5656; b) N. Kumaragurubaran, K. Juhl, W. Zhuang, A. Bøgevig, K. A. Jørgensen, *J. Am. Chem. Soc.* **2002**, *124*, 6254; c) A. Bøgevig, K. Juhl, N. Kumaragurubaran, W. Zhuang, K. A. Jørgensen, *Angew. Chem.* **2002**, *114*, 1868; *Angew. Chem. Int. Ed.* **2002**, *41*, 1790.

[9] For other notable examples of enantioselective organocatalytic reactions, see Diels–Alder reaction: a) K. A. Ahrendt, C. J. Borths, D. W. C. MacMillan, *J. Am. Chem. Soc.* **2000**, *122*, 4243; b) A. B. Northrup, D. W. C. MacMillan, *J. Am. Chem. Soc.* **2002**, *124*, 2458; hetero-Diels–Alder reaction: c) K. Juhl, K. A. Jørgensen, *Angew. Chem.* **2003**, *115*, 1536; *Angew. Chem. Int. Ed.* **2003**, *42*, 1498; nitrone cycloaddition: d) W. S. Jen, J. J. M. Wiener, D. W. C. MacMillan, *J. Am. Chem. Soc.* **2000**, *122*, 9874; pyrrole substitution: e) N. A. Paras, D. W. C. MacMillan, *J. Am. Chem. Soc.* **2001**, *123*, 4370; indole substitution: f) J. F. Austin, D. W. C. MacMillan, *J. Am. Chem. Soc.* **2002**, *124*, 1172; aniline substitution: g) N. A. Paras, D. W. C. MacMillan, *J. Am. Chem. Soc.* **2002**, *124*, 7894; Baylis–Hillman reaction: h) Y. Iwabuchi, M. Nakatani, N. Yokoyama, S. Hatakeyama, *J. Am. Chem. Soc.* **1999**, *121*, 10219.

[10] a) H. Fujieda, M. Kanai, T. Kambara, A. Iida, K. Tomioka, *J. Am. Chem. Soc.* **1997**, *119*, 2060; b) H. Ishitani, M. Ueno, S. Kobayashi, *J. Am. Chem. Soc.* **1997**, *119*, 7153; c) S. Kobayashi, H. Ishitani, M. Ueno, *J. Am. Chem. Soc.* **1998**, *120*, 431; d) H. Ishitani, M. Ueno, S. Kobayashi, *J. Am. Chem. Soc.* **2000**, *122*, 8180; e) S. Kobayashi, J. Kobayashi, H. Ishitani, M. Ueno, *Chem. Eur. J.* **2002**, *8*, 4185; f) E. Hagiwara, A. Fujii, M. Sodeoka, *J. Am. Chem. Soc.* **1998**, *120*, 2474; g) A. Fujii, E. Hagiwara, M. Sodeoka, *J. Am. Chem. Soc.* **1999**, *121*, 5450; h) D. Ferraris, B. Young, T. Dudding, T. Lectka, *J. Am. Chem. Soc.* **1998**, *120*, 4548; i) D. Ferraris, B. Young, C. Cox, W. J. Drury III, T. Dudding, T. Lectka, *J. Org. Chem.* **1998**, *63*, 6090; j) D. Ferraris, T. Dudding, B. Young, W. J. Drury III, T. Lectka, *J. Org. Chem.* **1999**, *64*, 2168; k) D. Ferraris, B. Young, C. Cox, T. Dudding, W. J. Drury III, L. Ryzhkov, A. E. Taggi, T. Lectka, *J. Am. Chem. Soc.* **2002**, *124*, 67.

[11] a) S. Matsunaga, N. Kumagai, S. Harada, M. Shibasaki, *J. Am. Chem. Soc.* **2003**, *125*, 4712; b) S. Yamasaki, T. Iida, M. Shibasaki, *Tetrahedron Lett.* **1999**, *40*, 307; c) S. Yamasaki, T. Iida, M. Shibasaki, *Tetrahedron* **1999**, *55*, 8857.

[12] K. Juhl, N. Gathergood, K. A. Jørgensen, *Angew. Chem.* **2001**, *113*, 3083; *Angew. Chem. Int. Ed.* **2001**, *40*, 2995.

[13] B. M. Trost, L. R. Terrell, *J. Am. Chem. Soc.* **2003**, *125*, 338.

[14] PMP = *para*-methoxyphenyl.

[15] a) N. B. Ambhaikar, J. P. Snyder, D. C. Liotta, *J. Am. Chem. Soc.* **2003**, *125*, 3690; b) F. Chemla, V. Hebbe, J. Normant, *Synthesis* **2000**, 75; c) M. Yamaguchi in *Comprehensive Organic Synthesis, Vol. 1* (Eds.: B. M. Trost, I. Fleming), Pergamon, Oxford, **1991**, p. 325.

[16] S. Kobayashi, S. Nagayama, *J. Am. Chem. Soc.* **1997**, *119*, 10049.

[17] H. Nakamura, H. Iwama, Y. Yamamoto, *J. Am. Chem. Soc.* **1996**, *118*, 6641.

[18] T. Akiyama, J. Takaya, H. Kagoshima, *Chem. Lett.* **1997**, 947.

[19] DMSO cannot be used at −20 °C because it solidifies.

[20] Crystal data: $C_{17}H_{20}ClNO_2$, monoclinic, space group $P2_1$, $a = 10.206(4)$, $b = 6.187(2)$, $c = 12.962(5)$ Å, $\beta = 97.838(6)°$, $V = 810.8(5)$ Å^3, $Z = 2$, $R1 = 0.1427$, $wR2 = 0.4094$ (refined on F^2 using SHELXL97). CCDC-212084 contains the supplementary crystallographic data for this paper. These data can be obtained free of charge via www.ccdc.cam.ac.uk/conts/retrieving.html (or from the Cambridge Crystallographic Data Centre, 12 Union Road, Cambridge CB2 1EZ, UK; fax: (+44) 1223-336-033; or deposit@ccdc.cam.ac.uk).

[21] S. Bahmanyar, K. N. Houk, *Org. Lett.* **2003**, *5*, 1249.

[22] HPLC conditions: Chiral AD-H column, *i*PrOH:hexane 1:30, 0.5 mL min^{-1}, retention times: 74.6 min (minor) and 80.4 min (major).

 © 2003 Wiley-VCH Verlag GmbH & Co. KGaA, Weinheim

Controlled Nanoparticle Growth

Highly Stable Metal Hydrous Oxide Colloids by Inorganic Polycondensation in Suspension**

Corine Gérardin, Nicolas Sanson, Frédéric Bouyer, François Fajula, Jean-Luc Putaux, Mathieu Joanicot, and Thierry Chopin*

The interest in finely dispersed particles with controlled properties significantly increased in recent years not only for fundamental reasons but also due to the various applications of well-defined nanoparticles (e.g., in catalysis, magnetism, microelectronics, optics, and medicine). The properties of nanoparticles depend not only on their chemical composition but also on their size and morphology. Hence, much effort has focused on the development of new strategies for the synthesis of particles with controlled characteristics. Nevertheless, further improvements are still required, especially with regard to size control over a wide range, shape design, and long-term stability of colloidal suspensions in the presence of additives.

Here we report on the preparation of highly stable suspensions of metal hydrous oxides. The most commonly used method of generating metal hydroxide nanoparticles is through precipitation from homogeneous solutions by hydrolysis of metal cations.[1–3] The key parameters in the synthesis are the pH value, the temperature, the nature of the counterions, the reactant concentrations, the aging time, and also processing conditions, such as the feed rate of reactants. Growth control can be achieved by the use of strong complexing agents[4] or polyelectrolytes. Particle suspensions thus produced are electrostatically stabilized and are unstable at high ionic strength. Nanoreactor-based methods of preparation using surfactant or amphiphilic block copolymer assemblies allow dispersions of uniform particles to be directly prepared.[5–8] They were mainly developed for the preparation of metallic or semiconducting nanoparticles, and are based on the use of preformed micelles in an organic solvent. The water-in-oil microemulsion method[9–10] is also used to prepare nanoparticles in the inner aqueous phase of reverse micelles.[11]

Here we present a direct method for the preparation of sterically stabilized colloids of metal hydroxides in aqueous media, based on the use of double hydrophilic block copolymers (DHBCs). The DHBCs do not self-assemble in water; they behave as soluble polymers or polyelectrolytes. To ensure simultaneous control of particle growth and stabilization, DHBCs with an anionic metal-binding block and a neutral stabilizing block were used. The metal-complexing block acts as a growth inhibitor, while the neutral block promotes colloidal stabilization. A review on the synthesis and applications of DHBCs was recently published by Cölfen.[12] Such polymers proved to be convenient for controlled precipitation of inorganic powders[13–16] and the preparation of nanosized metal particles[17] in polar solvents. DHBCs were also used to control the morphology of organic crystals and for separating racemates into enantiomers.[18] The aim of our approach has been to elucidate the mechanisms of the formation of nanoparticles from aqueous inorganic precursors in the presence of hydrophilic block copolymers. Knowledge of the mechanisms that combine induced structuring of the polymers and inorganic polycondensation is necessary for designing size- and shape-controlled particles with long-term colloidal stability.

The strategy of nanoparticle formation is summarized in Figure 1, which schematically presents the different steps involved in the synthesis. First, hybrid precursors are prepared by mixing inorganic species and hydrophilic block copolymers. The aqueous inorganic precursors can be either solutions of salts of metal ions, such as Al^{3+}, La^{3+}, and Cu^{2+} or condensed entities, such as polycationic clusters, prepared by controlled partial prehydrolysis of metal ions M^{n+}. Polymetallic species such as Al_{13}^{7+} and Al_{30}^{18+} have been prepared[19] and used as precursors. By varying the degree of partial prehydrolysis of the metal ions ($h_1 = [OH^-]_{added}/[M]$), the size and the charge density of the inorganic precursor were tuned. When copolymers and inorganic precursors are mixed, complexation of the metal ions by the polyelectrolyte block occurs. As will be shown, complexation induces the formation

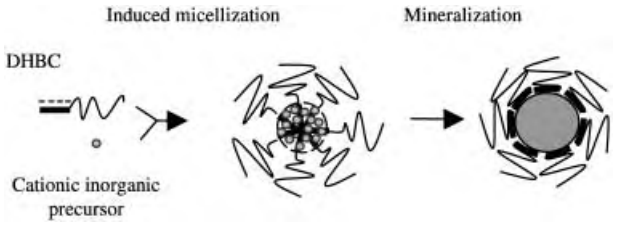


Figure 1. Schematic scenario of the different steps involved in nanoparticle formation.

[*] Dr. C. Gérardin, N. Sanson, Dr. F. Bouyer, Dr. F. Fajula
Laboratoire de Matériaux Catalytiques et Catalyse en Chimie Organique
UMR 5618 CNRS ENSCM
8, rue de L'Ecole Normale, 34296 Montpellier cedex 5 (France)
Fax: (+33) 4-6716-3465
E-mail: gerardin@cit.enscm.fr
Dr. J.-L. Putaux
Centre de Recherches sur les Macromolécules Végétales CNRS associated with the Joseph Fourier University of Grenoble (France)
Dr. M. Joanicot
CNRS Rhodia Complex Fluids Laboratory
Rhodia Inc.
Cranbury, NJ 08512 (USA)
Dr. T. Chopin
Rhodia Centre de Recherches d'Aubervilliers
93308 Aubervilliers (France)

[**] The authors acknowledge financial support provided by Rhodia. We thank M. Destarac (Rhodia Aubervilliers, France) for providing the copolymers, L. Auvray for help in neutron scattering measurements, performed at Laboratoire Leon Brillouin, CEA Saclay, France, J.-P. Selzner (Laboratoire de Microscopie Electronique, Université Montpellier II, France) for help in TEM measurements on the Jeol 1200 EXII microscope, and M. In (Montpellier) and J. P. Jolivet (Paris) for discussions.

 DOI: 10.1002/anie.200350917 © 2003 Wiley-VCH Verlag GmbH & Co. KGaA, Weinheim

of well-defined nanoaggregates. The aggregates are then direct precursors for particle formation. In a final step, mineralization of the core of the aggregate can occur by completing hydrolysis and condensation in suspension.

The block copolymers used in this study were poly(acrylic acid)-*b*-polyhydroxyethylacrylate (PAA-*b*-PHEA) and poly(acrylic acid)-*b*-polyacrylamide (PAA-*b*-PAM). Only asymmetric copolymers in which the anchoring block is much smaller than the stabilizing block were examined. The pH value of the copolymer solution was adjusted to 5.5, which corresponds to a degree of dissociation of the acrylic acid groups of about 50%, and then the solution was added to solutions of metal ions. Metal complexation by acrylate groups leads to the spontaneous formation of large aggregates. The degree of metal complexation is expressed as the number of acrylate groups added per metal atom ($R = [AA]/[M]$). The hydrodynamic diameter, determined by dynamic light scattering (DLS), was 40 nm for aggregates formed from Al_{13}^{7+} ions and PAA_{1900}-*b*-$PHEA_{8200}$, as opposed to 11 nm for the corresponding copolymer in solution.

Small-angle neutron scattering (SANS) experiments were performed to characterize the nanostructure of the assemblies. Figure 2 shows the scattering curve of an aggregate from

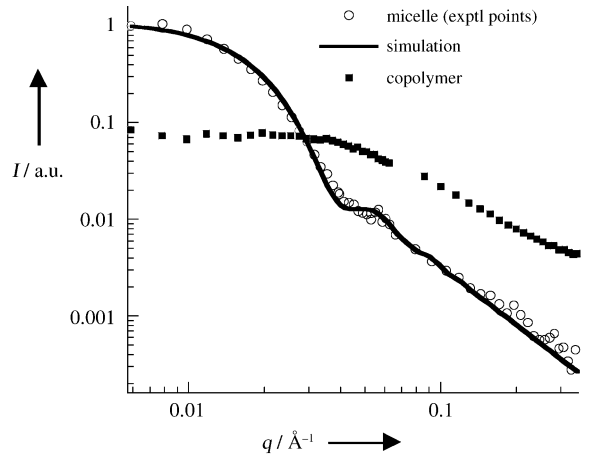


Figure 2. SANS curves of the nanoaggregate (○) obtained from the block copolymer PAA_{1900}-*b*-$PHEA_{8200}$ and Al_{13}^{7+} ions, and of the copolymer in water (■). The simulation (Pedersen's model) of the scattering curve of the nanoaggregate is shown as a full line.

Al_{13}^{7+} ions and PAA_{1900}-*b*-$PHEA_{8200}$, together with the scattering curve of the same copolymer in water. The two curves represent scattering from suspensions at the same copolymer concentration, in the absence and in the presence of metal polycations. Since the Al_{13} clusters were prepared in D_2O, the $Al_{12}(AlO_4)(OD)_{24}(D_2O)_{12}^{7+}$ species have scattering-length densities that practically match the scattering-length density of D_2O. Then, the scattered intensity of the cation/polymer mixture essentially arises from the polymer blocks. The scattering curve of the copolymer is characteristic of a polymer in a good solvent, whereas that of the cation/copolymer mixture reveals that supramolecular aggregates with a spherical core–corona structure were formed. At low values of q (the amplitude of the scattering vector), the observation of a much higher scattering intensity for the suspension with polycations compared to that of the polymer solution supports the formation of polymer aggregates. In the low-q regime, Guinier behavior allows the radii of gyration R_G of the copolymer and of the aggregate to be determined. The R_G value was 11 nm for micelles of PAA_{1900}-*b*-$PHEA_{8200}$ with Al_{13}^{7+} ions and 2.5 nm for the copolymer in solution. The high-q range of the scattering curve (Figure 2) characterizes the outer layer of the micelle; a power-law behavior of the intensity ($I(q) \propto q^{-3.9}$) indicates the presence of a diffuse corona consisting of polymer chains in a good solvent. The value of the power exponent is in good agreement with an excluded-volume model that accounts for self-avoidance and mutual avoidance of the chains in the corona. The sharp decrease in intensity ($I(q) \propto q^{-1.7}$) of the scattering curve of the aggregate in the intermediate q range ($0.025 < q < 0.045$ Å^{-1}) suggests that a dense core with a sharp interface is formed by the collapsed polyelectrolyte blocks. The scattering curve of the micelle was simulated (Figure 2) by using Pedersen's model,[20,21] which was developed for form factors of core–corona assemblies of block copolymers. The simulation gave a mean core diameter of the micelle of 12 nm. Figure 3 shows a cryo-TEM image of micelles formed from

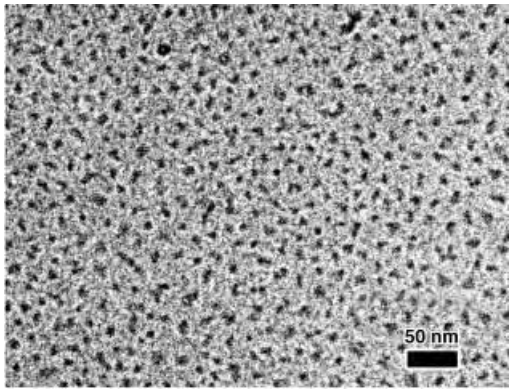


Figure 3. Cryo-TEM image of the micellar aggregates obtained from Al_{13}^{7+} ions and PAA_{2800}-*b*-$PHEA_{11\,100}$.

Al_{13}^{7+} ions and PAA_{2800}-*b*-$PHEA_{11\,100}$, embedded in a thin film of vitreous ice. Well-separated isotropic objects with a small size distribution around a mean diameter of 9 nm are observed; some larger and elongated aggregates can also be seen. The TEM image confirms the concentration of the inorganic ions in a dense central part of the aggregates, and the mean core diameter measured here is in agreement with the values obtained by simulation of the SANS curves. The micelles have a very small zeta potential (−3 mV), which is consistent with the neutral blocks forming the micelle corona. Suspensions were also investigated by ^{27}Al NMR spectroscopy in solution. The NMR signal at $\delta = 63$ ppm, characteristic of the tetrahedral site in Al_{13} clusters, disappeared on formation of micellar aggregates, and this is consistent with the formation of a dense insoluble core containing the Al species.

The characteristics of the nanoassemblies formed with various multivalent ions (e.g., Ca^{2+}, Cu^{2+}, Al^{3+}, La^{3+}) and

 © 2003 Wiley-VCH Verlag GmbH & Co. KGaA, Weinheim

various asymmetric anionic–neutral block copolymers were similar. Their microstructures are similar to those of core–corona micelles of amphiphilic block copolymers such as polyoxyethylene-*b*-polyoxybutylene in water.[22] They can also be compared to microstructures formed from DHBCs and oppositely charged surfactants.[23] In the present case, the formation of core–corona structures is explained by the formation of an insoluble complex whose macroscopic precipitation is inhibited by the presence of neutral blocks. It is well known that in the presence of multivalent ions, oppositely charged polymers precipitate into compact structures, due to condensation of ions with the polyelectrolyte chains.[24] The neutral blocks sterically stabilize the water-incompatible phase. Induced amphiphilicity of DHBCs was reported for the formation of polyion complex (PIC) micelles from charged diblock copolymers with oppositely charged polymers or surfactants.[25–27] The formation of aggregates between DHBCs and metal ions was also reported by several authors.[28,29] The hybrid analogues of the PIC micelles described here exhibit a major difference in stability to PIC aggregates. In the case of polymer PIC micelles, complex formation is triggered essentially by electrostatic interactions and entropy gain for the released counterions of the polymers. With metal cations, the coordinative bond is an additional stability factor, and this could explain why inorganic/polymeric micelles are more stable than PIC micelles towards addition of salts.

The hybrid nanoaggregates were used as precursors for nanoparticle formation. Particle growth and morphology control were investigated. Core mineralization was induced by hydroxylation of the metal cations. In this step, the hydrolysis ratio $h_2 = [OH^-]/[M^{n+}]$ was generally chosen to be equal to $n - h_1$. In the absence of copolymer, metal hydroxides obtained by hydroxylation are flocculated precipitates formed by the aggregation of particles. In the presence of copolymers, completion of metal hydrolysis in the aggregates leads to stable suspensions or settling precipitates, depending on two parameters: the prehydrolysis ratio $h_1 = [OH^-]/[M]$ and the degree of complexation R. The quantities R and h_1 are convenient means of controlling particle growth and stability. The mean particle size increases with increasing h_1 or decreasing R, as illustrated in Figure 4 for La^{3+}/PAA_{1000}-*b*-PAM_{10000} as a precursor for lanthanum-hydroxide-based nanoparticles. Figure 4 shows the hydrodynamic diameters of the particles and the corresponding micellar La^{3+}/PAA_{1000}-*b*-PAM_{10000} precursors as a function of the acrylate-to-metal ratio R. Three domains can be distinguished. Below a copolymer ratio R_1, flocculation occurs, and no stable colloids form. In addition, there is a minimum copolymer amount R_2 ($R_2 > R_1$) above which the hybrid precursor acts as a closed compartment for mineralization. Above R_2, particle sizes are similar to those of the corresponding precursor. In Figure 4, R_1 is 0.5 and R_2 about 2. Between R_1 and R_2, hydrodynamic diameters vary between 25 and 100 nm, and mineralization proceeds by enlargement of the core. Figure 5 shows TEM images of the particles for two values of R. For $R = R_1 = 0.5$, elongated particles about 80 nm long are obtained (Figure 5a). Electron diffraction studies revealed that cristalline lanthanum trihydroxide particles were formed. For $R = 3$, spherical particles with a mean diameter of about 8 nm are obtained (Figure 5b). For $R > R_2$, mineralization proceeds within the confined environment of the micellar precursors, and the particles retain the size and shape of the precursors.

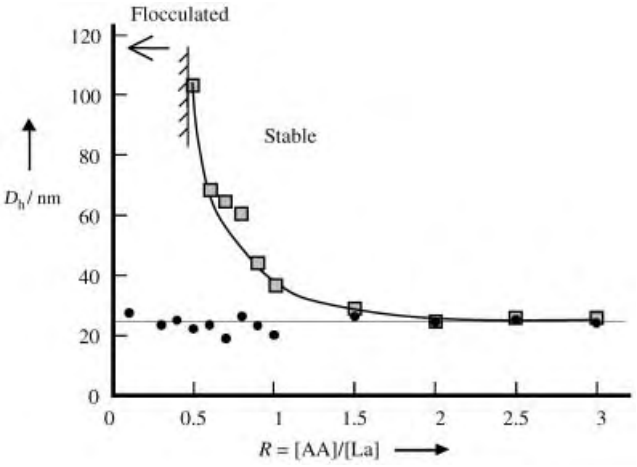


Figure 4. Hydrodynamic diameters as a function of the degree of complexation R = [AA]/[M] of the particles (■) and of the corresponding La^{3+}/PAA_{1000}-*b*-PAM_{10000} precursors (●).

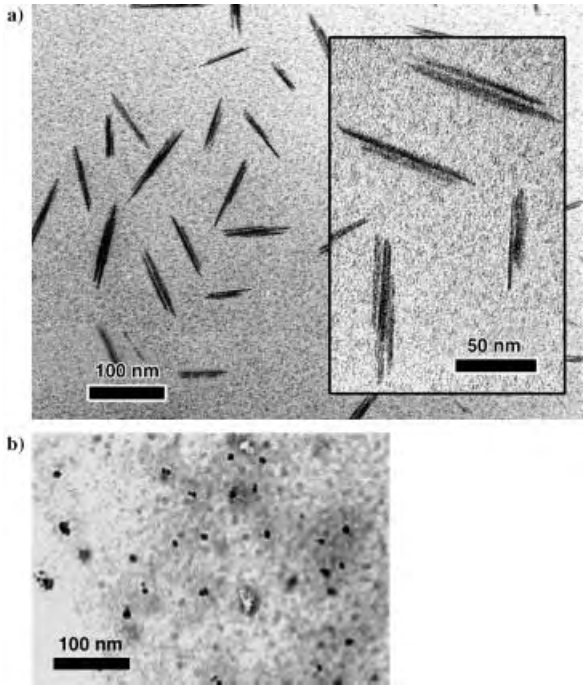


Figure 5. TEM images of the particles obtained from hydrolysis ($h_2 = 3$) of the mixtures La^{3+}/PAA_{1000}-*b*-PAM_{10000} for $R = 0.5$ (a) and $R = 3$ (b).

In the case of dispersed aluminum hydroxide particles prepared from Al_{13} clusters and PAA_{1900}-*b*-$PHEA_{8200}$, a similar dependence of size on R is observed. The average hydrodynamic diameter of the particles varies from 45 to 155 nm when R decreases from 1 to 0.6. Figure 6 shows TEM images of particles obtained for $R = R_1 = 0.6$ and $R = R_2 = 1$. Particles of aluminum hydroxide of varying size were

 © 2003 Wiley-VCH Verlag GmbH & Co. KGaA, Weinheim

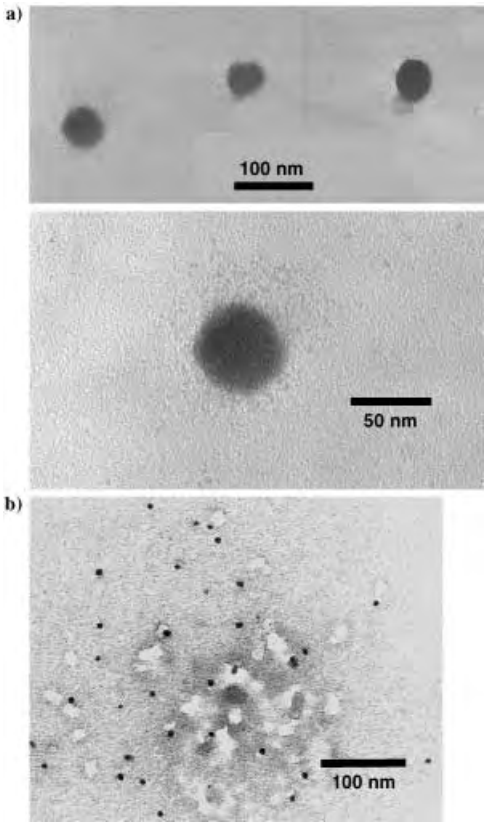


Figure 6. TEM images of the particles obtained by hydrolysis ($h_2 = 0.54$) of the mixtures Al_{13}^{7+}/PAA_{1900}-*b*-$PHEA_{8200}$ for $R = 0.6$ (a) and $R = 1$ (b).

obtained for intermediate values of R ($0.6 \leq R < 1$; Figure 6a), whereas for high R values ($R \geq 1$), metal hydrolysis and condensation reactions proceed within the restricted volume of the micellar core, and the particles remain small (8 nm) and spherical, as shown in Figure 6b.

In the case of copper-based precursors, stable polymer-protected platelets of copper hydroxide could be synthesized at low degrees of complexation, whereas high degrees of complexation led to spherical shapes. Moreover, by varying the prehydrolysis ratio h_1, it was also possible to change the shape. In all cases, the presence of the polymeric corona attached to the inorganic particle surface was checked by different techniques: SANS, TEM combined with DLS, IR spectroscopy, and electrophoresis.

The concept of a nanoreactor with a closed reservoir of metal ions can be used to explain the mechanisms of formation of the particles from the micelles only under conditions where a high degree of metal complexation ($R \geq R_2$) occurs. For intermediate degrees of complexation ($R < R_2$), the polyelectrolyte blocks act as surface-active agents during mineralization, while the neutral blocks provide the necessary steric stabilization of the particle. The complexation rate [AA]/[M] defines the degree of poisoning of inorganic polycondensation reactions. Therefore, it governs the total surface area of the particle suspension and controls the mean particle size. The particle size can also be tailored by varying the metal prehydrolysis ratio and the polymer block lengths, as will be detailed in a forthcoming paper. Finally, depending on the nature of the metal and the synthetic parameters, the preparation method can lead to different morphologies: spherical, elongated, or platelike particles.

A great advantage of the present method is that the colloids thus prepared are stable for months. The neutral polymer segments constitute an effective barrier against particle aggregation. In addition, suspension stability is neither affected by changes in pH value (at least in the range 5–11) nor by increases in electrolyte concentration. Both micelle and particle suspensions remained stable for ionic strengths up to 2.8 M. We also showed that the present block copolymers are better stabilizers than the corresponding homopolymers or random copolymers.

In summary, a method for the direct preparation of highly stable colloids of metal hydrous oxides was developed; hydrolysis and condensation of metal cations can be performed in suspension in the presence of double-hydrophilic block copolymers. Anionic–neutral copolymers simultaneously ensure control of growth and stabilization of the particles. Above a critical degree of complexation, particle size and shape correspond to those of the primary aggregates, whereas below that level, the particle size can be tuned by means of the degree of metal complexation. The present process directly produces sterically stabilized particles of metal hydroxides or metal basic salts with long-term stability. Since this preparation route was tested with Al^{3+}, La^{3+}, Cu^{2+}, Ni^{2+}, Zn^{2+}, and Ca^{2+} precursors, it can reasonably be speculated that it is applicable to many other metal ions. The direct precursors of the particles are micelle-like aggregates formed by inhibited precipitation of the insoluble ion/polyelectrolyte complex. For the first time, the core–corona microstructure of the assemblies has been extensively characterized. The hybrid micelles represent new supramolecular precursors for inorganic polycondensation reactions and should serve as model systems for reactions in confined environments. Since this preparation method is highly versatile and robust, it should open new opportunities for the preparation of nanomaterials and also for elucidating the mechanisms involved in soft aqueous chemistry of materials. Finally, the present suspensions may also be excellent candidates for fundamental studies of the phase behavior and dynamics of suspensions of stabilized plate-shaped or rodlike nanoparticles.

Experimental Section

$La(NO_3)_3 \cdot 6H_2O$ and $Al(NO_3)_3 \cdot 9H_2O$ were used as inorganic precursors. Pure solutions of Al_{13}^{7+} clusters were prepared by controlled prehydrolysis of an aqueous solution of $Al(NO_3)_3 \cdot 9H_2O$ (0.1 M) with a solution of sodium hydroxide (0.3 M) at 90 °C. A prehydrolysis ratio $h_1 = [OH^-]/[M]$ of 2.46 was used. The solution was analyzed by ^{27}Al NMR spectroscopy to ensure that it only contained Al_{13} species.[19] Ultrapure deionized water (MilliQ, Millipore, France) was used for the preparation of all solutions. PAA-*b*-PAM and PAA-*b*-PHEA copolymers were synthesized by free-radical polymerization at Rhodia (Aubervilliers, France); the synthesis has been described elsewhere.[30] The pH value of the polymer solutions was then adjusted to 5.5 before mixing with solutions of inorganic precursors, so that the PAA block is partially neutralized before mixing with

 © 2003 Wiley-VCH Verlag GmbH & Co. KGaA, Weinheim

inorganic cations. The concentrations of the mother copolymer solutions were approximately 5 wt%.

The particle suspensions were prepared at room temperature. The copolymer solution was added to the solution of the inorganic precursor, and the mixture vigorously stirred for 10 min. Particle suspensions were obtained by the addition of sodium hydroxide solution (1M). Metal concentrations in the final suspensions varied between 5×10^{-3} and 10^{-1}M.

Light-scattering measurements were carried out with a Zetasizer 3000HS instrument (Malvern, U.K.) with a 10 mW laser operating at 633 nm. Hydrodynamic diameters were obtained from measured diffusion coefficients by using the Stokes–Einstein equation. Small-angle neutron-scattering experiments were carried out at Laboratoire Leon Brillouin (Saclay, France). A q range from 0.004 to 0.5 $Å^{-1}$ was measured. Suspensions were prepared in D_2O to enhance the difference in scattering-length density between solvent and particles. The scattering data were corrected for background intensity.

Transmission electron microscopy (TEM) was performed on a Jeol 1200 EXII microscope operated at 80 kV. Cryo-TEM images were recorded on a Philips CM200 "Cryo" microscope operated at 80 kV. Dry specimens were prepared by depositing one droplet of the micelle or particle suspension onto glow-discharged carbon-coated copper grids. After 1 min the excess liquid was blotted with filter paper, and the remaining film allowed to dry. Cryo-TEM samples were prepared, as described elsewhere,[31] by quench-freezing a thin film of the micelle suspension into liquid ethane at −171 °C. The specimen was mounted onto a Gatan 626 cryo-holder and transferred into the microscope. The micelles were observed at low temperature (−180 °C) embedded in a thin layer of vitreous ice.

Received: January 9, 2003 [Z50917]

Keywords: block copolymers · colloids · metal hydroxides · micelles · nanostructures

[1] E. Matijevic, *Annu. Rev. Mater. Sci.* **1985**, *15*, 483.
[2] E. Matijevic, *Langmuir* **1994**, *10*, 8.
[3] J. P. Jolivet, *Metal Oxide Chemistry and Synthesis: From Solution to Solid State*, Wiley, Chichester, **2000**.
[4] W. Stumm, *Colloids Surf. A* **1993**, *73*, 1.
[5] M. Antonietti, S. Heinz, *Nachr. Chem. Tech. Lab.* **1992**, *40*, 308.
[6] M. Moffit, A. Eisenberg, *Chem. Mater.* **1995**, *7*, 1178.
[7] S. Forster, M. Antonietti, *Adv. Mater.* **1998**, *10*, 195.
[8] "Reactions and Synthesis in Surfactant Systems": C. Göltner, *Surfactant Sci. Ser.* **2001**, *100*, 797.
[9] M. P. Pileni, *Langmuir* **1997**, *13*, 3266.
[10] "Reactions and Synthesis in Surfactant Systems": L. Jeunieau, F. Debuigne, J. B. Nagy, *Surfactant Sci. Ser.* **2001**, 100.
[11] H. Sakai, H. Kawahara, M. Shimazaki, M. Abe, *Langmuir* **1998**, *14*, 2208.
[12] H. Cölfen, *Macromol. Rapid Commun.* **2001**, *22*, 219–252.
[13] J. M. Marentette, J. Norwig, E. Stockelmann, W. H. Meyer, G. Wegner, *Adv. Mater.* **1997**, *9*, 647.
[14] H. Cölfen, M. Antonietti, *Langmuir* **1998**, *14*, 582.
[15] L. Qi, H. Cölfen, M. Antonietti, *Chem. Mater.* **2000**, *12*, 2392.
[16] A. Taubert, D. Palms, O. Weiss, M.-T. Piccini, D. N. Batchelder, *Chem. Mater.* **2002**, *14*, 2594.
[17] S. N. Sidorov, L. M. Bronstein, P. M. Valetsky, J. Hartmann, H. Cölfen, H. Schnablegger, M. Antonietti, *J. Colloid Interface Sci.* **1999**, *212*, 107–211.
[18] Y. Matsai, M. Sedlak, H. Colfen, M. Antonietti, *Chem. Eur. J.* **2002**, *8*, 2429.
[19] L. Allouche, C. Gérardin, T. Loiseau, G. Férey, F. Taulelle, *Angew. Chem.* **2000**, *112*, 521–524; *Angew. Chem. Int. Ed.* **2000**, *39*, 511–514.
[20] J. S. Pedersen, M. C. Gerstenberg, *Macromolecules* **1996**, *29*, 1363.
[21] J. S. Pedersen, C. Svaneborg, *Curr. Opin. Colloid Interface Sci.* **2002**, *7*, 158.
[22] I. W. Hamley, J. S. Pedersen, C. Booth, V. M. Nace, *Langmuir* **2001**, *17*, 6386.
[23] P. Hervé, M. Destarac, J.-F. Berret, J. Lal, J. Oberdisse, I. Grillo, *Europhys. Lett.* **2002**, *58*, 912.
[24] C.-I. Huang, M. Olvera de la Cruz, *Macromolecules* **2002**, *35*, 976–986.
[25] A. V. Kabanov, T. K. Bronich, V. A. Kabanov, K. Yu, A. Eisenberg, *Macromolecules* **1996**, *29*, 6797.
[26] A. Harada, K. Kataoka, *Science* **1999**, *283*, 65.
[27] A. Harada, K. Kataoka, *Macromol. Symp.* **2001**, *172*, 1–9.
[28] L. M. Bronstein, S. N. Sidorov, P. Valetsky, J. Hartmann, H. Colfen, M. Antonietti, *Langmuir* **1999**, *15*, 6256.
[29] Y. Li, Y-K. Gong, K. Nakashima, Y. Murata, *Langmuir* **2002**, *18*, 6727.
[30] D. Taton, A.-Z. Wilczewska, M. Destarac, *Macromol. Rapid Commun.* **2001**, *22*, 1497–1503.
[31] J. L. Putaux, A. Buléon, R. Borsali, H. Chanzy, *Int. J. Biol. Macromol.* **1999**, *26*, 145.

 © 2003 Wiley-VCH Verlag GmbH & Co. KGaA, Weinheim

Ti-Catalyzed Tandem Reactions

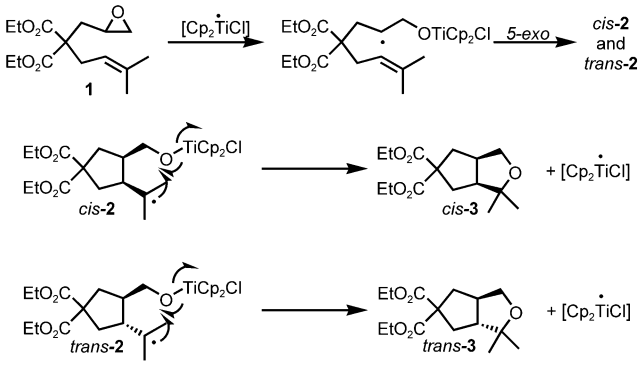
A Radical Tandem Reaction with Homolytic Cleavage of a Ti–O Bond**

Andreas Gansäuer, Björn Rinker, Marianna Pierobon, Stefan Grimme,* Mareike Gerenkamp, and Christian Mück-Lichtenfeld*

Dedicated to Professor Manfred T. Reetz on the occasion of his 60th birthday

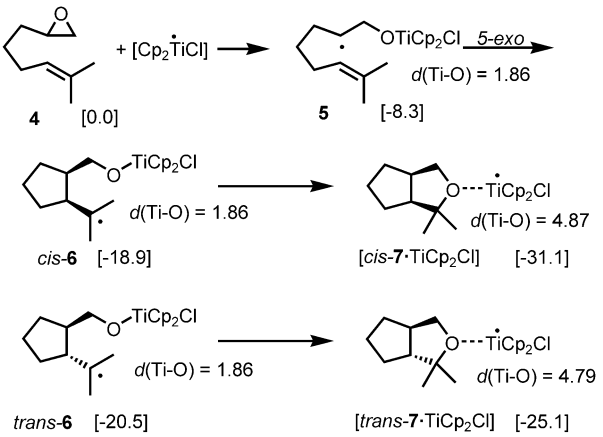
Over the last years radicals have been used increasingly in multistep syntheses due to the mild reaction conditions, high functional group tolerance, and broad accessibility of interesting structures, often obtained in sequential transformations.[1] In this context we wish to report our first results on a novel radical tandem reaction[1b] featuring an unprecedented formal homolytic substitution reaction at a Ti-O bond for the formation of tetrahydrofurans. The planned sequence is shown in Scheme 1. The initial step is based on the titanocene-mediated opening of **1** described by Nugent and RajanBabu,[2] which we have developed into a catalytic reaction,[3] to give the radicals *cis*- and *trans*-**2**.

The second and conceptually novel step of our tandem reaction constitutes the attack of the tertiary radical **2** on the Ti-O bond. Mechanistically, this can be viewed as a homolytic substitution of the [Cp_2TiCl] radical.[4] Our work therefore introduces metal–oxygen bonds as a very useful class of radical traps. As a consequence of this homolytic substitution the redox catalyst [Cp_2TiCl] is regenerated. To the best of our knowledge, this concept of a catalytic redox isomerization is unknown in the literature.



Scheme 1. General concept of the titanocene-catalyzed tandem reactions with tetrahydrofuran formation.

Because the second cyclization is counterintuitive, a supposedly strong Ti-O bond is cleaved and a C-O bond formed, we analyzed the transformation of model system **4** by density functional theory (DFT) calculations as shown in Scheme 2.[5] As expected[1c,6] both the ring opening of **4**



Scheme 2. Intermediates in the DFT model calculation of the reaction of epoxide **4**. The relative energies in brackets are given in kcal mol^{-1} and refer to the separated reactants (**4** and [$TiCp_2Cl$] radical); bond lengths are given in Å.[5]

(−8.3 kcal mol^{-1}) and the 5-*exo* cyclization of **5** (−12.2 kcal mol^{-1} for *trans*-**6**; −10.6 kcal mol^{-1} for *cis*-**6**) are exothermic. Despite this thermodynamic preference for *trans*-**6** the formation of *cis*-**6** should be kinetically favored according to the Beckwith–Houk rules[6] and our own calculations on related systems. A detailed analysis of the transition-state structures of titanocene-mediated cyclizations will be published in due course.

The key steps of our tandem reaction, formation of *cis*-**7** and *trans*-**7** complexed to [Cp_2TiCl], were also found to be exothermic by −12.2 and −4.6 kcal mol^{-1}. Thus, breaking of the Ti–O bond is predicted to be possible! The low energy of formation of *trans*-**7** compared to that of *cis*-**7** can be attributed to the strain in the resulting *trans*-fused bicyclo[3.3.0] system. The product complexes [**7**·$TiCp_2Cl$] shown in Scheme 2 are slightly more stable (−31.1 and −25.1 kcal mol^{-1}) than the separated molecules. Since entropy effects favor the dissociation of the product complex, ΔG will most likely be negative and the catalyst will be regenerated as desired for efficient catalysis.

The relative energies of the transition-state structure, **6**, and **7** were also confirmed by MP2 calculations. The transition-state structure for the formation of [*cis*-**7**·Cp_2TiCl] is shown in Figure 1. This final ring closure has a low barrier (+11.4 kcal mol^{-1}) and should therefore be viable even at low temperatures. The transition state exhibits similar Ti–O and O–C bond lengths. This indicates that a homolytic, concerted

[*] Prof. Dr. A. Gansäuer, B. Rinker, Dr. M. Pierobon
Kekulé-Institut für Organische Chemie und Biochemie
der Universität Bonn
Gerhard-Domagk-Strasse 1, 53127 Bonn (Germany)
Fax: (+49) 228-734760
E-mail: andreas.gansaeuer@uni-bonn.de
Prof. Dr. S. Grimme, M. Gerenkamp, Dr. C. Mück-Lichtenfeld
Organisch-Chemisches Institut der Universität Münster
Corrensstrasse 40, 49149 Münster (Germany)
Fax: (+49) 251-83-36515
E-mail: grimmes@uni-muenster.de

[**] We thank the Deutsche Forschungsgemeinschaft (Gerhard-Hess-Programm) and the Fonds der Chemischen Industrie for financial support.

 DOI: 10.1002/anie.200351240 © 2003 Wiley-VCH Verlag GmbH & Co. KGaA, Weinheim

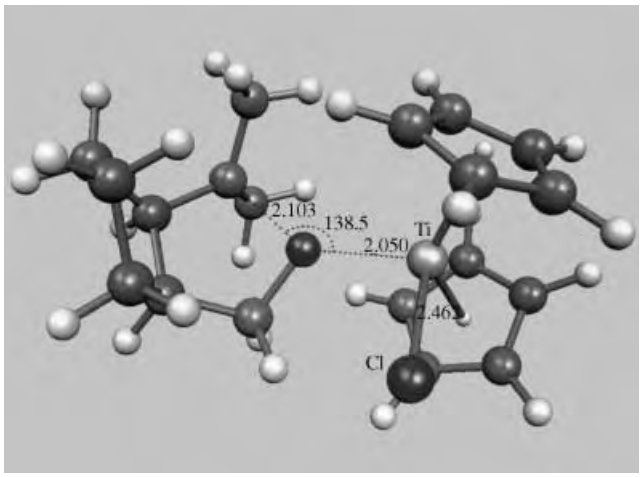


Figure 1. Transition-state structure for the ring closure of *cis*-**6** to *cis*-**7**·$TiCp_2Cl$ (bond lengths in Å).

substitution reaction[4] is taking place which resembles the S_N2 reaction with anionic nucleophiles. The calculated spin densities give a clear indication that the radical center is shifted from carbon to the metal (C +0.37, O −0.05, Ti + 0.70).

These findings suggest that only *cis*-**3** will be preparatively accessible for both kinetic and thermodynamic reasons. With substrates similar to **1** selectivities of 85:15 to 90:10 in favor of the *cis* isomer required here were typically observed[2a,d,3a,3b,3e] in accordance with the Beckwith–Houk rules.[1c,6] Epoxy olefin **1**, which is easily prepared, should therefore constitute a useful starting point for preparative investigations.

We have chosen the tertiary radical **2** as the key intermediate for the tandem reaction because it is relatively inert towards hydrogen-atom abstraction or reduction by a second equivalent of the titanium(III) reagent to yield an organometallic intermediate.[2,3] However, in the absence of other pathways this reduction has been observed.[7] This relative persistence under reducing conditions through exclusion of competing radical pathways should promote the desired tandem reaction.

Our results with **1** are summarized in Table 1. The reaction works well in THF or ethyl acetate in the presence of 10 mol% $[Cp_2TiCl_2]$ as the precatalyst and Mn or Zn dust (2.0–0.2 equiv) as the reductant, producing *cis*-**3** in up to 66% yield. No *trans*-**3** was formed as expected from the calculations. It made little difference whether Mn or Zn was used (entries 1–4). The experiments suggest that a low stationary concentration of the titanium(III) reagent under the highly reducing conditions is essential for better yields due to the deceleration of the undesired reductive trapping of the tertiary radical. Thus, the stoichiometric use of $[Cp_2TiCl]$ (entry 6) results in a reduced yield. The use of ethyl acetate (entry 4) is beneficial with Zn because the reduction of titanium(IV) is slowed down markedly.

The reaction of *trans*-**2** yielded products of simple reductive cyclization, and addition of collidine hydrochloride (0.5 equiv, not optimized) was needed to regenerate the catalyst by the usual protonation of Ti-O and C-O bonds.[2a,b,e]

Table 1: Optimization of the titanocene-catalyzed tandem reaction of **1**.[a][8]

Entry	Catalyst	Conditions	Yield [%]
1	$[Cp_2TiCl_2]$ (10 mol%)	THF, Zn (2 equiv), Coll·HCl (2.5 equiv)	57[b]
2	$[Cp_2TiCl_2]$ (10 mol%)	THF, Mn (2 equiv), Coll·HCl (2.5 equiv)	51[b]
3	$[Cp_2TiCl_2]$ (10 mol%)	THF, Mn (0.2 equiv), Coll·HCl (0.5 equiv)	66[c]
4	$[Cp_2TiCl_2]$ (10 mol%)	EA, Zn (0.2 equiv), Coll·HCl (0.5 equiv)	63[d]
5	$[Cp_2TiCl_2]$ (10 mol%)	THF, Mn (0.2 equiv), Coll·HCl (0.5 equiv)	66[e]
6	$[Cp_2TiCl_2]$ (100 mol%)	THF, Zn (2 equiv)	50[b]
7	$[CpTiCl_3]$ (10 mol%)	THF, Mn (0.2 equiv), Coll·HCl (0.5 equiv)	48[f]

[a] Coll = collidine, EA = ethyl acetate. [b] 24 h, room temperature (RT). [c] 20 h, RT. [d] 60 h, RT. [e] 4 h, 70°C. [f] 16 h, RT.

Entry 6 demonstrates that collidine hydrochloride is not necessary for the reaction to occur. Without reductant no product was formed. Thus, the transformation did indeed proceed under titanium(III) catalysis. The reaction could be accelerated by heating to 70°C without affecting the yield (entry 5). The observation that $[CpTiCl_3]$ led to distinctly inferior results (entry 7) lends support to our mechanistic proposal. Here the Ti-O bond should be stronger and hence more difficult to break because of the higher Lewis acidity of titanium and the reduced steric interaction of the alkoxide with only one bulky cyclopentadienyl ligand.

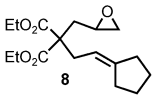
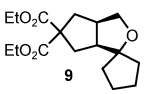
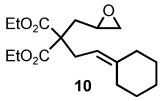
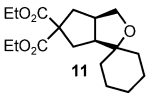
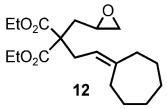
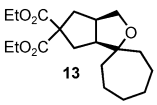
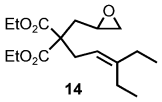
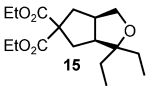
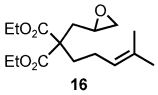
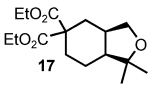
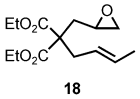
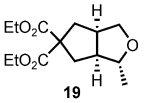
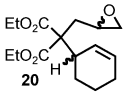
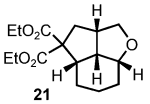
The reaction is not only catalytic but also atom-economical, a feature rarely displayed by radical reactions.[9] We also tested SmI_2, a powerful and frequently employed electron-transfer reagent,[10] $CrCl_2$,[11] and VCl_2,[12] but none of the desired product was obtained.

Some other tandem reactions are summarized in Table 2. The reaction works well for substrates with trisubstituted double bonds (entries 1–4). The spiro tricyclic compounds **9**, **11**, and **13** should be of special interest as there are no other simple approaches for these structurally complex units. The bicyclo[4.3.0] system **17** (entry 5) demonstrates the usefulness of our titanocene-catalyzed protocol. Usually *6-exo* cyclizations are distinctly less efficient than the corresponding *5-exo* cyclizations in contrast to our system.[1] The reaction also works well for substrates containing 1,2-disubstituted double bonds (entries 6 and 7). The diastereoconvergent synthesis of **21** creates a tricyclic system with complete selectivity in just three steps from commercially available starting materials and amply demonstrates the potential of our reaction for the synthesis of complex molecules.

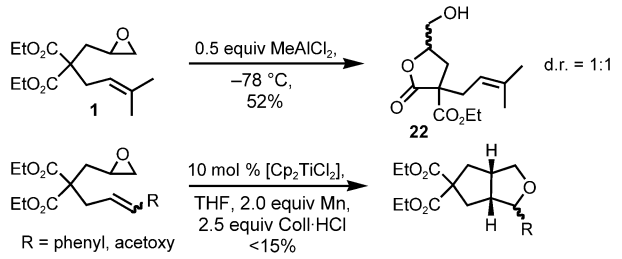
Although all the experimental evidence and the theoretical results support the proposed radical pathway, we also investigated the possibility of cationic pathways.[13,14] However, exposing **1** to $MnCl_2$, $ZnCl_2$, camphorsulfonic acid, $[Cp_2TiCl_2]$, and 2,4,6-collidine hydrochloride did not lead to **3**, whereas reaction with $BF_3{\cdot}Et_2O$ lead to extensive decomposition. In the case of $MeAlCl_2$[13] lactone **22** was the only product (52%) obtained besides recovered **1** (23%) as shown in Scheme 3. Thus, nucleophilic substitution is unlikely under

 © 2003 Wiley-VCH Verlag GmbH & Co. KGaA, Weinheim

Table 2: Scope of the titanocene-catalyzed tandem reaction.

Entry	Substrate	Product	Yield [%]
1	 8	 9	61[a]
2	 10	 11	62[b]
3	 12	 13	62[a]
4	 14	 15	64[b]
5	 16	 17	66[b], d.r. = 88:12
6	 18	 19	60[c], d.r. = 80:20
7	 20	 21	63[c], d.r. > 98:2

[a] 10 mol% $[Cp_2TiCl_2]$, Zn, EtOAc (0.02 M). [b] 10 mol% $[Cp_2TiCl_2]$, THF (0.1 M), Mn. [c] 20 mol% $[Cp_2TiCl_2]$, EtOAc (0.02 M), Zn.



Scheme 3. Experimental evidence against cationic intermediates in the reaction of **1**.

our conditions. The oxidation of radical *cis*-**2** to give a cation by a radical–polar crossover mechanism[14] and THF ring closure by an S_N1 reaction were rendered unlikely by the other two examples shown in Scheme 3. In both cases hardly any (< 15% as judged by NMR analysis of the crude mixture) of the desired product was formed. The phenyl and the acetoxy group should promote the putative oxidation by stabilizing the cation by mesomeric effects. Besides, this mechanism requires the presence of oxidants. This is unlikely under our reducing conditions because excess metal powder is always present.

Received: February 20, 2003
Revised: April 3, 2003 [Z51240]

Keywords: epoxides · homolytic substitution · radical reactions · tandem reactions · titanium

[1] a) *Radicals in Organic Synthesis* (Eds.: P. Renaud, M. Sibi), Wiley-VCH, Weinheim, **2001**; b) A. J. McCarroll, J. C. Walton, *Angew. Chem.* **2001**, *113*, 2282; *Angew. Chem. Int. Ed.* **2001**, *40*, 2225; c) D. P. Curran, N. A. Porter, B. Giese, *Stereochemistry of Radical Reactions*, VCH, Weinheim, **1996**; d) J. Fossey, D. Lefort, J. Sorba, *Free Radicals In Organic Synthesis*, Wiley, Chichester, **1995**.

[2] a) W. A. Nugent, T. V. RajanBabu, *J. Am. Chem. Soc.* **1988**, *110*, 8561; b) T. V. RajanBabu, W. A. Nugent, *J. Am. Chem. Soc.* **1989**, *111*, 4525; c) T. V. RajanBabu, W. A. Nugent, M. S. Beattie, *J. Am. Chem. Soc.* **1990**, *112*, 6408; d) T. V. RajanBabu, W. A. Nugent, *J. Am. Chem. Soc.* **1994**, *116*, 986.

[3] a) A. Gansäuer, M. Pierobon, H. Bluhm, *Angew. Chem.* **1998**, *110*, 107; *Angew. Chem. Int. Ed.* **1998**, *37*, 101; b) A. Gansäuer, H. Bluhm, M. Pierobon, *J. Am. Chem. Soc.* **1998**, *120*, 12849; c) A. Gansäuer, T. Lauterbach, H. Bluhm, M. Noltemeyer, *Angew. Chem.* **1999**, *111*, 3112; *Angew. Chem. Int. Ed.* **1999**, *38*, 2909; d) A. Gansäuer, H. Bluhm, *Chem. Rev.* **2000**, *100*, 2771; e) A. Gansäuer, M. Pierobon, H. Bluhm, *Synthesis* **2001**, 2500; f) A. Gansäuer, M. Pierobon, H. Bluhm, *Angew. Chem.* **2002**, *114*, 3341; *Angew. Chem. Int. Ed.* **2002**, *41*, 3206.

[4] a) C. H. Schiesser, L. M. Wild, *Tetrahedron* **1996**, *52*, 13265; b) J. C. Walton, *Acc. Chem. Res.* **1998**, *31*, 99.

[5] All DFT calculations were performed with the Turbomole program package.[5a] The geometries and energies were obtained with the BP functional[5b,c] and a TZVP basis set[5d] using unrestricted wavefunctions. The transition state was obtained using an eigenvector-following algorithm.[5e] Spin densities for the transition state were calculated using the Mulliken population analysis scheme. a) Turbomole 5.3: R. Ahlrichs, M. Bär, H.-P. Baron, R. Bauernschmitt, S. Böcker, M. Ehrig, K. Eichkorn, S. Elliot, F. Furche, F. Haase, M. Häser, H. Horn, C. Huber, U. Huniar, M. Kattanek, C. Kölmel, M. Kollwitz, K. May, C. Ochsenfeld, H. Öhm, A. Schäfer, U. Schneider, O. Treutler, M. von Armin, F. Weigend, P. Weis, H. Weiss, Universität Karlsruhe, **2002**; b) A. D. Becke, *Phys. Rev. B* **1988**, *38*, 3098; c) J. P. Perdew, *Phys. Rev. B* **1986**, *33*, 8822; d) A. Schäfer, C. Huber, R. Ahlrichs, *J. Chem. Phys.* **1994**, *100*, 5829; e) EF routine in Mopac 6: J. Baker, *J. Comput. Chem.* **1986**, *7*, 385.

[6] a) A. L. J. Beckwith, C. H. Schiesser, *Tetrahedron* **1985**, *41*, 3925; b) D. C. Spellmeyer, K. N. Houk, *J. Org. Chem.* **1987**, *52*, 959.

[7] A. F. Barrero, J. M. Cuerva, M. M. Herrador, M. V. Valdivia, *J. Org. Chem.* **2001**, *66*, 4074.

[8] Typical experimental procedure: Collidine hydrochloride (79 mg, 0.5 mmol, 0.5 equiv) was dried under vacuum by gentle heating. Dry THF (10 mL), $[Cp_2TiCl_2]$ (25 mg, 0.1 mmol, 0.1 equiv) and manganese powder (11 mg, 0.2 mmol, 0.2 equiv) were added, and the resulting suspension was stirred at room temperature until the reaction mixture turned green. After the addition of **1** (284 mg, 1.0 mmol) stirring was continued for further 16 h at room temperature. The reaction was quenched by addition of HCl (2 N, 30 mL), then methyl *tert*-butyl ether (30 mL) was added and the organic layer was separated. After extraction of the aqueous layer with CH_2Cl_2 (2 × 30 mL) the combined organic layers were washed with saturated aq. $NaHCO_3$ (30 mL), H_2O (2 × 30 mL), and saturated aq. NaCl (30 mL) and dried over $MgSO_4$. The solvent was removed under reduced pressure and the residue purified by SiO_2 flash chromatography to yield *cis*-**3** (189 mg, 66%).

[9] a) B. M. Trost, *Science* **1991**, *254*, 1471; b) B. M. Trost, *Angew. Chem.* **1995**, *107*, 285; *Angew. Chem. Int. Ed. Engl.* **1995**, *34*, 259.

[10] For some reviews on SmI_2 see: a) H. B. Kagan, J.-L. Namy, *Tetrahedron* **1986**, *42*, 6573; b) G. A. Molander, *Chem. Rev.* **1992**,

 © 2003 Wiley-VCH Verlag GmbH & Co. KGaA, Weinheim

92, 29; c) G. A. Molander, C. R. Harris, *Chem. Rev.* **1996**, *96*, 307; d) T. Skrydstrup, *Angew. Chem.* **1997**, *109*, 355; *Angew. Chem. Int. Ed. Engl.* **1997**, *36*, 345; e) A. Krief, A.-M. Laval, *Chem. Rev.* **1999**, *99*, 745.

[11] For a recent review see: A. Fürstner, *Chem. Rev.* **1999**, *99*, 991.

[12] a) J. H. Freudenberger, A. W. Konradi, S. F. Pedersen, *J. Am. Chem. Soc.* **1989**, *111*, 8014; b) A. W. Konradi, S. J. Kemp, S. F. Pedersen, *J. Am. Chem. Soc.* **1994**, *116*, 1316.

[13] Y. Mi, J. V. Schreiber, E. J. Corey, *J. Am. Chem. Soc.* **2002**, *124*, 11290, and references therein.

[14] For a recent review see: J. A. Murphy in *Radicals in Organic Synthesis, Vol. 2* (Eds.: P. Renaud, M. Sibi), Wiley-VCH, Weinheim, **2001**, 298, and references therein.

 © 2003 Wiley-VCH Verlag GmbH & Co. KGaA, Weinheim

Sterically Flexible Carbene Ligands

An N-Heterocyclic Carbene Ligand with Flexible Steric Bulk Allows Suzuki Cross-Coupling of Sterically Hindered Aryl Chlorides at Room Temperature **

*Gereon Altenhoff, Richard Goddard, Christian W. Lehmann, and Frank Glorius**

Dedicated to Professor Manfred T. Reetz on the occasion of his 60th birthday

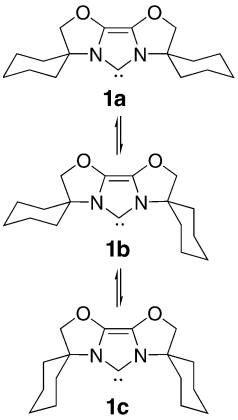
The Suzuki cross-coupling reaction has become a standard method for biaryl synthesis in both academia and industry.[1] Its popularity is based on its wide functional-group tolerance and the ready availability and low toxicity of the required boronic acids. Although aryl iodides or bromides usually serve as the substrates, the development of new catalyst systems has recently enabled the efficient coupling of aryl chlorides, which are cheaper and more readily available.[2] Most successful have been applications of palladium complexes of electron-rich, sterically demanding phosphane[3] or N-heterocyclic carbene (NHC)[4,5] ligands. Several factors are thought to be responsible for the success of the ligands used in these systems: 1) their electron-rich nature enhances the rate of oxidative addition, 2) the ligands coordinate tightly to the Pd, thus disfavoring the formation of Pd black, and 3) their steric bulk favors a monophosphane– or monocarbene–Pd species[6] and increases the rate of reductive elimination.[3b,4d]

[*] Dr. F. Glorius, Dipl.-Chem. G. Altenhoff, Dr. R. Goddard, Dr. C. W. Lehmann
Max-Planck-Institut für Kohlenforschung
Kaiser-Wilhelm-Platz 1, 45470 Mülheim an der Ruhr (Germany)
Fax: (+49) 208-306-2994
E-mail: glorius@mpi-muelheim.mpg.de

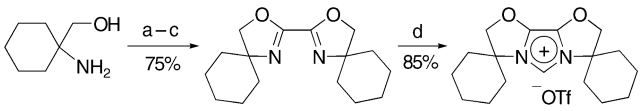
[**] We thank Prof. A. Fürstner for generous support and constant encouragement and the Fonds der Chemischen Industrie as well as the Deutsche Forschungsgemeinschaft for financial support.

Supporting information for this article is available on the WWW under http://www.angewandte.org or from the author.

However, despite considerable efforts, the coupling of aryl chlorides to give biaryl compounds with more than one *ortho* substituent at room temperature has not been realized to date.[7]

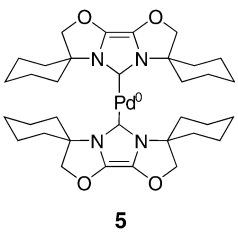


To overcome this problem, an electron-rich ligand is required that is *small* enough to accept sterically hindered substrates yet sufficiently *bulky* to support monoligation and promote reductive elimination. We rationalized that these stringent requirements could be met by new NHC **1**, which exhibits *flexible* steric bulk. Imidazolium salt **4** (Scheme 1) and the corresponding NHC **1** derived thereof are expected to exist in the form of three different conformers **a**, **b** and **c**. Conformation **a** should allow the coordinated Pd^0 to undergo oxidative addition, even with sterically hindered substrates, and facilitate transmetallation, whereas the sterically more demanding conformations **b** or **c** should enhance reductive elimination and favor a monocarbene Pd species.[8]



Scheme 1. Synthesis of imidazolium salt **4**. a) Diethyl oxalate, $(ClCH_2)_2$, toluene, 80 °C, 84 %; b) $SOCl_2$, toluene, 90 °C, 93 %; c) THF, EtOH, NaOH, 80 °C, 96 %; d) AgOTf, chloromethyl pivalate, CH_2Cl_2, 40 °C, 85 %.

The synthesis of imidazolium salt **4** was based on our recent finding that bioxazolines can be converted into imidazolium salts with AgOTf and chloromethyl pivalate.[9] The desired salt **4** was obtained in 64 % overall yield from diethyl oxalate and amino alcohol **2** (Scheme 1). The conformational flexibility of imidazolium salt **4** was confirmed by crystal structure and NMR spectroscopic analysis. The unit cell of **4** contains two independent cations, with conformations corresponding to that of **a** and **b** (Figure 1).[10] NMR spectroscopic analysis of **4** in CD_2Cl_2 revealed that **4a** and **4b** exist in a ratio of 2.4:1 at −80 °C, whereas only one set of signals is observed at room temperature, thus indicating rapid interconversion of **4a** and **4b** on the NMR timescale.



$Pd(NHC)_2$ complex **5**[11] (Figure 2) was synthesized from **4**, $[\{(\eta^3\text{-}C_3H_5)PdCl\}_2]$, and sodium malonate.[12] Interestingly, **5** proved to be catalytically inactive in the Suzuki coupling under the conditions employed (Table 1) and only became active at higher temperatures. However, a catalyst prepared from $Pd(OAc)_2$ and 1 equivalent of imida-

 © 2003 Wiley-VCH Verlag GmbH & Co. KGaA, Weinheim DOI: 10.1002/anie.200351325

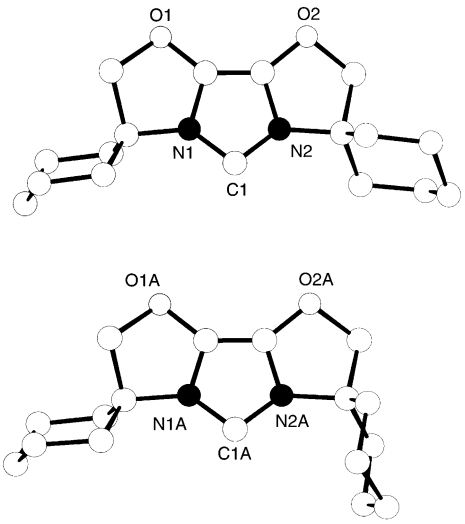


Figure 1. Structures of the two independent cations of **2** in the crystal.

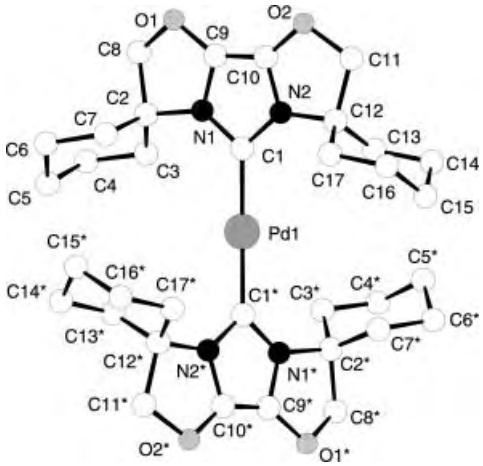


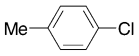
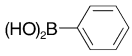
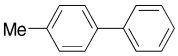
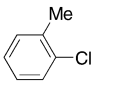
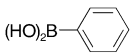
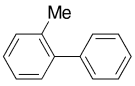
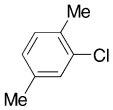
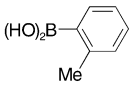
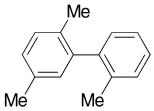
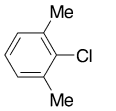
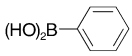
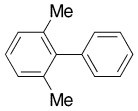
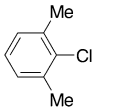
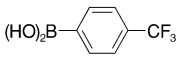
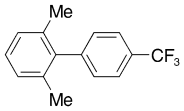
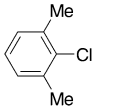
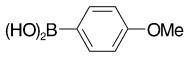
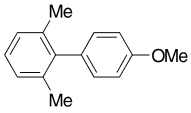
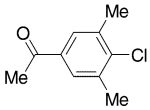
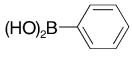
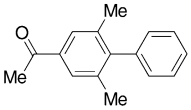
Figure 2. Structure of **5** in **5**·THF. Selected distances [Å] and angles [°]: Pd1-C1 2.001(2), C1-N1 1.367(3), C1-N2 1.373(3), C5···C13* 4.197(4), C6···C14* 4.293(4), C7···C15* 4.220(4); C1-N1-C2 135.0(2), C1-N2-C12 134.0(2), mean plane (C1, C9, C10, N1, N2, Pd1)/mean plane (C1*, C9*, C10*, N1*, N2*, Pd1) 62(1)°.

zolium salt **4** showed excellent catalytic activity at room temperature, thus indicating that a Pd^0(NHC) species may be the active catalyst.[6] To demonstrate the efficacy of this system, we prepared several biaryl derivatives from aryl chlorides and aryl boronic acids.[13] As shown in Table 1, unsubstituted, mono-*ortho*-, and di-*ortho*-substituted aryl chlorides can be coupled in good to excellent yields with a variety of aryl boronic acids in the presence of 3 mol% Pd. High turnover numbers of 1730 at room temperature and 3130 at 60°C were obtained in the coupling of a sterically hindered aryl chloride (Table 1, entries 7 and 8).

For sterically hindered boronic acids the use of a THF/H_2O mixture as solvent and KO*t*Bu as base was found to be optimal (Table 2). Remarkably, these reaction conditions allow the coupling of highly hindered 2,6-dimethylbenzeneboronic acid with unsubstituted, *ortho*-substituted, electron-deficient, and electron-rich aryl chlorides (Table 2, entries 1–5). To the best of our knowledge, these results represent the first room-temperature Suzuki cross-coupling of aryl chlorides with aryl boronic acids to give di- and tri-*ortho*-substituted biaryl compounds. Furthermore, the reaction of 2,6-dimethylchlorobenzene with 2-methylbenzeneboronic acid, which results mainly in homocoupling of the aryl boronic acid under standard conditions, was achieved by increasing the NHC/Pd ratio from 1 to 2 and heating at 60°C (Table 2, entry 6).[14]

Flexible steric bulk might be the key to success. Although Herrmann and co-workers showed that [Pd(**6**)$_2$] is an efficient catalyst for the Suzuki cross-coupling reaction of unhindered aryl chlorides at room temperature, *ortho* substitution is less well tolerated.[4a] A

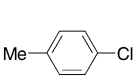
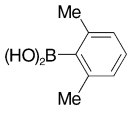
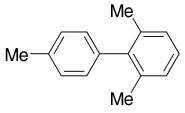
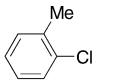
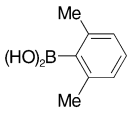
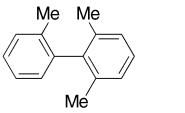
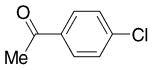
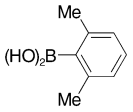
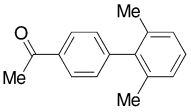
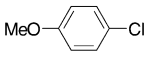
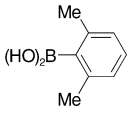
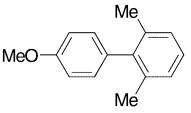
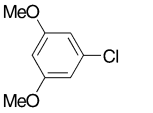
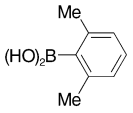
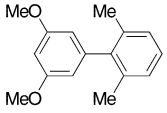
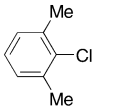
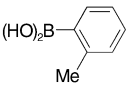
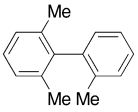
Table 1: Suzuki coupling of sterically hindered aryl chlorides.[a]

Entry	Aryl chloride	Boronic acid	Product	Yield [%][b]
1				82[c]
2				83
3				94
4				79[c]
5				85
6				87
7				52[d]
8				94[e]

[a] Standard conditions: $Pd(OAc)_2$ (3 mol%), **1** (prepared from **4** (3.1 mol%), KH (6.25 mol%), KO*t*Bu (0.67 mol%) in THF), aryl chloride (1 mmol, 1.0 equiv), boronic acid (1.1 equiv), CsF (2.0 equiv), THF (0.3 M), room temperature, 24 h (reaction times were optimized). [b] Yields of isolated products. [c] When **5** was used as catalyst, <5% of product was obtained. [d] Catalyst: 0.03 mol%. [e] Catalyst: 0.03 mol%, at 60°C.

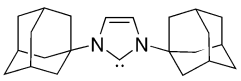
 © 2003 Wiley-VCH Verlag GmbH & Co. KGaA, Weinheim

Table 2: Suzuki coupling of sterically hindered boronic acids.[a]

Entry	Aryl chloride	Boronic acid	Product	Yield [%][b]
1				70
2				69
3				95
4				72
5				76
6				66[c]

[a] Standard conditions: $Pd(OAc)_2$ (3 mol%), **1** (prepared from **2** (3.1 mol%), KH (6.25 mol%), KO*t*Bu (0.67 mol%) in THF), aryl chloride (1 mmol, 1.0 equiv), boronic acid (1.1 equiv), KO*t*Bu (2.0 equiv), THF/H_2O (10:1, 0.3 M), room temperature, 24 h (reaction times were not optimized). [b] Yields of isolated products. [c] 60 °C.

comparison of the crystal structures of the $Pd(NHC)_2$ complexes of **1** and **6** indicates that **6** is bulkier than **1a**.[15] Although bulk aids reductive elimination, it impedes oxidative addition and transmetallation of sterically hindered substrates allowed by the more flexible **1**.



6

In conclusion, we have developed a general, highly efficient catalyst system for the room-temperature Suzuki coupling of hindered and unhindered, activated and deactivated aryl chlorides and aryl boronic acids. For the first time di- and tri-*ortho*-substituted biaryl compounds were formed under these conditions and high turnover numbers were obtained. We anticipate that other metal-catalyzed reactions will benefit from the application of the concept of flexible steric bulk.

Experimental Section

4: Chloromethyl pivalate (1.25 mL, 8.4 mmol) was added to a suspension of AgOTf (2.16 g, 8.4 mmol) in CH_2Cl_2 (30 mL), and the resulting suspension was stirred in the absence of light for 45 min. After filtration, the filtrate was added to bioxazoline **3** (1.60 g, 5.8 mmol), and the solution was stirred in a sealed tube in the absence of light at 40 °C for 20 h. After the solution was cooled to room temperature, the solvent was evaporated in vacuo and the resulting oil was purified by column chromatography (silica gel, 2.5 × 10 cm, CH_2Cl_2/MeOH 20:1→10:1). Subsequent crystallization from a solvent mixture of THF (10 mL), toluene (40 mL), and pentane (40 mL) gave imidazolium triflate **4** (2.15 g, 85%) as colorless crystals. $R_f = 0.58$ (CH_2Cl_2/MeOH 10:1); IR (KBr): $\tilde{\nu} = 3113$, 2945, 2862, 1727, 1516, 1459, 1266, 1224, 1151, 1031, 957, 913, 825, 754, 637 cm^{-1}; ^1H NMR (400 MHz, $CDCl_3$): $\delta = 9.12$ (s, 1H; NCHN), 4.80 (s, 4H; OCH_2), 2.32 (td, $J = 3.8$, 12.5 Hz, 4H; CH_2), 2.10–1.98 (m, 8H; CH_2), 1.74–1.58 (m, 4H; CH_2), 1.46–1.37 ppm (m, 4H; CH_2); ^{13}C NMR (100 MHz, $CDCl_3$): $\delta = 124.6$ (NCO), 120.8 (q, $J = 319$ Hz, CF_3), 113.9 (NCHN), 85.6 (OCH_2), 67.5 (CCH_2), 34.7 (CH_2), 23.5 (CH_2), 23.1 ppm (CH_2); ^{19}F NMR (300 MHz, $CDCl_3$): $\delta = -78.5$ ppm (CF_3); MS (EI): *m*/*z* (%): 289 (100), 261 (5), 194 (5), 166 (5), 122 (12), 95 (20); HRMS (EI): calcd for $C_{17}H_{25}N_2O_2$ (cation): 289.1916; found: 289.1918; elemental analysis: calcd for $C_{18}H_{25}F_3N_2O_5S$: C 49.31, H 5.75, N 6.39; found: C 49.52, H 5.75, N 6.31.

Received: March 4, 2003 [Z51325]

Keywords: biaryls · carbene ligands · C–C coupling · cross-coupling · palladium

[1] a) N. Miyaura, A. Suzuki, *Chem. Rev.* **1995**, *95*, 2457; b) A. Suzuki, *J. Organomet. Chem.* **1999**, *576*, 147; c) N. Miyaura, *Top. Curr. Chem.* **2002**, *219*, 11; d) S. Kotha, K. Lahiri, D. Kashinath, *Tetrahedron* **2002**, *58*, 9633.

[2] For a review, see: A. F. Littke, G. C. Fu, *Angew. Chem.* **2002**, *114*, 4350; *Angew. Chem. Int. Ed.* **2002**, *41*, 4176.

[3] For example, see: a) R. B. Bedford, C. S. J. Cazin, S. L. Hazelwood, *Angew. Chem.* **2002**, *114*, 4294; *Angew. Chem. Int. Ed.* **2002**, *41*, 4120; b) J. P. Wolfe, R. A. Singer, B. H. Yang, S. L. Buchwald, *J. Am. Chem. Soc.* **1999**, *121*, 9550; c) A. F. Littke, C. Dai, G. C. Fu, *J. Am. Chem. Soc.* **2000**, *122*, 4020; d) J. P. Stambuli, R. Kuwano, J. F. Hartwig, *Angew. Chem.* **2002**, *114*, 4940; *Angew. Chem. Int. Ed.* **2002**, *41*, 4746; e) A. Zapf, A. Ehrentraut, M. Beller, *Angew. Chem.* **2000**, *112*, 4315; *Angew. Chem. Int. Ed.* **2000**, *39*, 4153.

[4] a) C. W. K. Gstöttmayr, V. P. W. Böhm, E. Herdtweck, M. Grosche, W. A. Herrmann, *Angew. Chem.* **2002**, *114*, 1421; *Angew. Chem. Int. Ed.* **2002**, *41*, 1363; b) W. A. Herrmann, C.-P. Reisinger, M. Spiegler, *J. Organomet. Chem.* **1998**, *557*, 93; c) T. Weskamp, V. P. W. Böhm, W. A. Herrmann, *J. Organomet. Chem.* **1999**, *585*, 348; d) G. A. Grasa, M. S. Viciu, J. Huang, C. Zhang, M. L. Trudell, S. P. Nolan, *Organometallics* **2002**, *21*, 2866; e) C. Zhang, J. Huang, M. L. Trudell, S. P. Nolan, *J. Org. Chem.* **1999**, *64*, 3804; f) A. Fürstner, A. Leitner, *Synlett* **2001**, 290.

[5] For an excellent review on the use of NHC ligands in catalysis, see: a) W. A. Herrmann, *Angew. Chem.* **2002**, *114*, 1342; *Angew. Chem. Int. Ed.* **2002**, *41*, 1291; see also: b) A. J. Arduengo III, R. Krafczyk, *Chem. Unserer Zeit* **1998**, *32*, 6; c) D. Bourissou, O. Guerret, F. P. Gabbaï, G. Bertrand, *Chem. Rev.* **2000**, *100*, 39.

[6] The importance of monoligated Pd^0 complexes as catalytically active species in Suzuki cross-coupling has been proposed; for

 © 2003 Wiley-VCH Verlag GmbH & Co. KGaA, Weinheim

example, see: a) reference [3c]; b) reference [3d]; c) Q.-S. Hu, Y. Lu, Z.-Y. Tang, H.-B. Yu, *J. Am. Chem. Soc.* **2003**, *125*, 2856.
[7] For the synthesis of sterically hindered biaryl compounds by Suzuki cross-coupling at elevated temperatures, see: a) reference [3b]; b) reference [3c]; c) J. Yin, M. P. Rainka, X.-X. Zhang, S. L. Buchwald, *J. Am. Chem. Soc.* **2002**, *124*, 1162.
[8] For a mechanistic discussion of Pd/NHC catalyst systems in Suzuki cross-coupling reactions, see reference [4d].
[9] F. Glorius, G. Altenhoff, R. Goddard, C. Lehmann, *Chem. Commun.* **2002**, 2704.
[10] a) Crystal data for **4**:[11] $[C_{17}H_{25}N_2O_2]^+[CF_3O_3S]^-$, from THF/hexane, $M_r = 438.46$, crystal size: $0.18 \times 0.18 \times 0.18\ mm^3$, monoclinic, space group $P2_1/n$ (No. 14), $a = 12.6250(1)$, $b = 14.4420(1)$, $c = 22.1470(2)$ Å, $\beta = 98.289(1)°$, $V = 3995.88(6)$ Å^3, $Z = 8$, $\rho_{calcd} = 1.458\ g\,cm^{-3}$, $F(000) = 1840$, 99914 measured and 12665 independent reflections ($R_{int} = 0.068$), 9933 with $I > 2\sigma(I)$, $\theta_{max} = 30.96°$, $T_{min} = 0.958$, $T_{max} = 0.987$, 548 parameters, imidazolium H atoms were refined isotropically, otherwise riding, one anion slightly disordered (0.93:0.07), Chebychev weights, $R_1 = 0.0451$, $wR_2 = 0.1102$ (all data), $\Delta\rho_{max/min} = 0.454/-0.443\ e\,Å^{-3}$; b) Crystal data for **5**·THF:[11] $[C_{34}H_{48}N_4O_4Pd]\cdot[C_4H_8O]$, from THF/hexane, $M_r = 755.27$, crystal size: $0.24 \times 0.11 \times 0.10\ mm^3$, tetragonal, space group $I\bar{4}$ (No. 82), $a = 23.7110(2)$, $c = 12.6712(1)$ Å, $V = 7123.9(1)$ Å^3, $Z = 8$, $\rho_{calcd} = 1.408\ g\,cm^{-3}$, $F(000) = 3184$, 57202 measured and 11290 independent reflections ($R_{int} = 0.053$), 9227 with $I > 2\sigma(I)$, $\theta_{max} = 30.99°$, $T_{min} = 0.899$, $T_{max} = 0.950$, 434 parameters, absolute structure not determined (Pd atoms on Wyckhoff positions *e* and *f*), H atoms riding, Chebychev weights, $R_1 = 0.037$, $wR_2 = 0.085$ (all data), $\Delta\rho_{max/min} = 1.820/-0.673\ eÅ^{-3}$.
[11] General information for crystal-structure analysis: Data capture on a Nonius KappaCCD diffractometer at $T = 100\,°C$, $\lambda(Mo_{K\alpha}) = 0.71073$ Å, $\mu = 0.22$ (**4**), 0.57 mm^{-1} (**5**·THF); structure determination by direct methods (SHELXS-97), least-squares refinement (SHELXL-97) on F_0^2 (SHELXL-97); both programs from: G. Sheldrick, University of Göttingen, 1997; CCDC-204549 (**4**) and CCDC-204550 (**5**·THF) contain the crystallographic data (excluding structure factors) for this paper. These data can be obtained free of charge via www.ccdc.cam.ac.uk/conts/retrieving.html (or from the Cambridge Crystallographic Data Centre, 12 Union Road, Cambridge CB2 1EZ, UK; fax: (+44) 1223-336-033; or e-mail: deposit@ccdc.cam.ac.uk).
[12] S. Caddick, F. G. N. Cloke, G. K. B. Clentsmith, P. B. Hitchcock, D. McKerrecher, L. R. Titcomb, M. R. V. Williams, *J. Organomet. Chem.* **2001**, *617–618*, 635.
[13] All new compounds were fully characterized.
[14] A beneficial effect of increasing the ligand/Pd ratio was also observed by Buchwald and co-workers for Pd–phosphane-catalyzed cross-coupling reactions of sterically hindered substrates.[3b]
[15] Whereas the $C_{carbene}$-N-$C_{substituent}$ angle is 135° in **5**·THF, in [Pd(**6**)$_2$] it is 124°. Moreover, the favorable conformation of the spirocyclohexyl groups allows **5** to adopt an arrangement in which the two imidazolylidene ligands are more nearly coplanar. Thus, in [Pd(**6**)$_2$] the angle between the imidazolylidene ligands is 84.4(2)°, whereas in **5** it is 62(1)° (mean), despite a significantly shorter Pd–C distance (2.001(2) relative to 2.076(5) Å).[4a]

 © 2003 Wiley-VCH Verlag GmbH & Co. KGaA, Weinheim

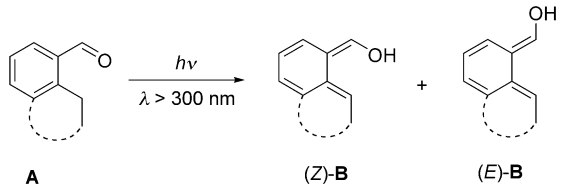
Asymmetric Photochemistry

Highly Enantioselective Diels–Alder Reaction of a Photochemically Generated *o*-Quinodimethane with Olefins**

*Benjamin Grosch, Caroline N. Orlebar, Eberhardt Herdtweck, Werner Massa, and Thorsten Bach**

Dedicated to Professor Manfred T. Reetz on the occasion of his 60th birthday

A highly reactive *ortho*-quinodimethane can be generated by intramolecular H-abstraction from a photochemically excited *ortho*-alkyl-substituted benzaldehyde **A** (Scheme 1). Its reaction with alkenes at low temperature represents a photochemical alternative to the classical Diels–Alder reaction between a diene and a dienophile.[1] The photochemical reaction was dicovered by Yang and Rivas in 1961[2] and was studied intensively thereafter. It was shown that only the *E* diastereoisomer ($\tau > 1$ s) of the two formed enols (*Z*)-**B** and (*E*)-**B** enters the cycloaddition reaction, while the *Z* diastereoisomer is subject to fast ($\tau = 30$ ns–1 μs) tautomerization.[3,4] As a consequence of this selectivity and due to the



Scheme 1. Photochemical formation of *o*-quinodimethanes **B** from *o*-substituted benzaldehydes **A**.

[*] Prof. Dr. T. Bach, Dipl.-Chem. B. Grosch
Lehrstuhl für Organische Chemie I
Technische Universität München
Lichtenbergstrasse 4, 85747 Garching (Germany)
Fax: (+49) 89-2891-3315
E-mail: thorsten.bach@ch.tum.de
C. N. Orlebar
Inorganic Chemistry Laboratory
University of Oxford
South Parks Road, Oxford OX1 3QR (UK)
Dr. E. Herdtweck
Lehrstuhl für Anorganische Chemie
Technische Universität München (Germany)
Prof. Dr. W. Massa
Fachbereich Chemie
Philipps-Universität Marburg
Hans-Meerwein-Strasse, 35032 Marburg (Germany)

[**] This project was supported by the Deutsche Forschungsgemeinschaft (Ba 1372-4/3) and the Fonds der Chemischen Industrie (FCI). B.G. is grateful to the FCI for a Kekulé-scholarship. E.H. thanks Mrs. Helena Keller for technical assistance.

 DOI: 10.1002/anie.200351567 © 2003 Wiley-VCH Verlag GmbH & Co. KGaA, Weinheim

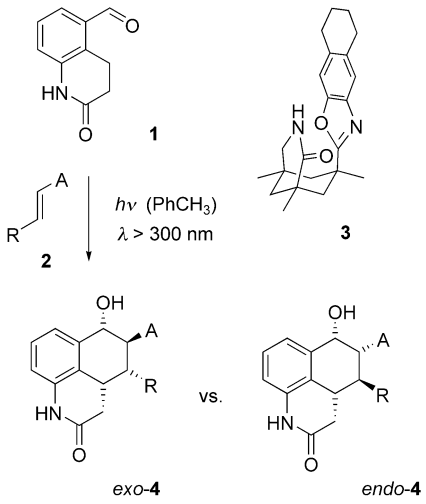
exo or *endo* selectivity determined by the choice of alkene, the product is formed with high diastereoselectivity. Up to four stereogenic centers can be created in a single step. Important applications of this reaction in the synthesis of highly substituted biologically relevant tetralins have been described.[1,5]

Despite its synthetic potential, no enantioselective example of the Diels–Alder reaction of *o*-quinodimethanes has been reported to the best of our knowledge. By employing substrate **1** (Scheme 2), which exhibits a lactam ring as noncovalent binding site for hydrogen bonds,[6] we envisaged a possible enantioselective version of the reaction. The required substrate was synthesized in a short sequence from *m*-aminobenzoic acid.[7]

Table 1: Enantioselective Diels–Alder reaction of compound **1** with dienophiles **2** (see Scheme 2) in the presence of the chiral complexing agent **3**.[9]

Entry	A	R	T[a] [°C]	**3** [equiv]	Product	d.r.[b]	Yield [%]	*ee*[c] [%]
1	CN	H	30	-	*exo*-**4a**	69:31	65	-
2	CN	H	30	2.5	*exo*-**4a**	71:29	69	70
3	CN	H	−35	2.5	*exo*-**4a**	65:35	62	92
4	CN	H	−60	1.2	*exo*-**4a**	63:37	69	91
5	CN	H	−60	2.5	*exo*-**4a**	75:25	68	96
6	COOMe	H	30	-	*endo*-**4b**	>95:5	47	-
7	COOMe	H	−60	1.2	*endo*-**4b**	>95:5	73	94
8	COOMe	H	−60	2.5	*endo*-**4b**	>95:5	68	97
9	COOMe	COOMe	30	-	*endo*-**4c**	56:44	76	-
10	COOMe	COOMe	−60	1.2	*endo*-**4c**	80:20	77	94
11	COOMe	COOMe	−60	2.5	*endo*-**4c**	83:17	78	96

[a] Irradiation temperature. [b] The diastereomeric ratio (d.r.) of the crude product mixture was determined by HPLC. [c] The *ee* values of the major diastereoisomer were determined by chiral GC (after derivatization with trimethylsilylchloride/hexamethyldisilazane) or by NMR shift experiments.



Scheme 2. Enantioselective Diels–Alder reaction of the *o*-quinodimethane derived from compound **1** with the dienophiles **2** to give products **4**.

In the presence of a chiral complexing agent of type **3**[8] the enantiotopic faces of the photochemically generated *o*-quinodimethane should be differentiated. Consequently, it was expected that in the reaction with appropriate dienophiles **2** the absolute and relative configuration of the products should be controlled. The regioselectivity is clearly defined for acceptor-substituted olefins (**2**, A = acceptor).

Indeed, our preliminary experiments with substrate **3** and alkenes **2** showed an extremely effective face differentiation (Table 1) simultaneous with perfect regioselectivity and good-to-excellent simple diastereoselectivity.[9] The reaction of acrylonitrile (**2a**) mainly gave the *exo* diastereoisomer *exo*-**4a** (entries 1–5), while the reactions of methyl acrylate (**2b**) and dimethyl fumarate (**2c**) showed a distinct *endo* selectivity in favor of *endo*-**4b** (entries 6–8) and *endo*-**4c** (entries 10, 11), respectively. The reaction is extraordinarily fast. At room temperature 95% of substrate **1** was converted after only 5–10 min, at −60°C the same conversion was reached after 30 min. The enantioselectivities were excellent and exceeded the selectivities we had previously obtained in other photocycloaddition[10] and photocyclization[11] reactions. Even with 1.2 equivalents of the chiral complexing agent at −60°C enantioselectivities of >90% *ee* were achieved (Table 1, entries 4, 7, 10). Alternatively, the reaction can be conducted at higher temperature (entry 3) in a highly enantioselective fashion by employing an excess of the complexing agent. In this context the almost quantitative recovery of the complexing agent **3** should be mentioned.[9] The enhancement of the *endo* selectivity of cycloaddition with dimethyl fumarate in the presence of the complexing agent **3** is remarkable (Table 1, entries 9–11). The electronic properties of the substrate might be altered by the hydrogen bonds in the complex with lactam **3**.

The direction of the face differentiation was proved by single-crystal X-ray analysis.[12] For the *exo* product *exo*-**4c**

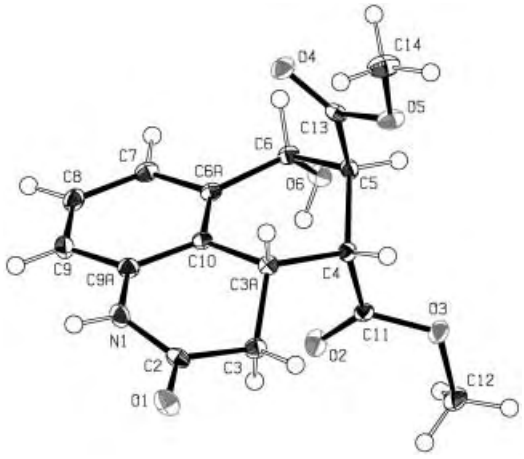


Figure 1. Absolute configuration of the enantiomerically pure cycloaddition product *exo*-**4c**.

 © 2003 Wiley-VCH Verlag GmbH & Co. KGaA, Weinheim

crystals were obtained which were suitable for the determination of the absolute configuration by anomalous X-ray diffraction (Figure 1). The structure proves a *Re*-face attack at the prostereogenic enol carbon atom, as expected owing to complexation of the enol to the complexing agent **3**. The circular dichroism (CD) spectrum of product *endo*-**4c** matches the calculated spectrum of this enantiomer, which can be considered additional proof of the absolute configuration.[13] The relative configuration of the products was fully elucidated by crystal structure analyses and NOE experiments.

In our current studies in this area we are investigating the effect of pressure on the cycloaddition reactions, examining experimental evidence for the reaction intermediates, and extending the range of products with potential applications of the reaction in organic synthesis.

Received: April 3, 2003 [Z51567]

Keywords: asymmetric synthesis · Diels–Alder reaction · enantioselectivity · enols · photochemistry

[1] Reviews: a) J. L. Segura, N. Martin, *Chem. Rev.* **1999**, *99*, 3199 – 3246; b) H. Nemoto, K. Fukumoto, *Tetrahedron* **1998**, *54*, 5425 – 5464; c) J. L. Charlton, M. M. Alauddin, *Tetrahedron* **1987**, *43*, 2873 – 2889; d) G. Quinkert, H. Stark, *Angew. Chem.* **1983**, *95*, 651 – 669; *Angew. Chem. Int. Ed. Engl.* **1983**, *22*, 637 – 655.

[2] N. C. Yang, C. Rivas, *J. Am. Chem. Soc.* **1961**, *83*, 2213.

[3] Reviews: a) A. C. Weedon in *The Chemistry of Enols* (Ed.: Z. Rappoport), Wiley, New York, **1990**, pp. 591 – 638; b) P. G. Sammes, *Tetrahedron* **1976**, *32*, 405 – 422.

[4] a) E. F. Zwicker, L. I. Grossweiner, N. C. Yang, *J. Am. Chem. Soc.* **1963**, *85*, 2671 – 2672; b) G. Porter, M. F. Tchir, *J. Chem. Soc. A* **1971**, 3772 – 3777; c) R. Haag, J. Wirz, *Helv. Chim. Acta* **1977**, *60*, 2595 – 2607; d) J. Gebicki, A. Krantz, *J. Chem. Soc. Perkin Trans. 1* **1984**, 1623 – 1627; e) W. C. Agosta, R. A. Caldwell, J. Jay, L. J. Johnston, B. R. Venepalli, J. C. Scaiano, M. Singh, S. Wolff, *J. Am. Chem. Soc.* **1987**, *109*, 3050 – 3057.

[5] Examples: a) B. J. Arnold, S. M. Mellows, P. G. Sammes, *J. Chem. Soc. Perkin Trans. 1* **1973**, 1266 – 1270; b) G. Quinkert, W.-D. Weber, U. Schwartz, H. Stark, H. Baier, G. Dürner, *Liebigs Ann. Chem.* **1981**, 2335 – 2371; c) G. Quinkert, U. Schwartz, H. Stark, W.-D. Weber, F. Adam, H. Baier, G. Frank, G. Dürner, *Liebigs Ann. Chem.* **1982**, 1999 – 2040; d) M. B. Glinski, T. Durst, *Can. J. Chem.* **1983**, *61*, 573 – 575; e) D. I. Macdonald, T. Durst, *J. Org. Chem.* **1986**, *51*, 4749 – 4750; f) J. L. Charlton, G. L. Plourde, K. Koh, A. S. Secco, *Can. J. Chem.* **1989**, *67*, 574 – 579; g) J. L. Charlton, K. Koh, *J. Org. Chem.* **1992**, *57*, 1514 – 1516; h) K. C. Nicolaou, D. Gray, *Angew. Chem.* **2001**, *113*, 783 – 785; *Angew. Chem. Int. Ed.* **2001**, *40*, 761 – 763; i) K. C. Nicolaou, D. Gray, J. Tae, *Angew. Chem.* **2001**, *113*, 3787 – 3790; *Angew. Chem. Int. Ed.* **2001**, *40*, 3675 – 3678; j) K. C. Nicolaou, D. Gray, J. Tae, *Angew. Chem.* **2001**, *113*, 3791 – 3795; *Angew. Chem. Int. Ed.* **2001**, *40*, 3679 – 3683.

[6] Example for selectivity control through hydrogen bonding in thermal Diels–Alder reactions: a) A. Wittkopp, P. R. Schreiner, *Chem. Eur. J.* **2003**, *9*, 407 – 414; b) C. Palomo, M. Oiarbide, J. M. Garcia, A. Gonzalez, A. Lecumberri, A. Linden, *J. Am. Chem. Soc.* **2002**, *124*, 10288 – 10289; c) E. J. Corey, T. W. Lee, *Chem. Commun.* **2001**, 1321 – 1329; d) T. Schuster, M. Kurz, M. W. Göbel, *J. Org. Chem.* **2000**, *65*, 1697 – 1701; e) A. Robertson, D. Philp, N. Spencer, *Tetrahedron* **1999**, *55*, 11365 – 11384, and references therein.

[7] a) L.-F. Tietze, H. Meier, E. Voß, *Synthesis* **1988**, 274 – 277; b) I. I. Kolodkina, K. V. Levshina, S. I. Sergievskaya, A. I. Kravchenko, *Zh. Org. Khim.* **1966**, *2*, 63 – 69; c) M. Tominaga, E. Yo, H. Ogawa, S. Yamashita, Y. Yabuuchi, K. Nakagawa, *Chem. Pharm. Bull.* **1986**, *34*, 682 – 693.

[8] T. Bach, H. Bergmann, B. Grosch, K. Harms, E. Herdtweck, *Synthesis* **2001**, 1395 – 1405.

[9] Representative experimental procedure: A solution of aldehyde **1** (0.29 mmol, 50 mg) and chiral complexing agent **3** (0.69 mmol, 241 mg) in toluene (150 mL) was degassed at room temperature by purging it with argon for 20 min, and the mixture was subsequently cooled to −60 °C. Dimethyl fumarate (14.3 mmol, 2.1 g) was added against a flow of argon. After 10 min of stirring the solution was irradiated for 30 min at −60 °C (light source: Original Hanau TQ 150, duran filter) and afterwards allowed to warm to room temperature. The toluene was removed under reduced pressure, and the residue was separated by column chromatography (CH_2Cl_2/MeOH = 97/3). Complexing agent **3** (224 mg, 93 %) and the products *exo*-**4c** (12 mg, 13 %) and *endo*-**4c** (59 mg, 65 %) were isolated. Selected analytical data for *endo*-**4c**: ^{1}H NMR (360 MHz, CD_3OD): $\delta = 2.46$ (dd, $^2J = 16.0$ Hz, $^3J = 14.2$ Hz, 1H, C*H*H), 2.57 (dd, $^2J = 16.0$ Hz, $^3J = 5.0$ Hz, 1H, CH*H*), 3.03–3.09 (m, 2H, $COCH_2CHCH$), 3.22 (dd, $^3J = 11.8$ Hz, $^3J = 3.4$ Hz, 1H, CHOHC*H*), 3.34 (s, 1H, NH), 3.75 (s, 3H, OCH_3), 3.77 (s, 3H, OCH_3), 5.07 (d, $^3J = 3.4$ Hz, 1H, C*H*OH), 6.86 (d, $^3J = 7.9$ Hz, 1H, CH_{Ar}), 7.08 (d, $^3J = 7.5$ Hz, 1H, CH_{Ar}), 7.24 ppm (virt. t, $^3J \cong {}^3J = 7.7$ Hz, 1H, CH_{Ar}); ^{13}C NMR (90.6 MHz, CD_3OD): $\delta = 34.6$ (CH_2), 34.7, 41.8, 48.5 (CH), 50.8, 50.9 (OCH_3), 66.6 (CHOH), 114.7 ($C_{Ar}H$), 120.4 ($C_{Ar,q}$), 124.0, 127.7 ($C_{Ar}H$), 135.9, 136.6 ($C_{Ar,q}$), 170.7, 172.0, 174.5 ppm (CO); HRMS (EI): calcd for $C_{16}H_{17}NO_6$: 319.10559, found: 319.10573.

[10] a) T. Bach, H. Bergmann, K. Harms, *Angew. Chem.* **2000**, *112*, 2391 – 2393; *Angew. Chem. Int. Ed.* **2000**, *39*, 2302 – 2304; b) T. Bach, H. Bergmann, *J. Am. Chem. Soc.* **2000**, *122*, 11525 – 11526; c) T. Bach, H. Bergmann, K. Harms, *Org. Lett.* **2001**, *3*, 601 – 603; d) T. Bach, H. Bergmann, B. Grosch, K. Harms, *J. Am. Chem. Soc.* **2002**, *124*, 7982 – 7990.

[11] a) T. Bach, T. Aechtner, B. Neumüller, *Chem. Commun.* **2001**, 607 – 608; b) T. Bach, T. Aechtner, B. Neumüller, *Chem. Eur. J.* **2002**, *8*, 2464 – 2475; c) T. Bach, B. Grosch, T. Strassner, E. Herdtweck, *J. Org. Chem.* **2003**, *68*, 1107 – 1116.

[12] Crystal structure analysis of compound *exo*-**4c**: $C_{16}H_{17}NO_6$, $M_r = 319.31$; colorless prisms ($0.43 \times 0.25 \times 0.20$ mm^3); orthorhombic, $P2_12_12_1$ (No. 19), $a = 9.0770(1)$, $b = 9.6510(1)$, $c = 16.2439(1)$ Å, $V = 1423.00(2)$ Å^3, $Z = 4$, $\rho_{calcd} = 1.490$ g cm^{-3}; $F_{000} = 672$; $\mu = 0.115$ mm^{-1}; Flack parameter $\varepsilon = -0.1(6)$. Preliminary examination and data collection were carried out on a Nonius-kappa-CCD device (Nonius Mach3) with an Oxford Cryosystems device at the window of a rotating anode (Nonius FR591) with graphite-monochromated $Mo_{K\alpha}$ radiation ($\lambda = 0.71073$ Å). Data collection were performed at 103 K within the range $2.45° < \Theta < 25.34°$. A total of 46619 reflections were integrated and corrected for Lorentz and polarization effects. A correction for absorption effects and/or decay was applied during the scaling procedure. After merging ($R_{int} = 0.033$), 2607 (2585: $I_o > 2\sigma(I_o)$) independent reflections remained, and all were used to refine 276 parameters. The structure was solved by a combination of direct methods and difference-Fourier syntheses. All non-hydrogen atoms were refined with anisotropic displacement parameters. All hydrogen atoms were found and refined with individual isotropic displacement parameters. Full-matrix least squares refinements were carried out by minimizing $\Sigma w(F_o^2 - F_c^2)^2$ and converged with $R1 = 0.0222$ ($I_o > 2\sigma(I_o)$), $wR2 = 0.0586$ (all data), GOF = 1.071, all parameters, and shift/error < 0.001. The final difference-Fourier map shows no striking features ($\Delta e_{min/max} = +0.17/-0.16$ e Å^{-3}). The absolute configuration (the trend was given correctly by the basic highly

 © 2003 Wiley-VCH Verlag GmbH & Co. KGaA, Weinheim

redundant measurement with molybdenum radiation) was determined exactly by 10 selected Friedel pairs with Bijvoet differences of highest significance. With copper radiation psi-scans of the reachable region in steps of 20° were collected for each Friedel pair and corrected numerically for absorption effects. All 10 pairs show the calculated sign of the given configuration and are therefore confirmed by the experiment. Crystallographic data (excluding structure factors) for the structure reported in this paper have been deposited with the Cambridge Crystallographic Data Centre as supplementary publication no. CCDC-209877 (*exo*-**4c**). Copies of the data can be obtained free of charge via www.ccdc.cam.ac.uk/conts/retrieving.html (or from the Cambridge Crystallographic Data Centre, 12, Union Road, Cambridge CB21EZ, UK; fax: (+44) 1223-336-033; or deposit@ccdc.cam.ac.uk). Data Collection Software for Nonius kappa-CCD devices, Delft (The Netherlands), **2001**; a) Z. Otwinowski, W. Minor, *Methods Enzymol.* **1997**, *276*, 307ff; b) A. Altomare, G. Cascarano, C. Giacovazzo, A. Guagliardi, M. C. Burla, G. Polidori, M. Camalli, SIR92, *J. Appl. Crystallogr.* **1994**, *27*, 435–436; c) *International Tables for Crystallography, Vol. C*, Tables 6.1.1.4, 4.2.6.8, and 4.2.4.2 (Ed.: A. J. C. Wilson), Kluwer Academic Publishers, Dordrecht (The Netherlands), **1992**; d) A. L. Spek, PLATON, *A Multipurpose Crystallographic Tool*, Utrecht University, Utrecht (The Netherlands), **2001**; e) G. M. Sheldrick, SHELXL-97, University of Göttingen, Göttingen (Germany), **1998**.

[13] We thank Prof. Dr. S. Grimme (Universität Münster) for carrying out the calculations: a) R. Bauernschmitt, R. Ahlrichs, *Chem. Phys. Lett.* **1996**, *256*, 454–464; b) F. Furche, R. Ahlrichs, A. Sobanski, F. Vögtle, C. Wachsman, E. Weber, S. Grimme, *J. Am. Chem. Soc.* **2000**, *122*, 1717–1724.

 © 2003 Wiley-VCH Verlag GmbH & Co. KGaA, Weinheim

Cover Picture



Eric F. Connor, Linda K. Sundberg, Ho-Cheol Kim, Jeroen J. Cornelissen, Teddie Magbitang, Phil M. Rice, Victor Y. Lee, Craig J. Hawker, Willi Volksen, James L. Hedrick,* and Robert D. Miller*

From Nanoscience to Nanotechnology Sacrificial micellar star-shaped polymers template their image in a thermosetting resin to generate a nanoporous film for the insulation of on-chip metal wiring. The uniform pore size and shape of the pores is solely determined by the molecular weight of the polymer, which is, in turn, controlled by using living polymerization techniques. More about this methodology is given in the Communication by R. D. Miller, J. L. Hedrick, and co-workers on page 3785 ff.

Contents

Angewandte EarlyView

The following articles are available online (in Wiley Interscience). You can find them at www.angewandte.org, under Full Text, Forthcoming Articles.

M. J. Thrippleton, J. Keeler:*
Elimination of Zero-Quantum Interference in Two-Dimensional NMR Spectra
DOI: 10.1002/anie.200351947
Published online: August 1, 2003

K. Inoue, K. Kikuchi, M. Ohba, H. Ōkawa:*
Structure and Magnetic Properties of a Chiral Two-Dimensional Ferrimagnet with T_c of 38 K
DOI: 10.1002/anie.200351888
Published online: August 1, 2003

M. D. Foster, O. Delgado Friedrichs, R. G. Bell, F. A. Almeida Paz, J. Klinowski*:*
Structural Evaluation of Systematically Enumerated Hypothetical Uninodal Zeolites
DOI: 10.1002/anie.200351556
Published online: August 1, 2003

K. Funabashi, M. Jachmann, M. Kanai, M. Shibasaki:*
Multicenter Strategy for the Development of Catalytic Enantioselective Nucleophilic Alkylation of Ketones: Me_2Zn Addition to α-Ketoesters
DOI: 10.1002/anie.200351650
Published online: August 1, 2003

Articles judged by the referees or the editor as being either very important or very urgent are immediately edited, proof-read, and electronically published once the manuscript has arrived in the editorial office in final form. As long as there is no page number available these articles should be cited in the following manner:

Author(s) *Angew. Chem. Int. Ed.*, online publication date, DOI.

News

Organic Chemistry: Jacobsen delivers Ruzicka Lecture ____ **3714**

Catalysis: Corma recognized ____ **3714**

Molecular Machines: Möller and Feringa honored ____ **3714**

Books

Bioinformatics and Genome Analysis ____ **3715**
Hans-Werner Mewes, Bertram Weiss, Henrik Seidel
reviewed by Dietlind L. Gerloff

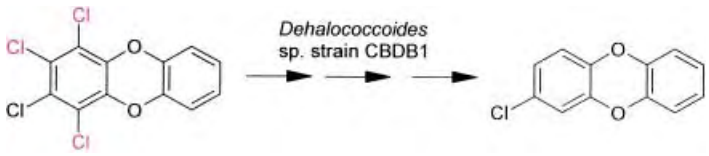
Industrial Dyes ____ **3716**
Klaus Hunger
reviewed by Günther Seybold

Highlights

Bacterial Degradation of Dioxin

K.-H. van Pée* ____ **3718 – 3720**

Dehalogenation of Polyhalogenated Dioxins



Bacterial combat on dioxins: A bacterial strain detected in a sediment sample from a creek contaminated with dioxins in the Bitterfeld region, Germany, dehalogenates different polyhalogenated dioxins under anaerobic conditions by reductive dehalogenation (see scheme). This reaction is coupled to the generation of energy and to growth (dehalorespiration).

Minireviews

Metal Carbonyl Pharmaceuticals

T. R. Johnson, B. E. Mann,* J. E. Clark, R. Foresti, C. J. Green, R. Motterlini* ——— **3722 – 3729**

Metal Carbonyls: A New Class of Pharmaceuticals?

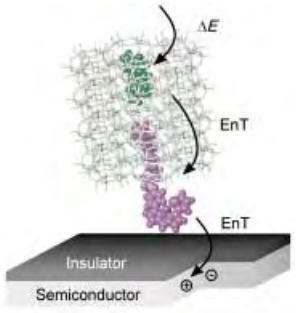
Carbon monoxide is an important signaling molecule in mammals. It is particularly active in the cardiovascular system and has been shown to be important in several areas of medicine, for example, in suppressing organ graft rejection and in reducing the damaging effects of ischemia. The importance of CO provides an opportunity for bioorganometallic chemistry to establish a new class of pharmaceuticals based on metal carbonyls.

Reviews

Light-Harvesting Antenna Materials

G. Calzaferri,* S. Huber, H. Maas, C. Minkowski ——— **3732 – 3758**

Host–Guest Antenna Materials



Dyeing Zeolites: Dye-zeolite antenna systems transporting excitation energy over large distances are discussed on the basis of three stages of organization: the supramolecular organization of dye molecules inside the zeolite channels, the organization of stopcock molecules plugging the channel entrances, and the coupling of stopcock-modified antenna systems to an external device (see picture; EnT = energy transfer).

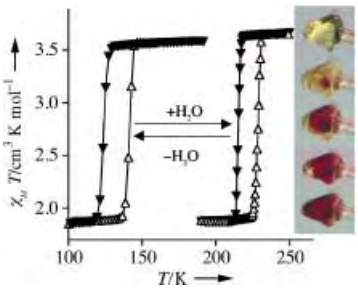
Communications

Hysteresis in Fe-CN-Ag/Au Networks

V. Niel, A. L. Thompson, M. C. Muñoz, A. Galet, A. E. Goeta, J. A. Real* ——— **3760 – 3763**

Crystalline-State Reaction with Allosteric Effect in Spin-Crossover, Interpenetrated Networks with Magnetic and Optical Bistability

A net change: A fully reversible ligand substitution involving coordination/uncoordination of gaseous water and pyrimidine induces the repetitive allosteric transformation of three interpenetrated nets into a single three-dimensional net. The transformation does not affect the crystallinity of the sample but alters significantly the spin-crossover transition; the compound shows magnetic and chromatic bistability (see picture).



For the USA and Canada:
ANGEWANDTE CHEMIE International Edition (ISSN 1433-7851) is published weekly by Wiley-VCH PO Box 191161, D 69451 Weinheim, Germany. Air freight and mailing in the USA by Publications Expediting Inc. 200 Meacham Ave., Elmont, NY 11003. Periodicals postage paid at Jamaica NY 11431. US POSTMASTER: send address changes to *Angewandte Chemie*, Wiley-VCH, 111 River Street, Hoboken, NJ 07030. Annual institutional subscription price for institutions: Europe € 2998.00/3148.00. Outside Europe US$ 3718.00/3904.00 (valid for print or electronic/print and electronic delivery); for individuals who are personal members of a national chemical society, or whose institution already subscribes, or who are retired or self-employed consultants, print only (including postage and handling charges): Europe € 248.00/Outside Europe US$ 348.00.

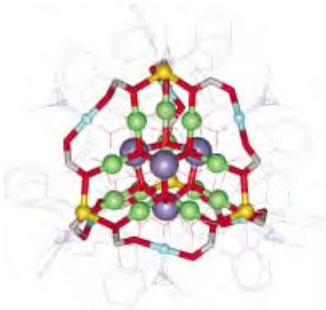
 © 2003 Wiley-VCH Verlag GmbH & Co. KGaA, Weinheim

Contents

Metallacryptate Magnets

C. Dendrinou-Samara, M. Alexiou, C. M. Zaleski, J. W. Kampf, M. L. Kirk,* D. P. Kessissoglou,* V. L. Pecoraro* ——— **3763 – 3766**

Synthesis and Magnetic Properties of a Metallacryptate that Behaves as a Single-Molecule Magnet



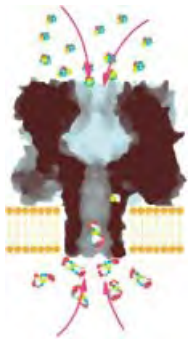
Crypt analysis: The reaction of manganese(II) chloride with sodium hydroxide, di-(2-pyridyl)-ketonoxime, and sodium azide yields a metallacryptate consisting of 26 manganese centers, namely, four Mn^{II} (see picture; gold spheres) and 22 Mn^{III} ions (green, aqua, and blue spheres). Results obtained from ac SQUID magnetic studies indicate that this molecule displays single-molecule magnetic behavior.

Single-Molecule Covalent Chemistry

T. Luchian,* S.-H. Shin, H. Bayley* ——— **3766 – 3771**

Single-Molecule Covalent Chemistry with Spatially Separated Reactants

In a recent study, the reversible covalent chemistry of a simple reaction was monitored at the single-molecule level by observing the current flowing through a protein pore, which acted as a nanoreactor. Now, a multistep reaction has been observed by an improved approach, in which two of the reactants are separated by the membrane that contains the pore and diffuse into the reaction zone (see picture).

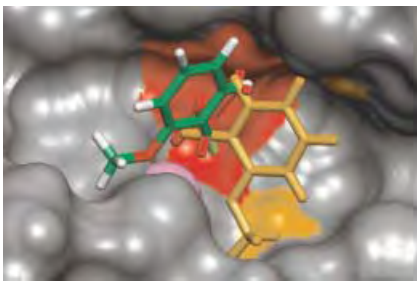


Structure-Based Drug Discovery

D. T. Puerta, J. R. Schames, R. H. Henchman, J. A. McCammon,* S. M. Cohen* ——— **3772 – 3774**

From Model Complexes to Metalloprotein Inhibition: A Synergistic Approach to Structure-Based Drug Discovery

A happy marriage: The combination of synthetic model chemistry with computational conformational analysis has revealed the binding of an inhibitor to a medically important metalloenzyme. $[(Tp^{Ph,Me})Zn(mbt)]$ ($Tp^{Ph,Me}$ = hydrotris(3,5-phenylmethylpyrazolyl)borate, mbt = 2-methoxybenzenethiol) was used to template the conformation of a known inhibitor in the active site of the metalloenzyme, as shown by the green ligand inside the active site of the protein (the Zn^{II} ion is shown in purple).

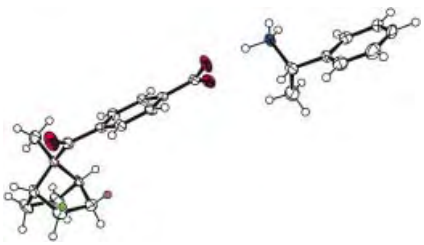


Photochemical Asymmetric Synthesis

B. O. Patrick, J. R. Scheffer,* C. Scott ——— **3775 – 3777**

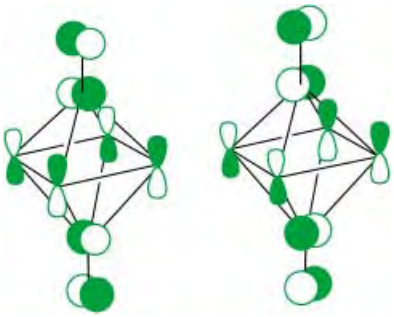
Preorganization of Achiral Molecules for Asymmetric Synthesis through Crystallization-Induced Immobilization in Homochiral Conformations

Enantioselective photochemistry: By forming salts with optically pure amines, achiral carboxylic acids can be induced to crystallize in chiral conformations that are preorganized for enantioselective photochemical reactions. Irradiation of crystals of the salt shown leads to selective Norrish type II abstraction of the nearer (green) γ-hydrogen atom, affording a diastereomerically pure cyclobutanol in 84–98% enantiomeric excess depending on the amine used.



 © 2003 Wiley-VCH Verlag GmbH & Co. KGaA, Weinheim

Three dimensional aromaticity: Polyhedral boranes with *para*-O, -NH, -S substituents should exhibit cylindrical π bonding on oxidation (see picture), with structural and reactivity consequences similar to benzoquinones.

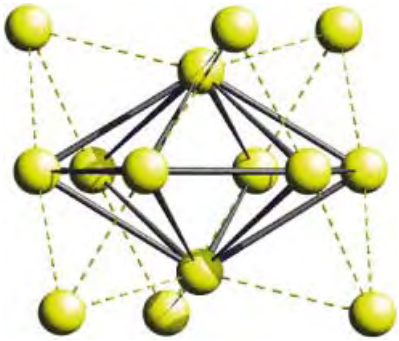


Polyhedral Boranes

M. M. Balakrishnarajan, R. Hoffmann* ——— **3777 – 3781**

Polyhedral Boranes with Exo Multiple Bonds: Three-Dimensional Inorganic Analogues of Quinones

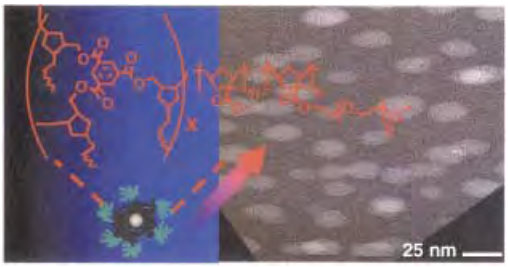
Solvothermal techniques allow the crystallization of high nuclearity products that are otherwise inaccessible by conventional techniques, directly from the reaction mixture. By this method, the reaction of the triangular species $[Fe_3O(OAc)_6(H_2O)_3]Cl$ with benzotriazole (BtaH) produces an $[Fe_{14}]$ cluster (depicted) with a very large spin ground state.



Iron Cluster with High Spin

D. M. Low, L. F. Jones, A. Bell, E. K. Brechin,* T. Mallah, E. Rivière, S. J. Teat, E. J. L. McInnes* – **3781 – 3784**

Solvothermal Synthesis of a Tetradecametallic Fe^{III} Cluster

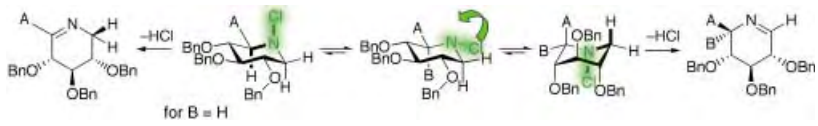


Nanopores created by micellar star polymers in amorphous organic silsequioxane thermosets produce morphologically controlled porous materials for semiconductor chip applications (see picture). Pore size is independent of concentration and processing conditions, but depends solely on the size of the polymer molecule.

Self-Organized Unimolecular Polymers

E. F. Connor, L. K. Sundberg, H.-C. Kim, J. J. Cornelissen, T. Magbitang, P. M. Rice, V. Y. Lee, C. J. Hawker, W. Volksen, J. L. Hedrick,* R. D. Miller* **3785 – 3788**

Templating of Silsesquioxane Cross-Linking Using Unimolecular Self-Organizing Polymers



A temperature-dependent relay of chirality is based on the inversion of the nitrogen lone pair in cyclic azasugars. Elimination from the conformation preferred at a given temperature leads to a cyclic imine, and in a subsequent nucleophilic attack the stereochemical information is relayed.

Azasugar Synthesis

M. A. T. Maughan, I. G. Davies, T. D. W. Claridge, S. Courtney, P. Hay, B. G. Davis* ——— **3788 – 3792**

Nitrogen Inversion as a Diastereomeric Relay in Azasugar Synthesis: The First Synthesis of Adenophorine

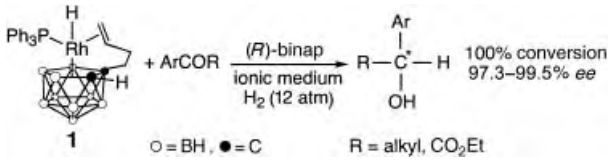
 © 2003 Wiley-VCH Verlag GmbH & Co. KGaA, Weinheim

Contents

Asymmetric Hydrogenation

Z. Yinghuai,* K. Carpenter, C. C. Bun, S. Bahnmueller, C. P. Ke,* V. S. Srid, L. W. Kee, M. F. Hawthorne* ——— **3792 – 3795**

(*R*)-Binap-Mediated Asymmetric Hydrogenation with a Rhodacarborane Catalyst in Ionic-Liquid Media



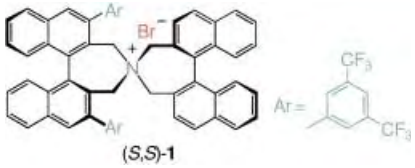
Unsymmetrical aryl ketones undergo asymmetric hydrogenation in ionic-liquid media in the presence of (*R*)-binap and a rhodacarborane catalyst derived from the suicide precursor **1** (see scheme). Ketones that are poor substrates for other methods can be hydrogenated in quantitative yields with very high enantioselectivities (97.3–99.5% *ee*). The novel ionic liquid (*N*-*n*-butylpyridinium)$^+$ (*closo*-$CB_{11}H_{12}$)$^-$ provides a superior medium for these reactions.

Stereoselective Alkylation

T. Ooi, T. Miki, M. Taniguchi, M. Shiraishi, M. Takeuchi, K. Maruoka* — **3796 – 3798**

Highly Enantioselective Construction of Quaternary Stereocenters on β-Keto Esters by Phase-Transfer Catalytic Asymmetric Alkylation and Michael Reaction

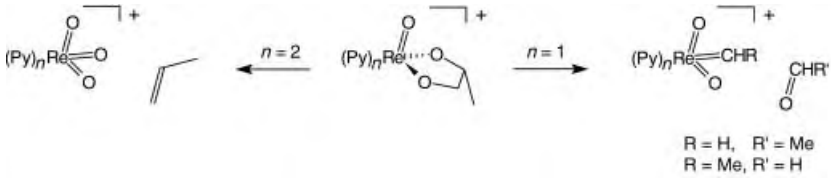
The designer ammonium salt (*S*,*S*)-1 catalyzes highly enantioselective phase-transfer alkylation and Michael reaction of β-keto esters. This approach provides a reliable route for the asymmetric synthesis of polyfunctionalized compounds having chiral quaternary carbon atoms.



High-Valent Rhenium Oxo Chemistry

X. Chen, X. Zhang, P. Chen* **3798 – 3801**

Metallaoxetanes and Carbenes from Diolates in High-Valent Rhenium Oxo Chemistry: The Importance of the Coordination Number

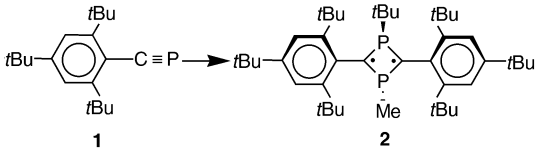


Re^V diolate complexes cleave to form either the Re^{VII} trioxo complex or a rhenium carbene, depending on the coordination number of the original diolate complex (see picture). The carbene complexes, detected by using collision induced mass spectrometry, are the best experimental indication to date for intermediate "metallaoxetanes", which would be the first-formed intermediate in [2+2] reactions of olefins with a d^0 oxo complex. This sharp dichotomy in reactivity can be explained by a qualitative π-strain model.

Stable Biradicals

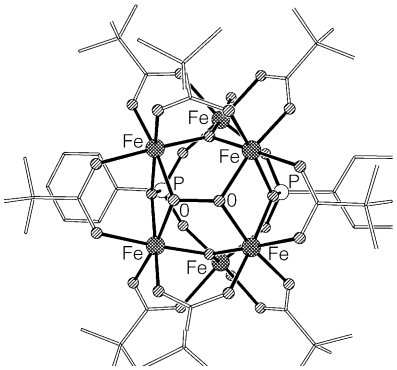
H. Sugiyama, S. Ito, M. Yoshifuji* ——— **3802 – 3804**

Synthesis of a 1,3-Diphosphacyclobutane-2,4-diyl from Mes*C≡P



A very stable biradical, **2**, was prepared from **1** (see picture). The deep-blue/violet biradical was stable in the air for several minutes. The sp^2-hybridized carbon radical centers of **2** were confirmed by X-ray crystallography and its reversible oxidation was characterized by cyclic voltammetry. Mes* = 2,4,6-$tBu_3C_6H_2$.

 © 2003 Wiley-VCH Verlag GmbH & Co. KGaA, Weinheim

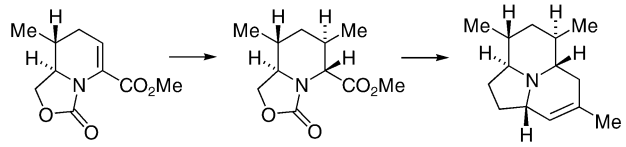


Sophisticated architectures can be built from oxo-centered carboxylate triangles linked together by phosphonates. This suggests that the phosphonate ligands could function as a means for building larger entities from carboxylate cages. The incorporation of a peroxide unit into the cage structures is also feasible, for example in the hexanuclear cage depicted.

Iron(III) Phosphonate Cage Complex

E. I. Tolis, M. Helliwell, S. Langley, J. Raftery, R. E. P. Winpenny* ——— **3804 – 3808**

Synthesis and Characterization of Iron(III) Phosphonate Cage Complexes



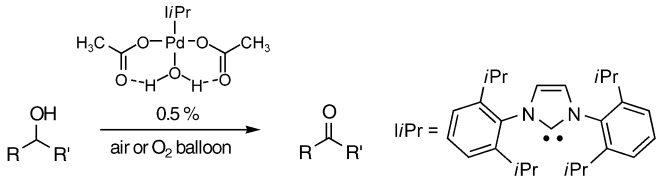
1

Forming the tetrasubstituted piperidine ring with stereocontrol in a Michael-type conjugate addition is a key step in the first enantioselective synthesis of the antipode **1** of alkaloid 205 B. The absolute stereochemistry of the natural product could be determined unambiguously by comparison of the optical rotations.

Alkaloid Total Synthesis

N. Toyooka,* A. Fukutome, H. Shinoda, H. Nemoto* ——— **3808 – 3810**

Total Synthesis of the Antipode of Alkaloid 205 B



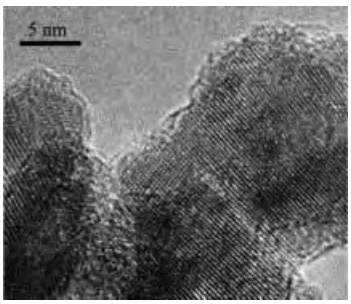
A breath of fresh air: A variety of alcohols are oxidized using 0.5–0.1 mol% of the catalyst, and in some cases the oxidation can simply be carried out open to the air (see scheme). Mechanistic insight into the mechanism is provided by a crystal structure that shows remarkable hydrogen bonds between the coordinated water and acetate ligands and an unprecedented large kinetic isotope effect.

Aerobic Oxidation of Alcohols

D. R. Jensen, M. J. Schultz, J. A. Mueller, M. S. Sigman* ——— **3810 – 3813**

A Well-Defined Complex for Palladium-Catalyzed Aerobic Oxidation of Alcohols: Design, Synthesis, and Mechanistic Considerations

A new purpose: Microreactors are commonly used in molecular high-throughput synthesis. Their use for the formation of catalysts through the precipitation of inorganic components is new. The product shows a high degree of nanostructuring (see electron microscopy image), which is at least partly retained in the subsequent production steps.



Optimized Heterogeneous Catalysts

M. Schur, B. Bems, A. Dassenoy, I. Kassatkine, J. Urban, H. Wilmes, O. Hinrichsen, M. Muhler, R. Schlögl* ——— **3815 – 3817**

Continuous Coprecipitation of Catalysts in a Micromixer: Nanostructured Cu/ZnO Composite for the Synthesis of Methanol

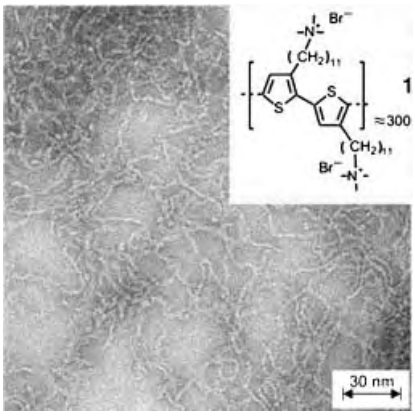
 © 2003 Wiley-VCH Verlag GmbH & Co. KGaA, Weinheim

Contents

Molecular Polymer Wires

G. Li, S. Bhosale, T. Wang, Y. Zhang, H. Zhu, J.-H. Fuhrhop* —— **3818 – 3821**

Gram-Scale Synthesis of Submicrometer-Long Polythiophene Wires in Mesoporous Silica Matrices

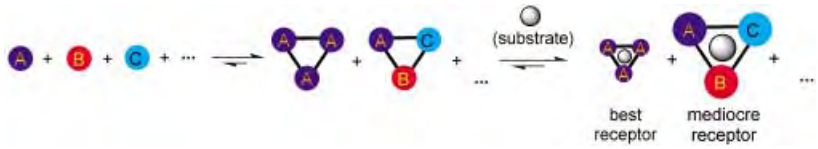


Mesoporous materials get wired: Micelles of the thienyl-substituted ammonium ion **1** in aqueous ammonia solution are applied as matrices for the formation of mesoporous silicate particles from tetraethylorthosilicate. After oxidation with $FeCl_3$ and treatment with HF, polymeric wires with a bimolecular diameter of 3 nm and average lengths of 100–200 nm (see TEM picture) are isolated. The yield of isolated material was consistently above 10% even in gram-scale reactions.

Libraries of Metal Complexes

Z. Grote, R. Scopelliti, K. Severin* —— **3821 – 3825**

Adaptive Behavior of Dynamic Combinatorial Libraries Generated by Assembly of Different Building Blocks

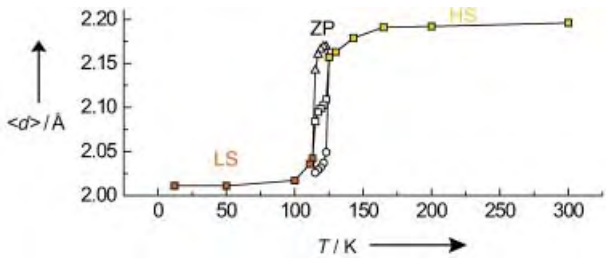


Democratic behavior: A strong bias for the amplification of assemblies, the composition of which reflects the overall composition of the library, can be observed in selection processes with dynamic combinatorial libraries. As a consequence, it is not necessarily the assembly with the highest affinity to a given target (for example, a substrate, see scheme) that is amplified the most.

Order and Disorder

D. Chernyshov, M. Hostettler, K. W. Törnroos, H.-B. Bürgi* **3825 – 3830**

Ordering Phenomena and Phase Transitions in a Spin-Crossover Compound—Uncovering the Nature of the Intermediate Phase of $[Fe(2\text{-pic})_3]Cl_2 \cdot EtOH$



From disorder to order and back: Contrary to all earlier studies on $[Fe(2\text{-pic})_3]Cl_2 \cdot EtOH$ (pic = picolylamine), an ordered phase (IP) with two crystallographically different iron sites was found between disordered high-spin (HS) and low-spin (LS) phases. The picture shows the average Fe–N distances of all three phases.

Communications labeled with this symbol have been judged by two referees as being "very important papers".

The publication of Communications labeled with this symbol has been accelerated because of their topical or highly competitive nature.

 © 2003 Wiley-VCH Verlag GmbH & Co. KGaA, Weinheim

Sources

Product and Company Directory

You can start the entry for your company in "Sources" in any issue of *Angewandte Chemie*.

If you would like more information, please do not hesitate to contact us.

Wiley-VCH Verlag – Advertising Department
Tel.: 0 62 01 - 60 65 65
Fax: 0 62 01 - 60 65 50
E-Mail: MSchulz@wiley-vch.de

Service

Keywords ____ *3832*

Authors ____ *3833*

Angewandte's Sister Journals ____ *3834 – 3835*

Vacancies ____ *3721*

Preview ____ *3837*

40 Years of Chemistry History



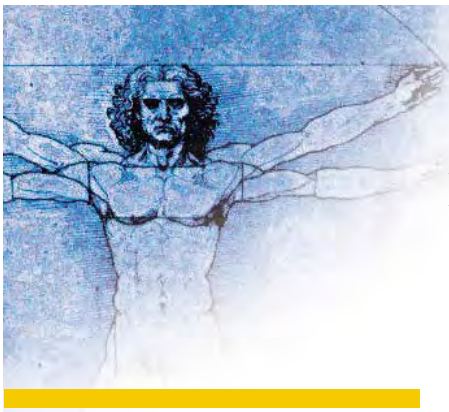
★ The basis for a **journey of discovery** through all the important developments in chemistry and related disciplines

★ The **authors** and **keywords** of all the reviews that have appeared in ***Angewandte Chemie*** in the last 40 years

★ ***Now available at a special price of € 19.80*** (including postage)

Only available directly from:
Angewandte Chemie
Postfach 10 11 61
69451 Weinheim (Germany)
Telephone: (+49) 6201-606-265
Fax: (+49) 6201-606-331
E-mail: angewandte@wiley-vch.de

 © 2003 Wiley-VCH Verlag GmbH & Co. KGaA, Weinheim



E. Jacobsen Gives Ruzicka Lecture

Invitations to give the Ruzicka Lecture, which is organized by the Laboratory for Organic Chemistry of the ETH Zurich[1], are made in an unusual way, namely, by the PhD students. Their selection committee decided on Eric N. Jacobsen (Harvard University) for 2003. Jacobsen gave the Lecture entitled "Privileged Ligands, Reactions, and Substrates in Asymmetric Catalysis" on June 30. A two-day workshop with the participation of PhD students was also organized.



E. Jacobsen

Jacobsen carried out PhD research from 1982 to 1986 at the University of California in Berkeley under the guidance of Robert G. Bergman on dinuclear transition-metal complexes with bridging ligands and their relevance to heterogeneous catalysis, then undertook postdoctoral research with Barry Sharpless at the MIT. From 1988 until 1993 he was a professor at the University of Illinois in Urbana–Champaign and he took up a position at Harvard University in 1993. His research is focused on the development of new synthetic methods,[2] in particular for asymmetric catalysis, and their use in natural-product synthesis. His research group also carries out physical-organic studies on reactivity and recognition phenomena in homogeneous catalysis. Jacobsen is a member of the Editorial Board of *Advanced Synthesis & Catalysis*.

Leopold Ruzicka (1887–1976) was a professor at the ETH when he was awarded the Nobel Prize for Chemistry for his work on polymethylenes and higher terpenes in 1939, together with Adolf Butenandt (Kaiser-Wilhelm-Institut für Biochemie, Berlin, for work on hormones).

A. Corma Receives Eugene Houdry Award



A. Corma

The North American Catalysis Society awards the Eugene Houdry Award annually in memory of the chemical engineer who introduced catalytic cracking to petrochemistry in 1920. This commercially and industrially oriented award is only rarely given to an academic researcher. In 2003 it goes to Avelino Corma, a professor at the Universidad Politécnica de Valencia (Spain), for his outstanding contributions in the field of heterogeneous catalysis, in particular for the development of catalysts and processes.

Corma received his PhD in 1976 from the Universidad Complutense de Madrid. After two years as a postdoctoral researcher at Queen's University in Kingston (Ontario, Canada) he returned to Spain. He has been a professor since 1987 and in 1989 founded the Instituto de Tecnología Química, where he is Scientific Director. His research is focused on acid–base and redox catalysis and molecular sieves. He is a member of the Editorial Advisory Board of *ChemPhysChem*, and his article on the modeling of catalysts through neural networks was the cover article in issue 11/2002 of that journal.[3]

Körber Prize to Nanotechnology Team

The Körber Foundation in Hamburg is awarding its Körber Prize, worth 750000 €, to an international and interdisciplinary team. The recipients are physicist Nieck F. van Hulst (Twente, the Netherlands), chemists Ben L. Feringa (Groningen, the Netherlands) and Martin Möller (RWTH Technical University of Aachen, Germany), and biologist Justin Molloy (MRC National Institute for Medical Research, London), whose research groups cooperate in the field of light-driven molecular machines.



B. L. Feringa

Feringa completed his PhD in 1978 in Groningen under the supervision of Hans Wynberg. After six years at Shell he returned as a lecturer to the University and was made a professor in 1988. He is a member of the Academic Advisory Board of *Advanced Synthesis & Catalysis*. His work focuses on organic stereochemistry,[4] and a Full Paper on molecular switches[5] appeared recently in *Chemistry—A European Journal*.[6]



M. Möller

Möller completed his PhD (1981) and habilitation (1988) in Freiburg (Germany). In 1981–1982 he undertook research at the University of Massachusetts in Amherst, MA (USA), in 1989 he moved as Professor of Macromolecular Chemistry to the University of Twente, and in 1993 he took up a position at the Universität Ulm (Germany). He has been Director of the Deutsche Wollforschungsinstitut (German Wool-Research Institute) at the RWTH Aachen since March 2003. His research encompasses macromolecular chemistry, in particular functional nanostructures.[7] Möller is a member of the Advisory Boards of *Macromolecular Chemistry and Physics* and of *Macromolecular Rapid Communications*.

[1] Eidgenössische Technische Hochschule (Swiss Federal Institute of Technology).
[2] S. N. Goodman, E. N. Jacobsen, *Angew. Chem.* **2002**, *114*, 4897; *Angew. Chem. Int. Ed.* **2002**, *41*, 4703.
[3] A. Corma, J. M. Serra, E. Argente, V. Botti, S. Valero, *ChemPhysChem* **2002**, *3*, 939.
[4] B. L. Feringa, R. A. van Elden, *Angew. Chem.* **1999**, *111*, 3624; *Angew. Chem. Int. Ed.* **1999**, *38*, 3418.
[5] *Molecular Switches* (Ed.: B. Feringa), Wiley-VCH, Weinheim, **2001**.
[6] R. A. van Delden, J. H. Hurenkamp, B. L. Feringa, *Chem. Eur. J.* **2003**, *9*, 2845.
[7] M. Jaumann, E. A. Rebrov, V. V. Kazakova, A. M. Muzafarov, W. A. Goedel, M. Möller, *Macromol. Chem. Phys.* **2003**, *13*, 271.

 © 2003 Wiley-VCH Verlag GmbH & Co. KGaA, Weinheim

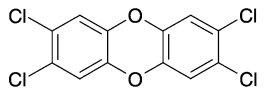
Bacterial Degradation of Dioxin

Dehalogenation of Polyhalogenated Dioxins

*Karl-Heinz van Pée**

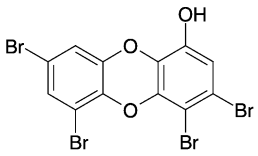
Keywords:
chlorine · dechlorination · dehalorespiration · dioxins · metabolism

In her book "The Silent Spring", which was published in 1962, Rachel Carson[1] described very impressively the consequences of the use of chlorinated herbicides for the environment and their hazards for mankind. This book prompted US president Kennedy to institute a commitee for the investigation of this problem. This commitee reached the same conclusions as Rachel Carson. However, it was also president Kennedy who approved the use of "Agent Purple" as a defoliant during the Vietnam War. "Agent Purple", like the later used "Agent Orange" contained not only the main components 2,4-dichlorophenoxyacetic acid (2,4-D) and 2,4,5-trichlorophenoxyacetic acid (2,4,5-T), but also 2,3,7,8-tetrachlorobenzo-*p*-dioxin (dioxin, **1**) and other polychlorinated



1

dibenzo-*p*-dioxins as contaminants. After an accident during the production of trichlorophenol in the village of Soveso near Milan in 1976, **1** in particular became tragically known as the "Seveso poison". It became evident during investigations following this industrial disaster that polychlorinated dioxins and dibenzofurans are not only extremely toxic, but that they can also be formed very easily during the incineration of organic compounds in the presence of chlorine. In addition, the natural production of polychlorinated dioxins (for example spongiadioxin A, **2**) was also observed.[2]

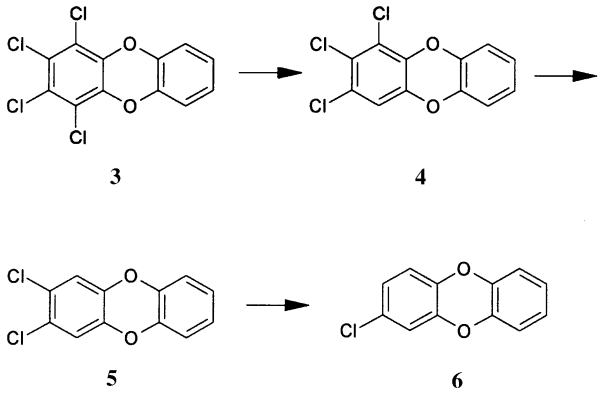


2

The dioxin problem became especially important because of the fact that polyhalogenated dioxins are extremely lipophilic and thus strongly adsorb onto hydrophobic material, such as humus, or they can get enriched in fatty tissue. During the 1980s the German federal government considered the dioxin problem so urgent that it was prepared to finance the building of special laboratories for the investigation of the biological degradation of polyhalogenated dioxins. At that time, data on the degradation of halogenated aromatic compounds by microorganisms and the direct elemination of chlorine atoms from aromatic compounds were already available,[3] however, nothing was known about the degradation of dioxin-like compounds. Early investigations on the degradation of dioxins by microorganisms were conducted under aerobic conditions.[4] Changes in the composition of dioxins in sediments were the first hints of anaerobic degradation of dioxins.[5]

The removal of halogen atoms from aromatic compounds under anaerobic conditions proceeds reductively. Reductive dehalogenation steps are also known from the degradation of pentachlorophenol; however, here oxidative as well as reductive dehalogenation steps occur.[6] A process called "dehalorespiration" plays an important role in the degradation of halogenated compounds in sediments and thus in the absence of oxygen. In this process reductive dehalogenation is coupled to the conservation of energy and cell growth. Such reactions have been known for quite some time for the dehalogenation of compounds such as tetrachloroethene and chlorophenols.[7,8]

Until now, investigations on the reductive dehalogenation of polychlorinated dioxins were performed with mixed cultures, such as in the investigations of the degradation of 1,2,3,4-tetrachlorodibenzo-*p*-dioxin (**3**, Scheme 1) by Bunge et al.[9] For this purpose,



3 **4** **5** **6**

Scheme 1. Proposed main pathway for the degradation of 1,2,3,4-tetrachloro-*p*-dioxin (**3**) according to Bunge et al.[10]

[*] Prof. Dr. K.-H. van Pée
Institut für Biochemie
Technische Universität Dresden
01062 Dresden (Germany)
Fax: (+49) 351-463-35506
E-mail:
karl-heinz.vanpee@chemie.tu-dresden.de

 © 2003 Wiley-VCH Verlag GmbH & Co. KGaA, Weinheim DOI: 10.1002/anie.200301662

bacterial cultures were isolated from sediments of the Spittelwasserbach, Bitterfeld region, Germany, since these sediments contain high concentrations of polyhalogenated dioxins. When **3** was added to these mixed cultures it was transformed into a mixture of 1,3- and 2,3-dichlorodibenzo-*p*-dioxin (**5**). During subsequent investigations,[10] these mixed cultures were transferred six times into a defined minimal medium without loss of dehalogenating activity. However, most of the transferred cultures now transformed 1,2,4-trichlorodibenzo-*p*-dioxin preferentialy to **5** and only to a lesser extent into 1,3-dichlorodibenzo-*p*-dioxin.

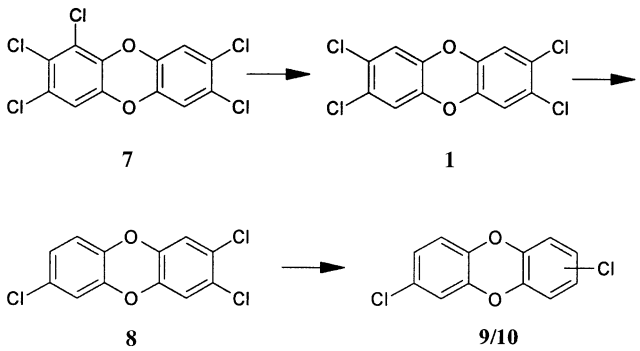
The structural similarity of chlorobenzene with chlorinated dioxins and the fact that *Dehalococcoides* sp. strain CBDB1 is the only bacterium known until now to dehalogenate chlorobenzene[11] meant that it did not seem far fetched to screen for related strains in the mixed cultures by using primers for 16S ribosomal DNA (rDNA). An additional *Dehalococcoides* strain, *D. ethenogenes* strain 195, dechlorinated tetrachloroethene to give ethene by dehalorespiration. Thus, 16S rDNA primers for this strain were also used. The 16S rDNA sequences could be amplified from the mixed cultures by employing specific PCR primers for these *Dehalococcoides* strains. These sequences were identical to the corresponding sequence of *Dehalococcoides* sp. strain CBDB1 and showed an identity of 98.5% to the corresponding sequence of *D. ethenogenes* strain 195. The identity of the same 16S rDNA sequence amplified from the mixed cultures with that of *Dehalococcoides* sp. strain CBDB1 implicates that a corresponding strain should be present in the mixed culture. Thus, the *Dehalococcoides* sp. strain CBDB1 isolated by Adrian et al.[11] was used to check whether this strain could also dehalogenate dioxins. It was found that this strain dechlorinates **3** to 2-monochlorodibenzo-*p*-dioxin (**6**) with **5** as an intermediary product. This intermediate was also detected during the degradation of 1,2,3-trichlorodibenzo-*p*-dioxin (**4**, Scheme 1). However, 1,3-dichlorodibenzo-*p*-dioxin was formed as an intermediate in up to 50 mol% during the degradation of 1,2,4-trichlorodibenzo-*p*-dioxin. In the course of the transfer of the mixed cultures, the preferred position for the dechlorination changed from the lateral to the *peri*-position. This result suggests that the original mixed culture contained additional organisms with the ability to dechlorinate dioxins and that the transfer resulted in enrichment of the *Dehalococcoides* sp. strain CBDB1.

1,2,3,7,8-Pentachlorodibenzo-*p*-dioxin (**7**) was used as a model substance for polychlorinated dioxins chlorinated on both benzene rings. This compound was dehalogenated very slowly (over 104 days) and only to an extent of 2.8 mol% to 2,3,7,8-tetrachlorodibenzo-*p*-dioxin (**8**), 2,7-dichlorodibenzo-*p*-dioxin (**9**) or 2,8-dichlorodibenzo-*p*-dioxin (**10**), and to a minor amount of 1,3,7,8-tetrachlorodibenzo-*p*-dioxin and 2,3,7-trichlorodibenzo-*p*-dioxin (Scheme 2).

The important novelties in the results of Bunge et al.[10] is the identification of a bacterial strain responsible for the dehalogenation of polychlorinated dioxins which originates from a sediment sample contaminated with dioxins, and the demonstration of the dehalogenation of polyhalogenated dioxins by a pure culture of a *Dehalococcoides* sp. strain which is part of a mixed culture. The fact that bacteria with the ability to degrade polyhalogenated dioxins are present in sediments contaminated with these compounds shows nature's adaptability and strengthens the hypothesis that compounds with structural similarity to compounds synthesized by living organisms, such as the polyhalogenated dioxin **2**,[2] can be detoxified and decomposed.

The results presented by Bunge et al.[10] give rise to the hope that detoxification of polychlorinated dioxins by anaerobic reductive dehalogenation reactions and subsequent further degradation of dioxins is possible in nature and that the decontamination of dioxin-contaminated soil can be accomplished by this means. This hope is especially strengthened by the finding that *Dehalococcoides* sp. strain CBDB1 cannot grow in a synthetic medium in the absence of a chlorinated electron acceptor. Since, according to these finding, *Dehalococcoides* sp. strain CBDB1 seems to be strictly dependent on dehalorespiration for energy conservation, it could be possible that this strain even dehalogenates polychlorinated dioxins in the presence of nonhalogenated nutrients. This could be a crucial advantage over the aerobic dehalogenation of polychlorinated dioxins.[12] However, the length of time required for the degradation and the degradation rates at about 60 mol% after 56 days for the transformation of **4** into **6** are still a long way from application. Molecular genetics to clone the dehalogenase genes and overexpression of the genes could be used to improve the degradation of polychlorinated dioxins in contaminated soil.

The repeated occurrence of contamination of feed stuff by polyhalogenated dioxins is only one example showing the necessity to find ways for the degradation and detoxification of polyhalogenated dioxins. However, in this respect it has to be mentioned that highest priority should be given to preventing the formation of polyhalogenated dioxins. The dehalogenation of dioxins is also a big challenge for basic research. Interesting research projects could involve the isolation of the dehalogenating enzymes



Scheme 2. Proposed main pathway for the degradation of 1,2,3,7,8-pentachlorodibenzo-*p*-dioxin (**7**) according to Bunge et al.[10]

 © 2003 Wiley-VCH Verlag GmbH & Co. KGaA, Weinheim

and their characterization or to find an answer to the question of why these *Dehalococcoides* strains are strictly dependent on halogenated electron acceptors. The low degradation rates and the long cultivation times required, however, indicate that it will take some time until we will see any progress towards these goals.

[1] R. Carson, *Der stumme Frühling*, Deutscher Taschenbuch Verlag, München, **1962**; R. Carson, *The Silent Spring*, Houghton Mifflin, Boston, MA, **1992**.

[2] N. K. Utkina, V. A. Denisenko, O. V. Scholokova, M. V. Virovaya, A. V. Gerasimenko, D. Y. Popov, V. B. Krasokhin, A. M. Popov, *J. Nat. Prod.* **2001**, *64*, 151–153.

[3] S. Fetzner, *Appl. Microbiol. Biotechnol.* **1998**, *50*, 633–657.

[4] J. A. Bumpus, G. Milewski, B. Brock, W. Ashbaugh, S. D. Aust in *Innovative Hazardous Waste Treatment Technology Series, Vol. 3* (Eds.: H. M. Freeman, P. R. Sferra), Technomic Publ. Co., Lancaster, PA, **1991**, pp. 47–54.

[5] J. E. M. Beurskens, G. A. J. Mol, H. L. Barreveld, B. van Munster, H. J. Winkels, *Environ. Toxicol. Chem.* **1993**, *12*, 1549–1566.

[6] M. Cai, L. Xun, *J. Bacteriol.* **2002**, *184*, 4672–4680.

[7] A. Neumann, G. Wohlfarth, G. Diekert, *Arch. Microbiol.* **1995**, *163*, 276–281.

[8] B. A. van de Pas, H. Smidt, W. R. Hagen, J. van der Oost, G. Schraa, A. J. M. Stams, W. M. de Vos, *J. Biol. Chem.* **1999**, *274*, 20287–20292.

[9] M. Bunge, H. Ballersted, U. Lechner, *Chemosphere* **2001**, *43*, 675–681.

[10] M. Bunge, L. Adrian, A. Kraus, M. Opel, W. G. Lorenz, J. R. Andreesen, H. Görisch, U. Lechner, *Nature* **2003**, *421*, 357–360.

[11] L. Adrian, U. Szewzyk, J. Wecke, H. Görisch, *Nature* **2000**, *408*, 580–583.

[12] H.-B. Hong, Y.-S. Chang, I.-H. Nam, P. Fortnagel, S. Schmidt, *Appl. Environ. Microbiol.* **2002**, *68*, 2584–2588.



Metal Carbonyl Pharmaceuticals

Metal Carbonyls: A New Class of Pharmaceuticals?**

Tony R. Johnson, Brian E. Mann, James E. Clark, Roberta Foresti, Colin J. Green, and Roberto Motterlini**

Keywords:
bioinorganic chemistry · carbon monoxide · cardiovascular agents · drug design · medicinal chemistry

It is now established that NO is a messenger molecule in mammals despite its high toxicity. As NO^+ and CO are isoelectronic, it should not be unexpected that CO could also have a role as a messenger. CO is produced naturally in humans at a rate of between 3 and 6 cm^3 per day, and this rate is increased markedly by certain inflammatory states and pathological conditions associated with red blood cell hemolysis. Over the last 10 years, the interest in the biological effects of CO has greatly increased, and it is now established in the medical literature that CO does have a major role as a signaling molecule in mammals. It is particularly active within the cardiovascular system, for example, in suppressing organ graft rejection and protecting tissues from ischemic injury and apoptosis. Recently it has been shown that metal carbonyls can also function as CO-releasing molecules and provide similar biological activities. This opens the possibility to develop pharmaceutically important metal carbonyls.

1. Introduction

Carbon monoxide (CO) is a colorless, odorless, tasteless, noncorrosive gas of about the same density as air, and is the most commonly encountered and pervasive poison in our environment.[1] Paradoxically, more than half a century ago, it was found that CO is constantly formed in humans in small quantities,[2] and that under certain pathophysiological conditions this endogenous production of CO may be considerably increased.[3] The discovery that hemoglobin, a heme-dependent protein, is required as a substrate for the production of CO in vivo,[4] and the identification of the enzyme heme oxygenase as the crucial pathway for the generation of this gaseous compound in mammals,[5] set the basis for the early investigation of an unexpected role of CO in the vasculature.[6] The succeeding cloning,[7] and characterization of constitutive (HO-2) and inducible (HO-1) isoforms of heme oxygenase,[8] as well as studies on the kinetics and tissue distribution of these enzymes,[9] started to reveal a major importance of this pathway in the physiological degradation of heme; that is, the end products of heme degradation (CO, biliverdin and bilirubin) might possess, after all, crucial biological activities.[10] This has led many research groups to examine the role of CO. A book describing the role of carbon monoxide in cardiovascular functions has been published,[11] and the role of CO as a signaling molecule has been reviewed.[12]

The role of CO in life may date from the prehistoric environments that were rich in CO,[13] and may be linked to biological pathways that developed during the origins of life. It has been recently proposed that CO made a significant contribution to the synthesis of the first amino and nucleic acids.[14]

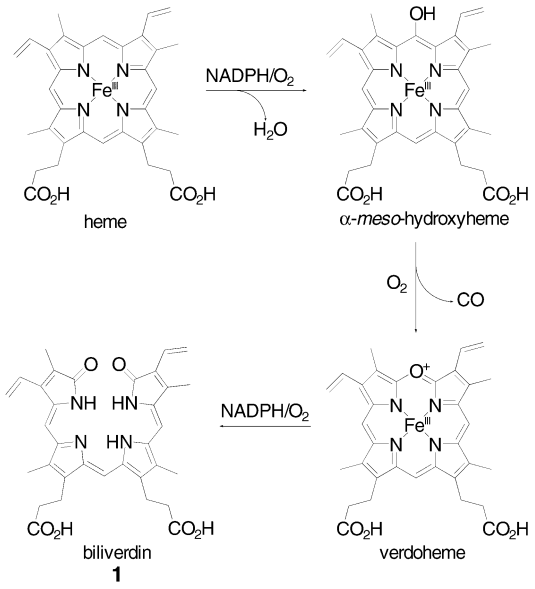
2. Sources of CO in the Human Body

The major source of CO (86%) in the human body arises from the oxidation of heme, catalyzed by heme oxygenase,[15] which was discovered in 1969.[16] The first step is the

[*] Prof. B. E. Mann, T. R. Johnson
Department of Chemistry
The University of Sheffield
Sheffield, S3 7HF (UK)
Fax: (44) 114-2738673
E-mail: b.mann@sheffield.ac.uk
Dr. R. Motterlini, J. E. Clark, R. Foresti, Prof. C. J. Green
Department of Surgical Research
Northwick Park Institute for Medical Research
Harrow, Middlesex, HA1 3UJ (UK)
Fax: (+44) 208-8693270
E-mail: r.motterlini@ic.ac.uk

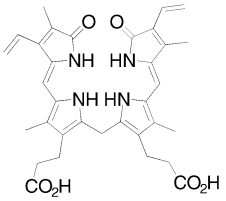
[**] We wish to thank MRC, British Heart Foundation, Dunhill Medical Trust, Northwick Park Institute for Medical Research, and the University of Sheffield for financial support.

 © 2003 Wiley-VCH Verlag GmbH & Co. KGaA, Weinheim DOI: 10.1002/anie.200301634



1

Scheme 1. Reaction intermediates in the heme oxygenase-catalyzed oxidation of heme to biliverdin.[17]



2

production of biliverdin (Scheme 1).[17] Biliverdin (**1**) is normally reduced to bilirubin (**2**) by biliverdin reductase and is excreted after conjugation with glucuronic acid.[18]

The action of heme oxygenase is commonly observed in bruises. During the injury causing the bruise, hemoglobin is liberated from lysed red blood cells leading to a dark red/purple area under the skin, which is associated with deoxygenated hemoglobin. Heme oxygenase in the vascular tissue then oxidizes the heme released from hemoglobin to biliverdin with the liberation of CO and iron ions. This has several obvious results: In the extravascular space, oxygen is consumed to give blue oxygen-free hemoglobin, and a green color, indicating the presence of biliverdin, appears in the underlying tissues. The reduction of biliverdin to bilirubin produces a yellow coloration, which then gradually fades (Figure 1). Some of the CO that is produced binds to the iron

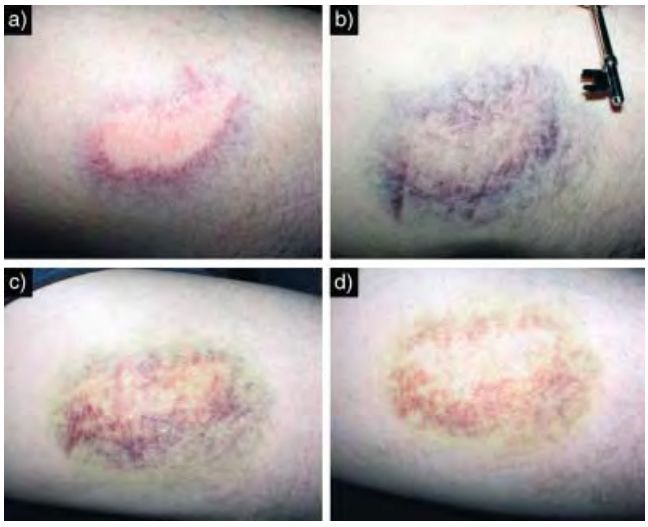


Figure 1. The changes in the appearance of a bruise with time. The pictures are of the thigh of an inline hockey player taken at various times after being hit by the puck. a) 12 h, showing the red and purple of heme; b) 2 days, showing green tinges because of the formation of biliverdin; c) 5 days showing yellow coloration resulting from the formation of bilirubin; d) 10 days, showing some residual bilirubin. The bright red color in (d) results from carboxyhemoglobin. Taken from LondonSkaters.com with permission.

center of hemoglobin to produce the bright-red carboxyhemoglobin that is very apparent in Figure 1d.

The remaining 14% of the generated CO comes from a mixture of sources, including photo-oxidation, lipid peroxidation, xenobiotics, and bacteria.[15]

The basal production of CO in the human body is approximately 20 $\mu mol\,h^{-1}$ under normal conditions; the majority of this originates from the turnover of the heme molecule and the degradation of heme-dependent proteins such as hemoglobin and myoglobin.[10] However, under stress conditions, the inducible isoform of heme oxygenase (HO-1), which is ubiquitously distributed in mammalian tissues, can be highly up-regulated leading to a significant increase in endogenously generated CO.[19] It is, therefore, not surprising that elevated CO levels can be detected in the breath of humans and can now be used as an indication of medical



Brian E. Mann graduated from Oxford (BA (1965), MA, DPhil (1968, all in Chemistry), DSc (1989)) and was at the University of Leeds (1968–1973) before moving to the University of Sheffield. He is the author or co-author of over 200 publications and three books. He has been a visiting Professor at eight universities. He ran the EPSRC High-Field NMR Service in Sheffield, 1980–1986.



Roberto Motterlini is Head of the Vascular Biology Unit at Northwick Park Institute for Medical Research and an Honorary Senior Lecturer at University College London. He obtained his doctoral degree in Biological Science from the University of Milan (1986) and was a Visiting Research Fellow at the University of California, San Diego (1991–1995). He has published several scientific papers on the biological role of heme oxygenase and its metabolites (carbon monoxide and bilirubin) in the control of cardiovascular function. He is a Fellow of the American Heart Association as well as a member of the American Society for Biochemistry and Molecular Biology.

 © 2003 Wiley-VCH Verlag GmbH & Co. KGaA, Weinheim

conditions. The levels of the gas correlate with the severity of a number of disease states,[20] such as asthma,[21] bronchiectasis,[22] cystic fibrosis,[23] diabetes,[24] and rhinitis.[25] The increased production of CO as a result of HO-1 induction during pathophysiological states must be viewed as the intrinsic capacity of the body to respond to stressful situations, as HO-1 is now regarded as the most sensitive inducible protein possessing cytoprotective and regulatory functions.[26]

3. Roles of Heme Oxygenase-1 (HO-1)

There have been extensive studies of the beneficial effects of HO-1.[27] These range over a wide variety of diseases and physiological functions including pulmonary, cardiovascular, renal, and neurological diseases. Research is centering on the breakdown products of heme, namely biliverdin, bilirubin, iron ions, and CO. The iron ions liberated during heme catabolism are promptly bound to ferritin. Except for the iron ions, all the products of heme degradation have an antioxidant and/or signaling function.[26] There are two approaches to exploit the beneficial role of heme oxygenase in medicine: The first method has been to induce and up-regulate HO-1 protein levels in tissues. The second approach is to deliver compounds which provide the breakdown products. In this review, some of the beneficial applications of CO are examined.

4. Medical Investigations of Beneficial Applications of CO Gas

The story of the investigations of the physiological function of CO began in the early 1990's and has predominantly involved the use of CO gas, although CH_2Cl_2 is also used as a precursor. In addition there is a substantial number of papers where heme oxygenase-1 has been induced to produce CO.

The recognition that CO possesses vasodilatory properties[28] is, perhaps, the most significant evidence in favor of a pharmacological function of CO. Although the molecular mechanisms and the chemical modifications that are required to transduce the signals mediated by CO into a specific biological effect need to be fully elucidated, convincing scientific reports have recently highlighted the signaling properties of endogenously generated CO.[29] There are now a wide range of documented physiological effects of CO:

1. It is anti-inflammatory.
   a) It attenuates endotoxic shock: Mice pre-exposed to CO gas followed by administration with lipopolysaccharide (LPS) displayed significantly less tumor necrosis factor-α levels in plasma and increased production of IL-10, a protective or anti-inflammatory cytokine.[30]
   b) It reduces allergic inflammation: CO gas administered to allergen-challenged mice blocks eosinophil efflux and IL-5 production.[31]
2. Organ graft rejection is suppressed by CO: A model of mouse-to-rat cardiac transplantation was performed. Rats were exposed to 400 ppm of CO gas for only 2 days following transplant and the graft survived for 50 days. In comparison, the control exposed to air survived only 5 to 7 days.[32]
3. It protects against hyperoxia: Pre-exposure of a rat to CO gas protected its lung from oxidative injury.[33]
4. It protects against ischemia: CO gas has been used recently to prevent ischemia/reperfusion injury in the liver.[34]
5. CO gas has been used to protect pancreatic beta cells from apoptosis.[35]
6. Leydig cells appear to use HO-1-derived CO to trigger apoptosis of premeiotic germ cells and thereby modulate spermatogenesis under conditions of stress.[36]
7. CO decreases perfusion pressure in isolated human placenta.[37]
8. CO has been shown to protect against septic shock and lung injury in animal models, and the mitogen-activated protein kinase system appears to mediate this cytoprotective effect.[38]
9. It modulates vascular smooth muscle tone.[19,39]
10. It regulates blood pressure under stress conditions.[19]
11. Carbon monoxide suppresses arteriosclerotic lesions associated with chronic graft rejection and with balloon injury.[40]

The scientific investigations of the role of CO in the body are still at an early stage. There is research that suggests that it may be significant in a number of other areas of medicine including transplant surgery, neuroprotection in strokes and Alzheimer's disease,[41] and ovulation.[42] Endogenous CO and bilirubin may have important roles in the control of placental vascular function.[43]

As a result of the beneficial role of CO in the body, three patent applications have recently appeared. One describes the application of CO gas in medicine.[44] A second covers both CO gas and the use of CH_2Cl_2.[45] The CH_2Cl_2 is metabolized to CO and thus provides a source of the gas. The third patent uses metal carbonyls as the source of the CO gas.[46]

5. Medical Investigations of the Beneficial Applications of CO-Releasing Metal Carbonyls

The investigation of applications of metal carbonyls as CO-releasing molecules (CO-RMs) is in its infancy. A paper has appeared reporting the use of $[Fe(CO)_5]$, $[Mn_2(CO)_{10}]$, and $[\{RuCl_2(CO)_3\}_2]$ to act as CO-RMs.[47] In the cases of $[Fe(CO)_5]$ and $[Mn_2(CO)_{10}]$, photolysis was necessary to release CO, but in the case of $[\{RuCl_2(CO)_3\}_2]$, which dissolved in DMSO, CO was released directly to myoglobin (Mb) to form CO-Mb. Further tests were performed and it was shown that CO-RMs:

1. Caused vasodilation of pre-contracted rat aortic rings.
2. Attenuated coronary vasoconstriction in hearts ex vivo.
3. Significantly reduced acute hypertension in vivo.

Recently a patent has been published which gives further developments in this work.[46] A wide range of $\{Ru^{II}(CO)_3\}$ complexes were shown to readily liberate one equivalent of

 © 2003 Wiley-VCH Verlag GmbH & Co. KGaA, Weinheim

CO in the presence of myoglobin and cause vasodilation in precontracted rat aortic rings. A number of Fe^{II} carbonyls were also shown to be active.

$[Ru(CO)_3Cl(glycinate)]$ was selected for further study. It releases CO rapidly when placed in a solution containing myoglobin and can be viewed as a rapid source of CO giving up one equivalent of CO within 5 min of mixing. Several medical applications of $[Ru(CO)_3Cl(glycinate)]$ were examined:

1. Ischemia was induced in an isolated rat heart by stopping the fluid supply for 30 min. When the fluid supply was restarted there was about 50% damage to the heart in the absence of $[Ru(CO)_3Cl(glycinate)]$ and no damage in its presence.
2. Heart transplantation was performed on mice. In the absence of $[Ru(CO)_3Cl(glycinate)]$ all the mice died within 8 days. In its presence, 40% of the mice were still alive after 50 days.
3. Blood platelet aggregation is partially inhibited by $[Ru(CO)_3Cl(glycinate)]$.
4. Macrophages pretreated with $[Ru(CO)_3Cl(glycinate)]$ followed by a challenge with LPS displayed significantly less NO production compared to LPS-treated macrophages.

$[Fe(bpy)(SPh)_2(CO)_2]$ is remarkable among the compounds so far examined. It does not release CO to myoglobin, but it does cause vasodilation. It would therefore appear that the CO is liberated within the cell in this case and raises the possibility of targeting tissues with metal carbonyls.

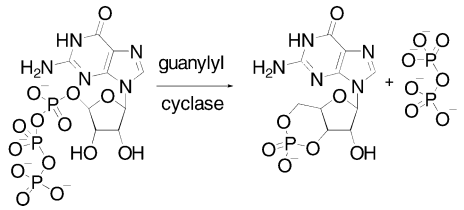
It is still early in the investigation of metal carbonyls as pharmaceuticals, but work on CO gas has shown the important role of CO in biology and these investigations of metal carbonyls have shown that there is a future for their use as a solid form of carbon monoxide. Their role may be enhanced by the presence of the metal. In humans, most of the CO is produced by the heme oxygenase enzymes that also produce iron ions. The iron ions could also be required for activity. Metal carbonyls are capable of providing both the CO and the metal ions.

6. Target Sites of CO in Mammals

Although there is strong evidence for the mechanism of action of NO, research into the mechanism of action of CO is in a much earlier state. Several targets for CO gas have been identified: guanylyl cyclase,[48] p38 mitogen-activated protein kinase,[30] and p51. However, what then happens is a matter of speculation.

6.1. Soluble Guanylyl Cyclase

The soluble guanylyl cyclase system (sGC) has been extensively investigated as it is an active site for the action of NO.[49] Guanylyl cyclase catalyses the conversion of guanosine 5′-triphosphate to cyclic guanosine 3′,5′-monophosphate (Scheme 2).

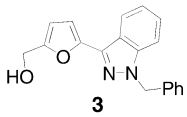


Scheme 2. The guanylyl cyclase-catalyzed conversion of guanosine 5′-triphosphate to cyclic guanosine 3′,5′-monophosphate.

The target for NO is probably the heme, and it is generally assumed that this is also the target for CO. This is the point at which mechanistic problems start. The reactions of NO and CO with heme are markedly different. The binding of NO to sGC is extremely fast ($k_{on} > 1.4 \times 10^8\,M^{-1}s^{-1}$ at 4 °C), to give a six-coordinate intermediate.[50] The reverse reaction is very slow ($k_{off} = 8.2 \times 10^{-4}\,s^{-1}$ at 25 °C[51] and $k_{off} = 1.7 \times 10^{-2}\,s^{-1}$ at 37 °C) resulting in a formation constant $> 10^{12}\,M^{-1}$.[52] There is then a subsequent reaction giving a five-coordinate complex with the loss of the histidine from coordination to the metal center. The rate of this reaction also depends on NO concentration, with a rate of $2.4 \times 10^5\,M^{-1}s^{-1}$ at 4 °C. The X-ray structure of the five-coordinate NO adduct of microbial cytochrome c′ shows that NO binds to the proximal side of the cytochrome, which displaces the histidine ligand.[53] This produces a substantial conformation change in the protein, and could provide the mechanism for the signaling.

In contrast, the binding of CO to sGC is much slower ($k_{on} \sim 10^5\,M^{-1}s^{-1}$ at 23 °C) to give a six-coordinate complex, with the precise rate depending on the buffer used.[51,54] The off-rate is faster than for NO ($k_{off} \sim 10\,s^{-1}$ at 23 °C) resulting in a formation constant $\sim 10^4\,M^{-1}$. Although a reliable formation constant for the six-coordinate NO complex was not determined, it is clear that the formation constant for NO is much larger than for CO. CO binds to the distal side of the microbial cytochrome c′ without displacing the histidine.[53] This is supported by measurements on the sGC system, which show that while in the NO-bound form the Fe–histidinyl bond is broken, it is intact in the CO adduct.[55] The difference between NO and CO in displacing the histidine is probably because of the *trans* influence. CO has a much smaller *trans* influence than NO and hence is unlikely to labilize the histidinyl group as effectively as does NO. The two ligands can be compared directly in the crystal structures of $[Fe(tpp)(NO)(1\text{-Me-imidazole})]^+$ and $[Fe(tpp)(CO)(1\text{-Me-imidazole})]$ (tpp = anion of 5,10,15,20-tetraphenylporphyrin). In $[Fe(tpp)(NO)(1\text{-Me-imidazole})]^+$, the Fe–N(imidazole) bond length is 2.180(4) Å,[56] while its counterpart in $[Fe(tpp)(CO)(1\text{-Me-imidazole})]$ is only 2.071(2) Å.[57]

As a result of this, there are marked differences between NO and CO in their ability to activate sGC; NO is about 80 times more effective than CO in activating sGC.[58] However, when combined with 1-benzyl-3-(5-hydroxymethyl-2-furyl)indazole (YC-1; **3**), the vasodilatory activity of CO increases to that of NO.[59] The mechanism is not understood, however, it is



3

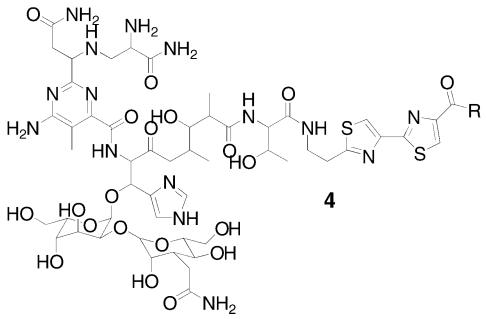
© 2003 Wiley-VCH Verlag GmbH & Co. KGaA, Weinheim

interesting to speculate whether there may be an endogenous physiological counterpart of YC-1.

When NO binds to microbial cytochrome c′, the removal of the histidinyl group from the coordination sphere produces a substantial change in conformation, which could act as the biological signal. In contrast, the binding of CO might be expected to produce little conformational change. However, when CO binds to cytochrome c′, there is considerable reorganization of the surrounding peptide; Leu 16 moves close to the CO moiety and the porphyrin ring flattens.[53] This could provide a mechanism for CO acting as a signaling molecule for sGC. As the bonding of CO to sGC produces a different conformational change to NO, the two signaling molecules could have different outcomes for their signal. This is an area that requires further investigation.

6.2. p38 Mitogen-Activated Protein Kinase and p51

p38 Mitogen-activated protein kinase and p51 are proteins that do not contain a heme residue. It is then difficult to see a mechanism of interaction of CO with these proteins. Most CO is generated by the heme oxygenase enzyme system, which liberates iron ions at the same time. This, therefore, gives a possible mechanism of CO interaction with the proteins. The bleomycin group of antibiotics (**4**) is closely related to peptides and is known to bind to iron ions.[60] The Fe^{II}–bleomycin complex coordinates CO.[61] In the light of this observation, it is possible that Fe^{II} binds to the protein and then binds CO.



4

6.3. Carbon Monoxide as a Reductant

Heme oxygenase produces CO when there is oxidative stress. The oxidation of heme removes oxygen and the CO produced is also a reductant, being oxidized to CO_2, and thus removing more oxygen. Carbon monoxide can act as a reducing agent in two ways: It can accept an oxygen atom and be oxidized directly to CO_2, as it does with cytochrome c oxidase. Alternatively, it can react with water and undergo the water–gas shift reaction, liberating H_2 or two electrons [Eq. (1)].[62]

Carbon monoxide is oxidized by cytochrome c oxidase to CO_2.[63] The X-ray structure of bovine[64] and bacterial[65] cytochrome c oxidase shows that there are two heme units and two copper centers. CO binds first to the Cu^I center and is then transferred to the Fe center in cytochrome cbb_3-CO.[66] The reaction of the oxidized forms of hemoglobin and myoglobin with peroxides generates intermediates containing ferryl (Fe^{IV}=O) groups.[67] Their oxygen atom is transferred to CO to produce CO_2.[68] Once reduced, the Fe^{II} cytochrome can coordinate CO, which would also help to block the action of cytochrome c oxidase.

$$\begin{aligned} &CO + H_2O \rightleftharpoons CO_2 + H_2 \\ \text{or } &CO + H_2O \rightleftharpoons CO_2 + 2e^- + 2H^+ \end{aligned} \qquad (1)$$

One of the clearest examples of the water–gas shift reaction in nature is with carbon monoxide dehydrogenases (CODH). The key mechanism derives from the oxidation of CO to CO_2 by CODH, with the production of two electrons [Eq. (1)].[69] The importance of this group can be judged from the estimate that 10^8 tons of environmental CO is oxidized to CO_2 every year by aerobic and anaerobic bacteria containing CODH enzymes.[70] The subject has been reviewed some years ago.[71]

The X-ray structures of the Ni-Fe-S carbon monoxide dehydrogenases of *Carboxydothermus hydrogenoformans*[72] and *Rhodospirillium rubrum*[73] have been determined; they contain a metal–sulfur cluster (Figure 2). The crystal structure shows the presence of a $\{Fe_3NiS_4\}$ core with an exo-cube Fe center. The suggested mechanism is a variation on the water–gas shift reaction.[62,74] It is proposed that CO coordinates to the vacant site on the Ni center. An hydroxide ion attacks CO to give $Ni{-}CO_2H$, which then decomposes to give CO_2, with the transfer of two electrons to the $\{Fe_3NiS_4\}$ core.

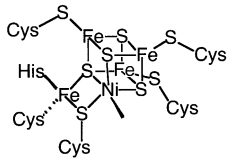
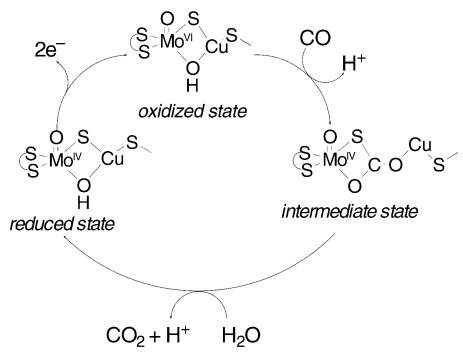


Figure 2. The metal core in Ni-Fe-S carbon monoxide dehydrogenases.

A different CO dehydrogenase has been identified from *Oligotropha carboxidovorans*[75,76] and *Hydrogenophaga pseudoflava*.[77] This enzyme contains a [CuSMo(=O)OH] cluster. The mechanism proposed for this enzyme involves activation of CO by copper, with the intermediate being trapped by using *n*BuNC in place of CO (Scheme 3).

Vitamin B_{12} has also been shown to be involved in the conversion of CO to CO_2 by CO dehydrogenase/CoA synthase.[78] Although its role appears to be that of a methyl transfer agent, earlier work has shown that several corrinoids are reduced by CO, presumably by a mechanism related to the



Scheme 3. The proposed mechanism for CO dehydrogenase from the eubacterium *Oligotropha carboxidovoran*.[75]

 © 2003 Wiley-VCH Verlag GmbH & Co. KGaA, Weinheim

water–gas shift reaction.[79] Hydroxycobalamin can also act as a source of CO.[80]

7. Other Possible Roles for Metal Carbonyls in Medicine

There have been reports of the investigation of metal carbonyls for roles in medicine other than the cardiovascular system. The CO vibration in the IR spectrum provides a method to detect metal carbonyls and this led to the development of the carbonylmetalloimmunoassay procedure.[81] Metal carbonyl moieties, such as $\{M(CO)_3\}$ (M = Cr, Mn, Re, Fe), are attached to molecules that are capable of molecular recognition, in order to label and assay specific biological receptors. When M = Tc or Re, the same idea is used to introduce radioactive ^{99m}Tc, ^{186}Re, or ^{188}Re at a receptor for radiopharmaceutical applications.[81b,82] There has been considerable interest in testing metal carbonyls for anticancer activity. For example, $[Co_2(CO)_6(HC_2CCH_2O_2CC_6H_4\text{-}2\text{-}OH)]$ has been shown to be more active than cisplatin on the human mammary tumor cell lines MCF-7 and MDA-MB-231.[83] Also $[\{\eta^5\text{-}(4\text{-}Me_2N\{CH_2\}_4OC_6H_4)(4\text{-}HOC_6H_4)CHCHEtC_5H_4\}Re(CO)_3]$ has been shown to behave in a similar manner to tamoxifen, and it appears that the observed antiproliferative effect is dependent on the oestradiol receptor α.[84]

8. Summary and Outlook

It appears that CO is of equal importance as NO as a signaling molecule in mammals; the mechanism of action is far from clear. One major target for CO is the iron center of heme in soluble guanylyl cyclase, but there are other targets with precedence for other coordination sites, including non-porphyrin iron, cobalt, nickel, and copper centers. There is much work needed from biochemists and bioinorganic modelers to understand how CO can have such an important biological role; there are many questions to answer: Although hemes and cytochromes are obvious binding sites for CO, p38 does not possess such a binding site; so, how does CO signal to CO-sensitive receptors such as p38? Once the CO group has bound to the receptor, is it the resulting conformational change that acts as the trigger, or does CO become involved chemically? Does the water–gas shift reaction play any significant role in mammal biochemistry and signal transduction mechanisms? Does the ability of CO to remove oxygen from a Fe=O bond in a cytochrome play a defensive role in mammals, or is this limited to being a mechanism for the destruction of CO? Does CO binding to cytochromes in mitochondria always play an inhibitory role? And finally, how is the specificity in CO-mediated regulation of cellular function achieved?

In view of the well-known toxicity of CO, it seems very unlikely that this gaseous compound could have beneficial medical applications. However, the toxicity of CO and NO are very similar,[85] and NO is now very important in the pharmaceutical industry, with a range of NO-releasing drugs currently available and under development with more than 70 US and World Patents on the applications of NO donors.[86]

It is probable that in the near future a range of new drugs will be developed based on CO-releasing molecules for the treatment of cardiovascular dysfunction, as well as neurodegenerative- and inflammatory-related diseases. This should open up a new floodgate of interest into the whole field of metal carbonyls and move the new field of bioorganometallic chemistry into a mature subject that needs to be taken seriously by the pharmaceutical industry.

Received: February 10, 2003 [M1634]

[1] "Toxicity of Carbon Monoxide: Hemoglobins vs. Histotoxic Mechanisms": C. A. Piantadosi in *Carbon Monoxide* (Ed.: D. G. Penney), CRC Press, Boca Raton, **1996**, chap. 8.
[2] T. Sjostrand, *Scand. J. Clin. Lab. Invest.* **1949**, *1*, 201–214.
[3] R. F. Coburn, W. S. Blakemore, R. E. Forster, *J. Clin. Invest.* **1963**, *42*, 1172–1178; R. F. Coburn, W. J. Williams, R. E. Forster, *J. Clin. Invest.* **1964**, *43*, 1098–1103; R. F. Coburn, W. J. Williams, S. B. Kahn, *J. Clin. Invest.* **1966**, *45*, 460–467.
[4] T. Sjostrand, *Acta Physiol. Scand.* **1952**, *26*, 328–333.
[5] M. D. Maines, *Heme Oxygenase: Clinical Applications, Functions*, CRC, Boca Raton, FL, **1992**.
[6] S. M. Scharf, S. Permutt, B. Bromberger-Barnea, *J. Appl. Physiol. Respir. Environ. Exercise Physiol.* **1975**, *39*, 752–758.
[7] S. Shibahara, R. Muller, H. Taguchi, T. Yoshida, *Proc. Natl. Acad. Sci. USA* **1985**, *82*, 7865–7869.
[8] M. D. Maines, G. M. Trakshel, R. K. Kutty, *J. Biol. Chem.* **1986**, *261*, 411–419; I. Cruse, M. D. Maines, *J. Biol. Chem.* **1988**, *263*, 3348–3353; G. M. Trakshel, M. D. Maines, *J. Biol. Chem.* **1989**, *264*, 1323–1328.
[9] M. D. Maines, *FASEB J.* **1988**, *2*, 2557–2568.
[10] G. S. Marks, J. F. Brien, K. Nakatsu, B. E. McLaughlin, *Trends Pharmacol. Sci.* **1991**, *12*, 185–188; R. Stocker, Y. Yamamoto, A. F. McDonagh, A. N. Glazer, B. N. Ames, *Science* **1987**, *235*, 1043–1046; A. F. McDonagh, *Clin. Perinat.* **1990**, *17*, 359–369.
[11] R. Motterlini, R. Foresti, C. J. Green in *Carbon Monoxide and Cardiovascular Functions* (Ed.: R. Wang), CRC, Boca Raton, FL, **2002**, p. 320.
[12] L. E. Otterbein, *Antioxid. Redox Signaling* **2002**, *4*, 309–319.
[13] J. F. Kasting, *Science* **1993**, *259*, 920–926.
[14] S. Miyakawa, H. Yamanashi, K. Kobayashi, H. J. Cleaves, S. L. Miller, *Proc. Natl. Acad. Sci. USA* **2002**, *99*, 14628–14631.
[15] H. J. Vreman, R. J. Wong, D. K. Stevenson in *Carbon Monoxide and Cardiovascular Functions* (Ed.: R. Wang), CRC, Boca Raton, FL, **2002**, chap. 15.
[16] R. Tenhunen, H. S. Marver, R. Schmid, *J. Biol. Chem.* **1969**, *244*, 6388–6394.
[17] Y. Liu, P. Moënne-Loccoz, T. M. Loehr, P. R. Ortiz de Montellano, *J. Biol. Chem.* **1997**, *272*, 6909–6917.
[18] R. Schmid, A. F. McDonagh, *The Porphyrins, Vol. VI* (Ed.: D. Dolphin), Academic Press, New York, **1979**, pp. 257–293.
[19] R. Motterlini, A. Gonzales, R. Foresti, J. E. Clark, C. J. Green, R. M. Winslow, *Circ. Res.* **1998**, *83*, 568–577; I. A. Sammut, R. Foresti, J. E. Clark, D. J. Exon, M. J. Vesely, P. Sarathchandra, C. J. Green, R. Motterlini, *Br. J. Pharmacol.* **1998**, *125*, 1437–1444.
[20] M. Scharte, H. G. Bone, H. Van Aken, J. Meyer, *Biochem. Biophys. Res. Commun.* **2000**, *267*, 423–426.
[21] K. Zayasu, K. Sekizawa, S. Okinaga, M. Yamaya, H. Sasaki, *Am. J. Respir. Crit. Care Med.* **1997**, *156*, 1140–1143; I. Horvath, L. E. Donelly, P. Paredi, S. A. Kharitonov, P. J. Barnes, *Thorax* **1998**, *53*, 668–672.

 © 2003 Wiley-VCH Verlag GmbH & Co. KGaA, Weinheim

[22] I. Horvath, S. Loukides, T. Wodehouse, S. A. Kharitonov, P. J. Cole, P. J. Barnes, *Thorax* **1998**, *53*, 867 – 870.
[23] J. D. Antuni, S. A. Kharitonov, D. Hughes, M. E. Hodson, P. J. Barnes, *Thorax* **2000**, *55*, 138 – 142; P. Paredi, S. A. Kharatonov, D. Leak, P. L. Shah, D. Cremer, M. E. Hodson, P. J. Barnes, *Am. J. Respir. Crit. Care Med.* **2000**, *161*, 1247 – 1251.
[24] P. Paredi, W. Biernacki, G. Invernizzi, S. A. Kharitonov, P. J. Barnes, *Chest* **1999**, *116*, 1007 – 1111.
[25] M. Monma, M. Yamaya, K. Sekizawa, K. Ikeda, N. Suzuki, T. Kikuchi, T. Takasaka, H. Sasaki, *Clin. Exp. Allergy* **1999**, *29*, 1537 – 1541.
[26] R. Foresti, R. Motterlini, *Free Radical Res.* **1999**, *31*, 459 – 475; J. E. Clark, R. Foresti, P. Sarathchandra, H. Kaur, C. J. Green, R. Motterlini, *Am. J. Physiol. Heart Circ. Physiol.* **2000**, *278*, H643 – H651; L. E. Otterbein, A. M. K. Choi, *Am. J. Physiol. Lung Cell. Mol. Physiol.* **2000**, *279*, L1029 – L1037.
[27] D. Morse, A. M. K. Choi, *Am. J. Respir. Cell. Mol. Biol.* **2002**, *27*, 8 – 16.
[28] F. Coceani, N. C. Hamilton, J. Labuc, P. M. Olley, *Am. J. Physiol.* **1984**, *246*, H640 – H643; Y. P. Vedernikov, T. Graser, A. F. Vanin, *Biomed. Biochim. Acta* **1989**, *48*, 595 – 597; R. F. Furchgott, D. Jothianandan, *Blood Vessels* **1991**, *28*, 52 – 61.
[29] T. Morita, M. A. Perrella, M. E. Lee, S. Kourembanas, *Proc. Natl. Acad. Sci. USA* **1995**, *92*, 1475 – 1479; N. Christodoulides, W. Durante, M. H. Kroll, A. I. Schafer, *Circulation* **1995**, *91*, 2306 – 2309; I. A. Sammut, R. Foresti, J. E. Clark, D. J. Exon, M. J. J. Vesely, P. Sarathchandra, C. J. Green, R. Motterlini, *Br. J. Pharmacol.* **1998**, *125*, 1437 – 1444; F. Coceani, *Circ. Res.* **2000**, *86*, 1184 – 1186.
[30] L. E. Otterbein, F. H. Bach, J. Alam, M. Soares, H. T. Lu, M. Wysk, R. J. Davis, R. A. Flavell, A. M. K. Choi, *Nat. Med.* **2000**, *6*, 422 – 428.
[31] J. T. Chapman, L. E. Otterbein, J. A. Elias, A. M. K. Choi, *Am. J. Physiol. Lung Cell Mol. Physiol.* **2001**, *281*, L209 – L215.
[32] K. Sato, J. Balla, L. Otterbein, R. N. Smith, S. Brouard, Y. Lin, E. Csizmadia, J. Sevigny, S. C. Robson, G. Vercellotti, A. M. Choi, F. H. Bach, M. P. Soares, *J. Immunol.* **2001**, *166*, 4185 – 4194.
[33] M. Stupfel, G. Bouley, *Ann. N. Y. Acad. Sci.* **1970**, *174*, 342 – 368.
[34] F. Amersi, X. D. Shen, D. Anselmo, J. Melinek, S. Iyer, D. J. Southard, M. Katori, H. D. Volk, R. W. Busuttil, R. Buelow, J. W. Kupiec-Weglinski, *Hepatology* **2002**, *35*, 815 – 823.
[35] L. Gunther, P. O. Berberat, M. Haga, S. Brouard, R. N. Smith, M. P. Soares, F. H. Bach, E. Tobiasch, *Diabetes* **2002**, *51*, 994 – 999.
[36] N. Ozawa, N. Goda, N. Makino, T. Yamaguchi, Y. Yoshimura, M. Suematsu, *J. Clin. Invest.* **2002**, *109*, 457 – 467.
[37] S. A. Bainbridge, A. E. Farley, B. E. McLaughlin, C. H. Graham, G. S. Marks, K. Nakatsu, J. F. Brien, G. N. Smith, *Placenta* **2002**, *23*, 563 – 569.
[38] D. Morse, J. Sethi, A. M. K. Choi, *Crit. Care Med.* **2002**, *30*, S12 – S17.
[39] S. P. Gaine, G. Booth, L. Otterbein, N. A. Flavahan, A. M. Choi, C. M. Weiner, *J. Vasc. Res.* **1999**, *36*, 114 – 119; T. Morita, S. A. Mitsialis, H. Koike, Y. Liu, S. Kourembanas, *J. Biol. Chem.* **1997**, *272*, 32804 – 32809.
[40] L. E. Otterbein, B. S. Zuckerbraun, M. Haga, F. Liu, R. Song, A. Usheva, C. Stachulak, N. Bodyak, R. N. Smith, E. Csizmadia, S. Tyagi, Y. Akamatsu, R. J. Flavell, T. R. Billiar, E. Tzeng, F. H. Bach, A. M. K. Choi, M. G. Soares, *Nat. Med.* **2003**, *9*, 183 – 190.
[41] D. E. Baranano, S. Dore, C. D. Ferris, S. H. Snyder, *Clin. Neurosci. Res.* **2001**, *1*, 46 – 52.
[42] W. Tschugguel, F. Stonek, Z. Zhegu, W. Dietrich, C. Schneeberger, T. Stimpfl, T. Waldhoer, W. Vycudilik, J. C. Huber, *J. Clin. Endocrinol. Metab.* **2001**, *86*, 3833 – 3839.
[43] M. McLean, M. Bowman, V. Clifton, R. Smith, A. B. Grossman, *J. Clin. Endocrinol. Metab.* **2000**, *85*, 2345 – 2349.
[44] A. M. Choi, P. J. Lee, L. E. Otterbein, , US Patent 2002155166, **2002** [*Chem. Abstr.* **2002**, *137*, 289059].
[45] R. Buelow, J. Woo, *PCT Int. Appl.* **2002**, 59; CODEN: PIXXD2 WO 0278684 [*Chem. Abstr.* **2002**, *137*, 273242].
[46] B. E. Mann, R. Motterlini, , World Patent Appl. WO 02092075 [*Chem. Abstr.* **2002**, *137*, 375272].
[47] R. Motterlini, J. E. Clark, R. Foresti, P. Sarathchandra, B. E. Mann, C. J. Green, *Circ. Res.* **2002**, *90*, e17 – e24.
[48] V. G. Kharitonov, V. S. Sharma, R. B. Pilz, D. Magde, D. Koesling, *Proc. Natl. Acad. Sci. USA* **1995**, *92*, 2568 – 2571.
[49] J. W. Denninger, M. A. Marletta, *Biochim. Biophys. Acta* **1999**, *1411*, 334 – 350.
[50] Y. Zhao, P. E. Brandish, D. P. Ballou, M. A. Marletta, *Proc. Natl. Acad. Sci. USA* **1999**, *96*, 14753 – 14758.
[51] V. G. Kharitonov, V. S. Sharma, D. Magde, D. Koesling, *Biochemistry* **1997**, *36*, 6814 – 6818.
[52] P. E. Brandish, W. Buechler, M. A. Marletta, *Biochemistry* **1998**, *37*, 16898 – 16907.
[53] D. M. Lawson, C. E. M. Stevenson, C. Andrew, R. R. Eady, *EMBO J.* **2000**, *19*, 5661 – 5671.
[54] V. G. Kharitonov, V. S. Sharma, D. Magde, D. Koesling, *Biochemistry* **1999**, *38*, 10699 – 10706; V. G. Kharitonov, M. Russwarn, D. Magde, V. S. Sharma, D. Koesling, *Biochem. Biophys. Res. Commun.* **1997**, *239*, 284 – 286.
[55] J. R. Stone, M. A. Marletta, *Biochemistry* **1994**, *33*, 5636 – 5640; T. Tomita, T. Ogura, S. Tsuyama, Y. Imai, T. Kitagawa, *Biochemistry* **1997**, *36*, 10155 – 10160; J. N. Burstyn, A. E. Yu, E. A. Dierks, B. K. Hawkins, J. H. Dawson, *Biochemistry* **1995**, *34*, 5896 – 5903; G. Deinum, J. R. Stone, G. T. Babcock, M. A. Marletta, *Biochemistry* **1996**, *35*, 1540 – 1570; A. E. Yu, S. Z. Hu, T. G. Spiro, J. N. Burstyn, *J. Am. Chem. Soc.* **1994**, *116*, 4117 – 4118; B. Fan, G. Gupta, R. S. Danziger, J. M. Friedman, D. L. Rousseau, *Biochemistry* **1998**, *37*, 1178 – 1184; J. R. Stone, R. H. Sands, W. R. Dunham, M. A. Marletta, *Biochem. Biophys. Res. Commun.* **1995**, *207*, 572 – 577.
[56] W. R. Scheidt, P. L. Piciulo, *J. Am. Chem. Soc.* **1976**, *98*, 1913 – 1919.
[57] R. Salzmann, C. J. Ziegler, N. Godbout, M. T. McMahon, K. S. Suslick, E. Oldfield, *J. Am. Chem. Soc.* **1998**, *120*, 11323 – 11334.
[58] J. R. Stone, M. A. Marletta, *Biochemistry* **1995**, *34*, 16397 – 16403.
[59] A. Friebe, G. Schultz, D. Koesling, *EMBO J.* **1996**, *15*, 6863 – 6868; A. Friebe, D. Koesling, *Mol. Pharmacol.* 1998, *53*, 123 – 127; J. R. Stone, M. A. Marletta, *Chem. Biol.* **1998**, *5*, 255 – 261; B. E. McLaughlin, M. L. Chretien, C. Choi, J. F. Brien, K. Nakatsu, G. S. Marks, *Can. J. Physiol. Pharmacol.* **2000**, *78*, 343 – 349.
[60] Y. Sugiura, T. Takita, H. Umezawa, *Met. Ions Biol. Syst.* **1985**, *19*, 81 – 108.
[61] Y. Sugiura, T. Suzuki, H. Kawabe, H. Tanaka, K. Watanabe, *Biochim. Biophys. Acta* **1982**, *716*, 38 – 44; Y. Sugiura, J. Kuwahara, T. Suzuki, *FEBS Lett.* **1985**, *182*, 39 – 42; N. J. Oppenheimer, L. O. Rodriguez, S. M. Hecht, *Proc. Natl. Acad. Sci. USA* **1979**, *76*, 5616 – 5620; Y. Sugiura, T. Suzuki, Y. Muraoka, Y. Umezawa, T. Takita, H. Umezawa, *J. Antibiot.* **1981**, *34*, 1232 – 1236.
[62] W. A. Herrmann in *Applied Homogeneous Catalysis with Organometallic Compounds, Vol. 2* (Eds.: B. Cornils, W. A. Herrmann), VCH, Weinheim, **1996**, pp. 957 – 963; R. M. Laine, R. B. Wilson, *Aspects Homogeneous Catal.* **1984**, *5*, 217 – 240.
[63] L. J. Young, W. S. Caughey, *Biochemistry* **1986**, *25*, 152 – 161; L. J. Young, W. S. Caughey, *J. Biol. Chem.* **1987**, *262*, 15019 – 15025; Ó. Einarsdóttir, M. G. Choc, S. Weldon, W. S. Caughey, *J. Biol. Chem.* **1988**, *263*, 13641 – 13654; Y. Kim, K. Shinzawa-Itoh, S. Yoshikawa, T. Kitagawa, *J. Am. Chem. Soc.* **2001**, *123*, 757 – 758.

 © 2003 Wiley-VCH Verlag GmbH & Co. KGaA, Weinheim

[64] T. Tsukihara, H. Aoyama, E. Yamashita, T. Tomizaki, H. Yamaguchi, K. Shinzawa-Itoh, R. Nakashima, R. Yaono, S. Yoshikawa, *Science* **1995**, *269*, 1069 – 1074.
[65] S. Iwata, C. Ostermeier, B. Ludwig, H. Michel, *Nature* **1995**, *376*, 660 – 669.
[66] S. Stavrakis, K. Koutsoupakis, E. Pinakoulaki, A. Urbani, M. Saraste, C. Varotsis, *J. Am. Chem. Soc.* **2002**, *124*, 3814 – 3815.
[67] P. George, D. H. Irvine, *Biochem. J.* **1952**, *52*, 511 – 517; J. J. Mieyal, *Rev. Biochem. Toxicol.* **1985**, *7*, 1; M. Chance, L. Powers, C. Kumar, B. Chance, *Biochemistry* **1986**, *25*, 1259 – 1265; C. E. Catalano, P. R. Ortiz de Montellano, *Biochemistry* **1987**, *26*, 8373 – 8380; M. B. Grisham, J. Everse in *Peroxidases in Chemistry and Biology, Vol. 1* (Ed.: J. Everse, K. E. Everse, M. B. Grisham), CRC, Boca Raton, FL, **1990**, p. 335; J. C. Alvarez, P. R. Ortiz de Montellano, *Biochemistry* **1992**, *31*, 8315 – 8322; A. J. Allentoff, J. L. Bolton, A. Wilks, J. A. Thompson, P. R. Ortiz de Montellano, *J. Am. Chem. Soc.* **1992**, *114*, 9744 – 9749.
[68] Q. Ji, C. R. Lloyd, W. R. Ellis, Jr., E. M. Eyring, *J. Am. Chem. Soc.* **1998**, *120*, 221 – 222.
[69] R. L. Uffen, *Proc. Natl. Acad. Sci. USA* **1976**, *73*, 3298 – 3302.
[70] G. W. Bartholomew, M. Alexander, *Appl. Environ. Microbiol.* **1979**, *37*, 932 – 937; J. C. Fontecilla-Camps, S. W. Ragsdale, *Adv. Inorg. Chem.* **1999**, *47*, 283 – 333.
[71] S. W. Ragsdale, M. Kumar, *Chem. Rev.* **1996**, *96*, 2515 – 2539.
[72] H. Dobbek, V. Svetlitchnyi, L. Gremer, R. Huber, O. Meyer, *Science* **2001**, *293*, 1281 – 1285.
[73] C. L. Drennan, J. Heo, M. D. Sintchak, E. Schreiter, P. W. Ludden, *Proc. Natl. Acad. Sci. USA* **2001**, *98*, 11 973 – 11 978.
[74] D. Qiu, M. Kumar, S. W. Ragsdale, T. G. Spiro, *J. Am. Chem. Soc.* **1996**, *118*, 10 429 – 10 435.
[75] H. Dobbek, L. Gremer, R. Klefersauer, R. Huber, O. Mayer, *Proc. Natl. Acad. Sci. USA* **1999**, *96*, 8884 – 8889.
[76] H. Dobbek, L. Gremer, R. Klefersauer, R. Huber, O. Mayer, *Proc. Natl. Acad. Sci. USA* **2002**, *99*, 15 971 – 15 976; M. Gnida, R. Ferner, L. Gremer, O. Meyer, W. Meyer-Klaucke, *Biochemistry* **2003**, *42*, 222 – 230.
[77] P. Hänzelmann, H. Dobbek, L. Gremer, R. Huber, O. Meyer, *J. Mol. Biol.* **2000**, *301*, 1221 – 1235.
[78] S. W. Ragsdale, M. Kumar, S. Zhao, S. Menon, J. Seravalli, T. Doukov in *Vitamin B_{12} and B_{12}-Protein* (Ed.: B. Kräutler, D. Arigoni, B. T. Golding), VCH, Weinheim, **1996**, p. 167.
[79] W. Friedrich, *Z. Naturforsch. B* **1970**, *25*, 1431 – 1434; G. N. Schrauzer, L. P. Lee, *Arch. Biochem. Biophys.* **1970**, *138*, 16 – 25; L. P. Lee, G. N. Schrauzer, *J. Am. Chem. Soc.* **1968**, *90*, 5274 – 5276.
[80] R. R. Engel, S. Modler, J. M. Matsen, Z. J. Petryka, *Biochim. Biophys. Acta* **1973**, *313*, 150 – 155.
[81] a) G. Jaouen, A. Vessières, I. S. Butler, *Acc. Chem. Res.* **1993**, *26*, 361 – 369; b) G. Jaouen, S. Top, A. Vessières, R. Alberto, *J. Organomet. Chem.* **2000**, *600*, 23 – 36; c) M. Salmain, A. Vessières, P. Brossier, I. S. Butler, G. Jaouen, *J. Immunol. Methods* **1992**, *148*, 65 – 75.
[82] R. Alberto, K. Ortner, N. Wheatley, R. Schibli, P. A. Schubiger, *J. Am. Chem. Soc.* **2001**, *123*, 3135 – 3136; S. S. Jurisson, J. D. Lydon, *Chem. Rev.* **1999**, *99*, 2205 – 2218; S. S. Jurisson, J. D. Lydon, *Inorg. Chem.* **2003**, *42*, 1014 – 1022; R. Schibli, P. A. Schubiger, *Eur. J. Nucl. Med. Mol. Imaging.* **2002**, *29*, 1529 – 1542.
[83] K. Schmidt, M. Jung, R. Keilitz, B. Schnurr, R. Gust, *Inorg. Chim. Acta* **2000**, *306*, 6 – 16.
[84] G. Jaouen, S. Top, A. Vessières, P. Pigeon, G. Leclercq, I. Laios, *Chem. Commun.* **2001**, 383 – 384.
[85] The rtecs web sites for NO and CO toxicity data are as follows: for NO; http://ccinfoweb.ccohs.ca/rtecs/Action.lasso?-database = rtecs&-layout = Display&-response = detail.html&-noresultserror = noresults.html&-op = eq&CAS + REGISTRY + NUMBER = 10102-43–9&-search; for CO; http://ccinfoweb.ccohs.ca/rtecs/Action.lasso?-database = rtecs&-layout = Display&-response = detail.html&-noresultserror = noresults.html&-op = eq&CAS + REGISTRY + NUMBER = 630-08-0&-search.
[86] P. G. Wang, M. Xian, X. Tang, X. Wu, Z. Wen, T. Cai, A. J. Janczuk, *Chem. Rev.* **2002**, *102*, 1091 – 1134; C. Napoli, L. J. Ignarro, *Annu. Rev. Pharmacol. Toxicol.* **2003**, *43*, 97 – 123.

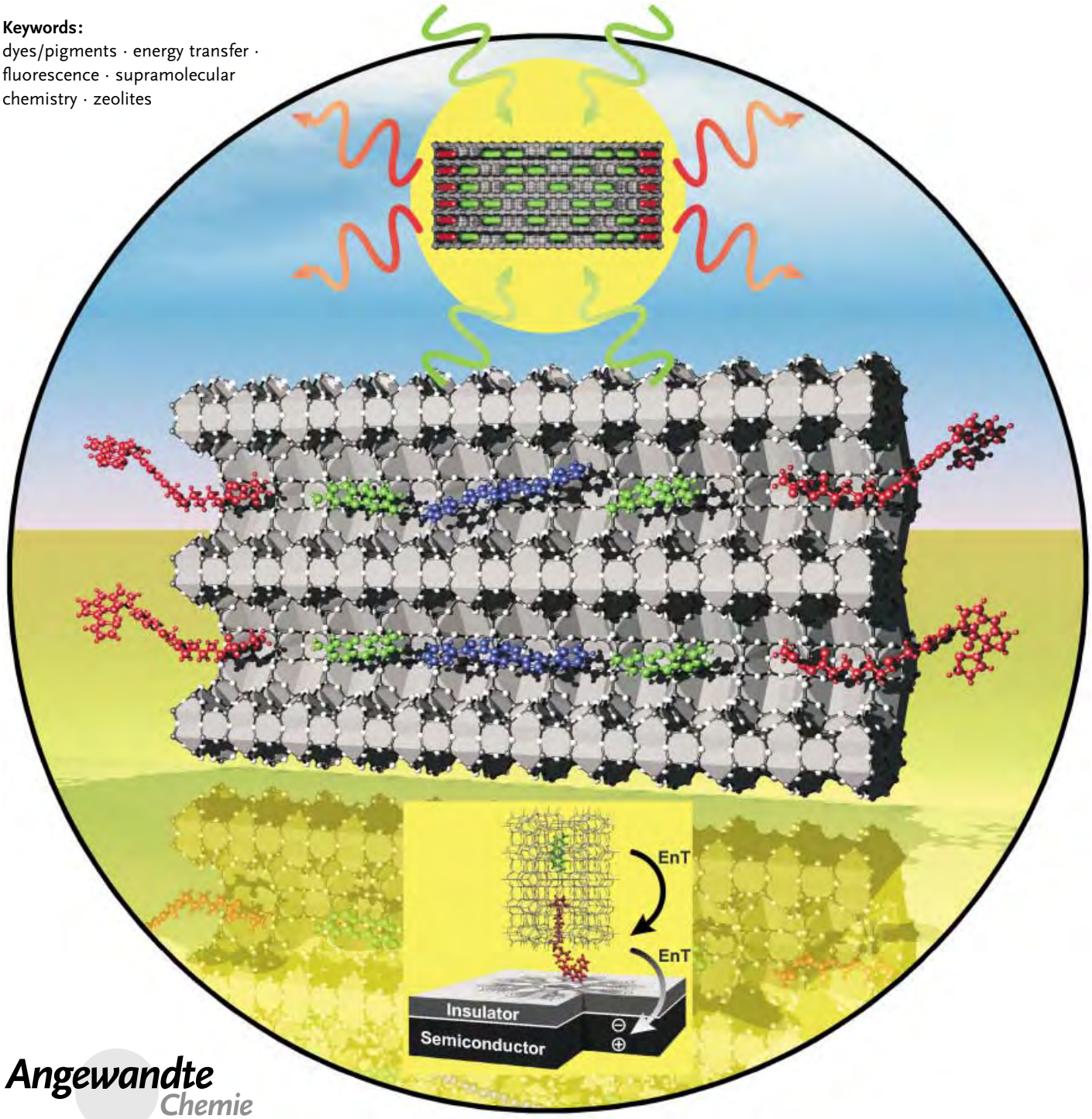
 © 2003 Wiley-VCH Verlag GmbH & Co. KGaA, Weinheim

Light-Harvesting Antenna Materials

Host–Guest Antenna Materials

Gion Calzaferri, Stefan Huber, Huub Maas, and Claudia Minkowski*

Keywords:
dyes/pigments · energy transfer · fluorescence · supramolecular chemistry · zeolites



© 2003 Wiley-VCH Verlag GmbH & Co. KGaA, Weinheim
DOI: 10.1002/anie.200300570

The focus of this review is on host–guest composites with photonic antenna properties. The material generally consists of cylindrical zeolite L crystals the channels of which are filled with dye molecules. The synthesis is based on the fact that molecules can diffuse into individual channels. This means that, under the appropriate conditions, they can also leave the zeolite by the same way. In some cases, however, it is desirable to block their way out by adding a closure molecule. Functionalization of the closure molecules allows tuning of, for example, wettability, refractive index, and chemical reactivity. The supramolecular organization of the dyes inside the channels is a first stage of organization. It allows light harvesting within a certain volume of a dye-loaded nanocrystalline zeolite and radiationless transport to both ends of the cylinder or from the ends to the center. The second stage of organization is the coupling to an external acceptor or donor stopcock fluorophore at the ends of the channels, which can trap or inject electronic excitation energy. The third stage of organization is the coupling to an external device through a stopcock molecule. The wide-ranging tunability of these highly organized materials offers fascinating new possibilities for exploring excitation-energy-transfer phenomena, and challenges for developing new photonic devices.

From the Contents

1. Introduction 3733
2. Hexagonal Zeolite Crystals as Hosts for Dyes 3734
3. Synthesis 3737
4. The Inner and Outer Surface of Zeolite L 3742
5. First Stage of Organization 3746
6. Second Stage of Organization 3752
7. Third Stage of Organization 3754
8. Intrazeolite Charge Transport 3756
9. Summary 3757

1. Introduction

Plants are masters of efficiently transforming sunlight into chemical energy. In this process, every plant leaf acts as a photonic antenna in which photonic energy in the form of sunlight is absorbed and transported by chlorophyll molecules. In natural photosynthesis, light is absorbed by a photonic antenna system of a few-hundred chlorophyll molecules arranged in a protein environment. These devices allow fast energy transfer from an electronically excited molecule to an unexcited neighboring molecule in such a way that the probability that the excitation energy reaches the reaction center is very high. Trapping occurs there. It has been reported that the anisotropic arrangement of chlorophyll molecules is important for efficient energy migration.[1]

Several attempts to build an artificial antenna are presented in the literature. Multinuclear luminescent metal complexes,[2,3] multichromophore cyclodextrins,[4] Langmuir–Blodgett films,[5–7] dyes in polymer matrices,[8–10] and dendrimers[11] have been investigated. In some cases aspects of artificial antenna systems are also found in sensitization processes in silver halide photographic materials[12] and the spectral sensitization of polycrystalline titanium dioxide films.[13,14] In natural antennae the formation of quenching aggregates is prevented by fencing the chlorophyll molecules in polypeptide cages.[15] A similar approach consists of enclosing dyes inside a nanoporous material and by choosing conditions such that the cavities are only able to uptake monomers but not aggregates.[16]

Our approach is based on using zeolites bearing a channel structure as a host. The light transport is made possible by specifically organized dye molecules which mimic the function of chlorophyll in the natural antennae. In most of our experiments we use zeolite L as a host because of its versatility. Zeolite L crystals consist of an extended one-dimensional tube system.[17,18] We have filled each individual tube with successive chains of various electronically non-interacting joined dye molecules. Light shining on the cylinder is first absorbed, and the energy is then transported by the dye molecules inside the tubes to the desired place. We have shown that photonic antenna materials can be prepared, not only for light harvesting within the volume of a dye loaded nanocrystalline zeolite L,[19,20] but also for radiationless transport of the electronic excitation energy to a target molecule fixed at the ends of the nanochannels or from an injector molecule fixed at the "entrances".[21] A schematic view of the photonic antenna invented by us[22,23] is illustrated in Figure 1. The monomeric dye molecules are represented by rectangles. The dye molecule which has been excited by absorbing an incident photon transfers its electronic excitation to a neighboring molecule. After a series of such steps the electronic excitation reaches a luminescent trap (dark rectangles). The energy migration is in competition with spontaneous emission, radiationless decay, quenching, and photochemically induced degradation. Fast energy migration is therefore crucial if a trap should be reached before other processes can take place. This means that a detailed understanding of the photochemical and photophysical processes

[*] Prof. Dr. G. Calzaferri, Dipl.-Chem. S. Huber, MSc H. Maas, Dipl.-Chem. C. Minkowski
Department of Chemistry and Biochemistry
University of Bern
3000 Bern 9 (Switzerland)
Fax: (+41) 31-631-3994
E-mail: gion.calzaferri@iac.unibe.ch

 DOI: 10.1002/anie.200300570 © 2003 Wiley-VCH Verlag GmbH & Co. KGaA, Weinheim

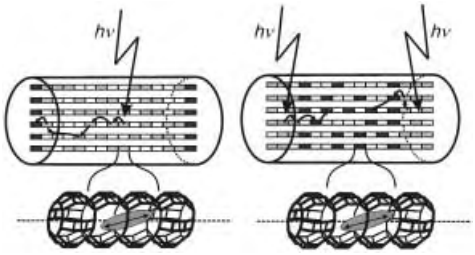


Figure 1. Representation of a cylindrical nanocrystal consisting of organized dye molecules acting as donors (gray rectangles) and acceptors (black rectangles). Left: The donors are in the middle part of the crystal and the acceptors at the ends of each channel. Right: The donors are at the ends of each channel and the acceptors are in the middle part. The enlargements show details of a channel with a dye and its electronic transition moment (double-headed arrow) which is parallel to the channel axis for long molecules and twisted for shorter ones. The diameter of the channel windows of zeolite L is 0.71 nm and the largest free diameter is 1.26 nm. The center-to-center distance between two channels is 1.84 nm.

taking place is important. Studies can be carried out on single crystals, or on crystals dispersed in a solvent, in a polymer matrix, but also on thin layers, for example, coated on a support.

We consider the supramolecular organization of the dyes inside the channels as a first stage of organization (Figure 1 and 2a). It allows light harvesting within a certain volume of a dye-loaded zeolite and radiationless energy transport to both ends of the cylinder or from the ends to the center. This first stage is well mastered as we will show below. A second stage of organization is the coupling to an external acceptor or donor stopcock fluorophore at the ends of the zeolite L channels (Figure 2b) which can trap electronic excitation energy from donor molecules inside the crystal or inject electronic excitation energy to acceptors inside the channels.[24] We have so far demonstrated that this works for three different stopcock fluorophores;[21,25] additional stopcock molecules are currently being explored. A third stage of organization is the coupling to an external device through a stopcock unit. We distinguish between the coupling to an artificial reaction center of 1) molecular dimensions, 2) macromolecular dimensions (photoconducting or conducting polymer, quantum dots), and 3) macroscopic dimensions (semiconductor, conductor, quantum wells). Figure 2c shows as an example the coupling to a semiconductor device, by which energy transfer from the photonic antenna through an insulating layer creates an electron-hole pair in the semiconductor.

Favorable conditions for realizing such a device are a high concentration of monomeric dye molecules with high luminescence quantum yield, an ideal geometrical arrangement of the chromophores, and an optimal size of the device. The type of host materials we are interested in are shown in Figure 3. Organic dyes have the tendency to form aggregates even at low concentration. Aggregates are known to cause fast thermal relaxation of electronic excitation energy. The role of the host is to prevent this aggregation and to superimpose a specific organization. The idea is to choose the diameter of the channels and the dyes such that the dyes cannot glide past each other. This arrangement allows the formation of highly anisotropic dye assemblies. Large amplitude motions of the dye molecules but also the diffusion of reactive molecules can be reduced or even completely suppressed because of the restricted space available and hence very stable materials can result. Host materials which meet the desired geometrical properties can be found among the zeolites.[18]

2. Hexagonal Zeolite Crystals as Hosts for Dyes

Examples of hexagonal zeolites with channels large enough to accommodate organic dye molecules (see Figure 3), are reported in Table 1. Our investigations have concentrated on zeolite L as a host. The reason for this is that neutral as well as cationic dyes can be inserted into the channels of zeolite L and that synthesis procedures for controlling the morphology of zeolite L crystals in the size regime of 30 nm to about 3000 nm are available.[19,26–30] Many results obtained with zeolite L are valid for other nanoporous materials as well.

Zeolite L is a crystalline aluminosilicate with hexagonal symmetry. Its anionic framework with the positions of the charge-compensating cations is illustrated in Figure 4. The crystals consist of so-called cancrinite cages (ε cages) linked



G. Calzaferri *S. Huber* *C. Minkowski* *H. Maas*

Gion Calzaferri received his Ph.D. at the University of Fribourg, Switzerland, 1971. After a postdoc period at the University of Basel and research position at Ciba-Geigy, Basel he moved to the University of Bern where he has been professor of physical chemistry since 1988. His current research interests concern supramolecularly organized molecules, clusters, and complexes in zeolite cavities, dye–zeolite materials as photonic antenna systems, photochemical transformation and storage of solar energy.

Stefan Huber studied chemistry at the University of Bern. After receiving his Diploma in 2001, he started a Ph.D. on the coupling of dye-loaded zeolite L antenna systems to a semiconductor.

Claudia Minkowski obtained her Diploma in chemistry in 2001 at the University of Bern, where she is now working as a Ph.D. student on the spectroscopic analysis of highly organized dye–zeolite composites.

Huub Maas studied Molecular Sciences at Wageningen University. After receiving his Masters in 1999, he moved to Switzerland and he is now working as a Ph.D. student at the University of Bern on the photochemistry at the internal–external surface interface of zeolite L.

 © 2003 Wiley-VCH Verlag GmbH & Co. KGaA, Weinheim

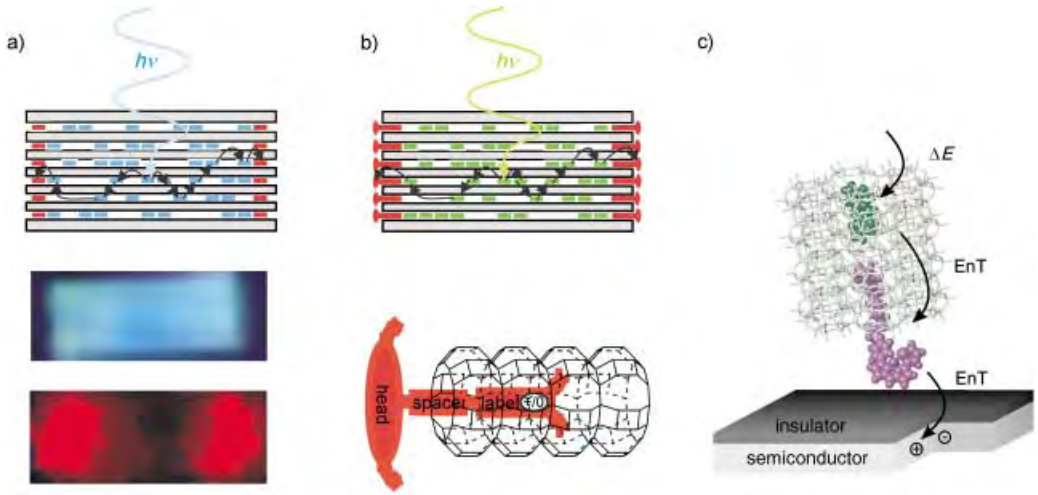


Figure 2. a) Top: dye-loaded zeolite L antenna; blue-emitting donors inside the zeolite L transfer electronic excitation energy to red-emitting acceptors at the ends of the cylindrical crystal. Middle and bottom: fluorescence microscope images of an approximately 2000-nm-long crystal containing DMPOPOP in the middle part (blue, polarizer parallel) and Ox^+ at both ends (red, polarizer perpendicular) on selective DMPOPOP excitation. b) Top: antenna system with stopcock molecules as external traps and bottom: a schematic representation of a stopcock at the end of a zeolite L channel. The stopcock consists of a head, a spacer, and a label. c) Energy transfer (EnT) from a photonic antenna to a semiconductor, creating an electron–hole pair in the semiconductor (radiationless near-field process).

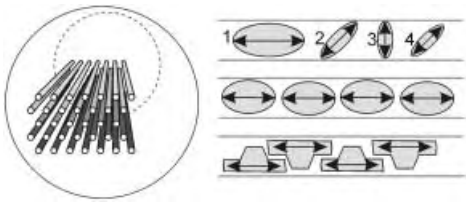


Figure 3. Left: schematic view of a host material bearing parallel channels into which dye molecules can be inserted. Right, top: four representative orientations of molecules and their electronic transition moments (double-headed arrow), middle: orientation of large molecules parallel to the channel axis and which because of their size and shape have no electronic interaction, bottom: orientation of large molecules which align parallel to the channel axis and which have some electronic interaction because of their shape.

Table 1: Lattice constants *a*, *b*, and *c* and free opening diameters *d* of hexagonal molecular sieves with linear channels (in nm).[18]

Material	$a=b$	c	d
Mazzite	1.84	0.76	0.74
$AlPO_4$-5	1.34	0.84	0.73
Zeolite L	1.84	0.75	0.71
Gmelinite	1.38	0.10	0.70
Offretite	1.33	0.76	0.68
CoAPO-50	1.28	0.90	0.61
Cancrinite	1.28	0.51	0.59
VPI-5	1.90	0.84	1.21

by double six-rings. These units form columns in the *c* direction which are connected and thus give rise to 12-rings in with a free diameter of 7.1 Å. As a consequence, zeolite L consists of one dimensional channels, which run through the whole crystal, with a largest free diameter of about 12.6 Å and a unit cell (u.c.) length of 7.5 Å. The main channels are linked by nonplanar eight-rings which form an additional two dimensional channel system with a ring opening of about 1.5 Å. The hexagonal structure of zeolite L material is visible in the scanning electron microscopy picture shown in Figure 4e. Four different cation sites (A, B, C, D) have been reported. Site A is in the center of the double six-ring unit, B is in the center of the ε cage, C lies midway between the centers of two adjacent ε cages, and D is inside the main channel near the wall of the eight-ring. Dehydrated zeolite L has an additional cation site located midway between two adjacent sites A and is indicated as E, see Figure 4c. The water molecules in the large cavities of zeolite L are reported to behave like an intracrystalline liquid, whereas in the smaller pores they seem to build clusters around the cations. The stoichiometry of zeolite L with monovalent cations M is $(M)_9[Al_9Si_{27}O_{72}]\cdot n\,H_2O$, where *n* equals 21 in fully hydrated materials and 16 at about 20% relative humidity.

Figure 4 illustrates that the shape of the crystals can be described reasonably well by assuming cylinder morphology. The primitive vector ***c*** corresponds to the channel axis while the primitive vectors ***a*** and ***b*** are perpendicular to it and make an angle of 60°. The channels run parallel to the central axis of the cylinder. The length, and the diameter of the cylinder are given as l_Z, and d_Z, respectively. The number of parallel channels (n_{ch}) in a hexagonal crystal that can be approximated by a cylinder of diameter d_Z is given by Equation (1), which

$$n_{ch} = \frac{\left(\frac{d_Z}{2}\right)^2 \pi}{|a|^2 \sin(60)} = \frac{\pi}{2\sqrt{3}}\left(\frac{d_Z}{|a|}\right)^2 \qquad (1)$$

 © 2003 Wiley-VCH Verlag GmbH & Co. KGaA, Weinheim

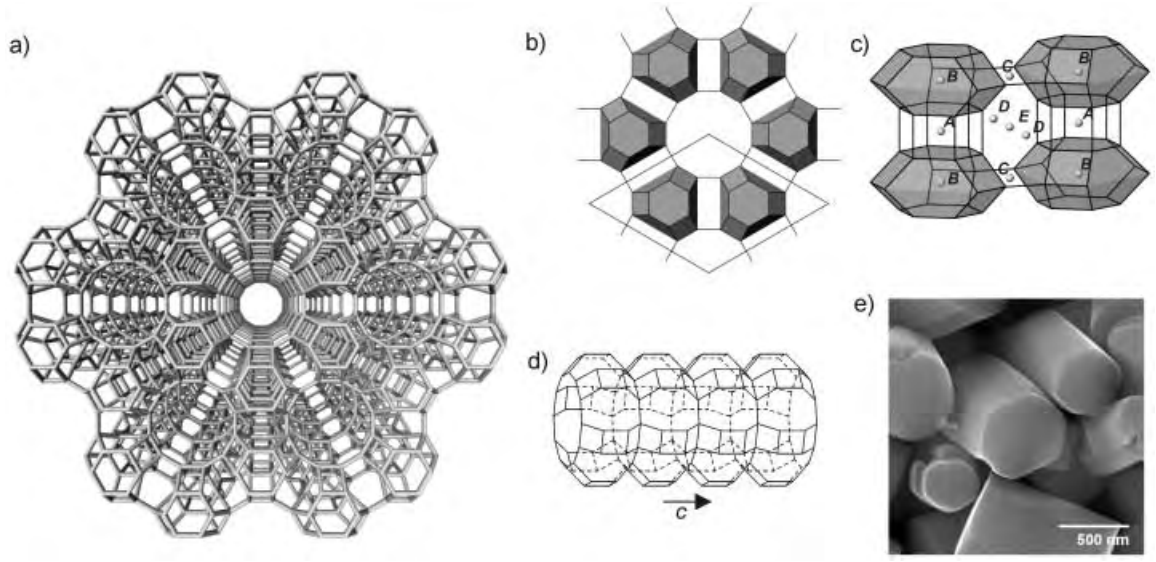


Figure 4. Zeolite L framework: a) projection along *c* axis, b) with the cancrinite cages highlighted as polyhedra, c) section showing the different cationic positions A to E; d) side view of the 12-ring channel along the *c* axis, e) scanning electron microscopy image of zeolite L crystals.

can be approximated for zeolite L as Equation (2), where d_Z is in units of nm.

$$n_{ch} \simeq 0.268 (d_Z)^2 \quad (2)$$

This means that a zeolite L of 500-nm diameter has about 67 000 parallel channels.

The dye molecules are positioned at sites along the linear channels. The length of a site is equal to a number n_s times the length of a unit cell (vector $\boldsymbol{c}$) so that one dye molecule fits into one site. Thus n_s is the number of unit cells which form a site. The value of n_s depends on the size of the dye molecules and on the length of the primitive unit cell. As an example, a dye with a length of approximately 1.5 nm in zeolite L (which has a primitive unit-cell length of 0.75 nm) requires two primitive unit cells, therefore n_s is equal to 2. In favorable cases the sites form a new (pseudo) Bravais lattice with the primitive vectors $\boldsymbol{a}$, $\boldsymbol{b}$, and $n_s\boldsymbol{c}$. Different types of sites exist: a) empty sites, b) sites occupied with luminescent dye molecules, or c) occupied with traps which may or may not be luminescent. In general we are interested in dye molecules with a large electronic-transition dipole moment $\mu(S_1 \leftarrow S_0)$. This means that the $S_1 \leftarrow S_0$ transition is of the $\pi^* \leftarrow \pi$ type.

Under equilibrium conditions, equivalent sites have the same probability of being occupied by a dye molecule. The occupation probability p is equal to the ratio between the occupied and the total number of equivalent sites. The number of unit cells n_{uc} is controlled by the host while n_s is determined by the size and shape of the guest. This means that p depends on purely geometrical (space filling) reasoning and that the dye concentration per unit volume, $c(p)$, of a zeolite crystal can be expressed as a function of p as in Equation (3),

$$c(p) = \frac{\rho_Z}{M_Z} \frac{p}{n_s} \quad (3)$$

where ρ_Z is the density and M_Z the molar mass of one unit cell. Using $\rho_Z = 2.17\ \mathrm{g\,cm^{-3}}$, $M_Z = 2883\ \mathrm{g\,mol^{-1}}$ for pure potassium zeolite L and $n_s = 2$, we obtain $c(p) = p\,0.376\ \mathrm{mol\,L^{-1}}$.

We usually assume that immediately after irradiation with a Dirac pulse each equivalent site i of a given crystal has the same probability of being occupied by an electronically excited molecule. Low-light-intensity experiments in which not more than one dye molecule per crystal is in an electronically excited state are discussed. We consider the case where the sites form a (pseudo)Bravis latice. This means that the position R_i of an n_s-site i can be expressed by the primitive vectors $\boldsymbol{a}$, $\boldsymbol{b}$, and $n_s\boldsymbol{c}$ of the hexagonal lattice and the integers $n_{a,i}$, $n_{b,i}$, and $n_{c,i}$ [Eq. (4), see also Figure 5]:

$$R_i = n_{a,i}\,\boldsymbol{a} + n_{b,i}\,\boldsymbol{b} + n_{c,i}\,n_c\,\boldsymbol{c} \quad (4)$$

This description is always precise for $n_s = 1$. Because it greatly simplifies the description, we will use this description as an approximation for $n_s > 1$, too. Some consequences of this have been discussed in the literature.[16,31,32]

Understanding the host allows us to describe, for example, the distribution of the dye molecules among the channels, the number of nearest-neighboring dye molecules, and the distribution of excitons at different illumination conditions. The distribution of distances between the dyes in the channels governs transport properties, for example, radiationless energy migration by dipole–dipole coupling, but also other types of interaction and communication between the molecules. Figure 6 illustrates the distribution h_S of empty sites S between two neighboring dyes for different dye loading as calculated by means of a Monte Carlo simulation. We found that this distribution can be expressed as an exponential distribution function $h(S)$ with mean $S_0 = 1/p - 1$ [Eq. (5)].[32]

$$h(S) = \frac{1}{S_0} e^{-S/S_0} \quad (5)$$

 © 2003 Wiley-VCH Verlag GmbH & Co. KGaA, Weinheim

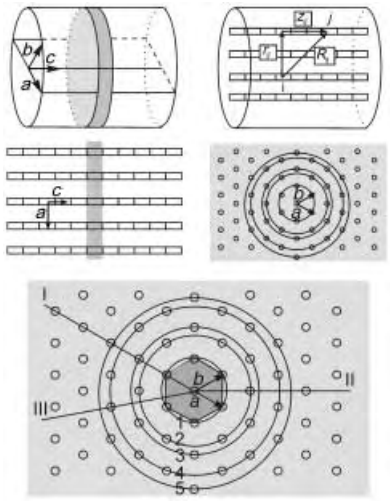


Figure 5. Geometrical situation of dye molecules in zeolite channels; the sites are marked by rectangles. Top: primitive vectors ***a***, ***b***, and ***c*** and definition of the distances R_{ij}, r_{ij}, and z_{ij} between sites i and j. Middle, left: section through the center of the hexagonal crystal with cylinder morphology along a and c. The sites of the shaded area belong to one slab. Middle, right: section vertical to c. The channels indicated by circles are arranged on rings around the central channel because of the hexagonal symmetry. Bottom: distances from one channel to the next channel along lines I, II, and III.

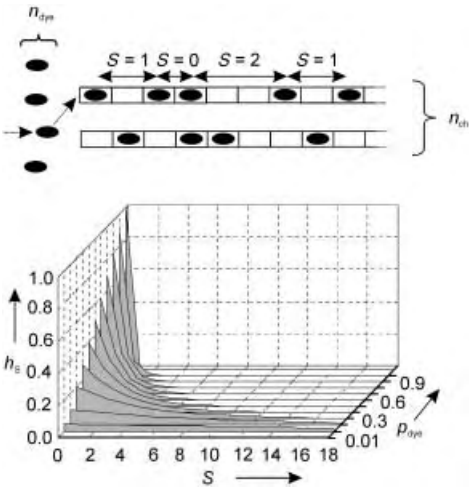


Figure 6. Distribution of empty sites S between two neighboring dye molecules for different dye loadings p. Top: Scheme which describes the simulation procedure; n_{dye} is the number of dye molecules which are to be distributed among the channels n_{ch}, each of them bearing n_s sites. S indicates the number of empty sites between two neighboring dye molecules in a channel. Bottom: Distribution h_S of empty sites between two neighboring dyes for different loadings p.[32]

3. Synthesis

3.1. Physical–Chemical Basis

Incorporation of chromophores into the cavities of zeolites can be achieved in different ways: from the gas phase,[20,33] by ion exchange if cations are involved,[22] by crystallization inclusion,[34] or by an in situ synthesis inside the zeolite cages (often called ship-in-a-bottle synthesis).[35] Many interesting materials have been prepared by means of the ship-in-a-bottle approach and the crystallization-inclusion syntheses. For the purpose of this work, however, the reversible methods, which are ion exchange, insertion from the gas phase, and insertion from a solution in a solvent where the solvent molecules are too large to enter the channels, are more important. We therefore focus on these methods. Solid–gas, displacement, ion-exchange, and adsorption equilibria play an important role in the reversible methods and we discuss them briefly.

Solid–gas equilibrium: Dye molecules D in the gas phase (g) are in equilibrium with dye molecules in the channels of zeolite L [Eq. (6)].

$$ZD_{r-1} + D(g) \rightleftharpoons ZD_r \tag{6}$$

The parameter r gives the number of sites occupied by dye molecules. Its values range from 0 to n_{box} where n_{box} is equal to the number of sites in one channel. As an example, n_{box} is equal to 200 in a 300-nm-long zeolite and a 1.5-nm-long dye which occupies two unit cells. ZD_r denotes the number of channels which contain r dye molecules D. The solid-gas the equilibrium constant (K_r^{SG}) is given by Equation (7).

$$K_r^{SG} = \frac{[ZD_r]}{[ZD_{r-1}]\,[D(g)]} \tag{7}$$

Displacement equilibrium: Molecules X can sometimes displace dye molecules D located inside of the zeolite. In a zeolite with the loading ZD_rX_{p-x} a dye molecule can also displace x molecules of X. The terms D(out) and X(out) refer to dyes and molecules that are outside the zeolite. The state of these species has in general to be specified [Eq. (8)].

$$ZD_{r-1}X_p + D(out) \rightleftharpoons ZD_rX_{p-x} + x\,X(out) \tag{8}$$

We express the equilibrium constant for displacement of D (K_r^{DI}) as in Equation (9).

$$K_r^{DI} = \frac{[ZD_rX_{p-x}]}{[ZD_{r-1}X_p]\,[D(out)]}\,[X(out)]^x \tag{9}$$

An example is the reversible displacement of *para*-terphenyl (*p*TP) by water.[20] This displacement was investigated by controlling the amount of coadsorbed water. Figure 7 shows the amount of *p*TP/u.c. located inside the zeolite channels as a function of the amount of coadsorbed water. Between one and about 10 H_2O/u.c., almost all the *p*TP is inside the channels. Thus, the first 8–10 equivalents of coadsorbed H_2O do not compete with the *p*TP. Then the displacement of the *p*TP by water starts. *p*TP moves to the outer surface, this process is reversible. When the water desorbs, the *p*TP moves back into the channels. The location of the *p*TP can reversibly be changed, according to Equation (8), by controlling the amount of coadsorbed water through its adsorption or desorption at temperatures between 25 °C and 200 °C.

Ion-exchange equilibrium: In most ion-exchange experiments monovalent cationic dyes have been used. D_S^+ and M_S^+

 © 2003 Wiley-VCH Verlag GmbH & Co. KGaA, Weinheim

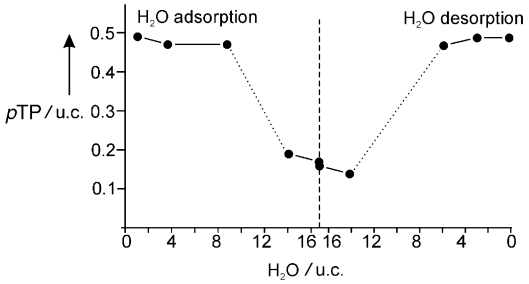


Figure 7. Amount of *p*TP/u.c. located inside the zeolite depending on the amount of coadsorbed H_2O/u.c. The water content of the sample was varied either by adsorption of water on the dry *p*TP-zeolite L sample (left side) or desorption of water from a water-containing *p*TP-zeolite L sample (right side). The dotted line indicates the region where it was difficult to obtain accurate data.[20]

denote, respectively, the dye and the alkali-metal cations in solution, Y is the cation concentration inside the zeolite. For monovalent cations and dyes which occupy two unit cells in zeolite L, for example, pyronine (Py^+) or oxonine (Ox^+) we use $Y_{n_{box}-r} = [M^+_{18}]_{n_{box}-r}[M^+_{17}]_r$ to describe the state of a given channel. An empty site contains 18 cations M^+, only one of which can be exchanged by a singly charged dye molecule D^+. By the exchange of $r\,D^+$ molecules the number of sites containing 18 cations is reduced by r, and r sites containing only 17 alkali-metal cations are formed [Eq. (10)].

$$ZY_{n_{box}-r-1}D_{r-1} + D^+_S \rightleftharpoons ZY_{n_{box}-r}D_r + M^+_S \qquad (10)$$

The equilibrium constant for ion exchange (K^{IE}_r) can thus be expressed as in Equation (11).

$$K^{IE}_r = \frac{[ZY_{n_{box}-r}D_r]}{[ZY_{n_{box}-r-1}D_{r-1}][D^+_S]}[M^+_S] \qquad (11)$$

The equations (7), (9), and (11) show that the equilibrium constants depend on r, a fact which has been discussed in ref. [36] If a dye to be inserted is very soluble in the chosen solvent it might occur that its affinity for entering the channels is low. Changing to a solvent in which it is less soluble might then be a better option. A parameter of interest is the total concentration $[D_Z]_{tot}$ of dye molecules in an ensemble of zeolite crystals dispersed in a solvent observed under equilibrium conditions. This parameter can be represented by an exchange isotherm. It is often convenient to express $[D_Z]_{tot}$ in terms of occupation probability as shown in Figure 8. Care has to be taken when analyzing such data. While methylviologen (MV^{2+}), and thionine (Th^+) are really inside of the channels of zeolite L, methylene blue (MB^+), and ethylene blue (EB^+) are only adsorbed at the outer surface of the crystals.

Adsorption equilibria at the outer surface: As the zeolite L crystals have a more or less cylindrical shape, we must distinguish between two external surfaces: the coat and the base. The coat is round and lacks channel entrances, whereas the base is flat and contains the channel openings. These chemical differences strongly influence the adsorption affinity of molecules with respect to these surfaces. A similar

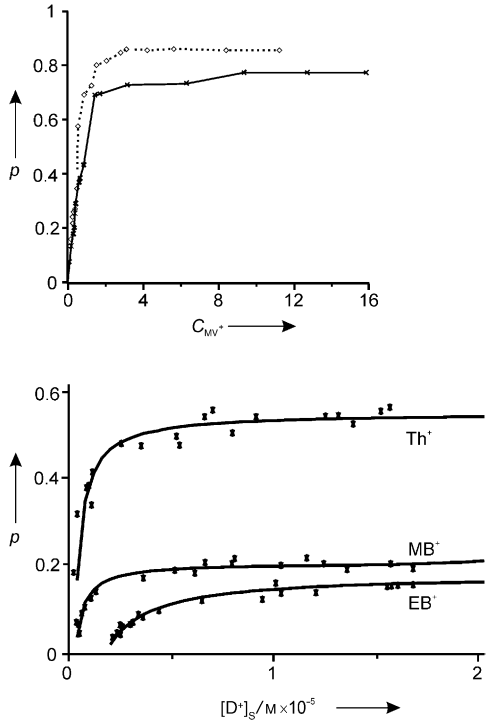


Figure 8. Exchange isotherms measured at room temperature in water. Top: Occupation probability p of the MV^{2+}-loaded zeolite L as a function of $C_{MV^{2+}}$ which is the number of mol of MV^{2+} per mol of zeolite L unit cells present in the aqueous suspension. Experiments with our synthesized zeolite L (dotted line) and with a commercial zeolite (solid line; Linde type ELZ-L, Union Carbide).[39] Bottom: Number of dye cations Th^+, MB^+ and EB^+ per two unit cells (p) versus the concentration of dye molecules in solution.[22]

effect has also been observed for MFI zeolite.[37,38] This difference is illustrated in Figure 9 where three different equilibria are shown. The insertion equilibrium A has already been discussed. Adsorption at the outer surface is important and it is usually the first step in any insertion reaction. We do not yet know any case in which it occurs specifically at the coat, as depicted in B in Figure 9. Preferential adsorption at the channel entrance (C) can be forced by choosing molecules of the right shape. Such molecules are head–tail compounds

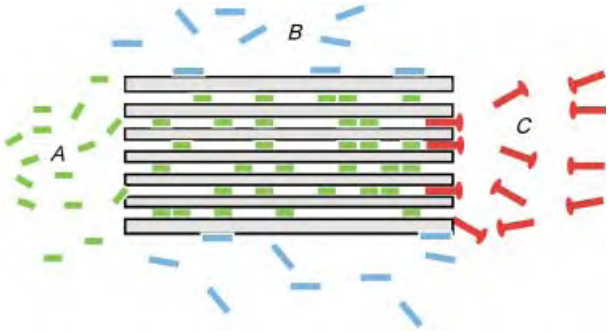


Figure 9. Three different kinds of molecule–zeolite equilibria; *A*) insertion equilibrium, *B*) adsorption at the coat, *C*) specific adsorption of a head-tail stopcock molecule at the channel entrance.

 © 2003 Wiley-VCH Verlag GmbH & Co. KGaA, Weinheim

which we name stopcock molecules. It has to be expected that these molecules also have some tendency to adsorb at the coat, but with lower affinity. Conditions to favor adsorption C with respect to B must be designed accordingly.[21,25] The picture has to be completed by including equilibria for dimer and higher-aggregate formation, which take place at the outer surface and also in solution.

3.2. Insertion from the Gas Phase

Insertion from the gas phase is carried out in two steps. Because the zeolite has a high affinity for water, the adsorption sites in the channels are occupied and have to be emptied first by drying the zeolite. In a second step, neutral dye molecules can be inserted following the solid–gas equilibrium [Eq. (6)]. A convenient way to do this is the double ampoule method (Figure 10), where clearly defined samples can be prepared under completely water-free conditions. To dehydrate the zeolite, it is filled in the cavity containing the glass spiral, heated (typically 400 °C, 10^{-2} mbar) for 12 h and sealed. If the zeolite is already loaded with another dye, the temperature has to be lowered and the dehydration time has to be increased. The neutral dye is filled in the other cavity that is then evacuated and also sealed. The glass hook can now be broken to link both cavities. The insertion is carried out at the sublimation temperature of the dye for a few hours up to a few days.

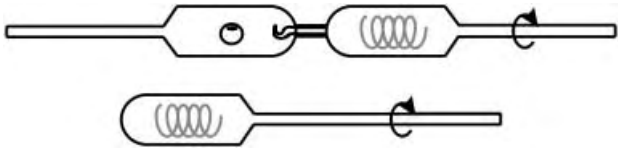


Figure 10. Schematic representation of ampoules used for the loading of zeolite L with neutral dye molecules. The glass spirals serve to mix the zeolite in a rotating furnace to gain a homogenous loading. Top: Double ampoule, the two cavities are separated by a hook that can be broken with the glass ball in the left cavity. Bottom: Single ampoule with a glass spiral.

If the amount of zeolite and/or the neutral dye is rather small, the single ampoule method (Figure 10) is advantageous, where the dehydration and the insertion are carried out simultaneously. The zeolite, together with the neutral dye (often solved in a volatile solvent) is filled in the cavity and dried under vacuum (10^{-2} mbar). The sample can be heated below the sublimation temperature of the neutral dye to accelerate the dehydration. Then, the ampoule is sealed and put in a rotating furnace, as in the double ampoule method. An overview of neutral dyes which have been studied with zeolite L to date is given in Table 2.

3.3. Insertion by Ion Exchange

The insertion of methylviologen (MV^{2+}), a well studied example, is especially simple from the experimental point of view, and illustrates many general features. Two reactions should be distinguished. The adsorption [Eq. (12)] and the

$$y\,MV^{2+} + (K^+)_n Z \rightleftharpoons (K^+)_{n-2y}\,Z[(MV^{2+})_y]_{ads} + 2\,y\,K^+ \quad (12)$$

insertion [Eq. (13)] reaction. The shape of MV^{2+} is such that one molecule occupies one unit cell and its affinity for entering the channels is high because MV^{2+} bears two positive charges. The restricted space inside the channels causes an

$$y\,MV^{2+} + (K^+)_{n-2y}\,Z[(MV^{2+})_y]_{channel} \rightleftharpoons (K^+)_{n-2(y+1)}\,Z[(MV^{2+})_{y+1}]_{channel} + 2(y+1)K^+ \quad (13)$$

entropy decrease which makes it difficult to fill 100 % of the sites. Figure 8 (top) shows that about 85 % of the sites can be filled in an aqueous dispersion at room temperature.[39]

Equation (13) also shows that the equilibrium can be shifted to higher MV^{2+} loading by removal of the exchanged potassium ions; this can be done in two ways. One is to separate the crystals from the solution, for example, by centrifugation, and to repeat the exchange with a fresh MV^{2+} solution. The second useful method for dyes which only reluctantly enter the zeolite channels, or which are insufficiently soluble or stable in aqueous solution, is to influence the equilibrium by means of an ionophore (crypt) [Eq. (14)].

$$K^+ + \text{crypt} \rightleftharpoons K^+\text{crypt} \quad (14)$$

For potassium zeolite L, cryptofix 222 and cryptofix 222BB can be used, for example.[40] The two methods can be combined if necessary. Table 3 shows the cationic dye molecules which have been explored to date.

The insertion of an anionic organic dye molecule was made possible by incorporating a neutral dye molecule [Eq. (15)] which is able to undergo an acid–base reaction.

$$Z + D(g) \rightleftharpoons ZD \quad (15)$$

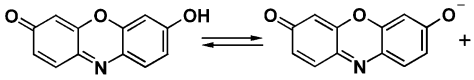
Once inside the channel, the neutral dye molecule can be deprotonated by the addition of a base, such as NH_3 [Eq. (16)]

$$ZD + NH_3(g) \rightleftharpoons ZD^- + NH_4^+(Z) \quad (16)$$

or by deprotonation with KOR (R = alkyl) [Eq. (17)]

$$ZD + KOR(solv) \rightleftharpoons ZD^- + (K^+)Z + ROH \quad (17)$$

The dye resorufin (ResH) possesses the desired properties and is known to undergo the acid–base reaction illustrated in Equation (18).

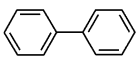
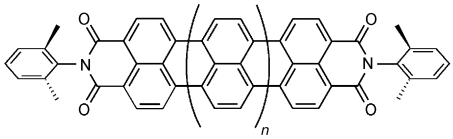
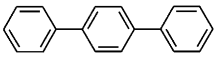
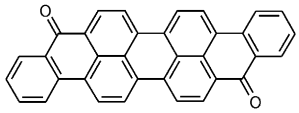
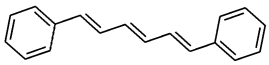
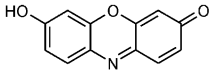
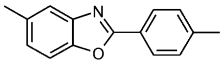
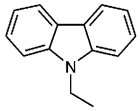
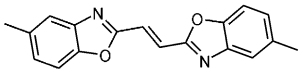
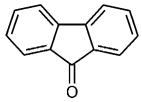
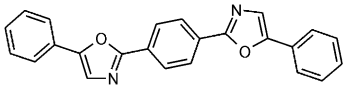
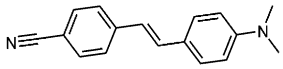
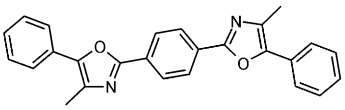
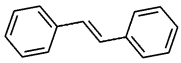
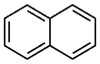
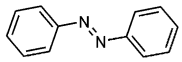
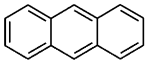


(18)

The pK_a value for this reaction is 5.5 in water and 6.1 in a 1:1 methanol/water mixture.[41] The electronic absorption spectra of the anionic and the neutral form of resorufin are

 © 2003 Wiley-VCH Verlag GmbH & Co. KGaA, Weinheim

Table 2: Neutral dyes that have been inserted in the channels of zeolite L from the gas phase.

Name/abbreviation	Structural formula	Name/abbreviation	Structural formula
BP		DXP ($n=0$), DXT ($n=1$)	
*p*TP		isoviolanthrone	
DPH		ResH	
PBOX		*N*-ethylcarbazole	
MBOXE		fluorenone	
POPOP		DCS	
DMPOPOP		stilbene	
naphthalene		azobenzene	
anthracene			

remarkably different, thus they can be easily distinguished. Incorporation of ResH into the channels of zeolite L and subsequent deprotonation to Res^--zeolite L allowed us to study the displacement of Res^- by different solvent molecules.[42]

3.4. Simultaneous Insertion of Two Species

Simultaneous insertion of two or more species, for example, from the gas phase but also by means of ion exchange leads to interesting materials. Many variations are possible. Figure 11 illustrates a simple case where two

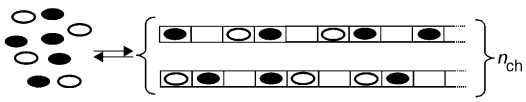


Figure 11. The competitive insertion of two different species from solution or the gas phase into the channels.

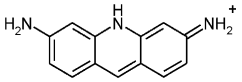
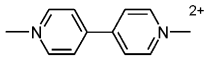
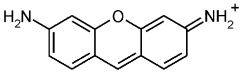
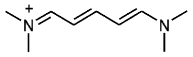
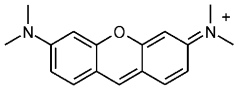
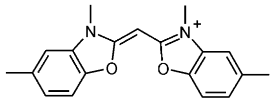
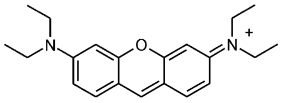
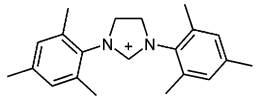
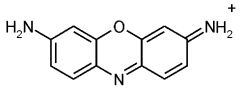
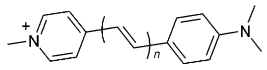
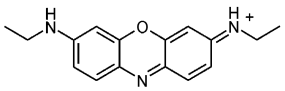
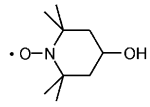
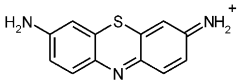
molecules of about the same shape and similar chemical properties compete to enter the channels. The material obtained can be altered to some extent by varying the ratio of the two species. Since molecules are always pushed from both sides deeper into the channels it is difficult or even impossible to achieve a thermodynamic equilibrium. This situation means that the result depends to a large extent on the kinetic step for entering the channels. If both types of molecules enter at about the same speed statistical mixing inside can be achieved. In Section 5 two experiments based on this are reported.

3.5. Consecutive Insertion of Different Molecules (Preparation of Sandwich Materials)

The fact that appropriately chosen dyes cannot glide past each other because the channels are too narrow is the underlying principle for preparing photonic antenna systems as illustrated in Figure 1. This feature was reported for the first time in 1998 for Py^+ and Ox^+[43] and later generalized in the manner illustrated in Figure 12[20] which has now become a standard method for preparing a large variety of sandwich materials with fascinating properties. The first step results in a material we name dye1-zeolite L. After removing the dyes which might eventually be adsorbed at the outer surface, a second dye, dye2 is inserted. Conditions must be chosen such

 © 2003 Wiley-VCH Verlag GmbH & Co. KGaA, Weinheim

Table 3: Cationic dyes and a radical which have been inserted in zeolite L.

Name/ abbreviation	Structural formula	Name/ abbreviation	Structural formula
Proflavin$^+$		MV^{2+}	
Py^+		BDP^+	
$PyGY^+$		MC^+	
PyB^+		$BTMPI^+$	
Ox^+		DSM^+ ($n=1$)	
$DEOx^+$		Hydroxy-TEMPO	
Th^+			

that dye1 has no chance to exit the channels at the beginning of this second step. Once a dye2 molecule has entered each channel from both sides, the dye1 molecules have no chance to escape. In fact, they are pushed deeper into the channels by the incoming dye2 species, and form the dye2,dye1-zeolite L material. The same procedure is repeated for dye3. The resulting material is the dye3,dye2,dye1-zeolite L material.

Different insertion methods can be combined. Dye1, for example, can be a cationic dye that is inserted by cation exchange, dye2 can be a neutral dye, inserted from the gas phase. Structures with more than three different dyes can be prepared but this is still to be explored.

While the stacking of the dyes is often easily visible in an optical microscope equipped with polarizer and appropriate optical filters for sufficiently large crystals, analysis of small crystals and correspondingly thin layers of the different dyes can be more difficult if the phase boundaries are not perpendicular but bent as shown for two dyes D1 and D2 in the lower part of Figure 12. However, a beautiful example which shows that we can even go beyond the resolution of an optical microscope is illustrated in Figure 13 where we show fluorescence microscopy pictures of an approximately 1000-nm long Py^+,DMPOPOP,Ox^+-zeolite L crystal (for DMPOPOP see Table 2). The middle of the crystal is filled with Ox^+, then towards the ends is a thin layer of DMPOPOP, and finally at both ends there is Py^+. Without using a special recording technique we would soon have a mixture of all colors under the fluorescence microscope owing to energy transfer from one dye to the other. But with some carefully developed analytical methods we can examine the different regions of one single crystal. After specific excitation of the Py^+ and detection through an interference filter around 550 nm the green Py^+ emission can clearly be seen. With a polarizer it is possible, after selective DMPOPOP excitation, to single out the blue DMPOPOP emission which is (unlike the Py^+ and Ox^+ emission) polarized along the crystal axis. Finally, the red Ox^+ emission can be detected by selectively exciting the Ox^+ molecules.

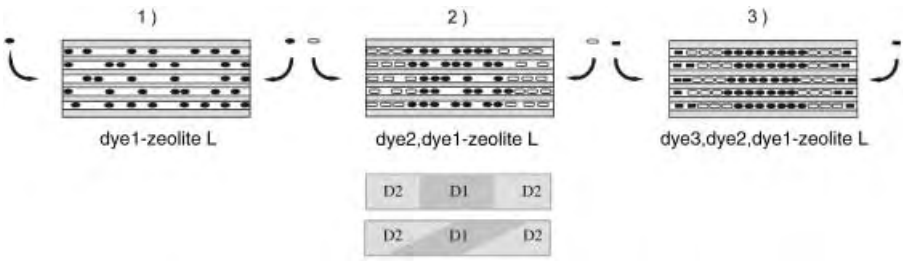


Figure 12. Successive insertion of three different dyes into the channels of a zeolite L crystal to form a sandwich material. Middle, bottom: for the material resulting in step (2) two kinds of mean phase boundaries for the two dyes D1 and D2 are possible. The phase boundaries are sorted according to their distance from both ends of the channels.

3.6. Extension to Longer Wavelengths

The spectral range extending from near UV to red is already covered by current matterials. Extension to the dark red and NIR region is desirable for many reasons. It can be done by selecting dyes which have been developed for other purposes.[44] In some cases the shape of the corresponding molecules must be adapted to fit into the channels. Suitable dyes are of the type of DXP and isoviolanthrone given in Table 2. Materials based on them or on similar dyes are still to be explored. We know already that DXP and isoviolanthrone can be inserted from the gas phase. Loading zeolite L with DXP results in a strongly luminescent material even at high loading with an emission maximum at 560 nm. These molecules are known to have very high fluorescence quantum yield, high absorptivity, and high chemical and photochemical stability.[45] Owing to the dimethylphenyl group that is turned out of the plane of the molecule, the DXP dye molecules have no possibility to overlap in the channels, which hin-

 © 2003 Wiley-VCH Verlag GmbH & Co. KGaA, Weinheim

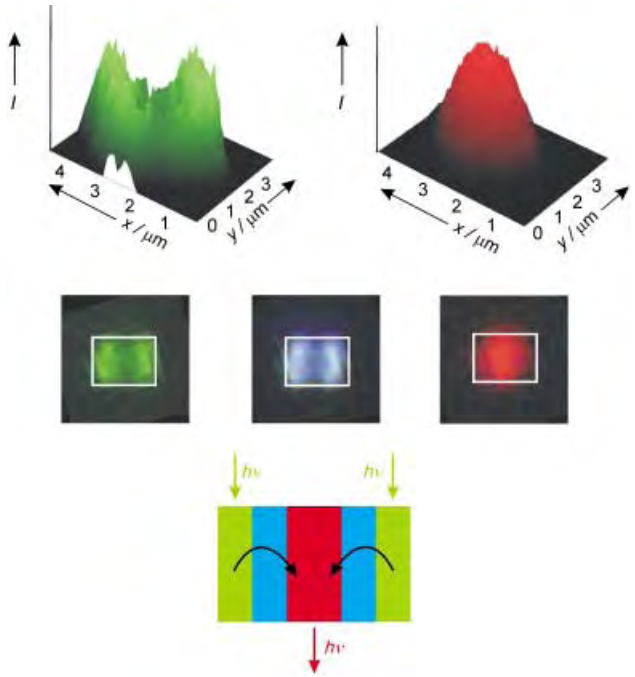


Figure 13. Top: two-dimensional intensity scan of the Py^+ and Ox^+ emission, recorded with an Olympus fluoview 300 confocal microscope. Middle: fluorescence microscope images of a single zeolite L crystal the edges of which are indicated by the white rectangle. To generate the green Py^+ emission, the crystal was excited at 470–490 nm and the emission was detected through a broad-band interference filter at 550 nm. The blue DMPOPOP emission was recorded by exciting the DMPOPOP at 330–385 nm and only transmitting emission polarized in the direction of the crystal axis. The red Ox^+ emission was detected after excitation at 545–580 nm. Bottom: a schematic picture of the crystal.

ders electronic coupling. Having the same shape but a larger π system than DXP, the terrylene dye DXT should lead to a material with high fluorescence intensities, absorption around 650 nm, and emission around 680 nm.

3.7. Addition and Fixation of Stopcocks

As already mentioned in the Introduction, a second step of organization can be realized by modifying zeolite L crystals with acceptor or donor dye molecules located at the entrances to the channels. These molecules have a narrow label which can penetrate into the channels of zeolite L, and a head which is too big to be inserted (see Figure 2b). The label and the head are connected by an inert flexible spacer. This shape enables them to plug the channel entrances in a champagne-cork manner. The stopcocks can be of reversible type when they are attached by adsorption, or of irreversible type when they are chemically bound to the zeolite crystals.

Stopcocks can be adsorbed on the zeolite only when the interactions between them and the zeolite surface are stronger than the interactions between the stopcocks and the solvent. If an excess of stopcock molecules is used, aggregation occurs. Aggregates usually quench the fluorescence and it is therefore necessary to work with well controlled amounts of dye so that only stopcock monomers are present. A safe way is to use the number of stopcocks needed to plug each channel end. This amount is usually relatively small which makes it possible to use a solvent in which the stopcocks are almost insoluble. For example, one can use polar stopcocks which like the polar surface of the zeolite channels and solve them in a nonpolar solvent.[21] When zeolite crystals are given to such a solution and the dispersion is sonicated for about half an hour, the dye molecules adsorb onto the zeolite surface. Because the adsorption process is reversible and thus equilibrium controlled, after some time the more preferred adsorption sites will be predominantly occupied. This means that a difference in adsorption affinity between the coat and the base of the zeolite L crystals will be decisive after the adsorption process has reached its equilibrium state. After centrifugation the zeolite crystals are colored and the supernatant is colorless, showing that the stopcocks have indeed adsorbed on the crystals.

For an irreversible attachment of stopcock molecules they have to be bound covalently to the zeolite framework. A stopcock with a reactive group is needed for this approach. A good choice is a stopcock with a triethoxysilane group that can tolerate being heated under reflux, for example, in toluene, which may be necessary for reaction with the zeolite framework. In the first step the stopcocks adsorb specifically at the base of the crystals and then they are fixed with a siloxane linkage. Figure 14 shows the irreversible binding of a coumarin derivative with a triethoxysilane group to zeolite L. The number of covalent siloxane linkages is not yet known. Depending on steric hindrance and the number of hydroxy groups on the zeolite surface there can be one, two, or even three bonds per coumarin derivative.

4. The Inner and Outer Surface of Zeolite L

4.1. Basic Principles

We have discussed how cationic dyes can be inserted by ion exchange (Section 3.3) and how neutral dyes can be inserted from the gas phase (Section 3.2). These dyes also

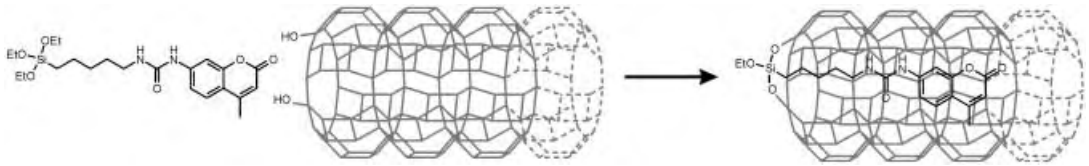


Figure 14. Coumarin-derived irreversible stopcock that can be covalently bound through a siloxane linkage.

 © 2003 Wiley-VCH Verlag GmbH & Co. KGaA, Weinheim

have some tendency to adsorb at the outer surface only. How can we distinguish between dye molecules which are inside the channels of a microcrystal and those adsorbed on its outer surface? This is an important question. Very powerful techniques such as X-ray diffraction, different kinds of NMR spectroscopy or SEM are not sensitive enough to detect a few molecules which might sit on the outer surface of a micro- or nanocrystal instead of being inside a channel. There is no single method available which could be applied in general. We now discuss a number of sensitive experiments which allow samples to be characterized with respect to this question and which allow very well specified materials to be prepared.

In some cases the very different spectral properties of the acidic and the basic form of a dye can be used[22] or alternatively the change in the luminescence behavior of a monomeric dye inside and outside of a channel.[36] The difference in the absorption spectra of the monomers compared to the aggregates, and especially the luminescence quenching of the aggregates (often very efficiently formed at the outer surface of the crystals), can be used. In addition solvatochromism effects in a solvent which can not enter the cavities of the zeolite and which thus only shows effects with molecules at the outer surface can be exploited as a sensitive probe.[46] Methods, based on specific transport properties, which arise from the restricted space of the channels or the negatively charged framework, and which occur when the zeolite crystals are suspended in a pure solvent or a solvent containing a specific reagent, can also be used as a tool for preparing dye-loaded zeolite microcrystals that do not have any dye molecules on their outer surface.

We can estimate how many molecules can adsorb as a monolayer on a certain amount of zeolite crystals of uniform size. We then calculate the ratio of molecules q inside the channels with respect to molecules at the outer surface under the assumption that all internal and external sites are occupied. The number of molecules needed for a monolayer n_{ML} on a single zeolite L cylinder of equal length and diameter can be expressed by Equation (19) where A_Z is the area of the

$$n_{ML} = \frac{A_Z}{A_D} = \frac{3}{2}\pi\frac{l_{cyl}^2}{A_D} \tag{19}$$

outer surface of a zeolite L cylinder, l_{cyl} is the length and diameter, and A_D is the surface required by one dye molecule lying flat on the zeolite (≈ 1.33 nm^2 for Py^+ or Ox^+).

The value n_D which is the number of dye molecules (in mol) per mass of zeolite L in grams (m_Z) for crystals with equal length and diameter and ρ_Z is the density of the crystal is given by Equation (20).

$$n_D = 6\frac{m_Z}{\rho_Z l_{cyl}}\frac{1}{A_D N_A} \tag{20}$$

Calculating n_D for crystals with a length and diameter of 600 nm this leads to Equation (21).

$$n_D \simeq m_Z\, 5.8 \times 10^{-6}\ \text{mol g}^{-1} \tag{21}$$

The number of unit cells n_{uc} of a zeolite L crystal of diameter d_{cyl} and length l_{cyl} is Equation (22) where

$$n_{uc} = \frac{\pi}{2\sqrt{3}} l_{cyl}\, d_{cyl}^2 \frac{1}{|c||a|^2} \tag{22}$$

$|c| = 0.75$ nm and $|a| = 1.84$ nm are the lengths of the unit cell along the corresponding crystal axis.

From this we find the ratio q with respect to the number of sites inside of the channels n_{uc}/n_s and n_{ML} [Eq. (23)].

$$q = \frac{n_{uc}}{n_{ML} n_s} = \frac{A_D}{2\sqrt{3} n_s} \frac{d_{cyl} l_{cyl}}{0.5 d_{cyl} + l_{cyl}} \frac{1}{|c||a|^2} \tag{23}$$

For the specific case of dyes of the size of Py^+ or Ox^+ ($n_s = 2$) and crystals of equal length and diameter, this simplifies to Equation (24).

$$q = \frac{d_{cyl}}{20\,\text{nm}} \tag{24}$$

From this we find, for example, that about 10^6 molecules form a monolayer on a 600-nm-long zeolite L crystal which consists of 7.7×10^7 unit cells. The ratio q is 30. For a 60-nm crystal it is only 3. This illustrates the importance of controlling the molecules adsorbed at the outer surface. In addition, the outer surface must be divided into the coat and the base which have distinctly different properties for adsorption. In the following Section we discuss some experiments which show that this differentiation is possible by making use of restricted transport, changes of the spectroscopic behavior, and the different affinities of well chosen molecules.

4.2. Restricted Transport

4.2.1. Exit Kinetics of Resorufin

Zeolite L containing the resorufin anion (Res^-) in its anionic framework can be prepared by incorporating the neutral ResH from the gas phase. Deprotonation to the Res^- ion can be achieved with NH_3 or a different base. The reversibility of the deprotonation/protonation reaction of resorufin can be monitored by measuring the UV/Vis absorption spectrum of the samples. While Res^- is strongly fluorescent in solution, the fluorescence is completely quenched when Res^- is located inside the channels of potassium zeolite L. This property allows the exit kinetics to be investigated as a function of the size of the solvent molecules which enter the zeolite channels and irreversibly displace the incorporated Res^-. Three cases can be distinguished concerning the mechanism of the displacement process: 1) the solvent molecules can pass a dye molecule inside the channel easily, 2) they are considerably hindered when passing a dye molecule inside the channel, and 3) they are too large to pass a dye molecule and hence the exit rate of dye molecules is zero.

Figure 15 illustrates the solvent dependence of the displacement of incorporated Res^- molecules. The reaction is fastest in water and decreases with the increasing size of the

 © 2003 Wiley-VCH Verlag GmbH & Co. KGaA, Weinheim

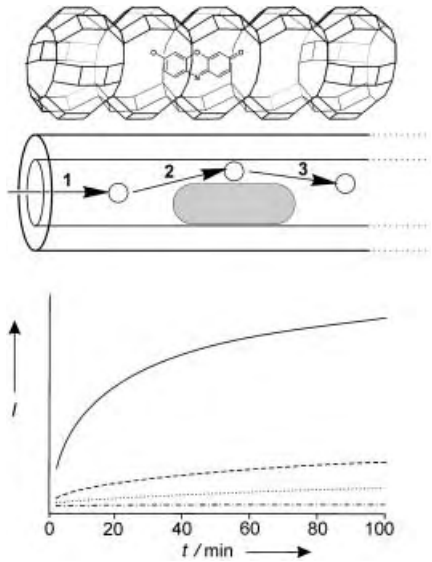


Figure 15. Top: mechanism of the displacement of the Res^- ion by solvent molecules from a channel of zeolite L. Bottom: experimental exit kinetics monitored by the fluorescence intensities of suspensions of Res^--zeolite L samples in different solvents: water (——), methanol (-----), ethanol (•••••), 1-propanol (–•–•).[42]

solvent molecules. There is virtually no displacement in 1-propanol, although a slight increase of fluorescence intensity with time can be observed. In 1-butanol there is no displacement and this measurement delivers the baseline for the experiment. The series: water $\gg$ methanol > ethanol > 1-propanol $\approx$ 1-butanol, outlines that the ability of solvent molecules to displace inserted Res^- ions is independent of the initial loading of the zeolite samples. However, the total displacement after a certain period of time depends on the loading.[42]

The displacement process in water, although starting very fast, levels off after a certain time. In a first step the solvent molecules penetrate into the channel until they find a Res^- ion. This process is probably very fast, since the diffusion of the penetrating solvent through the channel is only hindered by other solvent molecules. To further penetrate into the channel, the solvent must now pass the Res^- ion. This second step is decisive for the rate of displacement and its speed will depend on the size of the solvent molecules. After passing the Res^- ion, the solvent moves on until it encounters the next Res^- ion. All of the above processes of solvent diffusion are reversible and solvent molecules may also pass a Res^- molecule in the opposite direction and subsequently leave the channel. Most importantly, the second step results in an accumulation of diffusing solvent molecules in the void volume around the Res^- ions, which leads to the mobilization of the latter. The thereby initiated diffusion of the Res^- ion will, after a certain time, result in its release into the solution where it is strongly fluorescent. It follows that the rate of the increase of the concentration of Res^- ions in solution is a measure for the ability of the solvent molecules to pass the Res^- ions inside the zeolite main channel. Understanding the exit kinetics of a molecule in the one-dimensional channels of zeolite L is important for the handling of dye-zeolite materials.

4.2.2. *Destruction of Molecules on the Outside*

The molecules inside of the channels are not accessible to anionic species unless drastic conditions are applied. Being negatively charged themselves, anions have difficulty entering the negatively charged zeolite channels. This property can be used to specifically destroy molecules on the outer surface of the microcrystal by means of an anionic reagent, without affecting molecules that are inside.

Cationic dye molecules have the tendency to form aggregates on the zeolite surface as can be detected by means of UV/Vis and luminescence spectroscopy. When, for example, zeolite L is added to an aqueous Th^+ solution, aggregates on the zeolite surface are immediately formed, as indicated by the violet color (Figure 16). On boiling the

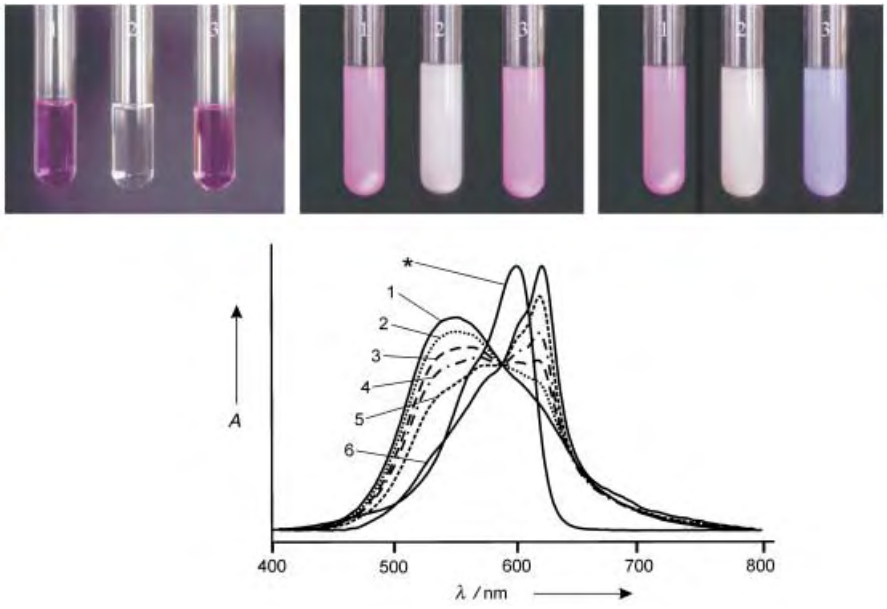


Figure 16. The formation of aggregates when zeolite L is added to a solution of Th^+ in water and the subsequent formation of monomers upon heating. Top left: test tubes 1 and 3 containing 4 mL of a 2×10^{-5} M aqueous solution of Th^+. Probe 2 contains pure water and serves as a reference. Top middle: addition of 2 mL of a zeolite suspension (0.2 g zeolite L in 10 mL water) to each of these test tubes results in immediate formation of Th^+ aggregates at the outer surface of the crystals (1 and 3). Top right: Probe 3 was heated to boiling for about 1 min. The color change observed is caused by the molecules entering the channels of the zeolite where they can exist only as monomers. Bottom: spectra of a Th^+ zeolite L suspension in water at 70 °C measured at different times after mixing. 1) 0 min, 2) 4 min, 3) 20 min, 4) 2 h, 5) 4 h, 6) 24 h. The spectrum of Th^+ in aqueous solution (2×10^{-5} M) at room temperature is given as a reference (marked *).

 © 2003 Wiley-VCH Verlag GmbH & Co. KGaA, Weinheim

sample for about 1 min a sudden color change from violet to blue is observed. The dye molecules slip into the zeolite L channels where owing to spatial constraints they can only exist as monomers. The blue color remains when the probe is cooled to room temperature. In an additional step we add a few drops of an acidic hypochlorite solution to the three test tubes on the right of Figure 16. The effect is striking: while the color of sample 1 on the left fades rapidly, nothing happens to sample 3 that was boiled. This experiment can be used as a convenient probe to check the success of a zeolite L synthesis.

4.2.3. ***Aggregates***

Aggregates are formed at the outer surface of the crystals immediately after addition of the zeolite crystals to a solution of dye molecules. The dyes then enter one by one into the channels where they can only exist as monomers because there is not enough space available for the formation of dimers. The spectrum in Figure 16 shows how the intense band 1 which is due to aggregates decreases upon insertion and eventually disappears completely when all the dye molecules have been inserted. Similar experiments can be performed, for example, with Ox^+, where the change of both the absorption and the fluorescence spectra upon the insertion can be observed (Figure 17). We observe a band at short wavelengths in the absorption spectrum which is due to H-aggregates and which disappears with time as adsorption proceeds, simultaneously the fluorescence intensity increases. This nicely illustrates that the aggregates quench the fluorescence. Considering the efficiency of this quenching one can see how important it is to remove aggregates from the surface when a strong fluorescing material is desired. This removal can be carried out by washing the material with an appropriate solvent, such as, 1-butanol (see Section 4.2.1), by destroying the molecules at the outer surface (see Section 4.2.2 for Th^+), but also by washing with a solution containing an appropriate detergent, which removes the molecules on the surface.

4.3. Dyes for probing the environment

4.3.1. ***Solvatochromism***

If dye-loaded zeolite L crystals are suspended in a solvent which for steric or polarity reasons cannot enter the zeolite cages, the dyes at the outer surface and those inside the cavities will experience a different environment. Hence they show different absorption spectra—also because dyes at the outside form aggregates. Figure 18 shows the electronic spectra of Ox^+ which can enter the zeolite L channels and MB^+ which is too large to enter under the same conditions. The absorption spectra of the Ox^+-zeolite L crystals are the same in water, CH_2ClBr, and cyclohexane. The spectra of MB^+-zeolite L samples are, however, significantly different depending upon the solvent. The change of the spectrum in water is large because the MB^+ ion is only adsorbed at the outer surface where it is surrounded by the water, under which conditions MB^+ forms aggregates[46]

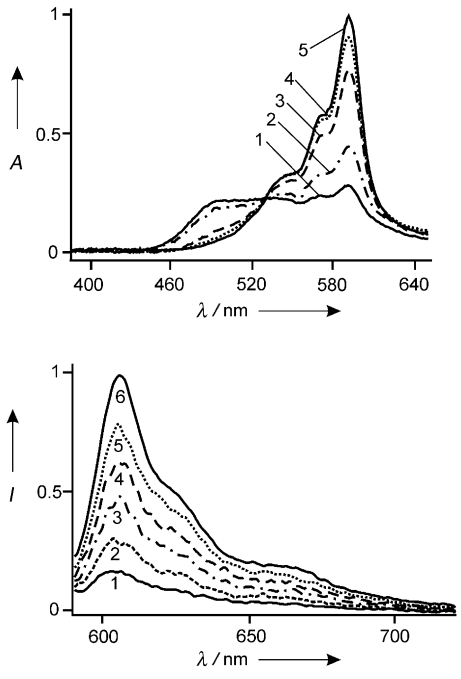


Figure 17. Top: absorption spectra measured under the same conditions at different times after mixing an aqueous zeolite suspension with Ox^+. 1) 30 s, 2) 9 min, 3) 190 min, 4) 1 day, 5) 7 days. Bottom: fluorescence spectra of Ox^+-zeolite L dispersions at room temperature measured at different times after mixing an aqueous zeolite suspension with the dye: 1) 10 s, 2) 30 s, 3) 90 s, 4) 4 min, 5) 4 h, 6) 18 h. The excitation wavelength was 580 nm.

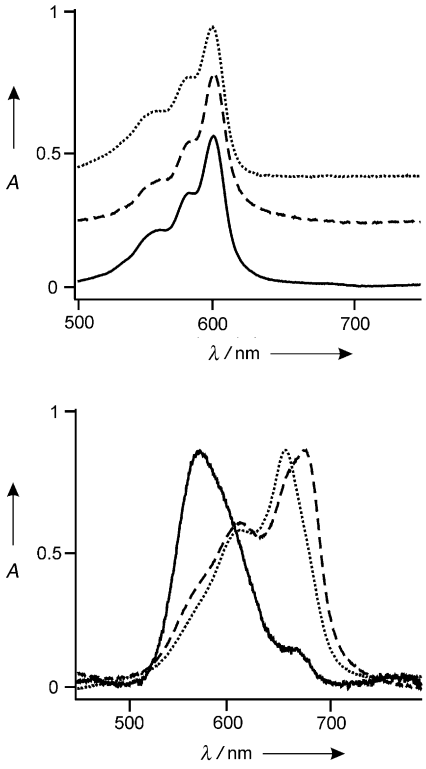


Figure 18. Absorption spectra of Ox^+-zeolite L (top) and of MB^+-zeolite L (bottom) suspensions in different solvents. Cyclohexane (-----), CH_2BrCl (•••••), water (——). The spectra of Ox^+-zeolite L are shifted because otherwise they would coincide.

 © 2003 Wiley-VCH Verlag GmbH & Co. KGaA, Weinheim

4.3.2. pH Value inside the Zeolite L Channels

The stoichiometric formula of a zeolite L with monovalent charge-compensating cations is $(M)_9(SiO_2)_{27}(AlO_2)_9{\cdot}21\text{-}H_2O$ in its fully hydrated form. For steric reasons only the cations belonging to the main channel can be exchanged by other cations. According to Breck,[17] 3.6 cations per unit cell belong to this channel on average. When exchanging some of these cations by protons, the pH value inside the main channel is expected to decrease dramatically because of the small unit-cell volume. An adequate approach to determine the pH value inside the main channel of a zeolite L is to insert a dye molecule which shows a change in the absorption spectrum when it is transferred from the basic to the acidic form. Two appropriate sensor molecules are Th^+ [Eq. (25)] and DSM^+ [Eq. (26)].

$$Th^+ + H^+ \rightleftharpoons ThH^{2+} \quad pK_a = -0.33^{[47]} \tag{25}$$

$$DSM^+ + H^+ \rightleftharpoons DSMH^{2+} \quad pK_a = 3.7 \tag{26}$$

Measuring the absorption spectra of a Th^+-exchanged potassium zeolite in a neutral aqueous surrounding results in a spectrum of the pure monomer with a redshift of about 20 nm compared to the spectrum of a highly diluted solution of Th^+. If the surrounding pH value is kept at 5.5 with HCl until equilibrium has reached, the resulting absorption spectrum is comparable with that of ThH^{2+} in 2.5 M HCl.[22] In 2.5 M HCl, the ratio of $[H_3O^+]/[H_2O] = 0.047$. There are 21 H_2O molecules per unit cell in a fully hydrated zeolite, thus, when one potassium ion per unit cell is exchanged for a proton the ratio $[H_3O^+]/[H_2O]$ is 1/21 which corresponds very well to this value of 0.047. This means that under the described conditions one cationic site per unit cell is occupied by a proton. The resulting pH value inside the channel is very sensitive to the number of exchangeable cations in the surrounding solution: measuring the absorption spectra of incorporated DSM^+ in different aqueous buffer solutions with high salt concentrations and a pH varying from 5 to 9, the pH value inside the channels remains constant at a value close to 3.5. The pH value inside the zeolite main channel is also affected by changing the type of metal co-cation owing to the different pK_a value of the hydrated ions [Eq. (27)].[48]

$$M(OH_2)_m^{n+} + H_2O \rightleftharpoons M(OH_2)_{m-1}(OH)^{(n-1)} + H_3O^+ \tag{27}$$

The pK_a values of some metal ions and the corresponding pH values measured in the metal-exchanged zeolite L probes are given in Table 4. The measured intrachannel pH values show the same trend as for the metal cations in aqueous solution.

Table 4: pK_a values of aqueous solutions of metal ions compared to the pH values measured inside metal-treated zeolites.

M^{n+}	pK_a[48]	pH (in zeolite)
Mg^{2+}	11.2	2.8
Ca^{2+}	12.7	3.1
Li^+	13.6	3.4
K^+	14	3.4

5. First Stage of Organization

5.1. Organization of Dye Molecules in Channels

Molecules can organize inside of the channels in different ways. We refer to this as the first stage of organization and we distinguish between three types of dye molecules: 1) Molecules small enough to fit into a single unit cell (e.g. BP, MV^{2+}, fluorenone, and naphtalene), 2) molecules the size of which makes it hard to guess if they align along the *c* axis, if they are tilted, or if they even find a way to fit into a single unit cell (e.g. Ox^+, Py^+, and Th^+), 3) molecules which are so large that they have no other choice but to align along the *c* axis. Many examples fit into this category (e.g. POPOP, DMPOPOP, MBOXE, *p*TP, and DPH). This third possibility is illustrated for POPOP in Figure 19 which shows that it adopts the idealized arrangement given in Figure 3 (right, middle). However, particularly at higher packing densities, some overlap of the phenyl groups cannot be excluded. For this to be avoided, the presence of specific substituents which shield both ends of the dye molecule is advantageous (as in DXP).

A good way to get information about the arrangement inside of the channels is to study the fluorescence polarization. For most dyes the double-cone distribution illustrated in Figure 20a is a good model. The arrows represent the transition moments of the dyes and α is the half open angle of the double cone. In Figure 20c the theoretical relative intensity of the observed fluorescence is plotted versus the

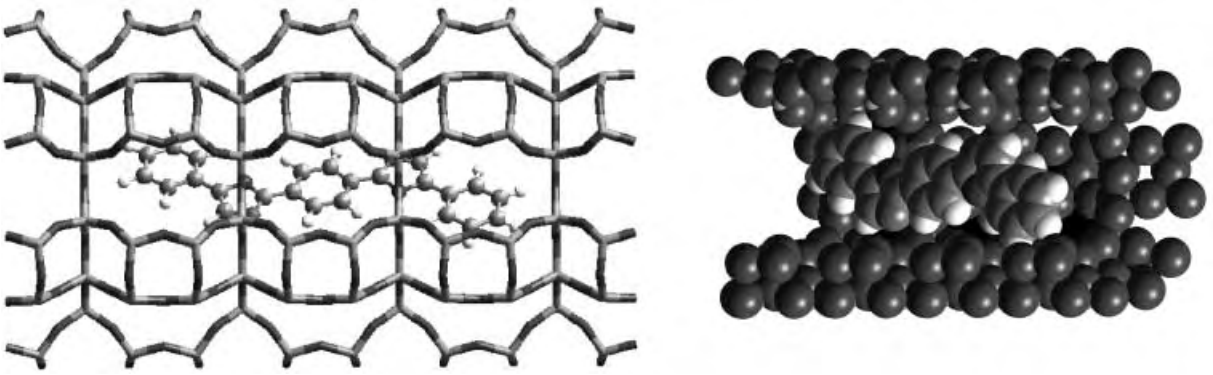


Figure 19. Line and space-filling illustrations of POPOP in zeolite L.

 © 2003 Wiley-VCH Verlag GmbH & Co. KGaA, Weinheim

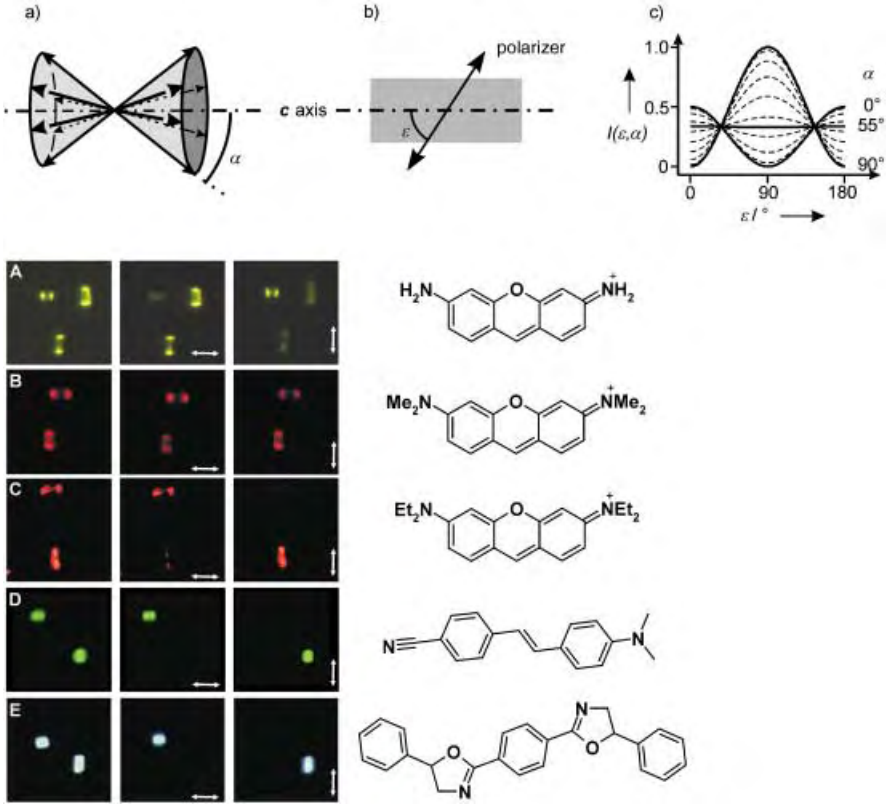


Figure 20. Fluorescence anisotropy of approximately 1500-nm long zeolite L crystals loaded with different dyes. Top: a) distribution of the transition moments on a double cone with a half-cone angle α, b) polarization direction observed, when a single crystal is examined with a polarizer, c) relative intensity of the observed fluorescence as a function of the observation angle ε with respect to the crystal c axis, for different angles α. A)–E): Fluorescence microscopy images of dye-loaded zeolite L single crystals, without polarizer (first column) and with polarizer (second and third column: the direction of the transmitted polarization is indicated by the arrows); A) Py^+-zeolite L, B) $PyGY^+$-zeolite L, C) PyB^+-zeolite L, D) DCS-zeolite L, E) POPOP-zeolite L.

angle ε between the observed polarization and the crystal c axis for different values of α. If $\alpha = 0°$, the transition moment of the molecule coincides with the crystal c axis and maximum fluorescence can be observed at $\varepsilon = 0°$ or 180°. Such a crystal emits most of its fluorescence parallel to the crystal axis and remains dark, if the polarizer is set perpendicular to it. If $\alpha = 90°$, then the maximum fluorescence is observed perpendicular to the c axis and the crystal emits no light parallel to it. Between $\alpha = 0°$ and 90° there is a transition from one of these extremes to the other, but the differences between the maximum and minimum fluorescence intensity levels off. At the magic angle of 54.7° no fluorescence anisotropy can be observed although the orientation of the transition moments is ordered and not statistically distributed in the crystal. For Ox^+ in zeolite L a half cone angle of $\alpha = 72°$ is observed.[49]

The lower part of Figure 20 shows fluorescence microscopy pictures of five different dye-loaded zeolite L single crystals. Each line consists of three pictures of the same sample, but each taken with different orientations of the polarizer. In the first column, the total fluorescence of the crystals is shown (that is, without the polarizer) and in the second and third columns the fluorescence observed with the polarizer oriented in the direction indicated by the arrows is displayed. The zeolite was loaded with Py^+, $PyGY^+$, PyB^+, DCS, and POPOP. Some crystals show a typical sandwich structure with fluorescent dyes at the crystal ends and a dark zone in the middle. This situation is observed when the diffusion of the dyes in the channels has not yet reached its equilibrium situation. It illustrates nicely how the molecules penetrate the crystals through the openings at each end of the one-dimensional channels. Py^+ is a molecule with similar dimensions as Ox^+ and therefore the behavior of the fluorescence polarization is the same as that already described for the Ox^+-zeolite L sample. $PyGY^+$, because of its methyl groups is slightly bigger than Py^+, and the fluorescence polarization changes accordingly. The maximum intensity in the $PyGY^+$-zeolite L sample is parallel to the c axis and the difference between maximum and minimum is rather small. From Figure 20c this situation indicates that the transition moments have changed to an angle α slightly below 55°. In the case of PyB^+ (with four ethyl groups) the intensity difference between minimum and maximum is more pronounced indicating an angle α near 0°. The series D and E show the fluorescence of DCS- and of POPOP-zeolite L crystals. The fluorescence polarization of these two dyes show very nicely that their transition moments are arranged parallel to the c axis, this means that $\alpha = 0°$.

The organization of molecules inside the channels can be used to study the mechanism of electronic excitation energy transfer and migration. In the next Sections six different experiments that we have set up for this purpose are presented.

5.2. Random Mixing of Donors and Acceptors

Competitive insertion of two different species from solution or from the gas phase into the channels is shown in Figure 11. If donors and acceptors enter at about the same speed, random mixing can be achieved (Figure 21 A). A visual demonstration of energy transfer is based on the observation that the dyes are inserted into zeolite L with about equal rates. It is therefore possible to control the mean distance between donors D (Py^+) and acceptors A (Ox^+) by varying the occupation probability. Electronically excited donors transfer their energy to the acceptors with a rate that depends on their mutual separation.

 © 2003 Wiley-VCH Verlag GmbH & Co. KGaA, Weinheim

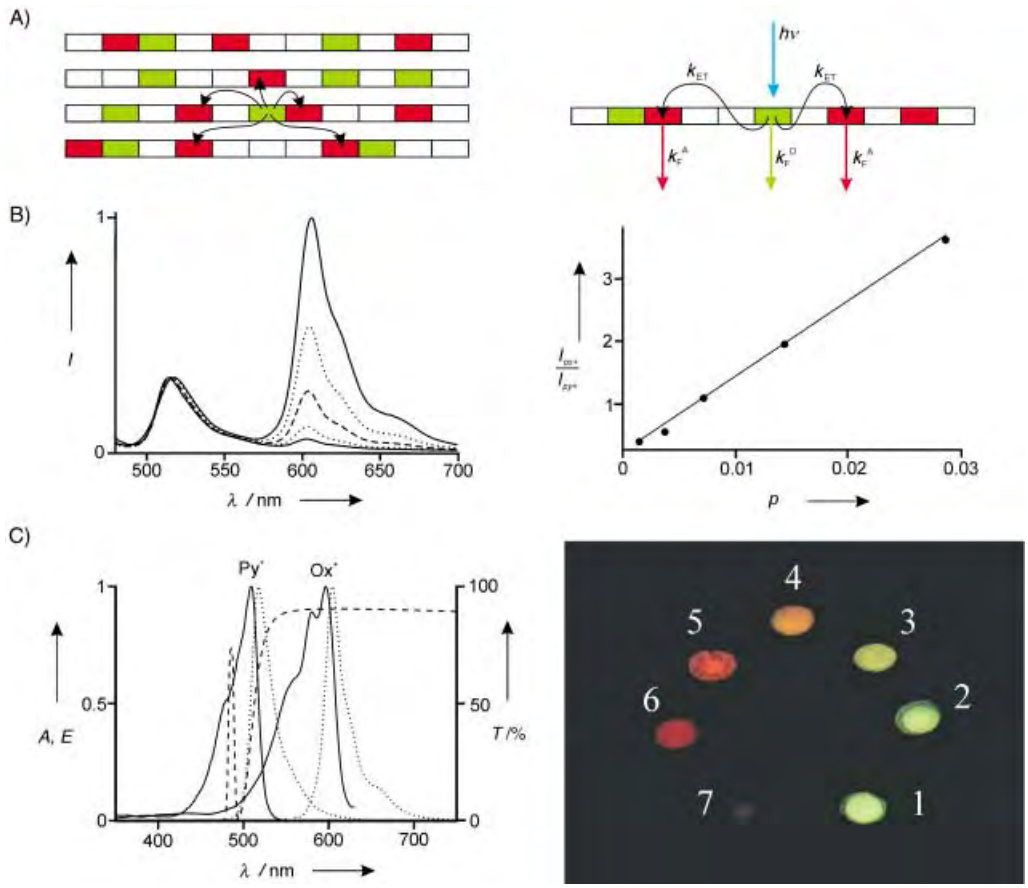


Figure 21. Energy-transfer experiment. A) Scheme of a zeolite L crystal containing acceptors A (red rectangles) and donors D (green rectangles). Each rectangle marks a dye site. The main processes taking place after excitation of a donor are indicated on the right. k_{ET} is the rate constant for energy transfer. k_F^A and k_F^D are the rate constants for fluorescence. B) Fluorescence of five suspensions with equal loading $p_{Py^+} = p_{Ox^+}$ (expressed in units of $p = 0.0014$: p, $2.5p$, $5p$, $10p$, and $20p$) after specific excitation of Py^+ at 465 nm. Left: fluorescence spectra, scaled to the same peak height for the Py^+ emission at approximately 520 nm. The intensity of the Ox^+ emission (band at around 600 nm) increases with increasing loading p. Right: ratio of the fluorescence intensity I_{Ox} of Ox^+ and I_{Py} of Py^+ as a function of the loading p. C) Visual demonstration of energy transfer; left: absorption (solid line) and emission spectra (dotted line) of Py^+ and Ox^+ in zeolite L. The dashed lines show the transmission T of the Schott DAD 8-1 interference filter and the Schott OG 515 cut-off filter we have used. Right: photograph of the fluorescence of dye-loaded zeolite L layers upon monochromatic irradiation at 485 nm and observation through a 500-nm cut-off filter. Probes 1 and 7 are references loaded with Py^+ and Ox^+. Probes 2 to 6 contain a 1:1 mixture of Py^+ and Ox^+ with the following loading for each dye: 2) p, 3) $2.5p$, 4) $5p$, 5) $10p$, and 6) $20p$.

The seven luminescent samples shown in Figure 21 C consist of zeolite L crystals of 300-nm average length filled with different amounts of Py^+ (donor D) and Ox^+ (acceptor A). In all the cases Py^+ was selectively excited at 485 ± 5 nm, a wavelength at which the absorption of Py^+ is strong and that of Ox^+ very weak (see Figure 21 C, left side). The two reference probes 1 and 7 are loaded with 5×10^{-3} M Py^+ and 5×10^{-3} M Ox^+, respectively. The other samples contain a 1:1 mixture of Py^+ and Ox^+ of the following concentrations: probe 2) 5.3×10^{-4}, 3) 1.3×10^{-3}, 4) 2.6×10^{-3}, 5) 5.2×10^{-3}, 6) 1.00×10^{-2} M. A rough estimate of the mean donor to acceptor distance R_{DA} (in Å) can be obtained, assuming isotropic conditions and equal concentrations of donors and acceptors, from Equation (28) where N_A is the Avogadro number and c_A is the concentration of Ox^+ in the zeolite nanocrystal.

$$R_{DA} = \left[\frac{3}{4\pi}\frac{10^{-3}}{c_A N_A}\right]^{1/3} \times 10^{10} \qquad (28)$$

From Equation (28) we obtain the following mean donor–acceptor separations: probe 2) 91, 3) 68, 4) 54; 5) 43, 6) 34 Å. The Förster radius for $Py^+ \rightarrow Ox^+$ energy transfer in a medium of refractive index of 1.4 is about 70 Å, based on the Py^+/Ox^+ spectral overlap which is 1.5×10^{-13} $cm^3 M^{-1}$. We observe in probe 2 mainly the green luminescence of Py^+, which indicates that energy transfer is insignificant. But the yellow color of probe 3 is due to a mixture of green and red luminescence which means that energy transfer is significant in this sample. It becomes more and more important with increasing concentration so that from probe 5 on, the red luminescence stemming from Ox^+ is dominant.

The same experiment can be carried out quantitatively. A linear relationship between the fluorescence intensity of the acceptor I_{Ox^+} and that of the donor I_{Py^+} as a function of the occupation probability (p_{Ox^+}) of the acceptor is expected to hold [Eq. (29) where C is a constant].[43]

 © 2003 Wiley-VCH Verlag GmbH & Co. KGaA, Weinheim

$$\frac{I_{Ox^+}}{I_{Py^+}} = C\,p_{Ox^+} \tag{29}$$

Figure 21 B shows the luminescence spectra measured in an aqueous Py^+/Ox^+ suspension. We observe that the acceptor emission is insignificant at low loading and that it becomes dominant at high loading. We also observe that the linear relationship between the acceptor and donor luminescence intensity and the acceptor loading is fulfilled.

5.3. Insertion Kinetics Monitored by Energy Transfer

Random mixing of Py^+ and Ox^+ can also be used for measuring the diffusion kinetics of these dyes inside the zeolite channels by using the distance dependence of the excitation energy transfer rate. We assume that at the beginning of an experiment, the situation illustrated in Figure 22 (top) can be prepared in all the channels. Immediately after all the dye molecules have entered the zeolite channels, the maximum energy transfer is observed because the donor-to-acceptor distance is short. When the molecules diffuse deeper into the channels this distance increases, and hence the energy transfer rate decreases. From this model, the relation for diffusion kinetics given in Equation (30) is found

$$\frac{I_{Ox^+}}{I_{Py^+}}(t) = C\frac{(p^0)^2}{\sqrt{8\pi}}\frac{1}{\sqrt{D_0\,t}} \tag{30}$$

under the condition that the initial distributions p^0 of the donors and the acceptors are the same, where C is a constant, t is the time, and D_0 the dye diffusion coefficient.

This Equation indicates that the ratio of the acceptor and donor fluorescence intensities is proportional to the inverse-square root of time. From this relationship, diffusion coefficients of the order of $10^{-15}\,cm^2\,s^{-1}$ at 80 °C have been determined in aqueous suspensions.[50]

Figure 22 shows fluorescence microscopy images of a sample after 20, 60, 470 min, and 162 h reaction time at 88 °C. The images were obtained by selectively exciting Py^+ with the exception of 3 b where Ox^+ was excited. Two selected crystals are framed, which represent the typical observations for most crystals. When comparing the images 1, 2, 3 a, and 4 (Figure 22; increasing reaction times), we first notice the progress of the insertion (1→2) of the dye molecules and then, from the size and the color of the fluorescent spots, their diffusion inside the channels. The fluorescence of Py^+ appears green and that of Ox^+ deep red, while yellow colors are due to mixtures of both colors. Since Py^+ was excited selectively, the red contribution is due to energy transfer from the exited Py^+ to Ox^+. Two yellow-red spots are observed on both sides of the crystals in image 1. In image 2 (Figure 22) the spots are red and, in the middle part, a weak green region appears. While this region is hardly visible in 2, it is clearly seen in 3 a. If Ox^+ is excited selectively its presence in the inner region of the channel can be detected (image 3 b). This result also shows that the mean distance between the donors and acceptors is greater in the middle than at the ends of the channels. The green color dominates after the very long reaction time and

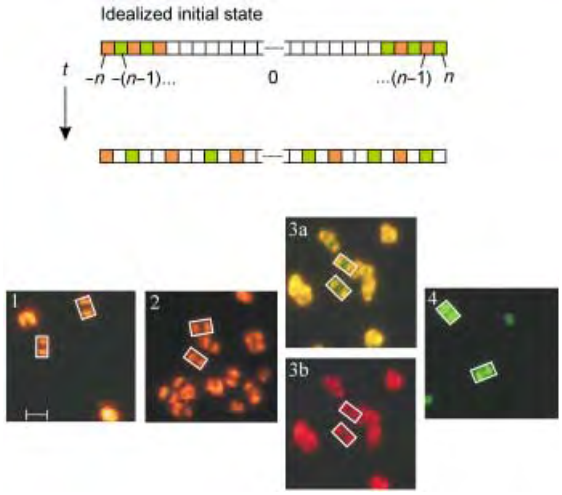


Figure 22. Diffusion of dye molecules in the channels of zeolite L. Top: idealized initial state of a channel and state after diffusion. Bottom: fluorescence microscopy pictures to visualize the diffusion of Ox^+ to Py^+ in zeolite L. The images were taken after 1) 20 min, 2) 60 min, 3) 470 min, and 4) 162 h. They were obtained by exciting Py^+ at 480 nm, with the exception of 3 b where Ox^+ was selectively excited at 565 nm. Two crystals of approximate length 1500 nm are framed in each image ($p_{Py^+} = p_{Ox^+} = 0.008$).

extends over the whole crystal (image 4). The intensity distribution shows that the equilibrium has not yet been reached. The same pattern of red fluorescence is observed if Ox^+ is excited selectively. This means that the distribution of Py^+ and Ox^+ in the crystals is the same or at least similar.

5.4. Ox^+,Py^+-Zeolite L Antenna Systems

The efficiency at which excitation energy is transferred by a Förster-type mechanism to acceptors placed at both ends of the crystals depends on two factors: the mean distances between the donors through which the energy migrates, which can be controlled by the donor loading, and on the length of the crystals. The longer both are, the more steps are needed and the higher the probability that the excitation energy can escape, either by spontaneous emission or by thermal relaxation. We carried out experiments at different loadings for crystals of equal average length and for crystals of different average length but equal loading. The results of such experiments are illustrated in Figure 23 (in which all spectra are scaled to the same height at the maximum of the donor emission). On the left the change of the relative fluorescence intensity is shown at Py^+ loadings varying from 0.007 to 0.182. The crystals were modified with, on average, two Ox^+ at both ends of each channel. The observed increase of acceptor emission with increasing donor loading is impressive. As expected if Förster energy transfer takes place, it shows that more and more excitation energy, initially located at the Py^+, reaches the Ox^+ under otherwise identical conditions. Figure 23 (right) illustrates the trapping efficiency as a function of the crystal lengths for otherwise constant parameters, specifically constant loading $p_{Py^+} = 0.11$ and with two

 © 2003 Wiley-VCH Verlag GmbH & Co. KGaA, Weinheim

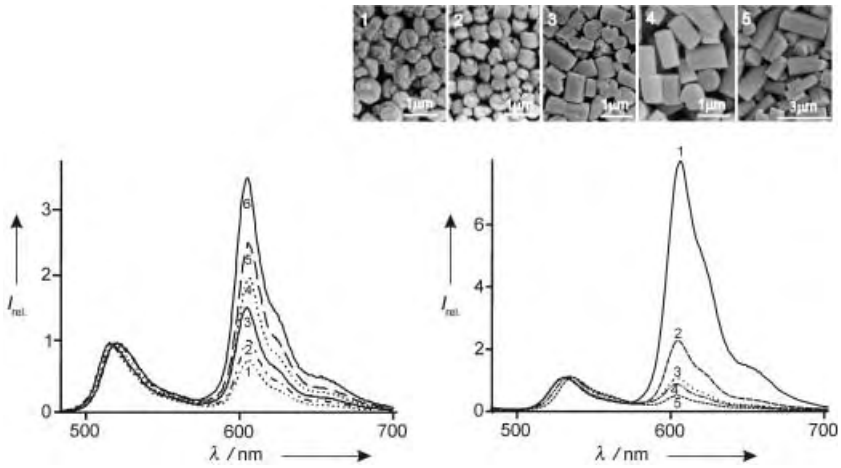


Figure 23. Antenna systems. Left: fluorescence intensity after selective excitation of only Py^+ at 470 nm (scaled to the maximum of the Py^+ emission) of Py^+-loaded and Ox^+-modified zeolite L crystals (length 600 nm, diameter 800 nm) as a function of Py^+ loading (p_{py}: 1) 0.007, 2) 0.012, 3) 0.031, 4) 0.057, 5) 0.106, 6) 0.182. The modification was the incorporation of on average two Ox^+ molecules at both ends of each channel. Right, top: electron micrographs of the zeolite L samples with different crystal length: 1) 300, 2) 500, 3) 850, 4) 1400, 5) 2400 nm. Bottom: fluorescence intensity after selective excitation of Py^+ at 460 nm (scaled to the maximum of the Py^+ emission) of Py^+-loaded and Ox^+-modified zeolite L crystals with constant Py^+ loading ($p_{Py^+}=0.11$) as a function of crystal length. The modification was the incorporation of on average two Ox^+ molecules at both ends of each channel.

Ox^+ molecules on average at both ends of the channels. Experiments with crystals of the average length of 1) 300, 2) 500, 3) 850, 4) 1400, and 5) 2400 nm are illustrated. The fluorescence of a thin layer on quartz was measured at room temperature after selective excitation of Py^+ at 460 nm. A strong increase of the front back-trapping efficiency with decreasing crystal length is clearly seen. In the 300-nm crystals about 90% of the emitted light is due to energy migration along the Py^+ and finally transfer to the luminescent traps Ox^+. This result is to be expected, if Förster energy transfer is the main process. There is a small shift of the Py^+ maximum, from 525 nm for the smallest crystals to 530 nm for the largest ones. This wavelength shift is due to self-absorption and re-emission because the absorption depth increases with increasing crystal size despite of the constant Py^+ loading. The maximum of the Ox^+ emission remains at 605 nm.

5.5. Inverse Antenna Systems

To change the scheme on the left of Figure 1 to the one shown on the right means the acceptors have to be placed in the middle part of the crystals and the donors have to be moved to both ends. Excitation energy can then be transported from both ends to the middle part, an option which extends the playground for the experimentalist exploring the energy migration mechanism. It is also of practical importance. Figure 24 illustrates such a system. It shows pictures of a single crystal with Ox^+ ($p=0.1$) located in the middle and DMPOPOP ($p=0.2$) located at both ends. Figure 24A illustrates the organization of the donors and acceptors and Figure 24B the shape of the crystal as seen by electron microscopy. The $S_1 \leftarrow S_0 \pi,\pi^*$ electronic transition moment of Ox^+ shows a double cone-shaped distribution with a half cone angle of 72° with respect to the channel axis while the moment for DMPOPOP is parallel to it. Observing crystals in a microscope equipped with polarizers, appropriate filters, and using an immersion lens gives the pictures in Figure 24C. The blue emission on the left is observed through a polarizer parallel to the cylinder axis when selectively exciting DMPOPOP at 360 nm, while the red emission in the middle is seen when the polarizer is turned into vertical position. The picture on the right side is observed without polarizer upon excitation of Ox^+ at 565 nm. Scanning the crystals results in the intensity profiles in Figure 24D. The profile on the left was observed when scanning the emission at 470 nm along the crystal axis in a confocal microscope upon excitation at 320 nm. The profile in the middle was observed when monitoring the emission at $\lambda > 610$ nm after excitation at 320 nm while the profile on the right was seen when the sample was excited at 490 nm. These data not only show that the organization of the dyes corresponds to Figure 24A but they also beautifully illustrate the energy transfer from the DMPOPOP to the Ox^+ and that the energy migration length of excited Ox^+ is not sufficient to fill the whole crystal homogeneously, as expected from Förster theory.[51]

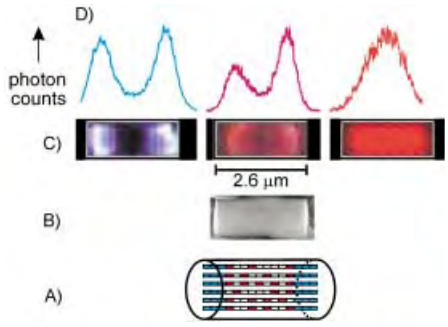


Figure 24. A) schematic representation of a crystal with donors (blue) at both ends and acceptors (red) in the middle, B) side view of a zeolite crystal observed by means of electron microscopy, C) immersion microscopy images, and D) scanning confocal optical microscopy results of a DMPOPOP,Ox^+-zeolite L crystal.

5.6. Antenna Systems with Spacers

A very elegant way for studying the distance dependence of excitation energy transfer and migration is to introduce a spacer between the donor and the acceptor. The energy-transfer rate constant k_{ET} from an excited donor D to an acceptor A can be written as Equation (31) in the point dipole

$$k_{ET} = \frac{9\ln(10)}{128\pi^5 N_A n^4}\frac{\Phi_D}{\tau_D} J_{DA}\, G_{DA}\, p_D\, p_A \qquad (31)$$

approximation,[31] where Φ_D and τ_D [s^{-1}] are the fluorescence quantum yield and the intrinsic fluorescence lifetime of the

 © 2003 Wiley-VCH Verlag GmbH & Co. KGaA, Weinheim

donor, N_A [mol^{-1}] is Avogadro's number, n is the refractive index of the medium, J_{DA} [cm^{3}M^{-1}] is the spectral overlap integral between the normalized donor emission and the acceptor absorption spectra, and p_D and p_A are the occupation probabilities of the sites with donors and acceptors.

The term G_{DA} [Å^{-6}] expresses the geometrical constraints of the sites in the crystal as a function of the distance R_{DA} between D and A and the relative orientation of the electronic transition moments κ_{DA} [Eq. (32)].

$$G_{DA} = \frac{\kappa_{DA}^2}{R_{DA}^6} \tag{32}$$

Therefore the distance R_{DA} has a strong effect on the energy-transfer rate constant for the donor–acceptor energy transfer and the donor–donor energy migration. The distance between the donors and acceptors can be varied by varying the loading (Figure 23, left) but also by placing spacer molecules Z between the donor and acceptor molecules to separate them locally. The spacer molecules must be chosen so that they do not participate in the energy-transfer process, that is, they should not absorb when the donor is excited and should not trap the energy from the donors. Figure 25 illustrates the construction of antenna systems with spacer molecules. This arrangement can be realized by first inserting Ox^+ ions, by ion exchange, then by adding DMPOPOP in a gas-phase reaction, and finally by adding Py^+ ions, again by ion exchange. The amount of inserted Py^+ and Ox^+ was kept constant, while the inserted amount of DMPOPOP was changed. Since the dyes were inserted consecutively, the zeolite crystal is divided into compartments where the density of one dye is dominant. We observe a very pronounced increase of energy transfer efficiency from D to A with decreasing thickness of the spacer layer, as expected from Förster theory. Systematic studies on such systems will help to find out experimentally at what distance the dipole–dipole approximation[52] must be replaced by, for example, an extended dipole–dipole approach, as described in refs. [53,54]

5.7. Time-Resolved Experiments on Ox^+,Py^+-zeolite L Antenna Materials

We have shown that the efficiency at which excitation energy is transferred by a Förster type mechanism to the acceptors placed at both ends of the crystals depends on the mean distances between the donors through which the energy migrates and which can be controlled by the loading. This effect should also be visible when carrying out time-resolved fluorescence experiments. The fluorescence decay of Ox^+ and Py^+ in ethanol at room temperature is 3.5 ns and 3.2 ns, respectively, and their fluorescence quantum yields are about one. When inserted in zeolite L crystals of average length 700 nm, the fluorescence decay of Ox^+ remains a single exponential at low loading ($p_{Ox+} = 0.001$, which corresponds to a concentration of 3.76×10^{-4} mol L^{-1}), and the lifetime is then 3.01 ns (measured under ambient conditions). For a ten-fold-higher loading, the decay is still strictly singly exponential with the same lifetime, if measured under oxygen-free conditions. Figure 26 shows the time-resolved fluorescence decay of Ox^+,Py^+-zeolite L after excitation of the Py^+ at 488 nm, for different Py^+ loadings but constant Ox^+ mod-

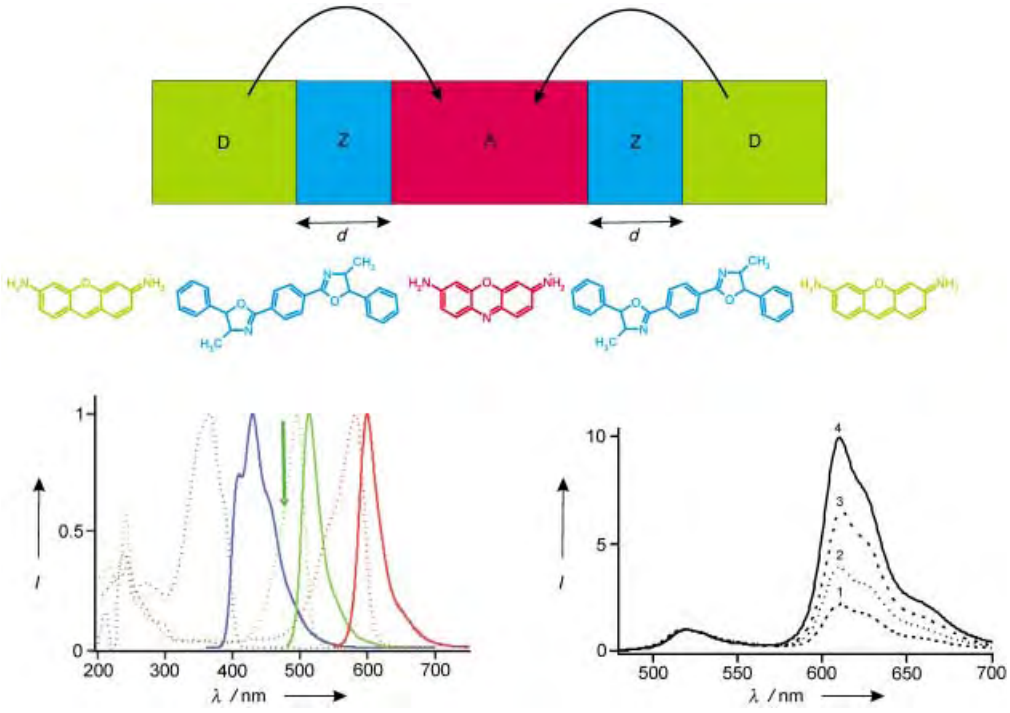


Figure 25. Antenna system with spacers. Top: the organization of the donors D, the spacer Z, and the acceptors A. Bottom, left: the excitation (dotted line) and the fluorescence (solid line) spectra of DMPOPOP (Z), Py^+ (D), and of Ox^+ (A). Right fluorescence spectra (scaled to the maximum of the Py^+ emission) for D,Z,A-zeolite L crystals (length 840 nm, diameter 750 nm) with different spacer loadings p_Z after selective excitation of Py^+ at 460 nm: 1) $p_Z = 0.12$, 2) $p_Z = 0.085$, 3) $p_Z = 0.06$, 4) $p_Z = 0.045$. The inserted amount of Py^+ and Ox^+ was kept constant.

© 2003 Wiley-VCH Verlag GmbH & Co. KGaA, Weinheim

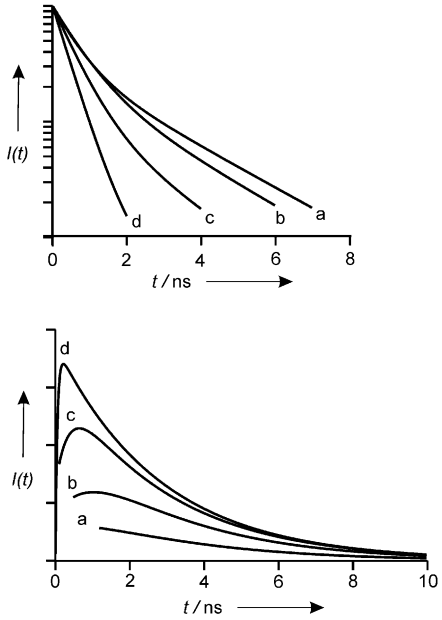


Figure 26. Experimental fluorescence decay of Ox^+,Py^+-zeolite L materials. Ox^+,Py^+-zeolite L, excited at 488 nm and observed at 520 nm (top), 605 nm (bottom) for different Py^+ loadings a) 0.01, b) 0.02, c) 0.08, d) 0.13).[32]

ification at both ends. The fluorescence observed at 520 nm, shown on the top, represents the evolution of the Py^+ luminescence in this material with time, while the values at 605 nm, shown on the bottom, represent the evolution of the luminescence of the Ox^+ acceptors under the same conditions. The Py^+ luminescence decays much faster than that of Py^+-zeolite L samples and it becomes faster and faster with increasing loading. The luminescence intensity of the Ox^+ rises and then decays. The time for the intensity rise becomes shorter and shorter with increasing donor loading, as expected from Förster theory.

The six experiments reported in this Sections 5.2–5.7 support the interpretation that Förster-type energy transfer occurs in the dye zeolite materials. It remains to be explored under what conditions the description of the main processes by the point dipole–dipole coupling is valid and when it must be substituted by, for example, the extended dipole–dipole approximation[32] or even more sophisticated models. The great versatility of the materials which can be prepared by the procedures explained allows the necessary experimental studies to be carried out.

6. Second Stage of Organization

6.1 General Remarks

The second stage of organization extends beyond modification of the interior of the zeolite crystals. A connection is made between the inside of a crystal and its environment. This can be done by the adsorption of stopcocks in the way described in Section 3.7. These stopcocks are meant to act as a link between the dye molecules inside the channels and the exterior of the zeolite crystals. They can also prevent small molecules, such as oxygen or water from diffusing into the interior of the crystals. We want to retain the one-dimensional character of the zeolite L crystals and therefore selective adsorption of the stopcocks at the channel entrances is desired (see Figure 2b). The goal is to have a champagne-cork manner of plugging the channels, where the label has penetrated inside the zeolite and the head is outside. A covalent link between the stopcock and the zeolite framework does significantly improve the stability of the system. Because we are interested in communication by energy transfer, it is important that the stopcocks are highly fluorescent. Depending on the requirements, a fluorophore can be located both on the head[21] or the label[25] of the stopcock. Fluorescent labels have the advantage of being chemically protected by the zeolite framework and they are prevented from forming dimers by the space restrictions. Fluorescent heads are closer to the external surface, which is desirable for communication with the environment.

6.2. Stopcock Location

To determine the location of the stopcocks that have adsorbed on the zeolite L external surface, the modified crystals are examined under a fluorescence microscope. The emitting parts of the crystals can be recognized directly and assigned to those parts of the crystal where the stopcocks have adsorbed. Figure 27 shows fluorescence microscope images of crystals modified with BTRX. From the fluorescence images it is clear that the BTRX dye molecules only adsorb on the base of the cylindrical zeolite crystals and not on the coat. If we consider the transmitted polarization direction then it turns out that the BTRX emission is polarized perpendicular to the zeolite channel axis. The $S_0 \leftarrow S_1$ transition dipole moment of the BTRX chromophore is mainly polarized perpendicular to its tail.[55] These results match with the picture of Figure 2B, where the stopcock tail has penetrated into the channel and the head is at the outside.

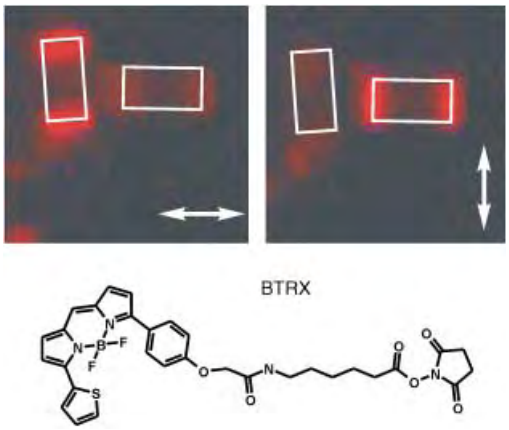


Figure 27. Fluorescence microscope images of BTRX modified zeolite L crystals of about 2000-nm length. The white rectangles indicate the edges of single zeolite L crystals. The double-headed arrows show the transmission direction of the polarizer.

 © 2003 Wiley-VCH Verlag GmbH & Co. KGaA, Weinheim

6.3. Trapping and Injecting Excitation Energy

Knowing the location of the stopcocks means we can start to consider using them to trap or inject electronic excitation energy. For that we need dye-loaded zeolite crystals which are modified with stopcocks. We can then investigate energy transfer between the stopcocks and the dye molecules inside the zeolite L channels.[21] In one case an energy donor (Py^+) is present in the zeolite channels and the stopcock (BTRX) acts as energy acceptor. This system enables excitation energy to be trapped at the external surface of the crystals. In a second case the stopcock (B493/503) acts as the energy donor and there are energy acceptors (Ox^+) inside the zeolite channels. With this second system excitation energy can be injected into the crystals. The two systems are shown schematically in Figure 28.

In both systems we can selectively excite the energy donors and there is considerable spectral overlap between the donor emission and the acceptor absorption spectra. Excitation of the donor molecules and detection of the emission gives the spectra shown in Figure 28 (bottom). For both systems a clear contribution of the acceptor emission near 16000 cm^{-1} is observed. This contribution is due to radiationless energy transfer. The energy injection from the B493/503 stopcock to Ox^+ acceptors works better than the trapping of energy from Py^+ by the BTRX stopcock . This can probably be attributed to the difference in length of the tails of the stopcock molecules. The shorter tail of B493/503 allows shorter donor–acceptor separations R_{DA}. This has a pronounced effect, since the Förster energy transfer rate falls off with R_{DA}^{-6}. Different kinds of stopcocks are still to be explored. To generate irreversible stopcocks one possibility is to have reactive labels which enter the zeolite channel and then undergo a chemical reaction. This reaction can be initiated by irradiation, heat, or a sufficiently small reactant. The penetration depth of the stopcock can be controlled by changing the length of the spacer, which at the same time has the function of changing the solubility of the stopcock.

The stopcock heads can be tuned to the function of interest which does not necessarily have to be energy transport. Some examples of stopcock heads are given in Figure 29. The head of Figure 29a has been used as a fluorescent chemosensor,[56] its emission spectrum shifts about 100 nm if the crown ether unit catches a cation. In Figure 29b a stopcock with a fullerene head is shown. As

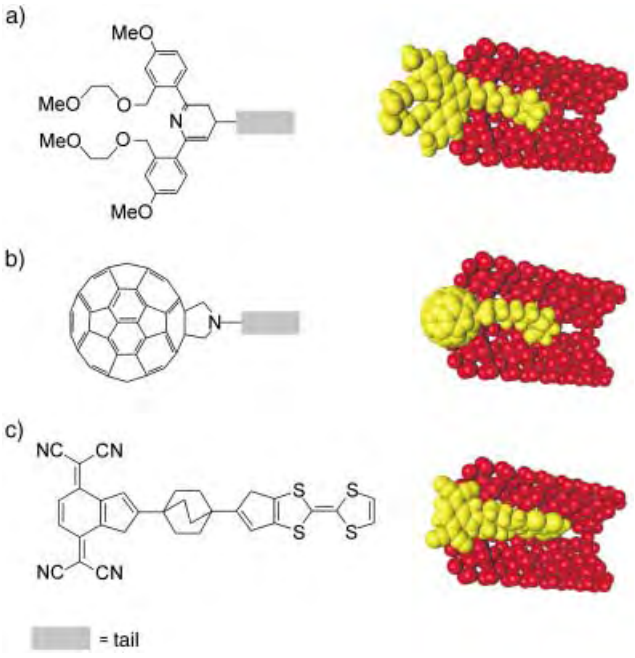


Figure 29. Examples for stopcock molecules. The space-filling models of a channel is shown (cut in half) with the stopcock to illustrate that the dimensions of the stopcock are appropriate. a) fluorescent chemosensor, b) C_{60}-based stopcock, c) molecular rectifier stopcock.

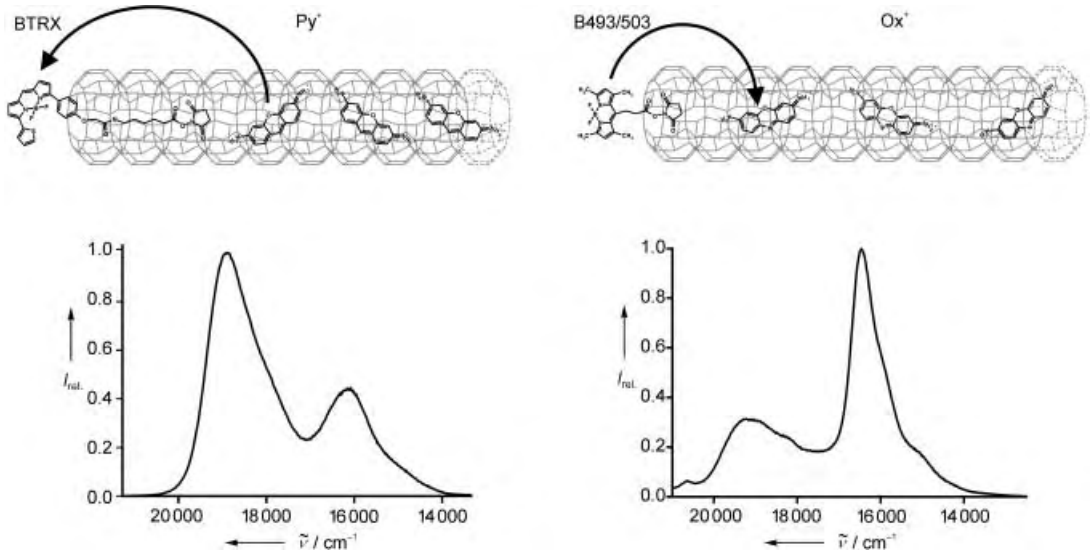


Figure 28. Left, top: Py^+-filled zeolite L channels, the ends of the channels are modified with BTRX stopcocks for external trapping of electronic excitation energy. Left, bottom: fluorescence spectrum after selective excitation of Py^+. Right, top: Ox^+-filled zeolite L channels, the ends of the channels are modified with B493/503 stopcocks for electronic excitation energy injection. Right, bottom: fluorescence spectrum after selective excitation of B493/503.

 © 2003 Wiley-VCH Verlag GmbH & Co. KGaA, Weinheim

fullerenes are generally known to be extremely good electron acceptors these stopcocks could be used for the electron-transfer experiments discussed in Section 8.[57,58] The last example (Figure 29c) is a molecule that has been used as a molecular rectifier,[59] and would be very interesting for charge transport measurements.

7. Third Stage of Organization

The third stage of organization concerns the coupling of the zeolite antenna to an external device by a stopcock. As described in the Introduction, we distinguish between the coupling to a device of molecular dimensions, of macromolecular dimensions, and of macroscopic dimensions.

7.1. Coupling to a Device of Molecular Dimensions

Molecules described in ref. [60,61], can be used to couple the zeolite antenna to an electron-transfer system which could be used to organize and to enhance the optical absorptivity of such systems.

7.2. Coupling to a Polymer

Bidirectional photonic antennae are of interest for coupling to a flexible material, such as a polymer (Figure 30a). Both, energy transfer from the antenna into a polymer but also from the polymer into the antenna are possible. Luminescent and also photoconductive polymers can be used. An additional feature is that the polymer can be used to protect and stabilize the antenna systems. Polymer light emitting diode (LED) research of the last decade has brought immense progress in the field of conjugated polymers. Therefore such a coupling is interesting for the development of new LED materials.

One way to combine the antennae with polymers is to embed the zeolite crystals in a polymer film (see Figure 30b). The stopcocks at the end of the channels act as communicators between the polymer and the antenna. They are the doorway in and out of the antenna systems. As polymer films are generally made from solution, it is important that the polymer solvent does not wash away the stopcocks. One must therefore either use an appropriate solvent which solves the polymer but not the stopcocks, or use irreversible stopcocks that cannot be washed away. Another issue is the contact area between the crystals and the polymer which should be as large as possible. Consequently, clustering of crystals in aggregates is unwanted and should be prevented. The contact area

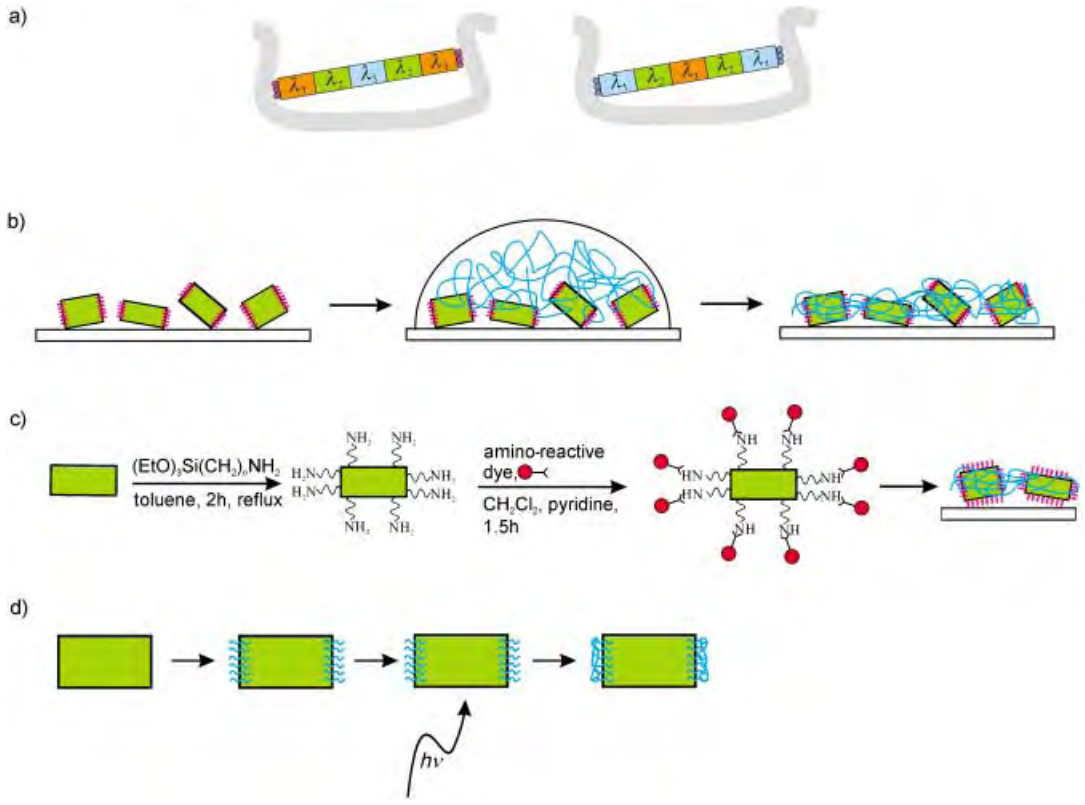


Figure 30. a) coupling of bidirectional dye-zeolite L materials to a polymer to give both normal and inverse antenna systems. The polymer is shown by the gray band, b) embedding of dye-loaded zeolite crystals in a polymer film. A layer of dye-loaded zeolites with adsorbed stopcocks is formed on quartz. Then a droplet of polymer solution is added and the solvent is evaporated, yielding in a polymer film, c) modifying the whole crystal surface with a reactive dye to maximize the contact between the external dye and the polymer, d) solid-state photopolymerization of adsorbed monomers, selectively yielding a polymer on the base of the crystals.

 © 2003 Wiley-VCH Verlag GmbH & Co. KGaA, Weinheim

between the dyes on the surface of the zeolite and the polymer can be enhanced when the whole surface of the zeolite crystal is modified with the external acceptor or injector molecules. One way to ensure the attachment of as many dye molecules as possible is to first cover the zeolite crystal with a silane reagent having an amino group that can be coupled to an amino-reactive fluorescent dye (Figure 30c).

An other approach, shown in Figure 30d is to start with photopolymerizable monomers. The monomers—just like the stopcocks—can be directly adsorbed from solution onto the zeolite L crystals, this gives selective adsorption at the base of the zeolite crystals. The monomers can then be photoirradiated to start a polymerization reaction. Photopolymerization in the solid state is a powerful method to afford polymers with controlled topochemical structure.[62,63] Because it is easy to adsorb the monomers in a sonicated suspension where the crystals are all separate, the contact area is then a minor issue.

7.3. Coupling to a Device of Macroscopic Dimensions

For linking the antenna to a device of macroscopic dimensions, such as a semiconductor or conductor, ordered monolayers of zeolite crystals are needed to minimize the distance between both units. Owing to the higher energy-transfer rate in the direction of the main channel (*c* axis),[31,32] it is desirable to have a monolayer of crystals standing on their bases (Figure 31a). This situation can be realized by using disc-shaped zeolite L crystals or by taking advantage of the chemical difference between the coat and the base of the cylindrical crystals. There are mainly three possibilities to achieve zeolite monolayers on flat surfaces: 1) Physisorption of zeolite crystals on surfaces, 2) noncovalent linkage between zeolites, and 3) covalent linkage of zeolites with surfaces.



Figure 31. Building up a monodirectional antenna system by a) consecutively inserting dyes into a fixed zeolite, b) layer-by-layer assembly of zeolite crystals with differently charged surfaces or stopcock molecules, c) insertion of an asymmetric dye entering the channel always with the same orientation.

7.3.1. Physisorption of Zeolite Crystals on Surfaces

Close-packed monolayers of zeolite crystals on a flat quartz surface are obtained by sedimentation. A calculated amount of a zeolite in a suspension is put on a quartz plate (or another substrate). The solvent slowly evaporates, leaving a homogeneous layer of closely packed zeolite crystals.[64] This method works best with zeolite A crystals (owing to their cubic shape), but can also be used to prepare zeolite L layers.

7.3.2. Noncovalent Linkage between Zeolites or to Surfaces

A stronger attachment to quartz is achieved by chemically modifying the zeolites and the quartz surface with differently charged groups. Further, a monolayer of charged zeolites can be converted into a bilayer, or multilayer, with zeolite crystals with opposite surface or stopcock charge (Figure 31b).[65] Alternatively layers of crystals having the same charge can be assembled by putting a differently charged polymer layer between them. With ZSM-5 crystals up to a pentalayer structure can be prepared. Noncovalent linkage can also be achieved by base pairing between adenine-modified quartz plates and thymine-modified ZSM-5 crystals.[66]

7.3.3. Covalent linkage of zeolites with surfaces

By chemically modifying the quartz surface or both quartz and zeolite surface with reactive groups, zeolite crystals can be linked covalently to a surface.[67a,b]

In monodirectional antenna systems the harvested energy is transported in one direction only. If we want to couple our photonic antenna with a macroscopic device, then such a system transporting the energy in only one direction is desired. The desired photonic monodirectional antenna can be formed by building up monolayers of crystals having the channels perpendicular to the substrate, and subsequently inserting dyes from only one channel end. Moreover by inserting a noncentrosymmetric dye, which fills up the crystal in its preferred orientation,[68] highly ordered systems can be created for nonlinear applications (Figure 31c). A monodirectional antenna can also be achieved by coupling acceptor-loaded zeolites with donor-loaded crystals by noncovalent or covalent linkages, as described above.

The next step is to use a semiconductor as an energy-transfer donor for LEDs or as an acceptor layer for antenna-sensitized solar cells.[16b] Electron-hole pairs in a semiconductor can also be produced by energy transfer.[69] The basic principle is shown in Figure 32. It is important that the semiconductor is covered with an insulating layer which makes electron-transfer impossible.

In this approach, the dye–zeolite composite acts as a light absorbing antenna, whereas the semiconductor is only responsible for the electron-hole-pair formation. Therefore, a very thin semiconductor layer of the order of only a few-hundred nanometers is sufficient. Furthermore, since the connection between the light-absorbing antenna and the semiconductor layer is realized by a dipole or higher multipole mechanism, and not by electron transfer, there is no need

 © 2003 Wiley-VCH Verlag GmbH & Co. KGaA, Weinheim

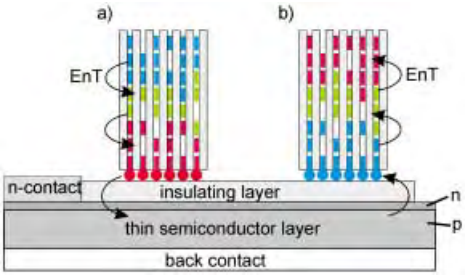


Figure 32. a) Principles of an antenna sensitized solar cell, where the semiconductor acts as an energy-transfer (EnT) acceptor and b) principles of a LED, where the semiconductor acts as energy-transfer donor. In both cases the energy transfer is nonradiative.

for regeneration of the antenna system. Energy transfer from the semiconductor to the dye is also possible, when the semiconductor acts as energy-transfer donor and the dye-loaded zeolite crystal as energy acceptor. While conventional organic LEDs are excited electrically, limiting the theoretical efficiency considerably,[70] the efficiency of an energy-transfer LED is only limited by the electron-hole-pair formation, the energy-transfer rate, and the fluorescence quantum yield of the dye.

8. Intrazeolite Charge Transport

Intrazeolite charge transport is of practical and fundamental importance but remains a controversial topic. We focus on "classical zeolites" of which the crystalline framework can be regarded as an enormous polyanionic system containing cations for charge compensation. The intrazeolite voids may contain solvent molecules, such as water or alcohol. In these materials the framework acts as an insulating host. This means that any charge transport is governed either by the charge-compensating cations or by guests which can be molecules, ions, complexes, conducting polymers, clusters, and quantum-sized particles. Different types of intrazeolite charge transport should be distinguished by the transport mechanism: 1) Ion conductivity is determined by the mobility of cations, such as Na^+, K^+ inside the channels,[71] 2) charge transport governed by intrazeolite redox processes is termed redox conductivity. In such a process the exchange of cations with the surroundings maintains charge neutrality.[72,73] 3) semiconductor conductivity is to be expected in materials in which the guests, such as nanosized particles or conducting polymers, form a sufficiently well developed band structure,[74] 4) metallic conductivity can occur if the band gap becomes small enough.[75] Combinations of these mechanisms are possible, depending on the composition and on the specific arrangement of the guests within the zeolite cavities.

The most delicate part for obtaining unambiguous results in charge-transport experiments on zeolite materials is the control of the interface. Intrazeolite charge transport on Cu^{2+}-Y zeolite, on Ag^+-A zeolite, and on MV^{2+}-Y zeolite electrodes, in which the zeolite microcrystals are deposited as monolayers on glassy carbon-disc electrodes, was reported by us.[73] Baker et al. questioned the importance of preparing zeolite electrodes as monolayers,[76] a question which we have countered.[73c] He and others later focussed mainly on conditions in which in the intrazeolite charge transport by the guest does not play a significant role.[77] Recently impressive progress on the preparation of zeolite monolayers has been made.[64,67,78–81] We feel that any further investigations on intrazeolite charge transport should concentrate on monolayers of the best possible quality. An other approach is to investigate single nanocrystals with, for example, atomic force microscopy(AFM), SEM, and confocal optical microscopy methods.

We now consider charge transport in one-dimensional channels which is challenging and we present a new idea for solving the interface problem. Among the many molecules which have been inserted into zeolite L we discuss only MV^{2+} as an example. About 85 % of the unit cells can be filled with this molecule. On the basis of Rietveld refinement of X-ray data and force-field calculations, the MV^{2+} location model shown in Figure 33 was derived. The MV^{2+} lies along the

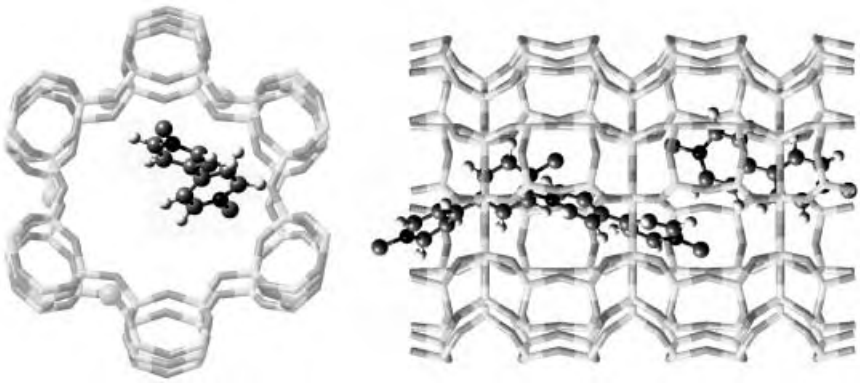


Figure 33. Location of the MV^{2+} cation inside the channel of zeolite L. Left: side view of the channel depicting the arrangement of the molecules along the one-dimensional channel. Right: view along the channel axis showing a position and orientation of a molecule.

channel wall, and the angle between the main MV^{2+} axis and the *c* axis of the zeolite is 27°.[39] We conclude that in such materials intrazeolite charge transfer along channels of MV^{2+} molecules is to be expected. Two problems have to be considered. Since MV^{2+} enters the zeolite channel by means of ion exchange, it can leave it by the same route. This must be prevented if a stable material should result. There are several ways to do this. We have shown for Res^-[42] that using a solvent, which cannot enter the channels of zeolites, prevents the exit of intrazeolite molecules. This means that using an appropriate solvent as the electrolyte, such as polycarbonates or an ionic liquid, should solve the problem. Another possibility is the use of a conductive polymer as a stopcock. The main problem is caused by the electrode–zeolite inter-

 © 2003 Wiley-VCH Verlag GmbH & Co. KGaA, Weinheim



Figure 34. Principle of the stopcock approach. The channels are filled with electron-conducting guests. An electron is injected on one side by the stopcock molecule. It travels along the channel to the other side if a corresponding voltage is applied.

face. We believe that it can be solved by applying the stopcock-molecule approach illustrated in Figure 34. The channels are therefore terminated in a plug-and-socket manner. Depending on the requirements, stopcocks can be either applied on both sides of the cylinders or only on one side. If redox conductivity is envisaged, care must be taken that the mobility of the cations, which is needed for charge compensation, is not hindered. It is clear that the success of this approach depends mainly on the skill of preparing zeolite crystals of the right morphology, of preparing monolayers on the electrode surface, and on applying the stopcock principle.

9. Summary

We have shown that the basic concept of filling luminescent dyes into hexagonal crystals, which consist of one-dimensional channels with molecular diameter and tunable length, leads to new inorganic–organic host–guest materials with fascinating properties and many options for chemical modification. The concepts described are not limited to zeolite L as a host. A nice feature of this zeolite is, however, that neutral as well as cationic dyes can be inserted and that methods for tuning the size and morphology of chemically pure crystals are known. For many dyes insufficient space is available in the zeolite channels for electronic overlap, so that the monomers properties of the dyes are maintained. Additionally, the entrance of the channels is chemically sufficiently different with respect to the coat, so that fine-tuning of stopcock molecules is feasible. The supramolecular organization of the dyes inside the channels is considered as the first stage of organization, which allows light harvesting within a certain volume of a dye-loaded nanocrystalline zeolite and radiationless transport to both ends of the cylinder or from the ends to the center. This first stage is well mastered. The second stage of organization is the coupling to an external acceptor or donor stopcock fluorophore at the ends of the zeolite L channels which can trap electronic excitation energy from donor molecules inside the crystal or inject electronic excitation energy to an acceptor inside the channels. Several such systems have already been prepared. The third stage of organization consists of coupling the organized micro- or nanocrystals to an external device. Preliminary experiments and theoretical reasoning let us expect that such materials/devices will soon be available. The wide-ranging tunability of these highly organized systems offers fascinating new possibilities for exploring excitation energy transfer phenomena and opportunities for developing new photonic devices. The strategy discussed may also result in a new twist in the long-discussed and controversial field of intrazeolite conductivity or photoconductivity.

This research was supported by the Swiss National Science Foundation Project NFP47 (4047-057481), NF 2000-053414/98/1 and by the Bundesamt für Energiewirtschaft Project 10441. We would like to thank Olivia Bossart for carrying out the measurements shown in Figure 23, Philippe Anliker for providing the data reported in Table 4, Dr. Antonio Currao for interesting discussions and his contributions to some Figures, and especially Prof. Peter Würfel (Karlsruhe) for stimulating discussions and suggestions.

Received: January 13, 2003 [A570]

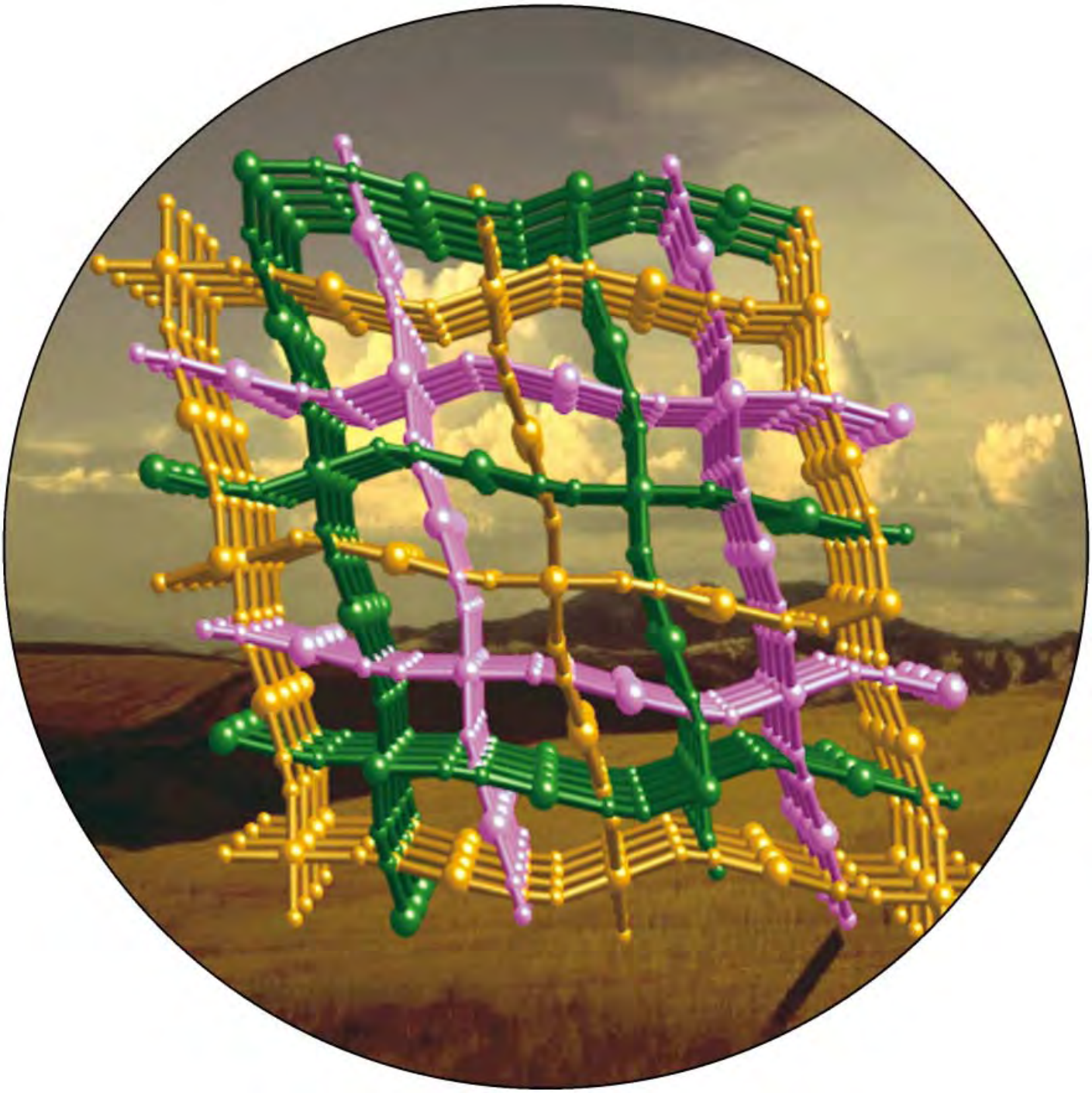
[1] T. Ritz, A. Damjanović, K. Schulten, *ChemPhysChem* **2002**, *3*, 243.
[2] V. Balzani, S. Campagna, G. Denti, A. Juris, S. Serroni, M. Venturi, *Sol. Energy Mater. Sol. Cells* **1995**, *38*, 159.
[3] V. Balzani, S. Campagna, G. Denti, A. Juris, S. Serroni, M. Venturi, *Acc. Chem. Res.* **1998**, *31*, 26.
[4] L. Jullien, J. Canceill, B. Valeur, E. Bardez, J.-M. Lehn, *Angew. Chem.* **1994**, *106*, 2582; *Angew. Chem. Int. Ed. Engl.* **1994**, *33*, 2438.
[5] H. Bücher, K. H. Drexhage, M. Fleck, H. Kuhn, D. Möbius, F. P. Schäfer, J. Sondermann, W. Sperling, P. Tillmann, J. Wiegand, *Mol. Cryst.* **1967**, *2*, 199.
[6] N. Tamai, T. Yamazaki, I. Yamazaki, *J. Phys. Chem.* **1987**, *91*, 841.
[7] J. A. Pescatore, Jr., I. Yamazaki, *J. Phys. Chem.* **1996**, *100*, 13333.
[8] B. A. Gregg, U. Resch, *J. Photochem. Photobiol. A* **1995**, *87*, 157.
[9] S. E. Webber, *Chem. Rev.* **1990**, *90*, 1469.
[10] D. M. Watkins, M. A. Fox, *J. Am. Chem. Soc.* **1996**, *118*, 4344.
[11] V. Balzani, P. Ceroni, S. Gestermann, M. Gorka, C. Kauffmann, M. Maestri, F. Vögtle, *ChemPhysChem* **2000**, *1*, 224.
[12] D. M. Sturmer, D. W. Heseltine in *The Theory of the Photographic Process*, 4th ed. (Ed.: T. H. James), Macmillan, New York, **1977**, p. 194.
[13] H. Tributsch in *Proceedings of the Ninth International Conference on Photochemical and Photoelectrochemical Conversion and Storage of Solar Energy* (Ed.: Z. W. Tian), International Academic Publishers, Peking, **1993**, p. 235.
[14] R. Memming, H. Tributsch, *J. Phys. Chem.* **1971**, *75*, 562.
[15] W. Kühlbrandt, D. N. Wang, *Nature* **1991**, *350*, 130.
[16] a) G. Calzaferri, H. Maas, M. Pauchard, M. Pfenniger, S. Megelski, A. Devaux, *Adv. Photochem.* **2002**, *27*, 1; b) G. Calzaferri, M. Pauchard, H. Maas, S. Huber, A. Khatyr, T. Schaafsma, *J. Mater. Chem.* **2002**, *12*, 1.
[17] D. W. Breck, *Zeolite Molecular Sieves*, Wiley, New York, **1974**.
[18] Ch. Baerlocher, W. M. Meier, D. H. Olson, *Atlas of Zeolite Framework Types*, 5th ed., Elsevier, Amsterdam, **2001**.
[19] S. Megelski, G. Calzaferri, *Adv. Funct. Mater.* **2001**, *11*, 277.
[20] M. Pauchard, A. Devaux, G. Calzaferri, *Chem. Eur. J.* **2000**, *6*, 3456.
[21] H. Maas, G. Calzaferri, *Angew. Chem.* **2002**, *114*, 2389; *Angew. Chem. Int. Ed.* **2002**, *41*, 2284.
[22] a) G. Calzaferri, N. Gfeller, *J. Phys. Chem.* **1992**, *96*, 3428; b) V. Ramamurthy, D. R. Sanderson, D. F. Eaton, *J. Am. Chem. Soc.* **1993**, *115*, 10438.
[23] F. Binder, G. Calzaferri, N. Gfeller, *Sol. Energy Mater. Sol. Cells* **1995**, *38*, 175.
[24] G. Calzaferri, International patent, WO 02/36490A1, **2002**, Int. Appl. Number PCT/CH01/00647, Priority data: 03.11.2000 [*Chem. Abstr.* **2002**, *136*, 371855].

 © 2003 Wiley-VCH Verlag GmbH & Co. KGaA, Weinheim

[25] A. Khatyr, H. Maas, G. Calzaferri, *J. Org. Chem.* **2002**, *67*, 6705.
[26] S. Ernst, J. Weitkamp, *Catal. Today* **1994**, *19*, 27.
[27] M. Lovallo, M. Tsapatsis, *Adv. Catal. Nanostruct. Mater.* **1996**, 307.
[28] J. M. Newsam, *J. Phys. Chem.* **1989**, *93*, 7689.
[29] X. Meng, Y. Zhang, C. Meng, W. Pang in *Proceedings of the 9th International Zeolite Conference* (Eds.: R. von Ballmoos, J. B. Higgins, M. M. J. Treacy), Butterworth-Heinemann, Boston, **1993**, p. 297.
[30] a) M. Tsapatsis, T. Okubo, M. Lovallo, M. E. Davis, *Mater. Res. Soc. Symp. Proc.* **1995**, *371*, 21; b) M. Tsapatsis, M. Lovallo, T. Okubo, M. E. Davis, M. Sadakata, *Chem. Mater.* **1995**, *7*, 1734.
[31] N. Gfeller, G. Calzaferri, *J. Phys. Chem. B* **1997**, *101*, 1396.
[32] M. M. Yatskou, M. Meyer, S. Huber, M. Pfenniger, G. Calzaferri, *ChemPhysChem* **2003**, *4*, 567.
[33] S. Hashimoto, M. Hagiri, N. Matsubara, S. Tobita, *Phys. Chem. Chem. Phys.* **2001**, *3*, 5043.
[34] a) M. Ganschow, G. Schulz-Ekloff, M. Wark, M. Wendschuh-Josties, D. Wöhrle, *J. Mater. Chem.* **2001**, *11*, 1823; b) C. Seebacher, C. Hellriegel, C. Bräuchle, *J. Phys. Chem. B* **2003**, *107*, 5445.
[35] a) G. Meyer, D. Wöhrle, M. Mohl, G. Schultz-Ekloff, *Zeolites* **1984**, *4*, 30; b) W. H. Quayle, J. H. Lunsford, *Inorg. Chem.* **1982**, *21*, 97; c) P. Lainé, M. Lanz, G. Calzaferri, *Inorg. Chem.* **1996**, *35*, 3514; d) G. Schulz-Ekloff, D. Wöhrle, B. Van Duffel, R. A. Schoonheydt, *Microporous Mesoporous Mater.* **2002**, *51*, 91.
[36] G. Calzaferri, D. Brühwiler, S. Megelski, M. Pfenniger, M. Pauchard, B. Hennessy, H. Maas, A. Devaux, U. Graf, *Solid State Sci.* **2000**, *2*, 421.
[37] N. J. Turro, X.-G. Lei, W. Li, Z. Liu, A. McDermott, M. F. Ottaviani, L. Abrams, *J. Am. Chem. Soc.* **2000**, *122*, 11649.
[38] M. F. Ottaviani, X.-G. Lei, Z. Liu, N. J. Turro, *J. Phys. Chem. B* **2001**, *105*, 7954.
[39] B. Hennessy, S. Megelski, C. Marcolli, V. Shklover, C. Bärlocher, G. Calzaferri, *J. Phys. Chem. B* **1999**, *103*, 3340.
[40] J. M. Lehn, J. P. Sauvage, *J. Am. Chem. Soc.* **1975**, *97*, 6700.
[41] H. Musso, C. Rathjen, *Chem. Ber.* **1959**, *92*, 751.
[42] D. Brühwiler, N. Gfeller, G. Calzaferri, *J. Phys. Chem. B* **1998**, *102*, 2923.
[43] N. Gfeller, S. Megelski, G. Calzaferri, *J. Phys. Chem. B* **1998**, *102* 2433.
[44] S. Stoyanov, *Pract. Spectrosc.* **2001**, *25*, 35 (Near IR Applications in Biotechnology).
[45] F. O. Holtrup, G. R. J. Müller, H. Quante, S. De Feyter, F. C. De Schryver, K. Müllen, *Chem. Eur. J.* **1997**, *3*, 219.
[46] F. Binder, G. Calzaferri, N. Gfeller, *Proc. Indian Acad. Sci. Chem. Sci.* **1995**, *107*, 753.
[47] U. Sommer, H. E. A. Kramer, *Photochem. Photobiol.* **1971**, *13*, 387.
[48] S. J. Hawkes, *J. Chem. Educ.* **1996**, *73*, 516.
[49] S. Megelski, A. Lieb, M. Pauchard, A. Drechsler, S. Glaus, C. Debus, A. J. Meixner, G. Calzaferri, *J. Phys. Chem. B* **2001**, *105*, 25.
[50] M. Pfenniger, G. Calzaferri, *ChemPhysChem* **2000**, *1*, 211.
[51] M. Pauchard, S. Huber, R. Méallet-Renault, H. Maas, R. Pansu, G. Calzaferri, *Angew. Chem.* **2001**, *113*, 2921; *Angew. Chem. Int. Ed.* **2001**, *40*, 2839.
[52] T. Förster, *Ann. Phys.* **1948**, *6*, 55.
[53] J. Grabowska, K. Sienicki, *Chem. Phys.* **1995**, *192*, 89.
[54] V. Czikklely, H. D. Forsterling, H. Kuhn, *Chem. Phys. Lett.* **1970**, *6*, 207.
[55] J. Karolin, L. B.-Å. Johansson, L. Strandberg, T. Ny, *J. Am. Chem. Soc.* **1994**, *116*, 7801.
[56] J. V. Mello, N. S. Finney, *Angew. Chem.* **2001**, *113*, 1584; *Angew. Chem. Int. Ed.* **2001**, *40*, 1536.
[57] L. Echegoyen, L. E. Echegoyen, *Acc. Chem. Res.* **1998**, *31*, 593.
[58] D. M. Guldi, M. Maggini, E. Menna, G. Scorrano, P. Ceroni, M. Marcaccio, F. Paolucci, S. Roffia, *Chem. Eur. J.* **2001**, *7*, 1597.
[59] A. Aviram, M. A. Ratner, *Chem. Phys. Lett.* **1974**, *29*, 277.
[60] H. Imahori, H. Yamada, D. M. Guldi, Y. Endo, A. Shimomura, S. Kundu, K. Yamada, T. Okada, Y. Sakata, S. Fukuzumi, *Angew. Chem.* **2002**, *114*, 2450; *Angew. Chem. Int. Ed.* **2002**, *41*, 2344.
[61] D. Gust, T. A. Moore, A. L. Moore, *Acc. Chem. Res.* **2001**, *34*, 40.
[62] A. Prock, M. L. Shand, R. R. Chance, *Macromolecules* **1982**, *15*, 238.
[63] A. Alekseev, I. Domnin, A. Grudinin, H. Lemmetyinen, A. Nikitenko, *Macromol. Chem. Phys.* **2000**, *201*, 1317.
[64] P. Lainé, R. Seifert, R. Giovanoli, G. Calzaferri, *New J. Chem*, **1997**, *21*, 453.
[65] G. S. Lee, Y.-J. Lee, K. B. Yoon, *J. Am. Chem. Soc.* **2001**, *123*, 9769.
[66] J. S. Park, G. S. Lee, Y.-J. Lee, Y. S. Park, K. B. Yoon, *J. Am. Chem. Soc.* **2002**, *124*, 13366.
[67] a) K. Ha, Y.-J. Lee, D.-Y. Jung, J. H. Lee, K. B. Yoon, *Adv. Mater.* **2000**, *12*, 1614; b) K. Ha, Y.-J. Lee, H. J. Lee, K. B. Yoon, *Adv. Mater.* **2000**, *12*, 1114; c) A. Kulak, Y.-J. Lee, Y. S. Park, K. B. Yoon, *Angew. Chem.* **2000**, *112*, 980; *Angew. Chem. Int. Ed.* **2000**, *39*, 950; d) K. Ha, Y.-J. Lee, Y. S. Chun, Y. S. Park, G. S. Lee, K. B. Yoon, *Adv. Mater.* **2001**, *13*, 594.
[68] J. Caro, F. Marlow, M. Wübbenhorst, *Adv. Mater.* **1994**, *6*, 413.
[69] D. L. Dexter, *J. Lumin.* **1979**, *18/19*, 779.
[70] V. Cleave, G. Yahioglu, P. Le Barny, R. H. Friend, N. Tessler, *Adv. Mater.* **1999**, *11*, 285.
[71] a) A. K. Jonscher, *Universal Relaxation Law*, Chelsea Dielectrics Press, London, **1996**; b) R. Gerhardt, *J. Phys. Chem. Solids* **1994**, *55*, 1491; c) T. Ohgushi, S. Sato, *J. Solid State Chem.* **1990**, *87*, 95; d) E. K. Andersen, I. G. K. Andersen, E. Skou, *Chem. Solid State Mater.* **1992**, *2*, 210.
[72] a) D. R. Rolison, *Chem. Rev.* **1990**, *90*, 867; b) D. R. Rolison, *Stud. Surf. Sci. Catal.* **1994**, *85*, 543 (Advanced Zeolite Science and Applications).
[73] a) J.-W. Li, G. Calzaferri, *J. Electroanal. Chem.* **1994**, *377*, 163; b) J.-W. Li, K. Pfanner, G. Calzaferri, *J. Phys. Chem.* **1995**, *99*, 2119; c) J.-W. Li, K. Pfanner, G. Calzaferri, *J. Phys. Chem.* **1995**, *99*, 12368; d) G. Calzaferri, M. Lanz, J.-W. Li, *J. Chem. Soc. Chem. Commun.* **1995**, 1313.
[74] D. Brühwiler, C. Leiggener, S. Glaus, G. Calzaferri, *J. Phys. Chem. B* **2002**, *106*, 3770.
[75] M. Brändle, G. Calzaferri, *Res. Chem. Intermed.* **1994**, *20*, 783.
[76] M. D. Baker, C. Senaratne, M. McBrien, *J. Phys. Chem.* **1995**, *99*, 12367.
[77] a) C. Senaratne, J. Zhang, J. Fox, I. Burgess, M. D. Baker, *Microporous Mesoporous Mater.* **1999**, *33*, 281; b) T.-W. Hui, M. D. Baker, *J. Phys. Chem. B* **2002**, *106*, 827.
[78] L. Huang, Z. Wang, J. Sun, L. Miao, Q. Li, Y. Yan, D. Zhao, *J. Am. Chem. Soc.* **2000**, *122*, 3530.
[79] S. Mintova, B. Schoeman, V. Valtchev, J. Sterte, S. Mo, T. Bein, *Adv. Mater.* **1997**, *9*, 585.
[80] S. Mintova, V. Valtchev, *Zeolites* **1996**, *16*, 31.
[81] P. Yang, T. Deng, D. Zhao, P. Feng, D. Pine, B. F. Chmelka, G. M. Whitesides, G. D. Stucky, *Science* **1998**, *282*, 2244.

 © 2003 Wiley-VCH Verlag GmbH & Co. KGaA, Weinheim

Communications



The three interpenetrated independent 3D spin-crossover networks in $[Fe(pdm)(H_2O)\{Ag(CN)_2\}_2]\cdot H_20$ transform into a single 3D network upon losing the coordinated water molecules. This process is reversible and is accompanied by drastic modifications of the spin-crossover switching properties. For more information see the following communication by J. A. Real and co-workers.

DOI: 10.1002/anie.200351853
© 2003 Wiley-VCH Verlag GmbH & Co. KGaA, Weinheim

Hysteresis in Fe-CN-Ag/Au Networks

Crystalline-State Reaction with Allosteric Effect in Spin-Crossover, Interpenetrated Networks with Magnetic and Optical Bistability**

*Virginie Niel, Amber L. Thompson, M. Carmen Muñoz, Ana Galet, Andrés E. Goeta, and José A. Real**

The versatility of metal–organic chemistry offers a unique opportunity to construct multifunctional materials based on the assembly of molecular building blocks. Such an approach can lead to the design of coordination polymers with specific network topologies and potentially interesting properties.[1] Incorporation of iron(II) spin crossover (SCO) building blocks in such framework structures is particularly suitable for these purposes as the labile electronic configurations of the iron units may be switched between the high- (HS) and low-spin (LS) states. This switching leads to distinctive changes in magnetism, color, and structure, which may be induced by variation of temperature and/or pressure and by light irradiation.[2] Strong signal generation and hysteresis (memory effect) may be achieved when rigid linkers, which allow communication between the SCO centers, propagate the structural changes cooperatively to the whole framework conferring a bistable character to the material.[3–5] The construction of sensory and memory devices is the ultimate goal.

Hofmann-like open frame coordination polymers have been the subject of much research for many years.[6] Nevertheless, incorporation of iron(II) SCO building blocks in such systems is relatively recent.[7] Following this strategy we have shown the suitability of cyano-metallate complexes as connectors between iron(II) SCO centers to build highly cooperative thermo-, piezo-, and photo-switchable two- and three-dimensional coordination polymers.[8–10] A further important aspect for developing multifunctional materials based on these polymers stems from their porous nature,[11] which opens opportunities for investigating the interplay between inclusion chemistry and SCO signal generation.[12,13] Herein we report on the incorporation of electronic SCO, molecular recognition, and crystalline-state reaction[14] switching events and their cooperative interactions in [Fe(pmd)-$(H_2O)\{M(CN)_2\}_2]\cdot H_2O$ (**1**) (pmd = pyrimidine; M = Ag (**1Ag**) or Au (**1Au**)). This is a cyanide-based bimetallic coordination polymer made up of triple interpenetrated, 4-connected, three-dimensional, open-frame networks.

Compound **1** is monoclinic (space group $P2_1/c$) whatever the spin state (the structural parameters reported below correspond to the HS state).[15] Two distinct iron atoms, Fe(1) and Fe(2) (see Figure 2), which define the inversion center of an elongated $\{Fe(1)N_6\}$ and a compressed $\{Fe(2)N_4O_2\}$ coordination octahedron, respectively, constitute the building blocks of the structure. The four equatorial positions are occupied by the cyanide nitrogen atoms of the $[M(CN)_2]^-$ groups while the apical positions are occupied by two nitrogen atoms of two pmd ligands (Fe(1)) and by two water molecules (Fe(2)). The $[M(CN)_2]^-$ groups link the Fe(1) and Fe(2) atoms generating {Fe(1)-NC-M(1)-CN-Fe(2)-NC-M(2)-CN-} groups which connect to form rectangular motifs. These rectangles have edges Fe(1)···Fe(1) = 20.5775(7) (**1Ag**), 20.3860(6) Å (**1Au**) and Fe(1)···Fe(2) = 10.6417(2) (**1Ag**), 10.5643(2) Å (**1Au**). The edge sharing rectangles define an infinite set of parallel layers pillared by $[M(CN)_2]^-$ groups. The resulting 4-connected 3D network corresponds to the expanded version of the prototypical $CdSO_4$ net decorated by the coordinating water molecules and the pmd ligands (Figure 1a).[16,17] The much larger intraframework spaces are occupied by two other identical but independent networks, which interpenetrate the first network and each other (Figure 1b). Communication between the three covalently bonded nets is through weaker metallophilic M···M interactions (average Ag···Ag and Au···Au distances 3.1813(3) and 3.2901(4) Å, respectively) and hydrogen bonds between the coordinated water molecules and the uncoordinated nitrogen atom of the pmd ligands (N(pmd)···H_20 = 2.805(3) Å (**1Ag**) and 2.762(6) Å (**1Au**); (Figure 2a, b). This arrangement accounts for the close proximity of the Fe(2) atom and the uncoordinated nitrogen atom, Fe(2)-OH_2···N(pmd), which provides favorable conditions for a topochemical reaction to take place (Figure 2a).

Complete and rapid loss of both ligated and nonbonded water molecules occurs simultaneously in the temperature range 345–399 K (**1Ag**) and 323–382 K (**1Au**). X-ray powder diffraction spectra (XRPD) were recorded on **1Au** at 290 K and 373 K at ambient pressure and at 290 K under vacuum. The data obtained clearly confirms that at 290 K at ambient pressure the sample is in the hydrated state, in agreement with results obtained from single-crystal measurements. The X-ray spectra taken at 373 K at ambient pressure and at 290 K under vacuum are essentially identical though different to the spectra of the hydrated sample, thus revealing the structural changes caused by the loss of the water molecules. Ab initio indexing of the powder pattern of the dehydrated sample clearly shows the massive cell-contraction (ca. 2.5 Å) taking place along the *a* axis, previously assumed from the observed shift of the 200 reflection from 12.3(2)° to 14.5(2)° (Supporting Information). This large and reversible structural modification involving not only the loss of an unbound water

[*] Prof. Dr. J. A. Real, Dr. V. Niel
Institut de Ciencia Molecular/Departament de Química Inorgànica
Universitat de València
Doctor Moliner 50, 46100 Burjassot, València (Spain)
Fax: (+34) 96-386-4322
E-mail: jose.a.real@uv.es
A. L. Thompson, Dr. A. E. Goeta
Department of Chemistry
University of Durham
South Road, Durham, DH1 3LE (UK)
Prof. Dr. M. C. Muñoz, A. Galet
Departament de Física Aplicada
Universitat Politécnica de València
Camino de Vera s/n, 46071 València (Spain)

[**] We are grateful for financial assistance from the Ministerio Español de Ciencia y Tecnología (project BQU 2001–2928), The Royal Society for a Study Visit and a Join Project awards. ALT thanks EPSRC for a Postgraduate Fellowship. AG thanks to the Universitat Politècnica de València for a predoctoral fellowship.

Supporting information for this article is available on the WWW under http://www.angewandte.org or from the author.

 © 2003 Wiley-VCH Verlag GmbH & Co. KGaA, Weinheim DOI: 10.1002/anie.200351853

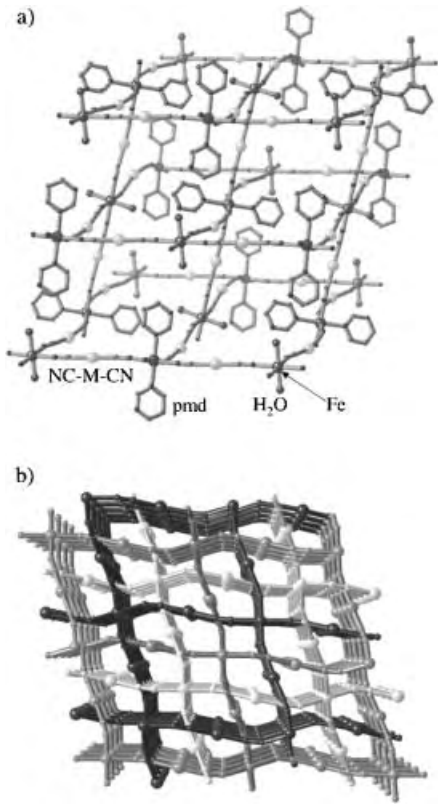


Figure 1. a) Fragment of the 3D network of **1** displaying the expanded version of the $CdSO_4$ structure. b) Perspective view of the three interlocked networks.

molecule but more importantly the loss of a coordinating water molecule, affects the integrity of the single crystals of **2** (they crack and become effectively a polycrystalline powder) precluding the in situ structure determination from single-crystal diffraction techniques. The structure determination of **2Au** was then carried out from a rigid-body Rietveld refinement of the hydrated model, excluding the water molecules, using the newly determined cell parameters.[18] No change in space group has been observed following the **1**↔**2** transformation. There are two crystallographically distinct $\{FeN_6\}$ distorted octahedrons in **2** whose Fe(1) and Fe(2) sites can be unambiguously identified with those corresponding to **1**. However, in contrast to **1**, the pmd ligand now bridges directly the Fe(1) and Fe(2) atoms defining a system of infinite chains {-Fe(1)-pmd-Fe(2)} running parallel to the *a* axis (Fe(1)···Fe(2) = 6.1927(4) Å) in **2**. The $[M(CN)_2]^-$ groups of one chain link with the equatorial positions of the iron centers, connecting adjacent chains and defining a single 3D network (Figure 2c, d). These significant structural changes are a consequence of the cooperative topochemical ligand substitution, which involves the concerted loss of the bonded water generating double coordination unsaturation at the Fe(2) centers and the coordination of the uncoordinated pmd nitrogen atom belonging to adjacent networks. A first example of topochemical conversion of a hydrogen-bonded into a covalent bonded supramolecular network was described for the binuclear $[\{Zn(sala)(H_2O)_2\}_2]\cdot 2H_2O$ compound (H_2sala = *N*-(2-hydroxybenzyl)-L-alanine), but this process was irreversible.[19] In contrast, when **1Au** and **1Ag** are exposed to an atmosphere of H_2O, selective absorption of this vapor induces the inverse reaction at the Fe(2) sites, regenerating the three independent 3D networks (Figure 2c, d). The system does not suffer any noticeable fatigue after repeating several **1**↔**2** cycles.

X-ray powder diffraction spectra of **1Ag** have also been recorded and it can be clearly observed that the behavior is similar to that described for the **1Au** compound. In spite of this, there are clear differences between **2Ag** and **2Au**, which point to either a different unit cell or a loss of symmetry from monoclinic to triclinic in **2Ag**. Further work is in progress to establish the cell parameters and space group for **2Ag**, with the aim of solving its crystal and molecular structure.

Figure 3 shows the temperature dependence of the $\chi_M T$ product for **1Ag** and **1Au**, χ_M being the molar magnetic susceptibility and T the temperature. At room temperature,

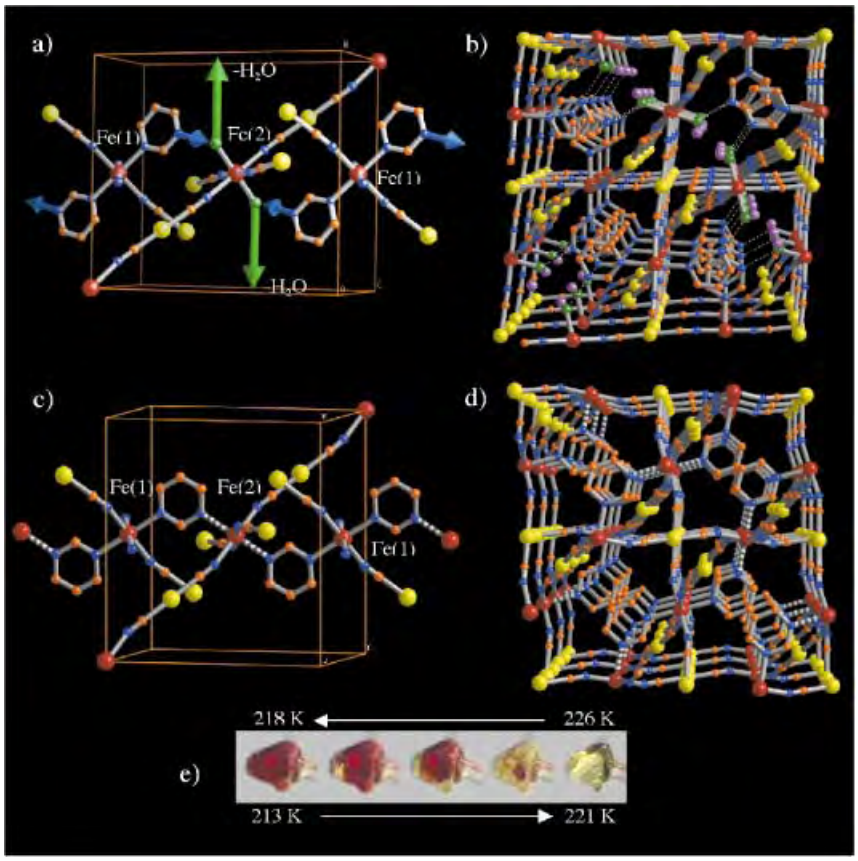


Figure 2. a) Unit cell of **1** showing fragments of three networks. Arrows on the uncoordinated nitrogen atoms (blue) and coordinated water molecules (green) indicate the dynamic event, which takes place during the topochemical solid-state reaction. b) Perspective view, [001], of the three nets showing the N(pmd)···H_2O hydrogen-bond system. c) Unit cell of **2Au** displaying the infinite chains defined by the bridging mode of the pmd ligand (striped bonds represent the new coordination bonds generated after dehydration. d) Perspective view of the new 3D network **2Au**. e) Photographs showing the color change of a **1Ag** single crystal around the critical region (yellow and deep red colors correspond to the high- and low-spin states, respectively).

 © 2003 Wiley-VCH Verlag GmbH & Co. KGaA, Weinheim

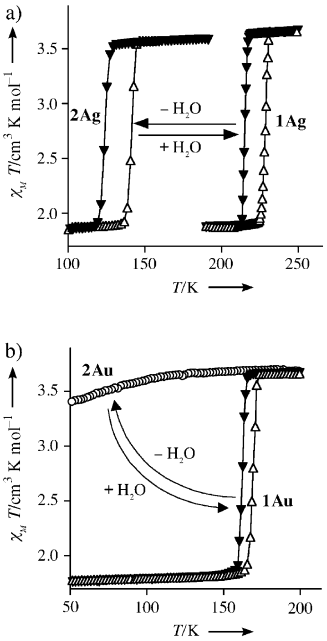


Figure 3. Magnetic susceptibility measurements displaying the first-order spin transition for a) **1Ag/2Ag** and b) **1Au/2Au**.

$\chi_M T$ is 3.7 for **1Ag** and 3.6 cm^3 K mol^{-1} for **1Au**. These values are consistent with the iron(II) ion in the HS state. Upon cooling, $\chi_M T$ remains almost constant up to 218 K (**1Ag**) and 165 K (**1Au**), below these temperatures the $\chi_M T$ value undergoes a sharp decrease that is characteristic of a first order SCO transition. The $\chi_M T$ value drops to 1.8 (**1Ag**) and 1.7 (**1Au**) cm^3 K mol^{-1} at 213 K and 159 K, respectively. The warming mode reveals the occurrence of thermal hysteresis. The critical temperatures for the cooling (T_c^{down}) and warming (T_c^{up}) modes (215 and 223 K (**1Ag**) and 163 and 171 K (**1Au**) respectively), indicate the occurrence of approximately 8 K wide hysteresis loops. At temperatures below T_c, the $\chi_M T$ value indicates that 50% of the iron(II) ions remains in the HS state for both compounds. As expected from their coordination environments, Fe(1) undergoes the HS↔LS transition while Fe(2) remains HS, which is in agreement with the structural data obtained at 120 K for both derivatives.

The temperature dependence of $\chi_M T$ was measured for the dehydrated **2Ag** and **2Au** forms (Figure 3a, b).For **2Ag** $\chi_M T$ is 3.6 cm^3 K mol^{-1} at room temperature and remains constant down to 125 K, which indicates that the iron(II) ion is in the HS state in **2Ag**. The subsequent sharp decrease of $\chi_M T$ to a value of 1.9 cm^3 K mol^{-1} is due to the occurrence of a spin transition. The warming mode reveals the occurrence of a 17 K wide thermal hysteresis loop. The critical temperatures are $T_c^{down} = 124$ K and $T_c^{up} = 141$ K. Compound **2Ag** has a hysteresis loop twice the width of **1Ag**, which denotes the expected increase of cooperativity when replacing the hydrogen-bonding internetwork interactions in **1** by stronger coordination bonds in the more rigid framework **2**. Compound **2Au** does not undergo a spin transition in the whole temperature range ($\chi_M T$ has a constant value of around 3.8 cm^3 K mol^{-1} between room temperature and 120 K). This difference in the behavior of **2Ag** and **2Au** may be supported by the differences in the diffraction patterns observed for each of the compounds upon dehydration, see above. The marked down shift of T_c in **2Ag** and disappearance of SCO in **2Au** indicate a decrease of the ligand-field strength at the Fe(1) site and may be ascribed to the bridging mode of the pmd ligand. Recovery of the original SCO behavior of **1Ag** and **1Au** occurs when **2Ag** and **2Au** are left in air atmosphere.

Compounds **1Ag**, **1Au**, and **2Ag** undergo a dramatic change of color from pale yellow (HS state) to deep red (LS state) accompanying the SCO (Figure 2e). This thermochromic effect, observed in other 2D and 3D Fe^{II}–M^{II} (M = Ni, Pd, Pt) Hofmann-like SCO compounds, is a consequence of the increase in intensity of the metal-to-ligand charge transfer (MLCT) band around 550 nm, associated with the electron delocalization from the t_{2g} orbitals of the iron(II) ion to the π^* orbitals of the ligands which is enhanced by the HS→LS spin change.[8]

In summary, the coordination polymers **1Au** and **1Ag** undergo thermally induced first-order, spin-crossover transitions with magnetic and chromatic bistability. They also participate in a controlled and fully reversible crystalline-state ligand substitution, involving coordination/uncoordination of gaseous water and pmd. This induces expansion/contraction of the nanoporous framework and the repeated allosteric transformation of the three interpenetrated nets into a single three-dimensional net (**2Ag** and **2Au**) without affecting their crystallinity but altering their SCO behavior significantly. Such a cooperative combination, in the same lattice, of different molecular events, such as recognition, allosterism, and electronic bistability is of fundamental significance for the generation of new switchable, multi-property materials.

Experimental Section

1Ag: was synthesized by slow diffusion, under an argon atmosphere, of two aqueous solutions containing stoichiometric amounts of $Fe(BF_4)_2 \cdot 6H_2O$ (0.185 mmol, 2 mL)/pyrimidine (0.374 mmol, 2 mL) in one side and $K[Ag(CN)_2]$ (0.374 mmol, 2 mL) in the other side of an H-shaped vessel. Pale yellow prismatic crystals were separated three weeks later. Yield approximately 50%. Elemental analysis (%) calcd for $C_8H_8N_6Ag_2O_2Fe$: C 19.54, H 1.61, N 17.09; found: C 20.05, H 1.98, N 16.76.

1Au: to an aqueous solution containing $FeCl_2$ (0.087 mmol, 4 mL) and pyrimidine (0.173 mmol, 4 mL) was added a water solution of $K[Au(CN)_2]$ (0.173 mmol, 6 mL). The resulting solution was stirred for 10 min and left at room temperature to evaporate under an argon stream. Pale yellow crystals were separated one week later. Yield approximately 70%. Elemental analysis (%) calcd for $C_8H_8N_6Au_2O_2Fe$: C 14.34, H 1.20, N 12.54; found: C 14.95, H 1.50, N 12.03.

2Ag and **2Au**: Dehydrated samples **2Ag** and **2Au** were prepared from **1Ag** and **1Au** in the SQUID sample holder. Hydrated samples placed in sealed containers in the SQUID sample holder and their magnetism checked. Small holes were then made in the lids of the sample containers and the samples left standing for 30 min at 380 K, dehydration under these conditions is confirmed by the thermogravimetric analysis (see Supporting Information).

Received: May 9, 2003 [Z51853]
Published online: July 28, 2003

 © 2003 Wiley-VCH Verlag GmbH & Co. KGaA, Weinheim

Keywords: allosterism · cooperative effects · crystalline-state reactions · N ligands · spin crossover

[1] a) J. M. Lehn, *Science* **2002**, *295*, 2400; b) M. D. Hollingsworth, *Science* **2002**, *295*, 2410.

[2] P. Gütlich, A. Hauser, H. Spiering, *Angew. Chem.* **1994**, *106*, 2109; *Angew. Chem. Int. Ed. Engl.* **1994**, *33*, 2024.

[3] J. A. Real, A. B. Gaspar, V. Niel, M. C. Muñoz, *Coord. Chem. Rev.* **2003**, *236*, 121.

[4] W. Vreugdenhill, J. H. Van Diemen, R. A. G. De Graaff, J. G. Haasnoot, J. Reedijk, A. M. Van der Kraan, O. Kahn, J. Zarembowitch, *Polyhedron* **1990**, *9*, 2971.

[5] O. Kahn, C. J. Martinez, *Science* **1998**, *279*, 44.

[6] T. Iwamoto in *Inclusion Compounds, Vol. 5* (Eds.: J. L. Atwood, J. E. D. Davies, D. D. MacNicol), Oxford University Press, London, UK, **1991**, p. 177.

[7] T. Kitazawa, Y. Gomi, M. Takahashi, M. Takeda, A. Enemoto, T. Miyazaki, T. Enoki, *J. Mater. Chem.* **1996**, *6*, 119.

[8] V. Niel, J. M. Martinez-Agudo, M. C. Muñoz, A. B. Gaspar, J. A. Real, *Inorg. Chem.* **2001**, *40*, 3838.

[9] V. Niel, M. C. Muñoz, A. B. Gaspar, A. Galet, G. Levchenko, J. A. Real, *Chem. Eur. J.* **2002**, *8*, 2446.

[10] V. Niel, A. Galet, A. B. Gaspar, M. C. Muñoz, J. A. Real, *Chem. Commun.* **2003**, 1248.

[11] a) B. Chen, M. Eddaoudi, S. T. Hyde, M. O'Keeffe, O. M. Yaghi, *Science* **2001**, *291*, 1021; b) O. M. Yaghi, G. Li, H. Li, *Nature* **1995**, *378*, 703.

[12] P. J. Langley, J. Hulliguer, *Chem. Soc. Rev.* **1999**, *28*, 279.

[13] a) G. J. Halder, C. J. Kepert, B. Moubaraki, K. S. Murray, J. D. Cashion, *Science* **2002**, *298*, 1762; b) J. A. Real, E. Andrés, M. C. Muñoz, M. Julve, T. Granier, A. Bousseksou, F. Varret, *Science* **1995**, *268*, 265.

[14] M. Albrecht, M. Lutz, A. L. Spek, G. van Koten, *Nature* **2000**, *406*, 970.

[15] Crystal for **1Ag**: Monoclinic, space group $P2_1/c$, $a = 14.7035(5)$, $b = 13.2962(5)$, $c = 7.3852(3)$ Å, $\beta = 91.441(2)°$, $Z = 4$, $V = 1443.35(9)$ Å^3, $T = 225$ K, $\rho_{calcd} = 2.263$ mg m^{-3}, $\mu = 3.683$ mm^{-1}, 19016 reflections measured, 3867 unique ($R_{int} = 0.0245$) which were used in all calculations and 3425 greater than $2\sigma(I)$. The final $R(F)$ was 0.0219 ($I > 2\sigma(I)$ data) and the $wR(F^2)$ was 0.0535 (all data). Crystal data for **1Au**: Monoclinic, space group $P2_1/c$, $a = 14.6157(5)$, $b = 13.3075(5)$, $c = 7.2272(3)$ Å, $\beta = 90.944(2)°$, $V = 1405.49(9)$ Å^3, $\rho_{calcd} = 3.166$ mg m^{-3}, $T = 180$ K, $\mu = 21.849$ mm^{-1}, 15805 reflections measured, 3072 unique ($R_{int} = 0.0545$) which were used in all calculations and 2441 greater than $2\sigma(I)$. The final $R(F)$ was 0.0241 ($I > 2\sigma(I)$ data) and the $wR(F^2)$ was 0.0474 (all data). CCDC-209792–209795 contain the supplementary crystallographic data for this paper. These data can be obtained free of charge via www.ccdc.cam.ac.uk/conts/retrieving.html (or from the Cambridge Crystallographic Data Centre, 12 Union Road, Cambridge CB2 1EZ, UK; fax: (+44) 1223-336-033; or deposit@ccdc.cam.ac.uk).

[16] L. Carlucci, G. Ciani, P. Macchi, D. M. Proserpio, *Chem. Commun.* **1998**, 1837.

[17] M. O'Keeffe, M. Eddaoudi, H. Li, T. Reineke, O. M. Yaghi, *J. Solid State Chem.* **2000**, *152*, 3.

[18] Crystal data for **2Au**: Monoclinic, space group $P2_1/c$, $a = 12.3855(7)$, $b = 13.6751(6)$, $c = 8.3348(4)$ Å, $\beta = 94.150(3)°$, $V = 1407.98(15)$ Å^3, $Z = 4$, $T = 293$ K. Final $wR_p = 7.46\%$, $R_F = 5.15\%$, GooF = 2.61, $\chi^2 = 6.827$ (see Supporting Information for structure refinement).

[19] J. D. Ranford, J. J. Vittal, D. Wu, *Angew. Chem.* **1998**, *110*, 1159; *Angew. Chem. Int. Ed.* **1998**, *37*, 1114.

 DOI: 10.1002/anie.200351246 © 2003 Wiley-VCH Verlag GmbH & Co. KGaA, Weinheim

Metallacryptate Magnets

Synthesis and Magnetic Properties of a Metallacryptate that Behaves as a Single-Molecule Magnet**

Catherine Dendrinou-Samara, Maria Alexiou, Curtis M. Zaleski, Jeff W. Kampf, Martin L. Kirk, Dimitris P. Kessissoglou,* and Vincent L. Pecoraro**

Metallamacrocyles have been intensively studied over the past decade. These molecules have already been used in applications as diverse as catalysis,[1] sensors,[2] or as chiral building blocks for two- and three-dimensional solids.[3] Metallamacrocyles include complexes such as metallacrowns,[3,4] molecular squares,[1,2] metallacalixarenes,[5] and metallahelicates.[6] Metallacrowns (MC), the inorganic structural and functional analogs to crown ethers, are usually formed with transition-metal ions incorporated into the metallamacrocyclic ring, thus providing the attractive feature that they concentrate a large number of metal ions per unit volume. This large metal-ion concentration may lead to interesting magnetic behavior.[4,7]

Since the recognition of single-molecule magnets (SMMs) in 1993, the field has gained considerable attention as a study of both classical and quantum effects.[8,9] SMMs of cobalt,[10] vanadium,[11] nickel,[12] iron,[13] and a mixed-metal system[14] have been studied. However, the best known and most intensely studied SMMs are the manganese carboxlyate clusters, which range in size from Mn_4 to Mn_{30}.[15] Herein we report the synthesis (Scheme 1) and characterization of the second[16] known Mn_{26} complex $[Mn^{II}_4Mn^{III}_{22}(pdol)_{12}(\mu_3\text{-}CH_3O)_{12}(\mu_3\text{-}O)_{10}(\mu_4\text{-}O)_6(N_3)_6]$ (**1**; $pdol^{2-}$ = dipyridylketone-

[*] Prof. M. L. Kirk
Department of Chemistry, The University of New Mexico
MSC03 2060, 1 University of New Mexico
Albuquerque, NM 87131-0001 (USA)
Fax: (+1) 505-277-2609
E-mail: mkirk@unm.edu

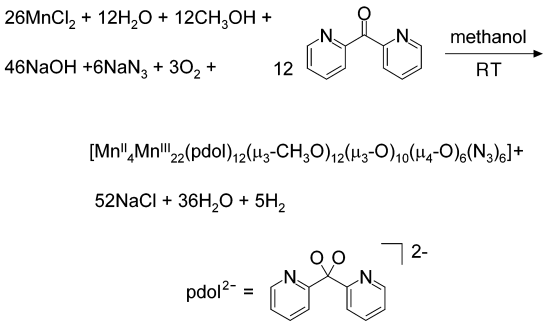
Prof. D. P. Kessissoglou, Dr. C. Dendrinou-Samara, M. Alexiou
Department of General and Inorganic Chemistry
Aristotle University of Thessaloniki
Thessaloniki, 54124 (Greece)
Fax: (+30) 231-099-7738
E-mail: kessisog@chem.auth.gr

Prof. V. L. Pecoraro, C. M. Zaleski, Dr. J. W. Kampf
Department of Chemistry
Willard H. Dow Laboratories, The University of Michigan
Ann Arbor, Michigan 48109–1055 (USA)
Fax: (+1) 734-936-7628
E-mail: vlpec@umich.edu

[**] This work was supported by NSF CHE-0111428 and NIH GM39406 to V.L.P. D.K. wishes to thank WG010 of COST action D21. This work was supported by ACS PRF 38086-AC3 and NIH GM057378-05 to M.L.K. The authors wish to thank the Physics and Astronomy Department at Michigan State University for the use of their Quantum Design dc and ac SQUID magnetometers.

Supporting information for this article is available on the WWW under http://www.angewandte.org or from the author.

 DOI: 10.1002/anie.200351246 © 2003 Wiley-VCH Verlag GmbH & Co. KGaA, Weinheim



Scheme 1.

diolate ion), a highly symmetric metallacryptate that exhibits an imaginary component in the low-temperature ac susceptibility data that is consistent with SMM behavior.[17]

The crystal structure of **1** is shown in Figure 1. A core composed of 16 Mn^{III} ions, 12 methoxide, and 16 oxide groups is surrounded by strands of Mn ions and $pdol^{2-}$ ligands, which

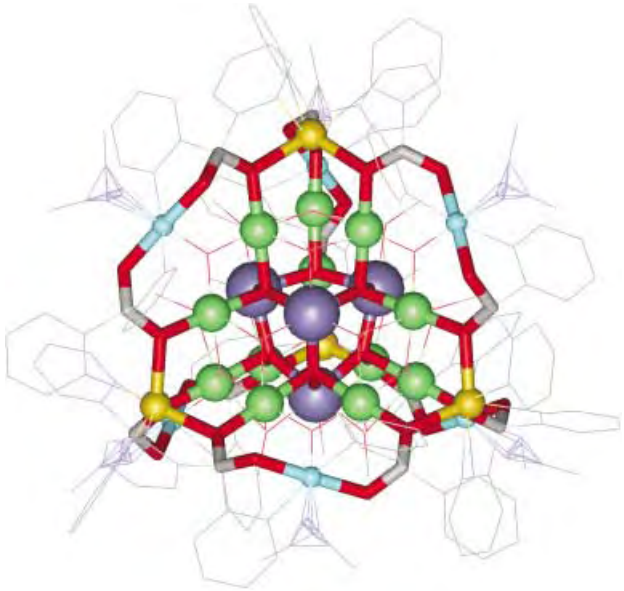


Figure 1. Crystal structure of **1**. The core and ring connectivity have been highlighted with thick tubes; Mn1 (gold spheres); Mn2 (aqua spheres); Mn3 (green spheres); Mn4 (navy blue spheres); C (gray tubes); O (red tubes). Bound azide groups are shown over all disordered positions.

form the metallacryptand (a three-dimensional version of a metallacrown). Figure 2 highlights the connectivity between the strands and the inner core. These strands, with the inner core removed, are shown as stereoviews oriented along the crystallographic twofold and threefold axes (Figure 3). The metallacryptand has an adamantoid structure[18] with four Mn^{II} ions on threefold axes that are bridged by pdol-Mn^{III}-pdol links; thus, **1** is a [4]metallacryptand, in which the $\{Mn_{16}(O^{2-})_{12}(MeO^{-})_{16}\}$ core is encapsulated (Figure 4). While **1** contains 26 metal ions, there are only four crystallographically unique manganese ions (Figure 5).

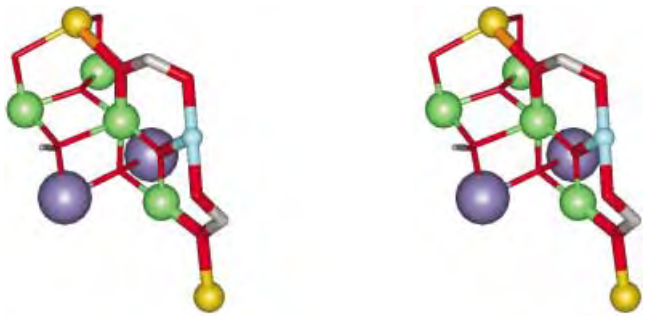


Figure 2. Steroview from the X-ray crystal structure of **1** highlighting the connectivity of strands to the core. The strand and connection points are represented by thick tubes, and the core connectivity is represented by thin tubes. The Mn3 atoms of the core are linked to the strand of the metallacrypate by a $pdol^{2-}$ ligand. Another link to the metallacryptate outer strand occurs through a μ_3-oxide bridge between one Mn2 and two Mn3 centers. Linkages within the core include a μ_3-oxide group that connects three Mn3 centers together and a μ_3-methoxide group that joins two Mn3 centers to one Mn4 center. A μ_4-oxide group links two Mn3 and two Mn4 centers. See Figure 1 for color scheme.

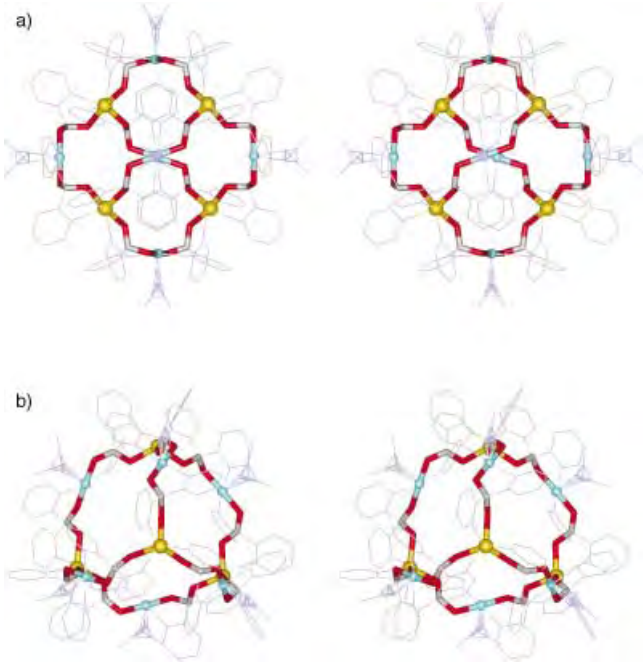


Figure 3. Stereoviews of **1** taken from its X-ray crystal structure, with the inner core removed. a) Along the twofold axis; b) along the threefold axis. See Figure 1 for color scheme.

Mn1, Mn2, and the 12 $pdol^{2-}$ ligands form the metallacryptand. The four seven-coordinate Mn1 centers (on threefold rotational axes) interact with three pyridyl nitrogen atoms (N1), three μ-oxygen atoms from the $pdol^{2-}$ ligand (O1), and a μ_3-oxide oxygen atom (O4) that links the metallacryptand to the core (Figure 5a). This face-capped octahedral polyhedron forms a Λ propeller, which results in a chiral molecule.[19] From the average Mn–N/O bond length of 2.32 Å, it appears that the manganese centers are in the +2 oxidation state. In comparison, seven-coordinate Mn^{III} ions

 © 2003 Wiley-VCH Verlag GmbH & Co. KGaA, Weinheim

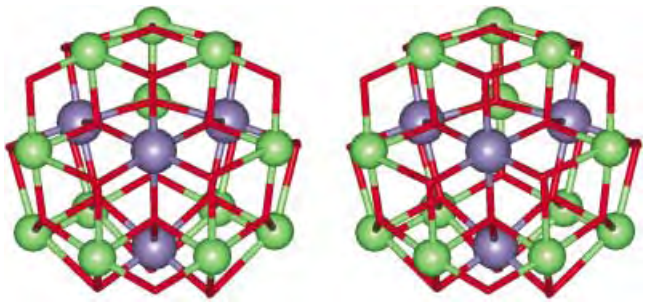


Figure 4. Steroview from the X-ray crystal structure of the core with carbon atoms of methoxide groups removed. See Figure 1 for color scheme.

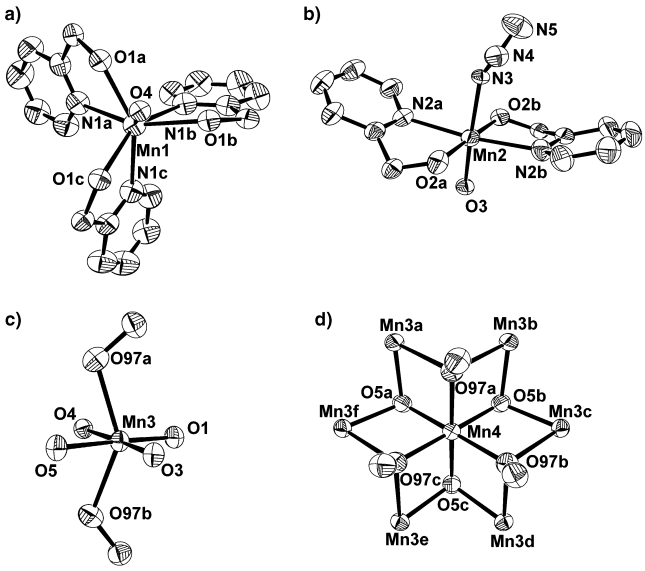


Figure 5. The first coordination sphere of each crystallographically unique manganese center is shown as an ORTEP diagram with thermal ellipsoids at 50% probability. a) Mn1, b) Mn2, c) Mn3, d) Mn4.

have an average separation of 2.13 Å.[18] The six Mn2 centers (on twofold axes) are six-coordinate, through interactions with two pyridyl nitrogen atoms (N2) and two oxygen atoms (O2) from the $pdol^{2-}$ ligand, a nitrogen atom from a disordered azide ligand (N3–N5), and a μ_3 oxygen atom (O3) that is part of the core (Figure 5b). The average bond length between Mn2 centers (2.05 Å) and the Jahn–Teller elongation along the N_{pyr}-Mn2-N_{pyr} axis (Mn2–N_{pyr} = 2.28 Å) support a +3 oxidation state.

The core of **1** also consists of two manganese species. The twelve Mn3 centers are six-coordinate, with one μ-oxygen atom from the $pdol^{2-}$ ligand (O1), two μ_3-oxide (O4 and O3), two μ_3-methoxide (O97), and a μ_4-oxide oxygen atoms (O5; Figure 2, 4, and 5c). The Mn3 ions are in the +3 oxidation state, as suggested by the average manganese separation of 2.05 Å, and the Jahn–Teller elongation along the O_{MeO}-Mn3-O_{MeO} axis (Mn3–O_{MeO} 2.31 Å). The four Mn4 centers (on a threefold axis) have an average manganese-to-ligand bond length of 2.02 Å. They are six-coordinated, with three μ_3-methoxide (O97) and three μ_4-oxide oxygen atoms (O5) (Figure 2, 4, and 5c).

Variable-temperature dc magnetic susceptibility data were collected on a powder sample mulled with eicosane over a 1.8–300 K temperature range at 2500 G under zero-field cooled conditions using a SQUID magnetometer. The effective magnetic moment (μ_{eff}) steadily decreased as the temperature was lowered from 300 K (μ_{eff} = 10.82) to 4.25 K (μ_{eff} = 3.02) indicating an overall antiferromagnetic interaction (Figure S1). Plots of the magnetization curves at 4.25 K and 10 K over the range of 200 G to 55000 G in an eicosane matrix (Figure S2) show no evidence for saturation, which precludes the determination of the ground-state spin.

We collected ac susceptibility data to probe the magnetization relaxation of the sample. Variable-temperature ac SQUID experiments were performed over the temperature range of 1.9–10 K at frequencies of 1–1000 Hz, with zero applied dc magnetic field and a 3.5 G oscillating ac magnetic field. The in-phase susceptibility (χ') begins to decrease and the out-of-phase susceptibility (χ'') begins to increase drastically near 2.5 K at all tested frequencies (Figure 6); this trend continues as the temperature is decreased. In addition, the out-of-phase susceptibility is frequency dependent as the onset temperature is slightly increased at higher frequencies. These observations provide strong evidence that **1** behaves as a single-molecule magnet. Unfortunately, the blocking temperature of the compound could not be determined and studies at lower temperatures are in progress.

In conclusion, we have synthesized a new member of the metallacrown family that structurally resembles a metallacryptate. The high nuclearity of the system coupled with

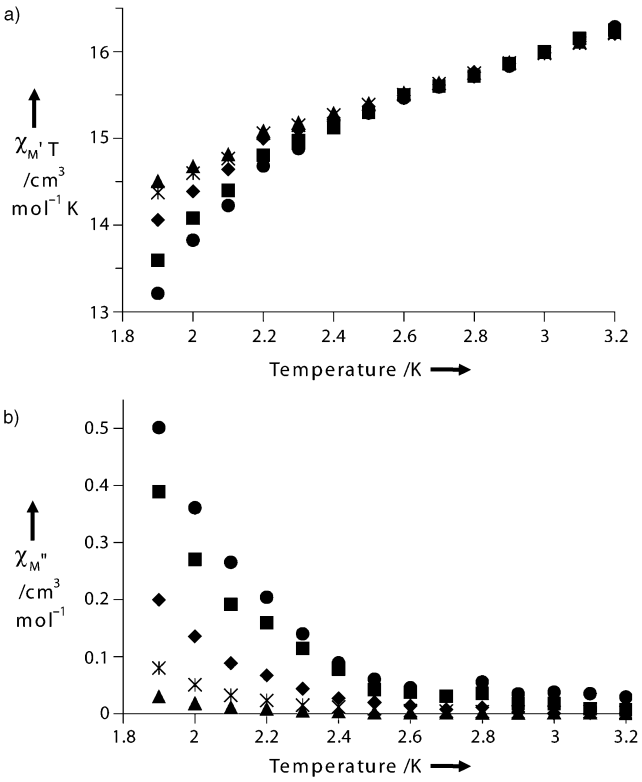


Figure 6. Temperature-dependent ac susceptibility measurements of **1**. a) In-phase susceptibility; b) out-of-phase susceptibility (■ 1 Hz; * 10 Hz; ◆ 100 Hz; ■ 500 Hz; ▲ 1000 Hz).

 © 2003 Wiley-VCH Verlag GmbH & Co. KGaA, Weinheim

significant magnetic exchange interactions between Mn ions results in the observation of single-molecule-magnet behavior. These observations suggest that metallacrown topologies may represent a novel class of molecular magnets.

Experimental Section

Complex **1** was synthesized by adding sodium hydroxide (10 mmol) and di-(2-pyridyl)-ketonoxime ligand (dpk; 10 mmol) to $MnCl_2 \cdot 4H_2O$ (15 mmol) in methanol (40 mL). NaN_3 (10 mmol) dissolved in methanol (10 mL) was then added. The resulting dark red-brown solution was reduced to a volume of 20 mL after stirring for 5 h. After 4 days, red-black octahedral crystals were deposited from the mother liquor.

Received: February 21, 2003
Revised: June 16, 2003 [Z51246]

Keywords: magnetic properties · manganese · metallacycles · metal–metal interactions · single-molecule studies

[1] M. Fujita, J. Y. Kwon, S. Washizu, K. Ogura, *J. Am. Chem. Soc.* **1994**, *116*, 1151 – 1152.
[2] H. Piotrowski, K. Polborn, G. Hilt, K. Severin, *J. Am. Chem. Soc.* **2001**, *123*, 2699 – 2700.
[3] a) J. J. Bodwin, V. L. Pecoraro, *Inorg. Chem.* **2000**, *39*, 3434 – 3435; b) M. Moon, I. Kim, M. S. Lah, *Inorg. Chem.* **2000**, *39*, 2710 – 2711.
[4] a) M. S. Lah, V. L. Pecoraro, *J. Am. Chem. Soc.* **1989**, *111*, 7258 – 7259; b) V. L. Pecoraro, A. J. Stemmler, B. R. Gibney, J. J. Bodwin, H. Wang, J. W. Kampf, A. Barwinski, *Prog. Inorg. Chem.* **1997**, *45*, 83 – 177.
[5] H. Rauter, E. C. Hillgeris, A. Erxleben, B. Lippert, *J. Am. Chem. Soc.* **1994**, *116*, 616 – 624.
[6] J. A. Johnson, J. W. Kampf, V. L. Pecoraro, *Angew. Chem./ Angew. Chem. Int. Ed.*, in press.
[7] A. J. Stemmler, J. W. Kampf, M. L. Kirk, B. H. Atasi, V. L. Pecoraro, *Inorg. Chem.* **1999**, *38*, 2807 – 2817.
[8] a) A. Caneschi, D. Gatteschi, R. Sessoli, *J. Am. Chem. Soc.* **1991**, *113*, 5873 – 5874; b) R. Sessoli, H, Tsai, A. R. Schake, S. Wang, J. B. Vincent, K. Folting, D. Gatteschi, G. Christou, D. N. Hendrickson, *J. Am. Chem. Soc.* **1993**, *115*, 1804 – 1816.
[9] J. R. Friedman, M. P. Sarachik, J. Tejada, R. Ziolo, *Phys. Rev. Lett.* **1996**, *76*, 3830 – 3833.
[10] E. Yang, D. N. Hendrickson, W. Wernsdorfer, M. Nakano, L. N. Zakharov, R. D. Sommer, A. L. Rheingold, M. Ledezma-Gairaud, G. Christou, *J. Appl. Phys.* **2002**, *91*, 7382 – 7384.
[11] Z. Sun, C. M. Grant, S. L. Castro, D. N. Hendrickson, G. Christou, *Chem. Commun.* **1998**, *6*, 721 – 722.
[12] H. Andres, R. Basler, A. J. Blake, C. Cadiou, G. Chaboussant, C. M. Grant, H. Gudel, M. Murrie, S. Parsons, C. Paulsen, F. Semadini, V. Villar, W. Wernsdorfer, R. E. P. Winpenny, *Chem. Eur. J.* **2002**, *8*, 4867 – 4876.
[13] A. L. Barra, P. Debrunner, D. Gatteschi, C. E. Schultz, R. Sessoli, *Europhys. Lett.* **1996**, *35*, 133 – 138.
[14] J. J. Sokol, A. G. Hee, J. R. Long, *J. Am. Chem. Soc.* **2002**, *124*, 7656 – 7657.
[15] a) G. Christou, D. Gatteschi, D. N. Hendrickson, R. Sessoli, *MRS Bull.* **2000**, *25*, 66 – 71; b) M. Soler, E. Rumberger, K. Folting, D. N. Hendrickson, G. Christou, *Polyhedron* **2001**, *20*, 1365 – 1369; c) C. Boskovic, W. Wernsdorfer, K. Folting, J. C. Huffman, D. N. Hendrickson, G. Christou, *Inorg. Chem.* **2002**, *41*, 5107 – 5118; d) D. Gatteschi, R. Sessoli, *Angew. Chem.* **2003**, *115*, 278 – 309; *Angew. Chem. Int. Ed.* **2003**, *42*, 268 – 297.
[16] L. F. Jones, E. K. Brechin, D. Collison, A. Harrison, S. J. Teat, W. Wernsdorfer, *Chem. Commun.* **2002**, *23*, 2974 – 2975.
[17] Crystals of **1** have been structurally characterized with the formula $Mn_{26}O_{16}(pdol)_{12}(N_3)_6(CH_3O)_{12}$. Elemental analysis (%) calcd for $C_{144}H_{132}N_{42}O_{52}Mn_{26}$: C 36.68, H 2.80, N 12.48; found: C 36.20, H 3.00, N 12.10; yield 20%. Crystal data for **1**: $M_W = 4711.36$, cubic, space group $Fd\bar{3}$ (no. 203), $a = 34.6619(13)$, $b = 34.6619(13)$, $c = 34.6619(13)$ Å, $V = 41644(3)$ Å^3, $Z = 8$, $\rho_{calcd} = 1.503$ mg m^{-3}, $2.88° < \theta < 28.30°$, crystal dimensions $0.34 \times 0.34 \times 0.34$ mm, $\mu = 1.590$ mm^{-1}, $T = 150(2)$ K; 4343 unique of 110229 reflections collected. 4343 reflections and 228 parameters were used for the full-matrix, least-squares refinement on F^2, $R1 = 0.0479$ ($I > 2\sigma(I)$), $R1 = 0.0709$ (all data); $wR2 = 0.1310$ ($I > 2\sigma(I)$), $wR2 = 0.1697$ (all data). Further details are given in the Supporting Information. CCDC-201416 (**1**) contains the supplementary crystallographic data for this paper. These data can be obtained free of charge via www.ccdc.cam.ac.uk/conts/retrieving.html (or from the Cambridge Crystallographic Data Centre, 12, Union Road, Cambridge CB2 1EZ, UK; fax: (+44) 1223-336-033; or deposit@ccdc.cam.ac.uk).
[18] R. W. Saalfrank, A. Stark, K. Peters, H. G. von Schnering, *Angew. Chem.* **1988**, *100*, 878 – 880; *Angew. Chem. Int. Ed. Engl.* **1988**, *27*, 851 – 853.
[19] The compound spontaneously resolves in each crystal; however, the bulk solid is racemic.
[20] S. Gupta, S. Pal, *Inorg. Chem.* **2002**, *41*, 4843 – 4845.

 © 2003 Wiley-VCH Verlag GmbH & Co. KGaA, Weinheim

Single-Molecule Covalent Chemistry

Single-Molecule Covalent Chemistry with Spatially Separated Reactants**

Tudor Luchian, Seong-Ho Shin, and Hagan Bayley**

The investigation of covalent chemistry at the single-molecule level offers several advantages including the ability to observe short-lived intermediates and the means to untangle complex reaction pathways. The available techniques of single-molecule detection have been brought to bear on single-molecule

[*] T. Luchian,[+] H. Bayley, S.-H. Shin[+]
Department of Medical Biochemistry & Genetics
The Texas A&M University System Health Science Center
440 Reynolds Medical Building, TAMU 1114
College Station, TX 77843-1114 (USA)
Fax: (+1) 979-847-9481
E-mail: tluchian@medicine.tamu.edu
bayley@tamu.edu

H. Bayley, S.-H. Shin[+]
Department of Chemistry
Texas A&M University
College Station, TX 77843 (USA)

[+] These authors contributed equally to this work.

[**] This work was supported by the Office of Naval Research, the U.S. Department of Energy, the Multidisciplinary University Research Initiative (ONR-1999), and the National Institutes of Health. We thank Sean Conlan for help with molecular modeling.

 © 2003 Wiley-VCH Verlag GmbH & Co. KGaA, Weinheim DOI: 10.1002/anie.200351313

chemistry. For example, the forces required to break individual covalent bonds between polymers and surfaces have been determined,[1] and optical methods have been used to investigate single turnovers of enzymes and ribozymes by using fluorescent substrates and probes.[2–5] Herein, we report the use of electrical measurements to observe the covalent chemistry of small untagged molecules inside a protein pore, which acts as a nanoreactor. Multiple turnovers were achieved through separating two reactants by the membrane containing the pore and allowing them to diffuse into the reaction zone. We demonstrate the utility of the approach by measuring the rate constant for breakdown of the short-lived intermediate ($RSSCH_2CH(OH)CH(OH)CH_2SH$, $k = 250\ s^{-1}$ as the thiolate) that is generated during disulfide reduction with dithiothreitol, a reagent commonly used in protein chemistry. Our approach is applicable to much of the covalent chemistry that occurs in aqueous solution. Further, it permits the development of sensors[6] for reactive molecules: for example, those found in chemical weapons, pesticides, and various pharmaceuticals and foodstuffs.

Force measurements and optical techniques are not well adapted for examining the covalent chemistry of individual unmodified small molecules. Scanning probe techniques can be applied to molecules lying on surfaces,[7] but not to molecules in solution. An alternative approach is to use electrical measurements to observe the chemistry of molecules tethered inside or near the mouth of a protein pore. The ionic current that is carried by the pore in an applied potential is highly sensitive to the size, shape, and polarity of the reactants. Hence, molecular rearrangements and bond cleavage can be monitored. The approach works with molecules of a few hundred daltons, does not require a tag (such as a fluorescent probe) or very low reagent concentrations, and has a time resolution of a few tens of microseconds under optimal conditions. The potential of the technique was recognized by Finkelstein and co-workers, who measured the rates of single-step modifications of cysteine residues in diphtheria toxin channels by observing multiple individual reactions.[8] We recently used the approach to investigate more complex chemistry. Two short-lived intermediates, a nitronate and a carbamate, were observed after the photolysis of an amine protected with a 4,5-dimethoxy-2-nitrobenzyloxycarbonyl group tethered inside the α-hemolysin (αHL) pore.[9] However, to obtain data of useful statistical significance, it was essential to perform many individual experiments. Multiple events in a single experiment were observed by Woolley and Jaikaran, who examined the reversible thermal isomerization of a carbamate group attached at the mouth of a gramicidin channel.[10] More recently, we observed reversible covalent-bond formation and cleavage between a single cysteine residue on the wall of an engineered αHL pore and an organoarsenic(III) compound in solution.[11] We now show that the versatility of this single-molecule approach can be enhanced by bringing about multiple turnovers of what, in solution, would be a rapid irreversible reaction. This is achieved by separating two reactants by the membrane containing the nanoreactor.

We measured the kinetics of the reaction of a cysteine residue on the lumenal wall of the αHL pore with 5,5′-dithiobis(2-nitrobenzoic acid) (DTNB, Ellman's reagent) to form a disulfide bond, and cleavage of that bond with dithiothreitol (DTT, threo-1,4-dimercapto-2,3-butandiol) to regenerate the cysteine residue. The short-lived intermediate in the DTT cleavage reaction, which is invisible to optical spectroscopy, was observed for the first time and the dependence of its lifetime on pH was measured. We used a heteroheptameric αHL pore, P_{SH}, in which one of the seven subunits contains a cysteine residue at position 117 and the other six are cysteine-free (Figure 1a).[11] Cys 117 in the lumen of the pore reacts with DTNB in a bimolecular reaction (step 1) with rate constant k_{1-obs} to form a mixed disulfide **1**, in which the sulfur atom proximal to the protein wall is activated towards attack by free thiolate groups because the aromatic thiolate is a good leaving group (Figure 1b). Disulfide **1** reacts with DTT in a bimolecular reaction (step 2) with rate constant k_{2-obs} to form the unstable disulfide **2**, which breaks down in a unimolecular reaction (step 3) in which P_{SH} is regenerated with rate constant k_{3-obs} (Figure 1b). In this way, P_{SH} is able to undergo multiple reaction cycles. In the first configuration we tested, DTNB was present in the *trans* chamber and DTT in the *cis* chamber. In single-channel recordings, three separate current levels representing P_{SH}, **1**, and **2** were observed as predicted (Figure 1c). Intermediate **2** was assigned the structure depicted because thiols other than DTT react with **1** to form intermediates or relatively stable molecules that are distinguished by distinct current levels, and also because the breakdown of **2** has the characteristics of a unimolecular reaction with the anticipated pH-dependence (see below).

The rate of reaction of DTNB with the cysteine residue of P_{SH} was measured in the DTNB(*trans*)/DTT(*cis*) configuration. Assuming that DTT(*cis*) reverses, but does not alter the rate of reaction of P_{SH} with DTNB (see below), the rate constant can be determined by analyzing the single-channel current trace. By using $k_{1-obs} = 1/(\tau_1[DTNB])$, where τ_1 is the lifetime of P_{SH} (Figure 2a), we calculated $k_{1-obs} = 4.9 \pm 0.5 \times 10^3\ M^{-1}s^{-1}$ (based on five independent experiments) in 2 M KCl, 30 mM 3-(4-morpholinyl)-1-propanesulfonic acid (MOPS), 100 μM ethylenediaminetetraacetic acid (EDTA), pH 8.5, at an applied potential of −50 mV, with 50 μM DTT(*cis*). The analysis assumes that the effective concentration of DTNB in the β barrel is the same as the concentration in the *trans* chamber. The analysis also assumes that although DTT(*cis*) can reverse the reaction with DTNB(*trans*) leading to multiple turnovers, it does not compete with the internal thiol (Cys 117) by reacting with DTNB in the barrel.[12] This lack of an effect of low concentrations of DTT(*cis*) on the rate of reaction with DTNB(*trans*) was demonstrated experimentally (Figure 2b).[13] Because the rate of reaction of **1** with DTT might have been affected by a reduced rate of diffusion of DTT(*cis*) through the central constriction of the pore (Figure 1a), we used the configuration DTNB(*cis*)/DTT(trans) to determine k_{2-obs}. By using $k_{2-obs} = 1/(\tau_2[DTT])$, we found $k_{2-obs} = 1.1 \pm 0.1 \times 10^4\ M^{-1}s^{-1}$ in 2 M KCl, 30 mM MOPS, 100 μM EDTA, pH 8.5, at an applied potential of −50 mV, in the presence of 50 μM DTNB(*cis*) (Figure 2c). As required, we demonstrated that low concentrations of DTNB(*cis*) do not affect the value of k_{2-obs} (Figure 2d).

 © 2003 Wiley-VCH Verlag GmbH & Co. KGaA, Weinheim

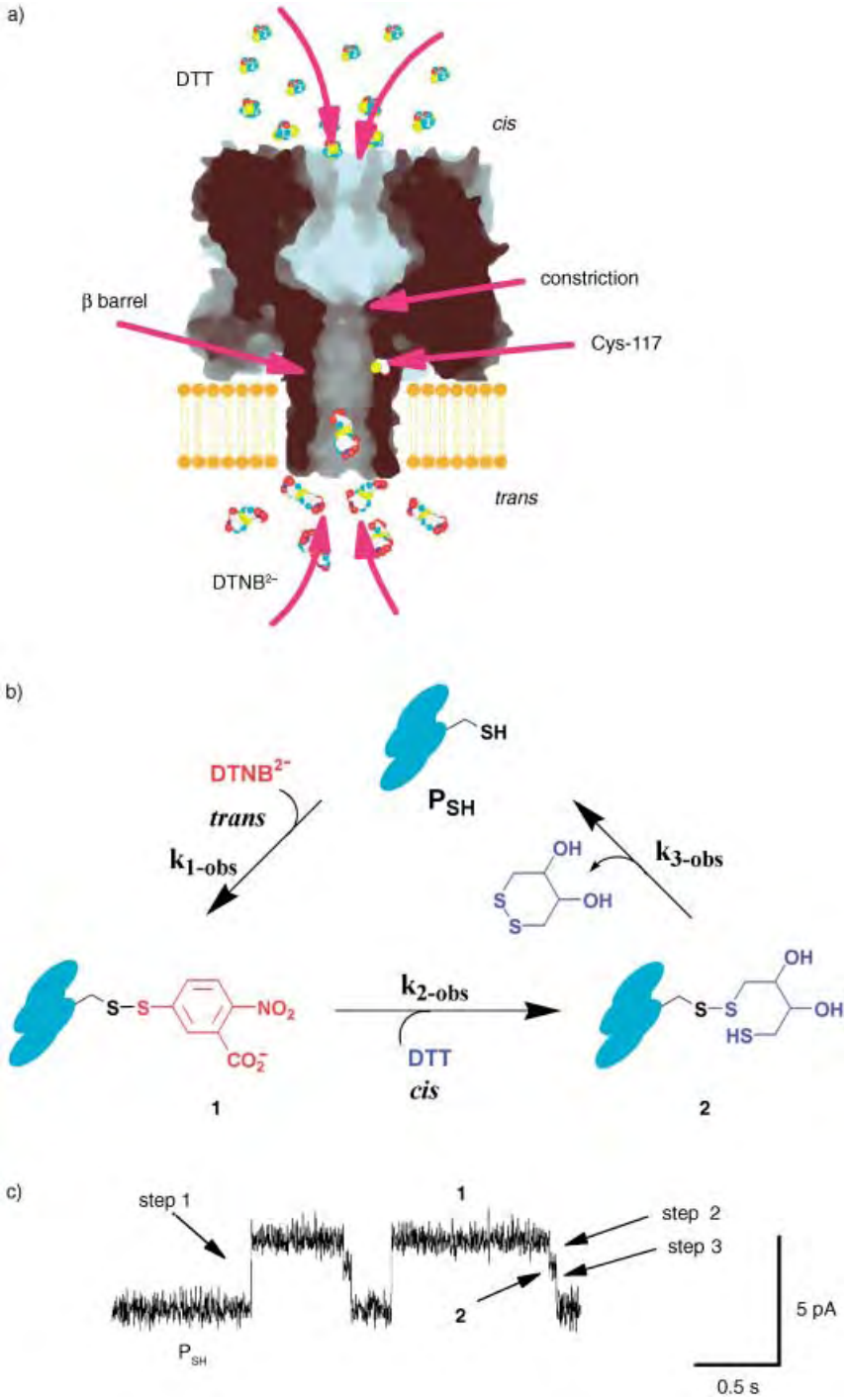


Figure 1. Single-molecule chemistry with spatially separated reactants. a) The orientation of the αHL pore (P_{SH}) and disposition of the reactants with respect to the bilayer are shown. The position of Cys 117 in the β barrel is indicated; this residue is present in one of the seven subunits of the P_{SH} heteromer. Small molecules are drawn to scale. The *cis* chamber of the bilayer apparatus was at zero potential. All experiments were conducted at an applied potential of −50 mV (*trans*) and positive current represents the flow of positive charge from *trans* to *cis*. The orientation of the pore was the same in all the experiments described here, while the *cis* or *trans* disposition of the reactants was varied. b) Details of the chemical cycle. Cys 117 reacts with DTNB in a bimolecular reaction, with rate constant k_{1-obs}, to form the mixed disulfide **1**. Disulfide **1** then reacts with DTT in a second bimolecular reaction (rate constant k_{2-obs}) to form the unstable disulfide **2**, which breaks down in a unimolecular reaction (rate constant k_{3-obs}) in which P_{SH} is regenerated. D,L-DTT was used throughout this work. c) Single-channel current recording. Two successive chemical cycles are shown; the levels representing P_{SH}, **1**, and **2** are indicated. See text for reaction conditions.

The breakdown of the unstable mixed disulfide **2** is a unimolecular reaction and therefore $k_{3-obs} = 1/\tau_3$, where τ_3 is the lifetime of the intermediate determined from current recordings.[14] By using the DTNB(*trans*)/DTT(*cis*) configuration, we found that $k_{3-obs} = 23 \pm 1\ s^{-1}$ (six experiments) in 2 M KCl, 30 mM MOPS, 100 μM EDTA, pH 8.5, at an applied potential of −50 mV. Because the reaction is unimolecular, k_3 should be independent of the concentrations of DTT and DTNB, and whether or not they are applied from the *trans* or *cis* sides of the bilayer; this was found to be the case (e.g., Figure 3a).

Intermediates with structures similar to **2** have not been observed directly in the reactions of disulfides with DTT. We examined the lifetime of the intermediate at various pH values and thereby derived k_{3-obs} as a function of pH value (Figure 3b). The data could be fitted (Figure 3b) to the equation: $k_{3-obs} = (k_3 K_a)/(K_a + [H^+])$. This result suggests that, as expected, the reactive form of **2** is the thiolate. The data yield a pK_a value of 9.5 ± 0.2 and $k_3 = 250 \pm 80\ s^{-1}$ in the deprotonated form. By comparison, the first pK_a value of DTT is 9.2, while that of mercaptoethanol is 9.5.[15]

Relatively little covalent chemistry of small molecules has been examined at the single-molecule level. The use of engineered protein pores to provide a nanoreactor for this purpose is a promising approach. Here, we have advanced previous efforts by using a system in which two reactants are separated by the lipid bilayer containing the engineered pore. In this way, multiple turnovers can be observed for a reaction that would be "short-circuited" in bulk solution by direct reaction of the two components. Vectorial chemistry in bilayer systems has been observed previously, and can be traced back to the ideas of Mitchell.[16,17] Despite this and related work, we know of no previous examples of single-molecule covalent chemistry utilizing spatially separated reactants.

The rates of reaction of a wide variety of thiols with DTNB have been investigated in solution.[15,18] The reactive species in both the initial reaction and the subsequent reaction of the intermediate mixed disulfide (equivalent to k_1 and k_2 in our case) are thiolates. Therefore, the observed rates

 © 2003 Wiley-VCH Verlag GmbH & Co. KGaA, Weinheim

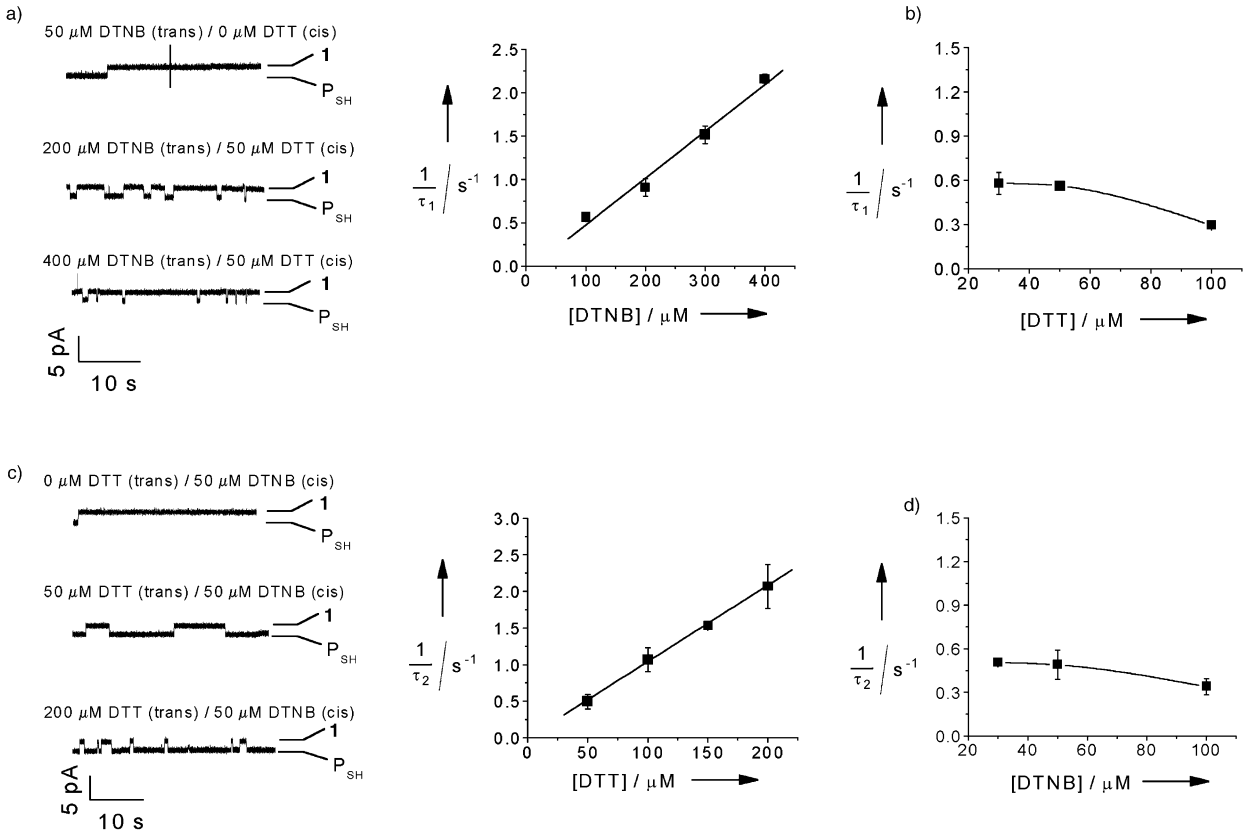


Figure 2. Bimolecular reactions within the P_{SH} pore. a) Dependence of $1/\tau_1$ on $[DTNB]_{trans}$, where τ_1 is the interval between step 3 and step 1, that is, the interval before the reaction of P_{SH} with DTNB. k_{1-obs} was obtained from the slope of the straight-line fit. The conditions were 2 M KCl, 30 mM MOPS, 100 μM EDTA, pH 8.5, at −50 mV, with 50 μM DTT(*cis*). Typical traces are shown on the left. The current level corresponding to the single unmodified pore (P_{SH}) was -82.2 ± 2.1 pA. b) Low concentrations of DTT(*cis*) do not affect $1/\tau_1$ for the reaction of P_{SH} with DTNB(*trans*). The conditions were as in a) with $[DTNB]_{trans} = 100$ μM. c) Dependence of $1/\tau_2$ on $[DTT]_{trans}$, where τ_2 is the interval between step 1 and step 2, that is, the interval before the reaction of **1** with DTT. k_{2-obs} was obtained from the slope of the straight-line fit. The conditions were 2 M KCl, 30 mM MOPS, 100 μM EDTA, pH 8.5, at −50 mV, with 50 μM DTNB(*cis*). Typical traces are shown on the left. d) Low concentrations of DTNB(*cis*) do not affect $1/\tau_2$ for the reaction of **1** with DTT(*trans*). The conditions were as in c) with $[DTT]_{trans} = 50$ μM.

depend on pH value according to the relationship $k_{obs} = (k K_a)/(K_a + [H^+])$, where k is the bimolecular rate constant for attack of the thiolate on the disulfide. For reactions with DTNB, values of k_1 are correlated with the pK_a values of the thiols with a Brønsted coefficient, β_{nuc}, of ≈ 0.5, which means that the thiolates formed from thiols with higher pK_a values are more reactive.[15,18] According to these studies, the value of k_{1-obs} for an unperturbed cysteine residue in a peptide ($pK_a = 8.7$ for glutathione)[19] should be $k_{1-obs} \approx 4 \times 10^4\,M^{-1}s^{-1}$ at pH 8.5 (calculated from $k_1 = 10^5\,M^{-1}s^{-1}$).[15,18,20] The value we obtain is about ten times lower. DTNB carries a charge of $z = -2$; it is expected to be driven into the pore at −50 mV and react more rapidly than it does in bulk solution. Therefore, the observed rate probably reflects several small perturbations of the kinetics, which will require additional work to resolve. For example, steric hindrance near the protein surface may occur, or Cys 117 may have a higher than expected pK_a value (although the residue has no charged neighbors). The dependence of k_2 on the structure of the thiol has been less thoroughly investigated. Nevertheless, it is clear that the values of k_2 are lower than those for k_1 and in the range $k_2 = 10^4\,M^{-1}s^{-1}$.[15,18] Therefore, in our case, we predict $k_{2-obs} \approx 1.7 \times 10^3\,M^{-1}s^{-1}$, by using $k_{2-obs} = (k_2 K_a)/(K_a + [H^+])$, $pK_a = 9.2$ (for DTT) and pH 8.5. The observed value of $1.1 \times 10^4\,M^{-1}s^{-1}$ is about six times higher.

No kinetic constants for a reaction related to step 3 (k_3) are available from the literature, although the reaction is clearly fast.[15] According to our data, the rate of breakdown of the deprotonated intermediate is $250\,s^{-1}$. By comparison, the bimolecular rate constant for the reaction of the thiolate of 2-mercaptoethanol with oxidized glutathione is $57\,M^{-1}s^{-1}$.[19] Therefore the effective concentration of the thiolate in **2** is about 4 M. These findings demonstrate how short-lived intermediates that would be invisible kinetically in an ensemble experiment can be characterized by using single-molecule chemistry.

The present approach rivals other advanced single-molecule methodologies.[5] For example, high reagent concentrations are tolerated and a bulky fluorophore is not required. We believe the approach can be expanded to examine much of the varied chemistry that occurs in aqueous solutions.[21,22] From one point of view, we might mimic, as closely as possible, reaction conditions in solution. Our results indicate that the environment inside the β barrel of the αHL

 © 2003 Wiley-VCH Verlag GmbH & Co. KGaA, Weinheim

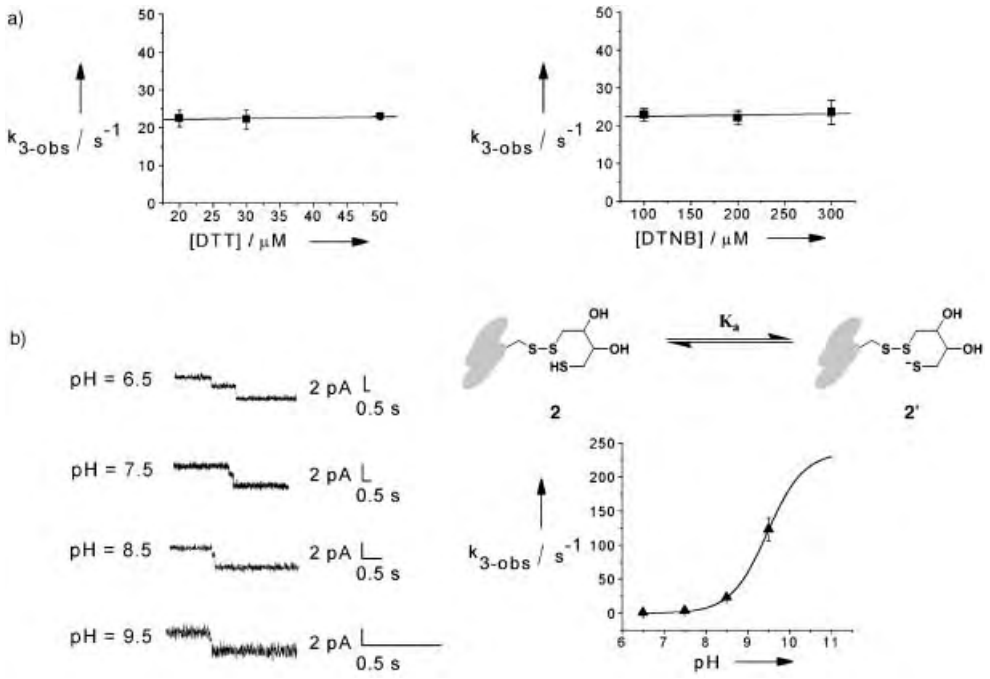


Figure 3. Rate of breakdown of the intermediate **2**. a) The lifetime of **2** is independent of the concentrations of the reactants DTT and DTNB. Left: k_{3-obs} as a function of $[DTT]_{cis}$. The conditions were as described in the legend of Figure 2 with $[DTNB]_{trans} = 50\ \mu M$; right: k_{3-obs} as a function of $[DTNB]_{trans}$. The conditions were as described in the legend of Figure 2 with $[DTT]_{cis} = 50\ \mu M$. b) pH-Dependence of the rate of breakdown of the intermediate **2**. Left: typical current traces at different pH values. The conditions were as before with $[DTNB]_{trans} = 50\ \mu M$ and $[DTT]_{cis} = 50\ \mu M$; right: k_{3-obs} as a function of pH value. The data were fitted to $k_{3-obs} = (k_3 K_a)/(K_a + [H^+])$.

pore at least approximates the conditions in solution. More might be done in this regard by replacing charged and hydrophobic side chains in the barrel with uncharged hydrophilic side chains such as Ser, Thr, Asn, and Gln. Surface charge effects can also be minimized by working at high salt concentrations, as we have done here. Greater attention might be paid to the applied potential, which can attract or repel charged and uncharged substrates, the latter through electro-osmotic flow.[23] From a second viewpoint, the approach can be used to study the effect of the protein environment on chemistry. In this case, residues that bind substrates or take part in the chemistry can be introduced onto the wall of the β barrel by mutagenesis, targeted chemical modification, or non-natural amino acid substitution. Catalysis in a synthetic barrel lined with histidine residues has been achieved by Matile and co-workers.[24,25] With the precise and diverse substitutions made feasible by protein engineering, it may be possible to improve turnover and even couple catalysis to transmembrane transport.

As with most other single-molecule techniques, a potential weakness of the approach described here is the inability to assign structures to intermediates by using spectroscopy. It would be dangerous to attribute the subtle changes in pore conductance to specific alterations in structure, such as the loss of a bulky group, and we have avoided doing so. Until now, our studies have involved chemistry where there is little doubt about the general reaction pathway. However, if unknown chemistry is to be investigated, it will be necessary to resort to non-spectroscopic approaches, well known in mechanistic organic chemistry to clarify the nature of reaction intermediates. They include the generation of intermediates by alternative routes, the trapping or diversion of intermediates,[14] the dependence of the lifetimes of intermediates on pH value (Figure 3b), the effects of temperature on reaction kinetics,[10,26] the use of isotope effects, and the investigation of substituents, for example, through linear free-energy relationships. In many cases, it may be necessary to supplement single-molecule studies with ensemble measurements. Indeed, the two approaches can be seen as complementary.

Experimental Section

P_{SH} is a heteromeric αHL pore, $(RL2)_6(T117C\text{-}D8)_1$, containing a single cysteine residue at position 117 of one of the seven subunits. P_{SH} was prepared as described,[11] except for the buffer that was used to elute the protein after preparative SDS-polyacrylamide gel electrophoresis, which was changed to 10 mM tris(hydroxymethyl)-aminoethane hydrochloride (Tris·HCl), 5 mM DTT, 1 mM EDTA, pH 7.5. The high concentration of DTT ensured that Cys117 in P_{SH} remained reduced during storage.

Single-channel recordings were carried out in a planar bilayer apparatus as previously described.[11] Both chambers contained 2 M KCl, 30 mM MOPS, 100 μM EDTA, titrated to pH 8.5 with aqueous KOH. For experiments at pH 9.5, MOPS was replaced by 3-(cyclohexylamino)-1-propanesulfonic acid (CAPS). A single pore was allowed to insert into the bilayer after the addition of a dilute solution of the P_{SH} to the *cis* chamber to give a final concentration of ≈0.5 ng protein per mL. The DTT from the storage buffer was diluted more than 10000 times in the chamber. The electrical current was filtered with a low-pass Bessel filter (80 dB/decade) with a corner frequency of 1 kHz and then digitized with a DigiData 1320 A/D converter (Axon Instruments) at a sampling frequency of 5 kHz. Data

 © 2003 Wiley-VCH Verlag GmbH & Co. KGaA, Weinheim

samples were stored on the hard disk of a computer. For further analysis and display, current traces were filtered digitally at 100 Hz. When fast transitions were observed (e.g., step 3 at high pH values), the filter was set at 5 kHz and the sampling frequency to 10 kHz. Event data files used to determine reaction rates were constructed by manual inspection of the experimental traces with Clampfit 9.0 software (Axon Instruments). The mean lifetime (τ_1, τ_2, τ_3) of each species (P_{SH}, **1**, or **2**) was used to calculate rate constants (k_1, k_2, k_3) as described in the text. At least 40 events were used to calculate each lifetime under each set of conditions. With the exception of some events used to determine k_3, single-channel recordings were used exclusively. Because k_3 is the rate constant of a unimolecular reaction, events observed in membranes containing two or three channels could be added to the data. The processed data were plotted using Origin 7.0 (Microcal Software). Individual values are presented as the mean ± standard deviation.

Preweighed samples of solid D,L-DTT (Gold Biotechnology) were prepared and stored at −20 °C. At the time of the experiment, buffer was added to the tube to generate a stock of 1 M DTT, which was kept on ice. Fresh stock solutions of DTT were prepared every two hours. DTNB (Aldrich) was dissolved in 200 mM sodium phosphate, pH 8.5, at 100 mM. Fresh DTNB stocks were made daily as it decomposes in basic solution.

Received: March 3, 2003
Revised: June 12, 2003 [Z51313]

Keywords: kinetics · nanoreactors · protein pores · single-molecule studies · thiols

[1] M. Grandbois, M. Beyer, M. Rief, H. Clausen-Schaumann, H. E. Gaub, *Science* **1999**, *283*, 1727 – 1730.
[2] A. Ishijima, H. Kojima, T. Funatsu, M. Tokunaga, H. Higuchi, H. Tanaka, T. Yanagida, *Cell* **1998**, *92*, 161 – 171.
[3] H. P. Lu, L. Xun, X. S. Xie, *Science* **1998**, *282*, 1877 – 1882.
[4] X. Zhuang, H. Kim, M. J. B. Pereira, H. P. Babcock, N. G. Walter, S. Chu, *Science* **2002**, *296*, 1473 – 1476.
[5] M. J. Levene, J. Korlach, S. W. Turner, M. Foquet, H. G. Craighead, W. W. Webb, *Science* **2003**, *299*, 682 – 686.
[6] H. Bayley, P. S. Cremer, *Nature* **2001**, *413*, 226 – 230.
[7] D. C. Jacobs, *Nature* **2003**, *423*, 488 – 489.
[8] J. A. Mindell, H. Zhan, P. D. Huynh, R. J. Collier, A. Finkelstein, *Proc. Natl. Acad. Sci. USA* **1994**, *91*, 5272 – 5276.
[9] T. Luchian, S.-H. Shin, H. Bayley, *Angew. Chem.* **2003**, *115*, 1970 – 1973; *Angew. Chem. Int. Ed.* **2003**, *42*, 1926 – 1929.
[10] D. C. J. Jaikaran, G. A. Woolley, *J. Phys. Chem.* **1995**, *99*, 13352 – 13355.
[11] S.-H. Shin, T. Luchian, S. Cheley, O. Braha, H. Bayley, *Angew. Chem.* **2002**, *114*, 3859 – 3861; *Angew. Chem. Int. Ed.* **2002**, *41*, 3707 – 3709.
[12] This is reasonable because the effective concentration of the thiol provided by Cys117 in the barrel (volume ≈14000 Å^3, as determined with the program HOLE)[27] is ≈0.12 M. In single-molecule terms, the probability of DTT being in the barrel, at a time when DTNB is also in the barrel, is $p \approx 3.6 \times 10^{-4}$ ($p \approx V_{barrel}/V_{DTT}$; where V_{barrel} is the volume inside the barrel and V_{DTT} is the volume of solution occupied by one DTT molecule, based on the external concentration).
[13] At high concentrations of DTT(*cis*), the reduction in rate most likely arises from depletion of DTNB(*trans*) by reaction with DTT that has reached the *trans* unstirred layer.
[14] To check whether the intermediate **2** was indeed formed from DTT, we carried out several controls. For example, in the absence of DTT, the reaction proceeded through the first step, but remained there indefinitely (> 60 s; Figure 2a, upper trace). Further, when DTT was replaced with 50 μM β-mercaptoethanol (βME, *cis*), a monothiol, the reaction took a different course. The first step with DTNB (50 μM, *trans*) was observed as before, but it was followed by a step to a level where the system remained for a prolonged period (> 60 s), which was distinct from the level representing **2**. We interpret the sequence as cleavage of **1** with βME to generate a mixed disulfide that reacts relatively slowly with a second molecule of βME.
[15] G. M. Whitesides, J. E. Lilburn, R. P. Szajewski, *J. Org. Chem.* **1977**, *42*, 332 – 338.
[16] P. Mitchell, *Nature* **1961**, *191*, 144 – 148.
[17] For example, an asymmetrically oriented "molecular triad" was used to transport Ca^{2+} ions across a lipid bilayer.[28] Intramolecular electron transfer was produced by excitation of the triad with visible light. A hydroquinone carrier in the bilayer was reduced on one side of the membrane, where Ca^{2+} ions are picked up, and oxidized on the other side, where they are released.
[18] J. M. Wilson, R. J. Bayer, D. J. Hupe, *J. Am. Chem. Soc.* **1977**, *99*, 7922 – 7926.
[19] R. P. Szajewksi, G. M. Whitesides, *J. Am. Chem. Soc.* **1980**, *102*, 2011 – 2026.
[20] J.-H. Ha, S. N. Loh, *Nat. Struct. Biol.* **1998**, *5*, 730 – 737.
[21] U. Lindström, *Chem. Rev.* **2002**, *102*, 2751 – 2772.
[22] S. J. Rowan, S. J. Cantrill, G. R. L. Cousins, J. K. M. Sanders, J. F. Stoddart, *Angew. Chem.* **2002**, *114*, 938 – 993; *Angew. Chem. Int. Ed.* **2002**, *41*, 898 – 952; Erratum: S. J. Rowan, S. J. Cantrill, G. R. L. Cousins, J. K. M. Sanders, J. F. Stoddart, *Angew. Chem.* **2002**, *114*, 1528; *Angew. Chem. Int. Ed.* **2002**, *41*, 1460.
[23] L.-Q. Gu, S. Cheley, H. Bayley, *J. Gen. Physiol.* **2001**, *118*, 481 – 494.
[24] B. Baumeister, N. Sakai, S. Matile, *Org. Lett.* **2001**, *3*, 4229 – 4232.
[25] B. Baumeister, S. Matile, *Macromolecules* **2002**, *35*, 1549 – 1555.
[26] S. Howorka, L. Movileanu, O. Braha, H. Bayley, *Proc. Natl. Acad. Sci. USA* **2001**, *98*, 12996 – 13001.
[27] O. S. Smart, J. G. Neduvelil, X. Wang, B. A. Wallace, M. S. P. Sansom, *J. Mol. Graphics* **1996**, *14*, 354 – 360.
[28] I. M. Bennett, H. M. V. Farfano, F. Bogani, A. Primak, P. A. Liddell, L. Otero, L. Sereno, J. J. Silber, A. L. Moore, T. A. Moore, D. Gust, *Nature* **2002**, *420*, 398 – 401.

 © 2003 Wiley-VCH Verlag GmbH & Co. KGaA, Weinheim

Structure-Based Drug Discovery

From Model Complexes to Metalloprotein Inhibition: A Synergistic Approach to Structure-Based Drug Discovery**

David T. Puerta, Julie R. Schames, Richard H. Henchman, J. Andrew McCammon, and Seth M. Cohen**

Matrix metalloproteinases (MMPs) are zinc-containing hydrolytic enzymes that are involved in the restructuring of connective tissue. The design of effective inhibitors of matrix metalloproteinases is a significant goal in chemotherapeutic development as a result of the correlation of MMP activity with a variety of illnesses, including cancer, arthritis, and inflammatory disease.[1–3] However, the design of inhibitors for MMPs and other metalloproteins is limited by the ability to predict the interaction of a given inhibitor with the metal ion at the active site. In most cases, the elucidation of a protein structure with the bound inhibitor, by using X-ray diffraction or NMR spectroscopy, is necessary for revealing the metal–inhibitor interactions.[4] Innovative approaches to increasing the efficiency and speed of the drug-discovery process may provide attractive, alternative routes to identifying new drug candidates. For example, the determination of a structure–activity relationship (SAR) by NMR[5] spectroscopy has been used to reveal probable binding modes of metal-ion chelators to facilitate the development of improved MMP inhibitors.[6,7] Despite being a very effective approach, the determination of SARs by NMR spectroscopy still requires substantial amounts of ^{15}N-labeled metalloprotein and is likely to be limited to metalloenzymes that contain diamagnetic metal ions.

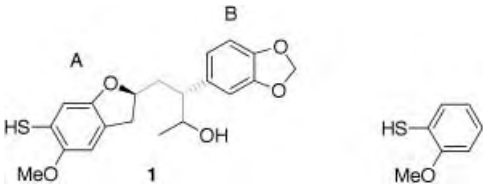
[*] Prof. J. A. McCammon, J. R. Schames, R. H. Henchman
Department of Chemistry and Biochemistry
Howard Hughes Medical Institute and
Department of Pharmacology
University of California, San Diego
9500 Gilman Drive, La Jolla, CA 92093-0358 (USA)
Fax: (+1) 858-534-7042
E-mail: jmccammon@ucsd.edu
Prof. S. M. Cohen, D. T. Puerta
Department of Chemistry and Biochemistry
University of California, San Diego
9500 Gilman Drive, La Jolla, CA 92093-0358 (USA)
Fax: (+1) 858-822-5598
E-mail: scohen@ucsd.edu

[**] We thank Stewart Adcock for writing the program to generate the initial conformers of **1** and for helpful discussions, and Accelrys for providing the Insight II 2000 software. This work was supported by the University of California, San Diego, a Chris and Warren Hellman Faculty Scholar award (S.M.C.), a Hellman Fellows award (S.M.C.), an American Cancer Society Grant (IRG-70-002-29 to S.M.C.), an NIH Grant (GM-60202-03 to D.T.P.), and, in part, by grants from the NIH, NSF, San Diego Supercomputer Center, Accelrys Inc., NBCR, and W. M. Keck Foundation (to J.A.M.).

Supporting information for this article is available on the WWW under http://www.angewandte.org or from the author.

Another approach for metalloprotein drug design is to reproduce the drug–metalloenzyme interactions by using small molecule models that can be readily characterized.[8–10] This strategy is effective for elucidating the interactions of an inhibitor with a metal ion, and we sought to augment this method so that the complete binding of an inhibitor to the active site of a metalloprotein could be predicted. Therefore, an integrated approach to metalloenzyme drug discovery that marries bioinorganic model chemistry with computational methods has been devised. This unique strategy involves the use of simple coordination complexes as active-site models to reveal metal–inhibitor interactions, followed by computational analysis using the model complex structure as a basis for drug docking. The model complex effectively overcomes the computational requirement for parameterization of the metal ion by directly providing the metal–ligand geometry. The result of this combined approach is the elucidation of the complete binding of an inhibitor to a metalloenzyme without the use of additional macromolecular NMR spectroscopic or X-ray crystallographic data.

Futoenones are natural products, derivatives of which are known to interfere with MMP activity;[11] however, the precise mode of binding for these compounds to MMPs has not been determined. Compound **1** was examined (Scheme 1), as it was shown in an earlier study to be the most effective inhibitor against MMP-3 ($IC_{50} = 600$ nM) from



Scheme 1. Futoenone derivative **1** (left, with ring systems labeled) and 2-methoxybenzenethiol (right).

a series of futoenone-derived compounds.[11] Compound **1** was selected because the mode of metal-binding and active-site conformation is unknown, it demonstrates significant selectivity for stromelysin (MMP-3) over other MMPs, and it does not possess a hydroxamate functional group as the metal-ion chelator. The limited number of heteroatoms in this compound indicated that the thiophenol ring moiety (ring system A, Scheme 1) was the most probable zinc-binding group.

2-Methoxybenzenethiol (MBT) was combined with $[(Tp^{Ph,Me})ZnOH]$ ($Tp^{Ph,Me}$ = hydrotris(3,5-phenylmethylpyrazolyl)borate)[10,12] to generate the complex $[(Tp^{Ph,Me})Zn(mbt)]$ as a model for the interaction between **1** and the zinc(II) ion at the MMP active site. The structure of $[(Tp^{Ph,Me})Zn(mbt)]$ was determined by single-crystal X-ray diffraction (Figure 1).[13] The three coordinated pyrazole nitrogen atoms recreate the highly conserved tris(histidine) coordination environment that is found in the active site of all MMPs.[1] The model complex clearly shows that the MBT ligand chelates the zinc ion in a bidentate fashion by utilizing both the sulfur and oxygen donor atoms.

 © 2003 Wiley-VCH Verlag GmbH & Co. KGaA, Weinheim DOI: 10.1002/anie.200351433

The modeling of **1** bound to stromelysin was performed in four stages. First, the structure of [(Tp^{Ph,Me})Zn(mbt)] was used to template the conformation of inhibitor **1** in the active site of MMP-3.[14] A portion of the structure (Figure 1) was inserted into the crystal structure of MMP-3[14] by aligning the three pyrazole nitrogen atoms (N2, N4, and N6) with the three histidine (H201, H205, H211) nitrogen atoms of the MMP active site. The overlay was performed in three different orientations because the pyrazole nitrogen donors do not specifically correlate with a particular histidine residue in the protein (Figure 2). Two of the conformations were immediately dismissed on the basis of steric conflicts between the MBT fragment and the protein. The remaining superposition showed no steric clashes with the protein, and was determined to be the most probable binding conformation. These steric evaluations are based only on the X-ray crystallographic data, and the role of protein mobility[15,16] on this analysis will be the subject of further investigations.

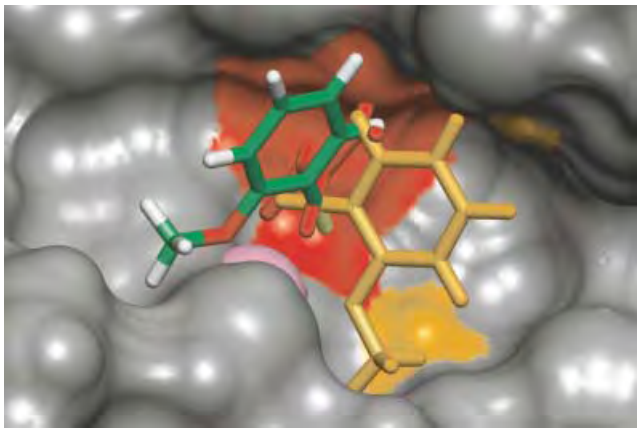


Figure 2. Three superpositions of the [(Tp^{Ph,Me})Zn(mbt)] fragment (Figure 1, bottom right) into the structure of MMP-3. The MBT ligand is shown in stick representations and the catalytic zinc(II) ion is shown as a purple sphere. The red and orange orientations clash with the protein in the areas as shown by the corresponding colors on the protein surface. Only the green orientation is free of steric conflicts.

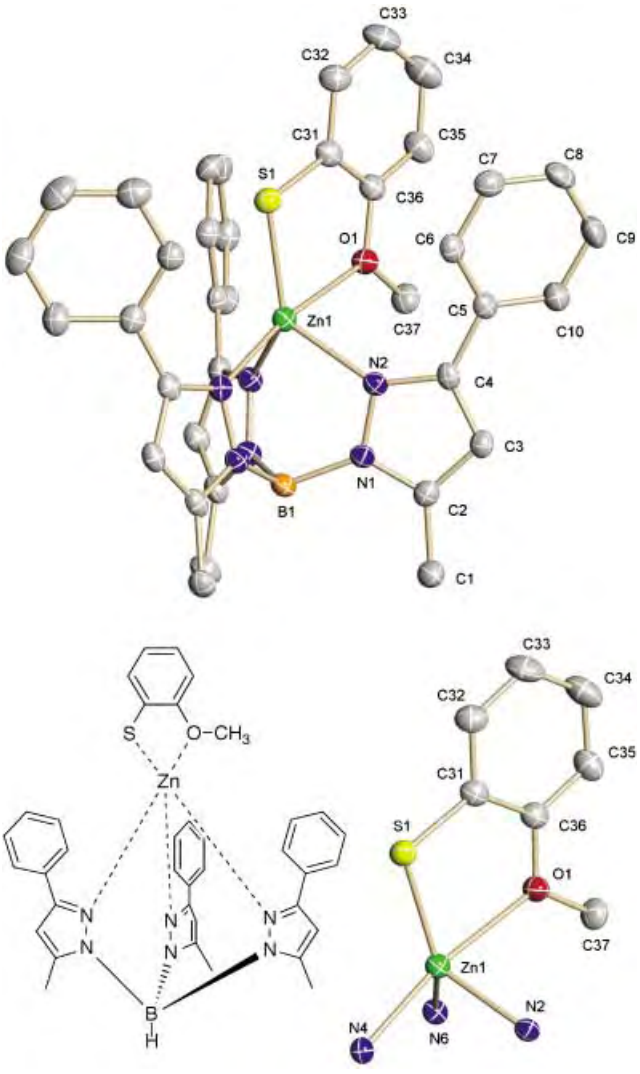


Figure 1. Top: Structural diagram of [(Tp^{Ph,Me})Zn(mbt)] with partial atom numbering schemes (ORTEP, 50% probability ellipsoids). Hydrogen atoms and solvent molecules have been omitted for clarity. Bottom left: A chemical drawing of the complex. Bottom right: A portion of this complex used as a template for computational analysis.

With the orientation of the MBT fragment resolved, the second step was to generate all possible conformers of **1** by varying each of four dihedral angles (Scheme 1, bonds in gray).[17] Of the conformers produced, 14559 were rejected on the basis of internal steric clashes between non-hydrogen atoms. Of the remaining 6177 conformers, every 60th conformation was chosen to obtain a uniform selection of 100 structures. Each structure was placed into the protein by superimposing ring A (Scheme 1) of the calculated conformers with that of the protein-imbedded MBT fragment.

In the third stage, AMBER parm99 and gaff force fields were used to model the protein and inhibitor, respectively.[18,19] Hydrogen atoms were added to the protein using the program WHAT IF.[20] Charges were derived using a Gaussian optimization (HF/6-31G*) and the AMBER 7 module Antechamber.[21] The process was completed by performing minimizations using the SANDER module of AMBER 7.[22] The ligand atoms not shared with the MBT fragment were allowed to move while the remaining atoms (including the protein) were kept rigid. Minimizations were run until the root-mean-square (RMS) deviation of the energy gradient was less than 1×10^{-4} kcal mol^{-1} Å^{-1}.

The strength of ligand binding was assessed according to the minimized energies (see the Supporting Information). A single conformation minimized to the lowest energy of 3.9 kcal mol^{-1}, followed by a cluster of less favorable conformations at 8–9 kcal mol^{-1}. It was apparent that the lowest energy structure relaxed in a unique position relative to the active site cleft (Figure 3). The remaining low-energy conformations minimized outside the protein subsites, thus making contacts predominantly with solvent space (see the Supporting Information).

The lowest energy minimized structure of **1** reveals several unusual features about the binding. Most MMP inhibitors have been designed to occupy the S′ subsites

 © 2003 Wiley-VCH Verlag GmbH & Co. KGaA, Weinheim

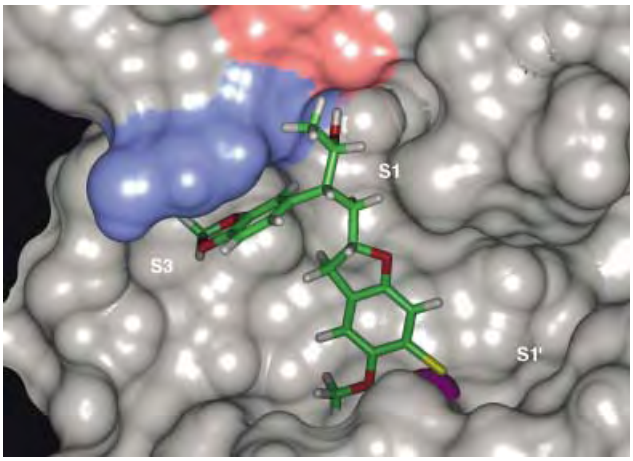


Figure 3. Lowest energy minimized structure of **1** in the active site of stromelysin (MMP-3). Y155 is shown in blue, P156 is shown in pink, and the catalytic zinc(II) ion is shown in purple.

(termed "right-handed" inhibitors), in particular the S1′ pocket (Figure 3).[1] However, the backbone portion of minimized **1** lies in the "left-handed" side of the active site (S subsites). There is a significant interaction in the open S1 and S3 subsites (Figure 3),[14,23] where π stacking is observed (π–π contact, 3.7 Å) between the phenyl group of ring system B of **1** and the side chain of Y155. The known efficacy of **1** against MMP-3 correlates well with other "left-handed" inhibitors that show preferential activity against MMP-3, where interactions with the hydrophobic residue Y155 play an important role.[23] For comparison, the corresponding residue in collagenase (MMP-1) is serine,[1] which thereby eliminates any possible π interactions. Another hydrophobic interaction occurs between the methyl group from the zinc-bound oxygen atom in **1** and a hydrophobic cleft created by the side chains of F86 and F210. Specific hydrogen-bonding interactions is also present between the backbone carbonyl group of P156 and the primary alcohol moiety of **1**.

Earlier attempts to model the binding of **1** relied on comparison to hydroxamate-based inhibitors[11] and failed to distinguish between binding in the S and S′ subsites. By applying a combined bioinorganic–computational technique to this system, we have demonstrated that the interactions of an MMP inhibitor with its target protein can be revealed. This approach is useful not only for known MMP inhibitors,[1] but also new MMP inhibitors that utilize unexplored zinc-binding groups and inhibitors of other medically relevant metalloproteins.

Received: March 18, 2003 [Z51433]

Keywords: bioinorganic chemistry · computer chemistry · drug design · metalloproteins · zinc

[1] M. Whittaker, C. D. Floyd, P. Brown, A. J. H. Gearing, *Chem. Rev.* **1999**, *99*, 2735.
[2] C. M. Overall, C. López-Otín, *Nat. Rev. Cancer* **2002**, *2*, 657.
[3] L. M. Coussens, B. Fingleton, L. M. Matrisian, *Science* **2002**, *295*, 2387.
[4] R. E. Babine, S. L. Bender, *Chem. Rev.* **1997**, *97*, 1359.
[5] S. B. Shuker, P. J. Hajduk, R. P. Meadows, S. W. Fesik, *Science* **1996**, *274*, 1531.
[6] P. J. Hajduk, G. Sheppard, D. G. Nettesheim, E. T. Olejniczak, S. B. Shuker, R. P. Meadows, D. H. Steinman, G. M. Carrerea, Jr., P. A. Marcotte, J. Severin, K. Walter, H. Smith, E. Gubbins, R. Simmer, T. F. Holzman, D. W. Morgan, S. K. Davidsen, J. B. Summers, S. W. Fesik, *J. Am. Chem. Soc.* **1997**, *119*, 5818.
[7] P. J. Hajduk, S. B. Shuker, D. G. Nettesheim, R. Craig, D. J. Augeri, D. Betebenner, D. H. Albert, Y. Guo, R. P. Meadows, L. Xu, M. Michaelides, S. K. Davidsen, S. W. Fesik, *J. Med. Chem.* **2002**, *45*, 5628.
[8] G. Parkin, *Chem. Commun.* **2000**, 1971.
[9] M. Ruf, K. Weis, I. Brasack, H. Vahrenkamp, *Inorg. Chim. Acta* **1996**, *250*, 271.
[10] D. T. Puerta, S. M. Cohen, *Inorg. Chem.* **2002**, *41*, 5075.
[11] L.-A. Yeh, J. Chen, F. Baculi, D. E. Gingrich, T. Y. Shen, *Bioorg. Med. Chem. Lett.* **1995**, *5*, 1637.
[12] D. T. Puerta, S. M. Cohen, *Inorg. Chim. Acta* **2002**, *337*, 459.
[13] Further details for the structure of [($Tp^{Ph,Me}$)Zn(mbt)] can be found in the Supporting Information. CCDC 199598 contains the supplementary crystallographic data for this paper. These data can be obtained free of charge via www.ccdc.cam.ac.uk/conts/retrieving.html (or from the Cambridge Crystallographic Data Centre, 12 Union Road, Cambridge CB21EZ, UK; fax: (+44) 1223-336-033; or deposit@ccdc.cam.ac.uk).
[14] L. Chen, T. J. Rydel, F. Gu, C. M. Dunaway, S. Pikul, K. M. Dunham, B. L. Barnett, *J. Mol. Biol.* **1999**, *293*, 545.
[15] F. J. Moy, P. K. Chanda, J. Chen, S. Cosmi, W. Edris, J. I. Levin, T. S. Rush, J. Wilhelm, R. Powers, *J. Am. Chem. Soc.* **2002**, *124*, 12658.
[16] J.-H. Lin, A. L. Perryman, J. R. Schames, J. A. McCammon, *J. Am. Chem. Soc.* **2002**, *124*, 5632.
[17] D. Weininger, *J. Chem. Inf. Comput. Sci.* **1988**, *28*, 31.
[18] J. Wang, P. Cieplak, P. A. Kollman, *J. Comput. Chem.* **2000**, *21*, 1049.
[19] J. Wang, R. M. Wolf, D. A. Case, P. A. Kollman, **2003**, unpublished results.
[20] G. Vriend, *J. Mol. Graphics* **1990**, *8*, 52.
[21] J. Wang, W. Wang, P. A. Kollman, **2003**, unpublished results.
[22] D. A. Case, D. A. Pearlman, J. W. Caldwell, T. E. Cheatham III, J. Wang, W. S. Ross, C. L. Simmerling, T. A. Darden, K. M. Merz, R. V. Stanton, A. L. Cheng, J. J. Vincent, M. Crowley, V. Tsui, H. Gohlke, R. J. Radmer, Y. Duan, J. Pitera, I. Massova, G. L. Seibel, U. C. Singh, P. K. Weiner, P. A. Kollman, University of California, San Francisco, AMBER 7, **2002**.
[23] B. C. Finzel, E. T. Baldwin, G. L. Bryant, Jr., G. F. Hess, J. W. Wilks, C. M. Trepod, J. E. Mott, V. P. Marshall, G. L. Petzold, R. A. Poorman, T. J. O'Sullivan, H. J. Schostarez, M. A. Mitchell, *Protein Sci.* **1998**, *7*, 2118.

 © 2003 Wiley-VCH Verlag GmbH & Co. KGaA, Weinheim

Photochemical Asymmetric Synthesis

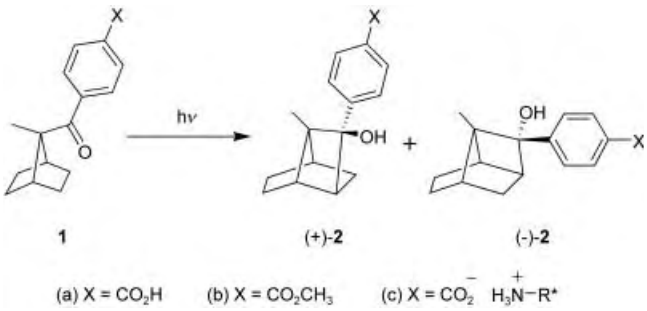
Preorganization of Achiral Molecules for Asymmetric Synthesis through Crystallization-Induced Immobilization in Homochiral Conformations**

Brian O. Patrick, John R. Scheffer, and Carl Scott*

The work described in this article represents the latest installment from our laboratory in a long-term program aimed at developing new methods of asymmetric synthesis in organic photochemistry,[1] a relatively unexplored field that has recently attracted widespread attention and interest.[2] By way of introduction, consider the common situation of a conformationally mobile molecule that is achiral in solution as a result of rapid equilibration between enantiomeric conformers. If such conformers could be immobilized and caused to react in enantiomerically pure form, this could be used to great advantage in asymmetric synthesis. The prevention of conformational equilibration is relatively straightforward and can be achieved through crystallization. Selective crystallization in an enantiomerically pure form, however, is more problematic, as the great majority of achiral, conformationally mobile molecules crystallize as racemic compounds containing equal amounts of both conformational enantiomers.[3]

Our approach to this problem has been to introduce a second element of chirality to the system in the form of an easily removed, enantiomerically pure chiral auxiliary. In this situation the conformers become diastereomers rather than enantiomers, and one diastereomer will generally crystallize out in a process known as a "crystallization-induced asymmetric transformation."[3,4] The crystals are then subjected to a chemical reaction that fixes the evanescent conformational chirality in the form of permanent molecular chirality; removal of the temporary chiral auxiliary completes the process, leaving the reaction product in enantiomerically enriched form.

Specifically, we consider here enantio- and diastereoselection in the photochemical conversion of 7-benzoylnorbornane derivatives initiated by hydrogen atom abstraction (**1**, Scheme 1) into the corresponding cyclobutanols (**2**), a new example of the well known Yang photocyclization reaction.[5] The application of the conformational preorganization technique described above leads to near-quantitative *de* and *ee* values in the crystalline state, even at very high conversions. A bonus was the finding that one of the reactions was a single crystal-to-single crystal process.[6] This allowed crystal structures to be obtained at the beginning, mid-point and end of the reaction and absolute configuration correlations to be established between reactant and product.[7]



Scheme 1. Photochemical conversion of 7-benzoylnorbornane derivatives into the corresponding cyclobutanols.

The key starting material, 7-methyl-7-benzoylnorbornane-*p*-carboxylic acid (**1a**) was synthesized in a straightforward fashion from 7-methyl-7-carboxynorbornane[8] by a) acid chloride formation ($(COCl)_2$, CH_2Cl_2, catalyst DMF), b) nucleophilic acyl substitution (*p*-FPhMgBr, THF, 0°, 43% overall for steps a and b), c) nucleophilic aromatic substitution (KCN, DMSO, △, 93%) and d) hydrolysis of the nitrile (KOH, aq. EtOH, 98%).

Prior to the asymmetric induction studies, the photochemistry of methyl ester **1b** was investigated in solution and the solid state. In both instances the reaction was remarkably clean, affording racemic cyclobutanol **2b** as the exclusive product; according to GC, no other photoproducts were formed in amounts greater than 0.5%. The structure and relative stereochemistry of cyclobutanol **2b** were established by detailed spectroscopic analysis and confirmed by an X-ray crystal structure of one of the corresponding ammonium salts, **2c** (see below).

For the asymmetric induction studies, chiral auxiliaries were introduced by the treatment of carboxylic acid **1a** with a series of optically pure amines to form the corresponding 1:1 ammonium salts (**1c**); Table 1 lists the amines used. Polycrystalline samples of the salts (1–2 mg) were sandwiched between pyrex microscope slides and irradiated to varying degrees of conversion under nitrogen. The chiral auxiliaries

Table 1: Asymmetric induction in the solid state photochemistry of salts **1c**.[a]

Entry	Amine	Conversion [%]	*ee* values of **2b** [%]	[α][b]
1	(*R*)-(+)-1-phenylethylamine	100	98	(−)
2	(*S*)-(−)-1-phenylethylamine	100	97	(+)
3	(1*S*,2*R*)-(−)-1-amino-2-indanol	94	96	(+)
4	(1*S*,2*S*)-(+)-2-amino-3-methoxy-1-phenyl-1-propanol	88	95	(−)
5	(*R*)-(−)-2-amino-1-butanol	100	84	(−)

[a] All photolyses were conducted at room temperature. Irradiation of the salts in solution invariably led to racemic **2b**. [b] Sign of rotation of predominant enantiomer of **2b** at the sodium D line.

[*] Prof. Dr. J. R. Scheffer, Dr. B. O. Patrick, C. Scott
Department of Chemistry
University of British Columbia
2036 Main Mall, Vancouver, B.C. V6T 1Z1 (Canada)
Fax: (+1) 604-822-3496
E-mail: scheffer@chem.ubc.ca

[**] We thank the Natural Sciences and Engineering Research Council of Canada for financial support.

Supporting information for this article is available on the WWW under http://www.angewandte.org or from the author.

 DOI: 10.1002/anie.200351609 © 2003 Wiley-VCH Verlag GmbH & Co. KGaA, Weinheim

were removed by treatment of the photolysis mixtures with ethereal diazomethane, and the resulting methyl esters were analyzed to obtain the *ee* values by chiral HPLC and for the extent of conversion by GC. As before, cyclobutanol **2b** was the sole GC-detectable photoproduct. The results are summarized in Table 1.

The data in Table 1 reveal that the *ee* values obtained for photoproduct **2b** in the solid state were excellent (84–98%), even at very high conversions. As expected for a well-behaved system, the use of (*R*)-(+)- and (*S*)-(−)-1-phenylethylamine as chiral auxiliaries (entries 1 and 2) led to the optical antipodes of cyclobutanol **2b** in equal *ee*. In contrast to the results in the solid state, photolysis of the salts in solution led to racemic **2b**, a result that highlights the critical role played by the reaction medium in controlling enantioselectivity.

To gain a greater understanding of the solid-state photochemistry, X-ray crystal-structure studies were undertaken. To date only the 1-phenylethylamine salt has given crystals suitable for X-ray analysis, but fortuitously, the solid state photoreaction in this case proved to be of the rare single crystal-to-single crystal variety,[6] which permitted the structure of both reactant and product to be obtained at various stages of reaction. Figure 1a shows the crystal structure of the (*S*)-(−)-1-phenylethylamine salt prior to photolysis, and Figure 1b and 1c depict the structure of the mixed crystal following 70% and 93% conversion to the corresponding cyclobutanol. The final ORTEP drawing (Figure 1d) shows the structure of the cyclobutanol photoproduct following its recrystallization from methanol.

The crystal structures reveal the source of the high enantio- and diastereoselectivity. Under the influence of the ionic chiral auxiliary, the reactant crystallizes in a homochiral conformation in which the carbonyl oxygen (red) is much closer to γ-hydrogen atom H_X (green, 2.70 Å) than to γ-hydrogen H_Y (purple, 3.43 Å). As a result, only H_X is abstracted,[9] leading to a 1,4-hydroxybiradical that undergoes least motion closure with "retention of configuration" at the carbonyl carbon. Closure of the biradical with inversion would require rotation of the aryl and hydroxyl groups about the C7-carbonyl carbon bond, a large amplitude motion that is topochemically forbidden in the crystalline state.[10] Enantioselectivity and diastereoselectivity are thus a direct consequence of conformational preorganization of the reactant in a rigid matrix that severely limits the range of motions available along the reaction coordinate.[11]

Figure 1b and 1c prove that H_X is, in fact, the hydrogen abstracted. Because the absolute configuration of the ionic chiral auxiliary is known, the absolute configuration of both reactant and product is established, which in turn allows us to state with certainty that abstraction of H_X leads to the experimentally observed photoproduct. We note that the reactant and product have nearly identical geometries, except for an upward movement of the γ-carbon to allow for cyclobutane ring formation and a change in orientation of the C–O bond accompanying the change in hybridization at the carbonyl carbon from sp^2 to sp^3. Presumably it is this close resemblance in size and shape between reactant and product that makes the single crystal-to-single crystal transformation possible.

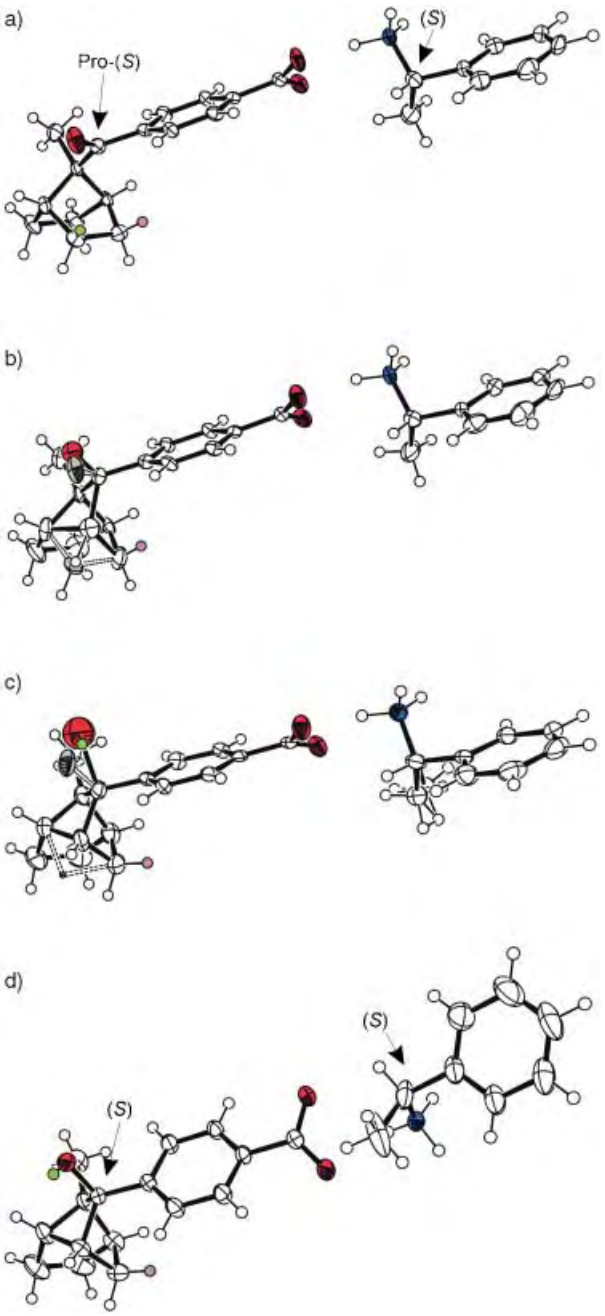


Figure 1. ORTEP representations of a) (*S*)-(−)-1-phenylethylamine salt **1c**; b) mixed crystal containing 70% **2c** and 30% **1c**; c) mixed crystal containing 93% **2c** and 7% **1c**; d) salt **2c** after recrystallization from methanol. The oxygen atoms are red, nitrogen blue, γ-H_X (most favored for abstraction) green and γ-H_Y purple. In (b) and (c) portions of salt **1c** are represented by dashed bonds and gray atoms. Ellipsoids are set at the 50% probability level.

An interesting question associated with single crystal-to-single-crystal transformations is whether the crystal structure of the "as formed" product is the same as that of the recrystallized material. Figure 1d shows that, in the present instance, it is not. Recrystallization has brought about not only a substantial change in molecular conformation (reorientation of the aromatic ring and its associated ionic auxiliary), but also a complete change in packing arrange-

 © 2003 Wiley-VCH Verlag GmbH & Co. KGaA, Weinheim

ment (from orthorhombic to monoclinic). Based on a very limited number of examples, such changes appear to be the rule rather than the exception when the products of single crystal-to-single crystal reactions are recrystallized.[12]

In summary, the use of ionic chiral auxiliaries to preorganize achiral organic molecules for asymmetric synthesis through crystallization-induced immobilization in homochiral conformations works well for the Yang photocyclization of 7-methyl-7-benzoylnorbornane derivatives. Related studies from our research group have shown the technique to give high *ee* values in a wide variety of excited state processes,[1] and it is clear that this approach represents one of the most powerful methods of asymmetric synthesis available in the field of organic photochemistry. Finally we point out that optically pure photoproducts, such as those formed in the present study, have potential as chiral synthons, and current efforts in our laboratory are directed along these lines. In addition, we are currently working toward extending the solid-state ionic chiral-auxiliary method to ground state as well as excited state processes.

Experimental Section

See the Supporting Information for the cell constants and related crystallographic data as well as the details of the synthesis of keto-acid **1a**, its conversion into an ionic chiral auxiliary-containing salt, the photolysis of the salt in the crystalline state, the diazomethane workup procedure and the characterization of cyclobutanol photoproduct **2b**.

Received: April 8, 2003 [Z51609]

Keywords: asymmetric synthesis · crystal engineering · photochemistry · solid-state reactions · topochemistry

[1] J. R. Scheffer, *Can. J. Chem.* **2001**, *79*, 349.
[2] H. Rau, *Chem. Rev.* **1983**, *83*, 535; H. Buschmann, H. D. Scharf, N. Hoffmann, P. Esser, *Angew. Chem.* **1991**, *103*, 480; *Angew. Chem. Int. Ed. Engl.* **1991**, *30*, 477; Y. Inoue, *Chem. Rev.* **1992**, *92*, 741; J. P. Pete, *Adv. Photochem.* **1996**, *21*, 135; S. R. L. Everitt, Y. Inoue in *Molecular and Supramolecular Photochemistry, Vol. 3* (Eds.: V. Ramamurthy, K. S. Schanze), Marcell Dekker, New York, **1999**, chap. 2.
[3] J. Jacques, A. Collet, S. Wilen, *Enantiomers, Racemates and Resolutions*, Wiley, New York, **1981**, chap. 6.
[4] E. Vedejs, R. W. Chapman, S. Lin, M. Müller, D. R. Powell, *J. Am. Chem. Soc.* **2000**, *122*, 3047; S. Caddick, K. Jenkins, *Chem. Soc. Rev.* **1996**, *25*, 447.
[5] N. C. Yang, D. H. Yang, *J. Am. Chem. Soc.* **1958**, *80*, 2913; Review: P. Wagner, B.-S. Park in *Organic Photochemistry, Vol. 11* (Ed.: A. Padwa), Marcell Dekker, New York, **1991**, chap. 4.
[6] For a discussion of the different types of photochemical solid-to-solid reactions (including single crystal-to-single crystal transformations), see A. E. Keating, M. A. Garcia-Garibay in *Molecular and Supramolecular Photochemistry, Vol. 2* (Eds.: V. Ramamurthy, K. S. Schanze), Marcell Dekker, New York, **1998**, chap. 5. For a discussion of the dynamics of single crystal-to-single crystal reactions, see G. Kaupp, *Curr. Opin. Solid State Mater. Sci.* **2002**, *6*, 131.
[7] For a review on absolute configuration correlation studies in solid state organic photochemistry, see M. Leibovitch, G. Olovsson, J. R. Scheffer, J. Trotter, *Pure Appl. Chem.* **1997**, *69*, 815.
[8] S. Beckmann, H. Geiger, *Chem. Ber.* **1961**, *94*, 48.
[9] There is now a large body of crystallographic evidence indicating that γ-hydrogen atom abstraction in the solid state occurs preferentially over distances near the sum of the van der Waals radii of oxygen and hydrogen (2.72 Å). See H. Ihmels, J. R. Scheffer, *Tetrahedron* **1999**, *55*, 885.
[10] 1,4-Hydroxybiradical ring closure involving retention of configuration at the hydroxyl-bearing carbon has been noted previously and appears to be a general feature of Yang photocyclization reactions conducted in the crystalline state. See for example A. D. Gudmundsdottir, T. J. Lewis, L. H. Randall, S. J. Rettig, J. R. Scheffer, J. Trotter, C.-H. Wu, *J. Am. Chem. Soc.* **1996**, *118*, 6167; M. Leibovitch, G. Olovsson, J. R. Scheffer, J. Trotter, *J. Am. Chem. Soc.* **1998**, *120*, 12755.
[11] Interestingly, the diastereoselectivity of the solution phase photoreaction is identical to that observed in the crystalline state. One explanation of this result is that, even in solution, rotation about the C7-carbonyl carbon bond in the initially formed biradical is slow relative to closure owing to unfavorable steric interactions developed between the aryl and methyl groups. In addition, the biradical (a triplet) may be formed in a conformation in which intersystem crossing to the singlet and closure is faster than rotation. For examples in which geometry-dependent intersystem crossing is thought to control the stereochemistry of 1,4-biradical closure, see A. G. Griesbeck, H. Heckroth, *J. Am. Chem. Soc.* **2002**, *124*, 396, and references therein.
[12] See for example, V. Buchholz, V. Enkelmann, *Mol. Cryst. Liq. Cryst.* **1998**, *313*, 309; K. Novak, V. Enkelmann, G. Wegner, K. B. Wagnener, *Angew. Chem.* **1993**, *105*, 1678; *Angew. Chem. Int. Ed. Engl.* **1993**, *32*, 1614. For a counter example, see K. Honda, *Bull. Chem. Soc. Jpn.* **2002**, *75*, 2383.

 © 2003 Wiley-VCH Verlag GmbH & Co. KGaA, Weinheim

Polyhedral Boranes

Polyhedral Boranes with Exo Multiple Bonds: Three-Dimensional Inorganic Analogues of Quinones**

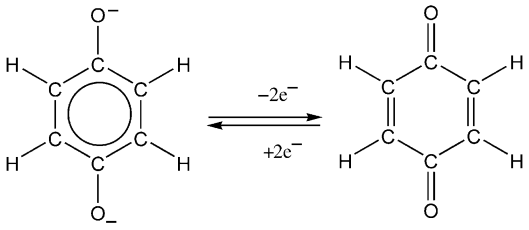
*Musiri M. Balakrishnarajan and Roald Hoffmann**

Something interesting and chemically significant happens in an organic aromatic system when it is substituted with lone-pair-bearing electronegative ligands, and then oxidized. Consider the dioxobenzene dianion—benzoquinone couple **1** and **2**. There is an easy oxidation/reduction connecting these two molecules, coupled with destruction/formation of the aro-

[*] Prof. Dr. R. Hoffmann, Dr. M. M. Balakrishnarajan
Department of Chemistry and Chemical Biology
Cornell University
Ithaca, NY 14853 (USA)
Fax: (+1) 607-255-5707
E-mail: rh34@cornell.edu

[**] We are grateful to the National Science Foundation (NSF) for its support of this research through its grant No. CHE-02 04841.

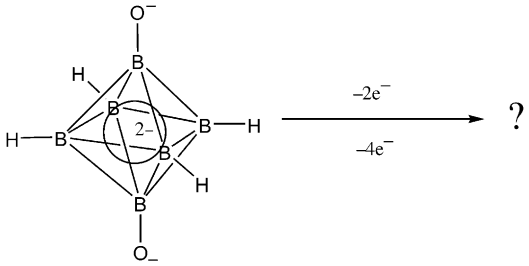
 DOI: 10.1002/anie.200351821 © 2003 Wiley-VCH Verlag GmbH & Co. KGaA, Weinheim



1 **2**

matic system, multiple bonding to the exocyclic substituent, and attendant strong skeletal deformation.

Polyhedral boranes are considered to be 3D aromatic systems.[1] Could something analogous take place in polyhedral boranes on substitution by lone-pair bearing ligands? And could the effect be even stronger than in organic molecules due to the cylindrical nature of the interaction? The idea is indicated schematically in **3**.



3

Our motivation for thinking about exohedral multiple bonds on a polyhedral skeleton was triggered by the observation of conjugative effects across ten and twelve vertex bi-*para*-substituted boranes and carboranes with phenyl, pyridinyl and dinitrogen substituents.[2–5] As electronic communication across the polyhedral skeleton essentially involves some π character in the bond connecting these substituents to the polyhedral skeleton, we wondered whether such partial π bonding could be maximized for a suitable electron count. Herein, we explore the relatively simple octahedral and pentagonal bipyramidal borane skeletons with exo multiple bonds. All the systems considered here are studied by using hybrid DFT calculations (B3LYP-6-311 + G**);[6] a fragment molecular-orbital (MO) analysis is performed by using extended Hückel calculations.[7] The extension of these to higher boranes and their energetics will be reported elsewhere.

We selected the disubstituted O, NH and S derivatives for the study. The substitution of these groups at the *para* positions of the *closo*-borane $B_6H_6^{2-}$ will result in $B_6H_4X_2^{4-}$ (X = O, NH, S), classical Wade systems. In fact, we had to carry out calculations on the di and tetraprotonated forms of these, as the parent tetraanion calculations failed to converge in the geometry optimization. To move toward multiple bonding, we removed one or two electron pairs from $B_6H_4X_2^{4-}$, leading to $B_6H_4X_2^{2-}$ or $B_6H_4X_2$, respectively. DFT calculations show that all of these dianions and neutrals are minima (Table 1). The various B–B distances calculated are given in Figure 1. In the dianions, there is pronounced bond alternation in the "belt" of the polyhedron, to which we will return later.

Table 1: The point group, and Wiberg Bond Orders (WBO) for B–X bonds, computed at B3LYP6-311 + G** level of theory for various $B_6H_4X_2^{y-}$, $B_7H_5X_2^{2-}$ and $B_6X_6^{2-}$ systems. The HOMO–LUMO gap (Gap) is obtained from eH calculations using the ab initio optimized geometry; LUMO = lowest-unoccupied molecular orbital.

No	Molecule	Symmetry	Gap(eV)	WBO
1	$B_6H_4O_2^{2-}$	D_{2h}	0.68	1.39
2	$B_6H_4(NH)_2^{2-}$	C_{2h}	0.66	1.38
3	$B_6H_4S_2^{2-}$	D_{2h}	0.53	1.52
4	$B_6H_4O_2$	D_{4h}	0.71	1.72
5	$B_6H_4(NH)_2$	D_{4h}	1.38	1.78
6	$B_6H_4S_2$	D_{4h}	1.01	1.91
7	$B_7H_5O_2^{2-}$	D_{5h}	0.28	1.38
8	$B_7H_5(NH)_2^{2-}$	C_1	0.26	1.34
9	$B_7H_5S_2^{2-}$	D_{5h}	0.19	1.47
10	$B_6O_6^{2-}$	O_h	3.35	1.57
11	$B_6S_6^{2-}$	O_h	2.35	1.81

The exopolyhedral B–X bond lengths decrease steadily and dramatically when the systems are oxidized (as in quinones). For example, the B–O bond length 1.574 Å in $B_6H_4(OH_2)$ (tetraprotonated $B_6H_4O_2^{4-}$) decreases to 1.296 Å in $B_6H_4O_2^{2-}$ and further decreased to 1.227 Å in $B_6H_4O_2$.[8] In all the oxidized systems, the bonds that connect the substituted boron atoms to the central B_4H_4 ring are also elongated compared to the unoxidized systems. This short–long–short alternation is parallel to what happens in quinones. In addition, the B–B bonds of the belt B_4H_4 ring fragment in the $B_6H_4X_2^{2-}$ series show pronounced bond alternation, much like cyclobutadiene. As we shall see, the relationship is not an accident.

A similar substitution sequence in the *closo*-B_7 skeleton gives $B_7H_5O_2^{2-}$, $B_7H_5(NH)_2^{2-}$and $B_7H_5S_2^{2-}$ ions—all of them characterized as stationary points at the same level of theory. In this case, however, further oxidation to the neutral species $B_7H_5X_2$ breaks the *closo*-B_7 the skeleton for all the substituents considered here. In the *closo*-B_7 skeletons of $B_7H_5X_2^{2-}$, bonds are elongated along the major symmetry axis and they also exhibit bond alternation in their belts (Figure 2); the B–B bond lengths of the central B_5H_5 ring in the pattern longer–short–long–short–longer.

To understand the origin of the fascinating bond alternation in $B_6X_4X_2^{2-}$ and $B_7H_5X_2^{2-}$, we studied the nature of π-orbital interactions between the borane skeleton and the exo substituent by extended Hückel calculations. Figure 3 shows the interaction of frontier orbitals of B_6H_4 and B_7H_5 fragments with $(O)_2$ π orbitals, building up $B_6H_4O_2^{4-}$ (D_{4h}) and $B_7H_5O_2^{4-}$, respectively.[9] All the levels shown in the figure are filled in the tetraanions. The triply degenerate highest-occupied molecular orbital (HOMO; t_{1g}) of the *closo*-$B_6H_6^{2-}$ borane[10] (which arises from the in-phase combination of tangential p orbitals of boron) splits into $b_{2g} + e_g$ due to the substitution by oxygen atoms (upper left of Figure 3). While b_{2g} by symmetry remains unaffected by oxygen π orbitals, the e_g set interacts with the out-of-phase combination (π_g) of $(O)_2$ to give a pair of bonding and antibonding MOs, the latter forming the HOMO of $B_6H_4O_2^{4-}$.

 © 2003 Wiley-VCH Verlag GmbH & Co. KGaA, Weinheim

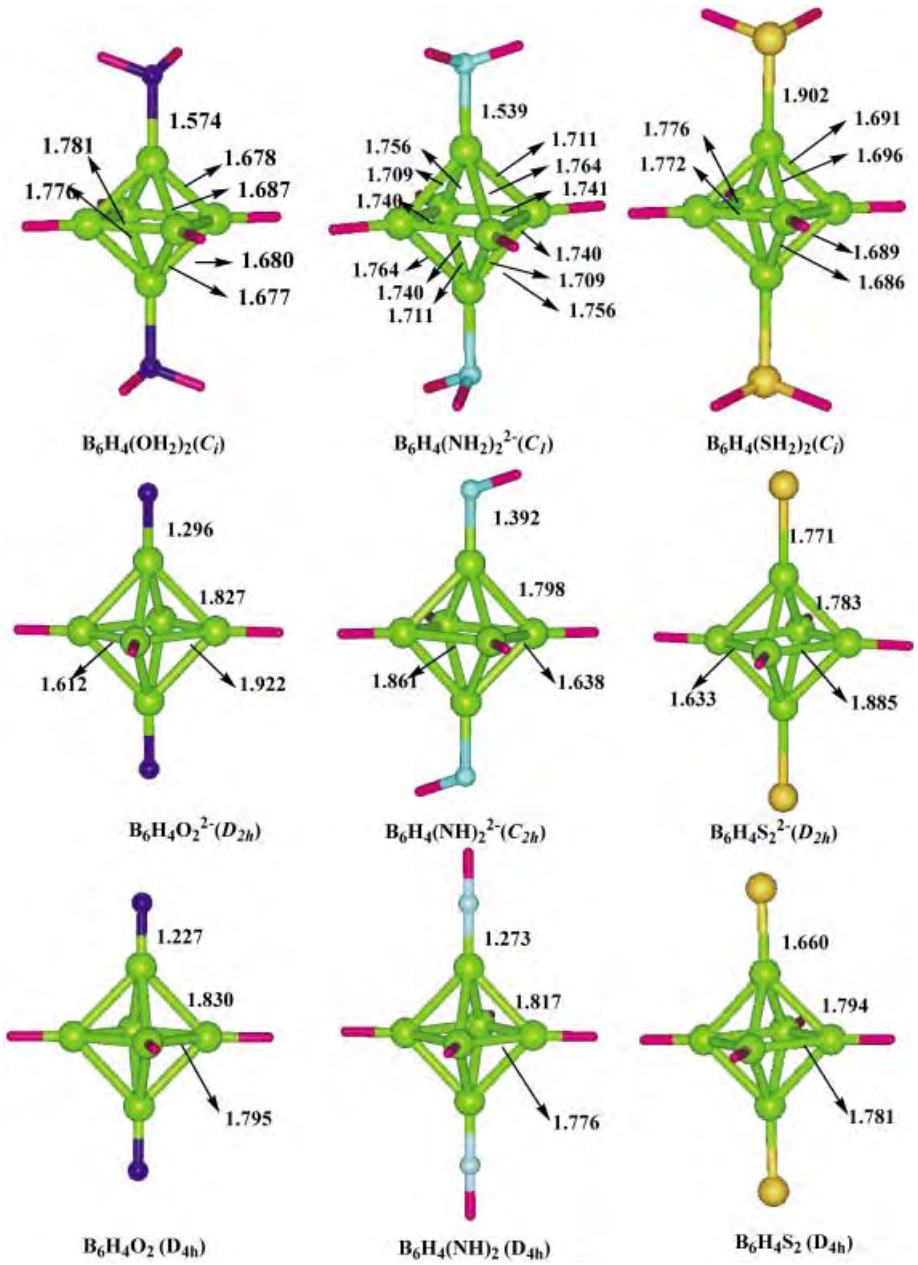


Figure 1. *Closo*-B_6 systems having exo multiple bonds, with their bond lengths (in Å) calculated at B3LYP6-311+G** level of theory.

Removal of an electron pair from the "Wadian" $B_6H_4O_2^{4-}$ to form $B_6H_4O_2^{2-}$ generates a classical Jahn–Teller situation; a distortion ensues, thus stabilizing one of the degenerate MOs. Figure 4 shows one representation of the degenerate pair of orbitals on the left, another combination on the right. Focusing on the equatorial B_4 ring in these orbitals, we see the direct parallel to the orbitals of cyclobutadiene. The outcome of the Jahn–Teller distortion, as in cyclobutadiene, is pronounced bond alternation within the square B_4H_4 ring.

The B_7H_5 fragment interacts with $(O)_2$ in a similar way. Though the π-type orbitals of the B_7H_5 fragment are slightly below the HOMO in $B_7H_7^{2-}$, they do mix strongly with the out-of-phase combination of the π orbitals of the exopolyhedral $(O)_2$ fragment, the antibonding combination forming the HOMO of $B_7H_5O_2^{4-}$. Again, removal of two electrons will generate a Jahn–Teller situation, resulting eventually in two of the bonds in $B_7H_5X_2$ systems being shorter than the other three.

In $B_6H_4X_2$, all four electrons are removed from the doubly degenerate HOMO, leading to a return to D_{4h} symmetry. Successive oxidation removes electrons from MOs that are antibonding between the borane skeleton and the substituents, and bonding within the polyhedron. This is reflected in the shortened B–X bond lengths, indicative of multiple bonding, and in bond expansion in the polyhedron (see Figure 1).

To assess the magnitude of multiple bonding, we calculated the Wiberg bond order (WBO)[11] by using NBO routines[12] in Gaussian 98 (Table 1). The WBO values of the B–X bond in the parent protonated forms are 0.56, 0.89 and 0.83 for -OH, $-SH_2$ and $-NH_2$ groups respectively. On oxidation, the WBO values are increased to more than one for $B_6H_4X_2^{2-}$ and further increased to more than 1.5 for the neutral $B_6H_4X_2$ series. This can be compared with the organic analogues $C_6H_4O_2^{2-}$ and $C_6H_4(OH)_2$, whose WBO values are 1.26 and 1.75, respectively, at the same level of theory.

Though the bond multiplicity of these B–X bonds is not provided by the B–X bond order values, the trends are indicative. There is clearly exopolyhedral multiple bonding.[13] In the case of neutral $B_6H_4(NH)_2$, the B-N-H bond angle is exactly 180°, which is also indicative of a cylindrical B≡N type interaction. The HOMO–LUMO gap, which is a fair measure of reactivity,[14] suggests that the dianionic systems are more reactive than the neutral systems. We believe the sum of the theoretical evidence supports the assertion that these systems are the natural 3D analogues of benzoquinone in polyhedral systems.

It is also possible to restore the octahedral geometry of the B_6 skeleton in $B_6H_6^{2-}$ with six multiply bonded exohedral substituents. DFT calculations on $B_6O_6^{2-}$ (O_h) and $B_6S_6^{2-}$ (O_h) show that they are indeed minima on their potential energy surface (Figure 5).

The two-electron requirement of these systems can be explained by analyzing the nature of the π-type interactions. The occupied levels of a classical Wade framework set for the

 © 2003 Wiley-VCH Verlag GmbH & Co. KGaA, Weinheim

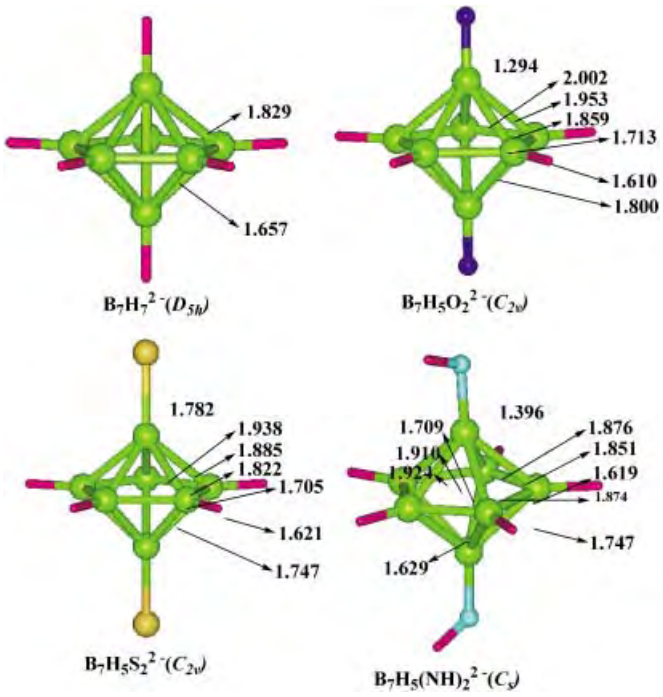


Figure 2. *Closo*-B_7 systems having exo multiple bonds, with bond lengths (in Å) as calculated at B3LYP6-311+G** level of theory. $B_7H_7^{2-}$ is included for calibration.

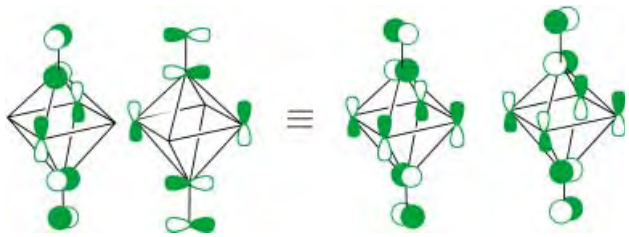


Figure 4. Two different ways of representing the e_g HOMO of $B_6H_4X_2^{4-}$, occupied only by two electrons in the dianions.

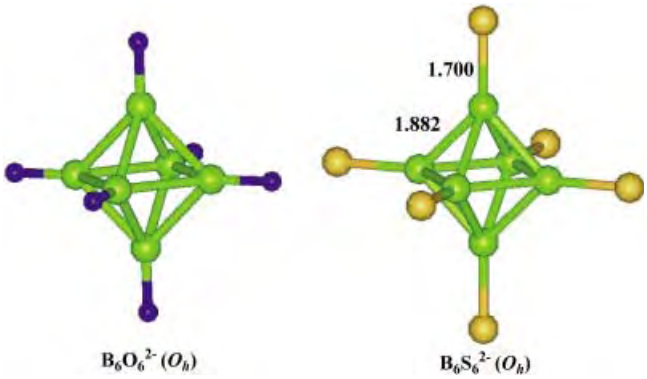


Figure 5. *Closo*-$B_6X_6^{2-}$ systems having exo multiple bonds, with bond lengths (in Å) as calculated at B3LYP6-311+G** level of theory.

B_6 cluster include two triply degenerate orbitals of tangential character; set up for interaction with external π systems; a purely tangential t_{2g}, and a t_{1u} that has a mixture of tangential and radial character. These are shown at left of Figure 6. The 12 π-type orbitals of the six external O substituents in a hypothetical $B_6O_6^{8-}$ ($B_6H_6^{2-}$ to $B(OH)_6^{2-}$ to $B_6O_8^{8-} + 6H^+$) transform as $t_{2g} + t_{1u} + t_{2u} + t_{1g}$. Of these t_{2u} and t_{1g} do not interact much with the polyhedron MOs. Cluster t_{2g} and t_{1u}

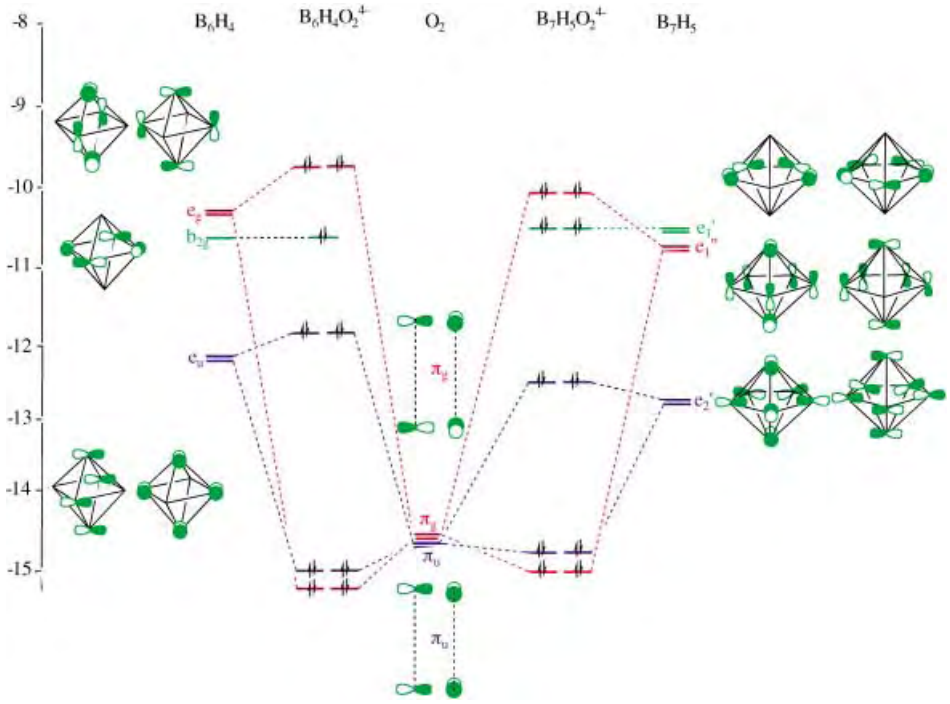


Figure 3. The interaction of the B_6H_4 (D_{4h}) and B_7H_5 (D_{5h}) fragments with two oxygen atoms ($D_{\infty h}$), leading to the bonding MOs of *closo*-$B_6H_4O_2^{-4}$ and *closo*-$B_7H_5O_2^{-4}$.

 © 2003 Wiley-VCH Verlag GmbH & Co. KGaA, Weinheim

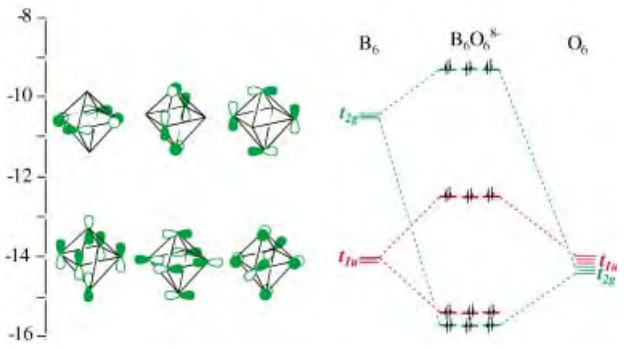


Figure 6. The interaction of $B_6(O_h)$ fragment with six oxygen atoms(O_h), resulting in the bonding MOs of *closo*-$B_6O_6^{2-}$.

MOs form antibonding combinations with the corresponding symmetry oxygen lone pair combinations, as illustrated in Figure 6. A good HOMO-LUMO gap results if the t_{2g} antibonding combination is unfilled, which implies a six electron oxidation of $B_6O_6^{8-}$ to $B_6O_6^{2-}$. The next closed shell structure is at $B_6O_6^{4+}$, which is not realistic. Since these MOs are antibonding between the two fragments, the removal of electrons results in π bonding.

These hypothetical polyhedral ions may be viewed as electronically equivalent to the oxocarbon dianions such as $C_3O_3^{2-}$, $C_4O_4^{2-}$, $C_5O_5^{2-}$ and $C_6O_6^{2-}$.[15] The boron systems show substantial HOMO–LUMO gaps (Table 1). Given all the useful chemistry of quinones and oxocarbon dianions, we believe that interesting structures and reactivity will be found in these 3D analogues.

Received: May 6, 2003 [Z51821]

Keywords: ab initio calculations · aromaticity · boranes · Jahn–Teller distortion · multiple bonds

[1] J. I. Aihara, *J. Am. Chem. Soc.* **1978**, *100*, 3339; b) I. Gutman, M. Milun, N. Trinajstic, *J. Am. Chem. Soc.* **1977**, *99*, 1692.
[2] P. Kaszynski, A. G. Doughlass, *J. Organomet. Chem.*, **1999**, *581*, 28.
[3] W. H. Knoth, *J. Am. Chem. Soc.* **1966**, *88*, 935.
[4] P. Kaszynski, J. Huang, G. S. Jenkins, K. A. Bairamov, D. Lipiak, *Mol. Cryst. Liq. Cryst.* **1995**, *260*, 315.
[5] M. A. Fox, J. A. H. Macbride, R. J. Peace, K. Wade, *J. Chem. Soc. Dalton Trans.* **1998**, 401.
[6] a) Gaussian 98 (Revision A.7), M. J. Frisch, G. W. Trucks, H. B. Schlegel, G. E. Scuseria, M. A. Robb, J. R. Cheeseman, V. G. Zakrzewski, J. A. Montgomery, R. E. Stratmann, J. C. Burant, S. Dapprich, J. M. Millam, A. D. Daniels, K. N. Kudin, M. C. Strain, O. Farkas, J. Tomasi, V. Barone, M. Cossi, R. Cammi, B. Mennucci, C. Pomelli, C. Adamo, S. Clifford, J. Ochterski, G. A. Petersson, P. Y. Ayala, Q. Cui, K. Morokuma, D. K. Malick, A. D. Rabuck, K. Raghavachari, J. B. Foresman, J. Cioslowski, J. V. Ortiz, B. B. Stefanov, G. Liu, A. Liashenko, P. Piskorz, I. Komaromi, R. Gomperts, R. L. Martin, D. J. Fox, T. Keith, M. A. Al-Laham, C. Y. Peng, A. Nanayakkara, C. Gonzalez, M. Challacombe, P. M. W. Gill, B. G. Johnson, W. Chen, M. W. Wong, J. L. Andres, M. Head-Gordon, E. S. Replogle, J. A. Pople, Gaussian, Inc., Pittsburgh, PA, **1998**; b) B3LYP is Becke's three parameter hybrid method with LYP correlation functional: c) A. D. Becke, *J. Chem. Phys.* **1993**, *98*, 5648; d) C. Lee, W. Yang, R. G. Parr, *Phys. Rev. B* **1988**, *37*, 785; e) S. H. Vosko, L. Wilk, M. Nusair, *Can. J. Phys.* **1980**, *58*, 1200; f) P. J. Stephens, F. J. Delvin, C. F. Chabalowski, M. J. Frisch, *J. Phys. Chem.* **1994**, *98*, 11623.
[7] a) R. Hoffmann, W. N. Lipscomb, *J. Chem. Phys.* **1962**, *36*, 2179; b) R. Hoffmann, *J. Chem. Phys.* **1963**, *39*, 1397.
[8] This can be compared with the polyhedral B–X bond lengths in experimentally known compounds: B-O = 1.480 ($B_{12}H_{11}OH^{2-}$), B-N = 1.521 ($B_{12}H_{11}$ $[NH_3]^{-1}$), B-S = 1.862 ($B_{12}H_{11}SH^{2-}$). I. B. Sivaev, V. I. Bregadze, S. SjÖberg, *Collect. Czech. Chem. Commun.* **2002**, *67*, 679.
[9] These orbital patterns are also seen in the DFT calculations.
[10] a) T. A. Albright, J. K. Burdett, M. Whangbo, *Orbital Interactions in Chemistry*, Wiley, New York, **1985**, chap. 22; b) M. A. Fox, K. Wade in *The Borane, Carborane, Carbocation continuum* (Ed.: J. Casanova), Wiley, New York, **1998**, p. 7.
[11] E. D. Glendening, A. E. Reed, J. E. Carpenter, F. Weinhold, NBO version 3.1, University of Wisconsin, WI, 1995.
[12] K. B. Wiberg, *Tetrahedron* **1968**, *24*, 1083.
[13] In the oxidized derivatives of $B_{12}(OR)_{12}^{2-}$ there is already some indication of exohedral multiple bonding and polyhedral deformation: T. Peymann, C. B. Knobler, S. I. Khan, M. F. hawthorne, *Angew. Chem.* **2001**, *113*, 1713; *Angew. Chem. Int. Ed.* **2001**, *40*, 1664; see also M. L. McKee, *Inorg. Chem.* **2002**, *41*, 1299.
[14] For comparison, the HOMO–LUMO gaps in $B_6H_6^{2-}$, $B_7H_7^{2-}$ and $B_{12}H_{12}^{2-}$ are 6.55 eV, 6.55 eV and 7.25 respectively.
[15] G. Seitz, P. Imming, *Chem. Rev.* **1992**, *92*, 1227.

 © 2003 Wiley-VCH Verlag GmbH & Co. KGaA, Weinheim

Iron Cluster with High Spin

Solvothermal Synthesis of a Tetradecametallic Fe^{III} Cluster**

David M. Low, Leigh F. Jones, Aidan Bell, Euan K. Brechin, Talal Mallah, Eric Rivière, Simon J. Teat, and Eric J. L. McInnes**

Polymetallic cluster complexes of paramagnetic transition-metal ions have attracted intense study since the discovery that such molecules can display the phenomenon of single-

[*] E. K. Brechin, E. J. L. McInnes, D. M. Low, L. F. Jones, A. Bell
Department of Chemistry
The University of Manchester
Oxford Road, Manchester, M13 9PL, (UK)
Fax: (+44) 161–275-7857
E-mail: euan.k.brechin@man.ac.uk
eric.mcinnes@man.ac.uk

Prof. T. Mallah, Dr. E. Rivière
Université Paris-Sud, Bat. 420
Laboratoire de Chimie Inorganique, UMR CNRS 8613
91405 Orsay (France)

Dr. S. J. Teat
CCLRC Daresbury Laboratory
Daresbury, Warrington, Cheshire, WA4 4AD (UK)

[**] This work was supported by the EPSRC (UK), Lloyd's of London Tercentenary Foundation and the European Community (contract HPRN-CT-1999–00012/TMR network "MolNanoMag").

 DOI: 10.1002/anie.200351865 © 2003 Wiley-VCH Verlag GmbH & Co. KGaA, Weinheim

molecule magnetism (SMM).[1] There is a barrier to relaxation of magnetisation in SMMs due to the combination of a large ground-state spin multiplicity and a significant negative zero-field splitting of that ground state, and this imparts a molecular magnetic memory effect. Unfortunately, all SMMs made to date only exhibit a memory effect at very low temperatures. Therefore, there is a huge effort in synthesizing larger clusters in an attempt to generate larger spin ground states and higher energy barriers to loss of magnetization.

To date, most cluster synthesis has involved "conventional" coordination chemistry techniques, that is, solution chemistry under atmospheric pressure and at temperatures limited to the boiling points of common solvents. We have been investigating the use of solvothermal techniques—chemistry in superheated solvents—towards cluster synthesis.[2] The solvothermal technique allows not only the application of high temperatures to reactions in low boiling solvents but is also a superb technique for crystallizing the products. We previously reported that superheating alcoholic solutions of trimetallic $[Cr_3O(O_2CMe)_6(H_2O)_3]Cl$ yields the decametallic Cr^{III} clusters $[Cr_{10}(OR)_{20}(O_2CMe)_{10}]$ (R = Me, Et).[2] We are now exploring the solvothermal chemistry of other simple basic metal acetates and report herein the isolation of a tetradecametallic Fe^{III} cluster by using the ligand benzotriazole (BtaH). Benzotriazole has previously been used to produce model compounds for corrosion inhibiton studies and in M^{II} cluster chemistry,[3] but until recently never in the synthesis of M^{III} clusters.[4]

A solution of $[Fe_3O(O_2CMe)_6(H_2O)_3]Cl$ in MeOH was superheated at 100 °C for 12 h to give a red solution, from which only insoluble powders could be isolated. However, an analogous reaction in the presence of the potential bridging ligand benzotriazole (BtaH) in MeOH followed by slow cooling gives a red crystalline product, **1**. The equivalent reaction at reflux under atmospheric pressure gives only solutions from which no clean product can be isolated. Single-crystal X-ray diffraction studies[5] of **1** reveals the structure to be the tetradecametallic Fe^{III} cluster $[Fe_{14}(bta)_6O_6(OMe)_{18}Cl_6]$ (Figure 1). Complex **1** has crystallographic C_i symmetry although there is pseudo threefold symmetry down the Fe1–Fe1A vector.

The metallic core of **1** can be described as a hexacapped hexagonal bipyramid with the caps on alternate faces (Figure 2). The three face capping iron ions [Fe2, Fe3, Fe4 and symmetry equivalents] and the apical iron [Fe1 and symmetry equivalents] on either half of the molecule form two $\{Fe_4(bta)_3Cl_3\}$ units each separated by nine μ_2-methoxides and three μ_4-oxides [O1, O2, and O3] from a central $\{Fe_6\}$ ring. The Bta^- ligands bind in a μ_3-fashion to generate $\{Fe_4(bta)_3\}$ fragments: the three "arrowhead" or central nitrogens in each fragment all bond to Fe1 (or symmetry equivalents) and the other two nitrogens on each Bta^- bind two of Fe2, Fe3, Fe4 (and symmetry equivalents). Each of the face caps also has a terminal chloride (Cl1, Cl2, and Cl3), with the coordination sphere of the apical Fe1 completed by three μ_4-oxides [O1,O2,O3] bridging it to each of Fe2, Fe3, and Fe4 and to the central $\{Fe_6\}$ ring [Fe5, Fe6, Fe7, and symmetry equivalents]. Remarkably, there is no carboxylate in the structure.

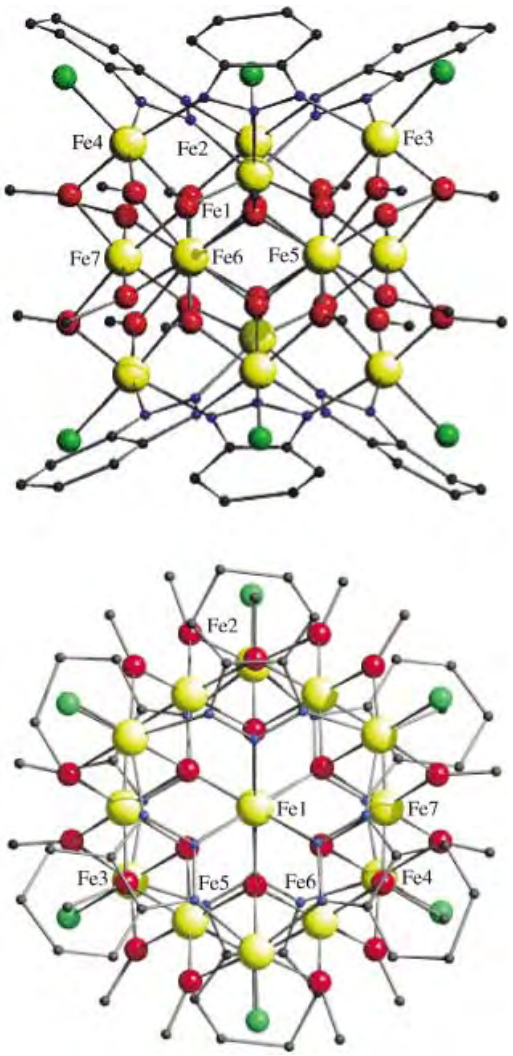


Figure 1. Molecular structure of $[Fe_{14}(bta)_6O_6(OMe)_{18}Cl_6]$ **1**. (top) Viewed perpendicular to the Fe1–Fe1A axis; (bottom) viewed down the Fe1–Fe1A axis. Bond length ranges: Fe-N 2.063–2.183 Å, Fe-Cl 2.235–2.267 Å, Fe-O(Me) 1.949–2.071 Å, Fe-μ_4O 1.935–2.174 Å. Colour scheme: Fe, yellow; O, red; N, blue; Cl, green.

The $\{Fe_6\}$ ring is near planar (0.0066 Å mean deviation from the best least-squares plane) with each iron ion bound to two μ_4-oxides, two μ_2-methoxides bridging to Fe1 and its symmetry equivalents, and two μ_2-methoxides bridging within the $\{Fe_6\}$ ring.

All the iron centers are Fe^{III}, as required by the charge balance of the formula, and the μ_4-oxides preclude any ambiguity of oxide versus hydroxide. This was also confirmed by Bond Valence Sum (BVS) calculations.[6] To our knowledge, complex **1** is the first example of an Fe_{14} cluster[17] and is amongst the highest nuclearity iron clusters reported to date, superseded only by Fe_{16}[7] and Fe_{18} wheels,[8] an Fe_{17} cluster,[9] the "captured rust" Fe_{17}/Fe_{19} clusters reported by Heath and Powell,[10] and a heterometallic species containing thirty Fe^{III} ions.[11]

The $\{Fe_4(bta)_3\}$ moiety resembles that formed between Bta^- and divalent metal cations, in which a centred tetrahedron of metal ions is held together by six μ_3-Bta^- ligands in a

 © 2003 Wiley-VCH Verlag GmbH & Co. KGaA, Weinheim

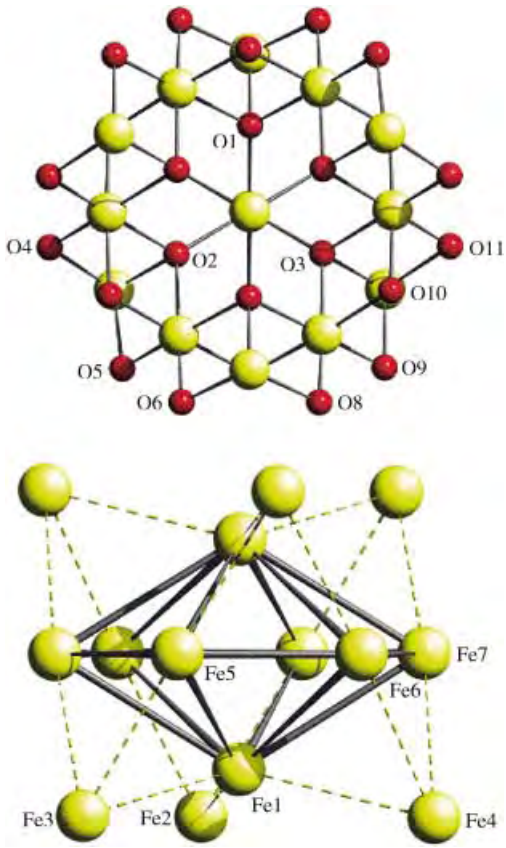


Figure 2. The metal–oxygen core viewed down the Fe1–Fe1A axis (top); The hexacapped hexagonal bipyramidal metallic skeleton (bottom). Fe···Fe distance ranges: Fe(3)···{Fe_6} ring 3.543–3.562 Å, Fe(3)···Fe(face caps) 3.147–3.425 Å, adjacent ions within {Fe_6} ring 3.023–3.043 Å, Fe(face cap)···{Fe_6} ring 3.095–3.129 Å.

similar fashion to give {$M_5(bta)_6$} cores.[12] Nonametallic Ni^{II} and hexaicosametallic Mn^{III} clusters, bound by μ_3-Bta^- type ligands, were also reported.[13,4] The {$Fe_4(bta)_3$} unit is flattened considerably with respect to a fragment of an idealized tetrahedron with Fe(face cap)-Fe(apex)-Fe(face cap) angles in the range 114.9–115.6°.

Solid-state dc magnetization measurements were performed on **1** in the range 2–300 K, in a field of 2.0 kG between 300 and 50 K and 0.5 kG below 50 K. The $\chi_M T$ value is equal to 57 emu mol^{-1} K at 300 K and it then increases steadily with decreasing temperature, reaching a maximum value of 163 emu mol^{-1} K at 17 K, before dropping dramatically below this temperature to a value of approximately 74 emu mol^{-1} K at 2 K (Figure 3). The value of the maximum in $\chi_M T$ suggests that the ground spin state is at least equal to 18. The collapse of $\chi_M T$ below 17 K may be a consequence of either zero-field splitting within the ground state as evidenced from M = f(H/T) data, or of the presence of intermolecular antiferromagnetic interactions between clusters at low temperature.

To determine the value of the spin ground state, magnetization measurements were performed at 3, 4 and 6 K between 0.1 and 5.5 Tesla. We attempted to fit the data assuming different spin states (S) between 21 and 24. The best fit (first made for each temperature independently and

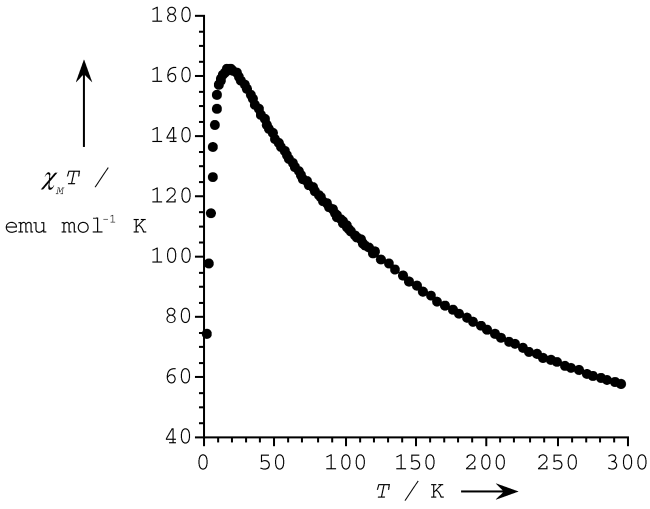


Figure 3. Plot of $\chi_M T$ vs T for **1**.

second by simultaneously fitting the data for the three temperatures) was obtained for $S = 23$ as the ground state with the following parameters: $g = 1.98$ and $D = 0.08\ cm^{-1}$ (Figure 4; $g = g$ factor, D = zero-field splitting parameter).

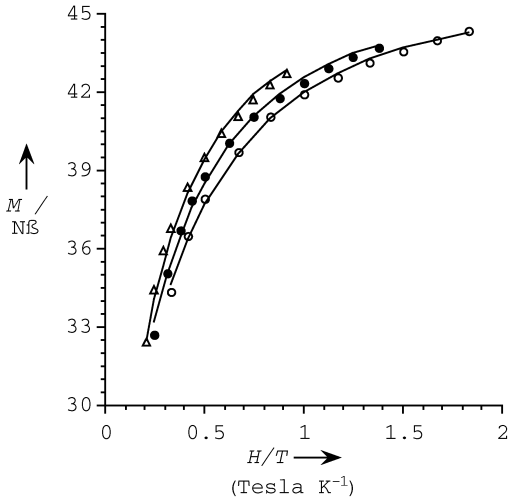


Figure 4. Plot of magnetization (M/Nβ) vs H/T for **1** in the ranges 0.1–5.5 T and 3 (o), 4 (●) and 6 (△) K. The solid lines are fits to $S = 23$, $g = 1.98$ and $D = 0.08\ cm^{-1}$.

This represents only a preliminary assignment of the spin ground state—a more detailed analysis will be reported in a full paper. Presumably the presence of such a large spin ground state is due to the presence of competing antiferromagnetic and ferromagnetic exchange coupling interactions between the Fe^{III} ions. A closer examination of the structure of **1** reveals that the Fe–O–Fe bridges fall into two clear categories: those that connect the apical Fe ions (Fe1 and Fe1A) to the face cap and equatorial Fe ions (through the μ_4-oxides) are characterized by angles of 113–125°, while those that connect all other Fe ions (through the μ_2-methoxides and the μ_4-oxides) are much smaller, characterized by angles less

 © 2003 Wiley-VCH Verlag GmbH & Co. KGaA, Weinheim

than 102°. If we assume that the larger angles will lead to the strongest antiferromagnetic exchange, thus dominating the other interactions, then we are left with a situation whereby the spins on Fe1 and Fe1A are antiferromagnetically coupled to all the other spins, which leads to twelve "spin up" $S = 5/2$ centers and two "spin down" $S = 5/2$ centers and an overall $S = 25$ ground state. While the best fit to the magnetic data is for an $S = 23$ ground state rather than $S = 25$, it is clear that a very large spin for this molecule can be rationalized.

Complex **1** would represent not only the highest spin Fe cluster yet reported but possibly the highest spin molecule known. The $S = 39/2$ Mn_9W_6 molecule reported by Hashimoto and co-workers[14] and the $S = 33/2$ Fe_{19} cluster[10] are the highest spin ground states reported, although an $S = 51/2$ ground state was suggested for a Mn_9Mo_6 cluster.[15] Ac susceptibility measurements, single-crystal studies and multi-frequency EPR experiments are currently underway to confirm the precise nature of S and the amplitude and sign of the zero-field splitting parameter D. These results will be reported at a later date.

This work highlights two significant advantages of the solvothermal technique for large paramagnetic cluster synthesis. The first is the synthesis of products different to those available from analogous reactions under conventional conditions—no cluster product was isolated after the reaction mixture had been heated at reflux. Second, solvothermal techniques allow the crystallization of high nuclearity products directly from the reaction mixture in good yield. Solvothermal techniques were originally developed by geochemists to mimic mineral growth, and have long been used for crystallization of inorganic materials.[16] This propensity for crystal growth will be hugely important in cluster chemistry given the reliance of this chemistry on X-ray diffraction for product identification.

Experimental Section

$[Fe_3O(CH_3CO_2)_6(H_2O)_3]Cl$ (0.32 mmol), BtaH (0.32 mmol) and MeOH (9 mL) were placed in a sealed Teflon container and heated for 12 h at 100 °C. X-ray quality crystals of **1** appeared on cooling the MeOH solution, in approximately 40% yield. Elemental analysis calcd(%)for $Fe_{14}C_{54}H_{78}O_{24}N_{18}Cl_6$: C 27.51, H 3.33, N 10.69, Fe 33.16; found: C 27.65, H 3.55, N 10.78, Fe 32.88. Selected IR data (KBr pellet): $\tilde{\nu}$2924(m), 2820(m) 1573(w), 1442(w), 1273(w), 1222(m), 1055(s), 787(m), 755(m), 573(m), 467 cm^{-1} (m).

Received: May 12, 2003 [Z51865]

Keywords: cluster compounds · iron · magnetic properties · N ligands · solvothermal chemistry

[1] a) R. Sessoli, H-L. Tsai, A. R. Schake, S. Wang, J. B. Vincent, K. Folting, D. Gatteschi, G. Christou, D. N. Hendrickson, *J. Am. Chem. Soc.* **1993**, *115*, 1804; b) R. Sessoli, D. Gatteschi, A. Caneschi, M. A. Novak, *Nature* **1993**, *365*, 141.

[2] E. J. L. McInnes, C. Anson, A. K. Powell, A. J. Thomson, R. Poussereau, R. Sessoli, *Chem. Commun.* **2001**, 89.

[3] M. Murrie, D. Collison, C. D. Garner, M. Helliwell, P. A. Tasker, S. S. Turner, *Polyhedron* **1998**, *17*, 3031.

[4] L. F. Jones, E. K. Brechin, D. Collison, A. Harrison, S. J. Teat, W. Wernsdorfer, *Chem. Commun.* **2002**, 2974.

[5] Crystal structure data for **1:** $C_{54}H_{78}C_{l6}Fe_{14}N_{18}O_{24}$, $M_r = 2357.94$, crystal size $0.05 \times 0.02 \times 0.01$ mm^3, monoclinic, space group, $P2(1)/n$ (no. 14) $a = 14.2255(6)$, $b = 19.4975(8)$, $c = 15.5833(7)$ Å, $\beta = 110.435(2)°$, $V = 4050.2(3)$ $Å^3$, $T = 150(2)$ K, $Z = 2$, $\rho_{calcd} = 1.933$ $g\,cm^{-3}$ $\mu(\lambda = 0.6845$ Å$) = 2.70$ mm^{-1}, 14319 reflections collected, 4178 unique ($R_{int} = 0.0567$), $R(F) = 0.0659$ and $wR2 = 0.1576$ using 3014 reflections with $I > 2\sigma(I)$. CCDC-209766 (**1**) contains the supplementary crystallographic data for this paper. These data can be obtained free of charge via www.ccdc.cam.ac.uk/conts/retrieving.html (or from the Cambridge Crystallographic Data Centre, 12 Union Road, Cambridge CB2 1EZ, UK; fax: (+44) 1223-336-033; or deposit@ccdc.cam.ac.uk).

[6] a) W. Liu, H. Thorp, *Inorg. Chem.* **1993**, *32*, 4102; b) I. D. Brown, D. Altermatt, *Acta Crystallogr. Sect. B* **1985**, *41*, 244.

[7] L. F. Jones, A. Batsanov, E. K. Brechin, D. Collison, M. Helliwell, T. Mallah, E. J. L. McInnes, S. Piligkos, *Angew. Chem.* **2002**, *114*, 4494; *Angew. Chem. Int. Ed.* **2002**, *41*, 4318.

[8] S. P. Walton, P. Fuhrmann, L. E. Pence, A. Caneschi, A. Cornia, G. L. Abbati, S. J. Lippard, *Angew. Chem.* **1997**, *109*, 2917; *Angew. Chem. Int. Ed. Engl.* **1997**, *36*, 2774.

[9] W. Micklitz, V. McKee, R. L. Rardin, L. E. Pence, G. C. Papaefthymiou, S. G. Bott, S. J. Lippard, *J. Am. Chem. Soc.* **1994**, *116*, 8061.

[10] a) S. L. Heath, A. K. Powell, *Angew. Chem.* **1992**, *104*, 191; *Angew. Chem. Int. Ed. Engl.* **1992**, *31*, 191; b) J. C. Goodwin, R. Sessoli, D. Gatteschi, W. Wernsdorfer, A. K. Powell, S. L. Heath, *J. Chem. Soc. Dalton Trans.* **2000**, 1835.

[11] A. Müller, S. Sarkar, S. Q. N. Shah, H. Bögge, M. Schmidtmann, S. Sarkar, P. Kögerler, B. Hauptfleisch, A. X. Trautwein, V. Schunemann, *Angew. Chem.* **1999**, *111*, 3435; *Angew. Chem. Int. Ed.* **1999**, *38*, 3238.

[12] see, for example, a) J. Handley, D. Collison, C. D. Garner, M. Helliwell, R. Docherty, J. R. Lawson, P. A. Tasker, *Angew. Chem.* **1993**, *105*, 1085; *Angew. Chem. Int. Ed. Engl.* **1993**, *32*, 1036; b) E. G. Bakalbassis, E. Diamantopoulou, S. P. Perlepes, C. P. Raptopoulou, V. Tangoulis, A. Terzis, T. F. Zafiropoulos, *J. Chem. Soc. Chem. Commun.* **1995**, 1347.

[13] V. Tangoulis, C. P. Raptopoulou, A. Terzis, E. G. Bakalbassis, E. Diamontopoulou, S. P. Perlepes, *Mol. Cryst. Liq. Cryst. Sci. Technol. Sect. A* **1999**, *335*, 463.

[14] Z. J. Zhong, H. Seino, Y. Mizobe, M. Hidai, A. Fujishima, S. Ohkoshi, K. Hashimoto, *J. Am. Chem. Soc.* **2000**, *122*, 2952.

[15] J. Larionova, M. Gross, M. Pilkington, H. Andres, H. Stoekli-Evans, H. U. Güdel, S. Decurtins, *Angew. Chem.* **2000**, *112*, 1667; *Angew. Chem. Int. Ed.* **2000**, *39*, 1605.

[16] see, for example, R. I. Walton, *Chem. Soc. Rev.* **2002**, *31*, 230.

[17] After the submission of this article, an Fe^{II}_{14} ellipse was reported: O. L. Sydora, P. T. Wolczanski, E. B. Lobkovsky, *Angewandte Chemie* **2003**, *115*, 2789; *Angew. Chem. Int. Ed.* **2003**, *42*, 2685

 © 2003 Wiley-VCH Verlag GmbH & Co. KGaA, Weinheim

Self-Organized Unimolecular Polymers

Templating of Silsesquioxane Cross-Linking Using Unimolecular Self-Organizing Polymers**

Eric F. Connor, Linda K. Sundberg, Ho-Cheol Kim, Jeroen J. Cornelissen, Teddie Magbitang, Phil M. Rice, Victor Y. Lee, Craig J. Hawker, Willi Volksen, James L. Hedrick, and Robert D. Miller**

The assembly of structures, molecule by molecule, into a defined macroscopic or mesoscale object is known as the "bottom-up" approach to nanomanufacturing.[1] This approach will become more important in the semiconductor field, as dimensions continue to decrease. Modern chips contain up to 10 km of copper wiring, which can connect between 200 and 500 million silicon transistors on a single centimeter-sized chip. As a direct result of increasing wiring and device densities, insulating materials with lower dielectric constants will be required to mitigate signal delays and crosstalk while simultaneously decreasing electrical power consumption. For materials with dielectric constants $k < 2.0$, porosity is required, a factor fueling the current interest in porous films.[2]

While the incorporation of air ($k = 1.01$) significantly lowers the dielectric constant of any matrix polymer, to be useful for on-chip dielectrics, the pores in the foam must be 5–10 times smaller than the minimum device features, currently approaching 100 nm. Typically, nanoporosity is introduced into amorphous spin-applied films using sacrificial organic materials (porogens or pore generators).[3] With most macromolecular porogens, nanoscopic domains develop by a liquid–solid phase separation caused by cross-linking of the thermosetting resin; a typical nucleation and growth (NG) process.[4] To prevent macroscopic phase separation, the porogen must be initially miscible in the matrix. Subsequent curing of the resin results in both chemical changes and accompanying molecular-weight increases in the matrix, which drive the phase separation of the porogen. Ideally these nucleated polymer domains, which may consist of many polymer chains, remain nanoscopic in scale with growth inhibited by the cross-linking matrix (kinetically arrested growth), a process that is typically difficult to control.[3] In this communication, we describe the generation of a nanoporous material from an amorphous thermosetting prepolymer, where the porosity is generated from single polymer molecules that exhibit unimolecular self-organization. The process requires a stimuli-responsive, star-shaped copolymer that creates a nanosized domain[5] through a matrix-mediated collapse of the interior core of the core-corona polymeric structure (Figure 1 a–c). The outer corona of the star renders the insoluble core compatible with the thermosetting resin and suppresses aggregation or precipitation of the insoluble interior, so that a single polymer molecule templates cross-linking and ultimately generates a single hole. Other processes produce nanoporous thin films,[6] however, this simple approach does not require concurrent monomer hydrolysis to produce a prematrix or dynamic reorganization of amphiphilic polymers to produce supermolecular aggregates, but is a system that conforms with the rapid spin-and-bake sequence required for semiconductor manufacturing, while incorporating a control for nanoscopic pore size.

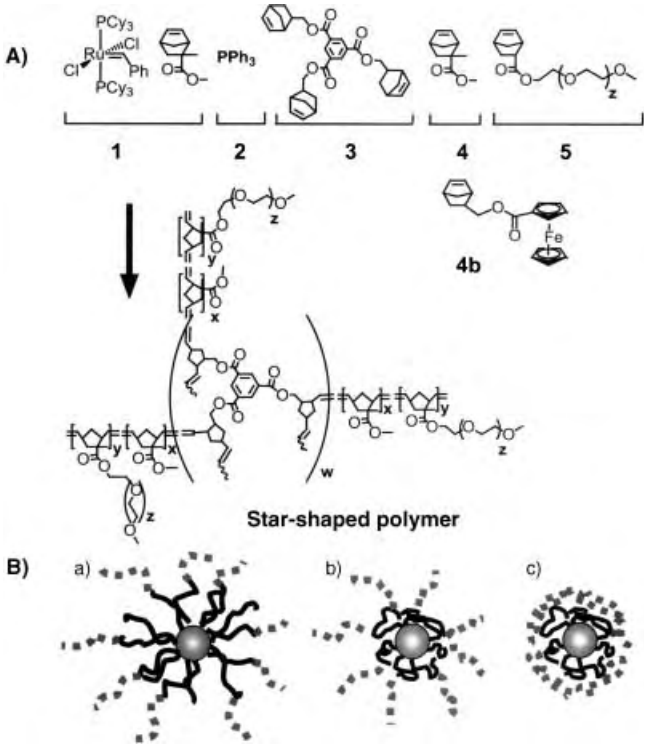


Figure 1. A) Outline of the stepwise synthesis of norbornene star-shaped copolymers (steps 1–5); B) solvent stimuli response of the unimolecular micelle: a) Swollen star polymer in good solvent for both the core and the corona; b) selective collapse of the hydrophobic core in a polar medium (e.g., MSSQ prepolymer); c) collapse of both the core and the corona in a poor solvent for both (e.g., cross-linked MSSQ).

A bottom-up route to unimolecular micellar star polymers using ruthenium-catalyzed ring-opening-metathesis polymerization (ROMP)[7] is described for the first time (details are provided in the Supporting Information). In a single pot,

[*] J. L. Hedrick, R. D. Miller, E. F. Connor, L. K. Sundberg, H.-C. Kim, J. J. Cornelissen, T. Magbitang, P. M. Rice, V. Y. Lee, C. J. Hawker, W. Volksen
IBM Almaden Research Center
650 Harry Road, San Jose, CA 95120 (USA)
Fax: (+1) 408-927-3310
E-mail: Hedrick@almaden.ibm.com
rdmiller@almaden.ibm.com

[**] Partial funding by the National Institute of Science and Technology (NIST) through an ATP cooperative agreement (70NANB8H4013) and the NSF Center for Polymeric Interfaces and Macromolecular Assemblies (CPIMA) is acknowledged. L.K.S. acknowledges partial financial support from JSR Microelectronics. The authors thank Eugene Delenia for expert assistance with TEM studies and Richard Siemens and Lucy Li for their definitive thermal analysis studies.

Supporting information for this article is available on the WWW under http://www.angewandte.org or from the author.

 DOI: 10.1002/anie.200350930 © 2003 Wiley-VCH Verlag GmbH & Co. KGaA, Weinheim

living oligomers (steps 1 and 2) are coupled to a polyfunctional cross-linking core (step 3) and the substructure is further elaborated by subsequent living polymerization (step 4), which generates additional arms (Figure 1). The reaction is completed by the addition of a norbornyl ester monomer containing a short polyethylene oxide (PEO) chain ($M_n = 2000$; step 5), to form the final "full star" that contains 30–40 wt % PEO incorporated in a comb architecture. The star polymers were subsequently hydrogenated for thermal and oxidative stability. By using a living polymerization technique, the molecular weight of the respective polymer chains can be controlled, a feature which ultimately governs both the size of the template and its relative hydrophilic/hydrophobic balance.

The size of the star polymer (as a solution in THF) was determined using dynamic light scattering (DLS).[8] In solution, a single star-shaped polymer assumes a solvent-swollen state and hence the values obtained by DLS represent the upper limit in size. The polymer samples (A and B, Table 1) were also studied by static light scattering (SLS), which provides both absolute molecular weights and the radius of gyration (R_g). The smaller star (polymer A) had an R_g value of 11.1 nm, while that of the larger star (polymer B) was 26.1 nm. The size distribution for both polymers was relatively narrow, consistent with the low-molecular-weight polydispersity index measured by both gel permeation chromatography (GPC) and SLS (Table 1). We used transmission electron microscopy (TEM) to estimate the sizes of the polymers in the dry state; under these conditions a single polymer molecule is assumed to be collapsed. To improve electron contrast for TEM imaging, star polymers analogous to samples A and B (GPC and DLS) that contained ferrocenyl monomer units were prepared. The ferrocenyl co-monomer (**4b**, Figure 1) was added after the core cross-linking step. From the TEM images of the star polymers, a number-average radius was calculated and taken as being representative of their templating size. The average radius for polymers A and B was 8.0 and 12.5 nm, respectively, with each sample showing a narrow size distribution (Figure 2). These particular micellar polymers are a convenient size for visualization by microscopy and to demonstrate the templating concept for the formation of amorphous porous materials.

The amphiphilic polymers (samples A and B) were dissolved in a solution containing methyl silsesquioxane (MSSQ) prepolymer in propylene glycol monomethyl ether and the resulting solution was spun on a silicon wafer to produce thin films. The sample was heated to 450 °C at a rate of 5 °C min^{-1}. During this process, the resin becomes progressively more cross-linked and hydrophobic as the initially present polar silanol end groups condense (150–250 °C). Upon further curing, the star polymer thermally degrades to low-molecular-weight products which vaporize (350–400 °C) to leave behind a hole or pore. For a true templated process,[9] the pore sizes should be independent of porogen concentration below the percolation threshold and reflect the actual size of the additive. This mechanism is distinguished from a NG process, where the domain sizes and shape depend strongly on porogen concentration, molecular weight, and processing conditions.[10a] Two cross-sectional TEM pictures illustrate the remarkable differences in the porous morphologies produced by NG and templating mechanisms (Figure 3). The NG morphology was generated using a linear methacrylate copolymer, which was initially miscible in the MSSQ resin.[10b] The pores generated through single-polymer templating (sample A) are clearly more regular in size and shape. Representative field-emission scanning electron microscopy (FE-SEM) of porous MSSQ produced from two different

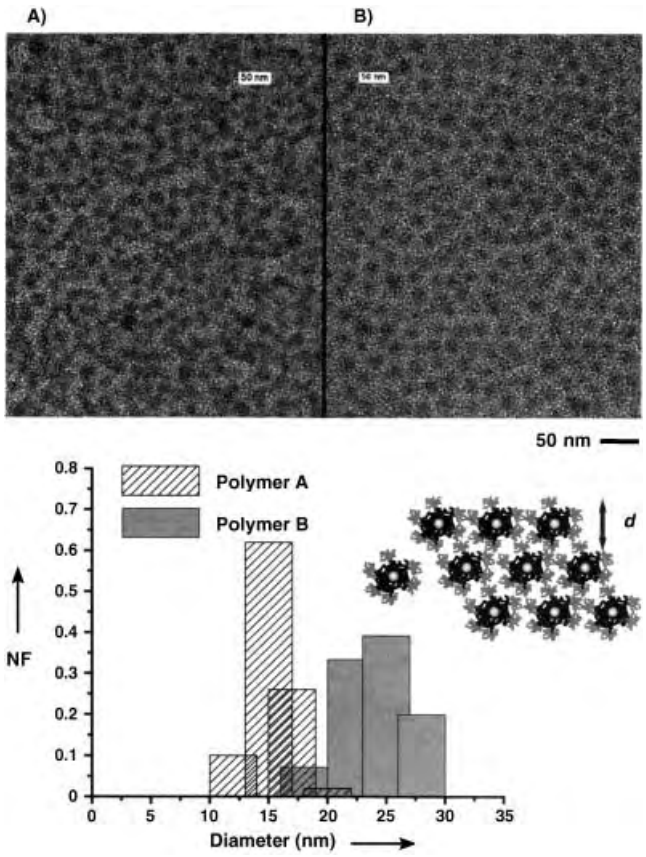


Figure 2. Above: TEM images of two different-sized star-shaped polynorbornene polymers (samples A and B, Table 1) containing ferrocene units (dark features) for contrast enhancement; below: size histograms produced from the TEM micrographs. NF = number fraction.

Table 1: Size characterization of the amphiphilic star polymer by dynamic light scattering, static light scattering, and TEM analysis.

Polymer sample	QR_n [nm]	R_g [nm]	R_{hs} [nm]	M_w [$\times 10^{-6}$ g mol^{-1}]	QR_w/R_n	SR_w/R_n	PD	TEM R_n [nm]
A	10.8	11.1	14.3	0.35	1.09	1.06	1.15	8.0
B	23.8	26.1	33.6	1.82	1.21	1.30	1.30	12.5

QR_n = hydrodynamic radius (DLS in tetrahydrofuran). R_g = radius of gyration (SLS in tetrahydrofuran). R_{hs} = hard sphere radius [$(5/3)^{0.5} \times R_g$]. QR_w/R_n = polydispersity determined by DLS. SR_w/R_n = polydispersity determined by SLS. M_w = molecular weight determined by SLS. PD = polydispersity determined by GPC. TEM R_n = number average radius, derived from transmission electron microscopy.

 © 2003 Wiley-VCH Verlag GmbH & Co. KGaA, Weinheim

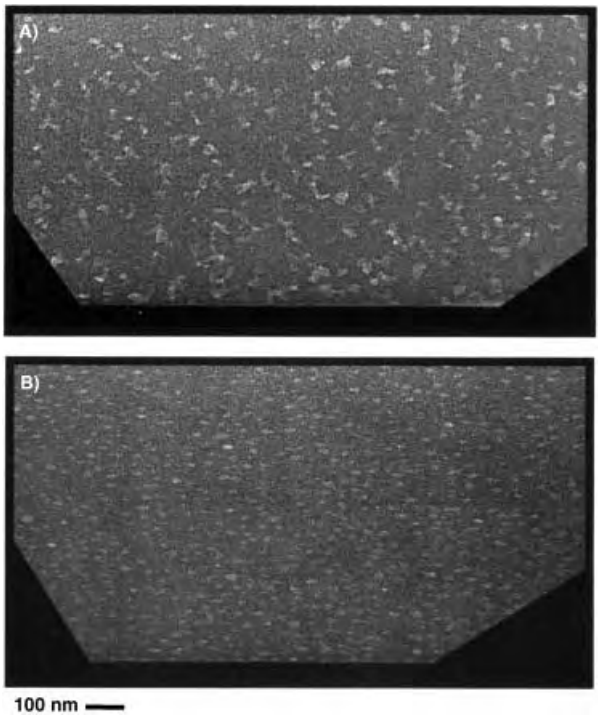


Figure 3. TEM pictures showing the differences in porous morphologies generated by: A) Nucleation and growth (NG),[9] and B) unimolecular templating techniques.

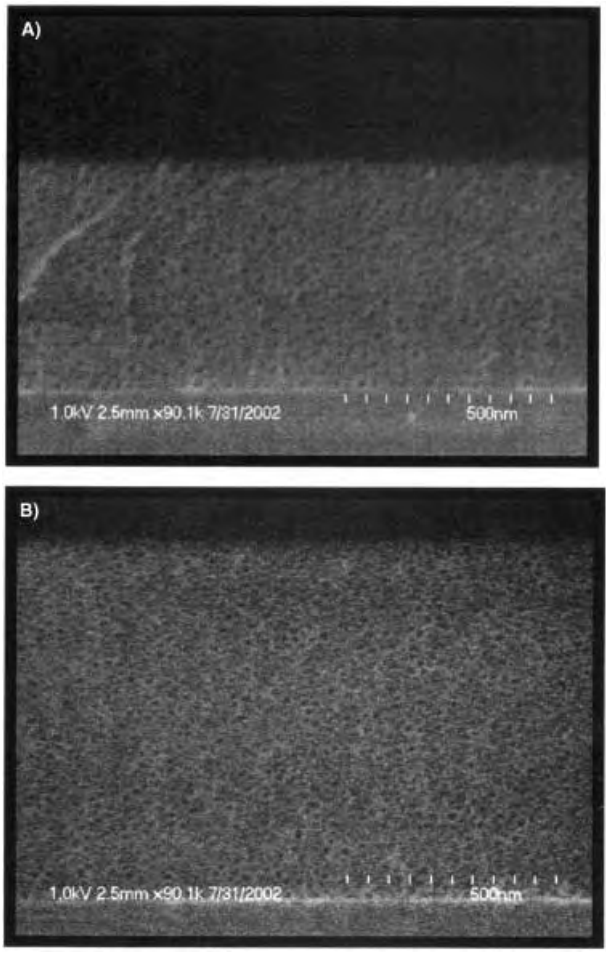


Figure 4. FE-SEM images of nanoporous MSSQ generated using different loadings of a unimolecular self-assembling star-shaped polymer (sample A, Table 1): A) 10 wt%; B) 30 wt%.

micellar poly(norbornene) loading levels (10 and 30 wt%) are shown in Figure 4 (the upper concentration limit for this star polymer/silsesquioxane system is around 35 wt%, above which aggregation begins to occur). The pore sizes in each sample are similar and a compositional invariance of morphology is observed; that is, only the pore density increases with loading level. For a templating process, two star polymers differing in size (for example, samples A and B, Table 1) should produce foams with hole sizes reflecting the respective porogen dimensions. Two cross-sectional TEM micrographs of these respective films are shown (Figure 5). Curiously, the pores are slightly elliptical, that is, elongated in the wafer plane, a feature that could result from a number of conditions; for example, the radial shear stresses produced during spinning, partial in-plane pore collapse, or perhaps as a result of the focussed ion beam (FIB) procedure used to prepare the sample (this effect is under investigation). The histograms generated for the porous films show that the hole sizes (measured along the longest axis) in the matrix resin (Figure 5) correlate with the dry size of the micellar polymers measured by TEM (Figure 4). Also, the distribution in pore size reflects the size dispersity of the polymer samples. These data collectively provide strong evidence that the star polymers behave as a unimolecular template during MSSQ vitrification. This particle-like behavior occurs in spite of the fact that cross-linking in the porogen is minimal and confined to a small molecular core.

Thermal analysis by dynamic mechanical analysis (DMA) of the micellar star polymers in the hybrid samples (see Supporting Information) confirms that at least the internal hydrophobic core of the micellar polymers is phase-separated

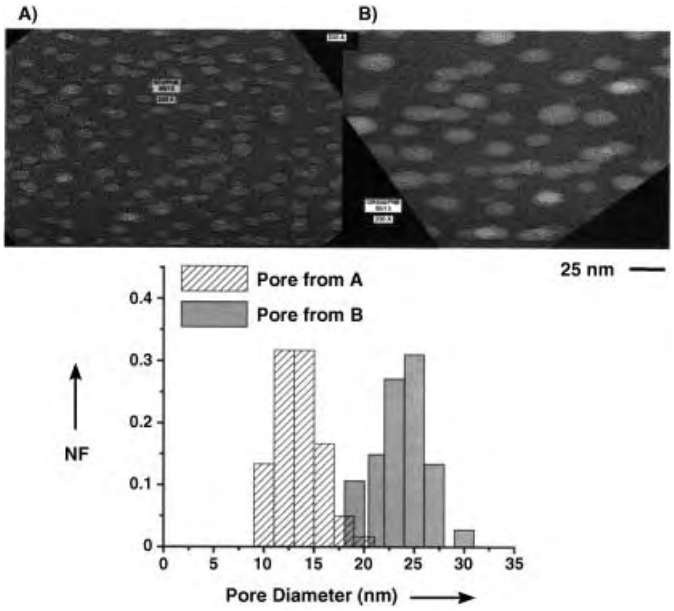


Figure 5. Above: TEM pictures of two porous MSSQ samples prepared from two different-sized star polymers (samples A and B, Table 1); below: size histograms produced from the TEM micrographs. NF = number fraction.

 © 2003 Wiley-VCH Verlag GmbH & Co. KGaA, Weinheim

from the MSSQ resin after soft curing (150 °C). The PEO arms are ultimately expelled during further curing (to 200 °C) by frustrated phase separation generating the single-polymer templating morphology.[11] The dielectric constants of the porous samples (see Supporting Information) decrease predictably from 2.8 to 1.7 with increasing porogen loading (0–50 %).

In summary, unimolecular amphiphilic star polymers, synthesized by ROMP procedures, provide a controlled templating effect during the thermal cure of amorphous silsesquioxane derivatives. The unimolecular nature of the polymeric micellar materials eliminates the complex dynamic assembly characterizing most amphiphilic systems. Porogen burnout results in nanoporous films where the pore sizes and distributions reflect the dimensions of single polymer molecules. By using controlled chemical synthesis to produce defined macromolecules, macroscopic nanostructured thin films of technological utility are produced providing a cogent example of the evolution from nanoscience to nanotechnology. Additional applications of unimolecular micellar templating will be discussed in future publications.

Received: January 13, 2003 [Z50930]
Published online: July 28, 2003

Keywords: metathesis · nanoporous materials · polymers · self-assembly · template synthesis

[1] H. Doumanidis, *Nanotechnology* **2002**, *13*, 248.
[2] R. D. Miller, *Science* **1999**, *286*, 421.
[3] a) J. L. Hedrick, T. Magbitang, E. F. Connor, T. Glauser, W. Volksen, C. J. Hawker, V. Y. Lee, R. D. Miller, *Chem. Eur. J.* **2002**, *8*, 3308; b) S. Yang, P. A. Mirau, C. S. Pai, O. Nalamasu, E. Reichmanis, J. C. Pai, Y. S. Obeng, J. Seputro, E. K. Lin, H. J. Lee, J. N. Sun, D. W. Gidley, *Chem. Mater.* **2002**, *14*, 369.
[4] J. Kiefer, J. L. Hedrick, J. G. Hilborn, *Adv. Polym. Sci.* **1999**, *147*, 161.
[5] a) M. Antonietti, R. Basten, S. Lohmann, *Macromol. Chem. Phys.* **1995**, *196*, 441; b) K. L. Wooley, *J. Polym. Sci. Part A* **2000**, *38*, 1397.
[6] S. Polarz, M. Antonietti, *Chem. Commun.* **2002**, *22*, 2593.
[7] a) T. M. Trnka, R. H. Grubbs, *Acc. Chem. Res.* **2001**, *34*, 18; b) C. W. Bielawski, R. H. Grubbs, *Macromolecules* **2001**, *34*, 8838.
[8] C. Graf, W. Schartl, K. Fischer, N. Hugenberg, M. Schmidt, *Langmuir* **1999**, *15*, 6170.
[9] D. Y. Zhao, J. L. Feng, Q. S. Huo, N. Melosh, G. H. Fredrickson, B. F. Chmelka, G. D. Stucky, *Science* **1998**, *279*, 548.
[10] a) E. Huang, M. F. Toney, W. Volkesen, D. Mecerreyes, P. Brock, H. C. Kim, C. J. Hawker, J. L. Hedrick, V. Y. Lee, T. Magbitang, R. D. Miller, *Appl. Phys. Lett.* **2002**, *81*, 2232; b) Q. R. Huang, W. Volksen, E. Huang, M. Toney, C. W. Frank, R. D. Miller, *Chem. Mater.* **2002**, *14*, 3676.
[11] E. A. Turi, *Thermal Characterization of Polymeric Materials, Vol. 1*, Elsevier/Academic Press, London, **1997**.

 © 2003 Wiley-VCH Verlag GmbH & Co. KGaA, Weinheim

Azasugar Synthesis

Nitrogen Inversion as a Diastereomeric Relay in Azasugar Synthesis: The First Synthesis of Adenophorine**

*Michael A. T. Maughan, Ieuan G. Davies, Timothy D. W. Claridge, Steve Courtney, Phil Hay, and Benjamin G. Davis**

Although amine nitrogen atoms are potential stereogenic centers, their configurational lability arising from lone-pair inversion[1] has typically prevented their utility in synthesis. *N*-Halogenation can dramatically slow lone-pair inversion[2] and therefore raise the temperature at which the configurational lability ceases. We therefore considered that if a suitable system could be found, *N*-chloramines might provide a new source of flexible, temperature-dependent stereogenesis. In turn, existing chiral information may then be relayed and exploited such that subsequent reactions are regio- or diastereoselective. Due to the often higher conformational lability of the acyclic N lone-pair isomers of *N*-haloamines, we selected cyclic amines for our study, which are typically, but not always, less labile due to angular constraint.[1] Cyclic systems have often been exploited for intramolecular relay of chirality.[3]

As our model chiral cyclic *N*-chloramine system we selected *N*-chloropiperidine azasugars. Polyhydroxylated nitrogen heterocycles such as deoxynojirimycin (DNJ, **1** in Scheme 1) may be considered to be mimics of sugars, for example, D-glucose, in which the ring oxygen has been replaced by a nitrogen atom.[4] The often potent inhibitory activity of many of these compounds towards carbohydrate-processing enzymes has suggested their use in a wide range of potential therapeutic strategies,[5–8] including the treatment of viral infections[9,10] and lysosomal storage diseases,[11,12] and as invaluable tools in the study of enzyme mechanism.[13]

[*] Dr. B. G. Davis, I. G. Davies, Dr. T. D. W. Claridge
Dyson Perrins Laboratory
Department of Chemistry
University of Oxford
South Parks Road, Oxford, OX1 3QY (UK)
Fax: (+44) 1865-275-674
E-mail: ben.davis@chem.ox.ac.uk

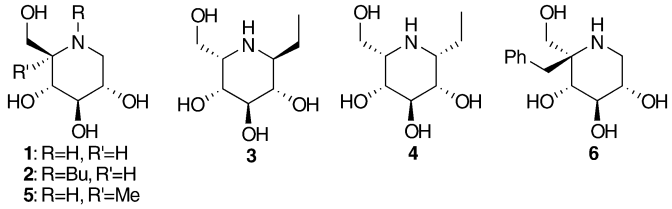
M. A. T. Maughan
Department of Chemistry
University of Durham
South Road, Durham, DH1 3LE (UK)

Dr. S. Courtney, Dr. P. Hay
Oxford Glycosciences Ltd.
The Forum
86 Milton Park, Abingdon, Oxfordshire, OX14 4RY (UK)

[**] This work was supported by the UK Engineering and Physical Sciences Research Council (EPSRC) and by Oxford Glycosciences Ltd. We would like to thank Dr. A. M. Kenwright for technical advice and Prof. N. Asano for spectroscopic data and the generous gift of an authentic sample of (+)-adenophorine.

Supporting information for this article is available on the WWW under http://www.angewandte.org or from the author.

 © 2003 Wiley-VCH Verlag GmbH & Co. KGaA, Weinheim DOI: 10.1002/anie.200351002

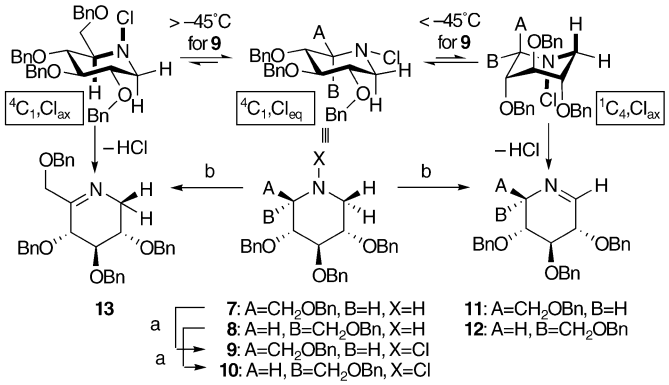


Scheme 1.

Azasugars carrying hydrophobic substituents, such as the butylated azasugar *N*-butyldeoxynojirimycin (**2**, NB-DNJ or Zavesca),[11] may show increased enzyme inhibition and enhanced bioavailability.[14] Therefore routes amenable to the ready installation of hydrophobic moieties are of high value.

Adenophorine, a rare example of a naturally occurring azasugar with hydrophobic substituents, was isolated from the roots of *Adenophora* spp. in 2000 by Asano and co-workers and was assigned the ethyl-substituted polyhydroxylated piperidine structure with the relative configuration shown in **3** (Scheme 1) on the basis of NMR investigations; its absolute configuration was not determined.[15] By virtue of its pseudoanomeric substituent,[16] adenophorine is a highly α-glycosidase-specific inhibitor (IC_{50} values for α-glucosidase: 32 μM, intestinal sucrase: 20 μM, α-galactosidase: 11 μM) that displays no detectable inhibition of β-glycosidases.[15]

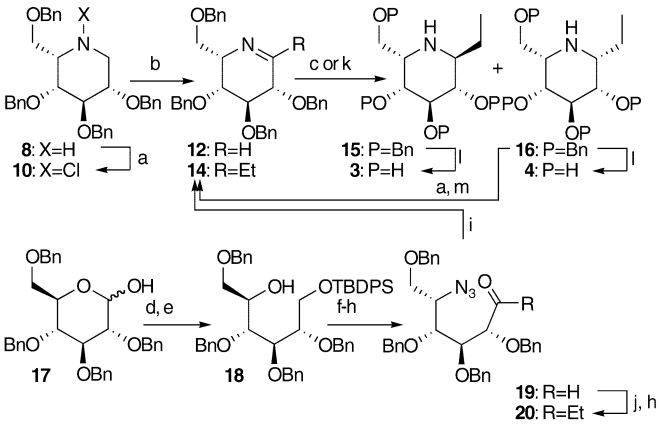
We reasoned that for the synthesis of adenophorine (**3**) a two-step process, consisting of regioselective elimination controlled by the switchable configuration at the chloramine nitrogen atom followed by addition of suitable nucleophiles to the resulting imine, might be used as a diastereomeric relay for the ready addition of hydrophobic functionality to a starting azasugar with regio- and stereocontrol (Scheme 2). We have shown previously that the highly functionalized piperidine azasugar **9** can undergo regioselective elimination.[17] In addition, building on the pioneering work of Horenstein and co-workers[18] and Furneaux and co-workers,[19] who demonstrated the addition of organometallic nucleophiles to a single pyrrolidine aldimine, we have recently shown that this is a general reaction that may be applied with high diastereoselectivity to several pyrrolidine aldimines.[17,20] We considered that addition of an ethyl nucleophile to idonojirimycin (INJ) aldimine **12** might provide convergent access to adenophorine (**3**) as well as ready access to analogues.[21]



Scheme 2. a) NCS, CH_2Cl_2, 97% for **9**, 93% for **10**; b) Base conditions for **9**→**11** < −45 °C: LiTMP, −78 °C, Et_2O; Base conditions for **9**→**13** > −45 °C: DBU, RT, Et_2O; Base conditions for **10**→**12**: DBU, reflux, Et_2O. DBU = 1,8-diazabicyclo[5.4.0]undec-7-ene, NCS = *N*-chlorosuccinimide, RT = room temperature, TMP = tetramethylpiperidine.

In this communication, we have applied this stereodynamic strategy to the first synthesis of adenophorine (**3**) and 1-*epi*-adenophorine (**4**) as well as hydrophobically modified DNJ variants **5** and **6**. To our knowledge this is the first example of a *N*-halogen stereogenic center in such a switchable, stereochemical relay.

Central to our approach (vide supra) we established the stereodynamics of the N–Cl bond in two piperidine systems. Tetrabenzyl DNJ **7**[22] and tetrabenzylidonojirimycin (tetrabenzyl INJ, **8**)[23] were prepared from D-glucose and smoothly *N*-chlorinated using *N*-chlorosuccinimide (NCS) to give DNJ-Cl **9** and INJ-Cl **10**, respectively, in excellent yields (Scheme 2 and Scheme 3). N-configurational exchange was evident by



Scheme 3. a) NCS, CH_2Cl_2, 93% for **10**; b) DBU, Et_2O, reflux; c) **12**→**16**: EtMgBr, Et_2O/dioxane, 47% over two steps from **10**; d) $NaBH_4$, THF/H_2O, 100%; e) TBDPSCl, imidazole, DMF, 99%; f) Method 1: MsCl, py, 97% then Bu_4N_3, toluene, reflux, 23% or Method 2: HN_3, DIAD, PPh_3, toluene, 87%; g) TBAF, THF, 100%; h) PCC, CH_2Cl_2, mol. sieves, 87% for **19**, 72% for **20**; i) PPh_3, Et_2O; j) EtMgBr, Et_2O, 70%; k) **14**→**15**/**16**: $NaBH_4$, MeOH, 17%:32% of **15**/**16** or $LiAlH_4$, THF, 69% of **15** only; l) H_2, $PdCl_2$, EtOH, 100% for **3**, 86% for **4**; m) LiTMP, −78 °C, Et_2O. DIAD = diisopropyl azodicarboxylate, PCC = pyridinium chlorochromate, py = pyridine, TBAF = tetrabutylammonium fluoride, TBDPSCl = *tert*-butyldiphenylsilyl chloride.

NMR in both **9** and **10** in the marked broadening of the resonances for C1 and C5 (Figure 1). Encouragingly, variable-temperature NMR experiments (VT-NMR) confirmed the existence at −55 °C of two species consistent with N-epimers of **9**, one of which was strongly dominant. When the sample was warmed from −55 °C to approximately −45 °C, a temperature that is accessible in standard synthesis, the signals of **9** started to broaden. Interestingly, signal broadening due to exchange was evident in **10** at much lower temperatures (< −80 °C);[24] only the control of the configurational exchange of **9** was required by our strategy (vide infra).

Gratifyingly and consistent with these observations, treatment of DNJ-Cl **9** with the base DBU at room temperature,

 © 2003 Wiley-VCH Verlag GmbH & Co. KGaA, Weinheim

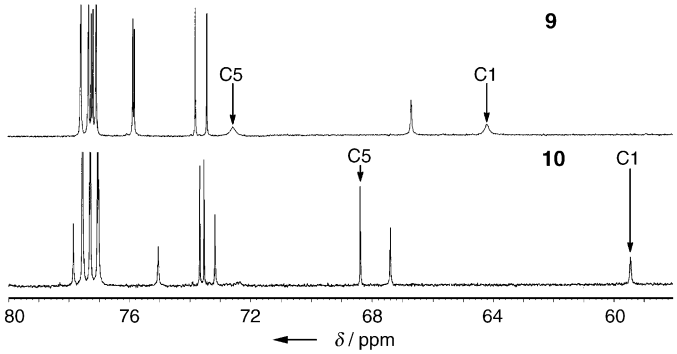
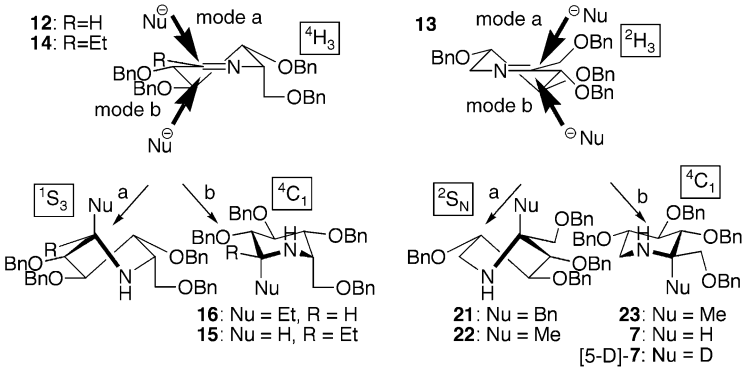


Figure 1. ^{13}C NMR spectra ($CDCl_3$, 125 MHz, 294 K) illustrating the dramatic broadening of the signals of the carbon atoms flanking the configurationally labile nitrogen atom in chloramines **9** and **10**.

above the point of N-configurational lability, yielded ketimine **13** (Scheme 2) (IR: $\tilde{\nu}=1667\ cm^{-1}$ (C=N), ^{13}C NMR: $\delta=168.5$ ppm (s, C5)), whereas treatment with LiTMP at −78 °C yielded DNJ-aldimine **11** (IR: $\tilde{\nu}=1654\ cm^{-1}$ (C=N), ^{13}C NMR: $\delta=162.3$ ppm (d, C1), ^1H NMR: $\delta=7.60$ ppm (br s, 1H, H1)). We interpret these results as being due to the relative accessibility of the conformational and configurational manifolds shown in Scheme 2. Above −45 °C elimination proceeds according to Curtin–Hammett principles via the $^4C_1, Cl_{ax}$ conformation that allows antiperiplanar elimination of $H5_{ax}$ and Cl_{ax}.[25] However, below −45 °C the $^4C_1, Cl_{eq} \rightleftarrows {}^4C_1, Cl_{ax}$ configurational manifold is inaccessible, and elimination proceeds via a conformation such as $^1C_4, Cl_{ax}$,[26,27] which allows elimination of $H1_{ax}$ and Cl_{ax}. To test these interpretations we studied the elimination of INJ-Cl **10**, for which the antiperiplanar elimination of H5 and Cl is not possible from its preferred $^4C_1$ conformation by virtue of the opposite configuration of **10** at C5. In accord with this model, elimination with DBU at reflux gave INJ-aldimine **12** as the exclusive product. To further confirm their identities imines **12** and **13** were also independently synthesized by novel routes employing Staudinger aza-Wittig reactions (Scheme 3).

Addition of EtMgBr to imine **12**, with the aim of synthesizing adenophorine, initially provided disappointing results, yielding only products consistent with intermediate tautomerization and/or elimination. To reduce the likelihood of these base-catalyzed processes, we added imine **12** to a solution of EtMgBr that had been pretreated with dioxane,[28] and gratifyingly obtained **16**. Subsequent deprotection gave protected 1-*epi*-adenophorine **4** as a single diastereomer (*de* > 98 %). Although we were pleased by the level of diastereoselectivity, our goal, the synthesis of adenophorine, required the opposite sense of selectivity, and this stimulated an investigation of the determining factors. An investigation of different nucleophile additions to ketimine **13**, as a near-enantiomeric substrate to INJ-aldimine **12**, revealed a graduation in the sense of selectivity (from mode a to b, Scheme 4) as the size of the nucleophile decreased, although electronic effects cannot be excluded.[29] Thus, addition of the bulky nucleophile BnMgCl yielded, exclusively by means of mode a, the highly substituted piperidine **21** as the only addition product albeit in low yield (19 %). The reaction with the smaller nucleophile MeMgBr yielded a mixture of products from mode a and mode b (d.r. 1:8, 17 %) **22** and **23**. Finally, reaction of **13** with yet smaller nucleophiles hydride and deuteride from $LiAlH_4$ and $LiAlD_4$ yielded, exclusively by means of mode b, **7** and [5-D]-**7** in 87 % and 93 % yield, respectively. We speculate that the two opposing modes may be influenced by two opposing factors: steric approach control[30] (mode a, H→S thereby developing strain, Scheme 4) and stereoelectronic control coupled with strain relief[31,32] (mode b, H→C, Scheme 4).[29]

The formation of protected *epi*-adenophorine **16** had indicated that Et_2Mg added to **12** exclusively by mode b.



Scheme 4. Competing modes a and b for the attack on polyhydroxylated imines are modulated by the size of the nucleophile (see Supporting Information for discussion).

Armed with the above information, we considered that only nucleophiles larger than Et^- would favor the desired addition mode a, and this appeared to block our convergent approach to the synthesis of adenophorine through addition of Et^- to **12**. However, according to this size-dependent model, addition of the small nucleophile hydride, again by means of mode b, to ethyl ketimine **14** as an alternative substrate would yield adenophorine. Ethyl ketimine **14** was synthesized in two ways: from **16** by our two-step chlorination–elimination approach and independently by means of a Staudinger aza-Wittig cyclization from ethylazidoketone **20**, which was in turn synthesized efficiently in 38 % yield from **17** in eight steps. Although the former provided a convenient way of converting **16** to **14**, the regioselectivity of the elimination step was poor and the latter route **17**→**14** was more efficient (overall yields: **16**→**15** 24 % over three steps, **17**→**15** 26 % over ten steps, vide infra). Reduction of **14** under various standard conditions ($NaBH_3CN$/AcOH, H_2/Pd, K-selectride) failed due to degradation or protecting-group incompatibilities. However, reduction with $NaBH_4$/MeOH yielded a mixture of mode-a and mode-b products (d.r. 1:2) **15** and **16**. The formation of **16** as a major mode b product highlighted the need for a yet smaller source of hydride. Gratifyingly, the use of $LiAlH_4$ yielded tetrabenzyladenophorine **15**

 © 2003 Wiley-VCH Verlag GmbH & Co. KGaA, Weinheim

in 69% yield ($de > 98\%$). Deprotection of **15** yielded (−)-adenophorine (**3**) ($[\alpha]_D^{22} = -52.3$ ($c = 0.20$ in water)) which was identical in all respects to a sample of the natural product save its opposite sense of rotation ($[\alpha]_D = +59.7$ ($c = 1.0$ in water)). On the basis of these results we have assigned the absolute configuration of the natural product (+)-adenophorine to the enantiomer of **3**.

In summary, we have exploited configurational dynamics at the nitrogen atom in azasugar chloramines to control the regiochemistry of elimination. Moreover, after the factors controlling stereoselectivity were determined, subsequent nucleophilic additions to the resulting imines were achieved with excellent diastereoselectivity. Together these represent, to the best of our knowledge, the first examples of a switchable, stereochemical relay from N to neighboring C1 or C5 positions. Furthermore, this imine methodology has enabled us to synthesize a number of novel hydrophobically modified azasugars. We were able to identify a good and highly selective inhibitor of human α-glucosidase[33] and completed the first synthesis of (−)-adenophorine, thereby allowing assignment of the configuration of the natural (+) isomer.

Received: January 23, 2003 [Z51002]

Keywords: asymmetric synthesis · azasugars · carbohydrates · glycosidase inhibitors · imines · stereodynamics

[1] A. Rauk, L. C. Allen, K. Mislow, *Angew. Chem.* **1970**, *82*, 453; *Angew. Chem. Int. Ed. Engl.* **1970**, *9*, 400.
[2] a) F. A. L. Anet, I. Yavari, *Tetrahedron Lett.* **1977**, *18*, 3207; b) H. Kessler, D. Leibfritz, *Tetrahedron Lett.* **1970**, *11*, 4297; c) J.-M. Lehn, J. Wagner, *J. Chem. Soc. D* **1970**, 414.
[3] S. D. Bull, S. G. Davies, D. J. Fox, A. C. Garner, T. G. R. Sellers, *Pure Appl. Chem.* **1998**, *70*, 1501.
[4] a) B. Winchester, G. W. J. Fleet, *Glycobiology* **1992**, *2*, 199; b) A. E. Stütz, *Iminosugars as Glycosidase Inhibitors*, Wiley-VCH, Weinheim, **1999**; c) N. Asano, R. J. Nash, R. J. Molyneux, G. W. J. Fleet, *Tetrahedron: Asymmetry* **2000**, *11*, 1645.
[5] Anticancer strategies: P. E. Goss, M. A. Baker, J. P. Carver, J. W. Dennis, *Clin. Cancer Res.* **1995**, *1*, 935.
[6] Antidiabetes strategies: K. A. Watson, E. P. Mitchell, L. N. Johnson, J. C. Son, C. J. F. Bichard, M. G. Orchard, G. W. J. Fleet, N. G. Oikonomakos, D. D. Leonidas, M. Kontou, A. C. Papageorgiou, *Biochemistry* **1994**, *33*, 5745.
[7] Antituberculosis strategies a) B. G. Davis, T. W. Brandstetter, L. Hackett, B. G. Winchester, R. J. Nash, A. A. Watson, R. C. Griffiths, C. Smith, G. W. J. Fleet, *Tetrahedron* **1999**, *55*, 4489; b) J. P. Shilvock, J. R. Wheatley, R. J. Nash, A. A. Watson, R. C. Griffiths, T. D. Butters, M. Muller, D. J. Watkin, D. A. Winkler, G. W. J. Fleet, *J. Chem. Soc. Perkin Trans. 1* **1999**, 2735.
[8] Antiparasite strategies: a) C. M. Li, P. C. Tyler, R. H. Furneaux, G. Kicska, Y. M. Xu, C. Grubmeyer, M. E. Girvin, V. L. Schramm, *Nat. Struct. Biol.* **1999**, *6*, 582; b) R. W. Miles, P. C. Tyler, G. B. Evans, R. H. Furneaux, D. W. Parkin, V. L. Schramm, *Biochemistry* **1999**, *38*, 13147.
[9] a) A. Karpas, G. W. J. Fleet, R. A. Dwek, S. Petursson, S. K. Namgoong, N. G. Ramsden, G. S. Jacob, T. W. Rademacher, *Proc. Natl. Acad. Sci. USA* **1988**, *85*, 9229; b) T. M. Block, X. L. Xu, F. M. Platt, G. R. Foster, W. H. Gerlich, B. S. Blumberg, R. A. Dwek, *Proc. Natl. Acad. Sci. USA* **1994**, *91*, 2235; c) N. Zitzmann, A. S. Mehta, S. Carrouee, T. D. Butters, F. M. Platt, J. McCauley, B. S. Blumberg, R. A. Dwek, T. M. Block, *Proc. Natl. Acad. Sci. USA* **1999**, *96*, 11878.
[10] R. A. Dwek, T. D. Butters, F. M. Platt, N. Zitzmann, *Nat. Rev. Drug Discovery* **2002**, *1*, 65.
[11] T. D. Butter, R. A. Dwek, F. M. Platt, *Chem. Rev.* **2000**, *100*, 4683. For example, *N*-butyldeoxynojirimycin (NB-DNJ or Zavesca) is a powerful glucosylceramide synthase (GCS) inhibitor and is now approved for use in Europe for the treatment of Gaucher disease, a glycolipid-storage disease.
[12] J. Q. Fan, S. Ishii, N. Asano, Y. Suzuki, *Nat. Med.* **1999**, *5*, 112.
[13] a) M. L. Sinnott, *Chem. Rev.* **1990**, *90*, 1171; b) G. Legler, *Adv. Carbohydr. Chem. Biochem.* **1990**, *48*, 319; c) A. E. Stütz, *Angew. Chem.* **1996**, *108*, 2054; *Angew. Chem. Int. Ed. Engl.* **1996**, *35*, 1926; d) T. D. Heightman, A. T. Vasella, *Angew. Chem.* **1999**, *111*, 794; *Angew. Chem. Int. Ed.* **1999**, *38*, 750.
[14] a) G. W. J. Fleet, S. K. Namgoong, C. Barker, S. Baines, G. S. Jacob, B. Winchester, *Tetrahedron Lett.* **1989**, *30*, 4439; b) F. M. Platt, G. R. Neises, G. B. Karlsson, R. A. Dwek, T. D. Butters, *J. Biol. Chem.* **1994**, *269*, 27108; c) Y. Blériot, C. R. Veighey, K. H. Smelt, J. Cadefau, W. Stalmans, K. Biggadike, A. L. Lane, M. Müller, D. J. Watkin, G. W. J. Fleet, *Tetrahedron: Asymmetry* **1996**, *7*, 2761; d) T. D. Butters, L. A. G. M. van den Broek, G. W. J. Fleet, T. M. Krulle, M. R. Wormald, R. A. Dwek, F. M. Platt, *Tetrahedron: Asymmetry* **2000**, *11*, 113.
[15] K. Ikeda, M. Takahashi, M. Nishida, M. Miyauchi, H. Kizu, Y. Kameda, M. Arisawa, A. A. Watson, R. J. Nash, G. W. J. Fleet, N. Asano, *Carbohydr. Res.* **2000**, *323*, 73.
[16] Depending on the absolute configuration of adenophorine, either C1 or C5 of structure **3** may be viewed as the pseudoanomeric center.
[17] B. G. Davis, M. A. T. Maughan, T. M. Chapman, R. Villard, S. Courtney, *Org. Lett.* **2002**, *4*, 103.
[18] B. A. Horenstein, R. F. Zabinski, V. L. Schramm, *Tetrahedron Lett.* **1993**, *34*, 7213.
[19] a) G. B. Evans, R. H. Furneaux, T. L. Hutchison, H. S. Kezar, P. E. Morris, V. L. Schramm, P. C. Tyler, *J. Org. Chem.* **2001**, *66*, 5723; b) G. B. Evans, R. H. Furneaux, G. J. Gainsford, V. L. Schramm, P. C. Tyler, *Tetrahedron* **2000**, *56*, 3053; c) R. H. Furneaux, V. L. Schramm, P. C. Tyler, *Bioorg. Med. Chem.* **1999**, *7*, 2599; d) R. H. Furneaux, G. Limberg, P. C. Tyler, V. L. Schramm, *Tetrahedron* **1997**, *53*, 2915.
[20] T. M. Chapman, S. Courtney, P. Hay, B. G. Davis, *Chem. Eur. J.* **2003**, in press.
[21] Additions of carbon nucleophiles to polyhydroxylated imines are rare. See T. Granier, A. Vasella, *Helv Chim. Acta* **1998**, *81*, 865 for the addition of trimethylsilyl cyanide.
[22] By the method of Vasella and co-workers: R. Hoos, A. B. Naughton, A. Vasella, *Helv. Chim. Acta* **1993**, *76*, 1802 and by additional methods that will be published elsewhere.
[23] By an adaptation of the method of Haines and co-workers: P. A. Fowler, A. H. Haines, R. J. K. Taylor, E. J. T. Chrystal, M. B. Gravestock, *Carbohydr. Res.* **1993**, *246*, 377 and by additional methods that will be published elsewhere.
[24] The signals of **10** may broaden more readily because of smaller differences, relative to those of **9,** in the chemical shifts of the two N-epimers in the slow-exchange limit, in addition to, or possibly instead of, differences in inversion exchange rates. Unfortunately, it was not possible to decoalesce the resonances of **10** and thus establish these shift differences.
[25] This Saytzev-sense elimination to form a more substituted imine is presumably favored by a high degree of double-bond character in the typically late transition states in imine-forming eliminations. For the formation of Saytzev products in base-catalyzed eliminations in six-membered-ring systems see: N. O. Brace, *J. Am. Chem. Soc.* **1964**, *86*, 2428 and M. Bartok, K. Felfoldi, G. Bozoki-Bartok, *Helv. Chim. Acta* **1980**, *63*, 2173–2178. For a primary example of the propensity of DBU to yield Saytzev

 © 2003 Wiley-VCH Verlag GmbH & Co. KGaA, Weinheim

elimination products see H. Oediger, F. Möller, *Angew. Chem.* **1967**, *79*, 53; *Angew. Chem. Int. Ed. Engl.* **1967**, *6*, 76.

[26] While conformers consistent with $^4C_1, Cl_{eq}$ and $^4C_1, Cl_{ax}$ were observed in NMR experiments, the $^1C_4, Cl_{ax}$ conformer was not directly observed. Assuming the $^1C_4$ conformer is disfavored over the $^4C_1$ by ~25 kJ mol^{-1} (based on the difference in ground-state energy for β-glucopyranose see P. L. Durette, D. Horton, *Adv. Carbohydr. Chem. Biochem.* **1971**, *26*, 49), this conformer would be present at $< 0.001\,\%$.

[27] Other conformations (e.g., $^{1,4}B$, $B_{N,3}$) that would also allow antiperiplanar alignment of NCl and only H1 or *syn* elimination (see N. O. Bruce, *J. Am. Chem. Soc.* **1964**, *86*, 2428) cannot be excluded. Estimates of the relative energy barriers of "ring-flip" conformational equilibria in cyclohexane of (~43.5 kJ mol^{-1} see M. Squillacote, R. S. Sheridan, O. L. Chapman, F. A. L. Anet, *J. Am. Chem. Soc.* **1975**, *97*, 3244), ring-substituted piperidines (~36–41 kJ mol^{-1} see V. M. Gittins, P. J. Heywood, E. Wyn-Jones, *J. Chem. Soc. Perkin Trans. 2* **1975**, 1642), and glucopyranose (~46 kJ mol^{-1}, see N. V. Joshi, V. S. R. Rao, *Biopolymers* **1979**, *18*, 2993) and the N-configurational equilibrium of *N*-chloropiperidine (~49–60 kJ mol see refs. [2a,b] and references therein) and ring-substituted *N*-chloropiperidines (~56–62 kJ mol^{-1} see J. V. Correia, M. N. Simões, A. C. Ferreira, L. R. Galveia, F. M. S. Brito Palma, *Heterocycl. Commun.* **2002**, *8*, 391) support the possibility of a situation in which a suitable ring-conformation manifold is energetically accessible while the N-inversion manifold is not. Initial estimates from line-shape analysis suggest that in **9** a barrier of ~48 kJ mol^{-1} to N-inversion exists at 248 K. Further investigations will be published in due course.

[28] We considered that displacement of the Schlenk equilibrium (W. Schlenk, W. Schlenk, Jr., *Ber. Dtsch. Chem. Ges. B* **1929**, *62*, 920) would provide Et_2Mg as a more suitable source of Et^- with reduced basicity.

[29] See Supporting Information for a more detailed discussion. Details of further investigations will be published in due course.

[30] W. G. Dauben, R. E. Bozak, *J. Org. Chem.* **1959**, *24*, 1596.

[31] a) R. B. Woodward, F. E. Bader, H. Bickel, A. J. Frey, R. W. Kierstad, *Tetrahedron* **1958**, 1; b) R. V. Stevens, *Acc. Chem. Res.* **1984**, *17*, 289.

[32] P. Deslongchamps, *Stereoelectronic Effects in Organic Chemistry*, Pergamon, Oxford, **1983**, pp. 211–221.

[33] The deprotected piperidine adducts produced here as hydrophobically modified azasugars were evaluated for their inhibitory activity towards panels of human glycoprocessing enzymes. These revealed that **5** is a good and highly selective inhibitor of human α-glucosidase (IC_{50}: 1 μM but no inhibition of GCS at 0.1 mM) that is more potent than the archetypal azasugar DNJ **1** (IC_{50}: 1.4 μM towards human α-glucosidase[14d]). This high α-glucosidase inhibitory power of **5** suggests it as a potential broad-spectrum antiviral agent.[9c] Further details will be published in due course.

 © 2003 Wiley-VCH Verlag GmbH & Co. KGaA, Weinheim

Asymmetric Hydrogenation

(*R*)-Binap-Mediated Asymmetric Hydrogenation with a Rhodacarborane Catalyst in Ionic-Liquid Media**

Zhu Yinghuai, Keith Carpenter, Ching Chi Bun, Stefan Bahnmueller, Chan Pek Ke,* Venugopal Shanmugham Srid, Leong Weng Kee, and M. Frederick Hawthorne**

The reduction of ketones to alcohols under homogeneous catalysis is an important synthetic step in the chemical industry, and recent emphasis placed upon the asymmetric hydrogenation of prochiral substrates as pharmaceutical precursors enhances the importance of this chemistry.[1] Aside from the discovery of new asymmetric hydrogenation reactions, there remains the challenge of separating the reaction products from an expensive chiral catalyst[2] for purposes of recycling. Novel reaction media or polymer-immobilized catalysts may play an important role in this regard. More specifically, salts that are liquids at ambient temperature have received much attention because of their potential as direct replacements for conventional solvents and as a means to immobilize transition-metal catalysts in biphasic processes.[3–5] Many organic reactions have been carried out in ionic liquids, such as hydrogenation,[6,7] oxidation,[8] epoxidation,[9] and hydroformylation reactions.[10] The use of ionic-liquid media for other classic transformations, such as Friedel–Crafts acylation[11] and alkylation[12] reactions, allylation,[13,14] Diels–Alder,[15] and Heck[16] reactions, as well as Suzuki[17] and Trost–Tsuji coupling[18] reactions in ionic liquids have also been reported. In contrast, relatively little attention has been given to the use of ionic-liquid reaction media in the catalytic hydrogenation of ketones.

As has been repeatedly demonstrated in the past, ketones do not easily undergo homogeneous hydrogenation in the presence of simple transition-metal catalysts. Rhodium was successfully employed for this purpose under 1 atm of H_2, in

[*] Z. Yinghuai, K. Carpenter, C. C. Bun, S. Bahnmueller
Institute of Chemical and Engineering Sciences, Block 28
Ayer Rajah Crescent, #02-08, Singapore 139959 (Singapore)
Fax: (+65) 6873-4805
E-mail: zhu_yinghuai@ices.a-star.edu.sg

C. P. Ke, V. S. Srid, L. W. Kee
Department of Chemistry, National University of Singapore
10 Kent Ridge Crescent, Singapore 119260 (Singapore)
Fax: (+65) 6779-1691
E-mail: chmlwk@nus.edu.sg

M. F. Hawthorne
Department of Chemistry and Biochemistry
University of California
Los Angeles, CA 90095 (USA)
Fax: (+1) 310-825-5490
E-mail: mfh@chem.ucla.edu

[**] This research was generously supported by an ICES grant, A* Star, Singapore (Z.Y.), and a U.S. National Science Foundation Grant CHE-0111718 (M.F.H.).

 © 2003 Wiley-VCH Verlag GmbH & Co. KGaA, Weinheim DOI: 10.1002/anie.200351273

complexes in which the metal center was made electron rich by using ligands of the fully alkylated bidentate diphosphane type.[1] In contrast with these results, we describe herein 1) the hydrogenation of aromatic ketones in the presence of a catalyst derived from a previously described rhodacarborane catalyst[19] precursor with a suicide alkene ligand: [*closo*-1,3-{μ-(η^2-3-CH_2=$CHCH_2CH_2$)}-3-H-3-PPh_3-3,1,2-$RhC_2B_9H_{10}$] (**1**); 2) the use of ionic-liquid reaction media: 1-methyl-3-octylimidazolium tetrafluoroborate ($OMIM^+BF_4^-$, **2**), 1-butyl-3-methylimidazolium hexafluorophosphate ($BMIM^+PF_6^-$, **3**), and the new liquid salt comprised of 1-carbadodecaborate ions[20] and *N*-*n*-butylpyridinium (BP) ions, $BP^+CB_{11}H_{12}^-$ (**4**); 3) the introduction of molecular asymmetry in the catalytic hydrogenation by complexation of the rhodium center of the catalyst with the optically active (*R*)-binap ligand, (*R*)-2,2′-bis(diphenylphosphanyl)-1,1′-binaphthyl (**5**); and 4) the comparison of these ionic liquids with tetrahydrofuran as reaction media, and comparison of the performance of the catalyst derived from **1** with that derived from [{Rh(cod)Cl}$_2$] (cod = 1,5-cyclooctadiene) under otherwise identical conditions.

The robust rhodacarborane catalyst systems developed by Hawthorne and co-workers,[21] such as [*closo*-3-H-3,3-$(Ph_3P)_2$-3,1,2-$RhC_2B_9H_{11}$], are understood mechanistically in the hydrogenation and isomerization of alkenes, as well as in the hydrogenolysis and hydrosilanolysis of alkenyl carboxylates. The complex **1** stands out among rhodacarborane catalyst precursors because of its η^2-3-CH_2=CH-$(CH_2)_2$ alkene ligand, which is linked to the *nido*-7,8-$C_2B_9H_{11}^{2-}$ dicarbollide module at the 7-vertex. Saturation of this alkenyl ligand under hydrogenation conditions removes it from the manifold of competitive ligands and creates a catalyst system that has only one triphenylphosphane ligand per rhodium atom, which results in its enhanced reactivity with alkene substrates. This alkene-hydrogenation catalyst is among the most reactive known.[19] The corresponding *closo* rhodacarborane catalyst systems, which contain two triphenylphosphane ligands per rhodium atom, are also quite active and robust in alkene hydrogenation.[21] As discussed below, **1** was used in this study because the bidentate ligand (*R*)-binap displaces all ligands originally attached to the rhodium center of **1** other than the hydride and the dicarbollide, in situ, to generate an active chiral catalyst. Hydrogenation of the coordinated suicide alkene ligand present in **1** simplifies this process.

The application of ionic-liquid media in the hydrogenation of aromatic ketones was explored by using the known liquid salts **2** and **3** as reaction media. The new liquid salt **4** was also prepared for use in this study, as it was thought that a beneficial interaction of the B–H bonds of the *closo*-$CB_{11}H_{12}^-$ ion with the rhodium center in the catalyst derived from **1** may occur, and that **4** should otherwise be chemically inert under the conditions used. The salt **4** was readily prepared by the metathesis reaction of *N*-*n*-butylpyridinium chloride with Cs^+*closo*-$CB_{11}H_{12}^-$ as a solution in CH_2Cl_2. Pure **4** is a colorless solid that melts at 21 °C.[22] This novel ionic liquid will undoubtedly find use in catalytic reactions other than those described herein.

The use of the catalyst precursor **1** in the hydrogenation of aromatic ketones in ionic-liquid reaction media provides both a potential new route to the corresponding alcohols and the opportunity to include optically active phosphanes, such as **5**, in the rhodacarborane catalyst system as structural components. This modification provided effective chiral catalysts that promoted the asymmetric hydrogenation of prochiral ketones under mild conditions. Both acetophenone and ethyl benzoylformate were hydrogenated in the presence of the catalyst precursor **1**[23] and (*R*)-binap (150 mol% relative to **1**), in the reaction media **2**, **3**, **4**, and tetrahydrofuran at 50 °C under H_2 (12 atm) within 12 h. In **2**, **3**, and **4**, the desired products (*R*)-phenylethanol and ethyl (*R*)-mandelate were formed in quantitative chemical yields and with very high *ee* values. The use of tetrahydrofuran led to both diminished chemical yields and diminished *ee* values. Reaction mixtures were monitored and product mixtures analyzed by GC.[24] Typical hydrogenation results for acetophenone are reported in Table 1, for which reaction rates are shown in Figure 1. The catalyst and (*R*)-binap were recycled in the ionic-liquid experiments by volatilization and removal of the reaction product under high vacuum, followed by the addition of fresh ketone. Six such cycles were carried out without degradation of catalyst activity or selectivity.

Table 1: Rhodium-catalyzed hydrogenation of acetophenone (A) and ethyl benzoylformate (B).[a]

Solvent	Conversion [%][b]	*ee* [%][c]	TOF [h^{-1}][d]
$OMIM^+BF_4^-$ **2**	100(A,B)	97.3(A), 99.3(B)	194(A), 201(B)
$BMIM^+PF_6^-$ **3**	100(A,B)	97.8(A), 98.2(B)	207(A), 213(B)
$BP^+CB_{10}H_{12}^-$ **4**	100(A,B)	99.1(A), 99.5(B)	239(A), 306(B)
tetrahydrofuran	82(A), 87(B)	91.3(A), 85.7(B)	96(A), 107(B)

[a] Mole ratio of catalyst/(*R*)-binap/acetophenone = 1:1.5:1000; reaction conditions: H_2 (12 atm), 50 °C, 12 h; [**1**] = 8.1×10^{-4} M; [**5**] = 1.21×10^{-3} M. [b] Determined by GC. [c] Determined by GC on a Chirasil DEX-CB column.[24] [d] Turnover frequency (= moles of hydrogenation product per mole of Rh per hour) was determined after 3 h.

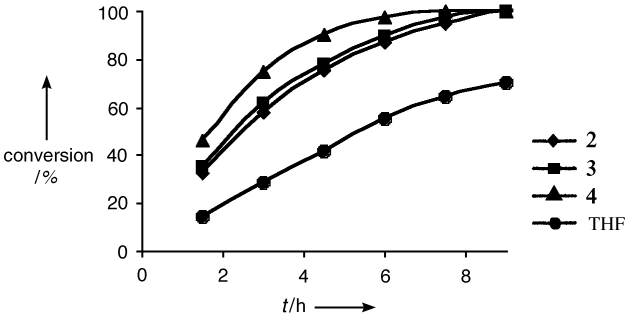


Figure 1. The course of acetophenone hydrogenation under standard conditions in the ionic-liquid media $OMIM^+BF_4^-$ (**2**), $BMIM^+PF_6^-$ (**3**), and $BP^+CB_{11}H_{12}^-$ (**4**), and in tetrahydrofuran.

The conversion, *ee* values, and turnover frequency observed when **1** and [{Rh(cod)Cl}$_2$] were used as catalyst precursors in the hydrogenation of acetophenone in the reaction media **2** and tetrahydrofuran are reported in Table 2. Thus, the replacement of **1** with [{Rh(cod)Cl}$_2$] as the catalyst precursor caused a severe decrease in performance in both reaction media examined. These observations strongly sug-

 © 2003 Wiley-VCH Verlag GmbH & Co. KGaA, Weinheim

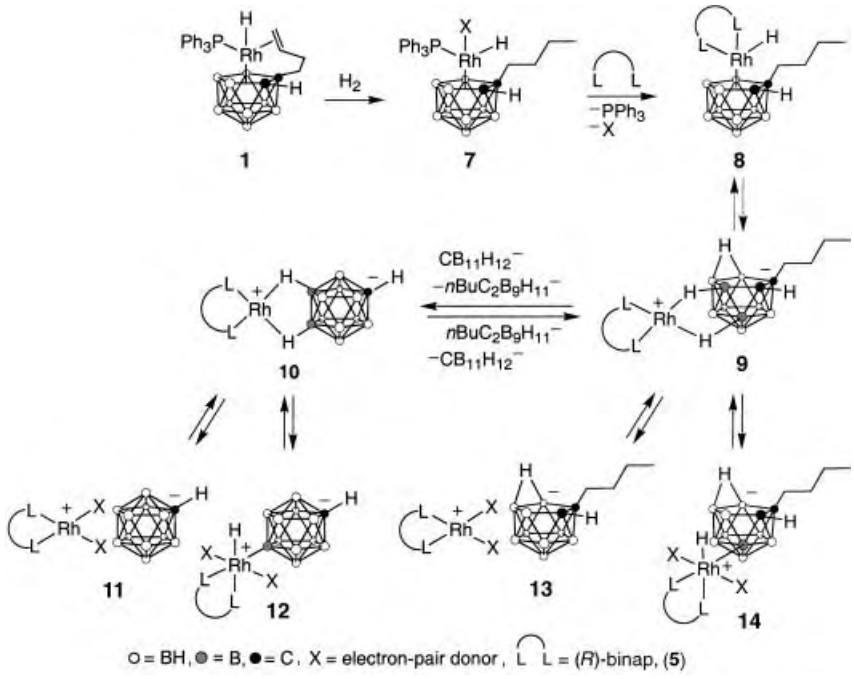
Table 2: Hydrogenation of acetophenone catalyzed by [{Rh(cod)Cl}$_2$] and by **1** in the ionic liquid OMIM$^+$BF$_4^-$ **2** (I) and in THF (II).[a]

Catalyst	Conversion [%][b]	*ee* [%][c]	TOF [h^{-1}][d]
1	100(I), 82(II)	97.3(I), 91.3(II)	194(I), 96(II)
[{Rh(cod)Cl}$_2$]	17(I), 8(II)	10.3(I), 5.7(II)	16(I), 11(II)

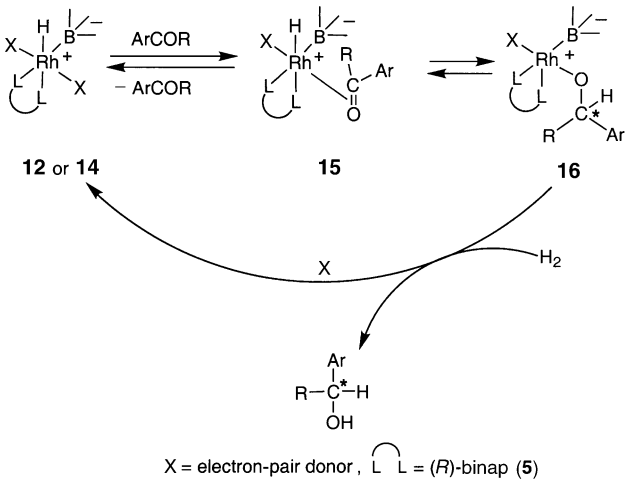
[a] Mole ratio of catalyst/(*R*)-binap/acetophenone = 1:1.5:1000; reaction conditions: H_2 (12 atm), 50 °C, 12 h. [b] Determined by GC. [c] Determined by GC on a Chirasil DEX-CB column.[24] [d] Turnover frequency was determined after 3 h.

gest that the hydrogenation processes in which **1** and [{Rh(cod)Cl}$_2$] serve as catalyst precursors differ in their mechanism. We are as yet unable to explain the significant increase in performance that results from the substitution of the ionic liquid **2** for tetrahydrofuran as the reaction medium for rhodacarborane-catalyzed reactions. However, it seems likely that an ionic medium better supports zwitterionic intermediates. The most efficient ionic-liquid reaction medium studied was **4**, which has a large number of available B–H bonds that may be involved in the reaction, as discussed below.

If it is assumed that ketone hydrogenation catalyzed by rhodacarboranes resembles rhodacarborane-catalyzed alkene hydrogenation and many other reactions that share its unusual mechanistic features,[21] the mechanisms shown in Schemes 1 and 2 can be proposed. The established mechanisms of rhodacarborane-catalyzed reactions[21] involve the presence of equilibrium concentrations of active zwitterionic [B-RhL$_2$-H] species formed by the oxidative addition of [L$_2$Rh]$^+$ to electron-rich terminal B–H bonds of the many isoelectronic, isomeric, and substituted variants of the parent *nido*-7,8-$C_2B_9H_{12}^-$ ion **6**.



Scheme 1. Fate of the rhodacarborane catalyst precursor **1** under the reaction conditions and equilibria leading to the possible catalytic species **12** and **14**.



Scheme 2. Proposed mechanism for the asymmetric hydrogenation of prochiral ketones in the presence of the rhodacarborane catalysts **12** and/or **14**.

As previously established, *closo*-rhodacarborane catalyst precursors, such as **8**, reductively eliminate Rh^{III} to produce mixtures of Rh^I *exo-nido* isomers, such as **9**, in which the [L$_2$Rh]$^+$ center is attached to the *nido* anion cage by a pair of three-center two-electron Rh–H–B bonds (Scheme 1). These species do not provide catalysis by dissociation to active [L$_2$RhX$_2$]$^+$ (X = electron pair donor) ion-pair species **13**, but rather undergo reversible oxidative addition of Rh^I to the coordinated terminal B–H bonds. The result is a set of catalytically active *exo-nido* Rh^{III} hydride derivatives **14**. Alkene hydrogenation and related reactions have been shown to proceed by a metathesis mechanism involving species such as **14**, which are regenerated in a separate catalytic cycle.[21] In reactions in which **4** was used as the ionic-liquid medium, reaction of the solvent *closo*-$CB_{11}H_{12}^-$ ion through its B–H donors with the [L$_2$RhX$_2$]$^+$ could possibly lead to the conversion of **9**, **13**, and **14** into the analogues **10**, **11**, and **12**, respectively. Of the latter group, species **12** would be expected, by analogy, to exhibit catalytic activity.

A generalized mechanism for the asymmetric hydrogenation of the aromatic ketones described in this study is proposed in Scheme 2. Species **12** and **14** are generalized, as shown, and the coordination of the ketone is followed by hydride transfer from the rhodium center of the catalyst to the carbonyl carbon atom of the ketone. Reversal of this last step is prevented by rapid irreversible H_2 metathesis, which regenerates the rhodium hydride species (either **12** or **14**). This metathesis step involves the formal addition of a proton to the complexed oxygen atom of the alkoxy group and the simultaneous formal addition of a hydride ion to Rh^{III}. This process is similar to the observed metathesis of the RhO(CO)CH$_3$ species involved in catalytic alkenyl acetate hydrogenolysis.[21] The precise stereochemical role of the (*R*)-binap

 © 2003 Wiley-VCH Verlag GmbH & Co. KGaA, Weinheim

ligand in these hydrogenation reactions is not yet understood. However, its remarkable effect can be seen in the essentially quantitative chemical yields and superb *ee* values recorded in Table 1. The observed reaction rates and *ee* data show that ketone hydrogenation is both more rapid and stereochemically more selective in the ionic liquid **4** than in the other reaction media studied (Figure 1 and Table 1). This suggests that **12** may play an important role under hydrogenation conditions.

In summary, we have synthesized a new carborane-based room-temperature ionic liquid **4**, and used this salt as the reaction medium in the asymmetric hydrogenation of unsymmetrical aryl ketones in the presence of the chelating ligand (*R*)-binap and a previously known[19] rhodacarborane catalyst. The extraordinary performance of this catalyst system warrants further synthetic and mechanistic studies, which are in progress.

Received: February 25, 2003 [Z51273]

Keywords: asymmetric catalysis · carboranes · hydrogenation · ionic liquids · P ligands · rhodium

[1] a) Q.-H. Fan, Y.-M. Li, A. S. C. Chan, *Chem. Rev.* **2002**, *102*, 3385 – 3466; b) T. Ohkuma, M. Koizumi, K. Muñiz, G. Hilt, C. Kabuto, R. Noyori, *J. Am. Chem. Soc.* **2002**, *124*, 6508 – 6509; c) R. Noyori, T. Ohkuma, *Angew. Chem.* **2001**, *113*, 41 – 75; *Angew. Chem. Int. Ed.* **2001**, *40*, 40 – 73.

[2] H. B. Kagan in *Comprehensive Organometallic Chemistry, Vol. 8* (Eds.: G. Wilkinson, F. G. A. Stone, E. W. Abel), Pergamon, Oxford, **1982**, pp. 463 – 498.

[3] J. D. Holbrey, K. R. Seddon, *Clean Prod. Processes* **1999**, *1*, 223 – 236.

[4] T. Welton, *Chem. Rev.* **1999**, *99*, 2071 – 2083.

[5] P. Wasserscheid, W. Keim, *Angew. Chem.* **2000**, *112*, 3926 – 3945; *Angew. Chem. Int. Ed.* **2000**, *39*, 3772 – 3789.

[6] C. J. Adams, M. J. Earle, K. R. Seddon, *Chem. Commun.* **1999**, 1043 – 1044.

[7] Y. Chauvin, L. Mussmann, H. Olivier, *Angew. Chem.* **1995**, *107*, 2941 – 2943; *Angew. Chem. Int. Ed. Engl.* **1995**, *34*, 2698 – 2700.

[8] J. Howarth, *Tetrahedron Lett.* **2000**, *41*, 6627 – 6629.

[9] G. S. Owens, M. M. Abu-Omar, *Chem. Commun.* **2000**, 1165 – 1166.

[10] C. C. Brasse, U. Englert, A. Salzer, H. Waffenschmidt, P. Wasserscheid, *Organometallics* **2000**, *19*, 3818 – 3823.

[11] C. J. Adams, M. J. Earle, G. Roberts, K. R. Seddon, *Chem. Commun.* **1998**, 2097 – 2098.

[12] C. E. Song, W. H. Shim, E. J. Roh, J. H. Choi, *Chem. Commun.* **2000**, 1695 – 1696.

[13] W. Chen, L. Xu, C. Chatterton, J. Xiao, *Chem. Commun.* **1999**, 1247 – 1248.

[14] C. M. Gordon, A. McCluskey, *Chem. Commun.* **1999**, 1431 – 1432.

[15] M. J. Earle, P. B. McCormac, K. R. Seddon, *Green Chem.* **1999**, *1*, 23 – 25.

[16] A. J. Carmichael, M. J. Earle, J. D. Holbrey, P. B. McCormac, K. R. Seddon, *Org. Lett.* **1999**, *1*, 997 – 1000.

[17] C. J. Mathews, P. J. Smith, T. Welton, *Chem. Commun.* **2000**, 1249 – 1250.

[18] C. de Bellefon, E. Pollet, P. Grenouillet, *J. Mol. Catal. A* **1999**, *145*, 121 – 126.

[19] a) M. S. Delaney, C. B. Knobler, M. F. Hawthorne, *Inorg. Chem.* **1981**, *20*, 1341 – 1347; b) M. F. Hawthorne, M. S. Delaney, US Patent 4363747, **1982**.

[20] A. S. Larsen, J. D. Holbrey, F. S. Tham, C. A. Reed, *J. Am. Chem. Soc.* **2000**, *122*, 7264 – 7272.

[21] J. A. Belmont, J. Soto, R. E. King, A. J. Donaldson, J. D. Hewes, M. F. Hawthorne, *J. Am. Chem. Soc.* **1989**, *111*, 7475 – 7486.

[22] **4**: A solution of (*N*-*n*-butyl-C_5H_5N)$^+Cl^-$ (1.40 g, 8.16 mmol) in dry CH_2Cl_2 (30 mL) was added to a stirred solution of $Cs^+CB_{11}H_{12}^-$ (2.26 g, 8.19 mmol) in dry methanol (120 mL), and the mixture was stirred at room temperature for 20 h. All solvents were then evaporated under reduced pressure, and the resulting viscous residue was dissolved in CH_2Cl_2 and purified by column chromatography (SiO_2; CH_2Cl_2/Et_2O 4:1). The solvent was removed under reduced pressure and the product was dried under high vacuum for 2 days to give (*N*-*n*-butylpyridinium)$^+$-*closo*-$CB_{11}H_{12}^-$ (**4**; 2.10 g, 92 %) as a colorless sticky liquid with the dynamic viscosity $\mu = 250$ cP (0.01 g cm^{-1} s^{-1}; measured on a CV-100 Caulking Viscometer at 20 °C; estimated error: ± 2 %). The liquid solidified at 21 °C to give **4** as a colorless waxy solid. Elemental analysis: calcd for $C_{10}H_{26}B_{11}N$ (279.246): C 43.01, H 9.39, N 5.02; found: C 43.10, H 9.41, N 5.08; ^{1}H NMR (400 MHz, $CDCl_3$): $\delta = 8.92$ (m, 2H, N-C_{py}-H), 8.18 (m, 1H, C_{py}-H), 7.75 (m, 2H; C_{py}-H), 4.46 (t, 2H; N-CH_2), 2.92 (s, 1H; B-CH), 1.65 (m, 2H; N-C-CH_2-), 1.03 (m, 2H; N-C-C-CH_2-), 0.56 (t, 3H; CH_3), 0.20–3.60 ppm (m, 11H; BH); ^{13}C NMR (100.6 MHz, $CDCl_3$): $\delta = 13.37$ (*C*-C-C-C-N), 19.24 (C-*C*-C-C-N), 33.59 (C-C-*C*-C-N), 55.67 (C-B), 61.89 (C-C-C-*C*-N), 128.58 (C_{py}), 144.72 (C_{py}), 145.41 ppm (C_{py}); IR (KBr): $\tilde{\nu} = 2955$ s, 2894 m, 2592 vs (νBH), 1588 m, 1501 m, 1455 m, 1409 m, 1322 s, 1250 vs, 1086 s, 927 s, 886 s, 835 vs, br, 692 s, 636 s, 518 s, 497 s cm^{-1}.

[23] Typical procedure: a solution of the catalyst precursor (8.1 μmol) in THF (2.53 mL), a solution of (*R*)-binap (12 μmol, 4.5 mM) in THF (2.64 mL), and an ionic liquid (10 mL) were placed in a 100-mL glass autoclave equipped with a magnetic stirring bar, a pressure gauge, and a gas inlet tube to be attached to a hydrogen source. The THF solvent was removed under reduced pressure, and the vessel was filled with argon. Acetophenone (975 mg, 8.12 mmol) was then added under a stream of argon, and the mixture was degassed by placing the autoclave under vacuum and filling it with argon three times, followed by evacuating it and filling it with hydrogen twice. After this procedure, the vessel was placed under H_2 pressure (12 atm) and the reaction mixture was stirred vigorously at 50 °C for 12 h. After the mixture had cooled to room temperature, the hydrogen gas was vented carefully. The yield and enantiomeric excess of the product was determined by GC analysis and the residue was distilled to give (*R*)-1-phenylethanol. The selective reduction of ethyl benzoylformate was carried out by a similar procedure to give ethyl-(*R*)-mandelate. When THF (15 mL) was used as the reaction medium, the degassing process was carried out at −78 °C. Chloro(1,5-cyclooctadiene)rhodium(I) dimer, [{Rh(cod)Cl}$_2$], was used as received from Sigma-Aldrich Pte., Ltd.

[24] GC column: Chirasil-DEX CB, 25 m, CHROMPACK; carrier gas: helium; column temperature: 105 °C; injection temperature: 200 °C; retention time, t_R, of (*R*)-1-phenylethanol: 17.8 min, (*S*)-1-phenylethanol: 20.5 min, acetophenone: 8.3 min, ethyl (*R*)-mandelate: 25.6 min, ethyl (*S*)-mandelate: 28.7 min, ethyl benzoylformate: 14.8 min.

 © 2003 Wiley-VCH Verlag GmbH & Co. KGaA, Weinheim

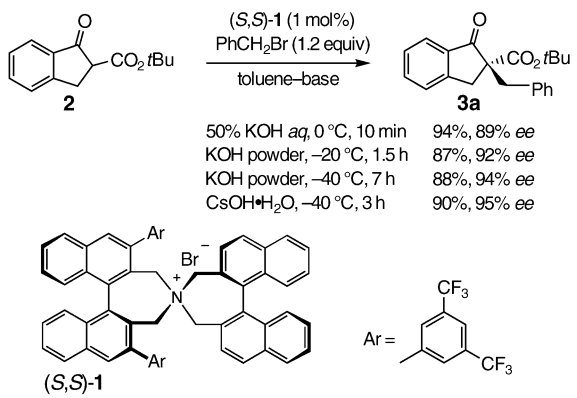
Stereoselective Alkylation

Highly Enantioselective Construction of Quaternary Stereocenters on β-Keto Esters by Phase-Transfer Catalytic Asymmetric Alkylation and Michael Reaction**

*Takashi Ooi, Takashi Miki, Mika Taniguchi, Misato Shiraishi, Mifune Takeuchi, and Keiji Maruoka**

The construction of organic molecules containing chiral quaternary carbon centers by catalytic enantioselective reactions represents a very challenging and demanding area in organic synthesis,[1] because in addition to the inherent difficulty of developing an appropriate catalyst system, chiral fully substituted carbon centers are often essential for the biological activity of natural products and pharmaceuticals. Among the various transformations suitable for this purpose, the catalytic asymmetric alkylation of β-keto esters facilitates the direct stereocontrolled formation of quaternary stereocenters with structurally diverse substituents, which offers ample opportunity for further structural elaboration. However, few examples have been demonstrated to date, and only palladium-catalyzed asymmetric allylic alkylation has proved to be promising as an alternative strategy.[2] Although a method for asymmetric alkylation under phase-transfer catalysis should provide a simple yet potential solution to this problem, it is far being a synthetically useful method.[3,4] Herein we wish to report highly enantioselective phase-transfer alkylation of β-keto esters catalyzed by *N*-spiro C_2-symmetric chiral quaternary ammonium salt **1**,[5] which results in the catalytic asymmetric establishment of a quaternary stereogenic center (Scheme 1). We also describe further utilization of our approach to establishing chirality by asymmetric Michael addition to α,β-unsaturated carbonyl compounds.

As expected based on the relatively low reactivity of metal enolates of 1,3-dicarbonyl compounds, attempted treatment of 2-*tert*-butoxycarbonyl-1-indanone (**2**) with benzyl bromide (1.2 equiv) in toluene/50% KOH aqueous solution at 0°C for several hours led to gradual formation of the alkylation product **3a** (13% yield after 6 h). In marked contrast, however, the benzylation in the presence of 1 mol% of chiral ammonium bromide **1** under otherwise similar conditions proceeded instantaneously to give **3a** in 94% yield and, fortunately, the selectivity was determined to be 89% *ee* (Scheme 1). To improve the enantioselectivity, we examined the effect of temperature on the reaction with solid inorganic bases and found that vigorous stirring of the mixture of **2**, benzyl bromide (1.2 equiv), **1** (1 mol%), and powdered KOH (5 equiv) in toluene at −20°C for 1.5 h afforded **3a** in 87% yield with 92% *ee*.[6] Even higher selectivity (94% *ee*) was achieved by conducting the reaction at −40°C, though the reaction was slower. The reactivity was improved when $CsOH{\cdot}H_2O$ was used as a base, leading to the production of **3a** in 90% yield with 95% *ee* after a reaction time of 3 h.[7]



Scheme 1. Optimization of the reaction conditions for the phase-transfer enantioselective benzylation of β-keto ester **2** in the presence of the catalyst (*S*,*S*)-**1**.

With these optimized conditions in hand, we explored the general applicability of the present phase-transfer catalytic asymmetric alkylation system; the results are summarized in Table 1. The catalytic asymmetric creation of quaternary carbon centers by introduction of methyl and allylic substituents to substrate **2** has been demonstrated with appropriate electrophiles. Excellent chemical yields as well as enantioselectivities were attained (entries 2–4). Introduction of a functionalized benzylic side chain was also successfully realized, and the desired product was obtained in 86% yield with 97% *ee* (entry 5). Not only cyclopentanone derivatives but also 2-alkoxycarbonylcyclohexanones appeared to be good candidates for this alkylation, and a high level of enantioselectivity was observed (entry 8). Moreover, enantiofacial differentiation of the enolate derived from an acyclic β-keto ester was feasible with our approach (entry 9).

Optically active α,α-dialkyl-β-keto esters can be readily converted to the corresponding β-hydroxy acid and β-amino acid derivatives without loss of chirality as exemplified in Scheme 2. Reduction of **4** (97% *ee*) with L-Selectride in THF at −78°C gave rise to the β-hydroxy ester **5** (97% *ee*) with a diastereomeric ratio of 86:14.[8] Further, reductive amination of **4** with benzyl amine and sodium cyanoborohydride in the presence of 4 Å molecular sieves in MeOH afforded the N-protected β-amino ester **6** almost quantitatively.[9]

Furthermore, our approach was found to be applicable to catalytic asymmetric Michael addition of β-keto esters to α,β-unsaturated carbonyl compounds, which is also a very

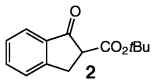
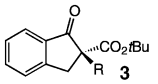
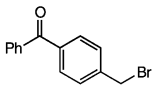
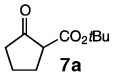
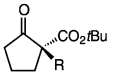
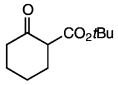
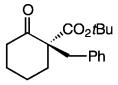
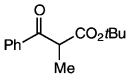
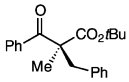
[*] Prof. Dr. K. Maruoka, Dr. T. Ooi, T. Miki, M. Taniguchi, M. Shiraishi, M. Takeuchi
Department of Chemistry
Graduate School of Science
Kyoto University
Sakyo, Kyoto, 606-8502 (Japan)
Fax: (+81) 75-753-4041
E-mail: maruoka@kuchem.kyoto-u.ac.jp

[**] This work was supported in part by a Grant-in-Aid for Scientific Research from the Ministry of Education, Culture, Sports, Science and Technology, Japan. M. Takeuchi is grateful to the Japan Society for the Promotion of Science for Young Scientists for a research fellowship.

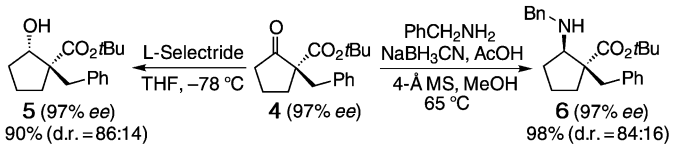
Supporting information for this article is available on the WWW under http://www.angewandte.org or from the author.

 © 2003 Wiley-VCH Verlag GmbH & Co. KGaA, Weinheim DOI: 10.1002/anie.200351469

Table 1: Catalytic enantioselective phase-transfer alkylation of β-keto esters.[a]

Entry	β-Keto ester	RX	Conditions [°C, h]	Product	Yield [%][b]	Sel. [% *ee*][c] (config)
1	 **2**	$PhCH_2Br$	−40, 3	 **3**	90	95 (*R*)[d]
2		Me_2SO_4	−30, 7		99	87 (*R*)[d,e]
3		$CH_2{=}CHCH_2Br$	−50, 12		94	91
4		$PhCH{=}CHCH_2Br$	−40, 5		93	96
5			−40, 7		86	97
6	 **7a**	$PhCH_2Br$	−40, 2.5		94	97 (*S*)[f]
7		$PhCH{=}CHCH_2Br$	−60, 9	80	92	
8		$PhCH_2Br$	−40, 4		88	92 (*S*)[f]
9		$PhCH_2Br$	−30, 9		96	85

[a] Unless otherwise specified, the reaction was carried out with 1.2 equiv RX and 5 equiv $CsOH{\cdot}H_2O$ in the presence of 1 mol% **1** in toluene under the given reaction conditions. [b] Yield of isolated product. [c] Enantiopurity was determined by HPLC analysis of the alkylated product with a chiral column: DAICEL Chiralcel OD-H (entries 1, 6–9), Chiralpak AS (entry 2), and Chiralpak AD (entries 3–5) with hexane/2-propanol or hexane/ethanol as eluent. [d] Absolute configuration was determined by comparison of the optical rotation of the corresponding methyl ester with the literature value.[15] [e] With 3 equiv Me_2SO_4. [f] Assigned by comparison of the HPLC retention time with that reported.[3b]



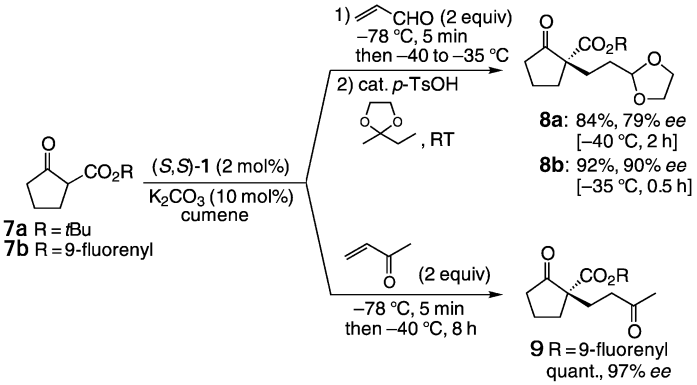
Scheme 2. Facile derivatization of optically active **4** to give the corresponding β-hydroxy ester **5** and β-amino ester **6**. MS = molecular sieves.

attractive tool for the synthesis of compounds with chiral quaternary carbon centers.[10] Particularly, in contrast to the previous methods elaborated for the reaction with α,β-unsaturated ketones and esters,[11] our system enabled the use of α,β-unsaturated aldehydes as a Michael acceptors, leading to the construction of quaternary stereocenter having three different functionalities of carbonyl origin. For instance, treatment of 2-*tert*-butoxycarbonylcyclopentanone (**7a**) with acrolein in the presence of **1** (2 mol%) and K_2CO_3 (10 mol%) in cumene at −78 °C followed by stirring at −40 °C for 2 h resulted in clean formation of the corresponding Michael adduct, which was isolated as its acetal **8a** in 84% yield with 79% *ee*.[12] Interestingly, use of fluorenyl ester **7b** as a substrate dramatically improved the enantioselectivity to 90% *ee* (92% yield) (Scheme 3). The reaction of **7b** with α,β-unsaturated ketones such as methyl vinyl ketone also proceeded smoothly under similar conditions, and the desired **9** was obtained quantitatively with 97% *ee*.[13]

In conclusion, we have accomplished the highly enantioselective phase-transfer catalytic alkylation and Michael reaction of β-keto esters by using a designer chiral quaternary ammonium salt as the catalyst, which allows efficient construction of fully substituted stereogenic centers. This provides a reliable route for the asymmetric synthesis of not only α,α-dialkyl-β-hydroxy acid and β-amino acid derivatives but also other useful building blocks with chiral quaternary carbon atoms.

Experimental Section

A representative procedure for enantioselective alkylation of β-keto ester **2** under solid–liquid phase-transfer conditions (entry 1 in Table 1): To a mixture of **2** (69.7 mg, 0.30 mmol) and (*S*,*S*)-**1** (3.2 mg, 0.003 mmol, 1 mol%) in toluene (2 mL) was added benzyl bromide (42.8 μL, 0.36 mmol) and $CsOH{\cdot}H_2O$ (252 mg, 1.5 mmol) at −40 °C under argon atmosphere, and the mixture was stirred for 4 h at the same temperature. The reaction mixture was diluted with water and extracted with Et_2O (three times). The combined extracts were washed with water and brine, and then dried over Na_2SO_4. Evaporation of solvent and purification of the residual crude products by column chromatography on silica gel (hexane/Et_2O = 5:1 as eluent) gave (*R*)-**3a** (86.0 mg, 0.27 mmol, 90% yield, 95% *ee*) as a colorless oil. $[\alpha]_D^{26} = +134.3°$ ($c = 1.2$, $CHCl_3$); ^1H NMR (400 MHz, $CDCl_3$): $\delta = 7.72$ (1H, d, $J = 7.2$ Hz, Ar-H), 7.51 (1H, t, $J = 7.2$ Hz, Ar-H), 7.33 (1H, d, $J = 7.2$ Hz, Ar-H), 7.31 (1H, t, $J = 7.2$ Hz, Ar-H), 7.20–7.06 (5H, m, Ph), 3.56 (1H, d, $J = 17.2$ Hz, CH_2), 3.43 (1H, d, $J = 17.6$ Hz, CH_2), 3.26 (1H, d, $J = 17.6$ Hz, CH_2), 3.12 (1H, d, $J = 17.2$ Hz, CH_2), 1.38 ppm (9H, s, *t*Bu); ^{13}C NMR (100 MHz, $CDCl_3$): $\delta = 202.4$, 169.5, 153.2, 136.7, 135.3, 134.9, 129.8, 128.0, 127.3, 126.5, 126.0, 124.4, 82.0, 62.4, 39.4, 35.7, 27.8 ppm; IR (liquid film): $\tilde{\nu} = 2978$, 2930, 1740, 1709, 1607,



Scheme 3. Catalytic asymmetric Michael addition of β-keto ester **7** to α,β-unsaturated carbonyl compounds under phase-transfer conditions. RT = room temperature.

 © 2003 Wiley-VCH Verlag GmbH & Co. KGaA, Weinheim

1456, 1369, 1254, 1215, 1151, 1026, 932, 847, 762, 739, 702 cm^{-1}. HRMS (ESI-TOF) calcd for $C_{21}H_{22}O_3Na$ ($[M+Na]^+$): 345.1461, found: 345.1470. HPLC conditions: DAICEL Chiralcel OD-H, hexane/*i*PrOH = 100:1, flow rate = 0.5 mL min^{-1}, retention times = 14.2 min (*R*), 17.1 min (*S*).

Received: March 24, 2003 [Z51469]

Keywords: alkylation · asymmetric synthesis · Michael addition · phase-transfer catalysis

[1] For a review on catalytic asymmetric synthesis of quaternary carbon centers, see: E. J. Corey, A. Guzman-Perez, *Angew. Chem.* **1998**, *110*, 402; *Angew. Chem. Int. Ed.* **1998**, *37*, 388. See also: J. Christoffers, A. Mann, *Angew. Chem.* **2001**, *113*, 4725; *Angew. Chem. Int. Ed.* **2001**, *40*, 4591.

[2] a) B. M. Trost, R. Radinov, E. M. Grenzer, *J. Am. Chem. Soc.* **1997**, *119*, 7879; b) J. M. Brunel, A. Tenaglia, G. Buono, *Tetrahedron: Asymmetry* **2000**, *11*, 3585; c) B. M. Trost, K. L. Sacchi, G. M. Schroeder, N. Asakawa, *Org. Lett.* **2002**, *4*, 3427; See also: d) B. M. Trost, X. Ariza, *J. Am. Chem. Soc.* **1999**, *121*, 10727; e) R. Kuwano, Y. Ito, *J. Am. Chem. Soc.* **1999**, *121*, 3236.

[3] a) K. Manabe, *Tetrahedron Lett.* **1998**, *39*, 5807; b) K. Manabe, *Tetrahedron* **1998**, *54*, 14465; c) E. V. Dehmlow, S. Düttmann, B. Neumann, H.-G. Stammler, *Eur. J. Org. Chem.* **2002**, 2087.

[4] For recent excellent reviews on asymmetric phase-transfer catalysis, see: a) T. Shioiri, S. Arai in *Stimulating Concepts in Chemistry* (Eds.: F. Vogtle, J. F. Stoddart, M. Shibasaki), Wiley-VCH, Weinheim, **2000**, p. 123; b) M. J. O'Donnell in *Catalytic Asymmetric Synthesis* (Ed.: I. Ojima), VCH, New York, **2000**, chap. 10.

[5] a) T. Ooi, M. Kameda, K. Maruoka, *J. Am. Chem. Soc.* **1999**, *121*, 6519; b) T. Ooi, M. Takeuchi, M. Kameda, K. Maruoka, *J. Am. Chem. Soc.* **2000**, *122*, 5228; c) T. Ooi, M. Kameda, H. Tannai, K. Maruoka, *Tetrahedron Lett.* **2000**, *41*, 8339; d) T. Ooi, K. Doda, K. Maruoka, *Org. Lett.* **2001**, *3*, 1273; e) T. Ooi, M. Takeuchi, K. Maruoka, *Synthesis* **2001**, 1716; f) T. Ooi, Y. Uematsu, M. Kameda, K. Maruoka, *Angew. Chem.* **2002**, *114*, 1621; *Angew. Chem. Int. Ed.* **2002**, *41*, 1551; g) T. Ooi, M. Takahashi, K. Doda, K. Maruoka, *J. Am. Chem. Soc.* **2002**, *124*, 7640; h) T. Ooi, M. Taniguchi, M. Kameda, K. Maruoka, *Angew. Chem.* **2002**, *114*, 4724; *Angew. Chem. Int. Ed.* **2002**, *41*, 4542; i) T. Ooi, E. Tayama, K. Maruoka, *Angew. Chem.* **2003**, *115*, 599; *Angew. Chem. Int. Ed.* **2003**, *42*, 579.

[6] The results of the benzylation of **2** with other alkaline metal hydroxides under similar conditions are as follows: 2% yield, 45% *ee* with LiOH; 40% yield, 83% *ee* with NaOH.

[7] Although a chiral ammonium bromide of type **1** having a 3,4,5-trifluorophenyl group (Ar = 3,4,5-F_3-Ph), a promising catalyst for the synthesis of α,α-dialkyl-α-amino acids,[5b] was also found to be effective, it lacked generality in the present system. A typical example is the benzylation of *tert*-butyl 2-benzoylpropanoate (43%, 70% *ee* with **1** (Ar = 3,4,5-F_3-Ph); see entry 9 in Table 1 for comparison).

[8] Absolute configuration of the hydroxy-bearing carbon center of **5** was determined to be *S* by ^{1}H NMR analysis of the corresponding (*R*) and (*S*) Mosher esters.[14]

[9] The stereochemistry of **6** was assigned by an NOE experiment.

[10] For recent reviews on catalytic asymmetric Michael reactions, see: a) N. Krause, A. Hoffman-Röder, *Synthesis* **2001**, 171; b) M. Sibi, S. Manyem, *Tetrahedron* **2000**, *56*, 8033; c) M. Kanai, M. Shibasaki in *Catalytic Asymmetric Synthesis*, 2nd ed. (Ed.: I. Ojima), Wiley, New York, **2000**, p. 569; d) K. Tomioka, Y. Nagaoka in *Comprehensive Asymmetric Catalysis, Vol. 3* (Eds.: E. N. Jacobsen, A. Pfaltz, H. Yamamoto), Springer, Berlin, **1999**, Chap. 31.1.

[11] For a recent successful example, see: a) Y. Hamashima, D. Hotta, M. Sodeoka, *J. Am. Chem. Soc.* **2002**, *124*, 11240 and related references cited therein. This type of reaction by chiral phase-transfer catalysis has so far been unsuccessful; see: b) G. Szöllösi, M. Bartók, *Chirality* **2001**, *13*, 614.

[12] With toluene as solvent, the enantioselectivity was slightly decreased (97% yield, 73% *ee* with **7a**).

[13] The absolute configuration of **9** was determined by comparison of the optical rotation with the reported value after conversion to the corresponding methyl ester.[10a]

[14] I. Ohtani, T. Kusumi, Y. Kashman, H. Kakisawa, *J. Am. Chem. Soc.* **1991**, *113*, 4092.

[15] For **3a**, see: a) H. Falk, W. Fröstl, K. Schlögl, *Tetrahedron Lett.* **1974**, 217; for the methylation product, see: b) K. Umemura, H. Matsuyama, M. Kobayashi, N. Kamigata, *Bull. Chem. Soc. Jpn.* **1989**, *62*, 3026.

 © 2003 Wiley-VCH Verlag GmbH & Co. KGaA, Weinheim

High-Valent Rhenium Oxo Chemistry

Metallaoxetanes and Carbenes from Diolates in High-Valent Rhenium Oxo Chemistry: The Importance of the Coordination Number**

*Xueyi Chen, Xiangyang Zhang, and Peter Chen**

Dedicated to Professor Jerome A. Berson on the occasion of his 80th birthday

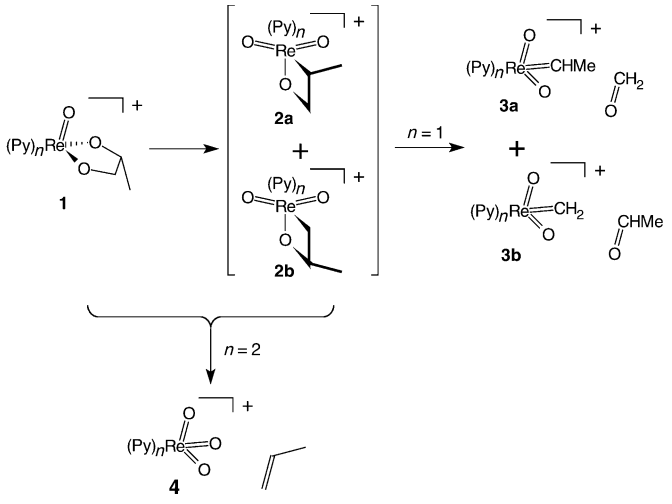
We report an electrospray ionization tandem mass spectrometric study of the chemistry of Re^{V} diolate complexes in which the intermediacy of the isomeric metallaoxetane complexes is implicated by dissociation of the diolates to rhenium carbene complexes instead of the expected oxo species (Scheme 1). Not only is the chemistry unprecedented for well-defined diolate complexes, but the marked dependence of the preferred reaction path upon coordination number in the original diolate complex supports a qualitative molecular orbital argument based on π-strain[1] that may be able to guide further design of new catalysts.

The chemistry of Re^{V} diolates and the corresponding Re^{VII} oxo complexes is closely related to that of OsO_4, and has been examined by other groups[2–5] in part as a model for the reactions of the latter complex, especially in connection to the catalytic asymmetric dihydroxylation reaction introduced by Sharpless and coworkers.[6] While the original mechanistic hypothesis by Böseken and De Graaft, and by Criegee and co-

[*] Prof. Dr. P. Chen, X. Chen, Dr. X. Zhang
Laboratorium für Organische Chemie
Eidgenossische Technische Hochschule
ETH Zürich, 8093 Zürich (Switzerland)
Fax: (41) 1-632-1280
E-mail: chen@org.chem.ethz.ch

[**] The authors acknowledge helpful discussions with Prof. K. Barry Sharpless and Prof. Kevin P. Gable. Financial support for this project was provided by the ETH Research Commission, the Swiss National Foundation, and the Robert Gnehm Foundation.

 © 2003 Wiley-VCH Verlag GmbH & Co. KGaA, Weinheim DOI: 10.1002/anie.200351496



Scheme 1. Schematic diagram of CID products of $(Py)_{1\text{-}2}ReO(OCHCH_3\text{-}CH_2O)$ cation upon the coordination number.

workers,[7] termed the [3+2] mechanism, had been accepted for decades, the mechanistic possibility of an alternative [2+2] mechanism[8] was investigated at length by stereochemical,[9,10] kinetic,[11,12] isotope effect,[13,14] and computational means.[1,15–17] A direct observation, however, of a metallaoxetane intermediate in high-valent Re or Os chemistry, or products uniquely derived from metallaoxetanes, has remained outstanding. The rhenium carbenes **3**, produced by dissociation of Re^{V} diolate **1**, are the first experimental evidence for the intermediacy of metallaoxetane intermediates based on observation of a product that may be uniquely associated with that intermediate. Furthermore, the results shed light on the activation reactions of metathesis reactions catalyzed by d^0 oxo complexes, for which the carbene formation step had been obscure.

The Re^{V} diolates were prepared by a route analogous to that reported by Paulo et al.[3] by the addition of one equivalent of the appropriate diol, 1,2-propanediol (in the work presented herein), and pyridine (in the first case) to $[ReOCl_3(SMe_2)(OPPh_3)]$ or $[(Py)_4ReO_2]Cl$ (Py = pyridine)[18] in CH_3Cl or CH_2Cl_2 solution at room temperature. The clean formation of the Re^{V} diolate complex in solution can be confirmed by ^1H NMR. Complex **1** was diluted to 10^{-5} M with CH_2Cl_2 and electrosprayed on a modified Finnigan MAT TSQ-700 tandem mass spectrometer as previously described.[19] The principal species in the electrospray mass spectrum is **1** ($n=2$) when desolvation conditions are gentle, for example, tube lens ~80 V. Collision-induced dissociation (CID) of **1** ($n=2$) in the radio-frequency (rf) 24-pole ion guide by collision with Xe under multiple collision conditions produces **1** ($n=1$) and further daughter products such as **3** or **4**. Each of the species, **1** ($n=2$), **1** ($n=1$), or **3** can be selected by m/z (usually the ^{187}Re isotopomer) in the first quadrupole mass filter and then presented for CID or reaction in a gas-filled (0.1 mbar of either Xe or *n*-propyl vinyl ether) rf octopole ion guide to distinguish between primary and secondary reactions of each ion. The products are then analyzed in the second quadrupole. CID and ion-molecule reactions were all performed at low collision energy, that is, −10 to −15 V in the laboratory frame.

While a variety of diols have been used in this study so that structure-activity relationships and substituent effects may be quantified, the salient result for the intermediacy of metallaoxetanes can already be seen for the simple alkyl substituted diolate **1**. For the five-coordinate complex **1** ($n=2$), CID with Xe induces two reactions: **1** ($n=2$) loses either propene to form the Re^{VII} trioxo complex **4**, or pyridine to form **1** ($n=1$). On the other hand, mass-selection of **1** ($n=1$), followed by CID, leads to mass spectrum in Figure 1.

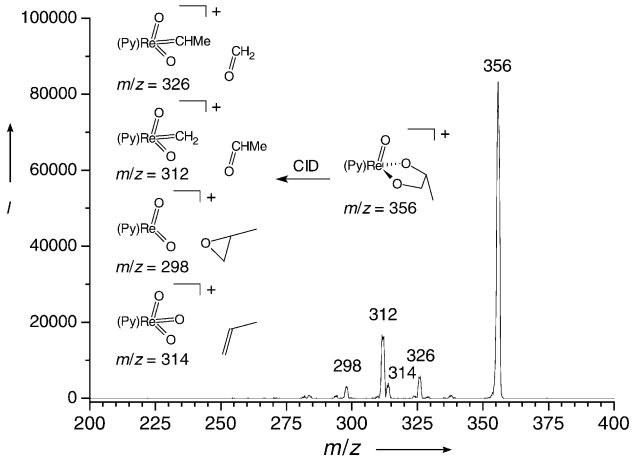


Figure 1. Daughter ion spectrum obtained by mass-selecting the ^{187}Re isotopomer of 1 ($n=1$) at $m/z=356$ and subjecting it to collision-induced dissociation with Xe at low collision energy. The major products at $m/z=326$ and 312 are shown to be carbene complexes by their subsequent reaction with *n*-propyl vinyl ether. *I* = intensity, arbitrary units

As is evident from Figure 1, the CID of four-coordinate **1** ($n=1$) gives ions with the masses of **3a**, $m/z=326$, and **3b**, $m/z=312$, as the major products, and a smaller amount of ions at $m/z=298$ and 314, which are assignable without doubt to $[(Py)ReO_2]^+$ and $[(Py)ReO_3]^+$. To establish the identity of the putative carbene complexes, the ion at $m/z=326$ was selected and reacted with *n*-propyl vinyl ether in the octopole ion guide to yield products at $m/z=298$ and 370. The former ion is again $[(Py)ReO_2]^+$; the latter is consistent with an assignment of $[(Py)ReO_2(=CHOPr)]^+$. From these ions, which would be the expected (ionic) products resulting from cyclopropanation and metathesis, respectively, of the vinyl ether, one can assign $m/z=326$ to the carbene complex **3a**. The experimental result can be simply formulated. For the two possible dissociation pathways that a preformed Re^{V} diolate can take, formation of carbene complexes **3** or formation of trioxo complex **4**, the former is the predominant reaction for **1** ($n=1$) and the latter for **1** ($n=2$). The sharp dichotomy is striking.

The mechanism of diolate formation in the asymmetric dihydroxylation of olefins by OsO_4, either concerted [3+2] cycloaddition or stepwise by [2+2] cycloaddition followed by ring expansion, has been the subject of intense discussion.[9–17]

 © 2003 Wiley-VCH Verlag GmbH & Co. KGaA, Weinheim

Arguments based on stereoselectivity, temperature effects, and isotope effects were made by both sides, with the interpretation of the same set of experimental results often diverging depending on one's point of view. The most convincing experimental study, a kinetic isotope effect study by using the method from Singleton, best fits expectations based on a [3+2] mechanism.[14] Quantum chemical calculations have been decisive in the entire story,[1,15–17] which have not only provided the basis for interpretation of experimentally determined isotope effects, but moreover predicted, in general, that the metallaoxetane intermediate in the [2+2] mechanism lay too high in energy, typically about 10–30 kcal mol^{-1}, above the isomeric diolate to be chemically significant. However, observation of the relevant metallaoxetane intermediates or products that could be uniquely associated has been wholly missing from the experimental side of the discussion. Recently, further experimental work on the closely related high-valent rhenium oxo complexes has provided some indirect support for the [2+2] mechanism.[5] Methyl trioxorhenium (MTO),[20] and other rhenium complexes[21,22] participates furthermore in a reaction, aldehyde olefination, for which a metallaoxetane intermediate has been proposed, although the intermediacy of metallaoxetanes in that reaction has been challenged by other experiments.[23,24]

Accordingly, we chose the chemistry of Re^{V} diolates as the most likely arena in which metallaoxetanes might appear. The Re^{V} diolates also allow a wide range of structural variation, which should be important if one wants to ultimately put together structure-activity models that may help clarify issues with OsO_4 and the corresponding Os^{VI} diolates. The observation of carbene complexes **3** from the diolate **1** ($n=1$) is unprecedented for well-defined complexes, although there have been reports of metathesis or ring-opening metathesis polymerization (ROMP) activity by Re_2O_7,[25] MTO,[26,27] some perrhenates,[28] and even OsO_4.[29] For Re_2O_7, an alkyl tin activator is not mandatory even though the "promoter" improves activity. For MTO, it was established definitively that the methyl group was not transformed into a carbene. For the perrhenates or OsO_4, there were no alkylating reagents to generate the metal alkyl that would be deprotonated to a carbene. It is difficult to establish the origin of the presumed carbene intermediates, especially given that there are only few reports of well-defined, high-valent rhenium carbenes.[30,31] The present experiment shows that simple Re^{V} diolates, which were shown[2] to be accessible by the reaction of Re^{VII} oxo complexes with olefins, can yield carbenes. By far the most probable mechanism involves the rearrangement of the diolate to a metallaoxetane, which then cleaves, that is, **1**→**2**→**3**. Observation of carbene products **3** therefore constitutes the best experimental evidence to date that metallaoxetanes are chemically significant intermediates in this manifold of structures. One should also note that the small amount of $[(Py)ReO_2]^+$ produced in the dissociation of **1** ($n=1$) is consistent with loss of an epoxide from either **1** ($n=1$) or **2** ($n=1$); epoxidation of olefins is a characteristic reaction of MTO, albeit in the presence of peroxides.[32] Lastly, the reaction sequence **4**→**2**→**3** or **4**→**1**→**2**→**3** provides a plausible mechanism for the metathesis activity of Re_2O_7, MTO, the perrhenates, and OsO_4.

It remains to explain why the observation of carbene products has remained outstanding up until now, and why the reactivity of **1** shows such a sharp dichotomy depending on whether one or two pyridine units are coordinated to the metal center. A rationale, which had in fact provided a part of the reasoning behind the experimental design, is inspired by a computational study by Rappé and co-workers.[1] For the reaction of an olefin with a model four-coordinate complex $LReO_3$, in which L ranges from a strong σ donor like $-CH_3$ to strong π donors, such as =O or Cp, Rappé and co-workers proposed that the thermodynamically favored product, either diolate or metallaoxetane, would be determined by release of π strain. They reasoned that the tetrahedral ligand field splits the d orbitals into bonding e_g and antibonding t_{2g} sets. With only two low-lying d orbitals, the complex can have only two strong π bonds to ligands. $LReO_3$ has either three or four π bonds, depending on the nature of L, so the electrons for the one or two "extra" π bonds necessarily go into antibonding (or at least substantially less bonding) orbitals. Accordingly, the more π-strained complexes, $LReO_3$, in which L is a π donor, prefer the product that reduces the total π bond order the most, that is, the diolate. For $LReO_3$, in which L is a σ donor, the preference for diolate over metallaoxetane is less, or perhaps even reversed. One additional point needs to be made. Whereas a four-coordinate tetrahedral ligand field gives only two low-lying d orbitals, both five-coordinate and six-coordinate complexes have at least three. Given that the coordination number of the metallaoxetane is one higher than that for the corresponding diolate, one expects therefore a relative stabilization of the metallaoxetane relative to the diolate when the two structures are five- and four-coordinate, respectively, as opposed to the case in which the metallaoxetane is six-coordinate and the diolate five-coordinate. Preliminary DFT calculations (B3LYPLACVP**, to be published) place **2** ($n=2$) approximately 30 kcal mol^{-1} above **1** ($n=2$), but **2** ($n=1$) a few kcal mol^{-1} below **1** ($n=1$), which is fully consistent with the expectations based on π strain, as well as the present experimental results. The working hypothesis says, therefore, that, the [2+2] mechanism is competitive with the [3+2] mechanism when the metallaoxetane is low enough in energy, which in turn requires a four-coordinate d^0 oxo complex, in which at least one of the ligands is a σ rather than π donor. While this is possible for $LReO_3$ systems, the [2+2] mechanism would not be competitive for OsO_4 with or without ligand acceleration.

We report a novel reaction in which Re^{V} diolate complexes cleave either to the Re^{VII} trioxo complex or a rhenium carbene, depending on the coordination number of the original diolate complex. The carbene complexes produced from diolates are the best experimental indication to date for intermediate metallaoxetanes, which would be the first-formed intermediate in [2+2] reactions of olefins with a d^0 oxo complex. The dichotomy in reactivity is surprisingly sharp and can be explained by a qualitative π-strain model. Further studies to investigate substituent and ligand effects are underway.

Received: March 26, 2003 [Z51496]

 © 2003 Wiley-VCH Verlag GmbH & Co. KGaA, Weinheim

Keywords: carbene ligands · diolate · mass spectrometry · reaction mechanisms · rhenium

[1] M. A. Pietsch, T. V. Russo, R. B. Murphy, R. L. Martin, A. K. Rappé, *Organometallics* **1998**, *17*, 2716.
[2] R. M. Pearlstein, A. Davison, *Polyhedron* **1988**, *7*, 1981.
[3] A. Paulo, A. Domingos, A. Pires de Matos, I. Santos, M. F. N. N. Carvalho, A. J. L. Pombeiro, *Inorg. Chem.* **1994**, *33*, 4729.
[4] K. P. Gable, T. N. Phan, *J. Am. Chem. Soc.* **1994**, *116*, 833; K. P. Gable, J. J. J. Juliette, *J. Am. Chem. Soc.* **1995**, *117*, 955; K. P. Gable, J. J. J. Juliette, *J. Am. Chem. Soc.* **1996**, *118*, 2625; K. P. Gable, *Adv. Organomet. Chem.* **1997**, *41*, 127; K. P. Gable, A. AbuBaker, K. Zientara, A. M. Wainwright, *Organometallics* **1999**, *18*, 173.
[5] K. P. Gable, F. A. Zhuravlev, *J. Am. Chem. Soc.* **2002**, *124*, 3970.
[6] For a review, see: H. C. Kolb, M. S. VanNieuwenhze, K. B. Sharpless, *Chem. Rev.* **1994**, *94*, 2483; Recent progress is described in: P. Dupau, R. Epple, A. A. Thomas, V. V. Fokin, K. B. Sharpless, *Adv. Synth. Catal.* **2002**, *344*, 421.
[7] J. Böseken, C. De Graaft, *Recl. Trav. Chim. Pays-Bas* **1922**, *41*, 199; R. Criegee, *Justus Liebigs Ann. Chem.* **1936**, *522*, 75; R. Criegee, *Angew. Chem.* **1937**, *50*, 153; R. Criegee, *Angew. Chem.* **1938**, *51*, 519; R. Criegee, B. Marchand, H. Wannowius, *Justus Liebigs Ann. Chem.* **1942**, *550*, 99.
[8] K. B. Sharpless, A. Y. Teranishi, J. E. Bäckvall, *J. Am. Chem. Soc.* **1977**, *99*, 3120.
[9] E. J. Corey, M. C. Noe, S. Sarshar, *J. Am. Chem. Soc.* **1993**, *115*, 3828; E. J. Corey, M. C. Noe, *J. Am. Chem. Soc.* **1993**, *115*, 12579; E. J. Corey, M. C. Noe, *J. Am. Chem. Soc.* **1996**, *118*, 11038; E. J. Corey, J. Zhang, *Org. Lett.* **2001**, *3*, 3211.
[10] P. O. Norrby, H. C. Kolb, K. B. Sharpless, *J. Am. Chem. Soc.* **1994**, *116*, 8470; H. Becker, P. T. Ho, H. C. Kolb, S. Loren, P. O. Norrby, K. B. Sharpless, *Tetrahedron Lett.* **1994**, *35*, 7315.
[11] E. J. Corey, M. C. Noe, *J. Am. Chem. Soc.* **1996**, *118*, 319.
[12] T. Göbel, K. B. Sharpless, *Angew. Chem.* **1993**, *105*, 1417; *Angew. Chem. Int. Ed. Engl.* **1993**, *32*, 1329; D. W. Nelson, A. Gypser, P. T. Ho, H. C. Kolb, T. Kondo, H. L. Kwong, D. V. McGrath, A. E. Rubin, P. O. Norrby, K. P. Gable, K. B. Sharpless, *J. Am. Chem. Soc.* **1997**, *119*, 1840.
[13] E. J. Corey, M. C. Noe, M. J. Grogan, *Tetrahedron Lett.* **1996**, *37*, 4899.
[14] A. J. DelMonte, J. Haller, K. N. Houk, K. B. Sharpless, D. A. Singleton, A. A. Thomas, *J. Am. Chem. Soc.* **1997**, *119*, 9907.
[15] P. O. Norrby, H. C. Kolb, K. B. Sharpless, *Organometallics* **1994**, *13*, 344; P. O. Norrby, H. Becker, K. B. Sharpless, *J. Am. Chem. Soc.* **1996**, *118*, 35.
[16] J. Haller, T. Strassner, K. N. Houk, *J. Am. Chem. Soc.* **1997**, *119*, 8031; P. O. Norrby, T. Rasmussen, J. Haller, T. Strassner, K. N. Houk, *J. Am. Chem. Soc.* **1999**, *121*, 10186.
[17] G. Ujaque, F. Maseras, A. Lledós, *J. Am. Chem. Soc.* **1999**, *121*, 1317; D. V. Deubel, G. Frenking, *J. Am. Chem. Soc.* **1999**, *121*, 2021; P. Gisdakis, N. Rösch, *J. Am. Chem. Soc.* **2001**, *123*, 697.
[18] $[(Py)_4ReO_2]^+$ Cl^- is prepared as described by: M. S. Ram, J. T. Hupp, *Inorg. Chem.* **1991**, *30*, 130.
[19] C. Hinderling, D. A. Plattner, P. Chen, *Angew. Chem.* **1997**, *109*, 272; *Angew. Chem. Int. Ed. Engl.* **1997**, *36*, 243; C. Hinderling, D. Feichtinger, D. A. Plattner, P. Chen, *J. Am. Chem. Soc.* **1997**, *119*, 10793; D. Feichtinger, D. A. Plattner, *Angew. Chem.* **1997**, *109*, 1796; *Angew. Chem. Int. Ed. Engl.* **1997**, *36*, 1718; D. Feichtinger, D. A. Plattner, P. Chen, *J. Am. Chem. Soc.* **1998**, *120*, 7125; C. Hinderling, C. Adlhart, P. Chen, *Angew. Chem.* **1998**, *110*, 2831; *Angew. Chem. Int. Ed.* **1998**, *37*, 2685; C. Hinderling, P. Chen, *Angew. Chem.* **1999**, *111*, 2393; *Angew. Chem. Int. Ed.* **1999**, *38*, 2253; Y. M. Kim, P. Chen, *Int. J. Mass Spectrom.* **1999**, *185-7*, 871; C. Hinderling, P. Chen, *Int. J. Mass Spectrom. Ion Processes* **2000**, *195/196*, 377; C. Hinderling, C. Adlhart, P. Chen, *Chimia* **2000**, *54*, 232; C. Adlhart, P. Chen, *Helv. Chim. Acta* **2000**, *83*, 2192; C. Adlhart, M. A. O. Volland, P. Hofmann, P. Chen, *Helv. Chim. Acta* **2000**, *83*, 3306; C. Adlhart, C. Hinderling, H. Baumann, P. Chen, *J. Am. Chem. Soc.* **2000**, *122*, 8204; M. A. O. Volland, C. Adlhart, C. A. Kiener, P. Chen, P. Hofmann, *Chem. Eur. J.* **2001**, *7*, 4621; G. Gerdes, P. Chen, *Organometallics*, in press; X. Zhang, P. Chen, *Chem. Eur. J.* **2003**, *9*, 1852 – 1859.
[20] W. A. Herrmann, M. Wang, *Angew. Chem.* **1991**, *103*, 1709; *Angew. Chem. Int. Ed. Engl.* **1991**, *30*, 1641; W. A. Herrmann, P. W. Roesky, M. Wang, W. Scherer, *Organometallics* **1994**, *13*, 4531.
[21] B. E. Ledford, E. M. Carreira, *Tetrahedron Lett.* **1997**, *38*, 8125.
[22] A. M. Santos, C. C. Romão, F. E. Kühn, *J. Am. Chem. Soc.* **2003**, *125*, 2414.
[23] O. Fujimura, T. Honma, *Tetrahedron Lett.* **1998**, *39*, 625; H. Lebel, V. Paquet, C. Proulx, *Angew. Chem.* **2001**, *113*, 2971; *Angew. Chem. Int. Ed.* **2001**, *40*, 2887; G. A. Mirafzal, G. Cheng, L. K. Woo, *J. Am. Chem. Soc.* **2002**, *124*, 176.
[24] X. Zhang, P. Chen, *Chem. Eur. J.* **2003**, *9*, 1852 – 1859.
[25] J. C. Mol, *Catal. Today* **1999**, *51*, 289.
[26] W. A. Herrmann, W. Wagner, U. N. Flessner, U. Volkhardt, H. Komber, *Angew. Chem.* **1991**, *103*, 1704; *Angew. Chem. Int. Ed. Engl.* **1991**, *30*, 1636; R. Buffon, A. Choplin, M. Leconte, J. M. Basset, R. Touroude, W. A. Herrmann, *J. Mol. Catal.* **1992**, *72*, L7; R. Buffon, A. Auroux, F. Lefebvre, M. Leconte, A. Choplin, J. M. Basset, W. A. Herrmann, *J. Mol. Catal.* **1992**, *76*, 287.
[27] Photochemical formation of a carbene tautomer of MTO has also been reported. L. J. Morris, A. J. Downs, T. M. Greene, G. S. McGrady, W. A. Herrmann, P. Sirsch, W. Scherer, O. Gropen, *Organometallics* **2001**, *20*, 2344.
[28] D. Commereuc, *J. Chem. Soc. Chem. Commun.* **1995**, 791; G. Doledec, D. Commereuc, *J. Mol. Catal. A* **2000**, *161*, 125.
[29] J. G. Hamilton, O. N. D. Mackey, J. J. Rooney, D. G. Gilheany, *J. Chem. Soc. Chem. Commun.* **1990**, 1600.
[30] R. Toreki, R. R. Schrock, *J. Am. Chem. Soc.* **1990**, *112*, 2448; R. Toreki, R. R. Schrock, W. M. Davis, *J. Am. Chem. Soc.* **1992**, *114*, 3367; R. Toreki, G. A. Vaughan, R. R. Schrock, W. M. Davis, *J. Am. Chem. Soc.* **1993**, *115*, 127; A. M. LaPointe, R. R. Schrock, *Organometallics* **1995**, *14*, 1875.
[31] M. Chabanas, A. Baudouin, C. Copéret, J. M. Basset, *J. Am. Chem. Soc.* **2001**, *123*, 2062.
[32] W. A. Herrmann, R. W. Fischer, W. Scherer, M. U. Rauch, *Angew. Chem.* **1993**, *105*, 1209; *Angew. Chem. Int. Ed. Engl.* **1993**, *32*, 1157; W. A. Herrmann, R. W. Fischer, M. U. Rauch, W. Scherer, *J. Mol. Catal.* **1994**, *86*, 243.

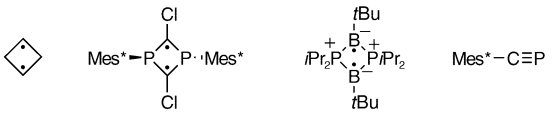
 © 2003 Wiley-VCH Verlag GmbH & Co. KGaA, Weinheim

Stable Biradicals

Synthesis of a 1,3-Diphosphacyclobutane-2,4-diyl from Mes*C≡P**

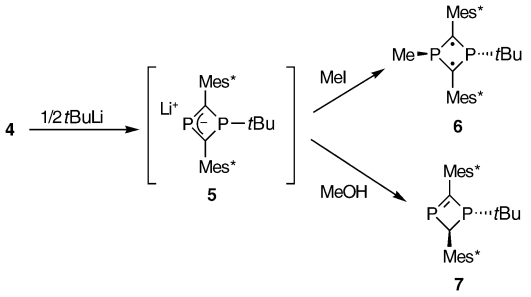
*Hiroki Sugiyama, Shigekazu Ito, and Masaaki Yoshifuji**

A biradical is defined as an even-electron molecular entity with two radical centers that act nearly independently of each other and they normally displays quite high reactivity.[1] Cyclobutane-1,3-diyl **1** is a biradical with a ring structure



and is observed at very low temperature.[2] More recently several stable "singlet" biradicals with a four-membered-ring skeleton by incorporating main-group elements, such as phosphorus were reported.[3] In 1995 Niecke and co-workers reported 2,4-dichloro-1,3-bis(2,4,6-tri-*tert*-butylphenyl)-1,3-diphosphacyclobutane-2,4-diyl (**2**)[4] as the first stable congener of singlet **1** and afterwards they prepared several derivatives from **2**.[5] In addition to the carbon-based 1,3-biradicals, a 1,3-dibora-2,4-diphosphacyclobutane-1,3-diyl compound **3** was reported by Bertrand and co-workers.[6] These successes in obtaining biradical compounds that can be handled at room temperature stimulated further efforts to explore similar curious molecules and their role as functional materials, such as magnets.[1,3,7] Niecke and co-workers used **2** to prepare several four-membered biradical derivatives, in which two Mes*P moieties are incorporated (Mes* = 2,4,6-tri-*tert*-butylphenyl).[5] In contrast to the biradicals of Niecke, we succeeded in preparing a novel 1,3-diphosphacyclobutane-2,4-diyl derivative from phosphaalkyne **4**. Herein we report the method of preparation of the 1,3-diphosphacyclobutane-2,4-diyl derivative and its properties, especially its high stability.

Phosphaalkyne **4** was prepared from 2,2-dibromo-1-(2,4,6-tri-*tert*-butylphenyl)-1-phosphaethene by a nickel-catalyzed [1,2] rearrangement.[8,9,10a] Compound **4** was allowed to react with half an equivalent of *tert*-butyllithium, to generate the corresponding anion intermediate **5**, and was then quenched with iodomethane. 1,3-Diphosphacyclobutane-2,4-diyl **6** was isolated as a deep-blue/violet solid almost quantitatively from **4**. On the other hand, 1,3-diphosphacyclobutene **7** was obtained in the reaction of **4** with *tert*-butyllithium and methanol,[11] thus indicating the formal ambident nature of the PCP anion system (Scheme 1).[12] 1,3-



Scheme 1. Reaction of **4** with *t*BuLi followed by quenching with iodomethane or methanol.

diphosphacyclobutane-2,4-diyl **6** was stable at room temperature and even in air. Indeed, **6** did not decompose for several minutes when it was treated with water or silica gel, and in the solid state it could be washed with ethanol. This lack of reactivity of **6** is in sharp contrast with **2** or **3**, which are reported to immediately decompose on contact with air.

A single crystal of **6** was used for X-ray crystallography and Figure 1 shows the molecular structure. The P_2C_2 four-membered ring is almost planar, to within 0.069 Å, whereas a butterfly conformation is observed in the structure of **7**.[11] C1 and C2 are sp^2 hybridized with a planar environment, and the sum of the bond angles around C1 and C2 are 360(1) and 358(1)°, respectively. There is no covalent bond between the C1 and C2 (C1···C2, 2.50 Å). The P1–C1 and P1–C2 bond lengths are shorter than the corresponding bond lengths for P2. The geometry around P1 is less pyramidal (more planar) than that of P2, as shown by the sum of bond angles (341(1)°

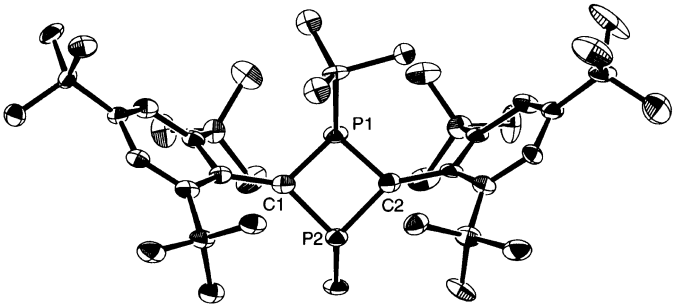


Figure 1. ORTEP drawing of **6** with 40% probability ellipsoids. Hydrogen atoms are omitted for clarity. The *tert*-butyl group on the P1 atom is disordered and the atoms with the predominant occupancy factor (0.53) are shown. Bond lengths (Å) and Angles (°): P1-C1 1.70(1), P1-C2 1.72(1), P1-C_{tBu} 1.877(10), P2-C1 1.77(1), P2-C2 1.79(1), P2-C_{Me} 1.85(1), C1-C_{Mes*} 1.50(1), C2-C_{Mes*} 1.49(1), C1-P1-C2 94.0(5), C1-P1-C_{tBu} 123.1(5), C2-P1-C_{tBu} 124.3(5), C1-P2-C2 89.1(5), C1-P2-C_{Me} 116.0(5), C2-P2-C_{Me} 113.9(5), P1-C1-P2 89.0(5), P1-C1-C_{Mes*} 127.5(7), P2-C1-C_{Mes*} 143.3(7), P1-C2-P2 87.6(5), P1-C2-C_{Mes*} 126.2(7), P2-C2-C_{Mes*} 144.4(7).

[*] Prof. Dr. M. Yoshifuji, H. Sugiyama, Dr. S. Ito
Department of Chemistry
Graduate School of Science
Tohoku University
Aoba, Sendai 980-8578 (Japan)
Fax: (+81) 22-217-6562
E-mail: yoshifj@mail.cc.tohoku.ac.jp

[**] This work was supported in part by Grants-in-Aid for Scientific Research (No. 13304049 and 14044012) from the Ministry of Education, Culture, Sports, Science and Technology, Japan.
Mes* = 2,4,6-$tBu_3C_6H_2$.

 © 2003 Wiley-VCH Verlag GmbH & Co. KGaA, Weinheim DOI: 10.1002/anie.200351727

for P1; 319(1)° for P2). This difference might indicate some influence of the dimethylenephosphorane structure on the P1 side,[5c] although the P1–C1/C2 bond lengths are indeed longer than the isolated dimethylenephosphoranes [1.65–1.67 Å].[13] The two Mes* rings make the mean angle to the P_2C_2 plane of 60(1)° (C1) and 59(1)° (C2), respectively. The lack of reactivity of **6** is due to the steric congestion around the radical centers formed by the bulky Mes* groups.

The NMR data was also used to characterize the singlet biradical structure of **6**. In the ^{13}C NMR spectrum, the (radical) sp^2 carbon was observed at $\delta_C = 111.3$, which is similar to that of **2** ($\delta_C = 98.8$)[4] and its derivatives.[5a,b] In the ^{31}P NMR spectrum of **6**, two kinds of phosphorus atoms were observed at $\delta_P = 55.9$ (*t*BuP) and −11.3 (MeP) with a large J(P,P) coupling constant (362.8 Hz). In ^1H NMR spectrum, a larger ^3J(P,H) value (13.6 Hz) was observed for the *t*BuP group rather than the ^2J(P,H) for the MeP part (5.8 Hz). In UV/Vis spectrum of **6** the absorption was observed at 612 nm, which is a large red shift compared with the absorptions of **2** (478 nm)[4] and **3** (446 nm).[6] This difference indicates that the energetic separation between the HOMO and LUMO in **6** is smaller than those of **2** and **3**. The ground state of 1,3-diphosphacyclobutane-2,4-diyl is theoretically assigned as a singlet due to the interaction between the symmetrical nonbonding molecular orbital (NBMO) and the lonepair of the phosphorus atoms.[4,5c] As discussed on cyclobutane-1,3-diyl, spin-multiplicity is controlled by substituents on the 2,4-positions,[14] and therefore the spin-multiplicity of 1,3-diphosphacyclobutane-2,4-diyl could operate to configure the triplet state. The red-shift absorption of **6** might indicate the small energetic gap between the singlet and triplet states.

We performed cyclic voltammetry (CV) on **6**. A reversible oxidation peak ($^1E^{ox}_{1/2}$) is observed at +0.35 V (versus Ag/AgCl, Figure 2) and an irreversible oxidation peak ($^2E^{ox}_p$) appears at +1.56 V. The first oxidation probably occurs at the radical centers, which corresponds to the HOMO, and the other irreversible oxidation peak might indicate the oxidation at the phosphorus atoms. Thus a stable cationic species is generated by the oxidation. In the case of **7**, an irreversible oxidation peak was observed at +1.36 V. As for the reduction, the irreversible peak E^{red}_p is observed at −0.70 V for **6**, which is similar to the corresponding value of **7** (−0.68 V).

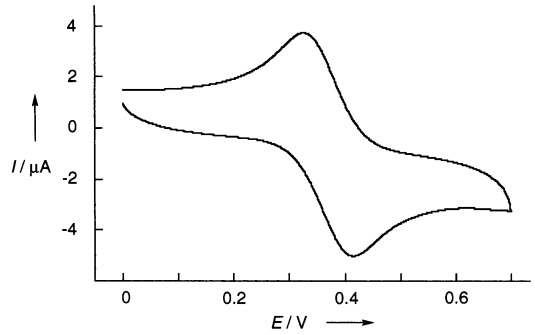


Figure 2. Cyclic volammogram of **6**: 1 mM in dichloromethane; supporting electrolyte: 0.1 M tetrabutylammonium perchlorate (TBAP); working electrode: glassy carbon; counter electrode: platinum wire; reference electrode: Ag/AgCl ($E_{1/2}$ (ferrocene/ferricinium) = +0.60 V) at 20 °C; scan rate: 50 mV s^{-1}; E = potential, I = current.

We were interested in the reactivity of **6** on thermolysis. The biradical **6** was heated to reflux in toluene to produce **4**, which was isolated in a moderate yield. This result, that is, the breaking of the P–C(alkyl) bond together with the breakup of the four-membered ring, are in sharp contrast to the reactivity of **2**.[4] Any other products, such as the eliminated *tert*-butyl or methyl group that would prove the reaction mechanism, have not been identified. We did not observe any isomerization of **6** upon irradiation (medium pressure 100 W Hg lamp at 0 °C for 15 h) but only recovered **6**.

In conclusion, we demonstrated an alternative method to prepare 1,3-diphosphacyclobutane-2,4-diyl from phosphaalkyne **4**, and the novel compound **6** showed quite high stability. The structural elucidation of **6** revealed the effective steric protection given by the Mes* groups around the radical centers. The small HOMO–LUMO gap found in **6**, indicated by the absorption spectrum, suggests a triplet state, as demonstrated by its carbon congener (cyclobutane-1,3-diyl). The present synthetic method should be a promising approach in the development of novel stable biradical species.

Experimental Section

Preparation of **6**: A solution of *tert*-butyllithium in pentane (0.56 mmol, 1.4 M) was added to a solution of **4** (300 mg, 1.0 mmol) in THF (8 mL) at −78 °C and stirred for 15 min. The solution was then warmed to room temperature, and stirred for 1 h, during which the solution turned blue. Iodomethane (0.64 mmol) was added to the reaction mixture and the solvent was removed in vacuo. The residue was extracted with hexane and the solvent was removed by evaporation to afford almost pure **6** (yield: 640 mg, 98 %). Compound **6** was crystallized in dichloromethane at 0 °C: deep-blue/violet prisms, mp 158–160 °C; $^{31}P\{^1H\}$ NMR (162 MHz, $CDCl_3$): $\delta = 55.9$ (d, $^2J(P,P) = 362.8$ Hz, *t*BuP), −11.3 ppm (d, $^2J(P,P) = 362.8$ Hz, MeP); ^1H NMR (400 MHz, $CDCl_3$): $\delta = 7.45$ (s, 2H, *m*-Mes*), 7.26 (s, 2H, *m*-Mes*), 1.86, (d, $^2J(P,H) = 5.8$ Hz, 3H, MeP), 1.68 (s, 18H, *o*-*t*Bu), 1.66 (s, 18H, *o*-*t*Bu), 1.36 (s, 18H, *p*-*t*Bu), 0.69 ppm (d, $^3J(P,H) = 13.6$ Hz, 9H, *t*BuP); $^{13}C\{^1H\}$ NMR (101 MHz, $CDCl_3$): $\delta = 150.2$ (pt, $(^2J(P,C) + {}^2J(P,C))/2 = 9.3$ Hz, *ipso*-Mes*), 148.0 (d, $^3J(P,C) = 9.3$ Hz, *o*-Mes*), 144.7 (s, *p*-Mes*), 133.8 (d, $^3J(P,C) = 2.8$ Hz, *o*-Mes*), 123.0 (s, *m*-Mes*), 120.0 (s, *m*-Mes*), 111.3 (dd, $^1J(P,C) = 10.7$ Hz, $^1J(P,C) = 3.3$ Hz, CP_2), 46.7 (dd, $^1J(P,C) = 52.9$ Hz, $^3J(P,C) = 15.8$ Hz, $PCMe_3$), 38.9 (s, *o*-CMe_3), 37.7 (s, *o*-CMe_3), 35.4 (s, *p*-CMe_3), 33.8 (s, *o*-CMe_3), 33.7 (s, *o*-CMe_3), 31.9 (s, *p*-CMe_3), 29.4 (dd, $^2J(P,C) = 5.6$ Hz, $^4J(P,C) = 3.7$ Hz, $PCMe_3$), 13.6 ppm (dd, $^1J(P,C) = 58.5$ Hz, $^3J(P,C) = 24.1$ Hz, PMe); UV-Vis (hexanes) λ_{max} (ε) = 326 (16700), 382 (17500), 612 (1500) nm.

Thermolysis of **6**: A solution of **6** (0.092 mmol) in toluene (8 mL) was heated to reflux for 3 h and the solution changed from blue/purple to yellow. The mixture was cooled to room temperature and analyzed by ^{31}P NMR spectroscopy, which indicated that **4** was the major product, although the spectrum also had unidentified trace resonance signals. The solvent was removed in vacuo and the residual product was purified by silica gel column chromatography (hexane) to afford **4** (14 mg, 0.049 mmol).

X-Ray data for **6**: $C_{43}H_{70}P_2$: $M_r = 648.97$, deep-blue/violet prism crystallized from dichloromethane at 0 °C. Crystal dimensions 0.30 × 0.25 × 0.10 mm^3, triclinic, space group $P\bar{1}$ (no. 2), $a = 14.553(2)$, $b = 14.480(3)$, $c = 8.878(3)$ Å, $\alpha = 96.64(1)$, $\beta = 104.94(2)$, $\gamma = 106.812(7)$°, $V = 2044.2(8)$ Å^3, $Z = 2$, $\rho_{calcd} = 1.054$ g cm^{-3}, $F(000) = 716.00$, $\mu = 0.133$ mm^{-1}, $T = 120$ K. A Rigaku RAXIS-IV imaging plate detector with graphite-monochromated $Mo_{K\alpha}$ radiation ($\lambda = 0.71070$ Å) was

 © 2003 Wiley-VCH Verlag GmbH & Co. KGaA, Weinheim

used. Of 8092 reflections measured ($2\theta_{max} = 55.0°$), 6027 were observed ($R_{int} = 0.062$). The structure was solved by direct methods (SIR92),[15] expanded by using Fourier techniques (DIRDIF94),[16] and then refined by full-matrix least squares on F for 404 variable parameters. The non-hydrogen atoms without the disordered atoms in the P*t*Bu group were refined anisotropically. Hydrogen atoms (calculated) were refined isotropically. $R1 = 0.099$ for $I > 3.0\sigma(I)$, and $R_w = 0.136$ for all data. Goodness of fit $S = 1.80$ for observed reflections. The maximum and minimum peaks on the final difference Fourier map corresponded to 0.97 and -0.34 e Å^{-3}, respectively. The data were corrected for Lorentz polarization effect. Structure solution, refinement, and graphical representation were carried out using the teXsan package.[17] CCDC-208433 contains the supplementary crystallographic data for this paper. These data can be obtained free of charge via www.ccdc.cam.ac.uk/conts/retrieving.html (or from the Cambridge Crystallographic Data Centre, 12, Union Road, Cambridge CB21EZ, UK; fax: (+44) 1223-336-033; or deposit@ccdc.cam.ac.uk).

Received: April 23, 2003 [Z51727]

Keywords: heterocycles · phosphaalkynes · protecting groups · radicals · structure elucidation

[1] a) "Diradicals": W. T. Borden in *Encyclopedia of Computational Chemistry* (Ed.: P. von R. Schleyer), Wiley-Interscience, NY, **1998**, p. 708; b) J. A. Berson, *Acc. Chem. Res.* **1997**, *30*, 238.
[2] a) R. Jain, M. B. Sponsler, F. D. Coms, D. A. Dougherty, *J. Am. Chem. Soc.* **1988**, *110*, 1356; b) K. A. Nguyen, M. C. Gordon, J. A. Boatz, *J. Am. Chem. Soc.* **1994**, *116*, 9241.
[3] a) H. Grützmacher, F. Brehler, *Angew. Chem.* **2002**, *114*, 4178; *Angew. Chem. Int. Ed.* **2002**, *41*, 4006; b) P. P. Power, *Chem. Rev.* **2003**, *103*, 789.
[4] E. Niecke, A. Fuchs, F. Baumeister, M. Nieger, W. W. Schoeller, *Angew. Chem.* **1995**, *107*, 640; *Angew. Chem. Int. Ed. Engl.* **1995**, *34*, 555. See also O. Schmidt, A. Fuchs, D. Gudat, M. Nieger, W. Hoffbauer, E. Niecke, W. W. Schoeller, *Angew. Chem.* **1998**, *110*, 995; *Angew. Chem. Int. Ed.* **1998**, *37*, 949.
[5] a) E. Niecke, A. Fuchs, M. Nieger, *Angew. Chem.* **1999**, *111*, 3213; *Angew. Chem. Int. Ed.* **1999**, *38*, 3028; b) E. Niecke, A. Fuchs, M. Nieger, O. Schmidt, W. W. Schoeller, *Angew. Chem.* **1999**, *111*, 3216; *Angew. Chem. Int. Ed.* **1999**, *38*, 3031; c) W. W. Schoeller, C. Begemann, E. Niecke, D. Gudat, *J. Phys. Chem. A* **2001**, *105*, 10731.
[6] D. Scheschkewitz, H. Amii, H. Gornitzka, W. W. Schoeller, D. Bourissou, G. Bertrand, *Science* **2002**, *295*, 1880.
[7] D. A. Dougherty, *Acc. Chem. Res.* **1991**, *24*, 88.
[8] M. Yoshifuji, S. Ito, *Top. Curr. Chem.* **2003**, *223*, 67.
[9] A mixture of 2,2-dibromo-1-(2,4,6-tri-*tert*-butylphenyl)-1-phosphaethene ($Mes^*P=CBr_2$, 6.0 g, 13 mmol),[10] $NiBr_2(PPh_3)_2$ (1.3 mmol), PPh_3 (2.7 mmol), Zn (14 mmol), and Et_4NI (13 mmol) in THF (180 mL) was heated at reflux for 24 h. After the mixture was cooled to room temperature, the solvent was removed in vacuo. The residue was diluted with hexane and the insoluble materials were filtered off. The solution was concentrated in vacuo and was purified by silica gel column chromatography (hexane) to give 2.7 g (9.4 mmol) of **4** (70% yield). See also H. Jun, V. G. Young, Jr., R. Angelici, *Organometallics* **1994**, *13*, 2444; V. D. Romanenko, M. Sanchez, T. V. Sarina, M. R. Maziéres, R. Wolf, *Tetrahedron Lett.* **1992**, *33*, 2981. Another preparation of **4** is described in ref. [8].
[10] a) S. J. Goede, F. Bickelhaupt, *Chem. Ber.* **1991**, *124*, 2677; b) S. J. Goede, M. A. Dam, F. Bickelhaupt, *Recl. Trav. Chim. Pays-Bas* **1994**, *113*, 278; c) R. Appel, C. Casser, M. Immenkeppel, *Tetrahedron Lett.* **1985**, *26*, 3551.
[11] S. Ito, H. Sugiyama, M. Yoshifuji, *Chem. Commun.* **2002**, 1744.
[12] S. Surana, S. Singh, R. K. Bansal, N. Peulecke, A. Spannenberg, J. Heinicke, *J. Organomet. Chem.* **2002**, *646*, 113.
[13] M. Regitz, O. J. Scherer, *Multiple Bonds and Low Coordination in Phosphorus Chemistry*, Georg Thieme, Stuttgart, **1990**.
[14] M. Abe, C. Ishihara, M. Nojima, *J. Org. Chem.* **2003**, *68*, 1618.
[15] A. Altomare, M. C. Burla, M. Camalli, M. Cascarano, C. Giacovazzo, A. Guagliardi, G. Polidori, *J. Appl. Crystallogr.* **1994**, *27*, 435.
[16] P. T. Beurskens, G. Admiraal, G. Beurskens, W. P. Bosman, R. de Gelder, R. Israel, J. M. M. Smits, The DIRDIF94 program system, Technical Report of the Crystallography Laboratory, University of Nijmegen, The Netherlands, **1994**.
[17] Crystal Structure Analysis Package, Molecular Structure Corporation, The Woodlands, TX, **1985** and **1999**.

 © 2003 Wiley-VCH Verlag GmbH & Co. KGaA, Weinheim

Iron(III) Phosphonate Cage Complex

Synthesis and Characterization of Iron(III) Phosphonate Cage Complexes**

*Evangelos I. Tolis, Madeleine Helliwell, Stuart Langley, James Raftery, and Richard E. P. Winpenny**

Many groups are now making polymetallic complexes, partly to study the unusual properties they can present, and partly because they represent a significant synthetic challenge. In this field two distinct approaches to synthesis can be found: designed assembly,[1] in which the use of ligands with strongly preferred binding modes leads to structures that could be predicted prior to synthesis, and self or "serendipitous" assembly,[2] in which the ligands are more flexible, and the resulting structures are not predictable. Typical ligands for serendipitous assembly are carboxylates or alkoxides.

Phosphonates are a family of ligands that should be ideal for serendipitous assembly, in that they have three O donors, and could, in principle, bind to up to nine metal centers. They have rarely been used in the synthesis of discrete molecules.[3] An important exception is the work by Zubieta and co-workers in which phosphonate is used to assemble vanadium cages.[4] The problem is the very limited solubility that metal phosphonates have, which results in phosphonates being frequently found in polymeric coordination complexes, for example, in 2D layered structures.[5] To produce cage complexes featuring phosphonates we have begun a project in which phosphonates are introduced with a coligand. In a related paper we report on reactions of cobalt salts involving

[*] Prof. R. E. P. Winpenny, Dr. E. I. Tolis, Dr. M. Helliwell, S. Langley, Dr. J. Raftery
Department of Chemistry
The University of Manchester
Oxford Road, Manchester, M13 9PL (UK)
Fax: (+44) 161-275-4616
E-mail: richard.winpenny@man.ac.uk

[**] This work was supported by the EU Research and Training Network "MolNanoMag" and by the EPSRC(UK).

 © 2003 Wiley-VCH Verlag GmbH & Co. KGaA, Weinheim DOI: 10.1002/anie.200351764

phosphonates and pyridonates;[6] herein we report reactions of phenylphosphonate with the well-known iron(III) carboxylate triangles $[Fe_3O(O_2CR)_6(H_2O)_3]X$, (R = H-, CH_3-, Ph- or -CMe_3; X = NO_3^- or Cl^-).

The variation of R, X, and reaction conditions allows access to a range of polynuclear cages. For example, treatment of $[Fe_3O(O_2CMe)_6(H_2O)_3](NO_3)$ with two equivalents of $PhPO_3H_2$ in pyridine (py) gives an orange-red solution. Vapor diffusion of Et_2O into this solution gives crystals of the hexa-iron cluster $[Fe_6O(OH)_3(O_2CMe)_3(O_3PPh)_4(py)_9](NO_3)_2$ **1** (Figure 1).[7] The structure consists of two iron

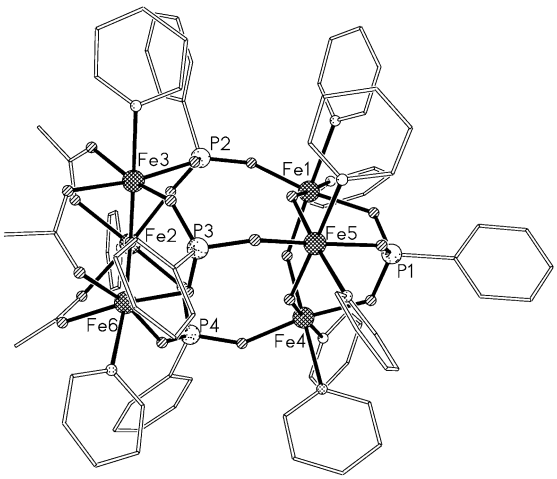


Figure 1. The structure of **1** in the crystal. Bond length ranges [Å]: Fe-O(oxide) 1.911–1.932, Fe-O(OH) 1.979–2.001, Fe-O(O_3PPh) 1.940–1.984, Fe-O(O_2CR) 2.007–2.055, Fe-N 2.164–2.231 (av. estimated standard deviation, esd, 0.005). Shading: Fe atoms, cross-hatched circle; P atoms, light shading; O atoms, diagonal top right–bottom left; N atoms dotted; C atoms drawn as lines. The same scheme is used for all figures.

triangles linked through the phosphonate. One triangle is clearly related to the precursor, which contains a μ_3-oxide and three carboxylates bridging the three iron(III) centers; however, three of the carboxylates in the original structure have been replaced by phosphonates. These ligands bridge within the triangle in an identical manner to the carboxylate, but the third O atom of each $PhPO_3$ unit binds to the second triangle. Each edge of the second triangle is bridged by a μ_2-hydroxide, and the "upper" face is occupied by a fourth phosphonate. By the Harris notation,[9] each phosphonate has a 3.111 binding mode. All Fe^{III} centers are six coordinate, with a single pyridine molecule attached to each iron atom in the first triangle, and two pyridine molecules bound to each iron atom of the second.

If the same reaction is performed starting with $[Fe^{III}_3O(O_2CPh)_6(H_2O)_3]Cl$, a tetranuclear iron cage is formed: $[Fe_4OCl(O_2CPh)_3(O_3PPh)_3(py)_5]$ **2** (Figure 2). Complex **2** again contains a triangle similar to that of the starting material, but from which three carboxylates have been displaced. In **2** the three O_3PPh units bind to a single Fe^{III} site, producing a capped tetrahedron. Two pyridine molecules and a chloride ion complete the coordination at this iron

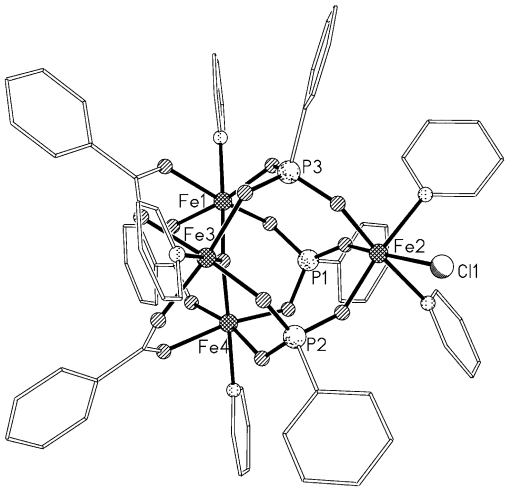


Figure 2. The structure of **2** in the crystal. Bond length ranges [Å]: Fe-O(oxide) 1.927–1.948, Fe-O(O_3PPh) 1.922–1.990, Fe-O(O_2CR) 2.032–2.067, Fe-N 2.177–2.291 (av esd 0.003).

center. The three phosphonates again show the 3.111 binding mode (Harris notation).

A reduction in the amount of pyridine present changes the reaction path. Thus the sequential addition of $[Fe_3O(O_2CMe)_6(H_2O)_3](NO_3)$, six equivalents of pyridine, and two equivalents of $PhPO_3H_2$ to $MeNO_2$ gave a red solution from which crystals of $[Fe_7O_2(O_2CMe)_9(O_3PPh)_4(py)_6]$ **3** could be grown by diffusion of Et_2O into the solution. Similar hepta-iron compounds $[Fe_7O_2(O_2CPh)_9(O_3PPh)_4(py)_6]$ **4** and $[Fe_7O_2(O_2CPh)_8(NO_3)(O_3PPh)_3(py)_6]$ **5** were formed when the iron(III) acetate triangle was replaced by $[Fe^{III}_3O(PhCOO)_6(H_2O)_3]Cl$ and $[Fe^{III}_3O(PhCOO)_6(H_2O)_3](NO_3)$ respectively.

Complexes **3**–**5** have similar structures (Figure 3). The structures are built from two oxo-centered triangles in which two carboxylates on one edge are replaced by phosphonates, which both bridge to a single Fe^{III} site. Thus this central iron site links the two triangles into a heptanuclear cage, and is bound to four O donors from four distinct phosphonates, and two further O donors from a chelating group. In **3** and **4**, this group is a carboxylate, while in **5** it is a nitrate. Pyridine ligands complete the coordination spheres of the iron atoms

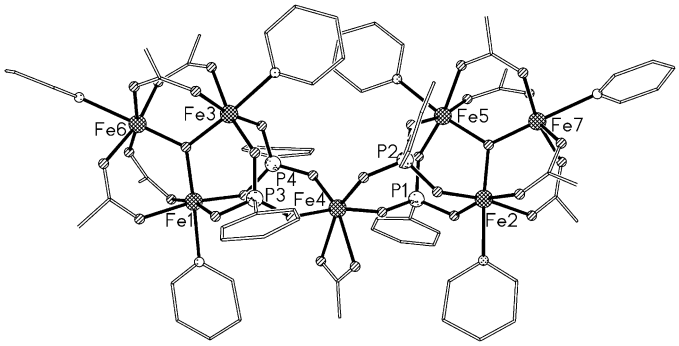


Figure 3. The structure of **3** in the crystal. Bond length ranges [Å]: Fe-O(oxide) 1.859–1.951, Fe-O(O_3PPh) 1.916–1.971, Fe-O(O_2CR) 2.007–2.203, Fe-N 2.171–2.262 (av. esd 0.011).

 © 2003 Wiley-VCH Verlag GmbH & Co. KGaA, Weinheim

within the triangles. As before the phosphonates show the 3.111 mode.

With pivalate as the carboxylate, and excluding pyridine entirely, the chemistry produces a much larger cluster. $[Fe_3O(O_2CCMe_3)_6(H_2O)_3](NO_3)$ was treated with one equivalent of $PhPO_3H_2$ in MeCN giving an orange-red solution, from which crystals of $[Fe_{14}O_4(O_2)_2(O_2CCMe_3)_{12}(O_3PPh)_8(H_2O)_{12}](NO_3)_2$ **6** were grown by the addition of Et_2O, followed by slow evaporation of the solvent. The structure (Figure 4) contains two "dimers of triangles", which form

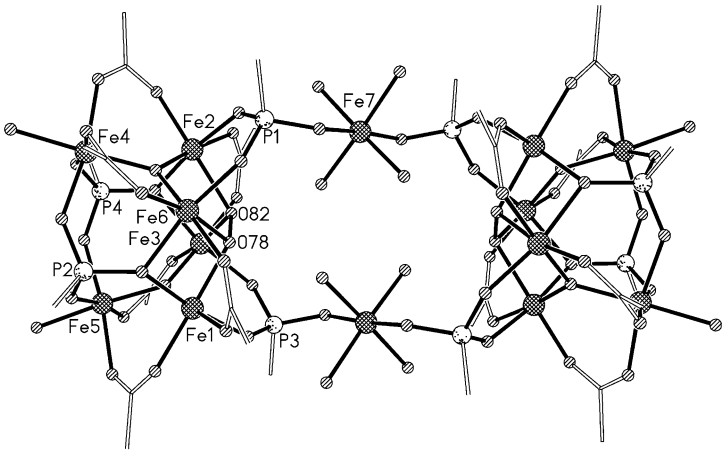


Figure 4. The structure of **6** in the crystal. Phenyl rings and methyl groups omitted for clarity. Bond length ranges [Å]: Fe-O(oxide) 1.879–1.925, Fe-O(peroxide) 2.083–2.101, Fe-O(O_3PPh) 1.938–1.996, Fe-μ_2-O(O_3PPh) 2.056–2.108, Fe-O(O_2CR) 1.963–2.052, Fe-O(H_2O) 2.006–2.095 (av. esd 0.005).

distorted trigonal prisms, with two phosphonates bridging in a 4.211 mode on two of the three "rectangular" sides of the prism, and with the μ_2 O-atom in each case bound to one Fe^{III} ion from each triangle. The third side of the prism is occupied by a peroxide binding in the 4.22 mode (O78 and O82 in Figure 4). Peroxides have been found previously in reactions of iron carboxylate triangles,[10] and have shown interesting reactivity in Gif type oxidations.[11]

The two trigonal prisms are linked through single Fe^{III} sites, which adopt a similar structural role to the linking sites in **3**–**5**. The phosphonates bridging to these sites adopt the 3.111 mode, and the coordination geometry of the Fe sites is completed by four molecules of H_2O in each case. Assignment of the bridging peroxide appears to be the only rational choice for a two-atom fragment adopting this binding motif. Raman spectroscopy of a solid sample of **6** shows a peak at 852 cm^{-1}, which is very close to ν(O–O) stretch reported previously for peroxides with 4.22 binding.[10]

The inclusion of peroxide in **6** was unexpected. We therefore repeated the experiment, but added a source of peroxide. On this occasion a hexanuclear iron cage formed: $[Fe_6O_2(O_2)(O_2CCMe_3)_8(O_3PPh)_2(H_2O)_2]$ **7**. The structure of **7** (Figure 5) is clearly related to **6**, and contains two oxo-centered Fe^{III} triangles bridged by two phosphonates binding in the 4.211 mode; phosphonates and a peroxide binding in the 4.22 mode. The pivalates binding in the 2.11 mode also bridge the two edges of the rectangular face containing the

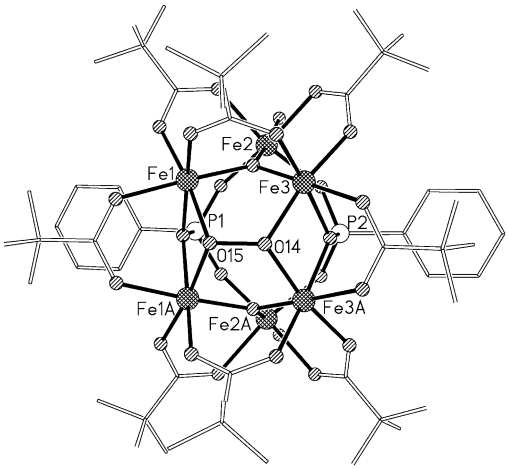


Figure 5. The structure of **7** in the crystal. Bond length ranges [Å]: Fe-O(oxide) 1.892–1.905, Fe-O(peroxide) 2.029–2.042, Fe-O(O_3PPh) 1.963–1.967, Fe-μ_2-O(O_3PPh) 2.089, Fe-O(O_2CR) 1.972–2.098, Fe-O(H_2O) 2.123 (av. esd 0.001).

peroxide, in addition to the pivalates bridging the edges of the triangular faces. The P atoms and the peroxide lie on a crystallographic mirror plane, making the cage much more regular than the equivalent units in **5**. We assign a Raman band at 859 cm^{-1} to the ν(O–O) stretch for **7**. The O–O bond is 1.468(2) Å long in **7**, compared with 1.480(5) Å in **6**.

The reactions reported show that phosphonate can be introduced into polynuclear iron(III) chemistry, without producing insoluble and intractable materials. This may be because of the presence of the carboxylate coligand. An interesting observation is that use of preformed clusters—triangles in this case—leads to structures in which the precursor cage motif is highly influential in the structure of the final complex. This result suggests that phosphonate could be used to link cages into larger arrays by displacement reactions with carboxylates.

Experimental Section

Iron oxo-centred carboxylate triangles were made by literature methods.[13]

1: $[Fe_3O(O_2CMe)_6(H_2O)_3](NO_3)$ (0.34 g, 0.49 mmol) and $PhPO_3H_2$ (0.16 g,0.99 mmol) were added to pyridine (10 mL) and the reaction stirred for 24 h. The solution was filtered, and Et_2O was allowed to diffuse into the red filtrate. This gave crystals of **1**. Yield: 0.11 g (19.4% based on Fe) Elemental analysis calcd (%) for **1**·0.5 py·8 H_2O ($C_{77.5}H_{95.5}Fe_6N_{11.5}O_{36}P_4$): C 41.87, H 4.33, N 7.25, Fe 15.07, P 5.57; found: C 41.56, H 3.51, N 7.74, Fe 14.79, P 5.48. IR (KBr): $\tilde{\nu}$ = 1604 (m), 1578 (s), 1567 (s), 1446 (s), 1384 (vs), 1119 (s), 1068 (s), 1014 (s), 994 (s), 697 (s), 550 cm^{-1} (m).

2: As for **1**, but replacing $[Fe_3O(O_2CMe)_6(H_2O)_3](NO_3)$ with $[Fe^{III}_3O(O_2CPh)_6(H_2O)_3]Cl$. Yield: 0.19 g (51.1% based on Fe) Elemental analysis calcd (%) for **2**·H_2O ($C_{64}H_{57}Fe_4N_5O_{17}ClP_3$): C 50.57, H 3.78, N 4.61, Cl 2.33, Fe 14.70, P 6.11; found: C 50.70, H 3.71, N 4.49, Cl 2.49, Fe 14.77, P 5.80. IR (KBr): $\tilde{\nu}$ = 1601 (s), 1561 (s), 1412 (vs), 1138 (s), 1095 (s), 1068 (s), 1011 (s), 994 (s), 719 (s), 696 (s), 547 (m), 470 cm^{-1} (s).

3: $[Fe_3O(O_2CMe)_6(H_2O)_3](NO_3)$ (0.42 g, 0.61 mmol), pyridine (0.29 ml, 3.7 mmol) and $PhPO_3H_2$ (0.19 g, 1.22 mmol) were added to $MeNO_2$ (10 ml) and the mixture stirred for 5 h, then filtered. Et_2O

 © 2003 Wiley-VCH Verlag GmbH & Co. KGaA, Weinheim

was allowed to diffuse into the red filtrate giving crystals suitable for X-Ray analysis. Yield: 0.12 g (20.1% based on Fe) Elemental analysis (%): calcd for **3**·3 CH_3NO_2 ($C_{75}H_{86}Fe_7N_9O_{38}P_4$): C 40.28, H 3.88; N 5.64; Fe 17.48, P 5.54, found: C 40.35, H 3.56, N 5.17, Fe 17.50, P 5.45. IR (KBr): $\tilde{\nu}$ = 1604 (vs), 1446 (vs), 1137 (m), 1089 (s), 1067 (s), 1010 (s), 994 (s), 718 (w), 697 (m), 547 (m), 473 cm^{-1} (w).

4: As for **3**, but replacing $[Fe_3O(O_2CMe)_6(H_2O)_3](NO_3)$ with $[Fe_3^{III}O(O_2CPh)_6(H_2O)_3]Cl$, and use of 1:1 CH_3CN/CH_2Cl_2 as the solvent in place of $MeNO_2$. Yield: 0.14 g (19.3% based on Fe) Elemental analysis calcd (%) for **4**·0.5 CH_2Cl_2 ($C_{117.5}H_{96}Fe_7N_6O_{32}ClP_4$): C 53.17, H 3.65, N 3.17, Fe 14.73, P 4.67; found: C 52.94, H 3.70, N 3.18, Fe 15.25, P 4.73. IR (KBr): $\tilde{\nu}$ = 1611 (s), 1570 (s), 1550 (s), 1411 (vs), 1136 (m), 1100 (s), 1067 (s), 1009 (s), 994 (s), 719 (s), 697 (s), 547 (s), 471 cm^{-1} (s).

5: As for **3**, but replacing $[Fe_3O(O_2CMe)_6(H_2O)_3](NO_3)$ with $[Fe_3^{III}O(O_2CPh)_6(H_2O)_3](NO_3)$, and use of 1:1 CH_3CN/CH_2Cl_2 as the solvent in place of $MeNO_2$. Yield: 0.05 g (10.0% based on Fe) Elemental analysis (%): calcd for **5**·0.5 CH_2Cl_2 ($C_{110.5}H_{91}Fe_7N_7O_{33}ClP_4$): C 51.14, H 3.53; N 3.78; Fe 15.06; found: C 51.32, H 3.58, N 3.82, Fe 15.16. IR (KBr): $\tilde{\nu}$ = 1611 (s), 1570 (s), 1548 (s), 1411 (vs), 1136 (m), 1098 (s), 1067 (s), 1011 (s), 994 (s), 719 (s), 697 (s), 547 (s), 471 cm^{-1} (s).

6: $[Fe_3O(piv)_6(H_2O)_3](NO_3)$(0.26 g, 0.28 mmol) and $PhPO_3H_2$ (45.1 mg,0.28 mmol) were added to CH_3CN (7 ml) and the solution stirred overnight. The solution was filtered, and Et_2O (5 ml) added before the solution was allowed to evaporate slowly. Yield: 0.04 g (18.0% based on Fe) Elemental analysis (%): calcd for **6** ($C_{96}H_{172}Fe_{14}N_2O_{74}P_8$): C 34.94, H 4.67, N 0.75; found: C 34.68, H 4.95, N 0.66. IR (KBr): $\tilde{\nu}$ = 2964 (m) 1530 (s), 1485 (s), 1426 (s) 1383 (s), 1141 (s), 1064 (s), 1012 (s), 995 (s), 752 (m) 721 (m), 696 (m), 603 (s), 556 (s), 440 cm^{-1} (s).

7. $[Fe_3O(piv)_6(H_2O)_3](NO_3)$(0.26 g, 0.28 mmol) and $PhPO_3H_2$ (45.1 mg,0.28 mmol) were added to CH_3CN (7 ml) and 2 drops of H_2O_2 (30% in H_2O) were added. The solution stirred for 1 h after which it turned red. Then the solution was allowed to stand undisturbed at 4°C for few days. Dark red crystals suitable for X-ray analysis formed. Yield: 0.1 g (31.6% based on Fe) Elemental analysis calcd (%) for **7**·0.5 MeCN ($C_{53}H_{87.5}Fe_6N_{0.5}O_{28}P_2$): C 40.37, H 5.59, N 0.44, P 3.93; found: C 39.88, H 5.61, N 0.47, P 4.02; IR (KBr): $\tilde{\nu}$ = 2963 (m) 1552 (s), 1485 (s), 1427 (s) 1380 (m), 1231 (m), 1130 (m), 1039 (w), 979 (s), 788 (w), 600 (m), 440 cm^{-1} (m).

Received: April 28, 2003 [Z51764]

Keywords: cage compounds · iron · phosphonates · supramolecular chemistry

[1] a) R. W. Saalfrank, B. Demleitner in *Transition Metals in Supramolecular Chemistry* (Ed.: J.-P. Sauvage), Wiley, Chichester, **1999**; b) J. Rojo, F. J. Romero-Salguero, J. M. Lehn, G. Baum, D. Fenske, *Eur. J. Inorg. Chem.* **1999**, 1421 – 1428; c) E. Breuning, U. Ziener, J. M. Lehn, E. Wegelius, K. Rissanen, *Eur. J. Inorg. Chem.* **2001**, 1515 – 1521; d) R. W. Saalfrank, U. Reimann, M. Goritz, F. Hampel, A. Scheurer, F. W. Heinemann, M. Buschel, J. Daub, V. Schunemann, A. X. Trautwein, *Chem. Eur. J.* **2002**, *8*, 3614 – 3619; d) R. W. Saalfrank, H. Glaser, B. Demleitner, F. Hampel, M. M. Chowdhry, V. Schunemann, A. X. Trautwein, G. B. M. Vaughan, R. Yeh, A. V. Davis, K. N. Raymond, *Chem. Eur. J.* **2002**, *8*, 493 – 497; e) M. Fujita, K. Umemoto, M. Yoshizawa, N. Fujita, T. Kusukawa, K. Biradha, *Chem. Commun.* **2001**, 509 – 518.

[2] R. E. P. Winpenny, *J. Chem. Soc. Dalton Trans.* **2002**, 1 – 10.

[3] a) V. Chandrasekhar, S. Kingsley, *Angew. Chem.* **2000**, *112*, 2410 – 2412; *Angew. Chem. Int. Ed.* **2000**, *39*, 2320 – 2322; b) M. G. Walawalkerm, H. W. Roesky, R. Murugavel, *Acc. Chem. Res.* **1999**, *32*, 117 – 126, and references therein; c) W. F. Ruettinger, G. C. Dismukes, *Inorg. Chem.* **2000**, *39*, 1021 – 1027; d) E. K. Brechin, R. A. Coxall, A. Parkin, S. Parsons, P. A. Tasker, R. E. P. Winpenny, *Angew. Chem.* **2001**, *113*, 2772 – 2775; *Angew. Chem. Int. Ed.* **2001**, *40*, 2700 – 2703.

[4] M. I. Khan, J. Zubieta, *Prog. Inorg. Chem.* **1995**, *43*, 1 – 149, and references therein.

[5] A. Clearfield, *Prog. Inorg. Chem.* **1998**, *47*, 371 – 510.

[6] M. Helliwell, S. Langley, J. Raftery, S. J. Teat, E. I. Tolis, R. E. P. Winpenny, unpublished results.

[7] Crystal data for **1**: ($C_{95}H_{94}Fe_6N_{14}O_{25}P_4$; M_r = 2290.82 g mol^{-1}): brown wedge, triclinic, space group $P\bar{1}$, a = 14.1201(13), b = 14.5564(14), c = 27.185(3) Å, α = 104.009(2)°, β = 100.447(2)°, γ = 98.644(2)°, V = 5219.9(9) Å^3, Z = 2, T = 100(2) K, ρ = 1.458 g cm^{-1}, $F(000)$ = 2356, $\mu(Mo_{K\alpha})$ = 0.951 mm^{-1}. Crystal data for **2**: ($C_{261}H_{210}Cl_3Fe_{12}N_{24}O_{54}P_9$; M_r = 5601.81 g mol^{-1}), brown prism, rhombohedral, space group $R\bar{3}$, $a = b$ = 41.1922(18), c = 29.1310(17) Å, V = 42807(4) Å^3, Z = 6, T = 100(2) K, ρ = 1.304 g cm^{-1}, $F(000)$ = 17244, $\mu(Mo_{K\alpha})$ = 0.742 mm^{-1}. Crystal data for **3**: ($C_{72}H_{64}Fe_7N_6O_{32}P_4$; M_r = 2040.12 g mol^{-1}): brown plate, triclinic, space group $P\bar{1}$, a = 16.104(2), b = 19.212(2), c = 20.976(3) Å, α = 66.906(2)°, β = 72.105(2)°, γ = 87.153(2)°, V = 5662.4(12) Å^3, Z = 2, T = 100(2) K, ρ = 1.197 g cm^{-1}, $F(000)$ = 2072, $\mu(Mo_{K\alpha})$ = 0.992 mm^{-1}. Crystal data for **4**: ($C_{119}H_{98}Fe_7N_7O_{32}P_4$; M_r = 2652.88 g mol^{-1}), orange plate, orthorhombic, space group $Pca2_1$, a = 27.865(3), b = 20.534(2), c = 20.583(3) Å, V = 11777(2) Å^3, Z = 4, T = 100(2) K, ρ = 1.496 g cm^{-1}, $F(000)$ = 5436, $\mu(Mo_{K\alpha})$ = 0.974 mm^{-1}. Crystal data for **5**: ($C_{113.5}H_{95.5}ClFe_7N_{8.5}O_{33}P_4$; M_r = 2656.76 g mol^{-1}), red rectangle, monoclinic, space group Cc, a = 22.4543(18), b = 19.9800(16), c = 26.985(2) Å, β = 96.270(2)°, V = 12034.0(17) Å^3, Z = 4, T = 100(2) K, ρ = 1.466 g cm^{-1}, $F(000)$ = 5436, $\mu(Mo_{K\alpha})$ = 0.976 mm^{-1}. Crystal data for **6**: ($C_{120}H_{130}Fe_{14}N_8O_{82}P_8$; M_r = 4025.96 g mol^{-1}), brown plate, orthorhombic, space group $Pnn2$, a = 23.3688(19), b = 26.584(2), c = 15.2904(12) Å, V = 9499.0(13) Å^3, Z = 2, T = 100(2) K, ρ = 1.408 g cm^{-1}, $F(000)$ = 4092, $\mu(Mo_{K\alpha})$ = 1.188 mm^{-1}. Crystal data for **7**: ($C_{56}H_{92}Fe_6N_2O_{28}P_2$; M_r = 1638.36 g mol^{-1}), brown plate, orthorhombic, space group $Pnma$, a = 17.0228(15), b = 18.6228(17), c = 22.836(2) Å, V = 7239.3(11) Å^3, Z = 4, T = 100(2) K, ρ = 1.503 g cm^{-1}, $F(000)$ = 3408, $\mu(Mo_{K\alpha})$ = 1.294 mm^{-1}. Data were collected on Bruker SMART CCD diffractometer ($Mo_{K\alpha}$, λ = 0.71069 Å). In all cases the selected crystals were mounted on a Hamilton cryoloop using Flombin oil and placed in the cold flow (100 K) produced with an Oxford Cryocooling device. Complete hemispheres or spheres of data were collected using ω-scans (0.3°, up to 30 seconds/frame). Integrated intensities were obtained with SAINT+[8] and when they were corrected for absorption SADABS was used.[8] Structure solution and refinement was performed with the SHELXTL-package.[8] The structures were solved by direct methods and completed by iterative cycles of ΔF syntheses and full-matrix least-squares refinement against F^2 to give: for **1**: using 1043 parameters, wR_2 = 0.3115 (23730 unique reflections), R_1 = 0.0933 (13448 reflections with $I > 2\sigma(I)$); for **2**: using 950 parameters, wR_2 = 0.2018 (22991 unique reflections), R_1 = 0.0579 (14468 reflections with $I > 2\sigma(I)$); for **3:** using 1022 parameters, wR_2 = 0.4381 (24767 unique reflections), R_1 = 0.1293 (7773 reflections with $I > 2\sigma(I)$); for **4:** using 1479 parameters and 1 restraint, wR_2 = 0.1194 (22844 unique reflections), R_1 = 0.0530 (17174 reflections with $I > 2\sigma(I)$); for **5:** using 1421 parameters and 776 restraints, wR_2 = 0.1515 (20236 unique reflections), R_1 = 0.0545 (17322 reflections with $I > 2\sigma(I)$); for **6:** using 913 parameters and 37 restraints, wR_2 = 0.1804 (19287 unique reflections), R_1 = 0.0599 (16810 reflections with $I > 2\sigma(I)$); for **7:** using 465 parameters, wR_2 = 0.0740 (7661 unique reflections), R_1 = 0.0269 (7010) reflections with $I > 2\sigma(I)$). CCDC 208769 to 208775 contain the supple-

 © 2003 Wiley-VCH Verlag GmbH & Co. KGaA, Weinheim

mentary crystallographic data for this paper. These data can be obtained free of charge via www.ccdc.cam.ac.uk/conts/retrieving.html (or from the Cambridge Crystallographic Data Centre, 12, Union Road, Cambridge CB21EZ, UK; fax: (+44) 1223-336-033; or deposit@ccdc.cam.ac.uk).

[8] SHELXTL-PC Package. Bruker Analytical X-ray Systems: Madison, WI, **1998**.

[9] Harris notation describes the binding mode as $[X.Y_1Y_2Y_3...Y_n]$, where X is the overall number of metals bound by the whole ligand, and each value of Y refers to the number of metal atoms attached to the different donor atoms. See: R. A. Coxall, S. G. Harris, D. K. Henderson, S. Parsons, P. A. Tasker, R. E. P. Winpenny, *J. Chem. Soc. Dalton Trans.* **2000**, 2349 – 2356.

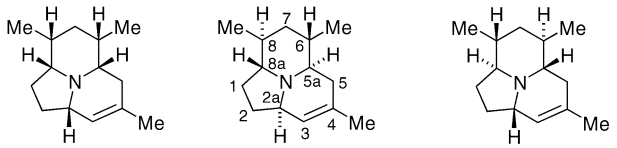
[10] a) W. Micklitz, S. G. Bott, J. G. Bentsen, S. J. Lippard, *J. Am. Chem. Soc.* **1989**, *111*, 372 – 374; b) I. Shweky, L. E. Pence, G. C. Papaefthymiou, R. Sessoli, J. W. Yun, A. Bino, S. J. Lippard, *J. Am. Chem. Soc.* **1997**, *119*, 1037 – 1042.

[11] R. Çelenligil-Çetin, R. J. Staples, P. Stavropolous, *Inorg. Chem.* **2000**, *39*, 5838 – 5846.

[12] M. Suzuki, T. Ishiguro, M. Kozuka, K. Nakamoto, *Inorg. Chem.* **1981**, *20*, 1993 – 1996.

[13] a) A. B. Blake, L. R. Fraser, *J. Chem. Soc. Dalton Trans.* **1975**, 193 – 197; b) M. K. Johnson, D. B. Powell, R. D. Cannon, *Spectrochim. Acta A* **1981**, *37*, 995 – 1006.

 © 2003 Wiley-VCH Verlag GmbH & Co. KGaA, Weinheim



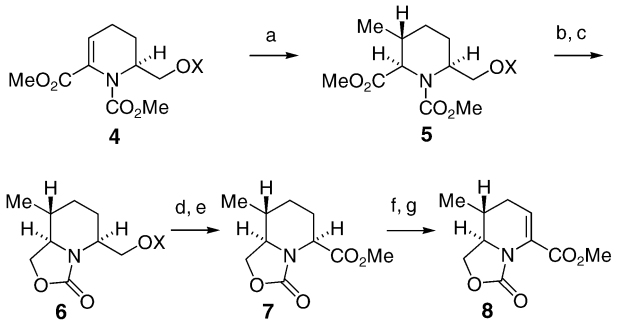
1 **2** **3**

Figure 1. Original (**1**) and revised (**2**) structures of alkaloid 205 B, and the structure of its antipode, **3**.

asymmetric centers in its compact, fourteen-carbon-atom frame; however, no synthesis of this unique alkaloid has been reported, and its absolute stereochemistry is still unknown.

As part of a program directed at studying the synthesis of biologically active alkaloids,[5] we report here the first total synthesis of **3** (see Figure 1), the antipode of natural 205 B, and the determination of the absolute stereochemistry of natural 205 B.

The synthesis began with enaminoester **4**,[6] which was treated with lithium dimethylcuprate to give adduct **5** as a single isomer (Scheme 1).[7] The oxazolizinone ring was constructed in a two-step sequence to provide **6**, which was transformed into the desired cyclic carbamate **8** via ester **7** by using the protocol developed by Matsumura et al.[8]



Scheme 1. Synthesis of enaminoester **8**. Reagents and conditions: a) $(Me)_2CuLi$, Et_2O, −78 to −30 °C (98 %); b) Lithium triethylborohydride, THF, 0 °C (92 %); c) NaH, THF, 0 °C (99 %); d) TBAF, THF, 0 °C–RT (99 %); e) 1. Swern oxidation, −78 °C to 0 °C, 2. $NaClO_2$, NaH_2PO_4, *t*BuOH/H_2O, 3. CH_2N_2, EtOAc (86 % over 3 steps); f) LiHMDS, PhSSPh, THF, −78–0 °C (99 %); g) *m*CPBA, 2,6-lutidine, CH_2Cl_2, RT (85 %). LiHMDS = lithium bis(trimethylsilyl)amide, *m*CPBA = *meta*-chloroperbenzoic acid, RT = room temperature, TBAF = tetrabutylammonium fluoride, X = *tert*-butyldiphenylsilyl.

The second and key Michael reaction of **8** with in situ generated lithium dimethylcuprate proceeded smoothly to afford adduct **9**, again as a single isomer (Scheme 2). The stereochemistry of **9** was confirmed by the NOE interactions indicated. The observed stereoselectivity of the Michael reaction of **8** can be explained by the stereoelectronic effect[9] illustrated in Figure 2.

An Arndt–Eistert sequence was used for carbon-chain extension of **9** to give the homologated ester **10**, which was transformed into ketone **11** by reaction with Weinreb's amide (Scheme 3).[10] Acid-catalyzed protection of the carbonyl group in **11** with ethylene glycol followed by hydrolysis of the oxazolidinone ring with base and protection of the

Alkaloid Total Synthesis

Total Synthesis of the Antipode of Alkaloid 205 B**

Naoki Toyooka, Ayako Fukutome, Hiroyuki Shinoda, and Hideo Nemoto**

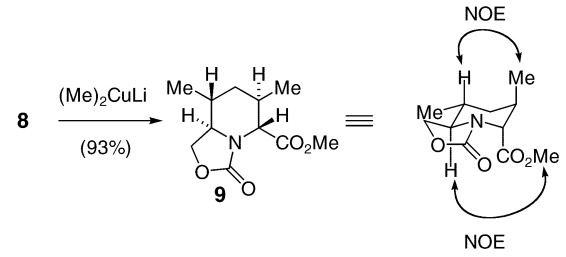
A remarkably diverse array of biologically active alkaloids, for example, blockers of neuromuscular-type, ganglionic-type, and nicotinic receptor channels, occurs in amphibian skin, and over 500 alkaloids have been isolated to date.[1] The structural diversity and pharmacological activity associated with these alkaloids have stimulated research in numerous synthetic groups.[2] Alkaloid 205 B, one of the compounds isolated from skin extracts of the Panamanian frog *Dendrobates pumilio*, possesses an unusual and unique 8b-azaacenaphthylene ring system (Figure 1). The structure of alkaloid 205 B was first reported to be **1**,[3] and recently revised to be **2** based upon FTIR, NMR, and MS data.[4] This alkaloid contains five

[*] Dr. N. Toyooka, Prof. Dr. H. Nemoto, A. Fukutome, Dr. H. Shinoda
Faculty of Pharmaceutical Sciences
Toyama Medical and Pharmaceutical University
Sugitani 2630, Toyama 930-0194 (Japan)
Fax: (+81) 76-434-4656
E-mail: toyooka@ms.toyama-mpu.ac.jp
nemotoh@ms.toyama-mpu.ac.jp

[**] We thank Professors Shigetoshi Kadota and Yasuhiro Tezuka for recording the NOE spectra of **14**.

Supporting information for this article is available on the WWW under http://www.angewandte.org or from the author.

 © 2003 Wiley-VCH Verlag GmbH & Co. KGaA, Weinheim DOI: 10.1002/anie.200351906



Scheme 2. Synthesis of tetrasubstituted piperidine **9**.

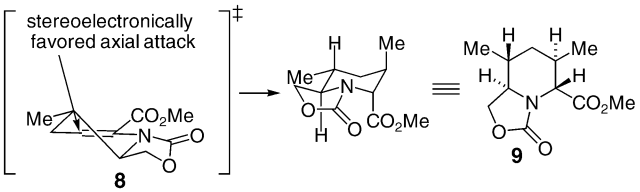
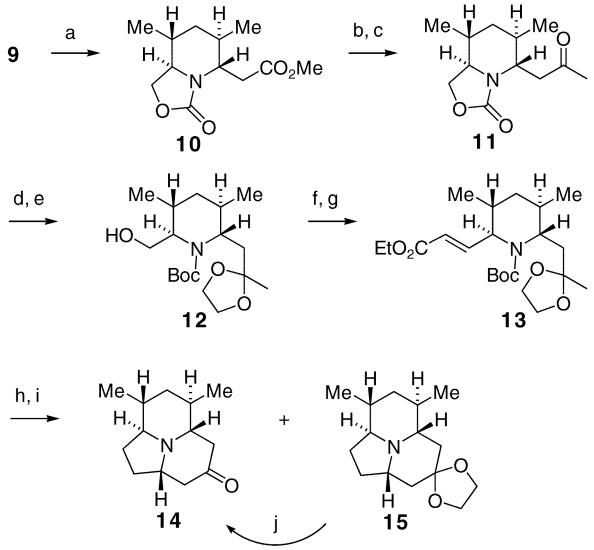


Figure 2. Stereochemical course of the Michael reaction of the enaminoester **8**.



Scheme 3. Synthesis of compound **14** with the tricyclic core. Reagents and conditions: a) 1. LiOH, $MeOH/H_2O$, reflux, 2. $ClCO_2Et$, Et_3N, THF, 0 °C, 3. CH_2N_2, Et_2O, 4. $PhCO_2Ag$, Et_3N, MeOH, RT (71 % over 4 steps); b) 1. LiOH, $MeOH/H_2O$, reflux, 2. 1,1′-carbonyldiimidazole, THF, RT, 3. Et_3N, (MeO)MeNH·HCl, THF, RT (98 % over 2 steps); c) MeMgBr, THF, 0 °C to RT (73 %); d) ethylene glycol, *p*TsOH, benzene, reflux (86 %); e) 1. 2 M KOH in *i*PrOH, 120 °C in a sealed tube, 2. Boc_2O, NaOH, dioxane/H_2O (74 % over 2 steps); f) Swern oxidation, −78 °C to 0 °C; g) $(EtO)_2P(O)CH_2CO_2Et$, NaH, THF (74 % over 2 steps); h) 1. 10 % Pd/C, H_2, EtOAc, 2. DIBAL, CH_2Cl_2, −78 °C; i) *p*TsOH, benzene/acetone, reflux (**14**; 62 %, **15**; 15 % over 3 steps); j) *p*TsOH, acetone, reflux (80 %). Boc = *tert*-butoxycarbonyl, DIBAL = diisobutylaluminum hydride, *p*TsOH = *para*-toluenesulfonic acid.

resulting amine with Boc_2O provided alcohol **12** in 74 % overall yield. Swern oxidation of **12** and Wittig–Horner reaction of the resulting aldehyde afforded the α,β-unsaturated ester **13**. Hydrogenation of **13** and reduction of the resulting ester with DIBAL followed by treatment with *p*TsOH in refluxing benzene/acetone provided the key tricyclic compound **14** in 62 % overall yield along with acetal **15** (15 %), which was transformed into **14** by treatment with acid.

The stereochemistry at the newly formed position in **14** was confirmed by the NOE (2 %) between H_{2a} and H_{5a}, and the stereoselectivity of the acid-catalyzed intramolecular Mannich-type cyclization is rationalized as depicted in Figure 3.

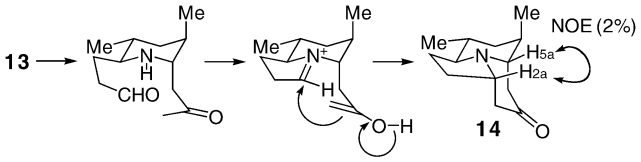
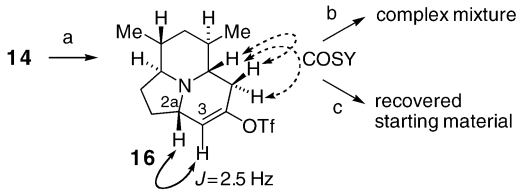


Figure 3. Stereochemical course of intramolecular Mannich-type cyclization reaction of **13** and the stereochemistry of **14**.

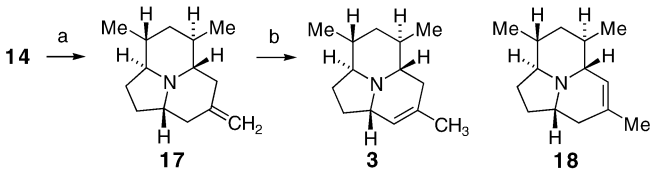
With the requisite tricyclic core **14** in hand, we next focused our attention on the final step for the completion of total synthesis of alkaloid 205B. First we examined the formation of the alkene unit by using triflate **16**. Thus treatment of **14** with chiral lithium amide base followed by Comins's triflating agent[11] provided triflate **16** in 54 % yield (Scheme 4). The structure of **16** was confirmed by the H,H COSY experiment and the coupling constant between H_{2a} and H_3. The cross-coupling reaction of **16** with trimethylaluminium in the presence of catalytic amounts of $[Pd(Ph_3P)_4]$[12] afforded a complex mixture and no desired compound was isolated. The coupling reaction with lithium dimethylcuprate[13] resulted in the complete recovery of starting material.



Scheme 4. Attempted synthesis of **3** via triflate **16**. Reagents and conditions: a) 1. *R*-(*R**,*R**)-(+)-bis(α-methylbenzyl)amine, *n*BuLi, THF, 2. [*N*,*N*-bis(trifluoromethylsulfonyl)amino]-5-chloropyridine (Comins's reagent), −78 to −40 °C (54 %); b) $[Pd(Ph_3P)_4]$, Me_3Al, $ClCH_2CH_2Cl$, 70 °C; c) $(Me)_2CuLi$, THF, 0 °C.

Thus, we were forced to introduce the C–C double bond by using the *exo*-alkene **17**. Wittig reaction of **14** afforded **17** in good yield (Scheme 5). Brief calculations (B3LYP method in Gaussian98, 6-31 + G** basis set) revealed that the desired isomer **3** is lower in energy than the other isomer **18**.[14] Thus, the acid-catalyzed isomerization of **17** provided the isomeric products in a ratio of 6.5:1 (from crude NMR), and the major isomer **3** was isolated in 63 % yield. The spectroscopic data (^1H and ^{13}C NMR, IR, MS) of **3** ($[\alpha]_D^{26} = +8.1$) were identical with those of the natural product ($[\alpha]_D = -8.5$), and the absolute stereochemistry was determined unambiguously to be 2a*R*,5a*R*,6*S*,8*S*,8a*R* by comparison of the optical rotations.

 © 2003 Wiley-VCH Verlag GmbH & Co. KGaA, Weinheim



Scheme 5. Completion of the total synthesis of **3**. Reagents and conditions: a) $MeP^{+}Ph_3I^{-}$, *n*BuLi, THF, 0 °C to RT (84 %); b) *p*TsOH, benzene, reflux (63 %).

In summary, we have demonstrated the first enantioselective total synthesis of the antipode **3** of the structurally unique alkaloid 205B. The key step in this synthesis is the stereocontrolled Micheal-type conjugate addition reaction of the enaminoester **8** to form the 2,3,5,6-tetrasubstituted piperidine ring system in **9**. Furthermore, we determined the absolute stereochemistry of the natural product to be 2a*R*,5a*R*,6*S*,8*S*,8a*R*.

Received: May 15, 2003 [Z51906]

Keywords: alkaloids · Michael addition · natural products · nitrogen heterocycles · stereoelectronic effects

[1] J. W. Daly, H. M. Garraffo, T. F. Spande in *Alkaloids*: *Chemical and Biological Perspective, Vol. 13* (Ed.: S. W. Pelletier), Pergamon, New York, **1999**, pp. 1–161; J. W. Daly in *The Alkaloids, Vol. 50* (Ed.: G. A. Cordell), Academic Press, New York, **1998**, pp. 141–169.

[2] C. J. Smith, A. B. Holmes, N. J. Press, *Chem. Commun.* **2002**, 1214–1215; S. Aoyagi, S. Hirashima, K. Saito, C. Kibayashi, *J. Org. Chem.* **2002**, *67*, 5517–5526; A. Wrobleski, K. Sahasrabudhe, J. Aubé, *J. Am. Chem. Soc.* **2002**, *124*, 9974–9975; F. A. Davis, B. Chao, A. Rao, *Org. Lett.* **2001**, *3*, 3169–3171; G. Kim, S. Jung, W-j. Kim, *Org. Lett.* **2001**, *3*, 2985–2987; C.-H. Tan, A. B. Holmes, *Chem. Eur. J.* **2001**, *7*, 1845–1854; D. L. Comins, S. Huang, C. L. McArdle, C. L. Ingalls, *Org. Lett.* **2001**, *3*, 469–471; L.-L. Wei, R. P. Hsung, H. M. Sklenicka, A. I. Gerasyuto, *Angew. Chem.* **2001**, *113*, 1564–1566; *Angew. Chem. Int. Ed.* **2001**, *40*, 1516–1518; D. Enders, C. Thiebes, *Synlett* **2000**, 1745–1748; P. Michel, A. Rassat, J. W. Daly, T. F. Spande, *J. Org. Chem.* **2000**, *65*, 8908–8918; G. M. Williams, S. D. Roughley, J. D. Davies, A. B. Holmes, J. P. Adams, *J. Am. Chem. Soc.* **1999**, *121*, 4900–4901; W. H. Pearson, H. Suga, *J. Org. Chem.* **1998**, *63*, 9910–9918; D. L. Comins, D. H. LaMunyon, X. H. Chen, *J. Org. Chem.* **1997**, *62*, 8182–8187, and references therein.

[3] T. Tokuyama, N. Nishimori, A. Shimada, M. W. Edwards, J. W. Daly, *Tetrahedron* **1987**, *43*, 643–657.

[4] T. Tokuyama, H. M. Garraffo, T. F. Spande, J. W. Daly, *An. Asoc. Quim. Argent.* **1998**, *86*, 291–298.

[5] N. Toyooka, H. Nemoto, *Drugs Future* **2002**, *27*, 143–158.

[6] N. Toyooka, A. Fukutome, H. Nemoto, J. W. Daly, T. F. Spande, H. M. Garraffo, T. Kaneko, *Org. Lett.* **2002**, *4*, 1715–1718; N. Toyooka, M. Okumura, H. Nemoto, *J. Org. Chem.* **2002**, *67*, 6078–6081.

[7] The stereoselectivity of the Micheal-type conjugate addition reaction of **4** to give **5** was controlled by $A^{(1,3)}$ strain and stereoelectronic effect; see: T. Momose, N. Toyooka, *J. Org. Chem.* **1994**, *59*, 943–945; N. Toyooka, K. Tanaka, T. Momose, J. W. Daly, H. M. Garraffo, *Tetrahedron* **1997**, *53*, 9553–9574.

[8] Y. Matsumura, M. Inoue, Y. Nakamura, I. L. Talib, T. Maki, O. Onomura, *Tetrahedron Lett.* **2000**, *41*, 4619–4622.

[9] R. W. Hoffmann, *Chem. Rev.* **1989**, *89*, 1841–1873.

[10] S. Nahm, S. M. Weinreb, *Tetrahedron Lett.* **1981**, *22*, 3815–3818.

[11] D. L. Comins, A. Dehghani, *Tetrahedron Lett.* **1992**, *33*, 6299–6302.

[12] K. Takai, M. Sato, K. Oshima, H. Nozaki, *Bull. Chem. Soc. Jpn.* **1984**, *57*, 108–115.

[13] J. E. McMurry, W. J. Scott, *Tetrahedron Lett.* **1980**, *21*, 4313–4316.

[14] Calculations were performed by using the B3LYP method in Gaussian98 with the 6-31 + G** basis set. The desired isomer **3** is more stable than isomer **18** by 2.01 kcal mol^{-1}.

 © 2003 Wiley-VCH Verlag GmbH & Co. KGaA, Weinheim

Aerobic Oxidation of Alcohols

A Well-Defined Complex for Palladium-Catalyzed Aerobic Oxidation of Alcohols: Design, Synthesis, and Mechanistic Considerations**

*David R. Jensen, Mitchell J. Schultz, Jaime A. Mueller, and Matthew S. Sigman**

The Pd^{II}-catalyzed oxidation of an alcohol using molecular oxygen as the terminal oxidant is potentially a powerful transformation for organic synthesis.[1–3] Of the reported oxidations, monodentate nitrogenous ligands in combination with $Pd(OAc)_2$ have generally provided active catalyst mixtures, yet many of these oxidations suffer from relatively high catalyst loadings, an excess of ligand or base, and/or high oxygen pressures. Mechanistic explanations for these trends have recently been sought in several studies.[4] Key findings include: 1) base is necessary for catalysis,[4a,b] 2) an excess of ligand is needed to prevent catalyst decomposition,[2a,4c] and 3) a ligand must dissociate to allow alcohol binding and/or β-hydride elimination.[2a,4,5] Unfortunately, the need for excess ligand to prevent decomposition of the catalyst leads to less-efficient oxidation as a result of inhibition of either alcohol binding or β-hydride elimination. Herein, we report the design, use, and preliminary mechanistic studies of a well-defined Pd complex for alcohol oxidation that circumvents

[*] Prof. Dr. M. S. Sigman, D. R. Jensen, M. J. Schultz, J. A. Mueller
Department of Chemistry
University of Utah
315 S. 1400 East, Salt Lake City, UT 84112 (USA)
Fax: (+1) 801-581-8433
E-mail: sigman@chem.utah.edu

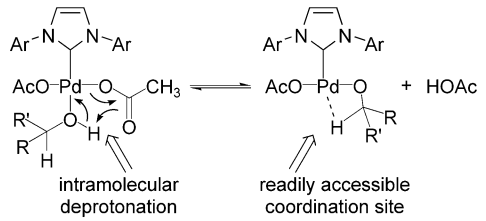
[**] This work was supported by the National Institutes of Health (NIGMS no. RO1 GM63540). D.R.J. is supported by an ACS Division of Organic Chemistry Graduate Fellowship sponsored by the Schering–Plough Research Institute. Pd salts were provided by Johnson Matthey. The crystal-structure analysis was performed by Atta Arif.

Supporting information for this article is available on the WWW under http://www.angewandte.org or from the author.

 © 2003 Wiley-VCH Verlag GmbH & Co. KGaA, Weinheim DOI: 10.1002/anie.200351997

this conflict and is consequently suitable for oxidation using lower catalyst loadings and an ambient air atmosphere.

Based on the above discussion, a highly effective Pd^{II}-catalyzed alcohol oxidation might be achieved using a well-defined complex that does not require excess ligand to prevent decomposition of the catalyst. Directed by our previous studies, we considered using a palladium(II) acetate complex with a single N-heterocyclic carbene (NHC) ligand, since the NHC should act as a strong ligand to stabilize Pd^{II} and Pd^0 intermediates without the need for excess ligand.[6] Furthermore, Pd^{II}–NHC complexes have been shown to facilitate alcohol oxidation with the tertiary diamine (−)-sparteine as base.[3c] The acetate ligands were envisioned to serve two purposes: as a ligand for the Pd^{II} center and as a base to deprotonate the Pd-bound alcohol.[7] Since the acetate base would be masked as an anionic ligand, an intriguing possibility is that the acetate group could facilitate an intramolecular deprotonation (Scheme 1). Not only should this enhance the rate of deprotonation, but the resulting Pd–alkoxide should also have a readily accessible coordination site for β-hydride elimination.

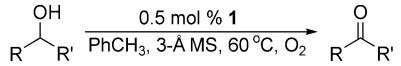


Scheme 1. Proposed intramolecular deprotonation.

To test these ideas complex **1** (Figure 1) was generated in situ from AgOAc and the requisite $PdCl_2$–NHC dimer and used for the oxidation of alcohol **2a.** The oxidation proved effective with 5 mol% of catalyst and gave >99% conversion in less than 2 h. [Pd(I*i*Pr)$(OAc)_2(H_2O)$] (**1**) was characterized by X-ray crystallography.[8] Our initial experiments were aimed at producing a reliable procedure at low catalyst loading, and, surprisingly, lowering the catalyst loading from 5 mol% to 0.5 mol% was found to give inconsistent results. However, the addition of a small amount of acetic acid to the reaction eliminated these inconsistencies and gave a reliable procedure under the following conditions: 0.5 M alcohol in toluene, 0.5 mol% **1**, 2.0 mol% HOAc, activated 3-Å molecular sieves, and a balloon of oxygen.

A variety of benzylic and allylic alcohols were cleanly oxidized to the corresponding aldehyde or ketone under these conditions, and high yields of the isolated products could be obtained by simple filtration through a plug of silica (Table 1, entries 1, 3, 5, and 7). The catalyst is capable of up to

Table 1: Oxidation of alcohols using pure O_2.



Entry[a]	Substrate	R	R′	*t* [h]	Yield [%][b,c]
1[d]	**2a**	Ph	CH_3	5	>99 (98)
2[e]	**2a**			13	>99
3[d]	**2b**	4-$MeOC_6H_4$	H	3.5	>99 (99)
4[d],[f]	**2b**			20	>99
5[d]	**2c**	3-$CF_3C_6H_4$	CH_3	12	>99 (99)
6[d],[g]	**2d**	Ph	*t*Bu	14	91
7[d]	**2e**	1-cyclohexenyl	CH_3	12	91 (84)
8[h]	**2f**	$CH_3(CH_2)_7$	CH_3	13	99 (93)
9[d]	**2g**	3-Me-cyclohexenol		12	92
10[h]	**2h**	*cis*-4-Me-cyclohexanol		13	>99
11[i]	**2i**	myrtenol		20	97
12[i],[j]	**2j**	$CH_3(CH_2)_{10}$	H	10	85 (76)
13[i],[j]	**2k**	$CH_3(CH_2)_{16}$	H	10	(85)

[a] See Supporting Information for details. [b] GC conversion. [c] Yield of isolated compound in parenthesis. [d] 2 mol% HOAc. [e] Catalyst prepared in situ using 0.5 mol% $Pd(OAc)_2$, 0.65 mol% I*i*Pr–HBF_4, 0.7 mol% KO*t*Bu. [f] 0.1 mol% **1**. [g] 1 mol% **1**. [h] 1 mol% HOAc. [i] 5.0 mol% Bu_4NOAc. [j] 0.75 mol% **1**. MS = molecular sieves.

1000 turnovers with the activated substrate **2b** (Table 1, entry 4). For synthetic simplicity, the catalyst can be pre-generated in the same reaction pot using $Pd(OAc)_2$, the I*i*Pr–HBF_4 salt, and KO*t*Bu, and applied successfully to the transformation (Table 1, entry 2). The sterically encumbered alcohol **2d** reacted slower but underwent good conversion by increasing the catalyst loading to 1.0 mol% (Table 1, entry 6). Only 1.0 mol% of acetic acid was needed for the clean oxidation of less reactive aliphatic alcohols to their corresponding ketones (Table 1, entries 8 and 10). Oxidation of non-benzylic, primary alcohols was accompanied by degradation of the aldehyde product which hindered catalysis. Several changes to the reaction conditions were required since auto-oxidation of aldehydes is possible under slightly acidic conditions. Removing the HOAc, adding Bu_4NOAc, and diluting the substrate to 0.125 M resulted in good yields of the aldehydic product (Table 1, entries 11–13).

A substantial practical improvement for aerobic oxidations is to replace the pure O_2 with air. Increasing the amount of acetic acid used enabled the oxygen balloon to be removed and the reaction carried out under the ambient atmosphere (no balloon necessary), with only slightly extended reaction times (Table 2). Increasing the amount of acetic acid to 5 mol% allowed the reaction to be scaled up to one gram in air, and gave >99% conversion in 14 h with the product isolated in a yield of 97% (Table 2, entry 1). Replacement of O_2 with air at ambient pressure usually leads to decomposi-

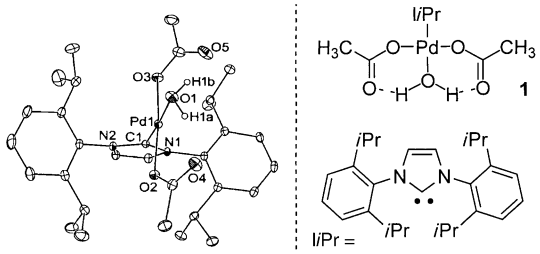
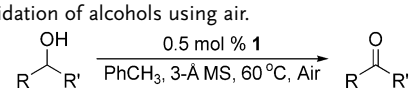


Figure 1. ORTEP and ChemDraw views of [Pd(I*i*Pr)$(OAc)_2(H_2O)$] (**1**). Hydrogen bond lengths [Å]: O(1)-H(1a) = 0.89(4), O(1)-H(1b) = 0.85(4), O(4)-H(1a) = 1.73(4), O(5)-H(1b) = 1.82(4), O(1)-O(4) = 2.571(3), O(1)-O(4) = 2.627 (3), and hydrogen bond angles [°]: O(1)-H(1A)···O(4) = 156(3), O(1)-H(1B)···O(5) = 159(3).

 © 2003 Wiley-VCH Verlag GmbH & Co. KGaA, Weinheim

Table 2: Oxidation of alcohols using air.



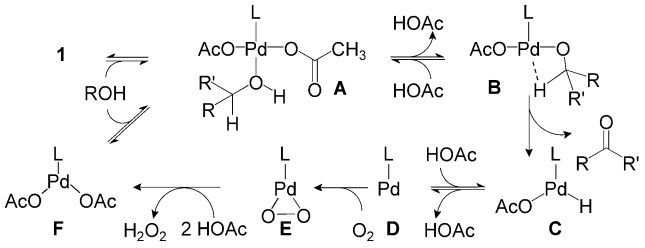
Entry[a]	Substrate	R	R′	*t* [h]	Yield [%][b,c]
1[d,e]	**2a**	Ph	CH_3	14	>99 (97)
2[f]	**2l**	4-$MeOC_6H_4$	CH_3	14	>99 (93)
3[f]	**2c**	3-$CF_3C_6H_4$	CH_3	20	>99
4[f]	**2m**	4-$CH_3C_6H_4$	H	14	>99
5[g]	**2f**	$CH_3(CH_2)_7$	CH_3	14	99 (91)
6[f]	**2n**	1-indanol		14	>99
7[f]	**2h**	*cis*-4-Me-cyclohexanol		14	96

[a] See Supporting Information for details. [b] GC conversion. [c] Yield of isolated product in parenthesis. [d] 5 mol% HOAc. [e] 1.0 g scale. [f] 4 mol% HOAc. [g] 2 mol% HOAc.

tion of the catalyst in Pd-catalyzed aerobic oxidation of alcohols, thus the use of air in the current reactions is notable and can be considered a tribute to the robustness of this catalyst system.[9]

The crystal structure lends credence to our initial hypothesis of the acetate group acting as an intramolecular base (Figure 1): when the complex forms, a molecule of water is captured by the complex, with formation of a dative bond to the Pd and a hydrogen bond to each acetate ligand.[10,11] The presence of the hydrogen bonds between the water and the acetate oxygen atoms is quite remarkable as they suggest that an acetate ligand could indeed facilitate an intramolecular deprotonation. With evidence to suggest that the acetate ligand could function as an intramolecular base, several mechanistic experiments were undertaken to determine what effect(s) this might have on catalysis. After determining a first-order dependence on both [alcohol] and [**1**], the kinetic isotope effect (KIE) for the β-hydride (deuteride) of **2a** was measured. In contrast to the typically small KIE (1.3–2.5) for rate-limiting elimination of a β-hydride from a Pd–alkoxide complex,[12] an unusually large primary KIE of 6.8 ± 0.7 was determined. The magnitude of this KIE is similar to the calculated value for a transition state with no C–H(D) bond vibration and is consistent with a readily accessible coordination site for β-hydride elimination. The lower KIEs measured in other systems may be attributed to agostic interactions needed to displace a relatively strong ligand (for example, pyridine or chloride).

A reasonable catalytic cycle can be proposed (Scheme 2) from the structural and mechanistic data. The catalytic cycle begins with the binding of the alcohol to **1** and concomitant loss of water. Intramolecular deprotonation of the Pd-bound alcohol **A** gives a Pd–alkoxide **B**. Rate-limiting transfer of a β-hydride to a readily accessible coordination site gives the carbonyl product and the Pd–hydride **C**. Reductive elimination of acetic acid from **C** gives a Pd^0–NHC complex **D**, which can be oxidized by molecular oxygen to give a Pd^{II}–NHC peroxo complex **E**.[4f] Protonation with two equivalents of acetic acid regenerates the $Pd(OAc)_2$–NHC complex **F** and completes the catalytic cycle. While the precise role(s) of added acetic acid is not defined, added acetic acid could affect the turnover of the Pd^0–NHC peroxo intermediate **E**, reprotonation of Pd–alkoxide **B**, or an equilibrium between Pd–hydride **C** and Pd^0 species **D**.[13]



Scheme 2. Proposed mechanism.

In conclusion, a robust and effective Pd catalyst for aerobic alcohol oxidation that is effective for a variety of alcohols with turnover numbers of up to 1000 has been discovered and studied. Using a slightly higher concentration of acetic acid and extending the reaction times, the oxidations can be carried out under an ambient atmosphere of air, as showcased by the oxidation of alcohol **2a** on a one-gram scale. Mechanistic and structural data support proposals of intramolecular deprotonation and transfer of a β-hydride to a readily accessible coordination site. Future directions for this project include identifying chiral NHC ligands and/or carboxylates for an asymmetric variant and applying this catalyst system to other Pd-catalyzed reactions. A full study of the mechanism will be reported in due course and should elucidate the role(s) of acetic acid in the current oxidation as well as an evolved understanding of β-hydride elimination from Pd complexes.

Received: May 28, 2003 [Z51997]
Published online: August 1, 2003

Keywords: alcohols · oxidation · oxygen · palladium · reaction mechanisms

[1] For recent reviews, see a) R. A. Sheldon, I. W. C. E. Arends, G. ten Brink, A. Dijksman, *Acc. Chem. Res.* **2002**, *35*, 774; b) R. A. Sheldon, I. W. C. E. Arends, A. Dijksman, *Catal. Today* **2000**, *57*, 157.

[2] For examples, see a) M. J. Schultz, C. C. Park, M. S. Sigman, *Chem. Commun.* **2002**, 3034; b) N. Kakiuchi, Y. Maeda, T. Nishimura, S. Uemura, *J. Org. Chem.* **2001**, *66*, 6620; c) K. Hallman, C. Moberg, *Adv. Synth. Catal.* **2001**, *343*, 260; d) G. ten Brink, I. W. C. E. Arends, R. A. Sheldon, *Science* **2000**, *287*, 1636; e) T. Nishimura, T. Onoue, K. Ohe, S. Uemura, *J. Org. Chem.* **1999**, *64*, 6750; f) K. P. Peterson, R. C. Larock, *J. Org. Chem.* **1998**, *63*, 3185.

[3] For the use of Pd-catalyzed alcohol oxidation for kinetic resolution, see a) S. K. Mandal, D. R. Jensen, J. S. Pugsley, M. S. Sigman, *J. Org. Chem.* **2003**, *68*, 4600; b) J. T. Bagdanoff, E. M. Ferreira, B. M. Stoltz, *Org. Lett.* **2003**, *5*, 835; c) D. R. Jensen, M. S. Sigman, *Org. Lett.* **2003**, *5*, 63; d) E. M. Ferreira, B. M. Stoltz, *J. Am. Chem. Soc.* **2001**, *123*, 7725; e) D. R. Jensen, J. S. Pugsley, M. S. Sigman, *J. Am. Chem. Soc.* **2001**, *123*, 7475.

[4] For mechanistic studies, see a) J. A. Mueller, M. S. Sigman, *J. Am. Chem. Soc.* **2003**, *125*, 7005; b) J. A. Mueller, D. R. Jensen, M. S. Sigman, *J. Am. Chem. Soc.* **2002**, *124*, 8202; c) B. A. Steinhoff, S. S. Stahl, *Org. Lett.* **2002**, *4*, 4179; d) B. A. Steinhoff, S. R. Fix, S. S. Stahl, *J. Am. Chem. Soc.* **2002**, *124*, 766; e) G. ten Brink, I. W. C. E. Arends, R. A. Sheldon, *Adv. Synth. Catal.*

 © 2003 Wiley-VCH Verlag GmbH & Co. KGaA, Weinheim

2002, *344*, 355; f) S. S. Stahl, J. L. Thorman, R. C. Nelson, M. A. Kozee, *J. Am. Chem. Soc.* **2001**, *123*, 7188.

[5] A notable exception is the phenathrolene-based catalyst.[2d] In this catalyst, a bidentate ligand is used. Since the solvent is H_2O at 100 °C and 30 atm, the oxidation precedes by dissociation of anionic ligands.

[6] For a review of NHC ligands, see W. A. Hermann, *Angew. Chem.* **2002**, *114*, 1342; *Angew. Chem. Int. Ed.* **2002**, *41*, 1290.

[7] For evidence of acetate acting as a base, see ref. [4b].

[8] CCDC-213715 contains the supplementary crystallographic data for this paper. These data can be obtained free of charge via www.ccdc.cam.ac.uk/conts/retrieving.html (or from the Cambridge Crystallographic Data Centre, 12 Union Road, Cambridge CB21EZ, UK; fax: (+44) 1223-336-033; or deposit@ccdc.cam.ac.uk). A yellow prism-shaped crystal $0.30 \times 0.23 \times 0.18$ mm in size was mounted on a glass fiber with traces of viscous oil and then transferred to a Nonius KappaCCD diffractometer equipped with $Mo_{K\alpha}$ radiation ($\lambda = 0.71073$ Å). Ten frames of data were collected at 150(1) K with an oscillation range of 1 deg/frame and an exposure time of 20 s/frame. Indexing and unit-cell refinement based on all observed reflection from those ten frames indicated a monoclinic *P* lattice. A total of 12906 reflections ($\lambda_{max} = 27.5°$) were indexed, integrated, and corrected for Lorentz, polarization, and absorption effects using DENZO-SMN and SCALEPAC. Post refinement of the unit cell gave $a = 9.59400(10)$, $b = 19.1341(3)$, $c = 17.1480(3)$ Å, $\beta = 92.3451(5)°$, and $V = 3145.27(8)$ Å^3. Axial photographs and systematic absences were consistent with the compound having crystallized in the monoclinic space group $P2_1/a$. The structure was solved by a combination of direct methods and heavy atom using SIR 97. All of the non-hydrogen atoms were refined with anisotropic displacement coefficients. Hydrogen atoms were located and refined isotropically except those on the C31 atom which were assigned isotropic displacement coefficients $U(H) = 1.5\,U(\text{C methyl})$, and their coordinates were allowed to ride on their respective carbon atoms using SHELXL97. The weighting scheme employed was $w = 1/[\sigma^2(F_o^2) + (0.0257\,P)^2 + 2.171\,P]$ where $P = (F_o^2 + 2F_c^2)/3$. The refinement converged to $R1 = 0.0303$, $wR2 = 0.0726$, and $S = 1.027$ for 6402 reflections with $I > 2\sigma(I)$, and $R1 = 0.0353$, $wR2 = 0.0758$, and $S = 1.027$ for 7162 unique reflections and 517 parameters. The maximum Δ/σ value in the final cycle of the least-squares was 0.001, and the residual peaks on the final difference-Fourier map ranged from -0.594 to 0.869 e Å^{-3}.

[9] For a homogeneous Pd catalyst using air, see ref. [2c]. For a heterogeneous Pd catalyst using air, see ref. [2b].

[10] The H_2O molecule binds when the complex is formed and not during recrystallization, as evidenced by identical ^{1}H NMR spectra for the complex formed in situ and after recrystallization.

[11] The hydrogen atoms of the water molecule were located and found to be within the van der Waal radii of the acetate and the water. See Supporting Information for details.

[12] See ref. [4b,c,e] and G. Noronha, P. M. Henry, *J. Mol. Catal. A* **1997**, *120*, 75.

[13] For the reversible formation of Pd^{II}–hydride species under acidic conditions, see C. Amatore, A. Jutand, G. Meyer, I. Carelli, I. Chiarotto, *Eur. J. Inorg. Chem.* **2000**, 1855.

 © 2003 Wiley-VCH Verlag GmbH & Co. KGaA, Weinheim

Optimized Heterogeneous Catalysts

Continuous Coprecipitation of Catalysts in a Micromixer: Nanostructured Cu/ZnO Composite for the Synthesis of Methanol

*Michael Schur, Bettina Bems, Alina Dassenoy, Igor Kassatkine, Joachim Urban, Hagen Wilmes, Olaf Hinrichsen, Martin Muhler, and Robert Schlögl**

Bulk catalysts are indispensable for the production of primary chemicals. A Cu/ZnO system, which has been tremendously improved through promotion with Al, is used for the low-pressure synthesis of methanol.[1–3] This material is synthesized through the coprecipitation of a hydroxycarbonate (HC) precursor followed by calcination to form CuO/ZnO.[4,5] The properties of the activated catalyst are dictated by the kinetic details of the synthesis of the solid, that is, by the properties of the precursor HC material;[3,5–7] the catalyst retains a "chemical memory".

The precipitation of large quantities of material is an ill-defined process. Even under "constant" precipitating conditions, the chemical potential of the reagents are neither spatially nor temporally constant when a drop of the precipitating agent is added to the reactor in which precipitate and dissolved ions already coexist. During ageing, washing, and drying of the catalyst precursor, complex exchange reactions occur, particularly between the anions (carbonate/hydroxide and hydroxide/nitrate). These exchange reactions are not controlled and thus result in variations in the properties of materials that are synthesized in a similar manner.[8]

A remedy for such a situation could be a continuous precipitation process in which, in the shortest possible time, a precipitate is formed in a small volume of solution, and is then collected under inert conditions (room temperature, water) followed by conventional processing. The kinetically controlled steps of nucleation and growth are thus carried out under much more reproducible boundary conditions. Furthermore, one can hope to minimize ensuing processes such as redissolution, reprecipitation, and ion exchange.

In our studies, a commercial microreactor designed for reactions in solution was used for the precipitation.[9] The reactor consists of a plate (with parallel channels approximately 100 mm long and about 200 μ wide), which is sealed between two temperature-controlled plates. The reagent solutions (0.15 M metal nitrate and 0.18 M sodium carbonate; pH = 7.0) are combined in the channels at a constant throughput (5 mL min^{-1}) under fully defined flow conditions (very short residence time and rapid, intense mixing in the reaction zone). Heat transfer is thus rapid and precise temperature control (328 K) is ensured. The product is collected in a cooled settling container and is processed with the conventional washing and drying steps, followed by calcination. In a future, improved version of this method, the postprecipitation steps of collection, washing, and drying could also be organized into a continuous processing system to produce an even more uniform product.

The fundamental experiments described herein demonstrate that such a production scheme, which above all distinguishes itself from standard batch precipitation in that the precipitate is rapidly isolated from the reactive mother liquor, does not produce a worse catalyst. Thus, such a continuous (parallel) precipitation technique is possible.

To avoid blockage of the microreactor with precipitate, a 0.15 M reagent solution was used. Therefore, two conventionally precipitated comparison samples were produced, one with the usual 1.0 M solution and one with a 0.15 M solution.

Powder X-ray diffraction analysis showed that the samples consisted mainly of rosasite with a small fraction of aurichalcite. The conventionally precipitated samples (constant pH 7.0) were largely X-ray amorphous. However, the crystalline fractions of all samples were similar in structure.

Table 1 contains some characteristic measurements for the samples. It is evident that the new precipitation technique results in a much better catalyst, although for the most part this improvement is due to the lower concentration necessary for the commercially available microreactor. The fact that a lower concentration of solution produces a better catalyst underscores the importance of kinetic control of the precipitation reaction. The high activity[10] per mass unit of the catalyst is traceable to the high dispersion of Cu sites. It seems that this dispersion can be connected with a high-temperature carbonate phase (HT-CO3). The existence of such a phase was detected by temperature-programmed decomposition with simultaneous analysis of the produced gas.[8] The data in Figure 1 show that the conventionally precipitated sample C-1m contains no HT-CO3. Both highly active samples produce desorption signatures with only minor differences.

Table 1: Characteristics of the HC product from microreactor precipitation (C-MR) and two conventionally precipitated comparison samples with similar nominal compositions (Cu/Zn 70:30).

Property	Units	C-1m	C-MR	C-0.15m
Methanol production per unit Cu metal surface area	μmol m^{-2} h^{-1}	0.29	1.72	1.58
Methanol production per unit mass of catalyst	μmol g^{-1} h^{-1}	22.8	334.5	265.2
Specific surface area of metallic Cu	m g^{-1}	8.0	21.4	15.0
Cu content as CuO	wt%	74.3	67.2	74.4
HT-CO3 species as fraction of total CO_2 emission	%	0	15	13
Temperature of the maximum emission of CO_2 from HT-CO3	K	–	783	755

[*] Prof. Dr. R. Schlögl, Dr. M. Schur, B. Bems, A. Dassenoy, Dr. I. Kassatkine, Prof. Dr. J. Urban
Abteilung Anorganische Chemie
Fritz-Haber-Institut der Max-Planck-Gesellschaft
Faradayweg 4–6, 14195 Berlin (Germany)
Fax: (+49) 30-8413-4401
E-mail: acsek@fhi-berlin.mpg.de
H. Wilmes, Priv.-Doz. Dr. O. Hinrichsen, Prof. Dr. M. Muhler
Lehrstuhl für Technische Chemie, Ruhr-Universität Bochum
44780 Bochum (Germany)

 DOI: 10.1002/anie.200250709 © 2003 Wiley-VCH Verlag GmbH & Co. KGaA, Weinheim

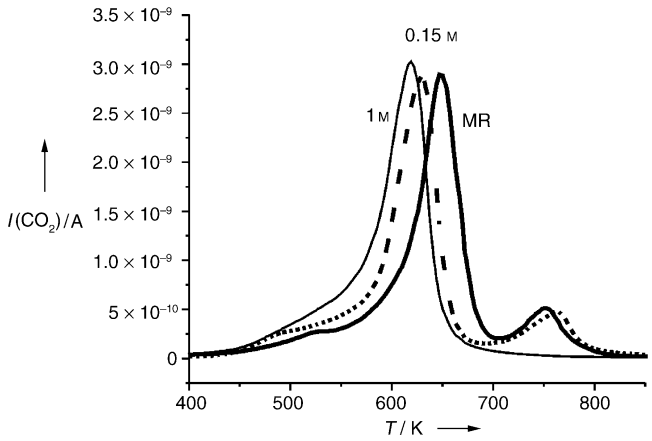


Figure 1. CO_2 evolution during thermogravimetric evolved-gas analysis of the catalyst samples (1 M and 0.15 M, conventional samples; MR: microreactor sample). Ordinate: Ion current at *m/e* 44.

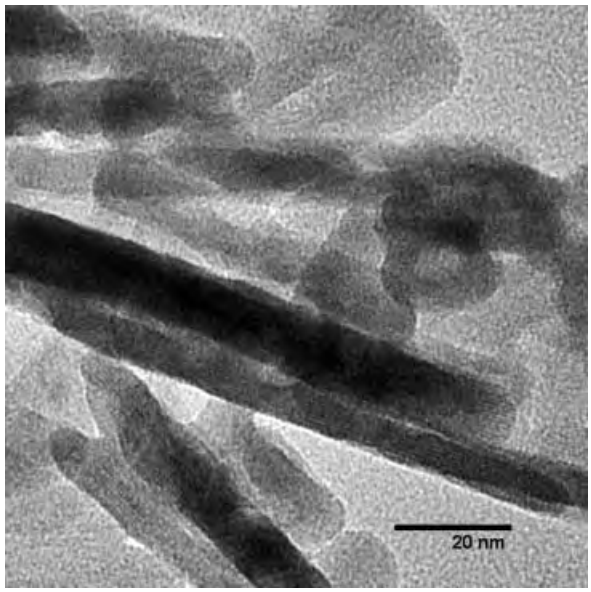


Figure 2. Transmission electron microscopy (TEM) image of the microreactor hydroxycarbonate product.

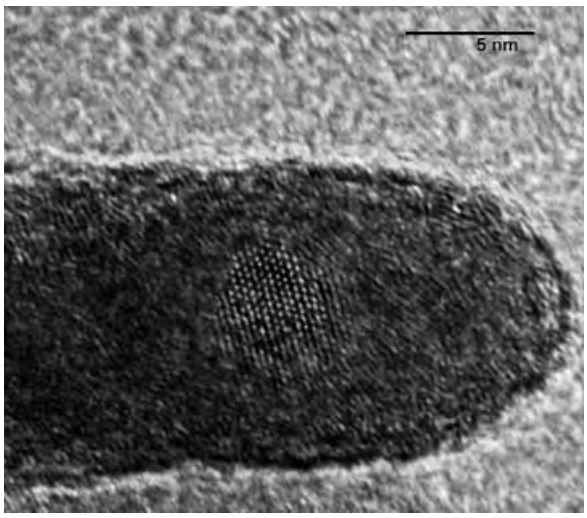


Figure 3. High-resolution TEM image of a needle structure of the sample in Figure 2. The nanocrystalline ZnO particle is observed from the [100] direction.

Through changes in the ageing, washing, and drying steps for a conventionally precipitated sample, a similar HT-CO3 species can be formed. This formation can be achieved through a significant increase in the pH value of the ageing mixture and is connected with a release of hydroxide ions. However, such a release was not observed during precipitation in the microreactor. Furthermore, there were no indications in this run of an exchange of nitrate for hydroxide ions that competes with the inclusion of carbonate.[8] Clearly, the constant run of the reaction in the microreactor causes the formation of a solid with the desired final structure, but without the necessity for any postprecipitation reactions.[8,11]

The significant change in the catalytic activity per unit of Cu surface area also indicates that either the density or the effectiveness of the active centers is increased with the new precipitation procedure. The required production of "catalytically active" copper has been extensively investigated for conventional catalysts.[5,12–15] An important factor in addition to the formation of the required Cu surface termination[2,16] is straining of the lattice of the Cu particles.[17,18] The formation of defects[19] in the copper through the inclusion of foreign atoms,[12] with a demonstrated effect on the binding energy of the relevant adsorbates[20,21] through corresponding nanorestructuring or initial incorporation of second phases[5,22,23] such as ZnO in CuO, are seen as the basis of the chemical memory.

Such structures are observable by electron microscopy. The HC material shown in Figure 2 consists of needlelike structures of about 100 nm length and 10 nm width. A closer inspection of the needle structures (Figure 3) shows that they are nanostructured and consist of clusters with dimensions of approximately 2 nm embedded in an amorphous matrix. The discernable lattice planes indicate ZnO. This is consistent with observations from the synthesis of nano-ZnO, in which the starting sol corresponds somewhat to the clusters observed in this case.[24] The complex anion chemistry of the Cu in this system[8] should hinder the formation of crystalline primary products.

The needles lose water in the electron microscope and then show radiation-sensitive lattice fringes with an average distance of 0.7 nm. The variability of the locally measured lattice spacing reflects the variation in the composition of the sample. Each needle is a mixture of the materials listed in Table 2.[25] A simulated calcination in which the sample was heated in an electron microscope gave rise to platelets consisting of a composite of $\approx$5-nm crystallites of Cu oxides[22,23] and ZnO. It is possible that through careful reduction, this nanostructured morphology remains at least partially intact and therefore allows the formation of the necessary defect structure[2,8,15,26,27] of active copper.

In conclusion, it has been shown that a change in the kinetic boundary conditions of a precipitation reaction through short reaction times, a small volume, and efficient temperature control, leads to a useable catalyst. Despite the

 © 2003 Wiley-VCH Verlag GmbH & Co. KGaA, Weinheim

Table 2: Lattice distances (D_m) and assignments from high-resolution TEM measurements of the HC product from the microreactor precipitation.

D_m [nm]	Composition [%]	D_{ref} [nm]	(*hkl*)	Formula
0.779	17	0.759	(110)	zinc hydroxide, $Zn(OH)_2$
		0.784	(202)	claraite, $(Cu,Zn)_3(CO_3)(OH)_4{\cdot}4H_2O$
0.723	69	0.741	(110)	rosasite, $CuZn(CO_3)(OH)_2$
		0.739	(110)	malachite, $Cu_2(CO_3)(OH)_2$
0.689	14	0.678	(200)	aurichalcite, $(Cu, Zn)_5(OH)_6(CO_3)_2$
		0.677	(200)	hydrozincite, $Zn_5(OH)_6(CO_3)_2$

different thermodynamic properties of the reactants, the short reaction time leads to a considerable approximation of the product that one would achieve in an ideal homogeneous coprecipitation, which could have a considerable meaning for other element combinations with large differences in their solution chemistry. The exclusion of uncontrollable reaction steps after the first precipitation technically improves the quality of the catalyst and allows a scientific explanation for the basis of the chemical memory of the system. This demonstrates that current efforts to improve the Cu/ZnO systems[26–28] by using conventional chemistry but with new reaction techniques has not yet run out of possibilities. Microreactor-directed synthesis of solids is not only an analytical technique for the improvement of the precipitation processes,[29] but is also an attractive synthesis technique for solids with kinetically controlled properties of their real structure.

Received: December 5, 2002
Revised: March 18, 2003 [Z50709]

Keywords: copper · electron microscopy · heterogeneous catalysis · methanol synthesis · microreactors

[1] T. Fujitani, J. Nakamura, *Appl. Catal. A* **2000**, *191*, 111 – 129.
[2] J. D. Grunwaldt, A. M. Molenbroek, N. Y. Topsoe, H. Topsoe, B. S. Clausen, *J. Catal.* **2000**, *194*, 452 – 460.
[3] J. G. Wu, M. Saito, M. Takeuchi, T. Watanabe, *Appl. Catal. A* **2001**, *218*, 235 – 240.
[4] M. S. Spencer, *Catal. Lett.* **2000**, *66*, 255 – 257.
[5] R. Brahmi, C. Kappenstein, J. Cernak, D. Duprez, A. Sadel, *J. Chim. Phys. Phys.-Chim. Biol.* **1999**, *96*, 487 – 497.
[6] S. Fujita, S. Moribe, Y. Kanamori, N. Takezawa, *React. Kinet. Catal. Lett.* **2000**, *70*, 11 – 16.
[7] Y. W. Suh, H. K. Rhee, *Korean J. Chem. Eng.* **2002**, *19* 17 – 19.
[8] B. Bems, M. Schur, A. Dassenoy, H. Junkes, D. Herein, R. Schlögl, *Chem. Eur. J.* **2003**, *9*, 2039 – 2052. Of particular relevance is the formation of a high-temperature carbonate (HT-CO3) phase that has a decomposition temperature greater than the maximum temperature experienced by the catalyst during its production or use.
[9] Fa. CPC Systems, CYTOS Lab System with a 1-mL capacity microstructured steel reactor. Further details of the patented reactor design can be obtained from Fa. CPC Systems. See also: T. Schwalbe, V. Autze, G. Wille, *Chimia* **2002**, 636 – 646.
[10] Methanol production was measured at atmospheric pressure, and thus heat- and mass-transport limitations are excluded; see also: H. Bielawa, M. Kurtz, T. Genger, O. Hinrichsen, *Ind. Eng. Chem. Res.* **2001**, *40*, 2793 – 2800.
[11] I. Melian-Cabrera, M. L. Granados, J. L. G. Fierro, *Phys. Chem. Chem. Phys.* **2002**, *4*, 3122 – 3127.
[12] N. Y. Topsoe, H. Topsoe, *Top. Catal.* **1999**, *8*, 267 – 270.
[13] Z. M. Hu, H. Nakatsuji, *Chem. Phys. Lett.* **1999**, *313*, 14 – 18.
[14] Y. W. Suh, S. H. Moon, H. K. Rhee, *Catal. Today* **2000**, *63*, 447 – 452.
[15] P. L. Hansen, J. B. Wagner, S. Helveg, J. R. Rostrup-Nielsen, B. S. Clausen, H. Topsoe, *Science* **2002**, *295*, 2053 – 2055.
[16] J. Nerlov, S. Sckerl, J. Wambach, I. Chorkendorff, *Appl. Catal. A* **2000**, *191*, 97 – 109.
[17] I. Böttger, T. Schedel-Niedrig, O. Timpe, R. Gottschall, M. Hävecker, T. Ressler, R. Schlögl, *Chem. Eur. J.* **2000**, *6*, 1870 – 1876.
[18] M. M. Günter, T. Ressler, B. Bems, C. Büscher, T. Genger, O. Hinrichsen, M. Muhler, R. Schlögl, *Catal. Lett.* **2001**, *71*, 37 – 44.
[19] F. W. Telgheder, J. Urban, *Phys. Chem. Chem. Phys.* **1999**, *1*, 4479 – 4483.
[20] H. A. Abdullah, C. H. Rochester, J. A. Anderson, J. E. Bailie, N. V. Richardson, G. J. Hutchings, *Phys. Chem. Chem. Phys.* **2000**, *2*, 3925 – 3932.
[21] S. Vollmer, G. Witte, C. Wöll, *Catal. Lett.* **2001**, *77*, 97 – 101.
[22] M. M. Günter, T. Ressler, R. E. Jentoft, B. Bems, *J. Catal.* **2001**, *203*, 133 – 149.
[23] M. M. Günter, B. Bems, R. Schlögl, T. Ressler, *J. Synchrotron Radiat.* **2001**, *8*, 619 – 621.
[24] C. Pacholski, A. Kornowski, H. Weller, *Angew. Chem.* **2002**, *114*, 1234 – 1237; *Angew. Chem. Int. Ed.* **2002**, *41*, 1188 – 1191.
[25] The composition data are the result of about 200 measurements and are in good agreement with X-ray diffraction data: P. Porta, S. de Rossi, G. Ferraris, L. Jacono, M. Minelli, M. Moretti, *J. Catal.* **1988**, *109*, 367; whether the rest of the phases or the variation in the cation composition plays a role in this spatially limited technique of structure analysis can not be determined because the sensitivity of the samples does not allow prolonged exposure to the beam for preview measurements or meticulous observation.
[26] E. K. Poels, D. S. Brands, *Appl. Catal. A* **2000**, *191*, 83 – 96.
[27] H. L. Castricum, H. Bakker, E. K. Poels, *Mater. Sci. Eng. A* **2001**, *304*, 418 – 423.
[28] Y. Ma, Q. Sun, D. Wu, W. J. Fan, J. F. Deng, *Appl. Catal. A* **1999**, *177*, 177 – 184.
[29] H. Wang, H. Nakamura, M. Uehara, M. Miyazaki, H. Maeda, *Chem. Commun.* **2002**, 1462 – 1463.

 © 2003 Wiley-VCH Verlag GmbH & Co. KGaA, Weinheim

Molecular Polymer Wires

Gram-Scale Synthesis of Submicrometer-Long Polythiophene Wires in Mesoporous Silica Matrices**

*Guangtao Li, Sheshanath Bhosale, Tianyu Wang, Yang Zhang, Hesun Zhu, and Jürgen-Hinrich Fuhrhop**

The mesoporous silica MCM-41 is characterized by ordered hexagonal arrays of uniform channels. The pore diameter can be controlled in the range of 2–10 nm by the synthetic procedures and the surface area is about 1000 m^2g^{-1}.[1–2] These attributes make the material attractive not only as sorbent, catalytic support, and separation membrane, but also as ideal host for rational nanomanufacturing,[3–7] especially as synthetic scaffolds for controlled polymerization.[8–13]

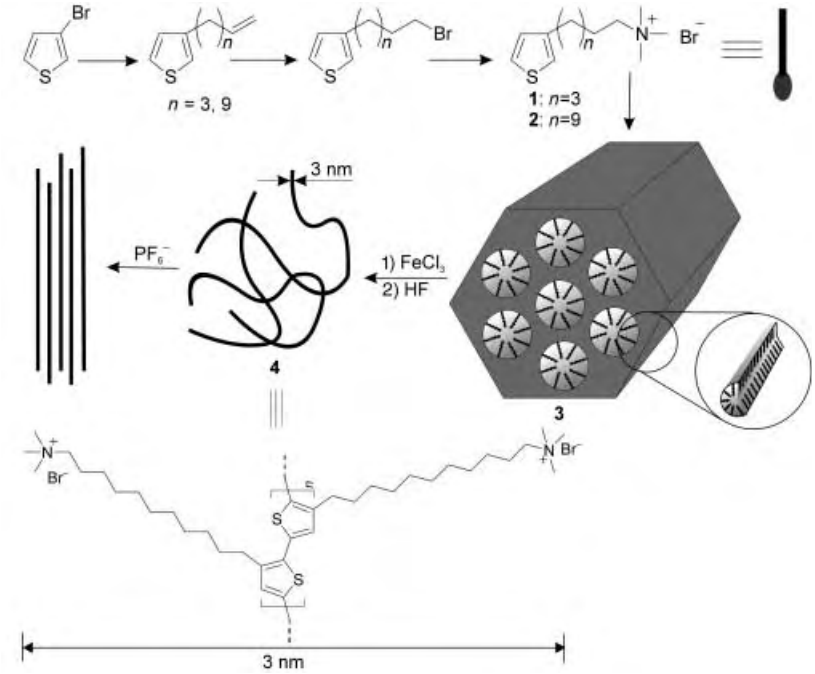


Figure 1. Schematic representation of the fabrication and organization of conjugated polythiophene molecular wires with mesoporous silica MCM-41.

[*] Prof. Dr. J.-H. Fuhrhop, Dr. G. Li, S. Bhosale, Dr. T. Wang
Freie Universität Berlin
Institut für Organische Chemie
Takustrasse 3, 14195-Berlin (Germany)
Fax: (+49) 30-8385-5589
E-mail: fuhrhop@chemie.fu-berlin.de
Dr. G. Li, Dr. Y. Zhang, Prof. Dr. H. Zhu
Department of Chemistry
Tsinghua University
Beijing (China)

[**] Financial support by the Deutsche Forschungsgemeinschaft (SFB 448 "Mesoscopic Systems"), the Fonds der Deutschen Chemischen Industrie, and by the FNK of the Free University is gratefully acknowledged.

Polyanilin and polyacryl fibers were first synthesized inside MCM-41 by oxidation and free-radical initiation of the corresponding monomers.[8–9] Contactless microwave conductivity measurements displayed a high conductivity of the encapsulated polymer as compared with the bulk polymer. Since then the polymerization of various monomers, such as styrene, alkyne, ethylene, and methylmethacrylate, have been reported within MCM-41.[3–13] The described polymerization processes occur in two steps, 1) loading of the monomer into preformed silica channels by chemical vapor deposition (CVD) or freeze-thaw cycles, and 2) polymerization by irradiation or oxidation.

It is conceivable that the structure-directing agents for the silicate, for example, cetyltrimethylammonium bromide, could also bear polymerizable units. Aida and Tajima applied this approach on polyacetylene, but obtained only a few macroscopic rods, with diameters between 15 and 25 μm.[13] We assumed that flexible thiophene units with pentyl or undecyl ammonium side chains may form more fluid, densely packed template monomers and could be directly polymerized in situ in a controllable fashion to linear macromolecular fibers. Using this strategy (Figure 1), we report herein the fabrication of submicrometer long conjugated polythiophene molecular wires of molecular thinness in gram-scale. The surfactants, which function both as template and monomer, trimethyl-(11-thiophen-3-yl-undecyl) ammonium bromide (**2**) and the pentyl homologue **1** were synthesized by standard methods.[14] Mesostructured silicates were synthesized following a slightly modified procedure reported by Ozin et al. for the preparation of mesoporous silica with functional organic groups within the channels.[15] In a typical synthesis, 1.0 g of tetraethylorthosilicate (TEOS) was added to an aqueous solution of NH_4OH containing monomer **2** under stirring. The molar ratio of 1.0 Si:114 H_2O:8.0 NH_4OH (28%):0.12 thiophene **2** was thus established in the reaction mixture. After 60 min stirring at room temperature, the solution was left standing at 90 °C for 5 h in a closed polyethylene bottle. A white powder was collected by filtration, washed thoroughly with millipore water, and dried in air. The yield was about 1 g. We assume that all of the thiophene **2** was entrapped in the material, because the filtrate seemed not to contain a detergent. The homologous monomer **1** was less useful as a template, presumably, because of its shorter chain length, it does not form micelles.

Figure 2A shows the powder X-ray diffraction (PXRD) pattern of the resultant material **3**. Three resolved peaks could be indexed as (100), (110), and (200) and are typical of the reflections of a well-ordered hexagonal mesoporous solid. The position of the intense (100) peak reflects a *d* spacing of approximately 3.6 nm, which is clearly larger than that of mesostructured silica prepared with tetradecyltrimethylammonium bromide (which has the same chain length as **2**) as template. Complementary to the XRD data, transmission electron microscopy (TEM) reveals micropores with a hexagonal symmetry throughout the sample with a center to

 © 2003 Wiley-VCH Verlag GmbH & Co. KGaA, Weinheim DOI: 10.1002/anie.200351158

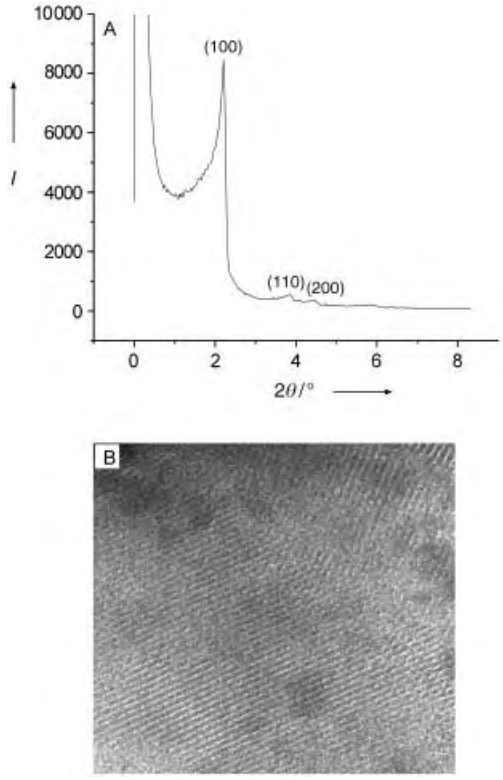


Figure 2. A) Powder X-ray diffraction pattern and B) TEM image of synthesized mesoporous silica using **2** as structure-directing agent.

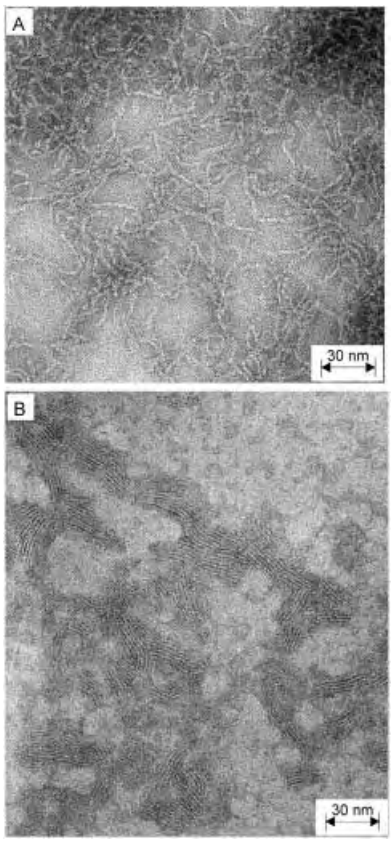


Figure 3. TEM images of A) the conjugated molecular wires from the polymerization of **2** and B) the organized wires upon the addition of PF_6^- ions.

center distance between the hexagon centers of 3.4–3.8 nm (Figure 2B). FT-IR spectra display bands close to 1500 cm^{-1} (1490, 1479, and 1467 cm^{-1}), which are characteristic for the stretching of thiophene ring.

The polymerization of densely packed thiophene monomer in MCM-41 was carried out in 10 mL of a CH_2Cl_2 dispersion containing 2 g of synthesized silica and 8 g of $FeCl_3$.[16,17] The reaction mixture was stirred at room temperature for 2 days and the solvent removed. The residue was then dispersed in 10 mL of 0.3 M HF in water. An orange solid **4** was formed, collected by filtration, washed thoroughly with water, and dried in air. We obtained 240 mg of the polymer from 2 g TEOS and 1.0 g from 10 g TEOS.

The polymer was very soluble in water and produced a broad absorption band in the UV/Vis spectrum with a maximum at 465 nm as well as a fluorescence band centered at 610 nm, which both indicate the formation of a conjugated polymer. The same polymer in the MCM-matrix showed an absorption maximum at 505 nm and an emission at 640 nm. The red-shift clearly indicates the confinement effect of the nanoscale silicate channel on the effective conjugation length of the polymer chain formed. This effect was also found for other semiconducting polymer chromophores which have been encapsulated into the hexagonally arrayed channels of mesoporous silica glass by a post-loading approach.[18,19] The IR-spectrum showed essentially the same thiophene bands as the monomer (1490, 1485, and 1467 cm^{-1}).

TEM provided direct visualization of the polythiophene wires formed. Figure 3A shows TEM images of a sample stained by 1% phosphotungstate (pH 7). It is clear that massive, coiled, individual strands are distributed over large areas. These strands have a tendency to entangle with each other. Attempts to obtain separated single strands by dilution and to detect clear-cut endings and thus determine the length of individual strands failed. The strands have, however, a uniform diameter of 3 nm (Figure 3A), which is in excellent agreement with the width of unidecylammonium thiophene repeating units in the *all-trans* conformation in a micellar double strand (Figure 1). This result suggests that the in situ polymerization in mesoporous silica produces well-resolved individual molecular wires. This is quite different from other studies, where analogous reactions in porous membranes gave nanorods or nanotubes with submicrometer diameters.[20–22] From the images, it was estimated that the average length of the conjugated chains is at least 100 nm corresponding to approximately 330 thiophene units. Attempts to obtain MALDI-TOF spectra gave no positive results (matrix: terthiophene).[23] The polymer was free of low-molecular-weight components. It was also found that upon the addition of PF_6^- to neutralize the ammonium groups the polymer changed from being in a disordered state into a semiordered state with chains of up to 150-nm in length (Figure 3B).

Thin polymer films were spin-coated from aqueous solutions containing about 10 mg of the polymer per 1 mL water onto various substrates and electrodes. Figure 4 shows

 © 2003 Wiley-VCH Verlag GmbH & Co. KGaA, Weinheim

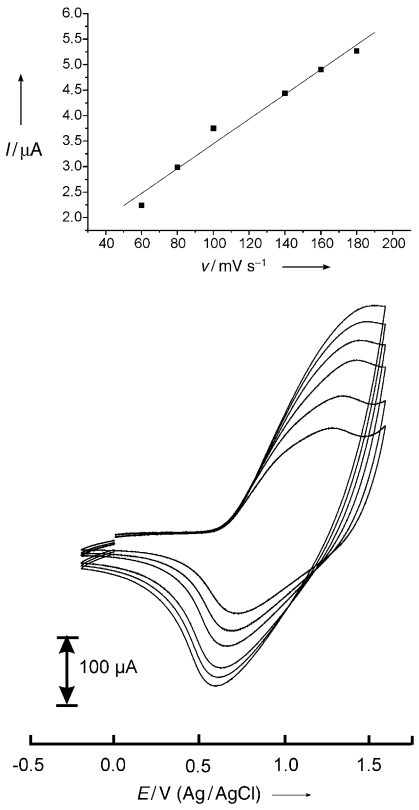


Figure 4. Cyclic voltammograms of spin-coated film of the polymer of **2** on ITO-electrode in 0.1 M Bu_4NPF_6/CH_2Cl_2 as a function of scan rates.

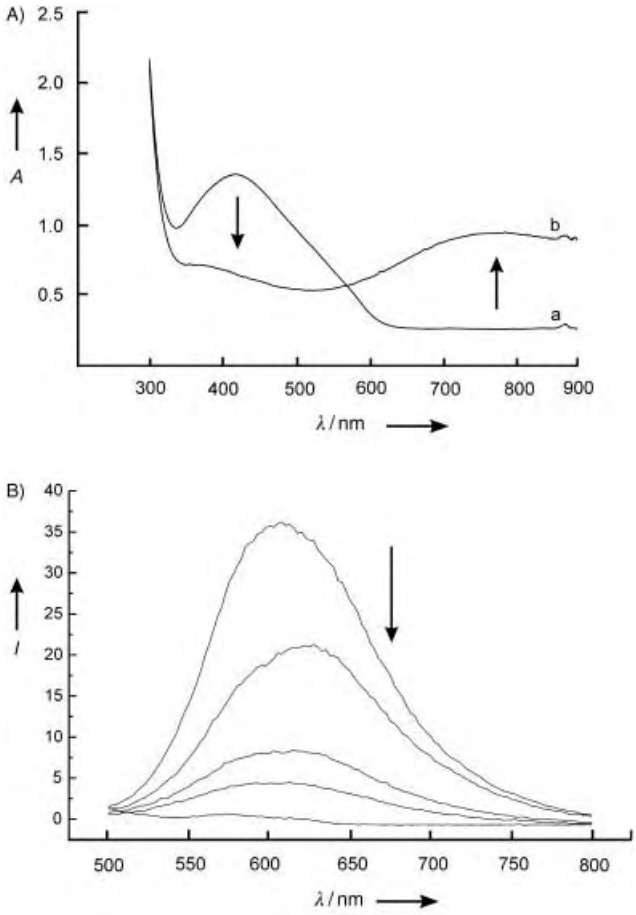


Figure 5. A) UV/Vis absorption spectra of spin-coated film of the polymer of **2** on ITO-plate: a) neutral state and b) oxidized state; B) fluorescence quenching of aqueous solution of synthesized polythiophene wires using 9,10-anthraquinone-2,6-disulphonic acid sodium salt (5 μL each of a 0.1 M solutions).

the cyclic voltammograms (CVs) of polymer films in CH_2Cl_2 with 0.1 M Bu_4NPF_6 using various scan rates. The polymer film displayed the typical reversible oxidative processes of conjugated polythiophene at a potential of 1.0 V (vs. Ag/AgCl). The current is linearly proportional to the scan rate (Figure 4), which indicates that the electroactive polymer was in contact with the electrode (electrode supported). The system was unusually stable; even after 20 CV cycles no decrease of the signal intensity was observed. Using interdigitated electrodes for the measurement we observed sigmoidal curves indicating a maximum conductivity of 2 $S\,cm^{-1}$ at room temperature and in the presence of air. This conductivity is comparable to that reported for polyalkylthiophene.[23]

Figure 5 illustrates the optoelectrochemical spectra obtained with synthesized polymer on an ITO-coated glass plate. The neutral-state polymer has its absorption maximum at 420 nm. Upon oxidation the maximum absorption is shifted to 780 nm which is accompanied by a color change from reddish violet to dark blue. This characteristic π–π* transition of conjugated polythiophenes is completely reversible in this polymer. The fluorescence can be effectively quenched by negative charged anthraquinone molecules (Figure 5B).

In conclusion, our method provides photoluminescent silica composite and also aligned conjugated 100-nm polymer chains on a gram scale. Since cetyltrimethylamonium bromide can been replaced by other detergent matrices in the synthesis of MCM-41,[24–26] one may also equip the thiophene bolaamphiphiles with different head groups (e.g. poly(ethylene glycol) or phosphonate). This would make conducting wires accessible, which can be combined in assemblies.

Received: February 11, 2003
Revised: May 2, 2003 [Z51158]

Keywords: mesoporous materials · molecular wires · polythiophene · silicates · template synthesis

[1] C. T. Kresge, M. E. Leonowicz, W. J. Roth, J. C. Vartuli, J. S. Beck, *Nature* **1992**, *359*, 710.
[2] J. S. Beck, J. C. Vartuli, W. J. Roth, M. E. Leonowicz, C. T. Kresge, K. D. Schmitt, C. T.-W. Chu, D. H. Olsen, E. W. Sheppard, S. B. McCullen, J. B. Higgins, J. L. Schlenker, *J. Am. Chem. Soc.* **1992**, *114*, 10835.
[3] F. Schüth, W. Schmidt, *Adv. Mater.* **2002**,*14*, 629.
[4] M. Ganschow, M. Wark, D. Wöhrle, G. Schulz-Ekloff, *Angew. Chem.*, **2000**, *112*, 167; *Angew. Chem. Int. Ed.* **2000**, *38*, 161.
[5] K. Moller, T. Bein, *Chem. Mater.* **1998**, *10*, 2950.
[6] J. Y. Ying, C. P. Mehnert, M. S. Wong, *Angew. Chem.* **1999**, *111*, 58; *Angew. Chem. Int. Ed.* **1999**, *38*, 56.

 © 2003 Wiley-VCH Verlag GmbH & Co. KGaA, Weinheim

[7] G. A. Ozin, E. Chomski, D. Khushalani, M. J. Maclachlan, *Curr. Opin. Colloid and Interface Sci.* **1998**, *3*, 181.
[8] Y. Lu, Y. Yang, A. Sellinger, M. Lu, J. Huang, H. Fan, R. Haddad, G. Lopez, A. R. Burns, D. Y. Sasaki, J. Shelnutt, C. J. Brinker, *Nature* **2001**, *410*, 913.
[9] C. G. Wu, T. Bein, *Science* **1994**, *266*, 1013.
[10] S. A. Johnson, D. Khushalani, N. Coombs, T. E. Mallouk, G. A. Ozin, *J. Mater. Chem.* **1998**, *10*, 1841.
[11] M. J. MacLachlan, P. Aroca, N. Coombs, I. Manners, G. A. Ozin, *Adv. Mater.* **1998**, *10*, 144.
[12] K. Kageyama, J. Tamazawa, T. Aida, *Science* **1999**, *285*, 2113.
[13] T. Aida, K. Tajima, *Angew. Chem.* **2001**, *113*, 3919; *Angew. Chem. Int. Ed.* **2001**, *40*, 3803.
[14] G. Li, G. Koßmehl, W. Kautek, W. Plieth, H. Zhu, S. C. Ng, *Macromol. Chem. Phys.* **2000**, *201*, 21.
[15] T. Asefa, M. J. MacLachlan, N. Coombs, G. A. Ozin, *Nature* **1999**, *402*, 867.
[16] M. Leclerc, *Adv. Mater.* **1999**, *11*, 1491.
[17] R. D. McCullough, *Adv. Mater.* **1998**, *10*, 93.
[18] T. Q. Nguyen, J. Wu, V. Doan, B. J. Schwartz, S. H. Tolbert, *Science* **2000**, *288*, 652.
[19] T. Q. Nguyen, J. Wu, V. Doan, S. H. Tolbert, B. J. Schwartz, *Adv. Mater.* **2001**, *13*, 609.
[20] S. D. Vito, C. R. Martin, *Chem. Mater.* **1998**, *10*, 1738.
[21] C. Jérôme, R. Jérôme, *Angew. Chem.* **1998**, *110*, 2639; *Angew. Chem. Int. Ed.* **1998**, *37*, 2488.
[22] M. Gao, S. Huang, L. Dai, G. Wallace, R. Gao, Z. Wang, *Angew. Chem.*, **2000**, *112*, 3810; *Angew. Chem. Int. Ed.* **2000**, *39*, 3664.
[23] *Handbook of Conducting Polymer* (Eds.: T. A. Skotheim, R. L. Elsenbaumer, J. R. Reynolds), 2nd Ed., Marcel Dekker, New York, **1998**.
[24] Q. Huo, D. I. Margolese, U. Ciesla, P. Feng, T. E. Gier, P. Sieger, R. Leon, P. M. Petroff, F. Schüth, G. D. Stucky, *Nature* **1994**, *368*, 317.
[25] P. Yang, D. Zhao, D. I. Margolese, B. F. Chmelka, G. D. Stucky, *Nature* **1998**, *396*, 152.
[26] P. T. Tanev, T. J. Pinnavaia, *Chem. Mater.* **1996**, *8*, 2068.

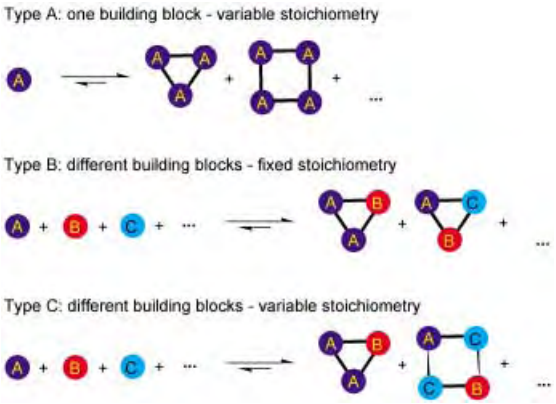
 © 2003 Wiley-VCH Verlag GmbH & Co. KGaA, Weinheim

Libraries of Metal Complexes

Adaptive Behavior of Dynamic Combinatorial Libraries Generated by Assembly of Different Building Blocks**

*Zacharias Grote, Rosario Scopelliti, and Kay Severin**

Combinatorial libraries in which the individual compounds are connected by dynamic equilibria are able to respond to the environment. If such a system is disturbed by addition of a target molecule (a receptor or a ligand), it will re-equilibrate with the concomitant amplification of compounds which bind to the target molecule. This offers the possibility to utilize dynamic combinatorial libraries (DCLs) for the fast detection of new ligands or new receptors, as demonstrated by several research groups in recent years.[1] Three different types of DCLs obtained by reversible assembly of reactive building blocks can be distinguished (Scheme 1). If only one kind of



Scheme 1. Different types of dynamic combinatorial libraries obtained by assembly of reactive building blocks.

subunit is employed, structural diversity can be generated by the formation of assemblies with different stoichiometries (Type A).[2] By using two or more structurally diverse building blocks it is possible to obtain libraries with uniform (Type B) or variable stoichiometry (Type C). All three types have been investigated experimentally.[3–5] In the following we show that DCLs of Type B and C can display a behavior fundamentally

[*] Prof. Dr. K. Severin, Z. Grote, Dr. R. Scopelliti[+]
Institut de Chimie Moléculaire et Biologique
École Polytechnique Fédérale de Lausanne
1015 Lausanne (Switzerland)
Fax: (+41) 21-693-9305
E-mail: kay.severin@epfl.ch

[+] X-ray structural analysis

[**] This work was supported by the Swiss National Science Foundation and by OMG.

Supporting information for this article (synthesis and characterization of the complexes **ccc** and the calculated steady-state concentration of different DCLs of types B and C) is available on the WWW under http://www.angewandte.org or from the author.

 DOI: 10.1002/anie.200351623 © 2003 Wiley-VCH Verlag GmbH & Co. KGaA, Weinheim

different from that of libraries of Type A. Importantly, we will demonstrate that there is no direct correlation between the relative amplification and the thermodynamic stability of the DCL members in such systems.

Our investigations started with calculations performed to study the effect of thermodynamic differences on the steady-state concentration of members of a library of Type B.[6] The results obtained for a dynamic mixture with the fixed stoichiometry X_3 using equimolar amounts of the three different building blocks A, B, and C are summarized in Table 1.[7]

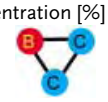
The data for a statistical mixture without thermodynamic preferences is given in entry 1. The following three entries describe the hypothetical[8] cases that only one member of the library is stabilized (for example, by selective binding of a guest molecule). If the assembly AAA is stabilized by a factor of 1000, it is amplified by a factor of $f_{AAA} = 7.6$ relative to the original equilibrium concentration and subsequently represents the dominant species in solution (entry 2). Upon selective stabilization of AAB (entry 3), a similar result is obtained: AAB is clearly the dominant species in solution (47.7%; $f_{AAB} = 4.3$). It should be noted, however, that in both cases species with a high content of B and C such as BBC and CCC are likewise amplified to a considerable extent (for example, entry 3: $f_{CCC} = 3.6$). A rather dramatic effect is observed upon selective stabilization of ABC (entry 4): the whole mixture collapses to give almost exclusively ABC. The steady-state concentrations of a mixture in which both AAA and ABC are stabilized relative to the other members are given in entry 5. Remarkably, only ABC is amplified and completely dominates the mixture (98.6%). The assembly AAA, on the other hand, becomes nearly extinct (0.4%). A more equilibrated situation is described in entry 6. The incorporation of A leads to an additive stabilization by a factor of 300. In this mixture, three species of moderate stability dominate, with the same amplification factor: ABB, ACC, and ABC ($f = 2.1$). The assembly AAA, however, is the species with the lowest concentration of all members (0.1%). We thus observe the quasi-extinction of the thermodynamically most stable species in the mixture.

This theoretical analysis demonstrates that a DCL can adapt in a way which is quite different from the paradigm "amplification of the fittest".[18] It is not necessarily the most stable member of the library which is amplified the most. On the contrary, it is possible that the most stable member becomes extinct and that members of mediocre or low stability are amplified. Further analyses of related model systems show that a behavior of this kind can also be found for DCLs of noncyclic assemblies and for libraries of Type C (see Supporting Information). Overall, our analyses predict that libraries of Type B and C should display the following characteristics: a) the selection of an assembly with a high content of one subunit will lead to the concomitant amplification of one or more assemblies comprised of the other subunit(s); b) there is an intrinsic bias for the selection of heteroassemblies, or more precisely, for assemblies whose composition reflects the overall composition of the library.[9] For libraries of Type A, on the other hand, these "restrictions" do not apply because the members compete for the same resource: the common building block. The same is true for DCLs, which are based on reversible conformational changes.[10]

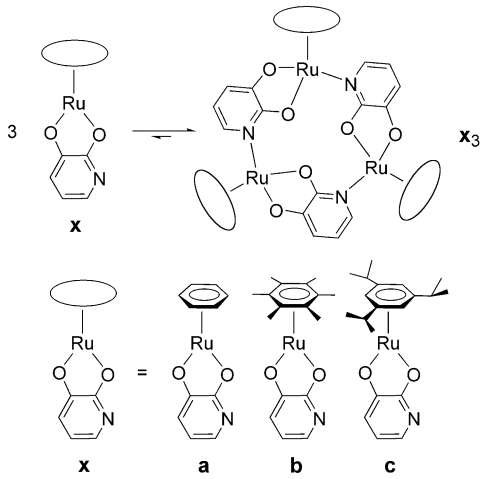
To demonstrate that the above-mentioned characteristics can indeed be found in synthetic DCLs, we have investigated the equilibrium concentrations of dynamic mixtures of metallamacrocycles. In a recent publication we have shown that the trinuclear complexes **aaa** and **bbb** can be easily obtained by the self-assembly of organometallic pyridonate complexes (Scheme 2).[11] These compounds were expected to be suitable starting materials for the generation of DCLs because their framework contains labile metal–ligand bonds.

Instead of using a target molecule to induce a selection process, we chose to utilize steric effects to introduce thermodynamic differences among the DCL members.[12] For this purpose, the new metallamacrocycle **ccc** with sterically demanding π ligands was synthesized. The structure of this complex in the crystal[13] shows that the three tris(isopropyl)benzene ligands are very close to each other (Figure 1). As a result of this steric congestion, the Ru···Ru distance of 5.40 Å is increased relative to that found in the

Table 1: Calculated steady-state concentrations of a dynamic mixture of macrocycles with the fixed stoichiometry X_3 obtained by assembly of three different building blocks ($\log K_{CCC} >> 5$; $[A]_{total} = [B]_{total} = [C]_{total}$).

Entry	Relative stability relative concentration [%]									
										
1	1	1	1	1	1	1	1	1	1	1
	3.7	11.1	11.1	3.7	11.1	11.1	3.7	11.1	11.1	22.2
2	1000	1	1	1	1	1	1	1	1	1
	28.1	0.5	3.4	7.2	21.5	21.5	7.2	0.5	3.4	6.8
3	1	1000	1	1	1	1	1	1	1	1
	0.0	47.7	0.5	1.9	11.1	21.2	13.5	0.1	1.9	2.0
4	1	1	1	1	1	1	1	1	1	1000
	0.0	0.1	0.1	0.0	0.1	0.1	0.0	0.1	0.1	99.6
5	1000	1	1	1	1	1	1	1	1	1000
	0.4	0.0	0.1	0.1	0.3	0.3	0.1	0.0	0.1	98.6
6	900	600	300	1	1	1	1	600	300	300
	0.1	2.1	22.8	0.5	1.6	1.6	0.5	2.1	22.8	45.7

 © 2003 Wiley-VCH Verlag GmbH & Co. KGaA, Weinheim



Scheme 2. The assembly of organometallic pyridonate complexes gives trinuclear metallamacrocycles.



Figure 1. Space-filling representation of the structure of complex **ccc** in the crystal.

Ru–benzene complex **aaa** (Ru···Ru: 5.32 Å). A similar expansion of the macrocycle was observed for the hexamethylbenzene complex **bbb** (Ru···Ru: 5.46 Å).[11] These data indicate that the macrocycles **bbb** and **ccc** are less stable than **aaa** because of steric repulsion of the π ligands.

We then investigated the conditions under which scrambling occurs. It was found that when a 1:1 mixture of the symmetrical complexes **aaa** and **ccc** in methanol is heated to 40 °C, the asymmetric complexes **aac** and **acc** can be observed within several minutes. The steady-state concentrations are reached after 12 h. The reaction can be conveniently followed by NMR spectroscopy if CD_3OD is employed as the solvent (Figure 2).

The equilibrium concentrations of all possible binary mixtures of **aaa**, **bbb**, and **ccc** are given in Table 2. A statistical distribution of 1:3:3:1 is expected for a hypothetical mixture with equally stable members. Concentrations approaching these theoretical values are found for a mixture of **bbb** and **ccc**: all four possible species can be detected in the mixture, with

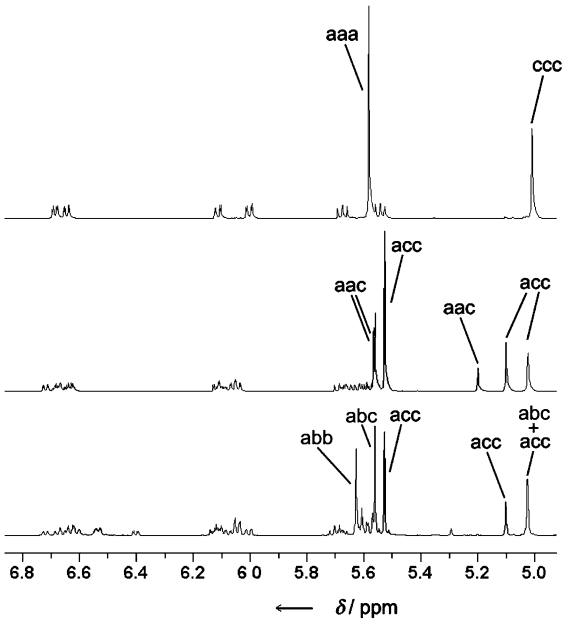


Figure 2. Aromatic region of the ^{1}H NMR spectrum (CD_3OD) of an equimolar mixture of **aaa** and **ccc** before equilibration (top), after equilibration (middle), and an equimolar mixture of **aaa**, **bbb**, and **ccc** after equilibration (bottom). The labeled signals correspond to the C_6H_6 ($\delta = 5.5$–5.7 ppm) and to the $C_6H_3i\mathrm{Pr}_3$ protons ($\delta = 5.0$–5.2 ppm) of the π ligands of **a** and **c**. The small signals between $\delta = 5.5$ and 6.8 ppm correspond to the protons of the bridging pyridonate ligands.

a slight preference for the mixed complex **bcc** (entry 1). This result points to the fact that the steric requirements of the large hexamethylbenzene and tris(isopropyl)benzene π ligands are comparable.

As soon as thermodynamic differences are introduced, the relative distribution changes substantially (entries 2 and 3). For mixtures with the small Ru–benzene complex **aaa**, the heteroassemblies completely dominate after equilibration and only traces of the homotrimeric complexes can be detected (Figure 2). Based on the size of the π ligands, complexes should become more stable the more **a** fragments they contain. In accordance with our theoretical predictions, this leads to the selection of the mixed species **aab**/**bcc** and **aac**/**acc**, respectively, and not of the most stable species **aaa**.

A DCL obtained by mixing all three complexes **aaa**, **bbb**, and **ccc** should display a behavior which resembles the theoretical model described in Table 1, entry 6, since only the incorporation of the fragment **a** will lead to stabilization. Consequently, the complexes **abb**, **acc**, and **abc** should be selected. This is exactly what we observed: the ^{1}H NMR

Table 2: Equilibrium concentrations of the four metallamacrocycles obtained by scrambling of equimolar amounts of two homotrimeric complexes in CD_3OD.[a]

Entry	Starting mixture	Equilibrium mixture
1	**bbb** + **ccc**	**bbb** (14%) **bbc** (19%) **bcc** (49%) **ccc** (18%)
2	**aaa** + **bbb**	**aaa** (<3%) **aab** (45%) **abb** (55%) **bbb** (<3%)
3	**aaa** + **ccc**	**aaa** (<3%) **aac** (45%) **acc** (55%) **ccc** (<3%)

[a] The relative concentration was determined by integration of selected ^{1}H NMR signals (CD_3OD). The error is estimated to be ±3%.

 © 2003 Wiley-VCH Verlag GmbH & Co. KGaA, Weinheim

spectrum of the equilibrium mixture showed that these three complexes clearly dominate in the mixture (Figure 2, bottom).[14] This result was confirmed by ^{13}C NMR spectroscopy. Again, it is not the most stable species **aaa**, **aab**, and **aac** which are amplified. On the contrary, we were not able to detect the signals of complex **aaa**. The competition within our DCL has thus led to the extinction of the most stable assembly.

There are possibile ways to circumvent or reduce the "problems", which may be encountered if DCLs of Type B and C are used for selection processes. First, one can conduct the experiment in a way so that it is possible to separate the target and the bound DCL members from the unbound members (for example, by using a target on a solid support).[15,16] This will eliminate the false positives, which arise from the concomitant amplification of species which do not bind to the target. However, this approach does not reduce the intrinsic bias for the selection of heteroassemblies. Secondly, the DCL can be designed in a way such that without a target it has an equilibrium distribution in which the monomeric building blocks represent the dominating species and the various aggregates are present in only small amounts. In this case, the selective stabilization of one or several aggregates of this virtual[1f] library will give rise to amplification factors which are not only significantly higher, but which also correspond much more closely to the relative thermodynamic stability. Furthermore, there will be no concomitant amplification of assemblies which do not bind to the target. Some experiments, which confirm this prediction, have been described recently;[17] a theoretical analysis analogous to that shown in Table 1 is given in the Supporting Information.

Received: April 9, 2003 [Z51623]

Keywords: combinatorial chemistry · compound libraries · metallamacrocycles · ruthenium complexes · self-assembly

[1] For reviews, see a) O. Ramström, T. Bunyapaiboonsri, S. Lohmann, J.-M. Lehn, *Biochim. Biophys. Acta* **2002**, *1572*, 178 – 186; b) S. J. Rowan, S. J. Cantrill, G. R. L. Cousins, J. K. M. Sanders, J. F. Stoddart, *Angew. Chem.* **2002**, *114*, 938 – 993; *Angew. Chem. Int. Ed.* **2002**, *41*, 898 – 952; c) S. Otto, R. L. E. Furlan, J. K. M. L. Sanders, *Curr. Opin. Chem. Biol.* **2002**, *6*, 321 – 327; d) S. Otto, R. L. E. Furlan, J. K. M. L. Sanders, *Drug Discovery Today* **2002**, *7*, 117 – 125; e) C. Karan, B. L. Miller, *Drug Discovery Today* **2000**, *5*, 67 – 75; f) J.-M. Lehn, *Chem. Eur. J.* **1999**, *5*, 2455 – 2463.

[2] The term "stoichiometry" is used simply to indicate the number of subunits of a certain assembly. It is not meant to characterize the nature of the subunits.

[3] For libraries of Type A, see a) S. L. Roberts, R. L. E. Furlan, S. Otto, J. K. M. Sanders, *Org. Biomol. Chem.* **2003**, *1*, 1625 – 1633; b) S. L. Roberts, R. L. E. Furlan, G. R. L. Cousins, J. K. M. Sanders, *Chem. Commun.* **2002**, 938 – 939; c) R. L. E. Furlan, Y.-F. Ng, G. R. L. Cousins, J. E. Redman, J. K. M. Sanders, *Tetrahedron* **2002**, *58*, 771 – 778; d) R. L. E. Furlan, Y.-F. Ng, S. Otto, J. K. M. Sanders, *J. Am. Chem. Soc.* **2001**, *123*, 8876 – 8877; e) G. R. L. Cousins, R. L. E. Furlan, Y.-F. Ng, J. E. Redman, J. K. M. Sanders, *Angew. Chem.* **2001**, *113*, 437 – 442; *Angew. Chem. Int. Ed.* **2001**, *40*, 423 – 428; f) R. L. E. Furlan, G. R. L. Cousins, J. K. M. Sanders, *Chem. Commun.* **2000**, 1761 – 1762; g) B. Hasenknopf, J.-M. Lehn, N. Boumediene, A. Dupont-Gervais, A. Can Dorsselaer, B. Kneisel, D. Fenske, *J. Am. Chem. Soc.* **1997**, *119*, 10956 – 10962; h) P. A. Brady, R. P. Bonar-Law, S. J. Rowan, C. J. Suckling, J. K. M. Sanders, *Chem. Commun.* **1996**, 319 – 320; i) B. Hasenknopf, J.-M. Lehn, B. O. Kneisel, G. Baum, D. Fenske, *Angew. Chem.* **1996**, *108*, 1987 – 1990; *Angew. Chem. Int. Ed. Engl.* **1996**, *35*, 1838 – 1840.

[4] For libraries of Type B, see a) Y. Ma, S. V. Kolotuchin, S. C. Zimmerman, *J. Am. Chem. Soc.* **2002**, *124*, 13757 – 13769; b) M. C. Calama, P. Timmerman, D. N. Reinhoudt, *Angew. Chem.* **2000**, *112*, 771 – 774; *Angew. Chem. Int. Ed.* **2000**, *39*, 755 – 758.

[5] For libraries of Type C, see a) B. Brisig, J. K. M. Sanders, S. Otto, *Angew. Chem.* **2003**, *115*, 1308 – 1311; Angew . *Chem. Int. Ed.* **2003**, *42*, 1270 – 1273; b) Y. Kubota, S. Sakamato, K. Yamaguchi, M. Fujita, *Proc. Natl. Acad. Sci. USA* **2002**, *99*, 4854 – 4856; c) S. Otto, R. L. E. Furlan, J. K. M. Sanders, *Science* **2002**, *297*, 590 – 593; d) S. Otto, R. L. E. Furlan, J. K. M. Sanders, *J. Am. Chem. Soc.* **2000**, *122*, 12063 – 12064.

[6] The calculations are based on the assumption that all assemblies are in equilibrium with their corresponding building blocks. The association constant of CCC was fixed to $K_{CCC} = 1 \times 10^5\ mM^{-2}$. The steady-state concentrations were calculated with the program Gepasi, version 3.30: a) P. Mendes, *Comput. Appl. Biosci.* **1993**, *9*, 563 – 571; b) P. Mendes, *Trends Biochem. Sci.* **1997**, *22*, 361 – 363.

[7] In some cases the sum of the relative concentrations deviates slightly from 100%. This is the result of an accumulation of rounding errors.

[8] The examples in Table 1, entries 2–5, describe extreme situations in which only one or two species of the DCL are stabilized. They were chosen because their results demonstrate the peculiar characteristics of a DCL of Type B. A balanced situation with a broader distribution of stability constants is more likely for "real" systems.

[9] A library of Type B composed of equal amounts of the building blocks A, B, and C, for example, will show a bias for the selection of the assembly ABC (see Table 1, entry 5).

[10] a) A. V. Eliseev, M. I. Nelen, *Chem. Eur. J.* **1998**, *4*, 825 – 834; b) A. V. Eliseev, M. I. Nelen, *J. Am. Chem. Soc.* **1997**, *119*, 1147 – 1148.

[11] a) H. Piotrowski, G. Hilt, A. Schulz, P. Mayer, K. Polborn, K. Severin, *Chem. Eur. J.* **2001**, *7*, 3196 – 3208; for structurally related macrocycles, see b) M.-L. Lehaire, R. Scopelliti, K. Severin, *Chem. Commun.* **2002**, 2766 – 2767; c) M.-L. Lehaire, R. Scopelliti, K. Severin, *Inorg. Chem.* **2002**, *41*, 5466 – 5474; d) M.-L. Lehaire, R. Scopelliti, H. Piotrowski, K. Severin, *Angew. Chem.* **2002**, *114*, 1477 – 1480; *Angew. Chem. Int. Ed.* **2002**, *41*, 1419 – 1422; e) H. Piotrowski, K. Severin, *Proc. Natl. Acad. Sci. USA* **2002**, *99*, 4997 – 5000; f) H. Piotrowski, K. Polborn, G. Hilt, K. Severin, *J. Am. Chem. Soc.* **2001**, *123*, 2699 – 2700; g) T. Habereder, M. Warchhold, H. Nöth, K. Severin, *Angew. Chem.* **1999**, *111*, 3422 – 3425; *Angew. Chem. Int. Ed.* **1999**, *38*, 3225 – 3228.

[12] For the present discussion, it is irrelevant whether the thermodynamic differentiation between the DCL members is caused by binding to a guest molecule, by binding to a receptor, or by steric effects.

[13] Crystal data for **ccc**:: $C_{60}H_{81}N_3O_6Ru_3 \cdot 0.5\,C_6H_{14} \cdot H_2O$, $M_r = 1304.59$, monoclinic, space group $P2_1/n$ (No. 14), $a = 13.4120(6)$, $b = 24.4988(13)$, $c = 18.6629(8)$ Å, $\beta = 100.255(4)°$, $V = 6040.4(5)$ Å^3, $Z = 4$, $\rho_{calcd} = 1.435\ g\,cm^{-3}$, $\mu = 0.794\ mm^{-1}$, $F(000) = 2708$, crystal dimensions $0.50 \times 0.36 \times 0.26\ mm^3$. Data collection: Oxford Diffraction KM4/Sapphire CCD, $T = 140(2)$ K, $Mo_{K\alpha}$ radiation, $\lambda = 0.71073$ Å, $\theta = 3.34$–$25.03°$, $-15 \le h \le 15$, $-29 \le k \le 29$, $-18 \le l \le 22$, 35584 reflections col-

 © 2003 Wiley-VCH Verlag GmbH & Co. KGaA, Weinheim

lected, 10064 independent reflections, $R_{int} = 0.0439$, 7606 observed reflections [$I > 2\sigma(I)$], empirical absorption correction, max./min. transmission: 0.902/0.663. Refinement: $N_{ref} = 10064$, $N_{par} = 709$, R_1 [$I > 2\sigma(I)$] = 0.0339, wR_2 (all data) = 0.0746, S = 0.961, the weighting scheme is $w^{-1} = [\sigma^2(F_o^2) + (0.0336P)^2]$ with $P = (F_o^2 + 2F_c^2)/3$, max. and average shift/error = 0.005, 0.000, largest difference peak 0.890 e Å^{-3}, largest difference minimum −0.640 e Å^{-3}. Structure solution and refinement by SHELX97 (G. M. Sheldrick, SHELX97, Programs for Crystal Structure Analysis, University of Göttingen, Göttingen (Germany), **1998**). H atoms were placed in calculated positions using the riding model. Disorder problems dealing with an isopropyl moiety have been handled with the split model and with geometrical (card DFIX) and "rigid bond" restraints (card DELU). CCDC-207895 contains the supplementary crystallographic data for this paper. These data can be obtained free of charge via www.ccdc.cam.ac.uk/conts/retrieving.html (or from the Cambridge Crystallographic Data Centre, 12 Union Road, Cambridge CB2 1EZ, UK; fax: (+44) 1223-336-033; or deposit@ccdc.cam.ac.uk).

[14] We were not able to differentiate the two possible isomers for **abc** by NMR spectroscopy.

[15] For DCL experiments where the target is immobilized on a solid support, see a) O. Ramström, J.-M. Lehn, *ChemBioChem* **2000**, *1*, 41 – 48; b) B. Klekota, B. L. Miller, *Tetrahedron* **1999**, *55*, 11687 – 11697; c) B. Klekota, M. H. Hammond, B. L. Miller, *Tetrahedron Lett.* **1997**, *38*, 8639 – 8642.

[16] The detection of DCL members with a high affinity for a given target can be facilitated by including a reaction which destroys unbound members: J. D. Cheeseman, A. D. Corbett, R. Shu, J. Croteau, J. L. Gleason, R. J. Kazlauskas, *J. Am. Chem. Soc.* **2002**. *124*, 5692 – 5701.

[17] a) M. Hochgürtel, R. Biesinger, H. Kroth, D. Piecha, M. W. Hofmann, S. Krause, O. Schaaf, C. Nicolau, A. V. Eliseev, *J. Med. Chem.* **2003**, *46*, 356 – 358; b) H. J. Cooper, M. A. Case, G. L. McLendon, A. G. Marshall, *J. Am. Chem. Soc.* **2003**, *125*, 5331 – 5339; c) M. Hochgürtel, H. Kroth, D. Piecha, M. W. Hofmann, C. Nicolau, S. Krause, O. Schaaf, G. Sonnenmoser, A. V. Eliseev, *Proc. Natl. Acad. Sci. USA* **2002**, *99*, 3382 – 3387; d) M. Case, G. L. McLendon, *J. Am. Chem. Soc.* **2000**, *122*, 8089 – 8090.

[18] M. Freemantle, *Chem. Eng. News* **2002** (sept. 2), 31 – 33.

 © 2003 Wiley-VCH Verlag GmbH & Co. KGaA, Weinheim

Order and Disorder

Ordering Phenomena and Phase Transitions in a Spin-Crossover Compound—Uncovering the Nature of the Intermediate Phase of $[Fe(2\text{-pic})_3]Cl_2 \cdot EtOH$**

*Dmitry Chernyshov, Marc Hostettler, Karl W. Törnroos, and Hans-Beat Bürgi**

Many properties of solid materials are intimately related to their crystal structures, and changes in properties are often accompanied by phase transitions. Here we show that a deeper understanding of the various phases of spin-crossover compounds, their phase transitions and properties, calls for multiple structure determinations as a function of external variables; the usual "one phase–one crystal structure" protocol is insufficient.

The spin state of several first-row transition-metal complexes may be switched between high and low under the influence of an external perturbation such as a change in temperature or pressure or irradiation with light. The characteristics of the bi- or multistable compounds, for example, transition temperatures, hysteresis properties, thermochromism, photochromism, and photomagnetism as well as thermodynamic and kinetic quantities, depend on the interplay between the ligand-field strength at the transition-metal ion and the interactions between the metal complex, the counterions, and solvate molecules, as governed by the crystal packing. The properties of spin-crossover complexes, especially of iron(II) complexes, have been widely studied over the last several decades. Many publications stress the potential—unproven so far—for applications of such compounds in nanotechnology, for example, in information storage, as sensors, or as molecular switches.[1–4]

In octahedral d^6 iron(II) complexes the conversion is between a low-spin (LS) and a high-spin (HS) state of nearly equal energies (LS, $S = 0$, $t_{2g}^6 e_g^0$; HS, $S = 2$, $t_{2g}^4 e_g^2$). Spin

[*] Prof. H.-B. Bürgi, Dr. D. Chernyshov, Dr. M. Hostettler, Prof. K. W. Törnroos[+]
Laboratorium für Kristallographie der Universität Bern
Freiestrasse 3, 3012 Bern (Switzerland)
Fax: (+41) 31-631-3996
E-mail: hans-beat.buergi@krist.unibe.ch

[+] Permanent address:
Department of Chemistry, University of Bergen
Bergen (Norway)

[**] This work was supported by the Swiss National Science Foundation. We thank the staff of the Swiss Norwegian Beam Lines (SNBL) at the European Synchrotron Research Facility for their support, Dr. A. Linden, University of Zürich, and Dr. T. Weber, ETHZ, for help with initial experiments, and Prof. A. Hauser, University of Geneva, Prof. G. M. Sheldrick, Universität Göttingen, Prof. P. Tolédano, Université de Picardie, and Prof. V. Dmitriev, SNBL, for advice and discussions. The Universities of Bern and Bergen provided the means and opportunity for a sabbatical leave for K.W.T. pic = picolylamine.

Supporting information for this article is available on the WWW under http://www.angewandte.org or from the author.

 DOI: 10.1002/anie.200351834 © 2003 Wiley-VCH Verlag GmbH & Co. KGaA, Weinheim

crossover is characterized by a transition curve which relates the relative concentrations of the two spin states to temperature. There are two main types of such curves which show either a continuous or discontinuous single step, or two such steps. The three plateaus of a double-step transition are associated with a HS phase, an intermediate phase (IP), and a LS phase at elevated, intermediate, and low temperatures, respectively. The IP is defined by the limiting temperatures $T_1 > T_2$ and is usually found at approximately equal populations of the HS and LS states.

The ordering of spin states in some mononuclear complexes displaying two-step transitions has been investigated by X-ray diffraction: an IP differing from the high-temperature phase has been described for $[Fe^{II}\{5\text{-}NO_2\text{-}sal\text{-}N(1,4,7,10)\}]$ which appears to show two, rather than one, iron sites in the asymmetric unit (the ligand is six-coordinating and prepared by Schiff base condensation of 5-NO_2-salicylaldehyde with 1,4,7,10-tetraazadecane).[5] The crystal structure of the HS phase of $[Fe^{II}\{HC(3,5\text{-}Me_2pz)_3\}_2](BF_4)_2$ shows a single iron site at room temperature. Upon cooling, the compound undergoes a transition to an IP with a 1:1 mixture of HS and LS states on each of two different metal sites.[6] $[Fe^{II}\{4,4'\text{-bis}(1,2,4\text{-triazole})\}_3](ClO_4)_2$ has two crystallographically independent iron sites at all temperatures. In the region of the plateau of the transition curve one of them is occupied by HS complexes, the other by LS complexes.[7] An ordered IP has also been suggested for some binuclear complexes showing a plateau in their transition curves.[1,8,9] The theoretical approaches hitherto developed to explain the magnetic behavior of compounds with two-step transitions assume an Ising-type[10,11] or Gorski–Bragg–Williams model that has been adapted to binary systems.[12] Both models account for the ordered IP in terms of two different iron lattices, one predominantly populated by HS molecules, the other predominantly by LS molecules.

The compound $[Fe^{II}(2\text{-pic})_3]Cl_2\cdot EtOH$ (**1**, pic = picolylamine) has been studied extensively during the last 20 years and has become the prototypical example of a two-step transition *not* associated with an ordered IP.[2,3] Optical[13] and magnetic data[14] as well as crystallographic unit-cell constants in the range 108–290 K[15] show a plateau between $T_1 = 122$ K and $T_2 = 114$ K (Figure 1a). Complete crystal structures were earlier determined at 298, 150, and 90 K[16] as well as at 227, 199, 171, 148, and 115 K.[17] All studies, including the one in the plateau at 115 K, report a single iron site in the asymmetric unit and no change of crystal symmetry. The theoretical interpretation of this observation is based on an Ising-type model with a single iron sublattice. Numerical analysis of the model by Monte Carlo[18] and cluster variation methods[19] reproduces the experimental transition curve qualitatively, and suggests an intermediate state built from ordered clusters of HS–LS pairs, whose correlation length has been estimated to be on the order of next-nearest neighbor distances, thereby excluding long-range ordering.[20]

We have reinvestigated **1** by X-ray diffraction with the aim of characterizing these short-range correlations. Instead of the expected diffuse scattering arising from short-range order—and contrary to all diffraction evidence reported so far—we have discovered additional Bragg reflections that

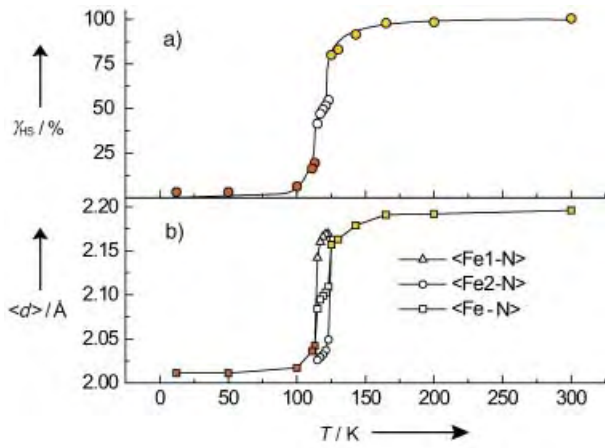


Figure 1. a) Comparison of spin-transition behavior from diffraction (circles) and magnetization experiments (line). The HS fraction $\gamma_{HS}(T)$ was estimated from the observed average Fe–N bond lengths $d(T)$ as $\gamma_{HS}(T) = 1-[(d_{HS}-d(T))/(d_{HS}-d_{LS})]$, with $d_{HS} = 2.195$ Å and $d_{LS} = 2.005$ Å. These values provide an overall agreement between $\gamma_{HS}(T)$ from the diffraction and magnetic data. Standard uncertainties are approximately equal to the symbol sizes. b) Temperature dependence of the average Fe–N bond lengths $\langle d \rangle$.[26] The bond lengths at the two iron sites differ in the intermediate phase (the lines are guides to the eye).

disclose an IP between two successive phase transitions at $T_1 \sim 124(1)$ and $T_2 \sim 114(1)$ K.[21] At temperatures higher than T_1 the asymmetric unit of the crystal structure comprises one pair of chloride ions, one ethanol molecule, and a single independent iron complex, the latter being predominantly, but not entirely, in the HS state.[16,17] The unit cell doubles in size between T_1 and T_2; the resulting superstructure contains four Cl^- ions, two EtOH molecules, and two different iron complexes: one predominantly HS, the other predominantly LS (Figure 1b). The third phase appears at temperatures below T_2, its structure reverting to a single iron complex, but now predominantly in the LS state.[16] Both phase transitions are of the order-disorder type. The sequence of three phases may be considered "re-entrant" in the sense that the unit cell of the HS structure reappears in the LS structure, but differs from that in the IP. Re-entrant behavior has so far not been described for spin-crossover compounds. These observations prompted us to characterize the transitions in **1** by means of 16 crystal structures obtained between 12 and 298 K.

At first glance the structure of the HS phase, crystals of which are yellow, and that of the LS phase, crystals of which are red (the same color schemes are used in the figures), appear to be the same: the unit cell dimensions are similar, the space groups the same, and all the iron atoms crystallographically equivalent. On closer inspection it becomes evident that the unit-cell constants and the atomic coordinates change discontinuously with temperature between the two phases. Figure 2 shows two typical examples: the monoclinic angle β and the x coordinates of the iron atoms. The intermolecular vibrational frequencies, Debye temperatures, and Grüneisen parameters are also different in the HS and LS phases.[22,23] If the transition between these phases were not separated by an IP, the discontinuous changes in the

 © 2003 Wiley-VCH Verlag GmbH & Co. KGaA, Weinheim

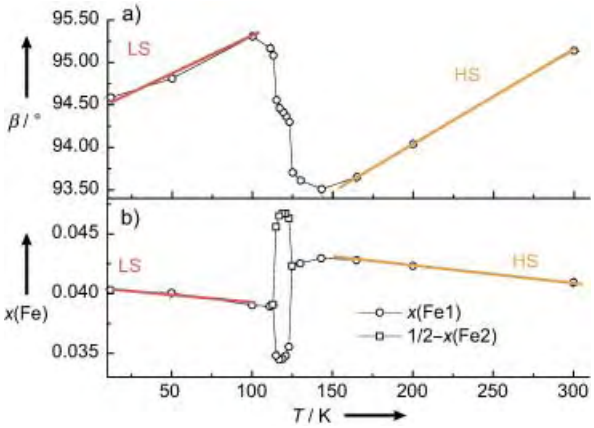


Figure 2. Monoclinic angle β (a) and x-coordinate of the Fe atoms (b) as a function of temperature. The coordinate of Fe2 in the IP is given as $^1/_2-x$(Fe2) for easier comparison with x(Fe1). The standard uncertainties are approximately equal to the symbol sizes.

structural parameters would indicate a so-called *isostructural* phase transition,[24] which is always of first order.[25]

The average Fe–N bond lengths of the two crystallographically independent iron complexes in the IP show that one of the two independent iron atoms is predominantly HS, the other predominantly LS (Figure 1b).[26] However, their positions coincide neither with those found in the HS nor those in the LS phases, but are displaced significantly from both (Figure 2b). The spin ordering, which is characterized by the difference in the HS populations at the two independent sites, is zero at both transition temperatures and goes through a maximum at $T_{1/2} \sim 119$ K, the temperature at which the crystal as a whole contains equal concentrations of the two spin states. On one site the HS population factor is about 0.85, on the other it is approximately 0.13, which implies an order parameter of 0.72.[27] The occurrence of a largely ordered IP implies that long-range correlations of HS and LS complexes are energetically more favorable than the short-range correlations postulated in the literature,[19,20] even though the ordering in the IP is not quite perfect.

It is worthwhile pointing out that distinguishing between the different iron sites in the IP by means of optic, magnetic, and Mössbauer data is very difficult, if not impossible. It is trivial, however, from multitemperature structure analyses (Figure 1). Furthermore, the characterization of the nature of the phase transitions required the determination of crystal structures over as large a range of temperatures as possible (Figure 2).

In all three phases the crystal structures are built from layers of hydrogen-bonded cationic complexes, chloride anions, and alcohol molecules (Figure 3, left). The layers are stacked through hydrophobic contacts between the hydrocarbon parts of the ligand and alcohol molecules (Figure 3, right). The oxygen atom of the ethanol molecule was found to be disordered over two sites between 298 and 100 K; occupation of the major site varies from about 0.73 to 0.94 between 298 and 125 K and from about 0.85 to 1.0 below 115 K. The occupations of the two major sites by the alcohol molecule in the IP are different: about 0.78 and 0.95.[28]

The two successive order-disorder transformations coincide with the two steps in the spin-transition curve (Figure 1) and with maxima in the specific heat function $c_p(T)$,[29] with the latter being typical for the latent heat and entropy changes associated with first-order phase transitions. The structural results presented here enable the HS/LS mixing entropy to be calculated as a function of temperature from the spin populations,[10,12] which in turn are derived from the observed average Fe–N bond lengths. The mixing entropy amounts to

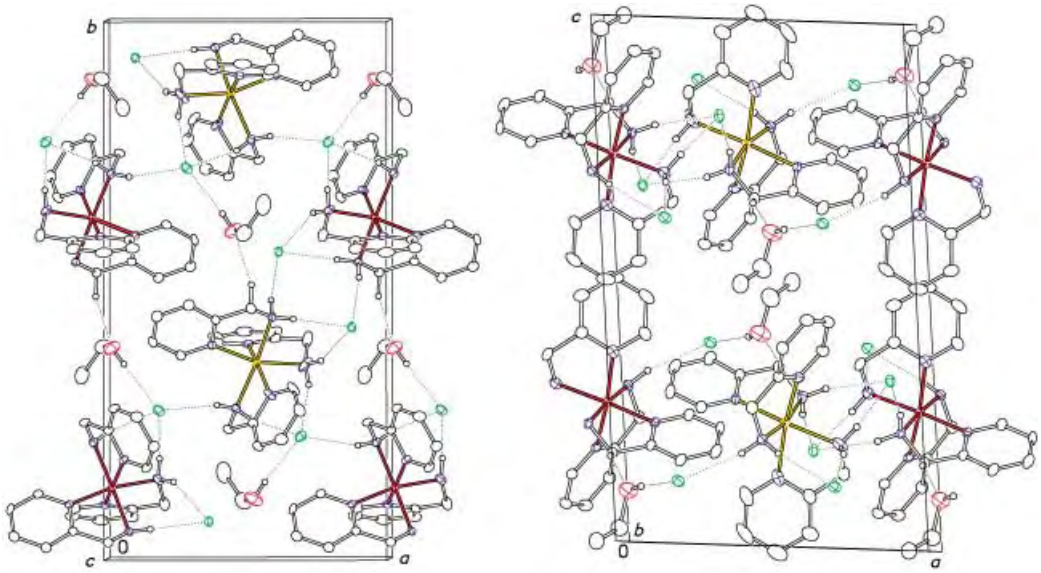


Figure 3. Left: projection of one layer of the IP down the c-axis showing hydrogen bonds (dotted lines). Right: projection of the structure of the IP down the b-axis showing the hydrophobic contacts at $c/2$ between layers of Fe complexes stacked along the c-axis. Only complexes between 0 and $b/2$ are shown. Black: C and H, blue: N, red: O, green: Cl. The illustrations are based on the structure determined at 115 K and 50% probability ellipsoids. The two different iron, chlorine, and ethanol sites become indistinguishable in the HS and LS phases (a-glide operation in the left picture, translation $(a+c)/2$ in the right picture).

 © 2003 Wiley-VCH Verlag GmbH & Co. KGaA, Weinheim

approximately 4 $J K^{-1} mol^{-1}$ at most. The entropy corresponding to the disorder of the oxygen atoms of EtOH is of similar magnitude to that of the spin-related one.[30] The entropies determined from the residual disorder in the structures together with those from spin multiplicities help to narrow down other contributions to the total entropy, for example, from phonons.

With the detailed experimental information reported here, models describing spin-crossover behavior, especially the occurrence of a plateau in the spin transition curve of **1** and related compounds may be assessed with respect to their ability for predicting transition curves, structural changes, and phase transitions as well as for interpreting the intermolecular—that is, supramolecular—interactions driving the transitions. All models include the notion of spatial correlations between the states of different molecules, but differ in their respective correlation lengths. Multitemperature diffraction experiments are well-suited to probe such differences: absence of correlation leads to a nearly homogenous background; short-range correlations extending over a few unit cells produce modulated diffuse intensities; correlations at the mesoscopic scale broaden the Bragg reflections whereas long-range order produces sharp reflections.

Even after careful processing of the diffraction patterns of freshly grown single crystals of **1**, no diffuse scattering could be discerned at any temperature, not even close to the phase-transition temperatures where disorder is most pronounced (Figure 1). The lack of observable diffuse scattering and the extra Bragg reflections in the IP suggest that the spin transition does not induce short-range order of any importance, but rather the long-range order characteristic of the IP.

The Ising-type, HS/LS models derived from a Gorski–Bragg–Williams or Slichter–Drickamer approach,[31,32] assume a single crystallographic iron site in a mean environment (mean field) and neglect correlation effects. These models allow for continuous or discontinuous spin crossover and are useful for describing the HS and LS parts of the transition curve of **1** and for rationalizing the absence of correlated diffuse scattering. They exclude the occurrence of an intermediate phase and cannot explain the formation of the plateau. Models abandoning the mean-field approximation interpret the plateau in the transition curve as an "intermediate phase" built from correlated HS/LS pairs with a short correlation length extending to next-nearest neighbor distances.[18,19] Since no modulated diffuse scattering has been detected, these models do not describe the behavior of **1**, but may well be applicable to other, as yet unidentified, compounds.

More general mean-field models with appropriately chosen numerical parameters account for disordered HS and LS phases as well as for ordered IPs with two crystallographically independent iron sites.[10–12] They predict additional Bragg reflections in the IP, as observed in this study of **1**. The maximum degree of order of 0.72 found in our experiment is somewhat higher than those calculated from two different two-sublattice models (0.65 from an Ising-type model,[11] or ca. 0.62 from a Gorski–Bragg–Williams model modified for binary mixtures[12]).

The parameters of Ising-like models—namely the energy difference and the interaction energy between HS and LS molecules—appear simple and physically transparent. However, interpretation of these parameters on a microscopic level is very difficult, because they do not explicitly take into account structural changes associated with the ordering of spin states (atomic shifts, ordering of solvent, variation of size and shape of unit cell), even though these changes do contribute to both transition entropy and enthalpy.

A convenient alternative to analyze phase transitions is Landau theory, which explicitly accounts for changes of crystal symmetry and the coupling of ordering and spin-transition processes. A Landau-type approach using a totally symmetric quantity as an order parameter, for example, the HS fraction γ_{HS} or associated scalar quantities such as metal–ligand distances, has been developed for isostructural phase transitions.[25] A discussion of the application of this approach to two-step crossover systems will be given elsewhere.

In summary, we have shown that the structure of $[Fe(2\text{-pic})_3]Cl_2 \cdot EtOH$ undergoes two first-order phase transitions on cooling from a high-spin phase via an intermediate phase to a low-spin phase. Comparisons of structural data over large ranges of temperature clearly show that the structural changes from the HS to the LS phase, both with a single iron site, are discontinuous. The relationship between the phases is isostructural. The IP reveals that, contrary to earlier assertions, the intermediate plateau in the two-step transition of this compound is the expression of a structure with two different iron sites showing long-range order, very much like that found for other compounds with two-step behavior. The absence of discernible diffuse scattering suggests that short-range correlations are very weak. The combination of the isostructural HS and LS phases with the ordered IP implies re-entrant phase-transition behavior, a relatively rare phenomenon.

The results presented here, probably the most detailed and accurate structural description of an order-disorder phase transition in a spin-crossover compound hitherto published, will serve as a basis for developing and testing new models of the coupling between spin-crossover processes and order-disorder phase transitions. Such models will help to better understand the many physical properties relevant for practical applications, for example, elastic, optical, and magnetic properties, the latent heat and entropy changes associated with the spin transition, as well as lattice and molecular vibration. Thus, the completeness of the new data not only corrects an oversight, but leads to new conclusions concerning the phase diagram of $[Fe(2\text{-pic})_3]Cl_2 \cdot EtOH$. Since the useful properties of new materials often depend on changes in crystal structure, phase transitions in particular, the approach outlined here for a molecular spin-crossover compound should be useful for other molecular materials as well.

Experimental Section

Magnetic susceptibility: Measurements between 2 and 298 K were performed with a SQUID MPMS-XL5 (Quantum Design) instrument on a freshly made[33] microcrystalline sample (13.3 mg) in field-cooling mode (1003 Oe). The measured susceptibilities were cor-

 © 2003 Wiley-VCH Verlag GmbH & Co. KGaA, Weinheim

rected for diamagnetic contributions,[14] and the paramagnetic susceptibilities $\chi_{HT}(T)$ and $\chi_{LT}(T)$ at high (230–300 K, HT) and low temperatures (2–5 K, LT) described in terms of Curie and Weiss constants (see Supporting Information). The high-spin fraction $\gamma_{HS}(T)$ follows from $\chi(T) = \gamma_{HS}(T)\chi_{HT}(T) + \chi_{LT}(T)$ (5–230 K). The temperature dependence of $\gamma_{HS}(T)$ agrees very well with that from our diffraction data and well with published values,[14] except for a shift of our T_1 and T_2 values to higher temperatures by about 1.5 K. This shift is essentially attributed to the larger temperature range used for modeling the $\chi_{LT}(T)$ function (2–300 versus 80–300 K in ref. [14]).

X-ray data: Single-crystal data were collected on the SNBL beam line BM1A at the ESRF synchrotron in Grenoble (France) with a MAR345 image-plate area detector at $\lambda = 0.7000(1)$ Å, with φ scans of 1.5–2.0°, and a readout pixel resolution of 150 μm. These measurements have been done on five different crystals: No. 1 at 12 K, no. 2 at 50 K, no. 3 at 100, 111, 113, 115, 117, 119, 121, 123, and 125 K, no. 4 at 130, and 200 K, and no. 5 at 165 K. Samples were cooled with N_2 and He cryostats (Oxford Cryostream series 600 and Oxford Diffraction HeliJet open-flow, respectively). Intensities were integrated with CrysAlis,[34] and reflections shadowed by the cryostats were removed from the data by means of locally written software. Additional data at 143 and 298 K were collected on a sixth crystal with a SMART 1 K CCD diffractometer by means of 0.3° ω scans with $Mo_{K\alpha}$ radiation ($\lambda = 0.71073$ Å) using SMART and integrated with SAINT.[35] Empirical absorption correction was made with SADABS[36] and the structures refined with SHELXL97.[37] The standard uncertainties of the cell constants reflect their precision and internal consistency for a given crystal (Table 1). Their accuracy is about an order of magnitude lower, because of the difficulties in determining the crystal-to-image plate distance accurately. The disordered oxygen atoms of the ethanol molecules were modeled with two positions. All non-hydrogen atoms except for the minor disorder component of the alcohol oxygen atom were refined anisotropically. Hydrogen atoms were input as riding atoms and the isotropic displacement parameters of these fixed at $1.2\,U_{eq}$(CH, CH_2) and $1.5\,U_{eq}$(CH_3, OH) of their respective parent atoms. The hydrogen atom of the minor disorder component was not accounted for.

To simplify the comparison between the HS/LS phases and the IP the nonconventional monoclinic space group description $B2_1/c$ was chosen for the former. The transformation matrix from the conventional HS/LS unit cell with space group $P2_1/c$ to that with $B2_1/c$ is $[001][010][\bar{2}0\bar{1}]$.

Further crystallographic data can be found in the Supporting Information. CCDC-209849–209864 contain the supplementary crystallographic data for this paper. These data can be obtained free of charge via www.ccdc.cam.ac.uk/conts/retrieving.html (or from the Cambridge Crystallographic Data Centre, 12 Union Road, Cambridge CB2 1EZ, UK; fax: (+44) 1223-336-033; or deposit@ccdc.cam.ac.uk).

Received: May 7, 2003 [Z51834]
Published online: July 28, 2003

Keywords: iron · low-temperature crystallography · N ligands · order–disorder phase transition · spin crossover

Table 1: Cell constants (a, b, c, β), cell volume (V), and measurement temperature (T) with crystal phase of **1** (HS = high spin, LS = low spin, both with space group $B2_1/c$, IP = intermediate phase with space group $P2_1/c$).

T [K]	a [Å]	b [Å]	c [Å]	β [°]	V [Å^3]
12 (LS)	11.3256(7)	21.5132(15)	19.1574(9)	94.589(7)	4652.7(5)
50 (LS)	11.3291(7)	21.5223(13)	19.1834(14)	94.812(8)	4661.0(5)
100 (LS)	11.3653(10)	21.581(2)	19.2469(13)	95.308(10)	4700.5(7)
111 (LS)	11.3888(8)	21.6325(18)	19.2601(13)	95.167(8)	4725.8(6)
113 (LS)	11.3871(7)	21.6310(16)	19.2593(12)	95.082(8)	4725.2(5)
115 (IP)	11.4075(5)	21.6979(15)	19.2636(11)	94.557(4)	4753.0(5)
117 (IP)	11.4109(5)	21.7112(15)	19.2669(10)	94.463(4)	4758.8(5)
119 (IP)	11.4129(5)	21.7181(14)	19.2727(10)	94.417(4)	4762.9(4)
121 (IP)	11.4146(5)	21.7307(16)	19.2777(11)	94.365(4)	4767.9(5)
123 (IP)	11.414(2)	21.734(4)	19.283(4)	94.30(3)	4770.4(17)
125 (HS)	11.4182(5)	21.8134(10)	19.3128(9)	93.705(6)	4800.2(4)
130 (HS)	11.4090(15)	21.814(3)	19.308(2)	93.612(10)	4795.7(10)
143 (HS)	11.426(2)	21.846(4)	19.335(4)	93.51(3)	4817.2(17)
165 (HS)	11.448(2)	21.891(4)	19.359(5)	93.58(3)	4842.1(17)
200 (HS)	11.4725(6)	21.9166(12)	19.4189(10)	94.041(4)	4870.5(4)
298 (HS)	11.571(2)	22.045(4)	19.626(4)	95.16(3)	4986.0(17)

[1] E. König, *Struct. Bonding (Berlin)* **1991**, *76*, 51.
[2] P. Gütlich, A. Hauser, H. Spiering, *Angew. Chem.* **1994**, *106*, 2109; *Angew. Chem. Int. Ed. Engl.* **1994**, *33*, 2024.
[3] P. Gütlich, Y. Garcia, H. Spiering, in *Magnetism: Molecules to Materials IV* (Eds.: J. S. Miller, M. Drillon), Wiley-VCH, **2002**.
[4] J. A. Real, A. B. Gaspar, V. Niel, M. C. Munoz, *Coord. Chem. Rev.* **2003**, *236*, 121.
[5] D. Boinnard, A. Bousseksou, A. Dworkin, J. M. Savariault, F. Varret, J.-P. Tuchagues, *Inorg. Chem.* **1994**, *33*, 271; 5-NO_2-sal-*N*(1,4,7,10) = 1,10-bis(5-nitrosalicylaldehyde)-1,4,7,10-tetra-azadecane-*O,O′,N,N′,N″,N‴*.
[6] D. L. Reger, C. A. Little, V. G. Young, Jr., M. Pink, *Inorg. Chem.* **2001**, *40*, 2870; HC(3,5-Me_2pz)$_3$ = tris(3,5-dimethylpyrazolyl)methane.
[7] Y. Garcia, O. Kahn, L. Rabardel, B. Chansou, L. Salmon, J.-P. Tuchagues, *Inorg. Chem.* **1999**, *38*, 4663.
[8] V. Ksenofontov, H. Spiering, S. Reiman, Y. Garcia, A. B. Gaspar, N. Moliner, J. A. Real, P. Gütlich, *Chem. Phys. Lett.* **2001**, *348*, 381.
[9] V. Ksenofontov, A. B. Gaspar, J. A. Real, P. Gütlich, *J. Phys. Chem. B* **2001**, *105*, 12266.
[10] H. Bolvin, *Chem. Phys.* **1996**, *211*, 101.
[11] A. Bousseksou, J. Nasser, J. Linares, K. Boukheddaden, F. Varret, *J. Phys. I* **1992**, *2*, 1381.
[12] A. B. Koudriavtsev, *Chem. Phys.* **1999**, *241*, 109.
[13] H. Romstedt, A. Hauser, H. Spiering, *J. Phys. Chem. Solids* **1998**, *59*, 265.
[14] R. Jakobi, H. Spiering, P. Gütlich, *J. Phys. Chem. Solids* **1992**, *53*, 267.
[15] L. Wiehl, G. Kiel, C. P. Köhler, H. Spiering, P. Gütlich, *Inorg. Chem.* **1986**, *25*, 1565.
[16] M. Mikami, M. Konno, Y. Saito, *Acta Crystallogr. Sect. B* **1980**, *36*, 275.
[17] B. A. Katz, C. E. Strouse, *J. Am. Chem. Soc.* **1979**, *101*, 6214.
[18] T. Kohlhaas, H. Spiering, P. Gütlich, *Z. Phys. B* **1997**, *102*, 455.
[19] H. Romstedt, H. Spiering, P. Gütlich, *J. Phys. Chem. Solids* **1998**, *59*, 1353.
[20] H. Spiering, T. Kohlhaas, H. Romstedt, A. Hauser, C. Brun-Yilmaz, J. Kusz, P. Gütlich, *Coord. Chem. Rev.* **1999**, *190–192*, 629.

 © 2003 Wiley-VCH Verlag GmbH & Co. KGaA, Weinheim

[21] These temperatures are redeterminations from a freshly prepared sample of **1**. They agree to within less than 0.5 K with our SQUID results (see Experimental Section).
[22] P. Gütlich, H. Köppen, R. Link, H. G. Steinhäuser, *J. Chem. Phys.* **1979**, *70*, 3977.
[23] E. Meissner, H. Köppen, C. P. Köhler, H. Spiering, P. Gütlich, *Hyperfine Interact.* **1987**, *36*, 1.
[24] The commonly used term "isostructural" phase transition does not imply "equal structures", but rather equal space groups and equal Wyckoff positions. The unit-cell volumes and atomic coordinates are generally different and their changes with temperature discontinuous, as expected for a first-order phase transition.[25]
[25] P. Tolédano, V. Dmitriev, *Reconstructive Phase Transitions in Crystals and Quasicrystals*, World Scientific, Singapore, **1996**.
[26] Occupation of the Fe sites by HS and LS molecules implies positional disorder amounting to about 0.2 Å. As the resolution of the diffraction experiments is only approximately 0.8 Å the disorder can not be resolved, but is modeled in terms of an average between HS and LS positions weighted with the respective population factors and a disorder contribution to the atomic displacement parameters (ADP). Mean positions imply that the experimentally determined Fe–N bond lengths reported in Figure 1b are to be interpreted as averages between a long (HS) and a short (LS) value. Disorder contributions have been gauged from the differences in ADPs along internuclear vectors, which tend to be largest where the mean distances deviate most from the LS and HS values (K. Chandrasekhar, H. B. Bürgi, *Acta Crystallogr. Sect. B* **1984**, *40*, 387).
[27] The order parameter is defined as the difference between the two populations.
[28] Where comparable our results are close to those published earlier.[15–17]
[29] K. Kaji and M. Sorai, *Thermochim. Acta* **1985**, *88*, 185.
[30] The calculation of entropies arising from spin disorder is given in ref. [10] for oxygen disorder $S/R = p\ln p + (1-p)\ln(1-p)$, where p is the occupation factor of the major site.
[31] C. P. Slichter, H. G. Drickamer, *J. Chem. Phys.* **1972**, *56*, 2142.
[32] R. Boča, W. Linert, *Monatsh. Chem.* **2003**, *134*, 199.
[33] M. Sorai, J. Ensling, P. Gütlich, *Chem. Phys.* **1976**, *18*, 199.
[34] CrysAlis Software System, Version 1.169, Oxford-diffraction Ltd. Oxford, England, **2001**.
[35] SMART, Version 5.059; SAINT, Version 6.02a Bruker AXS Inc., Madison, Wisconsin, USA, **2001**.
[36] G. M. Sheldrick, SADABS, Version 2.06, Empirical Absorption Correction Program, University of Göttingen, Göttingen (Germany), **2002**.
[37] G. M. Sheldrick, SHELXL97, University of Göttingen, Göttingen (Germany), **1997**.

 © 2003 Wiley-VCH Verlag GmbH & Co. KGaA, Weinheim

Cover Picture



Ivory D. Hills and Gregory C. Fu*

The enantioselective rearrangement of *O*-acylated benzofuranones and oxindoles with the generation of a quaternary stereocenter at C3 of the heterocycle is catalyzed by a planar-chiral derivative of 4-dimethylaminopyridine. As shown in the cover picture, the catalyst itself is red, whereas the resting state of the complex during the rearrangement of benzofurans is a green ion pair. Diazonamide A, an oxindole-derived natural product with potent anticancer activity, is shown in the background. More on the asymmetric syntheses of such heterocycles is provided by I. D. Mills and G. C. Fu on page 3921 ff.

Contents

Angewandte EarlyView

The following articles are available online (in Wiley Interscience). You can find them at www.angewandte.org, under Full Text, Early View.

F. Kraus, J. C. Aschenbrenner, N. Korber:*
P_4^{2-}: A 6π Aromatic Polyphosphide in Dicesium Cyclotetraphosphide–Ammonia (1/2)
DOI: 10.1002/anie.200351776
Published online: August 14, 2003

R. Shintani, G. C. Fu:*
Catalytic Enantioselective Synthesis of β-Lactams: Intramolecular Kinugasa Reactions and Interception of an Intermediate in the Reaction Cascade
DOI: 10.1002/anie.200352103
Published online: August 8, 2003

K. C. Nicolaou, C. J. N. Mathison, T. Montagnon:*
New Reactions of IBX: Oxidation of Nitrogen- and Sulfur-Containing Substrates To Afford Useful Synthetic Intermediates
DOI: 10.1002/anie.200352076
Published online: August 8, 2003

Articles judged by the referees or the editor as being either very important or very urgent are immediately edited, proof-read, and electronically published once the manuscript has arrived in the editorial office in final form. As long as there is no page number available these articles should be cited in the following manner:

Author(s) *Angew. Chem. Int. Ed.*, online publication date, DOI.

Obituary

Friedrich Cramer (1923–2003) — **3850** — Nucleic Acid Chemist and Philosopher — *Fritz Eckstein*

Books

Aromatic Chemistry — **3851** — John D. Hepworth, David R. Waring, Michael J. Waring — *reviewed by Herbert Mayr*

Surface Chemistry and Catalysis — **3851** — Albert F. Carley, Philip R. Davies, Graham J. Hutchings, Michael S. Spencer — *reviewed by Ulrich Heiz*

Solvents and Solvent Effects in Organic Chemistry — **3852** — Christian Reichardt — *reviewed by José Elguero*

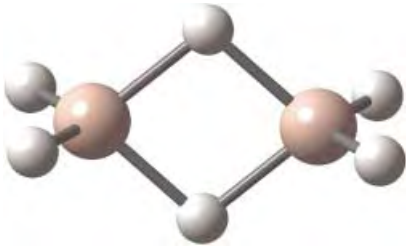
Highlights

Group 13 Binary Hydrides

N. W. Mitzel* — **3856–3858**

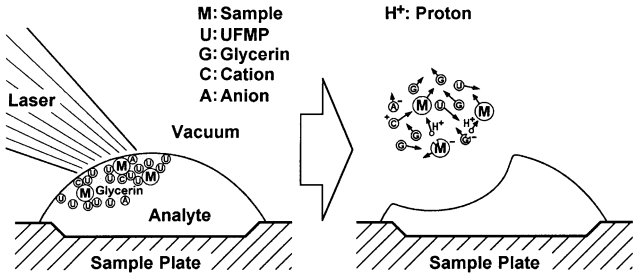
Molecular Dialane and Other Binary Hydrides

The dialane molecule (Al_2H_6, see structure) is highly unstable in the condensed phase, and hence it was more than half a century after the discovery of aluminum hydride that it was identified in a hydrogen matrix. Apart from such fundamental findings, the rapidly developing chemistry of the binary main-group hydrides is also aimed at synthetic applications.



© 2003 Wiley-VCH Verlag GmbH & Co. KGaA, Weinheim

Reviews



Without fragmentation: The mass spectrometric analysis of biological macromolecules can be achieved without fragmentation of the parent molecule by using the technique of soft laser (matrix-assisted laser desorption/ionization (MALDI; see scheme, UFMP = ultrafine metal-powder matrix). The development of this technique was greatly influenced by the work of Koichi Tanaka for which he was awarded the Nobel Prize for Chemistry in 2002.

Gentle Mass Spectrometry

K. Tanaka* _____ 3861 – 3870

The Origin of Macromolecule Ionization by Laser Irradiation (Nobel Lecture)



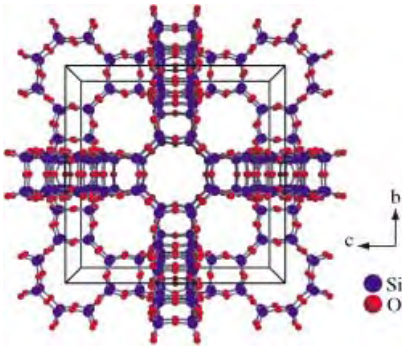
From flames to flying elephants: A few years ago the idea of making proteins or polymers "fly" by electrospray ionization (ESI) seemed as improbable as a flying elephant, but today it is a standard part of modern mass spectrometers. The key to this success was the development of free jet technology.

Electrospray Ionization

J. B. Fenn* _____ 3871 – 3894

Electrospray Wings for Molecular Elephants (Nobel Lecture)

Communications



Along theoretical channels: Although 139 distinct structural types of zeolite are currently known, the search for new structures with improved applications in catalysis and ion exchange is of extreme interest. Recent advances in mathematical tiling theory has given rise to the enumeration of 294 uninodal frameworks with an empirical formula SiO_2 (an energetically stable example of which is shown).

Zeolite Frameworks

M. D. Foster, O. Delgado Friedrichs, R. G. Bell,* F. A. Almeida Paz, J. Klinowski* _____ 3896 – 3899

Structural Evaluation of Systematically Enumerated Hypothetical Uninodal Zeolites

For the USA and Canada:
ANGEWANDTE CHEMIE International Edition (ISSN 1433-7851) is published weekly by Wiley-VCH PO Box 191161, D 69451 Weinheim, Germany. Air freight and mailing in the USA by Publications Expediting Inc. 200 Meacham Ave., Elmont, NY 11003. Periodicals postage paid at Jamaica NY 11431. US POSTMASTER: send address changes to *Angewandte Chemie*, Wiley-VCH, 111 River Street, Hoboken, NJ 07030. Annual institutional subscription price for institutions: Europe € 2998.00/3148.00. Outside Europe US$ 3718.00/3904.00 (valid for print or electronic/print and electronic delivery); for individuals who are personal members of a national chemical society, or whose institution already subscribes, or who are retired or self-employed consultants, print only (including postage and handling charges): Europe € 248.00/Outside Europe US$ 348.00.

 © 2003 Wiley-VCH Verlag GmbH & Co. KGaA, Weinheim

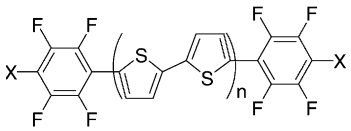
Contents

Semiconductors

A. Facchetti, M.-H. Yoon, C. L. Stern, H. E. Katz, T. J. Marks* ____ **3900 – 3903**

Building Blocks for n-Type Organic Electronics: Regiochemically Modulated Inversion of Majority Carrier Sign in Perfluoroarene-Modified Polythiophene Semiconductors

A new family of perfluoroarene-modified thiophene semiconductors **1**–**3** has been synthesized to assess the influence of perfluoroarene introduction and regiochemistry on molecular and thin-film transistor properties. Compound **1** is an n-type semiconductor with a mobility approaching 0.1 $cm^2V^{-1}s^{-1}$ whereas **2** and **3** exhibit p-type behavior. These results show that the origin of n-type carrier mobility is not solely a consequence of solution/film LUMO and HOMO energies.

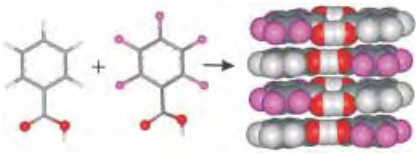


1: X = F, *n* = 2
2: X = 2-thienyl, *n* = 1
3: X = 5-(2,2'-dithienyl), *n* = 0

Crystal Engineering

M. Gdaniec,* W. Jankowski, M. J. Milewska, T. Połoński* **3903 – 3906**

Supramolecular Assemblies of Hydrogen-Bonded Carboxylic Acid Dimers Mediated by Phenyl–Pentafluorophenyl Stacking Interactions

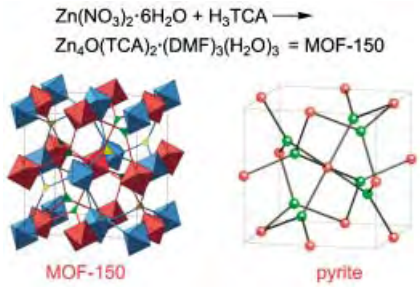


Stacks of acids: Pentafluorobenzoic acid forms heterodimers with benzoic acid and 2,4,6-trimethylbenzoic acid that assemble into π stacks with alternating phenyl and pentafluorophenyl residues (see picture). Cocrystals of these acids with 1,4-bisarylbutadiynes contain acid homodimers sandwiched between the diacetylene molecules.

Framework Design with Molecular Blocks

H. K. Chae, J. Kim, O. D. Friedrichs, M. O'Keeffe, O. M. Yaghi* ___ **3907 – 3909**

Design of Frameworks with Mixed Triangular and Octahedral Building Blocks Exemplified by the Structure of $[Zn_4O(TCA)_2]$ Having the Pyrite Topology



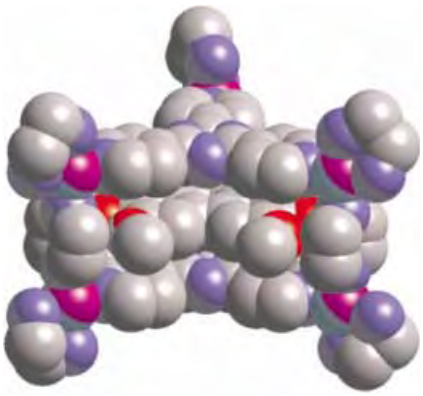
Building blocks, octahedral (basic zinc acetate units) and triangular (tritopic carboxylic acid), are assembled into a metal-organic framework (MOF-150) having the topology of the FeS_2 pyrite net (see picture). Two independent nets interpenetrate, forming the first example of a fully catenated structure with mixed coordination, an occurrence that is ascribed to the self-dual property of the pyrite net (TCA = 4,4′,4″-Tricarboxytriphenylamine).

Template Synthesis of Cages

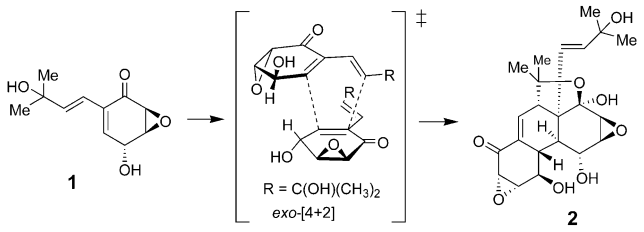
K. Kumazawa, K. Biradha, T. Kusukawa, T. Okano, M. Fujita* ____ **3909 – 3913**

Multicomponent Assembly of a Pyrazine-Pillared Coordination Cage That Selectively Binds Planar Guests by Intercalation

A prismlike cage composed of six end-capped Pt^{II} ions, two panel-like ligands, and three pyrazine pillars assembles quantitatively through the template effect of a planar aromatic guest (see space-filling structure). The cage thus obtained is stable even when the template is removed. Other large aromatic molecules are also strongly bound and a β-diketone is shown to exist only in a planar enol form in the cage with the keto–enol tautomerization being almost completely suppressed.



 © 2003 Wiley-VCH Verlag GmbH & Co. KGaA, Weinheim



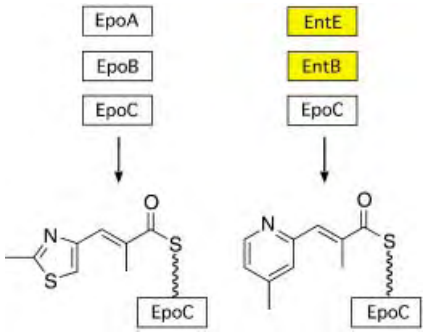
The [4+2] dimerization of epoxyquinol **1** is rendered irreversible by formation of a hemiacetal in the enantioselective total synthesis of the ubiquitin-activating enzyme inhibitor (+)-panepophenanthrin (**2**).

Panepophenanthrin Total Synthesis

X. Lei, R. P. Johnson, J. A. Porco, Jr.* ——— 3913 – 3917

Total Synthesis of the Ubiquitin-Activating Enzyme Inhibitor (+)-Panepophenanthrin

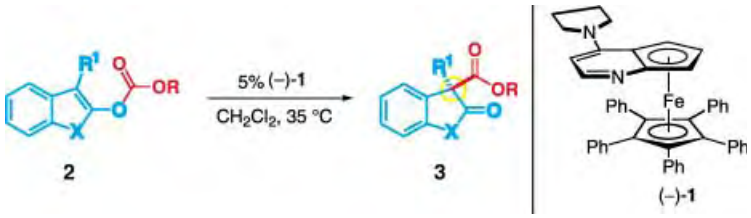
The early steps of epothilone biosynthesis were reprogrammed in vitro by incorporating enzyme subunits (e.g. EntB, EntE) from other biosynthetic pathways into the epothilone (Epo) assembly line (see scheme). Recognition sequences identified at the C termini of the epothilone biosynthetic proteins enabled heterologous enzyme transfer when fused to noncognate proteins, as a step toward the reengineering of biosythetic pathways to produce natural product analogues in vivo.



Reengineering Biosynthetic Pathways

S. E. O'Connor, C. T. Walsh,* F. Liu ——— 3917 – 3921

Biosynthesis of Epothilone Intermediates with Alternate Starter Units: Engineering Polyketide–Nonribosomal Interfaces

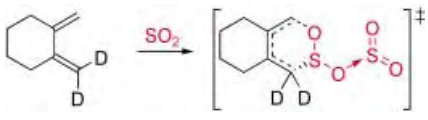


A common feature in indole- and benzofuran-derived natural products is a quaternary stereocenter in the 3-position of the heterocycle. The catalyst (–)-**1** promotes the asymmetric synthesis of such compounds **3** (with up to 99% *ee*) through the rearrangement of *O*-acylated benzofuranones (X = O) and oxindoles (X = NR^2) **2**.

Stereogenic Quaternary Centers

I. D. Hills, G. C. Fu* ——— 3921 – 3924

Catalytic Enantioselective Synthesis of Oxindoles and Benzofuranones That Bear a Quaternary Stereocenter



The C–S bond is formed to a greater extent than the C–O bond in the transition state of the [4+2] cycloaddition of SO_2 to dimethylidenecyclohexane (see scheme). Both deuterium isotope effects and quantum calculations lead to this conclusion.

Hetero-Diels–Alder Reaction

F. Monnat, P. Vogel,* R. Meana, J. A. Sordo* ——— 3924 – 3927

Equilibrium and Kinetic Deuterium Isotope Effects on the Hetero-Diels–Alder Addition of Sulfur Dioxide

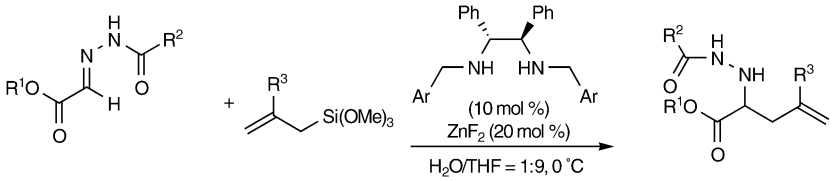
 © 2003 Wiley-VCH Verlag GmbH & Co. KGaA, Weinheim

Contents

Asymmetric Allylation

T. Hamada, K. Manabe,
S. Kobayashi* ——— **3927 – 3930**

Catalytic Asymmetric Allylation of Hydrazono Esters in Aqueous Media by Using ZnF_2–Chiral Diamine

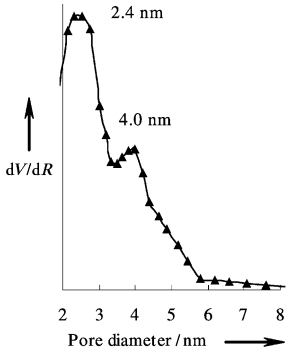


Chiral homoallylic hydrazines are synthesized by catalytic asymmetric allylation of acylhydrazono esters with allyltrimethoxysilane by using a chiral Zn catalyst (see picture). The reactions proceed smoothly in aqueous media to give the allylated products in good to high yields and selectivities. Water played an essential role in this reaction, and this is the first example of catalytic asymmetric allylation of C=N bonds in aqueous media. R^1 = Me, Et; R^2 = *p*-C_6H_4OMe, *p*-C_6H_4OEt; R^3 = H, Me, Ph.

Mesoporous Silica/Carbon Replicas

S. Che, A. E. Garcia-Bennett, X. Liu,
R. P. Hodgkins, P. A. Wright, D. Zhao,
O. Terasaki, T. Tatsumi* ——— **3930 – 3934**

Synthesis of Large-Pore *Ia*$\bar{3}$*d* Mesoporous Silica and Its Tubelike Carbon Replica



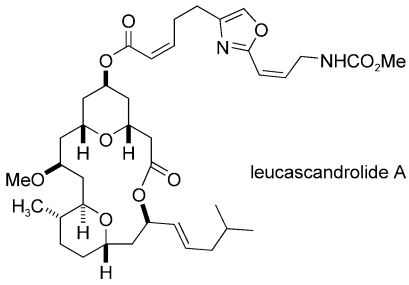
A synthetic route to tubelike mesoporous carbon materials with a cubic structure has been developed by using propylsulfonic acid groups anchored onto a silica wall, which act as an acid catalyst for carbon-source polymerization. Pores with diameters of 2.4 and 4.0 nm were recorded for the carbon replicas obtained after removing the silica walls (see isotherm).

Macrolide Synthesis

D. R. Williams,* S. V. Plummer,
S. Patnaik ——— **3934 – 3938**

Formal Synthesis of Leucascandrolide A

Asymmetric allylation reactions of stannane-derived allyl diazaborolanes, and the use of the Terashima reagent for the highly selective asymmetric hydride reduction of a β-alkoxy ketone are key features of a highly convergent, stereocontrolled formal synthesis of leucascandrolide A (see picture).

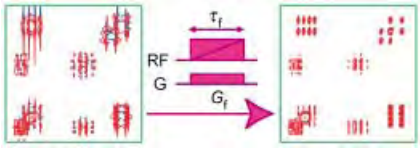


Two-Dimensional NMR Spectroscopy

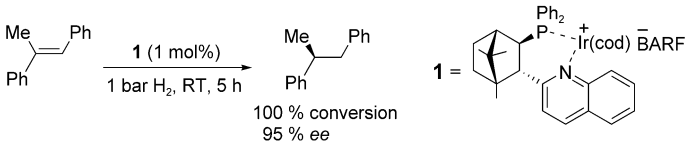
M. J. Thrippleton, J. Keeler* **3938 – 3941**

Elimination of Zero-Quantum Interference in Two-Dimensional NMR Spectra

The simultaneous application of a swept-frequency pulse and a gradient pulse G_f enables *z*-magnetization to be distinguished from zero-quantum coherence (see picture). This new and highly effective method enables the elimination of strong interference caused by zero-quantum coherence, which is often present in NOESY, TOCSY, and many other types of NMR spectra obtained by traditional methods of signal selection, and can be readily implemented on any modern NMR spectrometer.



© 2003 Wiley-VCH Verlag GmbH & Co. KGaA, Weinheim

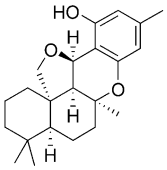


Asymmetric Hydrogenation

T. Bunlaksananusorn, K. Polborn, P. Knochel* ——— 3941 – 3943

New P,N Ligands for Asymmetric Ir-Catalyzed Reactions

Chiral Ir complexes such as **1** catalyze the hydrogenation of (*E*)-1,2-diphenylpropene at 1 bar of H_2 to give (*S*)-1,2-diphenylpropane with up to 95% *ee* and full conversion (see scheme). Methyl (*Z*)-α-(acetamido)cinnamate underwent enantioselective hydrogenation under similar conditions to the corresponding amino acid derivative with up to 96% *ee*. BARF = tetrakis(3,5-bis(trifluoromethyl)phenyl)borate, cod = 1,5-cyclooctadiene.



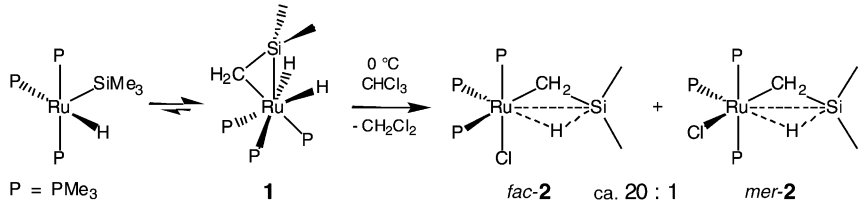
1

Biomimetic Total Synthesis

B. M. Trost,* H. C. Shen, J.-P. Surivet ——— 3943 – 3947

An Enantioselective Biomimetic Total Synthesis of (−)-Siccanin

A convergent asymmetric synthesis of the clinically important antifungal agent (−)-siccanin (**1**) mimics the proposed biosynthetic pathway. A Pd-catalyzed asymmetric allylic alkylation was used to establish the stereochemistry, and sequential radical processes (a Ti^{III}-promoted cyclization followed by diacetoxyiodobenzene-promoted tetrahydrofuran formation) led to the completion of the first asymmetric synthesis of **1**.



P = PMe_3 **1** *fac*-**2** ca. 20 : 1 *mer*-**2**

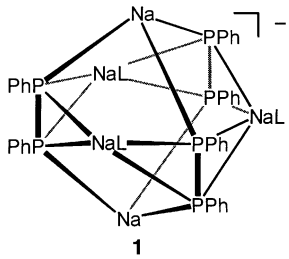
Agostic Si–H Interactions

V. K. Dioumaev, P. J. Carroll, D. H. Berry* ——— 3947 – 3949

Tandem β-C–H Activation/Si–H Elimination Reactions: Stabilization of C–H Activation Products by β-Agostic Si–H Interactions

Conversion of $[(Me_3P)_3Ru(H)SiMe_3]$ into **1** and further on into the structurally characterized *fac*- and *mer*-**2** (see scheme) is the first example of a transformation from a [M]$SiMe_3$ species into a β-agostic [M]CH_2SiMe_2-H complex; a reversal of the typical sequence observed in the rearrangement of silaalkyl metal complexes. This reversal is likely the result of Si–H coordination to the unsaturated metal center.

A new look into an old pot: A new cluster structure is found for the cage anion **1** (see picture, L = dme) in the salt $[Na(dme_3)]^+[Na_5(P_2Ph_2)(dme)_3]^-$. This (structurally characterized) ionic compound is obtained in excellent yield when $PhPCl_2$ is simply reduced with sodium in a toluene/tetramethylethylene mixture. This method delivers *catena*-oligophosphane-α,ω-diides with two, three, or four phosphorus atoms.



1

Cages of Phosphorus and Sodium

J. Geier, H. Rüegger, M. Wörle, H. Grützmacher* ——— 3951 – 3954

Sodium Oligophosphanediide Ions in the $PhPCl_2$/Na System: Syntheses and Structural Characterization

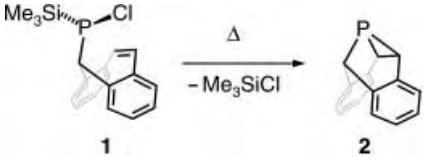
 © 2003 Wiley-VCH Verlag GmbH & Co. KGaA, Weinheim

Contents

Phosphorus Heterocycles

J. Geier, G. Frison, H. Grützmacher* ——— **3955 – 3957**

Dibenzophosphasemibullvalene



1 2

Strain is not to blame: Controlled thermolysis of **1** afforded dibenzo-1-phosphasemibullvalene **2** (see scheme). This unstable compound can be stabilized as a ligand in the complex $[W(CO)_5(\mathbf{2})]$. Although the sum of bond angles at phosphorus (220°) is very small, **2** is only a little strained.

DNA–Protein Interactions

C. Beuck, I. Singh, A. Bhattacharya, W. Hecker, V. S. Parmar, O. Seitz,* E. Weinhold* ——— **3958 – 3960**

Polycyclic Aromatic DNA-Base Surrogates: High-Affinity Binding to an Adenine-Specific Base-Flipping DNA Methyltransferase



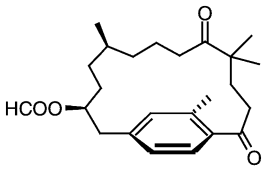
Filling the hole is a strategy that confers high-affinity DNA binding to the M·*Taq*I DNA methyltransferase. Aromatic base surrogates (e.g. pyrene, red in picture) were introduced into DNA by means of organocuprate-mediated C-glycosylations. A new competitive binding assay revealed that DNA with aromatic base surrogates placed opposite to the target base binds to M·*Taq*I with up to 400-fold-enhanced affinity.

Conformational Flexibility

S. Bäurle, T. Blume,* A. Mengel, C. Parchmann, W. Skuballa, S. Bäsler, M. Schäfer, D. Sülzle, H.-P. Wrona-Metzinger ——— **3961 – 3964**

From Rigidity to Conformational Flexibility: Macrocyclic Templates Derived from ansa-Steroids

More than a curiosity in the field of steroid derivatives, the 17-membered macrocycle **1** was obtained from a more rigid ansa-steroid. Compound **1** serves as a prototype of a template with differentiable functional groups, which can be used in the synthesis of libraries of novel macrocycles.



1

VIP Communications labeled with this symbol have been judged by two referees as being "very important papers".

The publication of Communications labeled with this symbol has been accelerated because of their topical or highly competitive nature.

The issues for August 2003 appeared online on the following dates
Issue 29: July 24. · Issue 30: July 30. · Issue 31: August 7. · Issue 32: August 13

Sources

Product and Company Directory

You can start the entry for your company in "Sources" in any issue of *Angewandte Chemie*.

If you would like more information, please do not hesitate to contact us.

Wiley-VCH Verlag – Advertising Department
Tel.: 0 62 01 - 60 65 65
Fax: 0 62 01 - 60 65 50
E-Mail: MSchulz@wiley-vch.de

Service

Keywords ——— *3966*

Authors ——— *3967*

Sources ——— *A67*

Vacancies ——— *A69*

Preview ——— *3969*

Friedrich Cramer (1923–2003): Nucleic Acid Chemist and Philosopher

Friedrich Cramer died on June 24, 2003 shortly before his 80th birthday. In him we have lost a colleague of great merit, particularly in the area of nucleic acid chemistry. Friedrich Cramer, or Fritz to his colleagues and friends, was born in Breslau on September 20, 1923. Having been badly wounded in Russia in October 1942, he started studying chemistry a year later in Breslau and continued his studies in Heidelberg from 1944. He received his PhD in 1949 with work on cyclodextrins under the supervision of Karl Freudenberg. He continued to work on this class of compounds for his habilitation, which he completed in 1953. This work formed the basis for the development of cyclodextrins as enzyme models. Cramer could show that compounds enclosed in a cyclodextrin cavity, as so-called inclusion compounds, become available for catalytic reactions through a key–lock interaction similar to that of an enzyme–substrate complex.[1] These results were of fundamental interest at the time, and Professor Alexander Todd invited Cramer for a one-year visit to his laboratory in Cambridge. This laboratory was prominent in the budding field of nucleic acid chemistry, and investigations into the type of linkage of the nucleotide monomers in DNA and RNA formed an active research program there.



Friedrich Cramer (Self-portrait)

Cramer returned to Heidelberg in 1954 and accepted the position of Professor of Organic Chemistry at the Technische Hochschule Darmstadt in 1959. There he built upon his experience gained in Cambridge and began work on the chemical synthesis of oligonucleotides. In 1962 he became a member of the Max-Planck-Gesellschaft and Director of the Department of Chemistry at the newly created Institute for Experimental Medicine in Göttingen. With the new opportunities available to him at this institute he focused on the study of nucleic acids. He was not only interested in the chemical synthesis of oligonucleotides, but he extended his research to *t*RNA and in particular to the enzymes that play a role in the aminoacylation of *t*RNA. These studies led to the first attempts to crystallize *t*RNA. Through probably the first use of nucleotide analogues it was also discovered that aminoacyl synthases occur in two classes, depending on whether they catalyze the binding of the amino acid residue to the 2′ or the 3′ hydroxy group.[2] This classification was later fully confirmed by X-ray structural analysis in another laboratory. Work on the specificity of aminoacylation formed the basis for a better understanding of this reaction, which is so important for cell function.[3] The work in Cramer's department in many respects formed a foundation for the bioorganic research of nucleic acids, particularly in such modern areas as RNA research.

Friedrich Cramer created a very stimulating and lively atmosphere in his department, to which his dislike of hierarchical structures certainly contributed, and he permitted the members of his department to work quite independently. The department was also enriched by the presence of many postdoctoral researchers from abroad at a time when this was not the rule in Germany. His contact with Professor Jan Michalski from Poland, who Cramer had met in Cambridge, laid the foundation for a lively exchange with Poland, which has continued to this day. These international relations also included close contacts with Israel. This stimulating and open environment served to encourage many members of the department to stay in research and to continue to work in the field of nucleic acids.

Friedrich Cramer had many varied interests and talents. For example, his sketchbook was a constant companion, and he produced portraits of colleagues and paintings. As the years went on his interest in the philosophical component of the sciences grew, and themes such as complexity, chaos, and the ethics of gene technology attracted his particular attention. These thoughts were the subject of many lectures, articles, and books. His concerns about the significance of science for society as a whole, not frequently encountered among scientists, led to his election as a Fellow of the Wissenschaftskolleg in Berlin for 1989/90 and as a member of the Göttinger Colloquium for Ethical Questions in Science and Technology.

Friedrich Cramer's death coincides with the end of an era following the Second World War during which the rebuilding of respect and recognition for Germany was of prime concern. Cramer contributed greatly to this endeavor, alongside his considerable contributions to nucleic acid research.[4]

Fritz Eckstein
Max-Planck-Institut für Experimentelle Medizin, Göttingen (Germany)

[1] F. Cramer, *Chem. Ber.* **1953**, *86*, 1576.
[2] M. Sprinzl, K. H. Scheit, H. Sternbach, F. von der Haar, F. Cramer, *Biochem. Biophys. Res. Commun.* **1973**, *51*, 881.
[3] F. von der Haar, F. Cramer *Biochemistry* **1976**, *15*, 4131.
[4] F. Cramer, W. Feist, *Angew. Chem.* **1993**, *105*, 198; *Angew. Chem. Int. Ed. Engl.* **1993**, *32*, 190.

 © 2003 Wiley-VCH Verlag GmbH & Co. KGaA, Weinheim

Group 13 Binary Hydrides

Molecular Dialane and Other Binary Hydrides

*Norbert W. Mitzel**

Keywords:
aluminum · density functional calculations · gallium · hydrides · indium

The simplest molecular compounds are often the greatest preparative challenges for chemists. This applies in particular to many binary compounds of hydrogen, the hydrides. Last year, Bürger and co-workers reproduced the synthesis of bismuthane and thus characterized BiH_3 in an unambiguous way from spectroscopic and structural analysis.[1] This contribution confirmed the work of Amberger 40 years earlier, whose study, which includes the description of an all-glass apparatus that could be cooled in its entirety, is a pleasure to read for those who are interested in the art of chemical experimentation.[2]

Of all the groups of the periodic table, the largest range of hydride complexes is found in the third main group. In contrast to some 100 known binary boranes,[3] only a handful of hydrides are well established for aluminum and gallium. The binary hydrides of indium and thallium (InH_3 and TlH_3) are currently unknown as isolated substances. Theoretical investigations found them to be thermodynamically unstable both in the gaseous and solid state, although the prediction of a level of kinetic stability suggests that there may yet be some success in this endeavor.[4]

The hydrides of aluminum originate from the work of Wiberg and Stecher, who obtained a mixture of hydridoalanes $R_{3-n}AlH_n$ from electrical-discharge reactions of trimethylaluminum and hydrogen gas.[5] The alanate ion $[AlH_4]^-$, discovered in 1947 by Schlesinger and co-workers,[6] has become well established in synthetic chemistry, whereas binary AlH_3, with an absence of suitable donors, does not represent a very useful reagent. In the solid state, AlH_3 exists as a polymeric compound and its α form is isostructural to AlF_3, which exhibits six-coordinate aluminum centers.[7]

Fifty years after the first report of the preparation of $(GaH_3)_n$ from $GaCl_3$ and $LiGaH_4$[8] or from $Ga_2H_2(CH_3)_4$ and NEt_3,[9] it was not until 1991 that Downs and co-workers obtained digallane (Ga_2H_6) by successive hydrogenation starting from $GaCl_3$. The first step of this synthesis is a dehalosilylation reaction of $GaCl_3$ with Me_3SiH, first discovered by Schmidbaur et al., which yields Cl_2GaH.[10] The addition of two equivalents of Me_3SiH yields the very sensitive $ClGaH_2$,[11] which then can be treated with lithium tetrahydrogallate to yield gallane in a solvent-free reaction that employs an all-glass apparatus at pressures below 10^{-4} Torr; gallane is stable only up to 240 K.[12]

Structural determination by gas-phase electron diffraction (Figure 1) required the construction of a special gas-inlet nozzle and was even then only possible with difficulty due to the reaction of gallane with the photographic emulsion at pressures of about 10^{-6} mbar. A determination of the solid-state structure of GaH_3 has not yet been possible because of thermal instability and the resulting difficulties with crystal growth from the liquid phase. However, from investigations on polymeric gallaborane $(GaBH_6)_n$,[13] one could be tempted to predict GaH_3 to be also polymeric in the solid state.

Large structural variations for the hydrides are expected, similar to those found for the chlorides of the same elements: BCl_3 is monomeric in the gas phase and the solid state, the polymeric solid $AlCl_3$ ($CN_{Al}=6$) gives dimeric Al_2Cl_6 ($CN_{Al}=4$) in the vapor phase upon heating, while Ga_2Cl_6 is dimeric in both phases. The simplest organometallic compounds, the dimeric Al_2Me_6 ($CN_{Al}=4$) and the monomeric $GaMe_3$ show a similar difference in coordination numbers of Al and Ga, but remain aggregated in both the solid state and in the gas phase.[14]

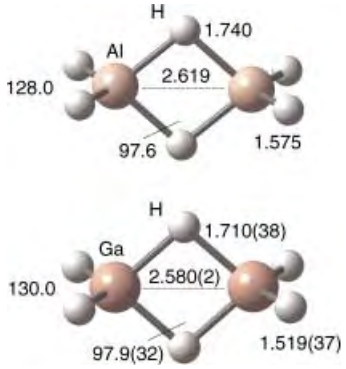


Figure 1. Molecular structures and geometric parameters (Å,°) of Al_2H_6 (B3LYP/6-311++G**) and Ga_2H_6 (gas-phase electron diffraction).

For the elusive dialane (Al_2H_6), its existence in the gas phase was supported only by vague hints and theoretical predictions. As early as 1964, Breisacher and Siegel suggested that traces of Al_2H_6 were formed in the reaction of a mixture of molecular and atomic hydrogen with molten aluminum, which could be detected by mass spectrometry.[15] Free, neutral Al_2H_6 was thus still not confirmed and could only be stabilized in the form of donor adducts, such as $PhMe_2N{-}H_2Al(\mu\text{-}H)_2AlH_2{-}NMe_2Ph$.[16]

In the very recent work of Andrews and Wang, Al_2H_6 has been unambigu-

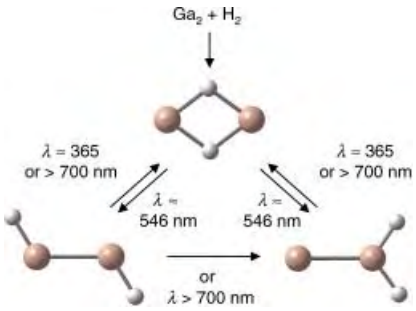
[*] Prof. Dr. N. W. Mitzel
Institut für Anorganische und Analytische Chemie
Westfälische Wilhelms-Universität Münster
Wilhelm-Klemm-Str. 8, 48149 Münster (Germany)
Fax: (+49) 251-83-36006
E-mail: mitzel@uni-muenster.de

 © 2003 Wiley-VCH Verlag GmbH & Co. KGaA, Weinheim DOI: 10.1002/anie.200301659

ously detected by means of vibrational spectroscopy in a matrix of solid hydrogen.[17] In these experiments, laser-ablated aluminum atoms were co-deposited with hydrogen on a cold substrate at 3.5 K (Scheme 1). Immediately after deposition, the AlH species is mainly detected in the infrared spectra, which has been identified earlier in the gas phase and in argon matrices. In addition, the radical $AlH_2^{\bullet}$ was detected. After increasing the temperature to 6.0 K and by subjecting the substrate to irradiation at $\lambda > 240$ nm, AlH was almost completely converted into AlH_3 in the H_2 matrix. The spectrum of AlH_3 had already been recorded from an argon matrix, in which the target species was obtained by the co-condensation of aluminum atoms and hydrogen atoms resulting from a gas discharge.[18]

At 6.5 K the matrix softens and the diffusion of AlH_3 units becomes possible, which leads to the exothermic dimerization of AlH_3 into Al_2H_6. To confirm these findings, the experiments were repeated using deuterium instead of hydrogen and the vibrational spectra were compared with results from DFT calculations (B3LYP/6-311++G**). At 6.8 K and above, hydrogen evaporates and the molecular aluminum hydrides AlH_3 and Al_2H_6 are transformed into polymeric $(AlH_3)_n$. In this step the stoichiometry is retained, but in contrast to the chemistry of the gallanes, the tendency to adopt higher coordination numbers dominates the processes.

Very recently the subhydrides Ga_2H_2 and In_2H_2 were generated in argon matrices[19] and compared with the known subhydrides HBBH and Al(μ-H)$_2$Al.[20] In these experiments H_2 adds spontaneously to matrix-isolated Ga_2 units, deposited from gallium vapor (Scheme 2). The analogous reaction with In_2 units only proceeds under photolytic conditions. The resulting dimers Ga(μ-H)$_2$Ga and In(μ-H)$_2$In undergo interesting photochemically induced rearrangement reactions, which yield the *trans*-bent species HGaGaH and HInInH; these species are of importance with respect to the ongoing discussion of multiple bonds in the organodigallenes RGaGaR (R = $Mes^*_2C_6H_3$, 2,4,6-*i*$Pr_3C_6H_3$).[21] In addition, Himmel et al. reported a photochemically induced pathway to a further isomer: H_2GaGa.[19] The fact that different isomers have been identified is due to the comparably small energy differences between them.

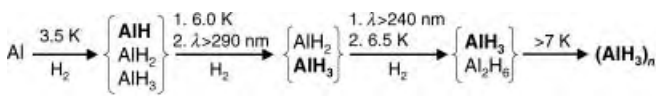


Scheme 2. Thermally and photochemically induced reactions of Ga_2 and H_2 in the matrix.

The fundamental investigations on binary compounds add much to our in-depth understanding of the chemistry of elemental hydrides and thus generally to our knowledge of the chemistry of group 13. However, the chemical stabilization of these unstable hydrides has generated a number of new results, which have great potential in synthetic applications. For example, the amine-stabilised gallium hydride $EtMe_2N{\cdot}GaH_3$ was used by Uhl et al. for the hydrogallation of tetramethyl-2,3-diazabutadiene.[22]

The elusive indium hydride InH_3 could be stabilized in many donor complexes, such as $Me_3N{\cdot}InH_3$ and the chinuclidine complex of InH_3 as monomeric compounds, the polymeric dabco complex $[\text{-}N(C_2H_4)_3N{\cdot}InH_3\text{-}]_n$, the mono- and diphosphane complexes $R_3P{\cdot}InH_3$ and $(R_3P)_2{\cdot}InH_3$, and even InH_3 adducts of Arduengo carbenes,[23] but some of these compounds are only stable at low temperatures. The direct application of indium hydrides in organic synthesis has been reported for the chemoselective reduction of functionalized benzaldehydes, conjugated alkenes (such as α,α-dicyanoalkenes), and α,β-unsaturated nitriles, as well as for hydroindation. The reagents for such reactions are dichloroindane ($HInCl_2$) which is obtained from the reaction of $InCl_3$ with Bu_3SnH or $NaBH_4$, and is found to be stable as a solution in THF at room temperature.[24]

There are many questions remaining to be answered. Will it be possible to isolate InH_3? Which form of aggregation does digallane adopt in the solid state? Which reactions will occur if small metal clusters are brought into contact with molecular hydrogen? Do hypervalent compounds of the type AlH_5 or GaH_5 exist? Deficiencies in the characterization of binary-earth-metal hydrides, and their diverse applications, both existent and foreseen, suggest that some surprises from this field of chemistry will be observed in the future.



Scheme 1. Synthesis of dialane.[17]

[1] W. Jerzembeck, H. Bürger, L. Constantin, L. Margulès, J. Demaison, J. Breidung, W. Thiel, *Angew. Chem.* **2002**, *114*, 2659–2661; *Angew. Chem. Int. Ed.* **2002**, *41*, 2550–2661.

[2] E. Amberger, *Chem. Ber.* **1961**, *94*, 1447–1452.

[3] N. N. Greenwood, *Chem. Soc. Rev.* **1992**, *21*, 49–57.

[4] P. Hunt, P. Schwerdtfeger, *Inorg. Chem.* **1996**, *35*, 2085–2088.

[5] E. Wiberg, O. Stecher, *Angew. Chem.* **1939**, *52*, 372–373.

[6] A. E. Finholt, A. C. Bond, H. I. Schlesinger, *J. Am. Chem. Soc.* **1947**, *69*, 1199–1203.

[7] a) J. W. Turley, H. W. Rinn, *Inorg. Chem.* **1969**, *8*, 18–22; b) F. M. Brower, N. E. Matzek, P. F. Reigler, H. W. Rinn, C. B. Roberts, D. L. Schmidt, J. Snover, K. Terada, *J. Am. Chem. Soc.* **1976**, *98*, 2450–2453.

[8] E. Wiberg, E. Amberger, *Hydrides of the Elements of Main Groups I–IV*, Elsevier, Amsterdam, **1971**.

[9] a) G. Brauer, *Handbuch der präparativen Anorganischen Chemie*, 2nd ed., Ferdinand Enke, Stuttgart, **1960**, p. 746; b) E. Wiberg, T. Johannsen, *Chemie* **1942**, *55*, 38.

[10] a) H. Schmidbaur, W. Findeiss, E. Gast, *Angew. Chem.* **1965**, *77*, 170; *Angew. Chem. Int. Ed. Engl.* **1965**, *4*, 152; b) S. Nogai, H. Schmidbaur, *Inorg. Chem.* **2002**, *41*, 4770–4774.

[11] M. J. Goode, A. J. Downs, C. R. Pulham, D. W. H. Rankin, H. E. Robertson, *J. Chem. Soc. Chem. Commun.* **1988**, 768–769.

 © 2003 Wiley-VCH Verlag GmbH & Co. KGaA, Weinheim

[12] C. R. Pulham, A. J. Downs, M. J. Goode, D. W. H. Rankin, H. E. Robertson, *J. Am. Chem. Soc.* **1991**, *113*, 5149–5162.
[13] a) A. J. Downs, S. Parsons, C. R. Pulham, P. F. Souter, *Angew. Chem.* **1997**, *109*, 910–911; *Angew. Chem. Int. Ed. Engl.* **1997**, *36*, 890–891.
[14] N. W. Mitzel, C. Lustig, R. J. F. Berger, N. Runeberg, *Angew. Chem.* **2002**, *114*, 2629–2633; *Angew. Chem. Int. Ed.* **2002**, *41*, 2519–2522.
[15] P. Breisacher, B. Siegel, *J. Am. Chem. Soc.* **1964**, *86*, 5053–5054.
[16] J. L. Atwood, K. W. Butz, M. G. Gardiner, C. Jones, G. A. Koutsantonis, C. L. Raston, K. D. Robinson, *Inorg. Chem.* **1993**, *32*, 3482–3487.
[17] L. Andrews, X. Wang, *Science* **2003**, *299*, 2049–2052.
[18] P. Pullumbi, Y. Bouteiller, L. Manceron, C. Mijoule, *Chem. Phys.* **1994**, *185*, 25–37.
[19] H.-J. Himmel, L. Manceron, A. J. Downs, P. Pullumbi, *J. Am. Chem. Soc.* **2002**, *124*, 4448–4452.
[20] a) T. J. Tague, L. Andrews, *J. Am. Chem. Soc.* **1994**, *116*, 4970–4976; b) J. C. Stephens, E. E. Bolton, H. F. Schaefer III, L. Andrews, *J. Chem. Phys.* **1997**, *107*, 119–123.
[21] N. J. Hardmann, R. J. Wright, A. D. Phillips, P. P. Power, *Angew. Chem.* **2002**, *114*, 2966–2969; *Angew. Chem. Int. Ed.* **2002**, *41*, 2842–2844.
[22] W. Uhl, J. Molter, B. Neumüller, *J. Organomet. Chem.* **2001**, *634*, 193–197.
[23] C. Jones, *Chem. Commun.* **2001**, 2293–2298.
[24] a) T. Miyai, K. Inoue, M. Yasuda, I. Shibata, A. Baba, *Tetrahedron Lett.* **1998**, *39*, 1929–1932; b) B. C. Ranu, S. Samanta, *Tetrahedron Lett.* **2002**, *43*, 7405–7407.



THE NOBEL PRIZE IN CHEMISTRY 2002



Proteins in close-up

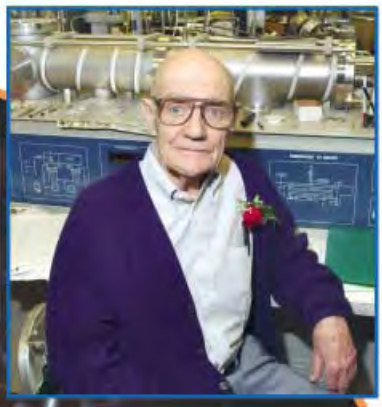
Living cells consist of myriads of molecules. The large molecules, which include the proteins, interact with one another and with other molecules in a never-resting molecular machinery. How can we understand what is happening inside the cell? One important step is to develop tools to "see" with, and this is what this year's Nobel Laureates in Chemistry have done.

Mass spectrometry: Of course proteins can fly!

With mass spectrometry we can now quickly identify a substance in a sample by accurately determining its molecular mass. Mass spectrometry is a very widely used method for small and medium-sized molecules. John B. Fenn and Koichi Tanaka showed, in different ways, that macromolecules could also be studied. The trick was to get the proteins to fly, or as John Fenn himself said, to give "wings to molecular elephants".

John B. Fenn

John B. Fenn is the chemist who invented the electrospray method. Today it is used in laboratories all over the world. Fenn has worked mainly as Professor of Chemistry at Yale University, USA, and at Virginia Commonwealth University, USA.



Mass spectrometry

WITH SPRAY TECHNIQUE

The protein solution is sprayed, using an electric field, towards a negatively charged plate.

Sample in solution

Minute charged droplets are formed.

The droplets evaporate and grow smaller and smaller.

3 000 V

5+ 9+ 25+

Soon the free protein ions appear entirely "naked", often strongly charged.

17+ 18+ 19+ 20+

The protein ions are accelerated by an electric field ...

... and their time of flight over a known distance is measured.

A computer calculates the exact mass of the protein.

A spectrum is formed, in which each peak represents a certain relationship between mass and charge.

WITH LASER TECHNIQUE

The sample is in a solid state in a matrix.

The sample erupts but thanks to the matrix the actual protein molecules do not break to pieces.

2+

The hovering, weakly charged, protein ions; or two or more proteins that are in a complex, are accelerated in an electrical field and their time of flight is measured as above.

The sample is shot with a laser beam.

laser

The height of the peaks in the spectrum reveals the quantities of the different proteins that were in the sample.

Copyright © The Royal Swedish Academy of Sciences. We thank the Academy for permission to reproduce parts of their poster (illustrations: Typoform).

Koichi Tanaka

Koichi Tanaka worked as a research engineer at Shimadzu Corp in Kyoto, Japan when he was telephoned by the Royal Swedish Academy of Sciences in Stockholm: "You have been awarded the Nobel Prize!" Tanaka's idea was to use the energy from laser light, ingeniously transferred to the proteins, to get them to let go of one another and hover freely. It worked!



 © 2003 Wiley-VCH Verlag GmbH & Co. KGaA, Weinheim

Angewandte Chemie

Gentle Mass Spectrometry

The Origin of Macromolecule Ionization by Laser Irradiation (Nobel Lecture)**

*Koichi Tanaka**

Keywords:
laser desorption · macromolecules · mass spectrometry · Nobel lecture

From the Contents

1. Introduction	*3861*
2. Mass Separation: Time-of-Flight Technology	*3862*
3. Reflectron Technology	*3862*
4. Time-Delayed Ion Extraction	*3863*
5. Ion Detection	*3863*
6. Ionization Technology	*3865*
7. Commercialization and Public Announcement	*3868*
8. Development of MALDI Technology	*3869*
9. Conclusion	*3869*

1. Introduction

When I was a student at university, my major field of study was electrical engineering. I did not specialize in chemistry in my studies at university, and my knowledge of chemistry overall was somewhat less than rich. Under those circumstances, upon entering the Shimadzu Corporation, I applied myself wholeheartedly to the study of chemistry to challenge and overcome a barrier in analytical chemistry considered at that time to be impenetrable. I am, of course, very pleased to receive the Nobel Prize and further, especially pleased that the Prize serves to acknowledge my efforts and results in the field of analytical chemistry, a field that while rather inconspicuous to the general population is indeed very important and useful to the world.

I am employed by the analytical instrument manufacturer, Shimadzu Corporation. I was assigned to a team charged with the task of designing and building a completely new mass spectrometer. The achievement of developing "a soft desorption ionization method for mass spectrometric analysis of biological macromolecules", for which I was awarded this prize, was one aspect of that project. At that period in the 1980s, four of my colleagues, whom I will introduce shortly, in addition to myself, were each in charge of developing a part of the instrument. I was responsible for developing the sample preparation and ionization technologies. Success of the instrument would not have been assured unless the other technologies were suitably provided, even with an excellent ionization technology. First, I will briefly describe the progress of development of the technologies for the other components at that time, other than that of ionization.

[*] K. Tanaka
Shimadzu Corporation
1 Nishinokyo-Kuwabaracho
Nakagyo-ku, Kyoto 604-8511 (Japan)
Fax: (+81) 75-823-3218
E-mail: koichi-t@shimadzu.co.jp

[**] Copyright© The Nobel Foundation 2003. We thank the Nobel Foundation, Stockholm, for permission to print this lecture.

 DOI: 10.1002/anie.200300585 © 2003 Wiley-VCH Verlag GmbH & Co. KGaA, Weinheim

2. Mass Separation: Time-of-Flight Technology

In mass spectrometry, it is necessary to use some method to separate the generated ions according to mass, and then perform detection of the ions. One of these methods is called Time-of-Flight Mass Spectrometry (TOF-MS), which involves separating ions according to mass by measuring their respective flight times. Figure 1 provides the simplest

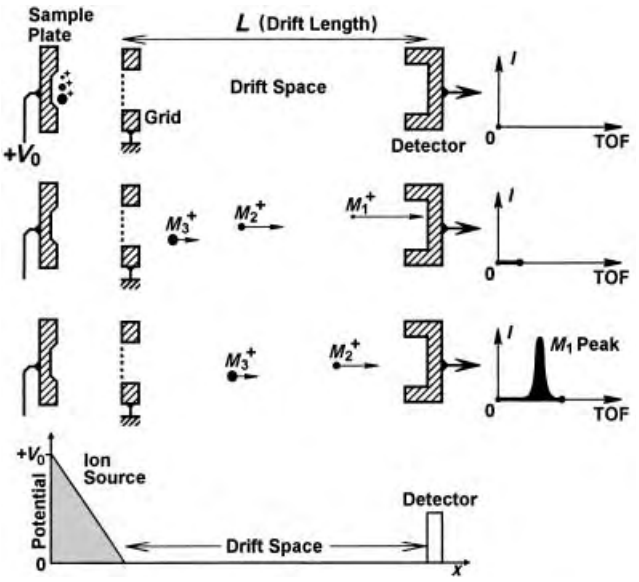


Figure 1. The principles of time-of-flight mass spectrometry.

representation of the principle behind TOF-MS. This assumes that equally charged ions of differing mass, M_1, M_2, and M_3 are generated instantly at the same time and starting position. Assume that M_1 is the lightest of the ions. The ions are generated at an electrical potential V_0, and have a potential energy of $z\,V_0$, where z is the charge of the ion and m the mass of the ion [Eq. (1)]. If all of the potential energy is converted

$$z\,V_0 = \frac{1}{2}mv^2 \tag{1}$$

into kinetic energy, the velocity v is expressed by Equation (2), based on the law of conservation of energy. In other

$$v = \sqrt{\frac{2\,z\,V_0}{m}} \tag{2}$$

words, the lighter ion travels at a higher speed, reaching the detector first [Eq. (3,4) L = length of drift space, t = flight time of ion in drift space, t' = flight time of ion in drift space with initial kinetic energy ε].

$$t = \frac{L}{v} = L\sqrt{\frac{m}{2\,z\,V_0}} \tag{3}$$

$$t' = L\sqrt{\frac{m}{2\,(z\,V_0 + \varepsilon)}} \tag{4}$$

This explanation is based on ideal conditions [Eq. (3)]. Since the ions actually possess a distribution of initial velocities, that is, of the initial kinetic energy ε, their arrival time t' at the detector will show some distribution, even among ions of equal mass [Eq. (4)]. This situation results in diminished mass resolution.

3. Reflectron Technology

To improve the resolution, it would be best if ions of the same mass and charge arrive at the detector at the same time, even if their initial kinetic energies are different. Specifically, a device referred to as a "reflectron" (an electrostatic ion "mirror"), first described by Boris Mamyrin et al.[1] in 1973, is used to reflect the ions midway in their flight back towards the detector. This turning back of the ions has the effect of adjusting the flight times of the ions in conjunction with their initial kinetic energies, to ensure that ions of the same mass and charge reach the detector at the same time (Figure 2).

The isochronism of the pendulum is very well known. Stated simply, even if the swing amplitude of the pendulum varies, the cycle times remain equal provided the cord length of the pendulum and the force of gravity stay the same.



Koichi Tanaka, born in 1959 in Toyama, Japan. After completion of his degree in Electrical Engineering at Tohoku University he took a position in the Central Research Laboratory of Shimadzu Corporation in 1983. His first task was the development of the ionization and data acquisition for the time-of-flight mass spectrometer (TOF-MS) group. In 1985, he established his idea of soft laser desorpsion/ionization together with the hardware of the TOF-MS for observing macromolecular ions. The results of the group were presented at Japanese and then at international conferences (1987) and in 1989 published in the journal Rapid Communications in Mass Spectrometry. He was transferred to Kratos Analytical Plc and Shimadzu Research Laboratory (Europe) Ltd. to develop TOF-MS methods further. In 2002 he shared the Nobel Prize in Chemistry with J. B. Fenn and K. Wutrich.

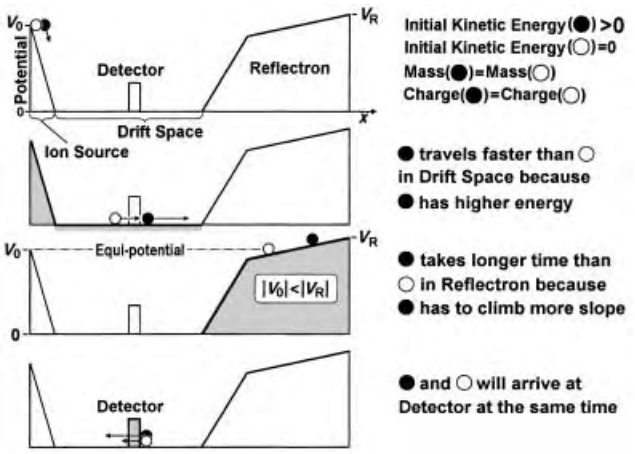


Figure 2. Improvement of mass resolution by reflectron.

 © 2003 Wiley-VCH Verlag GmbH & Co. KGaA, Weinheim

Applying this principle, an ideal reflectron was developed. In this case, the cord length corresponds to the ion mass, the swing amplitude corresponds to the initial kinetic and potential energy, and the cycle time corresponds to the time of flight. One method for this reflectron technology (Figure 3) was developed by one of my colleagues at that time, Mr. Yoshikazu Yoshida (Patent number: US4625112, 1986).

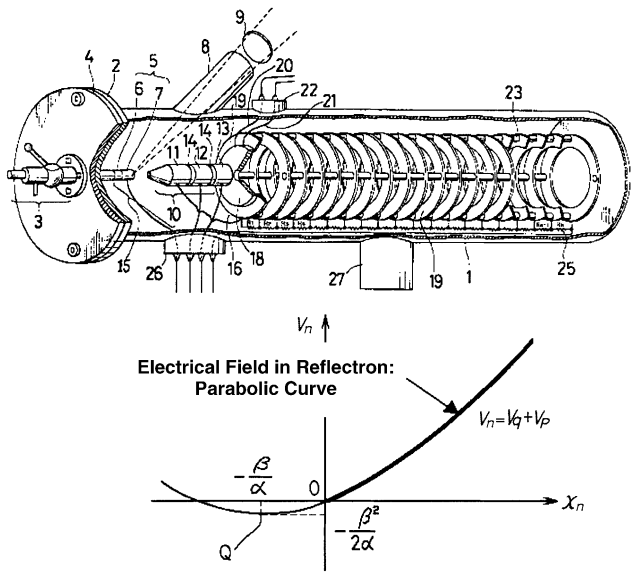


Figure 3. Improvement of mass resolution by ideal reflectron (Patent: US4625112).

4. Time-Delayed Ion Extraction

The principle behind TOF-MS assumes that ions are generated instantaneously, that is, in an infinitely short generation time. The time width of a laser pulse is extremely small, on the order of a few nanoseconds in the case of the N_2 laser. However, when the laser intensity is high enough to greatly exceed the ion-generation threshold, as shown in Figure 4, ions may continue to be generated even after the completion of laser irradiation. As a result, in the TOF model, the mass resolution decreases owing to the wider time width of ion generation.

One of my colleagues at that time, Dr. Tamio Yoshida, succeeded in improving the mass resolution by drawing out the time from ion generation to ion extraction, as shown in Figure 5. This is accomplished by maintaining equivalent voltages at the sample plate and the accelerating grid to prevent the ions from being extracted until generation is

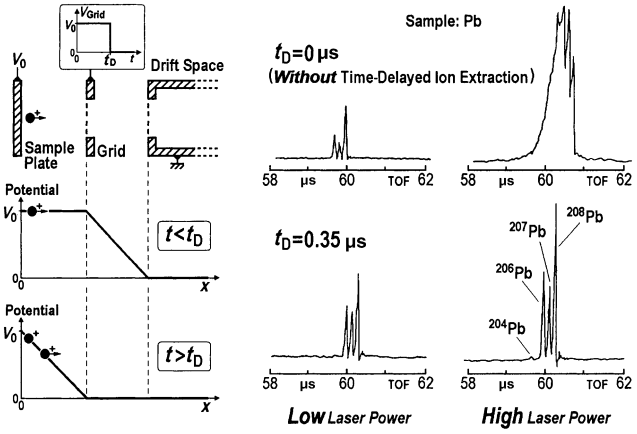


Figure 5. Improvement of mass resolution by time-delayed ion extraction.

complete, and then by creating a potential difference after t_D to cause extraction of all the ions at the same time (filed in Japan Patent Office S60035097, 1985). This method is the same in principle as the time-lag focusing method which was originally designed by William Wiley and Ian McLaren[2] to reduce the effect of initial spatial and kinetic-energy distributions, but is now applied specifically to minimize the effect of the prolonged laser-induced ion-generation time.

In addition, there is a heightened possibility that particles given a charge, for example, protons and cations, will collide and react with the normally uncharged sample molecules. Such processes are generally referred to as "chemical ionization", as originally described by Burnaby Munson and Frank Field.[3] Thus with time-delayed ion extraction the amount of molecular ions, such as $[M+Na]^+$ (Figure 6), formed is expected to increase.

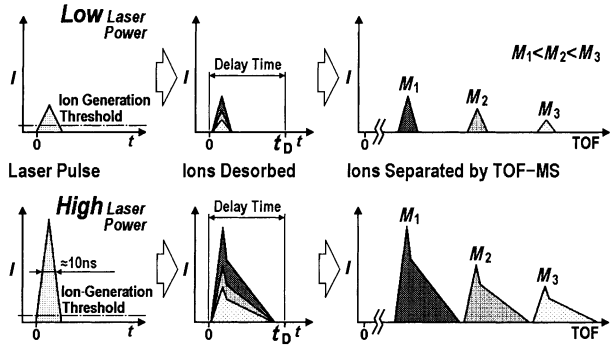


Figure 4. Measurement of TOF mass-spectrum with low and high laser power.

5. Ion Detection

The term detector here refers to the conversion of ions separated by the mass-separation mechanism into a flow of electrons, in other words, an electrical signal. The maximum mass number of ions that had been detected in the early 1980s was in the range of several thousand. In principle, the greater the molecular weight (M_W) of the ion, the lower the velocity of the ion, and thus the lower the ion-to-electron conversion efficiency, this conversion efficiency could even drop to zero.

The simplest method of raising sensitivity is to accelerate the ions even further after mass separation occurs (this is called "post acceleration"). As shown in Figure 7, the higher

 © 2003 Wiley-VCH Verlag GmbH & Co. KGaA, Weinheim

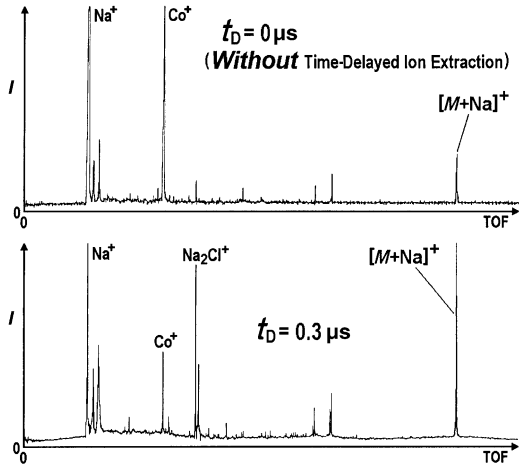


Figure 6. Increase in molecular-ion intensity by time-delayed ion extraction.

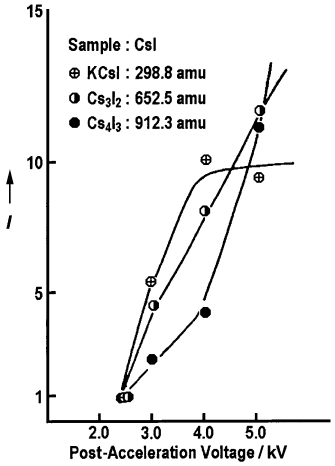


Figure 7. Ion detection with high-sensitivity by post acceleration; amu = atomic mass unit.

the post-acceleration voltage, the greater the intensity of the ions, and further, the higher the mass number, the greater will be the effect, especially when a high voltage is applied. Another method is the ion-to-electron conversion method. As shown in Figure 8, the intensity increases using this method as well.

One of my colleagues at that time, Mr. Yutaka Ido, developed a detector (Figure 9) that obtained the effects of both of these methods, which enables sufficiently sensitive detection even when ions of especially high molecular weight were generated.

5.1. Measurement Technology

5.1.1. Analog-to-Digital Conversion

Even with improved detector sensitivity, it can be assumed that the intensity of signals arising from macromolecular ions would be weak. In particular, when performing a single, one-shot measurement using a minute quantity of sample,

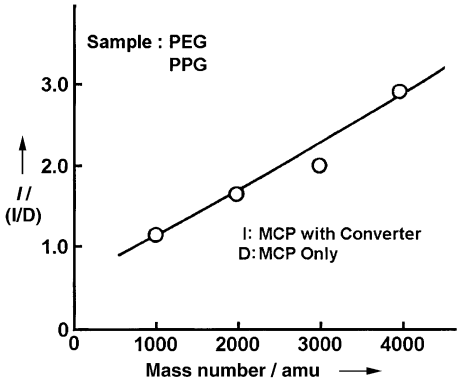


Figure 8. Ion detection with high-sensitivity by ion-to-electron conversion; PEG = polyethylene glycol, PPG = polypropylene glycol.

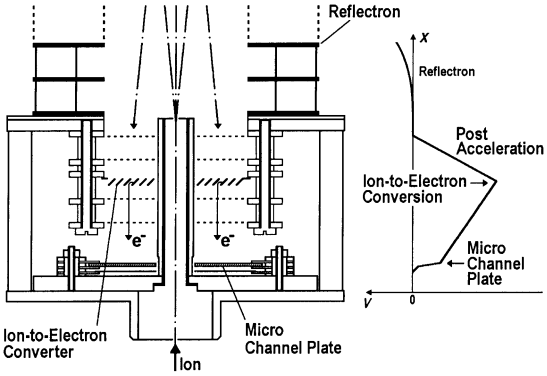


Figure 9. Detection of macromolecule ions by post acceleration and ion-to-electron conversion.

successful quantitative analysis may not be possible without a high enough signal-to-noise ratio. For this reason, a spectrum accumulation circuit is considered to be indispensable. To satisfy the demand for an instrument capable of high-speed measurement, our group developed a TOF spectrum measurement accumulation circuit.

One of my colleagues at that time, Mr. Satoshi Akita, developed an analog-to-digital converter (ADC) circuit adopting a "pipeline technique" to achieve the required speedup in measurement. The new ADC circuit provided a processing speed of 1 kHz with real-time accumulation of the spectrum at a maximum time resolution of 10 ns and intensity resolution of 24 bit (Figure 10). Moreover, to enable measurement of both low-mass high-intensity ions as well as high-mass low-intensity ions, an amplifier that could perform gain switching within one microsecond was developed and adopted to provide a wider dynamic range.

5.1.2. Time-to-Digital Converter

At that time, ADC circuits had a time resolution of 10 ns. It was our opinion that even this resolution would not be enough. Mr. Yoshikazu Yoshida developed a time-to-digital converter (TDC) circuit that could measure up to 255 events after one start signal (Multi-Stop-TDC), which allowed the flight time of the ions to be measured with great accuracy,

 © 2003 Wiley-VCH Verlag GmbH & Co. KGaA, Weinheim

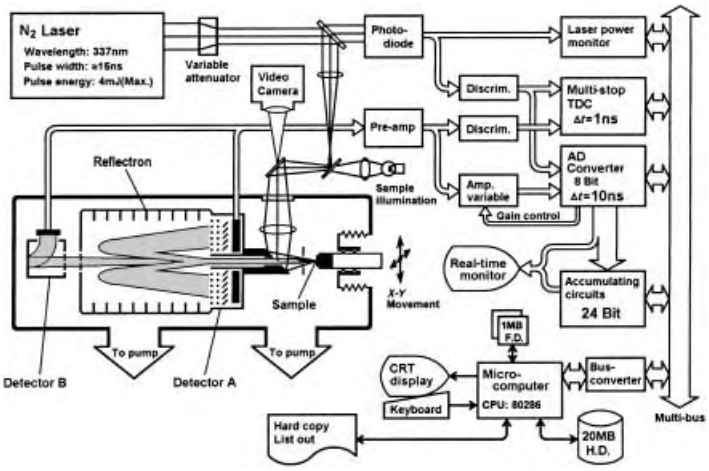


Figure 10. Schematic diagram of the Shimadzu LDI-TOF mass spectrometer.

although peak intensity information was sacrificed. As a result, we were able to measure the time of flight at a maximum time resolution of 1 ns (Figure 10).

All of these crucial developments further emphasize the certainty that if even one of our group of five were not there, we would not have been able to achieve the measurement of macromolecular ions. I am truly happy that the technologies we developed in the 1980s have been improved through their use in various instruments, and that they have played a role in bringing TOF technology into the mainstream of MS from the 1990s.

6. Ionization Technology

Long before the 1980s, there had been investigations into the use of optical energy, not limited to laser light, to achieve ionization of organic compounds.[4] However, for the most part, this ionization consisted of stripping electrons from compounds in the gas phase.[5] Because this was limited to compounds that could be vaporized without being decomposed, very few compounds could be ionized. When a solid-phase organic compound was irradiated with a laser, the organic compound absorbed the laser light, which provided enough energy for desorption. Further, when the positive and negative charges of the particle are not in balance, it could be measured as an ion. However, in this case, since the laser light is absorbed directly into the analyte, the molecular bonds may be broken owing to the increased internal energy. In other words, there is an increased risk that measurement would occur in the decomposed state (Figure 11). Because we wanted to measure the undecomposed, intact molecular ion, this was unsatisfactory.

At that time, the molecular weight of compounds that could be ionized by laser irradiation was about 1000 Dalton (Da), and ionization of compounds having a molecular weight exceeding 10000 Da was generally considered by chemists at the time to be impossible. However, not being a specialist in chemistry, I was unaware of the existence of this widely held belief.

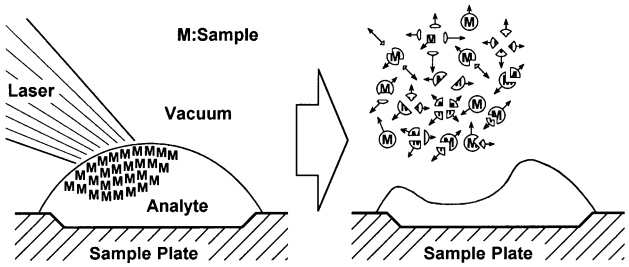


Figure 11. Laser desorption/ionization (LDI) from solid or liquid phase.

6.1 Rapid-Heating Technology

In the 1980s, "desorption to gas phase by rapid heating" gained attention through the efforts of several groups that had obtained some encouraging results. These include Franz Röllgen[6,7] of Germany, Mamoru Ohashi[8] of Japan, and Louis Friedman,[9] Don Hunt,[10] Burnaby Munson,[11] and Robert Cotter[12] of the USA. A simple description of the principle is depicted in Figure 12. In short, if a given compound AB is heated, it is assumed that AB will be released to the gas phase as intact AB as well as fragmented A and B [Eq. (5a,b)]. Respectively applying the well-known

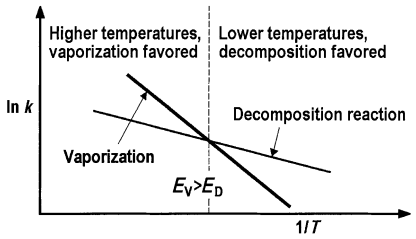


Figure 12. Temperature dependence of vaporization versus decomposition.[9]

$$\text{Vaporization}: \ AB \xrightarrow{K_V} AB \tag{5a}$$

$$\text{Decomposition}: \ AB \xrightarrow{K_D} A + B \tag{5b}$$

Arrhenius Equation [Eq. (6) where k = rate constant, f = frequency factor, E = activation energy, R = gas constant, T = absolute temperature] will give the logarithmic expressions shown in Equations 7a,b.

$$k = f \exp(-E/\mathrm{R}\,\mathrm{T}) \tag{6}$$

$$\ln K_V = \ln F_V - E_V/RT \tag{7a}$$

$$\ln K_D = \ln F_D - E_D/RT \tag{7b}$$

For compounds that are thermally labile and decompose easily, the rate constant for decomposition k_D is larger than that for vaporization k_V at low temperatures. Because the activation energy for vaporization E_V is higher than that for decomposition E_D, the slope of the vaporization reaction k_V in

 © 2003 Wiley-VCH Verlag GmbH & Co. KGaA, Weinheim

Figure 12 ($\ln k$ versus $1/T$) is steeper than that of the decomposition reaction. If this relationship is always correct, at high temperature, where $1/T$ is small, vaporization should be favored. In other words, reaching the highest possible temperature as quickly as possible should provide a high degree of vaporization.

6.1.1. *Use Of Ultrafine Metal Powder*

To perform this rapid heating, various heating methods were devised.[9] However, a high enough temperature could not be achieved quickly enough to obtain intact vaporization of macromolecules, such as proteins. Since the time width of a pulse laser itself is between a nanosecond to several microseconds, rapid heating would seem possible, that using a focused laser beam would generate energy at high density and high speed. However, this would require a medium to enable the conversion of the irradiating photons into thermal energy.

In Japan at that time in the 1980s, ultrafine metal powder (UFMP) received much attention in the field of metallurgy owing to its usefulness in the efficient production of alloys, and was referred to as "Japanese Powder". UFMP, as its name indicates, is an extremely fine metallic powder with particle diameters measuring a few tens of nanometers. The particle diameter of UFMP is about the same as a wavelength, thus when compared to bulk metal, there is an increasing possibility that scattered light could be taken up internally (Figure 13). In other words, light energy could be absorbed more efficiently. Even visually, UFMP is black in color.

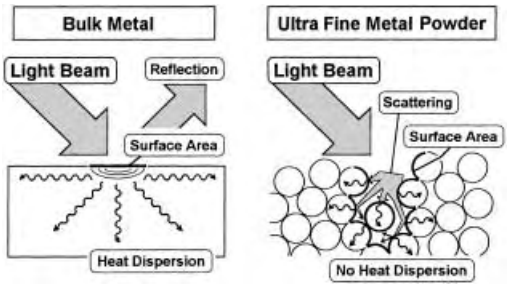


Figure 13. Differences between light absorption by bulk metal and ultrafine metal powder.

Moreover, the possibility that thermal energy would be dispersed and lost decreases owing to the interparticle spaces.

Mixing UFMP with an organic compound should allow the laser light to be efficiently absorbed into the UFMP, and to achieve a high UFMP temperature very quickly without the dispersion and loss of heat. This would efficiently achieve heating of the sample in the mixture. It was Mr. Yoshikazu Yoshida who proposed using UFMP as a matrix (that is, a substance used to assist ionization; Figure 14; Patent number: JP 01731501, filed in 1985, issued in 1993).

There was at that time an interest in using laser desorption for the analysis of polymers, such as in the reports by Charles Wilkins et al.[13] of the USA. The MS spectrum shown in the upper part of Figure 15 is obtained when the sample, consisting of a polymer mixture of polyethylene glycols

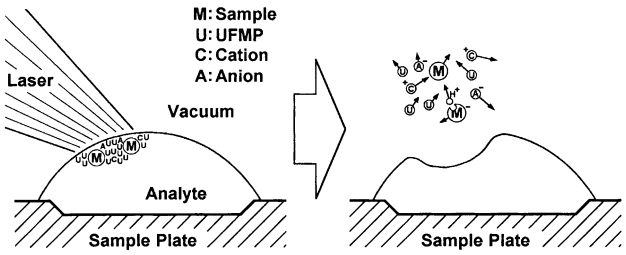


Figure 14. Molecular-ion desorption by using the UFMP matrix.

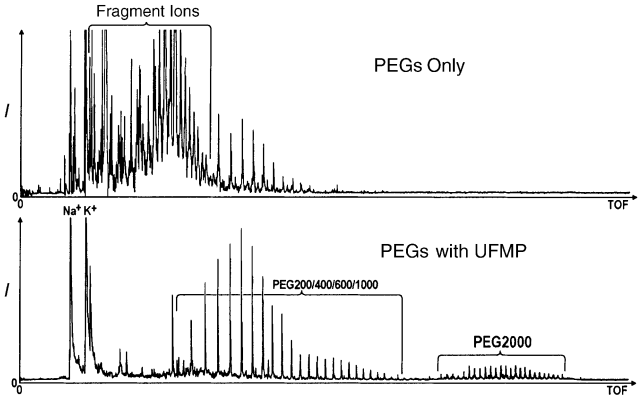


Figure 15. Spectra of polyethylene glycol probes with and without UFMP matrix.

(PEGs), is irradiated with a laser. The lower spectrum of Figure 15 shows that of the PEG sample mixed with UFMP. With PEG alone, fragment ion peaks of the PEG molecule are dominant, and no PEG2000 peaks are observed. On the other hand, not only are there almost no fragment peaks observed when PEG is mixed with UFMP, the peaks arising from the molecular ion, PEG2000, have become clearly evident.

With the use of this matrix, the molecular ions from many organic compounds that could not be measured previously could now be measured by mass spectrometry. However, according to our experimental results, this technique could not be applied to compounds with molecular weights in the tens of thousands.

6.1.2. *Glycerin Matrix Technology*

At that time in the 1980s, the fast atom bombardment (FAB) MS method was widely used to achieve ionization in thermally labile compounds. The FAB method was developed by Donald Sedgwick and colleagues,[14] and David Surman and John Vickerman[15] of the UK, and involved accelerating neutral particles, such as xenon, at high speed so as to collide with the sample and generate ions. In this method, the solid sample was maintained in a liquid state by using glycerin (glycerol) as a matrix (Figure 16).It is thought that since glycerin is a liquid at room temperature, it releases the solid sample from its crystalline state to dissolve in the liquid,

 © 2003 Wiley-VCH Verlag GmbH & Co. KGaA, Weinheim

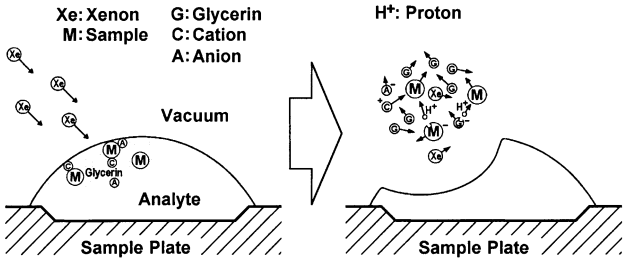


Figure 16. Molecule desorption/ionization by using a glycerin matrix in FAB-MS.

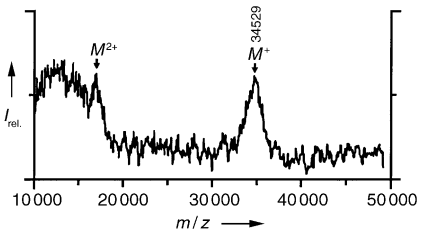


Figure 17. Molecular-ion measurement of carboxypeptidase A (molecular weight ≈ 35k Da).

thereby assisting ionization. We used glycerin as a matrix, just as it was used in FAB, but because the N_2 laser wavelength (337 nm) that we used was only slightly absorbed into the glycerin, no significant effect was seen on the enhancement of molecular-ion generation for organic compounds. However, this matrix was useful in improving reproducibility owing to its effectiveness in providing a uniform mixture

6.1.3. *UFMP–Glycerin Mixture Technology*

Here it can be said that I had come up against a brick wall. Soon after that, while preparing many trial-and-error UFMP suspensions, changing the organic solvent and concentration repeatedly to obtain even the slightest improvement in data, I committed a monumental blunder, which was followed by a series of fortuitous, arbitrary decisions. I was using ordinary acetone as a UFMP suspension, and one day, by mistake, 1) I used the glycerin instead of the acetone. Reasoning that it would be wasteful to discard the expensive UFMP, 2) I decided to use the "ruined" preparation as the matrix solution. Because glycerin gradually evaporates in a vacuum, I knew it would eventually disappear. However, instead of waiting, 3) I decided to speed up vaporization of the glycerine by continuing to irradiate the laser. On top of that, because I wanted to see the result as soon as possible, 4) I was monitoring the acquisition of the TOF spectrum. In this way, only after at least four factors fell into place could I observe a phenomenon never before seen.

I think that the sample first measured was vitamin B_{12}. I have tried recently to locate the original spectrum, but unfortunately I could not find it. Because vitamin B_{12} itself can absorb laser light with an extremely high degree of efficiency, up to then, only fragment ions could be measured with high sensitivity. However, by using the mixed UFMP–glycerin matrix, at the position where unfragmented ions (molecular ions) should have appeared, peaks which seemed to be noise were observed. No matter how many times I performed the measurement, these peaks were present. Molecular ions were observed even after changing the sample, and therefore must be the molecular ion of vitamin B_{12}.

After that, as a result of progressing to higher mass ions while optimizing the concentration, laser power, and other parameters, I was able to measure an ion having a molecular weight of 35 000 Da in 1985 (Figure 17) and in 1987 an ion cluster having a mass number exceeding 100 000 Da (Figure 18). The patent application for this ionization method was submitted in Japan in 1985, and was subsequently issued in 1993 (Patent number: JP 01769145).

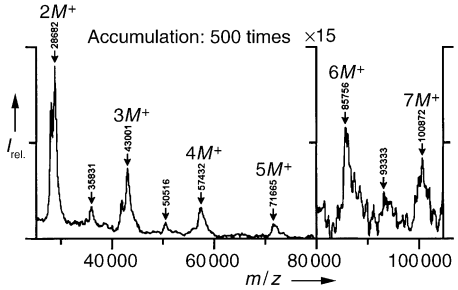


Figure 18. Molecular cluster-ion measurement of lysozyme (molecular weight = 14 306 Da).

6.2. *Why Did The Macromolecule Become Ionized Without Decomposing?*

Use of UFMP conveniently allows high temperatures to be reached at high speed. However, when this is mixed with a typical organic compound, it is difficult to achieve sufficient mixing. Even when viewing the mixture in an electron-microscope-generated photograph, the lack of uniformity is obvious (Figure 19, top). When glycerin is added to the mixture, however, the uniformity becomes evident (Figure 19, bottom). Moreover, glycerin may also serve to release the sample from its crystalline state. The ability to measure molecular ions from organic compounds even exceeding a molecular weight of 10 000 Da may indeed be due to these effects (Figure 20).

Herein I have suggested the principles by which laser-light irradiation is able to generate huge molecular ions. However, these principles are not necessarily correct because they have not yet been fully proven scientifically. Even with the knowledge of all the developments in MALDI (matrix-assisted laser desorption/ionization) technology that followed my discovery, I cannot yet claim to have correctly grasped the theoretical principles behind all of these phenomena. However, I am an engineer, an engineer employed in a business enterprise. So even if the principles are unverified, their application takes priority if they are useful and practical.

 © 2003 Wiley-VCH Verlag GmbH & Co. KGaA, Weinheim

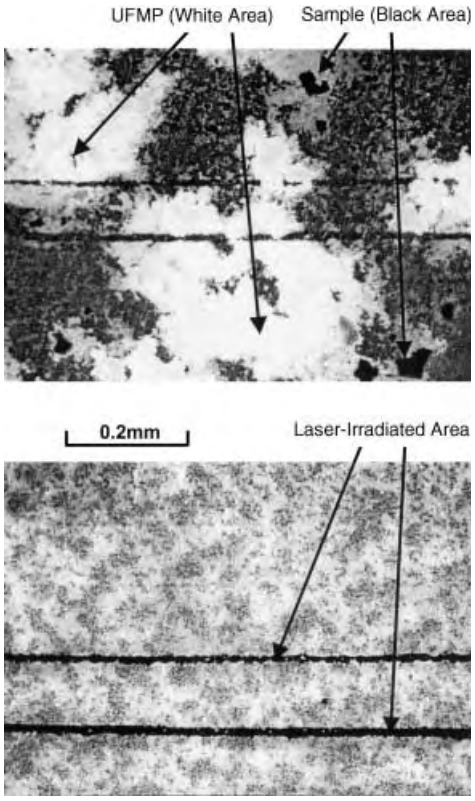


Figure 19. Electron microscope images of a) sample and UFMP matrix mixture without glycerin, b) sample and UFMP matrix mixture with glycerin.

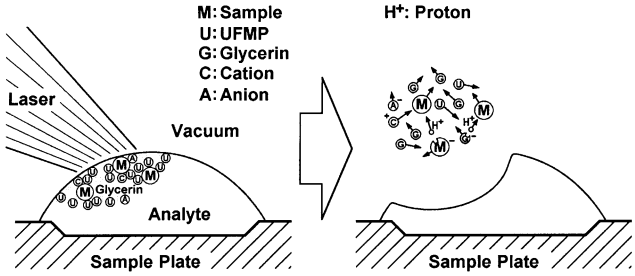


Figure 20. Desorption/Ionization of macromolecules by using the UFMP–glycerin mixed matrix.

7. Commercialization and Public Announcement

If a business organization does not consider that a technology is basically saleable, development would not be advanced and there would be no announcement regarding the technology outside of the company. If our technology had not been made into a product, it would have been buried in-house and forgotten. For example, similar technology might have been developed somewhere else in the world in the 1980s, but if it had not been introduced to the international scientific community, it would not have been further developed to become a useful technique worldwide.

Because this basic technology that we developed at the Central Research Laboratory of Shimadzu Corporation was to be incorporated into a product, I was transferred to the business division. However, this technology was not made known outside the company until it was decided to release the product. The five members of our group made the first announcement outside the company at the Annual Conference of the Japan Mass Spectrometry Society held in Kyoto in May of 1987 (Oral and poster presentations[16–20] were conducted in Japanese). The announcement caused some reverberations, however, almost no one believed that this technology would become so useful. Of course, we were just pleased and satisfied to confirm that we had made scientific progress, and further, that we had presented it to the public.

7.1 Technology Transfer to Europe and the USA

In September of 1987, I participated in the Second Japan–China Joint Symposium on Mass Spectrometry that was held in Takarazuka, Japan, and presented the result for the first time in English.[21] At that time in the 1980s, Plasma Desorption MS (PD-MS) was widely used as a method of measuring macromolecular compounds, such as proteins.[22] During his presentation there, Professor Robert Cotter stated that "PD-MS can measure higher masses than laser desorption/ionization (LDI) MS." Professor Cotter was an authority with respect to TOF-MS even at that time, but given my own recent results, which I would present the next day, I could not agree with his statement. I apparently indicated to Professor Cotter that I thought he must be mistaken, and that he should look at my data. Professor Cotter tells me that he was indeed impressed with the high-mass results. He later saw my poster presentation and he and Dr. Catherine Fenselau forwarded details of our ionization method and copies of the spectra to other researchers in Europe and the USA.

At that time, Dr. Takekiyo Matsuo, an assistant professor at Osaka University who was attending the symposium, strongly recommended that I write a formal paper in English. I reluctantly agreed, and in 1988, our contribution was published in *Rapid Communications in Mass Spectrometry*,[23] and is now referred to as one of the original sources of the MALDI technique.

7.2. Manufacture of the Instrument and then Termination of Sales

The analytical technology and the instrument became a commercial product. To sell the instrument, I traveled around Japan visiting many customers, and actually analyzed more than two hundred samples. However, the reaction was almost always, "There is little practical use." I then looked further afield and there was only one potential customer on whom we could pin our hopes. That was Dr. Terry D. Lee, employed at the City of Hope's Beckman Research Institute in the USA. The instrument that he bought was in fact the first and only instrument of our commercialized product that was sold, and we eventually halted development and sales of the instrument. Although the instrument could do what no other instrument was capable of, it seemed to have little practical use. Perhaps, it is fair to say that the sensitivity, accuracy, and resolution required improvement for use in pharmaceutical and medical diagnostic applications.

 © 2003 Wiley-VCH Verlag GmbH & Co. KGaA, Weinheim

8. Development of MALDI Technology

My research and development efforts on MALDI technology remained inactive until 1992 when I was transferred temporarily to KRATOS Analytical (a subsidiary company of Shimadzu Corporation from 1989) in Manchester, England. During that period, our technology that had been conveyed to Europe and the USA was steadily being improved upon and reformed through the efforts of Professor Cotter, Professor Fenselau, and many other researchers throughout the world. Special acknowledgement is warranted for the meritorious efforts of both Professor Michael Karas and Professor Franz Hillenkamp[24–26] of Germany. Were it not for their tremendous and continuous efforts and the achievements of thousands of other researchers, it is certain that subsequent development of this technology that has benefited so many people around the world would not have occurred.

9. Conclusion

Development of this macromolecule ionization technology was not accomplished by one genius or gifted person. It is a victory of teamwork, and I believe it is the result of a lot of honest activity by many individuals seeking to advance a good technology.

The history of chemistry is long and it is natural that the field is wide and deep. Because of this, there is a tendency to believe that chemistry-related technology is already well developed. It should be mentioned here that I strongly believe that building new theories and bringing them to useful roles in the world requires the total mobilization of knowledge in special fields. However, I think it can be said that the technique that I discovered and the subsequent technologies that originated throughout the world broke through the common thinking of chemistry. If I had been caught within the grasp of this thinking, I would not have been able to make this type of unique discovery. Even though I cannot claim to possess extraordinary intellectual abilities, and further, my academic specialization was in a field other than that of chemistry, there is enough proof that I was able to contribute to the development of chemistry-related technology. With this in mind, it would give me great pleasure if many people around the world, and especially engineers working in private business enterprises, would mobilize their courage and hold onto their dreams in the pursuit of scientific innovation for the benefit of all living beings.

I would like to express my thanks to Mr. Ralph Nesson for his tremendous efforts in helping me prepare for my Nobel Lecture presentation, and for his invaluable insight and patience in helping me express my thoughts in English. I would also like to thank Prof. Robert Cotter, Prof. Catherine Fenselau, Dr. Chris Sutton, and Dr. Andrew Bowdler for many stimulating discussions.

Received: February 17, 2003 [A585]

[1] "The Mass- Reflectron, a New Nonmagnetic Time-of-Flight Mass Spectrometer with High Resolution": B. A. Mamyrin, V. I. Karataev, D. V. Shmikk, V. A. Zagulin, *Sov. Phys. JETP* **1973**, *37*, 45–48.

[2] "Time-of-Flight Mass Spectrometer with Improved Resolution": W. C. Wiley, I. H. McLaren, *Rev. Sci. Instrum.* **1955**, *26*, 1150–1157.

[3] "Chemical Ionization Mass Spectrometry. I. General Introduction": M. S. B. Munson, F. H. Field, *J. Am. Chem. Soc.* **1966**, *88*, 2621–2630.

[4] "Photodissociation of Salt Molecules into Ions": A. Terrenin, B. Popov, *Phys. Z. Sowjetunion* **1932**, *2*, 299–318.

[5] "Mass Spectrometry of Aromatic Molecules with Resonance-Enhanced Multiphoton Ionization": D. M. Lubman, M. N. Kronick, *Anal. Chem.* **1982**, *54*, 660–665.

[6] "Ion Formation by $[Li]^+$ Ion Attachment in High Electric Fields": U. Giessmann, F. W. Röllgen, *Org. Mass Spectrom.* **1976**, *11*, 1094–1100.

[7] "Field Ion Emitters for Field Desorption of Salts": F. W. Röllgen, U. Giessmann, H. J. Heinen, S. J. Reddy, *Int. J. Mass Spectrom. Ion Phys.* **1977**, *24*, 235–238.

[8] "In-beam Electron Impact Mass Spectrometry of Amino Sugars": M. Ohashi, S. Yamada, H. Kudo, N. Nakayama, *Biomed. Mass Spectrom.* **1978**, *5*, 578–581.

[9] "Proton Transfer Mass Spectrometry of Peptides. A Rapid Heating Technique for Underivatized Peptides Containing Arginine": R. J. Beuhler, E. Flanigan, L. J. Greene, L. Friedman, *J. Am. Chem. Soc.* **1974**, *96*, 3990–3999.

[10] "Chemical Ionization Mass Spectrometry of Salts and Thermally Labile Organics with Field Desorption Emitters as Solids Probes": D. F. Hunt, J. Shabanowitz, F. K. Botz, D. A. Brent, *Anal. Chem.* **1977**, *49*, 1160–1163.

[11] "Surface Chemical Ionization Mass Spectrometry": G. Hansen, B. Munson, *Anal. Chem.* **1978**, *50*, 1130–1134.

[12] "The Effects of Heating Rate and Sample Size on the Direct Exposure/Chemical Ionization Mass Spectra of Some Biological Conjugates": R. J. Cotter, C. Fenselau, *Biomed. Mass Spectrom.* **1979**, *6*, 287–293.

[13] "High Mass Analysis by Laser Desorption Fourier Transform Mass Spectrometry": C. L. Wilkins, D. A. Weil, C. L. C. Yang, C. F. Ijames, *Anal. Chem.* **1985**, *57*, 520–524.

[14] "Fast Atom Bombardment of Solids (F.A.B.): A New Ion Source for Mass Spectrometry": M. Barber, R. S. Bordori, R. D. Sedgwick, A. N. Tyler, *J. Chem. Soc. Chem. Commun.* **1981**, 325–327.

[15] "Fast Atom Bombardment Quadrupole Mass Spectrometry": D. J. Surman, J. C. Vickerman, *J. Chem. Soc. Chem. Commun.* **1981**, 324–325.

[16] "Development of Laser Ionization Time of Flight Mass Spectrometer I—Curved Electric Field Ion Reflector": Y. Yoshida, K. Tanaka, Y. Ido, S. Akita, T. Yoshida, *Shitsuryo Bunseki Rengo Toronkai Yoshishu*, **1987**, 12–13 (in Japanese).

[17] "Development of Laser Ionization Time of Flight Mass Spectrometer II—High-speed, High-accuracy Measuring Circuit for TOF Spectrum": S. Akita, K. Tanaka, Y. Ido, Y. Yoshida, T. Yoshida, *Shitsuryo Bunseki Rengo Toronkai Yoshishu* **1987**, 14–15 (in Japanese).

[18] "Development of Laser Ionization Time of Flight Mass Spectrometer III—Sensitive Ion Detection in High Mass Range": Y. Ido, K. Tanaka, S. Akita, Y. Yoshida, T. Yoshida, *Shitsuryo Bunseki Rengo Toronkai Yoshishu*, **1987**, 20–21 (in Japanese).

[19] "Development of Laser Ionization Time of Flight Mass Spectrometer IV—Generation of Quasi-Molecular Ions from High Mass Organic Compound": T. Yoshida, K. Tanaka, Y. Ido, S. Akita, Y. Yoshida *Shitsuryo Bunseki Rengo Toronkai Yoshishu*, **1987**, 22–23 (in Japanese).

 © 2003 Wiley-VCH Verlag GmbH & Co. KGaA, Weinheim

[20] "High Molecular Ion Detection using Laser Ionization TOF Mass Spectrometer": T. Yoshida, K. Tanaka, Y. Ido, S. Akita, Y. Yoshida, *Shitsuryo Bunseki Rengo Toronkai Yoshishu*, **1987**, 30–31 (in Japanese).
[21] "Detection of High Mass Molecules by Laser Desorption Time-of-Flight Mass Spectrometry": K. Tanaka, Y. Ido, S. Akita, Y. Yoshida, T. Yoshida, *Proceedings of the Second Japan-China Joint Symposium on Mass Spectrometry* **1987**, 185–188.
[22] "Plasma Desorption Mass Spectrometry: Coming of Age": R. J. Cotter, *Anal. Chem.* **1988**, *60*, 781A-793A.
[23] "Protein and Polymer Analyses up to *m*/*z* 100000 by Laser Ionization Time-of-Flight Mass Spectrometry": K. Tanaka, H. Waki, Y. Ido, S. Akita, Y. Yoshida, T. Yoshida, *Rapid Commun. Mass Spectrom.* **1988**, *2*, 151–153.
[24] "Influence of the Wavelength in High-Irradiance Ultraviolet Laser Desorption Mass Spectrometry of Organic Molecules": M. Karas, D. Bachmann, F. Hillenkamp, *Anal. Chem.* **1985**, *57*, 2935–2939.
[25] "Laser Desorption Ionization of Proteins with Molecular Masses Exceeding 10000 Daltons": M. Karas, F. Hillenkamp, *Anal. Chem.* **1988**, *60*, 2299–2301.
[26] "Ultraviolet-Laser Desorption/Ionization Mass Spectrometry of Femtomolar Amounts of Large Proteins": M. Karas, Ingendoh, A. U. Bahr, F. Hillenkamp, *Biomed. Environ. Mass Spectrom.* **1989**, *18*, 841–843.

 © 2003 Wiley-VCH Verlag GmbH & Co. KGaA, Weinheim

Electrospray Ionization

Electrospray Wings for Molecular Elephants (Nobel Lecture)**

*John B. Fenn**

Keywords:
analytical chemistry · electrospray ionization · history of science · mass spectrometry · Nobel lecture

From the Contents

Upto 1952	3871
From Flames to Flying Elephants	3876

Upto 1952

My father, Herbert Bennett Fenn, the eldest of three children was born and raised on a farm in northern Delaware which his father operated but did not own. I never saw that farm but I vividly remember my Grandmother's frequent reference to a single chestnut tree in the front yard, so large and prolific that the nuts from that one tree paid the taxes on the farm every year! My mother was the sixth of ten children in the family of John Clarence Dingman, a country doctor in Spring Valley NY whose three surviving sons also became physicians. Dad worked his way through college, graduating in electrical engineering from Rutgers in 1910, the same year that mother received a degree in home economics and nutrition from Columbia. They were both hired by the Presbyterian Mission Board to teach at the Sheldon Jackson Mission School in Sitka, Alaska, originally settled by the Russians and sometime capital (until replaced by Juneau in 1900). The Chairman of that Board told each one about the other and warned them both not to fall in love, but if they did and got married he would provide them with a house for as long as they stayed in Sitka! They did and he did, after mother's death in 1990 (Dad had died in 1944) we found in her papers a clipping from the Sitka paper with a photograph of the "Honeymoon Cottage".



During a cruise in 1996 I spent a day in Sitka. The Mission School is now Sheldon-Jackson University. I visited the library, discovered a complete file of student newspapers, and found several articles about my parents! Moreover, the present Librarian was then living in the "Honeymoon Cottage" and gave me a tour so I was actually able to look out through its front windows and see the magnificent view of Sitka Bay that my parents used to rave about.

The newlyweds were very happy in Alaska and no doubt would have remained there indefinitely had it not emerged that mother would be unable to bear children except by Caesarian Section, a procedure not then available in Sitka. Determined to have family she persuaded Dad to move back to the States where he became manager of the Metacloth Company, a small enterprise in Lodi, New Jersey whose main product was cotton duck treated by immersion in a concentrated ammoniacal solution of copper hydroxide followed by a wash in acid. The deep blue "cuprammonium" solution dissolved some of the cellulose which reprecipitated during passage through the succeeding acid bath, filling the pores of the cloth enough to make it "water resistant" but not "waterproof". Residual copper provided a characteristic blue-green color along with a high resistance to attack by microorganisms and white ants. For these reasons, "Metacloth" was in fairly steady demand for tents and tarpaulins in tropical latitudes. My abrupt introduction to "chemistry" occurred on one of the treasured Saturdays when Dad took me to the plant. Nosing around outside I lifted a small flap on the cover

[*] Prof. Dr. J. B. Fenn
Department of Chemistry
College of Humanities and Sciences, Box 2006
Virginia Commonwealth University
1001 West Main Street, Richmond VA 23284-2006 (USA)
Fax: (+1) 804-367-8599
E-mail: jbfenn@vcu.edu

[**] Copyright© The Nobel Foundation 2003. We thank the Nobel Foundation, Stockholm, for permission to print this lecture.

DOI: 10.1002/anie.200300605
© 2003 Wiley-VCH Verlag GmbH & Co. KGaA, Weinheim

of a large tank half full of cuprammonium solution. I still recoil at the memory of that ammoniacal, and demoniacal, assault on my eyes and nose. It was a startling revelation on how and why a whiff of smelling salts can often revive people from a dead faint!

Our home was in Hackensack, N.J., next door to Lodi and County Seat of Bergen County. I was born in New York City in 1917 and three-plus years later my brother Norman arrived in Paterson, N.J. where two of mother's brothers were surgeons. The Metacloth company was sold in 1926 and Dad was unceremoniously dumped by the new owners. He was not a vindictive man but he got no little satisfaction out of the several occasions in the next two years when his help was needed in overcoming mistakes made by the new management. Meanwhile, approaching fifty and finding equivalent jobs scarce, he was paying the bills by working as a draftsman at the Fokker Aircraft Company in Teterboro, N.J. The value of having a trade as back-up for a profession was an enduring object lesson for a youngster on the eve of the Great Depression but there was for him a far more exciting consequence of the Fokker connection. When Lindbergh's "Spirit of St. Louis" was shipped back from Paris after its famous flight across the Atlantic, it was parked for a time in a hangar at the Teterboro airport. The thrill of a lifetime for a ten year old boy was when his Dad took him into that hangar where he was allowed to sit in the cockpit and move the controls, pretending to be pilot of that famous plane!

Meanwhile the family fortunes were going down hill, much further than my brother and I were aware. Just before Dad lost his job, he and mother had invested their life savings in a new (for us) house that everyone insisted was worth "every nickel" of the $15,000 that it cost! Unfortunately, after we had to move and before the house could be sold the great depression had begun. No prospective buyers had enough nickels so those savings disappeared in the meltdown of foreclosure. Meanwhile, a door of opportunity had opened in Berea, Kentucky, a small community of 3500 or so inhabitants at the edge of bluegrass country some 40 miles south of Lexington and roughly halfway between Cincinnati, Ohio, and Knoxville, Tennessee. The town of Berea was home for a remarkable institution known by the same name but officially entitled "Berea College and Allied Schools". Both the community and the school had their roots in a non-sectarian Union Church founded in 1848 by John G. Fee, on a ridge of land donated by Cassius Clay, a brother of Henry Clay, the famous orator and statesman from Lexington, Kentucky.

Fee was a Congregational Minister from Massachusetts and a fervent abolitionist determined to provide educational opportunities for needy students, whatever their race or creed. After decades of effort by himself and his followers his dream grew into what in 1928 comprised a coeducational student body of about 1700 divided among four schools: 1) The Foundation-Junior-High School with an ungraded program into which students with as little as two years of formal schooling could enroll and progress at their own rate up through the equivalent of eighth grade into a standard and accredited ninth-grade curriculum; 2) The Academy, with an accredited curriculum for grades 10 through 12, 3) the Normal School with a two-year program leading to a Teaching Certificate, and 4) the College which offered accredited curricula leading to BA degrees in the liberal arts and sciences as well as BS degrees in home economics and agriculture. Mother's sister was teaching in the College and knew that the Industrial Arts Department of the Foundation School and the Academy needed someone to teach auto mechanics and practical electricity. Dad was eminently qualified and got the job. We moved to Kentucky in time for me to enter the eighth grade in the "Training School" of Berea's Normal School in the fall of 1928. The next fall I entered ninth grade in the Foundation School and continued on through the Academy and College.

A lot of misgivings, pain, and confusion attended our passage through the newly opened door, including an automobile accident on the way to Kentucky, but life on the other side turned out to be rich and rewarding beyond what any of us had dreamed. In later years Dad and Mother both said time and again, that losing his "good" job in New Jersey turned out to be the greatest blessing that we could have received! To this day my brother and I share those sentiments and count ourselves especially privileged to have been reared in what was a truly remarkable community. Its soul was its President, William J. Hutchins, father of Robert Maynard Hutchins, the "boy wonder" of the American education scene who became Secretary of Yale at the age of 24, Dean of its Law School at 26 and President of the University of Chicago at 30! "William J", as the father was fondly known at his own institution, was truly one of nature's noblemen. A striking man of vision and patrician to the core, his Berea was a singular stage on which the play was always provocative and the message meaningful. Name an outstanding man or woman of letters, the arts, science, or religion, of those days and the odds are high that he or she came to Berea to talk at one of the thrice weekly "United Chapels" for students from all schools. Attendance was required of all, and resented by most, but at my 50th class reunion there was a remarkable consensus among my surviving classmates that the community experience of those United Chapel services were by far the most memorable and valuable components of their educational experience. Alas, that tradition has long since disappeared, one more victim of "students' rights" and television. Moreover, as the public education system improved in surrounding "Appalachia", over the years, the need for Berea's Foundation School, Academy, and Normal School faded so that the only survivor is a now a substantially larger Berea College.

A unique feature of Berea was and is a student-labor program that provided much of the manpower required to run the institution. Under the supervision of permanent staff, the dining halls, dormitories, offices, and yard work were all maintained and operated by student labor. In addition were several "industries" including a bakery, broom factory, dairy, large truck garden, sheep farm, piggery, a "woodwork department" that made fine furniture, and a weaving establishment. The normal work load was two hours a day by which a student could earn as much as half or two thirds of his or her out-of-pocket expenses that in the 1930s averaged only $250 to $300 per year because tuition was free! The system was very democratic because every student was

 © 2003 Wiley-VCH Verlag GmbH & Co. KGaA, Weinheim

required to work at least two hours a day. A fair fraction of the student body comprised so-called half-day students who worked four hours a day, earning enough to pay all expenses. I knew students who arrived at Berea with nothing but the clothes on their backs, having dropped out of school after the second grade, and worked their way through college! It is not surprising that competition to enter Berea, especially the college, was extremely keen. To avoid having to reject such a large fraction of applicants, the Trustees had established a policy requiring that 85 percent of the student body come from a region of Appalachia comprising some 500 or so counties in Virginia, West Virginia, Kentucky, Tennessee, and North Carolina. The remaining 15 percent of the students came from the rest of the world. Today's Berea is quite a different place because the growth of alternative educational opportunities in Berea's "territory", has decreased demand to the point that in 1987, at my 50th reunion, I learned there were only two applicants for every opening in the College compared to 20 or 30 in my day. Part of that decrease in demand is due to a higher level of average income in that "territory" so that fewer students can show that they cannot afford to go elsewhere, a requisite for admission.

When I graduated from the Academy in 1932 I was only 15, too young, my parents thought, to go to college, so I stayed in the Academy an extra year taking courses in mechanical drawing and shorthand. I also continued the piano lessons that I had started the year before and spent enough time practicing so that I actually gave a recital during my last year in college! Alas, whatever piano skills I had have faded until now I do well to play chopsticks with my grandchildren! When I entered College with the class of '38 I had not decided on a major but I leaned towards a science, probably because of my long affair with the "Book of Knowledge", an encyclopedia set for young people which my parents bought when I was around eight or nine. During the hours that I pored over them, its 20 volumes became a well-worn magic carpet to new and fascinating worlds. I have often quipped that "I got through college on the Book of Knowledge", a bit of rhyming hyperbole that contains an appreciable kernel of truth.

The College required at least one course in science for all students no matter what their major. Having enjoyed my chemistry course in the Academy I enrolled in "Introductory Chemistry" during my freshman year. It was taught by Professor Julian Capps, the senior of the two-member chemistry faculty. He was a wonderful teacher who made his subject live. I was so seduced that chemistry became my major even though gravimetric analysis gave me fits in my sophomore year. I repeated the lengthy phosphorous determination on three samples each of ten unknowns before I got one set of three results with acceptable agreement! It seems ironic that mass spectrometry, the center of my scientific life for the last 20 years, is really just an exercise in gravimetric analysis!

During that sophomore year an experiment in another kind of chemistry turned out to have a big effect on my chemical education. I fell in love with a girl in the junior class. Determined to catch up with her and graduate when she did, I went to summer school in 1936 at the University of Iowa because it had a 10-week session that allowed me to earn 12 semester hours of credit in organic chemistry under "Uncle Charlie" Raiford, and inorganic chemistry under Professors Jacob Cornog and Perry Bond. All in all it was a very hot and grueling summer. The romance that had blossomed in the spring and sent me off to summer school, withered the following fall. However, because I would be within two courses of finishing my degree requirements by end of that year, my third in college, I managed to get classified as a Senior and became a provisional member of Class of '37 at the June commencement, the objective inspired by a young man's fancy of the previous spring. My courses in chemistry thus far had required only some facility in simple algebra. Straight A's in all Professor Peck's courses in the Academy (plane geometry, advanced algebra, solid geometry, and trigonometry) had excused me from freshman math in college, all that was then required for a major in chemistry.

Fortunately for my future our next door neighbor, George Bent, was visited by his brother Henry, then an assistant professor of chemistry at Harvard. When Henry discovered that I was contemplating graduate work in chemistry, having had no college math, he was aghast and spent a couple of hours impressing me with the importance of mathematics in chemistry. As a result I spent much of my third and last year of college immersed in that subject. Fortune had tossed me another favor in the form of Berea's new curriculum based on four nine-week quarters instead of two 18-week semesters. So-called "intensive" courses met six hours a week for nine weeks while "running" courses met three hours a week for eighteen. Thus, a standard full load of 15 class hours per week comprised two intensive courses and one running course, an arrangement which I heartily endorse. One major advantage is that a student takes only three courses at any one time instead of five. It is much less distracting to be studying three subjects at a time rather than five. The particular advantage for me was that the calendar time for a three-credit-hour course was cut in half so that both Course B, and its prerequiste Course A, could be completed in two nine-week quarters instead of two eighteen week semesters. Thus, in my senior year I was able to take analytic geometry, differential calculus, integral calculus, and complex variable, all in that same year! It was pretty heavy going, but it enabled me to survive in graduate school where I took one more undergraduate course in advanced calculus. The record seems to say that I have also survived after graduate school but a lack of mathematical skills has been a great handicap throughout my life.

Though I had taken part in the June commencement exercises at Berea in 1937, I still had course requirements to complete before I could get my degree. I fulfilled those requirements at Purdue University that summer by taking physical chemistry with lectures by Roy Newton and laboratory under Hershel Hunt, along with a course in chemical microscopy under Ed F. Degering.

During that hectic last year in college I had applied to several universities for graduate study in chemistry. Yale and Northwestern responded with offers of teaching assistantships that would meet most of my expenses. I first leaned toward Northwestern but, for reasons I won't take space to enlarge

 © 2003 Wiley-VCH Verlag GmbH & Co. KGaA, Weinheim

on, I finally decided on Yale. That decision delayed by half a century my meeting Malcolm Dole who in 1937 was a young assistant professor of chemistry at Northwestern. It was the experiments he reported much later (in 1968) that changed the course of my scientific life.

At Yale I found myself in a new and different world. I had done time in two much larger universities and one much smaller college but I was completely unprepared for, and awed by, the splendor of Yale's campus. Its architectural theme has been disdainfully dubbed "Fifth Avenue Gothic" by the self-styled experts who sneer at such expensive imitation of the old world. But a wide-eyed small-town youth from Kentucky found it all fascinating and loved to wander around and through the gardens, gargoyles, and gates that were scattered throughout the campus. To me it was rewarding recreation to discover and explore the little nooks and courtyards where one could sit in the shade of a tree completely oblivious to the cacaphony of a busy city, only a few yards away but completely shut out by the thickest walls and heaviest masonry I had ever seen. Sterling Library, then said to be the largest in the world with open stacks, became a favorite haunt where I spent many winter weekend afternoons with a good book and an apple or a candy bar. My room in the Hall of Graduate Studies looked out on a forest of chimneys, slate roofs, and Gothic towers that resembled a Hollywood version of medieval London. I ate in an elegant dining hall, complete with menus and waiters—twenty one meals per week for a now incredible eight dollars! Even so, to save money I took advantage of an option in the board contract and "signed out" every week for dinner on Friday night along with breakfast and lunch on Saturday. This "fasting" saved me $1.15 every week and probably was good for my figure! My assistantship paid a total of $850 for nine months, of which $350 went for tuition and fees. By such frugalities as the weekly "fast" I could make the remaining $500 cover most of my other expenses. My parents were horrified when they later learned of my miserly existence at Yale but I was determined to get along without their support.

On the appointed day in September the six new graduate students in physical chemistry met in Sterling Chemistry Laboratory with Professor Herbert Harned, the ranking faculty member in that subject whose colleagues included Lars Onsager, Benton B. Owen, Rodney Smith, George Murphy, John Vance, and Gosta "Gus" Akerlof. With little or no ceremony, no introductions, and no opportunity to ask questions or indicate preferences, we were assigned to advisors. I recall "Herbie" as he was known but not addressed, saying to me: "Fenn, you might as well go with Gus." Thus, began what blossomed into a close friendship that lasted until the day Gus died, many years later, in Princeton.

The Yale curriculum for chemistry graduate students in those days was pretty cut and dried. During the first year we took four courses, spent 12 to 14 hours per week as assistants in undergraduate labs and the rest of the time getting our feet wet in the laboratory on what would become our dissertation research. At the end of that first year the faculty, on the basis of course grades and day to day observations, decided whether or not each student was Ph.D. material. Those for whom thumbs were down were given a Master's degree and dismissed. The others continued, almost always receiving a Ph.D. after two more years. The second year was much like the first except that we took only a couple of courses and spent much more time on our research projects. At the beginning of the third year we had to take a two day written comprehensive exam. While I was a student, all who took that exam passed it so I don't know what the consequences of failing would have been. One very big difference in the third year was that we could no longer be teaching assistants but were expected to spend full time on research. Thus, unless we were lucky enough to win one of the two fellowships available to third year students, we were on our own financially. My solution to this problem was to get married, not to my sophomore flame but to Margaret Wilson, who became supervisor of my student labor at Berea while I was working in the Registrar's Office. She was a beautiful woman by whom I (then in the tenth grade!) was smitten the first day she started work as Assistant Registrar. Always ten years older than I she seemed to be so far beyond my reach that I never dreamed she could ever be more than the close friend and confidante that she became. I had escorted her to several events while I was in college and when I was home after I graduated. Romance bloomed while I was at Yale and she finally agreed to become my bride at end of my second year. She also became my "fellowship" during that third year at Yale, supporting us both on the 50 cents per hour she earned at various odd jobs. To this day I marvel that the daughter of a very conservative minister had the courage to ignore the disapproval of her parents and the inevitable elevation of eyebrows by everybody, everywhere, at our flagrant departure from the social norm. One of my closest friends told us decades later that he had been sure our marriage would not last more than a year or so. In fact it was not until 1992 that I lost my bride of 53 years in a New Zealand car crash. She was then 85 but looked and acted ten years younger than the husband she had "snatched from the cradle."

The plain truth is that in matters of matrimony this society's norms are genetically out of joint. Women on average live about ten years longer than men and yet become the wives of husbands who are several years older. That is why widows greatly outnumber widowers. Some say that this imbalance in life expectancy will be redressed as women increasingly become exposed to the stresses of employment in the workplace. I am much more inclined to believe the geneticist who told me that the female of the species lived longer than the male because she is fundamentally tougher and more resistant to the ravages of age. In choosing a mate men should follow the advice of Ben Franklin in his letter of advice to a young man on choosing a mistress. His message? "be sure she is older than you are!"

Only in choosing a graduate school did I exert any influence on the research I would do for my thesis. That influence was unwitting because I knew nothing of the faculty research interests at either Yale or Northwestern. Indeed I had only the vaguest idea of what graduate study and research were all about. Thus, I felt neither joy nor apprehension when I was summarily assigned to Gus Akerlof's group. Most of the research by Harned and his colleagues was on the properties of electrolyte solutions, the more dilute the better. So narrow

 © 2003 Wiley-VCH Verlag GmbH & Co. KGaA, Weinheim

was this focus that when I left Yale I halfway believed the old cliche that "physical chemistry was the study of slightly contaminated water." Gus was a bit of a maverick because he had an interest in concentrated solutions. In essence what I had to do was measure the potential difference between electrodes of silver/silver chloride and platinum/hydrogen in solutions of HCl with molalities from 0.01 to 10.0 in solvents comprising methanol in water at concentration intervals of 10 per cent from 0 to 90% methanol, at temperatures every ten degrees from zero to 50 Celsius. As I remember the total number of acceptable electromotive force (emf) measurements was around 3000, taking into account that each measurement was made in duplicate. Thus, my routine every afternoon for most of two years was to prepare three pairs of cells with both cells of each pair containing the same solution. The cells were suspended in a large water bath or "thermostat" and allowed to equilibrate over night (i.e. with hydrogen bubbling over the Pt electrodes.) If by the next morning the emfs in each pair of cells agreed to within some forgotten small fraction of a millivolt, then I would haul some 80 pounds or so of ice from the basement to lower the bath temperature to near 273 K. The rest of the day would be spent recording emf values for all six cells at every 10 K as the thermostat was heated to 313 or 323 K depending on the vapor pressure (i.e. the methanol content) of the cell solvent. All the results were fitted by least squares to a quadratic curve for the dependence of emf on concentration. The least-square calculations were all carried out on a hand-cranked Monroe calculator, except when I was lucky enough to grab the one electrically driven machine in the calculating room. Clearly, I was less than inspired by this introduction to "original research". The experiments were a boring chore with few redeeming features. The results contained no surprises and nothing of much interest to anyone, least of all me. It was some years later before any of them found their way into the literature and then only as part of a table in a review article that Gus had been asked to write. My dissertation attested to the sterility of that project, consisting as it did of 45 pages of tables with only three pages of text! Although this first experience in "original research" shattered some illusions, my three years at Yale were a rewarding experience. I made many long lasting friendships with both fellow students and faculty. The physical chemists were a very congenial group and Herbie Harned was really a very interesting man, except in the class room. He came by almost every lab almost every day to chat with us students about almost everything. Sometimes his visits were inconveniently long and would interfere with experiments. One of the older graduate students had told me that Herbie would run for cover if he were asked to help, for example, by holding a light or a tool during some adjustment. That ploy worked like a charm and saved me many hours. Actually, the Harneds were very kind and warm hearted people. They held an open house every Friday night which both students and faculty felt obliged to attend more or less regularly. More often than not we ended up around the piano in a group sing-along with Roger Bates, then a Sterling Fellow and accomplished musician, at the keyboard.

I also learned a lot about life and lore outside of chemistry, for example, to play bridge, to drink beer, and to smoke a pipe during the mostly dull seminars every Tuesday night. I had many interactions with many interesting people. The weekly university calendar was filled with provocative events ranging from seminars to sermons and concerts to contests. My perspectives were stretched by memorable if abstruse encounters with great minds, including lectures on resonance by Linus Pauling, and two required courses in statistical mechanics under Lars Onsager (known to the students as Norwegian I and II!). Gus and his wife Rosalie, who was the sister of Joe Hirschfelder, looked after his students with great care and affection, making their house our home away from home. Rosalie took my new bride under her wing, showering us newlyweds with almost too much attention. I was extremely fond of Gus and most grateful for his always calm demeanor and seeming imperturbability. He strongly disapproved of marriage for graduate students but when I told him I wanted to take a wife he protested not at all and simply said "OK, we take it from here." He and "Magee" as my wife was later known, became extremely fond of each other and he later told me many times that marrying her was the smartest thing I ever did, an opinion shared by everyone who has known us both. All in all, my time at Yale was happy and rewarding but I left with a much diminished interest in "scholarly research", and no desire to return. I often think about how surprised and pleased Gus would have been to know that six decades later his son George Akerlof would share the 2001 Nobel Prize in economics and his student John Fenn would share the 2002 Prize in Chemistry!

My immediate and exciting prospect after graduation from Yale was a job in the research department of the Phosphate Division of Monsanto Chemical Company in Anniston, Alabama. The starting salary was $2700 per year, then the going rate for new Ph.D.'s in Industry and a mind-boggling jump from the $1000 or so a year Magee and I had been living on. I couldn't understand why my mother laughed when I once remarked that I didn't know how we could spend so much money!

Anniston, the county seat of Calhoun county and "Cast Iron Pipe Capital of the World", was located halfway between Atlanta and Birmingham. Living there was my introduction to the deep south where Cotton still grew and the Confederate Flag still flew. It was the home of Fort McClellan, a long-time army base that was already gearing up for America's forthcoming participation in World War II. Two of my mother's brothers had been medical officers at McClellan during World War I and two of our closest friends from New Haven passed through there after being drafted in the wake of Pearl Harbor. We had the chance to compensate them a wee bit with an occasional home-cooked meal. I was more fortunate because the army was not yet drafting husbands.

Monsanto had recently acquired the Anniston Plant when it bought Swann Chemical Company started by a legendary character named Theodore Swann. He had pioneered the production of phosphoric acid from elemental phosphorous shipped in by tank car from a plant in Columbia, Tennessee where it was produced by smelting "phos rock" in an electric furnace. At Anniston the phosphorous was burned in air to produce its pentoxide which could be hydrated to form acid of any desired concentration. Major customers for the acid

 © 2003 Wiley-VCH Verlag GmbH & Co. KGaA, Weinheim

per se included the soft-drink industry, especially the Coca Cola Company in nearby Atlanta. According to local folk lore, the first tank car of food-grade acid to be delivered was filtered through laboratory Buechner funnels because the filtration plant was not ready in time to meet the deadline on the sales contract! Much of the phosphoric acid left the plant in the form of sodium and potassium phosphates that among other applications were widely used as soap builders, water conditioners, and in food products, such as baking powders.

The other main product line, which some said was the main reason Monsanto bought Swann, comprised biphenyl and its chlorinated derivatives known as Arochlors, the now notorious PCBs (polychlorinated biphenyls). Biphenyl was produced by bubbling benzene vapor through large baths of molten lead at a temperature of around 800 °C, as I remember. Liquid metal as a heating agent provided a rapid rise and close control of the temperature, thus minimizing formation of byproducts which mostly comprised *ortho*, *meta*, and *para* diphenyl benzenes. The various Arochlors were characterized by their chlorine content which ranged from 10 % to 60 % by weight. One of their main uses was as transformer oils because they had very good heat-transfer characteristics, would not burn, and were very inert. Indeed, they were so inert and sticky that the chemists insisted that if Arochlor ever got into a laboratory some of it would remain forever! Because it was so inert we practically bathed in the stuff, never dreaming that it might be toxic. General Electric dumped PCB wastes into the Hudson River for many years and is now resisting Federal orders to dredge it all up. Recently, the press has reported growing anger in Anniston and threats of legal action as new surveys have shown the extent to which PCBs from the plant where I worked have contaminated the soil and waters around the town. My own substantial exposure seems to have had no ill effects, but I daresay that even today, sixty years later, the PCB content of my fatty tissue would horrify the EPA (environmental protection agency)! There is no doubt that PCBs in the environment accumulate in the fatty tissues of mammals and fish. The evidence of resulting toxicity is less convincing. I remember a paper by an Australian chemist claiming that the only documented evidence of significant toxicity stemmed from two cases in which PCBs, used as the heat-transfer medium in the heating coils of deep fat fryers, leaked into the fat. The resulting reaction produced highly toxic benzo compounds whose identity I have forgotten. I do know that sixty years ago I practically bathed in the stuff while operating a pilot plant in which PCB was produced in the vapor phase by reaction of biphenyl with HCl and air over a copper catalyst in a variation of the old Deacon process for producing chlorine by the oxidation of HCl. Occasionally I would get a slight skin rash, as did the other operators, but I have detected no lasting effects.

After I had been at Anniston for a year, James W. Mullen, II a young Ph.D. organic chemist from Princeton came aboard. He and I became good friends, sharing a growing dissatisfaction with the way things were being run at work. Jim insisted that someday he was going to start a research company and that when he did he wanted me to join him. Talking about what we might do was fun but it all seemed like pipe dreaming to me. Having become increasingly disenchanted with the work situation we both resigned and left Anniston on the same day in 1943. Jim went to Bell Labs in New Jersey. I took my family, which now included an 18 month old daughter, Marianne, to Wyandotte, Michigan where I had obtained a job in the research department of Sharples Chemicals, a relatively small producer of alcohols, amines, esters, and other derivatives of amyl chloride produced by the chlorination of pentane. One day in June of 1945 a letter came from Jim saying that he had finally started his company and wanted me to join him. I took a train down to Richmond to find out more. At Bell Labs he had become involved in Project Bumblebee, a large-scale effort by the Navy to develop a ramjet-powered anti-aircraft missile for the fleet. The ramjet depends upon ram pressure from high-speed-flight to compress air enough so that its expansion after heating by combustion could provide useful thrust. It was clear that supersonic flight velocities would be required to achieve substantial thrust but because there was little or no information on drag at such velocities, nobody knew whether that thrust could equal or exceed the drag. The Project name, Bumblebee, derived from a bit of aeronautical badinage to the effect that by all the laws of modern aerodynamics it is impossible for a bumblebee to fly, but the bumblebee doesn't know any aerodynamics so it goes ahead and flies anyway!

From Flames to Flying Elephants

Experiment, Inc., the name Jim Mullen gave his company, prospered over the next seven years. To watch and participate in its growth, from a total of three employees when I arrived to perhaps 45 or so when I left in 1952, was an exciting experience. Most of its business was based on research-and-development (R and D) contracts with government agencies for which the central theme was combustion and propulsion but we did pursue some commercial ventures. There were some important personal dividends from my investment of time at Experiment. One was that I learned a little bit about the dynamics and thermodynamics of compressible flow, a newly popular area of research spawned by the advent of jet propulsion and sometimes referred to as "aerothermodynamics", or "aerothermochemistry" if changes in chemical composition were involved. Another personal dividend was the opportunity to do some research in combustion, both applied and fundamental. Jim was a strong believer in publishing our results. Thus the first research publication of my life was a paper on ignition in high-speed flow, coauthored by Jim and a junior colleague, M. R. Irby. That paper appeared in 1949, almost a decade after I left graduate school.[1] Consequent to several more papers, visits to other labs, and attendance at various meetings, I began to get some recognition in the "combustion community". Moreover, in an about-face from my feelings at Yale, I found I enjoyed doing research and communicating with others about my findings and theirs.

My life in Berea had made me think that I would someday like to become a college professor. But I had also thought that I should get some of the real-world industrial experience that

 © 2003 Wiley-VCH Verlag GmbH & Co. KGaA, Weinheim

had seemed to help make Julian Capps, my chemistry professor at Berea, such an effective teacher. That desire to join a college faculty had faded somewhat at Yale but was revived a bit during my experience at Experiment, Inc. We obtained a number of provocative results on some properties of flames, in particular on stabilizing them in high-velocity flows. Both Jim and the sponsors of our studies were happy to have us attend technical meetings and to publish results of our studies, (so long as they didn't involve classified information.) Consequently, I got to know, and become known by, a number of people in the combustion community. One result of this new and limited "notoriety" was an offer from Princeton University to serve as Director of Project SQUID, a program of pure and applied research in "those fields of science relating to jet propulsion" including combustion, fluid flow, and heat transfer. Financed by the Office of Naval Research (ONR) and administered by Princeton, Project SQUID was named after the jet-propelled decapod of the sea. (That name had additional but unpremeditated relevance in that both the animal and its namesake project secreted ink, the former in clouds that confused predators, the latter in print in reports that confused readers!) SQUID's organizational structure comprised a prime contract between ONR and Princeton, with subcontracts at any one time between Princeton and from 12 to 20 or so university and industrial laboratories. The overall purpose was to cultivate interest and activity by students, faculty, and other investigators in combustion, fluid flow, and heat transfer.

One reason for my interest in Princeton was that by then I had learned that research could be a lot more fun than it had been when I was a student at Yale. Another reason was that my Yale mentor, Gus Akerlof, had set up a laboratory in its newly established James Forrestal Center to develop, with Navy (but not SQUID) support, an electrical-discharge process for the production of hydrazine, an attractive rocket propellant. Gus had once visited me in Richmond and in fact had put my name in the pot at Princeton when he learned that the previous director of SQUID was leaving. One of the "other reasons" for my interest was that Jim Mullen and many of his friends, were Princeton graduates. After seven years among those fiercely loyal alumni I had been brainwashed to the point of believing that maybe Old Nassau really was the "best old place of all." Moreover, as I have already noted, my life in Berea had long made me think that I would enjoy becoming a teacher and living in a college community.

At Princeton I would report directly to Sir Hugh Taylor, long-time Chairman of Princeton's Chemistry Department, then Dean of the Graduate School and Chairman of the University Research Board. The position was "with rank of Professor" and the Dean assured me that I would be welcomed as an active member of the academic community. And so, after much soul searching, Magee and I decided to leave the "Cradle of the Confederacy" for what was and is often called "the northernmost southern town in the country". That epithet stemmed from the substantial numbers of Princeton students that over the years have come from below the Mason Dixon line. Before the Civil War it had become customary for students from the south to celebrate graduation by freeing their personal servants. An interesting result is that Princeton has a much larger black population than do other towns of comparable size in that part of the country.

My new job turned out to be very interesting and highly educational. I had to travel a lot but was able to visit many laboratories and meet well-known scientists in many fields all over the country. I got to know the people in ONR pretty well and my circle of acquaintances included people in ARO (Army Research Office) and AFOSR (Air Force Office of Scientific Research) both of which were providing some support for Project SQUID and were represented on its Steering Committee. ONR had a branch in London (ONRL) that maintained a rotating corps of 12 to 15 Scientific Liaison Officers whose job was to promote interaction between scientists and engineers in Europe and America by visiting laboratories and attending scientific meetings. They would get to know the investigators, learn about what they were doing, help them establish contacts with their counterparts in America, arrange visits, find items of equipment, assist with travel arrangements, and the like. Research laboratories in Europe were beginning to recover from the trauma of World War II and they welcomed the communication links and the help with their needs that ONRL could provide. The SQUID office had occasionally been involved in making travel and visiting arrangements for some of the European scientists who came to America under ONRL's auspices. After I had been at Princeton for about three years I was invited to serve a year as an ONRL Liaison Officer in the areas of combustion and propulsion. My bosses in ONR Washington approved and I persuaded John Scott, who had just finished his Ph.D. in aeronautical engineering at Princeton, to mind the store at SQUID while I was gone. Thus, Magee and I and the children, then 9, 11, and 13, went to London for the calendar year of 1955. And what a wonderful year it was! The children still insist that living London was the high point in the Fenn family fortunes which have been going down hill ever since! I share some of those sentiments because that year was also a marvelous experience for the parents. The kids were in school so Magee was free to roam London during the day. I visited many laboratories in many countries, made many friends, and learned "more things than had been dreamt of in my philosophy."

Among these "things" was my stumbling on to something that was to set the stage for the rest of my scientific life. Up to that time flames and their behavior were the focal point of almost all efforts to elucidate the kinetics and mechanisms of the important reactions in high-temperature combustion. The general approach was mostly based on attempts to measure and interpret flame characteristics, such as propagation velocity, flammability limits, ignition temperatures and the like. I had become convinced that flames, with their extremely high gradients of temperature and composition, were much too complex to be useful as stages for the study of those reactions. I often recalled a comment by Philip Rudnick, Professor of Physics at Vanderbilt, who was active in the propulsion panel of Project Bumblebee. He said that the more he learned about flames the more he was convinced that they were organisms whose study properly belonged in the province of biology! I'm sure that view strikes a responsive note in many investigators who have been exasperated by the

 © 2003 Wiley-VCH Verlag GmbH & Co. KGaA, Weinheim

vagaries of flame behavior that seem to give them a life of their own. Indeed, the analogy can be extended. Flames, like organisms, are born, need fuel and oxidant for nourishment, grow and multiply to the extent that those necessities are accessible, and are poisoned unto death when immersed in their own waste products! Not only is their structure and behavior complex but the conversion of reactants to products involves sequences of different reactions over such short distances that to determine how the composition and temperature change with distance or time in real flames, that is, the relation between their "fine structure" and their behavior, was not experimentally feasible with the tools and techniques then available.

Thus, for some time I had been somewhat naively musing about whether and how it might be possible to study chemical reactions by the same approach that physicists so successfully use in the study of nuclear reactions. They build accelerators to produce beams of atomic nuclei with energies of mega to giga electron volts with which they bombard stationary targets comprising collision partners of interest. They then characterize the products from reactive collisions by analyzing the post-collision trajectories of the product particles as measured by appropriate detectors, for example, bubble or cloud chambers. I had been introduced to the possible uses of molecular-beam scattering experiments in chemistry by Professor I. "Izzy" Amdur, a colleague of the Professor Frederick Keyes at MIT whose elegant measurements on the transport properties of gases were being supported by Project SQUID. Amdur was using beam scattering experiments to characterize the intermolecular potentials of molecules. His approach was based on the electrostatic acceleration of ions to relatively high energies and then neutralizing them by charge-exchange collisions with neutral molecules for which the cross-sections are much larger than those for momentum exchange. In this way he could produce beams of neutral molecules with translational energies equal to those of the incident ions. Space–charge effects give rise to the Childs–Langmuir law by which the maximum intensity (current density) of an ion beam is proportional to the square root of its energy. Consequently, neutral beams with intensities high enough to provide good signal-to-noise ratio in a scattering experiment, must perforce have energies substantially higher than the intermolecular potentials that Amdur was trying to probe. His solution to this problem was to locate his detector so that it would "see" only the post-collision beam molecules whose trajectories differed by only a very small amount from their precollision values. This "small-angle scattering" approach allowed him to exploit the high intensities obtainable with beams of high-energy molecules (in laboratory coordinates) in the study of molecule–molecule interactions at low energies in center-of-mass coordinates of the colliding partners. Unfortunately, that approach did not seem to lend itself to the study of reactive collisions.

When I went to ONR London in late 1954, nobody had successfully carried out reactive scattering experiments with molecular beams on any chemical reaction, even one with a negligibly small activation energy. Moreover, activation energies for many combustion reactions were known to be as high as 30 kcal mol^{-1} or more. The energies of beam molecules from conventional effusive sources are always limited by the temperature at which the source could operated. The average translational energy of an oxygen molecule from a source at 3000 K would be only about 10 kcal mol^{-1} (but that temperature is well above the melting point of most materials from which the source might be made!). Any polyatomic molecules of interest in combustion would completely decompose even at much lower temperatures. In sum, the collision energies that can be reached simply by raising beam-source temperatures are severely limited. Even so, the possibility of bringing about reactive collisions by colliding a beam of reactant molecules with other gaseous molecules had been contemplated since the late 1920s. In spite of numerous attempts, no really convincing results had been obtained when we left for London at the end of 1954. However, shortly after we returned to Princeton in early 1956, the age of reactive scattering experiments with molecular beams dawned when Datz and Taylor reported that intersecting beams of K atoms and HBr molecules produced detectable amounts of KBr.[2] These results gave some substance to my musings but there was a fundamental problem with the idea of applying the same method to combustion reactions. Activation energies for the K plus HBr reaction are negligibly small. For many of the most interesting reactions in combustion the activation energies were thought to range from 0.5 to 2.0 or more eV, much much higher than for the reaction studied by Datz and Taylor. Amdur's charge–exchange technique could easily produce beams with much higher energies but because of space–charge effects could not provide useful intensities at energies as low as a few eV. Nor did Amdur's ploy of looking only at small-angle scattering seem applicable in the study reactive scattering. To produce beam molecules from classical effusive sources with energies of even 0.5 eV would require source temperatures of 3000 K. Neither materials of construction for the source, nor reactant molecules other than atoms, could endure such temperatures. The situation thus seemed hopeless.

One day in London I was calculating rocket exhaust velocities achievable with various propellants and suddenly realized that many reactant molecules at the velocities attainable with some such propellants would have translational energies as high as two or more eV. I began to fantasize about using micro-rockets in vacuum as molecular-beam sources, anticipating by 30 years an experiment we actually carried out for another purpose! I then remembered that rocket visionaries had often touted hydrogen as an ideal propellant fluid for nuclear-powered rockets because of its low molecular weight. The limiting maximum convective velocity that can be reached by a gas expanding into vacuum is equal to $(C_p/M T_0)^{1/2}$ where C_p is its constant pressure heat capacity, M its molecular weight, and T_0 its source temperature. Thus the maximum velocity reachable by helium is about 3.33 times that for argon. If the helium is "seeded" with one or two per cent argon, and if those argon atoms are swept along like dust particles in a wind storm, the translational kinetic energy of the argon atoms after free jet expansion of the mixture would be almost 10 times that of the helium atoms, if the two reached the same terminal flow velocity.

 © 2003 Wiley-VCH Verlag GmbH & Co. KGaA, Weinheim

A few days later I was browsing in ONRL's library and ran across the now famous paper by E. W. Becker and K. Bier reporting the production of intense beams of hydrogen molecules by expansion of the gas from high pressure through a small converging–diverging nozzle into vacuum.[3] That paper referenced the also now famous paper by Kantrowitz and Grey in the *Review of Scientific Instruments* which proposed the use of a converging–diverging nozzle to produce a jet of high-velocity molecules in a region of low pressure.[4] A small core portion of that jet would be admitted through a conical "skimmer" into a high-vacuum region to form a jet of molecules. The "static" temperature of the molecules (as measured by a thermometer traveling with the gas and at the same velocity) would be very low so that the divergence of the molecular trajectories downstream of the skimmer would be very small and the velocity distribution in the direction of flow would also be very narrow. In sum, the jet would comprise a very intense beam of molecules, all traveling at nearly the same velocity! Another paper in the same issue of that journal reported a not very successful attempt by Kistiakowsky and Schlichter to reduce the Kantrowitz–Grey idea to practice.[5] Both of those papers also happened to be in the ONRL library and when I read them I began to take my musings seriously. (I was told that Kistiakowsky and Schlicter had been so frustrated by troubles in their experiment that when Schlicter had suffered enough to deserve a degree, they vented their frustration by demolishing the apparatus with an axe!)

I later learned that 25 years earlier, T. H. Johnson, a Sterling Fellow at Yale, had produced intense beams of mercury atoms by expanding the vapor from a "boiler" at several hundred torr into vacuum.[6] Unfortunately this truly remarkable result had been ignored because it was at odds with the dogma from Otto Stern's lab in Hamburg that raising the source-gas pressure (density) would produce a sort of stagnant cloud of molecules at the exit of the source orifice. That mythical cloud would scatter a large fraction of the emerging molecules that might otherwise have contributed to beam intensity. Later in his career at the Franklin Institute Johnson found diffraction effects in the scattering of hydrogen from an LiF crystal, which confirmed the wave nature of particles much heavier than the electrons with which Davisson and Germer had earlier found diffraction effects. Unfortunately, some eight weeks earlier Estermann, Frisch, and Stern had found the same result in Goettingen[7] so Johnson's work again went unnoticed while Stern got the Nobel Prize! An able investigator who was 25 years too early with one landmark experiment and 8 weeks too late with another, Johnson had every right to feel frustrated by the fickleness of fate.

The results predicted by Kantrowitz and Grey in 1951, having been already achieved by Johnson in 1929, were confirmed in the above-mentioned paper by Becker and Bier in 1954. They showed that convective flow of gas through a small orifice from high pressure into vacuum could indeed produce molecular beams with much higher intensities than could the effusive sources introduced and exploited to great advantage by Otto Stern and his colleagues. Moreover, these "convective" beams had much narrower velocity distributions than did their effusive cousins. Consequently, the achievable intensity within a narrow velocity interval, a highly desirable feature, could be very much higher with convective beams. What had not yet been shown, nor apparently considered, was that heavy molecules could be accelerated to suprathermal translational energies by expansion of a light carrier gas, such as hydrogen or helium, in which those heavy molecules were present a low levels.

When I returned to Princeton after my year in London, I found that John Scott, who had run the SQUID Office during my absence, was going to the University of Virginia as an assistant professor of aeronautical engineering. He was wondering what research he ought to work on and I told him about my musings on molecular beams from high pressure sources. I also told him that if he would submit proposal on such work to Project SQUID I would try my best to get support for it. When he arrived at Virginia he found a group that was already using beam scattering experiments to characterize the exchange of energy and momentum between molecules and surfaces. Their goal was to understand and predict surface heat transfer and drag for aerodynamic bodies at very high altitudes where the particle flow was molecular rather than continuum. The high intensities achievable with beams from supersonic free jets (or "nozzle beams", as they came to be known) would be most useful in such surface scattering experiments. Moreover, the high velocities that seemed achievable with the seeded beams I was dreaming about, would make possible the study of drag and heat transfer in molecular flow at velocities much closer to those expected in ultrahigh-altitude flight. As a result of their enthusiasm and mine, the first nozzle-beam system in America was built in Charlottesville, Virginia[8] I should really say, the first to be built in America since the one which T. H. Johnson built at Yale in 1929 that produced high-intensity beams of mercury atoms but had been ignored. It now seems clear that the reason for Johnson's success was that the walls of his system were all water-cooled enough to condense most of the incident mercury atoms. The net result was an effective pumping speed, orders of magnitude higher than the nominal speed of his vacuum pumps or those of any of the other molecular-beam systems then in existence. (Fraser in his 1932 book on "Molecular Rays" refers to a system then being built with the "exorbitant" pumping speed of 100 liters per second.[9] The nominal speed of each of two 32-inch pumps that we bought "off the shelf" 45 years later was 30000 liters per second!) The real reason for the generally observed decrease in beam intensity with increasing source-gas density was scattering due not to the molecules in a "cloud" at the source-orifice exit but to those in the relatively high density of background gas throughout the system as a result of inadequate pumping speed.

Meanwhile, I was getting more and more intrigued with the problems and possibilities of beams from free jet sources and eager to become more directly involved. I had by this time learned that in spite of Dean Taylor's rosy assurances I could not become an active participant in academic research unless I had some direct association with a department. SQUID had been supporting research on two-phase flow by Shao Lee (Charlie) Soo, a young assistant professor of

 © 2003 Wiley-VCH Verlag GmbH & Co. KGaA, Weinheim

mechanical engineering. During a visit to Soo's lab one day I met Robert Drake, the new chairman hired to refurbish that department's image by expanding its research activities. I described my wild ideas on free jet beams and said: "If I write a proposal and get some support will your department provide a home for the project?" Bob had done his doctoral research in rarefied gas dynamics at UC Berkeley. Familiar with the molecular perspective on gas dynamics he immediately said yes. I prepared a proposal on which I was listed as a "Consultant" because I was not on the faculty and under university rules could not be a Principal Investigator. That role was assumed jointly by Bob Drake and Michel Boudart, my next-door neighbor and close friend who was interested in chemical kinetics and catalysis and was on the faculty of chemical engineering. I had been discussing my beam ideas with him and he too found them intriguing. The proposal was submitted to the National Science Foundation (NSF) who sent it for review to Immanuel Estermann, a co-author with Stern and Frisch of the landmark paper on diffractive scattering of hydrogen from LiF, one of the two papers cited when Stern won the Nobel prize in 1943. Estermann had become Director of ONR's Material Sciences Division (whose "power branch" was responsible for Project SQUID) and was thus my ultimate boss. He took his reviewing seriously and spent a day in Princeton discussing the proposal with me. (The fact that his daughter was then living in Princeton was no doubt something of an inducement for him to make the trip from Washington.) He had visited Becker's laboratory in Marburg, Germany and was aware of the difficulties Becker had encountered in fabricating the tiny converging–diverging nozzles prescribed by Kantrowitz and Grey. As he took his leave he said: "John, I'm afraid this research may be too difficult to pursue with graduate students but I think it is important so I'm going to recommend support." He apparently was as good as his word because NSF gave us the money we had sought and we began work in the fall of 1960. As it turned out, Estermann's fears about the difficulties of making very small Laval (converging–diverging) nozzles were groundless. The Marburg group discovered empirically, that beam intensities became higher when the diverging section of the nozzle was cut off![10] The lower intensities obtained with a diverging nozzle are due to viscosity effects which Kantrowitz and Grey had ignored in their analysis. Dave Miller's group in San Diego, later showed experimentally that for most practical purposes the jets from a simple orificea (hole in a flat plate), a simple converging nozzle, or a long tube, had almost identical properties as long as the flow was "choked", that is, reached sonic velocity, at the exit plane of the nozzle, tube, or orifice.[11]

Michel Boudart was then hosting Jacques Deckers, a young postdoc who had done his doctoral research on ions in flames with Van Tiggelen at the University of Louvain. Jacques had had experience with vacuum systems and was very excited about our beam project so Michel turned him over to my tender love and care, (or me to his, I'm not sure which!). With Bob Drake and Michel looking over our shoulders we began designing an apparatus. One of the lessons from the experiments of the Kistiakowsky and Becker groups was the need for lots of pumping speed. When the salesman from NRC showed us the performance characteristics of its 32-inch (diameter) oil diffusion pumps, Jacques' enthusiasm overcame my reticence (or timidity) so the main chamber of our system became a long horizontal tank resting on and evacuated by two of those big pumps. In retrospect I think that in choosing such big pumps as the heart of our system we were either much wiser or more fortunate than we knew. Those who work with vacuum systems learn early that there is no such thing as too much pumping speed. Sooner or later they always wish they had more. It's nice not to have to worry about the vapor pressure of finger prints, even nicer to be able to sustain disasters. We arrived one Monday morning to find the apparatus completely filled with some 700 gallons of water from a failed cooling coil! We drained the system and easily decanted the water from the silicone pump oil. After cleaning, the interior surfaces of the pumps, pipes, and chamber, all of which were made of mild steel, sported a beautifully uniform beige coat of rust! We then closed up the chamber and ran the forepumps for a couple of days, passing a small flow of air through the system to help dry things out. With fingers crossed we then started the diffusion pumps and got the best vacuum we had ever obtained! Figure 1 shows a picture of that apparatus after it was moved to Yale.



Figure 1. The "big" molecular-beam system, with two 32 inch diffusions pumps and one 16 inch "Jet Booster Pump", after it was moved from Princeton to Yale. The other people in the picture are S. P. Venkateshan (sitting) and S. B. Ryali (standing, center), both postdocs from India.

Meanwhile Dame Fortune had smiled at me in another way. Not long after the beam project started, Professor Soo, who had been teaching thermodynamics to the mechanical engineers, sudden1y announced he would leave at the end of the first semester. Bob Drake, not knowing I had barely passed the only course I had taken in the subject, asked me if I would accept a temporary appointment as a lecturer and teach the sophomore course on thermodynamics in the second semester. After a deep breath and a small prayer I said yes. Things must have gone pretty well because at the end of the term he asked if I would consider a permanent position on the faculty. All of a sudden I had the chance to realize what I had long hoped for, the opportunity to become a first-class citizen in the academic community. Moreover, because my appointment as SQUID's director was "with rank of profes-

 © 2003 Wiley-VCH Verlag GmbH & Co. KGaA, Weinheim

sor" I automatically became an instant full Professor of Mechanical Engineering, a transmutation that would be much more difficult in today's world. I also continued to run SQUID until 1962 when, by mutual agreement of all parties, its headquarters moved to the University of Virginia where John Scott became director.

After an extensive effort in design and construction we finally assembled the molecular-beam apparatus and got it working well. The first meaningful experiment was by Bob Koros, one of Michel Boudart's graduate students. He measured the sticking coefficient of water molecules on ice at liquid-nitrogen temperatures. The simplicity and success of the experimental design were strong evidence of both the achievability and utility of high beam intensities from free jet sources. Bob simply suspended a small target from a calibrated helical spring of glass and measured the time-dependent extension of the spring with a cathetometer viewing the target through a window in the vacuum system. Nearby baffles, filled with liquid nitrogen, maintained the target at low temperature. The beam flux of water molecules, from a source containing water vapor at pressure of a few torr, was sufficiently intense to deposit in a few hours enough mass of ice to extend the calibrated spring by measurable amounts. In a subsequent analogous experiment Jim Anderson, another Boudart student, found that oxygen molecules incident on a heated germanium wafer reacted to form a volatile GeO molecule. Above a threshold value that I've forgotten, the reaction probability of 0.04, was independent of the target temperature and the intensity of the incident beam. In that case we used the spring balance to measure the loss of mass in the germanium wafer. These preliminary experiments clearly demonstrated the utility of the apparatus whose design and performance were described and characterized in a 1963 paper.[12]

Over the next four years at Princeton and the following twenty at Yale this equipment gave rise to some 65 papers. We confirmed the high intensities of beam molecules predicted by Kantrowitz and Grey and first realized by Becker and Bier. Moreover, our hope that the seeding technique could produce beams of molecules with supra thermal translational energies was abundantly realized by ourselves and others.[13a]

An originally unanticipated virtue of free jet expansions was their ability to produce and maintain populations of molecules under non-equilibrium but steady-state conditions which some investigators have characterized as "new states of matter!"[14] For present purposes it will be useful to show the distribution of conditions encountered by molecules of a gas undergoing a free jet expansion from a simple orifice into vacuum. Such expansions are "self-similar" in that they scale in terms of the orifice diameter. That is to say, at any particular number of diameters along the jet axis, the equilibrium state of a particular gas will be the same, no matter what the diameter of the jet may be. Thus, at 5 mm downstream from an orifice 1 mm in diameter the equilibrium state of the jet gas is the same as in a jet of the same gas at 5 m downstream from an orifice 1 m in diameter. As it happens, however, the expansion rate from small-diameter orifices is so fast that the collision-induced processes and reactions involved in maintaining equilibrium in the jet gas may not be rapid enough for the gas to reach equilibrium before the gas density gets so low that the collision processes are arrested. The net result is that the terminal state of the jet gas may be far from equilibrium. This ability of free jet expansions from small nozzles to produce steady-state conditions in gases that are far removed from equilibrium is one of the reasons that these jets have proved to be such interesting research tools.

Figure 2 shows the axial distribution of density n/n_0 and temperature T/T_0 in supersonic free jets from a monatomic and a diatomic gas where subscript "0" refers to the value in the source when the gas is at rest. The curves show the values

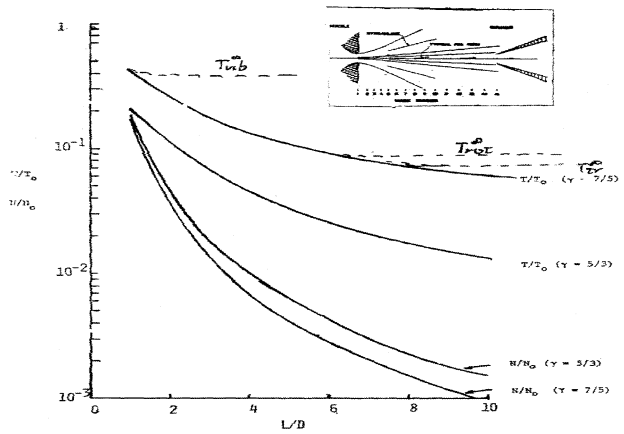


Figure 2. The axial distribution of gas properties in a supersonic free jet, normalized by their source values. The abscissa distance *L* from the nozzle is in terms of nozzle diameters *D*. The top two solid curves show the temperature distribution for a monatomic and a diatomic gas with rotational and vibrational degrees of freedom in equilibrium. Note that because the exchange of energy between translation and vibration is very slow, that is, requires many collisions per quantum, the "vibrational temperature" (for a diatomic gas such as nitrogen) "freezes" much earlier in the expansion than does the rotational temperature. The bottom pair of curves show the axial distribution of gas density for a monatomic and a diatomic gas.

first obtained by Owen and Thornhill from solutions of Euler's equation for monatomic species $C_p/C_v = {}^5/_3$ and for diatomic gases with rotational (but no vibrational) degrees of freedom $C_p/C_v = {}^7/_5$.[15] We had no means of measuring the gas density "n" but we could and did obtain values of the centerline temperature at any point by locating the skimmer at that point, and "chopping" the extracted beam into pulses with a rotating shutter. The signal-versus-time output from a fast-response detector located at a carefully measured distance downstream from the shutter was readily transformed into a velocity distribution and thus the translational temperature of the jet molecules at the skimmer entrance. From such velocity analysis at varying values of nozzle–skimmer distance we determined the axial distribution of translational temperatures of jet molecules along the jet axis. For monatomic and diatomic gases, for example, argon and nitrogen, the experimental values fell right on the theoretical curves out to distances at which the jet gas densities became so low that the collision frequency was not high enough to

 © 2003 Wiley-VCH Verlag GmbH & Co. KGaA, Weinheim

maintain equilibrium. Because the jet expansion is adiabatic, and because vibrational relaxation times for many species are much longer than the sojourn time of the molecules in the jet, the vibrational energies for such molecules remain "frozen" at the source values. By means of an energy balance on the jet molecules it is thus possible to determine the relaxation rates for rotational degrees of freedom in polyatomic molecules.[16] It turns out that this approach is extremely effective for measurement of such rates at much higher gas temperatures than can be accommodated in the widely used instrument measurements based on the velocity of sound. In the present context the important result of our extensive studies of free jet expansion by velocity analysis is that the translational-temperature distributions obtained analytically by Owen and Thornhill and shown in Figure 2 have been experimentally confirmed by ourselves and others. It will emerge in what follows that these findings played a crucial role in the development of electrospray ionization mass spectrometry.

Having developed the ability to measure velocity distributions at any point in the jet we, and subsequently others, were able to verify our hope that heavy molecules seeded at low levels into a light carrier gas could be accelerated to high velocities and thus high translational energy.[13a] Figure 3 shows some early examples of the acceleration and the energies we obtained. Compargue and his group in France have since achieved translational energies as high as 45 eV.[13b] An important result of this seeding technique has been that studies of molecule–molecule and molecule–surface interactions, by ourselves and others, reached new levels of energy, utility, and sophistication.

Free jet expansions have also revolutionized the optical spectroscopy of polyatomic molecules. Our studies showed that such expansions cool rotational degrees of freedom without affecting the vibrational modes. Thus, by performing absorption or emission spectroscopy on polyatomic molecules in a free jet, one can eliminate the rotational broadening of vibrational lines. Unfortunately, we were not knowledgeable enough to realize the spectroscopic implications of rotational cooling so it was Wharton, Smalley, and Levy who provided the earliest demonstration of this effect, obtaining the first-ever spectrum of NO_2 in which the vibrational lines could be clearly distinguished and identified without rotational broadening.[17] Now the free jets used in optical spectroscopy far outnumber those used as molecular-beam sources in scattering experiments!

Because they can produce extremely low temperatures in gases at fairly high densities, free jet expansions can bring about supersaturation of almost any gaseous mixture for very short periods of time. Thus they have become sources of a wide variety of uncommon species, such as HeBr and ArI, and all kinds of aggregates, pure and mixed, even including helium. Consequently, by 1984 free jet expansions had began to play what has turned out to be a major role in the rapid development of so-called "cluster science and technology".[18] Indeed, the Scoles group at Princeton[19] and later the Toennies group at Goettingen[20] have found remarkable effects in the emission spectra of species contained in clusters of superfluid liquid helium where the absence of viscosity means that atoms can rotate freely!

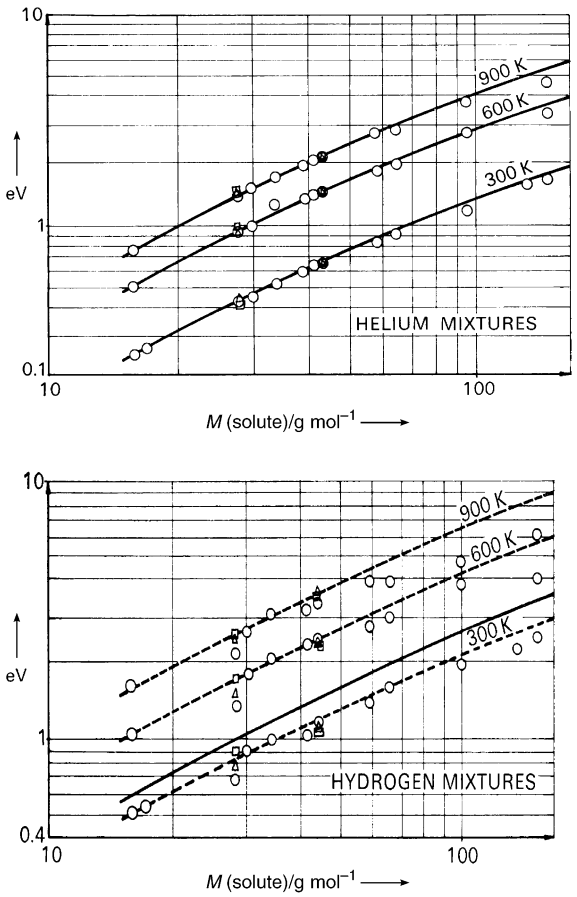


Figure 3. Some results on the acceleration of heavy molecules by a carrier gas comprising helium (top) and hydrogen (bottom). Note that, as is clear for hydrogen, with increasing difference in molecular weight between seed and carrier species there can be appreciable slip resulting in lower velocities for the seed species than would be the case if the velocities of the two species remained in velocity equilibrium. The dotted lines in the hydrogen data assume no relaxation of the rotational energy of hydrogen. The solid line at 300 K shows what would have happened if there were no slip and the rotational and translational "temperature" had remained in equilibrium. In Dole's experiments the differences in molecular weight between seed and carrier species were much greater than for any mixture in this Figure. We estimate that the actual velocities of some of his large polymer molecules were as much as 40% less than he thought they were.

In 1967, for a variety of reasons, I decided to accept an invitation to join the chemical engineering group in a newly organized "Department of Engineering and Applied Science" at Yale. The "beam machine" was dismantled in Princeton and reassembled at Yale in a somewhat different configuration. The picture in Figure 1 was in fact taken at Yale. The very large size of the apparatus had turned out to provide an unexpected dividend. Because our published results had many interesting implications in chemistry, many chemists visited our laboratory in both Princeton and New Haven. Frequently intimidated by the very size of our apparatus, they would listen to our story and say "Very nice, but not for us." The net result was that for a long time we enjoyed a relative absence of competition! In time, of course, we and others learned how to achieve similar results with much smaller and

 © 2003 Wiley-VCH Verlag GmbH & Co. KGaA, Weinheim

more compact gear so that free jet expansions have now become very commonplace tools in departments of chemistry and physics as well as engineering. It is perhaps appropriate to note that these supersonic free jets have played an important role in research that has helped at least five other investigators win Nobel prizes in Chemistry![21]

In 1968, the year after I arrived at Yale, Malcolm Dole published his now famous paper describing his attempt to measure the molecular weights of oligomers of synthetic polymers based on electrospray ionization.[22] He chose to look at polystyrene molecules because relatively monodisperse samples were readily available over a wide range of molecular weights. That paper caught the eye of Professor Seymour (Sandy) Lipsky in Yale's Medical School. With characteristic enthusiasm Sandy showed it to Csaba Horvath, one of my new Yale colleagues in chemical engineering who was working with Sandy on HPLC, then known as "High Pressure Liquid Chromatography." Sandy, who was also a mass spectrometrist, was quite excited because he thought that Dole's approach might make possible the mass-spectrometric analysis of proteins and other complex molecules of biochemical importance. This cherished but elusive goal had long seemed a nearly impossible dream because all the then common methods for ionizing any atom or molecule depended upon an appropriately energetic gas-phase encounter between a neutral molecule and an electron, photon, or ion of some other atom or molecule. But large polyatomic molecules, especially the complex and fragile species of biological interest, could not be vaporized without extensive fragmentation and decomposition. Noting the references to our Princeton papers Csaba told him that the John Fenn of those references had just moved to Yale so Sandy showed the paper to me. Always looking for new ways to apply our free jet technology I was readily seduced by Dole's results and Sandy's enthusiasm. Thus began a friendship with Sandy that lasted until his death and a romance with mass spectrometry that will doubtless last until mine. That romance led to the now popular Electrospray Ionization (ESI) which burst into prominence at about the same time as the other now most widely used method for ionizing large nonvolatile molecules, Matrix Assisted Laser Desorption Ionization (MALDI), began to show its potential. A brief history of each of these techniques will be summarized in the next two sections of this report. MALDI's story will be told first even though ESI's was the first to begin.

Ionization Based on "Energy-Sudden" Methods

One class of techniques for producing intact ions from complex and nonvolatile molecules was embodied in what might be called the "energy-sudden" approach, based on an idea originally proposed in 1974 by Beuhler et al.[23] On the grounds of rate theory for unimolecular decomposition they argued that sufficiently rapid heating could vaporize complex molecules before they had time to decompose. In some proof-of-principle experiments on the vaporization of small peptides they showed that decomposition indeed decreased with increasing heating rates but they never were able to heat rapidly enough to eliminate substantial fragmentation. The several techniques based on this idea include so-called "pyrolysis mass spectrometry" (PMS),[24] pre-MALDI versions of laser desorption (LD),[25] fast atom bombardment (FAB),[26] fast ion bombardment, (usually called SIMS for "secondary ionization mass spectrometry),[27] in which rapid energy addition is achieved by incidence of high-energy atoms, ions, or photons and plasma desorption (PD)[28] in which the sudden energy comes from the decay of a radioactive isotope, usually californium (^{252}Cf). Introduced by Macfarlane and Torgerson et al., PD was the first of these techniques to gain appreciable use.[28] Its name stems from the idea that the energy released by the nuclear disintegration formed a small blob of plasma on the sample-bearing surface. As many as 30 or more analyte ions are ejected from that plasma when the analyte is dispersed in an appropriate matrix, typically nitrocellulose. The ions are then accelerated through a drift region so that their masses can be determined by time of flight (TOF) analysis for which a convenient zero-time marker is provided by back-scattered decay products of the Cf disintegration.

All these energy-sudden methods depend on the nearly instantaneous achievement of high energy density in a sample dispersed in or on a solid or liquid surface. Thus they can be regarded as extensions of the rapid-heating idea of Beuhler et al. They all could produce intact ions from many complex molecules including peptides and small proteins. However, their procedures were complex and awkward, and because their processes were highly irreversible the yields of intact ions were very low. Even so, during the 1970s and 80s they provided substantial accumulations of mass-spectral data on a variety of complex, nonvolatile molecules, giving rise to a literature much too large for review or comment here.

By far the most important legacy of these energy-sudden methods is so-called matrix-assisted laser desorption ionization or MALDI introduced in 1987 by Tanaka[29] and expanded in 1988 by Karas and Hillenkamp.[30] In MALDI the analyte molecules are dispersed on a surface in a thin layer of matrix, usually an organic acid. The energy of an incident pulse of laser photons is absorbed mostly by the matrix to form a jet of matrix vapor that lifts analyte molecules from the surface and by mechanisms still not well understood, transforms some of them into ions that are mostly singly charged. Because those ions are all produced at a well-defined location in an exceedingly short time their mass analysis is most effectively achieved by time-of-flight methods, as in the case of PD. MALDI is one of the two ionization methods for biomolecules that promise to dominate the MS scene for the foreseeable future. Recently MALDI-TOF in vacuo has been supplemented by MALDI at atmospheric pressure with subsequent introduction of the resulting ions into any of several types of mass analyzers.

Ionization Based on Intense Electric Fields

In 1966, when Dole first had the idea that led to his 1968 paper, there was little evidence of any useful solution to the problem of vaporizing large polar molecules. However, in

 © 2003 Wiley-VCH Verlag GmbH & Co. KGaA, Weinheim

1951 the first step had been taken along one of two paths that ultimately led to successful "soft" ionization methods for complex molecules, though it was not fully appreciated at the time. In that year Mueller discovered that when a sharp metal point was at a sufficiently high voltage in vacuo, the electric field at the tip of that point could be intense enough to extract an electron from a nearby gaseous atom or molecule to form a positive ion,[31] a discovery that led to his development of field ion microscopy.[32] The first use of such points as sources of ions for mass analysis was reported three years later by Inghram and Gomer,[33] but only with gaseous molecules. The ion currents were too small to stir up much interest but they were larger than could be accounted for by the flux of molecules from the ambient gas into the region occupied by the point. Beckey then suggested that this apparent excess in ion-formation rate could be accounted for by molecules that struck the surface of the wire at some distance from its tip and then arrived at the tip region by surface diffusion. In 1963 he showed that arrays of "whiskers" on thin wires could produce much higher currents than single needles and that nonvolatile species present on the surfaces of such whiskers could migrate to the tip by surface diffusion to be desorbed as intact ions. Beckey went on to develop this discovery into "field desorption ionization mass spectrometry" (FDI-MS) and in 1977 published a book on the subject.[34] Emitter electrodes comprising wires with dense arrays of whiskers are now available off-the-shelf at relatively low cost, but dosing them with sample and positioning them in the vacuum system are time-consuming and tedious tasks. Moreover, ion currents depend so strongly upon both the temperature of the emitter and the applied voltage that substantial manual skill is required to find and maintain the right combination for a particular sample. That control function might now be made much less tedious by computers but solving the control problem does not deal with an even more important difficulty. The ions from field desorption are released from high voltage into high vacuum. Consequently, their kinetic energies are so high that their mass analysis requires relatively large and expensive magnetic sector instruments. For these and other reasons FDI-MS a la Beckey has never been widely practiced. However, from the perspective of history's hindsight one can argue that the ability of intense fields at the surface of a tiny charged droplet, which play a vital role in Dole's ESI, is simply an obvious extension of the discoveries by Mueller and Beckey on the nature of field ionization at a sharp tip, that is, a surface with a very small radius of curvature. Maybe so, but it is also quite clear that nobody recognized these possibilities at the time, and that Dole arrived at the ESI approach by a logic that depended in no way on the field-ionization ideas of Mueller and Beckey. In other words Dole was a true pioneer in that his ESI ideas were breaking brand-new ground.

Fields intense enough to desorb solute ions at useful rates from a condensed phase can also be achieved without the array of very sharp needles or "whiskers" required by Beckey's approach. In 1972 Evans and Hendricks found that a high voltage applied to the surface of a nonvolatile conducting liquid in vacuo would produce a sharply pointed cone.[35] The field at the tip of such a cone was intense enough to desorb charge-bearing molecules and clusters of the liquid. If the liquid was a solution, the desorbed ions included solute species. These observations led to so-called "electrohydrodynamic ionization" (EHI) that was introduced to the mass spectrometry community in 1974 by Simons et al.[36] In EHI a sample solution is electrosprayed from a small-bore tube maintained at high potential relative to the surroundings, just as had been taught by Zeleny and adopted by Dole. The difference is that in Dole's ESI the droplets are dispersed into gas at near atmospheric pressure. In EHI the sample solution is dispersed into vacuum. In that case the solvent must have a very low vapor pressure to avoid "freeze drying". But as Dole had recognized, evaporation of solvent is the *sine qua non* (essential feature) for the formation of solute ions from charged droplets and such evaporation requires a source of enthalpy. This dilemma has never been completely resolved in EHI because no satisfactory method has yet been found by which the enthalpy needed to vaporize solvent from a droplet can be supplied to such a droplet in vacuo. Moreover, as in the case of FDI, any ions produced by EHI in vacuo have such high kinetic energies that their mass analysis generally requires magnetic sector instruments which are large, heavy, and expensive. For these reasons EHI-MS has never become widely used despite fairly extensive research that has been reviewed in detail by Cook.[37]

In sum, Malcolm Dole's paper in 1968 was the seed which, after an extended period of germination, ultimately blossomed into electrospray ionization (ESI), one of the two "soft" ionization methods that have made the precision, sensitivity, and elegance of mass spectrometry readily available for the study of biomolecules and their reactions. The germination and development of Dole's ESI will be briefly described in what follows.

Electrospray Ionization

The other of the two dominant methods for ionizing large molecules is electrospray ionization (ESI), the subject of the 1968 paper by Malcolm Dole and his colleagues[22] that Sandy Lipsky showed me in 1969. In fact Dole had first proposed his electrospray idea two years earlier (1966) at the International Symposium on Macromolecular Chemistry in Tokyo. Those two communications comprise a testament to Dole's remarkable acumen in realizing that the production and behavior of highly charged droplets from solutions of nonvolatile solute species in volatile solvents might produce intact gaseous ions of those species. Perhaps even more remarkable was the extent of his insight on the roles of ESI's several component processes. For example, he clearly recognized the need to disperse the charged droplets in a gas at relatively high (atmospheric) pressure. Such gas would provide the enthalpy required to vaporize solvent from those highly charged droplets. Moreover, collisions of the ions with molecules of that gas would reduce their initially high kinetic energies to those of the ambient neutral gas molecules, thereby avoiding the need for mass analyzers capable of accommodating high-energy ions, for example, magnetic sector instruments.

As most mass spectrometrists now know, the essence of Dole's idea was to take advantage of what happens during the

 © 2003 Wiley-VCH Verlag GmbH & Co. KGaA, Weinheim

evaporation of solvent from a droplet that has a net electric charge. In 1882 Rayleigh had analyzed the behavior to be expected of such a droplet and found that as the solvent evaporated the density of charges on the droplet surface would increase to a critical value, now known as the "Rayleigh Limit", at which Coulomb repulsion would overcome surface tension. The resulting instability would cause the droplet to break up into a plurality of offspring droplets.[38] Thirty years later John Zeleny made the first reported observation of this "Rayleigh Instability" in pioneering experimental studies on the production and behavior of charged droplets carried out, first at the University of Minnesota and then at Yale.[39] He passed a stream of conducting volatile liquid through a small-bore thin-walled tube or "needle" (because it often comprised a short length of hypodermic needle tubing) maintained at a high potential relative to an opposing counter electrode. The resulting intense electric field at the tube tip dispersed the emerging liquid into a fine spray of charged droplets. Zeleny was able to see the break up of charged droplets as solvent evaporated, just as Rayleigh had predicted. Figure 4a is a schematic representation of the how droplets are formed. The emerging liquid at the tube exit forms a conical meniscus now known as a "Taylor Cone" because its formation was predicted theoretically in 1964 by G. I. Taylor.[41] In truth, Taylor's treatment applied to a nonconducting liquid of neutral molecules with dipole moments for which there is no electric current and no liquid flow. Even so, the Taylor name is still applied even when the liquid is a conductor because it contains anions and cations. In that case a thin jet emerges from the tip of the cone. As the result of another kind of instability, also first characterized by Rayleigh for uncharged liquids,[42] the interaction between viscosity and surface tension produces so-called "varicose waves" on the surface of such a liquid jet. Those waves grow in amplitude until they truncate the jet into a series of uniform droplets as illustrated in Figure 4 (top left). (That same kind of instability causes the break up into droplets of a solid jet of water issuing from a garden hose or, on a smaller scale, the tiny stream of water from a tap that is incompletely turned off.) In the electrospray

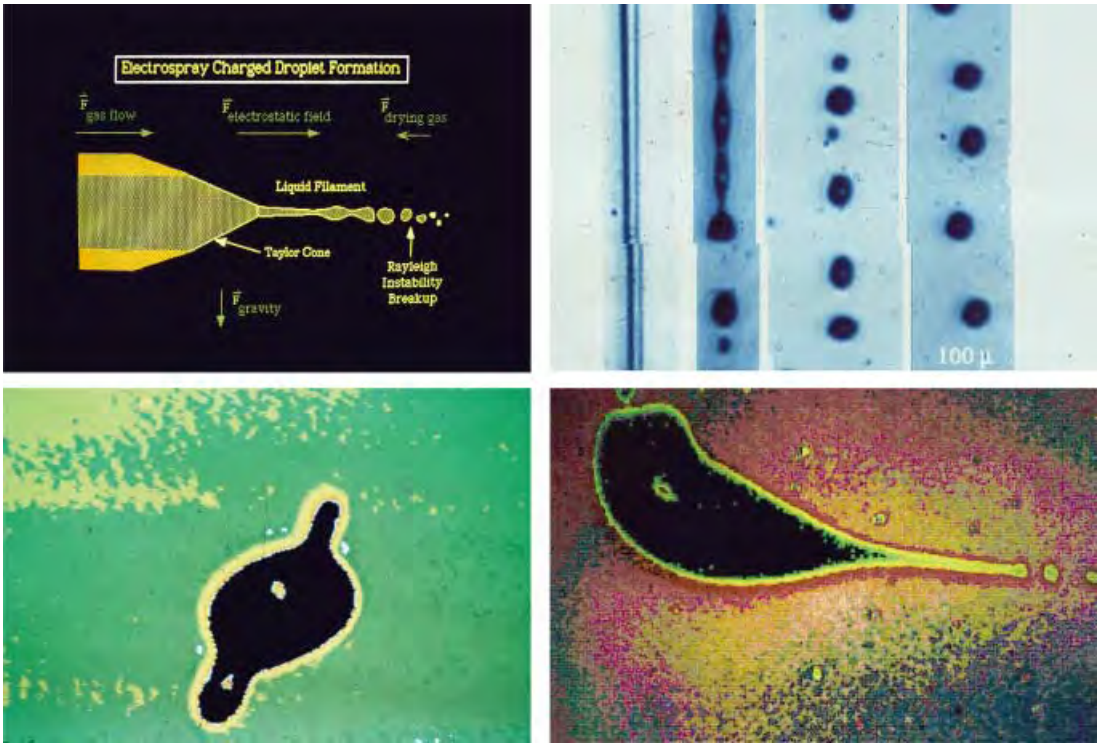


Figure 4. How a flow of conducting polar liquid is dispersed into highly charged droplets by an intense electric field at the exit tip of a small tube at high potential relative to an opposing electrode. Top left: schematic representation the conical meniscus formed by the emerging liquid as the result of competition between the surface tension of the liquid and forces owing to the interaction of dipoles in the liquid with the applied field. This meniscus is known as a "Taylor Cone".[41] When the liquid is electrically conducting, a small flow of the liquid emerges from the tip of the cone as a very narrow column or jet. Interaction between surface tension and viscosity produces so-called varicose waves which grow in amplitude until they truncate the jet into a sequence of segments of equal length that are molded by surface tension into droplets nearly uniform in size.[42] Because the droplets contain excess cations or anions on their surface, depending on the polarity of the field, they repel each other with the result that their trajectories diverge to form a conical "electrospray" of charged droplets. This sequence was captured in the photographs by Gomez and Tang (top right). If the liquid is volatile, evaporation shrinks the droplet thereby bringing the surface charges closer together until the resulting Coulomb repulsion overcomes surface tension and the droplets disrupt into a plurality of smaller droplets, a phenomenon characterized and predicted theoretically by Lord Raleigh in 1882. Two years more than a century later, Gomez and Tang captured on film, for the first time, the images in the lower two panels of Figure 4 showing a droplet in the throes of what is now known as a Rayleigh Instability, and sometimes referred to as a Coulomb explosion.

 © 2003 Wiley-VCH Verlag GmbH & Co. KGaA, Weinheim

case the droplets all have charges of the same sign (excess anions or cations, depending on the polarity of the applied field). Coulomb repulsion thus results in a divergence of their trajectories to form a conical "electrospray" of charged droplets. Figure 4b is a series of four photographs made by Tang and Gomez[40] illustrating, from left to right, the undisturbed jet, the appearance and growth of the varicose waves, the resulting droplets, and the beginning of the divergence of the droplet trajectories (as a result of Coulomb repulsion) to form a conical spray. We believe the two lower pictures in Figure 4 are of historic significance as the first ever photographs showing droplets undergoing a Rayleigh instability when the Coulomb repulsion of the surface charges overcomes the surface tension that tries to contain the droplet liquid in a spherical shape.

Dole's scenario further assumed that the "offspring" droplets resulting from a Rayleigh instability would continue to evaporate until they too would reach the Rayleigh limit and break up into still smaller droplets. If the original solution were sufficiently dilute, a succession of such Rayleigh instabilities would ultimately produce droplets so small that each one would contain only one solute molecule. That lone molecule would retain some of its droplet's charge to become a free gas-phase ion as the last of the solvent evaporated. The upper sequence in Figure 5 attempts to illustrate this process. (The lower sequence illustrates an alternative proposal by Iribarne and Thomson which will be described later.)

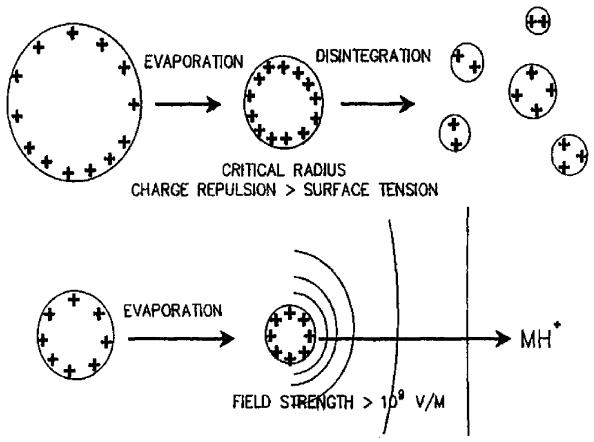


Figure 5. Top: Dole's idea of how solute ions are formed. He assumed that the offspring droplets resulting from a first Rayleigh Instability would continue to evaporate solvent so that they too would undergo a Rayleigh Instability and disrupt. If the original solution were sufficiently dilute, a sequence of such evaporation–disruption episodes would ultimately produce ultimate droplets so small that each would contain only one solute molecule. As the last of the solvent evaporated from the ultimate droplet the remaining solute molecules would retain some of the droplet charge and thus become a free gas-phase ion. This scenario embodies what is sometimes referred to as the "charged residue model" (CRM) for ES ion formation. The lower sequence of sketches portrays the so-called "ion evaporation model" scenario later proposed by Iribarne and Thomson[46]. It argues that before ultimate droplets containing only one solute molecules are formed, the field at a droplet's surface becomes sufficiently intense to lift a solute ion from the droplet surface into the ambient gas.

In the 1968 paper that described this scenario Dole also presented preliminary experimental results obtained in an attempt to reduce his idea to practice. As taught by Zeleny, a solution of polystyrene molecules was infused through a small-bore tube maintained at high potential relative to a counter electrode. Dole was always generous and conscientious in acknowledging the work of others so it is curious that though he refers to Rayleigh's analysis of droplet instability he never mentioned Zeleny in any of his papers, even though his method of producing charged droplets seems to derive directly from Zeleny's experiments. His account of the electrospray experiments in his autobiography simply says: "I got this idea from learning about the electrospraying of paint on to automobile bodies while working as a consultant for a paint company in Chicago".[43] Such "electrospraying" of paint consisted in maintaining a potential difference between the sprayer and the object being painted. The result was enough charge on the paint droplets to attract them toward the object being painted, thereby decreasing substantially the loss of paint to the surroundings by convection currents. Similar charging of droplets was practiced by "crop dusting" airplanes to decrease aggregation and increase adhesion of insecticides to the plants.

But Dole had another problem to solve. The mass spectrometers then available, even the most expensive magnetic sector instruments were unable to "weigh" singly charged ions with masses larger than about ten-thousand Daltons. The oligomer ions of interest to Dole could have molecular weights up to a million or more and he had apparently not taken into account the possibility of extensive multiple charging which then had not yet been discovered. The problem he thus faced was how to "weigh" such large ions after they had been produced. Moreover, as he also mentioned in his autobiography, he had found that the magnetic electron multiplier (MEM) on his Bendix mass spectrometer did not respond to his ES ions because "Although these ions had the same kinetic energy as light ions their velocity decreased in the ratio of the square root of their mass. We proved the mass limitation of the MEM in a separate experiment."[44] That comment strongly suggests that the ions Dole had produced from polystyrene oligomers did not have extensive multiple charging. Therefore, their mass/charge ratios were too high for available analyzers so he had to find another method for "weighing" them. That is how our free jet studies entered the picture.

As noted earlier, we had shown that during such free jet expansions of mixtures comprising a very dilute solution of heavy "seed" molecules in a light carrier gas, for example, argon in helium, the heavy seed species were accelerated like dust particles in a windstorm to almost the velocity that would be reached by the light carrier gas alone.[13] Consequently, the translational kinetic energy of the argon molecules after expansion was higher than would be achieved in a jet of pure argon by a factor roughly equal to the ratio of the molecular weights of the two species, that is, 10 in the case of argon accelerated by helium. This acceleration effect was important to Dole because it seemed to provide a way to weigh the large polymer ions he hoped to produce. As shown in the sketch of his apparatus in Figure 6 (from his 1968 paper) a variable-

 © 2003 Wiley-VCH Verlag GmbH & Co. KGaA, Weinheim

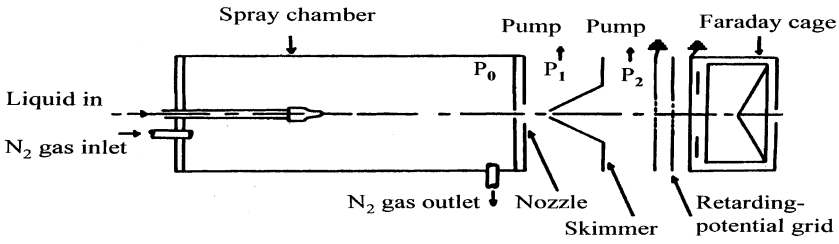


Figure 6. Schematic representation of Dole's original ESI apparatus. The electrospray forms at the tip of the tube through which liquid enters the spray chamber concurrent with the nitrogen bath gas. Most of that gas leaves the chamber near the end plate containing the nozzle through which a small portion of the mixture of bath gas and ions enters the vacuum system in the form of a supersonic free jet. A small fraction of the ion-bearing jet gas passes though a skimmer into a second vacuum stage, thence through a retarding-potential grid into a Faraday cage connected to a galvanometer.

potential grid was placed between the skimmer (that passed a collimated, ion-containing beam from the free jet source into a vacuum chamber) and a sensitive galvanometer in a Faraday cage contained in that chamber. The only ions that could pass through the grid and reach the galvanometer were those with a translational kinetic energy $mv^2/2$ exceeding the product of the charge on those ions and the potential on the grid. The translational velocity v of the stopped ions was equal to the readily calculated velocity reached by the carrier gas in the free jet. Thus, scanning the voltage applied to the grid should produce a current–voltage curve with a decrease in current to the galvanometer at every value of the voltage corresponding to the energy of an ion species in the beam. Figure 7 shows the curve Dole obtained with a fractionated sample of polystyrene having a nominal M_r of 51000 at a concentration of 0.01% by weight in 60:40 (v:v) benzene:acetone. Also reported were results with polystyrene having a nominal M_r of 411000 and with a mixture of the two. These results showed a certain consistency with expectations but, possibly for reasons to be described, were not convincing enough to persuade other investigators to confirm or extend them.

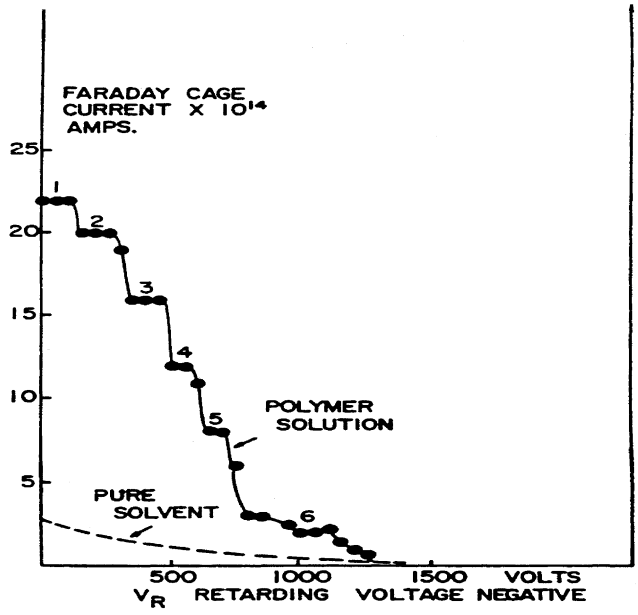


Figure 7. A current–voltage curve obtained by Dole when the electrosprayed solution comprised 0.005 wt% each of polystyrene samples having a molecular weight of 51000. The solvent comprised benzene:acetone (3:2 v/v). The distances from the needle to the first aperture, the first aperture to the second aperture, and the second aperture to the nozzle were respectively 2, 3, and 3 inches.

Electrospray Ionization at Yale

A year or so after Sandy showed me Dole's paper I persuaded a new graduate student, Mike Labowsky, to repeat Dole's experiments in our much bigger vacuum system with much faster pumps than Dole had. We also had a better understanding of free jet expansions and realized that Dole had overlooked two of their features which were crucial in his experiments: 1) For the very large differences in molecular weight between the carrier gas and the seed species that he was using, there would have been a substantial amount of "slip" as suggested by the results with hydrogen in Figure 3. Thus, the actual velocities of his heaviest ions could have been as much as 50% lower than he had reckoned. 2) During the adiabatic expansion that occurs in a free jet the temperature of the gas nose-dives. In the case of nitrogen, for example, at an axial distance downstream from the orifice of only ten nozzle diameters (ca. 1 mm in Dole's experiments) the absolute temperature of the gas drops to about 5% or less of its source value! Thus, the expanding gas rapidly becomes supersaturated with solvent vapor resulting from the evaporation of the ES droplets before the expansion. Ions are famously effective as condensation nuclei so that any ES ions in Dole's experiments must have been substantially resolvated to an unknown extent. Consequently, the actual masses of the unsolvated ions must have been much lower than Dole's measurements had indicated. To avoid such resolvation problems Mike modified the Dole arrangement so that the bath gas of dry nitrogen was introduced at the exit-nozzle end of the spray chamber. Consequently, drying gas flowed "upstream", counter-current to the flux of charged droplets and ions from the spray needle, leaving the spray chamber through an exit port at its "entrance end", that is, opposite to the end containing the nozzle leading into the vacuum system. Thus the solvent vapor from the evaporating droplets was carried out of the system so that the gas expanding into vacuum through the nozzle was free of solvent and any other "junk" that was not ionized. This counter-current flow of bath gas solved the problem of ion resolvation during the free jet expansion, greatly reduced system fouling, and has become a feature of the most successful ESI-MS systems. One can also avoid resolvation of ions during expansion by raising the temperature of the ion–gas mixture to a value high enough so that after free jet expansion the gas temperature remains above "the dew point" for the ions. This "fix" was demonstrated by Chowdhury et al.[45] and has been incorporated in some commercial instruments. It has had limited use because,

 © 2003 Wiley-VCH Verlag GmbH & Co. KGaA, Weinheim

unlike a counter-current gas flow, it does not prevent uncharged "junk" from entering the vacuum system. Much more frequent cleaning is therefore required.

As already mentioned, Dole's paper apparently failed to persuade other investigators to confirm his experiments which though simple in principle were really very difficult and demanding in practice. For example, large macroions incident on the first dynode of a multiplier do not produce secondary electrons unless their incident velocities are very high, either because of multiple charging or high accelerating voltages. As implied by reference [44] it seems highly likely that Dole's ions did not have many charges. Consequently, in his later experiments he used mobility measurements to characterize his macroions.

In 1969 at the age of 66, just two years before mandatory retirement at Northwestern, Dole had accepted an offer to become Welch Professor of Chemistry at Baylor University in Waco, Texas where he was assured there would be no mandatory retirement as there was at Northwestern. At Baylor he continued his electrospray experiments using mobility measurements rather than mass analysis to characterize the ions. He presented a short paper on that work at the 33rd Annual Meeting of American Society of Mass Spectrometery (ASMS) in San Diego in 1985 where I also gave a paper that included a discussion of the cooling and resultant resolvation that occurs in free jets. Dole came up to me afterward to introduce himself and to express his gratitude for finally understanding why there didn't seem to be any reasonable relation in his experiments between the size of the molecules and the mobilities of their ES ions. He said "Now I realize that we have been measuring the mobilities of highly solvated ions!" That was our only face-to-face encounter but we subsequently exchanged several letters and had a cordial relationship. I was delighted when he was later able to attend the first ASMS Workshop on ESI-MS which was in Chicago. I didn't see him there because I had not been invited but by that time the "electrospray revolution" was well on its way so Dole had the satisfaction of realizing how fruitful his ideas had become before he passed on to his ultimate reward some months later. He would have been amazed if he had known that by 2001 the number of papers per year on ESI in the archival journals would reach 1500 and still be growing!

There was a hiatus in ESI studies at Yale after 1975 when, for understandable reasons, Mike Labowsky got discouraged. The retarding-potential method of determining ion mass was most exasperating. The only available means for measuring the very small ion currents was an old vibrating-reed electrometer that on its best days was crankier than a model T Ford! Mike became interested in the evaporation behavior of the cloud of ES droplets and thus in the evaporation and combustion of a cloud of interacting fuel droplets, an important and challenging practical problem of interest to several of my colleagues in Chemical Engineering. He developed some unique computational techniques which together with several important papers on this classic problem comprised his Ph.D. thesis.

In 1982, Masamichi Yamashita, a young scientist I had met in Japan, came to my lab as a postdoc. When he arrived, "Gado" as he preferred to be called, asked for some suggestions about what he might work on. I mentioned that it might be interesting to take another look at ESI, but instead of trying to make ions out of big molecules, to explore whether Dole's idea would work with molecules of low-enough mass for their ions to be analyzed with a small quadrupole mass spectrometer that had been a detector in some of our molecular-beam experiments. It had an upper limit for m/z ratio of only 450. Gado liked the idea and off he went. Not only was he an extraordinary experimentalist, with sound instincts and magic hands, he knew everything from the biology of sea urchins to the practice of digital electronics (already in 1982!). In a relatively short time he assembled what was really the world's first ESI mass spectrometer from the bits and pieces of molecular-beam apparatus in our precious "junk pile". (My Scottish heritage of "Waste not, want not" makes it very difficult for me to throw anything away that might have some conceivable use!)

That first apparatus is shown schematically in Figure 8 and illustrates the arrangement for providing a counter-current flow of drying gas. We first tried electrospraying methanol–water mixtures and obtained spectra showing peaks corresponding, for example, to protons solvated by various combinations and numbers of methanol and water molecules that could be varied widely simply by adjusting the flow rate and/or temperature of the counter-current drying gas. We then added some solutes to the solvent and were rewarded with the spectrum shown Figure 9a. It was obtained with a solution of several tetra-alkyl ammonium (and one phosphonium) halides at concentrations of a few parts per million. These results were especially gratifying because those solutes cannot be vaporized without extensive, even catastrophic decomposition. Beginning to get excited, Gado dissolved a vitamin B tablet in methanol–water and obtained the spectrum in Figure 9b showing a clearly defined peak for intact ions of every species in that tablet (i.e. with an M_r value under 450.)

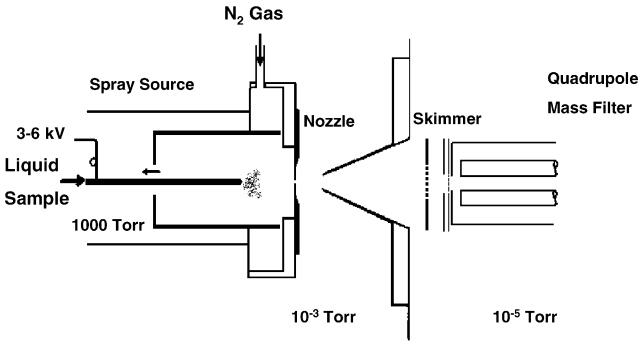


Figure 8. Schematic representation of the first electrospray mass spectrometer built at Yale. Sample solution was sprayed from the hypodermic needle into a counter-current flow of dry nitrogen. The needle was at high potential relative to the cylindrical electrode and the end plate containing the orifice into the vacuum system. A center portion of the resulting free jet passed through the skimmer into a second vacuum chamber containing a quadrupole analyzer.

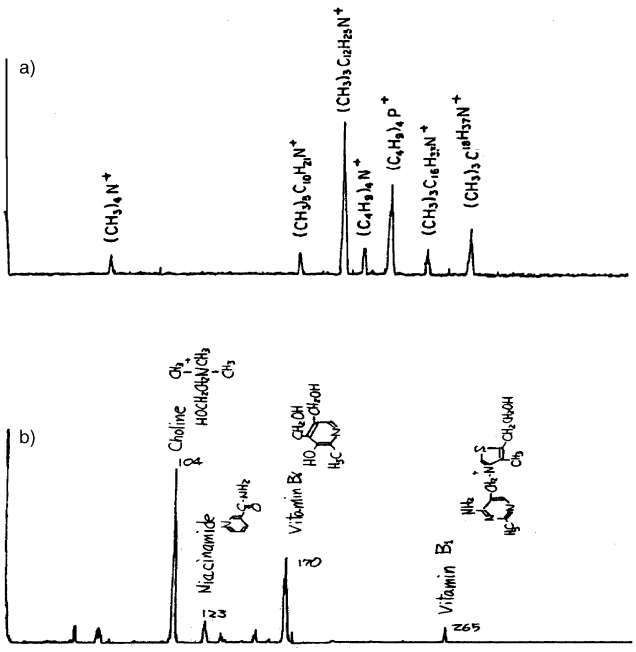


Figure 9. a) The ESI mass spectrum obtained with the apparatus of Figure 8 with a dilute solution (ppm) of quaternary ammonium halides and one quaternary phosphonium halide in methanol:water (50:50 v/v). b) The ESI mass spectrum obtained with a solution obtained by dissolving a vitamin B tablet in methanol:water (50:50 v/v).

The spectra in Figure 9a and Figure 9b were exciting to us because they clearly demonstrated that ESI could produce intact ions of each of several species in a plurality of fragile molecules in a dilute solution while avoiding both fragmentation and interference between them. The spectra also raised second thoughts about the mechanism of ionization. We had been tacitly assuming that Dole's "charged residue model" (CRM) accounted for the formation of the large ions he had found as well as the small ions that we had found in the results just described. In our early experiments, as well as in Dole's, there were always many more analyte (solute) molecules than charges in the ES flux. Consequently, as our results accumulated we had become increasingly uneasy about the adequacy of the CRM. The spectra in Figure 9 heightened that concern because we could not understand how the sequence of Rayleigh instabilities could produce, for each of several species in the same solution, singly charged ultimate droplets containing only one molecule of that species. Moreover, if the CRM model is to explain the results, the relative number of those droplets for each species would have had to be in direct proportion to the relative concentration of that species! How could the droplet know how to program its sequence of Rayleigh instabilities so as to produce a distribution of ultimate droplets such that the number of those ultimate droplets containing one molecule of any species X is always directly proportional to the concentration of species X in the original solution? Of course, that would happen if the droplet subdivision continued until all the droplets contained only one solute molecule. But that scenario somehow seems unlikely, especially when rapid evaporation from all droplets is occurring from the start. Moreover, if the subdivision process were to produce ultimate droplets for each ionizable species in a solution, one should then always find a spectral peak for every species in such a solution and that just doesn't happen.

These conceptual problems seemed to be resolved when we learned about some papers by Iribarne and Thomson, meteorologists at the University of Toronto.[46] Interested in the possibility that charged droplets of sea water might be a source of some of the ions found in the atmosphere, they had carried out experiments showing that evaporation of charged droplets could indeed produce gas-phase ions of solute species in those droplets. The charged droplets in those experiments were produced by pneumatically nebulizing a conducting liquid. In such nebulization the droplets become charged as a result of statistical fluctuations in the distribution of anions and cations among those droplets so that roughly equal numbers of positively and negatively charged droplets are formed. In their first experiments only aerodynamic forces were used to nebulize the liquid, as in a perfume atomizer. Then they found that 3.5 KV applied to an "induction electrode" (1 cm away from the nebulizing zone) would result in all the droplets, and the ions from their evaporation, having the same sign, positive or negative, depending on the polarity of that electrode. Iribarne and Thomson called their technique "atmospheric pressure ion evaporation" (APIE) a name which literally refers more to the mechanism of ion formation from charged droplets rather than to the method of producing the droplets. Moreover, both the earlier ESI of Dole and the later thermospray ionization (TSI) of Marvin Vestal,[47] also depend upon vaporization of charged droplets but their names do not identify any ion-forming mechanism. The essential differences between these three "spray" techniques consist mostly in the way the charged droplets are produced. Therefore, it seems more appropriate to give them names that relate to those characteristic differences, that is, "ESI" for electrospray ionization, "ASI" for aerospray ionization, and "TSI" for thermospray ionization. These names relate specifically to the way droplets are produced in terms of the kind of energy used to produce them, (i.e. electrical, aerodynamic, and thermal) and will be used hereafter.

The ASI technique of Iribarne and Thomson has never become as widely used as ESI. However, their ion evaporation mechanism (IEM) for ion formation from charged droplets, set forth in their papers, was a milestone contribution and has become a formidable competitor for Dole's charged residue model (CRM) with each one having its champions. Both models assume that a sequence of evaporation steps followed by Rayleigh instabilities leads to smaller and smaller droplets. In the CRM this sequence continues until the droplets become so small that each one contains a single solute molecule that becomes an ion by retaining some of its droplet's charge as the last of the solvent evaporates. The upper sequence of steps in Figure 5 attempts to illustrate this process. The IEM holds that before the droplets become small enough to contain only one solute molecule, the field strength at the droplet surface becomes intense enough to "lift" a surface ion from the droplet into the ambient gas. In other words the surface field can evaporate an ion from the

 © 2003 Wiley-VCH Verlag GmbH & Co. KGaA, Weinheim

droplet surface. The lower sequence of steps in Figure 5 attempts to represent this mechanism. There is no unanimity in the ESI community as to which model is correct. The feeling in this corner is that under most circumstances the IEM is more consistent with more experimental observations than is the CRM. However, sometimes the CRM seems more likely to apply, especially in the case of very large analyte molecules.

A bit more needs to be said about TSI, the thermospray ionization technique introduced by Marvin Vestal and his colleagues beginning in 1978. The last of the charged-droplet sources to appear, TSI became the first to be widely used, in part because of its effectiveness and in part because it was the first to become available commercially as an add-on to existing mass spectrometers. This sequence of events would seem to fulfill that passage in the scripture which says "The last shall be first." (That passage continues by saying "And the first shall be last", which apparently is being fulfilled by ESI because it was the first to be introduced and now would seem likely to be the last of the spray techniques to be abandoned, if it ever is!)

TSI consists in passing analyte solution through a capillary tube whose walls are hot enough to vaporize 90% or more of the solvent. The resulting expansion produces the same kind of shear and acceleration forces on the liquid that occur in aerodynamic nebulization, for example, as in ASI or a perfume atomizer. The result is a dispersion of droplets in vapor that emerges from the exit of the capillary as a supersonic jet into ambient solvent vapor at a pressure of 10 to 15 Torr in a chamber whose walls are hot enough to maintain the vapor in a superheated state. The already-mentioned statistical fluctuations in the distribution of cations and anions give rise to equal numbers of positively and negatively charged droplets as in ASI. Evaporation of the droplets in the superheated vapor brings about the sequence of Rayleigh instabilities common to all the techniques based on charged droplets. That sequence leads to the formation of gaseous ions by either the CRM of Dole or the IEM of Iribarne and Thomson. The mixture of ions in vapor flows past an aperture through which ions of the desired polarity are driven by an applied field into the vacuum chamber housing a mass analyzer. For several years in the 1980s TSI sources became the preferred "hyphen" in LC-MS, but they have now been almost completely replaced by ESI sources.

Meanwhile we were achieving ever better results with ESI as we climbed the learning curve and Sandy Lipsky was keeping in close touch with our progress. He was a good friend of Brian Green of VG Analytics, a British manufacturer of mass spectrometers that has since evolved into what is now Micromass, Ltd. Brian would stop by New Haven and visit Sandy every few months and on most of those visits Sandy brought him by our laboratory. As our results with small molecules began to get better and better, Brian became more and more intrigued and asked us if the technique would work with larger molecules. We said we thought it might but couldn't be sure because our little quadrupole analyzer had an upper limit of about 450 for m/z ratio. Brian then arranged for VG to lend us a used quadrupole analyzer that could weigh ions with m/z ratios up to 1500 or so. That instrument was incorporated in a new system for which much of the design and assembly was done by Craig Whitehouse. Craig had worked in Sandy's lab after finishing college and Sandy urged me to take him on for graduate study in chemical engineering. The design of this new system is shown schematically in Figure 10 and has some novel features that deserve comment.

In light of the results obtained with Gado's machine, and with Csaba and Sandy hovering in the background, we increasingly viewed ESI as a possibly more potent hyphen in LC-MS than the already widely used TSI. An electric field, sufficiently intense to disperse analyte solution emerging from the spray needle into a fine spray, required a potential difference of up to several kilovolts between that tip and the

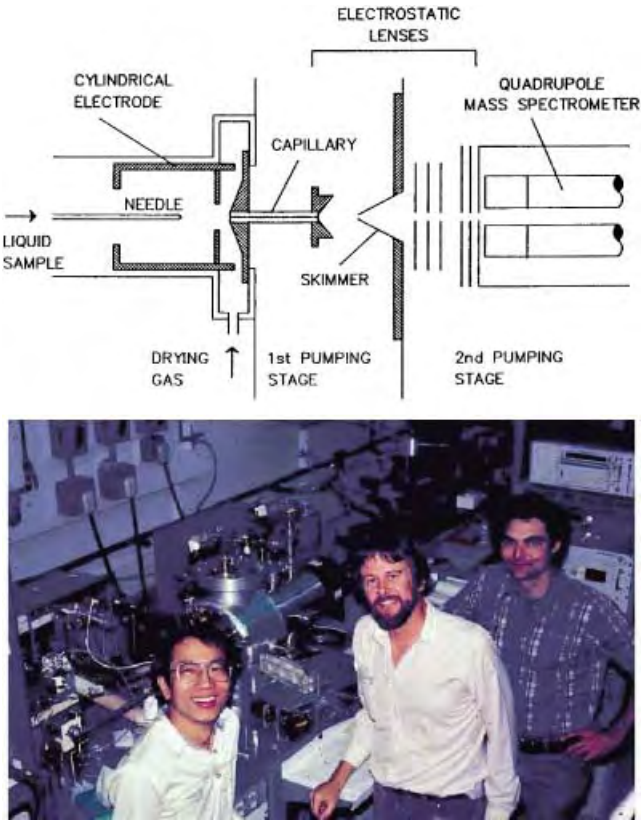


Figure 10. Top: Schematic diagram of the second ESI-MS apparatus. It features the same counter-current flow of drying gas shown in Figure 8 which excludes solvent vapor from the ion–gas mixture that enters the vacuum system by way of a free jet expansion. A novel feature of this apparatus is that the ion–gas mixture enters the free jet expansion at the exit of glass capillary rather than through the simple flat-plate orifice. Each end of that capillary is metallized so that it can be maintained at any desired potential. Thus the field required to "electrospray" the sample solution can be achieved with the spray needle while the metallized entrance of the capillary is at the required potential "below" ground. The ions entering the capillary are then in a potential well. The rapid flow of gas through the capillary then drags the ions out of that potential well to any desired potential at which the metallized exit end of the capillary is maintained. Thus, all external parts of the apparatus can be at ground, posing no hazard to an operator. Bottom: Photograph of the apparatus of Figure 10 showing (left to right) Chin Kai Meng (graduate student), Robert Dreyer (chromatographer from the Medical School) and Craig Whitehouse, (graduate student who did much of the design and assembly of the instrument).

 © 2003 Wiley-VCH Verlag GmbH & Co. KGaA, Weinheim

orifice leading into the vacuum system. Thus, one was faced with a trilemma in LC-MS operation. Either 1) the LC system would have to be maintained at several KV above ground, 2) the MS at several KV "below" ground, or 3) the power supply would require enough capacity to maintain the required potential difference in spite of the leak to ground of current through the conducting path comprising the flow of liquid from the LC. Options (1) and (2) were not feasible but option (3) was being used in some systems. We then had a wild idea that turned out to be a very effective solution to this problem. We replaced the simple orifice into the vacuum system by a glass capillary tube (see Figure 10). That glass tube was metallized at each end to provide an electrical contact. The inlet end of the capillary would be maintained at the required potential below ground so the ions entering the tube would be in a potential well. We guessed, correctly as it turned out, that the fairly high-velocity flow of bath gas through the glass (dielectric) tube into the vacuum system could drag the ions out of that potential well up to whatever potential might be desired at the metallized exit end of that tube. It worked like a charm. Indeed, the gas flow could raise the ions to an exit potential of several tens of KV, sufficient to inject the ions into a magnetic sector analyzer. At the same time all exposed external parts and surfaces of the instrument could be maintained at ground potential, thereby posing no hazard to an operator.

Eager to flex our muscles with the new apparatus we tried it out with a couple of cyclic peptide samples from friends in the Medical School, cyclosporin A and gramicidin S with molecular weights of 1184 and 1141 $g\,mol^{-1}$, respectively. Figure 11a shows the spectrum obtained with a solution of 1.0 $g\,L^{-1}$ of cyclosporin A in 85:15 (v:v) acetonitrile:water. The dominant peak at 1203 corresponds to singly protonated parent molecules M with one water of hydration $[M+H+H_2O]^+$. The small satellite peaks on either side are due to ions with one more and one less water molecule. The small triplet peak near m/z 600 is from doubly protonated ions of the same species $[M+2H]^{2+}$. (The right to left increase in m/z ratio is the opposite of custom owing to a quirk of the available chart recorder.) Figure 11b shows the spectrum for 1.0 $g\,L^{-1}$ of gramicidin S in 50:50 (v:v) methanol:water. Here the peak is much larger for the ions that are doubly rather than singly protonated. These differences can be understood in terms of the IEM mechanism and the greater hydrophobicity of cyclosporin. A hydrophobic molecule can be more easily removed from an aqueous environment than a hydrophilic one. Consequently, one charge can provide enough "lift" to remove the ion from the droplet surface. This observation seems to support the IEM of Iribarne and Thomson. As the droplet shrinks, the charges get close enough together so that two of them can attach to a single gramicidin molecule thus providing more lift, in part because of the two charges and in part because the surface field is stronger, owing to the higher surface charge density.

Peaks for doubly charged ions also dominated in similar spectra for the peptides bleomycin and "substance P". In the spectra for renin substrate and insulin chain B we found evidence of triple protonation. This propensity for multiple charging was quite provocative because the effective mass

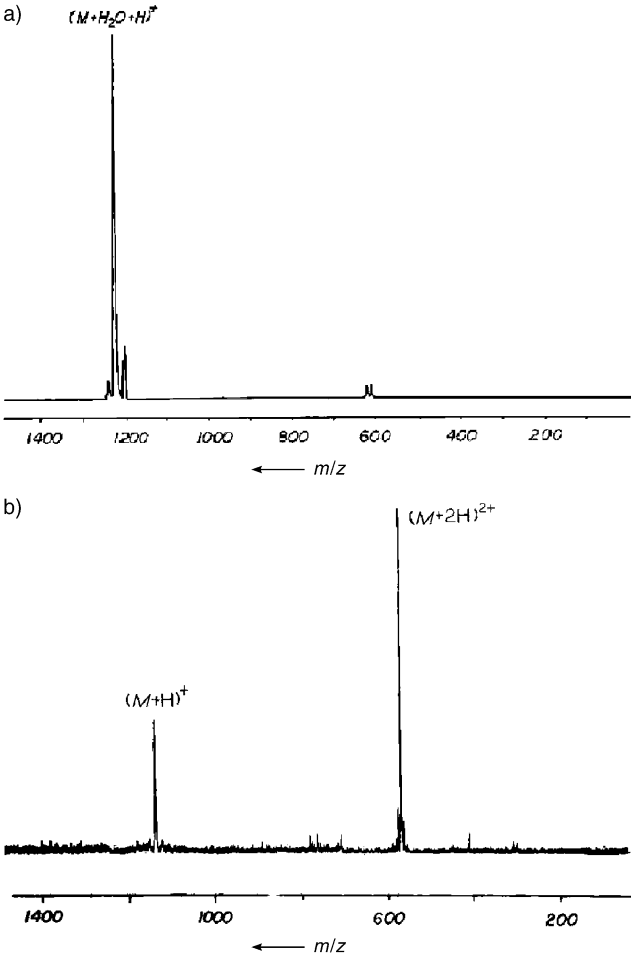


Figure 11. a) shows a mass spectrum obtained with a solution of the cyclic peptide, cyclosporin A, in methanol:water (50:50 v/v). The dominant peak is for a singly charged molecule with one adduct water molecule $[M+H+H_2O]^+$. The small peak on the right is due to the bare ion $[M+H]^+$. The tiny peak on the left is due to the parent molecule with two adduct water molecules $[M+H+2H_2O]^+$. b) The spectrum obtained with a solution of gramicidin S.

range of any analyzer increases by a factor equal to the number of charges per ion. To explore the extent to which such multiple charging can occur, and to identify and evaluate the controlling factors, we carried out an extensive study of ES ion formation with poly(ethylene glycol) (PEG) oligomers. Samples with a range of nominal molecular weights (M_r values) were kindly provided by Union Carbide and Chemical Corp. Each one comprised a mixture of oligomers with a Gaussian-like distribution of M_r values having a half width (FWHM) roughly 15% of the nominal M_r value of the most abundant oligomer. These species retain their chemical and structural similarity over a wide range of M_r values. Na^+ ions bind to the oxygen atoms in the oligomer chain with an energy of 2.05 eV and there is always enough sodium around so that spectra of samples from the manufacturer (Union Carbide and Chemical Corp) comprised oligomers with varying numbers of Na^+ adducts that increased with increasing molecular weight. (However, one can change these adducts by appropriate additions to the sample, for example, to K^+ by

 © 2003 Wiley-VCH Verlag GmbH & Co. KGaA, Weinheim

adding KOH or KCl) Figure 12 shows mass spectra for PEG samples having nominal M_r values from 400 to 3350 for which the individual peaks are clearly resolvable in the original spectra and correspond to oligomers with varying numbers of

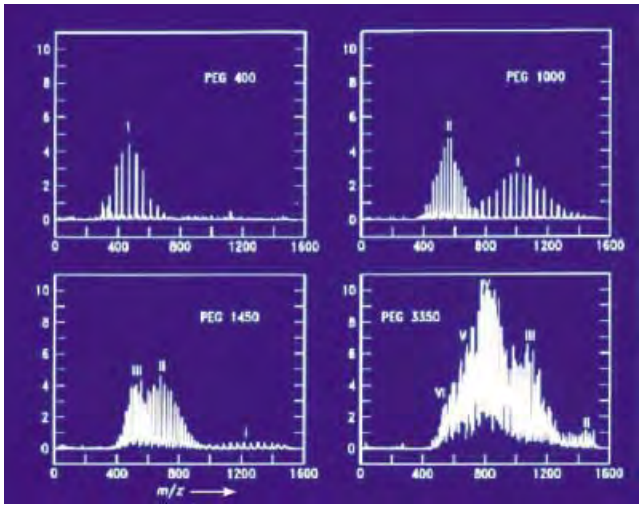


Figure 12. a) ESI spectra obtained with the apparatus of Figure 10 for poly(ethylene glycol) oligomers with nominal molecular weights of 400, 1000, 1450, and 3350.

Na^+ adducts. Figure 13 shows spectra for samples with nominal M_r values of 8000 and 17500 wherein the peaks are much too close together to be resolved (with our analyzer) because of the superposition of a wide distribution of oligomer sizes on a wide distribution of charge states for each oligomer.[48] A reviewer of that first paper on these results dismissed them outright, saying that the spectra in Figure 13 were "not mass spectra but were due to dirt in the

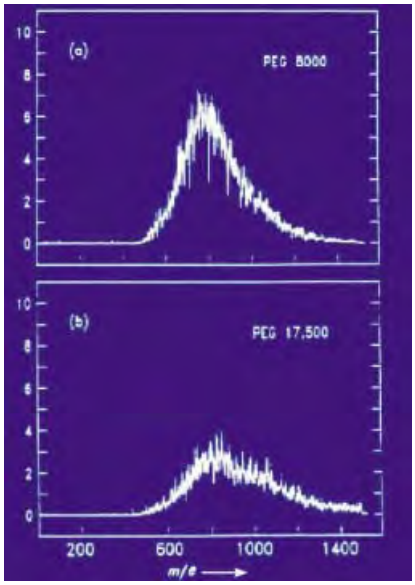


Figure 13. ESI spectra obtained with the apparatus of Figure 10 for poly(ethylene glycol) oligomers with nominal molecular weights of a) 8000 and b) 17500.

system!" However, we have found over the years that for polymers like these one can correctly and usefully assume that the m/z values at the maximum intensity of the envelope of the overlapping peaks is a reasonably reliable estimate of the most probable m/z value for the most abundant oligomer in the sample. We used this assumption to great advantage in a later study which showed that intact ions could be obtained from PEG oligomers with M_r values of at least 5000000![49] Others have since shown that ESI can produce intact ions of species with molecular weights of over 100 million![50]

The message of these PEG experiments was clearly that to study the ESI-MS behavior of large molecules we needed samples of pure compounds in which all the molecules had the same molecular weight. Obvious examples of such compounds are natural peptides and proteins which for many other reasons, of course, are far more interesting and rewarding subjects of study than synthetic polymers. We began to get promising results with such compounds in late 1987 and presented the results in June 1988 at the 36th ASMS Conference on Mass Spectrometry and Allied Topics in San Francisco. Inspection of those spectra showed that each peak in the spectrum for any one species differs from an adjacent peak only by one adduct charge, usually a proton in the case of these peptides and proteins. The first reviewer of a preliminary paper on these results asserted that they showed the method to be worthless for two reasons: 1) The total ion current was divided among so many peaks that the signal/noise ratio for any one peak would inevitably be low and 2) the multiplicity of peaks for each species in a mixture would inevitably make the spectra too congested to be interpreted.

As I have often done, and still do, that reviewer underestimated the power of a computer. One day I commented to my then student, Matthias Mann, that each peak in one of these multiple peak spectra was really an independent measure of the parent ion mass. Therefore, there should be some way of averaging those independent values to get a more reliable and accurate measure of the parent molecule mass than any single-peak spectrum could provide. Two days later he had worked out a computer algorithm that transformed the multiple peaks into a single peak that would be obtained if all the ions had a single massless charge. The m/z value for that peak is thus the M_r value for that species. Figure 14 shows the ESI mass spectrum for cytochrome C.

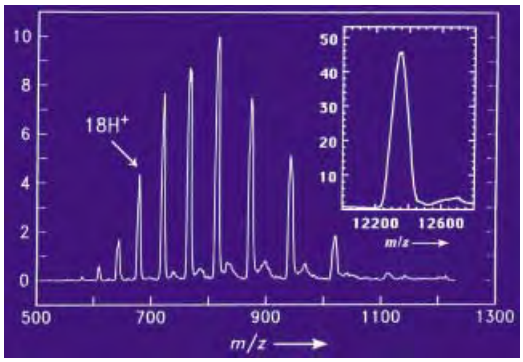


Figure 14. Spectrum for Cytochrome C. The insert shows the result of applying Matthias Mann's deconvolution algorithm.

 © 2003 Wiley-VCH Verlag GmbH & Co. KGaA, Weinheim

The insert shows the result of the deconvolution by the algorithm Matthias had worked out, that is, the peak that would be obtained if all the ions had a single massless charge. The m/z value on the abscissa for the apex of that peak is thus the true molecular weight of the parent neutral molecule. It is noteworthy that the scale for the ordinate value, which represents the relative abundance of the ions in any peak, is the same on the insert as in the multipeak spectrum. Clearly, values for both total signal and signal-to-noise ratio are much higher in the deconvoluted spectrum than in the parent spectrum as measured. It is now taken for granted that computers can deconvolute what seem to be hopelessly complex mass spectra to obtain precise and accurate M_r values for very large molecules in an extremely complex mixture of species.

Funding agencies were also generally somewhat less than enthusiastic in response to our proposals. For example, when we submitted one for research to extend the results shown in Figure 9 the reviewer simply said: "It is impossible for this man to obtain these results with his equipment!" I was reminded of the slogan once promoted by a company which said: "Difficult tasks we can finish quickly. The impossible ones take a little longer!"

There were only a handful of people at the session of the ASMS meeting at which we presented these results. Nor were there many questions or comments from the floor. However, when those results were published in 1989 (the first complete paper on the method and results appeared in the 10/6/89 issue of Science and is by far the most cited publication that ever came out of our lab[51]) they began what has become a "flood" of papers and ignited what has been referred to as the "electrospray revolution!" Some idea of the dimensions of that flood can be gained from Figure 15 which was prepared by my good friend and former colleague, Professor Juan de la Mora at Yale. It shows how the publications on ESI-MS have been increasing with time. The sudden rise began in 1990, a year or so after we first presented the protein results and reaching over 1500 per year in 2001 and still climbing! Moreover those numbers reflect only a small fraction of the total ESI-MS activity, most of which is being carried out by the pharmaceutical companies and is not published.

In view of the flood of papers on ESI-MS revealed in Figure 15, even a rudimentary summary of what they have taught would clearly take much more than a little longer.

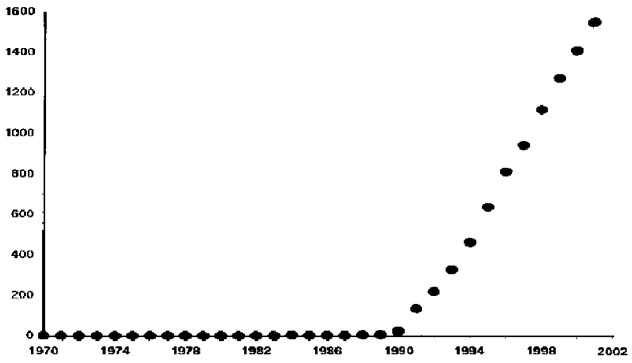


Figure 15. The number of publications each year on ESI-MS.

Consequently, I will stop here with a final word of appreciation to the many who have made possible the preparation of this paper. I would especially emphasize the extent of my gratitude and thanks to my eager and able colleagues without whose efforts I would not be here today (see Figures 10 and 16). Nor could I be writing this had I not had the support of numerous sponsors who over the years have provided the funds (albeit sometimes unwittingly!) without which we could have done nothing. They include the Department of Energy, the National Science Foundation, the National Institutes of Health, the Army Research Office, the American Cancer Society, the duPont Company, and the Jeffress Foundation. Finally, of course, I want to express my eternal gratitude to the Nobel Foundation and its marvelously helpful and gracious staff. They, along with what must have been generous and abundant approval from my peers and colleagues in the fellowship of scientists, have transformed my wildest dreams into a reality even more unbelievable than "flying elephants!"

Received: May 5, 2003 [A605]

[1] J. W. Mullen, M. R. Irby, J. B. Fenn, *Third International Symposium on Combustion, Flames and Explosive Phenomena*, Williams and Wilkins, Baltimore, **1949**.
[2] S. Datz, E. H. Taylor, *J. Chem. Phys.* **1956**, *25*, 395.
[3] E. W. Becker, K. Bier, *Z. Naturforsch. A* **1954**, *9*, 975.
[4] A. Kantrowitz, J. Grey, *Rev. Sci. Instrum.* **1951**, *22*, 328.
[5] G. B. Kistiakowsky, P. Schlichter, *Rev. Sci. Instrum.* **1951**, *22*, 333.
[6] T. H. Johnson, *Nature* **1928**, *31*, 103.



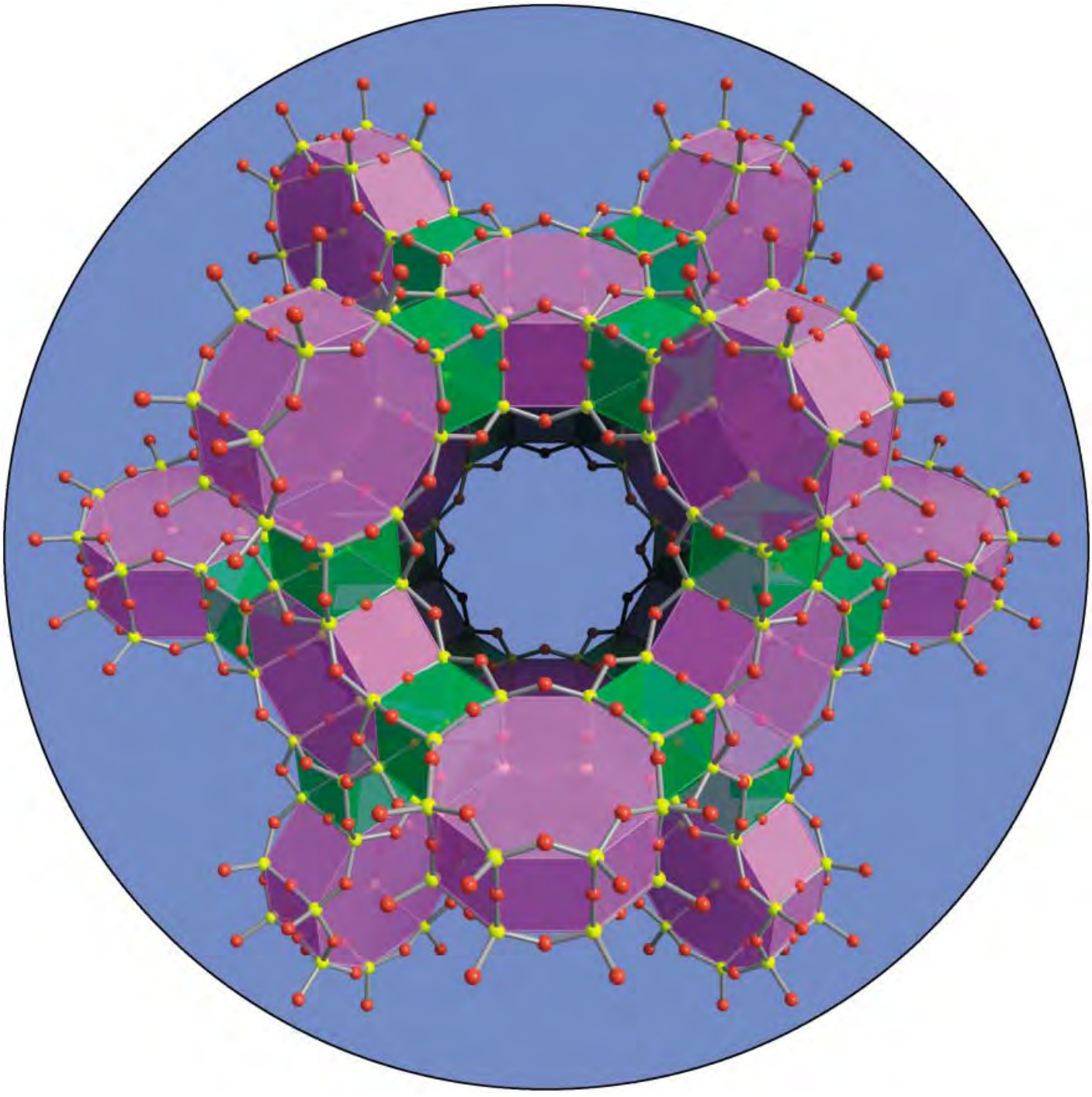
Figure 16. The colleagues, other than those shown in Figure 10, who played the most important roles in the development of electrospray ionization; from left: Mike Labowsky, Masamachi Yamashita, Matthias Mann, Shek Fu Wong

 © 2003 Wiley-VCH Verlag GmbH & Co. KGaA, Weinheim

[7] I. Estermann, O. Frisch, O. Stern, *Z. Phys.* **1931**, *73*, 348.
[8] J. E. Scott, Jr., J. E. Drewry, *Proceedings of the 3rd International Symposium on Rarefied Gas Dynamics, Vol. I*, (Paris) Academic Press, New York, **1963**, p. 516,.
[9] R. G. J. Fraser in *Molecular Rays*, Macmillan, New York, **1931**.
[10] E. W. Becker, K. Bier, H. Berghoff, *Z. Naturforsch. A* **1955**, *A10*, 565.
[11] H. R. Murphy, D. R. Miller, *J. Phys. Chem.* **1984**, *88*, 4474.
[12] J. Deckers, J. B. Fenn, *Rev. Sci. Instrum.* **1963**, *34*, 96.
[13] a) N. Abuaf, J. B. Anderson, R. P. Andres, J. B. Fenn, *Science* **1967**, *18*, 314; b) R. Campargue, J. B. Anderson, J. B. Fenn, B. B. Hamel, E. F. Muntz, J. R. White in *Nuclear Energy Maturity* (Ed.: P. Zaleski), Pergamon, Oxford, **1975**, p. 5.
[14] E. Kolb, D. R. Herschbach, *J. Phys. Chem.* **1984**, *88*, 4488.
[15] P. L. Owen, C. K. Thornhill, *Aeronautical Council Reports and Memoranda* No. 2616.
[16] R. J. Gallagher, *J. Chem. Phys.* **1974**, *60*, 3487.
[17] R. E. Smalley, L. Wharton, D. H. Levy, *J. Chem. Phys.* **1975**, *63*, 4977.
[18] S. B. Ryali, J. B. Fenn, *Ber. Bunsen-Ges.* **1984**, *88*, 245.
[19] S. Goyal, D. L. Schutt, G. Scoles, *Phys. Rev. Lett.* **1992**, *69*, 933.
[20] M. Hartmann, R. E. Miller, J. P. Toennies, A. Vilesov, *Phys. Rev. Lett.* **1995**, *75*, 1566.
[21] D. Herschbach, Y. Lee, J. Polanyi (1986); R. Smalley (1996); A. Zewail (1999).
[22] M. Dole, L. L. Mach, R. L. Hines, R. C. Mobley, R. C. Ferguson, M. B. Alice, *J. Chem. Phys.* **1968**, *49*, 2240.
[23] R. J. Beuhler, E. Flanigan, L. J. Greene, L. Friedman, *J. Am. Chem. Soc.* **1974**, *96*, 3990.
[24] H. L. C. Meuzelaar, M. A. Posthumus, P. G. Kistemaker, J. Kistemaker, *Anal. Chem.* **1973**, *45*, 1546.
[25] a) E. Unsoeld, F. Hillenkamp, R. Nitsche, *Analysis* **1976**, *4*, 115; b) M. A. Posthumus, P. G. Kistemaker, M. C. Ten Nover de Brauw, *Anal. Chem.* **1978**, *50*, 985.
[26] M. Barber, R. S. Baordolli, G. J. Elliot, R. D. Sedgwick, A. N. Tyler, *J. Chem. Soc. Chem. Commun.* **1981**, 325.
[27] A. Benninghoven, D. Jaspers, W. Sichtermann, *Appl. Phys.* **1976**, *11*, 35.
[28] a) D. F. Torgerson, A. R. P. Skowronski, R. D. Macfarlane, *Biochem. Biophys. Res. Commun.* **1974**, *60*, 616; b) B. U. R. Sundquist, R. D. Macfarlane, *Mass Spectrom. Rev.* **1985**, *4*, 421.
[29] K. H. Tanaka, H. Wake, Y. Ido, S. Akita, Y. Yoshida, I. Yoshida, *Rapid Commun. Mass Spectrom.* **1988**, *2*, 2.
[30] M. Karas, F. Hillenkamp, *Anal. Chem.* **1988**, *60*, 2299.
[31] E. W. Mueller, *Z. Phys.* **1951**, *131*, 136.
[32] E. W. Mueller, *Electronics and Electron Physics, Vol. 13*, Academic Press, New York, **1960**, p. 83..
[33] M. Ingram, R. Gomer, *J. Chem. Phys.* **1954**, *22*, 1279.
[34] H. D. Beckey in *Principles of Field Ionization and Field Desorption Mass Spectrometry*, Pergamon, Oxford, **1977**.
[35] C. A. Evans, Jr., C. D. Hendricks, *Rev. Sci. Instrum.* **1972**, *43*, 1527.
[36] D. W. Simons, B. N. Colby, C. A. Evans, Jr., *Int. J. Mass Spectrom. Ion Phys.* **1974**, *15*, 291.
[37] K. D. Cook, *Mass Spectrom. Rev.* **1986**, *5*, 467.
[38] J. W. Strutt (Lord Rayleigh), *Philos. Mag.* **1882**, *14*, 184.
[39] J. Zeleny, *Phys. Rev.* **1917**, *10*, 1.
[40] A. Gomez, K. Tang, *Phys. Fluids* **1994**, *6*, 404.
[41] G. I. Taylor, *Proc. R. Soc. London Ser. A* **1964**, *280*, 383.
[42] J. W. Strutt (Lord Rayleigh) in *The Theory of Sound*, Dover, New York, **1945**, chap. 20.
[43] M. Dole in *My Life in the Golden Age of America*, Vantage, New York, **1989,** p. 169.
[44] M. Dole in *My Life in the Golden Age of America*, Vantage, New York, **1989**, p. 167.
[45] S. K. Chowdhury, V. Katta, B. T. Chait, *Rapid Commun. Mass Spectrom.* **1990**, *4*, 53.
[46] J. V. Iribarne, B. A. Thomson, *J. Chem. Phys.* **1976**, *64*, 2287.
[47] a) C. R. Blakley, M. J. McAdams, M. L. Vestal, *J. Chromatogr.* **1980**, *102*, 5931.
[48] S. F. Wong, C. K. Meng, J. B. Fenn, *J. Phys. Chem.* **1988**, *92*, 546.
[49] T. Nohmi, J. B. Fenn, *J. Am. Chem. Soc.* **1992**, *114*, 3241.
[50] S. F. Fuerstenau, *J. Mass Spectrom. Soc. Jpn.* **2003**, *51*, 50.
[51] J. B. Fenn, M. Mann, C. K. Meng, S. F. Wong, C. M. Whitehouse, *Science* **1989**, *246*, 64.

 © 2003 Wiley-VCH Verlag GmbH & Co. KGaA, Weinheim

Communications



Through embracing some of the recent advances in mathematical tiling theory, R. G. Bell, J. Klinowski, et al. have calculated the hypothetical structures of a number of zeolitic frameworks. The use of this knowledge for the design of materials with improved applications is discussed on the following pages.

DOI: 10.1002/anie.200351556
© 2003 Wiley-VCH Verlag GmbH & Co. KGaA, Weinheim

Zeolite Frameworks

Structural Evaluation of Systematically Enumerated Hypothetical Uninodal Zeolites**

Martin D. Foster, Olaf Delgado Friedrichs, Robert G. Bell, Filipe A. Almeida Paz, and Jacek Klinowski**

The wide applications of zeolites as molecular sieves, ion exchangers, and catalysts, and their intrinsic academic interest have given rise to a large body of work on the characterization of zeolitic structures, of which 139 distinct structural types are known.[1] The design of new zeolite frameworks is a matter of considerable importance for two main reasons. Firstly, a list of chemically feasible hypothetical structures will permit the design of strategies leading to their synthesis. Secondly, X-ray diffraction patterns generated for hypothetical structures will be of considerable help in determining the structures of new materials.

The enumeration of zeolitic structures originates from the work of Wells.[2] New structures have been generated by linking together various structural subunits in new ways,[3–5] or by using computer search algorithms.[6,7] However, such methods can generate only a small fraction of possible networks, since the number of three-dimensional frameworks constructed from tetrahedral building blocks is infinite.

A completely new approach to the problem of systematic enumeration[8] is based on recent advances in mathematical tiling theory.[9] We now describe the use of simulation methods of computational chemistry to calculate the structure, lattice energy, framework density, and other structural parameters of such hypothetical frameworks. Each framework was assumed to have the empirical formula SiO_2 and optimized using a standard lattice-energy-minimization program GULP.[10] Accurate interatomic potential methods were used to calculate lattice energies of these structures relative to α-quartz. Based on relative lattice energy and on various structural features, we have devised criteria to identify frameworks that are likely to be feasible as zeolites. We describe the results for hypothetical uninodal structures (structures in which all tetrahedral sites are equivalent), which contain all 19 known uninodal zeolites, providing a control set to guide our selection of feasible structures, with the main criterion being the relative lattice energy.

A total of 294 uninodal frameworks were originally enumerated.[8] This set included nine uninodal frameworks derived from simple tilings (with tetrahedral vertex figures), and frameworks from quasi-simple tilings (with vertex figures derived from tetrahedra, but containing double edges). After removing duplicates and frameworks in which, after one initial Si–Si separation was set at 3.1 Å there remained more than three other next-neighbor Si atoms within 3.1 ± 0.2 Å, 166 uninodal structures were available for evaluation. Of these, all except two were refineable in the sense that we were able to carry out an energy-minimization calculation on their structure. Among the 164 minimized structures were 19 known zeolites, two minerals (tridymite and cristobalite) and 80 unknown zeolite topologies. The remaining structures were duplicates with the same framework topology but arising from different tilings which, in most cases, minimized to identical structures. In several cases, however, qualitatively different structures were obtained with the same topology, because different unit cell definitions can result in minimized structures with different symmetries. For example, several low- and high-symmetry forms of cristobalite and trydimite were found. While most of the structures have previously been found by model-building[4] or computer-based methods,[6] our enumeration is systematic, and ranking by relative lattice energies gives a different "order of preference" as compared to those of Boisen et al.[11] (who used a calculated force field) and Treacy et al.[6] (who relied on an empirical cost function based on the geometries of known silicate zeolites), thus giving prominence to a different subset of chemically feasible structures.

For framework-energy calculations (Figure 1), instead of considering only zeolites which exist in the purely siliceous form, we have treated all the known topologies as though they were realized as silica polymorphs. The three structures which substantially deviate from the rest are the non-silicate structure types WEI (a beryllophosphate), CZP (a zincophosphate), and OSO (a berylosilicate). OSO and WEI are frameworks containing three-membered rings, and the higher energy of these structures in the siliceous form indicates a strained framework. Figure 1 excludes structures CHI, CLO, PAR, RON, and WEN, which have interrupted frameworks. The straight line, showing the least-squares fit for all data except those for CZP, WEI and OSO, is similar to those reported by Henson et al.[12] and Aporiaye and Price,[13] and to those derived from calorimetric measurements.[14] The deviation of the relative lattice energy from the fit can be easily quantified. If the equation of the regression line is written as $y + ax + c = 0$ (where y = framework energy E_F and x = framework density D_F), then the distance of a point with coordinates (x_1, y_1) from the line is $\vartheta = |(ax_1 + y_1 + c)/a|$. Table S1 (Supporting Information) lists the values of the

[*] Dr. R. G. Bell, M. D. Foster
Davy Faraday Research Laboratory
The Royal Institution of Great Britain
21 Albemarle Street, London W1S 4BS (UK)
Fax: (+44) 20-7629-3569
E-mail: rob@ri.ac.uk
Prof. Dr. J. Klinowski, F. A. Almeida Paz
Department of Chemistry
University of Cambridge
Lensfield Road, Cambridge CB2 1EW (UK)
Fax: (+44) 1223-336-362
E-mail: jk18@cam.ac.uk
Dr. O. Delgado Friedrichs
Wilhelm Schickard Institut für Informatik und ZBIT Zentrum für Bioinformatik
Universität Tübingen
Sand 14, 72072 Tübingen (Germany)

[**] We are grateful to the EPSRC (UK) for support and to the Portuguese Foundation for Science and Technology (FCT) for the Ph.D. scholarship No. SFRH/BD/3024/2000 to F.A.A.P.

Supporting information for this article is available on the WWW under http://www.angewandte.org or from the author.

 © 2003 Wiley-VCH Verlag GmbH & Co. KGaA, Weinheim DOI: 10.1002/anie.200351556

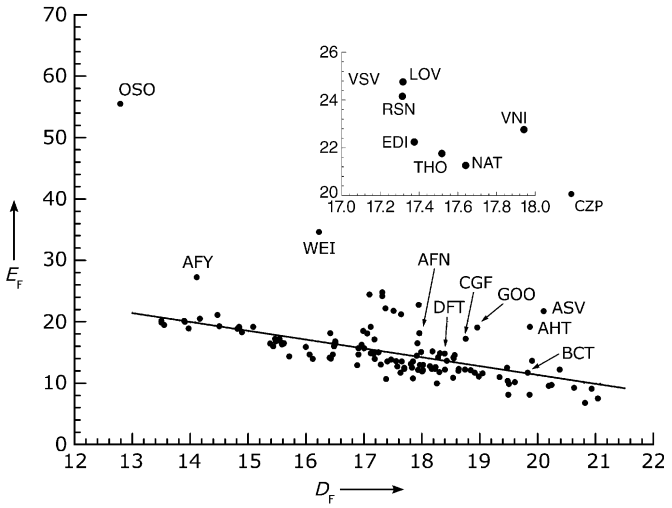


Figure 1. Framework energy (kJ mol^{-1}) with respect to α-quartz versus framework density (Si atoms per 1000 Å^3) for all known zeolitic structure types treated as silica polymorphs. The equation of the least-squares best fit line is $E_F = -1.4404 \times D_F + 40.126$ (correlation coefficient $R = -0.69$).

dimensionless deviation parameter ϑ for the structures which we consider as the most feasible.

Figure 2 gives the plot of relative framework energy versus the framework density for the known and hypothetical uninodal structures for energies below 35 kJ mol^{-1}. This identifies structures with energies falling within this range, which we consider as the most feasible. Some of these hypothetical structures have been singled out using several criteria.

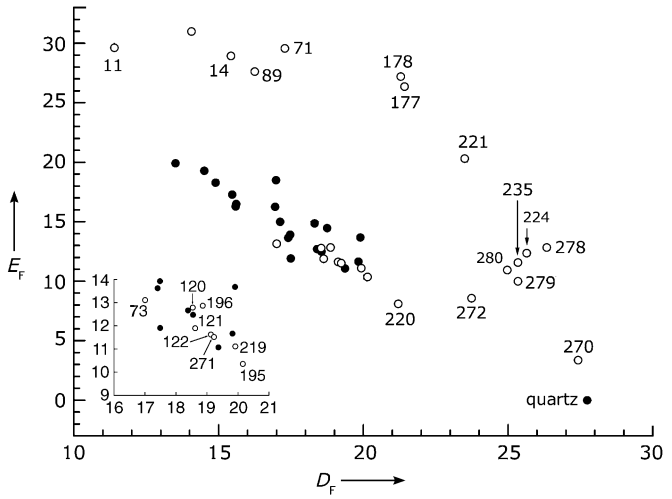


Figure 2. Framework energy with respect to α-quartz versus framework density for known (●) and hypothetical (○) uninodal zeolitic structures with framework energies below 35 kJ mol^{-1}.

Figure 3 shows the plot of relative framework density (Si atoms per 1000 Å^3) versus the number of Si atoms in the fourth coordination shell (N_4), a topological property directly related to framework density, for the known and hypothetical uninodal zeolites. For quartz, the most dense structure, $N_4 = 52$. Structures with low framework density contain large cavities and/or channels outlined by large rings. This occurs for low degrees of branching of the framework, and is reflected in the coordination sequence, which is thus a useful tool for identifying feasible zeolitic structures.[3,13]

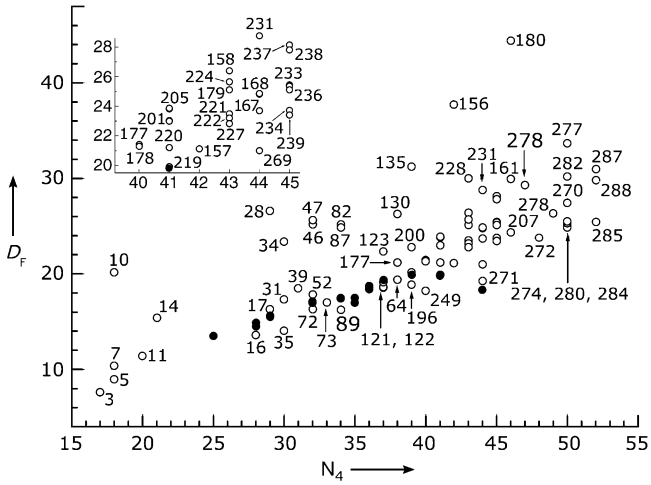


Figure 3. Framework density versus the number of Si atoms in the fourth coordination shell for known (●) and hypothetical (○) uninodal zeolitic structures.

The accessible free volume determined by a probe molecule with a radius of 1.4 Å (such as H_2O) gives an indication of the space that is available within each structure for applications in molecular sieving and catalysis. Known structures such as AST, MSO, and NON have zero accessible volume for the given size of the probe molecule. OSO has the highest accessible volume, closely followed by FAU, EMT, and SBT, all of which contain large cavities.

Low-framework-density structures are of particular interest, as they have very high accessible free volumes. Of the structures corresponding to points on the left of Figure 4, only structure 11 turns out to be energetically stable (Figure 5a).

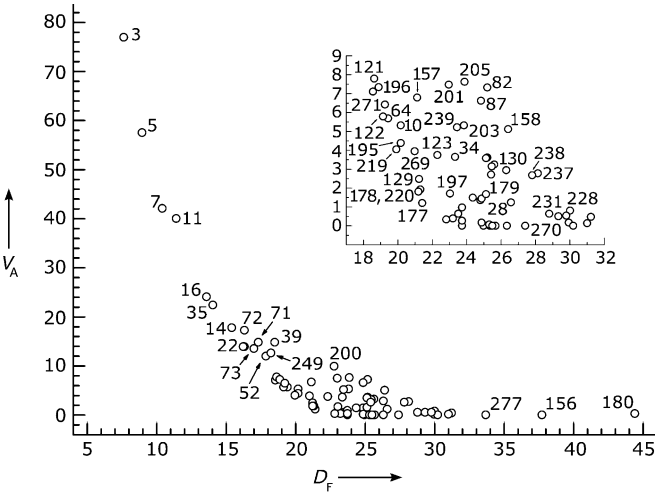


Figure 4. Accessible volume (Å^3 per Si atom) versus framework density for the hypothetical uninodal zeolites.

 © 2003 Wiley-VCH Verlag GmbH & Co. KGaA, Weinheim

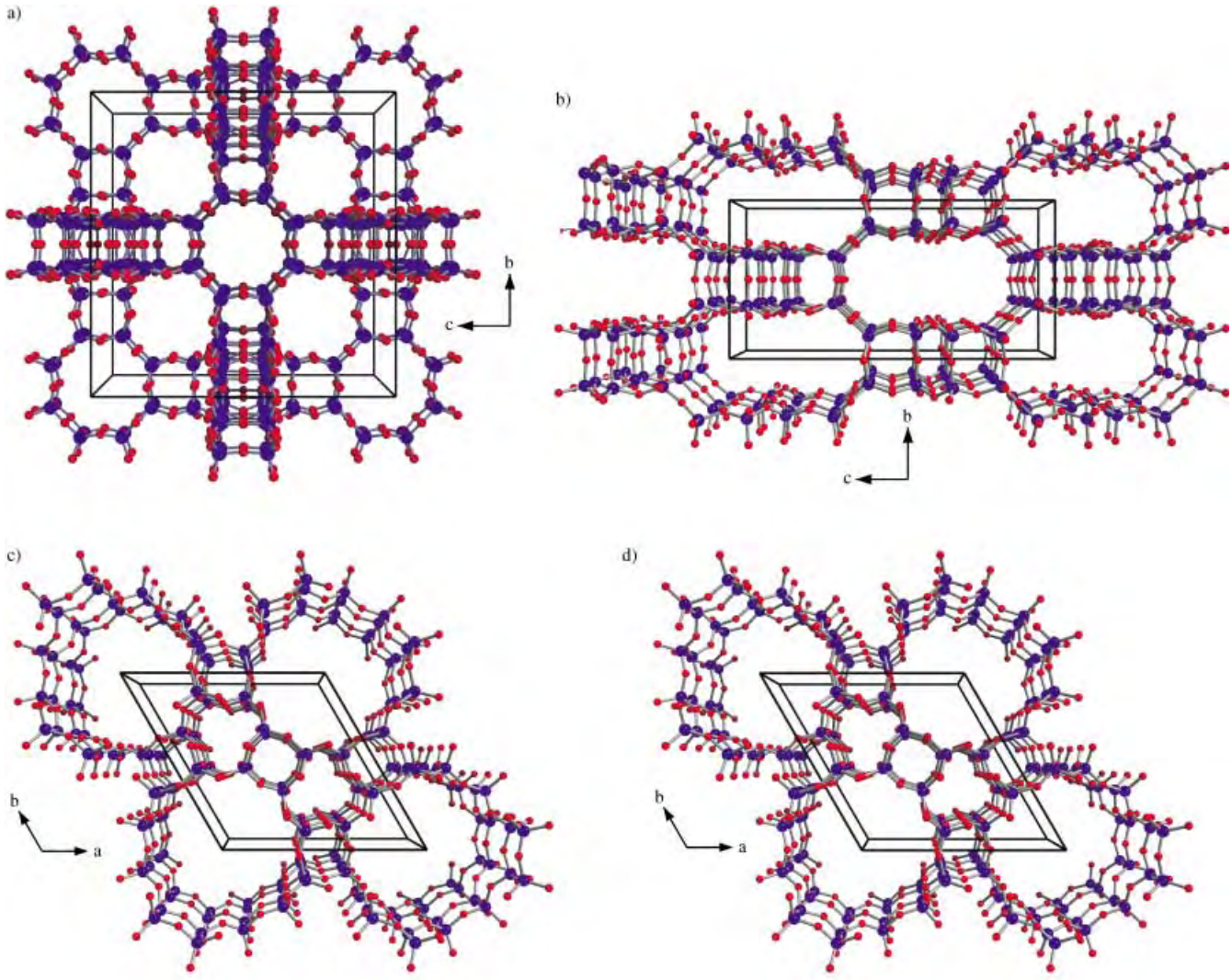


Figure 5. a) Structure 11 consists of cages connected by 4- and 8-membered rings; b) structure 14 contains two systems of elongated channels outlined by 12-membered rings (5.3×9.3 Å) running along the *a* and *b* directions of the unit cell; c) structure 71 consists of layers of 12-membered rings (7.2×7.2 Å) connected by 4- and 6-membered rings; d) structure 73 contains large channels of 12-membered rings, and narrower channels of 4- and 6-membered rings. When viewed along the *c* axis, the structure is similar to that of AFI, although the rings are connected in a different fashion along the *a* and *b* axes.

Although many of the hypothetical uninodal structures have dense frameworks, we observe a strong correlation between hypothetical structures and the known zeolite topologies. Thus one cannot rule out a structure just on the basis of the accessible free volume, even though a structure with no accessible free volume for such a small probe molecule will hardly be of interest to sorption, ion exchange, or catalysis. Figure 4 distinguishes between "favorable" hypothetical structures on the basis of their accessible free volume, but is not a suitable "filter" for feasible zeolitic topologies. Further structures of interest are: 14, 71, and 73 (Figure 5b–d and Table S1 in Supporting Information), as well as 35, 122, 195, and 196 (not shown).

Although some of the zeolite topologies only exist as aluminum phosphates (AlPOs) or other non-silica compositions, all hypothetical structures were evaluated on the assumption that a purely siliceous composition is a good indicator of energetic stability. Evaluation of the topologies with the AlPO composition suggests that their stability is similar to that of the SiO_2 compositions,[15] and atomistic modeling of known AlPO structures shows that the correlation between energy and density for purely siliceous systems is also valid for the AlPO systems.[16]

The synthesis of microporous materials is facilitated by the use of structure-directing agents (templates), typically organic bases incorporated in the reactive mixture, which will direct the shape of the resulting framework. A given microporous structure may then be targeted by adroit choice of the template using ZEBEDDE,[17] a computational method for the de novo design of template molecules, which are "grown" within the desired inorganic framework. ZEBEDDE is already being used with a view to synthesizing the hypothetical zeolitic structures, which we have enumerated and evaluated in this work.

 © 2003 Wiley-VCH Verlag GmbH & Co. KGaA, Weinheim

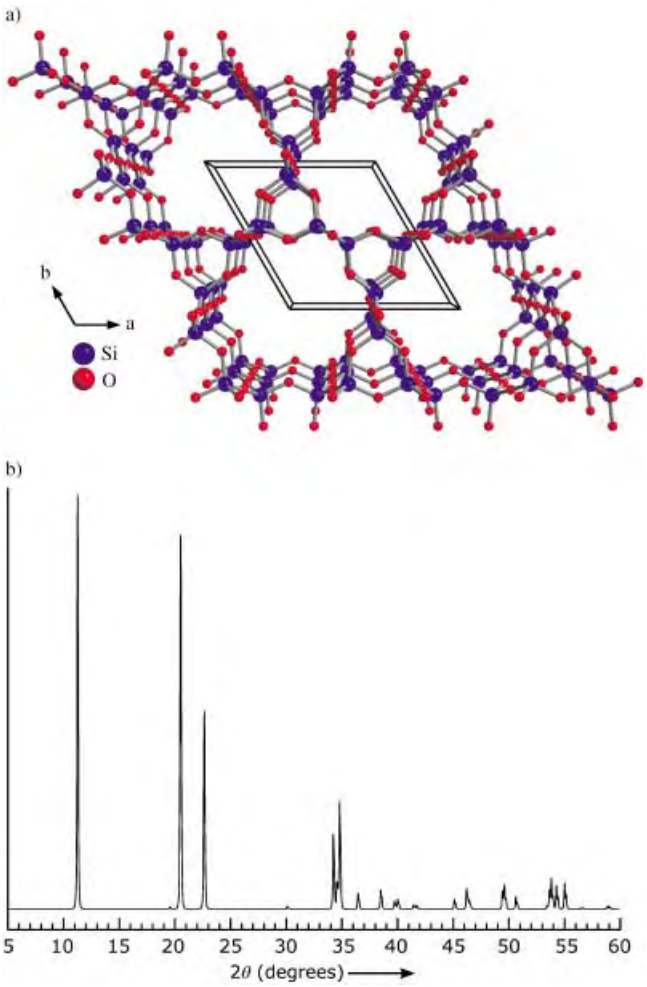


Figure 6. a) Structure 88; b) the calculated X-ray diffraction pattern for this structure.

Finally, we note that a zeolite-like material with the framework composed of phosphorus, nitrogen, and oxygen and the structure corresponding to our net 88 (Figure 6a), has recently been synthesized.[18] This was confirmed by comparing the calculated (Figure 6b) and experimental powder X-ray patterns.[18]

Received: April 2, 2003 [Z51556]
Published online: August 1, 2003

Keywords: computer chemistry · energy minimization · molecular modeling · silicates · zeolites

[1] C. Baerlocher, W. M. Meier, D. H. Olson, *Atlas of Zeolite Structure Types*, 5th ed., Elsevier, London, **2001** (updates on http://www.iza-structure.org/).
[2] A. F. Wells, *Three-Dimensional Nets and Polyhedra*, Wiley, New York, **1977**; A. F. Wells, *Further Studies of Three-Dimensional Nets, American Crystallographic Association Monograph No. 8, Vol. 9*, Polycrystal Book Service, Pittsburgh, **1979**; A. F. Wells, *Structural Inorganic Chemistry*, 5th ed., Oxford University Press, Oxford, **1984**.
[3] D. E. Akporiaye, G. D. Price, *Zeolites* **1989**, *9*, 23.
[4] J. V. Smith, *Chem. Rev.* **1988**, *88*, 149; M. O'Keeffe, B. G. Hyde, *Crystal Structures I: Patterns and Symmetry*, Mineralogical Association of America Monograph, Washington, DC, **1996**.
[5] K. J. Andries, H. J. Bosmans, *Acta Crystallogr.* **1990**, *46*, 847.
[6] M. M. J. Treacy, K. H. Randall, S. Rao, J. A. Perry, D. J. Chadi, *Z. Kristallogr.* **1997**, *212*, 768.
[7] J. Klinowski, *Curr. Opin. Solid State Mater. Sci.* **1998**, *3*, 79.
[8] O. Delgado Friedrichs, A. W. M. Dress, D. H. Huson, J. Klinowski, A. L. Mackay, *Nature* **1999**, *400*, 644.
[9] A. W. M. Dress, D. H. Huson, E. Molnár, *Acta Crystallogr. Sect. A* **1993**, *49*, 806; A. W. M. Dress in *Springer Lecture Notes In Mathematics, Vol. 1172*, Springer, Göttingen, **1985**, pp. 56; A. W. M. Dress, *Adv. Math.* **1987**, *63*, 196.
[10] J. D. Gale, *J. Chem. Soc. Faraday Trans.* **1997**, *93*, 629.
[11] M. B. Boisen, G. V. Gibbs, M. O'Keeffe, K. L. Bartelmehs, *Microporous Mesoporous Mater.* **1999**, *29*, 219.
[12] N. J. Henson, A. K. Cheetham, J. D. Gale, *Chem. Mater.* **1994**, *6*, 1647.
[13] D. E. Akporiaye, G. D. Price, *Zeolites* **1989**, *9*, 321.
[14] I. Petrovic, A. Navrotsky, M. E. Davis, S. I. Zones, *Chem. Mater.* **1993**, *5*, 1805; P. M. Piccione, C. Laberty, S. Y. Yang, M. A. Camblor, A. Navrotsky, M. E. Davis, *J. Phys. Chem. B* **2000**, *104*, 10001; Y. T. Hu, A. Navrotsky, C. Y. Chen, M. E. Davis, *Chem. Mater.* **1995**, *7*, 1816; P. M. Piccione, B. F. Woodfield, J. Boerio-Goates, A. Navrotsky, M. E. Davis, *J. Phys. Chem. B* **2001**, *105*, 6025; P. M. Piccione, S. Y. Yang, A. Navrotsky, M. E. Davis, *J. Phys. Chem. B* **2002**, *106*, 3629.
[15] A. Simperler, M. D. Foster, R. G. Bell, J. Klinowski, *J. Phys. Chem.* **2003**, submitted.
[16] N. J. Henson, A. K. Cheetham, J. D. Gale, *Chem. Mater.* **1996**, *8*, 664.
[17] D. W. Lewis, D. J. Willock, C. R. A. Catlow, J. M. Thomas, G. J. Hutchings, *Nature* **1996**, *382*, 604; D. W. Lewis, G. Sankar, J. K. Wyles, J. M. Thomas, C. R. A. Catlow, D. J. Willock, *Angew. Chem.* **1997**, *109*, 2791; *Angew. Chem. Int. Ed. Engl.* **1997**, *36*, 2675; D. J. Willock, D. W. Lewis, C. R. A. Catlow, G. J. Hutchings, J. M. Thomas, *J. Mol. Catal. A* **1997**, *119*, 415.
[18] S. Correll, O. Oeckler, N. Stock, W. Schnick, *Angew. Chem.* **2003**, *115*, 3674; *Angew. Chem. Int. Ed.* **2003**, *42*, 3549.

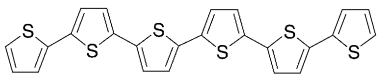
 © 2003 Wiley-VCH Verlag GmbH & Co. KGaA, Weinheim

Semiconductors

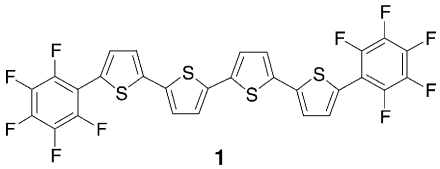
Building Blocks for n-Type Organic Electronics: Regiochemically Modulated Inversion of Majority Carrier Sign in Perfluoroarene-Modified Polythiophene Semiconductors**

*Antonio Facchetti, Myung-Han Yoon, Charlotte L. Stern, Howard E. Katz, and Tobin J. Marks**

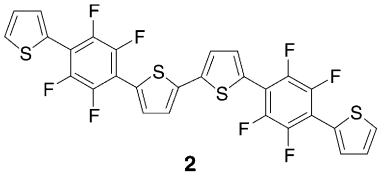
Electron-transporting (n-type) organic semiconductors[1] are relatively rare, but of great interest for "plastic electronics" such as thin-film transistors (TFTs), organic light-emitting diodes (OLEDs), and photovoltaics.[2] The most prominent examples of TFT n-type materials have been obtained by modifying known p-type cores with strongly electronegative fluoro/fluoroalkyl substituents. However, despite these advances, those factors underlying fluoro stabilization of the injected electrons are not fully understood, and have often been attributed to the reduction in LUMO energies. Of the known thiophene-based semiconductors, the vast majority[1a,b] exhibit hole-transporting (p-type) TFT activity. However, n-type thiophene-based oligomers and polymers would be extremely useful considering the stability and ready functionalizability of oligothiophene cores.[3]



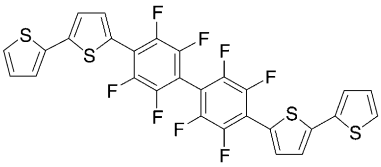
α6T



1



2



3

We report here on the surprising properties of the first fluoroarene-modified thiophene semiconductors **1**–**3**, which can be viewed as p-type **α6T** derivatives drastically reconstituted according to the following criteria: 1) Electronic: electron-deficient perfluoroarene substitution for electron-rich thiophene rings should lower LUMO energies, thus allowing more favorable electron injection. 2) Steric: nonbonded interactions accompanying five→six-membered ring substitution should destabilize ring coplanarity and additionally modulate orbital energies.[4] 3) Regiochemistry: systematic displacement of fluoroarene moieties from the periphery to embedded in the molecular core (**1**→**2**→**3**) can be achieved while preserving rodlike molecular architectures. This is impossible in other classes of molecular semiconductors. 4) Molecular packing: mixing electron-rich and electron-deficient π rings should favor close cofacial π-stacking versus slipped-stacking (herringbone) motifs, as suggested by packing in many 1:1 π-excessive/π-deficient molecular crystals.[5] The net result is a new family of closely packed polythiophene–fluoroarene conductors in which carrier mobility and sign can be drastically modulated by changing the molecular regiochemistry.

Compounds **1**–**3** were prepared in 60–80% yield by $Pd[PPh_3]_4$-catalyzed Stille coupling (Scheme 1), purified by gradient sublimation, and characterized by elemental analysis, mass spectrometry, multinuclear NMR, differential scanning calorimetry, thermogravimetric analysis, and single-crystal X-ray diffraction.[6]

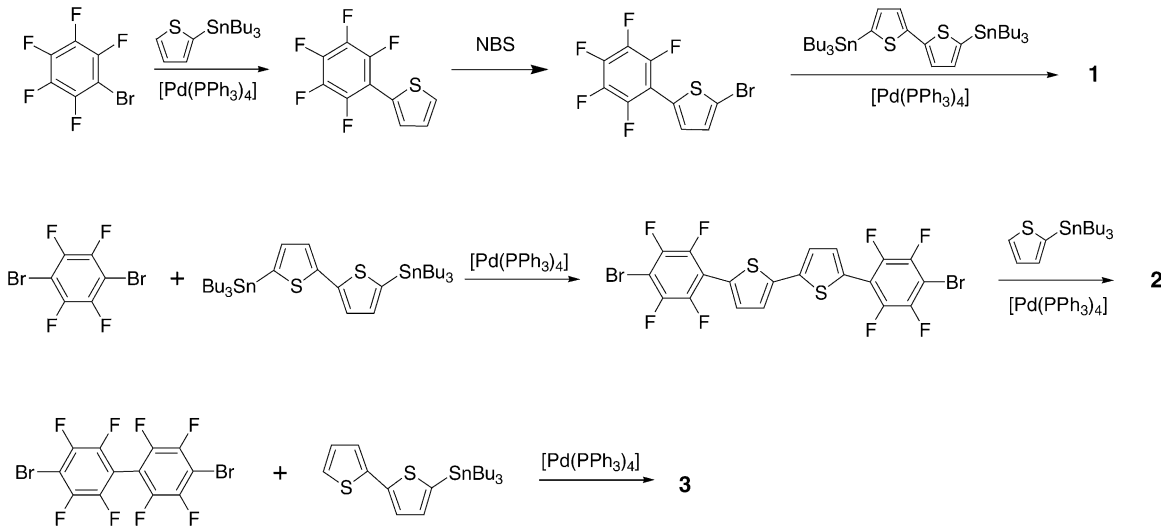
Interestingly, the crystal structures of **1**–**3** (Figure 1)[7] exhibit the common feature of close cofacial packing of electron-rich and electron-deficient subunits, in contrast to all previously reported unsubstituted oligothiophenes (terthiophene to octathiophene) in which a herringbone motif with twist angles of 60–70° between adjacent molecular planes is found. The latter arrangement reduces intermolecular orbital overlap and therefore should increase the barrier to charge transport versus an ideal, π–π overlapped structure. The structures of **1** and **2** reveal substantially planar cores with maximum thiophene–fluoroarene torsional angles between adjacent outer rings of 17.6° and 7.9°, respectively, versus 4.1° for **α6T**.[8] These angles are much smaller than the limiting ≈30° value required for the intramolecular π overlap of an efficient conduction band.[4a,9] Molecules of **1** exhibit an uncommon *syn* conformation between outer pairs of thiophene rings and are stacked in parallel layers along the *b* axis. System **2** packs along *c* in a zig-zag double layer motif, the first layer having an 18.31 Å ($^1/_2c$) repeat distance. Within each layer, the molecular units form slipped π–π stacks. To our

[*] Prof. Dr. T. J. Marks, Dr. A. Facchetti, M.-H. Yoon, Dr. C. L. Stern
Department of Chemistry and
the Materials Research Center
Northwestern University
2145 Sheridan Road, Evanston, IL, 60208-3113 (USA)
Fax: (+1) 847-491-2290
E-mail: tjmarks@casbah.acns.nwu.edu
Dr. H. E. Katz
Bell Laboratories
Lucent Technologies
Murray Hill, NJ 07974 (USA)

[**] We thank DARPA (N00421-98-1187), ONR (N00014-02-1-0909), and the NSF-MRSEC program through the Northwestern Materials Research Center (DMR-0076097) for support of this research.

Supporting information for this article is available on the WWW under http://www.angewandte.org or from the author.

 © 2003 Wiley-VCH Verlag GmbH & Co. KGaA, Weinheim DOI: 10.1002/anie.200351253



Scheme 1. Synthetic routes to compounds **1**–**3**.

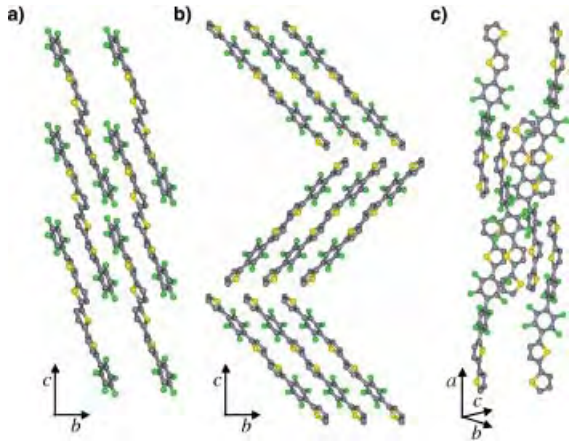


Figure 1. Crystal structures of fluoroarene-thiophene compounds **1** (a), **2** (b), and **3** (c). (C = gray, F = green, S = yellow,).

knowledge, the minimum cofacial π–π distances in **1** (3.20 Å) and **2** (3.37 Å) are the shortest so far reported for thiophene-based oligomers. In contrast, the structure of **3** exhibits a large intramolecular torsional angle (53.9°) between adjacent fluoroarene rings, hence interrupted π conjugation. The packing of **3** is also more complex, with waved layers having the long molecular axes extending along *c*.

Cyclic voltammetry[10] (Table 1) of **α6T** and **1**–**3** as THF solutions or as thin films on Au/glass reveal either two (solution) or one (50 nm films) chemically reversible reductive peaks. Electron affinity increases upon introduction of fluoroaryl rings as evidenced by anodic $E_{1/2}$(THF)/$E_{1/2}$(film) shifts from **α6T** to **1** (+0.20/+0.33 V), **2** (+0.17/+0.31 V), and **3** (+0.16/+0.17 V), respectively. Reversible oxidations are observed in solution for **α6T**, **1**, and **2**, but not for **3**. The film oxidative waves are irreversible as all films dissolve upon cation formation. LUMO energies were calculated directly from reductive $E_{1/2}$ values whereas HOMO energies were estimated from $E_{HOMO} = E_{LUMO} - E_{gap}$(optical).[11] The derived energy level orderings (Figure 2) demonstrate that fluoroarene substitution strongly lowers solution/film HOMO and LUMO energies. However, solution E_{HOMO} values strongly decrease on going from **1**→**2**→**3** (ΔE_{HOMO}(max) = 0.33 eV), whereas film E_{HOMO} and E_{LUMO} values remain in a narrower range (ΔE(max) = 0.16 eV). Therefore, relative stabilization at the molecular level of injected charge should be similar for all of these fluoroarene oligothiophenes, especially for **1** and **2**.

Film microstructure and morphology were investigated by XRD and SEM for 500 nm films vacuum-deposited on 60 °C Si/SiO_2 substrates. θ–2θ X-ray diffraction spectra of **1** and **3** exhibit only one set of Bragg reflections from the same family and a single strong peak, respectively, whereas **2** exhibits two sets of reflections with one being predominant. From the first reflection, interlayer spacings (*d*) of 25.07, 18.38 (14.96 for the second, less intense reflection set), and 5.98 Å are deduced for the films of **1**, **2**, and **3**, respectively, versus 23.3 Å for **α6T**.[12] From the **1**–**3** single-crystal cell parameters,[7] it can be surmised that preferential growth of **1**–**3** crystallites is with the *ab* plane parallel to the substrate surface. Since the molecular long axes are in the *c* direction for **1** and **2** and in the *a* direction for **3**, this corresponds to a preferential orientation of **1** and **2** molecules

Table 1: Solution and Film First Reduction Potentials ($E_{1/2}$),[a] Derived LUMO and HOMO Energies, and Transistor Data[b] for Oligomers α6T[c] and **1**–**3**.

Oligomers	$E_{1/2}$ [V]		E_{LUMO} [eV]		E_{HOMO} (eV)		μ (type)	*Ion*/*Ioff*
	THF	Film	THF	Film	THF	Film		
α6T	−1.71	−2.00	−2.65	−2.36	−5.20	−4.78	0.03 (p)	$>10^6$
1	−1.51	−1.67	−2.85	−2.69	−5.48	−5.27	0.08 (n)	$>10^5$
2	−1.54	−1.69	−2.82	−2.67	−5.64	−5.32	0.01 (p)	10^4
3	−1.55	−1.83	−2.81	−2.53	−5.81	−5.40	4×10^{-5}(p)	10^2

[a] Versus SCE. Ferrocene used as internal standard. [b] μ = mobility ($cm^2 V^{-1} s^{-1}$), *Ion*/*Ioff* = current on/off ratio. [c] Optimized device. See Ref. [2b].

 © 2003 Wiley-VCH Verlag GmbH & Co. KGaA, Weinheim

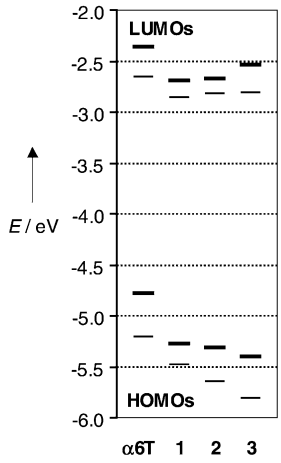


Figure 2. Molecular orbital energy (*E*) level diagram (solution = fine line; film = thick line) for molecules **α6T** and **1**–**3**.

with the long molecular axes along the substrate normal, while **3** molecules orient parallel to the oxide surface. SEM images of **1** and **2**-based films reveal similar morphologies, consisting of highly interconnected crystallites. Smoother and larger grains are found for films of **3**.

Electrical measurements (Table 1) were performed in top source, drain TFT configurations under moderate vacuum ($\approx$20 mTorr). No attempts were made to optimize performance through exhaustive variation in film morphology. Transistor responses are observed only for positive bias for **1**, and for negative bias for **2** and **3** (Figure 3), which means that these materials are n- and p-type semiconductors, respectively. These results combined with the solution/film CV and optical data clearly demonstrate that reduction of the LUMO energy is necessary but not sufficient to promote majority electron transport. The regiochemistry of fluoroarene electron-withdrawing moieties with respect to the π backbone plays a fundamental role in establishing the active

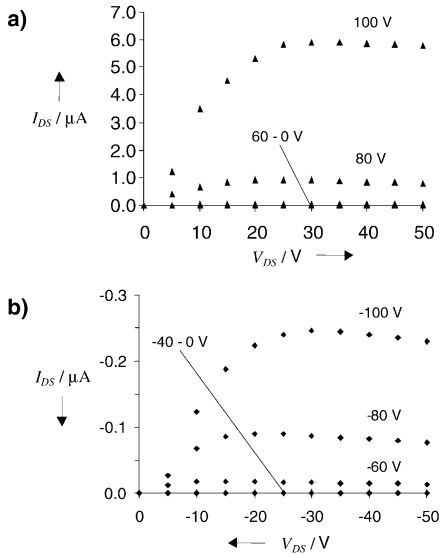


Figure 3. Output characteristics of TFT devices based on films of **1** (a) and **2** (b) at different gate bias.

conducting channel. As shown above, fluoroarene ring displacement along the molecular core dramatically affects packing characteristics and should therefore affect intermolecular orbital overlap.[13] This in turn modulates electronic coupling (bandwidth) between HOMO (for hole transport) and LUMO (for electron transport) levels of adjacent molecules and consequently may greatly affect the corresponding carrier mobilities. Another important factor may be localization of charge in polaronic structures. Maximum charge separation would result in charge localization on the end rings, fluoroarene for **1**, and thiophene for **2** and **3**. The former should preferentially accommodate a negative charge whereas the latter a positive charge. Finally, n- versus p-type transport may be influenced by the superior core screening by the end-fluoroarene groups in **1** against environmental electron traps (O_2, H_2O), probably at the grain boundaries.[1e]

Since the **1**–**3** film morphologies are similar, mobility trends within the series (μ ($cm^2V^{-1}s^{-1}$): **1** (0.08) > **2** (0.01) $\gg$ **3** (4×10^{-5})) can be explained by considering the single-crystal and film microstructural data. Closely π–π stacked planar **1** and **2** are more favorably organized for charge transport in the plane of the substrate than the poorly conjugated structure of **3**. In addition, the highly crystalline, textured films of **1** provide more favorable microstructures for charge transport than less ordered films of **2** having two sets of reflections, which presumably correspond to two crystallite growth orientations. However, both crystal and film microstructures are clearly superior to that of **3**.

In summary, a new polythiophene–fluoroarene conductor family allowing direct scrutiny of regiochemical effects on crystal structure, orbital energies, and charge transport has been synthesized. For the first time, n- and p-type activities have been achieved within the same series by manipulating relative building-block connectivity. Proper LUMO energy and molecular regiochemistry results in n-type activity only for **1**, with $\mu = 0.08\ cm^2V^{-1}s^{-1}$—the highest mobility yet reported in the thiophene series. Enclosing the fluoroaryl fragments within the thiophene(s) core results in more (**2**) or less (**3**) efficient p-type structures, depending on the corresponding film microstructure and molecular self-organization. This study therefore provides fundamental insight into the improved design and understanding of fluoroaromatic n-type semiconductors.

Received: February 24, 2003
Revised: May 16, 2003 [Z51253]

Keywords: conducting materials · electron transport · fluorine · semiconductors · thiophene oligomers

[1] a) A. Facchetti, M. Mushrush, H. E. Katz, T. J. Marks, *Adv. Mater.* **2003**, *15*, 33; b) T. M. Pappenfus, R. J. Chesterfield, C. D. Frisbie, K. R. Mann, J. Casado, J. D. Raff, L. L. Miller, *J. Am. Chem. Soc.* **2002**, *124*, 4184; c) A. Yassar, F. Demanze, A. Jaafari, M. El Idrissi, C. Coupry, *Adv. Funct. Mater.* **2002**, *12*, 699; d) P. R. L. Malenfant, C. D. Dimitrakopoulos, J. D. Gelorme, L. L. Kosbar, T. O. Graham, A. Curioni, W. Andreoni, *Appl. Phys. Lett.* **2002**, *80*, 2517; e) B. Crone, A. Dodabalapur, Y. Y. Lin, R. W. Filas, Z. Bao, A. LaDuca, R. Sarpeshkar, H. E. Katz,

 © 2003 Wiley-VCH Verlag GmbH & Co. KGaA, Weinheim

W. Li, *Nature* **2000**, *403*, 521; f) So. B. Heidenhain, Y. Sakamoto, T. Suzuki, A. Miura, H. Fujikawa, T. Mori, S. Tokito, Y. Taga, *J. Am. Chem. Soc.* **2000**, *122*, 10240; g) A. Facchetti, Y. Deng, A. Wang, Y. Koide, H. Sirringhaus, T. J. Marks, R. H. Friend, *Angew. Chem.* **2000**, *112*, 4721; *Angew. Chem. Int. Ed.* **2000**, *39*, 4547; h) M. L. Renak, G. P. Bartholomew, S. Wang, P. J. Ricatto, R. J. Lachicotte, G. C. Bazan, *J. Am. Chem. Soc.* **1999**, *121*, 7787; i) Z. Bao, A. J. Lovinger, J. Brown, *J. Am. Chem. Soc.* **1998**, *120*, 207.

[2] a) C. D. Dimitrakopoulos, P. R. L. Malenfant, *Adv. Mater.* **2002**, *14*, 99; b) F. Würthner, *Angew. Chem.* **2001**, *113*, 1069; *Angew. Chem. Int. Ed.* **2001**, *40*, 1037.

[3] a) *Handbook of Organic Conducting Molecules and Polymers, Vols. 1–4* (Ed.: H. S. Nalwa), Wiley, Chichester, **1997**.

[4] a) *Handbook of Conducting Polymers* (Eds.: T. A. Skotheim, R. L. Elsenbaumer, J. R. Reynolds), Marcel Dekker, New York, **1998**; b) K. Meerholz, J. Heinze, *Electrochim. Acta* **1996**, *41*, 1854.

[5] a) Online Cambridge Crystallographic Database; b) *Crystal Structure Determination* (Ed.: M. Warner), Teubner, Stuttgart, **1996**, and reference therein.

[6] The Supporting Information includes: Experimental details, TGA and CV plots, single crystal and film XRD data, SEM micrographs and *I–V* plot for compound **3**, cyclic voltammograms, and details of device fabrication.

[7] Single crystals of **1**–**3** were grown by either vacuum sublimation or cooling of saturated solutions. All measurements were made on a Bruker SMART CCD diffractometer with graphite monochromated $Mo_{K\alpha}$ (0.71073 Å) radiation. The data were collected at a temperature of 153(2) K and the structures were solved by direct methods and expanded using Fourier techniques using SHELXTL. All non-hydrogen atoms were refined anisotropically. Hydrogen atoms were included in idealized positions and not refined. Intensities were corrected for absorption. **1**. Crystal size: $0.160\times0.054\times0.032$ mm. Triclinic, $P\bar{1}$, $Z=1$. Cell dimensions: $a=6.3854(15)$ Å; $b=7.6862(18)$ Å; $c=12.502(3)$ Å; $\alpha=89.412(4)°$; $\beta=78.660(4)°$; $\gamma=80.760(4)°$. $V=593.7(2)$ Å^3, $2\theta_{max}=56.82$, $\rho_{calcd}=1.853\,g\,cm^{-3}$. Of 5530 reflections, 2751 were independent ($R_{int}=0.064$), 190 parameters, $R1=0.066$ (for reflections with $I>2\sigma(I)$), $wR2=0.160$ (for all reflections). **2**. Crystal size: $0.600\times0.136\times0.044$ mm. Monoclinic, $P2(1)/n$, $Z=2$. Cell dimensions: $a=6.258(2)$ Å; $b=5.0431(14)$ Å; $c=36.618(11)$ Å; $\alpha=90.00°$; $\beta=90.71(3)°$ $\gamma=90.00°$. $V=1155.6(6)$ Å^3, $2\theta_{max}=57.64$, $\rho_{calcd}=1.801\,g\,cm^{-3}$. Of 10121 reflections, 2835 were independent ($R_{int}=0.073$), 181 parameters, $R1=0.086$ (for reflections with $I>2\sigma(I)$), $wR2=0.272$ (for all reflections). **3**. Crystal size: $0.512\times0.076\times0.062$ mm. Orthorhombic, *Pbcn*, $Z=4$. Cell dimensions: $a=25.754(5)$ Å; $b=7.625(2)$ Å; $c=11.842(2)$ Å; $\alpha=90.00°$; $\beta=90.00°$; $\gamma=90.00°$. $V=2325.5(9)$ Å^3, $2\theta_{max}=57.92$, $\rho_{calcd}=1.790\,g\,cm^{-3}$. Of 20218 reflections, 2931 were independent ($R_{int}=0.047$), 188 parameters, $R1=0.048$ (for reflections with $I>2\sigma(I)$), $wR2=0.124$ (for all reflections). CCDC 207396 (**1**), CCDC 207397 (**2**), CCDC 207398 (**3**) contain the supplementary crystallographic data for this paper. These data can be obtained free of charge via www.ccdc.cam.ac.uk/conts/retrieving.html (or from the Cambridge Crystallographic Data Centre, 12, Union Road, Cambridge CB21EZ, UK; fax: (+44) 1223-336-033; or deposit@ccdc.cam.ac.uk).

[8] D. Fichou, *J. Mater. Chem.* **2000**, *10*, 571.

[9] a) R. D. McCullough, *Adv. Mater.* **1998**, *10*, 93; b) J.-L. Brédas, *J. Chem. Phys.* **1985**, *82*, 3809.

[10] Measurements performed in O_2- and moisture-free n-Bu_4NPF_6/THF in a one-compartment cell with a C disk working electrode, a bare Ag reference, and Pt wire counter electrodes.

[11] A. J. Bard, L. R. Faulkner, *Electrochemical Methods—Fundamentals and Applications*, Wiley, New York, **1984**. Note that **α6T**, **1**, and **2** E_{HOMO} values calculated from reversible oxidation potentials (−5.34, −5.55, and −5.64 eV, respectively) and optical E_{gap} data (see Table 1) are in excellent agreement. Solution (THF) optical E_{gap} (eV): 3.00 (**3**), 2.82 (**2**), 2.63 (**1**), 2.55 (**α6T**). Film optical E_{gap} (eV): 2.87 (**3**), 2.65 (**2**), 2.58 (**1**), 2.42 (**α6T**).

[12] A. J. Lovinger, L. J. Rothberg, *J. Mater. Res.* **1996**, *11*, 1581.

[13] J. Cornil, D. Beljonne, J.-P. Calbet, J.-L. Brédas, *Adv. Mater.* **2001**, *13*, 1053.

 © 2003 Wiley-VCH Verlag GmbH & Co. KGaA, Weinheim

Crystal Engineering

Supramolecular Assemblies of Hydrogen-Bonded Carboxylic Acid Dimers Mediated by Phenyl–Pentafluorophenyl Stacking Interactions

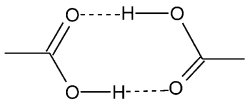
Maria Gdaniec, Wojciech Jankowski, Maria J. Milewska, and Tadeusz Połoñski**

Stacking between aryl and perfluoroaryl units is an important class of aromatic–aromatic interactions that has been attracting rapidly growing interest in recent years.[1–7] This phenomenon has been studied extensively since Patrick and Prosser demonstrated in 1960 that a 1:1 mixture of benzene and hexafluorobenzene forms a solid complex that melts at 24 °C.[1] In contrast to the crystals of the individual components, which show a herringbone packing, this complex consists of face-to-face stacks of alternating benzene and hexafluorobenzene molecules. Crystallographic studies of several 1:1 complexes of perfluorinated aromatic compounds with non-fluorinated arenes have revealed similar stacking motifs of alternating component molecules.[2–7] This kind of arrangement can be attributed to a quadrupolar interaction between electron-rich and electron-deficient aromatic rings.[8] The calculated binding energy between two aromatic rings (benzene and hexafluorobenzene) ranges from 3.7 to 4.7 kcal mol^{-1}.[9] Thus, this interaction has emerged as a very important synthon in crystal engineering that has a utility comparable to that of many robust hydrogen-bonding synthons. For example, the aryl–perfluoroaryl stacking interaction has been used to induce the crystal packing of monomers suitable for solid-state photopolymerization[2] and to stabilize liquid-crystalline phases.[3] It also seems to offer new possibilities for the modification of biologically important structures including peptides and oligonucleotides.[10]

[*] Prof. M. Gdaniec, W. Jankowski
Faculty of Chemistry
A. Mickiewicz University
60-780 Poznań (Poland)
Fax: (+48) 61-8656-008
E-mail: magdan@amu.edu.pl
Prof. T. Połoñski, Dr. M. J. Milewska
Department of Chemistry
Technical University
80-952 Gdañsk (Poland)
E-mail: tadpol@chem.pg.gda.pl

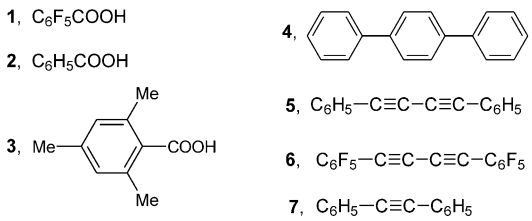
 DOI: 10.1002/anie.200351432 © 2003 Wiley-VCH Verlag GmbH & Co. KGaA, Weinheim

We were particularly interested as to whether the aryl–perfluoroaryl interaction could be effectively used in the construction of supramolecular aggregates from discrete hydrogen-bonded assemblies instead of covalently bonded units. Herein we report the structures of cocrystals obtained from benzoic acids, the self-assembly of which is controlled by phenyl–pentafluorophenyl π-stacking interactions. Since aromatic carboxylic acids are known to assemble through formation of the cyclic motif **I**,[11] we anticipated that



I

cocrystallization of pentafluorobenzoic acid (**1**) with benzoic (**2**) or 2,4,6-trimethylbenzoic acid (**3**, Scheme 1) should afford the corresponding homo- or heterodimers that assemble into



Scheme 1. Chemical structures of the substrates.

face-to-face stacks with alternating phenyl and pentafluorophenyl rings. Cocrystallization of the acids **1** and **2** from water as well as from CH_2Cl_2/heptane gave colorless plates that proved to be the 1:1 complex **1·2**. X-ray structural analysis of the complex revealed that two types of symmetry-independent heterodimers are formed in these monoclinic crystals (space group *Cc*): one with a nearly planar arrangement of the aryl rings and the carboxylic dimer system **I** (the corresponding dihedral angle is 8.9°) and a second one with system **I** twisted by 30.9° out of the plane of the neighboring aryl rings.[12] More importantly, the heterodimers are assembled into infinite stacks in a head-to-tail fashion such that the phenyl rings interact with the pentafluorophenyl moieties (Figure 1 a). These rings are not completely parallel (dihedral angles A/D 7.8° and B/C 4.6°) but, as usual for such systems, the aryl rings show offset face-to-face stacking. The slip angles of the stacks[13] are in the range of 19.7–27.7°.

A remarkably similar assembly of carboxylic acid molecules was observed for the 1:1 complex **1·3** that crystallized from water (triclinic, $P\bar{1}$; Figure 1 b).[12] Again, the acid heterodimers are packed in well-ordered columns with the 2,4,6-trimethylphenyl and pentafluorophenyl residues stacked in an alternating fashion. The creation of heterodimers is not unexpected in both of the above cases since it has been shown that a heterodimer is favored over either of the two homodimers by about 1 kcal mol^{-1} for a pair of aromatic carboxylic acids with substituents of different electronegativities.[14] This observation remains in accordance

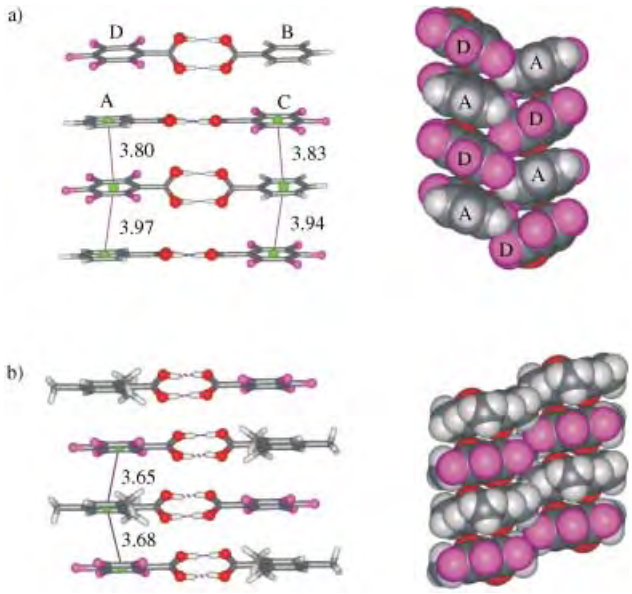


Figure 1. Stacking of carboxylic acid heterodimers and space-filling models of the adjacent binary stacks observed in a) the monoclinic cocrystal **1·2** and b) the triclinic cocrystal **1·3**. The distances between the phenyl-ring centroids are given in Å. The carboxylic hydrogen atoms are disordered.

with the principle that the strongest proton donor forms hydrogen bonds with the strongest proton acceptor.[15] It is important to note that the homodimers of **1**–**3** do not form π stacks in the crystals of the pure acids.[16]

Since the benzoic acid dimer can be regarded as a supramolecular analogue of *p*-terphenyl (**4**),[17] we tried to cocrystallize **1** with **4**. However, no cocrystals formed, probably because the size of the ring **I** does not match that of the central benzene ring in **4**; that is, the distance between the carboxylic carbon atoms in **I** is 3.81 Å, whereas the C-1 and C-4 atoms in the *p*-substituted benzene unit are separated by 2.80 Å, which makes interaction between the phenyl and pentafluorophenyl units in **4** and **1**, respectively, ineffective. Therefore, we used 1,4-diphenylbutadiyne (**5**),[18] where the separation of the phenyl rings almost exactly matches that in the benzoic acid dimer (the length of the diacetylene spacer is 3.78 Å). Cocrystallization of equimolar amounts of **1** (m.p. 101–102 °C) and **5** (m.p. 87–88 °C) from CH_2Cl_2/heptane produced colorless needles that melted at 136–137 °C. Interestingly, when a solution of **1** was mixed with a solution of **5** in the same solvent, precipitation of the 1:1 adduct **1·5** occurred spontaneously. The sharp and higher melting point of **1·5** compared to either of the two pure compounds indicated a possible phenyl–pentafluorophenyl interaction. X-ray structural analysis of **1·5** revealed that the dimers of **1** are sandwiched between the molecules of the diacetylene **5** which leads to formation of regular columns (Figure 2).[12] Analogously, the combination of acids **2** and **3** with 1,4-bis(pentafluorophenyl)butadiyne (**6**)[19] gave 1:1 cocrystals **2·6** and **3·6**, respectively, which are nearly isostructural with the complex **1·5**. Here again, the aryl–perfluoroaryl interaction mediates formation of infinite stacks similar to those

 © 2003 Wiley-VCH Verlag GmbH & Co. KGaA, Weinheim

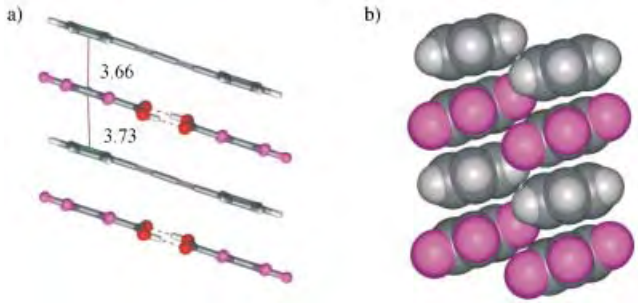


Figure 2. a) π Stacks of the homodimers of **1** and the diyne **5** in **1·5** and b) space-filling models of the adjacent binary stacks. The distances between phenyl-ring centroids are given in Å. The interplanar angle between the aromatic rings of the two components is 5.7° and the stack slip angles are 35 and 31°.

observed in **1·5**. The homodimer **2** remains nearly planar in the complex **2·6** as well as in the crystals of the pure acid **2**. However, complexation of **1** and **3** with 1,4-bisarylbutadiynes leads to a significant flattening of the corresponding carboxylic homodimers. Thus, the system **I** in **1·5** and **3·6** is twisted out of the plane of the neighboring aryl rings by 10.7 and 32.6°, respectively, whereas the corresponding dihedral angles found in the crystals of the pure acids **1** and **3** are 29.8 and 48.4°, respectively.[16]

The component molecules in all the complexes described above are arranged in a columnar fashion with the strongest intermolecular interactions within the infinite columns (Figure 3). Thus, we became interested in the possibility of constructing 2D assemblies stabilized by aryl–perfluoroaryl interactions in combination with hydrogen-bonding interactions between the carboxylic acid groups. Since **4** did not form a complex with **1**, we looked for molecules with a shorter spacer between the phenyl rings. For this purpose we studied the complexation of **1** with diphenylacetylene (**7**), where the spacer length is only 1.20 Å. We expected that the stacking between the phenyl and pentafluorophenyl units in these mismatching systems would lead to a "brick-wall" structure constructed of rows of alternating acid dimers **1** and acetylene **7** "bricks". The 1:1 prismatic crystals of the complex **1·7** were obtained from hexane, and X-ray structure analysis revealed that, indeed, the dimer **1** and the acetylene **7** aggregate in a simple brick-wall motif (Figure 4) with the carboxylic dimer **I** units located in a row just over the gap between the molecules of **7** in the row below.[12] The aryl rings within the wall are nearly parallel (dihedral angle 2.9°): they show an usual offset face-to-face stacking with an aryl–perfluoroaryl stack slip angle of 21.4°.

In conclusion, our results demonstrate that the phenyl–pentafluorophenyl interaction is a useful synthon, which in cooperation with hydrogen-bonding interactions, may enable supramolecular architectures to be controlled in a predictable way. Furthermore, as illustrated by the complexation of the carboxylic acid dimers with diphenylacetylene (**7**) and 1,4-bisarylbutadiynes **5** and **6**, these interactions allow the assembly of systems with extremely different chemical functionalities. However, some degree of size and shape compatibility between the supramolecular substrates is necessary to allow effective aryl–perfluoroaryl stacking within the molecular complexes.

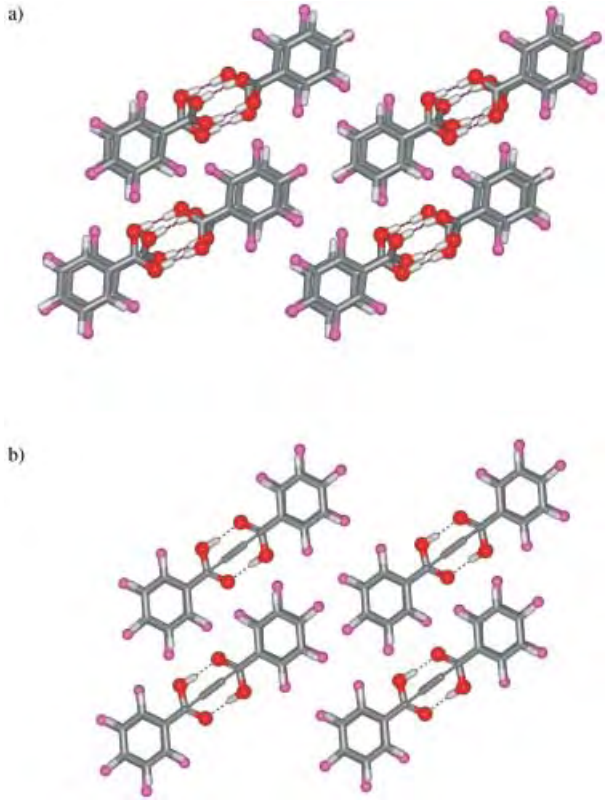


Figure 3. Projection of the crystal packing viewed along the stack axis in a) **1·2** and b) **1·5.**

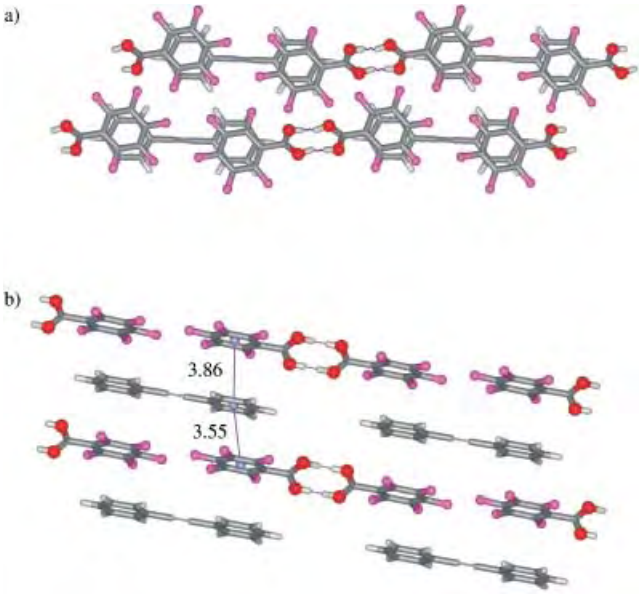


Figure 4. a) Projection of the crystal packing viewed along the stack axis in **1·7** and b) side view of the brick-wall construction in this complex**.** The distances between the phenyl-ring centroids are given in Å. The carboxylic hydrogen atoms are disordered.

Received: March 18, 2003 [Z51432]

 © 2003 Wiley-VCH Verlag GmbH & Co. KGaA, Weinheim

Keywords: crystal engineering · hydrogen bonds · pi interactions · self-assembly · supramolecular chemistry

[1] C. R. Patrick, G. S. Prosser, *Nature* **1960**, *187*, 1021.

[2] J. S. W. Overell, G. S. Pawley, *Acta Crystallogr. Sect. B* **1982**, *38*, 1966; J. H. Williams, J. K. Cockcroft, A. N. Fitch, *Angew. Chem.* **1992**, *104*, 1666; *Angew. Chem. Int. Ed. Engl.* **1992**, *31*, 1655.

[3] G. W. Coates, A. R. Dunn, L. M. Henling, D. A. Dougherty, R. H. Grubbs, *Angew. Chem.* **1997**, *109*, 290; *Angew. Chem. Int. Ed. Engl.* **1997**, *36*, 248; G. W. Coates, A. R. Dunn, L. M. Henling, J. W. Ziller, E. B. Lobkovsky, R. H. Grubbs, *J. Am. Chem. Soc.* **1998**, *120*, 3641.

[4] C. Dai, P. Nguyen, T. B. Marder, A. J. Scott, W. Clegg, C. Viney, *Chem. Commun.* **1999**, 2493; M. Weck, R. Dunn, K. Matsumoto, G. W. Coates, E. B. Lobkovsky, R. H. Grubbs, *Angew. Chem.* **1999**, *111*, 2909; *Angew. Chem. Int. Ed.* **1999**, *38*, 2741.

[5] D. G. Naae, *Acta Crystallogr. Sect. B* **1979**, *35*, 2765; M. L. Renak, G. P. Bartholomew, S. Wang, P. J. Ricatto, R. J. Lachicotte, G. C. Bazan, *J. Am. Chem. Soc.* **1999**, *121*, 7787; F. Ponzini, R. Zagha, K. Hardcastle, J. S. Siegel, *Angew. Chem.* **2000**, *112*, 2413; *Angew. Chem. Int. Ed.* **2000**, *39*, 2323; W. J. Feast, P. W. Lövenich, H. Puschmann, C. Taliani, *Chem. Commun.* **2001**, 505; T. Nishinaga, N. Nodera, Y. Miyata, K. Komatsu, *J. Org. Chem.* **2002**, *67*, 6091; V. R. Vangala, A. Nangia, V. M. Lynch, *Chem. Commun.* **2002**, 1304.

[6] C. M. Beck, J. Burdeniuc, R. H. Crabtree, A. L. Rheingold, G. P. A. Yap, *Inorg. Chim. Acta* **1998**, *270*, 559; C. J. Aspley, C. Boxwell, M. L. Buil, C. L. Higgitt, C. Long, R. N. Perutz, *Chem. Commun.* **1999**, 1027; E. Lork, R. Mews, M. M. Shakirov, P. G. Watson, A. V. Zibarev, *Eur. J. Inorg. Chem.* **2001**, 2123; D. B. Mitzi, D. R. Medeiros, P. R. L. Malenfant, *Inorg. Chem.* **2002**, *40*, 2134; J. A. C. Clyburne, T. Hamilton, H. A. Jenkins, *Cryst. Eng.* **2001**, *4*, 1; M. R. Haneline, M. Tsunoda, F. P. Gabbai, *J. Am. Chem. Soc.* **2002**, *124*, 3737; J. C. Collings, K. P. Roscoe, E. G. Robins, A. S. Batsanov, L. M. Stimson, J. A. K. Howard, S. J. Clark, T. B. Marder, *New J. Chem.* **2002**, *26*, 1740, and references therein.

[7] J. C. Collings, K. P. Roscoe, R. L. Thomas, A. Batsanov, L. M. Simon, J. A. K. Howard, T. B. Marder, *New J. Chem.* **2001**, *25*, 1410.

[8] J. H. Williams, *Acc. Chem. Res.* **1993**, *26*, 593; J. Hernandez-Ttrujillo, M. Costas, A. Vela, *J. Chem. Soc. Faraday Trans.* **1993**, *89*, 2441; M. Luhmer, K. Bartnik, A. Dejaegere, P. Bovy, J. Reisse, *Bull. Soc. Chim. Fr.* **1994**, *131*, 603.

[9] J. Hernandez-Ttrujillo, F. Colmenares, G. Cuevas, M. Costas, *Chem. Phys. Lett.* **1997**, *265*, 503; A. P. West, S. Mecozzi, D. A. Dougherty, *J. Phys. Org. Chem.* **1997**, *10*, 347; S. Lorenzo, G. R. Lewis, I. Dance, *New J. Chem.* **2000**, *24*, 295.

[10] S. Butterfield, P. R. Patel, M. L. Waters, *J. Am. Chem. Soc.* **2002**, *124*, 9751; G. Mathis, J. Hunziker, *Angew. Chem.* **2002**, *114*, 3335; *Angew. Chem. Int. Ed.* **2002**, *41*, 3203; K. A. Frey, S. A. Woski, *Chem. Commun.* **2002**, 2206.

[11] L. Leiserowitz, *Acta Crystallogr. Sect. B* **1976**, *32*, 775.

[12] X-ray crystal structure analyses: Kuma Diffraction KM4CCD diffractometer, $Mo_{K\alpha}$ radiation ($\lambda = 0.71073$ Å), Lorentz and polarization corrections, no absorption correction; the structures were solved by direct methods with SHELXS-97 and refined against F^2 with SHELXL-97. Hydrogen atoms were located on the ΔF maps and their positional and isotropic displacement parameters included in the refinement. a) Crystal structure data for **1·2**: $C_6H_5CO_2H{\cdot}C_6F_5CO_2H$, crystal size $0.5 \times 0.5 \times 0.2$ mm, $M_r = 334.20$, monoclinic, space group *Cc* (no. 9), $a = 24.7871(15)$, $b = 7.7160(3)$, $c = 14.3292(9)$ Å, $\beta = 108.571(4)°$, $V = 3741.0(9)$ Å^3, $T = 120$ K, $Z = 8$, $\mu(Mo_{K\alpha}) = 0.17$ mm^{-1}, $\theta_{max} = 26.37°$, 6923 reflections measured, 3349 unique ($R_{int} = 0.021$) which were used in all calculations. Final $R_1 = 0.0336$ and $wR(F^2) = 0.0890$ (all data). The carboxylic hydrogen atoms are disordered over two positions. b) Crystal structure data for **1·3**: $C_6F_5CO_2H{\cdot}C_9H_{11}CO_2H$, crystal size $0.45 \times 0.45 \times 0.25$ mm, $M_r = 376.27$, triclinic, space group $P\bar{1}$ (no. 2), $a = 7.1521(7)$, $b = 8.1727(8)$, $c = 15.2499(12)$ Å, $\alpha = 99.337(8)$, $\beta = 99.018(7)$, $\gamma = 107.234(9)°$, $V = 820.01(13)$ Å^3, $T = 293$ K, $Z = 2$, $\mu(Mo_{K\alpha}) = 0.144$ mm^{-1}, $\theta_{max} = 26.37°$, 5578 reflections measured, 3240 unique ($R_{int} = 0.027$) which were used in all calculations. Final $R_1 = 0.0675$ and $wR(F^2) = 0.1494$ (all data). The carboxylic hydrogen atoms are disordered over two positions. c) Crystal structure data for **1·5**: $(C_6F_5CO_2H)_2{\cdot}C_{16}H_{10}$, crystal size $0.6 \times 0.6 \times 0.6$ mm, $M_r = 626.40$, triclinic, space group $P\bar{1}$ (no. 2), $a = 7.3812(9)$, $b = 7.9939(8)$, $c = 11.6725(12)$ Å, $\alpha = 98.775(8)$, $\beta = 92.169(9)$, $\gamma = 112.861(11)°$, $V = 623.63(12)$ Å^3, $T = 130$ K, $Z = 1$, $\mu(Mo_{K\alpha}) = 0.160$ mm^{-1}, $\theta_{max} = 26.37°$, 5123 reflections measured, 2525 unique ($R_{int} = 0.026$) which were used in all calculations. Final $R_1 = 0.0445$ and $wR(F^2) = 0.1168$ (all data). d) Crystal structure data for **2·6**: $(C_6H_5CO_2H)_2{\cdot}C_{16}F_{10}$, crystal size $0.8 \times 0.3 \times 0.05$ mm, $M_r = 626.40$, triclinic, space group $P\bar{1}$ (no. 2), $a = 7.2876(10)$, $b = 7.6086(11)$, $c = 12.5006(13)$ Å, $\alpha = 94.933(10)$, $\beta = 90.670(10)$, $\gamma = 111.319(13)°$, $V = 642.63(14)$ Å^3, $T = 130$ K, $Z = 1$, $\mu(Mo_{K\alpha}) = 0.155$ mm^{-1}, $\theta_{max} = 26.37°$, 5804 reflections measured, 2616 unique ($R_{int} = 0.041$) which were used in all calculations. Final $R_1 = 0.0675$ and $wR(F^2) = 0.1370$ (all data). The carboxylic hydrogen atoms are disordered over two positions. e) Crystal structure data for **3·6**: $(C_9H_{11}CO_2H)_2{\cdot}C_{16}F_{10}$, crystal size $0.4 \times 0.4 \times 0.3$ mm, $M_r = 710.55$, triclinic, space group $P\bar{1}$ (no. 2), $a = 7.2150(4)$, $b = 8.1122(5)$, $c = 14.3128(6)$ Å, $\alpha = 97.488(4)$, $\beta = 100.135(4)$, $\gamma = 105.863(5)°$, $V = 779.04(7)$ Å^3, $T = 130$ K, $Z = 1$, $\mu(Mo_{K\alpha}) = 0.138$ mm^{-1}, $\theta_{max} = 26.37°$, 8805 reflections measured, 3123 unique ($R_{int} = 0.023$) which were used in all calculations. Final $R_1 = 0.0467$ and $wR(F^2) = 0.11508$ (all data). One of the methyl groups is disordered. f) Crystal structure data for **1·7**: $(C_6F_5CO_2H)_2{\cdot}C_{14}H_{10}$, crystal size $0.4 \times 0.4 \times 0.2$ mm, $M_r = 602.38$, triclinic, space group $P\bar{1}$ (no. 2), $a = 6.3760(5)$, $b = 7.3009(5)$, $c = 13.9240(11)$ Å, $\alpha = 104.681(6)$, $\beta = 101.092(6)$, $\gamma = 91.897(7)°$, $V = 613.00(8$ Å^3, $T = 125$ K, $Z = 1$, $\mu(Mo_{K\alpha}) = 0.159$ mm^{-1}, $\theta_{max} = 26.37°$, 4923 reflections measured, 2483 unique ($R_{int} = 0.016$) which were used in all calculations. Final $R_1 = 0.0435$ and $wR(F^2) = 0.1081$ (all data). The carboxylic hydrogen atoms are disordered over two positions. g) CCDC-199913–199917 and CCDC-205458 contain the supplementary crystallographic data for this paper. These data can be obtained free of charge via www.ccdc.cam.ac.uk/conts/retrieving.html (or from the Cambridge Crystallographic Data Centre, 12 Union Road, Cambridge CB2 1EZ, UK; fax: (+44) 1223-336-033; or deposit@ccdc.cam.ac.uk).

[13] For the definition of the π-stack parameters see reference [7].

[14] C. V. K. Sharma, K. Panneerselvam, T. Pilati, G. R. Desiraju, *J. Chem. Soc. Perkin Trans. 2* **1993**, 2209.

[15] M. C. Etter, *Acc. Chem. Res.* **1990**, *23*, 120.

[16] C. C. Wilson, N. Shankland, A. J. Florence, *J. Chem. Soc. Faraday Trans.* **1996**, *92*, 5051; V. Benghiat, L. Leiserowitz, *J. Chem. Soc. Perkin Trans. 2*, **1972**, 1778.

[17] G. R. Desiraju, *Angew. Chem.* **1995**, *107*, 2541; *Angew. Chem. Int. Ed. Engl.* **1995**, *34*, 2311; G. R. Desiraju, *Chem. Commun.* **1997**, 1475.

[18] A. S. Hay, *J. Org. Chem.* **1962**, *27*, 3320.

[19] Y. Zhang, J. Wen, *Synthesis* **1990**, 727.

 © 2003 Wiley-VCH Verlag GmbH & Co. KGaA, Weinheim

Framework Design with Molecular Blocks

Design of Frameworks with Mixed Triangular and Octahedral Building Blocks Exemplified by the Structure of $[Zn_4O(TCA)_2]$ Having the Pyrite Topology **

*Hee K. Chae, Jaheon Kim, Olaf Delgado Friedrichs, Michael O'Keeffe, and Omar M. Yaghi**

A prerequisite to the design of crystalline materials is the knowledge of the possible structures that potentially may form by linking together specific molecular shapes. In this context, we recently argued that, from the large number of possible structures that could in principle be assembled from various molecular shapes, those with the highest symmetry are most likely to form in practice. Thus it is particularly important to identify these special structures since they represent the default structures for the assembly of shapes.[1]

This approach has been useful in the chemistry of extended metal–organic frameworks (MOFs) in which 3D structures assembled entirely from triangles,[2] squares,[3] tetrahedra,[4] or octahedra[5] usually form structures based on the $SrSi_2$, NbO, diamond and primitive cubic nets, respectively. Indeed, these have the highest possible symmetry for their respective building block shapes and have become as important to crystal designers as the Platonic solids are to molecular chemists. Herein we point out that the FeS_2 (pyrite) net found in $[Zn_4O(TCA)_2]\cdot(DMF)_3(H_2O)_3$ (hereafter MOF-150; TCA = 4,4′,4″-Tricarboxytriphenylamine, DMF = *N*,*N*′-dimethylforamide), is the most regular net (and the most likely to form) for linking together triangles and octahedra and that it has some additional net properties that lead to its classification as a default net.

We use TCA and $[Zn_4O(CO_2)_6]$ as secondary building units (SBUs) (Figure 1a) to provide three- and six-coordinated vertices, respectively. The SBUs are produced by employing previously determined reaction parameters to effect their formation in situ.[5a,b] Thus, the reaction of zinc nitrate and TCA in DMF/EtOH/H_2O resulted in the formation of light brown truncated crystals, which were formulated by elemental microanalysis and single crystal X-ray diffraction studies.[6]

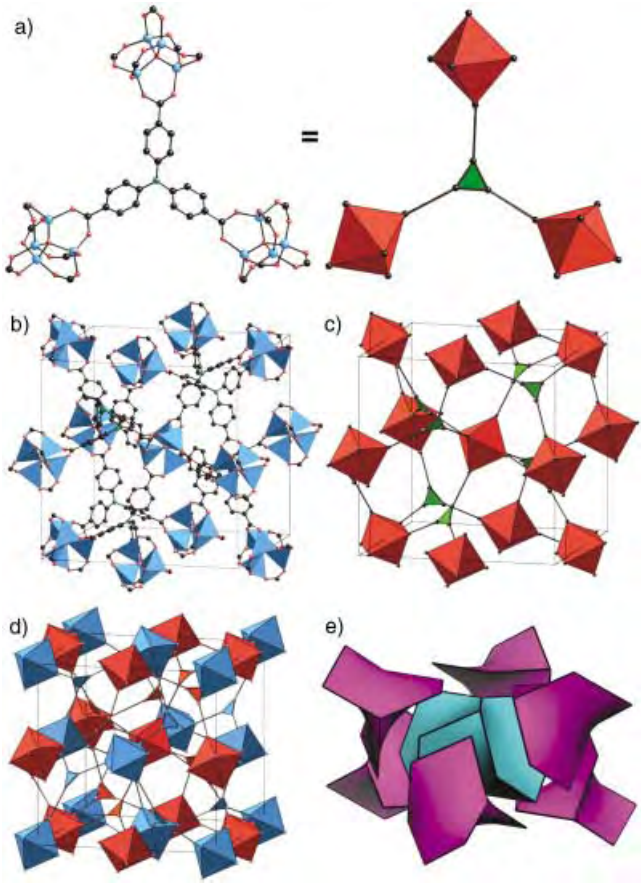


Figure 1. a) A TCA unit linked to three octahedral SBUs. Zn blue, O red, N green, C black. b) One net of MOF-150 with ZnO_4 tetrahedra (blue) filled in c) as (b) but stylized. d) Two intergrown nets as (c). e) Tiles of the pyrite net.

The structure consists of two identical interpenetrating nets, one of which is shown in Figure 1b. In this structure, the basic zinc acetate octahedral SBUs, each composed of four ZnO_4 tetrahedra sharing a common corner, are linked by the tritopic TCA to form a 6,3-coordinated net shown in stylized form in Figure 1c. The two interpenetrating frameworks are depicted in Figure 1d. The underlying 6,3-coordinated framework has symmetry $Pa\bar{3}$, and the two interpenetrating frameworks have symmetry $Ia\bar{3}$ (as found in the crystal, Figure 1d). The topology of each framework is related to the structure of the pyrite form of FeS_2; it has the same topology if the S–S bonding in pyrite is ignored, so we call it the pyrite net.[7] It has been observed, not interpenetrating, in a $[Hg(TPT)_3]^{3+}$ (TPT = 2,4,6-tri(4-pyridyl)-1,3,5-triazine) framework.[8] A cyanide with the pyrite topology (but now with the S–S link included) was also reported, again not interpenetrating.[9] We believe MOF-150 is the first example of a fully catenated structure (one in which all rings of one net are mechanically linked to rings of the other and vice versa) with mixed

[*] Prof. Dr. O. M. Yaghi, Dr. J. Kim
Materials Design and Discovery Group
Department of Chemistry
University of Michigan
Ann Arbor, MI 48109-1055 (USA)
Fax: (+1) 734-615-9751
E-mail: oyaghi@umich.edu
Prof. Dr. H. K. Chae
Department of Chemistry
Hankuk University of Foreign Studies
Yongin, Kyungki-Do, 449-791 (S. Korea)
Dr. O. D. Friedrichs, Prof. Dr. M. O'Keeffe
Department of Chemistry and Biochemistry
Arizona State University
Tempe, AZ 85287-1604 (USA)

[**] The National Science Foundation support to MO'K (DMR-0103036) and OMY (DMR-9980469) is gratefully acknowledged. HKC is supported by the Korean Science and Engineering Foundation (KOSEF 2000-1-12200-002-3). TCA = 4,4′,4″-Tricarboxytriphenylamine.

 DOI: 10.1002/anie.200351546 © 2003 Wiley-VCH Verlag GmbH & Co. KGaA, Weinheim

coordination. Interpenetration of nets of mixed coordination is well known,[3g,10] but they are never fully catenated.

Three DMF and three water molecules per formula unit fill the space remaining after interpenetration in the crystal. This space is calculated to be 52% of the crystal volume and it is in the form of small capsules of 7–8 Å diameter that are interconnected by 4 Å openings. The solvent guests can be removed from the pores in air: A sample (18.526 mg) heated at 10 °C min^{-1} in air from 30 to 700 °C showed a weight loss (20.9%) step at 240 °C corresponding to the loss of all guests (21.0% calcd for three DMF and three H_2O molecules per unit formula).

MOF-150 is important both in its intrinsic net properties and in the fact that it led to the identification of the pyrite net as the default structure for the assembly of triangles and octahedra. It is instructive to discuss the topology of the net in terms of tilings of space.[11] Figure 1e shows space-filling tiles (cages) that underlie the pyrite net. The tiling is composed of trihedral tiles (green) and hexahedral tiles (red) in the ratio 2:1 and the vertices and edges of the tiling are the vertices and edges of the pyrite net. The tiling is an example of a natural tiling in that all the rings of the net are faces of the tiles and vice versa.[12] Tilings are characterized by a transitivity *pqrs* which signifies that there are *p* kinds of vertex, *q* kinds of edge, *r* kinds of face (ring), and *s* kinds of tile.[13] The simple cubic network, which is derived from a tiling of space with congruent cubes, is an example of a net with transitivity 1111 (all vertices, edges, faces and tiles related by symmetry). The most regular net with two kinds of vertex is that of the fluorite (CaF_2) structure which has transitivity 2111; we believe that it is the only net in this class.[12]

The next most regular tilings with two kinds of vertex have transitivity 2112 and pyrite is a member of this very small class. The dual structure is obtained by placing new vertices inside the original tiles and allowing new edges to connect these new vertices in the interior of adjacent tiles. It should be clear that a net and its dual are fully catenated, and that for a net with transitivity *pqrs*, the dual has transitivity *srqp*. For a net to be self-dual the transitivity must be palindromic; and indeed the pyrite net is self-dual.

The pyrite net has other interesting properties that it shares only with the diamond net. All the rings are 6-rings and all are related by symmetry. There are two 6-rings per vertex and the average coordination number is four.

It is our thesis that unless specific information in the form of low-symmetry features of the SBU is provided, the default net will form for a given connectivity and indeed this is overwhelmingly the case.[1] Thus it might be expected that for 6,3-coordination the pyrite net would be the default net. However most framework materials with this connectivity reported to date have the rutile topology and in fact this was identified as the default structure,[1] but rutile is significantly less symmetric than pyrite having two kinds of edge and three kinds of ring (transitivity 2232). Most of the rutile-structured materials reported have been cyanides with interpenetrating, partly catenated, frameworks such as $\{M[C(CN)_3]_2\}$;[10,14] in some instances the three-coordinated vertex has more than one kind of link as in compounds with a $\{M[N(CN)_2]_2\}$ framework, so the appearance of a less-symmetrical network is less surprising in this instance.[15] The occurrence of the rutile net in bis(isonicotinate) Fe^{II} is understandable on the same grounds.[16] We also note that in the case of MOF-150, the "octahedral" SBU actually has tetrahedral (T_d) symmetry with the planes of opposite carboxylate groups at 90°. However, as can be seen from Figure 1c, opposite triangular groups have to be coplanar. TCA is flexible enough to provide the twist angle of 45° needed between the carboxylates and triangles. With less-flexible linkers we might expect to find other, less-symmetrical nets; we are exploring this possibility.

Experimental Section

A mixture DMF/C_2H_5OH/H_2O (1.00/0.25/0.25 mL) containing the acid form of TCA (H_3TCA)[17] (0.005 g, 1.32×10^{-5} mol) and $Zn(NO_3)_2\cdot6H_2O$ (0.017 g, 5.71×10^{-5} mol) was sealed under vacuum in a quartz tube (10 mm external diameter, 15 cm length, 6 mL capacity) and heated (0.5 °C min^{-1}.) to 90 °C for 20 h, then cooled at 0.1 °C min^{-1} to room temperature. The light brown truncated octahedral crystals were washed with a DMF/ethanol mixture (3–4 mL) to give MOF-150 (0.01 g 55% yield). Elemental analysis calcd (%) for $C_{51}H_{51}O_{19}N_5Zn_4 = [Zn_4O(TCA)_2]\cdot(DMF)_3\cdot(H_2O)_3$: C 47.14, H 3.96, N 5.39; found C 47.98, H 3.84, N 5.40.

Received: April 1, 2003 [Z51546]

Keywords: chelates · interpenetrating structures · metal–organic frameworks · solid-state structures · zinc

[1] M. O'Keeffe, M. Eddaoudi, H. Li, T. M. Reineke, O. M. Yaghi, *J. Solid State Chem.* **2000**, *152*, 3–20.

[2] a) O. M. Yaghi, C. E. Davis, G. Li, H. Li, *J. Am. Chem. Soc.* **1997**, *119*, 2861–2868; b) C. J. Kepert, M. J. Rosseinsky, *Chem. Commun.* **1999**, 375–376; c) S. V. Kolotuchin, P. A. Thiessen, E. E. Fenlon, S. R. Wilson, C. J. Loweth, S. C. Zimmerman, *Chem. Eur. J.* **1999**, *5*, 2537–2547; d) Y. H. Kiang, G. B. Gardner, S. Lee, Z. Xu, *J. Am. Chem. Soc.* **2000**, *122*, 6871–6883; e) J. S. Seo, D. Whang, H. Lee, S. I. Jun, J. Oh, Y. J. Jeon, K. Kim, *Nature* **2000**, *404*, 982–986; f) M. J. Horner, K. T. Holman, M. D. Ward, *Angew. Chem.* **2001**, *113*, 4169–4172; *Angew. Chem. Int. Ed.* **2001**, *40*, 4045–4048; g) S. Masaoka, S. Furukawa, H.-C. Chang, T. Mizutani, S. Kitagawa, *Angew. Chem.* **2001**, *113*, 3933–3935; *Angew. Chem. Int. Ed.* **2001**, *40*, 3817–3819; h) C. Inman, J. M. Knaust, S. W. Keller, *Chem. Commun.* **2002**, 156–157.

[3] a) H. Li, M. Eddaoudi, T. Groy, O. M. Yaghi, *J. Am. Chem. Soc.* **1998**, *120*, 8571–8572; b) M. Eddaoudi, J. Kim, M. O'Keeffe, O. M. Yaghi, *J. Am. Chem. Soc.* **2002**, *124*, 376–377; c) M. Eddaoudi, J. Kim, D. T. Vodak, A. Sudik, J. Wachter, M. O'Keeffe, O. M. Yaghi, *Proc. Natl. Acad. Sci. USA* **2002**, *99*, 4900–4904; d) J. Lu, A. Mondal, B. Moulton, M. Zaworotko, *Angew. Chem.* **2001**, *113*, 2171–2174; *Angew. Chem. Int. Ed.* **2001**, *40*, 2113–2116; e) F. A. Cotton, C. Lin, C. A. Murillo, *Acc. Chem. Res.* **2001**, *34*, 759–771; f) S. S. Y. Chu, S. M. F. Lo, J. P. H. Charmant, A. G. Orpen, I. D. Williams, *Science* **1999**, *283*, 1148–1150; g) B. Chen, M. Eddaoudi, S. T. Hyde, M. O'Keeffe, O. M. Yaghi, *Science* **2001**, *291*, 1021–1023; h) K. Biradha, Y. Hongo, M. Fujita, *Angew. Chem.* **2000**, *112*, 4001–4003; *Angew. Chem. Int. Ed.* **2000**, *39*, 3843–3845; i) M. E. Kosal, J.-H. Chou, S. R. Wilson, K. S. Suslick, *Nat. Mater.* **2002**, *1*, 118–121; j) C. Serre, F. Millange, C. Thouvenot, M. Nogues, G. Marsolier, D. Louer, G. Ferey, *J. Am. Chem. Soc.* **2002**, *124*, 13519–13526.

[4] a) J. Kim, B. Chen, T. M. Reineke, H. Li, M. Eddaoudi, D. B. Moler, M. O'Keeffe, O. M. Yaghi, *J. Am. Chem. Soc.* **2001**, *123*, 8239–8247; b) K. Barthelet, D. Riou, G. Férey, *Solid State Sci.*

 © 2003 Wiley-VCH Verlag GmbH & Co. KGaA, Weinheim

2002, *4*, 841 – 844; c) O. R. Evans, Z. Wang, R.-G. Xiong, B. M. Foxman, W. Lin, *Inorg. Chem.* **1999**, *38*, 2969 – 2973; d) L. Carlucci, G. Ciani, D. M. Proserpio, S. Rizzato, *CrystEngComm* **2002**, *4*, 1 – 13; e) K. Barthelet, D. Riou, G. Ferey, *Chem. Commun.* **2002**, 1492 – 1493; f) L. C. Tabares, J. A. R. Navarro, J. M. Salas, *J. Am. Chem. Soc.* **2001**, *123*, 383 – 387; g) C. Klein, E. Graf, M. W. Hosseini, A. D. Cian, *New J. Chem.* **2001**, *25*, 207 – 209; h) D. S. Reddy, T. Dewa, K. Endo, Y. Aoyama, *Angew. Chem.* **2000**, *112*, 4436 – 4438; *Angew. Chem. Int. Ed.* **2000**, *39*, 4266 – 4268.

[5] a) H. Li, M. Eddaoudi, M. O'Keeffe, O. M. Yaghi, *Nature* **1999**, *402*, 276 – 279; b) M. Eddaoudi, J. Kim, N. L. Rosi, D. T. Vodak, J. Wachter, M. O'Keeffe, O. M. Yaghi, *Science* **2002**, *295*, 469 – 472; c) H. K. Chae, M. Eddaoudi, J. Kim, S. I. Hauck, J. F. Hartwig, M. O'Keeffe, O. M. Yaghi, *J. Am. Chem. Soc.* **2001**, *123*, 11 482 – 11 483; d) T. M. Reineke, M. Eddaoudi, D. B. Moler, M. O'Keeffe, O. M. Yaghi, *J. Am. Chem. Soc.* **2000**, *122*, 4843 – 4844; e) S. Y. Yang, L. S. Long, Y. B. Jiang, R. B. Huang, L. S. Zheng, *Chem. Mater.* **2002**, *14*, 3229 – 3231; f) L. G. Beauvais, M. P. Shores, J. R. Long, *J. Am. Chem. Soc.* **2000**, *122*, 2763 – 2772.

[6] X-ray structure data: Siemens SMART CCD diffractometer, ω scans, graphite-monochromated $Mo_{K\alpha}$ radiation, SAINT for data integration, SADABS for absorption correction, XPREP for correction of Lorentz and polarization effects, and structure solution with direct methods and subsequent difference Fourier techniques by using SHELX-TL. Data collection for MOF-150: a) A brown octahedron crystal was analyzed: approximate dimensions: $0.16 \times 0.16 \times 0.14$ mm at $-115\,^{\circ}C$, cubic, space group $Ia\bar{3}$ No. 206) with $a = 22.328(4)$ Å, $V = 11\,132(4)$ Å^3, $Z = 8$, $d_{calc} = 1.551$ g cm^{-3}, and $\mu(Mo_{K\alpha}) = 17.80$ cm^{-1}, $F(000) = 5312$, 985 unique reflections within $2\theta_{max} = 41.70^{\circ}$, $T_{max} = 0.93$, $T_{min} = 0.59$. The Zn_4O cluster in the SBU consisted of two independent disordered Zn atoms (Zn(1) and Zn(2)) in the asymmetric unit, which generated eight Zn sites in the cluster. While Zn(1) atom with half occupancy was present in a general position, Zn(2) atom with half occupancy sit on a threefold crystallographic axis. The carboxylic oxygen atoms of the TCA link were also disordered over two sites with the same occupancies. A threefold axis penetrated through the center of the TCA link, the N(1) atom. Both guest molecules, the water and DMF molecules were disordered over two sites around a twofold crystallographic axis, which penetrated into the nitrogen atom, N(1S) in the DMF molecule. All non-hydrogen atoms were refined anisotropically. The hydrogen atoms of the TCA link were generated with idealized geometries. The final cycle of full-matrix least-squares refinement was based on 704 observed reflections ($I > 2.00\sigma(I)$) and 153 variable parameters and refined to convergence $R_1 = 0.0837$ and $R_w = 0.2266$. The maximum and minimum peaks on the final difference Fourier map corresponded to 0.769 and -0.732 e$^-$ Å^{-3}, respectively; b) All crystal structures in this report may be viewed and manipulated on the web: http://www.umich.edu/~yaghigrp/structures.html. CCDC-201056 (MOF-150) contains the supplementary crystallographic data for this paper. These data can be obtained free of charge via www.ccdc.cam.ac.uk/conts/retrieving.html (or from the Cambridge Crystallographic Data Centre, 12, Union Road, Cambridge CB21EZ, UK; fax: (+44) 1223-336-033; or deposit@ccdc.cam.ac.uk).

[7] The high-pressure form of PdF_2 has the structure without anion–anion bonds. A. Tressaud, J. L. Soubreyroux, H. Touhara, G. Demazeau, F. Langlais, *Mater. Res. Bull.* **1981**, *16*, 207 – 214.

[8] S. R. Batten, B. F. Hoskins, R. Robson, *Angew. Chem.* **1995**, *107*, 884 – 886; *Angew. Chem. Int. Ed. Engl.* **1995**, *34*, 820 – 822.

[9] S. Nishikiori, T. Iwamoto, *J. Chem. Soc. Chem. Commun.* **1993**, 1555 – 1556.

[10] a) S. R. Batten, R. Robson, *Angew. Chem.* **1998**, *110*, 1558 – 1595; *Angew. Chem. Int. Ed.* **1998**, *37*, 1460 – 1494; b) P. Kroll, R. Riedel, R. Hoffmann, *Phys. Rev. B* **1999**, *60*, 3126 – 3139; c) J. S. Miller, *Adv. Mater.* **2001**, *13*, 525 – 527.

[11] a) O. Delgado Friedrichs, A. W. M. Dress, D. H. Huson, J. Klinowski, A. L. Mackay, *Nature* **1999**, *400*, 644 – 647; b) M. O'Keeffe, *Nature* **1999**, *400*, 617 – 618.

[12] O. Delgado Friedrichs, M. O'Keeffe, O. M. Yaghi, *Acta Crystallogr. Sect. A* **2003**, *59*, 22 – 27.

[13] O. Delgado Friedrichs, D. H. Huson, *Discrete Comput. Geom.* **2000**, *24*, 279 – 292.

[14] S. R. Batten, B. F. Hoskins, B. Moubaraki, K. S. Murray, R. Robson, *J. Chem. Soc. Dalton Trans.* **1999**, 2977 – 2986.

[15] S. R. Batten, B. F. Hoskins, B. Moubaraki, K. S. Murray, R. Robson, *J. Chem. Soc. Dalton Trans.* **1999**, 2977 – 2986.

[16] R. G. Xiong, S. R. Wilson, W. Lin, *J. Chem. Soc. Dalton Trans.* **1998**, 4089 – 4090.

[17] The synthesis of H_3TCA was accomplished by using literature procedures. H. Schrage, F. Vogtle, E. Steckhan, *J. Inclusion Phenom.* **1988**, *6*, 157 – 165. Characterization data: ^{1}H NMR (400 MHz, [D$_6$]DMSO): $\delta = 7.904$ ($J = 8.8$ Hz), 7.137 ppm ($J = 8.8$ Hz). ^{13}C NMR (400 MHz, [D$_6$]DMSO): $\delta = 123.7$, 125.9, 131.2, 149.8, 166.7 ppm. Elemental analysis calcd (%) for $C_{21}H_{15}O_6N = H_3TCA$: C 66.83, H 4.01, N 3.71; found: C 66.37; H 4.30, N 3.40. FTIR (KBr, 3500–400): $\tilde{\nu} = 3071$ (br), 1687(s), 1597(vs), 1511(m), 1417(m), 1327(s), 1272(s), 1177 (m), 1107 (w), 1017 (w), 852 (w), 767 (m), 707 (w), 652 (w), 552 cm^{-1} (w)

 © 2003 Wiley-VCH Verlag GmbH & Co. KGaA, Weinheim

Template Synthesis of Cages

Multicomponent Assembly of a Pyrazine-Pillared Coordination Cage That Selectively Binds Planar Guests by Intercalation**

*Kazuhisa Kumazawa, Kumar Biradha, Takahiro Kusukawa, Takashi Okano, and Makoto Fujita**

Aromatic intercalation is an important phenomenon both in chemistry and biology. When large aromatic molecules are intercalated, their chemical and physical properties are expected to change significantly.[1] To exploit such unique properties, several molecular tweezers and boxes based on large π systems (for example, anthracene or porphyrin) have

[*] Prof. M. Fujita, K. Kumazawa, Dr. K. Biradha, Dr. T. Kusukawa
Department of Applied Chemistry
School of Engineering, The University of Tokyo
Bunkyoku, Tokyo 113-8656 (Japan)
Fax: (+81) 3-5841-7257
E-mail: mfujita@appchem.t.u-tokyo.ac.jp
Dr. T. Okano
Department of Applied Chemistry
Graduate School of Engineering, Nagoya University
Chikusaku, Nagoya 464-8603 (Japan)

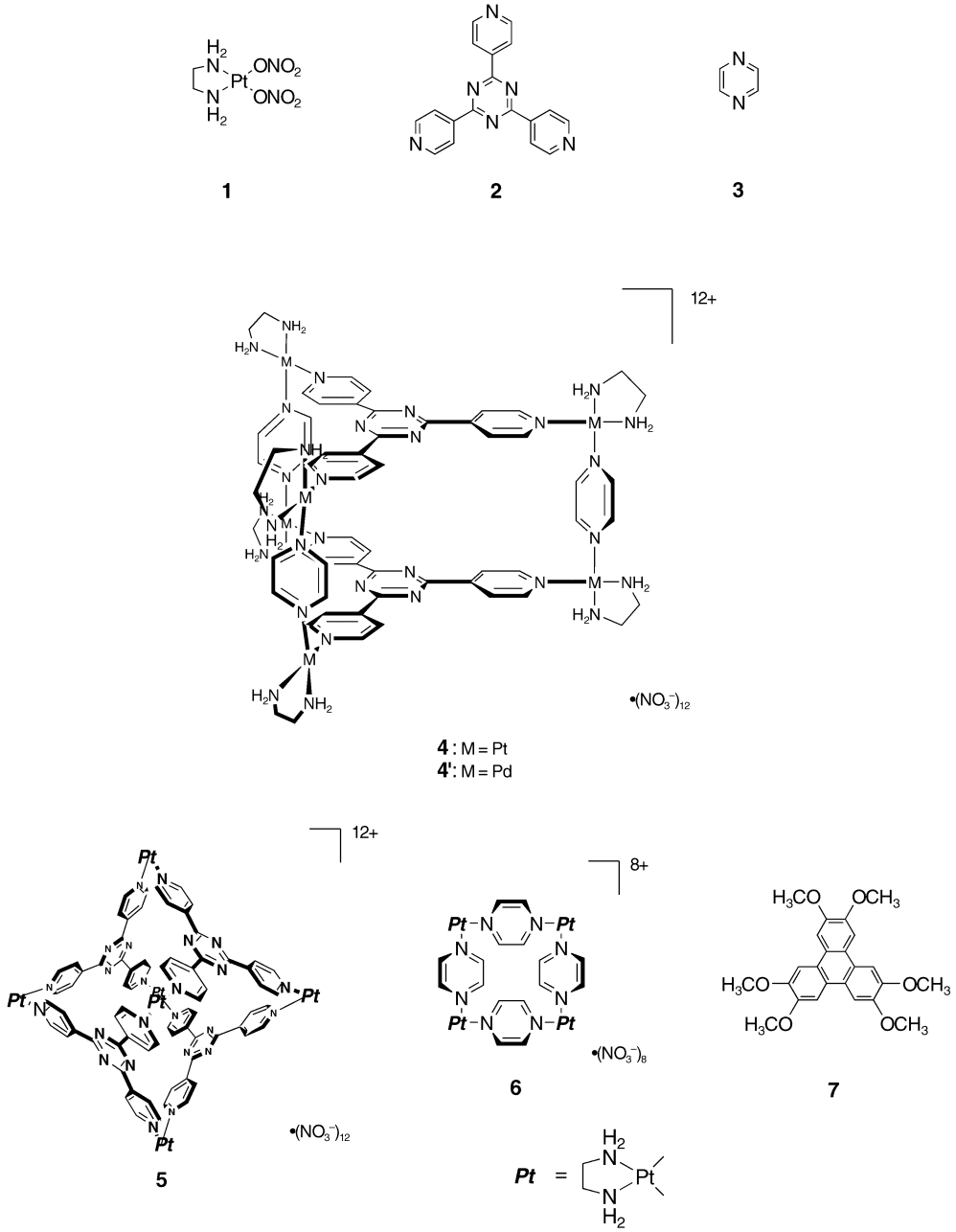
[**] This work was supported by the CREST (Core Research for Evolutional Science and Technology) project of the Japan Science and Technology Corporation.

Supporting information for this article is available on the WWW under http://www.angewandte.org or from the author.

 DOI: 10.1002/anie.200351797 © 2003 Wiley-VCH Verlag GmbH & Co. KGaA, Weinheim

been developed,[2] yet the precise construction of rigid, three-dimensional cages for efficient aromatic intercalation still remains tedious. We now discuss the self-assembly of large prismlike cage **4** in which end-capped Pt^{II} ions **1** link two panel-like ligands **2** with three pyrazine pillars **3** (Scheme 1). This cage is expected to bind aromatic guests since the predicted interplane separation is ideal for aromatic intercalation (about 3.5 Å). To selectively obtain the desired cage **4** from multicomponents (**1**–**3**), however, the assembly of homotopic discrete compounds **5** and **6** need to be avoided. In this regard, we have found a remarkable template effect of large aromatic molecules:[3] for example, triphenylene derivative **7** efficiently templates the selective multicomponent assembly of cage **4**. This cage is stable even when the template is removed and the empty cage strongly binds other large aromatic molecules. The multicomponent assembly of metal-linked cages has been previously reported by Lehn and co-workers,[4] Stang and co-workers,[5] and others,[6] but the binding of such large aromatic compounds has been not documented.

The guest-templated assembly of cage **4** from multicomponents **1**–**3** was clearly observed by NMR spectroscopic analysis. When components **1**–**3** were combined in a 6:2:3 ratio in D_2O, a complicated mixture was obtained which gave an NMR spectrum that was very difficult to interpret (Figure 1 a). However, the addition of hexamethoxytriphenylene **7** (an excess amount) as a suspension and on heating the mixture at 100 °C resulted in the appearance of prominent peaks and the spectrum became simpler within hours. After 48 h, we finally obtained a quite simple NMR spectrum that



Scheme 1. Building blocks and products.

 © 2003 Wiley-VCH Verlag GmbH & Co. KGaA, Weinheim

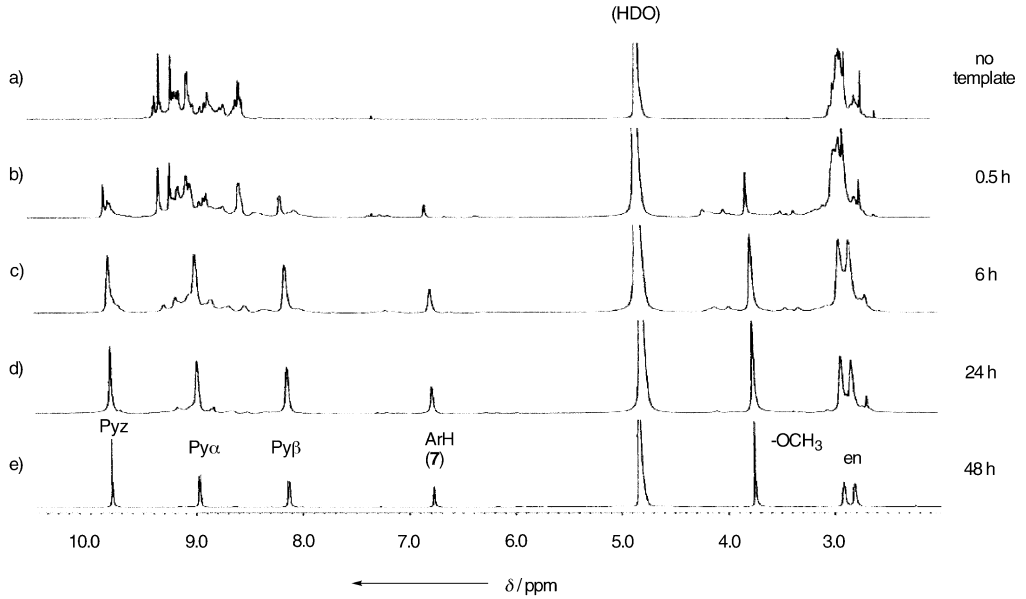


Figure 1. ^{1}H NMR spectra showing the guest-templated assembly of **7**⊂**4** complex (500 MHz, D_2O, 25 °C). a) A mixture of **1**, **2**, and **3**. Template **7** was added to this solution and the mixture was heated at 100 °C for b) 0.5 h, c) 6 h, d) 24 h, and e) 48 h. Pyz = pyrazine.

contained only four signals in the aromatic region: two doublets at $\delta = 8.96$ and 8.13 ppm for component **2**, a singlet at $\delta = 9.78$ ppm for component **3**, and another singlet at $\delta = 6.77$ ppm for guest **7** (Figure 1e). This spectrum was in accordance with the quantitative formation of complex **7**⊂**4**, where cage **4** accommodated guest **7** in the cavity. The signals of component **2** and guest **7** are shifted upfield as a result of face-to-face contact with each other, while that of component **3** is shifted downfield as a consequence of edge-to-face contact with the guest. The integral ratio indicated a 1:1 host–guest complexation. NOE correlation between the host and the guest in a NOESY spectrum is further support for the efficient complexation (see Supporting Information).

The template effect in the assembly of cage **4** is clearly apparent since, in the absence of the template, we could not observe the selective formation of **4** even after heating the solution for a few days; instead a mixture of **5**, **6** (ca. 1:0.7 ratio), and some uncharacterized components was obtained. We also examined the assembly of Pd^{II}-linked analogue **4′**. The formation of **4′** was dominant but not quantitative, presumably because of the weaker ligand field of Pd^{II} ions relative to the Pt^{II} ions.

It is noteworthy that homotopic cages **5** and **6**, which were not formed in the reaction of **1**–**3**, are thermodynamically stable. The quantitative formation of **5** from **1** and **2** has been well-documented;[7] square-shaped complex **6** was also found to efficiently assemble from **1** and **3** as confirmed by NMR spectroscopic and X-ray analysis (Figure 2).[8,9] Therefore, the exclusive formation of **4**, despite the sufficient stability of **5** and **6**, strongly shows the remarkable stabilization of **4** by the host–guest interaction.

The efficient intercalation of **7** in the cavity of **4** was evidenced by X-ray crystallographic analysis of single crystals obtained by slow evaporation of an aqueous solution of **7**⊂**4** (Figure 3).[10] The pyrazine pillars stand perpendicularly on a plane defined by three Pt^{II} ions which are connected to an



Figure 2. Crystal structure of **6**. Counterions and water molecules are omitted for clarity.

identical triazine ligand. The template molecule is intercalated in such a way that aromatic contact is maximized. As a result, the host–guest complex has D_{3h} symmetry. The face-to-face distance between the host and the guest is 3.3 Å, which is slightly shorter than the sum of the van der Waals distances, which suggests there are strong π-π interactions. A new absorption band appearing at 472 nm in the UV/Vis spectrum is attributed to charge transfer between **4** and **7**.

Cage **4** has kinetic stability and thus remained stable at room temperature even after the guest was removed by extraction with $CHCl_3$ (Figure 4a).[11] The empty cage of

 © 2003 Wiley-VCH Verlag GmbH & Co. KGaA, Weinheim

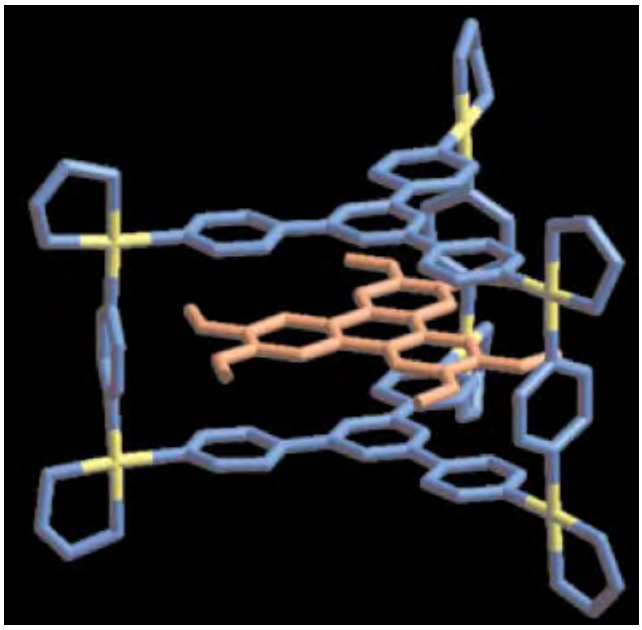


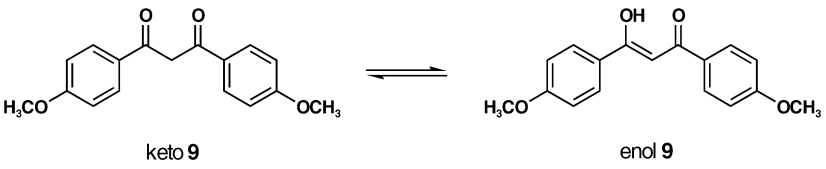
Figure 3. Crystal structure of **7**⊂**4**. Hydrogen atoms, other solvents, and counterions are omitted for clarity.

course was able to bind other neutral aromatic molecules well. For example, pyrene (**8**) was efficiently included inside the cage by suspending it in a D_2O solution of the empty cage **4** (Figure 4b). Though the host symmetry (D_{3h}) does not match the guest symmetry (D_{2h}), minimal numbers of signals were observed in the NMR spectrum, which suggests there is an unrestricted orientation of **8** in the cavity.

The efficient intercalation of planar guest molecules within the cage of **4** was applied to the control of the equilibration between planer and nonplaner molecules. Keto and enol tautomers of β-diketone **9**, which exist in a 15:85 ratio in CD_3CN, can never be separated because of rapid tautomerization. When complexed with cage **4**, however, this molecule was found to exist only in the enol form.[12] The exclusive enolization of **9** is interpreted by the selective intercalation of a planer enol form over a nonplaner keto form. H/D exchange of the CH proton of complexed **9** in D_2O was very slow ($t_{1/2} = 40$ h) relative to the rapid exchange in free **9**. This result clearly shows the inhibition of the keto–enol tautomerization of **9** in the cavity of cage **4**.[13]

Received: May 2, 2003 [Z51797]

Keywords: cage compounds · molecular recognition · palladium · self-assembly · template synthesis



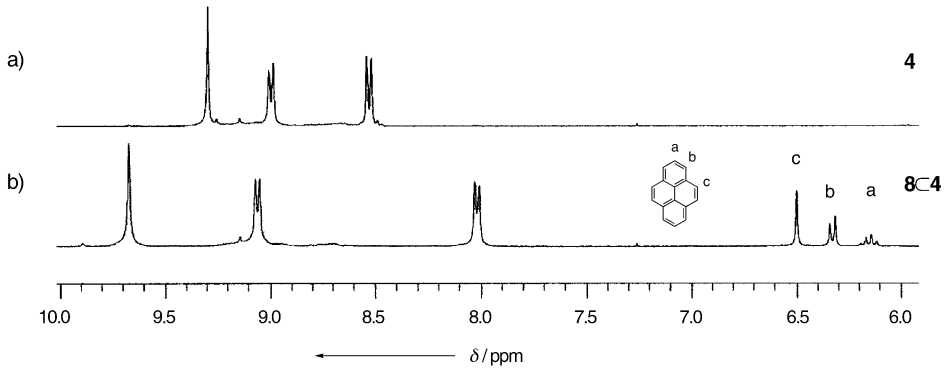


Figure 4. ^{1}H NMR spectra (300 MHz, D_2O, 25 °C) of aromatic regions of a) free **4** after extraction of template and b) **8**⊂**4** after the subsequent reinclusion of **8**.

[1] For Synthetic receptors for large aromatic molecules, see J.-M. Lehn, *Comprehensive Supramolecular Chemistry, Vol. 2* (Eds.: J. L. Atwood, J. E. D. Davis, D. D. Macnicol, F. Vögtle), Pergamon, Oxford, **1996**.

[2] a) S. C. Zimmerman, C. M. VanZyl, *J. Am. Chem. Soc.* **1987**, *109*, 7894–7896; b) F.-G. Klärner, U. Burkert, M. Kamieth, R. Boese, J. Benet-Buchholz, *Chem. Eur. J.* **1999**, *5*, 1700–1707; c) R. M. Sommer, A. L. Rheingold, A. J. Goshe, B. Bosnich, *J. Am. Chem. Soc.* **2001**, *123*, 3940–3952; d) A. J. Goshe, I. M. Steele, C. Ceccarelli, A. L. Rheingold, B. Bosnich, *Proc. Natl. Acad. Sci. USA* **2002**, *99*, 4823–4829; e) P. R. Ashton, T. T. Goodnow, A. E. Kaifer, M. V. Reddington, A. M. Z. Slawin, N. Spencer, J. F. Stoddart, C. Vicent, D. J. Williams, *Angew. Chem.* **1989**, *101*, 1404–1408; *Angew. Chem. Int. Ed. Engl.* **1989**, *28*, 1396–1400; f) N. Fujita, K. Biradha, M. Fujita, S. Sakamoto, K. Yamaguchi, *Angew. Chem.* **2001**, *113*, 1768–1771; *Angew. Chem. Int. Ed.* **2001**, *40*, 1718–1721; g) K. Tashiro, T. Aida, J.-Y. Zheng, K. Kinbara, K. Saigo, S. Sakamoto, K. Yamaguchi, *J. Am. Chem. Soc.* **1999**, *121*, 9477–9478.

[3] Template effect in self-assembly: a) M. Aoyagi, K. Biradha, M. Fujita, *J. Am. Chem. Soc.* **1999**, *121*, 7457–7458; b) M. Fujita, S. Nagao, K. Ogura, *J. Am. Chem. Soc.* **1995**, *117*, 1649–1650; c) Y. Kubota, S. Sakamoto, K. Yamaguchi, M. Fujita, *Proc. Natl. Acad. Sci. USA* **2002**, *99*, 4854–4856; d) B. Hasenknopf, J.-M. Lehn, G. Baum, B. O. Kneisel, D. Fenske, *Angew. Chem.* **1996**, *108*, 1987–1990; *Angew. Chem. Int. Ed. Engl.* **1996**, *35*, 1838–1840; e) B. Hasenknopf, J.-M. Lehn, N. Boumediene, A. Dupont-Gervais, A. V. Dorsselaer, B. Kneisel, D. Fenske, *J. Am. Chem. Soc.* **1997**, *119*, 10956–10962; f) M. Scherer, D. L. Caulder, D. W. Johnson, K. N. Raymond, *Angew. Chem.* **1999**, *111*, 1689–1694; *Angew. Chem. Int. Ed.* **1999**, *38*, 1588–1592; g) M. A. Houghton, A. Bilyk, M. M. Harding,

P. Turner, T. W. Hambley, *J. Chem. Soc. Dalton Trans.* **1997**, 2725 – 2733; h) A. C. Try, M. M. Harding, D. G. Hamilton, J. K. M. Sanders, *Chem. Commun.* **1998**, 723 – 724; i) E. Stulz, Y.-F. Ng, S. M. Scott, J. K. M. Sanders, *Chem. Commun.* **2002**, 524 – 525.

[4] a) A. M. Garcia, D. M. Bassani, J.-M. Lehn, G. Baum, D. Fenske, *Chem. Eur. J.* **1999**, *5*, 1234 – 1238; b) P. N. W. Baxter, J.-M. Lehn, G. Baum, D. Fenske, *Chem. Eur. J.* **1999**, *5*, 102 – 112; c) P. N. W. Baxter, J.-M. Lehn, B. O. Kneisel, G. Baum, D. Fenske, *Chem. Eur. J.* **1999**, *5*, 113 – 120; d) P. N. W. Baxter, J.-M. Lehn, A. DeCian, J. Fischer, *Angew. Chem.* **1993**, *105*, 764 – 766; *Angew. Chem. Int. Ed. Engl.* **1993**, *32*, 69 – 72.

[5] a) C. J. Kuehl, T. Yamamoto, S. R. Seidel, P. J. Stang, *Org. Lett.* **2002**, *4*, 913 – 915; b) C. J. Kuehl, Y. K. Kryschenko, U. Radhakrishnan, S. R. Seidel, S. D. Huang, P. J. Stang, *Proc. Natl. Acad. Sci. USA* **2002**, *99*, 4932 – 4936.

[6] a) K. D. Benkstein, J. T. Hupp, *Mol. Cryst. Liq. Cryst.* **2000**, *342*, 151 – 158; b) S.-S. Sun, A. Lees, *Chem. Commun.* **2001**, 103 – 104; c) B. Manimaran, T. Rajendran, Y.-L. Lu, G.-H. Lee, S.-M. Peng, K.-L. Lu, *Eur. J. Inorg. Chem.* **2001**, 633 – 636.

[7] a) M. Fujita, D. Oguro, M. Miyazawa, H. Oka, K. Yamaguchi, K. Ogura, *Nature* **1995**, *378*, 469 – 471; b) T. Kusukawa, M. Fujita, *J. Am. Chem. Soc.* **2002**, *124*, 13576 – 13582.

[8] Crystal data for **6**: $C_{24}H_{48}N_{24}O_{24}Pt_4 \cdot 4H_2O$, $M_r = 1909.29$, crystal dimensions $0.15 \times 0.15 \times 0.15$ mm^3, triclinic, space group $P\bar{1}$, $a = 8.0932(13)$, $b = 12.085(2)$, $c = 14.318(2)$ Å, $V = 1302.8(3)$ Å^3, $Z = 1$, $\rho_{calcd} = 2.434$ g cm^{-3}, $F(000) = 904$, $\lambda(Mo_{K\alpha}) = 0.71073$ Å, $T = -100$ °C, 6958 reflections collected, 4530 independent reflections observed; 361 number of parameters; $R_1 = 0.0568$; $wR_2 = 0.1587$.

[9] For related pyrazine bridged complexes, see the following: a) Re^{I}–pyrazine square complex: T. Rajendran, B. Manimaran, F.-Y. Lee, P.-J. Chen, S.-C. Lin, G.-H. Lee, S.-M. Peng, Y.-J. Chen, K.-L. Lu, *J. Chem. Soc. Dalton Trans.* **2001**, 3346; b) Ru^{II}/Ru^{III}–pyrazine square complex: C. Victor, C. C. Lau, L. A. Berben, J. R. Long, *J. Am. Chem. Soc.* **2002**, *124*, 9042 – 9043; c) Pt^{II}–pyrazine trianglar complex: M. Schweigner, S. R. Seidel, A. M. Arif, P. J. Stang, *Angew. Chem.* **2001**, *113*, 3575 – 3577; *Angew. Chem. Int. Ed.* **2001**, *40*, 3467 – 3469.

[10] a) Crystal data for **7**⊂**4**: $C_{84}H_{108}N_{42}O_{42}Pt_6 \cdot 9H_2O$, $M_r = 3723.91$, crystal dimensions $0.10 \times 0.10 \times 0.60$ mm^3, trigonal, $P\bar{3}$, $a = b = 19.8516$ (12), $c = 19.515(2)$ Å, $V = 6660.3(10)$ Å^3, $Z = 2$, $\rho_{calcd} = 1.857$ g cm^{-3}, $F(000) = 3626$, $\lambda(Mo_{K\alpha}) = 0.71073$ Å, $T = -100$ °C, 20206 reflections measured, 4033 independent reflections observed; 509 number of parameters; $R_1 = 0.0672$; $wR_2 = 0.1836$. Further refinement was unsuccessful because of the high degree of disorder of the counterions and water molecules.

[11] We have previously reported that Pt^{II}–pyridine bonds have dual nature: labile at elevated temperature but inert at ambient temperature. By exploiting the dual nature, thermodynamic structure assembled at elevated temperature can be kinetically "locked" at ambient temperature (referred to as molecular lock concept). a) M. Fujita, F. Ibukuro, K. Yamaguchi, K. Ogura, *J. Am. Chem. Soc.* **1995**, *117*, 4175 – 4176; b) F. Ibukuro, T. Kusukawa, M. Fujita, *J. Am. Chem. Soc.* **1998**, *120*, 8561 – 8562.

[12] Confirmed by ^{1}H, ^{13}C, and COSY NMR spectra. See Supporting Information.

[13] Keto–enol control through host–guest complexations: T. Chin, Z. Gao, I. Lelouche, Y. K. Shin, A. Purandare, S. Knapp, S. S. Isied, *J. Am. Chem. Soc.* **1997**, *119*, 12849 – 12858.

[14] CCDC-205061 (**6**) and CCDC-205062 (**7**⊂**4**) contains the supplementary crystallographic data for this paper. These data can be obtained free of charge via www.ccdc.cam.ac.uk/conts/retrieving.html (or from the Cambridge Crystallographic Data Centre, 12 Union Road, Cambridge CB21EZ, UK; fax: (+44) 1223-336-033; or deposit@ccdc.cam.ac.uk).

 © 2003 Wiley-VCH Verlag GmbH & Co. KGaA, Weinheim

Panepophenanthrin Total Synthesis

Total Synthesis of the Ubiquitin-Activating Enzyme Inhibitor (+)-Panepophenanthrin**

*Xiaoguang Lei, Richard P. Johnson, and John A. Porco, Jr.**

The ubiquitin-proteasome pathway (UPP) regulates a variety of cellular processes by degradation of targeted proteins.[1] Ubiquitin (Ub) is first activated by ubiquitin-activating enzyme (E1), and the activated ubiquitin is transferred by transacylation to an active cysteine residue of ubiquitin-conjugating enzymes (E2s). The E2 enzymes then cooperate with ubiquitin ligases (E3s) to attach Ub to the amino group of lysine residues on protein targets, leading ultimately to protein degradation by the proteasome. It has been shown that abnormal ubiquitination-mediated protein degradation may be associated with human cancers, inflammation, and neurodegenerative disease.[2] Small-molecule inhibitors of ubiquitination may thus find clinical applications, provided that selective compounds may be uncovered.[3] Recently, the first naturally occurring inhibitor of ubiquitin-activating enzyme, panepophenanthrin (**1**, Figure 1), was isolated from the mushroom strain *Panus rudis* Fr. IFO8994.[4] This molecule falls into a general class of epoxyquinoid natural products produced by Diels–Alder-type dimerization,[5] including torreyanic acid (**2**)[6] and epoxyquinols A (**3**) and B (**4**)[7] (Figure 1). Herein, we report the first total synthesis of (+)-panepophenanthrin, which utilizes a highly stereoselective Diels–Alder dimerization of an epoxyquinol dienol monomer, as well as initial experimental and computational studies to probe the dimerization mechanism.

Our retrosynthetic route for panepophenanthrin is depicted in Figure 2a. Target molecule **1**[28] may be derived from hemiacetal formation of the hydroxy ketone **5.** The propensity for epoxyquinol derivatives to form both hydrates and hemiacetals by reaction of water and alcohols with the electrophilic carbonyl has been documented.[8] The X-ray

[*] Prof. Dr. J. A. Porco, Jr., X. Lei
Department of Chemistry and
Center for Chemical Methodology and Library Development
Boston University, 590 Commonwealth Avenue
Boston, MA 02215 (USA)
Fax: (+1) 617-353-6466
E-mail: porco@chem.bu.edu
Prof. Dr. R. P. Johnson
Department of Chemistry, University of New Hampshire
Durham, NH 03824 (USA)

[**] We thank Chaomin Li for helpful discussions, Dr. Ryuichi Sekizawa (Showa Pharmaceutical University) for providing authentic panepophenanthrin, and Dr. Emil Lobkovsky (Cornell University) for X-ray crystal structure analysis. Financial support from the American Cancer Society (RSG-01-135-01, J.A.P, Jr.) and the NIH (P50 GM067041) is gratefully acknowledged. R.P.J. acknowledges the Norman and Anna S. Waite Professorship for support.

Supporting information for this article is available on the WWW under http://www.angewandte.org or from the author.

 DOI: 10.1002/anie.200351862 © 2003 Wiley-VCH Verlag GmbH & Co. KGaA, Weinheim

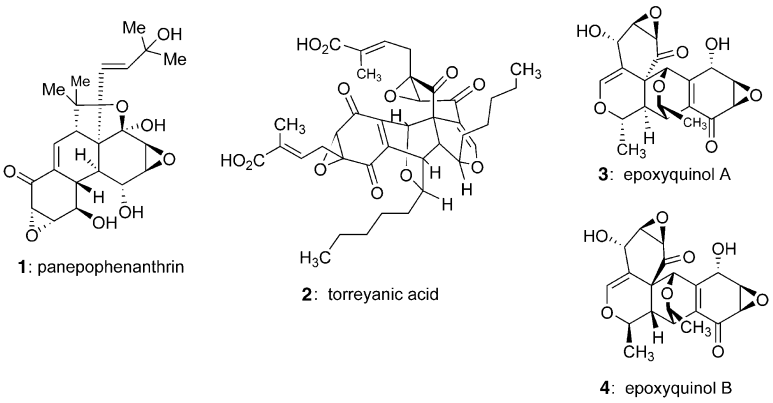


Figure 1. Dimeric epoxyquinoid natural products **1**–**4**.

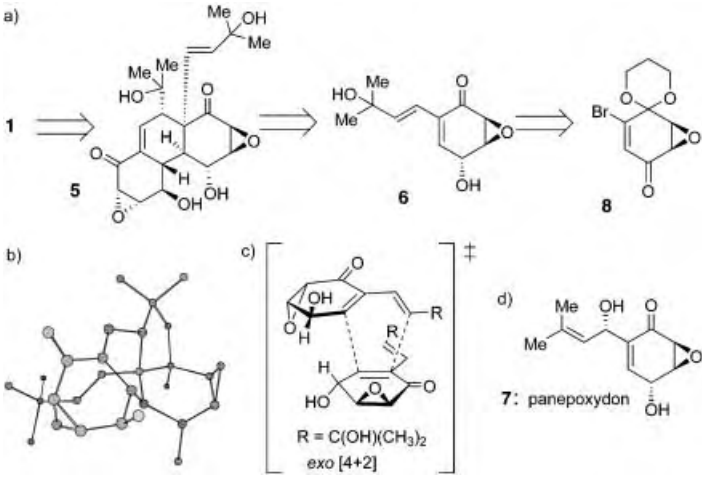
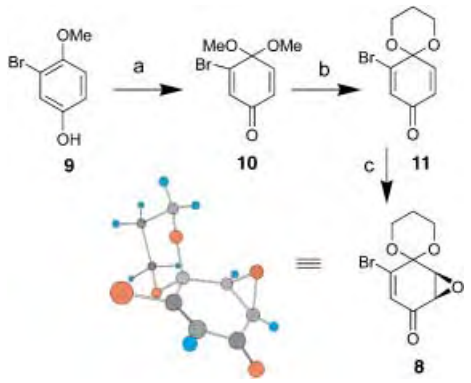


Figure 2. a) Retrosynthetic analysis for panepophenanthrin (**1**), b) X-ray crystal structure of **1**, c) transition state structure for the dimerization of **6**, d) panepoxydon (**7**).

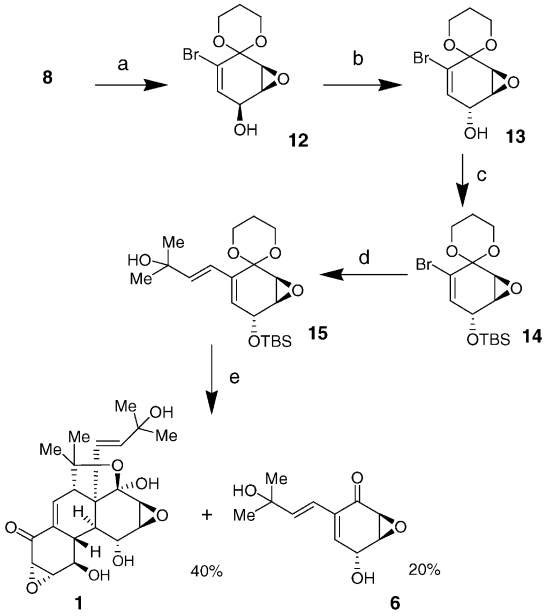
crystal structure of **1** (Figure 2b) also shows the close proximity of the tertiary hydroxy group and ketone, which should substantially favor formation of a hemiacetal bridge.[9] In principle, hemiacetal formation may precede intramolecular [4+2] cycloaddition.[10] The open-form precursor **5** may be derived from *exo*-Diels–Alder dimerization[11] of epoxyquinol monomer **6** (Figure 2c), the conjugated diene isomer of the natural product panepoxydon (**7**, Figure 2d).[12] Recent reports by Shotwell et al. have documented the facile rearrangement of **7** to give conjugated isomers such as **6** under mildly acidic conditions.[12c] Epoxyquinol diene monomer **6** may be derived from transformations of chiral, nonracemic epoxy ketone **8**, including a Heck-type coupling to install the dienol. Compound **8** may be prepared as either antipode by using tartrate-mediated asymmetric nucleophilic epoxidation[13] of a quinone monoketal precursor.

The synthesis of epoxyquinol diene monomer **6** was initiated by oxidation of the readily available monomethoxy hydroquinone **9**[14] with $PhI(OAc)_2$[15] to afford dimethoxyketal **10** (Scheme 1). Transketalization of **10** with 1,3-propanediol under Pirrung's conditions[16] afforded 1,3-dioxane **11**, which was found to be a suitable substrate for nucleophilic epoxidation. Tartrate-mediated nucleophilic epoxidation of **11** using NaHMDS as base cleanly produced epoxy ketone **8** (80% yield, 95% *ee*). The absolute stereochemistry of **8** was confirmed by X-ray crystal structure analysis[27] (Scheme 1) and is consistent with our proposed transition-state model for tartrate-mediated nucleophilic epoxidation.[13a]



Scheme 1. a) $PhI(OAc)_2$, MeOH, RT, 1 h, 96%; b) 1,3-propanediol, $BF_3{\cdot}Et_2O$, DME, RT, 2 h, 75%; c) Ph_3COOH, NaHMDS (1 M in THF), L-DIPT, 4-Å molecular sieves, toluene, −55 °C, 48 h, 80%, 95% *ee*. DIPT = diisopropyl tartrate, DME = dimethoxyethane, NaHMDS = sodium bis(trimethylsilyl)amide, RT = room temperature.

Advancement of **8** to the epoxyquinol monomer **6** is shown in Scheme 2. Attempted chelation-controlled reduction (with e.g. DIBAL-H[17] or $Zn(BH_4)_2$[18]) led to poor diastereoselectivity (1:1). In contrast, reduction of **8** with Super-Hydride cleanly afforded *syn*-epoxy alcohol **12**, which

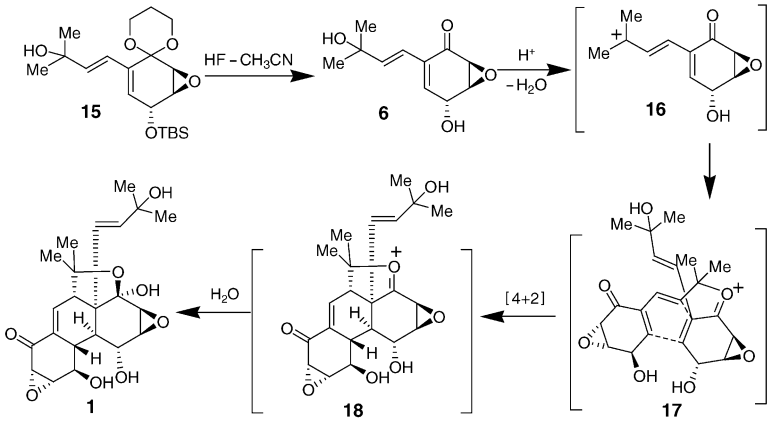


Scheme 2. a) $LiEt_3BH$, THF, −78 °C, 1 h, 98%; b) PPh_3, DIAD, 4-nitrobenzoic acid, THF, −50 °C→RT, 1 h; NaOMe 1 M, MeOH, RT, 30 m, 80%; c) TBSCl, imidazole, DMF, RT, 10 h, 90%; d) $Pd(OAc)_2$, Ag_2CO_3, 2-methyl-3-buten-2-ol, DMF, 90 °C, 16 h, 80%; e) 10% HF, CH_3CN/CH_2Cl_2, RT, 1 h. DIAD = diisopropyl diazodicarboxylate, DMF = dimethylformamide, TBS = *tert*-butyldimethylsilyl.

 © 2003 Wiley-VCH Verlag GmbH & Co. KGaA, Weinheim

was subsequently converted into the *anti* diastereomer **13** by a Mitsunobu protocol[19] (80%, two steps). Silylation of the secondary hydroxy group afforded **14**, which was subjected to Heck-type coupling with 2-methyl-3-buten-2-ol[12c] to afford dienol **15** (80%). Double deprotection of **15** with aqueous HF afforded the desired epoxyquinol monomer **6** (20%) and panepophenanthrin (**1,** 40%). Synthetic **1** was confirmed to be identical to natural panepophenanthrin by ^{1}H and ^{13}C NMR data, mass spectrometry, and optical rotation, and by TLC comparison in three solvent systems.

Our initial supposition was that the tandem deprotection/Diels–Alder dimerization (**15**→**1**)may proceed through an ionic process (Scheme 3).[20] Acid-catalyzed ionization of the tertiary allylic alcohol of epoxyquinol **6** could in principle lead

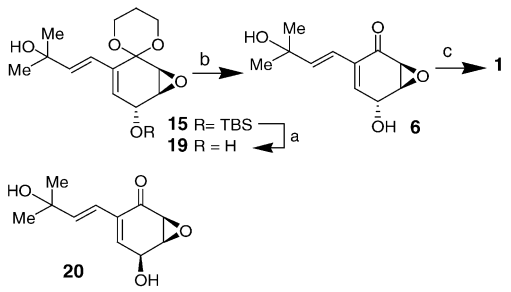


Scheme 3. Deprotection of **15** and subsequent Diels–Alder dimerization to give **1**.

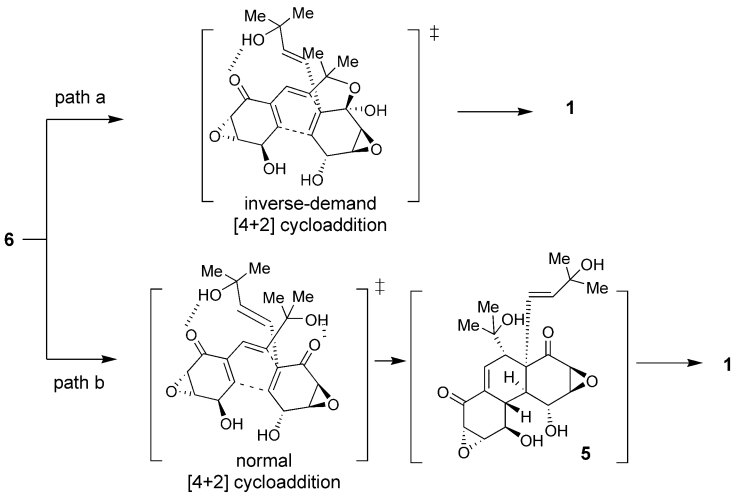
to allylic cation **16,** which may react with the carbonyl group of another monomer to produce the tethered intermediate **17**.[10,21] Intramolecular ionic Diels–Alder reaction of **17** to give **18** followed by addition of water *anti* to the epoxide would afford **1** directly. To further judge the validity of an ionic Diels–Alder process, we revised our synthetic approach in order to prepare **6** for alternative dimerization experiments (Scheme 4). Desilylation of **15** with TBAF cleanly produced epoxy alcohol **19** (90%). Gratifyingly, treatment of **19** with 0.2 M HCl in CH_3CN/CH_2Cl_2 (1:1) cleanly effected ketal hydrolysis to afford epoxyquinol monomer **6** (95%). Interestingly, Diels–Alder dimerization of **6** to give panepophenanthrin (**1**) also proceeded when the monomer was allowed to stand at 25 °C without solvent (24 h, 80%).[7d] The reaction was conducted effectively in both standard laboratory glassware and Teflon vials, which confirms that an ionic Diels–Alder process is not strictly required for the [4+2] dimerization. Subsequent experiments also revealed that *syn*-epoxyquinol monomer **20** (Scheme 4) did not undergo Diels–Alder dimerization under conditions reported for *anti* isomer **6** (neat, room temperature).

We next considered alternative mechanisms for the Diels–Alder dimerization of monomer **6** (Scheme 5). In one case (path a), the tertiary hydroxy group of one monomer adds to the carbonyl group of another to generate a hemiacetal intermediate. An intramolecular, inverse-demand Diels–Alder reaction then affords the dimeric natural product.[22] An alternative mechanism (path b) may involve transition-state hydrogen bonding[23] of the epoxyquinol monomers in a "pseudo-transannular,"[24] normal Diels–Alder cycloaddition. Subsequent ring closure to form a five-membered ring hemiacetal leads to **1**.

To further probe the role of the tertiary hydroxy group in the Diels–Alder dimerization of **6**, we prepared an epoxyquinol monomer lacking this functionality (Scheme 6). Heck-type coupling of **14** with 3,3-dimethylbutene afforded **21** (80%). Reaction of **21** with TBAF produced **22**, which was treated with 0.2 M HCl to effect ketal hydrolysis forming monomer **23**. Epoxyquinol **23** was cleanly dimerized to **24** (neat, 24 h). The regio- and stereochemistry of **24** was confirmed by X-ray structure analysis of bis-*para*-bromobenzoate **25**. Interestingly, **25** crystallized as a centrosymmetric racemate ($P\bar{1}$ space group).[25] Production of dimer **24** confirms that that tertiary hydroxy group of monomer **6** and hydrogen-bond organization is not essential for successful Diels–Alder dimerization. Acetylation of monomer **22** led to **26**, which was hydrolyzed to give monomer **27**. This com-

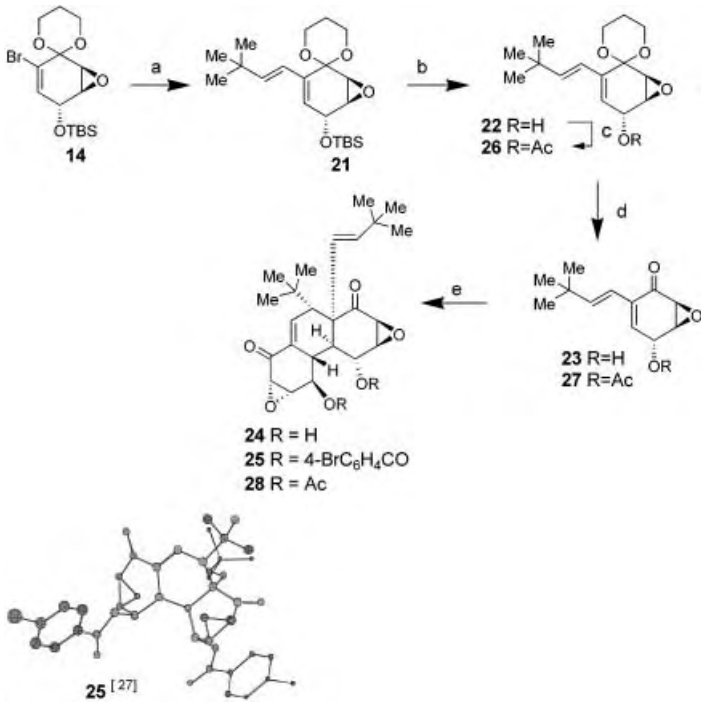


Scheme 4. a) TBAF 1 M in THF, THF, RT, 3 h, 90%; b) 0.2 M HCl, CH_3CN/CH_2Cl_2 (1:1), RT, 2 h, 95%; c) no solvent, RT, 24 h, 80%. TBAF = tetrabutylammonium fluoride.



Scheme 5. Possible mechanisms for the Diels–Alder dimerization.

 © 2003 Wiley-VCH Verlag GmbH & Co. KGaA, Weinheim



Scheme 6. Top: a) $Pd(OAc)_2$, Ag_2CO_3, 3,3-dimethylbutene, DMF, 90 °C, 24 h, sealed tube, 80%; b) TBAF 1 M in THF, THF, RT, 3 h, 90%; c) AcOH, DIC, DMAP, CH_2Cl_2, RT, 30 m, 91%; d) 0.2 M HCl, CH_3CN/CH_2Cl_2 (1:1), RT, 2 h, 95%; e) neat, RT, 24 h, 90%. DIC = 1,3-diisopropylcarbodiimide, DMAP = 4-dimethylaminopyridine. Bottom: X-ray structure of **25**.[27]

pound also dimerized to afford **28**, which was identical to material obtained by acetylation of **24**. These studies support the normal [4+2] pathway (Scheme 5, path b), in which Diels–Alder dimerization is followed by hemiacetal formation.

To further understand the timing of the [4+2] dimerization and hemiacetal formation, we performed computational studies by disconnecting panepophenanthrin in a retro-[4+2] fashion and optimizing each stage at the B3LYP/6-31G* level of theory.[26] Our results are summarized in Figure 3. Initial formation of the hemiacetal link provides the advantage of an intramolecular [4+2] reaction, but renders the dienophile much less reactive because it is no longer an enone. The predicted overall free-energy barrier is 39.2 kcal mol^{-1}. In

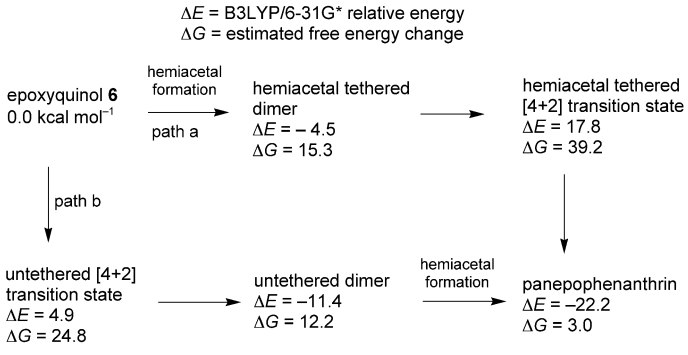


Figure 3. Relative energies (in kcal mol^{-1}, B3LYP/6-31G*) for the intermediates in the two paths for Diels–Alder dimerization.

contrast, direct intermolecular cycloaddition of two epoxyketones proceeds through a reactive dienophile and thus a much lower intrinsic barrier of 24.8 kcal mol^{-1}. Figure 4 shows the predicted transition-state structure. The initial stage of

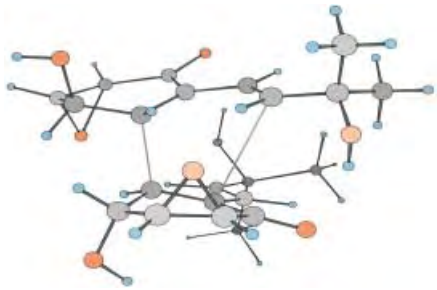
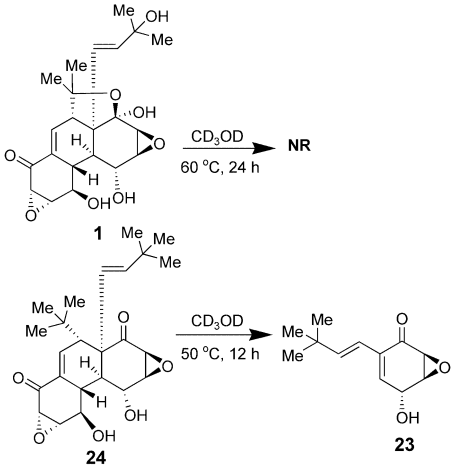


Figure 4. B3LYP/6-31G*-optimized transition-state structure for the formation of panepophenanthrin (**1**).

intermolecular cycloaddition is slightly endothermic, and presumably reversible, but hemiacetal formation "locks" the structure and thus renders panepophenanthrin isolable. Thermolysis experiments on panepophenanthrin are consistent with these general energetic considerations (Scheme 7). When dimer **1** was heated (CD_3OD, 60 °C, 24 h), starting material was recovered; however, thermolysis of untethered dimer **24** (CD_3OD, 50 °C, 12 h) led to quantitative production (^{1}H NMR) of monomer **23** in solution.



Scheme 7. Thermolysis of hemiacetal-bridged (**1**) and nonbridged (**24**) dimers.

In summary, the first enantioselective total synthesis of the ubiquitin-activating enzyme inhibitor (+)-panepophenanthrin (**1**) has been achieved employing tartrate-mediated asymmetric nucleophilic epoxidation and stereoselective Diels–Alder dimerization of an epoxyquinol dienol monomer. Modification of the epoxyquinol monomer leading to panepophenanthrin by replacing a tertiary hydroxy group with a methyl group gave mechanistic insight into the critical [4+2] dimerization. Additional experimental and computational studies related to panepophenanthrin and applications

 © 2003 Wiley-VCH Verlag GmbH & Co. KGaA, Weinheim

of the methodology to produce highly functionalized molecules are in progress and will be reported in due course.

Received: May 12, 2003 [Z51862]

Keywords: cycloaddition · epoxyquinoids · natural products · total synthesis

[1] For recent reviews on the ubiquitin-proteasome pathway, see: a) A. Hershko, A. Ciechanover, *Annu. Rev. Biochem.* **1998**, *67*, 425; b) J. Myung, K. B. Kim, C. M. Crews, *Med. Res. Rev.* **2001**, *21*, 245.

[2] For information regarding ubiqutin ligases and relevance to human disease, see: http://www.ligase.com/ligase/si_ligased-iseases.php

[3] D. C. Swinney, *Drug Discovery Today* **2001**, *6*, 244.

[4] R. Sekizawa, S. Ikeno, H. Nakamura, H. Naganawa, S. Matsui, H. Iinuma, T. Takeuchi, *J. Nat. Prod.* **2002**, *65*, 1491.

[5] For a recent review of Diels–Alder-type natural products, see: A. Ichihara, H. Oikawa, *Curr. Org. Chem.* **1998**, *2*, 365.

[6] a) C. Li, E. Lobkovsky, J. A. Porco, Jr., *J. Am. Chem. Soc.* **2000**, *122*, 10484; b) C. Li, R. P. Johnson, J. A. Porco, Jr., *J. Am. Chem. Soc.* **2003**, *125*, 5095.

[7] Isolation: a) H. Kakeya, R. Onose, H. Koshino, A. Yoshida, K. Kobayashi, S.-I. Kageyama, H. Osada, *J. Am. Chem. Soc.* **2002**, *124*, 3496; epoxyquinol B: b) H. Kakeya, R. Onose, A. Yoshida, H. Koshino, H. Osada, *J. Antibiot.* **2002**, *55*, 829; synthesis: c) C. Li, S. Bardhan, E. Pace, M. Liang, T. Gilmore, J. A. Porco, Jr., *Org. Lett.* **2002**, *4*, 3267; d) M. Shoji, J. Yamaguchi, H. Kakeya, H. Osada, Y. Hayashi, *Angew. Chem.* **2002**, *114*, 3324; *Angew. Chem. Int. Ed.* **2002**, *41*, 3192; e) M. Shoji, S. Kishida, M. Takeda, H. Kakeya, H. Osada, Y. Hayashi, *Tetrahedron Lett.* **2002**, *43*, 9155; f) G. Mehta, K. Islam, *Tetrahedron Lett.* **2003**, *44*, 3569.

[8] Cf.: P. Wipf, P. Jeger, Y. Kim, *Bioorg. Med. Chem. Lett.* **1998**, *8*, 351.

[9] For examples of molecules with a hemiacetal bridge formed from a tertiary hydroxy group, see: a) M. Matsuo, S. Matsumoto, Y. Iitaka, A. Hanaki, T. Ozawa, *Chem. Commun.* **1979**, 105; b) D. Martins, E. Osshiro, N. F. Roque, V. Marks, H. E. Gottlies, *Phytochemistry* **1998**, *48*, 677.

[10] For an ionic Diels–Alder reaction involving a hemiacetal tether, see: R. K. Haynes, K.-P. Lam, K.-Y. Wu, I. D. Williams, L.-L. Yeung, *Tetrahedron* **1999**, *55*, 89.

[11] The *endo* [4+2] dimerization appears to be precluded by steric interactions between the epoxide on the dienophile and the diene. For Diels–Alder reactions of 2-vinylcyclohexenones and related dienes, see: a) C. Spino, M. Pesant, Y. Dory, *Angew. Chem.* **1998**, *37*, 3454; *Angew. Chem. Int. Ed.* **1998**, *37*, 3262; b) J. T. Kuethe, C. A. Brooks, D. L. Comins, *Org. Lett.* **2003**, *5*, 321.

[12] a) Z. Kis, A. Closse, H. P. Sigg, L. Hruban, G. Snatzke, *Helv. Chim. Acta* **1970**, *53*, 1577; b) G. Erkel, T. Anke, O. Sterner, *Biochem. Biophys. Res. Commun.* **1996**, *226*, 214; c) J. B. Shotwell, S. Hu, E. Medina, M. Abe, R. Cole, C. M. Crews, J. L. Wood, *Tetrahedron Lett.* **2000**, *41*, 9639.

[13] a) C. Li, E. Pace, M. Liang, E. Lobkovsky, T. D. Gilmore, J. A. Porco, Jr., *J. Am. Chem. Soc.* **2001**, *123*, 11308; For tartrate-mediated epoxidation of acyclic enones, see: b) C. L. Elston, R. F. W. Jackson, S. J. F. MacDonald, P. J. Murray, *Angew. Chem.* **1997**, *36*, 379; *Angew. Chem. Int. Ed. Engl.* **1997**, *36*, 410; c) O. Jacques, S. J. Richards, R. F. W. Jackson, *Chem. Commun.* **2001**, 2712.

[14] A. B. Hughes, M. V. Sargent, *J. Chem. Soc. Perkin Trans. 1* **1989**, *10*, 1787.

[15] a) A. Pelter, S. Elgendy, *Tetrahedron Lett.* **1988**, *29*, 677; b) A. E. Fleck, J. A. Hobart, G. W. Morrow, *Synth. Commun.* **1992**, *22*, 179.

[16] M. C. Pirrung, D. S. Nunn, *Tetrahedron Lett.* **1992**, *33*, 6591.

[17] J. P. Ragot, C. Steeneck, M.-L. Alcaraz, R. J. K. Taylor, *J. Chem. Soc. Perkin Trans. 1* **1999**, 1073.

[18] T. Nakata, T. Tanaka, T. Oishi, *Tetrahedron Lett.* **1981**, *22*, 4723.

[19] S. F. Martin, J. A. Dodge, *Tetrahedron Lett.* **1991**, *32*, 3017.

[20] For a review on ionic Diels–Alder reactions, see: R. Sanghi, P. S. Vankar, Y. D. Vankar, *J. Indian Chem. Soc.* **1998**, *75*, 709.

[21] For ionic Diels–Alder reactions involving hydroxy dienes and cyclic enones, see: a) P. G. Gassman, D. A. Singleton, *J. Am. Chem. Soc.* **1984**, *106*, 6085; b) R. K. Haynes, G. R. King, S. C. Vonwiller, *J. Org. Chem.* **1994**, *59*, 4743.

[22] For a review, see: D. L. Boger, M. Patel, *Prog. Heterocycl. Chem.* **1989**, *1*, 30.

[23] a) R. Tripathy, P. J. Carroll, E. R. Thornton, *J. Am. Chem. Soc.* **1990**, *112*, 6743; b) Y. Huang, V. H. Rawal, *J. Am. Chem. Soc.* **2002**, *124*, 9662.

[24] Recent review: E. Marsault, A. Toro, P. Nowak, P. Deslongchamps, *Tetrahedron* **2001**, *57*, 4243.

[25] Analysis by chiral HPLC verified that the crystal was racemic, while the mother liquor was optically pure (see Supporting Information). For an example of a "racemic crystal" formed by crystallization of an optically enriched compound, see: A. Mishnev, I. Iovel, J. Popelis, I. Vosekalna, E. Lukevics, *J. Organomet. Chem.* **2000**, *608*, 1.

[26] All calculations were performed with Spartan'02, Wavefunction Inc., Irvine, CA, 2002; see Supporting Information.

[27] CCDC-206033 (**8**) and -206034 (**25**) contain the supplementary crystallographic data for this paper. These data can be obtained free of charge via www.ccdc.cam.ac.uk/conts/retrieving.html (or from the Cambridge Crystallographic Data Centre, 12, Union Road, Cambridge CB2 1EZ, UK; fax: (+44) 1223-336-033; or deposit@ccdc.cam.ac.uk).

[28] Note added in proof: A racemic synthesis of **1** was recently reported: J. E. Moses, L. Commeiras, J. E. Baldwin, R. M. Adlington, *Org. Lett.* **2003**, *5*, 2987.

 © 2003 Wiley-VCH Verlag GmbH & Co. KGaA, Weinheim

Reengineering Biosynthetic Pathways

Biosynthesis of Epothilone Intermediates with Alternate Starter Units: Engineering Polyketide–Nonribosomal Interfaces**

Sarah E. O'Connor, Christopher T. Walsh, and Fei Liu*

The epothilones, a class of antitumor macrolides,[1] are nonribosomal-peptide–polyketide natural products that are constructed by mixed enzyme assembly lines composed of nonribosomal-peptide synthetases (NRPS) and polyketide synthases (PKS).[2] In the early steps of the epothilone

[*] Prof. Dr. C. T. Walsh, Dr. S. E. O'Connor,[+] Dr. F. Liu[+]
Department of Biological Chemistry and Molecular Pharmacology
Harvard Medical School
Boston, MA 02215 (USA)
Fax: (+1) 617-432-0438
E-mail: christopher_walsh@hms.harvard.edu

[+] These authors contributed equally to this work.

[**] Funding for this work was provided by the NIH (GM20011, C.T.W.). F.L. is supported by a NIH Postdoctoral Fellowship (GM66456) and S.E.O. by an Irving Sigal Postdoctoral Fellowship (American Chemical Society).

 DOI: 10.1002/anie.200352077 © 2003 Wiley-VCH Verlag GmbH & Co. KGaA, Weinheim

biosynthetic pathway, the incipient methylthiazolyl group is formed by acetyl transfer from the PKS subunit EpoA to the cysteine residue of the NRPS subunit EpoB.[3] Subsequent cyclization, dehydration, and oxidation by the cyclization (Cy) and oxidase (Ox) domains of EpoB results in the methylthiazolyl species, which is then transferred from EpoB to the downstream PKS acceptor subunit EpoC by the ketosynthase (KS) domain of EpoC (Figure 1a).[4] As both EpoB and EpoC have demonstrated tolerance for unnatural upstream acyl substrates in vitro,[5] it was hypothesized that proteins from other biosynthetic pathways with novel substrate specificities could be used in place of EpoA and EpoB within the epothilone assembly line (Figure 1b).

This study demonstrates that EpoA or EpoB can be replaced in vitro with proteins from the rapamycin,[6] enterobactin,[7] or yersiniabactin[8] biosynthetic pathways. Fusion of a protein-recognition element to the C terminus of the noncognate protein is critical for substrate transfer, as observed in studies with PKS enzymes.[9] Although similar recognition domains have been proposed for mixed PKS/NRPS assembly lines,[10] this hypothesis has not been validated experimentally. A putative recognition sequence at the C terminus of the PKS EpoA appears to facilitate substrate transfer to EpoB, whereas a sequence at the C terminus of the NRPS EpoB facilitates substrate transfer to EpoC (Figure 2a).

When the acyl carrier protein from RapC of the rapamycin biosynthetic pathway was loaded with [^{3}H]acetyl-CoA (see Experimental Section) and incubated with cysteinyl-*S*-EpoB and methylmalonyl-*S*-EpoC, no substrate transfer occurred (Figure 3a, top). However, when the 39-residue EpoA recognition sequence was fused in place of the C terminus of RapC to yield RapC(EpoA) (Figure 2b) and this hybrid protein was used, formation of compound **1** was observed (Figure 3a, bottom).

The free-standing aryl carrier protein EntB from the enterobactin biosynthetic pathway,[7] primed with the methylthiazolyl-*S*-pantetheinyl moiety derived from methylthiazolyl-CoA, produced compound **1** when incubated with methylmalonyl-*S*-EpoC (Figure 3b, top). However, after fusion of the 32-residue EpoB linker to the enterobactin protein (EntB(EpoB), Figure 2b), the formation of product **1** was improved (Figure 3b, bottom). When Ybt-PCP2, a peptidyl carrier protein from the yersiniabactin biosynthetic pathway,[8] was primed with the methylthiazolyl-*S*-acyl group and incubated with methylmalonyl-*S*-EpoC, a small amount of product formation was again observed (Figure 4). However, replacement of the C-terminal sequence of Ybt-PCP2 by

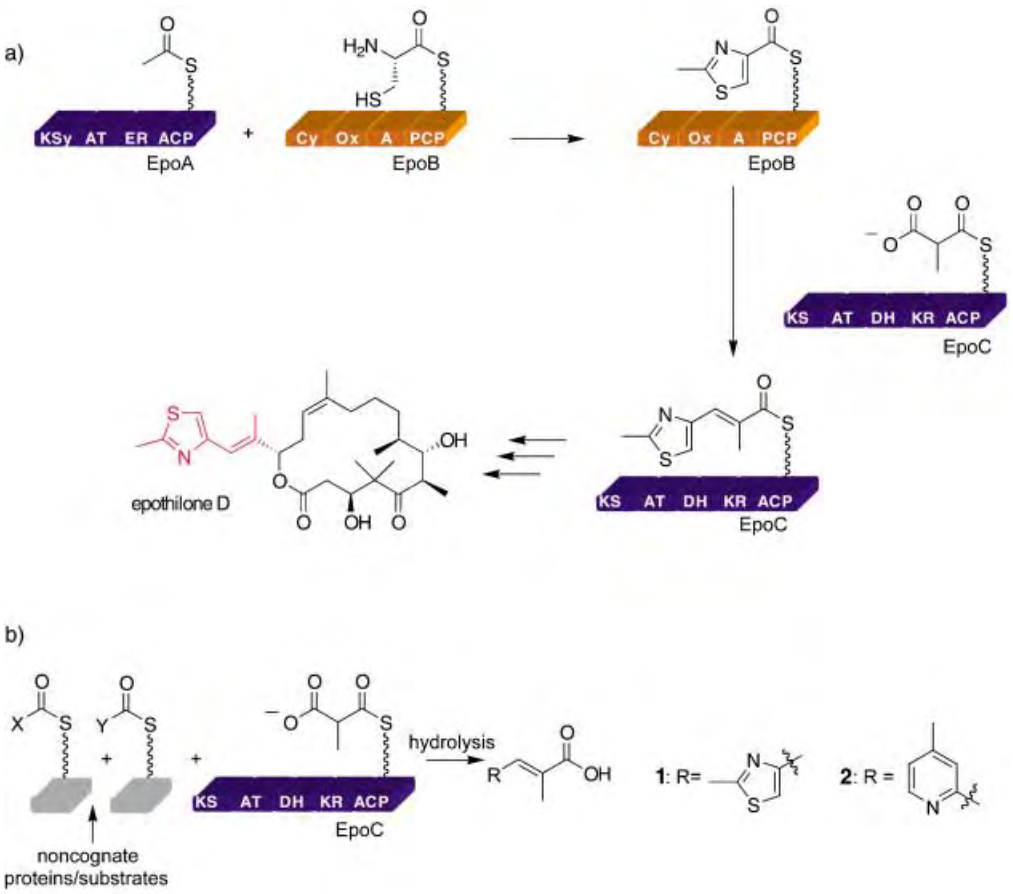


Figure 1. a) Early steps in the biosynthesis of epothilone. The EpoA, EpoB, and EpoC proteins are depicted with their catalytic modules. b) Integration of noncognate proteins into the epothilone assembly line. Use of noncognate proteins with different substrates. (X = methyl and Y = cysteine to make epothilone fragment **1**; alternatively the X-containing substrate was omitted from the enzymatic reaction, and the substrates Y = methylthiazole or methylpyridine were used to make epothilone fragments **1** or **2**, respectively.)

 © 2003 Wiley-VCH Verlag GmbH & Co. KGaA, Weinheim



Figure 2. a) Proposed C-terminal recognition sequences of EpoA (in blue) and EpoB (in red). b) Amino acid sequences of the C termini of the proteins used in this study. Underlined sequences in RapC and YbtPCP2 were removed and replaced with the EpoA or EpoB recognition sequence. Italicized letters indicate the serine residue that is pantetheinylated.

that of the EpoB recognition sequence (Ybt-PCP2(EpoB), Figure 2b)[11] greatly improved product yield (Figure 4). The use of the protein Ybt-PCP2(NS), which lacks the C-terminal residues of the wild-type carrier protein, also led to diminished product formation (decreased by 60% relative when Ybt-PCP2(EpoB) was used). These studies indicate that the recognition sequences that assist protein recognition in the PKS pathways[9a] are also observed in both PKS/NRPS and NRPS/PKS mixed interfaces. A preliminary study revealed that product formation in the presence of methylthiazolyl-*S*-EntB(EpoB) and methylmalonyl-*S*-EpoC is much slower than the rate of product formation that is observed with the cognate EpoB protein (Figure 3c). This suggests that the engineered partner protein, although viable, is not as efficient as the wild-type EpoB donor. Further optimization of the recognition sequence may lead to improved acyl-group transfer.

The use of noncognate proteins to deliver tethered acyl groups to NRPS or PKS assembly lines for the synthesis of unnatural products is an important goal. Therefore, we examined the ability of EntE,[7] the partner protein of EntB, to load aromatic acyl substrates onto the phosphopantetheinyl group of EntB(EpoB). Although the interaction of EntE with EntB(EpoB) is adversely affected by the addition of the linker sequence, a substantial extent of [^{14}C]salicylate-group loading (57%) was noted for the modified carrier protein (compared to 90% for the wild type). EntE can also activate and load the heteroaromatic substrate 4-methyl-2-pyridine carboxylic acid (picolinic acid), though at a significantly decreased rate (0.33 min^{-1}) to that of its activation and loading of the natural substrate 2,3-dihydroxybenzoate (330 min^{-1}).[7a] As a methylpyridine epothilone derivative has been shown to exhibit enhanced cytotoxic activity,[12] this substrate provides an interesting test case for further study. Acyl transfer, reduction, and dehydration on EpoC could be demonstrated with this novel substrate by incubating EntE, picolinic acid, EntB(EpoB), and EpoC, in the presence of [^{14}C]methylmalonyl-CoA and NADPH (Figure 5). The recognition sequence from EpoB appears to dramatically improve product formation when this noncognate substrate is used, thus suggesting that improvement of the protein–protein interaction by the recognition sequence is critical when unusual substrates are incorporated into the enzymatic assembly line.

This study demonstrates that proteins from rapamycin, yersiniabactin, and enterobactin biosynthetic pathways can interact productively with the epothilone assembly line, which suggests that short recognition sequences in hybrid PKS/NRPS systems may be fused to multiple proteins. Thus, the "linker hypothesis", which has enabled the mixing and matching of proteins within PKS systems,[9a] can also be used to mix PKS and NRPS systems and enable acyl transfer and subsequent reactions such as cyclization, reduction, or dehydration to build novel assembly-line intermediates. The rates for product formation in the hybrid system are decreased relative to that observed in the natural system, thus suggesting that the terminal recognition sequence is not the only element required for productive acyl transfer. Consistent with this observation, studies with the erythromycin biosynthetic pathway suggest that the entire protein may contribute to the protein–protein interaction.[9d] Nevertheless, addition of the C-terminal recognition sequence greatly improved substrate transfer in the three examples described herein. Although a coiled-coil protein interaction has been proposed for the PKS recognition elements,[9e] it is not known whether PKS/NRPS sequences interact in a similar manner. More detailed studies designed to elucidate the mechanism by which these recognition elements foster protein–protein interactions are currently underway.

Experimental Section

Carrier proteins were amplified by polymerase chain reaction (PCR) from existing constructs or from genomic DNA and ligated into pET28b (Novagen) to create constructs that contained an N-terminal His tag. The carrier protein of RapC consists of 151 amino acids (residues 6110–6260 of RapC); Ybt-PCP2 consists of the amino acids 1933–2041 of HMWP2. Carrier proteins with a linker sequence were

 © 2003 Wiley-VCH Verlag GmbH & Co. KGaA, Weinheim

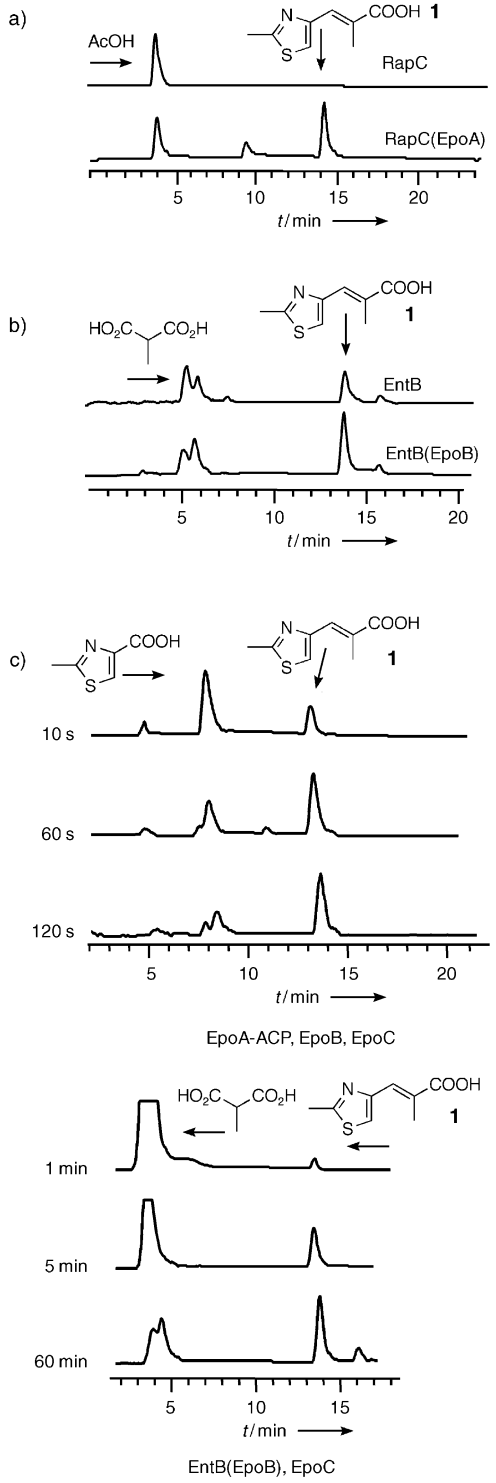


Figure 3. a) Radio-HPLC traces that indicate the formation of compound **1** from the incubation of cysteinyl-*S*-EpoB, methylmalonyl-*S*-EpoC, and either 1) [^{3}H]acetyl-*S*-RapC or 2) [^{3}H]acetyl-*S*-RapC(EpoB). b) Radio-HPLC traces that indicate the formation of compound **1** from the incubation of [^{14}C]methylmalonyl-*S*-EpoC and 1) methylthiazolyl-*S*-EntB or 2) methylthiazolyl-*S*-EntB(EpoB). c) Comparison of product formation from wild-type epothilone biosynthetic enzymes (acetyl-*S*-EpoA-carrier protein, [^{35}S]cysteine-*S*-EpoB, and methylmalonyl-*S*-EpoC) with product formation from enterobactin and epothilone biosynthetic pathways (methyl-thiazolyl-*S*-EntB(Epo) and [^{14}C]methylmalonyl-*S*-EpoC) over time. ACP = acyl carrier protein.

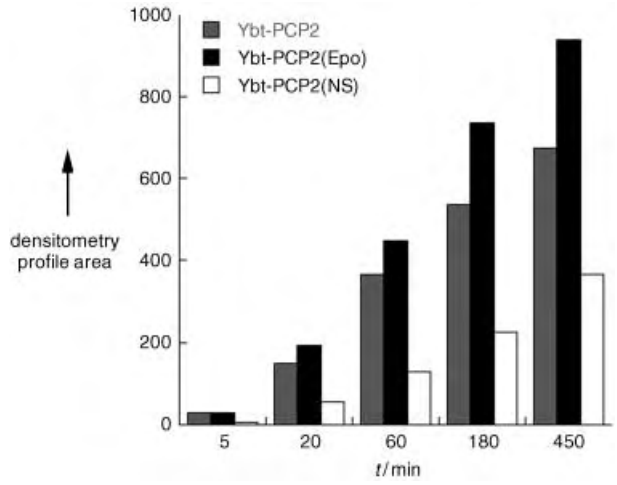


Figure 4. Comparison of the formation of compound **1** by the interfaces formed between [^{14}C]methylmalonyl-*S*-EpoC and methyl-thiazolyl-*S*-Ybt-PCP2, Ybt-PCP2(EpoB), and Ybt-PCP2(NS) over time.

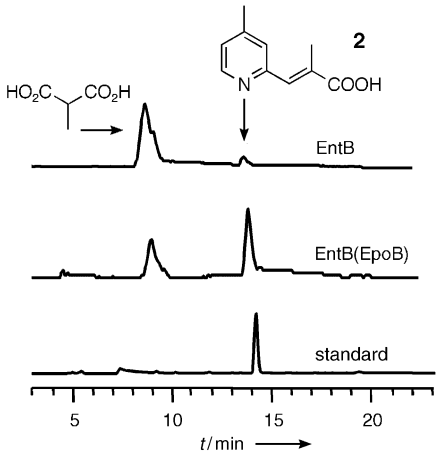


Figure 5. Radio-HPLC trace that indicates the product **2** formed upon incubation of [^{14}C]methylmalonyl-*S*-EpoC and picolinyl-*S*-EntB or picolinyl-*S*-EntB(EpoB), against the UV-HPLC trace (254 nm) of compound **2** as a chemical standard.

constructed by splicing-overlap-extension PCR.[13] Carrier proteins were expressed in the apo (nonpantetheinylated) form in BL21(DE3) *E. coli* cells under control of a T7 promoter at 25 °C and purified by nickel chromatography. Apo carrier proteins were modified by incubation with the broad-specificity phosphopantetheinyl transferase Sfp[14] and acetyl-CoA or methylthiazolyl-CoA. The Ybt proteins exhibited a loading capacity of 65 %, as judged by quantitation of covalent modification of the protein with the radiolabeled coenzyme [^{3}H]acetyl-CoA. EntB(EpoB) and RapC(EpoA) both exhibited approximately 50 % modification, whereas the wild-type counterparts RapC and EntB showed greater than 90 % priming. EpoB and EpoC were expressed and purified as reported previously.[3,4] In a representative assay, apo-EntB(EpoB) (5 μM) in a total volume of 100 μL was incubated at pH 7 with Sfp (0.5 μM) and methylthiazolyl-CoA (200 μM) in the presence of $MgCl_2$ (5 mM). EpoC (5 μM), NADPH (3 mM), and [^{14}C]methylmalonyl-CoA (10 μM) (total reaction volume 65 μL) were then added, and the reaction was left for 20 min at 25 °C. The reaction was quenched by the addition of trichloroacetic acid (10 %), and the product was hydrolyzed from the precipitated protein

 © 2003 Wiley-VCH Verlag GmbH & Co. KGaA, Weinheim

by heating with KOH (0.5 M, 60 °C) for 5 min. The methylthiazole methylacrylic acid **1** and picolinic methylacrylic acid **2** standards were made as previously reported and used to verify product formation in the reaction.[4,15] Reversed-phase HPLC (C_{18} Vydac column) with a UV detector and an online radioisotope detector was used for the assays. (**1**: MeCN (0–70 %) in aqueous TFA (0.1 %), 25 min; **2**: MeCN (0–25 %) in aqueous TFA (0.1 %), 25 min.) The formation of **1** was also assayed by radio-TLC (silica; 90:5:5 chloroform/ethanol/acetic acid). Rates for EntE activation were determined by using a PPi (inorganic pyrophosphatase) exchange assay as previously described.[7a] Quantitation of the loading onto EntB by EntE was performed by loading with [^{14}C]salicylate.

Received: June 6, 2003 [Z52077]

Keywords: antitumor agents · biosynthesis · enzyme catalysis · polyketides · protein modifications

[1] D. M. Bollag, P. A. McQueney, J. Zhu, O. Hensens, L. Koupal, J. Liesch, M. Goetz, E. Lazarides, C. M. Woods, *Cancer Res.* **1995**, *55*, 2325 – 2333.

[2] a) L. Tang, S. Shah, L. Chung, J. Carney, L. Katz, C. Khosla, B. Julien, *Science* **2000**, *287*, 640 – 642; b) I. Molnar, T. Schupp, M. Ono, R. E. Zirkle, M. , Milnamow, B. Nowak-Thompson, N. Engel, C. Toupet, A. Stratmann, D. D. Cyr, J. Gorlach, J. M. Mayo, A. Hu, S. Goff, J. Schmid, J. M. Ligon, *Chem. Biol.* **2000**, *7*, 97 – 109.

[3] H. Chen, S. O'Connor, D. E. Cane, C. T. Walsh, *Chem. Biol.* **2001**, *8*, 899 – 912.

[4] S. E. O'Connor, H. Chen, C. T. Walsh, *Biochemistry* **2002**, *41*, 5685 – 5694.

[5] T. L. Schneider, C. T. Walsh, S. E. O'Connor, *J. Am. Chem. Soc.* **2002**, *124*, 11 272 – 11 273.

[6] A. Konig, T. Schwecke, I. Molnar, G. A. Bohm, P. A. Lowden, J. Staunton, P. F. Leadley, *Eur. J. Biochem.* **1997**, *247*, 526 – 534.

[7] a) A. M. Gehring, K. A. Bradley, C. T. Walsh, *Biochemistry* **1997**, *36*, 8495 – 8503; b) F. Rusnak, W. S. Faraci, C. T. Walsh, *Biochemistry* **1989**, *28*, 6827 – 6835.

[8] a) D. A. Miller, L. Luo, N. Hillson, T. A. Keating, C. T. Walsh, *Chem. Biol.* **2002**, *9*, 333 – 344; b) H. Drechsel, H. Stephan, R. Lotz, H. Haag, H. Zaehner, K. Hantke, G. Jung, *Liebigs Ann.* **1995**, 1727 – 1733; c) A. M. Gehring, E. DeMoll, J. D. Fetherston, I. Mori, G. F. Mayhew, F. R. Blattner, C. T. Walsh, R. D. Perry, *Chem. Biol.* **1998**, *5*, 573 – 586.

[9] a) R. S. Gokhale, S. Y. Tsuji, D. E. Cane, C. Khosla, *Science* **1999**, *284*, 482 – 485; b) S. Y. Tsuji, D. E. Cane, C. Khosla, *Biochemistry* **2001**, *40*, 2326 – 2331; c) N. Wu, S. Y. Tsuji, D. E. Cane, C. Khosla, *J. Am. Chem. Soc.* **2001**, *123*, 6465 – 6474; d) N. Wu, D. E. Cane, C. Khosla, *Biochemistry* **2002**, *41*, 5056 – 5066; e) P. Kumar, Q. Li, D. E. Cane, C. Khosla, *J. Am. Chem. Soc.* **2003**, *125*, 4097 – 4102.

[10] L. Du, C. Sanchez, B. Shen, *Metab. Eng.* **2001**, *3*, 78 – 95.

[11] A previously reported definition of a PCP domain was used in this study to separate the linker region (the sequence after the fourth helix) from the minimal PCP domain: T. Weber, R. Baumgartner, C. Renner, M. A. Marahiel, T. A. Holak, *Structure* **2000**, *8*, 407 – 418.

[12] K. C. Nicolaou, R. Scarpelli, B. Bollbuck, B. Werschkun, M. M. A. Pereira, M. Wartmann, K. H, Altmann, D. Zaharevitz, R. Gussio, P. Giannakakou, *Chem. Biol.* **2000**, *7*, 593 – 599.

[13] R. M. Horton, Z. Cai, S. N. Ho, L. R. Pease, *BioTechniques* **1990**, *8*, 528.

[14] a) L. E. N. Quadri, P. H. Weinreb, M. Lei, M. M. Nakano, P. Zuber, C. T. Walsh, *Biochemistry* **1998**, *37*, 1585 – 1595; b) P. J. Belshaw, C. T. Walsh, T. Stachelhaus, *Science* **1999**, *284*, 486 – 489.

[15] Characterization of **2**. Reversed-phase HPLC (MeCN (0–25 %) in TFA (0.1 %) over 25 min, C18 Vydac column): retention time = 14.6 min; MALDI-MS: calcd: 178.08, found: 178.06; ^{1}H NMR (200.055 MHz, $CDCl_3$): $\delta = 8.63$ (1 H, d, $J = 4.81$ Hz; Ar), 7.76 (1 H, d, $J = 1.40$ Hz; Ar), 7.09 (1 H, d, $J = 4.80$ Hz; Ar), 2.40 (3 H, s; CH_3-Ar), 2.30 (3 H, d, $J = 1.60$ Hz; CH=C(CH_3)), 2.16 ppm (1 H, d, $J = 0.80$ Hz; C*H*=C); ^{13}C NMR (50.31 MHz, $CDCl_3$): $\delta = 172.6$, 154.5, 148.9, 148.5, 137.3, 132.7, 126.8, 124.1, 21.39, 14.35 ppm.

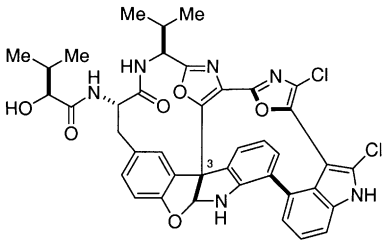
 © 2003 Wiley-VCH Verlag GmbH & Co. KGaA, Weinheim

Stereogenic Quaternary Centers

Catalytic Enantioselective Synthesis of Oxindoles and Benzofuranones That Bear a Quaternary Stereocenter**

*Ivory D. Hills and Gregory C. Fu**

A diverse array of indole alkaloids and benzofuran-derived natural products bear quaternary stereocenters in the 3-position of the heterocycle.[1,2] Although noteworthy progress has been described in the development of strategies for the enantioselective synthesis of such compounds,[3] there remains a need for additional approaches.



diazonamide A gelsemine

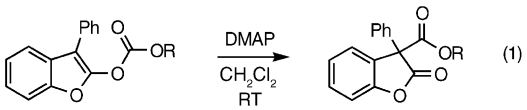
In 1986, Black et al. reported that 4-dimethylaminopyridine (DMAP) catalyzes the rearrangement of *O*-acylated benzofuranones to give their *C*-acylated isomers [Eq. (1)].[4] During the course of studies directed toward the synthesis of

[*] Prof. Dr. G. C. Fu, I. D. Hills
Department of Chemistry, Massachusetts Institute of Technology
Cambridge, MA 02139 (USA)
Fax: (+1) 617-324-3611
E-mail: gcf@mit.edu

[**] We thank Dr. J. Craig Ruble for preliminary experiments. Support has been provided by the American Chemical Society (Organic Division Fellowship to I.D.H., sponsored by Abbott Laboratories), the National Institutes of Health (National Institute of General Medical Sciences, R01-GM57034), Merck, and Novartis. Funding for the MIT Department of Chemistry Instrumentation Facility has been furnished in part by NSF CHE-9808061 and NSF DBI-9729592.

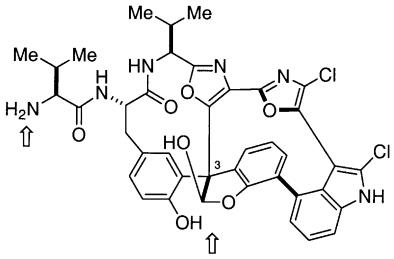
Supporting information for this article is available on the WWW under http://www.angewandte.org or from the author.

 DOI: 10.1002/anie.200351666 © 2003 Wiley-VCH Verlag GmbH & Co. KGaA, Weinheim



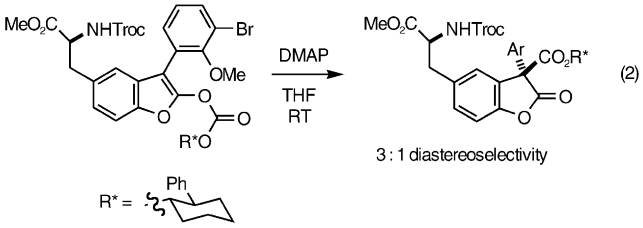
(1)

the originally assigned incorrect structure of the potent anticancer agent diazonamide A,[5] Moody et al. employed a non-asymmetric Black-type *C*-acylation to generate the



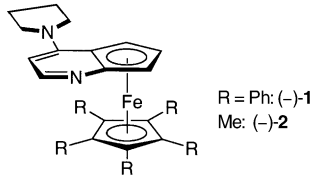
diazonamide A [incorrect] (initial structural assignment)

quaternary stereocenter of the benzofuran-derived core.[6] A few years later, also in the context of an approach to the synthesis of the incorrect structure of diazonamide A, Vedejs and Wang described a diastereoselective variant of the Black rearrangement reaction [Eq. (2)] (Troc = trichloroethoxycarbonyl).[7] Notably, for the correct structure of diazonamide A (above), a corresponding *C*-acylation strategy would employ an oxindole rather than a benzofuranone as the substrate.

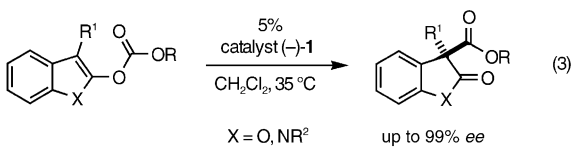


(2)

In recent years, we have been pursuing the development of applications of chiral derivatives of DMAP and PPY (PPY = 4-(pyrrolidino)pyridine; e.g., **1** and **2**) to a range of



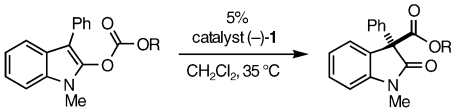
enantioselective nucleophile-catalyzed transformations.[8] In view of the potential significance of the reaction products, we decided to explore the use of these catalysts in asymmetric rearrangements of *O*-acylated benzofuranones and oxindoles. Herein we provide the first examples of enantioselective variants of these processes, demonstrating that catalyst **1** generates the new quaternary stereocenter with very good enantiomeric excess [Eq. (3)].



(3)

Our initial studies focused on *O*-acylated oxindoles, a family of compounds that had not previously been explored in the context of O-to-C rearrangements. We generated a representative substrate by treating an oxindole with methyl chloroformate, and we were pleased to discover that PPY derivative **1** did, indeed, catalyze the rearrangement of the resulting carbonate, thus providing a new quaternary stereocenter with promising enantioselectivity (Table 1, entry 1).

Table 1: Effect of the acyl group on the enantioselectivity of O-to-C rearrangements.



Entry	R	*ee* [%][a]
1	Me	58
2	Et	63
3	*t*Bu	–[b]
4		98

[a] The data are an average of two runs. [b] No rearrangement was observed.

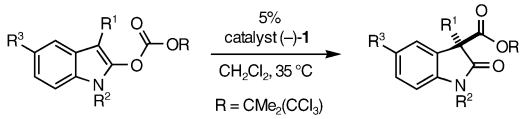
We subsequently determined that an increase in the bulk of the carbonate group (Me→Et) led to an increase in the enantioselectivity (Table 1, entries 1 and 2, 58→63% *ee*). Unfortunately, in the case of a *tert*-butyl substituent, the rearrangement did not proceed, presumably due to a steric effect (Table 1, entry 3). However, we were able to overcome this lack of reactivity through electronic activation, specifically, the use of a trichloro-*tert*-butyl group: rearrangement of this carbonate furnished the desired product with very good enantioselectivity (Table 1, entry 4, 98% *ee*).[9]

With the trichloro-*tert*-butoxycarbonyl substituent as the migrating group, catalyst **1** promotes the rearrangement of a variety of oxindole derivatives with high enantioselectivity (Table 2).[10,11] The reaction proceeds cleanly with either aromatic or heteroaromatic groups in the 3-position (Table 2, entries 1 and 2).[12] 3-Alkyl-substituted *O*-acylated oxindoles can also be employed as substrates, although these rearrangements are slower and require a 10% catalyst loading to obtain a good yield (Table 2, entries 3 and 4). Substitution on the six-membered ring is tolerated, furnishing a product suitable for further functionalization (Table 2, entry 5). Finally, the reaction is not limited to *N*-methyl-substituted oxindoles—catalyst **1** also promoted the rearrangement of an *N*-benzyl-protected heterocycle with high enantioselectivity (Table 2, entry 6).[13]

The conditions that we employed for O-to-C rearrangements of oxindole derivatives (Table 2) are directly applicable to the corresponding reactions of *O*-acylated benzofuranones

 © 2003 Wiley-VCH Verlag GmbH & Co. KGaA, Weinheim

Table 2: Catalytic enantioselective rearrangement of oxindole derivatives.

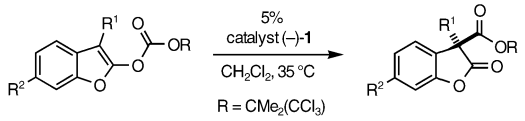


Entry	R^1	R^2	R^3	*ee* [%][a]	Yield [%][a]
1	Ph	Me	H	99	91
2	2-thienyl	Me	H	95	81
3[b]	benzyl	Me	H	94	82
4[b]	Me	Me	H	93	72
5	Ph	Me	I	98	94
6	Ph	Bn	H	98	88

[a] Yield of isolated products. The data are an average of two runs. [b] Catalyst loading: 10%.

(Table 3).[14] Thus, for both 3-aryl- and 3-alkyl-substituted compounds, catalyst **1** promotes the generation of the new quaternary stereocenter with very good enantioselectivity.[15,16]

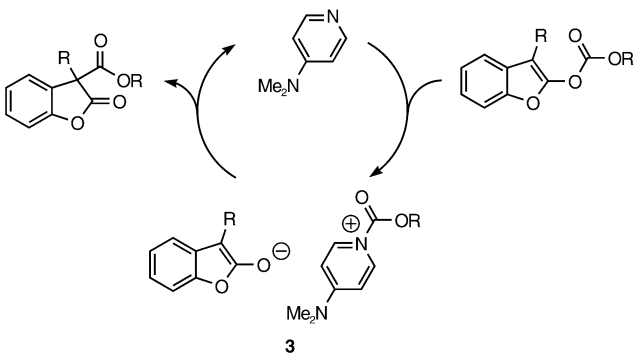
Table 3: Catalytic enantioselective rearrangement of benzofuranone derivatives.



Entry	R^1	R^2	*ee* [%]	Yield [%][a]
1	Ph	H	97	81
2	Bn	H	88	95
3[b]	Me	Me	90	93

[a] Yield of isolated product. [b] This reaction was run at −12 °C with 10% catalyst.

Black et al. suggested that DMAP-catalyzed rearrangements of *O*-acylated benzofuranones proceed through the mechanism illustrated in Scheme 1.[4] We believe that asymmetric reactions of *O*-acylated benzofuranones and oxindoles catalyzed by PPY derivative **1** follow an analogous pathway. Indeed, we have been able to obtain a low-resolution X-ray crystal structure of the ion pair corresponding to **3** (Figure 1).[17–19]



Scheme 1. Proposed mechanism for DMAP-catalyzed rearrangements of *O*-acylated benzofuranones.

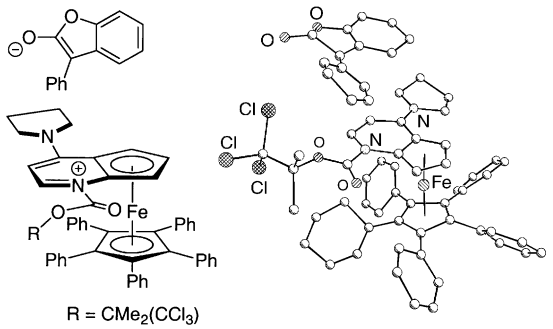


Figure 1. X-ray crystal structure of an ion pair derived from catalyst **1** and an *O*-acylated benzofuranone.

In summary, we have developed the first method for the catalytic enantioselective rearrangement of *O*-acylated benzofuranones and oxindoles, an efficient carbon–carbon bond-forming reaction that generates a quaternary stereocenter. On the mechanistic side, we have crystallographically characterized the presumed intermediate in this process. In view of the abundance of important indole- and benzofuran-derived natural products that bear a quaternary stereocenter in the 3-position of the heterocycle, we believe that this method may prove useful in asymmetric synthesis.

Received: April 15, 2003 [Z51666]
Published online: July 3, 2003

Keywords: asymmetric synthesis · heterocycles · homogeneous catalysis · ion pairs · rearrangements

[1] For a sampling of recent total syntheses, see: a) gelsemine: H. Lin, S. J. Danishefsky, *Angew. Chem.* **2003**, *115*, 38–53; *Angew. Chem. Int. Ed.* **2003**, *42*, 36–51; b) strychnofoline: A. Lerchner, E. M. Carreira, *J. Am. Chem. Soc.* **2002**, *124*, 14826–14827; c) alantrypinone: D. J. Hart, N. A. Magomedov, *J. Am. Chem. Soc.* **2001**, *123*, 5892–5899; d) spirotryprostatin B: L. E. Overman, M. D. Rosen, *Angew. Chem.* **2000**, *112*, 4768–4771; *Angew. Chem. Int. Ed.* **2000**, *39*, 4596–4599.

[2] For a review of catalytic asymmetric methods that generate quaternary stereocenters, see: a) E. J. Corey, A. Guzman-Perez, *Angew. Chem.* **1998**, *110*, 402–415; *Angew. Chem. Int. Ed.* **1998**, *37*, 388–401; see also: b) J. Christoffers, A. Mann, *Angew. Chem.* **2001**, *113*, 4725–4732; *Angew. Chem. Int. Ed.* **2001**, *40*, 4591–4597.

[3] For example, the intramolecular asymmetric Heck reaction has proved to be useful; for leading references, see: a) A. D. Lebsack, J. T. Link, L. E. Overman, B. A. Stearns, *J. Am. Chem. Soc.* **2002**, *124*, 9008–9009; b) Y. Donde, L. E. Overman in *Comprehensive Asymmetric Catalysis*; (Eds.: E. N. Jacobsen, A. Pfaltz, H. Yamamoto), Springer, New York, **1999**, pp. 675–697.

[4] a) T. H. Black, S. M. Arrivo, J. S. Schumm, J. M. Knobeloch, *J. Chem. Soc. Chem. Commun.* **1986**, 1524–1525; b) T. H. Black, S. M. Arrivo, J. S. Schumm, J. M. Knobeloch, *J. Org. Chem.* **1987**, *52*, 5425–5430.

[5] For the correct structural assignment of diazonamide A, see: a) J. Li, A. W. G. Burgett, L. Esser, C. Amezcua, P. G. Harran, *Angew. Chem.* **2001**, *113*, 4906–4909; *Angew. Chem. Int. Ed.* **2001**, *40*, 4770–4773; for an overview of diazonamide chemistry, see: b) T. Ritter, E. M. Carreira, *Angew. Chem.* **2002**, *114*, 2601–

 © 2003 Wiley-VCH Verlag GmbH & Co. KGaA, Weinheim

2606; *Angew. Chem. Int. Ed.* **2002**, *41*, 2489 – 2495; for the total synthesis of the corrected structure of diazonamide A, see: c) K. C. Nicolaou, M. Bella, D. Y.-K. Chen, X. Huang, T. Ling, S. A. Snyder, *Angew. Chem.* **2002**, *114*, 3645 – 3649; *Angew. Chem. Int. Ed.* **2002**, *41*, 3495 – 3499; K. C. Nicolaou, P. Bheema Rao, J. Hao, M. V. Reddy, G. Rassias, X. Huang, D. Y.-K. Chen, S. A. Snyder, *Angew. Chem.* **2003**, *115*, 1795 – 1800; *Angew. Chem. Int. Ed.* **2003**, *42*, 1753 – 1758.

[6] C. J. Moody, K. J. Doyle, M. C. Elliott, T. J. Mowlem, *J. Chem. Soc. Perkin Trans. 1* **1997**, 2413 – 2419.

[7] E. Vedejs, J. Wang, *Org. Lett.* **2000**, *2*, 1031 – 1032.

[8] For an early overview, see: a) G. C. Fu, *Acc. Chem. Res.* **2000**, *33*, 412 – 420; for intra- and intermolecular *C*-acylation reactions, see: b) J. C. Ruble, G. C. Fu, *J. Am. Chem. Soc.* **1998**, *120*, 11532 – 11533; A. H. Mermerian, G. C. Fu, *J. Am. Chem. Soc.* **2003**, *125*, 4050 – 4051; for additional applications, see: c) S. Arai, S. Bellemin-Laponnaz, G. C. Fu, *Angew. Chem.* **2001**, *113*, 240 – 242; *Angew. Chem. Int. Ed.* **2001**, *40*, 234 – 236; B. L. Hodous, G. C. Fu, *J. Am. Chem. Soc.* **2002**, *124*, 1578 – 1579.

[9] 2,2,2-Trichloro-1,1-dimethylethyl chloroformate is commercially available. The trichloro-*tert*-butoxycarbonyl group has been employed in kinetic resolutions of secondary alcohols by an *N*-acylated chiral derivative of DMAP: a) E. Vedejs, X. Chen, *J. Am. Chem. Soc.* **1996**, *118*, 1809 – 1810. Catalyst (−)-**2** affords essentially identical enantioselectivity as (−)-**1** (97% *ee*; same enantiomer of the product as (−)-**1**); we chose to focus our studies on catalyst **1**, since it is particularly stable.

[10] The absolute stereochemistry of the product of Table 2, entry 3 was determined by X-ray crystallography (see the Supporting Information); the other configurations were assigned by analogy.

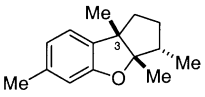
[11] General procedure: The substrate (1.00 equiv) and catalyst (−)-**1** (0.050 equiv) were added, exposed to the air, to a vial that contained a stirrer bar. The vial was sealed with a septum and purged with argon. CH_2Cl_2 ([substrate] = 1.0 M) was then added to the vial through a syringe, and the reaction mixture was heated at 35 °C for 48 h. The reaction mixture was then applied directly to a silica-gel column for purification by flash chromatography (typically, ~85% of the catalyst was recovered).

[12] The slight difference in enantiomeric excess between Table 1, entry 4 and Table 2, entry 1 is due to the difference in the scale of the reactions. See the Supporting Information for additional details.

[13] In preliminary studies, we selectively hydrolyzed (aqueous NaOH) and transesterified (NaOMe) the trichloro-*tert*-butyl ester group.

[14] The absolute stereochemistry of the product of Table 3, entry 1 was determined by X-ray crystallography (see the Supporting Information); the other configurations were assigned by analogy.

[15] We employed the product of Table 3, entry 3 in a formal total synthesis of debromoaplysin (I. D. Hills, unpublished results).



debromoaplysin

[16] Under our standard reaction conditions, the benzofuranone-derived substrates react more rapidly than do the oxindole-derived compounds.

[17] In the original studies of Black et al., a solid was generated under certain conditions and speculated to be the ion-pair intermediate. Unfortunately, the solid could not be characterized.[4]

[18] The quality of the crystal was sufficiently high to unambiguously assign the structure of the ion pair, but not sufficiently high to accurately determine bond lengths. CCDC-208287 contains the supplementary crystallographic data for **3**. These data can be obtained free of charge via www.ccdc.cam.ac.uk/conts/retrieving.html (or from the Cambridge Crystallographic Data Centre, 12, Union Road, Cambridge CB2 1EZ, UK; fax: (+44) 1223-336-033; or deposit@ccdc.cam.ac.uk).

[19] The *ee* of the product does not erode with time, indicating that *C*-acylation of the enolate is irreversible; ^{1}H NMR studies show that for the benzofuranone chemistry, the resting state of the catalyst is the *N*-acylated derivative, whereas for the oxindole chemistry, the resting state is the catalyst itself (not acylated).

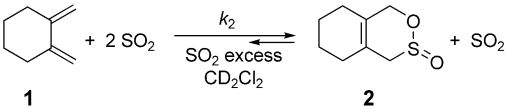
 © 2003 Wiley-VCH Verlag GmbH & Co. KGaA, Weinheim

Hetero-Diels–Alder Reaction

Equilibrium and Kinetic Deuterium Isotope Effects on the Hetero-Diels–Alder Addition of Sulfur Dioxide**

Frédéric Monnat, Pierre Vogel, Rubén Meana, and José A. Sordo**

At room temperature butadiene and alkyl-substituted 1,3-dienes that can adopt the *s-cis* conformation add to sulfur dioxide giving the corresponding sulfones (2,5-dihydrothiophene-1,1-dioxides),[1] which are about 10 kcal mol^{-1} more stable than the isomeric sultines (3,6-dihydro-1,2-oxathiin-2-oxides).[2][3] In the presence of acid catalysts and at temperatures below −40 °C the latter equilibrate with the 1,3-dienes, which results in hetero-Diels–Alder additions that are much faster than the corresponding cheletropic additions.[4] The hetero-Diels–Alder addition of 1,2-dimethylidenecyclohexane (**1**) to SO_2 does not require promotion by an acid [Eq. (1)]. However, we have demonstrated that the reaction is



1 **2** (1)

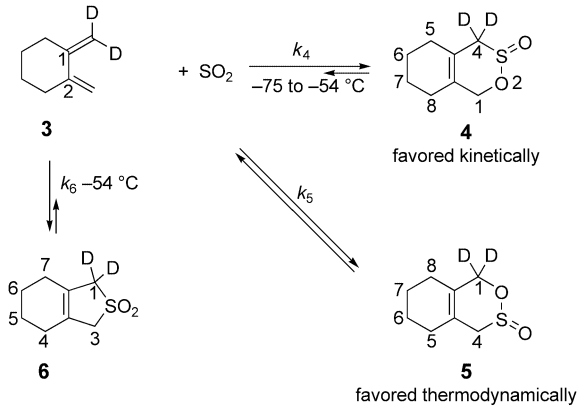
[*] Prof. Dr. P. Vogel, Dr. F. Monnat
Institute of Molecular and Biological Chemistry
Swiss Institute of Technology, BCH
1015 Lausanne-Dorigny (Switzerland)
Fax: (+41) 21-693-93-75
E-mail: pierre.vogel@epfl.ch.
Prof. Dr. J. A. Sordo, R. Meana
Laboratorio de Química Computacional
Departamento de Química Física y Analítica
Universidad de Oviedo
Oviedo, Principado de Asturias (Spain)
Fax: (+34) 98-523-78-50
E-mail: jasg@correo.uniovi.es

[**] This work was supported by the Swiss National Science Foundation, the Centro Svizzero di Calcolo Scientifica (Manno), the SOCRATES (Oviedo/EPFL) program, the Société Vaudoise des Sciences Naturelles (Lausanne), and DGI (BQU2001-3600-C02-01, Madrid, Spain).

Supporting information for this article is available on the WWW under http://www.angewandte.org or from the author.

 © 2003 Wiley-VCH Verlag GmbH & Co. KGaA, Weinheim DOI: 10.1002/anie.200351732

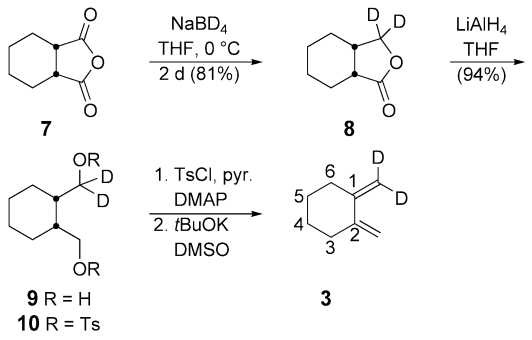
promoted by SO_2 itself (rate law of second order in $[SO_2]$).[5] The unstable sultine **2** resulting from that cycloaddition has been crystallized and analyzed by X-ray diffraction studies at −100 °C.[6] High-level quantum calculations[6,7] have suggested that the hetero-Diels–Alder addition of SO_2 to 1,2-dimethylidenecyclohexane is concerted and asynchronous, with the C–S bond formed to a greater extent than the C–O bond in the transition state. We confirm this hypothesis by measuring the kinetic deuterium isotope effect[8] of the reactions of **1** and its dideuterated derivative **3** with SO_2. Diene **3** equilibrates with the two regioisomeric adducts **4** and **5** (Scheme 1). The experimental kinetic isotope effects are



Scheme 1. The reaction of SO_2 with **3**.

compared with those estimated by quantum calculations. We have been able also to measure the deuterium isotope effect on the equilibrium **4**⇌**5** and have found that it is opposite to the kinetic deuterium isotope effect on the regioselectivity of the addition. This is the first example of Diels–Alder additions for which kinetic and equilibrium isotope effects are compared.

Diene **3** (98 % D_2) was prepared as outlined in Scheme 2, starting with the reduction of *cis*-cyclohexane-1,2-dicarboxylic anhydride (**7**) with one equivalent of $NaBD_4$ in THF at 0 °C. The resulting lactone **8** was reduced with $LiAlH_4$ to give diol **9**. Esterification with 4-toluenesulfonyl chloride (TsCl) gave **10**, which underwent double elimination of toluenesulfonic acid to provide **3** (26 % overall yield based on **7**).



Scheme 2. Synthesis of diene **3**. DMAP = dimethylaminopyridine, DMSO = dimethyl sulfoxide, pyr. = pyridine.

The rate laws $d[\mathbf{4}]/dt = k_4[\mathbf{3}][SO_2]^2$, $d[\mathbf{5}]/dt = k_5[\mathbf{3}][SO_2]^2$ (formation of regioisomeric sultines **4**, **5**), and $d[\mathbf{6}]/dt = k_6[\mathbf{3}][SO_2]^2$ (formation of sulfolene **6**) were followed between −75 and −54 °C and with a 10- to 40-fold excess of SO_2 in CD_2Cl_2. The third-order rate constants k_4, k_5, and k_6 are reported in Table 1. One finds a kinetic regioselectivity $k_4/k_5 = 1.11 \pm 0.01$ at −75 °C and 1.0798 ± 0.0003 at −54 °C. The thermodynamic

Table 1: Third-order rate constants [$M^2 s^{-1}$] determined by ^1H NMR spectroscopy with toluene as an internal reference.

T [K]	$k_4 \times 10^6$	$k_5 \times 10^6$	$k_6 \times 10^9$	k_4/k_5
198	2.13 ± 0.15	1.91 ± 0.13	76.9 ± 0.5	1.11 ± 0.001
219.1	4.03 ± 0.16	3.73 ± 0.15	338 ± 3	1.0798 ± 0.003

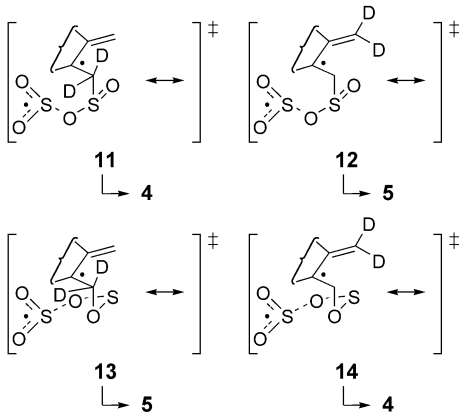
regioselectivity given by [**4**]/[**5**] could not be measured at −75 °C because equilibrium was reached too slowly. At −54 °C, however, it amounts to [**4**]/[**5**] = 0.73 ± 0.04 (no change in this product ratio after more than 300 h at −54 °C).

We have also measured the relative rate constants for the disappearance of dienes **1** and **3**. The ratio of rate constants $k_2/2k_4$ and $k_2/2k_5$ give the kinetic deuterium isotope effect for the formation of sultines **4** and **5**, respectively, where k_2 is the rate constant for the appearance of non-deuterated sultine **2**. This was done by following the reactions of a 1:1 mixture of dienes **1** and **3** ($[\mathbf{1}+\mathbf{3}] < 0.2$ M, 2.5–3 M SO_2 in CD_2Cl_2) at −75 °C by ^{13}C NMR spectroscopy (toluene as internal reference; because of the vicinal deuteration, the chemical shifts of C1 in **1** and **2** are different). The ratio $k_4/k_5 = 1.11 \pm 0.01$ (Table 1) led to $k_2/2k_4 = 0.89 \pm 0.04$ (k_H/k_D for the formation of **4**) and $k_2/2k_5 = 0.99 \pm 0.05$ (k_H/k_D for the formation of **5**) at −75 °C.

Equilibrium deuterium isotope effects have shown that C–D bonds at sp^3(C) centers are lower in energy than those at sp^2(C) centers .[9] It was thus expected that the transition structure **11** (in which the C–S bond is formed to a greater extent than the C–O bond) should be more stable than **12** and the corresponding transition structure arising from the non-deuterated dienes. On the contrary, if the C–O bond should be formed first, transition structure **13** is expected to be more stable than **14** and the transition structures of the SO_2 addition to **1** (Scheme 3). Our experimental data ($k_4/k_5 = 1.1$, $k_2/2k_4 = 0.89$, and $k_2/2k_5 = 0.99$ at −75 °C) are consistent only with transition structure **11**, as predicted by quantum calculations.[2] Although the calculations did not locate any intermediates along the reaction hypersurface of the hetero-Diels–Alder addition of butadiene $+2SO_2$,[5] we cannot exclude formally that **11** and **12** equilibrate with diradical or zwitterionic intermediates before the formation of sultines **4** and **5**, respectively.

Isotope effects were computed by means of the QUIVER program,[10] which employs the Bigeleisen–Mayer formulation[11] within the transition-state-theory approximation.[12] Scaling factors of 0.943 [MP2/6-31G(d)] and 0.9614 [B3LYP6-31G(d)] were used in the calculations.[13] The kinetic deuterium isotope effects calculated are reported in Table 2 for the hetero-Diels–Alder addition of **1**/**3** + $2SO_2$ and of butadiene (**15**)/1,1-dideuterobutadiene (**16**) + $2SO_2$ following concerted mechanisms.

 © 2003 Wiley-VCH Verlag GmbH & Co. KGaA, Weinheim



Scheme 3. Transition structures leading to products **4** and **5**.

Calculations predict smaller k_H/k_D values than those found experimentally, but the calculated kinetic regioselectivities k_4/k_5 are similar to the experimental values. This confirms that the C–S bond is formed to a greater extent than the C–O bond in the transition state of the hetero-Diels–Alder additions of sulfur dioxide (see Figure 1). Calculations made for the butadiene + SO_2 reaction predict the C–O bond to be formed to a greater extent in the transition state of the concerted mechanism. For the reaction involving a diradical intermediate $^{\bullet}OSOCH_2CH{=}CH_2CH_2^{\bullet}$ calculations lead to k_4/k_5 values much smaller than those observed (Table 3). Furthermore, the "energy of concert"[14] (the difference between the activation energies of the concerted and diradical transition states) is ca. 13 kcal mol^{-1} in favor of the concerted mechanism.

The theoretical prediction for the thermodynamic regioselectivity at the B3LYP6-31G(d) level of theory (0.758 and 0.718 for equilibria involving one and two molecules of SO_2, respectively) agrees rather well with the experimental measurements (0.73 ± 0.04).

The equilibrium deuterium isotope effect that renders **5** more stable than **4** can be interpreted in terms of the preference for dueterium to substitute at C–H moieties with the highest stretching vibration energy. In sultines **4** and **5** the acidifying effect of the S=O moiety makes the C4–H bond weaker than the C1–H bond. Thus deuterium prefers C1, rendering **5** more stable than **4**.The kinetic isotope effects are not dominated by the thermodynamic isotope effects (Dimroth principle: $\Delta H^{\neq} = \alpha \Delta H + \beta$), thus reinforcing the validity of the experimental test used here to define the asynchronous character of the concerted hetero-Diels–Alder additions of SO_2.[14]

Table 2: Calculated kinetic deuterium isotope effects for concerted hetero-Diels–Alder additions.

Reaction	Ratio	T [°C]		
		−75	−54	+25
1/3 + $2SO_2 \rightarrow$ [**11**] $\rightarrow$ **4** + SO_2	k_H/k_D[a]	0.692	0.725	0.816[b]
		(0.714)	(0.746)	(0.830)[c]
1/3 + $2SO_2 \rightarrow$ [**12**] $\rightarrow$ **5** + SO_2 k'_H/k'_D[d]		0.776	0.801	0.869[b]
		(0.734)	(0.763)	(0.841)[c]
Kinetic regioselectivity[i]:			1.12	1.10	1.06
15/16 + $2SO_2 \rightarrow$ [**11′**] $\rightarrow$ **4′** + SO_2	k_H/k_D[e]	0.707	0.741	0.829[b,j]
		(0.673)	(0.709)	(0.806)[c]
		0.658	0.695	0.796[f]
		(0.755)	(0.785)	(0.865)[g]
15/16 + $2SO_2 \rightarrow$ [**12′**] $\rightarrow$ **5′** + SO_2	k'_H/k'_D[h]	0.693	0.729	0.824[b]
		(0.721)	(0.754)	(0.842)[c,k]
		0.748	0.780	0.861[f]
		(0.647)	(0.685)	(0.789[g]

[a] $k_H/k_D \triangleq k_1/2k_4$. [b] B3LYP6-31G(d). [c] B3LYP6-31G(d) for the reaction with only one equivalent of SO_2. [d] $k'_H/k'_D \triangleq k_1/2k_5$. [e] $k_H/k_D \triangleq$ butadiene + $2SO_2$ vs. 1,1-D_2-butadiene + $2SO_2$ giving a sultine analogous to **4**. [f] MP2/6-31G(d). [g] MP2/6-31G(d) for reaction with only one equivalent of SO_2. [h] $k'_H/k'_D \triangleq$ butadiene + $2SO_2$ vs. 1,1-D_2-butadiene + $2SO_2$ giving sultine analogous to **5**. [i] k'_H/k'_D(**5**)/k_H/k_D(**4**) and k'_H/k'_{DD}(**5′**)/k_H/k_D(**4′**); calculated (B3LYP6-31G(d) including zero-point energy). [j] Energy barrier: 4.8 kcal mol^{-1}. [k] Energy barrier: 12.2 kcal mol^{-1}.

Table 3: Calculated kinetic deuterium isotope effects for nonconcerted hetero-Diels–Alder addition of SO_2 + butadiene $\rightarrow$ [$^{\bullet}OSOCH_2CHCH$-$CH_2^{\bullet}$][a].

Reaction	Ratio	T [°C]		
		−75	−54	+25
15, **16** + $SO_2 \rightarrow$ **4′**	k_H/k_D[b]	1.086	1.075	1.046[c]
15, **16** + $SO_2 \rightarrow$ **5′**	k'_H/k'_{DD}[d]	0.568	0.610	0.727[c]
Kinetic regioselectivity[e]:		0.52	0.56	0.69

[a] Calculated (B3LYP6-31G(d)) energy barrier: 25.3 kcal mol^{-1}, relative stability of the diradical intermediate: 18.5 kcal mol^{-1}, second energy barrier: 19.1 kcal mol^{-1}. [b] $k_H/k_D = k$(**15** + SO_2)/k(**16** + $SO_2 \rightarrow$ **4′**). [c] B3LYP6-31G(d). [d] $k'_H/k'_{DD} = k$(**15** + SO_2)/k(**16** + $SO_2 \rightarrow$ **5′**). [e] Ratio $(k'_H/k'_{DD})/(k_H/k_D)$.

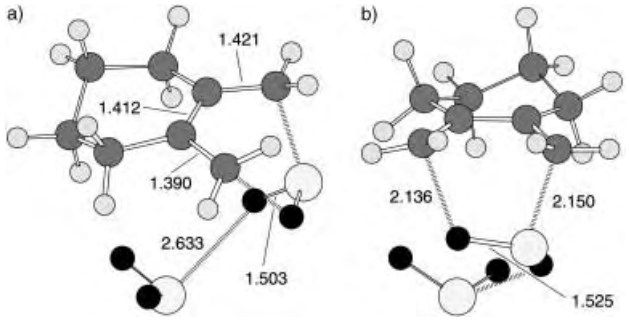


Figure 1. Calculated transition structure for the hetero-Diels–Alder addition **1** + $2SO_2$. a) Top view, b) side view. Large pale balls = sulfur, small black balls = oxygen, medium gray balls = carbon, small pale balls = hydrogen. Distances in Å.

Received: April 23, 2003 [Z51732]

Keywords: ab initio calculations · cycloaddition · heterocycles · isotope effects · sulfur dioxide

[1] G. de Bruin, *Proc. K. Ned. Akad. Wet.* **1914**, *17*, 585; H. J. Backer, J. Strating, *Recl. Trav. Chim. Pays-Bas* **1943**, *62*, 815.
[2] B. Deguin, P. Vogel, *J. Am. Chem. Soc.* **1992**, *114*, 9210; T. Fernández, D. Suárez, J. A. Sordo, F. Monnat, E. Roversi, A. Estrella de Castro, K. Schenk, P. Vogel, *J. Org. Chem.* **1998**, *63*, 9490; F. Monnat, P. Vogel, J. A. Sordo, *Helv. Chim. Acta* **2002**, *85*, 712.
[3] For early examples of hetero-Diels–Alder additions of SO_2, see: R. F. Heldeweg, H. Hogeveen, *J. Am. Chem. Soc.* **1976**, *98*, 2341; T. Durst, L. Tréteault-Ryan, *Tetrahedron Lett.* **1978**,

 © 2003 Wiley-VCH Verlag GmbH & Co. KGaA, Weinheim

2353; see also: J.-H. Liu, A.-T. Wu, M.-H. Huang, C.-W. Wu, W.-S. Chong, *J. Org. Chem.* **2000**, *65*, 3395.
[4] E. Roversi, F. Monnat, P. Vogel, K. Schenk, P. Roversi, *Helv. Chim. Acta* **2002**, *85*, 733; E. Roversi, R. Scoppelliti, E. Solari, R. Estoppey, P. Vogel, P. Braña, B. Menéndez, J. A. Sordo, *Chem. Eur. J.* **2002**, *8*, 1336.
[5] T. Fernández, J. A. Sordo, F. Monnat, B. Deguin, P. Vogel, *J. Am. Chem. Soc.* **1998**, *120*, 13276.
[6] D. Markovic, E. Roversi, R. Scoppelliti, P. Vogel, R. Meana, J. A. Sordo, *Chem. Eur. J.*, **2003**, in press..
[7] D. Suárez, T. L. Sordo, J. A. Sordo, *J. Am. Chem. Soc.* **1994**, *116*, 763; D. Suárez, T. L. Sordo, J. A. Sordo, *J. Org. Chem.* **1995**, *60*, 2848.
[8] For examples of kinetic deuterium isotope effects used to establish the synchronicity or asynchronicity of concerted Diels–Alder reactions: M. Taagepera, E. R. Thornton, *J. Am. Chem. Soc.* **1972**, *94*, 1168; J. J. Gajewski, K. B. Petersen, J. R. Kagel, Y. C. J. Huang, *J. Am. Chem. Soc.* **1989**, *111*, 9078; D. A. Singleton, S. R. Merrigan, B. R. Beno, K. N. Houk, *Tetrahedron Lett.* **1999**, *40*, 5817; D. A. Singleton, S. R. Merrigan, A. A. Thomas, *Tetrahedron Lett.* **1999**, *40*, 639; K. N. Houk, J. González, Y. Li, *Acc. Chem. Res.* **1995**, *28*, 81; N. Chronakis, M. Orfanopoulos, *Org. Lett.* **2001**, *3*, 545.
[9] J. J. Gajewski, N. D. Conrad, *J. Am. Chem. Soc.* **1979**, *101*, 6693.
[10] W. Saunders, K. E. Laidig, M. Wolfsberg, *J. Am. Chem. Soc.* **1989**, *111*, 8989.
[11] J. Bigeleisen, M. G. Mayer, *J. Chem. Phys.* **1947**, *15*, 261.
[12] K. J. Laidler, *Chemical Kinetics*, 3rd ed., Harper & Row, New York, **1987**.
[13] A. P. Scott, L. Radom, *J. Phys. Chem.* **1996**, *100*, 16502.
[14] For other studies on the hetero-Diels–Alder addition mechanisms, see e.g.: L. Kupczyk-Subotkowska, H. J. Shine, *J. Am. Chem. Soc.* **1993**, *115*, 5296; G. Orlova, J. D. Goddard, *J. Org. Chem.* **2001**, *66*, 4026; A. G. Leach, K. N. Houk, *J. Org. Chem.* **2001**, *66*, 5192; A. G. Leach, K. N. Houk, *Chem. Commun.* **2002**, 1243.

 © 2003 Wiley-VCH Verlag GmbH & Co. KGaA, Weinheim

Asymmetric Allylation

Catalytic Asymmetric Allylation of Hydrazono Esters in Aqueous Media by Using ZnF_2–Chiral Diamine**

*Tomoaki Hamada, Kei Manabe, and Shū Kobayashi**

Over the past several years, highly efficient methods for enantioselective addition to C=N double bonds by chiral Lewis acid catalysts have been developed.[1] Among them, enantioselective addition of allylmetal reagents to imino compounds[2] provides a useful route to optically active homoallylic amines, which are important building blocks in organic synthesis as the γ,δ-double bonds of homoallylic amines can be readily converted into many different functional groups. In spite of the synthetic utility of optically active homoallylic amines, however, examples of catalytic asymmetric allylation of imino compounds are limited.

Recently, we reported catalytic asymmetric Mannich-type reactions of acylhydrazono esters in H_2O/THF by using a combination of a stoichiometric amount of zinc fluoride and a catalytic amount of a chiral diamine and TfOH (TfOH = Trifluoromethanesulfonic acid).[3] Acylhydrazones are imine surrogates more stable than imines even in aqueous media.[4] Furthermore, hydrazines, such as the products in the Mannich reaction or allylation are interesting compounds, not only because hydrazines themselves can be used as unique building blocks,[5] but also because, if the N–N bond can be cleaved, amines are obtained. Accordingly, asymmetric allylation of hydrazones is considered to be a versatile methodology, although there are no examples of a catalytic version.[6] Herein, we describe the first catalytic asymmetric allylation of acylhydrazones, especially acylhydrazono esters. The reactions proceeded smoothly by using a chiral Zn catalyst in aqueous media.

We focused on allyltrimethoxysilane as an allylating agent,[7,8] because it can form a pentacoordinate silicate easily,[9] and is a preferable reagent compared with allyltin compounds from the standpoint of toxicity. As a chiral catalyst system, we initially used the combination of ZnF_2[10] (100 mol%), diamine **1** (10 mol%), and TfOH (1 mol%), which was effective for the previous Mannich-type reaction. The reaction of hydrazono ester **2** with allyltrimethoxysilane was conducted in H_2O/THF (1:9), to afford the corresponding allylated product **3** in moderate yield with a relatively high *ee* value (Table 1, entry 1). Interestingly, it was found that TfOH, which was essential in the Mannich-type reaction, was not needed in the allylation reaction (Table 1, entry 2). Moreover, even when only 20 mol% of ZnF_2 was used, the allylation proceeded with a good yield (Table 1, entry 3), although more than 50 mol% of ZnF_2 was necessary to achieve high yields in the Mannich-type reaction. These results indicate that a catalytic amount of the fluoride anion is sufficient for the allylation, while a stoichiometric amount of the fluoride anion is needed in the Mannich-type reaction. The fluoride anion is considered to be a key in this reaction, as $Zn(OTf)_2$ gave no product (Table 1, entry 5). Furthermore, it was found that **1** accelerated the reaction significantly[11] (Table 1, compare entries 2 and 6). From these results, it is concluded that the reaction mechanism including the catalytic cycle of the present asymmetric allylation may be different from that of the previous Mannich-type reaction.

We speculate that this reaction proceeds with double activation[12,13] in which Zn^{2+} acts as a Lewis acid to activate **2** and, at the same time, the fluoride anion acts as a Lewis base to attack the silicon atom of allyltrimethoxysilane. In other words, the zinc amide and $(MeO)_3SiF$ are formed first, and subsequent hydrolysis of the amide affords allylated product **3**

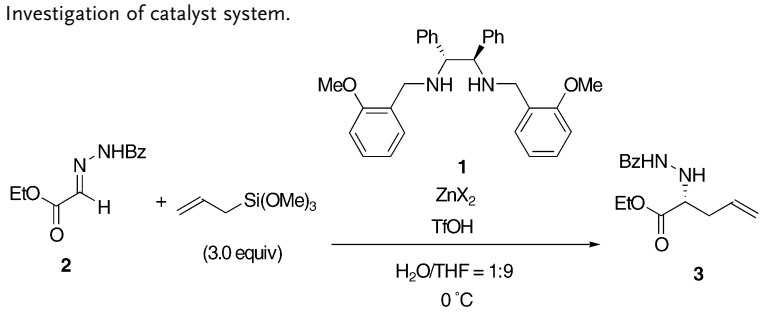
[*] Prof. Dr. S. Kobayashi, T. Hamada, Prof. Dr. K. Manabe
Graduate School of Pharmaceutical Sciences
The University of Tokyo
Hongo, Bunkyo-ku, Tokyo 113-0033 (Japan)
Fax: (+81) 3-5684-0634
E-mail: skobayas@mol.f.u-tokyo.ac.jp

[**] This work was partially supported by CREST and SORST, Japan Science and Technology Corporation (JST), and a Grant-in-Aid for Scientific Research from Japan Society of the Promotion of Science. T.H. thanks the JSPS fellowship for Japanese Junior Scientists.

Supporting information for this article is available on the WWW under http://www.angewandte.org or from the author.

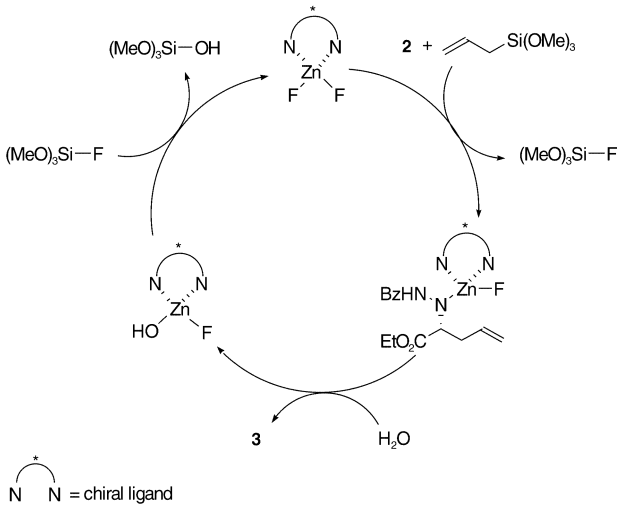
 DOI: 10.1002/anie.200351778 © 2003 Wiley-VCH Verlag GmbH & Co. KGaA, Weinheim

Table 1: Investigation of catalyst system.



Entry	ZnX_2 [mol%]	**1** [mol%]	TfOH [mol%]	*t* [h]	Yield [%]	*ee* [%][a]
1	ZnF_2 (100)	10	1	20	46	75
2	ZnF_2 (100)	10	0	20	51	76
3	ZnF_2 (20)	10	0	90	77	75
4	ZnF_2 (10)	12	0	36	33	74
5	$Zn(OTf)_2$ (10)	12	0	36	0	–
6	ZnF_2 (100)	0	0	20	2	–

[a] The absolute configuration is assumed to be *R* (see [5]).



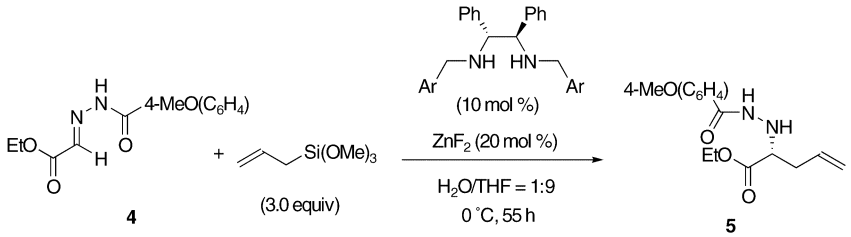
Scheme 1. Proposed reaction mechanism.

and Zn(OH)F (Scheme 1). It is considered that a catalytic amount of the fluoride anion gives a good yield in this reaction probably because catalytic turnover of the fluoride anion occurs. This apparently means that the Si–F bond of $(MeO)_3SiF$ is hydrolyzed by Zn(OH)F, regenerating ZnF_2. To elucidate this mechanism, we investigated the ability of $(MeO)_3SiF$ to regenerate ZnF_2 from Zn(OH)F. In fact, the reaction of **2** with allyltriethoxysilane did not proceed in the presence of Zn(OH)F[14] (100 mol%) and **1** (10 mol%) in H_2O/THF = 1:9 at 0 °C for 20 h. When $(EtO)_3SiF$ (100 mol%) was added, however, the reaction proceeded, and **3** was obtained in similar yield and selectivity to that of the reaction with ZnF_2 (33% yield, 76% *ee*, compare with Table 1, entry 2). These results indicate that the exchange of the fluoride anion between Zn(OH)F and $(EtO)_3SiF$ regenerates ZnF_2, which is active to catalyze the reaction.

Next, we examined the effect of chiral diamines on the enantioselectivity in the reaction of 4-methoxybenzoylhydrazone **4**.[15] Diamine **6**[16] without the methoxy group on the aromatic ring of **1** gave lower yield and *ee* (Table 2, entry 2). When **7** was employed, the yield was low, while the same *ee* value was obtained as that in the reaction with **1** (Table 2, entry 3). Diamine **8** afforded comparable yield and *ee* value to **1**, although **9** gave a disappointing result (Table 2, entries 4 and 5). The above results indicate that the MeO group in the chiral diamine ligand plays an essential role for attaining high yields and selectivities. Among the diamines examined in Table 2, **12** gave the highest *ee* value (Table 2, entry 8).

Several examples of the allylation reactions are shown in Table 3. The reactions were conducted in the presence of ZnF_2 (20 mol%) and a chiral diamine (10 mol%) in H_2O/THF (1:9) at 0 °C. When 4-methoxybenzoylhydrazone derived from methyl glyoxylate was used as a substrate, the *ee* value was slightly improved (Table 3, entries 1 and 2). An improvement in the yield was observed when the reaction of 4-ethoxybenzoylhydrazone derived from ethyl glyoxylate was performed (Table 3, entries 3 and 4). The reactions of 2-substituted allylsilanes gave the desired products with moderate to good yields and selectivities (Table 3, entries 5 and 6).

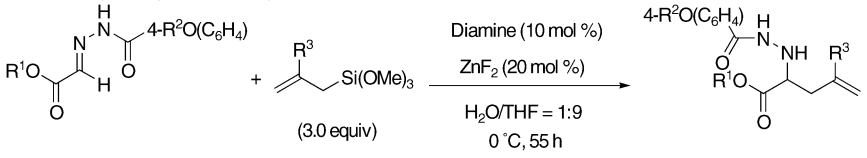
Table 2: Effect of chiral diamines.



Entry	Ar	Yield [%]	*ee* [%]
1	2-MeO-C_6H_4 (**1**)	84	81
2	C_6H_5 (**6**)	29	48
3	2-Me-C_6H_4 (**7**)	26	83
4	2,5-$(MeO)_2$-C_6H_3 (**8**)	81	76
5	3,5-$(MeO)_2$-C_6H_3 (**9**)	27	31
6	2-MeO-5-*t*Bu-C_6H_3 (**10**)	99	64
7	1-MeO-2-naphthyl (**11**)	19	70
8	8-MeO-2-naphthyl (**12**)	59	84

 © 2003 Wiley-VCH Verlag GmbH & Co. KGaA, Weinheim

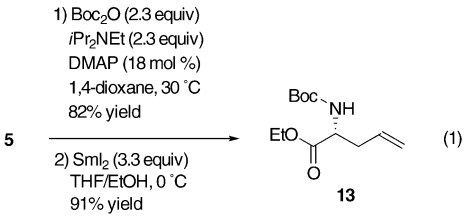
Table 3: Catalytic asymmetric allylation.



Entry	R^1	R^2	R^3	Diamine	Yield [%]	*ee* [%]
1	Me	Me	H	**1**	61	83
2[a]	Me	Me	H	**12**	60	86
3	Et	Et	H	**1**	92	81
4	Et	Et	H	**12**	81	85
5	Et	Et	Me	**1**	88	65
6[b]	Et	Et	Ph	**1**	62	78

[a] 96 h. [b] 162 h.

To highlight the importance of the allylated products obtained in this reaction, **5** (84% *ee*) was converted into synthetically important *N*-Boc (Boc = 1,1-dimethylethoxycarbonyl) α-amino acid **13** [Eq. (1)]; DMAP = 4-dimethylamino pyridine. N-Boc protection of **5** afforded *N*-Boc hydrazine[17]



in 82% yield, and the N–N bond of the hydrazine was cleaved with SmI_2[18] to afford **13** in 91% yield without significant loss of the enantiomeric purity.[19] Thus, this allylation reaction has been shown to be a versatile method to obtain not only the optically active α-amino ester hydrazine analogues but also *N*-protected α-amino esters.

(DMAP = N,N-dimethyl 1,3-propanediamine). Another important aspect of the present catalytic asymmetric allylation is that the reactions proceed smoothly in aqueous media. Recently, organic reactions in aqueous media have attracted a great deal of attention,[20] because water is a clean and safe solvent. In addition, the drying of substrates and solvents by dehydration is not required, and unique reactivities and selectivities are often observed by using water as a solvent. However, catalytic asymmetric carbon–carbon bond-forming reactions in aqueous media are extremely difficult to attain, because most chiral catalysts are not stable in the presence of even a small amount of water.[21] However, water plays a key role to obtain the product in the present allylation. Namely, it was shown that the reaction of **2** with allyltrimethoxysilane did not proceed at all in THF without water or MeOH/THF (1:9) in the presence of ZnF_2 (100 mol%) and **1** (10 mol%) at 0°C for 20 h.

In summary, the asymmetric allylation of acylhydrazono esters in aqueous media has been achieved by using a catalytic amount of ZnF_2 and a chiral diamine ligand. This reaction is the first example of catalytic asymmetric allylation of hydrazones. Furthermore, it should be noted that the catalytic asymmetric allylation to the C=N bond in aqueous media is unprecedented. Further investigations involving elucidation of the detailed reaction mechanism are currently in progress.

Received: April 30, 2003 [Z51778]

Keywords: allylation · asymmetric synthesis · fluorides · zinc

[1] a) S. Masumoto, H. Usuda, M. Suzuki, M. Kanai, M. Shibasaki, *J. Am. Chem. Soc.* **2003**, *125*, 5634; b) N. S. Josephsohn, M. L. Snapper, A. H. Hoveyda, *J. Am. Chem. Soc.* **2003**, *125*, 4018; c) S. Kobayashi, R. Matsubara, Y. Nakamura, H. Kitagawa, M. Sugiura, *J. Am. Chem. Soc.* **2003**, *125*, 2507; d) A. G. Wenzel, E. N. Jacobsen, *J. Am. Chem. Soc.* **2002**, *124*, 12964; e) S.-I. Murahashi, Y. Imada, T. Kawakami, K. Harada, Y. Yonemushi, N. Tomita, *J. Am. Chem. Soc.* **2002**, *124*, 2888; f) S. Kobayashi, H. Ishitani, *Chem. Rev.* **1999**, *99*, 1069, and references therein; g) A. E. Taggi, A. M. Hafez, T. Lectka, *Acc. Chem. Res.* **2003**, *36*, 10, and references therein.

[2] a) H. Nakamura, K. Nakamura, Y. Yamamoto, *J. Am. Chem. Soc.* **1998**, *120*, 4242; b) D. Ferraris, T. Dudding, B. Young, W. J. Drury III, T. Lectka, *J. Org. Chem.* **1999**, *64*, 2168; c) K. Nakamura, H. Nakamura, Y. Yamamoto, *J. Org. Chem.* **1999**, *64*, 2614; d) X. Fang, M. Johannsen, S. Yao, N. Gathergood, R. G. Hazell, K. A. Jørgensen, *J. Org. Chem.* **1999**, *64*, 4844; e) T. Gastner, H. Ishitani, R. Akiyama, S. Kobayashi, *Angew. Chem.* **2001**, *113*, 1949; *Angew. Chem. Int. Ed.* **2001**, *40*, 1896.

[3] S. Kobayashi, T. Hamada, K. Manabe, *J. Am. Chem. Soc.* **2002**, *124*, 5640.

[4] a) S. Kobayashi, T. Hamada, K. Manabe, *Synlett* **2001**, 1140; b) H. Oyamada, S. Kobayashi, *Synlett* **1998**, 249; c) K. Manabe, H. Oyamada, K. Sugita, S. Kobayashi, *J. Org. Chem.* **1999**, *64*, 8054.

[5] Hydrazine and its Derivatives in *Kirk-Othmer Encyclopedia of Chemical Technology, Vol. 13*, Wiley, New York, 4th ed., **1995**.

[6] Quite recently, we have developed asymmetric allylation of acylhydrazones with allyltrichlorosilanes using 3 equiv of chiral sulfoxide in dichloromethane. S. Kobayashi, C. Ogawa, H. Konishi, M. Sugiura, *J. Am. Chem. Soc.* **2003**, *125*, 6610.

[7] For early examples with allyltrimethoxysilane in organic synthesis, see: a) G. Cerveau, C. Chuit, R. J. P. Corriu, C. Reye, *J. Organomet. Chem.* **1987**, *328*, C17; b) A. Hosomi, S. Kohra, Y. Tominaga, *J. Chem. Soc. Chem. Commun.* **1987**, 1517; c) K. Sato, M. Kira, H. Sakurai, *J. Am. Chem. Soc.* **1989**, *111*, 6429.

[8] For catalytic allylation by using a combination of metal fluoride and allyltrimethoxysilane, see: a) A. Yanagisawa, H. Kageyama, Y. Nakatsuka, K. Asakawa, Y. Matsumoto, H. Yamamoto, *Angew. Chem.* **1999**, *111*, 3916; *Angew. Chem. Int. Ed.* **1999**, *38*, 3701; b) S. Yamasaki, K. Fujii, R. Wada, M. Kanai, M. Shibasaki, *J. Am. Chem. Soc.* **2002**, *124*, 6536; c) N. Aoyama, T. Hamada, K. Manabe, S. Kobayashi, *Chem. Commun.* **2003**, 676.

[9] Review: C. Chuit, R. J. P. Corriu, C. Reye, J. C. Young, *Chem. Rev.* **1993**, *93*, 1371.

[10] The results of the reaction of **2** with allyltrimethoxysilane in the presence of several metal fluorides (10 mol%) and **1** (12 mol%) in H_2O/THF (1:9) at 0°C for 48 h: ZnF_2, 40% yield, 73% *ee*; CdF_2, 49% yield, 5% *ee*; AgF, 93% yield, 1% *ee* (20 h); No reaction occurred with CuF_2 and ScF_3.

 © 2003 Wiley-VCH Verlag GmbH & Co. KGaA, Weinheim

[11] Quite recently, we reported that the ligand acceleration was observed in the allylation of carbonyl compounds by using allyltrimethoxysilane in aqueous media. See reference [8c].
[12] For a similar type of double activation, see: a) S. Kobayashi, H. Uchiro, I. Shiina, T. Mukaiyama, *J. Am. Chem. Soc.* **1991**, *113*, 4247; b) D. R. Gauthier, Jr., E. M. Carreira, *Angew. Chem.* **1996**, *108*, 2521; *Angew. Chem. Int. Ed. Engl.* **1996**, *35*, 2363.
[13] Diastereoselective allylsilane additions to acylhydrazones with double activation by fluoride and $In(OTf)_3$ have been reported. G. K. Friestad, H. Ding, *Angew. Chem.* **2001**, *113*, 4623; *Angew. Chem. Int. Ed.* **2001**, *40*, 4491.
[14] O. K. Srivastava, E. A. Secco, *Can. J. Chem.* **1967**, *45*, 579.
[15] 4-Methoxybenzoylhydrazone derived from ethyl glyoxylate afforded higher yield and *ee* (69% yield, 81% *ee*) than benzoylhydrazone did (51% yield, 76% *ee*) in the reaction with allyltrimethoxysilane in the presence of ZnF_2 (100 mol%) and **1** (10 mol%) in H_2O/THF (1:9) at 0°C for 20 h.
[16] A. Alexaxis, P. Mangeney, *Advanced Asymmetric Synthesis* (Ed.: G. R. Stephenson), Chapman & Hall, London, **1996**, p. 93, and references therein.
[17] This compound was highly crystalline, and one recrystallization from ethyl acetate/hexane afforded the enantiomerically almost pure material (from 70% *ee* to 98% *ee*).
[18] M. J. Burk, J. E. Feaster, *J. Am. Chem. Soc.* **1992**, *114*, 6266.
[19] The absolute configuration and the *ee* of **13** were determined by HPLC analysis after **13** had been converted to the corresponding *N*-tosylate (81% *ee*), which was reported by Jørgensen et al. See reference [2d].
[20] a) *Organic Synthesis in Water* (Ed.: P. A. Grieco), Blackie Academic and Professional, London, **1998**; b) C.-J. Li, T.-H. Chan, *Organic Reactions in Aqueous Media*, Wiley, New York, **1997**.
[21] a) D. Sinou, *Adv. Synth. Catal.* **2002**, *344*, 221; b) U. M. Lindström, *Chem. Rev.* **2002**, *102*, 2751; c) K. Manabe, S. Kobayashi, *Chem. Eur. J.* **2002**, *8*, 4094.

 © 2003 Wiley-VCH Verlag GmbH & Co. KGaA, Weinheim

Mesoporous Silica/Carbon Replicas

Synthesis of Large-Pore $Ia\bar{3}d$ Mesoporous Silica and Its Tubelike Carbon Replica**

*Shunai Che, Alfonso E. Garcia-Bennett, Xiaoying Liu, Robert P. Hodgkins, Paul A. Wright, Dongyuan Zhao, Osamu Terasaki, and Takashi Tatsumi**

Following the designed synthesis of mesoporous silica materials, such as MCM-41 and MCM-48 with small pore sizes (2–4 nm),[1] which are templated by quaternary ammonium cationic surfactants with different chain lengths, numerous ordered large-pore (8–30 nm) mesoporous silicas, such as SBA-15 and SBA-16,[2] have been synthesized by using block-copolymer nonionic surfactants as templates. Recently, a series of ordered rodlike mesoporous carbon materials have been synthesized by using mesoporous silica materials with a large range of pore diameters, such as MCM-48 and SBA-15, as hard templates.[3] Furthermore, it has been reported that new two-dimensional hexagonal mesoporous carbon materials with connected tubelike pores can be synthesized with large-pore mesoporous silica SBA-15.[4]

The mesoporous material, with a bicontinuous cubic structure of $Ia\bar{3}d$ symmetry, is one of the most interesting materials among the varied mesoporous silica materials reported to date. The independent and intricately interwoven three-dimensional networks of mesoporous channels are much more attractive for use as adsorbents and catalyst supports than the two-dimensional channels of hexagonal mesoporous silica MCM-41 and SBA-15. In spite of the recent discovery of large-pore cubic $Ia\bar{3}d$ mesoporous silica,[5a–c] the hydrothermal method for synthesizing a highly ordered material has not been fully developed. Therefore, the devel-

[*] Prof. Dr. T. Tatsumi, Dr. S. Che
Division of Materials Science & Chemical Engineering
Faculty of Engineering, Yokohama National University
79-5 Tokiwadai, Yokohama 240-8501 (Japan)
Fax: (+81) 45-339-3943
E-mail: ttatsumi@ynu.ac.jp

A. E. Garcia-Bennett, Prof. Dr. O. Terasaki
Arrhenius Laboratory
Stockholm University, 10691 Stockholm (Sweden)

X. Liu, Prof. Dr. D. Zhao
Laboratory of Molecular Catalysis and Innovative Materials
Department of Chemistry, Fudan University
Shanghai 200433 (P.R. China)

R. P. Hodgkins, Dr. P. A. Wright
School of Chemistry, The University of St. Andrews
St. Andrews, Fife KY16 9ST (UK)

[**] The authors are grateful to Makoto Watanabe (Hitachi Science System) and Yasushi Nakaizumi (Hitachi High-Technologies Corporation) for scanning electron micrography. S.C. thanks Prof. S. Iijima and Dr. M. Yudasaka (ICORP-JST) for their advice and comments. S.C. thanks the Japan Society for the Promotion of Science for a postdoctoral fellowship. X.Y.L. and D.Y.Z. thank NSFC support (No. 29925309 and 20173012). T.T. thanks Grant-in-aid for Priority Areas Research (No. 13134101) from the Ministry of Education, Culture, Sports, Science and Technology.

 © 2003 Wiley-VCH Verlag GmbH & Co. KGaA, Weinheim DOI: 10.1002/anie.200351752

opment of a controlled method for thermally and hydrothermally synthesizing stable, large-pore mesoporous silica materials with cubic $Ia\bar{3}d$ symmetry would seem to be important. The synthesis of rodlike mesoporous carbon monoliths with bicontinuous cubic $Ia\bar{3}d$ symmetry[5d] has been reported. However, to date, the synthesis of a tubelike mesoporous carbon with a bicontinuous cubic $Ia\bar{3}d$ structure has not been reported. Such novel architectures are of great technological interest for the development of advanced catalysts, adsorbents, and electrochemical systems.

In this paper, we present a hydrothermal synthetic route towards high-quality large-pore mesoprous silica with a cubic $Ia\bar{3}d$ structure by co-condensation of tetraethoxysilane (TEOS) and 3-mercaptopropyltrimethoxysilane (MPTS) using a block-copolymer surfactant as a template. We have developed a novel synthesis route to highly ordered mesoporous carbon using propylsulfonic acid groups anchored onto the silica wall,[6] which act as an acid catalyst for carbon-source polymerization; this synthesis route was found to be an excellent and simple method for carbonizing the carbon source. The acid catalyst can be obtained by a direct synthetic method, and the acidity can be controlled over a wide range, as compared with aluminosilicates. More importantly, tubelike mesoporous carbon materials with a bicontinuous cubic structure of $Ia\bar{3}d$ symmetry were synthesized by using the highly ordered large-pore silica as a hard template. This is the first report on the synthesis of a tubelike mesoporous carbon replica of a cubic mesoporous material. Selected structural properties of the silica templates and its tubelike carbon replicas are listed in Table 1.

Figure 1 A shows XRD patterns of the as-synthesized, extracted, oxidized, and neutralized materials obtained from the starting mixture of Pluronic P123 (4.0 g), TEOS (0.0394 mol), MPTS (0.0035 mol), HCl (0.08 mol), and H_2O (5.8 mol). To obtain the stable mesophase, the starting mixture was heated to 373 K for 48 h. All the samples showed two well-resolved sharp XRD diffraction peaks in the region of $2\theta = 0.5$–$1.5°$, which correspond to 211 and 220 reflections, based on the cubic system.[3a,7] The bicontinuous

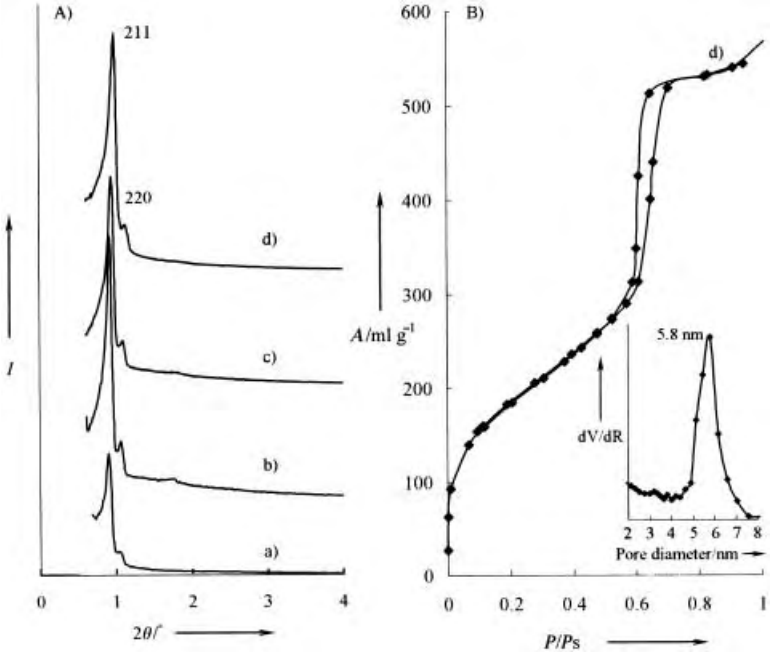


Figure 1. A) XRD patterns of the large-pore mesoporous silica with cubic $Ia\bar{3}d$ structure: a) as-synthesized, b) after extraction, c) after oxidation, and d) after neutralization with NH_4OH; B) nitrogen adsorption–desorption isotherm and pore-size distribution for material after neutralization (I = relative intensity).

cubic $Ia\bar{3}d$ symmetry was confirmed by combining the XRD pattern with SEM and HRTEM images, as shown below. After extracting, oxidizing, and neutralizing treatments, the high regularity of the pore arrangement was maintained, which indicates that this mesophase is very stable. In addition, the hydrothermal synthesis provided a large-pore cubic $Ia\bar{3}d$ silica with much improved structural integrity and thermal and hydrothermal stability. Figure 1 A shows that the three treatments were essentially unaccompanied by structural shrinkage. After the as-synthesized sample was calcined in air at 550 °C, the XRD patterns remained well-resolved despite a slight shrinkage. Very recently, Flodström synthesized the cubic $Ia\bar{3}d$ mesophase in the presence of NaI.[5c] In the course of our synthesis, which uses P123 as a template surfactant, it was found that the cubic $Ia\bar{3}d$ mesostructure could not be formed without MPTS, even when the synthesis conditions were varied over a wide range. Thus, such a mesostructure seems difficult to prepare without additives.

As can be seen in Figure 1 B, nitrogen adsorption–desorption isotherms for the silica template featured narrow capillary condensation steps, which indicate the high degree of pore-size uniformity. The mesoporous silica exhibited a unit cell size (a) of 22.5 nm, primary mesopore size (d_p) of 5.8 nm, and a wall thickness (b) of

Table 1: Properties of large-pore mesoporous silica with cubic $Ia\bar{3}d$ symmetry and its tube- and rodlike mesoporous carbon replicas.

Sample	Synthesis conditions		Unit cell a	S_{BET}[b]	V_p[c]	d_{BJH}[d]	b[d,e]
	FA/SiO_2	t [min][a]	[nm]	[$m^2 g^{-1}$]	[$mm^3 g^{-1}$]	[nm]	[nm]
Figure 1 (d)	–	–	22.5	740	791	5.8[f]	2.5[g]
Figure 2 (a_1)[h]	1.0	60	18.5	175	183	4.0[i]	–
Figure 2 (a_2)[j]	1.0	60	18.6	1421	1154	4.0	2.4
Figure 2 (b_1)[h]	2.4	–[j]	17.7	8.97	5.9	–	–
Figure 2 (b_2)[j]	2.4	–[j]	17.8	1324	734	–	2.4

[a] t = polymerization time. [b] Surface area calculated by the BET method. [c] Primary pore volume determined by using the high-resolution t-plot method. [d] Internal tube diameter calculated using the BJH method from the adsorption branch of the N_2 isotherm of the carbon replicas with silica walls. [e] Intertubular pore size; the pore was formed by removing the silica wall. [f] Pore diameter of mesoporous silica with cubic $Ia\bar{3}d$ symmetry. [g] Pore-wall thickness calculated by using an equation based on the pore volume.[8a] [h] Silica/carbon composite. [i] Pore diameter of silica/carbon composite. [j] Carbon material obtained after removing the silica wall. [k] Synthesized by a two-step FA polymerization and without evacuation.

 © 2003 Wiley-VCH Verlag GmbH & Co. KGaA, Weinheim

2.5 nm; the value of a is about twice that of MCM-48 synthesized using the longer quaternary ammonium cationic surfactant eicosyltrimethylammonium bromide ($(CH_3(CH_2)_{19}(CH_3)_3NBr$).[9]

Figure 2 shows scanning electron microscopy (SEM) images of the surfactant-extracted mesoporous silica. The samples were composed of particles that were uniform in shape (not shown); a typical morphology is shown in Figure 2a. The mesoporous silica particles in the SEM image suggest the growth of irregular shaped particles that display domains. The high-resolution SEM images of the apex reveal the regular pore distribution. The mesostructure was confirmed by EM observations to be bicontinuous with cubic $Ia\bar{3}d$ symmetry.

Figure 3A displays the XRD patterns of the mesoporous carbon replicas before and after removing the silica wall, which were synthesized by using sulfonic acid groups embedded in the silica wall as a catalyst. The tube- and rodlike mesoporous carbon materials were synthesized with different furfuryl alcohol (FA) to silica ratios and FA polymerization times (Table 1). Both samples synthesized with FA/silica ratios of 1.0 and 2.4 exhibited XRD patterns characteristic of the silica support used for their preparation. It has been reported that carbon replicas formed in an MCM-48 silica template of cubic $Ia\bar{3}d$ symmetry tend to undergo a transformation to cubic $I4_1/a$ symmetry as the template is removed. In this case, the structure of the carbon replicas were not altered upon removal the silica template. This result can be explained in terms of the presence of the micropores in the walls of the triblock-copolymer-templated materials, which make the replication of SBA-15 possible, and allow for the retention of the cubic $Ia\bar{3}d$ symmetry. The two carbon frameworks formed in the enantiometric channel systems of the silica with cubic $Ia\bar{3}d$ symmetry are likely to be connected to one another through the bridges formed in the micropores in the silica walls. In a similar manner to SBA-15,[4b] the intensity of the XRD pattern of the silica/carbon composite (before removal of the silica wall) decreased with an increase in the thickness of the carbon tubes formed within the silica channels (Figure 3 (a_1) and (b_1)) and vice versa for the carbon obtained by removing the silica wall (Figure 3 (a_2) and (b_2)). A more systematic study on the significant change in XRD intensity depending on the carbon thickness is ongoing, and the results will be reported elsewhere.

The nitrogen adsorption isotherms and the pore-size distribution of the silica/carbon composite (before removal of the silica wall) (Figure 3B) show that the inner diameter of the mesoporous carbon tube was 4.0 nm. For the carbon material obtained after

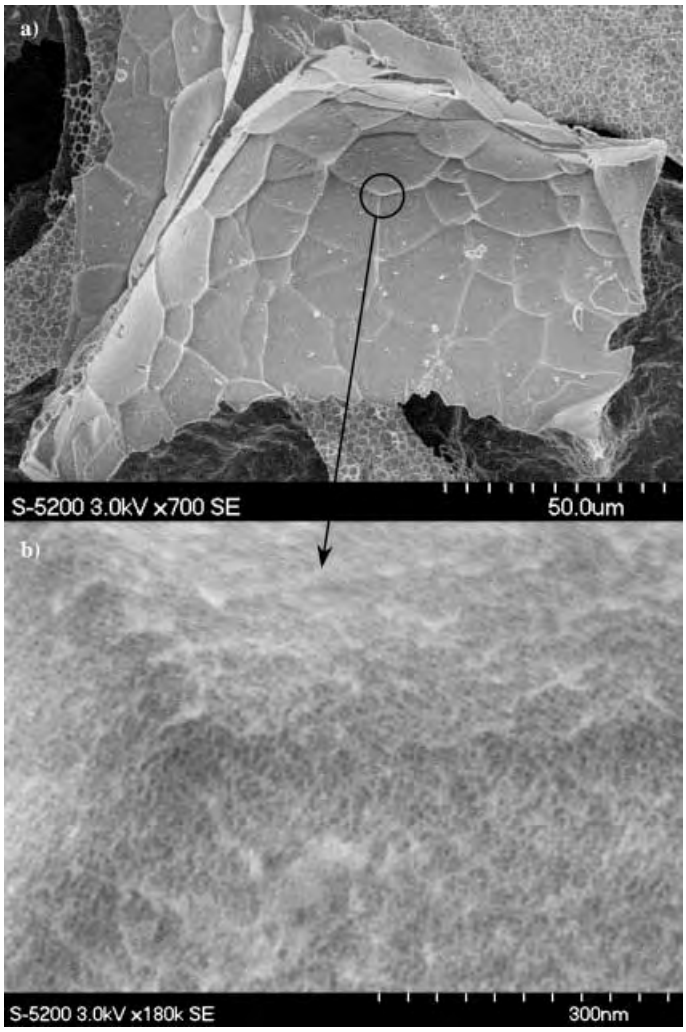


Figure 2. SEM images of mesoporous silica with a cubic $Ia\bar{3}d$ structure. Image b) shows the enlargement of the circled area in a).

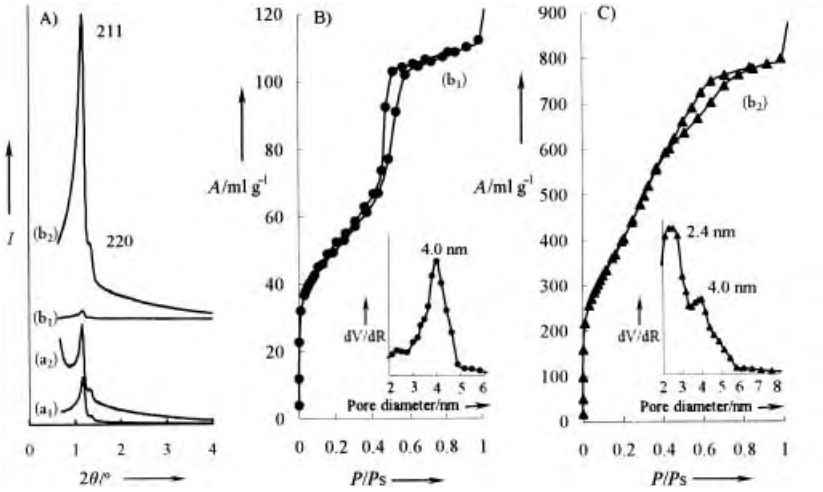


Figure 3. A) XRD patterns of silica/carbon composites (a_1) and (b_1) formed under different conditions (Table 1), and the resulting carbon materials (a_2) and (b_2) formed after removing the silica walls. B) and C) Nitrogen adsorption–desorption isotherms and pore-size distributions for carbon replicas before (B) and after (C) removing the silica wall (I = relative intensity; A = adsorbed amount).

 © 2003 Wiley-VCH Verlag GmbH & Co. KGaA, Weinheim

removing the silica wall, two capillary condensation steps were observed on the adsorption and desorption branches of the nitrogen isotherms in the pressure range of 0.1–0.3 and 0.4–0.6, which correspond to pore sizes of 2.4 and 4.0 nm (see inset of Figure 3C), respectively. The pore size of the silica/carbon composite is in agreement with the larger one of the carbon material, thus indicating that the mesoporous carbon replica, with pores of 4.0 nm inner diameter, and another pore system of 2.4 nm diameter that is formed between the tubes, was obtained by using cubic $Ia\bar{3}d$ mesostructured mesoprous silica with a pore diameter of 5.8 nm as the template. This result indicates that the thinnest possible tubes were 0.9 nm in wall thickness. In our previous work,[4b] we found that it was difficult to prepare carbon tubes with walls less than 1.6 nm thick by aluminosilicate-catalyzed FA polymerization. The mesostructure was not formed when the FA/silica ratio was smaller than 1.0, or when the polymerization time was shorter than 1 h, for the case where aluminosilicate acid was used as the catalyst of FA polymerization. Thus, much thinner carbon walls can be formed by sulfonic-acid-catalyzed FA polymerization. The silica/carbon composition synthesized with a higher (FA)/silica ratio of 2.4 and a two-step FA polymerization did not show any porosity (Table 1), which indicates that the rodlike mesoporous carbon material had been formed. Both carbon replica samples show the same morphology before and after removing the silica wall (not shown), which is a similar situation to that shown in Figure 2.

Figure 4 shows high-resolution transmission electron microscopy (HRTEM) images of the silica, silica/carbon composite, and tubelike mesoporous carbon materials obtained by removing the silica wall. The images show the structure of these materials parallel to the [111] direction. Insets show the corresponding Fourier diffractograms (FDs). The carbon materials synthesized with FA/silica ratios both higher and lower than 1.0 exhibit cubic $Ia\bar{3}d$ symmetry, identical to the silica template. However, we have not yet confirmed that the structure is tubular by TEM observation. A qualitative analysis of these and other images reveals differences in the contrast patterns before and after removal of the silica walls, with a reversal of contrast observed in the carbon replicas. Quantitative analysis of these contrast patterns is currently being conducted by means of Fourier analysis.[3c]

In conclusion, we have presented for the first time a hydrothermal synthesis route for stable large-pore mesoporous silica and its tubelike mesoporous carbon replica with a bicontinuous cubic structure displaying $Ia\bar{3}d$ symmetry, by using sulfonic acid incorporated into the silica during the synthesis step as a catalyst for carbon-source polymerization.

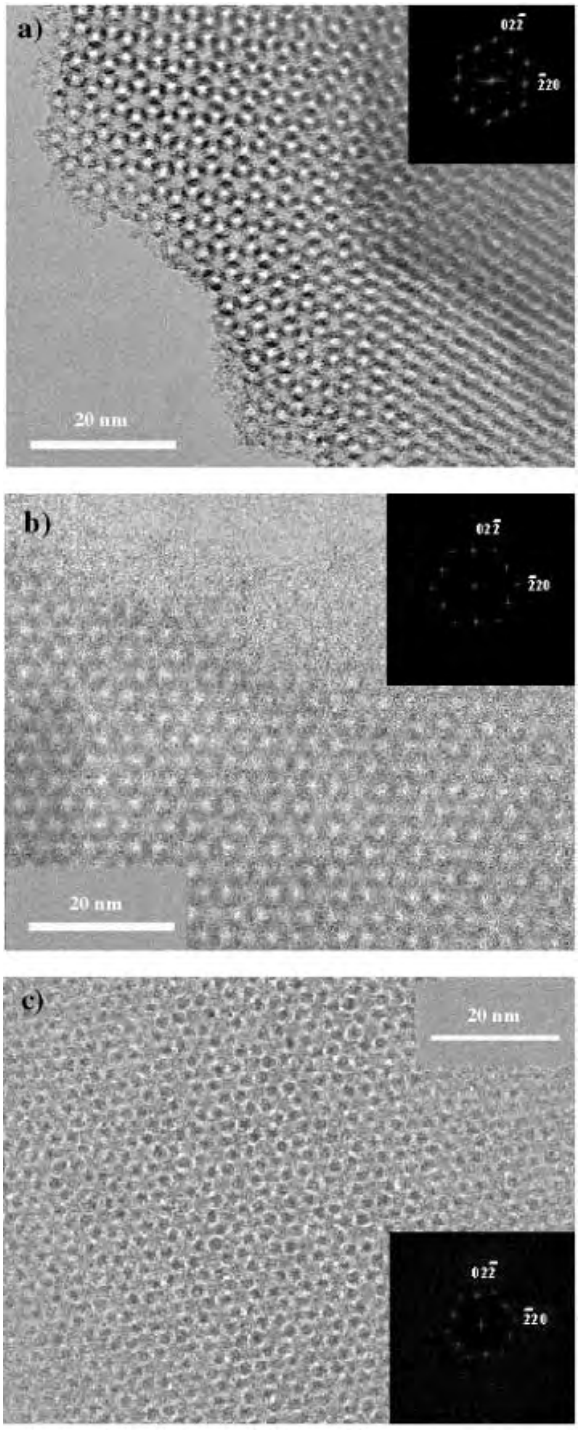


Figure 4. HRTEM images and their Fourier diffractograms of silica (a), a silica/carbon composite (b), and a tubelike mesoporous carbon replicas (c) with cubic $Ia\bar{3}d$ symmetry. The images were recorded along the [111] direction.

Experimental Section

Mesoporous silica with a cubic $Ia\bar{3}d$ mesostructure was synthesized by the co-condensation of TEOS and MPTS using triblock copolymer Pluronic P123 ($EO_{20}PO_{70}EO_{20}$, $M_{av} = 5800$, BASF) as a surfactant template. In a typical synthesis, a mixture of TEOS (8.19 g) and MPTS (0.69 g) was added to a mixture of P123 (4.0 g), HCl (8.0 g, 35 wt %), and deionized water (100 ml) at 40 °C. After the mixture was stirred for 24 h, the mesostructured product formed was cured at 100 °C for an additional 48 h. The products were filtered without washing and dried at 60 °C. The surfactant was removed by exhaustive solid–liquid extraction using 1N HCl/ethanol solution at 70 °C for 24 h.

The carbon replica was synthesized by using large-pore cubic $Ia\bar{3}d$ mesoporous silica as the template and furfuryl alcohol (FA, $C_5H_6O_2$) as a carbon source. First, oxidation of the mercaptopropyl group of the sulfonic acid was achieved by treating the extracted sample with

 © 2003 Wiley-VCH Verlag GmbH & Co. KGaA, Weinheim

H_2O_2 (33 vol%), followed by washing, acidification with 1M sulfuric acid, washing again, and drying at 60°C. Second, the sulfonic acid was partially neutralized by washing with 1N NH_4OH solution (because the acidity of the sulfonic acid was found to be too high to be used for the polymerization of FA). The pore volume of the mesoporous silica was filled with varying amounts of FA by the incipient-wetness technique. The sulfonic-acid-functionalized mesoporous silica containing FA was treated at 60°C for different polymerization times (Table 1), which resulted in the acid-catalyzed polymerization of FA in the form of a layer coating the pore walls. The unpolymerized FA remaining in the core of the template pores was removed by subsequent evacuation at 60°C. To obtain the rodlike carbon material, a two-step method was employed to fill the material with FA. Oxalic acid was used as an acid catalyst in the second step, because the sulfonic-acid-functionalized wall was covered with FA polymer in the first step and therefore could not catalyze the polymerization further. The polymerized FA was converted to carbon inside the silica template by pyrolysis at 900°C for 6 h under vacuum. The porous carbon was obtained after subsequent dissolution of the silica framework in 5% HF acid at room temperature.

XRD patterns were recorded on an MX Labo powder diffractometer equipped with $Cu_{K\alpha}$ radiation (40 kV, 20 mA) at the rate of 1.0 deg min^{-1} over the range of 1.5–10.0° (2θ). The samples were prepared as thin layers on glass slides.

Microscopic features of all the samples were observed by SEM (Hitachi, S-5200). The samples were observed without any metal coating. Using a low accelerating voltage, we were able to obtain selective information from the surface region.[4b,10]

HRTEM images were taken on a JEM-3010 microscope operating at an accelerating voltage of 300 kV. All samples were crushed in an agate mortar, dispersed in ethanol, and deposited on a microgrid.

The surface area and the pore size were measured at −196°C on a Belsorp 28SA sorptometer. Samples were pretreated for 2 h at 200°C and 1.33×10^{-4} Pa. The BET specific surface area, S_{BET}, was calculated from adsorption branches in the relative pressure range from 0.04 to 0.1. The primary mesopore volume V_p was determined by using the high-resolution t-plot method. The pore-size distribution was calculated from adsorption branches of isotherms by the BJH method.

Received: April 25, 2003 [Z51752]

Keywords: carbon · mesoporous materials · nanotubes · self-assembly · silica

[1] a) C. T. Kresge, M. E. Leonowicz, W. J. Roth, J. C. Vartuli, J. S. Beck, *Nature* **1992**, *359*, 710; b) J. S. Beck, J. C. Vartuli, W. J. Roth, M. E. Leonowicz, C. T. Kresge, K. D. Schmitt, C. T.-W. Chu, D. H. Olson, E. W. Sheppard, S. B. McCullen, J. B. Higgins, J. L. Schlenker, *J. Am. Chem. Soc.* **1992**, *114*, 10834.

[2] a) D. Zhao, J. Feng, Q. Huo, N. Melosh, G. H. Fredrickson, B. F. Chmelka, G. D. Stucky, *Science* **1998**, *279*, 548; b) D. Zhao, Q. Huo, J. Feng, B. F. Chmelka, G. D. Stucky, *J. Am. Chem. Soc.* **1998**, *120*, 6024.

[3] a) R. Ryoo, S. H. Joo, S. Jun, *J. Phys. Chem. B* **1999**, *103*, 7743; b) M. Kaneda, T. Tsubakiyama, A. Carlsson, Y. Sakamoto, T. Ohsuna, O. Terasaki, S. H. Joo, R. Ryoo, *J. Phys. Chem. B* **2002**, *106*, 1256; c) J. Lee, S. Yoon, S. M. Oh, C.-H. Shin, T. Hyeon, *Adv. Mater.* **2000**, *12*, 359; d) S. Jun, S. H. Joo, R. Ryoo, M. Kruk, M. Jaroniec, Z. Liu, T. Ohsuna, O. Terasaki, *J. Am. Chem. Soc.* **2000**, *122*, 10712; e) S. S. Kim, T. J. Pinnavaia, *Chem. Commun.* **2001**, 2418.

[4] a) S. H. Joo, S. J. Chol, I. Oh, J. Kwak, Z. Liu, O. Terasaki, R. Ryoo, *Nature* **2001**, *412*, 169; b) S. Che, K. Lund, T. Tatsumi, S. Iijima, S. H. Joo, R. Ryoo, O. Terasaki, *Angew. Chem./Angew. Chem. Int. Ed.* **2003**, in press.

[5] a) X. Liu, B. Tian, C. Yu, F. Gao, S. Xie, B. Tu, R, Che, L. Peng, D. Zhao, *Angew. Chem.* **2002**, *114*, 4032; *Angew. Chem. Int. Ed.* **2002**, *41*, 3876; b) Y. T. Chan, H. P. Lin, C. Y. Mou, S. T. Liu, *Chem. Commun.* **2002**, 2878; c) K. Flodström, V. Alfredsson, N. Källrot, *J. Am. Chem. Soc.* **2003**, *125*, 4402; d) H. Yang, Q. Shi, X. Liu, S. Xie, D. Jiang, F. Zhang, C. Yu, B. Tu, D. Zhao, *Chem. Commun.* **2002**, 2842.

[6] a) I. Díaz, C. Márquez-Alvarez, F. Mohino, J. Pérez-Pariente, E. Sastre, *J. Catal.* **2000**, *193*, 283; b) I. Díaz, C. Márquez-Alvarez, F. Mohino, J. Pérez-Pariente, E. Sastre, *J. Catal.* **2000**, *193*, 295.

[7] A. Carlsson, M. Kaneda, Y. Sakamoto, O. Terasaki, R. Ryoo, H. Joo, *J. Electron Microsc.* **1999**, *48*, 795.

[8] a) The pore thickness (b) for mesoporous silica with cubic $Ia\bar{3}d$ symmetry was calculated by the method proposed by Ravikovitch and Neimark[8b] using an equation based on the pore volume: $b = \left(1 - \frac{V_{sp}}{1+V_{sp}}\right)\frac{a}{x_0}$, where ρ is the pore-wall density (assumed to be 2.3 g cm^{-1}), a is the unit-cell parameter, and x_0 is a constant ($x_0 = 3.0910$); b) P. I. Ravikovitch, A. V. Neimark, *Langmuir* **2000**, *16*, 2419.

[9] M. Kruk, M. Jaroniec, R. Ryoo, S. H. Joo, *J. Phys. Chem. B* **2000**, *104*, 7960.

[10] "Structure and Structure Determination": O. Terasaki in *Electron Microscopy Studies in Molecular Sieve Science in Molecular Sieves-Science and Technology, Vol. 2* (Eds.: H. G. Karge, J. Weitkamp), Springer, Heidelberg, **1999**, pp. 71–112.

 © 2003 Wiley-VCH Verlag GmbH & Co. KGaA, Weinheim

Macrolide Synthesis

Formal Synthesis of Leucascandrolide A**

David R. Williams, Scott V. Plummer, and Samarjit Patnaik*

Extracts from the calcareous sponge *Leucascandra caveolata* were collected from waters along the northeastern coast of New Caledonia by Pietra and co-workers, and yielded the novel marine macrolide leucascandrolide A (**1**).[1] The structure of **1** was elucidated by extensive 2D NMR experiments and analysis of Mosher ester derivatives, which revealed an 18-membered macrolide containing two bridging trisubstituted tetrahydropyran rings and an ester side chain with a *Z*-α,β-unsaturated oxazole. The natural product displayed significant in vitro cytotoxicity against both KB oral epidermoid carcinoma and P388 leukemia cell lines ($IC_{50} = 0.05$ and $0.25\ \mu g\,mL^{-1}$, respectively), as well as antifungal activity against the pathogenic yeast *Candida albicans*. Attempts to isolate additional quantities of the natural product through subsequent harvesting of sponge samples proved unfruitful, which led to the suggestion that **1** may be derived from the

[*] Prof. D. R. Williams, S. V. Plummer, S. Patnaik
Department of Chemistry, Indiana University
800 East Kirkwood Avenue, Bloomington, IN, 47405 (USA)
Fax: (+1) 812-855-8300
E-mail: williamd@indiana.edu

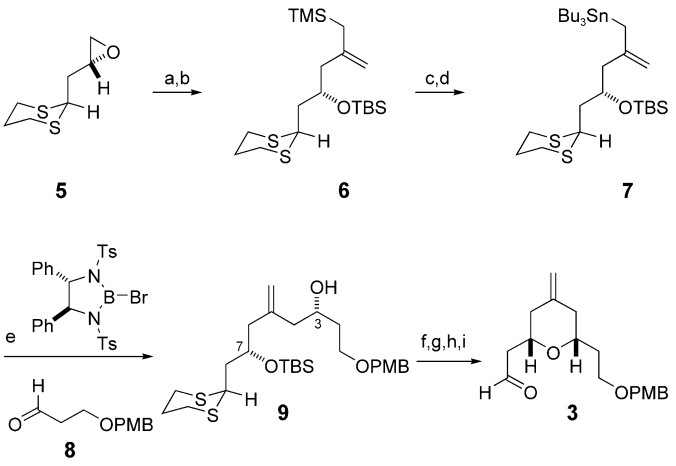
[**] Generous financial support for this research was provided by the NIH (GM-42897).

 © 2003 Wiley-VCH Verlag GmbH & Co. KGaA, Weinheim DOI: 10.1002/anie.200351817

metabolism of microbial species harbored within the sponge.[2] The biological activity and complex molecular architecture of **1** have provided the impetus for several studies toward its synthesis.[3] Recently, total[4] and formal syntheses[5] of leucascandrolide A have been reported by several groups. Herein we describe the culmination of our efforts, which have led to a convergent, highly stereocontrolled formal synthesis of **1** in the preparation of the macrolactone **2**.

Our retrosynthetic analysis of the leucascandrolide A macrolactone **2** inspired an asymmetric allylation strategy based on the nonracemic aldehyde **3** and the complex optically active allyl stannane **4** (Scheme 1). This efficient C9–C10 bond construction would directly incorporate all the carbon atoms necessary for macrocycle formation, and the major stereochemical features associated with the macrolide **2**. Late-stage incorporation of the C18–C23 side chain through an alkenyl zinc addition, and subsequent formation of the allylic alcohol at C17 through an asymmetric hydride reduction would precede the final macrolactonization step.

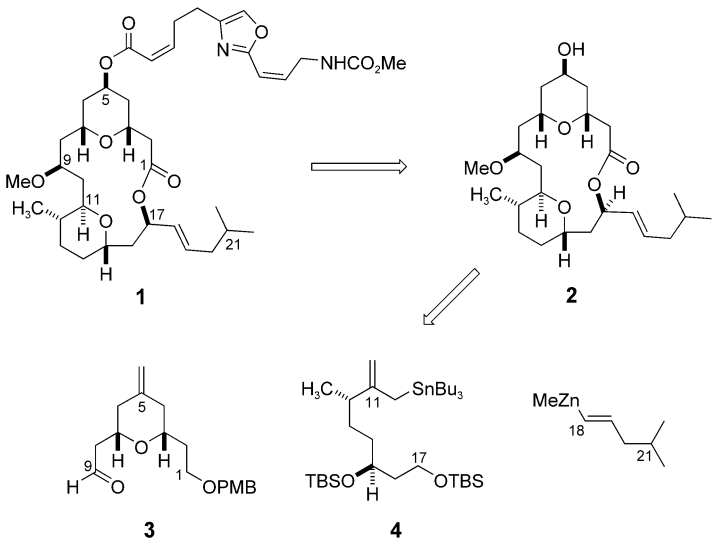
The preparation of the C1–C9 aldehyde **3** commenced with the conversion of the known epoxide **5** (readily available from (+)-epichlorohydrin)[6] into the allyl silane **6** through the copper-catalyzed addition of the Grignard reagent prepared from 2-bromo-3-trimethylsilylpropene (Scheme 2).[7] Subsequent protection of the resulting homoallylic alcohol gave the TBS ether **6**. Treatment of **6** with freshly recrystallized NBS at −78 °C led to the immediate formation of the labile corresponding allylic bromide, which was displaced directly with a tributylstannylcuprate to give the allyl stannane **7**. Asymmetric allylation was effected following the tin-to-boron transmetalation of the allylstannane **7** by using the boron bromide reagent developed by Corey et al., which is derived from a (*S*,*S*)-1,2-diamino-1,2-diphenylethane bis(sulfonamide) and boron tribromide.[8] Nucleophilic addition to the aldehyde **8**[9] provided the *S* homoallylic alcohol **9** as the major component of a mixture of diastereomers epimeric at C3 (100%, d.r. 11:1).[10] Ring closure of **9** to afford the 2,6-*cis*-tetrahydropyranyl moiety of **3** was carried out by conversion of the alcohol at C3 into the corresponding tosylate, removal of the silyl protecting group at C7, and internal backside displacement to yield an 11:1 ratio of diastereomers, which were separated by flash chromatography. Mild hydrolysis of the dithiane was promoted by methylation of the sulfur atoms,[11] which provided the aldehyde **3** in excellent overall yield.



Scheme 2. Reagents and conditions: a) Mg^0, THF, (2-bromoallyl)trimethylsilane; then **5**, CuI, −50 °C; −50→−10 °C, 2 h; 79%; b) TBSCl, imidazole, DMF; 100%; c) NBS, propylene oxide, CH_2Cl_2/DMF (2:3), −78 °C; d) Bu_3SnLi, CuBr·DMS, THF, −78°→−40 °C; 77% (2 steps); e) the (*S*,*S*)-1,2-diamino-1,2-diphenylethane bis(sulfonamide), BBr_3, CH_2Cl_2, 0 °C, 1 h; then **7**, room temperature, 10 h; then **8**, −78 °C, 1.5 h; 100%, d.r. 11:1; f) TsCl, Et_3N, DMAP, CH_2Cl_2; 100%; g) HF·pyr, CH_3CN; 99%; h) NaH, PhH, 90 °C; 75%; i) MeI, $CaCO_3$, CH_3CN/H_2O (9:1), 16 h; 100%. DMAP = 4-(dimethylamino)pyridine, DMF = *N*,*N*-dimethylformamide, DMS = dimethyl sulfide, NBS = *N*-bromosuccinimide, pyr = pyridine, TBS = *tert*-butyldimethylsilyl, Ts = *p*-toluenesulfonyl.

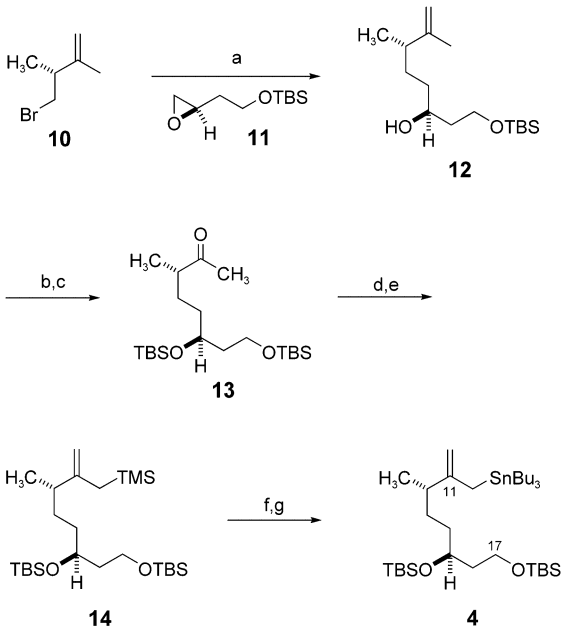
Preparation of the novel allyl stannane **4** began with the copper(I)-catalyzed addition of the Grignard reagent derived from (2*S*)-1-bromo-2,3-dimethyl-3-butene **10**[12] to the nonracemic epoxide **11**,[13] which led directly to the alcohol **12** in 80% yield (Scheme 3). Protection of the secondary alcohol in **12** as its TBS ether and subsequent oxidative cleavage of the terminal olefin by ozonolysis gave the methyl ketone **13** in excellent yield. Conversion of **13** into the corresponding enol triflate through kinetic deprotonation at low temperature and sulfonate formation by use of the Comins reagent[14] was followed by nickel-catalyzed cross-coupling with (trimethylsilylmethyl)magnesium chloride to provide the allyl silane **14**.[15] As we have noted previously,[10] the transmetalation of allyl silanes to allyl boranes tends to be ineffective. Thus, conversion of **14** into the allyl stannane, as described for **7**, led to the C10–C17 allyl stannane **4** in 77% yield after flash silica-gel chromatography.

Our convergent strategy toward **2** was to examine the selective introduction of asymmetry at C9. This feature was of particular interest for our studies of asymmetric allylation owing to the presence of adjacent asymmetry at C12 in the allyl component **4**, and



Scheme 1. Retrosynthetic analysis of the leucascandrolide A macrolactone **2**.

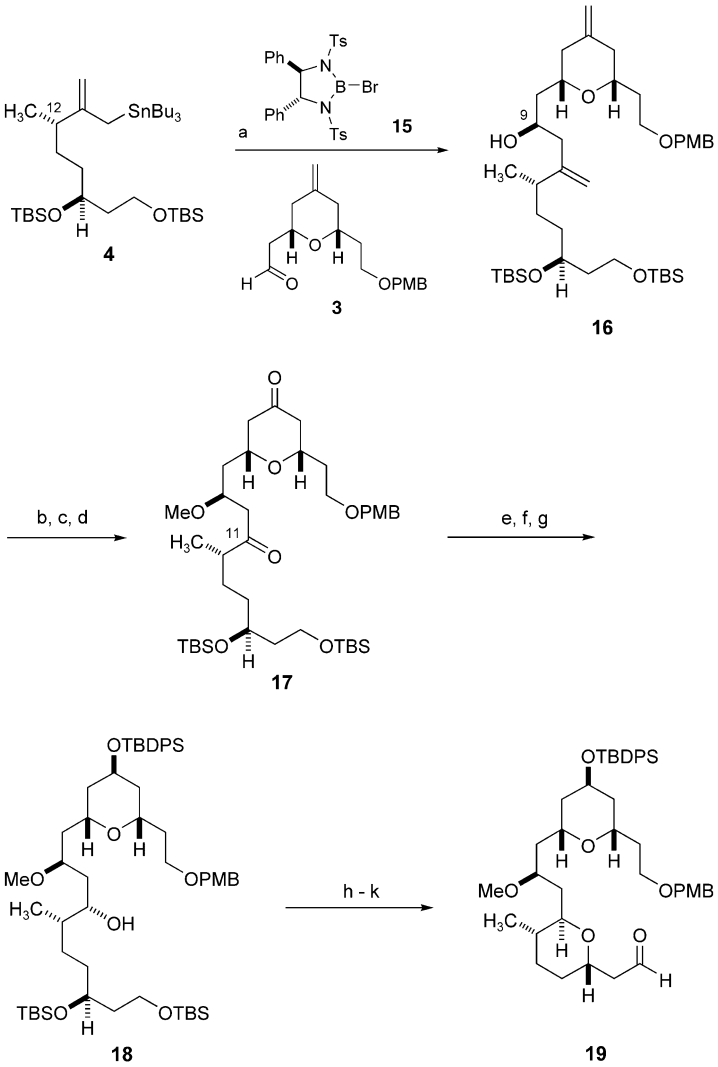
 © 2003 Wiley-VCH Verlag GmbH & Co. KGaA, Weinheim



Scheme 3. Reagents and conditions: a) Mg^0, THF, **10**; then CuBr·DMS, THF, −78 °C; then **11**, THF, −78 °C→RT; 80%; b) TBSCl, imidazole, DMF; 96%; c) O_3, CH_2Cl_2/MeOH (1:1), −78 °C; then DMS, −78 °C→RT; 98%; d) KHMDS, THF, −78 °C; then Comins reagent, THF; 87%; e) $[Ni(acac)_2]$, $TMSCH_2MgCl$, THF, room temperature; 75%; f) NBS, propylene oxide, CH_2Cl_2/DMF (3:2), −78→−10 °C; g) Bu_3SnLi, CuBr·DMS, THF, −78°→−40 °C; 77% (2 steps). acac = acetylacetone, Comins reagent = 2-[*N*,*N*-bis(trifluoromethylsulfonyl)amino]-5-chloropyridine, HMDS = hexamethyldisilazide.

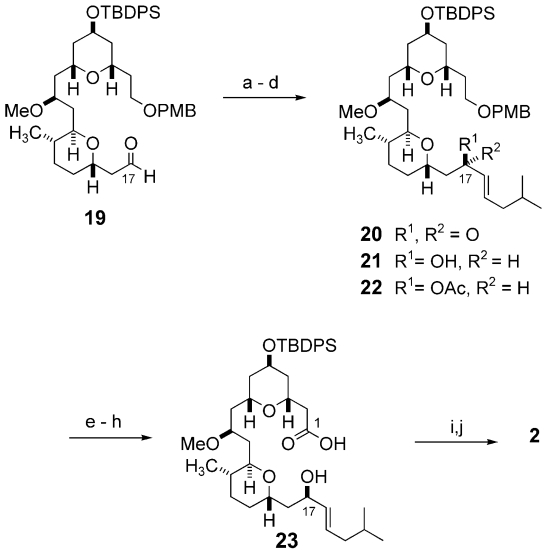
the possible formation of diastereotopic transition states in the reaction of the intermediate chiral allyl borane with the aldehyde **3**.[16] The homoallylic alcohol (9*R*)-**16** (95%, d.r. 8.5:1) was prepared by transmetalation of optically pure **4** with the *R*,*R* bromoborane **15** to yield an intermediate allylic borane for low-temperature condensation with the tetrahydropyranyl aldehyde **3** (Scheme 4). Facial selectivity of the nucleophilic addition was dominated by the chiral auxiliary, and the diastereomers were readily separated by flash chromatography. Methylation of the homoallylic alcohol at C9 in **16** was followed by oxidative cleavage (OsO_4, NMO; $NaIO_4$) to provide the corresponding diketone **17**. L-Selectride promoted selective reduction at C5 of the tetrahydropyranone **17**, which led to the corresponding axial alcohol in 84% yield (d.r. > 95:5), and this alcohol was protected as its TBDPS ether. Attention was then focused on the asymmetric reduction of the ketone at C11. The use of the Terashima reagent[17] for selective aluminum hydride reductions of acyclic β,β′-dialkoxy ketones has been reported recently from these laboratories.[18] In this case, the Terashima reduction of the ketone at C11 in the presence of the ligand (−)-*N*-methylephedrine resulted in an effective reagent-based hydride addition with excellent diastereofacial selectivity (d.r. > 95:5) to provide the anti-Felkin product **18** in high yield (95%). To ensure formation of the 2,6-*trans*-tetrahydropyran, tosylation of the alcohol **18** was followed by selective removal of the TBS groups and treatment with sodium hydride. The resulting internal backside displacement led to the exclusive formation of the desired six-membered ring, and Dess–Martin oxidation[19] of the primary alcohol yielded the aldehyde **19**.

To achieve our final objective we required efficient incorporation of the C18–C23 carbon chain and flexibility for the development of stereogenicity at C17.[20] To this end, the hydrozirconation of 4-methyl-1-pentyne with the Schwartz reagent was followed by transmetalation with dimethylzinc as adapted from the reports of Wipf et al.



Scheme 4. Reagents and conditions: a) the (*R*,*R*)-1,2-diamino-1,2-diphenylethane bis(sulfonamide), BBr_3, CH_2Cl_2, 0 °C, 1 h; then **4**, room temperature, 10 h; then **3**, −78 °C, 1.5 h; 96%, d.r. 8.5:1; b) Me_3OBF_4, proton sponge, 4-Å molecular sieves, CH_2Cl_2; 96%; c) OsO_4, NMO, acetone/H_2O (2:1), 16 h; d) $NaIO_4$, THF/phosphate buffer (pH 7; 1:1), 16 h; 80% (2 steps); e) L-Selectride, THF, −78 °C, 1.5 h; 84%; f) TBDPSCl, imidazole, DMF, 40 h; 73%; g) $LiAlH_4$ (2.0 equiv), (−)-*N*-methylephedrine (2.0 equiv), *N*-ethylaniline (4.0 equiv), Et_2O, −78 °C, 2 h; 95%; h) Ts_2O, pyridine, CH_2Cl_2; 100%; i) HF·pyr, pyridine, THF; 84%; j) NaH, PhH, 60 °C, 16 h; 73%; k) Dess–Martin periodinane, $NaHCO_3$, CH_2Cl_2; 95%. NMO = *N*-methylmorpholine *N*-oxide, L-Selectride = lithium tri-*sec*-butylborohydride, TBDPS = *tert*-butyldiphenylsilyl.

 © 2003 Wiley-VCH Verlag GmbH & Co. KGaA, Weinheim



Scheme 5. Reagents and conditions: a) 4-methyl-1-pentyne, CH_2Cl_2, $Cp_2Zr(H)Cl$, room temperature; then Me_2Zn, −78 °C; then **19**, −78 °→ 0 °C, 1 h; 87%; b) Dess–Martin periodinane, $NaHCO_3$, CH_2Cl_2; 75%; c) (*S*)-2-methyloxazaborolidine, BH_3·THF, −10 °C; 89%, d.r. 5:1; d) Ac_2O, pyridine, DMAP, CH_2Cl_2; 97%; e) DDQ, CH_2Cl_2/phosphate buffer (pH 7)/*t*BuOH (40:10:1), 1.5 h; quant.; f) Dess–Martin periodinane, $NaHCO_3$, CH_2Cl_2; g) $NaClO_2$, NaH_2PO_4, 2-methyl-2-butene, aqueous *t*BuOH, 0 °C, 45 min; 56% (2 steps); h) K_2CO_3, MeOH, 16 h; i) 2,4,6-trichlorobenzoyl chloride, Et_3N, DMAP, benzene; 63% (2 steps); j) TBAF, THF; 67%. DDQ = 2,3-dichloro-5,6-dicyano-1,4-benzoquinone.

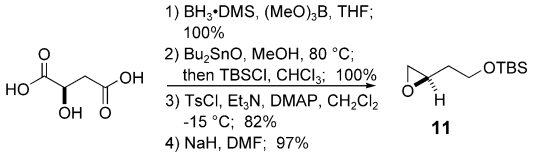
(Scheme 5).[21] Reactions of the resulting alkenyl zinc species with the aldehyde **19** resulted in the efficient formation of a mixture of diastereomeric allylic alcohols (1:1 ratio), which was oxidized directly to the enone **20** (75% yield over two steps). Interestingly, the asymmetric hydride reduction of the α,β-unsaturated ketone **20** under Terashima conditions gave rise to conjugate reduction as a major reaction pathway. This result is atypical as the Terashima conditions are generally utilized for the production of chiral allylic alcohols. However, Corey–Bakshi–Shibata (CBS) borohydride reduction[22] of **20** with the CBS reagent (*S*)-2-methyloxazaborolidine in the presence of borane–tetrahydrofuran complex gave an 89% yield of a 5:1 mixture of separable diastereomers, epimeric at C17, in favor of the *R* alcohol **21**. Acetylation to **22** was followed by oxidative deprotection of the alcohol at C1. The seco-acid **23** was obtained by oxidation of the resulting primary alcohol to the carboxylic acid and subsequent basic methanolysis of the acetate at C17. The crude product was subjected to the Yonemitsu-modified Yamaguchi[23] protocol to give the macrolide in good yield (63% over two steps). Finally, deprotection of the alcohol at C5 by treatment with fluoride provided the leucascandrolide A macrolactone **2**, whose physical and spectroscopic data were identical in all respects to those previously reported.[4a] Leighton and coworkers have also described the conversion of **2** into leucascandrolide A, and thus, our efforts constitute a formal synthesis of the natural product **1**.

In summary, our investigations into asymmetric allylation methodology have extended this fundamental technique to the efficient, convergent construction of complex molecules. Our studies have also provided unprecedented results for the use of the Terashima hydride reduction in the stereoselective formation of saturated, acyclic alcohols. Overall, we have carried out an efficient synthesis of the leucascandrolide A macrolactone **2** with a high level of stereoselectivity. Further studies are in progress in our laboratory.

Received: May 6, 2003 [Z51817]

Keywords: allylation · antitumor agents · asymmetric synthesis · macrolide · natural products

[1] M. D'Ambrosio, A. Guerriero, C. Debitus, F. Pietra, *Helv. Chim. Acta* **1996**, *79*, 51.
[2] M. D'Ambrosio, M. Tatò, G. Pocsfalvi, C. Debitus, F. Pietra, *Helv. Chim. Acta* **1999**, *82*, 347.
[3] a) M. T. Crimmins, C. A. Carroll, B. W. King, *Org. Lett.* **2000**, *2*, 597; b) S. A. Kozmin, *Org. Lett.* **2001**, *3*, 755; c) P. Wipf, T. H. Graham, *J. Org. Chem.* **2001**, *66*, 3242; d) L. A. Dakin, N. F. Langille, J. S. Panek, *J. Org. Chem.* **2002**, *67*, 6812.
[4] a) K. R. Hornberger, C. L. Hamblett, J. L. Leighton, *J. Am. Chem. Soc.* **2000**, *122*, 12894; b) A. Fettes, E. M. Carreira, *Angew. Chem.* **2002**, *114*, 4272; *Angew. Chem. Int. Ed.* **2002**, *41*, 4098; c) Y. Wang, J. Janjic, S. A. Kozmin, *J. Am. Chem. Soc.* **2002**, *124*, 13670; d) I. Paterson, M. Tudge, *Angew. Chem.* **2003**, *115*, 357; *Angew. Chem. Int. Ed.* **2003**, *42*, 343.
[5] a) D. J. Kopecky, S. D. Rychnovsky, *J. Am. Chem. Soc.* **2001**, *123*, 8420; b) P. Wipf, J. T. Reeves, *Chem. Commun.* **2002**, 2066.
[6] The synthesis of the epoxide **5** proceeds through the alkylation of 2-lithio-1,3-dithiane with (*R*)-epichlorohydrin (97% *ee*, Aldrich): a) M. Braun, D. Seebach, *Chem. Ber.* **1976**, *109*, 669; b) D. Seebach, I. Willert, A. Beck, B. T. Groebel, *Helv. Chim. Acta* **1978**, *61*, 2510.
[7] a) H. Nishiyama, H. Yokoyama, S. Narimatsu, K. Itoh, *Tetrahedron Lett.* **1982**, *23*, 1267; b) B. M. Trost, T. A. Grese, D. M. T. Chan, *J. Am. Chem. Soc.* **1991**, *113*, 7350.
[8] E. J. Corey, C. M. Yu, S. S. Kim, *J. Am. Chem. Soc.* **1989**, *111*, 5495.
[9] The synthesis of the aldehyde **8** proceeds by the mono-*p*-methoxybenzylation of 1,3-propanediol followed by Swern oxidation: A. J. Mancuso, D. Swern, *Synthesis* **1981**, 165.
[10] For the development of this asymmetric-allylation methodology, see: D. R. Williams, D. A. Brooks, K. G. Meyer, M. P. Clark, *Tetrahedron Lett.* **1998**, *39*, 7251.
[11] S. Takano, S. Hatakeyama, K. Ogasawara, *J. Chem. Soc. Chem. Commun.* **1977**, 68.
[12] The bromide **10** is available from the corresponding homoallylic alcohol by tosylation (TsCl, DMAP, pyridine; 98%), followed by exchange with lithium bromide (DMF, 50 °C; 65%). For the synthesis of the starting homoallylic alcohol, see: J. D. White, G. N. Reddy, G. O. Spessard, *J. Am. Chem. Soc.* **1988**, *110*, 1624.
[13] The epoxide **11** is available from D-malic acid in four steps.



[14] D. Comins, A. Dehghani, *Tetrahedron Lett.* **1992**, *33*, 6299.
[15] C. A. Busacca, M. C. Eriksson, R. Fiaschi, *Tetrahedron Lett.* **1999**, *40*, 3101. Contrary to the results reported in this paper, we

 © 2003 Wiley-VCH Verlag GmbH & Co. KGaA, Weinheim

found [Ni(acac)$_2$] to be an efficient catalyst for the conversion of the enol triflate into the allyl silane **14**.
[16] A complete study of matched and mismatched elements of stereochemistry will be detailed in further reports devoted to the asymmetric-allylation process.
[17] a) S. Terashima, N. Tanno, K. Koga, *J. Chem. Soc. Chem. Commun.* **1980**, 1026; b) S. Terashima, N. Tanno, K. Koga, *Chem. Lett.* **1980**, 981; c) N. Tanno, S. Terashima, *Chem. Pharm. Bull.* **1983**, *31*, 837.
[18] D. R. Williams, D. A. Brooks, M. A. Berliner, *J. Am. Chem. Soc.* **1999**, *121*, 4924.
[19] D. B. Dess, J. C. Martin, *J. Am. Chem. Soc.* **1991**, *113*, 7277.
[20] Either of the diastereomeric alcohols (*R* or *S* at C17) could potentially be a valuable intermediate toward lactone **2**, depending on the strategy chosen: macrocyclization with retention of configuration at C17 (Yamaguchi protocol) or Mitsunobu macrocyclization with inversion of configuration at C17. For example, compare the reports of references [4a] and [5b].
[21] a) P. Wipf, W. Xu, *Tetrahedron Lett.* **1994**, *35*, 5197; b) P. Wipf, S. Ribe, *J. Org. Chem.* **1998**, *63*, 6454.
[22] a) E. J. Corey, R. K. Bakshi, S. Shibata, C. P. Chen, V. K. Singh, *J. Am. Chem. Soc.* **1987**, *109*, 7925; b) D. J. Mathre, T. K. Jones, L. C. Xavier, T. J. Blacklock, R. A. Reamer, J. J. Mohan, E. T. T. Jones, K. Hoogsteen, M. W. Baum, E. J. J. Grabowski, *J. Org. Chem.* **1991**, *56*, 751.
[23] a) J. Inanaga, K. Hirata, H. Saeki, T. Katsuki, M. Yamaguchi, *Bull. Chem. Soc. Jpn.* **1979**, *52*, 1989; b) M. Hikota, Y. Sakurai, K. Horita, O. Yonemitsu, *Tetrahedron Lett.* **1990**, *31*, 6367.

 © 2003 Wiley-VCH Verlag GmbH & Co. KGaA, Weinheim

Two-Dimensional NMR Spectroscopy

Elimination of Zero-Quantum Interference in Two-Dimensional NMR Spectra**

*Michael J. Thrippleton and James Keeler**

High-resolution NMR experiments often contain periods during which the magnetization is placed along the z-axis. For example, the magnetization must be along the z-axis during the mixing time in a NOESY experiment so that cross-relaxation can take place. Either phase cycling or field gradient pulses are used to ensure that only the wanted z-magnetization ends up contributing to the spectrum. However, neither of these methods can distinguish between z-magnetization and homonuclear zero-quantum coherence, which is invariably present. The zero-quantum coherence gives rise to anti-phase dispersive components in the spectra, thereby reducing the effective resolution, introducing misleading correlations, and obscuring wanted features. Over the years a number of methods have been devised to suppress these zero-quantum contributions,[1–5] but it is fair to say that none of these methods have proved entirely satisfactory. Herein we present a new method for suppressing zero-quantum coherence; the method is widely applicable, does not extend the duration of the experiment significantly, and can be implemented easily on any modern spectrometer.

Our new method of zero-quantum suppression involves applying simultaneously a swept-frequency 180° pulse and a gradient. Figure 1a shows how this combination can be introduced into the NOESY pulse sequence. The way in which this swept-pulse/gradient pair works can be envisaged in the following way. The application of the gradient (along the z-axis) results in the Larmor frequency becoming a function of position in the NMR tube. The swept-frequency 180° pulse will therefore flip the spins at different positions in the sample at different times. Thus, the top of the sample

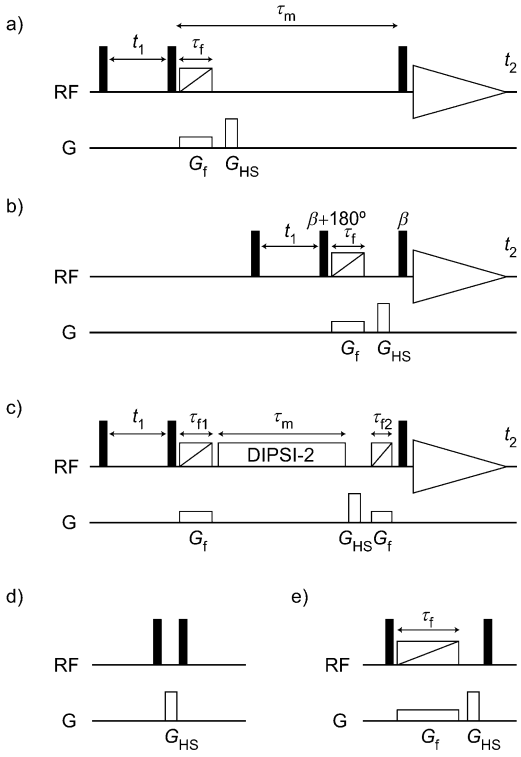


Figure 1. Pulse sequence timing diagrams for the a) NOESY, b) z-COSY, and c) TOCSY experiments incorporating swept-pulse/gradient pairs for the dephasing of zero-quantum coherence. Radiofrequency pulses are shown on the line marked RF. Unless otherwise specified, filled-in rectangles represent pulses of flip angle 90° and phase x, and swept-frequency 180° pulses are indicated by an open box containing a diagonal line. Gradient pulses are shown on the line marked G. G_{HS} denotes a homospoil gradient pulse. The z-filter pulse sequence element shown in (d) results in the selection of in-phase magnetization along the y-axis. Zero-quantum suppression can be introduced into this element as shown in (e); this modified z-filter appears in sequences (a)–(c). We note that the swept-frequency pulse may be considered as part of the mixing time in the NOESY pulse sequence (a).

[*] Dr. J. Keeler, M. J. Thrippleton
Department of Chemistry
University of Cambridge
Lensfield Road, Cambridge, CB2 1EW (UK)
Fax: (+44) 1223-336-362
E-mail: jhk10@cam.ac.uk

[**] This work was supported by the EPSRC, Procter & Gamble, and the Newton Trust. We are grateful to Dr. David Neuhaus for a generous allocation of spectrometer time at the MRC LMB.

Supporting information for this article is available on the WWW under http://www.angewandte.org or from the author.

 © 2003 Wiley-VCH Verlag GmbH & Co. KGaA, Weinheim DOI: 10.1002/anie.200351947

might experience the 180° pulse at the start of the sweep, the middle of the sample at time $\tau_f/2$, and the bottom at time τ_f, where τ_f is the duration of the sweep. In general, the 180° pulse occurs at time $\alpha\tau_f$, where α is 0 at the top of the sample and 1 at the bottom.

The 180° pulse forms a spin echo which refocuses the evolution of the zero-quantum coherence over a time $2\alpha\tau_f$; however, for the remainder of the time, $(1–2\alpha)\tau_f$, the zero-quantum continues to evolve. The result is that in different parts of the sample the zero-quantum has evolved for different times, and so has acquired a different phase. If the range of these phases across the sample is large enough, the net result will be cancelation of the zero-quantum coherence.

A simple calculation (see Supporting Information) shows that the degree of attenuation A of the zero-quantum depends on both its frequency, Ω_{ZQ} (in rad s^{-1}), and the length of the swept-pulse/gradient pair, τ_f, [Eq. (1)]:

$$A = \frac{\sin \Omega_{ZQ}\tau_f}{\Omega_{ZQ}\tau_f} \quad (1)$$

Ω_{ZQ} is simply $(\Omega_1-\Omega_2)$, where Ω_1 and Ω_2 are the frequencies of the two spins involved. If the oscillations produced by the sine term are ignored, the zero-quantum is attenuated by a factor $1/\Omega_{ZQ}\tau_f$. For example, for a zero-quantum frequency of 500 Hz (namely, with two spins separated by 1 ppm at 500 MHz) and a τ_f value of 30 ms, the attenuation factor will be 0.01, that is, the zero-quantum coherence is reduced to 1 % of its original size.

The key feature of our new method is that suppression of zero-quantum coherence is achieved in a single scan; no repetition of the experiment is necessary. This represents a very significant improvement over the usual method of zero-quantum suppression, which is to repeat the experiment for a range of mixing times of the order of $2\pi/\Omega_{ZQ}$.[1] Not only does this greatly extend the minimum required experiment time, but it is also difficult to choose a small set of mixing-time values which give adequate suppression over a range of zero-quantum frequencies. The alternative approach of varying the mixing time randomly from one t_1 increment to the next merely transforms the unwanted signals into t_1 noise.[1]

In a previous study we showed how spin-locking in the presence of an inhomogeneous B_0 or B_1 field can also result in the dephasing of zero-quantum coherence.[4] However, the technique proposed herein is far superior to our earlier work in that the new approach is simpler to implement, leads to faster dephasing of the zero-quantum coherence, and does not suffer from additional complications, such as unwanted TOCSY-type transfer.

Figure 2 compares part of the NOESY spectrum of strychnine recorded with and without the new zero-quantum suppression method; a short mixing time τ_m of 400 ms has been used, as it is under these conditions that the anti-phase contributions are most troublesome. Figure 2a shows a spectrum recorded without zero-quantum suppression; the significant phase distortions on both the diagonal- and cross-peak multiplets arise from the zero-quantum coherence present during the mixing time. Figure 2a′ shows a spectrum recorded using the new zero-quantum suppression method:

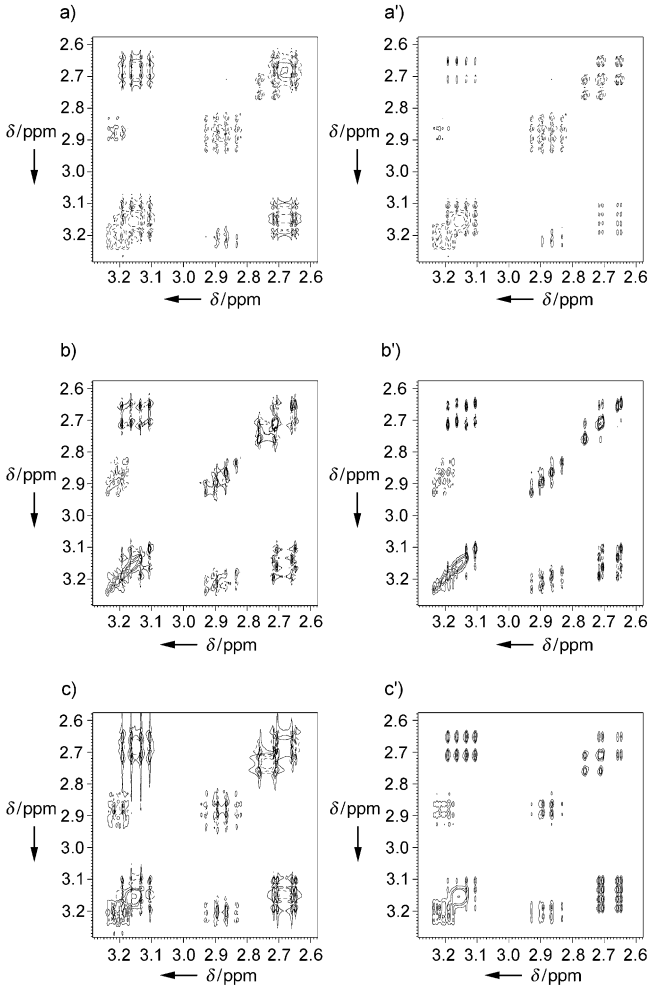


Figure 2. Comparison of spectra recorded without zero-quantum suppression (left) and with (right) the new swept-pulse/gradient method for the suppression of zero-quantum coherence; a, a′): NOESY spectra (mixing time 400 ms), b, b′): *z*-COSY spectra, and c, c′): TOCSY spectra (mixing time 23 ms). The same region of the spectrum of strychnine is shown in each case. The spectra on the left all show dispersive anti-phase contributions arising from zero-quantum coherence present during the mixing time. In the spectra shown on the right, these contributions have been removed by the new dephasing method; as a result, the spectra show pure absorption line shapes and are thus much easier to interpret. Positive contours are indicated by full lines, negative contours by dashed lines; the F_1-axis is vertical.

the anti-phase dispersive contributions are removed, which leaves all of the peaks in pure absorption—the improvement is dramatic (the remaining intensity distortions result from a combination of strong coupling and flip-angle effects). Clearly, one-dimensional NOE experiments, such as the double-pulsed field gradient spin echo (DPFGSE) NOE, which also require zero-quantum suppression, will benefit from the same approach.

There are other experiments in which the new zero-quantum suppression method can be used to good effect; here we consider just two: *z*-COSY and TOCSY. The *z*-COSY experiment is similar to NOESY except that the two pulses bracketing the mixing period have small flip angles, typically 20°.[6] In the resulting spectrum both the cross- and diagonal-

 © 2003 Wiley-VCH Verlag GmbH & Co. KGaA, Weinheim

peak multiplets have absorption-mode line shapes and, most importantly, the multiplets are "reduced", thus making it possible to measure both the size and relative sign of passive couplings.

Effective suppression of zero-quantum coherences that are present between the two small flip angle pulses is crucial to the success of the *z*-COSY experiment; the pulse sequence in Figure 1b shows how this can be achieved by using the new method. Figure 2b shows part of the *z*-COSY spectrum of strychnine recorded without zero-quantum suppression; significant dispersive contributions obscure the fine structure of the multiplets. Zero-quantum suppression gives the dramatic improvement shown in Figure 2b′: the line shapes are absorptive and the reduced multiplets can now clearly be seen.

Finally, we consider TOCSY (total correlation spectroscopy) experiments.[7] Again, the pulse sequence is similar to that used in NOESY experiments except that an isotropic mixing sequence (such as DIPSI-2) is applied during the mixing time. Such a sequence results in the interchange of *z*-magnetization between coupled spins via a state of zero-quantum coherence. To obtain spectra with pure phase, it is necessary to dephase zero-quantum coherence present both before and after the period of isotropic mixing; a suitable pulse sequence is shown in Figure 1c. Note that to avoid the zero-quantum coherence dephased by the first swept-pulse/gradient pair being rephased in the second, different durations (τ_{f1} and τ_{f2}) must be used.

Figure 2c shows part of the TOCSY spectrum of strychnine recorded without any suppression of the zero-quantum contributions; the presence of anti-phase dispersive contributions is clear, both for cross- and diagonal-peak multiplets. In contrast, the spectrum shown in Figure 2c′, recorded using the new zero-quantum suppression method, has multiplets that are both in-phase and with absorption-mode line shapes.

In fact, all of these experiments can be thought of as utilizing a *z*-filter, which is the pulse sequence element shown in Figure 1d; it is used to select one in-phase component of transverse magnetization by rotating it, temporarily, on to the *z*-axis. Figure 1e shows how the *z*-filter element can be modified to include our new method for zero-quantum suppression.

We are confident that the method presented here is also applicable to NMR spectroscopic analysis of biological macromolecules. Much shorter NOESY mixing times are typically used for such molecules, and the duration of the swept-frequency pulse will limit the shortest mixing-time available. The sweep will also need to be kept short in other *z*-filtered experiments to minimize relaxation losses. However, while a somewhat generous τ_f value of 50 ms was mainly used in this work, significantly shorter sweeps are likely to be feasible in biological applications. This is because such experiments are routinely performed at higher spectrometer frequencies than the 300 MHz used here; since the value of Ω_{ZQ} increases in proportion to field strength, the τ_f value can be reduced by the same factor. Furthermore, as the method does not use gradients for defocusing and refocusing, it is no more sensitive to the effects of diffusion and convection than the conventional experiments.

In conclusion, we have introduced a new method which, in a single scan, results in excellent suppression of zero-quantum coherence, thus leading to spectra with excellent phase properties. Furthermore, it is simple to implement on any modern spectrometer and we believe that its adoption will see an improvement in many NMR experiments. The key idea of generating spatially dependent evolution clearly has other applications in high-resolution NMR spectroscopy.[8,9]

Experimental Section

All experiments were performed at 300 MHz on a Bruker DRX300 spectrometer using a sample containing strychnine (11 mg) dissolved in $CDCl_3$ (1 mL). All two-dimensional spectra were recorded with two scans per increment and a simple two-step phase cycle in which the phase of the first pulse and receiver were simultaneously changed by 180°; coherence transfer pathway selection was completed using a homospoil gradient pulse of strength 50% of the maximum (60 G cm^{-1}) with a duration of 6–8 ms; frequency discrimination was achieved in the t_1/F_1 dimension using TPPI. The spectral width in each dimension was 2216 Hz, the acquisition time in t_2 was 1.8 s, and 1024 increments of t_1 were recorded to a maximum value of 0.23 s. Gaussian multiplication was used in processing the t_1/F_1 dimension to reduce truncation artifacts.

The swept-frequency pulses were adiabatic 180° CHIRP pulses;[10] the frequency was swept through 20 kHz in $\tau_f = 50$ ms (except for the TOCSY pulse sequence, where the frequency was swept through 20 kHz in $\tau_{f1} = 50$ ms for the first sweep and in $\tau_{f2} = 30$ ms for the second sweep); the strength of the radiofrequency field was constant at 1 kHz, except during the first and final tenths of the pulse, when the field was smoothed to zero according to a sine function. The gradient strength G_f was 4% of the maximum. Recommendations for the determination of the parameters for the swept-pulse and gradient are given in the Supporting Information.

The comparison experiments without zero-quantum suppression were run as described, but with the G_f value and the radiofrequency field strength for the swept-frequency pulses set to zero. In the conventional *z*-COSY experiment two pulses of flip angle β were used. However, in the version with zero-quantum suppression the first of these was increased to $\beta + 180°$ to compensate for the 180° sweep, which would otherwise alter the multiplet structures. A value of $\beta = 20°$ was used in this work.

To reduce line-shape distortions resulting from eddy currents, it may be beneficial to include a short delay between the last gradient pulse and the last radiofrequency pulse. Delays of 43.5 ms for the *z*-COSY experiment and 20 ms for the TOCSY experiment were used, although these values will depend on the performance of the spectrometer used.

Received: May 22, 2003 [Z51947]
Published online: August 1, 2003

Keywords: analytical methods · NMR spectroscopy · NMR theory · zero-quantum coherence

[1] S. Macura, Y. Huang, D. Suter, R. R. Ernst, *J. Magn. Reson.* **1981**, *43*, 259–281.
[2] S. Macura, K. Wüthrich, R. R. Ernst, *J. Magn. Reson.* **1982**, *46*, 269–282.
[3] M. Rance, G. Bodenhausen, G. Wagner, K. Wüthrich, R. R. Ernst, *J. Magn. Reson.* **1985**, *62*, 497–510.
[4] A. L. Davis, G. Estcourt, J. Keeler, E. D. Laue, J. J. Titman, *J. Magn. Reson. Ser. A* **1993**, *105*, 167–183.
[5] M. Baur, H. Kessler, *Magn. Reson. Chem.* **1997**, *35*, 877–882.

 © 2003 Wiley-VCH Verlag GmbH & Co. KGaA, Weinheim

[6] H. Oschkinat, A. Pastore, P. Pfändler, G. Bodenhausen, *J. Magn. Reson.* **1986**, *69*, 559 – 566.
[7] L. Braunschweiler, R. R. Ernst, *J. Magn. Reson.* **1983**, *53*, 521 – 528.
[8] N. M. Loening, J. Keeler, G. A. Morris, *J. Magn. Reson.* **2001**, *153*, 103 – 112.
[9] L. Frydman, T. Scherf, A. Lupulescu, *Proc. Natl. Acad. Sci. USA* **2002**, *99*, 15858 – 15862.
[10] J.-M. Böhlen, G. Bodenhausen, *J. Magn. Reson. Ser. A* **1993**, *102*, 293 – 301.

 © 2003 Wiley-VCH Verlag GmbH & Co. KGaA, Weinheim

Asymmetric Hydrogenation

New P,N Ligands for Asymmetric Ir-Catalyzed Reactions**

*Tanasri Bunlaksananusorn, Kurt Polborn, and Paul Knochel**

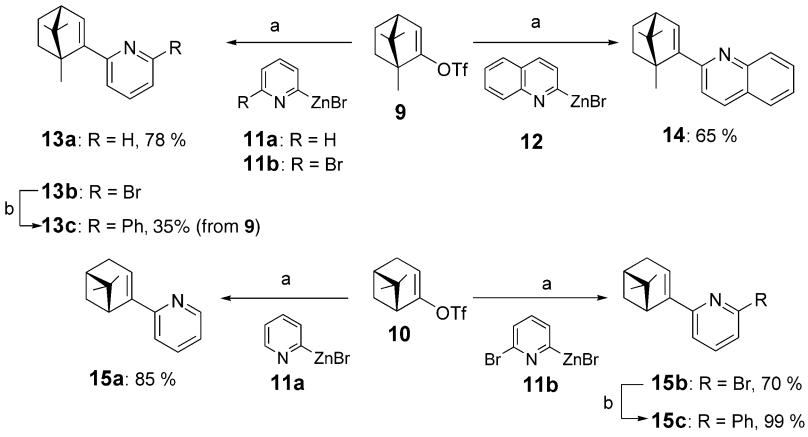
In memory of Alain Louis Rodriguez

The preparation of new ligands for asymmetric metal catalysis has led in recent years to the discovery of several new classes of chiral ligands.[1] Recently, we reported *t*BuOK-catalyzed addition reactions of nucleophiles (carbonyl derivatives and phosphanes) to a variety of functionalized alkenes.[2] Herein, we report the use of this method for the preparation of the new chiral P,N ligands[3] **1**–**6** (see Scheme 2) from readily available chiral building blocks such as D-(+)-camphor (**7**) and (*R*)-(+)-nopinone (**8**). We show that these ligands can be used for highly enantioselective Ir-catalyzed hydrogenations.

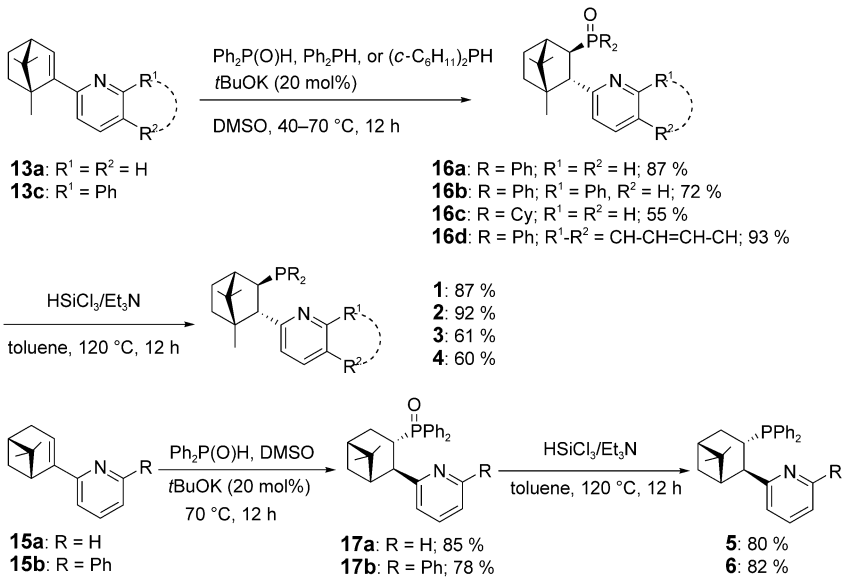
The known alkenyl triflate[4] **9** underwent smooth Negishi cross-coupling reactions[5] to afford the desired 2-alkenyl pyridines **13a**–**c** in 35–78% yield[6] and the 2-alkenyl quinoline **14** in 65% yield. Similarly, the alkenyl triflate **10** was converted into the 2-alkenyl pyridines **15a**–**c** in 69–85% yield (Scheme 1).

The treatment of these unsaturated pyridines with diphenylphosphane (Ph_2PH), dicyclohexylphosphane ($(c\text{-}C_6H_{11})_2PH$), or diphenylphosphane oxide ($Ph_2P(O)H$) in dimethyl sulfoxide (DMSO) or *N*-methylpyrrolidinone (NMP) in the presence of a catalytic amount of *t*BuOK (20 mol%) provided the phosphane oxides **16a**–**d** and **17a**–**b** in 55–93% yield.[2c] The phosphane oxides were reduced with $HSiCl_3/Et_3N$ in toluene[7] to give the desired P,N ligands **1**–**6** in 60–92% yield (Scheme 2). The relative stereochemistry of the P,N ligands was established by NOESY NMR experiments and by X-ray crystal-structure analysis (see Supporting Information).[8]

Although a number of terpene-derived ligands have been prepared and used in asymmetric catalysis,[9] these new modular ligands, in which a broad range of pyridyl and related heterocycles can be incorporated, display particularly high enantioselectivities in asymmetric iridium-catalyzed



Scheme 1. The synthesis of 2-alkenylpyridines **13**–**15**: a) $[Pd(dba)_2]$ (2 mol%), dppf (2 mol%), alkenyl triflate **9** or **10**, THF, LiCl, reflux, overnight; b) $[Pd(PPh_3)_4]$ (5 mol%), $PhB(OH)_2$, Na_2CO_3, toluene, MeOH, H_2O, 85 °C, overnight. dba = dibenzylideneacetone, dppf = 1,1′-bis-(diphenylphosphanyl)ferrocene.



Scheme 2. Preparation of the P,N ligands **1**–**6**.

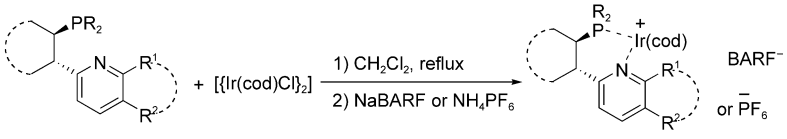
[*] Prof. Dr. P. Knochel, T. Bunlaksananusorn, Dr. K. Polborn
Department Chemie, Ludwig-Maximilians-Universität
Butenandtstrasse 5–13, Haus F,
81377 München (Germany)
Fax: (+49) 89-2180-77680
E-mail: paul.knochel@cup.uni-muenchen.de

[**] We thank the Fonds der Chemischen Industrie for financial support. We thank BASF AG (Ludwigshafen), Bayer AG (Leverkusen), and Chemetall GmbH (Frankfurt) for the generous gift of chemicals.

Supporting information for this article is available on the WWW under http://www.angewandte.org or from the author.

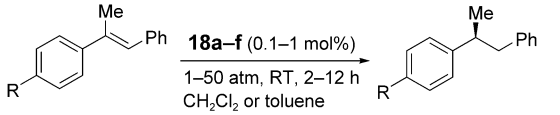
 DOI: 10.1002/anie.200351936 © 2003 Wiley-VCH Verlag GmbH & Co. KGaA, Weinheim

hydrogenations.[10,11] Thus, the P,N ligands **1–6** were heated with $[\{Ir(cod)Cl\}_2]$ in CH_2Cl_2 (40 °C, 1 h), and the reaction was quenched with sodium tetrakis(3,5-bis(trifluoromethyl)phenyl)borate (NaBARF) or with NH_4PF_6 in water to give the corresponding iridium complexes **18a–f** in 75–89% yield, according to the procedure of Pfaltz and co-workers (Scheme 3).[11]



1–6

18a: [Ir(**1**)(cod)]BARF; 89 %
18b: [Ir(**2**)(cod)]BARF; 88 %
18c: [Ir(**3**)(cod)]BARF; 75 %
18d: [Ir(**4**)(cod)]BARF; 88 %
18e: [Ir(**5**)(cod)]BARF; 85 %
18f: [Ir(**1**)(cod)]PF_6; 80 %



19a: R = H
19b: R = OMe

100 %; up to 96 % *ee*

20a: R = H
20b: R = OMe

Scheme 3. Preparation of the chiral Ir complexes **18a–f** and their use in the asymmetric hydrogenation of **19a** and **19b**. cod = 1,5-cyclooctadiene.

The Ir-catalyzed hydrogenation of (*E*)-1,2-diphenylpropene (**19a**) and 2-(4-methoxyphenyl)-1-phenyl-1-propene (**19b**) was performed at room temperature in the presence of complexes **18a–e** (0.1–1 mol%; Table 1). A slower reaction was observed in CH_2Cl_2, and excellent conversion was observed in toluene (see Table 1, entries 1 and 2). Remarkably, the use of complex **18d**, which contains a quinolyl group, led to high conversions and high enantioselectivities (Table 1, entries 8–13). As a result of the high activity of this catalyst, the reaction can be carried out at 1 bar of hydrogen (Table 1, entries 10, 11, and 12). Similar results were obtained with **19b** (Table 1, entries 15–18). Catalyst **18d** was the most active of those studied (see Table 1, entries 15 and 16). Other substrates, such as ethyl 3-phenylbut-2-enoate (**21**), 2-methyl-3-phenylallyl alcohol (**22**), and 2-methyl-3-phenylallyl acetate (**23**), were also hydrogenated in the presence of catalyst **18d** (1 mol%; H_2 (50 bar), room temperature, 12 h), and the desired reduced products were obtained with moderate to good enantioselectivities (58–80% *ee*; Scheme 4).

The hydrogenation of unsaturated enamides such as **24** to amino acid derivatives such as **25** is of special interest. This enantioselective hydrogenation has been studied extensively in the presence of Rh catalysts.[1] To our knowledge, no enantioselective Ir-catalyzed hydrogenation of this type has been reported.

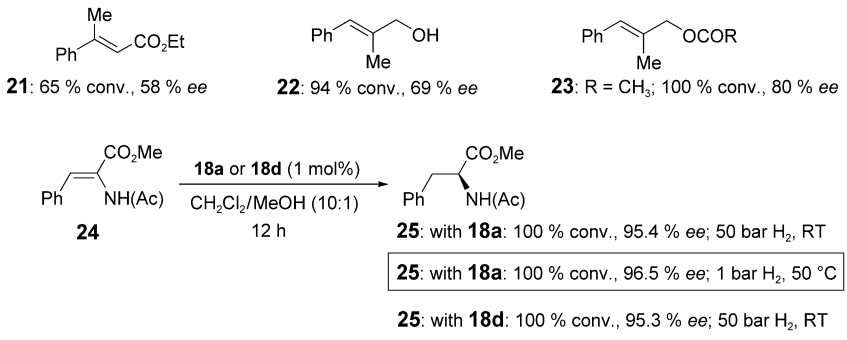
Table 1: Iridium-catalyzed enantioselective hydrogenation of **19a** and **19b** in toluene at 25 °C.

Entry	**18** (mol%)	**19**	*P* [bar][a]	*t* [h]	Conv. [%][b]	*ee* [%][c]
1	**a** (1.0)	**a**	50	12	44	93.5[d]
2	**a** (1.0)	**a**	50	12	100	95.0
3	**a** (0.5)	**a**	50	12	100	95.0
4	**a** (1.0)	**a**	1	5	91	95.0
5	**a** (0.5)	**a**	1	2	90	95.0
6	**b** (1.0)	**a**	50	12	6	–
7	**c** (1.0)	**a**	1	12	80	80.0
8	**d** (1.0)	**a**	50	12	100	95.0
9	**d** (1.0)	**a**	50	2	100	94.0
10	**d** (1.0)	**a**	1	5	100	95.0
11	**d** (0.5)	**a**	1	2	96	96.0
12	**d** (0.1)	**a**	1	12	1	–
13	**d** (0.1)	**a**	50	12	92	95.0
14	**e** (1.0)	**a**	50	2	26	80.0[e]
15	**a** (1.0)	**b**	50	2	87	91.0
16	**d** (1.0)	**b**	50	2	100	94.7
17	**d** (1.0)	**b**	1	2	76	94.0
18	**d** (1.0)	**b**	50	2	75	95.2[d]

[a] Reaction pressure. [b] Conversion. [c] The enantiomeric excess was determined by HPLC on a chiral phase (Daicel Chiracel OJ column). The products have the *S* configuration unless otherwise indicated. [d] This reaction was performed in CH_2Cl_2. [e] *R* configuration.

We found that the hydrogenation of **24** under our standard conditions (H_2 (50 bar), room temperature, 12 h) in CH_2Cl_2/MeOH (10:1) in the presence of the chiral Ir catalysts **18a** and **18d** provided the phenylalanine derivative **25** in 100% conversion and with 95.4% *ee* and 95.3% *ee*, respectively. Moreover, when the reaction was carried out the higher temperature of 50 °C and at just 1 bar of H_2, 100% conversion and an excellent 96.5% *ee* were observed (Scheme 4). These results show the potential of Ir complexes for new applications in the asymmetric synthesis of amino acids.

In summary, we have prepared a new type of P,N ligand, which facilitates the Ir-catalyzed enantioselective hydrogenation of unactivated stilbene derivatives and dehydroamino acid derivatives. Because of the modular synthesis[12] of these ligands, their stereochemical and electronic properties can be tuned to optimize the enantioselectivity of a given asymmetric reaction or for a particular substrate. Further applications in new asymmetric reactions are currently underway in our laboratories.[13]



21: 65 % conv., 58 % *ee*

22: 94 % conv., 69 % *ee*

23: R = CH_3; 100 % conv., 80 % *ee*

24

25: with **18a**: 100 % conv., 95.4 % *ee*; 50 bar H_2, RT

25: with **18a**: 100 % conv., 96.5 % *ee*; 1 bar H_2, 50 °C

25: with **18d**: 100 % conv., 95.3 % *ee*; 50 bar H_2, RT

Scheme 4. Ir-catalyzed hydrogenation of unsaturated substrates with catalysts **18a** and **18d**. conv. = conversion.

 © 2003 Wiley-VCH Verlag GmbH & Co. KGaA, Weinheim

Experimental Section

Preparation of (*S*)-**25**: An autoclave was charged with **18a** (4.7 mg, 3.0 μmol, 1 mol%), **24** (65 mg, 0.3 mmol), CH_2Cl_2 (3 mL), and MeOH (0.3 mL). The autoclave was then sealed and pressurized to 1 bar of H_2, and the reaction mixture was stirred at 50 °C for 2 h. The CH_2Cl_2 and MeOH were then removed and the crude product was passed through a short column of silica gel with diethyl ether as eluent. After evaporation of the solvent, (*S*)-**25** was obtained in quantitative yield and with 96.5% *ee*. The *ee* value was determined by GC on a chiral phase (Chiralsil L-Val); 140 °C: $t_r = 10.5$ (*R*), 11.5 min (*S*).

Received: May 20, 2003 [Z51936]

Keywords: asymmetric catalysis · cross-coupling · hydrogenation · iridium · N,P ligands

[1] a) R. Noyori, *Asymmetric Catalysis in Organic Synthesis*, Wiley, New York, **1994**; b) T. Ohkuma, M. Kitamura, R. Noyori in *Catalytic Asymmetric Synthesis* (Ed.: I. Ojima), Wiley-VCH, Weinheim, **2000**, p. 1; c) J. M. Brown in *Comprehensive Asymmetric Catalysis* (Eds.: E. N. Jacobsen, A. Pfaltz, H. Yamamoto), Springer, Berlin, **1999**, p. 121; d) M. Beller, M. Eckert, *Angew. Chem.* **2000**, *112*, 1026; *Angew. Chem. Int. Ed.* **2000**, *39*, 1010.

[2] a) A. L. Rodriguez, T. Bunlaksananusorn, P. Knochel, *Org. Lett.* **2000**, *2*, 3285; b) T. Bunlaksananusorn, A. L. Rodriguez, P. Knochel, *Chem. Commun.* **2001**, 745; c) T. Bunlaksananusorn, P. Knochel, *Tetrahedron Lett.* **2002**, *43*, 5817.

[3] a) G. Helmchen, A. Pfaltz, *Acc. Chem. Res.* **2000**, *33*, 336; b) A. Togni, N. Bieler, U. Burckhardt, C. Köllner, G. Pioda, R. Schneider, A. Schnyder, *Pure Appl. Chem.* **1999**, *71*, 1531; c) O. Loiseleur, M. Hayashi, M. Keenan, N. Schmees, A. Pfaltz, *J. Organomet. Chem.* **1999**, *576*, 16; d) P. W. Roesky, *Heteroat. Chem.* **2002**, *13*, 514.

[4] J. E. Mc Murry, W. J. Scott, *Tetrahedron Lett.* **1983**, *24*, 979.

[5] a) E.-I. Negishi, *Acc. Chem. Res.* **1982**, *15*, 340; b) E.-I. Negishi in *Metal-catalyzed Cross-coupling Reactions* (Eds.: F. Diederich, P. J. Stang), Wiley-VCH, Weinheim, **1998**, chap. 1.

[6] a) G. Chelucci, N. Culeddu, A. Saba, R. Valenti, *Tetrahedron: Asymmetry* **1999**, *10*, 3537; b) M. Alami, J.-F. Peyrat, L. Belachmi, J.-D. Brion, *Eur. J. Org. Chem.* **2001**, *22*, 4207; c) for an excellent recent review, see: A. F. Littke, G. C. Fu, *Angew. Chem.* **2002**, *114*, 4350; *Angew. Chem. Int. Ed.* **2002**, *41*, 4176.

[7] Y. Uozumi, T. Hayashi, *J. Am. Chem. Soc.* **1991**, *113*, 9887.

[8] CCDC 209753–209755 (borane complexes of **1, 16a**, and **17b**) contain the supplementary crystallographic data for this paper. These data can be obtained free of charge via www.ccdc.cam.ac.uk/conts/retrieving.html (or from the Cambridge Crystallographic Data Centre, 12, Union Road, Cambridge CB2 1EZ, UK; fax: (+44) 1223-336-033; or deposit@ccdc.cam.ac.uk).

[9] For some recent examples, see: a) S. Schleich, G. Helmchen, *Eur. J. Org. Chem.* **1999**, *10*, 2515; b) G. Knühl, P. Sennhenn, G. Helmchen, *J. Chem. Soc. Chem. Commun.* **1995**, 1845; c) A. V. Malkov, M. Bella, I. G. Stará, P. Kocovský, *Tetrahedron Lett.* **2001**, *42*, 3045; d) G. Chelucci, A. Saba, F. Soccolini, *Tetrahedron* **2001**, *57*, 9989; e) B. Goldfuss, M. Steigelmann, F. Rominger, *Angew. Chem.* **2000**, *112*, 4299; *Angew. Chem. Int. Ed.* **2000**, *39*, 4133; f) B. Goldfuss, T. Löschmann, F. Rominger, *Chem. Eur. J.* **2001**, *7*, 2028; g) B. Goldfuss, M. Steigelmann, F. Rominger, H. Urtel, *Chem. Eur. J.* **2001**, *7*, 4456; h) M. Steigelmann, Y. Nisar, F. Rominger, B. Goldfuss, *Chem. Eur. J.* **2002**, *8*, 5211.

[10] a) F. Menges, M. Neuburger, A. Pfaltz, *Org. Lett.* **2002**, *4*, 4713; b) H.-U. Blaser, *Adv. Synth. Catal.* **2002**, *344*, 17; c) J. Blankenstein, A. Pfaltz, *Angew. Chem.* **2001**, *113*, 4577; *Angew. Chem. Int. Ed.* **2001**, *40*, 4445; d) H.-U. Blaser, H.-P. Buser, R. Häusel, H.-P. Jalett, F. Spindler, *J. Organomet. Chem.* **2001**, *621*, 34; e) G. H. Bernardinelli, E. P. Kündig, P. Meier, A. Pfaltz, K. Radkowski, N. Zimmermann, M. Neuburger-Zehnder, *Helv. Chim. Acta* **2001**, *84*, 3233; f) P. G. Cozzi, N. Zimmermann, R. Hilgraf, S. Schaffner, A. Pfaltz, *Adv. Synth. Catal.* **2001**, *343*, 450; g) D. G. Blackmond, A. Lightfoot, A. Pfaltz, T. Rosner, P. Schnider, N. Zimmermann, *Chirality* **2000**, *12*, 442; h) R. Hilgraf, A. Pfaltz, *Synlett* **1999**, 1814; i) P. Schnider, G. Koch, R. Prétôt, G. Wang, F. M. Bohnen, C. Krüger, A. Pfaltz, *Chem. Eur. J.* **1997**, *3*, 887; j) M. C. Perry, K. Burgess, *Tetrahedron: Asymmetry* **2003**, *14*, 951; k) M. C. Perry, X. Cui, M. T. Powell, D.-R. Hou, J. H. Reibenspies, K. Burgess, *J. Am. Chem. Soc.* **2003**, *125*, 113; l) M. T. Powell, D.-R. Hou, M. C. Perry, X. Cui, K. Burgess, *J. Am. Chem. Soc.* **2001**, *123*, 8878; m) D.-R. Hou, J. H. Reibenspies, T. J. Colacot, K. Burgess, *Chem. Eur. J.* **2001**, *7*, 5391; n) D.-R. Hou, J. H. Reibenspies, K. Burgess, *J. Org. Chem.* **2001**, *66*, 206.

[11] A. Lightfoot, P. Schnider, A. Pfaltz, *Angew. Chem.* **1998**, *110*, 3047; *Angew. Chem. Int. Ed.* **1998**, *37*, 2897.

[12] a) C. A. Luchaco-Cullis, H. Mitzutani, K. E. Murphy, A. H. Hoveyda, *Angew. Chem.* **2001**, *113*, 1504; *Angew. Chem. Int. Ed.* **2001**, *40*, 1456; b) S. J. Degrado, H. Mitzutani, A. H. Hoveyda, *J. Am. Chem. Soc.* **2001**, *123*, 755; c) T. P. Yoon, E. N. Jacobsen, *Science* **2003**, *299*, 1691.

[13] The new ligands and their applications in asymmetric catalysis were patented in collaboration with Bayer AG.

 © 2003 Wiley-VCH Verlag GmbH & Co. KGaA, Weinheim

Biomimetic Total Synthesis

An Enantioselective Biomimetic Total Synthesis of (−)-Siccanin**

Barry M. Trost, Hong C. Shen, and Jean-Philippe Surivet*

Siccanin (**1**), a mold metabolite isolated from the culture broth of *Helminthosposium siccans* by Ishibashi in 1962,[1] possesses an unusual *cis*,*syn*,*cis*-fused alicyclic ring system. Siccanin exhibits potent antifungal activity, in particular against several pathogenic fungi,[2] and its clinical effectiveness against surface mycosis has also been established.[3]

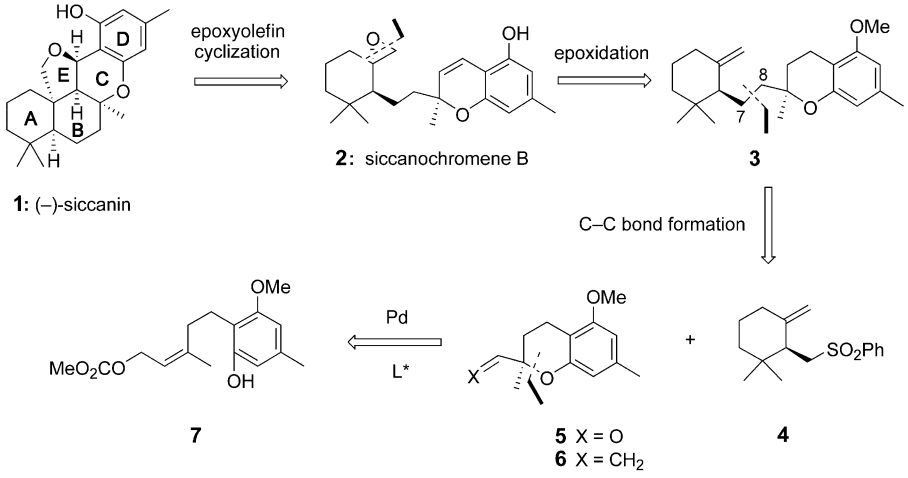
As a result of its interesting biological activity, siccanin has been the subject of a number of synthetic efforts.[4] However, only two successful racemic syntheses of this natural product have been reported to date.[4g–i] Herein we

[*] Prof. B. M. Trost, H. C. Shen, J.-P. Surivet
Department of Chemistry, Stanford University
Stanford, CA 94305-5080 (USA)
Fax: (+1) 650-725-0002
E-mail: bmtrost@stanford.edu

[**] We thank the National Science Foundation and the National Institutes of Health, General Medical Sciences (GM-13598) for their generous support of our programs. Mass spectra were provided by the Mass Spectrometry Regional Center of the University of California, San Francisco, supported by the NIH Division of Research Resources.

Supporting information for this article is available on the WWW under http://www.angewandte.org or from the author.

 DOI: 10.1002/anie.200351868 © 2003 Wiley-VCH Verlag GmbH & Co. KGaA, Weinheim



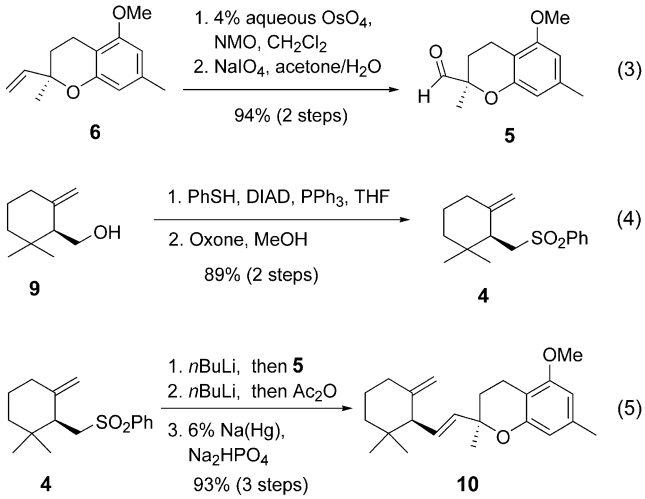
Scheme 1. Retrosynthetic analysis of (−)-siccanin (**1**). L = ligand.

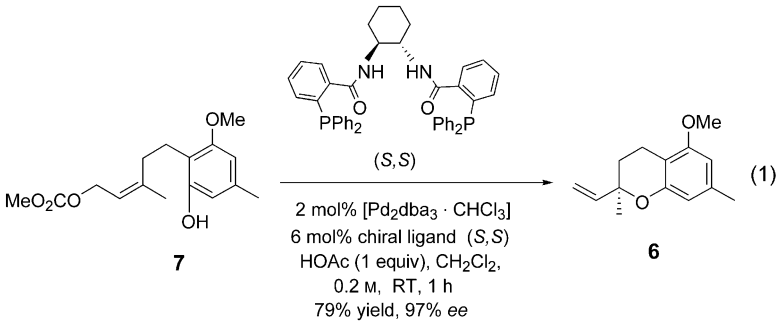
report the first enantioselective biomimetic total synthesis of (−)-siccanin (**1**), which has a Pd-catalyzed asymmetric allylic alkylation and an epoxyolefin radical cyclization as key steps (Scheme 1).

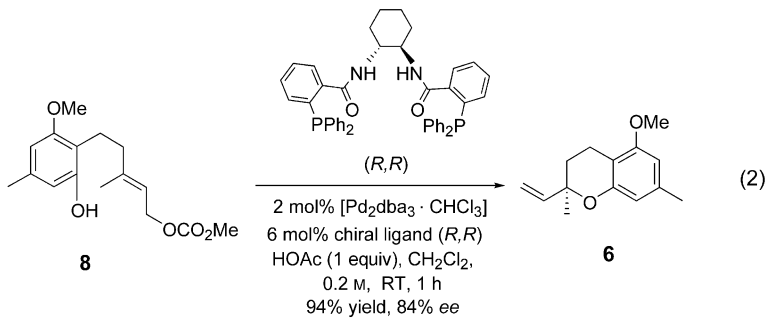
Inspired by the biosynthetic pathway of **1**,[5] we envisaged that its B and E rings could be formed through an epoxyolefin cyclization reaction of siccanochromene B (**2**), a proposed biosynthetic precursor of **1**. Siccanochromene B (**2**) can be seen to be derived from **3**, which itself could be prepared from a coupling reaction of chiral sulfone **4** with chiral chroman **5**. Chroman **6**, the precursor of **5**, is in turn available through a Pd-catalyzed asymmetric allylic alkylation reaction that has been developed recently by our group [Eq. (1) and (2)] (dba = dibenzylideneacetone).

Both the *Z* and the *E* allylic carbonates **7** and **8**, readily available through literature procedures,[6] can be used to prepare the same chiral chroman **6** by using ligands of opposite chirality [Eq. (1) and (2)]. Use of the *Z* allylic carbonate **7** afforded chiral chroman **6** with a substantially higher *ee* value (97%) than did use of its *E* counterpart **8** (84%). The resulting chiral chroman **6** underwent a dihydroxylation followed by oxidative cleavage to afford aldehyde **5** [Eq. (3)] (NMO = *N*-methylmorpholine *N*-oxide).

As shown in Equation (4), sulfone **4** can be prepared from the readily available chiral alcohol **9** in two steps (DIAD = diisopropyl azodicarboxylate.)[7] The subsequent Julia olefination[8] of chiral sulfone **4** with chiral chroman aldehyde **5** proceeded in high yield to give diene **10** [Eq. (5)].



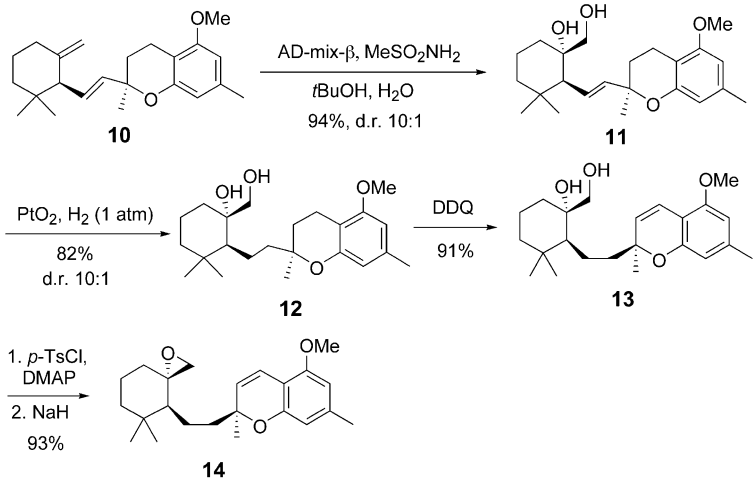




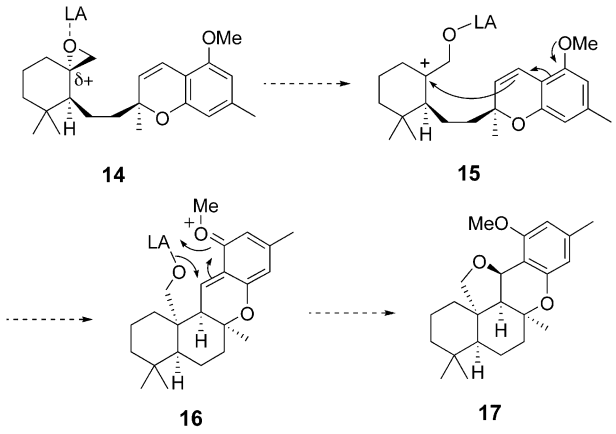
The epoxidation of diene **10** with *m*CPBA gave a complex mixture of products. In contrast, the dihydroxylation of **10** under the conditions of Sharpless and coworkers[9] took place chemo- and diastereoselectively to generate diol **11** (d.r. 10:1). The subsequent hydrogenation smoothly afforded chroman diol **12** (Scheme 2). DDQ oxidation[10] of diol **12** afforded chromene diol **13**, which was readily converted into epoxide **14**, the methyl ether of **2**.

Our first approach to the biomimetic synthesis of **1** involved a proposed novel cationic cyclization (Scheme 3). A Lewis acid should open epoxide **14** to generate a tertiary cation **15**, which could then be trapped by the electron-rich olefin to form the B ring of siccanin, as in **16**. The resulting oxygen nucleophile could undergo a 1,4-addition to the adjacent enone, facilitated by the Lewis acid (LA), to construct the tetrahydrofuran ring and form the siccanin methyl ether (**17**). This proposal would allow **17** to be built up in one pot, with the cleavage of one C–O bond and the formation of one C–C bond and one C–O bond. However, when **14** was treated with a variety of Lewis acids, only decomposition or formation of 1,2-hydride-shift product **18** were observed, and no cyclization products were isolated [Eq. (6)].

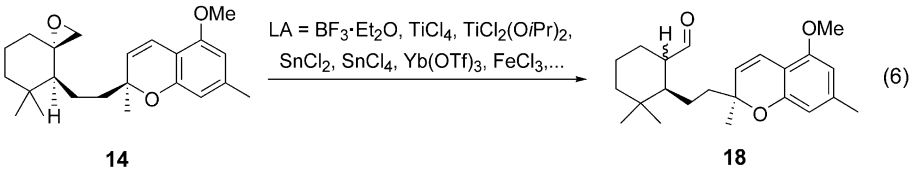
 © 2003 Wiley-VCH Verlag GmbH & Co. KGaA, Weinheim



Scheme 2. Synthesis of epoxide **14**. DDQ = 2,3-dichloro-5,6-dicyano-1,4-benzoquinone; DMAP = 4-(dimethylamino)pyridine; Ts = toluenesulfonyl.



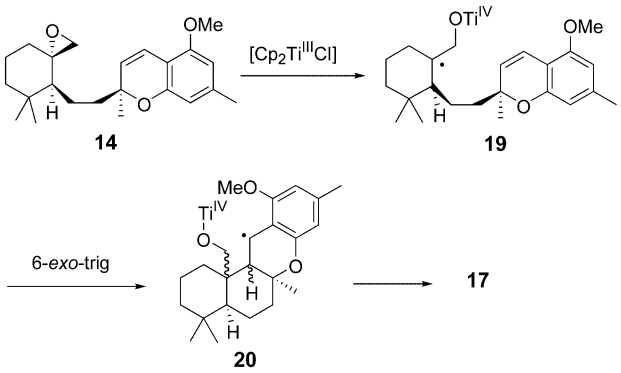
Scheme 3. Proposed biomimetic cationic cyclization.



(6)

To overcome this problem, we proposed a radical cyclization of epoxide **14** in the presence of $Cp_2Ti^{III}Cl$.[11] The resulting tertiary radical **19** should undergo a 6-*exo*-trig cyclization to form benzylic radical **20** (Scheme 4). After considerable experimentation, we were pleased to observe that the Ti^{III}-mediated cyclization of **14** afforded the desired tetracyclic compound **21**, and the 5-*epi*-siccanin methyl ether (**22**) as a side product, in a 3:1 ratio and 81% combined yield [Eq. (7)].

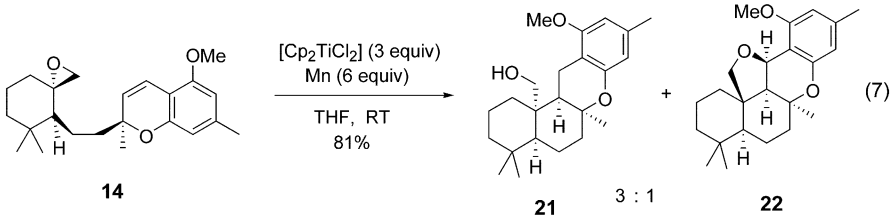
A mechanistic rationale for the formation of **21** and **22** is proposed in Scheme 5. The Ti^{III} species, generated in situ by the reduction of titanocene dichloride with manganese, opens epoxide **14** to form a tertiary radical **19**. Intermediate **19** then cyclizes in a 6-*exo*-trig fashion to form benzylic radical **23**, which reacts further with a second equivalent of the Ti^{III} species to form a C–Ti^{IV} bond. Subsequent hydrolysis leads to the formation of tetracyclic product **21** with the desired stereochemistry. Alternatively, **19** may undergo cyclization to benzylic radical **25**, which is diastereomeric with respect to **23**. It appears that the proximity of the Ti^{IV}-bonded oxygen atom to the benzylic carbon radical in **25** leads to a further cyclization. Radical recombination as illustrated liberates Ti^{III} and produces **22**.



Scheme 4. Proposed biomimetic radical cyclization. Cp = cyclopentadienyl.

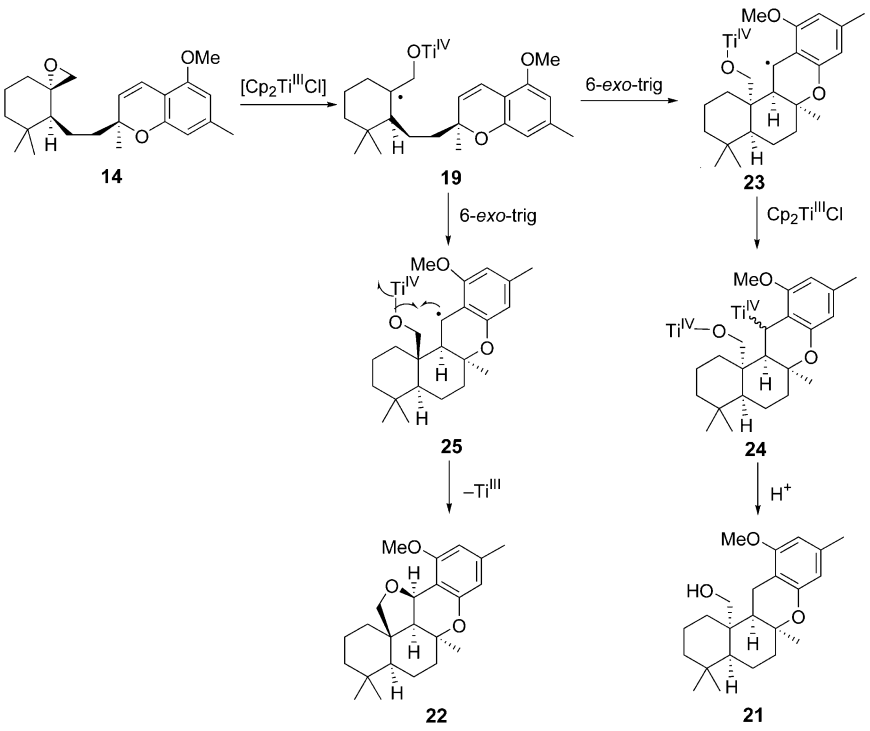
The final key step in the synthesis of siccanin involves a free-radical remote functionalization of **21** under conditions reported by Suarez and co-workers[12] to provide pentacyclic compound **28**, presumably via iodide **26** and oxonium ion **27**(Scheme 6). PM3 calculations showed that the energy of natural siccanin methyl ether (**28**) is 16.5 kcal mol^{-1} lower than that of 11-*epi*-siccanin methyl ether (**29**). The energy of the transition states that lead to **28** or **29** should reflect the strain energy of the product. Therefore, the product with significantly lower energy is formed preferentially. Furthermore, the preferred conformation of intermediate **27** acts as a constraint on the hydroxy nucleophile to attack **27** from the face that leads to the *cis*-fused ring system of the desired pentacyclic compound **28** (Scheme 6).

Finally, the pentacyclic compounds **28** and **22** were demethylated to afford (−)-siccanin (**1**) and (−)-5-*epi*-sicca-

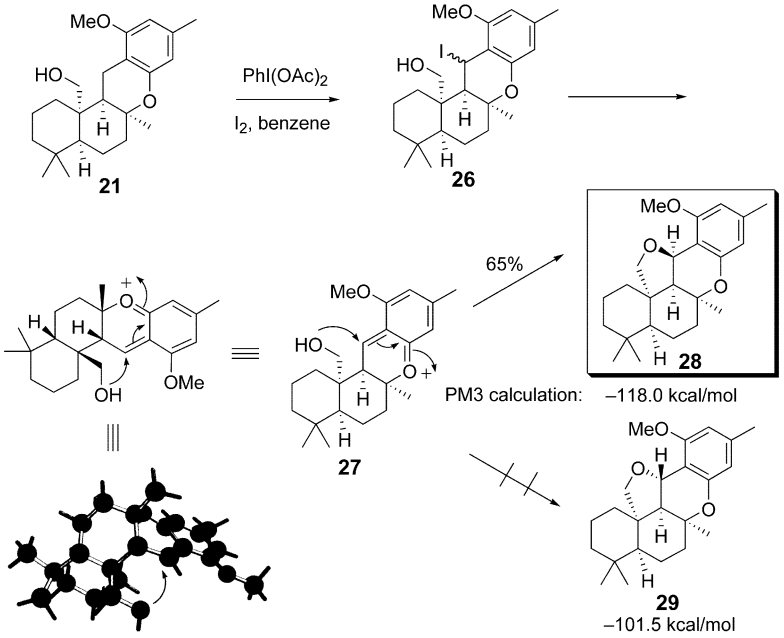


(7)

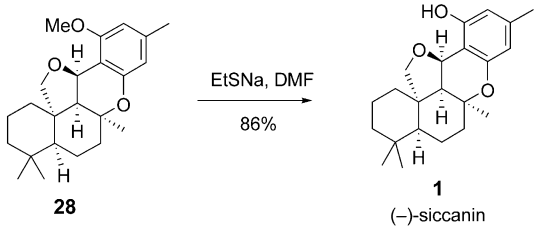
 © 2003 Wiley-VCH Verlag GmbH & Co. KGaA, Weinheim



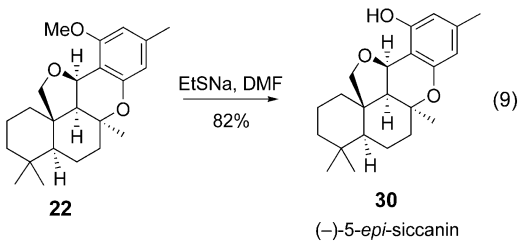
Scheme 5. Proposed mechanism for the radical cyclization.



Scheme 6. The synthesis of pentacyclic compound **28**.



(8)



(9)

nin (**30**), respectively [Eq. (8) and (9)] (DMF = *N*,*N*-dimethylformamide).

In summary, we have carried out the first enantioselective total synthesis of (−)-siccanin (**1**), inspired by the biosynthetic route and based on our development of the Pd-catalyzed asymmetric allylic alkylation and a novel radical epoxide cyclization. Our synthesis consists of 13 linear steps from allyl carbonate **7** or **8.** These results may have implications for the understanding of the biosynthetic pathway—that is, whether the corresponding biocyclization is cationic or radical in nature.

Received: May 12, 2003 [Z51868]

Keywords: asymmetric synthesis · biomimetic synthesis · cyclization · natural products · radical reactions

[1] K. J. Ishibashi, *J. Antibiot. Ser. A* **1962**, *15*, 161.
[2] a) K. Ishibashi, K. Hirai, M. Arai, S. Sugasawa, A. Endo, A. Yasumura, H. Matsuda, T. Muramatsu, *Annu. Rep. Sankyo Res. Lab.* **1970**, *22*, 1; b) M. G. Belloti, L. Riviera, *Chemioterapia* **1985**, *4*, 431.
[3] a) D. Crippa, C. G. Albanese, G. P. Sala, *G. Ital. Dermatol. Venereol.* **1985**, *120*, LVII and references therein; b) M. Arai, K. Ishibashi, H. Okazaki, *Antimicrob. Agents Chemother.* **1969**, 247; c) S. Sugawara, *Antimicrob. Agents Chemother.* **1969**, 253.
[4] a) S. Nozoe, K. Hirai, *Tetrahedron* **1971**, *27*, 6073; b) S. Oida, Y. Ohashi, A. Yoshida, E. Ohki, *Chem. Pharm. Bull.* **1972**, *20*, 2634; c) A. Yoshida, S. Oida, Y. Ohashi, C. Tamura, E. Ohki, *Chem. Pharm. Bull.* **1972**, *20*, 2642; d) S. Oida, Y. Ohashi, E. Ohki, *Chem. Pharm. Bull.* **1973**, *21*, 528; e) H. Liu, B. Ramani, *Tetrahedron Lett.* **1988**, *29*, 6721; f) M. Kato, Y. Matsuma, K. Heima, A. Yoshikoshi, *Bull. Chem. Soc. Jpn.* **1988**, *61*, 1991; g) M. Kato, K. Heima, Y. Matsuma, A. Yoshikoshi, *J. Am. Chem. Soc.* **1981**, *103*, 2434; h) M. Kato, Y. Matsuma, K. Heima, N. Fukamiya, C. Kabuto, A. Yoshikoshi, *Tetrahedron* **1987**, *43*, 711; i) B. M. Trost, F. J. Fleitz, W. J. Watkins, *J. Am. Chem. Soc.* **1996**, *118*, 5146.
[5] a) S. Nozoe, K. T. Suzuki, *Tetrahedron* **1971**, *27*, 6063; b) K. T. Suzuki, S. Nozoe, *Bioorg. Chem.* **1974**, *3*, 72; c) K. T. Suzuki, S. Nozoe, *J. Chem. Soc. Chem. Commun.* **1971**, 527; d) D. J. Goldsmith, C. F. Philips, *J. Am. Chem. Soc.* **1969**, *91*, 5862; e) D. J. Goldsmith, B. C. Clark, *Tetrahedron Lett.* **1967**, *8*, 1215.
[6] B. M. Trost, N. Asakawa, *Synthesis* **1999**, 1491.

 © 2003 Wiley-VCH Verlag GmbH & Co. KGaA, Weinheim

[7] H. Tanimoto, T. Oritani, *Tetrahedron* **1997**, *53*, 3527.
[8] a) M. Julia, J. M. Paris, *Tetrahedron Lett.* **1973**, 4833; b) P. Kocienski, *Phosphorus Sulfur Relat. Elem.* **1985**, *24*, 97.
[9] H. C. Kolb, M. S. VanNieuwenhze, K. B. Sharpless, *Chem. Rev.* **1994**, *94*, 2483.
[10] a) A. N. Starrat, A. Stoesl, *Can. J. Chem.* **1977**, *55*, 2360; b) V. K. Ahluwalia, R. S. Jolly, *Synthesis* **1982**, 74; c) D. R. Buckle, in *Encyclopedia of Reagents for Organic Synthesis, Vol. 3* (Ed.: L. A. Paquette), Wiley, New York, **1995**, p. 1699.
[11] a) T. V. RajanBabu, W. A. Nugent, M. S. Beattie, *J. Am. Chem. Soc.* **1990**, *112*, 6408; b) A. Gansauer, M. Pierobon, H. Bluhm, *Synthesis* **2001**, 2500; c) T. V. RajanBabu, W. A. Nugent, *J. Am. Chem. Soc.* **1994**, *116*, 986; d) S. C. Roy, K. K. Rana, C. Guin, *J. Org. Chem.* **2002**, *67*, 3242.
[12] J. T. Concepcion, C. G. Francisco, R. Hernandez, J. A. Salaza, E. Suarez, *Tetrahedron Lett.* **1984**, *25*, 1953.

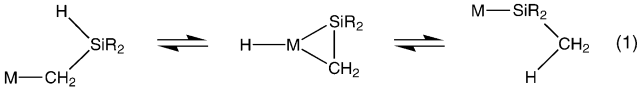
 © 2003 Wiley-VCH Verlag GmbH & Co. KGaA, Weinheim

Agostic Si–H Interactions

Tandem β-C–H Activation/Si–H Elimination Reactions: Stabilization of C–H Activation Products by β-Agostic Si–H Interactions**

*Vladimir K. Dioumaev, Patrick J. Carroll, and Donald H. Berry**

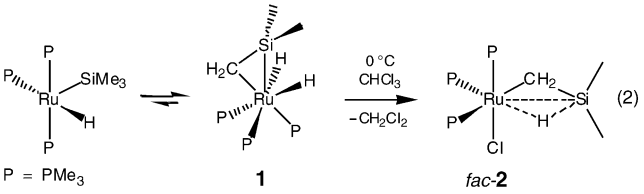
Organometallic complexes of silenes have been postulated and often observed to be intermediates in many C–H, Si–H, Si–C, and Si–Si bond-breaking and bond-forming processes.[1] Many isolated and characterized silene complexes have been synthesized via β-Si–H activation of CH_2SiR_2-H ligands, but this reaction often proceeds further to furnish the metal silyl ($MSiR_2CH_3$) as a more thermodynamically stable product [Eq. (1)].[1a] Interestingly, this preference of breaking SiH/MC



(1)

and forming CH/MSi bonds is not universal. For instance, the silene complex $[(\eta^5\text{-}C_5Me_5)Ru(P\mathit{i}Pr_3)(\eta^2\text{-}CH_2SiPh_2)H]$, formed via β-Si–H activation, in some cases reacts with hydrosilanes via Si–H instead of C–H reductive elimination, and the selection is triggered by subtle changes in the nature of the incoming silane.[2] Furthermore, selective isotope exchange in osmium and ruthenium silyl complexes suggests that the CH-activation stage of Equation (1) is also reversible.[3] Recent reports of the direct observation of aliphatic β-C–H bond elimination in 16-electron metal silyl complexes by us and by Klei et al.[4] conclusively establish the reversibility of C–H addition/elimination processes in some metal silyl complexes [Eq. (1)]. We now report the first example of conversion from $[M]SiMe_3$ to β-agostic $[M]CH_2SiMe_2$-H species, a total inversion of the usual left-to-right direction of the process in Equation (1).

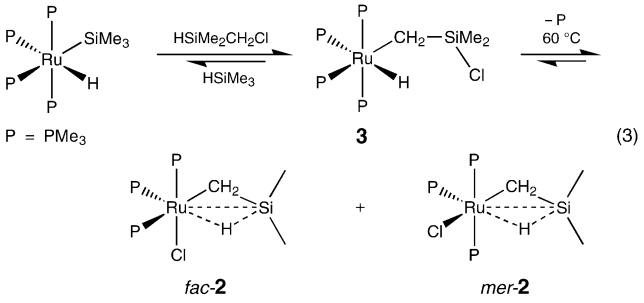
Treatment of a mixture of the 16-electron $[(Me_3P)_3Ru(SiMe_3)H]$, in equilibrium with the "silene dihydride" complex $[(Me_3P)_3Ru(\eta^2\text{-}CH_2SiMe_2)(H)_2]$ (**1**)[4a,b] with $CHCl_3$ between −40 and 0 °C leads to the chlorination of one hydride and the formation of $[(Me_3P)_3Ru(CH_2SiMe_2)(H)Cl]$, *fac*-(**2**) [Eq. (2)], which has been isolated in 86% yield and



(2)

fully characterized. That this complex is neither a simple η^2-silene hydride nor a η^1-alkyl is evident from strong Si–H scalar coupling (J(H,Si) = 75 Hz).[5] A very weak, low-frequency band in the IR spectrum (1615 cm^{-1}; absent in $[D_1]$*fac*-**2**) is also consistent with an agostic Si···H···Ru, but this assignment is tentative because of the very low intensity of the band.

A more convenient synthetic route to *fac*-**2** is based on *cis*-$[(Me_3P)_4Ru(CH_2SiMe_2Cl)H]$ (**3**), which in turn can be readily synthesized from $[(Me_3P)_4Ru(SiMe_3)H]$ and $HSiMe_2CH_2Cl$ [Eq. (3)]. Isotopically labeled material, $[D_1]$*fac*-**2** was synthe-



(3)

sized using $DSiMe_2CH_2Cl$. Note that the deuterium atom is only found as Si-D-Ru and no scrambling into C–H positions was observed. The structure of **3** was determined by single-crystal X-ray diffraction to be approximately octahedral, with all bond distances and angles within normal ranges. No evidence for nonclassical Si–Cl···Ru, Si···H–Ru, or Ru–H···Cl interactions was observed in the solid state or in solution

[*] D. H. Berry, V. K. Dioumaev, P. J. Carroll
Department of Chemistry and
Laboratory for Research on the Structure of Matter
University of Pennsylvania
Philadelphia, PA 19104-6323 (USA)
Fax: (+1) 215-573-3044
E-mail: dberry@sas.upenn.edu

[**] We are grateful to the National Science Foundation (CHE-9904798) and Tokyo Electron Massachusetts for support of this work.

Supporting information for this article is available on the WWW under http://www.angewandte.org or from the author.

 DOI: 10.1002/anie.200352078 © 2003 Wiley-VCH Verlag GmbH & Co. KGaA, Weinheim

(^{1}H NMR: J(H,Si) < 12 Hz; IR: $\tilde{\nu}$(RuH) = 1840 cm^{-1}; Si···H 3.34; Cl···Ru 4.86; H···Cl 4.54 Å).

Thermal (65 °C) or photochemical (350 nm) treatment of **3** in hydrocarbon solvents leads to phosphane loss and formation of *fac*-**2**. Under thermal conditions, *fac*-**2** is in equilibrium with **3**, although the product is strongly favored ($K_{eq} \approx 0.06$ mol L^{-1} at 25 °C). Removal of PMe_3 and addition of fresh solvent allows the isolation of **2** nearly quantitatively. In addition, approximately 5 % of the meridional isomer *mer*-(**2**) is also observed [Eq. (3)]. The structure of *mer*-**2** was determined from a pure sample obtained by fractional crystallization (see below). The spectroscopic data is also consistent with the meridional structure, and again, a strong SiH scalar coupling (J(H,Si) = 77.5 Hz) indicates a nonclassical Ru···H···Si linkage.[5] The formation of **3** from $HSiMe_2CH_2Cl$ and $[(Me_3P)_4Ru(SiMe_3)H]$ and the subsequent conversion of **3** to **2** is an interesting sequence of reactions. Initial exchange of silyl ligands on the metal center by SiH addition and Me_3SiH elimination seems likely, given that Me_3SiCH_2Cl, which lacks the SiH group, does not react after days at ambient temperature. The migration of the chloride ion from carbon to silicon in the synthesis of **3** may involve a dyotropic process as suggested in a similar case for $[CpFe(CO)_2(SiMe_2CH_2Cl)]$.[6] An alternative mechanism involving the oxidative addition of C–Cl and the elimination of Si–Cl cannot be completely excluded, however the intermediate would have to be a yet unknown isomer of **2**, as neither *fac*-**2** nor *mer*-**2** favor the recoordination of PMe_3 and the formation of **3**.

The rate of conversion of **3** to **2** is approximately halved in the presence of added $[D_9]PMe_3$ (10 equiv), and the labeled phosphane is nonselectively incorporated into both **3** and **2**. This suggests the reaction proceeds via initial PMe_3 dissociation, and SiCl oxidative addition would be a likely second step. Interestingly, there are relatively few clear precedents for the oxidative addition of SiCl.[7] It is also noteworthy that the strong Si–Cl bond is maintained in **3**, but cleaved in **2** in preference for Ru–Cl (and agostic Si···H) bonds. It is likely that Cl–Ru π-donation compensates for partial electronic unsaturation in **2**, whereas additional electron donation would contribute nothing to the stability of **3**, an unequivocally 18-electron species.

The solid-state structures of *fac*-**2** and *mer*-**2** can both be described as square pyramidal, with three phosphane groups, a Cl atom, and the CH_2 group positioned around the ruthenium center, and the agostic Si···H occupying a sixth coordination site (Figure 1 and 2). Disorder of the agostic {CSiH} fragment in *fac*-**2** was successfully modeled (see Experimental Section), and while the heavy-atom positions should be reliable, the location of the hydride is less precise than usual. The Ru–P, Ru–Cl, and Ru–C bond lengths and angles are within normal ranges, but the Ru–Si bond lengths (*fac*-**2**: 2.526(2); *mer*-**2**: 2.468(2) Å) are at the long end of the range for Ru–Si single bonds (approximately 2.3–2.58 Å; 2.39 Å on average).[8] Longer Ru–C and Ru–Si separations in *fac*-**2** than in the *mer* isomer may be due the stronger *trans* influence of phosphane versus Cl on the agostic CSiH ligand, but the crystallographic disorder may also contribute. The hydrides in *fac*-**2** and *mer*-**2** were located in positions bridging

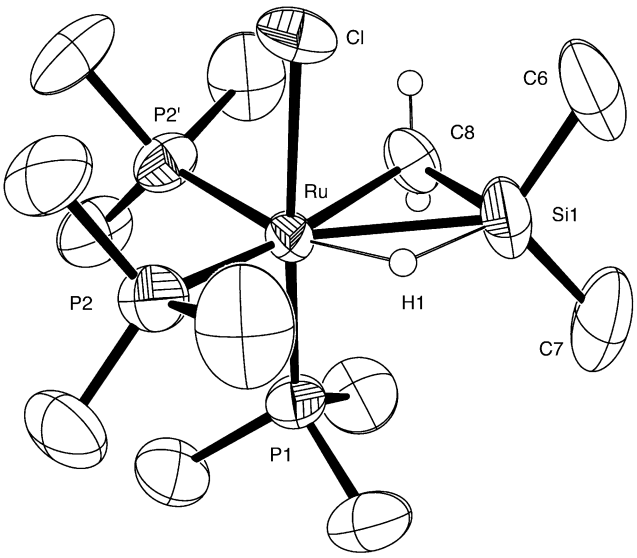


Figure 1. ORTEP diagram of complex *fac*-**2** (30 % probability ellipsoids). The second disordered position of the silene fragment is not shown. Selected bond lengths [Å] and angles [°]: Ru-C8 2.307(7), Ru-Si1 2.526(2), Si-C6 1.837(9), Si-C7 1.814(9), Si-C8 1.788(11), Ru-H1 1.550, Si-H1 1.664; Si1-C8-Ru 75.0(3), C8-Si1-Ru 61.9(2).

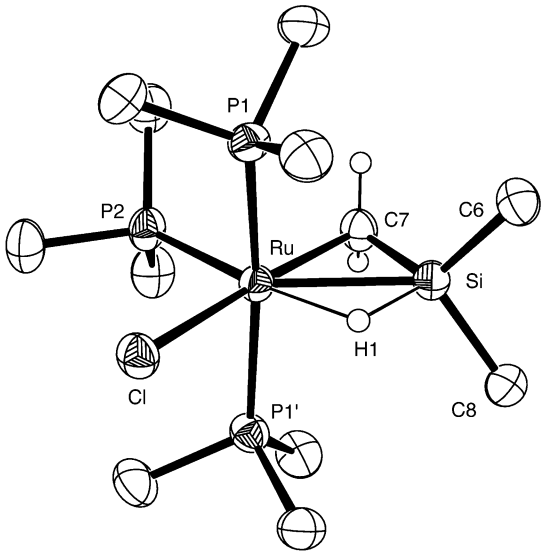


Figure 2. ORTEP diagram of complex *mer*-**2** (30 % probability ellipsoids). Selected bond lengths [Å] and angles [°]: Ru-C7 2.200(6), Ru-Si 2.468(2), Si-C6 1.878(4), Si-C7 1.790(6), Ru-H1 1.732, Si-H1 1.557; Si-C7-Ru 75.7(2), C7-Si-Ru 59.7(2).

the silicon and ruthenium centers (Ru···H/Si···H = 1.550/1.664 Å in *fac*-**2** and 1.732/1.557 Å in *mer*-**2**), consistent with agostic interactions indicated by the spectroscopic evidence. Silane σ-bond complexes can be viewed as products of "arrested" Si–H elimination on the pathway from metal(silyl)(hydride) complexes to silanes. Analogously, *fac*- and *mer*-**2** can be considered as being frozen during the intramolecular β-Si–H elimination from the ruthenium silene hydride complexes. The Si–C distances (*fac*-**2**: 1.788(11); *mer*-**2**: 1.790(6) Å) are shorter than normal Si–C single bonds (approximately 1.87–1.91 Å),[8] but are comparable to those in

 © 2003 Wiley-VCH Verlag GmbH & Co. KGaA, Weinheim

metal silene complexes (1.78–1.81 Å).[9] However, the Ru–Si bond lengths in both *fac*- and *mer*-**2** are much longer than in known silene complexes.[9a,b] On the other hand, short Si–C distances are also observed in ruthenium complexes reported by Jones and co-workers ([Cp*(Cy_3P)Ru{η^3-HSiMe_2-(C=CPh_2)}],[5a]) and Sabo-Etienne and co-workers ([(Cy_3P)$_2$RuH_2{η^4-HSiMe_2(CH=CHMe)}]).[5b] These β-agostic RuCSiH species also exhibit long Ru–Si and short Si–H bond lengths and can be viewed as an arrested stage of the reductive elimination from 1-silaallene and η^3-silaallyl complexes. Comparison with these compounds strongly supports the view that *fac*- and *mer*-**2** are better described as β-agostic rather than silene complexes. It is tempting to attribute the relative stability of the β-agostic motif entirely to the influence of chloride in **2**, but structural data is not available for **1**. Furthermore, spectroscopic evidence for **1** is consistent with some degree of Si···H interaction. Studies probing the similarities and differences in the structures of **1**, **2**, and substituted derivatives are currently in progress.

The reaction proceeding from [(Me_3P)$_3$Ru(H)SiMe_3] to **1** and further on to *fac*- and *mer*-**2** is the first example of a [M]SiMe_3 to β-agostic [M]CH_2SiMe_2-H conversion, a reversal of the typical sequence observed in the rearrangement of silaalkyl metal complexes. This reversal is likely the result of SiH coordination to the unsaturated metal center, which would provide greater stabilization than any potential agostic C–H binding in the metal silyl.

Experimental Section

Synthetic procedures and characterization data are included in the Supporting Information.

fac-**2**: 0.32 × 0.30 × 0.24 mm; orthorhombic; *Pnma* (no. 62); a = 18.7076(3), b = 10.6471(2), c = 10.5218(2) Å, V = 2095.75(7) Å^3, Z = 4, ρ_{calcd} = 1.388 g cm^{-3}; $2\theta_{max}$ = 50.7°; $Mo_{K\alpha}$ radiation (λ = 0.71069 Å); ∅ oscillations (Rigaku R-AXIS IIc); T = 200 K; 12 712 reflections, all 2027 unique reflections were used in the refinement; corrected for Lorentz and polarization effects but not for absorption (μ = 11.79 cm^{-1}); solution by direct methods (SIR92); refinement by full-matrix least-squares based on F^2 (SHELXL-93); 137 parameters; hydrogen atoms unrefined (H1 was located); R_1 = 0.0379 and wR_2 = 0.0991 for 1962 reflections for which $I > 2\sigma(I)$; residual electron density +0.492 and −0.527 e Å^{-3}; the molecule lies on a crystallographic mirror plane perpendicular to the Ru-C8-Si-H1 plane (disordered Si and C8 refined successfully at 50% occupancy). One PMe_3 (P2) was rotationally disordered about the Ru–P2 bond (55:45 relative populations).

mer-**2**: 0.44 × 0.22 × 0.12 mm; orthorhombic; *Cmc*2$_1$ (no. 36); a = 16.2940(4), b = 10.9748(2), c = 11.4191(3) Å, V = 2042.00(8) Å^3, Z = 4, ρ_{calcd} = 1.424 g cm^{-3}; $2\theta_{max}$ = 54.96°; $Mo_{K\alpha}$ radiation (λ = 0.71069 Å); ∅ oscillations (Rigaku R-AXIS IIc); T = 200 K; 8222 reflections, all 2173 unique reflections were used in the refinement; absorption correction by REQAB (μ = 11.79 cm^{-1}, min./max. transmission 0.693/1.000); solution by direct methods (SIR92); refinement by full-matrix least-squares based on F^2 (SHELXL-93); 97 parameters; hydrogen atoms unrefined (H1, H5a, H5b, and H7a were located); R_1 = 0.0358 and wR_2 = 0.0929 for 2144 reflections for which $I > 2\sigma(I)$; residual electron density +0.814 and −0.855 e Å^{-3}.

CCDC-166039 (*fac*-**2**), CCDC-166037 (*mer*-**2**), and CCDC-166038 (**3**) contain the supplementary crystallographic data for this paper. These data can be obtained free of charge via www.ccdc.cam.ac.uk/conts/retrieving.html (or from the Cambridge Crystallographic Data Centre, 12, Union Road, Cambridge CB2 1EZ, UK; fax: (+44) 1223-336-033; or deposit@ccdc.cam.ac.uk).

Received: June 6, 2003 [Z52078]

Keywords: agostic interactions · C–H activation · coordination modes · metallacycles · silene complexes

[1] a) H. K. Sharma, K. H. Pannell, *Chem. Rev.* **1995**, *95*, 1351–1374; b) P. D. Lickiss, *Chem. Soc. Rev.* **1992**, *21*, 271–279; c) T. D. Tilley in *Chemistry of Organic Silicon Compounds* (Ed.: S. Patai, Z. Rappoport), Wiley, New York, **1991**, pp. 245–364.

[2] B. K. Campion, R. H. Heyn, T. D. Tilley, *J. Chem. Soc. Chem. Commun.* **1992**, 1201.

[3] a) D. H. Berry, L. J. Procopio, *J. Am. Chem. Soc.* **1989**, *111*, 4099; b) P. I. Djurovich, P. J. Carroll, D. H. Berry, *Organometallics* **1994**, *13*, 2551.

[4] a) V. K. Dioumaev, K. Plössl, P. J. Carroll, D. H. Berry, *J. Am. Chem. Soc.* **1999**, *121*, 8391; b) V. K. Dioumaev, K. Ploessl, P. J. Carroll, D. H. Berry, *Organometallics* **2000**, *19*, 3374; c) S. R. Klei, T. D. Tilley, R. G. Bergman, *Organometallics* **2001**, *20*, 3220.

[5] a) J. Yin, J. Klosin, K. A. Abboud, W. M. Jones, *J. Am. Chem. Soc.* **1995**, *117*, 3298; b) F. Delpech, S. Sabo-Etienne, B. Donnadieu, B. Chaudret, *Organometallics* **1998**, *17*, 4926.

[6] C. Windus, S. Sujishi, W. P. Giering, *J. Am. Chem. Soc.* **1974**, *96*, 1951.

[7] a) A. A. Zlota, F. Frolow, D. Milstein, *J. Chem. Soc. Chem. Commun.* **1989**, 1826; b) J. Grobe, R. Martin, G. Huttner, L. Z. Zolnai, *Z. Anorg. Allg. Chem.* **1992**, *607*, 79.

[8] Determined by searching the Cambridge Structural Database, November 2002 update: F. H. Allen, J. E. Davies, J. J. Galloy, O. Johnson, O. Kennard, C. F. Macrae, E. M. Mitchell, C. F. Mitchell, J. M. Smith, D. G. Watson, *J. Chem. Inf. Comput. Sci.* **1991**, *31*, 187.

[9] a) B. K. Campion, R. H. Heyn, T. D. Tilley, A. L. Rheingold, *J. Am. Chem. Soc.* **1993**, *115*, 5527; b) B. K. Campion, R. H. Heyn, T. D. Tilley, *J. Am. Chem. Soc.* **1990**, *112*, 4079; c) T. S. Koloski, P. J. Carroll, D. H. Berry, *J. Am. Chem. Soc.* **1990**, *112*, 6405.

 © 2003 Wiley-VCH Verlag GmbH & Co. KGaA, Weinheim

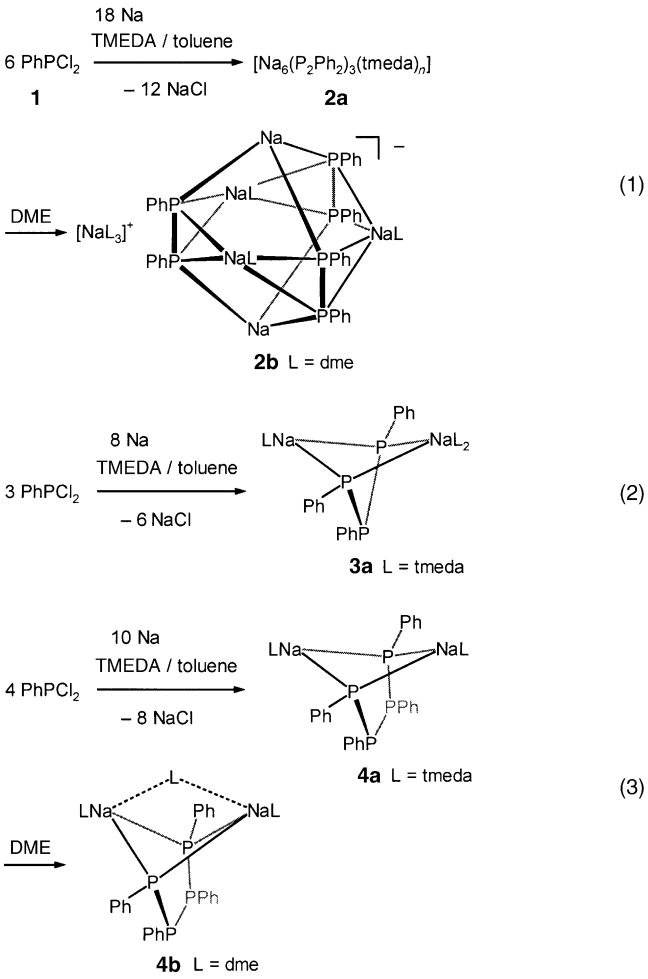
Cages of Phosphorus and Sodium

Sodium Oligophosphanediide Ions in the $PhPCl_2$/Na System: Syntheses and Structural Characterization**

*Jens Geier, Heinz Rüegger, Michael Wörle, and Hansjörg Grützmacher**

Although reductive bond coupling (RBC) of organophosphorus halides with reducing metals and subsequent reductive cleavage of the resulting oligophosphanes to give metal phosphanides have been intensively studied for more than 50 years,[1] the $PhPCl_2$/Na system which is of particular practical and fundamental importance is still insufficiently understood.[2] Phenylphosphonous acid dichloride, $PhPCl_2$ (**1**), is one of the cheapest organophosphorus compounds produced on a large scale and sodium is the most versatile among the strongly reducing metals. Structural information about disodium 1,2,3-triphenyltriphosphane-1,3-diide, $[Na_2(P_3Ph_3)]$, and 1,2,3,4-tetraphenyltetraphosphane-1,4-diide, $[Na_2(P_4Ph_4)]$, stems from the pioneering work of Baudler et al.[3] and Caulton et al.,[4] who studied THF solutions of these species by ^{31}P NMR spectroscopy. However, more precise structural information is not available for these compounds or for the shorter chain dianions, that is, the 1,2-diphenyldiphosphane-1,2-diide, $[Na_2(P_2Ph_2)]$,[5] and phenylphosphanediide, $[Na_2(PPh)]$. Moreover, the latter frequently seen[2] formulation $[Na_2(PPh)]$ is not yet fully confirmed.[6] Herein we report a simple method for the preparation of three sodium *catena*-oligophosphane-α,ω-diides which can be isolated from the $PhPCl_2$/Na system and the X-ray structure analyses of these compounds.[7] $[Na_2(P_2Ph_2)]$ in particular could be obtained in high yield and as the first structurally characterized s-block-metal diphosphanediide,[8] represents a new cluster type.

When ethers are used in the dehalogenation of organochlorophosphanes with sodium, ether-cleavage reactions provoked by the strongly basic sodium phosphanides impede the isolation of pure products. Moreover, the formation of insoluble NaCl deactivates the metal surface (in contrast to reactions with lithium, where LiCl readily dissolves in THF) an effect which becomes even more problematic in hydrocarbons as solvents.[2] We now found, that a 10:1.5 (v/v) mixture of toluene and tetramethylethylenediamine (TMEDA) is a suitable solvent system for a simple, high-yield synthesis (≈90%) of the disodium salt of 1,2-diphenyldiphosphane **2a**,**b** [Eq. (1) in Scheme 1].



Scheme 1. Syntheses of *catena*-oligophosphane-α,ω-diides **2**–**4**.

After a few hours of stirring $PhPCl_2$ (**1**) with three or more equivalents of molten sodium at temperatures above 100 °C (reflux) a bright yellow powder of **2a** precipitates rather suddenly. This powder contains no other phosphorus-based byproducts [$\delta(^{31}P) = -106.4$ ppm]. Compound **2a** is moderately soluble in dimethoxyethane (DME) or THF to give deeply red colored solutions, which are stable for a few days at room temperature (longer storage results in solvent deprotonation). Thus, **2a** can be separated from sodium chloride by extraction. The higher members of the family of the phenyl-substituted disodium *catena*-oligophosphane-α,ω-diides, **3a** and **4a**, are similarly obtained in satisfactory yields (55 and 73%) by choosing the stoichiometric ratios shown in Equations (2) and (3) of Scheme (1). Alternatively, the diphosphanediide **2a** can be treated with the *cyclo*-pentaphosphane $(PhP)_5$ in THF or DME solution to give **4a**, furthermore, the triphenyltriphosphanediide **3a** is obtained in a slow but almost quantitative synproportionation from **2a** and **4a**. All the compounds **2**–**4** are highly air-sensitive and **2a**,**b** are even pyrophoric.

[*] Prof. Dr. H. Grützmacher, Dipl.-Chem. J. Geier, Dr. H. Rüegger, Dr. M. Wörle
Department of Chemistry, HCI
ETH Hönggerberg
8093 Zürich (Switzerland)
Fax: (+41) 1-632-1032
E-mail: gruetzmacher@inorg.chem.ethz.ch

[**] This work was supported by the Ciba Speciality Chemicals and the ETH Zürich. We thank Prof. Dr. T. F. Fässler (TU Darmstadt (Germany)) and Dr. J. Richter (STOE & CIE GmbH, Darmstadt) for assistance with the structure determinations.

Supporting information for this article is available on the WWW under http://www.angewandte.org or from the author.

 DOI: 10.1002/anie.200250725 © 2003 Wiley-VCH Verlag GmbH & Co. KGaA, Weinheim

Rod-shaped, orange crystals of $[Na(dme)_3]^+$-$[Na_5(P_2Ph_2)_3(dme)_3]^-$ (**2b**) were obtained from a saturated DME solution of **2a**. The tri- and tetraphosphanediides $[Na_2(P_3Ph_3)(tmeda)_3]$ (**3a**) and $[Na_2(P_4Ph_4)(tmeda)_2]$ (**4a**), respectively, both crystallize, with TMEDA as coligands, as yellow cuboids from the reaction mixture after filtration and concentration. As with **2a**, recrystallization of **4a** from DME leads to a displacement of the TMEDA ligands by DME to give crystals of $[Na_2(P_4Ph_4)(dme)_3]$ (**4b**). The results of the X-ray structure analyses[9] of **2b**, **3a**, **4a**, and **4b** are shown Figure 1.

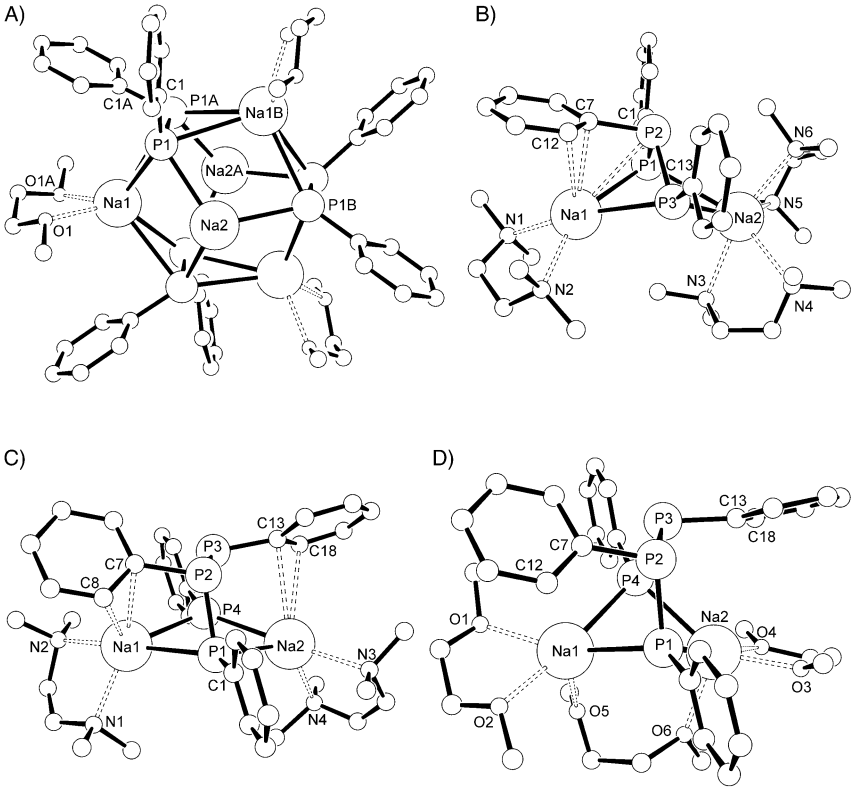


Figure 1. A) Structure of the cluster anion in **2b**. Selected separations [Å] and angles [°]: P1-P1A 2.205(10), Na1-P1 3.063(6), Na1-P1A 3.158(7), Na2-P1 2.831(5), Na1-Na2 3.669(7), Na1-Na1B 5.347(13), Na2-Na2A 3.965(13), P1-C1 1.835(11), Na2-P1-P1A 108.1(2), Na1-P1-Na1B 118.5(2), Na1-P1-C1 150.5(3), Na1B-P1-C1 85.7(4), P1-Na1-P1A 41.5(2), P1-Na1B-P1B 97.0(2), P1-Na2-P1B 110.8(1), C1-P1-P1A-C1A −71.6(7), Na2-P1-P1A-Na2A 4.2(4). B) Structure of **3a**. Selected separations [Å] and angles [°]: P1-P2 2.192(1), P2-P3 2.188(1), P1-P3 3.146(1), Na1-P1 2.968(1), Na1-P2 3.177(1), Na1-P3 2.966(1), Na2-P1 3.106(1), Na2-P2 3.759(1), Na2-P3 3.097(1), Na1-Na2 4.781(1), Na1-C7 2.728(2), Na1-C12 3.056(3), Na1-N1 2.452(2), Na1-N2 2.478(2), P1-C1 1.818(2), P2-C7 1.860(3), P3-C13 1.823(2), C1-P1-P2 103.44(8), P1-P2-P3 91.81(3), P2-P3-C13 103.62(8), P1-Na1-P3 64.03(2), P1-Na2-P3 60.94(2), C7-P2-P3-C13 −84.65(10), normal angle Na1-P1-P3/Na2-P1-P3 45.77(3). C) Structure of **4a**. Selected separations [Å] and angles [°]: P1-P2 2.162(3), P2-P3 2.185(3), P3-P4 2.156(3), Na1-P1 2.848(4), Na2-P1 2.829(4), Na1-P2 3.385(4), Na2-P2 3.611(5), Na1-P3 3.704(5), Na2-P3 3.372(4), Na1-P4 2.885(4), Na2-P4 2.972(5), Na1-Na2 4.587(5), P1-C1 1.813(7), P2-C7 1.837(8), P3-C13 1.845(8), P4-C19 1.816(7), Na1-N1 2.393(9), Na1-N2 2.431(8), Na1-C7 2.985(8), Na1-C8 3.100(9), Na2-C13 2.931(7), Na2-C18 2.901(8), C1-P1-P2 102.5(3), P1-P2-P3 105.3(1), P2-P3-P4 105.3(1), P3-P4-C19 102.1(3), P1-Na1-P4 72.9(1), P1-Na2-P4 71.9(1), N1-Na1-N2 73.3(3), P1-P2-P3-P4 20.3(1), normal angle Na1-P1-P4/Na2-P1-P4 19.2(1). (C19 = ipso-carbon bonded to P4). D) Structure of **4b**. Selected separations [Å] and angles [°]: P1-P2 2.168(4), P2-P3 2.190(4), P3-P4 2.167(4), Na1-P1 2.916(6), Na1-P4 2.933(6), Na2-P1 2.960(6), Na2-P4 2.849(6), Na2-C13 3.627(11), Na2-C18 3.695(12), Na1-Na2 3.948(7), P1-Na1-P4 74.0(1), P1-Na2-P4 74.6(1), P1-P2-P3-P4 27.8(2), normal angle Na1-P1-P4/Na2-P1-P4 63.7(2).

The crystal structure of **2b** has the rare[10] symmetry of the chiral space group $P6_322$ and consists of a ionic lattice built from octahedrally coordinate $[Na(dme)_3]^+$ ions and $[Na_5(P_2Ph_2)_3(dme)_3]^-$ cage anions. A view along the *c* axis (Figure 2) shows the stacking of the anions in columns, each anion cage being tilted by 60° with respect to the preceding one. The columns are trigonally surrounded by $[Na(dme)_3]^+$ ions which are situated in planes orthogonal to the columns. The $[Na_5(P_2Ph_2)_3(dme)_3]^-$ cage (and also the $[Na(dme)_3]^+$ ion) has D_3 symmetry with the C_3 axis pointing along the Na2-Na2A-vector (see Figure 1 A) and the three C_2 axes running through the Na1 atoms and the midpoints of the opposing P–P bonds (bond length: 2.21(1) Å). The $\{Na_5P_6\}$ polyhedron consists of a slightly distorted (Na2-P1-P1A-Na2A = 4.2(4)°) trigonal P_6 prism, composed of three $[P_2Ph_2]^{2-}$ units, which is fivefold capped by the sodium atoms. Note that the cage perimeter consists of three corner-sharing bicyclobutane("butterfly")-shaped $[Na_2(P_2)]$ units. These $A^+_2B^{2-}$ ion triples are a well-known structural motif in dicarbanion chemistry[11] and are also observed for *N*,*N*′-dilithiohydrazines.[12] The two apical sodium atoms Na2 and Na2A are only coordinated by three P atoms through short Na–P bonds (2.831(5) Å) in a pyramidal coordination environment (P1-Na2-P1B = 110.8(1)°). The three radial Na atoms (Na1 and its two symmetry equivalents) are six-coordinate being linked to four phosphorus and two DME oxygen atoms which results in a slightly distorted trigonal-prismatic coordination geometry and longer Na–P bonds (Na1-P1: 3.063(6) Å and Na1-P1A: 3.158(7) Å).

The structures of **3a** and **4a** are shown in Figure 1 B and C, respectively.[13,14] As has been reported for the reduction of $(PhP)_5$ in THF,[3,4] the formation of **4a** is diastereoselective and on the basis of steric considerations the product was correctly assumed to be the 2R,3R/2S,3S racemate[3]. In both, **3a** and **4a**, the two sodium atoms are located above and below the plane defined by the P_n chain ($n = 3$, 4) and the Na_2P_2 cycle is folded along the P–P vector by 45.8(1)° in **3a** and 19.2(1)° in **4a** (normal angles Na1-P1-P3/Na2-P1-P3 and Na1-P1-P4/Na2-P1-P4, respectively). With respect to the van der Waals radius of phosphorus, (1.8 Å)[15] a remarkable feature of the triphosphanediide **3a** is the short distance between the terminal P1 and P3 atoms (3.146(1) Å) and the small P1-P2-P3 angle (91.81(3)°)

In **3a** and **4a** intramolecular π solvation of the sodium cations by phenyl groups[16] occurs in an unsymmetrical η^2-fashion. In **4b**, the sodium atoms Na1 and Na2 are each chelated by one DME molecule and are additionally linked by a third one. This binding causes considerably more folding (63.7(2)°) of the Na_2P_2 ring in **4b**. The structural parameters of the different phenyl groups and the P–C bond lengths do not differ

 © 2003 Wiley-VCH Verlag GmbH & Co. KGaA, Weinheim

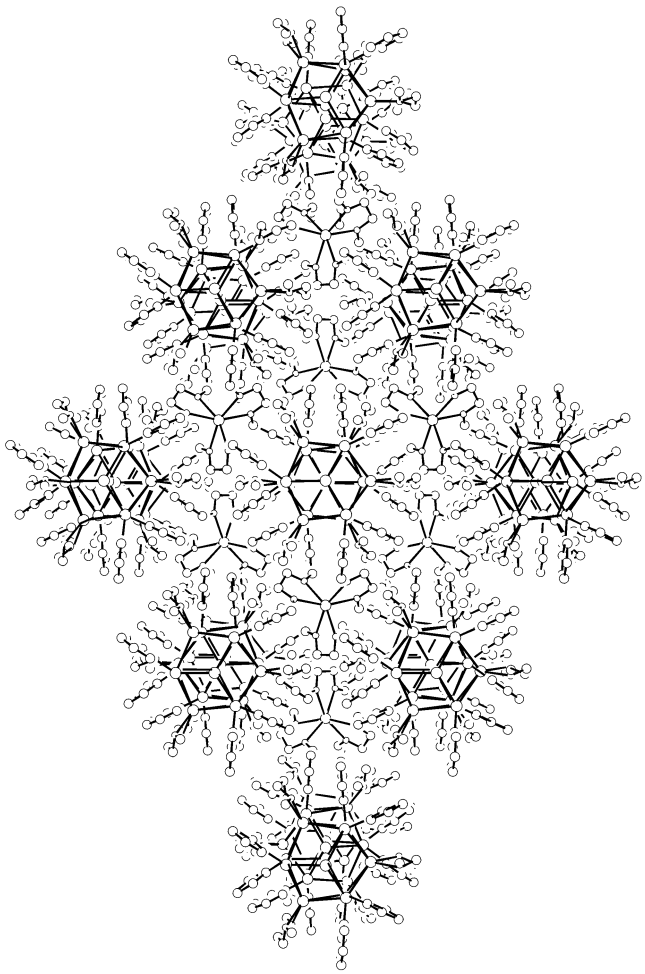


Figure 2. View along the *c* axis of the crystal structure of **2b** (four unit cells are shown). The six $[Na(dme)_3]^+$ ions visible around the central cage column are residing alternately in $c = {}^1/_4$ and ${}^3/_4$ respectively.

significantly and give no indication for delocalization of negative charge into the arene rings.

The ^{23}Na magic-angle spinning (MAS) NMR spectrum of crystalline **2b** shows the three signals expected, while the solution spectra, in THF or DME, have only one broad ($b_{1/2} \approx$ 1300 Hz) resonance signal at 248 K. The ^1H, ^{13}C and ^{31}P solution NMR spectra are well resolved at room temperature and show the presence one type of phosphorus and phenyl group. The isotropic chemical shift from ^{31}P cross-polarization (CP) MAS spectra ($\delta = -105$ ppm; principal components of the anisotropic shielding tensor: 0, −46, and −268 ppm) is nearly identical to the value in solution ($\delta = -106.4$ ppm). Furthermore, the spherical volume (1630 Å^3) calculated with the Stokes-equation from the diffusion coefficient of **2b** (5.9×10^{-10} m^{2}s^{-1}), which was measured by pulsed field-gradient spin echo NMR techniques[17] using the phenyl-proton resonances, corresponds well to the spherically approximated volume (1580 Å^3) from the solid-state structure. Thus the core of the cage anion of **2b** is retained in solution. The diffusion coefficient of the DME molecules, measured in the same way, is significantly larger (2.4×10^{-9} m^{2}s^{-1}) indicating that this ligand is replaced by the solvent THF. While the ^{31}P NMR spectrum of **3a** in THF shows a single AB_2 spin system (as was observed for the TMEDA-free compound[3b]) we find two exchanging major species to be present in THF solutions of the tetraphosphanediide $[Na_2(P_4Ph_4)(L)_n]$, which indicates an equilibrium according to Equation (4) between the C_2-

$$[Na_2(P_4Ph_4)(L)_n] \rightleftharpoons [Na(L)_k]^+ + [Na(P_4Ph_4)(L)_m]^- \quad (4)$$

symmetric bicyclic ion triple (left) with a structure similar to **4a** and **4b** and a asymmetric monocyclic ion pair consisting of a folded five-membered NaP_4 ring (right; see the Experimental Section and the Supporting Information for more details).

Experimental Section

All operations were performed under inert conditions. Sodium metal (**2a**: 3.86 g, 0.168 mol; **3a**: 3.43 g, 0.149 mol; **4a**: 3.21 g, 0.140 mol) was melted and dispersed with a magnetic stirring bar in a refluxing mixture of toluene (100 mL) and TMEDA (15 mL). **1** (10.00 g, 0.056 mol) was added cautiously. The formation of solid colorless NaCl was immediately apparent and the initial formation of the *cyclo*-phosphanes $(PPh)_n$ ($n = 3$–6) was indicated by ^{31}P NMR spectroscopy. Reflux was maintained for 4–6 h until the sodium had disappeared. **2a** precipitated as a yellow solid after 2–6 h and was isolated by filtration and drying in vacuum as yellow pyrophoric powder in approximately 90% yield (corresponding to a composition of $[Na_2(P_2Ph_2)(tmeda)_{0.5-1}]$ together with NaCl). Subsequent extraction with DME at room temperature gave a deep-red solution, which after evaporation under vacuum yielded an orange solid of composition $[Na_2(P_2Ph_2)(dme)_{0.5-1}]$. Single crystals of **2b** were obtained from a saturated DME solution of **2a** at room temperature within one day. Solid **2a** and **2b** are stable for several months.[18] ^{31}P NMR (121.49 MHz, [D$_8$]THF, 298 K): $\delta =$ −106.4 ppm (s).

The more soluble **3a** was obtained, after filtration and concentration of the above reaction mixture, by repeated recrystallizations from toluene/TMEDA as yellow crystals (55% yield), which contained less than 5 mol-% of **4a**. ^{31}P NMR (101.25 MHz, [D$_8$]THF, 298 K): 8 line AB_2 spin system, $\delta_A = -54.0$ ppm (P2), $\delta_B = -56.7$ ppm (P1,3), $^1J_{AB} = 242.4$ Hz.

4a crystallized in pure form directly from the hot filtered toluene/TMEDA reaction mixture as bright yellow crystals (73%). Ion triple $[Na_2(P_4Ph_4)(L)_n]$ (L = thf, tmeda) ^{31}P NMR (202.49 mHz, [D$_8$]THF, 183 K): $\delta = -25.7$ (br., A-part of AA′XX′ system; P-2,3), −89.7 ppm (br., X-part of AA′XX′ system; P1,4). The parameters $\delta_A = -24.9$ ppm, $\delta_B = -89.1$ ppm, $J_{AA'} = 310$ Hz, $J_{XX'} = 306$ Hz, $J_{AX'} = 11$ Hz, $J_{AX} = 322$ Hz were determined by simulation[19] of the well-resolved spectrum obtained at 253 K. $[Na(P_4Ph_4)(L)_m]^-$ ^{31}P NMR (202.49 mHz, [D$_8$]THF, 183 K): $\delta = -16.8$ (m, 1P; P3), −30.8 (td, $^1J_{1,2} = 340$ Hz, $^1J_{2,3} = 340$ Hz, $^2J_{2,4} = 148$ Hz, 1P; P2), −70.4 (dd, $^1J_{3,4} = 274$ Hz, 1P; P4), −73.3 ppm (br. d, 1P; P1).

The reactions of **2a** with **4a**, and **2a** with $(PhP)_5$, were performed in THF at room temperature and monitored by ^{31}P NMR spectroscopy. In reactions of **4a** with $(PhP)_5$ no indications for the formation of higher oligophosphane-α,ω-diides $[Na_2(P_nPh_n)]$ with $n > 4$ were obtained.

A detailed description of the experimental procedures and further comments on the X-ray structure analyses are given in the supporting information.

Received: December 9, 2002
Publication delayed at authors request [Z50725]

Keywords: alkali metals · anions · phosphorus · reduction

 © 2003 Wiley-VCH Verlag GmbH & Co. KGaA, Weinheim

[1] a) Reviews: K. Issleib, *Z. Chem.* **1962**, *6/7*, 163; b) K. Issleib, K. Krech, *Chem. Ber.* **1966**, *99*, 1310; c) A. Schisler, P. Lönnecke, U. Huniar, R. Ahlrichs, E. Hey-Hawkins, *Angew. Chem.* **2001**, *113*, 4345; *Angew. Chem. Int. Ed.* **2001**, *40*, 4217.

[2] a) F. Pass, H. Schindlbauer, *Monatsh. Chem.* **1959**, *90*, 148; b) L. Horner, P. Beck, H. Hoffmann, *Chem. Ber.* **1959**, *92*, 2088. Most of the sodium reductions described in the literature use $(PhP)_5$ rather than $PhPCl_2$ as educt, see refs. [3–5].

[3] a) M. Baudler, D. Koch, E. Tolls, K. M. Diedrich, B. Kloth, *Z. Anorg. Allg. Chem.* **1976**, *420*, 146; b) M. Baudler, D. Koch, *Z. Anorg. Allg. Chem.* **1976**, *425*, 227.

[4] P. R. Hoffman, K. G. Caulton, *J. Am. Chem. Soc.* **1975**, *97*, 6370.

[5] a) J. W. B. Reesor, G. F. Wright, *J. Org. Chem.* **1957**, *22*, 385. $[Li_2(P_2Ph_2)]$ and $[K_2(P_2Ph_2)]$ have been described in refs. [1b, 4] but no spectroscopic data were given.

[6] In many reactions where $[M_2(PPh)]$ (M = Li, Na, K) was supposed to be involved, the monometal salts of phenylphosphane, [M(PHPh)], could also have been the actual reagents. For a recent X-ray structure report of a substituted derivative see: V. L. Rudzevich, H. Gornitzka, K. Miqueu, J.-M. Sortiropoulos, G. Pfister-Guillouzo, V. D. Romanenko, G. Bertrand, *Angew. Chem.* **2002**, *114*, 1241; *Angew. Chem. Int. Ed.* **2002**, *41*, 1193, and references therein.

[7] Our attempts to isolate and characterize $[Na_2(PPh)]$ have failed to date. The preparation of insoluble (and hence not spectroscopically characterized) $[K_2(PPh)]$ is described in: a) H. Schumann, H. Benda, *Chem. Ber.* **1971**, *104*, 333; b) M. Baudler, A. Zarkadas, *Chem. Ber.* **1973**, *106*, 3970. Crystallographically characterized s-block-metal monophosphanediides are only known for magnesium (a $[Mg_6(PR)_6]$ prism and a $[Mg_4(PR)_4]$ cube): c) M. Westerhausen, M. Krofta, A. Pfitzner, *Inorg. Chem.* **1999**, *38*, 598; d) M. Westerhausen, S. Schneiderbauer, J. Knizek, H. Nöth, A. Pfitzner, *Eur. J. Inorg. Chem.* **1999**, 2215.

[8] The structural chemistry of other metal phosphanides has been intensively studied over the last decade, for reviews see: a) M. Driess, *Adv. Inorg. Chem.* **2000**, *50*, 236; b) K. Izod, *Adv. Inorg. Chem.* **2000**, *50*, 33; c) M. Driess, *Acc. Chem. Res.* **1999**, *32*, 1017.

[9] Data collection on Bruker AXS SMART CCD (**2b, 4a**), STOE IPDS I (**4b**) and II (**3a**) diffractometers. The structures were solved by direct methods, all atoms except hydrogen were refined anisotropically; G. M. Sheldrick, SHELX-97, University of Göttingen, Göttingen (Germany), **1997**. **2b**: $C_{60}H_{90}O_{12}Na_6P_6$; orange rod, crystal size $0.60\times0.35\times0.35$ mm; hexagonal, space group $P6_322$, $a=15.04(2)$, $c=20.93(4)$ Å, $V=4102(10)$ Å^3, $Z=2$, $\mu=0.21$ mm^{-1}; $\lambda(Mo_{K\alpha})=0.71073$ Å, $T=293$ K, detector distance = 60 mm, $t=40$ s, $2\theta_{max}/2\theta_{min}=38.22°/5.76°$, collected (independent) reflections = 10445 (1127), $R_{int}=0.0695$; 116 refined parameters, $R_1=0.0996$ for 747 reflections with $I>2\sigma$, $wR_2=0.2921$ for all data, GooF on $F^2=1.969$, max./min. residual electron density = 0.51/−0.29 e Å^{-3}. The C–C and C–O bond lengths of the severely disordered DME ligands were restrained to standard values; the benzene ring was constrained to a regular hexagon with d(C-C) = 1.39 Å. **3a**: $C_{36}H_{63}N_6Na_2P_3$; yellow cuboid, crystal size $0.62\times0.44\times0.42$ mm; monoclinic, space group $P2_1/c$, $a=10.500(1)$, $b=14.914(1)$, $c=27.046(1)$ Å, $\beta=91.890(4)°$, $V=4233.0(3)$ Å^3, $Z=4$, $\mu=0.19$ mm^{-1}; $\lambda(Mo_{K\alpha})=0.71073$ Å, $T=173$ K, detector distance = 120 mm, $t=3$ min, $2\theta_{max}/2\theta_{min}=52.74°/3.02°$, collected (independent) reflections = 52111(8656), $R_{int}=0.0774$; refined parameters = 425, $R_1=0.0513$ for 5712 reflections with $I>2\sigma$, $wR_2=0.1621$ for all data, GooF on $F^2=1.068$, max./min. residual electron density = 0.86/−0.82 e Å^{-3}. The central C–C bond length of one of the TMEDA ligands (C27–C28) was restrained to a standard value. **4a**: $C_{36}H_{52}N_4Na_2P_4$; yellow cuboid, crystal size $0.40\times0.20\times0.20$ mm; triclinic, space group $P1$, $a=10.17(1)$, $b=10.27(1)$, $c=11.94(1)$ Å, $\alpha=76.40(2)$, $\beta=71.33(2)$, $\gamma=62.14(2)°$, $V=1039(2)$ Å^3, $Z=1$, $\mu=0.23$ mm^{-1}; $\lambda(Mo_{K\alpha})=0.71073$ Å, $T=293$ K, detector distance = 40 mm, $t=30$ s, $2\theta_{max}/2\theta_{min}=46.62°/3.62°$, collected (independent) reflections = 4576(3655), $R_{int}=0.0304$; refined parameters = 425, $R_1=0.0484$ for 2576 reflections with $I>2\sigma$, $wR_2=0.1137$ for all data, GooF on $F^2=1.014$, max./min. residual electron density = 0.21/−0.18 e Å^{-3}. **4b**: $C_{36}H_{50}O_6Na_2P_4$; yellow cuboid, crystal size $0.26\times0.18\times0.17$ mm; orthorhombic, space group $Pna2_1$, $a=20.597(4)$, $b=12.301(3)$, $c=16.647(3)$ Å, $V=4218(2)$ Å^3, $Z=4$, $\mu=0.24$ mm^{-1}; $\lambda(Mo_{K\alpha})=0.71073$ Å, $T=293$ K, detector distance = 80 mm, $t=10$ min, $2\theta_{max}/2\theta_{min}=47.68°/3.86°$, collected (independent) reflections = 21216(5390), $R_{int}=0.2537$; refined parameters = 5387/433, $R_1=0.0755$ for 2349 reflections with $I>2\sigma$, $wR_2=0.1806$ for all data, GooF on $F^2=0.997$, max./min. residual electron density = 0.23/−0.18 e Å^{-3}. The 1,3-separations between methyl and methylene carbon atoms were restrained to be equal in the disordered μ_2-DME ligand. CCDC-203787 (**2b**), CCDC-203788 (**3a**), CCDC-203789 (**4a**), CCDC-203790 (**4b**) contain the supplementary crystallographic data for this paper. This data can be obtained free of charge via www.ccdc.cam.ac.uk/conts/retrieving.html (or from the Cambridge Crystallographic Data Centre, 12 Union Road, Cambridge CB2 1EZ, UK; fax: (+44) 1223-336-033; or deposit@ccdc.cam.ac.uk).

[10] Up to 26.06.2003 there are 20 entries in the Cambridge Structural Database.

[11] A. Streitwieser, Jr., *Acc. Chem. Res.* **1984**, *17*, 353.

[12] B. Gemünd, H. Nöth, H. Sachdew, M. Schmidt, *Chem. Ber.* **1996**, *129*, 1335. The nitrogen analogue of **2b** was structurally characterized in form of the adduct $[(Na_2N_2Ph_2)\text{-}(NaHN_2Ph_2)_2(dme)_4]$: J. Knizek, I. Krossing, H. Nöth, H. Schwenk, T. Seifert, *Chem. Ber.* **1997**, *130*, 1053.

[13] The only other structurally characterized disodium triphosphanediide is $[Na(NH_3)_5]^+[Na(NH_3)_3(P_3H_3)]^-$, which contains a single sodium-bridged $[P_3H_3]^{2-}$ chain with the hydrogen atoms in an *all-trans* arrangement. N. Korber, J. Aschenbrenner, *J. Chem. Soc. Dalton Trans.* **2001**, 1165.

[14] A disodium 1,4-tetraphosphanediide substructure was observed in the silyl-substituted compounds $[Na_4(P_8R_4)(dme)_4]$ and $[Na_2(P_5R_3)(thf)_4]$ (R = *t*Bu$_3$Si): a) N. Wiberg, A. Wörner, K. Karaghiosoff, D. Fenske, *Chem. Ber.* **1997**, *130*, 135 and b) N. Wiberg, A. Wörner, H.-W. Lerner, K. Karaghiosoff, H. Nöth, *Z. Naturforsch. B* **1998**, *53*, 1004.

[15] A. Bondi, *J. Phys. Chem.* **1964**, *68*, 441.

[16] π Solvation of alkali-metal cations by arene rings is a common phenomenon. For reviews see: a) C. Schade, P. von R. Schleyer, *Adv. Organomet. Chem.* **1987**, *27*, 169; b) H. Bock, K. Ruppert, C. Näther, Z. Havlas, H.-F. Herrmann, C. Arad, I. Göbel, A. John, J. Meuret, S. Nick, A. Rauschenbach, W. Seitz, T. Vaupel, B. Solouki, *Angew. Chem.* **1992**, *104*, 564; *Angew. Chem. Int. Ed. Engl.* **1992**, *31*, 550; c) J. D. Smith, *Adv. Organomet. Chem.* **1998**, *43*, 267.

[17] M. Valentini, H. Rüegger, P. S. Pregosin, *Helv. Chim. Acta* **2001**, *84*, 2833.

[18] After a few days of storage, **2a** and **b** decompose in ethereal solvents at room temperature whereby $Na[HP_2Ph_2]$ is formed as the first product [^{31}P{H}-NMR (101.25 MHz, DME, 298 K): $\delta=-63.0$ (dd, $^1J_{P,P}=375.9$ Hz, $^1J_{P,H}=208.9$ Hz; HPPh), −91.8 ppm (dd, $^1J_{P,P}=375.9$ Hz, $^2J_{P,H}=15.2$ Hz; PPh^-)] which then disproportionates to give equimolar amounts of Na[HPPh] [^{31}P NMR (101.25 MHz, DME, 298 K): $\delta=-107.9$ ppm (d, $^1J_{P,H}=157.5$ Hz)] and $Na_2[P_3Ph_3]$. The protonation/disproportionation is quantitative after two months.

[19] Program MEXICO (Version 3.0, A. D. Bain, http://www.chemistry.webmaster.ca/faculty/bain/exchange).

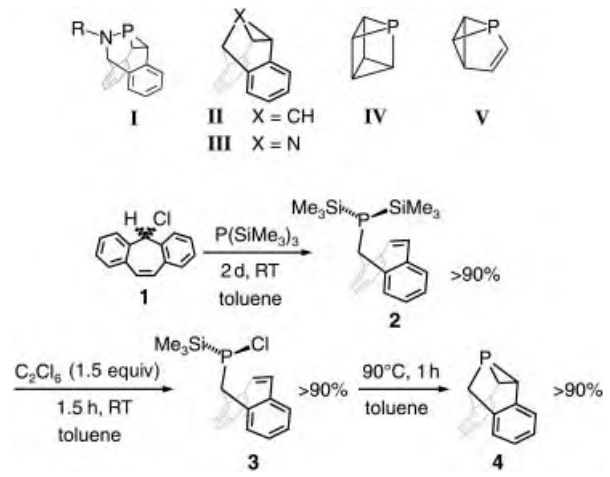
Phosphorus Heterocycles

Dibenzophosphasemibullvalene**

*Jens Geier, Gilles Frison, and Hansjörg Grützmacher**

Dedicated to Professor Horst Prinzbach on the occasion of his "70+" birthday

Because of their frequently unusual properties, small heterocycles are of constant interest.[1] They also remain a challenge to any synthetic chemist. Three-membered rings with phosphorus are less strained than their carbon analogues,[2] tetrahedral P_4 being the most prominent example.[2c] Baba-Phos (**I** Scheme 1), a remarkable stable polycyclic phosphirane,[3] has potential as a ligand for transition-metal complexes in homogeneous catalysis.[3–5] This situation prompted us to investigate the possibility of synthesizing the unknown phosphorus analogue of dibenzosemibullvalene **II** (X = CH).[6] Derivatives of dibenzoazasemibullvalene **III** (X = N)[7] have been described as quite stable compounds.



Scheme 1. Syntheses of tropp-type phosphanes **2** and **3** and the dibenzo-1-phosphasemibullvalene **4**.

For the synthesis of the dibenzo-1-phosphasemibullvalene (**4**), we adopted a method developed by Niecke et al. (Scheme 1).[8] As a precursor, we prepared the 5-bis-(trimethylsilyl)phosphanyl-5*H*-dibenzo[*a*,*d*]cycloheptene (tropp^{SiMe_3}, **2**)[9] which was converted into the highly air, moisture, and temperature sensitive unsymmetrical tropp$^{(Cl)SiMe_3}$ compound **3**. The yields of **2** and **3** are almost quantitative in both reactions.

The controlled thermolysis of **3** at 90 °C gives only one product, with a resonance in the ^{31}P NMR spectra at $\delta = -21.6$ ppm, in quantitative yield. A phosphinidene, trop-P, a plausible intermediate could not be trapped, however, and the mechanism of this reaction is uncertain.

The product **4** can be isolated as a colorless, air-sensitive solid but decomposes upon storage into a waxy insoluble material. The ^1H and ^{13}C NMR spectra show that **4** has a symmetric structure but the very unusual ^{31}P chemical shift left doubts that a dibenzo-1-phosphasemibullvalene was obtained. Phosphiranes with alkyl or aryl substitutents on the phosphorus atoms typically show ^{31}P chemical shifts at very low frequencies: $\delta = -150$–-250 ppm[1] (cage compounds such as phosphaprismanes **IV** ($\delta = -100$–-140 ppm) and phosphabenzvalenes **V** ($\delta = -80$–-90 ppm) are more deshielded).[10] The calculated ^1H, ^{13}C, and ^{31}P chemical shifts (GIAO-B3LYP/6-31+G(d)//B3LYP-6-31G(d) level)[11] are included in Figure 1 which shows the geometry optimized structure of **4**.[12] Selected bond lengths and angles are given in Table 1. The agreement between the experimental values and

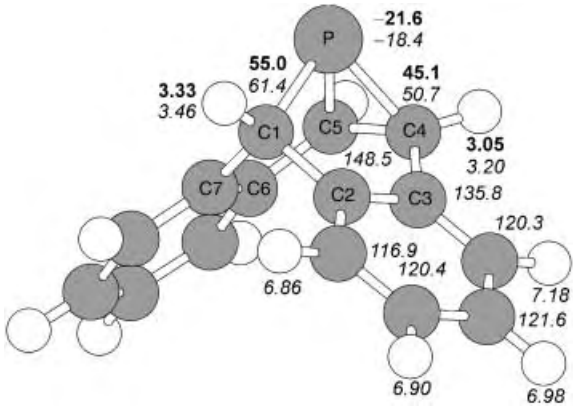
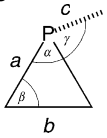


Figure 1. Calculated structure and NMR chemical shifts of **4**. Selected experimental data are shown in bold, calculated data are given in italics.

Table 1: Bond lengths and angles of PC_2 of **4** and as a ligand in **5**.



	a [Å]	*b* [Å]	*c* [Å]	α [°]	β [°]	γ [°]	Σ°(P)
4[a]	1.890	1.527	1.934	47.7	66.2	86.2	220.1
5[b]	1.83(1)	1.54(2)	1.88(1)	50.0(6)	65.0(7)	88.8(5)	227.6

[a] Calculated values. [b] Experimental average values for both molecules in the asymmetric unit.

[*] Prof. Dr. H. Grützmacher, Dipl.-Chem. J. Geier, Dr. G. Frison[+]
Department of Chemistry, HCI
ETH Hönggerberg
8093 Zürich (Switzerland)
Fax: (+41) 1-632-1032
E-mail: gruetzmacher@inorg.chem.ethz.ch

[+] Present address: Laboratoire des Mécanismes Réactionnels–DCMR
Ecole Polytechnique
91128 Palaiseau Cedex (France)

[**] This work was supported by the ETH Zürich. We are indebted to the Swiss Center for Scientific Computing (CSCS) and the Competence Centre for Computational Chemistry (C4) of the ETH Zürich for providing computer time.

Supporting information for this article is available on the WWW under http://www.angewandte.org or from the author.

 DOI: 10.1002/anie.200351388 © 2003 Wiley-VCH Verlag GmbH & Co. KGaA, Weinheim

calculated values is very satisfactory. Definitive proof for the assignment of **4** as dibenzo-1-phosphasemibullvalene was obtained in a complexation reaction with $[W(CO)_5(thf)]$ which gave the complex [**4**-$W(CO)_5$] (**5**). The result of the X-ray structure analysis for **5** is shown in Figure 2;[13] selected bond lengths and angles of **4** as ligand are listed in Table 1.

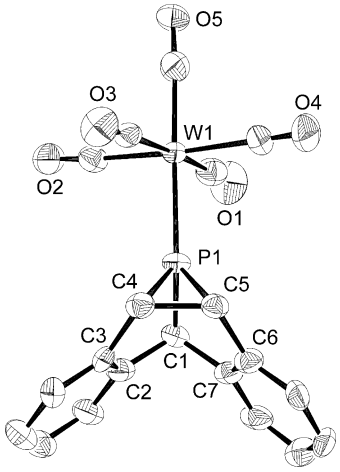


Figure 2. Molecular structure of **5**. Thermal ellipsoids at 50% probability. Hydrogen atoms have been omitted for clarity and only one of the two crystallographically independent molecules is shown. Selected mean values for the bond lengths [Å] and angles [°] of the {$W(CO)_5$} fragments in both molecules are listed: W-P 2.462(3), W-C_{eq} 2.06(2), W-C_{axial} 1.98(2), C_{eq}-O 1.12(2), C_{axial}-O 1.15(2), P-W-C_{axial} 177.7(4).

As observed for various Babar-Phos complexes, the P–C bonds *a* and *c* (see Table 1) are shortened and the basal C–C bond *b* of the PC_2 cycle is elongated in the complex.[14] In **4** and **5** the sum of bond angles at the phosphorus center, $\Sigma°(P)$, is about 20° smaller than in monocyclic phosphiranes[1] or Babar-Phos derivatives[14] and to our knowledge are the smallest values reported to date for any PC_2 heterocycle.

Noteworthy, the ^{31}P chemical shift does not change significantly when **4** serves as a ligand in **5** (^{31}P: $\delta = -20.7$ ppm) while the change in chemical shift in Babar-Phos complexes on coordination exceeds 50 ppm. The $^{183}W^{31}P$ coupling constant is used as a sensitive measure for the electronic properties of the phosphane ligands and increases with the electronegativity of the phosphorus-bonded substituents.[15] The coupling constant in **5** ($^1J(P,W) = 238$ Hz) compares well with ordinary tri-alkyl/aryl phosphanes and is significantly smaller than in $[W(CO)_5$(Babar-Phos)] complexes ($^1J(P,W) > 285$ Hz) which lie in the range of tris-(amino)- or tris(alkoxy)phosphane–$W(CO)_5$ complexes.[16] Also, the calculated Naturall Bond Orbitals (NBO) charge at the phosphorus center ($q_P = 0.75$ at the B3LYP6-31G(d) level) gives no indication that the electron density is especially depleted from the phosphorus atom in **4**. To this end, the unexpectedly deshielded ^{31}P resonance signal in phosphasemibullvalenes such as **4** cannot be satisfactorily explained.[17]

The ring strain of **4** (ca. 28 kJ mol^{-1}) was estimated by a set of bond-separation reactions and is about 30 kJ mol^{-1} lower than in the parent phosphirane, HPC_2H_4 (58 kJ mol^{-1} in our calculations, 51–55 kJ mol^{-1} in ref. [2a]; see the Supporting Information for details.) In conclusion, the polycyclic framework in **4** does not exert any particular strain. In fact because of conjugation of the PC_2 cycle with the hydrocarbon π system, **4** is even less strained and its instability must therefore have different origins.

Experimental Section

Inert conditions (high vacuum or argon atmosphere) were maintained throughout all operations. Additional spectroscopic data of **2**–**5** are given in the Supporting Information.

2: **1**[18] (5.00 g, 22.1 mmol) was stirred with tris(trimethylsilyl)-phosphane[19] (13.82 g, 55.1 mmol, 2.5 equiv) in toluene (100 mL) at room temperature for 2 days. After removal of the solvent and all other volatile compounds under high vacuum the residue was recrystallized from toluene/*n*-hexane to give 7.38 g (91%) of **2** as colorless, air-sensitive needles: ^{31}P NMR (121.49 MHz, C_6D_6, 298 K): $\delta = -146.6$ (s).

3: Compound **2** (500 mg, 1.4 mmol) was stirred at room temperature with hexachloroethane (355 mg, 1.5 mmol) in toluene (15 mL) until the ^{31}P NMR spectrum indicated quantitative conversion (1–2 h). After removal of all volatiles under high vacuum, **3** was obtained as spectroscopically pure, air-sensitive and thermally instable, colorless solid which was immediately used for the preparation of **4**. ^{31}P NMR (121.49 MHz, C_6D_6, 298 k): $\delta = 69.6$ ppm (s).

4: **3** was dissolved in toluene (10 mL) and heated to 90 °C until the ^{31}P NMR spectrum indicated quantitative conversion into **4** (1–2 h); longer heating results in decomposition. The dibenzophosphasemibullvalene **4** was isolated as a colorless, thermally unstable and air-sensitive solid by rapidly removing the solvent and the formed Me_3SiCl under high vacuum. However, it cannot be stored and decomposes within a few hours at room temperature: $^{31}P\{H\}$ NMR (101.25 MHz, C_6D_6, 298 K): $\delta = -21.6$ ppm (quintet, $^2J(P,H\text{-}1) = 27.8$ Hz, $^2J(P,H\text{-}4) = {}^2J(P,H\text{-}5) = 13.9$ Hz); ^1H NMR (300.13 MHz, C_6D_6, 298 K): $\delta = 3.05$ (d, $J = 13.9$ Hz, 2H, H-4/5), 3.33 (d, $J = 27.8$ Hz, 1H, H-1), 6.74–7.27 ppm (m, 8H, Ar-H).

5: Freshly prepared **4** was stirred with an excess of $[W(CO)_5(thf)]$[20] (1.5 equiv) in THF solution (200 mL) for 2 h at room temperature. The solvent was removed in vacuum and the brown residue was purified by column chromatography on neutral aluminium oxide. After washing the column with *n*-hexane, the product was eluted with toluene (^{31}P NMR control). After three recrystallizations from cyclopentane solution a rather low yield of crystalline colorless, air-sensitive **5** (184 mg, 24%) was obtained although the initial yield in the crude reaction mixture was quantitative (as judged from ^{31}P NMR). M.p. 139 °C (dec.); $^{31}P\{H\}$ NMR (101.25 MHz, C_6D_6, 298 K: $\delta = -20.7$ ppm (d with ^{183}W satellites, $^1J(P,W) = 238.3$ Hz, $^2J(P,H\text{-}1) = 11.2$ Hz); ^1H NMR (250.13 MHz, C_6D_6 298 K: $\delta = 3.02$ (s, 2H, H-4/5), 4.02 (d, $J = 11.2$ Hz, 1H, H-1), 6.71–7.02 ppm (m, 8H, Ar-H); ^{13}C NMR (75.48 MHz, C_6D_6, 298 K): $\delta = 42.8$ (d, $^1J(C\text{-}4/5,P) = 12.1$ Hz, C-4/5), 59.3 (d, $^1J(C\text{-}1,P) = 14.7$ Hz, C-1), 122.3 (d, $J(C,P) = 7.1$ Hz), 127.0 (two nearly superimposed s), 127.1 (s), 135.4 (d, $J(C,P) = 1.1$ Hz), 149.8 (d, $J(C,P) = 2.5$ Hz), 194.8 (d with ^{183}W satellites, $^2J(C,P) = 8.1$ Hz, $^1J(C,W) = 125.3$ Hz, *cis* CO), 198.7 ppm (d, $^2J(C,P) = 32.4$ Hz, *trans* CO); IR (neat): $\tilde{\nu} = 2074$s, 1996m, 1954w, 1889vs, 1600w, 1583w, 1474m, 1458m, 1340w, 1303w, 1260w, 934w, 880w, 789m, 755s, 588s, 569s, 562s cm^{-1}; MS (70 eV): *m*/*z* (%): 546 (33) [M^+], 191 (100) [$C_{15}H_{11}^+$].

Received: March 13, 2003 [Z51388]

Keywords: ab initio calculations · cycloaddition · heterocycles · phosphorus

 © 2003 Wiley-VCH Verlag GmbH & Co. KGaA, Weinheim

[1] a) For a discussion of the stability of strained heterocycles with main-group element centers see: M. Driess, H. Grützmacher, *Angew. Chem.* **1996**, *108*, 901; *Angew. Chem. Int. Ed. Engl.* **1996**, *35*, 828, and references therein; b) For reviews focusing on three-membered phosphorus heterocycles see: c) F. Mathey, M. Regitz in *Phosphorus Heterocyclic Chemistry: The Rise of a New Domain* (Ed.: F. Mathey), Pergamon, Amsterdam, **2001**, pp. 17–55; d) F. Mathey, *Chem. Rev.* **1990**, *90*, 997. For a recent computational work on the ring strain in three-membered rings see: M. Alcamí, O. Mó, M. Yañez, *J. Comput. Chem.* **1998**, *19*, 1072.

[2] a) M. T. Nguyen, A. Dransfeld, L. Landuyt, L. G. Vanquickenborne, P. von R. Schleyer, *Eur. J. Inorg. Chem.* **2000**, 103; b) M. T. Nguyen, E. Van Praet, L. G. Vanquickenborne, *Inorg. Chem.* **1994**, *33*, 1153; c) The low ring strain of P_4 can be ascribed to the phenomenon of Non-Orbital-Hybridisation (NOH), see: W. W. Schoeller, V. Staemmler, P. Rademacher, E. Niecke, *Inorg. Chem.* **1986**, *25*, 4382.

[3] J. Liedtke, S. Loss, G. Alcaraz, V. Gramlich, H. Grützmacher, *Angew. Chem.* **1999**, *111*, 1724; *Angew. Chem. Int. Ed.* **1999**, *38*, 1623.

[4] J. Liedtke, S. Loss, H. Grützmacher, *Tetrahedron* **2000**, *56*, 143.

[5] J. Liedtke, H. Rüegger, S. Loss, H. Grützmacher, *Angew. Chem.* **2000**, *112*, 2596; *Angew. Chem. Int. Ed.* **2000**, *39*, 2479.

[6] a) G. F. Emerson, L. Watts, R. Pettit, *J. Am. Chem. Soc.* **1965**, *87*, 131; b) E. Ciganek, *J. Am. Chem. Soc.* **1966**, *88*, 2882; c) For derivatives of dibenzosemibullvalene see: M. Böshar, H. Heydt, M. Regitz, *Tetrahedron* **1986**, *42*, 1815.

[7] M. J. Haire, *J. Org Chem.* **1980**, *45*, 1310.

[8] R. Streubel, E. Niecke, *Chem. Ber.* **1990**, *123*, 1245.

[9] For the nomenclature used for (tropylidenyl)phosphanes = tropp type phosphanes see: J. Thomaier, S. Boulmaâz, H. Schönberg, H. Rüegger, A. Currao, H. Grützmacher, H. Hillebrecht, H. Pritzkow, *New J. Chem.* **1998**, *22*, 947.

[10] a) K. Blatter, W. Rösch, U.-J. Vogelbacher, J. Fink, M. Regitz, *Angew. Chem.* **1987**, *99*, 67; *Angew. Chem. Int. Ed. Engl.* **1987**, *26*, 85; b) M. Regitz in *Multiple Bonds and Low Coordination in Phosphorus Chemistry* (Eds.: M. Regitz, O. J. Scherer), Thieme, Stuttgart, **1990**, pp. 78–80.

[11] R. Ditchfield, *Mol. Phys.* **1974**, *27*, 789.

[12] All calculations were carried out with the Gaussian 98 suite of programs: Gaussian 98 (Revision A.9), M. J. Frisch, G. W. Trucks, H. B. Schlegel, G. E. Scuseria, M. A. Robb, J. R. Cheeseman, V. G. Zakrzewski, J. A. Montgomery, R. E. Stratmann, J. C. Burant, S. Dapprich, J. M. Millam, A. D. Daniels, K. N. Kudin, M. C. Strain, O. Farkas, J. Tomasi, V. Barone, M. Cossi, R. Cammi, B. Mennucci, C. Pomelli, C. Adamo, S. Clifford, J. Ochterski, G. A. Petersson, P. Y. Ayala, Q. Cui, K. Morokuma, D. K. Malick, A. D. Rabuck, K. Raghavachari, J. B. Foresman, J. Cioslowski, J. V. Ortiz, B. B. Stefanov, G. Liu, A. Liashenko, P. Piskorz, I. Komaromi, R. Gomperts, R. L. Martin, D. J. Fox, T. Keith, M. A. Al-Laham, C. Y. Peng, A. Nanayakkara, C. Gonzalez, M. Challacombe, P. M. W. Gill, B. G. Johnson, W. Chen, M. W. Wong, J. L. Andres, M. Head-Gordon, E. S. Replogle, J. A. Pople, Gaussian, Inc., Pittsburgh, PA, **1998**. Further details are given in the Supporting Information.

[13] Crystal structure data for **5**: $C_{20}H_{11}O_5PW$, $M_r = 546.1\ g\,mol^{-1}$; colourless, irregular shaped, crystal size $0.40 \times 0.39 \times 0.37$ mm; monoclinic, space group $P2_1/c$, $a = 13.644(3)$, $b = 11.448(2)$, $c = 24.129(5)$ Å, $V = 3731(1)$ Å^3, $Z = 8$, $\rho_{calcd} = 1.945\ g\,cm^{-3}$, $F(000) = 2080$, $\mu = 6.31\ mm^{-1}$. The data were collected on a STOE IPDS I diffractometer in 300 frames separated by 1° in φ-direction: $\lambda(Mo_{K\alpha}) = 0.71073$ Å, $T = 293$ K, $2\theta_{max} = 47.94°$, $2\theta_{min} = 3.94°$, number of collected (independent) reflections = 13994 (5579), $R_{int} = 0.1042$. The structure was solved by direct methods and refined against F^2 with the full-matrix least-squares method (SHELXS-97, SHELXL-97; G. Sheldrick, Göttingen, Germany, **1997**). All non-hydrogen atoms were found in difference fourier synthesis and were refined anisotropically, while the hydrogen atoms were added to the structure at calculated positions and then refined according to a riding model. Number of refined parameters = 487, $R_1 = 0.0589$ for 3718 reflections with $I > 2\sigma$, $wR_2 = 0.1778$ for all data, GooF on $F^2 = 1.072$, max./min. residual electron density = 3.16/−1.73 e Å^{-3}. CCDC-209240 (**5**) contains the supplementary crystallographic data for this paper. These data can be obtained free of charge via www.ccdc.cam.ac.uk/conts/retrieving.html (or from the Cambridge Crystallographic Data Centre, 12 Union Road, Cambridge CB2 1EZ, UK; fax: (+44) 1223-336-033; or deposit@ccdc.cam.ac.uk).

[14] C. Laporte, G. Frison, H. Grützmacher, A. C. Hillier, W. Sommer, S. P. Nolan, *Organometallics* **2003**, *22*, 2202.

[15] The range is defined by the extremes $(Me_3Sn)_3P$: $^1J(W,P) = 142$ and PF_3: $^1J(W,P) = 485$ Hz; a) E. O. Fischer, L. Knauss, R. I. Keiter, J. G. Verkade, *J. Organomet. Chem.* **1972**, *37*, C7; b) H. Schumann, H.-J. Kroth, *Z. Naturforsch. B* **1972**, *32*, 768.

[16] J. Liedtke, Dissertation, ETH Zürich, No. 13688, **2000**. In this context, we mention that the A_1-symmetric CO stretching mode of **5** ($\tilde{\nu} = 2074\ cm^{-1}$) is comparable to $[W(CO)_5$(Babar-Phos)] complexes ($\tilde{\nu} = 2074$–$2078\ cm^{-1}$) and other $W(CO)_5$–phosphirane complexes and is, in general, a poor measure for the electronic properties of phosphanes.

[17] Note, that the benzo groups are unlikely to contribute to the deshielding since, a) a calculation of the ^{31}P chemical shift of the parent phosphasemibullvalene PC_7H_7 gives an even higher frequency shifted value ($\delta = -14.6$ ppm), and b) such an effect is not seen in Babar-Phos which shows usual low frequency ^{31}P resonances ($\delta = -140$–230 ppm).

[18] G. Berti, *J. Org. Chem.* **1957**, *22*, 230.

[19] H. H. Karsch, F. Bienlein, T. Rupprich, F. Uhlig, E. Herrmann, M. Scheer in *Synthetic Methods of Organometallic and Inorganic Chemistry, Vol. 3* (Eds.: W. A. Herrmann, G. Brauer), Georg Thieme, Stuttgart, **1996**, p. 58.

[20] For the preparation of $[W(CO)_5$(thf)] we used the method described in: G. Balázs, H. J. Breunig, E. Lork, *Z. Anorg. Allg. Chem.* **2001**, *627*, 1855.

 © 2003 Wiley-VCH Verlag GmbH & Co. KGaA, Weinheim

DNA–Protein Interactions

Polycyclic Aromatic DNA-Base Surrogates: High-Affinity Binding to an Adenine-Specific Base-Flipping DNA Methyltransferase**

Christine Beuck, Ishwar Singh, Anupam Bhattacharya, Walburga Hecker, Virinder S. Parmar, Oliver Seitz, and Elmar Weinhold**

DNA methylation is an important biological event that serves diverse cellular functions such as protection against endogenous restriction endonucleases, direction of DNA-mismatch repair, as well as regulation of gene expression and DNA replication.[1] DNA methylation is catalyzed by DNA methyltransferases (MTases), which bind to specific DNA sequences and transfer a methyl group from *S*-adenosyl-L-methionine to the exocyclic amino groups of adenine or cytosine or to C5 of cytosine.[2] Interestingly, methylation is commenced by flipping the target nucleotide completely out of the helix.[3] The energy cost for disrupting Watson–Crick hydrogen bonds and base-stacking interactions is mainly compensated by specific binding of the target bases within the active sites of the enzymes and by stabilizing the formed apparent abasic site. Three different mechanisms of abasic-site stabilization have been observed in crystal structures of DNA MTases complexed with DNA. The cytosine-specific DNA MTases M·*Hha*I[4] (Figure 1A) and M·*Hae*III[5] (Figure 1B) either only insert an amino acid side chain into the opened space or insert an amino acid side chain in addition to rearranging the base pairing. This is in contrast to the adenine-specific DNA MTase M·*Taq*I[6] (Figure 1C). In this case, the formed unpaired partner base is inserted into the opened space, resulting in interstrand stacking.

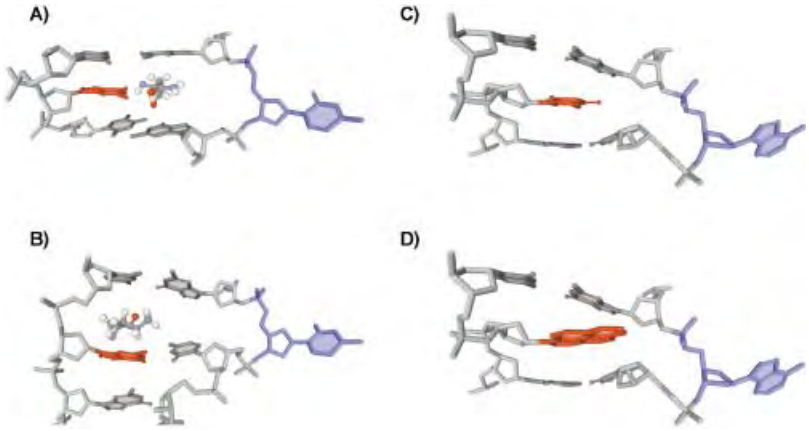


Figure 1. DNA structures found in MTase–DNA complexes with the target extrahelical nucleotide in blue and the orphaned nucleobase in red. A) In the M·*Hha*I structure, Gln237 (represented as a ball-and-stick model) partially occupies the opened space after cytosine flipping and forms hydrogen bonds with the orphaned guanine. B) M·*Hae*III inserts Ile221 (represented as a ball-and-stick model) into the DNA, and the orphaned guanine pairs with the 3′-cytosine that flanks the flipped target cytosine. C) In M·*Taq*I, the orphaned thymine is displaced towards the center of the DNA helix. As a result, interstrand stacking with the 5′ neighboring base of the target adenine occurs. D) A modeled replacement of the orphaned thymine in the M·*Taq*I-DNA structure suggests that aromatic base surrogates such as pyrene (red) fit well into the cavity left by the flipped target adenine and potentially improve interstrand stacking. This filling of the apparent abasic site is likely to contribute to a tightening of the enzyme–DNA complex.

[*] Prof. Dr. O. Seitz
Institut für Chemie
Humboldt-Universität zu Berlin
Brook-Taylor-Strasse 2, 12489 Berlin (Germany)
Fax: (+49) 30-2093-7266
E-mail: oliver.seitz@chemie.hu-berlin.de
Prof. Dr. E. Weinhold, C. Beuck
Institut für Organische Chemie, RWTH Aachen
Prof.-Pirlet-Strasse 1, 52056 Aachen (Germany)
Fax: (+49) 241-80-92528
E-mail: elmar.weinhold@oc.rwth-aachen.de
W. Hecker
Max-Planck-Institut für molekulare Physiologie
Otto-Hahn-Strasse 11, 44227 Dortmund (Deutschland)
I. Singh, A. Bhattacharya, Prof. Dr. V. S. Parmar
Bioorganic Laboratory, Department of Chemistry
University of Delhi
Delhi 110007 (India)

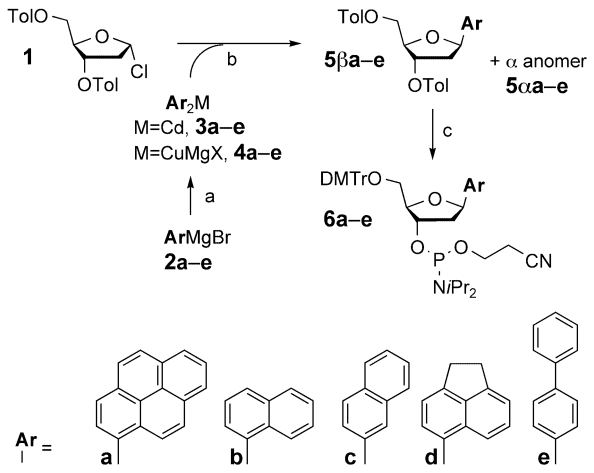
[**] This work was supported by the DAAD, the DFG, the Indian Department of Science and Technology, and the Fonds der Chemischen Industrie. O.S. is grateful for a DFG and Heisenberg fellowship and C.B. for a doctoral stipend from the Studienstiftung des Deutschen Volkes. We thank R. S. Goody for helpful discussions regarding the competitive DNA MTase binding assays.

Supporting information for this article is available on the WWW under http://www.angewandte.org or from the author.

Inspection of the crystal structure of M·*Taq*I suggested that interstrand stacking could be improved by replacing the partner thymine with larger aromatic DNA-base surrogates. It was expected that more complete filling of the apparent abasic site would lead to tightening of the M·*Taq*I–DNA complex (Figure 1D). In addition, we imagined that a polycyclic base surrogate could destabilize the innerhelical conformation of the opposing target adenine. The DNA MTase could thus bind to double-stranded DNA containing an unstacked target base without having to compensate for the energy required for disrupting Watson–Crick hydrogen bonds and base-stacking interactions. These hypotheses were investigated with DNA substrates that contained pyrenyl, 1-naphthyl, 2-naphthyl, acenaphthyl, and biphenyl residues (**a**–**e**, Scheme 1) opposite to the target position within the recognition sequence of M·*Taq*I.

The synthesis of the required known building blocks **6a**–**c** and of the new phosphoramidites **6d** and **6e** relies upon the formation of a C-glycosidic bond, which we[7] and others[8] performed by employing the 2-deoxyribose donor **1**[9] and cadmium–organic reagents such as **3a**–**e** as glycosyl acceptors (Scheme 1).[10] We sought an alternative C-glycosylation

 © 2003 Wiley-VCH Verlag GmbH & Co. KGaA, Weinheim DOI: 10.1002/anie.200219972



Scheme 1. a) M = Cd: $CdCl_2$, THF, 40–50 °C, 2–3 h; M = CuMgX: CuI, THF, 0 °C, 5 min; b) M = Cd: 0 °C–reflux, THF, 1–2 h; M = CuMgX: THF, 25 °C, 30 min; c) 1) NaOMe, MeOH, 4 h; 2) DMTr-Cl, DMAP, EtN*i*Pr$_2$, pyridine, CH_2Cl_2, 8 h; 3) (*i*Pr$_2$N)$_2$POCH$_2$CH$_2$CN, tetrazole, CH_2Cl_2, MeCN, 1–2 h, 59% (**6a**), 67% (**6b**), 40% (**6c**), 80% (**6d**), 51% (**6e**). DMTr = dimethoxytrityl, DMAP = dimethylaminopyridine.

method with the aims of replacing the toxic cadmium and improving the sometimes low glycosylation yields. Organocuprates are mild and versatile C-nucleophiles in the coupling with reactive alkyl chlorides.[11] Indeed, the C-glycosylation of the Normant reagents **4a–e** proved superior to the reaction with the organocadmium reagents **3a–e** in terms of both synthetic practicability and yields (Table 1). The synthesis of the building blocks **6a–e** was completed after removal of the tolyl protecting groups from **5a–e**, regioselective introduction of the trityl protecting group, and final phosphitylation.

Table 1: Yields of the C-glycosylation reactions.[a]

Organometallic reagent	5a	5b	5c	5d	5e
Ar$_2$Cd, **3a–e**	72% (4:1)	67% (4:1)	47% (2:1)	47% (2:1)	41% (2:1)
Ar$_2$CuMgX, **4a–e**	74% (3:1)	81% (4:1)	74% (3:1)		75% (2:1)

[a] The α/β ratio is given in parentheses.

The phosphoramidites **6a–e** were used in the automated solid-phase synthesis of oligonucleotides **7a–e** (Table 2).[7] First, we investigated whether the presence of the base surrogates could be tolerated in duplex DNA. The modified oligonucleotides **7a–e** were hybridized with the complementary strand **8A**, which contains a target adenine opposite to the base surrogates within the 5′-TCGA-3′ recognition sequence of M·*Taq*I (Table 2). In all cases the melting curves exhibited a sigmoid behavior. Substitution of thymine in **7T** by the aromatic base surrogates in **7a–e** led to a decrease in the melting temperature by 4.9–8.7 K.

After having secured the integrity of the duplexes **7a–e·8A**, their binding affinities to the M·*Taq*I DNA MTase were investigated in solution and compared with the binding

Table 2: Thermal stability of duplexes and binding affinities to the adenine-specific DNA MTase M·*Taq*I.[a]

```
5'-GCCGC T C G dRibX TGCCG-3'   8A, 8b
3'-CGGCG A G C dRibY ACGGC-5'   7T, 7C, 7G, 7A, 7a-e
```

Y	X = adenine, **8A**		X = H, **8b**	
	T_M [°C][b]	K_A [10^9 M^{-1}][c]	T_M [°C][b]	ΔT_M [K][d]
thymine, **7T**	65.9 ± 0.2	0.05 ± 0.02	49.8 ± 0.1	0.0
cytosine, **7C**	55.7 ± 0.1	0.03 ± 0.02	50.6 ± 0.1	+0.8
guanine, **7G**	61.0 ± 0.2	0.03 ± 0.02	48.7 ± 0.2	−1.1
adenine, **7A**	56.1 ± 0.2	0.04 ± 0.02	52.5 ± 0.2	+2.7
1-pyrenyl, **7a**	61.0 ± 0.3	20 ± 10	63.6 ± 0.4	+13.8
4-biphenyl, **7e**	57.5 ± 0.3	3.0 ± 1.0	59.0 ± 0.3	+9.2
acenaphthyl, **7d**	59.0 ± 0.4	2.0 ± 1.0	57.9 ± 0.3	+8.1
1-naphthyl, **7b**	57.2 ± 0.1	2.0 ± 1.0	56.0 ± 0.2	+6.2
2-naphthyl, **7c**	58.0 ± 0.1	1.0 ± 0.5	57.8 ± 0.2	+8.0

[a] The double-stranded recognition sequence of M·*Taq*I is boxed. [b] Measured as denaturation curves at a DNA concentration of 1 μM in a buffered solution (100 mM NaCl, 10 mM NaH_2PO_4, pH 7.0). [c] For experimental details, see Supporting Information. [d] ΔT_M values are based on the T_M value of **8b·7T**.

affinities of the matched duplex **7T·8A** and the duplexes **7C·8A**, **7G·8A**, and **7A·8A**, which contain a mismatched target adenine. The affinities were determined in a new competitive fluorescence binding assay by employing a competitor duplex that contained the fluorescent base analogue 2-aminopurine at the target position.[12,13] Owing to a partial overlap of the spectra of the 2-aminopurine and pyrene fluorophores, this binding assay was not suitable for the pyrene-containing duplex **7a·8A**. Therefore, a pyrene fluorescence binding assay was performed which employed a nonfluorescent duplex oligonucleotide as competitor.[13]

M·*Taq*I binds its unmodified substrate **7T·8A** with an affinity constant of $K_A = 5 \times 10^7$ M^{-1} and the duplexes **7C·8A**, **7G·8A**, and **7A·8A** containing a mismatched target adenine with almost the same affinity (Table 2). This similarity suggests that removal of the Watson–Crick hydrogen bonds within the target base pair has little effect. However, this finding differs from results with the cytosine-specific DNA MTase M·*Hha*I, in which an up to 20-fold enhanced binding affinity was observed with duplexes that contained a mismatched target cytosine.[14]

In contrast to the duplexes with natural nucleobases, duplexes with the naphthyl, acenaphthyl, and biphenyl base surrogates enhanced the binding affinity by a factor of 20–60. The ≈400-fold enhancement of DNA MTase binding affinity determined for the duplex **7a·8A** containing the pyrenyl residue was most remarkable. The observed affinity corresponds to a dissociation constant $K_D = 50$ pM.

In principle, the enhancement of binding affinity to M·*Taq*I could originate from unstacking the target adenine in the duplexes **7a–e·8A**. This possibility was explored in previous investigations.[7] Fluorescence studies suggested that the pyrenyl residue was rather ineffective in disrupting target base stacking. On the contrary, the biphenyl residue, which led to a sevenfold lower affinity to M·*Taq*I, was the most potent base surrogate in unstacking its partner base. These results suggest that although binding of DNA to M·*Taq*I might profit from an unstacked target base, it is not the

 © 2003 Wiley-VCH Verlag GmbH & Co. KGaA, Weinheim

decisive determinant for the observed order of binding affinities.

Binding of M·*Taq*I to its target DNA leads to the formation of an apparent abasic site, which is only partially filled by the interstrand stacked partner thymine (Figure 1C). Abasic sites, however, dramatically decrease duplex stability, as exemplified by the substantial decrease in the melting temperature that was observed when the target 2′-deoxyadenosine in **7T·8A** was replaced by the abasic-site analogue 1,2-dideoxy-D-ribose in **7T·8b** ($\Delta T_M = -16.1$ K). This destabilization also occurred with the other natural nucleobases, as evidenced by similar T_M values of duplexes **7C·8b**, **7G·8b**, and **7A·8b**. We explored whether the base surrogates opposite to an abasic site are capable of increasing duplex stability. Indeed, each of the duplexes **7a–e·8b**, which contain an abasic site opposite to any of the five base surrogates, displayed an enhanced thermal stability relative to the duplex **7T·8b** (Table 2). Most importantly, the thermal stabilities of the abasic site duplexes **7a–e·8b** correlate well with the binding affinities of duplexes **7a–e·8A** to M·*Taq*I (Table 2). The pyrene residue conferred the highest abasic-site stabilization and led to the highest binding affinity to M·*Taq*I. Thus, we propose that the pyrenyl residue enhances the M·*Taq*I-binding affinity mainly by an increased compensation of the energy penalty that arises from the enzyme-induced abasic-site formation.

Recently, studies of uracil DNA glycosylase (UDG) and variants with a duplex that contained the pyrenyl residue opposite to an unreactive uracil analogue were reported.[15,16] Similar to the cytosine-specific DNA MTase M·*Hha*I, UDG flips its target base out of the DNA helix and stabilizes the apparent abasic site by insertion of an amino acid side chain. In contrast to our binding studies with M·*Taq*I, only a minor change in the binding affinity to UDG was conferred by the pyrenyl residue, which is in agreement with the different mechanisms of stabilizing the apparent abasic sites. In M·*Taq*I, the pyrenyl residue fills the space formed by target base flipping better than the natural partner thymine, whereas in UDG a steric interference with the inserting amino acid side chain is expected. In line with this interpretation, the weak binding affinity of a UDG variant in which the critical amino acid side chain is deleted could be restored by incorporation of a pyrene nucleotide.[15,16] This comparison between M·*Taq*I and UDG illustrates that duplexes with extended aromatic base surrogates opposite to the target base could be very useful probes to analyze the mechanism of DNA base-flipping enzymes. In addition, the observed high-affinity binding the of duplex with a pyrenyl residue is of interest for the inhibition of adenine-specific DNA MTases from pathogenic bacteria which are essential for bacterial virulence.[17]

In conclusion, we have presented an improved and less toxic C-glycosylation that is expected to provide a reliable access to a variety of nonpolar nucleoside analogues. Our results point out that improved abasic-site stabilization is an important criterion for high-affinity binding to M·*Taq*I. Future work will concern the implementation of this design approach for the development of high-affinity binders to other adenine-specific DNA MTases, an endeavor ultimately aimed at the construction of inhibitors of these interesting enzymes.

Received: August 14, 2002
Revised: May 14, 2003 [Z19972]

Keywords: abasic sites · DNA methylation · DNA–protein interactions · enzymes · glycosides · nucleic acids

[1] A. Jeltsch, *ChemBioChem* **2002**, *3*, 275–293.
[2] X. Cheng, *Annu. Rev. Biophys. Biomol. Struct.* **1995**, *24*, 293–318.
[3] X. Cheng, R. J. Roberts, *Nucleic Acids Res.* **2001**, *29*, 3784–3795.
[4] S. Klimasauskas, S. Kumar, R. J. Roberts, X. Cheng, *Cell* **1994**, *76*, 357–369.
[5] K. M. Reinisch, L. Chen, G. L. Verdine, W. N. Lipscomb, *Cell* **1995**, *82*, 143–153.
[6] K. Goedecke, M. Pignot, R. S. Goody, A. J. Scheidig, E. Weinhold, *Nat. Struct. Biol.* **2001**, *8*, 121–125.
[7] I. Singh, W. Hecker, A. K. Prasad, V. S. Parmar, O. Seitz, *Chem. Commun.* **2002**, 500–501.
[8] A. K. Ogawa, Y. Q. Wu, M. Berger, P. G. Schultz, F. E. Romesberg, *J. Am. Chem. Soc.* **2000**, *122*, 8803–8804.
[9] M. Hoffer, *Chem. Ber.* **1960**, *93*, 2777–2781.
[10] R. X. F. Ren, N. C. Chaudhuri, P. L. Paris, S. Rumney, E. T. Kool, *J. Am. Chem. Soc.* **1996**, *118*, 7671–7678.
[11] Notably, the reaction of lithium dialkyl cuprates with glucopyranosyl halides has been reported: R. Bihovsky, C. Selick, I. Giusti, *J. Org. Chem.* **1988**, *53*, 4026–4031.
[12] B. Holz, S. Klimasauskas, S. Serva, E. Weinhold, *Nucleic Acids Res.* **1998**, *26*, 1076–1083.
[13] For procedures, see Supporting Information.
[14] S. Klimasauskas, R. J. Roberts, *Nucleic Acids Res.* **1995**, *23*, 1388–1395.
[15] Y. L. Jiang, K. Kwon, J. T. Stivers, *J. Biol. Chem.* **2001**, *276*, 42347–42354.
[16] Y. L. Jiang, J. T. Stivers, F. Song, *Biochemistry* **2002**, *41*, 11248–11254.
[17] D. M. Heithoff, R. L. Sinsheimer, D. A. Low, M. J. Mahan, *Science* **1999**, *284*, 967–970.

 © 2003 Wiley-VCH Verlag GmbH & Co. KGaA, Weinheim

Conformational Flexibility

From Rigidity to Conformational Flexibility: Macrocyclic Templates Derived from ansa-Steroids**

Stefan Bäurle, Thorsten Blume, Anne Mengel, Christian Parchmann, Werner Skuballa, Siegfried Bäsler, Martina Schäfer, Detlev Sülzle, and Hans-Peter Wrona-Metzinger*

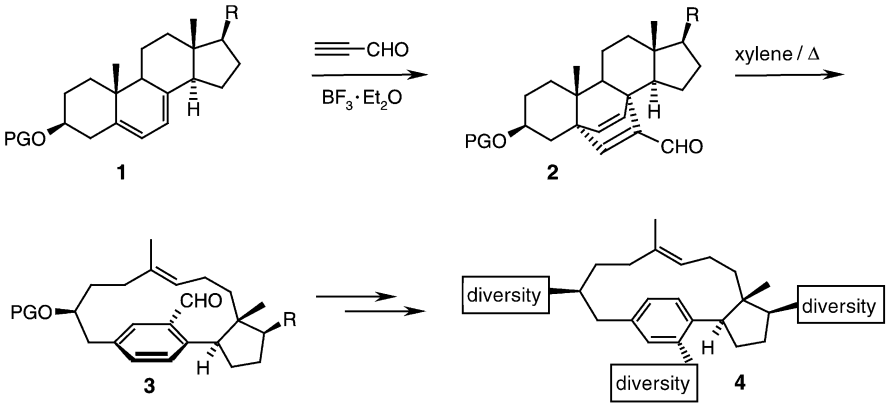
Dedicated to Professor Dr. Rudolf Wiechert on the occasion of his 75th birthday

The synthesis of natural product derivatives is a powerful approach for increasing the diversity of compound libraries to be screened with the goal of improving the chance of finding leads for drug discovery.[1] The original natural products can be modified by scaffold rearrangement, core decoration, or functional group transformation and derivatization reactions. This approach combines the principle of diverse libraries with the structural complexity of natural products.

Our concept of natural product derivatization is based on readily available steroids. Two approaches are known for the synthesis of macrocyclic structures by cleavage of the ABC ring system of steroids: the fragmentation of endoperoxides to obtain "steroklastanes"[2] and the Winterfeldt approach to yield "ansa-steroids".[3] In this paper we briefly present our approach to new diverse compound libraries from steroids and discuss the extension of the concept to larger ring sizes in more detail.

We started the synthesis with steroids of type **1** (Scheme 1). We chose the Winterfeldt tandem reaction[3] to create new compounds with the general structure **3** by scaffold rearrangement (Diels–Alder/retro-Diels–Alder sequence). Compound **3** was formed as one single regio- and atropisomer. Even under harsh conditions no atropisomerization was observed, which was expected due to the small ring size. By this economic route we were able to obtain multigram quantities of structurally complex templates offering high potential for diversification. Alterations of the side chain by means of parallel synthesis (to amines, esters), and modifications at the aryl ring (to ethers, amines, amides) and of the secondary hydroxy group resulted in compound libraries with the general structure **4**.[4] The first biologically active compounds were identified by screening with targets such as the androgen receptor and the tumor-relevant cell cycle phosphatase cdc25, for which we found inhibition in low micromolar range (3–10 μM).[5]

Calculation of energy-minimized conformations for the representative structure **5** at the HF/3-21G* level of theory[6] confirms the assumption of extremely low conformational flexibility comparable to that of the parent steroid (Figure 1). Owing to the rigid core structure of these macrocycles with their alterable functional groups, pharmacophoric groups can be presented in a defined way. The structures of the calculated conformers of lowest energy are in excellent agreement with the results of an X-ray structure analysis.[7]



Scheme 1. Synthesis of ansa-steroids. PG = protecting group.

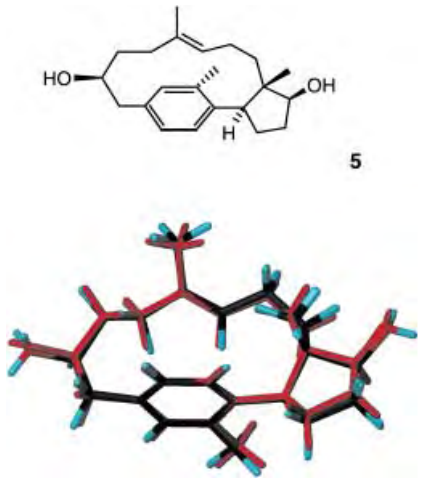


Figure 1. Compound **5** (top) and the superposition (bottom) of its X-ray structure (red) with two energy-minimized conformations of **5** (blue).

To access a variety of templates with different degrees of flexibility it was our aim to expand the ring size of the given macrocyclic system. The relationship between the ring size and the rigidity of the structure could then be examined by NMR studies and conformational analysis. The modulation of the conformational flexibility might improve the chances of finding suitable interactions between small molecules and

[*] Dr. T. Blume, Dr. S. Bäurle, Dr. A. Mengel, C. Parchmann, Prof. Dr. W. Skuballa, S. Bäsler, Dr. M. Schäfer, Dr. D. Sülzle, H.-P. Wrona-Metzinger
Schering AG
Research Center Europe
13342 Berlin (Germany)
Fax: (+49) 30-468-92531
E-mail: thorsten.blume@schering.de

[**] We thank Prof. Dr. E. Winterfeldt for numerous fruitful discussions.

 DOI: 10.1002/anie.200351385 © 2003 Wiley-VCH Verlag GmbH & Co. KGaA, Weinheim

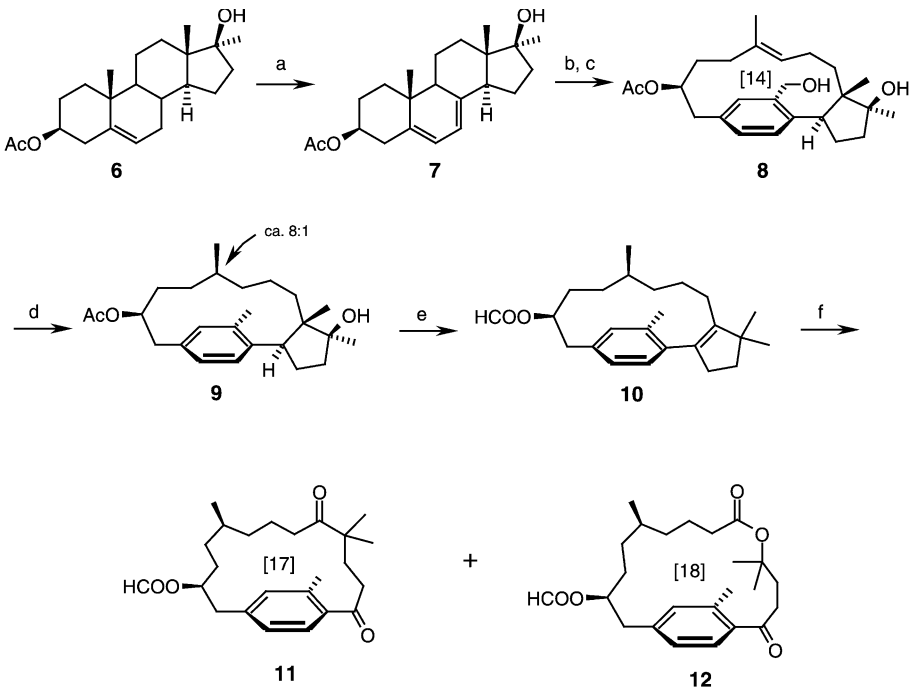
proteins. As a part of this program we here report for the first time on the synthesis of a 17-membered macrocycle derived from a steroid. Despite extensive research on steroids, the synthesis of such a compound has not been described before.

Since we had access to the 14-membered ansa-steroids of type **3**, the challenge was to open the remaining cyclopentane ring to give a structure in which all the transannular bonds of the original steroid are cleaved.[3a] To reach this goal, we applied a combination of the Winterfeldt sequence, a Wagner–Meerwein rearrangement, and an ozonolysis (Scheme 2). In addition, to obtain a compound comparable to the 14-membered structure **5** in terms of its conformational properties, we intended to reduce the aromatic aldehyde to a methyl group.

Starting from the readily available steroid **6** with a 17-β-hydroxy-17-α-methyl functionality,[9] we obtained the $\Delta^{5,7}$-steroid **7** in moderate yield by a bromination/dehydrobromination sequence.[10] Compound **7** was converted into the corresponding ansa-steroid by the Winterfeldt procedure, and the formyl group was reduced to a hydroxy group (→**8**). In the subsequent hydrogenation the benzyl alcohol was deoxygenated and the double bond saturated in one step to give **9**. The new stereogenic center was introduced with a selectivity of 8:1 (from the ^{1}H NMR spectrum of **11**) in favor of the *S* isomer shown (determined by X-ray structure analysis of **11**). The selectivity is a result of the rigid conformation of **8**. Since one of the diastereotopic faces of the double bond is shielded by the macrocycle, the hydrogenation occurs predominantly at the outer face. A similar approach using rigid ansa-type compounds for stereocontrolled additions to double bonds was described by Mulzer et al.[11]

Heating **9** in formic acid induced the Wagner–Meerwein rearrangement leading to compound **10**, which has a transannular double bond. Simultaneously the acetate was replaced by a formiate group.[12] The double bond was cleaved by ozonolysis.[13] The main product of this reaction was the desired 17-membered cyclic diketone **11** in which all 17 carbon atoms of the steroidal skeleton form one large ring. An interesting side product of the ozonolysis is ketolactone **12**, an 18-membered macrocycle in which the two carbonyl groups are already differentiated. Compound **12,** the favored product of the Baeyer–Villiger oxidation of **11,** is apparently readily formed under ozonolysis conditions. The analytical data of **11** and **12** are presented in Table 1.

The structure of **11** was confirmed by X-ray structure analysis (Figure 2). The energy-minimized conformations of



Scheme 2. a) 1. 1,3-Dibromo-5,5-dimethylhydantoin (0.76 equiv), AIBN (0.12 equiv), hexane, reflux, 10 min; 2. collidine (6 equiv), xylene, reflux, 1 h, 35%; b) 1. propargylaldehyde (2.5 equiv), BF_3/Et_2O (1.0 equiv), CH_2Cl_2, 0°C→RT, 1 h, 2. xylene, reflux, 1 h, 46%; c) $NaBH_4$ (2.0 equiv), CH_2Cl_2/EtOH, RT, 30 min, 65%; d) H_2, Pt/C, MeOH, RT, 85%; e) HCOOH, reflux, 10 min, 80%; f) O_3, −78°C, then PPh_3 (1.1 equiv), RT, 34% of **11** and 6% of **12** after preparative HPLC.[8] AIBN = 2,2′-azobisisobutyronitrile, RT = room temperature.

Table 1: Selected analytical data of **11** and **12** (steroid numbering).

11: m.p.: 129–132°C; HPLC: t_R = 10.3 min (Chiralcel OD(2) 10μ, hexane/EtOH 97:3); ^{1}H NMR (500 MHz, $CDCl_3$): δ = 0.68–0.77 (m, 2H, 9-H_2), 0.80 (d, J = 7 Hz, 3H, 19-H_3), 0.86–0.95 (m, 1H, 11-H_a), 0.97–1.07 (m, 1H, 1-H_a), 1.06 (s, 3H) and 1.08 (s, 3H) (18-H_3 and 20-H_3), 1.13–1.20 (m, 1H, 1-H_b), 1.20–1.28 (m, 2H, 11-H_b and 10-H), 1.33–1.42 (m, 2H, 2-H_2), 1.60–1.70 (m, 2H, 16-H_2), 1.98–2.06 (m, 2H, 12-H_2), 2.38 (s, 3H, Ar-CH_3), 2.55–2.65 (m, 2H, 15-H_2), 2.65 (dd, J = 10 Hz/13 Hz, 1H, 4-H_a), 3.10 (dd, J = 4 Hz/13 Hz, 1H, 4-H_b), 5.12–5.17 (m, 1H, 3-H), 7.10 (s, 1H, 6′-H), 7.11 (d, J = 8 Hz, 1H, 6-H), 7.30 (d, J = 8 Hz, 1H, 7-H), 8.12 ppm (s, 1H, formiate); ^{13}C NMR (125 MHz, $CDCl_3$): δ = 20.3 (C-19), 20.3 (Ar-CH_3), 20.8 (C-11), 22.9/24.2 (C-18/C-20), 28.1 (C-2), 30.2 (C-1), 30.8 (C-10), 34.4 (C-9), 35.1 (C-16), 37.1 (C-12), 38.3 (C-15), 39.9 (C-4), 47.5 (C-17), 73.8 (C-3), 126.9 (C-6), 128.0 (C-7), 132.4 (C-6′), 137.0/137.3/140.2 (C-5, C-8, C-7′), 160.8 (formiate), 205.9 (C-14), 214.4 ppm (C-13); MS (CI/NH_3): 404 $[M+NH_4]^+$, 387 $[M+H]^+$, $C_{24}H_{34}O_4$

12: HPLC: t_R = 8.2 min (Chiralcel OD(2) 10μ, hexane/EtOH 97:3); ^{1}H NMR (500 MHz, $CDCl_3$): δ = 0.71–0.93 (m, 2H, 9-H_2), 0.79 (d, J = 7 Hz, 3H, 19-H_3), 0.99–1.13 (m, 3H, 11-H_a and 1-H_2), 1.18–1.30 (m, 2H, 10-H and 11-H_b), 1.45 (s, 3H) and 1.46 (s, 3H) (18-H_3 and 20-H_3), 1.40–1.50 (m, 2H, 2-H_2), 1.74–1.80 (m, 1H, 12-H_a), 1.85–1.91 (m, 1H, 12-H_b), 2.03–2.11 (m, 1H, 16-H_a), 2.16–2.22 (m, 1H, 16-H_b), 2.49 (s, 3H, Ar-CH_3), 2.69 (dd, J = 10 Hz/13 Hz, 1H, 4-H_a), 2.73–2.79 (m, 1H, 15-H_a), 2.91–2.97 (m, 1H, 15-H_b), 3.13 (dd, J = 4 Hz/13 Hz, 1H, 4-H_b), 5.09–5.15 (m, 1H, 3-H), 7.12 (s, 1H, 6′-H), 7.17 (d, J = 8 Hz, 1H, 6-H), 7.59 (d, J = 8 Hz, 1H, 7-H), 8.14 ppm (s, 1H, formiate); ^{13}C NMR (125 MHz, $CDCl_3$): δ = 20.1 (C-19), 21.3 (Ar-CH_3), 22.2 (C-11), 25.7/26.3 (C-18/C-20), 28.5 (C-2), 30.7 (C-1), 31.0 (C-10), 34.5 (C-9), 35.6 (C-12), 36.1 (C-15), 36.9 (C-16), 40.3 (C-4), 74.0 (C-3), 81.4 (C-17), 126.9 (C-6), 128.9 (C-7), 133.1 (C-6′), 136.6/138.4/140.5 (C-5, C-8, C-7′), 160.8 (formiate), 172.7 (C-13), 204.7 ppm (C-14); MS (CI/NH_3): 420 $[M+NH_4]^+$, 403 $[M+H]^+$, $C_{24}H_{34}O_5$

 © 2003 Wiley-VCH Verlag GmbH & Co. KGaA, Weinheim

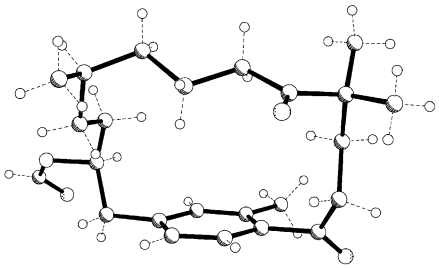


Figure 2. X-ray structure of the macrocyclic diketone **11**.[7]

11 show the structural features of the macrocycle. The ansa-aryl group, the two carbonyl groups, and the geminal dimethyl group generate still a quite rigid structure. However, in contrast to the smaller ring system of **5**, there is more flexibility within the carbon chain of **11** (Figure 3). According to the energy data obtained at the HF/3-21G* level of theory, rotation of the aryl group to form the other atropisomer is not expected. In fact, high-temperature NMR experiments (120 °C, [D_6]DMSO) showed no signs of isomerization, in line with the theoretical predictions.

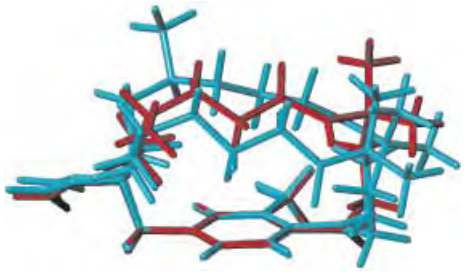


Figure 3. Superposition of the X-ray structure (red) of **11** with two energy-minimized[6] conformations (turquoise) of **11**.

In conclusion, we have succeeded in generating a conformationally more flexible structure by scaffold modification of our first-generation template. The new macrocyclic compound **11** is more than an interesting curiosity in the field of steroid derivatives; it is a prototype of a template with differentiable functional groups, which could be used in the synthesis of libraries of novel macrocyles. For this purpose all functional groups—such as double bond and benzyl alcohol of compond **8**—should be conserved in order to maintain all possible points of diversification. The ultimate goal is the generation of biologically active compounds as starting points for new lead structures.

Received: March 13, 2003 [Z51385]

Keywords: conformations · macrocycles · ring expansions · steroids

[1] a) R. Breinbauer, I. R. Vetter, H. Waldmann, *Angew. Chem.* **2002**, *114*, 3002–3015; *Angew. Chem. Int. Ed.* **2002**, *41*, 2878–2890; b) D. G. Hall, S. Manku, F. Wang, *J. Comb. Chem.* **2001**, *3*, 125–150; c) L. A. Wessjohann, *Curr. Opin. Chem. Biol.* **2000**, *4*, 303–309; d) "Role of Natural Products in Drug Discovery": S. Grabley, R. Thiericke, I. Sattler, Ernst Schering Research Foundation Workshop **2000**, *32*, pp. 217–252; e) S. L. Schreiber, *Science* **2000**, *287*, 1964–1969.

[2] a) L. Lorenc, L. Bondarenko, V. Pavlovic, H. Fuhrer, G. Rihs, J. Kalvoda, M. L. Mihailovic, *Helv. Chim. Acta* **1989**, *72*, 608–623; b) M. L. Mihailovic, L. Lorenc, V. Pavlovic, L. Bondarenko-Gheorghiu, *J. Serb. Chem. Soc.* **1989**, *54*, 459–464; c) L. Lorenc, L. Bondarenko-Gheorghiu, V. Pavlovic, H. Fuhrer, J. Kalvoda, M. L. Mihailovic, *Helv. Chim. Acta* **1992**, *75*, 203–209.

[3] a) E. Winterfeldt, *Chimia* **1993**, *47*, 39–45; b) A. Prelle, E. Winterfeldt, *Heterocycles* **1989**, *28*, 333–346; c) P.-K. Chowdhury, A. Prelle, D. Schomburg, M. Thielmann, E. Winterfeldt, *Liebigs Ann. Chem.* **1987**, 1095–1099; d) D. Schomburg, M. Thielmann, E. Winterfeldt, *Tetrahedron Lett.* **1985**, *26*, 1705–1706.

[4] About 500 compounds of type **4** have been synthesized so far mainly with carousel reactors. Solid-phase synthesis was also successfully established. All compounds were characterized by NMR spectroscopy and/or mass spectrometry.

[5] a) Detailed biological results including the inhibition of phosphatases will be published elsewhere; b) biological activity of ansa-steroids was described for the first time in the context of vitamin D_3 analogues: W. H. Okamura, S. Do, H. Kim, S. Jeganathan, T. Vu, G.-D. Zhu, A. W. Norman, *Steroids* **2001**, *66*, 239–247.

[6] In the conformational analysis the conformer distribution was calculated by the Monte Carlo method in the Alter Conformation module of SPARTAN'02 with the MMFF force field. Conformers thus obtained were further refined at the HF/3-21G* level of theory. The final characterization by frequency calculation revealed that the conformers of lowest energy thus obtained are true minima on the corresponding potential energy surface.

[7] a) Crystal data for **5**: $C_{22}H_{32}O_2 + C_7H_8$, $M_r = 420.67$, monoclinic, space group $P2(1)$, crystal dimensions $0.45 \times 0.2 \times 0.2$ mm^3, unit cell dimensions $a = 7.297(5)$, $b = 36.515(7)$, $c = 11.933(2)$ Å, $\alpha = 90.0$, $\beta = 97.22(3)$, $\gamma = 90°$, $V = 3154(2)$ Å^3, $Z = 6$, $\rho_{calcd} = 1.135$ mg m^{-3}, $F(000) = 1180$, $\mu(Mo_{K\alpha}) = 0.070$ mm^{-1}, $T = 173$ K, $\lambda = 0.71073$ Å, $4.10° \le 2\Theta \le 45.02°$, 4021 reflections collected of which 3641 are independent ($R_{int} = 0.0395$, Friedel mates are not merged). For the final refinement of the 739 parameters, 1042 restraints were used. R indices (all data) $R_1 = \Sigma | F_o - F_c | / \Sigma F_o = 0.0494$ for $I > 2\sigma(I)$ and $wR_2 = \Sigma[w(F_o^2 - F_c^2)^2 / \Sigma w F_o^4]^{1/2} = 0.1122$ for all data; min./max. electron density: 0.205/−0.228 e Å^{-3}, b) Crystal data for **11**: $C_{24}H_{34}O_4$, $M_r = 386.51$, monoclinic, space group $P2(1)$, crystal dimensions $0.8 \times 0.6 \times 0.02$ mm^3, unit cell dimensions $a = 11.8813(7)$, $b = 7.8734(5)$, $c = 12.3232(7)$ Å, $\alpha = 90$, $\beta = 108.090(4)$, $\gamma = 90°$, $V = 1095.81(11)$ Å^3, $Z = 2$, $\rho_{calcd} = 1.171$ mg m^{-3}, $F(000) = 420$, $\mu(Cu_{K\alpha}) = 0.620$ mm^{-1}, min./max. transmission 0.9877/0.6369, $T = 153$ K, $\lambda = 1.54178$ Å, $7.54° \le 2\Theta \le 129.56°$, 5885 reflections collected of which 2721 are independent ($R_{int} = 0.0238$, Friedel mates are not merged). For the final refinement of the 257 parameters, 1 restraint was used. $R_1 = \Sigma | F_o - F_c | / \Sigma F_o = 0.0775$ for $I > 2\sigma(I)$ and $wR_2 = \Sigma[w(F_o^2 - F_c^2)^2 / \Sigma w F_o^4]^{1/2} = 0.1903$ for all data; min./max. electron density: 0.386/−0.356 e Å^{-3}. Intensity data for **5** and **11** were recorded for shock-cooled crystals mounted in oil drops.[14] Data for **5** were collected on a Siemens four-circle P4 diffractometer using ω scans, whereas for **11** it was collected on a three-circle diffractometer with a Smart6000 CCD area detector using ω scans. Data for **5** were integrated using the Siemens Software XSCANS and no absorption correction was applied. Data for **11** was integrated using the program SAINT. All data were corrected semiempirically for systematic errors such as absorption using the program SADABS. The structures were solved by

 © 2003 Wiley-VCH Verlag GmbH & Co. KGaA, Weinheim

Direct Methods using the program SHELXS 96[15] and refined against F^2 by least squares.[16] All non-hydrogen atoms could be refined anisotropically. In **5** three crystallographically independent molecules in the asymmetric unit and one disordered molecule of toluene were refined using distance restraints and restraints for the anisotropic temperature factors. All hydrogen atoms in both structures were placed in geometrically ideal positions and refined using the riding model, in which the methyl groups could rotate about their local threefold axes. The isotropic temperature factors of all hydrogen atoms are 1.2 and 1.5 times the size of the temperature factors of the corresponding heavy atoms (for **5** and **11**, respectively). The absolute structure for both molecules could not be determined. CCDC-205757 (**5**) and -205756 (**11**) contain the supplementary crystallographic data for this paper. These data can be obtained free of charge via www.ccdc.cam.ac.uk/conts/retrieving.html (or from the Cambridge Crystallographic Data Centre, 12, Union Road, Cambridge CB21EZ, UK; fax: (+44) 1223-336-033; or deposit@ccdc.cam.ac.uk).

[8] Experimental procedures for the preparation of compounds **10**–**12**: Wagner-Meerwein rearrangement: Compound **9** (280 mg, 0.72 mmol) was dissolved in formic acid (15 mL) and heated to reflux for 30 min. The solution was cooled and partitioned between ethyl acetate and water. The organic phase was carefully neutralized with sat. $NaHCO_3$, washed with brine, and dried over Na_2SO_4. Chromatography on silica gel with hexane/ethyl acetate (6:1) yielded compound **10** (205 mg, 80%) as a colorless solid. ^{1}H NMR (300 MHz, $CDCl_3$): $\delta = 0.05$–0.25 (m, 1H), 0.32–0.46 (m, 1H), 0.63 (d, 3H), 0.65–0.95 (m, 4H), 1.03 (s, 3H), 1.06 (s, 3H), 1.17–1.35 (m, 2H), 1.45–1.70 (m, 2H), 1.72–1.88 (m, 3H), 2.19 (s, 3H), 2.45–2.70 (m, 2H), 2.84 (dd, 1H), 2.95 (dd, 1H), 5.10 (m, 1H), 6.98 (s, 1H), 7.04 (d, 1H), 7.10 (d, 1H), 8.11 ppm (s, 1H); ^{13}C NMR (75 MHz, $CDCl_3$): $\delta = 19.1$, 19.9, 24.6, 25.3, 26.9, 27.1, 29.2, 29.3, 30.4, 34.0, 37.4, 39.6, 41.4, 47.4, 73.8, 127.4, 128.8, 131.3, 135.0, 135.1, 135.9, 138.9, 148.1, 160.7 ppm; MS (CI): 309 [$M-HCO_2H+H$], 326 [$M-HCO_2H+NH_4$], 354 [M], 372 [$M+NH_4$]. Ozonolysis: A solution of compound **10** (175 mg, 0.49 mmol) in CH_2Cl_2 (30 mL) was cooled to −78 °C. Ozone was bubbled through the solution until the color it turned light blue. Excess ozone was removed by passage of oxygen and argon. PPh_3 (142 mg, 0.54 mmol) was added, the cooling bath removed, and the reaction mixture stirred for 1 h. Chromatography on silica gel with hexane/ethyl acetate (9:1 to 4:1) yielded a mixture of **11** and **12** (90 mg), which was separated by preparative HPLC (see Table 1).

[9] G. Ortar, A. Romeo, *J. Org. Chem.* **1976**, *41*, 4036–4038.

[10] D. Fischer-Henningsen, Dissertation, Universität Hannover, **1992**.

[11] a) J. Mulzer, K. Schein, J. W. Bats, J. Buschmann, P. Luger, *Angew. Chem.* **1998**, *110*, 1625–1628; *Angew. Chem. Int. Ed.* **1998**, *37*, 1566–1569; b) J. Mulzer, I. Böhm, J. W. Bats, *Tetrahedron Lett.* **1998**, *39*, 9643–9646.

[12] a) J. Toreilles, A. Crastes de Paulet, *Bull. Soc. Chim. Fr.* **1968**, 4112–4117; b) C. L. Hewett, S. G. Gibson, I. M. Gilbert, J. Redpath, D. S. Savage, T. Sleigh, R. Taylor, *J. Chem. Soc. Perkin Trans. 1* **1975**, 336–334.

[13] J. Toreilles, A. Crastes de Paulet, *Bull. Soc. Chim. Fr.* **1968**, 4892–4898.

[14] T. Kottke, D. Stalke, *J. Appl. Crystallogr.* **1993**, *26*, 615–619.

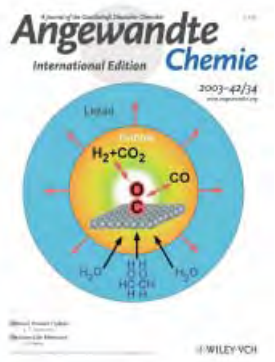
[15] "SHELXS-96, Program for Structure Solution": G. M. Sheldrick, *Acta Crystallogr. Sect. A* **1990**, *46*, 467–473.

[16] G. M. Sheldrick, T. R. Schneider, *Methods Enzymol.* **1997**, *277*, 319–343.

 © 2003 Wiley-VCH Verlag GmbH & Co. KGaA, Weinheim

Cover Picture

Rupali R. Davda and James A. Dumesic*



CO-poor hydrogen can be produced by reforming oxygenates, such as ethylene glycol, in water over Pt catalysts. The expansion of the gas bubbles formed in the process by the vaporization of water results in a decrease in the partial pressures of H_2 and CO_2, thereby favoring the water–gas shift and lowering the CO concentration. This process leads to the production of fuel-cell-grade H_2 at high pressures. For more information see the Communication by J. A. Dumesic and R. R. Davda on page 4068 ff.

Contents

Angewandte EarlyView

The following articles are available online (in Wiley Interscience). You can find them at www.angewandte.org, under Full Text, Early View.

K. Koh, K. Ohno, Y. Tsujii, T. Fukuda:*
Precision Synthesis of Organic/Inorganic Hybrid Nanocapsules with a Silanol-Functionalized Micelle Template
DOI: 10.1002/anie.200351398
Published online: August 25, 2003

D. B. Ramachary, N. S. Chowdari, C. F. Barbas III:*
Organocatalytic Asymmetric Domino Knoevenagel/Diels–Alder Reactions: A Bioorganic Approach to the Diastereospecific and Enantioselective Construction of Highly Substituted Spiro[5,5]undecane-1,5,9-triones
DOI: 10.1002/anie.200351916
Published online: August 25, 2003

M. Bois-Choussy, P. Cristau, J. Zhu:*
Total Synthesis of an Atropdiastereomer of RP-66453 and Determination of Its Absolute Configuration
DOI: 10.1002/anie.200351996
Published online: August 25, 2003

K. C. Nicolaou, P. K. Sasmal, H. Xu, K. Namoto, A. Ritzén:*
Total Synthesis of 1-O-Methyllateriflorone
DOI: 10.1002/anie.200351805
Published online: August 25, 2003

N. J. Adderley, D. J. Buchanan, D. J. Dixon, D. I. Lainé:*
Highly Diastereoselective Oxy-Michael Additions of Enantiopure δ-Lactol Anions to Nitroalkenes: Asymmetric Synthesis of 1,2-Amino Alcohols
DOI: 10.1002/anie.200352007
Published online: August 25, 2003

M. Chiesa, G. Amato, L. Boarino, E. Garrone, F. Geobaldo, E. Giamello:*
Reversible Insulator-to-Metal Transition in p$^+$-Type Mesoporous Silicon Induced by the Adsorption of Ammonia
DOI: 10.1002/anie.200352114
Published online: August 25, 2003

Articles judged by the referees or the editor as being either very important or very urgent are immediately edited, proof-read, and electronically published once the manuscript has arrived in the editorial office in final form. As long as there is no page number available these articles should be cited in the following manner:

Author(s) *Angew. Chem. Int. Ed.*, online publication date, DOI.

Web Sites

http://www.microarrays.org, www.biochipnet.de — **3982**	Microarrays: Everything Counts in Large Amounts	*R. Dahint, H. Sültzmann*

Books

Molecular Imprinting — **3983**	Makoto Komiyama, T. Takeuchi, T. Mukawa, H. Asanuma	*reviewed by I. Huc*
Introduction to Macromolecular Crystallography — **3984**	Alexander McPherson	*reviewed by D. Heinz*

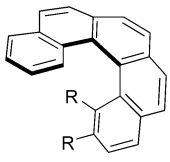
Highlights

Helicene-Like Molecules

A. Urbano* — **3986 – 3989**

Recent Developments in the Synthesis of Helicene-Like Molecules

Straightforward access to helicene-like molecules (see structure) is possible by short and efficient protocols that have emerged in the past few years. These transformations, as well as recent approaches to chiral nonracemic derivatives, constitute a significant advancement in synthetic methodology.



[*n*]helicenes

Essays



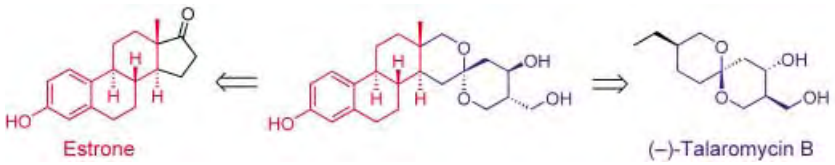
He counts as one of the co-founders of physical chemistry, contributor to scientific research and organization, scientific publicist, and color researcher. This year marks the 150th anniversary of the birth of Wilhelm Ostwald, Nobel Prize winner in 1909.

Wilhelm Ostwald

R. Zott* _____ **3990 – 3995**

Friedrich Wilhelm Ostwald (1853–1932), Now 150 Years Young...

Reviews



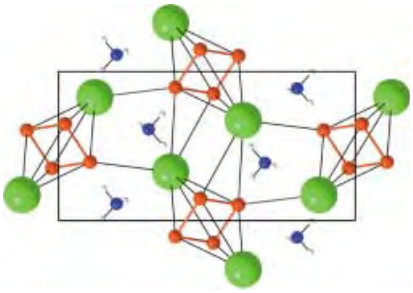
Unlimited options: The synthesis of natural product hybrids by combining structurally different, naturally occurring compounds that exhibit high biological activities appears to be a promising approach to increase the number and diversity of substances for pharmacological testing. An example is the hybrid of estrone and (−)-talaromycin (see picture).

Hybrids of Natural Products

L. F. Tietze,* H. P. Bell, S. Chandrasekhar _____ **3996 – 4028**

Natural Product Hybrids as New Leads for Drug Discovery

Communications



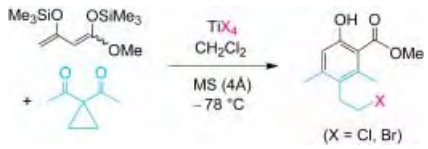
Aromatic P: Among the homoatomic polyanions of group 15 elements, Bi_4^{2-} and Sb_4^{2-} have been exotic curiosities for a long time, as they are potential 6π aromatic rings. As_4^{2-} joined as the lighter congener as recently as 2002. Considering the diagonal relationship of P to C, the cyclobutadienediide analogue P_4^{2-} would be expected naturally, but only now has it been prepared in the form of $Cs_2P_4 \cdot 2\,NH_3$ from diphosphane(4).

Aromatic Polyphosphides

F. Kraus, J. C. Aschenbrenner, N. Korber* _____ **4030 – 4033**

P_4^{2-}: A 6π Aromatic Polyphosphide in Dicesium Cyclotetraphosphide–Ammonia (1/2)

Domino reactions of 1,3-bis(silyl enol ether)s with 1,1-diacetylcyclopentane and 1,1-diacetylcyclopropane (see scheme) allow a new and convenient one-pot synthesis of spiro[5.4]cyclodecenones, bicyclo[4.4.0]deca-1,4-dien-3-ones, and functionalized salicylates, which are versatile intermediates for the synthesis of pharmacologically relevant natural product analogues. MS = molecular sieves.



Reactions of Bis(silyl enol ether)s

P. Langer,* G. Bose _____ **4033 – 4036**

[3+3] Cyclizations of 1,3-Bis(silyl enol ether)s with 1,1-Diacetylcyclopentane and 1,1-Diacetylcyclopropane

For the USA and Canada:
ANGEWANDTE CHEMIE International Edition (ISSN 1433-7851) is published weekly by Wiley-VCH PO Box 191161, D 69451 Weinheim, Germany. Air freight and mailing in the USA by Publications Expediting Inc. 200 Meacham Ave., Elmont, NY 11003. Periodicals postage paid at Jamaica NY 11431. US POSTMASTER: send address changes to *Angewandte Chemie*, Wiley-VCH, 111 River Street, Hoboken, NJ 07030. Annual institutional subscription price for institutions: Europe € 2998.00/3148.00. Outside Europe US$ 3718.00/3904.00 (valid for print or electronic/print and electronic delivery); for individuals who are personal members of a national chemical society, or whose institution already subscribes, or who are retired or self-employed consultants, print only (including postage and handling charges): Europe € 248.00/Outside Europe US$ 348.00.

 © 2003 Wiley-VCH Verlag GmbH & Co. KGaA, Weinheim

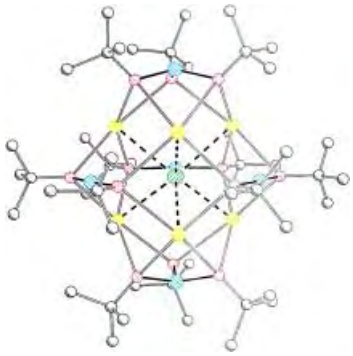
Contents

A Mixed-Valence Copper Alkoxide

R. Ahlrichs, C. E. Anson, D. Fenske,*
O. Hampe, A. Rothenberger,
M. Sierka ——— **4036 – 4039**

Template Synthesis and Theoretical Investigation of $[Cu^{II}_2Cu^{I}_3K_6(\mu_6\text{-}Cl)(\mu_3\text{-}O\mathit{t}Bu)_{12}]$: The First Mixed-Valence Copper Alkoxide

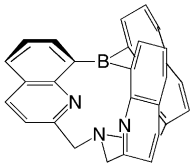
A prismatic prison for chloride: Partial disproportionation of CuCl during the reaction with KOtBu leads to the formation of a mixed-valence Cu^{I}/Cu^{II} alkoxido complex. The trigonal prismatic $K_6(\mu_6\text{-}Cl)$ template in the middle of the complex is capped by two $[Cu^{II}(OtBu)_3]^-$ and three $[Cu^{I}(OtBu)_3]^-$ units (see picture, Cl green, Cu light blue, K yellow, O red).



Proton Sponges

G. Bucher* ——— **4039 – 4042**

DFT Calculations on a New Class of C_3-Symmetric Organic Bases: Highly Basic Proton Sponges and Ligands for Very Small Metal Cations



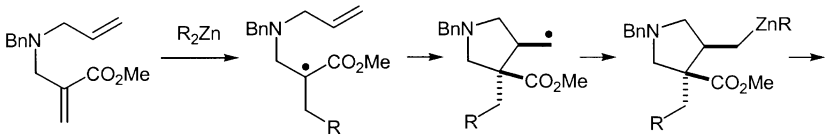
1

Back to bases: What happens, if three nitrogen lone pairs are forced to interact with each other? An extraordinary increase in basicity. This conclusion is the result of DFT calculations which, for example, predict a pK_a value (of the conjugate acid, in acetonitrile) of 30.2 for tris(8-quinolyl)borane **1**. The basicity is due to a strongly destabilizing interaction between the three quinoline lone pairs in the free bases.

Domino Reaction Mechanism

F. Denes, F. Chemla,*
J. F. Normant ——— **4043 – 4046**

Domino 1,4-Addition/Carbocyclization Reaction through a Radical–Polar Crossover Reaction

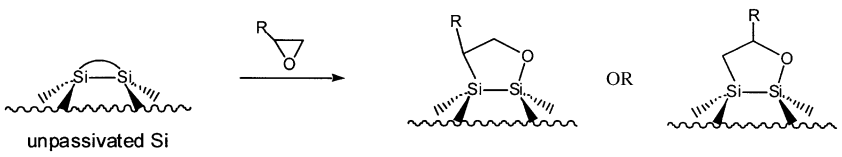


Radical processes explain the reactivity and selectivity observed in a one-pot, two- or three-component domino reaction, which consists of 1,4-addition, carbocyclization, and quenching with electrophiles. This radical–polar crossover reaction leads stereoselectively to 3,4-disubstituted 3-methoxycarbonylpyrrolidines (see scheme).

Reaction of Epoxides with Silicon

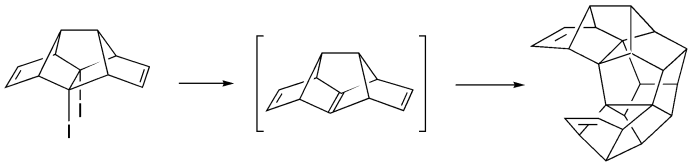
Y.-Y. Lua, M. V. Lee, W. J. J. Fillmore, R. Matheson, A. Sathyapalan, M. C. Asplund, S. A. Fleming, M. R. Linford* ——— **4046 – 4049**

Amine-Reactive Monolayers on Scribed Silicon with Controlled Levels of Functionality: Reaction of a Bare Silicon Surface with Mono- and Diepoxides



The reaction of epoxides with a bare silicon surface is reported (see scheme). Diepoxides yield amine-reactive monolayers on scribed silicon. Controlled levels of epoxide functionality are obtained in mixed monolayers of 1,2-epoxyoctane and 1,2,7,8-diepoxyoctane.

 © 2003 Wiley-VCH Verlag GmbH & Co. KGaA, Weinheim



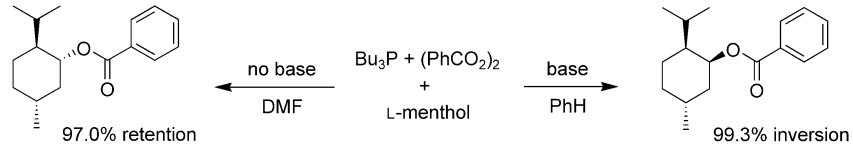
1 2

Highly Pyramidalized Alkenes

P. Camps,* J. A. Fernández, S. Vázquez, M. Font-Bardia, X. Solans — **4049 – 4051**

Generation, Trapping, and Dimerization of Pentacyclo[6.4.0.0^{2,10}.0^{3,7}.0^{4,9}]dodeca-5,8,11-triene: An Uncatalyzed Thermal [2+2+2+2] Cycloaddition

Simultaneous formation of four C–C bonds and three rings occurs in the unique uncatalyzed thermal [2+2+2+2] cycloaddition to give the tridecacyclotetracosane derivative **2**, which takes place when the highly pyramidalized alkene **1** is generated in the absence of a trapping agent (see scheme).

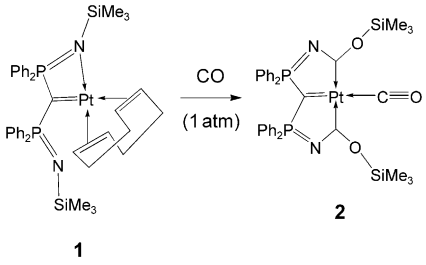


Acyloxyphosphonium Ion Trapping

J. McNulty,* A. Capretta, V. Laritchev, J. Dyck, A. J. Robertson — **4051 – 4054**

The Role of Acyloxyphosphonium Ions and the Stereochemical Influence of Base in the Phosphorane-Mediated Esterification of Alcohols

Intimate details of the Mitsunobu mechanism: The trapping of an acyloxytributylphosphonium ion with a chiral secondary alcohol leads to either retention or inversion of stereochemistry in the resulting ester depending on the exclusion or inclusion of a base (see scheme). Insight into the mechanism of phosphorane-mediated esterification processes is presented.



1 2

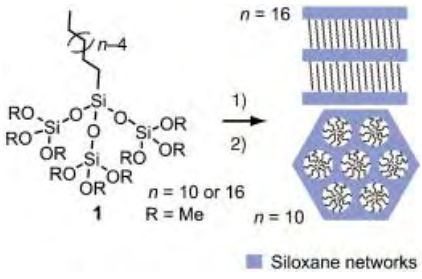
A Pt Tris(carbene) Pincer Complex

G. Lin, N. D. Jones, R. A. Gossage, R. McDonald, R. G. Cavell* — **4054 – 4057**

A Tris(carbene) Pincer Complex: Monomeric Platinum Carbonyl with Three Bound Carbene Centers

Carbon monoxide replaces cod in the mono carbene phosphane imine complex **1** (see picture) to form, through a double silyl migration reaction, the remarkable complex **2** containing three carbene centers bound to platinum (cod = cycloocta-1,5-diene).

Lamellar and hexagonal structures of new silica-based hybrids were directly formed from newly designed alkylsiloxane oligomers **1**. This approach based on the self-assembly of single precursors provides a novel pathway to ordered microporous silica as well as mesostructured silica-based hybrid materials (see scheme, 1) hydrolysis and polycondensation, 2) self-assembly).



Mesostructured Silica-Based Hybrids

A. Shimojima, K. Kuroda* — **4057 – 4060**

Direct Formation of Mesostructured Silica-Based Hybrids from Novel Siloxane Oligomers with Long Alkyl Chains

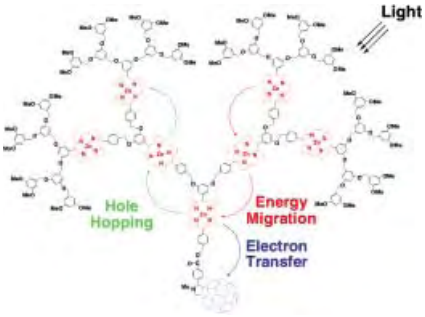
 © 2003 Wiley-VCH Verlag GmbH & Co. KGaA, Weinheim

Contents

Photoinduced Electron Transfer

M.-S. Choi, T. Aida,* H. Luo, Y. Araki, O. Ito* ——— **4060 – 4063**

Fullerene-Terminated Dendritic Multiporphyrin Arrays: "Dendrimer Effects" on Photoinduced Charge Separation

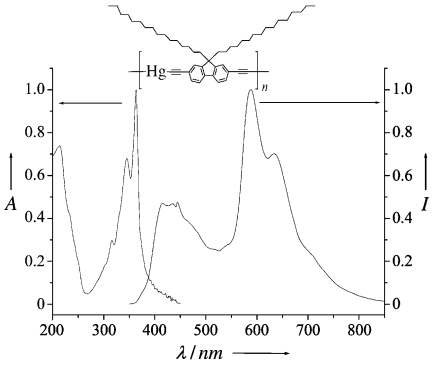


Energy funnels: A large dendritic zinc porphyrin heptamer ($7P_{Zn}$) in a C_{60}-terminated electron-transfer relay system $7P_{Zn}$-C_{60} (see picture) not only harvests visible light for the electron transfer to the C_{60} terminus, but also retards the back-electron-transfer process, thus resulting in a longer lifetime of the charge-separated state ($7P^{\cdot+}_{Zn}$-$C^{\cdot-}_{60}$).

Emission in Hg^{II} Polymers

W.-Y. Wong,* L. Liu, J.-X. Shi **4064 – 4068**

Triplet Emission in Soluble Mercury(II) Polyyne Polymers

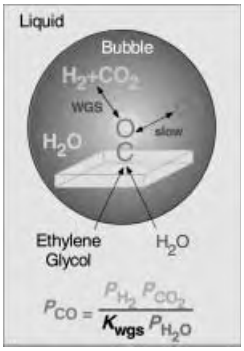


The light fantastic: The first examples of soluble high-molecular-weight d^{10} mercury(II) polyyne copolymers incorporating a 9,9-dialkylfluorene moiety have been prepared and photophysically characterized (see picture). These polymers have been shown to utilize a heavy-atom effect in exhibiting strong phosphorescence.

Fuel-Cell-Grade H_2 from Hydrocarbons

R. R. Davda, J. A. Dumesic* **4068 – 4071**

Catalytic Reforming of Oxygenated Hydrocarbons for Hydrogen with Low Levels of Carbon Monoxide



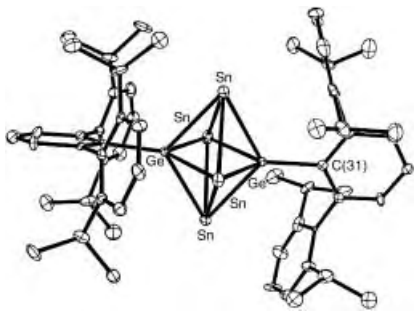
Vaporization of water leads to low levels of CO: Now, it is possible to produce low-CO-containing, H_2-rich streams by simple, aqueous-phase reforming of oxygenates. The schematic of ethylene glycol reforming on a Pt catalyst shows the composition of a gas bubble in the aqueous-phase reactor. Lowering the H_2 and CO_2 pressures, by increasing the water pressure, lowers the CO concentration in the product. WGS = water–gas shift.

Mixed-Metal Main-Group Clusters

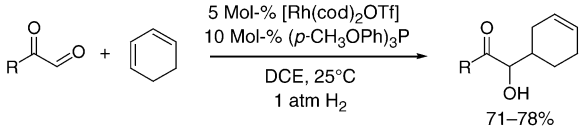
A. F. Richards, H. Hope, P. P. Power* ——— **4071 – 4074**

Synthesis and Characterization of Neutral, Homo and Heteronuclear Clusters with Unsubstituted Germanium or Tin Atoms

The first, well-characterized, polyhedral cluster with two different heavier group 14 elements is prepared (see picture). Low-valent group 14 halides are used to synthesize species in which the majority of the group 14 atoms carry no organic substituents.



 © 2003 Wiley-VCH Verlag GmbH & Co. KGaA, Weinheim

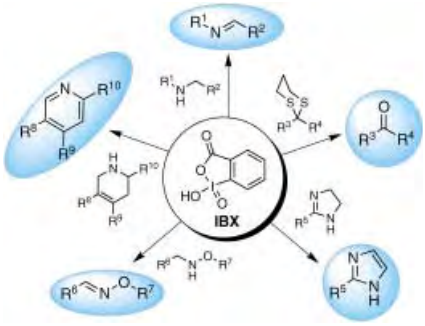


Reductive C–C Coupling Reaction

H.-Y. Jang, R. R. Huddleston, M. J. Krische* ——— 4074 – 4077

A New Catalytic C–C Bond-Forming Hydrogenation: Reductive Coupling of Dienes and Glyoxals under Catalytic Hydrogenation Conditions

Since the discovery of catalytic homogeneous hydrogenation in 1938, C–C bond formation has only been observed under hydrogenation conditions in alkene hydroformylation and Fischer–Tropsch-type processes, that is, in catalytic processes involving migratory insertion of carbon monoxide. As revealed in the present study, organometallic intermediates obtained upon diene hydrogenation are subject to electrophilic trapping by glyoxal partners, thus demonstrating catalytic C–C bond formation under hydrogenation conditions in the absence of carbon monoxide (see scheme). DCE: 1,2-dichloroethane. R = aryl, heteroaryl, alkyl.

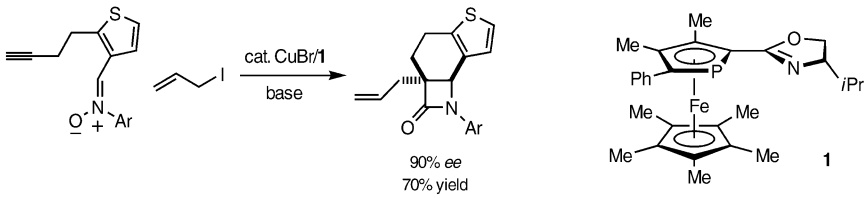


Reactions of IBX

K. C. Nicolaou,* C. J. N. Mathison, T. Montagnon ——— 4077 – 4082

New Reactions of IBX: Oxidation of Nitrogen- and Sulfur-Containing Substrates To Afford Useful Synthetic Intermediates

New reactions for the synthetic toolbox: 2-Iodoxybenzoic acid (IBX) was employed to access a diverse array of useful synthetic intermediates. Among other transformations, the developed chemistry converts amines into imines, dithianes into carbonyl groups, N-heterocycles into N-heteroaromatic compounds, and hydroxylamines into oximes in high yields.

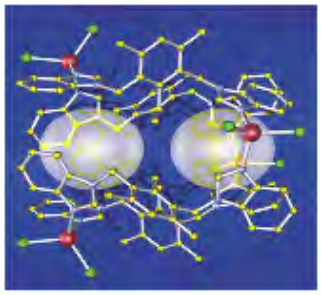


Chiral Tricyclic Lactams

R. Shintani, G. C. Fu* ——— 4082 – 4085

Catalytic Enantioselective Synthesis of β-Lactams: Intramolecular Kinugasa Reactions and Interception of an Intermediate in the Reaction Cascade

A planar-chiral Cu/phosphaferrocene–oxazoline catalyst mediates intramolecular Kinugasa reactions to give tricyclic β-lactams with good enantioselectivity. A variant of the process, in which a postulated enolate intermediate is intercepted with an electrophile in a transformation that generates two C–C bonds, a C–N bond, two new rings, a carbonyl group, and adjacent tertiary and quaternary stereocenters (see scheme), supports the proposed mechanism.



Coordination Nanotubes

C.-Y. Su, M. D. Smith, H.-C. zur Loye* ——— 4085 – 4089

Columnar Supramolecular Architecture Self-Assembled from S_4-Symmetric Coordination Nanotubes Encapsulating Neutral Guest Molecules

Self-cyclization of four $HgCl_2$ units and four ditopic 1,3-bis(benzimidazol-1-ylmethyl)-2,4,6-trimethylbenzene (bbimms) ligands has resulted in the assembly of the neutral nanotube $[Hg_4Cl_8(bbimms)_4]$ containing two compartments which can accomodate DMF and DMSO guest molecules (see picture). Crystal packing arranges all the tubes into an extended pipeline structure.

 © 2003 Wiley-VCH Verlag GmbH & Co. KGaA, Weinheim

Contents

Helical Zinc Phosphate

Y. Wang, J. Yu,* M. Guo, R. Xu* ——— **4089 – 4092**

[{$Zn_2(HPO_4)_4$}{$Co(dien)_2$}]·H_3O: A Zinc Phosphate with Multidirectional Intersecting Helical Channels

A twist in the tale: A racemic mixture of the chiral $[Co(dien)_2]Cl_3$ complex has been used as a template in preparing an open-framework zinc phosphate with multidirectional helical channels, consisting of alternate ZnO_4 and PO_4 tetrahedra. The framework contains 12-membered ring channels along the [100] direction, within which $[Co(dien)_2]^{3+}$ ions are located. Each channel is enclosed by chiral interpenetrating double helices (see picture; dien = diethylenetriamine).

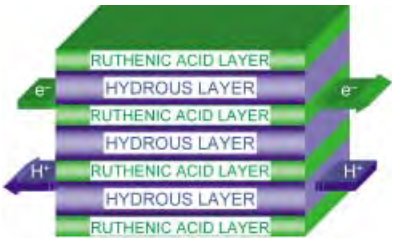


Ruthenic Acid Supercapacitors

W. Sugimoto,* H. Iwata, Y. Yasunaga, Y. Murakami, Y. Takasu ——— **4092 – 4096**

Preparation of Ruthenic Acid Nanosheets and Utilization of Its Interlayer Surface for Electrochemical Energy Storage

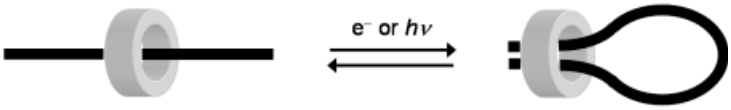
A layered compound composed of crystalline ruthenic acid sheets interleaved with layers of water can be exfoliated (delaminated) to yield colloidal nanosheets. This material is a mixed conductor where the crystalline nanosheets contribute to the electron conductivity and the hydrous interlayer supplies proton transport (see diagram). A large active surface area and a high specific capacitance is promising for electrochemical supercapacitor applications.



Molecular Machines

W. S. Jeon, A. Y. Ziganshina, J. W. Lee, Y. H. Ko, J.-K. Kang, C. Lee, K. Kim* ——— **4097 – 4100**

A [2]Pseudorotaxane-Based Molecular Machine: Reversible Formation of a Molecular Loop Driven by Electrochemical and Photochemical Stimuli



Picking up the thread: A large, reversible change in size as well as shape is observed in a [2]pseudorotaxane-based molecular machine composed of cucurbit[8]uril (CB[8]; bead) and a hexamethylene-bridged bisviologen (thread, see schematic representation) on application of external stimuli. The key feature of the machinelike behavior is the reversible formation of a molecular loop by intramolecular pairing of the terminal viologen radical cation units inside CB[8] upon electrochemical or photochemical reduction.

VIP Communications labeled with this symbol have been judged by two referees as being "very important papers".

The publication of Communications labeled with this symbol has been accelerated because of their topical or highly competitive nature.

 © 2003 Wiley-VCH Verlag GmbH & Co. KGaA, Weinheim

Deadline for recruitment adverts

38/2003	September 11	Publication date:	October 6
39/2003	September 18	Publication date:	October 13

Angewandte Chemie International Edition
Advertising Sales Department:
Marion Schulz
Phone: 0 62 01 – 60 65 65
Fax: 0 62 01 – 60 65 50
E-Mail: MSchulz@wiley-vch.de

Place an advert in the printed version
and have it made available online for 1 month, free of charge!

Service

Keywords ____ *4102*

Authors ____ *4103*

Angewandte's Sister Journals ____ *4104 – 4105*

Vacancies ____ *A47*

Preview ____ *4107*

Corrigenda

In the Communication "First Observation of Alkali Metal Ion Induced *Trans–Cis* Isomerization of Palladium(II) Phosphane Complexes Containing Crown Ether Moieties" by V. W.-W. Yam et al. (*Angew. Chem. Int. Ed.* **2003**, *42*, 3385) on page 3386 on the left column, 17 lines from the bottom, the ratio given should be 2.57:1 (not 3.57:1). The author apologizes for this error.

In the Communication "Highly Enantioselective Construction of Quaternary Stereocenters on β-Keto Esters by Phase-Transfer Catalytic Asymmetric Alkylation and Michael Reaction" K. Maruoka and co-workers (*Angew. Chem. Int. Ed.* **2003**, *42*, 3796) the values 80 and 92 in Table 1, entry 7 should be one column to the right (i.e., Yield 80%, Selectivity 92% *ee*. The editorial office apologizes for this error.

Warning

In the Communication "HIO_3 and I_2O_5: Mild and Selective Alternative Reagents to IBX for the Dehydrogenation of Aldehydes and Ketones" by Nicolaou et al. (*Angew. Chem.* **2002**, *114*, 1444; *Angew. Chem. Int. Ed.* **2002**, *41*, 1386), the HIO_3·DMSO and I_2O_5·DMSO complexes were disclosed as new reagents for the dehydrogenation of ketones and aldehydes to afford the corresponding enones and enals, respectively. The reagents were prepared by heating either iodic acid (HIO_3), or iodine pentoxide (I_2O_5) in DMSO (1 M solution) at 80 °C for 1 h. The resulting solution was then diluted with cyclohexene as cosolvent and employed in the oxidation of a ketone or enone at 45–65 °C. We undertook a large series of such reactions on a small scale (0.1–0.5 mmol) and also on many occasions made the reagents on a larger scale (up to 2.5 mmol), without incident.

Dr. S. Woodward (University of Nottingham) has subsequently reported to the authors that during the preparation of HIO_3·DMSO on a 42-mmol scale, the reaction exploded after heating for 30 min 80 °C. The reaction was being stirred using a circulator heater equipped with a safety cut-out, so accidental overheating could be eliminated as cause. No abnormalities were found in the reagents employed.

The authors would like to direct the attention of the reader to the adverse incident reported by Dr. S. Woodward and urge extreme *Caution!* in the large-scale implementation of the procedure for making HIO_3·DMSO. Until further investigation is completed, the authors suggest the same caution should be applied to the synthesis of the I_2O_5·DMSO complex.

Apology

In the Communication "Lewis Acid Catalyzed Room-Temperature Michaelis–Arbuzov Rearrangement" by **Renard**, **Mioskowski**, and co-workers (*Angew. Chem. Int. Ed.* **2003**, *42*, 2389–2392), the authors used the same introduction to the Michaelis–Arbuzov rearrangement as they did in their related article "Trimethylsilyl Halide-Promoted Michaelis-Arbuzov Rearrangement" (*Org. Lett.* **2003**, *5*, 1661–1664). Although the scientific purpose, mechanisms, scope, and limitations of the two reactions are completely different, the authors apologize for this duplication and for not citing the *Angewandte Chemie* paper in their *Organic Letters* article.

 © 2003 Wiley-VCH Verlag GmbH & Co. KGaA, Weinheim

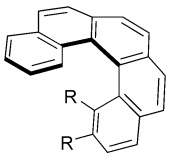
Helicene-Like Molecules

Recent Developments in the Synthesis of Helicene-Like Molecules

*Antonio Urbano**

Keywords:
arenes · asymmetric synthesis · helical structures · helicenes · synthetic methods

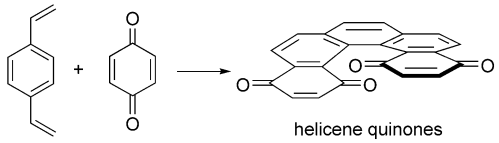
For many years [*n*]helicenes, nonplanar *ortho*-fused aromatic compounds that exhibit helical chirality, were regarded as little more than an academic curiosity.[1] More recently, helicene chemistry has grown from the stage of a descriptive field of aesthetic and curious molecules to an important field of research owing to the extraordinary optical and electronic properties of these compounds,[2] closely associated to their inherent chirality. Though useful, the classical synthesis of helicenes based on the oxidative photocyclization of stilbene-type precursors[3] has been hampered by fundamental drawbacks from evolving into a really convenient method for preparing these molecules. This has led to the development of several new methodologies during the last decade which provide useful alternatives for the synthesis of this type of helical skeleton. Among them, the pioneering work of Katz and Liu[4] led to the production of racemic helicene bisquinones through a Diels–Alder approach (Scheme 1),[5] supplemented by an efficient procedure for effecting the required resolutions.[6] Despite remarkable progress in helicene chemistry, the task of developing new, short, and efficient strategies to racemic and enantiopure helicenes which fulfill criteria of atom economy remains a challenge.



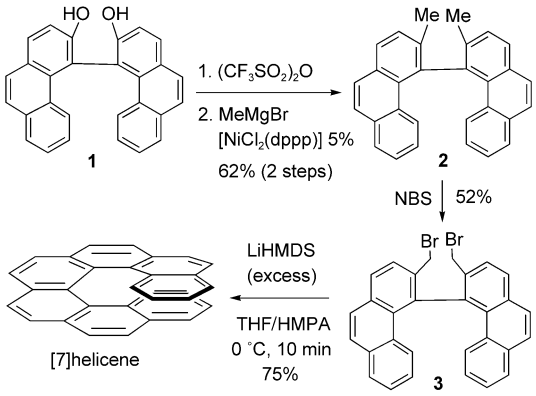
[*n*]helicenes

For example, the first nonphotochemical preparation of [7]helicene, which was the first carbohelicene to be synthesized by dehydrophotocyclization,[7] was not described until 1999 when Gingras and Dubois[8] reported a five-step approach using a "carbenoid coupling" strategy (Scheme 2). Biphenanthrol **1**, obtained by oxidative Cu-promoted coupling of 3-phenanthrol, was treated with triflic anhydride followed by addition of MeMgBr in the presence of a nickel catalyst to afford derivative **2** in 62% yield. After bromination of **2** and "carbenoid coupling" of dibromide **3** with excess LiHMDS, [7]helicene was obtained in 75% yield.

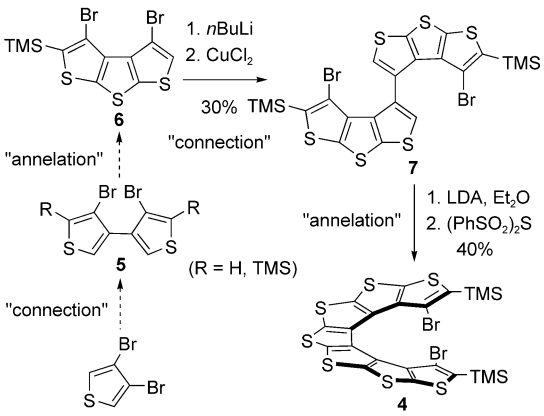
A related strategy was presented in 2000 by Rajca and co-workers[9] for the synthesis of a novel oligothiophene **4** (Scheme 3), in which the thiophene rings are cross-conjugated and annelated into a helix. The synthetic route consisted of two iterations using 3,4-dibromothiophene and compound **6** as the functionalized starting modules. In each iteration,



Scheme 1. Simple nonphotochemical route to helicene quinones by Katz and Liu.



Scheme 2. First nonphotochemical synthesis of [7]helicene by a "carbenoid coupling" strategy. dppp = 1,3-bis(diphenylphosphanyl)propane, NBS = *N*-bromosuccinimide, LiHMDS = lithium hexamethyldisilazide, HMPA = hexamethyl phosphoramide.



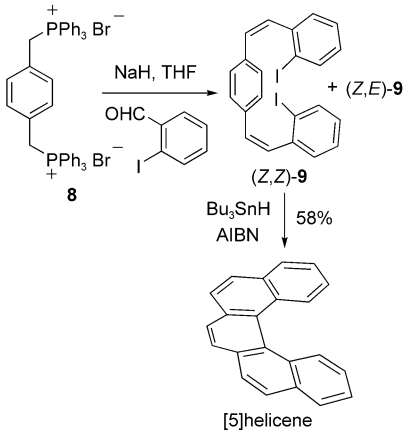
Scheme 3. Iterative ("connection"–"annelation") synthesis of racemic carbon–sulfur helicene **4**. TMS = trimethylsilyl, LDA = lithium diisopropylamide.

[*] Dr. A. Urbano
Departamento de Química Orgánica (C-I)
Universidad Autónoma de Madrid
Cantoblanco, 28049-Madrid (Spain)
Fax: (+34) 91-397-3966
E-mail: antonio.urbano@uam.es

 © 2003 Wiley-VCH Verlag GmbH & Co. KGaA, Weinheim DOI: 10.1002/anie.200301667

the modules were connected by means of a single Li/Br exchange followed by oxidative coupling with $CuCl_2$, and then "annelated" through the LDA-mediated dilithiation of the unprotected α positions of the thiophene rings in **5** and **7** and further reaction with bis(phenylsulfonyl)sulfide.

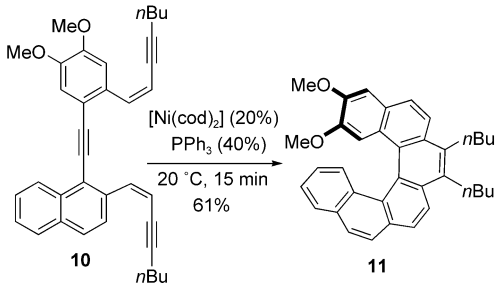
A new route to [5]helicenes, based on a tin-mediated, nonreducing tandem radical cyclization of (*Z*,*Z*)-1,4-bis(2-iodostyryl)-benzene derivatives was recently described by Harrowven et al.[10] The bisphosphonium salt **8** (Scheme 4), obtained from the corresponding dibromide, was subjected to a Wittig reaction with *o*-iodobenzaldehyde to give compound (*Z*,*Z*)-**9**, together with the *E*,*Z* isomer. After separation and treatment of **9** with tributyltin hydride under



Scheme 4. [5]Helicene by tandem radical cyclization of (*Z*,*Z*)-1,4-bis(2-iodostyryl)benzene (**9**). AIBN = azobisisobutyronitrile.

standard radical-forming conditions, [5]helicene was obtained in 58% yield. This short and easy protocol provided different substituted [5]helicenes with yields ranging from 35 to 58%.

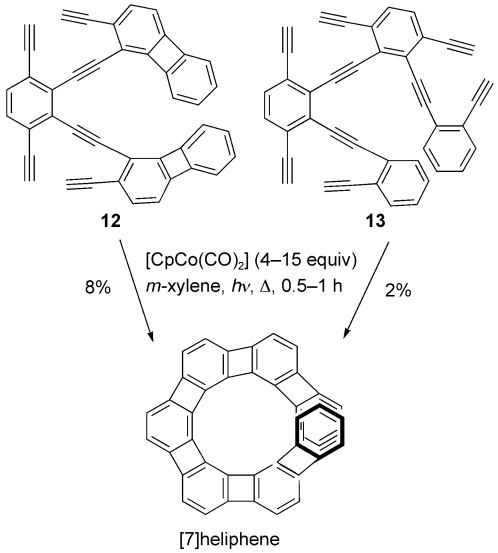
An important breakthrough in the field was reported in 2002 by Stará, Starý, and co-workers,[11] in an innovative approach to helicenes that exploited atom-economic isomerization of aromatic *cis*,*cis* dienetryines under transition-metal catalysis (Scheme 5). Thus, the nickel(0)-catalyzed [2+2+2] cycloisomerization of derivative **10** afforded substituted [6]helicene **11** in 61% yield, after formation of three new cycles in



Scheme 5. Nickel(0)-catalyzed [2+2+2] cycloisomerization of aromatic *cis*,*cis*-dienetryine **10**. cod = cycloocta-1,5-diene.

one step under very mild conditions. The scope of this efficient procedure was clearly demonstrated with the synthesis of different substituted [5], [6], and [7]helicenes with yields ranging from 60 to 83%.

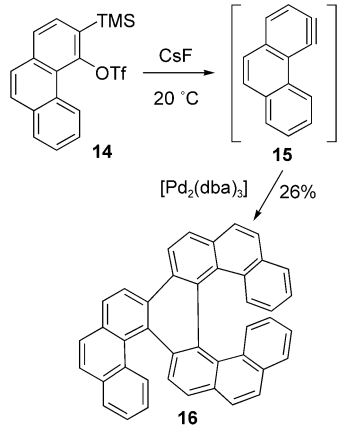
An impressive demonstration of the ability of transition-metal catalysis to build up helical frameworks is the recently described total synthesis of angular [*n*]phenylenes, comprised of *n* alternating benzene units fused with *n*−1 cyclobutadiene rings, the first helical phenylenes, called heliphenes by the authors Vollhardt et al.[12] A first approach to [7]heliphene (Scheme 6) was effected by a cobalt-catalyzed double cycloisomerization of hexayne intermediate **12** in 8% yield through the one-step formation of six new cycles.[12a] In an even more convergent approach, the nonayne precursor **13** was submitted



Scheme 6. Cobalt-catalyzed double and triple cycloisomerizations of aromatic hexayne **12** and nonayne **13**.

to an unprecedented cobalt-catalyzed triple cycloisomerization protocol to afford [7]heliphene in only 2% yield, but forming nine rings in one step, including all six of the component cyclobutadienes.[12b] Such methodology proved to be suitable for the preparation of [6], [7], [8], and [9]heliphenes. Surprisingly, none of these helical molecules could be resolved into their enantiomers, showing much lower barriers to racemization than those of the corresponding helicenes.[13]

A new palladium-catalyzed cyclotrimerization of arynes developed by Guitián and co-workers was very recently applied to the synthesis of **16** in 26% yield (Scheme 7), the first double heli-



Scheme 7. Palladium-catalyzed cyclotrimerization of aryne **15**. dba = dibenzylideneacetone.

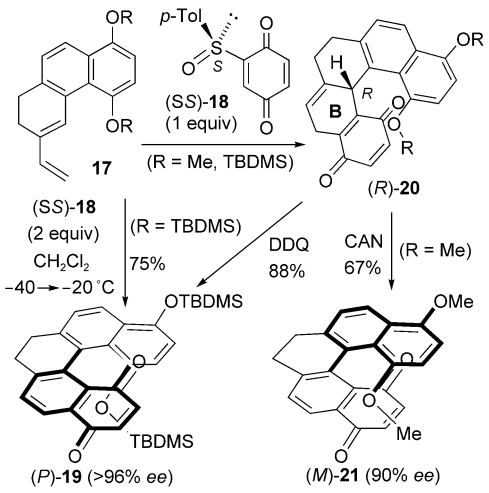
cene formed by a pentahelicene and a heptahelicene with two rings in common.[14]

Another major challenge in the chemistry of helicenes is the efficient preparation of the individual enantiomers with high enantioselectivity. Most of the asymmetric approaches reported to date were based on the resolutions of the racemic derivatives. Although several enantio- or diastereoselective syntheses have been described, only moderate asymmetric inductions have been achieved, except in a few cases. To extend the range of applications of functionalized helicenes, there is still a need for general, efficient, and versatile enantiose-

 © 2003 Wiley-VCH Verlag GmbH & Co. KGaA, Weinheim

lective approaches to both *M* and *P* helimers.

In this context, Carreño et al. described the first enantioselective synthesis of 7,8-dihydro[5]helicene quinones and bisquinones based on a three-step one-pot domino process (Scheme 8).[15] Thus, the reaction of vinyl 3,4-dihydrophenanthrene **17** (R = TBDMS) with 2 equivalents of enantiopure (S*S*)-2-(*p*-tolylsulfinyl)-1,4-benzoquinone (**18**) led, under very mild conditions, to 7,8-dihydro[5]-helicene quinone (*P*)-**19** in 75% yield, through a domino process comprising a Diels–Alder reaction and the elimination of the sulfoxide, followed by aromatization of the B ring of intermediate **20** (R = TBDMS) effected by excess quinone. Helicene **19** was obtained in optically pure form ($[\alpha]_D^{20} = +3700$ ($c = 0.015$, $CHCl_3$)) with the absolute configuration *P*.

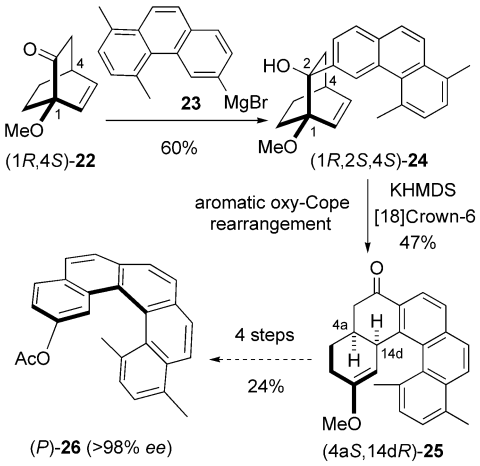


Scheme 8. Domino process for the enantiodivergent synthesis of 7,8-dihydro[5]helicene quinones (*P*)-**19** and (*M*)-**21**. TBDMS = *tert*-butyldimethylsilyl, DDQ = 2,3-dichloro-5,6-dicyano-1,4-benzoquinone, CAN = cerium ammonium nitrate.

The versatility of this methodology was probed, after isolation of the cycloaddition/sulfoxide-elimination product (*R*)-**20** (R = Me, TBDMS), with the enantiodivergent synthesis of either *P* or *M* helimers from such common intermediates by simply selecting the aromatizing reagent.[16] The aromatization of the B ring of **20** (R = TBDMS) with DDQ gave helicene (*P*)-**19** in 67% yield with 96% *ee*, whereas helicene (*M*)-**21** was obtained in 88% yield with 90% *ee* ($[\alpha]_D^{20} = -3030$ ($c = 0.003$, $CHCl_3$)) when the aromatization of **20** (R = Me) was effected with CAN.

In another asymmetric approach to helical conjugated molecules, Karikomi and co-workers developed a practical method for the synthesis of chiral [5]helicenes using an aromatic oxy-Cope rearrangement strategy (Scheme 9).[17] The chiral bicyclo[2.2.2]ketone (1*R*,4*S*)-**22**, obtained by enzymatic resolution, reacted with the Grignard reagent **23** to give (1*R*,2*S*,4*S*)-**24** as the major product. Aromatic oxy-Cope rearrangement afforded pentacyclic fused-ring derivative (4a*S*,14d*R*)-**25** in 47% yield. [5]Helicene (*P*)-**26** was obtained from **25** in 24% yield and in enantiomerically pure form ($[\alpha]_D^{20} = +1243$ ($c = 0.015$, $CHCl_3$)) in four steps (reduction, hydrolysis and dehydration, enol-acetylation, and aromatization). The same procedure was followed to synthesize the enantiomer (*M*)-**26** from (1*S*,4*R*)-**22**.

In summary, these recent protocols constitute a significant advancement of synthetic methodology that allows straightforward access to helicene-like molecules. The development of efficient asymmetric approaches should lead to further applications of chiral nonracemic helicenes, both in asymmetric synthesis and catalysis and in materials science.



Scheme 9. Synthesis of chiral [5]helicene (*P*)-**26** with an aromatic oxy-Cope rearrangement as the key step.

[1] a) For a recent highlight on a related topic, see: C. Schmuck, *Angew. Chem.* **2003**, *115*, 2552–2556; *Angew. Chem. Int. Ed.* **2003**, *42*, 2448–2452; for excellent reviews on helicenes, see: b) H. Hopf, *Classics in Hydrocarbon Chemistry*, Wiley-VCH, Weinheim, **2000**, p. 321–330; c) F. Vögtle, *Fascinating Molecules in Organic Chemistry*, Wiley, New York, **1992**, p. 156–180; d) K. P. Meurer, F. Vögtle, *Top. Curr. Chem.* **1985**, *127*, 1–76; e) W. H. Laarhoven, W. J. Prinsen, *Top. Curr. Chem.* **1984**, *125*, 63–120; f) R. H. Martin, *Angew. Chem.* **1974**, *86*, 727–738; *Angew. Chem. Int. Ed. Engl.* **1974**, *13*, 649.

[2] a) T. J. Katz, *Angew. Chem.* **2000**, *112*, 1997–1999; *Angew. Chem. Int. Ed.* **2000**, *39*, 1921–1923; b) S. Grimme, J. Harren, A. Sobanski, F. Vögtle, *Eur. J. Org. Chem.* **1998**, 1491–1509.

[3] L. Liu, B. Yang, T. J. Katz, M. K. Poindexter, *J. Org. Chem.* **1991**, *56*, 3769–3775.

[4] L. Liu, T. J. Katz, *Tetrahedron Lett.* **1990**, *31*, 3983–3986.

[5] For recent work, see: K. E. S. Phillips, T. J. Katz, S. Jockusch, A. J. Lovinger, N. J. Turro, *J. Am. Chem. Soc.* **2001**, *123*, 11 899–11 907, and references therein.

[6] T. Thongpanchang, K. Paruch, T. J. Katz, A. L. Rheingold, K. Lam, L. Liable-Sands, *J. Org. Chem.* **2000**, *65*, 1850–1856.

[7] M. Flammang-Barbieux, J. Nasielski, R. H. Martin, *Tetrahedron Lett.* **1967**, 743–744.

[8] M. Gingras, F. Dubois, *Tetrahedron Lett.* **1999**, *40*, 1309–1312.

[9] A. Rajca, H. Wang, M. Pink, S. Rajca, *Angew. Chem.* **2000**, *112*, 4655–4657; *Angew. Chem. Int. Ed.* **2000**, *39*, 4481–4483.

[10] a) D. C. Harrowven, M. I. T. Nunn, D. R. Fenwick, *Tetrahedron Lett.* **2002**, *43*, 7345–7347; b) D. C. Harrowven, M. I. T. Nunn, D. R. Fenwick, *Tetrahedron Lett.* **2002**, *43*, 3189–3191.

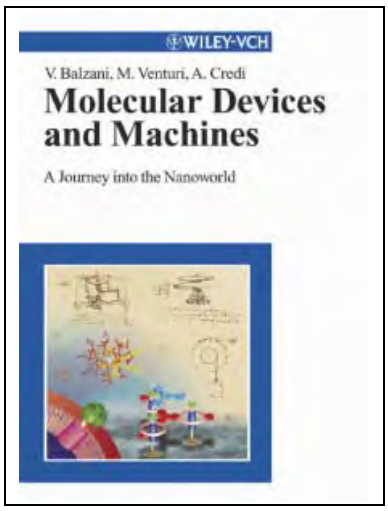
[11] a) F. Teplý, I. G. Stará, I. Starý, A. Kollárovič, D. Šaman, L. Rulíšek, P. Fiedler, *J. Am. Chem. Soc.* **2002**, *124*, 9175–9180; b) I. G. Stará, I. Starý, A. Kollárovič, F. Teplý, D. Šaman, P. Fiedler, *Collect. Czech. Chem. Commun.* **2003**, *68*, 917–930; c) F. Teplý, I. G. Stará, I. Starý, A. Kollárovič, D. Šaman, Š. Vyskočil, P. Fiedler *J. Org. Chem.* **2003**, *68*, 5193–5197.

[12] a) S. Han, A. D. Bond, R. L. Disch, D. Holmes, J. M. Schulman, S. J. Teat, K. P. C. Vollhardt, G. D. Whitener, *Angew. Chem.* **2002**, *114*, 3357–3361; *Angew. Chem. Int. Ed.* **2002**, *41*, 3223–3227; b) S. Han, D. R. Anderson, A. D. Bond, H. V. Chu, R. L. Disch, D. Holmes, J. M. Schulman, S. J. Teat,

 © 2003 Wiley-VCH Verlag GmbH & Co. KGaA, Weinheim

K. P. C. Vollhardt, G. D. Whitener, *Angew. Chem.* **2002**, *114*, 3361 – 3364; *Angew. Chem. Int. Ed.* **2002**, *41*, 3227 – 3230.
[13] R. H. Janke, G. Haufe, E. U. Würthwein, J. H. Borkent, *J. Am. Chem. Soc.* **1996**, *118*, 6031 – 6035.
[14] a) D. Peña, A. Cobas, D. Pérez, E. Guitián, L. Castedo, *Org. Lett.* **2003**, *5*, 1863 – 1866; b) D. Peña, D. Pérez, E. Guitián, L. Castedo, *Org. Lett.* **1999**, *1*, 1555 – 1557.
[15] a) M. C. Carreño, S. García-Cerrada, A. Urbano, *J. Am. Chem. Soc.* **2001**, *123*, 7929 – 7930; this methodology has also been successfully applied to the enantioselective synthesis of 7,8-dihydro[4]-helicene quinones: b) M. C. Carreño, S. García-Cerrada, A. Urbano, *Chem. Eur. J.* **2003**, *9*, 4118 – 4131; c) M. C. Carreño, M. J. Sanz-Cuesta, S. García-Cerrada, A. Urbano, *Chem. Commun.* **2001**, 1452 – 1453.
[16] M. C. Carreño, S. García-Cerrada, A. Urbano, *Chem. Commun.* **2002**, 1412 – 1413.
[17] a) Y. Ogawa, M. Toyama, M. Karikomi, K. Seki, K. Haga, T. Uyehara, *Tetrahedron Lett.* **2003**, *44*, 2167 – 2170; b) Y. Ogawa, T. Ueno, M. Karikomi, K. Seki, K. Haga, T. Uyehara, *Tetrahedron Lett.* **2002**, *43*, 7827 – 7829.

Key-Technologies of the Future



ISBN 3-527-30506-8
€ 99,- / sFr 146,-*

**The Euro price is only valid for Germany.*

VINCENZO BALZANI, Italy, ALBERTO CREDI, and MARGHERITA VENTURI, all of University of Bologna, Italy

Molecular Devices and Machines

A Journey into the Nanoworld
2003. XVII, 494 pp Hbk

The miniaturization of bulky devices and machines is a process that confronts us on a daily basis. However, nanoscale machines with varied and novel characteristics may also result from the enlargement of extremely small building blocks, namely individual molecules. This bottom-up approach to nanotechnology is already being pursued in information technology, with many other branches about to follow.
Written by Vincenzo Balzani and his team of co-authors, this book provides a comprehensive overview of this fascinating and multifarious topic, offering newcomers and experts alike a wealth of information.

- Most important new technologies for a broad audience
- Unifying, critical, and stimulating overview of red-hot topics

Wiley-VCH Verlag
Fax: +49 (0)6201 606 184
e-Mail: service@wiley-vch.de
www.wiley-vch.de

Register now for the free
WILEY-VCH Newsletter!
www.wiley-vch.de/home/pas

WILEY-VCH

50303032_kn

 © 2003 Wiley-VCH Verlag GmbH & Co. KGaA, Weinheim

Wilhelm Ostwald

Friedrich Wilhelm Ostwald (1853–1932), Now 150 Years Young…

*Regine Zott**

Keywords:
biographies · history of science · Ostwald, Wilhelm

He was versatile, successful, controversial—one of the fathers of physical chemistry as a scientific discipline, critic, founder of associations, journals, and of schools of science, author of text books and writings on the history of science and biographics, on creativity, scientific theory, philosophy, and color theory—and last but not least—writer and recipient of thousands of letters.

His literary bequest is considered to be one of the best documented, and his letter fund one of the most extensive, as, mindful of history, he himself kept nearly all his correspondence.[1]

Such superlatives give the impression that his work and life are already widely known—but there is an unchangingly wakeful and at the same time critical interest that springs from the diversity of his work and from changing historical perspectives.



Figure 1. Wilhelm Ostwald.

Background and Work up to 1909

Wilhelm Ostwald (Figure 1) was born on 2.9.1853 as the second son of a master cooper in Riga, where he grew up. He studied chemistry in Dorpat, mainly under the tutelage of Liebig's pupil Carl Schmidt (1822–1894), to whom he also owes his motivation to become involved with the history of science, Johannes Lemberg (1842–1902), who raised questions on physical chemistry, and Arthur von Oettingen (1836–1920), who imparted mathematical and physical stimulation. In 1877 he defended his master's dissertation "Volumchemische Studien über Affinität",[2] and was appointed Privatdozent when he gained his first experience in teaching. In 1880 he married; from his marriage with Helene von Reyher (1854–1946) there ensued three sons and two daughters (his son Wolfgang Ostwald (1883–1943) became a well-known colloid chemist).

He was appointed professor at the polytechnic in Riga in 1882 with a glowing recommendation from Dorpat. His areas of research were applications of the law of mass action, measurements of chemical reaction kinetics, and the conductivity of solutions. For this he specifically developed the pyknometer for the determination of the density of liquids and a thermostat, both of which were named after him. His spirited teaching and publication activities soon gave rise to a school of science in Riga which was recognizable by the constantly increasing number of students, and made the construction of a new institute necessary. From the beginning, he sought communication with colleagues, and he undertook journeys, principally to become familiar with laboratories in Germany—the first as early as 1882/83 ("laboratory travel"). In 1884 he became acquainted with Svante Arrhenius (1859–1927) and his ideas on the electrical conductivity of acids, which led to the dissociation theory of strong electrolytes (honored with the Nobel Prize in 1903). Their work together in Riga improved measurement methods and instrumental possibilities—in this way Ostwald developed his famous viscometer in 1885—and at the same time promoted Arrhenius's scientific recognition which initially had been denied him in his Swedish homeland because he could not be clearly identified as either a chemist or a physicist, and his outline of a future theory of electrolyte dissociation was not universally accepted because of its intellectual boldness. The new, specialist area of physical chemistry had aroused relatively little interest, even in Germany, partly because of the high mathematical demands and partly because of the much more favorable opportunities available at universities for organic chemists. Ostwald too had been warned by such highly experienced teachers as Hans Landolt (1831–1910) at the beginning of his career of the difficult path to physical chemistry (up to that time still not regarded as an independent specialist area) which was bristling with complicated questions of

[*] Dr. R. Zott
Ahornallee 21
12587 Berlin (Germany)
Fax: (+49) 30-6409-3697
E-mail: behladres@gmx.de

 © 2003 Wiley-VCH Verlag GmbH & Co. KGaA, Weinheim DOI: 10.1002/anie.200330059

methodology and mathematics. It was necessary to be ingenious and develop essential equipment or to get hold of special chemicals—hence, Ostwald's later "acid journey" of 1887 served mainly to collect acid samples—and moreover there were only a few books specially devoted to physical chemistry. Ostwald wanted to fill this gap with his Lehrbuch der allgemeinen Chemie, the first volume of which appeared in 1885 (the second volume appeared in 1887).[3] The work brought together the scattered knowledge on physical chemistry in a systematic way and pointed to outstanding problems, and thus gave stimulus to recognize research trends.

Once this overview was available, Ostwald considered a journal to be necessary. This approach, first to determine the current state of knowledge and questions still unanswered and then establish a scientific publication from this status quo, was retained as a methodic concept when in 1899 he justified his critical position against the "Archiv der wissenschaftlichen Photographie".[4]

In spite of the skepticism of a number of colleagues on matters such as the demand and availability of material, Ostwald pushed forward the founding of the "Zeitschrift für physikalische Chemie" with urgency in 1887[5] in order to establish his future claim as leader in this specialist area, especially as he learned of the founding of an analogous journal by a young colleague in Berlin and "did not wish to live as a lodger in his own house". He succeeded in winning over Jacobus Henricus van't Hoff (1852–1911) from Amsterdam as co-publisher, who was already recognized in this new specialist area through his work on the position of atoms in space and the optical isomerism of hydrocarbons. That was an important prerequisite for the future success of the journal. It became the most important journalistic forum for rapidly increasing physical-chemical debates, and one had to be familiar with it because it informed comprehensively and because Ostwald often reported very brusquely and arrogantly.

In the following years the intensity of direct communication between van't Hoff, Arrhenius, and Ostwald grew. They formed the elite corps of the "wild legion of ionists", so named, and thus cited gladly, by Ostwald to publicize the understanding of the new ionic theory more effectively in vigorous debate. The basis of this theory was that the molecules of a number of substances break down in more or less dilute solution into electropositive and electronegative particles (ions), which brought about electrical conductivity. The triumvirate undertook ground-breaking work in chemical kinetics, generally on the relationships between physical parameters and chemical properties, and succeeded in establishing physical chemistry as a chemical discipline equal in status to inorganic and organic chemistry.

van't Hoff developed the theory of dilute solutions on the basis of osmotic pressure, the laws for ideal solutions, and gas theory analogies of all thermodynamic derivations, Arrhenius extended the theory of the dissociation of electrolytes, undertook the calculation of the degree of dissociation and measurement of reaction rates, as well as of activation energy and the equilibrium between passive and active molecules, and Ostwald investigated the relationships between dissociation constants and chemical constitution, set out the mathematical calculation of the dilution law for molar conductivity named after him, and—last but not least—he contributed above all to the institutionalization of physical chemistry. For that reason his appointment to the professorship for physical chemistry at the University of Leipzig in 1887—at that time the only professorship in Germany explicitly with this designation—following the departure of Gustav Wiedemann (1826–1899), was an important event.

For Ostwald a second great creative epoch began, and a further school, the Leipzig school, grew up. His enthusiasm had an effect on students because of his didactically clear teaching, his electrifying lectures, and his richness of ideas. More books appeared from 1889 onwards, including the "Grundriß der allgemeinen Chemie".[6] With the series "Ostwalds Klassiker der exakten Naturwissenschaften",[7] also published in 1889 and still in existence today, in which newly printed key scientific publications could be more widely accessible and their content of ideas heuristically productive, he established himself as a scientific historian.

Since aids to methodology were then not available to the students of physical chemistry in a focused manner, Ostwald wrote them himself, including an introduction to physical chemical measurements.[8] Like many of his books, the clearly presented "Grundlagen der analytischen Chemie"[9] was published in several languages.

Ostwalds rise was steep and unmistakable. However, the rapidly growing quantity of publications, his claim to the leading role as central critic of physical chemistry, and his versatility appeared suspect to many. Indeed, with exaggeration and absolutization in his lectures and responses, Ostwald frequently gave cause for dispute, particularly during the early years.

In 1894 Ostwald contributed substantially to the scientific recognition of a further specialist area, was cofounder of the "Deutsche Elektrochemische Gesellschaft" (in 1902 he pushed through the name Deutsche Bunsen-Gesellschaft für angewandte physikalische Chemie), and the "Zeitschrift für Elektrotechnik und Elektrochemie" (from 1985 onwards "Zeitschrift für Elektrochemie"). Since, in Ostwalds view, an overview of knowledge should precede the founding of a specialist journal, the second edition of his textbook "Lehrbuch der allgemeinen Chemie", especially its second volume, and "Die wissenschaftlichen Grundlagen der analytischen Chemie" of 1894 may seemingly have assumed this role. In addition, fundamental work by Walther Nernst (1864–1941) and others were available. Ostwalds "Elektrochemie, Ihre Geschichte und Lehre" appeared in 1896.[10]

From the beginning of the 1890s he turned increasingly to philosophy. His ideas conflicted with atomic theory, which he had supported for many years, and he henceforth wanted to distance himself from the atomic hypothesis. Like Ernst Mach (1838–1916), Franz Wald (1861–1930), and other scholars, whose influence need not be discussed here, he too wanted to manage without the concept of the atom in the definition of chemically pure materials, and wanted instead to find a thermodynamic explanation. In place of the material postulate, he used the concept of energism as a central theme, and the use of

 © 2003 Wiley-VCH Verlag GmbH & Co. KGaA, Weinheim

the atom as a "picture" or hypothesis did not hinder him during the years of his teaching activities, in serving on the Atomic Weights Commission, etc.—His lecture "Die Überwindung des wissenschaftlichen Materialismus" at the meeting of the Gesellschaft Deutscher Naturforscher und Ärzte in Lübeck in 1895,[11] in which he introduced his concept of energism, met largely with rejection, particularly by Ludwig Boltzmann (1844–1906), but with some agreement, or at least some interested parties. In spite of all the debate, he later regarded Planck's quantum hypothesis and even Einstein's formula on the relationship of mass and speed as confirmation of his energism concept. On the basis of the research on radioactivity and Brownian Movement he allowed himself to be converted to atomism and regarded it "as a well-founded theory" in 1908, but he did not revise the relevant passages of his textbooks.

Over the next few years his scientific work concentrated increasingly on investigations into catalysis. He was able to derive a valid definition, according to which a catalyst does not induce a process, but accelerates it without appearing in the final product; in this way important advances in chemical kinetics were stimulated. It was mainly for his work on catalysis, but also in part for his work on chemical equilibria and rates of reaction, that he received the Nobel Prize in 1909. Ostwald developed an industrial catalytic process for the production of ammonia from free nitrogen and hydrogen, which he patented, but which proved not to be economic. His work on ammonia oxidation was considerably more promising; later Walther Nernst and principally Fritz Haber (1868–1934) continued the work under different conditions of pressure, temperature, etc.

From about 1897 Ostwald became involved in a science policy dispute to oppose the introduction of a state examination for chemists.[12] This was demanded by industry to ensure a generally demonstrable and testable level of scientific and relevant education. The universities saw this as an attack on their autonomy in regard to the determination of the teaching content and also as a threat to their traditional sole right to grant doctorates, and they feared corresponding demands for equality on the part of the technical high schools. Ostwald supported the position of the universities that it was for them alone to impart scientific principles and qualification for research. He formed an alliance with Adolf von Baeyer (1835–1917) and Victor Meyer (1848–1897) and organized questionnaires, etc. The threatened introduction of the examination was eventually dropped, but resulted in the formation of the Verband der Laboratoriumvorstände together with resolutions for unified examination regulations. A preliminary conclusion of the general debate on course content and examinations connected with this issue, and the question of prestige altogether, resulted finally in the introduction of the right for technical high schools to grant doctorates, for Berlin in 1899. "… The transfer of a specific right of universities (can) perhaps become dangerous", wrote von Baeyer to Ostwald, "Does this strike at the heart of the university? Perhaps! But can we prevent it?…".[13]

As the number of students continued to increase at Leipzig, Ostwald—as before at Riga—was able to set up a new institute. Opened in 1898, it soon became a Mecca of physical chemistry of international repute.

The pressure over many years of research, lectures, practical courses and examinations, criticisms, and the building of new institutes as well as the numerous organizational tasks in the university, journals, or organizations had led in the meanwhile to repeated states of exhaustion. Ostwald called it "overtaxing the brain", and he rejuvenated himself with numerous extended holidays. He also included his exhaustion syndrome as the subject of theoretical considerations in his theory formed after 1900 for the economic handling of one's own energy. He even developed a special formula for happiness.

From about 1900 Ostwald developed his energism concepts into an ethically characterized system, "energetic monism", held lectures and seminars on natural philosophy, and published the "Annalen der Naturphilosophie".[14] The rationale of these thoughts lay in the so-called "energetic imperative": "Do not squander energy, ennoble it!" The sole proven means to actually knowingly and rationally handle the potential of human energy is science, with which in principle all problems can be solved. His general promotion of a scientific conception of life, of the struggle against mysticism and religion, as well as the later takeover and leadership over many years by Ostwald of the Monist League founded by Ernst Haeckel (1834–1919), and his later public commitment to the question of church secession as well as in pacifism were totally resolute because stupidity, false belief, warlike destruction of cultural values, and energy-consuming disagreements meant a squandering of energy which mankind could not afford. His commitment to an international language (Esperanto, Ido) for the purposes of energy-conserving international communication also represented one of the consequences.

In order, for example, to be able to employ scientists according to their abilities, and thus to be able to utilize their energy resources more efficiently, that is, for the purpose of the "management" of intellect and genius, Ostwald made use of his biographical and historical ("psychographical") studies in "Große Männer"[15] to draft a typology of creative scholarly personalities which he divided, each according to depth of ideas, behavior, and productivity, into "classicist" and "romanticist", even when these were misleading and frequently coined terms (he also mentioned "organizers" and "mixed types").

The reflections on energism and natural philosophy matured as part of Ostwald's conceptions for a far-reaching systematic "science of science", the fundamental ideas of which he first presented in 1903. Concepts of scientific doctrine were a frequent topic amongst scholars within the context of the changes in the relationships between science and society since Georg W. F. Hegel (1770–1857). Ostwald knowingly connected with the positivist August Comte (1798–1857). He developed, however, a classification of sciences (1904)[16] which did not set the natural sciences against the humanities, but conceived them as interdependent aspects of the cognitive process. In a "science pyramid" the sciences are built up upon each other according to the degree of abstraction of their respective inherent fundamental concepts: at the

 © 2003 Wiley-VCH Verlag GmbH & Co. KGaA, Weinheim

base the disciplinary sciences such as mathematics, and above the sciences with increasingly diverse concepts up to sociology.

From about 1903 Ostwald's weariness for teaching increased, he ardently wished to be able to devote himself solely to natural philosophy, to questions of scientific theory and organization. He yearned for a research professorship of the type van't Hoff had enjoyed in Berlin since 1895/96 that was financed by academia and university and wanted to leave Leipzig altogether. In about 1905 it became clear that he was not going to take over Landolt's vacant professorship in Berlin—he could perhaps have been included in the list of nominees for the sake of honor, since his top position in Leipzig was regarded as unrivaled. His attempt to become an "academic" regarding questions of the philosophy of art also failed.

Abruptly, even brusquely, he henceforth ended his activities at Leipzig university, the place of long and successful involvement. The decision was regarded by many as incomprehensible. Prior to his change to a life as a private scholar, the prestigious invitation to work during 1905/06 as the first German exchange professor in the USA reached him.

Ostwald entered retirement on the 30.9.1906 to live in his country house "Energy" in Grossbothen, where he was extensively occupied with questions of scientific research and organization and the history of science, and was still frequently engaged publicly.

The year 1909 brought him the peak of achievement, for after many nominations, just in time according to the statutes, and justified by close reference to his research on catalysis, he finally received the Nobel Prize for Chemistry.

Ostwald and the Nobel Prize

Amongst his life's achievements were the already mentioned fundamental research on physical chemistry, the cooperation with van't Hoff and Arrhenius in the establishment of physical chemistry as a scientific discipline, the organization of journals, societies, and his journalism.

The Nobel Prize itself had been awarded since 1901; moreover Arrhenius had been significantly involved in formulating the statutes, which contributed amongst other things to the reasons for his dispute with Nernst.[17] The reason why Ostwald had not already received the prize together with Arrhenius was because it was only from 1904 that his name was put forward, but then was repeatedly done so each year by many nominators.[18] In the subsequent years the already twofold consideration of physical chemistry (van't Hoff, Arrhenius) as well as excellent results in other areas of chemistry (E. Fischer, von Baeyer, Buchner) and in other countries (Ramsay, Moisson, Rutherford), had to be taken into account.

It took until 1909 for the suggestion to be realized. Since he received the Nobel Prize for chemistry "for his work on catalysis and his ground-breaking investigations on chemical equilibrium relationships and rates of reactions" the honor came almost "too late". He had been away from the Leipzig university for over three years, away from chemistry teaching and research. According to the statutes of the Nobel Foundation, the prize was originally to be awarded in each case just a year following the achievement being honored, that is, it was not to represent a "reward for age", a condition which had already been criticized by the physicist Friedrich Kohlrausch (1840–1910) in 1900: "Those are remarkable requirements! Always from the current years! So often when something great sprang to mind it was already older than one year." In fact the requirement was soon proved to be unrealizable.

Besides, Ostwald's break with the university had also affected his chances, as Beckmann wrote in confidence to Arrhenius in 1906:

> "...unfortunately the general situation and opinion would appear to suggest that Ostwald's nomination be postponed. He is increasingly distancing himself from chemistry, and even his closest friends here and in wider circles do not support the nomination at the present time. In America O. had chosen philosophy, world language, and painting as a hobby horse, and in the Fall he intends to relinquish his chemistry professorship totally. Under these circumstances and in the present climate it is really for the better not to subject O. to further chemical criticism. Since I hear from you that merits lying further back are to be assessed fully, waiting brings with it no great risk..."

The prejudicial mood slowly faded, especially in view of Ostwald's further achievements for an effective functioning of science, and in 1907 Landolt wrote to Arrhenius that in his opinion Ostwald was now decidedly in line; in consultation with van't Hoff and Nernst he "had found no unfavorable response", and he also wanted to speak with E. Fischer. In his comprehensive justification to the Nobel Committee of 1908 Landolt emphasized Ostwald's "tremendously successful teaching activity in Riga, later in Leipzig, until "because of the state of his health" he had to give up his teaching post in 1906. Ostwald was one of the "most active and successful chemists of his time". His experimental investigations since 1877 followed on the one hand the investigation of the chemical relationship and affinity coefficients of acids and bases, measured by electrical conductivity and resulting in Ostwald's dilution law to express the relationship between conductivity and dilution of the solution, and on the other hand the investigations on catalytic phenomena, solubility relationships, and electrochemical studies, the development of physicochemical methods, the foundation of energism, and many other matters. As the most important journalistic achievements Landolt cited the two-volume "Lehrbuch der allgemeinen Chemie", "which has given a significant boost to the considerable development of this discipline which has occurred in modern times" and the "Wissenschaftliche Grundlagen der analytischen Chemie" of 1894 for the introduction of dissociation teaching, furthermore "Die Elektrochemie, ihre Geschichte und Lehre" of 1896, the "Grundriss der allgemeinen Chemie" of 1890, and the "Grundlinien der anorganischen Chemie 1900". In addition, Landolt praised Ostwald's lectures on natural philoso-

 © 2003 Wiley-VCH Verlag GmbH & Co. KGaA, Weinheim

phy of 1902 and the "Annalen der Naturphilosophie". Landolt thus based his recommendation both on the versatility of Ostwald's achievements and on certain results. In 1909 Landolt wrote happily to Arrhenius

"that Ostwald is being considered for the next Nobel Prize. He would certainly be deserving of it for he is truly the 'grandfather' of modern physical chemistry, whereas the title 'father' befits you yourself."

The emphasis on the versatility of the achievements of the candidate by Landholt differed from many other arguments for nomination for the respective Nobel prizes, which usually detailed specific achievements. Moreover, Ostwald for his part included such novel perspectives in his recommendations: with multidisciplinary conception he was the first to recommend Albert Einstein (1879–1955, Nobel Prize 1922 for 1921) in 1909, then repeatedly thereafter "his relativity principle presents the most far-reaching concept which has been effected since the discovery of the energy principle"; Einstein's "philosophically portentous view of nature" represents an epochal advance. Cleverly he commended the merit of the committee when it felt able to honor the importance of knowledge that had still to penetrate the common understanding of science or popular conception. When Ostwald proposed Ernst Mach (1838–1916) in 1914, already nominated by others in 1911 and 1912, he pointed to his experimental investigations and merits of the inclusion of epistemology and history in natural science thinking, and as one of the very few nominators he commented that the prize would be also materially very welcome for Mach, now living under much reduced circumstances, and it would be in accord with Nobel's behest also to prosper financially with the prize.

Ostwald marked his support of the new specialist area of colloid chemistry when in 1922 he nominated Richard Zsigmondy (1865–1929, Nobel Prize 1925) and Henry Siedentopf (1872–1940).

After Riga and Leipzig henceforth in Grossbothen

After leaving teaching, Ostwald developed numerous activities on the rationalization of scientific communication, in which support for the international languages Esperanto and Ido previously noted lay close to his heart. Apart from his own experience with time-consuming foreign language barriers, this was no random excursion into a spiritual enclave, but belonged to his broad concept of energetically effective organization and application of science. He felt that intellectual intercourse, that is communication, must itself become a subject of research to be organized rationally. A further, energetically conceived organizational measure was the founding of an association, the "Brücke", in 1911 for the purposes of the international organization and rationalization of intellectual work: unified formats should be introduced, publication printed uniformly in an international language, for example Ido, and scientific publications and all scientific installations of institutes, libraries, or associations registered uniformly. The intention was initially quite successful, but went into insolvency because of commercial errors of co-workers. In order to widely disseminate a scientific view of life and the conviction of scientific cognoscibility and solvability of all problems, he gladly assumed—as mentioned—the presidency of the Monist League (to 1915), wrote popular liberal tracts on a variety of questions ("Monistic Precepts"[19]), and was active for the church secession movement and for pacifism.

Ostwald was so serious about pursuing monism that in 1912 he used a considerable part of his Nobel Prize for the founding of a monist settlement where the humanitarianism of scientific ideology and ethic self control would be instilled, an enterprise which after a while did not meet his expectations, however, and fell apart.

With the beginning of the First World War, Ostwald's pacifism, that military force meant a waste of human energy and resources, failed. Like many others, he justified with chauvinistic argument the war as a defense of German culture. After the start of the war and a number of activities undertaken under the name of nationalism, for example, to promulgate a future prominent and leading international function for the German cultural nation, which brought him harsh criticism from many quarters, he withdrew, also from the Monistic League.

Thereafter he devoted himself to quantitative color research. For decades he had occupied himself both practically and theoretically with painting. He wanted to see his pictures recognized as an artistic achievement and not just for the technical skill in the handling of pastel colors or fixatives. For years he had occupied himself intensely with experimental and theoretical studies for a quantitative color science. In that way he wanted to open up the often mystifying artistic activity to scientific scrutiny. Artistic and commercial color selection and color gradation should be definable and reproducible. He considered his theoretical and experimental work on color a physical achievement with physiological background and placed it higher than his work as a physical chemist. Although he had already published a series of color atlases, books, and lectures on color measurement and color science, and had instituted the industrial production of color patterns and paint boxes[20] he was of the opinion that this part of his life's work during the war had not been recognized sufficiently. From 1919 onwards he repeatedly submitted the results of his color science for the Nobel Prize in physics, although he knew that the statutes excluded self-nomination.

Ostwald never quite gave up his activities on science theory and the history of science. As a result, a number of books appeared, such as "Die chemische Literatur und die Organisation der Wissenschaft" in 1919[21] (with appendices on the history of science, for example, on the role of the letter in the shaping of journals and papers and their significance for the opening up of science, etc.), "Die Pyramide der Wissenschaften" of 1929,[22] and individual contributions as well as many surviving manuscripts.

During 1926/27 he published his three-volume autobiography "Lebenslinien".[23] In spite of a certain degree of subjectivity, which as a matter of course

 © 2003 Wiley-VCH Verlag GmbH & Co. KGaA, Weinheim

characterizes almost all memoir texts, the numerous pictures and encounters in his life were illustrated in a very lively manner and also opened up important insights into the development of a discipline and its institutionalization as well as his fundamental ideas on energy and energism.

It has also to be noted that throughout his life he fostered music at home and himself played the viola.

Highly honored with decorations, medals, memberships of many scientific academies, and above all by the Nobel Prize, Ostwald died on 4.4.1932.

One of the friendliest tributes, which thoroughly summarized his claim to life, received by Ostwald on the occasion of his 75th birthday in 1928 came from his former pupil, later successor at the Riga Polytechnic and his first biographer and bibliographer, the chemist Paul Walden (1863–1957), in a manner Goethe might have formulated:[24]

Dem lieben, verehrten Meister,
Dem Jungen trotz Taufschein und Alter:
Noch lange wecke als Weiser die Geister
Und wirke als farbreichen Weltbilds Gestalter!

[1] Ostwald's written estate may be found in the central archives of the Berlin–Brandenburgische Akademie der Wissenschaften in Berlin.

[2] W. Ostwald, *Volumchemische Studien über Affinität*, Dorpat, **1877**.

[3] W. Ostwald, *Lehrbuch der allgemeinen Chemie*, 2 volumes, Vol 1 Leipzig **1885**, Vol 2 Leipzig **1887**. For revisions and expansions, new editions, and translations of this work and other writings of W. Ostwald, see G. Lotz, L. Dunsch, U. Kring, with cooperation from Brigitte Millik, *Forschen und Nutzen. Wilhelm Ostwald zur wissenschaftlichen Arbeit*, 2 ed., Berlin, **1982**, pp. 312–319.

[4] "Archiv für wissenschaftliche Photographie" appeared from 1899 to 1900, in total two volumes, editor Wilhelm Eugen Englisch (1869–1905).

[5] "Zeitschrift für physikalische Chemie, Stöchiometrie und Verwandtschaftslehre" was founded in 1887 and published together with J. H. van't Hoff.

[6] W. Ostwald, *Grundriß der allgemeinen Chemie*, Leipzig, **1889**.

[7] Foundation of the series "Ostwalds Klassiker der exakten Naturwissenschaften" in 1889.

[8] W. Ostwald, *Hand- und Hilfsbuch zur Ausführung physiko-chemischer Messungen*, Leipzig, **1893**.

[9] W. Ostwald, *Die wissenschaftlichen Grundlagen der analytischen Chemie. Elementar dargestellt*, Leipzig, **1894**.

[10] W. Ostwald, *Elektrochemie. Ihre Geschichte und Lehre*, Leipzig, **1896**.

[11] "Die Überwindung des wissenschaftlichen Materialismus": W. Ostwald, *Verhandlungen der Gesellschaft Deutscher Naturforscher und Ärzte*, 67. Versammlung, Leipzig, **1895**.

[12] For Ostwald's involvement in the state examination debate, see *Gelehrte im Für und Wider. Briefwechsel zwischen Adolf v. Baeyer und Wilhelm Ostwald* (Ed.: R. Zott), Münster, **2002** (with correspondence from and to Victor Meyer) as well as *Briefwechsel zwischen Wilhelm Ostwald und Richard Abegg* (with letters or extracts of letters from Fritz Haber and Clara Immerwahr and to Svante Arrhenius), with an introduction: *Chemieausbildung in Deutschland um die Wende vom 19. zum 20. Jahrhundert*.

[13] Letter from A. von Baeyer to W. Ostwald of 5.3.1899 in *Gelehrte im Für und Wider…* (Ed.: R. Zott), Münster, **2002**, p. 24 and p. 227.

[14] Foundation of "Annalen der Naturphilosophie" in 1901.

[15] W. Ostwald, *Große Männer. Studien zur Biologie des Genies*, Vol 1 of the series, which appeared in 12 volumes with different authors up to 1932.

[16] Articles and lectures of general content (1887–1903): W. Ostwald, *Biologie und Chemie*, Leipzig, **1904**, p. 286. In this lecture, which he gave at the University of California in Berkely in 1903, he developed his ideas of a future "science of science".

[17] *Wilhelm Ostwald und Walther Nernst in ihren Briefen sowie in denen einiger Zeitgenossen* (Ed.: R. Zott), Berlin, **1996**, p. 142 ff.

[18] The following correspondence citations on the Nobel prize nominations for Ostwald come from the aforementioned publication *Gelehrte im Für und Wider …* and the correspondence publication *Briefliche Begegnungen. Korrespondenzen von Wilhelm Ostwald, Friedrich Kohlrausch und Hans Landolt* (Ed.: R. Zott), Berlin, **2002**. Correspondence to Svante Arrhenius and from and to Karl Seubert is included with an essay: Scholar correspondence as a source of (scientific) history.

[19] W. Ostwald, *Monistische Sonntagspredigten*, Leipzig, **1911–1914**.

[20] W. Ostwald, *Die Farbenfibel*, Leipzig, **1917;** *Der Farbenatlas*, Leipzig, **1918**; *Die Farbenlehre*, in 5 volumes, Leipzig, **1918–1922** (volume 5 did not appear); *Farbnormen-Atlas*, Leipzig, **1920**.

[21] W. Ostwald, *Die chemische Literatur und die Organisation der Wissenschaft*, Leipzig, **1919** (Vol 1 of "Handbuch der allgemeinen Chemie").

[22] W. Ostwald, *Die Pyramide der Wissenschaften. Eine Einführung in wissenschaftl. Denken und Arbeiten*, Stuttgart, **1929**.

[23] W. Ostwald, *Lebenslinien. Eine Selbstbiographie*, 3 volumes, Leipzig, **1926/27**.

[24] Paul Walden to Wilhelm Ostwald on 31.8.1928 in *Wilhelm Ostwald und Paul Walden in ihren Briefen* (Ed.: R. Zott), Berlin, **1994**, p. 173. With accompanying text: "Paul Walden—Scientist between cultures".

The DOI printed for this paper was incorrect, the correct DOI is given in the electronic version here.

 © 2003 Wiley-VCH Verlag GmbH & Co. KGaA, Weinheim

Hybrids of Natural Products

Natural Product Hybrids as New Leads for Drug Discovery**

Lutz F. Tietze, Hubertus P. Bell, and Srivari Chandrasekhar*

Keywords:
biological activity · combinatorial chemistry · drug design · hybrids · natural products

Dedicated to Professor Helmut Schwarz on the occasion of his 60th birthday



© 2003 Wiley-VCH Verlag GmbH & Co. KGaA, Weinheim
DOI: 10.1002/anie.200200553

Angewandte Chemie

Natural products play an important role in the development of drugs, especially for the treatment of infections and cancer, as well as immunosuppressive compounds. However, the number of natural products is limited, whereas millions of hybrids as combinations of parts of different natural products can be prepared. This new approach seems to be very promising in the development of leads for both medicinal and agrochemical applications, as the biological activity of several new hybrids exceeds that of the parent compounds. The advantage of this concept over a combinatorial chemistry approach is the high diversity and the inherent biological activity of the hybrids.

From the Contents

1. Introduction	3997
2. Naturally Occurring Hybrid Molecules	3998
3. Synthetic Hybrid Molecules	4000
4. Conclusion	4024

1. Introduction

When modern synthetic chemistry came into being in the middle of the 19th century, Nature had already been generating a plethora of substances for millions of years. Many of those equipped the producing organism with an evolutionary advantage to survive in a more or less hostile environment, thus the percentage of biologically active substances in Nature is relatively high relative to substances from artificial sources. In fact, man has always taken advantage of Nature as a pharmacy: approximately 40% of the drugs that have been approved in the last years are either natural products or derivatives and analogues thereof.[1] Among anticancer and antiinfective agents, the percentage is even estimated to exceed 60%, including such well-known examples as penicillin G (**1**) and erythromycin A (**2**), as well as colchicine (**3**), vinblastine (**4a**), vincristine (**4b**), and paclitaxel (taxol, **5**). Organ transplantation would not have been possible without immunosuppressive natural products such as cyclosporin A (**6**), FK506 (**7**), or rapamycin (**8**). Natural products and their analogues have been put to use not only in pharmacology but also in modern crop protection.[2] They play an important role as highly potent insecticides, for example, pyrethrin (**9**), spinosyne A (**10a**), and spinosyne D (**10b**), or as fungicides, such as the derivatives of strobilurin A (**11**).

Modern combinatorial chemistry[3] allows the synthesis of millions of new compounds in a relatively short time. These libraries can be evaluated for their biological activity using high-throughput screening (HTS) techniques.[4] However, the success of such purely random approaches has been not very pronounced, which may especially be due to the lack of new chemical entities (NCEs) with high diversity. Bearing this in mind, the next logical step seems to be to profit from Nature's structural diversity by combining two or more natural products to form a hybrid.

Naturally, the question arises as to whether such an approach is of any use for the development of new biologically active therapeutic compounds with novel properties, or if there are any examples that demonstrate the potential of this methodology. Actually, from a general standpoint, the approach is not quite new, since even Nature employs such a strategy; for example, in the case of vitamin E, the terpenoid phytyl chain interacts with the cell membrane and the phenol moiety derived from shikimic acid forms a radical trap. Another naturally occurring hybrid, the indole alkaloid vincristine **4b** mentioned above, has completely changed the fate of young children afflicted with lymphatic leukemia: Previously, this disease was fatal, but vincristine is now used in its treatment with a success rate of over 60%. The compound is a dimeric indole alkaloid consisting of vindoline—an alkaloid of the *Aspidosperma* subgroup—and catharanthine—a member of the *Iboga* subgroup of indole alkaloids. It is of special interest that both monomeric alkaloids do not express any pronounced or useful biological activity. Artificial natural-product hybrids have not yet been used as drugs, as this idea is quite new, but several novel compounds of this type developed in the last years show promising biological activity, which will be discussed below.

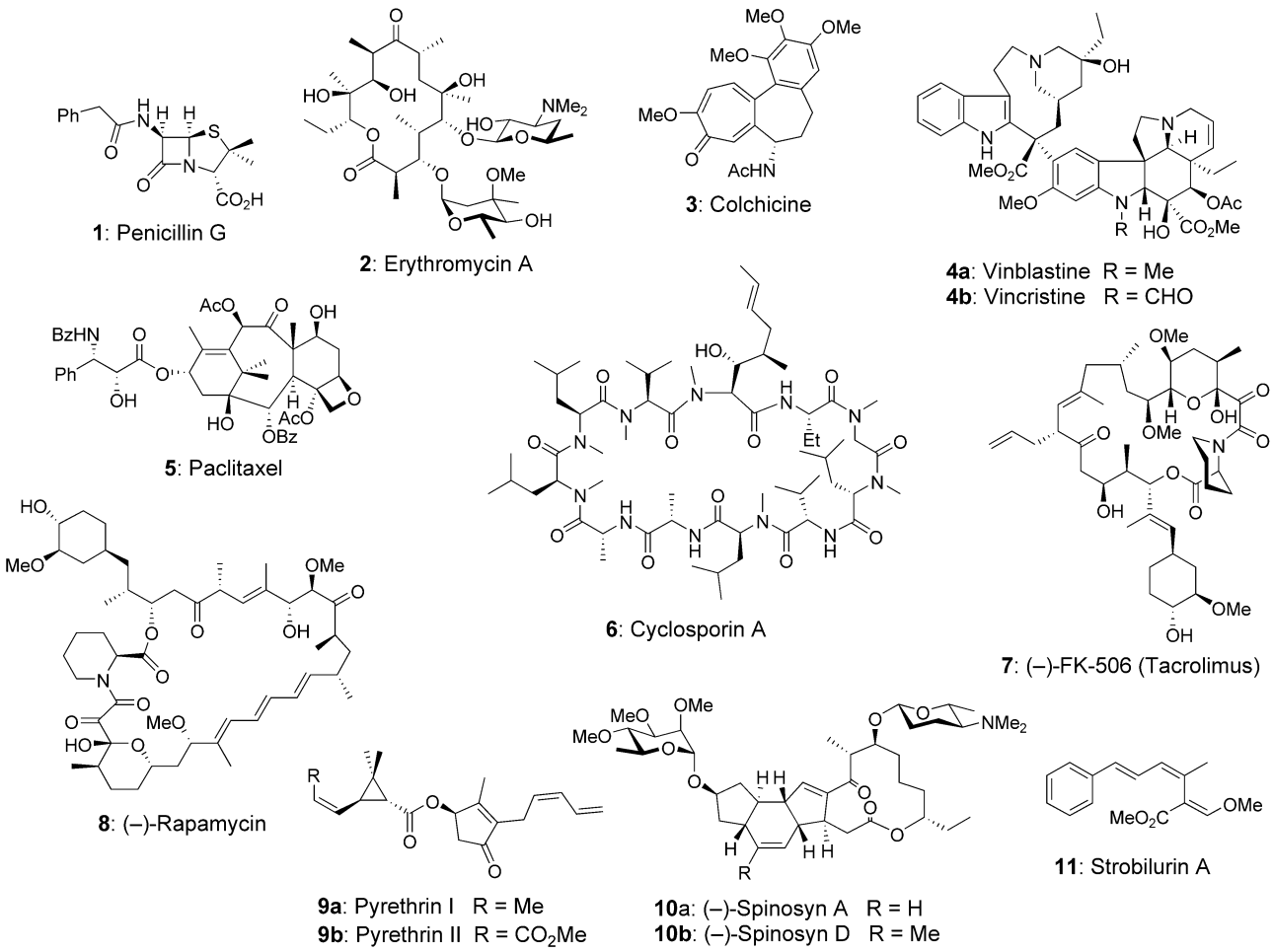
Such hybrids can be synthesized either by classical organic methods or by hybridization of the corresponding biosynthetic devices, namely by a transfer of gene clusters into a new host, which will then produce new "non-natural" natural products. This area has been applied mainly to the synthesis of polyketides and is often referred to as "combinatorial biosynthesis".[5]

The present review, for the first time,[6] tries to highlight the developments made over the past few years in the design, synthesis, and biological studies of natural product hybrids and related classes of molecules. As there already are excellent literature surveys that cover combinatorial biosynthesis and the production of hybrid molecules by employing genetically engineered organisms,[5] these fields will not be covered in this article.

[*] Prof. Dr. L. F. Tietze, Dipl.-Chem. H. P. Bell
Institut für Organische Chemie
Georg-August-Universität Göttingen
Tammannstrasse 2, 37077 Göttingen (Germany)
Fax: (+49) 551-39-9476
E-mail: ltietze@gwdg.de
Dr. S. Chandrasekhar
Indian Institute of Chemical Technology
Hyderabad, 500007 (India)

[**] A list of abbreviations can be found at the end of this article. The frontispiece shows Ganesha, the Indian god of wisdom and prosperity, in the center of a triangle of the natural products estrone and talaromycin B as well as a synthetic hybrid of both. According to legend, Shiva tore off the head of his son in a jealous rage and in remorse gave him the head of the first creature to pass by, an elephant.

 DOI: 10.1002/anie.200200553 © 2003 Wiley-VCH Verlag GmbH & Co. KGaA, Weinheim



We have divided natural product hybrids into four classes: 1) Naturally occurring hybrids of whole natural products or analogues, 2) naturally occurring hybrids of partial structures of natural products or analogues, 3) synthetic hybrids of whole natural products or analogues, and 4) synthetic hybrids of partial structures of natural products or analogues. This Review will mainly focus on the latter, but a few examples will also be presented for the other classes. Thus, emphasis will be given to artificial hybrid molecules, their synthesis, and a discussion of their biological properties, which often differ from those of the parent compounds.

2. Naturally Occurring Hybrid Molecules

2.1. Naturally Occurring Hybrids of Whole Natural Products or Analogues

An interesting example of this class of natural hybrids is the antimicrobial antibiotic thiomarinol (**12**), which was isolated from a culture broth of the marine bacterium *Alteromonas rava* sp. nov. SANK 73390 and was shown to be a hybrid of the pseudomonic acid C analogue **13b** and holothin (**14**).[7] Importantly, the antimicrobial spectrum of **14**

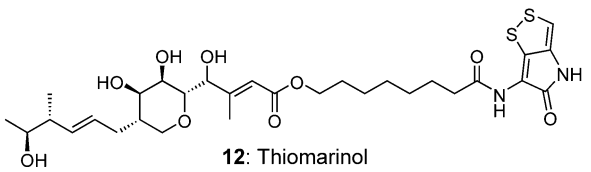


Lutz F. Tietze was born in 1942. He studied chemistry at the Universities of Kiel and Freiburg (Germany) and received his PhD in 1968 under the guidance of B. Franck. After postdoctoral studies with G. Büchi at MIT, Cambridge (USA) and A. R. Battersby in Cambridge (UK), he completed his Habilitation in 1975 at the University of Münster. In 1977 he was appointed professor at the University of Dortmund and one year later at the University of Göttingen. Among his recent honors and awards are the Literature Prize of the Fonds der Chemischen Industrie and an honorary doctorate from the University of Szeged (Hungary).

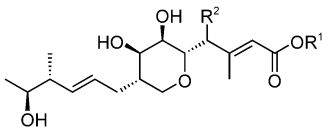


Srivari Chandrasekhar was born in 1964. He studied chemistry at the Osmania University, Hyderabad (India) and obtained his PhD in 1991 from the Indian Institute of Chemical Technology (IICT), Hyderabad under the supervision of A. V. Rama Rao. After postdoctoral studies with J. R. Falck at the University of Texas South-Western Medical School and with L. F. Tietze at the University of Göttingen, he became assistant director at the IICT in Hyderabad. He is a recipient of the Indian Young Scientist award. His research is focused on combinatorial chemistry and the total synthesis of bioactive molecules, including natural product hybrids.

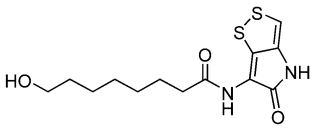
 © 2003 Wiley-VCH Verlag GmbH & Co. KGaA, Weinheim



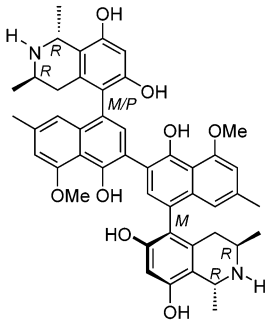
12: Thiomarinol



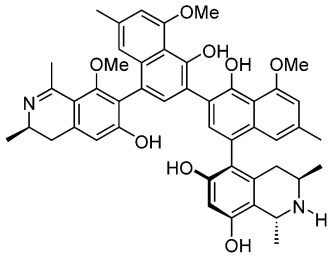
13a: Pseudomonic acid C
$R^1 = (CH_2)_8CO_2H$, $R^2 = H$
13b: $R^1 = H$, $R^2 = OH$



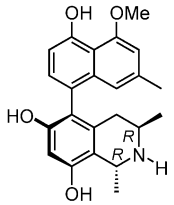
14: Holothin



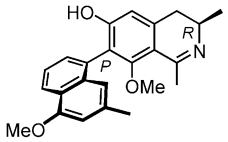
15a: (–)-Michellamine A (*P*,*P*)
15b: (–)-Michellamine B (*M*,*P*)



16: Korundamine A



17: Korupensamine A



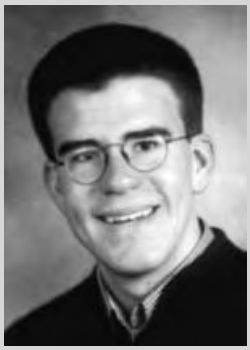
18: Yaoundamine A

shows characteristics of both parent compounds: it is active against Gram-positive and Gram-negative bacteria (e.g. multiresistant *Staphylococcus aurea* strains), and its effects are more pronounced than those of either parent compound.

The formation of dimers of natural products is a common feature in nature. The new hybrids usually exhibit a different biological activity to that of the monomer. Some of the best-known examples are the dimeric indole alkaloids vinblastine (**4a**) and vincristine (**4b**), which are both used clinically. Other examples are the bisbenzylisoquinoline alkaloids such as tubocurarine, which has been used for a long time in surgery as a muscle relaxant. It has now been replaced by amino steroid derivatives such as vecuronium bromide and rocuronium bromide.

Some new examples of dimeric natural product hybrids found in nature are the dimeric naphthylisoquinoline alkaloids michellamine A (**15a**), michellamine B (**15b**), and korundamine A (**16**).[8] Michellamine A (**15a**) is a homodimer of the alkaloid korupensamine A (**17**) in all respects, whereas michellamine B (**15b**) has the same constitution, but a different configuration at one of the two stereogenic axes. In contrast, korundamine A (**16**) is a heterodimer of korupensamine A (**17**) and yaoundamine A (**18**).

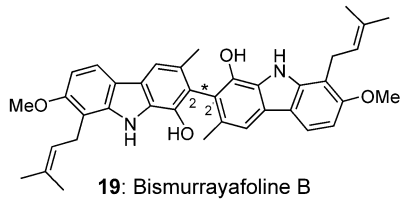
Whereas the monomeric naphthylisoquinoline alkaloids exist abundantly in the plant families *Ancistrocladaceae* and *Diocophyllaceae*, the dimeric compounds have so far only been found in a single species, *Ancistrocladus korupensis*.



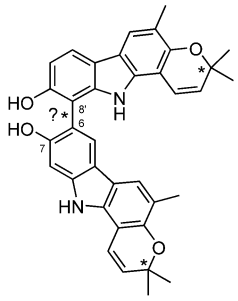
Hubertus P. Bell was born in 1976. He studied chemistry at the University of Göttingen and at the Ecole Nationale Supérieure de Chimie de Paris (ENSCP). He completed his diploma under the guidance of L. F. Tietze with a thesis on the "Synthesis of a haptene for a novel immunotherapy of tumors". He is currently completing his PhD.

Michellamine B (**15b**) and korundamine A (**16**) show strong anti-HIV activity ($EC_{50} \approx 2$ μM). In addition, korundamine A (**16**) is a potent antimalarial compound with an in vitro IC_{50} value of 1.1 μg mL^{-1} against *Plasmodium falciparum*.

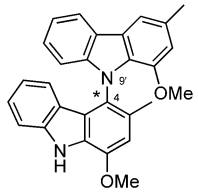
Another interesting class of dimeric compounds are the biaryl biscarbazole alkaloids such as **19** and **20**. Only 14 are currently known, all isolated from plants of two genera of the family *Rutaceae*: *Clausena* and *Murraya* S.[9] The unique feature of these alkaloids again is a stereogenic axis. However, dimeric compounds coupled through a C–N bond (e.g. **21**) are also found in these plants. The biological activity of the biaryl biscarbazole alkaloids is not as pronounced as that



19: Bismurrayafoline B



20: Bis-7-hydroxy-girinimbine-B



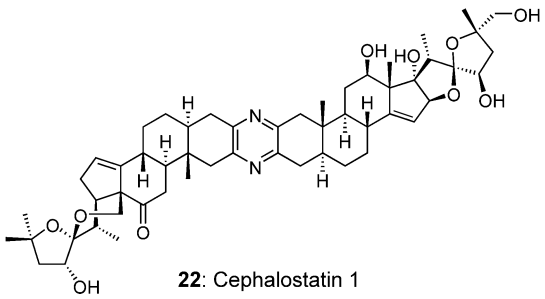
21: Murrastifoline-F

* configurationally stable

 © 2003 Wiley-VCH Verlag GmbH & Co. KGaA, Weinheim

of the dimeric naphthylisoquinoline alkaloids. However, some of the compounds are active against *Leischmania donovani*, the pathogenic agent of leishmaniasis, and exhibit a moderate fungicidal activity.

The cephalostatins and ritterazines are dimeric natural product hybrids with especially high biological activity; however, they have completely different properties to their monomers. Both types of compounds contain a pyrazine unit, which is connected to a highly oxygenated steroid moiety on each side. Cephalostatin 1 (**22**), the most potent compound of



22: Cephalostatin 1

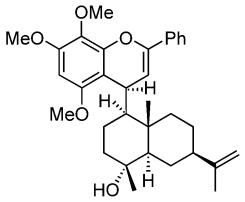
this type, was isolated from the marine worm *Cephalodiscus gilchristi*.[10] In an in vitro screening against a National Cancer Institute (NCI) panel of 60 human cancer cell lines, **22** was shown to have a GI_{50} value of about 2.20 nM.

Many other examples of the combination of natural products are known, for example, the cebetins,[11] some anthraquinone–xanthone conjugates, and the secalonic acids,[12] in which two xanthone units are bound to each other.

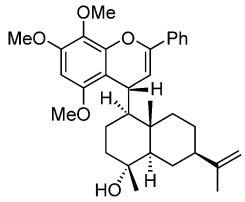
2.2. Naturally Occurring Hybrids of Partial Structures of Natural Products or Analogues

In this section we discuss a few natural product hybrids in which a part of at least one of the component molecules has been lost, for example, a hydroxy group or a carbon center. An example are the fissistigmatins A–D (**23**–**26**), which were isolated from *Fissistigma bracteolatum* Chatt. (*Annonaceae*), a creeper grown in North Vietnam, and characterized as hybrids composed of a flavonoid and a sesquiterpene moiety.[13] In South East Asia, the extract of this plant is used in traditional medicine, especially to stop wound bleeding and also as an antiinfective.[14] The biosynthesis has not been determined yet, but it has been proposed that a mixed biosynthetic pathway is involved in the combination of a chalcone unit **27** with either a germacrene- **28** or a bicyclogermacrene-type unit **29**.

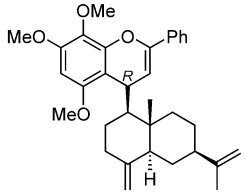
There are thousands of *O*- and *N*-glycosidic natural products, such as the saponines, flavones, ribonucleosides, and anthracyclic glycosides, which contain a carbohydrate and another natural compound (the aglycone) and may therefore also be considered as natural product hybrids. These substances are not covered in this Review, but we have included some C-glycosides. Several C-glycosidic antitumor antibiotics are hybrids of carbohydrates and tetracyclines. These compounds generally fall under the anthracycline class of natural products, which is amply covered in the literature.[15]



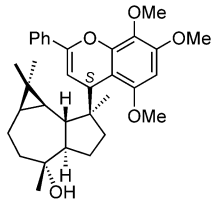
23: Fissistigmatin A



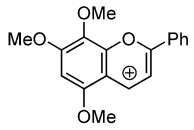
24: Fissistigmatin B



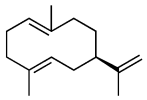
25: Fissistigmatin C



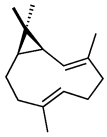
26: Fissistigmatin D



27

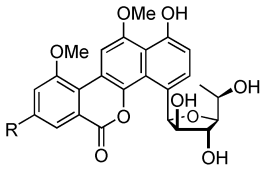


28

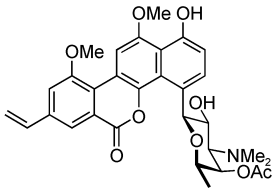


29

Gilvocarcin (**30**) and ravidomycin (**31**) represent a new class of aryl C-glycoside antitumor antibiotics that have a



30a: (–)-Gilvocarcin M
R = Me
30b: Gilvocarcin V
R = CH=CH$_2$



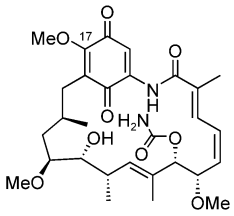
31: Ravidomycin

benzonaphthopyrone tetracycle in common and differ in the carbohydrate at C4 (a fucose unit in gilvocarcin and an amino sugar in ravidomycin).[16] It has been shown that the amino sugar congener is biologically more potent.

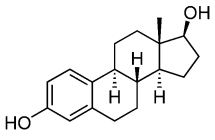
3. Synthetic Hybrid Molecules

3.1. Synthetic Hybrids of Whole Natural Products or Analogues

Geldanamycin (**32**), an ansamycin antibiotic first isolated from *Streptomyces hygroscopicus*, binds to the Hsp90 chaperone protein and causes the degradation of several important signalling proteins. Therefore, it was hoped that an appropriately fashioned hybrid drug of **32** and estradiol (**33**) would

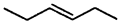
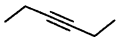


32: Geldanamycin



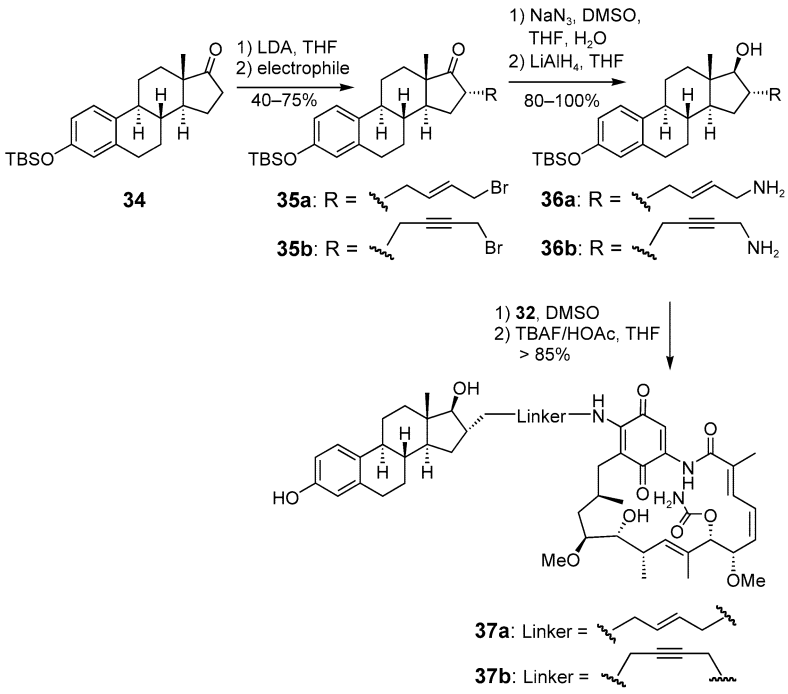
33: Estradiol

Table 1: The effects of geldanamycin (**32**) and the hybrids **37a, b** on steady-state levels of HER2, ER, and Raf-1 in MCF7 breast cancer cells.

Compound	Linker	IC_{50} (HER2) [μM]	IC_{50} (ER) [μM]	IC_{50} (Raf-1) [μM]
32	–	0.05	0.06	0.2
37a		0.1	0.08	1.5
37b		0.1	0.22	1.5

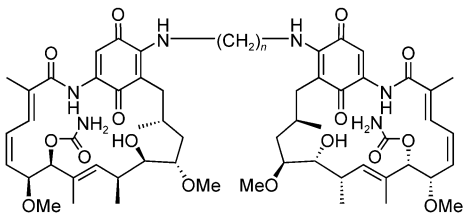
offer the ability to induce a selective degradation of the estrogen receptor (ER).[17]

A linker was attached to the protected estrone derivative **34** through α alkylation of the enolate with a 1,4-dihalide as the electrophile (Scheme 1). The required amino function was introduced by nucleophilic substitution with an azide followed by reduction with $LiAlH_4$. The coupling to geldanamycin (GDM, **32**) relied on its Michael acceptor character at C17. Cleavage of the phenolic TBS ether afforded the final estradiol–GDM hybrid **37**, which was subjected to biological tests. The concentrations necessary to reduce the expression of different tumor-relevant proteins in MCF7 breast cancer cells (HER2, ER, and Raf-1) is summarized in Table 1. A second assay on these proteins and IGF1R revealed that hybrid **37a** is more selective than geldanamycin (**32**) and estradiol (**33**) towards the degradation of HER2 and ER.



Scheme 1. Synthesis of hybrids of geldanamycin (**32**) and estradiol (**33**) connected through a linker.

As HER-kinases, which are inhibited very effectively by geldanamycin, undergo dimerization on activation, it was speculated that both units of the HER-kinase dimer interact with Hsp90.[18] Accordingly, it seemed reasonable that a geldanamycin dimer might be able to interact with both subunits of the HER-kinase dimers, which led to the synthesis of the homohybrids **38a–d**. The two monomers were connected by a diamino alkyl linker of variable length attached to the respective C17 atoms, since this is the only atom not buried in the binding pocket, as revealed by crystal-structure analysis. The selectivity was found to decrease with increasing chain length of the linker (Table 2). The best selectivity was exhibited by dimer **38a** with a butyl linker. It was especially active against SKBR-3, a cell line in which the *HER2* gene is amplified and the corresponding protein is highly overexpressed. As the GMD-4c dimer has a less pronounced effect on other key signalling proteins, it is likely to be less toxic than geldanamycin itself.



38a: GMD-4c $n = 4$
38b: GMD-7c $n = 7$
38c: GMD-9c $n = 9$
38d: GMD-12c $n = 12$

3.2. Synthetic Hybrids of Partial Structures of Natural Products or Analogues

3.2.1. Hybrids with a Steroid Substructure

The estrogen receptor is present in higher concentrations in breast cancer, ovarian adenocarcinoma, prostatic carcinoma, and endometrial carcinoma than in normal tissue. This discovery led to the establishment of estrogens as vectors for cytotoxic agents in the hope that an increased organ and/or tissue specificity could be achieved through a selective accumulation of the cytotoxic compound in the tumor cells.[19] As the C3 phenolic group and the β-oriented oxy-

 © 2003 Wiley-VCH Verlag GmbH & Co. KGaA, Weinheim

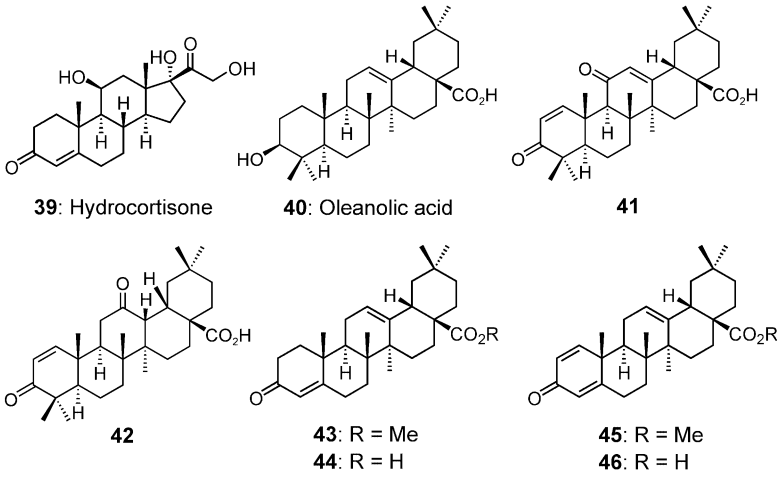
Table 2: The effects of various homohybrids of geldanamycin (**32**) on protein downregulation and cell growth.

Drug	MCF-7			SKBR-3
	IC_{50}[a] (HER-2) [nM]	IC_{50}[a] (Raf-1) [nM]	IC_{50}[b] (GI) [nM]	IC_{50}[b] (GI) [nM]
32	45	200	25	3
38a	60	2200	100	20
38b	70	500	600	200
38c	500	3800	700	500
38d	750	3500	700	650

[a] IC_{50} for each protein is defined as the concentration of each drug needed to decrease the steady-state level of either HER2 or Raf-1 to 50% of the control after 24 h of treatment. [b] IC_{50} (GI = growth inhibition) is defined as the concentration of each drug needed to inhibit cell growth to 50% of the control after the 4-day treatment.

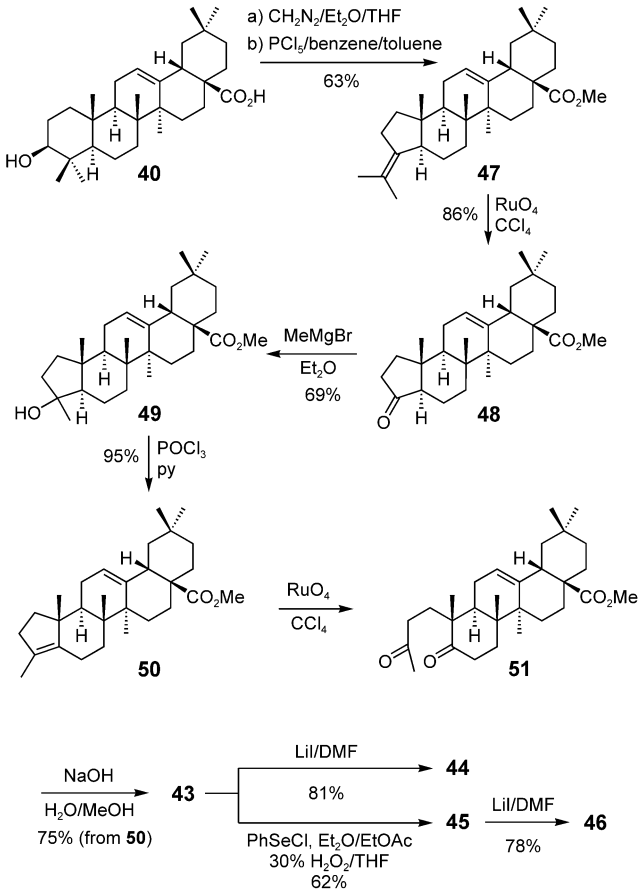
genated moiety at C17 seem to be crucial for the recognition process, these functions are kept in most newly developed hybrids.[20] However, the 17α and 16α positions can be modified without adversely affecting the molecular recognition.

Besides estrogens, other steroids such as the corticoids have also been used as vectors. Their biological activity is associated with a 4-en-3-one or a 1,4-dien-3-one functionality in ring A (e.g. in hydrocortisone (**39**) or dexamethasone). On the other hand, it was shown that derivatives of oleanolic acid (**40**), for example, **41** and **42,** with a 1-en-3-one functionality in ring A, exhibit significant inhibitory activity against interferon-γ-induced nitric oxide (NO) production in mouse macrophages.[21] Accordingly, the design of hybrid molecules



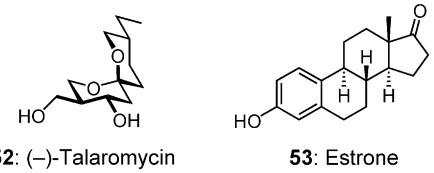
that contain parts of **39** and **40** was deemed to be interesting for structure–activity relationship studies.[22] Four such analogues **43**–**46** were synthesized and their biological activity evaluated in an inducible nitric oxide synthase (iNOS) assay, which revealed that compound **46** showed a moderate inhibitory activity at the 1 μM level.

For the synthesis of **43**–**46** (Scheme 2), acid **40** was converted into methyl oleanolate by treatment with diazomethane, and subsequent dehydration with rearrangement upon exposure to PCl_5 gave the desired ring contraction product **47**, which was oxidized with RuO_4 in CCl_4 to yield ketone **48**. Addition of methylmagnesium bromide led to the tertiary alcohol **49**, which upon treatment with $POCl_3$ produced alkene **50.** Oxidative ring opening with RuO_4 gave diketone **51**, which was cyclized by an aldol condensation with sodium hydroxide in methanol to yield **43**. The ester moiety was then cleaved with lithium iodide in DMF to give **44**. The desired second double bond in ring A was introduced by treatment of **43** with phenylselenyl chloride followed by oxidation with hydrogen peroxide. The dienone acid **46** was formed by treatment of **45** with lithium iodide, as before (**43**→**44**).



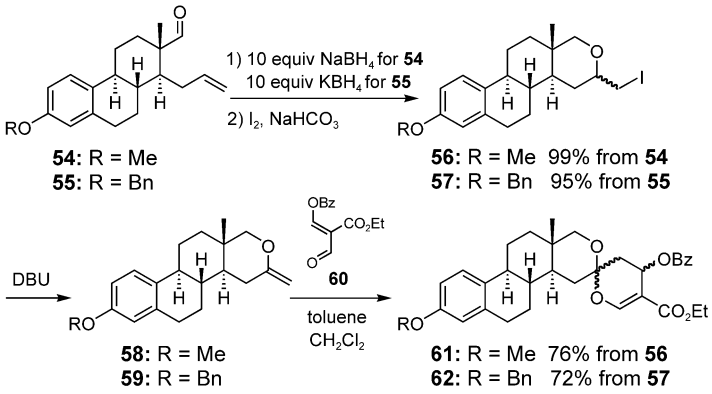
Scheme 2. Synthesis of hybrids of hydrocortisone (**39**) and oleanolic acid (**40**).

Talaromycin (**52**) is a biologically highly active spirocyclic mycotoxin.[23] Thus, the combination of this natural product with estrone (**53**) could lead to a new



 © 2003 Wiley-VCH Verlag GmbH & Co. KGaA, Weinheim

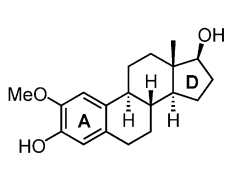
class of cytotoxic compounds.[24] The synthesis of the respective hybrids started from the D-secoestrone (**55**), which is easily available in five steps from estrone (**53**).[25] Reduction of **55** with potassium borohydride led to the corresponding alcohol, which upon subsequent iodoetherification afforded the iodoethers **57** as a 2.5:1 mixture of the two possible epimers (Scheme 3). The formation of stereoisomers is of little importance, since the new stereogenic center is destroyed in the following elimination step. The resulting enol ether **59** can act as a dienophile in a hetero-Diels–Alder reaction with heterodiene **60** to form the spiroacetal **62**.



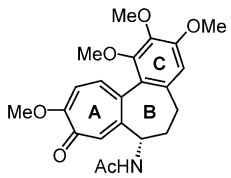
Scheme 3. Synthesis of precursors for various estrone–talaromycin hybrids.

Further transformations depicted in Scheme 4 led to the novel natural-product hybrids **69**–**71**. The methyl ethers **65** and **67** were prepared in a similar manner. The cytotoxicity of these compounds was determined by performing HTCFA (human tumor colony forming ability) tests with human lung cancer cells (A549). ED_{50} values of 23 (**65**), 30 (**67**), 95 (**70**), and 73 μM (**71**) were found and are comparable with those of the well-known anticancer agent cyclophosphamide.

2-Methoxyestradiol (**72**), a metabolite of estradiol (**33**), was found to be one of the most potent endogenous inhibitors of mammalian tubulin polymerization, probably through interaction at the colchicin-binding receptor of tubulin.[26] Much information on the structure–activity relationship was obtained from a series of estradiol–colchicine hybrids (estratropones, A-homoestranes) that contain a steroid nucleus and



72: 2-Methoxyestradiol



3: Colchicine

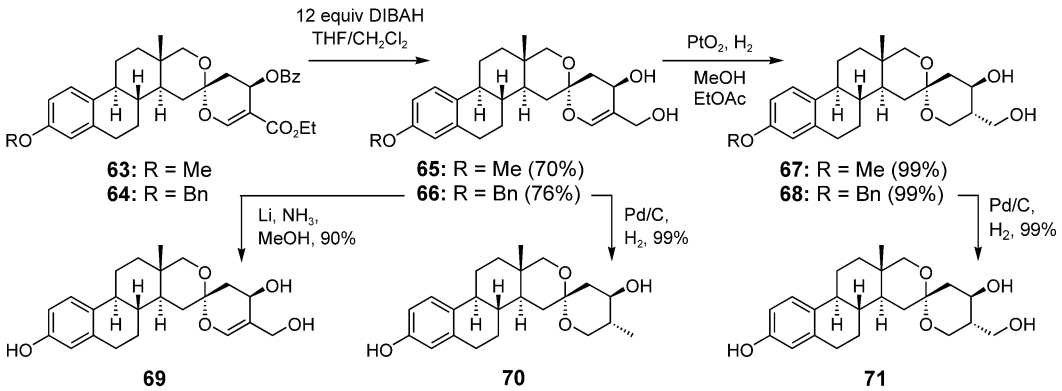
an A-ring tropone system similar to that of colchicine.[27] These so-called estratropones, for example, **76** and **78**, inhibit the polymerization of tubulin with greater potency than the natural products (Table 3). Several of the most active leads are under preclinical investigation for the treatment of disorders associated with abnormal angiogenesis.

The synthesis of the hybrids **76** and **78** followed a modified protocol previously reported[28] and began with the selective methylation of estradiol (**33**) and subsequent Birch reduction, which provided **73**. A base-catalyzed isomerization furnished **74** (Scheme 5). The two dienes **73** and **74** were treated with dibromocarbene and dichlorocarbene to obtain the corresponding cyclopropanes **75** and **77**, which were transformed into the homoestranes **76** and **78**. In a similar manner, the analogues **81**–**86** were prepared as shown in Scheme 6.

Another attempt to use steroids as vectors in the targeted development of drugs combined the anthra-

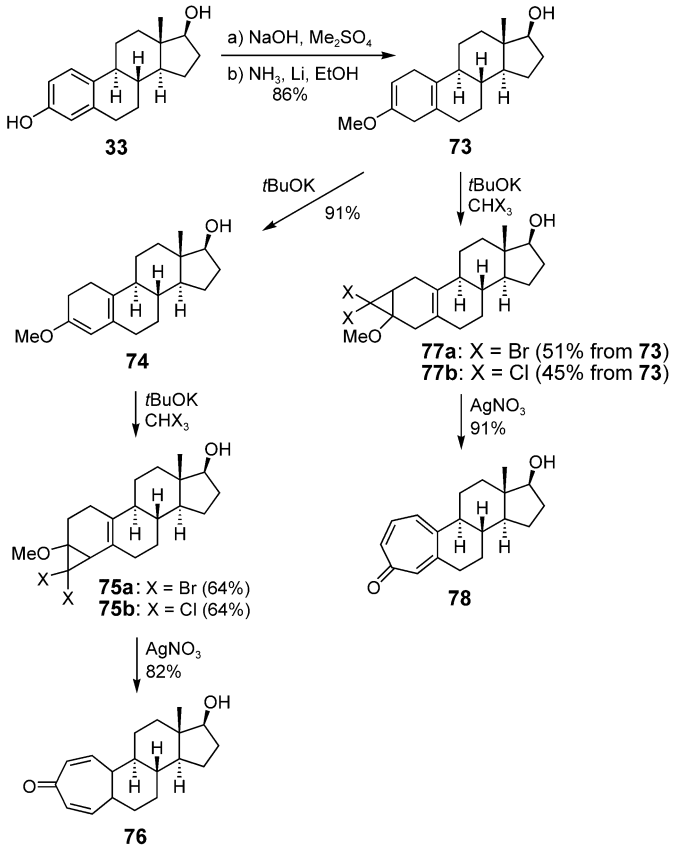
Table 3: Effect of estratropones on tubulin polymerization.

Compound	Inhibition of tubulin polymerization IC_{50} [μM]	Activity (IC_{50} colchicine/IC_{50} drug)
3	11.2±5.0	1
72	14.2±1.2	0.79
76	4.4±1.7	2.5
78	7.2±1.7	1.5
81	8.1±4.1	1.4
84a	2.1±0.5	5.3
84b	5.9±1.1	1.9
85	27.5±5.2	0.41
86	29.8±2.9	0.38

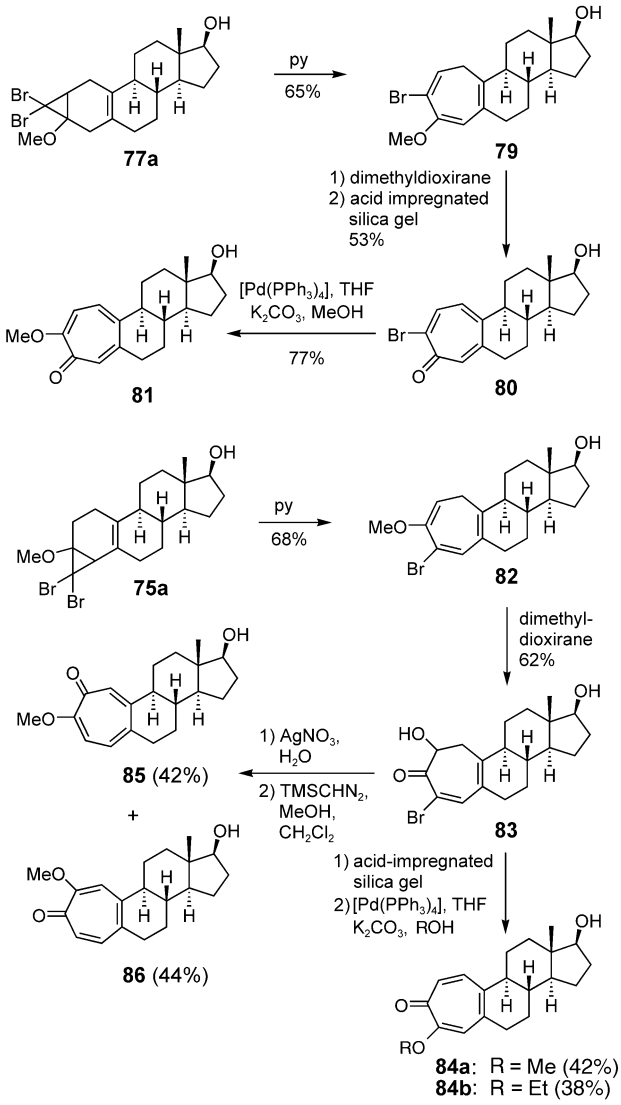


Scheme 4. Synthesis of various estrone–talaromycin hybrids.

 © 2003 Wiley-VCH Verlag GmbH & Co. KGaA, Weinheim

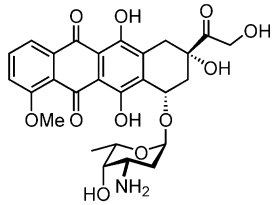


Scheme 5. Synthesis of hybrids of 2-methoxyestradiol (**72**) and colchicin (**3**), part 1.

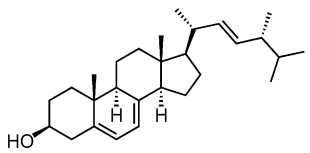


Scheme 6. Synthesis of hybrids of 2-methoxyestradiol (**72**) and colchicin (**3**), part 2.

quinone motif of powerful antineoplastic anthracycline antibiotics such as adriamycin (**87**) with steroidal elements.[29] For this purpose, the hybrids **98**–**101** (Scheme 8) were synthesized



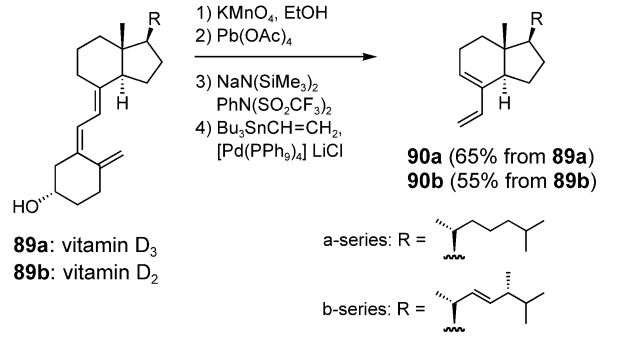
87: Adriamycin (Doxorubicin)



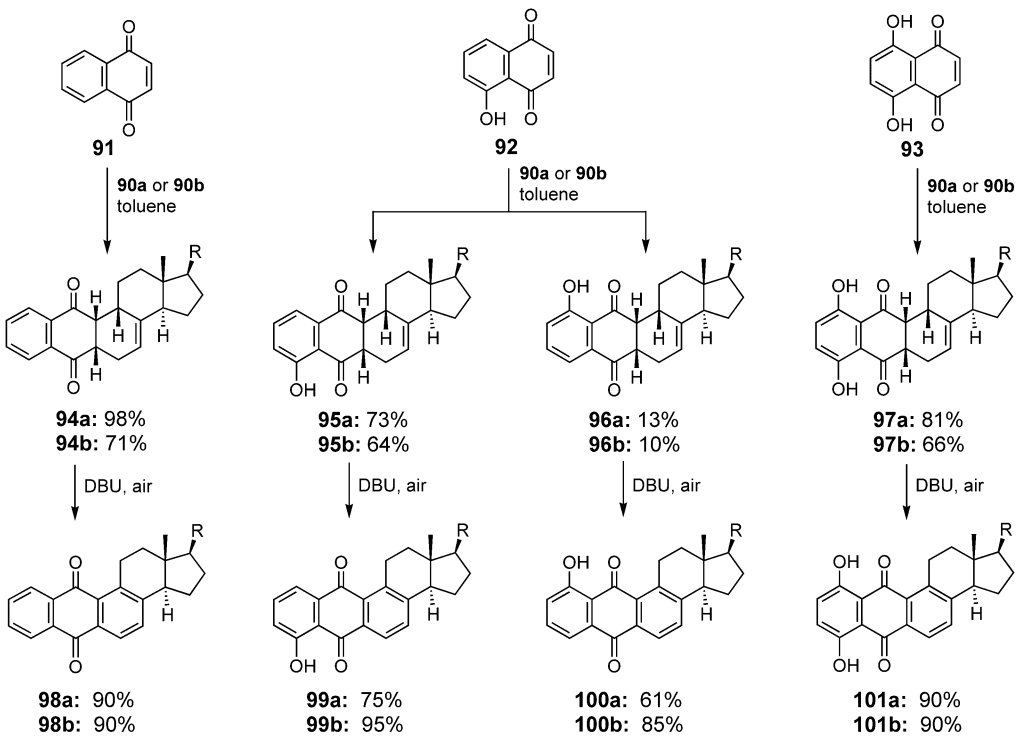
88: Ergosterol

by coupling two dienes **90a** and **90b**, obtained from vitamin D_3 (**89a**) and vitamin D_2 (**89b**), respectively, by oxidative cleavage (Scheme 7), with a series of naphthoquinones **91**–**93** in a Diels–Alder reaction to give the adducts **94**–**97** (Scheme 8). Subsequent aromatization led to the final compounds **98**–**101**, which were tested in vitro on four tumor cell lines to evaluate their potency relative to adriamycin (**87**) as a standard (Table 4). The hybrids **98b**–**101b** with the unsaturated side chain were generally more cytotoxic than their congeners **98a**–**101a** with the saturated side chain. Some of the compounds were even more potent than adriamycin (**87**).

The steroid motive has also been used for the design of new anticancer agents based on calicheamicin (**102**), neocarzinostatin (**103**), and similar antibiotics obtained from bacterial sources. These highly cytotoxic compounds contain an enediyne moiety, which can cause single- and double-stranded lesions of DNA by formation of a diyl radical



Scheme 7. Synthesis of indane derivatives **90**.

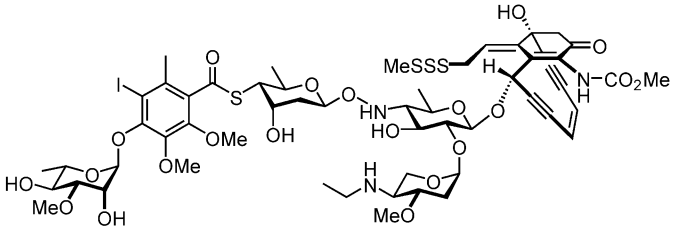


Scheme 8. Synthesis of steroid–anthraquinone hybrids **98**–**101**.

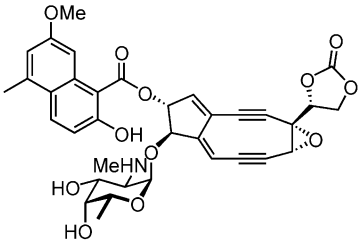
Table 4: In vitro cytotoxic activity of compounds **98**–**101** and adriamycin (**87**) on J774 (murine monocyte/macrophage), GM7373 (bovine aortic endothelial), IGR-1 (human melanoma), and P388 (murine leukemia) cell lines.

Cell line	**98a** [μM][a]	**98b** [μM]	**99a** [μM]	**99b** [μM]	**100a** [μM]	**100b** [μM]	**101a** [μM]	**101b** [μM]	**87** [μM]
J774	263	57	216	22	141	95	289	23	100
GM7373	167	79	192	49	114	120	96	34	32
IGR-1	n.d.[b]	100	250	67	44	191	502	23	21
P388	639	411	369	76	169	274	378	49	19

[a] IC_{50} is defined as the concentration of compound required to inhibit cellular growth by 50% after 48 h of drug exposure. [b] Not determined.



102: Calicheamicin γ_1^I

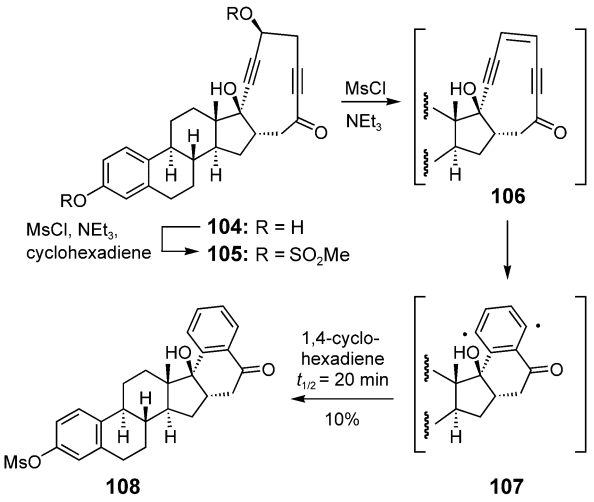


103: Neocarzinostatin chromophore

through a Bergman cycloaromatization. Unfortunately, the compounds have severe side effects owing to their toxicity.[30]

To improve efficiency and selectivity, there have been several efforts to link the diradical precursor enediyne moiety with DNA-binding agents[31] and also to couple it to an estradiol molecule.[32] Such a hybrid of estradiol and calicheamicin (estramicin) may allow a selective transfer into the nuclei of human mammary cancer cells, as these are usually rich in estrogen receptors (designated ERα and ERβ). In one of the studies, the estradiol–enediyne **106** was formed as an intermediate from the steroid–diynol derivative **104** via **105** by treatment with methanesulfonyl chloride in the presence of triethylamine (Scheme 9). Bergman cyclization then led to the diradical **107**, which in the presence of 1,4-cyclohexadiene gave the aromatic system **108** with a half-life $t_{1/2}$ of 20 min.

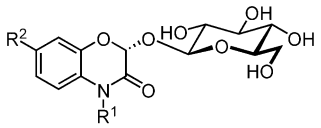
A second approach[33] started from the commercially available contraceptive ethynyl estradiol (**109**, Scheme 10). Monosilylation, carboxylation, EDC·HCl-catalyzed esterification with the protected enediyne alcohol **111** and deprotection yielded the hybrid **112**, whose binding affinity to hERα was determined to be 0.51 μM. The growth inhibition



Scheme 9. Synthesis and Bergman cyclization of the estradiol–enediyne hybrid **106**.

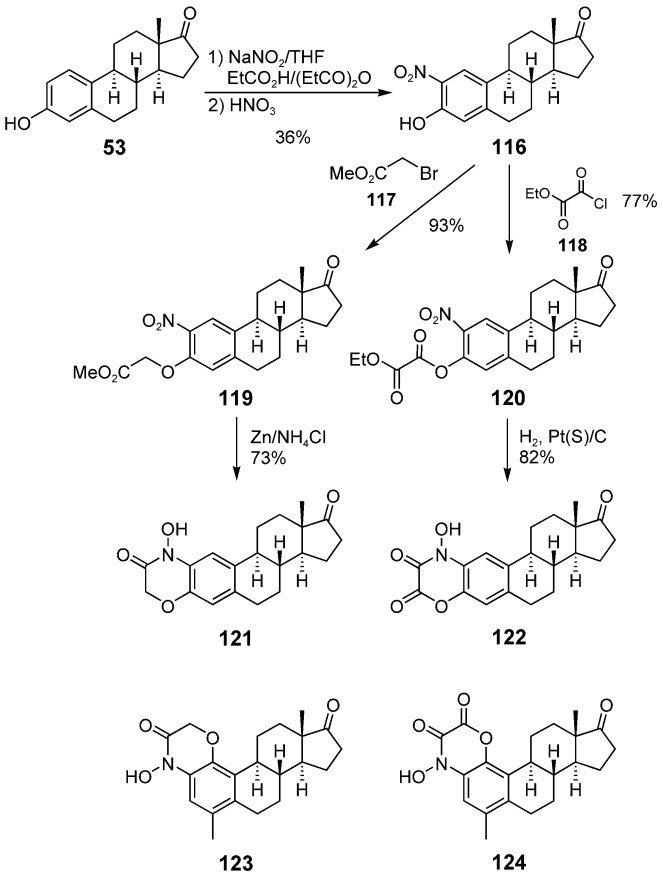
test with a hERα-rich cell line (MCF7: $IC_{50} = 31$ μM), a hERα-deficient cell line (MDB-231, $IC_{50} = 48$ μM), an androgen receptor (AR)-positive cell line (LNCCaP, $IC_{50} = 33$ μM), and an AR-negative cell line (HEK-293, $IC_{50} = 10$ μM) showed a more or less distinct inhibition in all four cases, thus suggesting an ER-independent mechanism for cytotoxicity.

Acetal glycosides such as **115a-c**, which contain a benzoxazine subunit as well as their aglycones, exhibit

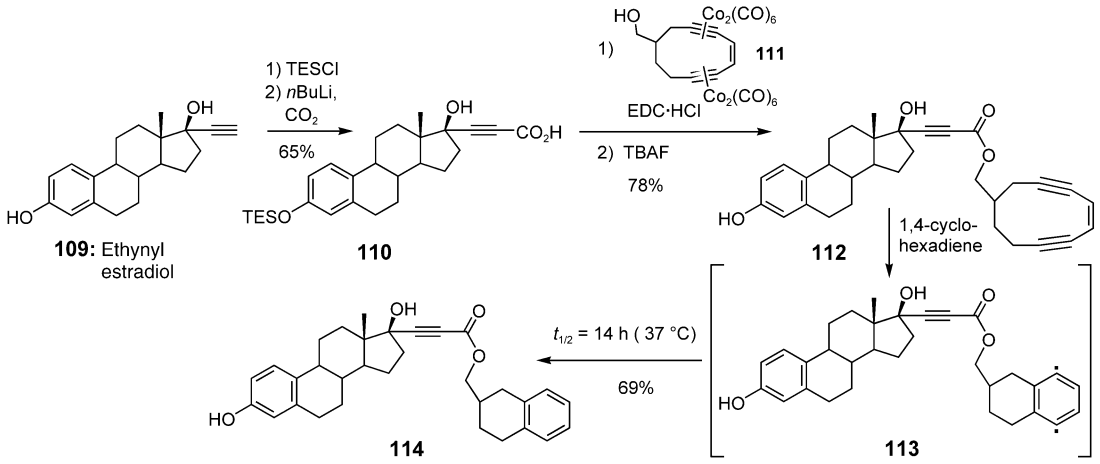


115a: R^1 = OH, R^2 = H
115b: R^1 = OH, R^2 = OMe
115c: R^1 = OMe, R^2 = OMe

interesting pharmacological and biological properties, such as antiinflammatory activity and inhibition of bacterial and fungal growth. They also act as a resistance factor, for example, in maize against the European corn borer. In spite of the importance of these compounds, their total synthesis had not been reported until the early 1990s.[34] Such a benzoxazine subunit has now been combined with the steroidal skeleton of two members of the estra-1,3,5(10)-triene series.[35] However, no biological data is yet available to show the usefulness of these hybrid products. For the synthesis of **121** and **122**, estrone **53** was treated with sodium nitrite and subsequently oxidized with nitric acid to provide the nitro compound **116** (Scheme 11). Alkylation with methyl 2-bromoacetate (**117**)



Scheme 11. Synthesis of steroidal benzoxazine hybrids **121**–**124**.

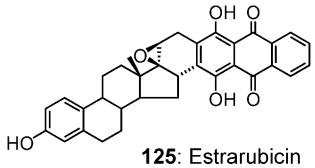


Scheme 10. Synthesis and Bergman cyclization of the estradiol–enediyne hybrid **112**.

 © 2003 Wiley-VCH Verlag GmbH & Co. KGaA, Weinheim

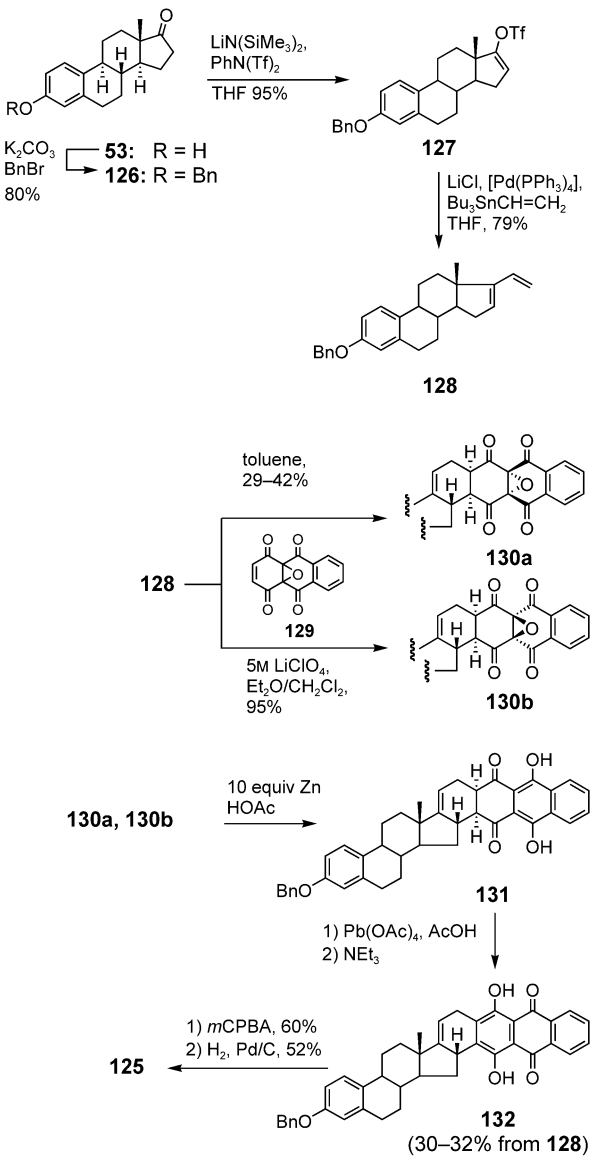
and ethyl 2-chloro-2-oxoacetate (**118**), respectively, and reduction of the nitro group led to the two desired compounds **121** and **122**, respectively, by an in situ cyclization of the intermediate aryl hydroxylamines. The other two hybrids **123** and **124** were prepared in a similar manner, starting from 1-hydroxy-4-methylestra-1,3,5(10)-trien-17-one.

The anthraquinone subunit is present in numerous bioactive molecules of a class of compounds that exhibit strong antineoplastic activity due to its DNA-strand-cleavage ability.[36] Therefore the synthesis of a hybrid estrogen–anthraquinone, estrarubicin (**125**) seemed to be attractive.[37]



125: Estrarubicin

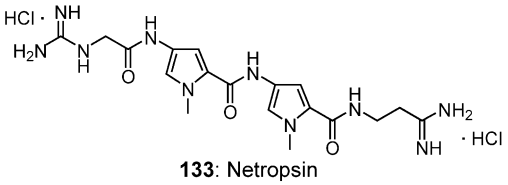
An eight-step sequence led to the synthesis of **125** starting from estrone (**53**), which was converted into the enol triflate **127** via **126** according to the McMurry procedure (Scheme 12).[38] Treatment of **127** with tributyl(vinyl)tin in the presence of Pd^0 provided the diene **128** for a Diels–Alder reaction with 4a,9a-epoxy-4a,9a-dihydroanthracene-1,4,9,10-tetrone (**129**).[39] Two different stereoisomers **130a** and **130b** with respect to the epoxide function were obtained, which, however produced the same compound **131** upon reduction with zinc in acetic acid. Oxidation with lead tetraacetate and tautomerization with triethylamine yielded the octacycle **132**, which was smoothly epoxidized with *m*CPBA and subsequently debenzylated with hydrogen and palladium on charcoal as catalyst to give the desired hybrid compound **125**. The results of the biological testing have not yet been published.



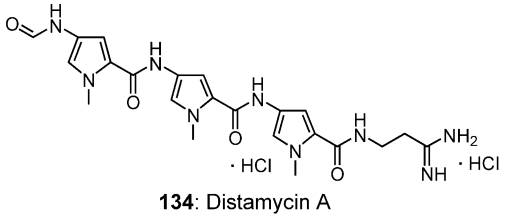
Scheme 12. Synthesis of estrarubicin (**125**).

3.2.2. *Hybrids with a DNA-Binding Lexitropsin Substructure*

Netropsin (**133**)[40] and distamycin A (**134**)[41] belong to the lexitropsin class of compounds. The two naturally occurring oligopeptides are structurally closely related in that two and three *N*-methylpyrrole-2-carboxamide units, respectively, are combined. They show a relatively strong affinity for A–T-rich DNA regions in the minor groove of double-stranded B-DNA. This selectivity was explained by the fact that A–T base pairs are associated with the narrow minor groove and the elongated crescent-shaped distamycin and netropsin molecules allow a tight fit. Furthermore, the presence of the N2 amino group of guanine serves as a major steric block that prevents the pyrrolamide chain from docking fully to the minor groove in G–C-rich segments.[42] However, netropsin and distamycin A themselves show only a weak cytotoxicity, which can be traced back to the absence of a covalent bonding to the DNA. Thus, only reversible binding occurs by electrostatic forces, van der Waals interactions, and hydrogen bonds.



133: Netropsin



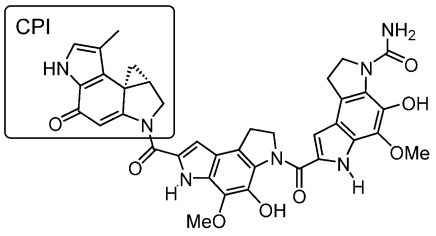
134: Distamycin A

In recent years there have been a number of efforts to use the lexitropsins ("information-reading" oligopeptides) as DNA-sequence-selective vehicles in conjunction with known antitumor compounds such as nitroso ureas, benzoyl mustards, CC-1065, psoralens, bleomycin, flavins, acridines, and many more in order to improve their selectivity.[43] In this

 © 2003 Wiley-VCH Verlag GmbH & Co. KGaA, Weinheim

Review we will only focus on hybrids of natural products or their derivatives. The distamycin-derived agents show, to different extents, a significant cytotoxicity that is stronger than that of the alkylating agent alone, thus suggesting a cooperative effect of both. However, this cannot always be predicted in a rational manner.

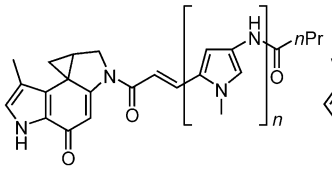
The antibiotic (+)-CC-1065 (**135**) is an antibiotic that was first isolated from *Streptomyces zelensis* and is one of the most



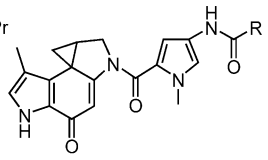
135: (+)-CC-1065

potent anticancer agents with an IC_{50} of about 30 pM on some cancer cell lines (e.g. L1210).[44] It contains a spirocyclopropanepyrroloindoline (CPI) moiety, which can alkylate the N3 position of adenine in A–T-rich parts of the minor groove of B-DNA. However, CC-1065 (**135**) exhibits a delayed hepatotoxicity and thus cannot be used in the clinical treatment of malignant tumors.[45] It was revealed that it is mainly the non-CPI part of the molecule that is responsible for these severe side effects. Consequently, there have been several efforts to combine the CPI unit or derivatives thereof with other DNA-binding moieties, among those, the lexitropsins. Interestingly, these CPI–lexitropsin hybrids are often much more water-soluble than the original natural product, which overcomes another problem of the clinical administration of CC-1065 (**135**).

Two recent examples of hybrids that combine the CPI moiety with various lexitropsins are the series **136a–b** and **137a-c**.[46] Among these CPI–lexitropsin



136a–b: *n* = 1–2



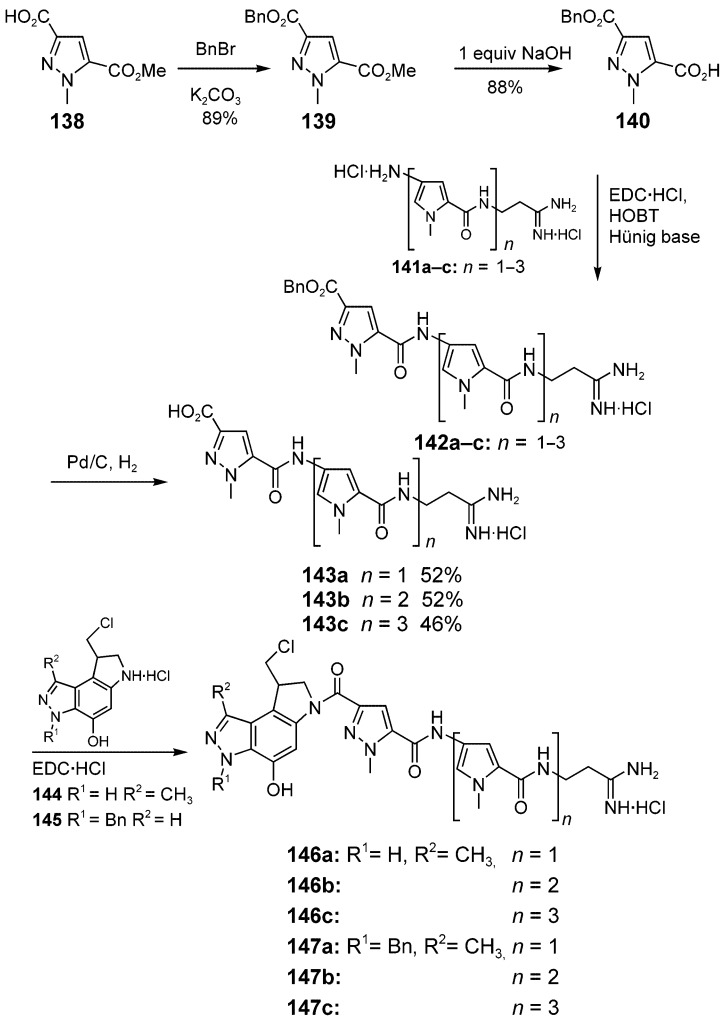
137a: R = Me
137b: R = Et
137c: R = *n*Pr

hybrids, the two most potent antineoplastic agents were **136a** and **136b**, in which the two parts are linked through a *trans* double bond. The reason for this is not well understood.

However, many examples are known in which the CPI unit is replaced by a seco-CPI unit with a chloromethyl group, as it has been shown that such seco derivatives usually show a similar activity to the corresponding spirocyclopropanecyclohexadienone moiety, which is formed in situ from the seco compound by a Winstein cyclization. A novel class of seco-CPI unit is represented by the compounds **144** and **145**, in which a pyrazoloindoline instead of the pyrroloindoline moiety is present.

For the synthesis of the corresponding seco-CPI hybrids **146–147**, the pyrazole derivative **138**[47] was benzylated to give **139**, and the methyl ester moiety was hydrolyzed with NaOH to afford the acid **140** (Scheme 13). Its coupling with the amines **141a–c**[48] to give **142a–c** followed by a deprotective hydrogenation step with Pd/C yielded the acids **143a–c**, which were coupled, again by using classical peptide synthesis conditions, with the seco-CPI derivatives **144** and **145** to afford the desired compounds **146–147**.

The results of the biological tests are displayed in Table 5. The hybrids **146a–c** have a significantly higher cytotoxicity than the individual parent molecules. This enhanced activity may be attributed to an efficient intercalation into the DNA followed by a covalent reaction with DNA at selected sites.[45] Especially **146c** showed a remarkable activity with an IC_{50} in the range between 7.4 and 71 nM, depending on the tumor cell



Scheme 13. Synthesis of hybrids **146–147** of seco-CC-1065 analogues and a lexitropsin moiety.

 © 2003 Wiley-VCH Verlag GmbH & Co. KGaA, Weinheim

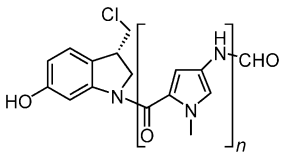
Table 5: In vitro activity of hybrids **146**–**147** and alkylating units **144** and **145** against the proliferation of murine leukemia (L1210), murine mammary carcinoma (FM3A), human T-lymphoblast (Molt/4 and CEM), and human B-lymphoblast (Daudi) cell lines.

Compound	IC_{50} [nM ± SE][a] L1210	FM3A	Molt/4	CEM	Daudi
144	520 ± 6.6	1400 ± 40	1740 ± 50	1260 ± 30	680 ± 150
145	2710 ± 490	18300 ± 200	8550 ± 280	6720 ± 1040	7520 ± 30
146a	58 ± 17	1600 ± 50	340 ± 20	230 ± 10	150 ± 40
146b	19 ± 2	190 ± 6	45 ± 1	39 ± 1	22 ± 10
146c	7.4 ± 0.4	31 ± 11	17 ± 4	71 ± 9	8.8 ± 0.1
147a	240 ± 30	4000 ± 1000	130 ± 20	70 ± 21	11 ± 6.0
147b	600 ± 90	5600 ± 1400	160 ± 60	210 ± 110	38 ± 7.0
147c	400 ± 16	19300 ± 3400	310 ± 70	400 ± 50	100 ± 10

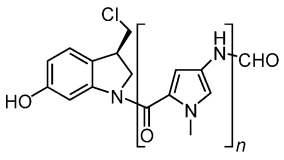
[a] Compound concentration required to inhibit tumor cell proliferation by 50%.

line used in the trials. However, the cytotoxicity is lower than that of CC-1065 (**135**) by a factor of about 1000.

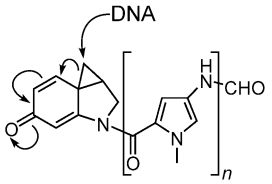
Although the CPI unit as well as its benzo analogue and their seco compounds show the highest biological activity, a smaller CPI unit—called CI—has been used for the synthesis of hybrids of **148a–c** and **149a–c** with a lexitropsin moiety.



148a–c: *n* = 1–3



149a–c: *n* = 1–3



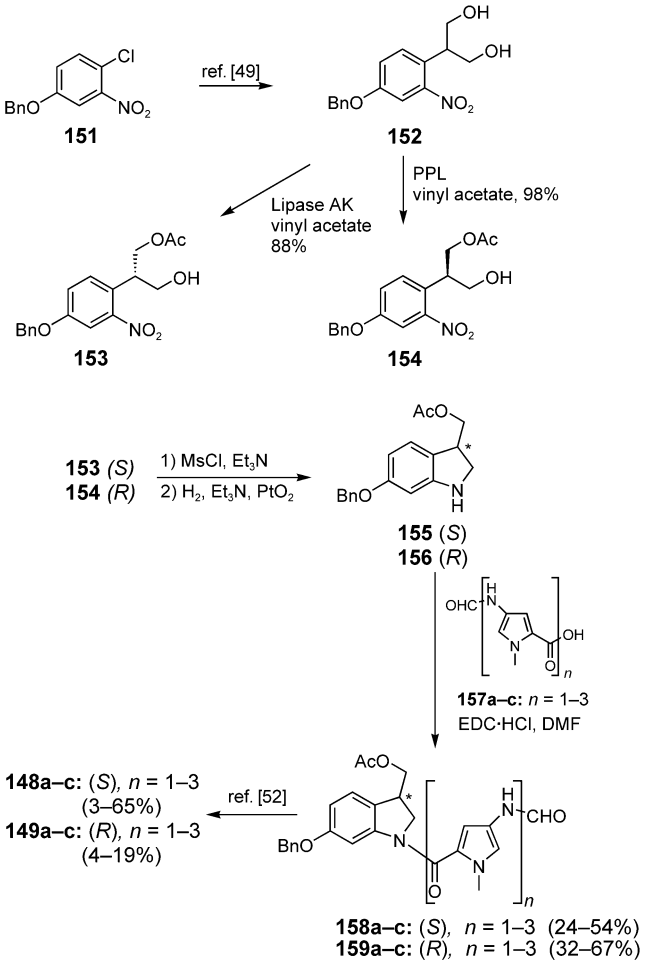
150a–c: *n* = 1–3

Again, the seco-CI unit containing a chloromethyl group was employed, from which **150a–c** are probably formed in vitro or in vivo as the final drugs.

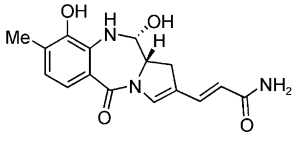
These hybrids were accessed in both enantiomeric forms through an asymmetric acetylation from the prochiral diol **152**,[49] which was obtained from **151** by using two different lipases (Scheme 14, (*S*)-**153**: 98% *ee*, (*R*)-**154**: 88% *ee*). Transformation of **153** and **154** into the corresponding methanesulfonates followed by reduction of the nitro group and subsequent nucleophilic ring closure gave the indole derivatives **155** and **156**, respectively. Condensation with the pyrrole carboxylic acids **157a–c**[50] in the presence of EDC·HCl led to compounds **158a–c** and **159a–c**, respectively. The final enantiomeric hybrids **148a–c** and **149a–c** were obtained after sequential hydrolysis, chlorination, and debenzylation. The DNA-cleaving activity of these compounds was assayed by using supercoiled plasmid Col E1. In these studies, the compound with the non-natural *R* configuration was found to be more potent than the one with the natural configuration.[51]

The natural compounds anthramycin (**160**) and DC-81 (**161**) belong to the pyrrolo[2,1-*c*][1,4]-benzodiazepine (PBD) group[52] and covalently bind to the C2-NH_2 group of guanine residues in the minor groove of DNA through the N,O-acetal and imine moiety, respectively, in the central B-ring. This affinity to G–C-rich DNA-sequences was combined with the opposite recognition pattern of the lexitropsins.[53]

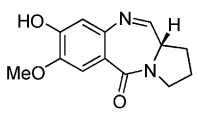
For the synthesis of the hybrid molecules **169a–c** and **170a–c**, vanillin (**162**) was functionalized



Scheme 14. Synthesis of seco-CI–lexitropsin hybrids **148**–**149**.



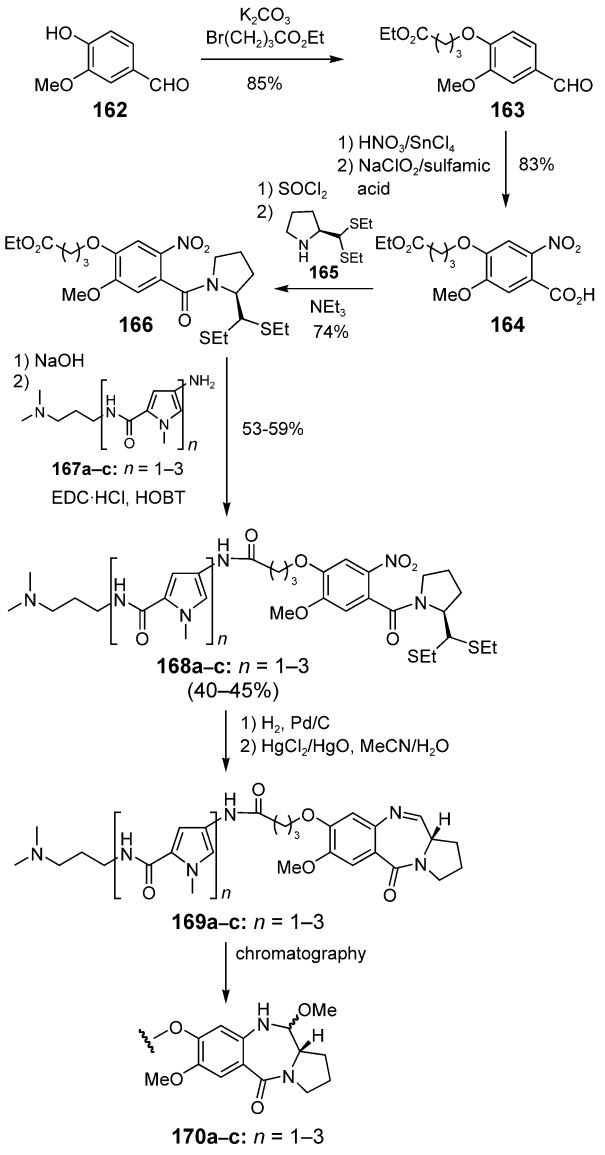
160: Anthramycin



161: DC-81

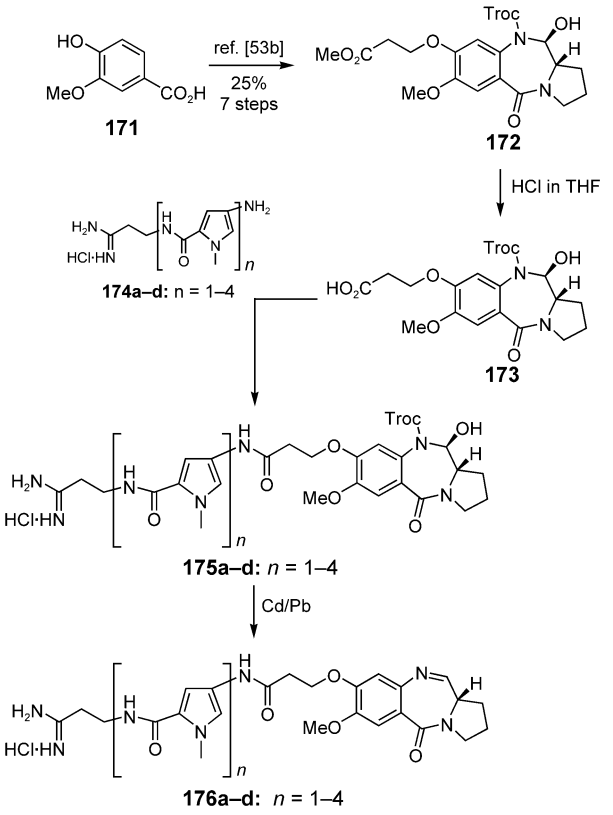
 © 2003 Wiley-VCH Verlag GmbH & Co. KGaA, Weinheim

by alkylation of the phenolic hydroxy group with ethyl γ-bromobutyrate, nitration, and oxidation of the aldehyde to give the carboxylic acid **164** via **163** (Scheme 15). Transformation into the acid chloride and coupling with pyrrolidine-2-carboxaldehyde diethyl thioacetal (**165**) afforded the amide **166**. Saponification of the ester moiety and combination with the respective lexitropsin amine **167a–c** in the presence of EDC·HCl and HOBT led to compounds **168a–c**, respectively, which upon hydrogenation of the nitro group with H_2 on Pd/C and subsequent deprotection with $HgCl_2$/HgO furnished the corresponding imines **169a–c**. The high polarity of these compounds made it necessary to use methanol in chloroform as the eluent for column chromatography, which partially led to the formation of the N,O-acetals **170a–c**. So far, biological tests of **169** and **170** are not available.



Scheme 15. Synthesis of anthramycin–lexitropsin hybrids **169–170**.

However, the four hybrids **176a–d** were synthesized and tested together with the parent compounds **134**, **161**, and **174d** for their in vitro biological effects (Scheme 16).[53c] The results of tests for antiproliferative activity against human chronic myeloid leukemia cells (K562) and T-lymphoblastoid Jurkat cells as well as the polymerase chain reaction (PCR) amplification of the human estrogen receptor (hER) gene, the c-myc oncogene, and the human immunodeficiency virus type 1 long terminal repeat (HIV-1 LTR) are summarized in Table 6. Again, the hybridization of the two natural products led to a dramatic increase of the potency of the drug,



Scheme 16. Synthesis of DC-81–lexitropsin hybrids **176a–d**.

Table 6: In vitro biological effects on K562 and Jurkat cell lines: PCR experiments on human estrogen receptor, human c-myc oncogene, and HIV-1 LTR.

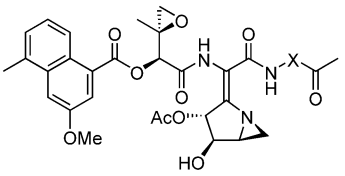
	IC_{50} [μM]		PCR IC_{50} [μM][a]		
Compound	Jurkat	K562	c-myc	ER	HIV-1 LTR
134	20	12	25	5	50
161	2.2	1	n.d.[b]	n.d.	n.d.
174d	25	12	12	0.5	20
176a	80	>100	4	3	1
176b	50	6	6	2	0.8
176c	0.8	0.7	2.5	0.8	2
176d	0.07	0.04	2	0.2	2

[a] IC_{50} is the inhibitory concentration necessary to obtain 50% inhibition of generation of PCR products of human c-myc, estrogen receptor (ER), and HIV-1 LTR sequences. [b] Not determined.

 © 2003 Wiley-VCH Verlag GmbH & Co. KGaA, Weinheim

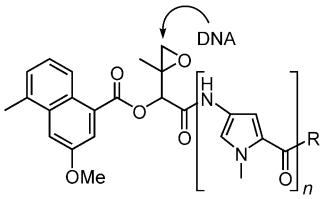
especially in the case of **176d**. In a general strategy for the synthesis of the anthramycin moiety in the hybrid compounds **176a–d**, vanillic acid (**171**) was transformed into ester **172** in seven steps (Scheme 16).[53b] Hydrolysis of **172** with acid afforded **173**, which was coupled with the aminopoly(pyrrolamide) moieties **174a,**[48a] **174b,**[48b] **174c**[54] and **174d**[55] in the presence of EDC·HCl as the condensing agent to give the conjugates **175a–d**, respectively. Final cleavage of the Troc group with a Cd/Pb couple furnished the desired hybrids **176a–d**.

The two antitumor antibiotics azinomycin A (**177**) and azinomycin B (**178**) were isolated from the culture broth of



177: Azinomycin A X = CH_2
178: Azinomycin B X = C=CH(OH)

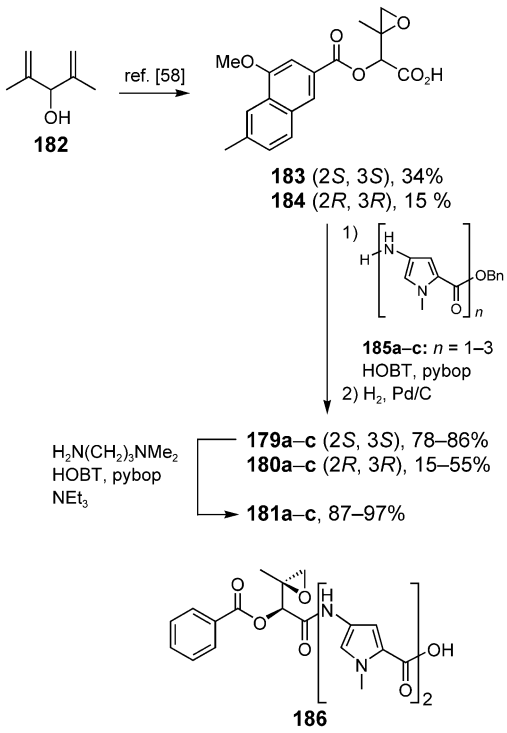
Streptomyces griseofuscus S42227.[56] As part of the development of artificial and potent DNA-cleaving agents based on natural products, the enantiopure azinomycin–lexitropsin hybrid molecules **179–181** were synthesized and their DNA-



179a–c: R = OH, (2*S*, 3*S*), *n* = 1–3
180a–c: R = OH, (2*R*, 3*R*), *n* = 1–3
181a–c: R = $NH(CH_2)_3NMe_2$, (2*S*, 3*S*), *n* = 1–3

cleaving activities evaluated.[57] For their preparation, the enantiopure carboxylic acids **183** and **184** were obtained from **182** by a known procedure[58] employing an asymmetric Sharpless epoxidation, condensation with 3-methoxy-5-methylnaphthalene-1-carboxylic acid in the presence of DCC, and oxidative cleavage of the remaining double bond (Scheme 17). The acids **183** and **184** were coupled with the *N*-methyl-4-aminopyrrole-2-carboxylic acids **185a–c** to generate the desired hybrids **179a–c** and **180a–c**, respectively. To introduce the dimethylaminopropyl appendage, **179a–c** were treated with 3-dimethylaminopropylamine in the presence of pybop, HOBT, and NEt_3 to yield **181a–c**.

The DNA-cleaving activities of the synthetic hybrids **179–181** were again assayed with supercoiled plasmid Col E1. It was found that the fastest and the most complete cleavage of the DNA was obtained with **181b** and especially **181c**. The compounds **180a–c**, which have the non-natural configuration, showed rather low cleaving activity. The derivative **186**,

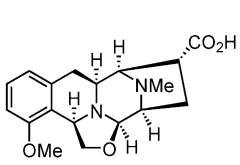


183 (2*S*, 3*S*), 34%
184 (2*R*, 3*R*), 15 %
185a–c: *n* = 1–3
HOBT, pybop
2) H_2, Pd/C
$H_2N(CH_2)_3NMe_2$
HOBT, pybop
NEt_3
179a–c (2*S*, 3*S*), 78–86%
180a–c (2*R*, 3*R*), 15–55%
181a–c, 87–97%
186

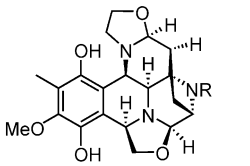
Scheme 17. Synthesis of hybrids **179–181** and structure of the reference compound **186**.

which has a phenyl instead of a naphthyl group, was not active at all, which suggests that both the left hand segment of azinomycin with the natural configuration and the trimeric pyrrole amide moiety from lexitropsin are indispensable for potent activity.[59]

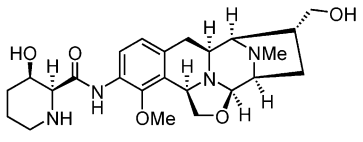
So far, most of the described natural product hybrids exhibited a higher biological activity than the parent compounds. This is not always the case, as is shown by the following example. The strong antitumor activity of the oxazolidine-containing natural products quinocarcin (**187**), the bioxalomycins (**188**), and tetrazomine (**189**), which were isolated from various *Actinomycetes* species, prompted the development of a hybrid **198** with netropsin (**133**).[60] The



187: Quinocarcin



188a: Biooxalomycin$_{\alpha 1}$ R = Me
188b: Biooxalomycin$_{\alpha 2}$ R = H

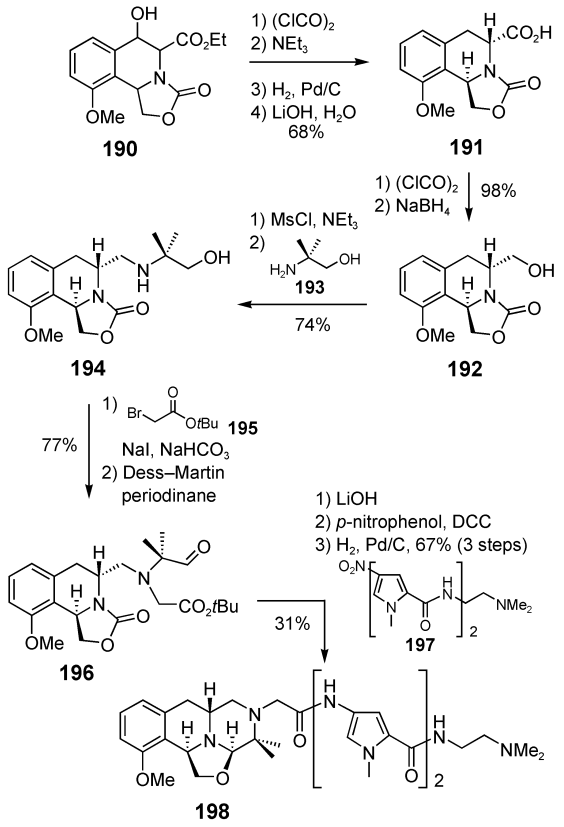


189: Tetrazomine

 © 2003 Wiley-VCH Verlag GmbH & Co. KGaA, Weinheim

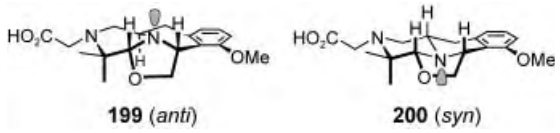
activity of the natural products **187**–**189** is believed to rely on a spontaneous disproportionation; in the presence of molecular oxygen, a superoxide radical anion is generated which could induce scission of DNA strands.

The synthesis of **198** began with the treatment of **190** with oxalyl chloride followed by elimination of the resulting β-chloroester to give the corresponding α,β-unsaturated ester, which was hydrogenated catalytically (Scheme 18). In this



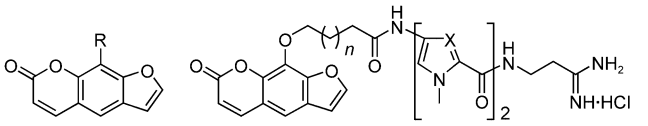
Scheme 18. Synthesis of the quinocarcin–netropsin hybrid **198**.

reaction a nearly 1:1 mixture of the two corresponding epimeric saturated esters was obtained. However, after saponification mainly the *anti* ester **191** was isolated as a result of an epimerization. Its acid moiety was transformed into the amino alcohol **194** via **192** by selective reduction of the corresponding acid chloride, followed by mesylation and nucleophilic substitution with 2-methyl-2-aminopropanol (**193**). Alkylation of **194** with *tert*-butyl bromoacetate **195** and subsequent Dess–Martin oxidation afforded the key aldehyde **196**. Addition of lithium hydroxide effected the cleavage of the oxazolidinone with loss of CO_2 and ring closure of the amino alcohol. Hydrolysis of the *tert*-butyl ester moiety of the resulting oxazolidine, was followed by coupling with compound **197** under reductive conditions to afford the final hybrid **198**. However, the evaluation of the ability of **198** and of the synthetic intermediate **199** to produce superoxide gave a negative result, whereas the corresponding *syn* analogue **200**, which was obtained in small amounts from the *syn* epimer of acid **191**, produced moderate amounts of



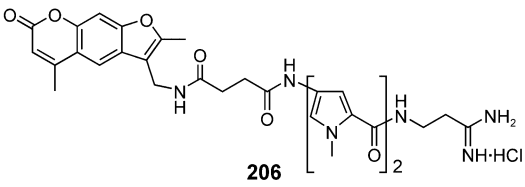
superoxide (0.82×10^{-9} M s^{-1}; in comparison, a 1.0 mM solution of quinocarcin produced 4.2×10^{-9} M s^{-1} superoxide). Furthermore no alkylation or oxidative cleavage of DNA was detectable in incubation experiments with **198**. Based on this result, the authors deduced that the stereoelectronic geometry of the nitrogen atom in **187**–**189** is of great importance for their biological activity, which is not matched in the *anti* compounds **198** and **199** and only to a much lower extent in the simple *syn* oxazolidine **200**.

Psoralen (**201**) is the prototype of a group of furocoumarins that occur naturally as phytoalexins in several plant



201: Psoralen R = H
202: R = OMe

203 *n* = 1, X = CH, R = –(CH$_2$)$_2$C(=NH·HCl)NH$_2$
204 *n* = 2, X = CH, R = –(CH$_2$)$_2$NMe$_2$
205 *n* = 2, X = N, R = –(CH$_2$)$_2$NMe$_2$

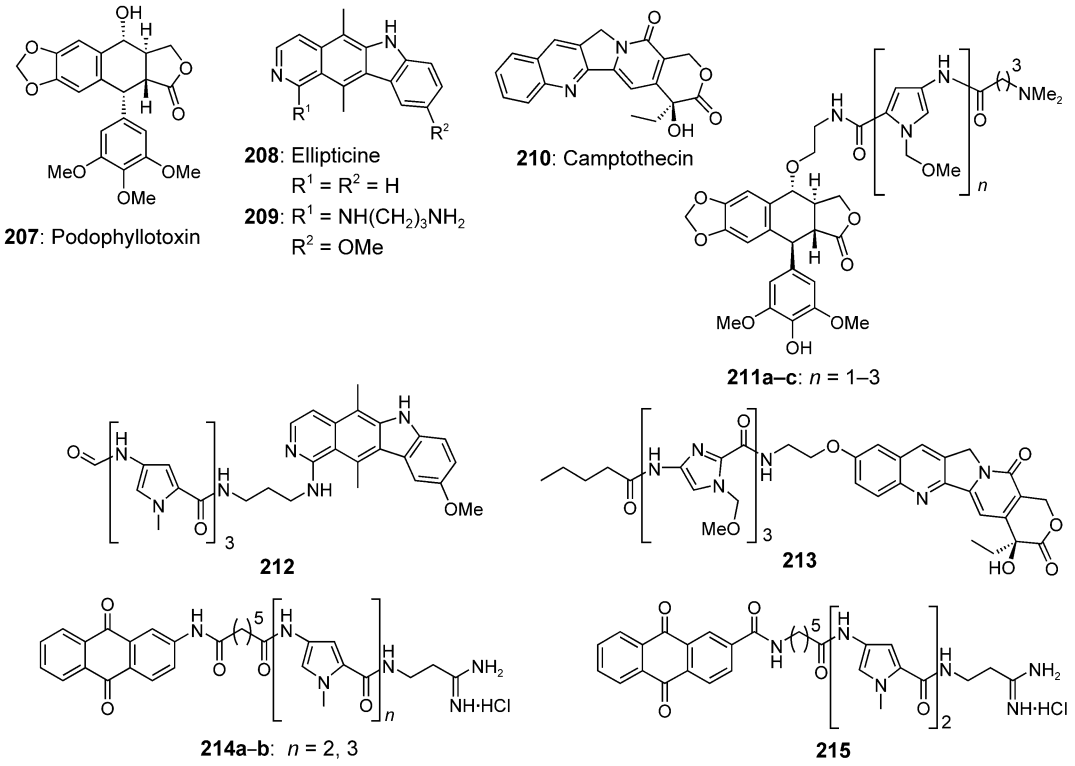


families. The psoralens, such as 8-methoxypsoralen (**202**), have been used in photochemotherapy for the treatment of psoriasis, vitiligo, and cutaneous T-cell lymphoma. They intercalate into DNA and react with the thymine residues, in particular with 5′-T–A sequences, under irradiation.[61]

To improve the interaction of the psoralens with DNA, lexitropsin conjugates have been prepared. Such psoralen–lexitropsin hybrids, for example, **203** and **206**, bind to poly(dA–dT) with K_{app} values of 2.8 and 0.9×10^{7} M^{-1}, respectively, that is, greater than or equal to that of netropsin ($K_{app}=1.0\times10^{7}$ M^{-1}). Their ability to mediate the photoinduced cross-linking of DNA, while efficient, is less pronounced than that of the psoralen derivative **202**.[62] In contrast, the hybrids **204** and **205** were 333- and 22-fold, respectively, more cytotoxic than **202** in photoinduction experiments with leukemic K562 cells. Although **202** is an efficient cross-linker under the conditions employed (plasmid DNA; UV light, $\lambda=366$ nm), compounds **204** and **205** are more than 300- and 10-fold, respectively, more efficient.[63]

Podophillotoxin (**207**) was originally isolated from the rhizomes of the North American plant *Podophyllum peltatum* L. Its semisynthetic analogue etoposide is used clinically as an antitumor chemotherapeutic that inhibits topoisomerase II. Therefore 4′-demethylepipodophyllotoxin–lexitropsin

 © 2003 Wiley-VCH Verlag GmbH & Co. KGaA, Weinheim



hybrids **211a–c** have been prepared, but they show rather poor topoisomerase II-inhibition activity.[64]

Another cytotoxic compound that was combined with distamycin A (**134**) is the ellipticine derivative **209**, which was chosen mainly because of its known anticancer properties.[65] The obtained hybrid **212** was evaluated for cytostatic and cytotoxic activities against L1210 leukemia cells in vitro. It exhibited marked cytostatic properties, but its cytotoxicity was approximately 10 times lower than that of the original ellipticine (**208**). Taking advantage of the fluorescence of the pyridocarbazole chromophore, fluorescence microscopy was used to compare the cellular uptake of the hybrid molecule **212** with that of compound **209**. Nuclei of hybrid treated cells were markedly less fluorescent than those of cells treated with **209**. Thus, a difference in intranuclear concentrations might explain the difference in cytotoxicities.

The hybrid **213** of camptothecin (**210**), an alkaloid isolated from the stem wood of the Chinese tree *Camptotheca acuminata*, and lexitropsin is one to two orders of magnitude less cytotoxic than camptothecin (**210**). However, it exhibits a significant topoisomerase I-inhibitory activity, which is only slightly lower than that of distamycin A (**134**).[66]

Antitumor anthraquinones such as adriamycin (**87**) and mitoxantrone can cleave DNA upon enzymatic activation.[67] Therefore the anthraquinone–lexitropsin hybrids **214a–b** and **215** were synthesized.[68] However, information on their biological activity has not yet been disclosed.

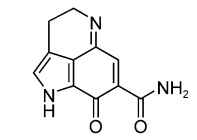
The conjugate **217** of makaluvamine A (**216**),[69] a representative of a class of cytotoxins found in marine sponges, and *N*-methoxymethylpyrrole oligopeptides exhibits a cytotoxicity comparable to that of **216** itself. Makaluvamine A (**216**) is known to inhibit topoisomerase II and to intercalate into DNA. Numerous enediyne–lexitropsin hybrids (e.g. **218**,[70] **219**,[70] **220**,[72b] **221**,[71] and **222**[72c]) were synthesized in the hope that such hybrids would increase the potency of synthetic enediynes by increasing their affinity for DNA, while minimizing cytoplasmic toxicity.[70] Their IC_{50} values ranged from about 14–48 μM following 96 h incubation in the presence of the test compound. Thus, the expected dramatic increase in potency is not observed. This might be due to the geometry of the hybrids not allowing the precise docking of the enediyne to the DNA, which is required to enable the radicals generated in situ to abstract hydrogen atoms from the DNA backbone.[72]

3.2.3. *Hybrids with an Enediyne Substructure.*

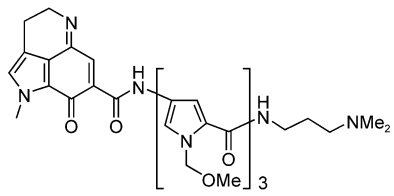
In Sections 3.2.1 and 3.2.2 we already presented some conjugates of enediynes with steroids and with lexitropsins. In this section, we describe enediyne hybrids with other natural products.

The enediyne class of anticancer antibiotics such as calicheamicin (**102**)[73] and dynemicin A (**223**)[74] has engendered excitement under chemists, biologists, and medical doctors owing to their unique structure, their unprecedented mechanism of action, and their high biological activity. Several efforts have been made to mimic, combine, or even outperform the biological actions of these natural products. In one attempt, the oligosaccharide fragment of calicheamicin γ^{I}_{1} (**102**) was combined with either the dynemicin substructure **224** or its enantiomer (as the "warhead" and triggering device) to give the complex hybrids **225** and **226**, respectively.[75] The evaluation of the anticancer activity of

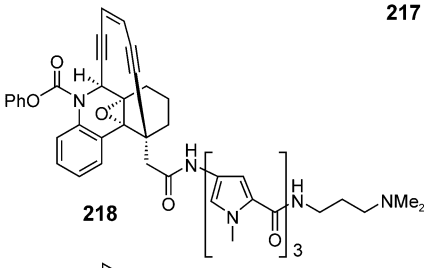
 © 2003 Wiley-VCH Verlag GmbH & Co. KGaA, Weinheim



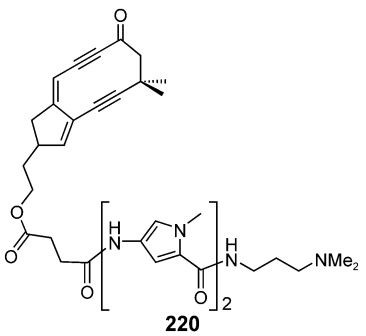
216: Makaluvamine A



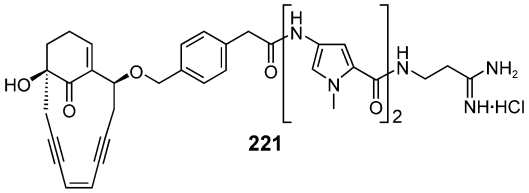
217



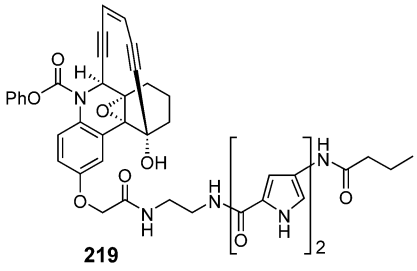
218



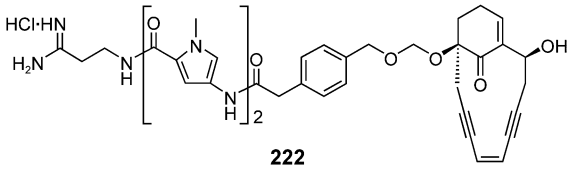
220



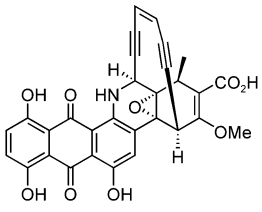
221



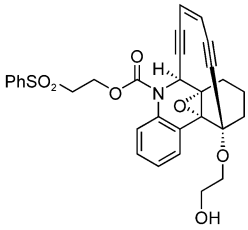
219



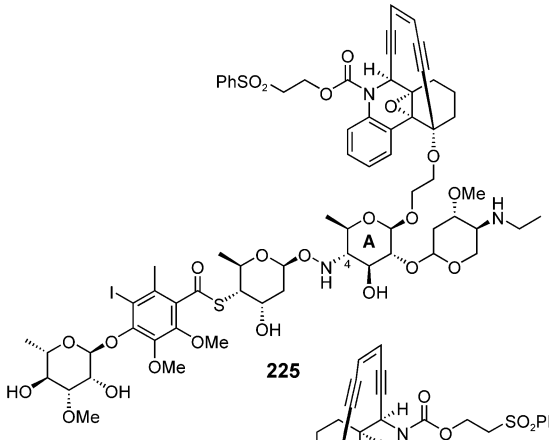
222



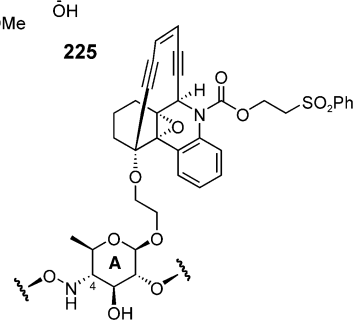
223: Dynemicin A



224



225

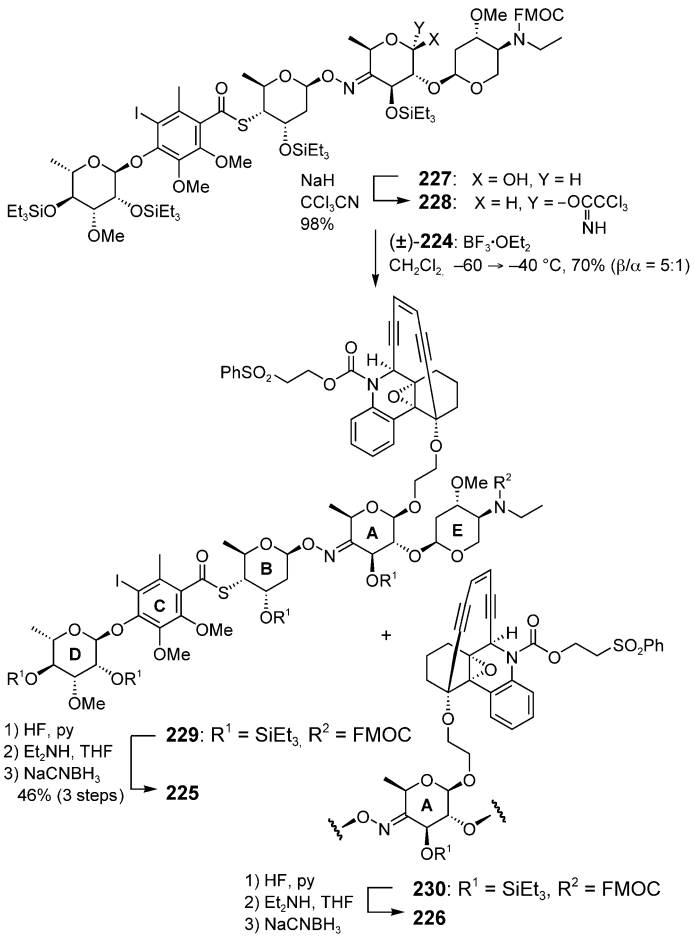


226

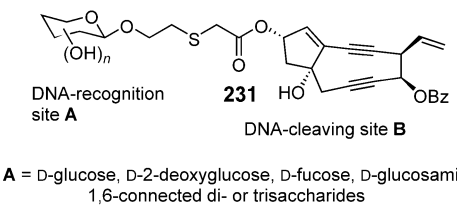
225 as well as of **226** (containing the enantiomer of **224**) against Molt-4 T-cell leukemia resulted in an gave IC_{50} values of approximately 0.1 and 1 nM, respectively; against UCLAP-3 lung carcinoma cells, IC_{50} values of about 0.16 μM and 78 nM, respectively, were observed. Thus, the natural enantiomer **224** is much more effective than its non-natural enantiomer. This finding is not quite surprising, but in some anticancer agents, such as CC-1065 (**135**) or the duocarmycins, both enantiomers have nearly the same activity. A much more pronounced difference in the biological activity as a result of different stereochemistries was found for the anomeric derivatives of **225** and **226** (the α-glycosides with respect to ring A); in this case, no significant biological effect was observed.

For the synthesis of the β-glycoside hybrids **225** and **226**, as well as of their corresponding α-glycosides, the protected oligosaccharide **227**[76] was converted into the corresponding trichloroacetimidate **228** and then coupled with the racemic **224**[77] in the presence of $BF_3{\cdot}OEt_2$. A mixture of four diastereomers (**229**, **230**, and their A-ring anomers) was obtained, with the β anomers **229** and **230** as the main products. The latter were then transformed into the desired hybrids and their C4 (ring A) epimers by following the sequence of reactions shown in Scheme 19.

A combinatorial approach to building a whole library of hybrids **231**, which incorporates a neocarzinostatin-like chromophore and various monosaccharides and 1,6-connected disaccharides and trisaccharides, made use of a new silyl linker (see **232**, Scheme 20), which was elaborated from 4-pentenoic acid.[78] The (2-sulfanylethyl)glycosides **232** were supported on a polymer through this silyl linker and then coupled with the enediyne by *S*-alkylation of the bromoacetate group of **233**. The hybrids **234** were then cleaved from the



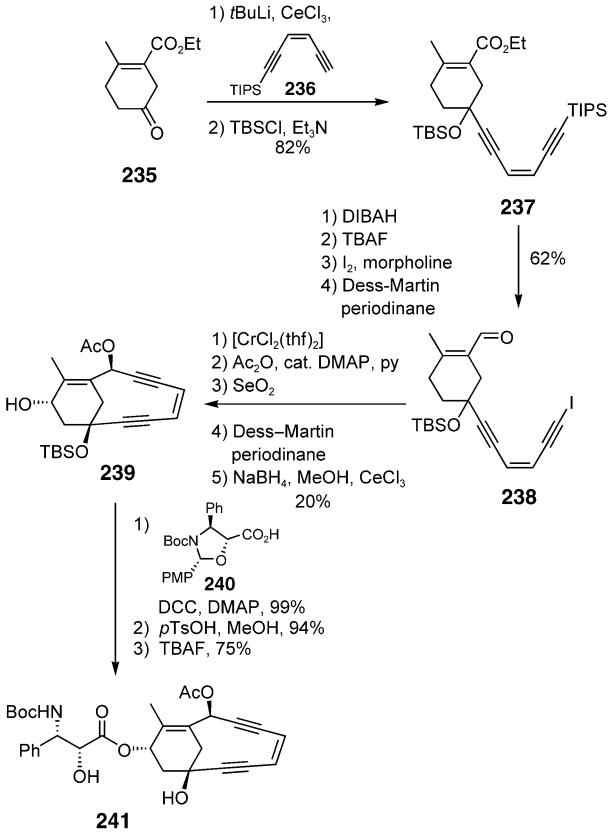
Scheme 19. Synthesis of calicheamicin–dynemicin hybrids **225** and **226**.



A = D-glucose, D-2-deoxyglucose, D-fucose, D-glucosamine, 1,6-connected di- or trisaccharides

polymeric support (Scheme 20). Biological tests of the new hybrids have not been disclosed yet.

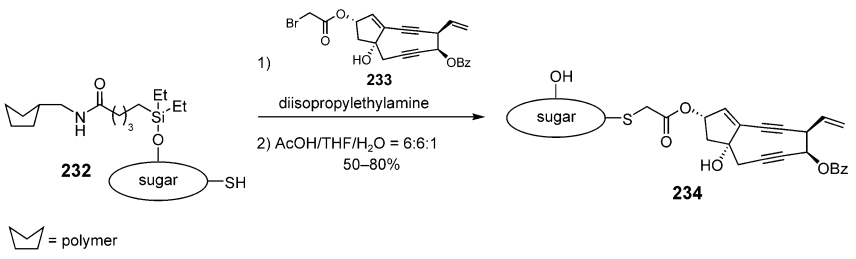
The hybrid **241** was designed in the hope that it would combine the tubulin-binding action of paclitaxel (taxol) and docetaxel (taxotere) with the cell-damaging effect of esperamicin and calicheamicin.[79] The synthesis is shown in Scheme 21 and involved the addition of the cerium acetylide of **236** to ketoester **235**, a Cr-catalyzed ring closure, and esterification with the oxazolidine **240** as the protected form of the docetaxel side chain. The hybrid **241** displayed only negligible effects on tubulin polymerization. Its cytotoxic activity was also relatively weak (70% cell death at 100 μM with the HT-29 human cancer cell line).



Scheme 21. Synthesis of the paclitaxel–esperamicin hybrid taxamicin (**241**).

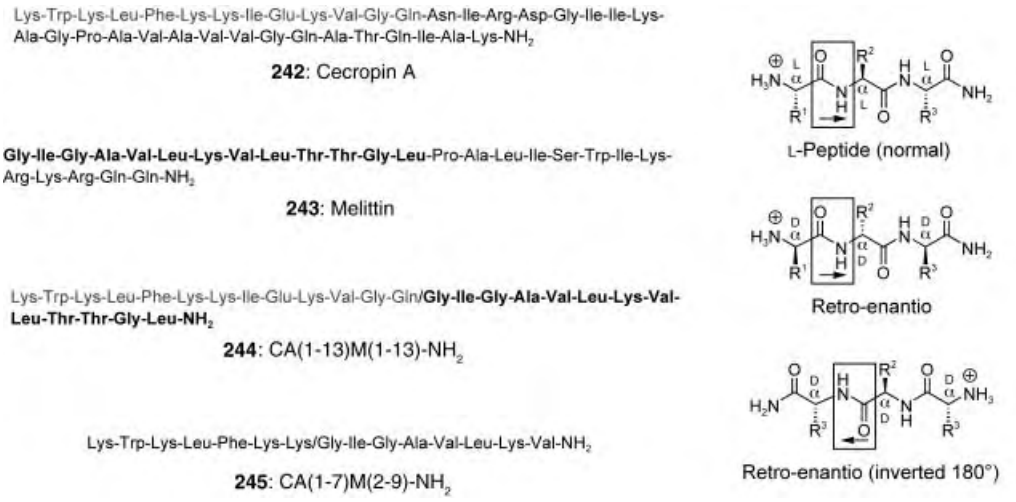
3.2.4. *Hybrids with a Peptide Substructure*

The synthesis of peptidic hybrids has also attracted some attention. Thus, hybrids of cecropin A (**242**)[80] and melittin (**243**),[81] two potent peptide antibiotics isolated from insects and pigs and from honeybees, respectively, were synthesized in a recent study (Scheme 22).[82] All analogues of CA(1-13)M(1-13)-NH_2 were as biologically active as the parent compounds against five bacterial strains. Surprisingly, even the retro and the retro-enantio derivatives, which are made up of the same amino acids as the natural peptide but in the other direction or with the opposite configuration, showed no significant loss of activity in most cases. It was concluded that the stereochemistry



Scheme 20. Solid-phase synthesis of carbohydrate–neocarzinostatin hybrids **234**.

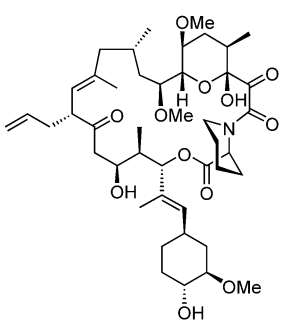
 © 2003 Wiley-VCH Verlag GmbH & Co. KGaA, Weinheim



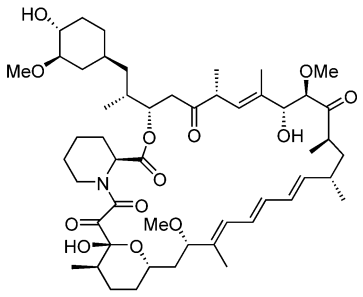
Scheme 22. Peptide sequence of cecropin A (**242**) and melittin (**243**), as well as of hybrids **244** and **245**.

of the peptide was not a critical feature, and full activity could be achieved with peptides containing either all-L- or all-D-amino acids in their respective right-handed or left-handed helical conformations.

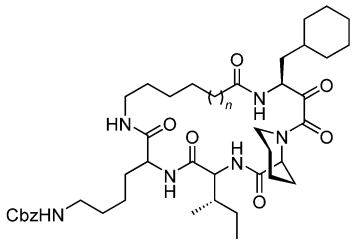
A possible explanation for the biological activity of some natural products is the assumption that the molecule mimics an endogenous peptide substance and thus exerts its action by binding to the corresponding receptor. This has long been proposed for the alkaloid morphine, which mimics the encephalin peptides. There is now some evidence that the natural macrocycle FK506 (**7**),[83] which shows high immunosuppressive and anticancer activity, uses nonpeptide structural elements to bind to its intracellular FKBP12 receptor. To gain some insight into the binding of this compound and rapamycin (**8**),[84] another potent immunosuppressor, to immunophilin receptors, several cyclic FK506 hybrids **246**–**248** were synthesized[85] in which parts of the compound were replaced by a peptide moiety. This approach is different from the well-known design of peptidomimetics in which an active peptide is mimicked by, for example, an N-heterocycle to avoid enzymatic cleavage by peptidases. For the synthesis of the hybrids **246**–**248**, tethers of variable lengths were introduced through a macrocyclization protocol. Interestingly, the X-ray crystallographic studies of the complex of the receptor with hybrid **247** show a nearly identical overall protein topology to that observed in the FKBP12–FK506 complex. However, as expected, the affinities of the hybrids **246**–**248** for the receptor were considerably lower than that of FK506 (**7**).



7: (–)-FK506 (tacrolimus)



8: (–)-Rapamycin

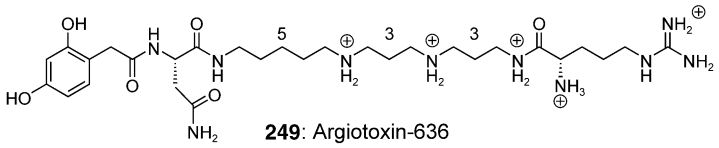


246: $n = 1$
247: $n = 2$
248: $n = 3$

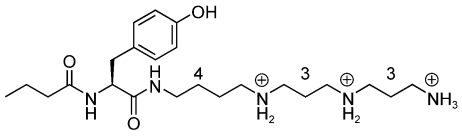
Glutamate receptors (Glu-R) comprise a class of excitatory amino acid receptors involved in signal transduction in the central nervous system of vertebrates.[86] Argiotoxin-636 (**249**, ArgTX, $M_r = 636$) is one of the polyaminoamides isolated from the venom of the spider *Argiope* and is a strong antagonist of Glu-R.[87] Philanthotoxin-433 (**250**, PhTX, numerals denote the number of methylene groups in the polyamine part) is the most active component of the venom of the solitary digger wasp, *Philanthus triangulum F.*[88] The observation that structural variations such as sequence and length of polyamine sequences and the nonpolyamine structures are major factors for the potency of Glu-R antagonists led to the design of ArgTX–PhTX hybrids **251**–**254**. In **254**, the 2,4-dihydroxyphenylacetyl group from ArgTx-636 was replaced with the nonpolyamine portion of PhTX-343.[89]

The syntheses of these hybrids and other analogues were based on routine transformations starting from the appropriate α,ω-diamines and the corresponding phenylacetic or cinnamic acid derivatives.[90] To measure the inhibitory activities of the hybrids, skeletal muscles of locusts were used as they are rich in glutamate receptors that are sensitive to quisqualate (QUIS-R). All these compounds antagonize

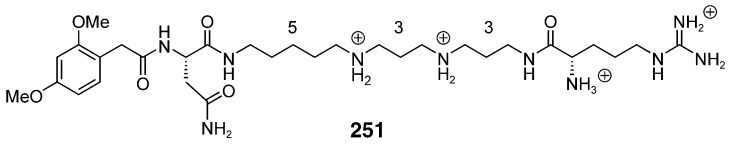
 © 2003 Wiley-VCH Verlag GmbH & Co. KGaA, Weinheim



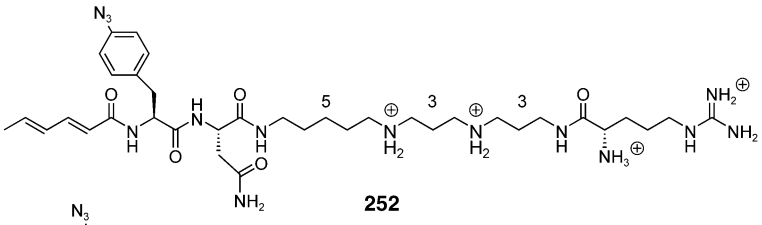
249: Argiotoxin-636



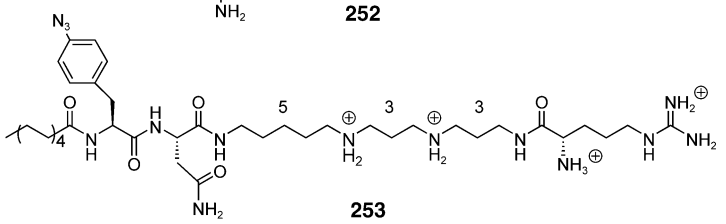
250: Philanthotoxin-433 (PTX433)



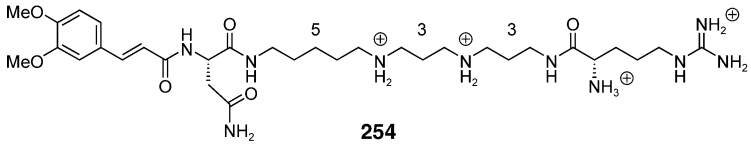
251



252



253



254

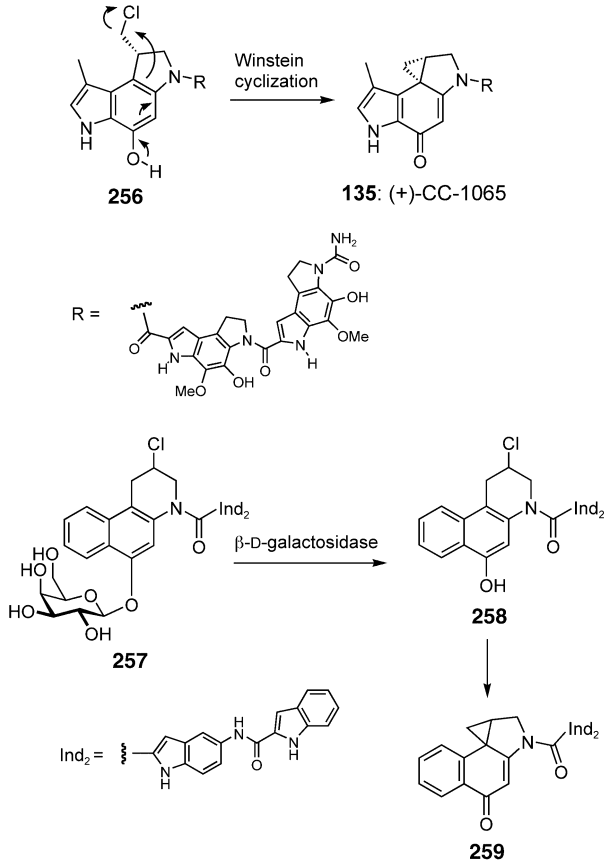
QUIS-R reversibly; **253** and **254** exhibit the highest activity (Table 7). After UV irradiation of the muscle preparations, which contained **252** or **253** with an azide moiety as a photoaffinity label, the antagonists became irreversible.

Table 7: Activity of ArgTX-636/PhTX-343 hybrids in a locust skeletal muscle assay against quisqualate-sensitive glutamate receptors (QUIS-R).

Compound	IC_{50} [μM]	Relative activity
PhTX-343	23	1
251	2.9	8
252	2.9	8
253	1.4	16
254	1.5	15

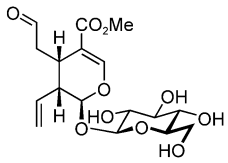
3.2.5. *Hybrids with a Carbohydrate Substructure*

As the transformation of the seco derivative **256** into the above-mentioned anticancer antibiotic CC-1065 (**135**), which includes an alkylating spirocycle) by a Winstein cyclization requires a free phenolic hydroxy group in the *para* position, it was proposed to protect this position with a sugar that should be cleavable selectively at the tumor site, but not in the rest of the body (Scheme 23).[91] Carbohydrates are also often used



Scheme 23. Winstein cyclization of seco analogues of CC-1065 (**135**). Enzymatic activation of the prodrug **257** to release the CC-1065 analogue **259**.

in Nature as protecting groups, for instance, in the case of secologanin (**255**). The latter is a hybrid of a monoterpene and glucose and is a key intermediate in the biosynthesis of the secoiridoids as well as of the indole, ipecacuanha, cinchona, and pyrroloquinoline alkaloids.[92]



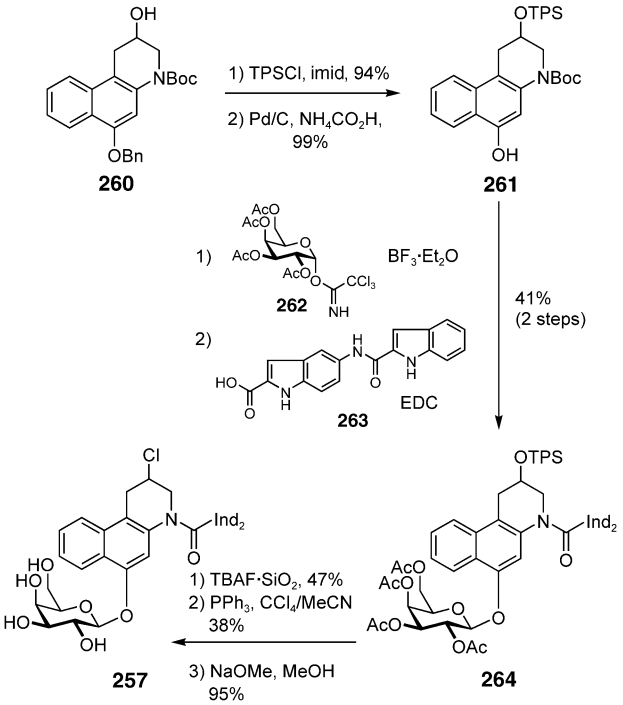
255: Secologanin

The selective and focused drug release from of a relatively nontoxic prodrug based on a seco CC-1065 analogue might be possible by using a conjugate of a monoclonal antibody that binds to tumor-associated antigens with an enzyme that performs the desired deprotection under physiological conditions. The prodrug **257**, a hybrid of galactose and a seco analogue of CC-1065, was developed for this purpose.[93] The enzymatic removal of the sugar moiety in **257** leads to the phenol **258**, which then cyclizes to give **259** (Scheme 23). Prodrug **257** was found to be much less cytotoxic than **259** or **257** in cultures of malignant

 © 2003 Wiley-VCH Verlag GmbH & Co. KGaA, Weinheim

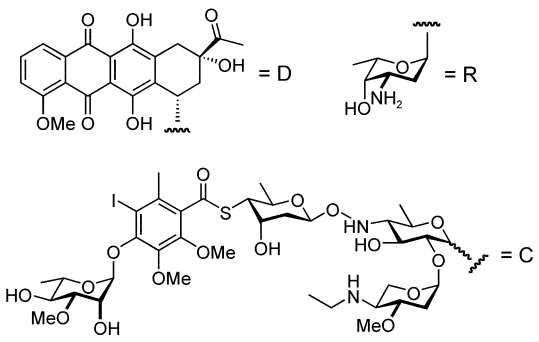
cells in the presence of galactosidase. Thus, in a cellular cytotoxicity assay, upon exposure to A549 cancer cell lines and the human pancreatic ductal adenocarcinoma cell line PancTu1, the prodrug **257** show IC_{50} values of 320 nM and 410 nM, respectively, whereas in the presence of β-D-galactosidase, IC_{50} values of 0.2 nM and 0.13 nM, respectively, were found. These results correspond to a selectivity factor of 1600 for the cell line A549 and of 3140 for the cell line PancTu1. In addition, treatment of a human bronchial carcinoma (A549) in a SCID mouse model with the prodrug **257** and a conjugate of galactosidase with a monoclonal antibody that binds to human epithelial cells showed complete remission of the tumor in several cases without any toxic effects on the mice.

The prodrug **257** was prepared from the racemic alcohol **260**, which was first transformed into a silyl ether (Scheme 24). Subsequently, the phenol moiety was deprotected by using Pd/C and ammonium formate as hydrogen source to give **261**, which was glycosylated with **262**, the trichloroacetimidate of tetraacetylgalactose, in the presence of $BF_3{\cdot}Et_2O$.[94] Under these conditions, the Boc group was also cleaved, and the resulting free amine was coupled with bisindolylcarboxylic acid **263** to afford **264**. The bisindolyl moiety from **263** serves as a DNA binder. Deprotection of the secondary alcohol, substitution of the hydroxy group with a chlorine atom,[95] and subsequent saponification led to the desired hybrid **257**.

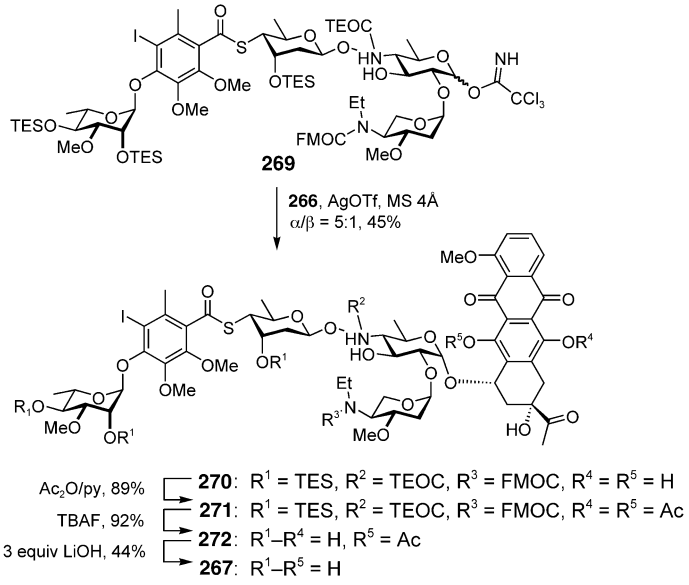


Scheme 24. Synthesis of the prodrug **257** for cancer therapy.

Another such hybrid was prepared by combining the calicheamicin sugar motif and the aglycon **D** of daunorubicin (**265**), an anthracycline antibiotic.[96] Daunorubicin (**265**) as well as the similar adriamycin (**86**) are potent anticancer agents that were isolated from *Streptomyces peucetius*.[97] For the synthesis of the hybrids calichearubicin A (**267**) and calichearubicin B (**268**), the trichloroacetimidate donor **269** ($\alpha/\beta = 5{:}1$) was used in the glycosylation of daunorubicinone (**266**) in the presence of Ag(OTf) (Scheme 25). Acetylation of the phenolic hydroxy groups, deprotection of the sugar moiety, and subsequent saponification led to **267**. A similar method was used to prepare calichearubicin B (**268**).



265: Daunorubicin, D-O-R
266: Daunorubicinone, D-OH
267: Calichearubicin A, α-C-O-D
268: Calichearubicin B, β-C-O-$(CH_2CH_2O)_2$-D



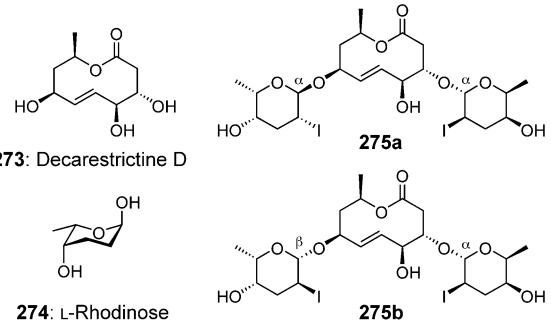
Scheme 25. Synthesis of the calicheamicin–daunorubicin hybrid, calichearubicin A (**267**). MS = molecular sieves.

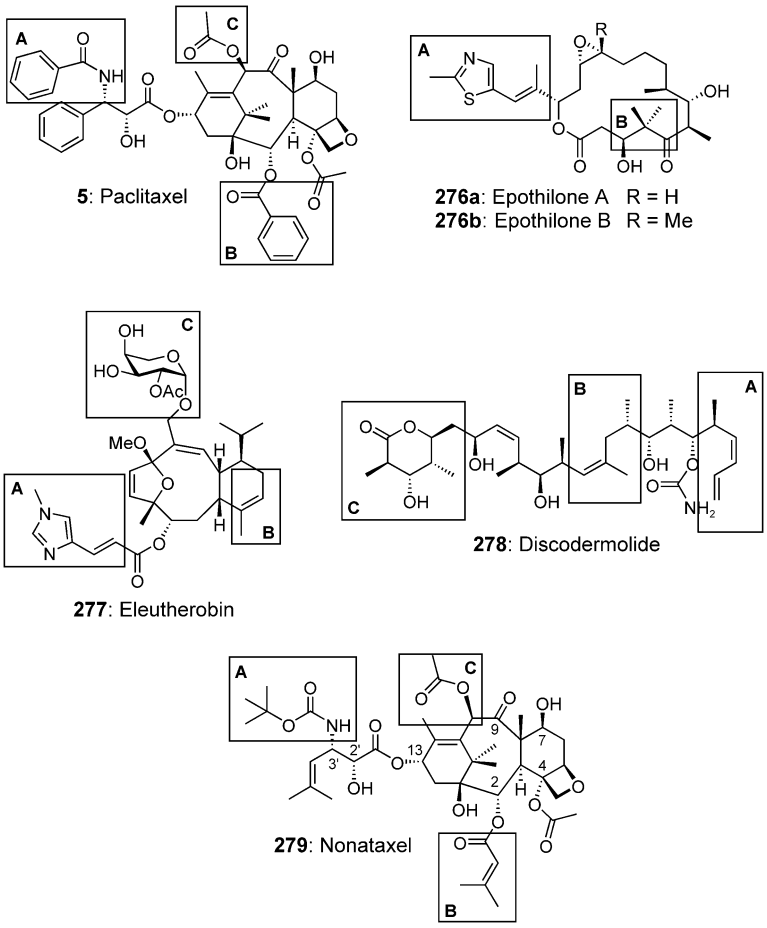
The measurement of UV absorption is used in the determination of the interactions of compounds with DNA.[98] As there is no substantial difference between the chromophores of daunorubicin (**265**) and its hybrids, the bathochromic shift of the hybrids in the presence of DNA allowed a comparison of the degree of intercalation. Whereas daunorubicin (**265**) evoked a red shift of 29 nm, compound **267** without a spacer did not display a measurable difference in the absorption maxima in the presence and absence of DNA. In contrast, compound **268** showed nearly the same result as daunorubicin; thus, as predicted by molecular

 © 2003 Wiley-VCH Verlag GmbH & Co. KGaA, Weinheim

modeling and NMR-based minimization studies, a β-glycosidic five-atom-spacer such as the ethoxy ethyl tether seems to allow a better intercalation into and interaction with the minor groove of DNA.

As the number of pathogens that are resistant towards existing antibiotics increases, the construction of new therapeutic agents by hybridization is regarded as an important approach in this field. The glycosylation of decarestrictine D (**273**), a naturally occurring 10-membered lactone with an iodo derivative of L-rhodinose (**274**), one of the rare sugars commonly found as constituents of angucycline antibiotics, led to the formation of the anomeric glycosides **275a** and **275b**.[99] In preliminary tests, these hybrids displayed DNA-binding properties.





3.2.6. *Hybrids with a Microtubule-Stabilizing Substructure*

Several natural products such as paclitaxel (taxol, **5**), eleutherobin (**277**), epothilone A (**276a**), epothilone B (**276b**), and discodermolide (**278**) as well as nonataxel (**279**), a nonaromatic analogue of paclitaxel (**5**), can induce the stabilization of microtubules, thus leading to mitotic arrest. Paclitaxel (taxol, **5**) is a particularly striking example, as it is a powerful agent in the treatment of cancer. Although the structures of **5** and **276–279** are quite dissimilar, it was proposed that as they all share a similar mode of action, they all might have a common pharmacophore that binds to the same receptor. Based on this idea, a hybrid construct SB-TE-1120 (**280**) was developed which demonstrated cytotoxic and tubulin-binding activity.[100] The construct **280** exhibited an IC_{50} value of 0.39 μM against the human breast cancer cell line MDA-435/LCC6-WT; furthermore, it exhibited 37% of the activity of taxol in a tubulin-polymerization assay. Interestingly, the cytotoxicity and tubulin-binding ability of **280** shows a similar sensitivity to the steric bulk of the substituent at the C2α position as found for **279**. Further work is aimed at the development of a new generation of tubulin-directed anticancer agents.

The synthesis of **280** (SB-TE-1120) started from the baccatin derivative **281**. A nucleophilic ring opening with 2-allyloxyphenyl magnesium bromide (**282**) followed by protecting-group manipulations yielded **284** via **283** (Scheme 26). Coupling with the β-lactam **285** to give **286** and subsequent ring-closing metathesis with the ruthenium complex **287** provided an 18-membered macrocycle, from which the hybrid construct **280** could be released by deprotection with HF–pyridine.

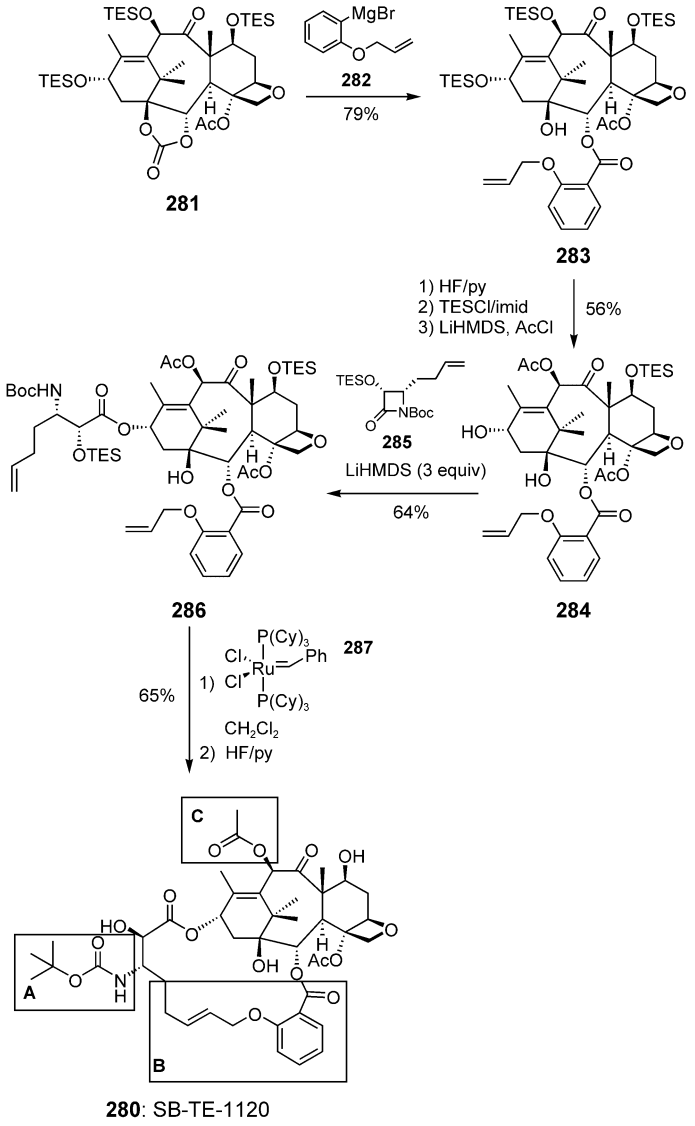
Another investigation involved the conjugate **289** of parts of discodermolide (**278**) and dictyostatin-1 (**288**) as another discodermolide-like macrocycle.[101] For comparison, a simplified analogue **290** of dictyostatin with an unfunctionalized alkyl chain bridging the lactone carbonyl group and the alkene was also prepared and tested. However, **290** showed only modest activity against a breast cancer and an ovary cancer cell line, whereas the hybrid **289**, which contains the more complex bottom part of dictyostatin-1 (**288**), was much more potent ($GI_{50} = 1.0–1.4$ μM). Furthermore, and unlike the analogue **290**, compound **289** displaced [^{3}H]paclitaxel stoichiometrically bound to microtubules at about one third of the potency of **278**. The synthesis involved the coupling of the three major building blocks **291**, **292**, and **293** through sequential Wittig transformations and a macrocyclization (Scheme 27).

3.2.7. *Hybrids with a Porphyrin Substructure*

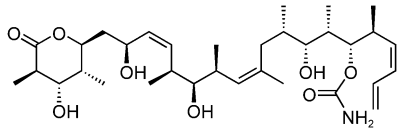
Although porphyrins are abundant in nature and play a dominant role in photosynthesis and in the respiratory chain, there are only a few examples up to now in which they were combined with other natural products.

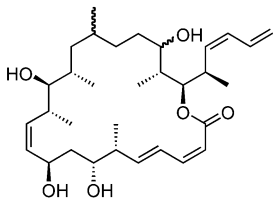
Some of these hybrids are aimed at photodynamic cancer therapy (PDT) and link porphyrins as a photosensitizer with

 © 2003 Wiley-VCH Verlag GmbH & Co. KGaA, Weinheim

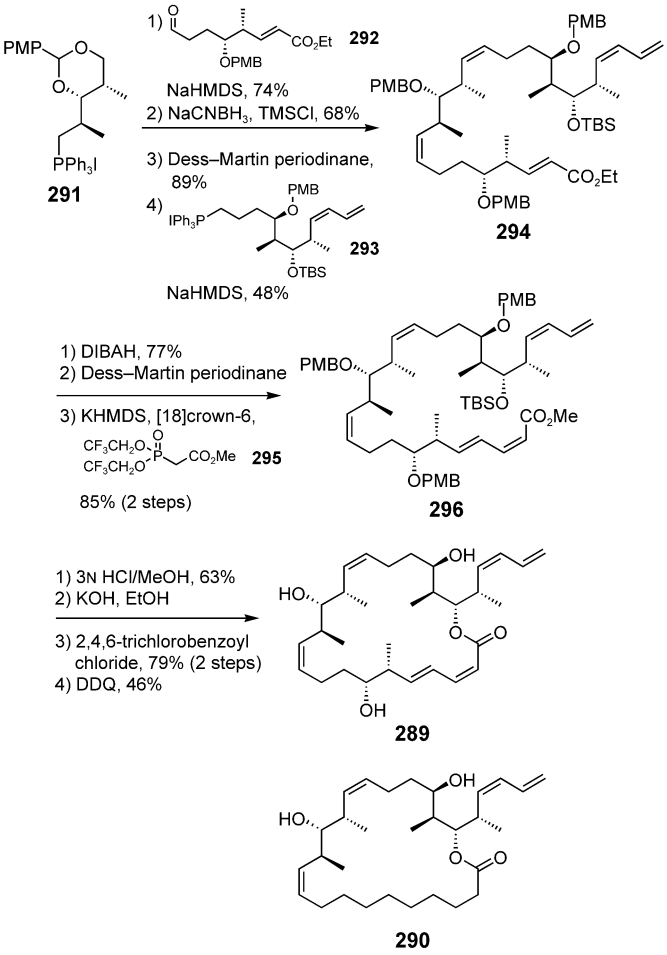


Scheme 26. Synthesis of hybrid **280**.





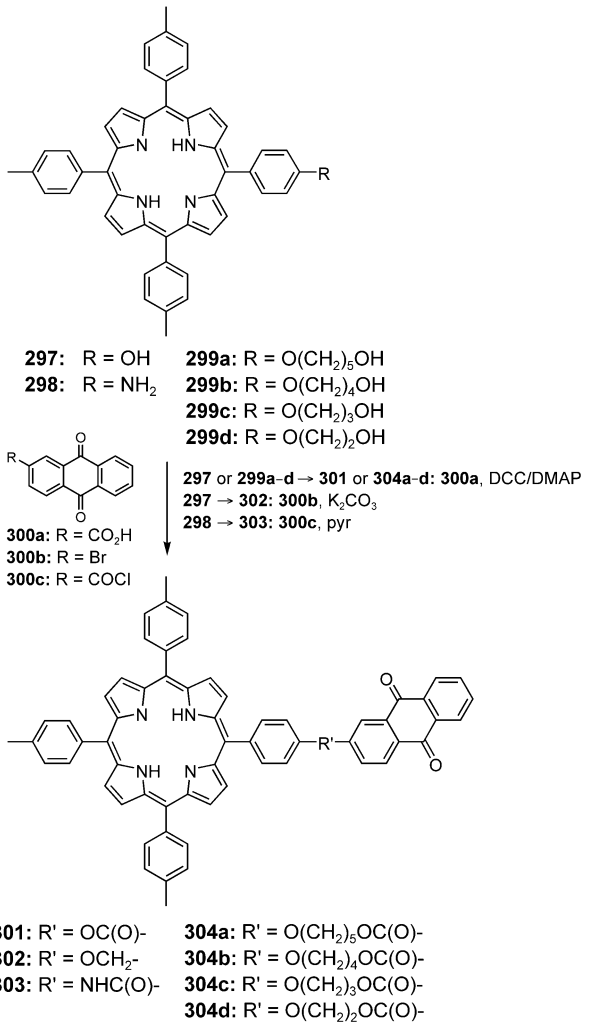
the DNA-binding or electron-transfer properties of other natural products. PDT is based on the activation of a photosensitizing drug with light to induce the production of cytotoxic $^1O_2$. Unfortunately, undesirable posttreatment phototoxic responses are observed quite often. Therefore a number of targeted-drug-delivery approaches are reported in the literature that combine photoactive porphyrins with moieties that bind selectively to DNA either by intercalation (e.g. acridinone, phenothiazine), binding to the minor groove (e.g. ellipticine), or by cross-linking (e.g. chlorambucil). Many natural anticancer drugs such as adriamycin (**86**) owe their potency to the electron transfer/H abstraction caused by an anthraquinone system. It thus seemed to be a promising approach to design hybrid molecules such as **301**–**304**, which comprise both structural entities.[102] The C2-functionalized anthraquinones **300** were combined with the corresponding porphyrin derivatives **297**–**299** to give the hybrids **301**–**304**, as shown in Scheme 28.



Scheme 27. Synthesis of the discodermolide–dictyostatin-1 hybrid **289**.

The fluorescence and singlet oxygen quantum yield data is lower for the hybrid compounds than for the reference compound **297** (Table 8). This might be attributed to a photoinduced electron transfer (PET). Interestingly, the hybrids act as wavelength-dependent DNA photonucleases.

Porphyrins also show in some cases a selective uptake into cancer cells. Therefore the combination of known potent anticancer agents such as paclitaxel (taxol, **5**) and ellipticine (**208**) with porphyrins might increase their selectivity. This



Scheme 28. Synthesis of the anthraquinone–porphyrin hybrids **301**–**304**.

was the rationale for the synthesis of the hybrids **305**[103] and **306**–**308**).[104] Data concerning the biological activity of these compounds is not available.

3.2.8. *Miscellaneous Hybrid Molecules*

Many acetogenins isolated from the *Annonaceae* (custard apple) family show interesting antitumor, immunosuppressive, pesticidal, and antimicrobial activities.[105] The characteristic feature of these compounds, for example, squamocin D (**309**)[106] and mucocin (**310**),[107] is a central ether unit that consists either of two tetrahydrofuranyl groups or of a tetrahydropyranyl group.

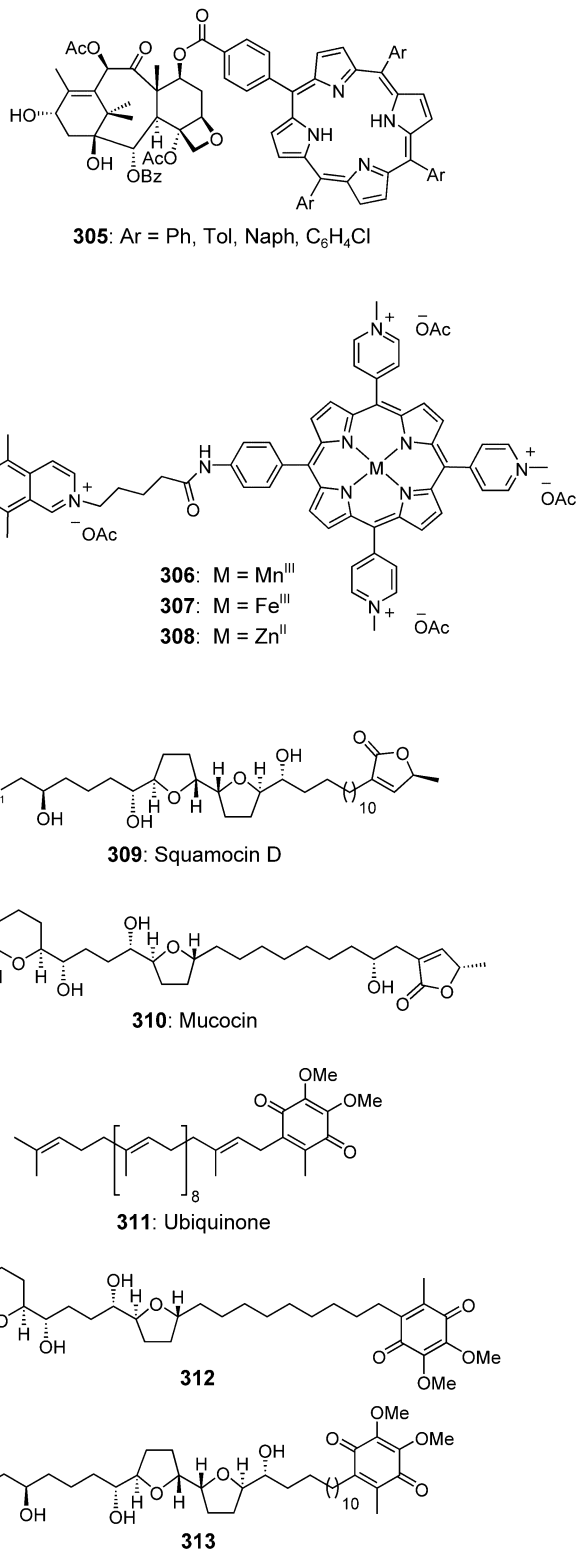


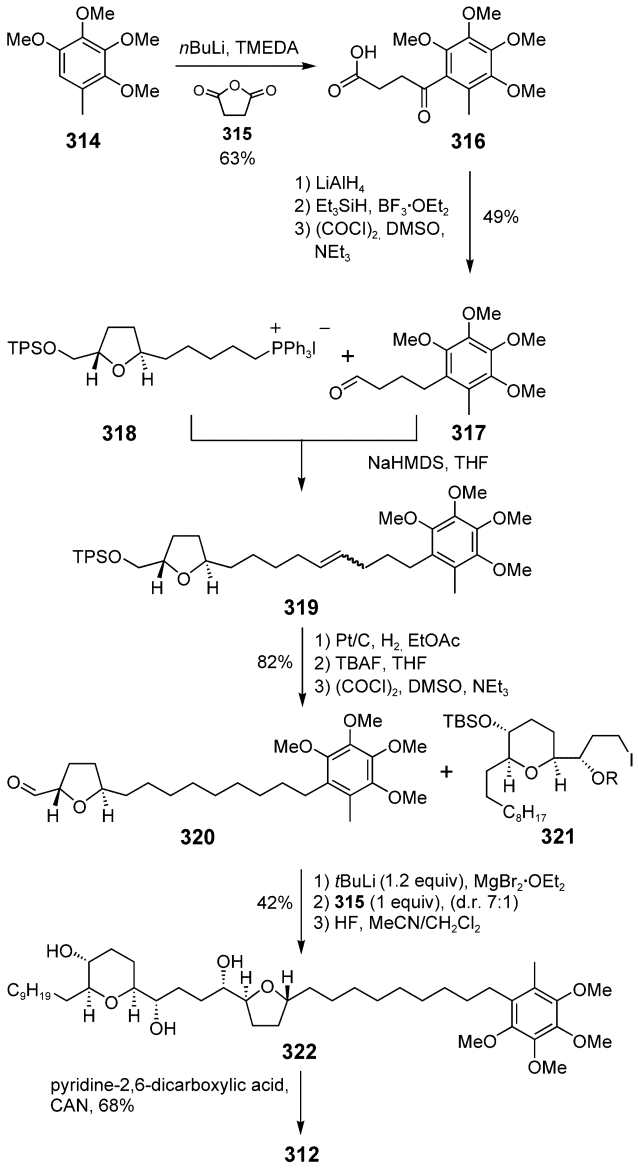
Table 8: Fluorescence (Φ_f) and singlet oxygen ($\Phi(^1O_2)$) quantum yield data for **297** and the hybrids **301**–**304**.

Compound	**297**	**301**	**302**	**303**	**304a**	**304b**	**304c**	**304d**
Φ_f	0.13	0.037	0.090	0.013	0.053	0.056	0.041	0.047
$\Phi(^1O_2)$	0.65	0.43	0.65	0.49	0.49	0.50	0.43	0.46

 © 2003 Wiley-VCH Verlag GmbH & Co. KGaA, Weinheim

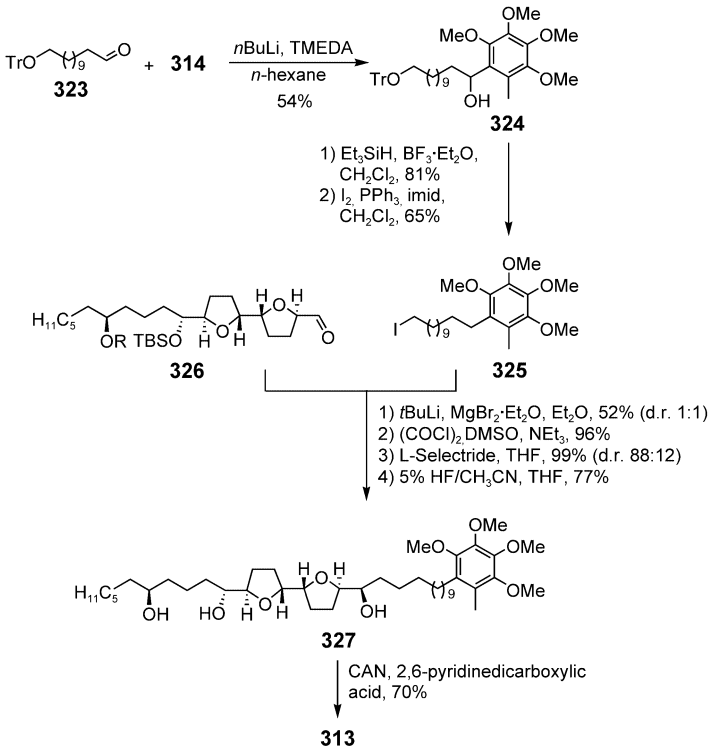
This central ether unit is flanked on both sides by two long alkyl chains, one of which bears a butenolide unit at the end. The mode of action is believed to be the blockage of the mitochondrial complex I (NADH: ubiquinone oxidoreductase).[108] For a better understanding and also to modify the activity, two hybrids **312** and **313** were designed as probes for studies with complex I. The hybrids **312** and **313** contain the quinone portion of the natural complex I substrate ubiquinone (**311**) instead of the α,β-unsaturated γ-butyrolactone found in the original acetogenins.[109a]

The synthetic strategy towards **312** involved the three building blocks **317**, **318**, and **321** (Scheme 29). The first, which was intended to become the quinone later on, was built from 2,3,4,5-tetramethoxytoluene (**314**)[110] by the addition of the lithiated species to succinic anhydride (**315**). The obtained γ-ketocarboxylic acid **316** was then transformed over three steps into the corresponding aliphatic aldehyde **317**, which was coupled in a Wittig olefination with the furan derivative **318** as the second building block.[109c] Hydrogenation, deprotection, and Swern oxidation yielded another aldehyde **320**, which was coupled with the third building block, the iodide **321**, in a chelation-controlled Grignard addition.[109d] Finally, deprotection and oxidation of the hydroquinone ether **322** gave the hybrid compound **312**.



Scheme 29. Synthesis of the mucocin–ubiquinone hybrid **312**.

The synthesis of the second hybrid **313** also started from tetramethoxytoluene **314** (Scheme 30). This time, the corresponding organolithium compound obtained from **314** was added to the dodecanal **323** to give **324**. The resulting alcohol and the trityl group were then removed simultaneously with $Et_3SiH/BF_3{\cdot}OEt_2$. Further transformation yielded the iodide **325**, which was added as the corresponding lithium compound to the bisfuran aldehyde **326**. Oxidation, followed by stereoselective reduction and deprotection provided compound **327**, which was oxidized with CAN to give the desired hybrid **313** with a ubiquinone moiety. Both hybrids **312** and **313** as well as some other compounds were examined in complex I-inhibition studies (Table 9). The quinone–mucocin **312** exhibited a K_{i50} value of 3.6 nM, about tenfold more active than mucocin (**310**) itself. In contrast, quinone–squamocin D **313** was slightly less potent than squamocin A.[109b]



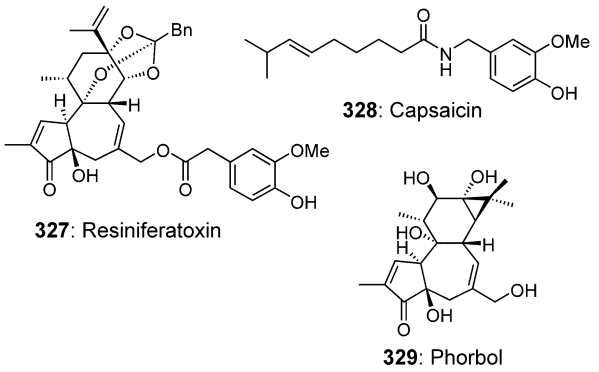
Scheme 30. Synthesis of the squamocin D–ubiquinone hybrid **313**.

Resiniferatoxin (RTX, **327**)[111] is a daphnane diterpene isolated from the resin of *Euphorbia resinifera*. RTX exhibits a unique mechanism of action and is under clinical trials for the relief of pain associated with diabetic neuropathy.[112] The discovery that RTX can be considered as a complex analogue of capsaicin (**328**), the pungent principle of hot pepper, led to the characterization of a specific receptor, whose activation

 © 2003 Wiley-VCH Verlag GmbH & Co. KGaA, Weinheim

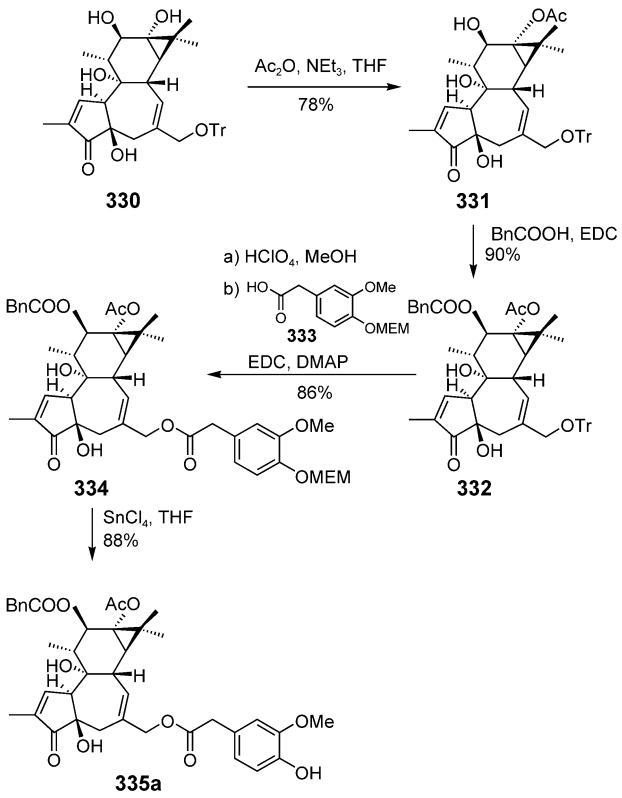
Table 9: Inhibition of the mitochondrial complex I by natural acetogenins and quinone–natural product hybrids **312** and **313**.

Compound	K_{i50} [nM]	IC_{50} [μmol mg^{-1} protein]	IC_{50} [μmol mg^{-1} protein]
squamocin A	1.0	1.3	
309			8.7
310	34	45	33.3
312	3.6	4.9	
313	1.7	2.3	
322	123	163	
327	4.7	6.2	
rotenone	1.0	1.3	



causes desensitization to capsaicin.[113] Both compounds share a vanillyl moiety and thus the receptor was named the vanilloid receptor. As RTX (**327**) is not readily available in the required quantities, the resiniferatoxin–phorbol hybrids **335a–f** were synthesized, in which the structurally similar core of phorbol (**329**) was combined with the homovanillyl moiety of RTX. For the synthesis of **335a**, phorbol (**329**) was protected at the primary alcohol site as a trityl ether to give **330**. The tertiary hydroxy function at the cyclopropane group of **330** was then protected as an acetate to form **331**. Finally, protection of the secondary hydroxy group of **331** provided phenyl acetate **332** (Scheme 31). After acid-catalyzed deprotection of the primary alcohol, esterification with the MEM-protected homovanillic acid **333** provided compound **334**, which upon cleavage of the MEM ether group, furnished the phorbol–RTX hybrid **335a**. Even though **335a** was not the initially envisaged compound, it turned out to be very interesting for the study of the vanilloid receptor: **335a** and several analogues **335b–f** showed a binding affinity to the vanilloid receptor comparable to that of capsaicin (Table 10).[114] However, one should bear in mind that capsaicin (**328**) is much simpler in structure than the hybrids **335** and that the activity of resiniferatoxin (**327**) is about 10000 times higher.

As already mentioned, one of the main problems in the treatment of infectious diseases caused by bacteria is the development of resistance of these organisms to the available antiinfective agents. Therefore several hybrids **340–344** were prepared in which the structural entities of well-known antibiotics such as chloramphenicol (**336**) (from *Streptomyces*



Scheme 31. Synthesis of the phorbol–RTX hybrid **335a**.

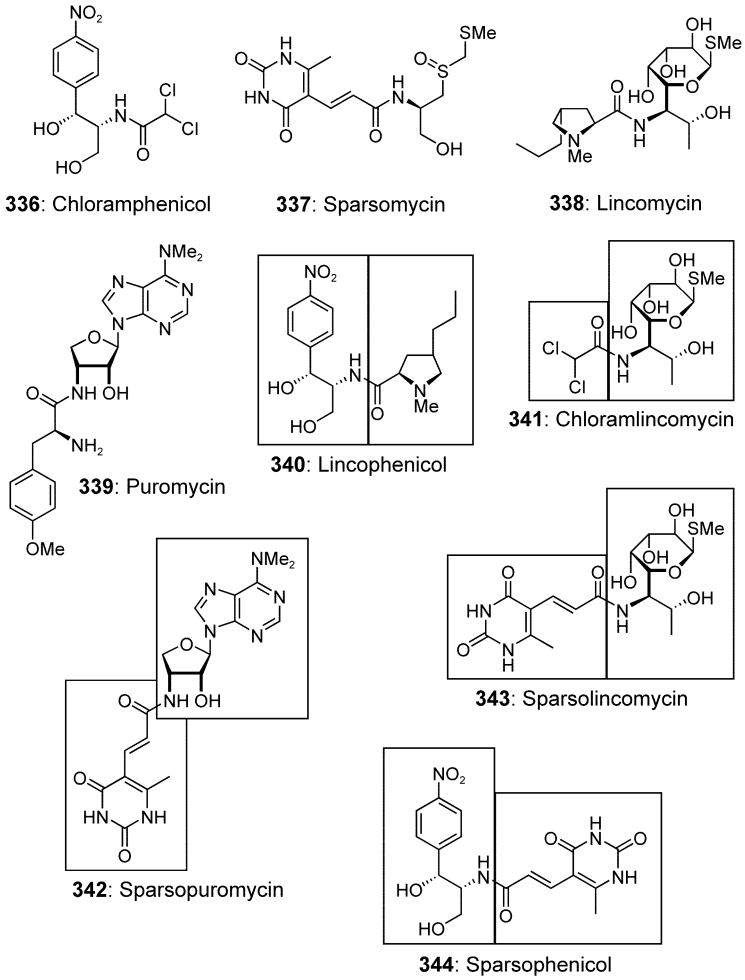
Table 10: Binding affinity to vanilloid receptors of the phorbol–RTX hybrids **335a–f** relative to RTX (**327**) and capsaicin (**328**).

Compound	R	Affinity K_i [μM]
335a	Bn	0.6 ± 0.3
335b	Ph	0.4 ± 0.2
335c	*p*-N_3PhCH_2	0.2 ± 0.1
335d	*p*-N_3Ph	0.2 ± 0.2
335e	$C_6H_{11}CH_2$	0.4 ± 0.1
335f	C_6H_{11}	2.2 ± 0.1
327	–	2×10^{-5}
328	–	2.0 ± 0.2

venezuelae), sparsomycin (**337**) (from *Streptomyces sparsogenes*), lincomycin (**338**) (from *Streptomyces lincolnensis*), and puromycin (**339**) (from *Streptomyces alboniger*)[115] were combined. The synthesis involved a simple amidation of either the appropriate carboxylic acids or their active esters with suitable amines. Their potency as inhibitors of certain processes involved in prokaryotic and eukaryotic protein biosynthesis was investigated.

However, the results of the biological tests were not very promising. The only active hybrids in the cell-free systems investigated are lincophenicol (**340**) and sparsophenicol (**344**), both derived from chloramphenicol (**336**). All other hybrids were inactive. Astonishingly, chloramlincomycin (**341**), which was completely inert in all cell-free systems, was the only hybrid to exhibit an activity comparable to that of the parent antibiotic chloramphenicol (**336**) in the screen-

 © 2003 Wiley-VCH Verlag GmbH & Co. KGaA, Weinheim



ing for antimicrobial activity. It inhibited the growth of *Streptococcus pyogenes* with a minimum inhibitory concentration (MIC) of 6.25 $\mu g\,mL^{-1}$. There are two reasons for the observation that the hybrids **340** and **344** were almost inactive, although they exhibited inhibitory activity in the *E. coli* and rat liver ribosome systems: either they do not penetrate the cell membrane through the active transport systems of the parent antibiotics and/or they are unable to inhibit the protein synthesis in the intact cells. Further investigations are necessary to shed some light on this problem.

4. Conclusion

In the fight against disease, society depends on the development of new biologically active compounds. One of the new approaches towards this goal is the development of natural product hybrids, of which nearly unlimited numbers can be accessed by the combination of fragments of naturally occurring substances. The advantage of this concept over combinatorial chemistry is the high diversity and the inherent biological activity of the hybrids. As this approach is rather new, only a small number of combinations have been explored, mainly for the development of new anticancer agents and antibiotics. Several of the new hybrids show promising activity, which in some cases exceeds that of the parent compounds. Thus, even a critical view would arrive at the conclusion that we have a promising approach in hand for the development of new lead structures for bioactive compounds for medicine and agriculture. However, in most cases so far, the development of hybrids has followed a rational design. In future, the combinatorial synthesis of hybrids as well as their testing in many different assays should also play a role.

List of Abbreviations

Bn	Benzyl
Boc	*tert*-butoxycarbonyl
Bz	Benzoyl
CAN	Cerium(IV) ammonium nitrate
Cbz	Benzyloxycarbonyl
CI	Cyclopropaneindoline
CPI	Cyclopropanepyrroloindoline
Cy	Cyclohexyl
DBU	1,8-Diazabicyclo[5.4.0]undec-7-ene
DCC	*N*,*N*′-Dicyclohexylcarbodiimide
DDQ	2,3-Dichloro-5,6-dicyano-*p*-benzoquinone
DIBAH	Diisobutylaluminum hydride
DMAP	4-Dimethylaminopyridine
DMF	*N*,*N*-Dimethylformamide
DMSO	Dimethyl sulfoxide
EC_{50}	effective drug concentration (see ED_{50})
ED_{50}	effective drug dosage, at which 50% of the maximum activity occurs or at which 50% of the test candidates show a particular reaction
EDC	*N*-(3-Dimethylaminopropyl)-*N*′-ethylcarbodiimide
FMOC	9-Fluorenylmethoxycarbonyl
GI_{50}	Drug concentration at which 50% growth inhibition occurs
Glu-R	Glutamate-sensitive receptor
(H)ER	(Human) estrogen receptor
HMDS	Hexamethyldisilazide
HOBT	1-Hydroxy-1*H*-benzotriazole
HTCFA	Human tumor colony forming ability
HTS	High-throughput screening
IC_{50}	Drug concentration at which 50% inhibition (e.g. of an enzyme) occurs
IGF	Insulin-like growth factor
imid	Imidazole
Ind	Indole
iNOS	Inducible NO Synthase
K_{i50}	See IC_{50}
LDA	Lithiumdiisopropylamide
Lipase AK	Free lipase from *Pseudomonas fluorescens*
*m*CPBA	*m*-Chloroperbenzoic acid
MEM	2-Methoxyethoxymethyl
MIC	Minimum inhibitory concentration
Ms	Mesyl (methanesulfonyl)
NADH	Nicotinamide adenine dinucleotide, reduced form

 © 2003 Wiley-VCH Verlag GmbH & Co. KGaA, Weinheim

PBD	Pyrrolo[2,1-*c*][1,4]benzodiazepine
PCR	Polymerase chain reaction
PDT	Photodynamic therapy
PET	Photoinduced electron transfer
PMB	*p*-Methoxybenzyl
PPL	porcine pancreatic lipase
pybop	(Benzotriazol-1-yloxy)-tripyrrolidinophosphonium hexafluorophosphate
py	Pyridine
RTX	Resiniferatoxin
SCID	severe combined immunodeficiency
TBAF	Tetra-*n*-butylammonium fluoride
TBS	*tert*-Butyldimethylsilyl
TEOC	2-(Trimethylsilyl)ethoxycarbonyl
TES	Triethylsilyl
Tf	Trifluoromethane sulfonyl
TIPS	triisopropylsilyl
TMEDA	*N*,*N*,*N*′,*N*′-Tetramethylethylenediamine
TMS	Trimethylsilyl
TPS	*tert*-Butyldiphenylsilyl
Troc	2,2,2-Trichloroethoxycarbonyl
Ts	*p*-toluenesulfonyl

We thank the Deutsche Forschungsgemeinschaft (SFB 416), the Fonds der Chemischen Industrie (FCI), and the Bundesministerium für Bildung, Wissenschaft, Forschung und Technologie for the generous support of our work discussed in this review. The continuous gifts of chemicals by Aventis, BASF AG, Bayer AG, Degussa AG, Dragoco Gerberding & Co. AG, Eli Lilly & Co., Organon, Schering AG, Solvay Fluor und Derivate GmbH, and Wacker-Chemie GmbH are gratefully acknowledged. The authors also wish to thank M. Pretor for help with the preparation of this manuscript and S. Hellkamp for the cover design. Furthermore S.C. thanks the Alexander-von-Humboldt-Stiftung for a research grant. H.P.B. thanks the Fonds der Chemischen Industrie and the Studienstiftung des deutschen Volkes for a PhD scholarship.

Received: August 15, 2002 [A553]

[1] a) G. M. Cragg, D. J. Newman, K. M. Snader, *J. Nat. Prod.* **1997**, *60*, 52–60; b) G. A. Cordell, *Phytochemistry* **2000**, *55*, 463–480; c) A. Zeeck, G. Bach, H. Terlau, *Internist* **2001**, *42*, 1422–1427.

[2] J. Stetter, F. Lieb, *Angew. Chem.* **2000**, *112*, 1792–1812; *Angew. Chem. Int. Ed.* **2000**, *39*, 1724–1744.

[3] a) L. A. Thompson, J. A. Ellman, *Chem. Rev.* **1996**, *96*, 555–600; b) *Combinatorial Chemistry and Molecular Diversity in Drug Discovery* (Eds.: E. M. Gordon, J. F. Kerwin, Jr.), Wiley-Liss, New York, **1998**; c) L. F. Tietze, M. Lieb, *Curr. Opin. Chem. Biol.* **1998**, *2*, 363–371; d) *Combinatorial Chemistry: A Practical Approach, Methods and Principles in Medicinal Chemistry, Vol. 9* (Eds.: W. Bannwarth, E. Felder), Wiley-VCH, Weinheim, **2000**; e) F. Guillier, D. Orain, M. Bradley, *Chem. Rev.* **2000**, *100*, 2091–2158; f) P. Arya, M. Baek, *Curr. Opin. Chem. Biol.* **2001**, *5*, 292–301.

[4] a) *High Throughput Screening: The Discovery of Bioactive Substances* (Ed.: J. P. Delvin), Dekker, New York, **1997**; b) S. L. Schreiber, *Science* **2000**, *287*, 1964–1969.

[5] a) C. J. Tsoi, C. Khosla, *Chem. Biol.* **1995**, *2*, 355–362; b) C. Khosla, *Chemtracts* **1998**, *11*, 1–15; c) A. C. W. Waugh, P. F. Long, *Sci. Prog.* **2002**, *85*, 73–88; d) L. Katz, R. McDaniel, *Med. Res. Rev.* **1999**, *19*, 543–558; e) J. Staunton, *Curr. Opin. Chem. Biol.* **1998**, *2*, 339–345; f) R. McDaniel, S. Ebert-Khosla, D. A. Hopwood, C. Khosla, *Science* **1993**, *262*, 1546; g) J. Rohr, *Angew. Chem.* **1995**, *107*, 963–967; *Angew. Chem. Int. Ed. Engl.* **1995**, *34*, 881–885; h) A. I. Scott, *J. Nat. Prod.* **1994**, *57*, 557–573; i) E. Rodriguez, R. McDaniel, *Curr. Opin. Microbiol.* **2001**, *4*, 526–534.

[6] After submission of the manuscript, a review was published that touches parts of this topic: G. Mehta, V. Singh, *Chem. Soc. Rev.* **2002**, *31*, 324–334.

[7] H. Shiozawa, T. Kagasaki, T. Kinoshita, H. Haruyama, H. Domon, Y. Utsui, K. Kodama, S. Takahashi, *J. Antibiot.* **1993**, *46*, 1834–1842.

[8] Y. F. Hallock, J. H. Cardellina II, M. Schäffer, G. Bringmann, G. Francois, M. R. Boyd, *Bioorg. Med. Chem. Lett.* **1998**, *8*, 1729–1734.

[9] S. Tasler, G. Bringmann, *Chem. Rec.* **2002**, *2*, 113–126.

[10] G. R. Pettit, M. Inoue, Y. Kamano, D. L. Herald, C. Arm, C. Dufresne, N. D. Christie, J. M. Schmidt, D. L. Doubek, T. S. Krupa, *J. Am. Chem. Soc.* **1988**, *110*, 2006–2007.

[11] a) M. A. F. Jalal, M. B. Hossain, D. J. Robeson, D. van der-Helm, *J. Am. Chem. Soc.* **1992**, *114*, 5967–5971; b) K. Matsuzaki, N. Tabata, H. Tomoda, Y. Iwai, H. Tanaka, S. Omura, *Tetrahedron Lett.* **1993**, *34*, 8251–8254.

[12] a) D. J. Aberhart, Y. S. Chen, P. De Mayo, J. B. Stothers, *Tetrahedron* **1965**, *21*, 1417–1432; b) B. Franck, G. Baumann, *Chem. Ber.* **1966**, *99*, 3863–3874.

[13] A. Porzel, T. P. Lien, J. Schmidt, S. Drosihn, C. Wagner, K. Merzweiler, T. Van Sung, G. Adam, *Tetrahedron* **2000**, *56*, 865–872.

[14] L. M. Perry, *Medicinal Plants of East and Southeast Asia*, MIT-Press, Cambridge, MA, **1980**, p. 19.

[15] a) *Anthracycline antibiotics: New analogues, methods of delivery and mechanisms of action*: *ACS Symp. Ser.* **1995**, *574*; b) C. Monneret, *Eur. J. Med. Chem.* **2001**, *36*, 483–493.

[16] a) K. Suzuki, *Pure Appl. Chem.* **2000**, *72*, 1783–1786; b) T. Matsumoto, T. Hosoya, K. Suzuki, *J. Am. Chem. Soc.* **1992**, *114*, 3568–3570; c) S. Futagami, Y. Ohashi, K. Imura, K. Hosoya, K. Ohmori, T. Matsumoto, K. Suzuki, *Tetrahedron Lett.* **2000**, *41*, 1063–1067.

[17] S. D. Kuduk, F. F. Zheng, L. Sepp-Lorenzino, N. Rosen, S. J. Danishefsky, *Bioorg. Med. Chem. Lett.* **1999**, *9*, 1233–1238.

[18] F. F. Zheng, S. D. Kuduk, G. Chiosis, P. N. Münster, L. Sepp-Lorenzino, S. J. Danishefsky, N. Rosen, *Cancer Res.* **2000**, *60*, 2090–2094.

[19] a) J. Raus, G. Le Clercq, H. Martens in *Cytotoxic Estrogens in Hormone Receptive Tumors*, Academic Press, London, **1980**; b) G. Le Clercq, J. C. Heuson, *Anticancer Res.* **1981**, *1*, 217–228, and references therein; c) G. Le Clercq, J. C. Heuson, *Biochim. Biophys. Acta* **1979**, *560*, 427–455.

[20] T. Ojasoo, J. P. Raynaud, J.-P. Mornon in *Comprehensive Medicinal Chemistry, Vol. 3* (Eds.: C. Hansch, P. G. Sammes, J. B. Taylor, J. C. Emmett), Pergamon, Oxford, **1990**, p. 1175.

[21] a) D. Kunz, G. Walker, W. Eberhardt, J. Pfeilschifter, *Proc. Natl. Acad. Sci. USA* **1996**, *93*, 255–259; b) T. Honda, H. J. Finlay, G. W. Gribble, N. Suh, M. B. Sporn, *Bioorg. Med. Chem. Lett.* **1997**, *7*, 1623–1628.

[22] T. Honda, G. W. Gribble, *J. Org. Chem.* **1998**, *63*, 4846–4849.

[23] a) D. G. Lynn, N. J. Phillips, W. C. Hutton, J. Shabanowitz, D. I. Fennell, R. J. Cole, *J. Am. Chem. Soc.* **1982**, *104*, 7319–7322; b) for a review on spiroketals, see: F. Perron, K. F. Albizati, *Chem. Rev.* **1989**, *89*, 1617–1661.

 © 2003 Wiley-VCH Verlag GmbH & Co. KGaA, Weinheim

[24] L. F. Tietze, G. Schneider, J. Wölfling, T. Nöbel, C. Wulff, I. Schubert, A. Rübeling, *Angew. Chem.* **1998**, *110*, 2644 – 2646; *Angew. Chem. Int. Ed.* **1998**, *37*, 2469 – 2470.
[25] L. F. Tietze, G. Schneider, J. Wölfling, A. Fecher, T. Nöbel, S. Petersen, I. Schuberth, C. Wulff, *Chem. Eur. J.* **2000**, *6*, 3755 – 3760.
[26] R. J. D'Amato, C. M. Lin, E. Flynn, J. Folkman, E. Hamel, *Proc. Natl. Acad. Sci. USA* **1994**, *91*, 3964 – 3968.
[27] T. A. Miller, A. L. Bulman, C. D. Thompson, M. E. Garst, T. L. Macdonald, *J. Med. Chem.* **1997**, *40*, 3836 – 3841.
[28] A. J. Birch, G. S. R. S. Rao, *Tetrahedron* **1966**, Suppl. *7*, 391 – 395.
[29] F. De Riccardis, I. Izzo, M. Di Filippo, G. Sodano, F. D'Acquisto, R. Carnuccio, *Tetrahedron* **1997**, *53*, 10871 – 10882.
[30] a) K. K. Wang, *Chem. Rev.* **1996**, *96*, 207 – 222; b) R. L. Funk, E. R. R. Young, R. M. Williams, M. F. Flanagan, T. L. Cecil, *J. Am. Chem. Soc.* **1996**, *118*, 3291 – 3292; c) C. Meert, J. Wang, P. J. De Clercq, *Tetrahedron Lett.* **1997**, *38,* 2179 – 2182; d) J. Wang, P. J. De Clercq, *Angew. Chem.* **1995**, *107*, 1898 – 1901; *Angew. Chem. Int. Ed. Engl.* **1995**, *34*, 4202 – 4204.
[31] K. C. Nicolaou, W.-M. Dai, *Angew. Chem.* **1991**, *103*, 1453 – 1481; *Angew. Chem. Int. Ed. Engl.* **1991**, *30*, 1387 – 1416.
[32] J. W. Grissom, G. U. Gunawardena, D. Klingberg, D. Huang, *Tetrahedron* **1996**, *52*, 6453 – 6518.
[33] G. B. Jones, G. Hynd, J. M. Wright, A. Purohit, G. W. Plourde II, R. S. Huber, J. E. Mathews, A. Li, M. W. Kilgorl, G. J. Bubley, M. Yancisin, M. A. Brown, *J. Org. Chem.* **2001**, *66*, 3688 – 3695.
[34] L. F. Tietze, M. Beller, A. Terfort, A. Dölle, *Synthesis* **1991**, 1118 – 1120.
[35] I. Scherlitz-Hofmann, M. Dubs, R. Krieg, B. Schönecker, M. Kluge, D. Sicker, *Helv. Chim. Acta* **1997**, *80*, 2345 – 2351.
[36] S. A. Islam, S. Neidle, B. M. Gandecha, M. Partridge, L. H. Patterson, J. R. Brown, *J. Med. Chem.* **1985**, *28*, 857 – 864, and references therein.
[37] F. De Riccardis, D. Meo, I. Izzo, M. Di Filippo, A. Casapullo, *Eur. J. Org. Chem.* **1998**, 1965 – 1970.
[38] J. E. McMurry, W. J. Scott, *Tetrahedron Lett.* **1983**, *24*, 979 – 982.
[39] M. Chandler, R. J. Stoodley, *J. Chem. Soc. Perkin Trans. 1* **1980**, 1007 – 1012.
[40] F. Arcamone, S. Penco, P. Orezzi, V. Nicolella, A. Pirelli, *Nature* **1964**, *203*, 1064 – 1065.
[41] a) F. Arcamone, A. Di Marco, M. Gaetani, T. Scotti, *G. Microbiol.* **1961**, *9*, 83 – 90; b) C. Zimmer, *Prog. Nucleic Acid Res. Mol. Biol.* **1975**, *15*, 285 – 318.
[42] a) M. Coll, C. A. Frederick, A. H. Wang, A. Rich, *Proc. Natl. Acad. Sci. USA* **1987**, *84*, 8385 – 8389; b) H. Iida, G. Jia, J. W. Lown, *Curr. Opin. Biotechnol.* **1999**, *10*, 29 – 33.
[43] a) P. Cozzi, N. Mongelli, *Curr. Pharm. Des.* **1998**, *4*, 181 – 201; b) P. G. Baraldi, B. Cacciari, A. Guiotto, R. Romagnoli, A. N. Zaid, G. Spalluto, *Curr. Pharm. Des.* **1998**, *4*, 249 – 276; c) F. Zunino, F. Animati, G. Capranico, *Curr. Pharm. Des.* **1995**, *1*, 83 – 94; d) S. M. Sondhi, B. S. P. Reddy, J. W. Lown, *Curr. Med. Chem.* **1997**, *4*, 313 – 358.
[44] L. J. Hanka, A. Dietz, S. A. Gerpheide, S. L. Kuentzel, D. G. Martin, *J. Antibiot.* **1978**, *31*, 1211 – 1217.
[45] P. G. Baraldi, G. Balboni, M. G. Pavani, G. Spalluto, M. A. Tabrizi, E. D. Clercq, J. Balzarini, T. Bando, H. Sugiyama, R. Romagnoli, *J. Med. Chem.* **2001**, *44*, 2536 – 2543.
[46] a) N. L. Fregeau, Y. Wang, R. T. Pon, W. A. Wylie, J. W. Lown, *J. Am. Chem. Soc.* **1995**, *117*, 8917 – 8925; b) Y. Wang, R. Gupta, L. Huang, W. Luo, J. W. Lown, *Anti-Cancer Drug Des.* **1996**, *11*, 15 – 34.
[47] H. H. Lee, B. F. Cain, W. A. Denny, J. S. Buckleton, G. R. Clark, *J. Org. Chem.* **1989**, *54*, 428 – 431.
[48] a) M. Lee, J. W. Lown, *J. Org. Chem.* **1987**, *52*, 5717 – 5721; b) J. W. Lown, K. Krowicki, *J. Org. Chem.* **1985**, *50*, 3774 – 3779.
[49] M. A. Warpehoski, I. Gebhard, R. C. Kelly, W. C. Krueger, L. H. Li, J. P. McGovren, M. D. Prairie, N. Wicnienski, W. Wierenga, *J. Med. Chem.* **1988**, *31*, 590 – 603.
[50] E. Nishiwaki, S. Tanaka, H. Lee, M. Shibuya, *Heterocycles* **1988**, *27*, 1945 – 1952.
[51] K. Shishido, S. Haruna, C. Yamamura, H. Iitsuka, H. Nemoto, Y. Shinohara, M. Shibuya, *Bioorg. Med. Chem. Lett.* **1997**, *7*, 2617 – 2622.
[52] D. E. Thurston, D. S. Bose, *Chem. Rev.* **1994**, *94*, 433 – 465.
[53] a) P. G. Baraldi, B. Cacciari, A. Guiotto, A. Leoni, R. Romagnoli, G. Spalluto, N. Mongelli, P. W. Howard, D. E. Thurston, N. Bianchi, R. Gambari, *Bioorg. Med. Chem. Lett.* **1998**, *8*, 3019 – 3024; b) Y. Damayanthi, B. S. P. Reddy, J. W. Lown, *J. Org. Chem.* **1999**, *64*, 290 – 292; c) P. G. Baraldi, G. Balboni, B. Cacciari, A. Guiotto, S. Manfredini, R. Romagnoli, G. Spalluto, D. E. Thurston, P. W. Howard, N. Bianchi, C. Rutigliano, C. Mischiati, R. Gambari, *J. Med. Chem.* **1999**, *42*, 5131 – 5141.
[54] F. Arcamone, P. Orezzi, W. Barbieri, V. Nicolella, S. Penco, *Gazz. Chim. Ital.* **1967**, *97*, 1097 – 1109.
[55] R. D'Alessio, C. Geroni, G. Biasioli, E. Pesenti, M. Grandi, N. Mongelli, *Bioorg. Med. Chem. Lett.* **1994**, *4*, 1467 – 1472.
[56] K. Nagaoka, M. Matsumoto, J. Ono, K. Yokoi, S. Ishizeki, T. Nakashima, *J. Antibiot.* **1986**, *39*, 1527 – 1532; K. Yokoi, K. Nagaoka, T. Nakashima, *Chem. Pharm. Bull.* **1986**, *34*, 4554 – 4561.
[57] K. Shishido, S. Haruna, H. Iitsuka, M. Shibuya, *Heterocycles* **1998**, *49*, 109 – 112.
[58] K. Shishido, T. Omodani, M. Shibuya, *J. Chem. Soc. Perkin Trans. 1* **1992**, 2053 – 2054.
[59] a) E. Nishiwaki, H. Lee, T. Matsumoto, K. Toyooka, H. Sakurai, M. Shibuya, *Tetrahedron Lett.* **1990**, *31*, 1299 – 1302; b) Y. Sakai, Y. Bando, K. Shishido, M. Shibuya, *Tetrahedron Lett.* **1992**, *33*, 957 – 960.
[60] B. Herberich, J. D. Scott, R. M. Williams, *Bioorg. Med. Chem.* **2000**, *8*, 523 – 532.
[61] a) H. B. Gamper, J. Piette, J. E. Hearst, *Photochem. Photobiol.* **1984**, *40*, 29 – 34; b) W. P. Zhen, C. Jeppesen, P. E. Nielsen, *FEBS Lett.* **1988**, *229*, 73 – 76; c) W. P. Zhen, D. Buchardt, H. Nielsen, P. E. Nielsen, *Biochemistry* **1986**, *25*, 6598 – 6603; d) E. Sage, E. Moustacchi, *Biochemistry* **1987**, *26*, 3307 – 3314.
[62] K. E. Rao, G. Gosselin, D. Mrani, C. Périgaud, J.-L. Imbach, C. Bailly, J.-P. Hénichart, P. Colson, C. Houssier, J. W. Lown, *Anti-Cancer Drug Des.* **1994**, *9*, 221 – 237.
[63] J. A. Hartley, S. R. McAdam, S. Das, M. C. Roldan, M. K. Haskell, M. Lee, *Anti-Cancer Drug Des.* **1994**, *9*, 181 – 197.
[64] R. Gupta, N. H. Al-Said, B. Oreski, J. W. Lown, *Anti-Cancer Drug Des.* **1996**, *11*, 325 – 338.
[65] C. Bailly, V. Leclere, N. Pommery, P. Colson, C. Houssier, C. Rivalle, E. Bisagni, J. P. Hénichart, *Anti-Cancer Drug Des.* **1993**, *8*, 145 – 164.
[66] R. Zhao, N. H. Al-Said, D. L. Sternbach, J. W. Lown, *J. Med. Chem.* **1997**, *40*, 216 – 225.
[67] G. Powis, B. A. Svingen, P. Appel, *Mol. Pharmacol.* **1981**, *20*, 387 – 394.
[68] P. Helissey, C. Bailly, J. N. Vishwakarma, C. Auclair, M. J. Waring, S. Giorgi-Renault, *Anti-Cancer Drug Des.* **1996**, *11*, 527 – 551.
[69] a) L. R. Barrows, D. C. Radisky, B. R. Copp, D. S. Swaffar, R. A. Kramer, R. L. Warters, C. M. Ireland, *Anti-Cancer Drug Des.* **1993**, *8*, 333 – 347; b) R. Zhao, J. W. Lown, *Heterocycles* **1995**, *41*, 337 – 344; c) R. Ahao, B. Oreski, J. W. Lown, *Bioorg. Med. Chem. Lett.* **1996**, *6*, 2169 – 2172.
[70] Y. Xie, G. G. Miller, S. A. Cubitt, K.-J. Soderlind, M. J. Allalunis-Turner, J. W. Lown, *Anti-Cancer Drug Des.* **1997**, *12*, 169 – 179.

 © 2003 Wiley-VCH Verlag GmbH & Co. KGaA, Weinheim

[71] M. D. Wittman, D. Langley, J. F. Kadow (Bristol-Myers Squibb), US Patent 5395849, **1995** [*Chem. Abstr.* **1995**, *123*, 32861].

[72] a) K. C. Nicolaou, A. L. Smith, E. W. Yue, *Proc. Natl. Acad. Sci. USA* **1993**, *90*, 5881–5888; b) M. Tokuda, K. Fujiwara, T. Gomibuchi, M. Hirama, M. Uesugi, Y. Sugiura, *Tetrahedron Lett.* **1993**, *34*, 669–672; c) M. D. Wittman, J. F. Kadow, D. R. Langley, D. M. Vyas, W. C. Rose, W. Solomon, N. Zein, *Bioorg. Med. Chem. Lett.* **1995**, *5*, 1049–1052.

[73] a) M. D. Lee, T. S. Dunne, M. M. Siegel, C. C. Chang, G. O. Morton, D. B. Borders, *J. Am. Chem. Soc.* **1987**, *109*, 3464–3466; b) M. D. Lee, T. S. Dunne, C. C. Chang, G. A. Ellestad, M. M. Siegel, G. O. Morton, W. J. McGahren, D. B. Borders, *J. Am. Chem. Soc.* **1987**, *109*, 3466–3468.

[74] a) M. Konishi, H. Ohkuma, K. Matsumoto, T. Tsuno, H. Kamei, T. Miyaki, T. Oki, H. Kawaguchi, *J. Antibiot.* **1989**, *42*, 1449–1452; b) M. Konishi, H. Ohkuma, T. Tsuno, T. Oki, G. D. Van Duyne, J. Clardy, *J. Am. Chem. Soc.* **1990**, *112*, 3715–3716.

[75] K. C. Nicolaou, E. P. Schreiner, Y. Iwabuchi, T. Suzuki, *Angew. Chem.* **1992**, *104*, 317–319; *Angew. Chem. Int. Ed. Engl.* **1992**, *31*, 340–342.

[76] K. C. Nicolaou, R. D. Groneberg, T. Miyazaki, N. A. Stylianides, T. J. Schultze, W. Stahl, *J. Am. Chem. Soc.* **1990**, *112*, 8193–8195.

[77] a) K. C. Nicolaou, E. P. Schreiner, W. Stahl, *Angew. Chem.* **1991**, *103*, 566–568; *Angew. Chem. Int. Ed. Engl.* **1991**, *30*, 585–590; b) K. C. Nicolaou, C.-K. Hwang, A. L. Smith, S. V. Wendeborn, *J. Am. Chem. Soc.* **1990**, *112*, 7416–7418; c) K. C. Nicolaou, A. L. Smith, S. V. Wendeborn, C.-K. Hwang, *J. Am. Chem. Soc.* **1991**, *113*, 3106–3114.

[78] A. Matsuda, T. Doi, H. Tanaka, T. Takahashi, *Synlett* **2001**, 1101–1104.

[79] S. Py, C. W. Harwig, S. Banerjee, D. L. Brown, A. G. Fallis, *Tetrahedron Lett.* **1998**, *39*, 6139–6142.

[80] a) D. Hultmark, H. Steiner, T. Rasmuson, H. G. Boman, *Eur. J. Biochem.* **1980**, *106*, 7–16; b) J. Y. Lee, A. Boman, C. X. Sun, M. Andersson, H. Jornvall, V. Mutt, H. G. Boman, *Proc. Natl. Acad. Sci. USA* **1989**, *86*, 9159–9162.

[81] E. Habermann, J. Jentsch, *Hoppe-Seyler's Z. Physiol. Chem.* **1967**, *348*, 37–50.

[82] R. B. Merrifield, P. Juvvadi, D. Andreu, J. Ubach, A. Boman, H. G. Boman, *Proc. Natl. Acad. Sci. USA* **1995**, 92, 3449–3453.

[83] A. B. Smith III, S. M. Condon, J. A. McCauley, *Acc. Chem. Res.* **1998**, *31*, 35–46.

[84] A. Farooq, S. Anjum, M. I. Choudhary, Atta-ur-Rahman, *Curr. Org. Chem.* **1998**, *2*, 281–328.

[85] Y. Ikeda, L. W. Schultz, J. Clardy, S. L. Schreiber, *J. Am. Chem. Soc.* **1994**, *116*, 4143–4144.

[86] a) E. R. Kandel, J. H. Schwartz, Thomas M. Jessell, *Principles of Neural Science,* 4th ed., McGraw-Hill, New York, **2000**; b) C. Braestrup, P. Krogsgaard-Larsen in *A Textbook of Drug Design and Development* (Eds.: P. Krogsgaard-Larsen, H. Bundgaard), Harwood, Chur, **1991**, pp. 335–433.

[87] a) E. V. Grishin, T. M. Volkova, A. S. Arseniev, O. S. Reshetova, V. V. Onoprienko, L. G. Magazanik, S. M. Antonov, I. M. Fedorova, *Bioorg. Khim.* **1986**, *12*, 1121–1124; b) E. V. Grishin, T. M. Volkova, A. S. Arseniev, *Toxicon* **1989**, *27*, 541–549; c) M. E. Adams, R. L. Carney, F. E. Enderlin, E. T. Fu, M. A. Jarema, J. P. Li, C. A. Miller, D. A. Schooley, M. J. Shapiro, V. J. Venema, *Biochem. Biophys. Res. Commun.* **1987**, *148*, 678–683.

[88] A. T. Eldefrawi, M. E. Eldefrawi, K. Konno, N. A. Mansour, K. Nakanishi, E. Oltz, P. N. R. Usherwood, *Proc. Natl. Acad. Sci. USA* **1988**, *85*, 4910–4913.

[89] S.-K. Choi, K. Nakanishi, P. N. R. Usherwood, *Tetrahedron* **1993**, *49*, 5777–5790.

[90] a) V. J. Jasys, P. R. Kelbaugh, D. M. Nason, D. Phillips, N. A. Saccomano, R. A. Volkman, *Tetrahedron Lett.* **1988**, *29*, 6223–6226; b) T. L. Shih, J. Ruiz-Sanchez, H. Mrozik, *Tetrahedron Lett.* **1987**, *28*, 6015–6018.

[91] a) L. F. Tietze, M. Lieb, T. Herzig, F. Haunert, I. Schuberth, *Bioorg. Med. Chem.* **2001**, *9*, 1929–1939; b) L. F. Tietze, T. Herzig, A. Fecher, F. Haunert, I. Schuberth, *ChemBioChem* **2001**, *2*, 758–765.

[92] a) L. F. Tietze, *Angew. Chem.* **1983**, *95*, 840–853; *Angew. Chem. Int. Ed. Engl.* **1983**, *22*, 828–841; b) L. F. Szabo, *Stud. Nat. Prod. Chem.* **2002**, *26*, 95–148 (Bioactive Natural Products, Part G); c) J. Leonard, *Nat. Prod. Rep.* **1999**, *16*, 319–338.

[93] L. F. Tietze, T. Feuerstein, A. Fecher, F. Haunert, O. Panknin, U. Borchers, I. Schuberth, F. Alves, *Angew. Chem.* **2002**, *114*, 785–787; *Angew. Chem. Int. Ed.* **2002**, *41*, 759–761.

[94] R. R. Schmidt, *Angew. Chem.* **1986**, *98*, 213–236; *Angew. Chem. Int. Ed. Engl.* **1986**, *25*, 212–235; b) W. Dullenkopf, J. C. Castro-Palomino, L. Manzoni, R. R. Schmidt, *Carbohydr. Res.* **1996**, *296*, 135–147.

[95] R. Appel, *Angew. Chem.* **1975**, *87*, 863–874; *Angew. Chem. Int. Ed. Engl.* **1975**, *14*, 801–812.

[96] K. M. Depew, S. M. Zeman, S. H. Boyer, D. J. Denhart, N. Ikemoto, S. J. Danishefsky, D. M. Crothers, *Angew. Chem.* **1996**, *108*, 2972–2975; *Angew. Chem. Int. Ed. Engl.* **1996**, *35*, 2797–2800.

[97] G. Cassinelli, P. Orezzi, *G. Microbiol.* **1963**, *11*, 167–174.

[98] a) E. J. Gabbay, D. Grier, R. E. Fingerle, R. Reimer, R. Levy, S. W. Pearce, W. D. Wilson, *Biochemistry* **1976**, *15*, 2062–2070; b) A. Di Marco, F. Zunino, R. Silvestrini, C. Gambarucci, R. A. Gambetta, *Biochem. Pharmacol.* **1971**, *20*, 1323–1328.

[99] G. Dräger, A. Garming, C. Maul, M. Noltemeyer, R. Thiericke, M. Zerlin, A. Kirschning, *Chem. Eur. J.* **1998**, *4*, 1324–1332.

[100] I. Ojima, S. Chakravarty, T. Inoue, S. Lin, L. He, S. B. Horwitz, S. D. Kuduk, S. J. Danishefsky, *Proc. Natl. Acad. Sci. USA* **1999**, *96*, 4256–4261.

[101] a) Y. Shin, N. Choy, R. Balachandran, C. Madiraju, B. W. Day, D. P. Curran, *Org. Lett.* **2002**, *4*, 4443–4446; Corrigendum: Y. Shin, N. Choy, T. R. Turner, R. Balachandran, C. Madiraju, B. W. Day, D. P. Curran, *Org. Lett.* **2003**, *5*, 603; b) for a recent review article on discodermolide, see: I. Paterson, G. J. Florence, *Eur. J. Org. Chem.* **2003**, 2193–2208.

[102] G. Mehta, S. Muthusamy, B. G. Maiya, S. Arounaguiri, *Tetrahedron Lett.* **1997**, *38*, 7125–7128.

[103] G. Mehta, B. G. Maiya, S. Muthusamy, M. Chanon, M. Julliard, FR 2764605, **1998** [*Chem. Abstr.* **1999**, *130*, 153827], available under http://ep.espacenet.com.

[104] L. Ding, G. Etemad-Moghadam, S. Cros, C. Auclair, B. Meunier, *J. Chem. Soc. Chem. Commun.* **1989**, 1711–1713.

[105] a) F. Q. Alali, X.-X. Liu, J. L. McLaughlin, *J. Nat. Prod.* **1999**, *62*, 504–540; b) M. C. Zafra-Polo, B. Figadère, T. Gallardo, J. R. Tormo, D. Cortes, *Phytochemistry* **1998**, *48*, 1087–1117.

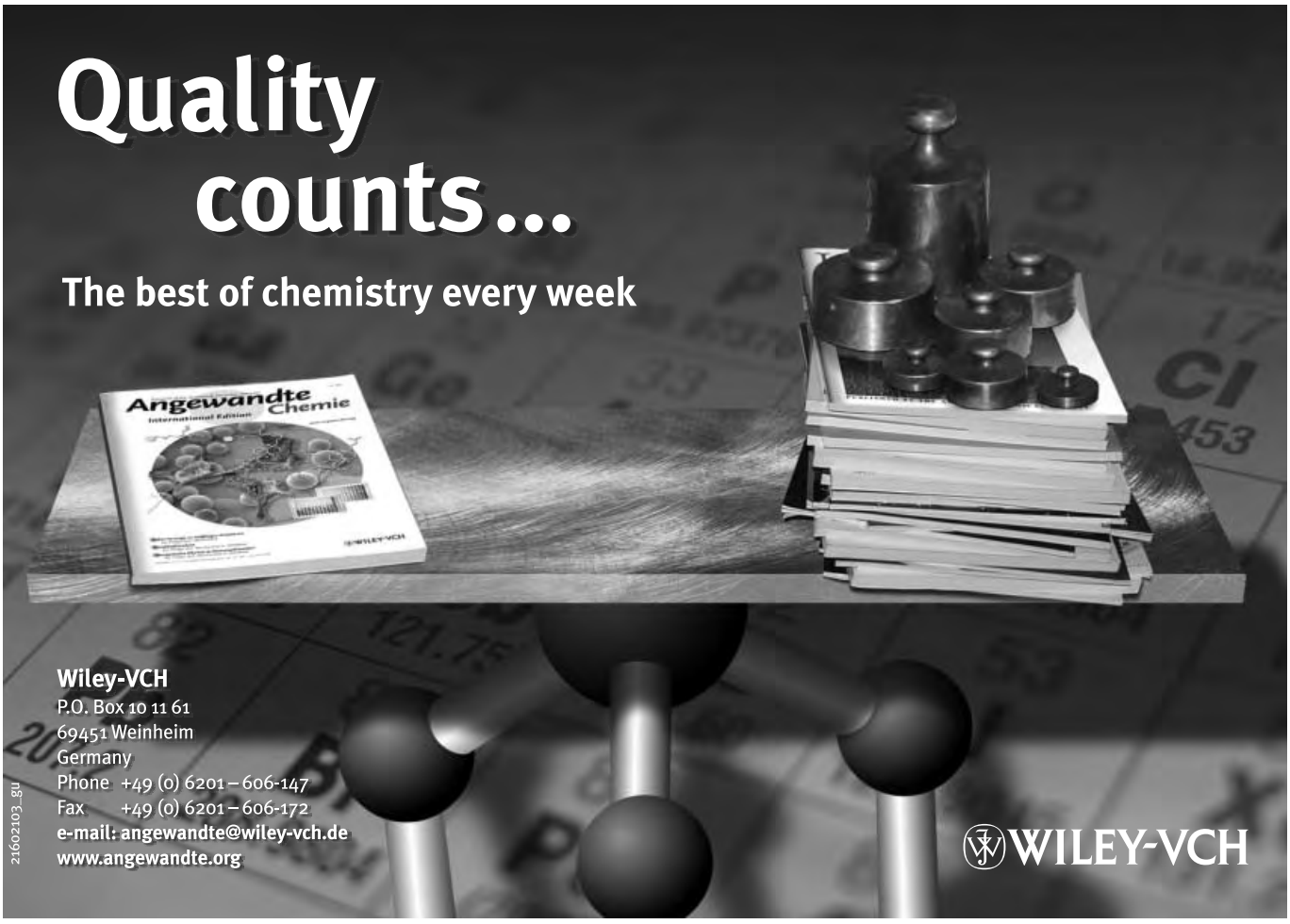
[106] a) G.-X. Zhao, L. R. Miesbauer, D. L. Smith, J. L. McLaughlin, *J. Med. Chem.* **1994**, *37*, 1971–1974; b) M. Sahai, S. Singh, M. Singh, Y. K. Gupta, S. Akashi, R. Yuji, K. Hirayam, H. Asaki, H. Araya, N. Hara, T. Eguchi, K. Kakinuma, Y. Fujimoto, *Chem. Pharm. Bull.* **1994**, *42*, 1163–1174.

[107] G. Shi, D. Alfonso, M. O. Fatope, L. Zeng, Z.-m. Gu, G.-x. Zhao, K. He, J. M. MacDougal, J. L. McLaughlin, *J. Am. Chem. Soc.* **1995**, *117*, 10409–10410.

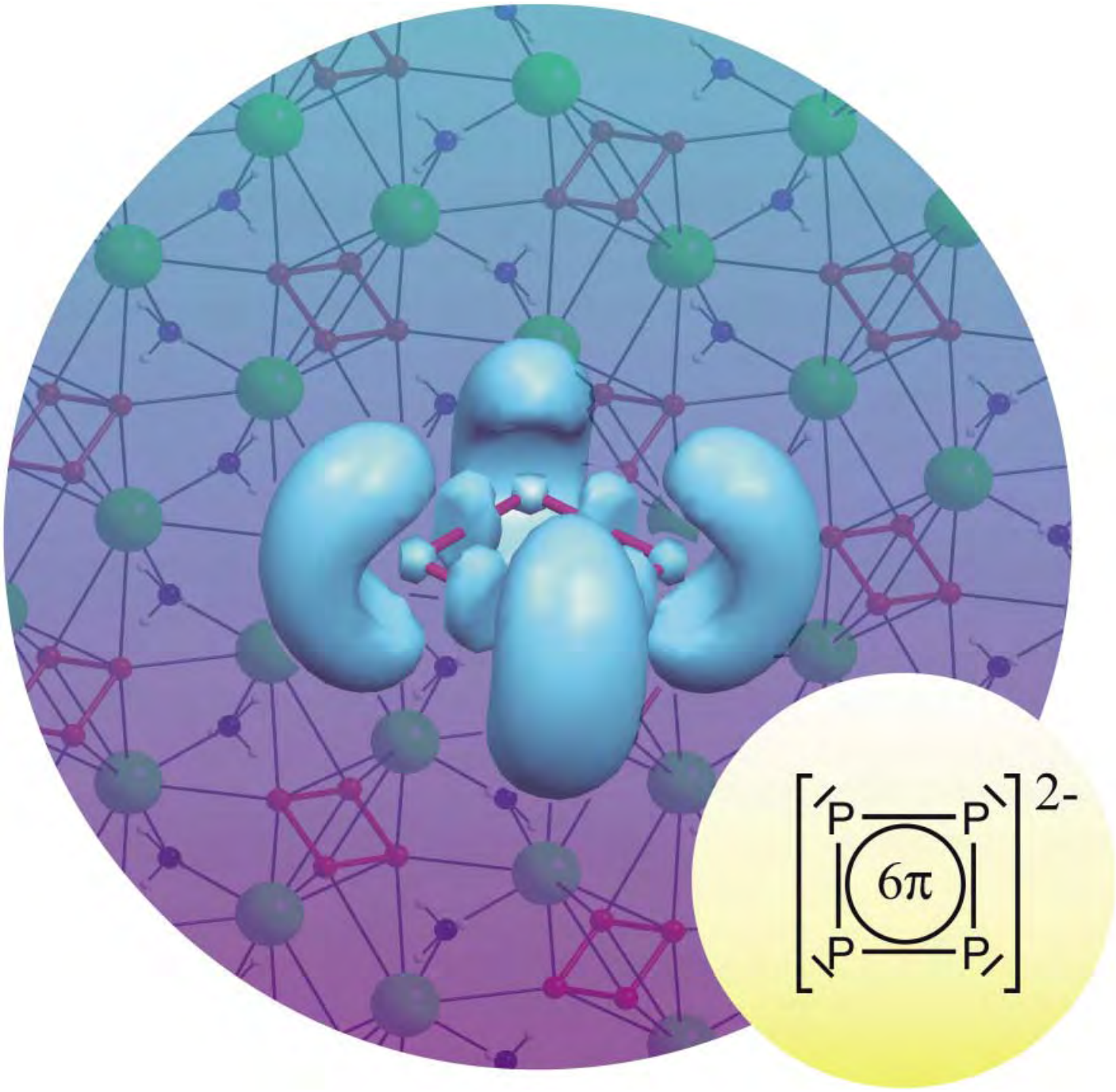
[108] a) M. D. Esposti, *Biochim. Biophys. Acta* **1998**, *1364*, 222–235; b) J. R. Tormo, M. C. Gonzales, D. Cortes, E. Estornell, *Arch. Biochem. Biophys.* **1999**, *369*, 119–126; c) H. Miyoshi, M. Ohshima, H. Shimada, T. Akagi, H. Iwamura, J. L. McLaughlin, *Biochim. Biophys. Acta* **1998**, *1365*, 443–452; d) H. Shimada, J. B. Grutzner, J. F. Kozlowski, J. L. McLaughlin, *Biochemistry* **1998**, *37*, 854–866.

 © 2003 Wiley-VCH Verlag GmbH & Co. KGaA, Weinheim

[109] a) S. Hoppen, U. Emde, T. Friedrich, L. Grubert, U. Koert, *Angew. Chem.* **2000**, *112*, 2181 – 2184; *Angew. Chem. Int. Ed.* **2000**, *39*, 2099 – 2102; b) S. Arndt, U. Emde, S. Bäurle, T. Friedrich, L. Grubert, U. Koert, *Chem. Eur. J.* **2001**, *7*, 993 – 1005; c) U. Koert, M. Stein, H. Wagner, *Liebigs Ann.* **1995**, 1415 – 1426; d) S. Bäurle, S. Hoppen, U. Koert, *Angew. Chem.* **1999**, *111*, 1341 – 1344; *Angew. Chem. Int. Ed.* **1999**, *38*, 1263 – 1266.
[110] L. Syper, K. Kloc, J. Mlochowski, Z. Szulc, *Synthesis* **1979**, 521 – 522.
[111] M. Hergenhahn, W. Adolf, E. Hecker, *Tetrahedron Lett.* **1975**, 1595 – 1598.
[112] G. Appendino, A. Szallasi, *Life Sci.* **1997**, *60*, 681 – 696.
[113] A. Szallasi, P. M. Blumberg, *Neuroscience* **1989**, *30*, 515 – 520.
[114] G. Appendino, *Gazz. Chim. Ital.* **1997**, *127*, 461 – 469.
[115] J. Zemlicka, M. C. Fernandez-Moyano, M. Ariatti, G. E. Zurenko, J. E. Grady, J. P. G. Ballesta, *J. Med. Chem.* **1993**, *36*, 1239 – 1244.



Communications



By using diphosphane (P_2H_4) as the source of phosphorus N. Korber and co-workers have succeeded in isolating a compound that contains a 6π aromatic P_4^{2-} unit, shown, which was missing in the series of E_4^{2-} ions of group 15. For more information, see the Communication on the following pages.

DOI: 10.1002/anie.200351776
© 2003 Wiley-VCH Verlag GmbH & Co. KGaA, Weinheim

Aromatic Polyphosphides

P_4^{2-}: A 6π Aromatic Polyphosphide in Dicesium Cyclotetraphosphide–Ammonia (1/2)**

*Florian Kraus, Jürgen C. Aschenbrenner, and Nikolaus Korber**

In memory of Marianne Baudler

The diagonal relationship between carbon and phosphorus is especially evident in the analogies of hydrocarbons with polyphosphanes or polyphosphides, which have been reviewed by Baudler and Glinka in seminal articles.[1–3] However, these analogies cover mainly saturated systems with element–element single bonds. Polyphosphorus compounds with multiple bonds are, as one may expect, very rare. Possible exceptions to this observation could be the particularly stable aromatic representatives. If the aromatic hydrocarbons $C_4H_4^{2-}$, $C_5H_5^-$, and C_6H_6 are considered, the diagonal relationship predicts their phosphorus homologues to be P_4^{2-} (cyclotetraphosphide dianion), P_5^- (cyclopentaphosphide anion) and P_6 (hexaphosphorus).

The existence of the cyclopentaphosphide anion P_5^- was verified by NMR spectroscopy in solution;[4–7] P_5^- is also well known as a ligand in organometallic complexes.[8] No saltlike compounds that contain an isolated P_5^- anion have been characterized so far. Recently, neutral P_6 molecules were observed in the gas phase by mass spectrometry but there is still no reliable information about their structure;[9,10] the use of hexaphosphabenzene, P_6, as a ligand is well-known.[11] The cyclotetraphosphide dianion, P_4^{2-}, and NaP_4^- were the subjects of theoretical[12,13] and photoelectron-spectroscopical investigations in the gas phase.[13] Until now, the approximately square planar P_4^{2-} ion is known only as a ligand in organometallic complexes. In one case, the P_4^{2-} ion has D_{2h} symmetry with two different P–P bond lengths,[14] whereas in another case it shows a kitelike distortion.[15,16] Isolated P_4^{2-} ions outside the ligand sphere of a transition-metal ion have yet not been reported in the solid state. However, the homologous E_4^{2-} anions of group 15 elements are known. In 1977, Corbett and co-workers synthesized Bi_4^{2-} by using 2,2,2-crypt (4,7,13,16,21,24-hexaoxa-1,10-diazabicyclo[8.8.8.]hexacosane) in ethylenediamine and K_3Bi_5 or K_3Bi_2.[17] This was followed in 1984 by the synthesis of Sb_4^{2-}, which was prepared from KGeSb and 2,2,2-crypt in en.[18] In 2002, the reduction of arsenic by sodium in liquid ammonia yielded the As_4^{2-}-containing compound $[Na(NH_3)_5]_2As_4{\cdot}2\,NH_3$.[19] However, the use of this approach with white or red phosphorus and an alkali metal (M) dissolved in liquid ammonia has not yielded ammoniates of M_2P_4; only ammoniates of the more stable neighbor phase M_3P_7 are found.

Starting from diphosphane(4) (P_2H_4, **1**) as a new source of phosphorus, we succeeded in synthesizing dicesium cyclotetraphosphide–ammonia(1/2) ($Cs_2P_4{\cdot}2\,NH_3$, **2**) in liquid ammonia; **2** contains an approximately square, perfectly planar P_4^{2-} unit.

To obtain **2**, compound **1** is treated with cesium at −78 °C and, after the evolution of gas has ceased, dry ammonia is condensed into the reaction vessel. After storage of the reaction mixture at −40 °C for a few days, the main product, **2**, precipitates in the form of transparent, yellow, cube-shaped crystals, which were characterized by low temperature X-ray crystal-structure analysis (Figures 1 and 2).[20] NMR spectroscopic analysis of the yellow supernatant only shows the presence of $CsPH_2$, which gives rise to a signal at $\delta =$ −260.6 ppm in the $^{31}P\{^1H\}$-NMR spectrum.[21] Consequently, the following formal reaction equation may be written, in which ammonia is omitted for sake of clarity:

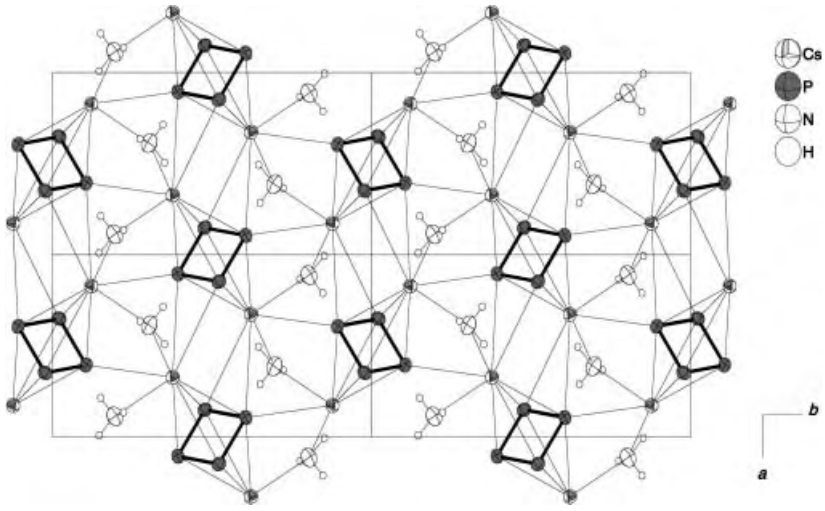


Figure 1. Projection of the crystal structure of $Cs_2P_4{\cdot}2\,NH_3$ along the *c* axis; atoms are shown at the 70% probability level.

$$6\,P_2H_4 + 10\,Cs \rightarrow Cs_2P_4 + 8\,CsPH_2 + 4\,H_2\uparrow \quad (1)$$

The P–P bond lengths in **2** are 2.146(1) Å and 2.1484(9) Å. These distances are shorter than the P–P single bond in diphosphane(4) (2.219 Å) but significantly longer than the P=P bond in bis(2,4,6-tri-tert-butylphenyl)diphos-

[*] Prof. Dr. N. Korber, Dipl.-Chem. F. Kraus, J. C. Aschenbrenner
Institut für Anorganische Chemie, Universität Regensburg
Universitätsstrasse 31, 93053 Regensburg (Germany)
Fax: (+49) 941-943-1812
E-mail: nikolaus.korber@chemie.uni-regensburg.de

[**] This work was supported by the Deutsche Forschungsgemeinschaft and the Fonds der Chemischen Industrie. We appreciate the generous donation of calcium phosphide by Chemische Fabrik Wülfel. F. K. thanks the Studienstiftung des Deutschen Volkes for a fellowship.

Supporting information for this article is available on the WWW under http://www.angewandte.org or from the author.

 © 2003 Wiley-VCH Verlag GmbH & Co. KGaA, Weinheim DOI: 10.1002/anie.200351776

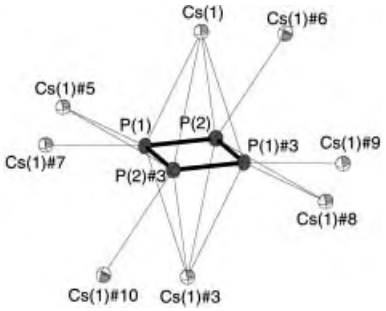


Figure 2. Coordination sphere of P_4^{2-}; atoms are shown at the 50% probability level; selected bond lengths [Å] and angles [°]: P(1)-P(2) 2.146(1), P(1)-P(2)#3 2.1484(9), P(1)-Cs(1) 3.7665(8), P(1)-Cs(1)#3 3.7023(7), P(1)-Cs(1)#5 3.8937(8), P(1)-Cs(1)#7 3.7529(8), P(2)-Cs(1) 3.7089(8), P(2)-Cs(1)#3 3.7651(7), P(2)-Cs(1)#6 3.7587(7), P(2)-Cs(1)#8 3.6742(9); P(1)-P(2)-P(1)#3 89.76(4), P(2)-P(1)-P(2)#3 90.24(4) Symmetry operations for generating equivalent atoms: #3 $-x+1, -y, -z$; #5 $-x, -y, -z$; #6 $x+{}^1/_2, -y+{}^1/_2, z$; #7 $x, y, z-1$; #8 $x+1, y, z$; #9 $-x+1, -y, -z+1$; #10 $-x+{}^1/_2, y-{}^1/_2, -z$.

phene (2.034 Å).[22] In other homoatomic polyphosphorus anions, for example, P_7^{3-} (Figure 3), P–P bond lengths span a range from 2.12 to 2.29 Å, with the shorter bonds being those from the triangular P-P-P plane to the formally negatively charged, two coordinate phosphorus atoms.[23] Thus, the P–P bond length in P_4^{2-} is not valid as a criterion of aromaticity.

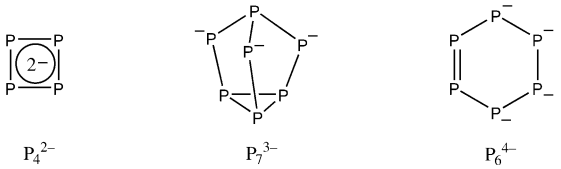


Figure 3. Anionic units in $Cs_2P_4{\cdot}2\,NH_3$ (**2**), $Cs_3P_7{\cdot}3\,NH_3$ (**3**), and K_4P_6 (**4**).

Further preparative investigations showed that **2** is also accessible by treating white phosphorus with cesium in THF, followed by solvation in liquid ammonia. In this reaction, however, $Cs_3P_7{\cdot}3\,NH_3$ (**3**) is the major product and **2** is only a by-product. The ^{31}P NMR spectrum of the supernatent solution[24] (Figure 4) shows one singlet at $\delta = 349.1$ ppm (−35 °C) or 345.8 ppm (−60 °C). With this chemical shift the singlet can not originate from P_7^{3-},[1,23,25] and we assigned it to the P_4^{2-} ion.

A very similar chemical shift was observed and assigned previously to a different polyphosphide. Von Schnering et al. reported the ^{31}P NMR spectra of M_4P_6 (M = K, Rb, Cs) in ethylenediamine at 10 °C and observed, among other signals, singlets in the range between $\delta = 331$ (M = K) and 348 ppm (M = Cs). Those chemical shifts were assigned to the "valence tautomeric 10π system" P_6^{4-}, which is the only other known cyclic polyphosphide with partial multiple bonding in an ionic solid.[26] To resolve this discrepancy, we also performed solvation experiments with K_4P_6 (**4**, Figure 3) in liquid ammonia. Characterization of the solutions by NMR spectroscopy[27] yields three signals (A, B, C). Signals C and B

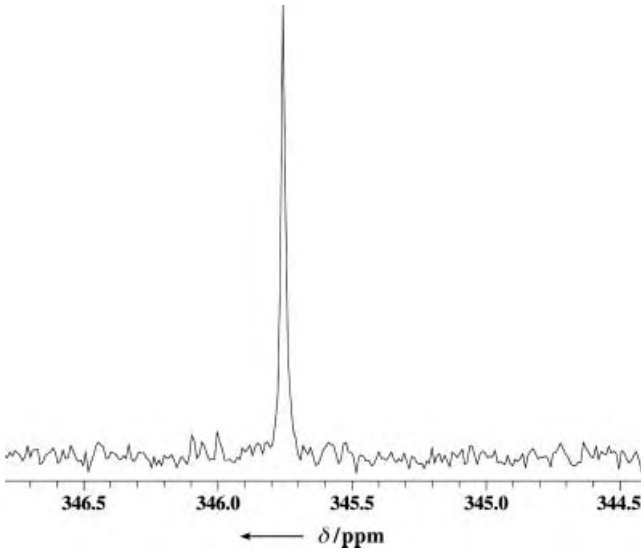


Figure 4. ^{31}P NMR spectrum: solution of the product of the reaction between cesium and white phosphorus in liquid ammonia at −60 °C.

were unambiguously assigned to the PH_2^- anion and to the P_7^{3-} anion, respectively (Figure 5). In the $^{31}P\{^1H\}$-NMR as well as in the ^{31}P NMR spectra signal A is a singlet at $\delta =$ 330.3 ppm (−35 °C) or $\delta = 327.3$ ppm (−60 °C). As the dependence of the chemical shift on the alkali-metal counterion was demonstrated previously,[26] it is likely that the identity of this polyphosphorus species is the same as that in the solution of $Cs_2P_4{\cdot}2NH_3$.

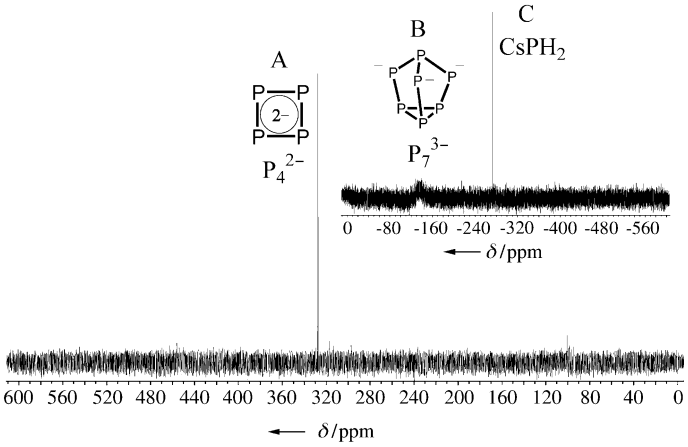


Figure 5. $^{31}P\{^1H\}$ NMR spectrum of the solvation products of K_4P_6 in liquid ammonia at −60 °C.

As the formation of a P_6^{4-} ion from P_4^{2-} in liquid ammonia does not seem plausible, we reassigned the signal at approximately $\delta = 348$ ppm to the cyclotetraphosphide dianion P_4^{2-}. It is unlikely that the fourfold negatively charged P_6 cycle containing only one formal P=P bond causes a downfield shift of that magnitude. On the other hand, this downfield shift is in agreement with the aromatic 6π system of P_4^{2-}. For comparison, the chemical shift of the 6π aromatic system P_5^- is approximately $\delta = 468$ ppm (in THF at 25 °C).[4–7]

 © 2003 Wiley-VCH Verlag GmbH & Co. KGaA, Weinheim

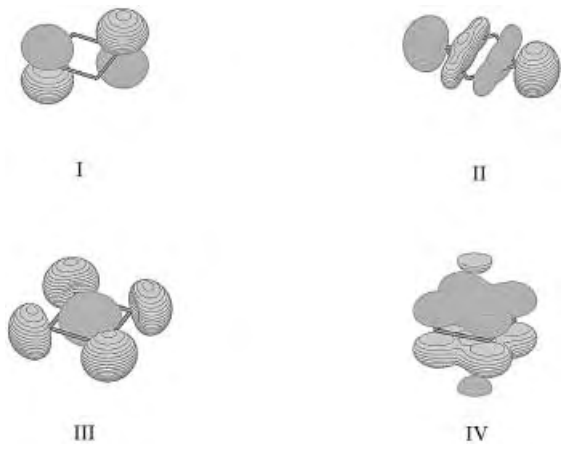


Figure 6. Contour plots of molecular orbitals of Cs_2P_4 (D_{4h} symmetry); I) doubly degenerate HOMO, $E = -0.225$ H; II) doubly degenerate HOMO-1, $E = -0.240$ H; III) HOMO-2, $E = -0.352$ H; IV) HOMO-3, $E = -0.358$ H.

By using quantum-chemical calculations[28] at different levels[29] we were able to obtain information on the form of the molecular orbitals of Cs_2P_4 and P_4^{2-} (Figure 6).[30] As Cs_2P_4 and P_4^{2-} have the same set of π molecular orbitals as known aromatic species such as C_6H_6, $C_5H_5^-$, $C_4H_4^{2-}$, P_5^-, or the isoelectronic cyclotetrasulfur dication, S_4^{2+}, the aromaticity of the system was confirmed.[13] A calculation of the bond order in P_4^{2-} at the HF/6-311++G** level by using the AIM method[31,32] yields 1.53, which also agrees well with a simple Frost–Musulin model. By using the GIAO method at the HF/aug-cc-pVQZ level for chemical shift calculations, one obtains for P_4^{2-} $\delta = 359.6$ ppm, which deviates by only 11 ppm from the experimental value.[33–37] The chemical shift of the comparison species P_5^- was calculated to be $\delta =$ 428.1 ppm and differs by 40 ppm from the experimental value. Thus, the assignment of the signal at about $\delta = 348$ ppm to P_4^{2-} is substantiated.

From the synthesis of the cyclotetraphosphide dianion P_4^{2-}, the expected final member in the series of E_4^{2-} anions of group 15 elements has been prepared. However, for N_4^{2-}, only theoretical investigations have been reported, which, for example, predict the stability of Li_2N_4.[38]

Experimental Section

All work was carried out under the exclusion of moisture and air in an atmosphere of purified argon. Diphosphane(4) was produced by hydrolyzing calcium phosphide in a modified apparatus according to Baudler et al.[39] All operations with diphosphane(4) were performed in a dark room under only dim red light. A Schlenk tube was charged with distilled cesium (1.1 g, 8.27 mmol), and diphosphane(4) (2 mL) was condensed into the tube at −78 °C. After the evolution of gas had ceased, dry ammonia (10 mL) was condensed onto the product, to yield a yellow solution. The reaction mixture was stored at −40 °C for several days; yellow cube-shaped crystals formed, which were subjected to X-ray crystal-structure analysis.

NMR spectra were recorded with a variable temperature, multicore Avance Bruker spectrometer (^{1}H: 400 MHz). All samples for ^{31}P NMR spectroscopy used liquid ammonia (300 μL) with [D$_8$]THF (100 μL) as the solvent and spectra were taken in the range of $\delta =$ +600 ppm to −600 ppm at −60 and −35 °C. Phosphoric acid (85 %) and TMS were used as external reference standards for ^{31}P NMR or ^{1}H NMR spectra, respectively.

Received: April 30, 2003 [Z51776]

Keywords: aromaticity · phosphanes · phosphorus rings · polyphosphides

[1] M. Baudler, K. Glinka, *Chem. Rev.* **1993**, *93*, 1623–1667.
[2] M. Baudler, K. Glinka, *Chem. Rev.* **1994**, *94*, 1273–1297.
[3] M. Baudler, *Angew. Chem.* **1987**, *99*, 429–451; *Angew. Chem. Int. Ed. Engl.* **1987**, *26*, 419–441.
[4] M. Baudler, D. Düster, D. Ouzounis, *Z. Anorg. Allg. Chem.* **1987**, *544*, 87–94.
[5] M. Baudler, S. Akpapoglou, D. Ouzounis, F. Wasgestian, B. Meinigke, H. Budzikiewicz, H. Münster, *Angew. Chem.* **1988**, *100*, 288–289; *Angew. Chem. Int. Ed. Engl.* **1988**, *27*, 280–281.
[6] M. Baudler, D. Ouzounis, *Z. Naturforsch. B* **1989**, *44*, 381–382.
[7] M. Baudler, T. Etzbach, *Chem. Ber.* **1991**, *124*, 1159–1160.
[8] O. J. Scherer, *Nachr. Chem. Tech. Lab.* **1987**, *35*, 1140–1144.
[9] D. Schröder, H. Schwarz, M. Wulf, H. Sievers, P. Jutzi, M. Reiher, *Angew. Chem.* **1999**, *111*, 3723–3726; *Angew. Chem. Int. Ed.* **1999**, *38*, 3513–3515.
[10] M. Reiher, D. Schroder, *Chem. Eur. J.* **2002**, *8*, 5501–5506.
[11] O. J. Scherer, H. Sitzmann, G. Wolmershäuser, *Angew. Chem.* **1985**, *97*, 358–359; *Angew. Chem. Int. Ed. Engl.* **1985**, *24*, 351–353.
[12] A. F. Cuthbertson, C. Glidewell, *Inorg. Chim. Acta* **1981**, *49*, 91–97.
[13] A. E. Kuznetsov, H. J. Zhai, L. S. Wang, A. I. Boldyrev, *Inorg. Chem.* **2002**, *41*, 6062–6070.
[14] M. Scheer, C. Troitzsch, P. G. Jones, *Angew. Chem.* **1992**, *104*, 1395–1397; *Angew. Chem. Int. Ed. Engl.* **1992**, *31*, 1377–1379.
[15] M. Scheer, E. Herrmann, J. Sieler, M. Oehme, *Angew. Chem.* **1991**, *103*, 1023–1025; *Angew. Chem. Int. Ed. Engl.* **1991**, *30*, 969–971.
[16] O. J. Scherer, J. Vondung, G. Wolmershäuser, *Angew. Chem.* **1989**, *101*, 1395–1397; *Angew. Chem. Int. Ed. Engl.* **1989**, *28*, 1355–1357.
[17] A. Cisar, J. D. Corbett, *Inorg. Chem.* **1977**, *16*, 2482–2487.
[18] S. C. Critchlow, J. D. Corbett, *Inorg. Chem.* **1984**, *23*, 770–774.
[19] N. Korber, M. Reil, *Chem. Commun.* **2002**, 84–85.
[20] Crystallographic data of **2**: $H_6N_2Cs_2P_4$, monoclinic, $P2_1/a$ (No. 14), $a = 6.6580(7)$, $b = 12.579(1)$, $c = 6.7026(7)$ Å, $\beta = 106.18(1)°$, $V = 539.11(9)$ Å^3, $\rho_{calcd} = 2.611$ g cm^{-3}, $\mu(Mo_{K\alpha}) = 7.287$ mm^{-1}, $Z = 2$. Stoe-IPDS-Diffractometer (graphite monochromator) $Mo_{K\alpha}$ radiation $\lambda = 0.71073$ Å, $T = 123(1)$ K, 2θ scan, 9093 measured reflections ($3.16° < \theta < 25.96°$), 1259 independent reflections, 1189 reflections with $I > 2\sigma(I)$ ($R_{int} = 0.0575$). The structure was solved by using direct methods (SHELXS97) and refined on F^2 (SHELXL97). H atoms were localized by Fourier methods and refined isotropically, 49 refined parameters, the refinement converged at $wR_2 = 0.0477$ (all reflections), conventional $R = 0.0206$ for $I > 2\sigma(I)$. Further details on the crystal structure investigation(s) may be obtained from the Fachinformationszentrum Karlsruhe, 76344 Eggenstein-Leopoldshafen, Germany (fax: (+49) 7247-808-666; e-mail: crysdata@fiz-karlsruhe.de), on quoting the depository number CSD-413072.
[21] NMR data (solution of the Cs/P_2H_4 reaction in NH_3): ^{1}H NMR (400 MHz, NH_3, [D8]THF, −60 °C, TMS ext.): $\delta = -1.31$ ppm (d, $^1J(P,H) = 141$ Hz); ^{1}H{^{31}P} NMR (400 MHz, NH_3, [D$_8$]THF, −60 °C, TMS ext.): $\delta = -1.31$ ppm (s); ^{31}P NMR (162 MHz, NH_3, [D$_8$]THF, −60 °C, H_3PO_4 ext.): $\delta = -260.6$ ppm (t, $^1J(P,H) = 141$ Hz); ^{31}P{^{1}H} NMR (162 MHz, NH_3, [D$_8$]THF, −60 °C, H_3PO_4 ext.): $\delta = -260.4$ ppm (s).

 © 2003 Wiley-VCH Verlag GmbH & Co. KGaA, Weinheim

[22] M. Yoshifuji, I. Shima, N. Inamoto, *J. Am. Chem. Soc.* **1981**, *103*, 4587 – 4589.
[23] V. Manriquez, W. Hönle, H. G. von Schnering, *Z. Anorg. Allg. Chem.* **1986**, *539*, 95 – 109.
[24] NMR data (solution of the Cs/P_4 reaction in NH_3): ^1H NMR (400 MHz, NH_3, $[D_8]$THF, −60 °C, TMS ext.): $\delta = 5.34$ ppm (s; OH^- from H_2O coordinated to P_4); ^{31}P NMR (162 MHz, NH_3, $[D_8]$THF, −60 °C, H_3PO_4 ext.): $\delta = 345.8$ ppm (s); $^{31}P\{^1H\}$-NMR (162 MHz, NH_3, $[D_8]$THF, −60 °C, H_3PO_4 ext.): $\delta = 345.8$ ppm (s).
[25] M. Baudler, H. Ternberger, W. Faber, J. Hahn, *Z. Naturforsch. B* **1979**, *34*, 1690 – 1697.
[26] H. G. von Schnering, T. Meyer, W. Hönle, W. Schmettow, U. Hinze, W. Bauhofer, G. Kliche, *Z. Anorg. Allg. Chem.* **1987**, *553*, 261 – 279.
[27] NMR data: (solution of **4** in NH_3): ^1H NMR (400 MHz, NH_3, [D8]THF, TMS ext.):$\delta = -1.48/-1.46$ ppm (−35/−60 °C) (d, $^1J(P,H) = 140$ Hz); ^{31}P-NMR (162 MHz, NH_3, $[D_8]$THF, H_3PO_4 ext.): $\delta = -273.3/-270.6$ (−35/−60 °C) (t, $^1J(P,H) = 140$ Hz, PH_2^-), −135/−145 (−35/−60 °C) (m, P_7^{3-}), 330.3/327.3 ppm (−35/−60 °C) (s); $^{31}P\{^1H\}$-NMR (162 MHz, NH_3, [D8]THF, H_3PO_4 ext.): $\delta = -273.3/-270.6$ (−35/−60 °C) (s), −135/−145 (−35/−60 °C) (m, P_7^{3-}), 330.3/327.3 ppm (−35/−60 °C) (s).
[28] Gaussian 98 (Revision A.7), M. J. Frisch, G. W. Trucks, H. B. Schlegel, G. E. Scuseria, M. A. Robb, J. R. Cheeseman, V. G. Zakrzewski, J. A. Montgomery, R. E. Stratmann, J. C. Burant, S. Dapprich, J. M. Millam, A. D. Daniels, K. N. Kudin, M. C. Strain, O. Farkas, J. Tomasi, V. Barone, M. Cossi, R. Cammi, B. Mennucci, C. Pomelli, C. Adamo, S. Clifford, J. Ochterski, G. A. Petersson, P. Y. Ayala, Q. Cui, K. Morokuma, D. K. Malick, A. D. Rabuck, K. Raghavachari, J. B. Foresman, J. Cioslowski, J. V. Ortiz, A. G. Baboul, B. B. Stefanov, G. Liu, A. Liashenko, P. Piskorz, I. Komaromi, R. Gomperts, R. L. Martin, D. J. Fox, T. Keith, M. A. Al-Laham, C. Y. Peng, A. Nanayakkara, C. Gonzalez, M. Challacombe, P. M. W. Gill, B. G. Johnson, W. Chen, M. W. Wong, J. L. Andres, M. Head-Gordon, E. S. Replogle, J. A. Pople, Gaussian, Inc., Pittsburgh, PA, **1998**.
[29] The calculation shown of molecular Cs_2P_4 in D_{4h} symmetry was done at the CCSD(T)/LanL2DZ level. Calculation at the MP4 level yielded identical orbital energies. For HF, CISD, MP2, and B3LYP, calculated energies were less negative. After full geometry optimization, vibration analysis was used to confirm the ground states. The cyclotetraphosphide anion was calculated at the HF/6-311++G**, HF/6-311++G(3df,3pd), and HF/aug-cc-pVTZ levels of theory. The form of the molecular orbitals did not change. Higher levels of theory (MP2, MP4) also showed no change in shape. Orbital eigenvalues of the two highest molecular orbitals are positive, as is expected for a dianion. The P_4^{2-} ion was shown to be a minimum on the potential energy surface of the system in reference [13].
[30] G. Schaftenaar, J. H. Noordik, *J. Comput.-Aided Mol. Des.* **2000**, *14*, 123 – 134.
[31] R. F. W. Bader, *Chem. Rev.* **1991**, *91*, 893 – 928.
[32] R. F. Bader, *Atoms in Molecules: A Quantum Theory*, Oxford University Press, Oxford, **1994**.
[33] R. Ditchfield, *J. Chem. Phys.* **1972**, *56*, 5688 – 5691.
[34] R. Ditchfield, *Mol. Phys.* **1974**, *27*, 789 – 807.
[35] T. M. Alam, *Int. J. Mol. Sci.* **2002**, *3*, 888 – 906.
[36] C. van Wullen, *Phys. Chem. Chem. Phys.* **2000**, *2*, 2137 – 2144.
[37] T. Helgaker, M. Jaszunski, K. Ruud, *Chem. Rev.* **1999**, *99*, 293 – 352.
[38] G. van Zandwijk, R. A. J. Janssen, H. M. Buck, *J. Am. Chem. Soc.* **1990**, *112*, 4155 – 4164.
[39] M. Baudler, H. Standeke, M. Borgardt, H. Strabel, J. Dobbers, H. Muntenbeck, C. P. Schoner, W. Faber, U. M. Krause, W. Kronenberg, *Z. Anorg. Allg. Chem.* **1995**, *621*, 1133 – 1139.

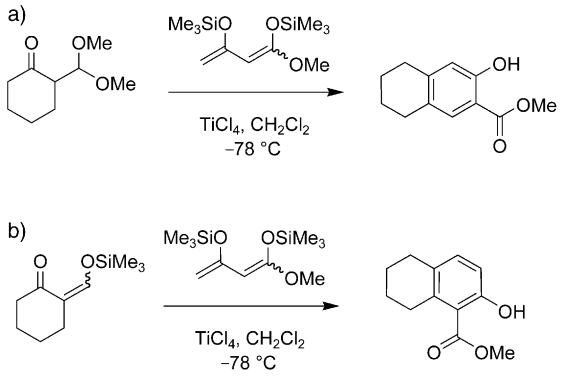
 © 2003 Wiley-VCH Verlag GmbH & Co. KGaA, Weinheim

Reactions of Bis(silyl enol ether)s

[3+3] Cyclizations of 1,3-Bis(silyl enol ether)s with 1,1-Diacetylcyclopentane and 1,1-Diacetylcyclopropane**

Peter Langer and Gopal Bose*

Domino reactions facilitate the rapid assembly of complex products in a one-pot process.[1] Despite the simplicity of the idea, domino cyclizations of 1,3-dicarbonyl dianions[2] with dielectrophiles are relatively rare.[3] As a result of their high negative charge density, ambident dianions are very reactive compounds, and many side reactions can occur, such as polymerization, decomposition, deprotonation, formation of open-chain products, elimination, and single-electron-transfer processes. A number of base-mediated cyclization reactions of activated (symmetrical) 1,3,5-tricarbonyl compounds (e.g. diethyl acetone-1,3-dicarboxylate) with enolizable 1,3-dicarbonyl derivatives have been reported.[4] In contrast, many side reactions, such as deprotonation or reduction of the dielectrophile, can interfere with the direct cyclization of (unsymmetrical) 1,3-dicarbonyl dianions with enolizable and non-enolizable 1,3-diketones.[5] A solution to this problem was developed by Chan and co-workers. They reported the synthesis of benzene derivatives and salicylic acid esters by the Lewis acid mediated cyclization of acetals of β,β-ketoaldehydes, β-ketocarboxylic acid esters, and β-ketocarboxylic acid chlorides (Scheme 1a), and of 3-silyloxyalk-2-en-1-ones (Scheme 1b) with 1,3-bis(silyl enol ether)s. 1,3-Bis-



Scheme 1. Cyclizations of 1,3-bis(silyl enol ether)s reported by Chan et al.[6b,8]

[*] Prof. Dr. P. Langer, Dr. G. Bose
Institut für Chemie und Biochemie
Ernst-Moritz-Arndt Universität Greifswald
Soldmannstr. 16, 17487 Greifswald (Germany)
Fax: (+49) 3834-86-4373
E-mail: peter.langer@uni-greifswald.de

[**] This work was supported by the Deutsche Forschungsgemeinschaft (Heisenberg Fellowship to P. L. and regular funding). We are grateful to Dr. M. Noltemeyer for the X-ray crystal-structure analysis.

Supporting information for this article is available on the WWW under http://www.angewandte.org or from the author.

 DOI: 10.1002/anie.200351263 © 2003 Wiley-VCH Verlag GmbH & Co. KGaA, Weinheim

(silyl enol ether)s can be regarded as electroneutral 1,3-dicarbonyl dianion equivalents.[6–8]

Herein, we report the first cyclizations, to the best of our knowledge, of 1,3-bis(silyl enol ether)s with 1,1-diacetylcyclopentane and 1,1-diacetylcyclopropane. The reaction of 1,3-bis(silyl enol ether)s with 1,1-diacetylcyclopentane afforded spiro[5.4]cyclodecenones, which underwent a domino rearrangement upon treatment with trifluoroacetic acid (TFA). This transformation provided efficient access to functionalized bicyclo[4.4.0]deca-1,4-dien-3-ones with an angular methyl group. The products are of considerable pharmacological relevance and represent useful precursors for the synthesis of steroids (e.g. corticoids) and terpene analogues.[9] Furthermore, we report a novel [3+3] cyclization of 1,3-bis(silyl enol ether)s with 1,1-diacetylcyclopropane, which allows an efficient one-pot synthesis of salicylates that contain a halogenated side chain. The strategic placement of the latent functionality in these products makes them versatile intermediates for the synthesis of natural product analogues and electron-rich styrenes.[10]

The $TiCl_4$-mediated cyclization of the bis(silyl enol ether) **1a** ($R^1 = H$, $R^2 = OEt$) with 1,1-diacetylcyclopentane (**2a**)[11] afforded the spiroannulated 3-hydroxycyclohex-5-en-1-one **3a** in good yield (Scheme 2). The choice of Lewis acid, the temperature (−78→20 °C), and the presence of molecular sieves (4 Å) proved to be important parameters in the optimization of this reaction. The reaction of **3a** with TFA gave **5a** in high yield. The structure of **5a** was established by NMR spectroscopy (coupling constants, H,H COSY) and was independently confirmed by X-ray crystal-structure analysis (Figure 1).[12] The saturated six-membered ring has a distorted chair conformation; the cyclohexadienone moiety is slightly distorted from planarity. The formation of **5a** can be explained by an acid-catalyzed Wagner–Meerwein rearrangement (Scheme 2).[13] The intermediacy of the spiro compound **4** is supported by the fact that **4** could be isolated when the reaction was stopped after just 3 h. The structurally related isomer **6** was not isolated from the reaction mixture.

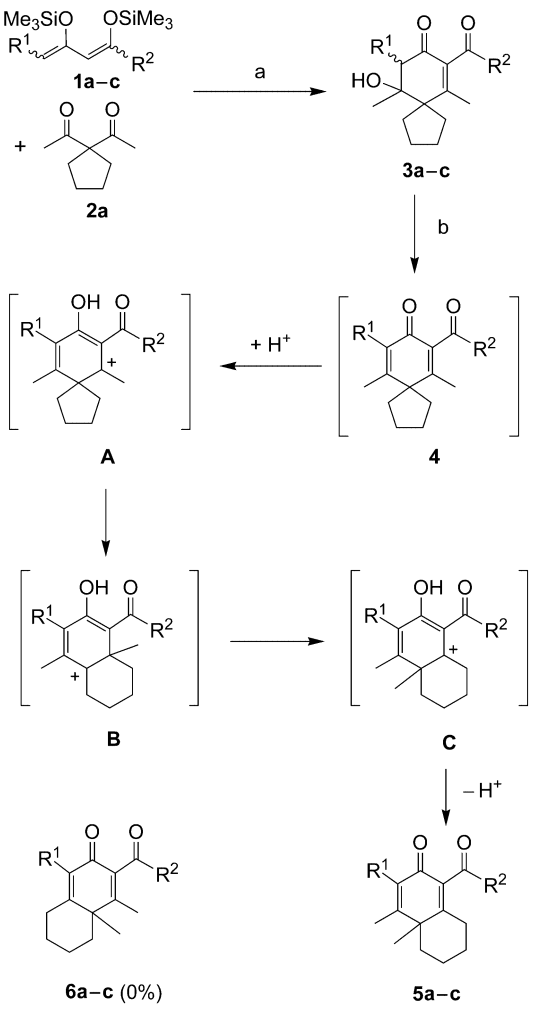
The 1,3-bis(silyl enol ether)s **1b** and **1c**, derived from acetylacetone and ethyl 3-oxohexanoate, respectively, were also used successfully as starting materials. The reaction of **2a** with **1b** and **1c** gave the spiro compounds **3b** and **3c**, which were transformed into the bicyclo[4.4.0]deca-1,4-dien-3-ones **5b** and **5c** in the presence of TFA (Table 1).

The reaction of the bis(silyl enol ether)s **1a** and **1b** with 2,2-diacetylindane (**2b**) afforded the spiro compounds **3d** and **3e**, respectively, in good yields (Scheme 3). Treatment of **3d** and **3e** with TFA afforded the interesting tricyclic products **5d** and **5e**, respectively, which can be regarded as 9,9a-dihydroanthracenes. The products were formed via inter-

Table 1: Synthesis of **3a–c** and **5a–c**.

Entry	R^1	R^2	Yields [%][a]	
			3	**5**
a	H	OEt	78	97
b	H	Me	67	95
c	Et	OEt	41[b]	88

[a] Yields of isolated products. [b] Diastereomeric mixture (4:1, assignment unclear).



Scheme 2. Cyclizations of 1,3-bis(silyl enol ether)s **1** with 1,1-diacetylcyclopentane (**2a**); a) 1. $TiCl_4$ (2.0 equiv), CH_2Cl_2, molecular sieves (4 Å), −78→20 °C, 2. H^+, H_2O; b) TFA, CH_2Cl_2, 72 h.

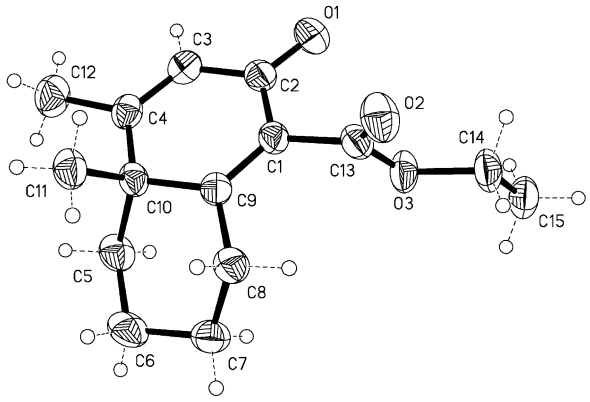
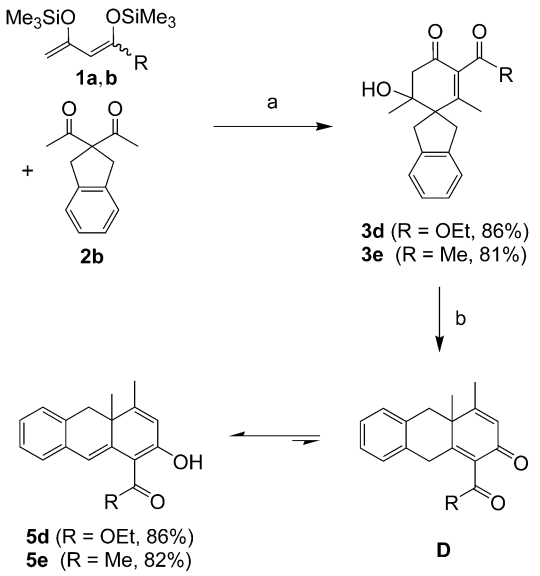


Figure 1. ORTEP plot of **5a**. Non-hydrogen atoms are represented by thermal ellipsoids of 50% probability. Selected bond lengths [Å] and angles [°]: O1-C2 1.227(2), C1-C9 1.345(2), C1-C2 1.473(2), C3-C4 1.335(3), C4-C10 1.509(2), C5-C6 1.520(3), C6-C7 1.517(3), C7-C8 1.532(2); C9-C1-C2 122.16(15), C1-C2-C3 122.52(17), C4-C3-C2 123.21(17), C6-C5-C10 113.67(14), C6-C7-C8 110.96(15).

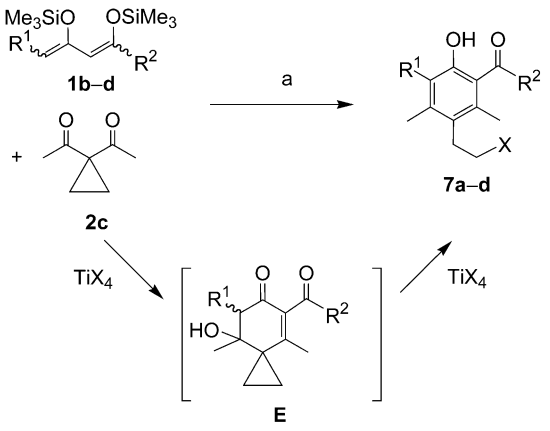
 © 2003 Wiley-VCH Verlag GmbH & Co. KGaA, Weinheim



Scheme 3. Cyclizations of 1,3-bis(silyl enol ether)s **1** with 2,2-diacetylindane (**2b**); a) 1. $TiCl_4$ (2.0 equiv), CH_2Cl_2, molecular sieves (4 Å), −78→20 °C, 2. H^+, H_2O; b) TFA, CH_2Cl_2, 72 h.

mediate **D** and reside in the thermodynamically more stable enol tautomeric form as a result of conjugation of the enol with the aryl ring.

An unexpected cyclization was observed in the reaction of the silyl enol ether **1d** with 1,1-diacetylcyclopropane (**2c**)[11] in the presence of $TiCl_4$ (Scheme 4).[14] The functionalized salicylic ester **7a**, which contains a chloro-substituted side



Scheme 4. Cyclizations of 1,3-bis(silyl enol ether)s **1** with 1,1-diacetylcyclopropane (**2c**); a) 1. TiX_4 (X = Cl, Br; 2.0 equiv), CH_2Cl_2, molecular sieves (4 Å), −78→20 °C, 2. H^+, H_2O.

chain, was isolated in 82 % yield. The use of $TiBr_4$ (in place of $TiCl_4$) resulted in the formation of the bromo-substituted salicylate **7b** in 80 % yield (Table 2).

The formation of **7a** can be explained by a $TiCl_4$-mediated cyclization with formation of the intermediate **E**. A subsequent $TiCl_4$-mediated cyclopropylcarbinyl→homoallyl rearrangement[14] and elimination of water afforded product **7a**.

Table 2: Synthesis of **7a–d**.

1	7	X	R^1	R^2	Yield of **7** [%][a]
d	**a**	Cl	H	OMe	82
d	**b**	Br	H	OMe	80
b	**c**	Cl	H	Me	68
c	**d**	Cl	Et	OEt	40

[a] Yields of isolated products.

The spiro[5.2]cyclooctenone **E** could be isolated in up to 55 % yield when only a small amount of $TiCl_4$ (0.5–0.7 equiv) was used. The use of larger quantities of the Lewis acid resulted in the formation of significant amounts of **7a**. The reaction of **2c** with the bis(silyl enol ether)s **1b** and **1c** afforded the functionalized salicylates **7c** and **7d** in good yields (Table 2). Further studies related to the scope and limitations of the cyclization reactions presented herein and their application in organic synthesis are in progress.

Experimental Section

Typical procedure for **3**: **3a**: $TiCl_4$ (0.22 mL, 2.0 mmol) was added dropwise at −78 °C under an argon atmosphere to a stirred solution of **2a** (0.154 g, 1.0 mmol) and **1a** (0.415 g, 1.5 mmol) in CH_2Cl_2 (100 mL) in the presence of molecular sieves (4 Å; 1.0 g). The reaction mixture was allowed to warm to 20 °C over 6 h, was stirred for an additional 6 h at 20 °C, and was then filtered. The filtrate was poured into an aqueous solution of HCl (10 %, 100 mL). The organic layer was collected, and the aqueous layer was extracted with CH_2Cl_2 (3 × 100 mL). The combined organic layers were dried (Na_2SO_4) and filtered, and the filtrate was concentrated in vacuo. The residue was purified by column chromatography (silica gel; hexane/ethyl acetate 3:2) to give **3a** (0.208 g, 78 %) as colorless crystals; m.p. 107–108 °C; $R_f = 0.35$ (hexane/ethyl acetate 1:1); IR (KBr): $\tilde{\nu} = 3410$ s, 2966 s, 1724 s, 1663 s, 1619 s, 1470 m, 1385 s, 1342 s, 1237 s, 1205 s, 1089 s, 1026 cm^{-1} m; ^1H NMR ($CDCl_3$, 300 MHz): $\delta = 4.29$ (q, 2H, $J = 7.2$ Hz; OCH_2), 2.64 (br, 2H; CH_2), 2.16 (br, 2H; CH_2), 1.98 (s, 3H; CH_3), 1.88 (br, 1H; OH), 1.76 (brs, 6H; CH_2), 1.32 (t, 3H, $J = 7.2$ Hz; CH_3), 1.26 ppm (s, 3H; CH_3); ^{13}C NMR ($CDCl_3$, 75 MHz): $\delta = 194.2$, 167.5, 164.6, 131.7 (C), 75.7 (C-OH), 61.5 (CH_2), 56.4 (C), 50.0, 33.5, 33.5, 28.5, 28.5 (CH_2), 25.1, 18.0, 14.4 ppm (CH_3); MS (EI, 70 eV): *m*/*z* (%): 266 (M^+, 9), 220 (52), 162 (100); elemental analysis: calcd for $C_{15}H_{22}O_4$: C 67.64, H 8.32; found: C 67.38, H 8.45. All compounds were characterized by spectroscopic methods and gave correct elemental analyses and/or high-resolution mass spectra.

Typical procedure for **5**: **5a**: TFA (0.4 mL, 5.2 mmol) was added dropwise at 20 °C to a stirred solution of **3a** (0.134 g, 0.5 mmol) in CH_2Cl_2 (0.4 mL) and the mixture was stirred until all the starting material had disappeared (72 h; monitored by TLC). The solvent and TFA were then removed in vacuo, and the residue was purified by column chromatography (silica gel; hexane/ethyl acetate 3:2) to give **5a** (0.120 g, 96 %) as colorless crystals; m.p. 79–80 °C; $R_f = 0.30$ (hexane/ethyl acetate 3:2); IR (KBr): $\tilde{\nu} = 2941$ s, 1730 s, 1658 s, 1630 m, 1447 m, 1390 m, 1324 w, 1265 s, 1245 s, 1050 cm^{-1} m; ^1H NMR ($CDCl_3$, 300 MHz): $\delta = 6.14$ (q, 1H, $^4J = 1.2$ Hz; C=CH), 4.33 (q, 2H, $J = 7.2$ Hz; OCH_2), 2.47–2.41 (m, 2H; CH_2), 2.12–1.98 (m, 2H; CH_2), 2.01 (d, 3H, $^4J = 1.2$ Hz; CH_3), 1.78–1.71 (m, 2H; CH_2), 1.44–1.37 (m, 2H; CH_2), 1.36 (s, 3H; CH_3), 1.34 ppm (t, 3H $J = 7.2$ Hz; CH_3); ^{13}C NMR ($CDCl_3$, 75 MHz): $\delta = 182.0$, 167.2, 166.0, 163.8, 131.1 (C), 126.3 (CH), 61.3 (CH_2), 43.2 (C), 37.6, 29.8, 28.1 (CH_2), 22.6 (CH_3), 21.2 (CH_2), 19.0, 14.2 ppm (CH_3); MS (EI, 70 eV): *m*/*z* (%): 248 (M^+, 71), 233 (46), 203 (72), 178 (100); elemental analysis: calcd for $C_{15}H_{20}O_3$: C 72.55, H 8.11; found: C 72.59, H 8.39.

 © 2003 Wiley-VCH Verlag GmbH & Co. KGaA, Weinheim

Typical procedure for **7**: **7a**: Compound **2c** (0.136 g, 1.1 mmol) was treated with **1d** (0.421 g, 1.6 mmol) in the presence of $TiCl_4$ (0.22 mL, 2.0 mmol), as described for the synthesis of **3**. Chromatography: silica gel; hexane/ethyl acetate 4:1. Compound **7a** (0.251 g, 82%) was obtained as colorless crystals; m.p. 73–74 °C; $R_f = 0.53$ (hexane/ethyl acetate 4:1); IR (KBr): $\tilde{\nu} = 3026$ m, 2906 s, 1657 s, 1601 m, 1574 m, 1468 m, 1437 s, 1355 s, 1239 s, 1151 m, 1072 m, 804 cm^{-1} s; ^1H NMR ($CDCl_3$, 300 MHz): $\delta = 10.68$ (s, 1H; OH), 6.70 (s, 1H; ArH), 3.95 (s, 3H; OCH_3), 3.51–3.46 (m, 2H; CH_2Cl), 3.12–3.06 (m, 2H; CH_2), 2.48 (s, 3H; CH_3), 2.32 ppm (s, 3H; CH_3); ^{13}C NMR ($CDCl_3$, 75 MHz): $\delta = 171.8$, 160.3, 144.2, 139.0, 127.1, 117.2, 111.9, 52.1, 42.2, 33.0, 21.0, 18.5 ppm; MS (EI, 70 eV): *m/z* (%): 244.5 ([*M*+2]$^+$, 15), 242.5 (M^+, 47), 212.5 (41), 210.4 (93), 161.4 (100); elemental analysis: calcd for $C_{12}H_{15}O_3Cl$: C 59.39, H 6.22; found: C 59.56 H 6.50.

Received: February 24, 2003
Revised: June 3, 2003 [Z51263]

Keywords: cyclizations · cyclopropanes · rearrangements · silyl enol ethers · spiro compounds

[1] L. F. Tietze, U. Beifuss, *Angew. Chem.* **1993**, *105*, 137; *Angew. Chem. Int. Ed. Engl.* **1993**, *32*, 131.
[2] L. Weiler, *J. Am. Chem. Soc.* **1970**, *92*, 6702.
[3] P. Langer, *Chem. Eur. J.* **2001**, *7*, 3858.
[4] a) V. Prelog, J. Würsch, K. Königsbacher, *Helv. Chim. Acta* **1951**, *34*, 258; b) M. Beringer, I. Kuntz, *J. Am. Chem. Soc.* **1951**, *73*, 364; c) S. H. Bertz, G. Dabbagh, *Angew. Chem.* **1982**, *94*, 317; *Angew. Chem. Int. Ed. Engl.* **1982**, *21*, 306; for intramolecular reactions of unsymmetrical derivatives, see: d) M. Yamaguchi, K. Hasebe, T. Minabi, *Tetrahedron Lett.* **1986**, *27*, 2401; e) S. G. Gilbreath, C. M. Harris, T. M. Harris, *J. Am. Chem. Soc.* **1988**, *110*, 6172.
[5] For the cyclization of a 1,3-dicarbonyl dianion with 3-(*N,N*-dimethylamino)-2-ethylacrolein, see: D. H. R. Barton, G. Dressaire, B. J. Willis, A. G. M. Barrett, M. Pfeffer, *J. Chem. Soc. Perkin Trans. 1* **1982**, 665.
[6] a) T.-H. Chan, P. Brownbridge, *J. Chem. Soc. Chem. Commun.* **1979**, 578; b) T.-H. Chan, P. Brownbridge, *J. Am. Chem. Soc.* **1980**, *102*, 3534; c) G. A. Molander, K. O. Cameron, *J. Am. Chem. Soc.* **1993**, *115*, 830.
[7] Review: P. Langer, *Synthesis* **2002**, 441.
[8] a) T. H. Chan, T. Chaly, *Tetrahedron Lett.* **1982**, *23*, 2935; b) P. Brownbridge, T.-H. Chan, M. A. Brook, G. J. Kang, *Can. J. Chem.* **1983**, *61*, 688.
[9] a) N. Ezaki, T. Shomura, M. Koyama, T. Niwa, M. Kojima, S. Inouye, T. Niida, *J. Antibiot.* **1981**, *34*, 1363; b) M. Kaneda, S. Nakamura, N. Ezaki, Y. Iitaka, *J. Antibiot.* **1981**, *34*, 1366; c) N. Ezaki, M. Koyama, T. Shomura, T. Tsuruoka, S. Inouye, *J. Antibiot.* **1983**, *36*, 1263; d) G. T. Carter, J. A. Nietsche, J. J. Goodman, M. J. Torrey, T. S. Dunne, M. M. Siegel, D. B. Borders, *J. Chem. Soc. Chem. Commun.* **1989**, 1271.
[10] *Römpp Lexikon Naturstoffe* (Eds.: B. Fugmann, S. Lane-Fugmann, W. Steglich), Thieme, Stuttgart, **1997**.
[11] The starting materials were prepared according to known procedures: a) N. S. Zefirov, S. I. Kozhushkov, T. S. Kuznetsova, R. Gleiter, M. Eckert-Maksic, *J. Org. Chem. USSR (Engl. Transl.)* **1986**, 95; b) O. Itoh, N. Iwakoshi, T. Saitoh, H. Katano, Y. Fujisawa, *Bull. Chem. Soc. Jpn.* **1982**, *55*, 177; c) W. Adam, T. Heidenfelder, C. Sahin, *Synthesis* **1995**, 1163; d) K. Beck, S. Hünig, *Chem. Ber.* **1987**, *120*, 477.
[12] CCDC 211439 (**5a**) contains the supplementary crystallographic data for this paper. These data can be obtained free of charge via www.ccdc.cam.ac.uk/conts/retrieving.html (or from the Cambridge Crystallographic Data Centre, 12, Union Road, Cambridge CB21EZ, UK; fax: (+44) 1223-336-033; or deposit@ccdc.cam.ac.uk).
[13] For acid-mediated dienone–phenol rearrangements, see: B. Hagenbruch, S. Hünig, *Chem. Ber.* **1983**, *116*, 3884.
[14] "Carbocyclic Three-Membered Ring Compounds": *Methods Org. Chem.* (Houben-Weyl) 4th ed. 1952–, *Vol. E17*, **1996**.

 © 2003 Wiley-VCH Verlag GmbH & Co. KGaA, Weinheim

A Mixed-Valence Copper Alkoxide

Template Synthesis and Theoretical Investigation of $[Cu^{II}_2Cu^{I}_3K_6(\mu_6\text{-}Cl)(\mu_3\text{-}O\mathit{t}Bu)_{12}]$: The First Mixed-Valence Copper Alkoxide**

Reinhart Ahlrichs, Christopher E. Anson, Dieter Fenske, Oliver Hampe, Alexander Rothenberger, and Marek Sierka*

In recent years we have investigated the syntheses, structures, and properties of a variety of copper–chalcogen clusters.[1] The general synthetic route to these species involves the reaction of CuX (X = halide, carboxylate) salts with tertiary phosphanes and subsequent reaction with trimethylsilyl chalcogenides. Recently, we have started to investigate the reactivity of copper alkoxides with trimethylsilyl chalcogen derivatives. A new feature of using alkoxides instead of copper(I) halides is the solubility and reactivity of the starting materials in organic solvents in the absence of tertiary phosphanes. These fundamentally different reaction conditions could thus give rise to a range of novel copper complexes.

In the course of these investigations we attempted to prepare CuO*t*Bu using an alternative procedure to the ones reported by Weiss et al. and Saegusa et al.[2] Our reaction of KO*t*Bu with copper(I) chloride in THF at room temperature afforded a dark green solution together with a red precipitate.

[*] Prof. Dr. D. Fenske, Dr. C. E. Anson, Dr. A. Rothenberger
Institut für Anorganische Chemie
Universität Karlsruhe
Engesserstrasse 15, 76131 Karlsruhe (Germany)
Fax: (+49) 721-608-8440
E-mail: dieter.fenske@chemie.uni-karlsruhe.de

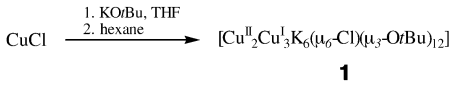
Prof. Dr. R. Ahlrichs, Dr. M. Sierka
Institut für Physikalische Chemie
Universität Karlsruhe
Fritz-Haber-Weg 4, 76131 Karlsruhe (Germany)

Dr. O. Hampe
Institut für Nanotechnologie (INT)
Forschungszentrum Karlsruhe GmbH
Postfach 3640, 76021 Karlsruhe (Germany)

[**] We gratefully acknowledge the DFG (Zentrum für funktionelle Nanostrukturen) and the Fonds der Chemischen Industrie for financial support. Thanks are due to Dr. A. Eichhöfer for the powder diffraction experiments.

 © 2003 Wiley-VCH Verlag GmbH & Co. KGaA, Weinheim DOI: 10.1002/anie.200351395

X-ray powder diffraction of the precipitate shows that it consists of a mixture of residual CuCl, copper, and the desired product Cu*O*t*Bu* (identified by X-ray analysis) together with KCl and other copper alkoxides, which were observed in the ESI-MS but could not be identified unambiguously. The green solution was collected by filtration and removal of solvent gave a green solid. From the hexane extract of this solid, single crystals of $[Cu^{II}_2Cu^{I}_3K_6(\mu_6\text{-}Cl)(\mu_3\text{-}O\textit{t}Bu)_{12}]\cdot$THF (**1a**) and $[Cu^{II}_2Cu^{I}_3K_6(\mu_6\text{-}Cl)(\mu_3\text{-}O\textit{t}Bu)_{12}]\cdot$hexane (**1b**) in a combined yield of approximately 4% were obtained (Scheme 1; see Experimental Section).



Scheme 1. Formation of **1** (**1a** = 1·THF, **1b** = 1·hexane).

The initial characterization of compounds **1** was hindered by the poor solubility of the complexes once isolated. Because of the green color and the deposition of copper during the reaction it was assumed that disproportion had resulted in a mixture of copper(I/II) alkoxides or $Cu(O\textit{t}Bu)_2$.[2]

The true nature of these species only became apparent once structurally characterized by X-ray crystallography.[13] Because **1b** has similar structural parameters, only the structural data for **1a** are discussed (Figure 1). Compound **1a** crystallizes in the space group $P6_3/m$ with two molecules in the unit cell.

The cage complex **1a** consists of a central trigonal prismatic K_6Cl unit in which the trigonal faces are each capped by a $[Cu^{II}(O\textit{t}Bu)_3]^-$ ion. The three tetragonal faces are bridged by three $[Cu^{I}(O\textit{t}Bu)_2]^-$ ions resulting in a mixed-valence copper(I/II) alkoxide.[3] The central chloride anion Cl(1) was unequivocally identified by its isotope pattern (ESI-MS); this ion acts as a template for the formation of the cluster. In contrast to the octahedral (NaCl structure) of KCl, the coordination environment around Cl(1) is a trigonal-prismatic arrangement of six potassium ions [K(1A)-Cl(1) 3.1202(8) Å in **1a**], an arrangement which maximizes the electrostatic interactions between the central K_6Cl unit and the monoanionic copper moieties $[Cu^{I}(O\textit{t}Bu)_2]^-$ and $[Cu^{II}(O\textit{t}Bu)_3]^-$ ions. All the oxygen atoms of the O*t*Bu ligands are μ^3-bridging between one copper atom and two potassium atoms. K–O separations in **1a** range from 2.641(5)–3.074(5) Å and are similar to K–O bond lengths observed in other potassium alkoxide complexes.[4] The two-coordinate Cu^{I} centers in **1a** have a slightly distorted linear coordination geometry (Cu-O 1.837(3) and 1.838(3) Å; O-Cu-O 174.40(14)°), a structural motif also found in other Cu^{I} alkoxides.[5] The O*t*Bu ligands of the $[Cu^{II}(O\textit{t}Bu)_3]^-$ units in **1a** show twofold disorder, which results from a Jahn–Teller distortion of the trigonal environment about Cu(1). The O-Cu^{II}-O bond angles in **1a** (O-Cu-O 102.2(6), 115.90(17), and 135.1(6)°) differ from the ones observed in $[KCu(\mu_2\text{-}O\textit{t}Bu)_3]\cdot$THF (O-Cu-O 91.9(2), 133.7(1)°) as a consequence of the coordination mode of the $[Cu(\mu_3\text{-}O\textit{t}Bu)_3]^-$ ion in **1a**.[6]

Investigation of the magnetic properties of **1a** suggested a very weak interaction between unpaired electrons of the $[Cu^{II}(O\textit{t}Bu)_3]^-$ units. SQUID measurements over the temperature range 2–300 K showed 85% of the molecules with spin $^1/_2$ with an indication of antiferromagnetic coupling only at low temperatures (below 10 K). A possible explanation for this behavior is that the $[Cu^{II}(O\textit{t}Bu)_3]^-$ units interact weakly enough to be detected independently most of the time. UV/Vis measurements, however, show weak d–d transitions at 683 nm indicating the presence of Cu^{II} centers.[7]

Quantum chemical calculations using density functional theory (DFT) were performed on the model complex $[Cu^{II}_2Cu^{I}_3K_6(\mu_6\text{-}Cl)(\mu_3\text{-}OMe)_{12}]$ **A**.[8] Test calculations on model compounds $[KCu^{I}(OMe)_2]$ (**2**) and $[KCu^{II}(OMe)_3]$ (**3**; Figure 2) and their *t*Bu analogues showed that the structural effects of this replacement of *t*Bu by Me are small.[9]. Additionally, the performance of the DFT method was

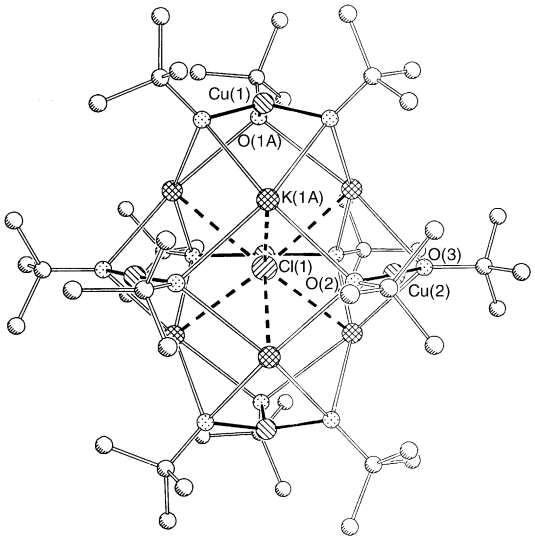


Figure 1. Molecular structure of **1a**. Selected bond lengths [Å] and angles [°] (hydrogen atoms and disordered components are omitted for clarity): Cl(1)-K(1A) 3.1202(8), K(1A)-O(2) 2.743(2), K(1A)-O(3) 2.732(3) Cu(1)-O(1A) 1.752(9), Cu(2)-O(2) 1.837(3), Cu(2)-O(3) 1.838(3), O(1A)-Cu(1)-O(1AA) 115.90(17), K(1)-Cl(1)-K(1) 131.458(11).

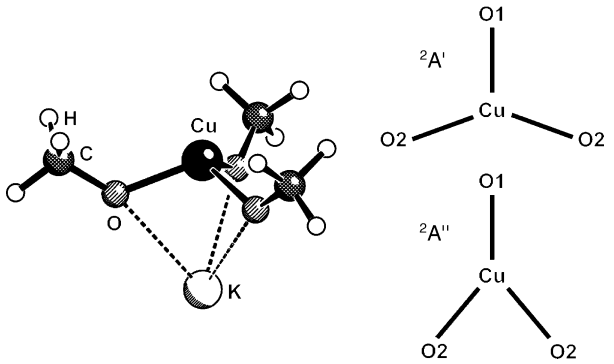


Figure 2. Left: calculated structure of the model compound $KCu^{II}(OMe)_3$ (**3**) in C_{3v} symmetry (Cu-O 1.91 Å, O-Cu-O 109°). Right: structural distortions of the CuO_3 unit because of the Jahn–Teller effect for $^2A'$ (distortion D1) and $^2A''$ (distortion D2) states. In $^2A'$ state: Cu-O1 1.96 Å, Cu-O2 1.86 Å; O2-Cu-O2 135°, O1-Cu-O2 102°. In the $^2A''$ state: Cu–O 1.9 Å; O2-Cu-O2 104°, O1-Cu-O2 114°.

 © 2003 Wiley-VCH Verlag GmbH & Co. KGaA, Weinheim

assessed by comparing with the results of MP2 calculations.[10] This comparison shows that Cu–O bond lengths obtained at the DFT level are overestimated by up to 0.07 Å.

The electronic structure of **A** is mainly determined by the weakly interacting d^9 copper atoms of the two $[Cu^{II}(OMe)_3]^-$ units. Calculations using C_{3v} symmetry constraints yielded a ^2E ground state arising from $Cu(3d_{x^2-y^2}, 3d_{xy})^3$ occupation with slight delocalization into 2p orbitals on oxygen atoms. According to Mulliken population analysis the unpaired electron is distributed over the CuO_3 unit with spin populations of 0.18 on the oxygen atoms and 0.4 on the Cu^{II} center. Owing to the partially filled degenerate e orbital, **3** is expected to show a first-order Jahn–Teller effect. Indeed, by lowering the symmetry to C_s we could identify two distorted structures containing a three-coordinate Cu^{II} center, which were 24 kJ mol^{-1} more stable than the ^2E state.[11] We classify the structural distortions as D1 and D2 (Figure 2).

The Jahn–Teller distortions of **A** were investigated by DFT calculations using various symmetries D_{3h}, C_{2v}, C_s, and C_1. In D_{3h} symmetry the three $[Cu^{I}(OMe)_2]^-$ and two $[Cu^{II}(OMe)_3]^-$ units show the same Cu–O bond lengths as in the compounds **2** in C_{2v} and **3** in C_{3v} symmetry.[12] This result indicates that the local electronic structure of these units is preserved in **A**. Whereas $[Cu^{I}(OMe)_2]^-$ units form a closed-shell subsystem, the two unpaired d electrons of the $[Cu^{II}(OMe)_3]^-$ units can now occupy two levels, e′ and e″, which can be viewed as combinations of two doubly degenerated e orbitals of $[Cu^{II}(OMe)_3]^-$ units with a local C_{3v} symmetry. Indeed, we found two $^3A_2'$ states, the lowest arising from $(e'')^2$ and a 4.7 kJ mol^{-1} higher state with $(e')^2$ occupation. Additionally, the results of Mulliken population analysis show significant spin populations only on the $[Cu^{II}(OMe)_3]^-$ units, 0.14–0.15 on the oxygen atoms and 0.4 on the copper atoms. Thus the electronic states of **A** are determined by the two weakly interacting d^9 copper atoms of the $[Cu^{II}(OMe)_3]^-$ moieties.

The Jahn–Teller distortions of the two $[Cu^{II}(OMe)_3]^-$ units in **A** can be classified in terms of D1 and D2 distortions observed in **3**. In C_{2v} symmetry we found two distorted structures with energies lower by 23.7 and 22.9 kJ mol^{-1} than the most stable D_{3h} structure. In the first structure the $[Cu^{II}(OMe)_3]^-$ moieties show D1, and in the second D2 distortions. The two unpaired electrons show occupations $(a_1)^1(b_2)^1$ and $(a_2)^1(b_1)^1$, respectively (both structures have a $^3B_2$ ground state).

In C_s symmetry a third structure is found where the coordination environment of the two copper(II) centers differs, one has D1 and the other D2 distortion. It has a $^3A''$ ground state and is 25 kJ mol^{-1} more stable than the most stable D_{3h} structure. We could also identify a $^1A''$ state only 0.7 kJ mol^{-1} higher in energy. It arises from antiparallel electron coupling of the two d^9 Cu^{II} centers and has a structure very similar to the $^3A''$ state. Finally, lowering symmetry to C_1 yielded virtually degenerate ^3A and ^1A states with almost identical structures. They are 38 kJ mol^{-1} more stable than the most stable D_{3h} structure and show two D1 distortions which are rotated with respect to each other.

Table 1 shows selected structural parameters calculated for the model complex **A** and compares them with experimental results obtained from X-ray analysis of **1a**. Except for the Cu(1)-O(1A) bond all the other bond lengths agree within 0.05 Å to the experimental values. The overestimation of the Cu^{II}–O bond by the DFT method in comparison to MP2 results was also observed for complexes **2** and **3**, and explains the deviation in the Cu(1)-O(1A) bond length.

Table 1: Comparison of selected calculated bond lengths [Å] with experimentally determined (see Figure 1 and 2).

Parameter	DFT (**A**)	Experimental (**1a**)
Cu(1)-O(1A)	1.86–1.88	1.752(9)
Cu(1)-O(1B)	1.91–1.93	1.915(13)
Cu(2)-O(2)	1.85–1.86	1.837(3)
Cu(2)-O(3)		1.838(3)
K(1A)-O(2)	2.72–2.82	2.743(2)
K(1A)-O(3)		2.732(3)
K(1A)-Cl(1)	3.15–3.27	3.1202(8)

Both experimental and theoretical investigations suggest that the $[Cu^{II}(tBu)_3]^-$ units in **1a** are very flexible ligands and can distort in a variety of ways to stabilize a coordination environment which is unprecedented for Cu^{II} alkoxy ligands. Copper(I) halides can undergo disproportion in reactions with alkali-metal alkoxides providing an easy access to mixed-valence copper(I/II) alkoxides stabilized by a halide template. Only recently we obtained the KBr analogue of **1** showing that the route chosen should be applicable to a range of alkali-metal halide templates.

Experimental Section

All operations were carried out in an atmosphere of purified Argon. THF was heated to reflux over potassium and freshly distilled before use. Hexane was dried over $LiAlH_4$. KO*t*Bu was purchased from Aldrich and used without further purification. Commercially available CuCl was suspended in dilute hydrochloric acid, collected by filtration, and washed with degassed water, ethanol, and absolute diethyl ether.

1: A solution of KO*t*Bu (5.60 g, 50.0 mmol) in THF (80 mL) was added to a suspension of CuCl (4.90 g, 50.0 mmol) in THF (80 mL) and stirred at room temperature for about 8 h. The dark green solution was separated by filtration from the red precipitate and the solvent removed under reduced pressure. The residue (ca. 4.8 g) is extracted with hexanes (200 mL). Storage of the green solution for a week at −40 °C produced ellipsoidal crystals of **1a** and green blocks of **1b** suitable for X-ray diffraction studies. Yield 0.65 g (4%) single crystals. Yield of solid after hexane extraction and subsequent removal of solvent approximately 2.7 g **1** (18%). M.p. 190 °C (decomp.); ESI-MS (hexane, THF) *m/z* 209 $[Cu(OtBu)_2]^-$ other peaks were observed up to *m/z* 843 but could not be assigned. Distances between peaks indicated decomposition of higher Cu-alkoxide species into isobutene [$\Delta_{peaks}m/z$ 56] and copper oxide; a chlorine isotope pattern was observed in the cation ESI-MS *m/z* 466.6; UV/Vis (hexane): λ_{max} (ε) 689.06 (ca. 1729), 750 (1453); IR (CsI and Nujol) $\tilde{\nu}$ = 974 (C-O), 478, 428, 351 cm^{-1} [O-CMe]; Elemental analysis (%) calcd for **1a** $C_{52}H_{116}ClCu_5K_6O_{13}$: C 40.6, H 7.6; found: C 40.6, H 7.9.

Received: March 13, 2003
Revised: June 2, 2003 [Z51395]

 © 2003 Wiley-VCH Verlag GmbH & Co. KGaA, Weinheim

Keywords: copper · density functional calculations · mixed-valence compounds · template synthesis · X-ray diffraction

[1] S. Dehnen, A. Eichhöfer, D. Fenske, *Eur. J. Inorg. Chem.* **2002**, 279 – 317, and references therein.

[2] a) T. Tsuda, T. Hashimoto, T. Saegusa, *J. Am. Chem. Soc.* **1972**, *94*, 658 – 659; b) T. Greiser, E. Weiss, *Chem. Ber.* **1976**, *109*, 3142 – 3146.

[3] For other examples of mixed-valence Cu^{I}/Cu^{II} complexes see D. D. LeCloux, R. Davydov, S. J. Lippard, *Inorg. Chem.* **1998**, *37*, 6814 – 6826, and references therein.

[4] see, for example, a) W. Clegg, A. M. Drummond, S. T. Liddle, R. E. Mulvey, A. Robertson, *Chem. Commun.* **1999**, 1569 – 1570; b) P. C. Andrews, G. D. Fallon, M. Maguire, A. C. Peatt, *Angew. Chem.* **2000**, *112*, 4690 – 4692; *Angew. Chem. Int. Ed.* **2000**, *39*, 4516 – 4518.

[5] a) A. P. Purdy, C. F. George, *Polyhedron* **1995**, *14*, 761 – 769; b) A. P. Purdy, C. F. George, J. H. Callahan, *Inorg. Chem.* **1991**, *30*, 5013 – 5015; c) B. Borup, W. E. Streib, K. G. Caulton, *Inorg. Chem.* **1997**, *36*, 5058 – 5063.

[6] R. Becker, J. Weiß, M. Winter, K. Merz, R. A. Fischer, *J. Organomet. Chem.* **2001**, *630*, 253 – 262.

[7] A. B. P. Lever, *Inorganic Electronic Spectroscopy*, 2nd ed., Elsevier, Amsterdam, **1984**, p. 554.

[8] All calculations were performed with the TURBOMOLE program package. a) R. Ahlrichs, M. Bär, M. Häser, H. Horn, C. Kölmel, *Chem. Phys. Lett.* **1989**, *162*, 165 – 169; b) O. Treutler, R. Ahlichs, *J. Chem. Phys.* **1995**, *102*, 346 – 354. We used the Becke-Perdew (BP86) exchange-correlation functional within the resolution of the identity (RI) approximation; c) A. D. Becke, *Phys. Rev. A* **1988**, *38*, 3098 – 3100; d) S. H. Vosko, L. Wilk, M. Nusair, *Can. J. Phys.* **1980**, *58*, 1200 – 1211; e) J. P. Perdew, *Phys. Rev. B* **1986**, *33*, 8822 – 8824; erratum: J. P. Perdew, *Phys. Rev. B* **1986**, *34*, 7406; f) K. Eichkorn, O. Treutler, H. Öhm, M. Häser, R. Ahlrichs, *Chem. Phys. Lett.* **1995**, *242*, 652. The basis and auxiliary basis set used in the DFT calculations was triple-valence basis and auxiliary basis sets with one polarization function (TZVP); g) A. Schäfer, H. Horn, R. Ahlrichs, *J. Chem. Phys.* **1992**, *97*, 2571 – 2577; h) A. Schäfer, C. Huber, R. Ahlrichs, *J. Chem. Phys.* **1994**, *100*, 5829 – 5835; i) K. Eichkorn, F. Weigend, O. Treutler, R. Ahlrichs, *Theor. Chem. Acc.* **1997**, *97*, 119 – 124.

[9] Calculations on **2** in C_{2v} and **3** in C_{3v} symmetry. Differences of Cu–O bond distances are less than 0.01 Å and of O-Cu-O bond angles less than 2°.

[10] The MP2 calculations with frozen-core approximation were carried out using the RI-MP2 method and TZVPP basis and auxiliary basis sets on all atoms. a) F. Weigend, M. Häser, *Theor. Chem. Acc.* **1997**, *97*, 331 – 340; b) F. Weigend, *Phys. Chem. Chem. Phys.* **2002**, *4*, 4285 – 4291.

[11] Additionally, two even more stable structures were found with almost planar CuO_3 unit and twofold coordinate potassium atom. However, the threefold coordinate potassium structures correspond closer to the $[Cu^{II}(OMe)_3]$ units in **A**.

[12] Only the O-Cu-O bond angles change owing to a different coordination of potassium atoms. The O-Cu^{I}-O bond angles increase from 138° to 174° and the O-Cu^{II}-O bond angles from 109° to 117°.

[13] Crystallography: Data were measured on a Stoe IPDS II image-plate diffractometer using graphite-monochromated $Mo_{K\alpha}$ radiation ($\lambda = 0.71073$ Å). The structures were solved by direct methods and refined by full-matrix least-squares on F^2 (all data) using the SHELXTL software package.[14] Hydrogen atoms were placed in calculated positions, non-hydrogen atoms were assigned anisotropic thermal parameters. Crystal data for **1a**; $C_{52}H_{116}ClCu_5K_6O_{13}$; $M_r = 1537.20$; hexagonal, space group $P6_3/m$; $Z = 2$; $a = 14.764(2)$, $c = 19.966(4)$ Å; $V = 3769.3(11)$ Å^3; $T = 100(2)$ K; $F(000) = 1616$; $\rho_{calcd} = 1.354$ g cm^{-3}. 15547 reflections measured, of which 3150 unique ($R_{int} = 0.0572$). 213 parameters; final $wR_2 = 0.1468$, $S = 1.146$ (all data); $R_1 = 0.0495$ {3035 data with $I > 2\sigma(I)$}; largest difference peak and hole +0.62, −0.70 e Å^{-3}. The O*t*Bu ligand coordinated to Cu(1) showed twofold disorder. K(1) was also disordered over two positions, and this disorder correlated with that of the O*t*Bu ligand, the occupancies were fixed with a 2:1 ratio. Attempts to refine an ordered structure in monoclinic $P2_1/m$ with threefold twin ("Drilling") were unsuccessful. The THF molecule lies on a $\bar{3}$ site, and is heavily disordered. Crystal data for **1b**; $C_{54}H_{122}ClCu_5K_6O_{12}$; $M_r = 1551.27$; triclinic, space group $P\bar{1}$; $Z = 2$; $a = 14.4730(6)$, $b = 15.1819(7)$, $c = 18.0926(10)$ Å; $\alpha = 93.411(4)$, $\beta = 91.313(4)$, $\gamma = 91.833(3)$°; $V = 3965.1(3)$ Å^3; $T = 100(2)$ K; $F(000) = 1636$; $\rho_{calcd} = 1.299$ g cm^{-3}. 17628 reflections measured, of which 13965 unique ($R_{int} = 0.0349$). 936 parameters; final $wR_2 = 0.1695$, $S = 1.026$ (all data); $R_1 = 0.0586$ {12280 data with $I > 2\sigma(I)$}; largest difference peak and hole +0.84, −0.88 e Å^{-3}. Eleven of the O*t*Bu ligands were disordered, and, as in **1a**, this generally involved a pivoting about the tertiary carbon. Refinement of occupancies resulted in an approximately 7:3 ratio for all the ligands coordinated to the Cu^{II} centers, Cu(1) and Cu(2), and also for three of those coordinated to the Cu^{I} center. Consideration of intermolecular steric interactions between *t*Bu groups indicated that the disorder of these nine ligands was correlated, two other ligands showed 50:50 disorder. CCDC-205464 (**1a**) and CCDC-205465 (**1b**) contain the supplementary crystallographic data for this paper. These data can be obtained free of charge via www.ccdc.cam.ac.uk/conts/retrieving.html (or from the Cambridge Crystallographic Data Centre, 12 Union Road, Cambridge CB2 1EZ, UK; fax: (+44) 1223-336-033; or deposit@ccdc.cam.ac.uk).

[14] G. M. Sheldrick, SHELXTL-97, University of Göttingen, Göttingen (Germany), **1997**.

 © 2003 Wiley-VCH Verlag GmbH & Co. KGaA, Weinheim

Proton Sponges

DFT Calculations on a New Class of C_3-Symmetric Organic Bases: Highly Basic Proton Sponges and Ligands for Very Small Metal Cations

*Götz Bucher**

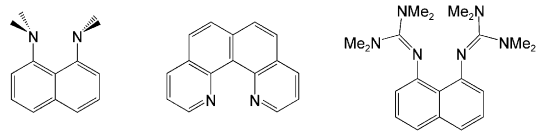
The design and synthesis of strong organic bases has long been an active field of research.[1–4] Extremely high basicity can be achieved by different strategies. Spatial overlap of lone

[*] Dr. G. Bucher
Lehrstuhl für Organische Chemie II
Ruhr-Universität Bochum
Universitätsstrasse 150, 44780 Bochum (Germany)
Fax: (+49) 234-3214-353
E-mail: goetz.bucher@rub.de

Supporting information for this article is available on the WWW under http://www.angewandte.org or from the author.

 DOI: 10.1002/anie.200351648 © 2003 Wiley-VCH Verlag GmbH & Co. KGaA, Weinheim

pairs leads to destabilization and thus enhanced basicity. This concept has repeatedly been employed with nitrogen bases. It led to the synthesis of proton sponges, such as 1,8-bis(dimethylamino)naphthalene (**1**)[5] and derivatives or quino[7,8-*h*]quinoline (**2**).[6] The basicity of these compounds does not



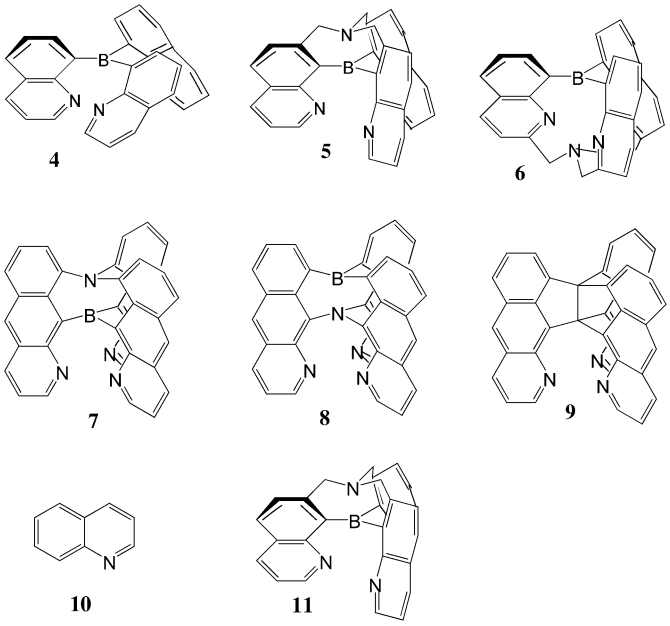
1 **2** **3**

only derive from the overlap of two nitrogen lone pairs in the free bases, but is also due to the formation of a strong intramolecular hydrogen bridge in the monoprotonated compounds.

The conjugate acids of certain organic bases, such as guanidines, are more strongly stabilized by resonance than the free bases which also leads to compounds of significantly increased basicity.[7a,b] The systematic exploitation of this strategy has led to the synthesis of exceedingly basic species, such as vinamidines[7c] or polyphosphazenes.[8] The two concepts can also be combined, as has recently been demonstrated by the synthesis of the highly basic 1,8-bis(tetramethylguanidino)naphthalene (**3**).[9]

To date, all known examples of proton sponges involve two nitrogen lone pairs. Herein the possibility of achieving even more basic systems through the interaction of three or four nitrogen lone pairs, and of possibly obtaining a C_3-symmetric hydrogen bridge is addressed. Molecules with threefold symmetry can be obtained by joining three identical ligands with a nitrogen or boron atom.

The bases introduced herein build on the framework of *syn*-tris-8-quinolylborane (**4**). Additional bridging of **4** by a C_3-symmetric $(CH_2)_3N$ bridge either in the 7-position (→**5**) or in 2-position (→**6**) reduces the conformational flexibility of



4 **5** **6**

7 **8** **9**

10 **11**

tris-8-quinolylborane unit and forces the nitrogen lone pairs into close proximity. The use of a nitrogen and a boron atom as molecular axis of threefold symmetry offers the advantage of a stabilizing intramolecular N–B donor–acceptor bond.[10] The benzoquinolines **7**–**9** were calculated to investigate the influence of a more rigid molecular framework. The choice of B and N in different sequence (**7** or **8**) or of two C atoms (**9**) as central atoms makes it possible to vary the space between the N atoms. To investigate the influence of the third lone pair, the bridged bis(quinolyl)phenylborane **11** was calculated. While having a similar structure of the basic center, in compound **11** an interaction of only two lone pairs takes place.

The geometries and vibrational spectra of **4**–**9** as well as of quinoline **10** and quino[7,8-*h*]quinoline **2** as reference compounds, each in different stages of protonation, were calculated by standard density functional theory (B3LYP/6-31G(d)). For the calculation of gas-phase proton affinities single-point calculations employing a larger basis set were performed (see Methods Section). Proton affinities in acetonitrile ($PA(CH_3CN)$) were calculated according to the isodensity surface polarized continuum model (ipcm).[11] The pK_a values of the conjugate acids in acetonitrile were obtained from $PA(CH_3CN)$ by Equation (1).[12]

$$pK_a(\text{theor}) = 0.72888\,PA(CH_3CN) - 189.5 \quad (1)$$

The results are displayed in Table 1. Relevant geometric parameters chosen are the N–H and N–N separations which are important for characterization of the intramolecular hydrogen bridges, as well as the $\alpha_{N\text{-}H\text{-}N'}$ bond angles. If applicable, the B–N (or C–C in the case of **9**) bond lengths and the dihedral around the central N–B unit (δ_{CNBC}) are also tabulated. The latter indicates the degree of propeller-shape assumed by the molecule.

The results show that in **5**–**9** the forced proximity of three nitrogen atoms leads to a basicity that is far greater than that of **2**, although the N–N separation (which is a determining factor for the destabilizing interaction of the lone pairs) is shorter in **2** (274 pm) than in **5**–**9** (between 289 pm in **6** and 343 pm in **5**). While the pK_a value of the conjugate acid of **2** ($pK_a(MeCN) = 19.2$) exceeds the pK_a value of the conjugate acid of the reference compound **10** (12.2) by 7 units, the C_3-symmetric proton sponges have pK_a values, that are higher by 6.8 (**5**, 26.0) to 11 units (**6**, 30.2). In particular **6** is predicted to show a basicity approaching that of the most basic known neutral nitrogen bases.[12,7] Taking the *syn* conformer of **4** ($pK_a(MeCN) = 14.5$) as reference compound reveals that the additional bridging in **5** or **6** results in a gain in basicity of 11.5 (**5**) to 15.7 (**6**) units. This, however, only applies to the free bases. The differences are significantly less pronounced for the monoprotonated compounds, while in the case of the diprotonated compounds the more flexible system **4** shows a higher basicity than **5** or even **6** (**6**/2H$^+$: $pK_a = -15.2$).

The bases **4**–**9** are propeller-shaped and thus have C_3 and not D_{3d} symmetry. For **5** and **6**, the deviation from D_{3d} symmetry is defined over the dihedral angle δ_{CNBC}, which is given by C(H_2)-N-B-C8.[13] In **7** it is defined by C9, N, B, and C10. In general, δ_{CNBC} ranges between 15.2° (**7**) and 34.0° (**6**).

 © 2003 Wiley-VCH Verlag GmbH & Co. KGaA, Weinheim

Table 1: Calculated geometric parameters, proton affinities (PA), and pK_a values of bases **2** and **4**–**11** and their conjugate acids.[a]

Compound	δ_{CNBC}	$R_{B\text{-}N}$	$R_{N\text{-}H}$	$R_{N'\text{-}H}$	$R_{N'\text{-}N}$	$A_{N\text{-}H\text{-}N'}$	PA(Gas)[b]	PA(MeCN)[c]	pK_a(theor)[d]
10	–	–	–	–	–	–	228.0	276.7	12.2
10/H$^+$	–	–	102	–	–	–	–	–	–
2	–	–	–	–	274	–	253.7	286.3	19.2
2/H$^+$	–	–	105	173	263	140.4	–	n.c.[e]	n.c.[e]
4		–	–	–		–	251.8	279.9	14.5
4/H$^+$	–	–	105	179	282	163.8	175.3	273.0	9.5
4/2H$^+$	–	–	104	197	297	161.8	112.8	269.1	6.6
			104	195	298	176.3			
4/3H$^+$	–	–	102	394	488	155.6	–	–	–
5	28.1	172	–	–	343	–	265.6	295.6	26.0
5/H$^+$	21.6	170	105	189	288	154.8	185.8	273.7	10.0
5/2H$^+$	19.6	169	104	191	294	164.0	102.4	263.3	2.4
			104	193	294	174.0			
5/3H$^+$	31.9	165	102	309	408	162.5	–	–	–
5/Be^{++}	17.3	166	167[f]	–	289	120.0[g]	–	–	–
5/Mg^{++}	25.7	164	204[h]	–	353	119.9[i]	–	–	–
6	34.0	457	–	–	289	–	268.1	301.4	30.2
6/H$^+$	18.6	456	105	199	284	136.2	176.7	270.5	7.7
	20.2			206	285	119.8			
6/2H$^+$	1.2	460	103	186	288	169.0	79.9	239.2	−15.2
6/3H$^+$[k]	27.0	449	101	212	312	170.0	–	–	–
7	15.2	183	–	–	337	–	264.5	292.5	23.7
7/H$^+$	4.4	179	105	194	288	148.2	n.c.[e]	n.c.[e]	n.c.[e]
8	22.1	180	–	–	303	–	255.4	290.3	22.1
8/H$^+$	17.1	188	106	171	272	159.6	n.c.[e]	n.c.[e]	n.c.[e]
9	19.3	162[j]	–	–	313	–	262.3	290.2	22.0
9/H$^+$	11.0	164[j]	105	176	275	156.7	n.c.[e]	n.c.[e]	n.c.[e]
11	25[l]	173	–	–	335	–	257.4	290.3	22.1
11/H$^+$	20[l]	170	105	181	284	165.4	–	–	–

[a] All bond lengths [pm] and bond angles [°] calculated with B3LYP/6-31G(d). [b] Calculated with B3LYP/6-311+G(d,p)//B3LYP/6-31G(d), in kcal mol^{-1}. [c] Calculated with ipcm B3LYP/6-31G(d), in kcal mol^{-1}. [d] pK_a value of conjugate acid. [e] n.c. = not calculated. [f] $R_{N\text{-}Be}$. [g] $\alpha_{N\text{-}Be\text{-}N'}$. [h] $R_{N\text{-}Mg}$. [i] $\alpha_{N\text{-}Mg\text{-}N'}$. [j] C–C bond length of the central bond of the triquinacene framework. [k] Protonation of the quinoline nitrogen atoms [l] Average of all three δ_{CNBC}.

The values are smaller for the benzoquinolines **7**–**9** than for the bridged methylquinolines **5** and **6**, which is due to the lower flexibility of the benzoquinolines. The benzoquinolines can only avoid D_{3d} symmetry by giving up planarity of the benzoquinoline unit. Some of the mono- and diprotonated compounds are predicted to show significantly reduced values of δ. In particular the dication of **6** (**6**/2H$^+$) is almost C_S symmetric ($\delta = 1.2°$). The intramolecular N-H-N hydrogen bridges of the monoprotonated compounds of **5**–**9** are generally unsymmetrical. The N–H bond lengths are only slightly elongated compared to the reference compound **10**/H$^+$. The N–N′ separations of the monoprotonated compounds (ranging from 275 pm (**9**/H$^+$) to 288 pm (**5**/H$^+$)) are slightly longer than the N–N′ separations of the reference proton sponge **2**/H$^+$ (263 pm). Also, the N-H-N bond angles of the monoprotonated compounds deviate from the ideal value of 180° (A ranges from 136.2° (**6**/H$^+$) to 159.6° (**8**/H$^+$)).

A comparison with the model compound **11** is of particular interest. In the case of **11**, the interaction of two nitrogen lone pairs leads to a high basicity (pK_a(MeCN) = 22.1). This value lies four units below the pK_a value of the analogous tris(quinoline) base **5**. A comparison of the N-H-N′ bond angle of the intramolecular hydrogen bridge in **5**/H$^+$ ($\alpha = 154.8°$) and **11**/H$^+$ ($\alpha = 165.4°$) shows that the presence of a third nitrogen lone pair in **5**/H$^+$ results in a stronger deviation from the ideal value of $\alpha = 180°$. Also, N′–H separation is larger in **5**/H$^+$ than in **11**/H$^+$, while the N–H separation is the same in both systems. The fact that **5** is predicted to be a stronger base than **11** thus shows that the destabilizing interaction of three lone pairs is more pronounced for the free bases than for the monoprotonated species.

In the case of proton sponge **6**, four nitrogen lone pairs are in close proximity. In this system, the tertiary amine should have basic character too, as an intramolecular donor–acceptor bond to boron cannot be formed. Protonation of **6** should thus also be possible at the tertiary amine moiety, in both *endo* and *exo* positions. The pK_a(MeCN) value for *exo*-protonation is calculated as 6.8 which corresponds to a PA(CH_3CN) = 269.3 kcal mol^{-1}. This extremely low basicity is because the nitrogen atom of the tris(quinolylmethyl)amine moiety in **6** has almost trigonal-planar coordination (calculated dihedral angle C-N-C-C = 174°). The lone pair thus has almost pure p character.[14] In *exo*-monoprotonated **6**/H$^+$(*exo*) the dihedral angle C-N-C-C is calculated to be 140°, thus deviating strongly from the ideal value of 120°. *Endo*-monoprotonation of the tertiary nitrogen atom is not possible according to the calculations. An attempted geometry optimization instead gave the geometry of **6**/H$^+$ (monoprotonation in the tris(quinoline) system).

 © 2003 Wiley-VCH Verlag GmbH & Co. KGaA, Weinheim

The proton is bound by **5**–**9** through an unsymmetrical N-H···N hydrogen bridge. C_3-symmetric coordination of the three quinoline nitrogen atoms should be possible in the case of metal cation complexation in the cavity of **5**–**9**. Owing to the small size of the cavity (N–N = 343 pm for **5**) only the smallest metal cations have to be considered. Selected geometric parameters for **5**/Be^{2+} and **5**/Mg^{2+} are given in Table 1. The data show that complexation of a Be^{2+} ion should lead to similar changes of the host geometry as protonation, whereas complexation of the larger Mg^{2+} ion should result in larger N–N separations and in a more pronounced twisting of the molecule. Nevertheless, a perfectly shielded beryllium ion is only expected to be found in the gas phase or in aprotic solvents. Semiempirical calculations (PM3)[15] for the system **5** + Be^{2+} + 6 H_2O indicate, that the presence of water should lead to the formation of additional O-H-N hydrogen bridges, to a more pronounced twisting of the molecule, and to larger N–N separations.

In conclusion, interaction of three nitrogen lone pairs should lead to a dramatic increase of the basicity of quinoline derivatives. Furthermore, the tris(quinolyl)boranes **5** and **6** should be interesting three-dimensional chelating ligands for very small metal cations such as Be^{2+} or Mg^{2+}. The synthesis of **5** and **6** is in preparation.

Methods Section

All calculations were performed with the Gaussian 98 suite of programs.[16] All stationary points were unambiguously characterized as minima by calculating their vibrational spectra. The calculated energies include a zero-point vibrational-energy correction. The B3LYP hybrid functional[17] in connection with a 6-31G(d) basis was employed for geometry optimizations and calculations of IR spectra. In addition, for all molecules investigated a single-point-calculation employing a larger basis set (B3LYP/6-311 + G(d,p)//B3LYP/6-31G(d)) was performed. Proton affinities in acetonitrile were calculated according to the isodensity surface polarized continuum model (method: B3LYP/6-31G(d)).[11]

Received: April 14, 2003 [Z51648]

Keywords: density functional calculations · organic bases · proton sponges

[1] F. Hibbert, *Acc. Chem. Res.* **1984**, *17*, 115 – 120.
[2] H. A. Staab, T. Saupe, *Angew. Chem.* **1988**, *100*, 895 – 1040; *Angew. Chem. Int. Ed. Engl.* **1988**, *27*, 865 – 879.
[3] R. W. Alder, *Chem. Rev.* **1989**, *89*, 1215 – 1223.
[4] R. W. Alder, *Tetrahedron* **1990**, *46*, 683 – 713.
[5] a) W. G. Brown, N. J. Netang, *J. Am. Chem. Soc.* **1941**, *63*, 358 – 361; b) R. W. Alder, P. S. Bowman, W. R. S. Steele, D. R. Winterman, *Chem. Commun.* **1968**, 723 – 724; c) R. W. Alder, N. C. Goode, N. Miller, F. Hibbert, K. P. Hunte, H. J. Robbins, *J. Chem. Soc. Chem. Commun.* **1978**, 89 – 90; d) R. W. Alder, M. R. Bryce, N. C. Goode, N. Miller, J. Owen, *J. Chem. Soc. Perkin Trans. 1* **1981**, 2840 – 2847; e) R. W. Alder, M. R. Bryce, N. C. Goode, *J. Chem. Soc. Perkin Trans. 2* **1982**, 477 – 483; f) F. Hibbert, K. P. Hunte, *J. Chem. Soc. Perkin Trans. 2*, **1983**, 1895 – 1899.
[6] M. A. Zirnstein, H. A. Staab, *Angew. Chem.* **1987**, *99*, 460 – 461; *Angew. Chem. Int. Ed. Engl.* **1987**, *26*, 460 – 461.
[7] a) Z. B. Maksic, B. Kovacevic, *J. Org. Chem.* **2000**, *65*, 3303 – 3309; b) B. Kovacevic, T. Glasovac, Z. B. Maksic, *J. Phys. Org. Chem.* **2002**, *15*, 765 – 774; c) R. Schwesinger, M. Mißfeldt, K. Peters, H. G. von Schnering, *Angew. Chem.* **1987**, *99*, 1210 – 1212; *Angew. Chem. Int. Ed. Engl.* **1987**, *26*, 1165 – 1166.
[8] a) R. Schwesinger, H. Schlemper, *Angew. Chem.* **1987**, *99*, 1212 – 1214; *Angew. Chem. Int. Ed. Engl.* **1987**, *26*, 1167 – 1169; b) R. Schwesinger, H. Schlemper, C. Hasenfratz, J. Willaredt, T. Dambacher, T. Breuer, C. Ottaway, M. Fletschinger, J. Boele, H. Fritz, D. Putzas, H. W. Rotter, F. G. Bordwell, A. V. Satish, G.-J. Ji, E.-M. Peters, K. Peters, H. G. von Schnering, L. Walz, *Liebigs Ann.* **1996**, 1055 – 1081.
[9] a) V. Raab, J. Kipke, R. M. Gschwind, J. Sundermeyer, *Chem. Eur. J.* **2002**, *8*, 1682 – 1693; b) B. Kovacevic, Z. B. Maksic, *Chem. Eur. J.* **2002**, *8*, 1694 – 1702.
[10] This does not apply to **6**. In this molecule the N and B atoms are too far apart to form a N–B donor/acceptor bond.
[11] J. B. Foresman, T. A. Keith, K. B. Wiberg, J. Snoonian, M. J. Frisch, *J. Phys. Chem.* **1996**, *100*, 16098 – 16104.
[12] a) B. Kovacevic, Z. B. Maksic, *Org. Lett.* **2001**, *3*, 1523 – 1526; b) Equation (1) was derived analogous to in ref. [12a] by correlating the calculated (ipcm B3LYP/6-31G(d)) proton affinities (in acetonitrile) of a series of 13 bases with the experimentally determined pK_a values of the conjugate acids (in acetonitrile). The basis set of the ipcm calculations presented here is smaller than the basis set used in ref. [12a]. For that reason, the correlation is not as good ($r^2 = 0.960$) as in ref. [12a]. The calculated pK_a values differ from the experimentally determined pK_a values by a maximum of 1.5 units. A scheme showing the bases calculated for deriving Equation (1), as well as a plot of PA(MeCN) vs. pK_a(MeCN), is given in the Supporting Information.
[13] C8 belongs to the same methylenequinoline subunit as $C(H_2)$.
[14] By planarizing the tertiary nitrogen atom, the distance between the quinoline lone pairs is maximized.
[15] a) J. J. P. Stewart, *J. Comput. Chem.* **1989**, *10*, 209 – 220; b) J. J. P. Stewart, *J. Comput. Chem.* **1989**, *10*, 221 – 264.
[16] Gaussian 98 (Revision A.7), M. J. Frisch, G. W. Trucks, H. B. Schlegel, G. E. Scuseria, M. A. Robb, J. R. Cheeseman, V. G. Zakrzewski, J. A. Montgomery, R. E. Stratmann, J. C. Burant, S. Dapprich, J. M. Millam, A. D. Daniels, K. N. Kudin, M. C. Strain, O. Farkas, J. Tomasi, V. Barone, M. Cossi, R. Cammi, B. Mennucci, C. Pomelli, C. Adamo, S. Clifford, J. Ochterski, G. A. Petersson, P. Y. Ayala, Q. Cui, K. Morokuma, D. K. Malick, A. D. Rabuck, K. Raghavachari, J. B. Foresman, J. Cioslowski, J. V. Ortiz, B. B. Stefanov, G. Liu, A. Liashenko, P. Piskorz, I. Komaromi, R. Gomperts, R. L. Martin, D. J. Fox, T. Keith, M. A. Al-Laham, C. Y. Peng, A. Nanayakkara, C. Gonzalez, M. Challacombe, P. M. W. Gill, B. G. Johnson, W. Chen, M. W. Wong, J. L. Andres, M. Head-Gordon, E. S. Replogle, J. A. Pople, Gaussian, Inc., Pittsburgh, PA, **1998**.
[17] A. D. Becke, *J. Chem. Phys.* **1993**, *98*, 5648 – 5652.

 © 2003 Wiley-VCH Verlag GmbH & Co. KGaA, Weinheim

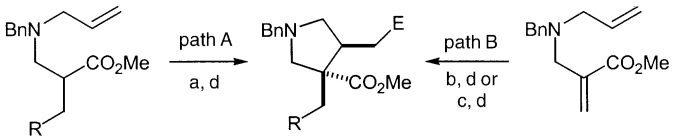
Domino Reaction Mechanism

Domino 1,4-Addition/Carbocyclization Reaction through a Radical–Polar Crossover Reaction**

Fabrice Denes, Fabrice Chemla, and Jean F. Normant*

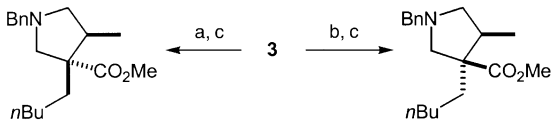
Dedicated to Professor Reinhardt W. Hoffmann on the occasion of his 70th birthday

We have recently shown that 3,4-disubstituted 3-methoxycarbonylpyrrolidines **1** can be constructed diastereoselectively by carbocyclization[1] of the zinc enolates derived from β-*N*-allyl aminoesters **2** (Scheme 1, path A) or by the domino 1,4-addition/carbocyclization/functionalization[2] of zincates and copper–zinc mixed organometallic compounds with the Michael acceptor **3a** (Scheme 1, path B). In the course of our studies on the latter domino reaction (which involves the stereoselective formation of three carbon–carbon bonds in a two- or three-step, one-pot sequence), we have examined the reactivity of dialkylzinc reagents. We were very surprised to see that with di-*n*-butylzinc, a smooth domino reaction occurs leading predominantly to the pyrrolidine derivative *cis*-**4a**, diastereoisomeric to *trans*-**4a** which is produced by the domino reaction with the copper–zinc reagents (Scheme 2).



2 **1** **3a**

Scheme 1. Diastereoselective formation of pyrrolidines **1**. a) 1. LDA, Et_2O, 2. $ZnBr_2$; b) $RCu(CN)ZnBr$, LiBr, $ZnBr_2$; c) 1. R_3ZnLi, 2. $ZnBr_2$; d) Electrophile (E). LDA = lithium diisopropyl amide.



trans-**4a** **4a** (*cis* / *trans* = 75 : 25)

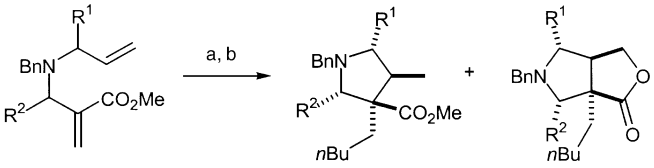
Scheme 2. Diastereodivergency in the domino reaction of **3** with zinc *n*-butylcyanocuprate and di-*n*-butylzinc. a) *n*BuCu(CN)ZnBr, LiBr, $ZnBr_2$; b) $(nBu)_2Zn$; c) NH_4OH.

[*] Prof. F. Chemla, F. Denes, J. F. Normant
Laboratoire de Chimie Organique
UMR 7611, Bte 183, Tour 44-45 2ème étage
Université Pierre et Marie Curie
4 Place Jussieu, 75252 Paris Cedex 05 (France)
Fax: (+33) 1-4427-7567
E-mail: fchemla@ccr.jussieu.fr

[**] Thanks are due to Prof. Philippe Renaud (University of Bern) for helpful discussions.

Product **4a** is obtained as a mixture of *cis/trans* diastereomers in a 75:25 ratio and in good overall yield (88%).

The same smooth domino reaction occurs with di-*n*-butylzinc and the substituted Michael acceptors **3b–e**, leading after hydrolysis to the *cis* pyrrolidines **4b–e** in good yields (Scheme 3). It should be noted that the *cis* and *trans*



3b: R^1 = H, R^2 = Me — **4b**: 49 %, *cis* / *trans* = 87 : 13 — **5b**: 9 %

3c: R^1 = Me, R^2 = H — **4c**: 64 %, *cis* / *trans* = 85 : 15 — **5c**: 5 %

3d: R^1 = Ph, R^2 = H — **4d**: 64 %, *cis* / *trans* = 92 : 8 — **5d**: 14 %

3e: R^1 = *i*Pr, R^2 = H — **4e**: 56 %, *cis* / *trans* = 96 : 4 — **5e**: 7 %

Scheme 3. Domino reaction of **3b–e** with di-*n*-butylzinc. a) $(nBu)_2Zn$; b) NH_4OH.

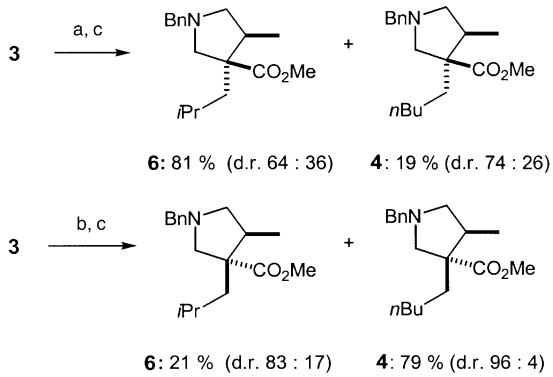
diastereomers of compounds **4a–e** can be separated easily by chromatography on silica gel. The diasteroselectivity of the reaction is better with these substituted Michael acceptors than with **3a**, and small amounts of the lactones **5b–e** can also be isolated.

The diastereoselectivity in the domino reaction with zincates and copper–zinc reagents was attributed to a chelation of a zinc species with the nitrogen and the sp^2 oxygen atoms of the ester moiety.[1,2] The reversal in the diastereoselectivity with di-*n*-butylzinc could be attributed to its weaker Lewis acidity. However, we examined the reaction of **3a** with di-*n*-butylzinc in various solvents (pentane, ether, THF, and DMF). Surprisingly, the polarity and the Lewis basicity of the solvent did not affect the diastereoselectivity, rate, or yield of the domino reaction.

This negligible influence of the solvent was intriguing, as 1,4-addition of organozinc reagents has been reported[3] to occur only in polar solvents (THF/*N*-methylpyrrolidone) in the presence of trimethylsilyl chloride or under the activation of a strong Lewis acid.[4] On the other hand, radical-mediated 1,4-addition of dialkylzinc reagents to unsaturated ketones,[5a,b] *N*-enoyloxazolidinones,[5c] and imines[6] has been reported. However, these radical 1,4-additions fail with unsaturated esters.[5a,c] These reactions are considered to be initiated by oxygen[5,7] or by light.[8] The small amounts of lactones **5b–e** obtained in the domino reaction could be an indication of mediation by molecular oxygen. Indeed, when our reaction was conducted in rigorously degassed solvents, the rate was very slow and the reaction reached 60% conversion only after 48 h. On the other hand, when the reaction was conducted in THF under dry air, total conversion was observed after two hours, thus providing good evidence for radical involvement in the overall process.

To determine which step of this domino reaction proceeds via radicals, we conducted the reaction of **3a** with di-*n*-butylzinc in the presence of isopropyl iodide (top reaction in Scheme 4). The major product was pyrrolidine **6** bearing the

 DOI: 10.1002/anie.200250474 © 2003 Wiley-VCH Verlag GmbH & Co. KGaA, Weinheim

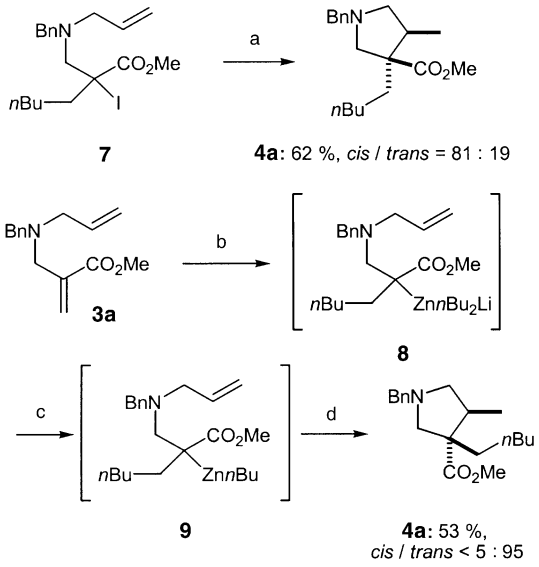


Scheme 4. Competition reactions in the domino reaction. a) nBu$_2$Zn, iPrI (10 equiv); b) nBuCu(CN)ZnBr, LiBr, ZnBr$_2$, iPrI (10 equiv); c) NH_4OH.

iPr moiety, which was obtained as a mixture of two diastereomers. By contrast, the same competition reaction with nBuCu(CN)ZnBr (bottom reaction in Scheme 4) gave predominantly the pyrrolidine *trans*-**4a** accompanied by a small amount of **6**. It should be noted that in the second reaction compound **6** was obtained as a 83:17 mixture of diastereomers, with the diastereoselectivity opposite to that of the first reaction.

These cross experiments give strong evidence of the radical character of the 1,4-addition of di-n-butylzinc to the substrate **3**, as well as of the strong anionic character of the 1,4-addition of nBuCu(CN)ZnBr. In the first case, radical exchange occurs between the nBu$_2$Zn and the iPrI, leading to the more stable isopropyl radical and its major reaction to give **6**. In the case of the copper–zinc reagent, this exchange takes place to a much lower extent, as the resulting isopropyl carbanion is less stable than the incipient n-butyl carbanion. The same type of cross experiments have been used to establish the radical nature of the 1,4-addition of dialkylzinc compounds to other Michael acceptors.[5]

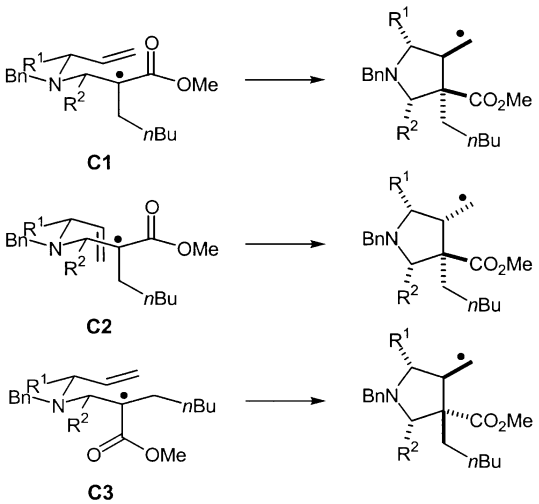
Having thus established the radical nature of the 1,4-addition, we examined the carbocyclization step in greater detail. It was reported very recently that in the radical 1,4-additions of dialkyzinc reagents to Michael acceptors, the resulting radical is further reduced by dialkylzinc to a zinc enolate.[5c] On the other hand, 5-*exo*-trig cyclization reactions of radicals have been widely reported. To determine whether the carbocyclization step occurs by a radical or an anionic mechanism, we have conducted a pure radical cyclization reaction starting from iodide **7** (Scheme 5). Pyrrolidine **4a** was obtained with a diastereoselectivity similar to that observed in the domino reaction with di-n-butylzinc. On the other hand, the 1,4-addition step was performed with **3a** and tri-n-butyl lithium zincate, as described previously.[2] The resulting zincate enolate **8** was allowed to react with n-butylzinc bromide. The diorganozinc enolate **9** (Scheme 5) formed through Schlenk equilibrium should be the same as that obtained if the reduction of the radical formed after the 1,4-addition would occur. However, the carbocyclization reaction gave, after hydrolysis, the *trans* pyrrolidine *trans*-**4a** as a single diastereomer, without any trace of the *cis* isomer obtained by the domino reaction.



Scheme 5. a) Bu_3SnH (1.5 equiv), Et_3B (0.15 equiv), THF, RT; b) nBu$_3$ZnLi (2 equiv), ether; c) nBuZnBr (2 equiv), THF; d) NH_4OH. RT = room temperature.

Finally, the domino reaction was conducted with **3d** and **3e** at −70 °C, and the yields and diastereoselectivities of **4d** and **4e** were the same as in Scheme 3, although the reaction was slower. This reactivity at low temperature is not compatible with an anionic cyclization, as this process is not observed below 0 °C.[2] All these results show unambiguously that the mechanism of the carbocyclization step is of a radical nature.

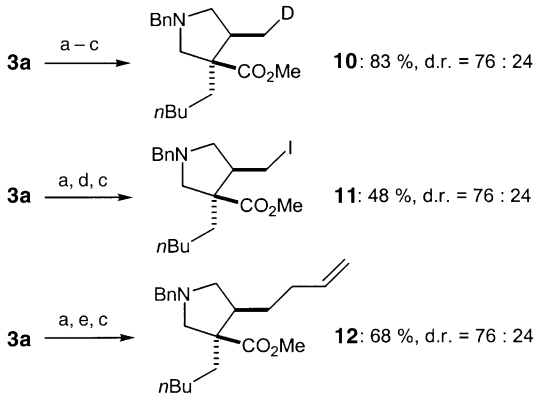
The diastereoselectivity of the 5-*exo*-trig cyclization can be interpreted in terms of conformational preferences of the enol radical in the cyclization. The major pyrrolidine is obtained from the cyclization of conformer **C1** (Scheme 6), which follows the Beckwith–Houk model[9] and minimizes the $A^{1,3}$ strain.[10] The minor diastereomer is obtained by the cyclization of conformer **C2**, as the other possible conformer **C3** is disfavored by the strong $A^{1,3}$ strain and dipolar interactions.[11]



Scheme 6. Diastereoselection in the 5-*exo*-trig cyclization.

 © 2003 Wiley-VCH Verlag GmbH & Co. KGaA, Weinheim

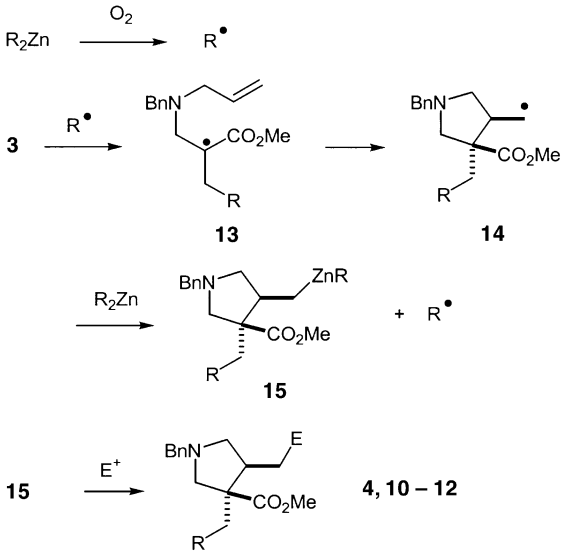
Since both the 1,4-addition and carbocyclization reactions follow a radical pathway, the question of the behavior of the final pyrrolidinylmethyl radical arises. This radical could be quenched through hydrogen abstraction from the solvent or reduced by di-*n*-butylzinc to promote the radical chain. The species resulting from the domino reaction was allowed to react with various electrophiles (Scheme 7). We were pleased



Scheme 7. Reactions of the pyrrolidinylzinc species with electrophiles. a) nBu$_2$Zn (2 equiv); b) D_2O; c) NH_4OH; d) I_2; e) CuCN (0.25 equiv), then allylbromide.

to obtain the substituted pyrrolidines **10**–**12** in good yields. Thus the pyrrolidinyl radical formed from the cascade 1,4-addition/5-*exo*-trig cyclization is further reduced to a pyrrolidinylmethylzinc species, which can be quenched by electrophiles. This remarkable reduction seems to be thermoneutral and disfavored, but the driving force of the reaction could be the chelation of the resulting organozinc species by the methoxycarbonyl moiety.[12]

The overall process can then be depicted as follows. Oxygen initiation produces an alkyl radical from dialkylzinc (Scheme 8). This radical adds to the enoate moiety of **3** to produce the enol radical **13**. This radical undergoes a 5-exo-trig cyclization to form stereoselectively the alkyl radical **14**, which is further reduced by dialkylzinc to produce the pyrrolidinylmethylzinc compound **15** and an alkyl radical which can promote the radical chain. This compound **15** can be further functionalized by electrophiles. This unusual mechanism has a number of very interesting features. First, radical addition of dialkylzincs on unsaturated esters can occur. Second, the reduction of **14** to give **15** occurs at a faster rate than the quenching of **14** by an alkyl iodide in the reaction mixture. Third, the reduction of **13** to give zinc enolate **8** is slower than the 5-*exo*-trig cyclization to give **14**.



Scheme 8. Mechanism of the radical domino reaction.

In conclusion, we have shown that the reaction of dialkylzinc reagents with Michael acceptors **3** occurs through a radical 1,4-addition/5-*exo*-trig cyclization/reduction reaction with electrophiles and results in the formation of 3,4-disubstituted 3-methoxycarbonylpyrrolidines with interesting diastereoselectivity. This procedure constitutes a novel example of a one-pot, two- or three-component, radical–polar crossover reaction and one of the few examples[5c,13–16] of a radical reaction that begins with an organometallic species and is ended by the reduction of another organometallic species. The viability of this process suggests application to intermolecular reactions as well as living polymerization processes. Further studies in this field will be reported in due course.

Received: November 4, 2002
Revised: May 9, 2003 [Z50474]

Keywords: cyclization · domino reactions · Michael addition · multicomponent reactions · zinc

[1] F. Denes, F. Chemla, J.-F. Normant, *Synlett* **2002**, 919–922.
[2] F. Denes, F. Chemla, J.-F. Normant, *Eur. J. Org. Chem.* **2002**, 3536–3542.
[3] a) A. Devasagayaraj, P. Knochel, K. Reddy, *Tetrahedron Lett.* **1996**, *37*, 4495–5598; b) S. Berger, P. Knochel, F. Langer, C. Lutz, A. Mobley, K. Reddy, *Angew. Chem.* **1997**, *109*, 1605–1607; *Angew. Chem. Int. Ed. Engl.* **1997**, *36*, 1496–1498; c) P. Knochel, P. Jones, K. Reddy, *Tetrahedron* **1998**, *54*, 1471–1490.
[4] a) S. Kim, J.M. Lee, *Tetrahedron Lett.* **1990**, *31*, 7627–7630; b) M. Hanson, R. D. Rieke, *J. Am. Chem. Soc.* **1995**, *117*, 10775–10776.
[5] a) M. P. Bertrand, R. Feray, R. Nouguier, P. Perfetti, *J. Org. Chem.* **1999**, *64*, 9189–9193; b) B. L. Feringa, R. M. Kellog, H. van der Deen, *Org. Lett.* **2000**, *2*, 1593–1595; c) S. Bazin, L. Feray, D. Siri, J.-V. Naubron, M. P. Bertrand, *Chem. Commun.* **2002**, 2506–2507.
[6] a) M. P. Bertrand, L. Feray, R. Nouguier, P. Perfetti, *Synlett* **1999**, 1148–1150; b) M. P. Bertrand, S. Coantic, L. Feray, R. Nouguier, P. Perfetti, *Tetrahedron* **2000**, *56*, 3951–3961.
[7] I. Ryu, F. Araki, S. Minakata, M. Komatsu, *Tetrahedron Lett.* **1998**, *39*, 6335–6336.
[8] A. B. Charette, A. Beauchemin, J.-F. Marcoux, *J. Am. Chem. Soc.* **1998**, *120*, 5114–5115.
[9] a) D. P. Curran in *Comprehensive Organic Chemistry, Vol. 4* (Eds.: B. M. Trost, I. Fleming), Pergamon, Oxford, **1991**, pp. 779–831; b) T. V. Rajanbabu, *Acc. Chem. Res.* **1991**, *24*, 139–145.
[10] a) R. W. Hoffmann, *Chem. Rev.* **1989**, *89*, 1841–1860; b) D. J. Hart, R. Krishnamurthy, *Synlett* **1991**, 412–414; c) M. Bulliard, B. Giese, H. G. Zeitz, *Synlett* **1991**, 425–427; d) W. Smadja, *Acc.*

 © 2003 Wiley-VCH Verlag GmbH & Co. KGaA, Weinheim

Chem. Res. **1994**, *27*, 1–26; e) R. Batra, W. Damm, B. Giese, *Chemtracts Org. Chem.* **1994**, *7*, 355–370.
[11] a) L. Boisvert, D. Delorme, Y. Guindon, J.-F. Lavallée, R. Lemieux, C. Yoakim, *Tetrahedron Lett.* **1990**, *31*, 2845–2848; b) L. Boisvert, C. Chabot, D. Delorme, Y. Guindon, D. Hall, J.-F. Lavallée, R. Lemieux, B. Simoneau, C. Yoakim, *Tetrahedron Lett.* **1991**, *32*, 27–30; c) L. Boisvert, D. Durkin, Y. Guindon, J.-F. Lavallée, J. Liotta, J. Rancourt, *J. Am. Chem. Soc.* **1992**, *114*, 4912–4914.
[12] We thank a referee for this proposed explanation.
[13] For examples involving diethylzinc and Ni^{II} or Pd^{II} complexes, see: a) W. Dörner, R. Lentz, H. Stadtmüller, T. Stüdemann, C. Tucker, P. Knochel, *J. Am. Chem. Soc.* **1993**, *115*, 7027–7028; b) P. Knochel, A. Vaupel, *Tetrahedron Lett.* **1994**, *35*, 8349–8352; c) P. Knochel, A. Vaupel, *J. Org. Chem.* **1996**, *61*, 5743–5753.
[14] For examples involving Grignard reagents, see: a) A. Inoue, K. Oshima, H. Shinokubo, *Org. Lett.* **2000**, *2*, 651–653; b) K. Oshima, K. Wakabayashi, H. Yorimitsu, *J. Am. Chem. Soc.* **2001**, *123*, 5374–5375.
[15] For examples involving Sm^{III} intermediates, see: a) H. Bluhm, A. Gansaüer, *Chem. Rev.* **2000**, *100*, 2771–2788; b) C. R. Harris, G. A. Molander, *Tetrahedron* **1998**, *54*, 3321–3354.
[16] For examples involving Ti^{III} intermediates, see: D. Lenoir, *Synthesis* **1989**, 883–898; b) J. Schwartz, R. P. Spencer, *J. Org. Chem.* **1997**, *62*, 4204–4205.

 © 2003 Wiley-VCH Verlag GmbH & Co. KGaA, Weinheim

Reaction of Epoxides with Silicon

Amine-Reactive Monolayers on Scribed Silicon with Controlled Levels of Functionality: Reaction of a Bare Silicon Surface with Mono- and Diepoxides**

*Yit-Yian Lua, Michael V. Lee, William J. J. Fillmore, Reija Matheson, Amarchard Sathyapalan, Matthew C. Asplund, Steven A. Fleming, and Matthew R. Linford**

Herein we report a significant advance in the preparation of patterned and functionalized silicon surfaces by showing that epoxides react with scribed silicon to yield monolayers with even greater efficiency than was reported for 1-alkenes,[1–5] 1-alkynes,[2,3] 1-halo- and α,ω-dihalo- alkanes,[3,6] and alcohols.[1] But more importantly we demonstrate that amine-reactive mixed monolayers with controlled levels of functionality can be formed on scribed silicon from mixtures containing an α,ω-diepoxide. As before,[1–4,6] monolayer formation simply consisted of wetting a dry, native oxide coated silicon surface with a reactive liquid, which had not been degassed, and scribing it in the air with a diamond tipped instrument. To our knowledge this is the first report of the reaction of an epoxide and a bare silicon surface (scribed or unpassivated). We are only aware of one other independent, unpublished study of the reaction of ethylene oxide with Si(100)-(2 × 1).[7]

The epoxide ring is an important functionality for industry, as well as organic and bioconjugate[8] chemistry because of its reactivity with amines, sulfhydryls, and other nucleophiles. Other researchers have also recognized the importance of epoxide-terminated,[9,10] and otherwise amine-reactive[11–13] or amine-terminated,[14,15] monolayers. Warning: Many epoxides and diepoxides are suspected carcinogens. Appropriate care should be exercised in their use.

We have considered several mechanistic pathways on model Si(100)-2 × 1 and $(H_3Si)_3Si^{\bullet}$ structures that could account for the reaction between scribed silicon and mono-substituted epoxides (see Figure 1). If one assumes that the silicon surface has zwitterionic reactivity, then two modes of addition can be considered. In many respects the most logical of these paths would involve nucleophilic attack of the epoxide oxygen onto an oxyphilic silicon. Unfortunately, the polar intermediate that is formed from the first step suffers from poor orbital overlap between the silyl anion and the antibond of the weak carbon–oxygen bond. This would lead to a disfavored 5-*endo*-tet reaction according to Baldwin's rules.[16] Formation of a high energy secondary cabocation is necessary for the eventual formation of the disilaoxane shown in path A.

The alternative zwitterionic reaction has nucleophilic silicon attacking the electrophilic epoxide in an S_N2 fashion (see path B). The resulting alkoxide would rapidly close to give a disilaoxane. The position of the alkyl group, R, by path B may allow better chain packing than the products of paths A and C. Therefore, the high C1s:Si2p X-ray photoelectron spectroscopy (XPS) ratios observed for epoxides support this mechanism. However, it does not take advantage of the silicon–oxygen bond strength in the first step, the rate-determining step.

A recent theoretical study shows that alkenes bind to Si(100)-2 × 1 through a diradical mechanism.[17] The weakness of the Si=Si banana bond in Si(100)-2 × 1, which "has been estimated at values between 1 and 31 kJ mol^{-1}, with most estimates clustering between 20 and 30 kJ mol^{-1},"[18] suggests that a diradical should be a good resonance structure for it, and further suggests that scribed silicon may have significant radical character. A surface silyl radical would be expected to bond to an epoxide through its oxygen, as shown in path C. The strong silicon–oxygen bond that would be formed concomitantly with the opening of the epoxide ring would be an energetically favorable event. Our ab initio calculations on $(H_3Si)_3Si^{\bullet}$ are consistent with radical ring opening to give the more stable secondary radical intermediate. This species

[*] Dr. M. R. Linford, Y.-Y. Lua, M. V. Lee, W. J. J. Fillmore, R. Matheson, Dr. A. Sathyapalan, Dr. M. C. Asplund, Dr. S. A. Fleming
Department of Chemistry and Biochemistry
Brigham Young University
Provo, UT 84602 (USA)
Fax: (1) 801-422-0153
E-mail: mrlinford@chemdept.byu.edu

[**] Acknowledgment is made to the Donors of The Petroleum Research Fund, administered by the American Chemical Society, to the Research Corporation, and to the David M. Kennedy Center at BYU for their support of this research.

Supporting information for this article is available on the WWW under http://www.angewandte.org or from the author.

 © 2003 Wiley-VCH Verlag GmbH & Co. KGaA, Weinheim DOI: 10.1002/anie.200250846

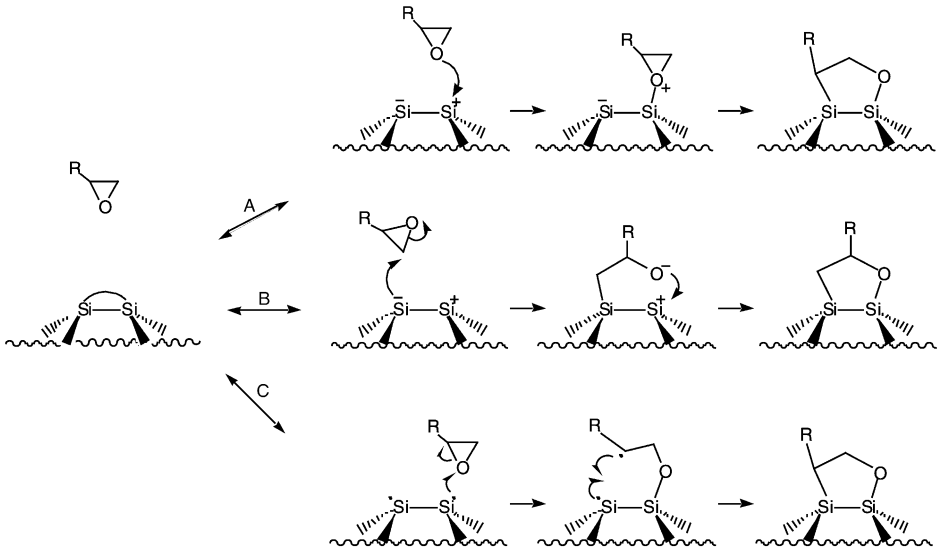


Figure 1. Possible mechanisms for the reaction of scribed silicon with epoxides. Path A: Nucleophilic attack by the epoxide oxygen. Path B: Nucleophilic attack by the silicon surface. Path C: Radical attack by the silicon surface.

would rapidly close with the silicon surface to give the ring structure shown.

The nature of the scribed silicon surface (radicaloid versus zwitterionic), the orientation(s) of the alkyl groups, the effect of the heat generated during scribing on the surface reaction, and the possibility that more than one type of mechanism accounts for bonding on scribed silicon are issues that deserve further analysis.

Figure 2 shows XPS and wetting results from surfaces prepared by scribing Si in the presence of different 1,2-epoxyalkanes and also 1,2,7,8-diepoxyoctane. The C1s:Si2p XPS ratio (Figure 2a) increases as the number of carbon atoms in the monoexpoxide increases. This result is in accord with alkyl monolayer formation by chemisorption of epoxides. A slightly larger C1s:Si2p ratio is found for 1,2,7,8-diepoxyoctane compared to 1,2-epoxyoctane. This result is consistent with a higher concentration of oxirane rings in 1,2,7,8-diepoxyoctane, compared to 1,2-epoxyoctane, thus leading to a higher surface concentration of alkyl chains. Figure 2b shows a steady increase in the ratio of chemically unshifted carbon (carbon bonded only to carbon or hydrogen) versus carbon bonded to one oxygen atom. As expected, 1) the fraction of chemically shifted carbon from the monolayers decreases as the chain length of the monoepoxide increases, and 2) there is more chemically shifted carbon on the surface prepared by scribing under 1,2,7,8-diepoxyoctane than under 1,2-epoxyoctane.

The sessile water contact angle measurements of the surfaces prepared from monoepoxides shown in Figure 2c increase as the number of methylene units in the monoepoxide increases. As before,[1] the unusually high contact angles for these surfaces is attributed to surface roughness. These results suggest increasingly thick and dense alkyl monolayers. The relatively low contact angle from the surface prepared with 1,2,7,8-diepoxyoctane is consistent with a polar head group, that is, an oxirane ring, at the monolayer surface, and

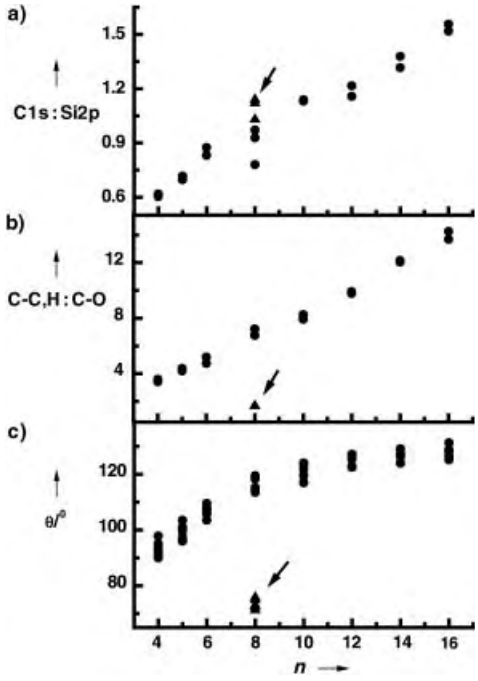


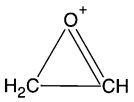
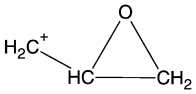
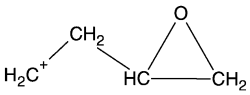
Figure 2. Physical properties of silicon scribed under 1,2-epoxyalkanes (circles) and 1,2,7,8-diepoxyoctane (triangles, note arrows) as a function of the number of carbon atoms, *n*, in the reactive liquid: a) C1s:Si2p XPS uncorrected area ratio, b) XPS ratio of carbon (bonded to carbon or hydrogen) to carbon bonded to one oxygen atom, and c) sessile water contact angles, θ, (in degrees).

attachment of diepoxides to surfaces through a single epoxide ring.

Monolayers prepared from 1,2-epoxyoctane and 1,2,7,8-diepoxyoctane were also characterized by time-of-flight secondary ion mass spectrometry (ToF-SIMS). Table 1 shows peak areas of selected masses from the resulting spectra. As expected, 1) more $(CH_2)_nC_2H_3O^+$ ($n=0$, 1, 2), CHO^+, and CH_2O^+ appear in the mass spectra of surfaces

 © 2003 Wiley-VCH Verlag GmbH & Co. KGaA, Weinheim

Table 1: Intensities of cationic fragments in ToF-SIMS of Si scribed under 1,2-epoxyoctane and 1,2,7,8-diepoxyoctane.

Fragment (with proposed structure)	1,2-epoxyoctane[a]	1,2,7,8-diepoxyoctane[a]
	0.023 ± 0.003	0.066 ± 0.002
	0.014 ± 0.003	0.023 ± 0.006
	0.0043 ± 0.0016	0.0070 ± 0.0014
$C_5H_9O^+$	0	0
CHO^+	0.0104 ± 0.0012	0.0527 ± 0.0147
CH_2O^+	0.0002 ± [b]	0.0031 ± 0.0004
CH_3^+	0.0569 ± 0.0092	0.0648 ± 0.0128
$CH_2CH_3^+$	0.1866 ± 0.0281	0.0976 ± 0.0122
$(CH_2)_2CH_3^+$	0.1234 ± 0.0247	0.0659 ± 0.0068
H^+	0.0178 ± 0.0048	0.0374 ± 0.0067

[a] Values are the ratio of the area of the fragment in question to the area of the $^{28}Si^+$ peak in the same spectrum. [b] In three of four measurements no signal was observed. Errors are $\frac{ts}{\sqrt{N}}$, where $t = 3.18$ for 95% confidence with three degrees of freedom, s is the standard deviation of four measurements, and $N = 4$.

prepared by scribing under 1,2,7,8-diepoxyoctane than under 1,2-epoxyoctane, and 2) the yield of $CH_3CH_2^+$ and $CH_3CH_2CH_2^+$ is greater in surfaces derived from the monoepoxide than from the diepoxide.

An important method of tailoring surface reactivity and properties is to create mixed monolayers through chemisorption of more than one reactive species.[19,20] Figure 3 shows the physical properties of mixed monolayers that were prepared by scribing silicon in the presence of mixtures of 1,2,7,8-diepoxyoctane and 1,2-epoxyoctane. As expected from the results in Figure 2, the C1s:Si2p XPS ratio increases (see Figure 3a) and the sessile water contact angles decrease (see Figure 3c) as the mole fraction of 1,2,7,8-diepoxyoctane increases. As before,[1] these results suggest kinetic, and not thermodynamic control in monolayer formation.

The amine reactivity of epoxides is used to couple proteins in bioconjugate chemistry[8] as well as in many industrial processes. Figure 3 shows the reaction of mixed monolayers prepared from 1,2,7,8-diepoxyoctane and 1,2-epoxyoctane with 1-aminooctane. After this reaction, the C1s:Si2p (Figure 3a) and N1s:Si2p (Figure 3b) XPS ratios, as well as the water contact angles (Figure 3c) increase above initial levels with increasing 1,2,7,8-diepoxyoctane concentration in the scribing liquid. Thus, amine-reactive surfaces with controlled degrees of available functionality are prepared on scribed silicon by using a mixture of a mono- and a bifunctional epoxide.

Epoxides react with gaseous HCl, and this reaction has been used to label them for XPS studies.[21,22] Functionalized patches[1] prepared from neat 1,2,7,8-diepoxyoctane and from neat 1,2-epoxyoctane were exposed to fumes of concentrated HCl for 1 hr at room temperature. Following this exposure

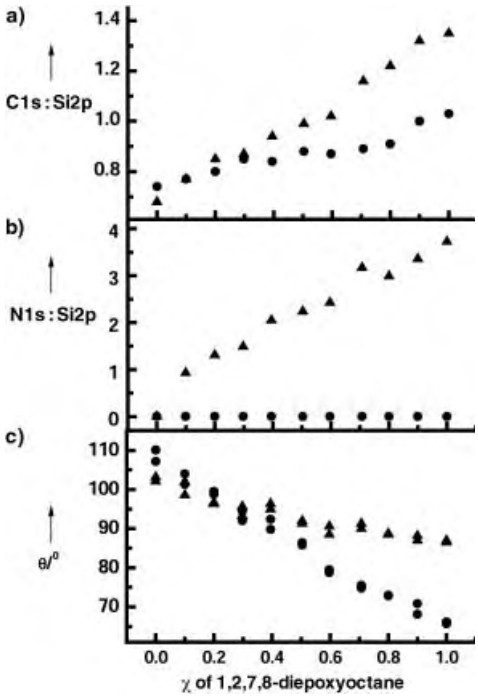


Figure 3. Physical properties of mixed monolayers prepared by scribing silicon under binary solutions of 1,2-epoxyoctane and 1,2,7,8-diepoxyoctane before (circles) and after (triangles) reaction with 1-aminooctane: a) C1s:Si2p XPS uncorrected area ratio, b) N1s:Si2p XPS uncorrected area ratio, and c) sessile water contact angles. χ = molar fraction.

the surfaces derived from 1,2-epoxyoctane had no Cl by XPS but those derived from 1,2,7,8-diepoxyoctane showed significant amounts of Cl (~27 C atoms per Cl atom, or ~3.5 alkyl chains per Cl atom). After HCl exposure, ToF-SIMS of the diepoxide surface showed pairs of fragments with the same ratio and spacing as naturally occurring ^{35}Cl and ^{37}Cl; these masses were attributable to CH_2Cl^+, $CHOHCH_2Cl^+$, and CH_2Cl^-. Corresponding pairs of peaks were neither obtained from the monoepoxide surface after HCl exposure, nor in the mass spectra of the surfaces prior to reaction.

Thus, a combination of instrumental characterization and chemical studies indicate that scribed silicon reacts with mono- and di-epoxides to produce alkyl monolayers. Materials and methods for the amine reaction, the surface characterization, and semiempirical calculations are given in the Supporting Information.

Received: December 27, 2002
Revised: June 17, 2003 [Z50846]

Keywords: chemisorption · monolayers · nucleophilic addition · radical reactions · silicon

[1] T. L. Niederhauser, Y.-Y. Lua, G. Jiang, S. D. Davis, R. Matheson, D. A. Hess, I. A. Mowat, M. R. Linford, *Angew. Chem.* **2002**, *114*, 2459–2462; *Angew. Chem. Int. Ed.* **2002**, *41*, 2353–2356.

 © 2003 Wiley-VCH Verlag GmbH & Co. KGaA, Weinheim

[2] T. L. Niederhauser, G. Jiang, Y.-Y. Lua, M. J. Dorff, A. T. Woolley, M. C. Asplund, D. A. Berges, M. R. Linford, *Langmuir* **2001**, *17*, 5889 – 5900.
[3] Y.-Y. Lua, T. L. Niederhauser, R. Matheson, C. Bristol, I. A. Mowat, M. C. Asplund, M. R. Linford, *Langmuir* **2002**, *18*, 4840 – 4846.
[4] Y.-Y. Lua, T. L. Niederhauser, B. A. Wacaser, I. A. Mowat, A. T. Woolley, R. C. Davis, H. A. Fishman, M. R. Linford, *Langmuir* **2003**, *19*, 985 – 988.
[5] B. A. Wacaser, M. J. Maughan, I. A. Mowat, T. L. Niederhauser, M. R. Linford, R. C. Davis, *Appl. Phys. Lett.* **2003**, *82*, 808 – 810.
[6] T. L. Niederhauser, Y.-Y. Lua, Y. Sun, G. Jiang, G. S. Strossman, P. Pianetta, M. R. Linford, *Chem. Mater.* **2002**, *14*, 27 – 29.
[7] R. A. Wolkow, **2002**, personal communication.
[8] G. T. Hermanson, *Bioconjugate Techniques*, Academic Press, SanDiego, **1996**.
[9] J. M. Abad, M. Vélez, C. Santamaría, J. M. Guisán, P. R. Matheus, L. Vázquez, I. Gazaryan, L. Gorton, T. Gibson, V. M. Fernández, *J. Am. Chem. Soc.* **2002**, *124*, 12 845 – 12 853.
[10] D. G. Kurth, G. K. Broeker, C. P. Kubiak, T. Bein, *Chem. Mater.* **1994**, *6*, 2143 – 2150.
[11] R. G. Chapman, E. Ostuni, L. Yan, G. M. Whitesides, *Langmuir* **2000**, *16*, 6927 – 6936.
[12] R. L. Cicero, P. Wagner, M. R. Linford, C. J. Hawker, R. M. Waymouth, C. E. D. Chidsey, *Polym. Prepr. Am. Chem. Soc. Div. Polym. Chem.* **1997**, *38*, 904 – 905.
[13] P. Wagner, S. Nock, J. A. Spudich, W. D. Volkmuth, S. Chu, R. L. Cicero, C. P. Wade, M. R. Linford, C. E. D. Chidsey, *J. Struct. Biol.* **1997**, *119*, 189 – 201.
[14] N. Balachander, C. N. Sukenik, *Langmuir* **1990**, *6*, 1621 – 1627.
[15] A. B. Sieval, R. Linke, G. Heij, G. Meijer, H. Zuilhof, E. J. R. Sudhölter, *Langmuir* **2001**, *17*, 7554 – 7559.
[16] J. E. Baldwin, R. C. Thomas, L. T. Kruse, L. Silberman, *J. Org. Chem.* **1977**, *42*, 3846 – 3852.
[17] X. Lu, *J. Am. Chem. Soc.* **2003**, *125*, 6384 – 6385.
[18] R. J. Hamers, Y. Wang, *Chem. Rev.* **1996**, *96*, 1261 – 1290.
[19] J. P. Folkers, P. E. Laibinis, G. M. Whitesides, *Langmuir* **1992**, *8*, 1330 – 1341.
[20] D. A. Offord, C. M. John, M. R. Linford, J. H. Griffin, *Langmuir* **1994**, *10*, 883 – 889.
[21] L. J. Gerenser, J. F. Elman, M. G. Mason, J. M. Pochan, *Polymer* **1985**, *26*, 1162 – 1166.
[22] J. M. Pochan, L. J. Gerenser, J. F. Elman, *Polymer* **1986**, *27*, 1058 – 1062.

 © 2003 Wiley-VCH Verlag GmbH & Co. KGaA, Weinheim

Highly Pyramidalized Alkenes

Generation, Trapping, and Dimerization of Pentacyclo[6.4.0.0^{2,10}.0^{3,7}.0^{4,9}]dodeca-5,8,11-triene: An Uncatalyzed Thermal [2+2+2+2] Cycloaddition**

Pelayo Camps, José A. Fernández, Santiago Vázquez, Mercè Font-Bardia, and Xavier Solans*

Pyramidalized alkenes are compounds that contain carbon–carbon double bonds in which one or both of the sp^2-hybridized carbon atoms does not lie in the same plane as the attached atoms.[1] Such alkenes are interesting targets for both synthetic and theoretical organic chemists owing to their intriguing physical properties and fascinating reactivity.[2] In recent years, we have been engaged in the synthesis, chemical trapping, dimerization, and cross-coupling of several highly pyramidalized alkenes that contain the bisnoradamantane skeleton.[3]

Herein we report the generation of pentacyclo[6.4.0.0^{2,10}.0^{3,7}.0^{4,9}]dodeca-5,8,11-triene (**4**), its trapping with 1,3-diphenylisobenzofuran, and its unusual dimerization to the polycyclic compound **6** by an uncatalyzed thermal [2+2+2+2] cycloaddition process with formation of four new carbon–carbon bonds (Scheme 1).

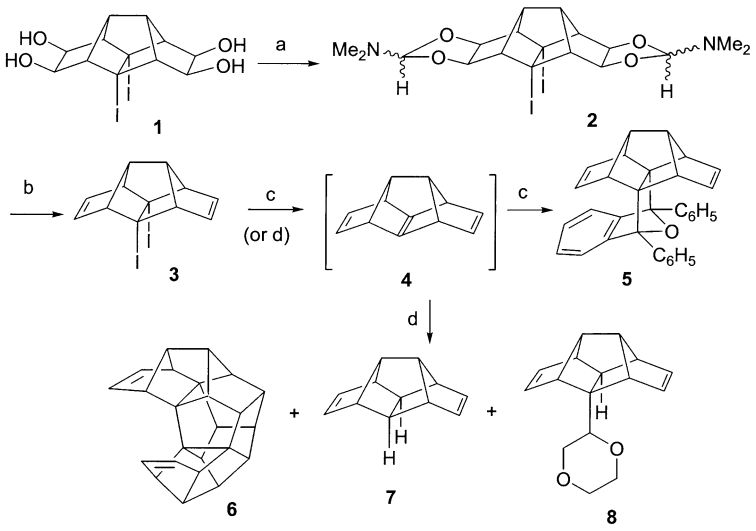
Previous work in this field showed that vicinal diiodo compounds are suitable precursors for highly pyramidalized alkenes,[2,3] so the generation of **4** was envisioned from the diiodo derivative **3**, whose preparation from the known compound **1** appeared to be straightforward.[4] The double bisdehydroxylation of **1** to **3** was accomplished by following the procedure of Eastwood et al.[5] Reaction of **1** with neat *N*,*N*-dimethylformamide dimethyl acetal gave bis(dimethylformamide cyclic acetal) **2** as a mixture of diastereomers. Heating **2** with acetic anhydride yielded **3** as a white solid in 83% overall yield. As expected, reaction of **3** with *tert*-butyllithium in THF at −67°C in the presence of 1,3-

[*] Prof. Dr. P. Camps, J. A. Fernández, Dr. S. Vázquez
Laboratori de Química Farmacèutica (Unitat Associada al CSIC)
Facultat de Farmàcia, Universitat de Barcelona
Av. Diagonal s/n, 08028 Barcelona (Spain)
Fax: (+34) 93-403-5941
E-mail: camps@farmacia.far.ub.es
Dr. M. Font-Bardia, Prof. Dr. X. Solans
Serveis Cientifico-Tècnics, Universitat de Barcelona
Av. Martí i Franqués s/n, 08028 Barcelona (Spain)

[**] Financial support from the Ministerio de Ciencia y Tecnología (Project PPQ2002-01080) and the Comissionat per a Universitats i Recerca (Project 2001-SGR-00085) is gratefully acknowledged. S.V. thanks the Ministerio de Ciencia y Tecnología for a fellowship (Programa Ramón y Cajal). We thank the Serveis Cientifico-Tècnics of the University of Barcelona for recording the NMR spectra, the Centre de Supercomputació de Catalunya (CESCA) for computational facilities, and Ms. P. Domènech from IIQAB (CSIC, Barcelona, Spain) for carrying out the elemental analyses.

Supporting information for this article is available on the WWW under http://www.angewandte.org or from the author.

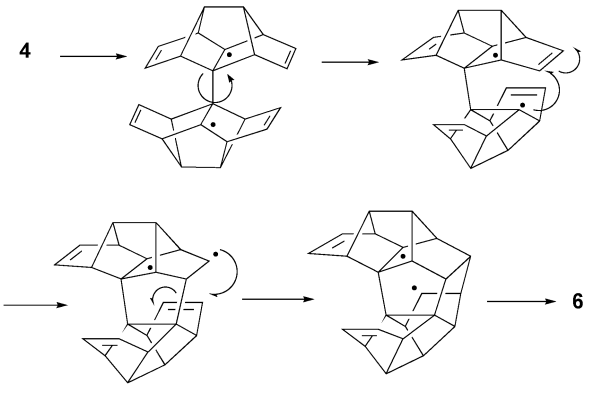
 DOI: 10.1002/anie.200351070 © 2003 Wiley-VCH Verlag GmbH & Co. KGaA, Weinheim



Scheme 1. Generation, trapping, and dimerization of triene **4**. a) $(MeO)_2CHNMe_2$, Δ; b) Ac_2O, reflux, 16 h, 83% of **3** from **1**; c) *t*BuLi, THF, 1,3-diphenylisobenzofuran, −67°C, 63% of **5**. d) Na, dioxane, reflux, 4 h, 24% yield of pure **6**.

diphenylisobenzofuran gave Diels–Alder adduct **5** (63% yield). Reaction of **3** with 8 equivalents of molten sodium in 1,4-dioxane under reflux for 4 h gave a mixture of three main products (GC–MS). The product eluted first ($t_r = 12.7$ min, $M = 156$, 19.5% area ratio) corresponded to the known reduction product **7** (^{1}H NMR);[6] according to our previous results on related substrates,[4] the second product ($t_r =$ 22.9 min, $M = 242$, 15.3% area ratio) could be **8**, derived from the addition of the intermediate pyramidalized alkene and the solvent (1,4-dioxane), and the third product ($t_r =$ 29.3 min, $M = 308$, 62.6% area ratio) is a dimer of **4**. Column chromatography of this mixture (neutral aluminum oxide, hexane), allowed us to isolate dimer **6** in 24% yield. The ^{1}H and ^{13}C NMR spectra of this dimer showed the lack of the C_{2v} symmetry characteristic of the expected cyclobutane or derived dimers,[3,4] and the presence of C_2 symmetry, which led us to propose structure **6**, in which the two halves are orthogonally fused. X-ray diffraction analysis unequivocally established **6** as the structure of the isolated dimer.[7]

Dimer **6** is the result of a [2+2+2+2] cycloaddition of two molecules of triene **4**. A possible mechanism for the dimerization of **4** to **6** is shown in Scheme 2. Two units of **4** are first connected by forming a C–C single bond and, after rotation around the new C–C bond, a cascade radical process would give dimer **6** with formation of four new C–C bonds and three new rings.



Scheme 2. Possible pathway for the dimerization of **4**.

This proposal was based on a) the fact that, some time ago, Eaton and Lukin provided the first demonstration of the intermediacy of biradicals in the dimerization of strained olefins by using 1-iodoadamantane as a probe in the dimerization of cubene,[2a] and b) the biradical character of 11% for **4**, calculated by using the two-configuration self-consistent field (TCSCF) procedure of Gaussian 98[8] and the 6-31G(d) basis set with the HF/6-31G(d) optimized geometry.

The first [2+2+2+2] cycloaddition was discovered 55 years ago by Reppe, and several additional examples were described later.[9] All these reactions are stepwise processes catalyzed by complexes of Ni,[9] Fe, Mo, or Rh.[10] Although a pericyclic process of the type $[_\pi 2_s + _\pi 2_s + _\pi 2_s + _\pi 2_s]$ is not thermally allowed according to the Woodward–Hoffman rules, photochemically it would be allowed. However, to the best of our knowledge, examples of [2+2+2+2] cycloadditions in the absence of a metal catalyst, either thermally or photochemically induced, have never been described, with the exception of the tetramerization of 1,2-cyclohexadiene to give, among other products, two isomeric cyclooctane derivatives.[11]

In conclusion, the dimerization of the highly pyramidalized alkene **4**[12] to its dimer **6** described herein is a unique example of an uncatalyzed thermal [2+2+2+2] cycloaddition. Moreover, this type of process may be extended to more complex transformations; for instance, the dimerization of a triquinacene derivative that contains a highly pyramidalized C=C bond with its opened face in an *endo* arrangement could provide a dodecahedrane derivative by a [2+2+2+2+2+2] cycloaddition, a type of transformation that many have tried without success till now with triquinacene and numerous triquinacene derivatives under different reaction conditions.

Received: January 30, 2003
Revised: May 7, 2003 [Z51070]

Keywords: cycloaddition · dimerization · domino reactions · polycycles · strained molecules

[1] a) W. T. Borden, *Chem. Rev.* **1989**, *89*, 1095–1109; b) W. Luef, R. Keese, *Top. Stereochem.* **1991**, *20*, 231–318; c) W. T. Borden, *Synlett* **1996**, 711–719; d) H. Hopf, *Classics in Hydrocarbon Chemistry*, VCH, Weinheim, **2000**, pp. 122–137; e) I. V. Komarov, *Russ. Chem. Rev.* **2001**, *70*, 991–1016.

[2] For some leading recent references on pyramidalized alkenes, see a) K. Lukin, P. E. Eaton, *J. Am. Chem. Soc.* **1995**, *117*, 7652–7656; b) K. Rosendorfer, O. Jarosch, K. Polborn, G. Szeimies, *Liebigs Ann. Chem.* **1995**, 1765–1771; c) G. Dyker, J. Körning, P. G. Jones, P. Bubenitschek, *Angew. Chem.* **1995**, *107*, 2743–2745; *Angew. Chem. Int. Ed. Engl.* **1995**, *34*, 2502–2504; d) R. Haag, F.-M. Schüngel, B. Ohlhorst, T. Lendvai, H. Butenschön, T. Clark, M. Noltemeyer, T. Haumann, R. Boese, A. de Meijere,

 © 2003 Wiley-VCH Verlag GmbH & Co. KGaA, Weinheim

Chem. Eur. J. **1998**, *4*, 1192 – 1200; e) A. G. Griesbeck, T. Deufel, G. Hohlneicher, R. Rebentisch, J. Steinwascher, *Eur. J. Org. Chem.* **1998**, 1759 – 1762; f) A. P. Marchand, I. N. N. Namboothiri, B. Ganguly, W. H. Watson, S. G. Bodige, *Tetrahedron Lett.* **1999**, *40*, 5105 – 5109; g) H. Irngartinger, A. Altreuther, T. Sommerfeld, T. Stojanik, *Eur. J. Org. Chem.* **2000**, 4059 – 4070; h) J. Reinbold, E. Sackers, T. Oßwald, K. Weber, A. Weiler, T. Voss, D. Hunkler, J. Wörth, L. Knothe, F. Sommer, N. Morgner, B. von Issendorff, H. Prinzbach, *Chem. Eur. J.* **2002**, *8*, 509 – 524.

[3] a) P. Camps, M. Font-Bardia, F. Pérez, X. Solans, S. Vázquez, *Angew. Chem.* **1995**, *107*, 1011 – 1012; *Angew. Chem. Int. Ed. Engl.* **1995**, *34*, 912 – 914; b) P. Camps, M. Font-Bardia, F. Pérez, Ll. Solà, X. Solans, S. Vázquez, *Tetrahedron Lett.* **1996**, *37*, 8601 – 8604; c) P. Camps, F. J. Luque, M. Orozco, F. Pérez, S. Vázquez, *Tetrahedron Lett.* **1996**, *37*, 8605 – 8608; d) P. Camps, M. Font-Bardia, N. Méndez, F. Pérez, X. Pujol, X. Solans, S. Vázquez, M. Vilalta, *Tetrahedron* **1998**, *54*, 4679 – 4696; e) P. Camps, X. Pujol, S. Vázquez, *Org. Lett.* **2000**, *2*, 4225 – 4228; f) P. Camps, X. Pujol, S. Vázquez, *Tetrahedron* **2002**, *58*, 10081 – 10086.

[4] P. Camps, X. Pujol, S. Vázquez, M. A. Pericàs, C. Puigjaner, Ll. Solà, *Tetrahedron* **2001**, *57*, 8511 – 8520.

[5] F. W. Eastwood, K. J. Harrington, J. S. Josan, J. L. Pura, *Tetrahedron Lett.* **1970**, 5223 – 5224.

[6] L. A. Paquette, M. J. Wyvratt, *J. Am. Chem. Soc.* **1974**, *96*, 4671 – 4673.

[7] Crystal data of **6**: A prismatic crystal was selected and mounted on an Enraf-Nonius CAD4 four-circle diffractometer. Unit-cell parameters were determined from automatic centering of 25 reflections ($12 < \theta < 21°$) and refined by the least-squares method. Intensities were collected with graphite-monochromated $Mo_{K\alpha}$ radiation by using the $\omega/2\theta$ scan technique. 2195 reflections were measured in the range $2.92 = \theta = 29.97°$, 2090 of which were nonequivalent by symmetry (R_{int}(on I) = 0.026) and 1111 reflections were assumed as observed ($I > 2\sigma(I)$). Three reflections were measured every 2 hours as orientation and intensity control; significant intensity decay was not observed. Corrections were made for Lorentzian polarization but not for absorption. The structure was solved by direct methods with the SHELXS computer program (G. M. Sheldrick, *Acta Crystallogr. Sect. A* **1990**, *46*, 467 – 473) and refined by full-matrix least-squares methods with the SHELX97 computer program (G. M. Sheldrick, SHELX-97, A computer Program for the Determination of Crystal Structure, University of Göttingen, Göttingen, Germany, **1998**), using 2090 reflections (very negative intensities were not assumed). The function minimized was $\Sigma w ||F_o|^2 - |F_c|^2|^2$, where $w = [\sigma^2(I) + (0.0728P)^2]^{-1}$, and $P = (|F_o|^2 + 2|F_c|^2)/3$, *f*, *f*′ and *f*″ were taken from the literature (*International Tables of X-ray Crystallography, Vol. IV* (Eds.: J. A. Ibers, W. C. Hamilton), Kynoch, Birmingham, **1974**, pp. 99 – 100, 149). All H atoms were located from a difference synthesis and refined with an overall isotropic temperature factor. GOF = 0.950 for all observed reflections. Max. shift/esd = 0.00, mean shift/esd = 0.00, max./min. peaks in final difference synthesis: 0.248/−0193 e Å^{-3}. $C_{24}H_{20}$, $M_r = 308.40$, monoclinic, space group *C*2/*c*, $a = 16.268(2)$, $b = 7.718(3)$, $c = 11.686(2)$ Å, $\alpha = 90$, $\beta = 93.85(2)$, $\gamma = 90°$, $V = 1463.9(6)$ Å^3, $Z = 4$, $F(000) = 656$, $\rho_{calcd} = 1.399$ g cm^{-3}; crystal dimensions, $0.1 \times 0.1 \times 0.2$ mm; $\mu(Mo_{K\alpha}) = 0.079$ mm^{-1}; $Mo_{K\alpha}$ radiation ($\lambda = 0.71069$ Å), $T = 293(2)$ K; 2090 reflections and 131 parameters were used for the full matrix, least-squares refinement on F^2, $R1 = 0.0571$, and $wR2 = 0.1184$. CCDC-199680 contains the supplementary crystallographic data for this paper. These data can be obtained free of charge via www.ccdc.cam.ac.uk/conts/retrieving.html (or from the Cambridge Crystallographic Data Centre, 12, Union Road, Cambridge CB2 1EZ, UK; fax: (+44) 1223-336-033; or deposit@ccdc.cam.ac.uk).

[8] Gaussian 98 (Revision A.7), M. J. Frisch, G. W. Trucks, H. B. Schlegel, G. E. Scuseria, M. A. Robb, J. R. Cheeseman, V. G. Zakrzewski, J. A. Montgomery, R. E. Stratmann, J. C. Burant, S. Dapprich, J. M. Millam, A. D. Daniels, K. N. Kudin, M. C. Strain, O. Farkas, J. Tomasi, V. Barone, M. Cossi, R. Cammi, B. Mennucci, C. Pomelli, C. Adamo, S. Clifford, J. Ochterski, G. A. Petersson, P. Y. Ayala, Q. Cui, K. Morokuma, D. K. Malick, A. D. Rabuck, K. Raghavachari, J. B. Foresman, J. Cioslowski, J. V. Ortiz, B. B. Stefanov, G. Liu, A. Liashenko, P. Piskorz, I. Komaromi, R. Gomperts, R. L. Martin, D. J. Fox, T. Keith, M. A. Al-Laham, C. Y. Peng, A. Nanayakkara, C. Gonzalez, M. Challacombe, P. M. W. Gill, B. G. Johnson, W. Chen, M. W. Wong, J. L. Andres, M. Head-Gordon, E. S. Replogle, J. A. Pople, Gaussian, Inc., Pittsburgh, PA, **1998**.

[9] M. Lautens, W. Klute, W. Tam, *Chem. Rev.* **1996**, *96*, 49 – 92 and references therein.

[10] T. J. Chow, *Proc. Natl. Sci. Counc. Repub. China Part A* **1992**, *16*, 89 – 107.

[11] W. R. Moore, W. R. Moser, *J. Am. Chem. Soc.* **1970**, *92*, 5469 – 5474.

[12] The pyramidalization angle Φ of the C8–C9 double bond of **4** was calculated to be 62.6 and 63.7° at the B3LYP6-31G(d) and MP2/6-31G(d) levels, respectively, by using the Gaussian 98 program,[8] in good agreement with values previously calculated for related highly pyramidalized alkenes that contain the tricyclo[3.3.0.0^{3,7}]oct-1(5)-ene skeleton.[3d]

 © 2003 Wiley-VCH Verlag GmbH & Co. KGaA, Weinheim

Acyloxyphosphonium Ion Trapping

The Role of Acyloxyphosphonium Ions and the Stereochemical Influence of Base in the Phosphorane-Mediated Esterification of Alcohols**

James McNulty, Alfredo Capretta, Vladimir Laritchev, Jeff Dyck, and Al J. Robertson*

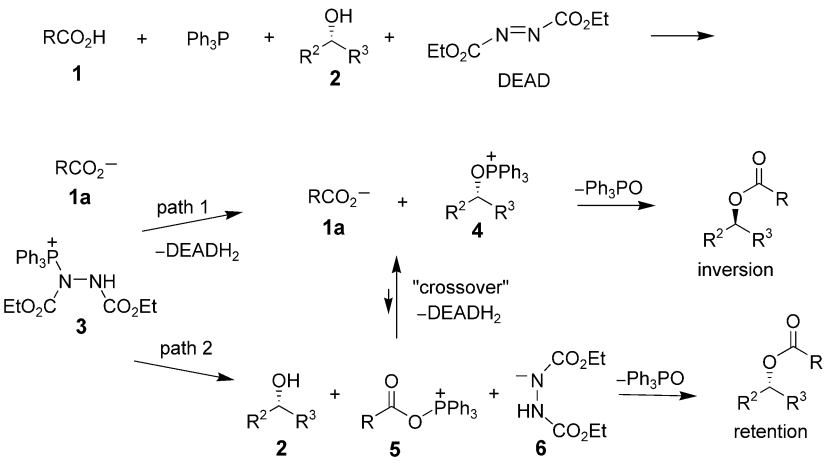
The Mitsunobu reaction[1–4] is widely employed in both condensation and displacement reactions of alcohols with various nucleophiles and normally proceeds with inversion of stereochemistry when chiral secondary alcohols are used. The mechanism of the reaction continues to receive attention and the present view is summarized in Scheme 1. Although the

[*] Dr. J. McNulty, Dr. A. Capretta, Dr. V. Laritchev
Department of Chemistry, McMaster University
1280 Main Street West, Hamilton, Ontario, L8S 4M1 (Canada)
Fax: (+1) 905-522-2509
E-mail: mcnulty@chemistry.mcmaster.ca
J. Dyck
Department of Chemistry, Brock University
St. Catharines, Ontario, L2S 3A1 (Canada)
A. J. Robertson
Cytec Canada Inc.
P.O. Box 240, Niagara Falls, Ontario, L2E 6T4 (Canada)

[**] Financial support was provided by the Natural Sciences and Engineering Research Council of Canada.

Supporting information for this article is available on the WWW under http://www.angewandte.org or from the author.

 DOI: 10.1002/anie.200351209 © 2003 Wiley-VCH Verlag GmbH & Co. KGaA, Weinheim



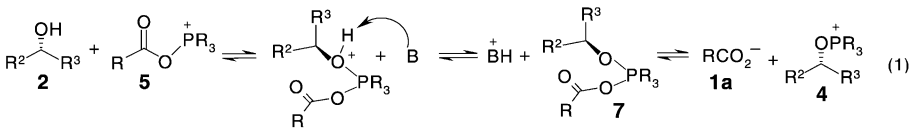
Scheme 1. Mechanism of the Mitsunobu esterification.

initiation and termination steps of the reaction seem clear cut, there is still debate concerning the exact details involved in the intermediate stages of the reaction. The reaction proceeds through the rapid addition[3a] of triphenylphosphane to an azodicarboxylate such as diethyl azodicarboxylate (DEAD), followed by proton transfer from the carboxylic acid to give **1a** and **3** as shown. As the esters obtained are the product of inversion of stereochemistry in the vast majority of cases, it appears that the reaction normally terminates through nucleophilic displacement by **1a** of triphenylphosphane oxide from the activated alkoxyphosphonium ion **4**.

Recent evidence from several laboratories has challenged the original mechanistic hypothesis put forward by Mitsunobu and Yamada,[1,2a] wherein the reaction proceeds directly to the alkoxyphosphonium salt **4** (Scheme 1, path 1). Evidence for the involvement of acyloxyphosphonium ion intermediates **5** has been obtained indirectly over a number of years.[5] Hughes et al.[3b] and Jenkins and co-workers[6] independently reported the isolation of anhydrides from the reaction of acids with DEAD and attributed this to the intermediacy of acyloxyphosphonium ions **5** that Jenkins[6] postulated were in equilibrium with **4**. More recently, DeShong and co-workers,[7] Smith et al.,[8] and De Brabander and co-workers[9] have reported the isolation of products of retention of configuration from the reactions of certain sterically hindered chiral secondary alcohols under standard Mitsunobu conditions.

Retention of stereochemistry is thought to arise through the direct attack of the alcohol at the carbonyl carbon atom of an intermediate acyloxyphosphonium salt. It has been postulated that the normal product obtained from the Mitsunobu reaction may be the result of a competitive crossover reaction mediated by basic species present or generated (such as the hydrazide anion **6**) during the reaction.[7a,10] According to this hypothesis (Scheme 1, path 2), an initial acyloxyphosphonium ion **5** is generated by the attack of the more nucleophilic carboxylate anion **1a**, rather than the alcohol, at the phosphorus center in **3**. The details of the postulated base-mediated crossover to **4** are described in Equation (1). We now report the independent generation of the benzoyloxytributylphosphonium ion, which could be trapped with chiral secondary alcohols under both neutral and basic conditions in the synthesis of esters with either retention or inversion of configuration. Clear evidence was thus obtained for both direct acylation and the postulated base-mediated crossover step.

Acyloxyphosphonium ions have been generated through the addition of a peroxide to a tertiary phosphane, for example, the addition of benzoyl peroxide (BPO) to a solution of triphenylphosphane.[11] When a solution of BPO in *N*,*N*-dimethylformamide



(1)

(DMF) was added dropwise to a mixture of L-menthol and tributylphosphane at 70 °C under argon, menthol benzoate was isolated from the reaction mixture in 50 % yield. Spectral analysis of the product showed 97 % retention of stereochemistry, which indicates that direct attack of menthol at the carbonyl carbon of the benzoyloxyphosphonium intermediate had occurred predominantly. These results concur with the postulated intermediacy of acyloxytrialkylphosphonium ions in esterification reactions, generated alternatively by using our recently described phosphorane method.[10] When this method was used, L-menthol reacted with 4-nitrobenzoic acid in DMF to give the corresponding menthol ester with 99.2 % retention of configuration (76 % yield). Recently, Burke and co-workers reported a further independent route to acyloxyphosphonium ions, from trihaloethyl esters. These species also reacted in DMF with L-menthol under nonbasic conditions to provide the corresponding esters with retention of configuration.[12]

Having demonstrated that the benzoyloxytributylphosphonium ion can be trapped with menthol to yield the desired ester with retention of configuration, we now focused on developing a more synthetically useful process that could provide access to esters with inversion of stereochemistry. We screened a large variety of bases for their ability to effect the postulated crossover step that might lead to inversion. Although essentially any amine added increased the amount of the product of inversion obtained, we quickly determined that bulky primary amines, such as *tert*-butylamine or 1,1,3,3-tetramethylbutylamine, were superior both in terms of the product of inversion/product of retention ratio observed and in terms of the yield of the desired product. The results with L-menthol show that high selectivity in favor of the product of inversion might be anticipated when such hindered bases are present (Table 1, entries 1 and 2), whereas retention of configuration is favored in the absence of a base (Table 1,

 © 2003 Wiley-VCH Verlag GmbH & Co. KGaA, Weinheim

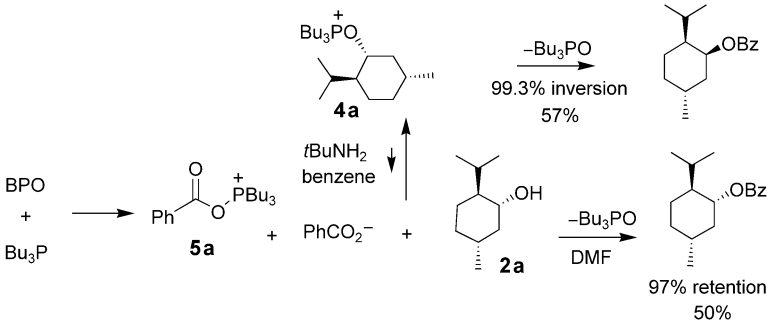
Table 1: Esterification reactions of chiral alcohols promoted by BPO/Bu_3P alone and in the presence of bulky primary amines.

Entry	Alcohol	Base	Method[a]	Ret./inv.[b]	Conv.[c]
1	L-menthol	Me_3CNH_2	A	0.7:99.3	57%
2	L-menthol	$Me_3CCH_2CMe_2NH_2$	A	1.1:98.9	55%
3	L-menthol	–	B	97.0:3.0	50%
4	(2*S*)-hexanol	$Me_3CCH_2CMe_2NH_2$	A	1.9:98.1	73%
5	(2*S*)-hexanol	–	B	55.0:45.0	67%
6	(1*R*)-1-phenyl propanol	$Me_3CCH_2CMe_2NH_2$	A	2.7:97.3	54%
7	(1*R*)-1-phenyl propanol	–	B	43.7:56.3	56%
8	ethyl (*S*)-(−)-lactate	$Me_3CCH_2CMe_2NH_2$	A	5.6:94.4	73%
9	ethyl (*S*)-(−)-lactate	–	B	72.3:27.7	70%

[a] BPO (1.5 equiv) was dissolved in 1.5 mL of benzene (protocol A) or DMF (protocol B) and added dropwise over 70 min to a stirred solution of tributylphosphane (1.5 equiv), the alcohol (1.0 equiv), and the appropriate base (2.5 equiv) in 0.5 mL of benzene or DMF at 70 °C. [b] Product of retention/product of inversion ratio determined by NMR spectroscopy and GC on a chiral phase in comparison with authentic samples. [c] Unoptimized conversion based on mass of purified ester product obtained under standard conditions described.

entry 3). These results are evidence for the base-mediated crossover step proposed in Equation (1). To the best of our knowledge, this is the first report of clear independent evidence for the involvement of a base in such a redox condensation leading to esters with inversion of configuration. These results proved to be general for the chiral secondary alcohols investigated: (2*S*)-2-hexanol (98.1% inversion), (1*R*)-1-phenyl-1-propanol (97.3% inversion), and (2*S*)-ethyl lactate (94.4% inversion).

A relatively clear mechanism can now be proposed to explain the dichotomous results obtained. In contrast with standard Mitsunobu[1] and phosphorane-mediated esterification processes,[11] in the new esterification protocol with inversion of stereochemistry in the presence of BPO/Bu_3P, direct formation of the alkoxyphosphonium ion **4a** is not possible, and the reaction must proceed via **5a** (Scheme 2).



Scheme 2. Generation and trapping of the benzoyloxytributylphosphonium ion **5a** with L-menthol.

When an alcohol is present and in the absence of base, direct acylation of the alcohol predominates, which leads to esters with retention of configuration. This process is also facilitated by the use of DMF as the solvent. In the presence of a base the crossover path becomes dominant, thus leading to the alkoxyphosphonium ion **4a**, and then to esters with inversion of configuration. The function of the base must be either to generate a continuous low concentration of alkoxide to facilitate the crossover step, or to remove a proton with formation of the phosphorane intermediate **7** [Eq. (1)], followed by dissociation to give the required alkoxyphosphonium ion **4**. In either case, the function of the base is to shift the equilibrium shown in Equation (1) to the right and promote the formation of **4**.[12]

In conclusion, we have demonstrated the independent generation of the benzoyloxytributylphosphonium ion and shown that it can be directly trapped with chiral alcohols to yield esters with retention of configuration, or can be converted into an alkoxyphosphonium ion through the addition of a base to yield esters predominantly with inversion of configuration. These studies confirm the existence of a base-induced crossover step and highlight the significance of basic species with regard to the stereochemical outcome of an esterification when such a redox condensation reaction that proceeds via an acyloxytrialkylphosphonium intermediate is used. Attention has often been drawn to the subtle interplay of factors that contribute to the stereochemical outcome in a given case.[6,7a,9,13] The results presented here show that the nature of any basic species present or generated during the reaction can have a profound effect on the stereochemistry of the esterification and thus requires due consideration.

Received: February 18, 2003 [Z51209]

Keywords: acylation · amines · peroxides · phosphanes · synthetic methods

[1] O. Mitsunobu, M. Yamada, *Bull. Chem. Soc. Jpn.* **1967**, *40*, 2380.
[2] For comprehensive reviews, see: a) O. Mitsunobu, *Synthesis* **1981**, 1; b) D. L. Hughes, *Org. React.* **1992**, *42*, 335.
[3] a) D. L. Hughes, R. A. Reamer, J. J. Bergan, E. J. J. Grabowski, *J. Am. Chem. Soc.* **1988**, *110*, 6487; b) D. L. Hughes, R. A. Reamer, *J. Org. Chem.* **1996**, *61*, 2967.
[4] For further mechanistic discussions, see: a) M. Varasi, K. A. M. Walker, M. L. Maddox, *J. Org. Chem.* **1987**, *52*, 4235; b) D. Camp, I. D. Jenkins, *Aust. J. Chem.* **1988**, *41*, 1835; c) D. Crich, H. Dyker, R. J. Harris, *J. Org. Chem.* **1989**, *54*, 257; d) D. Camp, I. D. Jenkins, *J. Org. Chem.* **1989**, *54*, 3045; e) J. A. Dodge, J. I. Trujillo, M. Presnell, *J. Org. Chem.* **1994**, *59*, 234; f) D. L. Hughes, *Org. Prep. Proced. Int.* **1996**, *28*, 127.
[5] For early reports on the involvement of acyloxyphosphonium ions in Mitsunobu-type processes, see: a) H. Kunz, P. Schmidt, *Chem. Ber.* **1979**, *112*, 3886; b) W. Adam, N. Narita, Y. Nishizawa, *J. Am. Chem. Soc.* **1984**, *106*, 1843; c) D. Camp, I. D. Jenkins, *J. Org. Chem.* **1989**, *54*, 3049.
[6] P. J. Harvey, M. von Itzstein, I. D. Jenkins, *Tetrahedron* **1997**, *53*, 3933.

 © 2003 Wiley-VCH Verlag GmbH & Co. KGaA, Weinheim

[7] a) C. Ahn, R. Correia, P. DeShong, *J. Org. Chem.* **2002**, *67*, 1751; addendum: C. Ahn, R. Correia, P. DeShong, *J. Org. Chem.* **2003**, *68*, 1176; b) C. Ahn, P. DeShong, *J. Org. Chem.* **2002**, *67*, 1754.
[8] A. B. Smith III, I. G. Safonov, R. M. Corbett, *J. Am. Chem. Soc.* **2002**, *124*, 11102.
[9] X. Liao, Y. Wu, J. K. De Brabander, *Angew. Chem.* **2003**, *115*, 1686; *Angew. Chem. Int. Ed.* **2003**, *42*, 1648.
[10] J. McNulty, A. Capretta, V. Laritchev, J. Dyck, A. J. Robertson, *J. Org. Chem.* **2003**, *68*, 1597.
[11] a) A. M. Pautard, S. A. Evans Jr. , *J. Org. Chem.* **1988**, *53*, 2300; b) M. A. Greenbaum, D. B. Denney, A. K. Hoffman, *J. Am. Chem. Soc.* **1956**, *78*, 2563.
[12] J. J. Hans, R. W. Driver, S. D. Burke, *J. Org. Chem.* **2000**, *65*, 2114.
[13] M. E. Lizarzaburu, S. J. Shuttleworth, *Tetrahedron Lett.* **2002**, *43*, 2157.

 © 2003 Wiley-VCH Verlag GmbH & Co. KGaA, Weinheim

A Pt Tris(carbene) Pincer Complex

A Tris(carbene) Pincer Complex: Monomeric Platinum Carbonyl with Three Bound Carbene Centers**

*Guanyang Lin, Nathan D. Jones, Robert A. Gossage, Robert McDonald, and Ronald G. Cavell**

Transition-metal carbene complexes are currently the focus of intense research because of their wide-ranging application in olefin metathesis[1–3] and organic synthesis.[4] Since 1999, we have been developing a series of novel "pincer" carbene complexes of the group four metals[5–9] and lanthanides,[10,11] as well as a number of bimetallic Cr[12] and Al[13] compounds containing bridging carbenes. The latter species are very efficient transition-metal-free ethylene polymerization catalyst precursors when activated by only one equivalent of trityl borate.[14] These new pincer-type complexes incorporate N,C,N chelates or bridges, with the carbene C atom being substituted by two $Ph_2P{=}NSiMe_3$ groups.

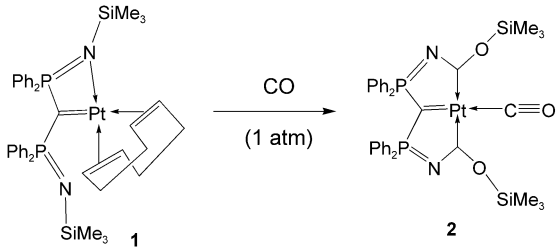
[*] Prof. Dr. R. G. Cavell, Dr. G. Lin, Dr. N. D. Jones, Prof. Dr. R. A. Gossage,[+] Dr. R. McDonald[+]
Department of Chemistry
University of Alberta
Edmonton, Alberta T6G 2G2 (Canada)
Fax: (+1) 780-492-8231
E-mail: ron.cavell@ualberta.ca

[+] Permanent Address: Department of Chemistry
Acadia University
Wolfville, Nova Scotia B4P 2B3 (Canada)

[+] X-ray Crystallography Laboratory.

[**] The authors are indebted to the Natural Sciences and Engineering Research Council of Canada (NSERC), the Petroleum Research Fund (PRF), the Izaak Walton Killam Foundation and the University of Alberta for financial support. We also thank NOVA Chemicals Ltd. (Calgary, Canada) for support of the initial work on pincer complexes. N.D.J. Izaak Walton Killam Postdoctoral Fellow (2002–2004). R.A.G. PRF Summer Research Fellow (2002).

Recently, we extended this chemistry to the late transition metals and reported the synthesis, characterization and some reactivity of a novel Pt–olefin–carbene complex, [(η^4-cod)Pt{=C($Ph_2P{=}NSiMe_3$)$_2$-$\kappa C,\kappa N$}] (**1**; cod = cycloocta-1,5-diene), in which only one of the N atoms is coordinated to the metal center.[15] Herein we report that **1** reacts with CO to give the remarkable compound [(CO)Pt{=$C(Ph_2P{=}NCO\text{-}SiMe_3)_2$-$\kappa C$, $\kappa C'$, $\kappa C''$}] (**2**) which contains a tridentate pincer ligand in which all three donors are carbenes (Scheme 1).



Scheme 1. The reaction of **1** with CO to give **2**.

The treatment of a pentane or hexanes suspension of **1** with 1 atm of CO gas at room temperature resulted in the rapid and quantitative conversion of **1** to **2**.[16] Interrogation of **2** by solution ^{1}H and ^{13}C{^{1}H} NMR and solid-state IR spectroscopies, mass spectrometry and elemental analysis revealed that **2** did not contain cod, and that it incorporated three molecules of CO, one of which was a terminal CO ligand and the other two had been chemically transformed and were related by a mirror plane.

An X-ray crystallographic study revealed the structure of **2** to be that shown in Figure 1.[17] The molecule contains a

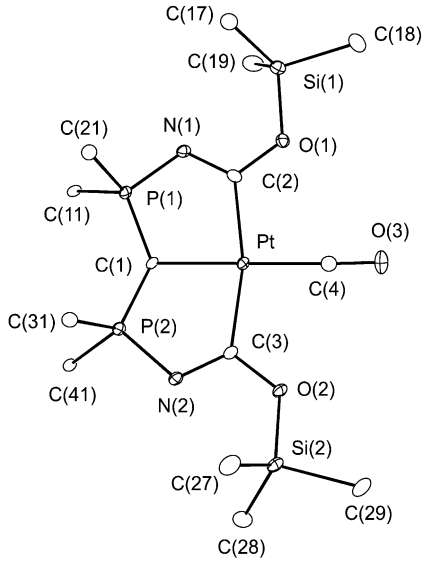


Figure 1. An ORTEP representation (ellipsoids set at the 20% probability level) of the molecular structure of **2**. Only the ipso carbon atoms of the phenyl rings are shown, and hydrogen atoms have been omitted. Selected bond lengths (Å) and angles (°): Pt-C(1) 2.002(5), Pt-C(2) 2.059(6), Pt-C(3) 2.048(6), Pt-C(4) 1.868(6), C(4)-O(3) 1.139(7); P(1)-C(1)-P(2) 133.3(3), P(1)-C(1)-Pt 111.6(3), C(1)-Pt-C(4) 179.2(3), C(2)-Pt-C(3) 166.9(2).

 © 2003 Wiley-VCH Verlag GmbH & Co. KGaA, Weinheim DOI: 10.1002/anie.200351320

total of three CO fragments, consistent with the mass spectrometric and elemental analytical data, including one terminal CO ligand, as revealed by the IR and NMR spectroscopic data. The other two CO groups have been inserted into both of the N–Si bonds with concomitant formation of two Fischer-type N,O-carbenes. The good correspondence between the solid-state and solution data shows that the molecular structure as revealed by X-ray crystallography is essentially maintained in solution.

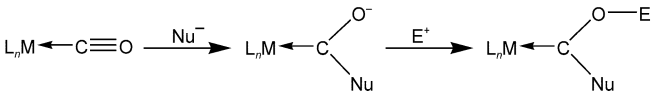
The bond angles surrounding C(1), C(2) and C(3) range from 111.6(3)° to 133.3(3)° and the sums of the angles around these centers are 356.8(3)°, 360.0(4)° and 359.9(4)°, respectively, suggesting sp^2 hybridization at these carbon atoms. The Pt–C(1) bond length (2.002(5) Å) is significantly shorter than those of Pt–C(2) and Pt–C(3) (2.059(6) and 2.048(6) Å, respectively), and slightly shorter than the corresponding bond length found in **1** (2.021(5) Å).[15] All of these lengths are significantly longer than those typically found for both N-heterocyclic carbene complexes of two- and four-coordinate Pt centers (1.93–1.97 Å),[18–20] and the Fischer carbene complexes of four-coordinate Pt centers (1.87–1.96 Å).[21–25] Indeed, the Pt–C(1) bond length in **2** is unusual in that it is more akin to those found for Fischer carbene complexes of five-[26] and six-coordinate[27] Pt centers (1.99–2.01 Å). Nevertheless, all of the the Pt–C(carbene) bonds in **2** are shorter than typical Pt–C(alkyl) single bonds (2.07–2.15 Å).[28]

It is interesting to note that the Pt–C(4) (carbonyl) bond in **2** (1.868(6) Å) is significantly shorter than those found in typical four-coordinate Pt^{II}-carbonyl complexes, for example, those in *cis*-$[PtCl_2(CO)_2]$ are 1.901(5) and 1.893(5) Å.[29] In addition, the C(4)–O(3) distance in **2** (1.139(7) Å) is longer than the corresponding lengths in *cis*-$[PtCl_2(CO)_2]$ (1.110(7) and 1.121(6) Å), and its $\tilde{\nu}$(C≡O) is much lower (2038 *vs.* 2170 and 2128 cm^{-1}, respectively). In contrast, these distances in **2** are comparable to those found in Pt(0) carbonyl complexes, for example, $[Pt(CO)(PPh_3)_3]$ has Pt–C bond lengths of 1.86(3)[30] and 1.84(2)[31] Å (two polymorphs) and corresponding C–O distances of 1.12(4) and 1.13(3) Å. The comparative data suggest that the metal center in **2** is appreciably electron rich, as we have suggested previously for the Pt center in **1**,[15] and that there is significant π-backbonding to the terminal CO ligand. Given that Pt^{II}- and Pd^{II}-CO bonds have been considered repeatedly to be almost pure σ-type interactions,[29,32] a zero oxidation state of the Pt center in **2** is possible, and **2**, as drawn, is an 18-electron species. However, its square-planar coordination geometry strongly suggests a 16-electron Pt^{II} configuration.

The apparent electron-count/coordination geometry discrepancy may be resolved either by describing **2** in terms of 16-electron resonance structures incorporating two Pt–C covalent bonds and one Pt–C dative bond, or by reference to restricted Hartree-Fock calculations by Nakamura and Morokuma. These researchers have found that their 18-electron carbene carbonyl model complex *cis*-$[Pt(PH_3)_2(CO)(CH_2)]$ adopts a square-planar structure as its most stable coordination geometry, with the C–H bonds in the plane.[33] They attribute the stability of the square-planar structure over a tetrahedral one to $CH_2(\pi)$-Pt(pπ) overlap, which constitutes the HOMO in their complex. Carbene complex **2** may likewise be an 18-electron Pt^{II} compound whose square-planar geometry is the result of such an overlap.

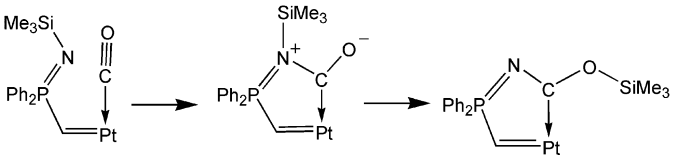
Phosphorus substituted carbene (P,P-carbene) metal complexes are rare. In addition to compounds developed by us, only a few examples have been reported previously, and almost all of these are based on the carbodiphosphoranes $R_3P{=}C{=}PR_3$ (R=Me,[34] Ph[35]). Apart from **1** and **2**, only three structurally characterised Group 10 P,P-carbene complexes have so far appeared in the literature: $[(OC)_nNi\{{=}C(PPh_3)_2\}]$ ($n=2$, 3)[36] and $[Pd(\mu\text{-}Cl)_2Pt\{{=}C(PPh_2)_2\}]_\infty$.[37] Other examples of $Ph_3P{=}C{=}PPh_3$ complexes of Pt have been characterized spectroscopically.[38,39] Aside from **2**, we are not aware of any Group 10 complexes bearing P,P- as well as classical Fischer carbene ligands.

Fischer carbene complexes are typically made from metal-carbonyl or metal-isonitrile complexes by the stepwise addition of a strong nucleophile and an electrophile according



Scheme 2. The formation of carbene complexes by the stepwise addition of a nucleophile and electrophile to a metal carbonyl.

to Scheme 2.[2] It is therefore reasonable to postulate that the reaction of CO with **1** to generate **2** may proceed analogously, with the mechanism containing steps that are outlined in Scheme 3 (only the crucial atoms are shown). Nucleophilic attack on a coordinated CO ligand by the N-atom of a



Scheme 3. Postulated mechanism for the formation of **2**.

"dangling" $Ph_2P{=}NSiMe_3$ group, and subsequent N-to-O trimethylsilyl migration generates an N,O-carbene. This sequence of steps must occur on both "sides" of the molecule to generate the final product.

Because **1** may also be drawn in one resonance form as an alkyl amido complex, insertion of CO into the Pt–N bond is also possible in the formation of **2**. However, because such insertions are rare (though not unprecedented) for late transition-metal amides[40,41] and because **1** does not behave like a typical complex in this class (the Pt–N bond is not hydrolyzed, for example), we favor the route outlined in Scheme 3.

The first step in this proposed mechanism has precedence in reports of intramolecular attack by Ru-coordinated 2-amino[42] or 2-acetamido pyridine[43] on the α-carbon atom of a vinylidene ligand, and in those describing the ring-closing of W-, Mo-, Cr- and Fe-coordinated 2-hydroxyphenyl isonitrile

 © 2003 Wiley-VCH Verlag GmbH & Co. KGaA, Weinheim

by attack of the hydroxy group on the bound C-atom in the same ligand.[44–46] In all of these cases, Fischer carbenes ultimately result by N-to-C or O-to-N proton transfer, respectively.

Literature precedence for the second step is found in our own observations of N-to-O trimethylsilyl migration reactions,[47] as well as those of other groups.[48–50] Of particular relevance to this system is our recent finding that the reaction of **1** with CO_2 produced [Pt(η^4-cod){=C(Ph_2P=NSiMe_3)(Ph_2P=NC(O)OSiMe_3)}-κC,κN}].[15]

To the best of our knowledge, **2** represents the first example of a tris(carbene) pincer complex, although the homoleptic Fischer carbene complex $[Pt\{C(N(H)CH_3)_2\}_4]^{2+}$ has long been known.[51] We are aware neither of other instances in which a carbene complex is thought to be generated in the first step by intramolecular attack on coordinated CO (rather than on vinylidene[42,43] or isonitrile[44–46]), nor have we found instances of trimethylsilyl as opposed to proton migration as the second step in the carbene formation process. We are currently investigating the onward reactivity of **2**.

Received: March 3, 2003
Revised: May 12, 2003 [Z51320]

Keywords: carbenes · carbonyl ligands · imines · phosphorus · platinum

[1] R. R. Schrock, *Chem. Rev.* **2002**, *102*, 145 – 179.
[2] T. M. Trnka, R. H. Grubbs, *Acc. Chem. Res.* **2001**, *34*, 18 – 29.
[3] A. M. Rouhi, in *Chemical and Engineering News, Vol. 80*, **2002**, pp. 29 – 38.
[4] K. H. Dötz, *Angew. Chem.* **1984**, *96*, 587 – 608; *Angew. Chem. Int. Ed. Engl.* **1984**, *23*, 587 – 608
[5] R. P. Kamalesh Babu, R. McDonald, S. A. Decker, M. Klobukowski, R. G. Cavell, *Organometallics* **1999**, *18*, 4226 – 4229.
[6] R. P. Kamalesh Babu, R. McDonald, R. G. Cavell, *Organometallics* **2000**, *19*, 3462 – 3465.
[7] R. P. Kamalesh Babu, R. McDonald, R. G. Cavell, *Chem. Commun.* **2000**, 481 – 482.
[8] R. G. Cavell, R. P. Kamalesh Babu, A. Kasani, R. McDonald, *J. Am. Chem. Soc.* **1999**, *121*, 5805 – 5806.
[9] K. Aparna, R. P. Kamalesh Babu, R. McDonald, R. G. Cavell, *Angew. Chem. Int. Ed.* **2001**, *40*, 4400 – 4402; *Angew. Chem.*, **2001**, *113*, 4535 – 4537.
[10] A. Kasani, M. Ferguson, R. G. Cavell, *J. Am. Chem. Soc.* **2000**, *122*, 726 – 727.
[11] R. G. Cavell, R. P. Kamalesh Babu, K. Aparna, *J. Organomet. Chem.* **2001**, *617*, 158 – 169.
[12] A. Kasani, R. McDonald, R. G. Cavell, *Chem. Commun.* **1999**, 1993 – 1994.
[13] A. Kasani, R. McDonald, M. Ferguson, R. G. Cavell, *Organometallics* **1999**, *18*, 4241 – 4243.
[14] R. G. Cavell, K. Aparna, R. P. Kamalesh Babu, Q. Wang, *J. Mol. Catal. A* **2002**, *189*, 137 – 143.
[15] N. D. Jones, G. Lin, R. A. Gossage, R. McDonald, R. G. Cavell, *Organometallics* **2003**, *22*, 2832 – 2841.
[16] A suspension of **1** (62 mg, 0.072 mmol) in pentane was solidified at liquid N_2 temperature in an Schlenk flask. The flask was evacuated, allowed to warm to room temperature and filled with 1 atm of CO gas. The red orange suspension of **1** became green after 15 min of stirring. Centrifugation gave a crystalline solid, which was washed with pentane (2 × 5 mL) and dried under vacuum. Yield: 53 mg (88 %). A ^{13}C-enriched sample of **2** was made in exactly the same manner by using ^{13}CO gas. Elemental anal calcd (%) for $C_{34}H_{38}N_2O_3P_2PtSi_2$: C 48.85, H 4.58, N 3.35; found: C 48.92, H 4.46, N 3.25. ^{1}H NMR ([D$_8$]THF): 0.22 (s, 18 H, Si(CH_3)$_3$), 7.19 (m, 8 H, *o*-Ph-*H*), 7.37 ppm (m, 12 H, *m*- and *p*-Ph-*H*). ^{31}P{^{1}H} ([D$_8$]THF): 46.9 ppm (s, $^2J_{PPt}$ = 35 Hz). ^{13}C{^{1}H} NMR ([D$_8$]THF, ^{13}C-enriched): 1.1 (s, Si(CH_3)$_3$), 128.8 (m, Ph-*C*), 131.6 (m, Ph-*C*), 132.5 (m, Ph-*C*), 133.8 (m, Ph-*C*), 177.3 (s, *C*O, $^1J_{CPt}$ = 1370 Hz, $^2J_{CC}$ = 0 Hz), 207.1 ppm (apparent (second-order) triplet, N*C*O, $^2J_{CP}$ = 39 Hz, $^2J_{CC}$ = 0 Hz (both derived by simulation), $^1J_{CPt}$ = 871 Hz). FTIR (KBr pellet) :ν = 2038 (CH_2Cl_2); 2038 cm^{-1} . MS (EI, *m/z*): 836.1 ([M]$^+$, 21.2 %), 820.8 ([M-CH_3]$^+$, 10.8 %), 807.6 ([M-CO]$^+$, 68.8 %), 779.8 ([M-2 CO]$^+$, 100.0 %), 751.4 ([M-3 CO]$^+$, 15.2 %).
[17] Crystallographic data for **2**: triclinic, space group P$\bar{1}$(No. 2), a = 12.3685(7), b = 13.1635(7), c = 13.1789(7) Å, α = 118.2869(10), β = 108.3633(11), γ = 93.0971(11)°, V = 1739.37(16) Å^3, Z = 2. The structure was solved by direct methods and refined by full-matrix least-squares procedures: R_1 = 0.0405 [$F_0^2 \geqq 2\sigma F_0^2$] and wR_2 = 0.0951 [$F_0^2 \geqq -3\sigma F_0^2$]. Extra details about the structure of **2** have been deposited with the Cambridge Crystallographic Data Center as supplementary publication no. CCDC-204403 . These data can be obtained free of charge via www.ccdc.cam.ac.uk/conts/retrieving.html (or from the Cambridge Crystallographic Data Centre, 12 Union Road, Cambridge CB2 1EZ, UK; fax: (+44) 1223-336-033; or deposit@ccdc.cam.ac.uk).
[18] M. Hasan, I. V. Kozhevnikov, M. Rafiq, H. Siddiqui, C. Femoni, A. Steiner, N. Winterton, *Inorg. Chem.* **2001**, *40*, 795 – 800.
[19] R.-Z. Ku, J.-C. Huang, J.-Y. Cho, F.-M. Kang, K. R. Reddy, Y.-C. Chen, K.-J. Lee, J.-H. Lee, G.-H. Lee, C.-M. Peng, S.-T. Liu, *Organometallics* **1999**, *18*, 2145 – 2154.
[20] A. J. Arduengo III, S. F. Gamper, J. C. Calabrese, F. Davidson, *J. Am. Chem. Soc.* **1994**, *116*, 4391 – 4394.
[21] G. Ferguson, Y. Li, A. J. McAlees, R. McCrindle, E. Zang, *J. Organomet. Chem.* **2001**, *617–618*, 671 – 680.
[22] S. Tollari, S. Cenini, A. Penoni, G. Granata, G. Palmisano, F. Demartin, *J. Organomet. Chem.* **2000**, *608*, 34 – 41.
[23] G. Ferguson, Y. Li, A. J. McAlees, R. McCrindle, K. Xiang, *Organometallics* **1999**, *18*, 2428 – 2439.
[24] E. K. Barefield, A. M. Carrier, D. J. Sepelak, D. G. V. Derveer, *Organometallics* **1982**, *1*, 103 – 110.
[25] G. K. Anderson, R. J. Cross, L. Manojlovic-Muir, K. W. Muir, R. A. Wales, *J. Chem. Soc. Dalton Trans.* **1979**, 684 – 690.
[26] M. E. Cucciolito, A. Panunzi, F. Ruffo, *Organometallics* **1999**, *18*, 3482 – 3489.
[27] L. M. Redina, J. J. Vittal, R. J. Puddephatt, *Organometallics* **1995**, *14*, 1030 – 1038.
[28] A. G. Orpen, L. Brammer, F. H. Allen, O. Kennard, D. G. Watson, R. Taylor, *J. Chem. Soc. Dalton* **1989**, *1*-83.
[29] F. Bagnoli, D. B. Dell′Amico, F. Calderazzo, U. Englert, F. Marchetti, G. E. Herberich, N. Pasqualetti, S. Ramello, *J. Chem. Soc. Dalton* **1996**, 4317 – 4318.
[30] V. G. Albano, G. M. Basso Ricci, P. L. Bellon, *Inorg. Chem.* **1969**, *8*, 2109 – 2115.
[31] V. G. Albano, P. L. Bellon, M. Sansoni, *Chem. Commun.* **1969**, 899.
[32] D. Belli Dell′Amico, F. Calderazzo, C. A. Veracini, N. Zandona, *Inorg. Chem.* **1984**, *23*, 3030 – 3033.
[33] S. Nakamura, K. Morokuma, *Organometallics* **1988**, *7*, 1904 – 1909.
[34] O. Gasser, H. Schmidbauer, *J. Am. Chem. Soc.* **1975**, *97*, 6281 – 6282.
[35] G. E. Hardy, J. C. Baldwin, J. I. Zink, W. C. Kaska, P.-H. Liu, L. DuBois, *J. Am. Chem. Soc.* **1977**, *99*, 3552 – 3558.
[36] W. Petz, F. Weller, J. Uddin, G. Frenking, *Organometallics* **1999**, *18*, 619 – 626.

 © 2003 Wiley-VCH Verlag GmbH & Co. KGaA, Weinheim

[37] S. I. Al-Resayes, P. B. Hitchcock, J. F. Nixon, *J. Chem. Soc. Chem. Commun.* **1986**, 1710 – 1711.
[38] J. C. Baldwin, W. C. Kaska, *Inorg. Chem.* **1979**, *18*, 686 – 691.
[39] W. C. Kaska, D. K. Mitchell, R. F. Reichelderfer, *J. Organomet. Chem.* **1973**, *47*, 391 – 402.
[40] M. D. Fryzuk, C. D. Montgomery, *Coord. Chem. Rev.* **1989**, *95*, 1 – 40.
[41] P. L. Holland, R. A. Andersen, R. G. Bergman, *J. Am. Chem. Soc.* **1996**, *118*, 1092 – 1104.
[42] E. Ruba, A. Hummel, K. Mereiter, R. Schmid, K. Kirchner, *Organometallics* **2002**, *21*, 4955 – 4959.
[43] C. Slugovc, K. Mereiter, R. Schmid, K. Kirchner, *Organometallics* **1998**, *17*, 827 – 831.
[44] F. E. Hahn, M. Tamm, *J. Organomet. Chem.* **1993**, *456*, C11-C14.
[45] F. E. Hahn, M. Tamm, *J. Chem. Soc. Chem. Commun.* **1993**, 842 – 844.
[46] F. E. Hahn, M. Tamm, *J. Chem. Soc. Chem. Commun.* **1995**, 569 – 570.
[47] K. V. Katti, R. G. Cavell, *Inorg. Chem.* **1989**, *28*, 3033 – 3036.
[48] R. R. Schrock, C. Rosenberger, S. W. Seidel, K.-Y. Shih, W. M. Davis, A. L. Odom, *J. Organomet. Chem.* **2001**, *617–618*, 495 – 501.
[49] C. P. Gerlach, J. Arnold, *Inorg. Chem.* **1996**, *35*, 5770 – 5780.
[50] M. D. Fryzuk, P. A. MacNeil, S. J. Rettig, *J. Organomet. Chem.*, **1987**, *332*, 345 – 360.
[51] J. S. Miller, A. L. Balch, *Inorg. Chem.*, **1972**, *11*, 2069 – 2074.

 © 2003 Wiley-VCH Verlag GmbH & Co. KGaA, Weinheim

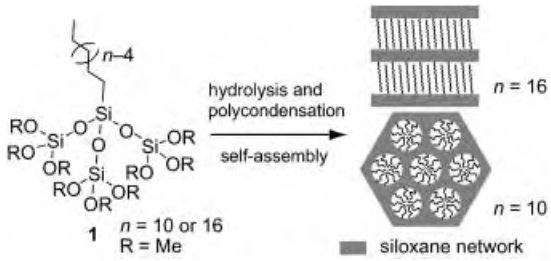
Mesostructured Silica-Based Hybrids

Direct Formation of Mesostructured Silica-Based Hybrids from Novel Siloxane Oligomers with Long Alkyl Chains**

*Atsushi Shimojima and Kazuyuki Kuroda**

Silica-based hybrids derived from organoalkoxysilanes have been extensively studied because of their potential for novel nanomaterials as well as their scientific significance. Although a wide variety of hybrids can be designed at a molecular scale by the modification of the precursors, the control of their nanostructures is still an important subject of research.[1,2] Recently, intensive efforts have been made in the synthesis of mesostructured (lamellar, hexagonal, or cubic) hybrids by using surfactant assemblies as structure directors.[3–7] However, their formations are governed by weak interactions between surfactant molecules and silicate or organosiloxane species. The control of the hybrid nanostructures without the use of surfactants is a great challenge, and the preparation of a novel building block with self-organizing ability should be important. The design of such a single precursor would open up the possibility of creating nanohybrid materials that are not accessible through surfactant-directed processes.

Herein we report an innovative method for the formation of ordered silica-based hybrids by using newly designed siloxane-based oligomers **1**, consisting of an alkylsilane core and three branched trimethoxysilyl groups ($C_nH_{2n+1}Si(OSi(OMe)_3)_3$, $n = 10$ or 16), as single precursors. The self-assembly of **1** during the hydrolysis and polycondensation leads to the formation of lamellar or hexagonal-like mesostructures that are controlled by changing the length of the alkyl chain (Scheme 1).



Scheme 1. Formation of mesostructured hybrids from siloxane-based oligomers **1** with two different chain lengths.

The ability of organoalkoxysilanes to self-organize during hydrolysis and polycondensation was recently explored.[8–14] This is an attractive feature based on the weak interactions of the organic groups and the hydrophilic nature of the silanol groups. However, all attempts to prepare ordered hybrids through self-assembly have resulted in layered structures, except for the specific case in which a precursor bearing a surfactant molecule with a Si–C bond was employed.[12] We have reported the formation of multilayered hybrids from alkyltrialkoxysilanes.[13] Although the morphological control of the transparent films was attained by cocondensation of alkyltrialkoxysilane with tetraalkoxysilane, oligomeric species with well-defined structures have never been formed in precursor solutions,[14] which implies that highly organized nanoarchitectures are formed with difficulty.

The precursors **1** ($n = 10$ and 16) were synthesized by the reaction of corresponding *n*-alkylsilanetriols and tetrachlorosilane, followed by methanolysis of Si–Cl groups. Hydrolysis and polycondensation reactions of **1** were performed in the solutions with a molar composition of **1**/THF/H_2O/HCl = 1:50:18:0.002. The mixtures were stirred at 25 °C for 12 h, and water (H_2O:**1** = 32) was then added. The resulting

[*] Prof. Dr. K. Kuroda, Dr. A. Shimojima
Department of Applied Chemistry
Waseda University
Ohkubo 3–4–1, Shinjuku-ku, Tokyo 169–8555 (Japan)
Fax: (+81) 3-5286-3199
E-mail: kuroda@waseda.jp
Prof. Dr. K. Kuroda
Kagami Memorial Laboratory for Materials Science and Technology
Waseda University
Nishiwaseda 2–8–26, Shinjuku-ku, Tokyo 169–0051 (Japan)
and
CREST, Japan Science and Technology Corporation (JST)

[**] The authors are grateful to Prof. Y. Sugahara (Waseda University) for discussion. The work was partially supported by a Grant-in-Aid for COE research, MEXT, Japan. A. S. thanks a financial support by a Grant-in-Aid for JSPS Fellows from MEXT.

Supporting information for this article is available on the WWW under http://www.angewandte.org or from the author.

 DOI: 10.1002/anie.200351419 © 2003 Wiley-VCH Verlag GmbH & Co. KGaA, Weinheim

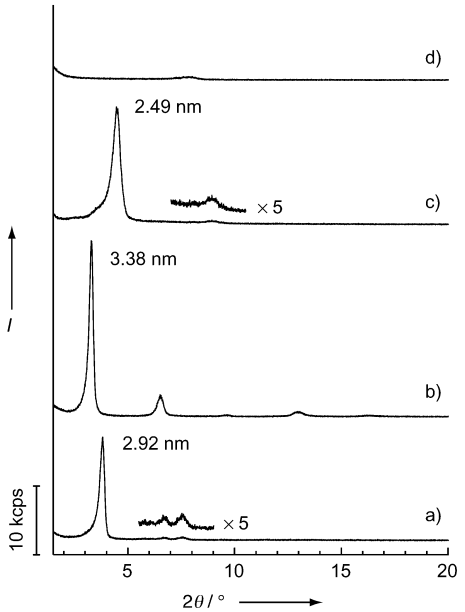


Figure 1. Powder XRD patterns of the products derived from **1**: a) $n=10$ (as-synthesized), b) $n=16$ (as-synthesized), c) $n=10$ (calcined), and d) $n=16$ (calcined). The patterns were recorded on a Mac Science M03XHF[22] diffractometer with Mn-filtered $Fe_{K\alpha}$ radiation.

precursor solutions were cast on glass substrates, and air-dried at room temperature for 2 days. The resulting platelike solids were pulverized before characterization.

The powder X-ray diffraction (XRD) patterns of the hybrids ($n=10$ and 16) exhibit low-angle diffraction peaks corresponding to the d spacings of 2.92 and 3.38 nm, respectively (Figure 1a, b). In the case of $n=16$, all the peaks observed at higher angles ($2\theta=6$–$17°$) are attributed to higher order diffractions, thus indicating the well-ordered layered structure of the product. This ordering was revealed by the increase of the d value to about 4.7 nm upon adsorption of *n*-decyl alcohol. The interlayer chains appear to take a monolayer arrangement, because the d value (3.38 nm) is much smaller than that for lamellar alkylsiloxanes with a bilayer structure ($d=4.80$ nm).[13] On the other hand, the pattern for $n=10$ (Figure 1a) shows quite a different profile with several small peaks at the higher region, and the structure of the product can tentatively be assigned as 2D hexagonal.

Figure 2 shows the transmission electron microscopic (TEM) images of the products. The hybrid with $n=16$ exhibits exclusively well-defined striped patterns whose periodicity is close to the d spacing. In contrast, a hexagonal-like structure is observed for the hybrid with $n=10$, in agreement with the XRD data. The structure is slightly distorted, possibly due to the anisotropic shrinkage of the siloxane frameworks during the polycondensation process. Although a future detailed structural study is needed, the present results evidently show that the precursors have the ability to form both lamellar and hexagonal mesophases through self-assembly.

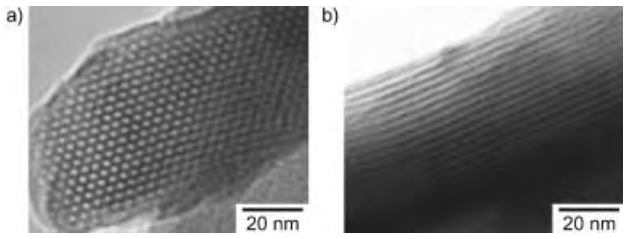


Figure 2. Typical TEM images of the as-synthesized hybrids derived from **1**: a) $n=10$ and b) $n=16$. The images were obtained by a JEOL JEM-100CX microscope at an accelerating voltage of 100 kV.

The formation of the siloxane networks was confirmed by ^{29}Si MAS NMR spectroscopy of the hybrids (Figure 3). The

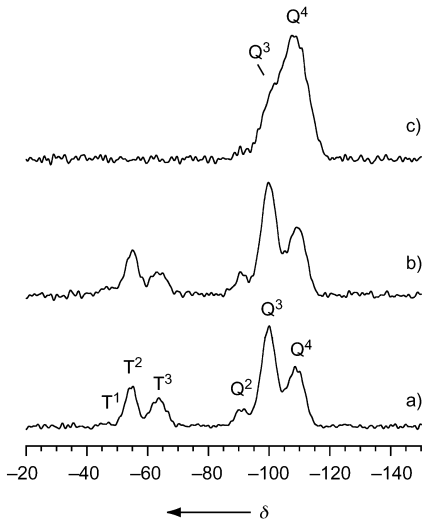


Figure 3. Solid-state ^{29}Si MAS NMR spectra of the products derived from **1**: a) $n=10$ (as-synthesized), b) $n=16$ (as-synthesized), and c) $n=10$ (calcined). The spectra were recorded on a JEOL JNM-CMX-400 spectrometer at a resonance frequency of 79.42 MHz with a 45° pulse and a recycle delay of 100 s. The relative intensity ratios of the signals are listed in the Supporting Information.

spectra for $n=10$ and 16 are similar and display signals corresponding to the T^1, T^2, and T^3 units (T^x, $CSi(OSi)_x(OH)_{3-x}$), and also to the Q^2, Q^3, and Q^4 units (Q^x, $Si(OSi)_x(OH)_{4-x}$). The presence of the T^1 and T^2 units suggests the partial cleavage and the rearrangement of the original Si–O–Si bonds in the precursor **1** during hydrolysis and polycondensation. We confirmed that the signals arising from the Q^0 species did not appear in the ^{29}Si NMR spectra of the solution during the reaction, thus suggesting a very slow rate of the hydrolysis of Si–O–Si bonds in **1** to form smaller species. Further work to investigate the detailed reaction process is underway and will be reported subsequently.

These results prove the formation of two types of nanostructured hybrids as depicted in Scheme 1. The products are structurally unique because organic regions are filled with alkyl chains covalently attached to nanostructured-silica frameworks. The formation of these products depends on the self-assembly of the single precursor, and is quite different from conventional methods, including cocondensation of organotrialkoxysilane and tetraalkoxysilane in the presence of surfactants, or postmodification of mesoporous silica or layered silicates with organosilanes.[4,5]

 © 2003 Wiley-VCH Verlag GmbH & Co. KGaA, Weinheim

The difference in the nanostructures was further confirmed by the calcination of the hybrids at 500 °C for 8 h to remove organic components. The ^{29}Si NMR spectra of the calcined samples mainly showed the Q^3 and Q^4 signals (Figure 3c), which suggests the conversion of the T units to Q units by thermal degradation of the organic moieties. While the layered structure ($n = 16$) collapsed upon calcination (Figure 1d), the ordered structure was retained in the case of $n = 10$ with a decrease in the d spacing (Figure 1c), which was also supported by TEM (see Supporting Information). The nitrogen adsorption measurement revealed that the calcined hybrid ($n = 10$) was a microporous solid with a Brunauer–Emmett–Teller (BET) surface area of 1070 $m^2 g^{-1}$, the average Barrett–Joyner–Halenda (BJH) pore diameter of about 1.7 nm, and pore volume of 0.41 $cm^3 g^{-1}$, while the as-synthesized hybrid was nonporous (see Supporting Information). Although several researchers have proposed the idea of using organoalkoxysilanes as organic templates to prepare microporous silica,[15–18] this work is truly the first synthesis of the hexagonally ordered porous silica. Such a method has the advantage of producing relatively small pores compared to those obtained by using surfactants with the corresponding chain length.[19]

The siloxane oligomers formed by the hydrolysis and polycondensation of **1** can be regarded as a polyhydroxy amphiphile containing a hydrophobic alkyl chain and hydrophilic silanol groups.[20] It is plausible that the nanostructured hybrids are formed by the self-assembly of the alkylsiloxane species upon evaporation of the solvents, followed by siloxane formation. The difference in the nanostructures of the hybrids depending on the alkyl chain length can be explained in terms of the geometrical packing of alkylsiloxane oligomers.[21] In contrast to the several reports on the formation of lamellar hybrids from organoalkoxysilanes with the general formula of $RSi(OR')_3$ or $(R'O)_3Si{-}R{-}Si(OR')_3$ (R, R′ = organic groups),[9–11,13] this example is the first self-assembly of organosilane molecules into a hexagonal structure, which is apparently due to the large occupying volume of the hydrophilic headgroup in the precursor **1** compared to that of a single $Si(OH)_3$ group. It should be noted that such mesostructures cannot be obtained by the random cocondensation of alkylalkoxysilane-tetraalkoxysilane mixtures,[14] thus suggesting the importance of well-designed molecular structure of the precursor.

Furthermore, the control of the macroscopic morphology of the hybrids was achieved because of the high cross-linking ability of **1**. Transparent thin films with the thickness of about 450–600 nm were obtained by spin coating (3000 rpm, 10 s) the precursor solutions on glass substrates. The XRD patterns of the films ($n = 10$ and 16) are shown in Figure 4. Both patterns show the smaller d spacings than those of powdered samples, which may in part be ascribed to the difference in the degree of polycondensation. It is noteworthy that the film for $n = 10$ exhibits a very sharp and intense peak with only second and third order diffractions, which is typical for the well-ordered 2D hexagonal structures in which cylindrical assemblies are oriented parallel to the substrate.[22,23] Evidence for the hexagonal structure of the film was obtained from the cross-sectional TEM image (Figure 4 inset).

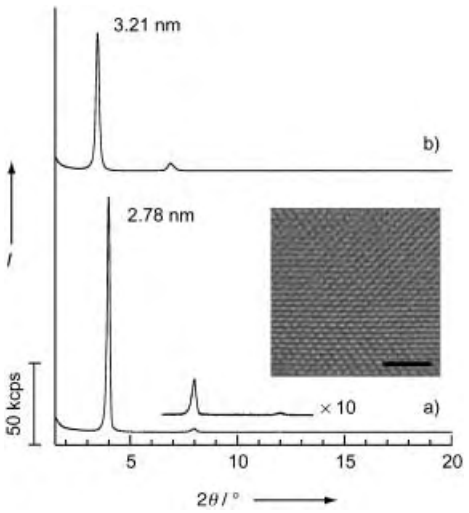


Figure 4. XRD patterns of the as-synthesized hybrid films derived from **1**: a) $n = 10$ and b) $n = 16$. Inset shows the cross-sectional TEM image of the film with $n = 10$ (scale bar; 20 nm). The image was obtained by a JEOL JEM-2010 microscope at an accelerating voltage of 200 kV.

In conclusion, we have demonstrated the successful formation of silica-based hybrids with highly ordered lamellar and 2D hexagonal nanostructures by using novel alkylsiloxane oligomers as single precursors. Such a method proves to lead to the better control of composition, mesostucture, and morphology of silica-based hybrids. It is of great interest that a hexagonally ordered hybrid is prepared for the first time without the use of surfactants and any other silica source, thus providing a novel pathway to ordered porous silica. The further design of precursors based on the organic group and/or the siloxane part will allow functionalization as well as variations of the architecture at molecular and nanometer scales.

Experimental Section

n-Alkylsilanetriols ($n = 10$ and 16) were synthesized by the hydrolysis of decyltrichlorosilane ($C_{10}H_{21}SiCl_3$) and hexadecyltriethoxysilane ($C_{16}H_{33}Si(OEt)_3$). Detailed procedures are described in the Supporting Information. In a typical synthesis of **1**, 12.0 g of alkylsilanetriol dissolved in THF (600 mL) was added to a vigorously stirred mixture of $SiCl_4$ (100 mL) and hexane (240 mL) at room temperature. Removal of the solvents and unreacted $SiCl_4$ under reduced pressure afforded a slightly turbid liquid which contained mainly $RSi(OSiCl_3)_3$ (R = alkyl) and a small amount of $RSiCl(OSiCl_3)_2$. $RSi(OSiCl_3)_3$ was isolated by vacuum distillation, and the conversion of Si–Cl groups to Si–OMe groups was performed by the addition of methanol with degassed HCl under reduced pressure. The precursor **1** was obtained as a clear and colorless liquid. The spectroscopic data are contained in the Supporting Information.

Received: March 17, 2003
Revised: May 5, 2003 [Z51419]

Keywords: nanostructures · organic–inorganic hybrid composites · self-assembly · sol–gel processes · thin films

 © 2003 Wiley-VCH Verlag GmbH & Co. KGaA, Weinheim

[1] a) R. J. P. Corriu, D. Leclercq, *Angew. Chem.* **1996**, *108*, 1524 – 1540; *Angew. Chem. Int. Ed. Engl.* **1996**, *35*, 1420 – 1436; b) R. J. P. Corriu, *Angew. Chem.* **2000**, *112*, 1432 – 1455; *Angew. Chem. Int. Ed.* **2000**, *39*, 1376 – 1398.

[2] C. Sanchez, G. J. de A. A. Soler-Illia, F. Ribot, T. Lalot, C. R. Mayer, V. Cabuil, *Chem. Mater.* **2001**, *13,* 3061 – 3083.

[3] A. Sellinger, P. M. Weiss, A. Nguyen, Y. Lu, R. A. Assink, W. Gong, C. J. Brinker, *Nature* **1998**, *394,* 256 – 260.

[4] A. Stein, B. J. Melde, R. C. Schroden, *Adv. Mater.* **2000**, *12,* 1403 – 1419, and references therein.

[5] A. Sayari, S. Hamoudi, *Chem. Mater.* **2001**, *13,* 3151 – 3168, and references therein.

[6] Y. Lu, H. Fan, N. Doke, D. A. Loy, R. A. Assink, D. A. LaVan, C. J. Brinker, *J. Am. Chem. Soc.* **2000**, *122,* 5258 – 5261.

[7] S. Inagaki, S. Guan, T. Ohsuna, O. Terasaki, *Nature* **2002**, *416,* 304 – 307.

[8] B. Boury, R. J. P. Corriu, *Chem. Commun.* **2002**, 795 – 802, and references therein.

[9] a) J. J. E. Moreau, L. Vellutini, M. W. C. Man, C. Bied, *J. Am. Chem. Soc.* **2001**, *123*, 1509 – 1510; b) J. J. E. Moreau, L. Vellutini, M. W. C. Man, C. Bied, J.-L. Bantignies, P. Dieudonné, J.-L. Sauvajol, *J. Am. Chem. Soc.* **2001**, *123*, 7957 – 7958.

[10] N. Liu, K. Yu, B. Smarsly, D. R. Dunphy, Y. B. Jiang, C. J. Brinker, *J. Am. Chem. Soc.* **2002**, *124,* 14540 – 14541.

[11] K. Katagiri, K. Ariga, J. Kikuchi, *Chem. Lett.* **1999**, 661 – 662.

[12] a) Q. Huo, D. I. Margolese, G. D. Stucky, *Chem. Mater.* **1996**, *8,* 1147 – 1160; b) E. Ruiz-Hitzky, S. Letaïef, V. Prévot, *Adv. Mater.* **2002**, *14*, 439 – 443.

[13] A. Shimojima, Y. Sugahara, K. Kuroda, *Bull. Chem. Soc. Jpn.* **1997**, *70,* 2847 – 2853.

[14] a) A. Shimojima, K. Kuroda, *Langmuir* **2002**, *18,* 1144 – 1149; b) A. Shimojima, N. Umeda, K. Kuroda, *Chem. Mater.* **2001**, *13,* 3610 – 3616.

[15] N. K. Raman, M. T. Anderson, C. J. Brinker, *Chem. Mater.* **1996**, *8,* 1682 – 1701.

[16] Y. Lu, G. Cao, R. P. Kale, S. Prabakar, G. P. López, C. J. Brinker, *Chem. Mater.* **1999**, *11,* 1223 – 1229.

[17] M. Park, S. Komarneni, W. T. Lim, N. H. Heo, J. Choi, *J. Mater. Res.* **2000**, *15,* 1437 – 1440.

[18] G. Büchel, K. K. Unger, A. Matsumoto, K. Tsutsumi, *Adv. Mater.* **1998**, *10,* 1036 – 1038.

[19] R. Ryoo, I. S. Park, S. Jun, C. W. Lee, M. Kruk, M. Jaroniec, *J. Am. Chem. Soc.* **2001**, *123*, 1650 – 1657, and references therein.

[20] C. Tschierske, *J. Mater. Chem.* **1998**, *8,* 1485 – 1508.

[21] J. N. Israelachvili, D. J. Mitchell, B. W. Ninham, *J. Chem. Soc. Faraday Trans. 1* **1976**, *72,* 1525 – 1568.

[22] H. Yang, A. Kuperman, N. Coombs, S. Mamiche-Afara, G. A. Ozin, *Nature* **1996**, *379,* 703 – 705.

[23] P. C. A. Alberius, K. L. Frindell, R. C. Hayward, E. J. Kramer, G. D. Stucky, B. F. Chmelka, *Chem. Mater.* **2002**, *14,* 3284 – 3294.

 © 2003 Wiley-VCH Verlag GmbH & Co. KGaA, Weinheim

Photoinduced Electron Transfer

Fullerene-Terminated Dendritic Multiporphyrin Arrays: "Dendrimer Effects" on Photoinduced Charge Separation

Myung-Seok Choi, Takuzo Aida, Hongxia Luo, Yasuyuki Araki, and Osamu Ito**

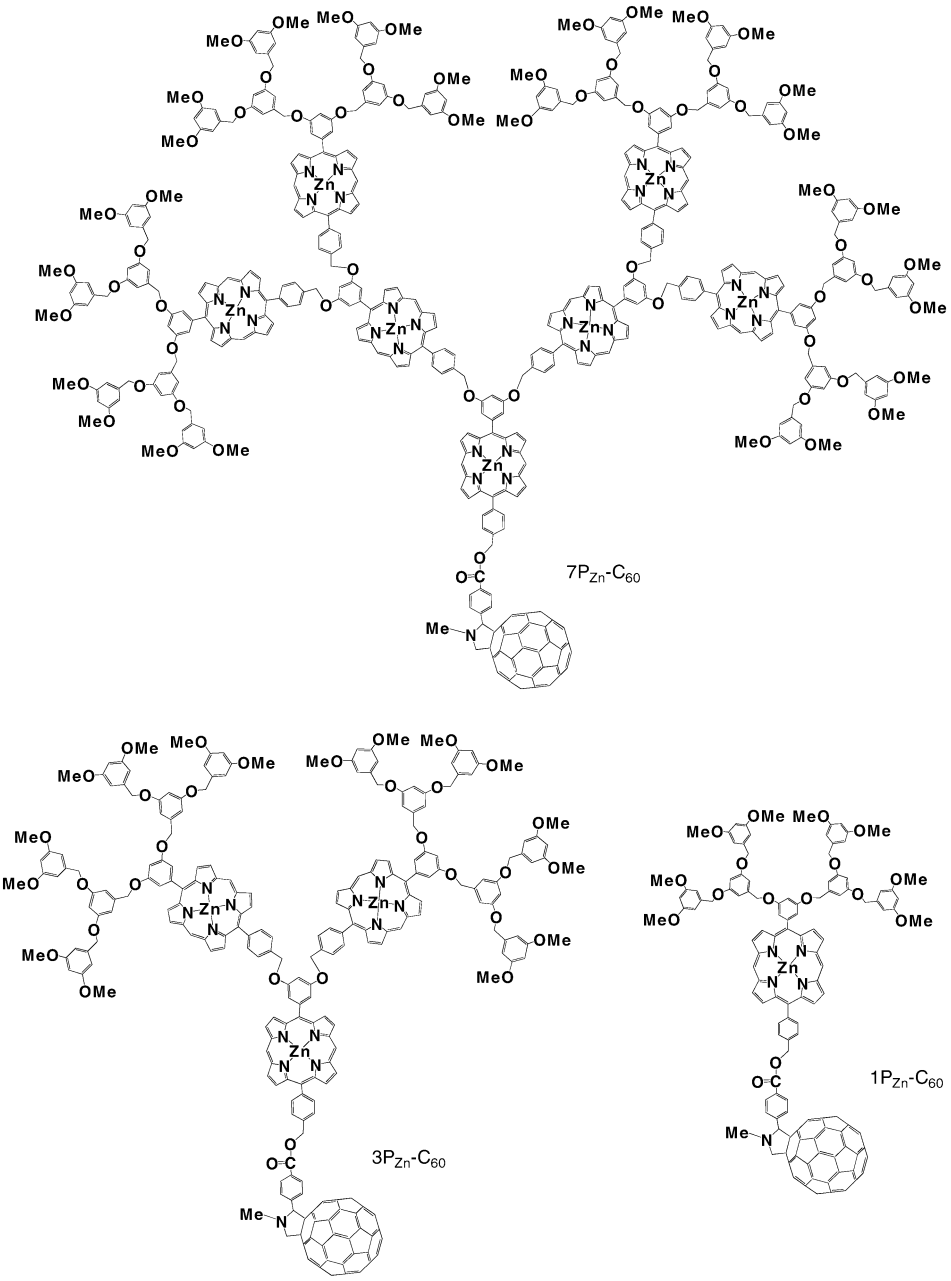
The development of light-harvesting antenna molecules for visible photons is one of the important subjects in the basic issue of solar-energy conversion in natural photosynthesis and also to their potential applications to molecular electronics.[1] Recently, we reported light-harvesting dendritic zinc porphyrin arrays which can efficiently capture visible photons and channel the excitation energy to the focal core.[2,3] This observation prompted us to integrate such dendritic dye molecules as light-harvesting antennas into electron-transfer relay systems. Here we report the molecular design and photoinduced electron-transfer properties of a series of fullerene-terminated dendritic zinc-porphyrin arrays $n\mathrm{P_{Zn}}$-$\mathrm{C_{60}}$ (Scheme 1).[4] Covalently linked porphyrin–$\mathrm{C_{60}}$ dyads (P-$\mathrm{C_{60}}$) have attracted a great deal of attention as novel photoinduced electron-transfer units,[5–7] in which the charge-separated (CS) state ($\mathrm{P^{\bullet+}}$-$\mathrm{C_{60}^{\bullet-}}$), which results from electron transfer from the porphyrin moiety to $\mathrm{C_{60}}$, can take advantage of the low reorganization energy of $\mathrm{C_{60}}$. Thus, the present study featuring $\mathrm{C_{60}}$-terminated multiporphyrin arrays $n\mathrm{P_{Zn}}$-$\mathrm{C_{60}}$ can make use of the well-established photochemistry of covalently linked porphyrin–$\mathrm{C_{60}}$ dyads. Herein, we highlight a unique effect of a large dendritic array ($7\mathrm{P_{Zn}}$) on the lifetime of the CS state.

The arrays $n\mathrm{P_{Zn}}$-$\mathrm{C_{60}}$ ($n = 1$, 3, and 7) were synthesized from hydroxy-terminated zinc-porphyrin dendrons ($n\mathrm{P_{Zn}}$-OH) and a carboxylic acid appended $\mathrm{C_{60}}$ derivative ($\mathrm{C_{60}}$-$\mathrm{CO_2H}$), by using azodicarboxylic acid diethyl ester as a condensation agent, and unambiguously characterized by ^{1}H NMR and UV/Vis spectroscopies, as well as with MALDI-TOF-MS spectrometry.[8] For example, a solution of $7\mathrm{P_{Zn}}$-$\mathrm{C_{60}}$ in benzonitrile (PhCN) showed an intense Soret absorption band at 417 nm arising from the zinc-porphyrin units and a weak $\mathrm{C_{60}}$ absorption band at 700 nm.[8] Comparison of this spectral profile with those of $7\mathrm{P_{Zn}}$-OH and $\mathrm{C_{60}}$-$\mathrm{CO_2H}$ as reference compounds showed only a slight broadening of the

[*] Prof. Dr. T. Aida, Dr. M.-S. Choi
ERATO Nanospace Project
Japan Science and Technology Corporation (JST)
2-41 Aomi, Koto-ku, Tokyo 115-0064 (Japan)
Fax: (+81) 3-5841-7310
E-mail: aida@macro.t.u-tokyo.ac.jp
Prof. Dr. O. Ito, Dr. H. Luo, Dr. Y. Araki
Institute of Multidisciplinary Research for Advanced Materials
Tohoku University
Katahira 2-1-1, Aoba-ku, Sendai, 980-8577 (Japan)
Fax: (+81) 22-217-5608
E-mail: ito@tagen.tohoku.ac.jp

Supporting information for this article is available on the WWW under http://www.angewandte.org or from the author.

 © 2003 Wiley-VCH Verlag GmbH & Co. KGaA, Weinheim DOI: 10.1002/anie.200351460



Scheme 1. Schematic structures of nP_{Zn}-C_{60}.

Soret absorption band (difference in the full-width at half-maximum (ΔFWHM) = +54 cm^{-1}) without any shift, which indicates there is a negligibly weak ground-state interaction between the zinc-porphyrin units and the C_{60} terminus. Although $3P_{Zn}$-C_{60} and $1P_{Zn}$-C_{60} showed essentially the same characteristics in the absorption spectra as $7P_{Zn}$-C_{60}, the Soret absorption band became broader (FWHM increases from 572 to 947 cm^{-1}) as the generation number of the dendritic wedge increased, which suggests there is an electronic interaction among the P_{Zn} moieties in $7P_{Zn}$-C_{60}.

Excitation of a solution of $1P_{Zn}$-C_{60} in PhCN at 544 nm resulted in a zinc-porphyrin fluorescence with two major bands at 590 and 645 nm, while no fluorescence was detected from the C_{60} terminus.[8] The fluorescence of $1P_{Zn}$-C_{60} was clearly quenched by 84 ± 1 % relative to the reference system of $1P_{Zn}$-OH. As expected, the one-generation-higher $3P_{Zn}$-C_{60}, when $3P_{Zn}$-OH was used as the reference, showed a lower quenching efficiency (60 ± 2 %) than $1P_{Zn}$-C_{60}.[8] On the other hand, the quenching efficiency of $7P_{Zn}$-C_{60}, the largest homologue of the series, stayed at the same level as that of $3P_{Zn}$-C_{60} (62 ± 2 %; $7P_{Zn}$-OH as reference).[8] A similar trend was observed for the analysis by time-resolved spectroscopy. Excitation of solutions of nP_{Zn}-C_{60} (n = 1, 3, and 7) in PhCN under argon at 22 °C at 410 nm resulted in the fluorescence monitored at 610 nm (Figure 1a) having dual-exponential decay characteristics, where the relatively long-lived fluorescing components are assignable to residual components after the photochemical communication between the nP_{Zn} and C_{60} units.[8] The average rate constant for the fluorescence decay ($k_{CS} = [1/\tau_{FL}^{av}]_{sample} - [1/\tau_{FL}]_{ref}$) became smaller by a factor of

 © 2003 Wiley-VCH Verlag GmbH & Co. KGaA, Weinheim

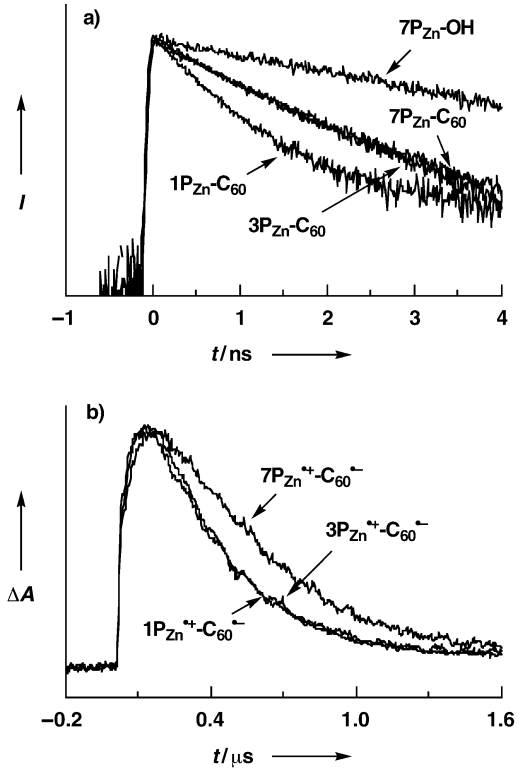


Figure 1. a) Fluorescence decay profiles of nP$_{Zn}$-C$_{60}$ ($n=1$, 3, and 7) at 610 nm upon excitation at 410 nm, and b) absorption decay profiles of C$_{60}^{\bullet-}$ at 1020 nm, generated upon excitation of nP$_{Zn}$-C$_{60}$ ($n=1$, 3, and 7) at 532 nm, in PhCN at 22 °C under argon.

four as the zinc-porphyrin array increased from 1P$_{Zn}$-C$_{60}$ (1.55×10^9 s^{-1}) to 3P$_{Zn}$-C$_{60}$ (0.40×10^9 s^{-1}; Figure 2, gray bars). On the other hand, the k_{CS} value (0.43×10^9 s^{-1}) of the largest homologue of the family (7P$_{Zn}$-C$_{60}$) was comparable to that of 3P$_{Zn}$-C$_{60}$, in spite of the fact that 7P$_{Zn}$-C$_{60}$ has a greater number of the zinc-porphyrin units located away from the C$_{60}$ terminus.

We found that the fluorescence quenching observed arises from a photoinduced electron-transfer reaction from the zinc-porphyrin units to the C$_{60}$ terminus. Formation of an ion pair (P$_{Zn}^{\bullet+}$-C$_{60}^{\bullet-}$) was confirmed by means of picosecond time-resolved absorption spectroscopy. For example, excitation of a solution of 7P$_{Zn}$-C$_{60}$ in PhCN at 388 nm with a 150-fs laser pulse resulted in an absorption band at 450 nm corresponding to the singlet-excited state ^{1}P$_{Zn}^*$, which decayed with a rate constant of 0.50×10^9 s^{-1}.[8] This value is almost identical to the fluorescence decay rate constant (k_{CS}) observed for 7P$_{Zn}$-C$_{60}$ (0.43×10^9 s^{-1}) in PhCN. The transient absorption spectroscopy also showed a rise of the P$_{Zn}^{\bullet+}$ absorption at 650 nm, whose rate constant (0.50×10^9 s^{-1}) was again in agreement with the k_{CS} value of 7P$_{Zn}$-C$_{60}$. The characteristic absorption band of the C$_{60}^{\bullet-}$ species appeared at 1020 nm.[8] These observations clearly indicate that the photoexcitation of the P$_{Zn}$ units in 7P$_{Zn}$-C$_{60}$ is followed by an electron transfer from the resultant ^{1}P$_{Zn}^*$ species to the C$_{60}$ terminus to generate a charge-separated (CS) state (P$_{Zn}^{\bullet+}$-C$_{60}^{\bullet-}$). Hence, as shown in Figure 2, the rate constants for fluorescence decay (k_{CS}; gray bars) allowed evaluation of the quantum efficiencies of nP$_{Zn}$-C$_{60}$ ($n=1$, 3, and 7) for charge separation (Φ_{CS}, black bars).[8] Interestingly, the Φ_{CS} value of 7P$_{Zn}$-C$_{60}$ (51 %), which is smaller than that of 1P$_{Zn}$-C$_{60}$ (80 %), is comparable to the Φ_{CS} value of lower generation 3P$_{Zn}$-C$_{60}$ (49 %). This trend suggests that the large dendritic 7P$_{Zn}$ array may serve as a better energy funnel than the lower generation 3P$_{Zn}$, and allow the excitation energy to flow more efficiently into the focal core.

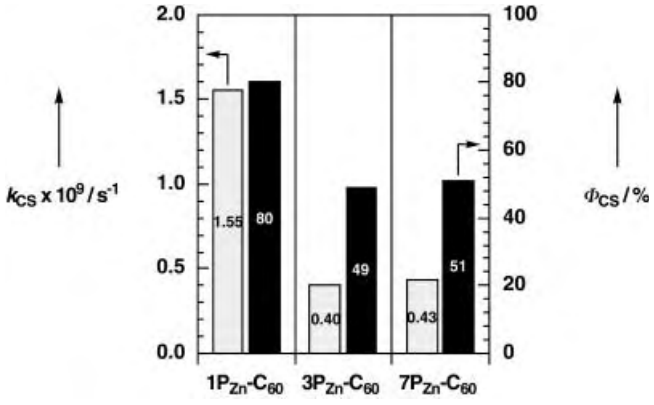


Figure 2. Fluorescence decay rate constants (k_{CS}) at 610 nm and quantum efficiencies of the charge separation (Φ_{CS}) of nP$_{Zn}$-C$_{60}$ ($n=1$, 3, and 7) upon excitation at 410 nm in PhCN at 22 °C under argon.

We investigated the charge recombination (CR) process by nanosecond time-resolved absorption spectroscopy of nP$_{Zn}$-C$_{60}$ ($n=1$, 3, and 7) at 600–1200 nm. Excitation of a solution of 7P$_{Zn}$-C$_{60}$ in PhCN at 532 nm with a 6-ns laser pulse gave an absorption band at 1020 nm, which correspond to C$_{60}^{\bullet-}$, and bands centered at 850 and 740 nm, which correspond to the triplet-excited ^{3}P$_{Zn}^*$ and ^{3}C$_{60}^*$ species,[9] respectively.[8] The time profile of the absorption corresponding to C$_{60}^{\bullet-}$ at 1020 nm (Figure 1b) was analyzed for determination of the lifetime of the charge-separated state (τ_{CS}), and the decay curve nicely fitted with dual-exponential components. The slow-decaying component corresponded to the triplet-excited species, while a radical ion pair P$_{Zn}^{\bullet+}$-C$_{60}^{\bullet-}$ was identified as the fast-decaying component, whose τ_{CS} value was evaluated to be as long as 0.66 μs in PhCN at 22 °C. Very interestingly, 3P$_{Zn}$-C$_{60}$ and 1P$_{Zn}$-C$_{60}$ also showed similar transient absorption spectral characteristics in PhCN, but their τ_{CS} values (0.41 and 0.35 μs, respectively) were clearly shorter than that of 7P$_{Zn}$-C$_{60}$. Accordingly, 7P$_{Zn}$-C$_{60}$ showed a smaller CR rate constant ($k_{CR}=(1.5\pm0.2)\times10^6$ s^{-1}) than 1P$_{Zn}$-C$_{60}$ ($(2.9\pm0.3)\times10^6$ s^{-1}) and 3P$_{Zn}$-C$_{60}$ ($(2.4\pm0.3)\times10^6$ s^{-1}; Figure 3, gray bars).

We consider that the electron-transfer reaction in nP$_{Zn}$-C$_{60}$ most likely takes place from the zinc-porphyrin unit directly connected to the C$_{60}$ terminus, while the energy for the electron transfer is acquired by the dendritic antenna. We also propose another interesting role of the large dendritic antenna in the electron-transfer event. From the slowest back electron transfer process, observed for the largest dyad 7P$_{Zn}$-C$_{60}$, we assume that the P$_{Zn}^{\bullet+}$ species, which is generated at the focal point of 7P$_{Zn}$-C$_{60}$ upon electron transfer, should move away from the C$_{60}^{\bullet-}$ terminus towards the periphery by an intramolecular hole hopping mechanism.[8] In relation to this proposal, the first oxidation potential (E_{ox}^1) of 7P$_{Zn}$-C$_{60}$ (0.29 V) was lower than those of 1P$_{Zn}$-C$_{60}$ (0.33 V) and 3P$_{Zn}$-

 © 2003 Wiley-VCH Verlag GmbH & Co. KGaA, Weinheim

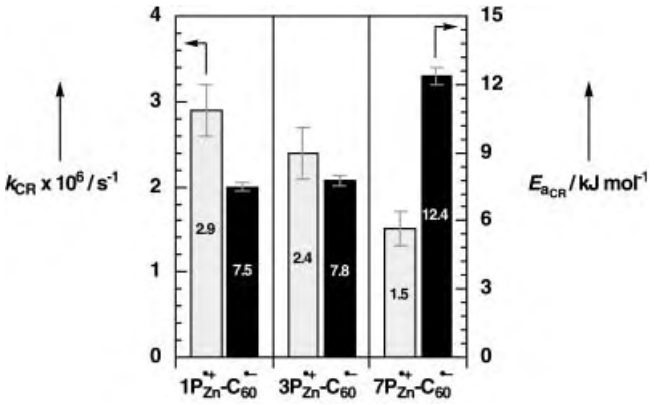


Figure 3. Charge recombination rate constants (k_{CR}, 22 °C) and activation energies (E_a^{CR}) for nP$_{Zn}^{+}$-C$_{60}^{-}$ (n = 1, 3, and 7) in PhCN under argon.

C_{60} (0.31 V).[10] As already suggested from the analysis of the band widths in the absorption spectra, this result may again indicate a large electronic interaction among the densely packed chromophores in 7P$_{Zn}$-C$_{60}$. We also investigated the temperature dependencies of the k_{CR} values of nP$_{Zn}$-C$_{60}$ (n = 1, 3, and 7), which gave activation energies (E_a) for the charge recombination process (Figure 3, black bars). Quite interestingly, the E_a value for 7P$_{Zn}$-C$_{60}$ (12.4 kJ mol^{-1}) was much greater than those for the lower generation homologues (7.5 and 7.8 kJ mol^{-1} for 1P$_{Zn}$-C$_{60}$ and 3P$_{Zn}$-C$_{60}$, respectively). This trend is consistent with the above proposal, since a thermally activated conformational motion of the dendritic chromophore array possibly allows folding of the large 7P$_{Zn}^{+}$-C$_{60}^{-}$ dyad, thereby facilitating the collision of even topologically distant P$_{Zn}^{+}$ and C$_{60}^{-}$ species.

In conclusion, we have demonstrated with studies on the photoinduced electron transfer properties of the C$_{60}$-terminated dendritic zinc porphyrin arrays (nP$_{Zn}$-C$_{60}$; n = 1, 3, and 7) that the large dendritic antenna (7P$_{Zn}$) not only harvests visible light for the electron transfer to the C$_{60}$ terminus, but also retards the back-electron-transfer process. These results indicate a new potential of dendronized dye molecules for the efficient conversion of solar energy into chemical potentials. Application of fullerene-terminated dendritic multiporphyrin arrays to solar cells is one of the subjects worthy of further investigation.

Experimental Section

1P$_{Zn}$-C$_{60}$, 3P$_{Zn}$-C$_{60}$, and 7P$_{Zn}$-C$_{60}$ were prepared by coupling of the hydroxy-terminated zinc porphyrin dendrons 1P$_{Zn}$-OH, 3P$_{Zn}$-OH, and 7P$_{Zn}$-OH with C$_{60}$-CO$_2$H, respectively.[8] Time-resolved fluorescence spectra were measured by a single-photon-counting method using a second harmonic generation (SHG, 410 nm) of a Ti:sapphire laser (Spectra-Physics, Tsunami 3950-L2S, FWHM = 1.5 ps) and a streakscope (Hamamatsu Photonics, C43334-01) equipped with a polychromator (Action Research, SpectraPro 150) as an excitation source and a detector, respectively. Picosecond transient absorption spectra were recorded by a pump and probe method, whereby samples were excited with a second harmonic generation (SHG, 388 nm) of an output from a femtosecond Ti:sapphire regenerative amplifier seeded by SHG of an Er-doped fiber (Clark-MXR CPA-2001 plus, 1 kHz, FWHM = 150 fs). The excitation light was depolarized, while the monitor white light was generated by focusing the fundamental of the laser light on a flowing D_2O/H_2O cell. The transmitted monitor light was detected with a dual MOS linear image sensor (Hamamatsu Photonics, C6140) or a InGaAs photodiode array (Hamamatsu Photonics, C5890-128). Nanosecond transient absorption spectroscopy was carried out using SHG (532 nm) of a Nd:YAG laser (Spectra-Physics, Quanta-Ray GCR-130, FWHM = 6 ns) as an excitation source. For obtaining transient absorption spectra in the near-IR region (600–1200 nm), the monitor light from a pulsed Xe lamp was detected with a Ge-APD (Hamamatsu Photonics, B2834). All the samples in a quartz cell (1 × 1 cm) were deaerated by bubbling the solutions with argon for 15 min. Cyclic voltammograms were obtained by using a conventional three-electrode system on a BAS CV-50W potentiostat/galvanostat. A platinum disk electrode was used as a working electrode, while a platinum wire served as a counter electrode. An Ag/AgCl electrode was used as a reference electrode. The potentials were referenced to an internal ferrocene/ferrocenium redox couple.

Received: March 24, 2003
Revised: June 17, 2003 [Z51460]

Keywords: dendrimers · electron transfer · fullerenes · photosynthesis · porphyrinoids

[1] a) D. Gust, T. A. Moore in *The Porphyrin Handbook, Vol. 8* (Eds.: K. M. Kadish, K. M. Smith, R. Guilard), Academic Press, New York, **2000**, p. 153; b) H. Imahori, Y. Sakata, *Adv. Mater.* **1997**, *9*, 537; c) D. M. Guldi, M. Prato, *Acc. Chem. Res.* **2000**, *33*, 695; d) D. M. Guldi, *Chem. Commun.* **2000**, 321.

[2] a) M.-S. Choi, T. Aida, I. Yamazaki, T. Yamazaki, *Angew. Chem.* **2001**, *113*, 3294; *Angew. Chem. Int. Ed.* **2001**, *40*, 3194; b) M.-S. Choi, T. Aida, I. Yamazaki, T. Yamazaki, *Chem. Eur. J.* **2002**, *8*, 2667.

[3] M.-S. Choi, T. Yamazaki, I. Yamazaki, T. Aida, *Angew. Chem.* **2003**, *115*, in press; *Angew. Chem. Int. Ed.* **2003**, *42*, in press, and references therein.

[4] J.-F. Nierengarten, N. Armaroli, G. Accorsi, Y. Rio, J.-F. Eckert, *Chem. Eur. J.* **2003**, *9*, 37, and references therein.

[5] a) P. A. Liddell, D. Kuciauskas, J. P. Sumida, B. Nash, D. Nguyen, A. L. Moore, T. A. Moore, D. Gust, *J. Am. Chem. Soc.* **1997**, *119*, 1400; b) D. Carbonera, M. Di Valentin, C. Corvaja, G. Agostini, G. Giacometti, P. A. Liddell, D. Kuciauskas, A. L. Moore, T. A. Moore, D. Gust, *J. Am. Chem. Soc.* **1998**, *120*, 4398; c) M. Fujitsuka, O. Ito, H. Imahori, K. Yamada, H. Yamada, Y. Sakata, *Chem. Lett.* **1999**, 721; d) D. Kuciauskas, P. A. Liddell, S. Lin, S. G. Stone, A. L. Moore, T. A. Moore, D. Gust, *J. Phys. Chem. B* **2000**, *104*, 4307.

[6] a) D. Kuciauskas, P. A. Liddell, S. Lin, T. E. Johnson, S. J. Weghorn, J. S. Lindsey, A. L. Moore, T. A. Moore, D. Gust, *J. Am. Chem. Soc.* **1999**, *121*, 8604; b) C. Luo, D. M. Guldi, H. Imahori, K. Tamaki, Y. Sakata, *J. Am. Chem. Soc.* **2000**, *122*, 6535; c) D. M. Guldi, C. Luo, A. Swartz, M. Scheloske, A. Hirsch, *Chem. Commun.* **2001**, 1066; d) H. Imahori, K. Tamaki, Y. Araki, Y. Sekiguchi, O. Ito, Y. Sakata, S. Fukuzumi, *J. Am. Chem. Soc.* **2002**, *124*, 5165; e) G. Kodis, P. A. Liddell, L. Garza, P. C. Clausen, J. S. Lindsey, A. L. Moore, T. A. Moore, D. Gust, *J. Phys. Chem. A* **2002**, *106*, 2036.

[7] Gust and co-workers have reported the photochemical properties of a fullerene-appended star-shaped porphyrin pentamer (see refs. [6a] and [6e]).

[8] See Supporting Information.

[9] The decay of this absorption band was accelerated on introduction of O_2 as a triplet quencher.

[10] [nP$_{Zn}$-C$_{60}$] = 0.1 mM in PhCN containing 0.05 M Bu_4NClO_4 as a supporting electrolyte; scan rate = 0.1 V s^{-1}.

 © 2003 Wiley-VCH Verlag GmbH & Co. KGaA, Weinheim

Emission in Hg^{II} Polymers

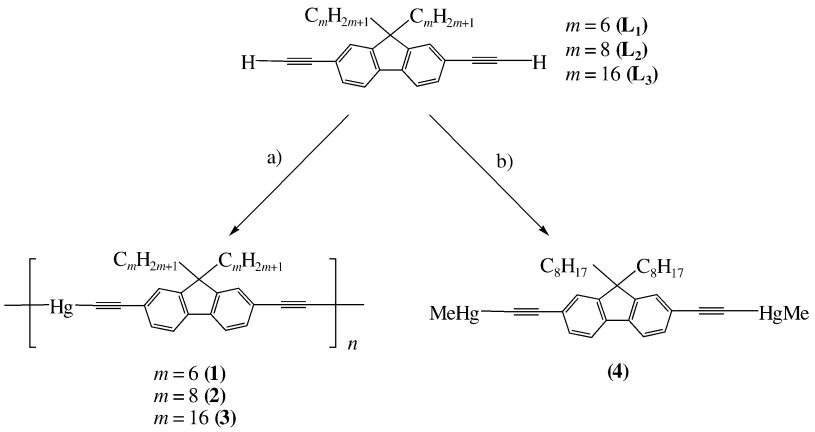
Triplet Emission in Soluble Mercury(II) Polyyne Polymers**

Wai-Yeung Wong, Li Liu, and Jian-Xin Shi*

Dedicated to Professor The Lord Lewis on the occasion of his 75th birthday

Following the report of the first soluble metal polyyne oligomers by Hagihara et al.[1a], there is growing interest in the chemical and photophysical properties of conjugated polymetallaynes of group 8, 9, and 10 transition metals. These metal-based polymers provide model systems to explain the electronic properties of conjugated organic polymers used in light-emitting diodes.[1] In the past two decades, much has been discovered about the photoluminescent behavior of oligomeric and polymeric acetylides of platinum(II) and gold(I) complexes, where spin-forbidden triplet emissions (phosphorescence) can be identified clearly.[2,3] However, there is relatively little understood about the d^{10} mercury(II) system. To our knowledge, there are no literature reports on the photophysics and structural properties of soluble mercury-based polyynes. Although linear polymeric copper and mercury acetylides of the form $[\text{-M-C}\equiv\text{C-}p\text{-C}_6\text{H}_4\text{-C}\equiv\text{C-}]_n$ were reported as early as 1960, these materials were often found to be insoluble and intractable, which hampered their purification and characterization.[1a] The group 12 heavy mercury atom, with its propensity to enhance spin–orbit coupling, could be an ideal candidate for harvesting the energy of triplet excitons.[1b,4] We report here the first examples of soluble well-defined high-molecular-weight mercury(II) polyyne polymers with 9,9-dialkylfluorene groups, from which we have been able to directly trigger $^3(\pi\pi^*)$ emissions localized on the organic system through efficient intersystem crossing (ISC) by ligation to the Hg^{II} moiety.

The synthesis of the new polymers **1**–**3** is shown in Scheme 1. Mercuration of 9,9-dialkyl-2,7-diethynylfluorenes $\mathbf{L_1}$–$\mathbf{L_3}$ with $HgCl_2$ using methanolic NaOH at room temperature produced a pale-yellow suspension and the solids were collected by filtration to afford off-white air-stable products **1**–**3** in high yields and purity. Their excellent film-forming properties suggest a macromolecular nature for the materials, and their good solubilities in CH_2Cl_2 and $CHCl_3$ render them amenable to spectroscopic studies and readily solution-processable for optical characterization. Estimates of the molecular weights using GPC in THF indicate a high degree of polymerization (DP = 24–47) in these polyynes (Table 1) and the absence of end-group NMR resonances is evidence of their high molecular weight. A similar synthetic route using 2,7-diethynylfluorene ($m = 0$ in Scheme 1) only afforded an intractable solid and thus the use of long alkyl chains is crucial in achieving highly soluble polymers. Complex **4**, as a model complex of polymer **2**, was also synthesized by treatment of $\mathbf{L_2}$ with two equivalents of MeHgCl, in which one coordination site is protected by a Me group, under similar basic conditions.[5] The symmetrical nature of the molecules was ascertained by NMR studies. Notably, two distinct ^{13}C NMR signals for the sp carbon atoms of the acetylenic units were observed for **1**–**4**, and they are shifted downfield with respect to the free alkynes, consistent with the formation of Hg–C(sp) bond. Only six peaks appeared in the aromatic region of their ^{13}C NMR spectra, which relate to the 12 aromatic carbon atoms in the structures of **1**–**4**; these data indicate high structural regularity in the polymers. Complex **4** displayed a single ^{199}Hg NMR peak at $\delta = -453$ (compared with $\delta = -847$ for MeHgCl), which reflects the polarization of the Hg–C≡ bonds.[6] The molecular structure of **4**, as confirmed by X-ray crystallography,[7] also helped to establish polymer structures in the solid state and to correlate the photophysical properties with the structural data. The structure of **4** consists of dinuclear molecules in which the mercury centers adopt a two-coordinate linear geometry in a rigid-rod manner (Figure 1). The lattice structure is highlighted by the presence of weak intermolecular noncovalent Hg···Hg interactions (3.738 and 4.183 Å), which link the molecular units together to form a loose polymeric structure in a 3D network (Figure 2).[5b,c] The Hg···Hg separations in **4** are comparable to the values of 3.71–4.25 Å for $[Hg(C\equiv CR)_2]$ (R = Ph, $SiMe_3$) and are toward the upper limit of those accepted as representing metallophilic interactions.[8]



Scheme 1. Synthesis of **1**–**4**: a) $HgCl_2$, NaOH, MeOH; b) MeHgCl, NaOH, MeOH.

[*] Dr. W.-Y. Wong, L. Liu, Dr. J.-X. Shi
Department of Chemistry
Hong Kong Baptist University
Waterloo Road, Kowloon Tong, Hong Kong (P.R. China)
Fax: (+852) 3411-7348
E-mail: rwywong@hkbu.edu.hk

[**] This work was supported by a CERG Grant from the Research Grants Council of the Hong Kong SAR, P.R. China (Project No. HKBU 2048/01P) and a Faculty Research Grant from Hong Kong Baptist University (FRG/01-02/II-48).

Supporting information for this article is available on the WWW under http://www.angewandte.org or from the author.

 © 2003 Wiley-VCH Verlag GmbH & Co. KGaA, Weinheim DOI: 10.1002/anie.200351672

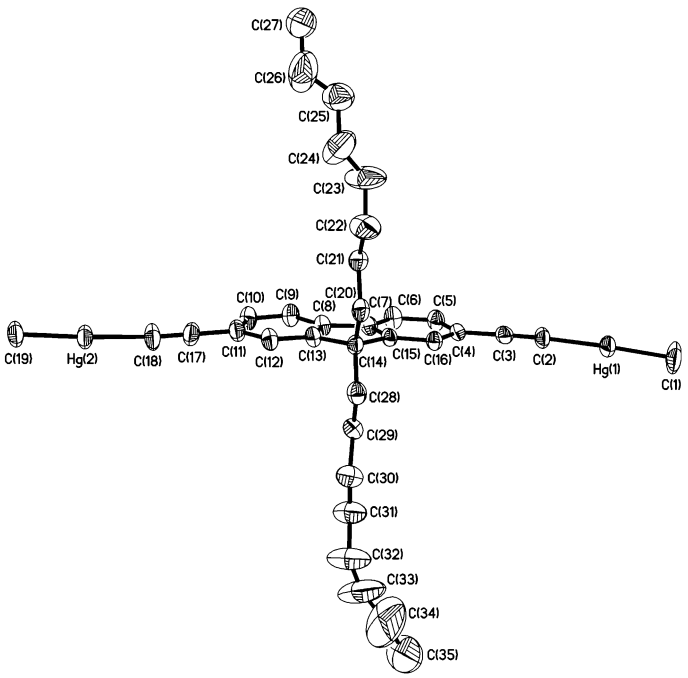


Figure 1. Molecular structure of the model complex **4**, with thermal ellipsoids shown at the 25% probability level. Hydrogen atoms are omitted for clarity. Selected bond lengths [Å] and angles [°]: Hg(1)-C(1) 2.080(11), Hg(1)-C(2) 2.045(8), Hg(2)-C(18) 2.044(9), Hg(2)-C(19) 2.059(9), C(2)-C(3) 1.186(11), C(17)-C(18) 1.209(13); C(1)-Hg(1)-C(2) 177.6(7), Hg(1)-C(2)-C(3) 176.8(8), C(18)-Hg(2)-C(19) 177.7(5), Hg(2)-C(18)-C(17) 176.1(12).

Table 1: Structural and thermal properties of **1**–**3**.

polymer	M_w[a]	M_n[a]	M_w/M_n	DP	T_{decomp} [°C][b]
1	28720	27100	1.06	47	282 ± 5
2	18320	15090	1.22	24	220 ± 5
3	38650	36250	1.07	42	200 ± 5

[a] Calibration against polystyrene. [b] Onset temperature.

The thermal properties of the polymers were examined by thermogravimetric analysis (TGA) and differential scanning calorimetry (DSC; heating rate 20 °C min^{-1}). Polymers **1**–**3** displayed moderate thermal stability with decomposition temperatures greater than 200 °C (Table 1), and exhibited an exotherm coincident with the mass lost due to decomposition. Polymer **3** showed the lowest onset decomposition temperature, while **1** and **2** with shorter alkyl chains exhibited increasing decomposition temperatures with decreasing *m* value. Each showed two stepwise losses in the thermogravimetric curve, which correspond to the elimination of two alkyl groups from their respective molecules.

The photophysical data of **1**–**4** are shown in Table 2. They all display similarly structured absorption bands in the near-UV region. These bands are mainly associated with the organic $^1(\pi\pi^*)$ transitions, possibly with some admixture of metal orbitals, and

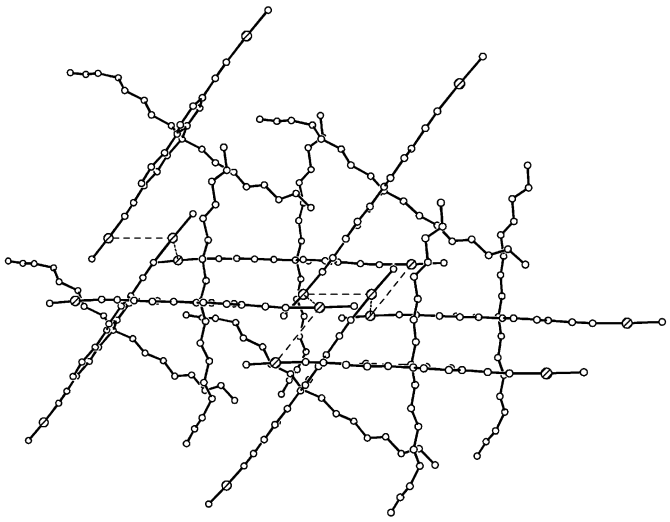


Figure 2. Crystal packing diagram for **4** showing the weak intermolecular Hg···Hg contacts in a 3D network.

the 0–0 absorption peak is assigned as the $S_0 \rightarrow S_1$ transition.[5b,9] As compared with $\mathbf{L_1}$–$\mathbf{L_3}$, we noted a red-shift in the absorption and emission bands of **1**–**4** after the inclusion of a heavy metal atom, which indicates an increase in π-conjugation. The C-9 substituents on the fluorene ring exert a minimal effect on the absorption energies, and comparable optical band gaps (E_{gap}) are noted for **1**–**3** (Figure 3a). The transition energies of polymer **2** are lowered with respect to those of the monomer **4**, which suggests that a well-extended singlet excited state exists in the polymers.[1c,9b,9d] Bathochromic shifts of about 10 nm are observed for the lowest-energy absorption bands of **1**–**4** in the solid state. Examination of the absorption behavior of the polymers in $CHCl_3$, $CHCl_3$/MeOH solutions, and in the solid state, corroborates the presence of solid-state aggregates in thin films.[10] For instance, the addition of a nonsolvent (MeOH) to a $CHCl_3$ solution of **2** leads to the development of a new band centered at 365 nm, which corresponds to the strongest absorption observed in the solid state (Figure 4). Further support for the red shift is provided by the observation of solid-state mercuriophilic interactions in the crystal structure of the model compound **4** (see above).[5b,8]

Table 2: Photophysical data for **1**–**4**.

	λ_{max} [nm] CH_2Cl_2	λ_{max} [nm] film	E_{gap} [eV]	λ_{em} [nm] CH_2Cl_2 (290 K)[b]	film (290 K)	film (11 K)
1	313, 341, 355	316, 345, 365	3.32	381, 406* (0.003)[c]	475br	427, 570, 610*
2	313, 340, 355	316, 345, 364	3.31	382, 406* (0.004)[c]	477br	426, 583, 630*
3	313, 338, 355	316, 345, 364	3.32	385*, 409 (0.007)[c]	478br	429, 590, 634*
4	311 (4.7), 330 (4.9), 346 (5.0)[a]	316, 339, 358	3.38	374 (0.02)[d]	417, 435, 477br	416, 438, 544*, 591*

[a] logε. [b] Fluorescence quantum yields in parentheses are measured relative to quinine sulfate in 0.1 N H_2SO_4 ($\Phi = 0.54$). [c] $\lambda_{ex} = 328$ nm. [d] $\lambda_{ex} = 340$ nm. Asterisks indicate that emission peaks appear as shoulders or weak bands. br = broad.

 © 2003 Wiley-VCH Verlag GmbH & Co. KGaA, Weinheim

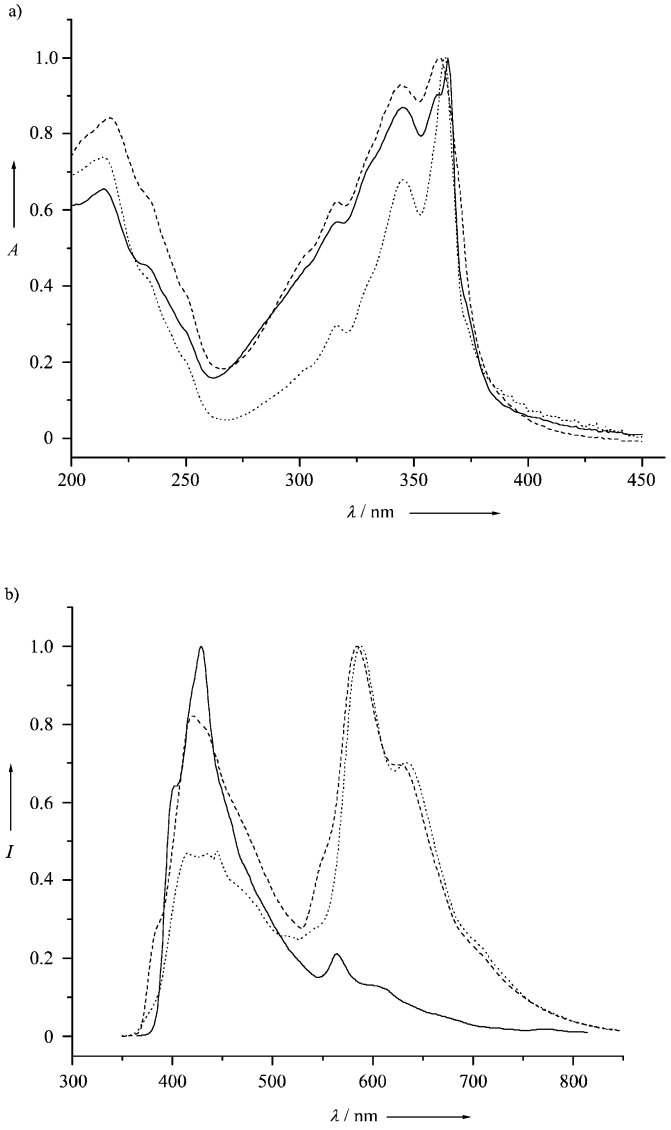


Figure 3. a) Absorption and b) emission spectra (11 K) of thin solid films of **1** (——), **2** (-----) and **3** (•••••).

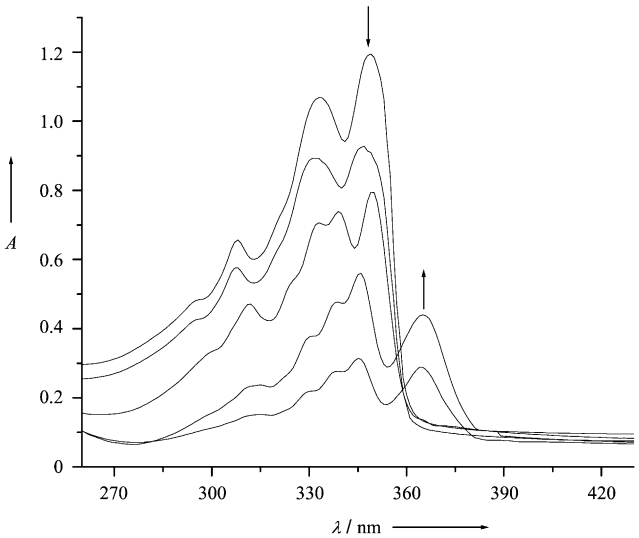


Figure 4. Absorption spectrum of **2** ($CHCl_3$) upon the addition of MeOH (top to bottom: 0, 20, 40, 80, 90%).

The long side chains in polymers **1**–**3** should suppress aggregation or at least delay its onset, and indeed, changes in absorptions are observed for **2** after the addition of approximately 80% methanol. The behavior of **1**–**3** is analogous to that of the poly[(9,9-dialkyl)fluoren-2,7-yleneethynylene]s, 2,5-dialkylpoly(*p*-phenylene-ethynylenes), and polydiacetylenes, where similar aggregate bands are described.[10]

The photoluminescence (PL) spectra display a red shift on going from binuclear to polynuclear structures (e.g., **2** versus **4**), which implies that the excited state is stabilized by the greater degree of delocalization in the polymers. However, we cannot rule out the possibility that the shifts are related to the number and/or strength of the Hg···Hg interactions in the polymers. In dilute fluid solutions, we observe an intense $^1(\pi\pi^*)$ emission peak near 400 nm for **1**–**4** due to fluorescence ($S_1 \rightarrow S_0$), which is in line with the small Stokes shift observed between the bands in the absorption and the emission spectra.[2,9] Comparing these results with the solution PL data, the thin-film singlet emissions in **1**–**4** appear broad at 290 K and are red-shifted, which is consistent with their absorption features, and is likely to be a result of interchain interactions due to aggregate formation.[11] At 11 K, another well-resolved lower-lying emission emerges at around 570–590 nm for polymers **1**–**3** and the large Stokes shifts of these peaks from the dipole-allowed absorptions (approximately 1.2–1.3 eV), plus the long emission lifetimes at 11 K (28 ± 0.2 (**1**), 35 ± 0.2 (**2**), and 42 ± 0.2 μs (**3**)) are indicative of their triplet parentage; thus, they are assigned to the $^3(\pi\pi^*)$ excited states of the diethynylfluorenes (Figure 3b).[9] The triplet emission ($T_1 \rightarrow S_0$) bands increase in intensity with decreasing temperature for **1**–**3** (see Supporting Information) and show vibronic structure at low temperatures, typical of the phosphorescence observed in related Pt^{II} and Au^{I} polyynes.[2,3,9] We found that the intensity of the phosphorescence relative to fluorescence increases as the value of *m* increases from **1** ($m = 6$) to **3** ($m = 16$); this phenomenon probably results from a reduced number of quenching sites through mono- or bimolecular decay processes in **3**, which has longer alkyl chains.[2a] To assess the relative ISC efficiency based on the peak height ratio from triplet emission to singlet emission at 11 K, we note that the order of S_1–T_1 crossover efficiency is **3** > **2** > **1** (Figure 3b). The ISC rate is also higher in the polymers than in the monomers (that is, **2** versus **4**). Considering the spatial extent of the singlet and triplet excitons in our systems, values of $\Delta E(S_0$–$T_1)$ (energy gap between S_0 and T_1) were found to be 2.10–2.23 eV for **1**–**3**, which can be compared to those observed in dialkoxy-substituted poly(*p*-phenyleneethynylene)s (PPEs, 1.90 eV),[12] [Cy_3PAu]-capped PPEs (1.98–2.04 eV),[3a] and Pt-containing poly[(9,9-dialkyl)fluoren-2,7-yleneethynylene]s (2.20 eV).[9a,b] The $\Delta E(S_1$–$T_1)$ values for **1**–**3** lie within the range of 0.73–0.79 eV, which corresponds well with the S_1–T_1 energy gap of 0.7 ± 0.1 eV for similar π-conjugated Pt and Au polyynes,[2,3a] and are close to the gaps estimated for a series of related organic polymers.[13] We attribute such a constant $\Delta E(S_1$–$T_1)$ value to the exchange energy and possibly some additional

 © 2003 Wiley-VCH Verlag GmbH & Co. KGaA, Weinheim

constant contribution which results from the admixture of the Hg orbitals.[2b] Similar to the Pt polyynes, the use of mercury in **1**–**3** together with their associated large optical band gaps can offer a good route towards the enhancement of the ISC rate, and we have shown for the first time that the organic triplet emissions of fluorenyleneethynylenes have been "illuminated" by the heavy-atom effect of mercury. The present investigation is desirable for applications that harvest the T_1 state for light emission and will provide impetus for future study.

Experimental Section

1–**3**: A solution of $HgCl_2$ (0.60 g, 2.21 mmol) in MeOH (10 mL) was mixed with $\mathbf{L_2}$[9a,b] (0.97 g, 2.21 mmol) in MeOH (10 mL). To this mixture, 28 mL of basic MeOH (5.60 mmol; prepared by dissolving 0.40 g of NaOH in 50 mL of MeOH) was added. Within a few minutes, a light-yellow solid precipitated from the homogeneous solution. The solid was then collected by filtration after stirring for 12 h, washed with MeOH (2 × 20 mL), and air-dried to furnish **2** in 87% yield (1.23 g). IR (KBr): $\tilde{\nu} = 2140\ cm^{-1}$ (C≡C); ^1H NMR (400 MHz, $CDCl_3$, 298 K, TMS): $\delta = 7.58$–7.55 (m, 2H; Ar), 7.43–7.40 (m, 4H; Ar), 1.87 (m, 4H; $CH_2(CH_2)_5$), 1.18–0.86 (m, 20H; $(CH_2)_5$), 0.76 (t, 6H; CH_3, $^3J(H,H) = 7.2$ Hz), 0.51 ppm (m, 4H; CH_2CH_3); $^{13}C\{^1H\}$ NMR (100.6 MHz, $CDCl_3$, 298 K, TMS): $\delta =$ 151.03, 140.83, 131.43, 126.65, 120.80 (Ar), 119.98 (Ar), 106.83 (C≡C), 84.51 (C≡C), 55.27 (quat C), 40.35, 31.85, 30.07, 29.32, 23.82, 22.68, and 14.21 ppm (C_8H_{17}); elemental analysis calcd (%) for $(C_{33}H_{40}Hg)_n$: C 62.20, H 6.33; found: C 61.98, H 6.20. Polymers **1** and **3** were prepared similarly from $\mathbf{L_1}$ and $\mathbf{L_3}$; they were both isolated as off-white solids in 93 and 82% yields, respectively. **1**: IR (KBr): $\tilde{\nu} =$ 2135 cm^{-1} (C≡C); ^1H NMR (400 MHz, $CDCl_3$, 298 K, TMS): $\delta =$ 7.65–7.62 (m, 2H; Ar), 7.50–7.47 (m, 4H; Ar), 1.94 (m, 4H; $CH_2(CH_2)_3$), 1.11–0.91 (m, 12H; $(CH_2)_3$), 0.78 (t, 6H; CH_3, $^3J(H,H) = 7.3$ Hz), 0.57 ppm (m, 4H; CH_2CH_3); $^{13}C\{^1H\}$ NMR (100.6 MHz, $CDCl_3$, 298 K, TMS): $\delta = 150.92$, 140.74, 131.43, 126.61, 120.85 (Ar), 119.90 (Ar), 107.04 (C≡C), 84.52 (C≡C), 55.20 (quat C), 40.30, 31.57, 29.70, 23.75, 22.67, and 14.09 ppm (C_6H_{13}); elemental analysis calcd (%) for $(C_{29}H_{32}Hg)_n$: C 59.93, H 5.55; found: C 59.77, H 5.29. **3**: IR (KBr): $\tilde{\nu} = 2140\ cm^{-1}$ (C≡C); ^1H NMR (400 MHz, $CDCl_3$, 298 K, TMS): $\delta =$ 7.64–7.61 (m, 2H; Ar), 7.49–7.46 (m, 4H; Ar), 1.96 (m, 4H; $CH_2(CH_2)_{13}$), 1.25–1.04 (m, 52H; $(CH_2)_{13}$), 0.87 (t, 6H; CH_3, $^3J(H,H) = 7.2$ Hz), 0.58 ppm (m, 4H; CH_2CH_3); $^{13}C\{^1H\}$ NMR (100.6 MHz, $CDCl_3$, 298 K, TMS): $\delta = 151.02$, 140.84, 131.43, 126.64, 120.75 (Ar), 119.96 (Ar), 106.83 (C≡C), 84.51 (C≡C), 55.33 (quat C), 40.36, 32.00, 30.11, 29.78, 29.76, 29.69, 29.44, 29.41, 29.36, 23.82, 22.79, and 14.24 ppm ($C_{16}H_{33}$); elemental analysis calcd (%) for $(C_{49}H_{72}Hg)_n$: C 68.30, H 8.42; found: C 68.05, H 8.21.

4: The diyne $\mathbf{L_2}$ (0.44 g, 1.00 mmol) in MeOH (10 mL) was first combined with MeHgCl (0.50 g, 2.00 mmol) in MeOH (10 mL). 0.20 M basic MeOH (13 mL) was subsequently added to give a pale-yellow suspension. The solvents were then decanted and the light-yellow solid **4** (0.69 g, 80%) was washed with MeOH (2 × 20 mL) and air-dried. IR (KBr): $\tilde{\nu} = 2120\ cm^{-1}$ (C≡C); ^1H NMR (400 MHz, $CDCl_3$, 298 K, TMS): $\delta = 7.58$–7.55 (m, 2H; Ar), 7.43–7.29 (m, 4H; Ar), 1.86 (m, 4H; $CH_2(CH_2)_5$), 1.21–0.82 (m, 20H; $(CH_2)_5$), 0.80 (t, 6H; CH_2CH_3, $^3J(H,H) = 8.0$ Hz), 0.68 (s, 6H; CH_3), 0.54 ppm (m, 4H; CH_2CH_3); $^{13}C\{^1H\}$ NMR (100.6 MHz, $CDCl_3$, 298 K, TMS): $\delta =$ 151.00, 140.49, 131.13, 126.49, 121.58 (Ar), 119.82 (Ar), 106.42 (C≡C), 84.48 (C≡C), 55.06 (quat C), 40.35, 31.75, 30.02, 29.26, 23.68, 22.56, and 14.08 ppm (C_8H_{17}); ^{199}Hg (48.2 MHz, $CDCl_3$, 298 K, Me_2Hg): $\delta =$ −453 ppm; positive FAB-MS: m/z 868 $[M]^+$; elemental analysis calcd (%) for $C_{35}H_{46}Hg_2$: C 48.44, H 5.34; found: C 48.28, H 5.23.

Received: April 15, 2003 [Z51672]

Keywords: aggregation · alkyne ligands · luminescence · mercury · polymers

[1] a) Y. Fujikura, K. Sonogashira, N. Hagihara, *Chem. Lett.* **1975**, 1067—1070; b) P. Nguyen, P. Gómez-Elipe, I. Manners, *Chem. Rev.* **1999**, *99*, 1515–1548; c) A. Köhler, J. S. Wilson, R. H. Friend, *Adv. Mater.* **2002**, *14*, 701–707; d) D. Beljonne, H. F. Wittmann, A. Köhler, S. Graham, M. Younus, J. Lewis, P. R. Raithby, M. S. Khan, R. H. Friend, J. L. Brédas, *J. Chem. Phys.* **1996**, *105*, 3868–3877.

[2] a) J. S. Wilson, N. Chawdhury, M. R. A. Al-Mandhary, M. Younus, M. S. Khan, P. R. Raithby, A. Köhler, R. H. Friend, *J. Am. Chem. Soc.* **2001**, *123*, 9412–9417; b) J. S. Wilson, A. Köhler, R. H. Friend, M. K. Al-Suti, M. R. A. Al-Mandhary, M. S. Khan, P. R. Raithby, *J. Chem. Phys.* **2000**, *113*, 7627–7634; c) N. Chawdhury, A. Köhler, R. H. Friend, W.-Y. Wong, J. Lewis, M. Younus, P. R. Raithby, T. C. Corcoran, M. R. A. Al-Mandhary, M. S. Khan, *J. Chem. Phys.* **1999**, *110*, 4963–4970; d) W.-Y. Wong, C.-K. Wong, G.-L. Lu, A. W.-M. Lee, K.-W. Cheah, J.-X. Shi, *Macromolecules* **2003**, *36*, 983–990.

[3] a) H.-Y. Chao, W. Lu, Y. Li, M. C. W. Chan, C.-M. Che, K.-K. Cheung, N. Zhu, *J. Am. Chem. Soc.* **2002**, *124*, 14696–14706; b) W. Lu, H.-F. Xiang, N. Zhu, C.-M. Che, *Organometallics* **2002**, *21*, 2343–2346; c) C.-M. Che, H.-Y. Chao, V. M. Miskowski, Y. Li, K.-K. Cheung, *J. Am. Chem. Soc.* **2001**, *123*, 4985–4991.

[4] a) X. Gong, M. R. Robinson, J. C. Ostrowski, D. Moses, G. C. Bazan, A. J. Heeger, *Adv. Mater.* **2002**, *14*, 581–585; b) C. Adachi, M. A. Baldo, M. E. Thompson, S. R. Forrest, *J. Appl. Phys.* **2001**, *90*, 5048–5051; c) X. Gong, J. C. Ostrowski, G. C. Bazan, D. Moses, A. J. Heeger, M. S. Liu, A. K.-Y. Jen, *Adv. Mater.* **2003**, *15*, 45–49; d) W. Lu, B.-X. Mi, M. C. W. Chan, Z. Hui, N. Zhu, S.-T. Lee, C.-M. Che, *Chem. Commun.* **2002**, 206–207.

[5] a) D. Fabbri, M. Lombardo, C. Trombini, I. Vassura, *Appl. Organomet. Chem.* **1995**, *9*, 713–718; b) W.-Y. Wong, K.-H. Choi, G.-L. Lu, Z. Lin, *Organometallics* **2002**, *21*, 4475–4481; c) P. Li, B. Ahrens, K.-H. Choi, M. S. Khan, P. R. Raithby, P. J. Wilson, W.-Y. Wong, *CrystEngComm* **2002**, *4*, 405–412; d) W.-Y. Wong, K.-H. Choi, G.-L. Lu, J.-X. Shi, P.-Y. Lai, S.-M. Chan, Z. Lin, *Organometallics* **2001**, *20*, 5446–5454.

[6] A. Sebald, B. Wrackmeyer, *Spectrochim. Acta Part A* **1982**, *38*, 163–173.

[7] Crystal data for **4**: $C_{35}H_{46}Hg_2$, $M_w = 867.90$, crystal dimensions $0.32 \times 0.19 \times 0.17\ mm^3$, monoclinic, space group *Cc*, $a =$ 21.8830(13), $b = 17.6803(13)$, $c = 9.2053(6)$ Å, $\beta = 107.840(2)°$, $V = 3390.3(4)$ $Å^3$, $Z = 4$, $\rho_{calcd} = 1.700\ g\,cm^{-3}$, $\mu(Mo_{K\alpha}) =$ $9.065\ mm^{-1}$, $F(000) = 1664$, $T = 293$ K, $2\theta_{max} = 56.6°$. 10015 reflections measured, of which 5992 were unique ($R_{int} =$ 0.0419). Final $R_1 = 0.0317$ and $wR_2 = 0.0702$ for 4357 observed reflections with $I > 2\sigma(I)$. CCDC-208083 contains the supplementary crystallographic data for this paper. These data can be obtained free of charge via www.ccdc.cam.ac.uk/conts/retrieving.html (or from the Cambridge Crystallographic Data Centre, 12, Union Road, Cambridge CB21EZ, UK; fax: (+44) 1223-336-033; or deposit@ccdc.cam.ac.uk).

[8] a) S. J. Faville, W. Henderson, T. J. Mathieson, B. K. Nicholson, *J. Organomet. Chem.* **1999**, *580*, 363–369; b) P. Pyykkö, *Chem. Rev.* **1997**, *97*, 597–636; c) S. S. Batsanov, *J. Chem. Soc. Dalton Trans.* **1998**, 1541–1546.

[9] a) M. S. Khan, M. R. A. Al-Mandhary, M. K. Al-Suti, B. Ahrens, M. F. Mahon, L. Male, P. R. Raithby, C. E. Boothby, A. Köhler, *J. Chem. Soc. Dalton Trans.* **2003**, 74–84; b) W.-Y. Wong, G.-L. Lu, K.-H. Choi, J.-X. Shi, *Macromolecules* **2002**, *35*, 3506–3513; c) M. Younus, A. Köhler, S. Cron, N. Chawdhury, M. R. A. Al-Mandhary, M. S. Khan, J. Lewis, N. J. Long, R. H. Friend, P. R. Raithby, *Angew. Chem.* **1998**, *110*, 3180–3183; *Angew. Chem.*

 © 2003 Wiley-VCH Verlag GmbH & Co. KGaA, Weinheim

Int. Ed. **1998**, *37*, 3036 – 3039; d) N. Chawdhury, A. Köhler, R. H. Friend, M. Younus, N. J. Long, P. R. Raithby, J. Lewis, *Macromolecules* **1998**, *31*, 722 – 727; e) W.-Y. Wong, C.-K. Wong, G.-L. Lu, K.-W. Cheah, J.-X. Shi, Z. Lin, *J. Chem. Soc. Dalton Trans.* **2002**, 4587 – 4594; f) W.-Y. Wong, K.-H. Choi, G.-L. Lu, J.-X. Shi, *Macromol. Rapid Commun.* **2001**, *22*, 461 – 465.

[10] a) U. H. F. Bunz, *Chem. Rev.* **2000**, *100*, 1605 – 1644, and references therein; b) J. L. Foley, L. Li, D. J. Sandman, M. J. Vela, B. M. Foxman, R. Albro, C. J. Eckhardt, *J. Am. Chem. Soc.* **1999**, *121*, 7262 – 7263; c) C. E. Halkyard, M. E. Rampey, L. Kloppenburg, S. L. Studer-Martinez, U. H. F. Bunz, *Macromolecules* **1998**, *31*, 8655 – 8659; d) N. G. Pschirer, U. H. F. Bunz, *Macromolecules* **2000**, *33*, 3961 – 3963.

[11] R. J. Puddephatt, *Coord. Chem. Rev.* **2001**, *216*–217, 313 – 332.

[12] A. Köhler, J. S. Wilson, R. H. Friend, M. K. Al-Suti, M. S. Khan, A. Gerhard, H. Bässler, *J. Chem. Phys.* **2002**, *116*, 9457 – 9463.

[13] a) D. Hertel, S. Setayesh, H. G. Nothofer, U. Scherf, K. Mullen, H. Bässler, *Adv. Mater.* **2001**, *13*, 65 – 70; b) A. P. Monkman, H. D. Burrows, L. J. Hartwell, L. E. Horsburgh, I. Hamblett, S. Navaratnam, *Phys. Rev. Lett.* **2001**, *86*, 1358 – 1361; c) Y. V. Romanovskii, A. Gerhard, B. Schweitzer, U. Scherf, R. I. Personov, H. Bassler, *Phys. Rev. Lett.* **2000**, *84*, 1027 – 1030.

 © 2003 Wiley-VCH Verlag GmbH & Co. KGaA, Weinheim

Fuel-Cell-Grade H_2 from Hydrocarbons

Catalytic Reforming of Oxygenated Hydrocarbons for Hydrogen with Low Levels of Carbon Monoxide**

*Rupali R. Davda and James A. Dumesic**

The production of fuel-cell-grade hydrogen, containing very low levels of CO, is critical for the global transition to a hydrogen society. In spite of ongoing efforts to make fuel cells more CO-tolerant,[1] the use of hydrogen fuel-cells in portable applications (e.g., automobiles, battery replacement devices) is particularly challenging, as the production of hydrogen by steam-reforming of hydrocarbons[2] requires a complex combination of multiple processes[3–7] to achieve the required low CO levels (e.g., 100–500 ppm).[1] An important step toward a simple process for the production of hydrogen containing low levels of CO is made possible by the discovery[8] that hydrogen can be produced by catalytic reforming of biomass-derived oxygenated hydrocarbons in liquid water at temperatures near 500 K. This process has the advantage that the reforming of oxygenated hydrocarbons and the water–gas shift (WGS) reaction are both thermodynamically favorable at the same low temperatures, thus making it possible to conduct both reactions in one reactor. These low levels of CO, combined with the fact that our low-temperature process uses biomass-derived renewable feedstocks, makes aqueous-phase reforming of oxygenates an attractive process for applications in portable devices.

Herein, we show results from studies of the aqueous-phase reforming of ethylene glycol (EG) to produce H_2, with specific emphasis on the levels of CO produced as a function of the process conditions. We show the importance of the reaction operating conditions for achieving low levels of CO in the effluent gas from our single-reactor reforming process, and we elucidate the factors that control the ultimate levels of CO that can be attained.

Aqueous-phase reforming of oxygenates to produce H_2 takes place on metal catalysts[9] through C–C cleavage to make CO and H_2, [Eq. (1)].

$$C_2H_6O_2 \rightleftharpoons 2\,CO + 3\,H_2 \tag{1}$$

(Undesired alkanes are formed through C–O cleavage.) Adsorbed CO undergoes WGS [Eq. (2)], which increases the

$$CO + H_2O \rightleftharpoons CO_2 + H_2 \tag{2}$$

amount of H_2 produced and removes CO from the catalyst surface.[10]

The lowest partial pressure of CO that can be achieved depends on the thermodynamics of the WGS reaction and the operating conditions, [Eq. (3)].

$$P_{CO} = \frac{P_{CO_2} P_{H_2}}{K_{WGS} P_{H_2O}} \tag{3}$$

K_{WGS} is the equilibrium constant for the vapor-phase WGS and P_j are partial pressures. Since H_2, CO_2, and small amounts of alkanes (primarily CH_4) are produced by aqueous-phase reforming,[8] gas bubbles are formed within the liquid-phase flow reactor. The pressure in these bubbles can be approximated to be equal to the system pressure, [Eq. (4)].

$$P_{bubble} \approx P_{system} = P_{H_2O} + \sum_{products} P_j \tag{4}$$

The partial pressures of the reaction products and water vapor are dictated by the feed concentrations, system pressure and temperature, as outlined below.

For dilute product concentrations and system pressures above the saturation pressure of water, the bubbles contain water vapor at a pressure equal to its saturation pressure at the reactor temperature, and the remaining pressure is the sum of the partial pressures of the product gases. The extent of vaporization, y, is defined as the percent of water in the vapor phase relative to the total amount of water flowing into the reactor. In contrast, for systems operated at pressures that are near the saturation pressure of water, all the liquid water

[*] Prof. Dr. J. A. Dumesic, R. R. Davda
Chemical Engineering Department
University of Wisconsin
Madison, WI 53706 (USA)
Fax: (+1) 608-262-5434
E-mail: dumesic@engr.wisc.edu

[**] This work was supported by U.S. Department of Energy (DOE), Office of Basic Energy Sciences, Chemical Sciences Division. We thank Sibongile Nkosi and Jonathon Tomshine for help in collecting reaction kinetics data.

Supporting information for this article is available on the WWW under http://www.angewandte.org or from the author.

 © 2003 Wiley-VCH Verlag GmbH & Co. KGaA, Weinheim DOI: 10.1002/anie.200351664

may vaporize, and the composition of the bubble is dictated by the stoichiometry of the feed stream. At this condition, the partial pressure of water is below its saturation pressure because the water vapor is diluted by the reforming product gases. Higher concentrations of EG lead to lower partial pressures of water because of greater dilution from H_2 and CO_2 produced by reforming reactions. As the system pressure is increased, the partial pressure of water vapor increases until it reaches the saturation pressure of water, at which point any further increase in the system pressure leads to partial condensation of water.

The above arguments indicate that the conditions which favor the lowest levels of CO from reforming of oxygenates are those which lead to the lowest partial pressures of H_2 and CO_2 in the reforming gas bubbles; and, these conditions are achieved by operating at system pressures that are near the saturation pressure of water and at low EG feed concentrations. As the system pressure increases and the extent of vaporization decreases below 100%, the partial pressures of H_2 and CO_2 in the bubble increase, thereby leading to higher equilibrium concentrations of CO. Similarly, as the EG concentration in the feed increases, higher partial pressures of H_2 and CO_2 are developed, even for the case of complete vaporization, again leading to higher equilibrium CO concentrations. This dependence of the CO concentration on the operating conditions for EG reforming has been corroborated with detailed experiments, as outlined below.

Table 1 summarizes results for aqueous-phase reforming of EG at feed concentrations of 2 wt% (runs 1–7), 5 wt% (runs 8–13) and 10 wt% (run 14). The upflow reactor (1.27 cm (0.5 inch) stainless-steel tube) containing the Pt/Al_2O_3 catalyst was divided into two separately heated reaction zones. Reforming reactions were carried out in the lower section (denoted as the reforming zone), maintained at 498 K (see Supporting Information for further details). The temperature of the top section (denoted as the shift zone), system pressure, feed concentration, and feed flow rate were varied in the different runs listed in Table 1. The weight hourly space velocity (WHSV) of EG, defined as the grams of EG per gram of catalyst per hour, was maintained such that complete conversion to gas phase products was achieved for all runs. The performance of the catalyst was stable for long periods of time on stream (e.g., 2 weeks). Results from replicate runs agreed to within $\pm 10\%$.

The data in Table 1 show that the dry effluent gas stream (after condensation of water) for each reaction condition consists primarily of H_2 and CO_2. The CO concentration in the effluent gas and the corresponding equilibrium concentration are reported for each condition. For the 2% and 5% EG feeds, detailed studies were conducted for system pressures of 25.8, 32.0 and 36.2 bar, with the shift zone of the reactor controlled at various temperatures. For the 10% feed, data were collected at 25.8 bar with the shift zone at 498 K. Higher system pressures lead to lower reaction rates,[11] resulting in a slightly lower conversion of the 10% EG feed.

As the saturation pressure of water at 498 K is equal to 25.1 bar, liquid water is completely vaporized at a system pressure of 25.8 bar. For 2% EG at this pressure (run 1), the H_2 pressure in the bubble is calculated to be 0.77 bar, and this condition leads to a low equilibrium CO concentration of 66 ppm in the reactor effluent. At system pressures of 32 and 36.2 bar (runs 2 and 3, respectively), the H_2 pressures are 4.60 and 7.53 bar, respectively, with only 18 and 11% vaporization of water occurring in each case. These conditions lead to higher equilibrium CO concentrations of 380 and 617 ppm, respectively. For the 5% EG feed at a system pressure of 25.8 bar (run 8), complete vaporization leads to a H_2 partial pressure of 1.79 bar, which results in a higher equilibrium CO concentration (163 ppm) compared to run 1 for the 2% feed. The effect of increasing system pressure for the 5% feed is similar to the behavior of 2% EG, as presented in runs 9 and 10 of Table 1.

The effect of H_2 pressure on the equilibrium CO concentration is illustrated in Figure 1a and 1b for the 2 and 5% feeds, respectively. It can be seen that the observed concentrations of CO are slightly lower than the calculated equilibrium values, especially for experiments conducted at higher system pressures. These lower values of CO concentrations are not caused by consumption of CO through methanation reactions. In particular, we conducted experi-

Table 1: Results for ethylene glycol (EG) reforming over 3% Pt/γ-Al_2O_3.

Run Number	1	2	3	4	5	6	7	8	9	10	11	12	13	14
EG Feed Concentration [wt%]	2	2	2	2	2	2	2	5	5	5	5	5	5	10
WHSV [g/gcat/hr]	0.0054	0.0054	0.0054	0.0054	0.0054	0.0027	0.0081	0.0135	0.0135	0.0135	0.0135	0.0135	0.0054	0.0270
Shift Temperature, T_s [K]	498	498	498	508	515	498	498	498	498	498	505	512	498	498
System Pressure [bar]	25.8	32.0	36.2	32.0	36.2	32.0	32.0	25.8	32.0	36.5	32.0	36.2	32.0	25.8
% Vaporization of Water, γ	100	18	11	91	90	16	16	100	41	22	100	100	42	100
H_2 Pressure in Vapor Phase [bar]	0.77	4.60	7.53	1.05	1.14	4.51	4.66	1.79	4.62	7.87	2.20	2.33	4.63	3.40
H_2O Pressure in Vapor Phase [bar]	24.4	25.1	25.1	30.1	34.1	25.1	25.1	22.6	25.1	25.1	28.5	32.4	25.1	20.7
H_2 [mol%]	69.8	69.6	70.0	69.1	68.9	68.3	70.4	69.9	69.7	70.9	69.3	69.0	70.0	69.6
CO_2 [mol%]	28.7	28.7	28.6	28.9	28.8	29.3	28.4	28.5	28.9	28.3	29.1	29.0	28.3	28.9
CH_4 [mol%]	1.38	1.43	1.06	1.64	2.02	1.66	0.99	1.35	1.09	0.51	1.34	1.70	1.37	1.34
C_2H_6 [mol%]	0.16	0.25	0.32	0.28	0.36	0.32	0.23	0.20	0.26	0.27	0.27	0.35	0.28	0.14
Experimental CO [ppm]	**60**	**326**	**564**	**84**	**89**	**363**	**328**	**118**	**305**	**558**	**163**	**183**	**341**	**196**
Equilibrium CO [ppm]	**66**	**380**	**617**	**88**	**95**	**380**	**379**	**163**	**382**	**638**	**185**	**195**	**377**	**341**

 © 2003 Wiley-VCH Verlag GmbH & Co. KGaA, Weinheim

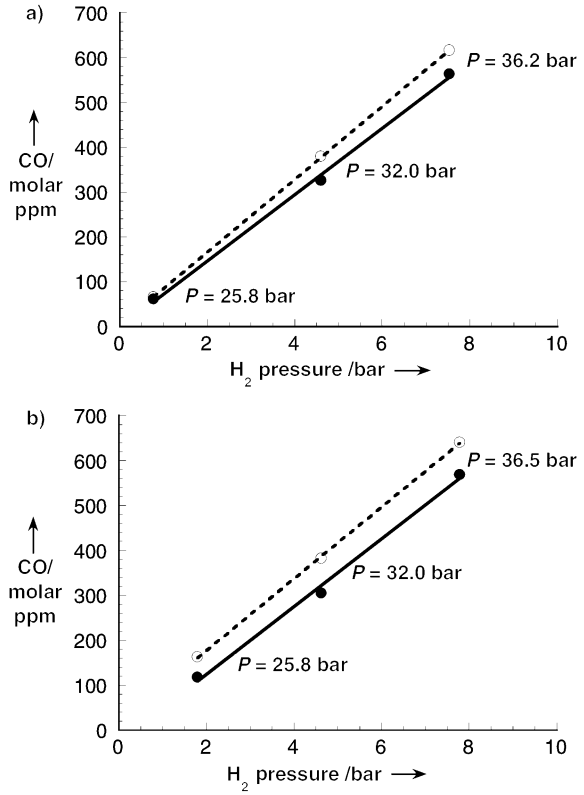


Figure 1. Effect of H_2 pressure on CO concentration for a) 2% EG (WHSV = 0.0054 h^{-1}) and b) 5% EG (WHSV = 0.0135 h^{-1}). Each point corresponds to a shift temperature of 498 K. Open symbols represent equilibrium CO and filled symbols represent observed CO.

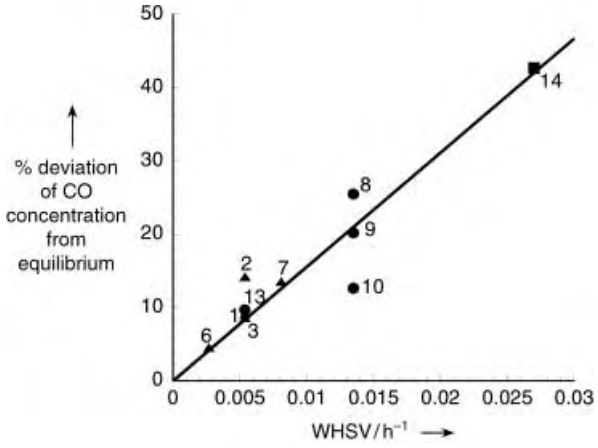


Figure 2. Effect of WHSV on the % deviation of CO concentration from equilibrium. The numbers alongside each point correspond to the run numbers (see Table 1). Triangles: 2% EG (runs 1–3, 6–7); Circles: 5% EG (runs 8–10, 13); and Squares: 10% EG (run 14).

ments in which water was co-fed with a simulated reformer gas (containing 1000 ppm CO in a 30:70 CO_2:H_2 mixture) over the Pt/Al_2O_3 catalyst at 498 K and a system pressure of 25.8 bar, such that the partial pressures of water and H_2 in the reactor were 21.6 and 2.95 bar, respectively (conditions similar to run 14). Under these conditions, we did not detect any measurable amounts of CH_4 and the concentration of CO in this simulated reformer gas was converted to the WGS equilibrium value of 298 ppm.

Our previous studies of EG reforming over Pt/Al_2O_3[11] have shown that reaction rates are lower at higher system pressures. Hence, we suggest that lower values of observed CO concentrations (compared to equilibrium values) at higher system pressures are caused by lower WGS rates. Accordingly, we conducted experiments to study the effect of WHSV on the deviations of the effluent CO concentrations from the equilibrium values. The WHSV was altered for 2 and 5% feeds at 32 bar (runs 6–7 and run 13) by changing the feed flow rate through the reactor. Also, for a particular volumetric flow rate, the WHSV is different for the three feed concentrations. Figure 2 shows the deviation of the observed CO concentration from the equilibrium value (expressed as a percentage of the equilibrium value) as a function of WHSV for runs conducted at 498 K. Higher temperatures (runs 4, 5, 11 and 12) were not included in this plot, because the resulting higher rates reduced the CO deviations from equilibrium. It is seen from Figure 2 that the CO deviations from equilibrium increase with increasing space velocity, thus suggesting that these deviations may be caused by reaction kinetics effects involving the WGS reaction, such as adsorbed CO species react more rapidly with water to form CO_2 and H_2, compared to the slower desorption to form gaseous CO. Aupretre, et al.[12] have shown that H_2 and CO_2 were the primary gaseous products from steam reforming of ethanol, and CO was produced by the reverse WGS reaction.

Although the lowest levels of CO are obtained when the reactor is operated near the saturation pressure of water, this condition is not feasible for larger, nonvolatile feeds such as sorbitol and glucose, which undergo undesirable decomposition reactions when vaporized.[13] It thus becomes imperative to operate the reformer at system pressures above the saturation pressure of water to maintain liquid phase conditions. We now propose a new process, which we denote as ultra shift, to achieve very low levels of CO in the product gas from aqueous-phase reforming of oxygenated hydrocarbons, conducted at pressures above the saturation pressure of water. This process involves the vaporization of liquid water (in the shift zone) to dilute the H_2 and CO_2 in the bubbles, thereby favoring increased conversion of the WGS reaction and leading to lower CO concentrations.

Experiments were designed to demonstrate the feasibility of the ultra-shift process, and these data are included in Table 1. Reforming of a 2% EG feed, conducted at a system pressure of 32 bar with the shift-zone at 498 K (run 2), resulted in a CO concentration of 326 ppm. When the temperature of the shift zone was increased to 508 K (run 4), 91% of the water vaporized, thereby decreasing the H_2 pressure to 1.05 bar, and lowering the measured CO concentration to 84 ppm. In the case where the system pressure was 36.2 bar (runs 3 and 5), increasing the temperature of the shift zone from 498 to 515 K decreased the H_2 pressure from 7.53 to 1.14 bar and the measured CO concentration from 564 to 89 ppm. At the higher temperatures, the effect of diluting the H_2 and CO_2 pressures with water vapor supersedes the less favorable thermodynamics, leading to

 © 2003 Wiley-VCH Verlag GmbH & Co. KGaA, Weinheim

ultra shift. Similar effects were observed for 5% EG, as seen in runs 9–12.

Figure 3a and 3b shows the effects of ultra shift on the levels of CO attained from reforming of 2 and 5% EG feeds. It is seen that when the shift temperature is maintained at the reforming temperature of 498 K, the effluent concentration of

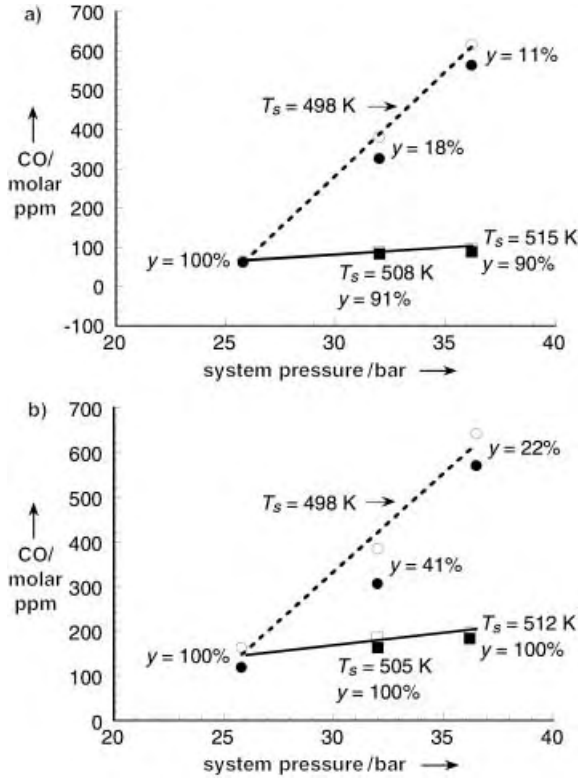


Figure 3. Effect of system variables on CO concentration for a) 2% EG (WHSV = 0.0054 h^{-1}) and b) 5% EG (WHSV = 0.0135 h^{-1}). Circles: CO concentration versus system pressure at shift temperature T_s = 498 K, Squares: Ultra shift at higher shift temperatures. Open symbols represent equilibrium CO and filled symbols represent observed CO.

CO increases as the system pressure is increased. When the shift temperature is increased such that a majority of the water vaporizes, then the product CO concentration, even at the higher pressures, decreases to below 100 ppm for 2% EG and below 200 ppm for 5% EG. Importantly, when the effluent from the reactor is subsequently cooled to a lower temperature to condense water, then the pressure of the noncondensable gases increases and approaches the system pressure. This process of ultra shift, involving initial vaporization followed by condensation of water, thus leads to the desirable production of fuel-cell-grade H_2 at high pressures and containing very low levels of CO.

Received: April 15, 2003 [Z51664]

Keywords: carbon monoxide · fuel cells · heterogeneous catalysis · hydrogen · water–gas shift

[1] M. Murthy, M. Esayian, W. Lee, J. W. Van Zee, *J. Electrochem. Soc.* **2003**, *150*, A29.
[2] J. Rostrup-Nielsen, *Phys. Chem. Chem. Phys.* **2001**, *3*, 283.
[3] H. Gunardson, *Industrial Gases in Petrochemical Processing*, Marcel Dekker, New York, **1998**.
[4] G. J. Grashoff, C. E. Pilkington, C. W. Corti, *Platinum Met. Rev.* **1983**, *27*, 157.
[5] P. G. Gray, M. I. Petch, *Platinum Met. Rev.* **2000**, *44*, 108.
[6] A. N. J. Van Keulen, in *US 6,207,307* USA, **2001**.
[7] C. S. Gittleman, R. Gupta, in *US 2002110503* USA, **2002**.
[8] R. D. Cortright, R. R. Davda, J. A. Dumesic, *Nature* **2002**, *418*, 964.
[9] R. R. Davda, J. W. Shabaker, G. W. Huber, R. D. Cortright, J. A. Dumesic, *Appl. Catal. B*, **2003**, *43*, 13.
[10] J. Novakova, L. Kubelkova, *Appl. Catal. B* **1997**, *14*, 273.
[11] J. W. Shabaker, R. R. Davda, G. W. Huber, R. D. Cortright, J. A. Dumesic, *J. Catal.*, **2002**, *215*, 344.
[12] F. Aupretre, C. Descorme, D. Duprez, *Catal. Commun.* **2002**, *3*, 263.
[13] B. M. Kabyemela, T. Adschiri, R. M. Malaluan, K. Arai, *Ind. Eng. Chem. Res.* **1999**, *38*, 2888.

 © 2003 Wiley-VCH Verlag GmbH & Co. KGaA, Weinheim

Mixed-Metal Main-Group Clusters

Synthesis and Characterization of Neutral, Homo and Heteronuclear Clusters with Unsubstituted Germanium or Tin Atoms**

*Anne F. Richards, Håkon Hope, and Philip P. Power**

Stable polyhedral clusters of the formula M_nR_m ($n > m$; M = Si–Pb (tetrel; a tetrel is a group 14 element); R = organo or related group) that contain several tetrels unsubstituted by organic or related groups are rare.[1–4] The synthesis of such species is of interest as it could allow the crystallization of well-defined larger tetrel clusters of nanometer dimensionality that may have unusual electronic properties. Generally speaking, most currently known tetrel clusters can be categorized as either Zintl anions,[5] for example M_5^{2-} or M_9^{n-} (M = Ge, Sn or Pb; $n = 2$, 3 or 4), or as neutral clusters of the formula M_nR_n (M = Si–Pb, $n = 4$, 6, 8 or 10)[6] where each tetrel carries one substituent. In contrast, the substituent poor polyhedral tetrel clusters are represented only by the compounds $Sn_8\{Si(SiMe_3)_3\}_6$,[2] $Sn_8\{C_6H_3\text{-}2,6\text{-}Mes_2\}_4$[3] and the germanium species $Ge_8\{N(SiMe_3)_2\}_6$[4] that was recently reported by Schnepf and co-workers. The tin compounds

[*] Prof. Dr. P. P. Power, Dr. A. F. Richards, Prof. Dr. H. Hope
Department of Chemistry
University of California Davis
One Shields Avenue, Davis, CA 95616 (USA)
Fax: (+1) 530-752-8995
E-mail: pppower@ucdavis.edu

[**] This work was supported by the Donors of the Petroleum Research Fund Administered by the American Chemical Society.

 DOI: 10.1002/anie.200351907 © 2003 Wiley-VCH Verlag GmbH & Co. KGaA, Weinheim

were obtained either by thermolysis[2] or by reduction/ligand stripping of an aryl tin(II) halide precursor $Sn(Cl)C_6H_3$-2,6-Mes_2.[3] The more recent synthesis of $Ge_8\{N(SiMe_3)_2\}_6$ represented a new departure in that it employed germanium(I) bromide trapped at low temperature as the germanium source.[4] This approach is analogous to that employed by Schnöckel and co-workers[7] for the synthesis of numerous aluminum and gallium clusters with unsubstituted metals through the use of low oxidation state Al^I and Ga^I halides. It is believed that the disproportionation of these generally unstable species provides a pathway through which clusters involving unsubstituted metal atoms are formed and trapped by ligands attached to the cluster surface. The reduction of the low valent aryl tin(II) halide $Sn(Cl)C_6H_3$-2,6-Mes_2 near room temperature to give the cluster $Sn_8\{C_6H_3$-2,6-$Mes_2\}_4$[3] suggested to us that it might be possible to use the low valent tetrel(II) halides themselves to introduce unsubstituted tetrel atoms into a cluster. We now describe a new strategy for the synthesis of tetrel clusters of this type and show that it can be used to synthesize species in which the majority of tetrel atoms carry no organic substituent. Furthermore, we show that this approach allows the synthesis and the first detailed structural characterization of a stable species in which two different tetrels comprise the cluster framework.[8]

The clusters $Ge_6Ar'_2$ (**1**) or $Sn_4(GeAr')_2$ (**2**) ($Ar' = C_6H_3$-2,6-$Dipp_2$; $Dipp = C_6H_3$-2,6-$i Pr_2$) were synthesized by the reduction of a 1:1 proportion of Ge(Cl)Ar′[9] and $GeCl_2$·dioxane or $SnCl_2$ with three equivalents of KC_8 in THF at room temperature. The Ge_6 derivative **1** (Figure 1) was isolated as orange crystals, and the Sn_4Ge_2 cluster **2** (Figure 2) was obtained as red crystals in about 40% and 20% yields, respectively. Both compounds were characterized by X-ray crystallography;[10] the structures are broadly similar with distorted octahedral hexatetrel cores in which two of the six vertices are substituted by Ar′ groups. The unsubstituted Ge_4 (**1**) and Sn_4 (**2**) atom sets comprise almost perfectly square arrays which have Ge–Ge and Sn–Sn separations that average 2.86(1) Å and 3.12(1) Å. The average Ar′Ge–Ge and Ar′Ge–Sn distances in **1** and **2** are 2.50(2) in 2.72(2) Å. The orientation of the central aryl rings of the terphenyl substituents is coplanar with respect to each other in **1** and almost perpendicular in **2** but this is probably a packing effect. ^1H, ^{13}C NMR and UV/Vis data for **1** and **2** are unremarkable. The solution ^{119}Sn NMR spectrum of **2** displayed a downfield signal at $\delta = 1583$.

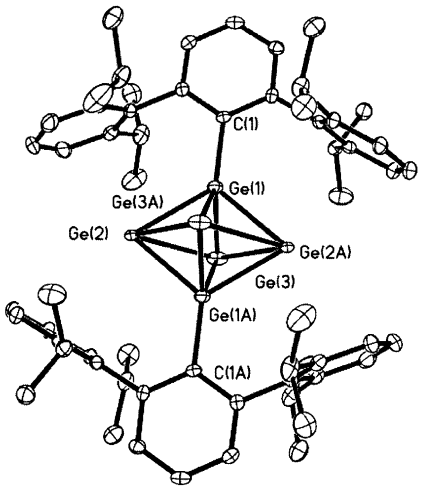


Figure 1. Structure of **1**; H atoms are not shown. Representative bond lengths [Å] and angles [°]: Ge1-Ge2 2.546(1), Ge1-Ge3 2.498(2), Ge1-Ge2A 2.532(1), Ge1-Ge3A 2.503(2), Ge2-Ge3 2.883(2), Ge2-Ge3A 2.886(2), Ge1-C1 1.974(6), C1-Ge1-Ge3 125.0(2), C1-Ge1-Ge2 126.0(2), Ge2-Ge1-Ge3 68.70(5), Ge3-Ge2-Ge3A 88.66(5), Ge2-Ge3-Ge2A 91.34(5)°.

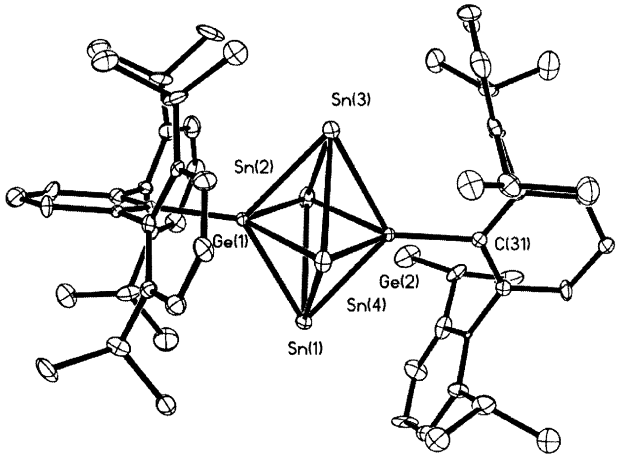


Figure 2. Structure of **2**; H atoms are not shown. Representative bond lengths [Å] and angles [°]: Ge1-Sn1 2.763(2), Ge1-Sn2 2.714(2), Ge1-Sn3 2.728(2), Ge1-Sn4 2.704(2), Sn1-Sn2 3.098(2), Sn1-Sn4 3.135(2), Sn2-Sn3 3.115(2), Sn3-Sn4 3.143(2), Ge2-C3(1) 1.98(1), Sn1-Ge1-C11 128.3(4), Sn3-Ge1-C11 128.3(4), Sn1-Ge1-Sn2 69.10(5), Sn2-Ge1-Sn3 69.85(5), Sn2-Sn1-Sn4 90.19(4), Sn1-Sn2-Sn3 90.60(4), Sn2-Sn3-Sn4 89.72(4), Sn1-Sn4-Sn3 89.41(4).

The observation of unsubstituted germanium or tin atoms in the structures clearly arises from the inclusion of $GeCl_2$ or $SnCl_2$ in the reaction mixtures as similar experiments involving the reduction of Ge(Cl)Ar′ or Sn(Cl)Ar′ or Sn(Cl)Ar′ without $GeCl_2$ or $SnCl_2$ give the alkyne analogues Ar′MMAr′ (M = Ge[11] or Sn[12]) exclusively. The distorted octahedral core of **1** or **2** is their most conspicuous structural feature. It is plausible to view this finding to be in agreement with Wade's Rules[13] which predict a closo structure for the hypothetical Ge_6^{2-} or $Ge_2Sn_4^{2-}$ clusters since they have $n+1$ electron pairs (n = no. of vertices) available for cluster bonding in **1** and **2**. Thus, each unsubstituted tetrel provides two electrons and each substituted moiety provides three electrons to afford a total of seven electron pairs. Recent calculations by King and co-workers for Ge_6^{2-} have predicted that a regular octahedral structure with a Ge–Ge bond lengths of 2.687 Å as the global minimum for Ge_6^{2-}.[14] This value can be compared to the average of 2.63 Å for the twelve Ge–Ge bond lengths in **1**. The substitution of organic groups at two of the six germanium atoms in **1** introduces large distortions to the octahedron. The separation of the four unsubstituted germanium atoms is over 0.3 Å greater than the Ar′Ge–Ge bond lengths, and although the angles within the plane formed by Ge(2), Ge(3), Ge(2A) and Ge(3A) are near 90°, the corresponding Ge(2)-Ge(1)-Ge(2A) and Ge(3)-Ge(1)-

 © 2003 Wiley-VCH Verlag GmbH & Co. KGaA, Weinheim

Ge(3A) angles associated with the substituted germanium atoms have opened out to 107.75(3) and 106.33(3)°. The Ge–Ge distances may be compared with those observed in the substituted clusters Ge_6R_6 (R = Dipp[15] or $CH(SiMe_3)_2$[16]); Ge–Ge range 2.465(1)–2.584(2) Å), $[PPh_4]_2[Ge_6\{M(CO)_5\}_6]$ (M = Cr, Mo, or W, Ge–Ge = 2.541(1)–2.592(4) Å,[17] and in the species $Ge_8[N(SiMe_3)_2]_6$ where bond lengths of about 2.67 and 2.50 Å were observed for the R_2NGe–$Ge(NR_2)$ and Ge–$Ge(NR_2)$ (R = $SiMe_3$) germanium bonds. A similar pattern of distortion is seen in the structure of **2** where the distances between the unsubstituted tin atoms average 3.12(2) Å and the Ge–Sn distances are in the range 2.701(2)–2.746(2) Å. The latter distances are longer than the two center-two-electron Ge–Sn bonds in compounds of the type $R_3MM'R_3$ (M = Ge; M = Sn; R = organic group; range 2.573(2)–2.652(2) Å.[18] The unsubstituted Ge–Ge and Sn–Sn bond lengths in **1** and **2** lie at the longer end of the ranges generally found in Zintl anions and approach the distances seen in the square M_4 moieties of the $[M_9]^{4-}$ Zintl species[19,20] or the "long" Sn–Sn contacts (3.107(2) Å) in $Sn_8(C_6H_3\text{-}2,6\text{-}Mes_3)_4$.[3] The weak M–M contacts within the M_4 squares receive support from the ^{119}Sn NMR chemical shift which lies well downfield toward a region most commonly associated with two coordinate tin(II) species.[21] The NMR data suggest that writing the structures of **1** or **2** with the bonds between the unsubstituted germanium or tin atoms omitted also is a plausible representation of their bonding environment. Work to isolate a wider range of stable group 14 clusters with larger numbers of unsubstituted atoms (nanosized clusters) and the extension of the range of stable heteronuclear neutral clusters to other heavier main group elements is in hand.

Experimental Section

All manipulations were carried out under anaerobic and anhydrous conditions.

1: Ar′GeCl (0.505 g, 1 mmol)[4] and $GeCl_2$(dioxane), (0.232 g, 1 mmol) was added dropwise to a suspension of KC_8 (0.111 g, K) in THF (20 mL). After the reaction had been stirred for 16 h, the THF was removed under reduced pressure and the resultant red solid was extracted into hexanes (40 mL). The volume was reduced to incipient crystallization and storage of the solution at about −5 °C for 48 h afforded **1** as orange crystals. m.p. 69–71 °C; ^{1}H NMR (C_6D_6, 399.7 MHz, 25 °C): δ = 0.94 (d, $^3J_{HH}$ = 6.8 Hz, 24 H; *o*-C$(CH_3)_2$), 1.24 (d, $^3J_{HH}$ = 6.8 Hz, 24 H; *o*-CH(C$H_3)_2$), 2.709 (sept, $^3J_{H,H}$ = 6.8 Hz, 18 H; *o*-C$H$$(CH_3)_2$)), 6.98 (d, $^3J_{H,H}$ = 7.2, Hz, 4 H; *m*-C_6H_3), 7.08 (d, $^3J_{H,H}$ = 8.0 Hz, 8 H; *m*-Dipp), 7.20 (t, $^3J_{H,H}$ = 7.2 Hz, 4 H; *p*-C_6H_3), 7.22 ppm (t, $^3J_{H,H}$ = 8.0 Hz, 4 H; *p*-Dipp); ^{13}C{^{1}H} NMR (C_6D_6, 100.59 MHz, 25 °C): δ = 24.31 (*o*-CH(C$H_3)_2$), 25.76 (*o*-CH(C$H_3)_2$), 31.06 (*o*-C$H$$(CH_3)_2$), 122.69 (*m*-Dipp), 123.01 (*p*-C_6H_3), 136.75 (*m*-C_6H_3), 140.49 (*p*-Dipp), 146.57 (*i*-Dipp), 146.68 (*i*-C_6H_3), 147.22 (*o*-Dipp), 150.76 ppm (*o*-C_6H_3); UV/Vis (hexane): λ_{max}, (ε) 500 nm (69,800).

2: A mixture of Ar′GeCl (0.505 g, 1 mmol)[9] and $SnCl_2$ (0.19 g, 1 mmol) in THF solution (20 mL) was added dropwise to a suspension of KC_8 (0.117 g, K) in THF (20 mL). After the reaction had been stirred for 16 h the THF was removed under reduced pressure and the resultant red solid was extracted into hexanes (40 mL). The solution was concentrated and stored at room temperature for 2 weeks, which afforded deep red cyrstals of **2** in 17 % yield. m.p. 100–110 °C, ^{1}H NMR (C_6D_6, 399.7 MHz, 25 °C): δ = 1.016 (d, $^3J_{H,H}$ = 6.8 Hz, 24 H; *o*-CH(C$H_3)_2$), 1.137 (d, $^3J_{H,H}$ = 6.8 Hz, 24 H; *o*-CH(C$H_3)_2$), 2.84 (sept, $^3J_{H,H}$ = 6.8 Hz, 18 H; *o*-C$H$$(CH_3)_2$)), 6.979 (d, $^3J_{H,H}$ = 7.2 Hz, 4 H; *m*-C_6H_3), 7.1535 (d, $^3J_{H,H}$ = 8.0 Hz, 8 H; *m*-Dipp), 7.174 (t, $^3J_{H,H}$ = 7.2 Hz, 4 H; *p*-C_6H_3), 7.234 ppm (t, $^3J_{H,H}$ = 8.0 Hz, 4 H; *p*-Dipp); ^{13}C{^{1}H} NMR (C_6D_6, 100.59 MHz, 25 °C): δ = 24.18 (*o*-CH(C$H_3)_2$), 24.42 (*o*-CH(C$H_3)_2$), 34.71 (*o*-C$H$$(CH_3)_2$), 120.56 (*m*-Dipp), 122.67 (*p*-C_6H_3), 137.41 (*m*-C_6H_3), 141.08 (*p*-Dipp), 146.66 (*i*-Dipp), 148.21 (*o*-Dipp), 149.92 ppm (*o*-C_6H_3), (*i*-C_6H_3 carbon was not observed); ^{119}Sn NMR (C_6D_6), δ = 1583.5 ppm.

Received: May 15, 2003 [Z51907]

Keywords: cluster compounds · germanium · terphenyls · tin

[1] Two neutral tin clusters, Sn_5Ar_6 and Sn_7Ar_8 (Ar = C_6H_3-2,6-Et_2)$_2$, that contain two unsubstituted tin atoms are known, but the number of organic substituents exceeds that of the metal atoms as some metal atoms carry two organic substituents. They were obtained from the thermolysis of $(SnAr_2)_3$. See; L. R. Sita, *Adv. Organomet. Chem.* **1995**, *38*, 187 for an account of this and related work. In addition, a cationic germanium cluster containing unsubstituted germanium atoms $[(t\text{Bu}_3\text{Si})_6Ge_{10}I]^+$ has been structurally characterized: A. Sekiguchi, Y. Ishida, Y. Kabe, M. Ichinohe, *J. Am. Chem. Soc.* **2002**, *124*, 8776.

[2] N. Wiberg, H.-W. Lerner, S. Wagner, H. Nöth, T. Seifert, *Z. Naturforsch. B* **1999**, *54*, 877.

[3] B. E. Eichler, P. P. Power, *Angew. Chem.* **2001**, *113*, 818; *Angew. Chem. Int. Ed.* **2001**, *40*, 796.

[4] A. Schnepf, R. Köppe, *Angew. Chem.* **2003**, *115*, 940; *Angew. Chem. Int. Ed.* **2003**, *42*, 911.

[5] J. D. Corbett, *Angew. Chem.* **2000**, *112*, 682; *Angew. Chem. Int. Ed.* **2000**, *39*, 670.

[6] A. Sekiguchi, H. Sakurai, *Adv. Organomet. Chem.* **1995**, *37*, 1.

[7] A. Schnepf, H. Schnöckel, *Angew. Chem.* **2002**, *114*, 3682; *Angew. Chem. Int. Ed.* **2002**, *41*, 3532.

[8] The extraction of Zintl phases such as $Sn_{9-x}E_x^{4-}$ (E = Ge or Pb; x = 0–9) with ethylene diamine, and their study by ^{119}Sn NMR spectroscopy, have proven the existence of mixtures of anionic heteronuclear tetrel clusters. No crystal structures have been determined, however. See: R. W. Rudolph, W. L. Wilson, R. C. Taylor, *J. Am. Chem. Soc.* **1981**, *103*, 2480.

[9] M. Stender, A. D. Phillips, R. J. Wright, P. P. Power, *Angew. Chem.* **2002**, *114*, 1863; *Angew. Chem. Int. Ed.* **2002**, *41*, 1785.

[10] Crystal data for **1** and **2**·hexane with $Mo_{K\alpha}$ (λ = 0.7107 Å) radiation at 90 K: **1**, monoclinic, *P*2(1)/*n*, orange block, a = 10.9496(11), b = 19.2684(19), c = 13.7857(14) Å, β = 98.547(2)°, V = 2876.2(5) Å^3, Z = 2, *R1* (obs data) = 0.0589, *wR2* (all data) = 0.1523, GOF = 0.966; **2**·hexane: monoclinic, $P2_1/c$, red block, a = 16.928(4), b = 15.442(4), c = 25.196(7) Å, β = 103.857(5)°, V = 6395(3) Å^3, Z = 4, *R*1 (obs data) = 0.1001, *wR*2 (all data) = 0.2465, GOF = 1.146. CCDC-210326 (**1**) and CCDC-210327 (**2**) contains the supplementary crystallographic data for this paper. These data can be obtained free of charge via www.ccdc.cam.ac.uk/conts/retrieving.html (or from the Cambridge Crystallographic Data Centre, 12 Union Road, Cambridge CB2 1EZ, UK; fax: (+44) 1223-336-033; or deposit@ccdc.cam.ac.uk). The structure of **1** displayed disorder problems involving the unsubstituted Ge_4 array such that three plausible Ge_4 arrangements are possible. The major (70 %) array features an almost square Ge_4 unit similar in structure to the Sn_4 moiety in the tin counterpart. The remaining 30 % is divided between two rectangular Ge_4 arrays that have "short" bond lengths in the range 2.71–2.73 Å and longer (probably non-bonded) Ge–Ge separations in the range 3.41–3.64 Å. The positions of the minority Ge atoms were clearly shown on a difference electron-density map. Distances between the main Ge atoms and minority atoms are too large to allow a description based on large amplitudes of motion. The

 © 2003 Wiley-VCH Verlag GmbH & Co. KGaA, Weinheim

final R index for **2** is higher than normal for a correct structure. The reason for this is an overlap of parts of the main reciprocal lattice and an extraneous lattice, either from a twin component or a misoriented crystal fragment. By removing reflections with large I_o/I_c discrepancies, it was possible to lower R and reduce the magnitude of the largest difference peak. These operations are purely cosmetic, however, as they resulted in no discernible structural changes. Final refinement was therefore performed with the offending reflections included.

[11] M. Stender, A. D. Phillips, R. J. Wright, P. P. Power, *Angew. Chem.* **2002**, *114*, 1863; *Angew. Chem. Int. Ed.* **2002**, *41*, 1785.
[12] A. D. Phillips, R. J. Wright, M. M. Olmstead, P. P. Power, *J. Am. Chem. Soc.* **2002**, *124*, 5930.
[13] K. Wade, *Adv. Inorg. Chem. Radiochem.* **1976**, *18*, 1.
[14] R. B. King, I. Silaghi-Dumitrescu, A. Kun, *J. Chem. Soc. Dalton Trans.* **2002**, 3999.
[15] A. Sekiguchi, T. Yatabe, C. Kabuto, H. Sakurai, *J. Am. Chem. Soc.* **1993**, *115*, 5853.
[16] A. Sekiguchi, C. Kabuto, H. Sakurai, *Angew. Chem.* **1989**, *101*, 97; *Angew. Chem. Int. Ed. Engl.* **1989**, *28*, 55.
[17] G. Renner, P. Kirchen, G. Huttner, P. Rutsch, K. Heinze, *Eur. J. Inorg. Chem.* **2001**, 973.
[18] K. H. Pannell, L. Parkanyi, H. Sharma, F. Cervantes-Lee, *Inorg. Chem.* **1992**, *31*, 522.
[19] C. H. E. Belin, J. D. Corbett, A. Cisar, *J. Am. Chem. Soc.* **1977**, *99*, 7163.
[20] J. D. Corbett, P. A. Edwards, *J. Am. Chem. Soc.* **1977**, *99*, 3313.
[21] B. Wrackmeyer, *Annu. Rep. NMR Spectrosc.* **1999**, *38*, 203.

 © 2003 Wiley-VCH Verlag GmbH & Co. KGaA, Weinheim

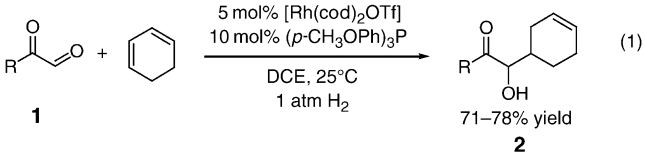
Reductive C–C Coupling Reaction

A New Catalytic C–C Bond-Forming Hydrogenation: Reductive Coupling of Dienes and Glyoxals under Catalytic Hydrogenation Conditions**

*Hye-Young Jang, Ryan R. Huddleston, and Michael J. Krische**

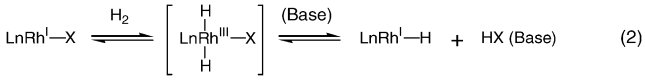
Catalytic reductive C–C bond formation is emerging as an important class of chemical transformation.[1–5] Recently, progress has been made with regard to the nucleophilic activation of diverse precursors containing π bonds (alkenes,[1] alkynes,[2] enones,[3,8] and dienes[4,5]) in regard to catalytic reductive couplings to carbonyl partners. Hydrometallative transformations of this type employ silanes, alanes, and boranes as the terminal reductant, which results in the generation of stoichiometric by-products. While use of elemental hydrogen as the terminal reductant would enable completely atom-economical variants of these catalytic transformations, C–C bond formation has only been observed under hydrogenation conditions in the case of alkenes hydroformylation and Fischer–Tropsch-type processes, that is, catalytic processes involving migratory insertion of carbon monoxide.[6,7]

Recently, we described a catalytic method for the intra- and intermolecular reductive coupling of enone pronucleophiles with aldehyde and ketone partners under hydrogenation conditions.[8] These results demonstrate that the organometallic intermediates obtained in the course of catalytic hydrogenation are subject to electrophilic trapping, thus establishing nucleophilic activation under hydrogenation conditions as a novel pattern of reactivity and encouraging us to explore related catalytic C–C bond-forming hydrogenations. Here, we describe a new example of this uncommon reaction type: the reductive coupling of dienes to aryl and alkyl glyoxal partners under hydrogenation conditions [Eq. (1)]. In addition we report on mechanistic studies that support an unusual catalytic mechanism.



1 2 (1)

In the course of developing the rhodium-catalyzed reductive coupling of enones to aldehydes and ketones under hydrogenation conditions, it was recognized that simple conjugate reduction manifolds are attenuated upon adoption of monohydride-based catalytic cycles induced through formal heterolytic activation of elemental hydrogen [Eq. (2)].[8] Cationic rhodium complexes are especially effective at promoting heterolytic activation of elemental hydrogen,[9,10] owing to the acidity of the dihydride intermediates that result upon oxidative addition.[11]



(2)

Given the elegant studies of Osborn and Schrock, who reported the selective hydrogenation of conjugated dienes to monoolefins using cationic rhodium catalysts,[10a] we were interested in determining whether the organometallic intermediates derived upon hydrogenation of dienes are subject to electrophilic trapping by exogenous carbonyl partners. Consequently, the reductive condensation of 1,3-cyclohexadiene and phenyl-substituted glyoxal **1a** (R = Ph) was examined under hydrogenation conditions. Initial studies employing

[*] Prof. M. J. Krische, H.-Y. Jang, R. R. Huddleston
Department of Chemistry and Biochemistry
University of Texas at Austin
1 University Station–A5300, Austin, TX 78712-1167 (USA)
Fax: (+1) 512-471-8696
E-mail: mkrische@mail.utexas.edu

[**] This research was supported in part by the Research Corporation Cottrell Scholar Award (CS0927), the Alfred P. Sloan Foundation, the Dreyfus Foundation, and Eli Lilly. We thank Dr. Ben Shoulders for skillful assistance in the characterization of deuterated materials by one- and two-dimensional ^{1}H NMR analysis. We thank Dr. Vincent Lynch for skillful assistance in the characterization of **2a** by X-ray crystallographic analysis.

Supporting information for this article is available on the WWW under http://www.angewandte.org or from the author.

 © 2003 Wiley-VCH Verlag GmbH & Co. KGaA, Weinheim DOI: 10.1002/anie.200351986

Wilkinson's catalyst reveal simple reduction of both 1,3-cyclohexadiene and glyoxal **1a** (Table 1, entry 1). In accordance with the aforementioned analysis, rhodium complexes with cationic character should promote monohydride-based catalytic cycles, thus attenuating simple reduction manifolds.

Table 1: Reductive condensation of 1,3-cyclohexadiene and **1a** (R = Ph) [Eq. (1)].[a]

Entry	Catalyst (mol%)	Ligand (mol%)	Yield [%][b]
1	$[Rh(PPh_3)_3Cl]$ (10)	–	–[c]
2	$[Rh(cod)_3OTf]$ (10)	Ph_3P (20)	61
3	$[Rh(cod)_3OTf]$ (10)	$(p\text{-}CF_3Ph)_3P$ (20)	24
4	$[Rh(cod)_3OTf]$ (10)	$(p\text{-}CH_3OPh)_3P$ (20)	77
5	$[Rh(cod)_3BF_4]$ (10)	$(p\text{-}CH_3OPh)_3P$ (20)	79
6	$[Rh(cod)_3OTf]$ (5)	$(p\text{-}CH_3OPh)_3P$ (20)	76

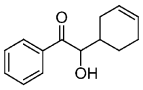
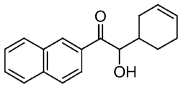
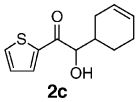
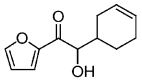
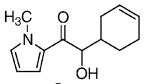
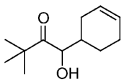
[a] In all cases, 1 equiv phenyl glyoxal **1a** and 5 equiv 1,3-cyclohexadiene were employed. [b] Yield of product after purification by silica gel chromatography. [c] Simple reduction of **1a** was observed.

Indeed, the reductive coupling product **2a** (R = Ph) is obtained in 61% yield when $[Rh(cod)_2OTf]$ (cod = cyclooctadiene, Tf = trifluoromethanesulfonyl) is used in conjunction with PPh_3 (Table 1, entry 2). Profound ligand electronic effects are observed in reactions with several *para*-substituted triphenylphosphane derivatives. Whereas reactions with $(p\text{-}CF_3Ph)_3P$ as the ligand provide **2a** in 24% yield, use of $(p\text{-}CH_3OPh)_3P$ provides **2a** in 77% yield (Table 1, entries 3 and 4). Precatalysts derived from other cationic rhodium sources, such as $[Rh(cod)_2BF_4]$, exhibit similar efficiencies when used in conjunction with $(p\text{-}CH_3OPh)_3P$ (Table 1, entry 5). Comparable yields are obtained with 5-mol% loadings of the commercially available precatalyst $[Rh(cod)_2OTf]$ with $(p\text{-}CH_3OPh)_3P$ (Table 1, entry 6). In all cases **2a** was obtained as a roughly equimolar mixture of diastereomers. The structure of **2a** was corroborated by single-crystal X-ray diffraction analysis. Bidentate phosphane ligands were found to retard the rate of reaction, resulting in diminished yields of **2a**.

Under these optimized conditions (5 mol% $[Rh(cod)_2OTf]$, 10 mol% $(p\text{-}CH_3OPh)_3P$, ambient temperature and pressure, 1,2-dichloroethane (DCE)), the catalytic reductive coupling of 1,3-cyclohexadiene with diverse glyoxal partners was examined. Both aryl and heteroaryl glyoxals provide reductive coupling products **2a**–**2e** (Table 2) in good yield. Aliphatic glyoxal partners also participate in the reaction, as evidenced by the formation of *tert*-butyl-substituted α-hydroxy ketone **2f**. Reductive condensation of 1,3-cyclohexadiene with ethyl glyoxalate does not occur under these conditions. Additionally, the use of acyclic dienes gave reductive coupling products in diminished yield; for example, the coupling of 2,4-hexadiene with phenyl glyoxal proceeds in 52% yield. In all cases reductive condensation products **2a**–**2f** were obtained as roughly equimolar mixtures of diastereomers (Table 2).

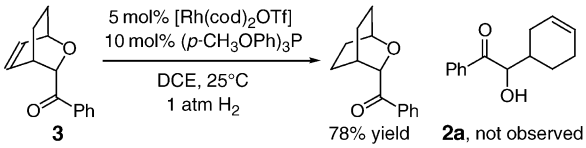
To address the design of second-generation catalyst systems, an understanding of the catalytic mechanism is required. As Rh-catalyzed reductive ring-opening of oxabicyclic alkenes is well known,[12] it was important to determine whether the reductive coupling proceeds through initial

Table 2: Reductive condensation of 1,3-cyclohexadiene and assorted glyoxals.[a]

Product	Yield	Ratio of isomers
 **2a**	76%	1:1.6
 **2b**	77%	1:1.5
 **2c**	74%	1:1.4
 **2d**	78%	1:1.3
 **2e**	73%	1:1.4
 **2f**	71%	1:1.6

[a] Procedure: To a solution of glyoxal (100 mol%) and 1,3-cyclohexadiene (500 mol%) in DCE at ambient temperature was added $[Rh(cod)_2OTf]$ (5 mol%) and $(p\text{-}CH_3OPh)_3P$ (10 mol%). The system was purged with hydrogen gas, and the reaction was allowed to stir at 25 °C under 1 atm H_2 until the substrate was completely consumed. The reaction mixture was evaporated onto silica gel and the product was purified by silica gel chromatography.

hetero-Diels–Alder cycloaddition. Exposure of 1,3-cyclohexadiene to phenyl glyoxal in dichloroethane at ambient temperature does not produce the Diels–Alder adduct. Nor is the Diels–Alder adduct obtained upon exposure of 1,3-cyclohexadiene to phenyl glyoxal under standard coupling conditions but without hydrogen. Unreacted starting materials were observed in these experiments. An independent synthesis of the Diels–Alder adduct of phenyl glyoxal and 1,3-cyclohexadiene was carried out.[13] Subjection of the Diels–Alder adduct **3** to the reductive coupling conditions does not provide **2a**. Instead, the simple alkene hydrogenation product is obtained in 78% yield [Eq. (3)]. These results



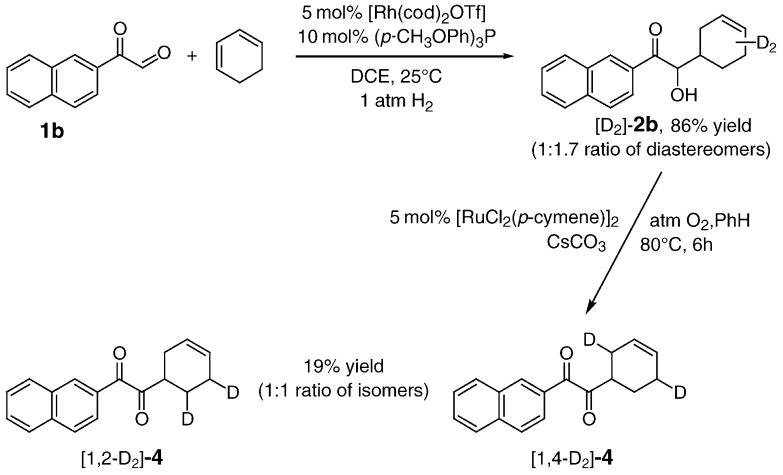
(3)

suggest that catalytic reductive coupling under hydrogenation conditions does not proceed through the intermediacy of a Diels–Alder adduct.

Surprisingly, the reductive condensation of 1,3-cyclohexadiene with naphthyl glyoxal **1b** under one atmosphere of D_2

 © 2003 Wiley-VCH Verlag GmbH & Co. KGaA, Weinheim

results in the incorporation of precisely two deuterium atoms, as revealed by high-resolution mass spectrometric analysis of the product of reductive condensation, [D_2]-**2b** (Scheme 1). The regio- and stereochemistry of the deuterium incorporation could not be determined by two-dimensional ^{1}H NMR analysis. Thus, for the purpose of structural assignment, [D_2]-**2b** was converted into the corresponding α-diketone,[14] which was shown to be an equimolar mixture of the 1,2- and 1,4-dideuterated isomers [1,2-D_2]-**4** and [1,4-D_2]-**4** (Scheme 1). The relative stereochemistry of these compounds could not be assigned.



Scheme 1. Catalytic reductive condensation of **1b** with 1,3-cyclohexadiene under an atmosphere of D_2.

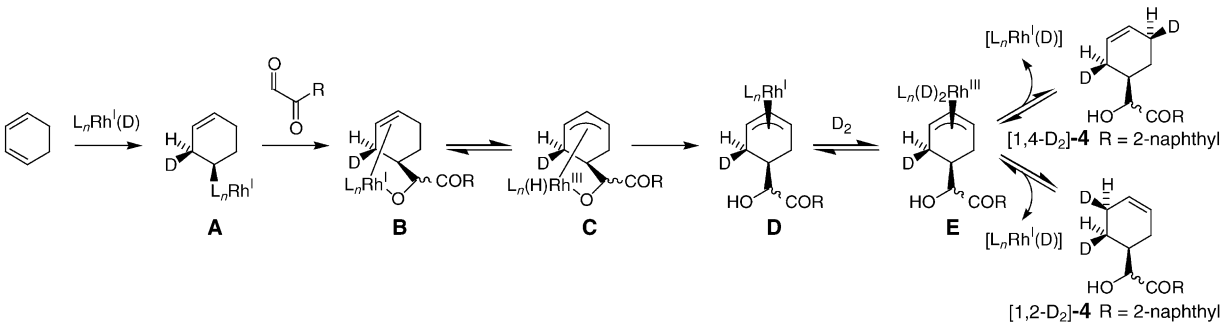
Based on the collective results, the catalytic cycle proposed in Scheme 2 serves as a working mechanistic hypothesis. The starting Rh^I deuteride complex is derived as illustrated in Equation (2). Deuteriometalation of the diene affords the homoallyl rhodium intermediate **A**, which adds to the glyoxal to afford the rhodium alkoxide **B**. The indicated regiochemistry of the C–C bond formation is consistent with that observed by Loh et al. in the nickel-catalyzed reductive coupling of 1,3-cyclohexadiene with aldehydes.[5e] Allylic C–H insertion gives the π-allyl intermediate **C**, which upon O–H reductive elimination gives intermediate **D**. Finally, the catalytic cycle is completed by oxidative addition of elemental deuterium to give dideuteride **E** followed by C–D reductive elimination. The intermediacy of π-allyls **C**–**E** is required to account for the incorporation of precisely two deuterium atoms in the equimolar mixture of 1,2- and 1,4-dideuterated isomers. As [1,2-D_2]-**4** and [1,4-D_2]-**4** may be regarded as alkene isomers, it is noteworthy that the isomerization of alkenes through the intermediacy of π-allyls has been documented.[15]

Subjecting **2b** to standard conditions for catalytic reductive coupling under an atmosphere of D_2 does not provide [D_2]-**2b**. Nor does exposure of [Rh(**2b**)(cod)]$_2$ in dichloroethane solvent to an atmosphere of D_2 provide [D_2]-**2b**. Rather, in each case, the product of alkene hydrogenation is obtained. These results are consistent with the notion that 1,3-cyclohexadiene serves as a ligand for the catalytically active metal complex in the reductive coupling of 1,3-cyclohexadiene with glyoxals. The fact that reductive coupling product **2b** is not overreduced under the conditions in which it is formed, yet is readily hydrogenated when resubmitted to the reductive coupling conditions in the absence of 1,3-cyclohexadiene is also consistent with this hypothesis. Indeed, Mori et al. have observed that the addition of exogenous 1,3-cyclohexadiene induces 1,4-regiochemistry in related nickel-promoted diene/aldehyde cyclizations.[4b]

In summary, while catalytic homogeneous hydrogenation has been practiced routinely since Calvin's initial discovery in 1938,[16] to our knowledge, the present studies are the first examples of the catalytic nucleophilic activation of simple π-unsaturated precursors under the conditions of catalytic hydrogenation in the absence of carbon monoxide. The scope of this transformation with the present catalyst system appears limited to the reductive coupling of cyclohexadiene to aryl, heteroaryl, and alkyl glyoxals. Future studies will be devoted to expanding the scope of this new reaction type, including the development of related reductive couplings to alkyne and alkene partners.

Received: May 27, 2003 [Z51986]

Keywords: C–C coupling · hydrogenation · reduction · rhodium



Scheme 2. A plausible catalytic cycle accounting for the formation of [1,2-D_2]-**4** and [1,4-D_2]-**4**.

 © 2003 Wiley-VCH Verlag GmbH & Co. KGaA, Weinheim

[1] For use of alkenes as nucleophilic partners in catalytic reductive couplings, see: a) N. M. Kablaoui, S. L. Buchwald, *J. Am. Chem. Soc.* **1995**, *117*, 6785 – 6786; b) W. E. Crowe, M. J. Rachita, *J. Am. Chem. Soc.* **1995**, *117*, 6787 – 6788; c) N. M. Kablaoui, S. L. Buchwald, *J. Am. Chem. Soc.* **1996**, *118*, 3182 – 3191.

[2] For use of alkynes as nucleophilic partners in catalytic reductive couplings, see: a) X. Q. Tang, J. Montgomery, *J. Am. Chem. Soc.* **1999**, *121*, 6098 – 6099; b) W.-S. Huang, J. Chen, T. F. Jamison, *Org. Lett.* **2000**, *2*, 4221 – 4223; c) E. A. Colby, T. F. Jamison, *J. Org. Chem.* **2003**, *68*, 156 – 166; d) K. M. Miller, W.-S. Huang, T. F. Jamison, *J. Am. Chem. Soc.* **2003**, *125*, 3442 – 3443; e) K. Takai, S. Sakamoto, T. Isshiki, *Org. Lett.* **2003**, *5*, 653 – 655.

[3] For use of enones as nucleophilic partners in catalytic reductive couplings, see: a) A. Revis, T. K. Hilty, *Tetrahedron Lett.* **1987**, *28*, 4809 – 4812; b) S. Isayama, T. Mukaiyama, *Chem. Lett.* **1989**, 2005 – 2008; c) I. Matsuda, K. Takahashi, S. Sato, *Tetrahedron Lett.* **1990**, *31*, 5331 – 5334; d) S. Kiyooka, A. Shimizu, S. Torii, *Tetrahedron Lett.* **1998**, *39*, 5237 – 5238; e) S. J. Taylor, J. P. Morken, *J. Am. Chem. Soc.* **1999**, *121*, 12202 – 12203; f) T. Ooi, K. Doda, D. Sakai, K. Maruoka, *Tetrahedron Lett.* **1999**, *40*, 2133 – 2136; g) S. J. Taylor, M. O. Duffey, J. P. Morken, *J. Am. Chem. Soc.* **2000**, *122*, 4528 – 4529; h) C.-X. Zhao, M. O. Duffey, S. J. Taylor, J. P. Morken, *Org. Lett.* **2001**, *3*, 1829 – 1831; i) T.-G. Baik, A. L. Luis, L.-C. Wang, M. J. Krische, *J. Am. Chem. Soc.* **2001**, *123*, 5112 – 5113; j) L.-C. Wang, H.-Y. Jang, V. Lynch, M. J. Krische, *J. Am. Chem. Soc.* **2002**, *124*, 9448 – 9453; k) R. R. Huddleston, M. J. Krische, *J. Org. Chem.* **2003**, *68*, 11 – 14.

[4] For use of dienes as nucleophilic partners in intramolecular catalytic reductive couplings, see: a) Y. Sato, M. Takimoto, K. Hayashi, T. Katsuhara, K. Tagaki, M. Mori, *J. Am. Chem. Soc.* **1994**, *116*, 9771 – 9772; b) Y. Sato, M. Takimoto, M. Mori, *Tetrahedron Lett.* **1996**, *37*, 887 – 890; c) Y. Sato, T. Takanashi, M. Hoshiba, M. Mori, *Tetrahedron Lett.* **1998**, *39*, 5579 – 5582; d) Y. Sato, N. Saito, M. Mori, *J. Am. Chem. Soc.* **2000**, *122*, 2371 – 2372; e) K. Shibata, M. Kimura, M. Shimizu, Y. Tamaru, *Org. Lett.* **2001**, *3*, 2181 – 2183.

[5] For use of dienes as nucleophilic partners in intermolecular catalytic reductive couplings, see: a) M. Kimura, A. Ezoe, K. Shibata, Y. Tamaru, *J. Am. Chem. Soc.* **1998**, *120*, 4033 – 4034; b) M. Kimura, H. Fujimatsu, A. Ezoe, K. Shibata, M. Shimizu, S. Matsumoto, Y. Tamaru, *Angew. Chem.* **1999**, *111*, 410 – 413; *Angew. Chem. Int. Ed.* **1999**, *38*, 397 – 400; c) M. Kimura, K. Shibata, Y. Koudahashi, Y. Tamaru, *Tetrahedron Lett.* **2000**, *41*, 6789 – 6793; d) M. Kimura, A. Ezoe, S. Tanaka, Y. Tamaru, *Angew. Chem.* **2001**, *113*, 3712 – 3614; *Angew. Chem. Int. Ed.* **2001**, *40*, 3600 – 3602; e) T.-P. Loh, H.-Y. Song, Y. Zhou, *Org. Lett.* **2002**, *4*, 2715 – 2717.

[6] For recent reviews on alkene hydroformylation, see: a) B. Breit, *Acc. Chem. Res.* **2003**, *36*, 264 – 275; b) B. Breit, W. Seiche, *Synthesis* **2001**, 1 – 36.

[7] For reviews on the Fischer–Tropsch reaction, see: a) W. A. Herrmann, *Angew. Chem.* **1982**, *94*, 118 – 131; *Angew. Chem. Int. Ed. Engl.* **1982**, *21*, 117 – 131; b) C.-K. Rofer-Depoorter, *Chem. Rev.* **1981**, *81*, 447 – 474.

[8] a) H.-Y. Jang, R. R. Huddleston, M. J. Krische, *J. Am. Chem. Soc.* **2002**, *124*, 15156 – 15157; b) R. R. Huddleston, M. J. Krische, *Org. Lett.* **2003**, *5*, 1143 – 1146.

[9] For a review on the heterolytic activation of elemental hydrogen, see: P. J. Brothers, *Prog. Inorg. Chem.* **1981**, *28*, 1 – 61.

[10] Formation of monohydride complexes by deprotonation of cationic rhodium dihydrides has been postulated: a) R. R. Schrock, J. A. Osborn, *J. Am. Chem. Soc.* **1976**, *98*, 2134 – 2143; b) R. R. Schrock, J. A. Osborn, *J. Am. Chem. Soc.* **1976**, *98*, 2143 – 2147; c) R. R. Schrock, J. A. Osborn, *J. Am. Chem. Soc.* **1976**, *98*, 4450 – 4455.

[11] For a review of the acidity of metal hydrides, see: J. R. Norton in *Transition Metal Hydrides* (Ed.: A. Dedieu), VCH, New York, **1992**, chap. 9.

[12] For a recent review, see: M. Lautens, K. Fagnou, S. Hiebert, *Acc. Chem. Res.* **2003**, *36*, 48 – 58.

[13] S. Oi, E. Terada, K. Ohachi, T. Kato, Y. Tachibana, Y. Inoue, *J. Org. Chem.* **1999**, *64*, 8660 – 8667.

[14] S. Chang, M. Lee, S. Ko, P.-H. Lee, *Synth. Commun.* **2002**, *32*, 1279 – 1284.

[15] For a recent discussion, see: T. C. Morrill, C. A. D'Souza, *Organometallics* **2003**, *22*, 1626 – 1629, and references therein.

[16] M. Calvin, *Trans. Faraday Soc.* **1938**, *34*, 1181 – 1191.

 © 2003 Wiley-VCH Verlag GmbH & Co. KGaA, Weinheim

Reactions of IBX

New Reactions of IBX: Oxidation of Nitrogen- and Sulfur-Containing Substrates To Afford Useful Synthetic Intermediates**

K. C. Nicolaou, Casey J. N. Mathison, and Tamsyn Montagnon*

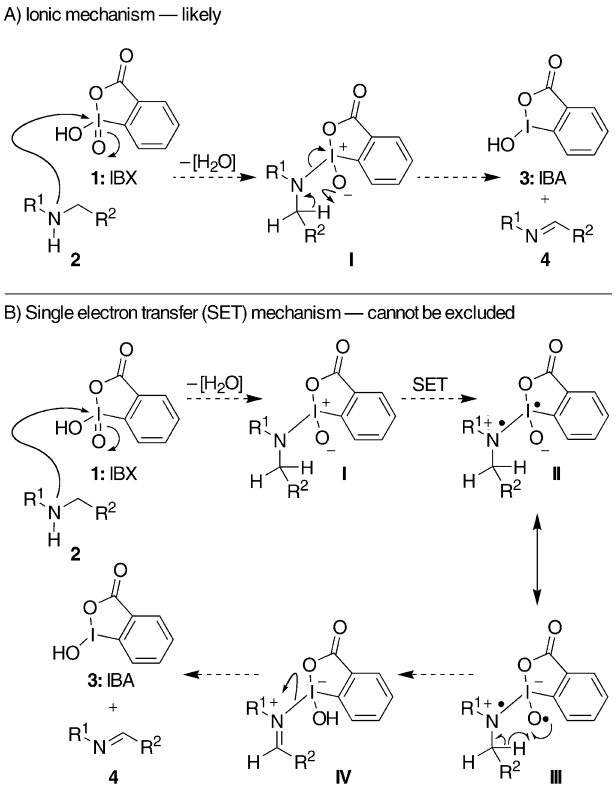
Despite its early description (1893),[1] *o*-iodoxybenzoic acid (**1**, IBX) languished, essentially forgotten, until the 1980s when the seminal works of Dess and Martin initiated a renaissance in interest in the chemistry of hypervalent iodine(v) reagents.[2] Within the past decade, the use of IBX as a reagent has grown dramatically, a surge driven by an improved method for its synthesis,[3] and by explorations into its chemistry that have unveiled its versatility in mediating a wide array of transformations with far-reaching synthetic applicability.[4] In particular, investigations from our own laboratories have revealed that IBX is a powerful single-electron-transfer (SET) agent that readily accepts new heteroatom-based ligands and, thus, can 1) effect the oxidation of ketones, aldehydes, and silyl enol ethers to the corresponding α,β-unsaturated carbonyl compounds,[5–7] 2) oxidize benzylic positions,[5] and 3) facilitate the cyclization of *N*-aryl amides, (thio)carbamates, and ureas to afford

[*] Prof. Dr. K. C. Nicolaou, C. J. N. Mathison, Dr. T. Montagnon
Department of Chemistry and The Skaggs Institute for Chemical Biology
The Scripps Research Institute
10550 North Torrey Pines Road, La Jolla, CA 92037 (USA)
Fax: (+1) 858-784-2469
E-mail: kcn@scripps.edu
and
Department of Chemistry and Biochemistry
University of California, San Diego
9500 Gilman Drive, La Jolla, CA 92093 (USA)

[**] We thank Dr. D. H. Huang and Dr. G. Siuzdak for NMR spectroscopic and mass spectrometric assistance, respectively. Financial support for this work was provided by the National Institutes of Health (USA) and the Skaggs Institute for Chemical Biology.

 DOI: 10.1002/anie.200352076 © 2003 Wiley-VCH Verlag GmbH & Co. KGaA, Weinheim

various heterocycles and amino sugars.[8–11] These developments prompted us to further postulate that reactions with other heteroatom-containing compounds might be feasible. For example, we rationalized, through the mechanism delineated in Scheme 1, that it might be possible to employ

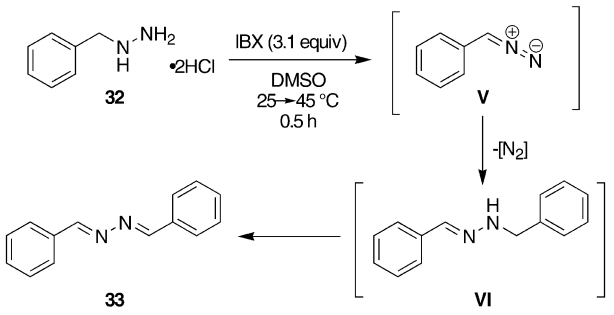


Scheme 1. Proposed A) ionic and B) single-electron-transfer (SET) mechanisms for the oxidation of amines to imines mediated by IBX (**1**). IBA = iodosobenzoic acid.

this reagent to oxidize unhindered amines to their imine counterparts. Herein, we report the successful direct oxidation of multifarious amines to the corresponding imines and oximes by IBX under mild conditions and in excellent yields, as well as a series of related transformations, including new entries into certain aromatic heterocycles, and the deprotection of dithianes to yield the corresponding carbonyl compounds.

Imines and oximes are ubiquitous and useful intermediates within the domain of synthesis, acting as electrophilic participants in a plethora of reactions including alkylations, condensations, or aza-Diels–Alder and other cycloadditions. A series of diverse protocols describing the oxidation of a limited range of amines to the corresponding imines have already been reported in the literature,[12–23] emphasizing synthetic interest in this transformation. The disparate nature of these procedures and the narrow range of amine substrates utilized, however, also serve to accentuate the shortcomings associated with each of these methods.[24]

In this context we were, therefore, gratified to observe, as we proceeded to investigate the potential of IBX in this transformation, that a diverse range of amine substrates could be smoothly and rapidly oxidized in excellent yield and under mild conditions as shown in Table 1. The inclusion of a cyanide, a halide, an *O*-benzyl group, or even a primary hydroxy group did not hinder the desired reaction (Table 1, entries 2, 5, 6, and 9). Among these examples, entry 5 is particularly remarkable, as IBX is perhaps best known as a mild and rapid oxidant for the conversion of alcohols into the corresponding carbonyl compounds[3] (see below), yet in this instance the primary hydroxy group remained unaltered over the course of the reaction (**14**→**15**). Interestingly, hydroxylamine **26** and hydroxylamine ether **28** were rapidly transformed into the oxime **27** and oxime ether **29**, respectively, in excellent yields under very mild conditions (Table 1, entries 12 and 13). The high yields observed in these reactions are notable because IBX has been reported to facilitate the rapid cleavage of various oximes to afford the corresponding carbonyl-containing compounds at room temperature.[25] When a hydrazine, such as **32**, rather than an hydroxylamine, was employed, oxidation with IBX was accompanied by concomitant dimerization and gas evolution (Table 1, entry 15). It is presumed that this dimerization proceeds through initial double oxidation to afford diazo intermediate **V**, followed by loss of nitrogen and insertion of the resultant carbene into the terminal N–H bond of a second molecule of **32**, perhaps organized by precoordination of several N-based ligands around an iodine center. The product **33** may then be obtained after a final IBX-mediated oxidation of the hydrazone **VI** (Scheme 2).



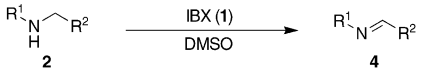
Scheme 2. Proposed mechanism for the IBX-induced conversion of hydrazine derivative **32** into dimeric product **33**. DMSO = dimethyl sulfoxide.

When a primary amine (**34**) was subjected to this procedure, the resultant imine could not be isolated as it was apparently hydrolyzed in situ to afford the corresponding ketone **35** directly (Table 1, entry 16). In substrate **18**, the secondary activated amine reacted rapidly, whereas the tertiary amine moiety remained unaltered over the course of the reaction (Table 1, entry 8). In general, this useful transformation does not necessarily require the elevated temperature (45 °C) used in the standard protocol. High yields can also be obtained when the reaction is conducted at room temperature (Table 1, entry 7); inevitably, however, significantly longer reaction times are required.

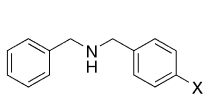
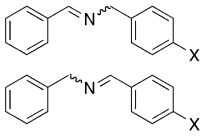
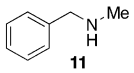
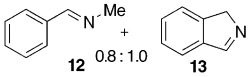
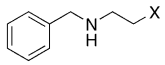
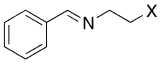
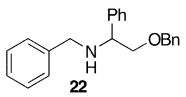
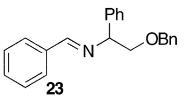
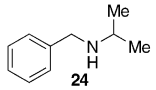
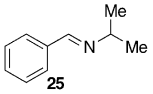
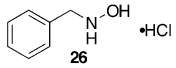
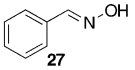
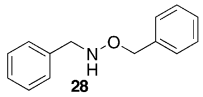
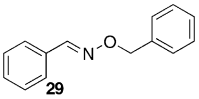
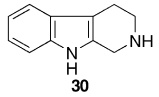
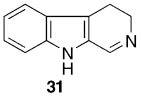
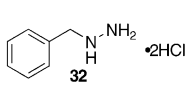
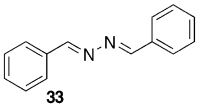
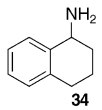
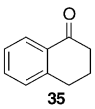
The observed transformations were, for the most part, regioselective when unsymmetrical secondary amines were

 © 2003 Wiley-VCH Verlag GmbH & Co. KGaA, Weinheim

Table 1: Oxidation of amines with IBX. Synthesis of substituted imines, oximes, azines, and ketones.[a]



2 **4**

Entry	Starting material	Product(s)	t [h]	T [°C]	Yield [%]
					
1	**5**: X = H	**6**: X = H	0.5	45	83
2	**7**: X = Br	**8**: X = Br[b]	0.5	45	91
3	**9**: X = OMe	**10**: X = OMe[b]	0.5	45	95
4	 **11**	 **12** 0.8 : 1.0 **13**	0.5	45	70
					
5	**14**: X = OH	**15**: X = OH	0.5	45	79
6	**16**: X = OBn	**17**: X = OBn	0.5	45	89
7	**16**: X = OBn	**17**: X = OBn	9	25	81
8	**18**: X = NMe_2	**19**: X = NMe_2	0.5	45	77
9	**20**: X = CN	**21**: X = CN	0.5	45	89
10	 **22**	 **23**	14	45	49[c]
11	 **24**	 **25**	1	45	88
12	 **26**	 **27**	0.5	45	97
13	 **28**	 **29**	0.5	45	98
14	 **30**	 **31**	0.5	45	98
15	 **32**	 **33**	0.5	45	94
16	 **34**	 **35**	40	25	79

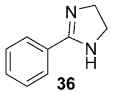
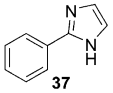
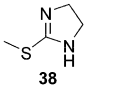
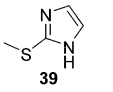
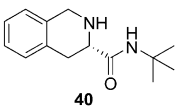
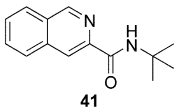
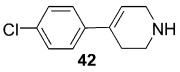
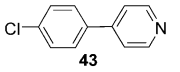
[a] Reactions were conducted on a 0.2–0.5-mmol scale in DMSO with 1.1 equivalents of IBX. [b] Mixture of isomers observed by ^{1}H NMR spectroscopy. [c] Unreacted starting material was also recovered (37%).

employed. Generally, the reaction proceeded to form the conjugated *N*-benzylidene preferentially rather than occurring at the alternative unactivated site to furnish the imine (Table 1, entries 5–9, 11, and 14). This finding contrasts with previous protocols, which were not as discriminating and thus afforded regioisomeric mixtures.[15] (Activation of the methylene to be oxidized is not, however, a prerequisite: see Table 1, entry 4 and Table 2, entries 1 and 2). There are two exceptions to this observation of regioselectivity: The first instance is when differentiation is exhibited by remote substitution on one of the two phenyl rings of an *N*-dibenzylamine. In examples of this case, the relative rates conspired to afford a mixture of regioisomers in the imine product (Table 1, entries 2 and 3), despite the electronic differences in the aromatic rings derived from substitution with bromide or methoxy groups. The second example in which a lack of regioselectivity is observed involved *N*-benzylmethylamine (**11**), which upon treatment with IBX, gave a mixture of products (**12**/**13** ≈ 0.8:1.0; Table 1, entry 4). Imine **12** arises from simple oxidation at the benzylic position of the starting material **11**, whereas the formation of its partner, **13**, is initiated when oxidation of the methyl group is followed by cyclization of the so-formed electrophile onto the proximal aromatic ring, and concludes with a final benzylic oxidation. This transformation, if adopted, holds promise for the synthesis of isoquinolines and other heterocycles.

The abundance of aromatic heterocycles in nature and their prominence in medicinal chemistry inspired us to consider using IBX-mediated oxidation of nitrogen-containing cyclic compounds as a means to access such systems. The concept was initially examined by treating imidazoline **36** (Table 2) with IBX (1.5 equiv) in DMSO for 14 h at 45 °C. Despite requiring oxidation at an unactivated α-methylene group with respect to the nitrogen atom (i.e. not a benzylic methylene; compare with examples in Table 1), the reaction proceeded smoothly to furnish the corresponding imidazole (**37**) in high yield (Table 2, entry 1). Likewise, 2-methylsulfanylimidazoline (**38**) was transformed into the corresponding 2-methylsulfanylimidazole (**39**) in excellent yield (Table 2, entry 2), suggesting that the presence of a sulfur substituent is not necessarily detrimental to the success of the reaction (see below). Isoquinoline **41** and pyridine **43** could also be obtained from terahydroisoquinoline **40** and tetrahydropyridyl compound **42**, respectively (Table 2, entries 3 and 4). In these examples, it is presumed that the initial IBX-mediated oxidation step is followed by rapid aerobic autoxidation (IBA-mediated oxi-

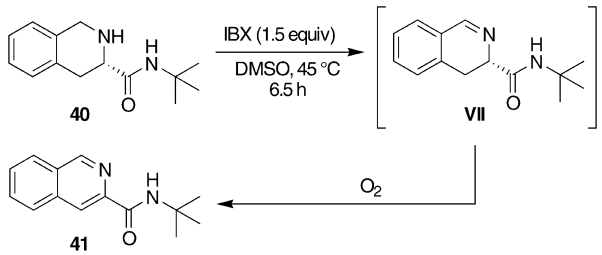
 © 2003 Wiley-VCH Verlag GmbH & Co. KGaA, Weinheim

Table 2: Synthesis of substituted imidazoles, isoquinolines, and pyridines from precursor cyclic amines mediated by IBX (**1**).[a]

Entry	Starting material	Product	*t* [h]	Yield [%][b]
1	 **36**	 **37**	14	71
2	 **38**	 **39**	16	81
3	 **40**	 **41**	6.5	95
4	 **42**	 **43**	48	76

[a] Reactions were conducted on a 0.3–0.5-mmol scale in DMSO with 1.5 equivalents of IBX at 45 °C. [b] Yield of isolated product, with no purification required.

dation cannot be excluded), as less than 2 equivalents of IBX were employed in both cases and the sole product was the fully aromatized heterocycle (Scheme 3). The proposed aerial oxidation is in line with precedent set by a similar observation

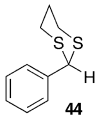
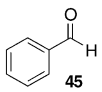
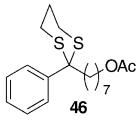
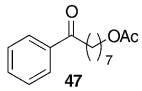
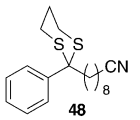
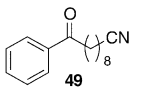
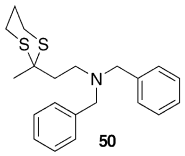
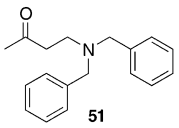
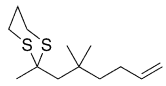
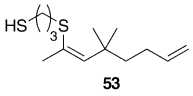
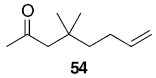


Scheme 3. Aromatization of tetrahydroisoquinoline substrate **40** through initial IBX-mediated oxidation followed by (presumed) autoxidation to afford isoquinoline **41**.

in analogous compounds.[21] It is of interest to contrast these last two examples with the oxidation of **30** (Table 1, entry 14) in which no products derived from a second oxidation were observed.

With the knowledge acquired from these investigations and previous reports[4] describing the behavior of IBX in reactions in which the presence of oxygen and nitrogen is crucial, it now seemed prudent to evaluate the reactivity of some common sulfur-containing substrates in order to obtain a fuller understanding of the reactivity profile of this reagent. To this end, it should be noted that iodine has, for some time, been known to be thiophilic, a feature that has previously been exploited in a number of protocols for the deprotection of dithianes.[26–28] Indeed, the hypervalent iodine(III) reagent, bis(trifluoroacetoxy)iodobenzene, may be employed for the rapid removal of dithiane protecting groups to generate the corresponding carbonyl group (or furnish directly the *O*-acetal/ketal counterpart), albeit under relatively acidic conditions. Initially, the dithiane derivative of benzaldehyde **44** was treated with IBX in wet DMSO to evaluate whether IBX would offer a milder alternative to bis(trifluoroacetoxy)iodobenzene (Table 3, entry 1). Rapid dithiane cleavage was followed by isolation of benzaldehyde (**45**) in essentially quantitative yield after a simple workup procedure. Similar

Table 3: IBX-induced cleavage of dithianes to the corresponding carbonyl compounds.[a]

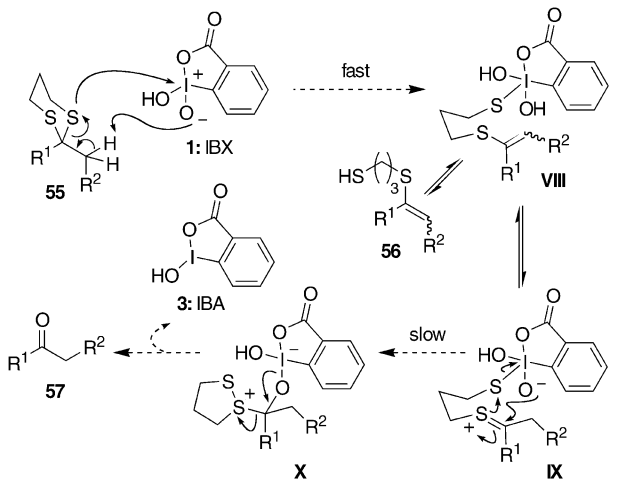
Entry	Starting material	Product	*t* [h]	Yield [%][b]
1	 **44**	 **45**	0.3	99
2	 **46**	 **47**	1	95[c]
3	 **48**	 **49**	1	98[c]
4	 **50**	 **51**	6	96[c]
5	 **52**	 **53**	0.1	98
6		 **54**	6	96[c]

[a] Reactions were carried out on 0.1–1.0 mmol scale in H_2O:DMSO (1:9) with 2.0 equiv of IBX at 25 °C. [b] Isolated yield with no purification required. [c] 1–10 mol% AcOH added.

facile deprotections were carried out with a number of other benzylic dithianes (Table 3, entries 2 and 3), including a substrate bearing a tertiary amine substituent (Table 3, entry 4), a function that is known to retard the IBX-mediated oxidations of alcohols (see below).[6,29] Interestingly, when alkyl dithiane **52** (Table 3, entry 5) was subjected to the new protocol, the intermediate compound **53** could be isolated after a short reaction time, giving some insight into the mechanism of this cleavage process (Scheme 4). When **53** was resubjected to the reaction conditions, the parent ketone **54** was isolated in high yield (Table 3, entry 6).

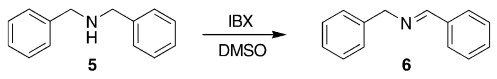
Having established the new IBX-mediated transformations reported above, it was now necessary to compare the relative rates of these reactions so that selectivity parameters could be secured. A series of competition experiments was, therefore, conducted (Table 4). Remarkably, in the presence of secondary alcohol **58**, saturated ketone **59**, or dithiane **60**,

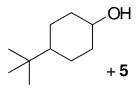
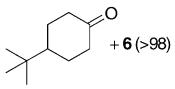
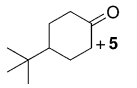
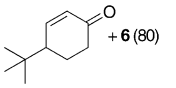
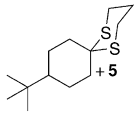
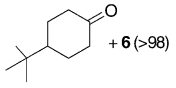
 © 2003 Wiley-VCH Verlag GmbH & Co. KGaA, Weinheim



Scheme 4. Postulated mechanistic rationale for the deprotection of dithianes by IBX under neutral conditions.

Table 4: Relative reactivity of IBX towards secondary amine **5** versus alcohol **58**, ketone **59**, and dithiane **60**.[a]



Entry	Starting materials[b]	Conditions	Conversion ([%])[c]
1	 **58** + **5**	IBX (1.5 equiv), DMSO	 + **6** (>98) (not observed)
2	 **59** + **5**	IBX (1.0 equiv), DMSO	 + **6** (80) (not observed)
3	 **60** + **5**	IBX (1.5 equiv), DMSO/CH_2Cl_2 (10:1)[d]	 + **6** (>98) (not observed)

[a] Reactions were carried out on a 0.2–0.5-mmol scale at 45 °C for 45 min. [b] 1 equivalent each of **5** and **58**, **59**, or **60** was used. [c] Determined by ^{1}H NMR spectroscopy. [d] Dichloromethane was added to improve substrate solubility.

the formation of imine **6** was convincingly favored in each case. In the case in which ketone α,β-unsaturation was evaluated in the presence of dibenzylamine **5** (Table 1, entry 2), *N*-benzylidene formation could not be driven to completion, as substrate degradation became a factor with increased amounts of IBX.

In conclusion, we have discovered a number of new reactions of IBX with heteroatom-containing substrates and demonstrated their utility in organic synthesis. Specifically, we have developed general IBX-induced procedures for the generation of imines from secondary amines under mild conditions and in notably high yields. Furthermore, the oxidative aromatization of nitrogen heterocycles from simple substrates, including those with no activating groups, has been realized. Finally, a new mild procedure for the cleavage of dithianes with IBX has been unveiled. Although these novel reactions induced by IBX are expected to find considerable applications in organic synthesis, new modes of reactivity for this rather old reagent are still anticipated.

Experimental Section

Typical oxidation procedure: IBX (1.0–1.5 equiv) was added to a solution of the amine substrate (1.0 mmol) dissolved in DMSO (2.5 mL, 0.4 M) at ambient temperature. The resulting mixture was heated (45 °C) and the reaction progress was monitored by ^{1}H NMR spectroscopy ([D_6]DMSO). Upon completion, the reaction mixture was diluted with saturated aqueous $Na_2S_2O_3$ (2.5 mL) and an equal volume of EtOAc. The suspension was stirred for about 5 min, and, if necessary, any remaining solids were filtered off through a pad of celite and washed with EtOAc (3 × 1 mL). The combined solution was basified with saturated aqueous $NaHCO_3$ (2.5 mL) and subsequently extracted with EtOAc (2 × 2.5 mL). The organic solution was then washed with saturated aqueous $NaHCO_3$ (2 × 5 mL) and brine (5 mL). After drying ($MgSO_4$), the solvent was removed in vacuo to yield the crude product, which rarely required further purification.

Received: June 6, 2003 [Z52076]

Keywords: imines · nitrogen heterocycles · oxidation · oximes · synthetic methods

[1] C. Hartman, V. Meyer, *Ber. Dtsch. Chem. Ges.* **1893**, *26*, 1727.
[2] For a leading reference, see: D. B. Dess, J. C. Martin, *J. Am. Chem. Soc.* **1991**, *113*, 7277.
[3] M. Frigerio, M. Santagostino, S. Sputore, *J. Org. Chem.* **1999**, *64*, 4537.
[4] K. C. Nicolaou, T. Montagnon, P. S. Baran in *Electronic Encyclopedia of Reagents for Organic Synthesis (e-EROS)* (Ed.: L. A. Paquette), Wiley-VCH, Weinheim, in press, and references therein. See also references [5–11] as leading references.
[5] K. C. Nicolaou, T. Montagnon, P. S. Baran, Y.-L. Zhong, *J. Am. Chem. Soc.* **2002**, *124*, 2245.
[6] K. C. Nicolaou, T. Montagnon, P. S. Baran, *Angew. Chem.* **2002**, *114*, 1035; *Angew. Chem. Int. Ed.* **2002**, *41*, 993.
[7] K. C. Nicolaou, D. L. F. Gray, T. Montagnon, S. T. Harrison, *Angew. Chem.* **2002**, *114*, 1038; *Angew. Chem. Int. Ed.* **2002**, *41*, 996.
[8] K. C. Nicolaou, Y.-L. Zhong, P. S. Baran, *Angew. Chem.* **2000**, *112*, 639; *Angew. Chem. Int. Ed.* **2000**, *39*, 625.
[9] K. C. Nicolaou, P. S. Baran, R. Kranich, Y.-L. Zhong, K. Sugita, N. Zou, *Angew. Chem.* **2001**, *113*, 208; *Angew. Chem. Int. Ed.* **2001**, *40*, 202.
[10] K. C. Nicolaou, P. S. Baran, Y.-L. Zhong, J. A. Vega, *Angew. Chem.* **2000**, *112*, 2625; *Angew. Chem. Int. Ed.* **2000**, *39*, 2525.
[11] K. C. Nicolaou, P. S. Baran, Y.-L. Zhong, S. Barluenga, K. W. Hunt, R. Kranich, J. A. Vega, *J. Am. Chem. Soc.* **2002**, *124*, 2233.
[12] a) T. Sueda, D. Kajishima, S. Goto, *J. Org. Chem.* **2003**, *68*, 3307; b) M. Ochiai, D. Kajishima, T. Sueda, *Heterocycles* **1997**, *46*, 71.
[13] K. Yamaguchi, N. Mizuno, *Angew. Chem.* **2003**, *115*, 1518; *Angew. Chem. Int. Ed.* **2003**, *42*, 1480.
[14] A. Goti, M. Romani, *Tetrahedron Lett.* **1994**, *35*, 6567.
[15] J. Yamaguchi, T. Takeda, *Chem. Lett.* **1992**, 1933.
[16] J. Larsen, K. A. Jørgensen, *J. Chem. Soc. Perkin Trans. 2* **1992**, 1213.
[17] K. Maruyama, T. Kusukawa, Y. Higuchi, A. Nishinaga, *Chem. Lett.* **1991**, 1093.

 © 2003 Wiley-VCH Verlag GmbH & Co. KGaA, Weinheim

[18] A. Nishinaga, S. Yamazaki, T. Matsuura, *Tetrahedron Lett.* **1988**, *29*, 4115.
[19] D. Keirs, K. Overton, *J. Chem. Soc. Chem. Commun.* **1987**, 1660.
[20] J. J. Cornejo, K. D. Larson, G. D. Mendenhall, *J. Org. Chem.* **1985**, *50*, 5382.
[21] J. P. Marino, R. D. Larsen, *J. Am. Chem. Soc.* **1981**, *103*, 4642.
[22] P. A. Wehrli, B. Schaer, *Synthesis* **1974**, 288.
[23] E. F. Pratt, T. P. McGovern, *J. Org. Chem.* **1964**, *29*, 1540.
[24] Amongst the known procedures for this transformation is the notably mild method utilizing catalytic tetra-*N*-propylammonium perruthenate (TPAP), and *N*-methylmorpholine-*N*-oxide (NMO) as a stoichiometric cooxidant.[14] This procedure was shown to convert a small number of simple benzylamines successfully into the corresponding imines. Ruthenium catalysis is also involved in a more recent procedure in which oxygen is employed as the stoichiometric cooxidant.[13] Alternative transition-metal-based protocols include employing expensive cobalt Schiff base complexes,[18] a copper bromide–lithium *tert*-butoxide combination,[15] manganese salen and iron porphyrins,[16] and manganese dioxide in refluxing benzene,[23] but again the substrate range reported was rather limited. Oxidations with diphenylselenium bis(trifluoroacetate)[21] or Fremy's salt[22] have been explored in the oxidation of simple tetrahydroisoquinoline systems. Furthermore, other methods employing Swern conditions,[19] di-*tert*-butyliminoxyl radicals,[20] iodosobenzene[16] or hypervalent *tert*-butylperoxyiodanes[12] for accomplishing this reaction can justifiably be described as restricted with regard to their scope and efficiency.
[25] D. S. Bose, P. Srinivas, *Synlett* **1998**, 977.
[26] B. M. Choudary, Y. Sudha, *Synth. Commun.* **1996**, *26*, 2993.
[27] N. F. Langille, L. A. Dakin, J. S. Panek, *Org. Lett.* **2003**, *5*, 575.
[28] G. Stork, K. Zhao, *Tetrahedron Lett.* **1989**, *30*, 287.
[29] M. Frigerio, M. Santagostino, S. Sputore, G. Palmisano, *J. Org. Chem.* **1995**, *60*, 7272.

Chiral Tricyclic Lactams

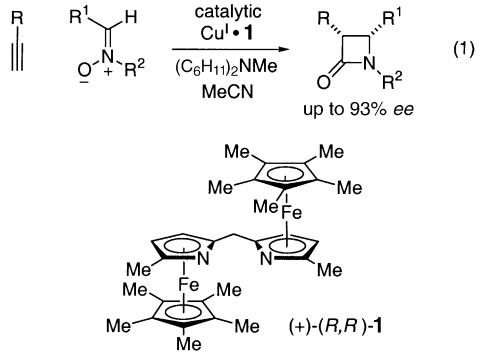
Catalytic Enantioselective Synthesis of β-Lactams: Intramolecular Kinugasa Reactions and Interception of an Intermediate in the Reaction Cascade**

*Ryo Shintani and Gregory C. Fu**

β-Lactams have been intensely investigated as a result of both their biological activity and their utility as synthetic intermediates.[1,2] For example, in the pharmaceutical arena, penicillins and cephalosporins are widely prescribed antibiotics,[1] ezetimibe (zetia) serves as a potent hypocholesterolemic agent,[3] and a β-lactam is employed in the commercial synthesis of the anticancer drug paclitaxel (taxol) to install a β-amino acid derived side chain.[4]

Because of the wide-ranging significance of β-lactams, the development of efficient methods for their enantioselective synthesis is an important objective. A number of noteworthy strategies have been described, almost all of which rely upon the generation of chiral, nonracemic precursors, followed by formation of the four-membered ring.[1,2] In contrast, very few catalytic enantioselective routes to β-lactams from achiral precursors have been reported.[5]

Based on the pioneering work of Kinugasa et al.,[6] Miura et al.,[7] and others,[8] we recently described a copper/bisazaferrocene-catalyzed method for the asymmetric coupling of alkynes with nitrones (the Kinugasa reaction; [Eq. (1)] and Figure 1).[9] This mild approach to the generation of β-lactams is very attractive owing to its convergence, its high functional-group tolerance, and the ready availability and stability of alkynes and nitrones. In our initial study, planar-chiral bisazaferrocene **1** proved to be the most effective ligand among those that we examined.



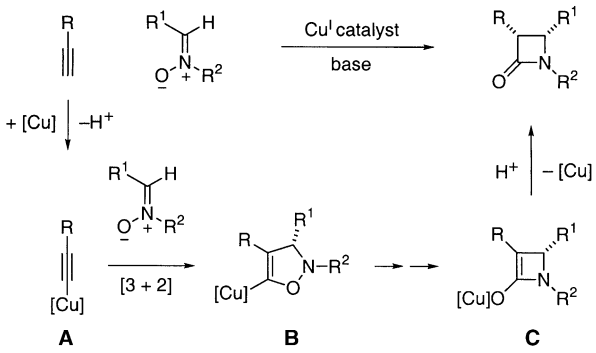


Figure 1. Outline of a possible mechanism for the Kinugasa reaction.

This early investigation explored the generation of monocyclic β-lactams exclusively. Bicyclic and polycyclic β-lactams also constitute important targets, both as endpoints (e.g., penicillins[1] and trinems/tribactams[10]) and as synthetic intermediates.[11] Although, in principle, an intramolecular Kinugasa reaction would provide efficient access to these classes of compounds, to the best of our knowledge no

[*] Prof. Dr. G. C. Fu, R. Shintani
Department of Chemistry, Massachusetts Institute of Technology
Cambridge, MA 02139 (USA)
Fax: (+1) 617-324-3611
E-mail: gcf@mit.edu

[**] Support has been provided by the National Institutes of Health (National Institute of General Medical Sciences, R01-GM066960), Merck, and Novartis. Funding for the MIT Department of Chemistry Instrumentation Facility has been furnished in part by NSF CHE-9808061 and NSF DBI-9729592. We thank Ivory D. Hills for an X-ray crystallographic study.

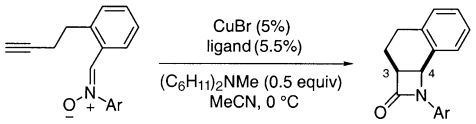
Supporting information for this article is available on the WWW under http://www.angewandte.org or from the author.

 © 2003 Wiley-VCH Verlag GmbH & Co. KGaA, Weinheim DOI: 10.1002/anie.200352103

examples of such a process have been reported. We therefore turned our attention to the development of intramolecular Kinugasa reactions, ideally with a chiral catalyst, with a view to preparing enantioenriched bi- and polycyclic β-lactams. Herein we demonstrate that a copper/phosphaferrocene–oxazoline catalyst mediates asymmetric intramolecular Kinugasa reactions to produce two new rings with very good stereoselectivity. Furthermore, we establish that one of the presumed intermediates in the catalytic cycle (**C** in Figure 1) can be intercepted with an electrophile to generate an additional C–C bond and a quaternary stereocenter.

Our initial investigations focused on the intramolecular Kinugasa reaction of alkyne–nitrone **2** (Table 1) to produce

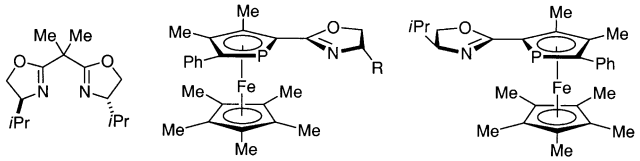
Table 1: Ligand effects for an intramolecular Kinugasa reaction.[a]



2 Ar = *p*-carboethoxyphenyl **3**

Entry	Ligand	*ee* [%]	Configuration	Yield [%]
1	**1**	6	3*S*,4*S*	30
2	**4**	62	3*R*,4*R*	39
3	**5a**	88	3*S*,4*S*	74 ←
4	**5b**	90	3*S*,4*S*	47
5	**6**	58	3*S*,4*S*	52

[a] All data are the average of two runs.



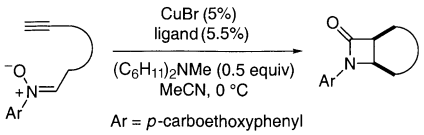
4 **5a**: R = *i*Pr; **5b**: R = *t*Bu **6**

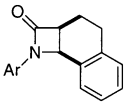
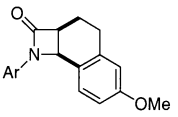
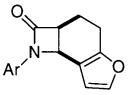
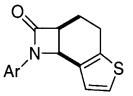
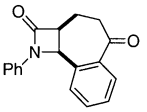
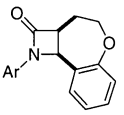
the tricyclic β-lactam framework employed by Merck for the synthesis of melanocortin receptor agonists.[12] Disappointingly, planar-chiral bisazaferrocene **1**, which had been useful for intermolecular processes [Eq. (1)], furnished the desired β-lactam **3** with poor enantioselectivity and in low yield (6% *ee* and 30% yield; Table 1, entry 1). We therefore decided to explore alternative ligand architectures. Chiral bisoxazolines have proved to be effective for a wide variety of transformations, including an array of copper-catalyzed reactions.[13] Unfortunately, the use of bisoxazoline ligand **4** afforded **3** with only moderate stereoselectivity and in modest yield (62% *ee* and 39% yield; Table 1, entry 2).[14]

During the past few years, we have begun to explore the use of a new family of ligands, planar-chiral phosphaferrocene–oxazolines, in asymmetric catalysis (e.g., **5a**, **5b**, and **6** in Table 1).[15] When we applied ligand **5a** in the copper-catalyzed intramolecular Kinugasa reaction of alkyne–nitrone **2**, we were pleased to observe that the desired β-lactam **3** was furnished with markedly improved stereoselectivity and yield (88% *ee* and 74% yield; Table 1, entry 3). Ligand **5b**, in which the *i*Pr group of the oxazoline has been replaced with a *t*Bu group, promoted a similar level of enantioselectivity but a lower yield (90% *ee* and 47% yield; Table 1, entry 4). Finally, phosphaferrocene–oxazoline **5a** is superior to the diastereomeric ligand **6** with respect to both enantioselectivity and yield (Table 1, entry 3 vs. entry 5).[16,17]

Having established that a Cu/phosphaferrocene–oxazoline catalyst not only promotes an intramolecular Kinugasa reaction, but does so with very good enantioselectivity, we explored the application of our method to the synthesis of a range of tricyclic compounds containing a 6,4 or a 7,4 ring system (Table 2).[18] The *i*Pr-substituted ligand **5a** was typically found to be the ligand of choice for the generation of β-lactams fused to a six-membered ring (86–90% *ee*; Table 2, entries 1–3), whereas for seven-membered rings the *t*Bu-substituted analogue **5b** gave superior results (85–91% *ee*; entries 5 and 6).[19]

Table 2: Copper-catalyzed intramolecular Kinugasa reactions in the presence of planar-chiral phosphaferrocene–oxazoline ligands: Enantioselective synthesis of two new rings.[a]



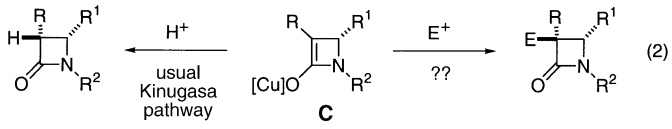
Entry	Product	Ligand	*ee* [%]	Yield [%]
1		**5a**	88	74
2		**5a**	86	60
3[b]		**5a**	90	46
4[b]		**5b**	90	64
5[b]		**5b**	85	53
6		**5b**	91	68

[a] All data are the average of two runs. [b] The reaction was run at room temperature.

The proposed mechanism for the Kinugasa reaction is illustrated in Figure 1.[6–8] It is believed that the terminal alkyne is converted into copper acetylide **A** in the presence of Cu^I and a base (e.g., $(C_6H_{11})_2NMe$),[6] and that **A** participates in a [3+2] dipolar cycloaddition with the nitrone. The resulting heterocycle **B** then rearranges to afford the conjugate base of a β-lactam (enolate **C**).[20] Protonation (e.g., by $[(C_6H_{11})_2NHMe]^+$) furnishes the desired product and releases the copper catalyst.

 © 2003 Wiley-VCH Verlag GmbH & Co. KGaA, Weinheim

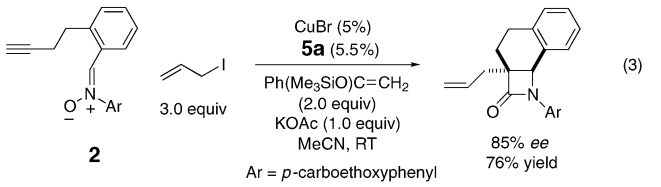
It occurred to us that the utility of the Kinugasa reaction would be further enhanced if we could intercept intermediate **C** by adding an electrophile to the reaction mixture, thereby generating a quaternary stereocenter [Eq. (2)].[21] This is not a



(2)

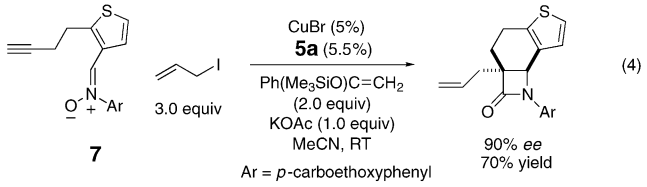
trivial objective, as energetically favorable proton transfers often proceed with remarkable facility relative to other bond-forming reactions.[22] Indeed, when allyl iodide was added to the reaction mixture under our otherwise standard conditions for the cyclization of alkyne–nitrone **2**, a negligible amount of the α-allylated β-lactam was obtained.

After considerable effort, we were pleased to discover conditions under which the desired α functionalization occurred. In the presence of a mixture of a silyl enol ether and KOAc as the base (rather than $(C_6H_{11})_2NMe$), alkyne–nitrone **2** underwent cyclization followed by α alkylation with good stereoselectivity and in good yield (85% *ee* and 76% yield; Eq. (3)).[23] Similarly, the heterocyclic substrate **7** was effi-



(3)

ciently converted into the desired enantioenriched β-lactam (90% *ee* and 70% yield; Eq. (4)). Thus, two carbon–carbon bonds, a carbon–nitrogen bond, two new rings (including a β-lactam), a carbonyl group, and adjacent tertiary and quaternary stereocenters can be generated in a single cyclization–alkylation sequence.



(4)

In summary, we have demonstrated that an intramolecular Kinugasa reaction can be used to prepare fused tricyclic ring systems efficiently with very good levels of enantioselectivity in the presence of a planar-chiral Cu/phosphaferrocene–oxazoline catalyst. Other ligands, including bisoxazolines and bisazaferrocenes, led to the formation of the desired β-lactam in significantly lower yields and with lower *ee* values. Based on the postulated mechanism for the Kinugasa reaction, we have devised a variant of the process in which a presumed intermediate in the catalytic cycle (an enolate) is intercepted with an electrophile. The viability of this variant provides support for the suggested mechanism and enhances the remarkable utility of the Kinugasa reaction. Additional studies of this and related transformations are underway.

Received: June 10, 2003 [Z52103]

Keywords: asymmetric catalysis · copper · cyclizations · domino reactions · nitrogen heterocycles

[1] For discussions of the biological activity of β-lactams, see: a) *Comprehensive Heterocyclic Chemistry II* (Eds.: A. R. Katritzky, C. W. Rees, E. F. V. Scriven), Pergamon, New York, **1996**, chap. 1.18–1.20; b) *The Chemistry of* β*-Lactams* (Ed.: M. I. Page), Blackie Academic & Professional, New York, **1992**; c) *Chemistry and Biology of* β*-Lactam Antibiotics, Vol. 1–3* (Eds.: R. B. Morin, M. Gorman), Academic Press, New York, **1982**.

[2] For reviews on the synthetic organic chemistry of β-lactams, see: a) *Synthesis of* β*-Lactam Antibiotics: Chemistry, Biocatalysis and Process Integration* (Ed.: A. Bruggink), Kluwer, Dordrecht, Netherlands, **2001**; b) *Enantioselective Synthesis of* β*-Amino Acids* (Ed.: E. Juaristi), VCH, New York, **1997**; c) I. Ojima, F. Delaloge, *Chem. Soc. Rev.* **1997**, *26*, 377–386; d) *The Organic Chemistry of* β*-Lactams* (Ed.: G. I. Georg), VCH, New York, **1993**.

[3] a) S. B. Rosenblum, T. Huynh, A. Afonso, H. R. Davis, Jr., N. Yumibe, J. W. Clader, D. A. Burnett, *J. Med. Chem.* **1998**, *41*, 973–980; b) M. J. M. Darkes, R. M. Poole, K. L. Goa, *Am. J. Cardiovasc. Drugs* **2003**, *3*, 67–76; c) http://custom.marketwatch.com/custom/excite-com/news-story.asp?guid={4EB90E73-AC13–43B8–841D-E907016B2F85}.

[4] For leading references, see: a) D. G. I. Kingston, *Chem. Commun.* **2001**, 867–880; b) D. G. I. Kingston, P. G. Jagtap, H. Yuan, L. Samala, *Prog. Chem. Org. Nat. Prod.* **2002**, *84*, 53–225.

[5] For leading references, see: a) P. A. Magriotis, *Angew. Chem.* **2001**, *113*, 4507–4509; *Angew. Chem. Int. Ed.* **2001**, *40*, 4377–4379; b) B. L. Hodous, G. C. Fu, *J. Am. Chem. Soc.* **2002**, *124*, 1578–1579.

[6] Their original report describes the stoichiometric reaction of a copper acetylide with a nitrone: M. Kinugasa, S. Hashimoto, *J. Chem. Soc. Chem. Commun.* **1972**, 466–467.

[7] M. Miura, M. Enna, K. Okuro, M. Nomura, *J. Org. Chem.* **1995**, *60*, 4999–5004.

[8] For examples of applications of the Kinugasa reaction by others, see: a) L. K. Ding, W. J. Irwin, *J. Chem. Soc. Perkin Trans. 1* **1976**, 2382–2386; b) D. K. Dutta, R. C. Boruah, J. S. Sandhu, *Indian J. Chem. Sect. B* **1986**, *25*, 350–353; D. K. Dutta, R. C. Boruah, J. S. Sandhu, *Heterocycles* **1986**, *24*, 655–658; c) A. Basak, G. Bhattacharya, H. M. M. Bdour, *Tetrahedron* **1998**, *54*, 6529–6538; d) A. Basak, S. C. Ghosh, T. Bhowmich, A. K. Das, V. Bertolasi, *Tetrahedron Lett.* **2002**, *43*, 5499–5501.

[9] M. M.-C. Lo, G. C. Fu, *J. Am. Chem. Soc.* **2002**, *124*, 4572–4573.

[10] For reviews of the chemistry and the biology of trinems/tribactams, see: a) M. Gomez-Gallego, M. J. Mancheno, M. A. Sierra, *Tetrahedron* **2000**, *56*, 5743–5774; b) C. Ghiron, T. Rossi, *Targets Heterocycl. Syst.* **1997**, *1*, 161–186; c) S. Biondi, *Spec. Publ. R. Soc. Chem.* **1997**, *198*, 86–100; d) A. Perboni, B. Tamburini, T. Rossi, D. Donati, G. Tarzia, G. Gaviraghi, *Spec. Publ. R. Soc. Chem.* **1993**, *119*, 21–35.

[11] For an overview of the biological activity and the synthesis of 2-aminocycloalkyl carboxylic acid derivatives, see: F. Fülöp, *Chem. Rev.* **2001**, *101*, 2181–2204.

[12] a) R. K. Bakshi, K. J. Barakat, Y. Lai, R. P. Nargund, B. L. Palucki, M. K. Park, A. A. Patchet, I. Sebhat, Z. Ye, WO US

 © 2003 Wiley-VCH Verlag GmbH & Co. KGaA, Weinheim

25757 20010817, **2001**; b) R. K. Bakshi, R. P. Nargund, Z. Ye, WO US 17014 20010525, **2001**.

[13] a) For a review of applications of C_2-symmetric bisoxazolines in asymmetric catalysis, see: A. K. Ghosh, P. Mathivanan, J. Cappiello, *Tetrahedron: Asymmetry* **1998**, *9*, 1–45; b) for some leading references to copper-catalyzed reactions, see: T. Rovis, D. A. Evans, *Prog. Inorg. Chem.* **2001**, *50*, 1–150.

[14] Similarly, in the only study by others of a catalytic asymmetric Kinugasa reaction, Miura et al. found bisoxazoline **4** to be only modestly effective as a chiral ligand for copper-catalyzed intermolecular couplings of alkynes with nitrones (maximum *ee* value: 57%).[7]

[15] a) R. Shintani, M. M.-C. Lo, G. C. Fu, *Org. Lett.* **2000**, *2*, 3695–3697; b) R. Shintani, G. C. Fu, *Org. Lett.* **2002**, *4*, 3699–3702.

[16] The data for ligands **5a** and **6** in Table 1 (entries 3 and 5) indicate that the central chirality of the oxazoline subunit is the dominant stereocontrol element and that the planar chirality of the phosphaferrocene subunit plays a subordinate, although significant, role.

[17] The absolute configuration of the product was determined through X-ray crystallographic analysis of the bis(amide) that is produced upon the reaction of β-lactam **3** with excess 2-bromobenzylamine (see Supporting Information).

[18] Notes for Table 2, entry 1: 1) When CuBr is used, the product is furnished with somewhat higher *ee* values than with CuCl, CuI, Cu(OTf), $Cu(MeCN)_4BF_4$, or Cu(SCN). 2) The course of the coupling is highly dependent on the $(C_6H_{11})_2NMe$/Cu ratio (e.g., a 20:1 ratio leads to a substantial increase in side reactions). 3) The use of bases such as $K_3PO_4{\cdot}H_2O$, K_2CO_3, 1,4-diazabicyclo[2.2.2]octane (dabco), 2,6-lutidine, KF, NEt_3, 1,8-diazabicyclo[5.4.0]undec-7-ene (DBU), and KOH results in an erosion in enantioselectivity and/or yield. 4) The use of MeCN as the solvent gives rise to much cleaner reactions than the use of CH_2Cl_2, THF, dioxane, *N,N*-dimethylformamide (DMF), acetone, or 2-methylbutan-2-ol. 5) Kinugasa reactions of *N*-phenyl and *N*-(4-carboethoxyphenyl)-substituted nitrones lead to β-lactams with similar *ee* values, but couplings of *N*-(4-carboethoxyphenyl)-substituted nitrones generally proceed in somewhat better yield. In the case of an *N*-benzyl- rather than an *N*-(4-carboethoxyphenyl)-substituted nitrone, the *ee* value and the yield of the β-lactam are lower. We have not attempted to optimize these processes. 6) Recrystallization of the β-lactam from Et_2O enhances the *ee* value (> 99% *ee*; 53% recovery).

[19] Ligands **5a** and **5b** promote similar enantioselectivity in the synthesis of 6,4 bicyclic systems (Table 2, entries 1–4). However, the yields are generally higher when **5a** is employed. For the synthesis of 7,4 bicyclic systems (Table 2, entries 5 and 6), comparable yields were observed when ligands **5a** or **5b** were used, but somewhat better *ee* values (up to 15% higher) were observed in the presence of ligand **5b**.

[20] We believe that this proceeds through ring-opening fragmentation to a ketene, followed by recyclization; see: C. Ahn, J. W. Kennington, Jr., P. DeShong, *J. Org. Chem.* **1994**, *59*, 6282–6286.

[21] For a recent review of catalytic asymmetric methods for the generation of quaternary stereocenters, see: E. J. Corey, A. Guzman-Perez, *Angew. Chem.* **1998**, *110*, 402–415; *Angew. Chem. Int. Ed.* **1998**, *37*, 388–401; see also: J. Christoffers, A. Mann, *Angew. Chem.* **2001**, *113*, 4725–4732; *Angew. Chem. Int. Ed.* **2001**, *40*, 4591–4597.

[22] Another potential complication is the reaction of a nucleophilic Brønsted base (e.g., a tertiary amine) with the electrophile (E^+).

[23] When $KOAc/Ph(Me_3SiO)C{=}CH_2$ is used instead of $(C_6H_{11})_2NMe$, acetophenone is presumably generated, rather than a trialkylammonium salt. Acetophenone is a poor proton donor compared to a trialkylammonium salt.

 © 2003 Wiley-VCH Verlag GmbH & Co. KGaA, Weinheim

Coordination Nanotubes

Columnar Supramolecular Architecture Self-Assembled from S_4-Symmetric Coordination Nanotubes Encapsulating Neutral Guest Molecules**

*Cheng-Yong Su, Mark D. Smith, and Hans-Conrad zur Loye**

Synthetic tubular architectures are of broad interest in the fields of materials science, nanotechnology, molecular sieves, ion sensors, and fluidic transport systems. Inorganic nanotubes consisting of pure carbon,[1] boron nitride,[2] metal dichalcogenides,[3] and other layered materials[4] have been the focus of many research efforts and, similarly, many advances have been reported in the realm of organic nanotubular ensembles.[5] For example, open-ended hollow nanotubes have been created from cyclic peptides,[6] lipids,[7] oligocyclodextrins,[8] and related organic systems,[9] and have been investigated for their potential applications. Inorganic/organic coordination nanotubes, on the other hand, remain largely unexplored in spite of the fast moving developments in the area of self-assembled inorganic/organic molecular and polymeric architectures.[10]

Recently, the columnar channels in a number of tubular coordination networks were created by the connection of macrocyclic molecules.[11] To date, and to the best of our knowledge, discrete coordination nanotubes have only been reported by Fujita and co-workers.[12] These tubular structures, templated by rod-shaped guest molecules, were obtained by the reaction between oligo(3,5-pyridine)s and ethylenediamine-protected Pd^{II} ions. We report herein a similar discrete coordination nanotube formed from Hg^{II} ions and a semirigid ditopic ligand.

In recent studies we demonstrated control over product formation—either coordination polymers or metallamacrocycles—by utilizing semirigid di- or tritopic benzimidazolyl-based ligands. The choice of ligand structure and morphology provided us with selective control over the product type, and was accomplished by the designed adjustment of the location and spatial extent of the tethered benzimidazolyl rings by using a variety of different cores or spacers.[13] Herein we describe the synthesis and characterization of a novel coordination architecture—a neutral tetranuclear nanotube $[Hg_4Cl_8(bbimms)_4]$ (**1**)—assembled from $HgCl_2$ and the semi-

[*] Prof. Dr. H.-C. zur Loye, Dr. C.-Y. Su, Dr. M. D. Smith
Department of Chemistry and Biochemistry
University of South Carolina
Columbia, SC 29208 (USA)
Fax: (+1) 803-777-8508
E-mail: zurloye@mail.chem.sc.edu

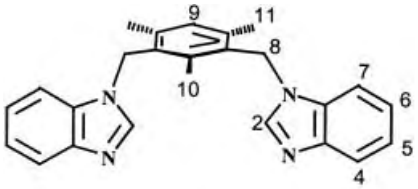
[**] Acknowledgement is made to the Donors of the Petroleum Research Fund, administered by the American Chemical Society, for partial support through grant PRF no. 36822 and to the National Science Foundation, through award DMR no. 0134156.

Supporting information for this article is available on the WWW under http://www.angewandte.org or from the author.

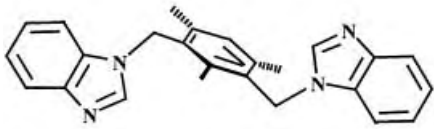
 DOI: 10.1002/anie.200351353 © 2003 Wiley-VCH Verlag GmbH & Co. KGaA, Weinheim

rigid ditopic ligand 1,3-bis(benzimidazol-1-ylmethyl)-2,4,6-trimethylbenzene (bbimms).

The semi-rigid bbimms ligand is capable of adopting either the *syn* or the *anti* conformation depending on the orientation of the two benzimidazolyl arms. These two



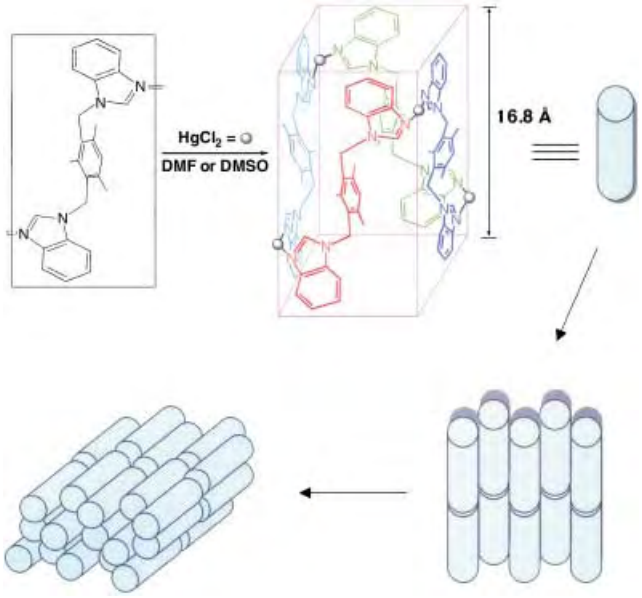
syn conformation



anti conformation

conformations lead to the formation of complexes with completely different structural topologies that are further shaped by the coordination preference of the metal ion used. When metal ions with inherent C_2 (linear) or C_4 (square-planar) symmetry, such as Ag^{I} or Pd^{II}, were used without blocking ligands, the bbimms ligand was found to take on the *syn* conformation and generate dinuclear metallacycles with a rectangular or tetragonal prismatic shape.[14] On the other hand, when metal cations that favor bent coordination environments, such as Hg^{II}, were treated with bbimms, it was observed that the ligand inevitably bridges the ions in an *anti* conformation to form discrete tubular tetramers by self-cyclization, as in **1** (Scheme 1).

Under carefully controlled conditions the straightforward reaction is nearly quantitative. Combining bbimms with $HgCl_2$ in a MeOH/MeCN (1:1 v/v) solution leads to the rapid precipitation of a solid crystalline product whose structure has not been fully characterized.[15] However, this poorly crystalline intermediate has a structure different from that of **1**, as evident from the analysis of powder X-ray diffraction data (see Supporting Information). The addition of DMF or DMSO while heating results in the rapid dissolution of this precipitate, and the subsequent formation of colorless octahedral-shaped crystals suitable for single-crystal X-ray analysis occurs upon letting the solution sit for several days at ambient conditions. The uniform appearance (see Supporting Information) of all the crystals suggested the presence of one single phase, an assumption that was validated by powder X-ray diffraction measurements. The observed diffraction pattern closely matches the intensities and exactly matches the peak positions of the pattern



Scheme 1.

simulated using the single-crystal structure data (see Supporting Information).

The tubular structure of **1** was unambiguously established by single-crystal X-ray diffraction analysis, which also determined that **1**·2 DMF and **1**·2 DMSO are isostructural and differ only in the nature of guest molecules (DMF or DMSO). In both cases, systematic absences in the intensity data were consistent with the space group $I4_1/a$. The $[Hg_4Cl_8(bbimms)_4]$ cage is situated about a $\bar{4}$ site (0,1/4,1/8), and consequently has crystallographically imposed S_4 point symmetry. The asymmetric unit contains one $HgCl_2$ unit, one bbimms ligand, and half of one encapsulated DMF or DMSO molecule of crystallization that is disordered over a twofold rotational axis. Thus, as shown in Figure 1, a neutral tubular structure $[Hg_4Cl_8(bbimms)_4]$ is generated by self-cyclization of four $[HgCl_2(bbimms)]$ subunits whose orientation alternates successively up and down. This molecular tube consists of an approximately rectangular-prismatic shape with four S_4-symmetrically arranged Hg^{II} ions occupying the four edges while four bbimms ligands occupy the four faces of the rectangular prism. The bbimms ligand has to take on the *anti* conformation to achieve this structural topology. In fact the two benzimidazolyl rings of the ligand are nearly coplanar (dihedral angle 16.8°) and perpendicular to the bridging mesityl group (dihedral angles 95.6 and 79.0°, respectively), and exist in the expected *anti* conformation. The Hg^{II} ions are in the common distorted tetrahedral geometry[16] with a Cl-Hg-Cl angle of 115.97(3)° and an N-Hg-N angle of 101.96(10)°, which is necessary for completing this rectangular tube structure.

The overall dimensions of the molecular tube can be estimated from the length of the ligand and the separation between the parallel benzimidazolyl rings, and yields an approximate interior cavity of $4.6 \times 8.6 \times 16.8$ Å after consideration of the van der Waals radii (C 1.71, H 1.16, N 1.52 Å).

 © 2003 Wiley-VCH Verlag GmbH & Co. KGaA, Weinheim

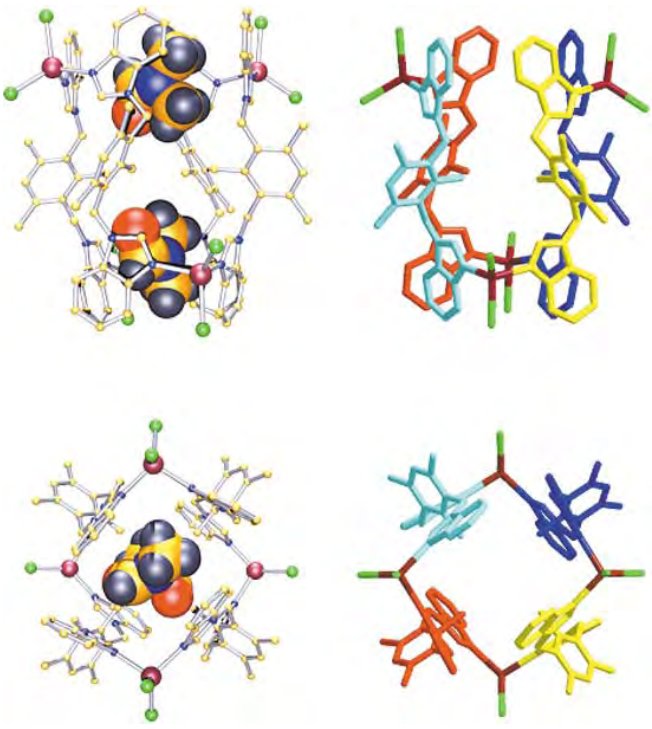


Figure 1. Representation of the $[Hg_4Cl_8(bbimms)_4]$ nanotube with (left) or without (right) guest molecules, which are shown in a space-filling mode.

Consequently, the diameter of a molecule that can enter the cavity is on the order of 4 Å. This cavity is further subdivided into two rectangular compartments (see Supporting Information) that are separated by four methyl groups (5.9 Å apart) pointing to the center of the tube, thus restricting the passage of large guest molecules through this bottleneck. One disordered guest molecule, either DMF or DMSO, is found in each compartment and leads to a stoichiometry of **1**·2 DMF or **1**·2 DMSO, respectively. Despite the disorder, identification of the guest molecules is readily accomplished by other characterization techniques. The IR spectra of **1**·2 DMF and **1**·2 DMSO display almost identical patterns of absorption peaks that can be assigned to the ligand. As expected, there is a strong $\tilde{\nu}_{C=O}$ vibration observed at 1670 cm^{-1} for **1**·2 DMF and a $\tilde{\nu}_{S=O}$ vibration at 1061 cm^{-1} observed for **1**·2 DMSO, which is indicative of DMF and DMSO molecules, respectively. Further information supporting the structure was obtained by ^{1}H NMR spectroscopy: while **1**·2 DMF exhibits two CH_3 signals at 2.88 and 2.76 ppm in its spectrum **1**·2 DMSO exhibits one CH_3 signal at 2.519 ppm. Thermogravimetric (TGA) analysis of **1**·2 DMF and **1**·2 DMSO suggests that the tubes are thermally stable up to 200 °C. The guest molecules are lost between 200–220 °C, and a massive weight loss in the 220–360 °C range is indicative of sample decomposition.

It is evident from the above discussion that the guest molecules, either DMSO or DMF, play an important role in the formation and stabilization of the tube structures. In addition to dissolving the intermediates formed in the MeOH/MeCN mixture, they appear to participate in what Fujita et al. termed "guest-induced assembly,"[17] which can be monitored by NMR spectroscopy.

The ^{1}H NMR spectra of **1** and **2** recorded in warm CD_3CN exhibit a single set of well-resolved proton signals (slightly broadened relative to those of the free ligands). All of the proton resonances are shifted downfield except for those of the H10 atoms belonging to the methyl groups pointing into the center of the tube, which are shifted upfield. These data support both the hypotheses that metal complexation occurs and that, based on the unusual upfield shift of H10, the tube structure is retained in the CD_3CN solution. Interestingly, the chemical shifts of DMSO or DMF remain unchanged relative to those of the free molecules, which indicates that the guest molecules are free to move. Any conclusion concerning the retention of the tube structure in solution based on ^{1}H NMR spectroscopy alone is, of course, rendered less certain by the known lability of the Hg–N bond. The experiment of choice to settle this issue, electrospray mass spectroscopy analysis, proved uninformative, and alternative investigations of the solution structure and dynamics by temperature-dependent NMR spectroscopy are precluded by the sparing solubility of **1** and **2** in common solvents. Nonetheless, the available data, plus the fact that these complexes form only in the presence of DMSO and DMF (numerous other solvents were tried unsuccessfully), favor the suggestion that these tube structures, once formed by guest-induced assembly, can survive in solution even after removal of the guest.

In addition to the intrinsic interest in this type of discrete molecular tube $[Hg_4Cl_8(bbimms)_4]$, there are other notable features resulting from its crystal packing mode. Figure 2 shows an extended view of the crystal packing in the [100] and [001] planes. It is fascinating to observe that all the tubes line-up to generate a pipeline structure that extends along the *c* direction. These pipes stack side-by-side in the [100] plane to form a layer, and the overlap of such layers in the *b* direction generates a three-dimensional columnar architecture. One potential driving force for the alignment of the tubes might be the weak Cl···H–C hydrogen-bonding interactions[18] (Cl1···H1 2.786 Å, Cl1···H1–C1 165.6°, Cl2···H6 2.735 Å, Cl2···H6-C6 152.6°) that exists between adjacent tubes. In fact, every tube is held in place by sixteen Cl···H–C hydrogen bonds that stabilize the resulting columnar architecture. The tubular stacking arrangement in $[Hg_4Cl_8(bbimms)_4]$ represents potential transport pathways for small molecules, which is of interest in the context of natural and artificial membrane structures.[5]

In summary, a neutral coordination nanotube was assembled from four $HgCl_2$ units and four ditopic bbimms ligands in a highly concerted fashion. Two directional binding sites on the Hg^{II} ion direct the assembly which is facilitated by the *anti* conformation adopted by the ligand. The molecular tube exhibits relatively high thermal stability and is capable of encapsulating guest molecules such as DMF or DMSO in its two rectangular compartments. Most exciting, however, is the fact that the tubes are aligned to resemble a pipeline and that these pipelines are arranged into a three-dimensional columnar architecture. To the best of our knowledge, such a columnar supramolecular architecture constructed from neu-

 © 2003 Wiley-VCH Verlag GmbH & Co. KGaA, Weinheim

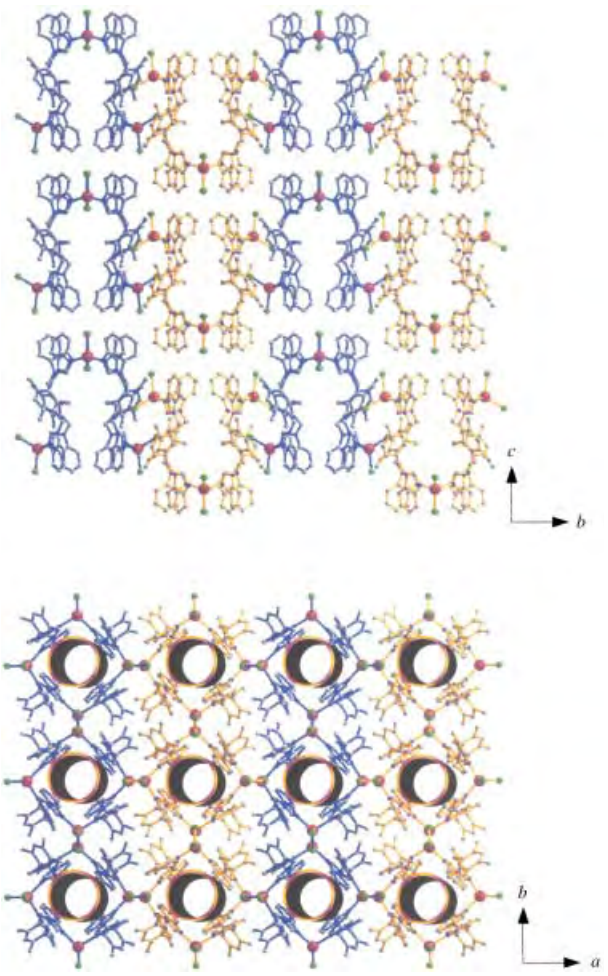


Figure 2. The extended alignment and "pipeline" formation of the molecular tubes in the [001] plane (top) and of the columnar architecture in the [100] plane with open cylinders in the cavities highlighting the "pipeline" nature of the architecture (bottom).

tral coordination tubes has not been reported before, and the synthetic strategy employed in its construction provides a means of expanding the general knowledge of tubular coordination networks[11] and cationic nanotubes.[12]

Experimental Section

General procedure for the preparation of **1**·2 DMF and **1**·2 DMSO: A solution of MeOH containing an equal molar amount of bbimms was added to a solution of $HgCl_2$ in MeCN and a colorless crystalline product appeared in a short time. DMF (or DMSO) was added on heating until the precipitate had dissolved completely and a clear solution was obtained again. The mixture was filtered and left to stand at room temperature for several days to yield colorless crystals having a pseudo-octahedral shape.

1·2 DMF: ^{1}H NMR (300 MHz, CD_3CN): $\delta = 7.92$ (s, 1 H, -COH), 7.58 (s, 4 H, H2), 7.75 (ddd, 4 H, H4), 7.60 (ddd, 4 H, H7), 7.29–7.39 (m, 8 H, H5,6), 7.19 (s, 2 H, H9), 5.41 (s, 8 H, H8), 2.88 (s, 3 H, CH_3 (DMF)), 2.76 (s, 3 H, CH_3 (DMF)), 2.31 (s, 12 H, H11), 1.89 ppm (s, 6 H, H10). IR (KBr): $\tilde{\nu} = 3086$, 2970, 1670, 1609, 1504, 1462, 1396, 1327, 1296, 1234, 1196, 1092, 1015, 910, 752, 717, 575, 513 cm^{-1}.

1·2 DMSO: ^{1}H NMR (300 MHz, CD_3CN): $\delta = 7.57$ (s, 4 H, H2), 7.78 (ddd, 4 H, H4), 7.59 (ddd, 4 H, H7), 7.27–7.39 (m, 8 H, H5,6), 7.19 (s, 2 H, H9), 5.38 (s, 8 H, H8), 2.52 (s, 6 H, CH_3 (DMSO)) 2.34 (s, 12 H, H11), 1.90 ppm (s, 6 H, H10). IR (KBr): $\tilde{\nu} = 3086$, 2966, 1609, 1504, 1462, 1396, 1327, 1296, 1234, 1196, 1060, 1011, 910, 752, 718, 575, 513 cm^{-1}.

X-ray crystallographic analysis: X-Ray intensity data were measured at 150 K on a Bruker SMART APEX CCD diffractometer ($Mo_{K\alpha}$, graphite monochromator). Empirical absorption corrections were applied (SADABS). The structures were solved by Patterson methods followed by difference Fourier synthesis (SHELXS97) and refined anisotropically by full-matrix least-squares against F^2 using all data (SHELXTL).[19] Hydrogen atoms were included in calculated positions as riding atoms except where noted. Crystal data for **1**·2 DMF: Colorless octahedron, $M_r = 2754.08$, $0.40 \times 0.36 \times 0.32$ mm^3, tetragonal, space group $I4_1/a$, $a = 24.7294(8)$, $c = 17.3830(8)$ Å, $V = 10630.5(7)$ Å^3, $Z = 4$, $\mu = 6.02$ mm^{-1}, $\rho_{calcd} = 1.721$ g cm^{-3}. 41495 reflections measured; 5446 independent ($R_{int} = 0.0370$); 4794 with $I > 2\sigma I$. $R1$ (F, all data) = 0.0294, $wR2$ (F^2) = 0.0627, GOF = 1.067. Min./max. residual electron density, +1.08/−0.34 e Å^{-3}. The DMF guest is disordered over a twofold rotational axis. Crystal data for **1**·2 DMSO: Colorless octahedron, $M_r = 2764.14$, $0.26 \times 0.24 \times 0.18$ mm^3. tetragonal, space group $I4_1/a$, a = 24.7502(8), $c = 17.1254(7)$ Å, $V = 10490.5(6)$ Å^3, $Z = 4$, $\mu = 6.14$ mm^{-1}, $\rho_{calcd} = 1.750$ g cm^{-3}. 25295 reflections measured; 4635 independent ($R_{int} = 0.0549$); 3838 with $I > 2\sigma I$. R1 (F, all data) = 0.0374, $wR2$ (F^2) = 0.0969, GOF = 1.049. Min./max. residual electron density, +1.70/−1.14 e Å^{-3}. The DMSO guest is disordered over a twofold rotational axis. H atoms were not located or calculated. CCDC-196335–196336 contain the supplementary crystallographic data for this paper. These data can be obtained free of charge via www.ccdc.cam.ac.uk/conts/retrieving.html (or from the Cambridge Crystallographic Data Centre, 12 Union Road, Cambridge CB2 1EZ, UK; fax: (+44) 1223-336-033; or deposit@ccdc.cam.ac.uk).

Received: March 7, 2003 [Z51353]

Keywords: coordination modes · mercury · nanotubes · self-assembly · supramolecular chemistry

[1] a) S. Iijima, *Nature* **1991**, *354*,56; b) P. M. Ajayan, T. W. Ebbeson, *Rep. Prog. Phys.* **1997**, *60*, 1025; c) J. Chen, H. Y. Liu, W. A. Weimer, M. D. Halls, D. H. Waldeck, G. C. B. Walker, *J. Am. Chem. Soc.* **2002**, *124*, 9034; d) H. W. Zhu, C. L. Xu, D. H. Wu, B. Q. Wei, R. Vajtai, P. M. Ajayan, *Science* **2002**, *296*, 884.

[2] a) N. G. Chopra, R. J. Luyken, K. Cherrey, V. H. Crespi, M. L. Cohen, S. G. Louie, A. Zettl, *Science* **1995**, *269*, 966; b) A. Loiseau, F. Willaime, N. Demoncy, G. Hug, H. Pascard, *Phys. Rev. Lett.* **1996**, *76*, 4737.

[3] a) R. Tenne, L. Margulis, M. Genut, G. Hodes, *Nature* **1992**, *360*, 444; b) Y. Feldman, E. Wasserman, D. J. Srolovitch, R. Tenne, *Science* **1995**, *267*, 222; c) R. Tenne, *Mater.* **1995**, *7*, 965; d) M. Nath, A. Govindaraj, C. N. R. Tao, *Adv. Mater.* **2001**, *13*, 283; e) M. Nath, C. N. R. Rao, *Angew. Chem.* **2002**, *114*, 3601; *Angew. Chem. Int. Ed.* **2002**, *41*, 3451.

[4] M. Terrones, W. K. Hsu, H. W. Kroto, D. R. M. Walton, *Top. Curr. Chem.* **1999**, *199*, 189, and references therein.

[5] a) D. T. Bong, T. D. Clark, J. R. Granja, M. R. Ghadiri, *Angew. Chem.* **2001**, *113*, 1016; *Angew. Chem. Int. Ed.* **2001**, *40*, 989, and references therein.

[6] a) J. D. Hartgerink, T. D. Clark, M. R. Ghadiri, *Chem. Eur. J.* **1998**, *4*, 1367; b) T. D. Clark, J. M. Buriak, K. Kobayashi, M. P. Isler, D. E. McRee, M. R. Ghadiri, *J. Am. Chem. Soc.* **1998**, *120*, 8949; c) J. D. Hartgerink, J. R. Granja, R. A. Milligan, M. R. Ghadiri, *J. Am. Chem. Soc.* **1996**, *118*, 43; d) D. T. Bong, M. R. Ghadiri, *Angew. Chem.* **2001**, *113*, 2221; *Angew. Chem. Int. Ed.* **2001**, *40*, 2163.

 © 2003 Wiley-VCH Verlag GmbH & Co. KGaA, Weinheim

[7] a) J. M. Schnur, *Science* **1993**, *262*, 1669; b) Y.-S. Lee, J.-Z. Yang, T. M. Sisson, D. A. Frankel, J. T. Gleeson, M. Aksay, S. L. Keller, S. M. Gruner, D. F. O'Brien, *J. Am. Chem. Soc.* **1995**, *117*, 5573.
[8] a) A. Harada, J. Li, M. Kamachi, *Nature* **1993**, *364*, 516; b) T. Kraus, M. Budesínský, I. Císarová, J. Závada, *Angew. Chem.* **2002**, *114*, 1791; *Angew. Chem. Int. Ed.* **2002**, *41*, 1715.
[9] a) H. Fenniri, P. Mathivanan, K. L. Vidale, D. M. Sherman, K. Hallenga, K. V. Wood, J. G. Stowell, *J. Am. Chem. Soc.* **2001**, *123*, 3854; b) B. F. Abrahams, B. F. Hoskins, D. M. Michall, R. Robson, *Nature* **1994**, *369*, 272; c) D. Venkataraman, S. Lee, J. Zhang, J. S. Moor, *Nature* **1994**, *371*, 591; d) C. F. van Nostrum, S. J. Picken, A.-J. Schouten, R. J. M. Nolte, *J. Am. Chem. Soc.* **1995**, *117*, 9957; e) V. Sidorov, F. W. Kotch, M. El-Kouedi, J. T. Davis, *Chem. Commun.* **2000**, 2369; f) D. Ranganathan, M. P. Samant, I. L. Karle, *J. Am. Chem. Soc.* **2001**, *123*, 5619; g) V. Semetey, C. Didierjean, J.-P. Briand, A. Aubry, G. Guichard, *Angew. Chem.* **2002**, *114*, 1975; *Angew. Chem. Int. Ed.* **2002**, *41*, 1895.
[10] a) S. Leininger, B. Olenyuk, P. J. Stang, *Chem. Rev.* **2000**, *100*, 853; b) M. Fujita, K. Umemoto, M. Yoshizawa, N. Fujita, T. Kusukawa, K. Biradha, *Chem. Commun.* **2001**, 509; c) D. L. Caulder, K. N. Raymond, *Acc. Chem. Res.* **1999**, *32*, 975; d) R. W. Saalfrank, E. Uller, B. Demleitner, I. *Bernt, Struct. Bonding (Berlin)* **2000**, *96*, 149; e) B. Moulton, J. Lu, A. Mondal, M. J. Zaworotko, *Chem. Commun.* **2001**, 863.
[11] a) M. Loï, M. Hosseini, A. Jouaiti, A. De Cian, J. Fischer, *Eur. J. Inorg. Chem.* **1999**, 1981; b) C. Kleina, E. Gtaf, M. W. Hosseini, A. De Cian, J. Fischer, *Chem. Commun.* **2000**, 239; c) M. C. Hong, Y. J. Zhao, W. P. Su, R. Cao, M. Fujita, Z. Y. Zhou, A. S. C. Chan, *Angew. Chem.* **2000**, *112*, 2586; *Angew. Chem. Int. Ed.* **2000**, *39*, 2468; d) Y. Liu, C.-C. You, H.-Y. Zhang, S.-Z. Kang, C.-F. Zhu, C. Wang, *Nano Lett.* **2001**, *1*, 613; e) C. Daiguebonne, O. Guillou, K. Boubekeur, *Inorg. Chim. Acta* **2000**, *304*, 161.
[12] M. Aoyagi, K. Biradha, M. Fujita, *J. Am. Chem. Soc.* **1999**, *121*, 7457.
[13] a) C.-Y. Su, Y.-P. Cai, C.-L Chen, F. Lissner, B.-S. Kang, W. Kaim, *Angew. Chem.* **2002**, *114*, 3519; *Angew. Chem. Int. Ed.* **2002**, *41*, 3371; b) C.-Y. Su, X.-P. Yang, B.-S. Kang, T. C. W. Mak, *Angew. Chem.* **2001**, *113*, 1775; *Angew. Chem. Int. Ed.* **2001**, *40*, 1725; c) C.-Y. Su, Y.-P. Cai, C.-L. Chen, B.-S. Kang, *Inorg. Chem.* **2001**, *40*, 2210; d) C.-Y. Su, B.-S. Kang, H.-Q. Liu, Q.-C. Wang, T. C. W. Mak, *Chem. Commun.* **1998**, 1551.
[14] a) C.-Y. Su, Y.-P. Cai, C.-L. Chen, H.-X. Zhang, B.-S. Kang, *J. Chem. Soc. Dalton Trans.* **2001**, 359; b) C.-Y. Su, Y.-P. Cai, C.-L. Chen, M. D. Smith, W. Kaim, H.-C. zur Loye, *J. Am. Chem. Soc.* **2003**, *125*, 8595.
[15] Elemental analysis indicates a stoichiometric formula of [$HgCl_2$(bbimms)], calcd for $C_{25}H_{24}N_4HgCl_2$ (%): C 46.06, H 3.71, N 8.59; found: C 46.24, H 3.90, N 8.64. IR (KBr): $\tilde{\nu} = 3099$, 2929, 1610, 1500, 1460, 1389, 1363, 1290, 1186, 1011, 912, 744, 617 cm^{-1}.
[16] Y.-B. Dong, M. D. Smith, H.-C. zur Loye, *Angew. Chem.* **2000**, *112*, 4441; *Angew. Chem. Int. Ed.* **2000**, *39*, 4271.
[17] a) M. Fujita, S. Nagao, K. Ogura, *J. Am. Chem. Soc.* **1995**, *117*, 1649; b) M. Yoshizawa, Y. Takeyama, T. Kusukawa, M. Fujita, *Angew. Chem.* **2002**, *114*, 1403; *Angew. Chem. Int. Ed.* **2002**, *41*, 1347.
[18] a) P. K. Thallapally, A. Nangia, *CrystEngComm* **2001**, *27*; b) L. Brammer, E. A. Bruton, P. Sherwood, *Cryst. Growth Des.* **2001**, *1*, 227.
[19] SHELXTL Version 5.1; Bruker Analytical X-ray Systems, Inc., Madison, Wisconsin, USA, **1997**.

 © 2003 Wiley-VCH Verlag GmbH & Co. KGaA, Weinheim

Helical Zinc Phosphate

$[\{Zn_2(HPO_4)_4\}\{Co(dien)_2\}]\cdot H_3O$: A Zinc Phosphate with Multidirectional Intersecting Helical Channels**

Yu Wang, Jihong Yu, Min Guo, and Ruren Xu**

Chiral inorganic materials with helical pores are particularly desirable because of their promising applications in enantioselective catalysis and separation. It is recognized that both zeolite beta[1,2] and ETS-10[3] are heavily intergrown, with one of the polymorphs being chiral. However, an optically pure chiral zeolite material has been never found. The occurrence of inorganic materials with helical character is particular rare. Among the vast variety of open-framework materials,[4–6] only a few are known to have such structural features. For instance, the vanadium phosphate $[\{(CH_3)_2NH_2\}K_4\{V_{10}O_{10}(H_2O)_2(OH)_4(PO_4)_7\}]$ contains chiral interpenetrating double helices,[7] the zinc phosphate $[\{NH_3(CH_2)_2NH_2(CH_2)_2NH_3\}\{Zn_4(PO_4)_3(HPO_4)\}]\cdot H_2O$ contains intersecting helical channels,[8] UCSB-7 frameworks contain cross-linked helical pores,[9] and metal borophosphates contain 6_1 or 6_5 helices.[10] Recently, we reported the layered zinc phosphite $[(C_5H_6N_2)Zn(HPO_3)]$, which consists of left-handed and right-handed helical chains. The guest templating molecules are found to be important for the formation of the helical -Zn-O-P- chains.[11]

Employing chiral metal complexs as templating agents has proven to be a possible approach to induce a chiral environment in the host framework.[12] Several metal phosphates templated by an optically pure or a racemic mixture of chiral metal complexes have been reported, including aluminophosphates,[12–16] gallium phosphates $[\{d\text{-}Co(en)_3\}\{H_3Ga_2P_4O_{16}\}]$[17] (en = ethylenediamine) and $[\{Co(en)_3\}\{Ga_3(H_2PO_4)_6(HPO_4)_3\}]$,[18] boron phosphate $[\{Co(en)_3\}\{B_2P_3O_{11}(OH)_2\}]$,[19] and zinc phosphates $[\{Co^{II}(en)_3\}_2\{Zn_6P_8O_{32}H_8\}]$ and $[\{Co^{III}(en)_3\}\{Zn_8P_6O_{24}Cl\}]\cdot 2H_2O$.[20] Interestingly, the use of the $[Co(dien)_2]^{3+}$ ion as a template (dien = diethylenetriamine) led to the formation of a layered aluminophosphate $[\{trans\text{-}Co(dien)_2\}\{Al_3P_4O_{16}\}]\cdot 3H_2O$, which has layers that stack in a helical fashion. In this work, by using a racemic mixture of a chiral $[Co(dien)_2]Cl_3$ complex as the template, we have successfully prepared a new open-framework zinc phosphate, $[\{Zn_2(HPO_4)_4\}\{Co(dien)_2\}]\cdot H_3O$ (**1**) with multidirectional helical channels. Of particular interest is the existence of chiral intertwined double helices in its structure. Furthermore, the

[*] Prof. J. Yu, Prof. R. Xu, Y. Wang, M. Guo
State Key Laboratory of Inorganic Synthesis and Preparative Chemistry
College of Chemistry, Jilin University
Changchun 130023 (P. R. China)
Fax: (+86) 431-567-1974
E-mail: jihong@mail.jlu.edu.cn
rrxu@mail.jlu.edu.cn

[**] This work is supported by the National Natural Science Foundation of China and the State Basic Research Project of China (G2000077507).

 DOI: 10.1002/anie.200351643 © 2003 Wiley-VCH Verlag GmbH & Co. KGaA, Weinheim

role of a chiral complex template in inducing the asymmetric environment in the host framework has been investigated.

Compound **1** crystallizes in the orthorhombic space group *Fdd*2 (No. 43). Its structure consists of a macroanionic $[Zn_2(HPO_4)_4]^{4-}$ framework. Charge neutrality is achieved by the complex cation $[Co(dien)_2]^{3+}$ and the protonated water molecule H_3O^+. Each asymmetric unit contains two unique Zn atoms that reside on the twofold symmetry axis, two unique P atoms in general positions, and one Co atom, also located on the twofold axis. Each Zn atom is tetrahedrally coordinated, sharing four vertex oxygen atoms with adjacent P atoms. The Zn–O bond lengths are in the range of 1.914(5) to 1.960(5) Å. Each HPO_4^{2-} tetrahedron shares two oxygen atoms with adjacent Zn atoms, with two oxygen atoms in terminal positions. The $P–O_{bridging}$ bond lengths are in the range of 1.497(6)–1.522(5) Å. The hydroxyl groups have longer P–O bond lengths in the range of 1.555–1.592(6) Å. The Zn-centered tetrahedra and P-centered tetrahedra alternate to form a three-dimensional open-framework. The framework density is 9.7 T per 1000 Å^3 (T = tetrahedrally coordinated atoms, that is, Zn or P), which is one of the lowest values known for open-framework materials.[21–28]

The framework of **1** consists solely of 12-membered rings. Each tetrahedrally coordinated Zn atom is associated with six 12-rings. Each 12-ring consists of six Zn and six P atoms, and has C_2 symmetry. Such structural units are connected together through vertex oxygen atoms to form a very open framework with a multidirectional helical pore system. Figure 1a shows the framework viewed along the [100] direction. It contains 12-membered ring channels that run along this direction. Each 12-ring accommodates one $[Co(dien)_2]^{3+}$ ion. Note that the $[Co(dien)_2]^{3+}$ ions in alternating rows I and II are a pair of enantiomers which are related by the *d* glide-plane operation. Interestingly, each 12-membered ring channel is enclosed by two intertwined helices of the same handedness, which are connected through Zn-O-P linkages (Figure 1b). Such chiral interpenetrating double helices are particularly rare in inorganic materials, with one notable example being $[\{(CH_3)_2NH_2\}K_4\{V_{10}O_{10}(H_2O)(OH)_4(PO_4)_7\}]\cdot 4H_2O$.[7]

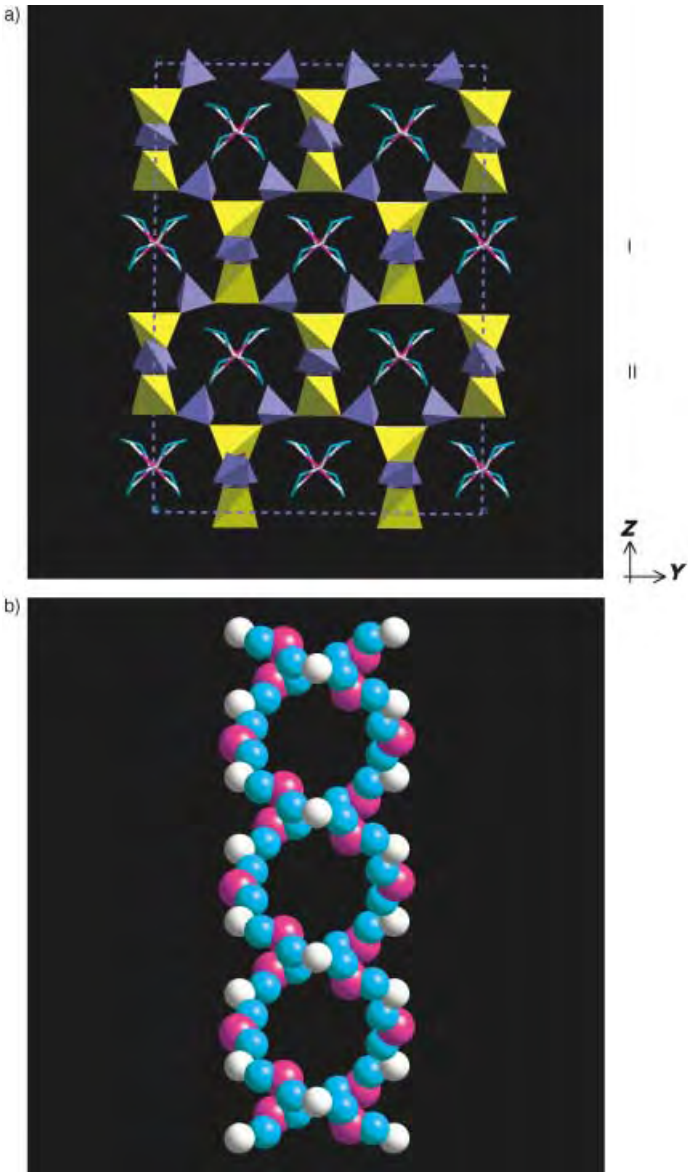


Figure 1. a) A polyhedral view of the framework along the [100] direction (the water molecules in the channels are not shown). The $[Co(dien)_2]^{3+}$ ions reside in the 12-membered ring channels. A pair of enantiomers of $Co(dien)_2^{3+}$ cations alternate in rows I and II (color code: Zn yellow, P blue, Co pink, N white, C light blue); b) a space-filling diagram of two intertwined helices that enclose the 12-membered ring channel (color code: Zn white, P pink, O light blue).

Figure 2a shows the framework of **1** viewed along the [110] direction. Besides the 12-membered ring channels, channels that appear to have an 8-membered ring opening can be seen. In fact, they are enclosed by two types of helical chains as seen in Figure 2b. Furthermore, there are helical channels along the $[1\bar{1}0]$, [411], $[41\bar{1}]$, [011], $[0\bar{1}1]$, [031], $[0\bar{3}1]$, [101], and $[10\bar{1}]$ directions. Thus **1** possesses a multidirectional helical pore system.

Alternatively, it is helpful to view the framework of **1** as being built up from a simple structural motif composed of a Zn(1)-centered tetrahedron with four dangling PO_4 groups (Figure 3a). These units are connected through Zn(2) atoms to form the 3D open framework. It is notable that such a structural motif is chiral and that it has the same C_2 symmetry as the chiral complex cation $[Co(dien)_2]^{3+}$. As has been demonstrated in the work by Morgan et al.[12] and by us,[20] a chiral microenvironment can be induced by the chiral complex template because of molecular recognition between the host and guest complexes. Examination of the hydrogen-bonding network in the metal complex and the inorganic structural motifs can help to understand the observed chiral molecular recognition. Figure 3b shows the H-bonding arrangement between the complex cations and the host framework. Each $[Co(dien)_2]^{3+}$ ion forms a total of 10 H-bonds to the water molecules and the bridging and terminal oxygen atoms in the structural motif. The N···O separations are in the range 2.939(9)–3.124(8) Å. Furthermore, the H-bonding between the chiral metal complex and the chiral

 © 2003 Wiley-VCH Verlag GmbH & Co. KGaA, Weinheim

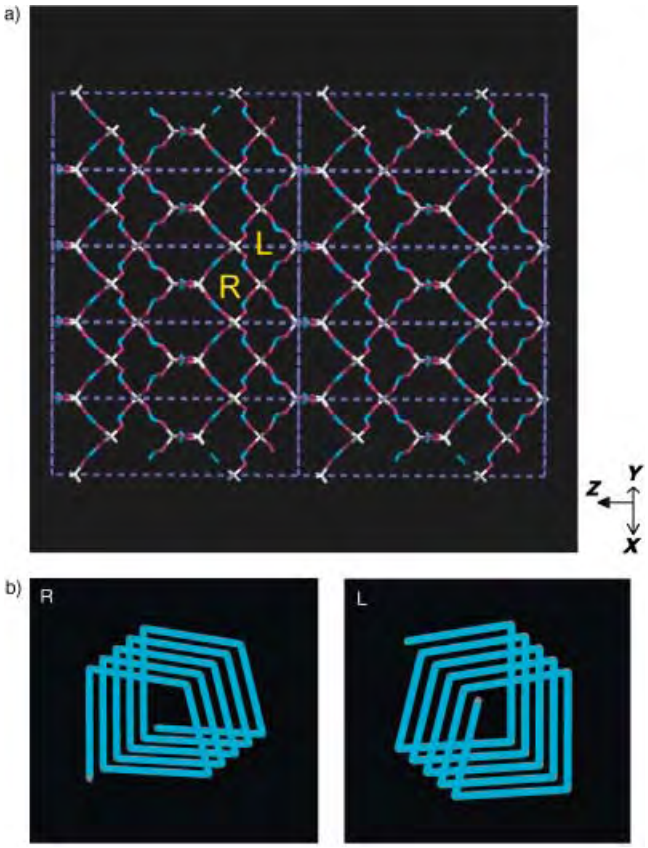


Figure 2. a) The framework viewed along the [110] direction showing the 12-membered ring channels and two types of helical channels; b) the right-handed (R) and left-handed (L) helical channels (color code: Zn white, P light blue, O pink).

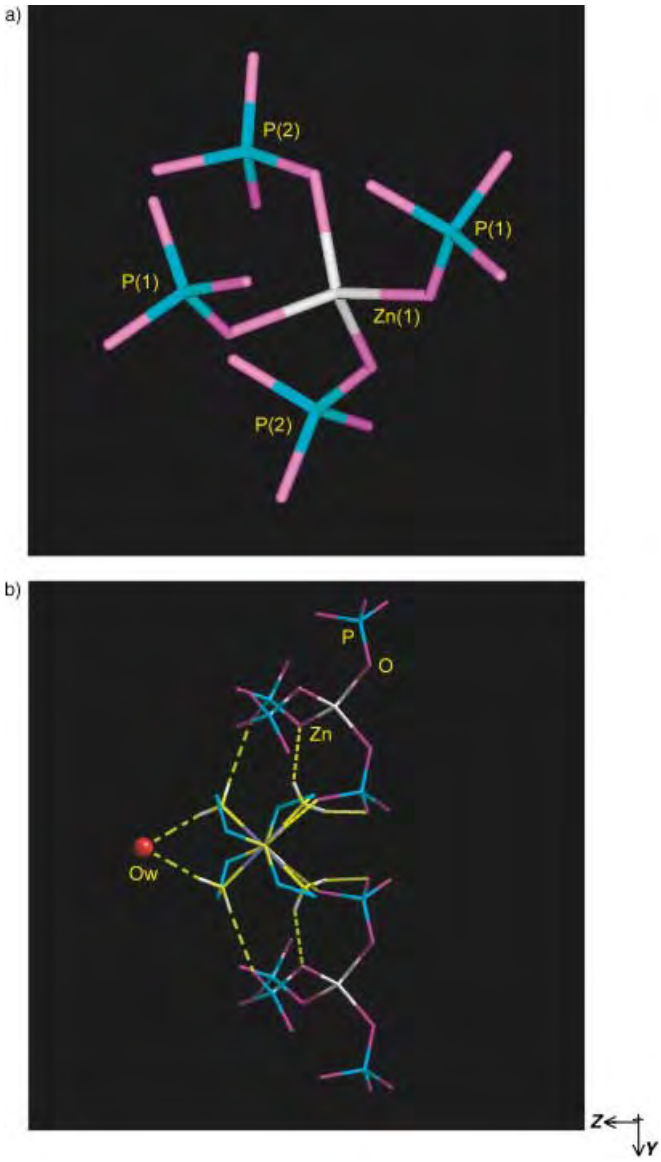


Figure 3. a) Zn(1)-centered tetrahedral structural motif with four dangling PO_4 groups; b) H-bonding arrangement between the chiral complex cation $[Co(dien)_2]^{3+}$ and the chiral structural motif (Zn white, P light blue, O pink).

structural motifs are related by a twofold symmetry axis. This suggests that the H-bonding imposes the C_2 symmetry operation of the chiral complex template onto the chiral structural motif. It is believed that chiral molecular recognition between the guest and host occurs through H-bonds. We are continuing to investigate the role of the chiral metal-complex template in determining the chirality of the inorganic framework. These studies have so far found that such H-bonding is the common origin for inducing chirality transfer in open frameworks templated with chiral metal complexes.

Experimental Section

1: $Zn(OAc)_2{\cdot}2H_2O$ (0.5 g) was dissolved in H_2O (10 mL) and then H_3PO_4 (0.46 mL, 85 wt % in water) and $[Co(dien)_2]Cl_3$ (0.58 g) were subsequently added while stirring. Finally, Me_4NOH (6.0 mL, 10 wt % aqueous solution) was added to the reaction mixture. A homogeneous gel (pH ≈ 7) was formed after stirring for 1 h, which was then sealed in a teflon-lined stainless steel autoclave and heated at 130 °C for 6 days under static conditions. Orange rod-shaped single crystals were separated from the remainder of the product by sonication, washed with distilled water, and then dried in air.

X-ray powder diffraction (XRD) data were collected on a Siemens D5005 diffractometer using $Cu_{K\alpha}$ radiation ($\lambda = 1.5418$ Å). Inductively coupled plasma (ICP) analysis (Perkin-Elmer Optima 3300 DV ICP instrument): Zn 16.21, Co 7.30, P 15.38 % (calcd: Zn 16.29, Co 7.35, P 15.43 %). Elemental analysis (Perkin-Elmer 2400 elemental analyzer): C 12.00, H 4.62, N 10.12 % (calcd: C 12.04, H 4.14, N 10.47 %).

The valence state of +3 for Co in the complex was confirmed by magnetic measurements carried out on a Quantum-Design MPMS-XL SQUID magnetometer.

Thermogravimetric analysis was performed on a Perkin-Elmer TGA7 unit in air. A weight loss of approximately 26.0 % was observed over the 260–580 °C temperature range, which indicated decomposition of the metal complex. XRD analysis indicated that the weight loss was associated with a loss of crystallinity.

Structure determination: A suitable single crystal with dimensions of $0.60 \times 0.20 \times 0.10$ mm was selected for single-crystal X-ray diffraction analysis. Structural analysis was performed on a Siemens SMART CCD diffractometer using graphite-monochromated $Mo_{K\alpha}$ radiation ($\lambda = 0.71073$ Å). The data were collected at temperature of 20 ± 2 °C. Data processing was accomplished with the SAINT

 © 2003 Wiley-VCH Verlag GmbH & Co. KGaA, Weinheim

processing program.[29] The structure was solved by direct methods and refined on F^2 by full-matrix least-squares using SHELXTL97.[30] All Zn, Co, P, and O atoms were located from the difference map. H atoms associated with the hydroxyl groups and the metal-complex cation were placed geometrically and refined in a riding model. The non-hydrogen atoms were refined anisotropically.

Crystal data: $[\{Zn_2(HPO_4)_4\}\{Co(dien)_2\}]\cdot H_3O$, **1**, $M_r = 802.86$, orthorhombic, space group *Fdd*2 (No. 43), $a = 9.271(4)$, $b = 19.781(9)$, $c = 27.045(8)$ Å, $V = 4960(3)$ Å^3, $Z = 8$, $\mu = 2.932$ mm^{-1}, $\rho_{calcd} = 2.150$ g cm^{-3}, 2751 reflections measured, 1781 unique ($R_{int} = 0.0656$). The final $wR(F^2_{all\ data})$ was 0.1254 and $R(F_{all\ data})$ was 0.0503. CCDC-208125 contains the supplementary crystallographic data for this paper. These data can be obtained free of charge via www.ccdc.cam.ac.uk/conts/retrieving.html (or from the Cambridge Crystallographic Data Centre, 12, Union Road, Cambridge CB2 1EZ, UK; fax: (+44) 1223-336-033; or deposit@ccdc.cam.ac.uk).

Received: April 14, 2003 [Z51643]

Keywords: helical structures · host–guest systems · hydrothermal synthesis · phosphates · zinc

[1] M. M. J. Treacy, J. M. Newsam, *Nature* **1988**, *332*, 249 – 251.
[2] a) M. E. Davis, R. F. Lobo, *Chem. Mater.* **1992**, *4*, 756 – 768; b) M. E. Davis, *Acc. Chem. Res.* **1993**, *26*, 111 – 115.
[3] M. W. Anderson, O. Terasaki, T. Ohsuna, A. Philippou, S. P. MacKay, A. Ferreira, J. Rocha, S. Lidin, *Nature* **1994**, *367*, 347 – 351.
[4] A. K. Cheetham, G. Férey, T. Loiseau, *Angew. Chem.* **1999**, *111*, 3466 – 3492; *Angew. Chem. Int. Ed.* **1999**, *38*, 3268 – 3292, and references therein.
[5] C. N. R. Rao, S. Natarajan, A. Choudhury, S. Neeraj, A. A. Ayi, *Acc. Chem. Res.* **2001**, *34*, 80 – 87, and references therein.
[6] J. Yu, R. Xu, *Acc. Chem. Res.* **2003**, in press.
[7] V. Soghomonian, Q. Chen, R. C. Haushalter, J. Zubieta, C. J. O'Connor, *Science* **1993**, *259*, 1596 – 1599.
[8] S. Neeraj, S. Natarajan, C. N. R. Rao, *Chem. Commun.* **1999**, 165 – 166.
[9] T. E. Gier, X. Bu, P. Feng, G. D. Stucky, *Nature* **1998**, *395*, 154 – 157.
[10] a) R. Kniep, H. G. Will, I. Boy, C. Röhr, *Angew. Chem.* **1997**, *109*, 1052 – 1054; *Angew. Chem. Int. Ed. Engl.* **1997**, *36*, 1013 – 1014; b) A. Yilmaz, X. Bu, M. Kizilyalli, G. D. Stucky, *Chem. Mater.* **2000**, *12*, 3243 – 3245.
[11] J. Liang, Y. Wang, J. Yu, Y. Li, R. Xu, *Chem. Commun.* **2003**, 882 – 883.
[12] K. Morgan, G. Gainsford, N . Milestone, *J. Chem. Soc. Chem. Commun.* **1995**, 425 – 426.
[13] M. J. Gray, J. D. Jasper, A. P. Wilkinson, *Chem. Mater.* **1997**, *9*, 976 – 980.
[14] D. A. Bruce, A. P. Wilkinson, M. G. White, J. A. Bertrand, *J. Solid State Chem.* **1996**, *125*, 228 – 233.
[15] D. A. Bruce, A. P. Wilkinson, M. G. White, J. A. Bertrand, *J. Chem. Soc. Chem. Commun.* **1995**, 2059 – 2060.
[16] D. J. Williams, J. S. Kruger, A. F. McLeroy, A. P. Wilkinson, J. C. Hanson, *Chem. Mater.* **1999**, *11*, 2241 – 2249.
[17] S. M. Stalder, A. P. Wilkinson, *Chem. Mater.* **1997**, *9*, 2168 – 2173.
[18] Y. Wang, J. Yu, Y. Li, Z. Shi, R. Xu, *J. Solid State Chem.* **2003**, *170*, 176 – 181.
[19] G. Yang, S. C. Sevov, *Inorg. Chem.* **2001**, *40*, 2214 – 2215.
[20] J. Yu, Y. Wang, Z. Shi, R. Xu, *Chem. Mater.* **2001**, *13*, 2972 – 2978.
[21] G. Yang, S. C. Sevov, *J. Am. Chem. Soc.* **1999**, *121*, 8389 – 8390.
[22] Q. Huo, R. Xu, S. Li, Z. Ma, J. M. Thomas, R. H. Jones, A. M. Chippindale, *J. Chem. Soc. Chem. Commun.* **1992**, 875 – 876.
[23] M. Estermann, L. B. McCusker, C. Baerlocher, A. Merrouche, H. Kessler, *Nature* **1991**, *352*, 320 – 322.
[24] C.-H. Lin, S.-L. Wang, K.-H. Lii, *J. Am. Chem. Soc.* **2001**, *123*, 4649 – 4650.
[25] T. A. William, L. Hannooman, *Angew. Chem.* **1997**, *109*, 663 – 665; *Angew. Chem. Int. Ed. Engl.* **1997**, *36*, 640 – 641.
[26] Z.-E. Lin, Y.-W. Yao, J. Zhang, G.-Y. Yang, *J. Chem. Soc. Dalton Trans.* **2002**, 4527 – 4528.
[27] M. I. Khan, M. I. Meyer, R. C. Haushalter, A. L. Schweitzer, J. Zubieta, J. L. Dye, *Chem. Mater.* **1996**, *8*, 43 – 53.
[28] J. Plevert, T. M. Gentz, A. Laine, H. Li, V. G. Young, O. M. Yaghi, M. O'Keeffe, *J. Am. Chem. Soc.* **2001**, *123*, 12706 – 12707.
[29] SMART and SAINT software package; Siemens Analytical X-ray Instruments Inc., Madison, WI, **1996**.
[30] G. M. Sheldrick, SHELXL Program, version 5.1, University of Göttingen, Göttingen (Germany), **1998**; Siemens Industrial Automation, Inc, Madison, WI, **1997**.

 © 2003 Wiley-VCH Verlag GmbH & Co. KGaA, Weinheim

Ruthenic Acid Supercapacitors

Preparation of Ruthenic Acid Nanosheets and Utilization of Its Interlayer Surface for Electrochemical Energy Storage**

Wataru Sugimoto, Hideki Iwata, Yutaka Yasunaga, Yasushi Murakami, and Yoshio Takasu*

Recent advances in materials science have evoked the importance of combining protonics[1–4] and electronics in various applications, such as electrocatalysts for polymer electrolyte fuel cells[5] and electrode materials for electrochemical energy storage.[6–8] This has initiated a challenging search for mixed proton–electron conducting materials containing liquid or liquidlike regions of water to facilitate proton conduction within an electroconducting matrix. The object is to maintain a continuous electroconducting network while incorporating water molecules into the network structure so that the electrolyte can diffuse into the bulk of the electrode material. Crystalline ruthenium oxide is a metallic conductor and is known for its high electrical conductivity, catalytic activity, and excellent chemical, electrochemical, and photochemical stability.[9] It has been used as the main component in commercial Cl_2 evolution electrocatalysts,[10] and has attracted increased interest as bottom-electrode materials,[11] CO oxidizing catalysts,[12,13] and electrode materials for electrochemical supercapacitors.[6–8] Proton conductivity in

[*] Dr. W. Sugimoto, H. Iwata, Y. Yasunaga, Dr. Y. Murakami, Prof. Dr. Y. Takasu
Department of Fine Materials Engineering
Faculty of Textile Science and Technology
Shinshu University, 3-15-1 Tokida, Ueda, Nagano 386-8567 (Japan)
Fax: (+81) 268-22-9048
E-mail: wsugi@giptc.shinshu-u.ac.jp

[**] This work was partially funded by a NEDO Industrial Technology Research Grant Program and a MEXT 21st Century COE Program.

 © 2003 Wiley-VCH Verlag GmbH & Co. KGaA, Weinheim DOI: 10.1002/anie.200351691

ruthenium-oxide-based materials is an important factor, especially in cases where reactions occur at the solid/liquid interface, as in electrochemical energy devices.[5,6] So far, proton conductivity has been appended to ruthenium-oxide-based materials by the synthesis of hydrous ruthenium oxide with an amorphous structure either by electrochemical oxidation of ruthenium metal or by a sol–gel method. The hydrous structure allows facile proton conduction through the bulk of the material. However, the electrical conductivity of the amorphous phase is slightly lower than in the crystalline phase,[7] which is due to the noncontinuous oxide framework. We recently reported a layered ruthenate that may be a candidate as an electrochemical supercapacitor material.[14] This material consists of an electroconducting crystalline network of ruthenium oxide layers interleaved with a hydrous layer on the nanometer scale.

Here we report the intercalation and exfoliation behavior, and the electrochemical supercapacitor properties of layered ruthenic acid and exfoliated ruthenic acid nanosheets. The layered ruthenic acid is capable of accommodating alkyl ammonium molecules in the interlayer space, and can be exfoliated into individual sheets with lateral dimensions in the order of micrometers and thicknesses in the order of nanometers. This material exhibits a specific capacitance of 658 $F g^{-1}_{(RuO_2)}$, which is a tenfold increase compared to conventional three-dimensional RuO_2,[7,8,14] and comparable to amorphous ruthenium oxide hydrate.[6,7] The high specific capacitance was attributed to the utilization of the interlayer surface for (pseudo)electric double-layer capacitance, which results in an extremely high electrochemical active surface area ($\approx 250\ m^2 g^{-1}$) and utilization of the surface active sites for redox capacitance.

Acid treatment of a potassium ruthenate with a layered structure resulted in a decrease in the basal spacing from 0.7321(1) to 0.457(1) nm (Figure 1). The cation ratio of the products before and after the acid treatment decreased from K/Ru = 0.22:1 to < 0.05:1. Thermoanalysis of the acid-treated product revealed an exothermic reaction between 100–270 °C accompanied by a mass loss of 3 wt %, which can be attributed to dehydroxylation of the interlayer protons. The interlayer proton content based on the mass loss (H/Ru = 0.2:1) is in agreement with the cation ratio of K/Ru = 0.22:1 of the parent potassium ruthenate. These results indicate that the acid treatment of the layered potassium ruthenate yielded a layered ruthenic acid (hereafter designated as HRO) by a topotactic proton-exchange reaction. The composition of HRO based on X-ray photoelectron spectroscopy, inductively-coupled plasma spectroscopy, and thermogravimetry can be expressed as $H_{0.22}RuO_{2.11}{\cdot}nH_2O$, where n is the interlayer water content and varies with the drying conditions; typically $n \approx 0.9$ for a sample dried at room temperature. The lamellar structure and the crystalline nature of the ruthenium oxide layers was confirmed by electron diffraction (ED) and high-resolution transmission electron microscopy (HRTEM), as shown in Figure 2. The periodicity between the alternating layers of dark and light contrast observed by HRTEM was 0.45 nm, consistent with the basal spacing observed by XRD. The ED patterns of the acid-treated product could be indexed as $a = 0.47$, $b = 0.30$, $c = 0.45$ nm.

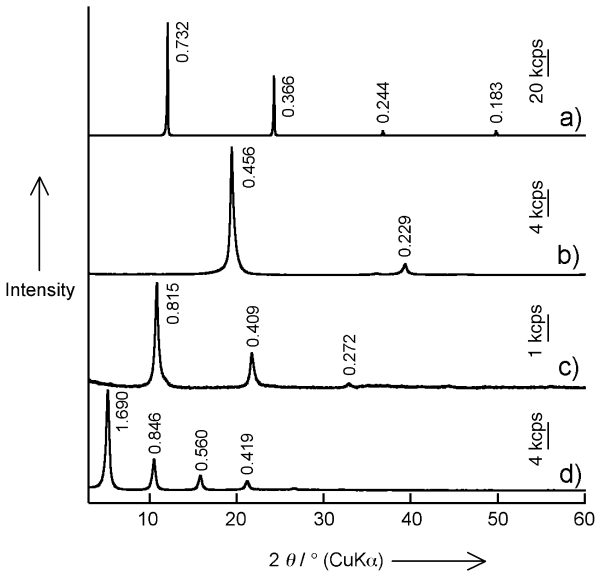


Figure 1. XRD patterns of a) the initial layered potassium ruthenate; b) the product obtained after drying at 120 °C and then undergoing acid treatment; c) the reaction of this product with an aqueous solution of ethylamine; d) the product formed through the subsequent reaction with aqueous tetrabutylammonium hydroxide. The numbers represent the *d* values (units in nm) for each peak.

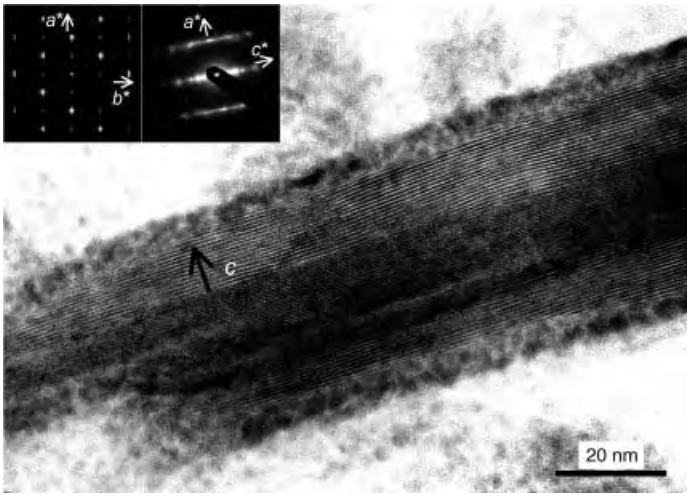


Figure 2. TEM image and ED patterns of layered ruthenic acid.

The lattice parameters suggest that the oxide layer is composed of double-octahedral layers sharing common edges.[15]

Reaction of HRO with aqueous ethylammonium hydroxide resulted in an expansion of the interlayer spacing to 0.816(2) nm, which indicates the formation of an ethylammonium–HRO intercalation compound (Figure 1c). The intercalated ethylammonium ion could be further exchanged with a bulky tetrabutylammonium ion to form a tetrabutylammonium–HRO intercalation compound (basal spacing = 1.68(1) nm) as shown in Figure 1d. The capability of HRO to accommodate alkyl ammonium ions strongly supports the layered structure.

 © 2003 Wiley-VCH Verlag GmbH & Co. KGaA, Weinheim

Suspending the tetrabutylammonium–HRO intercalation compound in water resulted in spontaneous exfoliation (delamination) of the ruthenic acid layers into colloidal ruthenic acid nanosheets. After centrifugation at 2000 rpm to separate the relatively large particles and agglomerates, the supernatant-containing exfoliated HRO nanosheets were stable for periods of months with no sedimentation. This stability is due to the weak interaction between the positively charged tetrabutylammonium ions and the negatively charged ruthenium oxide sheets, similar to the exfoliation behavior of layered titanates.[16,17] Figure 3 shows a typical

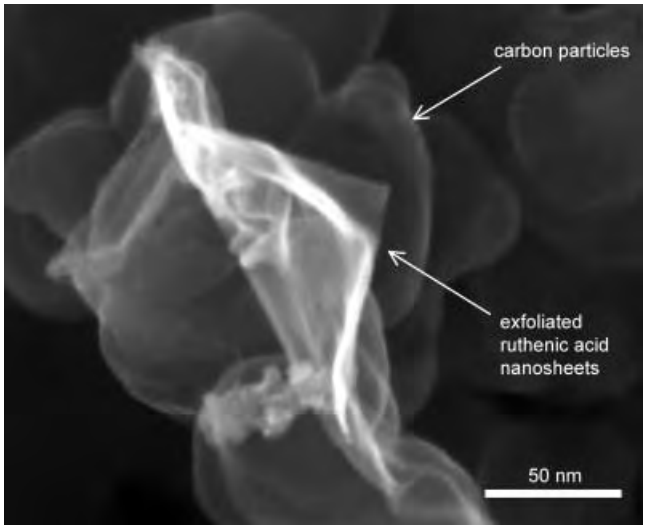


Figure 3. SEM image of exfoliated ruthenic acid nanosheets supported on carbon particles.

scanning electron micrograph of the exfoliated HRO nanosheets supported on carbon particles, which reveal platelike sheets with lateral dimensions in the range of micrometers and thicknesses in the order of nanometers. The exfoliated HRO nanosheets can be reassembled into a *c*-axis-oriented thin film of the tetrabutylammonium–ruthenic acid intercalation compound by casting the material onto a flat substrate.

Cyclic voltammagrams of pristine (non-exfoliated) HRO recorded at sweep rates between 2 and 500 $mV\,s^{-1}$ are shown in Figure 4. The square-shaped "background" of the CV (shaded region) is characteristic of (pseudo)electric double-layer capacitance (outer- and inner-Helmholtz plane charging) and is independent of the sweep rate. In addition to the (pseudo)electric double-layer capacitance, multiple redox peaks characteristic of surface redox reactions can be observed. Such redox peaks are typical features of crystalline RuO_2, and are not observed in amorphous ruthenium oxide hydrate. The specific capacitance at 2 $mV\,s^{-1}$ was 392 $F\,g^{-1}_{(RuO_2)}$. Even at a fast sweep rate of 500 $mV\,s^{-1}$, the specific capacitance was 329 $F\,g^{-1}_{(RuO_2)}$, which is representative of excellent fast charge/discharge properties (Figure 4). These results indicate that HRO is a mixed proton–electron conductor, in which the ruthenate layers contribute to the electrical conductivity and the hydrated interlayer allows

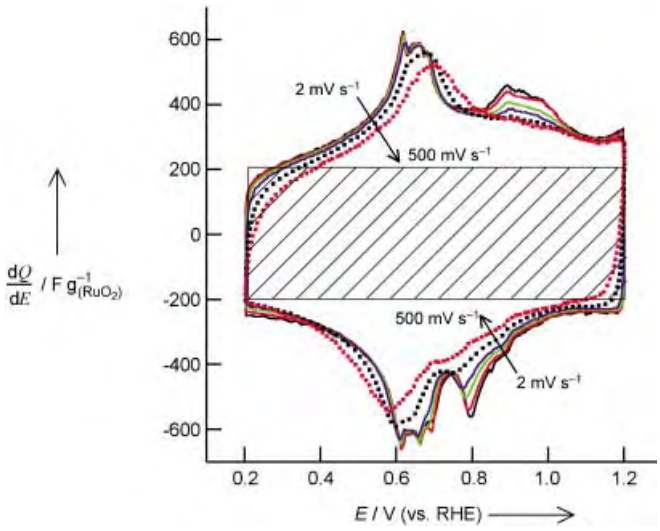


Figure 4. Steady-state cyclic voltammograms of layered ruthenic acid hydrate in 0.5 M H_2SO_4 (25 °C) at scan rates of 2 to 500 $mV\,s^{-1}$. The contribution from the (pseudo)electric double-layer capacitance is shown in the shaded region (dQ/dE = differential capacitance).

diffusion of the electrolyte (proton conductivity) into the bulk of the material.

The (pseudo)electric double-layer capacitance (shaded region in Figure 4) was independent of the sweep rate at approximately 200 $F\,g^{-1}_{(RuO_2)}$. By using a surface charge density of 80 $\mu C\,cm^{-2}$ as a measure for evaluation of the electrochemically active surface area,[18] this specific capacitance value gives an electrochemically active surface area of 250 $m^2\,g^{-1}$. This is much higher than the BET surface area of 57 $m^2\,g^{-1}$ determined by N_2 adsorption/desorption measurements. The difference is attributed to the fact that the BET surface area is a measurement of the outer surface area of anhydrous HRO, and does not include the hydrated interlayer surface area. Using the density of rutile-type RuO_2 ($\approx$7.1 $g\,cm^{-3}$), a specific surface area of 250 $m^2\,g^{-1}$ will yield a rectangular particle with a thickness of $\approx$0.6 nm, in good agreement with the observed thickness of ruthenic acid layers. The remarkably high specific capacitance can only be explained by assuming that the interlayer surface is utilizable for electrochemical charge storage. As shown in Figure 5 the capacitance loss after 10000 consecutive cycles was negligible, a fact that reveals the excellent electrochemical stability of HRO.

Cyclic voltammograms of the exfoliated HRO nanosheets are shown in Figure 6. The general electrochemical behavior of the exfoliated HRO nanosheets is comparable to that of the pristine HRO. However, the redox peaks are more well-defined for the exfoliated HRO nanosheets; that is, the contribution from the redox capacitance is more pronounced for the exfoliated nanosheets. This results in a significantly higher specific capacitance (658 and 601 $F\,g^{-1}_{(RuO_2)}$ at 2 and 50 $mV\,s^{-1}$, respectively) as shown in Figure 7. The (pseudo)-electric double-layer capacitance for both pristine HRO and exfoliated HRO nanosheets is $\approx$200 $F\,g^{-1}_{(RuO_2)}$, which illustrates that the electrochemically active surface area is the same (250 $m^2\,g^{-1}$) for both systems. The increase in the surface

 © 2003 Wiley-VCH Verlag GmbH & Co. KGaA, Weinheim

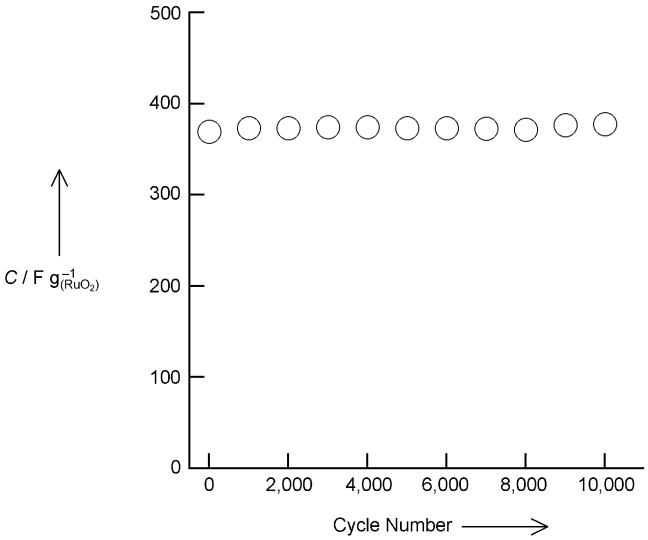


Figure 5. The specific capacitance of layered ruthenic acid hydrate in 0.5 M H_2SO_4 (25 °C) at scan rates of 50 mV s^{-1} as a function of the cycle number (C = specific capacitance).

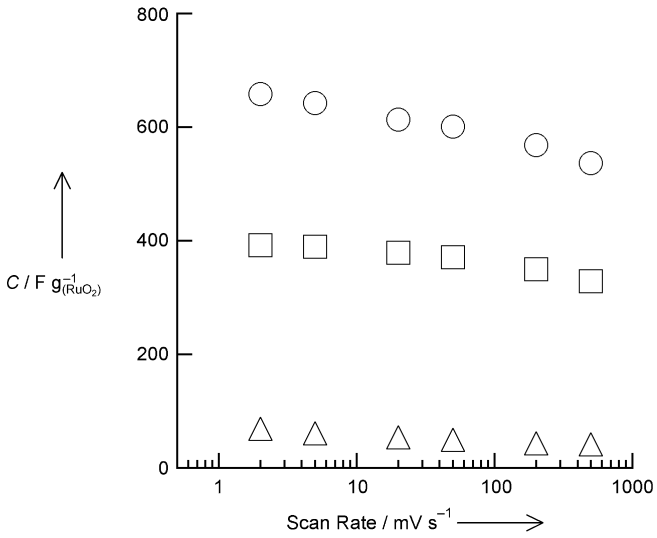


Figure 7. The specific capacitance as a function of the scan rate for rutile-type RuO_2 (△), layered ruthenic acid (□), and exfoliated ruthenic acid nanosheets (○) in 0.5 M H_2SO_4 at 25 °C.

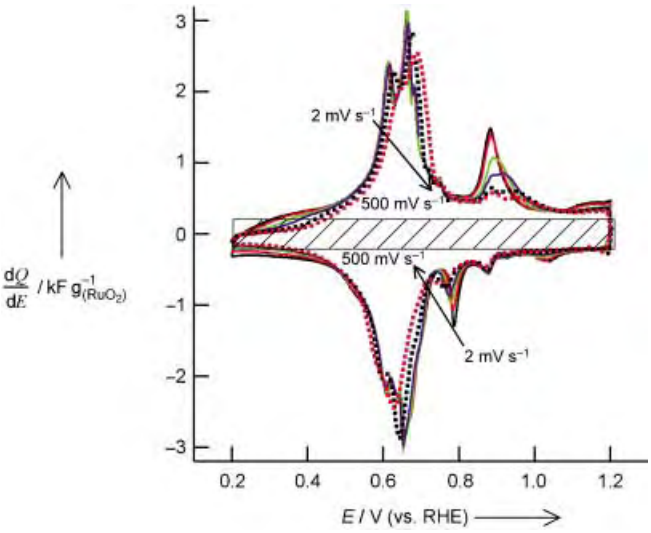


Figure 6. Steady-state cyclic voltammograms of exfoliated ruthenic acid nanosheets in 0.5 M H_2SO_4 (25 °C) at scan rates of 2 to 500 mV s^{-1}. The contribution from the (pseudo)electric double-layer capacitance is shown in the shaded region.

redox capacitance may be due to an increase in diffusion-limited capacitance owing to the more open framework of the exfoliated ruthenium oxide nanosheets compared to pristine HRO. The specific capacitance of the exfoliated HRO nanosheets is 10 times higher than nanocrystalline rutile-type RuO_2 (68 F $g^{-1}_{(RuO_2)}$ at 2 mV s^{-1}) with a similar BET surface area (52 $m^2 g^{-1}$).[19,20] The specific capacitance is comparable to that of sol–gel-derived or commercial amorphous ruthenium oxide hydrate (≈700 F g^{-1} at 2 mV s^{-1}).[6,7] The specific capacitance of HRO, exfoliated HRO nanosheets, and rutile-type RuO_2 decreases only slightly with increasing scan rate, as shown in Figure 7. The decreasing ratio is similar for the three systems, that is approximately 60–80% of the capacitance addressable at a scan rate of 2 mV s^{-1} can be achieved at 500 mV s^{-1}. Such observations indicate that the iR loss (voltage drop) due to inter- and inner-particle resistance of HRO is similar to rutile-type RuO_2. Thus it can be presumed that the electronic conductivity of HRO is similar to rutile-type RuO_2, and the electrochemical accessibility of the interlayer of HRO is comparable to the surface of rutile-type RuO_2.

In conclusion, we have demonstrated the synthesis of a mixed proton–electron conductor consisting of a crystalline ruthenium oxide layer interleaved with layers of water (Figure 8). The layered ruthenic acid is electrochemically stable, and has an extremely large electrochemically active surface area. The layered ruthenic acid has an expandable interlayer and can be delaminated into colloidal ruthenic acid nanosheets. The present material is a promising electrode material for electrochemical supercapacitors that can provide high energy density even at high-power specifications. From

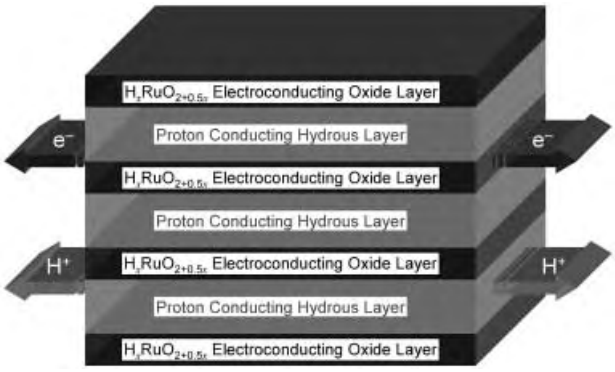


Figure 8. A schematic drawing of the concept of the mixed proton–electron conductivity of layered ruthenic acid.

 © 2003 Wiley-VCH Verlag GmbH & Co. KGaA, Weinheim

the viewpoint of materials chemistry, the present results should unearth a new class of mixed proton–electron conductors. The new layered ruthenium oxide hydrate adds a new dimension to the rapidly growing toolbox of layered compounds for novel soft-chemistry reactions.[21,22] The use of crystalline layered oxides will permit synthetic conditions that will furnish compositional and structural variety by traditional ceramic processing methods. Based on existing materials, one can postulate that partial substitution of Ru with transition metals such as Ti, V, Ir, etc. in the crystalline structure can be accomplished. Furthermore, the versatility of the oxide sheets to exfoliate into multilamellar to unilamellar nanosheets allows further flexibility for morphological control (thin films, "house-of-cards" structures, exfoliated nanosheets, etc.).[22,23]

Experimental Section

The layered potassium ruthenate was synthesized by calcination of a pelletized mixture of K_2CO_3 and RuO_2 (5:8 molar ratio) at 850 °C for 12 h under a flow of Ar. The product was ground into a fine powder then washed with copious amounts of water and dried at 120 °C. The layered ruthenic acid was prepared by acid treatment of the potassium ruthenate at 60 °C for 48 h, followed by washing with copious amounts of water and drying at 120 °C.

An ethylammonium-layered ruthenic acid intercalation compound was prepared by reaction of the layered ruthenic acid with an aqueous solution (50 %) of ethylamine at room temperature for 24 h. The solid product was centrifugally collected (15000 rpm), washed with acetone, and vacuum dried. A tetrabutylammonium-layered ruthenic acid intercalation compound was prepared by reaction of the ethylammonium–ruthenic acid intercalation compound with an aqueous solution (10 %) of tetrabutylammonium hydroxide at room temperature for 50 h. The solid product was centrifugally collected (15000 rpm). The solid product (the tetrabutylammonium-layered ruthenic acid intercalation compound) was then dispersed in distilled water and subjected to ultrasonification for 15 min. The supernatant containing exfoliated HRO nanosheets and other relatively large particles and agglomerates were centrifugally separated at 2000 rpm. The supernatant was then used for further investigation.

Electrochemical measurements were conducted in 0.5 M H_2SO_4 at 25 °C with a half-cell set up. A beaker-type electrochemical cell equipped with the working electrode, a platinum mesh counter electrode, and a Ag/AgCl reference electrode was used for electrochemical measurements. A Luggin capillary faced the working electrode at a distance of 2 mm. The working electrode was prepared by the thin-film electrode method.[24] For the characterization of pristine (non-exfoliated) HRO particles, HRO (20 mg) was dispersed in distilled water (10 mL) and then subjected to ultrasonification for 30 min. Then, while stirring, 20 μL of the HRO dispersion was extracted using a micropipette and dropped onto a mirror-polished glassy carbon rod (5-mm diameter). After drying the HRO-modified glassy carbon rod at 60 °C, 20 μL of a 1 wt % nafion ionomer solution was dropped onto the rod and dried at 60 °C to affix the active material onto the glassy carbon surface. For the exfoliated HRO nanosheets, 20 μL was extracted from a 1:10 diluted supernatant containing exfoliated HRO nanosheets (1.8 mg of RuO_2 per 10 mL of distilled water) and dropped onto a mirror-polished glassy carbon rod. The tetrabutylammonium intercalant should exchange with protons (deintercalate) in the acidic electrolyte. Cyclic voltammetry was conducted in a 0.5 M H_2SO_4 electrolyte with scan rates between 2 and 500 mV s^{-1} at 25 °C. The voltammagrams were recorded after 500 break-in cycles at 50 mV s^{-1}. The specific capacitance was determined by integration of the enclosed area of the anodic and cathodic curves in the cyclic voltammagrams between 0.20–1.20 V (versus a reversible hydrogen electrode (RHE)). The average of the anodic and cathodic charges was used to calculate the specific capacitance, which are reported in units of farads per unit mass of RuO_2 ($F g^{-1}_{(RuO_2)}$) to allow uncomplicated comparison between different systems.

Received: April 17, 2003 [Z51691]

Keywords: electrochemistry · intercalations · layered compounds · mixed conductors · supercapacitors

[1] H. Iwahara, *Proceedings 17th Risø International Symposium of Material Science* (Eds.: F. W. Poulsen, N. Bonanos, S. Linderoth, M. Mogenson, B. Zachau-Christiansen), Risø National Laboratories, Roskilde, Denmark, **1996**, p. 13.
[2] H. L. Tuller, *J. Phys. Chem. Solids* **1994**, *55*, 1393.
[3] K. D. Kreuer, *Chem. Mater.* **1996**, *8*, 610.
[4] Ph. Colomban, *Proton Conductors*, Cambridge Universitry Press, Cambridge, **1992**.
[5] J. W. Long, R. M. Stroud, K. E. Swider-Lyons, D. R. Rolison, *J. Phys. Chem. B* **2000**, *104*, 9772.
[6] J. P. Zheng, T. R. Jow, *J. Electrochem. Soc.* **1995**, *142*, L6.
[7] J. P. Zheng, P. J. Cygan, T. R. Jow, *J. Electrochem. Soc.* **1995**, *142*, 2699.
[8] B. Conway, *Electrochemical Supercapacitors*, Kluwer Academic/Plenum Publishers, New York, **1999**.
[9] S. Trasatti in *Electrodes of Conducting Metal Oxides*, (Ed.: S. Trasatti), Elsevier, Amsterdam, **1980**, p. 301 – 358.
[10] S. Trasatti, *Electrochim. Acta* **1991**, *36*, 225.
[11] R. Dat, D. J. Lichtenwalner, O. Auciello, A. I. Kingon, *Appl. Phys. Lett.* **1994**, *64*, 2673.
[12] H. Over, Y. D. Kim, A. P. Seitsonen, S. Wendt, Lundgren, M. Schmid, P. Varga, A. Morgante, G. Ertl, *Science* **2000**, *287*, 1474.
[13] L. Zang, H. Kisch, *Angew. Chem.* **2000**, *112*, 4075; *Angew. Chem. Int. Ed.* **2000**, *39*, 3921.
[14] Y. Takasu, Y. Murakami, *Electrochim. Acta* **2000**, *45*, 4135.
[15] B. Raveau, *Rev. Inorg. Chem.* **1987**, *9*, 37.
[16] T. Sasaki, M. Watanabe, H. Hashizume, H. Yamada, H. Nakazawa, *J. Am. Chem. Soc.* **1996**, *118*, 8329.
[17] W. Sugimoto, O. Terabayashi, Y. Murakami, Y. Takasu, *J. Mater. Chem.* **2002**, *12*, 3814.
[18] P. Siviglia, A. Daghetti, S. Trasatti, *Colloids Surf.* **1983**, *7*, 15.
[19] W. Sugimoto, T. Shibutani, Y. Murakami, Y. Takasu, *Electrochem. Solid-State Lett.* **2002**, *5*, A170.
[20] W. Sugimoto, T. Kizaki, K. Yokoshima, Y. Murakami, Y. Takasu, unpublished results.
[21] W. Sugimoto, M. Shirata, Y. Sugahara, K. Kuroda, *J. Am. Chem. Soc.* **1999**, *121*, 11601.
[22] R. E. Schaak, T. E. Mallouk, *Chem. Mater.* **2002**, *14*, 1455.
[23] C. N. R. Rao, J. Gopalakrishnan, *New Directions in Solid State Chemistry*, 2nd ed., Cambridge University Press, Cambridge, **1997**.
[24] T. J. Schmidt, H. A. Gasteiger, G. D. Stäb, P. M. Urban, D. M. Kolb, R. J. Behm, *J. Electrochem. Soc.* **1998**, *145*, 2354.

 © 2003 Wiley-VCH Verlag GmbH & Co. KGaA, Weinheim

Molecular Machines

A [2]Pseudorotaxane-Based Molecular Machine: Reversible Formation of a Molecular Loop Driven by Electrochemical and Photochemical Stimuli**

*Woo Sung Jeon, Albina Y. Ziganshina, Jae Wook Lee, Young Ho Ko, Jin-Koo Kang, Chongmok Lee, and Kimoon Kim**

Artificial molecular machines,[1] which can be defined as assemblies of a distinct number of molecular components designed to perform machinelike motions in response to appropriate external stimuli, such as light, electrons, or pH changes, are of great interest because of their potential applications in the creation of nanometer-scale molecular devices.[2] Mechanically interlocked molecules such as catenanes and rotaxanes have received a great deal of attention in the design of molecular machines because of their ability to switch between two or more states as a result of induced relative movement of their noncovalently interacting components on application of external stimuli. A number of prototype molecular machines based on rotaxanes,[3] pseudorotaxanes,[4] and catenanes,[5] which exploit shuttling, threading/dethreading, and circumrotational motions, respectively, have been reported over the past decade.

Cucurbituril (or cucurbit[6]uril),[6] a macrocycle comprised six glycoluril units, has been employed in the construction of a wide variety of interlocked molecules[7] and, more recently, rotaxane-based molecular machines and switches as well.[8] The recent discovery of cucurbituril homologues[9] containing a different number of glycoluril units has further widened the scope of cucurbituril chemistry.[10,11] In particular, cucurbit[8]uril (CB[8]) with a cavity comparable to that of γ-cyclodextrin can include two identical guest molecules to form a 1:2 complex,[9] or two different guest molecules to form a 1:1:1 complex.[10a] Furthermore, the guest-binding stoichiometry of CB[8] can be reversibly controlled by the redox chemistry of the guest.[10e] For example, CB[8] and methylviologen (MV^{2+}) form a 1:1 inclusion complex which can convert completely and reversibly into the 2:1 inclusion complex $(MV^{+\bullet})_2 \subset CB[8]$ upon one-electron reduction of the guest. The formation of the stable methylviologen radical cation dimer ($(MV^{+\bullet})_2$) in the cavity of CB[8] appears to be the driving force for the redox-triggered transformation. This interesting observation prompted us to design a new type of electrochemically controllable molecular machine. Here we report a [2]pseudorotaxane-based molecular machine that can reversibly form a molecular loop in response to electrochemical as well as photochemical stimuli (Figure 1).

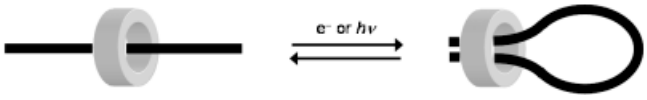
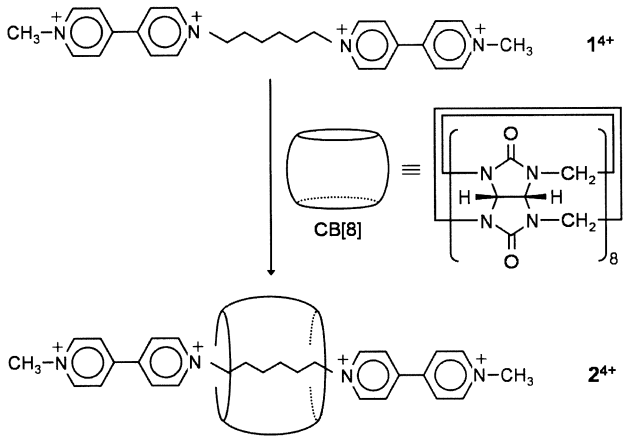


Figure 1. Novel [2]pseudorotaxane-based molecular machine that can reversibly form a molecular loop in response to external stimuli.

The hexamethylene-bridged bisviologen $\mathbf{1}^{4+}$ and CB[8] readily form a stable 1:1 inclusion complex or [2]pseudorotaxane ($\mathbf{2}^{4+}$; Scheme 1) in water which has been characterized by elemental analysis and various spectroscopic methods. The ^{1}H NMR spectrum and the parent ion peak at



Scheme 1. Synthesis of [2]pseudorotaxane $\mathbf{2}^{4+}$.

$m/z = 1754$ in the MALDI-TOF mass spectrum of $\mathbf{2}^{4+}$ confirmed the formation of a stable 1:1 host–guest complex. The formation constant of $\mathbf{2}^{4+}$ is estimated to be $2.3 \times 10^5\,\text{M}^{-1}$ from UV/Vis spectroscopic titration experiments. The large up-field shift of the aliphatic proton signals in the NMR spectrum of $\mathbf{2}^{4+}$ indicates that CB[8] mainly resides on the hexamethylene unit (see Supporting Information). The major

[*] Prof. Dr. K. Kim, W. S. Jeon, Dr. A. Y. Ziganshina, Dr. J. W. Lee,[+] Dr. Y. H. Ko, J.-K. Kang
National Creative Research Initiative Center for Smart Supramolecules and Department of Chemistry
Division of Molecular and Life Sciences
Pohang University of Science and Technology
San 31 Hyojadong, Pohang 790-784 (Republic of Korea)
Fax: (+82) 54-279-8129
E-mail: kkim@postech.ac.kr
Prof. Dr. C. Lee
Department of Chemistry
Ewha Womans Univeristy
11-1 Daehyundong, Seoul 120-750 (Republic of Korea)
[+] Current address: Department of Chemistry
Dong-A University
840 Hadandong, Busan 604–714 (Republic of Korea)

[**] We gratefully acknowledge the Creative Research Initiative Program and the International R&D Cooperation Program of the Korean Ministry of Science and Technology for support of this work and the Brain Korea 21 Program of the Korean Ministry of Education for graduate studentships (to W.S.J. and J.-K.K.). C.L. also thanks the Korea Science and Engineering Foundation for support (grant no. R01-2000-00050). We thank Dr. S. Samal for his help in the preparation of the manuscript.

Supporting information for this article is available on the WWW under http://www.angewandte.org or from the author.

 DOI: 10.1002/anie.200351925 © 2003 Wiley-VCH Verlag GmbH & Co. KGaA, Weinheim

driving force for the stable [2]pseudorotaxane formation appears to be the charge–dipole interaction between the pyridinium nitrogen atoms of $\mathbf{1}^{4+}$ and the portal oxygen atoms of CB[8] as well as the hydrophobic interaction between the aliphatic chain of $\mathbf{1}^{4+}$ and the inner cavity of CB[8].

The machinelike behavior of $\mathbf{2}^{4+}$ has been investigated by cyclic voltammetry. Typical cyclic voltammograms of $\mathbf{1}^{4+}$ and $\mathbf{2}^{4+}$ are shown in Figure 2. As expected, the bisviologen thread

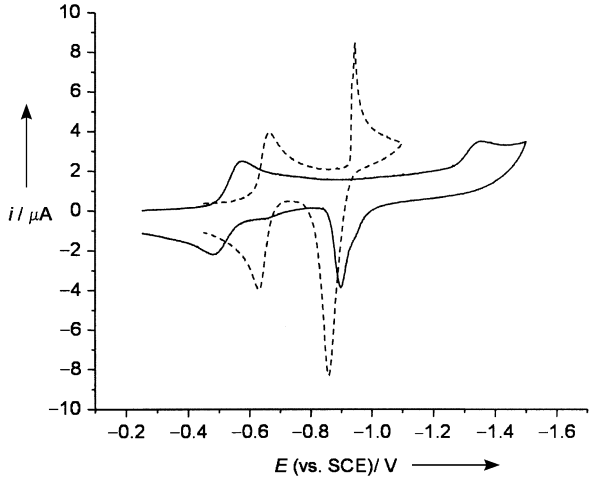
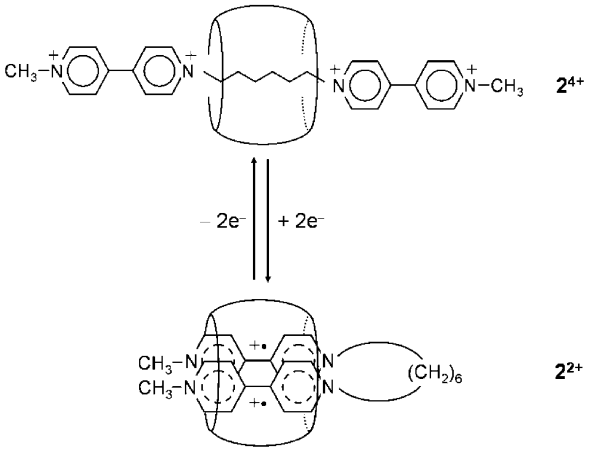


Figure 2. Cyclic voltammograms of $\mathbf{1}^{4+}$ (0.25 mM, dashed line) and $\mathbf{2}^{4+}$ (0.25 mM, solid line) in 0.1 M phosphate buffer solution (pH 7.0). Scan rate = 25 $mV s^{-1}$.

$\mathbf{1}^{4+}$ undergoes two consecutive two-electron reduction processes, with a sharp second wave that indicates strong adsorption of the fully reduced species (**1**) on the electrode surface. Compared to $\mathbf{1}^{4+}$, however, $\mathbf{2}^{4+}$ exhibits a large positive shift of the first reduction peak and a very large negative shift of the second reduction peak. This cyclic voltammetric behavior is quite similar to that of the 1:1 inclusion complex formed between MV^{2+} and CB[8],[10e] where the similar potential shifts for the reduction process have been attributed to facile formation of the stable methylviologen radical cation dimer $(MV^{+\bullet})_2$ inside CB[8] after one-electron reduction of MV^{2+}. Thus, the cyclic voltammetric behavior of $\mathbf{2}^{4+}$ suggests that the two-electron reduction of $\mathbf{2}^{4+}$ results in the generation of a species containing two terminal viologen radical cation units, which then undergo a rapid intramolecular pairing process inside CB[8] to form the stable inclusion species $\mathbf{2}^{2+}$—a molecular loop (Scheme 2).[12] This conjecture has been supported by a spectroelectrochemical study: the absorption spectrum (Figure 3) of the species $\mathbf{2}^{2+}$ generated by the two electron reduction of $\mathbf{2}^{4+}$ (applied potential: −0.8 V versus the saturated calomel electrode (SCE)) is essentially identical to that of $(MV^{+\bullet})_2 \subset$CB[8].[10e] A two-electron oxidation of the intramolecular viologen radical cation pair in CB[8] ($\mathbf{2}^{2+}$) regenerates the [2]pseudorotaxane $\mathbf{2}^{4+}$ with the initial linear structure. Taken together, these studies support a machinelike behavior of **2** in which an electrochemically triggered reversible folding/unfolding motion of the thread occurs. This operation mechanism is unprecedented in molecular machines based on mechanically interlocked systems.[13]



Scheme 2. Electrochemically triggered interconversion between $\mathbf{2}^{4+}$ with a linear structure and $\mathbf{2}^{2+}$ with a loop structure.

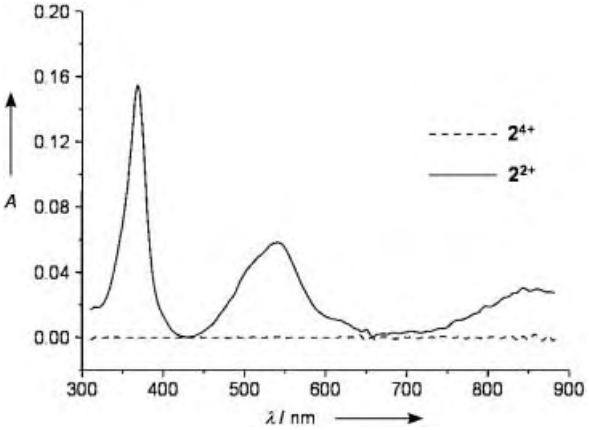


Figure 3. Absorption spectra of $\mathbf{2}^{4+}$ and $\mathbf{2}^{2+}$; the latter was generated by two-electron reduction of the former (applied potential, −0.8 V versus SCE).

Figure 4 shows the energy-minimized structures of $\mathbf{2}^{4+}$ and $\mathbf{2}^{2+}$ obtained by a semiempirical calculation,[14] which are in accord with the observation described above. Most importantly, the supermolecule undergoes a dramatic change not only in shape but also in size in response to electrochemical stimuli: the molecular dimension of $\mathbf{2}^{4+}$ with a linear structure is approximately 28 × 18 Å whereas that of $\mathbf{2}^{2+}$ with a loop

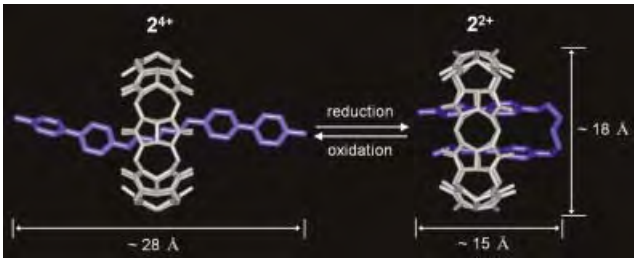
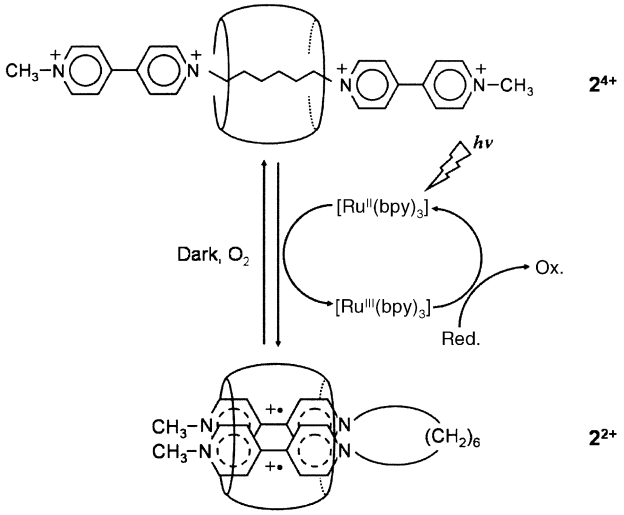


Figure 4. Energy-minimized structures of $\mathbf{2}^{4+}$ and $\mathbf{2}^{2+}$ obtained by a semiempirical calculation.

 © 2003 Wiley-VCH Verlag GmbH & Co. KGaA, Weinheim

structure is only about 15×18 Å. The hydrodynamic volumes of $\mathbf{2}^{4+}$ and $\mathbf{2}^{2+}$ measured by diffusion NMR (DOSY) studies[15] (see Supporting Information) are 1.7 and 1.4 times, respectively, as large as that of CB[8],[16] and consistent with the computational results. Such a large, reversible structural change triggered by electrochemical stimuli is rare in supramolecular systems.[13]

The [2]pseudorotaxane $\mathbf{2}^{4+}$ also behaves as a light-driven molecular machine. Irradiation of an aqueous solution of $\mathbf{2}^{4+}$ with a visible light ($\lambda > 350$ nm) in the presence of $[Ru(bpy)_3]^{2+}$ (bpy = 2,2′-bipyridine), which is capable of a photoinduced transfer of electrons to viologen,[17] and triethanolamine (sacrificial reductant) causes noticeable spectral changes which indicate that the terminal viologen units of $\mathbf{2}^{4+}$ are reduced. After 5 h, the absorption spectrum of the solution is almost the same as that observed in the spectroelectrochemical experiment described above: the characteristic absorption bands of the dimeric viologen radical cation are mainly observed (see Supporting Information). Furthermore, the absorbance at 368 nm increases linearly with increasing concentration of $\mathbf{2}^{4+}$ in the range from 7.5×10^{-6} to 1.0×10^{-3} M (see Supporting Information). This linear dependence of the absorbance on concentration, along with the above diffusion NMR results, suggests that the spectral change is predominantly a result of intramolecular pairing of the terminal viologen radical cation units inside CB[8] rather than intermolecular dimerization.[18] Thus, $\mathbf{2}^{4+}$ changes from a linear to a loop structure upon photochemical reduction (Scheme 3). When the irradiation is stopped and oxygen is allowed to enter the irradiated solution, the spectral changes are reversed and the initial absorption spectrum is restored, thus indicating the regeneration of $\mathbf{2}^{4+}$ with the linear structure.



Scheme 3. Photochemically driven interconversion between $\mathbf{2}^{4+}$ with a linear structure and $\mathbf{2}^{2+}$ with a loop structure.

In summary, we have designed and constructed a novel [2]pseudorotaxane-based molecular machine in which the folding and unfolding of the thread can be reversibly controlled by electrochemical and photochemical stimuli. The key feature of the machinelike behavior is the reversible formation of a molecular loop by intramolecular pairing of the terminal viologen radical cation units inside CB[8] upon reduction. The large, reversible change in its size as well as shape on application of external stimuli may provide an insight into the designing of molecular actuators with useful applications.

Experimental Section

2: The tetrabromide salt of *N*′,*N*″-(hexylene)bis(1-methyl-4,4′-bipyridinium) ($\mathbf{1}^{4+}\cdot 4Br^-$) was prepared by the literature procedure[19] with a minor modification. A mixture of $CB[8]\cdot H_2SO_4\cdot 16H_2O$ (34 mg, 20 μmol) and $\mathbf{1}^{4+}\cdot 4Br^-$ (15 mg, 18 μmol) in water (20 mL) was stirred at 50 °C overnight. After the undissolved solid had been filtered off, the volume of the filtrate was reduced to 2 mL under a reduced pressure. It was then allowed to stand in a refrigerator overnight to produce a yellow precipitate which was filtered, washed, and dried to afford $\mathbf{2}^{4+}\cdot 4Br^-$ (38 mg, 80 %). ^{1}H NMR (500 MHz, D_2O): $\delta = 0.87$ (m, 4H), 1.46 (m, 4H), 4.26 (d, $J = 15$ Hz, 16H), 4.53 (s, 6H), 5.56 (s, 16H), 5.80 (d, $J = 15$ Hz, 16H), 8.52 (m, 4H), 8.66 (m, 4H), 8.82 (d, $J = 6$ Hz, 4H), 9.09 ppm (d, $J = 6$ Hz, 4H); MALDI-MS: 1754 [M^+]; elemental analysis calcd (%) for $(C_{28}H_{34}N_4^{4+})\cdot 4Br^-\subset(C_{48}H_{48}N_{32}O_{16})\cdot H_2SO_4\cdot 25H_2O$: C 34.79, H 5.15, N 19.22; found: C 34.74, H 5.42, N 19.45.

Received: May 19, 2003
Revised: June 30, 2003 [Z51925]

Keywords: electrochemistry · molecular devices · photochemistry · rotaxanes · supramolecular chemistry

[1] a) V. Balzani, A. Credi, F. M. Raymo, J. F. Stoddart, *Angew. Chem.* **2000**, *112*, 3484; *Angew. Chem. Int. Ed.* **2000**, *39*, 3348; b) molecular machines special issue: *Acc. Chem. Res.* **2001**, *34*, 409–522.

[2] Electronic devices based on molecular machines have been reported, see a) C. P. Collier, E. W. Wong, M. Belohradský, F. M. Raymo, J. F. Stoddart, P. J. Kuekes, R. S. Williams, J. R. Heath, *Science* **1999**, *285*, 391; b) C. P. Collier, G. Mattersteig, E. W. Wong, Y. Luo, K. Beverly, J. Sapaio, F. M. Raymo, J. F. Stoddart, J. R. Heath, *Science* **2000**, *289*, 1172.

[3] a) R. A. Bissell, E. Córdova, A. E. Kaifer, J. F. Stoddart, *Nature* **1994**, *369*, 133; b) J.-P. Collin, P. Gaviña, J.-P. Sauvage, *New J. Chem.* **1996**, *20*, 25; c) P.-L. Anelli, M. Asakawa, P. R. Ashton, R. A. Bissell, G. Clavier, R. Górski, A. E. Kaifer, S. J. Langford, G. Mattersteig, S. Menzer, D. Philp, A. M. Z. Slawin, N. Spencer, J. F. Stoddart, M. S. Tolley, D. J. Williams, *Chem. Eur. J.* **1997**, *3*, 1113; d) H. Murakami, A. Kawabuchi, K. Kotoo, M. Kinitake, N. Nakashima, *J. Am. Chem. Soc.* **1997**, *119*, 7605; e) N. Armaroli, V. Balzani, J.-P. Collin, P. Gaviña, J.-P. Sauvage, B. Ventura, *J. Am. Chem. Soc.* **1999**, *121*, 4397; f) D. A. Leigh, A. Troisi, F. Zerbetto, *Angew. Chem.* **2000**, *112*, 358; *Angew. Chem. Int. Ed.* **2000**, *39*, 350; g) Y. Kawaguchi, A. Harada, *Org. Lett.* **2000**, *2*, 1353; h) A. M. Brouwer, C. Frochot, F. G. Gatti, D. A. Leigh, L. Mottier, F. Paolucci, S. Roffia, G. W. H. Wurpel, *Science* **2001**, *291*, 2124.

[4] a) R. Ballardini, V. Balzani, M. T. Gandolfi, L. Prodi, M. Venturi, D. Philp, H. G. Ricketts, J. F. Stoddart, *Angew. Chem.* **1993**, *105*, 1362; *Angew. Chem. Int. Ed. Engl.* **1993**, *32*, 1301; b) P. R. Ashton, R. Ballardini, V. Balzani, E. C. Constable, A. Credi, O. Kocian, S. J. Langford, J. A. Preece, L. Prodi, E. R. Schofield, N. Spencer, J. F. Stoddart, S. Wenger, *Chem. Eur. J.*

 © 2003 Wiley-VCH Verlag GmbH & Co. KGaA, Weinheim

1998, *4*, 2413; c) E. Ishow, A. Credi, V. Balzani, F. Spadola, L. Mandolini, *Chem. Eur. J.* **1999**, *5*, 984.

[5] a) P. R. Ashton, T. T. Goodnow, A. E. Kaifer, M. V. Reddington, A. M. Z. Slawin, N. Spencer, J. F. Stoddart, C. Vincent, D. J. Williams, *Angew. Chem.* **1989**, *101*, 1402; *Angew. Chem. Int. Ed. Engl.* **1989**, *28*, 1396; b) A. Livoreil, C. O. Dietrich-Buchecker, J.-P. Sauvage, *J. Am. Chem. Soc.* **1994**, *116*, 9399; c) D. J. Cárdenas, A. Livoreil, J.-P. Sauvage, *J. Am. Chem. Soc.* **1996**, *118*, 11980; d) A. Andrievsky, F. Ahuis, J. L. Sessler, F. Vögtle, D. Gudat, M. Moini, *J. Am. Chem. Soc.* **1998**, *120*, 9712; e) J. O. Jeppesen, J. Perkins, J. Becher, J. F. Stoddart, *Angew. Chem.* **2001**, *113*, 1256; *Angew. Chem. Int. Ed.* **2001**, *40*, 1216.

[6] For reviews on cucurbituril, see a) W. L. Mock in *Comprehensive Supramolecular Chemistry, Vol. 2* (Ed.: F. Vögtle), Pergamon, Oxford, **1996**, p. 477; b) P. Cintas, *J. Inclusion Phenom. Mol. Recognit. Chem.* **1994**, *17*, 205.

[7] a) K. Kim, *Chem. Soc. Rev.* **2002**, *31*, 96; b) D. Whang, Y.-M. Jeon, J. Heo, K. Kim, *J. Am. Chem. Soc.* **1996**, *118*, 11333; c) D. Whang, K. Kim, *J. Am. Chem. Soc.* **1997**, *119*, 451; d) D. Whang, K.-M. Park, J. Heo, K. Kim, *J. Am. Chem. Soc.* **1998**, *120*, 4899; e) S.-G. Roh, K.-M. Park, G.-J. Park, S. Sakamoto, K. Yamaguchi, K. Kim, *Angew. Chem.* **1999**, *111*, 672; *Angew. Chem. Int. Ed.* **1999**, *38*, 638; f) E. Lee, J. Heo, K. Kim, *Angew. Chem.* **2000**, *112*, 2811; *Angew. Chem. Int. Ed.* **2000**, *39*, 2699; g) E. Lee, J. Kim, J. Heo, D. Whang, K. Kim, *Angew. Chem.* **2001**, *113*, 413; *Angew. Chem. Int. Ed.* **2001**, *40*, 399; h) J. W. Lee, Y. H. Ko, S.-H. Park, K. Yamaguchi, K. Kim, *Angew. Chem.* **2001**, *113*, 768; *Angew. Chem. Int. Ed.* **2001**, *40*, 746; i) K.-M. Park, D. Whang, E. Lee, J. Heo, K. Kim, *Chem. Eur. J.* **2002**, *8*, 498; j) K.-M. Park, S.-Y. Kim, J. Heo, D. Whang, S. Sakamoto, K. Yamaguchi, K. Kim, *J. Am. Chem. Soc.* **2002**, *124*, 2140; k) S. W. Choi, J. W. Lee, Y. H. Ko, K. Kim, *Macromolecules* **2002**, *35*, 3526; l) Y. Tan, S. W. Choi, J. W. Lee, Y. H. Ko, K. Kim, *Macromolecules* **2002**, *35*, 7161; m) K.-M. Park, S.-G. Roh, E. Lee, J. Kim, H.-J. Kim, J. W. Lee, K. Kim, *Supramol. Chem.* **2002**, *14*, 153; n) Y.-b. Lim, T. Kim, J. W. Lee, S. Kim, H.-J. Kim, K. Kim, J. Park, *Bioconjugate Chem.* **2002**, *13*, 1181.

[8] a) W. L. Mock, J. Pierpont, *J. Chem. Soc. Chem. Commun.* **1990**, 1509; b) S. I. Jun, J. W. Lee, S. Sakamoto, K. Yamaguchi, K. Kim, *Tetrahedron Lett.* **2000**, *41*, 471; c) J. W. Lee, K. Kim, K. Kim, *Chem. Commun.* **2001**, 1042; d) J. W. Lee, S. W. Choi, Y. H. Ko, S.-Y. Kim, K. Kim, *Bull. Korean Chem. Soc.* **2002**, *23*, 1347; e) K. Kim, W. S. Jeon, J.-K. Kang, J. W. Lee, S. Y. Jon, T. Kim, K. Kim, *Angew. Chem.* **2003**, *115*, 2395; *Angew. Chem. Int. Ed.* **2003**, *42*, 2293.

[9] a) J. Kim, I.-S. Jung, S.-Y. Kim, E. Lee, J.-K. Kang, S. Sakamoto, K. Yamaguchi, K. Kim, *J. Am. Chem. Soc.* **2000**, *122*, 540; b) J. W. Lee, S. Samal, N. Selvapalam, H.-J. Kim, K. Kim, *Acc. Chem. Res.* in press.

[10] a) H.-J. Kim, J. Heo, W. S. Jeon, E. Lee, J. Kim, S. Sakamoto, K. Yamaguchi, K. Kim, *Angew. Chem.* **2001**, *113*, 1574; *Angew. Chem. Int. Ed.* **2001**, *40*, 1526; b) S.-Y. Kim, I.-S. Jung, E. Lee, J. Kim, S. Sakamoto, K. Yamaguchi, K. Kim, *Angew. Chem.* **2001**, *113*, 2177; *Angew. Chem. Int. Ed.* **2001**, *40*, 2119; c) S. Y. Jon, Y. H. Ko, S. H. Park, H.-J. Kim, K. Kim, *Chem. Commun.* **2001**, 1938; d) H.-J. Kim, W. S. Jeon, Y. H. Ko, K. Kim, *Proc. Natl. Acad. Sci. USA* **2002**, *99*, 5007; e) W. S. Jeon, H.-J. Kim, C. Lee, K. Kim, *Chem. Commun.* **2002**, 1828; f) J. W. Lee, K. Kim, S. W. Choi, Y. H. Ko, S. Sakamoto, K. Yamaguchi, K. Kim, *Chem. Commun.* **2002**, 2692; g) Y. J. Jeon, P. K. Bharadwaj, S. W. Choi, J. W. Lee, K. Kim, *Angew. Chem.* **2002**, *114*, 4654; *Angew. Chem. Int. Ed.* **2002**, *41*, 4474.

[11] a) W. Ong, M. Gómez-Kaifer, A. E. Kaifer, *Org. Lett.* **2002**, *4*, 1791; b) A. I. Day, R. J. Blanch, A. P. Arnold, S. Lorenzo, G. R. Lewis, I. Dance, *Angew. Chem.* **2002**, *114*, 285; *Angew. Chem. Int. Ed.* **2002**, *41*, 275; c) R. J. Blanch, A. J. Sleeman, T. J. White, A. P. Arnold, A. I. Day, *Nano Lett.* **2002**, *2*, 147.

[12] In the absence of CB[8], the two-electron reduction of the "thread" ($\mathbf{1}^{4+}$) generates the bis(radical cation) species which exists as a complicated mixture of a monomeric species with a linear structure, a monomeric species with a folded structure derived from intramolecular pairing of the terminal viologen radical cation units, and dimeric (and/or oligomeric) species produced by intermolecular pairing as judged by a spectroelectrochemical study.

[13] Controlled threading-dethreading in self-complexing systems, which may be viewed as a folding/unfolding motion, has been reported, see a) P. R. Ashton, R. Ballardini, V. Balzani, S. E. Boyd, A. Credi, M. T. Gandolfi, M. Gómez-López, S. Iqbal, D. Philp, J. A. Preece, L. Prodi, H. G. Ricketts, J. F. Stoddart, M. S. Tolly, M. Venturi, A. J. P. White, D. J. Whiliams, *Chem. Eur. J.* **1997**, *3*, 152; b) L. Fabbrizzi, M. Licchelli, P. Pallavicini, L. Parodi, *Angew. Chem.* **1998**, *110*, 838; *Angew. Chem. Int. Ed.* **1998**, *37*, 800; c) V. Balzani, P. Ceroni, A. Credi, M. Gómez-López, C. Hamers, J. F. Stoddart, R. Wolf, *New J. Chem.* **2001**, *25*, 25.

[14] Semiempirical AM1 calculations were carried out by using GAMESS-USA: M. W. Schmidt, K. K. Baldridge, J. A. Boatz, S. T. Elbert, M. S. Gordon, J. H. Jensen, S. Koseki, N. Matsunaga, K. A. Nguyen, S. J. Su, T. L. Windus, M. Dupuis, J. A. Montgomery, *J. Comput. Chem.* **1993**, *14*, 1347.

[15] C. S. Johnson, Jr., *Prog. Nucl. Magn. Reson. Spectrosc.* **1999**, *34*, 203.

[16] The hydrodynamic volume of $\mathbf{2}^{2+}$ is almost the same as that of an intramolecular charge-transfer complex formed inside CB[8], which has a similar loop structure.[10f]

[17] a) A. Juris, V. Balzani, F. Barigelletti, S. Campagna, P. Belser, A. von Zelewsky, *Coord. Chem. Rev.* **1988**, *84*, 85; b) V. Balzani, A. Juris, M. Venturi, S. Campagna, S. Serroni, *Chem. Rev.* **1996**, *96*, 759; c) P. R. Ashton, R. Ballardini, V. Balzani, A. Credi, K. R. Dress, E. Ishow, C. J. Kleverlaan, O. Kocian, J. A. Preece, N. Spencer, J. F. Stoddart, M. Venturi, S. Wenger, *Chem. Eur. J.* **2000**, *6*, 3558.

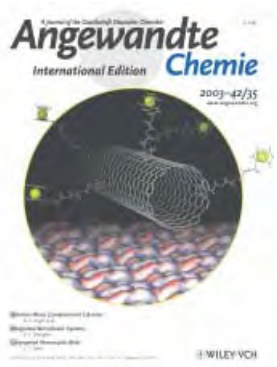
[18] The formation of intermolecular violgen radical cation dimers such as a 2:2 complex with a face-to-face dimer structure cannot be ruled out completely, but the decrease in the hydrodynamic volume of $\mathbf{2}^{4+}$ revealed by diffusion NMR studies upon two-electron reduction and the linear dependence of the absorbance on concentration over two orders of magnitude favors the intramolecular pairing of the terminal viologen radical cation units within CB[8] leading to the loop structure.

[19] a) M. Furue, S.-I. Nozakura, *Chem. Lett.* **1980**, 821; b) S. K. Lee, S. Y. Shin, S. Lee, C. Lee, J. W. Park, *J. Chem. Soc. Perkin Trans. 2* **2001**, 1983.

 © 2003 Wiley-VCH Verlag GmbH & Co. KGaA, Weinheim

Cover Picture

Dirk M. Guldi,* Massimo Marcaccio, Demis Paolucci, Francesco Paolucci,* Nikos Tagmatarchis, Dimitrios Tasis, Ester Vázquez, and Maurizio Prato*



Carbon Nanotubes are currently a subject of particular interest in materials chemistry. In the Communication by D. M. Guldi, F. Paolucci, M. Prato, and co-workers on page 4206 ff., the preparation of a single-wall nanotube–ferrocene (SWNT–Fc) nanohybrid is described. Photoinduced electron transfer gives rise to a long-lived charge-separated state ($SWNT^{\bullet-}$–$Fc^{\bullet+}$); the radical anionic form of the nanotube has been detected by laser flash photolysis.

Contents

Angewandte EarlyView

The following articles are available online (in Wiley InterScience). You can find them at www.angewandte.org, under Full Text, Early View.

G. Höfner, K. T. Wanner:*
Competitive Binding Assays Made Easy with a Native Marker and Mass Spectrometric Quantification
DOI: 10.1002/anie.200351806
Published online: September 1, 2003

D. G. Shchukin, G. B. Sukhorukov, H. Möhwald:*
Smart Inorganic/Organic Nanocomposite Hollow Microcapsules
DOI: 10.1002/anie.200352068
Published online: September 1, 2003

S. Ahlert, W. Klein, O. Jepsen, O. Gunnarsson, O. K. Andersen, M. Jansen:*
$Ag_{13}OsO_6$: A Silver Oxide with Interconnected Icosahedral Ag_{13}^{4+} Clusters and Dispersed $[OsO_6]^{4-}$ Octahedra
DOI: 10.1002/anie.200351740
Published online: September 1, 2003

G. Dyker, D. Hildebrandt, J. Liu, K. Merz:*
Gold(III) Chloride Catalyzed Domino Processes with Isobenzopyrylium Cation Intermediates
DOI: 10.1002/anie.200352160
Published online: September 1, 2003

V. S. Iyer, K. P. C. Vollhardt, R. Wilhelm:*
Near-Quantitative Solid-State Synthesis of Carbon Nanotubes from Homogeneous Diphenylethynecobalt and –Nickel Complexes
DOI: 10.1002/anie.200352201
Published online: September 1, 2003

F. M. H. de Groot, C. Albrecht, R. Koekkoek, P. H. Beusker, H. W. Scheeren:*
"Cascade-Release Dendrimers" Liberate All End Groups upon a Single Triggering Event in the Dendritic Core
DOI: 10.1002/anie.200351942
Published online: September 1, 2003

Articles judged by the referees or the editor as being either very important or very urgent are immediately edited, proof-read, and electronically published once the manuscript has arrived in the editorial office in final form. As long as there is no page number available these articles should be cited in the following manner:

Author(s) *Angew. Chem. Int. Ed.*, online publication date, DOI.

Web Sites

http://interscience.wiley.com	**4122**	Wiley InterScience Relaunched	*M. Müller*

Books

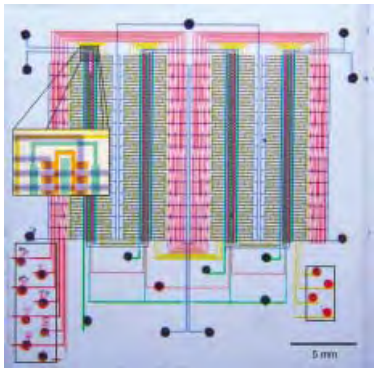
The Art of Chemistry	**4125**	Arthur Greenberg	*reviewed by H. Hopf*
The Road to Stockholm	**4126**	István Hargittai	*reviewed by G. B. Kauffman, L. M. Kauffman*

Highlights

Microfluidic Systems

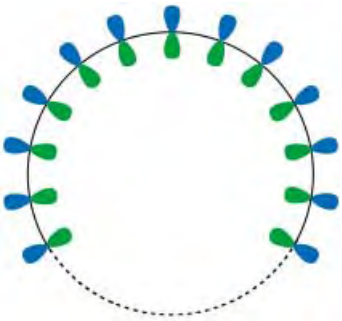
R. F. Ismagilov* ——— **4130 – 4132**

Integrated Microfluidic Systems



Microchips: Multistep reactions may be catalyzed by enzymes immobilized on microbeads trapped inside microfluidic channels. Large integrated microfluidic circuits can be created by using multilayer soft lithography in poly(dimethylsiloxane). These circuits (see schematic representation) can be used to perform hundreds of different reactions simultaneously, and can be applied to a range of problems, from enzymatic assays to crystallization of proteins.

Undeterred by the propensity of trigonal carbon atoms to strive for planarity, synthetic chemists have recently succeeded in constructing novel macrocycles with inward-pointing p orbitals (see picture). Individual metal ions are too small to fill the cavity, but fullerenes are just the right size for some of these electron-rich, π-lined hosts.

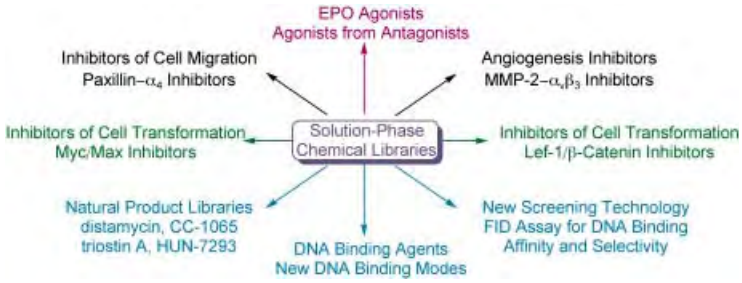


Conjugated Belts

L. T. Scott* ——— 4133 – 4135

Conjugated Belts and Nanorings with Radially Oriented p Orbitals

Reviews



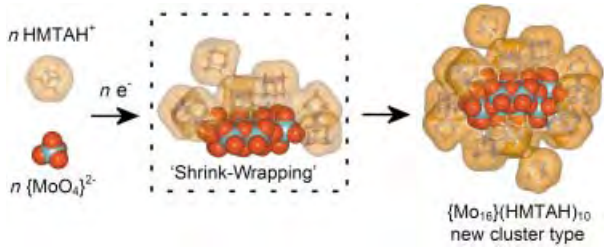
To bead or not to bead? This is the question posed at the start of the construction of every combinatorial library. The pros and cons of solid-phase and solution-phase library synthesis are discussed along with the authors personal experiences in constructing and using solution-phase libraries (see scheme) to study the modulation of protein–protein and protein–DNA interactions in cellular signal transduction.

Combinatorial Chemistry

D. L. Boger,* J. Desharnais, K. Capps ——— 4138 – 4176

Solution-Phase Combinatorial Libraries: Modulating Cellular Signaling by Targeting Protein–Protein or Protein–DNA Interactions

Communications



A mixed-valence polyoxomolybdate cluster $[H_2Mo^{VI}_{12}Mo^{V}_{4}O_{52}]^{10-}$ was isolated by a new "shrink-wrapping" approach to trap clusters that display low symmetry and nonspherical topology (see scheme; HMTAH = protonated hexamethylenetetraamine). The unprecedented cluster topology results from the restriction of the reorganization of the cluster framework to more symmetrical clusters, yet it reacts with electrophiles, such as Fe^{II}.

Small Polyoxomolybdates

D.-L. Long, P. Kögerler, L. J. Farrugia, L. Cronin* ——— 4180 – 4183

Restraining Symmetry in the Formation of Small Polyoxomolybdates: Building Blocks of Unprecedented Topology Resulting From "Shrink-Wrapping" $[H_2Mo_{16}O_{52}]^{10-}$-Type Clusters

For the USA and Canada:
ANGEWANDTE CHEMIE International Edition (ISSN 1433-7851) is published weekly by Wiley-VCH PO Box 191161, D 69451 Weinheim, Germany. Air freight and mailing in the USA by Publications Expediting Inc. 200 Meacham Ave., Elmont, NY 11003. Periodicals postage paid at Jamaica NY 11431. US POSTMASTER: send address changes to *Angewandte Chemie*, Wiley-VCH, 111 River Street, Hoboken, NJ 07030. Annual institutional subscription price for institutions: Europe € 2998.00/3148.00. Outside Europe US$ 3718.00/3904.00 (valid for print or electronic/print and electronic delivery); for individuals who are personal members of a national chemical society, or whose institution already subscribes, or who are retired or self-employed consultants, print only (including postage and handling charges): Europe € 248.00/Outside Europe US$ 348.00.

 © 2003 Wiley-VCH Verlag GmbH & Co. KGaA, Weinheim

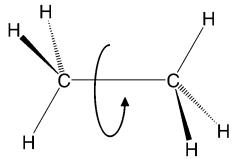
Contents

Rotational Barrier in Ethane (1)

F. M. Bickelhaupt,
E. J. Baerends* ——— **4183 – 4188**

The Case for Steric Repulsion Causing the Staggered Conformation of Ethane

The barrier to rotation in ethane (see picture) is considered a prototypical case of steric hindrance. This view has been recently contradicted, and hyperconjugation has been put forward as the right explanation. The authors argue that there is no reason to abandon the steric repulsion explanation, and discuss why



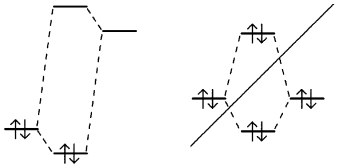
different electronic structure analyses yield different views.

Rotational Barrier in Ethane (2)

F. Weinhold* ——— **4188 – 4194**

Rebuttal to the Bickelhaupt–Baerends Case for Steric Repulsion Causing the Staggered Conformation of Ethane

Two tenets of qualitative MO theory suggest contradictory explanations of ethane torsional barriers, but only one stands up to rigorous examination (see energy level diagrams). Bickelhaupt and Baerends' defense of the neo-steric "four-electron destabilization" concept (right) is shown to be as illusory as its predecessors.

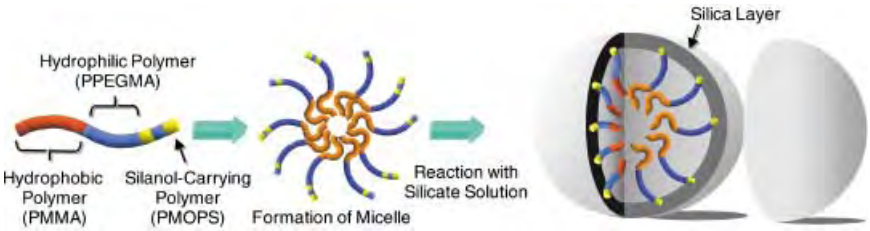


VIP

Organic/Inorganic Nanocapsules

K. Koh, K. Ohno, Y. Tsujii,
T. Fukuda* ——— **4194 – 4197**

Precision Synthesis of Organic/Inorganic Hybrid Nanocapsules with a Silanol-Functionalized Micelle Template

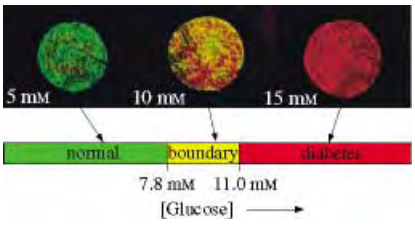


In a nutshell: An amphiphilic block copolymer that bears protected silanol groups was synthesized by atom-transfer radical polymerization, and the amphiphile was assembled to form a micelle in an aqueous medium. The micelle was mixed with a solution of active silicate, which resulted in the formation of a silica layer on the micelle surface to produce a novel type of organic/inorganic hybrid nanocapsule (see scheme).

Colorimetric Glucose Sensor

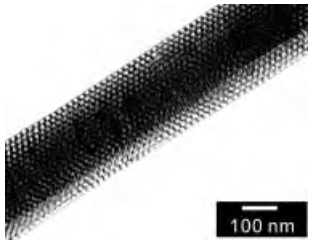
D. Nakayama, Y. Takeoka,* M. Watanabe,*
K. Kataoka ——— **4197 – 4200**

Simple and Precise Preparation of a Porous Gel for a Colorimetric Glucose Sensor by a Templating Technique



Red for danger! A glucose-sensitive gel is systematically prepared by careful control of the gel recipe to produce the desired swelling ratio at a given glucose concentration. Subsequently, a periodically ordered porous gel is obtained from the bulk gel by using a closest-packing colloidal crystal as a template; this template is subsequently removed. The gel exhibits expected structural color at certain glucose concentrations and thus can be used as a colorimetric glucose sensor, which may applied as a test for diabetes (see picture).

 © 2003 Wiley-VCH Verlag GmbH & Co. KGaA, Weinheim

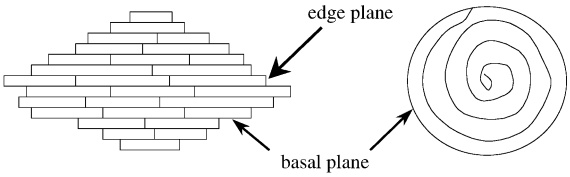


Taking control: One-dimensional mesostructured silica materials and their arrays are prepared in anodic alumina membranes. By adjusting the wettability of the alumina pore wall, nanofibers and nanotubes are prepared in a controlled way. The mesostructured silica morphology (see picture) can be adjusted by changing the surfactant concentration. Both the mesopores and the tubular cavities can be incorporated with functional materials, thus forming hierarchical nanocomposites.

1D Mesostructured Silica Materials

Z. Yang, Z. Niu, X. Cao, Z. Yang,* Y. Lu,* Z. Hu, C. C. Han ——— **4201 – 4203**

Template Synthesis of Uniform 1D Mesostructured Silica Materials and Their Arrays in Anodic Alumina Membranes

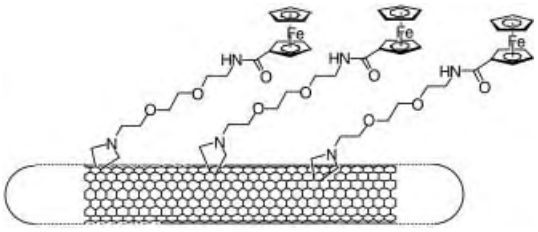


Lithium-ion batteries are the most convenient form of electrical storage. But their natural-graphite anodes are not compatible with propylene carbonate-based electrolytes. The edge planes of the graphite are attacked by the electrolyte, whereas the basal planes remain inert. A technique can be applied to form spherical graphite particles, which maximize the basal-plane exposure while the edge planes remain hidden (see picture). Thus only a small amount of carbon coating is now needed to protect the graphite core from the electrolyte.

Material for Lithium-Battery Anodes

M. Yoshio,* H. Wang, K. Fukuda ——— **4203 – 4206**

Spherical Carbon-Coated Natural Graphite as a Lithium-Ion Battery-Anode Material



A long-lived charge-separated state, $SWNT^{\bullet-}$–$Fc^{\bullet+}$, is formed by photoinduced electron transfer in a novel single-wall carbon nanotube–ferrocene (SWNT–Fc) nanohybrid. The presence of $SWNT^{\bullet-}$, detected by laser flash photolysis, was confirmed by time-resolved pulse radiolysis and steady-state bulk electrolysis.

Carbon Nanotube–Ferrocene Hybrids

D. M. Guldi,* M. Marcaccio, D. Paolucci, F. Paolucci,* N. Tagmatarchis, D. Tasis, E. Vázquez, M. Prato* ——— **4206 – 4209**

Single-Wall Carbon Nanotube–Ferrocene Nanohybrids: Observing Intramolecular Electron Transfer in Functionalized SWNTs

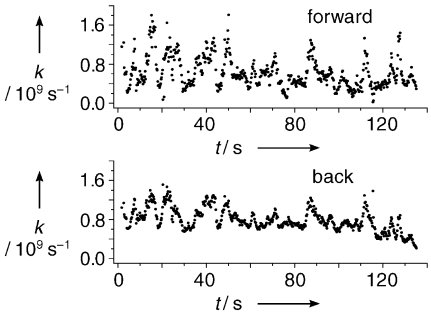
 © 2003 Wiley-VCH Verlag GmbH & Co. KGaA, Weinheim

Contents

Single-Molecule Electron Transfer

R. Gronheid, A. Stefan, M. Cotlet, J. Hofkens, J. Qu, K. Müllen, M. Van der Auweraer, J. W. Verhoeven, F. C. De Schryver* ——— **4209 – 4214**

Reversible Intramolecular Electron Transfer at the Single-Molecule Level

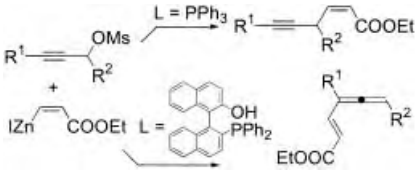


Fluctuating electron-transfer rates, both forward and back (see picture), were measured at the single-molecule level for a triphenylamine–perylenediimide donor–acceptor dendrimer. These fluctuations, reminiscent of those seen for forward electron transfer in some large biomolecules and so far not documented for synthetic systems, are induced by the local environment and conformational changes in the dendrimer.

Controlling Regioselectivity

S. Ma,* G. Wang ——— **4215 – 4217**

Regioselectivity Control by a Ligand Switch in the Coupling Reaction Involving Allenic/Propargylic Palladium Species

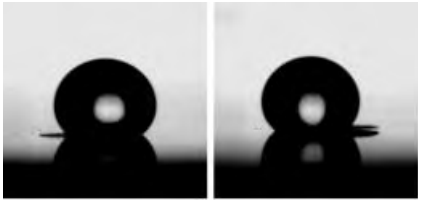


Tuning the regioselectivity of the Pd-catalyzed coupling reaction of propargylic mesylates and (*Z*)-2-ethoxycarbonylethenyl zinc iodide or PhZnBr is acheived by subtle choice of the ligand. When PPh_3 is the ligand, alkynes are formed, whereas when 2-diphenylphosphanyl-2′-hydroxy-1,1′-binaphthalene is the ligand, allenes are formed.

Superhydrophobic Carbon Films

L. Feng, Z. Yang, J. Zhai, Y. Song, B. Liu, Y. Ma, Z. Yang,* L. Jiang,* D. Zhu ——— **4217 – 4220**

Superhydrophobicity of Nanostructured Carbon Films in a Wide Range of pH Values

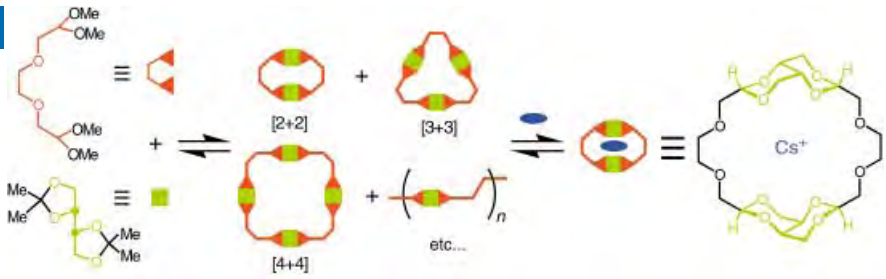


Nanostructured graphitelike carbon films are prepared through a simple pyrolysis method. The as-prepared films are superhydrophobic for not only pure water but also corrosive liquids, such as acidic and basic solutions. The picture shows water droplets with pH values of 1.07 (left) and 13.76 (right) in contact with a nanostructured carbon film. This is the first example of superhydrophobicity over the whole range of pH values, without the presence of fluorine-containing compounds.

Dynamic Covalent Chemistry

B. Fuchs, A. Nelson, A. Star, J. F. Stoddart,* S. Vidal ——— **4220 – 4224**

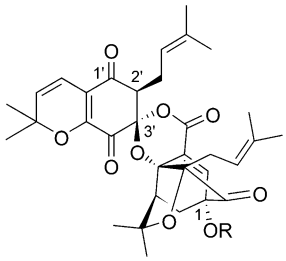
Amplification of Dynamic Chiral Crown Ether Complexes During Cyclic Acetal Formation



The dynamic duo: A more than tenfold increase in the yield of the chiral macropolycyclic polyether containing two 2,6-disubstituted 1,3,5,7-*cis*-tetraoxadecalin systems was obtained under thermodynamic conditions from a dynamic combinatorial virtual library with templating cesium ions (> 95% yield, see schematic representation) relative to kinetic syntheses (< 8% yields in their macropolycyclization steps), even when the same template was used.

 © 2003 Wiley-VCH Verlag GmbH & Co. KGaA, Weinheim

The unique spiroxalactone framework of lateriflorone (**1**) consists of a prenylated dihydrobenzoquinone moiety and a trioxatetracyclotetradecane system. A tandem Claisen rearrangement/Diels–Alder cascade was the key step in the synthesis of the complex tetradecane system, which was then used to prepare 1-*O*-methyllateriflorone (**2**).



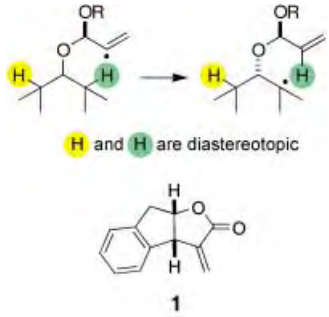
1 (R = H): lateriflorone
2 (R = Me): 1-*O*-methyllateriflorone

Natural Product Synthesis

K. C. Nicolaou,* P. K. Sasmal, H. Xu, K. Namoto, A. Ritzén ——— **4225 – 4229**

Total Synthesis of 1-*O*-Methyllateriflorone

A tin-free radical tandem reaction leads to optically active α-methylenelactones (e.g. **1**). The initial radical-mediated hydrogen-atom abstraction from a chiral acetal is highly stereoselective (see scheme). The stereochemical outcome of such reactions is governed by rules similar to those developed for related cyclization processes.

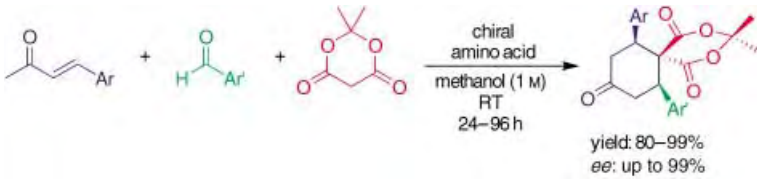


1

Stereoselective Radical Reactions

P. Renaud,* F. Beaufils, L. Feray, K. Schenk ——— **4230 – 4233**

Diastereoselective Radical-Mediated Hydrogen-Atom Abstraction

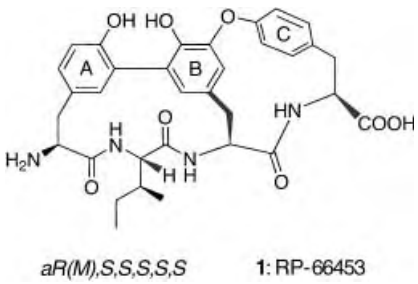


A practical and environmentally friendly organocatalytic process for the synthesis of optically active highly substituted spiro[5,5]undecane-1,5,9-triones was achieved through the reaction of an aldehyde, an enone, and Meldrum's acid in the presence of a catalytic amount of chiral amino acid (see scheme). The Diels–Alder products were obtained as single diastereomers in excellent yields and enantiomeric excesses.

Organocatalytic Domino Reactions

D. B. Ramachary, N. S. Chowdari, C. F. Barbas III* ——— **4233 – 4237**

Organocatalytic Asymmetric Domino Knoevenagel/Diels–Alder Reactions: A Bioorganic Approach to the Diastereospecific and Enantioselective Construction of Highly Substituted Spiro[5,5]undecane-1,5,9-triones



aR(M),S,S,S,S,S **1**: RP-66453

The absolute configuration (*aR*, *S*, *S*, *S*, *S*, *S*) was assigned to the natural product RP-66453 (**1**) after the total synthesis of its atropdiastereomer and spectroscopic studies on the two compounds. A sequence of S_NAr-based cycloetherification and an intramolecular atropdiastereoselective Suzuki–Miyaura coupling were used for the construction of the elusive A-B-O-C bicyclic skeleton of RP-66453.

Natural Product Synthesis

M. Bois-Choussy, P. Cristau, J. Zhu* ——— **4238 – 4241**

Total Synthesis of an Atropdiastereomer of RP-66453 and Determination of Its Absolute Configuration

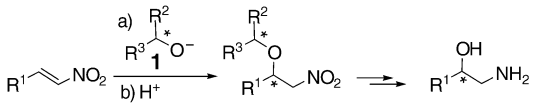
 © 2003 Wiley-VCH Verlag GmbH & Co. KGaA, Weinheim

Contents

Asymmetric Oxy-Michael Addition

N. J. Adderley, D. J. Buchanan, D. J. Dixon,* D. I. Lainé ____ **4241 – 4244**

Highly Diastereoselective Oxy-Michael Additions of Enantiopure δ-Lactol Anions to Nitroalkenes: Asymmetric Synthesis of 1,2-Amino Alcohols

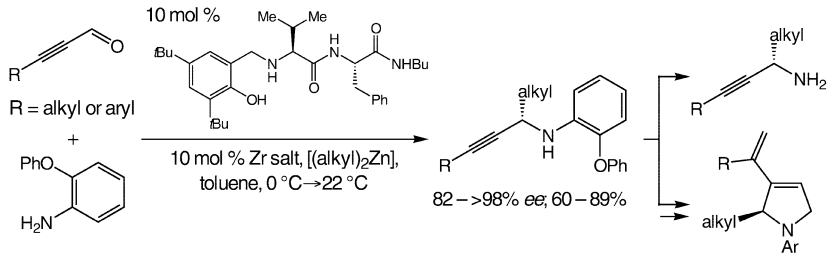


The "naked" alkoxide 1 of (*S*)-6-methyl-δ-lactol acts as an excellent chiral hydroxide equivalent in highly diastereoselective oxy-Michael additions to nitroalkenes (see scheme). The excellent stereoinduction arises from what becomes a superb protecting group in the resulting 1,2-amino alcohol products. R^1 = alkyl, aryl, furanyl, thiophenyl; $R^2,R^3 = -(CH_2)_3CHCH_3O-$.

Synthesis of Propargylamines

L. C. Akullian, M. L. Snapper,* A. H. Hoveyda* ____ **4244 – 4247**

Three-Component Enantioselective Synthesis of Propargylamines through Zr-Catalyzed Additions of Alkyl Zinc Reagents to Alkynylimines

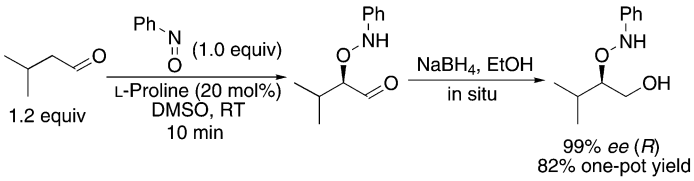


Readily available amino acid based chiral ligands are used in a three-component Zr-catalyzed enantioselective synthesis of propargylamines (see schemes). The reaction affords important enantiomerically enriched building blocks that are not conveniently accessible by alternative catalytic methods.

Asymmetric Catalysis

G. Zhong* ____ **4247 – 4250**

A Facile and Rapid Route to Highly Enantiopure 1,2-Diols by Novel Catalytic Asymmetric α-Aminoxylation of Aldehydes

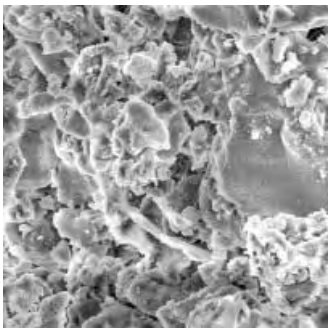


***R*- or *S*-configured 1,2-diol precursors** are formed in good yields (54–86%) and with excellent enantioselectivities (94 to 99% *ee*) by using a simple one-pot sequence—catalytic α-aminoxylation of aldehydes followed by in situ reduction with $NaBH_4$—with L- or D-proline as the catalyst and nitrosobenzene as the oxygen source (see scheme).

High-Surface-Area Aluminum Fluoride

E. Kemnitz,* U. Groß, S. Rüdiger, C. S. Shekar ____ **4251 – 4254**

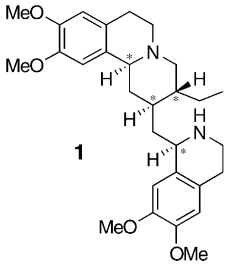
Amorphous Metal Fluorides with Extraordinary High Surface Areas



Super acidic solids: A new two-step route to high-surface-area metal fluorides is reported, by which amorphous AlF_3 can be prepared having a BET(N_2) surface area of more than 200 $m^2 g^{-1}$ (see SEM image). This HS-AlF_3 shows a very high Lewis acidity and consequently a high catalytic activity.

 © 2003 Wiley-VCH Verlag GmbH & Co. KGaA, Weinheim

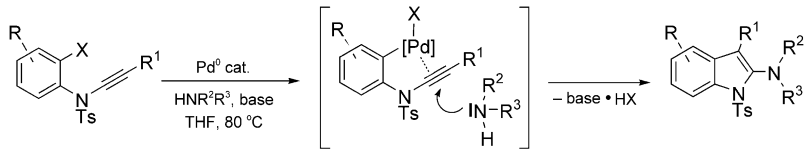
Stereochemical diversity as a novel concept in combinatorial chemistry for the synthesis of nonpeptidic biologically active compounds is introduced. As an example, the combination of the hydrogenation of imines in the presence of either enantiomer of a chiral Ru catalyst with a domino reaction led to the targeted construction of 12 of the 16 possible stereoisomers of emetine (**1**).



Combinatorial Synthesis

L. F. Tietze,* N. Rackelmann, G. Sekar ——— **4254 – 4257**

Catalyst-Controlled Stereoselective Combinatorial Synthesis

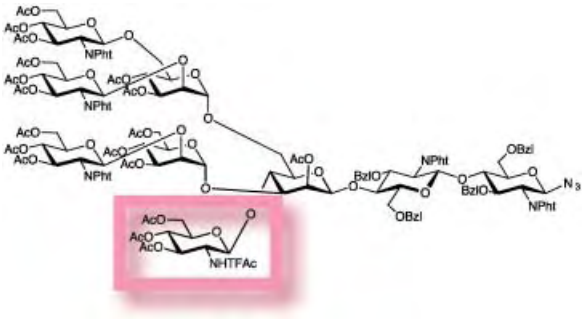


Chelates are the key: A conceptually novel indole ring forming reaction through heteroanulation is available through the palladium-catalyzed reaction of *N*-alkenylanilides with primary or secondary amines. The key feature is the formation of an unprecedented σ,π-chelated palladium species (see scheme); nitrogen nucleophiles can add to the activated alkyne unit of this species to form the indole skeleton. (X = I, Br; HNR^2R^3 = prim. or sec. amine; Ts = tosyl.)

Pd-Catalyzed Heteroanulation

B. Witulski,* C. Alayrac, L. Tevzadze-Saeftel ——— **4257 – 4260**

Palladium-Catalyzed Synthesis of 2-Aminoindoles by a Heteroanulation Reaction



Squeezing in a sugar: A modular building-block approach was the strategy used in a clever general synthesis of the sterically crowded triantennary N-glycans bearing an additional bisecting GlcNAc motif (see formula). Key steps include the use of the small trifluoroacetyl protective group and the late introduction of the α1,6-arm.

Antennary Oligosaccharides

H. Weiss, C. Unverzagt* ——— **4261 – 4263**

Highly Branched Oligosaccharides: A General Strategy for the Synthesis of Multiantennary N-Glycans with a Bisected Motif

VIP Communications labeled with this symbol have been judged by two referees as being "very important papers".

The publication of Communications labeled with this symbol has been accelerated because of their topical or highly competitive nature.

 © 2003 Wiley-VCH Verlag GmbH & Co. KGaA, Weinheim

Contents

Looking for outstanding employees?

Do you need another expert for your excellent team?
... Chemists, PhD Students, Managers, Professors, Sales Representatives...

Place an advert in the printed version and have it made available online for 1 month, free of charge!

Angewandte Chemie International Edition
Advertising Sales Department: Marion Schulz
Phone: 0 62 01 - 60 65 65
Fax: 0 62 01 - 60 65 50
E-Mail: MSchulz@wiley-vch.de

Service

Keywords ____ *4264*

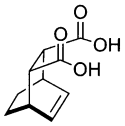
Authors ____ *4265*

Vacancies ____ *4121*

Preview ____ *4267*

Corrigendum

A reader has noticed that in the Review by **E. A. Meyer**, **R. K. Castellano**, and **F. Diederich**, in *Angew. Chem. Int. Ed.* **2003**, *42*, 1210, the structural formula for compound **31b** in Figure 26 is incorrect. The correct formula is given here. Furthermore, this receptor was not developed by Dvornikovs and Smithrud, as stated in the accompanying text, but, as correctly cited, was developed by Thompson and Smithrud.



31b

 © 2003 Wiley-VCH Verlag GmbH & Co. KGaA, Weinheim

Microfluidic Systems

Integrated Microfluidic Systems**

*Rustem F. Ismagilov**

Keywords:
analytical methods · enzymes · microfluidics · microreactors · protein structures

Microfluidic systems use networks of channels thinner than a human hair to manipulate nanoliter volumes of reagents. The goal of microfluidics is challenging: to integrate, on a chip smaller than a credit card, all operations normally performed in a chemical or medical laboratory. Synthesis, purification, analysis, and diagnostics would be performed by such a "lab on a chip" rapidly, economically, and with minute volumes of samples. This scale-down approach is inspired by, and often compared to, the success of the miniaturization in the computer industry, namely, the miniaturization and integration of thousands of transistors on a silicon chip that has led to a rapid increase in performance and decrease in the cost of computers. This highlight describes two significant steps towards these ambitious goals.

Multistep Catalytic Reactions using Microbeads

Seong and Crooks[1] have reported a microfluidic system that relies on microscopic beads trapped in microfluidic channels to perform sequential catalytic chemical reactions. It is remarkable that the microbeads serve two functions simultaneously: they induce rapid mixing of the reagents (Figure 1) and serve as the support for immobilized enzymatic catalysts (Figure 2).

Mixing solutions in microfluidic channels is difficult—two streams, injected into a microchannel, co-flow with slow mixing only through diffusion. Efficient mixing occurs when these streams are split into thin substreams ("laminae") and then recombined in such a way that the laminae of the two different fluids come in contact. Mixing is accelerated because diffusion through the thin laminae is fast, and because the laminae are in contact over a large total surface area. This splitting and recombination does not occur in simple geometries in a steady laminar flow, but it has been induced using several methods. For example, three-dimensional microfabrication may be used to induce multilaminar mixing directly[2] or to induce chaotic advection,[3] which repetitively splits and recombines the streams to achieve thinner and thinner laminae.[4,5] Alternatively, time may be used as the third dimension,[3] and chaotic advection may be induced in unsteady, time-periodic flows in droplets moving through channels fabricated by conventional two-dimensional methods.[6]

Seong and Crooks reported the remarkable observation that such splitting and recombination (distributive mixing) can be achieved simply by flowing solutions through beads packed inside a microfluidic channel (Figure 1); these beads are only a few times (ca. 10) smaller than the channel. The flow around a single large bead in a channel can be modeled easily. One would expect that such a bead would not induce significant mixing. The flow through a channel containing thousands of perfectly packed beads can be modeled by mean-field approximations. One would expect that a large number of very small beads perfectly packed in a channel would not induce such mixing either. The intermediate regime, with just a few beads across the width of the channel, may be especially challenging from a theoretical point of view because the flow patterns would strongly depend on packing defects that are likely to be present when rectangular channels are packed with spherical beads of inter-

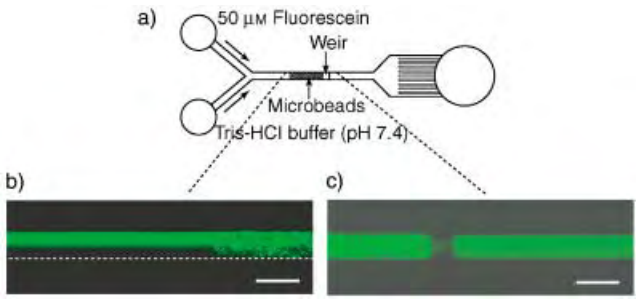


Figure 1. The mixing of two laminar streams by microbeads trapped inside a microfluidic channel.[1] a) A schematic drawing of the microfluidic device. b) A fluorescent microphotograph of distinct laminar streams of fluorescein and buffer entering the bead-packed region of the microchannel. c) A fluorescent microphotograph illustrating that the two streams are completely mixed upon exiting the bead-packed region of the microchannel. Scale bars are 200 μm. Tris = tris(hydroxymethyl)aminomethane. Reprinted (in part) with permission from the American Chemical Society. Copyright 2002.

[*] Prof. Dr. R. F. Ismagilov
Department of Chemistry
The University of Chicago
5735 S. Ellis Avenue
Chicago, IL 60637 (USA)
Fax: (+1) 773-702-0805
E-mail: r-ismagilov@uchicago.edu

[**] Original figures were generously provided by Prof. Richard Crooks and by Prof. Stephen Quake. Support by ONR is gratefully acknowledged.

 © 2003 Wiley-VCH Verlag GmbH & Co. KGaA, Weinheim DOI: 10.1002/anie.200301660

mediate size (especially if the beads are not uniform). An interesting possibility is that a three-dimensional network of these defects could effectively split and recombine the flows; presumably, mixing could be further enhanced by inducing and controlling these defects. These results are certain to stimulate exciting theoretical and experimental work, and it is rewarding to see new developments in chemistry posing new questions for physics.

Microbeads bearing immobilized enzymes[7] and heterogeneous catalysts[8] can be used to carry out reactions efficiently because they provide the high surface-to-volume ratio required for heterogeneous reactions.[8] An attractive feature of the system described by Seong and Crooks is the ability to carry out multistep transformations. To demonstrate this capability, they created microfluidic channels with two regions packed with trapped beads: the first with immobilized glucose oxidase and the second with immobilized horseradish peroxidase (HRP; Figure 2). The flow of a solution of glucose through the channels resulted in the catalytic oxidation of glucose by glucose oxidase and the generation of H_2O_2. A solution of the nonfluorescent dye amplex red was added downstream from the first pack of microbeads. Horseradish peroxidase immobilized on the second pack of beads used the H_2O_2 liberated in the first reaction to catalytically oxidize this dye and produce red fluorescent resorufin. This system will open many exciting opportunities in biochemical analysis and synthesis that involves multistep catalytic reactions.

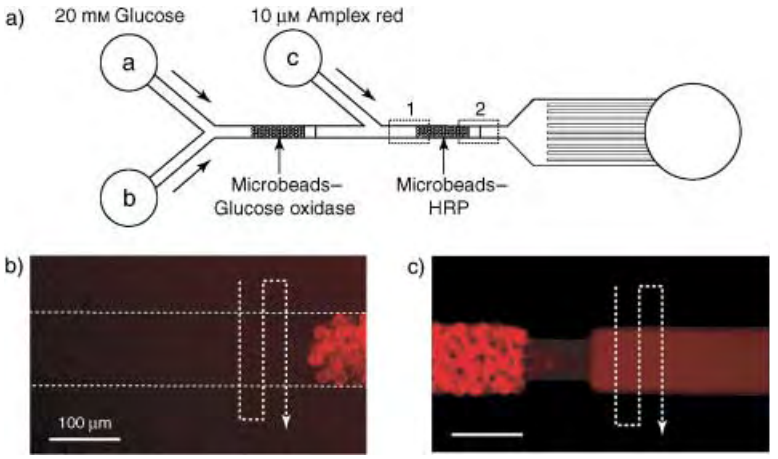


Figure 2. Two-step chemical transformation using catalyst-bearing microbeads in a microfluidic channel.[1] a) A schematic illustration of the microfluidic device. b) A fluorescent microphotograph of the fluid entering the second bead-packed region (rectangle 1 in a). c) A fluorescent microphotograph of the bright fluorescence of the fluid exiting the second bead-packed region (rectangle 2 in a). Fluorescent resorufin was formed by enzyme-catalyzed oxidation of amplex red by H_2O_2, which is produced in turn by glucose oxidase immobilized in the first bead-packed region. Reprinted (in part) with permission from the American Chemical Society. Copyright 2002.

Microfluidic Large-Scale Integration

The development reported by Quake and co-workers[9] provides a strong corroboration to the analogy between the miniaturization of computers systems and the miniaturization of microanalytical systems. Their work presented a solution for the large-scale integration (LSI) problem of microfluidic networks. In computer terminology, the term LSI refers to the ability to create large networks of transistors on a computer chip. The biggest problem in operating a computer chip with an array of millions of transistors is addressability, that is, being able to control (address) all the transistors using a minimal number of electrical connections to the outside world. The problem is similar in operating a microfluidic system containing thousands of microscopic reaction volumes: filling these reaction volumes with reagents using a minimal number of channels that have to be controlled.

The first problem solved by Quake and co-workers is microfluidic multiplexing, which is the ability to control flow through a large number (F) of flow channels using only a small number (C) of control channels. The fundamental form of control is on/off switching of the flow in the flow channel using a valve. Small systems can be easily controlled by introducing a valve in each flow channel. However, the number of the control elements equals the number of flow channels ($C = F$) and becomes prohibitively large as the size of the system is increased. Quake and co-workers solved this problem by using microfluidic multiplexing, an elegant analogy to the multiplexors used in computer chips. These systems rely on the ability to fabricate three-dimensional structures in poly(dimethylsiloxane) (PDMS) and the ability to create valves at crossings of microchannels by using the elastomeric properties of PDMS.[10] The principle of multiplexing is simple and is illustrated for eight flow channels controlled by three pairs of control channels (Figure 3). One control channel within a pair operates valves that can close half (4 out of 8) of the flow channels, while the other control channel closes the remaining half of the flow channels. In the same way as any number from zero to seven can be represented by a three-bit binary code, any of the eight channels can be left open (addressed) using three pairs of

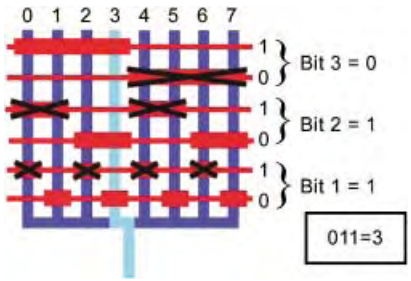


Figure 3. A schematic diagram illustrating the principle of microfluidic multiplexing.[9] Fluid flow through the eight vertical "flow channels" can be controlled using three pairs of horizontal "control channels". The wide sections of the control channels correspond to valves that can close off flow channels. Each pair of control channels may be described as one binary bit, and each binary three-bit number corresponds to the opening of one of the eight flow channels. Excerpted with permission from the American Association for the Advancement of Science. Copyright 2002.

 © 2003 Wiley-VCH Verlag GmbH & Co. KGaA, Weinheim

control channels. Since $C = 2\log_2 F$, the decrease in the number of control elements for small networks is modest, and six control channels are required for eight flow channels. For larger networks, the decrease is substantial—only 20 control channels are needed for 1024 flow channels.

To demonstrate the functionality of their system an array of 256 individually addressable microreactors was created. Figure 4 demonstrates that each microreactor can be filled with two different solutions, allowed to mix and react, and then the products can be selectively isolated. This system was then used to perform a high-throughput detection of single bacterial cells expressing recombinant cytochrome c peroxidase.

In a subsequent paper,[11] Quake and co-workers have shown how this method may be applied to the screening of conditions that induce the crystallization of proteins, a problem which is both difficult and important. Screening is very common in protein crystallization, but involves either expensive automation or extensive manual labor. In addition, prohibitively large volumes of concentrated solutions of proteins are required for screening. Microfluidic systems have the potential to solve all of these problems at once: they are inexpensive, could be automated, and consume minimal amounts of proteins. For example, this microfluidic chip performed 144 trials in parallel and each of the trials required only 10 nL of the protein solution. Manual dispensing would have required approximately 100 times larger amounts of proteins. The solutions of the protein and a precipitant were combined in each compartment of this chip (Figure 4) and crystals formed as the solutions mixed slowly by diffusion—the free-interface diffusion method. It is significant that prior to this microfluidic method, crystallization by the free-interface diffusion method had not been possible under Earth's gravity.

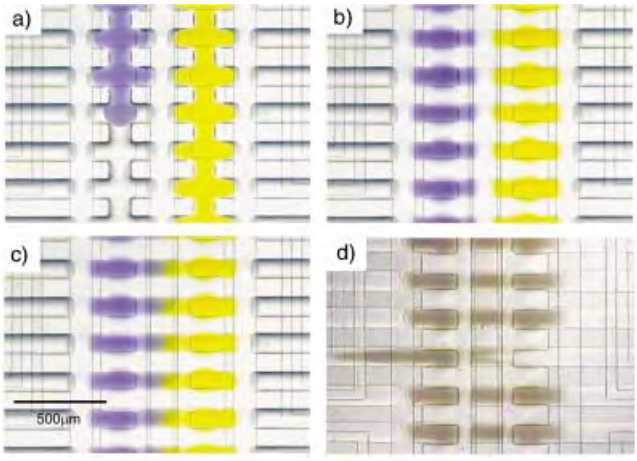


Figure 4. Complex manipulation of multiple solutions on a microfluidic chip using microfluidic multiplexing.[9] Hundreds of samples can be loaded (a), compartmentalized (b), allowed to mix and react (c), and then individual samples can be isolated (d) for further analysis or characterization. Reprinted with permission from the American Association for the Advancement of Science. Copyright 2002.

Conclusion and Outlook

Microfluidics is an exciting interdisciplinary field where chemistry, biology, physics, and engineering synergistically come together. The work discussed here clearly shows that the approach of miniaturization and integration is bearing fruit. Microfluidics is stimulating new chemistry—from the control of surface chemistry and development of new materials to the development of new analytical and synthetic methodologies that take full advantage of the new microscale technologies. It is especially exciting that microfluidics is also enabling chemistry to be carried out.

[1] G. H. Seong, R. M. Crooks, *J. Am. Chem. Soc.* **2002**, *124*, 13360–13361.
[2] F. G. Bessoth, A. J. deMello, A. Manz, *Anal. Commun.* **1999**, *36*, 213–215.
[3] J. M. Ottino, *The Kinematics of Mixing: Stretching, Chaos, and Transport*, Cambridge University Press, Cambridge, **1989**.
[4] R. H. Liu, M. A. Stremler, K. V. Sharp, M. G. Olsen, J. G. Santiago, R. J. Adrian, H. Aref, D. J. Beebe, *J. Microelectromech. Syst.* **2000**, *9*, 190–197.
[5] A. D. Stroock, S. K. W. Dertinger, A. Ajdari, I. Mezić, H. A. Stone, G. M. Whitesides, *Science* **2002**, *295*, 647–651.
[6] H. Song, J. D. Tice, R. F. Ismagilov, *Angew. Chem.* **2003**, *115*, 792–796; *Angew. Chem. Int. Ed.* **2003**, *42*, 768–772.
[7] T. Richter, L. L. Shultz-Lockyear, R. D. Oleschuk, U. Bilitewski, D. J. Harrison, *Sens. Actuators B* **2002**, *81*, 369–376.
[8] M. W. Losey, M. A. Schmidt, K. F. Jensen, *Ind. Eng. Chem. Res.* **2001**, *40*, 2555–2562.
[9] T. Thorsen, S. J. Maerkl, S. R. Quake, *Science* **2002**, *298*, 580–584.
[10] M. A. Unger, H. P. Chou, T. Thorsen, A. Scherer, S. R. Quake, *Science* **2000**, *288*, 113–116.
[11] C. L. Hansen, E. Skordalakes, J. M. Berger, S. R. Quake, *Proc. Natl. Acad. Sci. USA* **2002**, *99*, 16531–16536.

 © 2003 Wiley-VCH Verlag GmbH & Co. KGaA, Weinheim

Conjugated Belts

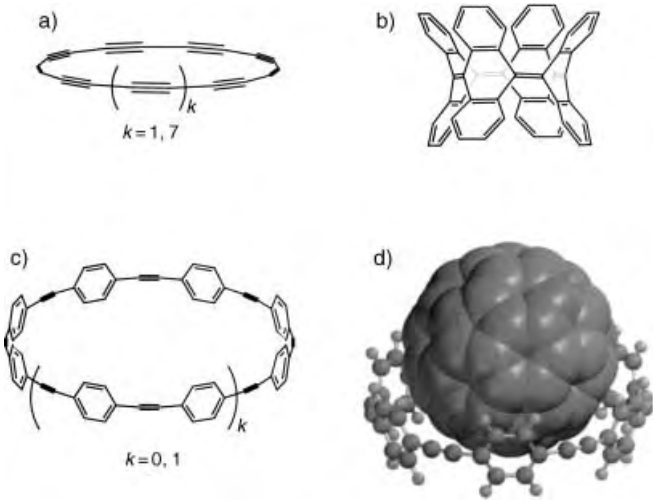
Conjugated Belts and Nanorings with Radially Oriented p Orbitals

*Lawrence T. Scott**

Keywords:
conjugation · fullerenes · pi interactions · strained molecules · supramolecular chemistry

Closed loops of p orbitals have captured the imagination of chemists since the dawn of quantum mechanics.[1] Even before p orbitals and delocalized π bonding had emerged as concepts, rings of atoms with alternating single and double bonds already intrigued and confounded our scientific forefathers.[1] Many of us know the story of Kekulé's famous dream about the structure of benzene,[2] but the first real step toward new π systems of theoretical interest can be traced to Willstätter's landmark synthesis in 1911 of cyclooctatetraene,[3] the next higher homologue of benzene. Half a century later, the synthesis and study of nonbenzenoid aromatic compounds played a prominent role in the advancement of organic chemistry.[1,4] More recently, the discovery of fullerenes sparked a flurry of activity, not only concerning the closed geodesic polyarenes and their endohedral complexes,[5] but also concerning their open geodesic fragments.[6] Today, a fascinating new class of conjugated π systems is taking shape; it comprises conjugated belts and nanorings with p orbitals oriented radially rather than perpendicular to the plane of the macrocycle.

First on the scene were the [*n*]cyclocarbons, namely, monocyclic arrays of alternating single and triple bonds (Scheme 1 a). No representative of this family of carbon allotropes has yet been isolated as a stable entity; however, such macrocycles are believed to play pivotal roles as reactive intermediates in the mechanism of formation of fullerenes from vaporized carbon.[7] Several [*n*]cyclocarbons have been generated from well-defined synthetic precursors and detected as transient species by mass spectrometry, thanks to the pioneering syntheses of Diederich and co-workers.[7]



Scheme 1. Nanorings: a) Representative all-carbon rings C_{18} and C_{30}, both of which have been generated and detected as transient species. b) A hydrocarbon picotube. c) [6]Cyclo- and [8]cycloparaphenyleneacetylene. d) Stable complex of C_{60} with [6]CPPA.

The spectacular "picotube" reported by Herges and co-workers[8a] (Scheme 1 b) was the first compound with fully conjugated radially oriented p orbitals to be put in a bottle as a pure, stable crystalline substance. This strained hydrocarbon can be viewed formally as a fully benzannulated derivative of the still unknown parent [4]cycloparaphenylene, which is a monocyclic array of alternating benzene rings and single bonds. A preliminary X-ray crystal structure of the picotube prepared by Herges and co-workers confirms the gross structure; however, it is not sufficiently refined to provide accurate experimental bond lengths and bond angles. Most likely, benzannulation perturbs the π bonding sufficiently to favor a structure that is best described as four benzannulated cyclohexa-1,4-diene units joined by double bonds with radially oriented p orbitals. Preliminary chemical transformations, complexation with silver ions, and reduction with lithium metal to a tetraanion have all been reported.[8b–d] Attempts to close up all eight fjord regions by cyclodehydrogenation reactions to transform this picotube into a [4.4]nanotube segment have, unfortunately, not yet met with success.[8e] All-carbon single-walled nanotubes (SWNTs) are also character-

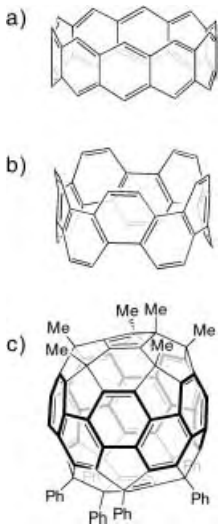
[*] Prof. Dr. L. T. Scott
Department of Chemistry
Merkert Chemistry Center
Boston College
Chestnut Hill, MA 02467-3860 (USA)
Fax: (+1) 617-552-6454
E-mail: lawrence.scott@bc.edu

DOI: 10.1002/anie.200301671
© 2003 Wiley-VCH Verlag GmbH & Co. KGaA, Weinheim

ized by radially oriented p orbitals, of course, and they constitute a large and immensely important new family of substances all by themselves.[9]

By remarkable coincidence, in the same issue of *Angewandte Chemie* that carried the first report of the picotube, with a picture on the cover, Oda and coworkers described new macrocycles composed of *para*-phenylenes alternating with alkyne units, compounds that they refer to as cyclic paraphenyleneacetylenes or simply [*n*]CPPAs (Scheme 1c).[10a] Very recently, the ability of these π-lined macrocycles to encircle hydrocarbon guests has been demonstrated,[10b] and [6]CPPA has been found to form a remarkably strong complex with C_{60} (Scheme 1d, $K_{assoc} = 1.6 \times 10^4\ L\,mol^{-1}$).[10c] The electron-rich inner surface of the macrocycle is both geometrically and electronically complementary to the electron-deficient convex exterior of C_{60}. A particularly exciting recent development in this area of research has been the synthesis of larger nanorings that complex larger fullerenes in preference to C_{60}.[10d] It is tantalizing to imagine a future series of fullerene-selective nanoring hosts, analogous to the known series of ion-selective crown ethers, which could be used as fullerene-specific sensors or in affinity chromatography. Related macrocycles having *para*-phenylenes alternating with 1,3-diyne units are now also known.[10e]

Fully unsaturated belts have been sought by synthetic organic chemists for many years,[11] but their preparation has not been easy. Unlike the nanorings illustrated in Scheme 1, true "belts" in this family are distinguished by the presence of upper and lower edges that are conjugated but never coincide (that is, they share no atoms in common). The [*n*]cyclacenes and the isomeric [*n*]cyclophenacenes (Scheme 2) represent two families of such belts in which every component ring spans the distance from one edge to the other. Wider belts would have two or more unsaturated rings between the edges, at least in some places. In the extreme, the distance separating the top and bottom edges can exceed the diameter of the belt many fold, and such belts are better known as carbon nanotubes. There is no clear dividing line between wide belts and short nanotubes, nor is one needed.



Scheme 2. Belts: a) [10]cyclacene (unknown). b) [10]Cyclophenacene (unknown). c) The first fully unsaturated hydrocarbon belt, a doubly capped [10]cyclophenacene.

Earlier this year, the first fully unsaturated belt, a [10]cyclophenacene, was finally reported by Nakamura et al.[12] Rather than assemble the belt de novo from smaller building blocks, the Tokyo group developed special methods for the controlled addition of organometallic reagents to C_{60} that preserved an electronically isolated [10]cyclophenacene around the equator of the ball, while converting all of the attached carbon atoms into saturated quaternary centers (Scheme 2c). The electronic absorption and emission spectra associated with this novel belt of radially oriented p orbitals have now been investigated, and X-ray crystallographic analysis confirms that the sp^2-sp^2 carbon–carbon bonds range in length from 1.37 to 1.44 Å, which is in agreement with theoretical predictions.

The coming years will undoubtedly bring forth new conjugated belts and nanorings with radially oriented p orbitals. Significant efforts in this direction have already been reported by the research groups of Stoddart,[13a] Cory,[13b] Bodwell,[13c] Iyoda,[13d] and even by students from my own laboratory.[13e,f] Schlüter and his co-workers in Berlin, however, are probably the closest to completing the first synthesis of a fully unsaturated hydrocarbon belt from small building blocks.[13g] Learning how to understand the molecular and supramolecular chemistry and properties of these novel macrocycles will add another dimension to our knowledge about molecular strain, π bonding, electron delocalization, intermolecular π/π interactions, and excited-state energy surfaces. A new frontier has been opened, and the exploration has now begun.

[1] For an overview, see P. J. Garratt, *Aromaticity*, Wiley, New York, NY, **1986**; see also H. Hopf, *Classics in Hydrocarbon Chemistry*, Wiley-VCH, Weinheim, **2000**.

[2] Quoted in many text books, for example: R. T. Morrison, R. N. Boyd, *Organic Chemistry*, 6th ed., Prentice Hall, Englewood Cliffs, NJ, **1992**, p. 495.

[3] For a summary with commentary, see I. Fleming, *Selected Organic Syntheses*, Wiley, New York, NY, **1973**, p. 24.

[4] *Nonbenzenoid Aromatic Compounds* (Ed.: D. Ginsburg), Interscience, New York, NY, **1959**.

[5] R. Taylor, *Lecture Notes on Fullerene Chemistry: A Handbook for Chemists*, Imperial College Press, London, **1999**.

[6] L. T. Scott, H. E. Bronstein, D. V. Preda, R. B. M. Ansems, M. S. Bratcher, S. Hagen, *Pure Appl. Chem.* **1999**, *71*, 209, and references therein.

[7] a) S. W. McElvany, M. M. Ross, N. S. Goroff, F. Diederich, *Science* **1993**, *259*, 1594; b) N. S. Goroff, *Acc. Chem. Res.* **1996**, *29*, 77, and references therein.

[8] a) S. Kammermeier, P. G. Jones, R. Herges, *Angew. Chem.* **1996**, *108*, 2834; *Angew. Chem. Int. Ed. Engl.* **1996**, *35*, 2669; b) R. Herges, M. Deichmann, T. Wakita, Y. Okamoto, *Angew. Chem.* **2003**, *115*, 1202; *Angew. Chem. Int. Ed.* **2003**, *42*, 1170; c) S. Kammermeier, P. G. Jones, I. Dix, R. Herges, *Acta Crystallogr. Sect. C* **1998**, *54*, 1078; d) N. Treitel, M. Deichmann, T. Sternfeld, T. Sheradsky, R. Herges, M. Rabinovitz, *Angew. Chem.* **2003**, *115*, 1204; *Angew. Chem. Int. Ed.* **2003**, *42*, 1172; e) M. Deichmann, C. Naether, R. Herges, *Org. Lett.* **2003**, *5*, 1269.

[9] For leading references, see *Acc. Chem. Res.* **2002**, *35*, 997 (special issue devoted to carbon nanotubes, Ed.: R. C. Haddon).

[10] a) T. Kawase, H. R. Darabi, M. Oda, *Angew. Chem.* **1996**, *108*, 2803; *Angew. Chem. Int. Ed. Engl.* **1996**, *35*, 2664; b) T. Kawase, Y. Seirai, H. R. Darabi, M. Oda, Y. Sarakai, K. Tashiro, *Angew. Chem.* **2003**, *115*, 1659; *Angew. Chem. Int. Ed.* **2003**, *42*, 1621; c) T. Kawase, K. Tanaka, N. Fujiwara, H. R. Darabi, M. Oda, *Angew. Chem.* **2003**, *115*, 1662; *Angew. Chem. Int. Ed.* **2003**, *42*, 1624; d) T. Kawase, K. Tanaka, Y. Seirai, N. Shiono, M. Oda, *Angew. Chem.* **2003**,

 © 2003 Wiley-VCH Verlag GmbH & Co. KGaA, Weinheim

115, in press; *Angew. Chem. Int. Ed.* **2003**, *42*, in press; e) M. Ohkita, K. Ando, T. Tsuji, *Chem. Commun.* **2001**, 2570.

[11] a) S. Kivelson, O. L. Chapman, *Phys. Rev. B* **1983**, *28*, 7236; b) A. Schröder, H.-B. Mekelburger, F. Vögtle, *Top. Curr. Chem.* **1994**, *172*, 179.

[12] E. Nakamura, K. Tahara, Y. Matsuo, M. Sawamura, *J. Am. Chem. Soc.* **2003**, *125*, 2834.

[13] a) U. Girreser, D. Giuffrida, F. H. Kohnke, J. P. Mathias, D. Philp, J. F. Stoddart, *Pure Appl. Chem.* **1993**, *65*, 119; b) R. M. Cory, C. L. McPhail, *Adv. Theor. Interesting Mol.* **1998**, *4*, 53; c) G. J. Bodwell, D. O. Miller, R. J. Vermeij, *Org. Lett.* **2001**, *3*, 2093; d) Y. Kuwatani, T. Yoshida, A. Kusaka, M. Oda, K. Hara, M. Yoshida, H. Matsuyama, M. Iyoda, *Tetrahedron* **2001**, *57*, 3567; e) M. A. Brooks, PhD thesis, Boston College (Chestnut Hill, MA), **1998**; f) H. M. St. Martin-Davis, PhD thesis, Boston College (Chestnut Hill, MA), **2002**; g) W. D. Neudorff, D. Lentz, M. Anibarro, A. D. Schlüter, *Chem. Eur. J.* **2003**, *9*, 2745; the Supporting Information for this paper proposes a detailed system of nomenclature for fully conjugated belts of this type.

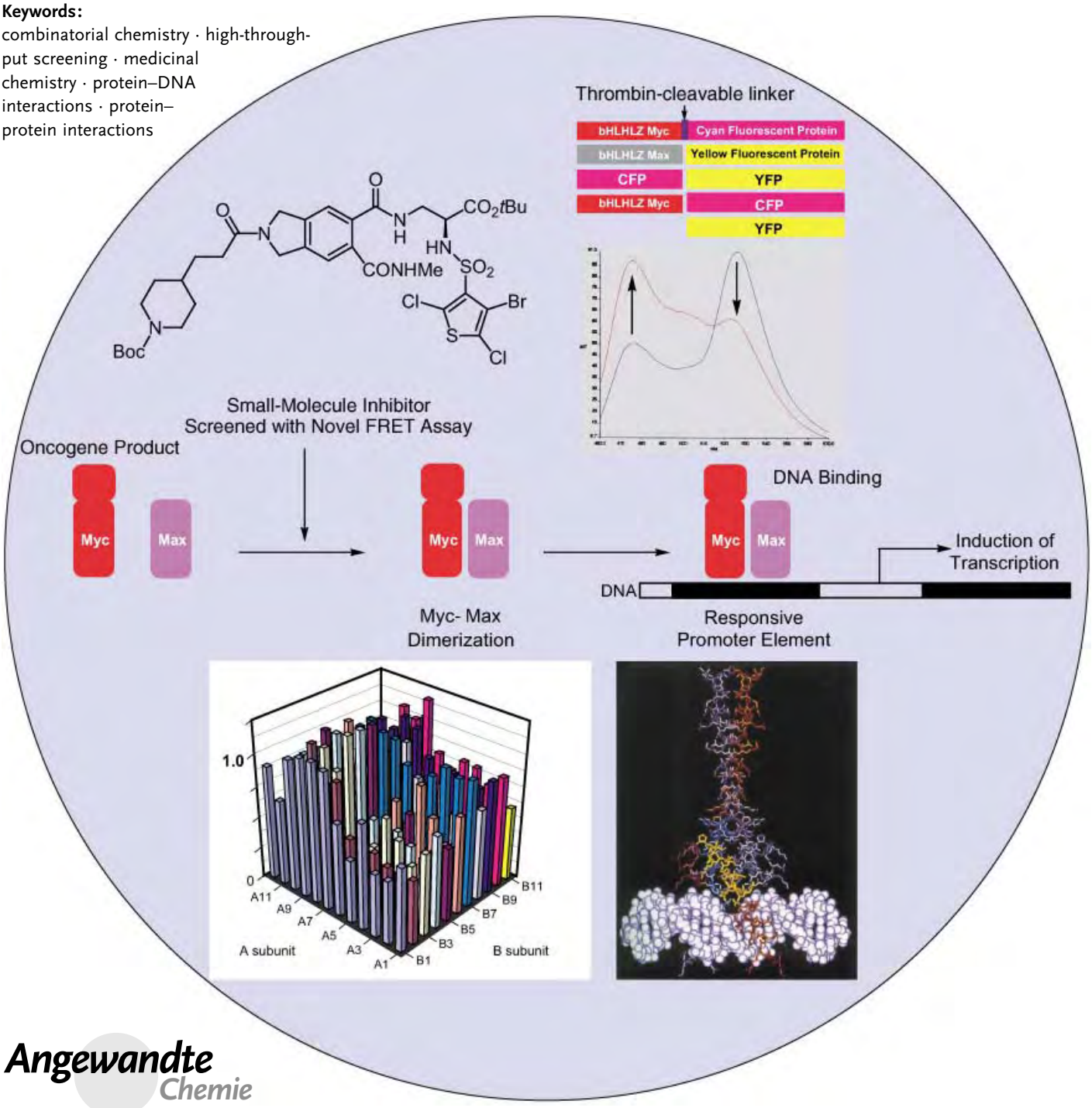
 © 2003 Wiley-VCH Verlag GmbH & Co. KGaA, Weinheim

Combinatorial Chemistry

Solution-Phase Combinatorial Libraries: Modulating Cellular Signaling by Targeting Protein–Protein or Protein–DNA Interactions

Dale L. Boger, Joel Desharnais, and Kevin Capps*

Keywords:
combinatorial chemistry · high-throughput screening · medicinal chemistry · protein–DNA interactions · protein–protein interactions



 © 2003 Wiley-VCH Verlag GmbH & Co. KGaA, Weinheim DOI: 10.1002/anie.200300574

The high-throughput synthesis and screening of compound libraries hold tremendous promise for drug discovery and powerful methods for both solid-phase and solution-phase library preparation have been introduced. The question of which approach (solution-phase versus solid-phase) is best for the preparation of chemical libraries has been replaced by which approach is most appropriate for a particular target or screen. Herein we highlight distinctions in the two approaches that might serve as useful considerations at the onset of new programs. This is followed by a more personal account of our own focus on solution-phase techniques for the preparation of libraries designed to modulate cellular signaling by targeting protein–protein or protein–DNA interactions. The screening of our libraries against a prototypical set of extracellular and intracellular targets, using a wide range of assay formats, provided the first small-molecule modulators of the protein–protein interactions studied, and a generalized approach for conducting such studies.

From the Contents

1. Introduction 4139

2. Solution-Phase versus Solid-Phase Combinatorial Chemistry 4139

3. Solution-Phase Library Preparation: Cyclic Anhydride Templates 4143

4. Targeting Protein–Protein Interactions 4146

5. Targeting Protein–DNA Interactions 4158

6. Natural Product Libraries 4163

7. Summary and Outlook 4168

1. Introduction

Combinatorial chemistry has undergone rapid development and has provided an important approach for target validation and drug discovery. As a consequence of its extension from peptide and oligonucleotide synthesis, the majority of approaches have relied on solid-phase synthesis techniques and many reviews have treated this emerging science.[1–16] A complement to adapting solution-phase chemistry to polymer-supported combinatorial synthesis is the development of protocols for solution-phase combinatorial synthesis.[17–31] A number of approaches have been introduced for this purpose including dynamic combinatorial chemistry,[32,33] soluble polymer-supported combinatorial synthesis (pioneered by Janda et al.),[34–38] fluorous-phase synthesis (FPS)[39,40] and other tagging strategies,[41] precipitation techniques,[42–45] and resin-bound,[46–52] soluble polymer-bound,[53] and fluorous-phase bound[30,40] catalysts, reagents, or scavenging reagents.[46–52] Preceding this work, we introduced a simple approach that permits the multistep solution-phase synthesis of chemical libraries employing liquid–liquid and liquid–solid (ion-exchange resin) extractions to remove residual starting materials, reagents, and reagent byproducts providing the purified product (>95% pure) irrespective of the reaction efficiency.[57–70] It has been implemented in formats for the parallel synthesis of individual compounds[62,68] (1000-member libraries), modest-sized libraries composed of small mixtures (1000–10000-member libraries, 10–50 compounds per mixture) including positional-scanning and deletion-synthesis libraries,[63–65] or combinatorially assembled to provide large libraries (25000–1000000-member libraries, 10000–28000 compounds per mixture).[65] This flexibility allows the method to be adopted in a format compatible with any screening objective. Thus, its implementation is convenient for either lead discovery or lead optimization and produces the library members on a scale that allows their repeated use in screening without resynthesis. Such libraries have been prepared in which members have been found to interfere with (antagonists) or mimic (agonists) extracellular or intracellular protein–protein interactions, inhibit intracellular enzymes, or modulate intranuclear protein–DNA interactions. The chemistry has proven applicable to natural product scaffolds, and cyclic (depsi)peptides and possesses a scope that exceeds what one might initially imagine based on its simplicity.[57–99]

This technology is being developed as an integral component of efforts to modulate cellular signaling by inhibiting, promoting, or mimicking protein–protein or protein–DNA interactions, especially those that lack existing small-molecule leads and target structural information. Despite the prevailing bias that such targets might not prove viable for small-molecule intervention,[100,101] the screening of our libraries provided the first small-molecule modulators of the protein–-protein interactions being studied, validated the targets for therapeutic intervention, and provided a generalized approach to conducting such investigations.[102] Herein, we review these efforts by first detailing methodology introduced for the solution-phase synthesis of chemical libraries followed by a more personal summary of our applications in the validation of a series of new therapeutic targets.

2. Solution-Phase versus Solid-Phase Combinatorial Chemistry

2.1. Key Distinctions of Solution-Phase Combinatorial Approaches

Solid-phase combinatorial chemistry has been widely implemented for lead discovery and lead optimization

[*] Prof. D. L. Boger, J. Desharnais, K. Capps
Department of Chemistry and
The Skaggs Institute for Chemical Biology
The Scripps Research Institute
10550 North Torrey Pines Road, La Jolla, CA 92037 (USA)
Fax: (+1) 858-784-7550
E-mail: boger@scripps.edu

 DOI: 10.1002/anie.200300574 © 2003 Wiley-VCH Verlag GmbH & Co. KGaA, Weinheim

because of the simplicity by which the compounds can be isolated once they are attached to solid supports. Several advances in the implementation of solid-phase library synthesis paved the way for its widespread acceptance including the spatially arrayed multipin peptide synthesis of Geysen et al.,[103,104] the tea-bag method of peptide synthesis introduced by Houghten et al.,[105] phage display from Smith et al.,[106,107] the spot or disc synthesis developed by Frank et al.,[108,109] and especially the (portion-mixing) split-and-mix solid-phase synthesis on beads introduced by Furka et al.[110–112] and also disclosed by Houghten et al.[113] (divide, couple, and recombine), and Lam et al.[114–116] (split synthesis), and Affymax's light-directed, spatially addressable, immobilized parallel synthesis.[117] Further promoting the widespread acceptance of split-and-mix solid-phase synthesis, several identification techniques were introduced including iterative[110,118,119] and recursive[120] deconvolution, or nucleotide-,[121,222] peptide-,[123–125] chemical-,[126–128] radiofrequency-,[129,130] color-,[131] and shape-encoded[132] solid-supported libraries. Similarly, advances in microarray synthesis continue to improve large-scale spatially arrayed parallel synthesis on a variety of solid supports.[133–136] In addition to the many merits of solid-phase synthesis, the isolation of the immobilized product by simple filtration permits the use of large reagent excesses to effect high-yield conversions for each of the steps (Table 1). However, its scale can be restricted by the amount of required solid support and its loading capacity and the production of significant quantities of each library member can be cumbersome and expensive for large libraries. Its use requires functionalized substrates and solid supports for attachment, compatible spacer linkers, orthogonal attachment and detachment techniques often with the release of spectator functional groups, specialized methods for monitoring the individual steps of a multistep synthesis often including orthogonal capping strategies for blocking residual substrate, and does not permit the purification of resin-bound intermediates. This last feature necessarily produces the released product of a multistep sequence in an impure state and requires that each step of a multistep synthesis on each substrate proceed with high efficiency. Advances addressing each of these limitations have been made which continue to improve the implementation of solid-phase synthesis. Some of the most notable introductions include traceless linkers,[137–139] the resin release of product only upon successful synthesis,[140,141] resin-capture of only the desired reaction products,[142] the introduction of safety-catch linker[143–145] and backbone amide linker[146,147] strategies, multidirectional resin-cleavage methods,[148,149] and improved resin properties and loading capacities.[34–38] Limitations that cannot be altered are that solid-phase synthesis is incompatible with the use of heterogeneous catalysts or reagents, is necessarily restricted to a linear (as opposed to convergent) synthetic strategy, is not easily amenable to the synthesis of mixture libraries, and is not amenable to selection or dynamic library screening[4] involving target-assisted synthesis.[150–154] These latter limitations are discussed in more detail in the following sections.

Table 1: Advantages (+) and disadvantages (−) of solution-phase and solid-phase combinatorial synthesis.

	Solid-phase		Solution-phase
+	Simple removal of excess reagents and reactants	−	Removal of excess reagents and reactants limits scope
+	Automation straightforward	+	Automation by liquid–liquid techniques
+	Split and mix synthesis simplifies preparation of large libraries	+	Mixture synthesis simplifies preparation of large libraries
+	Pseudo−dilution effects	+	Chemistry not limited by support
−	Adapt chemistry to solid phase and develop linking/cleavage strategies	+	Avoids extra steps for linking/cleavage
−	Reaction monitoring difficult	+	Monitor by traditional techniques
−	No purification possible	+	Purification possible after each step
−	Linear, but not convergent synthesis	+	Convergent or linear synthesis
−	Limited scale	+	Unlimited amounts (scales) available
−	Cannot conduct mixture synthesis	+	Mixture or parallel synthesis

At the time we initiated our efforts, no reports of the extension of the solid-supported synthesis of chemical libraries to solution-phase libraries had been described and a series of related studies including those of Smith et al.,[155] Rebek, et al.,[156–159] Pirrung et al.,[160] and Nielsen et al.,[161] and the popularization of multicomponent solution-phase



Dale L. Boger received his B.Sc. from the University of Kansas (1975) and Ph.D. degree from Harvard University (1980). He returned to the University of Kansas (Department of Medicinal Chemistry) then in 1985 moved to Purdue University (Department of Chemistry). Since 1991 he is the Richard and Alice Cramer Professor of Chemistry at The Scripps Research Institute. His research interests include synthetic methods, the total synthesis of natural products, heterocyclic, bioorganic, medicinal chemistry, and combinatorial chemistry, DNA–agent and protein–ligand interactions, and antitumor agents.



Joel Desharnais received a B.Sc. degree in Chemistry from the University of Montreal (1995) and his Ph.D. degree in Chemistry from the University of Montreal (2000) working with Professor James. D. Wuest in the field of supramolecular chemistry. Following this he was a postdoctoral fellow at The Scripps Research Institute working with Professor Boger, where his research interests entailed the synthesis of small-molecule agonists/antagonists of protein–protein interactions using solution-phase combinatorial chemistry and the synthesis of new folate-based enzyme inhibitors. He joined Acidophil (San Diego) in 2003.

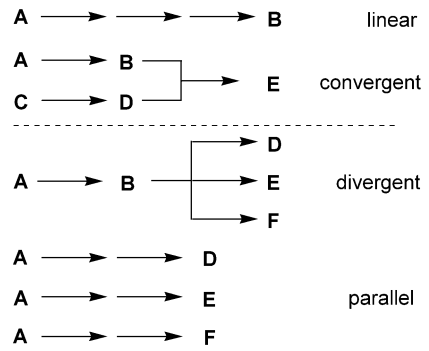
 © 2003 Wiley-VCH Verlag GmbH & Co. KGaA, Weinheim

reactions by Ugi et al.[162] and Armstrong et al.[163] were disclosed around the time of our initial contributions. The distinction of our work being that it constituted a multistep, not a single-step, strategy for the solution-phase synthesis of chemical libraries.

Given that both solution-phase and solid-phase sample manipulation are easily automated, the major limitation to the solution-phase synthesis of chemical libraries is the isolation or purification[164] of the library members. If the advantages of sample isolation characteristic of solid-phase synthesis can be incorporated into a solution-phase synthesis, its less limiting scale, expanded repertoire of chemical reactions, direct production of soluble intermediates and final products for purification or assay, and the lack of required linking, attachment and detachment, or capping steps make solution-phase library synthesis especially attractive (Table 1). It is the only approach readily amenable to convergent synthetic strategies, the synthesis of mixture libraries, or use of dynamic libraries. Consequently, we considered a number of techniques that are available for simplifying the isolation of solution-phase samples and focused on one of the most attractive involving isolation and purification by liquid–liquid or solid–liquid (ion-exchange resins) acid–base extractions. Descriptions of the initial libraries generated and their subsequent extensions, which included the introduction of solid-supported reagents,[57–63] solid-supported workup reagents (scavengers,[165] ion-exchange resins[57–59]) including the introduction of immobilized scavengers and reagents conducted within CombiChem in collaboration with L. Caporale,[165] purification by size-exclusion chromatography filtration,[62,63] and the generation of non-amide libraries have been detailed.[71]

2.2. Synthetic Strategies: Linear, Convergent, and Divergent Synthesis

Traditional organic synthesis has provided two widely recognized strategies for synthetic design: linear versus convergent synthesis (Scheme 1). The merits of a convergent synthesis are widely recognized; it typically provides a shorter (number of steps), more efficient (higher overall yield), and more effective (larger sample size) approach that is technically simpler (material balance) to execute than a linear synthesis. Since solid-phase synthesis is limited to a linear synthetic strategy, it is not surprising that it did not find widespread use in traditional organic synthesis. In fact, the applications where solid-phase synthesis did find widespread acceptance prior to the advent of combinatorial chemistry (solid-phase peptide and oligonucleotide synthesis) are those ideally suited for linear synthesis involving the repetitive use of a single highly optimized reaction. A third, less widely recognized, synthetic strategy is the divergent synthesis where a class of compounds is prepared from a single common intermediate. Although widely used, the formalization (definition) of this strategy was first detailed along with a strategy for divergent aromatic annulations.[166–168] Today, the divergent introduction of diversity is the basis of most combinatorial chemistry strategies.[169] The advantages of such a late-stage divergent approach relative to the parallel synthesis of a series of related compounds are analogous to those of a convergent versus linear synthesis (more efficient, larger sample size, material balance).



Scheme 1. Linear versus convergent and divergent versus parallel synthesis.

The strategies are not mutually exclusive for diversity-oriented synthesis. Either a linear or convergent synthetic strategy can be employed (Figure 1). Solid-phase synthesis is necessarily limited to a linear synthetic strategy whereas solution-phase synthesis may be adapted for either a linear or

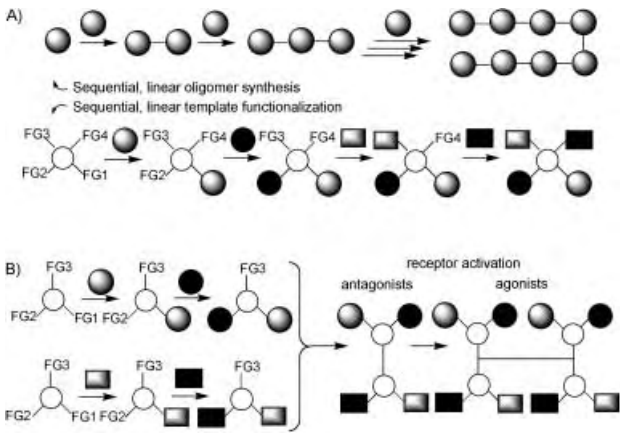


Figure 1. Convergent versus linear synthesis. A) Linear, divergent synthesis with multiplication of diversity (solid or solution phase), B) convergent synthesis with multiplication of diversity (solution phase only).



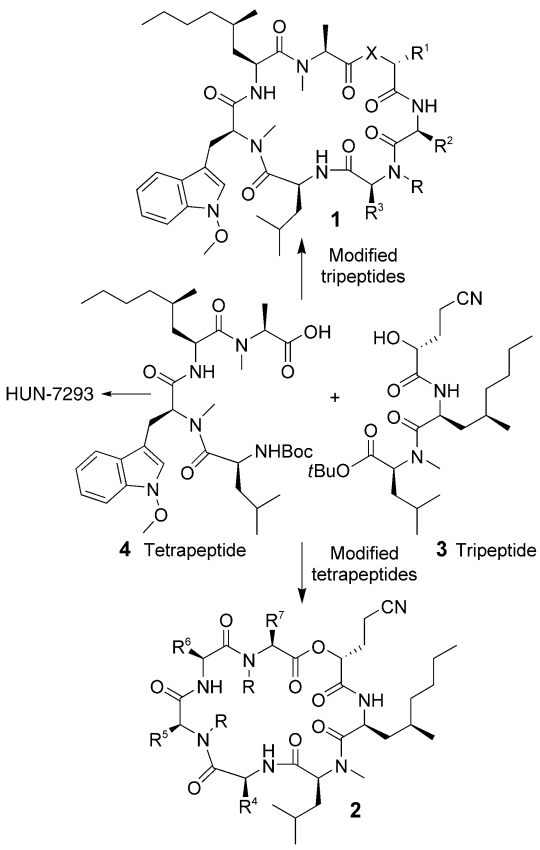
Kevin Capps graduated with a B.Sc. in Chemistry from the University of Maryland in 2000 while conducting undergraduate research in the laboratory of Professor Jeffery Davis. He is currently a graduate student at Scripps.

 © 2003 Wiley-VCH Verlag GmbH & Co. KGaA, Weinheim

convergent synthetic strategy. Moreover, the convergent synthesis is especially well suited for solution-phase synthesis and would be precluded by solid-phase techniques where the combining components are on mutually exclusive solid phases.

From the start, an important element of our efforts to probe protein–protein or protein–DNA interactions was the ability to screen for binding agents for each macromolecular partner (screen for antagonists) which could then be linked to promote the protein–protein interaction in the absence of an endogenous ligand (e.g., agonists for receptor homo- and heterodimerization; Figure 1). This was the genesis of the use of the iminodiacetic acid template for the synthesis of libraries and it has provided the first generalizable approach for the discovery or development of agonists from antagonists.[61,63,67,73,170,171] This convergent mix-and-match dimerization linkage of macromolecular binders was effected by a variety of techniques including diamide formation, olefin metathesis,[60,61,64] palladium-catalyzed biaryl coupling,[62] and Stille acetylenic–aryl couplings[63] and can only be accommodated by solution-phase, not solid-phase techniques.

An additional example of the superimposition of a divergent, diversity-oriented synthesis onto a convergent synthetic strategy may be found in work that provided a library of HUN-7293 analogues (**1** and **2**, Scheme 2) which was used to explore each structural detail of the natural product.[76] As discussed in Section 6.1, a solid-phase synthesis of the library would require a parallel linear synthesis of each analogue, whereas the implementation of a solution-phase convergent synthesis allowed the single synthesis of the key tri- and tetrapeptide subunits of the natural product (**3** and **4**) and their respective combination with diversified tetra- and tripeptides containing single-point changes in the HUN-7293 structure (Scheme 2). Thus, the advantages commonly associated with a convergent synthesis were combined with those of a divergent synthesis to provide a family of closely related structures.



Scheme 2. Convergent synthetic strategy for the generation of a library of HUN-7293 analogues. Boc = *tert*-butoxycarbonyl X = O, NH.

2.3. Solid-Phase Split-and-Mix versus Solution-Phase Mixture Synthesis and Deconvolution (Identification) Methods

Libraries of modest size can be prepared easily by either parallel solid-phase or solution-phase synthesis, both of which can provide individual compounds. The advent of split-and-mix solid-phase synthesis and the related tea-bag methods which provide one-compound-per-bead libraries made large libraries accessible by solid-phase synthesis. The concurrent introduction of the identification (tagging) methods detailed in Section 2.1[121–132] greatly enhanced the value of such strategies by providing an immediate identification of screening hits. The most valuable of these encoding technologies being those that do not add complexity to the library synthesis (Table 2).

Mixture synthesis provides for solution-phase synthesis what split-and-mix synthesis provided for solid-phase techniques (Table 2).[172] Unlike solid-phase synthesis where the polymer-bound substrate must be the stoichiometrically limiting reaction partner, either the substrate or the reacting attachment groups may be limiting in solution-phase chemistry. This situation dictates the use of split-and-mix synthesis in

Table 2: Comparison of library techniques.

Technique	Single compound or mixture	Speed of synthesis	SAR[a] retrieval	Utility
parallel synthesis	single	slow	fast	lead optimization
mixture synthesis (scanning/deletion deconvolution)	mixture	fast (fast)	slow (fast)	lead identification
parallel, spacial array	single	moderate	fast	lead identification or optimization
split and mix	mixture (one compound per bead)	moderate	slow	lead identification or optimization
encoded split and mix	mixture (one compound per bead)	moderate	moderate	lead identification or optimization
mix and sort (microreactors)	single	moderate	fast	lead identification or optimization

[a] SAR = structure activity relationship.

 © 2003 Wiley-VCH Verlag GmbH & Co. KGaA, Weinheim

the solid-phase synthesis to accommodate different reaction rates,[173] whereas the simpler method of mixture synthesis with limiting attachment-group stoichiometry may be used in solution to ensure all library members are generated in equal amounts. The cases where mixture synthesis has been conducted on the solid-phase enlists an excess of the reacting attachment groups in adjusted concentrations to accommodate the different reaction rates and requires that this rate information be available at the onset of the mixture synthesis. In contrast, the implementation of solution-phase mixture synthesis only requires the ability to remove residual substrate. Although this is not possible with solid-phase synthesis, it is readily accomplished in our efforts by simple acid–base liquid–liquid or liquid–solid extraction.

Analogous to encoding strategies for solid-phase split-and-mix synthesis of large libraries, the two important and complementary techniques of positional scanning[173] and deletion synthesis[64,65] permit the immediate identification of active leads from large mixture libraries (Figure 2). Because the preparation of positional-scanning and deletion-synthesis libraries entails implementing mixture synthesis, they are not easily adapted to solid-phase techniques. Typically, global observations are detected with a positional-scanning library and useful lead structures (although not necessarily the most potent member)[79,86,175] with defined properties are identified. Deconvolution with positional-scanning libraries is more sensitive because an increase in activity is measured, and this allows the identification of less-active lead structures. Deletion synthesis, on the other hand, screens for a loss of activity, provides less global information, but is better at identifying a uniquely potent library member.[64,65,174] The combination is more powerful than either technique alone.[64] Importantly, the lead identification is deduced from a single round of screening. Thus, not only are positional-scanning or deletion-synthesis libraries much less time intensive to prepare than the parallel synthesis of individual compounds or small mixtures and technically less demanding than spacially arrayed or encoded split-and-mix library synthesis, but they produce depository libraries for use in multiple screens capable of immediate deconvolution in a single round of testing. Although a subtle distinction and not typically a consideration, the convergent synthesis of dimeric libraries providing symmetrical and unsymmetrical combinations cannot be carried out with positional scanning libraries, but must use deletion synthesis to identify active unsymmetrical dimers.[64] Relative to the screening of individual compounds or small mixtures, the more subtle structure–activity relationship information contained in a library is often missed. However, the disadvantages associated with the loss of this information is balanced against the ease of synthesis of the parent libraries and must be judged in light of the screening objectives (lead identification or lead optimization), and the nature of the target.

A number of analytical techniques have also emerged as useful approaches to lead identification from complex mixtures, and these include assay (detection) and identification by mass spectrometry,[176] NMR spectroscopy,[177,178] and capillary electrophoresis,[179] and have expanded the utility and dynamic range for screening such mixture libraries.

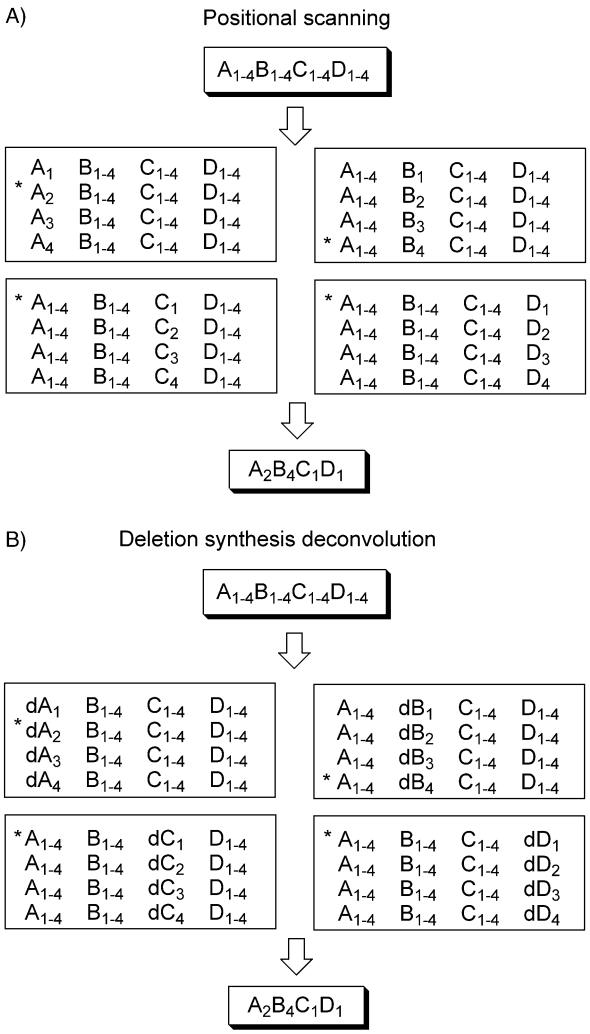
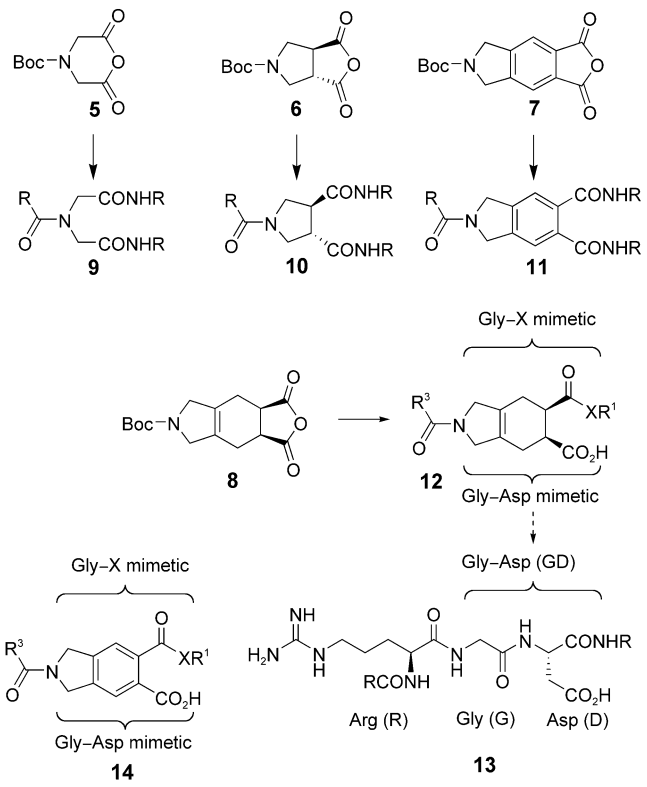


Figure 2. Examples of positional-scanning and deletion-synthesis deconvolution techniques for a library that contains four variable positions with four substitutions at each position. Positional scanning: In each sublibrary, an individual component is placed in one position but mixtures are used in all other positions. The most active sublibrary in each set (*) indicates the optimal substituent for that position. Deletion synthesis: In each sublibrary, an individual component is missing in one position (e.g. $\mathbf{dA_2}$ signifies all **A** substituents except $\mathbf{A_2}$), but full mixtures are used in all other positions. The least active sublibrary in each set (*) indicates the optimal substituent for that position, that is, the missing component is the most active.

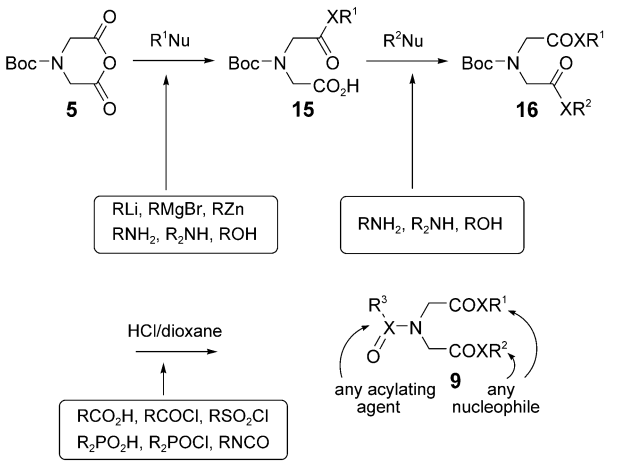
3. Solution-Phase Library Preparation: Cyclic Anhydride Templates

A summary of all the work on solution-phase libraries is beyond the scope of this article and excellent coverage is provided in a number of recent reviews.[17–31] However, we would like to briefly describe the basis of our own library preparations highlighting the design elements considered in the context of the biological targets we addressed. Template **5** (Scheme 3), the first of a representative set of five- and six-membered cyclic anhydride-based templates that have been examined, consists of a densely functionalized core which imposes little structural or conformational bias that might

 © 2003 Wiley-VCH Verlag GmbH & Co. KGaA, Weinheim



Scheme 3. Representative templates.



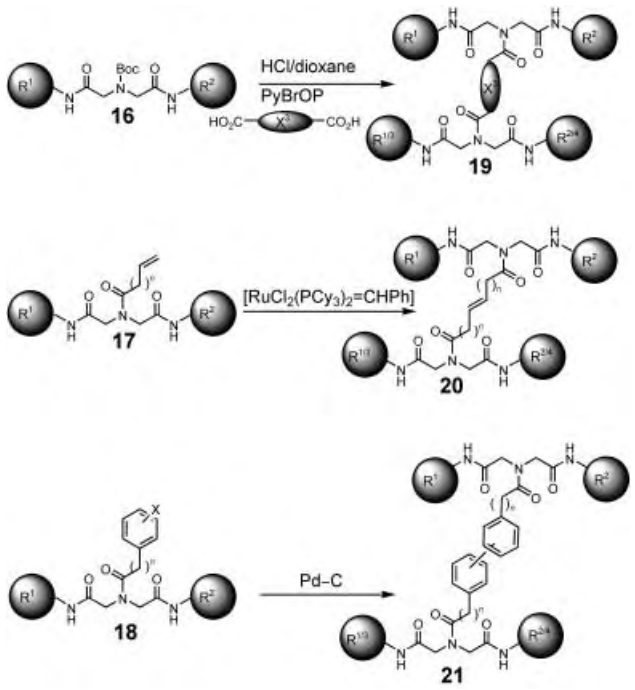
Scheme 4. Three-step solution-phase synthesis of iminodiacetic acid chemical libraries. Compound **15** is purified by washing with acid, **16** and **9** by washing with acid and base. (The R groups of the reagents in boxes become R^1, R^2, R^3.)

limit its use.[57,58] Interesting examples of alternative templates include the dipeptidomimetic template **8**, which contains a rigid bicyclic core with a plane of symmetry that allows it to function as a Gly–Asp or more general Gly–X mimetic.[57,59] Its symmetrical structure, like that of **5**, contains three positions that can be sequentially functionalized enabling the synthesis of libraries with up to three variable groups. A more rigid variant of a Gly–X mimetic **14**, isoindoline-5,6-dicarboxylic acid (**11**), has also been examined.[69] Importantly, an array of such templates, such as **5**–**7** (Scheme 3), displays the introduced diversity in conformationally constrained or different spacially defined locations providing rich structure–activity relationship information on the target of interest in a single round of testing.

The anhydride template is activated for the first functionalization, which is conducted by nucleophilic addition, and generates a free carboxylic acid group as its second functionalization site (Scheme 4). Although a subtle design element, this release of the second functionalization site concurrent with the first diversification not only provides an isolation and purification handle, but it avoids a separate deprotection step for the subsequent diversification. In addition, the use of symmetrical anhydrides insures only a single regioisomer of the product is generated simplifying the potential complexity of the library. The final diversification entails deprotection of the secondary amine which unmasks a third coupling position. At each step, the released functionality aids not only the isolation, but provides a method for separation of each of the intermediates and final products from starting materials, reactants, reagents, and their byproducts by simple liquid–liquid or liquid–solid acid–base extraction providing pure materials (typically $>95\,\%$) independent of reaction efficiencies, and a number of classes of nucleophiles and electrophiles can be used to functionalize the template (Scheme 4).[71]

This approach has been used to provide libraries in a variety of formats (individual compounds, small mixtures, large mixtures, positional-scanning, deletion-synthesis libraries) applicable to both lead generation or lead optimization. In fact, it was in this context that deletion-synthesis libraries[64] were introduced and compared with other library formats including positional scanning.[65,79,86] Although this work is most often cited for its isolation and purification by liquid–liquid acid–base extraction, the initial disclosures[57–59,68] detailed one of the first applications of polymer-bound immobilized reagents in solution-phase library synthesis (polymer supported EDCI (PS-EDCI), EDCI = 1-ethyl-3-(3-dimethylaminopropyl)carbodiimide) and also described the first use of ion-exchange resins in liquid–solid "extraction" workups.[58] The approach has been shown to dependably deliver pure compounds in 5–150 mg quantities ($>95\,\%$ pure) and multiple libraries have been assembled providing over 40000 compounds to date. It avoids the disadvantages of solid-supported synthesis, including the more restrictive scale, the required functionalized substrates and supports, compatible linkers, and the requirements for orthogonal attachment and detachment chemistry. It does not require specialized methods for monitoring each step of multistep syntheses, allows the purification of intermediates, and provides the final pure products directly for use in binding or functional assays. Extensions of these studies for generating symmetrical or unsymmetrical chemical libraries suitable for probing receptor and protein homo- and heterodimerization events were described (Scheme 5). The dimerization linkage was accomplished not only through amide-bond formation with dicarboxylic acids, but also by Stille coupling,[63] by the first application of an intermolecular

 © 2003 Wiley-VCH Verlag GmbH & Co. KGaA, Weinheim

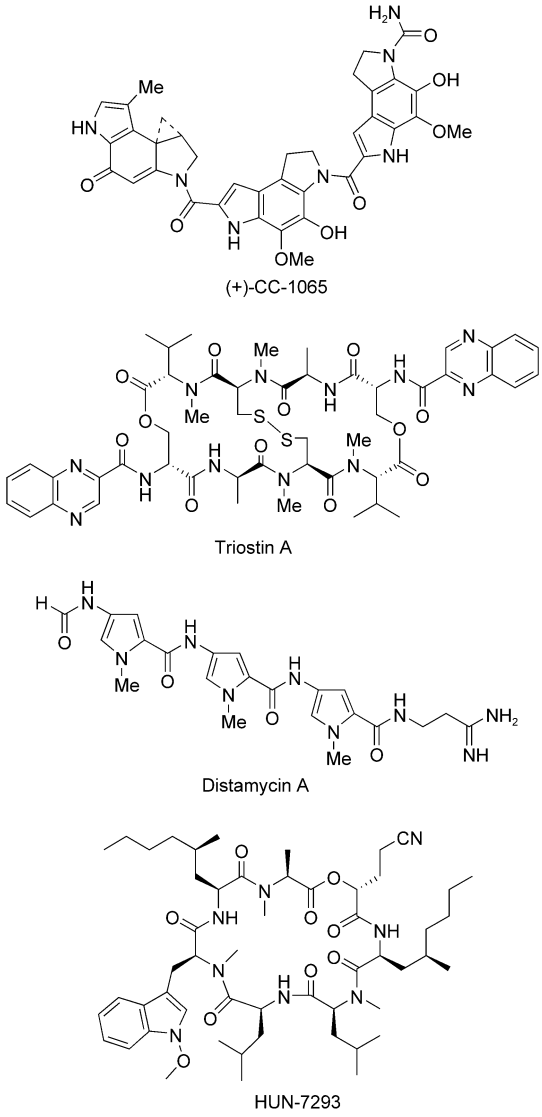


Scheme 5. Homo- or heterodimerization of libraries for protein–protein dimerization. The deconvolution of the unsymmetrical dimerization products is by scanning or deletion synthesis. Cy = cyclohexyl, PyBrOP = bromotris(pyrrolidino)phosphonium hexafluorophosphate.

olefin-metathesis reaction in the generation of chemical libraries,[60,61,64] and by one of the first disclosed applications of solid-supported catalysts (Pd-C) in solution-phase library preparation that was used to promote a biaryl coupling (see Scheme 5).[62] In this context, the use of size exclusion chromatography (filtration) for the rapid purification of such dimer, or higher oligomer, libraries was also demonstrated.[62]

Thus, the preparation and dimerization linkage of iminodiacetic acid diamides can be conducted in a reaction sequence that requires only three steps. In addition to the multiplication of the diversity that arises through the combinatorial dimerization linkage of the iminodiacetic acid diamides, the solution-phase synthesis of the intermediates permits their direct linkage which would be precluded by solid-phase synthesis techniques. As such, the strategy is uniquely suited for taking advantage of such dimerization (convergent) strategies utilizing a limited number of synthetic steps. This modular approach to the generation of libraries is especially well-suited for the discovery of antagonists or agonists of receptor and protein homo- and heterodimerization. Simple binders (i.e., **16**–**18**, Scheme 5) can serve as antagonists of ligand-induced receptor or protein dimerization. Covalently linked symmetrical dimers (i.e., **19**–**21**) can be utilized to promote receptor or protein homodimerization whereas unsymmetrical dimers can be utilized to promote receptor or protein heterodimerization. Thus, both antagonists and agonists may be developed depending on the therapeutic application and this was a major factor in our adaptation of this approach. Notably, the size and characteristics (cell permeability) of compounds targeting intracellular macromolecules may place restrictions on the library composition, whereas libraries of compounds addressing extracellular targets including cell surface receptors and proteins may not be influenced by such limitations.

One might arguably suggest from an examination of the anhydride templates that the structural complexity, available diversity, and drug-like properties of the library members, or scope of the technology may be restricted producing libraries of limited value. However, the present 40000-member library has been remarkably siccessful in providing leads for essentially any target it has been screened against. Counter to the prevailing trend of preparing libraries of increasing molecular rigidity and complexity, it may well be that this success can be attributed to the library's appropriate "intermediate" complexity where each library member embodies multiple pharmacophores more suited for lead discovery.[180] It should also be emphasized that alternatives to the amide couplings even for the initial library generations have been disclosed.[71] In addition and although this is discussed in



Scheme 6. Natural product templates where analogues were synthesized using the solution-phase combinatorial approach.

 © 2003 Wiley-VCH Verlag GmbH & Co. KGaA, Weinheim

greater detail in Sections 5 and 6, complex natural product libraries (Scheme 6) have been assembled using this technology indicating that the scope extends well beyond what one might initially suspect.

4. Targeting Protein–Protein Interactions

As attractive as the potential is for modulating aberrant cellular signaling[181–190] by inhibiting, promoting, or mimicking protein–protein[100,101,181,182] or protein–DNA interactions, the general consensus has been that such targets represent stubborn problems for small-molecule therapeutic intervention. The challenges posed by such targets arise from the large surface area generally covered by the two interacting proteins (approximately 800 Å^2 per protein on average), the relatively flat interface between binding proteins, and the range of affinities between proteins depending on their physiological function.[181] Although there are many examples of antibodies, dominant negative proteins, and medium-sized peptides that inhibit protein–protein interactions, the disclosure of small molecules has not been as extensive. Because the nature of protein–protein interactions differ widely (hydrophobic versus hydrophilic, the surfaces can be relatively flat and/or have buried crevices), since the affinities span a considerable range (K_d = 10^{-6}–10^{-12} M), and the response to inhibition may vary considerably (the need to simply perturb the equilibrium versus need for complete inhibition), it is fair to assume that some protein–protein interactions may prove to be better targets than others for small-molecule intervention. Table 3[191–225] summarizes many of the recent promising results of investigations on a range of targets and Scheme 7 shows the structures of some of the small-molecule modulators. It is clear that a reevaluation of the prevailing bias against such pro-

Table 3: Small molecule modulators of protein–protein interactions.

Protein–protein Interaction	Compound Source	Screen	Lead Structure[a]	Activity	Ref.
Ribonucleotide Reductase (dimerization)	Peptide analogue	Competitive binding assay	BILD 1263	Antagonist IC_{50} = 0.3 nM	[197]
iNOS (dimerization)	Encoded solid-phase library	Functional assay	iNOS inhibitor	IC_{50} = 0.6 nM	[198]
HIV Protease (dimerization)	Designed inhibitor	Enzyme inhibition	HIV-1 protease inhibitor	K_i = 310 nM	[199a]
HIV Protease (dimerization)	Natural product	Enzyme inhibition	Didemnaketal A	IC_{50} = 2 μM	[199b]
HIV-1 Integrase (dimerization)	Interface peptides	Enzyme inhibition	–	IC_{50} = 2–4 μM	[200]
CaM/smMLCK	α-helix mimetic	Enzyme inhibition	CaM antagonist	IC_{50} = 9 nM	[201]
MMP-2/$\alpha_v\beta_3$	Solution phase library	Radiolabeled binding assay	**27** (Figure 11)	Angiogenesis inhibitor	[77, 78]
Paxillin/α4	Positional scanning library	ELISA	**A7B7C7** (Figure 13)	Antagonist IC_{50} = 300 nM	[79]
Bax/Bcl-x_L	16320 compound library	Fluorescence polarization assay	BH3I-1 BH3I-1′ BH3I-2	Antagonist IC_{50} = 8–16 μM	[202]
Bax/Bcl-x_L	Natural product	Functional assay	Antimycin	Antagonist	[203]
Bax/Bcl-x_L	Virtual screening of 193383 compounds	Fluorescence polarization assay	HA14-1	Antagonist IC_{50} = 9 μM	[204]
Bax/Bcl-x_L	Designed α-helix mimetic	Fluorescence polarization assay	Bax antagonist-1	K_D = 114 nM	[205a]
Bax/Bcl-x_L	Designed α-helix mimetic	Fluorescence polarization assay	Bax antagonist-2	K_i = 1.6 μM	[205b]
MDM2/p53	Natural product	ELISA	Chlorofusin	Antagonist IC_{50} = 4.6 μM	[206a]
MDM2/p53	Unknown	ELISA, NMR	Chalcone B Antagonist	IC_{50} = 49 μM K_D = 90 μM	[206b]
HDM2/p53	Designed inhibitor	ELISA	HDM2 Antagonist	IC_{50} = 5 nM	[207]
Myc/Max	Solution phase library	FRET	**28** (Figure 17)	Antagonist IC_{50} = 20 μM	[80]
LEF-1/β-catenin	Solution phase library	Reporter assay	**A1B2C8** (Figure 18)	Antagonist	[71]
NGF/p75 NGF/TrkA	Commercial libraries	Radiolabeled binding assay	ALE-0540	IC_{50} = 6 μM IC_{50} = 4 μM	[208]
HIV-1 (RANTES)/CCR5	Corporate library	Radiolabeled binding assay (RANTES)	TAK-779	Antagonist IC_{50} = 1.4 nM	[209]
IL-2/IL-2R	Designed inhibitor	Radiolabeled binding assay	Ro26-4550	Antagonist IC_{50} = 3 μM	[210a]
IL-2/IL-2R	Structure-based design + fragment assembly	Competitive binding	IL-2 Antagonist	IC_{50} = 60 nM, K_d = 100 nM	[210b]
IL-1/IL-1R	Designed inhibitor	Scintillation proximity assay	IL-1 Antagonist	IC_{50} < 10 μM	[211]
EPO/EPOR	Phage display	Radiolabeled binding assay	EMP1 (Figure 20)	EPO Agonist IC_{50} = 0.2 μM	[319–321]
EPO/EPOR	Corporate library	Radiolabeled binding assay	EPO antagonist	IC_{50} = 60 μM	[330]
	Modified to	Radiolabeled binding assay	EPO agonist	EPO Agonist IC_{50} = 4.4 μM	[330]
EPO/EPOR	Solution phase library	Radiolabeled binding assay	**30** (Figure 19)	EPO Agonist EC_{50} = 8 μM	[82]
TPO/TPOR	Phage display	ELISA	TPO Agonist	EC_{50} = 400 nM	[212]
	Modified to	ELISA	AF13948 (dimer)	EC_{50} = 100 pM	[212]

 © 2003 Wiley-VCH Verlag GmbH & Co. KGaA, Weinheim

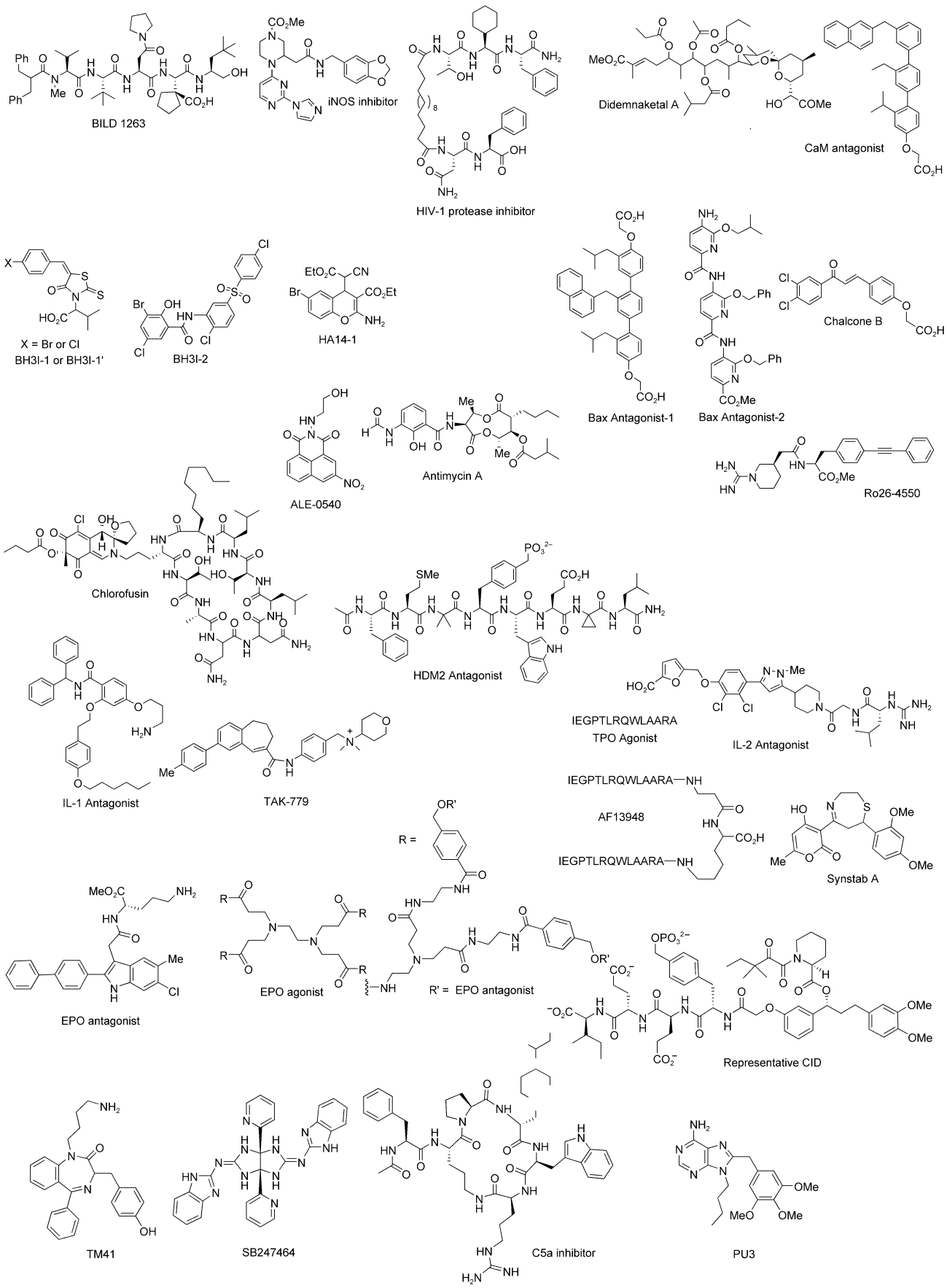
Table 3: (Continued)

Protein–protein Interaction	Compound Source	Screen	Lead Structure[a]	Activity	Ref.
TPO/TPOR	Corporate library	Radiolabeled binding assay	TM41	TPO Agonist	[213]
GCSF/GCSFR	Corporate library	Functional assay	SB247464	Agonist	[214]
C5a/C5aR	Design inhibitor	Radiolabeled binding assay	C5a antagonist	$IC_{50} = 300$ nM	[215]
FKBP/Cn	Natural product	–	FK506	Cn inhibitor	[216]
Cyclophilin/Cn	Natural product	–	Cyclosporin A	Cn inhibitor	[216217]
FKBP/FRAP	Natural product	–	Rapamycin	Immunosuppressant	[218]
Chemical inducers of dimerization (CIDs)	Synthetic constructs	Various	Representative CID	Various	[192–196]
Ribosome (RNA)/protein	Natural products	Various	Macrolides Tetracycline Oxazolidinones Streptogramin Chloramphenicol TAN 1057 Pestalone Cycloheximide Hygromycin Blasticidin Virginamycin Sparsomycin Puromycin Clindamycin	Antibiotics	[219]
Hsp90/Client Protein	Natural products	Various	Geldanamycin Herbimycin Radidicol 17-AAG	Antitumor compounds	[220a]
Hsp90/Client Protein	Designed ligand	Competitive binding	PU3	$EC_{50} = 15$–20 μM	[220b]
α/β tubulin	Natural products	Various	Colchicines Vincristine Taxol Epothilones	Mitotic inhibitors	[221a]
α/β tubulin	Commercial Library	Cell-based screen	Synstab A	Mitotic Inhibitors	[221b]
Topoisomerase/DNA	Natural product	Various	Camptothecin	Antitumor compounds	[222]
PG/Transpeptidase	Natural product	Various	Vancomycin	Antibiotic	[223a]
LI II/Transglycosylase	Natural product	Various	Ramoplanin	Antibiotic	[,223b]
Nuclear hormone receptors	Various	Various	Various	Agonists and antagonists	[224]
RGD mimetics	Various	Various	Various	Antagonists	[240–252]
SH2 domains	–	–	–	–	[181, 225a]
SH3 domains	–	–	–	–	[225b]
WW domains	–	–	–	–	[225c]
PDZ domains	–	–	–	–	[225d]

[a] Lead structure is shown in Scheme 7 unless indicated otherwise.

tein–protein interaction targets is warrented.[100–102,171,181,182] Interestingly, fewer of these examples represent results derived from screening combinatorial libraries than might be expected and most that do relied on phage display to generate initial peptide leads. The examples in Table 3 represent a wide range of strategies despite the commonality of all in perturbing a protein–protein interaction. For example, those that entail the inhibition of enzyme action do so by a range of mechanisms including directly preventing their homodimerization (HIV protease) or heterodimerization (ribonucleotide reductase), or inducing a conformational change that precludes dimerization (iNOS), effecting their localization (MMP-2, CaM), access to the substrate (transpeptidase, transglycosylase), stabilization of an intermediate ternary complex (topoisomerase), or promoting inhibitory ternary complexes with additional proteins (calcineurin (Cn)). Not included in this summary are enzyme active-site inhibitors that block a peptide or protein substrate binding to the enzyme, small-molecule agonists and antagonists of G-protein-coupled receptors, and all the cell surface integrin inhibitors based on the RGD recognition motif. The G-protein-coupled receptor antagonists typically bind the receptor transmembrane domain and do not directly (perhaps allosterically) perturb a receptor–ligand interaction. In contrast, the cell surface integrin inhibitors have been the subject of several reviews[240–252] and constitute a beautiful example of the discovery of a simple, small, and general protein–protein interaction motif that lends itself to subsequent antagonist development. Similarly, Src-homology 2 domains (SH2), SH3, WW, and PDZ domains constitute common protein–protein binding sites with small, focused interfaces for protein localization or signal transduction that have been the subject of small-molecule screening or design efforts.[101,181,225] In addition, there are several historically important modulators of protein–-protein interactions that have defined in such discussions important therapeutic targets. Although these are often neglected, they are superb examples of achieving productive therapeutic endpoints by interfering with a protein–protein (or protein–DNA) interaction. Notably, there may be significant distinctions in the work, design of the library, screening methods, and challenge of the investigations depending on whether it is an antagonist or agonist of a protein–protein interaction that is sought. To date, the consensus is that the discovery of antagonists may be much

 © 2003 Wiley-VCH Verlag GmbH & Co. KGaA, Weinheim



Scheme 7. Representative small-molecule modulators of protein–protein interactions listed in Table 3.

 © 2003 Wiley-VCH Verlag GmbH & Co. KGaA, Weinheim

easier than an agonist.[73,170,171] As such, the efforts related to the discovery of EPO, TPO, and GCSF agonists (mimetics; Table 3) constitute remarkable achievements. Finally, the development of general methods for establishing the selectivity of such antagonists or agonists is a challenge that still has not been faced by the field and that may constitute a major reason for the reluctance to address protein–protein interactions as useful therapeutic targets.

Several very clever ways of enlisting chemically prepared bifunctional protein binders that induce dimerization to achieve a biological endpoint or objective have been detailed.[191] These chemical inducers of protein dimerization (CIDs) pioneered by Schreiber and Crabtree et al. have been used to modulate cell membrane receptor signaling,[192] to control gene expression,[192c,193] to selectively antagonize cellular processes,[194] to identify protein–ligand partners,[195] and even to target protein heterodimers with no established ligand.[196]

Cell growth, differentiation, migration, and apoptosis are regulated in part by growth factors or cytokines. These factors are unable to penetrate the cell membrane and exert their effects by binding to cell surface receptors. In many instances, such receptors are activated by ligand-induced dimerization or oligomerization.[183–186] In addition, several components of the intracellular signal-transduction pathways are also regulated by dimerization. For instance, certain cytoplasmic signal-transduction molecules dimerize after activation, and the active form of a transcription factor is often a dimer.[187–190] Thus, protein dimerization has emerged as a general mechanism for the initiation and downstream regulation of signal transduction. The targets listed below that we selected to pursue were chosen not only for their therapeutic importance, but also because each constitutes a distinct stage at which to modulate cellular signaling by controlling such protein–protein or protein–DNA interactions:

- Promote a cell surface receptor homodimerization that is required for activation (EPO agonist).
- Inhibit an extracellular cell surface integrin–protein interaction (MMP-2/$\alpha_v\beta_3$).
- Inhibit an intracellular cell surface integrin–protein interaction (Paxillin/$\alpha_4\beta_1$).
- Inhibit the intracellular heterodimerization of a transcription factor (Myc/Max, LEF-1/β-catenin).
- Inhibit the protein–DNA interaction of a transcription factor (LEF-1/β-catenin, androgen receptor).

The more personal account of our own studies on this series of targets that follows highlights some important aspects of target selection, screening technology, and library generation.

4.1. MMP-2/$\alpha_v\beta_3$

MMP-2 (gelatinase A), a member of the matrix metalloproteinase family, is secreted by vascular endothelial cells and plays a crucial role in degrading the extracellular matrix during tumor-induced angiogenesis.[226] Consequently, MMP-2 inhibitors have been extensively pursued and developed which diminish tumor growth and metastasis.[226–231] Another key participant in angiogenesis is the integrin[232] $\alpha_v\beta_3$, which

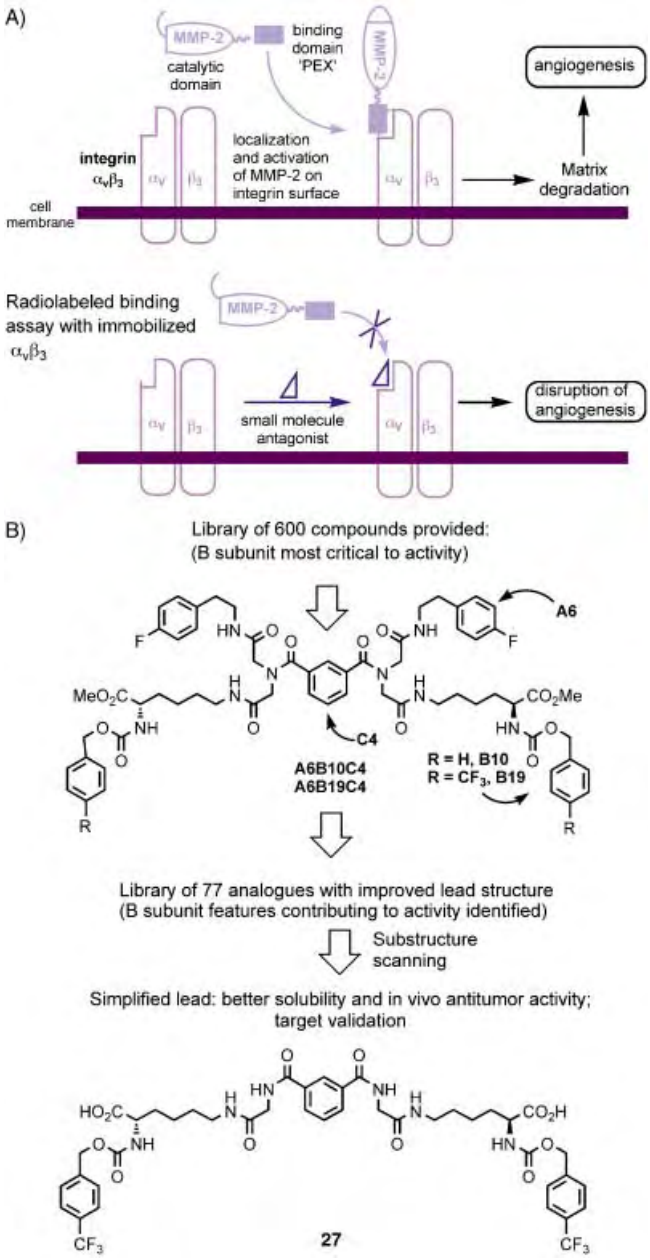


Figure 3. A) Disruption of angiogenesis by blocking matrix metallo proteinase 2 (MMP-2) binding to integrin $\alpha_v\beta_3$. B) Developing the angiogenesis inhibitor **27**.

mediates cellular interactions with the extracellular matrix.[231,233–239] This heterodimeric cell surface receptor recognizes certain matrix proteins containing the RGD (Arg-Gly-Asp) peptide sequence, which leads to integrin clustering, and ultimately supporting the migration and survival of endothelial cells. Soluble RGD peptides, nonpeptide RGD mimetics, and antibodies that disrupt $\alpha_v\beta_3$ ligation have been shown to inhibit angiogenesis and tumor growth.[240–252] Conservative estimates indicate that at least 40 pharmaceutical firms are developing angiogenesis inhibitors directed at these two targets with at least 27 drugs currently in clinical trials.[231,253–258]

Recently, a novel interaction between MMP-2 and integrin $\alpha_v\beta_3$ was observed by Cheresh et al. when these

 © 2003 Wiley-VCH Verlag GmbH & Co. KGaA, Weinheim

proteins were found to colocalize on the surface of angiogenic blood vessels in vivo.[259] Integrin $\alpha_v\beta_3$ binds MMP-2, and this interaction is a requisite step in the cellular utilization of the enzyme on the surface of invasive endothelial cells.[260] A noncatalytic, 193-residue C-terminal fragment of MMP-2, termed PEX, was found to inhibit MMP-2 binding to $\alpha_v\beta_3$ and to indirectly block its cell surface proteolytic activity.[261] PEX was further shown to disrupt angiogenesis and tumor growth in the chick chorioallantoic membrane (CAM). A naturally occurring form of PEX can be detected in vivo in association with cells expressing $\alpha_v\beta_3$, which implicates the role of PEX as an endogenous regulator of angiogenesis. These observations suggested that disrupting the extracellular binding of MMP-2 to integrin $\alpha_v\beta_3$ may be a promising approach to controlling angiogenesis, and could provide a novel therapeutic target for angiogenesis-dependent diseases including cancer (Figure 3).

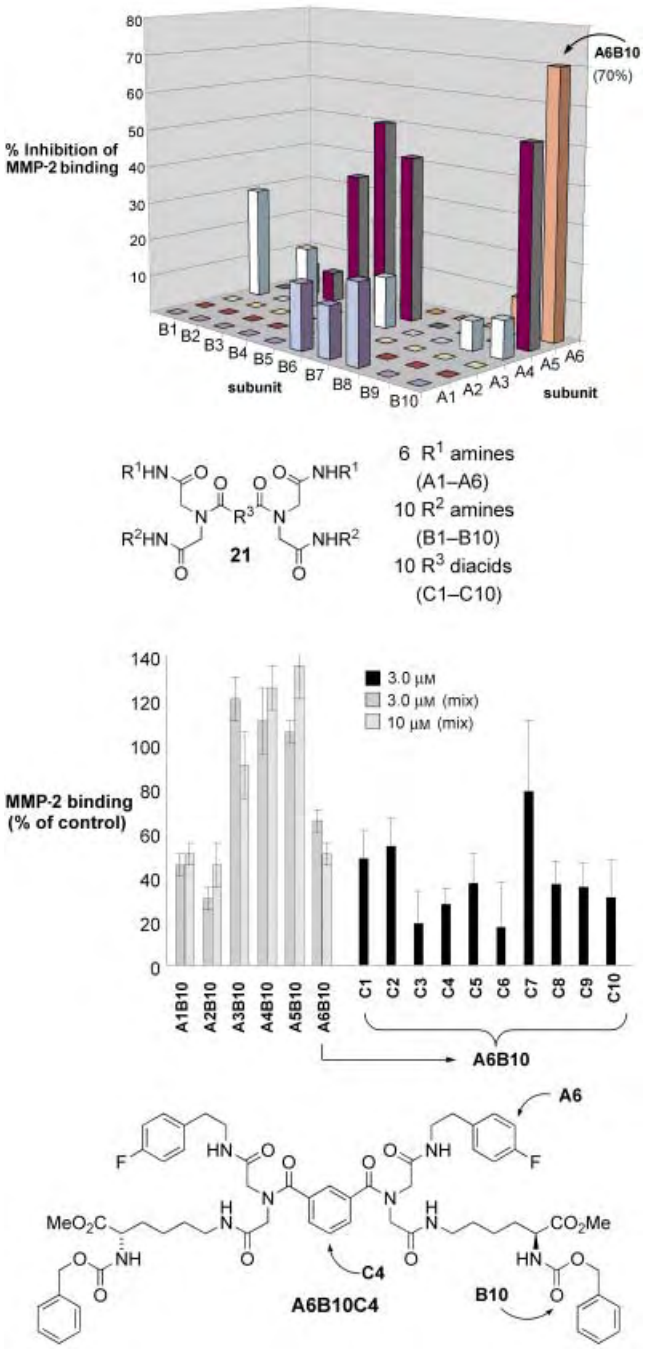


Figure 4. Screening of a 600-compound library that provided the initial lead **A6B10C4** for inhibition of MMP-2 binding to $\alpha_v\beta_3$.

The structural details of the MMP-2/$\alpha_v\beta_3$ interaction are unknown, although it has been established that the integrin binding site is distinct from that which recognizes the RGD sequence in traditional high-affinity ligands (e.g., vitronectin).[260] In the absence of further knowledge of the target structure, a combinatorial chemistry approach was used to identify small-molecule MMP-2/$\alpha_v\beta_3$ antagonists. This approach provided the first members of a new class of anti-angiogenic compounds that derive their activity by inhibiting this protein–protein interaction, and validated this extracellular target for therapeutic intervention.[77,78]

The initial lead came from a library that was screened as 60 mixtures of 10 compounds (Figure 4). The most effective inhibitors contained the **B10** subunit and each of the individual compounds in several of these mixtures was prepared for identification of the active constitutents. Because the 10-compound mixture was generated in the last step of the library synthesis, this entailed simply repeating the last step of the synthesis with individual (instead of mixture) C subunits on the archived samples of the immediate precursor.

Thus, the screening of the compound libraries in a radiolabel binding assay using the immobilized integrin led to the initial identification of **A6B10C4**, its refinement to **A6B19C4** and its subsequent simplification to provide **27** which also possesses improved solubility and in vivo activity (Figure 3). The inhibitor **27** was shown to bind $\alpha_v\beta_3$ and disrupt the binding of MMP-2, but not the integrin ligand vitronectin. It inhibits collagen-matrix degradation without directly inhibiting MMP-2 enzymatic activity, was shown to be a potent inhibitor of angiogenesis in a chick CAM model, and led to near complete reduction in the growth of CS-1 melanoma tumors in vivo in a chick CAM model. Notably, a close analogue of **27** (the benzamide rather than the carbamate) was inactive and used as a control.[77,78]

4.2. Paxillin/α_4: A Successful Use of Positional Scanning

The integrin $\alpha_4\beta_1$ (also know as VLA4, Very Late Antigen 4) is a cell surface receptor that plays an important role in embryogenesis, hematopoiesis, and the immune response.[262–267] It binds natural ligands including vascular cell adhesion molecule 1 (VCAM-1) and an alternatively spliced connecting segment (CS-1) from the extracellular matrix protein fibronectin. It mediates cellular adhesion and activation through a variety of cell–cell and cell–matrix interactions that regulates leukocyte migration into tissues during inflammatory responses and lymphocyte trafficking.[262–267] This integrin is believed to regulate cellular functions differently from other integrins because the α_4 cytoplasmic tail binds tightly to the signaling adapter protein Paxillin through a short conserved sequence motif dominated by two residues (Glu 983 and Tyr 991).[268] The α_4/Paxillin

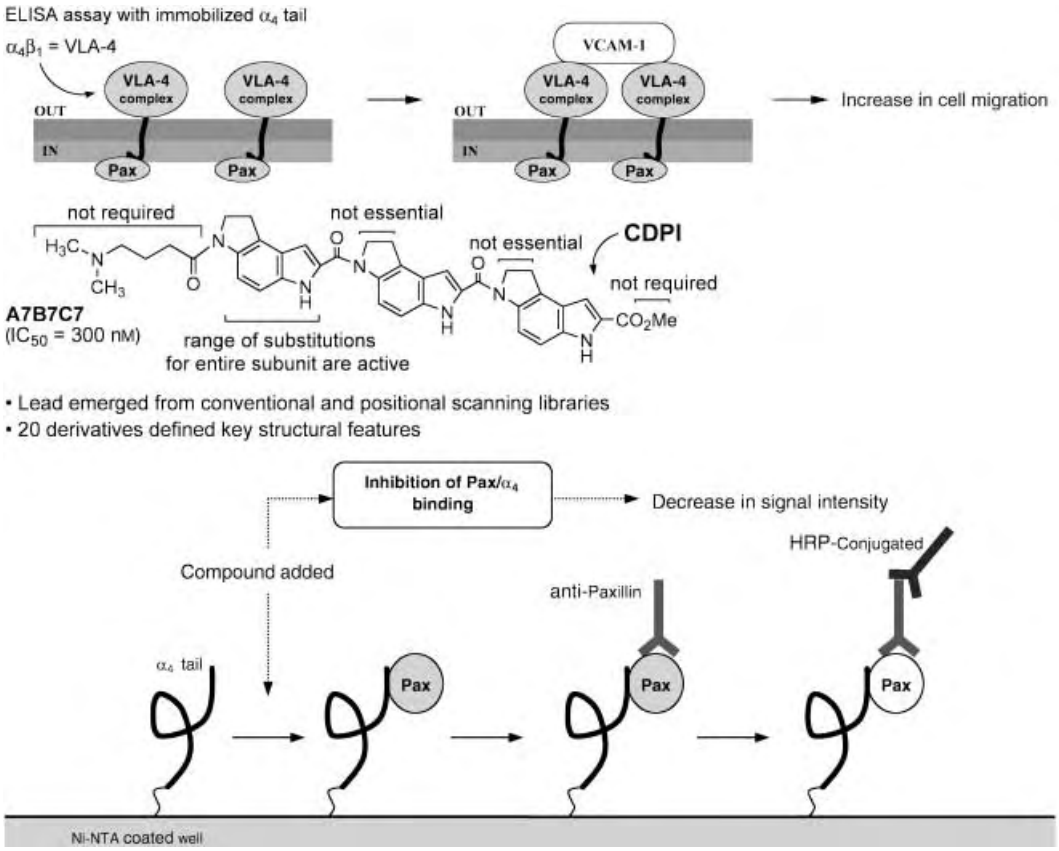


Figure 5. Top: Inhibition of cell migration by blocking intracellular paxillin/α4 binding, middle: identification of the lead structure **A7B7C7** through high-throughput screening using an ELISA assay and bottom: description of the high-throughput screen (ELISA). VLA-4 = very late antigen 4, Pax = paxillin, HRP = horseradish peroxidase

interaction leads to enhanced rates of cell migration and reduced rates of cell spreading, focal adhesion, and stress fiber formation (Figure 5).[269,270] These biological responses to integrin-mediated cell adhesion contribute to leukocyte migration and changes in gene expression important in chronic inflammation. While extracellular inhibitors for this class of integrins are under development for the treatment of asthma and multiple sclerosis,[271–273] inhibitors targeting the unique cytoplasmic Paxillin/α_4 interaction had not been explored.

The target protein–protein interaction again represents one in which no structural information is available and no existing inhibitors had been disclosed. The examination of our libraries (ca. 40000 compounds) in an ELISA assay enlisting the immobilized α_4 cytoplasmic tail and screening for inhibition of Paxillin binding provided the first and potent inhibitors of this protein–protein interaction (Figure 5). The preparation of key substructure analogues of **A7B7C7** identified structural features required for activity, those available for further modifications, and those which may be removed or modified without significantly changing the activity. The most potent lead structure was shown to inhibit $\alpha_4\beta_1$-mediated human Jurkat T cell migration in a dose-dependent manner validating the intracellular Paxillin/α_4 interaction as a useful and unique target for therapeutic intervention. Notably, such target validation is often first established by biological techniques or with monoclonal antibodies or peptide consensus sequences derived from the receptor or its ligands. Consequently, it is of note that even the initial target validation as well as its suitability for small-molecule therapeutic intervention came from the screening of small-molecule libraries. Moreover, the lead structure emerged from a library of 1000 compounds that had been prepared in two formats: 1) a traditional small-mixture format composed of 100 mixtures of 10 compounds, and 2) a less traditional positional-scanning library. Parallel testing of both libraries provided the rare opportunity to critically compare the results derived from the two approaches.[79]

Thus, an important feature in this work rested with the parallel screening of a positional-scanning library for which every component contained in a traditional compound library was also present, but assembled such that immediate deconvolution was possible. Scanning for the best subunit at position A by screening sublibrary **AxBC** showed that the greatest inhibition was observed for mixture **A7BC**, identifying the CDPI subunit as the best subunit at position A (Figure 6). Using the same procedure, CDPI was also identified as the most effective subunit at positions B and C (Figure 6). Immediate deconvolution of the results identified the **A7B7C7** combination as a potent Paxillin/α4 binding antagonist. This same lead compound (**A7B7C7**) was identified from the simultaneous and more traditional library screening. This unbiased screening success must be tempered by the fact that the positional-scanning-library screening and

 © 2003 Wiley-VCH Verlag GmbH & Co. KGaA, Weinheim

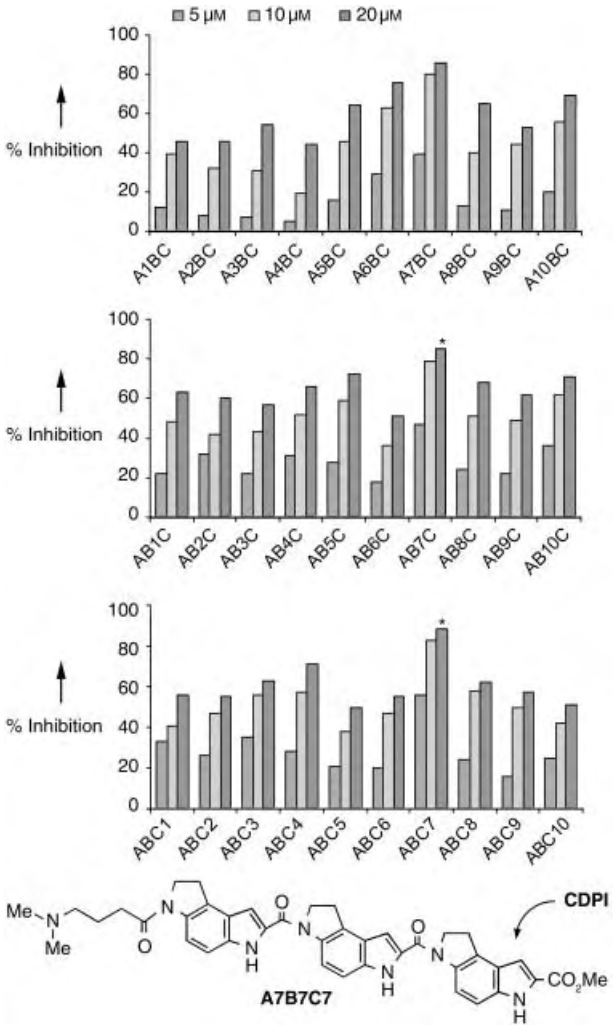
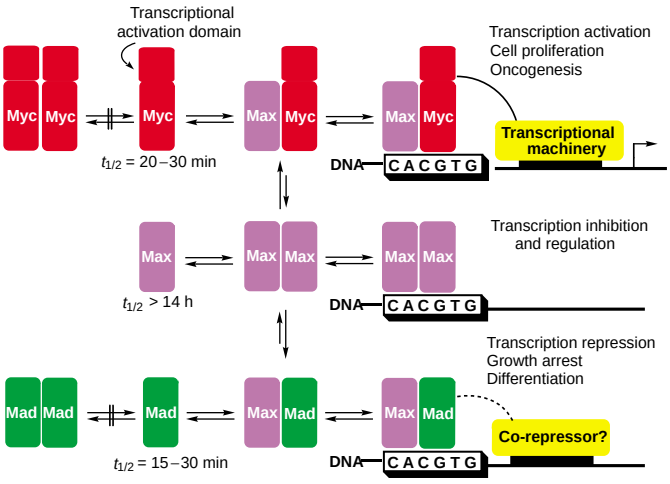


Figure 6. Inhibition of paxillin/α4 binding by the positional scanning libraries AxBC (top, A scan), AByC (middle, B scan), and ABCz (bottom, C scan). Each mixture of 100 compounds was tested in triplicate at 5, 10, and 20 μM (total compound).

direct deconvolution did not identify all candidate inhibitors which were identified from the traditional library. This situation is a natural consequence of testing larger 100-compound mixtures and the relative insensitivity of the assay to the contribution of any single, uniquely acting compound in the mixture. Thus, the global observations were effectively detected with the positional-scanning library, and a useful lead structure with defined properties was identified.[79] However, more subtle discoveries within the libraries were not identified. Thus, the disadvantages associated with the loss of their detection and this information contained within the library must be balanced against the advantages of the ease of synthesis of the parent libraries and judged in light of the objectives of the library screening. As in this case, the positional-scanning libraries typically would be only effective for lead identification and would be less suitable for lead optimization.

4.3. Myc/Max

The *c-myc* proto-oncogene is involved in the progression of a wide-range of human tumors.[274–284] Proteins in the immediate Myc network are essential regulators of cell growth and differentiation. Activation and transformation occur mainly through elevated expression of its gene product Myc, a short-lived nuclear protein and an important member of the basic helix-loop-helix leucine zipper (bHLHLZ) transcription factors (Figure 7).[285,286] The oncogenic potential of *c-myc* has been demonstrated in transgenic animals, reconstituted organs or cell culture, and typically requires the action of at least one additional oncogene, such as *ras* or *bcl-2* (inhibits apoptosis).[274–284] In normal cells, Myc is required for cell proliferation and prevents differentiation. It is transiently expressed in response to mitogenic stimuli and it has a short half-life ($t_{1/2}$ = 20–30 min). Its aberrant expression in the



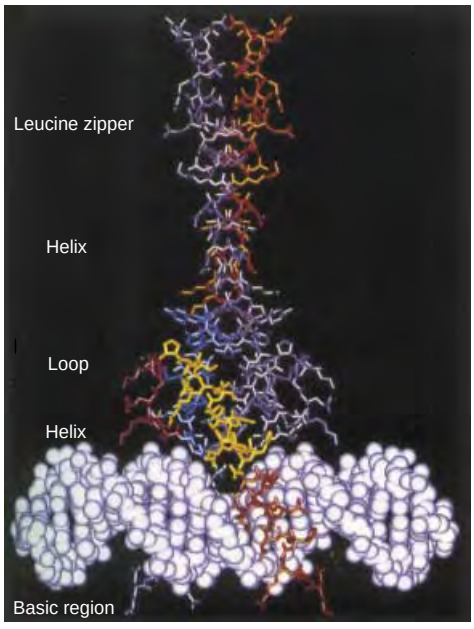


Figure 7. Top: Myc-Max-Mad network of transcription control: cell proliferation versus differentiation Max = Myc associated factor X. Bottom: Max(22-113) dimer complexed with DNA. Reproduced with permission from *Nature*, reference [285].

© 2003 Wiley-VCH Verlag GmbH & Co. KGaA, Weinheim

absence of such growth factors drives cells into cell cycle but also induces apoptosis unless co-oncogenic mechanisms are present (i.e., inhibition by constitutive *bcl-2* overexpression).

All known activities of Myc require heterodimerization with Max,[285–293] a constitutively expressed bHLHLZ protein that is stable ($t_{1/2} = > 14$ h) and always present. The Myc/Max heterodimer binds the DNA sequence CACGTG (E box element) and activates transcription through the transactivation domain of Myc. DNA binding occurs through the basic region while both the HLH and the leucine zipper form the dimerization interface.[285,286] Max, but not Myc, forms homodimers which bind the same DNA site and inhibit transcription. In part, this results from the competition for Max and for the common DNA site. In addition, Max heterodimerizes with another family of bHLHLZ proteins that include Mad (Mad-1), Mxi-1, Mad-3, and Mad-4 that are transiently expressed ($t_{1/2} = 15$–30 min) and signal growth arrest and differentiation.[296,297] Their dimerization behavior is similar to that of Myc in that they do not homodimerize or interact with Myc family members, but readily form heterodimers with Max that bind the CACGTG core consensus sequence. Mad and Myc compete for Max with approximately equal affinities and the heterodimers are formed in preference to Max homodimerization. Mad/Max heterodimers repress or antagonize Myc/Max transcriptional activation. In normal cells, the expression of Mad is induced by differentiating stimuli while Myc expression is repressed.[274–283] Thus, Myc/Max dimers induce proliferation and apoptosis in nontransformed cells while Max/Max and Mad/Max are involved in growth arrest, differentiation, and cell survival. At the center of this network lies Max which is metabolically stable ($t_{1/2} = > 14$ h) and constitutively expressed. Its heterodimer partners, Myc ($t_{1/2} = 20$–30 min) and Mad ($t_{1/2} = 15$–30 min), are rapidly degraded and highly regulated. Mitogenic stimulation induces a rapid rise in Myc levels, and a shift in the equilibrium to Myc/Max dimers and transcriptional activation. In transformed cells, when accompanied by oncogenic events inhibiting apoptosis, constitutive Myc expression maintains the cell proliferation state and prevents growth arrest and differentiation.[274–283] Thus, the function of the Myc-Max-Mad network relies on four major features:

1) Max is a required dimerization partner for Myc (or Mad) to bind DNA and execute its biological functions.
2) Myc/Max and Mad/Max heterodimers form in preference to Max/Max homodimers.
3) The highly regulated expression levels of Myc and Mad induce rapid changes in the equilibrium between the dimers. The Myc/Max heterodimer activates transcription throughout all stages of the cell cycle and maintains the cell in a state of cell growth and proliferation while the Mad/Max heterodimer signals an exit from the cell cycle, growth arrest, and differentiation.
4) All dimers compete for common target DNA sites, and the Myc/Max transcription activation is antagonized by the other dimers. Thus, the aberrant expression of Myc that leads to transformation may be addressed through inhibition of Myc/Max heterodimerization and its subsequent transcriptional activation. This provides an attractive therapeutic target for the treatment of cancer that is central to the disease.

A novel FRET assay for monitoring Myc/Max dimerization was developed specifically for this work (Figure 8). Thus, the fusion proteins (MycCFP and MaxYFP) consisting of the

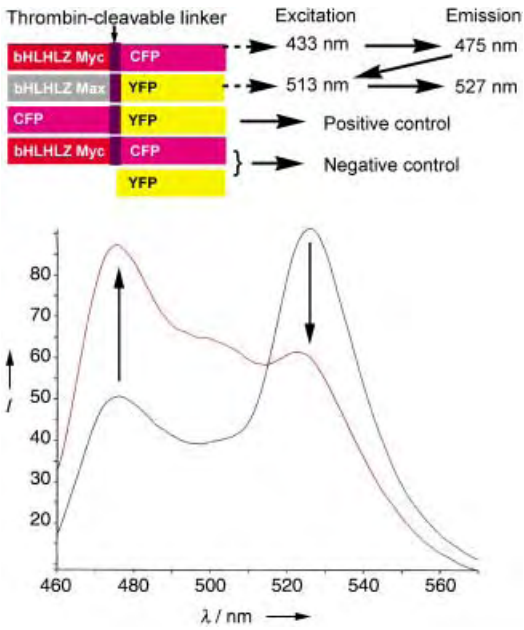


Figure 8. Fluorescence resonance energy transfer (FRET) assay. Addition of dimerization inhibitors induces a decrease in the intensity at 527 nm (dimer) and an increase in intensity at 475 nm (monomer). Compounds that give rise to a large ratio I_{475}/I_{527} are selected. CFP = cyan fluorescent protein, YFP = yellow fluorescent protein.

bHLHLZip domain of human *c-myc* linked to the N-terminus of cyan fluorescent protein (CFP) and the bHLHLZip domain of Max fused to the N-terminus of yellow fluorescent protein (YFP) were cloned, expressed, and purified for use in the assay. Inhibition of dimerization is measured as a loss of the FRET signal emission at 527 nm (YFP) following excitation of CFP at 433 nm. Using this assay, our library of 40 000 compounds was screened for inhibition of Myc/Max dimerization. Two closely related leads emerged from an isoindoline library of 240 compounds (Figure 9). These remarkably small inhibitors (38 % FRET inhibition at 25 μM for **28**) were subsequently shown to inhibit Myc/Max binding in a conventional ELISA assay and to inhibit Myc/Max DNA binding in a gel-shift assay confirming the observations made through use of the novel FRET assay. Impressively, the two most potent leads were shown to inhibit Myc-induced transformation of chicken embryo fibroblasts ($IC_{90} = 20$ μM) establishing functional activity of the compounds in a cellular assay.[80]

4.4. LEF-1/β-catenin

The majority of colorectal tumors contain mutations in the tumor-suppressor protein, adenomatous polyposis coli

 © 2003 Wiley-VCH Verlag GmbH & Co. KGaA, Weinheim

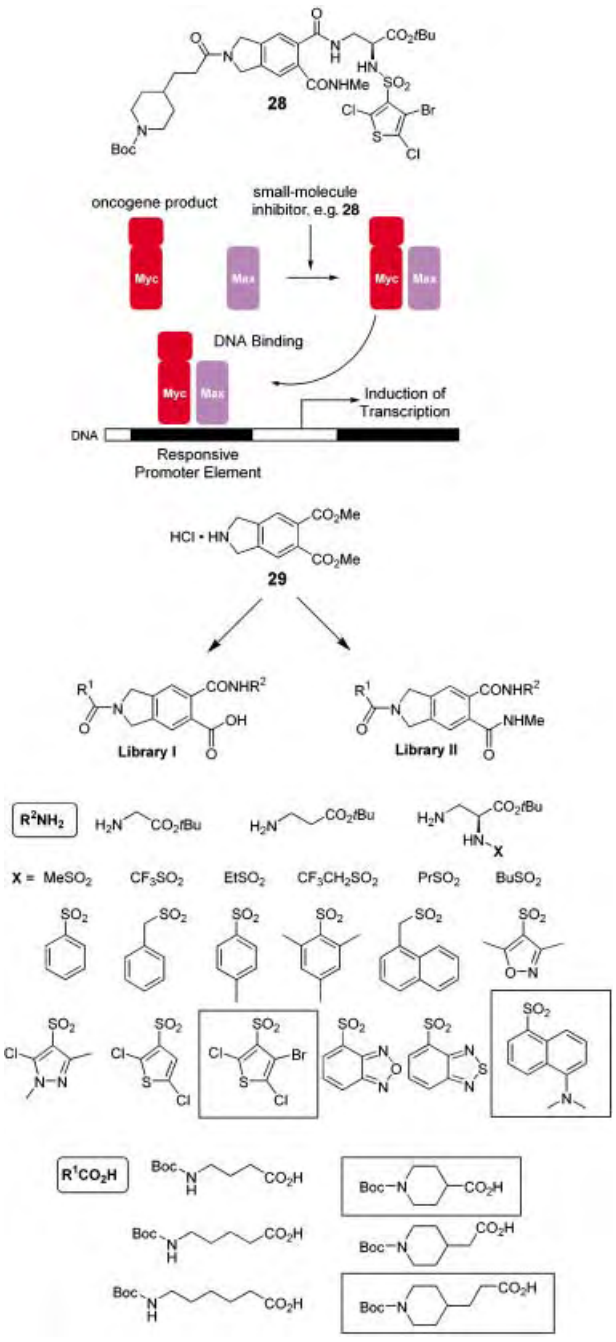


Figure 9. Inhibition of Myc-Max heterodimerization and aberrant gene transcription: antitumor target validation.

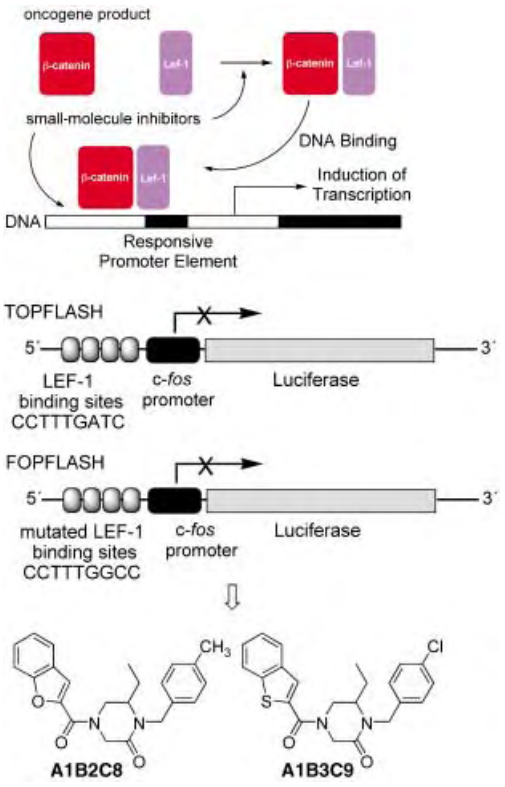


Figure 10. Inhibition of LEF-1/β-catenin-mediated gene transcription: controlling aberrant gene transcription and antitumor target validation. More than 40000 compounds were screened for inhibition of LEF-1 mediated gene transcription in a TOPFLASH luciferase reported assay. Two leads **A1B2C8** and **A1B3C9** exhibit TOPFLASH selectivity, they are derived from a 150-member non-amide based IDA library of piperazinones.

(APC) of the colon, that result in the release and accumulation of β-catenin in the cell nucleus. β-Catenin binds to and activates transcription factors including LEF-1 (Lymphoid-enhancers binding factor 1).[298–301] This results in upregulated and aberrant gene expression which is a key step in the development of colon cancer (Figure 10). The LEF-1 transcription factors (TCF) that interact with β-catenin share an identical DNA-binding domain referred to as the high mobility group (HMG) domain recognizing the sequence 5′-CTTTGWW-3′ (W = A or T). Importantly, LEF-1 binds the DNA minor groove[302] through its HMG domain making it an ideal target for libraries of DNA minor-groove binding ligands. When β-catenin interacts with the amino terminus of LEF-1, it activates transcription. In the absence of β-catenin, LEF-1 actively represses transcription. It is thought that LEF-1 bound β-catenin displaces corepressors and β-catenin binds LEF-1 through a domain distinct from that of the corepressors. The oncogenic potential of β-catenin through its interaction with LEF-1 has been demonstrated by Vogt et al.[303]

Initial studies were conducted screening our library of 40000 compounds enlisting a TOPFLASH/FOPFLASH cell-based reporter assay[298] transiently transfected into a colon cancer cell line (SW480) that has an APC mutation which allows β-catenin to accumulate in the nucleus. The use of a luciferase reporter assay permits the detection of leads that act by disrupting the LEF-1/β-catenin binding interaction or that inhibit LEF-1/DNA binding. This approach led to the identification of two classes of small molecules that inhibit LEF-1/β-catenin-mediated gene transcription. The first class, of which **A1B2C8** (3.7-fold inhibition at 10 μM) and **A1B3C9** (4.8-fold inhibition at 10 μM) are representative, proved to be a surprising class of small molecules that probably do not act by inhibiting LEF-1/DNA binding, but rather by inhibiting LEF-1/β-catenin binding (Figure 10). Their evaluation in a functional cellular assay revealed that they inhibit the β-

 © 2003 Wiley-VCH Verlag GmbH & Co. KGaA, Weinheim

catenin-induced tumor cell transformation of the colon cell line SW480. The initial library of 150 members from which the lead emerged was expanded to more than 350 members with the identification of structural features important for activity in the reporter and functional assays.[71] These studies are now being expanded to larger libraries based on **A1B2C8** and **A1B3C9** and with the development of a FRET assay capable of directly screening for disruption of LEF-1/β-catenin binding. This assay will serve to define the site of action of the leads related to **A1B2C8** and should provide new candidate lead structures through the screening of future libraries. The second class of selective TOPFLASH inhibitors emerged from a library of minor-groove DNA binding compounds and are discussed in detail in Section 5.3.

4.5. EPO/EPOR: Agonists from Antagonists

Erythropoietin (EPO), a 34-kDa monomeric glycoprotein composed of 165 amino acid residues and an almost equivalent mass of carbohydrate, is the principle factor regulating red blood cell production.[304–311] EPO exerts its effects by controlling the proliferation, differentiation, and maturation of erythroid progenitors. The EPO gene, which shows no homology with other known genes, is a single-copy gene and highly conserved across different species. Recombinant human EPO has found clinical applications in the treatment of anemias particularly those resulting from renal disease including kidney damage, anemia resulting from malignancy, AIDS or AIDS treatment, and anemia associated with myelodysplastic syndromes.[308–311] While EPO is presently the most important biotechnology product and its use has evolved into a $>$\$7 billion/year market, its administration requires intravenous or subcutaneous injection. This situation has led to an interest in developing small-molecule mimics of EPO to replace the recombinant human protein. More recently, EPO itself is thought to be a potentially useful antitumor agent,[312] although the mechanism is not yet well understood. Prompted by observations that EPO-treated patients experience longer survival times and more complete remissions than untreated patients, the in vivo evaluation of EPO itself for antitumor efficacy was successfully conducted.[312] EPO elicits its response through binding and homodimerization of its receptor EPOR[313–316] which is a member of the Class I cytokine receptors (Table 4).[183–185] The Class I cytokine receptors are characterized by the presence of one or two conserved 200-amino acid fibronectin type III-like domains, four conserved cysteine residues, and the conserved motif Trp-Ser-Xaa-Trp-Ser (WSXWS) in the extracellular domain. The intracellular domains of the cytokine receptors, unlike the receptor tyrosine kinases, lack intrinsic enzymatic activities. Ligand binding induces dimerization or oligomerization and this allows the interaction (dimerization) and activation (cross phosphorylation) of noncovalently associated tyrosine kinases (Janus Kinases; JAKs), Figure 11.[47,71,188,318] In turn, the activated JAKs phosphorylate cytoplasmic domain tyrosines of the receptor enlisted to recruit signaling proteins including STATs (Signal Transducers and Activators of Transcription).[187,188] Recruitment of STATs results in their phosphorylation, homo- or heterodimerization, and subsequent translocation to the nucleus where they directly activate gene transcription. This is the most direct signal-transduction pathway known and beautifully enlists coordinated protein–protein homo- or heterodimerization of signaling molecules to link the initiation receptor-dimerization event directly to gene transcription. Notably, receptor homodimerization enlists JAK and STAT homodimers (JAK2/JAK2 and STAT5/STAT5 for EPOR) that bind a unique DNA sequence and upregulate the target genes, whereas receptor heterodimerization enlists JAK and STAT heterodimers (i.e., STAT4/STAT5) that target a different DNA sequence for upregulating a different set of targets genes. Thus, this combinatorial dimerization strategy is enlisted in the natural signaling cascade to maximize the diversity of signals with a limited number of proteins.

The approach we adopted is generalizable to all cytokine receptors. Because of the scale on which the synthesis is conducted, the libraries could be enlisted to screen for agonists or antagonists against multiple receptors. Although not an objective of present work, their availability should allow such studies in the future. As detailed earlier, homo- or heterodimerization linkage of ligand binding antagonists can be enlisted to develop ligand agonists.[170] Potential applications of such studies with the cytokine receptors are summarized in Table 4.

Table 4: Class I cytokine receptors and approved or potential therapeutic applications of cytokine agonists and antagonists.

Class I cytokine receptors		
Family	Examples	Activation Characteristics
GH receptor	GHR, EPOR, TPOR, PRLR, G-CSFR	homodimers
IL-3 receptor	IL-3R, GM-CSFR, IL-5R	heterodimerization with β_c
IL-6 receptor	IL-6R, LIFR, CNTFR, IL-11R	heterodimerization with gp130
IL-2 receptor	IL-2Rα, IL-2Rβ, IL-4R, IL-7R	heterodimerization with IL-2Rγ
Therapeutic applications of cytokine agonists and antagonists		
Cytokine	Agonist	Antagonist
EPO	anemias, selective blood donation, cancer	
TPO	thrombocytopenia	
IL-2	cancer	histoincompatibility
IL-3	leukopenia, myeloid reconstitution	leukemia
IL-4	inflammation, cancer	allergy
IL-6	thrombocytopenia	cancer, osteoporosis, inflammation
IL-11	thrombocytopenia	
IL-12	cancer, infections	histoincompatibility, autoimmunity
G-CSF	neutropenia, myeloid reconstitution	leukemia
GM-CSF	leukopenia, myeloid reconstitution	leukemia
IFN α/β	cancer, viral infections, autoimmunity	inflammation
IFN γ	chronic granulonatous disease, infections	inflammation, autoimmunity

 © 2003 Wiley-VCH Verlag GmbH & Co. KGaA, Weinheim

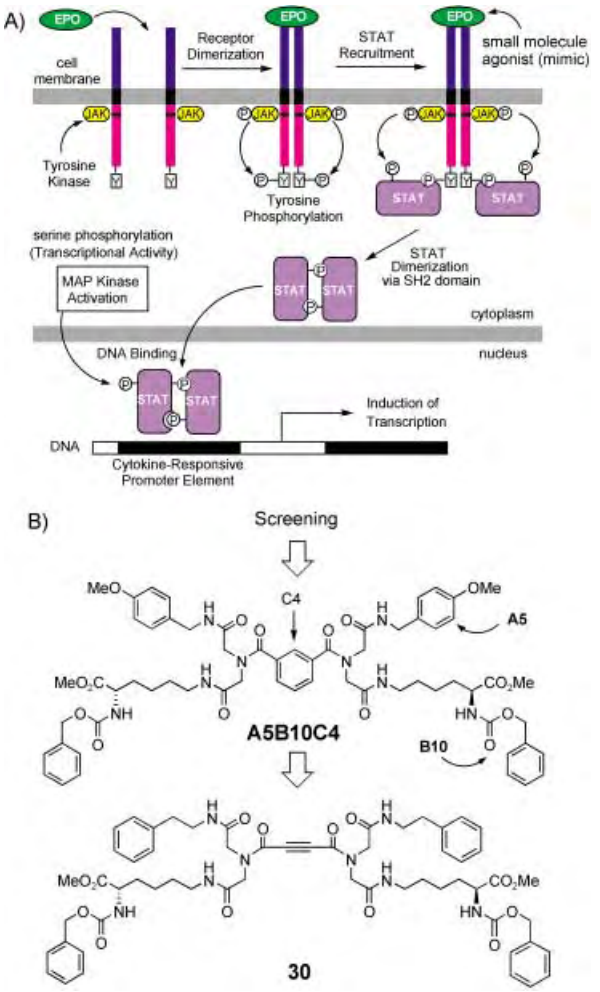


Figure 11. Top: EPO agonists (mimics) that function by promoting EPOR dimerization. Bottom: Development of EPO agonist **30** which is active in cellular functional assay, step 1: over 100 000 molecules were screened for EPOR binding, the B subunit is shown to be the most critical for binding activity. Step 2: A library of 115 A analogues provided an improved lead structure. The B subunit features contributing to activity were identified (77 analogues). A library of 70 C analogues provided an improved lead structure, three 1000-member libraries with alternative templates were examined. Higher order IDAs examined: binders examined in functional assay.

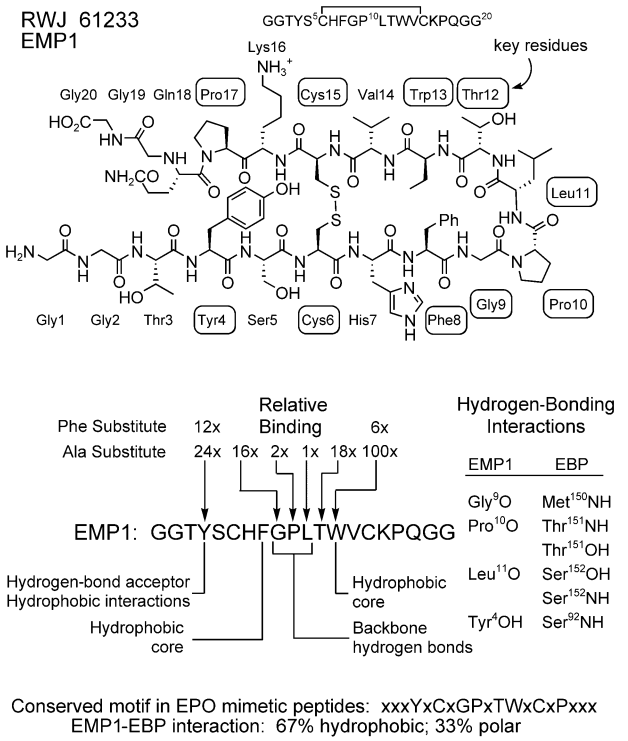


Figure 12. Structure of EPO mimetic peptide (EMP1), summary of relative EPOR binding, and summary of key contacts derived from the X-ray crystal structure of the complex with EBP (EPOR).

The disclosure of a 20-amino acid cyclic peptide RWJ 61233 (EMP1) identified in a phage library that binds to and activates EPOR ($K_D = 200$ nM versus $K_D = 200$ pM for EPO)[319,320] along with the X-ray structure determination of the peptide–receptor complex[321] revealed in detail how two molecules of the peptide dimerize EBP (EPO binding protein, the extracellular domain of EPOR; Figure 12 and 13).[322] The structure of the complex revealed a peptide dimer flanked by two molecules of the EBP and also reveals a striking structural homology to the growth hormone and prolactin receptors.[323,324] Interestingly, in the stem regions the two molecules of EBP have very little contact (ca. 75 Å^2) and, contrary to expectations, the WSXWS motif is not involved in ligand binding nor located in or near the ligand binding site or dimerization interface. Consistent with mutational studies of growth hormone and its receptor[325–328] which revealed that the majority of the intermolecular binding stabilization is derived from a few residues in the contact interface, the dimeric peptide binds EBP drawing upon a limited number of contacts for binding and dimerization. Further support for the key contacts has been derived through modifications of the cyclic peptide (Figure 12).[319,320] This result suggested that relatively small ligands may be devised as EPO agonists even though the cyclic peptide dimer itself is quite large. The cyclic peptide contains a single disulfide bond Cys 6/Cys 15 which links two short β-strands (residues 4–7 and 13–16) that are connected by a type I β-turn (Gly 9-Pro 10-Leu 11-Thr 12).[329] The dimerized cyclic peptide forms a hydrophobic clamp that slides into a receptor dimerization interface making contacts with both receptor molecules. Central to this binding is a hydrophobic interface, Pro 149-His 153, which houses residues engaged in main-chain and side-chain hydrogen bonds to Gly 9-Thr 12/Trp 13 of the peptide. Critical and also central to the binding dimerization is the receptor Phe 93 which provides key contacts with Trp 13 and Tyr 4 complementing the adjacent Ser 92/Tyr 4-OH hydrogen bond. Similarly, Phe 8 spans the binding sites defined by Leu 33, Met 150, and Phe 205 which contributes significantly to the stabilization of the dimer complex. Our candidate library agonists were selected on the basis of maintaining and spanning these critical interactions. Although space precludes a detailed description of the modeling efforts that went into the design of our initial libraries, it is perhaps sufficient to indicate that effective EPOR binding ligands were obtained in the first libraries and their further exploration has provided even better binders.

 © 2003 Wiley-VCH Verlag GmbH & Co. KGaA, Weinheim

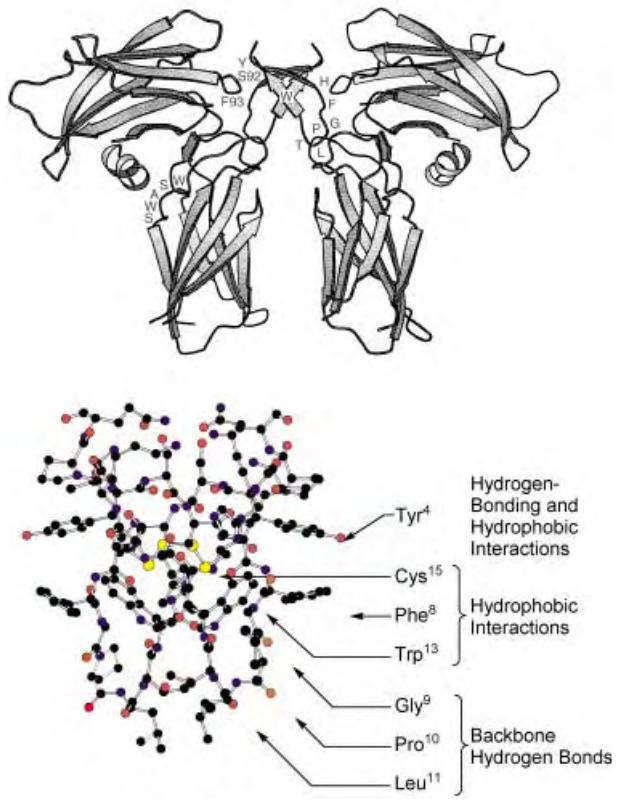


Figure 13. Top: X-ray structure of the EBP-EMP1 complex. Bottom: Key residues involved in the peptide–EBP interaction.

Employing libraries prepared from *N*-Boc-iminodiacetic acid anhydride and a three- or four-step solution-phase reaction with acid–base extractions for purification, numerous libraries were prepared (roughly 100 000 compounds) and evaluated for EPOR binding. A number of EPOR binding agents were identified that inhibited I^{125}-EPO binding to EPOR ($IC_{50} = 1$–$80\ \mu M$). These antagonists of EPO binding were covalently linked to provide C_2 symmetric dimers capable of receptor dimerization and activation. Several of the most active compounds were found to be weak agonists and induced concentration-dependent proliferation of an EPO-dependent cell line (UT-7/EPO) exhibiting the characteristic bell-shaped dose response curve while having no effect on a similar cell line (FDC-P1) lacking the EPOR (Figure 11 and 14).[82]

To date, only three reports of EPO agonists have been disclosed[82,319,330] and those reported above[82] are only about 10-fold less potent than EMP1[319] ($IC_{50} = 5$–10 versus $0.5\ \mu M$). They are substantially more efficacious than a recently reported Merck agonist[330] (15–20% versus 4% of activity of EPO), considerably smaller than EMP1 ($M_r \approx 2100$, but functions as dimer of $M_r \approx 4200$) or the Merck agonist ($M_r \approx 6400$), and are substantially more accessible (four synthetic steps). Key binding elements have been identified allowing for further potential reductions in the size of the identified leads.

Since the agents act on the extracellular domain of the receptor, they need not be permeable to the cell. As such, the relative size of the agonist structures need not be as significant a concern as it is with an intracellular target. Similarly, one can anticipate that the amide bonds present in the existing leads can be engineered out of the structures (Figure 14). Finally, one can anticipate that the size of the agonist structures may be reduced and their affinity increased through examination of the X-ray structures of complexes with EBP. These studies should allow the design of additional key interactions into the leads, the trimming away of non-productive elements of the compounds, and permit the design of rigid structures embodying the EBP bound conformation. Finally, it is now clear that simple dimerization of the EPO receptor is insufficient for receptor activation.[170,316,331–334] This dimerization, or conformational reorganization of a cell surface receptor dimer, must occur in a manner that

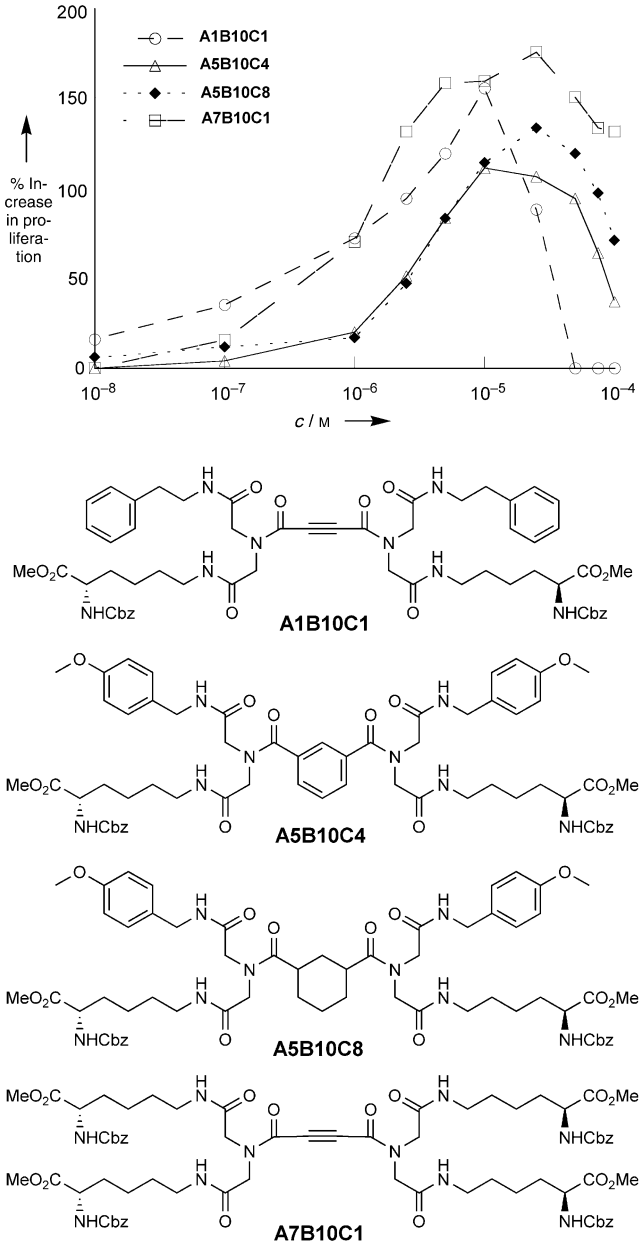


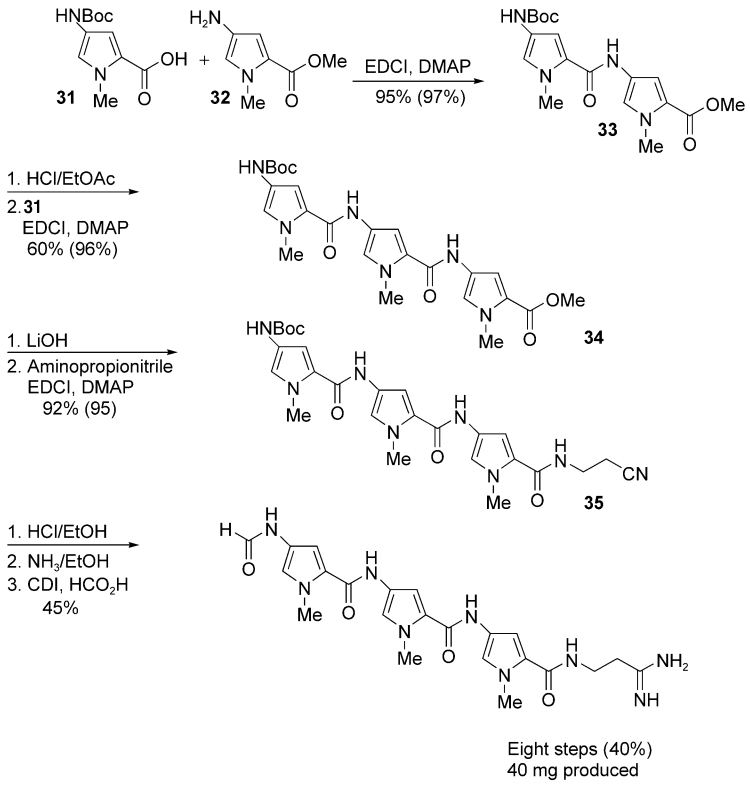
Figure 14. Concentration-dependent proliferation activity in an EPO-dependent cell line exhibiting a bell-shaped dose-response curve.

 © 2003 Wiley-VCH Verlag GmbH & Co. KGaA, Weinheim

brings the receptor cytoplasmic domains in close proximity to one another permitting the JAK cross phosphorylation and initiation of the signaling cascade. Thus, rigid variants of the lead structures that not only bind the ligand site and stabilize receptor dimerization, but that also more effectively induce the active conformation of the receptor dimer may help convert the partial agonists into full agonists.

5. Targeting Protein–DNA Interactions

Studies on the high-throughput synthesis and screening of DNA binding compounds[72,84–88] have also been detailed that are related to interests in understanding and exploiting their properties.[89–96] Our approach integrates the solution-phase techniques for the synthesis of libraries with a technique we introduced for rapid high-throughput screening for DNA binding affinity or sequence selectivity.[87,97,98] These techniques can be combined to rapidly explore and define the structural features responsible for the sequence-selective DNA binding properties of known agents, to discover new patterns for small-molecule recognition of DNA (new base-pair (bp) codes), and to screen for compounds that selectively target consensus sequences of transcription factors for controlling aberrant gene transcription (i.e., LEF-1/β-catenin, androgen receptor).



Scheme 8. Solution-phase synthesis of distamycin A. Optimized yields in parentheses. All the compounds were obtained in >95% purity after acid–base extraction, Chromatographic purification was not used. DMAP = 4-*N*,*N*-dimethylaminopyridine, Boc-Pyr-OH = **31**, EDCI = 1-ethyl-3-(3-dimethylaminopropyl)carbodiimide, CDI = 1,1′-carbonyldiimidazole.

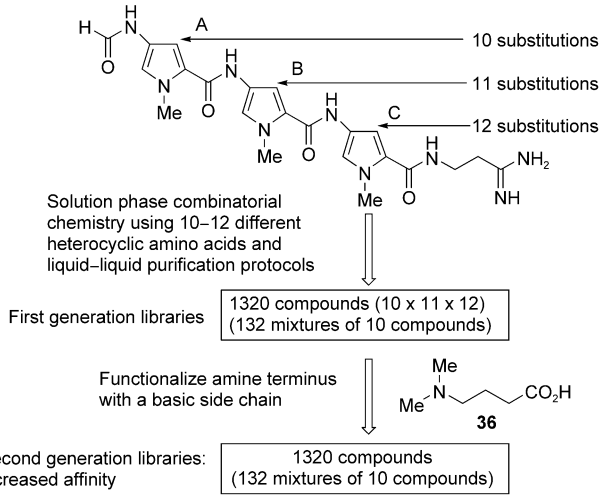
The regulation of gene expression is based on the sequence-selective recognition of nucleic acids by repressor, activator, and enhancer proteins. Selective control of such processes has been a long-standing goal and small molecules that selectively bind DNA and activate (block a repressor) or inhibit (block an activator) gene expression hold great promise as therapeutics.[335–356] Complicating such studies is the recognition that it is often not a single sequence that is ideally targeted, but rather an ensemble of related sites that compose the consensus binding sequence of a nuclear receptor or transcription factor. Consequently, the discovery of such agents has been slow owing to the complexity associated with understanding small-molecule/DNA interactions, the iterative process of designing and synthesizing individual compounds targeted towards specific DNA sequences, and the technically demanding techniques involved in the determination of their binding affinity for any given sequence, much less an ensemble of related sequences.

5.1. High-Throughput Synthesis of DNA-Binding Compounds Using Solution-Phase Library Techniques

5.1.1. Distamycin and a Library of 2640 Analogues

A rapid, parallel synthesis of distamycin A analogues was developed enlisting the simple, acid–base liquid–liquid extraction for purification and isolation of each intermediate and final product (Scheme 8). The utility of this method was first demonstrated with the preparation of distamycin A (eight steps, 40% overall yield), a naturally occurring antitumor antibiotic, where each of the reaction products was isolated in at least 95% purity.[87] A prototypical library of 2640 analogues was assembled in a small-mixture format of two libraries of 132 mixtures of 10 compounds providing each compound in multimilligram quantities sufficient for repetitive screening in multiple assays (Scheme 9). Screening the initial library in a functional assay for cytotoxic activity (L1210) revealed two uniquely active compounds which were found to be 1000-times more potent than distamycin A.[87] A complementary rapid, high-throughput screen for DNA binding affinity was also developed which is applicable for assessing binding to DNA homopolymers or specific sequences (discussed in Section 5.2). Using this technique, alternative AT-rich binding agents were identified establishing the usefulness of the approach and providing two new and effective DNA-binding distamycin A analogues. In addition, a comparison of several distamycin analogues established substituent contributions to AT-rich binding that may be safely implemented in future libraries. Extension of these studies to identify effective binders to predefined sequences was conducted in the context of the androgen response elements PSA-ARE-3 and the ARE-consensus sequences, the latter of which contains an AT-rich sequence interrupted by a GC base pair, and for which effective binders might prove useful in the treatment of resistant prostate cancer.

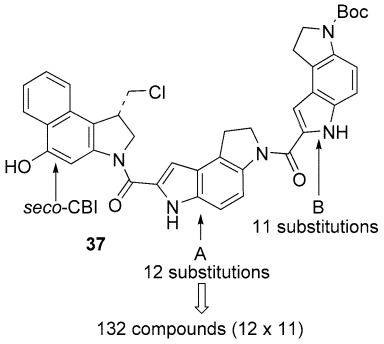
 © 2003 Wiley-VCH Verlag GmbH & Co. KGaA, Weinheim



Scheme 9. Solution-phase synthesis of a library of 2640 potential DNA-binding distamycin analogues.

5.1.2. *CC-1065 and the Duocarmycins: A 132-Membered Library Defining the Role of the DNA-Binding Domain*

A library of 132 CBI (1,2,9,9a-tetrahydrocyclopropa[*c*]-benzo[*e*]indol-4-one) analogues of CC-1065 and the duocarmycins, potent antitumor antibiotics that alkylate duplex DNA, was prepared utilizing the solution-phase technology of acid–base liquid–liquid extraction for the isolation and purification steps (Scheme 10).[88] The 132 analogues consti-



Scheme 10. Solution-phase synthesis of 132 CC-1065 analogues based on CBI. All the compounds were purified by liquid–liquid acid–base extraction.

tuted a systematic study of the DNA binding domain with the incorporation of dimers composed of monocyclic, bicyclic, and tricyclic (hetero)aromatic subunits. From their examination, clear trends in cytotoxic potency and DNA alkylation efficiency emerged highlighting the importance of the first-attached DNA-binding subunit (A subunit): tricyclic is more active than bicyclic, which in turn is far more active than monocyclic (hetero)aromatic subunits (Figure 15). Notably, the trends observed in the cytotoxic potencies paralleled those observed in the relative efficiencies of DNA alkylation.

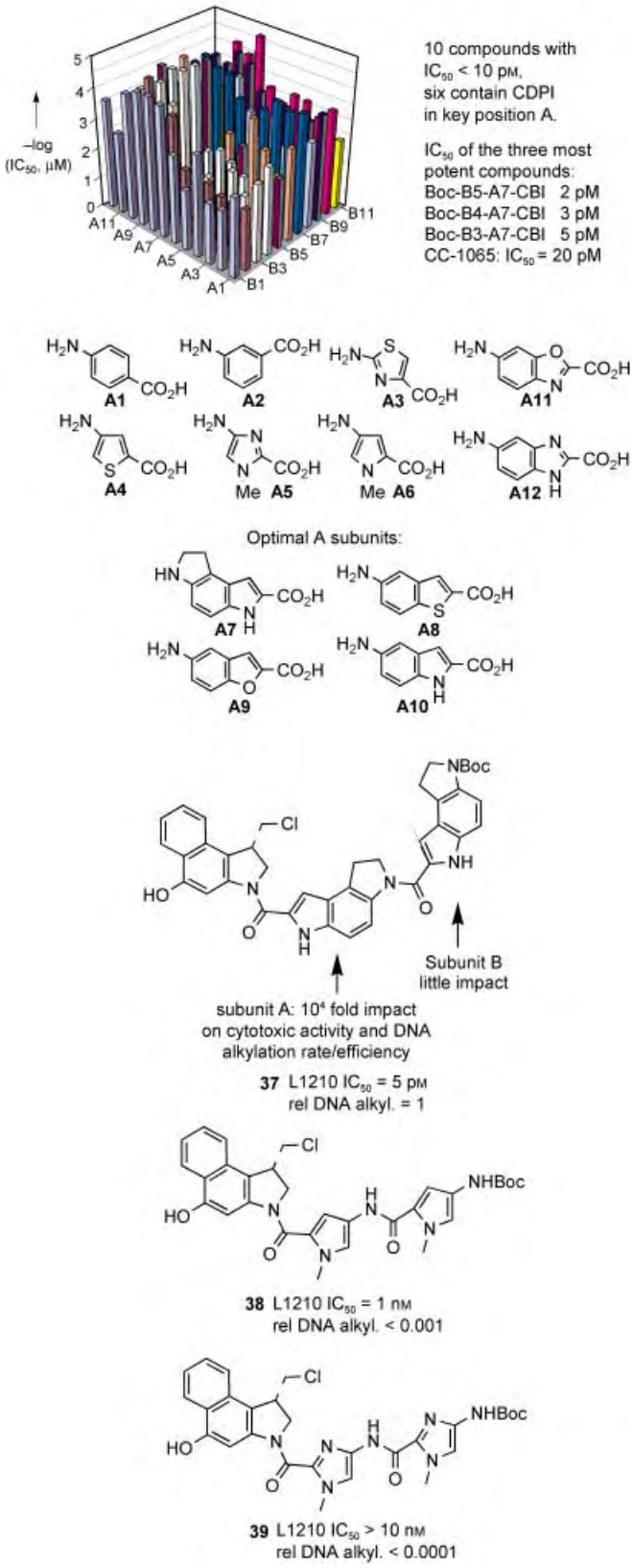


Figure 15. L1210 Cytotoxic activity of the CC-1065 analogues.

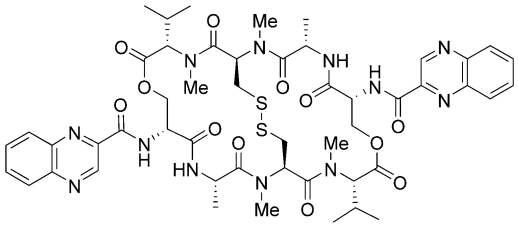
Our interpretation of these results is that the trends represent the partitioning of the role of the DNA-binding subunit(s) into two distinct contributions. The first of which is derived

 © 2003 Wiley-VCH Verlag GmbH & Co. KGaA, Weinheim

from an increase in DNA-binding selectivity and affinity which leads to property enhancements of 10–100-fold and is embodied in the monocyclic series. The second, which is additionally embodied in the bicyclic and tricyclic heteroaromatic subunits, is a contribution to the catalysis of the DNA alkylation reaction that provides additional enhancements of 100–1000-fold. The total enhancement thus exceeds 25000-fold. Aside from the significance of these observations in the design of future CC-1065/duocarmycin analogues, their importance to the design of hybrid structures containing the CC-1065/duocarmycin alkylation subunit should not be underestimated. Those that lack an attached bicyclic or tricyclic A subunit, that is, duocarmycin/distamycin hybrids, can be expected to be intrinsically poor or slow DNA alkylating agents.

5.1.3. A Prototype Triostin A Analogue Solution-Phase Synthesis

A solution-phase synthesis of azatriostin A, a key analogue of the DNA bisintercalator triostin A (Scheme 11), was developed such that libraries of triostin A analogues could be



Scheme 11. Triostin A: naturally occurring DNA bisintercalator.

prepared.[72] This work, in conjunction with the distamycin A and CC-1065 analogue libraries, highlights the ease with which natural product libraries targeting DNA can be constructed using solution-phase technology to rapidly identify the key structural components of the natural product as well as to discover and develop new therapeutics.

5.2. The FID Assay: A High-Resolution, High-Throughput Assay for Establishing DNA-Binding Affinity and Selectivity

A variety of techniques are commonly used to establish the DNA-binding properties of small molecules.[357] Most are technically challenging and require the knowledge of specialized biochemical procedures and assay reproducibility comes only with experience.[358,359] Prior to our efforts, none were applicable to the high-throughput screening required for assaying a library of compounds against an ensemble or complete library of sequences. The most widely utilized methods are footprinting or affinity cleavage and both have been used qualitatively and quantitatively to establish DNA-binding selectivity or affinity. Intrinsic in the methods employed in the destructive assays is the binding characterization at the highest affinity sites within an incomplete set of sites contained in a 100–200-bp segment of DNA, and modest- or low-affinity sites are not easily probed. As a consequence, the full DNA-binding profile of candidate ligands is not easily assessed or compared using these techniques.

The nondestructive fluorescent intercalator displacement (FID) assay, which addresses these issues of ease of use and information content, utilizes the displacement of ethidium bromide (or thiazole orange) from hairpin deoxyoligonucleotides (Figure 16).[72,87] A hairpin deoxyoligonucleotide con-

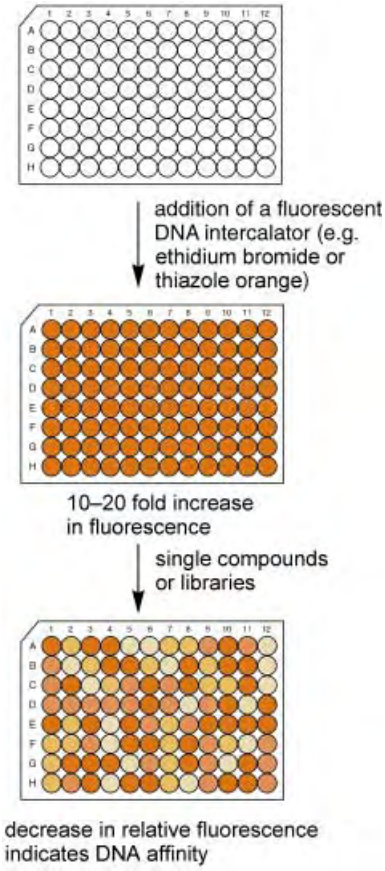


Figure 16. Fluorescent intercalator displacement (FID) assay. The method is suitable for screening a library to identify a single compound with affinity for a given DNA sequence, or, for screening DNA libraries to establish the sequence preference of a DNA binding agent.

taining the sequence of interest, or a library of hairpin deoxyoligonucleotides containing all four bp (136 hairpins) or five bp (512 hairpins) sequences individually displayed in 96-well plates are treated with the intercalator, yielding a fluorescence increase upon DNA binding.[360] Addition of a DNA-binding compound results in a decrease in fluorescence owing to displacement of the bound intercalator. The decrease in fluorescence is directly related to the extent of DNA binding, which provides relative DNA binding affinities and a rank-order binding. This rank-order binding profile can be used in the assay of a library of compounds against a single sequence to identify the best candidate ligands for a targeted sequence. Alternatively, it can entail the assay of a single compound against a library of hairpin DNAs containing all possible sequences thereby establishing a high-resolution profile of its DNA-binding selectivity.

 © 2003 Wiley-VCH Verlag GmbH & Co. KGaA, Weinheim

5.2.1. *Assaying Libraries of Compounds Against a Target Sequence Exemplified with the Discovery of Inhibitors of Androgen Receptor-Mediated Gene Transcription*

The FID assay can be used to rapidly screen a library of compounds against any target sequence or ensemble of sequences in a 96-well format. This approach was utilized to identify potent and selective inhibitors of androgen receptor-mediated gene transcription (Figure 17). The emergence of hormone-independent, constituently active androgen receptor dimer, which is unresponsive to competitive antagonist treatment, is responsible for prostate-cancer relapse that is resistant to chemotherapeutic treatment. A potentially effective treatment for such resistant prostate cancer could entail administration of a DNA-binding agent selective for the androgen response element (ARE)-consensus sequences. Such a treatment would competitively inhibit the constitutively active androgen receptor DNA binding and its transcription activation.

We used the FID assay with two hairpin deoxyoligonucleotides containing two related sequences of the androgen response element (ARE), the 14-bp ARE-consensus and PSA-ARE-3 sequences. The latter sequence contains a five-bp AT-rich sequence that could be anticipated to bind distamycin-like structures while the former contains a similar sequence interrupted by a GC bp. In the screening of our library, several candidates were identified which bound the AT-rich site of the PSA-ARE-3 sequence. One analogue (**49**, Figure 17) maintained the high-affinity binding to the ARE-consensus sequence. Compound **49** appeared suitable as an inhibition of the gene transcription initiated by hormone insensitive androgen-receptor dimerization and DNA binding characteristic of therapeutic-resistant prostate cancer.[87] Notably, **49** exhibited potent ($IC_{50} = 8$ nM) and selective (ca. 40-fold) inhibition of androgen receptor-mediated gene transcription in a cell-based reporter assay, albeit requiring liposome delivery of the compound for cell penetration and observation of the activity.

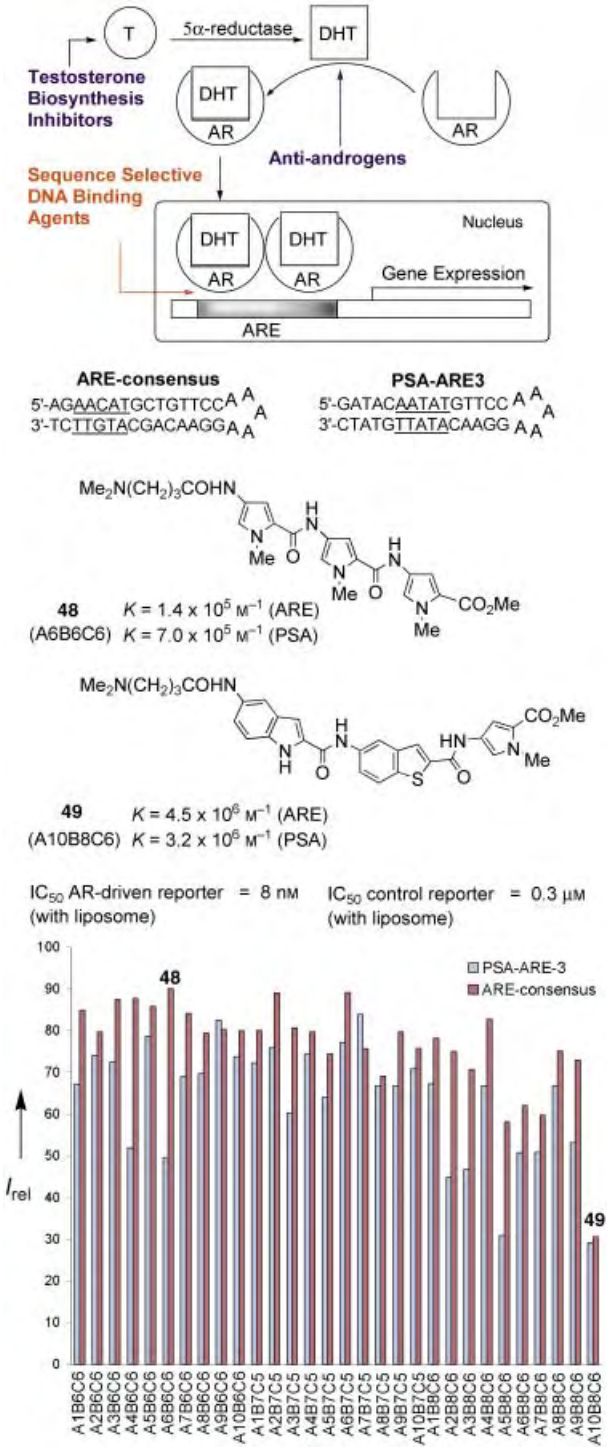


Figure 17. FID assay used in the screening for inhibitors of androgen receptor (AR) mediated gene transcription by evaluating the affinity to PSA-ARE3 and ARE-consensus sequences.

5.2.2. *High-Resolution Definition of Sequence Selectivity*

This FID assay is especially powerful for establishing the complete sequence selectivity of a DNA-binding agent. The technique entails the measurement of the loss of fluorescence derived from the displacement of ethidium bromide from hairpin deoxyoligonucleotides containing all possible five (512 hairpins) or four-bp sequences (136 hairpins) displayed in a 96-well format (Figure 18). In selected instances, the change in fluorescence of the DNA-binding compound itself can be monitored. This includes characterization of modest and nonbinding sequences not accessible by other techniques (i.e., footprinting), and such binding profiles may prove instrumental in distinguishing candidate ligands that display selectivity for an ensemble of related sequences characteristic of the consensus sequences of transcription factors. Technical issues associated with the use of the assay were investigated, multiple compounds of varying affinities were examined, and its use in comparing the DNA binding properties of distamycin A, netropsin, DAPI, Hoechst 33258, and berenil were disclosed.[97] The cost of the 512 hairpins for a single assay is about \$100 (ethidium bromide) or less (for thiazole orange).[98] The technique is nondestructive indicating that immobilization of the hairpins (chips, beads, glass slides) could permit their rinsing and reuse in subsequent assays. This hairpin immobilization and reuse would remove the barrier to

 © 2003 Wiley-VCH Verlag GmbH & Co. KGaA, Weinheim

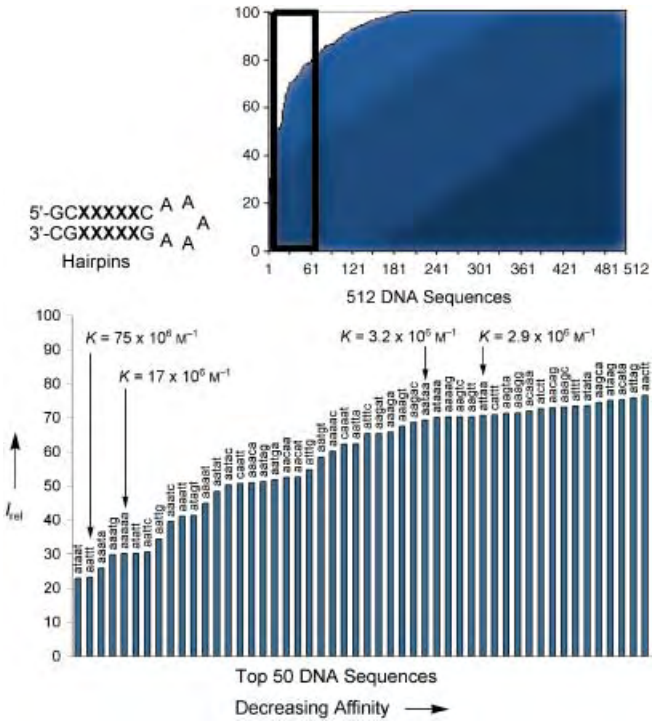


Figure 18. Determination of distamycin A sequence selectivity in one experiment by using the FID assay. The relative affinity for a given DNA sequence is proportional to the decrease in fluorescence. The affinity decreases with increasing AT content. The absolute binding constants obtained are comparable to those obtained with other techniques.

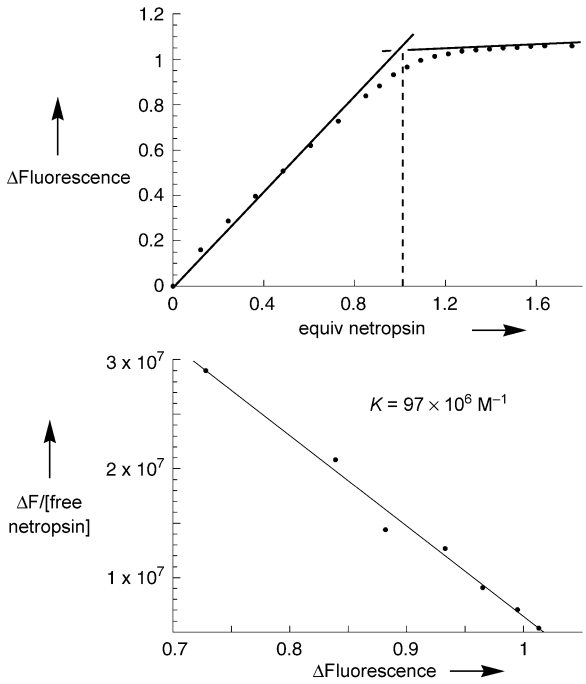


Figure 19. Top: Titration of netropsin versus the hairpin containing 5′-AATTT-3′ at 1.1 μM (8.8 μM/bp), the intersection is at 1.05 equivalents which indicates a 1:1 binding and bottom: Scatchard plot (Slope = $-K$).

examining libraries of longer sequences (> 5 bp) and extend the use of the technology to binding site sizes typical of proteins.

5.2.3. *Scatchard Analysis of Titration Curves: Absolute Binding Constants and Stoichiometry of Binding*

The FID assay may be used to establish binding constants for any given sequence through quantitative titration. Several methods of establishing binding constants were examined and the most reliable is a Scatchard analysis of the titration binding curve which also determines the stoichiometry of binding (Figure 19).[97] Direct measurement of binding constants of fluorescent DNA-binding compounds (DAPI, Hoechst 33258) compared favorably to those derived from the indirect displacement of ethidium bromide and thiazole orange (Table 5). As a demonstration of the power of this technique, the absolute binding constants for netropsin with each four-bp AT sequence were determined establishing its full relative and absolute selectivity (Table 6).[98]

Table 5: Binding constants of DAPI and Hoechst 33258.

A. Ethidium bromide and thiazole orange binding constants		
Hairpin	K_{EB} [$\times 10^6$ M^{-1}][a]	K_{TO} [$\times 10^6$ M^{-1}][a]
5′-AAAAA-3′	0.27 (4.5)[b]	1.2 (3.5)[b]
5′-AATTT-3′	0.42 (3.6)	1.3 (3.3)
5′-ATTAA-3′	0.87 (3.3)	1.0 (3.3)
5′-AATAA-3′	0.73 (3.3)	1.1 (3.3)

DAPI binding constants						
DNA Sequence	K [$\times 10^6$ M^{-1}][c]		K [$\times 10^6$ M^{-1}][d]		K [$\times 10^6$ M^{-1}][e]	
5′-AATTT-3′	58	(0.91)	110	(0.94)	120	(1.1)
5′-AATAA-3′	26	(0.83)	59	(0.98)	87	(0.94)
5′-ATTAA-3′	24	(0.83)	52	(0.88)	77	(1.0)
5′-AAAAA-3′	n.d.[f]	n.d.[f]	50	(0.95)	65	(0.99)

Hoechst 33258 binding constants						
DNA Sequence	K [$\times 10^6$ M^{-1}][c]		K [$\times 10^6$ M^{-1}][d]		K [$\times 10^6$ M^{-1}][e]	
5′-AATTT-3′	75	(0.90)	88	(0.96)	177	(0.98)
5′-AAAAA-3′	36	(0.86)	72	(0.98)	145	(0.92)
5′-AATAA-3′	28	(0.77)	34	(1.06)	83	(1.01)
5′-ATTAA-3′	13	(0.89)	19	(0.91)	47	(1.05)

[a] Established for the hairpin deoxyoligonucleotides containing the indicated sequence by direct titration. [b] Stoichiometry of binding established experimentally. [c] Thiazole orange displacement (experimental stoichiometry of binding). [d] Ethidium bromide displacement (experimental stoichiometry of binding). [e] Direct fluorescence titration (experimental stoichiometry of binding). [f] n.d. = not determined.

5.2.4. *Rapid Characterization of DNA Binding Modes*

The FID assay has been utilized to distinguish between and establish binding modes and binding-site sizes. This work has permitted the first characterization of a novel substituted β-alanine hairpin polyamide and the cooperative 2:1 side-by-side parallel (versus antiparallel) binding of iminodiacetic acid linked pyrrole polyamides. Polyamides composed of *N*-methylpyrrole, *N*-methylimidazole, and a growing set of structural analogues bind in the DNA minor groove with predictable sequence selectivity and high affinity.[350,361–363] The head-to-tail linkage of such polyamides with the five-atom linker γ-aminobutyric acid (γ) has been shown to

 © 2003 Wiley-VCH Verlag GmbH & Co. KGaA, Weinheim

Table 6: Comparative binding constants.

Titrant	DNA Sequence	K [$\times 10^6$ M^{-1}]	Binding stoichiometry
ethidium bromide	5′-AATT	2.7	2.92
thiazole orange	5′-AATT	15	3.05
Titrant	DNA Sequence	Ethidium bromide K [$\times 10^6$ M^{-1}]	Thiazole orange K [$\times 10^6$ M^{-1}]
Netropsin	5′-AAAT	127	113
	5′-AAAA	92	71
	5′-AATT	65	54
	5′-AATA	64	44
	5′-ATTA	45	35
	5′-ATAT	41	33
	5′-ATAA	34	18
	5′-TAAA	26	15
	5′-TTAA	11	8
	5′-TATA	11	8

provide hairpin polyamides that mimic the 2:1 side-by-side antiparallel binding of the unlinked polyamides (Figure 20), enhance the binding affinity 100 to 10000-fold, and improve the binding selectivity.[364] In contrast, polyamides incorporating a one-carbon-atom shorter head-to-tail linker, β-alanine (β), bind preferentially in an extended conformation forming 1:1 or side-by-side antiparallel 2:1 complexes.[364,365] By using the FID assay and a series of DNA hairpins containing a AT-rich binding site, the size of which was systematically varied, the stoichiometry of binding (1:1 vs 2:1) and the binding mode (hairpin vs extended) for such distamycin-derived polyamides can be rapidly and easily established (Figure 20).[83,84]

Using this approach, appropriate substitution of a β-alanine linker was established to induce hairpin instead of extended binding providing an alternative hairpin linker to γ (Figure 21).[83,84] These polyamide analogues were obtained using a parallel solution-phase approach involving a series of EDCI-mediated coupling reactions (Scheme 12).

As a natural extension of these studies, the behavior of head-to-head iminodiacetic acid (IDA) linked polyamides was characterized. Not only was IDA the template on which many other libraries had been generated (see Section 3), but it constituted a unique five-atom linker bearing an additional functionalization site at the central nitrogen atom of its structure, and represented an unusual head-to-head as opposed to head-to-tail linkage of the polyamides. The candidate IDA-linked pyrrole polyamides were prepared with solution-phase synthesis methodology (Scheme 13) and found to bind in a unique manner exhibiting cooperative extended 2:1 binding across a 9–10-bp site in what appears to be the first well-characterized example of parallel, side-by-side binding of such polyamides (Figure 22).[84]

5.3. LEF-1/β-Catenin

A second class of inhibitors of LEF-1/β-catenin mediated gene transcription (see Section 4.4 for the first class) were derived from the libraries of DNA minor-groove-binding

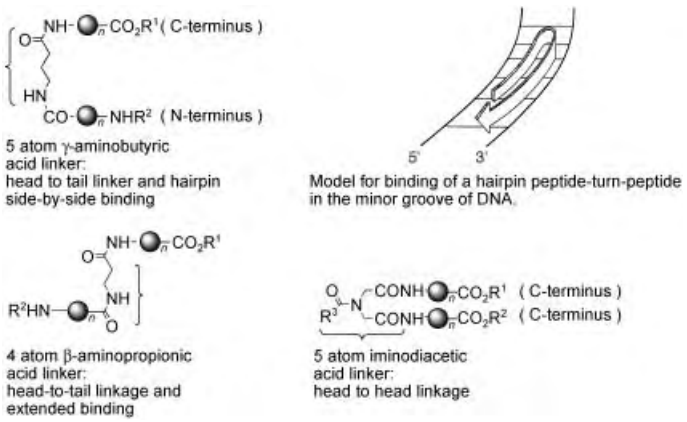


Figure 20. Linked polyamides for DNA binding.

ligands.[87] The unpublished results of the screening of one such library are shown in Figure 23 resulting in the identification of two closely related lead structures **69** and **70** that inhibit TOPFLASH transcription 10-fold, exhibit a ≧ three-fold TOPFLASH-FOPFLASH selectivity, inhibit LEF-1 DNA binding in a gel-shift assay, and inhibit the β-catenin induced transformation of the colon cancer cell line SW480. Their DNA-binding selectivities were established in our FID assay.[87] This constitutes only the second example of a small-molecule inhibitor of LEF-1/DNA binding (protein–DNA interaction) leading to inhibition of gene transcription, the first being a polyamide from Dervan et al.[366,367]

6. Natural Product Libraries

Natural product leads for existing or new targets often emerge as superb starting points for drug development. The merits of enlisting a natural product lead have been chronicled in many reviews and monographs,[368] and may be attributed to several features. They have emerged from a biological milieu in which they express their properties ensuring that they embody many drug-like qualities. No doubt, it is the integration of many functions into a single compact structure that distinguishes natural product leads from those created in the laboratory. As the exploration of the properties of complex natural products becomes increasingly more sophisticated with the technological advances being made in their screening and evaluation and as structural details of their interaction with biological targets becomes more accessible, the opportunities for providing unique solutions to complex biological problems have grown. A powerful complement to the examination of the naturally derived agents themselves is the preparation and subsequent examination of key partial structures, and agents containing deep-seated structural modifications. Well conceived deep-seated structural modifications may be used to address the structural basis of the natural product's interactions with biological targets and the define fundamental relationships between structure, functional reactivity, and properties. In these studies, the challenging problem is to understand the beautiful solutions and subtle design elements that nature has provided in the form of a natural product and work to extend

 © 2003 Wiley-VCH Verlag GmbH & Co. KGaA, Weinheim

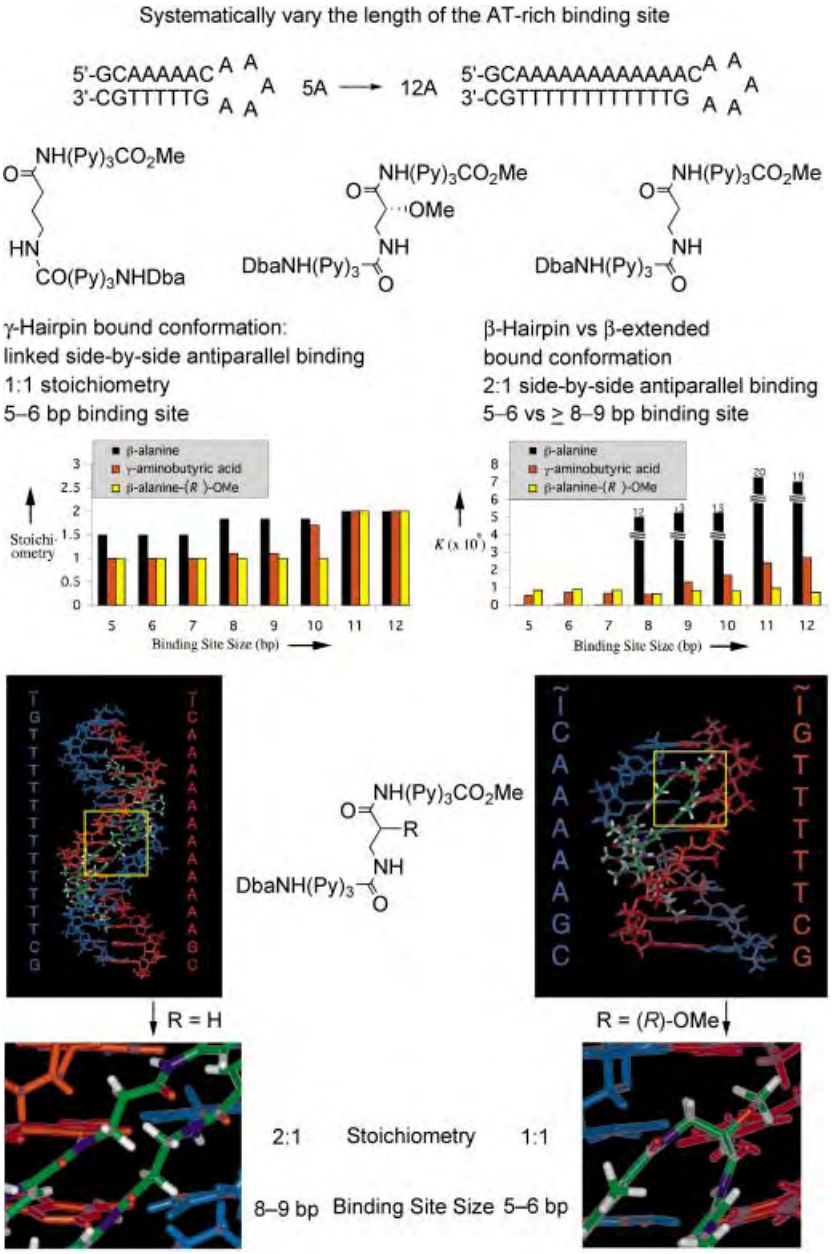


Figure 21. Hairpin binding of a substituted β-alanine linked polyamide. Bottom left: β-alanine extended antiparallel 2:1 side-by-side binding. Bottom right: $\beta^{(R)\text{-OMe}}$-alanine: antiparallel 1:1 side-by-side hairpin binding.

the solution through rational design elements to provide more selective, more efficacious, or more potent agents designed specifically for the problem or target under investigation.

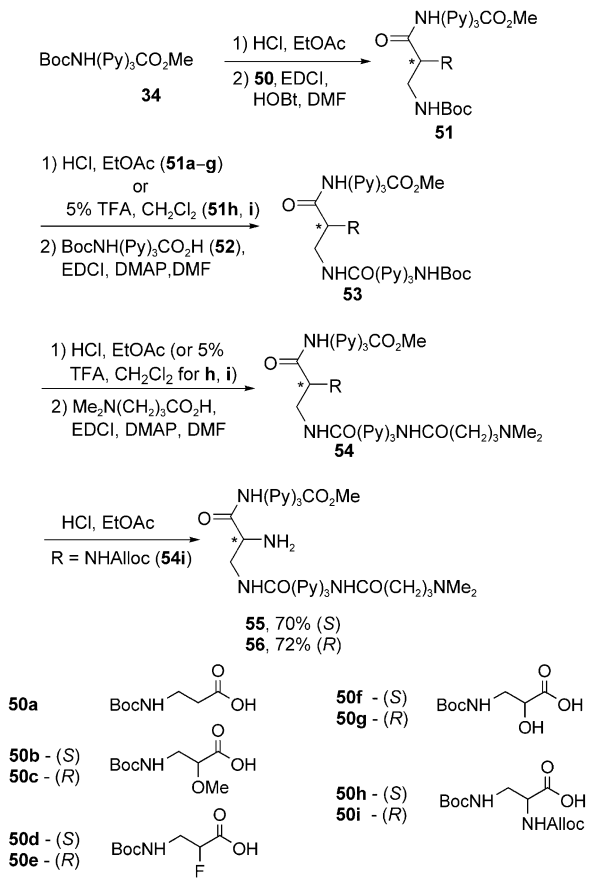
Still today, nine of top-20 best-selling drugs were derived or developed from natural product leads with combined sales of $>$ \$16 billion (1999).[407] Consequently, natural products are arguably one of the most successful approaches to modern drug discovery, and it is not surprising that combinatorial methods have been evolved to exploit the importance of such leads (Table 7).[369–407] The solution-phase synthesis approach we developed has proven successful for the generation of libraries of selected natural products. In addition to the synthesis of 2640 analogues of distamycin (Section 5.1.1), 132 analogues of CC-1065 and the duocarmycins (Section 5.1.2), and a prototype analogue of triostin A (Section 5.1.3), the approach was used to create a library of HUN-7293 analogues exploring each structural detail of the natural product. This example is one in which the biological target for the natural product has not been established. Even in the absence of a known target, a functional screen and a library of analogues was used to define the pharmacophore of the natural product.

6.1. HUN-7293: Single-Point Changes Introduced by Total Synthesis of a Library of Analogues: A "Chemical" Mutagenesis Approach to Defining Structure–Function Relationships

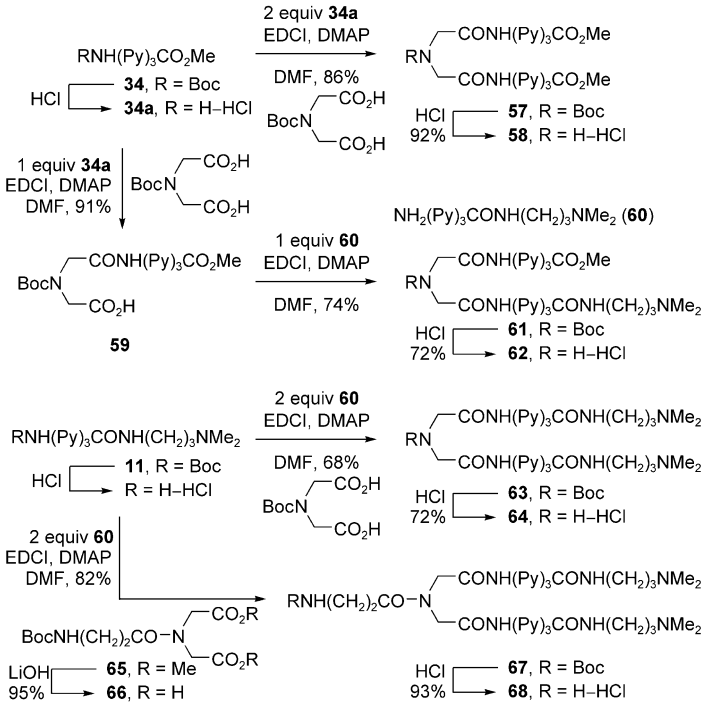
The naturally occurring cyclic heptadepsipeptide HUN-7293 (Scheme 14) was first isolated in 1992 from a fungal broth in a screen for inhibitors of inducible cell adhesion molecule expression.[408] Its structure was subsequently established by ^{1}H NMR spectroscopic methods and confirmed by X-ray analysis.[408] Independently, the same cyclic depsipeptide was isolated by a Japanese group from a different fungal species based on a screen for anti-HIV compounds.[409] Molecules that bind with endothelial cells, which include intercellular adhesion molecule 1 (ICAM-1), vascular cell adhesion molecule 1 (VCAM-1), and E-selectin play important roles in the immune response by recruiting and regulating leukocyte migration and cell-to-cell interactions at a site of inflammation. Modulation of these interactions through the inhibition of such cell adhesion molecule expression should prove useful for the treatment of chronic inflammatory and autoimmune diseases characterized by their overexpression or upregulation. As detailed in recent studies,[410] diverse signals act on endothelial cells to activate members of the nuclear factor of the Kappa B (NF-κB) transcription factor family. NF-κB family members are cytoplasmic homo- or heterodimer proteins inactive when complexed with members of a family of inhibitor proteins, IκB. Phosphorylation of IκB, releasing the active NF-κB, results in translocation to the nucleus and initiation of transcription of its targeted genes including the cell surface adhesion molecules. Few other groups have detailed work on small-molecule inhibitors of the expression[413–415] of cell surface adhesion molecules, aside from antisense[411] and antibody[412] approaches, and unlike HUN-7293, each target the NF-κB signal transduction pathway.

The first total synthesis of HUN-7293 was disclosed using a convergent approach which served to define several subtle elements essential to its preparation including backbone ester formation by a Mitsunobu displacement and the identification of MLEU^3-LEU^4 as an effective macrocyclization site (Scheme 14).[74] The subsequent implementation of this

 © 2003 Wiley-VCH Verlag GmbH & Co. KGaA, Weinheim



Scheme 12. The parallel synthesis of β-alanine linked pyrrole polyamides. Py = *N*-methylpyrrole, Im = *N*-methylimidazole, HOBt = 1-hydroxybenzotriazole, TFA = trifluoroacetic acid, Alloc = allyloxycarbonyl.



Scheme 13. Synthesis of pyrrole polyamides linked with an IDA scaffold.

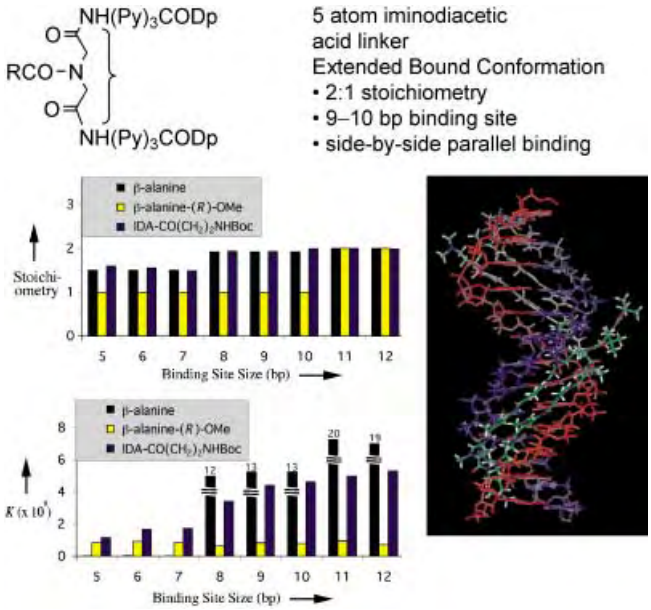


Figure 22. Extended 2:1 parallel side-by-side binding of IDA-linked polyamides. The best results are obtained with R = $(CH_2)_2$NHBoc.

approach in the convergent parallel synthesis of a library of key analogues of HUN-7293 was used to define in detail the structure–function relationships of the natural product (Scheme 15).[75,76]

A solution-phase approach to the simultaneous preparation of the library was utilized enlisting simple acid–base liquid–liquid extractions for isolation and purification of the synthetic intermediates and final products (Scheme 16). Notably, this approach provided each intermediate and final product sufficiently pure for subsequent use even in the multistep synthesis of HUN-7293 and its structurally challenging analogues. The library included an alanine scan of the seven residues, an *N*-methyl deletion of the three *N*-methyl residues, and fundamental simplifications in each of the nonstandard amino acid side chains allowing the identification of key residues and structure features contributing to the biological properties. The simultaneous inclusion of simplified analogues of the nonstandard amino acid side chains permitted the identification of not only essential structural features, but also non-obvious and subtle structural features.

Alanine-scanning mutagenesis is an informative method for defining epitopes in proteins.[416] By replacing each amino acid side chain with a methyl group while retaining the stereochemistry of the peptide backbone, the significance of each individual side chain can be identified. Although this approach has its limitations, it has been used to provide a general insight into structure–function relationships of a protein, especially when the functional mechanism is unknown or its 3D structure is unavailable.[416] Similarly, in the absence of a defined target, the importance of each residue of HUN-7293 could not be anticipated. Along with additional modifications and simplifications in each of the individual side chains, an alanine scan of the structure was conducted. The results of their examination are sum-

 © 2003 Wiley-VCH Verlag GmbH & Co. KGaA, Weinheim

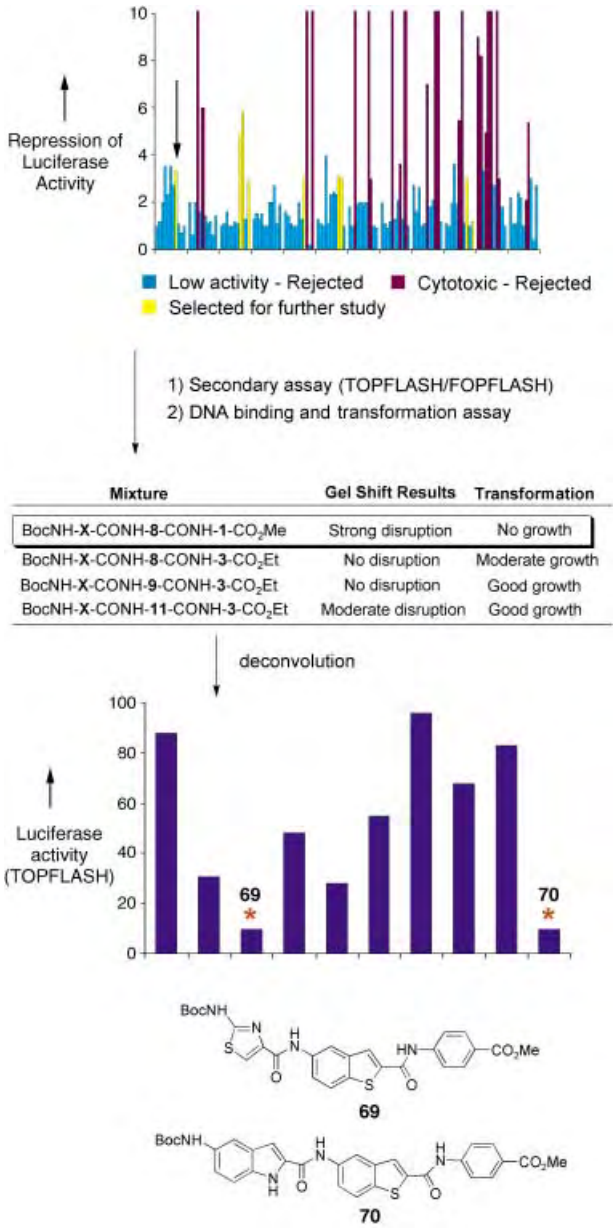


Figure 23. Disruption of LEF-1 DNA binding and inhibition of LEF-1/β-catenin-mediated gene transcription. The lead structures **69** and **70** have a tenfold transcription repression (TOPFLASH) and threefold selectivity (TOPFLASH/FOPFLASH)

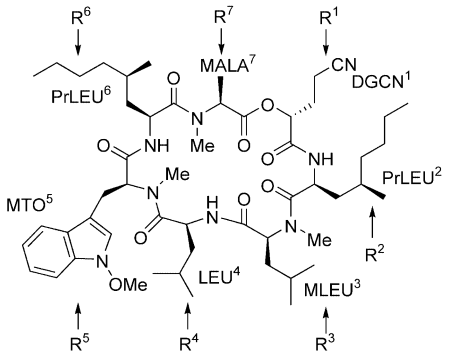
marized in Table 8 and they provided an initial, albeit surprisingly incomplete, overview of the relative importance of each residue. With the exception of residue 7, which already contains a methyl group in the natural product (R^7 = Me), the replacement of each side chain with a methyl group led to a reduction in potency. However, the magnitude of this loss in activity varied over a 1000-fold range with the R^1 replacement being only about two-times lower, the R^2–R^4 replacements leading to 10–100-fold reductions, and the R^5 and R^6 replacements leading to even larger, over 100–1000-fold, reductions with R^5 being by far the most significant residue. Just as interesting and despite the potency reductions, the methyl substitutions for the R^1–R^4 side chains enhanced the VCAM-1 versus ICAM-1 selectivity indicating that the changes in this half of the molecule affected inhibition of ICAM-1 expression more significantly, whereas this selectivity was lost along with the activity with methyl substitutions at R^5 and R^6 with the change at R^5 again being especially detrimental. From these results alone, one could anticipate that substantial changes in the R^1 side chain could be tolerated including efforts to enhance selectivity or physiochemical, distribution, stability, and toxicity profiles, whereas changes to R^2–R^4 might prove more challenging, and those to R^5 (a complete set of modifications of R^5 is

Table 7: Natural product libraries.

Natural product	Library format	Size	Reference
Lavendustin A	Solid Phase	61	[370]
Balanol	Solid Phase	32	[371]
Olomoucine	Solution and Solid Phase	364	[372]
Rauwolfa Alkaloids	Solid Phase	792	[373]
Epothilones	Solid Phase	180	[374]
Prostaglandin E_2 and $F_{2\alpha}$	Soluble Polymer Support	2/16/6	[375]
Taxoids	Solid Phase	400	[376]
Oscillamide Y	Solid Phase	4	[377]
(*S*)-Zearalenone	Solid Phase	1	[378]
Cycloserine	Solid Phase	80	[379]
Flavones	Solution Phase	36	[380]
Muscone	Solid Phase	12	[381]
Sarcodictyin	Solution Phase	15/53	[382]
Taxoids	Solution Phase	26	[383]
Prostaglandin E and F	Solid Phase	26	[384]
Fumitremorgin C	Solid Phase	42	[385]
Indolactam V	Solid Phase	31	[386]
Vitamin D_3	Solid Phase	1	[387]
Kramerixin	Solution Phase	120	[388]
Vancomycin	Solution and Solid Phase	39,304	[389]
HUN-7293	Solution Phase	1/40	[75, 76]
Carpanone	Solid Phase	6	[390]
Distamycin A	Solution Phase	2640	[87]
Distamycin A	Positional Scanning	1000	[86]
Triostin A	Solution Phase	1	[72]
Fumiquinazoline	Solid Phase	27	[391]
Benzopyrans	Solution and Solid Phase	>10000	[392]
Steroids	Solid Phase	20	[393]
Curacin A	Solution Phase	18	[394]
Stipiamide	Solution Phase	42	[395]
CC-1065	Solution Phase	132	[88]
Galanthamine	Solid Phase	2527	[397]
Mappicine	Solution Phase	112/560	[396]
Tambjamine	Solution Phase	10	[398]
Vitamin D_3	Solid Phase	72	[399]
Vitamin D_3	Solution and Solid Phase	5	[400]
Psammaplin A	Solution Phase	3828	[401]
Hapalosin	Solution and Solid Phase	6	[402]
Nakijiquinones	Solution Phase	56	[403]
Steroids	Solution Phase	298	[404]
Ceramide	Solid Phase	528	[405]
Dysidolide	Solid Phase	8	[406]
Natural product-like	–	–	[369] (review)

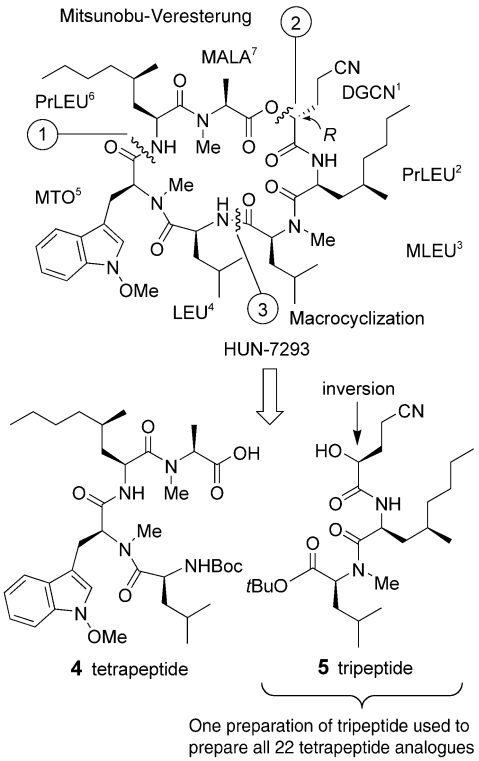
 © 2003 Wiley-VCH Verlag GmbH & Co. KGaA, Weinheim

Table 8: Alanine scan of HUN-7293. Inhibitory activity (IC_{50} [nM]) for VCAM-1 and ICAM-1 protein expression in human microvascular cell line (HMEC-1).[a]



Compound	VCAM-1	ICAM-1	Selectivity	Rel. potency
HUN-7293[b]	1	24	24	1
79, R^1 = Me	2.3 ± 0.5	178 ± 18	77	0.4
80, R^2 = Me	100 ± 34	6300 ± 370	63	0.01
81, R^3 = Me	56 ± 11	4100 ± 2500	73	0.02
82, R^4 = Me	16 ± 1.4	700 ± 20	43	0.06
83, R^5 = Me	1800 ± 10	2800 ± 210	1.6	0.0006
84, R^6 = Me	270 ± 40	1400 ± 300	5.2	0.004

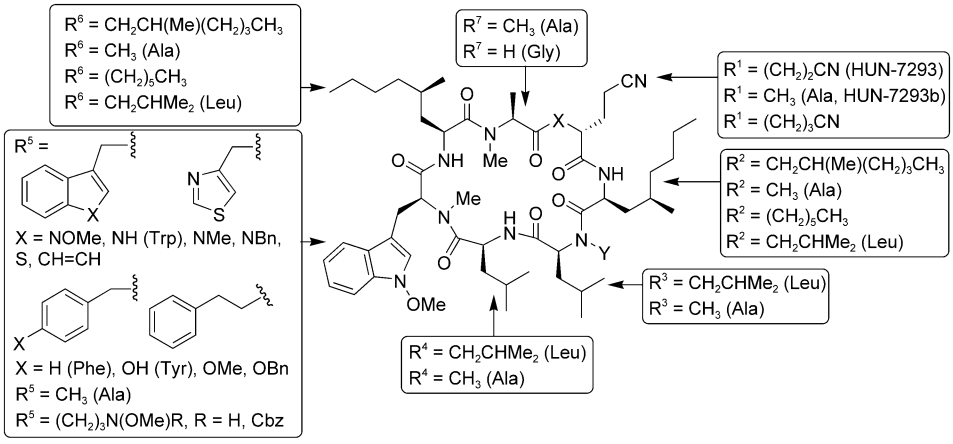
[a] Unless otherwise indicated, the substituents are those found in HUN-7293. [b] R^7 = Me, HUN-7293.



Scheme 14. Parallel synthesis of a library of HUN-7293 analogues: divergent preparation of a library by using a convergent total synthesis. All the intermediates and products were isolated and purified by liquid–liquid acid–base extraction. ①–③ indicate disconnections.

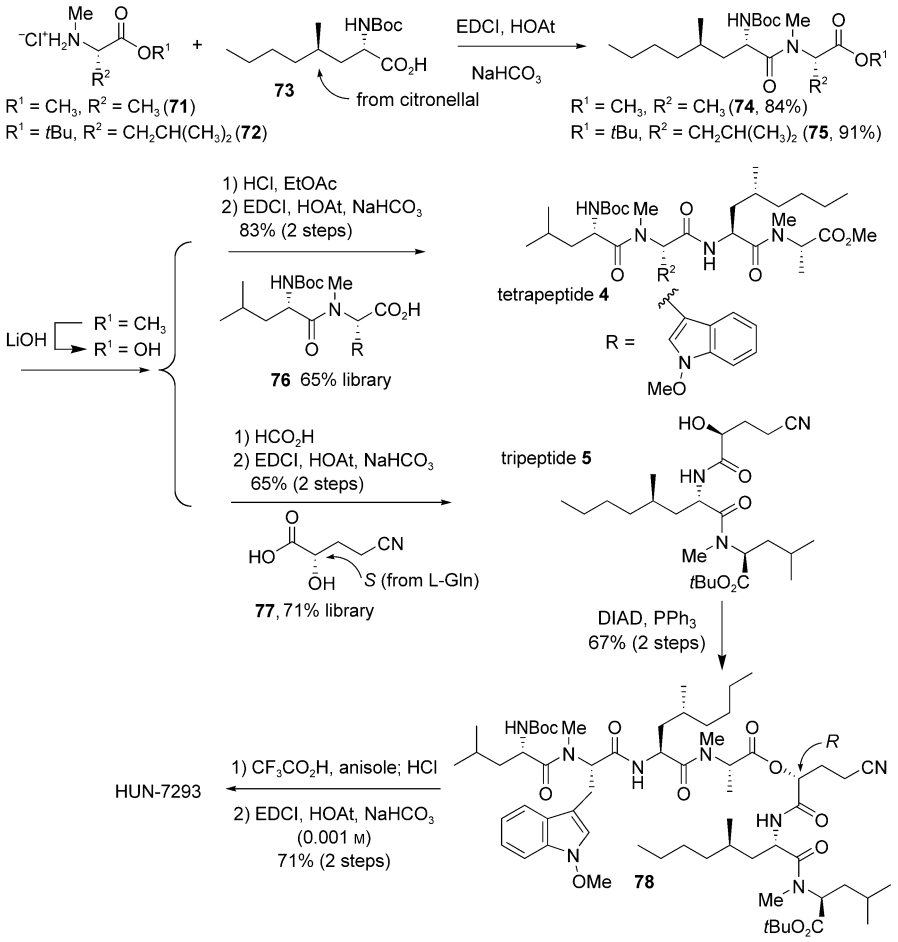
presented in Table 9) and R^6 are likely to be especially detrimental. Consequently, the results of the more subtle side-chain modifications proved especially valuable at addressing inaccuracies in interpreting such an incomplete data set from the alanine scan.

An assessment of the impact of each residue, each side chain, and each structural feature of HUN-7293 was established enlisting a complete library of analogues composed of systematic single-point changes in the structure prepared by parallel solution-phase synthesis. Over 40 new compounds were assembled by superimposing a divergent synthetic strategy onto a convergent total synthesis. The combination of the beneficial attributes of a conventional convergent synthetic strategy with the divergent preparation of a series of structurally related analogues can only be conducted using solution-phase, not solid-phase, techniques and avoids the more repetitive independent linear synthesis of each analogue. This generalized library approach of chemical mutagenesis of the cyclic depsipeptide provided a detailed first level structure–activity study that subsequent optimization efforts can be confidently based on. One of the most striking conclusions of the study was that a simple alanine scan of the naturally occurring depsipeptide may provide a sense of the



Scheme 15. Construction of HUN-7293 pharmacophore library via solution-phase parallel synthesis; X = O, NH; Y = H, Me; Bn = benzyl, Cbz = benzyloxycarbonyl. For more details see text.

 © 2003 Wiley-VCH Verlag GmbH & Co. KGaA, Weinheim



Scheme 16. Synthesis of HUN-7293 and analogues. A Mitsunobu esterification permits the use of the L-Gln-derived alcohol precursor **77** and avoids the racemization observed with activation of the NMe-Ala C-terminus. With **78** epimerization upon macrolactamization is minimized with DPPA (diphenylphosphorylazide). HOAt = 1-hydroxy-7-azabenzotriazole, DIAD = diisopropyl azodicarboxylate.

importance of each residue, but it provides an incomplete data set that is problematic to draw substantive conclusions from since each nonstandard residue or side chain, including residues 5 and 6, could be simplified without substantially influencing the potency. Although similar approaches have been disclosed to optimize or explore a single residue within a naturally occurring cyclic peptide, we are not aware of an instance where all the residues were examined simultaneously. Moreover, a more common approach to initial structure–activity relationship studies of such natural products has been systematic derivatization or degradation studies to establish the structural features important for activity. These efforts, like an alanine scan, provide an incomplete data set on which to base further studies.

7. Summary and Outlook

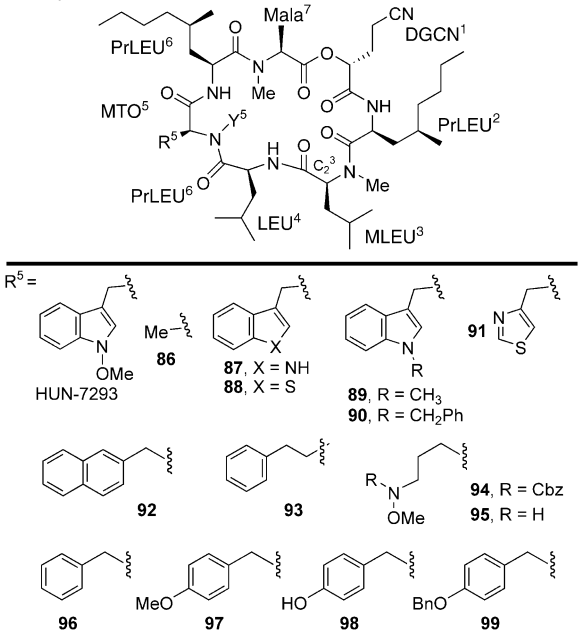
The complementary techniques of solid-phase and solution-phase combinatorial chemistry provide rare opportunities to rapidly probe challenging targets, especially those for which no known small-molecule leads exist and for which there is little or no structural information available. Split-and-mix solid-phase synthesis and solution-phase mixture synthesis have substantially increased the capacity for preparing candidate libraries and their value has increased as deconvolution techniques for rapidly or easily identifying screening leads have been introduced. Among its many attributes, solution-phase library synthesis permits the utilization of the widely accepted convergent synthesis strategy, easily accommodates mixture synthesis, is adaptable to dynamic- or selection-screening including target-assembled ligands, and is generally not limited by scale. Moreover, the advances in soluble polymer-supported synthesis and the widespread success of strategies enlisting polymer-supported reagents, scavengers, and workup reagents (inverse solid-phase synthesis)[165] suggest that the common assumption that library synthesis is best conducted on solid phase may not always be accurate and that the value of solution-phase library synthesis may still be underestimated.

Our present library of approximately 40000 compounds is in the process of being expanded to 1000000 compounds with a focus on assembling a series of libraries capable of adequately, if not fully, exploring pharmacophore space in a single round of screening, incorporating specific design elements for targeting protein–protein interactions (e.g. RGD mimetics, α-helix and β-sheet mimetics), exploring new templates, and implementing new solution-phase techniques including target-assisted synthesis for selection of candidate ligands. The fact that the libraries are generated on a scale permitting their repeated use in new assays as the opportunities arise ensures their value will only increase over time.

It is likely that the years ahead will be characterized by an increasing focus on the application of the technology more than the methodology itself, and this may very well be the era in which the most useful approaches naturally emerge. It will also mark a time where the problem selection may distinguish the notable contributions from those that are overlooked. The future issue may well be not just the identification of effective modulators (inhibitors or mimics) of target protein–protein or protein–DNA interactions, but the identification of selective modulators. A first step in such an analysis for protein–DNA interactions was taken with the introduction of the FID assay which permits the simultaneous examination of all possible DNA sequences. This allows an assessment of affinity for not

 © 2003 Wiley-VCH Verlag GmbH & Co. KGaA, Weinheim

Table 9: R^5 modification of HUN-7293. Inhibitory activity (IC_{50} [nM]) for VCAM-1 and ICAM-1 protein expression in human microvascular cell line (HMEC-1).[a]



Compound	VCAM-1	ICAM-1	Selectivity	Rel. potency
HUN-7293	1	24	24	1
85, $Y^5 = H$	>10000	>10000	n.d.[b]	<0.0001
86	1800 ± 10	2800 ± 210	1.6	0.0006
87	44 ± 11	510 ± 140	12	0.02
88	1.7 ± 1.6	19 ± 1.2	11	0.6
89	21 ± 1.6	186 ± 3	9	0.05
90	19 ± 1.2	16 ± 13	0.8	0.05
91	38 ± 5	2100 ± 170	55	0.03
92	11 ± 2.6	71 ± 35	6	0.09
93	29 ± 6	94 ± 13	3	0.03
94	380 ± 120	890 ± 340	2.3	0.003
95	1400 ± 230	>7000	>5	0.0007
96	2.3 ± 0.6	43 ± 6	19	0.4
97	63 ± 4	720 ± 90	11	0.02
C_2^3-epi-**97**	190 ± 20	9700 ± 3300	51	0.005
98	810 ± 130	8200 ± 120	10	0.001
99	280 ± 7	480 ± 65	1.7	0.004
C_2^3-epi-**99**	1100 ± 240	2600 ± 440	2.4	0.0009

[a] $Y^5 = Me$ (HUN-7293 unless otherwise stated). [b] n.d. = not determined.

only the desired target (sequence), but also a simultaneous assessment of selectivity among all targets (sequences) that may be used to distinguish between otherwise similar leads. Proteomics approaches towards examining ligand interactions with all proteins are emerging[417] that may be used to establish ligand selectivity,[99] and analogous approaches to simultaneous or parallel screening for modulating protein–protein interactions[418] are on the horizon.

We gratefully acknowledge the financial support of the National Institutes of Health (CA78045, CA41986, CA41101, EY14174), the Department of Army (DAMD17-02-1-0135), the Skaggs Institute for Chemical Biology, and predoctoral fellowship for K.C. (Thomas and Sharon Bauce Foundation Fellowship). K.C. is a Skaggs Fellow.

Received: January 24, 2003 [A574]

[1] M. R. Pavia, T. K. Sawyer, W. H. Moos, *Bioorg. Med. Chem. Lett.* **1993**, *3*, 387–396.
[2] M. A. Gallop, R. W. Barrett, W. J. Dower, S. P. A. Fodor, E. M. Gordon, *J. Med. Chem.* **1994**, *37*, 1233–1251.
[3] E. M. Gordon, R. W. Barrett, W. J. Dower, S. P. A. Fodor, M. A. Gallop, *J. Med. Chem.* **1994**, *37*, 1385–1401.
[4] N. K. Terrett, M. Gardner, D. W. Gordon, R. J. Kobylecki, J. Steele, *Tetrahedron* **1995**, *51*, 8135–8173.
[5] J. S. Früchtel, G. Jung, *Angew. Chem.* **1996**, *108*, 19–46; *Angew. Chem. Int. Ed. Engl.* **1996**, *35*, 17–42.
[6] J. A. Ellman, *Acc. Chem. Res.* **1996**, *29*, 132–143.
[7] E. M. Gordon, M. A. Gallop, D. V. Patel, *Acc. Chem. Res.* **1996**, *29*, 144–154.
[8] L. A. Thompson, J. A. Ellman, *Chem. Rev.* **1996**, *96*, 555–600.
[9] F. Balkenhohl, C. von dem Bussche-Hünnefeld, A. Lansky, C. Zechel, *Angew. Chem.* **1996**, *108*, 2436–2487; *Angew. Chem. Int. Ed. Engl.* **1996**, *35*, 2288–2337.
[10] I. M. Chaiken, K. D. Janda, *Molecular Diversity and Combinatorial Chemistry: Libraries and Drug Discovery,* American Chemical Society, Washington, DC, **1996**.
[11] G. Jung, *Combinatorial Peptide and Nonpeptide Libraries: a Handbook*, VCH, Weinheim, **1996**.
[12] A. W. Czarnik, S. H. DeWitt, *A Practical Guide to Combinatorial Chemistry*, American Chemical Society, Washington, DC, **1997**.
[13] A. Nefzi, J. M. Ostresh, R. A. Houghten, *Chem. Rev.* **1997**, *97*, 449–472.
[14] N. K. Terrett, *Combinatorial Chemistry*, Oxford University Press, Oxford, UK, **1998**.
[15] D. Obrecht, J. M. Villalgordo, *Solid-Supported Combinatorial and Parallel Synthesis of Small-Molecular-Weight Compound Libraries*, Pergamon/Elsevier, Oxford, UK, **1998**.
[16] B. Agnew, R. F. Sevice, M. Enserink, D. Normile, E. Marshal, C. Sander, M. R. Reich, *Science* **2000**, *287*, 1951–1981.
[17] R. Storer, *Drug Discovery Today* **1996**, *1*, 248–254.
[18] A. Chucholowski, T. Masquelin, D. Obrecht, J. Stadlwieser, J. M. Villalgordo, *Chimia* **1996**, *50*, 525–530.
[19] D. M. Coe, R. Storer, *Annu. Rep. Comb. Chem. Mol. Diversity* **1997**, *1*, 50–58.
[20] N. Bailey, A. W. J. Cooper, M. J. Deal, A. W. Dean, A. L. Gore, M. C. Hawes, D. B. Judd, A. T. Merritt, R. Storer, S. Travers, S. P. Watson, *Chimia* **1997**, *51*, 832–837.
[21] L. M. Gayo, *Biotechnol. Bioeng.* **1998**, *61*, 95–106.
[22] H. An, P. D. Cook, *Recent Res. Dev. Org. Chem.* **1998**, *2*, 473–488.
[23] R. Ferritto, P. Seneci, *Drugs Future* **1998**, *23*, 643–654.
[24] D. M. Coe, R. Storer, *Annu. Rep. Comb. Chem. Mol. Diversity* **1999**, *2*, 1–8.
[25] D. M. Coe, R. Storer, *Mol. Diversity* **1999**, *4*, 31–38.
[26] V. Austel, *Comb. Chem.* **1999**, 77–123.
[27] M. J. Suto, *Curr. Opin. Drug Discovery Dev.* **1999**, *2*, 377–384.
[28] A. Ganesan, *Drug Discovery Today* **2002**, *7*, 47–55.
[29] H. An, *Front. Biotechnol. Pharm.* **2000**, *1*, 83–113.
[30] C. M. Baldino, *J. Comb. Chem.* **2000**, *2*, 89–103.
[31] H. An, P. D. Cook, *Chem. Rev.* **2000**, *100*, 3311–3340.
[32] O. Ramström, J.-M. Lehn, *Nat. Rev. Drug Discovery* **2002**, *1*, 26–36.
[33] S. Otto, R. L. E. Furlan, J. K. M. Sanders, *Curr. Opin. Chem. Biol.* **2002**, *6*, 321–327.
[34] H. Han, M. M. Wolfe, S. Brenner, K. D. Janda, *Proc. Natl. Acad. Sci. USA* **1995**, *92*, 6419–6423.

 © 2003 Wiley-VCH Verlag GmbH & Co. KGaA, Weinheim

[35] D. J. Gravert, K. D. Janda, *Chem. Rev.* **1997**, *97*, 489 – 509.
[36] P. Wentworth, Jr., K. D. Janda, *Chem. Commun.* **1999**, 1917 – 1924.
[37] P. H. Toy, K. D. Janda, *Acc. Chem. Res.* **2000**, *33*, 546 – 554.
[38] N. A. Boyle, K. D. Janda, *Curr. Opin. Chem. Biol.* **2002**, *6*, 339 – 346.
[39] D. P. Curran, *Angew. Chem.* **1998**, *110*, 1230 – 1255; *Angew. Chem. Int. Ed.* **1998**, *37*, 1174 – 1196, Erratum: D. P. Curran, *Angew. Chem.* **1998**, *110*, 2569; *Angew. Chem. Int. Ed.* **1998**, *37*, 2292.
[40] D. P. Curran, *Med. Res. Rev.* **1999**, *19*, 432 – 438.
[41] J. Yoshida, K. Itami, *Chem. Rev.* **2002**, *102*, 3693 – 3716.
[42] R. A. Fecik, K. E. Frank, E. J. Gentry, L. A. Mitscher, M. Shibata, *Pure Appl. Chem.* **1999**, *71*, 559 – 564.
[43] H. Perrier, M. Labelle, *J. Org. Chem.* **1999**, *64*, 2110 – 2113.
[44] X. Wang, J. J. Parlow, J. A. Porco, Jr., *Org. Lett.* **2000**, *2*, 3509 – 3512.
[45] T. Bosanac, C. S. Wilcox, *J. Am. Chem. Soc.* **2002**, *124*, 4194 – 4195.
[46] S. W. Kaldor, M. G. Siegel, *Curr. Opin. Chem. Biol.* **1997**, *1*, 101 – 106.
[47] R. J. Booth, J. C. Hodges, *Acc. Chem. Res.* **1999**, *32*, 18 – 26.
[48] J. J. Parlow, R. V. Devraj, M. S. South, *Curr. Opin. Chem. Biol.* **1999**, *3*, 320 – 336.
[49] S. V. Ley, I. R. Baxendale, R. N. Bream, P. S. Jackson, A. G. Leach, D. A. Longbottom, M. Nesi, J. S. Scott, R. I. Storer, S. J. Taylor, *J. Chem. Soc. Perkin Trans. 1* **2000**, *23*, 3815 – 4195.
[50] S. V. Ley, I. R. Baxendale, *Nat. Rev. Drug Discovery* **2002**, *1*, 573 – 586.
[51] C. A. McNamara, M. J. Dixon, M. Bradley, *Chem. Rev.* **2002**, *102*, 3275 – 3300.
[52] D. E. Bergbreiter, *Chem. Rev.* **2002**, *102*, 3345 – 3384.
[53] T. J. Dickerson, N. N. Reed, K. D. Janda, *Chem. Rev.* **2002**, *102*, 3325 – 3344.
[54] D. L. Flynn, R. V. Devraj, J. J. Parlow, *Curr. Opin. Drug Discovery Dev.* **1998**, *1*, 41 – 50.
[55] D. L. Flynn, R. V. Devraj, W. Naing, J. J. Parlow, J. J. Weidner, S. Yang, *Med. Chem. Res.* **1998**, *8*, 219 – 243.
[56] D. L. Flynn, *Med. Res. Rev.* **1999**, *19*, 408 – 431.
[57] D. L. Boger, C. M. Tarby, L. H. Caporale, *J. Am. Chem. Soc.* **1996**, *118*, 2109 – 2110.
[58] S. Cheng, D. D. Comer, J. P. Williams, D. L. Boger, *J. Am. Chem. Soc.* **1996**, *118*, 2567 – 2573.
[59] S. Cheng, C. M. Tarby, D. D. Comer, J. P. Williams, L. H. Caporale, D. L. Boger, *Bioorg. Med. Chem.* **1996**, *4*, 727 – 737.
[60] D. L. Boger, W. Chai, R. S. Ozer, C.-M. Andersson, *Bioorg. Med. Chem. Lett.* **1997**, *7*, 463 – 468.
[61] D. L. Boger, W. Chai, *Tetrahedron* **1998**, *54*, 3955 – 3970.
[62] D. L. Boger, J. Goldberg, C.-M. Andersson, *J. Org. Chem.* **1999**, *64*, 2422 – 2427.
[63] D. L. Boger, W. Jiang, J. Goldberg, *J. Org. Chem.* **1999**, *64*, 7094 – 7100.
[64] D. L. Boger, W. Chai, Q. Jin, *J. Am. Chem. Soc.* **1998**, *120*, 7220 – 7225.
[65] D. L. Boger, J. K. Lee, J. Goldberg, Q. Jin, *J. Org. Chem.* **2000**, *65*, 1467 – 1474.
[66] D. L. Boger, R. S. Ozer, C.-M. Andersson, *Bioorg. Med. Chem. Lett.* **1997**, *7*, 1903 – 1908.
[67] D. L. Boger, P. Ducray, W. Chai, W. Jiang, J. Goldberg, *Bioorg. Med. Chem. Lett.* **1998**, *8*, 2339 – 2344.
[68] D. L. Boger, J. Goldberg, W. Jiang, W. Chai, P. Ducray, J. K. Lee, R. S. Ozer, C.-M. Andersson, *Bioorg. Med. Chem.* **1998**, *6*, 1347 – 1378.
[69] "Multi-step solution-phase combinatorial chemistry": D. L. Boger, J. Goldberg in *Combinatorial Chemistry: A Practical Approach* (Ed.: H. Fenniri), Oxford University Press, Oxford, UK, **2000**, pp. 303 – 326.
[70] D. L. Boger, B. E. Fink, M. P. Hedrick, *Bioorg. Med. Chem. Lett.* **2000**, *10*, 1019 – 1020.
[71] D. L. Boger, J. Goldberg, S. Satoh, Y. Ambroise, S. B. Cohen, P. K. Vogt, *Helv. Chim. Acta* **2000**, *83*, 1825 – 1845.
[72] D. L. Boger, J. K. Lee, *J. Org. Chem.* **2000**, *65*, 5996 – 6000.
[73] D. L. Boger, J. Goldberg, *Bioorg. Med. Chem.* **2001**, *9*, 557 – 562.
[74] D. L. Boger, H. Keim, B. Oberhauser, E. P. Schreiner, C. A. Foster, *J. Am. Chem. Soc.* **1999**, *121*, 6197 – 6205.
[75] D. L. Boger, Y. Chen, C. A. Foster, *Bioorg. Med. Chem. Lett.* **2000**, *10*, 1741 – 1744.
[76] Y. Chen, M. Bilban, C. A. Foster, D. L. Boger, *J. Am. Chem. Soc.* **2002**, *124*, 5431 – 5440.
[77] S. Silletti, T. Kessler, J. Goldberg, D. L. Boger, D. A. Cheresh, *Proc. Natl. Acad. Sci. USA* **2001**, *98*, 119 – 124.
[78] D. L. Boger, J. Goldberg, S. Silletti, T. Kessler, D. A. Cheresh, *J. Am. Chem. Soc.* **2001**, *123*, 1280 – 1288.
[79] Y. Ambroise, B. Yaspan, M. H. Ginsberg, D. L. Boger, *Chem. Biol.* **2002**, *9*, 1219 – 1226.
[80] T. Berg, S. B. Cohen, J. Desharnais, C. Sonderegger, D. J. Maslyar, J. Goldberg, D. L. Boger, P. K. Vogt, *Proc. Natl. Acad. Sci. USA* **2002**, *99*, 3830 – 3835.
[81] D. L. Boger, M. Searcey, W. C. Tse, Q. Jin, *Bioorg. Med. Chem. Lett.* **2000**, *10*, 495 – 498.
[82] J. Goldberg, Q. Jin, Y. Ambroise, S. Satoh, J. Desharnais, K. Capps, D. L. Boger, *J. Am. Chem. Soc.* **2002**, *124*, 544 – 555.
[83] C. R. Woods, T. Ishii, B. Wu, K. W. Bair, D. L. Boger, *J. Am. Chem. Soc.* **2002**, *124*, 2148 – 2152.
[84] C. R. Woods, T. Ishii, D. L. Boger, *J. Am. Chem. Soc.* **2002**, *124*, 10676 – 10682.
[85] C. R. Woods, N. Faucher, B. Eschgfaller, K. W. Bair, D. L. Boger, *Bioorg. Med. Chem. Lett.* **2002**, *12*, 2647 – 2650.
[86] D. L. Boger, M. A. Dechantsreiter, T. Ishii, B. E. Fink, M. P. Hedrick, *Bioorg. Med. Chem.* **2000**, *8*, 2049 – 2057.
[87] D. L. Boger, B. E. Fink, M. P. Hedrick, *J. Am. Chem. Soc.* **2000**, *122*, 6382 – 6394.
[88] D. L. Boger, H. W. Schmitt, B. E. Fink, M. P. Hedrick, *J. Org. Chem.* **2001**, *66*, 6654 – 6661.
[89] D. L. Boger, *Chemtracts: Org. Chem.* **1991**, *4*, 329 – 349.
[90] D. L. Boger, *Acc. Chem. Res.* **1995**, *28*, 20 – 29.
[91] D. L. Boger, D. S. Johnson, *Proc. Natl. Acad. Sci. USA* **1995**, *92*, 3642 – 3649.
[92] D. L. Boger, D. S. Johnson, *Angew. Chem.* **1996**, *108*, 1542 – 1580; *Angew. Chem. Int. Ed. Engl.* **1996**, *35*, 1438 – 1474.
[93] D. L. Boger, R. M. Garbaccio, *Bioorg. Med. Chem.* **1997**, *5*, 263 – 276.
[94] D. L. Boger, R. M. Garbaccio, *Acc. Chem. Res.* **1999**, *32*, 1043 – 1052.
[95] D. L. Boger, H. Cai, *Angew. Chem.* **1999**, *111*, 470 – 500; *Angew. Chem. Int. Ed.* **1999**, *38*, 448 – 476.
[96] S. E. Wolkenberg, D. L. Boger, *Chem. Rev.* **2002**, *102*, 2477 – 2495.
[97] D. L. Boger, B. E. Fink, S. R. Brunette, W. C. Tse, M. P. Hedrick, *J. Am. Chem. Soc.* **2001**, *123*, 5878 – 5891.
[98] D. L. Boger, W. C. Tse, *Bioorg. Med. Chem.* **2001**, *9*, 2511 – 2518.
[99] D. Leung, C. Hardouin, D. L. Boger, B. F. Cravatt, *Nat. Biotechnol.* **2003**, *23*, 687 – 691.
[100] A. G. Cochran, *Chem. Biol.* **2000**, *7*, R85 – R94.
[101] A. G. Cochran, *Curr. Opin. Chem. Biol.* **2001**, *5*, 654 – 659.
[102] D. L. Boger, *Bioorg. Med. Chem.* **2003**, *11*, 1607-—1613.
[103] H. M. Geysen, R. H. Meloen, S. J. Barteling, *Proc. Natl. Acad. Sci. USA* **1984**, *81*, 3998 – 4002.
[104] H. M. Geysen, S. J. Barteling, R. H. Meleon, *Proc. Natl. Acad. Sci. USA* **1985**, *82*, 178 – 182.
[105] R. A. Houghten, *Proc. Natl. Acad. Sci. USA* **1985**, *82*, 5131 – 5135.

 © 2003 Wiley-VCH Verlag GmbH & Co. KGaA, Weinheim

[106] J. K. Scott, G. P. Smith, *Science* **1990**, *249*, 386 – 390.
[107] G. P. Smith, V. A. Petrenko, *Chem. Rev.* **1997**, *97*, 391 – 410.
[108] R. Frank, *Tetrahedron* **1992**, *48*, 9217 – 9232. See also: R. Frank, *Nucleic Acids Res.* **1983**, *11*, 4365.
[109] Cut and combine membrane-supported synthesis: F. Dittrich, W. Tegge, R. Frank, *Bioorg. Med. Chem. Lett.* **1998**, *8*, 2351 – 2356.
[110] Á. Furka, F. Sebestyén, M. Asgedom, G. Dibó, *Int. J. Peptide Prot. Res.* **1991**, *37*, 487 – 493; Á. Furka, F. Sebestyén, M. Asgedom, G. Dibó, *Abstr. 10th Intl. Symp. Med. Chem.*, Budapest, Ungarn, **1988**, S. 288.
[111] F. Sebestyén, G. Dibó, A. Kovács, Á. Furka, *Bioorg. Med. Chem. Lett.* **1993**, *3*, 413 – 418.
[112] Á. Furka, *Drug Dev. Res.* **1995**, *36*, 1 – 12.
[113] R. A. Houghten, C. Pinilla, S. E. Blondelle, J. R. Appel, C. T. Dooley, J. H. Cuervo, *Nature* **1991**, *354*, 84 – 86.
[114] K. S. Lam, S. E. Salmon, E. M. Hersh, V. J. Hruby, W. M. Kazmierski, R. J. Knapp, *Nature* **1991**, *354*, 82 – 84.
[115] S. E. Salmon, K. S. Lam, M. Lebl, A. Kandola, P. S. Khattri, S. Wade, M. Pátek, P. Kocis, V. Krchòák, D. Thorpe, S. Felder, *Proc. Natl. Acad. Sci. USA* **1993**, *90*, 11708 – 11712.
[116] K. S. Lam, M. Lebl, V. Krchòák, *Chem. Rev.* **1997**, *97*, 411 – 448.
[117] S. P. A. Fodor, L. J. Read, M. C. Pirrung, L. Stryer, A. T. Lu, D. Solas, *Science* **1991**, *251*, 767 – 773.
[118] D. J. Ecker, T. A. Vickers, R. Hanecak, V. Driver, K. Anderson, *Nucleic Acids Res.* **1993**, *21*, 1853 – 1856.
[119] S. M. Freier, D. A. M. Konings, J. R. Wyatt, D. J. Ecker, *J. Med. Chem.* **1995**, *38*, 344 – 352.
[120] E. Erb, K. D. Janda, S. Brenner, *Proc. Natl. Acad. Sci. USA* **1994**, *91*, 11422 – 11426.
[121] S. Brenner, R. A. Lerner, *Proc. Natl. Acad. Sci. USA* **1992**, *89*, 5381 – 5383.
[122] J. Nielsen, S. Brenner, K. D. Janda, *J. Am. Chem. Soc.* **1993**, *115*, 9812 – 9813.
[123] J. M. Kerr, S. C. Banville, R. N. Zuckermann, *J. Am. Chem. Soc.* **1993**, *115*, 2529 – 2531.
[124] V. Nikolaev, A. Stierandova, V. Krchnák, B. Seligmann, K. S. Lam, S. E. Salmon, M. Lebl, *Pept. Res.* **1993**, *6*, 161 – 170.
[125] E. R. Felder, G. Heizmann, I. T. Matthews, H. Rink, E. Spieser, *Mol. Diversity* **1996**, *1*, 109 – 112.
[126] M. H. J. Ohlmeyer, R. N. Swanson, L. W. Dillard, J. C. Reader, G. Asouline, R. Kobayashi, M. Wigler, W. C. Still, *Proc. Natl. Acad. Sci. USA* **1993**, *90*, 10922 – 10926.
[127] H. P. Nestler, P. A. Bartlett, W. C. Still, *J. Org. Chem.* **1994**, *59*, 4723 – 4724.
[128] W. C. Still, *Acc. Chem. Res.* **1996**, *29*, 155 – 163.
[129] K. C. Nicolaou, X.-Y. Xiao, Z. Parandoosh, A. Senyei, M. P. Nova, *Angew. Chem.* **1995**, *107*, 2476 – 2479; *Angew. Chem. Int. Ed. Engl.* **1995**, *34*, 2289 – 2291.
[130] E. J. Moran, S. Sarshar, J. F. Cargill, M. M. Shahbaz, A. Lio, A. M. M. Mjallim, R. W. Armstrong, *J. Am. Chem. Soc.* **1995**, *117*, 10787 – 10788.
[131] J. W. Guiles, C. L. Lanter, R. A. Rivero, *Angew. Chem.* **1998**, *110*, 967 – 970; *Angew. Chem. Int. Ed.* **1998**, *37*, 926 – 932.
[132] A. R. Vaino, K. D. Janda, *Proc. Natl. Acad. Sci. USA* **2000**, *97*, 7692 – 7696.
[133] R. Frank, S. Hoffmann, M. Kiess, H. Lahmann, W. Tegge, C. Behn, H. Gausepohl, *Combinatorial Peptide and Nonpeptide Libraries* (Ed.: G. Jung), VCH, Weinheim, **1996**, pp. 363 – 386.
[134] C. M. Niemeyer, D. Blohm, *Angew. Chem.* **1999**, *111*, 3039 – 3043; *Angew. Chem. Int. Ed.* **1999**, *38*, 2865 – 2869.
[135] G. MacBeath, A. N. Koehler, S. L. Schreiber, *J. Am. Chem. Soc.* **1999**, *121*, 7967 – 7968.
[136] K. S. Lam, M. Renil, *Curr. Opin. Chem. Biol.* **2002**, *6*, 353 – 358.
[137] M. J. Plunkett, J. A. Ellman, *J. Org. Chem.* **1997**, *62*, 2885 – 2893.
[138] A. B. Reitz, *Curr. Opin. Drug Discovery Dev.* **1999**, *2*, 358 – 364.
[139] P. Blaney, R. Grigg, V. Sridharan, *Chem. Rev.* **2002**, *102*, 2607 – 2624.
[140] J. I. Crowley, H. Rapoport, *J. Am. Chem. Soc.* **1970**, *92*, 6363 – 6365.
[141] S. H. DeWitt, J. S. Kiely, C. J. Stankovic, M. C. Schroeder, D. M. R. Cody, M. R. Pavia, *Proc. Natl. Acad. Sci. USA* **1993**, *90*, 6909 – 6913.
[142] A. R. Brown, D. C. Rees, Z. Rankovic, J. R. Morphy, *J. Am. Chem. Soc.* **1997**, *119*, 3288 – 3295.
[143] G. W. Kenner, J. R. McDermott, R. C. Sheppard, *J. Chem. Soc. D* **1971**, 636 – 637.
[144] L. M. Gayo, M. J. Sato, *Tetrahedron Lett.* **1997**, *38*, 211 – 214.
[145] B. J. Backes, J. A. Ellman, *J. Org. Chem.* **1999**, *64*, 2322 – 2330.
[146] G. T. Bourne, W. D. F. Meutermans, M. L. Smythe, *Tetrahedron Lett.* **1999**, *40*, 7271 – 7274.
[147] K. J. Jensen, J. Alsina, M. F. Songster, J. Vágner, F. Albericio, G. Barany, *J. Am. Chem. Soc.* **1998**, *120*, 5441 – 5452.
[148] T. Masquelin, D. Sprenger, R. Baer, F. Gerber, Y. Mercadal, *Helv. Chim. Acta* **1998**, *81*, 646 – 660.
[149] C. O. Kappe, *Bioorg. Med. Chem. Lett.* **2000**, *10*, 49 – 51.
[150] A. Ganesan, *Angew. Chem.* **1998**, *110*, 2989 – 2992; *Angew. Chem. Int. Ed.* **1998**, *37*, 2828 – 2831.
[151] J.-M. Lehn, *Chem. Eur. J.* **1999**, *5*, 2455 – 2463.
[152] B. Klekota, B. L. Miller, *Trends Biotechnol.* **1999**, *17*, 205 – 209.
[153] G. R. L. Cousins, S.-A. Poulsen, J. K. M. Sanders, *Curr. Opin. Chem. Biol.* **2000**, *4*, 270 – 279.
[154] J.-M. Lehn, A. V. Eliseev, *Science* **2001**, *291*, 2331 – 2332.
[155] P. W. Smith, J. Y. Q. Lai, A. R. Whittington, B. Cox, J. G. Houston, C. H. Stylli, M. N. Banks, P. R. Tiller, *Bioorg. Med. Chem. Lett.* **1994**, *4*, 2821 – 2824.
[156] T. Carell, E. A. Wintner, A. Bashir-Hashemi, J. Rebek, Jr., *Angew. Chem.* **1994**, *106*, 2159 – 2162; *Angew. Chem. Int. Ed. Engl.* **1994**, *33*, 2059 – 2061.
[157] T. Carell, E. A. Wintner, A. J. Sutherland, J. Rebek, Jr., Y. M. Dunayevskiy, P. Vouros, *Chem. Biol.* **1995**, *2*, 171 – 183.
[158] Y. Dunayevskiy, P. Vouros, T. Carell, E. A. Wintner, J. Rebek, Jr., *Anal. Chem.* **1995**, *67*, 2906 – 2915.
[159] G. W. Shipps, Jr., U. P. Spitz, J. Rebek, Jr., *Bioorg. Med. Chem.* **1996**, *4*, 655 – 657.
[160] M. C. Pirrung, J. Chen, *J. Am. Chem. Soc.* **1995**, *117*, 1240 – 1245. M. C. Pirrung, J. H.-L. Chau, J. Chen, *Chem. Biol.* **1995**, *2*, 621 – 626.
[161] J. Nielsen, P. H. Rasmussen, *Tetrahedron Lett.* **1996**, *37*, 3351 – 3354.
[162] I. Ugi, A. Domling, W. Horl, *Endeavour* **1994**, *18*, 115 – 122.
[163] R. W. Armstrong, A. P. Combs, P. A. Tempest, S. D. Brown, T. A. Keating, *Acc. Chem. Res.* **1996**, *29*, 123 – 131.
[164] W. C. Ripka, G. Barker, J. Krakover, *Drug Discovery Today* **2001**, *6*, 471 – 477.
[165] "Inverse Solid Phase Synthesis": L. H. Caporale (Combichem, Inc.), US 5767238, **1998**; [*Chem. Abstr.* **1998**, *129*, 67693], filed 6/7/1995 (US application 95-483143).
[166] D. L. Boger, C. E. Brotherton, *J. Org. Chem.* **1984**, *49*, 4050 – 4055.
[167] D. L. Boger, M. D. Mullican, *J. Org. Chem.* **1984**, *49*, 4033 – 4044.
[168] D. L. Boger, M. D. Mullican, *J. Org. Chem.* **1984**, *49*, 4045 – 4050.
[169] S. L. Schreiber, *Science* **2000**, *287*, 1964 – 1969; L. Weber, *Curr. Opin. Chem. Biol.* **2000**, *4*, 295 – 302.
[170] B. Seed, *Chem. Biol.* **1994**, *1*, 125 – 129.
[171] A. Whitty, C. W. Borysenko, *Chem. Biol.* **1999**, *6*, R107 – R118.
[172] Reviews: R. A. Houghten, C. Pinilla, J. R. Appel, S. Blondelle, C. T. Dooley, J. Eichler, A. Nefzi, J. M. Ostresh, *J. Med. Chem.* **1999**, *42*, 3743 – 3778; C. Pinella, J. R. Appel, E. Borras, R. A. Houghten, *Nat. Med.* **2003**, *9*, 118 – 122.

 © 2003 Wiley-VCH Verlag GmbH & Co. KGaA, Weinheim

[173] C. Pinilla, J. R. Appel, P. Blanc, R. A. Houghten, *Biotechniques* **1992**, *13*, 901 – 905; C. T. Dooley, R. A. Houghten, *Life Sci.* **1993**, *52*, 1509 – 1517.
[174] Omission libraries: E. Câmpian, M. L. Peterson, H. H. Saneii, Á. Furka, *Bioorg. Med. Chem. Lett.* **1998**, *8*, 2357 – 2362; T. Carell, E. A. Wintner, J. Rebek, Jr., *Angew. Chem.* **1994**, *106*, 2162 – 2164; *Angew. Chem. Int. Ed. Engl.* **1994**, *33*, 2061 – 2064.
[175] R. A. Houghten, C. T. Dooley, *Bioorg. Med. Chem. Lett.* **1993**, *3*, 405 – 412.
[176] Y. M. Dunayevskiy, J.-J. Lai, C. Quinn, F. Talley, P. Vouros, *Rapid Commun. Mass Spectrom.* **1997**, *11*, 1178 – 1184. Y.-Z. Zhao, R. B. van Breemen, D. Nikolic, C.-R. Huang, C. P. Woodbury, A. Schilling, D. L. Venton, *J. Med. Chem.* **1997**, *40*, 4006 – 4012.
[177] P. J. Hajduk, R. P. Meadows, S. W. Fesik, Q. *Rev. Biophys.* **1999**, *32*, 211 – 240.
[178] M. Pellecchia, D. S. Sem, K. Wüthrich, *Nat. Rev. Drug Discovery* **2002**, *1*, 211 – 219.
[179] Y.-H. Chu, D. P. Kirby, B. L. Karger, *J. Am. Chem. Soc.* **1995**, *117*, 5419 – 5420; A. V. Eliseev, *Curr. Opin. Drug Discovery Dev.* **1998**, *1*, 106 – 115.
[180] M. M. Hann, A. R. Leach, G. Harper, *J. Chem. Inf. Comput. Sci.* **2001**, *41*, B56 – B64.
[181] P. L. Toogood, *J. Med. Chem.* **2002**, *45*, 1543 – 1558. M. W. Peczuh, A. D. Hamilton, *Chem. Rev.* **2000**, *100*, 2479 – 2494.
[182] R. Zutshi, M. Brickner, J. Chmielewski, *Curr. Opin. Chem. Biol.* **1998**, *2*, 62 – 66.
[183] C.-H. Heldin, *Cell* **1995**, *80*, 213 – 223.
[184] J. Schlessinger, *Cell* **2002**, *110*, 669 – 672.
[185] N. Stahl, G. D. Yancopoulos, *Cell* **1993**, *74*, 587 – 590.
[186] Further reviews: H. Ogiso, R. Ishitani, O. Nureki, S. Fukai, M. Yamanaka, J.-H. Kim, K. Saito, A. Sakamoto, M. Inoue, M. Shirouzu, S. Yokoyama, *Cell* **2002**, *110*, 775 – 787; A. L. F. Mui, A. Miyajima, *Prog. Growth Factor Res.* **1994**, *5*, 15 – 35; C.-H. Heldin, A. Oestman, *Cytokine Growth Factor Rev.* **1996**, *7*, 3 – 10; C.-H. Heldin, *Cancer Surv.* **1996**, *27*, 7 – 24; M. A. Lemmon, J. Schlessinger, *Methods Mol. Biol.* **1998**, *84*, 49 – 71; K. Schulze-Osthoff, D. Ferrari, M. Los, S. Wesselborg, M. E. Peter, *Eur. J. Biochem.* **1998**, *254*, 439 – 459; M. Onishi, T. Nosaka, T. Kitamura, *Int. Rev. Immunol.* **1998**, *16*, 617 – 634; F. P. Ottensmeyer, D. R. Beniac, R. Z.-T. Luo, C. C. Yip, *Biochemistry* **2000**, *39*, 12103 – 12112; B. M. Baker, D. C. Wiley, *Immunity* **2001**, *14*, 681 – 692; P. T. Daniel, T. Wieder, I. Sturm, K. Schulze-Osthoff, *Leukemia* **2001**, *15*, 1022 – 1032; S. R. George, B. F. O'Dowd, S. P. Lee, *Nat. Rev. Drug Discovery* **2002**, *1*, 808 – 820; R. C. Patel, U. Kumar, D. C. Lamb, J. S. Eid, M. Rocheville, M. Grant, A. Rani, T. Hazlett, S. C. Patel, E. Gratton, Y. C. Patel, *Proc. Natl. Acad. Sci. USA* **2002**, *99*, 3294 – 3299.
[187] J. N. Ihle, B. A. Witthuhn, F. W. Quelle, K. Yamamoto, W. E. Thierfelder, B Kreider, O. Silvennoinen, *Trends Biochem. Sci.* **1994**, *19*, 222 – 227.
[188] P. Lamb, H. M. Seidel, R. B. Stein, J. Rosen, *Annu. Rep. Med. Chem.* **1996**, *31*, 269 – 278; A. H. Brivanlou, J. E. Darnell, Jr., *Science* **2002**, *295*, 813 – 818.
[189] D. S. Aaronson, C. M. Horvath, *Science* **2002**, *296*, 1653 – 1655.
[190] Additional reviews K. Muegge, S. K. Durum, *Cytokine* **1990**, *2*, 1 – 8; L. A. Neuhold, B. Wold, *Cell* **1993**, *74*, 1033 – 1042. E. C. B. Jøergensen, H. Autrup, *Carcinogenesis* **1996**, *17*, 435 – 441; D. S. Latchman, *Int. J. Biochem. Cell Biol.* **1997**, *29*, 1305 – 1312; T. Hoey, *Science* **1997**, *278*, 1578 – 1579; P. A. Clemons, *Curr. Opin. Chem. Biol.* **1999**, *3*, 112 – 115; A. Stephanou, D. S. Latchman, *Gene Expression* **1999**, *7*, 311 – 319; Z. Yu, D. Zhou, G. Cheng, M. P. Mattson, *J. Mol. Neurosci.* **2000**, *15*, 31 – 44; P. S. Subramaniam, B. A. Torres, H. M. Johnson, *Cytokine* **2001**, *15*, 175 – 187; H. van Dam, M. Castellazzi, *Oncogene* **2001**, *20*, 2453 – 2464; T. E. Battle, D. A. Frank, *Curr. Mol. Med.* **2002**, *2*, 381 – 392.
[191] Reviews: a) J. D. Klemm, S. L. Schreiber, G. R. Crabtree, *Annu. Rev. Immunol.* **1998**, *16*, 569 – 592; b) S. L. Schreiber, G. R. Crabtree, *Harvey Lect.* **1997**, *91*, 99 – 114; c) G. R. Crabtree, S. L. Schreiber, *Trends Biochem. Sci.* **1996**, *21*, 418 – 422; d) D. J. Austin, G. R. Crabtree, S. L. Schreiber, *Chem. Biol.* **1994**, *1*, 131 – 136.
[192] a) D. M. Spencer, T. J. Wandless, S. L. Schreiber, G. R. Crabtree, *Science* **1993**, *262*, 1019 – 1024; b) D. M. Spencer, P. J. Belshaw, L. Chen, S. N. Ho, F. Randazzo, G. R. Crabtree, S. L. Schreiber, *Curr. Biol.* **1996**, *6*, 839 – 847; c) P. J. Belshaw, S. N. Ho, G. R. Crabtree, S. L. Schreiber, *Proc. Natl. Acad. Sci. USA* **1996**, *93*, 4604 – 4607; d) B. R. Stockwell, S. L. Schreiber, *Curr. Biol.* **1998**, *8*, 761 – 770.
[193] S. N. Ho, S. R. Biggar, D. M Spencer, S. L. Schreiber, G. R. Crabtree, *Nature* **1996**, *382*, 822 – 826.
[194] R. Briesewitz, G. T. Ray, T. J. Wandless, G. R. Crabtree, *Proc. Natl. Acad. Sci. USA* **1999**, *96*, 1953 – 1958.
[195] J. Huang, S. L. Schreiber, *Proc. Natl. Acad. Sci. USA* **1997**, *94*, 13396 – 13401.
[196] K. Koide, J. M. Finkelstein, Z. Ball, G. L. Verdine, *J. Am. Chem. Soc.* **2001**, *123*, 398 – 408.
[197] M. Liuzzi, R. Deziel, N. Moss, P. Beaulieu, A. M. Bonneau, C. Bousquet, J. G. Chafouleas, M. Garneau, J. Jaramillo, R. L. Krogsrud, *Nature* **1994**, *372*, 695 – 698.
[198] K. McMillan, M. Adler, D. S. Auld, J. J. Baldwin, E. Blasko, L. J. Browne, D. Chelsky, D. Davey, R. Dolle, K. A. Eagen, S. Erickson, R. I. Feldman, C. B. Glaser, C. Mallari, M. M. Morrissey, M. H. Ohlmeyer, G. Pan, J. F. Parkinson, G. B. Phillips, M. A. Polokoff, N. H. Sigal, R. Vergona, M. Whitlow, T. A. Young, J. J. Devlin, *Proc. Natl. Acad. Sci. USA* **2000**, *97*, 1506 – 1511.
[199] a) M. D. Shultz, M. J. Bowman, Y.-W. Ham, X. Zhao, G. Tora, J. Chmielewski, *Angew. Chem.* **2000**, *112*, 2822 – 2825; *Angew. Chem. Int. Ed.* **2000**, *39*, 2710 – 2713; b) X. Fan, G. R. Flentke, D. H. Rich, *J. Am. Chem. Soc.* **1998**, *120*, 8893 – 8894.
[200] a) L. Zhao, M. K. O'Reilly, M. D. Schultz, J. Chmielewski, *Bioorg. Med. Chem. Lett.* **2003**, *13*, 1175 – 1177; b) R. G. Maroun, S. Gayet, M. S. Benleulmi, H. Porumb, L. Zararian, H. Merad, H. Leh, J.-F. Mouscadet, F. Troalen, S. Fermandjian, *Biochemistry* **2001**, *40*, 13840 – 13848.
[201] B. P. Orner, J. T. Ernst, A. D. Hamilton, *J. Am. Chem. Soc.* **2001**, *123*, 5382 – 5383.
[202] A. Degterev, A. Lugovsky, M. Cardone, B. Mulley, G. Wagner, T. Mitchison, J. Yuan, *Nat. Cell Biol.* **2001**, *3*, 173 – 182.
[203] S.-P. Tzung, K. M. Kim, G. Basañez, C. D. Giedt, J. Simon, J. Simmerberg, K. Y. J. Zhang, D. M. Hockenbery, *Nat. Cell Biol.* **2001**, *3*, 183 – 191.
[204] J.-L. Wang, D. Liu, Z.-J. Zhang, S. Shan, X. Han, *Proc. Natl. Acad. Sci. USA* **2000**, *97*, 7124 – 7129.
[205] a) O. Kutzki, H. S. Park, J. T. Ernst, B. P. Orner, H. Yin, A. D. Hamilton, *J. Am. Chem. Soc.* **2002**, *124*, 11838 – 11839; b) J. T. Ernst, J. Becerril, H. S. Park, H. Yin, A. D. Hamilton, *Angew. Chem.* **2003**, *115*, 553 – 557; *Angew. Chem. Int. Ed.* **2003**, *42*, 535 – 539.
[206] a) S. J. Duncan, S. Gruschow, D. H. Williams, C. McNicholas, R. Purewal, M. Hajek, M. Gerlitz, S. Martin, S. K. Wrigley, M. Moore, *J. Am. Chem. Soc.* **2001**, *123*, 554 – 560; b) R. Stoll, C. Renner, S. Hansen, S. Palme, C. Klein, A. Belling, W. Zeslawski, M. Kamionka, T. Rehm, P. Muhlhahn, R. Schumacher, F. Hesse, B. Kaluza, W. Voelter, R. A. Engh, T. A. Holak, *Biochemistry* **2001**, *40*, 336 – 344.
[207] C. Garcia-Echeverria, P. Chene, M. J. Blommer, P. Furet, *J. Med. Chem.* **2000**, *43*, 3205 – 3208.
[208] J. B. Owolabi, G. Rizkalla, A. Tehim, G. M. Ross, R. J. Riopelle, R. Kamboj, M. Ossipov, D. Bian, S. Wegert, F. Porreca, D. K. H. Lee, *J. Pharmacol. Exp. Ther.* **1999**, *289*, 1271 – 1276.

 © 2003 Wiley-VCH Verlag GmbH & Co. KGaA, Weinheim

[209] M. Baba, O. Nishimura, N. Kanzaki, M. Okamoto, H. Sawada, Y. Iizawa, M. Shiraishi, Y. Aramaki, K. Okonogi, Y. Ogawa, K. Megurp, M. Fujino, *Proc. Natl. Acad. Sci. USA* **1999**, *96*, 5698 – 5702.

[210] a) J. W. Tilley, L. Chen, D. C. Fry, S. D. Emerson, G. D. Powers, D. Biondi, T. Varnell, R. Trilles, R. Guthrie, F. Mennona, G. Kaplan, R. A. LeMahieu, M. Carson, R.-J. Han, C.-M. Liu, R. Palermo, G. Ju, *J. Am. Chem. Soc.* **1997**, *119*, 7589 – 7590; b) A. C. Braisted, J. D. Oslob, W. L. Delano, J. Hyde, R. S. McDowell, N. Waal, C. Yu, M. R. Arkin, B. C. Raimundo, *J. Am. Chem. Soc.* **2003**, *125*, 3714 – 3715.

[211] R. Sarabu, J. P. Cooper, C. M. Cook, P. Gillespie, A. V. Perrotta, G. L. Olson, *Drug Des. Discovery* **1998**, *15*, 191 – 198.

[212] S. E. Cwirla, P. Balasubramanian, D. J. Duffin, C. R. Wagstrom, C. M. Gates, S. C. Singer, A. M. Davis, R. L. Tansik, L. C. Mattheakis, C. M. Boytos, P. J. Schatz, D. P. Baccanari, N. C. Wrighton, R. W. Barrett, W. J. Dower, *Science* **1997**, *276*, 1696 – 1699.

[213] T. Kimura, H. Kaburaki, T. Tsujino, Y. Ikeda, H. Kato, Y. Watanabe, *FEBS Lett.* **1998**, *428*, 250 – 254.

[214] S. S. Tian, P. Lamb, A. G. King, S. G. Miller, L. Kessler, J. I. Luengo, L. Averill, R. K. Johnson, J. G. Gleason, L. M. Pelus, S. B. Dillon, J. Rosen, *Science* **1998**, *281*, 257 – 259.

[215] a) A. Finch, A. K. Wong, N. J. Paczkowski, S. K. Wadi, D. J. Craik, D. P. Fairlie, S. M. Taylor, *J. Med. Chem.* **1999**, *42*, 1965 – 1974; b) A. J. Strachen, T. M. Woodruff, G. Haaima, D. P. Fairlie, S. M. Taylor, *J. Immunol.* **2000**, *164*, 6560 – 6565.

[216] J. Liu, J. D. Farmer, W. S. Lane, J. Friedman, I. Weissman, S. L. Schreiber, *Cell* **1991**, *66*, 807 – 815.

[217] H. M. Ke, L. D. Zydowsky, J. Liu, C. T. Walsh, *Proc. Natl. Acad. Sci. USA* **1991**, *88*, 9483 – 9487.

[218] a) E. J. Brown, M. W. Albers, T. B. Shin, K. Ichikawa, C. T. Keith, W. S. Lane, S. L. Schreiber, *Nature* **1994**, *369*, 756 – 758; b) J. Choi, J. Chen, S. L. Schreiber, J. Clardy, *Science* **1996**, *273*, 239 – 242.

[219] N. Ban, P. Nissen, J. Hansen, P. B. Moore, T. A. Steitz, *Science* **2000**, *289*, 905 – 920; N. Ban, P. Nissen, J. Hansen, P. B. Moore, T. A. Steitz, *Science* **2000**, *289*, 920 – 930.

[220] a) Reviews: T. Scheibel, J. Buchner, *Biochem. Pharmacol.* **1998**, *56*, 675 – 682; J. S. Isaacs, W. Xu, L. Neckers, *Cancer Cell*, **2003**, *3*, 213 – 217; b) G. Chiosis, M. N. Timaul, B. Lucas, P. M. Minster, F. F. Zheng, L. Sepp-Lorenzino, N. Rosen, *Chem. Biol.* **2001**, *8*, 289 – 299.

[221] a) Reviews: K. H. Downing, *Emerging Ther. Targets* **2000**, *4*, 219 – 237; J. R. Peterson, T. J. Mitchison, *Chem. Biol.* **2002**, *9*, 1275 – 1285; b) S. J. Haggarty, T. U. Mayer, D. T. Miyamoto, R. Fathi, R. W. King, T. J. Mitchison, S. L. Schreiber, *Chem. Biol.* **2000**, *7*, 275 – 286.

[222] Review: Y. Pommier, *Biochimie* **1998**, *80*, 255 – 270.

[223] Reviews: a) B. K. Hubbard, C. T. Walsh, *Angew. Chem.* **2003**, *115*, 752 – 789; *Angew. Chem. Int. Ed.* **2003**, *42*, 730 – 765; b) D. G. McCafferty, P. Cudic, M. K. Yu, D. C. Behenna, R. Kruger, *Curr. Opin. Chem. Biol.* **1999**, *3*, 672 – 680.

[224] a) J. A. Katzenellenbogen, B. S. Katzenellenbogen, *Chem. Biol.* **1996**, *3*, 529 – 536; b) D. Santiso-Mere, D. P. McDonnell, *Chem. Today*, **1994**, *12*, 29 – 36.

[225] a) T. K. Sawyer, *Biopolymers* **1998**, *47*, 243 – 261; b) J. K. Chen, S. L. Schreiber, *Bioorg. Med. Chem. Lett.* **1994**, *4*, 1755 – 1760; c) M. Sudol, T. Hunter, *Cell* **2000**, *103*, 1001 – 1004; d) A. Y. Hung, M. Sheng, *J. Biol. Chem.* **2002**, *277*, 5699 – 5702; M. Zhang, W. Wang, *Acc. Chem. Res.* **2003**, *36*, 530 – 538.

[226] J.-M. Chen, R. T. Aimes, G. R. Ward, G. L. Youngleib, J. P. Quigley, *J. Biol. Chem.* **1991**, *266*, 5113 – 5121.

[227] V.-M. Kahari, U. Saarialho-Kere, *Ann. Med.* **1999**, *31*, 34 – 45.

[228] M. A. Rudek, J. Venitz, W. D. Figg, *Pharmacotherapy* **2002**, *22*, 705 – 720.

[229] M. Lein, K. Jung, B. Ortel, C. Stephan, W. Rothaug, R. Juchem, M. Johannsen, S. Deger, D. Schnorr, S. Loening, H.-W. Krell, *Oncogene* **2002**, *21*, 2089 – 2096.

[230] L. M. Coussens, B. Fingleton, L. M. Matrisian, *Science* **2002**, *295*, 2387 – 2392.

[231] A. Matter, *Drug Discovery Today* **2001**, *6*, 1005 – 1024.

[232] For a review on integrins, see: R. O. Hynes, *Cell* **2002**, *110*, 673 – 687.

[233] P. C. Brooks, R. A. F. Clark, D. A. Cheresh, *Science* **1994**, *264*, 569 – 571.

[234] P. C. Brooks, A. M. P. Montgomery, M. Rosenfeld, R. A. Reisfeld, T. Hu, G. Klier, D. A. Cheresh, *Cell* **1994**, *79*, 1157 – 1164.

[235] F. Carreiras, B. Thiebot, J. Leroy-Dudal, S. Maubant, M.-F. Breton, H. Darbeida, *Int. J. Cancer* **2002**, *99*, 800 – 808.

[236] N. E. Tsopanoglou, P. Andriopoulou, M. E. Maragoudakis, *Am. J. Physiol.* **2002**, *283*, C1501 – C1510.

[237] M. A. Arnaout, *Immunol. Rev.* **2002**, *186*, 125 – 140.

[238] J. Takagi, B. M. Petre, T. Walz, T. A. Springer, *Cell* **2002**, *110*, 599 – 611.

[239] For a review of endogenous ligand binding to integrins, see: E. F. Plow, T. A. Haas, L. Zhang, J. Loftus, J. W. Smith, *J. Biol. Chem.* **2000**, *275*, 21785 – 21788.

[240] E. Ruoslahti, *Annu. Rev. Cell Biol.* **1996**, *12*, 697 – 715.

[241] R. Haubner, R. Gratias, B. Diefenbach, S. L. Goodman, A. Jonczyk, H. Kessler, *J. Am. Chem. Soc.* **1996**, *118*, 7461 – 7472.

[242] R. Bruck, H. Shirin, R. Hershkoviz, O. Lider, G. Kenet, H. Aeed, Z. Matas, L. Zaidel, Z. Halpern, *Gut* **1997**, *40*, 133 – 138.

[243] R. Pasqualini, E. Koivunen, E. Ruoslahti, *Nat. Biotechnol.* **1997**, *15*, 542 – 546.

[244] A. Giannis, F. Rübsam, *Angew. Chem.* **1997**, *109*, 606 – 609; *Angew. Chem. Int. Ed. Engl.* **1997**, *36*, 588 – 590.

[245] E. Ruoslahti, *Kidney Int.* **1997**, *51*, 1413 – 1417.

[246] K. Sunassee, R. Vile, *Curr. Biol.* **1997**, *7*, R282 – R285.

[247] C. D. Eldred, B. D. Judkins, *Prog. Med. Chem.* **1999**, *39*, 29 – 90.

[248] C. D. Buckley, D. Pilling, N. V. Henriquez, G. Parsonage, K. Threlfall, D. Scheel-Toellner, D. L. Simmons, A. N. Akbar, J. M. Lord, M. Salmon, *Nature* **1999**, *397*, 534 – 539.

[249] K. Kurohane, Y. Namba, N. Oku, *Life Sci.* **2000**, *68*, 273 – 281.

[250] C. D. Anuradha, S. Kanno, S. Hirano, *Cell Biol. Toxicol.* **2000**, *16*, 275 – 283.

[251] Y. Chen, X. Xu, S. Hong, J. Chen, N. Liu, C. B. Underhill, K. Creswell, L. Zhang, *Cancer Res.* **2001**, *61*, 2434 – 2438.

[252] Y. Yamamoto, Y. Tsutsumi, T. Mayumi. *Curr. Drug Targets* **2002**, *3*, 123 – 130.

[253] V. Brower, *Nat. Biotechnol.* **1999**, *17*, 963 – 968.

[254] W. D. Klohs, J. M. Hamby, *Curr. Opin. Biotechnol.* **1999**, *10,* 544 – 549.

[255] S. R. Kerbel, *Carcinogenesis* **2000**, *21*, 505 – 515.

[256] R. D. Connell, J. S. Beebe, *Expert Opin. Ther. Pat.* **2001**, *11*, 1919 – 1945.

[257] S. Madhusudan, A. L. Harris, *Curr. Opin. Pharmacol.* **2002**, *2*, 403 – 414.

[258] W. W. Li, V. W. Li, D. Tsakayannis, *New Angioth.* **2002**, 547 – 571.

[259] P. C. Brooks, S. Strömblad, L. C. Sanders, T. L. von Schalscha, R. T. Aimes, W. G. Stetler-Stevenson, J. P. Quigley, D. A. Cheresh, *Cell* **1996**, *85*, 683 – 693.

[260] S. Silletti, D. A. Cheresh, *Fibrinolysis Proteolysis* **1999**, *13*, 226 – 238.

[261] P. C. Brooks, S. Silletti, T. L. von Schalscha, M. Friedlander, D. A. Cheresh, *Cell* **1998**, *92*, 391 – 400.

[262] R. O. Hynes, *Cell* **1992**, *69*, 11 – 25.

[263] R. L. Juliano, S. Haskill, *J. Cell Biol.* **1993**, *120*, 577 – 585.

[264] T. A. Springer, *Cell* **1994**, *76*, 301 – 314.

[265] R. R. Lobb, M. E. Hemler, *J. Clin. Invest.* **1994**, *94*, 1722 – 1728.

 © 2003 Wiley-VCH Verlag GmbH & Co. KGaA, Weinheim

[266] M. Stewart, M. Thiel, N. Hogg, *Curr. Opin. Cell Biol.* **1995**, *7*, 690 – 696.
[267] Y. Shimizu, D. M. Rose, M. H. Ginsberg, *Adv. Immunol.* **1999**, *72*, 325 – 380.
[268] S. Liu, M. H. Ginsberg, *J. Biol. Chem.* **2000**, *275*, 22736 – 22742.
[269] S. Liu, S. M. Thomas, D. G. Woodside, D. M. Rose, W. B. Kiosses, M. Pfaff, M. H. Ginsberg, *Nature* **1999**, *402*, 676 – 681.
[270] M. E. Hemler, P. D. Kassner, B. M. C. Chan, *Cold Spring Harbor Symp. Quant. Biol.* **1992**, *57*, 213 – 220.
[271] K.-C. Lin, A. C. Castro, *Curr. Opin. Chem. Biol.* **1998**, *2*, 453 – 457.
[272] J. W. Tilley, A. Sidduri, *Drugs Future* **2001**, *26*, 985 – 998.
[273] H. Yusuf-Makagiansar, M. E. Anderson, T. V. Yakovleva, J. S. Murray, T. J. Siahaan, *Med. Res. Rev.* **2002**, *22*, 146 – 167.
[274] B. Amati, H. Land, *Curr. Opin. Genet. Dev.* **1994**, *4*, 102 – 108.
[275] B. Amati, S. R. Frank, D. Donjerkovic, S. Taubert, *Biochim. Biophys. Acta* **2001**, *1471*, M135 – M145.
[276] L. Ratner, S. F. Josephs, F. Wong-Staal, *Annu. Rev. Microbiol.* **1985**, *39*, 419 – 449.
[277] C. Lavialle, N. Modjtahedi, T. Lamonerie, T. Frebourg, R. M. Landin, N. Fossar, G. Lhomond, R. Cassingena, O. Brison, *Anticancer Res.* **1989**, *9*, 1265 – 1279.
[278] J. K. Field, D. A. Spandidos, *Anticancer Res.* **1990**, *10*, 1 – 22.
[279] K. B. Marcu, S. A. Bossone, A. J. Patel, *Annu. Rev. Biochem.* **1992**, *61*, 809 – 860.
[280] M. Henriksson, B. Lüscher, *Adv. Cancer Res.* **1996**, *68*, 109 – 182.
[281] B. Calabretta, T. Skorski, *Anti-Cancer Drug Des.* **1997**, *12*, 373 – 381.
[282] R. Eisenman, *Genes Dev.* **2001**, *15*, 2023 – 2030.
[283] W. Lutz, J. Leon, M. Eilers, *Biochim. Biophys. Acta* **2002**, *1602*, 61 – 71.
[284] S. K. Oster, C. S. W. Ho, E. L. Soucie, L. Z. Penn, *Adv. Cancer Res.* **2002**, *84*, 81 – 154.
[285] A. R. Ferré-d'Amaré, G. D. Prendergast, E. B. Ziff, S. K. Burley, *Nature* **1993**, *363*, 38 – 45.
[286] P. Brownlie, T. A. Ceska, M. Lamers, C. Romier, G. Stier, H. Teo, D. Suck, *Structure* **1997**, *5*, 509 – 520.
[287] G. C. Prendergast, D. Lawe, E. B. Ziff, *Cell* **1991**, *65*, 395 – 407.
[288] E. M. Blackwood, R. N. Eisenman, *Science* **1991**, *251*, 1211 – 1217.
[289] E. M. Blackwood, B. Lüscher, R. N. Eisenman, *Genes Dev.* **1992**, *6*, 71 – 80.
[290] L. Kretzner, E. M. Blackwood, R. N. Eisenman, *Nature* **1992**, *359*, 426 – 429.
[291] G. J. Kato, W. M. F. Lee, L. Chen, C. V. Dang, *Genes Dev.* **1992**, *6*, 81 – 92.
[292] B. Amati, S. Dalton, M. W. Brooks, T. D. Littlewood, G. I. Evan, H. Land, *Nature* **1992**, *359*, 423 – 426.
[293] B. Amati, M. W. Brooks, N. Levy, T. D. Littlewood, G. I. Evan, H. Land, *Cell* **1993**, *72*, 233 – 245.
[294] B. Amati, T. D. Littlewood, G. I. Evan, H. Land, *EMBO J.* **1993**, *12*, 5083 – 5087.
[295] M. Tsuneoka, F. Nakano, H. Ohgusu, E. Mekada, *Oncogene* **1997**, *14*, 2301 – 2311.
[296] D. E. Ayer, L. Kretzner, R. N. Eisenman, *Cell* **1993**, *72*, 211 – 222.
[297] A. S. Zervos, J. Gyuris, R. Brent, *Cell* **1993**, *72*, 223 – 232.
[298] V. Korinek, N. Barker, P. J. Morin, D. van Wichen, R. de Weger, K. W. Kinzler, B. Vogelstein, H. Clevers, *Science* **1997**, *275*, 1784 – 1787.
[299] J. Behrens, *Cancer Metastasis Rev.* **1999**, *18*, 15 – 30.
[300] Q. Eastman, R. Grosschedl, *Curr. Opin. Cell Biol.* **1999**, *11*, 233 – 240.
[301] A. Novak, S. Dedhar, *Cell. Mol. Life Sci.* **1999**, *56*, 523 – 537.
[302] J. J. Love, X. Li, D. A. Case, K. Giese, R. Grosschedl, P. Wright, *Nature* **1995**, *376*, 791 – 795.
[303] M. Aoki, A. Hecht, U. Kruse, R. Kemler, P. K. Vogt, *Proc. Natl. Acad. Sci. USA* **1999**, *96*, 139 – 144.
[304] S. B. Krantz, *Blood* **1991**, *77*, 419 – 434.
[305] M. J. Koury, M. C. Bondurant, *Eur. J. Biochem.* **1992**, *210*, 649 – 663.
[306] H. Youssoufian, G. Longmore, D. Neumann, A. Yoshimura, H. F. Lodish, *Blood* **1993**, *81*, 2223 – 2236.
[307] J. E. Damen, G. Krystal, *Exp. Hematol.* **1996**, *24*, 1455 – 1459.
[308] P. Foa, *Acta Haematol.* **1991**, *86*, 162 – 168.
[309] J. W. Fisher, *Proc. Soc. Exp. Biol. Med.* **1997**, *216*, 358 – 369.
[310] O. Ifudu, *Nephron* **2001**, *88*, 1 – 5.
[311] J. Seidenfeld, M. Piper, C. Flamm, V. Hasselblad, J. O. Armitage, C. L. Bennett, M. S. Gordon, A. E. Lichtin, J. L. Wade III, S. Woolf, N. Aronson, *J. Natl. Cancer Inst.* **2001**, *93*, 1204 – 1214.
[312] M. Mittelman, D. Neumann, A. Peled, P. Kanter, N. Haran-Ghera, *Proc. Natl. Acad. Sci. USA* **2001**, *98*, 5181 – 5186.
[313] S. S. Watowich, A. Yoshimura, G. D. Longmore, D. J. Hilton, Y. Yoshimura, H. F. Lodish, *Proc. Natl. Acad. Sci. USA* **1992**, *89*, 2140 – 2144.
[314] J. S. Philo, K. H. Aoki, T. Arakawa, L. O. Narhi, J. Wen, *Biochemistry* **1996**, *35*, 1681 – 1691.
[315] D. J. Matthews, R. S. Topping, R. T. Cass, L. B. Giebel, *Proc. Natl. Acad. Sci. USA* **1996**, *93*, 9471 – 9476.
[316] S. J. Frank, *Endocrinology* **2002**, *143*, 2 – 10.
[317] M. A. Lemmon, J. Schlessinger, *Trends Biochem. Sci.* **1994**, *19*, 459 – 463.
[318] B. A. Witthuhn, F. W. Quelle, O. Silvennoinen, T. Yi, B. Tang, O. Miura, J. N. Ihle, *Cell* **1993**, *74*, 227 – 236.
[319] N. C. Wrighton, F. X. Farrell, R. Chang, A. K. Kashyap, F. P. Barbone, L. S. Mulcahy, D. L. Johnson, R. W. Barrett, L. K. Jolliffe, W. J. Dower, *Science* **1996**, *273*, 458 – 463.
[320] D. L. Johnson, F. X. Farrell, F. P. Barbone, F. J. McMahon, J. Tullai, D. Kroon, J. Freedy, R. A. Zivin, L. S. Mulcahy, L. K. Joliffe, *Chem. Biol.* **1997**, *4*, 939 – 950.
[321] O. Livnah, E. A. Stura, D. L. Johnson, S. A. Middleton, L. S. Mulcahy, N. C. Wrighton, W. J. Dower, L. K. Joliffe, I. A. Wilson, *Science* **1996**, *273*, 464 – 471.
[322] I. A. Wilson, L. K. Joliffe, *Curr. Opin. Struct. Biol.* **1999**, *9*, 696 – 702
[323] A. M. de Vos, M. Ultsch, A. A. Kossiakoff, *Science* **1992**, *255*, 306 – 312.
[324] W. Somers, M. Ultsch, A. M. de Vos, A. A. Kossiakoff, *Nature* **1994**, *372*, 478 – 481.
[325] B. C. Cunningham, M. Ultsch, A. M. de Vos, M. G. Mulkerrin, K. R. Clauser, J. A. Wells, *Science* **1991**, *254*, 821 – 825.
[326] G. Fuh, B. C. Cunningham, R. Fukunaga, S. Nagata, D. V. Goeddel, J. A. Wells, *Science* **1992**, *256*, 1677 – 1680.
[327] B. C. Cunningham, J. A. Wells, *J. Mol. Biol.* **1993**, *234*, 554 – 563.
[328] J. A. Wells, *Proc. Natl. Acad. Sci. USA* **1996**, *93*, 1 – 6.
[329] N. J. Skelton, S. Russell, F. de Sauvage, A. G. Cochran, *J. Mol. Biol.* **2002**, *316*, 1111 – 1125.
[330] S. A. Qureshi, R. M. Kim, Z. Konteatis, D. E. Biazzo, H. Motamedi, R. Rodrigues, J. A. Boice, J. R. Calaycay, M. A. Bednarek, P. Griffin, Y.-D. Gao, K. Chapman, D. F. Mark, *Proc. Natl. Acad. Sci. USA* **1999**, *96*, 12156 – 12161.
[331] O. Livnah, D. L. Johnson, E. A. Stura, F. X. Farrell, F. P. Barbone, Y. You, K. D. Liu, M. A. Goldsmith, W. He, C. D. Krause, S. Pestka, L. K. Jolliffe, I. A. Wilson, *Nat. Struct. Biol.* **1998**, *5*, 993 – 1004.
[332] O. Livnah, E. A. Stura, S. A. Middleton, D. L. Johnson, L. K. Jolliffe, I. A. Wilson, *Science* **1999**, *283*, 987 – 990.
[333] R. S. Syed, S. W. Reid, C. Li, J. C. Cheetham, K. H. Aoki, B. Liu, H. Zhan, T. D. Osslund, A. J. Chirino, J. Zhang, J. Finer-Moore, S. Elliott, K. Sitney, B. A. Katz, D. J. Matthews, J. J. Wendoloski, J. Egrie, R. M. Stroud, *Nature* **1998**, *395*, 511 – 516.

 © 2003 Wiley-VCH Verlag GmbH & Co. KGaA, Weinheim

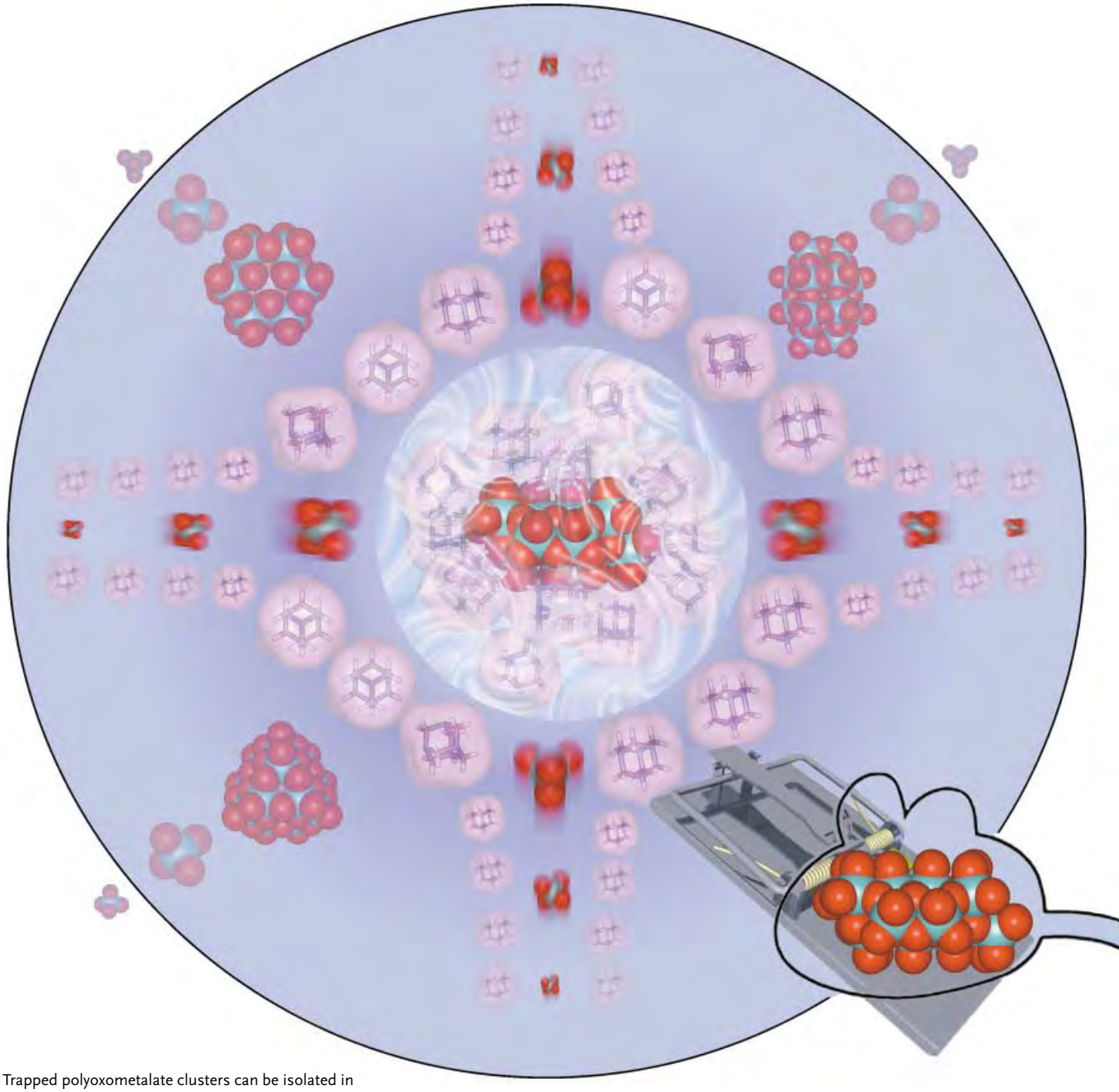
[334] I. Remy, I. A. Wilson, S. W. Michnick, *Science* **1999**, *283*, 990 – 993.
[335] Y. Choo, I. Sánchez-García, A. Klug, *Nature* **1994**, *372*, 642 – 645.
[336] S. Neidle, D. E. Thurston in *New Targets for Cancer Chemotherapy* (Eds.: D. J. Kerr, P. Workman), CRC Press, Boca Raton, FL, **1994**.
[337] S. Neidle, *Anti-Cancer Drug Des.* **1997**, *12*, 433 – 442.
[338] M. Mrksich, M. E. Parks, P. B. Dervan, *J. Am. Chem. Soc.* **1994**, *116*, 7983 – 7988.
[339] J. W. Trauger, E. E. Baird, P. B. Dervan, *Nature* **1996**, *382*, 559 – 561.
[340] D. Mercola, J. S. Cohen, *Cancer Gene Ther.* **1995**, *2*, 47 – 59.
[341] M. J. Browne, P. L. Thurlbey, *Genomes, Molecular Biology and Drug Discovery*, Academic Press, London, **1996**.
[342] H. Knudsen, P. E. Nielsen, *Nucleic Acids Res.* **1996**, *24*, 494 – 500.
[343] L. Good, P. E. Nielsen, *Antisense Nucleic Acid Drug Dev.* **1997**, *7*, 431 – 437.
[344] A. J. Gutierrez, M. D. Matteucci, D. Grant, A. Matsumura, R. W. Wagner, B. C. Froehler, *Biochemistry* **1997**, *36*, 743 – 748.
[345] G. W. Shipps, Jr., K. E. Pryor, J. Xian, D. A. Skyler, E. H. Davidson, J. Rebek, Jr., *Proc. Natl. Acad. Sci. USA* **1997**, *94*, 11 833 – 11 838.
[346] B. Klekota, M. H. Hammond, B. L. Miller, *Tetrahedron Lett.* **1997**, *38*, 8639 – 8642.
[347] B. Klekoka, B. L. Miller, *Tetrahedron* **1999**, *55*, 11 687 – 11 697.
[348] G. Werstuck, M. R. Green, *Science* **1998**, *282*, 296 – 298.
[349] T. Lescrinier, C. Hendrix, L. Kerremans, J. Rozenski, A. Link, B. Samyn, A. Van Aerschot, E. Lescrinier, R. Eritja, J. Van Beeumen, P. Herdewijn, *Chem. Eur. J.* **1998**, *4*, 425 – 433.
[350] C. Bailly, J. B. Chaires, *Bioconjugate Chem.* **1998**, *9*, 513 – 538.
[351] S.-Y. Chiang, J. C. Azizkhan, T. A. Beerman, *Biochemistry* **1998**, *37*, 3109 – 3115.
[352] D. E. Thurston, *Br. J. Cancer* **1999**, *80*, 65 – 85 (Suppl. 1).
[353] A. Simoncsits, M.-L. Tjornhammar, S. Wang, S. Pongor, *Genetica* **1999**, *106*, 85 – 92.
[354] C. M. Drain, X. Gong, V. Ruta, C. E. Soll, P. F. Chicoineau, *J. Comb. Chem.* **1999**, *1*, 286 – 290.
[355] V. M. Guelev, M. T. Harting, R. S. Lokey, B. L. Iverson, *Chem. Biol.* **2000**, *7*, 1 – 8.
[356] Md. R. Alam, M. Maeda, S. Sasaki, *Bioorg. Med. Chem.* **2000**, *8*, 465 – 473.
[357] Wechselwirkungen zwischen DNA und Wirkstoffen: *Methods in Molecular Biology, Vol. 90* (Ed.: K. R. Fox), Humana Press, Totowa, NJ, **1997**.
[358] H. R. Drew, A. A. Travers, *Cell* **1984**, *37*, 491 – 502.
[359] P. Hardenbol, J. C. Wang, M. W. Van Dyke, *Bioconjugate Chem.* **1997**, *8*, 616 – 620.
[360] J.-B. LePecq, C. Paoletti, *J. Mol. Biol.* **1967**, *27*, 87 – 106.
[361] B. S. P. Reddy, S. M. Sondhi, J. W. Lown, *Pharmacol. Ther.* **1999**, *84*, 1 – 111.
[362] S. Neidle, *Nat. Prod. Rep.* **2001**, *18*, 291 – 309.
[363] P. B. Dervan, *Bioorg. Med. Chem.* **2001**, *9*, 2215 – 2235.
[364] J. W. Trauger, E. E. Baird, M. Mrksich, P. B. Dervan, *J. Am. Chem. Soc.* **1996**, *118*, 6160 – 6166.
[365] R. P. Lamamie de Clairac, C. J. Seel, B. H. Geierstanger, M. Mrksich, E. E. Baird, P. B. Dervan, D. E. Wemmer, *J. Am. Chem. Soc.* **1999**, *121*, 2956 – 2964.
[366] J. W. Trauger, E. E. Baird, P. B. Dervan, *Nature* **1997**, *382*, 559 – 561.
[367] L. A. Dickinson, R. J. Gulizia, J. W. Trauger, E. E. Baird, D. E. Mosier, J. M. Gottesfeld, P. B. Dervan, *Proc. Natl. Acad. Sci. USA* **1998**, *95*, 12 890 – 12 895.
[368] Reviews: a) L. H. Caporale, *Proc. Natl. Acad. Sci. USA* **1995**, *92*, 75 – 82; b) R. P. Borris, *J. Ethnopharmacol.* **1996**, *51*, 29 – 38; c) D. G. I. Kingston in *The Practice of Medicinal Chemistry* (Ed.: C. G. Wermuth), Academic Press, London **1996**, pp. 101 – 116; d) G. M. Cragg, D. J. Newman, K. M. Snader, *J. Nat. Prod.* **1997**, *60*, 52 – 60; e) D. J. Newman, G. M. Cragg, K. M. Snader, *Nat. Prod. Rep.* **2000**, *17*, 215 – 234; f) Y.-Z. Shu, *J. Nat. Prod.* **1998**, *61*, 1053 – 1071; g) C. A. Montanari, V. da S. Bolzani, *Quim. Nova* **2001**, *24*, 105 – 111; h) A. B. Da Rocha, R. M. Lopes, G. Schwartsmann, *Curr. Opin. Pharmacol.* **2001**, *1*, 364 – 369; i) J. Mann, *Nat. Rev. Cancer* **2002**, *2*, 143 – 148.
[369] P. Arya, R. Joseph, D. T. H. Chou, *Chem. Biol.* **2002**, *9*, 145 – 156.
[370] a) J. Green, *J. Org. Chem.* **1995**, *60*, 4287 – 4290; b) R. Devraj, M. Cushman, *J. Org. Chem.* **1996**, *61*, 9368 – 9373.
[371] J. Nielsen, L. O. Lyngso, *Tetrahedron Lett.* **1996**, *37*, 8439 – 8442.
[372] a) T. C. Norman, N. S. Gray, J. T. Koh, P. G. Schultz, *J. Am. Chem. Soc.* **1996**, *118*, 7430 – 7431; b) N. S. Gray, L. Wodicka, A.-M. W. H. Thunnissen, T. C. Norman, S. Kwon, F. Herman Espinoza, D. O. Morgan, G. Barnes, S. LeClerc, L. Meijer, S.-H. Kim, D. J. Lockhart, P. G. Schultz, *Science* **1998**, *281*, 533 – 538; c) J. I. Armstrong, A. R. Portley, Y.-T. Chang, D. M. Nierengarten, B. N. Cook, K. G. Bowman, A. Bishop, N. S. Gray, K. M. Shokat, P. G. Schultz, C. R. Bertozzi, *Angew. Chem.* **2000**, *112*, 1359 – 1362; *Angew. Chem. Int. Ed.* **2000**, *39*, 1303 – 1306; d) Y.-T. Chang, N. S. Gray, G. R. Rosania, T. C. Kwon, R. Sarohira, M. Leost, L. Meijer, P. G. Schultz, *Chem. Biol.* **1999**, *6*, 361 – 375; e) G. R. Rosania, Y.-T. Chang, O. Perez, D. Sutherlin, H. Dong, D. J. Lockhart, P. G. Schultz, *Nat. Biotechnol.* **2000**, *18*, 304 – 308.
[373] A. Atubega, D. Maclean, C. Nguyen, E. M. Gordon, J. W. Jacobs, *Bioorg. Med. Chem.* **1996**, *4*, 1097 – 1106.
[374] a) K. C. Nicolaou, N. Winssinger, J. Pastor, S. Ninkovic, F. Sarabia, Y. He, D. Vourloumis, Z. Yang, T. Li, P. Giannakakou, E. Hamel, *Nature* **1997**, *387*, 268 – 272; b) K. C. Nicolaou, D. Vourloumis, T. Li, J. Pastor, N. Winssinger, Y. He, S. Ninkovic, F. Sarabia, H. Vallberg, F. Roschangar, N. P. King, M. R. V. Finlay, P. Giannakakou, P. Verdier-Pinard, E. Hamel, *Angew. Chem.* **1997**, *109*, 2181 – 2187; *Angew. Chem. Int. Ed. Engl.* **1997**, *36*, 2097 – 2103.
[375] a) S. Chen, K. D. Janda, *J. Am. Chem. Soc.* **1997**, *119*, 8724 – 8725; b) S. Chen, K. D. Janda, *Tetrahedron Lett.* **1998**, *39*, 3943 – 3946; c) K. J. Lee, A. Angulo, P. Ghazal, K. D. Janda, *Org. Lett.* **1999**, *1*, 1859 – 1862; d) J. A. López-Pelegrín, K. D. Janda, *Chem. Eur. J.* **2000**, *6*, 1917 – 1922.
[376] X. Y. Xiao, Z. Parandoosh, M. P. Nova, *J. Org. Chem.* **1997**, *62*, 6029 – 6033.
[377] T. R. Marsh, M. Bradley, S. J. Teague, *J. Org. Chem.* **1997**, *62*, 6199 – 6203.
[378] K. C. Nicolaou, N. Winssinger, J. Pastor, F. Murphy, *Angew. Chem.* **1998**, *110*, 2677 – 2680; *Angew. Chem. Int. Ed.* **1998**, *37*, 2534 – 2537.
[379] M. F. Gordeev, G. W. Luehr, H. C. Hui, E. M. Gordon, D. V. Patel, *Tetrahedron* **1998**, *54*, 15 879 – 15 890.
[380] M. Marder, H. Viola, J. A. Bacigaluppo, M. I. Colombo, C. Wasowski, C. Wolfman, J. H. Medina, E. A. Ruveda, A. C. Paladini, *Biochem. Biophys. Res. Commun.* **1998**, *249*, 481 – 485.
[381] K. C. Nicolaou, J. Pastor, N. Winssinger, F. Murphy, *J. Am. Chem. Soc.* **1998**, *120*, 5132 – 5133.
[382] a) K. C. Nicolaou, N. Winssinger, D. Vourloumis, T. Ohshima, S. Kim, J. Pfefferkorn, J.-Y. Xu, T. Li, *J. Am. Chem. Soc.* **1998**, *120*, 10 814 – 10 826; b) K. C. Nicolaou, S. Kim, J. A. Pfefferkorn, J. Xu, T. Ohshima, S. Hosokawa, D. Vourloumis, T. Li, *Angew. Chem.* **1998**, *110*, 1484 – 1487; *Angew. Chem. Int. Ed.* **1998**, *37*, 1418 – 1421.
[383] L. Bhat, Y. Liu, S. F. Victory, R. H. Himes, G. I. Georg, *Bioorg. Med. Chem. Lett.* **1998**, *8*, 3181 – 3186.
[384] a) D. R. Dragoli, L. A. Thompson, J. O'Brien, J. A. Ellman, *J. Comb. Chem.* **1999**, *1*, 534 – 539; b) L. A. Thompson, F. L.

 © 2003 Wiley-VCH Verlag GmbH & Co. KGaA, Weinheim

Moore, Y.-C. Moon, J. A. Ellman, *J. Org. Chem.* **1998**, *63*, 2066 – 2067.
[385] A. V. Loevezijn, J. H. V. Maarseveen, K. Stegman, G. M. Visser, G.-J. Koomen, *Tetrahedron Lett.* **1998**, *39*, 4737 – 4740.
[386] B. Meseguer, D. Alonso-Díaz, N. Griebenow, T. Herget, H. Waldmann, *Angew. Chem.* **1999**, *111*, 3083 – 3087; *Angew. Chem. Int. Ed.* **1999**, *38*, 2902 – 2906.
[387] H. Doi, I. Hijikuro, T. Takahashi, *J. Am. Chem. Soc.* **1999**, *121*, 6749 – 6750.
[388] R. A. Fecik, K. E. Frank, E. J. Gentry, L. A. Mitscher, M. Shibata, *Pure Appl. Chem.* **1999**, *71*, 559 – 564.
[389] R. Xu, G. Greiveldinger, L. E. Marenus, A. Cooper, J. A. Ellman, *J. Am. Chem. Soc.* **1999**, *121*, 4898 – 4899.
[390] C. W. Lindsey, L. K. Chan, B. C. Goess, R. Joseph, M. D. Shair, *J. Am. Chem. Soc.* **2000**, *122*, 422 – 423.
[391] H. Wang, A. Ganesan, *J. Comb. Chem.* **2000**, *2*, 186 – 194.
[392] a) K. C. Nicolaou, J. A. Pfefferkorn, A. J. Roecker, G.-Q. Cao, S. Barluenga, H. J. Mitchell, *J. Am. Chem. Soc.* **2000**, *122*, 9939 – 9953; b) K. C. Nicolaou, J. A. Pfefferkorn, H. J. Mitchell, A. J. Roecker, S. Barluenga, G.-Q. Cao, R. I. Affleck, J. E. Lillig, *J. Am. Chem. Soc.* **2000**, *122*, 9954 – 9967; c) K. C. Nicolaou, J. A. Pfefferkorn, S. Barluenga, H. J. Mitchell, A. J. Roecker, G.-Q. Cao, *J. Am. Chem. Soc.* **2000**, *122*, 9968 – 9976.
[393] R. Maltais, M. R. Tremblay, D. Poirier, *J. Comb. Chem.* **2000**, *2*, 604 – 614.
[394] P. Wipf, J. T. Reeves, R. Balachandran, K. A. Giuliano, E. Hamel, B. W. Day, *J. Am. Chem. Soc.* **2000**, *122*, 9391 – 9395.
[395] M. B. Andrus, T. M. Turner, Z. E. Sauna, S. V. Ambudkar, *J. Org. Chem.* **2000**, *65*, 4973 – 4983.
[396] a) O. de Frutos, D. P. Curran, *J. Comb. Chem.* **2000**, *2*, 639 – 649; b) W. Zhang, Z. Luo, C. H. Chen, D. P. Curran, *J. Am. Chem. Soc.* **2002**, *124*, 10443 – 10450.
[397] H. E. Pelish, N. J. Westwood, Y. Feng, T. Kirchhausen, M. D. Shair, *J. Am. Chem. Soc.* **2001**, *123*, 6740 – 6741.
[398] R. A. Davis, A. R. Carroll, R. J. Quinn, *Aust. J. Chem.* **2001**, *54*, 355 – 359.
[399] I. Hijikuro, T. Doi, T. Takahashi, *J. Am. Chem. Soc.* **2001**, *123*, 3716 – 3722.
[400] T. Hanazawa, T. Wada, T. Masuda, S. Okamoto, F. Sato, *Org. Lett.* **2001**, *3*, 3975 – 3977.
[401] K. C. Nicolaou, R. Hughes, J. A. Pfefferkorn, S. Barluena, A. J. Roecker, *Chem. Eur. J.* **2001**, *7*, 4280 – 4295.
[402] C. Herman, C. Giammasi, A. Geyer, M. E. Maier, *Tetrahedron* **2001**, *57*, 8999 – 9010.
[403] a) P. Stahl, L. Kissau, R. Mazitschek, A. Huwe, P. Furet, A. Giannis, H. Waldmann, *J. Am. Chem. Soc.* **2001**, *123*, 11586 – 11593; b) P. Stahl, L. Kissau, R. Mazitschek, A. Giannis, H. Waldmann, *Angew. Chem.* **2002**, *114*, 1222 – 1226; *Angew. Chem. Int. Ed.* **2002**, *41*, 1174 – 1178.
[404] R. Maltais, V. Luu-The, D. Poirier, *J. Med. Chem.* **2002**, *45*, 640 – 653.
[405] Y.-T. Chang, J. Choi, S. Ding, E. E. Prieschl, T. Baumruker, J.-M. Lee, S.-K. Chung, P. G. Schultz, *J. Am. Chem. Soc.* **2002**, *124*, 1856 – 1857.
[406] D. Brohm, S. Metzger, A. Bhargava, O. Muller, F. Lieb, H. Waldmann, *Angew. Chem.* **2002**, *114*, 319 – 323; *Angew. Chem. Int. Ed.* **2002**, *41*, 307 – 311.
[407] Reviews: a) D. G. I. Kingston, D. J. Newman, *Curr. Opin. Drug Discovery Dev.* **2002**, *5*, 304 – 316; b) J. Nielsen, *Curr. Opin. Chem. Biol.* **2002**, *6*, 297 – 305; c) S. P. Manly, R. Padmanabha, S. E. Lowe, *Methods Mol. Biol.* **2002**, *190*, 153 – 168; d) T. Paululat, Y.-Q. Tang, S. Grabley, R. Thiericke, *Chim. Oggi* **1999**, *17*, 52 – 56; e) S. Bertels, S. Frormann, G. Jas, K. U. Bindseil, *Drug Discovery from Nature*, Springer, Berlin, **1999**, pp. 72 – 105; f) L. A. Wessjohann, *Curr. Opin. Chem. Biol.* **2000**, *4*, 303 – 309; g) D. G. Hall, S. Manku, F. Wang, *J. Comb. Chem.* **2001**, *3*, 125 – 150; h) K. C. Nicolaou, J. A. Pfefferkorn, *Biopolymers* **2001**, *60*, 171 – 193; i) U. Abel, C. Koch, M. Speitling, F. G. Hannsske, *Curr. Opin. Chem. Biol.* **2002**, *6*, 453 – 458.
[408] a) C. A. Foster, M. Dreyfuss, B. Mandak, J. G. Meingassner, H. U. Naegeli, A. Nussbaumer, L. Oberer, G. Scheel, E.-M. Swoboda, *J. Dermatol.* **1994**, *21*, 847 – 854; b) U. Hommel, H.-P. Weber, L. Oberer, H. U. Naegeli, B. Oberhauser, C. A. Foster, *FEBS Lett.* **1996**, *379*, 69 – 73.
[409] H. Itazaki, T. Fujiwara, A. Sato, Y. Kawamura, K. Matsumoto, JP 07109299, **1995**.
[410] a) D. Thanos, T. Maniatis, *Cell* **1995**, *80*, 529 – 532; b) T. Collins, M. A. Read, A. S. Neish, M. Z. Whitley, D. Thanos, T. Maniatis, *FASEB J.* **1995**, *9*, 899 – 909; c) M. J. May, S. Ghosh, *Immunol. Today* **1998**, *19*, 80 – 88.
[411] a) J. M. Glover, J. M. Leeds, T. G. K. Mant, D. Amin, D. L. Kisner, J. E. Zuckerman, R. S. Geary, A. A. Levin, W. R. Shanahan, Jr., *J. Pharmacol. Exp. Ther.* **1997**, *282*, 1173 – 1180; b) B. R. Yacyshyn, M. B. Bowen-Yacyshyn, L. Jewell, J. A. Tami, C. F. Bennett, D. L. Kisner, W. R. Shanahan, Jr., *Gastroenterology* **1998**, *114*, 1133 – 1142.
[412] A. F. Kavanaugh, H. Schulze-Koops, L. S. Davis, P. E. Lipsky, *Arthritis Rheum.* **1997**, *40*, 849 – 853.
[413] a) D. H. Boschelli, J. B. Kramer, S. S. Khatana, R. J. Sorenson, D. T. Connor, M. A. Ferin, C. D. Wright, M. E. Lesch, K. Imre, G. C. Okonkwo, D. J. Schrier, M. C. Conroy, E. Ferguson, J. Woelle, U. Saxena, *J. Med. Chem.* **1995**, *38*, 4597 – 4614; b) D. H. Boschelli, D. T. Connor, M. E. Lesch, D. J. Schrier, *Bioorg. Med. Chem.* **1996**, *4*, 557 – 562.
[414] R. W. Sullivan, C. G. Bigam, P. E. Erdman, M. S. S. Palanki, D. W. Anderson, M. E. Goldman, L. J. Ransone, M. J. Suto, *J. Med. Chem.* **1998**, *41*, 413 – 419.
[415] A. O. Stewart, P. A. Bhatia, C. M. McCarty, M. V. Patel, M. A. Staeger, D. L. Arendsen, I. W. Gunawardana, L. M. Melcher, G.-D. Zhu, S. A. Boyd, D. G. Fry, B. L. Cool, L. Kifle, K. Lartey, K. C. Marsh, A. J. Kempf-Grote, P. Kilgannon, W. Wisdom, J. Meyer, W. M. Gallatin, G. F. Okasinski, *J. Med. Chem.* **2001**, *44*, 988 – 1002.
[416] E. Di Cera, *Adv. Protein Chem.* **1998**, *51*, 59 – 119, and references therein.
[417] D. D. Ryu, D. H. Nam, *Biotechnol. Prog.* **2000**, *16*, 2 – 16.
[418] H. Lin, V. W. Cornish, *Angew. Chem.* **2002**, *114*, 4580 – 4606; *Angew. Chem. Int. Ed.* **2002**, *41*, 4402 – 4425.

 © 2003 Wiley-VCH Verlag GmbH & Co. KGaA, Weinheim

Communications



Trapped polyoxometalate clusters can be isolated in a novel and simple synthetic approach which "shrink-wraps" unstable, unsymmetrical polyoxometalate clusters with large organic cations. This prevents their rearrangement and aggregation to more symmetrical, well known structures. Initial results and reactivities of clusters trapped in this way are presented by L. Cronin et al. on the following pages.

DOI: 10.1002/anie.200351615
© 2003 Wiley-VCH Verlag GmbH & Co. KGaA, Weinheim

Small Polyoxomolybdates

Restraining Symmetry in the Formation of Small Polyoxomolybdates: Building Blocks of Unprecedented Topology Resulting From "Shrink-Wrapping" $[H_2Mo_{16}O_{52}]^{10-}$-Type Clusters**

*De-Liang Long, Paul Kögerler, Louis J. Farrugia, and Leroy Cronin**

Dedicated to Professor Achim Müller on the occasion of his 65th Birthday

The structural diversity and potential for the formation of nanoscopic molecules in the field of polyoxomolybdate (POMo) cluster chemistry has been recently demonstrated in dramatic fashion.[1] Sparked by these discoveries and the many applications found and proposed for POMo-based clusters,[2–4] interest in their rational synthesis has been increasing rapidly. For example, the concept of generating a set of linkable nucleophilic building blocks that can be condensed together according to their intrinsic geometric and electronic properties has been stimulating research on the design of POMos with both high[5] and low[6] nuclearities. A range of smaller polyanions have themselves been incorporated as building blocks into hybrid and network solids,[7] however, there has been little advance in the generation of fundamentally new types of pure Mo–O cluster frameworks in the small-to-medium nuclearity range (Mo_{10}–Mo_{18}). Therefore, to expand this building-block concept further, the construction of structurally diverse cluster and cluster-based network geometries calls for the generation and isolation of low-nuclearity polyoxometalates that substantially deviate from the well-known "classical" polyoxometalate prototypes. These prototypes include clusters with spherical structures and high symmetry, such as the Lindqvist, Keggin, or Dawson anions.[8] Access to new types of nonspherical, low-symmetry clusters that can be used as building blocks (i.e., that display high negative charge and nucleophilicity) will be significant as their low symmetries are a crucial prerequisite for the emergence of structural complexity when tiling or linking these building blocks to larger aggregates.[9] To accomplish this, we have adopted a simple strategy to prevent the rapid aggregation of metal-oxide-based polyhedra to clusters with a stable uniform spherical topology. This approach relies on trapping and stabilizing nonspherical polyanions of low nuclearity and symmetry before their aggregation and rearrangement to more uniform and stable structures.

By adopting this approach we have synthesized a mixed-valence cluster anion which results when the formation of symmetrical aggregates appears to be restrained by "shrink-wrapping" the anionic POMo cluster. As such the cluster comprises a type of polyoxometalate cluster framework that displays an unprecedented topology, low symmetry, and high negative charge, and is isolated as:

$$(C_6H_{13}N_4)_{10}[H_2Mo_{16}O_{52}]\cdot 34\,H_2O \quad \mathbf{1}.$$

The anion in compound **1** demonstrates a high nucleophilicity and can bind two divalent transition-metal ions (Fe^{II}, Mn^{II}, Co^{II}, Ni^{II}, or Zn^{II}) to its framework. This yields a family of isostructural complexes, as confirmed by powder diffraction studies, and we have been able to determine the structure of an iron-adduct cluster **2**, which shows that the basic topology found for the anion in compound **1** is maintained. Hence, **2** can be formulated as:

$$(C_6H_{13}N_4)_6[Fe_2(H_2O)_8H_2Mo_{16}O_{52}]\cdot 8\,H_2O \quad \mathbf{2}$$

By using protonated hexamethylenetetraamine ($HMTAH^+$ or $C_6H_{13}N_4^+$) as counterions, the cluster compounds **1** and **2** were isolated as crystalline precipitates from an acidified molybdate solution in the presence of a reducing agent in around 20–30% yield.[10] Compounds **1** and **2** were characterized by single-crystal X-ray structure analyses,[11] bond valence sum (BVS) calculations, redox titrations, and elemental analyses, to aid in the determination of the (formal) number of Mo^V centers and protonation sites,[12] and also using IR and UV/Vis spectroscopy, and magnetic susceptibility measurements. In addition, the purity of the bulk phase of compounds **1** and **2** has also been confirmed by X-ray powder diffraction.

X-ray crystallographic analysis of **1** reveals that the anions present consist of a highly negatively charged framework of the composition $[H_2Mo_{16}O_{52}]^{10-}$ (Figure 1). The cluster framework displays an unusual flat shape and despite its high charge and nonspherical structure, this mixed-valence cluster compound is stable in the solid state as the salt **1**. Redox titrations, bond valence sum calculations, and elemental analysis reveal the formal oxidation numbers of the Mo centers to be $Mo^V{}_4Mo^{VI}{}_{12}$. The four Mo^V centers comprise two centrosymmetrically related $Mo^V{}_2$ groups (located in the central part of the $[H_2Mo^V{}_4Mo^{VI}{}_{12}O_{52}]^{10-}$ cluster core) which display a short Mo(2)-Mo(3) contact of 2.6427(4) Å, which is characteristic of Mo–Mo single bonds, and also explains the brown color[12] that is associated with clusters containing these groups.[13] The shape of the cluster resembles that of a "bat" and its main "body" consists of a central unit with twelve molybdenum atoms and two "wings" each with two molybdenum centers (according to the formulation $[\{Mo_{12}\} + 2\{Mo_2\}]$). In contrast to known polyoxomolybdates, **1** has a

[*] Dr. L. Cronin, Dr. D.-L. Long, Dr. L. J. Farrugia
Department of Chemistry
Joseph Black Building, The University of Glasgow
University Avenue, Glasgow, G12 8QQ (UK)
Fax: (+44) 141 330 4888
E-mail: L.Cronin@chem.gla.ac.uk
Dr. P. Kögerler
Ames Laboratory and Department of Physics & Astronomy
Iowa State University
Ames, IA 50011 (USA)

[**] This work was supported by the Leverhulme Trust (London), The Royal Society, and The University of Glasgow. The EPSRC provided funds for the X-ray diffractometer. We would like to acknowledge Dr. B. M. Kariuki (University of Birmingham (UK)) for help with initial crystallographic studies.

 © 2003 Wiley-VCH Verlag GmbH & Co. KGaA, Weinheim DOI: 10.1002/anie.200351615

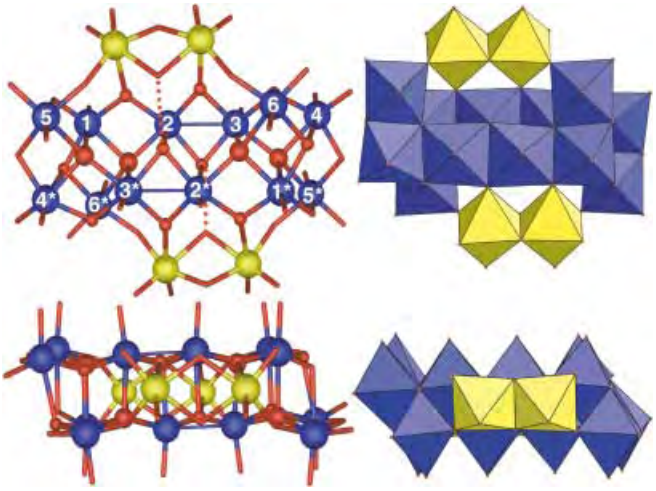


Figure 1. Ball-and-stick (left) and polyhedral representations (right) of the crystal structure of the $[H_2Mo^{V}_4Mo^{VI}_{12}O_{52}]^{10-}$ anion in **1** (top views above and side views below). The Mo positions 1 to 4 and 1* to 4* form the two $\{Mo_4\}$ backbones, in which 2, 2*, 3, and 3* are the reduced Mo^{V} centers (centrosymmetrically equivalent positions are indicated by a star). The Mo positions 5, 5*, 6, and 6* cap the ends of the backbones. The μ_4-oxo groups are shown by the large red spheres, the μ_3-oxo groups by smaller red spheres, and the μ_2-oxo bridging and terminal oxo ligands as red sticks. Finally, the two $\{Mo_2\}$ "wings" are shown in yellow and the hydrogen bonds are indicated by red dotted lines. The bond lengths for all terminal Mo=O bonds range from 1.687(3) to 1.730(3) Å, while the bridging O–Mo bonds range from 1.752(2) to 2.394(2) Å.

flat structure with approximate dimensions of $13 \times 11 \times 6$ Å. Of the twelve molybdenum centers which form the main body of the "bat", eight molybdenum centers are arranged in two lines of four to form two $\{Mo_4\}$ "backbones", which are highly condensed. This is illustrated by the large number of bridging oxo ligands in this central fragment, which comprises 18 (four μ_4-oxo, ten μ_3-oxo, and four μ_2-oxo ligands) of the 52 oxo ligands in total. The two protons in the $[H_2Mo^{V}_4Mo^{VI}_{12}O_{52}]^{10-}$ anion are involved in hydrogen-bonding interactions between the backbone and the wings, highlighted in Figure 1 as red dotted lines (O···O: 2.732(5) Å).[11]

Complex **2** can be isolated as the salt $(C_6H_{13}N_4)_6[Fe_2(H_2O)_8H_2Mo_{16}O_{52}]\cdot 8H_2O$ and consists of $[Fe_2(H_2O)_8H_2Mo^{V}_4Mo^{VI}_{12}O_{52}]^{6-}$ cluster anions, $HMTAH^+$ cations, and solvent water molecules. The polyoxomolybdate anion present in **2** (Figure 2) is derived from the cluster $[H_2Mo^{V}_4Mo^{VI}_{12}O_{52}]^{10-}$ anion in **1** with its structural features retained, and in **2** the two $[Fe^{II}(H_2O)_4]$ units are each coordinated to two terminal oxo ligands attached to $Mo^{VI}(4)$ and $Mo^{V}(3)$ (as labeled in the parent anion shown in Figure 1) at the opposite ends of the central $\{Mo_{12}\}$ body of the polyoxomolybdate anion. The coordination of the Fe^{II} centers to these particular sites is unexpected as semiempirical and preliminary DFT calculations of the cluster anion suggest that, among all terminal neighbored oxygen positions in the cluster anion in **1** that allow both steric access and a bidentate chelating coordination to a M^{2+} ion, the particular O(Mo3) and O(Mo4) positions actually display the lowest negative partial charges.[14]

While compound **1** is diamagnetic because of strong antiferromagnetic exchange within each of the two pairs of Mo^{V}_2 units (with $\chi_{dia/TIP} = -1.1 \times 10^{-3}$ emu mol^{-1}; TIP = temperature independent paramagnetism), the magnetic properties of **2** indicate weak, yet significant, intramolecular antiferromagnetic exchange interactions between the two Fe^{II} centers, despite their wide spatial separation of 1.18 nm. The observed temperature dependence of the susceptibility (2 K $< T <$ 290 K, 0.5 T, corrected for $\chi_{dia} = -9.0 \times 10^{-4}$ emu mol^{-1}) is best fitted to a Heisenberg model, employing the spin Hamiltonian $\mathscr{H} = -J\hat{S}_1\hat{S}_2 + \hat{S}_1\boldsymbol{D}\hat{S}_1 + \hat{S}_2\boldsymbol{D}\hat{S}_2$, with an exchange constant $J = -0.8$ K and a single-ion anisotropy $D =$ 8 K (reflecting the zero-field splitting of the $^5T_2$ term of the high-spin $3d^6$ Fe^{II} centers in an octahedral field). This exemplifies the efficiency of reduced polyoxomolybdates to act as superexchange ligands, where in the present case the superexchange pathways involve at least six centers and both $\{Mo^{V}_2\}$ dimers of the $\{Mo_{16}\}$ framework. The encapsulation of the cluster anion also effectively prevents any significant intercluster exchange interactions. Antiferromagnetic (yet weaker) coupling is also observed for the other magnetic derivatives $\{Mn^{II}_2Mo_{16}\}$ and $\{Ni^{II}_2Mo_{16}\}$ in the isostructural series of **2**.

An interesting aspect of the encapsulation is that it appears to also cause a high degree of condensation; the relative content of μ_4- and μ_3-oxo ligands is around twice that found for $\{Mo_{18}\}$-type Dawson or $\{Mo_{12}\}$-type Keggin anions. The significance of the encapsulation for the solid state is furthermore reflected by the very close interaction between surface oxo ligands of the anions present in **1** and **2** and the $HMTAH^+$ cations; there are 18 short hydrogen-bonded cluster surface oxygen-to-cation interactions for the anion

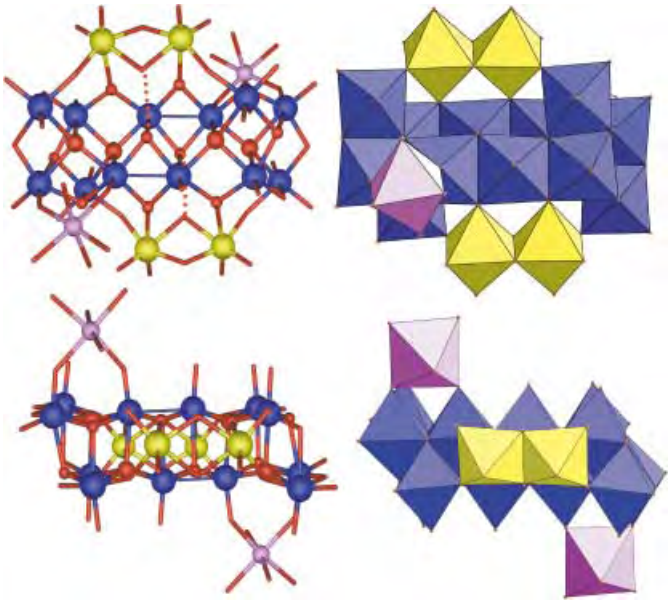


Figure 2. Ball-and-stick (left) and polyhedral representations (right) of the crystal structure of the $[Fe_2(H_2O)_8H_2Mo^{V}_4Mo^{VI}_{12}O_{52}]^{6-}$ anion in **2** (top views above and side views below). The main $\{Mo_{12}\}$ body is shown in blue, the two $\{Mo_2\}$ "wings" in yellow, and the Fe positions in purple. The oxo ligands and the hydrogen-bonded interactions are represented in the same style as Figure 1.

 © 2003 Wiley-VCH Verlag GmbH & Co. KGaA, Weinheim

present in **1** and 14 for the anion in **2**. These interactions are in the range $2.581(7) \le d[\mathrm{E(-H)\cdots O(Mo)}] \le 3.140(5)$ Å, where E = N, C; there are an additional 18 longer contacts for **1** and 10 for **2** in the range $3.157(5) \le d[\mathrm{E(-H)\cdots O(Mo)}] \le 3.296(3)$ Å. Furthermore, while the anion layers in **1** are effectively separated from each other by two cation layers, the separation in **2** involves only one cation layer, which permits limited cluster A-cation-cluster B contacts: In **2** the $HMTAH^+$ cations are associated via strong (N)H···O(Mo) hydrogen bonds to cluster A and via weak (C)H···O(Mo) contacts to a neighboring cluster B. This analysis shows that both of the clusters are extensively linked to the $HTMAH^+$ cations via hydrogen bonds; Figure 3 illustrates that the cluster anions are effectively covered, or "shrink-wrapped" by the $HTMAH^+$ cations in the solid state.

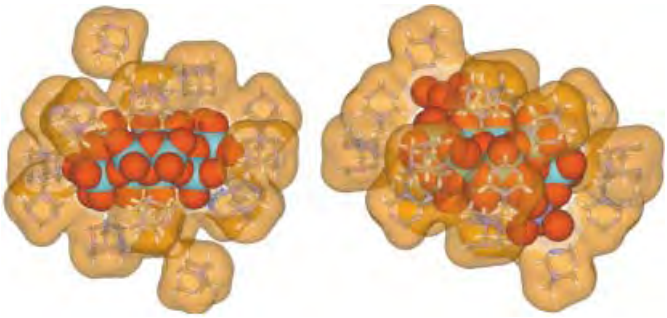


Figure 3. A representation of the extent of the encapsulation of the cluster anions present in compounds **1** (left) and **2** (right). The cluster anion is shown by a space-filling representation and the $HMTAH^+$ cluster cations are shown as sticks with a transparent space-filling surface over the cations.

Although cation–anion association will be present in solution, encouraged by both electrostatic and hydrogen-bonding effects, the extent of the interactions seen in the solid state also appears to play a crucial role in solution. This is because experiments attempting to synthesize the $\{Mo_{16}\}$ cluster under similar reaction conditions (e.g., pH value, concentrations, ionic strength, and temperature), but with different large cations (e.g., $[HN(CH_2CH_2OH)_3]^+$), result in the formation of well-known spherical-type POMo clusters of the Dawson type.[15] Furthermore, the isolation of compounds **1** and **2** is only possible in a narrow pH range (4.0–4.5) at room temperature in the presence of a large excess of $HMTAH^+$ ($HMTAH^+$:$\{Mo_{16}\}$ = 60:1). Dissolving compounds **1** and **2** in the presence of different cations appears to result in the decomposition of the cluster anions.[10]

The importance of the encapsulation event in the "shrink-wrapping" synthesis of these clusters is also supported by the fact that there is only one other structural type comprising an $\{Mo_{16}\}$ nuclearity framework reported previously,[16] $[X_nMo_{16}(OH)_{12}O_{40}]^{(8-n)-}$ (where X_n is Na or H_2) but, in contrast to the fundamentally new topology presented here, this $\{Mo_{16}\}$ framework is based upon the well-known spherical topology and adopts the high T_d symmetry of the inner ε-Keggin motif.[8] In this case the highly charged central, compact, and fully reduced $\{Mo^{V}_{12}\}$ ε-Keggin unit is stabilized by the condensation of four corner-sharing $Mo^{VI}O_6$ units. Although the cluster types in **1** and **2** bear no geometrical resemblance to the ε-Keggin-type $\{Mo_{16}\}$ ion,[17] in analogy their two $\{Mo_2\}$ wing fragments are also linked to their backbone fragments exclusively in a corner-sharing mode. Therefore it is interesting to note that the removal of those $\{Mo^{VI}{}_2O_6\}$ wings would produce an $\{Mo_{12}\}$ cluster, yet to be isolated, with the same nuclearity of a classical Keggin ion, but with a new topology for an $\{Mo_{12}\}$ fragment (shown in blue in Figures 1 and 2).

In summary, this work demonstrates that it is possible to redefine the structures of lower-nuclearity POMos away from the symmetrical spherical structures. In further work we will attempt to incorporate other types of electrophiles, for example Eu^{III}, in addition to studies that aim to exploit our new cluster topology in the formation of large clusters based on this interesting building block, that utilize the nonspherical nature of this new class of POMo clusters. There are certainly many other interesting structural types to be trapped and characterized using the approach outlined here, and we expect that this will provide access to a fundamentally more diverse set of POMo-based building blocks.

Experimental Section

1: Hexamethylenetetraamine (2.2 g, 15.7 mmol) was dissolved in water (20 mL) at room temperature and the resulting solution was acidified with 1.2 mL hydrochloric acid (37 %). To the resulting solution $Na_2MoO_4{\cdot}2H_2O$ (0.96 g, 4.0 mmol) and $Na_2S_2O_4$ (0.07 g, 0.44 mmol) were added simultaneously while stirring. After addition the color of the solution changed firstly to green, then to yellowish green, and finally to brown (the pH of the solution was 4.0–4.5). The solution mixture was filtered and sealed in a small vial, from which brown crystals of **1** formed over a period of two days in a yield of 0.20 g (18 %; all yields calculated based on Mo[10]). IR (KBr disk): $\tilde{\nu}$ = 3443, 1631, 1461, 1400, 1378, 1308, 1289, 1253, 1203, 1018, 1009, 978, 926, 817, 794, 658 cm^{-1}; elemental analysis calcd for $C_{60}H_{200}Mo_{16}N_{40}O_{86}$: C 16.40, H 4.59, N 12.75; found: C 16.28, H 4.13, N 12.77 %.

2: The brown solution obtained in the synthesis of **1** was left undisturbed for 6 h at room temperature. After this period the solution was added to a solution of $FeSO_4{\cdot}7H_2O$ (0.18 g, 0.65 mmol) in water (50 mL), which had previously been acidified with 0.2 mL hydrochloric acid (37 %). The mixture was stirred for two minutes and quickly filtered. Subsequently the color of the solution changed slightly from brown to reddish brown, and dark-brown crystals of **2** formed overnight. Yield: 0.25 g (28 %). IR (KBr disk): $\tilde{\nu}$ = 3426, 1637, 1462, 1401, 1384, 1259, 1017, 980, 925, 887, 639 cm^{-1}; elemental analysis calcd for $C_{36}H_{112}Fe_2Mo_{16}N_{24}O_{68}$: C 11.96, H 3.12, N 9.30; found: C 11.90, H 3.00, N 8.96 %.

Received: April 9, 2003 [Z51615]

Keywords: cluster compounds · molybdenum · polyoxometalates · self-assembly · supramolecular chemistry

[1] A. Müller, E. Beckmann, H. Bögge, M. Schmidtmann, A. Dress, *Angew. Chem.* **2002**, *114*, 1210–1215; *Angew. Chem. Int. Ed.* **2002**, *41*, 1162–1167; L. Cronin, C. Beugholt, E. Krickemeyer, M. Schmidtmann, H. Bögge, P. Kögerler, T. K. K. Luong, A. Müller, *Angew. Chem.* **2002**, *114*, 2929–2932; *Angew. Chem. Int. Ed.* **2002**, *41*, 2805–2808; A. Müller, E. Krickemeyer, H. Bögge,

 © 2003 Wiley-VCH Verlag GmbH & Co. KGaA, Weinheim

M. Schmidtmann, P. Kögerler, C. Rosu, E. Beckmann, *Angew. Chem.* **2001**, *113*, 4158 – 4161; *Angew. Chem. Int. Ed.* **2001**, *40*, 4034 – 4037; A. Müller, S. Q. N. Shah, H. Bögge, M. Schmidtmann, *Nature* **1999**, *397*, 48 – 50; A. Müller, E. Krickemeyer, H. Bögge, M. Schmidtmann, F. Peters, *Angew. Chem.* **1998**, *110*, 3567 – 3571; *Angew. Chem. Int. Ed.* **1998**, *37*, 3360 – 3363; A. Müller, E. Krickemeyer, J. Meyer, H. Bögge, F. Peters, W. Plass, E. Diemann, S. Dillinger, F. Nonnenbruch, M. Randerath, C. Menke, *Angew. Chem.* **1995**, *107*, 2293 – 2295; *Angew. Chem. Int. Ed. Engl.* **1995**, *34*, 2122 – 2124.

[2] H. D. Zeng, G. R. Newkome, C. L. Hill, *Angew. Chem.* **2000**, *112*, 1842 – 1844; *Angew. Chem. Int. Ed.* **2000**, *39*, 1772 – 1774.

[3] T. F. Otero, S. A. Cheng, E. Coronado, E. M. Ferrero, C. J. Gomez-Garcia, *ChemPhysChem* **2002**, *3*, 808 – 811.

[4] D. A. Judd, J. H. Nettles, N. Nevins, J. P. Snyder, D. C. Liotta, J. Tang, J. Ermolieff, R. F. Schinazi, C. L. Hill, *J. Am. Chem. Soc.* **2001**, *123*, 886 – 897.

[5] A. Müller, P. Kögerler, C. Kuhlmann, *Chem. Commun.* **1999**, 1347 – 1358.

[6] E. Cadot, F. Sécheresse, *Chem. Commun.* **2002**, 2189 – 2197; R. J. Errington, R. L. Wingad, W. Clegg, M. R. J. Elsegood, *Angew. Chem.* **2000**, *112*, 4042 – 4044; *Angew. Chem. Int. Ed.* **2000**, *39,* 3884 – 3886.

[7] P. Wang, Y. Yuan, Z. B. Han, G. Y. Zhu, *J. Mater. Chem.* **2001**, *11*, 549 – 553.

[8] a) P. Mialane, A. Dolbecq, L. Lisnard, A. Mallard, J. Marrot, F. Sécheresse, *Angew. Chem.* **2002**, *114*, 2504 – 2507; *Angew. Chem. Int. Ed.* **2002**, *41*, 2398 – 2401; b) J. F. Keggin, *Nature* **1933**, *131*, 908 – 909; A search of the CSD database revealed that all of the pure POMo-based clusters in the Mo_{10}–Mo_{18} range have spherical topologies.

[9] M. T. Pope, A. Müller, *Angew. Chem.* **1991**, *103*, 56 – 70; *Angew. Chem. Int. Ed. Engl.* **1991**, *30*, 34 – 48.

[10] a) The work presented here is the first example of the isolation of a nonspherical "shrink-wrapped" cluster-type using bulky cations, however HMTA has been utilized in the synthesis of POM-based clusters previously. For example, see: T. Duraismy, N. Ojha, A. Ramanan, J. J. Vittal, *Chem. Mater.* **1999**, *11*, 2339 – 2349. b) The relatively low yield of **1** could be explained by the fact that the by-product, $Na_2(HTMAH_2)_2[Mo_7O_{24}]$, was found to be produced in a yield of approximately 60 %, as verified by crystallographic analysis. This by-product is either produced during the formation of **1** in a competing reaction or by decomposition of **1** in the presence of the mother liquor; this decomposition appears to be accelerated upon heating.

[11] Crystal data and structure refinements for **1** and **2**: $(C_6H_{13}N_4)_{10}[H_2Mo_{16}O_{52}]\cdot 34\,H_2O$ **1**: $C_{60}H_{200}Mo_{16}N_{40}O_{86}$, $M_r = 4393.64$, a platelike crystal ($0.25 \times 0.20 \times 0.09$ mm) was analyzed with a Kappa CCD diffractometer using $Mo_{K\alpha}$ radiation ($\lambda = 0.71073$ Å) at 150(2) K; triclinic, space group $P\bar{1}$, $a = 13.81780(10)$, $b = 16.1705(2)$, $c = 17.0835(2)$ Å, $\alpha = 95.1180(10)$, $\beta = 112.5320(10)$, $\gamma = 96.7450(10)°$, $V = 3463.68(6)$ Å^3, $Z = 1$, $\rho_{calcd} = 2.106$ g cm^{-3}, $\mu(Mo_{K\alpha}) = 1.513$ cm^{-1}, $F(000) = 2200$, 76303 reflections measured, of which 20204 were independent, 910 refined parameters, $R1 = 0.0368$, w$R2 = 0.0886$. For $(C_6H_{13}N_4)_6[Fe_2(H_2O)_8H_2Mo_{16}O_{52}]\cdot 8\,H_2O$ **2**: $C_{36}H_{112}Fe_2Mo_{16}N_{24}O_{68}$, $M_r = 3616.24$ g mol^{-1}; $0.47 \times 0.35 \times 0.03$ mm; monoclinic, space group $P2_1/a$, $a = 13.87320(10)$, $b = 25.6770(2)$, $c = 15.80270(10)$ Å, $\beta = 108.8090(10)°$, $V = 5328.66(7)$ Å^3, $Z = 2$, $\rho_{calcd} = 2.254$ g cm^{-3}, $\mu(Mo_{K\alpha}) = 2.182$ cm^{-1}, $F(000) = 3528$, 79325 reflections measured, of which 10413 were independent, 758 refined parameters, $R1 = 0.0371$, w$R2 = 0.1066$. In both structures the distance between the two oxygen atoms (indicated by the dotted lines in Figures 1 and 2) is 2.732(5) Å, which is consistent with the presence of a medium-to-strong hydrogen-bonded interaction between the two atoms. Although these protons could not be located unambiguously from the crystallographic data (although a very small peak could be identified in the Fourier difference map), the two μ_3-oxo ligands bridging the Mo^V atoms are the only positions that could support a proton. CCDC-205853 (**1**) and CCDC-205854 (**2**) contain the supplementary crystallographic data for this paper. These data can be obtained free of charge via www.ccdc.cam.ac.uk/conts/retrieving.html (or from the Cambridge Crystallographic Data Centre, 12, Union Road, Cambridge CB2 1EZ, UK; fax: (+44) 1223-336-033; or deposit@ccdc.cam.ac.uk).

[12] I. D. Brown in *Structure and Bonding in Crystals, Vol. II* (Eds.: M. O'Keeffe, A. Navrotsky), Academic Press, New York, **1981**, pp. 1 – 30; N. E. Breese, M. O'Keeffe, *Acta Crystallogr. Sect. B* **1991**, *47*, 192 – 197; The UV/Vis spectrum for complex **1** shows a broad absorption band with $\lambda_{max} \approx 311$ nm (sh).

[13] H. K. Chae, W. G. Klemperer, T. A. Marquart, *Coord. Chem. Rev.* **1993**, *128*, 209 – 224.

[14] The partial charges on O(Mo3) and O(Mo4) were deduced by extended Hückel–MO and preliminary DFT studies and further computational and synthetic work, which examines the nature of the addition of electrophiles to O(Mo3) and O(Mo4), is ongoing and the results will be reported in due course.

[15] Replacement of $HMTAH^+$ by, for instance, $[HN(CH_2CH_2OH)_3]^+$, results in a Dawson-type POMo cluster containing heteroatoms which appear to originate from the reducing agent. (D.-L. Long, P. Kögerler, L. J. Farrugia, L. Cronin, unpublished results).

[16] M. I. Khan, A. Müller, S. Dillinger, H. Bögge, Q. Chen, J. Zubieta, *Angew. Chem.* **1993**, *105*, 1811 – 1813; *Angew. Chem. Int. Ed. Engl.* **1993**, *32*, 1780 – 1782; M. I. Khan, Q. Chen, J. Salta, C. J. O'Connor, J. Zubieta, *Inorg. Chem.* **1996**, *35*, 1880 – 1901.

[17] A. Müller, J. Meyer, E. Krickemeyer, C. Beugholt, H. Bögge, F. Peters, M. Schmidtmann, P. Kögerler, M. J. Koop, *Chem. Eur. J.* **1998**, *4*, 1000 – 1006.

 © 2003 Wiley-VCH Verlag GmbH & Co. KGaA, Weinheim

Rotational Barrier in Ethane (1)

The Case for Steric Repulsion Causing the Staggered Conformation of Ethane

*F. Matthias Bickelhaupt and Evert Jan Baerends**

It has recently been argued[1,2] that the barrier to rotation around the C–C bond in ethane is not to be explained by the generally accepted picture of steric hindrance between vicinal C–H bonds in the eclipsed conformation but is caused by more favorable orbital interaction in the staggered conformation. In that conformation the C–H bonds at opposite ends of the molecule have an in-plane *trans* conformation which is favorable for interaction of the σ* antibonding orbital of one C–H unit with the occupied σ_{C-H} bonding orbital at the other side (six such pairs). This view has been advocated with

[*] Prof. E. J. Baerends, Dr. F. M. Bickelhaupt
Afdeling Theoretische Chemie
Faculty of Science, Vrije Universiteit
Scheikundig Laboratorium, De Boelelaan 1083
1081 HV Amsterdam (The Netherlands)
Fax: (+31) 20-444-7629
E-mail: baerends@chem.vu.nl

 DOI: 10.1002/anie.200350947 © 2003 Wiley-VCH Verlag GmbH & Co. KGaA, Weinheim

natural bond orbital (NBO) analyses for a long time by Weinhold and co-workers.[3–6] Pophristic and Goodman[1] deleted the σ–σ* NBO interactions and found that the ethane preferred structure reverts to eclipsed, thus providing substantiation of the orbital-interaction view within the NBO framework.

The issue is interesting and important[7–9] but also controversial. We have reinvestigated the rotation around the C–C bond in ethane employing a widely used and straightforward electronic-structure analysis method (see below). It turns out that it is very important to take carefully into account the effect of geometry changes during rotation around the C–C bond, notably the C–C bond stretching when going towards the eclipsed conformation, as indeed already stressed by England and Gordon[14] and Goodman and co-workers.[15] We will see that the interpretation of the barrier as caused by steric repulsion between vicinal C–H bonds is fully corroborated by this analysis, and we conclude it is perfectly valid for organic chemists to adhere to this view. We comment on the possible source of the difference between our analysis and the NBO one.

Our electronic-structure analysis of the eclipsed versus staggered conformations uses a few well-defined terms, which can be used with exact wavefunctions of the interacting fragments, or with approximate wavefunctions. We start the formation of the C–C bond between two methyl fragments by employing the wavefunctions Ψ^A and Ψ^B of the isolated fragments to build a "zeroth-order" wavefunction Ψ^0 in which only the Pauli exclusion principle is enforced by antisymmetrization ($\hat{A}$) and renormalization (N) of the product function $\Psi^A\Psi^B$: $\Psi^0 = N\hat{A}[\Psi^A\Psi^B]$. In our case we use a determinantal wavefunction with the (overlapping) Kohn–Sham orbitals of the fragments. The antisymmetrization, which is usually performed after orthogonalization of the fragment orbitals, which does not change the wavefunction, see ref. [19], leads to a density ρ^0 which differs from the superposition $\rho^A + \rho^B$. One usually separates the electrostatic interaction (ΔV_{elstat}) between the (unmodified, interpenetrating) electronic charge cloud (ρ^A) and nuclei of one fragment with those of the other (ρ^B) from the total ΔE^0, defining the Pauli repulsion ΔE_{Pauli} as in Equation (1).

$$\Delta E^0 = E[\Psi^0] - E[\Psi^A] - E[\Psi^B] = \Delta E_{Pauli} + \Delta V_{elstat} \quad (1)$$

ΔE^0 is repulsive owing to the strongly repulsive ΔE_{Pauli} term. The repulsion is caused by an increase in the kinetic energy, which is an effect of the antisymmetrization (usually calculated by orthogonalization) among the occupied orbitals ("orthogonality tails"). This outweighs a generally more negative potential energy, see ref. [19] for detailed discussion of the various energy contributions. The energy lowering as a result of the formation of the electron-pair bond is not contained in ΔE^0. This energy, and in addition the occupied-virtual-orbital interactions which account for the polarization of the methyl fragments and for the possible vicinal charge-donation type of interaction from a σ_{C-H} orbital on fragment A to a σ^*_{C-H} orbital on fragment B, are included in the relaxation or orbital-interaction step with energy contribution ΔE_{oi} which describes the energy relaxation from $E[\Psi^0]$ to the final energy $E[\Psi^{AB}]$ of the wavefunction Ψ^{AB} of the ethane molecule. The total bond energy ΔE will be given by Equation (2).

$$\Delta E = \Delta E_{Pauli} + \Delta V_{elstat} + \Delta E_{oi} \quad (2)$$

The relaxation energy $\Delta E_{oi} = E[\Psi^{AB}] - E[\Psi^0]$ is defined for exact wavefunctions but also for the Hartree–Fock model and for Kohn–Sham DFT. Since we use these orbital models we refer to it as the orbital-interaction term ΔE_{oi}. These same terms are also used in the scheme originally introduced by Morokuma and co-workers[10–13] at the Hartree–Fock level, but we do not apply Morokuma's further break-down of the ΔE_{oi} term in the basis-set-dependent charge-transfer and polarization (and mix) terms. The same scheme, but with a different partitioning (symmetry based) of the ΔE_{oi} term, was used by Ziegler and co-workers[16–19] in a DFT context, which has the advantage of providing us with rather accurate energetics. We use an extension to open-shell systems where an electron-pair bond is formed.[20]

We stress that this energy decomposition, apart from being well established and widely practiced, is also general in the sense that the terms are defined also for high-quality (fully correlated) fragment and total wavefunctions. The definition of Pauli repulsion (or exchange repulsion) used here is generally used, for example, in the theory of intermolecular forces.

The total barrier height going from staggered to eclipsed ethane is calculated with the Becke 88–Perdew 86 functional of DFT to be 2.54 kcal mol^{-1}, with full optimization of C–C bond lengths and CH_3 geometry in both conformations. This situation compares reasonably with the experimental value of 2.875 kcal mol^{-1}.[21] Basis-set superposition errors (BSSE) are very small for the large STO basis sets we are using, and totally insignificant for the barrier height (correction for BSSE changes the barrier by 0.04 kcal mol^{-1}). To analyze the origin of the barrier we build ethane from two "prepared" methyl fragments. This preparation involves deforming the planar methyl radicals to exactly the optimized geometries they have in the two conformations. Although the difference in bending and C–H bond lengths for the two optimum CH_3 conformations (which we denote as CH_3(e) for eclipsed and CH_3(s) for staggered ethane, respectively) is quite small (0.5° larger ∢C-C-H angle, 0.001 Å shorter C–H bonds for eclipsed than staggered), the preparation energy for two CH_3(e) (19.32 kcal mol^{-1}) is 1.1 kcal mol^{-1} higher than for two CH_3(s) (18.24 kcal mol^{-1}). This difference is not insignificant compared to the barrier energy, and the effect of CH_3 deformation will be discussed later, but first we address the crucial role played by the C–C bond length. Figure 1 shows the behavior of the Pauli repulsion energy between the prepared methyl fragments as a function of the rotation angle φ. The ΔE_{Pauli} versus φ curves are given for both the optimum C–C separation for the staggered (upper curve) and the eclipsed (lower curve) conformations (the CH_3 geometries are also fixed at staggered and eclipsed values). At both separations the Pauli repulsion is a minimum for the staggered conformation, and goes to a maximum which is 2.35–2.60 kcal mol^{-1} higher at the eclipsed conformation. This

 © 2003 Wiley-VCH Verlag GmbH & Co. KGaA, Weinheim

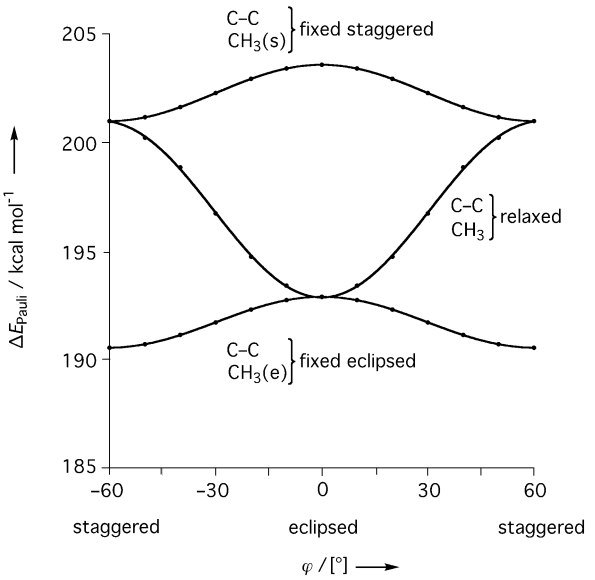


Figure 1. The Pauli repulsion energy between two CH_3 radicals as a function of the dihedral ∢HCCH angle φ. Upper curve: the C–C separation and the geometric parameters of the two CH_3 fragments are fixed to the values for staggered ethane (R_{eq}(staggered) and CH_3(s)). Lower curve: the C–C separation and geometric parameters of the two CH_3 fragments are fixed at the values for eclipsed ethane (R_{eq}(eclipsed) and CH_3(e)). Middle curve: the fully optimized geometry at each value of φ.

result would seem to indicate that Pauli repulsion is the origin of the barrier, as assumed in the standard view. However, we have to be careful with the strong effect of the C–C bond length on the Pauli repulsion. Even though the optimal C–C separations differ only a little (1.5315 Å for staggered and 1.5455 Å for eclipsed), it is to be noted that the energies of the Pauli repulsion at the longer bond length R_{eq}(eclipsed) are over the whole φ range some 10 kcal mol^{-1} lower than at the shorter bond length. In Figure 1 we also show the Pauli repulsion as a function of φ when we optimize the C–C bond length (and also the CH_3 geometries) at each φ value. Owing in particular to the C–C bond lengthening, the Pauli repulsion is lowest along this curve in the eclipsed conformation. However, it would not be logically correct to infer that steric repulsion favors the eclipsed conformation (and that therefore an alternative mechanism has to be invoked to explain the preference for the staggered conformation). Such a conclusion cannot be drawn from the behavior of ΔE_{Pauli} along a single path through the molecular configuration space (such as the middle curve of Figure 1). For instance, the lower curve shows that when the C–C separation is fixed at the longer bond length (R_{eq}(eclipsed)) of the eclipsed conformation, the Pauli repulsion would still favor rotation to the staggered conformation.

How, then, can we understand the behavior of the Pauli repulsion as a function of φ when all other geometry parameters are fully optimized (i.e. the middle curve in Figure 1)? Let us take staggered ethane at its optimum geometry and first rotate it with fixed R(C–C) and CH_3(s) geometry to the eclipsed conformation (upper curve), which leads to 2.60 kcal mol^{-1} more Pauli repulsion. The sum of ΔE_{oi} and ΔV_{elstat} adds only 0.07 kcal mol^{-1} to the barrier energy with these geometry constraints. When we keep the molecule in the eclipsed conformation but relax the other geometry parameters, the molecule responds by lowering the total energy slightly (the final barrier is 2.54 kcal mol^{-1}) by lengthening the C–C bond and bending back the CH_3 units. The individual energy components change much more, which is possible since their changes with C–C bond lengthening have opposite signs. The Pauli repulsion lowers by approximately 10 kcal mol^{-1}, in fact much more than the initial rise of only 2.6 kcal mol^{-1}. In Figure 2 we show the various terms—Pauli repulsion, electrostatic interaction, and orbital interaction—as a function of C–C separation, which is the most important

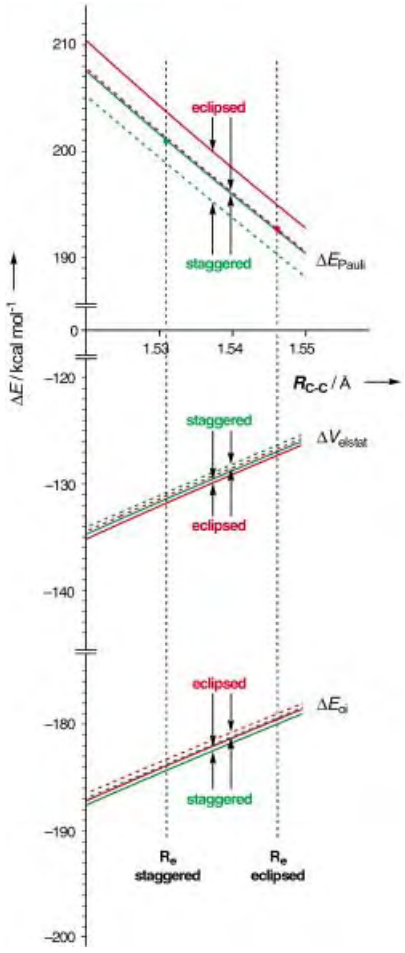


Figure 2. The three contributions ΔE_{Pauli}, ΔV_{elstat}, and ΔE_{oi} (see text) to the total bond energy between two CH_3 radicals, as a function of the C–C separation. The full lines are for CH_3(s) (optimized CH_3 geometry in staggered ethane); red for eclipsed conformation, green for staggered conformation. The broken lines are for CH_3(e) (optimized CH_3 geometry in eclipsed ethane); red for eclipsed conformation, green for staggered conformation. The Pauli repulsion in the equilibrium conformation of staggered ethane is denoted by a green dot, and the Pauli repulsion in the equilibrium conformation of eclipsed ethane by a red dot. Since accidentally the Pauli repulsion curves for staggered ethane with CH_3(s) (solid green line) and eclipsed ethane with CH_3(e) (broken red line) practically coincide, one has been shifted up and the other shifted down by 0.1 kcal mol^{-1} for clarity.

 © 2003 Wiley-VCH Verlag GmbH & Co. KGaA, Weinheim

geometric parameter. To separate the effect of C–C bond-length change from the effect of CH_3 flexing we first focus on the curves for fixed CH_3(s) geometry (solid line, green for staggered ($\varphi = 60°$), red for eclipsed ($\varphi = 0°$)). At all distances shown the Pauli repulsion is strongest in the eclipsed case. The difference in Pauli repulsion between eclipsed and staggered ethane is considerably larger than the differences for the other energy terms, ΔV_{elstat} and ΔE_{oi}. A crucial observation is that also the increase of the Pauli repulsion with the shortening bond length is greater in the eclipsed case, that is, at the shorter distance R_{eq}(staggered) the gradient of the red line is larger than of the green line. The equilibrium bond length is not determined by the absolute values of the total energy or its components, but simply by the requirement that the derivative of the total energy with respect to the C–C bond length be zero. Since the other energy components (ΔE_{oi} and ΔV_{elstat}) are virtually parallel for eclipsed and staggered ethane, the larger gradient of the steric repulsion curve in the eclipsed case, at shorter bond length, such as R_{eq}(staggered), will drive the molecule in that conformation to a state with a longer equilibrium C–C bond length. This situation explains why R_{eq}(eclipsed) is longer, as indicated in Figure 2. The resulting steric repulsion in the eclipsed conformation at that long equilibrium bond length (red dot in Figure 2) is lower than in the staggered conformation at its shorter equilibrium bond length (green dot). This should not be mistaken as a contradiction of the intuitive notion that the eclipsed conformation suffers from stronger steric repulsion, which we see is true at any given C–C bond length.

When we now consider the effect of CH_3 flexing (broken lines for CH_3(e)), the picture remains essentially the same. The flexing of CH_3 towards CH_3(e) reduces the overlap between the orbitals of the vicinal C–H bond, hence it reduces the Pauli repulsion. So the ΔE_{Pauli} curves for CH_3(e) are lowered with respect to the curves for CH_3(s) (Figure 2). Starting again with rotation of fixed CH_3(s) at R_{eq}(staggered) from staggered to eclipsed (from green dot to solid red line), the Pauli repulsion does not only increase, but will also get a steeper gradient for CH_3 bending, as it did for C–C bond lengthening. So the Pauli repulsion and its gradient will become lower by bending CH_3 back to CH_3(e). Accidentally, going from CH_3(s) to CH_3(e) in the eclipsed conformation (from solid red line to broken red line) lowers the Pauli repulsion practically by the same amount as rotation of CH_3(s) from staggered to eclipsed conformation made it rise.

The optimized geometry (C–C separation and CH_3 bending) in the eclipsed conformation is solely determined by the zero gradient of the total energy with respect to the allowed nuclear displacements. This point, at R_{eq}(eclipsed) and CH_3(e) (red dot Figure 2), is reached at a lower value of the Pauli repulsion than is obtained in the equilibrium geometry of the staggered conformation (green dot). This result does not present a paradox with the finding that the Pauli repulsion is always higher when going to the eclipsed conformation with all other geometry parameters fixed. It only signals the important increase of also the gradient of the Pauli repulsion when going to the eclipsed conformation. This is just one more example of the frequently encountered situation, that the values of the energy terms in the "final" equilibrium geometries may give a misleading picture; the full behavior along the relevant geometry changes has to be considered, see for example, ref. [22].

Let us now turn to the other energy terms, ΔV_{elstat} and ΔE_{oi}. It is interesting to observe that the electrostatic interaction ΔV_{elstat} is slightly more attractive in the eclipsed conformation (red lines below corresponding green lines). The effect is small in this case, but it is generally true that stronger overlap of the charge distributions of the fragments leads not only to higher steric repulsion, but also to a more attractive electrostatic interaction. The attractive nature of the electrostatic term is discussed in refs. [18, 19] In short, the electron–electron repulsion and the nucleus–nucleus repulsion between the two methyl fragments are both large and positive, but the negative electron–nucleus attraction is stronger. It is a general phenomenon (for neutral fragments)[18] that when we let two fragment charge distributions interpenetrate, the total electrostatic interaction is attractive since the electron–nucleus attraction outweighs the repulsive terms. This phenomenon first of all explains the more negative ΔV_{elstat} with shortening C–C separation. Furthermore, when one rotates to the eclipsed conformation with a fixed geometry CH_3, all the terms in ΔV_{elstat} become larger in an absolute sense, but the attractive one slightly more so, hence the more attractive electrostatic interaction for the eclipsed conformation. Similarly, when one bends CH_3 from CH_3(e) to CH_3(s), at a given C–C separation and a given rotation angle, the stronger interpenetration of charges for CH_3(s) than for CH_3(e) leads to more attractive ΔV_{elstat} (solid lines below broken lines in Figure 2). These observations underline the quite general fact that the origin of steric repulsion is not electrostatic repulsion between electron charge clouds and nuclei, on the contrary, the electrostatic term favors steric crowding! It is the quantum mechanical Pauli exclusion principle (which leads to a rise in kinetic energy) that is at the origin of the steric repulsion.

The ΔE_{oi} energy of approximately 180 kcal mol^{-1} largely consists of the electron-pair bonding energy of the C–C σ bond, which we find to be invariant under rotation to at least 0.01 kcal mol^{-1}. There are small additional contributions from the admixing of virtual fragment orbitals (notably σ* C-H) to the orbital interaction term ΔE_{oi}. This term is usually also more attractive when the overlap of the charge clouds is larger, since then not only the occupied–occupied orbital overlaps are larger, but the occupied–unoccupied orbital overlaps are also larger, which leads to stronger donor–acceptor interactions. Remarkably, in this case we find this situation reversed: the orbital interaction is more favorable in the case of the staggered conformation. The preference of about 0.4 kcal mol^{-1} for the staggered conformation arises from the unoccupied/occupied orbital mixing and must be due to the more favorable vicinal σ–σ* overlap in the staggered conformation that has been stressed by Weinhold and others.[1–6] However, we do not find this effect to be quantitatively very important, it is only 0.4 kcal mol^{-1} and it is almost canceled by the approximately 0.3 kcal mol^{-1} preference of ΔV_{elstat} for the eclipsed conformation. The Pauli repulsion clearly stands out as the energy component that discriminates between eclipsed and staggered conforma-

 © 2003 Wiley-VCH Verlag GmbH & Co. KGaA, Weinheim

tions, both because of the relatively large difference it makes for the two conformations at all C–C separations, and because of its steeper gradient for eclipsed ethane at shorter separations.

We conclude that our results are in full agreement with the textbook explanation for the preference for the staggered conformation as being due to steric hindrance. At all C–C separations in the range of interest, and for both CH_3(s) and CH_3(e), the steric repulsion is larger for eclipsed ethane. In fact, the steric repulsion is not only weaker in the staggered conformation at each C–C separation and CH_3 conformation, it also increases less steeply with shortening C–C separation and decreasing ∢C-C-H angle (softer repulsive wall). The equilibrium C–C separation therefore becomes shorter in the staggered case, and the ∢C-C-H angle smaller, with the result (only seemingly paradoxical) that an equilibrium geometry is attained where the steric repulsion has reached a higher value than it has at the equilibrium geometry of eclipsed ethane.

The barrier to rotation has been ascribed to Pauli repulsion between vicinal C–H bonds on the basis of more approximate methods a long time ago, notably by Hoyland,[23] Sovers et al.[24] and by Lowe[25] (see refs. [5,6] for extensive references to earlier work). Why does NBO analysis yield a different picture? This is basically because it does not leave the occupied orbital space of canonical orbitals untouched, but mixes the occupied and virtual spaces when transforming to bond orbitals and antibonding counterparts. (We take a single determinantal wavefunction (Hartree–Fock) as reference, which is the level of theory that has been used mostly in the NBO analyses.) The bond orbitals (and core and lone-pair orbitals) are associated with the bonds (and cores and lone pairs) of the Lewis structure. Owing to the procedure for their construction, the NBOs differ from the localized orbitals that can be obtained from the Hartree–Fock wavefunction by a localization procedure. The localized orbitals are nothing but a unitary transformation of the HF orbitals and leave the electron density and total energy unchanged. In contrast, the NBO determinantal wavefunction containing the strongly occupied NBOs ("Lewis determinant"), even though it approximates the density and HF wavefunction rather closely (to better than 99.7%), still is considerably higher in energy than Hartree–Fock (in the case of ethane some 30–40 kcal mol^{-1} higher,[5] that is, an order of magnitude more than the barrier height). Mixing of the antibonding orbitals (such as the σ^*_{C-H} orbitals in ethane) into the bonding orbitals in the NBO determinant leads to energy lowering (called delocalization energy, E_{deloc}) from the Lewis determinant energy E_{Lewis} to the HF energy E_{HF}. This mixing makes the unoccupied (in the Lewis determinant) σ* orbitals weakly occupied, and the bonding orbitals no longer fully (but still strongly) occupied. So the NBO scheme introduces a reference state (the Lewis determinant) which is destabilized compared to the Hartree–Fock determinant, and puts considerable emphasis on the σ* orbitals of the model, as is evident from the energy lowering coming from their admixing. In the present case we note, from the detailed analysis by Goodman et al.,[15] that when we perform a rigid rotation of staggered ethane to eclipsed ethane, keeping the C–C separation and the CH_3 conformation fixed, the energy E_{Lewis} of the Lewis determinant becomes more favorable by 2.68 kcal mol^{-1} (step I in table III of ref. [15]). We would expect at least some steric hindrance effect, and it is unfortunate that a wavefunction that is supposed to correspond to the Lewis structure, does not exhibit the expected steric repulsion between electron pairs when rotating towards a more sterically crowded conformation. This situation would put into jeopardy the very concept of steric hindrance. Of course, when the admixing of the σ* orbitals is allowed in the next step (E_{deloc}), the HF energy and therefore the barrier that is known to exist at the HF level, will be restored. So one can calculate that E_{deloc}, which is large (ca. 35 kcal mol^{-1}), will provide 5.52 kcal mol^{-1} more energy lowering in the staggered conformation. Conversely, when leaving this σ* admixing out, the eclipsed conformation will be preferred.[1] This leads to the contention that it is hyperconjugation and not steric repulsion that causes the barrier in ethane.

Our analysis scheme on the contrary identifies steric repulsion as the cause of the barrier. We prefer this analysis method for the following reasons. It uses the canonical orbitals of the two CH_3 fragments. This has the advantage that these orbitals are unambiguously defined (within the model used, Hartree–Fock for instance, or Kohn–Sham). They diagonalize the fragment one-electron Hamiltonian, that is, they have meaningful orbital energies and there are no zeroth-order couplings between the unoccupied (e.g. σ*) orbitals and the occupied orbitals on the same fragment. The stronger Pauli repulsion we find in the eclipsed conformation fits in with expectations from the steric crowding in that conformation. The behavior of the terms ΔE_{Pauli}, ΔV_{elstat} and ΔE_{oi} is physically completely understandable and is as expected (the trends and observations seen here recur in many applications[19]). The relative unimportance of the σ* orbitals that we find, fits in with the known high energy of these (canonical) orbitals in the CH_3 fragments. Weinhold and co-workers[26] have criticized the use of a virtual orbital space orthogonal to the occupied fragment orbital space, as used by Morokuma[12] to obtain charge-transfer and polarization energies and which we use to obtain the ΔE_{oi} term. It is indeed true that when we allow the bond orbitals in a localized orbital representation of the Hartree–Fock wavefunction to distort slightly to a Lewis structure NBO wavefunction, at the cost of a rise in energy of E_{Lewis} with respect to E_{HF}, the NBO antibonding orbitals, even if orthogonal to the occupied NBOs, can "occupy" some of the space of the occupied canonical orbitals (i.e. the Hartree–Fock orbitals; the equivalent localized orbitals span the same space). So they will without doubt become more "chemically active". However, this raises the issue of the right balance. In particular, when the Lewis determinant shows a reversed steric repulsion effect (i.e. attraction) for the more sterically crowded situation, this begs the question whether the generation procedure for the NBOs has struck the right balance between the "steric" (in E_{Lewis}) and "orbital interaction" or "hyperconjugation" (in E_{deloc}) components of the energy.

Since the concepts we are dealing with in these electronic structure analyses (steric repulsion, bond orbitals, hyperconjugation) are not observables, and not even sharply defined in terms of wavefunctions, we cannot conceive of a

 © 2003 Wiley-VCH Verlag GmbH & Co. KGaA, Weinheim

definitive experimental test to decide which model is "right" and which is "wrong". That hyperconjugation is the cause of the barrier in ethane is "true" within the NBO method of electronic-structure analysis. Steric repulsion is the "true" cause in our analysis. When deciding between electronic-structure analysis schemes, one weighs virtues, such as simplicity, physical transparency, lack of arbitrariness. The analysis should also preferably conform to intuitive chemical notions, and should serve the purpose of quantifying and sharpening those. If the electronic-structure analysis method identifies one of its quantities with an intuitive chemical concept, and subsequently finds the quantitative results to be in conflict with accepted notions, one has to face the question whether this quantity in the theory is rightfully identified with the chemical concept, and whether a different quantity from quantum chemical theory might correspond more closely to the concept. Apparently, the use of occupied canonical fragment orbitals to define the steric repulsion is not only simple and unambiguous, it also conforms in this case, as it unfailingly does,[19] to the notion of increasing steric repulsion with more steric crowding. The Lewis structure wavefunction of the NBO analysis in the case of ethane does not do so.

In conclusion, our analysis, which has been applied in many different situations, in the present case fully corroborates the intuitive expectation of steric repulsion as driving force for the barrier in ethane. These results confirm the association of the term ΔE_{Pauli} of Equation (1) with the Pauli repulsion to be meaningful. We conclude that there is no compelling reason for the chemical community to abandon the explanation of the barrier in ethane as arising from steric repulsion.

Received: January 15, 2003 [Z50947]

Keywords: conformation analysis · electronic structure · ethane · rotation barrier · steric hindrance

[1] V. Pophristic, L. Goodman, *Nature* **2001**, *411*, 565.
[2] F. Weinhold, *Nature* **2001**, *411*, 539.
[3] T. K. Brunck, F. Weinhold, *J. Am. Chem. Soc.* **1979**, *101*, 1700.
[4] G. T. Corcoran, F. Weinhold, *J. Chem. Phys.* **1980**, *72*, 2866.
[5] A. E. Reed, F. Weinhold, *Isr. J. Chem.* **1991**, *31*, 277.
[6] J. K. Badenhoop, F. Weinhold, *Int. J. Quantum Chem.* **1999**, *72*, 269.
[7] S. Borman, *Chem. Eng. News* **2001**, *79(50)*, 53.
[8] C. Henry, *Chem. Eng. News* **2001**, *79(23)*, 10.
[9] P. R. Schreiner, *Angew. Chem.* **2002**, *114*, 3729; Angew. *Chem. Int. Ed.* **2002**, *41*, 3579.
[10] K. J. Morokuma, *J. Chem. Phys.* **1971**, *55*, 1236.
[11] K. Kitaura, K. Morokuma, *Int. J. Quantum Chem.* **1976**, *10*, 325.
[12] K. Morokuma, *Acc. Chem. Res.* **1977**, *10*, 294.
[13] K. Morokuma, H. Umeyama, *Chem. Phys. Lett.* **1977**, *49*, 333.
[14] W. England, M. S. Gordon, *J. Am. Chem. Soc.* **1971**, *93*, 4649.
[15] L. Goodman, H. Gu, V. Pophristic, *J. Chem. Phys.* **1999**, *110*, 4269.
[16] T. Ziegler, A. Rauk, *Inorg. Chem.* **1979**, *18*, 1558.
[17] T. Ziegler, A. Rauk, *Inorg. Chem.* **1979**, *18*, 1755.
[18] "Cluster Models for Surface and Bulk Phenomena": E. J. Baerends, *NATO ASI Ser. Ser. B* **1992**, 189.
[19] F. M. Bickelhaupt, E. J. Baerends in *Reviews in Computational Chemistry, Vol. 15* (Eds.: K. B. Lipkowitz, D. R. Boyd), Wiley, New York, **2000**.
[20] F. M. Bickelhaupt, N. M. M. Nibbering, E. M. van Wezenbeek, E. J. Baerends, *J. Phys. Chem.* **1992**, *96*, 4864.
[21] J. D. Kemp, K. S. Pitzer, *J. Chem. Phys.* **1936**, *4*, 749.
[22] F. M. Bickelhaupt, R. L. DeKock, E. J. Baerends, *J. Am. Chem. Soc.* **2002**, *124*, 1500.
[23] J. R. Hoyland, *J. Am. Chem. Soc.* **1968**, *90*, 2227.
[24] O. J. Sovers, C. W. Kern, R. M. Pitzer, M. Karplus, *J. Chem. Phys.* **1968**, *49*, 2592.
[25] J. P. Lowe, *J. Am. Chem. Soc.* **1970**, *92*, 3799.
[26] A. E. Reed, L. A. Curtiss, F. Weinhold, *Chem. Rev.* **1988**, *88*, 899.

 © 2003 Wiley-VCH Verlag GmbH & Co. KGaA, Weinheim

Rotational Barrier in Ethane (2)

Rebuttal to the Bickelhaupt–Baerends Case for Steric Repulsion Causing the Staggered Conformation of Ethane**

*Frank Weinhold**

Introduction

In the preceding article, Bickelhaupt and Baerends [1] present arguments and numerical calculations in support of the concept (still all too pervasive[2] in organic chemistry textbooks) that torsional barriers in ethane-like molecules are primarily a result of steric repulsions. This concept is usually rationalized[3] in terms of the qualitative molecular orbital (MO) diagram for "four-electron (4e) destabilizing interactions," as shown in Figure 1. This diagram originates[4] in a simple observation concerning diagonalization of a 2×2 matrix $\underline{\underline{\mathbf{H}}}$ [Eq. (1)] in a nonorthogonal basis set ϕ_a, ϕ_b with

$$\underline{\underline{\mathbf{H}}} = \begin{pmatrix} \epsilon_a & h_{ab} \\ h_{ab} & \epsilon_b \end{pmatrix} \xrightarrow{\text{diagonalize}} \begin{pmatrix} E_1 & 0 \\ 0 & E_2 \end{pmatrix} \tag{1}$$

overlap $S_{ab} = \langle \phi_a | \phi_b \rangle$ where $\varepsilon_a = \langle \phi_a | \mathscr{H} | \phi_a \rangle$, $\varepsilon_b = \langle \phi_b | \mathscr{H} | \phi_b \rangle$, and $h_{ab} = \langle \phi_a | \mathscr{H} | \phi_b \rangle$ for the relevant orbital Hamiltonian (e.g., Fock or Kohn–Sham operator), and E_1, E_2 are

[*] Prof. Dr. F. Weinhold
Theoretical Chemistry Institute and
Department of Chemistry
University of Wisconsin
Madison, WI 53706 (USA)
Fax: (+1) 208–262–9918
E-mail: weinhold@chem.wisc.edu

[**] I thank Lionel Goodman, John Herbert, Melissa Lucero, Bob McMahon, and Ron Raines for helpful comments.

Supporting information for this article is available on the WWW under http://www.angewandte.org or from the author.

 © 2003 Wiley-VCH Verlag GmbH & Co. KGaA, Weinheim DOI: 10.1002/anie.200351777

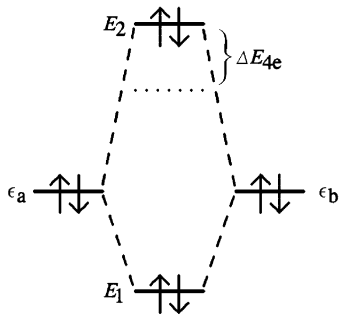


Figure 1. Four-electron destabilizing interaction (see Supporting Information Section A.1), expressed in terms of nonorthogonal "unperturbed" orbitals ϕ_a, ϕ_b (for which there is no imaginable Hermitian perturbation theory).

the final eigenvalues. It is found (see Supporting Information Section A.1 for algebraic details) that the sum of final eigenvalues $E_1 + E_2$ is raised ("destabilized") relative to the initial diagonal elements $\varepsilon_a + \varepsilon_b$, which leads to net destabilization [Eq. 2] when the MOs are fully occupied by four

$$\Delta E_{4e} = +4|S_{ab}\,h_{ab}| \qquad (2)$$

electrons, as schematically depicted in the "perturbative splitting diagram" of Figure 1. (Equation (2) gives the leading-order result for $h_{ab} \neq 0$, but significantly, a net "destabilization effect" is obtained whether the interaction element h_{ab} is zero or non-zero!)

For the ethane barrier problem, ϕ_a, ϕ_b are identified as filled C–H bond orbitals ($\phi_a = \sigma_{C-H}$, $\phi_b = \sigma_{C'-H'}$) on opposite ends of the torsional C–C axis, and the four electrons occupying these orbitals are considered to experience stronger "destabilizations" as they rotate into the eclipsed (*cis*-like) alignments where S_{ab} is strongest. Because the same model applies with equal aptness to the repulsive interactions of two closed-shell helium atoms (generally attributed to "steric repulsions"), it is inferred[3] that the ethane torsional barrier may similarly be assigned a steric origin.

It is no accident that the Bickelhaupt–Baerends (BB) analysis leads to a similar conclusion. Their method,[5] as implemented in the ADF package,[6] was expressly developed to be a bridge between modern density function theory (DFT) calculations and the qualitative MO concepts outlined in ref. [3] (as cited also by Bickelhaupt and Baerends[5]). For this purpose they developed a modification of Kitaura–Morokuma (KM)-type self consistant field (SCF)–MO analysis[7] (following related work of Ziegler and Rauk[8]) which may be identified as the "BB–KM method." The philosophical, mathematical, and numerical basis of the BB–KM method is outlined with admirable clarity and thoroughness in Ref. [5], and we shall quote this reference as the definitive exposition of the technical details underlying the BB case.

Critique of BB–KM Analysis

Bickelhaupt and Baerends characterize their method as "widely used and simple," "well-established and straightforward," and so forth. This characterization is far from accurate. The original KM method (and related nonorthogonal energy decomposition schemes) were severely criticized from the Natural Bond Orbital (NBO) perspective[9] as well as on grounds of basis-related numerical instabilities.[10] Natural Energy Decomposition Analysis (NEDA)[11] has emerged as a clear alternative, with strengthened interpretive foundations, better convergence to asymptotic classical quantities, and improved agreement with empirical chemical concepts (such as the uniqueness of hydrogen-bonding and the traditional σ-bonding/π-backbonding picture of transition-metal coordination). Recent experimental and theoretical evidence strongly suggests the erroneous physical picture that is presented by older KM-type analyses with regard to the important effects of intermolecular charge transfer and cooperative resonance-type phenomena in hydrogen-bonding interactions.[12] We need not reiterate here the specific criticisms of KM analysis,[9] but we emphasize that they apply with equal force to the BB–KM reformulation.

The BB–KM extension actually goes far beyond the original KM formulation by attempting a similar nonorthogonal decomposition in the short-range region of covalent bonding where the overlap-related interpretational ambiguities increase dramatically. As outlined by Bickelhaupt and Baerends in Equations (1) and (2) of the preceding communication, ref. [1] and detailed in ref. [5], the BB–KM method employs Slater determinants Ψ^A, Ψ^B of isolated fragments (e.g., two CH_3 radicals) to construct an "unperturbed" product function $\Psi^0 = \eta \det|\Psi^A\Psi^B|$ and energy ΔE^0 for overlapping fragments brought up to the final bonding geometry. Ziegler and Rauk[8] formerly labeled ΔE^0 as the "steric-interaction" energy, but BB identify it as the sum of "electrostatic" (ΔV_{elstat}) and "Pauli or steric repulsion" (ΔE_{Pauli}) contributions, where "ΔV_{elstat}" is evaluated (rather inconsistently) as the Coulombic interaction between the interpenetrating fragment densities $\rho_A + \rho_B$ (not the same as the density of Ψ^0, owing to the non-vanishing overlaps between Ψ^A, Ψ^B). "ΔE_{Pauli}" is then evaluated by difference from ΔE^0, and a final "orbital-interaction" term ΔE_{oi} is evaluated by difference from the actual fragment binding energy ΔE to give the basic BB–KM energy decomposition [Eq. (3)]. The same overlap inconsistencies that render the electrostatic label questionable are of course propagated into the Pauli and orbital-interaction labels.

$$\Delta E = \Delta E_{Pauli} + \Delta V_{elstat} + \Delta E_{oi} \qquad (3)$$

The BB–KM labeling ambiguities naturally propagate into Bickelhaupt and Baerends' verbal arguments. The issue of verbal imprecision is quite material in the present case, for it has been shown[13] that the ethane barrier can be made to appear or disappear by slightly varying the treatment of nonorthogonality in a manner that lies wholly within the uncertainties of the verbiage. (The fact that overlap ambiguities involve the unfilled as well as filled fragment orbitals will be discussed below.) The imprecision of terminology is therefore of the same order as the phenomenon to be analyzed.

 © 2003 Wiley-VCH Verlag GmbH & Co. KGaA, Weinheim

The inaccuracies of the BB–KM labels can also be judged by considering the simplest case of H_2. In this case the "unperturbed" Ψ^0 wavefunction is practically equivalent (differing at most by a possible triplet spin contamination term) to the original Heitler–London valence bond (VB) wavefunction, with the spatial part constructed from the product of overlapping hydrogen-atom orbitals. The apparent conclusion that a Heitler–London-type wavefunction contains no "orbital-interaction component" is implausible, casting profound doubt on the BB–KM definitional scheme.

Critique of Four-Electron Destabilizing Rationale

Let us nevertheless pass over these difficulties and proceed directly to the original 4e destabilizing MO diagram (Figure 1) that was the intended goal of BB–KM development. For this purpose we can agree to substitute Kohn–Sham MOs and matrix elements for the presumed SCF–MOs of earlier treatments, as BB suggest is valid. We can also stipulate the relevance for the ethane case of analyzing the energies E_1, E_2 of doubly degenerate *e*-type MOs (e'', e' in D_{3d} geometry, or e_g, e_u in D_{3h}), which are recognized[14] to carry the major torsional dependence. With these stipulations we shall now consider the possible physical interpretation (if any) that may be assigned to the "perturbation diagram" Figure 1. We shall also address how the *same* torsional dependence of E_1, E_2 can be alternately interpreted, in a more consistent and accurate perturbative framework, in hyperconjugative terms.

It is useful to first outline the hyperconjugative "two-electron (2e) stabilizing" rationale in a manner that can be most directly contrasted with the four-electron destabilizing rationale of Figure 1. Figure 2 presents the corresponding hyperconjugative diagram, showing how a doubly occupied orbital ϕ_a (e.g., σ_{C-H}) interacts with an unfilled orbital ϕ_{b^*} (e.g., the vicinal $\sigma^*_{C'-H'}$) of energy $\varepsilon_{b^*} = \langle \phi_{b^*} | \mathscr{H} | \phi_{b^*} \rangle$, with associated interaction and overlap matrix elements $h_{ab^*} = \langle \phi_a | \mathscr{H} | \phi_{b^*} \rangle$, $S_{ab^*} = \langle \phi_a | \phi_{b^*} \rangle$. An analysis similar to that for Figure 1 (see Supporting Information Section A.2 for details) leads to the familiar expression for the two-electron stabilization energy ΔE_{2e} [Eq. (4)] for $\phi_a \rightarrow \phi_{b^*}$ (vicinal $\sigma_{C-H} \rightarrow \sigma^*_{C'-H'}$) interaction.

$$E_{2e} = -2\frac{h^2_{ab^*}}{\varepsilon_{b^*} - \varepsilon_a} \tag{4}$$

(Note that Equation (4) is independent of overlap S_{ab^*}, although the expression is formally correct up through terms of order $O(S^2_{ab^*})$ To express ΔE_{2e} in a form somewhat more parallel to ΔE_{4e}, we can employ a Mulliken-type approximation to express the approximate proportionality of h_{ab^*} to the overlap S_{ab^*} [Eq. (5)] where k is a constant of order unity in atomic units.

$$h_{ab^*} = -k\, S_{ab^*} \tag{5}$$

We can also recognize that the orbital energy difference $\varepsilon_{b^*} - \varepsilon_a$ is nearly constant (torsionally insensitive) and of order unity in atomic units (1 a.u. $\approx$ 627 kcal mol^{-1}). Hence, we can rewrite Equation (4) in the approximate form given by Equation (6) (where k' is a new composite constant of order unity) to display the clear contrast with ΔE_{4e} in Equation (2).

$$\Delta E_{2e} \simeq -2\, k' |S_{ab^*}\, h_{ab^*}| \tag{6}$$

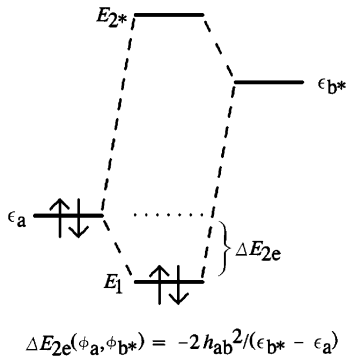


Figure 2. Two-electron stabilizing interaction (See Supporting Information Section A.2) for filled orbital ϕ_a and unfilled orbital ϕ_{b^*} (taken orthogonal, but leading to the same splitting diagram, to leading order in S_{ab^*}, whether ϕ_a, ϕ_b are orthogonal or nonorthogonal).

On a purely numerical level, Equation (1) or Figure 1 present no paradox, for matrix diagonalization in a chosen basis is a purely mathematical operation with no physical or chemical interpretation per se. The difficulty arises when one attempts to attach "perturbative" significance to the splitting diagram. As expressed by Bickelhaupt and Baerends (ref. [5], p. 4), the BB–KM analysis aims to provide an improved description of "changes of the one-electron energies of the orbitals in response to the perturbations" by means of such qualitative MO diagrams, while freeing them "from the double odium of inaccuracy and frequent empiricism." However, the difficulties of achieving a logically and physically consistent interpretation of these diagrams go far deeper.

What are the objections to such a "perturbative" interpretation of Equation (1) and Figure 1? Two major difficulties can be identified, the first quite general and the second somewhat specific to the ethane barrier problem:

1) If the orbitals ϕ_a and ϕ_b are overlapping, they cannot be considered to be the eigenfunctions of any underlying Hermitian Hamiltonian operator with energies ε_a, ε_b. Thus, there is no imaginable physical (Hermitian) Hamiltonian $\mathscr{H}^{(0)}$ that can serve as the "unperturbed system" for such analysis.[15]
2) Overlap integrals S_{ab^*} between filled and unfilled orbitals are often comparable to those S_{ab} between filled orbitals; in such cases (as for ethane), it is physically and numerically inconsistent to include one type of overlap without the other.

We can judge from the first objection that the "unperturbed Hamiltonian" which leads to the outer levels of the splitting diagram (Figure 1) must suffer from the profoundly unphysical pathologies of non-Hermitian operators (such as non-conservation of probability and violation of Fermi–Dirac commutation relations[9b]). We can also judge that the second objection is highly relevant in ethane by evaluating the

 © 2003 Wiley-VCH Verlag GmbH & Co. KGaA, Weinheim

numerical overlaps between vicinal C–H bond and antibond orbitals, for example, $S_{ab} = -0.0847$, $S_{ab^*} = -0.0743$ calculated at the RHF/6-31G* level in staggered geometry, a difference of less than 15%.[16] The superficial 4e-destabilizing interpretation of Figure 1 must therefore be reformulated to take account of both $\phi_a - \phi_b$ and $\phi_a - \phi_{b^*}$ interactions as well as to remove the overlap that prevents consistent Hermitian formulation of an unperturbed $\mathscr{H}^{(0)}$ system Hamiltonian.

The first difficulty can be removed by employing Löwdin's symmetric orthogonalization procedure,[17] which leads to orthonormal orbitals $\bar{\phi}_a$, $\bar{\phi}_b$ that differ as little as possible (in the least-squares sense) from ϕ_a, ϕ_b. The matrix diagonalization problem now takes the form of Equation (7) where $\bar{\varepsilon}_a = \langle \bar{\phi}_a \,|\, \mathscr{H} \,|\, \bar{\phi}_a \rangle$, $\bar{\varepsilon}_b = \langle \bar{\phi}_b \,|\, \mathscr{H} \,|\, \bar{\phi}_b \rangle$, $\bar{h}_{ab} = \langle \bar{\phi}_a \,|\, \mathscr{H} \,|\, \bar{\phi}_b \rangle$.

$$\underline{\underline{\mathbf{H}}} = \begin{pmatrix} \bar{\varepsilon}_a & \bar{h}_{ab} \\ \bar{h}_{ab} & \bar{\varepsilon}_b \end{pmatrix} \xrightarrow{\text{diagonalize}} \begin{pmatrix} E_1 & 0 \\ 0 & E_2 \end{pmatrix} \tag{7}$$

(Recall that the final MO energies E_1, E_2 are unchanged, since we have only performed a non-singular basis transformation.) The resulting splitting diagram (see Supporting Information Section A.3 for details) is shown in Figure 3, which leads to no net energy change when the MOs are fully occupied [Eq. (8)].

$$\Delta E_{4e}(\bar{\phi}_a, \bar{\phi}_b) = 0 \tag{8}$$

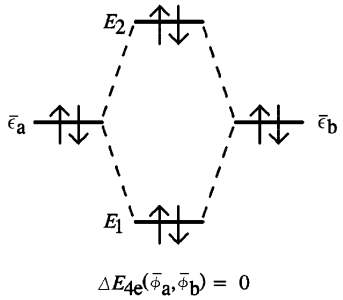


Figure 3. Four-electron nonstabilizing interaction (Supporting Information Section A.3), expressed in terms of orthogonalized unperturbed orbitals $\bar{\phi}_a$, $\bar{\phi}_b$ (for which there exists a valid Hermitian $\mathscr{H}^{(0)}$).

A proper physical (Hermitian) perturbative interpretation can now be given for the splitting diagram in Figure 3, but the physical "effect" on the torsion barrier has vanished!

However, as noted in Objection (2) above, an accurate description of the actual MO energy levels E_1, E_2 must actually involve the unfilled ϕ_{b^*} ($\sigma^*_{C'-H'}$) as well as filled ϕ_b ($\sigma_{C^-H'}$) neighbor orbitals of ϕ_a. Let us therefore extend the basis to three orbitals,[18] transforming these to orthonormal form by the Löwdin symmetric orthogonalization procedure as before [Eq. (9)]. To leading order in the overlaps S_{ab}, S_{ab^*},

$$(\phi_a, \phi_b, \phi_{b^*}) \xrightarrow{\text{Löwdin}} (\bar{\phi}_a, \bar{\phi}_b, \bar{\phi}_{b^*}) \tag{9}$$

the relationship between nonorthogonal and Löwdin-orthogonalized basis orbitals is found to be (see Supporting Information Section A.4 for details) given by Equations (10a–c)].

$$\phi_a = \bar{\phi}_a + {}^1\!/_2\, S_{ab}\, \bar{\phi}_b + {}^1\!/_2\, S_{ab^*}\, \bar{\phi}_{b^*} \tag{10a}$$

$$\phi_b = \bar{\phi}_b + {}^1\!/_2\, S_{ab}\, \bar{\phi}_a \tag{10b}$$

$$\phi_{b^*} = \bar{\phi}_{b^*} + {}^1\!/_2\, S_{ab^*}\, \bar{\phi}_a \tag{10c}$$

Only the expressions for ϕ_a, ϕ_b are needed to make comparisons with the original splitting diagram in Figure 1. Substitution of these quantities into the original matrix diagonalization problem, Equation (1), leads to the splitting diagram shown in Figure 4, in which the net perturbative effect, denoted $\Delta E_{4e}(\bar{\phi}_a, \bar{\phi}_b, \bar{\phi}_{b^*})$ is now of stabilizing form [Eq. (11)].

$$\Delta E_{4e}(\bar{\phi}_a, \bar{\phi}_b, \bar{\phi}_{b^*}) = -2|S_{ab^*}\, h_{ab^*}| \tag{11}$$

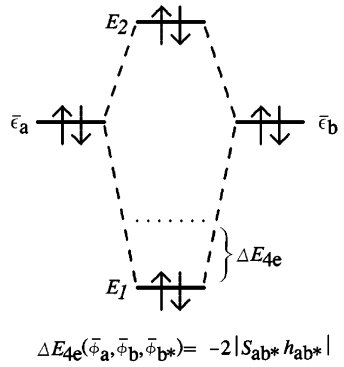


Figure 4. Four-electron stabilizing interaction (see Supporting Information Section A.4), for a proper three-term description of E_1, E_2 in terms of Löwdin-orthogonalized basis orbitals $\bar{\phi}_a$, $\bar{\phi}_b$, $\bar{\phi}_{b^*}$).

Comparison with Equation (6) shows that this stabilizing effect is essentially identical to that predicted by the two-electron $\phi_a \rightarrow \phi_{b^*}$ hyperconjugative interaction! The clear implication is that the numerical values are equivalent because the physical effects are equivalent. We can therefore conclude that hyperconjugative $\sigma_{C^-H} \rightarrow \sigma^*_{C'-H'}$ interactions are responsible for the torsional variations of E_1, E_2 in each case, whether deeply concealed as in Figure 1 (by orbital overlap and superficial "bond" labels that are inadequate to express the ambiguities of nonorthogonal orbital composition), or clearly isolated and identified as in Figure 2.

We re-emphasize that Figure 1, Figure 2, Figure 3, and Figure 4 describe the same final MO energies E_1 and E_2 and torsional variations, merely referred to different "unperturbed systems" $\mathscr{H}^{(0)}$ (manifestly non-Hermitian in Figure 1, Hermitian in other cases). The fact that four-electron destabilization (Figure 1) and two-electron stabilization (Figure 2) can be ascribed a common physical origin implies that the former is somewhat superfluous in this case. The key distinction between the two "effects" is that the former is explicitly overlap-dependent (with resultant lack of unitary invariance to basis transformations), and thus vanishes as

 © 2003 Wiley-VCH Verlag GmbH & Co. KGaA, Weinheim

soon as ϕ_{b^*} mixing is prevented by choosing an orthogonal basis, whereas the latter is not. (As remarked in the Introduction, the unphysical nature of the supposed four-electron destabilizing effect is also indicated by the fact that it persists even if the interaction $h_{ab}=0$.) It is remarkable that this somewhat flimsy theoretical construct has enjoyed such beguiling influence on a generation of organic chemists and their textbook writers.

True Steric Effects?

For comparison, it is useful to examine the case where interactions with unfilled orbitals ϕ_{b^*} are truly negligible compared to those with filled orbitals ϕ_b. An example is the interaction of two helium atoms, each in their $(1s)^2$ ground state. The nearest unfilled orbital is 2*s*, too high in energy and too radially and angularly diffuse to serve as an effective acceptor orbital. We may therefore safely neglect the interactions of filled donor orbitals ϕ_a, ϕ_b with acceptor orbitals ϕ_{a^*}, ϕ_{b^*}, which reduces the problem to 2×2 form. Although ϕ_a, ϕ_b are nodeless 1*s* orbitals at infinite separation, at finite separation they evolve into the corresponding orthogonalized orbitals $\bar{\phi}_a$, $\bar{\phi}_b$ that preserve the Pauli exclusion principle. Weisskopf[19] has lucidly described the manner in which this orbital orthogonalization leads to the "kinetic-energy pressure" that opposes interpenetration of matter. As the orbitals ϕ_a, ϕ_b begin to overlap, the physically required orthogonalization leads to additional oscillatory and nodal features in the orbital waveform, which correspond to increased wavefunction curvature and kinetic energy, the essential "destabilization" that opposes interpenetration. The energies $\bar{\varepsilon}_a$, $\bar{\varepsilon}_b$ of the Pauli-preserving orbitals $\bar{\phi}_a$, $\bar{\phi}_b$ are thereby raised with respect to the long-range asymptotic values ε_a, ε_b [Eq. (12a,b)].

$$\bar{\varepsilon}_a = \varepsilon_a + |S_{ab}\, h_{ab}| \tag{12a}$$

$$\bar{\varepsilon}_b = \varepsilon_b + |S_{ab}\, h_{ab}| \tag{12b}$$

As in Figure 3, the MO energy levels E_1, E_2 are split symmetrically with respect to the proper physical orbital energies $\bar{\varepsilon}_a$, $\bar{\varepsilon}_b$, but the energy raising in Equations (12a,b) gives an apparent unsymmetrical pattern (see Figure 1) when expressed with respect to the long-range asymptotic values ε_a, ε_b. This situation is completely consistent with Coulson's original remark.[4]

The Weisskopf picture of steric repulsion is the conceptual and numerical foundation of the Natural Steric Analysis method,[20] as implemented in the general NBO analysis program.[21] This method was employed by Pophristic and Goodman[2] to evaluate the ethane barrier steric effects directly (not by difference from a putative "electrostatic" contribution, as in the BB method). Consistent with the hyperconjugative picture[13b] (and results of other workers[22]) the "steric effect" is found to be of much smaller magnitude and opposite sign, acting to favor the eclipsed conformation![23] (The principal steric effect appears to involve the "backside" lobes of the C–H bond orbitals, which protrude toward one another in eclipsed conformation but sidestep one another in staggered conformation.) Thus, the steric rationalization of ethane barriers is doubly nonsensical.

Of course, as the steric bulk of pendant groups increases, "true" steric effects can increasingly dominate the conformational potential. Nevertheless it remains true that hyperconjugative delocalizations impose an innate preference of the skeletal geometry for staggered conformations,[24] subject to modulation by steric or coordinative interactions between more complex pendant groups, but exposed in relatively pure form in ethane and ethane-like molecules.

Concluding Remarks

In focussing on the logic of the BB method, we have bypassed details of the NBO-based algorithms for evaluating steric and hyperconjugative contributions; Supporting Information Section A.5 replies to Bickelhaupt and Baerends' two specific technical points on NBO methodology. We emphasize that the bond-antibond picture of barrier origins is rather insensitive to details of bond-orbital construction, and indeed was originally developed[13b] and critically tested[13a] in the framework of crude bond-orbital models[25] of pre-NBO vintage. Nevertheless, NBOs have become the preferred method for quantifying and visualizing hyperconjugative interactions in modern ab initio (single- or multi-configurational) and density functional descriptions, as illustrated in Figure 5.

To summarize, we conclude that proper mathematical formulation of the four-electron destabilizing-interaction diagram (Figure 1) exposes the superficiality of the supposed steric interpretation of the E_1, E_2 torsional variations in ethane, and demonstrates that these variations should instead be attributed to hyperconjugative two-electron stabilizing interactions (Figures 2 and 5) that are easily obscured through loose treatment of nonorthogonality. While Figure 1 may be a useful mnemonic for representing 2×2 matrix diagonalization in a nonorthogonal basis set, it should not be envisioned as a physical interpretation of any imaginable physical

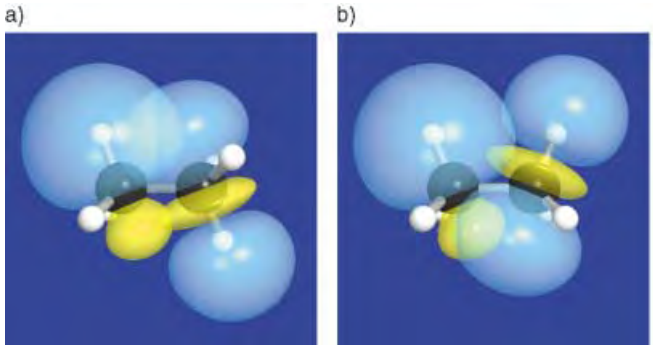


Figure 5. Vicinal σ_{C^-H}–$\sigma^*_{C'-H'}$ NBO interactions in a) staggered (-2.59 kcal mol^{-1}) and b) eclipsed (-0.89 kcal mol^{-1}) conformers of ethane (optimized, B3LYP/6-311++G** level), which show the more favorable 2e stabilization $\Delta E_{2e}(\sigma_{C^-H}\rightarrow\sigma^*_{C'-H'})$, Equation (4), in the staggered case.

 © 2003 Wiley-VCH Verlag GmbH & Co. KGaA, Weinheim

process. By exhibiting the mathematical relationship that converts a four-electron destabilizing effect into a two-electron stabilizing effect, we have demonstrated explicitly that these two "effects" generally share a common mathematical origin. In this circumstance, attempts to assign distinct physical interpretations to Figures 1 and 2 are illusory.

The preceding arguments essentially echo and complement the numerical conclusions that were drawn long ago[13] concerning earlier versions[25] of the "Pauli repulsions" rationale for ethane barriers. Because this literature and its implications seem to have largely escaped the notice of qualitative MO theory adherents, it seemed preferable to address the BB case directly in the language and iconography that is apparently still favored by many organic-chemistry textbook writers.

It should be emphasized that these criticisms make no reference to the numerical validity of standard LCAO-MO variational calculations in nonorthogonal basis sets. Because these calculations are invariant with respect to non-singular transformations that span the same Hilbert space, there can be no numerical distinction between one type of basis set or another; the choice is dictated solely by numerical convenience. Nor do these arguments detract from the general usefulness of Mulliken-type approximations [cf. Eq. (5)] to visualize bonding interactions in terms of orbital overlap (that is, in terms of pre-orthogonal PNBOs that differ from orthonormal NBOs only in omission of the final interatomic orthogonalization;[26] see Figure 5). Such overlap imagery can be a powerful conceptual guide to the actual Hamiltonian interaction strengths, without encouraging the frequent misconception that spatial orbital overlaps (rather than kinetic and potential energy terms in the Hamiltonian operator) are somehow "causing" chemical bonding.

The recognition that energy-level variations which are commonly attributed to four-electron destabilizing effects can instead be understood in terms of hyperconjugative $\phi_a - \phi_{b^*}$ interactions suggests how one can ultimately simplify and unify the understanding of phenomena that might otherwise seem to require distinct "effects." In effect, the stability of the staggered conformer can be attributed to resonance-type delocalization of the form (Figure 6) which imparts slight

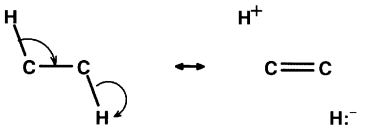


Figure 6. Resonance-type hyperconjugative delocalization in ethane

double-bond character to the C–C torsional bond and is maximized in antiperiplanar alignments.[27] The ethane-like rotation barriers are thus seen to have an intimate connection to anomeric and gauche effects, anionic hyperconjugation, stereoelectronic beta-elimination, and other conjugative and hyperconjugative phenomena in which $\phi_a - \phi_{b^*}$ donor–acceptor (generalized Lewis base–Lewis acid) interactions play a dominant role.[28] The four-electron destabilizing concept therefore seems to play a somewhat dubious and superfluous role in the present theory of torsional and stereoelectronic phenomena. Judicious de-emphasis of this concept would have the desirable effect of promoting conceptual economy and heightening general appreciation of the pervasive role of conjugative and hyperconjugative effects in chemistry.

Received: April 23, 2003 [Z51777]

Keywords: conformation analysis · ethane · hyperconjugation · NBO methods · steric hindrance

[1] F. M. Bickelhaupt, E. J. Baerends, *Angew. Chem.* **2003**, *115*, 4315; *Angew. Chem. Int. Ed.* **2003**, *42*, 4183 (preceding Communication).
[2] V. Pophristic, L. Goodman, *Nature* **2001**, *411*, 565; P. R. Schreiner, *Angew. Chem.* **2002**, *114*, 3729; *Angew. Chem. Int. Ed.* **2002**, *41*, 3579.
[3] See, for example, I. Fleming, *Frontier Orbitals and Organic Chemical Reactions*, Wiley, London, **1976**; T. A. Albright, J. K. Burdett, M.-H. Whangbo, *Orbital Interactions in Chemistry*, Wiley-Interscience, New York, **1985**; A. Rauk, *Orbital Interaction Theory of Organic Chemistry*, Wiley-Interscience, New York, **1994**. Much of the early development of perturbative molecular orbital (PMO) concepts can be credited to M. J. S. Dewar (see, for example, M. J. S. Dewar, R. C. Dougherty, *The PMO Theory of Organic Chemistry*, Plenum, New York, **1975**).
[4] C. A. Coulson, *Mol. Phys.* **1968**, *15*, 317.
[5] F. M. Bickelhaupt, E. J. Baerends in *Reviews in Computational Chemistry, Vol. 15* (Eds.: K. B. Lipkowitz, D. B. Boyd), Wiley-VCH, New York, **2000**, pp. 1–86.
[6] G. te Velde, F. M. Bickelhaupt, S. J. A. van Gisbergen, C. Fonseca Guerra, E. J. Baerends, J. G. Snijders, T. Ziegler, *J. Comput. Chem.* **2001**, *22*, 931.
[7] K. Kitaura, K. Morokuma, *Int. J. Quantum Chem.* **1976**, *10*, 325; K. Morokuma, *Acc. Chem. Res.* **1977**, *10*, 294.
[8] T. Ziegler, A. Rauk, *Inorg. Chem.* **1979**, *18*, 1558, 1755.
[9] a) A. E. Reed, L. A. Curtiss, F. Weinhold, *Chem. Rev.* **1988**, *88*, 899 (particularly Section IV.B); b) F. Weinhold, J. E. Carpenter, *J. Mol. Struct. (Theochem)* **1988**, *165*, 189.
[10] S. M. Cybulski, S. Scheiner, *Chem. Phys. Lett.* **1990**, *166*, 57.
[11] E. D. Glendening, A. Streitwieser, *J. Chem. Phys.* **1994**, *100*, 2900.
[12] See, for example, N. S. Golubev, I. G. Shenderovich, S. N. Smirnov, G. S. Denisov, H.-H. Limbach, *Chem. Eur. J.* **1999**, *5*, 492; G. Cornilescu, J.-S. Hu, A. Bax, *J. Am. Chem. Soc.* **1999**, *121*, 1601; E. D. Isaacs, A. Shulkla, P. M. Platzman, D. R. Hamann, B. Barbiellini, C. A. Tulk, *Phys. Rev. Lett.* **1999**, *82*, 600; W. H. Thompson, J. T. Hynes, *J. Am. Chem. Soc.* **2000**, *122*, 6278; A. van der Vaart, K. M. Merz, Jr., *J. Chem. Phys.* **2002**, *116*, 7380.
[13] a) C. T. Corcoran, F. Weinhold, *J. Chem. Phys.* **1980**, *72*, 2866; b) For the general hyperconjugative picture of ethane-type barriers and its relationship to previous work, see T. K. Brunck, F. Weinhold, *J. Am. Chem. Soc.* **1979**, *101*, 1700; c) After development of the NBO method (cf. refs. [26], [21]), the hyperconjugative picture was given quantitative ab initio confirmation by A. E. Reed, F. Weinhold, *Isr. J. Chem.* **1991**, *31*, 277.
[14] J. P. Lowe, *J. Am. Chem. Soc.* **1970**, *92*, 3799.
[15] This follows immediately from the elementary theorem (see, for example, I. N. Levine, *Quantum Chemistry*, 5th ed., Prentice-Hall, Upper Saddle River, NJ, **2000**, pp. 167–168) that the eigenfunctions of any Hermitian operator are (or can be taken) orthogonal.

 © 2003 Wiley-VCH Verlag GmbH & Co. KGaA, Weinheim

[16] Indeed, these two integrals can *never* differ by more than a factor of ≈ 2, because the principal contribution arises from the overlap between the adjacent carbon hybrids, which is identical in S_{ab} and S_{ab^*}. The quoted numerical values are for RHF/6-31G* PNBOs (pre-orthogonal NBOs), but any reasonable conjecture for the bond orbital forms leads to similar estimates.
[17] P.-O. Löwdin, *J. Chem. Phys.* **1950**, *18*, 365.
[18] In ethane, a proper symmetric treatment would include also ϕ_{a^*}, leading to an obvious 4×4 modification of the present 3×3 result. The simplified 3×3 model could represent a lone pair (ϕ_a) interacting with a vicinal bond and antibond (ϕ_b, ϕ_{b^*}), as in methylamine.
[19] V. W. Weisskopf, *Science* **1975**, *187*, 605.
[20] J. K. Badenhoop, F. Weinhold, *J. Chem. Phys.* **1997**, *107*, 5406, 5422; J. K. Badenhoop, F. Weinhold, *Int. J. Quantum Chem.* **1999**, *72*, 269.
[21] a) NBO 5.0. E. D. Glendening, J. K. Badenhoop, A. E. Reed, J. E. Carpenter, J. A. Bohmann, C. M. Morales, F. Weinhold, Theoretical Chemistry Institute, University of Wisconsin, Madison **2001**; b) For a comprehensive bibliography of NBO-based methods and recent applications, see http://www.chem.wisc.edu/~nbo5.
[22] R. F. W. Bader, J. R. Cheeseman, K. E. Laidig, K. B. Wiberg, C. Breneman, *J. Am. Chem. Soc.* **1990**, *112*, 6530.
[23] Even the BB analysis suggests that the "Pauli" term is smaller in the eclipsed conformer, when non-torsional variables are properly optimized at each torsion angle (see 4th paragraph of ref. [1],). BB's attempts to explain this paradox reveal that E_{Pauli} (and other "components") are varying by many times the flexing energy difference itself, an unmistakable sign of unphysical cause/effect dependencies in their analysis.
[24] J. Michl, R. West, *Acc. Chem. Res.* **2000**, *33*, 821.
[25] O. J. Sovers, C. W. Kern, R. M. Pitzer, M. Karplus, *J. Chem. Phys.* **1968**, *49*, 2592, and references therein.
[26] "Natural Bond Orbital Methods": F. Weinhold in *Encyclopedia of Computational Chemistry, Vol. 3* (Eds.: P. von R. Schleyer, N. L. Allinger, T. Clark, J. Gasteiger, P. A. Kollman, H. F. Schaefer III, P. R. Schreiner), Wiley, Chichester, **1998**, pp. 1792–1811. For further information on (P)NBO overlap images, see the *NBO-View* link of the NBO 5.0 website, ref. [21b].
[27] F. Weinhold, *Nature* **2001**, *411*, 539.
[28] As illustrative examples, see "The Anomeric Effect and Associated Stereoelectronic Effects": P. Petillo, L. Lerner, *ACS Symp. Ser.* **1993**, *539*; "Hyperconjugation": C. J. Cramer in *Encyclopedia of Computational Chemistry, Vol. 2* (Eds.: P. von R. Schleyer, N. L. Allinger, T. Clark, J. Gasteiger, P. A. Kollman, H. F. Schaefer III, P. R. Schreiner), Wiley, Chichester, **1998**, pp. 1294–1298; L. E. Bretscher, C. L. Jenkins, K. M. Taylor, M. L. DeRider, R. T. Raines, *J. Am. Chem. Soc.* **2001**, *123*, 777.

 © 2003 Wiley-VCH Verlag GmbH & Co. KGaA, Weinheim

Organic/Inorganic Nanocapsules

Precision Synthesis of Organic/Inorganic Hybrid Nanocapsules with a Silanol-Functionalized Micelle Template**

*Kyoungmoo Koh, Kohji Ohno, Yoshinobu Tsujii, and Takeshi Fukuda**

There has been increasing interest in the encapsulation of substances into confined spaces on the molecular to micrometer scale, as they have a wide variety of applications.[1,2] The related techniques can be classified into two types: 1) molecular assemblies with an internal cavity are used such as micelles, liposomes, and hollow spheres;[1–3] 2) substances are wrapped by organic and/or inorganic gels.[4] Herein we focus on the former type of system.

Self-assemblies of amphiphilic block copolymers in selective solvents commonly result in micelles with a core of the block that is insoluble in the solvent and a shell of the block that is swollen by the solvent.[5,6] Although micelle formation is among the most popular techniques for the construction of encapsulants in polymer science, the combination of micelle formation with some other techniques may lead to a new development in encapsulation technology. In the work described herein, we have attempted to coat the surface of a block copolymer micelle with a thin silica layer. In other words, we have used the micelle as a template to prepare a hollow silica nanoparticle. Such an organic/inorganic hybrid with its stable and confined nanoscale cavity would have many potential applications.

Our strategy consists of three steps, as shown in Figure 1: First, an amphiphilic block copolymer that bears several protected silanol groups near the free end of the hydrophilic block is synthesized. Second, the amphiphile is assembled into a micelle, with the silanol groups situated at the outermost layer of the micelle. Third, the micelle is coated with a silicon dioxide layer, which grows from the reactive points of the silanol groups near the micelle surface.

The amphiphilic block copolymer of the type PMMA-*b*-PPEGMA-*b*-poly(PEGMA-*r*-MOPS) was prepared by atom-transfer radical polymerization[7] (ATRP), as described in the experimental section. Figure 2 shows the gel-permeation chromatographic (GPC) traces for the polymerization steps. The polymerization of PEGMA using the purified PMMA macroinitiator proceeded smoothly: no shoulder peak was detected at the elution position of the macroinitiator and the

[*] Prof. Dr. T. Fukuda, K. Koh, Dr. K. Ohno, Dr. Y. Tsujii
Institute for Chemical Research, Kyoto University
Uji, Kyoto 611-0011 (Japan)
Fax: (+81) 774-38-3170
E-mail: fukuda@scl.kyoto-u.ac.jp

[**] This work was supported in part by a Grant-in-Aid for Scientific Research (Grant-in-Aid 14205131, 14750695) from the Ministry of Education, Culture, Sports, Science, and Technology, Japan.

Supporting information for this article is available on the WWW under http://www.angewandte.org or from the author.

 © 2003 Wiley-VCH Verlag GmbH & Co. KGaA, Weinheim DOI: 10.1002/anie.200351398

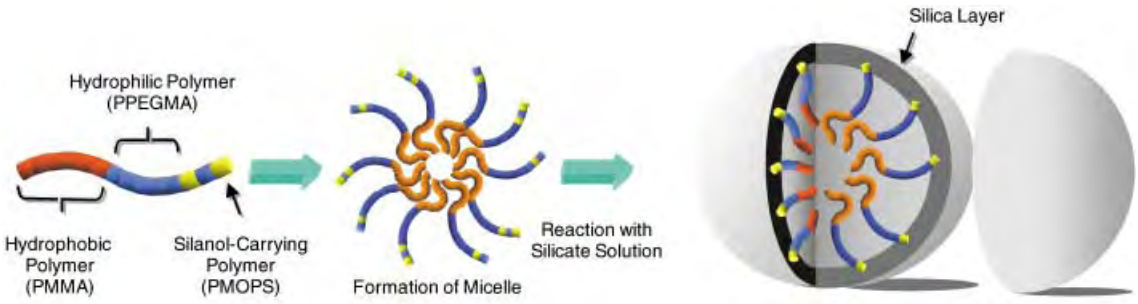


Figure 1. Strategy for the synthesis of an organic/inorganic hybrid nanocapsule.

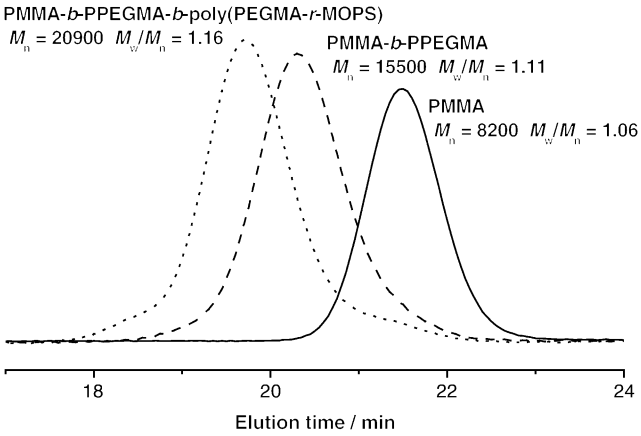


Figure 2. GPC traces for the PMMA macroinitiator, the PMMA-*b*-PPEGMA block copolymer, and the PMMA-*b*-PPEGMA-*b*-poly(PEGMA-*r*-MOPS) block copolymer.

molecular weight distribution was kept narrow. The GPC trace after the sequential addition of MOPS shows a shift of the peak position to a higher-molecular-weight region; again no shoulder peak was detected and the polydispersity index was kept low, as indicated in the figure.

Figure 3 represents the ^{1}H NMR spectrum (300 MHz) of the purified block copolymer PMMA-*b*-PPEGMA-*b*-poly(PEGMA-*r*-MOPS) with tentative assignments of the peaks. The peaks b, d, and i were assigned to the methyl protons of the polymethacrylate backbone, the methylene protons of PPEGMA, and the methylene protons of PMOPS, respectively, and were used to calculate the molar composition of the block copolymer as MMA/PEGMA/MOPS = 11.7:5.1:1. We also analyzed the composition of the random (statistical) copolymer poly(PEGMA-*r*-MOPS) independently prepared under similar conditions,[8] and estimated the molar composition of the last sequence poly(PEGMA-*r*-MOPS) in the block copolymer as PEGMA/MOPS = 1:0.84. With these molar ratios and the known number-average degrees of polymerization (DP_n) of the macroinitiator PMMA ($DP_n = 82$), the DP_n values of the PMMA, PPEGMA, and poly(PEGMA-*r*-MOPS) blocks were estimated to be 82, 28, and 15, respectively, and the molar composition of poly(PEGMA-*r*-MOPS) was assumed to be (1:0.84 ≈ 8:7). The $M_{n,NMR}$ of the block copolymer estimated in this way was 20700, which (accidentally, to some extent) agreed well with the PMMA-calibrated GPC value ($M_{n,GPC}$ = 20900). These results confirm the successful formation of the amphiphilic block copolymer, which bears several protected silanol groups near the free end of the hydrophilic block.

The polymeric micelle was prepared as described in the Experimental Section. The hydrodynamic diameter of the micelle was estimated to be about 30 nm by dynamic light scattering (DLS). This micelle is probably composed of a core of the hydrophobic PMMA block and a shell of the hydrophilic PPEGMA sequence, so that the MOPS moieties of the poly(PEGMA-*r*-MOPS) segment are preferentially distributed near the micelle surface. Moreover, hydrolysis of the trimethoxysilyl groups of the MOPS moieties under aqueous environment would result in silanol groups, which should be populated near the micelle surface.

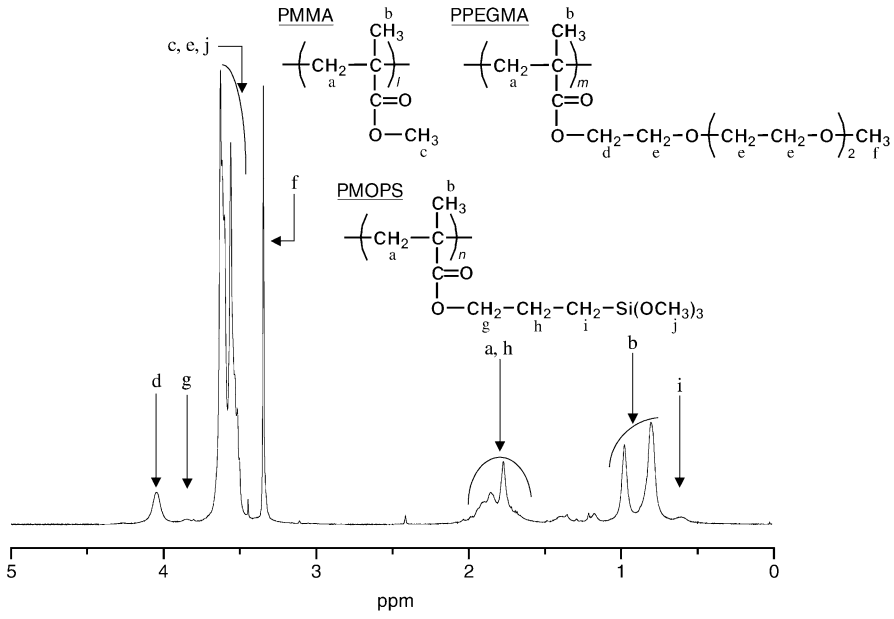


Figure 3. Typical ^{1}H NMR spectrum of the purified PMMA-*b*-PPEGMA-*b*-poly(PEGMA-*r*-MOPS) block copolymer in $CDCl_3$.

 © 2003 Wiley-VCH Verlag GmbH & Co. KGaA, Weinheim

Liz-Marzán et al.[9] previously reported a method for the homogeneous silica coating of a silanol-modified gold nanoparticle by active silica to produce a fairly monodisperse particle composed of a gold core and a silica shell. We applied this method to coat the silanol-carrying micelle with a silica layer (see Experimental Section). As shown in Figure 4, the



Figure 4. TEM image of the organic/inorganic hybrid nanocapsule.

transmission electron microscopic (TEM) image of the micelle after treatment with active silica reveals black rings with a mean diameter about 25 nm, which is roughly comparable to the diameter of the original micelle estimated by DLS. No such black rings were observed for the micelle before treatment with silica or for the micelle formed from the PMMA-*b*-PPEGMA block copolymer (without silanol groups) after treatment with silica. These results show the successful formation of a silica layer growing from the anchor points of the silanol groups near the micelle surface. We also synthesized a nanocapsule with a relatively large diameter (about 42 nm) by changing the molecular weight of the block copolymer (see Supporting Information).

With its unique structural features, the organic/inorganic hybrid nanocapsule obtained is potentially useful in many applications: for example, trapping substances in a micelle followed by coating with a silica layer will prove to be an efficient, yet stable form of encapsulation. (In fact, we performed a model experiment on a hydrophobic fluorescence dye, pyrene, to show that it could be contained within a nanocapsule (see Supporting Information).) Moreover, coating the micelle surface with a silica layer will offer a flexible method for further functionalization of the micelle by a variety of reactions with the silica surface.

To conclude, we precisely synthesized a silanol-functionalized amphiphilic block copolymer of the type PMMA-*b*-PPEGMA-*b*-poly(PEGMA-*r*-MOPS) by ATRP and produced the silanol-carrying micelle of the polymeric amphiphile. The micelle was mixed with a solution of active silicate to give a silica layer surrounding the micelle surface, thus producing an organic/inorganic hybrid nanocapsule. Because of the unique structural features of the nanocapsule, this chemistry will find many interesting applications. Studies on the incorporation of a reactive compound into the nanocapsule for use as a nanoscale reactor is in progress in our laboratory.

Experimental Section

Formation of the block copolymer: A solution of methyl methacrylate (MMA; 20.8 g) in diphenyl ether (19.46 g) was polymerized in the presence of *p*-toluenesulfonyl chloride (TsCl; 198 mg), copper(I) bromide (143 mg), and L-sparteine (Sp; 456 mg) at 70 °C for 4 h to obtain chlorine-terminated poly(methyl methacrylate) (PMMA; $M_n = 8200$, $M_w/M_n = 1.06$; M_n and M_w/M_n are number-average molecular weight and polydispersity index, respectively). Next, a Schlenk tube was charged with a magnetic stirrer bar and CuBr (5.2 mg), to which was quickly added a mixture of the chlorine-terminated PMMA (0.3 g) as a macroinitiator, poly(ethylene glycol) methyl ether methacrylate (PEGMA; Aldrich, $M_n \approx 300$, 2.2 g) as a hydrophilic monomer, diphenyl ether (3.8 g), and Sp (17 mg). The system was immediately degassed by three freeze–pump–thaw cycles and finally purged with argon. The polymerization was carried out in an oil bath under thermostat control at 70 °C. After 2 h, a mixture of methacryloxypropyltrimethoxysilane (MOPS; Chisso Co., Yokohama, Japan, 1.8 g), CuBr (16 mg), and Sp (51 mg), which had been degassed and charged with argon beforehand, was added into the Schlenk tube through a cannula. The polymerization was allowed to proceed at 70 °C for 2 h to obtain a block copolymer of the type PMMA-*b*-PPEGMA-*b*-poly(PEGMA-*r*-MOPS).The block copolymer was purified by passing through an activated alumina column and then by reprecipitation with *n*-hexane.

Preparation of the polymeric micelle: The block copolymer (100 mg) was dissolved in a mixture of *N*,*N*-dimethylacetamide (1 mL) and acetone (4 mL), to which Milli-Q-purified water (20 mL) was added dropwise at a rate of 1 mL min^{-1} with gentle stirring. The mixture was then sonicated in an ultrasound bath for 2 min to ensure complete dispersion of the amphiphile. The resultant cloudy solution was placed in a dialysis tube (Spectra/Por, molecular weight cutoff 15 000) and dialyzed against Milli-Q water for 3 days. The cloudy micellar solution remaining in the tube was passed through a membrane filter (pore size 0.45 μm) and stored in clean glassware.

Coating of the micelle: An aqueous solution of sodium silicate (0.5 wt %, pH 9; 20 mL) was added to the silanol-carrying micelle solution (20 mL). The mixture was left at room temperature for 40 h and then dialyzed against distilled water to remove unreacted active silica.

Received: March 14, 2003 [Z51398]
Published Online: August 25, 2003

Keywords: block copolymers · micelles · nanostructures · self-assembly · silicates

[1] a) M. Moffitt, K. Khougaz, A. Eisenberg, *Acc. Chem. Res.* **1996**, *29*, 95; b) S. E. Webber, *J. Phys. Chem. B* **1998**, *102*, 2618.
[2] a) F. Hof, S. L. Craig, C. Nuckolls, J. Rebek, Jr., *Angew. Chem.* **2002**, *114*, 1556; *Angew. Chem. Int. Ed.* **2002**, *41*, 1488; b) D. M. Rudkevich, *Bull. Chem. Soc. Jpn.* **2002**, *75*, 393.
[3] *Liposomes: A Practical Approach* (Ed.: R. R. C. New), IRL, Oxford, UK, **1990**.
[4] a) I. Gill, A. Ballesteros, *J. Am. Chem. Soc.* **1998**, *120*, 8587; b) M. L. Ferrer, F. del Monte, D. Levy, *Chem. Mater.* **2002**, *14*, 3619; c) C. Lei, Y. Shin, J. Liu, E. J. Ackerman, *J. Am. Chem. Soc.* **2002**, *124*, 11 242; d) N. Murthy, Y. X. Thng, S. Schuck, M. C. Xu, J. M. J. Fréchet, *J. Am. Chem. Soc.* **2002**, *124*, 12 398.
[5] a) L. Zhang, A. Eisenberg, *J. Am. Chem. Soc.* **1996**, *118*, 3168; b) Y. Maeda, N. Taniguchi, I. Ikeda, *Macromol. Rapid Commun.* **2001**, *22*, 1390; b) K. Kataoka, A. Harada, Y. Nagasaki, *Adv. Drug Delivery Rev.* **2001**, *47*, 113.
[6] a) K. B. Thurmond II, T. Kowalewski, K. L. Wooley, *J. Am. Chem. Soc.* **1996**, *118*, 7239; b) V. Bütün, A. B. Lowe, N. C. Billingham,

 © 2003 Wiley-VCH Verlag GmbH & Co. KGaA, Weinheim

S. P. Armes, *J. Am. Chem. Soc.* **1999**, *121*, 4288; c) J. Ding, G. Liu, *Macromolecules* **1998**, *31*, 6554.
[7] a) J. S. Wang, K. Matyjaszewski, *J. Am. Chem. Soc.* **1995**, *117*, 5614; b) K. Ohno, Y. Tsujii, T. Fukuda, *J. Polym. Sci. Part A* **1998**, *36*, 2473.
[8] The random copolymerization of MOPS (4.48 g) and PEGMA (5.56 g) was carried out in the presence of TsCl (7 mg), CuBr (42 mg), Sp (139 mg), and diphenyl ether (9.76 g) at 70 °C under argon. At low monomer conversions below 10 %, three different aliquots of the mixture were periodically sampled. The purified copolymers were analyzed by ^{1}H NMR spectroscopy, so that the average mole ratio of PEGMA/MOPS in the copolymer was estimated to be 1:0.84.
[9] L. M. Liz-Marzán, M. Giersig, P. Mulvaney, *Langmuir* **1996**, *12*, 4329.

 © 2003 Wiley-VCH Verlag GmbH & Co. KGaA, Weinheim

Colorimetric Glucose Sensor

Simple and Precise Preparation of a Porous Gel for a Colorimetric Glucose Sensor by a Templating Technique**

Daisuke Nakayama, Yukikazu Takeoka, Masayoshi Watanabe,* and Kazunori Kataoka*

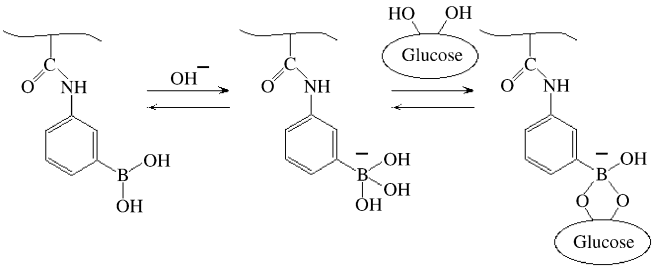
An inverse opal structure having a periodically ordered interconnecting porosity endows hydrogels with structural colors (i.e., colors that arise from physical optics as opposed chromophores) based on the Bragg diffraction of light.[1] Additionally, the porous hydrogels exhibit a rapid change in volume responding to environmental variations.[1,2] Consequently, the structural colors of the gels are quickly synchronized with their characteristic volume change. Such gels have the potential for applications in chemical sensing.[1c] Herein, we report the precision design and simple preparation of a colorimetric sensor for level of glucose in blood by using structurally colored gel.

[*] Dr. Y. Takeoka, Prof. Dr. M. Watanabe, Dr. D. Nakayama
Department of Chemistry and Biotechnology
Yokohama National University
Yokohama, Kanagawa 240-8501 (Japan)
Fax: (+81) 45-339-3956
E-mail: ytakeoka@ynu.ac.jp
Prof. Dr. K. Kataoka
Department of Materials Science
The University of Tokyo,
Tokyo 113-0033 (Japan)

[**] This work was supported by the Shiseido Fund for Science and Technology and a Grant-in-Aid for Scientific Research on Priority Areas of "Dynamic Control of Strongly Correlated Softmaterials" (No. 413) to Y.T. from the Ministry of Education, Culture, Sports, Science, and Technology, Japan.

Most existing glucose sensors use glucose-sensitive proteins, such as glucose oxidize enzyme, immobilized on films or in hydrogels.[3] However, such proteins will denature under prolonged storage and use, because of their high fragility towards environmental changes. Additionally, their response depends on the dissolved oxygen concentration. For commercial applications, especially, there is a strong demand for a more stable and simpler sensor. Synthetic compounds are among the leading candidates for such a system.[4]

It is well known that phenylboronic acid and its derivatives can form covalent complexes with glucose reversibly. In alkalescent aqueous solutions the phenylboronic acid compounds are in equilibrium between the undissociated and the dissociated states (Scheme 1). In this system, complexes with



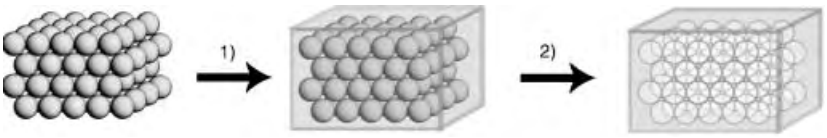
Scheme 1. Equilibria associated with complex formation between phenylboronic acid derivative and glucose under a basic condition.

glucose molecules are mainly formed with the dissociated state. Thus, the addition of glucose in the system causes a shift in the equilibrium in the direction of increasing the presence of charged phenylborates. Hence, if one prepares a hydrogel of a phenylboronic acid derivative, complexation with glucose causes the volume of the hydrogel to increase through positive osmotic pressure in the hydrogel.[4a,b,e] In this project, we attempted to introduce this mechanism into the structurally colored gel to produce a colorimetric glucose sensor. It follows that such a gel can be expected to display glucose-dependent changes in structural color.

A periodically ordered interconnecting porous gel exhibiting a desired structural color can be prepared by using a closest-packing colloidal crystal as a template (Scheme 2).[1] A pregel solution can easily be infiltrated into an open structure between each contact particle of the closest-packing colloidal crystal as a narrow vessel for making the gel. After the removal of the crystal component from the gel obtained, the porous gel exhibits a brilliant structural color under white light illumination[1b] and undergoes fast and drastic changes in color in response to a variety of environments.[1a]

The interval of time required for the volume of a gel to change is governed by the collective diffusion of the polymer network forming the gel.[5a,b] The time is proportional to the square of a characteristic length of a gel such as the diameter for a spherical or cylindrical gel and the thickness for a slab gel. Thus, the period needed for volume change reduces as the size of the gel becomes smaller. A bulk gel forms a dense polymer skin layer, which prevents the permeability of solvent molecules when a drastic change in the environment comes about.[5c] The result is a very slow deswelling of the

 DOI: 10.1002/anie.200351746 © 2003 Wiley-VCH Verlag GmbH & Co. KGaA, Weinheim



Scheme 2. Preparation of a periodically ordered interconnecting porous gel by using a closest-packing silica colloidal crystal as a template. 1) Pregel solution, polymerization; 2) immersion into aqueous HF to remove the silica component.

bulk gel. In contrast to the bulk gel, porous gel exhibits a very fast response time, attributable to the interconnecting porous structure which makes solvent discharge easier.

The peak values of reflection spectra, λ_{max}, for the porous gel are obtained by Equation (1):[1,6]

$$\lambda_{max} = 1.633\,(d/m)\,(D/D_0)\,(n_a^2 - \sin^2\theta)^{1/2} \quad (1)$$

in which d is the diameter of a colloidal particle, m is a constant, D/D_0 is the equilibrium swelling degree of the gel (D and D_0 are diameters of the gel in the equilibrium state at a certain condition and in the reference state, respectively.), n_a is the refractive index of the porous gel at a certain condition, and θ is the angle measured from the normal to the plane of the gel. In this report, d and θ are fixed at 220 nm and 0°, respectively, to reduce the parameters for this experiment. Consequently, we have only to experimentally determine the environmental dependence of the gel's swelling ratio (D/D_0), and refractive index to presurmise its observed value of λ_{max}. The swelling ratio can be estimated by monitoring the diameter of a cylindrical gel prepared in a capillary with a diameter of 100 μm. In the present case, D_0 is the inside diameter of the capillary. The change in the refractive index of the porous gel with varying conditions is then measured by a refractmeter. Although the rate of change in n_a for the porous thermosensitive chemical gel composed of *N*-isopropylacrylamide (NIPA) was less than 1% when the temperature was changed from 15 °C to 60 °C, the swelling ratio changed by about a few times.[1b] Therefore, the swelling ratio is dominant over λ_{max} of the observed reflection spectrum for the porous NIPA gel.

It follows from what has been said that a periodically ordered interconnecting porous gel based on NIPA and a phenylboronic acid derivative would reveal a shift in λ_{max} to a higher wavelength with an increase in the glucose concentration at certain temperature. To fabricate a visual sensor, λ_{max} should land somewhere between 400 nm to 700 nm. To obtain a sensor exhibiting visible color in any conditions, the value of D/D_0 should be kept between about 0.9 and 1.5 based on equation (1). As our prototype, we designed a colorimetric sensor for checking urine or blood glucose levels. If a person's blood glucose level on an empty stomach is more than about 11.0 mM, the person is diagnosed as diabetic. When the blood glucose level is between 7.8 mM to 11.0 mM, the person is borderline diabetic. In such a case, a sensor that signals these concentrations through distinctive colors would be useful in diagnosis. As, red, yellow, and green are used internationally in traffic signals, we introduced this color variation in our gel system in an easy-to-understand manner, thus aiming for a structurally colored gel that is yellow when the glucose concentration is from 7.8 mM to 11.0 mM, and red when the concentration is more than 11.0 mM. To realize this system, it was crucial that the desired swelling ratio of the gel could be systematically obtained by using precise recipes. If $n_a = 1.4$, D/D_0 should be from 1.15 to 1.17 for the gel to display yellow (580–590 nm) at the appropriate glucose concentration.

According to the theory,[7] the swelling ratio of a gel comes to equilibrium when the osmotic pressure difference between the inside and outside of the gel becomes zero. The total osmotic pressure of the gel is determined by the mixing between monomers and solvent, the elastic contribution, and ion concentration differences in and out of the gel. Based on the assumption that gelation proceeds perfectly, it is technically possible to prepare a gel membrane that exhibits a desired swelling ratio by controlling the recipe.[8] It follows that a porous gel reflecting a specific color at a certain condition may also be systematically obtained.

With the desired properties in mind, we carefully selected the monomer species, their concentrations and ratio, the concentration of cross-linker, and the solvent for making the gel. We used 3-acrylamidophenylboronic acid (AAPBA) as a sensing monomer to prepare the glucose-sensitive gel.[4a,b] Figure 1 shows the degree of swelling of NIPA-*co*-AAPBA

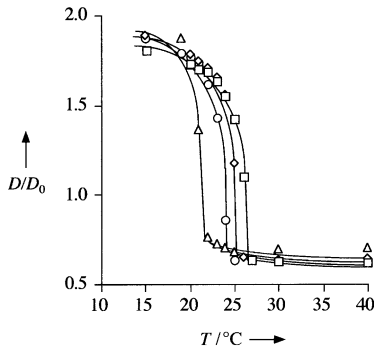


Figure 1. Degree of swelling of poly(NIPA-*co*-AAPBA) gel as a function of temperature in a CHES buffer aqueous solution. The total monomer concentrations ([NIPA] + [AAPBA]) in the recipes for these gels were fixed at 1.65 M, while [AAPBA] was changed: (□) [AAPBA] = 50 mM, (◇) [AAPBA] = 75 mM, (○) [AAPBA] = 100 mM, (△) [AAPBA] = 165 mM. [BIS] was also fixed at 2 mol% of the total monomer concentration. DMSO was used as the solvent.

gels that were prepared by using dimethylsulfoxide (DMSO) as a function of temperature in a 2-(cyclohexylamino)-ethanesulphonic acid (CHES) buffer. The monomer ratio between NIPA and AAPBA was changed, while the total monomer concentration ([NIPA] + [AAPBA]) and the cross-linker concentration were fixed. The ionic strength and pH value of the buffer were adjusted at 0.15 and 9.0, respectively. Although all gels underwent drastic volume changes, the transition temperature became lower as the AAPBA concentration was increased. It is known that transition temperature of NIPA copolymer gel having ionic sites increases as the amount of ionic sites increases.[7b,c] However, the swelling

 © 2003 Wiley-VCH Verlag GmbH & Co. KGaA, Weinheim

behavior of NIPA-*co*-AAPBA gels is not consistent with that of the typical ionized NIPA gel.[7d] This may be due to the hydrophobicity of the AAPBA monomer or to the hydrogen bonding between monomers.

Swelling curves measured on a series of NIPA-*co*-AAPBA gels in buffer solutions including different amounts of glucose are shown in Figure 2. An increase in glucose concentration shifts the transition temperature upward in every case. The change in the volume with increasing the glucose concentration can be observed clearly at certain temperatures. The region where the remarkable change can be observed widens with as the quantity of AAPBA increases.

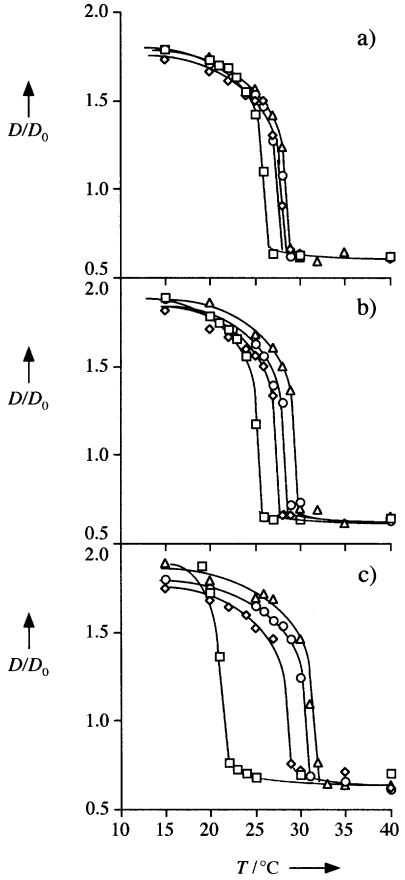


Figure 2. Degree of swelling of poly(NIPA-*co*-AAPBA) gels as a function of temperature in a CHES buffer aqueous solution including different concentrations of glucose: (□) [glucose] = 0 mM, (◇) [glucose] = 5 mM, (○) [glucose] = 10 mM, (△) [glucose] = 20 mM. The total monomer concentrations ([NIPA] + [AAPBA]) in the recipes for these gels were fixed at 1.65 M, while [AAPBA] was changed: a) [AAPBA] = 50 mM, b) [AAPBA] = 75 mM, c) [AAPBA] = 165 mM. [BIS] was also fixed at 2 mol% of the total monomer concentration. DMSO was used for the solvent.

The ratio of monomer concentration to cross-linker concentration for a pregel solution is a strong determinant of the swelling ratio of a gel obtained.[8] The more cross-linkers there are in a solution with a given amount of monomers, the smaller the swelling ratio of the gel is in its swollen state. The swelling ratio of NIPA-*co*-AAPBA gel at lower temperatures also decreased with the amount of the cross-linker. As indicated above, D/D_0 should be within the range between 1.15 to 1.17 for glucose concentrations at from 7.8 mM to 11 mM to obtain the desired property at about room temperature. Hence, for the gels displayed in Figure 2, it was clear that we needed to increase the amount of the cross-linker in the recipe.

1,4-Dioxane (DOx), the polarity of which is significantly lower than that of DMSO, was also used as a solvent. However, the gel obtained by DOx was not sensitive to the concentration of glucose (Figure 3). The hydrogen bond between NIPA and an acidic monomer such as an acrylic acid can be formed during polymerization in a nonpolar solvent.[9] The copolymer gels obtained often have microdomain structures produced by the hydrogen bond: the structures are maintained even after the displacement of the nonpolar solvent to water. It is possible to infer that the boronic acid site in the gel must be inactive to react with glucose, as the acid part participates in forming the microdomain through the hydrogen bond.

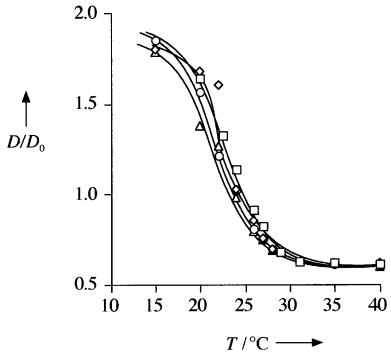


Figure 3. Degree of swelling of poly(NIPA-*co*-AAPBA) gel as a function of temperature in a CHES buffer aqueous solution including different concentration of glucose: (□) [glucose] = 0 mM, (◇) [glucose] = 5 mM, (○) [glucose] = 10 mM, (△) [glucose] = 20 mM. [NIPA] was 1.55 M of the recipe for the gel, while [AAPBA] was 100 mM. [BIS] was 2 mol% of the total monomer concentration. DOx was used for the solvent.

Eventually, we arrived at the following recipe for the pregel solution: [NIPA] = 1485 mM, [AAPBA] = 165 mM, [*N*,*N*′-methylene-bis-acrylamide (BIS: cross-linker)] = 5 mol% of a total monomer concentration ([NIPA] + [AAPBA]), and [*N*,*N*-azobisisobutyronitril (AIBN: initiator)] = 0.4 mol% of [NIPA] + [AAPBA]. DMSO was used for the solvent. The swelling ratios of the gel obtained by the recipe as a function of glucose concentration at 28 °C are shown in Figure 4a. The swelling curve suggests favorable terms for our desired property of exhibiting traffic signal colors. Practically, the tailor-made porous gel displays a yellow color when the glucose level is borderline diabetic (Figure 4b). The color of the gel turns red in the higher glucose concentrations associated with a clear-cut diagnosis of diabetes.

In conclusion, we demonstrated the creation of a colorimetric glucose sensor that can provide the desired monitoring of glucose levels by the naked eye. This new approach to

 © 2003 Wiley-VCH Verlag GmbH & Co. KGaA, Weinheim

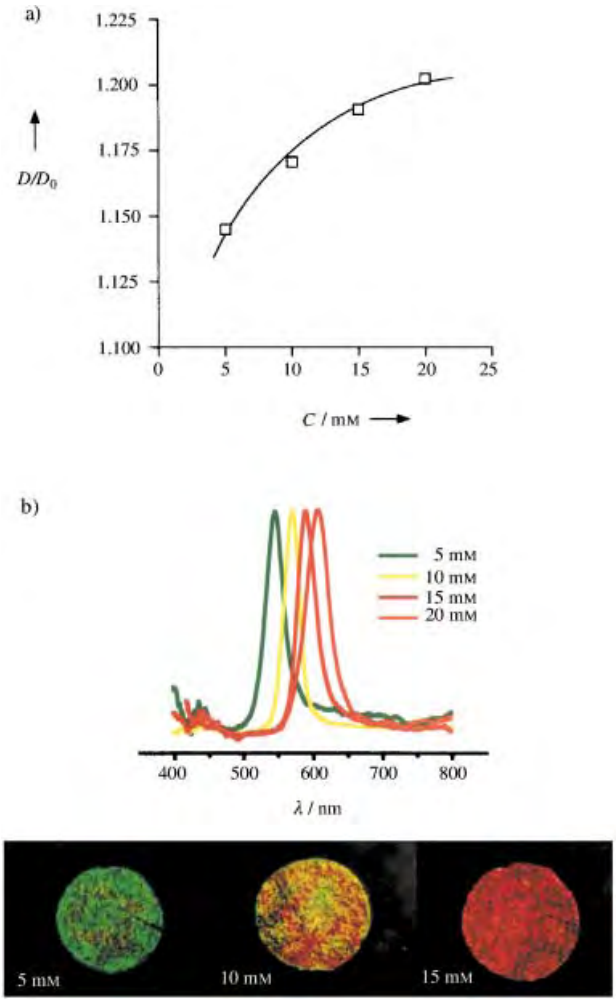


Figure 4. a) Degree of swelling of poly(NIPA-*co*-AAPBA) gel as a function of glucose concentration in a CHES buffer aqueous solution at 28 °C. [NIPA] was 1.485 M in the recipe for the gel, while [AAPBA] was 165 mM. [BIS] was 5 mol % of the total monomer concentration. DMSO was used for the solvent. b) Reflection spectra and photographs of periodically ordered interconnecting porous poly(NIPA-*co*-AAPBA) gel in a CHES buffer aqueous solution including different concentrations of glucose at 28 °C.

preparing colorimetric porous gel can be applied to many sensor systems. Similar colorimetric systems for sensing glucose, composed of a liquid crystal[4d] or a nonclosest packing colloidal crystal immobilized by polymer gels,[4e] were reported. However, our system is easier to fabricate and to control than those systems. Furthermore, the time required for porous gels to reach swelling equilibrium is shorter. These points give our method the advantage for development and use in sensor systems.

Experimental Section

To prepare the porous gels, we used closest-packing colloidal crystals composed of silica sphere particles 220 nm in diameter (Nippon Shokubai). The growth of the crystal was reported.[1b] The resulting crystal structure was confirmed by an atomic force microscope and a scanning electron microscope. Glucose-sensitive gels were prepared by free-radical polymerization as follows. First, certain amounts of NIPA, AAPBA, BIS, and AIBN, were dissolved in degassed and nitrogen-saturated DMSO or DOx to a final volume of 50 mL. The solutions were then infiltrated into the colloidal crystal in a Petri dish, and the polymerizations were conducted at 60 °C for 24 h. Afterward the samples were immersed in a 3wt % HF aqueous solution to remove the SiO_2. Cylindrical gels for swelling measurement were also prepared in glass micropipettes of 100 μm diameter. The resulting gels were washed carefully with distilled water for 1 week. Swelling was measured by monitoring the diameter of the cylindrical gel in a CHES buffer by using an inverted microscope. The reflection spectra of the disk-shaped porous gels (5 mm in diameter) were obtained by an Ocean Optics USB2000 fiber optic spectrometer. The temperature in the measurements was controlled by using a circulating water temperature control system.

Received: April 25, 2003 [Z51746]

Keywords: colloids · colorimetry · glucose sensors · polymers · porous gels

[1] a) Y. Takeoka, M. Watanabe, *Langmuir* **2002**, *18*, 5977; b) Y. Takeoka, M. Watanabe, *Adv. Mater.* **2003**, *15*, 199; c) Y.-J. Lee, P. V. Braun, *Adv. Mater.* **2003**, *15*, 563.
[2] a) B. Zhao, J. S. Moore, *Langmuir* **2001**, *17*, 4758; b) X.-Z. Zhang, Y.-Y. Yang, T.-S. Chung, K.-X. Ma, *Langmuir* **2001**, *17*, 6094.
[3] S. J. Updike, G. P. Hicks, *Nature* **1967**, *214*, 986.
[4] a) K. Kataoka, H. Miyazaki, M. Bunya, T. Okano, Y. Sakurai, *J. Am. Chem. Soc.* **1998**, *120*, 12694; b) H. Otsuka, E. Uchimura, H. Koshino, T. Okano, K. Kataoka, *J. Am. Chem. Soc.* **2003**, *125*, 3493; c) T. D. James, T. Harada, S. Shinkai, *J. Chem. Soc. Chem. Commun.* **1993**, 857; d) K. R. A. Samankumara Sandanayake, S. Shinkai, *J. Chem. Soc. Chem. Commun.* **1994**, 1083; e) S. A. Asher, V. L. Alexeev, A. V. Goponenko, A. C. Sharma, I. K. Lednev, C. S. Wilcox, D. N. Finegold, *J. Am. Chem. Soc.* **2003**, *125*, 3322.
[5] a) T. Tanaka, L. O. Hocker, G. B. Benedek, *J. Chem. Phys.* **1973**, *59*, 5151; b) T. Tanaka, D. J. Fillmore, *J. Chem. Phys.* **1979**, *70*, 1214; c) Y. Kaneko, S. Nakamura, K. Sakai, T. Aoyagi, A. Kikuchi, Y. Sakurai, T. Okano, *Macromolecules* **1998**, *31*, 6099.
[6] a) S. H. Park, Y. Xia, *Langmuir* **1999**, *15*, 266; b) Y. Xia, B. Gates, Y. Yin, U. Lu, *Adv. Mater.* **2000**, *12*, 693.
[7] a) P. J. Flory, *Principle of Polymer Chemistry*, Cornell University Press, Ithaca, New York, **1953**; b) T. Tanaka, *Sci. Am.* **1981**, *244*, 124; c) T. Tanaka, *Phys. Rev. Lett.* **1978**, *40*, 820; d) S. Hirotsu, Y. Hirokawa, T. Tanaka, *J. Chem. Phys.* **1987**, *87*, 1392.
[8] a) L. Bromberg, A. Y. Grosberg, E. S. Matsuo, Y. Suzuki, T. Tanaka, *J. Chem. Phys.* **1997**, *106*, 2906; b) J. P. Baker, L. H. Hong, H. W. Blanch, J. M. Prausnitz, *Macromolecules* **1994**, *27*, 1446; c) A. Y. Grosberg, A. R. Khokhlov, *Statistical Physics of Macromolecules*, AIP Press, New York, **1994**.
[9] a) G. Vlatakis, L. I. Anderson, R. Muller, K. Mosbach, *Nature* **1993**, *361*, 645; b) G. Wulff, *Angew. Chem.* **1995**, *107*, 1958; *Angew. Chem. Int. Ed. Engl.* **1995**, *34*, 1812.

 © 2003 Wiley-VCH Verlag GmbH & Co. KGaA, Weinheim

1D Mesostructured Silica Materials

Template Synthesis of Uniform 1D Mesostructured Silica Materials and Their Arrays in Anodic Alumina Membranes**

Zhenglong Yang, Zhongwei Niu, Xinyu Cao, Zhenzhong Yang, Yunfeng Lu,* Zhibing Hu, and Charles C. Han*

Mesostructured materials are useful in many fields such as in catalysis, separation, sensors, and optical materials. Since the pioneering work by Mobil scientists,[1] template synthesis has been extensively used to prepare mesostructured materials from several to tens of nanometers long.[2] Hereafter the mesostructured materials have been processed into various macroscopic morphologies such as spheres[3,4] and thin films.[5,6]

Besides, 1D mesostructured materials are interesting because of their hierarchically organized structure and potential applications such as waveguides and laser materials. Mesostructured silica fibers have been grown in a two-phase system.[7,8] They can also be prepared by spinning.[9] Mesostructured silica tubes have been obtained at an aqueous–oil (or air) interface.[8d,e,10] Recently, "tubules-within-a-tubule" hierarchical silica tubes were prepared by acidification induced membrane curvature.[11] However, if the acidification rate is fast, microparticles are unavoidably formed. It remains a challenge to control the diameter and aspect ratio of 1D mesostructured materials.

Well-distributed tubular porous media such as porous anodic alumina membranes have been extensively used as templates to prepare uniform 1D materials with controlled diameter and aspect ratio.[12] Recent work has shown the method's simplicity in preparing polymer nanotubes from polymer melts or solutions by a preferential wetting mechanism.[13] It is important to render the 1D materials a hierarchical structure.

Herein we report the preparation of 1D hierarchically mesostructured silica materials and their arrays in porous anodic alumina membranes. Silica nanotubes and nanofibers can be obtained by varying the pore-wall wettability. Both the interior cavity of the tubes and the mesopores can be used as mesocontainers to incorporate active components forming 1D nanocomposites.

The alumina membrane used became transparent after being immersed in the sol for 5 min, which means the pores were completely filled. After the sol–gel process induced by solvent evaporation, 1D mesostructured silica materials formed in the pores and arranged in an ordered array. When the alumina membranes without modification were used, silica preferentially coated the pore wall resulting in the formation of nanotubes. After the removal of the surfactant by calcination and the alumina with hydrochloric acid, long uniform silica nanotubes and their ordered arrays were obtained (Figure 1a and b). The interior cavity is clearly

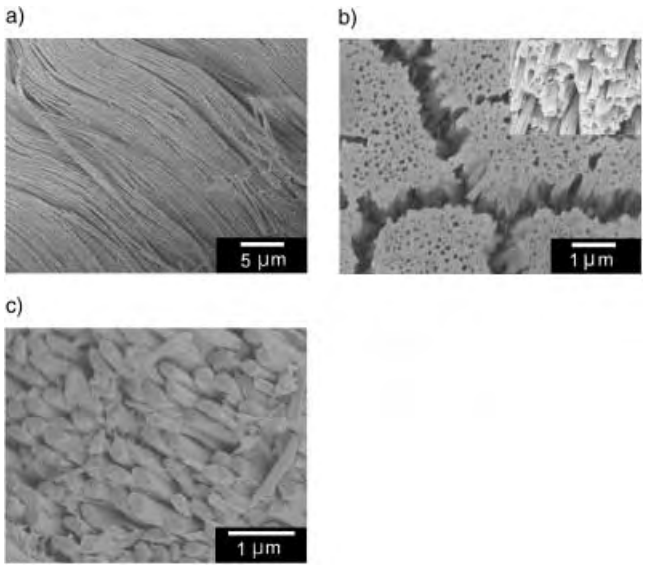


Figure 1. Scanning electron micrographs of 1D mesostructured silica materials and their arrays after being calcined at 450 °C for 3 h. a) Side and b) top views of the mesostructured silica tubular arrays prepared in the porous alumina membrane. c) Top view of the mesostructured silica fibril arrays prepared in the hydrophobically modified porous alumina membrane.

discerned in the broken nanotubes (inset Figure 1b). The sheath thickness is 50 nm, and the cavity diameter is 150 nm. The sheath became thinner by lowering the sol concentration. The as-prepared silica before calcination is also tubular, thus confirming that the interior cavity does not originate from contraction during calcination. The sheath thickness was less influenced by prolonging the immersion time, which is in contrast to that previously reported.[12] It is time consuming to prepare silica fibers by using the unmodified alumina

[*] Prof. Dr. Z. Yang, Z. Yang, Z. Niu, Dr. X. Cao, Prof. Dr. C. C. Han
State Key Laboratory of Polymer Physics and Chemistry
Joint Laboratory of Polymer Science and Materials
Institute of Chemistry
Chinese Academy of Sciences
Beijing 100080 (China)
Fax: (+86) 10-6255-9373
E-mail: yangzz@iccas.ac.cn
Prof. Dr. Y. Lu
Department of Chemical Engineering
Tulane University
New Orleans, LA 70118-5674 (USA)
Fax: (+1) 504-865-6744
E-mail: ylu@tulane.edu
Prof. Dr. Z. Hu
Departments of Physics
Chemistry and Materials Science
University of North Texas
Denton, TX 76203 (USA)

[**] This work was supported by the National Natural Science Foundation of China (Grant No. 90206025 and 20128004) and 973 Project (G1999022500). We thank Prof. Jiayong Yu for the fruitful discussion about the mesostructured silica materials internal morphology.

Supporting information for this article is available on the WWW under http://www.angewandte.org or from the author.

 DOI: 10.1002/anie.200250808 © 2003 Wiley-VCH Verlag GmbH & Co. KGaA, Weinheim

membrane because the membrane has to be immersed in the sol and undergo the whole bulk sol–gel process for a few days. As an alternative, we have developed a new method to prepare solid mesostructured-silica nanofibers and their arrays by exposing the sol-filled hydrophobically modified alumina membrane[14] to air. The diameter of the resulting nanofiber is about 250 nm (Figure 1c). The process time is substantially reduced from days to hours.

The ordered arrays were easily broken into 1D individuals by ultrasonication. As shown in Figure 2a, uniform mesopores of about 12 nm in diameter are hexagonally arranged over the whole nanotube sheath. The pore size decreases to 8–9 nm in diameter after calcination at high temperature above 600 °C. The ordered structure is preserved even at 900 °C. For the nanofibers, the center area looks dark with the ordered porous structure discernable at the edge (Figure 2b) with the diameters of the pores being about 7 nm. The *d* spacings of the mesostructures in the silica tubes and fibers (see Supporting Information) are 12.3 nm and 9.8 nm respectively, which are consistent with TEM observations. The difference in the sizes of the pores found in the tubes and in the fibers is likely to be related to the pore-wall wettability and the sol–gel starting sites. Hexagonally ordered pores can also be found in the whole longitudinal ultra-microtomed sections of the tubes and fibers (see Supporting Information). Circular structures are found in the ultra-microtomed cross sections (Figure 2c, d), which is similar to the mesostructured fibers reported.[8b–d] The fingerprint-like structure (Figure 2c) results from the deformation of the concentric circular structure of the nanotubes owing to the stress during microtoming. The nanotubes and nanofibers have high specific surface areas and large pore volumes,[15] thus indicating the mesopores are interconnected. With an increase in surfactant concentration, some morphologies of coexisting pores and stripes, and parallel stripes along the longitudinal tube axis are found (see Supporting Information). If the surfactant concentration is decreased by 20%, the mesopores are disordered.

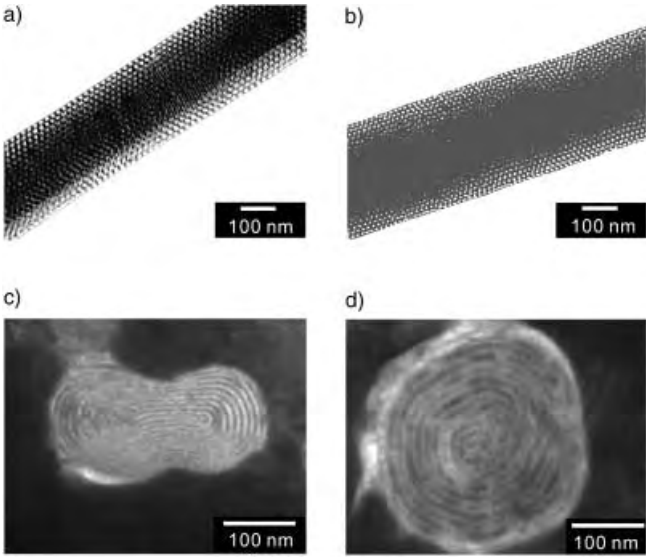


Figure 2. Transmission electron micrographs of the 1D mesostructured silica materials after being calcined at 450 °C for 3 h. a) b) Side views of the mesostructured silica nanotube and nanofiber prepared at Pluronic F-127/TEOS (wt/wt 1:3.2) by using the porous alumina membrane and the hydrophobically modified alumina membrane, respectively. c) d) Ultramicrotomed cross-sections of the same mesostructured silica nanotube (a) and nanofiber (b).

The alumina membrane with the pore wall that has been coated with mesostructured silica tubes becomes a new well-distributed tubular membrane. A variety of 1D materials can be prepared in the new membrane, thus forming 1D mesostructured silica-sheathed core hierarchical composites and their arrays. As an example, mesoporous silica-sheathed titania nanofibers and their arrays were prepared to demonstrate the methodology. The alumina membrane filled with mesostructured silica tubes was immersed in pure tetrabutyltianate (TBT) in a sealed system for 12 h at ambient temperature. After the sol–gel process was complete, the surfactant was removed by calcination at 450 °C and the silica nanotubes (Figure 1b) had become solid nanofibers similar to those of Figure 1c. A TEM image of the product (Figure 3a) shows the black interior. The area selected electron-diffraction pattern indicated that the anatase phase was formed. The composite-fiber edge is smooth and the ordered mesoporous structure preserved. When the composite was calcined at high temperature, for example 600 °C, the titania transformed into coexisting crystals of anatase and rutile, and contracted remarkably. The interior titania nanofibers could slip out of the broken shorter tubes (see Supporting Information), whilst the mesoporous structure of the sheath kept the same appearance as that before the loading of the titania (Figure 2a). This finding confirms that titania predominantly forms in the interior cavity of the silica nanotubes. When a membrane coated with mesoporous silica nanotubes after calcination was used, titania was formed both in the interior cavity and in the mesopores of the silica sheath (Figure 3b). Many 1D nanocomposites based on silica nanotubes and nanofibers may be prepared by incorporating functional components into the mesopores.[16]

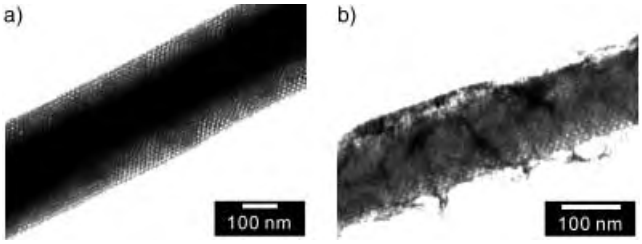


Figure 3. Transmission electron micrographs of the calcined (450 °C) mesostructured silica-sheathed titania composite nanofibers prepared by using the porous alumina membranes coated with different nanotubes. a) With surfactant/silica nanotubes. b) With mesoporous silica nanotubes.

In summary, 1D mesostructured silica materials and their ordered arrays have been prepared in anodic alumina membranes. By adjusting the wettability of the alumina pore wall, nanofibers and nanotubes are prepared in a controlled way. Both mesopores and tubular cavities can be incorporated with functional materials forming 1D hierarchical nanocomposites and their arrays.

 © 2003 Wiley-VCH Verlag GmbH & Co. KGaA, Weinheim

Experimental Section

1D mesostructured silica materials and their arrays: Anodic alumina membranes (Anodisc 47) about 60 μm thick were purchased from Whatman International Ltd. The average pore diameter was 250 nm as specified. They were hydrophobically modified with octachlorosilane by heating to reflux at 60 °C for 3 h under decreased pressure.[14] A block copolymer Pluronic F-127 ($EO_{106}PO_{70}EO_{106}$) was purchased from BASF and used as received. A typical preparation process was given to form a silica–surfactant sol. Pluronic F-127 (1.0 g) was dissolved in ethanol (2.3 g) followed by the addition of nitric acid (0.54 g 0.3 mol L^{-1})to the stirring mixture. Tetraethyl orthosilicate (TEOS; 3.2 g) was added to the mixture, which was stirred for 2 h at room temperature forming the sol. Two typical anodic alumina membranes before and after modification were then immersed in the sol for 12 h to ensure complete infiltration. After the membranes had been taken out from the sol, the residual sol on the membrane surface was completely scratched away. The sol–gel process was undertaken in air for 2 h followed by the aging at 60 °C for 1 h. The silica filled alumina membranes were calcined at 450 °C for 3 h to remove the surfactant. Alumina membranes were dissolved in hydrochloric acid (5 mol L^{-1}) at 60 °C and the residual product was washed with a large amount of water. 1D materials were obtained by ultrasonication.

Mesostructured silica-sheathed titania nanofibers: The alumina membrane filled with mesostructured silica tubes was immersed in pure TBT in a sealed system at ambient temperature for 12 h, the TBT swollen composite was then exposed to a moist atmosphere about 90 % relative humidity at 25 °C for 48 h to allow the TBT sol–gel process. The surfactant was removed by calcination at 450 °C for 3 h.

Characterization: JEOL JSM-6700F field emission scanning electron microscope at the acceleration voltage of 3 kV was used to record the morphology. The mesostructured silica materials were suspended in ethanol after ultrasonication for 15 min. A drop of the suspension was placed on a carbon-coated copper grid for transmission electron microscopy observation using JEM-100CX with EDX apparatus at the acceleration voltage of 75 kV. Ultramicrotomed sections were obtained by cutting the mesostructured samples embedded in copper followed by ion milling. A JEOL JEM-2010 electron microscope at the acceleration voltage of 200 kV was used to observe the section morphology. Rigaku D/max-2500 wide angle goniometer was used to measure the interpore distance of the samples. Nitrogen adsorption isothermal was performed on a Micromeritics OMNISORP 100CX porosimeter.

Received: December 19, 2002
Revised: June 17, 2003 [Z50808]

Keywords: alumina · mesoporous materials · nanostructures · nanotubes · silica

[1] C. T. Kresge, M. E. Leonowicz, W. J. Roth, J. C. Vartuli, J. S. Beck, *Nature* **1992**, *359*, 710 – 712.
[2] D. Zhao, J. Feng, Q. Huo, N. Melosh, G. H. Fredrickson, B. F. Chmelka, G. D. Stucky, *Science* **1998**, *279*, 548 – 552.
[3] a) S. Schacht, Q. Huo, I. G. Voigt-Martin, G. D. Stucky, F. Schüth, *Science* **1996**, *273*, 768 – 771; b) Q. Huo, J. Feng, F. Schüth, G. D. Stucky, *Chem. Mater.* **1997**, *9*, 14 – 17.
[4] Y. Lu, H. Fan, A. Stump, T. L. Ward, T. Rieker, C. J. Brinker, *Nature* **1999**, *398*, 223 – 226.
[5] M. Ogawa, *Chem. Commun.* **1996**, 1149 – 1150.
[6] Y. Lu, R. Ganguli, C. A. Drewien, M. T. Anderson, C. J. Brinker, W. Gong, Y. Guo, H. Soyez, B. Dunn, M. H. Huang, J. I. Zink, *Nature* **1997**, *389*, 364 – 368.
[7] Q. Huo, D. Zhao, J. Feng, K. Weston, S. K. Buratto, G. D. Stucky, S. Schacht, F. Schüth, *Adv. Mater.* **1997**, *9*, 974 – 978.
[8] a) F. Marlow, M. D. McGehee, D. Zhao, B. F. Chmelka, G. D. Stucky, *Adv. Mater.* **1999**, *11*, 632 – 636; b) F. Marlow, B. Splieth-off, B. Tesche, D. Zhao, *Adv. Mater.* **2000**, *12*, 961 – 965; c) F. Marlow, D. Zhao, G. D. Stucky, *Microporous Mesoporous Mater.* **2000**, *39*, 37 – 42; d) F. Marlow, F. Kleitz, *Microporous Mesoporous Mater.* **2001**, *44–45*, 671 – 677; e) F. Kleitz, F. Marlow, G. D. Stucky, F. Schüth, *Chem. Mater.* **2001**, *13*, 3587 – 3595.
[9] a) P. J. Bruinsma, A. Y. Kim, J. Liu, S. Baskaran, *Chem. Mater.* **1997**, *9*, 2507 – 2512; b) P. Yang, D. Zhao, B. F. Chmelka, G. D. Stucky, *Chem. Mater.* **1998**, *10*, 2033 – 2036; c) K. T. Jung, Y. H. Chu, S. Haam, Y. G. Shul, *J. Non-Cryst. Solids* **2002**, *298*, 193 – 201.
[10] a) S. M. Yang, I. Sokolov, N. Coombs, C. T. Kresge, G. A. Ozin, *Adv. Mater.* **1999**, *11*, 1427 – 1431; b) F. Kleitz, U. Wilczok, F. Schüth, F. Marlow, *Phys. Chem. Chem. Phys.* **2001**, *3*, 3486 – 3489.
[11] a) H. P. Lin, C. Y. Mou, *Science* **1996**, *273*, 765 – 768; b) H. P. Lin, S. Cheng, C. Y. Mou, *Microporous Mater.* **1997**, *10*, 111 – 121; c) H. P. Lin, S. Cheng, C. Y. Mou, *Chem. Mater.* **1998**, *10*, 581 – 589.
[12] J. C. Hulteen, C. R. Martin, *J. Mater. Chem.* **1997**, *7*, 1075 – 1087.
[13] M. Steinhart, J. H. Wendorff, A. Greiner, R. B. Wehrspohn, K. Nielsch, J. Schilling, J. Choi, U. Gösele, *Science* **2002**, *296*, 1997 – 1997.
[14] Z. Yang, Z. Niu, *Chem. Commun.* **2002**, 1972 – 1973.
[15] The silica nanotube (Figure 2a) has a BET specific surface area of 420 $m^2 g^{-1}$ and pore volume of 0.59 $cm^3 g^{-1}$. The nanofiber (Figure 2b) has a BET specific surface area of 453 $m^2 g^{-1}$ and pore volume of 0.42 $cm^3 g^{-1}$.
[16] C. J. Brinker, Y. Lu, A. Sellinger, H. Fan, *Adv. Mater.* **1999**, *11*, 579 – 585.

 © 2003 Wiley-VCH Verlag GmbH & Co. KGaA, Weinheim

Material for Lithium-Battery Anodes

Spherical Carbon-Coated Natural Graphite as a Lithium-Ion Battery-Anode Material

Masaki Yoshio, Hongyu Wang, and Kenji Fukuda*

The great demand for high-energy-density rechargeable lithium-ion batteries has spurred extensive research on electrode materials. Natural graphite is an important anode material for Li-ion batteries by virtue of its advantages such as

[*] Prof. Dr. M. Yoshio
Department of Applied Chemistry
Saga University
Honjo 1, Saga 840-8502 (Japan)
Fax: (+81) 952-28-8591
E-mail: yoshio@ccs.ce.saga-u.ac.jp
Dr. H. Wang
Department of Energy and Hydrocarbon Chemistry
Graduate School of Engineering
Kyoto University
Sakyo-ku, Kyoto 606-8501 (Japan)
Dr. K. Fukuda
Research Center
Mitusi Mining Co. Ltd.
1-3 Hibikimachi, Wakamatsu-ku, Kitakyushu 808-0021 (Japan)

 DOI: 10.1002/anie.200351203 © 2003 Wiley-VCH Verlag GmbH & Co. KGaA, Weinheim

a flat and low voltage range, high reversible capacity (372 mA h g^{-1} with the stoichiometry of LiC_6), and low cost.[1–2] However, it has one big disadvantage that may obstruct its further use. That is, its sensitivity to propylene carbonate (PC)-based electrolytes.[3–7] PC is an essential solvent for the electrolytes of lithium-ion batteries for low-temperature use because of its low melting point of about −49 °C. But graphite electrodes are exfoliated in most PC-based electrolytes, and thus give rise to a very drastic decomposition of the electrolyte, which leads to a big irreversible capacity as well as low coulombic efficiency. Moreover, the product of PC decomposition, propylene gas, is potentially explosive. Thus, obtaining a method to effectively and safely use natural graphite in PC-based electrolytes is urgent.

In recent years, we have applied the thermal vapor decomposition (TVD) technique to coat carbon onto natural graphite surfaces to keep the natural graphite surface from direct contact with the electrolyte.[8–10] We found that the carbon coating can suppress the electrolyte decomposition remarkably and the carbon-coated natural graphite shows excellent electrochemical performance in lithium-ion batteries. Although "common" TVD carbon-coated natural graphite can meet most of the practical needs for anode materials in lithium-ion batteries and so has been commercialized, there is still a wide margin for improvement of its comprehensive performance. For example, it was proven that the inertness of the carbon-coated graphite to the electrolytes increases with an increase in the amount of carbon coating. Nevertheless, as the density of the carbon coating (about 1.86 g cm^{-3}) is lower than that of graphite (2.27 g cm^{-3}) the electrode density will decrease with an increase in the amount of carbon coating. The electrode density is also a very important factor for practical lithium-ion batteries, because it determines the energy density of the batteries. Therefore the trade-off between the electrode density and the inertness towards the electrolyte decomposition becomes problematic for carbon-coated natural graphite anode materials.

In this kind of core–shell structured composite, a small amount of carbon coating is favored in terms of a higher density, and the cost of TVD process is reduced if the inertness of the graphite core towards electrolyte decomposition could be guaranteed by itself to some extent. Besides, too much carbon coating will decrease the discharge capacity of the composite electrode material. So in this study we turned our attention to the carbon-coating shell, and initially focused on the design of the natural graphite core.

There are two kinds of planes on graphite crystallite surface, edge and basal. Edge planes show much more activities towards chemical reactions than basal planes. The exfoliation and decomposition of the electrolyte mainly occur on edge planes rather than basal planes. Figure 1 schematically compares the morphology designs of the natural graphite core of our previous work and the present one.

In our previous studies,[8–11] we tore natural graphite flakes into thin planar sheets and then stacked the planar graphite fragments into a shuttle-shaped core by vibration-rod milling before applying the TVD carbon-coating process. In such a case, there are considerable edge planes on the outer surface

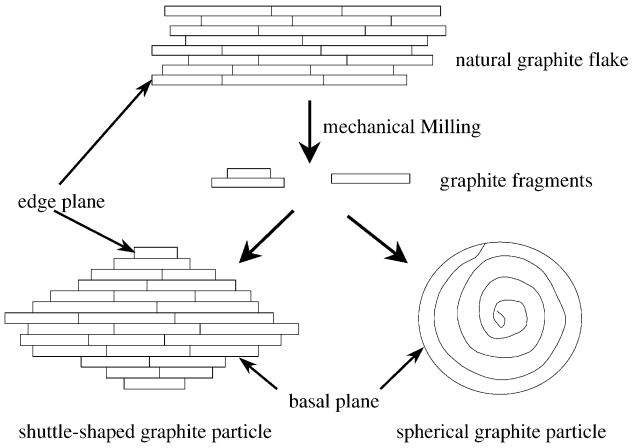


Figure 1. Schematic views for graphite morphology designs.

of the graphite core, and thus greater amounts of carbon coating is needed to cover these edge planes. In contrast, in the work presented herein, we succeeded in folding graphite fragments into a compact ball by applying pressure from both sides of the planar graphite fragments through impact milling. Considerable parts of the edge planes are bound inside the graphite balls and, predominantly, basal planes are exposed outside. Thus, only a very small amount of carbon coating is needed to cover the residue edge planes and the decomposition of the electrolytes is effectively suppressed.

Figure 2 shows the SEM images for the cross-sectional view of a spherical natural-graphite particle before TVD

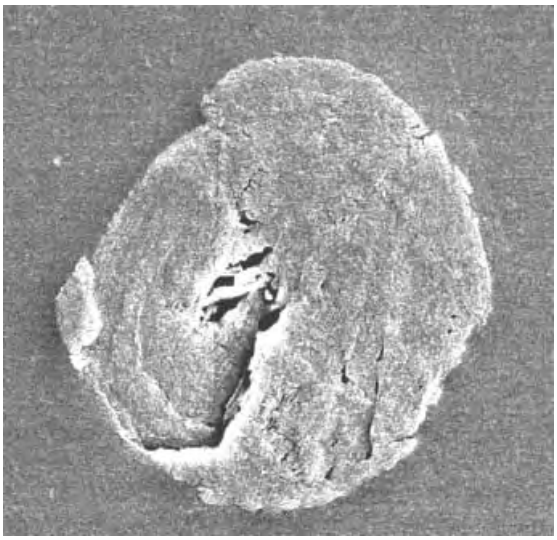


Figure 2. SEM images for the cross-section view of the spherical natural graphite core before TVD-carbon coating.

carbon coating. The concentric alignment of the graphite texture can be clearly observed in this compact natural graphite core, which is in good agreement with the structure model we proposed in Figure 1. The particle size of the

 © 2003 Wiley-VCH Verlag GmbH & Co. KGaA, Weinheim

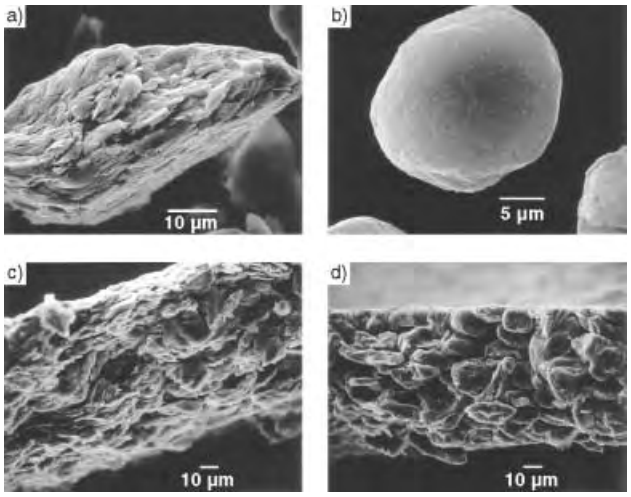


Figure 3. SEM images of TVD-carbon coated natural graphite particles: a) Shuttle-shaped and b) spherical graphite particles; c) shuttle-shaped and d) spherical-shaped graphite particles spread on a current substrate.

spherical natural-graphite core is about 20 μm. Figure 3 shows a comparison of the SEM images of the spherical carbon-coated natural graphite with the shuttlelike carbon-coated natural graphite. After TVD carbon coating, the surface of the spherical carbon-coated natural graphite particle is very smooth with respect to the surface morphology of shuttle-shaped one.

Because of the concentric alignment of planar graphite fragments in the core of spherical carbon-coated natural graphite, it is expected that each particle is isotropic, which is in contrast with the well-known anisotropic graphite flakes received directly from coal mines. Common natural graphite particles that are spread on a current substrate (such as copper foil) are highly orientated, with the basal planes parallel to the current substrate.[12] This kind of morphology may retard the rate capacity significantly, as the current flows in the direction perpendicular to the substrate whereas Li^+ intercalation and de-intercalation occur at edge planes from the directions parallel with the substrate. Therefore, the spherical carbon-coated natural graphite is more favorable than anisotropic graphite flakes in terms of the rate capacity.

Figure 4 shows a comparison of the XRD-patterns of the spherical and shuttle-shaped carbon-coated natural-graphite samples. The intensities of their (004) diffraction peaks were deliberately drawn equally. In the case of spherical sample, the diffraction peaks of (100), (101), (102), (103), (104), (110) and (112) can be clearly observed, which verifies the 3D structure. For the shuttle-shaped sample, these peaks are too weak to be labeled, mainly the (002), (004), and (006) peaks arising from the layered structure can be seen. If we take the intensity ratio of (002) to (110) as an orientation index, the shuttle-shaped sample has the value of 344.9 while the spherical sample has the value of 81.3. These values mean that graphitic layers in the spherical carbon-coated natural graphite are much less orientated than those in the shuttle-shaped carbon-coated natural graphite. Thus the rate capacity is likely to be increased in the former.

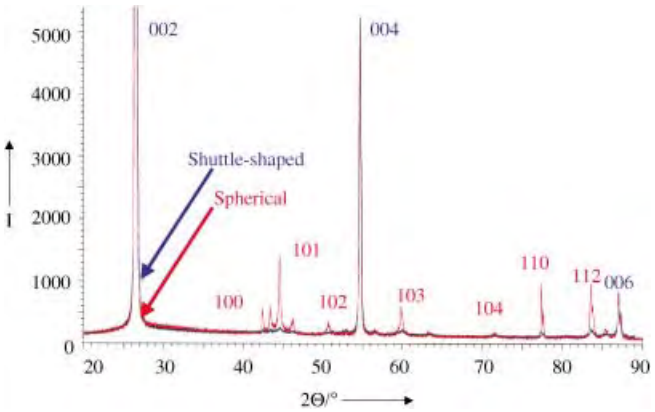


Figure 4. XRD-patterns of the spherical and shuttle-shaped TVD carbon-coated natural graphite samples. I = intensity.

Some preliminary electrochemical studies of spherical natural-graphite samples with different amounts of carbon coating have been carried out in both ethylene carbonate-(EC) and PC-based electrolytes. The reversible (discharge) capacity of the spherical graphite samples are as high as around 360 $mA\,h\,g^{-1}$, which is very near to the theoretical value of 372 $mA\,h\,g^{-1}$. Moreover, most of the coulombic efficiencies are over 90%, so the spherical carbon-coated natural graphite is a very promising material for use as anodes in lithium-ion batteries.

Figure 5 shows the relationship between coulombic efficiency and the amount of carbon coating for both spherical

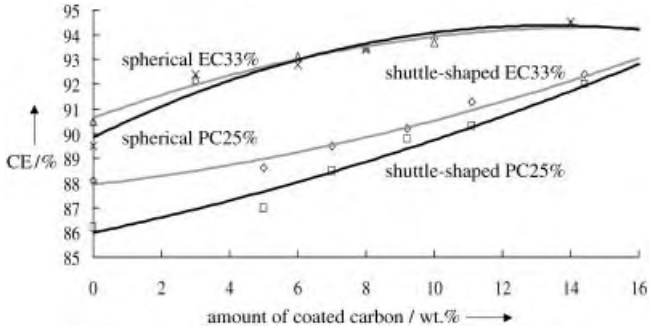


Figure 5. Relationship between coulombic efficiency and carbon-coating amount for both spherical and shuttle-shaped TVD-carbon coated natural graphite samples. Note: EC33% = the electrolyte of 1 M $LiPF_6$ dissolved in EC/DMC (1:2 by volume); PC25% = the electrolyte of 1 M $LiPF_6$ dissolved in PC/DMC (1:3 by volume). CE = coulombic efficiency.

and shuttle-shaped natural graphite samples. For both kinds of samples, the coulombic efficiency increases with the amount of carbon coating, in either EC-based or PC-based electrolytes. In addition, the spherical graphite samples demonstrate much higher coulombic efficiency values than the corresponding shuttle-shaped graphite samples with similar amounts of carbon coating. The curves for spherical graphite level off once the amount of carbon coating rises to about 10 wt.%, which means that this quantity of coating is

 © 2003 Wiley-VCH Verlag GmbH & Co. KGaA, Weinheim

sufficient to cover all the edge planes on the surface of the graphite core. On the other hand, the curves of shuttle-shaped graphite continue to climb even after the amount of carbon coating reaches 15 wt. %, which shows that more TVD carbon coating is needed to cover all the edge planes completely.

In conclusion, the spherical carbon-coated natural graphite is a promising candidate for use as an anode for lithium-ion battery, as it has high coulombic efficiency, high rate capacity, and low cost because of the abundance of natural graphite and low amount of carbon coating required.

Received: February 17, 2003 [Z51203]

Keywords: batteries · carbon · energy conversion · lithium

[1] M. Fujimoto, Y. Shoji, Y. Kida, R. Ohshita, T. Nohma, K. Nishio, *J. Power Sources* **1998**, *72*, 226 – 230.
[2] K. Fukuda, K. Kikuya, K. Isono, M. Yoshio, *J. Power Sources* **1997**, *69*, 165 – 168.
[3] A. N. Dey, B. P. Sullivan, *J. Electrochem. Soc.* **1970**, *117*, 222 – 224.
[4] M. Arakawa, J. Yamaki, *J. Electroanal. Chem.* **1987**, *219*, 273 – 280.
[5] R. Fong, U. von Sacken, J. R. Dahn, *J. Electrochem. Soc.* **1990**, *137*, 2009 – 2013.
[6] D. Aurbach, Y. Ein-Eli, O. Chusid, Y. Carmeli, M. Babai, H. Yamin, *J. Electrochem. Soc.* **1994**, *141*, 603 – 611.
[7] H. Nakamura, H. Komatsu, M. Yoshio, *J. Power Sources* **1996**, *62*, 219 – 222.
[8] M. Yoshio, H. Wang, K. Fukuda, Y. Hara, Y. Adachi, *J. Electrochem. Soc.* **2000**, *147*, 1245 – 1250.
[9] H. Wang, M. Yoshio, *J. Power Sources* **2001**, *93*, 123 – 129.
[10] H. Wang, M. Yoshio, T. Abe, Z. Ogumi, *J. Electrochem. Soc.* **2002**, *149*, A499 – A503.
[11] H. Wang, T. Ikeda, K. Fukuda, M. Yoshio, *J. Power Sources* **1999**, *83*, 141 – 147.
[12] Z. X. Shu, R. S. McMillan, J. J. Murray, *J. Electrochem. Soc.* **1993**, *140*, 922 – 927.

 © 2003 Wiley-VCH Verlag GmbH & Co. KGaA, Weinheim

Carbon Nanotube–Ferrocene Hybrids

Single-Wall Carbon Nanotube–Ferrocene Nanohybrids: Observing Intramolecular Electron Transfer in Functionalized SWNTs**

Dirk M. Guldi, Massimo Marcaccio, Demis Paolucci, Francesco Paolucci,* Nikos Tagmatarchis, Dimitrios Tasis, Ester Vázquez, and Maurizio Prato**

Dedicated to Professor Dan Meyerstein on the occasion of his 65th birthday

Since their discovery, carbon single-wall nanotubes (SWNTs) have drawn considerable attention, not only due to their unique chemical and physical properties, but also because of their promise in the area of materials chemistry.[1] A central aspect of nanotube chemistry, which yet awaits exploration, is their functionality and performance in donor–acceptor ensembles. Our recent success in SWNT functionalization,[2] based on the 1,3-dipolar cycloaddition of azomethine ylides to the double bonds of SWNTs, led us to pursue the covalent linkage of an electron donor, namely ferrocene, to the all-carbon network. Here we report for the first time on intramolecular electron transfer reactions in a novel SWNT-based donor–acceptor ensemble.

The SWNTs were produced by Carbon Nanotechnology, Inc., by the HIPco process (http://cnanotech.com). The functionalized SWNTs were synthesized by following our recently published procedure.[2] Accordingly, *N*-functionalized glycines **1a,b** and paraformaldehyde were heated to

[*] Dr. D. M. Guldi
Radiation Laboratory
University of Notre Dame
Notre Dame, IN 46556 (USA)
Fax: (+1) 574-631-8068
E-mail: guldi.1@nd.edu

Prof. Dr. F. Paolucci, Dr. M. Marcaccio, Dr. D. Paolucci
Dipartimento di Chimica "G. Ciamician"
Università di Bologna
Via Selmi 2, 40126 Bologna (Italy)
Fax: (+39) 051-2099-456
E-mail: paolucci@ciam.unibo.it

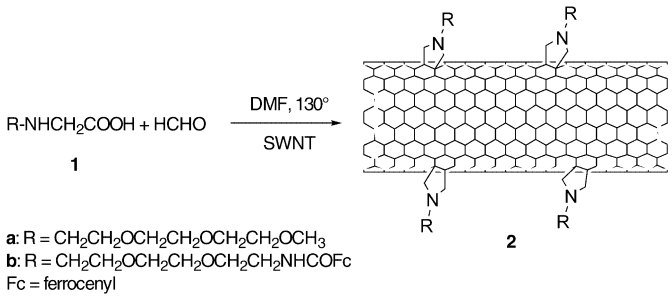
Prof. Dr. M. Prato, Dr. N. Tagmatarchis, Dr. D. Tasis, Dr. E. Vázquez
Dipartimento di Scienze Farmaceutiche
Università di Trieste
Piazzale Europa 1, 34127 Trieste (Italy)
Fax: (+39) 040-52-572
E-mail: prato@units.it

[**] This work was carried out with partial support from the EU (RTN networks "FUNCARS" and "CASSIUSCLAYS"), MIUR (PRIN 2002, nos. 2002032171 and 2002035735), the Universities of Trieste and Bologna, and the Office of Basic Energy Sciences of the U.S. Department of Energy. This is document NDRL-4468 from the Notre Dame Radiation Laboratory. We thank Mr. Claudio Gamboz and Prof. Maria Rosa Soranzo (CSPA, Trieste) for kind help with the TEM experiments. SWNT = single-wall nanotube.

Supporting information for this article is available on the WWW under http://www.angewandte.org or from the author.

 © 2003 Wiley-VCH Verlag GmbH & Co. KGaA, Weinheim DOI: 10.1002/anie.200351289

130 °C in dimethylformamide in which SWNTs were suspended (Scheme 1). After five days, the solvent was evaporated under reduced pressure, and the residue was washed several times with diethyl ether. (See Supporting Information for experimental details.)



Scheme 1. Synthesis of functionalized SWNTs.

Whereas SWNTs **2a** were identical to those reported recently,[2] the newly synthesized SWNTs **2b** were soluble in most organic solvents without sonication. They were characterized by common analytical techniques, such as FTIR, UV/Vis, and ^{1}H NMR spectroscopy, and transmission electron microscopy (TEM). In the ^{1}H NMR spectrum, the pyrrolidine and ethylenedioxy protons ($\delta = 2$–4 ppm) gave rise to rather broad peaks, whereas the ferrocenyl protons ($\delta = 4.7$, 4.3, 4.2 ppm) retained their fine structure. Therefore, since the ferrocenyl groups are rather remote from the SWNT core, it is reasonable to assume that they are less affected by the π-electron cloud of the SWNT. In the FTIR spectrum, the characteristic absorptions of the amide bond of **2b** at 1725 and 1667 cm^{-1} are present.

Differential scanning calorimetry (DSC) showed a loss of 25 wt % when a sample of SWNT **2b** was heated to 350 °C. This is in full agreement with the extent of functionalization we found earlier in **2a**, that is, approximately one ferrocene group per hundred carbon atoms of the SWNT (see Supporting Information for experimental details).[2,3]

The transmission electron micrograph of **2b** (Figure 1) shows functionalized SWNTs in relatively thin bundles. This bundling is a consequence of the way in which the TEM grid is prepared for the experiments. For the deposition of SWNTs we use diethyl ether, a solvent that does not dissolve **2a** and **2b** well and thus keeps the SWNT in bundles, which are easier to identify under the microscope.

The UV/Vis spectrum of **2b** in dichloromethane showed a broad band around 250 nm, which monotonically decreases in intensity with increasing wavelength, and shoulders at 326 and 431 nm. The observed absorbance is linearly dependent on the concentration of the measured sample, that is, no aggregation of the organic functionalized nanotubes takes place. Since the absorption cross section of ferrocene in the visible region is much smaller than that of the SWNTs, the absorption spectra of **2a** and **2b** are virtually identical. However, the most important characteristic of functionalized SWNT **2a,b** is the absence of appreciable near-IR (NIR) band-gap transitions (van Hove singularities), which is a clear indication of functionalization.[2,3]

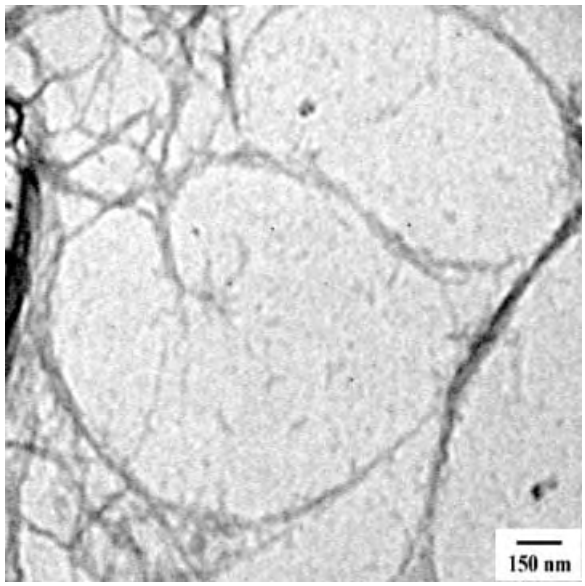


Figure 1. TEM image of SWNTs **2b**.

The cyclic voltammetric (CV) curve of **2b** (see Supporting Information) shows a reversible oxidation peak with $E_{1/2} = +0.53$ V, which results from diffusion-controlled Fc→Fc$^{\bullet+}$ oxidation. No discrete redox steps, associated with a single-electron charge transfer in SWNT, were evident in CV or differential-pulse voltammetric experiments. The CV curve was instead characterized by a continuous increase in current with potential, indicative of multiple-electron charge transfers, similar to those reported in recent work.[4] The onset of reduction of the functionalized SWNTs is at around −0.5 V. Thus, the lowest energy level of (SWNT)$^{\bullet-}$–(Fc)$^{\bullet+}$ is expected to lie around 1.0 eV. Owing to the low-lying (SWNT)$^{\bullet-}$–(Fc)$^{\bullet+}$ state, **2b** can be considered a promising material for photo-induced electron transfer.

For electron-transfer interactions in photoexcited SWNTs, changes in fluorescence[5] and transient absorption served as sensitive and meaningful probes. As mentioned above, the weak absorption of the ferrocene units led us to focus primarily on the deactivation of SWNTs (**2a**,**b**) excited with light of different wavelengths.[6]

For the SWNT band gap fluorescence in the range 800–2000 nm, some interesting observations were made. The room-temperature fluorescence of SWNT–TEG (**2a**) in dichloromethane with excitation at 355 nm is depicted in Figure 2. Several transitions are discernable, some in the form of well-resolved strong bands, while others appear as bands with lower oscillator strength and/or shoulders. Light scattering, as a possible origin of the NIR transitions, was ruled out by probing various excitation wavelengths (i.e., 300–550 nm). Overall, the NIR transitions lack the remarkable fine structure reported recently for individual, isolated nanotubes of different diameters.[7] It is possible that the extensive functionalization obtained in our case strongly affects the properties of the excited state and the band-gap fluorescence of the SWNTs, with concomitant loss of fine structure in the absorption spectrum.[2,3,8]

 © 2003 Wiley-VCH Verlag GmbH & Co. KGaA, Weinheim

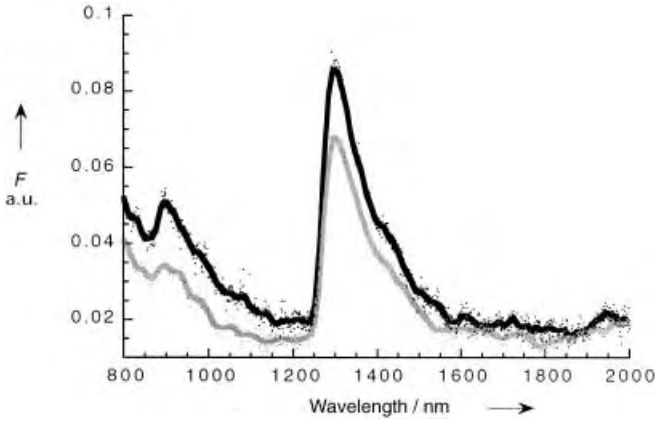


Figure 2. Fluorescence spectra of SWNT–TEG (**2a**; black) and SWNT–Fc (**2b**; gray) in deoxygenated dichloromethane following excitation at 355 nm. The optical density at the excitation wavelength ($OD_{355\ nm} = 0.5$) was matched to obtain comparable fluorescence spectra.

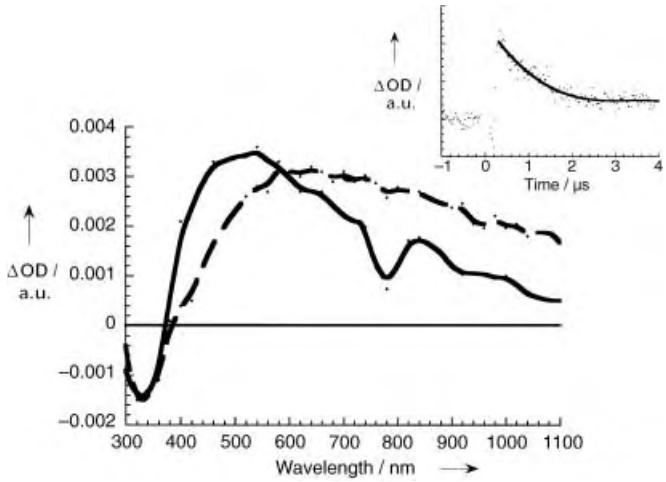


Figure 3. Transient absorption spectrum (UV/Vis/NIR part) of SWNT–TEG (**2a**; dashed spectrum) and SWNT–Fc (**2b**; solid spectrum) in deoxygenated dichloromethane, recorded 50 ns after a 355 nm laser pulse (8 ns), which shows the characteristic features of photoexcited SWNTs with $\lambda_{max} \approx 650$ nm and a $(SWNT)^{\bullet-}$ fingerprint with $\lambda_{max} \approx 500$ nm. The inset shows the decay of $(SWNT)^{\bullet-}$–$(Fc)^{\bullet+}$ at 450 nm.

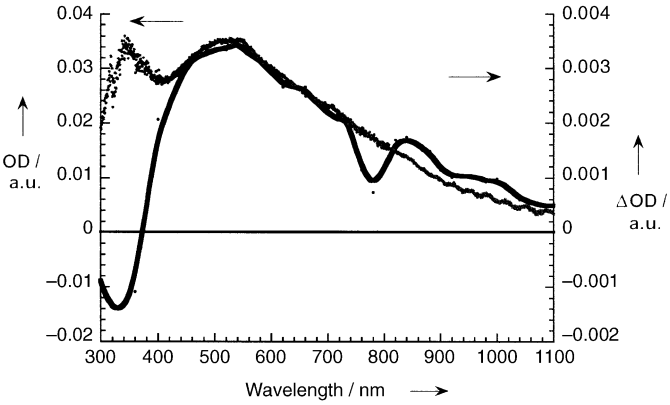


Figure 4. Absorption spectrum recorded after bulk electrolysis at −1.8 V of SWNT–Fc (**2b**), overlaid with the transient absorption spectrum following photoexcitation of **2b** (see also Figure 3). Experimental conditions: Bu_4NPF_6 (0.05 M), saturated THF solution, $T = -32\,^{\circ}C$, working electrode: Pt, quartz OTTLE cell with a 0.03 cm path length.

The fluorescence in SWNT–Fc (**2b**), in a sample that displays matching absorbances at the 350 nm excitation wavelength to **2a**, is quenched relative to that in **2a**. While the high-energy bands (i.e., < 1000 nm) give rise to about 50% quenching, the quenching of the corresponding low-energy bands (> 1300 nm) is more moderate, with an efficiency of only about 25%. The different excited-state energies are primarily responsible for this trend, since the driving force for an intramolecular electron transfer ($-\Delta G_{ET}$) is markedly reduced in the lower energy region.[9]

To gather evidence for possible quenching of electron transfer, as opposed to intrinsically faster deactivation of the excited state in **2b** (0.2 ns),[9] we carried out transient absorption spectroscopy with dichloromethane solutions of **2a** and **2b**. On laser excitation of **2a**, a long-lived transient ($\tau = 20$ μs) was observed, the features of which are displayed in Figure 3. This intermediate decayed quantitatively to the ground state in the absence and presence of molecular oxygen (O_2) without involving the formation of singlet oxygen ($^1O_2$). This finding implies that the energy of the excited state is too low for reaction with molecular oxygen, a hypothesis that was corroborated by the lack of $^1O_2$ phosphorescence.

Figure 3 also displays the transient obtained on irradiation of **2b** in solution. Clearly, the spectrum is different from that of **2a**, especially in the range between 375 and 500 nm, where the transient for **2a** shows minimal absorption changes. This leads us to postulate intramolecular electron transfer to give $(SWNT)^{\bullet-}$–$(Fc)^{\bullet+}$. The analysis of the decay component of $(SWNT)^{\bullet-}$–$(Fc)^{\bullet+}$ throughout the 400–700 nm region yields a lifetime of 1110 ± 100 ns (see inset to Figure 3).

With the aid of bulk electrolysis and pulse radiolysis the formation of the reduced SWNT in $(SWNT)^{\bullet-}$–$(Fc)^{\bullet+}$ was confirmed. In particular, bulk electrolysis at an applied potential of −1.8 V and pulse-radiolytic reduction with hydrated electrons (e^-_{aq}) led to the formation of a species whose UV/Vis/NIR absorption is identical to that reported in Figure 3, and thus confirms the assignment to $(SWNT)^{\bullet-}$. Figure 4 shows the UV/Vis/NIR spectrum recorded after exhaustive bulk electrolysis of **2b** at −1.8 V. The spectrum shows a very broad band in the visible region, centered at 445 nm.[10] The pristine absorption spectrum was recovered upon re-oxidation (at 0 V), showing the reversibility of the reduction process on the timescale of the electrolysis experiment. Similarly, radiolytic reduction with e^-_{aq} led to differential absorption changes which closely resemble those seen in the photolytic and electrolytic experiments with a maximum (450 nm) and a shoulder (550 nm). The spectra of the radiolytically and photolytically generated species are shown in the Supporting Information.

To resolve the dynamics of formation of photoexcited SWNT-TEG and $(SWNT)^{\bullet-}$–$(Fc)^{\bullet+}$, we used picosecond laser spectroscopy. The transient spectra recorded 50 ps after laser excitation of **2a** are compared with those of **2a** and **2b** at a time delay of 4000 ps in the Supporting Information. Impor-

 © 2003 Wiley-VCH Verlag GmbH & Co. KGaA, Weinheim

tantly, the two spectra at 4000 ps are qualitative matches to those recorded with a time delay of 50 ns, as displayed in Figure 3. In **2a**, the species is formed with a time constant of 1.65 ± 0.1 ns, while in **2b** the kinetics give rise to a much faster formation (0.28 ± 0.05 ns), which corresponds to an electron transfer rate of $3.6 \times 10^9\ s^{-1}$.

In summary, we have succeeded for the first time in demonstrating photoinduced electron transfer within a novel SWNT–ferrocene nanohybrid. The photoexcitation of SWNT–Fc with visible light leads to electron transfer that yields a long-lived $SWNT^{\bullet-}$–$Fc^{\bullet+}$ species, the spectral features of which were confirmed by steady-state electrolysis and time-resolved pulse radiolysis. These results, and especially the slow kinetics of charge recombination, appear promising in light of further developments of SWNT–Fc nanohybrids in solar-energy conversion.

Received: February 27, 2003 [Z51289]
Published Online: July 28, 2003

Keywords: carbon · electron transfer · fluorescence · nanotechnology · nanotubes

[1] a) Special issue on carbon nanotubes *Acc. Chem. Res.* **2002**, *35*, 997; b) J. L. Bahr, J. M. Tour, *J. Mater. Chem.* **2002**, *12*, 1952 – 1958; c) A. Hirsch, *Angew. Chem.* **2002**, *114*, 1933 – 1939; *Angew. Chem. Int. Ed.* **2002**, *41*, 1853 – 1859.

[2] a) V. Georgakilas, K. Kordatos, M. Prato, D. M. Guldi, M. Holzinger, A. Hirsch, *J. Am. Chem. Soc.* **2002**, *124*, 760 – 761; b) V. Georgakilas, N. Tagmatarchis, D. Pantarotto, A. Bianco, J.-P. Briand, M. Prato, *Chem. Commun.* **2002**, 3050 – 3051.

[3] V. Georgakilas, D. Voulgaris, E. Vázquez, M. Prato, D. M. Guldi, A. Kukovecz, H. Kuzmany, *J. Am. Chem. Soc.* **2002**, *124*, 14318 – 14319.

[4] L. Kavan, P. Rapta, L. Dunsch, M. J. Bronikowski, P. Willis, R. E. Smalley, *J. Phys. Chem. B* **2001**, *105*, 10764 – 10771.

[5] a) J. E. Riggs, Z. Guo, D. L. Carroll, Y.-P. Sun, *J. Am. Chem. Soc.* **2000**, *122*, 5879 – 5880; b) Y.-P. Sun, B. Zhou, K. Henbest, K. F. Fu, W. J. Huang, Y. Lin, S. Taylor, D. L. Carroll, *Chem. Phys. Lett.* **2002**, *351*, 349 – 353; c) Y. Sun, S. R. Wilson, D. I. Schuster, *J. Am. Chem. Soc.* **2001**, *123*, 5348 – 5349.

[6] The emission in the visible region—see for example earlier work by Sun et al.[5]—exhibited no quenching when comparing **2a** and **2b** with matching absorbances at the excitation wavelength. Similarly, no changes were noted in the underlying radiative lifetime (approximately 3.0 ns).

[7] a) M. J. O'Connell, S. M. Bachilo, C. B. Huffman, V. C. Moore, M. S. Strano, E. H. Haroz, K. L. Rialon, P. J. Boul, W. H. Noon, C. Kittrell, J. P. Ma, R. H. Hauge, R. B. Weisman, R. E. Smalley, *Science* **2002**, *297*, 593 – 596; b) S. M. Bachilo, M. S. Strano, C. Kittrell, R. H. Hauge, R. E. Smalley, R. B. Weisman, *Science*, **2002**, *298*, 2361 – 2366; c) A. Hagen, T. Hertel, *Nano Lett.* **2003**, *3*, 383 – 388.

[8] Excitation of the 890 and 1300 nm fluorescence transitions led to rather poorly resolved spectra with a series of broad maxima. For example, for the emission maximum at 890 nm excitation maxima were found at 440 nm, 600 nm, and 790 nm.

[9] The radiative decay constants were determined for both **2a** and **2b** by time-resolved fluorescence measurements. By following the emission up to 850 nm (i.e., the upper limit of our strobe detection system) we noticed that the lifetime, which in **2a** is about 1.8 ns and agrees well with published data,[6] is substantially shorter in **2b** (major component of 0.2 ns).

[10] Similar features were obtained on electrolysis of **2a** (see Supporting Information). The spectroelectrochemical experiments were carried out in a quartz OTTLE cell with a 0.03 cm path length.

 © 2003 Wiley-VCH Verlag GmbH & Co. KGaA, Weinheim

Single-Molecule Electron Transfer

Reversible Intramolecular Electron Transfer at the Single-Molecule Level**

*Roel Gronheid, Alina Stefan, Mircea Cotlet, Johan Hofkens, Jianqiag Qu, Klaus Müllen, Mark Van der Auweraer, Jan W. Verhoeven, and Frans C. De Schryver**

Investigation of the photophysical and photochemical processes that occur in single molecules by means of fluorescence microscopy has rapidly developed over the last decade.[1,2] We have focused on the photophysics of synthetic multichromophore systems and have shown evidence for intramolecular (excitation) energy migration, that is, energy hopping[3,4] and directional Förster energy transfer.[5] Photoinduced electron transfer is another fundamental physical process, but it is more difficult to monitor by single-molecule spectroscopy. Electron transfer is usually an efficient mechanism for fluorescence quenching which leaves no signal to be detected at the single-molecule level. In some special cases, charge-transfer fluorescence may be observed after photoinduced electron transfer,[6] but its quantum yield is usually quite low and therefore less suited for single-molecule detection.

Despite this difficulty some reports on forward electron transfer in single molecules exist in the literature. Interfacial electron transfer from a single molecule of a cresyl violet dye to the indium–tin oxide surface on which it was physisorbed was shown by Lu and Xie.[7] Weaker fluorescence and a decreased fluorescence lifetime with respect to the same molecule on a glass surface demonstrated the occurrence of electron transfer. In a similar way electron transfer between a guanine base and a dye linked to a DNA molecule could also

[*] Prof. Dr. F. C. De Schryver, R. Gronheid, A. Stefan, M. Cotlet, J. Hofkens, M. Van der Auweraer, J. W. Verhoeven
Department of Chemistry
Katholieke Universiteit Leuven
Celestijnenlaan 200F, 3001 Heverlee (Belgium)
Fax: (+32) 16-327-989
E-mail: frans.deschryver@chem.kuleuven.ac.be
J. Qu, K. Müllen
Max-Planck-Institut für Polymerforschung
Ackermannweg 10, 55128 Mainz (Germany)

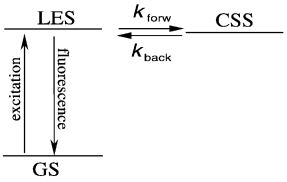
[**] This work was supported by the FWO, the Flemish ministry of education through GOA/1/2001, and the DWTC (Belgium) through IAP-V-03. R.G. thanks KU Leuven for a postdoctoral fellowship. The DFG and the BMBF are thanked for financial support.

 DOI: 10.1002/anie.200351430 © 2003 Wiley-VCH Verlag GmbH & Co. KGaA, Weinheim

be monitored, and conformational changes of DNA molecules were observed.[8–10]

Intramolecular electron transfer in a synthetic system was recently demonstrated by Zang et al.[11] in a compound in which a perylenediimide dye that serves as the electron acceptor upon excitation is connected to an aniline donor. On a sufficiently polar substrate, no fluorescence from single molecules could be observed, but after protonation of the amine by treatment of the sample with hydrogen chloride, the molecules could be visualized. This experiment nicely demonstrated the occurrence of electron transfer, but it still does not allow details of the photophysics to be investigated at the single-molecule level as the molecules are "invisible" under conditions for which electron transfer is possible.

In principle, this limitation can be overcome if the energy levels of the locally excited state (LES) and charge-separated state (CSS) can be tuned such that they are close in energy and, moreover, nonradiative decay from the CSS to the ground state (GS) is slow and inefficient (Scheme 1). Competition of charge transfer with prompt fluorescence will result in a fast component in the fluorescence decay. In the ideal case, nonradiative decay from the CSS to the GS should not compete with back electron transfer from the CSS to the LES. The competition may be mediated by the presence of oxygen.[12] If the CSS decays mainly by back electron transfer to the LES, this will result in delayed fluorescence from the LES, and hence the fluorescence spectrum remains unchanged.



Scheme 1. Jablonski diagram of the CSS near the LES. The corresponding triplets of the CT and the LE states have been omitted for clarity.

We recently reported a system that showed all the above properties in diethyl ether.[12] The dendritic electron donor–acceptor molecule consists of a triphenylamine core as donor and a perylenemonoimide chromophore as acceptor at the rim of the dendrimer. As electron transfer can be observed in this case by monitoring a state with high fluorescence quantum efficiency, we realized that such systems provide ideal subjects for studying electron transfer at the single-molecule level.

The present study involved the electron donor–acceptor dendrimer **1**, which contains a perylenediimide, a very promising chromophore for single-molecule spectroscopy, as "acceptor" core and a rigid polyphenylene skeleton of the second generation that prohibits backfolding and bears 16 triphenylamine units (donors) at the rim. A perylenediimide-core dendrimer of the same generation but without the triphenylamine arms (**2**) is used as model compound. The synthesis and some of the photophysical aspects will be reported separately.[13] From modeling studies of **1**, the distance from the nitrogen donor to the edge of the acceptor in the energy-optimized structure is calculated to be between 18 and 23 Å. However, upon rotation about single bonds "rotational isomers" can be constructed with a donor–acceptor distance as short as 13 Å. Since the positive charge on the amino group will be delocalized over the adjacent phenyl rings,[14] the edge-to-edge distances between donor and acceptor will be even shorter. However, since the degree of delocalization will strongly depend on the conformation, the edge-to-edge distance between donor and acceptor, used to describe distances for electron transfer, is difficult to define. These distances are certainly shorter than the values given above. In nonpolar solvents, both compounds show the same absorption and emission spectra (Figure 1). In toluene there is a small red shift for **1** and **2** in both the absorption and emission spectra with respect to methylcyclohexane (MCH); this indicates better solvation of the LES of the dendrimer.

The fluorescence quantum yields of **1** and **2** in different solvents under deaerated conditions are given in Table 1. The quantum yield of **1** drops drastically with increasing solvent polarity, whereas that of **2** does not. This is attributed to electron transfer from one of the triphenylamine groups at the rim of the dendrimer to the perylenediimide chromophore in the core.

Table 1: Fluorescence quantum yields of **1** and **2** ($\lambda_{exc} = 543$ nm) in degassed methylcyclohexane (MCH), toluene, and ethyl acetate (EtAc). For toluene the quantum yields under aerated conditions are given in parentheses.

Solvent	**1**	**2**
MCH	0.91	0.99
Toluene	0.65 (0.51)	0.95 (0.91)
EtAc	0.036	0.81

The fluorescence quantum yield of **1** in aerated toluene solution is 0.51, whereas that of **2** is barely affected (0.91), in line with previous observations.[12] The fluorescence spectrum of **1** does not change with solvent polarity, that is, all emission originates from the locally excited state and not from a charge transfer state. The effect of oxygen on the quantum yield of **1** in toluene suggests the occurrence of back electron transfer in this solvent. The more efficient quenching in ethyl acetate (EtAc) is due to a combination of faster electron transfer and more efficient back electron transfer to the GS. This was further explored by means of time-correlated single-photon counting (TCSPC).

The results of the TCSPC measurements (all under degassed conditions) are largely in line with the previously studied electron donor–acceptor dendritic structure.[12] The fluorescence decay of model compound **2** measured at the emission maximum is monoexponential in all solvents.[15] Fluorescence lifetimes of 6.4, 5.9, and 6.3 ns were found for MCH, toluene, and EtOAc respectively. The decay of the donor–acceptor compound **1** is also monoexponential in the apolar solvent MCH with a decay time of 6.4 ns (emission detected at $\lambda_{max} = 585$ nm), identical to that of the model compound. In EtOAc, the most polar solvent employed, only

 © 2003 Wiley-VCH Verlag GmbH & Co. KGaA, Weinheim

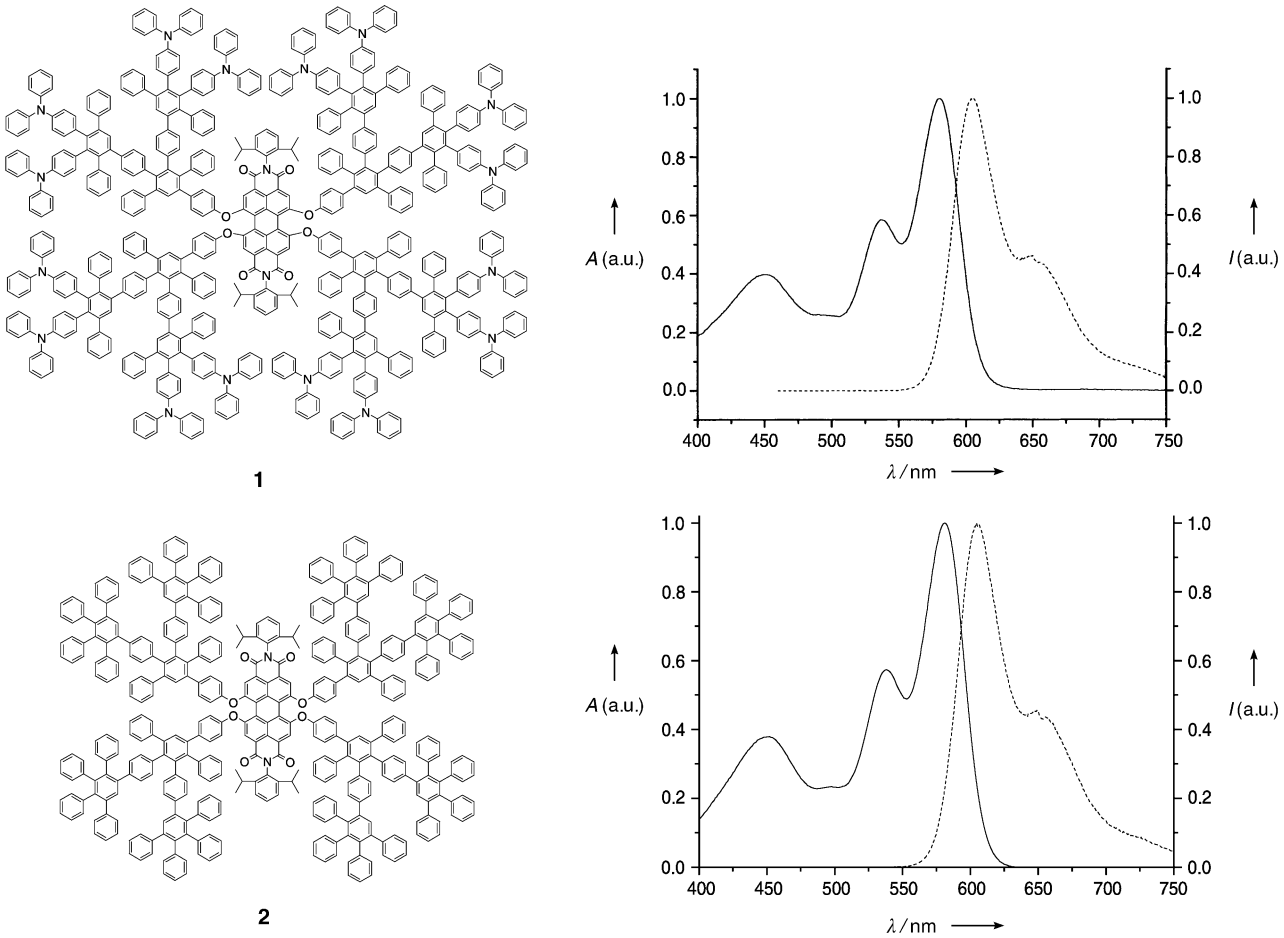


Figure 1. Structures and absorption and emission spectra ($\lambda_{exc} = 540$ nm) in toluene at room temperature of the electron donor–acceptor dendrimer **1** with the chromophore (acceptor) in the center and the donors at the rim, and its model compound **2**, consisting of just the chromophore and the dendritic skeleton.

very fast decay components are observed (triexponential decay, all components < 700 ps). The absence of any long-decay components indicates that back electron transfer to the LES does not occur, probably because it is a strongly endothermic process, and back electron transfer to the GS becomes faster in this solvent. This suggests that the drop in quantum yield in EtOAc is caused by fluorescence quenching by forward electron transfer.

In toluene, of intermediate polarity, the fluorescence decay of **1** can be fitted by four exponentials. Apart from the normal fluorescence decay time of about 6 ns (0.65) of the perylenediimide chromophore, two fast (0.14 (0.15) and 1.6 ns (0.14)) and one slow decay component (ca. 12 ns (0.06)) are observed for 543 nm excitation and 650 nm detection. (The values in parentheses are the respective contributions.)

Considering the complexity of the fluorescence decay dynamics in the case of reversible electron transfer between one donor and one acceptor site,[12] we will not attempt to give a quantitative analysis of these decay times for a mixture of conformational isomers of a compound that contains 16 donor sites and one acceptor site. Most important for the present discussion is the attribution of the component with the short decay times to the forward electron transfer and that with the long decay time (i.e., longer than the fluorescence decay time of **2**) to the back electron transfer. As previously discussed, this permits the direct detection of electron transfer at the single-molecule level.

The detection of single molecules at room temperature for prolonged times (several minutes) requires immobilization of the molecules. This is most conveniently done by embedding them in a polymer matrix. The polymeric equivalents in terms of polarity and polarizability of the solvents used in this study are Zeonex (comparable with MCH), polystyrene (PS, comparable with toluene), and poly(methyl methacrylate), PMMA (comparable with EtOAc).

No significant differences between the fluorescence intensity traces (Figure 2A and B) or the single-molecule emission spectra of **1** and **2** were observed in either Zeonex or PS. For most (~90%) of the traces, one stable level was observed until one-step photobleaching occurred. Both compounds are very robust in both matrices. Photobleaching of the compounds usually took 30 min or more, which corresponds to more than 10^{10} excitation/emission cycles for a single chromophore. However, for efficiency reasons, most measurements were stopped after a fixed measurement time (1–3 min).

As argued above, the single-molecule decay kinetics should give insight into electron transfer at the single-

 © 2003 Wiley-VCH Verlag GmbH & Co. KGaA, Weinheim

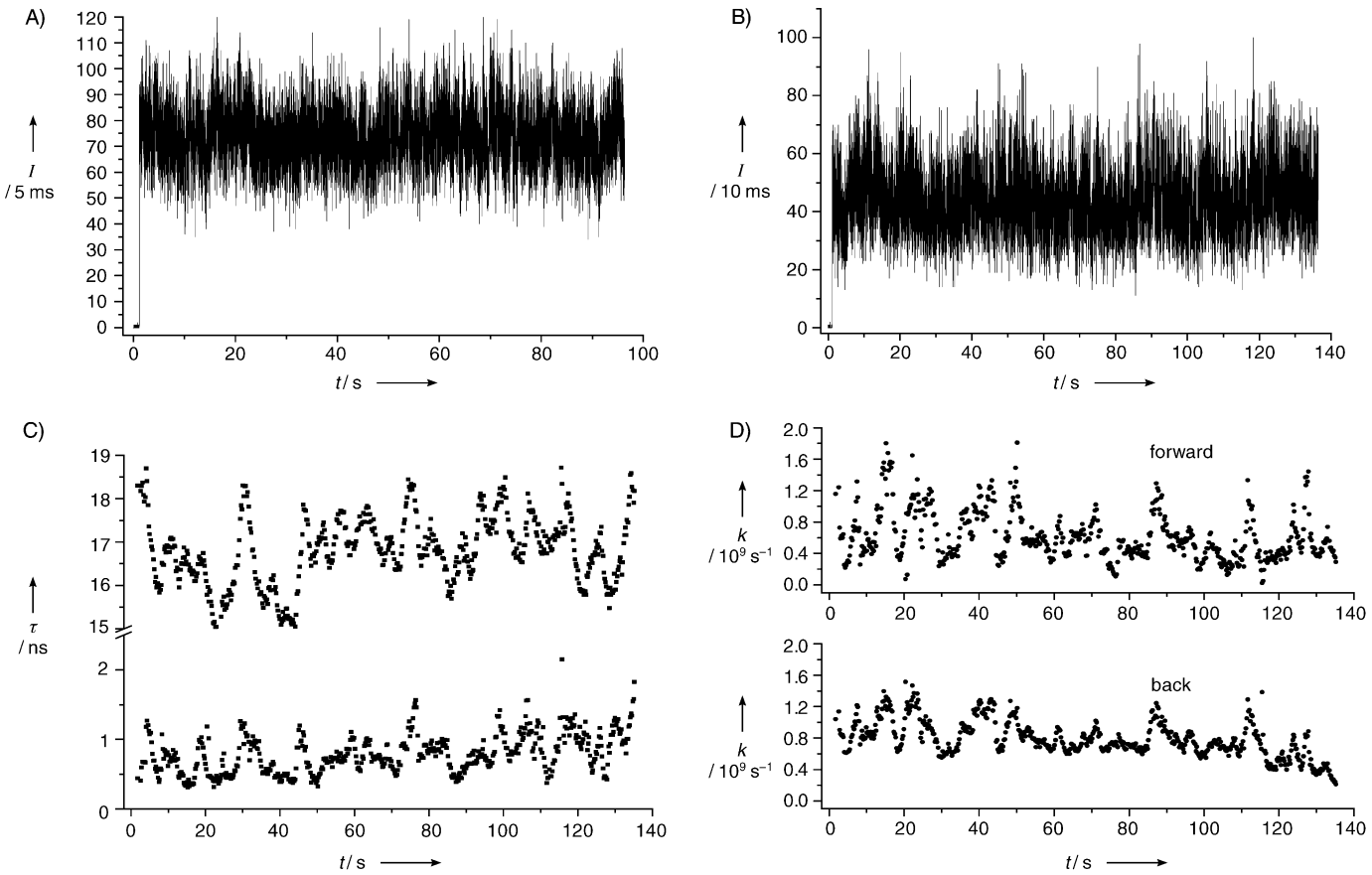


Figure 2. Fluorescence intensity traces for single molecules of **2** (A) and **1** (B) in PS. *I* is the number of counts per time unit. The latter exhibits electron-transfer behavior and fluctuations of the short and long fluorescence decay components (bin size = 10000 photons), which are shown in (C). τ is the decay time. From these data the rate constants for the back and forward electron transfer steps were calculated (D).[12]

molecule level. Although in our experimental setup the rigorous exclusion of oxygen is not possible, the oxygen concentration was lowered by a stream of nitrogen flowing over the sample. For the model compound **2** in Zeonex and in PS, the fluorescence decays monoexponentially, and the decay time is constant over the entire trace for all studied molecules. The histograms of model compound **2** in Zeonex and in PS (Figure 3B and D) give broad (2.5–10 ns) monomodal distributions at about 6 ns, close to the value of the ensemble in solution. This broad distribution of decay times near 6 ns has already been reported for a zeroth-generation dendrimer with a perylenediimide core and phenoxy substituents in the bay area.[16] It was argued that the twisted central chromophore that gives the 6-ns decay time is sensitive to perturbations in the local environment.

The same broad distribution of decay times at about 6 ns is observed for **1** in Zeonex (Figure 3A), but in this case about 33% of the molecules account for a second distribution at about 3 ns. For none of the investigated molecules were jumps between the 3 and 6 ns levels observed under the present conditions. A similar bimodal distribution was previously observed for the zeroth-generation perylenediimide dendrimer in Zeonex matrix[15] and attributed to different conformations of the phenoxy arms and a corresponding planar or twisted conformation of the central chromophore. However, this 3-ns component is absent in the decay histograms of the model compound **2**, so it must be related to the presence of the amine groups at the rim of the dendrimer. Since the TCSPC measurements show that electron transfer does not occur in **1** in the corresponding solvent MCH, it is unlikely that it occurs in Zeonex. Furthermore, a single exponential decay of 3 ns would suggest an irreversible and hence slightly exergonic electron-transfer process, which is not compatible with the low ion-solvating power of Zeonex. We suggest that these short decay times are caused by molecules close to the glass–polymer interface. Owing to the amine groups at the rim of the dendritic structure of **1**, this compound may be more strongly absorbed on the glass surface than **2**. Possibly, electron transfer near the polar glass surface may occur even in Zeonex, and back electron transfer for this subset of the molecules occurs only to the GS. Alternatively, the adsorption of **1** on the glass surface may induce a conformational change of the core, which also changes the decay time.[16] This point is still under investigation and is not the main focus of this paper. For the present investigation it is important that no decay times longer than 10 ns are observed for **1** in Zeonex.

For **1** in PS (Figure 3C) the histograms show the same two distributions of decay times as observed for **1** in Zeonex, one at about 3 ns (ca. 43% of the molecules) and the other at

 © 2003 Wiley-VCH Verlag GmbH & Co. KGaA, Weinheim

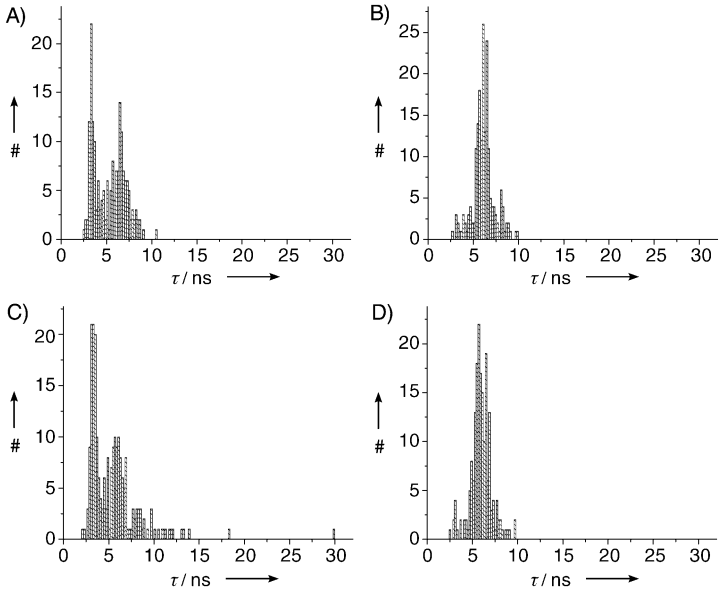


Figure 3. Histograms of the decay times τ of individual molecules of **1** and **2** in Zeonex (A and B, respectively) and in PS (C and D, respectively). For each compound–polymer combination, about 200 molecules were studied. In both matrices, **1** shows a multimodal distribution of decay times, whereas for **2** it is monomodal. The combination of **1** with PS has the only histogram displaying long (>10 ns) decay times indicative of the electron-transfer process. All molecules were analyzed with a monoexponential model, except for some of the molecules of C (especially those with longer decay times), which had to be fitted biexponentially. In this case, only the long decay times are included in the histogram.

about 6 ns. However, for **1** in Zeonex or **2** in PS or Zeonex the longest observed decay times are about 10 ns, whereas for compound **1** in PS decay components of up to 29.9 ns are observed. Whereas for **1** in Zeonex all decays were monoexponential, some of those in PS (ca. 10%) show a biexponential decay, in particular those with long decay times. As argued above, these long decay times and biexponential decay are indicative for the occurrence of back electron transfer.

In general it is expected that all molecules that show reversible electron transfer display a biexponential decay. However, when forward electron transfer is too fast, the fast component can not be resolved owing to the time resolution of our setup (ca. 400 ps).

For those molecules of **1** that show reversible electron transfer in PS, dynamic changes in the decay time were observed. Dynamic fluctuations of the decay times of the short and the long component could be observed. An example for one molecule is given in Figure 2C. The fluctuations are larger than the expected statistical noise (standard deviation $\sigma = \sim 0.06$ ns for the example given).[17] There appears to be a correlation between the changes in the short and long components. During the fluctuations no changes in the fluorescence intensity were observed (Figure 2B).

From the fluctuations in the decay times and their contributions, the fluctuations in the rate constants for forward and back electron transfer can be calculated.[12,18] These values are given in Figure 2D as a function of time for the same molecule. From these values the corresponding free energy change for charge separation ΔG_{CS} is calculated to vary between -250 and $+500$ cal mol^{-1}. The energy separation between the LES and the CSS is thus small; this was mentioned as a prerequisite for the observation of long decay times. Apparently, the charge-separation process is slightly endothermic for **1** in a PS matrix. The fluctuations observed in Figure 2C may have various origins. They may be caused by fluctuations in the polarity or polarizability of the local environment of the donor and/or acceptor. However, as the local environment mainly affects the relative position of the LES and CSS energy levels, they should be anticorrelated, because for a lower CSS, a faster forward and a slower back rate of energy transfer is expected. Figure 2D shows that this is not the case; instead, they are correlated. Therefore, the fluctuations must be caused, at least to some extent, by changes in the dendrimer itself. A possible explanation is a variation in the donor–acceptor orientation or distance. If we take the asymptotic quenching rate k_0^{ET} to be 10^{12} s^{-1} (for ΔG_{CS} close to zero) and the damping factor β as 0.7 Å^{-1},[19] then the edge-to-edge donor–acceptor distance ranges between 9.5 and 11 Å in the case of the rate constants for the molecule of Figure 2D. Given the large influence of β, the importance of these values lies not in the absolute distances, although they fit reasonably well with the shortest distances obtained from modeling, but in that they show that the fluctuations can be explained by very small variations in the donor–acceptor distance. The relatively long timescale (ms to s) on which the fluctuations occur indicates that there are local minima on the energy surface which are probed by the molecule. This situation is reminiscent of large biomolecules, such as enzymes[20] and RNA,[21] which also show such "rugged energy landscapes".

In a more polar polymer matrix than PS, such as PMMA, no fluorescence from single molecules of **1** in samples of the same concentrations as those used for Zeonex and PS could be observed. On the other hand, compound **2** could still be normally imaged. This proves that irreversible electron transfer in a medium of this polarity is too fast to compete with fluorescence.

We have demonstrated for the first time forward and back intramolecular electron transfer in a synthetic system at the single-molecule level by observing long decay times (i.e., longer than those of the model compound) and biexponential fluorescence decay. Dynamics in the forward and back electron-transfer steps were observed and a rationale has been presented. These fluctuations are attributed to changes in the local environment of the dendrimer, as well as to changes in the dendritic structure itself. The fluctuations are reminiscent of those previously observed in biological systems, and thus the polyphenylene denrimers with a triphenylamine–perylenediimide donor–acceptor function are models for studying the details of such single-molecule dynamics.

 © 2003 Wiley-VCH Verlag GmbH & Co. KGaA, Weinheim

Experimental Section

The synthesis of the dendrimers will be published separately.[13] Samples for ensemble measurements in solution were degassed by at least three freeze–pump–thaw cycles. Single-molecule samples were prepared by spin-coating solutions of **1** or **2** (10^{-10} M) and polymer (5 mg mL^{-1}) in chloroform (Aldrich, spectrophotometric grade) on a cover glass at 2000 rpm. This yields 100–150 nm thick polymer films. Before spin-coating, cover glasses were carefully cleaned by sonication in acetone, sodium hydroxide (10%), and MilliQ water and by irradiation with UV light.

Steady-state spectroscopy was performed on a Perkin-Elmer Lambda 40 spectrophotometer and a Spex Fluorolog-3 fluorimeter. Fluorescence quantum yields were determined by using cresyl violet in ethanol as reference compound ($\Phi_F = 0.51$).[22]

The setup for the single-molecule experiments has been described elsewhere.[23] In brief, samples were mounted on an inverted microscope (Olympus IX 70) equipped with a scanning stage (Physics Instruments). Excitation with an 8.13 MHz picosecond laser occurred at 543 nm through an oil-immersion objective (Olympus, 1.4 N.A., ×60). Fluorescence was collected by the same objective, passed through a dichroic mirror, filtered with a notch filter (Kaiser Optics), and detected with an avalanche photodiode (APD, SPCM 15, EG&G). The signal from the APD was registered by a time-correlated single-photon counting card (SPC 630, Picoquant) in the FIFO (first in, first out) mode. From the FIFO data fluorescence intensity traces and decay histograms were built.

In the picosecond time-correlated single-photon counting measurements, histograms were built by collecting the fluorescence in 4096 channels. To accurately determine the long and short components, time increments of 2, 7.5, and 15 ps were used. The resulting histograms were fitted globally by convolution with the instrumental response function (30 ps, full width at half maximum) by using an exponential model.

Received: March 18, 2003 [Z51430]

Keywords: dendrimers · donor–acceptor systems · electron transfer · fluorescence · single-molecule studies

[1] W. E. Moerner, *J. Phys. Chem. B* **2002**, *106*, 910 – 927.
[2] M. F. Garcia-Parajo, J. A. Veerman, R. Bouwhuis, R. Vallee, N. F. Van Hulst, *ChemPhysChem* **2001**, *2*, 347 – 360.
[3] J. Hofkens, M. Maus, T. Gensch, T. Vosch, M. Cotlet, F. Köhn, A. Herrmann, K. Müllen, F. C. De Schryver, *J. Am. Chem. Soc.* **2000**, *122*, 9278 – 9288.
[4] T. Vosch, J. Hofkens, M. Cotlet, F. Köhn, H. Fujiwara, R. Gronheid, K. Van der Biest, T. Weil, A. Herrmann, K. Müllen, S. Mukamel, M. Van der Auweraer, F. C. De Schryver, *Angew. Chem.* **2001**, *113*, 4779 – 44784; *Angew. Chem. Int. Ed.* **2001**, *40*, 4643 – 4648.
[5] R. Gronheid, J. Hofkens, F. Köhn, T. Weil, E. Reuther, K. Müllen, F. C. De Schryver, *J. Am. Chem. Soc.* **2002**, *124*, 2418 – 2419.
[6] M. Goes, M. De Groot, M. Koeberg, J. W. Verhoeven, N. R. Lokan, M. J. Shephard, M. N. Paddon-Row, *J. Phys. Chem. A* **2002**, *106*, 2129 – 2134.
[7] H. P. Lu, X. S. Xie, *J. Phys. Chem. B* **1997**, *101*, 2753 – 2757.
[8] a) L. Edman, Ü. Mets, R. Rigler, *Proc. Natl. Acad. Sci. USA* **1996**, *93*, 6710 – 6715; b) S. Wennmalm, L. Edman, R. Rigler, *Proc. Natl. Acad. Sci. USA* **1997**, *94*, 10641 – 10646.
[9] a) J. P. Knemeyer, N. Marme, M. Sauer, *Anal. Chem.* **2000**, *72*, 3717 – 3724; b) M. Sauer, *Angew. Chem.* **2003**, *115*, 1834 – 1837; *Angew. Chem. Int. Ed.* **2003**, *42*, 1790 – 1793; c) H. Neuweiler, A. Schulz, A. C. Vaiana, J. C. Smith, S. Kaul, J. Wolfrum, M. Sauer, *Angew. Chem.* **2002**, *114*, 4964 – 4968; *Angew. Chem. Int. Ed.* **2002**, *41*, 4769 – 4773.
[10] C. Eggeling, J. R. Fries, L. Brand, R. Gunther, C. A. M. Seidel, *Proc. Natl. Acad. Sci. USA* **1998**, *95*, 1556 – 1561.
[11] L. Zang, R. Liu, M. W. Holman, K. T. Nguyen, D. M. Adams, *J. Am. Chem. Soc.* **2002**, *124*, 10640 – 10641.
[12] M. Lor, J. Thielemans, L. Viaene, M. Cotlet, J. Hofkens, T. Weil, C. Hampel, K. Müllen, J. W. Verhoeven, M. Van der Auweraer, F. C. De Schryver, *J. Am. Chem. Soc.* **2002**, *124*, 9918 – 9925.
[13] J. Qu, A. Stefan, L. Doajun, F. C. De Schryver, K. Müllen, unpublished results..
[14] W. Verbouwe, L. Viaene, M. Van der Auweraer, F. C. De Schryver, H. Masuhara, R. Pansu, J. Faure, *J. Phys. Chem. A* **1997**, *101*, 8157 – 8165.
[15] If globally analyzed over the whole emission spectrum, the decay of **2** shows a rise component with a small contribution at the high-energy end of the emission spectrum. The detailed photophysics of these molecules will be reported elsewhere.
[16] J. Hofkens, T. Vosch, M. Maus, F. Köhn, M. Cotlet, T. Weil, A. Herrmann, K. Müllen, F. C. De Schryver, *Chem. Phys. Lett.* **2001**, *333*, 255 – 263.
[17] M. Maus, M. Cotlet, J. Hofkens, T. Gensch, F. C. De Schryver, J. Schaffer, C. A. M. Seidel, *Anal. Chem.* **2001**, *73*, 2078 – 2086.
[18] For each combination of decay times it is possible to calculate the rate constants of charge separation, back reaction, and recombination to the ground state or to a triplet state and the free-energy change ΔG_{CS} of the charge separation.[12] These parameters can be calculated from the decay times τ_i, τ_j, the ratio of the amplitudes $\frac{a_i}{a_j}$ of the two components of the corresponding biexponential fluorescence decay, $I(t) = a_i \exp(-\lambda_i t_i) + a_j \exp(-\lambda_j t_j)$, and the fluorescence lifetime τ_0 of the unquenched acceptor with the following set of equations ($\lambda_i = 1/\tau_i$, $\lambda_j = 1/\tau_j$, $k_{01} = 1/\tau_0$): $\lambda_i = \{(X+Y) + \sqrt{[X-Y]^2 + 4k_{21}k_{12}}\}/2$ and $\lambda_j = \{(X+Y) - \sqrt{[X-Y]^2 + 4k_{21}k_{12}}\}/2$ with $\frac{a_i}{a_j} = \frac{\lambda_i - Y}{Y - \lambda_j}$; and $X = k_{01} + k_{21}$ and $Y = k_{02} + k_{12}$ (k_{21} is the forward electron transfer rate constant, k_{12} the back electron transfer rate constant, k_{01} the reciprocal lifetime of the LES, and k_{02} the overall rate constant for deactivation of the CSS state to the ground state).
[19] "Electron Transfer—From Isolated Molecules to Biomolecules": J. W. Verhoeven in *Advances in Chemical Physics, Vol. 106, Part 1* (Eds.: J. Jortner, M. Bixon), Wiley, New York, **1999**, pp. 603 – 644.
[20] a) H. P. Lu, L. Xun, X. S. Xie, *Science* **1998**, *282*, 1877 – 1882; b) X. S. Xie, *J. Chem. Phys.* **2002**, *117*, 11024 – 11032.
[21] X. Zhuang, L. E. Bartley, H. P. Babcock, R. Russell, T. Ha, D. Herschlag, S. Chu, *Science* **2000**, *288*, 2048 – 2051.
[22] J. Olmsted, *J. Phys. Chem.* **1979**, *83*, 2581 – 2584.
[23] M. Cotlet, J. Hofkens, M. Maus, F. C. De Schryver, *Fluorescence Spectroscopy, Imaging and Probes, New Tools in Chemical, Physical and Life Sciences* (Eds.: R. Kraayenhof, A. J. W. G. Visser, H. C. Gerritsen), Springer, Heidelberg, **2002**, pp. 131 – 152.

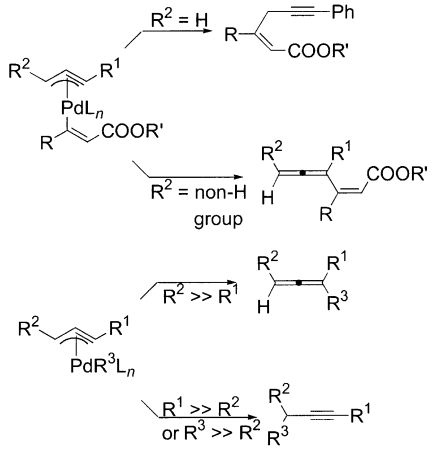
 © 2003 Wiley-VCH Verlag GmbH & Co. KGaA, Weinheim

Controlling Regioselectivity

Regioselectivity Control by a Ligand Switch in the Coupling Reaction Involving Allenic/Propargylic Palladium Species**

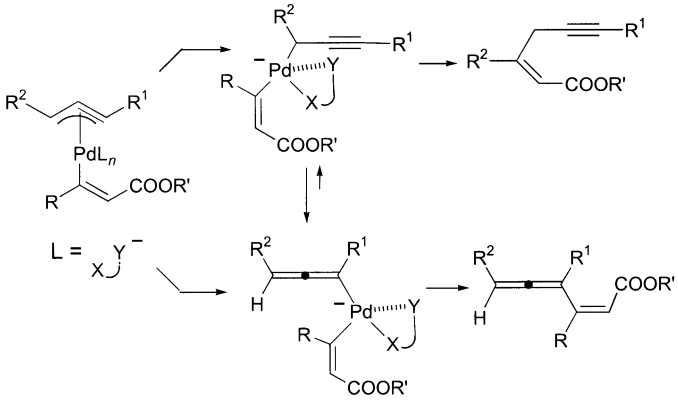
Shengming Ma and Guangwei Wang*

Transition-metal-catalyzed coupling reactions are becoming one of the most important approaches for the construction of C–C single bonds.[1] Usually, there is no regioselectivity problem as it is a "dummy" connection between an organometallic reagent and an organic compound with an appropriate leaving group. However, in the coupling reaction involving allenic and propargylic species,[2–5] although the formation of allenes is observed in most cases, in principle, the reaction could also afford alkynes. Regioselectivity in these coupling reactions depends on many parameters, such as the solvent and the steric/electronic properties of the substituents of both reactants.[6,7] Recently, we observed the highly regioselective formation of alkynes in the coupling reaction of propargylic/allenic zinc complexes with 3-halo-2-alkenoates.[5b] So far we have shown that the regioselectivity can be nicely tuned by the electronic and steric effects of the substrates (Scheme 1).[5c] Herein, we report the first example of the successful catalytic tuning of the regioselectivity[8] in the coupling reaction between propargylic mesylates and alkoxycarbonylethenyl zinc complexes or PhZnBr by the electronic effect of a new catalyst system resulting from 2-diphenylphosphino-2′-hydroxy-1,1′-binaphthalene[9] (**L3**) and $[\{PdCl(\pi\text{-}C_3H_5)\}_2]$.[10]



Scheme 1. Regioselectivity control by the electronic and steric effects.

We wanted to use bidentate ligands with one neutral coordination atom and a negatively charged coordination center, which may play a role for tuning the electronic property of Pd to influence the equilbrium between the propargyl and allenyl palladium as it is generally believed that an sp^2-carbon centered allenylic group is more electron-withdrawing than that of a sp^3-carbon centered propargylic group (Scheme 2).[6a,11]



Scheme 2. Regioselectivity control by the electronic effect of Pd.

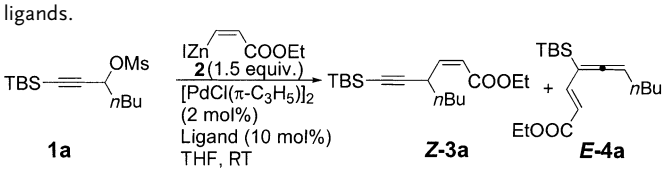
A primary investigation of the coupling reaction between propargylic carbonate, acetate, or mesylate and (*Z*)-(2)-ethoxycarbonylethenyl zinc iodide (**2**)[12] with the catalyst $[Pd(PPh_3)_4]$ in THF showed that the mesylate afforded the enyne **3a** as the major product in 68% yield (Table 1, entry 1) while the reaction of other two substrates did not occur at room temperature. Thus, we used this coupling reaction as the model and 2-diphenylphosphinophenyl carboxylic acid **L1**[13] as the ligand to test the concept shown in Scheme 2. It is noteworthy that although the yield is low (25%), the regioselectivity is reversed (**3a**/**4a** = 12:88; Table 1, entry 2). The reaction with 4-hydroxybutyldiphenylphosphane (**L2**)[14] as the ligand gave a 43% combined yield of products with a similar reversed regioselectivity of 16:84 (**3a**/**4a**; Table 1, entry 3). Although the result is not satisfactory, it proved that our initial assumption shown in Scheme 2 may be feasible. To our delight, when we used 2-diphenylphosphino-2′-hydroxy-1,1′-binaphthalene (**L3**) as the ligand together with $[PdCl(\pi\text{-}C_3H_5)]_2$ as the precatalyst in THF the allenyl product **4a** was formed with a good reversed selectivity(**4a**/**3a** > 97:3) and a moderate yield (49%) (Table 1, entry 5). Furthermore, it is noteworthy that 1) with binaphthol, **L4**, no coupling product was formed while with extra addition of PPh_3 the reaction afforded **3a** in 65% yield, thus indicating the importance of a phosphane ligand (Table 1, entries 7 and 8); 2) with a combination of $[PdCl(\pi\text{-}C_3H_5)]_2$ with PPh_3 and *i*PrOH or phenol (10 mol%) the reaction afforded the enyne product **3a** as the major product, which indicates the importance of the intramolecular interaction of the bidenate ligand with Pd (Table 1, entries 4 and 6); 3) with the methoxy analogue **L5** the reaction proceeded with the steric effect-controlled regioselectivity to give the alkyne as the major product (**3a**/**4a** > 92:8) in 45% combined yield, thus indicating the importance of the anionic oxygen (Table 1, entry 9).

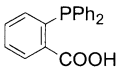
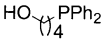
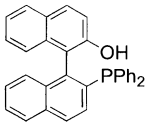
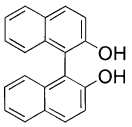
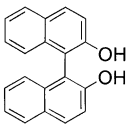
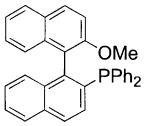
[*] Prof. Dr. S. Ma, G. Wang
State Key Laboratory of Organometallic Chemistry
Shanghai Institute of Organic Chemistry
Chinese Academy of Sciences
354 Fenglin Lu, Shanghai 200032 (P. R. China)
Fax: (+86) 21-6416-7510
E-mail: masm@pub.sioc.ac.cn

[**] Financial supports from National Natural Science Foundation of China, the Major State Basic Research Development Program (Grant No. G2000077500), and Chinese Academy of Sciences are greatly appreciated.

 DOI: 10.1002/anie.200351522 © 2003 Wiley-VCH Verlag GmbH & Co. KGaA, Weinheim

Table 1: Pd-catalyzed coupling reaction of **1a** with **2** with different ligands.



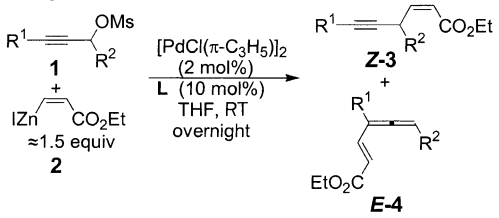
Entry	Ligand	*t* [h]	Yield [%]	**3a/4a**
1	[a]	26	68	>97:3
2	 **L1**	24	25	12:88
3	 **L2**	24	43	16:84
4	PPh_3[b]	24	46	96:4
5	 **L3**	16	49	<3:97
6	PPh_3[c]	9	59	>97:3
7	 **L4**	48	NR	–
8	 **L4**	12	65	>97:3
9	 **L5**	48	43	92:8

[a] $[Pd(PPh_3)_4]$ was used as the catalyst. [b] *i*PrOH (10 mol%) was added. [c] PhOH (10 mol%) was added. [d] PPh_3 (10 mol%) was added.

With different precatalysts such as $Pd_2(dba)_3$ (dba = dibenzylideneacetone) and $PdCl_2$, the same regioselectivity control was observed. When the reaction was preformed in other common solvents, such as CH_2Cl_2, CH_3CN, DMF or 1, 4-dioxane yielded complicated results.

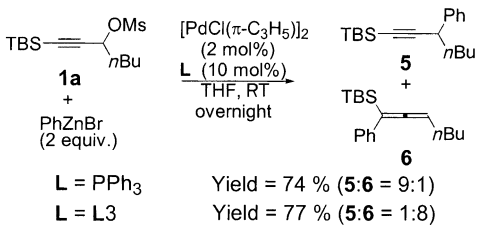
With this strategy, we tried other substrates to study its generality for the catalytic control of regioselectivity in the coupling reaction of propargylic mesylates and organozinc **2**. The results show that in the presence of PPh_3, enyne **3** is the predominant product while when **L3** was applied, allene **4** was formed highly selectively. In this case, R^1 can be the steric demanding TMS, TBS, *t*Bu as well as an ordinary alkyl group

Table 2: Ligand-controlled regioselective coupling of propargylic mesylates and organozinc **2**.



Entry	**1** R^{1}[a]	R^{2}[a]	L	Yield [%]	**3/4**
1	TBS	*n*-C_4 (**1a**)	PPh_3	68 (**3a**)	>97:3
2	TBS	*n*-C_4 (**1a**)	**L3**	49 (**4a**)	3:97
3	TMS	*n*-C_8 (**1b**)	PPh_3	68 (**3b**)	94:6
4	TMS	*n*-C_8 (**1b**)	**L3**	82 (**4b**)	5:95
5	TMS	allyl (**1c**)	PPh_3	44 (**3c**)	95:5
6	TMS	allyl (**1c**)	**L3**	51 (**4c**)	4:96
7	TMS	Bn (**1d**)	PPh_3	42 (**3d**)	>93:7
8	TMS	Bn (**1d**)	**L3**	66 (**4d**)	<3:97
9	[b]	*n*-C_8 (**1e**)	**L3**	68 (**4e**)	<3:97
10	*t*Bu	*n*-C_4 (**1f**)	PPh_3	69 (**3f**+**4f**)	50:50
11	*t*Bu	*n*-C_4 (**1f**)	**L3**	64 (**4f**)	0:100
12	*n*-C_5	H (**1g**)[c]	**L3**	63 (**4g**)	0:100

[a] $C_m = C_mH_{2m+1}$. [b] $R^1 = TBSOCH_2$. [c] Bromide was used instead of mesylate.



Scheme 3. Regioselectivity control in the coupling reaction with PhZnBr.

such as *n*-C_5H_{11} (see Table 2). A similar regioselectivity control was also observed with PhZnBr prepared from the transmetalation of PhMgBr with $ZnBr_2$ in THF (Scheme 3).

In summary, we have shown the first example of ligand control of regioselectivity in the coupling reactions involving allenic/propargylic palladium species leading to allenylsilanes[15] or 1-alkynylsilanes with different ligands. Because of the easy availability of the starting compounds and the synthetic utility of allenes[16] and alkynes,[17] this research will show its potential in organic synthesis and may open up a new area for catalytic regioselectivity control in transition metal-catalyzed coupling reaction. Further studies in this area are being pursued in our laboratory.

Experimental Section

$[PdCl(\pi\text{-}C_3H_5)]_2$ (2% mmol) and ligand (10% mmol) were added to a solution of propargylic mesylate **1b** in THF, and the mixture was stirred at room temperature for 20 min. Then *Z*-(2)-ethoxycarbonylethenyl zinc iodide (1.5 equiv) was added and the reaction mixture was stirred at room temperature overnight. After the reaction was complete, as monitored by TLC, it was quenched with water, and the mixture was extracted with diethyl ether and washed with water and brine. The product solution was dried over $MgSO_4$, the solvent was removed by rotary evaporation, and the product was purified by column chromatography on silica gel (hexane/diethyl ether = 50:1).

 © 2003 Wiley-VCH Verlag GmbH & Co. KGaA, Weinheim

3b: The reaction of **1b** (60 mg, 0.19 mmol), **2** (0.28 mL, 1.0 M in THF, 0.28 mmol), $[PdCl(\pi\text{-}C_3H_5)]_2$ (1.4 mg, 0.0038 mmol), and PPh_3 (4.9 mg, 0.019 mmol) in 5 mL THF afforded 41.4 mg (68%) of **3b**. **3b:** ^{1}H NMR (300 MHz, $CDCl_3$): $\delta = 6.10$ (dd, $J = 10.0$, 11.1 Hz, 1H), 5.75 (dd, $J = 0.88$, 11.4 Hz, 1H), 4.48 ~4.40 (m, 1H), 4.16 (q, $J = 7.1$ Hz, 2H), 1.62–1.25 (m, 17H), 0.87 (t, $J = 6.7$ Hz, 3H), 0.13 ppm (s, 9H); ^{13}C NMR (75.4 MHz, $CDCl_3$): $\delta = 165.82$, 148.73, 119.18, 107.44, 85.60, 60.08, 35.20, 31.85, 31.34, 29.42, 29.21, 29.20, 26.82, 22.66, 14.20, 14.10, 0.11 ppm; MS *m*/*z* 322 (M^+, 1), 73 (100); IR (neat): $\tilde{\nu} = 2927$, 2171, 1721, 1647 cm^{-1}; HRMS calcd for $C_{19}H_{34}SiO_2$: 322.2328, Found: 322.2362.

4b: The reaction of **1b** (73.2 mg, 0.23 mmol), **2** (0.46 mL, 1.0 M in THF, 0.46 mmol), $[PdCl(\pi\text{-}C_3H_5)]_2$ (1.8 mg, 0.0046 mmol), and **L3** (10.4 mg, 0.023 mmol) in 5 mL THF afforded 60.4 mg (82%) of **4b**. **4b:** ^{1}H NMR (300 MHz, $CDCl_3$): $\delta = 7.27$ (dd, $J = 1.2$, 15.9 Hz, 1H), 5.88 (dd, $J = 1.2$, 15.9 Hz, 1H), 5.12 (tt, $J = 1.2$, 6.7 Hz, 1H), 4.19 (q, $J = 7.2$ Hz, 2H), 2.02 (q, $J = 7.0$ Hz, 2H), 1.43–1.26 (m, 15H), 0.87 (t, $J = 7.0$ Hz, 3H), 0.19 ppm (s, 9H); ^{13}C NMR (75.4 MHz, $CDCl_3$) δ 213.79, 166.99, 144.98, 119.15, 97.62, 86.73, 60.15, 31.83, 29.40, 29.35, 29.18, 27.61, 22.63, 14.30, 14.06, −0.97 ppm; MS *m*/*z* 322 (M^+, 4.3), 73 (100); IR (neat): $\tilde{\nu} = 2926$, 1920, 1714, 1618 cm^{-1}; HRMS calcd for $C_{19}H_{34}O_2Si$: 322.2328, Found: 322.2322.

Received: March 31, 2003 [Z51522]

Keywords: alkynes · allenes · C—C coupling · ligand effects · regioselectivity

[1] For a most recent review, see: E. Negishi, F. Liu in *Metal-Catalyzed Cross-Coupling Reactions* (Eds.: P. Stang, F. Diederich), VCH, Weiheim, **1998**, pp. 1–47.
[2] For a review of reactions proceeding via η^3-proparyl intermediates, see: J. Tsuji, T. Mandai, *Angew. Chem.* **1995**, *107*, 2830; *Angew. Chem. Int. Ed. Engl.* **1995**, *34*, 2589.
[3] a) T. Mandai, T. Nakata, H. Murayama, H. Yamaoki, M. Ogawa, M. Kawada, J. Tsuji, *Tetrahedron Lett.* **1990**, *31*, 7179; b) T. Moriya, N. Miyaura, A. Suzuki, *Synlett* **1994**, 149; c) Y. Colas, B. Cazes, J. Core, *Tetrahedron Lett.* **1984**, *25*, 845; d) Y. Tsuji, M. Taniguchi, T. Yasuda, T. Kawamura, Y. Obora, *Org. Lett.* **2000**, *2*, 2635; e) S. Gueugnot, G. Linstrumelle, *Tetrahedron Lett.* **1993**, *34*, 3853.
[4] a) J. A. Marshall, *Chem. Rev.* **2000**, *100*, 3163; b) Y. Tamaru, S. Goto, A. Tanaka, M. Shimizu, M. Kimura, *Angew. Chem.* **1996**, *108*, 962; *Angew. Chem. Int. Ed. Engl.* **1996**, *35*, 878; c) J. A. Marshall, N. D. Adams, *J. Org. Chem.* **1998**, *63*, 3812; d) J. A. Marshall, M. A. Wolf, E. M. Wallace, *J. Org. Chem.* **1997**, *62*, 367; e) J. A. Marshall, N. D. Adams, *J. Org. Chem.* **1999**, *64*, 5201; f) J. A. Marshall, C. M. Grant, *J. Org. Chem.* **1999**, *64*, 696; g) J. A. Marshall, C. M. Grant, *J. Org. Chem.* **1999**, *64*, 8214.
[5] a) S. Ma, A. Zhang, *J. Org. Chem.* **1998**, *63*, 9601; b) S. Ma, A. Zhang, Y. Yu, W. Xia, *J. Org. Chem.* **2000**, *65*, 2287; c) S. Ma, A. Zhang, *J. Org. Chem.* **2002**, *67*, 2287.
[6] a) K. Tsutsumi, S. Ogoshi, K. Kakiuchi, S. Nishiguchi, H. Kurosawa, *Inorg. Chim. Acta* **1999**, *296*, 37; b) K. Tsutsumi, S. Ogoshi, S. Nishiguchi, H. Kurosawa, *J. Am. Chem. Soc.* **1998**, *120*, 1938; c) S. Ogoshi, K. Tsutsumi, M. Ooi, H. Kurosawa, *J. Am. Chem. Soc.* **1995**, *117*, 10415; d) S. Ogoshi, Y. Fukunishi, K. Tsutsumi, H. Kurasawa, *J. Chem. Soc. Chem. Commun.* **1995**, 2485; e) S. Ogoshi, T. Nishida, T. Shinagawa, H. Kurosawa, *J. Am. Chem. Soc.* **2001**, *123*, 7164; f) S. Ogoshi, T. Nishida, K. Tsutsumi, M. Ooi, T. Shinagawa, T. Akasaka, M. Yamane, H. Kurosawa, *J. Am. Chem. Soc.* **2001**, *123*, 3223; g) C. J. Elsevier, H. Kleijn, J. Boersma, P. Vermeer, *Organometallics* **1986**, *5*, 716.
[7] E. Keinan, E. Bosch, *J. Org. Chem.* **1986**, *51*, 4006.
[8] For the steric effect of ligands on the regioselectivity in the hydrogenolysis of secondary propargylic formats or carbonates, see: R. Radinov, S. D. Hutchings *Tetrahedron Lett.* **1999**, *40*, 8955.
[9] For the synthesis of L3, see: Y. Uozumi, A. Tanahashi, S.-Y. Lee, T. Hayashi, *J. Org. Chem.* **1993**, *58*, 1945; R. Kadyrov, J. Heinicke, M. K. Kindermann, D. Heller, C. Fischer, R. Selke, A. K. Fischer, P. G. Jones, *Chem. Ber.* **1997**, *130*, 1663.
[10] Y. Tatsuno, T. Yoshida, S. Otsuka, *Inorg. Synth.* **1990**, *28*, 342.
[11] A. Streitwieser, Jr., C. H. Heathcock, *Introduction to Organic Chemistry*, 3rd ed., Macmillan, New York, **1985**, chap. 11.
[12] M. W. Baize, P. W. Blosser, V. Plantevin, D. G. Schimpff, J. C. Gallucci, A. Wojcicki, *Organometallics* **1996**, *15*, 164; P. Knochel, C. J. Rao, *Tetrahedron* **1993**, *49*, 29.
[13] F. Refosco, F. Tisato, G. Bandoli, E. Deutsch, *J. Chem. Soc. Dalton Trans.* **1993**, 2901.
[14] O. Houille, T. Schmittberger, D. Uguen, *Tetrahedron Lett.* **1996**, *37*, 625.
[15] H. Westmijze, P. Vermeer, *Synthesis* **1979**, 390.
[16] D. A. Evans, Z. K. Sweeney, T. Rovis, J. S. Tedrow, *J. Am. Chem. Soc.* **2001**, *123*, 12095, and references therein.
[17] a) Y. Nishihara, K. Ikegashira, K. Hirabayashi, J.-I. Ando, A. Mori, T. Hiyama, *J. Org. Chem.* **2000**, *65*, 1780; b) H. Ito, A. Arimoto, H.-O. Sensui, A. Hosomi, *Tetrahedron Lett.* **1997**, *38*, 3977; c) J. A. Marshall, H. R. Chobanian, M. M. Yanik, *Org. Lett.* **2001**, *3*, 4107.

 © 2003 Wiley-VCH Verlag GmbH & Co. KGaA, Weinheim

Superhydrophobic Carbon Films

Superhydrophobicity of Nanostructured Carbon Films in a Wide Range of pH Values**

Lin Feng, Zhenglong Yang, Jin Zhai, Yanlin Song, Biqian Liu, Yongmei Ma, Zhenzhong Yang, Lei Jiang,* and Daoben Zhu*

Superhydrophobic surfaces whose water contact angle (CA) is larger than 150° has aroused great interest.[1–4] Over the past 60 years there have been numerous reports concerning the

[*] Prof. L. Jiang, Dr. L. Feng, Dr. J. Zhai, Prof. Y. Song, Dr. B. Liu, Dr. Y. Ma, Prof. D. Zhu
Organic Solid Laboratory
Center for Molecular Sciences
Institute of Chemistry
Chinese Academy of Sciences
Beijing 100080 (P.R. China)
Fax: (+86) 10-8262-7566
E-mail: jianglei@iccas.ac.cn
Prof. Z. Yang, Dr. Z. Yang
State Key Laboratory of Polymer Physics and Chemistry, Joint Laboratory of Polymer Science and Materials
Center for Molecular Sciences
Institute of Chemistry
Chinese Academy of Sciences
Beijing 100080 (P.R. China)
Fax: (+86) 10-6255-9373
E-mail: yangzz@iccas.ac.cn

[**] The authors thank the State Key Project Fundamental Research (G1999064504) and the Special Research Foundation of the National Nature Science Foundation of China (29992530, 20125102, and 90206025) for continuing financial support.

Supporting information for this article is available on the WWW under http://www.angewandte.org or from the author.

 DOI: 10.1002/anie.200351539 © 2003 Wiley-VCH Verlag GmbH & Co. KGaA, Weinheim

study of such surfaces.[5–17] It is concluded that a superhydrophobic surface can be effectively fabricated by combining appropriate surface roughness with materials of low surface energy, and the presence of a compound that contains fluorine is often necessary. Among the reported studies, we have also made some progress. For example, we reported that nanostructured aligned carbon nanotube films with a fluoroalkysilane coating show "superamphiphobic" properties, that is, CAs for both water and oil are larger than 150°.[18] Based on this study, we recently demonstrated the preparation of polymer nanofibers, whose surfaces have superhydrophobic properties with CAs larger than 170° even without any modification, by using materials of low surface energy.[19] A coating consisting of nanofibers exhibits a surface structure that is believed to cause superhydrophobicity. This effect can be observed in nature on the leaves of the lotus.[20] The as-prepared superhydrophobic surfaces have great potential in not only fundamental research but also practical applications. For example, they can be effectively used for textiles, traffic signs, hulls of ships, tubes or pipes, building glass, windshields of cars, satellite antenna, and conductors with a self-cleaning surface.[5,21] However, such surfaces are not available in different pH environments. Although polytetrafluoroethylene (PTFE) films are chemically resistant, they are only reported to be superhydrophobic for pure water.[22] Until now, no superhydrophobic surfaces suitable for all pH environments have been prepared.

Herein we report the formation of nanostructured carbon films through a facile and typical pyrolysis pathway.[23] Nanosturctured polyacrylonitrile (PAN) films prepared according to reported procedures[19a] were used as the precursor. Interestingly, the as-prepared films show superhydrophobic property in the pH range from 1.07 to 13.76. That is, water CAs are larger than 150° for not only pure water but also corrosive liquids, such as acidic and basic solutions. It is believed that the formation of nanostructured graphitelike structures causes this unique property. From the point of practical applications, this kind of surface will be more useful in the fabrication of chemical engineering materials and microfluidic devices.[24–26]

Figure 1 a shows the scanning electron microscopic (SEM) image of the top view of the as-prepared nanostructured carbon films. The average diameter of the carbon fibers and the interfiber distance are about 39 ± 3 nm and 50 ± 4 nm, respectively. Carbon nanofibers that consist of films are perpendicular to the substrate of the anodic aluminum oxide membrane, and the thickness of the films can be controlled in the range from 7 to 15 μm. These nanostructured films are rough enough and are regarded as a composite consisting of fibers and air, the latter is present in the troughs between individual carbon nanofibers. As such a rough structure can induce superhydrophobicity,[4–21] these films are expected to have special wettability properties. Figure 1 b shows the shape of water droplet (about 1.5 mm in diameter, pH 7.08) on the carbon films, the CA here is about $161.2 \pm 2.7°$, namely, the obtained films are superhydrophobic. Figure 1 c and 1 d show the shapes of aqueous solution droplets with pH values of 1.07 and 13.76, respectively, on the nanostructured carbon films. Surprisingly, these two droplets remain spherical with CAs

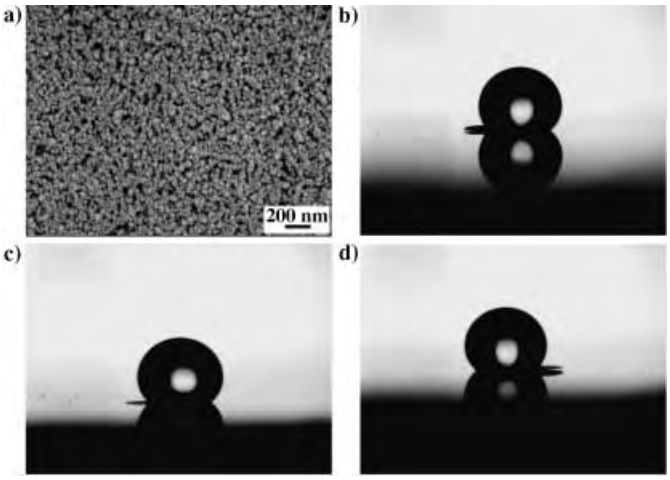


Figure 1. a) SEM image of the top view of the as-prepared nanostructured carbon films; pictures showing the water contact angles of the nanostructured carbon films; the pH values are: b) pH 7.08, c) pH 1.07, and d) pH 13.76.

larger than 150° ($158.9 \pm 2.3°$ and $159.3 \pm 1.7°$, respectively). High CAs for both the acidic and basic droplets on any kind of solid surfaces have never been reported before. It is very important that the superhydrophobic carbon films can be used in all pH environments for corrosive liquids.

To determine the effect of pH values on CAs for the nanostructured carbon films, further studies were developed in detail. Figure 2 shows the relationship between pH values and CAs on the nanostructured carbon films. There is no

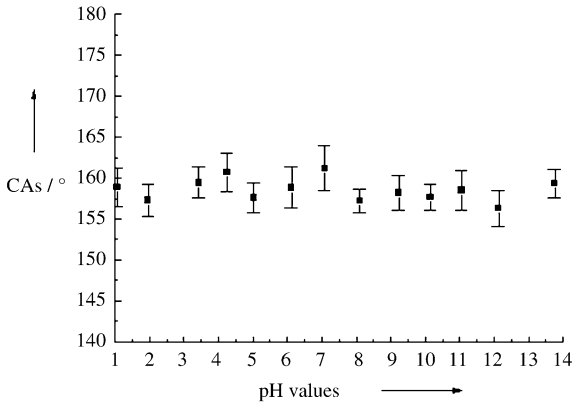


Figure 2. Graph showing the relationship between pH values and contact angles on the nanostructured carbon films.

obvious fluctuation of the CA value within the errors. All CA values are in the range from about 154.1° to 164.2°, with little difference coming from experimental error. This result indicates that pH values of the aqueous solution have little or no effect on CAs for as-synthesized carbon films. It confirms that the nanostructured carbon films are superhydrophobic in the pH range from 1.07 to 13.76.

The formation process of carbon films can be characterized by Fourier transform infrared (FTIR) spectroscopy (Figure 3).[27] The pyrolysis temperature employed in our

 © 2003 Wiley-VCH Verlag GmbH & Co. KGaA, Weinheim

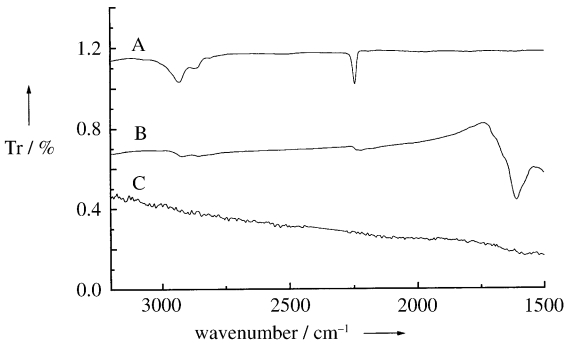


Figure 3. FTIR spectra of the representative samples: A) PAN nanofiber films, B) Cyclized PAN nanofiber films after treatment at 220 °C for 1 h in air, C) Carbon films after carbonization at 900 °C for 1 h under a nitrogen atmosphere. Tr = transmittance

study was 900 °C, which is far below the graphite formation temperature ranging from 1500–2000 °C. Therefore, the carbon materials formed here are in a graphitelike state. X-ray photoelectron spectroscopy (XPS) spectra (Figure 4)

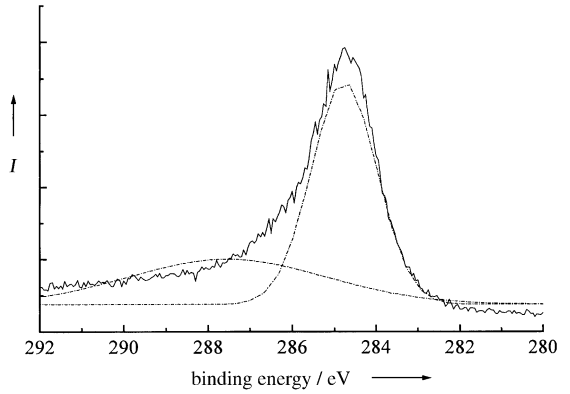


Figure 4. X-ray photoelectron spectra illustrating the C_{1s}-core of nanostructured carbon films. *I* = intensity (arbitrary units); —— real XPS spectra; –•–• fit to a Gauss–Lorenz function.

show a main asymmetric peak centered at 284.6 eV with a long tail extended to the higher energy region, which is characteristic graphite.[28] This peak can originate from both sp^2-hybridized graphitelike carbon atoms and from carbon atoms bonded to hydrogen atoms, and has been explained in terms of many electron interactions of the metallic conduction electrons, induced by low energy electron-hole excitations, which result from the absorption of the X-rays. The other broad peak, shown in Figure 4, which corresponds to a higher binding energy at 287.8 eV, is considered to originate from carbon atoms bonded to one, two, and three oxygen atoms because the electronegative oxygen atoms induce a positive charge on a carbon atom. According to the calculated result from the real XPS spectra, the relative intensity of the peak representing graphite is greater than 91 %, which is close to the ideal for purified multiwall carbon nanotubes with a graphitelike structure.[29] Therefore, we conclude that the as-synthesized carbon films have graphitelike structure.

Graphitelike carbon has intrinsic properties of thermal and chemical resistance, which can be used in strongly acidic or basic liquids. The results of wettability measurement indicate that CAs on the surface of a fresh graphite plane are all in the range of 80–85° for pure water, acidic and basic solutions (see Supporting Information). Nanostructured graphitelike carbon films were reported to be stable in an acidic or basic solution at normal temperature, and oxidized only when subjected to strong oxidation treatment, such as reflux at 140 °C in a mixture of concentrated nitric and sulphuric acid (1:3 in volume ratio).[30] In our study, no changes, including both structure and hydrophobicity, are found when the nanostructured carbon films are dipped into strong alkali and acid for 24 h (See Supporting Information). The contact angles of these films remain larger than 150° after dipping them in alkaline and acidic solutions (within the instrument and measurement error). In contrast, the precursor of PAN nanofiber films is easily eroded, and the nanostructures are destroyed.

In conclusion, nanostructured graphitelike carbon films were prepared through a simple pyrolysis method. The as-prepared films are superhydrophobic for not only pure water but also corrosive liquids, such as acidic and basic solutions. This is the first example of superhydrophobicity over the whole range of pH values without the presence of fluorine-containing compounds, and might open up new perspectives in preparing novel nanoscale interfacial materials.

Experimental Section

The formation processes of nanostructured carbon films included cyclization and carbonization: PAN nanofiber films were first cyclized at 220 °C for 1 h in air, followed by further carbonization at 900 °C for 1 h under a nitrogen atmosphere.[23] PAN nanofibers films prepared according to reference [19a] were used as the precursor to obtaining carbon films.

SEM image was obtained with a JEOL JSM-6700 scanning electron microscopic at 3 kV. CAs were measured on a dataphysics OCA20 contact-angle system at ambient temperature. Water droplets (about 5 μL) with different pH values were dropped carefully onto the nanostructured carbon films. The average CA value was obtained by measuring at five different positions of the same sample. FTIR spectra were performed on a Bruker EQUINOX55 Fourier transform infrared spectrometer. XPS spectra were recorded by using a VG ESCALAB MKII spectrometer with an $Al_{K\alpha}$ monochromatic X-ray source.

Received: March 31, 2003 [Z51539]

Keywords: carbon · hydrophobicity · nanostructures · surface chemistry · wettability

[1] a) L. Jiang, R. Wang, B. Yang, T. J. Li, D. A. Tryk, A. Fujishima, K. Hashimoto, D. B. Zhu, *Pure Appl. Chem.* **2000**, *72*, 73; b) P. Aussillous, D. Quéré, *Nature* **2001**, *411*, 924.
[2] a) R. N. Wenzel, *Ind. Eng. Chem.* **1936**, *28*, 988; b) A. B. D. Cassie, *Discuss. Faraday Soc.* **1948**, *3*, 11.
[3] a) G. Wolansky, A. Marmur, *Langmuir* **1998**, *14*, 5292; b) P. S. Swain, R. Lipowsky, *Langmuir* **1998**, *14*, 6772.
[4] S. Herminghaus, *Europhys. Lett.* **2000**, *52*, 165.
[5] A. Nakajima, K. Hashimoto, T. Watanable, *Monatsh. Chem.* **2001**, *132*, 31.

 © 2003 Wiley-VCH Verlag GmbH & Co. KGaA, Weinheim

[6] S. H. Li, H. J. Li, X. B. Wang, Y. L. Song, Y. Q. Liu, L. Jiang, D. B. Zhu, *J. Phys. Chem. B* **2002**, *106*, 9274.
[7] J. Genzer, K. Efimenko, *Science* **2000**, *290*, 2130.
[8] a) T. Onda, S. Shibuichi, N. Satoh, K. Tsujii, *Langmuir* **1996**, *12*, 2125; b) S. Shibuichi, T. Onda, N. Satoh, K. Tsujii, *J. Phys. Chem.* **1996**, *100*, 19512.
[9] H. Y. Erbil, A. L. Demirel, Y. Avci, O. Mert, *Science* **2003**, *299*, 1377.
[10] D. Öner, T. J. McCarthy, *Langmuir* **2000**, *16*, 7777.
[11] a) Y. Wu, H. Sugimura, Y. Inoue, O. Takai, *Chem. Vap. Deposition* **2002**, *8*, 47; b) A. Hozumi, O. Takai, *Thin Solid Films* **1997**, *303*, 222.
[12] a) K. Tsujii, T. Yamamoto, T. Onda, S. Shibuichi, *Angew. Chem.* **1997**, *109*, 1042; *Angew. Chem. Int. Ed. Engl.* **1997**, *36*, 1011; b) S. Shibuichi, T. Yamamoto, T. Onda, K. Tsujii, *J. Colloid Interface Sci.* **1998**, *208*, 287.
[13] a) A. Nakajima, A. Fujishima, K. Hashimoto, T. Watanabe, *Adv. Mater.* **1999**, *11*, 1365; b) A. Nakajima, K. Abe, K. Hashimoto, T. Watanable, *Thin Solid Films* **2000**, *376*, 140.
[14] a) K. Tadanaga, N. Katata, T. Minami, *J. Am. Ceram. Soc.* **1997**, *80*, 1040; b) K. Tadanaga, N. Katata, T. Minami, *J. Am. Ceram. Soc.* **1997**, *80*, 3213.
[15] J. Bico, C. Marzolin, D. Quéré, *Europhys. Lett.* **1999**, *47*, 220.
[16] H. Tada, H. Nagayama, *Langmuir* **1995**, *11*, 136.
[17] Z. Z. Gu, H. Uetsuka, K. Takahashi, R. Nakajima, H. Onishi, A. Fujishima, O. Sato, *Angew. Chem.* **2003**, *115*, 922; *Angew. Chem. Int. Ed.* **2003**, *42*, 894.
[18] H. J. Li, X. B. Wang, Y. L. Song, Y. Q. Liu, Q. S. Li, L. Jiang, D. B. Zhu, *Angew. Chem.* **2001**, *113*, 1793; *Angew. Chem. Int. Ed.* **2001**, *40*, 1743.
[19] a) L. Feng, S. H. Li, H. J. Li, J. Zhai, Y. L. Song, L. Jiang, D. B. Zhu, *Angew. Chem.* **2002**, *114*, 1269; *Angew. Chem. Int. Ed.* **2002**, *41*, 1221; b) L. Feng, Y. L. Song, J. Zhai, J. Xu, L. Jiang, D. B. Zhu, *Angew. Chem.* **2003**, *115*, 824; *Angew. Chem. Int. Ed.* **2003**, *42*, 800.
[20] a) L. Feng, S. H. Li, Y. S. Li, H. J. Li, L. J. Zhang, J. Zhai, Y. L. Song, B. Q. Liu, L. Jiang, D. B. Zhu, *Adv. Mater.* **2002**, *14*, 1857; b) W. Barthlott, C. Neinhuis, *Planta* **1997**, *202*, 1; c) C. Neinhuis, W. Barthlott, *Ann. Bot.* **1997**, *79*, 667.
[21] D. Cyranoski, *Nature* **2001**, *414*, 240.
[22] a) B. D. Washo, *Org. Coat. Appl. Polym. Sci. Proc.* **1982**, *47*, 69; b) J. P. Youngblood, T. J. McCarthy, *Macromolecules* **1999**, *32*, 6800; c) J. D. Miller, S. Veeramasuneni, J. Drelich, M. R. Yaamanchili, G. Yamauchi, *Polym. Eng. Sci.* **1996**, *36*, 1849.
[23] H. Bu, J. Rong, Z. Yang, *Macromol. Rapid Commun.* **2002**, *23*, 460.
[24] C. M. Henry, *Chem. Eng. News* **2001**, *79* (10), 35.
[25] H. Kind, J. M. Bonard, C. Emmenegger, L. O. Nilsson, K. Hermadi, S. E. Maillard, L. Schlapbach, L. Forro, K. Kern, *Adv. Mater.* **1999**, *11*, 1285.
[26] H. Gau, S. Herminghaus, P. Lenz, R. Lipowsky, *Science* **1999**, *283*, 46.
[27] Two stretching vibration bands from CH_2 stretching ($\sim 2931\ cm^{-1}$) and C=N ($\sim 2243\ cm^{-1}$) are observed in sample A. Both bands are strong, revealing the presence of PAN. The corresponding absorptions are weak in the spectrum of sample B, and a new band appear at $\sim 1594\ cm^{-1}$ originating from the C=N bond after cyclization. In the spectrum of sample C, all characteristic bands disappear, thus indicating the carbonization from the cyclized structure.
[28] P. M. Th. M. van Attekum, G. K. Wetheim, *Phys. Rev. Lett.* **1979**, *43*, 1896.
[29] H. Ago, T. Kugler, F. Cacialli, W. R. Salaneck, M. S. P. Shaffer, A. H. Windle, R. H. Friend, *J. Phys. Chem. B* **1999**, *103*, 8116.
[30] K. Esumi, M. Ishigami, A. Nakajima, K. Sawada, H. Honda, *Carbon* **1996**, *34*, 279.

 © 2003 Wiley-VCH Verlag GmbH & Co. KGaA, Weinheim

Dynamic Covalent Chemistry

Amplification of Dynamic Chiral Crown Ether Complexes During Cyclic Acetal Formation**

Benzion Fuchs, Alshakim Nelson, Alexander Star, J. Fraser Stoddart, and Sébastien Vidal*

Dynamic covalent chemistry[1] relates to the study of chemical reactions carried out under thermodynamic control. Labile coordinative bonds associated with certain metal–ligand interactions,[2] ring-opening/ring-closing metathesis reactions,[3] and protocols for the formation of imines[4] and disulfides[5] have all been exploited in the strict self-assembly of catenanes and rotaxanes.[6] A wide range of other functionalities[7–11] have also been explored in the creation of dynamic combinatorial libraries (DCLs). We describe here the efficient and selective acid-catalyzed formation of a chiral macropolycyclic polyether constituted of multiple [24]crown-8 frameworks, which incorporate either two D- or two L-threitol residues as bicyclic diacetals, by using dynamic template-directed approaches[12] to amplify the production of the most thermodynamically preferred complex(es).

Carbohydrates command a unique status[13] in the realm of dynamic covalent chemistry.[1] Acid-catalyzed formation[13,14] of cyclic acetals from alditols and aldehydes or ketones provides a well-known reaction[15] in which covalent (C–O) bonds are made and broken with varying degrees of ease under thermodynamic control. The constitutions of the configurationally isomeric *erythro*- and *threo*-1,2,3,4-butanetetraols result[16] in their undergoing three different kinds of acetal ring closures with aldehydes and ketones: 1) 1,3:2,4-diacetal formation yields "6/6" bicycles, 2) 1,2:3,4-diacetal formation affords "5/5" bicycles, and 3) 1,4:2,3-diacetal formation yields "5/7" bicycles. With aldehydes, "6/6" or 1,3,5,7-tetraoxadecalin (TOD) formation usually predominates at equilibrium, whereas with ketones, "5/5" bicycles are invariably the major products. The TOD-forming reactions involving aldehydes (RCHO) are completely diastereospecific, that is, erythritol gives *trans*-TOD and threitol affords *cis*-TOD. The latter has long attracted the interest of stereochemists because of its highly distinctive stereoelectronic properties.[17]

[*] Prof. J. F. Stoddart, A. Nelson, Dr. A. Star, Dr. S. Vidal
Department of Chemistry and Biochemistry
University of California, Los Angeles
405 Hilgard Avenue, Los Angeles, CA 90095-1569 (USA)
Fax: (+1) 310-206-1843
E-mail: stoddart@chem.ucla.edu
Prof. B. Fuchs
School of Chemistry
(Raymond and Beverly Sackler Faculty of Exact Sciences)
Tel-Aviv University, Ramat-Aviv, 69978 Tel-Aviv (Israel)

[**] We thank the National Science Foundation (CHE 9910199) for funding this research, which was also supported in part by equipment grants (CHE 9974928 and CHE 0092036) from the National Science Foundation.

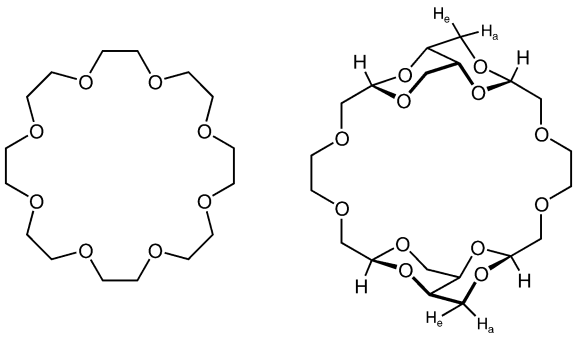
Supporting information for this article is available on the WWW under http://www.angewandte.org or from the author.

 © 2003 Wiley-VCH Verlag GmbH & Co. KGaA, Weinheim DOI: 10.1002/anie.200351558

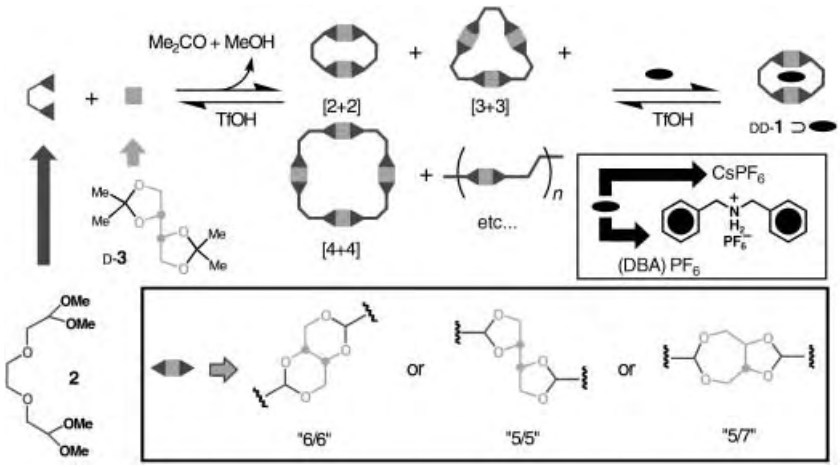
It is beyond any doubt that the O-inside conformations of *cis*-TOD with equatorial substituents (R) prevail at equilibrium.

In a recent quest for chiral [24]crown-8 derivatives that will form either complexes (pseudorotaxanes) or interlocked molecular compounds (catenanes or rotaxanes) with secondary dialkylammonium ($R'_2NH_2^+$) ions,[18] we have identified (Scheme 1) the macropolycyclic polyether DD-**1** containing two 2,6-disubstituted *cis*-TOD residues with O-inside conformations which is derived from D-threitol and linked in a macrocyclical manner by linkers containing bismethylenedioxy units. Numerous [24]crown-8 constitutions can be identified within DD-**1**. Inspection of molecular models reveals that all 12 of the oxygen atoms in DD-**1** can orient themselves toward the center of the relatively rigid host, thus creating an electron-rich environment for the complexation of electron-deficient guests, for example, $R'_2NH_2^+$ ions.

An initial attempt to react D-threitol[19] with the diacetal **2**[20] failed because of the insolubility of the former in organic solvents. We therefore decided to use a soluble derivative of D-threitol—namely the diacetonide D-**3**, which was prepared[21] by stirring the tetraol in Me_2CO in the presence of H_2SO_4. In the absence of a template, transacetalations (Scheme 2) between **2** and D-**3** proceed rapidly at room temperature in both CD_3CN and $CDCl_3$, after addition of an acid catalyst (triflic acid, TfOH) to give a complex mixture of products, including [2+2] TOD-containing [24]crown-8 derivatives, as indicated (Supporting Information) by mass spectrometry and ^{1}H NMR spectroscopy. The transacetalations are expected to occur with both enthalpic and entropic gains. For example, when DD-**1** is a product, the thermodynamically more stable "6/6" bicycles (TODs) should be formed in preference to "5/5" bicycles, such as is present in D-**3**. Entropy should increase during the reaction of two molecules of **2** with two molecules of D-**3** to give DD-**1** with the expulsion of four molecules of Me_2CO and eight molecules of MeOH.



Scheme 1. Structural formulas of [24]crown-8 and the [2+2] TOD-containing macropolycyclic polyether DD-**1**.



Scheme 2. The dynamic combinatorial virtual library (DCVL) generated in $CDCl_3$ solution from the diacetal **2** and the diacetonide D-**3**, prior to the addition of $CsPF_6$, after which [DD-**1**⊃Cs]$^+$ becomes amplified from a mixture which could, in principle, contain bicycles with "6/6", "5/5", and "5/7" constitutions in all possible permutations. Although the use of (DBA)PF_6 as a template did amplify the formation of [2+2] macropolycycles in CD_3CN, it did not produce [DD-**1**⊃DBA]$^+$ as a pure [2]pseudorotaxane.

The outcome of the reaction changed completely when dibenzylammonium hexafluorophosphate ((DBA)PF_6) was employed as the template. When this salt (1 equiv) was added to a solution of dry $CDCl_3$ containing equimolar amounts (40 mM) of **2** and D-**3**, a dynamic process could be initiated by addition of TfOH. Equilibrium was established after 3 days at 45 °C, and, while mass spectrometry revealed that the major products are [2+2] macropolycycles, ^{1}H NMR spectroscopy indicated that they are also a complex mixture of isomers that contain different bicyclic diacetals. The region in the ^{1}H NMR spectrum where signals for the acetal methine protons appear ($\delta = 4.4$–5.5 ppm) shows that, among the several products present, no more than 64% of the diacetal units[22] are "6/6" bicycles. Nonetheless, while a mixture of bicyclic diacetals was present in the reaction products, the MALDI-TOF mass spectrum revealed a relatively intense peak at m/z 662.32 which corresponds to the [2]pseudorotaxane composed of a DBA^+ ion template encircled by a [2+2] macropolycycle. Although it is possible that the various complexes are kinetically stable under the conditions of the reaction, and so do not equilibrate, it is more likely that [2+2] macropolycycles containing "6/6" and other bicycles form close to isoenergetic [2]pseudorotaxanes.

Changing the template[23] to $CsPF_6$ had a significantly beneficial effect upon the outcome (Scheme 2) of the dynamic transacetalations. The reaction between equimolar proportions (40 mM) of the diacetal **2** with the diacetonide D-**3** in dry $CDCl_3$ at 45 °C, using Cs^+ ions as the template, was initiated by addition of TfOH as a catalyst. The equilibration process was monitored (Figure 1) by ^{1}H NMR spectroscopy, primarily by focusing on the region ($\delta = 4.4$–5.5 ppm) where the acetal methine protons resonate in the spectrum. As the initially observed methine proton triplet at $\delta = 4.52$ ppm arising from the starting diacetal **2** decreases over several days, numerous new acetal methine signals begin to appear further downfield beyond $\delta = 4.8$ ppm. Presumably, a com-

 © 2003 Wiley-VCH Verlag GmbH & Co. KGaA, Weinheim

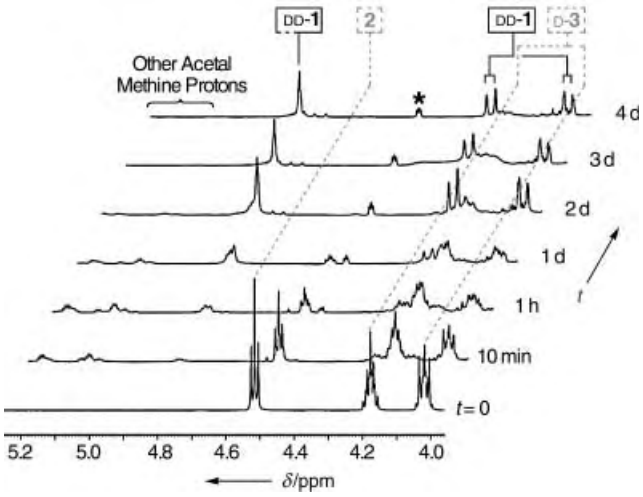


Figure 1. Stack of partial ^{1}H NMR spectra (500 MHz, $CDCl_3$, 298 K) recorded with time of an equilibrating equimolar (40 mM) mixture of the diacetal **2** and the diacetonide D-**3** in which Cs^+ ions are employed as the template. The slanting scale entries display the times after addition of the catalyst (TfOH) to initiate the equilibration process, which is complete after four days. The product is identified by solid lines and the reactant by dashed ones. The signal centered around $\delta = 4.5$ ppm and indicated by the asterisk results from a by-product formed during the reaction. It is removed during purification.

plex mixture containing isomeric bicyclic diacetals with "5/5", "6/6", and "5/7" constitutions is formed (Figure 2) under kinetic control. Subsequently and concomitantly, the resonances for these initially formed kinetic products decrease and a single predominantly broad singlet at $\delta = 4.86$ ppm, associated with the acetal methine protons in the "6/6" bicycle, begins to experience an increase in its relative intensity. Signals for the H_a and H_e protons (Scheme 1) in DD-**1** were also characteristically present in the spectrum as a broadened pair of doublets, centered on $\delta = 4.01$ ppm and 4.22 ppm, respectively. Thus, it is clear (Figure 2) that, as the resonances for the kinetic products undergo a decrease in their relative intensities, those associated with the macropolycyclic polyether containing two "6/6" bicycles increase in

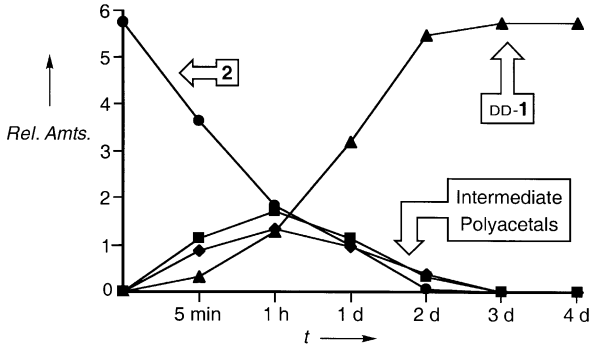


Figure 2. A graphical representation of the relative integrals (Rel. Amts.) for the acetal proton signals with time illustrating the consumption of the diacetal **2** (●), the production of two other intermediate polyacetals (■ and ◆) formed under kinetic control, and the formation of the macropolycyclic polyether DD-**1** from **2** and D-**3**, both 40 mM in $CDCl_3$ at 318 K.

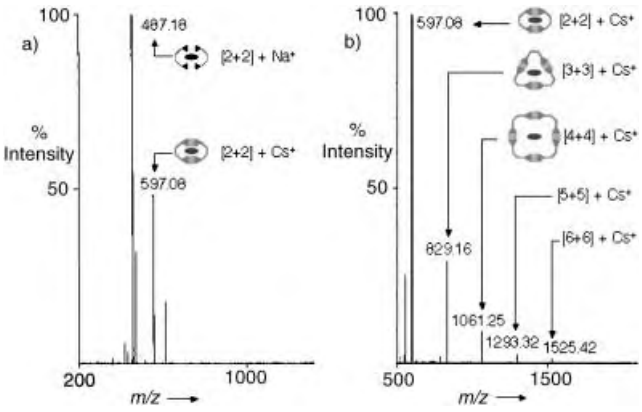


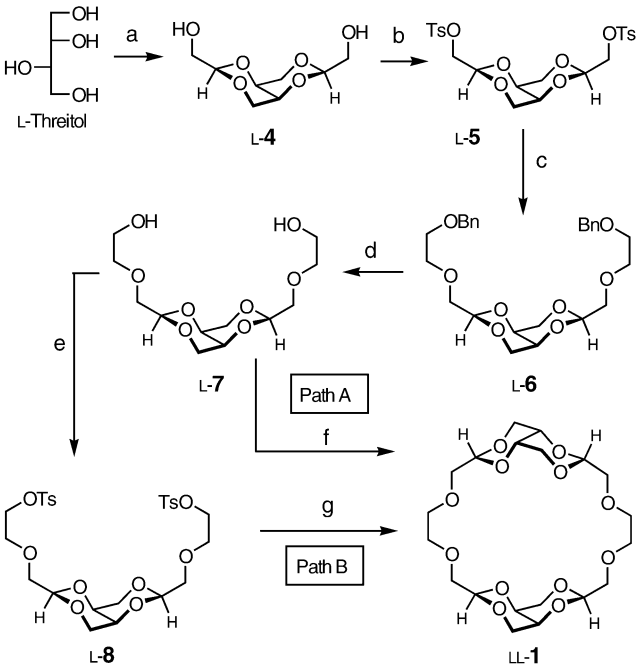
Figure 3. MALDI-TOF mass spectra of the equilibrium mixtures, obtained when the diacetal **2** and the diacetonide D-**3** were equilibrated for nine days in a) $CDCl_3$ and b) CD_3CN in the presence of $CsPF_6$ as template and TfOH as catalyst.

their relative intensities, which indicates that DD-**1** is being amplified in the presence of the Cs^+ ion template. ^{1}H NMR spectroscopy indicates that the conversion[24] of **2** and D-**3** into DD-**1** is all but quantitative after 3 days, that is, $> 95\%$ in dry $CDCl_3$ at 45 °C. The MALDI-TOF mass spectrum (Figure 3 a) of the equilibrated reaction mixture showed molecular ion peaks for both $[M+Na]^+$ (Na^+ ions are present in the matrix) and $[M+Cs]^+$ arising from the [2+2] macropolycycle. Peaks for higher polycyclic oligomers were absent to all intents and purposes. When this dynamic reaction was scaled up (see Experimental Section), DD-**1** was isolated in a 58% (unoptimized) yield and fully characterized as the [2+2] TOD-containing [24]crown-8 derivative by mass spectrometry and 2D NMR spectroscopy.[25] Interestingly, when CD_3CN is used as the reaction solvent, the Cs^+ ion template is not nearly as effective in amplifying DD-**1** from the dynamic mixture. In addition to this [2+2] macropolycyclic polyether, there is evidence for the presence of higher polycyclic oligomers.

To establish beyond any shadow of a doubt that the structure of the [2+2] macropolycyclic polyether corresponds to DD-**1**, and to be in a position to compare the efficiency of the dynamic approach with kinetic ones, we have synthesized LL-**1** in a conventional manner (Scheme 3). L-Threitol was treated with the glycoaldehyde dimer[26] to give L-**4** in 70% yield. The ditosylate L-**5** was obtained from L-**4** in high yield and was used to alkylate, rather inefficiently, 2-(benzyloxy)-ethanol[27] to afford the dibenzyl ether L-**6** in modest yield. Following near quantitative catalytic hydrogenolysis to give the diol L-**7**, it was tosylated to give the ditosylate L-**8** in a good yield. Macropolycyclization to form LL-**1** was achieved by means of two alternative pathways (Paths A and B) in the presence of base, under high dilution conditions using Cs^+ ions as templates to facilitate[28] the formation of LL-**1**. Reaction (Path A) of the diol L-**7** with the ditosylate L-**5** gave LL-**1** in 6.7% yield, whereas reaction (Path B) of the diol L-**4** with the ditosylate L-**8** gave LL-**1** in 5.8% yield.

Clearly, the isolated overall yields of DD/LL-**1** starting from D/L-threitol using the kinetic approach is considerably lower (1.4% over five steps along Path A and 0.8% over six steps along Path B) than for the thermodynamic approach (mini-

 © 2003 Wiley-VCH Verlag GmbH & Co. KGaA, Weinheim



Scheme 3. a) Glycoaldehyde dimer, 1 M HCl, 70%; b) TsCl, NaH, THF, 85 °C, 88%; c) 2-(benzyloxy)ethanol, NaH, DMF, 90 °C, 35%; d) H_2, Pd-C, EtOH, H_2O, 92%; e) TsCl, Et_3N, CH_2Cl_2, 68%; f) L-**5**, CsOTs, NaH, DMF, 100 °C, 6.9%; g) L-**4**, CsOTs, NaH, DMF, 100 °C, 5.8%. Ts = toluene-4-sulfonyl, Bn = benzyl.

mally 30% over two steps), thus proving the superiority of dynamic covalent chemistry[1] over the more conventional procedures (Scheme 3). These preliminary results lay the foundations for the creation of much more intricate transacetalations[29] and DCVLs, which will include many different components in the virtual library, as well as a range of templates, both reusable and consumable.

Experimental Section

2: $HOCH_2CH_2OH$ (5 mL, 90 mmol) was added dropwise to a suspension of NaH (95%, 6.80 g, 269 mmol) in $ClCH_2CH(OMe)_2$ (100 mL, 896 mmol) at 0 °C. The reaction mixture was heated (140 °C) under reflux for 24 h and the resulting brown gum was dissolved in H_2O (100 mL). The aqueous solution was concentrated under high vacuum and then diluted again with H_2O (250 mL). The aqueous layer was extracted with CH_2Cl_2 (3 × 250 mL). The organic layers were combined, dried (Na_2SO_4), filtered, and concentrated under vacuum. The resulting oil was subjected to column chromatography (basic Al_2O_3, hexanes then CH_2Cl_2) to give **2** (19 g, 90%) as a pale yellow liquid. ^{1}H NMR (500 MHz, CD_3OD): $\delta = 3.37$ (s, 12H), 3.50 (d, $J = 5.2$ Hz, 4H), 3.63 (s, 4H), 4.49 ppm (t, $J = 5.2$ Hz, 2H); ^{13}C NMR (125 MHz, CD_3OD): $\delta = 54.3$, 71.8, 104.1 ppm; FABMS: *m*/*z*: 499.3 $[2M+Na]^+$, 261.3 $[M+Na]^+$, 207.2 $[M-OMe]^+$; HRMS (FAB) *m*/*z* calcd for $C_{10}H_{22}NaO_6$ $[M+Na]^+$: 261.1314, found: 261.1314.

General procedure for NMR experiments. Compounds **2** (9.5 mg, 40 μmol) and D-**3** (8.1 mg, 40 μmol), in addition to either $(DBA)PF_6$ (8.8 mg, 22 μmol) or $CsPF_6$ (6.1 mg, 22 μmol) as the template, were added to an NMR tube and dissolved in either $CDCl_3$ or CD_3CN (1 mL). TfOH (2 μL, 0.02 μmol) was added to the mixture to initiate the dynamic process while the solutions were maintained at 45 °C. The equilibrations and amplifications of the products in the DCVLs were monitored by ^{1}H NMR spectroscopy and mass spectrometry.

DD-**1**: A mixture of **2** (181 mg, 0.80 mmol), DD-**3** (160 mg, 0.80 mmol), and $CsPF_6$ (122 mg, 0.44 mmol) was added to dry $CHCl_3$ (20 mL) and TfOH (40 μL, 0.45 μmol) was introduced into the stirred solution. The reaction mixture was maintained at 45 °C for 3 days and then quenched with iPr_2NEt. The solvents were removed under vacuum and the resulting oil was subjected to column chromatography (SiO_2, CH_2Cl_2/MeOH (9:1)) to afford DD-**1** (108 mg, 58%) as a foamy solid. $[\alpha]_D = -18.0$ ($c = 1$, $CHCl_3$). ^{1}H NMR (500 MHz, $CDCl_3$): $\delta = 3.60$–3.78 (m, 20H), 3.79 (s, 4H), 3.98 (d, $J =$ 12.8 Hz, 4H), 4.28 (d, $J = 12.8$ Hz, 4H), 4.86 ppm (br s, 4H); ^{13}C NMR (125 MHz, $CDCl_3$): $\delta = 69.1$, 69.6, 69.9, 70.6, 98.6 ppm; MALDI-TOF-MS *m*/*z* calcd for $C_{20}H_{32}NaO_{12}$ $[M+Na]^+$: 487.1786, found: 487.1786.

Received: April 2, 2003 [Z51558]

Keywords: combinatorial chemistry · macrocycles · supramolecular chemistry · template synthesis · transacetalation

[1] a) P. A. Brady, R. P. Bonar-Law, S. J. Rowan, C. J. Suckling, J. K. M. Sanders, *Chem. Commun.* **1996**, 319–320; b) P. A. Brady, J. K. M. Sanders, *Chem. Soc. Rev.* **1997**, *26*, 327–336; c) J.-M. Lehn, *Chem. Eur. J.* **1999**, *5*, 2455–2463; d) J. K. M. Sanders, *Pure Appl. Chem.* **2000**, *72*, 2265–2274; e) G. R. L. Cousins, S.-A. Poulsen, J. K. M. Sanders, *Curr. Opin. Chem. Biol.* **2000**, *4*, 270–279; f) L. M. Greig, D. Philp, *Chem. Soc. Rev.* **2001**, *30*, 287–302; g) I. Huc, R. Nguyen, *Comb. Chem. High Throughput Screening* **2001**, *4*, 109–130; h) R. L. E. Furlan, S. Otto, J. K. M. Sanders, *Proc. Natl. Acad. Sci. USA* **2002**, *99*, 4801–4804; i) S. J. Rowan, S. J. Cantrill, G. R. L. Cousins, J. K. M. Sanders, J. F. Stoddart, *Angew. Chem.* **2002**, *114*, 938–993; *Angew. Chem. Int. Ed.* **2002**, *41*, 898–952.

[2] For examples of catenanes incorporating metal–ligand coordination within their macrocyclic components, see a) M. Fujita, F. Ibukuro, H. Hagahira, K. Ogura, *Nature* **1994**, *367*, 720–723; for examples of rotaxanes incorporating metal–ligand interactions within their dumbbell-shaped components that are formed by threading-followed-by-stoppering approaches, see b) A. J. Baer, D. H. Macartney, *Inorg. Chem.* **2000**, *39*, 1410–1417; c) K. Chichak, M. C. Walsh, N. R. Branda, *Chem. Commun.* **2000**, 847–848; d) M. J. Gunter, N. Bampos, K. D. Johnstone, J. K. M. Sanders, *New J. Chem.* **2001**, *25*, 166–173; for examples of rotaxanes incorporating metal–ligand interactions within their macrocyclic components that are formed by clipping reactions, see e) S.-Y. Chang, J. S. Choi, K.-S. Jeong, *Chem. Eur. J.* **2001**, *7*, 2687–2697; f) C. A. Hunter, C. M. R. Low, M. J. Packer, S. E. Spey, J. G. Vinter, M. O. Vysotsky, C. Zonta, *Angew. Chem.* **2001**, *113*, 2750–2754; *Angew. Chem. Int. Ed.* **2001**, *40*, 2678–2682; for recent examples of metal–ligand coordination guiding other molecular self-assembly processes, see g) E. Stulz, Y.-F. Ng, S. M. Scott, J. K. M. Sanders, *Chem. Commun.* **2002**, 524–525; h) Y. Kubota, S. S. Sakamoto, K. Yamaguchi, M. Fujita, *Proc. Natl. Acad. Sci. USA* **2002**, *99*, 4854–4856.

[3] For an example of a [2]catenane synthesis employing ring-opening and ring-closing metathesis (RORCM) and operating under thermodynamic control, see a) T. J. Kidd, D. A. Leigh, A. Wilson, *J. Am. Chem. Soc.* **1999**, *121*, 1599–1600; for an example of a [2]catenane synthesis utilizing ring-closing metathesis (RCM), see b) M. Weck, B. Mohr, J.-P. Sauvage, R. H. Grubbs, *J. Org. Chem.* **1999**, *64*, 5463–5471; for examples of [2]rotaxane syntheses using RCM, see c) J. A. Wisner, P. D. Beer, M. G. B. Drew, M. R. Sambrook, *J. Am. Chem. Soc.* **2002**, *124*, 12469–12476; d) A. F. M. Kilbinger, S. J. Cantrill, A. W. Waltman, M. W. Day, R. H. Grubbs, *Angew. Chem.* **2003**, *115*, 3403–3407; *Angew. Chem. Int. Ed.* **2003**, *42*, 3281–3285.

 © 2003 Wiley-VCH Verlag GmbH & Co. KGaA, Weinheim

[4] For stoppering approaches to rotaxanes incorporating imine-containing dumbbells, see a) S. J. Cantrill, S. J. Rowan, J. F. Stoddart, *Org. Lett.* **1999**, *1*, 1363 – 1366; b) S. J. Rowan, J. F. Stoddart, *Org. Lett.* **1999**, *1*, 1913 – 1916; for rotaxanes incorporating an imine-containing macrocycle formed by clipping, see c) P. T. Glink, A. I. Oliva, J. F. Stoddart, A. J. P. White, D. J. Williams, *Angew. Chem.* **2001**, *113*, 1922 – 1927; *Angew. Chem. Int. Ed.* **2001**, *40*, 1870 – 1875; d) M. Horn, J. Ihringer, P. T. Glink, J. F. Stoddart, *Chem. Eur. J.* **2003**, *17*, 4046 – 4054; for a recent example of the use of imines in other molecular self-assembly processes, see e) M. Hochgürtel, R. Biesinger, H. Kroth, D. Piecha, M. W. Hofmann, S. Kraus, O. Schaaf, C. Nicolau, A. V. Eliseev, *J. Med. Chem.* **2003**, *46*, 356 – 358.

[5] For rotaxanes containing disulfide units in their dumbbell-shaped components that are formed by riveting and stoppering approaches, see a) A. G. Kolchinski, N. W. Alcock, R. A. Roesner, D. H. Busch, *Chem. Commun.* **1998**, 1437 – 1438; b) Y. Furusho, T. Hasegawa, A. Tsuboi, N. Kihara, T. Takata, *Chem. Lett.* **2000**, 18 – 19; c) T. Oku, T. Furush, T. Takata, *J. Polym. Sci. Part A* **2003**, *41*, 119 – 123; for examples of the use of disulfide groups in other molecular self-assembly processes, see d) H. Hioki, W. C. Still, *J. Org. Chem.* **1998**, *63*, 904 – 905; e) S.-W. Tam-Chang, J. S. Stehouwer, J. Hao, *J. Org. Chem.* **1999**, *64*, 334 – 335; f) S. Otto, R. L. E. Furlan, J. K. M. Sanders, *J. Am. Chem. Soc.* **2000**, *122*, 12063 – 12064; g) O. Ramström, J.-M. Lehn, *ChemBioChem* **2000**, *1*, 41 – 48; h) S. Otto, R. L. E. Furlan, J. K. M. Sanders, *Science* **2002**, *297*, 590 – 593; i) for the use of disulfide groups in the amplification of a catalyst from a DCL, see B. Brisig, J. K. M. Sanders, S. Otto, *Angew. Chem.* **2003**, *115*, 1308 – 1311; *Angew. Chem. Int. Ed.* **2003**, *42*, 1270 – 1273.

[6] a) D. B. Amabilino, J. F. Stoddart, *Chem. Rev.* **1995**, *95*, 2725 – 2828; b) *Molecular Catenanes, Rotaxanes, and Knots* (Eds.: J.-P. Sauvage, C. Dietrich-Buchecker), Wiley-VCH, Weinheim, **1999**.

[7] For an example of the use of acetals in the synthesis of natural products, see A. Nadin, K. C. Nicolaou, *Angew. Chem.* **1996**, *108*, 1732 – 1766; *Angew. Chem. Int. Ed. Engl.* **1996**, *35*, 1622 – 1656.

[8] For examples of the use of esters in DCLs, see a) P. A. Brady, J. K. M. Sanders, *J. Chem. Soc. Perkin Trans. 1* **1997**, 3237 – 3253; b) S. J. Rowan, J. K. M. Sanders, *J. Org. Chem.* **1998**, *63*, 1536 – 1546; c) G. Kaiser, J. K. M. Sanders, *Chem. Commun.* **2000**, 1763 – 1764; d) P. S. Lukeman, J. K. M. Sanders, *Tetrahedron Lett.* **2000**, *41*, 10171 – 10174.

[9] For examples of the use of hydrazones in DCLs, see a) G. R. L. Cousins, S.-A. Poulsen, J. K. M. Sanders, *Chem. Commun.* **1999**, 1575 – 1576; b) R. L. E. Furlan, G. R. L. Cousins, J. K. M. Sanders, *Chem. Commun.* **2000**, 1761 – 1762; c) T. Bunyapaiboonsri, O. Ramström, S. Lohmann, J.-M. Lehn, L. Peng, M. Goeldner, *ChemBioChem* **2001**, *2*, 438 – 444; d) R. L. E. Furlan, Y.-F. Ng, S. Otto, J. K. M. Sanders, *J. Am. Chem. Soc.* **2001**, *123*, 8876 – 8877; e) G. R. L. Cousins, R. L. E. Furlan, Y.-F. Ng, J. E. Redman, J. K. M. Sanders, *Angew. Chem.* **2001**, *113*, 437 – 442; *Angew. Chem. Int. Ed.* **2001**, *40*, 423 – 428; f) R. L. E. Furlan, Y.-F. Ng, G. R. L. Cousins, J. E. Redman, J. K. M. Sanders, *Tetrahedron* **2002**, *58*, 771 – 778; g) S. L. Roberts, R. L. E. Furlan, S. Otto, J. K. M. Sanders, *Org. Biomol. Chem.* **2003**, *1*, 1625 – 1633.

[10] For an example of the use of anhydrides of hydroxyboraza-aromatic compounds in DCLs, see P. J. Comina, D. Philp, B. M. Kariuki, K. D. M. Harris, *Chem. Commun.* **1999**, 2279 – 2280.

[11] For an example of the use of oximes in DCLs, see V. A. Polyakov, M. I. Nelen, N. Nazarpack-Kandlousy, A. D. Ryabov, A. V. Eliseev, *J. Phys. Org. Chem.* **1999**, *12*, 357 – 363.

[12] A number of dioxadiazadecalin–salen tautomeric macrocycles and complexes have been shown to constitute dynamic combinatorial virtual libraries (DCVLs); see A. Star, I. Goldberg, B. Fuchs, *Angew. Chem.* **2000**, *112*, 2797 – 2801; *Angew. Chem. Int. Ed.* **2000**, *39*, 2685 – 2689.

[13] J. F. Stoddart, *Stereochemistry of Carbohydrates*, Wiley-Interscience, New York, **1971**.

[14] a) S. A. Barker, E. J. Bourne, *Adv. Carbohydr. Chem.* **1952**, *7*, 137 – 207; b) J. A. Mills, *Adv. Carbohydr. Chem.* **1955**, *10*, 1 – 53; c) R. U. Lemieux, J. Howard, *Can. J. Chem.* **1963**, *41*, 393 – 398.

[15] A good example is the acid-catalyzed reaction between glycerol and isobutyraldehyde. Since the activation energy is less for the formation of the five-membered (1,3-dioxolane) ring acetals, they are formed faster under kinetic control than the six-membered (1,3-dioxane) ring acetals—both the *cis* and the *trans* isomers. However, since both reactions are reversible and the dioxanes are more stable than the dioxolanes, the former eventually constitute the major products of the reaction. Moreover, the acid-catalyzed equilibration of the dioxolane–dioxane system proceeds via an oxycarbenium ion and does not necessarily require water; see a) R. J. Abraham, H. D. Banks, E. L. Eliel, O. Hofer, M. K. Kaloustian, *J. Am. Chem. Soc.* **1972**, *94*, 1913 – 1918; b) E. L. Eliel, S. H. Wilen, *Stereochemistry of Organic Compounds*, Wiley, New York, **1994**, pp. 678 – 682.

[16] I. J. Burden, J. F. Stoddart, *J. Chem. Soc. Perkin Trans. 1* **1975**, 666 – 674 and 675 – 682.

[17] a) R. B. Jensen, O. Buchardt, S. E. Jorgensen, J. U. R. Nielsen, G. Schroll, C. Altona, *Acta Chem. Scand. Ser. B* **1975**, *29*, 373 – 378; b) J.-L. Gras, A. Poncet, *Synth. Commun.* **1992**, *22*, 405 – 409; c) H. Senderowitz, A. Linden, I. Golender, S. Abramsom, B. Fuchs, *Tetrahedron* **1994**, *50*, 9691 – 9706; d) H. Senderowitz, I. Golender, B. Fuchs, *Tetrahedron* **1994**, *50*, 9707 – 9728; e) H. Jatzke, K. Frische, M. Greenwald, I. Golender, B. Fuchs, *Tetrahedron* **1997**, *53*, 4821 – 4834; f) A. Linden, H. Beckhaus, S. P. Verevkin, C. Rückardt, B. Ganguly, B. Fuchs, *J. Org. Chem.* **1998**, *63*, 8205 – 8211; g) M. Grabarnik, N. G. Lemcoff, R. Madar, S. Abramson, S. Weinman, B. Fuchs, *J. Org. Chem.* **2000**, *65*, 1636 – 1642; h) S. Abramson, E. Ashkenasi, K. Frische, I. Goldberg, L. Golender, M. Greenwald, N. G. Lemcoff, R. Madar, S. Weinman, B. Fuchs, *Chem. Eur. J.*, in press.

[18] For a recent review, see S. J. Cantrill, A. R. Pease, J. F. Stoddart, *J. Chem. Soc. Dalton Trans.* **2000**, 3715 – 3734.

[19] a) P. W. Feit, *J. Med. Chem.* **1964**, *7*, 14 – 17; b) M. Carmack, C. J. Kelley, *J. Org. Chem.* **1968**, *33*, 2171 – 2173; c) J. Bourson, L. Oliveros, *Bull. Soc. Chim. Fr.* **1977**, *11*, 1241.

[20] R. Fahrang, D. Sinou, *Bull. Soc. Chim. Belg.* **1989**, *98*, 387 – 393.

[21] A. B. Foster, A. H. Olavesen, J. M. Webber, *J. Chem. Soc.* **1961**, 5095 – 5097.

[22] This percentage conversion is based on a comparison of the integrals for all the acetal methine proton resonances in the $\delta = 4.4$–5.5 ppm range.

[23] $CsPF_6$ was obtained by adding a saturated aqueous solution of NH_4PF_6 to an aqueous solution of CsCl. The resulting precipitate was filtered off and dried under vacuum.

[24] This estimate of the extent of the conversion is based on the integration of all the acetal methine proton signals in the ^1H NMR spectrum.

[25] The dynamic approach was equally successful in providing LL-**1** starting from L-threitol. The optical rotation was approximately equal to its enantiomer (DD-**1**), but of opposite sign ($[\alpha]_D = +19.0$ ($c = 1$, $CHCl_3$)).

[26] K. Frische, M. Greenwald, E. Ashkenasi, N. G. Lemcoff, S. Abramson, L. Golender, B. Fuchs, *Tetrahedron Lett.* **1995**, *36*, 9193 – 9196.

[27] J. A. Marshall, J. D. Trometer, B. E. Blough, T. D. Crute, *J. Org. Chem.* **1988**, *53*, 4274 – 4282.

[28] G. Dijkstra, W. H. Kruizinga, R. M. Kellogg, *J. Org. Chem.* **1987**, *52*, 4230 – 4234.

[29] Transacetalation has been used succesfully in the synthesis of dendritic polyacetals; see N. G. Lemcoff, B. Fuchs, *Org. Lett.* **2002**, *4*, 731 – 734.

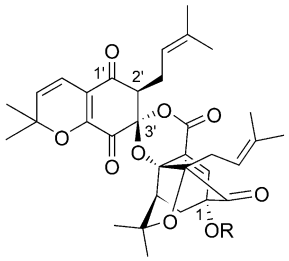
 © 2003 Wiley-VCH Verlag GmbH & Co. KGaA, Weinheim

Natural Product Synthesis

Total Synthesis of 1-*O*-Methyllateriflorone**

K. C. Nicolaou, Pradip K. Sasmal, Hao Xu, Kenji Namoto, and Andreas Ritzén*

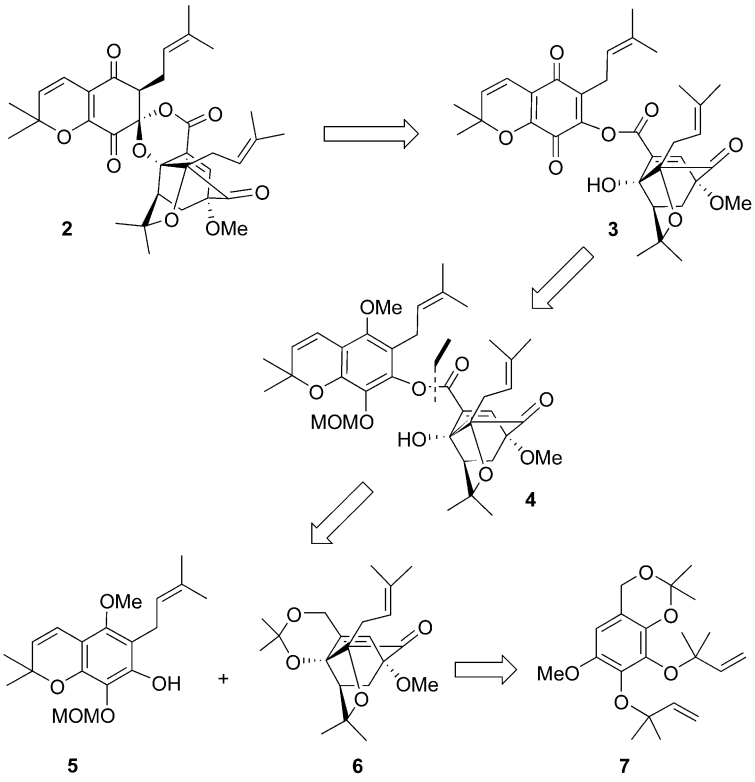
With its unique spiroxalactone framework carrying a prenylated dihydrobenzoquinone moiety and a trioxatetracyclo[7.4.1.$0^{2,7}$.$0^{2,11}$]tetradecane system, lateriflorone (**1**) represents an unusual synthetic challenge. Reported in 1999, this



1 (R = H): lateriflorone
2 (R = Me): 1-*O*-methyllateriflorone

novel natural product[1] was isolated from the stem bark of *Garcinia Lateriflora Bl* (*Guttiferae*) collected from Indonesia, and it exhibits potent cytotoxicity against the P388 cancer cell line ($ED_{50} = 5.4\ \mu g\,mL^{-1}$). Its seemingly fragile structure was secured by spectroscopic and X-ray crystallographic analysis. The secret of its stability, particularly at the spiroxalactone–dihydroquinone junction, is probably due to the *syn* arrangement between the C2′ proton and the C3′ ester grouping which locks the leaving group in place, avoiding the β-elimination pathway that may lead to its rupture. The intriguing structural features of lateriflorone, coupled with its biological activity, prompted us to seek a possible pathway for its construction in the laboratory. Herein we report our findings thus far in this project, including the first total synthesis of 1-*O*-methyllateriflorone (**2**).

We planned our synthesis of 1-*O*-methyllateriflorone (**2**) based on the expectation that the ester bond would be the easier bridge to forge between the two domains of the molecules. The retrosynthetic analysis began with the disconnection of the spiroxalactone moiety by rupturing its ethereal C–O bond, thus unraveling prenylated quinone **3** as a possible precursor (Scheme 1). The next rational disconnections, namely retro-aromatization of **3** and disassembly of its precursor **4** at the ester bond led to fragments **5** and **6** as suitable starting materials. Given our previous studies on forbesione,[2,3] a naturally occurring substance related to the present target, the cage ring system **6**[4] can be traced to the benzenoid compound **7**. The coupling partner **5** can be obtained from a simple benzene derivative.



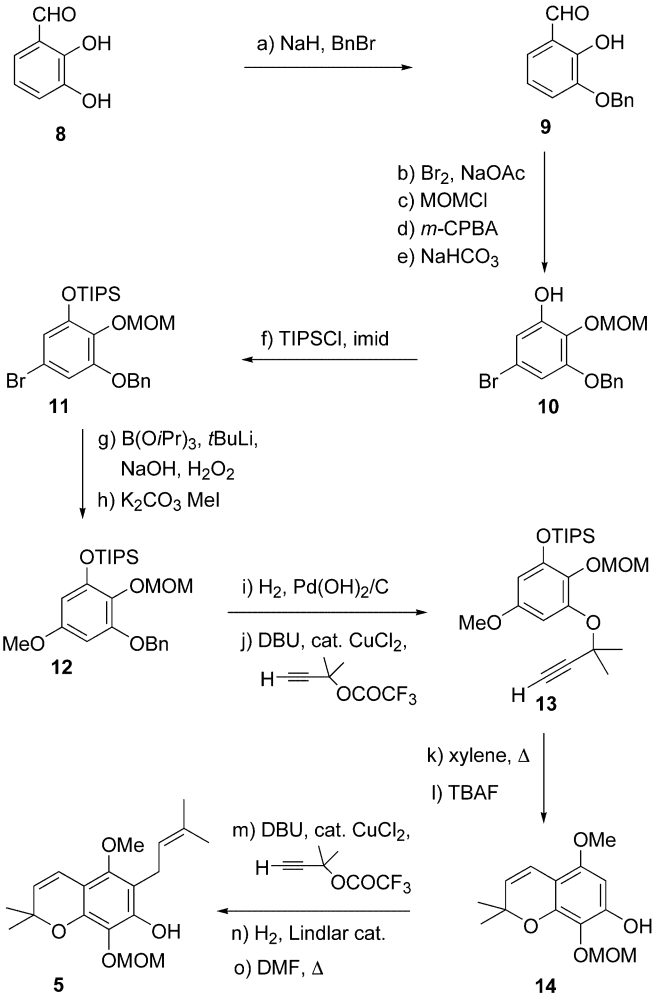
Scheme 1. Retrosynthetic analysis of lateriflorone (**1**).

The required prenylated 2,2′-dimethybenzopyran fragment **5** was synthesized as summarized in Scheme 2. Thus, 2,3-dihydroxybenzaldehyde (**8**) was selectively benzylated at the 3-position according to a literature procedure[5] to afford compound **9**, which was converted into bromophenol **10** in 61% overall yield by the following sequence: a) bromination *para* to the phenolic group; b) protection as a MOM ether, c) oxidation with *m*-CPBA; and d) cleavage of the resulting formate ester with $NaHCO_3$ (for abbreviations of reagents and protecting groups, see legends in schemes). Protection of the phenolic group in **10** as a TIPS ether to form **11** proceeded smoothly under standard conditions (TIPSCl, imid, 96%). Boronation of **11** required premixing of the substrate with $B(OiPr)_3$ prior to addition of *t*BuLi in Et_2O at −78 °C. The resulting borate derivative was then oxidized with H_2O_2 under basic conditions (NaOH), and the resulting phenolic product was methylated to afford **12** in 76% overall yield from **11**.

[*] Prof. Dr. K. C. Nicolaou, Dr. P. K. Sasmal, H. Xu, Dr. K. Namoto, Dr. A. Ritzén
Department of Chemistry and
The Skaggs Institute for Chemical Biology
The Scripps Research Institute
10550 North Torrey Pines Road, La Jolla, CA 92037 (USA)
Fax: (+1) 858-784-2469
E-mail: kcn@scripps.edu
and
Department of Chemistry and Biochemistry
University of California, San Diego
9500 Gilman Drive, La Jolla, CA 92093 (USA)

[**] We thank Dr. D H. Huang and Dr. G. Siuzdak for NMR spectroscopic and mass spectrometric assistance, respectively, and Dr. R. K. Chadha for X-ray crystallographic analysis. Financial support for this work was provided by The Skaggs Institute for Chemical Biology and the National Institutes of Health (USA).

 DOI: 10.1002/anie.200351805 © 2003 Wiley-VCH Verlag GmbH & Co. KGaA, Weinheim



Scheme 2. Synthesis of prenylated 2,2′-dimethylbenzopyran fragment **5**: a) NaH (2.5 equiv), BnBr (1.0 equiv), THF, 25 °C, 48 h, 72%; b) Br_2 (1.1 equiv), NaOAc (1.2 equiv), AcOH, 25 °C, 2 h; c) Et_3N (5.0 equiv), 4-DMAP (0.1 equiv), MOMCl (3.0 equiv), 25 °C, 16 h; d) *m*-CPBA (1.1 equiv), 0→25 °C, CH_2Cl_2, 6 h; e) aqueous saturated $NaHCO_3$, 16 h, 61% for four steps; f) TIPSCl (1.5 equiv), imid (2.0 equiv), DMF, 25 °C, 2 h, 96%; g) premix **11** and $B(OiPr)_3$ (2.2 equiv) in diethyl ether; then *t*BuLi (2.2 equiv) at −78 °C, 2 h, −78→0 °C, 1 h; then MeOH, aqueous NaOH (10%; 4.8 equiv), H_2O_2 (5.0 equiv), 0 °C, 30 min, 86%; h) K_2CO_3 (10 equiv), MeI (10 equiv), acetone, 25 °C, 16 h, 88%; i) $Pd(OH)_2/C$ (10 wt%; 10%), H_2 (1 atm), EtOAc/EtOH (1:1), 25 °C, 30 min, 100%; j) propargyl alcohol (1.3 equiv), DBU (1.5 equiv), TFAA (1.2 equiv), MeCN, 0 °C, 30 min; DBU (1.35 equiv), $CuCl_2$ (0.01% equiv), 10 min; then TFA propargyl ester, 4 h, 0 °C, 76% (90% based on 84% conversion); k) xylene, 140 °C, 30 min; l) TBAF (1.5 equiv), THF, 0 °C, 5 min, 93% for two steps; m) propargyl alcohol (1.3 equiv), DBU (1.5 equiv), TFAA (1.2 equiv), MeCN, 0 °C, 30 min; DBU (1.35 equiv), $CuCl_2$ (0.01% equiv), 10 min; then TFA propargyl ester, 4 h, 0 °C, 80% (90% based on 86% conversion); n) Lindlar catalyst (10 wt%), H_2 (1 atm), EtOAc, quinoline (3 equiv), 25 °C, 2 h, 95%; o) DMF, 120 °C, 1 h, 70%. Bn = benzyl, 4-DMAP = 4-dimethylaminopyridine, MOM = methoxymethyl, *m*-CPBA = *m*-chloroperbenzoic acid, TIPS = triisopropylsilyl, imid = imidazole, DMF = *N*,*N*-dimethylformamide, DBU = 1,8-diazabicyclo[5.4.0]undec-7-ene, TFAA = trifluoracetic anhydride, TBAF = tetra-*n*-butylammonium fluoride.

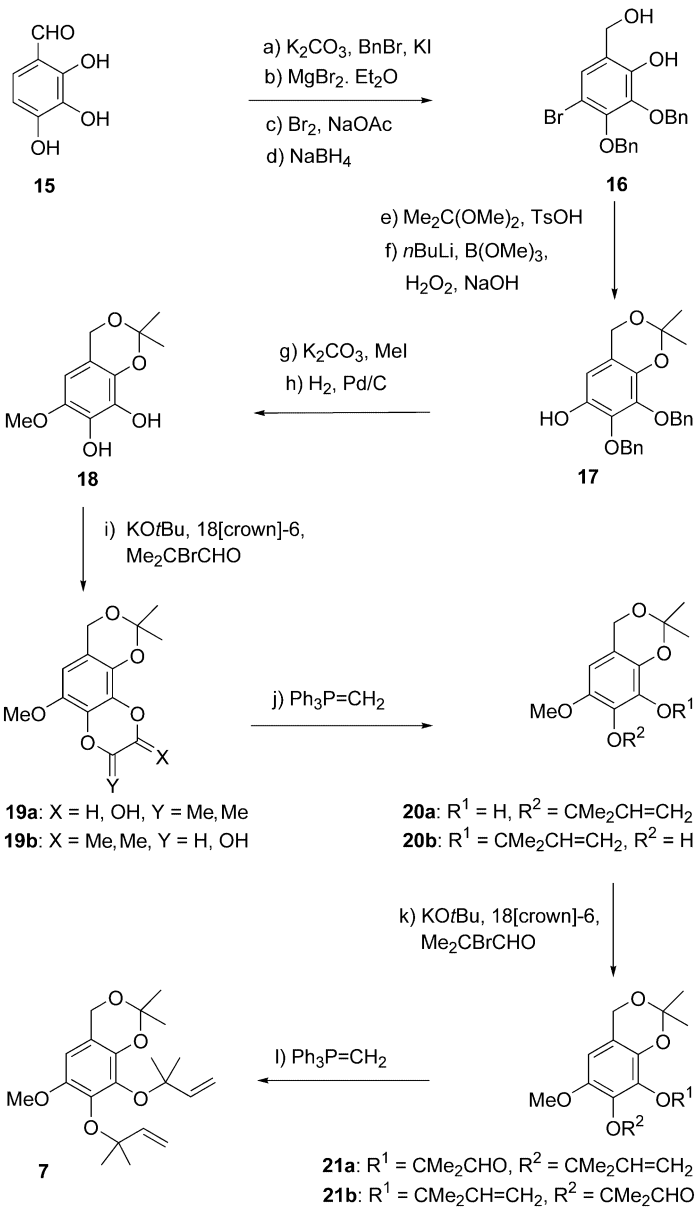
Hydrogenolysis of the benzyl group in this new product followed by reaction with $CH{\equiv}CC(Me)_2OCOCF_3$[6] in the presence of DBU and $CuCl_2$ resulted in the formation of propargylic ether **13** in 76% overall yield. Heating of the latter compound in refluxing xylene induced a Claisen rearrangement,[7] furnishing, after desilylation with TBAF, benzopyran derivative **14** in 93% overall yield. Finally, a second propargyl ether was introduced in **14**; selective reduction (H_2, Lindlar catalyst) of the acetylenic group to the corresponding olefin and Claisen rearrangement under thermal conditions provided the targeted prenylated benzopyran segment **5** in 53% overall yield.

The sequence devised and executed for the synthesis of precursor **7** is shown in Scheme 3. Thus, 2,3,4-trihydroxybenzaldehyde (**15**) was perbenzylated (K_2CO_3, BnBr, KI) and then selectively debenzylated at the position adjacent to the aldehyde group by the action of $MgBr_2{\cdot}Et_2O$. Subsequent *para* bromination (Br_2, NaOAc) and reduction of the aldehyde with $NaBH_4$ afforded dihydroxy compound **16** in 57% overall yield. Acetonide formation ($Me_2C(OMe)_2$, TsOH) followed by lithium–halogen exchange (*n*BuLi), borate formation ($B(OMe)_3$), and oxidation (H_2O_2, NaOH) led to phenolic substrate **17** in 86% overall yield. Methylation of **17** followed by hydrogenolysis of its benzyl ethers led to dihydroxy derivative **18** in 97% overall yield. The dipotassium salt of **18**, generated by addition of KO*t*Bu, was suspended in acetonitrile and treated with bromoisobutyraldehyde in the presence of 18[crown]-6 to afford a mixture of regioisomeric lactols **19a**,**b** (ca. 1:1, 70% yield), which reacted with methylene phosphorane ($MeP^+Ph_3Br^-$, NaHMDS) to provide olefins **20a**,**b** (ca. 1:1, 75% yield). Reiteration of the last two steps furnished, via **21a**,**b**, the required dialkene **7** in 60% overall yield.

Upon heating in DMF at 120 °C, the methoxy derivative **7** entered into the expected Claisen rearrangement/Diels–Alder cascade[3,8] leading through the indicated intermediate products to **6** and **6′** in 47 and 42% yields, respectively (Scheme 4). X-ray crystallographic analysis of **6′**[9] (see ORTEP drawing, Scheme 4) revealed its structure, and, by extension, that of **6**; both structures **6** and **6′** were also supported by NOE studies (see Scheme 4). Selective removal of the acetonide group from **6** (TsOH, MeOH), followed by a two-step oxidation protocol (1) DMP, 2) $NaClO_2$), led to hydroxy carboxylic acid **22** in 91% overall yield. An analogous sequence to that shown in Schemes 3 and 4 was originally employed to construct the dihydroxy acid **22a**. Attempted coupling of this fragment, **22a**), with the phenolic domain **5** (see Scheme 2), however, proved futile, presumably as a result of complications instigated by the free hydroxy group adjacent to the ketone moiety. Thus, this problem led to the targeting and adoption of the methoxy counterpart of this compound, substrate **22**, for our subsequent studies. The coupling of **22** with benzopyran system **5** (see Scheme 2) was smoothly realized under the influence of EDC and 4-DMAP (64% yield) to furnish the required advanced intermediate **4** as shown in Scheme 4.

Having assembled the entire lateriflorone carbon skeleton as expressed in compound **4**, its MOM group was selectively cleaved upon exposure to acidic conditions (HCl, MeOH/Et_2O) leading to a rapidly and spontaneously equilibrating mixture of phenolic esters **23a**,**b** (ca. 1:1, 96% yield) (Scheme 4). Oxidation of this mixture under a variety of

 © 2003 Wiley-VCH Verlag GmbH & Co. KGaA, Weinheim



Scheme 3. Synthesis of intermediate **7**: a) K_2CO_3 (5.0 equiv), BnBr (5.0 equiv), KI (0.1 equiv), DMF, 25 °C, 24 h, 85 %; b) $MgBr_2{\cdot}Et_2O$ (1.1 equiv), diethyl ether, 25 °C, 10 h, 83 %; c) Br_2 (1.1 equiv), NaOAc (1.15 equiv), AcOH, 25 °C, 2 h, 89 %; d) $NaBH_4$ (1.5 equiv), EtOH, 0→25 °C, 30 min, 91 %; e) 2,2-dimethoxypropane (5.0 equiv), TsOH (0.01 equiv), CH_2Cl_2, 1 h, 95 %; f) *n*BuLi (1.1 equiv), diethyl ether, −78 °C, 2 h; then $B(OMe)_3$ (3.0 equiv), 1 h, −78→0 °C; then aqueous NaOH (10 %; 4.8 equiv), H_2O_2 (5.0 equiv), 0 °C, 30 min, 90 %; g) K_2CO_3 (5.0 equiv), MeI (10.0 equiv), DMF, 0→25 °C, 16 h, 99 %; h) Pd/C (10 wt %; 10 %), H_2 (1 atm), EtOAc, 25 °C, 45 min, 98 %; i) *t*BuOK (2.2 equiv), THF, 0 °C; then concentrated and suspended in MeCN; then 18[crown]-6 (2.2 equiv), 15 min, bromoisobutyraldehyde (5.0 equiv), 0→25 °C, 1 h, 70 %; j) $CH_3P^+Ph_3Br^-$ (3.0 equiv), NaHMDS (3.0 equiv), THF, 0 °C, 1 h, 75 %; k) *t*BuOK (1.1 equiv), THF, 0 °C; then concentrated and suspended in MeCN; then 18[crown]-6 (1.1 equiv), 15 min, bromoisobutyraldehyde (5.0 equiv), 0→25 °C, 1 h, 75 %; l) $CH_3P^+Ph_3Br^-$ (2.0 equiv), NaHMDS (2.0 equiv), THF, 0 °C, 1 h, 80 %. Ts = *p*-toluenesulfonyl, HMDS = hexamethyldisilazane.

conditions[10] did not lead directly to the desired lateriflorone molecular framework, but rather to an array of other products, among which the most interesting were those shown in Scheme 5. Thus, exposure of **23a**,**b** to $PhI(OCOCF_3)_2$ in CH_2Cl_2 led to benzoquinone **3** (Table 1) in 43 % yield. Attempts to cyclize this substance under

Table 1: Selected data for compounds **2**, **3**, and **25**.

2: R_f = 0.19 (silica gel, EtOAc/hexanes 3:7); m.p. = 173–174 °C (Et_2O/hexane, uncorrected); ^{1}H NMR (600 MHz, $CDCl_3$): δ = 7.50 (s, 1 H), 6.49 (d, J = 9.8 Hz, 1 H), 5.78 (d, J = 9.8 Hz, 1 H), 5.32 (br t, J = 7.0 Hz, 1 H), 4.66 (br t, J = 7.0 Hz, 1 H), 3.53 (s, 3 H), 3.20 (dd, J = 8.3, 3.1 Hz, 1 H) 2.83 (m, 1 H), 2.79 (m, 1 H), 2.56 (m, 1 H), 2.39 (dd, J = 14.5, 7.0 Hz, 1 H), 2.16 (d, J = 13.0 Hz, 1 H), 1.89 (d, J = 9.9 Hz, 1 H), 1.69 (s, 3 H), 1.68 (s, 3 H), 1.60 (dd, J = 13.0, 9.9 Hz, 1 H), 1.56 (s, 3 H), 1.55 (s, 3 H), 1.48 (s, 3 H), 1.45 (s, 3 H), 1.16 ppm (s, 3 H), 1.14 ppm (s, 3 H); ^{13}C NMR (150 MHz, $CDCl_3$): δ = 200.7, 189.0, 186.7, 158.0, 150.9, 139.0, 136.5, 133.6, 134.0, 125.2, 123.0, 121.6, 116.0, 115.4, 101.3, 85.6, 84.7, 84.0, 82.8, 81.3, 57.4, 54.1, 48.6, 31.9, 30.0, 29.1, 28.3, 28.2, 27.8, 25.9, 25.8, 21.6, 18.1, 17.9 ppm; HRMS (MALDI): calcd for $C_{34}H_{40}O_9Na^+$: 615.2564 [M+Na^+], found 615.2549

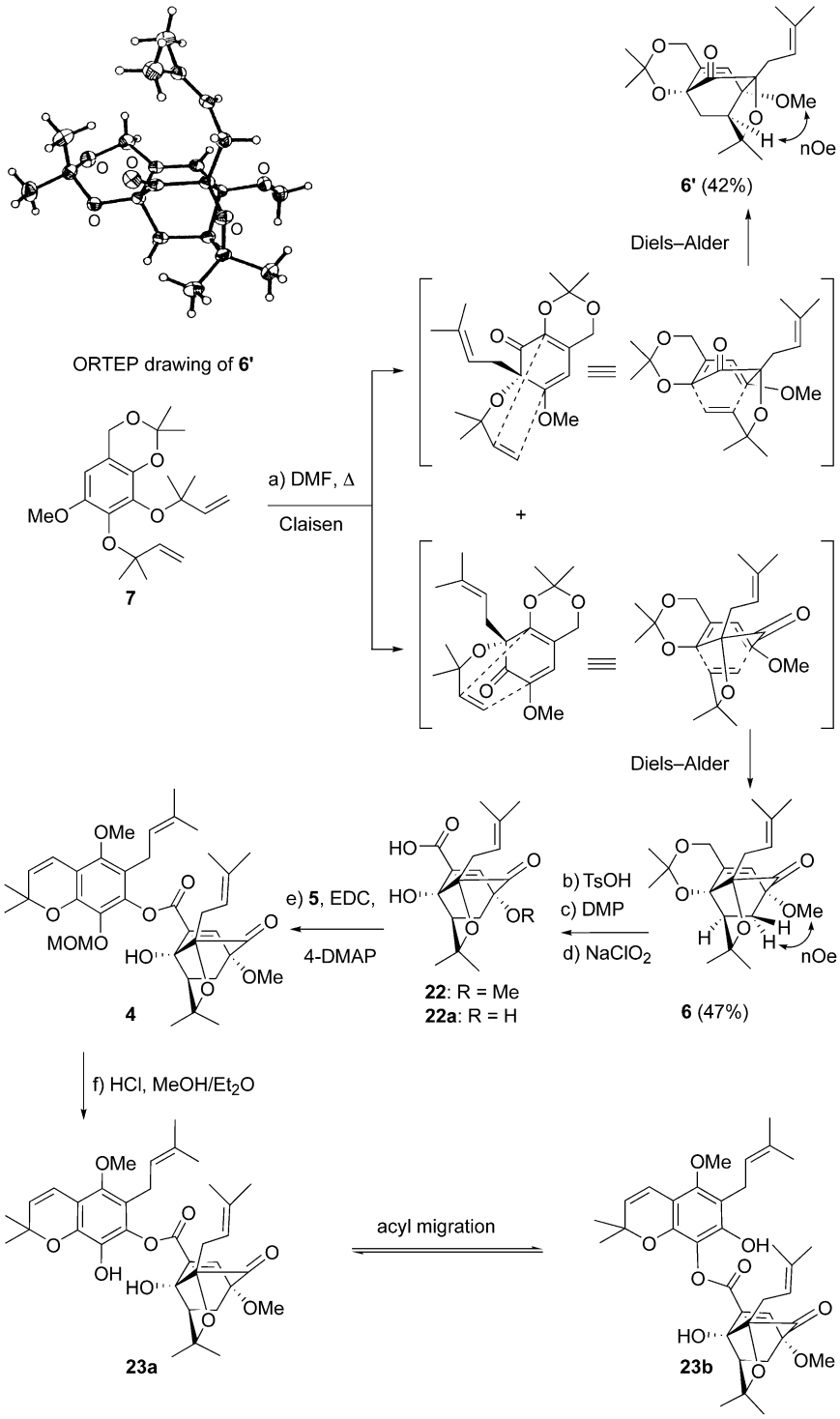
3: R_f = 0.32 (silica gel, EtOAc/hexanes 3:7); ^{1}H NMR (600 MHz, $CDCl_3$): δ = 7.50 (s, 1 H), 6.45 (d, J = 10.1 Hz, 1 H), 5.63 (d, J = 10.1 Hz, 1 H), 5.43 (s, 1 H, OH, D_2O exchangeable), 4.99 (br t, J = 7.5 Hz, 1 H), 4.84 (br t, J = 7.2 Hz, 1 H), 3.57 (s, 3 H), 3.09–3.17 (m, 2 H), 2.68 (dd, J = 14.0, 6.9 Hz, 1 H), 2.61 (dd, J = 14.0, 7.9 Hz, 1 H), 2.37 (d, J = 13.0 Hz, 1 H), 2.35 (d, J = 10.1 Hz, 1 H), 1.69 (s, 3 H), 1.68 (dd, J = 13.0, 10.1, Hz, 1 H), 1.67 (s, 3 H), 1.61 (s, 3 H), 1.60 (s, 3 H), 1.59 (s, 3 H), 1.51 (s, 3 H), 1.50 (s, 3 H), 1.27 ppm (s, 3 H); ^{13}C NMR (100 MHz, $CDCl_3$): δ = 202.8, 182.8, 174.7, 162.5, 149.7, 146.7, 144.2, 135.6, 135.4, 135.3, 130.6, 128.7, 118.4, 117.2, 116.1, 115.0, 84.6, 84.2, 83.5, 82.7, 81.2, 54.0, 50.1, 31.4, 30.1, 29.2, 28.54, 28.53, 28.3, 26.1, 25.9, 23.5, 18.1, 17.9 ppm; HRMS (MALDI): calcd for $C_{34}H_{40}O_9Na^+$: 615.2564 [M+Na^+], found 615.2594

25: R_f = 0.24 (silica gel, EtOAc/hexanes 3:7); m.p. = 154 °C (Et_2O/hexane, uncorrected); ^{1}H NMR (500 MHz, $CDCl_3$): δ = 7.47 (s, 1 H), 6.25 (d, J = 10.0 Hz, 1 H), 5.84 (d, J = 10.0 Hz, 1 H), 5.24 (br t, J = 6.5 Hz, 1 H), 4.75 (br t, J = 8.0 Hz, 1 H), 3.60 (s, 3 H), 3.53 (s, 3 H), 3.24 (dd, J = 15.0, 8.0 Hz, 1 H), 2.99 (dd, J = 15.0, 6.5 Hz, 1 H), 2.84 (dd, J = 13.5, 8.0 Hz, 1 H), 2.40 (dd, J = 13.5, 6.0 Hz, 1 H), 2.13 (d, J = 13.0 Hz, 1 H), 2.08 (d, J = 9.5 Hz, 1 H), 1.75 (dd, J = 13.0, 9.5 Hz, 1 H), 1.68 (s, 6 H), 1.56 (s, 3 H), 1.49 (s, 3 H), 1.48 (s, 3 H), 1.44 (s, 3 H), 1.34 (s, 3 H), 1.16 ppm (s, 3 H); ^{13}C NMR (125 MHz, $CDCl_3$): δ = 201.5, 188.7, 159.0, 149.2, 140.4, 136.6, 136.1, 135.6, 132.6, 126.2, 124.7, 123.4, 121.7, 117.1, 116.2, 97.3, 85.2, 84.9, 84.0, 82.8, 78.0, 60.4, 54.0, 48.4, 31.9, 29.9, 28.3, 28.0, 27.7, 27.2, 26.0, 25.8, 24.5, 17.9, 17.8 ppm; HRMS (MALDI): calcd for $C_{35}H_{43}O_9$: 607.2901 [M+H^+], found 607.2886

a variety of conditions failed to produce the desired lateriflorone skeleton, leading instead to a number of other compounds whose description will have to await the full account of this work.

Having failed to construct the desired 1-*O*-methyllateriflorone (**2**) from quinone **3**, we then proceeded to investigate the possibility of casting this structural motif from **23a**,**b** via benzoquinone monoketal **24**. To this end, **23a**,**b** was exposed to $PhI(OCOCF_3)_2$ in $MeOH/CH_2Cl_2$ (1:1), which led to the formation of **24** (60 % yield) through the participation of a molecule of methanol. Upon subsequent treatment with PPTS in refluxing benzene under azeotropic conditions, **24** led to **25**

 © 2003 Wiley-VCH Verlag GmbH & Co. KGaA, Weinheim



Scheme 4. Construction of advanced intermediate **23a,b**: a) DMF, 120 °C, 1 h, **6′** (42%) and **6** (47%); b) TsOH (20 mol%), MeOH, 25 °C, 16 h, 98%; c) DMP (2.0 equiv), $NaHCO_3$ (2.0 equiv), CH_2Cl_2, 25 °C, 30 min, 93%; d) $NaClO_2$ (6.0 equiv), NaH_2PO_4 (6.0 equiv), 2-methyl-2-butene (75.0 equiv), THF/*t*BuOH/H_2O (2:4:1), 30 min, 100%; e) EDC (1.5 equiv), 4-DMAP (1.5 equiv), **5** (2.0 equiv), CH_2Cl_2, 0→25 °C, 16 h, 64%; f) HCl (0.25 M) in MeOH/Et_2O (1:1), 0→25 °C, 1 h, 96%. DMP = Dess–Martin periodinane, EDC = 1-ethyl-(3-dimethylaminopropyl)carbodiimide hydrochloride.

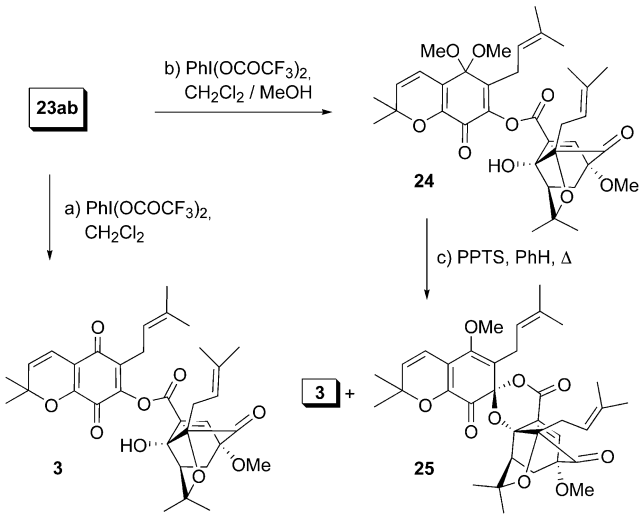
(Table 1) in 69% yield, together with quinone **3**, which was obtained in 11% yield (Scheme 5). Pleasantly, compound **25** crystallized as beautiful yellow crystals whose X-ray crystallographic analysis[9] revealed its lateriflorone-like molecular architecture, including the correct stereochemistry at C3′ (see ORTEP drawing, Scheme 5). However, an attempt to hydrolyze the enol methyl ether within **25** under acidic conditions (HCl (aq.)/THF) led to red quinone ether carboxylic acid **3′** (80%), which after methylation with diazomethane, afforded red quinone methyl ester **26** (81%, Scheme 6). The structurally intriguing isomeric quinones **3** (Scheme 5) and **3′** (Scheme 6) may well be related to biogenetic precursors and/or in vivo degradation products of lateriflorone. As such, these novel compounds, **3** and **3′**, may exhibit biological activity, and so could 1,1′-*O*,*O*-dimethyllateriflorone (**25**).

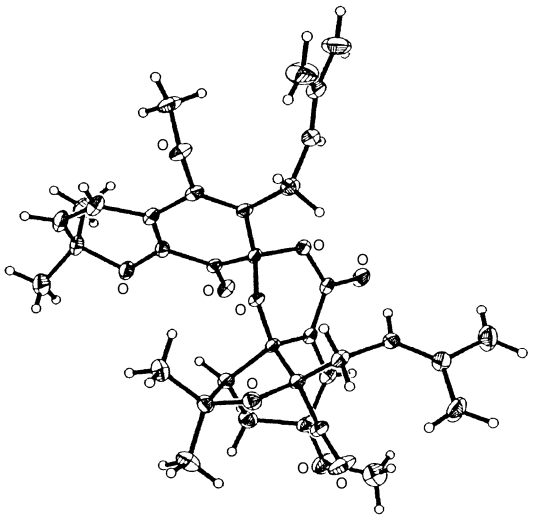
At this juncture, we felt that benzoquinone carboxylic acid **3′** presented a new opportunity for a final attempt to reach the lateriflorone framework. Indeed, exposure of **3′** to PPTS in refluxing benzene under anhydrous conditions led, in 83% yield, to a single yellow substance whose spectral data strongly suggested the lateriflorone-like structure **2** (Scheme 6). Pleasingly, X-ray crystallographic analysis[9] of the crystalline **2** (Table 1) confirmed its identity as 1-*O*-methyllateriflorone, ending the quest for this highly unusual molecular architecture. The completely stereoselective manner in which both **3′** and **24** cyclize to the corresponding lateriflorone frameworks is noteworthy. It is not impossible that both reactions are under thermodynamic control, leading to the natural stereochemistry, which may represent the most stable configuration of this system.

The described chemistry opens a facile entry into the novel lateriflorone molecular architecture and underscores the importance of careful strategy design for its construction. Future studies in the field will include further methodological explorations and chemical biology investigations with the synthesized compounds.

Received: May 5, 2003 [Z51805]

 © 2003 Wiley-VCH Verlag GmbH & Co. KGaA, Weinheim

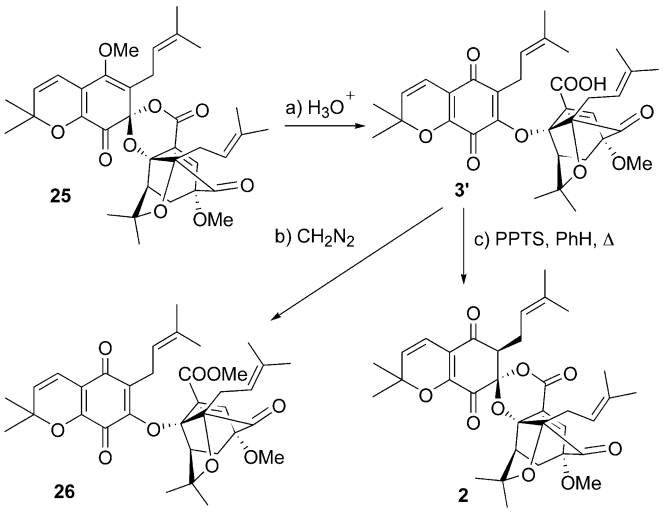


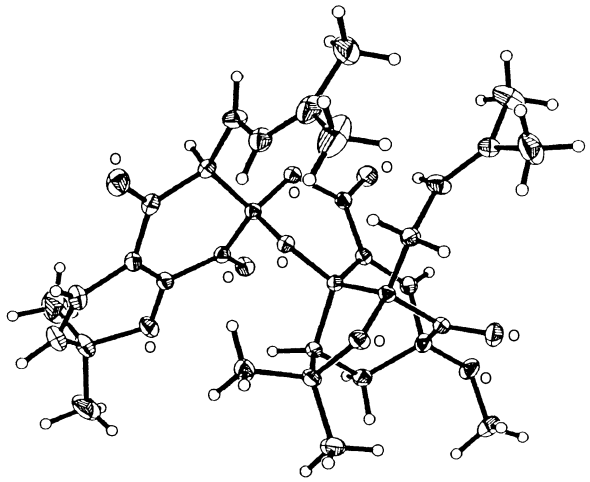


ORTEP drawing of **25**

Scheme 5. Synthesis and ORTEP drawing of 1,1′-*O*,*O*-dimethyllateriflorone (**25**): a) $PhI(OCOCF_3)_2$ (1.2 equiv), CH_2Cl_2, −78→25 °C, 2 h, 43%; b) $PhI(OCOCF_3)_2$ (1.2 equiv), CH_2Cl_2/MeOH (1:1), −78→25 °C, 2 h, 60%; c) PPTS (1.0 equiv), benzene, reflux, 4 h, **3** (11%) and **25** (69%). PPTS = pyridinium *p*-toluenesulfonate.

Keywords: cascade reactions · Claisen rearrangement · Diels–Alder reactions · electrocyclic reactions · natural products · quinones





ORTEP drawing of **2**

Scheme 6. Synthesis and ORTEP drawing of 1-*O*-methyllateriflorone (**2**): a) aqueous HCl (1 N), THF, 0→25 °C, 16 h, 80%; b) CH_2N_2, diethyl ether, 0 °C, 30 min, 81%; c) PPTS (1.0 equiv), benzene, reflux, 4 h, 83%.

[1] S. Kosela, S.-G. Cao, X.-H. Wu, J. J. Vittal, T. Sukri, Masdianto, S.-H. Goh, K.-Y. Sim, *Tetrahedron Lett.* **1999**, *40*, 157–160.

[2] For the isolation and structure elucidation, see: Y.-W. Leong, L. J. Harrison, G. J. Bennett, H. T.-W. Tan, *J. Chem. Res. Synop.* **1996**, 392–393.

[3] For the total synthesis of 1-*O*-methyl forbesione, see: K. C. Nicolaou, J. Li, *Angew. Chem.* **2001**, *113*, 4394–4398; *Angew. Chem. Int. Ed.* **2001**, *40*, 4264–4268.

[4] For related synthetic studies on lateriflorone, see: a) E. J. Tisdale, C. Chowdhury, B. G. Vong, H. Li, E. A. Theodorakis, *Org. Lett.* **2002**, *4*, 909–912; b) E. J. Tisdale, H. Li, B. G. Vong, S. H. Kim, E. A. Theodorakis, *Org. Lett.* **2003**, *5*, 1491–1494; c) E. J. Tisdale, B. G. Vong, H. Li, S. H. Kim, C. Chowdhury, E. A. Theodorakis, *Tetrahedron*, in press.

[5] K. A. Parker, A. T. Georges, *Org. Lett.* **2000**, *2*, 497–499.

[6] J. D. Godfrey, Jr., R. H. Mueller, T. C. Sedergran, N. Soundararajan, V. J. Colandrea, *Tetrahedron Lett.* **1994**, *35*, 6405–6408.

[7] A. J. Quillinan, F. Scheinmann, *J. Chem. Soc. Perkin Trans. 1* **1972**, 1382–1387.

[8] CCDC-209801 (**6′**), CCDC-209802 (**4**), and CCDC-209803 (**2**) contain the supplementary crystallographic data for this paper. These data can be obtained free of charge via www.ccdc.cam.ac.uk/conts/retrieving.html (or from the Cambridge Crystallographic Data Centre, 12, Union Road, Cambridge CB21EZ, UK; fax: (+44) 1223-336-033; or deposit@ccdc.cam.ac.uk).

[9] A. J. Quillinan, F. Scheinmann, *J. Chem. Soc. Chem. Commun.* **1971**, 966–967.

[10] For related applications of hypervalent iodine reagents to dearomatize benzenoid systems, see: a) A. Varvoglis, *Tetrahedron* **1997**, *53*, 1179–1255; b) Y. Kita, H. Tohma, K. Kikuchi, M. Inagaki, T. Yahura, *J. Org. Chem.* **1991**, *56*, 435–438; c) G. Scheffler, H. Seike, E. J. Sorensen, *Angew. Chem.* **2000**, *112*, 4785–4788; *Angew. Chem. Int. Ed.* **2000**, *39*, 4593–4596; d) A. Pelter, R. S. Ward, *Tetrahedron* **2001**, *57*, 273–282; e) H. Tohma, H. Morioka, S. Takizawa, M. Arisawa, Y. Kita, *Tetrahedron* **2001**, *57*, 345–352; f) S. Canesi, P. Belmont, D. Bouchu, L. Rousset, M. A. Ciufolini, *Tetrahedron Lett.* **2002**, *43*, 5193–5195.

 © 2003 Wiley-VCH Verlag GmbH & Co. KGaA, Weinheim

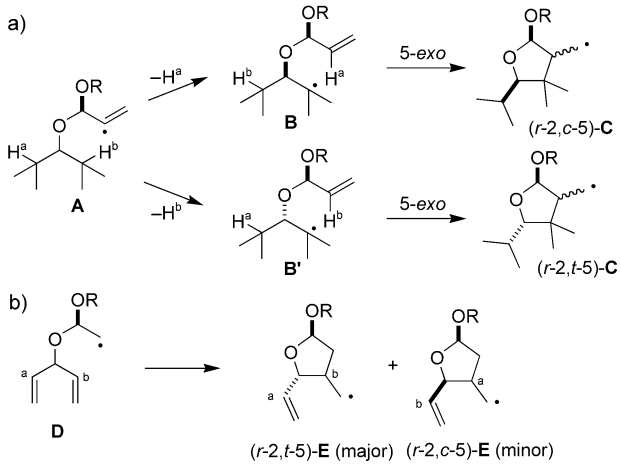
Stereoselective Radical Reactions

Diastereoselective Radical-Mediated Hydrogen-Atom Abstraction**

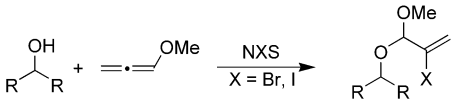
Philippe Renaud, Florent Beaufils, Laurence Feray, and Kurt Schenk*

Radical reactions are becoming a very valuable tool for organic synthesis.[1] The mildness of the reaction conditions, their complementary nature to ionic processes, and the possibility of carrying out sequential reactions (cascade reactions) are some of the key factors of their success. Radical reactions can be used for highly stereoselective bond-forming reactions.[2] The stereochemistry of radical cyclizations has been studied extensively and reliable stereoselectivity rules (the Beckwith–Schiesser–Houk model) have been proposed.[3,4] Hydrogen-atom abstraction (also called radical translocation) is a bond-breaking–bond-forming process that is frequently encountered in radical reactions.[5] With proper design of substrates, radical translocation represents a unique mode for remote functionalization of unreactive C–H bonds. Until now, stereoselective hydrogen-atom abstractions have been considered as curiosities.[6–8] Herein we report examples of diastereoselective hydrogen-atom abstractions from chiral acetals and show that the stereochemical outcome is governed by rules similar to those developed for related cyclization processes.

We decided to investigate vinyl radicals of type **A** as model systems (Scheme 1 a).[9] The two hydrogen atoms H^a and H^b are diastereotopic, and hydrogen-atom abstraction can produce two diastereomeric radicals **B** and **B′** that cyclize to produce the tetrahydrofurans (*r*-2,*c*-5)-**C** and (*r*-2,*t*-5)-**C**, respectively.[10] The stereochemical outcome of these reactions will be then compared with that of the selective cyclization of the related systems **D** to **E**, which has been thoroughly investigated by us (Scheme 1 b).[11–13] The radical precursors were readily prepared from the corresponding alcohols, 1-methoxyallene, and *N*-bromo- or *N*-iodosuccinimide, according to Equation (1).[14]

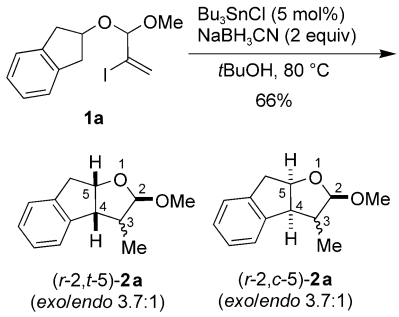


Scheme 1. a) Proposed radical 1,5-H abstraction and cyclization; b) stereoselective cyclization of a related system.



(1)

The reaction conditions for the hydrogen abstraction were optimized with substrate **1a** [Eq. (2)]. Attempts to carry out the reaction in benzene with the slow addition of tributyltin



(2)

hydride were unsuccessful, presumably because of the reaction of the intermediate alkenyl radical with benzene. Very reliable results were obtained by using the method of Stork et al. for the in situ generation of tin hydride in *tert*-butyl alcohol.[15] The best results were obtained by using Bu_3SnCl (5–10 mol%) in the presence of 2 equivalents of $NaBH_3CN$ in refluxing *tert*-butyl alcohol. A mixture of four diastereomers of **2a** was obtained. The two major diastereomers had the configuration *r*-2,*t*-5, and both result from the same diastereoselective hydrogen-atom abstraction. The stereoselectivity of the H-abstraction step (84:16) was determined from the ratio (*r*-2,*t*-5)-**2a**/(*r*-2,*c*-5)-**2a**. The cyclization step is stereoselective at C4 (*r*-2,*t*-4, *cis* ring junction) but not at C3 ((*r*-2,*c*-3)/(*r*-2,*t*-3) or *exo*/*endo* 3.7:1).

The stereochemistry of the hydrogen-atom abstraction is best explained by the chairlike model **F** depicted in Scheme 2. This model closely parallels model **G**, which has been

[*] Prof. Dr. P. Renaud, F. Beaufils
Department of Chemisty and Biochemistry, University of Berne
Freiestrasse 3, 3000 Berne 9 (Switzerland)
Fax: (+41) 31-631-3426
E-mail: philippe.renaud@ioc.unibe.ch
Dr. L. Feray
Department of Chemistry, University of Fribourg
Pérolles, 1700 Fribourg (Switzerland)
Dr. K. Schenk
Institute of Crystallography, BP, University of Lausanne
1015 Lausanne (Switzerland)

[**] This work was supported by the Swiss National Science Foundation (grant 21-67106.01). We thank A. Saxer for measuring the *ee* value of (+)-**5** by gas chromatography and for his assistance in the separation of the enantiomers of **3**.

Supporting information for this article is available on the WWW under http://www.angewandte.org or from the author.

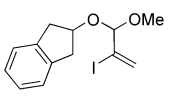
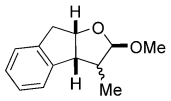
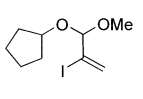
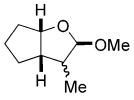
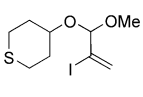
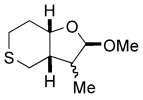
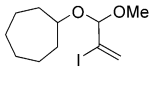
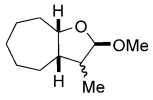
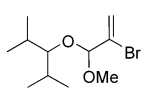
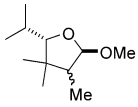
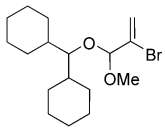
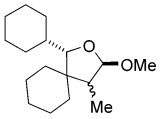
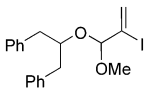
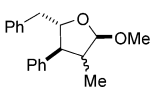
 © 2003 Wiley-VCH Verlag GmbH & Co. KGaA, Weinheim DOI: 10.1002/anie.200351829

proposed based on experimental results and ab initio calculations for the Ueno–Stork cyclization reaction.[12] The 2-methoxy group occupies an axial position as a result of the anomeric effect, and the nonreacting group at C5 is in a pseudoequatorial position. The observed level of stereoselectivity at 80 °C is very similar for both processes (H-abstraction 84:16, cyclization 86:14).[9] The stereochemical outcome of the subsequent cyclization step can be rationalized by model **H**, whereby the major diastereomer results from a chairlike transition state and the minor from a boatlike transition state.

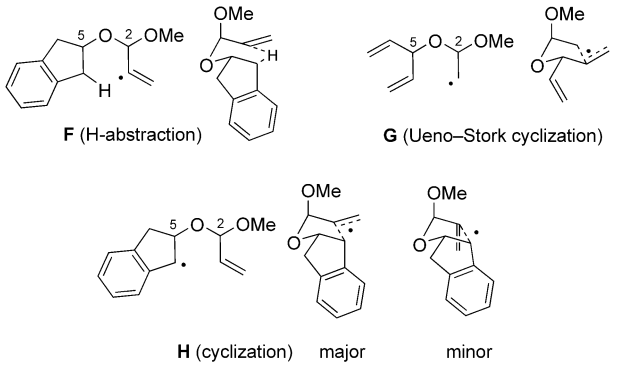
The reaction was then tested on several other haloacetals, and the results are described in Table 1. In the reactions of the cyclic alcohols **1b–d**, the stereoselectivity proved to be good for the five-, six- and seven-membered rings (**2b**: d.r. 89:11; **2c**: d.r. 94:6; **2d**: d.r. 86:14). The acyclic alcohols **1f–h** were also examined, and these underwent cyclization to the desired tetrahydrofurans **2f–h** with a similar level of stereoselectivity (d.r. 86:14) for the hydrogen-abstraction step.

This stereoselective hydrogen-atom-abstraction–cyclization is of synthetic interest and may find application in the preparation of diverse polysubstituted tetrahydrofurans. To demonstrate this point, we prepared the α-methylenelactone **5** with a tin-free hydrogen-atom-abstraction–cyclization as a key step (Scheme 3).[16,17] The propynal acetal **3**, which is readily available from the iodoacetal **1a**, was treated with thiophenol/AIBN to give the cyclic tetrasubstituted tetrahydrofuran (*r*-2,*t*-5)-**4** in 67% yield as a 2:1 mixture of *endo*/*exo* or (*r*-2,*t*-3)/(*r*-2,*c*-3) isomers.[18] Both products result from the same stereoselective hydrogen abstraction. The products of the minor H-abstraction were not isolated.[19] Oxidation of the cyclic acetal **4** with

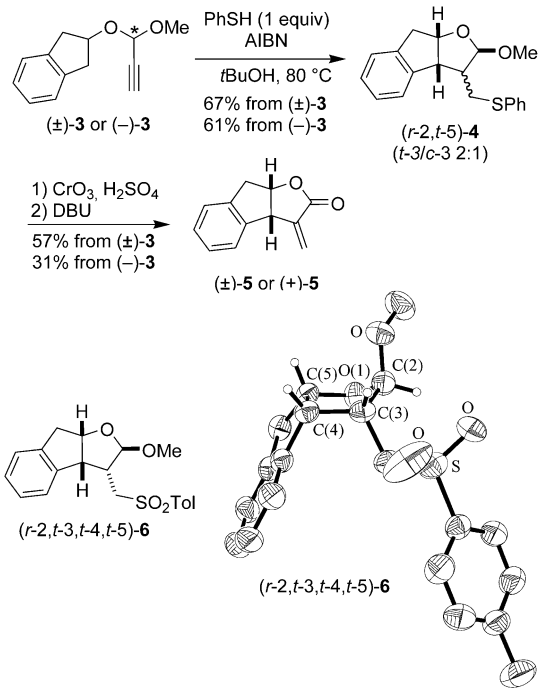
Table 1: Synthesis of polysubstituted tetrahydrofurans **2** through an initial stereoselective hydrogen abstraction and subsequent cyclization.[a]

	1	2[b]	(*r*-2,*t*-5)/(*r*-2,*c*-5)[c]	(*r*-2,*c*-3,*t*-5)/(*r*-2,*t*-3,*t*-5)[d]	Yield [%]
a			84:16	3.7:1	66
b			89:11	2.3:1	44
c			94:6	1.8:1	44
d			86:14	2.9:1	78
e			86:14	1.5:1	80
f			86:14	2.3:1	81
g			86:14	3.3:1	74

[a] See Equation (2) for reaction details. [b] Major isomer *r*-2,*t*-5 is shown. [c] d.r. for the hydrogen-atom abstraction. [d] d.r. for the cyclization of the radical intermediate resulting from the major H-abstraction product; stereochemistry at C4 is entirely controlled as indicated.



Scheme 2. Transition-state conformations for radical hydrogen-atom abstractions and radical cyclizations.



Scheme 3. Synthesis of racemic and nonracemic **5**, and X-ray crystal structure of **6**; AIBN = azobisisobutyronitrile, DBU = 1,8-diazabicyclo[5.4.0]undec-7-ene.

 © 2003 Wiley-VCH Verlag GmbH & Co. KGaA, Weinheim

an excess of CrO_3/H_2SO_4 followed by treatment of the crude oxidation product with DBU afforded the diastereomerically pure α-methylenelactone **5** in 57% yield. The relative configuration of the two stereoisomers of compound **4** were determined from NOE difference spectra. This result was confirmed by X-ray crystal-structure analysis of the sulfone **6**, prepared from **3** by reaction with thiocresol followed by oxidation of the major diastereomer with magnesium monoperphthalate.[20]

At this point, it was interesting to demonstrate that the transformation of **3** into **5** described above is applicable to the preparation of the nonracemic α-methylenelactone **5**. For this purpose, the racemic propynal acetal **3** was resolved by HPLC separation (Daicel Chiralcel OJ column; see Supporting Information). The α-methylenelactone (+)-**5** was obtained in 88% *ee* from enantiomerically enriched (−)-**3** (96% *ee*) according to the reaction sequence described above for (±)-**5**. As no separation of the diastereomers of the intermediate cyclized product **4** was attempted, the diastereoselectivity of the hydrogen-abstraction step can be estimated to be greater than 95:5. This is in agreement with the results obtained in the racemic series, for which only two diastereomers of **4** were detected resulting from a diastereoselective (>95:5) hydrogen abstraction.

In conclusion, we have demonstrated that hydrogen-atom abstraction can be highly stereoselective. The stereochemical outcome of the hydrogen abstractions can be explained by a model related to that developed for radical cyclizations. These results represent a step toward the development of stereoselective processes for the remote activation of centers that are usually unreactive under classical reaction conditions. For instance, by using acetals of type **1** and **3**, it is possible to activate alcohols at the β position. The chromatographic resolution of the starting acetals and the use of a chiral auxiliary to control the absolute stereochemistry at the acetal chiral center[11,13,21–23] should facilitate access to optically pure polysubstituted tetrahydrofurans and γ-lactones. Further work toward this goal is currently underway.

Experimental Section

Tin hydride mediated H-abstraction: Tributyltin chloride (13 μL, 0.05 mmol) and sodium cyanoborohydride (126 mg, 2.00 mmol) were added to a solution of the iodoacetal (1.00 mmol) in *t*BuOH (100 mL) at room temperature under a nitrogen atmosphere. The reaction mixture was stirred at reflux for 5 h. After disappearance of the starting iodoacetal (monitored by TLC), the solution was cooled, and the *t*BuOH was evaporated under reduced pressure. The residue was filtered through silica gel, and the filtrate was evaporated under reduced pressure. Flash chromatography (AcOEt/hexane or Et_2O/pentane) of the residue afforded the desired cyclic compounds. The isomeric ratio was determined from ^{1}H NMR spectra of the crude product.

Thiophenol-mediated H-abstraction: A solution of AIBN (164 mg, 1.00 mmol) in benzene (2 mL) and a solution of thiophenol (110 mg, 1.00 mmol) in benzene (2 mL) were added by a syringe pump over 20 h to a solution of the dialkoxypropyne **3** (202 mg, 1.00 mmol) and AIBN (80 mg, 0.5 mmol) in refluxing *t*BuOH (100 mL). After disappearance of the starting acetal **3** (monitored by TLC), the solution was cooled, then concentrated under reduced pressure. The residue was filtered through silica gel, and the filtrate was concentrated under reduced pressure. Flash chromatography (AcOEt/hexane) of the residue afforded **4** (209 mg, 67% yield). The isomeric ratio was determined from ^{1}H NMR spectra of the crude product.

See Supporting Information for experimental procedures and characterization of compounds **1**–**6**.

Received: May 7, 2003 [Z51829]

Keywords: acetals · asymmetric synthesis · hydrogen transfer · lactones · radical reactions

[1] P. Renaud, M. P. Sibi, Wiley-VCH, Weinheim, **2001**.
[2] D. P. Curran, N. A. Porter, B. Giese, *Stereochemistry of Radical Reactions*, VCH, Weinheim, **1995**.
[3] A. L. J. Beckwith, C. H. Schiesser, *Tetrahedron* **1985**, *41*, 3925.
[4] D. C. Spellmeyer, K. N. Houk, *J. Org. Chem.* **1987**, *52*, 959.
[5] L. Feray, N. Kouznetsov, P. Renaud, in *Radicals in Organic Synthesis, Vol. 2* (Eds.: P. Renaud, M. P. Sibi), Wiley-VCH, Weinheim, **2001**, p. 246.
[6] For a remarkable example of a diastereoselective hydrogen-atom-abstraction process, see: S. Bogen, M. Gulea, L. Fensterbank, M. Malacria, *J. Org. Chem.* **1999**, *64*, 4920.
[7] Diastereoselective hydrogen-atom abstractions have been reported for *o*-bromophenyl sulfoxides: C. Imboden, F. Villar, P. Renaud, *Org. Lett.* **1999**, *1*, 873.
[8] For an example of a hydrogen-atom abstraction involving a diastereotopic hydrogen atom, see: T. Sugimura, S. Goto, K. Koguro, T. Futagawa, S. Misaki, Y. Morimoto, N. Yasuoka, A. Tai, *Tetrahedron Lett.* **1993**, *34*, 505.
[9] Radical translocation of vinyl radicals is a well-documented process, and a qualitative parallel between substituent effects on 1,5-hydrogen transfer and 5-*exo* radical cyclization processes has been emphasized: D. P. Curran, W. Shen, *J. Am. Chem. Soc.* **1993**, *115*, 6051.
[10] For the stereochemical nomenclature used in this paper, see: R. Panico, W. H. Powell, J.-C. Richer, *A Guide to IUPAC Nomenclature of Organic Compounds, Recommendation 1993*, Blackwell, Oxford, **1993**.
[11] F. Villar, O. Equey, T. Kolly-Kovac, P. Renaud, *Chem. Eur. J.* **2003**, *9*, 1566.
[12] O. Corminboeuf, P. Renaud, C. H. Schiesser, *Chem. Eur. J.* **2003**, *9*, 1578.
[13] F. Villar, O. Equey, P. Renaud, *Org. Lett.* **2000**, *2*, 1061.
[14] Y. Ueno, O. Moriya, K. Chino, M. Watanabe, M. Okawa, *J. Chem. Soc. Perkin Trans. 1* **1986**, 1351.
[15] G. Stork, P. M. Sher, *J. Am. Chem. Soc.* **1986**, *108*, 303.
[16] Thiophenol has been used in a related synthesis of 2,3-disubstituted tetrahydrofurans: S. D. Burke, K. W. Jung, *Tetrahedron Lett.* **1994**, *35*, 5837.
[17] Preliminary investigations in our laboratory showed that this tin-free procedure is very general. This highly attractive method will be discussed elsewhere.
[18] The relative configurations at C3 of the major and minor products are reversed relative to **2a**. This is presumably a result of steric interactions between the OMe and the CH_2SPh groups that destabilize the chairlike transition state of the cyclization (see Scheme 2, model **H**).
[19] Several unidentified isomeric side products with a combined yield of less than 15% were removed during the chromatographic purification of **4**.
[20] The tolyl sulfone **6** is a colorless crystalline compound, whereas the corresponding phenyl sulfone is an oil. CCDC-209583 contains the supplementary crystallographic data for this paper. These data can be obtained free of charge via www.ccdc.cam.ac.uk/conts/retrieving.html (or from the Cambridge Crystallographic Data Centre, 12, Union Road, Cam-

 © 2003 Wiley-VCH Verlag GmbH & Co. KGaA, Weinheim

bridge CB21EZ, UK; fax: (+44) 1223-336-033; or deposit@ccdc.cam.ac.uk).
[21] F. Villar, P. Renaud, *Tetrahedron Lett.* **1998**, *39*, 8655.
[22] R. McCague, R. G. Pritchard, R. J. Stoodley, D. S. Williamson, *Chem. Commun.* **1998**, 2691.
[23] M. S. Idris, D. S. Larsen, R. G. Pritchard, A. Schofield, R. J. Stoodley, P. D. Tiffin, *J. Chem. Soc. Perkin Trans. 1* **2000**, 2195.

 © 2003 Wiley-VCH Verlag GmbH & Co. KGaA, Weinheim

Organocatalytic Domino Reactions

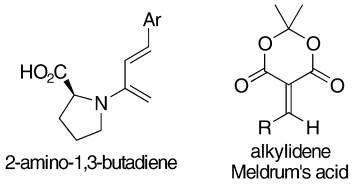
Organocatalytic Asymmetric Domino Knoevenagel/Diels–Alder Reactions: A Bioorganic Approach to the Diastereospecific and Enantioselective Construction of Highly Substituted Spiro[5,5]undecane-1,5,9-triones**

*D. B. Ramachary, Naidu S. Chowdari, and Carlos F. Barbas III**

One of the ultimate goals in organic chemistry is the catalytic asymmetric assembly of simple and readily available precursor molecules into stereochemically complex products. In this regard, the Diels–Alder reaction is one of the most powerful synthetic methodologies for the construction of cyclic six-membered rings, and tremendous efforts have been directed to expand the scope of this cycloaddition reaction with various combinations of dienes, dienophiles, catalysts, and reaction conditions.[1] Recently organocatalysis has emerged as a promising synthetic tool for constructing C–C and C–N bonds in aldol,[2] Michael,[3] Mannich,[4] Diels–Alder,[5] and related reactions[6] with high diastereoselectivity and enantioselectivity. Structurally simple and stable chiral organoamines typically facilitate iminium- and enamine-based transformations with carbonyl compounds and may be used as catalysts in operationally simple, and in some cases environmentally friendly, experimental protocols. Previously we extended our studies of organoamine-catalyzed aldol,[2a–d] Michael,[3a,b] Mannich,[4a–f] and related reactions[6c,e] founded on enamine catalysis, and reported the first direct asymmetric Diels–Alder reactions of α,β-unsaturated ketones with nitro olefins.[5a]

In continuation of our interest in organocatalytic assembly or multicomponent reactions,[2c,d,4c,6e] we herein report the first organocatalytic diastereospecific and enantioselective direct asymmetric domino Knoevenagel/Diels–Alder reactions that produce highly substituted spiro[5,5]undecane-1,5,9-triones **5** from commercially available 4-substituted-3-buten-2-ones **1a–e**, aldehydes **2a–d**, and 2,2-dimethyl-1,3-dioxane-4,6-dione (Meldrum's acid, **3**; Scheme 1). Spirocyclic ketones **5** are attractive intermediates in the synthesis of natural products and in medicinal chemistry,[7] and are the starting materials for the synthesis of exotic amino acids which are used to modify the physical properties and biological activities of peptides, peptidomimetics, and proteins.[8]

In our reaction we envisioned that an amino acid would catalyze the domino Knoevenagel condensation[9] of aldehyde **2** with Meldrum's acid **3** to provide the alkylidene derivative of Meldrum's acid, which would then undergo a concerted [4+2] cycloaddition with a 2-amino-1,3-butadiene generated in situ from enone **1** and an amino acid to form substituted



spiro[5,5]undecane-1,5,9-triones **5** in a highly enantioselective and diastereospecific manner.[10] The domino Knoevenagel/Diels–Alder reaction would then generate a quaternary center with formation of three new carbon–carbon σ bonds through amino acid catalysis. This proposal was reflective of the pioneering studies of Tietze and Beifuss[11a,b] and our recent disclosure of the first direct asymmetric Knoevenagel/Michael reactions with ketones, aldehydes, and malonates involving alkylidene malonates generated under organocatalysis that subsequently react as electrophiles with ketone-derived enamines also generated under organocatalysis.[3a] In contrast to this early study where asymmetric induction was compromised by the use of the cyclic malonate Meldrum's acid, the alkylidene derivative of Meldrum's acid proved to be more efficient in the Diels–Alder reaction than the alkylidene formed from alkyl malonates.

We were pleased to find that the three-component reaction of *trans*-4-phenyl-3-buten-2-one (**1a**), 4-nitrobenzaldehyde (**2a**), and Meldrum's acid (**3**) with a catalytic amount of L-proline in methanol at ambient temperature furnished the Diels–Alder product **5aa** as a single diastereomer in 85% yield with 60% *ee* after 48 h (Table 1, entry 6). This product was accompanied by an unexpected symmetric spirocyclic ketone **6aa** in 7% yield.[12] The stereochemistry of products **5aa** and **6aa** was established by NMR analysis.

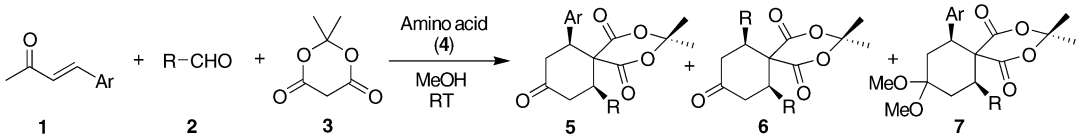
In the asymmetric three-component Diels–Alder (ATCDA) reaction of **1a**, **2a**, and **3** catalyzed directly by L-proline, we found that the solvent (dielectric constant) had a

[*] Prof. Dr. C. F. Barbas III, Dr. D. B. Ramachary, Dr. N. S. Chowdari
The Skaggs Institute for Chemical Biology
The Scripps Research Institute
10550 North Torrey Pines Road
La Jolla, CA 92037 (USA)
Fax: (+1) 858-784-2583
E-mail: carlos@scripps.edu

[**] This study was supported in part by the National Institutes of Health (CA27489) and the Skaggs Institute for Chemical Biology. We thank Dr. Raj K. Chadha for X-ray structural analysis.

Supporting information (experimental procedures and analytical data for all new compounds) for this article is available on the WWW under http://www.angewandte.org or from the author.

 DOI: 10.1002/anie.200351916 © 2003 Wiley-VCH Verlag GmbH & Co. KGaA, Weinheim



Scheme 1. Amino acid catalyzed asymmetric, three-component Diels–Alder reactions.

Table 1: Effect of solvent on the direct amino acid catalyzed ATCDA reaction of **1a**, **2a**, and **3**.[a]

Entry	Amino acid	Solvent	Dielectric constant [ε]	t [h]	Products	Yield [%][b]	Ratio[c] **5aa**:**6aa**	*ee* for **5aa** [%][d]
1	L-proline	C_6H_6	2.3	72	**5aa**	$\leq$10	100:0	nd[e]
2	L-proline	$CHCl_3$	4.8	72	**5aa**	24	100:0	71
3	L-proline	THF	7.6	72	**5aa**	70	100:0	65
4	L-proline	CH_2Cl_2	8.9	72	**5aa**	35	100:0	59
5	L-proline	C_2H_5OH	25	48	**5aa**, **6aa**	95	18:1	38
6	L-proline	CH_3OH	33	48	**5aa**, **6aa**	92	12:1	60
7	L-proline	CH_3CN	38	72	**5aa**	65	100:0	9
8	L-proline	[bmim]BF_4	–	24	**5aa**	95	100:0	6
9	thiaproline	*n*-C_3H_7OH	21.8	96	**5aa**, **6aa**	70	20:1	19
10	thiaproline	*iso*-C_3H_7OH	18.3	96	**5aa**, **6aa**	65	20:1	39
11[f]	DL-proline	(*S*)-$CH_3CHPhOH$	13	96	**5aa**	71	100:0	37

[a] Experimental conditions: Amino acid (0.1 mmol) was added to a stirred solution of enone (1 mmol), **2a** (0.5 mmol), and **3** (0.5 mmol) in the solvent (1 mL) at ambient temperature (see Supporting Information). [b] Yield refers to the purified product obtained by column chromatography. [c] Ratio based on isolated products. [d] Enantiomeric excesses determined by using chiral-phase HPLC. [e] not determined. [f] In this reaction, 0.75 mL of (*S*)-1-phenylethanol was used.

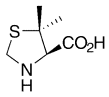
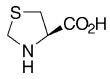
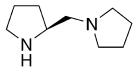
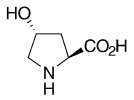
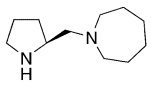
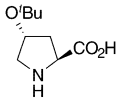
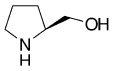
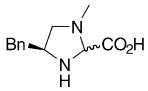
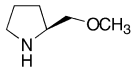
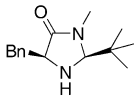
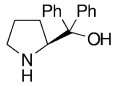
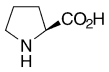
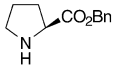
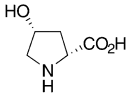
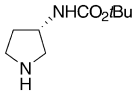
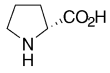
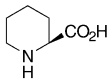
significant effect on the rates, yields, and *ee* values (Table 1). These results indicated that the domino Knoevenagel/Diels–Alder reaction catalyzed by L-proline produces products **5aa** and **6aa**[12] with low yields and good *ee* values in aprotic nonpolar solvents (Table 1, entries 2–4) and with excellent yields and good to moderate *ee* values in protic solvents (Table 1, entries 5 and 6). The same reaction in the ionic liquid [bmim]BF_4 (bmim = 1-butyl-3-methylimidazolium) provided **5aa** in 95% yield, albeit with a low *ee* value of 6% (Table 1, entry 8). The rates of both the Knoevenagel and Diels–Alder reactions catalyzed by L-proline were faster in protic/polar solvents than in nonprotic/nonpolar solvents presumably because of enhanced stabilization of charged intermediates and more-facile proton-transfer reactions. The transition state of the bimolecular Diels–Alder reaction is also effected by protic/polar solvents through hydrogen bonding.[1d,e]

To understand the role of solvent in this reaction aldehyde **2a**, Meldrum's acid (**3**), and enone **1a** were reacted in the chiral solvent (*S*)-1-phenylethanol, under DL-proline catalysis. The expected spiro product **5aa** was obtained in 71% yield, with an *ee* value of 37% (Table 1, entry 11). Thus, asymmetric induction can be effected by interactions with a chiral solvent. This finding supports a potential role of intermolecular hydrogen bonding, in standard achiral solvents, as a conduit for both transmission of chiral information from the prolyl-2-amino-1,3-butadiene and catalysis by lowering the activation barrier in a diastereotopic bimolecular Diels–Alder transition state. Intermolecular hydrogen bonding with the solvents serves these roles in the chiral protic solvent.

Next we probed the structure and reactivity relationships among a family of 19 pyrrolidine-based catalysts by monitoring the reaction yields and *ee* values of the ATCDA reaction of **1a**, **2a**, and **3** in methanol (Table 2). The structurally simple amine pyrrolidine catalyzed the ATCDA reaction to produce **5aa** in 14% yield and **6aa** in 17% yield (Table 2, entry 1). An imidazoline-type catalyst also catalyzed the ATCDA reaction (Table 2, entry 15). Among the catalysts screened, 5,5-dimethyl thiazolidinium-4-carboxylate (DMTC) proved to be the most efficient catalyst with respect to yield, and provided **5aa** in 88% yield and 86% *ee* (Table 2, entry 11), which is significantly better than L-proline in both respects (Table 2, entry 17). The overall structure/activity relationship garnered from the catalyst screen of the ATCDA reaction was similar to that which we reported for the aldol,[2b] with optimal yield and enantioselectivity being provided by pyrrolidine-amines substituted at the α-position with an acid functionality, that is, proline-like catalysts. Notable improvement in the enantioselectivity of the reaction beyond L-proline catalysis was found in the ATCDA reactions catalyzed by L-thiaproline, L-DMTC, and *trans*-4-hydroxy-L-proline. These amino acids catalyze the preferential addition of the in situ generated benzylidene derivative of Meldrum's acid **8** to the *exo* face of the in situ generated 2-amino-1,3-butadiene. It should

 © 2003 Wiley-VCH Verlag GmbH & Co. KGaA, Weinheim

Table 2: Effect of the structure/reactivity of the amino acid on the direct amino acid catalyzed ATCDA reaction of **1a**, **2a**, and **3** in methanol at 25 °C.[a]

Entry	Amine	*t* [h]	Yield [%][b] **5aa**	Yield [%][b] **6aa**	*ee* for **5aa** [%][c]	Entry	Amine	*t* [h]	Yield [%][b] **5aa**	Yield [%][b] **6aa**	*ee* for **5aa** [%][c]
1		48	14	17	–	11		72	88	trace	86
2		120	10	8	41	12		84	65	trace	89
3[d]		72	56	12	45	13		96	50	4	91
4		72	80	13	24	14		84	84	trace	76
5		96	12	17	68	15[e]		96	64	14	70
6		120	12	17	65	16		72	–	–	–
7		120	10	9	32	17		48	85	7	60
8		96	23	trace	35	18		84	70	trace	60
9		48	40	34	40	19		72	80	trace	34
10		120	7	17	60						

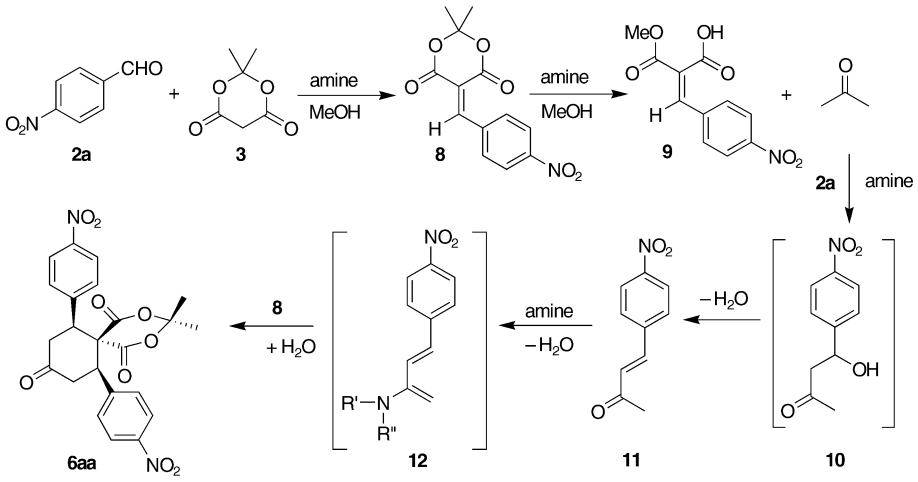
[a] See Supporting Information. [b] Yield refers to the column purified product. [c] Enantiomeric excesses were determined by using chiral-phase HPLC. [d] Reaction was performed in THF. [e] Reaction performed at 4 °C.

be noted that L-DMTC was also found to be generally more efficient than L-proline in aldol reactions involving aromatic acceptors.[2b]

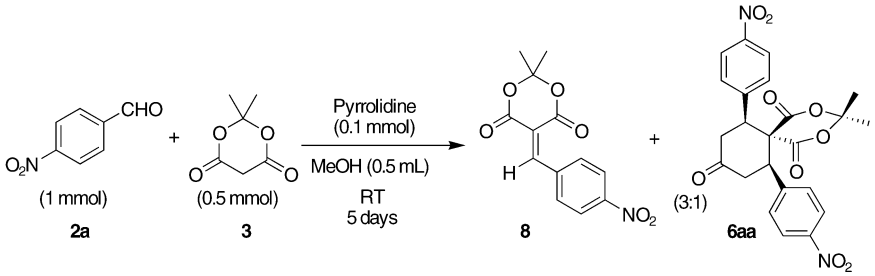
Formation of the unexpected symmetric triketone **6aa** in the reaction of **1a**, **2a**, and **3** can be explained as shown in Scheme 2. Amine-catalyzed Knoevenagel condensation of **2a** with **3** provides the 4-nitrobenzelidene derivative of Meldrum's acid **8**, which undergoes a Diels–Alder or a double Michael reaction with the soft nucleophilic 2-amino-1,3-butadiene generated in situ from enone **1a** and an amine to produce product **5aa.** Otherwise the in situ generated hard nucleophile methoxide (MeO^-) can react with **8** to regenerate acetone; the yield of this regeneration will depend on the basicity of the amine catalyst. Acetone undergoes amine-catalyzed aldol condensation with aldehyde **2a** to furnish enone **11**, which reacts with an amine to form reactive 2-amino-1,3-butadiene **12**, which undergoes a diastereospecific Diels–Alder reaction with dienophile **8** to furnish the ketone **6aa**. Regeneration of acetone and formation of prochiral ketone **6aa** were confirmed by the pyrrolidine-catalyzed reaction between **2a** and **3** in methanol (Scheme 3).

We further explored the scope of the DMTC-catalyzed ATCDA reaction with various aldehydes **2a–d** and enones **1a–e**. The spirotriones **5** were obtained as single diastereomers with good yields and excellent *ee* values together with the accompanying corresponding acetals **7**[13] in low yields. The reaction of benzaldehyde (**2c**), piperonal (**2d**), and Meldrum's acid (**3**) with enones **1a** and **1b** furnished the prochiral spirotriones **5ac** and **5bd**, respectively, in excellent yields (Table 3, entry 1 and 2). In the same manner, the reaction of *para*-substituted benzaldehydes **2a–b** and Meldrum's acid (**3**) with a variety of enones **1a–e** in methanol

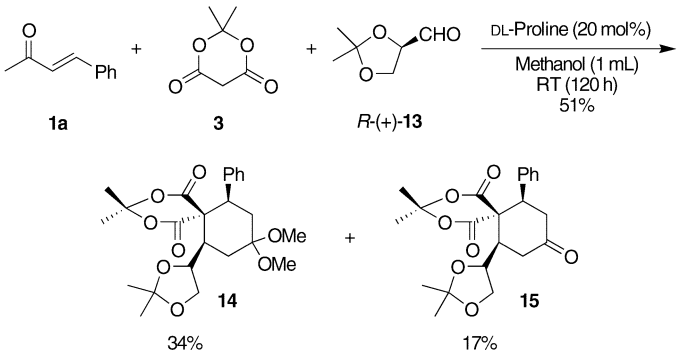
 © 2003 Wiley-VCH Verlag GmbH & Co. KGaA, Weinheim



Scheme 2. Proposed reaction mechanism for the formation of the unexpected product: prochiral cyclohexanone **6aa**.



Scheme 3. Formation of prochiral spirocyclic ketone **6aa** from 4-nitrobenzaldehyde (**2a**) and Meldrum's acid (**3**).



Scheme 4. Proline-catalyzed diastereoselective three-component Diels–Alder reaction of enone **1a** and Meldrum's acid (**3**) with chiral aldehyde **13**.

Table 3: Direct DMTC-catalyzed ATCDA reaction of different aldehydes **2a–d** and enones **1a–e** with Meldrum's acid (**3**).[a]

Entry	Enone	Aldehyde	*t* [h]	Products	Yield [%][b]	Ratio **5**:**7**	*ee* for **5** [%][c]
1[d]	**1a**	**2c**	96	**5ac**, **7ac**	85	16:1	prochiral
2[d]	**1b**	**2d**	96	**5bd**	99	>100:1	prochiral
3	**1a**	**2a**	72	**5aa**, **7aa**	95	13:1	86
4	**1a**	**2b**	96	**5ab**, **7ab**	85	16:1	84
5	**1c**	**2a**	72	**5ca**	93	>100:1	99
6	**1d**	**2a**	72	**5da**, **7da**	92	12:1	88
7	**1e**	**2a**	72	**5ea**, **7ea**	80	15:1	99

[a] See Supporting Information. [b] Yield of the combined isolated products. [c] Enantiomeric excesses were determined using chiral-phase HPLC. [d] Reaction catalyzed by L-proline (0.1 mmol).

furnished the spirotriones **5** as single diastereomers in good yields with excellent *ee* values together with the corresponding acetals **7** in low yields (Table 3). Formation of acetals **7** from ketones **5** is most likely the result of acid or base catalysis of the bifunctional acid/base catalyst DMTC in methanol. Spirotrione **5bd** should be an attractive starting material for the synthesis of endothelin receptor antagonists.[7d]

The diastereoselective ATCDA reaction of α,β-unsaturated ketone **1a** and Meldrum's acid (**3**) with chiral aldehyde (*R*)-2,2-dimethyl-[1,3]dioxolane-4-carbaldehyde (**13**) in methanol at room temperature produced the expected Diels–Alder product acetal **14** and ketone **15** as the major products (Scheme 4). Thus, optically pure aldehydes can be used to effect diastereoselective synthesis of chiral, substituted cyclohexanones under organocatalysis.

The absolute configuration of product **5aa** prepared under DMTC catalysis was established by using X-ray crystallography.[14] Product **5aa** was obtained as colorless, block-shaped crystals from hexane-chloroform. Crystallization enriched the *ee* value to 99%. On the basis of X-ray structural analysis and AM1 calculations we propose a transition state for the DMTC-catalyzed direct ATCDA reaction (Figures 1 and 2).

In summary, we have developed the first direct ATCDA reaction catalyzed by an amino acid. This experimentally simple and environmentally friendly approach can be used to construct highly substituted spiro[5,5]undecane-1,5,9-triones in a diastereospecific and enantioselective fashion. Selective reactions of this type inspire analogies with enzyme-catalyzed reaction and compliment traditional Diels–Alder reactions. As we have suggested previously, the synthesis of polyfunctionalized molecules under organocatalysis provides a unique and under-

 © 2003 Wiley-VCH Verlag GmbH & Co. KGaA, Weinheim

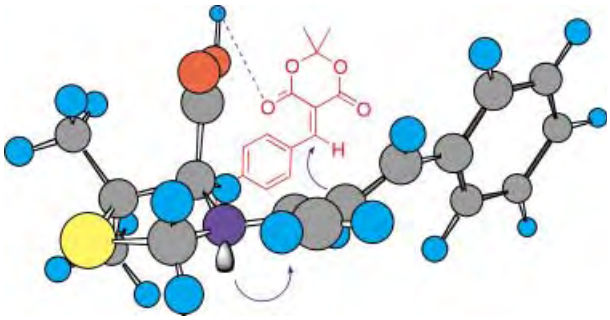


Figure 1. Proposed transition state for the DMTC-catalyzed ATCDA reaction based on AM1 calculations.

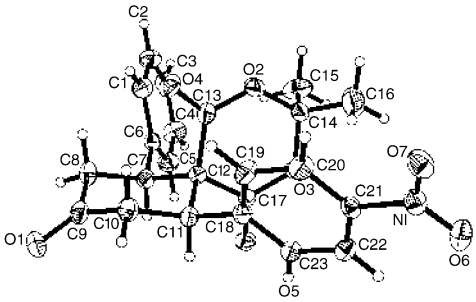


Figure 2. X-ray crystal structure of chiral spiro[5,5]undecane-1,5,9-trione **5aa**.

explored perspective on prebiotic synthesis. Given the efficiency of the organocatalysis of the Diels–Alder reaction, consideration should be given to the utilization of these types of reaction mechanisms in extant biological systems.

Received: May 16, 2003 [Z51916]

Keywords: amino acids · asymmetric catalysis · cycloaddition · domino reactions · enantioselectivity

[1] See for example a) D. A. Evans, J. S. Johnson, *Comprehensive Asymmetric Catalysis, Vol. III* (Eds.: E. N. Jacobsen, A. Pfaltz, H. Yamamoto), Springer, New York, **1999**, p. 1177; b) H. B. Kagan, O. Riant, *Chem. Rev.* **1992**, *92*, 1007; c) E. J. Corey, A. G. Perez, *Angew. Chem.* **1998**, *110*, 402; *Angew. Chem. Int. Ed.* **1998**, *37*, 388; d) Y. Huang, V. H. Rawal, *J. Am. Chem. Soc.* **2002**, *124*, 9662; e) P. R. Schreiner, A. Wittkopp, *Org. Lett.* **2002**, *4*, 217.

[2] a) B. List, R. A. Lerner, C. F. Barbas III, *J. Am. Chem. Soc.* **2000**, *122*, 2395; b) K. Sakthivel, W. Notz, T. Bui, C. F. Barbas III, *J. Am. Chem. Soc.* **2001**, *123*, 5260; c) A. Cordova, W. Notz, C. F. Barbas III, *J. Org. Chem.* **2002**, *67*, 301; d) N. S. Chowdari, D. B. Ramachary, A. Cordova, C. F. Barbas III, *Tetrahedron Lett.* **2002**, *43*, 9591; e) A. B. Northrup, D. W. C. MacMillan, *J. Am. Chem. Soc.* **2002**, *124*, 6798.

[3] a) J. M. Betancort, K. Sakthivel, R. Thayumanavan, C. F. Barbas III, *Tetrahedron Lett.* **2001**, *42*, 4441; b) J. M. Betancort, C. F. Barbas III, *Org. Lett.* **2001**, *3*, 3737; c) N. A. Paras, D. W. C. MacMillan, *J. Am. Chem. Soc.* **2002**, *124*, 7894; d) A. Alexakis, O. Andrey, *Org. Lett.* **2002**, *4*, 3611; e) N. Halland, R. G. Hazell, K. A. Jorgensen, *J. Org. Chem.* **2002**, *67*, 8331; f) B. List, C. Castello, *Synlett* **2001**, *11*, 1687.

[4] a) A. Cordova, W. Notz, G. Zhong, J. M. Betancort, C. F. Barbas III, *J. Am. Chem. Soc.* **2002**, *124*, 1842; b) A. Cordova, S. Watanabe, F. Tanaka, W. Notz, C. F. Barbas III, *J. Am. Chem. Soc.* **2002**, *124*, 1866; c) S. Watanabe, A. Cordova, F. Tanaka, C. F. Barbas III, *Org. Lett.* **2002**, *4*, 4519; d) A. Córdova, C. F. Barbas III, *Tetrahedron Lett.* **2002**, *43*, 7749; e) A. Córdova, C. F. Barbas III, *Tetrahedron Lett.* **2003**, *44*, 1923; f) W. Notz, K. Sakthivel, T. Bui, C. F. Barbas III, *Tetrahedron Lett.* **2001**, *42*, 199.

[5] a) R. Thayumanavan, D. B. Ramachary, K. Sakthivel, F. Tanaka, C. F. Barbas III, *Tetrahedron Lett.* **2002**, *43*, 3817; b) D. B. Ramachary, N. S. Chowdari, C. F. Barbas III, *Tetrahedron Lett.* **2002**, *43*, 6743; c) A. B. Northrup, D. W. C. MacMillan, *J. Am. Chem. Soc.* **2002**, *124*, 2458.

[6] a) Z. G. Hajos, D. R. Parrish, *J. Org. Chem.* **1974**, *39*, 1615; b) U. Eder, G. Sauer, R. Wiechert, *Angew. Chem.* **1971**, *83*, 492; *Angew. Chem. Int. Ed. Engl.* **1971**, *10*, 496; c) T. Bui, C. F. Barbas III, *Tetrahedron Lett.* **2000**, *41*, 6951; d) A. Bøgevig, K. Juhl, N. Kumaragurubaran, W. Zhuang, K. A. Jorgensen, *Angew. Chem.* **2002**, *114*, 1868; *Angew. Chem. Int. Ed.* **2002**, *41*, 1790; e) N. S. Chowdari, D. B. Ramachary, C. F. Barbas III, *Org. Lett.* **2003**, *5*, 1685.

[7] a) C. Hongchao, J. Xixian, L. Zhichang, *Huaxi Yaoxue Zazhi* **1995**, *10*, 150; b) C. Hongchao, *Faming Zhuanli Shenqing Gongkai Shuomingshu* **1999**, p. 7 CODEN: CNXXEV CN 1217330 A 19990526 (patent written in Chinese); c) D. R. Schroender, F. R. Stermitz, *Tetrahedron* **1985**, *41*, 4309; d) J. N. Xiang, P. Nambi, E. H. Ohlstein, J. D. Elliott, *Bioorg. Med. Chem.* **1998**, *6*, 695.

[8] a) D. R. Zitsane, I. T. Ravinya, I. A. Riikure, Z. F. Tetere, E. Y. Gudrinietse, U. O. Kalei, *Russ. J. Org. Chem.* **1999**, *35*, 1457; b) D. R. Zitsane, I. T. Ravinya, I. A. Riikure, Z. F. Tetere, E. Y. Gudrinietse, U. O. Kalei, *Russ. J. Org. Chem.* **2000**, *36*, 496; c) I. Bonnard, M. Rolland, C. Francisco, B. Banaigs, *Lett. Pept. Sci.* **1997**, *4*, 289.

[9] a) R. Tanikaga, N. Konya, K. Hamamura, A. Kaji, *Bull. Chem. Soc. Jpn.* **1988**, *61*, 3211; b) "The Knoevenagel reaction": L. F. Tietze, U. Beifuss in *Comprehensive Organic Synthesis, Vol. 2* (Eds.: B. M. Trost, I. Fleming), Pergamon, Oxford, **1991**, chap. 1.11, p. 341.

[10] For stoichiometric Diels–Alder reactions using iminium activated dienophiles, see M. E. Jung, W. D. Vaccaro, K. R. Buszek, *Tetrahedron Lett.* **1989**, *30*, 1893; for stoichiometric Diels–Alder reactions involving chiral 2-amino-1,3-butadienes, see J. Barluenga, A. S. Sobirino, L. A. Lopez, *Aldrichimica Acta* **1999**, *32*, 4. In both cases, the reaction rates are high but stoichiometric amounts of chiral amine are required for the additional synthetic step of preparing the isolable imine or diene.

[11] a) L. F. Tietze, U. Beifuss, *Angew. Chem.* **1993**, *105*, 137; *Angew. Chem. Int. Ed. Engl.* **1993**, *32*, 131; b) L. F. Tietze, *Chem. Rev.* **1996**, *96*, 115; c) Y. Oikawa, H. Hirasawa, O. Yonemitsu, *Chem. Pharm. Bull.* **1982**, *30*, 3092.

[12] Symmetric ketone **6aa** was generated only in alcoholic solvents and in low yields.

[13] Compounds **7da** and **7ea** are mixtures of acetal and methyl enol ethers (see Supporting Information).

[14] Crystal structure data for **5aa**: $C_{23}H_{21}NO_7$, $M_r = 423.41$, monoclinic, space group $P2_1/c$ (No. 14, C_{2h}^5), $a = 18.571(3)$, $b = 9.6564(16)$, $c = 11.9942(19)$ Å, $\alpha = 90$, $\beta = 106.511(3)$, $\gamma = 90°$, $V = 2062.2(6)$ Å^3, $T = 296(2)$ K, 17946 reflections collected. CCDC-205429 contains the supplementary crystallographic data for this paper. These data can be obtained free of charge via www.ccdc.cam.ac.uk/conts/retrieving.html (or from the Cambridge Crystallographic Data Centre, 12 Union Road, Cambridge CB21EZ, UK; fax: (+44) 1223-336-033; or deposit@ccdc.cam.ac.uk).

 © 2003 Wiley-VCH Verlag GmbH & Co. KGaA, Weinheim

Natural Product Synthesis

Total Synthesis of an Atropdiastereomer of RP-66453 and Determination of Its Absolute Configuration**

*Michèle Bois-Choussy, Pierre Cristau, and Jieping Zhu**

RP-66453 (**1**), a secondary metabolite, was isolated from an *Actinomycetes* strain by Helynck and co-workers at Rhône–Poulenc Rorer.[1] This new bicyclic compound binds very selectively to the neurotensin receptor from guinea pigs ($IC_{50} = 30\ \mu g\,mL^{-1}$). Subsequent structural modification has led to the discovery of potent neurotensin antagonists claimed to be useful for treating psychosis and Alzheimer's and Parkinson's diseases.[2] Structurally, RP-66453 belongs to a growing family of macrocycles that include the vancomycin class of antibiotics,[3] chloropeptin,[4] and kistamine.[5] The presence of strained macrocycles with both *endo* aryl–aryl and aryl–aryl ether bonds is the common structural feature of these complex and medicinally relevant natural products.

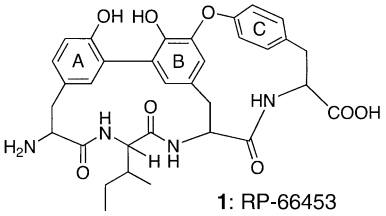
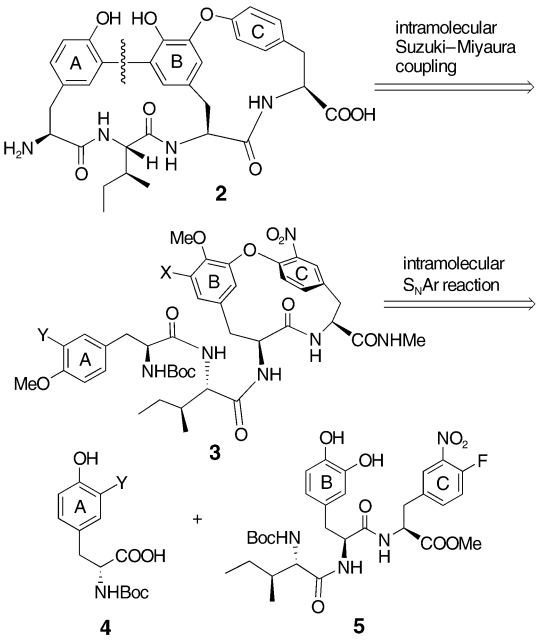


Figure 1. Structure of RP-66453 (**1**).

The connectivity of RP-66453 (**1**) was deduced from detailed spectroscopic studies. However, the absolute configuration of the five asymmetric carbon centers as well as the possible atropisomerism of the biaryl axis remained to be solved. Intrigued by its potent bioactivity and with the hope to determine its absolute configuration, we and Boger's group embarked on the total synthesis of RP-66453.[6,7] From a synthetic perspective, RP-66453 (**1**) is a challenging target because of the inherent ring strain associated with its two bridged macrocyclic ring systems. We communicate herein the first total synthesis of all-*S*-configured RP-66453, which, in combination with spectroscopic studies, also led to the assignment of the absolute configuration of the natural product as *aR(M),S,S,S,S,S*.

Our approach is depicted retrosynthetically in Scheme 1. In forward sense, a sequence of S_NAr-based cycloetherification[8] for the formation of the highly strained 14-membered



Scheme 1. Retrosynthetic analysis of RP-66453 (**1**).

B-O-C cyclophane **3** followed by an intramolecular Suzuki–Miyaura coupling reaction[9] for the construction of the 15-membered ring in **2** would complete the construction of the elusive A-B-O-C bicyclic skeleton of RP-66453. To proceed with the synthesis, we arbitrarily assigned all asymmetric carbon centers the *S* configuration, keeping in mind that the convergent approach would facilitate the incorporation of each fragment with desired stereochemistry.

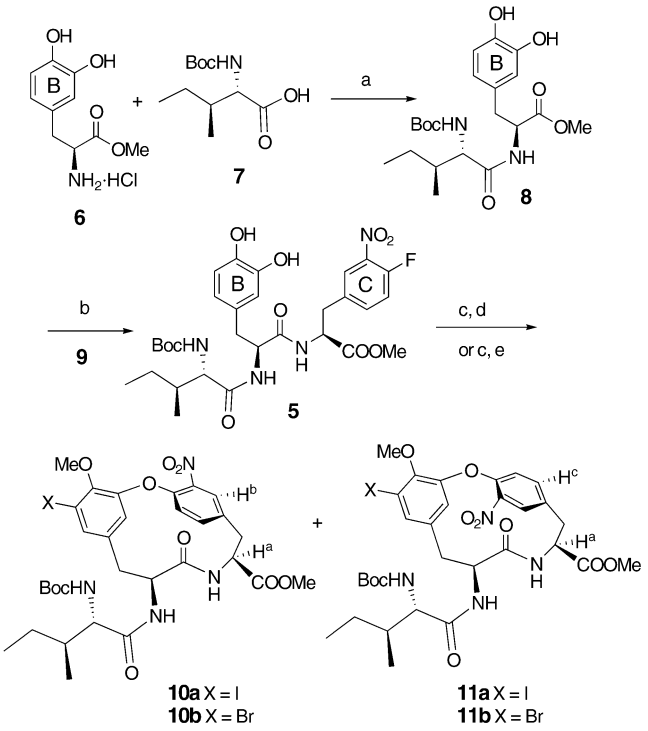
The synthesis began with commercially available (*S*)-dopa and (*S,S*)-isoleucine (Scheme 2). Coupling of (*S*)-dopa methyl ester (**6**) with (*S,S*)-*N*-Boc isoleucine (**7**) provided the dipeptide **8** in 94% yield. Subsequent hydrolysis of the methyl ester followed by amidation with the hydrochloride salt of (*S*)-methyl 4-fluoro-3-nitrophenylalanate (**9**)[10] afforded the tripeptide **5** in 78% overall yield. The size-selective ring-forming process based on the intramolecular S_NAr reaction proceeded smoothly.[11] Thus, stirring a solution of **5** (0.0026 M) in DMSO in the presence of cesium fluoride at room temperature gave the corresponding 14-membered *meta,para*-cyclophane. Without purification, the crude reaction mixture was submitted to one-pot sequential iodination and methylation to provide the two separable atropisomers **10a** and **11a** in 48% overall yield (1.3:1 ratio) from the linear tripeptide **5**. Similarly, a sequence of cycloetherification/bromination/methylation provided the two atropisomers **10b** and **11b** in 62% overall yield. It is worthy of note that the halogenation reaction must be performed before the O-methylation, otherwise the halogenation takes place exclu-

[*] Dr. J. Zhu, Dr. M. Bois-Choussy, P. Cristau
Institut de Chimie des Substances Naturelles
CNRS
91198 Gif-sur-Yvette Cedex (France)
Fax: (+33) 1-6907-7247
E-mail: zhu@icsn.cnrs-gif.fr

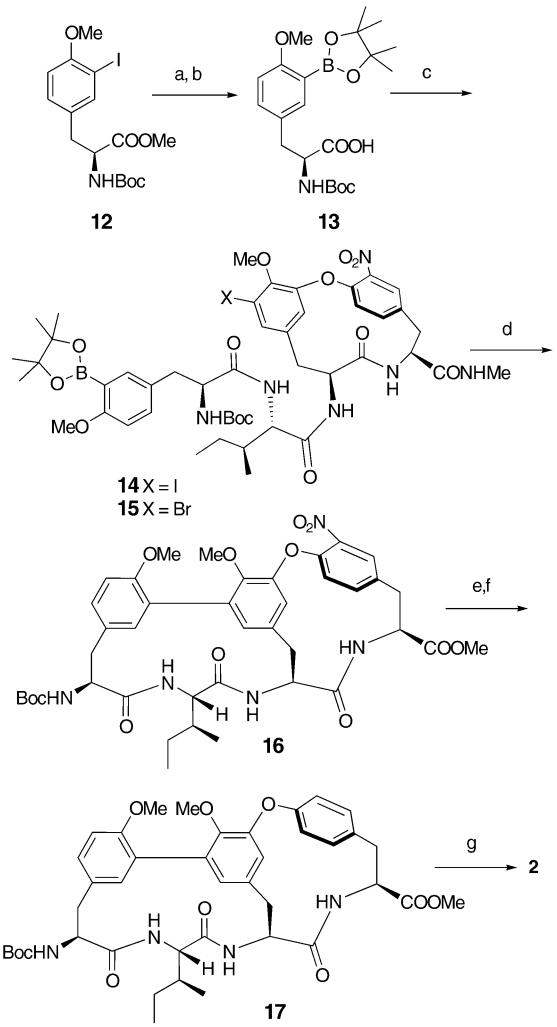
[**] We thank Dr. G. Helynck for helpful discussions. We are grateful to Drs. G. Helynck and J. C. Cavalier of Aventis Pharma S.A. for an authentic sample of RP-66453. We are grateful to J. F. Gallard for recording the NMR spectra of our final compounds. Financial support from CNRS is gratefully acknowledged.

Supporting information for this article is available on the WWW under http://www.angewandte.org or from the author.

 © 2003 Wiley-VCH Verlag GmbH & Co. KGaA, Weinheim DOI: 10.1002/anie.200351996



Scheme 2. Synthesis of the B-O-C ring. a) EDC, HOBt, Et_3N, CH_2Cl_2, RT, 94%; b) LiOH, THF/H_2O, RT, then compound **9**, EDC, HOBt, Et_3N, DMF, RT, 77%; c) CsF, DMSO (0.0026 M), RT, 2 h; d) NIS, DMF, then K_2CO_3, MeI, 48% overall yield of **10a** and **11a** from **5**; e) NBS, DMF, then MeI, 62% overall yield of **10b** and **11b** from **5**. Abbreviations: DMF = *N*,*N*-dimethylformamide, DMSO = dimethyl sulfoxide, EDC = 1-ethyl-(3-dimethylaminopropyl)carbodiimide hydrochloride, HOBt = 1-hydroxybenzotriazole hydrate, NBS = *N*-bromosuccinimide, NIS = *N*-iodosuccinimide, RT = room temperature.



Scheme 3. Completion of the synthesis of bicycle **2**. a) [$PdCl_2$(dppf)], bis(pinacolato)diboron, KOAc, DMSO, 80%; b) LiOH, THF/H_2O (1:1), RT, quantitative; c) 1) **11a**, 7% HCl in MeCN, RT, aqueous ($KHCO_3$) workup, then **13**, EDC, HOBt, Et_3N, DMF, RT, 87%; d) [$PdCl_2$(dppf)], toluene/H_2O (30:1), K_2CO_3, 90°C, 40%; e) Pd/C, H_2, MeOH; f) $NaNO_2$, H_3PO_2, Cu_2O, THF/H_2O (6:1), 42%; g) $AlBr_3$, EtSH, 55%. Abbreviation: dppf = 1,1′-bis(diphenylphosphano)ferrocene.

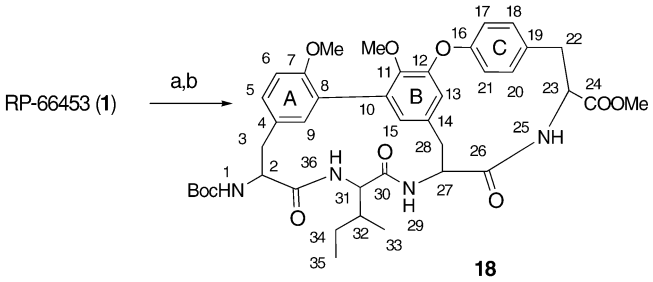
sively at the position *para* to the diaryl ether linkage.[12] Thus judicious selection of the reaction sequence allowed us to use the readily available and cheap (*S*)-dopa as starting material, reducing significantly the length of the overall synthetic sequence.[13]

The production of two atropisomers is of no consequence since the planar chirality will be destroyed in subsequent synthetic operations. We nevertheless determined their planar chirality by NOE studies[14] and continued the synthesis with the atropisomerically pure compounds **10a** and **11a**. Removal of the *N*-Boc function from **10a** followed by coupling with arylboronate **13**, obtained in turn from the (*S*)-3-iodotyrosine derivative **12** by the method of Miyaura et al.,[15] furnished the tetrapeptide **14** (Scheme 3). Due to the high ring strain imposed by the B-O-C ring, closing the second ring by means of an intramolecular Suzuki–Miyaura coupling was expected to be difficult.[16,17] In the event, the best results were obtained when we heated a solution of **14** in toluene/H_2O to 90°C in the presence of potassium carbonate and a catalytic amount of [$PdCl_2$(dppf)]. Under these conditions the desired bicycle **16** was obtained reproducibly in about 40% yield as a single atropstereoisomer. The choice of solvent was critical since the cyclization carried out in other solvents (DMF, DMSO, toluene/methanol) but under otherwise identical conditions afforded a complex reaction mixture. Finally, reductive removal of the nitro function provided the fully protected all-*S*-configured bicycle **17**. Following the same sequence, the atropisomer **11a** was converted into **17** in a similar overall yield. On the other hand, cyclization of bromide **15** gave the bicycle **16** in only about 5% yield under identical conditions. Treatment of **17** with $AlBr_3$ in the presence of EtSH removed all the protecting groups (two methyl ethers, one methyl ester, and one *N*-Boc function) to provide the desired bicyclic compound **2** in 55% yield.

The spectroscopic data (^{1}H NMR, COSY) and the high-resolution mass spectrum of bicycle **2** are in accord with its structure, but they, as well as the optical rotation, differ from those of the natural product (**2**: +208 (c = 1, MeOH); RP-66453 (**1**): −181 (c = 1, MeOH)). However, a simple experiment demonstrated that **1** and **2** differ only in their axial chirality and that the chiral carbon centers of the natural product **1** are all *S*-configured as in compound **2**. Indeed,

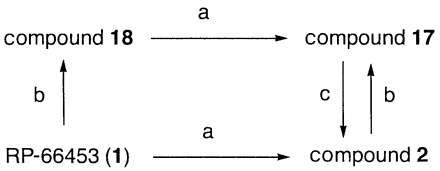
 © 2003 Wiley-VCH Verlag GmbH & Co. KGaA, Weinheim

heating a solution of **1** in DMSO at 150 °C for 3 h gave exclusively the compound **2** without any detectable decomposition. Conversely, compound **2** was perfectly stable at the same temperature, indicating that compound **2** is the thermodynamically more stable atropstereoisomer. Similarly, compound **18**, which was synthesized from the natural product by a two-step sequence (Scheme 4) was irreversibly converted



Scheme 4. Derivatization of RP-66453 (**1**). a) Boc_2O, MeOH, Et_3N; b) CsF, DMF, MeI, 50 °C, 80 %. Boc_2O = di-*tert*-butyl dicarbonate.

into **17** when a a solution in DMSO was heated at 150 °C. The similarity of the spectra of the pairs **1** and **18**, **2** and **17** indicated that there was no major conformational perturbation upon protection of the peripheral functional groups of the bicyclic structure. These results demonstrate that axial chirality was preserved during the deprotection of **17** to give **2**. Scheme 5 summarizes the chemical transformations that



T[K]	k[h^{-1}]	$t_{1/2}$[h]
405.15	0.27	2.53
420.15	0.58	1.19

Scheme 5. Evidence of atropisomerism between RP-66453 (**1**) and compound **2**. a) DMSO, 150 °C, 3 h, quantitative; b) Boc_2O, MeOH, Et_3N, then CsF, DMF, MeI, 50 °C, 80 %; c) $AlBr_3$, EtSH, CH_2Cl_2, 55 %.

proved the atropisomerism between RP-66453 (**1**) and the synthetic compound **2**. The activation energy (E_a) for the isomerization of **1** to **2** was calculated to be 16.9 kcal mol^{-1}.

The ^{1}H NMR spectra of both **1** and **2** exhibit a single set of signals in [D_6]DMSO or in CD_3OD indicating that they exist as single conformers. Based on the known absolute configuration of the peptide chain, the axial chirality of both compounds **17** and **18** was deduced from NOE studies as shown in Figure 2.[18] For compound **18**, it is evident from the ROESY spectrum that all amide bonds are *trans* by observing the NOEs between NH^{36}–H^2, NH^{29}–H^{31}, NH^{25}–H^{27}. The *aR*(M) configuration of the axial chirality of compound **18**,

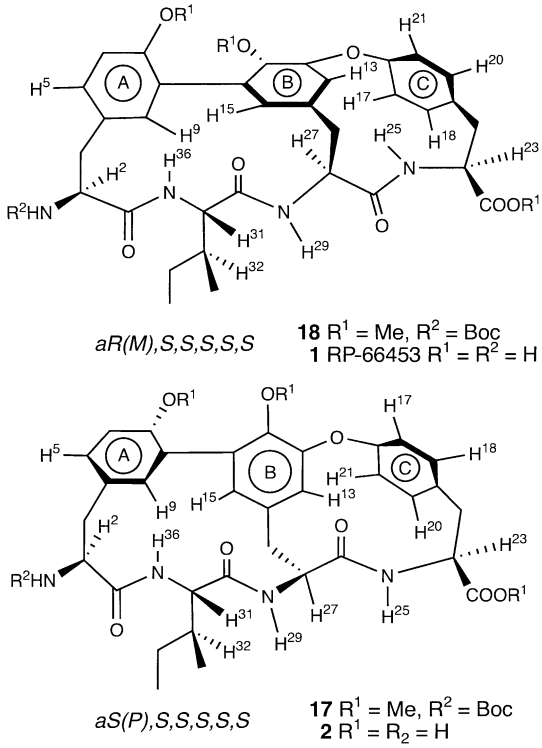


Figure 2. Stereochemistry of the natural product RP-66453 (**1**): (*aR*, *S*, *S*, *S*, *S*) and the synthetic compound **2**: (*aS*, *S*, *S*, *S*, *S*, *S*).

hence that of RP-66453 (**1**), was evidenced by the following characteristic NOEs: H^{27} with H^{23}, H^{25}, H^{13}, H^{15}, H^9; H^{13} with H^{27}, $H^{28'}$, H^{25}, H^{17}, H^{20}, H^{21} and H^{15} with H^{28}, H^{27}, H^{31}, H^9. This stereochemical assignment also nicely explains the unusual upfield shift of protons H^{27} ($\delta = 3.63$ ppm in [D_6]DMSO) and NH^{25} ($\delta = 4.22$ ppm in [D_6]DMSO) of RP-66453, both of which are located under the aromatic C ring. Although the ROESY spectra of compound **17** did not provide useful NOE correlations for the determination of its axial chirality, an *aS*(P) configuration was assigned, since chemical experiments indicated that **17** is an atropisomer of **18**. Drieding models showed that for atropisomer **17**, the proton H^{27} is completely out of the influence of aromatic ring current in contrast to that of **18**.

In conclusion, we have developed a convergent synthesis of all *S*-configured diastereoisomer of RP-66453 (*aS*,*S*,*S*,*S*,*S*,*S*). The synthesis is notable for its brevity, partly because functionalized amino acids can be used directly in our approach. By combination of chemical evidence and NMR data, the absolute configuration of RP-66453 (**1**) was determined to be (*aR*,*S*,*S*,*S*,*S*,*S*). It is interesting to note that nature created RP-66453 with a thermodynamically less stable atropisomer, while laboratory synthesis using intramolecular Suzuki–Miyaura coupling as the last ring-closure step produced the thermodynamically more stable isomer.

Received: May 28, 2003 [Z51996]

Keywords: atropisomerism · macrocycles · structure elucidation · Suzuki–Miyaura reaction · total synthesis

 © 2003 Wiley-VCH Verlag GmbH & Co. KGaA, Weinheim

[1] G. Helynck, C. Dubertret, D. Frechet, J. Leboul, *J. Antibiot.* **1998**, *51*, 512 – 514.

[2] F. F. Clerc, M. C. Dubroeucq, G. Helynck, J. Leboul, J. P. Martin , FR 2720066 (WO 9532218), **1995** [*Chem. Abstr.* **1996**, *124,* 233154x and 124, 233155y].

[3] a) D. H. Williams, B. Bardsley, *Angew. Chem.* **1999**, *111*, 1264 – 1286; *Angew. Chem. Int. Ed.* **1999**, *38*, 1173 – 1193; b) K. C. Nicolaou, C. N. C. Boddy, S. Bräse, N. Winssinger, *Angew. Chem.* **1999**, *111*, 2230 – 2287; *Angew. Chem. Int. Ed.* **1999**, *38*, 2096 – 2152; c) J. Zhu, *Expert Opin. Ther. Pat.* **1999**, *9*, 1005 – 1019.

[4] K. Matsuzaki, H. Ikeda, T. Ogino, A. Matsumoto, H. B. Woodruff, H. Tanaka, S. Omura, *J. Antibiot.* **1994**, *47*, 1173 – 1174.

[5] N. Naruse, M. Oka, M. Konishi, T. Oki, *J. Antibiot.* **1993**, *46*, 1812 – 1818.

[6] a) S. Boisnard, A.-C. Carbonnelle, J. Zhu, *Org. Lett.* **2001**, *3*, 2061 – 2064; b) S. Boisnard, J. Zhu, *Tetrahedron Lett.* **2002**, *43*, 2577 – 2580.

[7] a) P. J. Krenitsky, D. L. Boger, *Tetrahedron Lett.* **2002**, *43*, 407 – 410; b) P. J. Krenitsky, D. L. Boger, *Tetrahedron Lett.* **2003**, *44*, 4019 – 4022.

[8] a) J. Zhu, *Synlett* **1997**, 133 – 144; b) J. S. Sawyer, *Tetrahedron* **2000**, *56*, 5045 – 5065.

[9] N. Miyaura, A. Suzuki, *Chem. Rev.* **1995**, *95*, 2457 – 2483.

[10] C. Vergne, M. Bois-Choussy, J. Ouazzani, R. Beugelmans, J. Zhu, *Tetrahedron: Asymmetry* **1997**, *8*, 391 – 398.

[11] a) A. Bigot, J. Zhu, *Tetrahedron Lett.* **1998**, *39*, 551 – 554; b) A. Bigot, E. Tran Huu Dau, J. Zhu, *J. Org. Chem.* **1999**, *64*, 6283 – 6296.

[12] Bromination of (S)-dopa gave exclusively the undesired (*S*)-2-bromo-4,5-dihydroxyphenylalanine, see: S. Kirschbaum, H. Waldmann, *J. Org. Chem.* **1998**, *63*, 4936 – 4946.

[13] For the synthesis of selective protected L-dopa from tyrosine, see ref. [7] and a) D. L. Boger, D. Yohannes, *J. Org. Chem.* **1987**, *52*, 5283 – 5286; b) M. E. Jung, T. I. Lazarova, *J. Org. Chem.* **1997**, *62*, 1553 – 1555; c) C. Chen, Y.-F. Zhu, K. Wilcoxen, *J. Org. Chem.* **2000**, *65*, 2574 – 2576.

[14] In the NOESY spectra, characteristic NOE crosspeaks between protons H^a and H^b, between protons H^a and H^c were observed for compounds **10** and **11**, respectively.

[15] T. Ishiyama, M. Murata, N. Miyaura, *J. Org. Chem.* **1995**, *60*, 7508 – 7510.

[16] Aryl–Aryl bond formation by intramolecular Suzuki–Miyaura coupling see: a) A. M. Elder, D. H. Rich, *Org. Lett.* **1999**, *1*, 1443 – 1446; b) W. Li, K. Burgess, *Tetrahedron Lett.* **1999**, *40*, 6527 – 6530; c) A.-C. Carbonnelle, J. Zhu, *Org. Lett.* **2000**, *2*, 3477 – 3480; d) V. Lobrégat, G. Alcaraz, H. Bienaymé, M. Vautier, *Chem. Commun.* **2001**, 817 – 818.

[17] In our hands formation of the B-O-C cyclophane followed by macrolactamization failed to afford the complete A-B-O-C bicycle (S. Boisnard, Ph.D. Thesis, Université Paris-Sud, **2001**), although the 15-membered A-B ring can be prepared efficiently by macrolactamization (refs. [6a, 7b]).

[18] Due to the overlap of several key signals in the ^{1}H NMR spectra of RP-66453 (**1**) and **2** in DMSO, we performed NOE studies on their derivatives **18** and **17**, respectively.

 © 2003 Wiley-VCH Verlag GmbH & Co. KGaA, Weinheim

Asymmetric Oxy-Michael Addition

Highly Diastereoselective Oxy-Michael Additions of Enantiopure δ-Lactol Anions to Nitroalkenes: Asymmetric Synthesis of 1,2-Amino Alcohols**

Nicola J. Adderley, David J. Buchanan, Darren J. Dixon, and Dramane I. Lainé*

The abundance of bioactive natural and unnatural products that contain the 1,2-amino alcohol motif continues to stimulate the development of new methods for their efficient asymmetric synthesis. Whereas 1,2-amino alcohols derived from proteinogenic amino acids are readily accessible, non-proteinogenic amino acid derived amino alcohols require efficient enantioselective routes.[1] Methods for the asymmetric synthesis of 1,2-amino alcohols with a stereogenic hydroxy-substituted carbon center are relatively uncommon, even though these materials and their derivatives are widespread in nature and routinely exploited in asymmetric synthesis.[2]

Stimulated by the utility of 1,2-amino alcohols and encouraged by the lack of a general synthetic approach to such compounds, we recently became interested in developing asymmetric methods for their synthesis. Although a logical retrosynthetic disconnection is based on an asymmetric nitroaldol reaction,[3] our approach relies on the stereoselective Michael addition of a chiral water equivalent **1** to readily available nitroalkenes **2**. As in many asymmetric catalytic processes, the levels of asymmetric induction in the nitroaldol reaction are substrate dependent, and in the worst cases there is no way of increasing the enantiopurity of the product. In the oxy-Michael addition approach the chirality in the nucleophile allows the separation of the diastereomeric products **3** and hence the isolation of enantiopure material after auxiliary removal. However, ideally the chirality of the nucleophile will induce high levels of stereoselectivity in the formation of the stereogenic center β to N, and subsequent nitro-group manipulation and nondestructive removal of the auxiliary will free the deprotected oxy-Michael product **4** (Scheme 1).

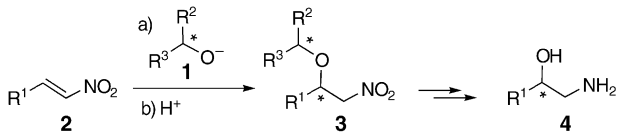
The strength of this concept was recognized previously by Enders et al.,[4] who used the sodium salt of *N*-formylnor-

[*] Dr. D. J. Dixon, N. J. Adderley, D. J. Buchanan
Department of Chemistry, University of Cambridge
Lensfield Road, Cambridge CB2 1EW (UK)
Fax: (+44) 1223-336-362
E-mail: djd26@cam.ac.uk
Dr. D. I. Lainé
GlaxoSmithKline, RI CEDD
709 Swedeland Road, P.O. Box 1539
King of Prussia, PA 19406-0939 (USA)

[**] We gratefully acknowledge the support of GlaxoSmithKline and Prof. S. V. Ley. We are also indebted to Dr. John E. Davis for the X-ray structure determinations and Dr. D. Hepworth for useful discussions.

Supporting information for this article is available on the WWW under http://www.angewandte.org or from the author.

 DOI: 10.1002/anie.200352007 © 2003 Wiley-VCH Verlag GmbH & Co. KGaA, Weinheim



Scheme 1. The diastereoselective oxy-Michael addition to nitroalkenes for the asymmetric synthesis of 1,2-amino alcohols.

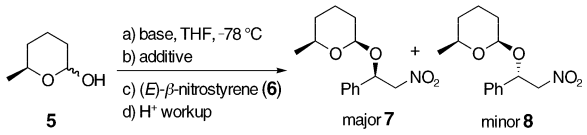
ephedrine as a chiral hydroxide equivalent in reactions with aliphatic nitroalkenes and observed excellent diastereoselectivities. However, when aryl nitroalkene acceptors were used, both the diastereoselectivities and the yields were low. Furthermore, the approach required a dissolving-metal Birch-type deprotection at the end of the sequence to free the amino alcohol products. This was not compatible with some aryl groups and led to partial reduction. Herein we report that enantiopure 6-substituted δ-lactols, when converted into the corresponding "naked" alkoxides, act as effective chiral water equivalents in Michael addition reactions to nitroalkenes, thus allowing the rapid synthesis of enantiomerically enriched 1,2-amino alcohols after subsequent manipulation of the nitro group and removal of the 6-methyltetrahydropyran (THP*) auxiliary.

The highly *cis*-selective O-alkylation and O-acylation of the anions of 6-substituted δ-lactols with bromoacetates and acid anhydrides has been reported previously.[5] This work and the availability of 6-alkyl δ-lactols in racemic and enantiopure form[5a,6] prompted us to test lactol anions in the oxy-Michael reaction and assess their potential as chiral water equivalents. Lactols such as these were attractive candidates from the outset, because the chirality source—the 6-substituted tetrahydropyran ring—is also an exceptional protecting group, which is used exhaustively in synthetic methodologies and total syntheses alike.[7]

Preliminary studies were performed with readily available enantiopure (*S*)-6-methyl-δ-lactol (**5**) as the chiral water equivalent and commercially available (*E*)-β-nitrostyrene (**6**) as the Michael acceptor. Typically the reactions were carried out in THF at −78 °C with an excess of the lactol anion and were quenched at the same temperature with glacial acetic acid. Whereas high yields were obtained when the potassium or the sodium alkoxides were used, the observed stereoinduction at the center β to the nitro group was moderate in the former case and poor in the latter. Importantly however, only two of the possible four diastereoisomers, the *cis*-tetrahydropyranyl ether products **7** and **8**, were observed in the crude reaction mixtures. The use of the potassium salt of the lactol with toluene as the solvent also led to a decrease in the diastereoselectivity of the reaction, as well as in the yield, and led us to the conclusion that tight ion pairing of the metal and the alkoxide was detrimental to the reaction in all respects. Accordingly, 1 equivalent of [18]crown-6 was added to the potassium alkoxide in THF, and the reaction was performed as before. To our delight the selectivity at the center β to the nitro group for the *cis*-THP* isomer soared to ⩾99:1, as measured by ^{1}H NMR spectroscopy. Similarly, when the sodium salt of the alkoxide was treated with 1 equivalent of [15]crown-5 prior to the Michael addition, the observed selectivity at the β center was excellent[8] (Table 1).

To ascertain the generality of the reaction, a range of commercially available or readily prepared *E*-nitroalkene acceptors were treated with the "naked" lactol alkoxide formed from KHMDS (HMDS = hexamethyldisilazide) and [18]crown-6 (Table 2). When the β substituent was aryl, heteroaryl, or alkyl the observed selectivity at the β center and the yields of the reactions were uniformly excellent. The reaction products were readily purified by chromatography on silica gel, and the stereochemistry of the major isomer was established unambiguously by single-crystal X-ray diffraction

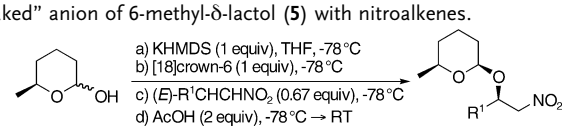
Table 1: Diastereoselective oxy-Michael addition reactions of 6-methyl-δ-lactol (**5**) with (*E*)-β-nitrostyrene (**6**) and variation in d.r. with metals and additives.

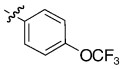


Entry	Base	Solvent	Additive	**7**/**8**[a]	Yield [%]
1	LiHMDS	THF	none	–	0
2	NaHMDS	THF	none	1:1	88
3	KHMDS	THF	none	4.2:1	89
4	KHMDS	THF	[18]crown-6	⩾99:1	99
5	NaHMDS	THF	[15]crown-5	56:1	97

[a] d.r. of the *cis*-THP* isomers **7** and **8**, determined by examination of ^{1}H NMR spectra of the crude product.

Table 2: Highly diastereoselective oxy-Michael addition reactions of the "naked" anion of 6-methyl-δ-lactol (**5**) with nitroalkenes.



Entry	R^1	d.r.[a]	Product	Yield [%]
1		>99:1	**7**	99
2		>99:1	**9**[b]	81
3		>99:1	**10**	72
4		>99:1	**11**	82
5		52:1	**12**[c]	94
6		45:1	**13**	99
7		>40:1[d]	**14**	83

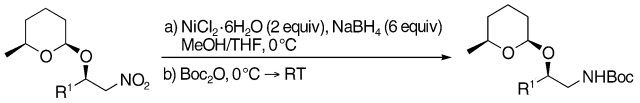
[a] d.r. of the *cis*-THP* isomers, determined by examination of the ^{1}H NMR spectrum of the crude product. [b] Configuration determined by single-crystal X-ray analysis. [c] Workup with ammonium chloride. [d] Approximated by peak-height measurements in the ^{13}C NMR spectrum of the crude product.

 © 2003 Wiley-VCH Verlag GmbH & Co. KGaA, Weinheim

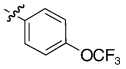
in the case of **9** and by chemical correlation methods for **12** and **13**.

Reductive manipulation of the nitro group and non-destructive removal of the THP* group was necessary to confirm the effectiveness of this reaction as an asymmetric method for the synthesis of amino alcohols. It was eventually found that the most reliable way to reduce the nitro group was a one-pot nickel boride reduction[9] with concomitant in situ *tert*-butyloxycarbonyl (Boc) protection. The THP* group functions as both a protecting group and a stereochemical marker: Any epimerization of the newly formed stereogenic center would be observable in the ^{1}H NMR spectra of the products. Gratifyingly, no epimerization was observed, and the *N*-Boc-protected amine products **15**–**21** were afforded in good to excellent yields in all cases (Table 3).

Table 3: Nickel boride reduction and in situ *N*-Boc-protection of the oxy-Michael adducts **7** and **9**–**14**.



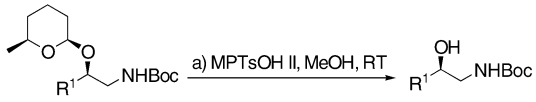
7, 9–14 **15–21**

Entry	R^1	Product	Yield [%]
1		**15**	98
2		**16**	57
3		**17**	80
4		**18**	81
5		**19**	85
6		**20**	90
7		**21**	83

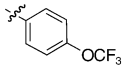
Removal of the THP* group in the presence of methanol and polymer-bound acid resin (MPTsOH II) was straightforward and afforded the *N*-Boc-protected amino alcohol products **22**–**28** in good to excellent yields in all cases following filtration and concentration in vacuo. Owing to the high efficiency of the reaction and high volatility of the 6-methyltetrahydropyranyl methyl ether side products, no further purification was required. The *ee* values of the products were determined by derivatization as their Mosher esters[10] and were found to be superior to or equivalent to the diastereomeric ratios obtained in the oxy-Michael addition reactions (Table 4).

In summary, the "naked" alkoxide of 6-methyl-δ-lactol, formed by deprotonation with KHMDS and sequestering with [18]crown-6, undergoes highly diastereoselective oxy-Michael additions to a range of nitroalkene acceptors to give the *O*-protected Henry products in good yields. Subsequent reduction of the nitro group and acidic methanolysis of the THP* group affords the desired enantiomerically enriched 1,2-amino alcohols. Further studies to ascertain the origin of stereoselectivity and the scope of the reaction are ongoing.

Table 4: Acid-mediated methanolysis of the THP* auxiliary and production of amino alcohols **22**–**28**.



15–21 **22–28**

Entry	R^1	Product	Yield [%]	*ee* [%]	$[\alpha]_D^{25}$ (*c*)[a]
1		**22**	97	>98	−57.5 (1.01)
2		**23**	94	>98	−19.9 (1.45)
3		**24**	99	>98	−20.0 (1.00)
4		**25**	84	>98	−37.8 (1.03)
5		**26**	74	>97	−27.4 (1.06)[b]
6		**27**	84	>96	−19.2 (1.00)[c]
7		**28**	99	>97	−10.2 (1.00)

[a] Measured in $CHCl_3$. [b] Ref. $[\alpha]_D^{25} = -28.8$ ($CHCl_3$, $c = 1.19$)[4b]. [c] Ref. $[\alpha]_D^{25} = -19.4$ ($CHCl_3$, $c = 0.94$)[4b].

Received: May 30, 2003 [Z52007]

Keywords: amino alcohols · diastereoselectivity · lactols · Michael addition · nitroalkenes

[1] a) S. C. Bergmeier, *Tetrahedron* **2000**, *56*, 2561–2576; b) N. Kise, N. Inakoshi, Y. Matsumura, *Tetrahedron Lett.* **1995**, *36*, 909–912; c) G. B. Fisher, C. T. Goralski, L. W. Nicholson, D. L. Hasha, D. Zakett, B. Singaram, *J. Org. Chem.* **1995**, *60*, 2026–2034; d) R. E. Marti, J. Heinzer, D. Seebach, *Liebigs Ann.* **1995**, 1193–1215; e) D. Enders, U. Reinhold, *Liebigs Ann.* **1996**, 11–26; f) D. Enders, U. Reinhold, *Angew. Chem.* **1995**, *107*, 1332–1334; *Angew. Chem. Int. Ed. Engl.* **1995**, *34*, 1219–1222; g) T. Wirth, *Angew. Chem.* **1996**, *108*, 65–67; *Angew. Chem. Int. Ed. Engl.* **1996**, *35*, 61–63; h) G. K. S. Prakash, M. Mandal, S. Schweizer, N. A. Petasis, G. A. Olah, *J. Org. Chem.* **2002**, *67*, 3718–3723; i) W. Oppolzer, O. Tamura, G. Sundarababu, M. Signer, *J. Am. Chem. Soc.* **1992**, *114*, 5900–5902; j) M. Brunner, L. Mußmann, D. Vogt, *Synlett* **1993**, 893–894; k) C. E. Harris, G. B. Fisher, D. Beardsley, L. Lee, C. T. Goralski, L. W. Nicholson, B. Singaram, *J. Org. Chem.* **1994**, *59*, 7746–7751; l) H.-T. Chang, K. B. Sharpless, *Tetrahedron Lett.* **1996**, *37*, 3219–3222; m) E. N. Jacobsen, *Acc. Chem. Res.* **2000**, *33*, 421–431; n) J. L. Leighton, E. N. Jacobsen, *J. Org. Chem.* **1996**, *61*, 389–390; o) C. H. Senanayake, R. D. Larsen, L. M. DiMichele, J. Liu, P. H. Toma, R. G. Ball, T. R. Verhoeven, P. J. Reider, *Tetrahedron: Asymmetry* **1996**, *7*, 1501–1506; p) G. Li, H.-T. Chang, K. B. Sharpless, *Angew. Chem.* **1996**, *108*, 449–452; *Angew. Chem. Int. Ed. Engl.* **1996**, *35*, 451–454; q) A. V. Gontcharov, H. Liu, K. B. Sharpless, *Org. Lett.* **1999**, *1*, 783–786; r) K. L. Reddy, K. R. Dress, K. B. Sharpless, *Tetrahedron Lett.* **1998**, *39*, 3667–3670; s) Z. P. Demko, M. Bartsch, K. B. Sharpless, *Org. Lett.* **2000**, *2*, 2221–2223; t) L. J. Goossen, H. Liu, K. R. Dress, K. B. Sharpless, *Angew. Chem.* **1999**, *111*, 1149–1152; *Angew. Chem. Int. Ed.*

 © 2003 Wiley-VCH Verlag GmbH & Co. KGaA, Weinheim

1999, *38*, 1080 – 1083; u) C. T. Goralski, D. L. Hasha, L. W. Nicholson, D. Zakett, G. B. Fisher, B. Singaram, *Tetrahedron Lett.* **1994**, *35*, 3251 – 3254.
[2] See, for example: J. M. Klunder, S. Y. Ko, K. B. Sharpless, *J. Org. Chem.* **1986**, *51*, 3710 – 3712.
[3] a) H. Sasai, N. Itoh, T. Suzuki, M. Shibasaki, *Tetrahedron Lett.* **1993**, *34*, 855 – 858; b) H. Sasai, T. Suzuki, N. Itoh, S. Arai, M. Shibasaki, *Tetrahedron Lett.*, **1993**, *34*, 2657 – 2660; c) R. Chinchilla, C. Nájera, P. Sanchez-Agulló, *Tetrahedron: Asymmetry* **1994**, *5*, 1393 – 1402; d) M. Shibasaki, H. Sasai, T. Arai, *Angew. Chem.* **1997**, *109*, 1290 – 1310; *Angew. Chem. Int. Ed. Engl.* **1997**, *36*, 1236 – 1256; e) H. Sasai, T. Tokunaga, S. Watanabe, T. Suzuki, N. Itoh, M. Shibasaki, *J. Org. Chem.* **1995**, *60*, 7388 – 7389; f) B. M. Trost, V. S. C. Yeh, H. Ito, N. Bremeyer, *Org. Lett.* **2002**, *4*, 2621 – 2623.
[4] a) D. Enders, A. Haertwig, G. Raabe, J. Runsink, *Angew. Chem.* **1996**, *108*, 2540 – 2542; *Angew. Chem. Int. Ed. Engl.* **1996**, *35*, 2388 – 2390; b) D. Enders, A. Haertwig, G. Raabe, J. Runsink, *Eur. J. Org. Chem.* **1998**, 1771 – 1792; c) D. Enders, A. Haertwig, J. Runsink, *Eur. J. Org. Chem.* **1998**, 1793 – 1802.
[5] a) M. F. Buffet, D. J. Dixon, S. V. Ley, E. W. Tate, *Synlett* **1998**, 1091 – 1092; b) D. J. Dixon, S. V. Ley, E. W. Tate, *Synlett* **1998**, 1093 – 1095; c) D. J. Dixon, S. V. Ley, E. W. Tate, *J. Chem. Soc. Perkin Trans. 1* **1999**, 2665 – 2667.
[6] a) D. J. Dixon, S. V. Ley, E. W. Tate, *J. Chem. Soc. Perkin Trans. 1* **1998**, 3125 – 3126; b) D. J. Dixon, S. V. Ley, E. W. Tate, *J. Chem. Soc. Perkin Trans. 1* **2000**, 2385 – 2394.
[7] *Protective Groups in Organic Synthesis, Vol. 3* (Eds.: T. W. Greene, P. G. M. Wuts), Wiley, New York, **1999**, pp. 49 – 55.
[8] For a related system with an oxazolidinone chiral nucleophile, see: a) D. Lucet, L. Toupet, T. Le Gall, C. Mioskowski, *J. Org. Chem.* **1997**, *62*, 2682 – 2683; b) S. Sabelle, D. Lucet, T. Le Gall, C. Mioskowski, *Tetrahedron Lett.* **1998**, *39*, 2111 – 2114; c) D. Lucet, S. Sabelle, O. Kostelitz, T. Le Gall, C. Mioskowski, *Eur. J. Org. Chem.* **1999**, 2583 – 2591; d) O. M. Berner, L. Tedeschi, D. Enders, *Eur. J. Org. Chem.* **2002**, 1877 – 1894.
[9] a) A. Nose, T. Kudo, *Chem. Pharm. Bull.* **1981**, *29*(4), 1159 – 1161; b) A. Nose, T. Kudo, *Chem. Pharm. Bull.* **1988**, *36*(4), 1529 – 1533; c) A. Nose, T. Kudo, *Chem. Pharm. Bull.* **1989**, *37*(3), 816 – 818; d) J. O. Osby, B. Ganem, *Tetrahedron Lett.* **1985**, *26*, 6413 – 6416.
[10] J. A. Dale, H. S. Mosher, *J. Am. Chem. Soc.* **1973**, *95*, 512.

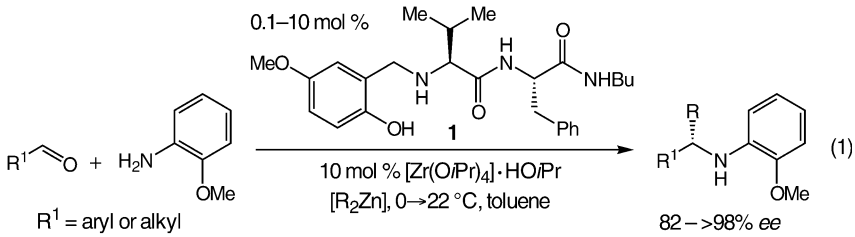
 © 2003 Wiley-VCH Verlag GmbH & Co. KGaA, Weinheim

Synthesis of Propargylamines

Three-Component Enantioselective Synthesis of Propargylamines through Zr-Catalyzed Additions of Alkyl Zinc Reagents to Alkynylimines**

Laura C. Akullian, Marc L. Snapper, and Amir H. Hoveyda**

Design and development of new methods for the synthesis of enantiomerically enriched amines is a critical objective in modern organic chemistry. We recently disclosed efficient catalytic methods for enantioselective alkylation of aryl- and alkylimines with alkyl zinc reagents promoted by chiral ligand **1** and $[Zr(OiPr)_4]\cdot HOiPr$ [Eq. (1)].[1,2] These asymmetric



(1)

amine syntheses do not require initial preparation of the imine substrates, which are typically difficult to isolate. The Zr-catalyzed asymmetric processes are effected by treatment of an aromatic or aliphatic aldehyde with *o*-methoxyaniline and an alkyl zinc reagent, as well as 1–10 mol % of **1** and the Zr salt.

Another class of chiral N-containing compounds are propargylamines. Several approaches involving chiral controllers[3] and auxiliaries[4,5] have been developed for the preparation of these synthetically[6] and biologically[3,7] important compounds. Two catalytic methods have been outlined involving addition of alkynyl nucleophiles to imines. One protocol is by Knochel and co-workers,[8] regarding Cu-catalyzed addition of alkynes to enamines (bearing *N*-allyl or *N*-Bn groups). Starting materials that contain larger substituents (i.e., Cy) can be converted into products with up to 90 % *ee*, whereas enantioselectivities range from 55–86 % *ee* with substrates bearing *n*-alkyl substituents. Another method was disclosed by Wei and Li,[9] in which addition of phenylacetylene to various arylimines in the presence of 10 mol % of

[*] Prof. Dr. M. L. Snapper, Prof. Dr. A. H. Hoveyda, L. C. Akullian
Department of Chemistry
Merkert Chemistry Center, Boston College
Chestnut Hill, MA 02467 (USA)
Fax: (+1) 617-552-1442
E-mail: marc.snapper@bc.edu
amir.hoveyda@bc.edu

[**] This research was supported by the United States National Institutes of Health (GM-57212). We are grateful to J. R. Porter and J. F. Traverse for helpful discussions and experimental advice.

Supporting information for this article is available on the WWW under http://www.angewandte.org or from the author.

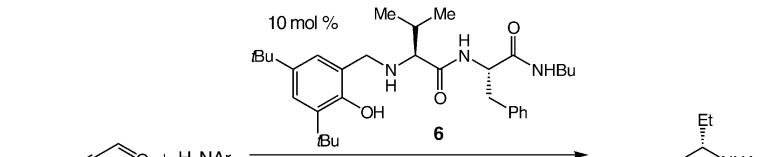
 © 2003 Wiley-VCH Verlag GmbH & Co. KGaA, Weinheim DOI: 10.1002/anie.200352081

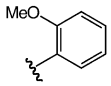
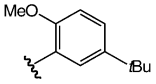
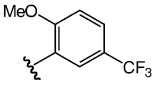
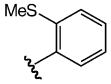
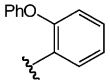
a chiral Cu complex proceeds in 78–96% *ee*; however, reactions are limited to a single nucleophile and methods for conversion of the *N*-arylamines into the corresponding free amines were not described.

Herein we report a Zr-catalyzed protocol for the enantioselective synthesis of propargylamines which, in contrast to the previous approaches, involves addition of alkyl metal reagents to alkynylimines [Eq. (2); G = *o*-methoxyphenyl].[10] Peptidic ligands, composed of commercially available and inexpensive amino acids, can be used to promote an efficient, three-component, and enantioselective (82→98% *ee*) synthesis of α-alkynylamines. Asymmetric synthesis of products obtained by the present method have not been covered by the previously mentioned reports.[8,9]

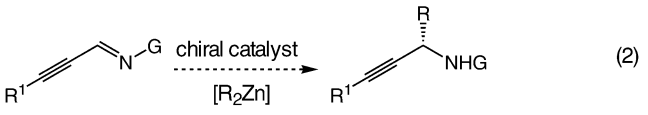
Initially, we examined the ability of **1**, the chiral ligand used in asymmetric additions to aliphatic and aromatic imines [Eq. (1)], in promoting similar transformations involving alkynyl substrates. As the representative examples in Equation (3) indicate, we discovered that although the desired propargylamines form efficiently, low levels of enantioselectivity are attained.

Table 1: Effect of arylamine structure on the enantioselectivity and efficiency of propargylamine formation.[a]

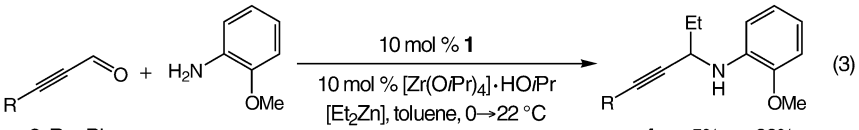


Entry	Ar	Product	*ee* [%]	Yield [%]
1		**5**	68	n.d.
2		**7**	54	n.d.
3		**8**	70	n.d.
4		**9**	92	61
5		**10**	94	84

[a] Conditions: alkyl zinc reagent (6 equiv), 4 h. [b] Enantioselectivities determined by HPLC (chiralcel OD). [c] Yields of products isolated after silica-gel chromatography; >98% conversion in all cases. n.d. = not determined.



(2)



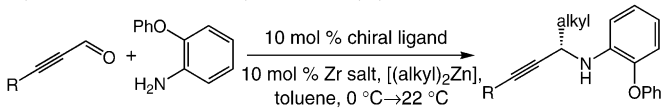
(3)

To improve asymmetric induction, we turned to modifications of the chiral ligand. Since the amino acid units in **1** are among the most readily available and inexpensive,[11] we decided to focus on altering other structural features of the peptidic system. Accordingly, a brief survey of chiral ligands varying in the structure of the aromatic terminus was carried out.[12] These studies established that, as illustrated in entry 1 of Table 1, dipeptide **6** catalyzes formation of **5** with improved enantioselectivity (68% *ee* versus 47% *ee*; >98% conversion). Next, we varied the structure of the aryl group in the imine substrate. This was based on our prior investigations [cf. Eq. (1)], which indicated that the structure of the aryl group attached to the imine can exert a strong influence on reaction outcomes. For example, in contrast to transformations involving *o*-anisidyl imines, the derived phenyl or *p*-methoxy derivatives are inert under the same reaction conditions. As the data in Table 1 illustrate, in the reaction of imines derived from aldehyde **3** in the presence of 10 mol% **6** and [Et_2Zn], levels of enantiofacial selectivity vary significantly as a function of the nature of the arylimine, with the phenoxyphenyl-bearing imine proving to be optimal (entry 5; 94% *ee*, 84%).

The data in Table 2 illustrate that three-component asymmetric alkylations can be performed with a variety of alkynylimines and alkyl zinc reagents to afford propargylamines (**15**–**19**, **21**, and **23**–**26**) efficiently and enantioselectively. Several important issues in connection with the data in Table 2 deserve mention: With the more reactive [Et_2Zn] (Table 1 and Table 2, entries 4–6 and 8) higher selectivity is obtained when [Zr(O*i*Pr)$_4$]·HO*i*Pr is used. With the less reactive [Me_2Zn] and longer chain dialkyl zinc reagents (Table 2, entries 1–3, 7, and 9–10), significantly higher enantioselectivities are attained with [Zr(O*t*Bu)$_4$].[13] As an example, in the reaction shown in entry 7 in Table 2, under otherwise identical conditions but in the presence of [Zr(O*i*Pr)$_4$]·HO*i*Pr, propargylamine **23** is obtained with only 40% *ee* (>98% conversion); in the presence of [Zr(OEt)$_4$], racemic product is formed (>98% conversion). It should be noted that in reactions of [Et_2Zn], use of [Zr(O*t*Bu)$_4$] does not result in improved selectivity. In spite of the diminished Lewis basicity of the *o*-phenoxy group (versus *o*-methoxy used previously), preliminary evidence suggests that the aryloxy heteroatom may be involved in metal chelation. Attempted catalytic alkylation of **27** with [Et_2Zn] in the presence of 10 mol% of **6** and [Zr(O*i*Pr)$_4$]·HO*i*Pr (identical conditions as shown in

 © 2003 Wiley-VCH Verlag GmbH & Co. KGaA, Weinheim

Table 2: Zr-catalyzed enantioselective alkylation of alkynylamines.[a]

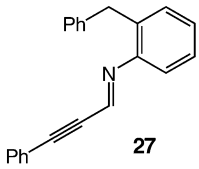


Entry	R		[(alkyl)$_2$Zn]	Zr salt	Product	Chiral ligand	Yield [%]	*ee* [%]
1	*n*Pent	**3**	[Me_2Zn]	[Zr(O*t*Bu)$_4$]	**15**	**6**	87	82
2	*n*Pent	**3**	[{$Me_2CH(CH_2)_3$}$_2$Zn]	[Zr(O*t*Bu)$_4$]	**16**	**6**	60	98
3		**11**	[Me_2Zn]	[Zr(O*t*Bu)$_4$]	**17**	**6**	75	92
4	TBSO	**11**	[Et_2Zn]	[Zr(O*i*Pr)$_4$]·HO*i*Pr	**16**	**6**	70	>98
5	TMSO, Me, Me	**12**	[Et_2Zn]	[Zr(O*i*Pr)$_4$]·HO*i*Pr	**19**	**20**	86	84
6		**13**	[Et_2Zn]	[Zr(O*i*Pr)$_4$]·HO*i*Pr	**21**	**22**	89	86
7	Ph	**2**	[Me_2Zn]	[Zr(O*t*Bu)$_4$]	**23**	**6**	84	80
8	Ph	**2**	[Et_2Zn]	[Zr(O*i*Pr)$_4$]·HO*i*Pr	**24**	**6**	85	>98
9	Ph	**2**	[{$Me_2CH(CH_2)_3$}$_2$Zn]	[Zr(O*t*Bu)$_4$]	**25**	**6**	81	91
10	F, O	**14**	[Me_2Zn]	[Zr(O*t*Bu)$_4$]	**26**	**6**	75	93

[a] Conditions: alkyl zinc reagent (6 equiv), 4 h for reactions with [Et_2Zn], 24 h for other alkyl zinc reagents. [b] Yields of product isolated after silica-gel chromatography; >98% conversion in all cases. [c] Enantioselectivities determined by HPLC (chiralcel OD).

Table 2) leads to the formation of a mixture of unidentified compounds.

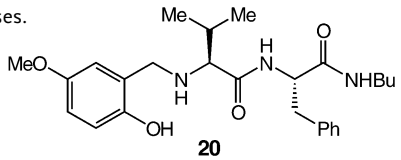
In the majority of cases shown in Table 2 dipeptide amine **6** delivers the highest *ee* values. However, in two instances, propargylamines **19** (Table 2, entry 5) and **21** (Table 2, entry 6) are obtained with 70 and 74% *ee*, respectively, when ligand **6** is used. In search of enhanced selectivity, we again took advantage of the modular character of this class of ligands to screen additional structures. These studies indicated that **19** can be obtained with 84% *ee* (versus 70% *ee*) when dipeptide amine **20** is employed (Table 2, entry 5); moreover, with Schiff base **22**, propargylamine **21** is isolated with 86% *ee* (versus 74% *ee*).



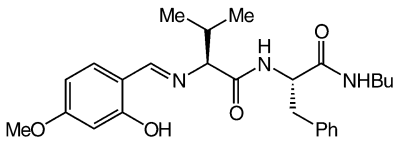
27

That a different ligand might be required for optimal selectivity with a particular substrate should not be viewed as a shortcoming of this or any other method. With less easily modifiable systems, although a single chiral ligand is utilized (and such could be the case here as well), levels of selectivity at times vary significantly and cannot be easily improved.[14]

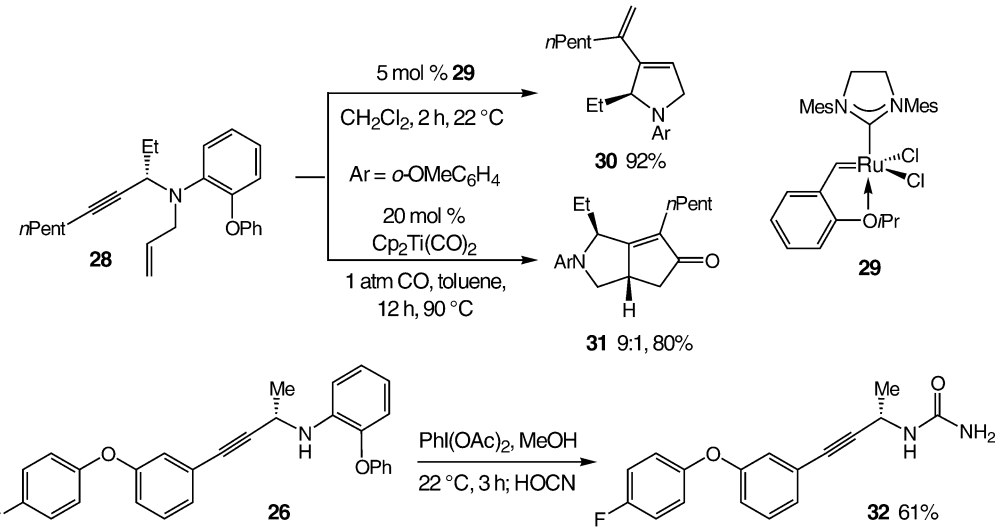
Propargylamines accessible through Zr-catalyzed alkylation can be functionalized in a variety of ways to afford chiral cyclic and acyclic N-containing compounds in high enantiomeric purity. Several representative examples are depicted in Scheme 1.



20



22



Scheme 1. Representative functionalization of nonracemic propargylamines. Mes = mesityl = 2,4,6-trimethylphenyl.

 © 2003 Wiley-VCH Verlag GmbH & Co. KGaA, Weinheim

Optically enriched enyne **28**, obtained from allylation of propargylamine **10** (Table 1, entry 5), readily undergoes Ru-catalyzed ring closure in the presence of 5 mol% of **29**[15] to afford diene **30**, a compound that may be further functionalized through [4+2] cycloaddition with dienophiles. Efficient and diastereoselective formation of bicycle **31** is achieved through a Ti-catalyzed intramolecular Pauson–Khand[16] reaction. The propargyl amines are unmasked and functionalized through oxidative cleavage of the N–aryl bond (e.g., **26**→**32**).[1b]

In summary, we have disclosed an efficient method for alkylation of alkynylimines that lead to a range of chiral enantiomerically enriched propargylamines. Several of the products (e.g., **15**–**17**, **23**, and **26**) obtained cannot be accessed readily or with high enantioselectivity by existing catalytic protocols. The chiral catalyst can be prepared conveniently from commercially available and inexpensive amino acids and Zr salts in significant quantities. Such attributes, together with the significance of propargylamines in the synthesis of compounds of therapeutic importance, render the present approach of notable synthetic utility.

Received: June 6, 2003 [Z52081]

Keywords: alkyl zinc reagents · asymmetric catalysis · enantioselectivity · propargylamines · zirconium

[1] a) J. R. Porter, J. F. Traverse, A. H. Hoveyda, M. L. Snapper, *J. Am. Chem. Soc.* **2001**, *123*, 984–985; b) J. R. Porter, J. F. Traverse, A. H. Hoveyda, M. L. Snapper, *J. Am. Chem. Soc.* **2001**, *123*, 10409–10410; for related studies from other laboratories, see: c) S. E. Denmark, C. M. Stiff, *J. Org. Chem.* **2000**, *65*, 5875–5878, and references therein; d) H. Fujihara, K. Nagai, K. Tomioka, *J. Am. Chem. Soc.* **2000**, *122*, 12055–12056; e) S. Dahmen, S. Brase, *J. Am. Chem. Soc.* **2002**, *124*, 5940–5941; f) A. A. Boezio, A. B. Charrette, *J. Am. Chem. Soc.* **2003**, *125*, 1692–1693; g) X.-M. Zhang, H.-L. Zhang, W.-Q. Lin, L.-Z. Gong, A.-Q. Mi, X. Cui, Y.-Z. Jiang, K.-B. Yu, *J. Org. Chem.* **2003**, *68*, 4322–4330.

[2] For reviews on catalytic asymmetric additions to imines, see: a) D. Enders, U. Reinhold, *Tetrahedron: Asymmetry* **1997**, *8*, 1895–1946; b) S. Kobayashi, H. Ishitani, *Chem. Rev.* **1999**, *99*, 1069–1094.

[3] M. A. Huffman, N. Yasuda, A. E. DeCamp, E. J. J. Grabowski, *J. Org. Chem.* **1995**, *60*, 1590–1594.

[4] a) M. Kolb, A. Barth, *Angew. Chem.* **1980**, *92*, 753–754; *Angew. Chem. Int. Ed. Engl.* **1980**, *19*, 725–726; b) K. Hattori, M. Miyata, H. Yamamoto, *J. Am. Chem. Soc.* **1993**, *115*, 1151–1152; c) D. Enders, J. Schankat, *Helv. Chim. Acta* **1995**, *78*, 970–992; d) J. Blanchet, M. Bonin, A. Chiaroni, L. Micouin, C. Riche, H.-P. Husson, *Tetrahedron Lett.* **1999**, *40*, 2935–2938; e) J. Blanchet, M. Bonin, L. Micouin, H.-P. Husson, *J. Org. Chem.* **2000**, *65*, 6423–6426; f) R. Fassler, D. E. Frantz, J. Oetiker, E. M. Carreira, *Angew. Chem.* **2002**, *114*, 3180–3182; *Angew. Chem. Int. Ed.* **2002**, *41*, 3054–3056.

[5] For an alternative approach to the synthesis of optically pure propargylamines through the corresponding optically pure propargyl alcohols, see: J. A. Marshall, M. A. Wolf, *J. Org. Chem.* **1996**, *61*, 3238–3239.

[6] For example, see: B. M. Trost, M. T. Rudd, *Org. Lett.* **2003**, *5*, 1467–1470.

[7] For example, see: a) F. N. Shirota, E. G. DeMaster, H. T. Nagasawa, *J. Med. Chem.* **1979**, *22*, 463–464; b) P. H. Yu, B. A. Davis, A. A. Boulton, *J. Med. Chem.* **1992**, *35*, 3705–3713.

[8] a) C. Koradin, K. Polborn, P. Knochel, *Angew. Chem.* **2002**, *114*, 2651–2654; *Angew. Chem. Int. Ed.* **2002**, *41*, 2535–2538; b) C. Koradin, N. Gommermann, K. Polborn, P. Knochel, *Chem. Eur. J.* **2003**, *9*, 2797–2811.

[9] C. Wei, C.-J. Li, *J. Am. Chem. Soc.* **2002**, *124*, 5638–5639.

[10] For an alternative method involving additions of alkynyl zinc reagents to arylimines catalyzed by this class of peptidic chiral ligands, see: J. T. Traverse, A. H. Hoveyda, M. L. Snapper, *Org. Lett.* **2003**, *5*, in press.

[11] Boc-L-Val and Boc-L-Phe are commercially available at US$0.15 and 0.19, respectively, per mmol from Advanced Chemtech; the corresponding D-isomers can be purchased at US$1.22 and 0.86 per mmol.

[12] See the Supporting Information for details.

[13] For similar observations in connection to Ti-catalyzed additions of [Me_2Zn] to α,β-unsaturated aldehydes, see: S. Nowotny, S. Vettel, P. Knochel, *Tetrahedron Lett.* **1994**, *35*, 4539–4540.

[14] a) C. A. Krueger, K. W. Kuntz, C. D. Dzierba, W. G. Wirschun, J. D. Gleason, M. L. Snapper, A. H. Hoveyda, *J. Am. Chem. Soc.* **1999**, *121*, 4284–4285; b) K. D. Shimizu, M. L. Snapper, A. H. Hoveyda, *Chem. Eur. J.* **1998**, *4*, 1885–1889.

[15] S. B. Garber, J. S. Kingsbury, B. L. Gray, A. H. Hoveyda, *J. Am. Chem. Soc.* **2000**, *122*, 8168–8179; for related discussions and additional data, see: F. Royer, C. Vilain, L. Elkaim, L. Grimaud, *Org. Lett.* **2003**, *5*, 2007–2009.

[16] a) F. A. Hicks, S. L. Buchwald, *J. Am. Chem. Soc.* **1999**, *121*, 7026–7033; b) S. J. Sturla, S. L. Buchwald, *J. Org. Chem.* **1999**, *64*, 5547–5550.

 © 2003 Wiley-VCH Verlag GmbH & Co. KGaA, Weinheim

Asymmetric Catalysis

A Facile and Rapid Route to Highly Enantiopure 1,2-Diols by Novel Catalytic Asymmetric α-Aminoxylation of Aldehydes**

*Guofu Zhong**

Enantioselective routes to optically active 1,2-diols are of considerable interest since this structural moiety is widely found in biologically active natural products and synthetic pharmaceuticals.[1] A number of methods for their synthesis have been developed and, among them, the Sharpless asymmetric dihydroxylation of olefins is most often

[*] Prof. Dr. G. Zhong
The Skaggs Institute for Chemical Biology and
The Department of Molecular Biology
The Scripps Research Institute
10550 North Torrey Pines Road, La Jolla, CA 92037 (USA)
Fax: (+1) 858-784-2582
E-mail: gzhong@scripps.edu

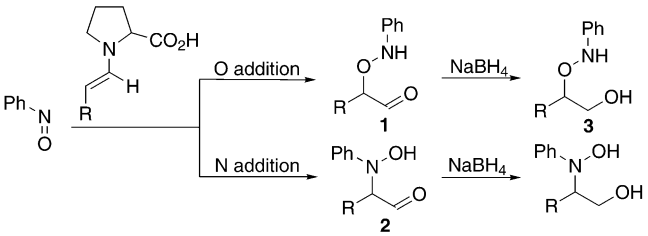
[**] We gratefully acknowledge Prof. R. Lerner and The Scripps Research Institute for support. We thank R. M. Gordley for helpful discussions.

Supporting information for this article is available on the WWW under http://www.angewandte.org or from the author.

 DOI: 10.1002/anie.200352097 © 2003 Wiley-VCH Verlag GmbH & Co. KGaA, Weinheim

used.[1c,2] Another potential route to chiral 1,2-diols is the asymmetric α-hydroxylation of aldehydes and subsequent reduction. However, a direct chemical method for the α-hydroxylation of aldehydes has not been reported.[3] This is because of the facile aldol reactions that occur during enolate formation. The only example leading to α-hydroxyaldehydes in high enantiomeric purity is shown by the oxidation of preformed enolates from aldehydes derivatized with chiral auxiliaries.[4] For these reasons, the development of new methodologies for the direct catalytic enantioselective α-hydroxylation of aldehydes has become an intriguing target in organic synthesis. Recent studies in enamine chemistry in which chiral amines were employed to mimic enzymatic catalysis[5] have led to the utilization of aldehydes as donors to form C–C bonds (for example, in aldol,[6] Mannich,[7] Michael,[8] and Diels–Alder[9] reactions) and C–N bonds (in Michael-like amination[10]). In contrast to the classic preformed enolates, these reactions are believed to proceed through the direct in situ production of enamines from aldehydes, in a similar way to natural enzymes.[11] These findings prompted us to investigate whether the amine catalysts could be applied to the formation of a C–O bond in the asymmetric α-aminoxylation of aldehydes.

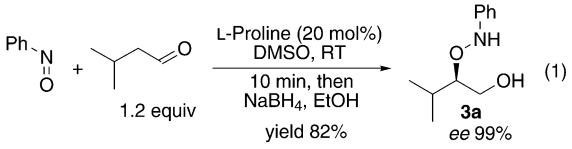
Herein, we report the first direct catalytic enantioselective α-aminoxylation of aldehydes by using enantiopure proline as the catalyst and nitrosobenzene as the oxygen source. This method provides a simple, yet efficient, route to chiral 1,2-diol precursers (O addition products in Scheme 1) in a one-pot sequence with excellent enantioselectivities (*ee* values from 94 to 99%) and good yields (54–86%).



Scheme 1. Possible nucleophilic addition of the enamine intermediate on the nitroso double bond.

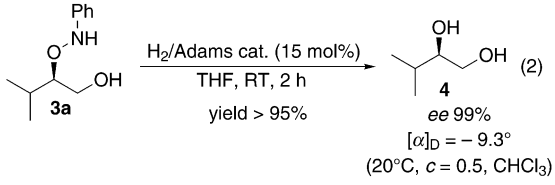
On the basis of previous results, we suspected that the highly reactive enamine intermediates formed between aldehydes and proline might serve as nucleophiles and add stereoselectively to the nitroso functional group, either on the oxygen atom or the nitrogen atom. Nucleophilic O attacks of the enamines on the nitroso double bond might give the α-aminoxy product **1**. While nucleophilic N attacks would afford the α-*N*-hydroxyamino product **2**. It was anticipated that this organocatalysis might provide a solution to the synthetic challenge if nucleophilic attacks could be directed to the oxygen side of the nitroso compounds.

We initially tested the reaction using isovaleraldehyde as the donor. The superior reactivity of nitrosobenzene over the aldehyde itself as the acceptor meant that the concurrent self-aldolization[6a,b] of the aldehyde was remarkably minimized. Only a small excess of the aldehyde (1.2 equiv) was required to accomplish the reaction. Initial experiments were conducted with the reaction of isovaleraldehyde (1.2 equiv), nitrosobenzene (1.0 equiv), and L-proline (20 mol%) in DMSO under fast stirring. To our delight, this reaction was completed in just 10 min. The reaction course can be easily monitored by observation of its color change from green to orange. The isolation and characterization of the main product by flash column chromatograghy over silica gel showed that an O-regioselective addition product **1** (Scheme 1; R = isopropyl) was formed, but the yield of the isolated product was not satisfying (less than 50%). The N-selective product **2** (R = isopropyl) was not found. This O-selective attack of the in situ generated enamine on the nitroso group clearly differs from that found in N-selective "nitroso-aldol reactions"[12] using preformed ketone enolates in the absence of catalysts, where the reactions give exclusively N-addition products, namely, α-N-hydroxyamino products. However, it is similar to that in the O-selective reactions of the preformed ketone enolates with catalysts.[13] Since longer reaction times caused a decrease in yield, we suspected that the poor yield obtained by flash chromatography might be a consequence of the labile properties of the product on silica gel as a result of the co-existence of both aldehyde and amine functions. We next tried in situ conversion of the intermediate **1** into the more stable 2-aminoxy alcohol **3a** (Scheme 1; R = isopropyl) by reduction with sodium borohydride in the mixed solvent of DMSO and ethanol. The corresponding product **3a** was then isolated in good yield (82%, one pot in two steps) and with excellent enantioselectivity by column chromatography on silica gel [Eq. (1), the



99% *ee* of the product **3a** was determined by chiral-phase HPLC on a chiracel AD column using hexane/isopropanol]. In addition to DMSO, a solvent screening with DMF, THF, diethyl ether, 1,4-dioxane, EtOH, CH_2Cl_2, $CHCl_3$, and EtOAc was performed under the same reaction conditions. It was found that DMSO afforded the best reaction rate, yield, and enantioselectivity than any other solvent. Accordingly, DMSO was utilized as the solvent in all subsequent studies.

The stereochemistry of this transformation was determined by conversion of 2-aminoxy alcohol **3a** into 1,2-diol **4**, the absolute configuration and optical rotation of which are known.[1b,c] Catalytic hydrogenation of the alcohol **3a** over platinum dioxide (Adams catalyst with 83% Pt) in THF cleaved cleanly the O–N bond of **3a** to furnish diol **4** with a yield greater than 95%. The absolute configuration of the diol **4** was assigned *R* [Eq. (2)] from optical rotation measure-

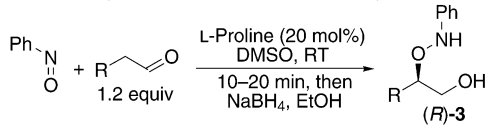


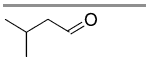
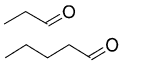
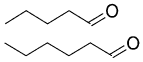
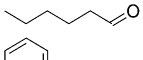
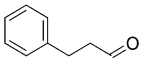
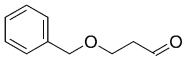
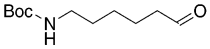
 © 2003 Wiley-VCH Verlag GmbH & Co. KGaA, Weinheim

ments. It should be noted that the removal of the phenylamino group from the O–N bond did not result in any loss in optical purity.

Encouraged by these initial results, we further explored the scope of these novel transformations with a series of aliphatic aldehydes under the same reaction conditions. In every case, the reaction proceeded rapidly. Typically it was done in 10 to 20 minutes. After in situ reduction with $NaBH_4$, the reactions afforded O-regioselective products **3b–3h** with excellent enantioselectivities (94–99% *ee*) in good overall yields (54–86%; Table 1). The racemic analogues required to establish the HPLC conditions were made by using racemic proline.

Table 1: Direct catalytic enantioselective α-aminoxylation of aldehydes.



Aldehyde	Product	Yield[a] [%]	*ee*[b] [%]
	**3a**	82	99
	**3b**	60	97
	**3c**	71	99
	**3d**	75	99
	**3e**	86	99
	**3f**	73	99
	**3g**	54	99
	**3h**	61	94

[a] Yields of isolated products. [b] The *ee* values were determined by chiral-phase HPLC using Chiracel AD column. Boc = *tert*-butoxycarbonyl.

The observed enantioselectivitiy of the catalytic α-aminoxylation of aldehydes can be rationalized by invoking an enamine mechanism operating through a chair transition state where the *Si* face of an *E* enamine formed from the aldehyde and L-proline approaches the less-hindered oxygen atom of nitrosobenzene to provide a chiral α-aminoxyaldehyde with *R* configuration (Figure 1). This mechanism is completely in accord with the previously proposed models for proline-catalyzed aldol reactions.[6e,14]

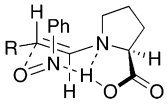


Figure 1. Proposed transition state of the reaction.

In summary, we have discovered the first direct catalytic enantioselective α-aminoxylation of aldehydes which provides a facile route to enantiopure α-aminoxyaldehyde intermediates. This novel reaction proceeds rapidly and is typically completed in 10–20 minutes in the presence of 20% equivalents of the proline catalyst. Since proline is commercially available in both enantiopure forms, a one-pot sequence—catalytic α-aminoxylation of aldehydes followed by in situ reduction with $NaBH_4$—affords *R*- or *S*-configured 1,2-diol units (the secondary alcohol "protected" by an O-amino group) with excellent enantioselectivities and in good yields which are important building blocks in natural product synthesis.[1c] The operational procedure is very simple and generally involves mixing and stirring the reaction components together at ambient temperature. The reaction does not require anhydrous or oxygen-free conditions. The process is ideally suited for industrial-scale preparation because of its wide scope and excellent enantioselectivity. The nitroso group has been found to be a good oxygen source for the formation of C–O bonds.[15] Studies addressing the mechanism and the synthetic scope of this new asymmetric transformation are ongoing.

Received: June 10, 2003 [Z52097]

Keywords: alcohols · aldehydes · asymmetric catalysis · enantioselectivity · proline

[1] a) H. Hanessian, *Total Synthesis of Natural Products: the "Chiron" Approach*, Pergamon, Oxford, **1983**; b) B. T. Cho, Y. S. Chun, *J. Org. Chem.* **1998**, *63*, 5280–5282; c) B. T. Cho, Y. S. Chun, *Tetrahedron*: *Asymmetry* **1999**, *10*, 1843–1846.

[2] H. C. Kolb, M. S. VanNieuwenhze, K. B. Sharpless, *Chem. Rev.* **1994**, *94*, 2483–2547.

[3] For the enzymatic synthesis, see M. D. Burkart, Z. Zhang, S.-C. Hung, C.-H. Wong, *J. Am. Chem. Soc.* **1997**, *119*, 11743–11746.

[4] a) D. Enders in *Asymmetric Synthesis, Vol.* 3 (Ed.: J. D. Morrison), Academic Press, Orlando, **1984**, p. 275; b) D. Enders, P. Fey, H. Kipphardt, *Org. Synth.* **1987**, *65*, 173–178, 183–194; c) D. Enders, V. Bhushan, *Tetrahedron Lett.* **1988**, *29*, 2437–2440; d) A. Job, C. F. Janeck, W. Bettray, R. Peters, D. Enders, *Tetrahedron* **2002**, *58*, 2253–2329.

[5] For antibody mimics, see a) J. Wagner, R. A. Lerner, C. F. Barbas III, *Science* **1995**, *270*, 1797–1800; b) G. Zhong, T. Hoffmann, R. A. Lerner, S. Danishefsky, C. F. Barbas III, *J. Am. Chem. Soc.* **1997**, *119*, 8131–8132; c) C. F. Barbas III, A. Heine, G. Zhong, T. Hoffmann, S. Gramatikova, R. Björnestedt, B. List, J. Anderson, E. A. Stura, E. A. Wilson, R. A. Lerner, *Science* **1997**, *278*, 2085–2092; d) T. Hoffmann, G. Zhong, B. List, D. Shabat, J. Anderson, S. Gramatikova, R. A. Lerner, C. F. Barbas III, *J. Am. Chem. Soc.* **1998**, *120*, 2768–2779; f) G. Zhong, D. Shabat, B. List, J. Anderson, S. C. Sinha, R. A. Lerner, C. F. Barbas III, *Angew. Chem.* **1998**, *110*, 2609–2612; *Angew. Chem. Int. Ed.* **1998**, *37*, 2481–2484; g) G. Zhong, R. A. Lerner, C. F. Barbas III, *Angew. Chem.* **1999**, *111*, 3957–3960; *Angew. Chem. Int. Ed.* **1999**, *38*, 3738–3741.

[6] a) A. Northrup, D. W. C. MacMillan, *J. Am. Chem. Soc.* **2002**, *124*, 6798–6799; b) A. Cordova, W. Notz, C. F. Barbas III, *J. Org. Chem.* **2002**, *67*, 301–303; c) Z. G. Hajos, D. R. Parrish, *J. Org. Chem.* **1974**, *39*, 1615–1621; d) U. Eder, G. Sauer, R. Wiechert, *Angew. Chem.* **1971**, *83*, 492–493; *Angew. Chem. Int. Ed. Engl.* **1971**, *10*, 496–497; e) K. Sakthivel, W. Notz, T. Bui, C. F. Barbas III, *J. Am. Chem. Soc.* **2001**, *123*, 5260–5267; f) B. List, R. A. Lerner, C. F. Barbas III, *J. Am. Chem. Soc.* **2000**, *122*, 2395–2396.

[7] a) A. Cordova, S.-i. Watanabe, F. Tanaka, W. Notz, C. F. Barbas III, *J. Am. Chem. Soc.* **2002**, *124*, 1866–1867; b) A. Cordova, W Notz, G. Zhong, J. M. Betancort, C. F. Barbas III, *J. Am. Chem. Soc.* **2002**, *124*, 1842–1843; c) B. List, P. Polarjiev, W. T. Biller, H. J. Martin, *J. Am. Chem. Soc.* **2002**, *124*, 827–833.

[8] a) J. M. Betancort, C. F. Barbas III, *Org. Lett.* **2001**, *3*, 3737–3740; b) A. Enders, A. Seki, *Synlett* **2002**, 26–28.

 © 2003 Wiley-VCH Verlag GmbH & Co. KGaA, Weinheim

[9] K. Juhl, K. A. Jørgensen, *Angew. Chem.* **2003**, *115*, 1536 – 1539; *Angew. Chem. Int. Ed.* **2003**, *42*, 1498 – 1501, and references therein.
[10] a) A. Bøgevig, K. Juhl, N. Kumaragurubaran, W. Zhuang, K. A. Jørgensen, *Angew. Chem.* **2002**, *114*, 1868 – 1871; *Angew. Chem. Int. Ed.* **2002**, *41*, 1790 – 1793; b) B. List, *J. Am. Chem. Soc.* **2002**, *124*, 5656 – 5657; c) N. Kumaragurubaran, K. Juhl, W. Zhuang, A. Bøgevig, K. A. Jørgensen, *J. Am. Chem. Soc.* **2002**, *124*, 6254 – 6255.
[11] For studies using natural class I aldolases in organic synthesis, see H. J. M. Gijsen, L. Qiao, W. Fitz, C.-H. Wong, *Chem. Rev.* **1996**, *96*, 443 – 473.
[12] N. Momiyama, H. Yamamoto, *Org. Lett.* **2002**, *4*, 3579 – 3582.
[13] a) N. Momiyama, H. Yamamoto, *J. Am. Chem. Soc.* **2003**, *125*, 6038 – 6039; b) N. Momiyama, H. Yamamoto, *Angew. Chem.* **2002**, *114*, 3112 – 3114; *Angew. Chem. Int. Ed.* **2002**, *41*, 2986 – 2988.
[14] S. Bahmanyar, K. N. Houk, *J. Am. Chem. Soc.* **2001**, *123*, 11 273 – 11 283.
[15] Nitroso compounds have been used to generate C–O bonds in Diel–Alder reactions, see P. F. Vogt, M. J. Miller, *Tetrahedron* **1998**, *54*, 1317 – 1348.

 © 2003 Wiley-VCH Verlag GmbH & Co. KGaA, Weinheim

High-Surface-Area Aluminum Fluoride

Amorphous Metal Fluorides with Extraordinary High Surface Areas**

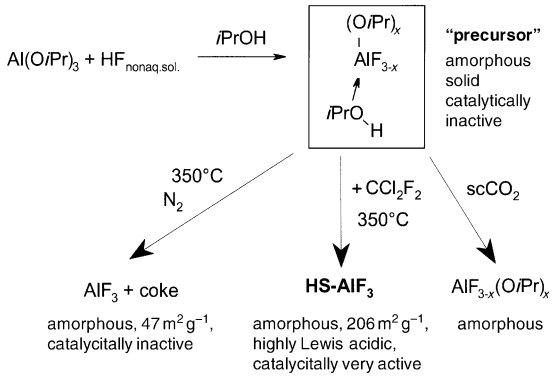
Erhard Kemnitz, Udo Groß, Stephan Rüdiger, and Chandra S. Shekar*

Inorganic materials having high surface areas are of interest, for example, in heterogeneous catalysis where the activity of a catalyst depends largely on its surface.[1] Metal oxides with very high surface areas can be prepared by sol–gel routes, by freeze-drying, or under supercritical conditions as xerogels or aerogels.[2] However, no such synthetic routes exist to date for metal fluorides, which because of their high lattice energy tend to form regular crystalline structures. Thus, aluminum trifluoride prepared conventionally by precipitation in aqueous media exhibits surface areas in the range from 10 to 60 $m^2 g^{-1}$ only.[3] In spite of this, AlF_3 is widely used as catalyst,[4] and other metal fluorides, such as magnesium fluoride, are used as supports for catalytically active materials.[5] By a sophisticated NF_3 plasma-etching treatment of aluminum-rich zeolites it could be shown that AlF_3 with surface areas of up to 190 $m^2 g^{-1}$ is in principal accessible.[6]

Herein we report a novel facile non-aqueous synthesis route to X-ray amorphous metal fluorides that have high surface areas. First a solid, fluoridated metal compound is prepared, which is structurally highly distorted because of the presence of bulky groups in stoicheiometrical quantities. This precursor is then fully fluorinated under soft conditions, that is, below crystallization temperature to preserve the distortion.

As in case of the sol–gel syntheses of metal oxides where the final removal of the alcohol from the metal–alkoxide precursor (aerogels vs. xerogels) is crucial for the development of their specific morphological properties, for high-surface-area metal fluorides the final fluorinating treatment of the partially fluorinated precursor is the determining step of the synthesis. For metal oxides, high-surface materials have unusual properties, particularly when it comes to catalysis. The same is true for metal fluorides. Thus, aluminum fluoride prepared as described below, has not only a very high surface area but is also an extremely strong Lewis acid, comparable with some of the strongest known Lewis acids SbF_5[7] and aluminum chlorofluoride (ACF).[8]

The route, which will be detailed for AlF_3, consists of two consecutive steps. First, aluminum triisopropoxide ($Al(OiPr)_3$) was treated in water-free isopropanol with a moderate excess of anhydrous hydrogen fluoride dissolved in isopropanol or diethyl ether. After removing all volatile material at elevated temperature in vacuum a white powdery solid remained; the precursor of the target fluoride. The precursor had a ratio of fluorine to aluminum of about 2:1, and a carbon content of about 30%. Thus, despite having treated the $Al(OiPr)_3$ with an excess of HF, there was obviously some isopropylate together with some coordinatively bound isopropanol in the compound (Scheme 1).



Scheme 1. Route used to prepare HS-AlF_3.

The second step comprises treatment of the precursor with a fluorinating agent, such as CCl_2F_2 at 350 °C, to remove the organic component by replacing it fully by fluorine. The final product obtained had a ratio of fluorine to aluminum of 3:1 and the carbon content was less than 0.5%. There is also a small amount of chlorine present, which becomes zero if CHF_3 is used instead of CCl_2F_2 (analysis (%) calcd for AlF_3: Al 32.13, F 67.87; found: Al 31.2, F 67.2, C 0.4, Cl 0.3). Strikingly, the aluminum fluoride prepared this way has a surface area of about 200 $m^2 g^{-1}$ and showed a very high Lewis acidity and corresponding catalytic activity. Because of its high specific surface area we denote it HS-AlF_3. In a similar way, other metal fluorides with very high surface areas can also be prepared. Thus, for example, magnesium fluoride prepared accordingly had a BET(N_2) surface area of 190 $m^2 g^{-1}$.

In case of aluminum fluoride, both the precursor and the final product, HS-AlF_3, were X-ray amorphous, but thermal analysis of both compounds revealed the exothermic formation of a crystalline phase at 540–570 °C identified by X-ray powder diffraction as α-AlF_3. The presence of *i*PrO units in the precursor was confirmed by (in addition to carbon analysis) the IR spectra of the solid, and also by ^1H NMR spectrum of a suspension in CD_3CN. Attempts to remove the organic from the precursor with supercritical CO_2 failed; more than two thirds of the organic remained (Scheme 1). Heating the precursor to 350 °C in a nitrogen flow gave an amorphous product with only 1% carbon content and a BET surface area of 47 $m^2 g^{-1}$, but which was not catalytically active. These results together with the elemental analysis indicate that the precursor has a composition corresponding to the formula $AlF_{3-x}(OiPr)_x \cdot (iPrOH)_y$ with $x \approx 1$ and $y < 1$. Only the loosely bound alcohol can be removed by super-

[*] Prof. Dr. E. Kemnitz, Dr. U. Groß, Dr. S. Rüdiger, Dr. C. S. Shekar
Institute of Chemistry
Humboldt University
Brook-Taylor-Strasse 2, 12489 Berlin (Germany)
Fax: (+49) 30-2093-7277
E-mail: erhard.kemnitz@chemie.hu-berlin.de

[**] We would like to thank Dr. M.-M. Pohl, ACA Berlin, for recording the TEM micrographs.

 DOI: 10.1002/anie.200351278 © 2003 Wiley-VCH Verlag GmbH & Co. KGaA, Weinheim

critical CO_2, whereas the alkoxy groups can be gently removed by a soft fluorination under preservation of the high morphological disorder. Hence, the presence of alkoxy groups in the precursor is decisive for obtaining high-surface-area metal fluorides.

The BET(N_2) surface properties were compared for HS-AlF_3, its precursor, and β-AlF_3, a common AlF_3-type, which is often used as a Lewis acid catalyst in fluorine chemistry. The specific surface area (S_{BET}) of β-AlF_3 is only $33\,m^2g^{-1}$, treatment with CCl_2F_2 at 350 °C did not improve that value. The HS-AlF_3 has a BET surface area of $206\,m^2g^{-1}$ (BJH adsorption cumulative surface area $251\,m^2g^{-1}$, BJH desorption cumulative surface area $281\,m^2g^{-1}$; all data obtained with N_2 using an ASAP 2010, Micrometrics) and the values for the precursor are even higher (Table 1). In addition, HS-AlF_3 had a much narrower pore size distribution than β-AlF_3 (Figure 1).

Table 1: Properties of selected aluminum fluorides.

Sample	Crystallinity	S_{BET} [m^2g^{-1}]	F:Al	C Content [%]
precursor	amorphous	430	≈2:1	31
HS-AlF_3	amorphous	206	3:1	0.4
β-AlF_3	crystalline	33	3:1	n.a.[a]
AlF_3[b]	crystalline	113	3:1	0.15

[a] n.a. = not applicable; [b] Obtained conventionally by an aqueous route; treated with CCl_2F_2 at 350 °C.

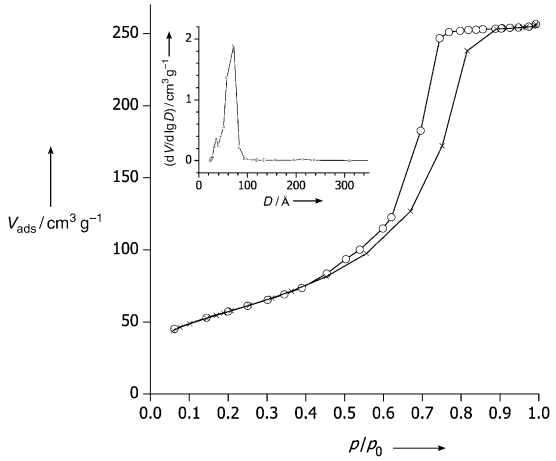


Figure 1. HS-AlF_3 adsorption/desorption isotherms and pore size distribution, obtained by N_2 adsorption technique. ⋆ adsorption, ○ desorption; p/p_0 = relative pressure, V_{ads} = adsorbed volume, D = pore diameter, $dV/dlgD$ = pore volume.

SEM micrographs (Figure 2) show the amorphous HS-AlF_3 as well as its precursor to be composed of particles, which according to BET results are mesoporous, and which are probably agglomerates of much smaller particles of irregular shape. In TEM micrographs well-defined domains of about 10 nm diameter can be seen (Figure 3), some of which are regular, that is, lattice planes could be detected in some regions. However these areas are too small to be detected by X-ray diffraction. For both the precursor and HS-AlF_3, interlattice-plane separations of approximately 3.5 Å were estimated, which are typical for aluminum fluorides.

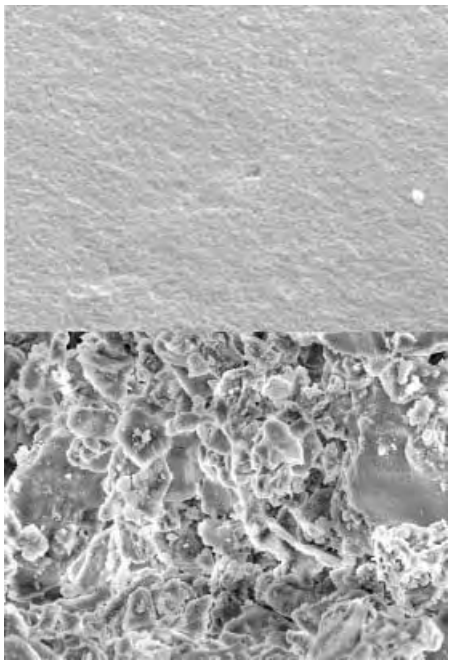


Figure 2. SEM micrographs of HS-AlF_3, view: $2\times2\,\mu m^2$ (upper) and $100\times100\,\mu m^2$ (lower section).

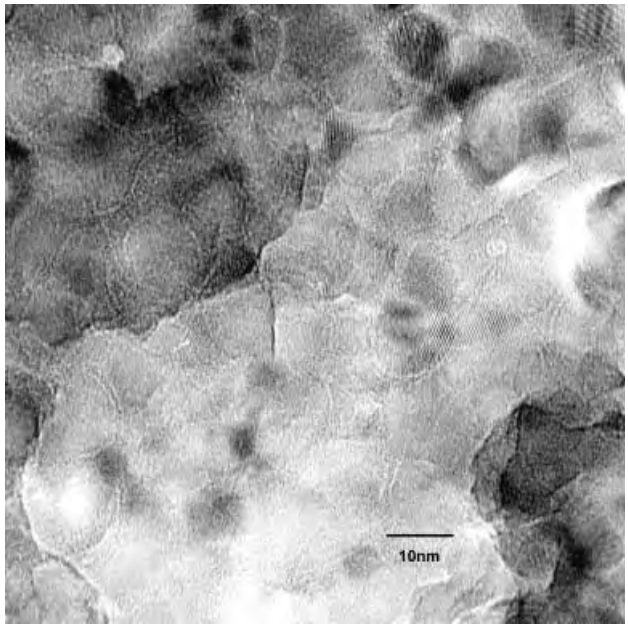


Figure 3. TEM micrograph of HS-AlF_3.

Energy-dispersive X-ray spectroscopy (EDX) confirms the elemental analysis of the HS-AlF_3 (after the fluorination/activation treatment) that it consists of Al, F, and some O. The oxygen content might be a result of surface hydration when the solid was handled in open atmosphere. IR- and ^{27}Al-magic angle spinning (MAS)-NMR-spectra of the solid HS-AlF_3 were recorded (Figure 4). The ^{27}Al-MAS-NMR-spectra were collected at 132.2 MHz at a spinning rate of 10 kHz and allow the short-range order at Al atoms to be described and enable discrimination of different Al species. The chemical shift of

 © 2003 Wiley-VCH Verlag GmbH & Co. KGaA, Weinheim

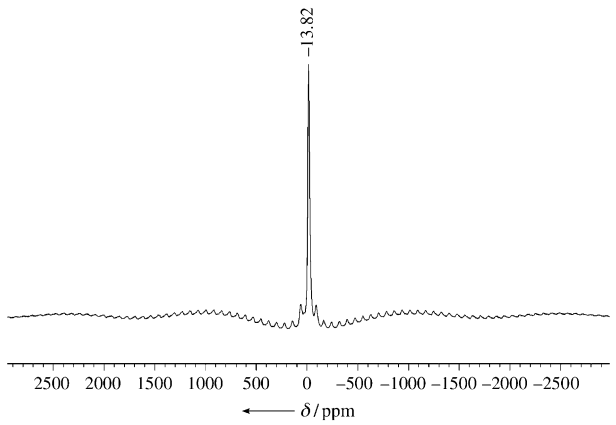


Figure 4. ^{27}Al-MAS-NMR spectrum of HS-AlF_3.

$\delta = -13.8$ ppm is indicative to an octahedral environment around the Al sites of a polymorphous solid. Compared with crystalline aluminum fluoride, for example, α-AlF_3, the resonance is shifted down field, that is, it is indicative of a more coordinatively unsaturated species.

The large sideband manifold of the satellite transitions of the quadrupolar aluminum nucleus (Figure 4) indicates large quadrupole coupling constants (QCCs) for aluminum, consistent with a stronger distortion of the octahedral environments. Clear discontinuities because of first-order QCCs were not found because of the wide distribution of the QCCs. Sideband simulations indicate QCCs of about 1.5 MHz which is much larger than that of the highly symmetric α-AlF_3, but comparable with the estimated 1.4 MHz of the nearly amorphous material.[6]

The IR spectra of HS-AlF_3 support these findings. In the region from $\tilde{\nu} = 700$–4000 cm^{-1}, there should be no absorption bands for AlF_3. In fact, only one band at 667 cm^{-1} (Al-F valence vibration ν_3) could be seen, which was very broad owing to the amorphous state of the compound. Laser-Raman analysis was not successful because of fluorescence phenomena, clearly a result of the carbon present. The chemical properties of the surface of HS-AlF_3 are demonstrated by its pyridine absorption, by temperature programmed desorption of NH_3 (NH_3-TPD), and more importantly by its catalytic properties. After treatment with pyridine and subsequent heating in an N_2 stream at 150 °C the photoacoustic IR spectra of the solid showed intense bands at $\tilde{\nu} = 1454$ and 1492 cm^{-1} which indicate Lewis acid sites. The NH_3 TPD profile resembles that of β-AlF_3, which shows two distinct maxima at about 150 and 375 °C, and the end of the desorption at about 500 °C.[9] HS-AlF_3, however, shows maxima at about 200 and 450 °C and desorption is complete at about 600 °C which gives evidence for much stronger Lewis acid sites than in β-AlF_3. The catalytic activity was compared to the precursor, to β-AlF_3, and to an amorphous AlF_3 prepared conventionally by an aqueous route from $AlF_3 \cdot 3\,H_2O$ desiccated at 200 °C in vacuum followed by subsequent CCl_2F_2 treatment at 350 °C. As test reaction the temperature dependence of catalytic CCl_2F_2 dismutation [Eq. (1)] was studied in a

$$5\,CCl_2F_2 \xrightarrow{\text{cat.}} CCl_3F + 3\,CClF_3 + CCl_4 \qquad (1)$$

flow reactor under conditions that equilibrium is reached (ca. 0.5 g of catalyst in a Ni tube of 0.5 cm i.d., CCl_2F_2 flow 2 mL min^{-1}, contact time ca. 2 s). Upon varying the contact time no change in product composition could be observed above 0.5 sec.

Further, the catalytic isomerization of 1,2-dibromohexafluoropropane to 2,2-dibromohexafluoropropane was studied.[10] According to the data in Table 2, the dismutation of CCl_2F_2 proceeds over HS-AlF_3 even at very low temperatures with much higher conversion rates than over the amorphous AlF_3 from the aqueous synthesis route, which also has a high surface area compared to other metal fluorides. This difference in reactivity is clearly founded in the presence of substantially more acidic sites in HS-AlF_3, as demonstrated by the NH_3-TPD curves shown in Figure 5. Although their profile is rather similar, the NH_3 desorption from the amorphous AlF_3 is completed at around 500 °C, as found for β-AlF_3 (see above)[9] whereas with HS-AlF_3 completion is around 600 °C. The heterogeneity of the acidic strength of the surface sites is the reason for the different temperature dependencies of this reaction in which the energy of activation for HS-AlF_3 is apparently higher than for amorphous AlF_3. The extraordinarily strongly acidic sites in HS-AlF_3 are clearly those at which the isomerization of 1,2-

Table 2: Catalytic activity of selected aluminum fluorides.

Sample	CCl_2F_2 Dismutation [%]					$C_3Br_2F_6$ Isomerization [%]
T [°C]	300	250	200	150	100	25
precursor	0		0		0	0
HS-AlF_3	96	96	87	59	22	>90
β-AlF_3	93		47			0
AlF_3[a]	96	90	55	20	8	5

[a] Obtained conventionally by an aqueous route; treated with CCl_2F_2 at 350 °C.

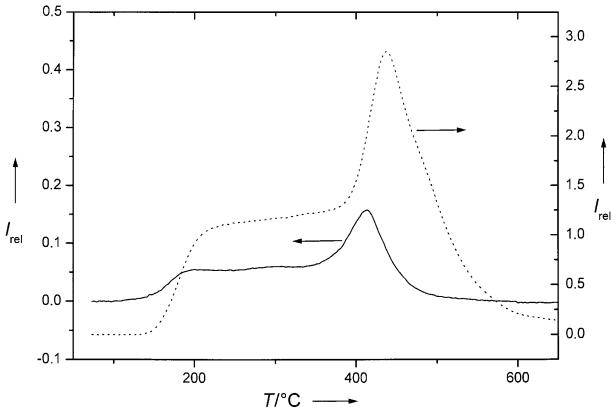


Figure 5. Temperature programmed desorption of NH_3 (NH_3-TPD) from HS-AlF_3 (----) and amorphous AlF_3 (——).

 © 2003 Wiley-VCH Verlag GmbH & Co. KGaA, Weinheim

dibromohexafluoropropane, which is only catalyzed by the strongest known Lewis acids (SbF_5 and ACF), is activated. Consequently, with amorphous AlF_3 nearly no conversion occurs.

However, and in striking contrast to ACF, HS-AlF_3 is not destroyed by contact with moisture, it completely regains its original catalytic activity after removing the adsorbed water at higher temperatures. Thus, it is suited for industrial application.

To conclude, the new two-step fluorination method is a powerful tool with which to prepare metal fluorides that have extraordinarily high specific surface areas and, depending on the metal, exhibit very high Lewis acidity.

Received: February 25, 2003
Revised: June 25, 2003 [Z51278]

Keywords: aluminum fluoride · heterogeneous catalysis · materials science · super-acidic systems

[1] M. Boudart in *Handbook of Heterogeneous Catalysis* (Eds.: G. Ertl, H. Knözinger, J. Weitkamp), VCH, Weinheim, **1997**.
[2] J. B. Miller, E. I. Ko in *Advanced Catalysts and Nanostructered Materials* (Ed.: W. R. Moser), Academic Press, San Diego, **1996**.
[3] E. Kemnitz, D.-H. Menz, *Prog. Solid State Chem.* **1998**, *26*, 97.
[4] L. E. Manzer, V. N. M. Rao, *Adv. Catal.* **1993**, *39*, 329.
[5] M. Wojciechowska, J. Goslar, W. Kania, M. Pietrowski, *J. Fluorine Chem.* **1998**, *91*, 141.
[6] J. L. Delattre, P. J. Chupas, C. P. Grey, A. M. Stacey, *J. Am. Chem. Soc.* **2001**, *123*, 5364.
[7] K. O. Christe, D. A. Dixon, D. McLemore, W. W. Wilson, J. A Sheehy, J. A. Boatz, *J. Fluorine Chem.* **2000**, *101*, 151.
[8] V. A. Petrov, C. G. Krespan, B. E. Smart, *J. Fluorine Chem.* **1996**, *77*, 139.
[9] A. Hess, E. Kemnitz, *J. Catal.* **1994**, *149*, 449.
[10] V. A. Petrov, C. G. Krespan, B. E. Smart, *J. Fluorine Chem.* **1998**, *89*, 125.

 © 2003 Wiley-VCH Verlag GmbH & Co. KGaA, Weinheim

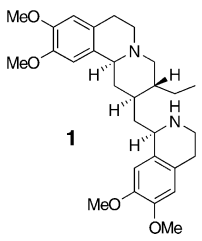
Combinatorial Synthesis

Catalyst-Controlled Stereoselective Combinatorial Synthesis**

Lutz F. Tietze, Nils Rackelmann, and Govindasamy Sekar*

Dedicated to Professor Ernst Schaumann on the occasion of his 60th birthday

Combinatorial chemistry[1] is an important method for the development of pharmaceuticals,[2] agrochemicals,[3] catalysts,[4] and materials.[5] It can be performed either on a solid phase or in solution and in some cases, the advantages of solid- and liquid-phase synthesis may be combined, if the products can be precipitated as salts.[6] The aim of combinatorial chemistry is the preparation of a multitude of organic compounds with constitutional diversity. Stereochemical aspects have so far played only a minor role, although the configuration of a molecule can have a considerable effect on its biological activity; this applies to both the absolute as well as the relative configuration.[7] Herein we present a method to access stereochemical diversity of nonpeptidic active compounds as a new combinatorial strategy.[8] By using enantiomerically pure catalysts, several stereogenic centers are constructed in a catalyst-controlled manner.[9] This general concept is introduced with the example of the synthesis of 12 stereoisomers of the biologically highly active ipecacuanha alkaloid emetine (**1**), which contains four stereogenic centers. The ruthenium complexes (*R*,*R*)-**5** and (*S*,*S*)-**5** developed by Noyori and co-workers[10] were used as catalysts. The key step of the synthesis is the enantio- or diastereoselective hydrogenation of imines, which can be prepared either by oxidation of a secondary amine or by a Bischler–Napieralski reaction.



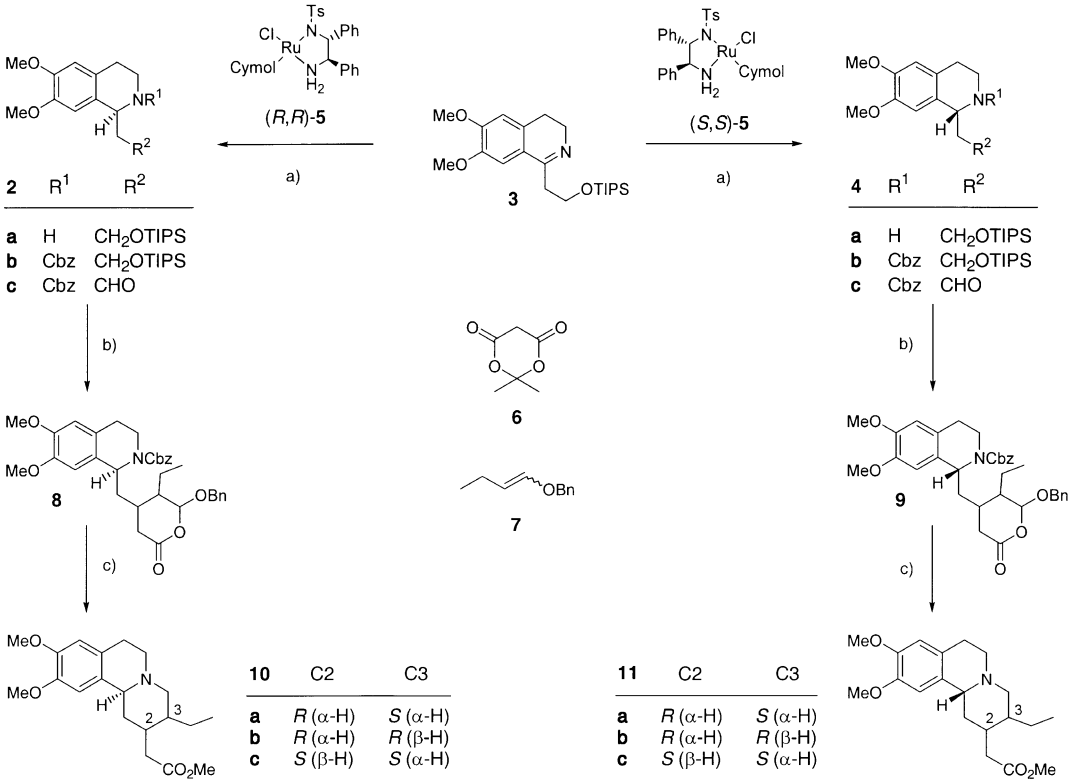
1

Oxidation of the racemic mixture of **2a** and **4a** with potassium permanganate led to the imine **3** in very good yields,[11] which was hydrogenated to the almost enantiomerically pure tetrahydroisoquinolines **2a** and **4a** by transfer hydrogenation with formic acid in the presence of the catalysts (*R*,*R*)-**5** and (*S*,*S*)-**5**, respectively (Scheme 1).[12] Protection of the secondary amino group in **2a** and **4a** with benzyloxycarbonyl chloride, cleavage of the silyl group, and subsequent oxidation of the primary alcohol yielded the

[*] Prof. Dr. L. F. Tietze, Dipl.-Chem. N. Rackelmann, Dr. G. Sekar
Institut für Organische Chemie
Georg-August-Universität Göttingen
Tammannstrasse 2, 37077 Göttingen (Germany)
Fax: (+49) 551-399-476
E-mail: ltietze@gwdg.de

[**] The investigations were supported by the Deutsche Forschungsgemeinschaft (SFB 416) and the Fonds der Chemischen Industrie. We thank BASF, Bayer, Degussa, Symrise, and Wacker Chemie for providing us with chemicals.

 © 2003 Wiley-VCH Verlag GmbH & Co. KGaA, Weinheim DOI: 10.1002/anie.200351129



Scheme 1. Synthesis of benzoquinolidizines **10a–c** and **11a–c**: a) **3** (1 equiv), (*R*,*R*)-**5** or (*S*,*S*)-**5**, respectively, (2.5 mol%), HCO_2H/NEt_3, DMF, room temperature, 60 min, 93%, >95% *ee*; b) **2c** or **4c** (1.1 equiv), **6** (1 equiv), **7** (10 equiv), EDDA (1 mol%), benzene, 60°C, ultrasound, 17 h, 86%; c) K_2CO_3 (0.5 equiv), MeOH; then Pd/C, H_2, 77%. DMF = *N*,*N*-dimethylformamide, EDDA = ethylenediammonium diacetate, Bn = benzyl, Cbz = benzyloxycarbonyl, TIPS = triisopropylsilyl, Ts = *p*-toluenesulfonyl, cymene = 4-isopropyltoluene.

aldehydes **2c** and **4c,** respectively. A domino reaction[13] of **2c** with Meldrum acid (**6**) and the enol ether **7** in the presence of catalytic amounts of ethylenediammonium diacetate (EDDA) led to the formation of the lactone **8**, which was treated directly with methanol/potassium carbonate and then hydrogenated with Pd/C as catalyst. In this sequence, cleavage of the lactone **8** occurs first with the formation of a methyl ester and an aldehyde, which after hydrogenolysis of the Cbz protecting group reacts with the formed secondary amino function to give an enamine. This enamine is hydrogenated under the reaction conditions to form the benzoquinolizidine framework of emetine (**1**). The mixture of the three diastereomers **10a–c** (1.5:1.0:1.8) can be separated chromatographically.[14] The conversion of the enantiomeric aldehyde **4c** under identical conditions afforded the diastereomers **11a–c**.

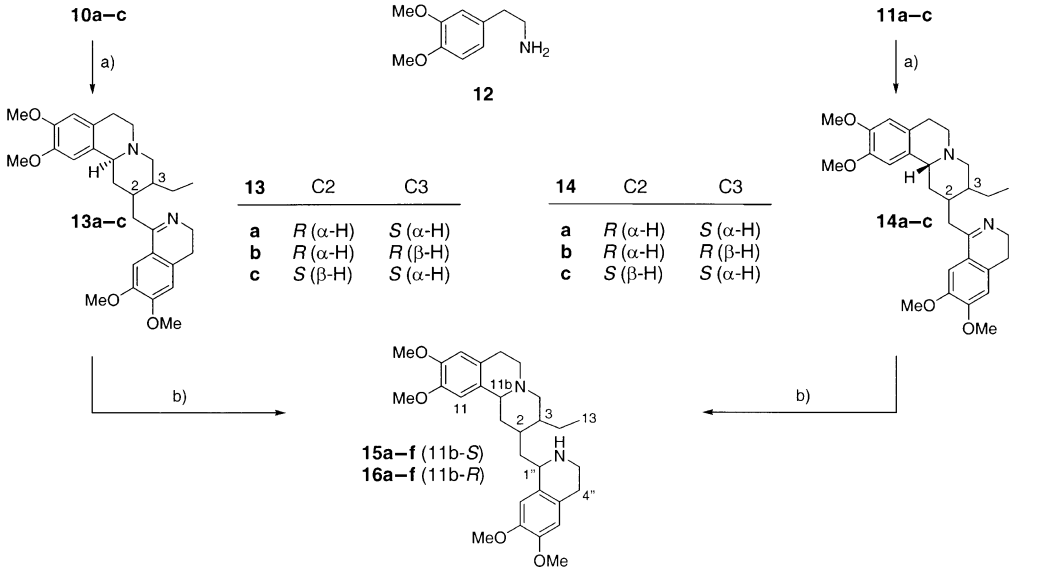
The condensation of the diastereomeric benzoquinolizidines **10a–c** with 2-(3,4-dimethoxyphenyl)ethylamine (**12**) gave the corresponding amides, which were converted into the imines **13a–c** in a Bischler–Napieralski reaction in 60–78% yield (Scheme 2). In a similar manner, the imines **14a–c** were prepared from **11a–c**. Hydrogenation of **13a–c** with (*S*,*S*)-**5** led to **15a–c**, whereas the diastereomers **15d–f** were obtained in the presence of (*R*,*R*)-**5**.[15] Analogously, the stereoisomers **16a–c** and the corresponding diastereomers **16d–f** were obtained from **14a–c** with (*S*,*S*)-**5** and (*R*,*R*)-**5**, respectively. The yields in all hydrogenations were greater than 71%, the diastereoselectivities were, however, slightly different because of the presence of *matched* and *mismatched* combinations: Thus, in the transfer hydrogenation of **13a** with (*S*,*S*)-**5**, selectivities >98:2 were found (that is, the other possible diastereomer could not be detected), whereas in the worst case, in the reaction of **13a** with (*R*,*R*)-**5**, a ratio of 91:9 was observed.

The concept of stereoselective combinatorial synthesis, which is introduced by means of the synthesis of 12 stereoisomers of emetine (**1**), makes a large number of stereoisomers of a chiral compound accessible in a targeted manner. The reactions introduced may be varied in many ways. Thus we have also used 2-phenylethylamine, 2-(2-methoxyphenyl)-ethylamine, 2-(2,5-dimethoxyphenyl)ethylamine, and a serotonin derivative as amino components instead of **12**. The described strategy is generally applicable, and good results can be expected if the enantiomeric catalysts or reagents allow high stereochemical control, independent of the substrate.

Received: February 7, 2003 [Z51129]

Keywords: asymmetric catalysis · combinatorial chemistry · domino reactions · hydrogenation · imines

 © 2003 Wiley-VCH Verlag GmbH & Co. KGaA, Weinheim



13	C2	C3
a	*R* (α-H)	*S* (α-H)
b	*R* (α-H)	*R* (β-H)
c	*S* (β-H)	*S* (α-H)

14	C2	C3
a	*R* (α-H)	*S* (α-H)
b	*R* (α-H)	*R* (β-H)
c	*S* (β-H)	*S* (α-H)

15	C2	C3	C1"	Catalyst
a	*R* (α-H)	*S* (α-H)	*R*	(*S*,*S*)-**5**
b	*R* (α-H)	*R* (β-H)	*R*	(*S*,*S*)-**5**
c	*S* (β-H)	*S* (α-H)	*R*	(*S*,*S*)-**5**
d	*R* (α-H)	*S* (α-H)	*S*	(*R*,*R*)-**5**
e	*R* (α-H)	*R* (β-H)	*S*	(*R*,*R*)-**5**
f	*S* (β-H)	*S* (α-H)	*S*	(*R*,*R*)-**5**

16	C2	C3	C1"	Catalyst
a	*R* (α-H)	*S* (α-H)	*R*	(*S*,*S*)-**5**
b	*R* (α-H)	*R* (β-H)	*R*	(*S*,*S*)-**5**
c	*S* (β-H)	*S* (α-H)	*R*	(*S*,*S*)-**5**
d	*R* (α-H)	*S* (α-H)	*S*	(*R*,*R*)-**5**
e	*R* (α-H)	*R* (β-H)	*S*	(*R*,*R*)-**5**
f	*S* (β-H)	*S* (α-H)	*S*	(*R*,*R*)-**5**

Scheme 2. Stereoselective synthesis of 12 stereoisomers of **1** (**15a–f** and **16a–f**): a) **10a–c** or **11a–c**, **12**, $AlMe_3$, reflux, 4.5 h, 60–78%; then $POCl_3$, benzene, reflux, 45 min, 60–82%; b) (*R*,*R*)-**5** or (*S*,*S*)-**5** (10 mol%), HCO_2H/NEt_3, DMF, room temperature, 60 min, 71–82%, d.r. 91:9 to >98:2.

[1] a) A. Kirschning, H. Monenschein, R. Wittenberg, *Angew. Chem.* **2001**, *113*, 670–701; *Angew. Chem. Int. Ed.* **2001**, *40*, 650–679; b) S. Senkan, *Angew. Chem.* **2001**, *113*, 322–344; *Angew. Chem. Int. Ed.* **2001**, *40*, 312–329; c) F. Balkenhohl, C. von dem Bussche-Hünnefeld, A. Lansky, C. Zechel, *Angew. Chem.* **1996**, *108*, 2436–2487; *Angew. Chem. Int. Ed. Engl.* **1996**, *35*, 2288–2337.

[2] a) J. Rademann, G. Jung, *Science* **2000**, *287*, 1947–1948; b) K. C. Nicolaou, R. Hughes, S. Y. Cho, N. Winssinger, C. Smethurst, H. Labischinski, R. Endermann, *Angew. Chem.* **2000**, *112*, 3473–3478; *Angew. Chem. Int. Ed.* **2000**, *39*, 3823–3828; c) P. N. Kaul, *Prog. Drug Res.* **1998**, *50*, 9–105.

[3] W. A. Kleschick, L. N. Davis, M. R. Dick, J. R. Garlich, E. J. Martin, N. Orr, S. C. Ng, D. J. Pernich, S. H. Unger, G. B. Watson, R. N. Zuckermann, *ACS Symp. Ser.* **2001**, *774*, 205–213.

[4] a) M. T. Reetz, *Angew. Chem.* **2001**, *113*, 292–320; *Angew. Chem. Int. Ed.* **2001**, *40*, 284–310; b) B. Jandeleit, D. Schaefer, T. S. Powers, H. W. Turner, W. H. Weinberg, *Angew. Chem.* **1999**, *63*, 2494–2532; *Angew. Chem. Int. Ed.* **1999**, *111*, 2648–2689; c) P. P. Pescarna, J. C. van der Waal, I. E. Maxwell, T. Maschmeyer, *Catal. Lett.* **1999**, *63*, 1–11.

[5] a) W. F. Maier, *Angew. Chem.* **1999**, *111*, 1294–1296; *Angew. Chem. Int. Ed.* **1999**, *38*, 1216–1218; b) E. W. McFarland, W. H. Weinberg, *Trends Biotechnol.* **1999**, *17*, 107–115.

[6] L. F. Tietze, H. Evers, E. Töpken, *Angew. Chem.* **2001**, *113*, 903–905; *Angew. Chem. Int. Ed.* **2001**, *40*, 927–929.

[7] a) G. Ekatodromis, A. Borgeat, *Curr. Top. Med. Chem.* **2001**, *1*, 205–206; b) B. Testa, M. Reist, P.-A. Carrupt, *Ann. Pharm. Fr.* **2000**, *58*, 239–246; c) S. Schiffman, K. Sennewald, J. Gagnon, *Physiology and Behavior* **1981**, *27*, 51–59; d) G. Blaschke, H. P. Kraft, K. Fickentscher, F. Koehler, *Arzneim.-Forsch.* **1979**, *29*, 1640–1642.

[8] For a further approach to stereochemical combinatorial synthesis, see: U. Müllenmeister, W.-D. Fessner in *Innovation and Perspectives in Solid Phase Synthesis and Combinatorial Libraries* (Ed.: R. Epten), Mayflower Worldwide Ltd, Birmingham (UK), **2001**, p. 149–152.

[9] Reagent-controlled reactions in which enantiomerically pure auxiliaries are used are likewise possible.

[10] N. Uematsu, A. Fujii, S. Hashiguchi, T. Ikariya, R. Noyori, *J. Am. Chem. Soc.* **1996**, *118*, 4916–4917.

[11] A solution of a racemic mixture of **2a** and **4a** (27.6 g, 70.2 mmol) in CH_3CN (650 mL) was treated at −7 °C with $KMnO_4$ (23.3 g, 147 mmol) in small portions over a period of 15 min and then stirred for 70 min at −5 °C. The reaction mixture was diluted with ice-cold Et_2O (2.5 L), the organic phase was washed with saturated NaCl solution until the solution was colorless, and dried over Na_2SO_4. The solvent was removed under reduced pressure to yield the dihydroisoquinoline **3** as a pale yellow oil, which was used without further purification (24.7 g, 90%).

[12] A solution of dimeric dichloro(*p*-cymene)ruthenium(II) (403 mg, 0.66 mmol), 1,2-(*R*,*R*)-*N*-tosyl-1,2-diphenylethylenediamine (530 mg, 1.45 mmol), and NEt_3 (0.37 mL, 2.63 mmol) in DMF (6.1 mL) was stirred under argon for 60 min at 80 °C. The warm solution was added to the dihydroisoquinoline **3** (21.5 g, 55 mmol) in DMF (103 mL) and the mixture was cooled to 0 °C. A mixture of HCO_2H and NEt_3 (5:2; 27.5 mL) was then added dropwise, and the reaction mixture was stirred for 2 h at 25 °C. The reaction was worked up by the addition of a saturated solution of K_2CO_3, the mixture was diluted with H_2O, the aqueous phase extracted with ethyl acetate, and the combined organic phases dried over Na_2SO_4. After removal of the solvent under reduced pressure, the brown crude product was purified by chromatography on silica gel ($AcOEt/NEt_3$, 100:1) to yield **2a** as a yellow oil (20.2 g, 93%, >95% *ee*).

[13] a) L. F. Tietze, A. Modi, *Med. Res. Rev.* **2000**, *20*, 304–322; b) L. F. Tietze, F. Haunert in *Stimulating Concepts in Chemistry* (Eds. F. Vögtle, J. F. Stoddart, M. Shibasaki, Wiley-VCH, Weinheim,

 © 2003 Wiley-VCH Verlag GmbH & Co. KGaA, Weinheim

2000, p. 39 – 64; c) L. F. Tietze, M. Lieb, *Curr. Opin. Chem. Biol.* **1998**, *2*, 363 – 371; d) L. F. Tietze, *Chem. Rev.* **1996**, *96*, 115 – 136; e) L. F. Tietze, U. Beifuss, *Angew. Chem.* **1993**, *105*, 137 – 170; *Angew. Chem. Int. Ed. Engl.* **1993**, *32*, 131 – 163.

[14] **10a**: ^{1}H NMR (300 MHz, C_6D_6, TMS): $\delta = 0.82$ (t, ^3J(H,H) = 7.5 Hz, 3H; 13-H), 1.10 (m, 1H; 12-H), 1.26 (ddd, ^2J(H,H) = 13.0 Hz, ^3J(H,H) = 11.5, 11.5 Hz, 1H; 1-H_{ax}), 1.34 (m, 1H; 3-H), 1.63 (m, 1H; 12-H), 1.94 (ddd, ^2J(H,H) = 13.0 Hz, ^3J(H,H) = 3.0, 3.0 Hz, 1H; 1-H_{eq}), 2.00–2.32 (m, 6H; CH_2CO$_2$Me, 2-H; 4-H_{ax}, 6-H, 7-H), 2.55 (ddd, ^2J(H,H) = 11.5 Hz, ^3J(H,H) = 5.5, 5.5 Hz, 1H; 6-H), 2.77 (dd, ^2J(H,H) = 11.5 Hz, ^3J(H,H) = 3.5 Hz, 1H; 4-H_{eq}), 2.90–3.10 (m, 2H, 7-H; 11b-H), 3.27 (s, 3H; OMe), 3.38 (s, 3H; OMe), 6.31 (s, 1H; 8-H), 6.62 ppm (s, 1H; 11-H); ^{13}C NMR (75 MHz, C_6D_6, TMS): $\delta = 12.69$ (C13), 18.13 (C12), 29.95 (C7), 34.10 (C1), 37.73 (C3), 38.24 (*C*H$_2$CO$_2$Me), 39.48 (C2), 50.95 (OMe), 53.39 (C4), 55.63 (OMe), 56.13 (OMe), 59.14 (C6), 63,71 (C11b), 110.0 (C8), 112.8 (C1), 127.5 (C11a), 130.8 (C7a), 148.5 (C10), 148.8 (C9), 172.7 ppm (C=O); $[\alpha]_D^{20} = -57.9$ ($c = 0.60$ in $CHCl_3$). **10b**: ^{1}H NMR (300 MHz, C_6D_6, TMS): $\delta = 0.81$ (t, ^3J(H,H) = 7.5 Hz, 3H; 13-H), 1.00 (m, 1H; 12-H), 1.41–1.52 (m, 3H; 1-H, 12-H, 3-H), 1.80 (m, 1H; CH_2CO$_2$Me), 1.92 (dd, ^2J(H,H) = 15.5 Hz, ^3J(H,H) = 15.5 Hz; 1H, 4-H_{ax}), 2.01 (dd, ^2J(H,H) = 22.0 Hz, ^3J(H,H) = 12.0 Hz; 1H, CH_2CO$_2$Me), 2.35–2.48 (m, 4H; 1-H, 2-H, 6-H, 7-H), 2.77(m; 1H, 6-H), 2.93 (dd, ^2J(H,H) = 15.5 Hz, ^3J(H,H) = 5.5 Hz; 1H, 4-H_{eq}), 3.10–3.14 (m, 2H; 7-H, 11b-H), 3.34 (s, 3H; OMe), 3.42 (s, 3H; OMe), 3.44 (s, 3H; OMe), 6.45, (s, 1H; 8-H), 6.77 ppm (s, 1H; 11-H); ^{13}C NMR (75 MHz, C_6D_6): $\delta = 11.20$ (C13), 23.75 (C12), 30.00 (C7), 38.85 (C1), 38.52 (C3), 38.24 (*C*H$_2$CO$_2$Me), 41.79 (C2), 50.93 (OMe), 52.77 (C4), 55.64 (OMe), 56.00 (OMe), 61.43 (C6), 63,00 (C11b), 110.1 (C8), 112.8 (C1), 127.4 (C11a), 130.8 (C7a), 148.5 (C10), 148.8 (C9), 172.9 ppm (C=O); $[\alpha]_D^{20} = -22.0$ ($c = 1.04$ in $CHCl_3$). **10c**: ^{1}H NMR (300 MHz, C_6D_6, TMS): $\delta = 0.88$ (t, $J = 7.5$ Hz, 3H; 13-H), 1.26 (m, 1H; 3-H), 1.54–1.80 (m, 2H; 12-H), 1.88 (ddd, ^2J(H,H) = 13.5 Hz, ^3J(H,H) = 4.0, 4.0 Hz, 1H; 1-H_{eq}), 2.04 (ddd, ^2J(H,H) = 13.5 Hz, ^3J(H,H) = 10.0, 4.5 Hz, 1H; 1-H_{ax}) 2.22 (m, 1H; 2-H), 2.28–2.45 (m, 3H; CH_2CO$_2$Me, 7-H) 2.57 (t, J = 4.0 Hz, 2H; 4-H_2), 2.53 (dd, ^2J(H,H) = 12.5 Hz, ^3J(H,H) = 4.0 Hz, 1H; 6-H), 2,71 (ddd, ^2J(H,H) = 12.5 Hz, ^3J(H,H) = 6.0, 1.0 Hz, 1H; 6-H), 3.04 (ddd, ^2J(H,H) = 17.0 Hz, ^3J(H,H) = 13.0, 6.5 Hz, 1H; 7-H), 3.43 (m, 1H; 11b-H), 3.39 (s, 3H; OMe), 3.44 (s, 3H; OMe), 6.43, (s, 1H; 8-H), 6.77 ppm (s, 1H; 11-H); ^{13}C NMR (75 MHz, C_6D_6): $\delta = 12.32$ (C13), 25.65 (C12), 28.44 (C7), 32.68 (C1), 33.72 (C2), 37.92 (*C*H$_2$CO$_2$Me), 40.76 (C3), 50.97 (OMe), 53.09 (C6), 54.35 (C4), 55.61 (OMe), 55.65 (OMe), 58.20 (C11b), 109.8 (C8), 112.8 (C11), 127.3 (C11a), 130.1 (C7a), 148.6 (C10), 148.7 (C9), 173.0 ppm (C=O); $[\alpha]_D^{20} = -81.5$ ($c = 0.46$ in $CHCl_3$).

[15] **15d**: ^{1}H NMR (600 MHz, $CDCl_3$, TMS): $\delta = 0.97$ (t, ^3J(H,H) = 7.5 Hz, 3H; 13-H), 1.32–1.43 (m, 2H, 1-H; 12-H), 0.97 (t, ^3J(H,H) = 7.5 Hz, 3H; 13-H), 1.58–1.67 (m, 2H, 1′-H; 3-H), 1.71 (m, 1H; 12-H), 1.83–1.93 (m, 2H; 1-H, 1′-H), 2.08 (m, 1H; 2-H), 2.32 (dd, ^2J(H,H) = 11.5 Hz, ^3J(H,H) = 1.5 Hz, 1H; 4-H), 2.42 (ddd, ^2J(H,H) = 11.5 Hz, ^3J(H,H) = 11.5, 3.5 Hz, 1H; 6-H), 2.55 (m, 1H; 7-H), 2.71 (m, 2H, 4″-H; 7-H), 2.83 (ddd, ^2J(H,H) = 11.5 Hz, ^3J(H,H) = 6.5, 1.5 Hz, 1H; 6-H), 2.95–3.05 (m, 4H; 3″-H, 4-H, 4″-H, 11b-H), 3.23 (m, 1H; 3″-H), 3.78 (s, 3H; OMe), 3.80 (s, 3H; OMe), 3.82 (s, 3H; OMe), 3.83 (s, 3H; OMe), 3.96 (m, 1H; 1″-H), 6.54, 6.55, 6.57, 6.61 ppm (s, 4H; 5″-H, 8-H, 8″-H, 11-H); ^{13}C NMR (150 MHz, $CDCl_3$): $\delta = 12.56$ (C13), 17.45 (C12), 29.30, 29.33 (C4″, C7), 34.82 (C1), 36.61 (C2), 37.30 (C3), 39.83 (C1′), 40.62 (C3″), 52.00 (C2″), 52.95 (C6), 55.72, 55.85, 55.96 (OMe), 58.86 (C4), 63.34 (C11b) 107.8, 109.1, 111.4, 111.7 (C5″, C8, C8″, C11), 126.8, 127.0, 130.6, 131.8 (C4a″, C7a″, C8a, C11a), 146.9, 147.1, 147.1, 147.2 ppm (C6″, C7″, C9, C10); $[\alpha]_D^{20} = -82.3$ ($c = 0.40$ in $CHCl_3$).

 © 2003 Wiley-VCH Verlag GmbH & Co. KGaA, Weinheim

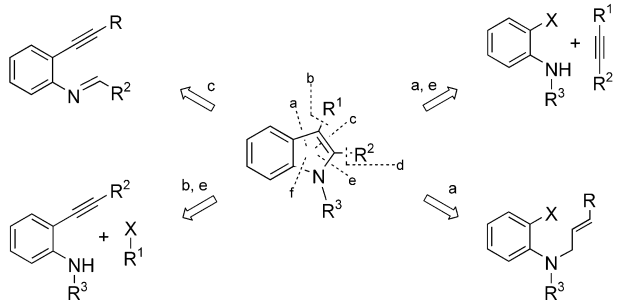
Pd-Catalyzed Heteroanulation

Palladium-Catalyzed Synthesis of 2-Aminoindoles by a Heteroanulation Reaction**

Bernhard Witulski, Carole Alayrac, and Lali Tevzadze-Saeftel*

The diversity of indole-based molecules found in naturally occurring alkaloids as well as their biological and pharmaceutical relevance have stimulated research into the development of new synthetic strategies for the synthesis of readily functionalized indole ring systems.[1] Although numerous procedures have been established for this purpose, palladium-catalyzed heteroannulation reactions have proven to be most powerful and many of them have found applications in target- or diversity-oriented syntheses.[2]

Previous palladium-based strategies for the assembly of the indole framework are summarized in Scheme 1: Palladium-induced cycloadditions of 2-haloanilines with terminal or internal alkynes (disconnection path a,e)[3] and intra- as



Scheme 1. Retro-synthetic representation of Palladium-catalyzed indole syntheses.

well as intermolecular reactions with 2-alkynyl anilides path b,e) give either 2-, or 2,3-disubtituted indoles.[4] Other approaches are based on Heck-type cyclization reactions (path a),[5] reactions of alkynes with imines (path c),[6] or on heteroannulation sequences achieved through palladium-catalyzed aryl amination reactions (disconnection f).[7]

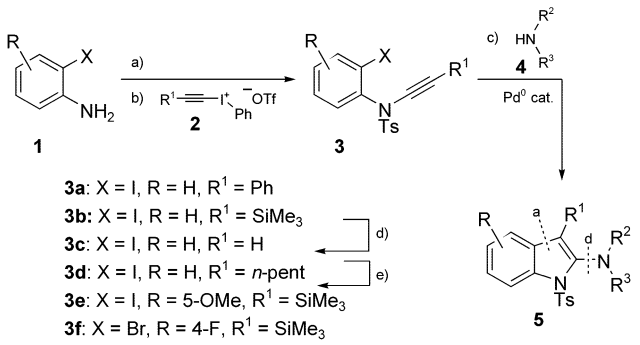
Herein we report an entirely new and straightforward route to 2,3-substituted indoles that is characterized by the following features: 1) the indole-ring formation relies on the unprecedented disconnection pattern a,d; 2) a unique σ,π-chelated palladium species is exploited as the key intermediate for a diversity-tolerant assembly of the indole nucleus.

[*] Priv.-Doz. Dr. B. Witulski, Dr. C. Alayrac, Dr. L. Tevzadze-Saeftel
Fachbereich Chemie
Universität Kaiserslautern
Erwin-Schrödinger-Strasse, 67663 Kaiserslautern (Germany)
Fax: (+49) 631-205-3921
E-mail: witulski@rhrk.uni-kl.de

[**] This work was supported by the Deutsche Forschungsgemeinschaft. C.A. is grateful to the Alexander von Humboldt Foundation for a Research Fellowship.

Supporting information for this article is available on the WWW under http://www.angewandte.org or from the author.

 DOI: 10.1002/anie.200351977 © 2003 Wiley-VCH Verlag GmbH & Co. KGaA, Weinheim

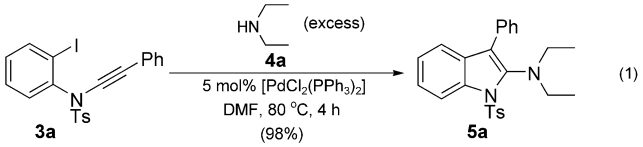


Scheme 2. a) TsCl, pyridine, THF, room temperature, 85–90%; b) KHMDS, toluene, 0°C, then addition of **2** (1.3 equiv), room temperature, 80–98%; c) see Table 2 and Table 3; d) TBAF, THF, 0°C, 93%; e) LiHMDS, *n*-pentyl bromide, THF, −50 to room temperature, 50%. KHMDS = potassium hexamethyldisilazane; OTf = $[CF_3SO_3]^-$, Ts = *p*-tolylsulfonyl, MHMDS = metal hexamethyldisilylazide, TBAF = tetrabutylammoniumfluoride.

Our approach is based on the palladium-catalyzed reaction of alkynyl-2-halogenanilides **3** with primary or secondary amines **4** affording a wide range of 2-aminoindoles ((1*H*-indol-2-yl)amines) **5** (Scheme 2). Although the 2-aminoindole moiety can be found in naturally occurring alkaloids,[8] its access by known methods is quite limited.[9]

Generation of the required starting material was accomplished by tosylation of readily available 2-iodo- or 2-bromoanilines **1** followed by an N-ethynylation reaction with the alkynyliodonium salts **2** (R^1 = Ph or $SiMe_3$) to give the alkynylhalogenanilides **3** in 80–90% yield.[10] Additional modifications of the ynamide functionality were then made by first desilylation of **3b** to **3c**, and subsequent alkylation of the thus obtained terminal alkyne moiety (**3c**→**3d**).

In a preliminary study, we observed that **3a** in the presence of 5 mol% of $[PdCl_2(PPh_3)_2]$ and a large excess of diethyl amine **4a** was readily converted into the 2-aminoindole **5a** [Eq. (1)]. 2-Aminoindoles are quite sensitive

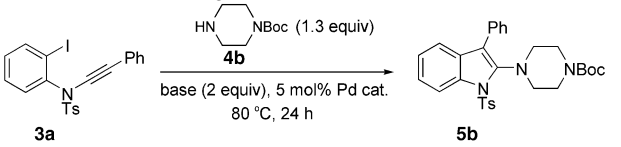


towards hydrolysis. However, product **5a** bearing a tosyl group at the indole nitrogen atom withstood an aqueous workup and could be isolated by silica-gel column chromatography (petroleum ether/diethyl ether) in 98% yield.

To reduce the amount of the amine component **4** and with the aim to create a general catalytic method, the influences of a series of additional bases, solvents, and Pd^{II}- or Pd^0-based precatalysts were studied (Table 1).

Amongst all additional bases tested, K_2CO_3 and Cs_2CO_3 proved to be the most efficient ones. In the presence of a twofold excess of either K_2CO_3 or Cs_2CO_3 the amount of the amine component **4b** could be reduced to 1.3 equivalents for the formation of the 2-aminoindole **5b**.[11] THF was found to be more suitable than DMF or toluene as the solvent. Higher yields were obtained with the precatalyst $[PdCl_2(PPh_3)_2]$ than with $[Pd(PPh_3)_4]$ (Table 1, entries 7–10). Based on these

Table 1: Influence of base, catalyst precursor, and solvent on the catalytic reaction of **3a** and **4b** to give 2-aminoindole **5b**.



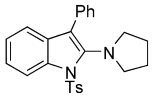
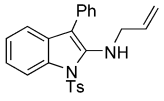
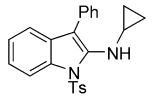
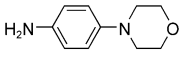
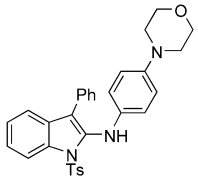
Entry	Base	Solvent	Catalyst	Yield [%][a]
1	DABCO[b]	DMF	$[PdCl_2(PPh_3)_2]$	23
2	Cs_2CO_3	DMF	$[PdCl_2(PPh_3)_2]$	64
3	K_2CO_3	DMF	$[PdCl_2(PPh_3)_2]$	76
4	KOH	DMF	$[PdCl_2(PPh_3)_2]$	75
5	*t*BuOK	DMF	$[PdCl_2(PPh_3)_2]$	8
6	Cs_2CO_3	toluene	$[PdCl_2(PPh_3)_2]$	64
7	Cs_2CO_3	THF	$[PdCl_2(PPh_3)_2]$	98
8	K_2CO_3	THF	$[PdCl_2(PPh_3)_2]$	95
9	Cs_2CO_3	THF	$[Pd(PPh_3)_4]$	79
10	K_2CO_3	THF	$[Pd(PPh_3)_4]$	69

[a] Yields refer to products obtained after column chromatography on silica gel. [b] DABCO = diazabicyclo[2.2.2]octane

results we assume that the active catalyst is a palladium(0) species, that is generated in situ from $[PdCl_2(PPh_3)_2]$—a process also found in other palladium catalyzed cross-couplings employing similar reaction conditions.[12] The lower yield obtained with the catalyst precursor $[Pd(PPh_3)_4]$ is presumably an effect of its higher phosphane content, which reduces the activity of the actual palladium(0) catalyst.

The scope of this 2-aminoindole synthesis is not limited to simple amines (Table 2). Besides secondary amines (**4a–c**), primary amines—such as allylamine (**4d**) and cyclopropyl-

Table 2: Palladium-catalyzed reaction of **3a** with the primary and secondary amines **4c–f**.[a]

Entry	Amine (equiv.)	Indole	Yield [%][b]
1	 **4c** (100)[c]	 **5c**	94[c]
2	 **4d** (5)	 **5d**	98
3	 **4e** (10)	 **5e**	94
4	 **4f** (2)	 **5f**	77

[a] Reaction conditions: 5 mol% $[PdCl_2(PPh_3)_2]$, THF, K_2CO_3 (2 equiv), 80°C, 2–24 h. [b] Yields refer to products obtained after column chromatography on silica gel (**5c–e**) or neutral Al_2O_3 (**5f**). [c] No K_2CO_3 was added because a large excess of amine was used.

 © 2003 Wiley-VCH Verlag GmbH & Co. KGaA, Weinheim

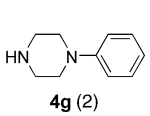
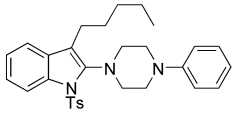
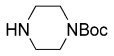
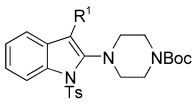
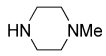
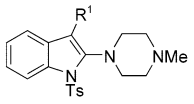
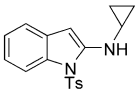
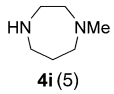
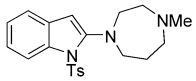
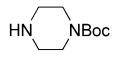
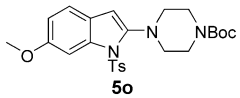
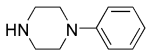
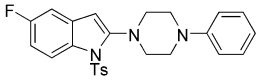
amine (**4e**)—were accepted by the catalytic process without any loss in the overall efficiency (Table 2, entries 2 and 3).[11] Furthermore, the less basic aniline **4f** could be introduced successfully to give **5f** in 77% yield (entry 4).

The 2-aminoindole synthesis was extended to the anilides **3b** and **3d–f** bearing either an alkylalkynyl or (trimethylsilyl)-alkynyl group leading to a wide range of substituted 2-aminoindoles in good to excellent yields (Table 3). The use of silylated ynamides (**3b**, **3e**, and **3f**) offered a synthetic handle for additional modifications of the indole nucleus. For example, a complete desilylation of **5h** and **5j** was readily achieved with TBAF in wet THF at room temperature to give the 2-aminoindoles **5i** and **5k** in 84% and 91% yield, respectively (Table 3, entries 2 and 3). Furthermore, the replacement of the silyl group by an iodine atom was accomplished by treatment of **5j** with NIS/KF (NIS = *N*-iodosuccinimide) in methanol resulting in iodoindole **5l** (entry 3)—thus offering the opportunity for further elaboration by transition-metal catalyzed cross-coupling reactions. Finally, the viability of the reaction was not limited to the use of *ortho*-iodoanilides. The catalytic process was preserved with anilide **3f** bearing an *ortho*-bromine substituent and indole **5p** was obtained in 99% yield following desilylation of the crude reaction product (entry 7).

A proposed mechanism is shown in Scheme 3. Initially, the Pd^0 center formed in situ inserts into the aryl–halogen bond of **3** to give the σ,π-chelated palladium intermediate **A**. Addition of amine **4** to the activated ynamide triple bond in **A** leads to the σ-vinylpalladium intermediate **B**. Subsequently, the positively charged nitrogen atom in **B** is deprotonated (**B**→**C**) by the base (K_2CO_3 or excess amine **4**) and thereby preparing the final reductive elimination step (**C**→**5**) by which the catalytic active Pd^0 species is regenerated.

The key step in this proposed mechanism is the formation of the σ,π-chelated palladium species **A**, that induces an alkyne activation and allows the addition of external amines to the carbon–carbon triple bond. The complementary version of such a heteroannulation—the formation of the externally bound σ,π-palladium complex **D** that gives 2,3-substituted indoles by an *endo-dig* type cyclization—is considered to play a key role in the well-explored palladium-mediated indole synthesis along disconnection path b, e in Scheme 1.[4] However, the σ,π-chelation controlled alkyne activation for the assembly of the indole scaffold, as effected by the palladium intermediate **A**, is unprecedented and it should offer further options for the introduction of other nucleophiles, such as enolates, thiols, or alcohols into the 2-position of the indole ring.

Table 3: Palladium-catalyzed synthesis of the 2-aminoindoles **5g–p**.[a]

Entry	3	Amine (equiv)	Indole	Yield [%][b]
1	**3d**	 **4g** (2)	 **5g**	97[c]
2	**3b**	 **4b** (2)	 **5h**: R^1 = $SiMe_3$ **5i**: R^1 = H TBAF (84%)	83
3	**3b**	 **4h** (10)	 **5j**: R^1 = $SiMe_3$ **5k**: R^1 = H **5l**: R^1 = I TBAF (91%) NIS, KF (65%)	95
4	**3b**	 **4e** (10)	 **5m**	66[c,d]
5	**3b**	 **4i** (5)	 **5n**	75[d]
6	**3e**	 **4b** (4)	 **5o**	89[d]
7	**3f**	 **4g** (4)	 **5p**	99[d]

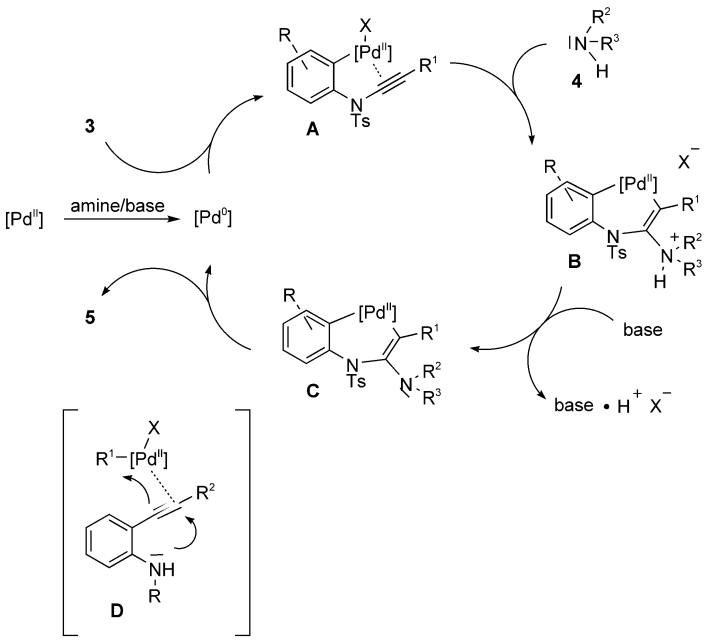
[a] Reaction conditions: 5 mol% $[PdCl_2(PPh_3)_2]$, THF, K_2CO_3 (2 equiv), 80°C, 5–24 h. [b] Yields refer to products obtained after column chromatography on silica gel or neutral Al_2O_3. [c] 10 mol% palladium catalyst was used. [d] yield over both steps, after desilylation with TBAF in wet THF at room temperature.

In conclusion, we have developed an efficient and diversity-tolerant synthesis of otherwise difficult to obtain 2-aminoindoles **5** based on a novel palladium-catalyzed cross-coupling sequence between *N*-alkynyl-2-halogenanilides **3** and primary, as well as secondary amines **4**. Further studies on synthetic applications and mechanistic investigations are in progress.

Experimental Section

Representative procedure: A dry Schlenk flask with screw cap was charged under argon with amine **4b** (26 mg, 0.14 mmol), alkynylanilide **3a** (50 mg, 0.11 mmol), $[PdCl_2(PPh_3)_2]$ (4 mg, 5 mol%), K_2CO_3 (29 mg, 0.21 mmol), and THF (1.5 mL). The resulting mixture was stirred at 80°C until the starting material was consumed (20 h, thin layer chromatography (TLC)). Workup was by addition of CH_2Cl_2 and brine, followed by extraction with CH_2Cl_2, extraction with brine, drying ($MgSO_4$), and filtration through celite. Purification by column chromatography (silica gel, petroleum ether:diethyl ether = 75:25 (v/v)) afforded the pure indole **5b** (54 mg, 95% yield).

 © 2003 Wiley-VCH Verlag GmbH & Co. KGaA, Weinheim



Scheme 3. Proposed mechanism for the palladium-catalyzed formation of 2-aminoindoles **5**, (X = Br, I). **D** = proposed intermediate of the palladium-catalyzed indole synthesis along disconnection path b, e in Scheme 1.

Further experimental details, as well as spectroscopic and analytic data of the 2-aminoindoles **5a–p** can be found in the Supporting Information.

Received: May 26, 2003 [Z51977]

Keywords: homogeneous catalysis · indoles · nitrogen heterocycles · palladium · ynamides

[1] a) H. Döpp, D. Döpp, U. Langer, B. Gerding, *Methoden Org. Chem. (Houben-Weyl) 4th ed. 1952–, Vol. E6b1*, **1994** pp. 145–172; b) R. J. Sundberg in *Indoles*, Academic Press, London, **1996**; c) J. A. Joule in *Science of Synthesis, Vol. 10* (Ed.: E. J. Thomas), Thieme, Stuttgart, **2000**, pp. 261–652; d) G. W. Gribble, *J. Chem. Soc. Perkin Trans. 1* **2000**, 1045.

[2] a) L. S. Hegedus, *Angew. Chem.* **1988**, *100*, 1147; *Angew. Chem. Int. Ed. Engl.* **1988**, *27*, 1113; b) T. Sakamoto, Y. Kondo, H. Yamanaka, *Heterocycles* **1988**, *27*, 2225; c) *Palladium in Heterocyclic Chemistry* (Eds.: J. J. Li, G. W. Gribble), Pergamon, Oxford, **2000**.

[3] a) R. C. Larock, E. K. Yum, *J. Am. Chem. Soc.* **1991**, *113*, 6689; b) R. C. Larock, E. K. Yum, M. D. Refvik, *J. Org. Chem.* **1998**, *63*, 7652; c) K. R. Roesch, R. C. Larock, *Org. Lett.* **1999**, *1*, 1551; d) H.-C. Zhang, K. K. Brumfield, B. E. Maryanoff, *Tetrahedron Lett.* **1997**, *38*, 2439; e) H.-C. Zhang, H. Ye, A. F. Moretto, K. K. Brumfield, B. E. Maryanoff, *Org. Lett.* **2000**, *2*, 89; f) X. Liu, J. R. Deschamp, J. A. Cook, *Org. Lett.* **2002**, *4*, 3339; g) N. Gathergood, P. J. Scammells, *Org. Lett.* **2003**, *5*, 921.

[4] Pd-induced *endo-dig* cyclizations: a) K. Iritani, S. Matsubara, K. Utimoto, *Tetrahedron Lett.* **1988**, *29*, 1799; b) A. Arcadi, S. Cacchi, F. Marinelli, *Tetrahedron Lett.* **1992**, *33*, 3915; c) S. Cacchi, G. Fabrizi, F. Marinelli, L. Moro, P. Pace, *Synlett* **1997**, 1363; d) S. Cacchi, G. Fabrizi, P. Pace, *J. Org. Chem.* **1998**, *63*, 1001; e) A. Arcadi, S. Cacchi, G. Fabrizi, F. Marinelli, *Synlett* **2000**, 394; f) S. Cacchi, G. Fabrizi, D. Lamba, F. Marinelli, L. M. Parisi, *Synthesis* **2003**, 728; g) S. Cacchi, G. Fabrizi, L. M. Parsi, *Heterocycles* **2002**, *58*, 667; h) G. Battistuzzi, S. Cacchi, G. Fabrizi, *Eur. J. Org. Chem.* **2002**, 2671; for a related cyclization employing (2-alkynyl)phenyl isocyanates, see: i) S. Kamijo, Y. Yamamoto, *Angew. Chem.* **2002**, *114*, 3364; *Angew. Chem. Int. Ed.* **2002**, *41*, 3230; for a base-induced 5-endo dig cyclization, see: j) A. L. Rodriguez, C. Koradin, W. Dohle, P. Knochel, *Angew. Chem.* **2000**, *112*, 2607; *Angew. Chem. Int. Ed.* **2000**, *39*, 2488; for a very recently disclosed Ipy_2BF_4-promoted (Ipy_2 = bis(pyridine)iodium(I)) assembly of the 3-iodoindole core, see: k) J. Barluenga, M. Trincado, E. Rubio, J. M. González, *Angew. Chem.* **2003**, *115*, 2508; *Angew. Chem. Int. Ed.* **2003**, *42*, 2406.

[5] a) L. S. Hegedus, G. F. Allen, E. L. Waterman, *J. Am. Chem. Soc.* **1976**, *98*, 2674; b) L. S. Hegedus, G. F. Allen, J. J. Bozell, E. L. Waterman, *J. Am. Chem. Soc.* **1978**, *100*, 5800; c) M. Mori, K. Chiba, Y. Ban, *Tetrahedron Lett.* **1977**, 1037; d) R. C. Larock, S. Babu, *Tetrahedron Lett.* **1987**, *28*, 5291; for a related strategy using *N*-vinyl-2-haloanilines, see: e) A. Kasahara, T. Izumi, S. Murakami, H. Yanai, M. Takatori, *Bull. Chem. Soc. Jpn.* **1986**, *59*, 927; f) T. Sakamoto, T. Nagano, Y. Kondo, H. Yamanaka, *Synthesis* **1990**, 215.

[6] A. Takeda, S. Kamijo, Y. Yamamoto, *J. Am. Chem. Soc.* **2000**, *122*, 5662.

[7] a) A. J. Peat, S. L. Buchwald, *J. Am. Chem. Soc.* **1996**, *118*, 1028; b) S. Wagaw, B. H. Yang, S. L. Buchwald, *J. Am. Chem. Soc.* **1999**, *121*, 10251; c) M. Watanabe, T. Yamamoto, M. Nishiyama, *Angew. Chem.* **2000**, *112*, 2620; *Angew. Chem. Int. Ed.* **2000**, *39*, 2501; d) J. A. Brown, *Tetrahedron Lett.* **2000**, *41*, 1623.

[8] see for example "Asperlicin, Flustramine, Fumiquinazoline, Physostigmin und Roquefortine"*RÖMPP-Lexikon Naturstoffe* (Eds.: B. Fugmann, S. Lang-Fugmann, W. Steglich), Georg Thieme, Stuttgart, **1997**. This book is also available in English as the *RÖMPP Encyclopedia Natural Products*, Georg Thieme, Stuttgart.

[9] a) T. Hino, M. Nakagawa, S. Akaboshi, *J. Chem. Soc. Chem. Commun.* **1967**, 656; b) A. Deberly, J. Bourdais, *Tetrahedron Lett.* **1971**, 3049; c) T. Hino, M. Nakagawa, T. Hashizume, N. Yamaji, Y. Miwa, K. Tsuneoka, S. Akaboshi, *Tetrahedron* **1971**, *27*, 775; d) K. Ishizumi, S. Inaba, H. Yamamoto, *J. Org. Chem.* **1974**, *39*, 2581; e) G. M. Coppola, G. E. Hardtmann, *J. Heterocycl. Chem.* **1977**, *14*, 1117; f) E. Foresti, P. Spagnolo, P. Zanirato, *J. Chem. Soc. Perkin Trans. 1* **1989**, 1354.

[10] a) B. Witulski, T. Stengel, *Angew. Chem.* **1998**, *110*, 495; *Angew. Chem. Int. Ed.* **1998**, *37*, 489; b) B. Witulski, T. Stengel, *Angew. Chem.* **1999**, *111*, 2521; *Angew. Chem. Int. Ed.* **1999**, *38*, 2426; c) B. Witulski, M. Gößmann, *Chem. Commun.* **1999**, 1879; d) B. Witulski, N. Buschmann, U. Bergsträßer, *Tetrahedron* **2000**, *56*, 8473; e) B. Witulski, M. Gößmann, *Synlett* **2000**, 1793; f) B. Witulski, C. Alayrac, *Angew. Chem.* **2002**, *114*, 3415; *Angew. Chem. Int. Ed.* **2002**, *41*, 3281; g) B. Witulski, J. Lumtscher, U. Bergsträßer, *Synlett* **2003**, 708; for other contributions to the chemistry of alkynylamides, see: h) R. W. Hoffmann, D. Brückner, *New J. Chem.* **2001**, *25*, 369; i) J. D. Rainier, J. E. Imbriglio, *J. Org. Chem.* **2000**, *65*, 7272; j) J. A. Mulder, R. P. Hsung, M. O. Frederick, M. R. Tracey, C. A. Zificsak, *Org. Lett.* **2002**, *4*, 1383; k) L.-L. Wei, J. A. Mulder, H. Xiong, C. A. Zificsak, C. J. Douglas, R. P. Hsung, *Tetrahedron* **2001**, *57*, 459; l) N. Saito, Y. Sato, M. Mori, *Org. Lett.* **2002**, *4*, 803; m) R. Tanaka, S. Hirano, H. Urabe, F. Sato, *Org. Lett.* **2003**, *5*, 67; n) M. O. Frederick, J. A. Mulder, M. R. Tracey, R. P. Hsung, J. Huang, K. C. M. Kurtz, L. Shen, C. J. Douglas, *J. Am. Chem. Soc.* **2003**, *125*, 2368.

[11] In the case of the use of volatile amines such as **4d** or **4e** a slight excess of 5–10 equivalents of amine was beneficial especially when the reaction was carried out on a small scale. No optimization of the amine content was undertaken in these cases.

[12] *Metal-catalyzed Cross-Coupling Reactions* (Eds.: F. Diederich, P. J. Stang), Wiley-VCH, London, **1998**.

 © 2003 Wiley-VCH Verlag GmbH & Co. KGaA, Weinheim

Antennary Oligosaccharides

Highly Branched Oligosaccharides: A General Strategy for the Synthesis of Multiantennary N-Glycans with a Bisected Motif**

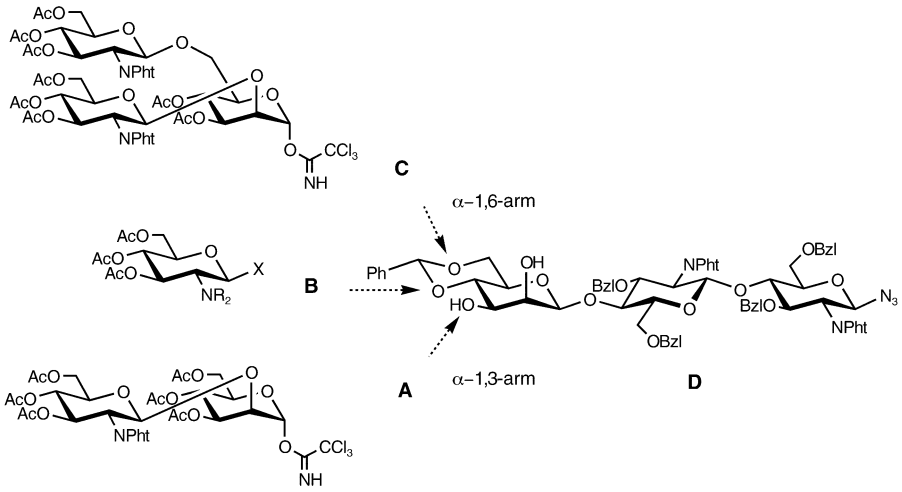
*Harald Weiss and Carlo Unverzagt**

Dedicated to Professor Peter Welzel on the occasion of his 65th birthday.

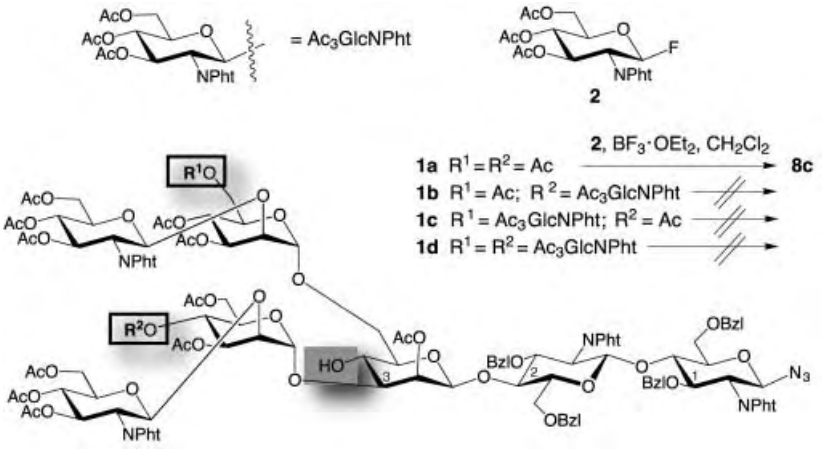
The majority of eukaryotic proteins found on cell surfaces and in blood serum are glycosylated, mostly with asparagine-linked oligosaccharides (N-glycans).[1] It has been shown that glycoprotein function is closely associated with the presented N-glycans; however, explicit structure–function studies[2] are scarce. Since homogeneous N-glycans for biological studies are available in only small amounts from natural sources, several groups have developed synthetic approaches to this important class of compounds.[3] The family of N-glycans, which has been the most difficult to synthesize, contains an additional β1,4-linked bisecting GlcNAc residue,[4–7] leading to a sterically crowded central β-mannoside. Bisected N-glycans have been shown to be involved in tumor progression,[8–10] cell development,[11] and the function of receptors.[12] We have developed a general approach to bisected N-glycans based on a modular system of building blocks and have synthesized the previously inaccessible tri- and tetraantennary compounds.

The β-mannoside in the trisaccharide building block **D**[13] contains a single benzylidene protective group (Scheme 1). This core unit was used for the straightforward assembly of multiantennary N-glycans following a double regio- and stereoselective glycosylation sequence.[14] To adapt that methodology to bisected N-glycans the three substituents **A**–**C** must be coupled efficiently to the β-mannoside of the acceptor **D**. In principle, this can be accomplished by six different strategies, depending on the sequence of introduction.

In our initial approach to multiantennary bisected N-glycans we planned a "late" introduction of the bisecting GlcNAc moiety to the triantennary N-glycan **1c** (Scheme 2). Compound **1c**[14] was obtained from the building blocks **A**, **C**, and **D** and should be suitable for the attachment of a bisecting residue at the unprotected OH-4[3] group. This approach had been applied successfully to biantennary compounds.[7] However, when the triantennary acceptor **1c** was treated with ten equivalents of donor **2**, the desired reaction at OH-4[3] was sluggish and gave only a low yield of a mixture of products, which could not be separated by chromatography. A similar



Scheme 1. Regioselective linkage of the building blocks **A**–**D** to obtain bisected N-glycans. Building block **B** contains the bisecting GlcNAc unit. Bzl = benzyl, Pht = phthaloyl.



Scheme 2. Late introduction of the bisecting residue **2** was accomplished only with the biantennary acceptor **1a** (56% yield of **8c**).

outcome was observed for the reactions of the homologous tri- and tetraantennary N-glycans **1b** and **1d**, respectively.

We assumed that by improving the reactivity of donor **2** and reducing steric demand these difficulties could be overcome. Thus the "late" introduction of the bisecting GlcNAc residue was optimized by using the corresponding biantennary acceptor **1a** and by varying donor **2**. Replacing the phthalimido group with a succinyl moiety or a 2,2,2-trichloro-

[*] Prof. Dr. C. Unverzagt, H. Weiss
Bioorganische Chemie, Gebäude NW1
Universität Bayreuth
95440 Bayreuth (Germany)
Fax: (+49) 921-555-365
E-mail: carlo.unverzagt@uni-bayreuth.de

[**] We thank the Deutsche Forschungsgemeinschaft and the Fonds der Deutschen Chemischen Industrie for funding.

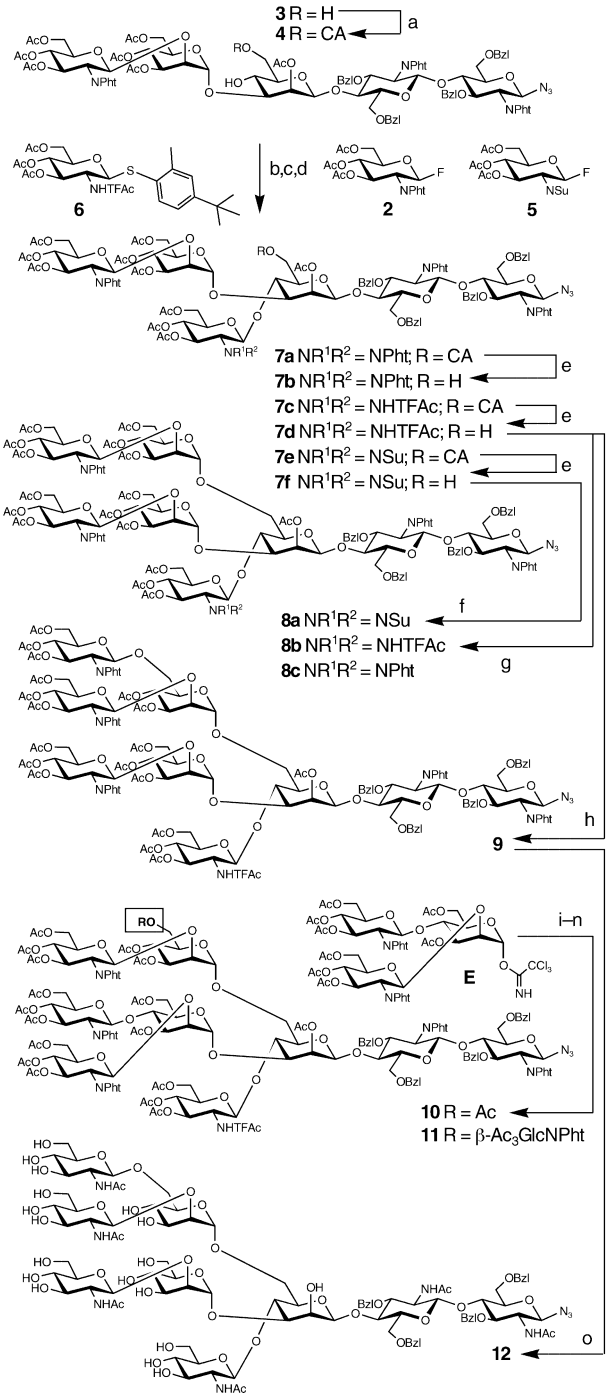
 DOI: 10.1002/anie.200351625 © 2003 Wiley-VCH Verlag GmbH & Co. KGaA, Weinheim

ethoxycarbonyl group[15] and the acetates with benzyl ether groups did not increase the yields beyond the level of 56% obtained with the parent compound **2**.[7] Apparently the introduction of the bisecting residue at a late stage is critical.

We thus envisioned introducing the bisecting GlcNAc residue before the α1,6-arm. This should reduce the steric hindrance for the attachment of donor **B**. However, this change of strategy required the selective introduction of a temporary protective function at the primary OH-6^3 group after removal of the benzylidene acetal. The required chemistry was developed for the pentasaccharide **3** as a model compound (Scheme 3). The pentasaccharide diol **3** was obtained by regioselective α1,3-glycosylation of the core trisaccharide **D** with the donor **A** followed by acetylation and removal of the benzylidene acetal.[16] At first the primary hydroxy function was protected with a *tert*-butyldimethylsilyl group. However, the resulting compound could not be equipped with the bisecting GlcNAc residue (reactions with donors **2** and **6**), presumably due to steric hindrance of the bulky silyl protecting group. Therefore the chloroacetyl group,[17] a much smaller protective function, was introduced regioselectively by using a small excess of chloroacetic acid anhydride at 0°C under dilute conditions (98% yield of **4**). Several donors with various protective groups on the amino function were tested for the introduction of the bisecting GlcNAc residue. The best yields were obtained for donor **2** (79%) followed by the trifluoroacetyl-protected[18] thioglycoside **6** (70%), and the succinimido derivative **5** (55%). Selective removal of the chloroacetyl group from the hexasaccharides **7a**, **7c**, and **7e** was accomplished by mild saponification with K_2CO_3 in MeOH/CH_2Cl_2 to give **7b**, **7d**, and **7f**, respectively.

With this homologous series of acceptors in hand we attempted to introduce the α1,6-arm. Glycosylation with the disaccharide donor **A** was highly dependent on the protective group at the amino function of the bisecting residue. The phthalimido derivative **7b** did not react, whereas **7f**, which has with the smaller succinimido function, and the trifluoroacetamide **7d** gave the corresponding bisected octasaccharides **8a** (43%) and **8b** (76%), respectively. This confirms earlier findings of Paulsen et al. on the blocking effect associated with a phthalimido function at position 2 of the bisecting residue.[5] To solve this steric problem a series of reactions was required to replace the phthalimido protective groups by acetamides prior to the final attachment of the α-1,6 arm.[5] However, with the trifluoroacetylated donor **6** this change of protective groups can be avoided and the phthaloyl groups typically employed with glucosamine moietes can be maintained. Phthalimido-protected building blocks for N-glycans have been shown to give higher yields and fewer side reactions in glycosylations than their *N*-acetylated derivatives.[16]

To prove that this novel approach is also suitable for the assembly of the sterically demanding triantennary bisected compounds, the acceptor **7d** was reacted with the branched donor **C**. To our delight the triantennary bisected N-glycan **9** was obtained in pure form (16% yield). The structure of **9**[19] was confirmed by 2D NMR experiments[20] (COSY, NOESY, HMQC, HMQC-COSY[21]) and by electrospray ionization



Scheme 3. a) Chloroacetic anhydride, pyridine, CH_2Cl_2, 98%; b) **4**, **2**, CH_2Cl_2, $BF_3{\cdot}OEt_2$, 79%; c) **4**, **6**, CH_2Cl_2, *N*-iodosuccinimide, TfOH, 71%; d) **4**, **5**, CH_2Cl_2, $BF_3{\cdot}OEt_2$, 55%; e) K_2CO_3, MeOH/CH_2Cl_2 (1:10), **7b** 70%, **7d** 74%, **7f** 83%; f) **A**, CH_2Cl_2, $BF_3{\cdot}OEt_2$, 43%; g) **A**, CH_2Cl_2, $BF_3{\cdot}OEt_2$, 76%; h) **C**, CH_2Cl_2, $BF_3{\cdot}OEt_2$, 16%; i) 1. **D**, CH_2Cl_2, $BF_3{\cdot}OEt_2$; 2. acetic anhydride, pyridine; 3. *p*TsOH, CH_3CN, 75% (steps 1–3); k) chloroacetic anhydride, pyridine, CH_2Cl_2, 85%; l) **6**, CH_2Cl_2, *N*-iodosuccinimide, TfOH, 34%; m) K_2CO_3, MeOH/CH_2Cl_2, 87%; n) **A**, CH_2Cl_2, $BF_3{\cdot}OEt_2$, 20%; o) 1. ethylenediamine, *n*BuOH, 80°C; 2. Ac_2O, pyridine; 3. 41% $MeNH_2$ in H_2O, 75% (steps 1–3). CA = chloroacetyl, *p*TsOH = *para*-toluenesulfonic acid, NSu = succinimido, TFAc = trifluoroacetyl, TfOH = trifluoromethanesulfonic acid.

 © 2003 Wiley-VCH Verlag GmbH & Co. KGaA, Weinheim

mass spectrometry. Based on this glycosylation sequence a second triantennary bisected N-glycan (**10**) was obtained starting from the building blocks **E** and **D**, followed by reaction with the bisecting GlcNAc donor **6** (34% yield) and the building block **A** (20% yield). When donor **C** was reacted instead in the final glycosylation step, the tetraantennary compound **11** was obtained (12% yield). The yields for the attachment of the α1,6-arm to produce the multiantennary bisected N-glycans are considerably lower than those for the analogous reaction with the reactive parent N-glycans (70–90% yield).[14] This indicates that steric hindrance substantially impairs this final step and demonstrates the inherent limitations of chemical oligosaccharide synthesis with extensive use of protective groups.

To ensure that the bisected N-glycans carrying the *N*-trifluoroacetyl group can be deprotected, compound **9** was subjected to a three-step sequence involving treatment with ethylene diamine[22] followed by peracetylation and O-deacetylation. This one-pot procedure gave the compound **12** in 75% yield after purification by solid-phase extraction.

We have thus shown for the first time that N-glycans with a bisecting residue flanked by three or four antennae can be obtained by a convenient building-block strategy. For the synthesis of these sterically congested oligosaccharides the sequence of introduction and the steric demand of the building blocks are crucial. Only a combination of a small protective function at the amino group of the bisecting residue and the final introduction of the α1,6-arm permitted the synthesis of these highly complex oligosaccharides.

Received: April 10, 2003 [Z51625]

Keywords: carbohydrates · glycosylations · N-glycans · polysaccharides

[1] B. Lowe, A. Varki, *Essentials in Glycobiology*, Cold Spring Harbour Laboratory Press, Cold Spring Harbour, NY, **1999**.
[2] P. M. Rudd, H. C. Joao, E. Coghill, P. Fiten, M. R. Saunders, G. Opdenakker, R. A. Dwek, *Biochemistry* **1994**, *33*, 17–22.
[3] B. G. Davis, *Chem. Rev.* **2002**, *102*, 579–602.
[4] F. Yamazaki, T. Kitajima, T. Nukada, Y. Ito, T. Ogawa, *Carbohydr. Res.* **1990**, *201*, 15–30.
[5] H. Paulsen, M. Heume, H. Nürnberger, *Carbohydr. Res.* **1990**, *200*, 127–166.
[6] S. Weiler, R. R. Schmidt, *Tetrahedron Lett.* **1998**, *39*, 2299–2302.
[7] C. Unverzagt, J. Seifert, *Tetrahedron Lett.* **2000**, *41*, 4549–4553.
[8] A. Rebbaa, P. M. Chou, I. Vucic, B. L. Mirkin, T. Tomita, E. G. Bremer, *Clin. Cancer Res.* **1999**, *5*, 3661–3668.
[9] J. J. Priatel, M. Sarkar, H. Schachter, J. D. Marth, *Glycobiology* **1997**, *7*, 45–56.
[10] X. Yang, M. Bhaumik, R. Bhattacharyya, S. Gong, C. E. Rogler, P. Stanley, *Cancer Res.* **2000**, *60*, 3313–3319.
[11] M. Yoshimura, Y. Ihara, T. Nishiura, Y. Okajima, M. Ogawa, H. Yoshida, M. Suzuki, K. Yamamura, Y. Kanakura, Y. Matsuzawa, N. Taniguchi, *Biochem. J.* **1998**, *331*, 733–742.
[12] Y. Ihara, Y. Sakamoto, M. Mihara, K. Shimizu, N. Taniguchi, *J. Biol. Chem.* **1997**, *272*, 9629–9634.
[13] a) C. Unverzagt, *Angew. Chem.* **1994**, *106*, 1170–1173; *Angew. Chem. Int. Ed. Engl.* **1994**, *33*, 1102–1104; b) C. Unverzagt, *Chem. Eur. J.* **2003**, *9*, 1369–1376.
[14] C. Unverzagt, *Angew. Chem.* **1997**, *109*, 2078–2081; *Angew. Chem. Int. Ed. Engl.* **1997**, *36*, 1989–1992.
[15] T. B. Windholz, D. B. R. Johnston, *Tetrahedron Lett.* **1967**, 2555–2557.
[16] C. Unverzagt, *Angew. Chem.* **1996**, *108*, 2507–2510; *Angew. Chem. Int. Ed. Engl.* **1996**, *35*, 2350–2353.
[17] C. P. J. Glaudemans, M. J. Bertolini, *Methods Carbohydr. Chem.* **1980**, *8*, 271–275.
[18] D. J. Silva, H. Wang, N. M. Allanson, R. K. Jain, M. J. Sofia, *J. Org. Chem.* **1999**, *64*, 5926–5929.
[19] Compound **9**: $R_f = 0.24$ (silica gel, hexane/acetone 1:1); $[\alpha]_D^{23} = +1.9$ ($c = 0.5$, CH_2Cl_2); ^{1}H NMR (500 MHz, [D$_6$]DMSO, 298 K): $\delta = 9.78$ (d, $J_{NH,2} = 7.8$ Hz, 1H, NH), 8.13–7.70 (m, 20H, Pht), 7.35–7.10 (m, 10H, Bzl), 6.87–6.74 (m, 10H, Bzl), 5.65 (dd, $J_{2,3} = J_{3,4} = 10.1$ Hz, 1H, H-3^5), 5.52 (m, 2H, H-3$^{5'}$, H-3^7), 5.48 (m, 2H, H-3^1, H-3^2) 5.42 (d, $J_{1,2} = 8.3$ Hz, 1H, H-1$^5\beta$), 5.37 (d, $J_{1,2} < 1.0$ Hz, 1H, H-1^4) , 5.24 (d, $J_{1,2} = 9.9$ Hz, 1H, H-1$^1\beta$), 5.16 (d, $J_{1,2} = 8.4$ Hz, 1H, H-1$^{5'}\beta$), 5.05–5.02 (m, 4H, H-4^2, H-4^1, H-1^7, H-3$^{5'}$), 4.83 (dd, $J_{2,3} = J_{3,4} = 10.3$ Hz, 1H, H-3^6), 4.83–4.78 (m, 4H, H-3^3, H-4$^{5'}$, CH_2O), 4.76 (dd, $J_{3,4} = J_{4,5} = 9.6$ Hz, 1H, H-4^4), 4.72 (dd, $J_{3,4} = J_{4,5} = 9.9$ Hz, 1H, H-4$^{4'}$), 4.68–4.65 (m, 2H, H-1^6, H-1^3), 4.63 (d, $J_{1,2} < 1.0$ Hz, H-1$^{4'}$), 4.35 (dd, $J_{1,2} = J_{2,3} = 8.9$ Hz, 1H, H-1^2), 4.33 (dd, $J_{1,2} = J_{2,3} = 9.1$ Hz, 1H, H-2$^{4'}$), 4.31–4.25 (m, 5H, H-6a$^{5'}$, H-2$^{4'}$, H-4^6, CH_2O), 4.21–4.19 (m, 3H, H-6b$^{5'}$, CH_2O), 4.17 (dd, $J_{3,4} = J_{4,5} = 7.3$ Hz, 1H, H-2^4), 4.11–3.95 (m, 7H, H-3$^{4'}$, H-2^2, H-2^1, H-5$^{4'}$, H-5^6, CH_2O), 3.86–3.76 (m, 10H, H-4^7, H-6a,b^7, H-5$^{5'}$, H-6a^2, H-5^1, H-6 a/b^3, H-2^3), 3.64 (m, 1H, H-5^5), 3.52–3.42 (m, 5H, H-5^5, H-6a$^{4'}$,H-6a^4, H-5^4, H-6a^1), 3.32–3.25 (m, 2H, H-6b$^{4'}$, H-6a^5), 3.24–3.17 (m, 3H, H-6b^4, H-5^7, H-6b^1), 2.99–2.88 (m, 2H, H-5^3, H-6b^5), 2.04, 2.03, 2.02, 2.01, 2.004, 2.003, 1.99, 1.98, 1.96, 1.94, 1.91, 1.89, 1.80, 1.78, 1.76, 1.75, 1.69 ppm (17 s, 54H, OAc); ^{13}C NMR (125 MHz, [D$_6$]DMSO, 298 K): $\delta = 170.16$, 170.03, 169.95, 169.82, 169.66, 169.52, 169.22, 169.12, 169.01, 167.64, 167.15, 166.32 (C=O), 156.43 (q, C=O, NTFAc), 139.44, 139.14, 138.52, 138.45 (C_i-Ar), 128.34–126.66 (C-Ar), 117.43 (q, CF_3), 100.98 (C-1^6, $J_{C\text{-}1,H\text{-}1} = 171.3$ Hz from a coupled HMQC spectrum), 97.46 (C-1$^{5'}$), 97.45 (C-1^3), 96.70 (C-1^7), 96.15 (C-1^5), 95.44 (C-1$^4\alpha$, $J_{C\text{-}1,H\text{-}1} = 172$ Hz from a coupled HMQC spectrum), 95.06 (C-1$^{4'}\alpha$, $J_{C\text{-}1,H\text{-}1} = 172$ Hz from a coupled HMQC spectrum), 92.01 (C-1^2), 84.83 (C-1^1), 76.33 (C-5$^{5'}$), 75.95 (C-5^4), 73.90 (C-5^7), 73.81 (C-2$^{4'}$), 72.38 (C-6^6), 72.19 (C-4^6), 71.85 (C-6$^{5'}$), 71.84 (C-4^5), 71.83 (C-5^5), 71.72 (C-3^2), 71.71 (C-3^1), 70.51 (C-3^4), 70.44 (C-3^7), 70.17 (C-3^5), 69.25 (C-4^3), 68.65 (C-4$^{5'}$), 68.63 (C-3^3), 68.57 (C-3^6), 68.53 (C-4^4), 68.47 (C-4^1), 68.43 (C-3$^{5'}$), 67.83 (C-6^7), 67.63 (C-4^2), 67.58 (C-6^1), 67.56 (C-6^4), 67.55 (C-6$^{4'}$), 67.46 (C-4^7), 67.37 (C-6^5), 67.17 (C-2^2), 62.14 (C-6^3), 62.04 (C-6^2), 62.03 (C-4$^{4'}$), 62.01 (C-5^2), 61.94 (C-5^3), 61.76 (C-5^6), 61.73 (C-3$^{4'}$), 61.72 (C-5$^{4'}$), 55.73 (C-2$^{5'}$), 54.70 (C-2^1), 54.62 (C-2^5), 54.19 (C-2^4), 53.98 (C-2^7), 53.88 (C-2^6), 53.84 (C-2^3), 20.55, 20.42, 20.35, 20.01, 19.96, 19.82 ppm (OAc) ESI-MS: *m*/*z* calcd for $C_{160}H_{166}F_3N_9O_{68}$: 3357.98 [$M^+$], *m*/*z* found: 3380.9 [M+Na]$^+$.
[20] H. Kessler, M. Gehrke, C. Griesinger, *Angew. Chem.* **1988**, *100*, 507–554; *Angew. Chem. Int. Ed. Engl.* **1988**, *27*, 490–536.
[21] H. Kessler, P. Schmieder, M. Kurz, *J. Magn. Reson.* **1989**, *85*, 400–405.
[22] O. Kanie, S. C. Crawley, M. M. Palcic, O. Hindsgaul, *Carbohydr. Res.* **1993**, *243*, 139–164.

 © 2003 Wiley-VCH Verlag GmbH & Co. KGaA, Weinheim

Cover Picture

Virgil Percec,* Martin Glodde, Gary Johansson, Venkatachalapathy S. K. Balagurusamy, and Paul A. Heiney



The mode of the self-assembly of **(3,4,5)^{2}G2-CO_2Me** monodendrons changes from a spherical to a pyramidal supramolecular dendrimer upon replacement of the aliphatic chains by partially fluorinated chains. This metamorphosis was verified with a combination of small- and wide-angle X-ray diffraction, electron density calculations, and molecular modeling studies. For more information on this process, see the Communication by V. Percec et al. on page 4338 ff.

Contents

Angewandte EarlyView

The following articles are available online (in Wiley InterScience). You can find them at www.angewandte.org, under Full Text, Early View.

P. Comba, A. Hauser, M. Kerscher, H. Pritzkow:*
Bond-Stretch Isomerism: Trapped Isomeric Structures of Hexacoordinate Copper(II) Bispidine Chromophores along a Jahn–Teller Active Vibrational Coordinate
DOI: 10.1002/anie.200351900
Published online: September 8, 2003

R. J. Amir, N. Pessah, M. Shamis, D. Shabat:*
Self-Immolative Dendrimers
DOI: 10.1002/anie.200351962
Published online: September 8, 2003

M. P. Sibi, J. Zimmerman, T. Rheault:*
Enantioselective Conjugate Radical Addition to β-Acyloxy Acrylate Acceptors: An Approach to Acetate Aldol-Type Products
DOI: 10.1002/anie.200352096
Published online: September 8, 2003

H. Xu, W. A. Goedel:*
Mesoscopic Rings by Controlled Wetting of Particle Imprinted Templates
DOI: 10.1002/anie.200351428
Published online: September 8, 2003

Articles judged by the referees or the editor as being either very important or very urgent are immediately edited, proof-read, and electronically published once the manuscript has arrived in the editorial office in final form. As long as there is no page number available these articles should be cited in the following manner:

Author(s) *Angew. Chem. Int. Ed.*, online publication date, DOI.

News

Royal Society of Chemistry Awards **4282**

Books

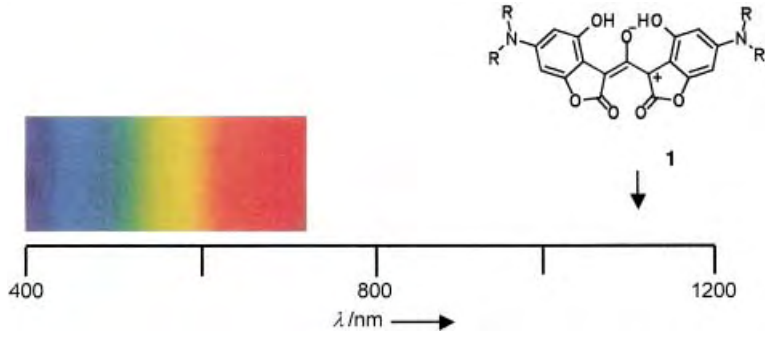
Makromoleküle — **4283**	Hans-Georg Elias	*reviewed by H. W. Schnecko*
Wandering in the Gardens of the Mind — **4284**	John Prebble, Bruce Weber	*reviewed by R. J. P. Williams*
Meilensteine der Wissenschaft — **4284**	Peter Tallack	*reviewed by H. Hopf*

Highlights

NIR Dyes

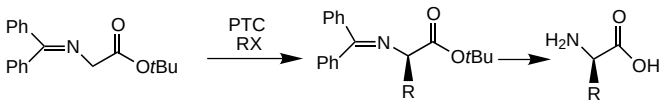
H. Langhals* — **4286 – 4288**

An Unexpectedly Simple NIR Dye for 1.1 μm with a Central Mesoionic Structure



Predictable with the color rules? The NIR dye **1** has a novel, mesoionic structure that exhibits a "super acceptor" function and an absorption far in the near infrared within a remarkably small chromophore.

Minireviews



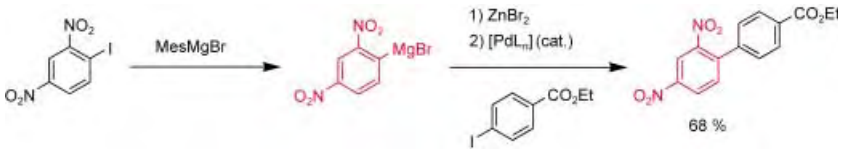
Optically appealing: Catalytic asymmetric methods should allow the synthesis of large amounts of optically active α- and β-amino acids using only small amounts of optically active catalysts (see picture; PTC = phase-transfer catalyst). This contribution highlights some of the recent developments in this area involving chiral organometallic catalysts and metal-free organic catalysts.

Synthesis of Amino Acids

J.-A. Ma* ——— **4290 – 4299**

Recent Developments in the Catalytic Asymmetric Synthesis of α- and β-Amino Acids

Reviews



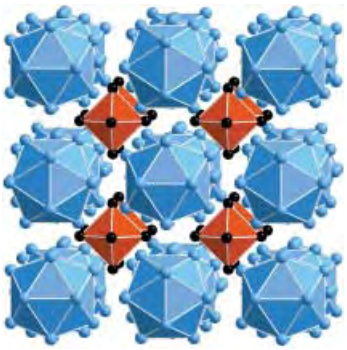
New perspectives in organic synthesis have been opened by the halogen–magnesium exchange reaction. It appears that many more functional groups than previously thought are compatible with magnesium organometallic reagents under the mild conditions required for halogen–magnesium exchange. The central role of Grignard reagents and recent developments in the application of organomagnesium reagents are described.

Grignard Reagents in Synthesis

P. Knochel,* W. Dohle, N. Gommermann, F. F. Kneisel, F. Kopp, T. Korn, I. Sapountzis, V. A. Vu ——— **4302 – 4320**

Highly Functionalized Organomagnesium Reagents Prepared through Halogen–Metal Exchange

Communications



The tendency for silver-rich compounds to form higher agglomerates of silver atoms or ions is well known. The synthesis of $Ag_{13}OsO_6$ represents the first compound in the Ag/Os/O system. Besides $[OsO_6]^{4-}$ octahedra, the compound contains icosahedrally shaped Ag_{13}^{4+} clusters (see picture), which are observed for the first time in solid silver oxides.

Subvalent Ternary Silver Oxide

S. Ahlert, W. Klein, O. Jepsen, O. Gunnarsson, O. K. Andersen, M. Jansen* ——— **4322 – 4325**

$Ag_{13}OsO_6$: A Silver Oxide with Interconnected Icosahedral Ag_{13}^{4+} Clusters and Dispersed $[OsO_6]^{4-}$ Octahedra

For the USA and Canada:
ANGEWANDTE CHEMIE International Edition (ISSN 1433-7851) is published weekly by Wiley-VCH PO Box 191161, D 69451 Weinheim, Germany. Air freight and mailing in the USA by Publications Expediting Inc. 200 Meacham Ave., Elmont, NY 11003. Periodicals postage paid at Jamaica NY 11431. US POSTMASTER: send address changes to *Angewandte Chemie*, Wiley-VCH, 111 River Street, Hoboken, NJ 07030. Annual institutional subscription price for institutions: Europe € 2998.00/3148.00. Outside Europe US$ 3718.00/3904.00 (valid for print or electronic/print and electronic delivery); for individuals who are personal members of a national chemical society, or whose institution already subscribes, or who are retired or self-employed consultants, print only (including postage and handling charges): Europe € 248.00/Outside Europe US$ 348.00.

 © 2003 Wiley-VCH Verlag GmbH & Co. KGaA, Weinheim

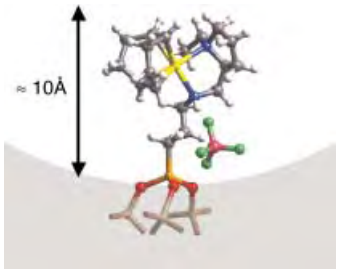
Contents

Asymmetric Heterogeneous Catalysis

M. D. Jones, R. Raja,* J. M. Thomas,* B. F. G. Johnson,* D. W. Lewis, J. Rouzaud, K. D. M. Harris _____ **4326 – 4331**

Enhancing the Enantioselectivity of Novel Homogeneous Organometallic Hydrogenation Catalysts

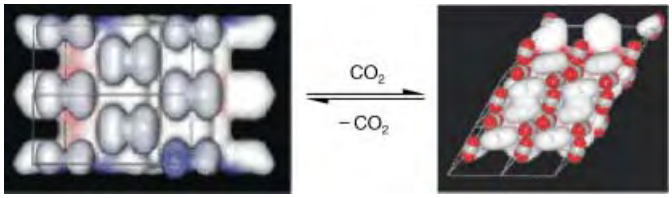
By designing well-defined, single-site asymmetric organometallic complexes anchored to a concave siliceous support (see picture) high *ee* values may be obtained in heterogeneous catalytic hydrogenations. O red, Si orange, Rh yellow, C grey, N blue, F green, B pink, H white.



CO_2 Inclusion in Crystals

S. Takamizawa,* E.-i. Nakata, H. Yokoyama, K. Mochizuki, W. Mori _____ **4331 – 4334**

Carbon Dioxide Inclusion Phases of a Transformable 1D Coordination Polymer Host $[Rh_2(O_2CPh)_4(pyz)]_n$



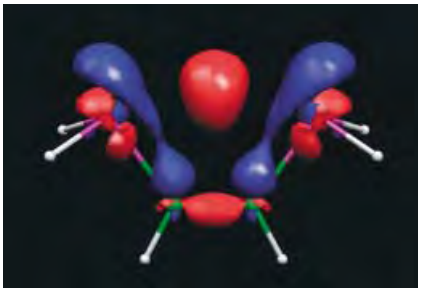
CO_2 is included: The one-dimensional coordination polymer host $[Rh_2(O_2CPh)_4(pyz)]_n$ (pyz = pyrazine; see picture, left) undergoes a reversible phase transition under cooling that is induced by CO_2 adsorption to give an inclusion complex, in which up to three CO_2 molecules per polymer unit reside within channels (right).

Spin–Spin Coupling Pathways

O. L. Malkina,* V. G. Malkin* _____ **4335 – 4338**

Visualization of Nuclear Spin–Spin Coupling Pathways by Real-Space Functions

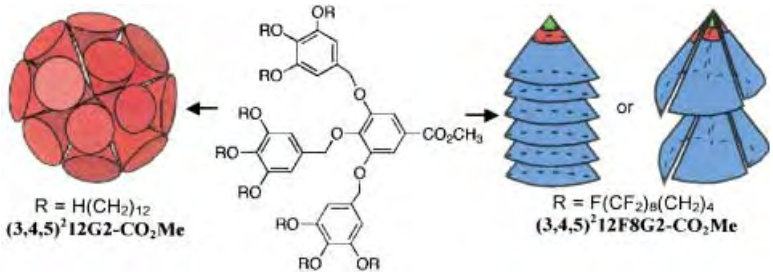
Spin, a yarn: A new approach for the visualization of indirect nuclear spin–spin coupling is presented, which allows for a clear judgement on the importance of the different possible coupling pathways that exist. For example, it is possible to examine coupling through space or through hydrogen-bond interactions (the picture describes the $^3J_{P,P}$ coupling energy density in the $C_2H_2(PH_2)_2$ molecule).



Dendrimer Shape Control

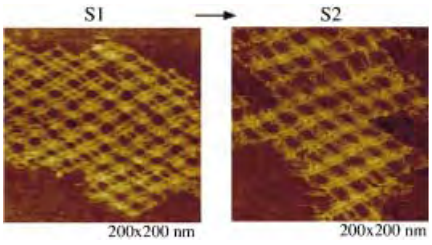
V. Percec,* M. Glodde, G. Johansson, V. S. K. Balagurusamy, P. A. Heiney _____ **4338 – 4342**

Transformation of a Spherical Supramolecular Dendrimer into a Pyramidal Columnar Supramolecular Dendrimer Mediated by the Fluorophobic Effect



Shape control: Fluorination of the *n*-dodecan-1-yloxy groups of the amphiphilic **(3,4,5)²G2-CO_2Me** monodendron changes the shape of the monodendron from an all-*trans*-conical to an all-*gauche*-crown or all-*trans*-tapered conformation as well as the mode of self-assembly from a spherical to a pyramidal columnar supramolecular dendrimer (see schematic representation).

 © 2003 Wiley-VCH Verlag GmbH & Co. KGaA, Weinheim

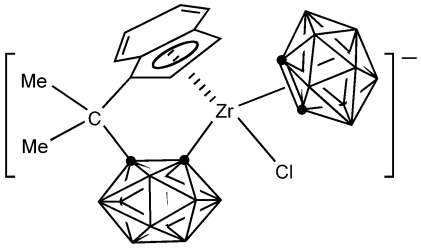


Changing the dimensions of the mesh. A robust sequence-dependent DNA device termed a nanoactuator was incorporated into a 2D parallelogram DNA lattice. Conversion of the DNA nanoactuator between two well-defined states (S1 and S2, see picture) results in controlled motion of the lattice.

Nanomechanical Device

L. Feng, S. H. Park, J. H. Reif, H. Yan* ——— **4342 – 4346**

A Two-State DNA Lattice Switched by DNA Nanoactuator

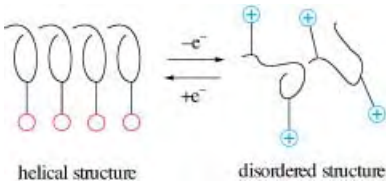


1,2-Dehydro-*o*-carborane, a three-dimensional relative of benzyne, has been successfully prepared and structurally characterized for the first time in the form of a zirconocene complex (see picture). This carborane molecule exhibits unique η^3-bonding characteristics, with an unprecedented Zr-H-B agostic interaction, as well as two Zr—C bonds, which serve to stabilize the cage.

Zirconocene–Carborane Complex

H. Wang, H.-W. Li, X. Huang, Z. Lin,* Z. Xie* ——— **4347 – 4349**

Synthesis, Structure, and Bonding of a Zirconocene–1,2-Dehydro-*o*-carborane Complex

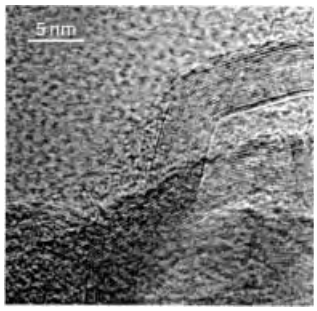


Winding up helices: The title compounds are prepared by a living polymerization of optically active ferrocenyl isocyanides initiated with a dinuclear Pt–Pd complex. Electrolytic CD and UV spectra suggest that the polymers exhibit reversible conformational change in response to oxidation and reduction of the ferrocenyl pendants (see scheme).

Electroresponsive Polymers

N. Hida, F. Takei, K. Onitsuka, K. Shiga, S. Asaoka, T. Iyoda, S. Takahashi* ——— **4349 – 4352**

Helical, Chiral Polyisocyanides Bearing Ferrocenyl Groups as Pendants: Synthesis and Properties



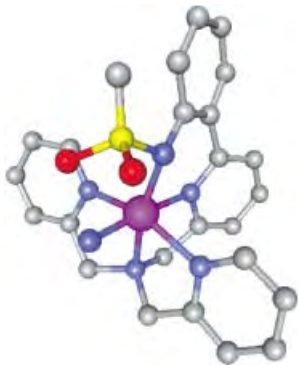
Carbon nanocoils with nanometer-thick graphitic fibers (see picture) were synthesized by the simple heat treatment of nanocomposites of a carbon precursor, silica, and a transition-metal salt. The carbon nanocoils exhibited a high surface area and a highly graphitized structure. The nanocoils were then successfully applied as catalyst supports for direct methanol fuel cell electrodes.

Carbon Nanocoils

T. Hyeon,* S. Han, Y.-E. Sung, K.-W. Park, Y.-W. Kim ——— **4352 – 4356**

High-Performance Direct Methanol Fuel Cell Electrodes using Solid-Phase-Synthesized Carbon Nanocoils

An iron(III) anilide complex can be formed through the reaction of phenyl-*N*-tosylimidoiodinane with the non-heme iron complex $[(6\text{-PhTPA})Fe^{II}(NCCH_3)_2](ClO_4)_2$ (TPA = tris(2-pyridylmethyl)amine), in which an efficient transfer of the nitrene moiety to the *ortho* position of the α-phenyl substituent is achieved (a hypothetical structure of the complex is illustrated, in which the tolyl ring, except for the *ipso* carbon atom, is excluded for clarity; Fe pink, S yellow, O red, N blue).



Iron-Mediated Aminations

M. P. Jensen, M. P. Mehn, L. Que, Jr.* ——— **4357 – 4360**

Intramolecular Aromatic Amination through Iron-Mediated Nitrene Transfer

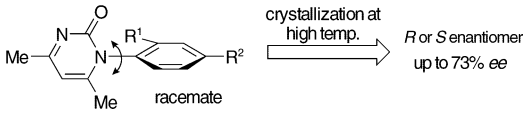
 © 2003 Wiley-VCH Verlag GmbH & Co. KGaA, Weinheim

Contents

Chiral Resolution

M. Sakamoto,* N. Utsumi, M. Ando, M. Saeki, T. Mino, T. Fujita, A. Katoh, T. Nishio, C. Kashima ——— **4360 – 4363**

Breaking the Symmetry of Axially Chiral *N*-Aryl-2(1*H*)-pyrimidinones by Spontaneous Crystallization



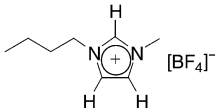
No outside source of chirality was needed to resolve the racemate of an axially chiral pyrimidinone (see scheme). Crystallization at high temperatures gave optically active material in up to 73 % *ee*. The resolved product could be reduced with $NaBH_4$ with high enantioselectivity.

Structure of Ionic Liquids

A. Mele,* C. D. Tran, S. H. De Paoli Lacerda ——— **4364 – 4366**

The Structure of a Room-Temperature Ionic Liquid with and without Trace Amounts of Water: The Role of C–H···O and C–H···F Interactions in 1-*n*-Butyl-3-Methylimidazolium Tetrafluoroborate

Solvated solvents: Water molecules interact with the imidazolium cation and $[BF_4]^-$ ion (see picture) of the molten ionic-liquid salt 1-*n*-butyl-3-methylimidazolium tetrafluoroborate. Evidence for short C–H···O and C–H···F interactions is provided by $^1H\{^1H\}$ and $^1H\{^{19}F\}$ NMR spectroscopy nuclear Overhauser enhancements.

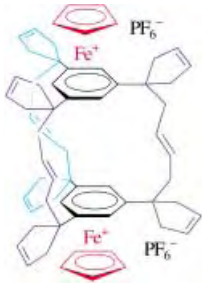


Rings Cages and Polymers

V. Martinez, J.-C. Blais, D. Astruc* ——— **4366 – 4369**

A Fast Organometallic Route from *p*-Xylene, Mesitylene, and *p*-Diisopropylbenzene to Organoiron and Polycyclic Aromatic Cyclophanes, Capsules and Polymers

New organic and organoiron polycyclic paracyclophane cages (see picture) and polymers are rapidly formed using two different, extremely efficient C–C bond coupling reactions from *p*-xylene, mesitylene and *p*-diisopropylbenzene: the η^5-C_5H_5-Fe^+-induced perallylation- or peralkenylation reaction followed by Ru-catalyzed ring-closing and cross-coupling metathesis by using the commercially available Grubbs catalysts.

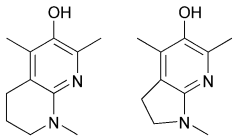


Pyridinol-Based Antioxidants

M. Wijtmans, D. A. Pratt,* L. Valgimigli,* G. A. DiLabio, G. F. Pedulli,* N. A. Porter* ——— **4370 – 4373**

6-Amino-3-Pyridinols: Towards Diffusion-Controlled Chain-Breaking Antioxidants

The incorporation of nitrogen in the phenolic ring leads to compounds with very low phenolic O–H bond dissociation enthalpies, and thus high reactivities towards peroxyl radicals, but which are reasonably stable to direct reactions with air. The 3-pyridinols **1** and **2** are extremely effective peroxyl-radical-trapping chain-breaking antioxidants.

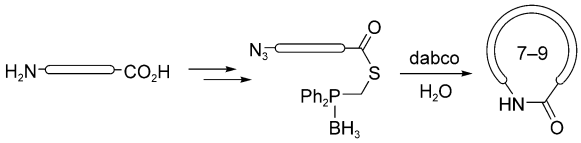


1 **2**

Intramolecular Staudinger Ligation

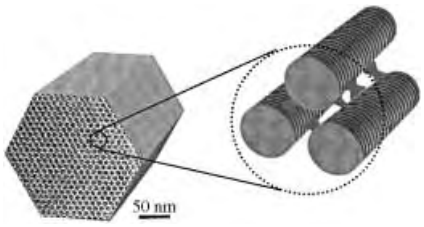
O. David, W. J. N. Meester, H. Bieräugel, H. E. Schoemaker, H. Hiemstra, J. H. van Maarseveen* ——— **4373 – 4375**

Intramolecular Staudinger Ligation: A Powerful Ring-Closure Method To Form Medium-Sized Lactams



Efficient access to medium-sized lactams from ω-amino acids that are resistant to ring-closure by traditional strategies is enabled by an intramolecular Staudinger ligation approach. An undesired premature Staudinger reaction is avoided by protecting the phosphane-containing auxiliary as a borane complex (see scheme; dabco = 1,4-diazabicyclo[2.2.2]-octane).

 © 2003 Wiley-VCH Verlag GmbH & Co. KGaA, Weinheim



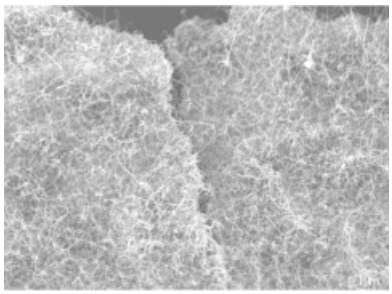
Carbonization of aromatic sources in an aluminosilicate mesoporous template yields mesoporous carbon materials with highly graphitic framework structures and excellent mechanical strength and thermal stability (see picture). TEM analysis shows discoid graphitic layers that are packed so that the most preferred orientation of the *c* axes is along the direction of the template channels.

Mesoporous Carbon Materials

T.-W. Kim, I.-S. Park, R. Ryoo* ——— **4375 – 4379**

A Synthetic Route to Ordered Mesoporous Carbon Materials with Graphitic Pore Walls

Free-standing films of multiwalled carbon nanotubes (see scanning electron micrograph) encapsulating crystalline metal particles are obtained by the solid-state thermolytic conversion of commercial homogeneous organometallic systems with a defined metal-to-carbon ratio.

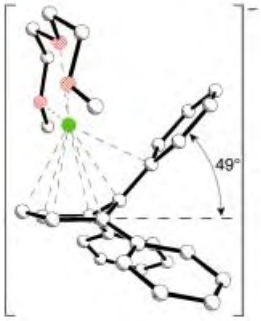


Synthesis of Carbon Nanotubes

V. S. Iyer, K. P. C. Vollhardt,* R. Wilhelm ——— **4379 – 4383**

Near-Quantitative Solid-State Synthesis of Carbon Nanotubes from Homogeneous Diphenylethynecobalt and -Nickel Complexes

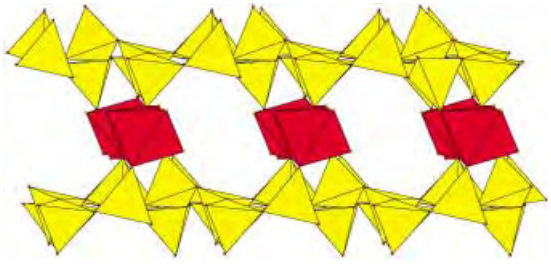
Ioning in distortions: Severe ionic distortions of phenyl-substituted hydrocarbon anions are observed on coordination to Na^+ or K^+ ions. Alkali-metal salts of 1,2-diphenylbenzene (see picture: Na green, O red) and 1,2,3-triphenylbenzene dianions are prepared by reduction, structurally characterized, and analyzed by density functional and natural bond order calculations. The reduction and subsequent cation coordination of the phenylbenzene ions dramatically distorts the structures of the hydrocarbon skeletons.



Contact Ion Pairs and Triples

H. Bock,* Z. Havlas,* K. Gharagozloo-Hubmann, S. Holl, M. Sievert ——— **4385 – 4389**

1,2-Diphenylbenzene Dianion: Alkali-Metal Salts with Drastically Spread C_6 Rings



Two metals in one net: GeO_4 tetrahedra and InO_6N_2 octahedra are primary building units in a new indium germanate. The germanium layers (yellow) are linked by the InO_6N_2 units (red) to form a 3D network. The compound is prepared by a hydrothermal synthesis using GeO_2 and $In(OH)_3$ in an aqueous solution of ethylenediamine.

Mixed In/Ge Oxide

D. Pitzschke, W. Bensch* — **4389 – 4391**

$In_2Ge_6O_{15}(en)_2$: A In–Ge Compound Composed of Germanate Layers Linked by Pillars of $In_2O_6N_4$ Double Octahedra

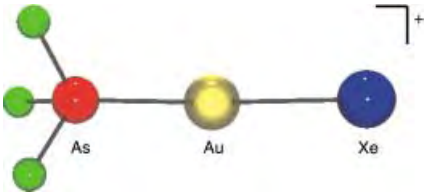
 © 2003 Wiley-VCH Verlag GmbH & Co. KGaA, Weinheim

Contents

Coordination of Noble-Gas Atoms

I.-C. Hwang, S. Seidel, K. Seppelt* ——— 4392 – 4395

Gold(I) and Mercury(II) Xenon Complexes



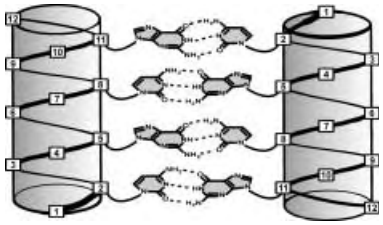
Noble-gas ligands: For the first time it has been possible to prepare a gold(I) xenon complex ($[(F_3As)AuXe]^+$, see picture) and a mercury(II) xenon complex. The syntheses of these compounds start from precursors with weakly coordinated metal ions and take place in a superacid medium.

Organization of Peptide Helices

A. M. Brückner, P. Chakraborty, S. H. Gellman,* U. Diederichsen* ——— 4395 – 4399

Molecular Architecture with Functionalized β-Peptide Helices

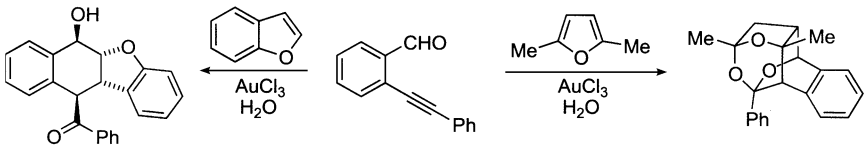
Specific recognition of β-peptide helices can be achieved by the incorporation of nucleo-β-amino acids in every third position of β-peptide oligomers. Pairing complexes (see picture) are formed with extraordinary high stabilities in aqueous buffer. A major contribution comes from the high preorganization of the nucleobases by the 14-helix backbone.



Cycloadditions and Domino Reactions

G. Dyker,* D. Hildebrandt, J. Liu, K. Merz ——— 4399 – 4402

Gold(III) Chloride Catalyzed Domino Processes with Isobenzopyrylium Cation Intermediates



A potpourri of remarkable reactions is initiated by the $AuCl_3$-catalyzed cyclization of an *ortho*-alkynyl benzaldehyde. In the presence of an olefin or an electron-rich heteroarene as a dienophile or nucleophile, this cyclization provides selective access to a broad variety of polycyclic structures (see scheme).

VIP Communications labeled with this symbol have been judged by two referees as being "very important papers".

The publication of Communications labeled with this symbol has been accelerated because of their topical or highly competitive nature.

Looking for outstanding employees?

Do you need another expert for your excellent team?
...Chemists, PhD Students, Managers, Professors, Sales Representatives...

Place an advert in the printed version and have it made available online for 1 month, free of charge!

Angewandte Chemie International Edition
Advertising Sales Department: Marion Schulz
Phone: 0 62 01 - 60 65 65
Fax: 0 62 01 - 60 65 50
E-Mail: MSchulz@wiley-vch.de

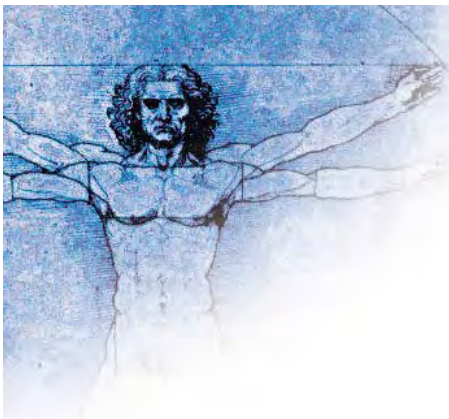
Service

Keywords ——— 4404

Authors ——— 4405

Angewandte's Sister Journals ——— 4406 – 4407

Preview ——— 4409



Royal Society of Chemistry Awards

The Royal Society of Chemistry (RSC, UK) gives numerous awards annually. Some of the latest recipients, who have also recently published in *Angewandte Chemie* or one of its sister journals, are presented below with their work.

Duncan Graham (University of Strathclyde, UK) has received the Society for Analytical Chemistry Silver Medal for young researchers (under 35) for his innovative syntheses of new analytical reagents for sensitive and specific measurements. He completed his Ph.D. in 1996 in Edinburgh under the guidance of Tom Brown and has worked since 2002 as a lecturer and senior lecturer in Glasgow.[1a,b]



D. Graham

The Spiers Memorial Lectureship of the Faraday Discussion has been awarded to Professor **Bruce Bursten** (Ohio State University, Columbus, USA) for his outstanding contributions to quantum inorganic chemistry, in particular of the actinoids. Bursten studied in Chicago and Madison (with Richard Fenske), then moved to Texas to work with F. Albert Cotton as a postdoctoral researcher. His research group is involved with the correlation of theoretical and experimental electronic-structure data with the bonding and reactivity patterns of transition-metal complexes.[2]



B. Bursten

Andrew Holmes, a professor at the University of Cambridge (UK), has been awarded a Tilden Lectureship. His research is focused on the synthesis of natural products and polymers, and he is being honored by the RSC for the breadth of this research.[3] Holmes was born in Australia, carried out his Ph.D. at University College London, and undertook postdoctoral research with Albert Eschenmoser (ETH Zürich, Switzerland).



A. Holmes

Professor **David Parker** (University of Durham, UK) has also been awarded a Tilden Lectureship for his elegant syntheses of supramolecular systems that are suited for use as electroanalytical sensors or paramagnetic contrast agents or that selectively bind and transport metal ions. His research group is concerned with complex chiral systems, and in particular with their complexation in aqueous media.[4] Parker was a Ph.D. student of John M. Brown (Oxford, UK) and a postdoctoral researcher with J.-M. Lehn.



D. Parker



H. Gray

The Geoffrey Wilkinson Lectureship goes to **Harry Gray** of the California Institute of Technology (USA) in recognition of his outstanding contributions to several areas of inorganic chemistry. He has been recognized in particular for his work on spectroscopy, photochemistry, and the mechanisms of electron transfer in coordination complexes and of electron transfer involving metal centers in proteins.[5]

Shankar Balasubramanian, a lecturer at the University of Cambridge (UK), is a recipient of a Corday-Morgan Medal for young scientists (under 38). His research interests include organic synthesis, chemical biology, and molecular biophysics. This distinction has been awarded in recognition of his excellent work at the interface of biology and chemistry: fluorescence resonance energy transfer in biomolecules, the synthesis and characterization of nucleic acids, including the catalytically active region of human telomerase, and the development of a photochemical linker for use in combinatorial chemistry.[6]



S. Balasubramanian

[1] a) D. Graham, B. J. Mallinder, W. E. Smith, *Angew. Chem.* **2000**, *112*, 1103; *Angew. Chem. Int. Ed.* **2000**, *39*, 1061; b) D. Graham, B. J. Mallinder, D. Whitcombe, W. E. Smith, *ChemPhysChem* **2001**, *2*, 746.

[2] L. Andrews, B. Liang, J. Li, B. E. Bursten, *Angew. Chem.* **2000**, *112*, 4739; *Angew. Chem. Int. Ed.* **2000**, *39*, 4565.

[3] a) S. A. Haque, T. Park, A. B. Holmes, J. R. Durrant, *ChemPhysChem* **2003**, *4*, 89; *ChemPhysChem* **2003**, *4*, 230; b) C.-H. Tan, A. B. Holmes, *Chem. Eur. J.* **2001**, *7*, 1845.

[4] M. Botta, S. Aime, A. Barge, G. Bobba, R. S. Dickins, D. Parker, E. Terreno, *Chem. Eur. J.* **2003**, *9*, 2102.

[5] G. Golubkov, J. Bendix, H. B. Gray, A. Mahammed, I. Goldberg, A. J. DiBilio, Z. Gross, *Angew. Chem.* **2001**, *113*, 2190; *Angew. Chem. Int. Ed.* **2001**, *40*, 2131.

[6] Y. Krishnan-Ghosh, S. Balasubramanian, *Angew. Chem.* **2003**, *115*, 2221; *Angew. Chem. Int. Ed.* **2003**, *42*, 2171.

 © 2003 Wiley-VCH Verlag GmbH & Co. KGaA, Weinheim

NIR Dyes

An Unexpectedly Simple NIR Dye for 1.1 μm with a Central Mesoionic Structure

*Heinz Langhals**

Keywords:
chromophores · color rules · donor–acceptor systems · dyes · mesoionic compounds

Introduction

Dyes[1,2] by strict definition are substances absorbing visible light. The term was extended to the invisible ultraviolet region later on; fluorescent whitening agents are the most prominent examples of this class of substances. In contrast to this, dyes for the invisible infrared region[3,4] have only been developed comparably recently. Novel technologies, especially the development of NIR semiconductor lasers, induced rapid progress in this field which comprises functional dyes for optical storage and substances for several applications in medicine. Dyes for applications in the NIR region require small differences in the energy between HOMO and LUMO. To date this situation was attained with extended π systems, sometimes with the additional incorporation of heavy elements, such as selenium and tellurium. The majority of such substances are difficult to synthesize and many of them are labile. Complex structures have been developed such as the combination of two perylene units with one diaminoanthraquinone unit and quite a number of donor groups.[5] The anellation of non-alternate heterocycles[6,7] is a further interesting approach for the development of such dyes. However, a concept for attaining bathochromic (long wavelength) absorption with simple dyes is still lacking.

[*] Prof. Dr. H. Langhals
Department Chemie
University of Munich
Butenandtstrasse 13
81377 Munich (Germany)
Fax: (+49) 89-2180-77740
E-mail: Langhals@lrz.uni-muenchen.de

A Dye with "Super Acceptor Groups"

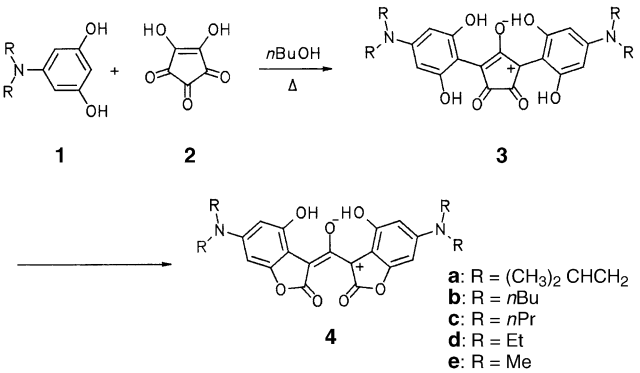
With a compound of surprisingly simple structure Tian and co-workers succeeded in attaining an absorption at 1100 nm (1.1 μm).[8] An even further bathochromic shift of the absorption to 1228 nm was then obtained by J-aggregation[9] of the new dye **4** (Scheme 1); this absorption is of special interest for optical components.

The expected croconate **3a** was obtained by the condensation of croconic acid (**2**) with 5-diisobutylbenzene-1,3-diol (**1a**) and exhibits a pronounced bathochromic absorption[4] at 860 nm. Dye **4a** was then formed as a product of the oxidation of **3a** in a slow reaction. The authors assumed that a disproportionation reaction of **3a** was responsible. The necessary reduction product of **3a** was not found, however, and mechanistic studies are difficult with a yield of only 7.4% of **4a**. The *n*-alkyl derivatives **4b**–**4d** could be also synthesized, however, with even lower yields.

The unusually long-wavelength absorption of **4a** is surprising. The remark of the authors[8] concerning a strongly shortened *N*-aryl bond length by pronounced mesomeric effects is important for the understanding of the special electronic conditions in **4a**. Its chromophoric structure can be interpreted in terms of the donor–acceptor–concept established by König[10] and Ismailsky,[11] and further developed by Dilthey and Wizinger[12–15] and incorporated into the perturbation molecular orbital theory (PMO) model by Dewar.[16] According to this a long-wavelength absorption is expected if π systems are substituted with donor (Do) and acceptor (A) groups. Very strong donor and acceptor groups can by applied in a double arrangement according to building principle (1) and cause long-wavelength absorption.

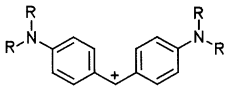
$$\mathrm{Do} - \pi - \mathrm{A} - \pi - \mathrm{Do} \qquad (1)$$

Michler's hydrole blue (**5e**, R = CH_3, $\lambda_{max} = 625$ nm) is a simple compound with the building principle (1) and forms the basic structure of malachite green. The two benzene rings of **5e** are the π systems, the dialkyl amino



Scheme 1. Synthesis of the NIR dyes **4**: yields **4a** 7.4, **4b** 2.5, **4c** 0.5, **4d** 0.2, **4e** 0%.

 © 2003 Wiley-VCH Verlag GmbH & Co. KGaA, Weinheim DOI: 10.1002/anie.200301642

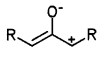


5

structures are the donor groups and the central, formal carbenium ion **6** the



6



7

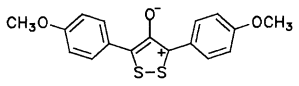
acceptor group. An even more bathochromic shift results by the replacement of the acceptor **6** by a squaric acid (see the comment of the authors,[8] compare also ref. [17]). Squaric acid contains two formal positive charges in the four-membered ring (mesomeric formula of squaric acid not shown). If the croconic acid unit is employed, which contains three formal positive charges in the central 2π aromatic ring (mesomeric formula of **3a** not shown) this shifts the absorption into the NIR at 860 nm.

The central unit in **4a** exceeds the acceptor properties of the croconate unit of **3a** by far. As the electronic properties of the donor groups in **5**, **3a**, and **4a** are identical and the substitution of the benzene rings in **3a** and **4a** remains unchanged, it is clearly the central mesoionic unit **7**, aided by the two carbonyl groups of the lactone rings, that acts as a "super acceptor group". The special arrangement of charges and carbonyl groups seems to be very strongly electron withdrawing and also causes the above mentioned shortening of the C–N bond. Quantum chemical calculations (AM1 or PM3)[18] verify the special situation of the π system of **4a**, for example, appreciably smaller differences in energy between HOMO and LUMO are calculated for **4e** than for **3e** or **5e** (Table 1).

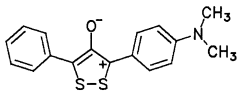
Table 1: Quantum chemically calculated energies of excitation (ΔE).

Method	ΔE [kcal mol^{-1}]		
	1e	**2e**	**5e**
AM1	44.6	50.4	73.8
PM3	42.2	47.7	70.0

The entire mesoionic structure **7** in **4a** was unknown in dyes. However, the strong acceptor properties of such arrangements could have been noticed because the heterocyclic compound **8**[19] with a similar central structure



8



9

absorbs at remarkably long wavelength, $\lambda_{max} = 571$ nm (1,4-dioxane) although the methoxy substituents are only weak donor groups. Compound **9** absorbs at 617 nm (1,4-dioxane),[19] even though the second donor group (according to building principle (1)) is missing.

The high molar absorptivity is the second remarkable property of **4a**. Especially for small molecules with π systems of similar dimensions a decrease in the absorption coefficient for bathochromic shifted absorption maxima is expected, because the mismatch between molecular dimensions and the wavelength of the absorbed radiation becomes more pronounced (see, for example, ref. [20]). A Gaussian analysis of the UV/Vis absorption spectrum of **4a** published in ref. [8] was made according to ref. [21]. The published spectrum can be constructed[22] in high precision (R value 1.4 %) from Gaussian bands[23] (Figure 1 and Table 2). Two neighboring absorptions were found in

Table 2: Gaussian functions for the simulation of the UV/Vis spectrum of **1a**; see text.

λ_{max} [nm]	ε_{max} [L^{-1} mol^{-1} cm^{-1}]	$2\sigma^2$ [kK]
1101	13 300	0.17
1092	45 500	0.75
1027	23 700	2.66
671	2 700	1.29
546	9 700	5.03
473	4 200	11.47

the long-wavelength region of the spectrum of **4a**, the overlap of these bands is responsible for the high absorption coefficients observed experimentally.

Conclusions and Outlook

A "super acceptor group" for dyes seems to be found with the central mesoionic structure of **4a**. Thus, novel classes of dyes can be expected where long-wavelength absorptions can be obtained with comparably small π systems. The color rules of König and Ismailsky and their further developments are a useful tool, even for completely novel structures.

The counterpart to the "super acceptor groups" are the recently discovered α-effect donor groups[24] which could be correspondingly named "super donor groups". A combination of such

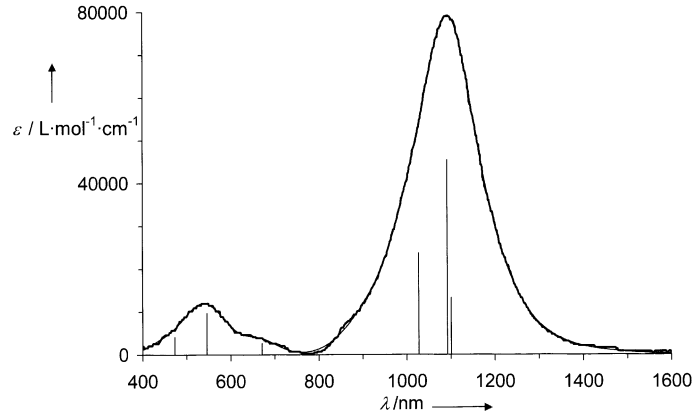


Figure 1. UV/Vis absorption spectrum of **4a** in 1,2-dichloroethane from ref. [8] (thick line) and simulated spectrum of a Gaussian analysis (thin line, nearly completely covered by the experimental spectrum). Bars: positions and intensities of the single Gaussian bands.

 © 2003 Wiley-VCH Verlag GmbH & Co. KGaA, Weinheim

extreme donor and acceptor groups according to the building principle (1) is expected to result in novel effects of interest in dye chemistry.

[1] H. Zollinger, *Color Chemistry*, 2nd ed., VCH, Weinheim, **1991**, ISBN 3-527-28352-8, LCC 91-23858.

[2] W. Herbst, K. Hunger, *Industrielle Organische Pigmente*, 2nd ed., VCH, Weinheim, **1995**, ISBN 3-527-28744-2.

[3] "Near-Infrared Dyes for High Technology Applications": S. Daehne, U. Resch-Genger, O. S. Wolfbeis, *NATO ASI Ser. Ser. 3* **1998**, 52, ISBN 0-7923-5101-0.

[4] J. Fabian, H. Nakazumi, M. Matsuoka, *Chem. Rev.* **1992**, *92*, 1197 – 1226.

[5] C. Kohl, S. Becker, K. Müllen, *Chem. Commun.* **2002**, 2778 – 2779.

[6] Dongfeng Hou, H. Balli, *Helv. Chim. Acta* **1992**, *75*, 2608 – 2612.

[7] H. Balli, M. Zeller, *Helv. Chim. Acta* **1983**, *66*, 2135 – 2139.

[8] M. Tian, S. Tatsuura, M. Furuki, I. Iwasa, L. S. Pu, *J. Am. Chem. Soc.* **2003**, *125*, 348 – 349.

[9] E. Jelley, *Nature* **1936**, *138*, 1009.

[10] W. König, *J. Prakt. Chem.* **1925**, *112*, 1 – 36.

[11] W. Ismailsky, Dissertation, Universität Dresden, **1913**.

[12] W. Dilthey, R. Wizinger, *J. Prakt. Chem.* **1928**, *118*, 321 – 348.

[13] R. Wizinger, *Chimia* **1961**, *15*, 89 – 105.

[14] J. Griffiths, *Colour and Constitution of Organic Molecules*, Academic Press, London, **1976**; ISBN 0-12-303550-3, LCCC 76-016971.

[15] S. Dähne, S. Kulpe, *Structural Principles of Unsaturated Organic Compounds*, Akademie Verlag, Berlin, **1977** (Abh. Akad. Wiss. DDR Nr. 8).

[16] M. J. S. Dewar, R. C. Dougherty, *The PMO Theory of Organic Chemistry*, 1st ed., Plenum, New York, **1975**, pp. 410 – 418, ISBN 0-306-20010-4.

[17] J. Fabian, H. Hartmann, *Light Absorption of Organic Colorants*, Springer, Berlin, **1980**, ISBN 3-540-09914-X.

[18] Parameters: PRECISE, XYZ; the vertically exited state was calculated from the optimized geometry of the ground state and the additional parameters EXCITED and 1SCF.

[19] D. Bariller, *Phosphorus Sulfur Relat. Elem.* **1980**, *8*, 79 – 85.

[20] E. F. McCoy, I. G. Ross, *Aust. J. Chem.* **1962**, *15*, 573 – 590.

[21] H. Langhals, *Spectrochim. Acta Part A* **2000**, *56*, 2207 – 2210.

[22] $\varepsilon(\lambda) = \Sigma\varepsilon(\lambda_{max})\exp(-(1/\lambda - 1/\lambda_{max})^2/2\sigma^2)$.

[23] The replacement of the two most bathochromic Gaussian functions by a Lorentzian function lowers the quality of the fit and increases the *R* value to 12%. The use of a lower number of Gaussian functions lowers the quality of the *R* value appreciably. Additional Gaussian functions do not give a significant improvement.

[24] H. Langhals, P. Blanke, *Dyes Pigm.*, **2003**, *59*, 109–116.

Synthesis of Amino Acids

Recent Developments in the Catalytic Asymmetric Synthesis of α- and β-Amino Acids**

*Jun-An Ma**

Keywords:
amino acids · asymmetric catalysis · chirality · diastereoselectivity · enantioselectivity

The stereoselective synthesis of amino acids is of great importance for the construction of optically active natural products and pharmaceuticals. Apart from enzymes, a broad repertoire of chiral reagents, auxiliaries, and catalysts can be used for the formation of amino acids. Asymmetric reactions using catalytic amounts of chiral molecules provide efficient methods for the generation of optically active proteinogenic and nonproteinogenic amino acids. This minireview collects recent work on catalytic asymmetric synthesis of α- and β-amino acids.

1. Introduction

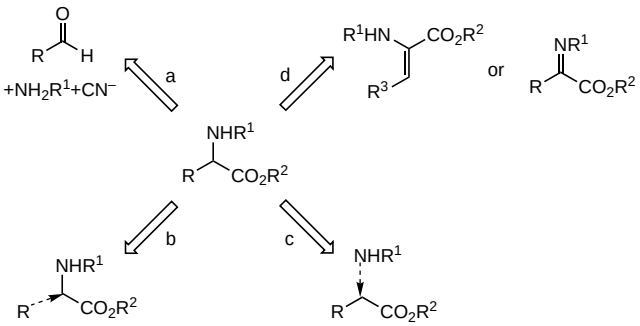
Optically active α- and β-amino acids are fundamental building blocks for the preparation of pharmaceutical and agrochemical target molecules, such as, peptides, proteins, and many other natural products.[1] Furthermore, amino acids are extensively used as chiral starting materials, auxiliaries, and catalysts in modern organic synthesis.[2] There are four main approaches to obtaining optically active amino acids, namely biotechnological methods, chemical synthesis using compounds from the chiral pool, resolution of a racemic mixture, and asymmetric synthesis. Asymmetric synthesis may be carried out by the use of chiral reagents or auxiliaries. The catalytic asymmetric synthesis have clear advantages over the reagents and auxiliaries approach since a catalytic amount of chiral material can produce large quantities of enantiomerically enriched or enantiopure products. This minireview collects recent work for synthesis of α- and β-amino acids including the use of organometallic catalysts and metal-free organic catalysts.

[*] Dr. J.-A. Ma
Institute and State Key Laboratory
of Elemento-Organic Chemistry
Nankai University, Tianjin 300071 (P.R. China)
Fax: (+86) 22-2350-3438
E-mail: majun_an68@yahoo.com

[**] The author thanks Professor Run-Qiu Huang and Professor Zheng-Zhi Zhang for the helpful suggestions and criticisms. The author gratefully acknowledges Professor Qi-Lin Zhou's encouragement of his research work.

2. Catalytic Asymmetric Synthesis of α-Amino Acids

Several different catalytic asymmetric approaches to α-amino acids involving carbon–carbon, carbon–nitrogen, and carbon–hydrogen bond-forming reactions have been developed (Scheme 1, paths a–d).[3] Recent publications have highlighted catalytic asymmetric Strecker reactions[4] (path a) and catalytic asymmetric hydrogenation of dehydroamino acids[5] (path d). Several advances involving carbon–carbon bond-forming events have emerged for the catalytic asymmetric synthesis of α-amino acids (path b), and also for asymmetric carbon–nitrogen bond-forming reactions (path c).



Scheme 1. Methods for the synthesis of α amino acids.

2.1. Asymmetric Carbon–Carbon Bond-Forming Reactions

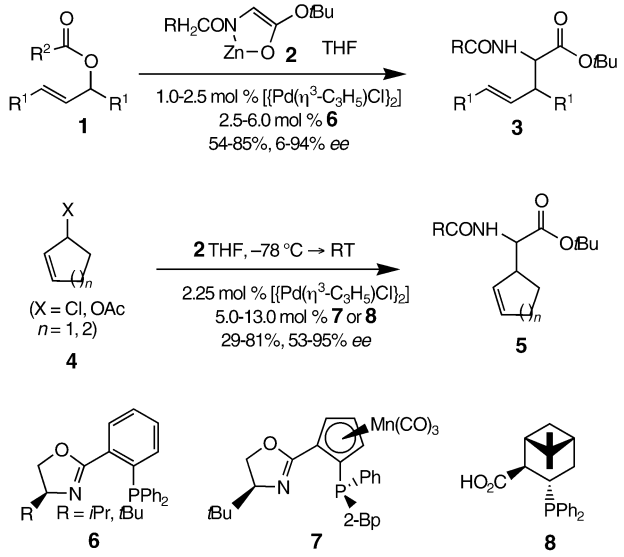
2.1.1. Glycine α-Anion Equivalents

Recently Helmchen and co-workers investigated Pd^{II}-catalyzed asymmetric allylic substitutions in which they utilized the Zn^{II} enolates **2** of glycine ester as nucleophiles

 © 2003 Wiley-VCH Verlag GmbH & Co. KGaA, Weinheim DOI: 10.1002/anie.200301600

to give α-alkylated γ,δ-unsaturated amino acids **3** with moderate to high levels of enantioselectivity (Scheme 2).[6] However, the diastereoselectivity of the substitution is strongly dependent on the ligand employed. Chiral P,N ligands **6** were particularly suited for acyclic substrates **1** whereas cymantrene derivative **7** and phosphanylmyrtanic acid **8** were better suited for cyclic compounds **4**.

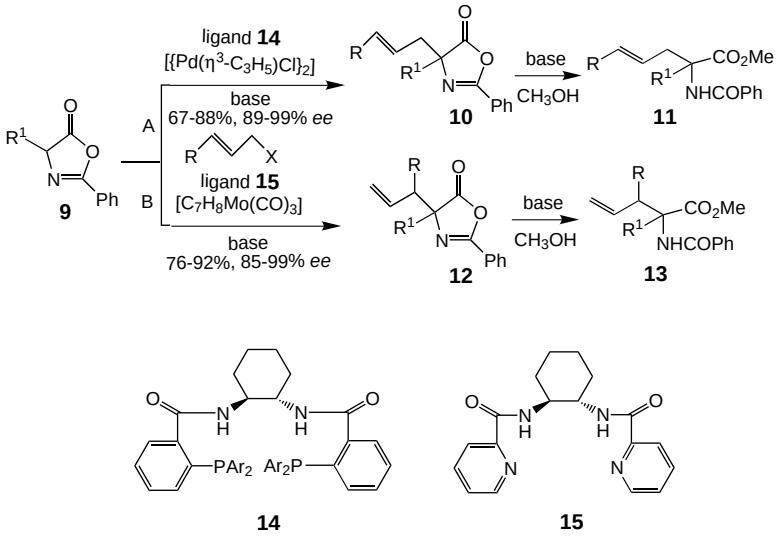
In the asymmetric allylic alkylation (AAA) reaction, the Trost group employed substituted azlactones **9** as nucleophiles to make α,α-disubstituted α-amino acids.[7] Depending on which of the catalytic systems is used the AAA reactions can go through two different routes (Scheme 3, path A and B). The Pd^{II}-catalyzed AAA reaction yields the linear product **10** in the reaction of azlactones **9** (as nucleophiles) with cinnamyl substrates (path A), while an alternative Mo-catalyzed AAA procedure (path B) leads to branched compounds **12**, with a high level of regio-, diastereo-, and enantioselectivity. The azlactones **10** and **12** were easily dissolved in methanol to afford the desired protected α-amino acids (**11**, **13**) in high yields.



Scheme 2. Asymmetric allylic substitution with the glycine ester zinc enolates **2** as nucleophiles. 2-Bp = 2-biphenylyl.



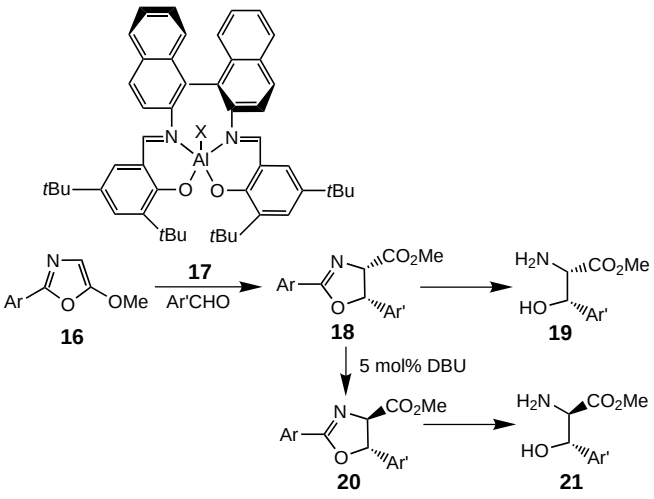
Jun-An Ma was born in Henan Province, China. He received his B.Sc. degree from Henan University in 1991 and his M.Sc. degree from Nankai University in 1994. Later he joined Guangzhou Baihua Flavor & Fragrance Company as a senior research fellow before he obtaining his Ph.D. in 1999 under the supervision of Professor Run-Qiu Huang at Nankai University. He stayed there to work with Professor Qi-Lin Zhou before taking up a postdoctoral fellowship with Dr. D. Cahard at Rouen University, France. His research interests focus on new methods for asymmetric synthesis, chiral catalysis, and bioorganic chemistry.



Scheme 3. Asymmetric allylic alkylation with azlactones **9** as nucleophiles.

Based on work by Suga and co-workers,[8] the research group of Evans recently disclosed a chiral salen–Al^{III} complex catalyst **17** (salen = bis(salicylidene)ethylenediamine) and its application in an aldol-addition/acyl-transfer process in which the 5-methoxyoxazoles **16** were employed as the glycine enolate synthon (Scheme 4).[9] This addition reaction afforded the versatile *cis*-2-oxazoline-4-carboxylates **18** in high yield (90–100%) and good stereoselectivity (74:26–99:1 d.r., 92–99% *ee*) from a range of aromatic aldehydes. The substrates **18** were cleanly isomerized to their *trans* counterparts **20** by DBU, thus providing access to both diastereomers of α-amino-β-hydroxy acids **19** and **21**. Solvents and salt additives were shown to have an effect on the catalytic efficiency. However, aliphatic aldehydes were found to be unreactive under the standard reaction conditions.

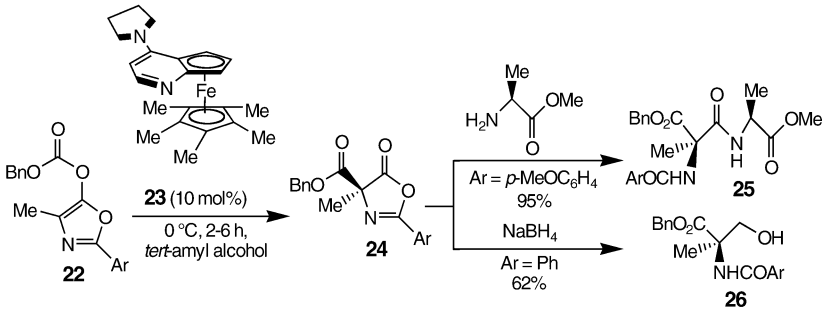
In 1970 Steglich and Höfle reported that DMAP (4-dimethylaminopyridine) served as a nucleophilic catalyst for the rearrangement of O-acylated azlactones to the corre-



Scheme 4. Lewis acid catalyzed asymmetric aldol reaction. X = SbF_6, DBU = 1,8-diazabicyclo[5.4.0]undeca-7-ene.

 © 2003 Wiley-VCH Verlag GmbH & Co. KGaA, Weinheim

sponding C-acylated oxazolinones.[10] Based on this report, Fu and co-workers introduced the first catalytic asymmetric version of this 1,2-acyl shift (Scheme 5).[11] Substrates, such as **22**, were converted in the presence of the planar-chiral DMAP derivative **23**, into the oxazoline derivatives **24** in excellent yields (93–95%) and with high enantioselectivities (88–92% *ee*). These rearrangement products **24** could be readily converted into α,α-dialkylated α-amino acids derivatives **25** and **26**.

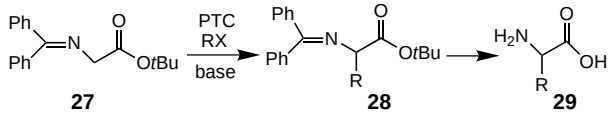


22 24 25 26

Scheme 5. Asymmetric rearrangement catalyzed by planar-chiral DMAP derivative **23**.

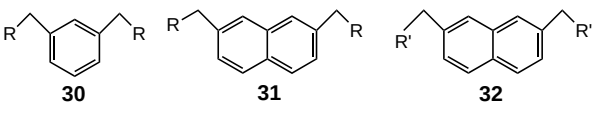
Since the enantioselective alkylation of *tert*-butyl glycinate benzophenone Schiff base **27** with the cinchona alkaloid-type phase-transfer catalyst was first reported by O'Donnell and co-workers (Scheme 6),[12] more efficient catalysts have been developed independently by the Lygo[13] and Corey research groups[14] by the introduction of the 9-anthracenylmethyl group.

Based on the fact that the introduction of a bulky subunit at the quinuclidine nitrogen atom of cinchona alkaloids leads to an enhancement of the stereoselectivity, Park and co-workers prepared the dimeric cinchona alkaloid ammonium salts (**30**–**32**; Scheme 7) as very efficient phase-transfer

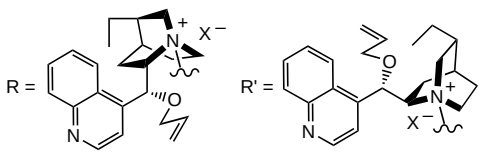


27 28 29

Scheme 6. Asymmetric synthesis of α-amino acids by the phase-transfer catalytic alkylation of glycine Schiff bases; PTC = phase-transfer catalyst.



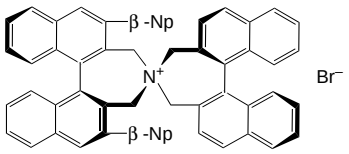
30 31 32



Scheme 7. Dimeric cinchona alkaloid ammonium salts as phase-transfer catalysts.

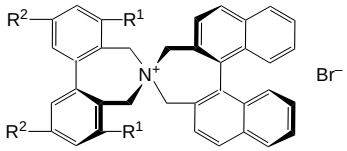
catalysts.[15] The catalytic enantioselective alkylation of glycinate derivate **27** using 1–5 mol% of catalyst (**30**–**32**) and 50% aqueous KOH in toluene/$CHCl_3$ gives the desired products **28** with high yields (50–96%) and excellent enantioselectivities (90–99% *ee*). Cinchona alkaloids are commercially available and relatively inexpensive, thus even the derivatives containing two cinchona moieties are relatively easy to prepare.

The Maruoka group developed a very efficient non-cinchona catalyst **33**, a chiral C_2-symmetric ammonium salt with a chiral binaphthyl structure, for the alkylation of glycine derivate **27** (Scheme 6).[16] With this



33 Np = naphthyl

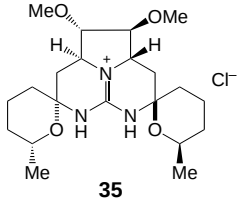
catalyst a high enantiomeric excess of alkylated compounds **28** could be prepared under mild conditions in a short reaction time. However, it imposed clear limitations on the catalyst design as two chiral binaphthyl moieties are required and modifications to the structure proved to be difficulty. Quite recently, Maruoka et al. described a new and simple strategy for the molecular design of chiral phase-transfer catalysts by introducing a new C_2-symmetric chiral quaternary ammonium salt **34** with a simple chiral binaphthyl moiety and an easily



34 a R^1 = 3,5-diphenylphenyl, R^2 = H
b R^1 = 3,5-diphenylphenyl, R^2 = Ph

modifiable achiral biphenyl substituent.[17] The phase-transfer catalytic alkylation of **27** was catalyzed smoothly by **34** in good to high yield (61–95%) in a highly enantioselective manner (92–95% *ee*).

Nayasawa and co-workers designed the new type of C_2-symmetric chiral pentacyclic guanidine derivative **35** as a phase-transfer catalyst for the enantioselective alkylation of **27**.[18] The alkylation products were obtained in good yields (61–90%) with high enantiomeric excesses (76–90% *ee*). Although the large amount of catalyst (30 mol%) was

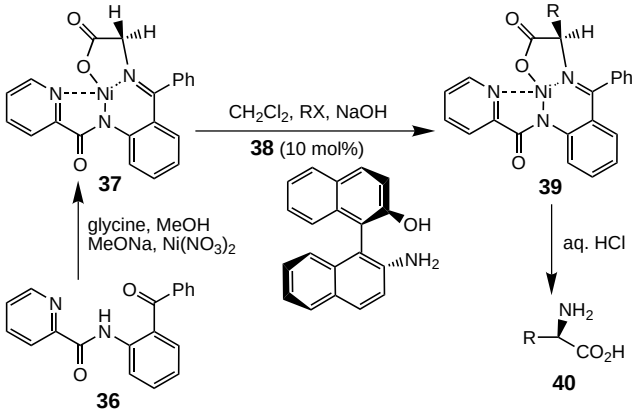


35

 © 2003 Wiley-VCH Verlag GmbH & Co. KGaA, Weinheim

required for to give a suitable level of reactivity and enantioselectivity, this catalyst could be recovered easily in almost quantitative yield by the use of silica-gel column chromatography.

Belokon et al. have developed a new substrate/catalyst pair for the efficient and simple asymmetric synthesis of a broad range of α-amino acids (Scheme 8).[19] Complex **37**,



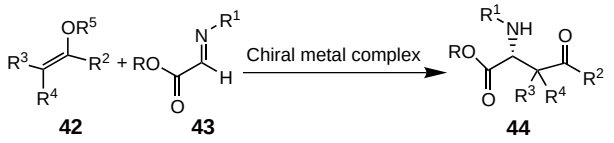
Scheme 8. Asymmetric synthesis of α-amino acids by the phase-transfer catalytic alkylation of metal complex **37**.

prepared from the condensation of *N*-(2-benzoylphenyl)pyridine-2-carbamide (**36**) with glycine and $Ni(NO_3)_2$, was employed as a substrate in the asymmetric phase-transfer-catalyst alkylation reactions to prepare the desired α-amino acids **40**. With activated alkyl halides the reaction gave the alkylated products **39** in good yields and high *ee* values (90–98.5%). Unactivated alkyl halides were less reactive, and relatively low yields of alkylated products were obtained. The role of the primary amino group of the catalyst **38** (nobin: 2-amino-2′-hydroxy-1,1′-binaphthyl) is crucial, since substitution of this group led to a drastic decrease in asymmetric induction.

2.1.2. Glycine α-Cation Equivalents

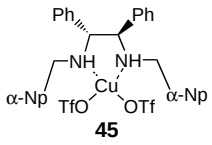
Since Weinreb's ground-breaking research work,[20] the potential utility of α-imino esters for the synthesis of optically active α-amino acids has been recognized, and a number of methods for the catalytic asymmetric addition of a variety of carbon-based nucleophiles to α-imino esters (Mannich-type reaction) have been developed.

Sodeoka and co-workers reported the first example of a Pd^{II}-catalyzed asymmetric addition of enol silyl ethers to α-imino esters.[21] The chiral binuclear μ-hydroxo palladium binap complex **41** (binap: 2,2′-bis(diphenylphosphino)-1,1′-binaphthyl) was shown to be effective in the Mannich-type addition of enol silyl ethers **42** to *N*-aryl α-imino esters **43**, and optically active γ-oxo-α-amino esters **44** were obtained with modest to high enantioselectivity (53–90% *ee*; Scheme 9).

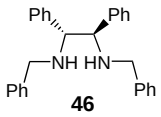


Scheme 9. Asymmetric alkylation of α-imino ester with chiral metal complexes as the catalyst: catalyst **41**, substrate: R^1 = aryl, $R^5 = SiMe_3$ or SiMe; catalyst **45**, substrate R^1 = acyl, $R^5 = SiR'_3$; catalyst **46**·ZnF_2, substrate: $R^1 = NHC(O)Ph$, $R^5 = SiR'_3$.

Kobayashi and co-workers descried catalytic asymmetric Mannich-type reactions of *N*-acylimine esters **43** (R^1 = acyl; Scheme 9) with enolates for the direct formation of *N*-acylated amino acid derivatives **44** by using a chiral Cu^{II} catalyst **45** (OTf = $[CF_3SO_3]^-$).[22a] Silyl enol ethers as well as an alkyl vinyl ether reacted smoothly to afford the desired amino esters in high yields (76–97%) with high enantioselective excess (90–97% *ee*).

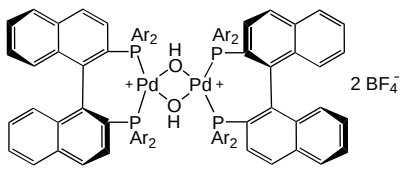


Quite recently, the Kobayashi group also disclosed the catalytic asymmetric alkylation reaction of hydrazono ester **43** (R = NHBz, Bz = benzoyl) with enol silyl ethers **42** using a catalyst formed from ZnF_2 and the chiral diamine ligand **46** in aqueous media (Scheme 9).[22b] The use of water and a small amount of TfOH was essential for the reactions to proceed. Enol silyl ethers **42** derived from aromatic and aliphatic ketones gave the hydrazines **44** (R = NHBz) in good yields (30–91%) with high stereoselection (*syn*/*anti* 9:1–19:1, *syn*: 86–91% *ee*), which were converted into the corresponding amino acids with SmI_2.

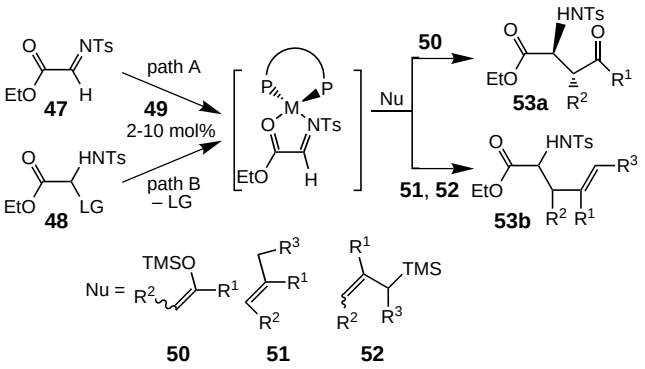


Lectka and co-workers summarized and described their methods for asymmetric alkylation of α-imino esters **47** and *N*,*O*-acetals **48** with enol silyl ethers **50**, alkenes **51**, and allylsilanes **52** using (*R*)-tol-binap/$CuClO_4$ complexes **49** (Scheme 10).[23] A variety of enol silyl ethers **50** were evaluated in the alkylation reaction catalyzed by complex **49** to give γ-oxo-α-amino esters **53a** with high enantioselectivity (up to 99% *ee*) and diastereoselectivity (*anti*:*syn* up to 25:1). In general, aliphatic enol silyl ethers gave slightly lower *ee* values. The same authors also presented the first example of a catalytic enantioselective imino–ene reaction with alkenes **51** and allylsilanes **52** to generate allylic amino esters **53b** in high yields and excellent enantioselectivity. Additionally, they developed a practical, preparative-scale synthesis of α-imino acid derivatives using hydrolytically stable N,O-acetals **48** (Scheme 10, path B) instead of α-imino esters with minimal loss in selectivity or yield.

Johannsen and Jørgensen et al. independently applied the combination of $CuPF_6$ and (*R*)-tol-binap in the addition

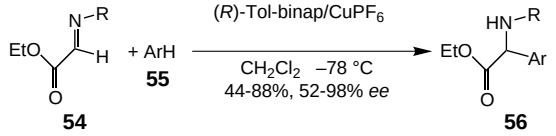


 © 2003 Wiley-VCH Verlag GmbH & Co. KGaA, Weinheim



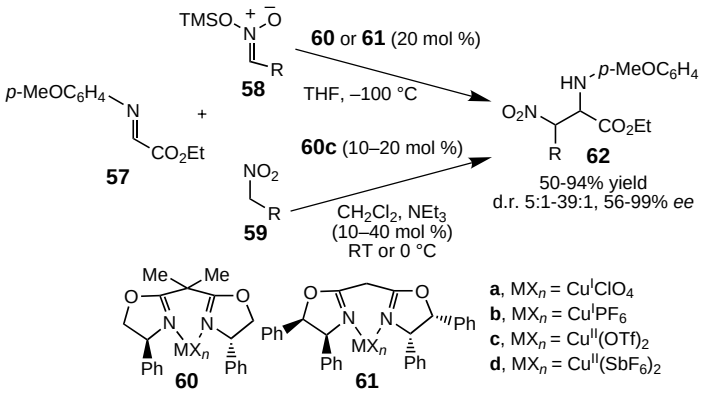
Scheme 10. Asymmetric alkylation of α-imino ester or *N*, *O*-acetal with Cu^{II}-(*R*)-Tol-binap complex **49**; Ts = *p*-toluenesulfonyl, LG = leaving group, TMS = trimethylsilyl.

reaction of imino ester **54** to the electron-rich aromatic compounds **55**. The reaction led to protected optically active α-aryl α-amino acid esters **56** generally in good to high yield, high regioselectivity and enantioselectivity (up to 98% *ee*; Scheme 11).[24] The limitation with this addition reaction is, however, the restriction to electron-rich aromatic compounds.



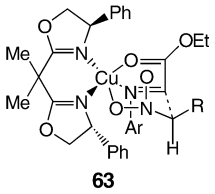
Scheme 11. The catalytic asymmetric arylation of α-imino esters.

Recently, the Jørgensen group developed the catalytic asymmetric nitro-Mannich reactions of α-imino esters **57** with silyl nitronates **58** and nitro compounds **59** in the presence of chiral bisoxazoline Cu^{I} or Cu^{II} complexes (**60**, **61**) to give optically active β-nitro-α-amino esters **62** (Scheme 12), which could be converted into synthetically valuable α, β-diamino acid derivatives.[25] In the catalytic asymmetric addition of silyl nitronates **58** to α-imino esters **57**, the reaction proceeded at −100 °C in the presence of copper–bisoxazoline catalysts **60** or **61**. For nitro compounds **59**, however, the reaction was

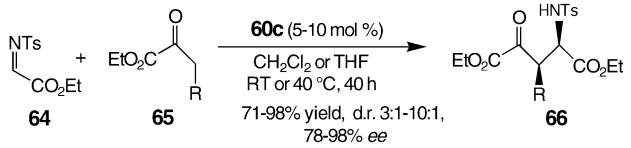


Scheme 12. The catalytic asymmetric alkylation of an α-imino ester with silyl nitronates **58** and nitro compounds **59**.

performed under ambient conditions using triethylamine and catalyst **60c** to give the desired products **62** in good yields and high diastereo- and enantioselectivities. A six-membered cyclic transition state **63** with a pentacoordinate copper center could account for the catalytic activity, diastereo- and enantioselectivity of the reactions.

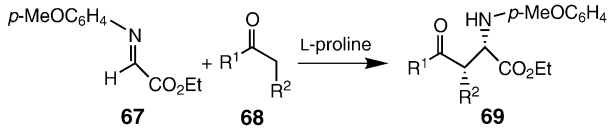


Jørgensen and co-workers also employed **60c** as the catalyst in a simple synthetic transformation of α-imino esters **64** with activated carbonyl compounds **65** to obtain highly functionalized γ-oxo-α-amino acid esters **66** in high yield and diastereoselectivity, and excellent enantioselectivity. (Scheme 13).[26] This new development provides an efficient process for the formation of optically active α-amino acid derivatives by using readily available carbonyl compounds rather than often troublesome enol silyl ethers or silyl ketene acetals.



Scheme 13. The catalytic asymmetric alkylation of α-imino ester **64** with α-keto esters **65**.

Barbas III and co-workers reported L-proline-catalyzed asymmetric Mannich-type reactions of the α-imino ester **67** with a variety of unmodified aldehydes and ketones **68** to provide functionalized α-amino acid esters **69** in moderate to high yields with excellent enantioselectivities (Scheme 14).[27] A number of aliphatic aldehydes **68** ($R^1 = H$) were investigated and high diastereoselectivities were achieved by increasing the bulkiness of the substitutents R^2. For asymmetric ketones, the major diastereomer is formed from regioselective nucleophilic attack at the more substituted α-carbon atom of the ketone. This method is conceptually novel and opens new horizons in synthesis of amino acids.



Scheme 14. L-proline-catalyzed asymmetric Mannich-type reaction of α-imino esters.

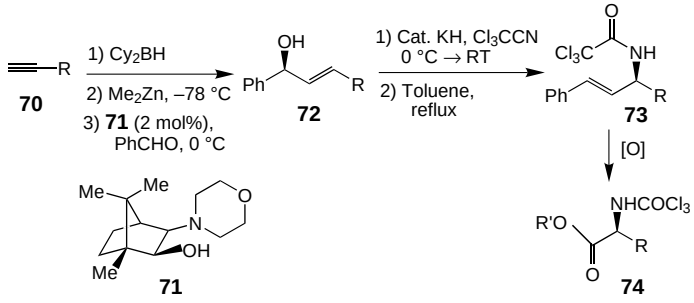
2.2. Catalytic Asymmetric Carbon–Nitrogen Bond-Forming Reactions

2.2.1. Nucleophilic Amination

The generation of α-amino acids by introducing the NH_2 group through the use of nucleophilic aminating reagents is generally based on S_N2 substitutions. Chirality is introduced

 © 2003 Wiley-VCH Verlag GmbH & Co. KGaA, Weinheim

prior to the nucleophilic amination. Versatile intermediates for this purpose are chiral epoxides and chiral α-halo or α-hydroxy carboxylates.[3b] Walsh and co-workers recently disclosed an efficient and highly enantioselective synthesis for protected α-amino acids from terminal alkynes (Scheme 15).[28] Asymmetric vinylation of benzaldehyde with

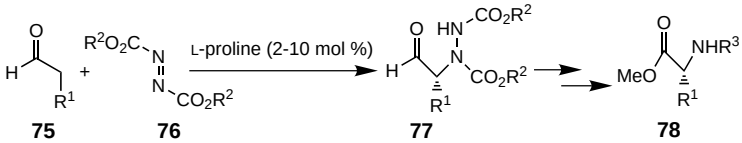


Scheme 15. Catalytic asymmetric synthesis of α-amino acids from terminal alkynes; Cy = cyclohexyl.

terminal alkynes **70** catalyzed by the ligand **71** gave allylic alcohols **72** in high yields (65–94%) and enantioselectivities (88–97% *ee*), which were converted into the protected allylic amines **73** by an Overman [3,3]-sigmatropic rearrangement. Then oxidative cleavage of the allylic amines gave the desired amino acids **74** in good yields (57–92%) without loss of optical purity. An attractive feature of this method is that it provides entry to bulkily substituted nonproteinogenic α-amino acids, such as *tert*-leucine, and (1-adamantyl)glycine (> 99% *ee*).

2.2.2. Electrophilic Amination of Enolates

Asymmetric electrophilic amination of enolates is a relatively uncommon approach to amino acids because of the paucity of electrophilic sources of nitrogen.[3] Evans, Oppolzer, and others have contributed in this area (see ref. [3] and references therein). Recently, the research groups of Jørgensen and List independently reported the L-proline-catalyzed asymmetric α-amination of unmodified aldehydes **75** with azodicarboxylates **76** as the nitrogen source (Scheme 16)[29] to give the corresponding chiral α-aminated



Scheme 16. L-proline-catalyzed asymmetric α-amination of aldehydes.

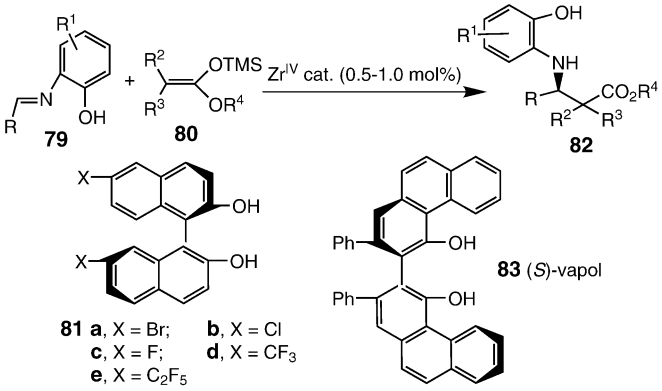
adducts **77** in high yields with excellent enantioselectivities (89–97% *ee*). A very attractive aspect of the α-amination reaction is the easy access that it gives to optically active α-amino acid derivatives **78** through oxidation of the α-aminated adducts.

3. Catalytic Asymmetric Synthesis of β-Amino Acids

Traditional diastereoselective synthesis of β-amino acids has been achieved by using stoichiometric chiral reagents or auxiliaries; however, the number of catalytic asymmetric methods is relatively small.[30] In recent months, several research groups have described many efficient catalytic asymmetric procedures for synthesis of β-amino acids.

3.1. Asymmetric Carbon–Carbon Bond-Forming Reactions

Kobayashi and co-workers reported the first example of catalytic enantioselective Mannich-type reactions of aldimines **79** with silyl enolates **80** using a chiral Zr^{IV} catalyst prepared from $Zr(OtBu)_4$, *N*-methylimidazole, and binol derivatives **81** (binol = 1,1′-binaphth-2-ol) (Scheme 17).[31a] These reactions afforded optically active β-amino acid derivatives **82** in high yields (70–100%) and enantioselectivities (83–98% *ee*). (*E*)-ke-



Scheme 17. Reactions of aldimines **79** with silyl enolates **80** with Zr^{IV} catalysts.

tene silyl acetal **80** (R^1 = *o*-Me, R^2 = H, R^3 = Me, R^4 = Ph) was employed and the *anti* product was preferred to the *syn* product in *anti*:*syn* ratios of up to 98:2, the optimized enantioselectivities obtained was *anti* 96% *ee*.[31b] The key elements responsible for the high yields, selectivities, and turnover of the catalysts were the presence of N-substituted hydroxyphenyl moiety at the aldimine groups and the electron-withdrawing groups at the 6,6′-positions of the binol ligands **81**. With this catalytic system, aldimines derived from aliphatic aldehydes generally gave lower yields (45–65%) and enantioselectivities (80–83% *ee*). It was also found that enantioselectivities were often temperature dependent: The asymmetric induction dropped for the bromine-substituted catalyst **81a** when the temperature was raised from −45 °C to room temperature.

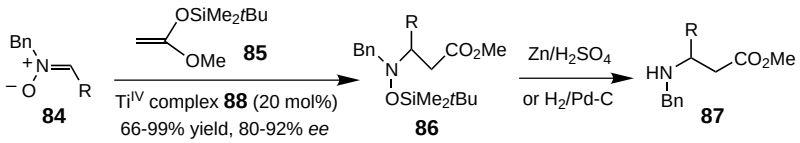
The same research group developed an air-stable, storable, and chiral zirconium catalyst with powdered molecular sieves as a support material (ZrMS) for asymmetric Mannich-type reactions.[31c] This catalyst was prepared from Zr(O*t*-

 © 2003 Wiley-VCH Verlag GmbH & Co. KGaA, Weinheim

Bu)$_4$, (*R*)-6,6′-C_2F_5-binol (**81e**), *N*-methylimidazole, and powdered 5-Å molecular sieve (MS) in benzene at 80 °C for 2 h.[31c] ZrMS was successfully applied to Mannich-type reactions by using various imines derived from not only aromatic and heterocyclic but also aliphatic aldehydes. The desired products were obtained in high yields (60–100 %) with high enantiomeric excess (85–96 % *ee*).

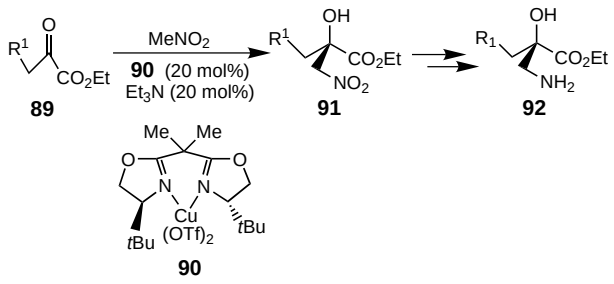
The Wulff group developed the chiral vapol (**83**; vapol = vaulted biphenanthrol) derived zirconium catalyst for the Mannich-type reactions.[32] It was quite striking to observe that the asymmetric induction with aldimines **79** (R = Ar) with this catalyst showed no temperature dependence over the range −45 to 40 °C. The aldimines **79** underwent catalytic asymmetric aldol reactions to give β-amino esters **82** in high yields (83–100 %) and excellent enantioselectivities (86–99.8 % *ee*). The origin of excellent induction was attributed to the presence of a methyl group *ortho* to the phenol hydroxy function. However, both Kobayashi and Wulff et al. found that suitable substrates were limited to aldimines.

Murahashi and co-workers disclosed the catalytic asymmetric synthesis of optically active β-amino acid derivatives **86** and **87** from benzyl nitrones **84** and silyl enolates **85** in high yields and enantioselectivities (Scheme 18).[33] The condensation reaction was catalyzed by a chiral Ti^{IV} complex **88**, which was prepared from Ti(O*i*Pr)$_4$, (*S*)-binol, and 4-*tert*-butylcatechol. The addition of 4-*tert*-butylcatechol was found to have a dramatic and beneficial effect on the activity and stereoselectivity of the reaction.



Scheme 18. Reactions of nitrones **84** with silyl enolates **85** in the presence of a Ti^{IV} complex; Bn = benzyl.

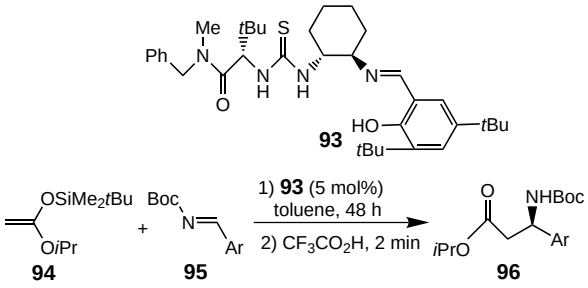
Jørgensen and co-workers developed a catalytic asymmetric Henry reaction of α-keto esters **89** with nitromethane in the presence of Brønsted base using a chiral Lewis acid as the catalyst (Scheme 19).[25c,34] The chiral Lewis acid/Brønsted base ratio was very crucial to the outcome of the reaction. It was demonstrated that equimolar amounts of Cu^{II} complex **90** and Et_3N constituted the best catalytic system in terms of yield and enantioselectivity. The reaction gave optically active



Scheme 19. Reactions of the α-keto esters **89** with nitromethane in the presence of a Cu^{II} catalyst.

β-nitro-α-hydroxy esters **91** in good to high yields (46–99 %) and enantioselectivities (57–94 % *ee*), which could be converted into β-amino-α-hydroxy esters **92** in high yields and without loss of optical purity.

More recently, Jacobsen and Wenzel described a highly efficient route to β-amino acid esters in which they utilized chiral organic-molecule catalyst **93** in the addition of silyl enolates **94** to *N*-*tert*-butoxycarbonyl aldimines **95** (Scheme 20).[35] Aldimines **95**, derived from aromatic aldehydes, gave products **96** in high yields (84–99 %) with high enantiomeric excess (86–98 % *ee*). This method is particularly suited for the highly enantioselective synthesis of thienyl-, furyl-, pyridyl-, and quinolinyl-substituted β-amino propionic esters. However, the successful use of aliphatic aldehyde derivatives in this addition reaction was not reported.



Scheme 20. Reactions of the imines **95** with silyl enolates **94** by using the chiral thiourea catalyst **93**; Boc = *tert*-butoxycarbonyl.

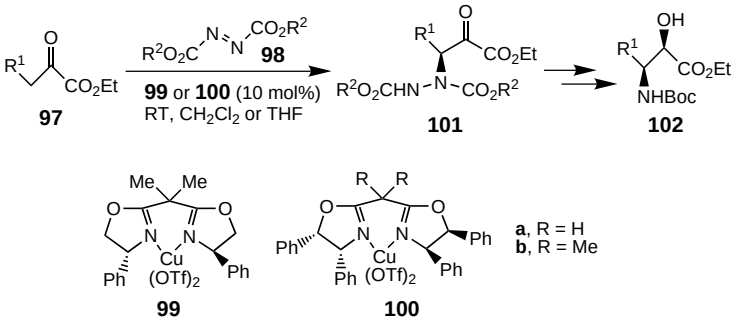
3.2. Asymmetric Carbon–Nitrogen Bond-Forming Reactions

As carbon–nitrogen bond-forming reactions go, the enantioselective aza Michael addition of azide and *O*-benzylhydroxylamino to α,β-unsaturated amides is one of the simplest and most direct approaches to β-amino acid derivatives. The groups of Sibi and Jacobsen among others have contributed to this area.[36] A catalytic asymmetric acyl halide/aldehyde cyclocondensation/amine ring-opening sequence was reported by Nelson's research group as an additional strategy for enantioselective β-amino acid synthesis.[36]

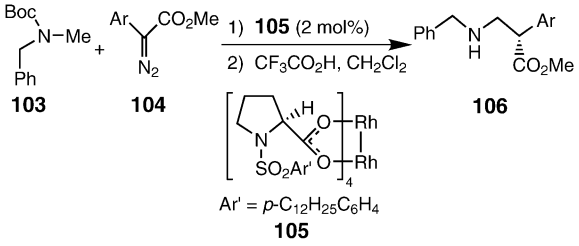
Jørgensen and Juhl presented a catalytic asymmetric α-amination reaction of α-keto esters **97** with commercially available azodicarboxylates **98** (Scheme 21).[37] The reactions catalyzed by chiral bioxazoline Cu^{II} complexes **99** and **100** gave the adducts **101** in moderate to good yields (29–78 %) with high enantioselectivites (70–96 % *ee*). The adducts **101** could be readily converted into optically active *syn*-β-amino-α-hydroxy acid esters **102**. Being able to use activated carbonyl compounds rather than often troublesome silyl enolates in this reaction is an advantage.

Somewhat later, a very interesting publication by Davies and Venkataramani described the Rh^{II}-catalyzed asymmetric synthesis of substituted β-amino acids (Scheme 22).[38] The

 © 2003 Wiley-VCH Verlag GmbH & Co. KGaA, Weinheim



Scheme 21. Reactions of α-keto esters with azodicarboxylates by using Cu^{II} catalysts.

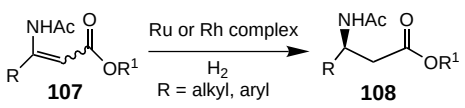


Scheme 22. Rh^{II}-catalyzed asymmetric synthesis of substituted β-amino acids.

reaction is an asymmetric C–H activation of *N*-Boc-protected methylamine **103** by means of a $[Rh_2\{(S)\text{-dosp}\}_4]$ (**105**; dosp = *N*-[(*p*-dodecylphenyl)sulfonyl]prolinate) induced C–H insertion. The intermolecular insertion into a C–H bond of **103** is a general process; various substituted aryl diazoacetates **104** can be used in this reaction to give the corresponding products **106**, with good yields (55–67%) and high enantioselectivities (87–96% *ee*), which are readily converted into useful amino acids and peptides.

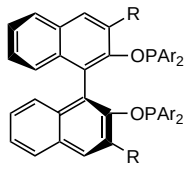
3.3. Asymmetric Hydrogenation of β-Aminoacrylic Acid Derivatives

Catalytic asymmetric hydrogenation of β-aminoacrylic acid derivatives **107** (Scheme 23) is the simplest and most straightforward way to β-amino acids. However, the previous trials of this reaction gave only moderate to good enantioselectivity.[39] The crucial problem is the different behaviors of *Z* and *E* isomeric substrates under catalysis. While good to excellent enantioselectivities have been reported for the ruthenium- or rhodium-catalyzed hydrogenation of the *E* isomer of β-aminoacrylic acid derivatives **107** by using chiral bisphosphane ligands, the results of hydrogenation of *Z* isomers are less than satisfying.

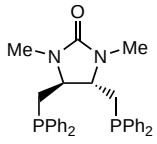


Scheme 23. Asymmetric hydrogenation of β-aryl-substituted β-(acylamino)acrylates **107** with Ru^{II} or Rh^{I} catalysts.

A remarkable study of the Ru^{II}-catalyzed asymmetric hydrogenation was published by Zhang and co-workers at the beginning of this year (Scheme 23).[40] The reaction was carried out in EtOH with 2 mol% $[\{(p\text{-Cymene})RuCl_2\}_2]$ and 4.2 mol% ligands **109**. A variety of β-aryl-substituted β-(acylamino)acrylates **107** were employed as substrates for the ruthenium-catalyzed hydrogenation reaction. High enantiomeric excesses (96–99% *ee*) were achieved with the exception of the *o*-methoxyl substituted enamide (80% *ee*). It is noteworthy that this catalytic system could tolerate an *E*/*Z* mixture of substrates. However, the catalytic efficiencies were relatively low (less than 100 turnovers).

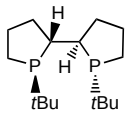


109a R = 3,5-$Me_2C_6H_3$, Ar = Ph
b R = Ph, Ar = 3,5-$Me_2C_6H_3$



110

Lee and Zhang have developed Rh^{I} complexes of the 1,4-bisphosphane ligand **110** as effective catalysts for the asymmetric hydrogenations of the *E* and *Z* isomers of β-aminoacrylic acid derivatives **107**. With these catalysts the conversion of the *Z* isomers exhibits the same or even higher *ee* values than the corresponding *E* isomers.[41] The catalytic system is also effective for the hydrogenation of a 1:1 *E*/*Z* mixture (89–95% *ee*). Quite recently, Zhang and Tang reported an efficient Rh^{I}-catalyzed system with the electron-rich bisphosphane ligand **111** for hydrogenation of *E*/*Z* mixtures of both β-alkyl and β-aryl β-(acylamino)acrylates.[42] Excellent enantioselectivities (92–99.6% *ee*) and high turnover number (TON 1000) have been obtained. Under these conditions, a variety of chiral β-alkyl and β-aryl β-amino acids can be efficiently synthesized. These findings open up the practical hydrogenation of *E*/*Z* substrate mixtures.



111

4. Summary and Outlook

All the publications discussed in this article indicate that catalytic asymmetric synthesis of various α- and β-amino acids is still under investigation. Several methods seem to be impressive and promising. In addition, the enantioselective organocatalysis, in which the reaction is mediated by a catalytic amount of a chiral organic molecule, is becoming a powerful tool for the synthesis of α- and β-amino acids. Despite these new developments, there is still a great demand for new processes and for the optimization of the known ones, since they do not always meet the requirements of modern

 © 2003 Wiley-VCH Verlag GmbH & Co. KGaA, Weinheim

synthetic organic chemistry. What is more, the industrial application of these methods to the large-scale production of optically active α- and β-amino acids is the ultimate goal of these investigations.

Received: October 11, 2002 [M1600]

[1] For α-amino acids: a) G. C. Barrett, *Chemistry and Biochemistry of the Amino Acids*, Chapman and Hall, London, **1985**; b) J. H. Jones, *Amino Acids and Peptides, Vol. 23*, The Royal Society of Chemistry, London, **1992** (Specialist Periodical Report). For β-amino acids: c) "The Chemistry and Biology of β-Amino Acids": (Ed: W. J. Hoekstra), *Curr. Med. Chem.* **1999**, *6*, 905 – 1004; d) C. A. Bewley, D. J. Faulkner, *Angew. Chem.* **1998**, *110*, 2280 – 2297; *Angew. Chem. Int. Ed.* **1998**, *37*, 2162 – 2178; e) A. H. Berks, *Tetrahedron* **1996**, *52*, 331 – 375.

[2] J. Seyden-Penne, *Chiral Auxiliaries and Ligands in Asymmetric Synthesis*, Wiley, New York, **1995**.

[3] Reviews: a) R. M. Williams, *Synthesis of Optically Active α-Amino Acids*, Pergamon, Oxford, **1989**; b) R. O. Duthaler, *Tetrahedron* **1994**, *50*, 1539 – 1650; c) L. S. Hegedus, *Acc. Chem. Res.* **1995**, *28*, 299 – 305; d) T. Wirth, *Angew. Chem.* **1997**, *109*, 235 – 237; *Angew. Chem. Int. Ed. Engl.* **1997**, *36*, 225 – 227; e) C. Cativiela, M. D. Diaz-de-Villegas, *Tetrahedron: Asymmetry* **1998**, *9*, 3517 – 3599; f) C. Cativiela, M. D. Diaz-de-Villegas, *Tetrahedron: Asymmetry* **2000**, *11*, 645 – 732.

[4] L. Yet, *Angew. Chem.* **2001**, *113*, 900 – 902; *Angew. Chem. Int. Ed.* **2001**, *40*, 875 – 877.

[5] a) Highlight: K. Rossen, *Angew. Chem.* **2001**, *113*, 4747 – 4749; *Angew. Chem. Int. Ed.* **2001**, *40*, 4611 – 4613; b) Review: R. Noyori, T. Ohkuma, *Angew. Chem.* **2001**, *113*, 41 – 75; *Angew. Chem. Int. Ed.* **2001**, *40*, 40 – 73; c) M. J. Burk, *Acc. Chem. Res.* **2000**, *33*, 363 – 372.

[6] T. D. Weiß, G. Helmchen, U. Kazmaier, *Chem. Commun.* **2002**, 1270 – 1271.

[7] a) B. M. Trost, K. Dogra, *J. Am. Chem. Soc.* **2002**, *124*, 7256 – 7257; b) review: B. M. Trost, *Chem. Pharm. Bull.* **2002**, *50*, 1 – 14.

[8] H. Suga, K. Ikai, T. Ibata, *J. Org. Chem.* **1999**, *64*, 7040 – 7047.

[9] D. A. Evans, J. M. Janey, N. Magomedov, J. S. Tedrow, *Angew. Chem.* **2001**, *113*, 1936 – 1940; *Angew. Chem. Int. Ed.* **2001**, *40*, 1884 – 1888.

[10] W. Steglich, G. Höfle, *Tetrahedron Lett.* **1970**, 4727 – 4730.

[11] a) J. C. Ruble, G. C. Fu, *J. Am. Chem. Soc.* **1998**, *120*, 11532 – 11533; b) G. C. Fu, *Acc. Chem. Res.* **2000**, *33*, 412 – 420.

[12] a) M. J. O'Donnell, W. D. Bennett, *J. Am. Chem. Soc.* **1989**, *111*, 2353 – 2355; b) Highlight: A. Nelson, *Angew. Chem.* **1999**, *111*, 1685 – 1687; *Angew. Chem. Int. Ed.* **1999**, *38*, 1583 – 1585.

[13] a) B. Lygo, P. G. Wainwright, *Tetrahedron Lett.* **1997**, *38*, 8595 – 8598; b) B. Lygo, J. Crosby, J. A. Peterson, *Tetrahedron Lett.* **1999**, *40*, 1385 – 1388; c) B. Lygo, *Tetrahedron Lett.* **1999**, *40*, 1389 – 1392.

[14] a) E. J. Corey, F. Xu, M. C. Noe, *J. Am. Chem. Soc.* **1997**, *119*, 12414 – 12415; b) E. J. Corey, Y. Bo, J. Busch-Petersen, *J. Am. Chem. Soc.* **1998**, *120*, 13000 – 13001.

[15] a) S.-s. Jew, B.-s. Jeong, M.-s. Yoo, H. Huh, H.-g. Park, *Chem. Commun.* **2001**, 1244 – 1245; b) H.-g. Park, B.-s. Jeong, M.-s. Yoo, J.-h Lee, M.-k Park, Y.-j Lee, M.-j Kim, S.-s. Jew, *Angew. Chem.* **2002**, *114*, 3162 – 3164; *Angew. Chem. Int. Ed.* **2002**, *41*, 3036 – 3038.

[16] a) T. Ooi, M. Kameda, K. Maruoka, *J. Am. Chem. Soc.* **1999**, *121*, 6519 – 6520; b) T. Ooi, M. Takeuchi, M. Kameda, K. Maruoka, *J. Am. Chem. Soc.* **2000**, *122*, 5228 – 5239.

[17] T. Ooi, Y. Uematsu, M. Kameda, K. Maruoka, *Angew. Chem.* **2002**, *114*, 1621 – 1624; *Angew. Chem. Int. Ed.* **2002**, *41*, 1551 – 1554.

[18] T. Kita, A. Georgieva, Y. Hashimoto, T. Nakata, K. Nagasawa, *Angew. Chem.* **2002**, *114*, 2956 – 2958; *Angew. Chem. Int. Ed.* **2002**, *41*, 2832 – 2834.

[19] Y. N. Belokon, K. A. Kochetkov, T. D. Churkina, N. S. Ikonnikov, O. V. Larionov, S. R. Harutyunyan, Š. Vyskočil, M. North, H. B. Kagan, *Angew. Chem.* **2001**, *113*, 2002 – 2005; *Angew. Chem. Int. Ed.* **2001**, *40*, 1948 – 1951.

[20] S. M. Weinreb, *Top. Curr. Chem.* **1997**, *190*, 131.

[21] E. Hagiwara, A. Fujii, M. Sodeoka, *J. Am. Chem. Soc.* **1998**, *120*, 2474 – 2475.

[22] a) S. Kobayashi, R. Matsubara, H. Kitagawa, *Org. Lett.* **2002**, *4*, 143 – 145; b) S. Kobayashi, T. Hamada, K. Manabe, *J. Am. Chem. Soc.* **2002**, *124*, 5640 – 5641.

[23] D. Ferraris, B. Young, C. Cox, T. Dudding, W. J. D. Lev Ryzhkov III, A. E. Taggi, T. Lectka, *J. Am. Chem. Soc.* **2002**, *124*, 67 – 77, and references therein.

[24] a) M. Johannsen, *Chem. Commun.* **1999**, 2233 – 2234; b) S. Saaby, X. Fang, N. Gathergood, K. A. Jørgensen, *Angew. Chem.* **2000**, *112*, 4280 – 4282; *Angew. Chem. Int. Ed.* **2000**, *39*, 4114 – 4116; c) S. Saaby, P. Bayón, P. S. Aburel, K. A. Jørgensen, *J. Org. Chem.* **2002**, *67*, 4352 – 4361.

[25] a) K. R. Knudsen, T. Risgaard, N. Nishiwaki, K. V. Gothelf, K. A. Jørgensen, *J. Am. Chem. Soc.* **2001**, *123*, 5843 – 5844; b) N. Nishiwaki, K. R. Knudsen, K. V. Gothelf, K. A. Jørgensen, *Angew. Chem.* **2001**, *113*, 3080 – 3083; *Angew. Chem. Int. Ed.* **2001**, *40*, 2992 – 2995; c) Highlight: B. Westermann, *Angew. Chem.* **2003**, *115*, 161 – 163; *Angew. Chem. Int. Ed.* **2003**, *42*, 151 – 153.

[26] K. Juhl, N. Gathergood, K. A. Jørgensen, *Angew. Chem.* **2001**, *113*, 3083 – 3085; *Angew. Chem. Int. Ed.* **2001**, *40*, 2995 – 2997.

[27] a) A. Córdova, W. Notz, G. Zhong, J. M. Betancort, C. F. Barbas III, *J. Am. Chem. Soc.* **2002**, *124*, 1842 – 1843; b) A. Córdova, S. Watanabe, F. Tanaka, W. Notz, C. F. Barbas III, *J. Am. Chem. Soc.* **2002**, *124*, 1866 – 1867.

[28] Y. K. Chen, A. E. Lurain, P. J. Walsh, *J. Am. Chem. Soc.* **2002**, *124*, 12225 – 12231.

[29] a) A. Bøgevig, K. Huhl, N. Kumaragurubaran, W. Zhang, K. A. Jørgensen, *Angew. Chem.* **2002**, *114*, 1868 – 1871; *Angew. Chem. Int. Ed.* **2002**, *41*, 1790 – 1793; b) B. List, *J. Am. Chem. Soc.* **2002**, *124*, 5656 – 5657.

[30] a) E. Juaristi, *Enantioselectivie Synthesis of β-Amino Acids*, Wiley-VCH, New York, **1997**; b) S. Kobayashi, H. Ishitani, *Chem. Rev.* **1999**, *99*, 1069 – 1094; c) H. Ishitani, M. Ueno, S. Kobayashi, *J. Am. Chem. Soc.* **1997**, *119*, 7153 – 7154; d) M. P. Sibi, J. J. Shay, M. Liu, C. P. Jasperse, *J. Am. Chem. Soc.* **1998**, *120*, 6615 – 6616; e) J. K. Myers, E. N. Jacobsen, *J. Am. Chem. Soc.* **1999**, *121*, 8959 – 8960.

[31] a) H. Ishitani, M. Ueno, S. Kobayashi, *J. Am. Chem. Soc.* **2000**, *122*, 8180 – 8186; b) S. Kobayashi, J. Kobayashi, H. Ishitani, M. Ueno, *Chem. Eur. J.* **2002**, *8*, 4185 – 4190; c) M. Ueno, H. Ishitani, S. Kobayashi, *Org. Lett.* **2002**, *4*, 3395 – 3397.

[32] S. Xue, S. Yu, Y. Deng, W. D. Wulff, *Angew. Chem.* **2001**, *113*, 2331 – 2334; *Angew. Chem. Int. Ed.* **2001**, *40*, 2271 – 2274.

[33] S.-i. Murahashi, Y. Imada, T. Kawakami, K. Harada, Y. Yonemushi, N. Tomita, *J. Am. Chem. Soc.* **2002**, *124*, 2888 – 2889.

[34] a) C. Christensen, K. Juhl, K. A. Jørgensen, *Chem. Commun.* **2001**, 2222 – 2225; b) C. Christensen, K. Juhl, R. G. Hazell, K. A. Jørgensen, *J. Org. Chem.* **2002**, *67*, 4875 – 4881.

[35] A. G. Wenzel, E. N. Jacobsen, *J. Am. Chem. Soc.* **2002**, *124*, 12964 – 12965.

[36] Highlight on the enantioselective synthesis of β-lactams: P. A. Magriotis, *Angew. Chem.* **2001**, *113*, 4507 – 4509; *Angew. Chem. Int. Ed.* **2001**, *40*, 4377 – 4379, and references therein.

[37] K. Juhl, K. A. Jørgensen, *J. Am. Chem. Soc.* **2002**, *124*, 2420 – 2421.

[38] H. M. L. Davies, C. Venkataramani, *Angew. Chem.* **2002**, *114*, 2301 – 2303; *Angew. Chem. Int. Ed.* **2002**, *41*, 2197 – 2199.

 © 2003 Wiley-VCH Verlag GmbH & Co. KGaA, Weinheim

[39] a) W. D. Lubell, M. Kitamura, R. Noyori, *Tetrahedron: Asymmetry* **1991**, *2*, 543 – 554; b) G. Zhu, Z. Chen, X. Zhang, *J. Org. Chem.* **1999**, *64*, 6907 – 6910; c) M. Yasutake, I. D. Gridnev, N. Higashi, T. Imamoto, *Org. Lett.* **2001**, *3*, 1701 – 1704; d) D. Heller, J. Holz, H.-J. Drexler, H.-P. Krimmer, A. Börner, *J. Org. Chem.* **2001**, *66*, 6816 – 6817.

[40] Y.-G. Zhou, W. Tang, W.-B. Wang, W. Li, X. Zhang, *J. Am. Chem. Soc.* **2002**, *124*, 4952 – 4953.

[41] S.-g. Lee, Y. J. Zhang, *Org. Lett.* **2002**, *4*, 2429 – 2431.

[42] a) W. Tang, X. Zhang, *Org. Lett.* **2002**, *4*, 4159 – 4161; see also: b) J. You, H.-J. Drexler, S. Zhang, C. Fischer, D. Heller, *Angew. Chem.* **2003**, *115*, 942 – 945; *Angew. Chem. Int. Ed.* **2003**, *42*, 913 – 916.



 © 2003 Wiley-VCH Verlag GmbH & Co. KGaA, Weinheim

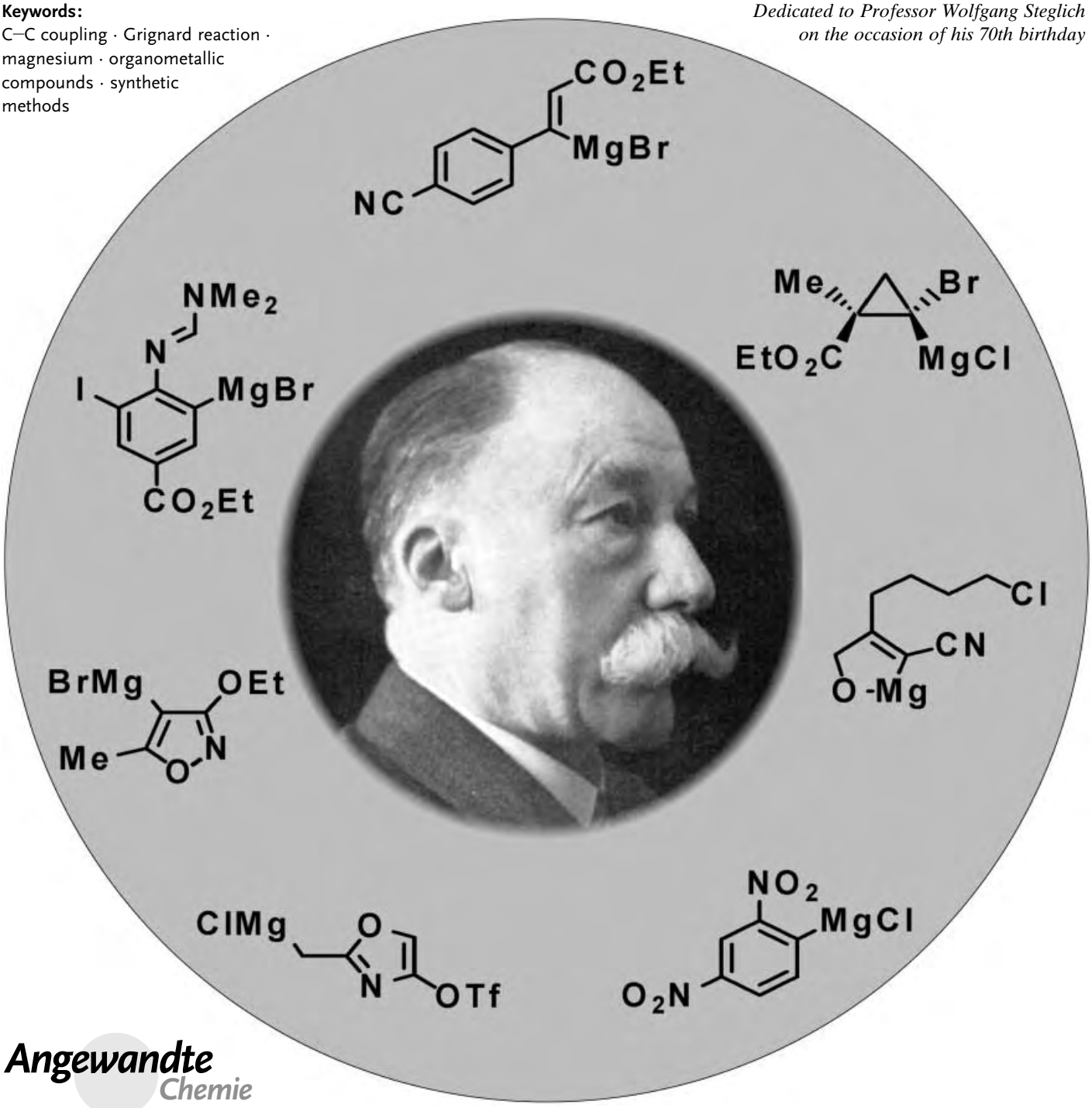
Grignard Reagents in Synthesis

Highly Functionalized Organomagnesium Reagents Prepared through Halogen–Metal Exchange

Paul Knochel, Wolfgang Dohle, Nina Gommermann, Florian F. Kneisel, Felix Kopp, Tobias Korn, Ioannis Sapountzis, and Viet Anh Vu*

Keywords:
C–C coupling · Grignard reaction · magnesium · organometallic compounds · synthetic methods

Dedicated to Professor Wolfgang Steglich on the occasion of his 70th birthday



© 2003 Wiley-VCH Verlag GmbH & Co. KGaA, Weinheim
DOI: 10.1002/anie.200300579

Organomagnesium reagents occupy a central position in synthetic organic and organometallic chemistry. Recently, the halogen–magnesium exchange has considerably extended the range of functionalized Grignard reagents available for synthetic purposes. Functional groups such as esters, nitriles, iodides, imines, or even nitro groups can be present in a wide range of aromatic and heterocyclic organomagnesium reagents. Also various highly functionalized alkenyl magnesium species can be prepared. These recent developments as well as new applications of organomagnesium reagents in cross-coupling reactions and amination reactions will be covered in this Review.

From the Contents

1. Introduction 4303

2. The Halogen–Magnesium Exchange 4303

3. Summary and Outlook 4317

1. Introduction

Access to functionalized organometallic compounds has considerably increased the scope of these nucleophilic reagents in organic synthesis.[1] The presence of sensitive functional groups makes their preparation more complicated, and a number of conventional methods are often not appropriate or not general. The direct oxidative addition of activated metals to organic halides,[2,3] carbometallation,[4] hydrometallation,[5] or selective deprotonation[6] have been used successfully, but generally have limited functional-group tolerance. The halogen–lithium exchange reaction discovered by Wittig et al.[7] and Gilman and co-workers[8] allows the preparation of a broad range of organolithium compounds,[9] although the functional-group tolerance is modest. In contrast, the halogen–magnesium exchange has been found to be the method of choice for preparing new functionalized organomagnesium reagents of considerable synthetic utility.

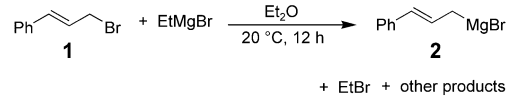
Herein, we wish to give an overview of the dramatic advances in the synthesis of functionalized Grignard reagents and to demonstrate its broad applicability. Organomagnesium reagents were first prepared over 100 years ago by Grignard and still occupy a central place in organic chemistry. Organomagnesium compounds have an excellent reactivity towards a wide range of electrophiles and readily undergo transmetallation to provide a variety of organometallic reagents,[10] particularly organocopper reagents, which react especially well with soft electrophiles and display excellent chemoselectivity.[11]

2. The Halogen–Magnesium Exchange

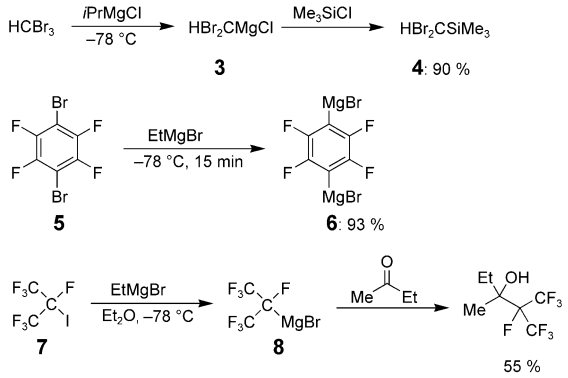
2.1. Early Work

Whereas the direct reaction of magnesium metal with organic halides is the most common method used to prepare organomagnesium compounds, the first example of a bromine–magnesium exchange reaction was briefly reported in 1931 by Prévost.[12] Thus, the reaction of cinnamyl bromide (**1**) with EtMgBr furnished cinnamylmagnesium bromide (**2**), albeit in a moderate yield (Scheme 1).[12]

The halogen–magnesium exchange reaction was the first general approach to magnesium carbenoids.[13] Villiéras and co-workers found that the reaction of *i*PrMgCl with $CHBr_3$ at −78 °C furnished the corresponding magnesium carbenoid **3**, which could be trapped with electrophiles to provide products of type **4** (Scheme 2). This pioneering work opened the way to the systematic study of magnesium carbenoids[14] and demonstrated that the halogen–magnesium exchange rate is enhanced by the presence of electronegative substituents. This behavior was confirmed a few years later by the work of Tamborski and Moore,[15] who found that 1,4-dibromo-2,3,5,6-tetrafluorobenzene (**5**) is readily converted into the corresponding 1,4-dimagnesium species **6** with EtMgBr (Scheme 2). Similarly, Furukawa et al. showed that



Scheme 1. First example of a halogen–magnesium exchange.



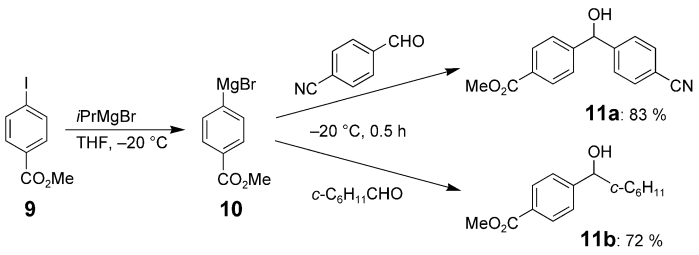
Scheme 2. Bromine–magnesium exchange of polyhalogenated compounds.

[*] Prof. Dr. P. Knochel, Dr. W. Dohle, Dipl.-Chem. N. Gommermann, Dipl.-Chem. F. F. Kneisel, Dipl.-Chem. F. Kopp, Dipl.-Chem. T. Korn, Dipl.-Chem. I. Sapountzis, Dipl.-Chem. V. A. Vu
Department Chemie
Ludwig-Maximilians-Universität München
Butenandtstrasse 5–13, Haus F, 81377 München (Germany)
Fax: (+49) 89-2180-77680
E-mail: paul.knochel@cup.uni-muenchen.de

DOI: 10.1002/anie.200300579
© 2003 Wiley-VCH Verlag GmbH & Co. KGaA, Weinheim

2-iodopyridine leads to the corresponding Grignard reagent within 30 min by the reaction with EtMgBr at 25 °C.[16] Interestingly, perfluoroalkyl iodides such as **7** undergo iodine–magnesium exchange at −78 °C to give the perfluorinated Grignard reagent **8**, which reacts well with carbonyl compounds (Scheme 2).[17]

These early results demonstrate the synthetic potential of the halogen–magnesium exchange reaction.[18] The reactivity of organomagnesium reagents is strongly dependent on the reaction temperature: Only reactive electrophiles such as aldehydes and most ketones react rapidly at temperatures below 0 °C. Thus, performing the halogen–magnesium exchange at temperatures below 0 °C has the potential for the preparation of magnesium organometallic reagents that bear reactive functional groups. Access to functionalized Grignard reagents will considerably expand the current scope of organomagnesium reagents in organic synthesis with the added benefit inherent to bifunctional reagents.



Scheme 3. The reaction of ester-containing aryl magnesium reagents with aldehydes.

2.2. Functionalized Aryl Magnesium Reagents

Functionalized aryl iodides react readily with *i*PrMgBr or *i*PrMgCl in THF below 0 °C, leading to a range of functionalized aryl magnesium iodides.[19] Sensitive carbonyl group derivatives such as nitriles, esters, or amides are tolerated. Typically, treatment of methyl 4-iodobenzoate (**9**) with *i*PrMgBr in THF at −20 °C for 1 h produces the functionalized Grignard reagent **10**, which is stable for several hours below −10 °C, but reacts smoothly with aldehydes at −20 °C leading to the expected alcohols **11a**,**b** in 72 and 83 % yields, respectively (Scheme 3).[20]

Aromatic iodides such as **12** that bear electron-donating groups undergo iodine–magnesium exchange only at higher temperatures (25 °C).[19,21] The addition of the resulting aryl magnesium species to diethyl *N*-Boc-iminomalonate (**13**)[22] furnishes the adduct **14** in 79 % yield. Saponification followed by decarboxylation provides the α-amino acid **15** in 81 % yield (Scheme 4).[21] Whereas aldehyde-containing aryl iodides preferentially react with the aldehyde group during attempted iodine–magnesium exchange, the corresponding imine (**16**) undergoes a smooth exchange reaction, leading to the Grignard reagent **17**. The imino group of **13** is considerably more reactive than that of **16**, which explains the compatibility of the later under the conditions used for forming the magnesium reagent **17**. The addition of $BiCl_3$ followed by purification by silica-gel column chromatography provides the resulting functionalized triarylbismuthane **18** (Scheme 4).[23]



Paul Knochel was born in 1955 in Strasbourg (France). He completed his undergraduate studies at the University of Strasbourg and his PhD at the ETH Zürich with Prof. D. Seebach (1982). He spent 4 years with Prof. J.-F. Normant (Paris) and 1 year with Prof. M. F. Semmelhack (Princeton) as a postdoctoral researcher. After professorships at the University of Michigan (Ann Arbor) and the Philipps-Universität (Marburg), he moved to the Ludwig-Maximilians-Universität (Munich) in 1999. His research interests include the development of new synthetic methods with organometallic reagents, new asymmetric catalysts, and natural product synthesis.



Nina Gommermann was born in Kassel (Germany) in 1978. After undergraduate studies at the Philipps-Universität in Marburg and at the Ludwig-Maximilians-Universität in Munich (1997–2002), she joined Prof. Knochel in 2001 for her diploma thesis and started her PhD in the same group in 2002. Her work is concentrated on enantioselective synthesis.

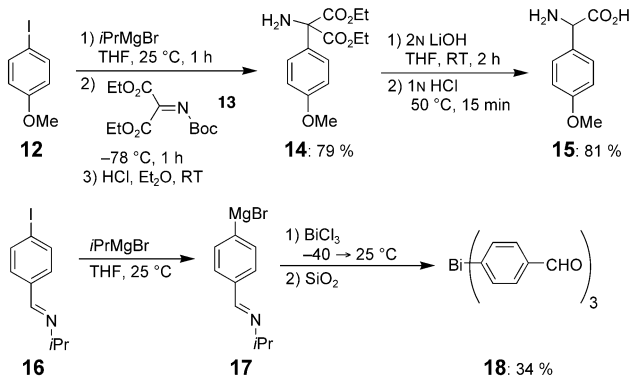


Wolfgang Dohle was born in Winterberg (Germany) in 1970. He completed his undergraduate studies at the Philipps-Universität in Marburg (1992–99). He joined Prof. Knochel in 1998 for his diploma thesis, and moved with him to the Ludwig-Maximilians-Universität in Munich, where he finished his PhD at the end of 2002. His work was focused on functionalized Grignard reagents for the synthesis of heterocycles and transition-metal-catalyzed cross-coupling reactions.



Florian Felix Kneisel was born 1975 in Darmstadt (Germany). He studied chemistry at the Philipps-University of Marburg (Germany) and at the University of Cambridge (UK). He completed his diploma thesis (2000) on macromolecular chemistry under the supervision of Prof. W. Heitz (Philipps-Universität, Marburg). In the same year he began his PhD with Prof. Dr. P. Knochel, dealing with intramolecular cross-coupling reactions, allylic substitutions, and new syntheses of organometallic reagents.

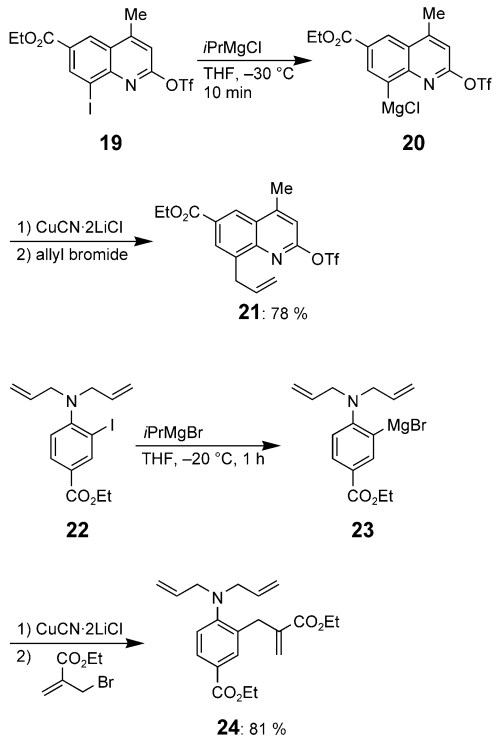
 © 2003 Wiley-VCH Verlag GmbH & Co. KGaA, Weinheim



Scheme 4. Reactivity and compatibility of imine groups within an aryl magnesium reagent. Boc = *tert*-butoxycarbonyl.

A wide range of basic nitrogen functionalities are compatible with the iodine–magnesium exchange. Thus, the functionalized iodoquinoline **19** is converted at −30 °C in 10 min into the corresponding magnesium reagent **20**. Transmetallation with CuCN·2 LiCl[24] and the reaction with allyl bromide furnishes the allylated quinoline **21** in 78% yield (Scheme 5).[25] Similarly, the diallylaniline **22** is allylated via the intermediate Grignard reagent **23**, leading to the functionalized aniline derivative **24** in 81% yield (Scheme 5).[20]

Labile amidine[26] and imine protecting groups are stable to magnesium–halogen exchange and are convenient derivatives for introducing primary amine functions in a molecule. Thus, the diiodoamidine **25** is converted within 5 min at −20 °C into the aryl magnesium species **26**. Remarkably, only one iodine–magnesium exchange reaction takes place. After the first I/Mg exchange the electron density of the aromatic ring increases which hampers a second exchange. Transmetallation of **26** with CuCN·2 LiCl provides the aryl copper derivative **27**, which readily undergoes an addition–elimination reaction with various β-iodocarbonyl compounds such as



Scheme 5. Aryl magnesium compounds containing nitrogen functional groups. Tf = trifluoromethanesulfonyl.



Felix Kopp was born in 1978 in Augsburg (Germany). He studied chemistry at the Ludwig-Maximilians-Universität in Munich and joined Prof. Knochel for his diploma thesis on new amination reactions using functionalized Grignard reagents. He is now working on his PhD in the same group.



Ioannis Sapountzis was born in Pforzheim (Germany) in 1975. After his undergraduate studies at the Ludwig-Maximilians-Universität in Munich (1996–2001), he joined Prof. Knochel for his diploma thesis and started his PhD thesis in the same group in 2001. His work is focused on reactions of nitroarenes and related nitrogen derivatives with organomagnesium reagents as well as the generation of functionalized alkenyl Grignard reagents.



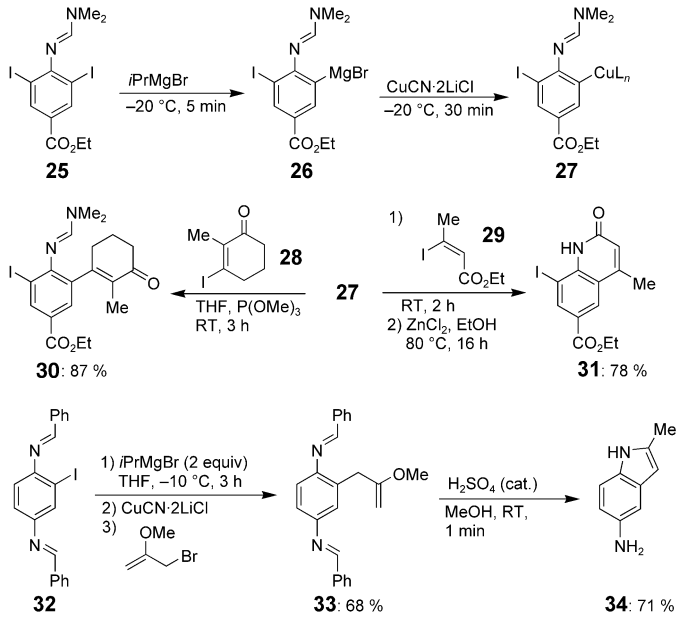
Tobias Korn, born in 1976 in Dachau (Germany), completed his undergraduate studies at the Ludwig-Maximilians Universität in Munich (1997–2002). After his diploma thesis with Prof. Gerhard Hilt, he started his PhD in December 2002 under the supervision of Prof. Knochel. His work is focused on transition-metal-catalyzed cross-coupling reactions.



Viet Anh Vu was born in 1974 in Hanoi (Vietnam). He completed his undergraduate studies at the Ho chi Minh University of Medicine and Pharmacy (Vietnam, 1991–96). After his MSc at the Vrije Universiteit Brussel (Belgium, 1998–2000), he started his PhD with Prof. Knochel in 2000. His work is focused on the preparation of new functionalized organomagnesium compounds.

 © 2003 Wiley-VCH Verlag GmbH & Co. KGaA, Weinheim

28 or **29** to furnish either directly the corresponding α,β-unsaturated carbonyl compound **30**[27] in 87% yield, or, after the removal of the amidine function and cyclization, the heterocycle **31**[28] in 78% yield (Scheme 6). Likewise, the

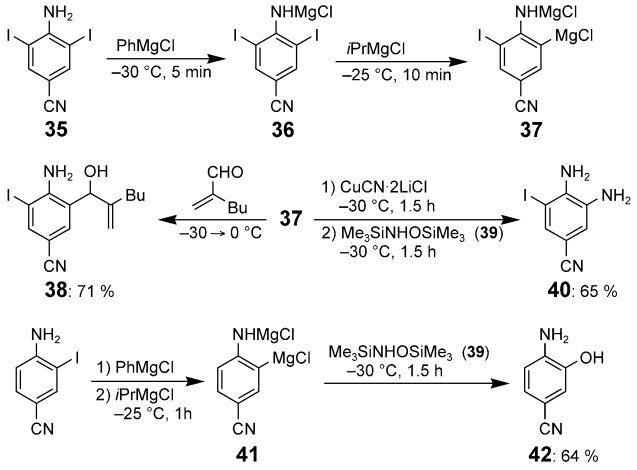


Scheme 6. Preparation of iminoaryl magnesium reagents for the synthesis of heterocycles. $L_n = MgX_2$, LiX.

diimine **32** undergoes an iodine–magnesium exchange with *i*PrMgBr (2 equiv) at −10°C in 3 h. Transmetallation to the copper derivative by treatment with CuCN·2 LiCl[24] and allylation with 2-methoxyallyl bromide gives the diimine **33** in 68% yield. Deprotection of the two amino functions, and of the vinylic ether, with concentrated H_2SO_4 furnishes the indole **34** in 71% yield.[29]

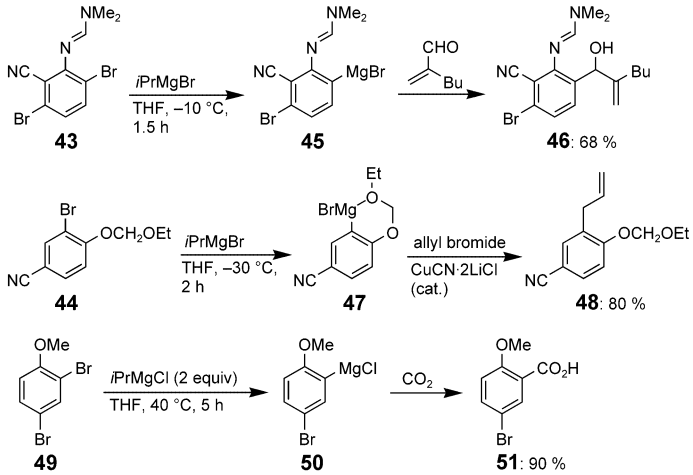
Unprotected functionalized iodoanilines can also be used to prepare Grignard reagents. The successive addition of PhMgCl (−30°C, 10 min) and *i*PrMgCl (−25°C, 10 min) to the diiodoaniline **35** gives, via the magnesium amide **36**, the dimagnesium derivative **37**, which reacts in satisfactory yields with an aldehyde to give the polyfunctionalized benzylic alcohol **38** (Scheme 7).[30] Interestingly, after transmetallation with CuCN·2 LiCl,[24] the resulting copper reagent reacts with *N*,*O*-bis(trimethylsilyl)hydroxylamine (**39**) to afford the diamine **40** in 65% yield. The direct reaction of **39**[31] with an aryl magnesium reagent such as **41** provides the corresponding 2-hydroxyaniline **42** in 64% yield (Scheme 7).[30] Collectively, these I/Mg exchanges demonstrate a versatile preparation of a range of aminated aryl magnesium reagents that is not complicated by the deactivation of magnesium metal in the more standard preparation of aryl magnesium species from aryl halides and magnesium turnings.

The Br/Mg exchange reaction, although slower than I/Mg exchange, is sufficiently fast below 0°C for preparing functionalized aryl magnesium bromides that bear electron-



Scheme 7. Reactions of unprotected aminoaryl magnesium reagents.

withdrawing groups. Therefore, Br/Mg exchange is suitable for the preparation of Grignard reagents that bear sensitive functional groups. The exchange rate depends strongly on the electron density of the aromatic ring. Thus, whereas bromopentafluorobenzene undergoes complete Br/Mg exchange at −78°C within 30 min, 1-bromo-2,4,5-trifluorobenzene requires 1 h at −10°C for a full conversion into the corresponding magnesium reagent.[32] Polyfunctionalized aromatic bromides such as **43**[27] and **44**[32] (Scheme 8) that bear a



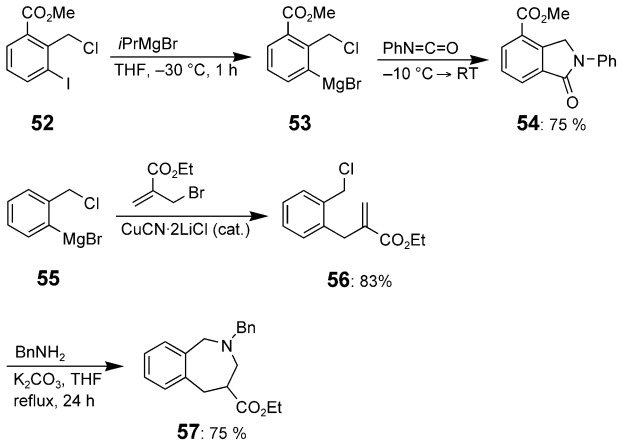
Scheme 8. Br/Mg exchange of functionalized aromatic bromides.

chelating group at the *ortho* position, rapidly undergo Br/Mg exchange. The chelating group complexes *i*PrMgBr prior to the Br/Mg exchange, which facilitates this exchange through an intramolecular reaction. Thus, the dibromide **43** undergoes a chemoselective Br/Mg exchange, leading only to the reagent **45**, in which the MgBr group is *ortho* to the amidine functionality. After the addition to 2-butylacrolein, the expected alcohol **46** is formed in 68% yield.[27] An oxygen chelating functional group such as an ethoxymethyl group in the aryl bromide **44** enhances the Br/Mg exchange rate,

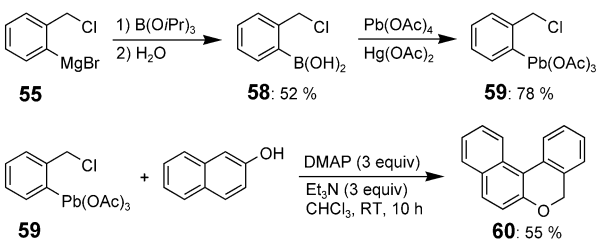
 © 2003 Wiley-VCH Verlag GmbH & Co. KGaA, Weinheim

allowing the preparation of the magnesium derivative **47** at −30 °C within 2 h. In the presence of a catalytic amount of CuCN·2 LiCl (10 mol %), **47** undergoes an allylation with allyl bromide to provide the aromatic nitrile **48** in 80 % yield.[32] Less effective chelating groups such as a methoxy function require higher reaction temperatures. For example, 2,4-dibromoanisole (**49**) is converted into the corresponding aryl magnesium compound **50** by treatment with *i*PrMgCl (2 equiv) in THF at 40 °C for 5 h. After the addition of CO_2, the corresponding carboxylic acid **51** is obtained in 90 % yield (Scheme 8).[18d]

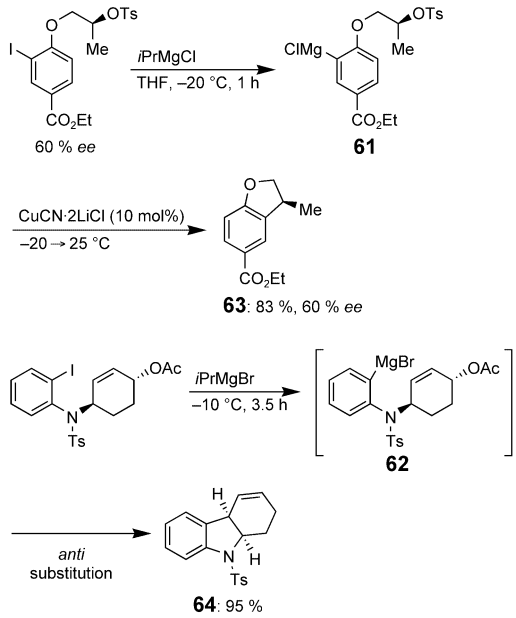
The incorporation of electrophilic functional groups *ortho* to the carbon–magnesium bond allows two sequential alkylations, leading to ring closure (Scheme 9). Treatment of the



Scheme 9. Reaction of chloromethyl-substituted aryl magnesium species.



Scheme 10. Preparation and reaction of chloromethyl-substituted aryl organometallic compounds. DMAP = 4-dimethylaminopyridine.



Scheme 11. Stereoselective ring closure of aryl magnesium intermediates. Ts = *p*-toluenesulfonyl.

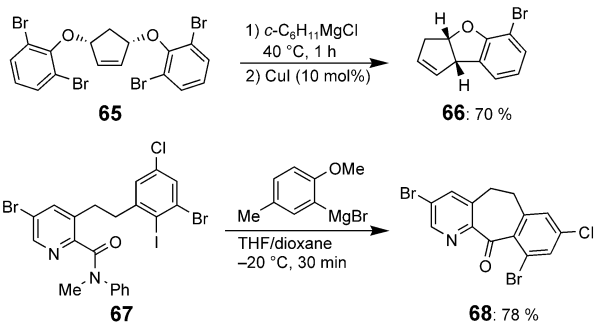
benzylic chloride **52** with *i*PrMgBr in THF (−30 °C, 1 h) furnishes the corresponding Grignard reagent **53**, which reacts at −10 °C with phenyl isocyanate to give the functionalized *N*-phenylphthalimide derivative **54** in 75 % yield.[33] The reaction of the related aryl magnesium species **55** with ethyl 2-(bromomethyl)acrylate[34] furnishes the polyfunctionalized product **56** in 83 % yield. Subsequent treatment of **56** with benzylamine in the presence of K_2CO_3 in refluxing THF provides the benzoazepine **57** in 75 % yield.[33]

In strong contrast to the corresponding lithium reagent, which is stable only at −100 °C,[35] the magnesium species **55** is stable for several hours at −30 °C. The reagent **55** was recently transmetallated to the boronic acid **58** by the reaction with $B(OiPr)_3$ and subsequent hydrolysis. The boronic acid **58** reacted with $Pb(OAc)_4$ to give the lead derivative **59**, allowing an expeditious preparation of **60** in 55 % yield (Scheme 10).[35] Complementary cyclizations can be achieved with functionalized aryl magnesium reagents that bear a more remote leaving group such as a tosylate (e.g. **61**) or an allylic acetate (e.g. **62**). In both cases, a stereoselective substitution reaction was observed (Scheme 11).[36] The S_N2 ring closure of **61** is catalyzed by CuCN·2 LiCl[24] and proceeds with complete inversion of configuration; **63** was obtained without eroding the original 60 % *ee*. An *anti* S_N2' substitution is observed with **62**, providing the *cis*-tetrahydrocarbazole **64** in quantitative yield. In this case, the Grignard reagent undergoes ring closure in the absence of a catalyst.[36]

*i*PrMgCl is the magnesium reagent of choice for the halogen–magnesium exchange. However, in some cases, the use of more (or less) reactive organomagnesium compounds is advantageous. Thus, a Br/Mg exchange reaction between cyclohexylmagnesium chloride and allylic tetrabromo ether **65** at 40 °C with a subsequent copper-catalyzed *syn* S_N2' substitution reaction furnishes the benzofuran derivative **66** in 70 % yield.[18d] In the synthesis of a potent farnesyl protein transferase inhibitor, the polyfunctionalized amide **67** needed to be converted into the tricyclic product **68**. This was achieved through an iodine–magnesium exchange reaction with 2-methoxy 5-methyl-phenylmagnesium bromide in a THF:dioxane mixture. The reaction was complete within 30 min at −20 °C and led to the cyclized product **68** in 78 % yield (Scheme 12).[37]

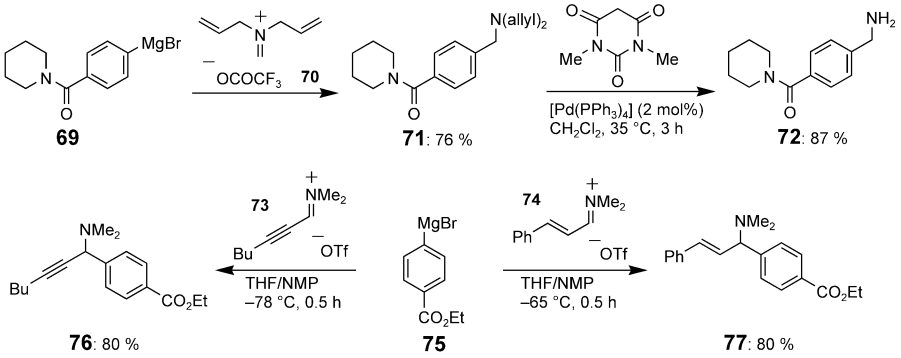
Functionalized aryl magnesium compounds allow direct aminomethylation reactions with various carbonyl compounds. Thus, the Grignard reagent **69** adds to the iminium trifluoroacetate **70** in THF/CH_2Cl_2 at −60 °C within 30 min, providing the diallylamine **71** in 76 % yield. Deallylation by

 © 2003 Wiley-VCH Verlag GmbH & Co. KGaA, Weinheim



Scheme 12. Cyclizations mediated by halogen–magnesium exchange.

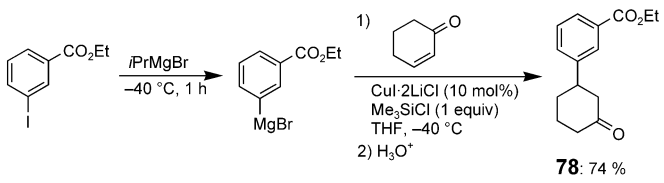
the method of Guibé and co-workers[38] provides the aminomethylation product **72** in 87% yield.[39] Various unsaturated iminium salts such as **73** and **74** react with functionalized aryl magnesium halides, for example, **75**, to furnish the expected benzylic amines **76** and **77**, respectively, in yields of 80% (Scheme 13).[40]



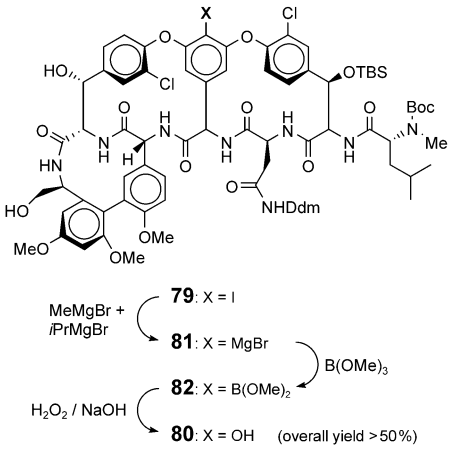
Scheme 13. Reaction of functionalized aryl magnesium compounds with iminium salts. NMP = *N*-methylpyrrolidinone.

In the presence of catalytic amounts of CuI·2 LiCl and Me_3SiCl (1 equiv),[41] functionalized aryl magnesium compounds can be added to various cyclic and acyclic enones, providing Michael-addition products of type **78** (Scheme 14).[42]

The iodine–magnesium exchange can be applied to the synthesis of complex natural products. A selective conversion by Nicolaou and co-workers of the aryl iodide **79** (X = I) into the corresponding phenol **80** (X = OH) was needed in the final steps of the synthesis of the antibiotic vancomycin (Scheme 15).[43] The aryl iodide **79** was converted into the corresponding Grignard reagent **81** by the reaction with a



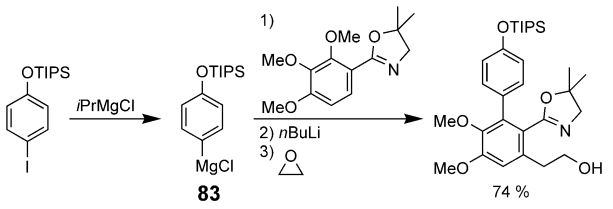
Scheme 14. Cu^I-catalyzed addition of functionalized aryl magnesium compounds to enones.



Scheme 15. Formation of a functionalized aryl magnesium compound during the synthesis of vancomycin. Ddm = 4,4′-dimethoxyphenylmethyl, TBS = *tert*-butyldimethylsilyl.

combination of MeMgBr and *i*PrMgBr (excess) at −40 °C followed by the addition of $B(OMe)_3$, leading to the boronic ester **82**. The reaction of **82** with an alkaline solution of H_2O_2 furnished the desired phenol **80** in approximately 50% overall yield.

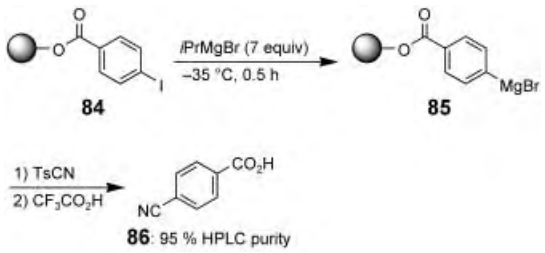
Functionalized aryl magnesium chlorides such as **83**, prepared by I/Mg exchange, readily undergo addition reactions to aryl oxazolines. The addition–elimination of **83** to a trimethoxyaryl oxazoline followed by *ortho* lithiation and substitution with ethylene oxide led to a polyfunctionalized aromatic intermediate that was required in the synthesis of an alkaloid (Scheme 16).[44]



Scheme 16. Formation of a functionalized aryl magnesium compound in the course of the synthesis of an alkaloid. TIPS = triisopropylsilyl.

Polyfunctionalized organomagnesium reagents on a resin can be generated readily by using an iodine– or bromine–magnesium exchange.[19] Various functionalized iodobenzoic acids have been attached to Wang resins through the carboxy group. The immobilized ester **84**, when treated with excess *i*PrMgBr at −30 °C for 15–30 min, generates the corresponding aryl magnesium compound **85** in high yield. It can be quenched successfully with a range of electrophiles and the resulting adduct, for example, 4-cyanobenzoic acid (**86**), is released from the resin by treatment with trifluoroacetic acid (Scheme 17). This method has an excellent generality and the

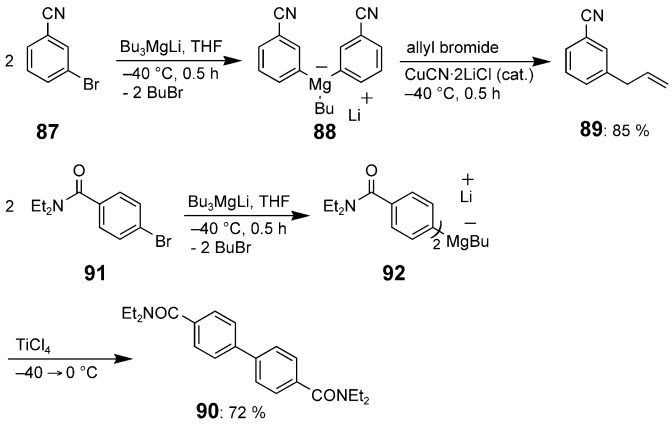
 © 2003 Wiley-VCH Verlag GmbH & Co. KGaA, Weinheim



Scheme 17. Immobilized functionalized aryl magnesium reagents for combinatorial synthesis.

yields and purities (HPLC) of products obtained via immobilized organomagnesium reagents prepared by a halogen–magnesium exchange are usually excellent, thus allowing their application in combinatorial chemistry.[45,46]

Oshima and co-workers have shown that besides alkyl magnesium halides, lithium trialkyl magnesiates (R_3MgLi) readily undergo iodine– or bromine–magnesium exchange reactions.[47,48] Lithium trialkyl magnesiates are prepared by the reaction of an organolithium reagent (RLi; 2 equiv) with an alkyl magnesium halide (RMgX; 1 equiv) in THF at 0 °C. Either 1 or 0.5 equivalents of the lithium magnesiate (Bu_3MgLi), relative to the aromatic halide (X = I or Br), can be used, which shows that two of the three butyl groups undergo the exchange reaction. Thus, the reaction of 3-bromobenzonitrile (**87**) provides the lithium diaryl butylmagnesiate **88**, which is allylated in the presence of CuCN·2 LiCl[24] to give the nitrile **89** in 85 % yield (Scheme 18). The



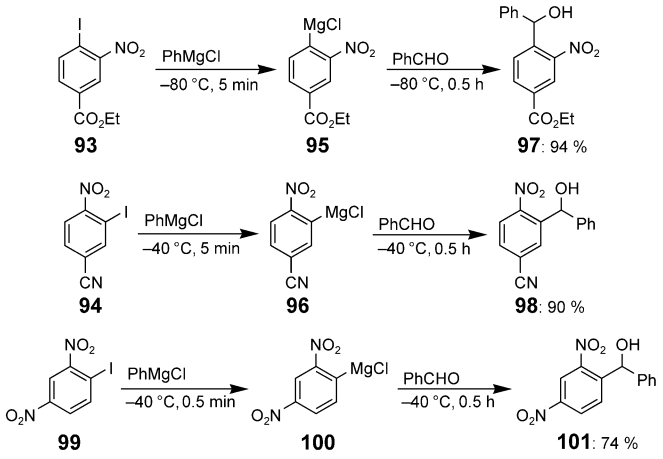
Scheme 18. Br/Mg exchange for the preparation of functionalized aryl magnesium reagents.

exchange reaction with lithium trialkyl magnesiates is generally faster than the halogen–magnesium exchange reaction with *i*PrMgBr and is less sensitive to the electronic density of the aromatic ring. Importantly, trialkyl magnesiates react more rapidly with aryl bromides than does *i*PrMgCl. However, the resulting lithium triorganomagnesiates of type **88** are more sensitive to the presence of electrophilic functional groups and thus exhibit a reactivity that is intermediate between organolithium and organomagnesium species. Therefore the greater reactivity limits the number of functional groups usually tolerated in these exchange reagents. The presence of an extra butyl group in **88** may also complicate the quenching of the reactions owing to competitive reactivity with electrophiles. However, Bu_3MgLi is an excellent reagent for preparing functionalized biaryl compounds of type **90**. Thus, lithium tributylmagnesiate induced bromine–magnesium exchange of the amide **91** provides the magnesiate species **92**, which undergoes a smooth titanium(IV)-mediated homocoupling reaction, leading to the biphenyl derivative **90** in 72 % yield (Scheme 18).[49]

2.3. Reactions of Nitroarene Derivatives with Organomagnesium Reagents

The reaction of nitroarenes with Grignard reagents was first investigated in the pioneering work of Wieland in 1903.[50] Several reactions between nitroaromatic and organometallic compounds were carefully investigated by Bartoli and coworkers.[51] Owing to the high electrophilicity of the nitro functionality, organometallic species can trigger either nucleophilic attack or electron-transfer reactions. However, it has been shown that *ortho*-lithiated nitrobenzene is stable at very low temperature.[52] Interestingly, the corresponding zinc and copper species obtained by transmetallation with zinc(II) or copper(I) salts, exhibit excellent stability and show, under appropriate reaction conditions, no tendency to undergo electron-transfer reactions.[53]

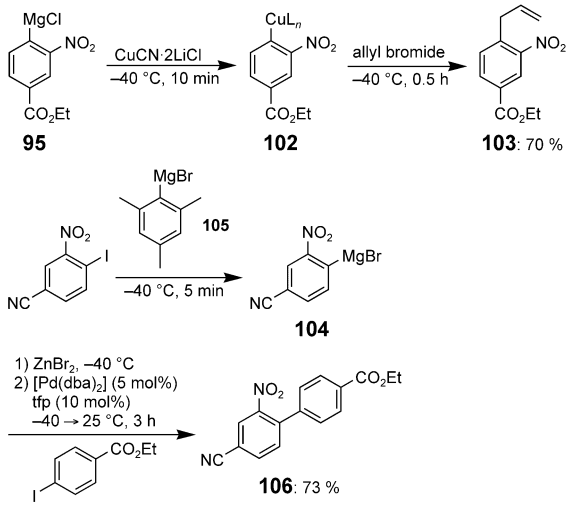
A broad range of functionalized aryl magnesium compounds that bear a nitro function at the *ortho* position can be prepared by iodine–magnesium exchange.[54] Thus, the nitro-substituted aryl iodides **93** and **94** undergo a smooth I/Mg exchange with phenylmagnesium chloride within a few minutes at −80 and −40 °C, respectively, leading to the expected Grignard reagents **95** and **96**. After the addition of benzaldehyde, the benzylic alcohols **97** and **98** are obtained respectively in 94 % and 90 % yields.[54] Even an electron-poor aryl iodide such as the dinitro derivative **99** cleanly provides the corresponding Grignard reagent **100**, which reacts with benzaldehyde to give the benzylic alcohol **101** in 74 % yield (Scheme 19).



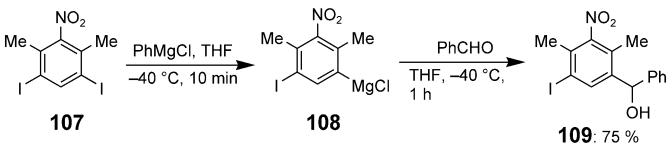
Scheme 19. Preparation of polyfunctionalized aryl magnesium compounds bearing a nitro function.

 © 2003 Wiley-VCH Verlag GmbH & Co. KGaA, Weinheim

Transmetallation of the Grignard reagent **95** with CuCN·2 LiCl[24] furnishes the corresponding copper reagent **102**, which can be trapped by several electrophiles, such as acyl halides or allylic halides, to afford products of type **103** (Scheme 20).[54] These results indicate that, contrary to general belief, single-electron-transfer reactions between nitro groups and organometallic species, especially organomagnesium compounds, is less favorable than the halogen–magnesium exchange reaction. Palladium(0)-catalyzed Negishi cross-coupling[55] can be performed by converting the magnesium reagents into the corresponding zinc reagents. The nitro-substituted aryl magnesium species **104** is best prepared by using the sterically hindered mesitylmagnesium bromide (**105**). Thus, the reaction of the zinc derivative of **104** with ethyl *p*-iodobenzoate (THF, −40 °C→RT, 3 h) in the presence of [Pd(dba)$_2$] (5 mol %) and tri-*o*-furylphosphane (10 mol %)[56] provides the biaryl compound **106** in 73 % yield (Scheme 20).[54] The *ortho* relationship between the carbon–magnesium bond and the nitro function is essential for a clean and fast exchange reaction. *Meta*- and *para*-substituted iodonitroarenes lead to unselective reactions with addition of the organometallic species to the nitro group. The *o*-nitro-substitution pattern facilitates the I/Mg exchange by precomplexation of the Grignard reagent to the nitro function prior to I/Mg exchange. I/Mg exchange of *meta*- and *para*-substituted iodonitroarenes is only possible in cases in which the nitro group is sterically hindered. Thus, the reaction of the diiodonitrobenzene derivative **107** with PhMgCl (THF, −40 °C, 10 min) furnishes the corresponding Grignard compound **108**, that reacts with benzaldehyde to afford the expected benzylic alcohol **109** in 75 % yield (Scheme 21).[57]

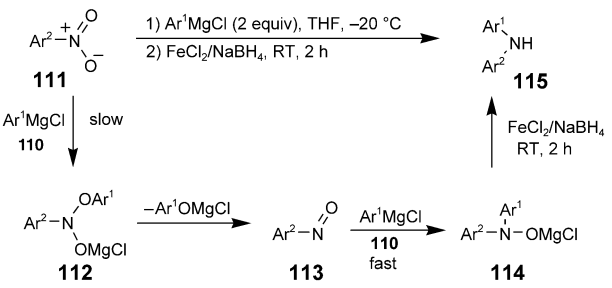


Scheme 20. Transmetallation of nitro-substituted aryl magnesium compounds. dba = Dibenzylideneacetone, tfp = tri-*ortho*-furylphosphane.

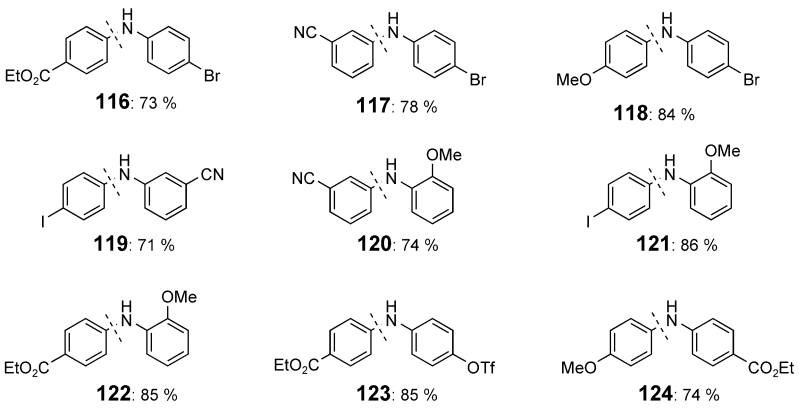


Scheme 21. Preparation of *meta*-nitroaryl magnesium compounds.

In the absence of sterically hindered systems such as **107**, phenylmagnesium chloride reacts with nitroarenes.[50,51] This reaction proceeds according to the mechanism originally proposed by Köbrich and co-workers (Scheme 22).[52a] The aryl magnesium reagent **110** adds first to the oxygen atom of the nitro function of arene **111** to furnish the adduct **112**, which eliminates one equivalent of a magnesium phenolate (Ar^1OMgCl), providing the arylnitroso derivative **113**. The addition of a second equivalent of Ar^1MgCl to **113** furnishes the magnesium salt of a diaryl hydroxylamine **114**. Diaryl hydroxylamines are air-sensitive and difficult to isolate in pure form. To make this reaction of preparative interest, a subsequent reduction with $FeCl_2/NaBH_4$ is required, providing the diaryl amine **115** (Scheme 22).[58] The method allows arylation of nitrobenzene derivatives and therefore is ideal for preparing a range of functionalized diaryl amines such as **116**–**124** (Scheme 23).[59] This reaction complements recently developed palladium(0)-catalyzed amination reactions[60] and



Scheme 22. Mechanism of the reaction of aryl magnesium compounds with nitroarenes leading to diaryl amines.

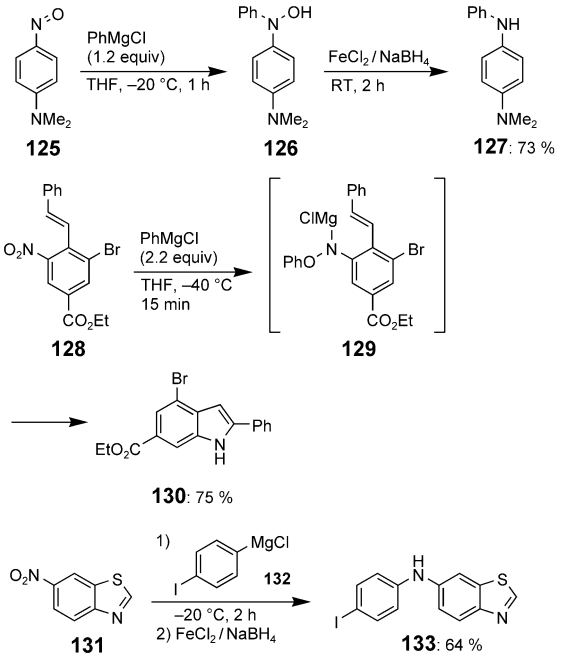


Scheme 23. Polyfunctionalized diaryl amines obtained by the reaction of a functionalized aryl magnesium compound with nitroarenes. The dotted lines indicate the newly formed C–N bond.

 © 2003 Wiley-VCH Verlag GmbH & Co. KGaA, Weinheim

related amination procedures that use a copper(I)[61] or nickel(0)[62] catalysis. As indicated above, the mild reaction conditions are compatible with a range of functional groups.

The Grignard reagent can bear electron-withdrawing groups (**116, 117, 120, 122, 123**) or electron-donating groups (**118, 124**). The same remark is true for the nitroarene. Interestingly, sensitive functions such as an iodine, bromine, or triflate[59] group can be present in either reaction partner, which is normally problematic in transition-metal-catalyzed amination procedures.[60–62] As shown in the mechanistic pathway described in Scheme 22, 2 equivalents of the aryl magnesium compound are required to produce amines of type **115**; 1 equivalent of the aryl magnesium reagent is wasted in the formation of the magnesium phenolate. This can be avoided by using a nitrosoarene instead of a nitroarene as the electrophilic reagent. The reaction of 4-dimethylaminonitrosobenzene (**125**) with PhMgCl (1.2 equiv) provides the expected[63,64] diaryl hydroxylamine **126**, which after reductive treatment ($FeCl_2/NaBH_4$), gives the diaryl amine **127** in 73% yield (Scheme 24). Sterically hindered, electron-poor nitroarenes such as **128** react with PhMgCl to generate an aryl

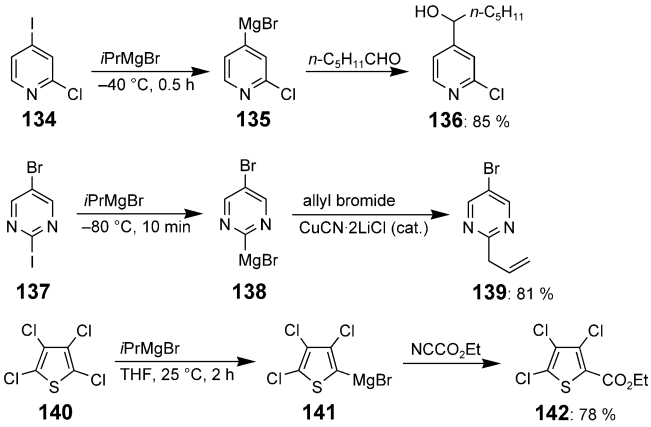


Scheme 24. The reaction of aryl magnesium reagents with nitro- and nitrosoarenes.

nitroso intermediate, which undergoes a reaction at the oxygen atom of the nitroso functional group, providing a magnesium nitrenoid[65] of type **129**. An intramolecular C–H insertion is triggered to give the polyfunctionalized indole **130** in 75% yield.[66] Finally, the reaction of heterocyclic benzothiazoles **131** with functionalized aryl magnesium species **132** provides the functionalized heterocycle **133** in 64% yield (Scheme 24).[59]

2.4. Preparation of Functionalized Heteroaryl Magnesium Reagents

A variety of functionalized heterocyclic Grignard reagents can be prepared by using an iodine– or bromine–magnesium exchange reaction.[32,67] The electronic nature of the heterocycle influences the halogen–magnesium exchange rate: electron-poor heterocycles react faster and electron-withdrawing substituents strongly accelerate the exchange. 2-Chloro-4-iodopyridine (**134**) reacts with *i*PrMgBr at −40 °C within 30 min[32,68] to furnish selectively the magnesium species **135**. The latter species adds to hexanal, leading to the alcohol **136** in 85% yield (Scheme 25). If instead of a

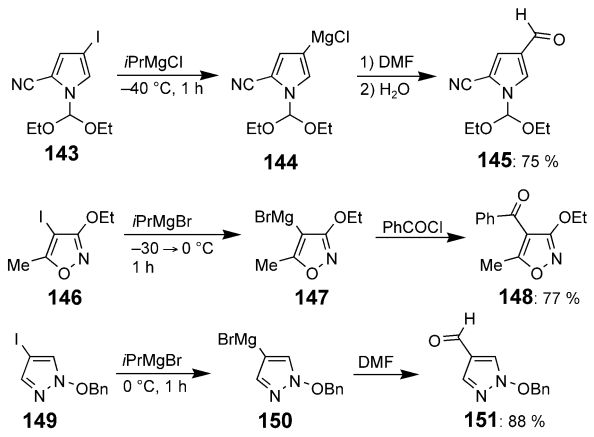


Scheme 25. The rate of the halogen–magnesium exchange reaction is dependent on the nature of the heterocycle.

pyridine, a pyrimidine derivative such as **137** is used, a selective iodine–magnesium exchange occurs at −80 °C within 10 min, providing the organomagnesium compound **138**. The subsequent reaction of **138** with allyl bromide in the presence of CuCN·2 LiCl[24] gives the 2-allylpyrimidine **139** in 81% yield.[32] Although a chlorine–magnesium exchange is a very slow reaction, the presence of four chlorine atoms in tetrachlorothiophene (**140**) accelerates this exchange (25 °C, 2 h), leading to the magnesiated heterocycle **141**, which reacts with ethyl cyanoformate to provide the thienylester **142** in 78% yield (Scheme 25).[32b]

A range of functionalized iodoheterocycles have been magnesiated through an iodine–magnesium exchange, thus allowing a rapid synthesis of polyfunctionalized heterocycles.[69,70] Thus, the protected iodopyrrole **143** undergoes an iodine–magnesium exchange at −40 °C within 1 h, leading to the magnesiated pyrrole **144**, which reacts with DMF to furnish the formyl derivative **145** in 75% yield (Scheme 26).[71] 4-Iodo-3-ethoxy-5-methylisoxazole (**146**) is converted into the corresponding Grignard reagent **147**, which reacts directly with benzoyl chloride to give the ketone **148** in 77% yield.[72] Also 4-iodopyrazoles such as **149** are converted at 0 °C into the intermediate organomagnesium reagent **150**. The subsequent reaction of **150** with DMF furnishes the formylated derivative **151** in 88% yield (Scheme 26).[73]

 © 2003 Wiley-VCH Verlag GmbH & Co. KGaA, Weinheim

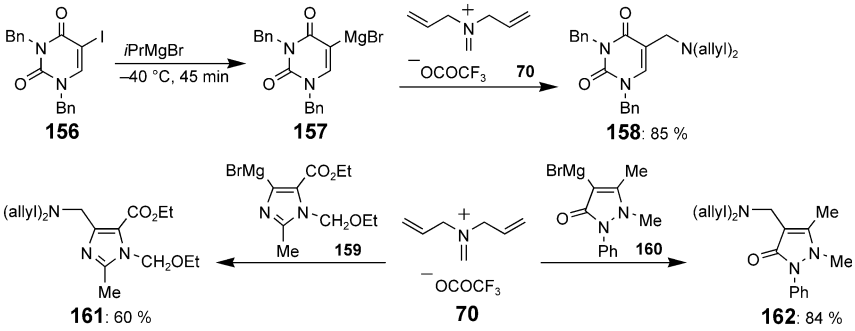


Scheme 26. Magnesiation of five-membered heterocycles. DMF = *N*,*N*-dimethylformamide.

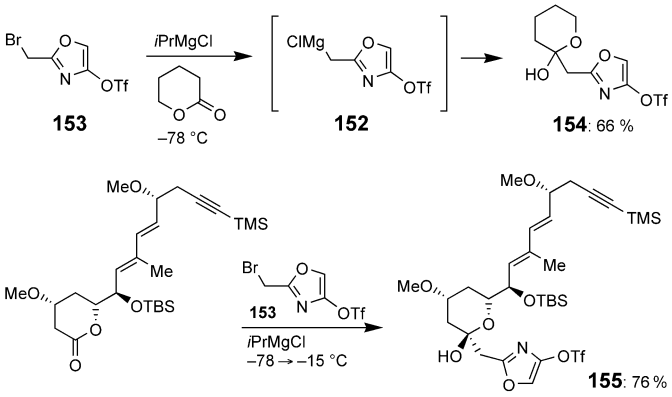
Polyhalogenated substrates usually undergo a single, selective halogen–magnesium exchange (Scheme 29). After the first magnesiation, the electron density of the heterocycle increases to such an extent that a subsequent second exchange is very slow. This very general behavior leads to the high chemoselectivity of the Br/Mg exchange reaction. The first exchange reaction of tribromoimidazole **163**[78] occurs at C2. Copper-catalyzed allylation leads to the 4,5-dibromoimidazole **164** (Scheme 29). Treatment of **164** with a second equivalent of *i*PrMgBr leads to an exchange reaction only at C5, as the intermediate Grignard reagent is stabilized by chelation. After quenching with ethyl cyanoformate (−40 → 25 °C, 2 h), the corresponding 4-bromo-5-carbethoxyimidazole **165** is obtained in 55 % yield (Scheme 29).[32] The presence of chelating groups strongly influences the regioselectivity of the Br/Mg exchange. Thus, the dibromothiazole

Sensitive heterocyclic "benzylic" magnesium species such as **152** are readily obtained by a bromine–magnesium exchange from the bromomethyloxazole **153** (Scheme 27). Grignard reagent **152** is generated at −78 °C in the presence of δ-valerolactone (to minimize self-condensation), leading to the hemiketal **154** in 66 % yield. This reaction was used to prepare advanced building blocks such as **155** for the total synthesis of (+)-phorboxazole A (Scheme 27).[74]

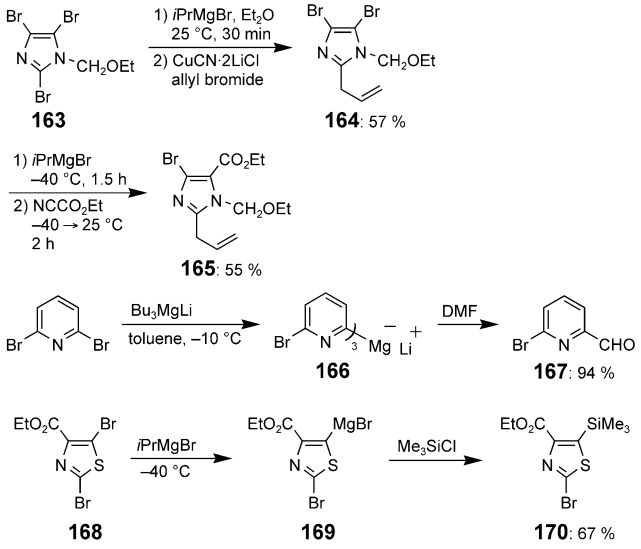
The preparation of functionalized uracils is of interest owing to the potential biological properties of this important class of heterocycles.[75] Starting from various protected 5-iodouracils such as **156**, the addition of *i*PrMgBr (−40 °C, 45 min) leads to the formation of the corresponding magnesium compound **157**, which can be trapped by various aldehydes, ketones, and acid chlorides. The use of the iminium salt **70**[39,40] leads to the diallylaminomethyl product **158** in 85 % yield (Scheme 28).[76] Various magnesiated imidazoles such as **159** or antipyrines such as **160** react with the iminium reagent **70** to afford the diallylaminomethylated products **161** and **162**, respectively, in satisfactory yields.[77]



Scheme 28. Aminomethylation of heterocyclic magnesium reagents.



Scheme 27. Preparation of (+)-phorboxazole A intermediates by using a Br/Mg exchange. TMS = trimethylsilyl.



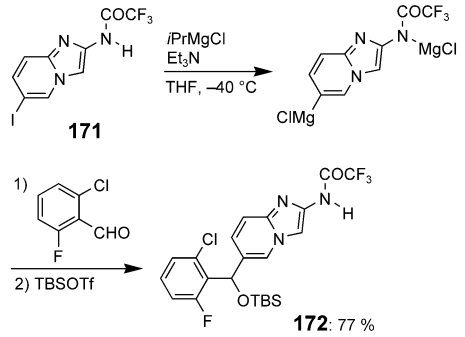
Scheme 29. Regioselective Br/Mg-exchange reactions.

168 undergoes a selective exchange at C5 owing to the chelating effect of the ethoxycarbonyl group, leaving the bromide at C2 unaffected. The reaction of the intermediate Grignard reagent **169** with Me_3SiCl provides the expected product **170** in 67 % yield (Scheme 29).[32b] This selectivity has been used to convert 4,5-diiodoimidazoles into the corre-

 © 2003 Wiley-VCH Verlag GmbH & Co. KGaA, Weinheim

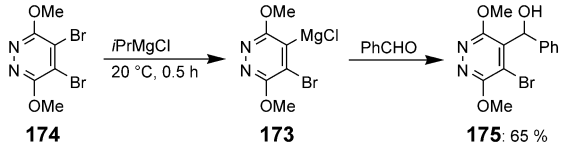
sponding 4-iodoimidazoles by using an I/Mg exchange followed by protonation.[79] Similarly, 2,6-dibromopyridine has been selectively exchanged with *i*PrMgX to generate the monomagnesium species.[32,80] The use of the magnesiate species Bu_3MgLi proves to be advantageous for performing this exchange reaction, leading to the ate complex **166**, which rapidly reacts with DMF to furnish the aldehyde **167** in 94% yield.[81] The use of magnesiate reagents for the preparation of various pyridyl magnesium species generally requires 1 equivalent of $BuMe_2MgLi$.[48]

Imidazo[1,2-*a*]pyridines are potentially a pharmaceutically useful class of heterocycles. The preparation of a range of functionalized 2-aminoimidazo[1,2-*a*]pyridines of type **172** has been realized starting from the heterocyclic iodide **171** and performing an I/Mg exchange at −40 °C (Scheme 30).[82]



Scheme 30. Preparation of imidazo[1,2-*a*]pyridines by using a I/Mg-exchange reaction.

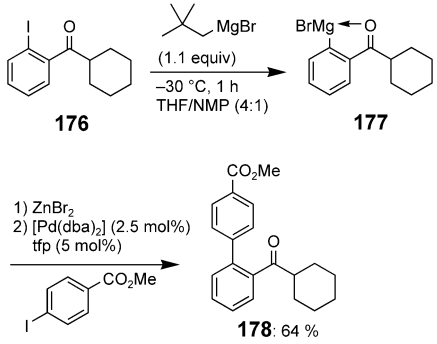
Quéguiner and co-workers have developed reaction conditions that allow the synthesis of magnesiated diazines such as **173**. The addition of *i*PrMgCl to the 4,5-dibromopyridazine **174** at 20 °C furnishes, within 1 h, the heterocyclic magnesium species **173**, which affords a range of new functionalized pyridazines such as **175** after quenching with an electrophile (Scheme 31).[80b]



Scheme 31. Magnesiation of pyridazine derivatives through a Br/Mg-exchange reaction.

Finally, a number of these heterocyclic Grignard reagents can be generated with solid-phase reagents and reacted with typical electrophiles in excellent yield.[19] As numerous heterocyclic bromides are available, this exchange method is anticipated to become a major method for the functionalization of sensitive polyfunctionalized heterocycles. The carbon–magnesium bond possesses a good intrinsic reactivity, which can be enhanced by appropriate transmetallations. The presence of electron-poor substituents attached to the heterocyclic ring somewhat reduces the reactivity of a neighboring carbon–magnesium bond and further improves the functional-group compatibility of this carbon–metal bond.

How far can this functional group tolerance be extended? A keto group usually reacts with a Grignard reagent, even at −70 °C. In fact, *i*PrMgCl reacts with benzophenone to afford the addition product and a large amount of diphenylmethanol, which results from a β-hydrogen reductive transfer. Nevertheless, by tuning the reaction conditions, the preparation of ketone-containing aryl magnesium species can be achieved. To avoid side reactions, a sterically hindered but reactive Grignard reagent was chosen: neopentylmagnesium bromide (NpMgBr)[83] in conjunction with *N*-methylpyrrolidinone (NMP) as a polar cosolvent to increase the rate of the iodine–magnesium exchange. Based on these modifications, 2-iodophenyl cyclohexyl ketone (**176**) reacts with NpMgBr (1.1 equiv) at −30 °C within 1 h in THF/NMP (4:1) to afford the aryl magnesium reagent **177** (Scheme 32). The *ortho*-keto



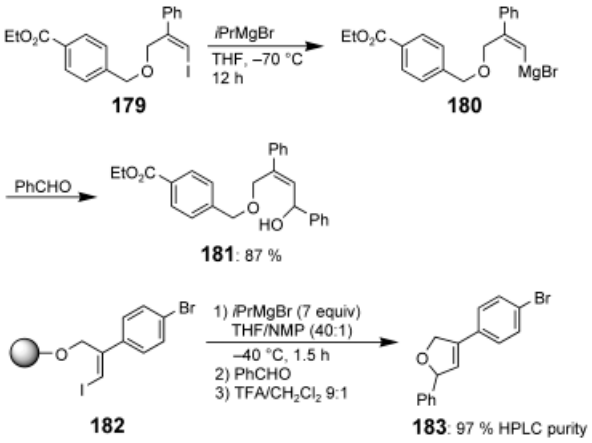
Scheme 32. Preparation of the aryl magnesium compound **177** bearing a keto group.

function facilitates formation of the Grignard reagent by precoordination of NpMgBr and stabilizes the resulting aryl magnesium species by chelation. Transmetallation of **177** with $ZnBr_2$ followed by Negishi cross-coupling,[55] furnishes the ketoester **178** in 64% yield (Scheme 32).[84]

2.5. Preparation of Functionalized Alkenyl Magnesium Reagents

Alkenyl iodides undergo I/Mg exchange upon reaction with *i*PrMgBr or iPr_2Mg. However, this exchange reaction is slower than with aryl iodides. Thus, (*E*)-1-iodo-1-octene only undergoes the exchange reaction at 25 °C and the reaction requires 18 h, therefore precluding the presence of functionality at a remote position in iodoalkenes.[85] However, the presence of a chelating heteroatom or of an electron-withdrawing functionality directly linked to the double bond greatly enhances its propensity for undergoing iodine–magnesium exchange. Thus, the functionalized *Z* allylic ether **179** reacts at −78 °C with *i*PrMgBr, providing the corresponding alkenyl magnesium reagent **180**. The reaction of **180** with PhCHO gives the *Z* alcohol **181** in 87% yield (Scheme 33).[85] Similarly, the resin-attached allylic ether **182** reacts smoothly with *i*PrMgBr in THF/NMP (40:1) within 1.5 h at −40 °C, leading to the desired Grignard reagent. In the absence of

 © 2003 Wiley-VCH Verlag GmbH & Co. KGaA, Weinheim

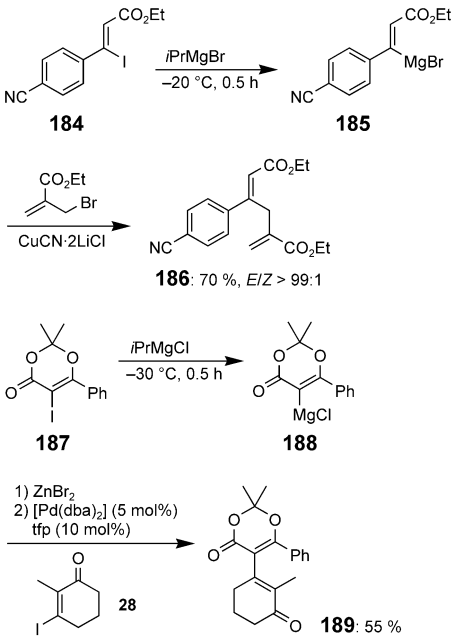


Scheme 33. Preparation of functionalized alkenyl magnesium reagents. TFA = trifluoroacetic acid.

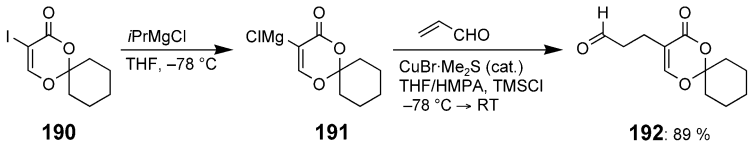
NMP, the exchange reaction is considerably slower. Quenching with benzaldehyde and cleavage from the resin with TFA in CH_2Cl_2 provides the dihydrofuran **183** (97% purity).[85,46b]

The presence of an electron-withdrawing group attached to the double bond considerably facilitates the iodine–magnesium exchange reaction. A range of β-iodoenoates such as **184** are converted into the corresponding Grignard reagent **185** (−20°C, 30 min). The reaction with an allylic bromide in the presence of CuCN·2 LiCl[24] leads to the *E* enoate **186**, which demonstrates a high configurational stability of the intermediate alkenyl magnesium species **185**.[86] Whereas alkenyl magnesium compounds that bear a leaving group such as a halide or an alkoxide at the β position are elusive reagents,[87] the incorporation of the leaving group in a ring system leads to more robust reagents. The reaction of **187** with *i*PrMgCl at −30°C furnishes the desired Grignard reagent **188**, which has a half-life of ≈2 h at −30°C. After transmetallation with $ZnBr_2$, **188** undergoes a smooth Negishi cross-coupling with 3-iodo-2-methyl-cyclohex-2-enone (**28**), leading to the enone **189** in 55% yield (Scheme 34).[88,89] The preparation of related carbonyl-containing alkenyl magnesium reagents was reported by Hiemstra and co-workers in the course of synthetic studies toward the synthesis of solanoeclepin A.[90,91] Treatment of the cyclic alkenyl iodide **190** with *i*PrMgCl in THF at −78°C furnished the desired Grignard reagent **191**, which reacts with acrolein and catalytic CuBr·Me_2S in THF/HMPA in the presence of TMSCl to furnish the Michael adduct **192** in 89% yield (Scheme 35).[91]

If the sp^2-hybridized carbon atom bears an electron-withdrawing group *and* a bromine atom, a very fast Br/Mg exchange reaction is usually observed (−40°C, 15–60 min). This behavior is very general for alkenyl bromides of type **193** (Y = CN, SO_2Ph, CO_2tBu, and $CONEt_2$), which readily react with *i*PrMgBr to affording Grignard reagents of type **194**. The reaction of **194** with electrophiles is not always stereoselective,[92] and produce a mixture of diastereoisomers of type **195**, although this method provides an efficient synthesis of tri- and tetrasubstituted alkenes **195a–d** (Scheme 36).[93,94]

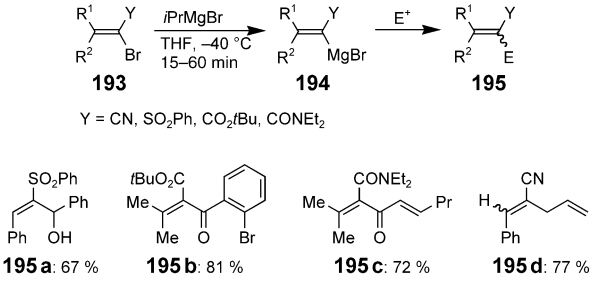


Scheme 34. Preparation of carbonyl-containing alkenyl magnesium compounds.



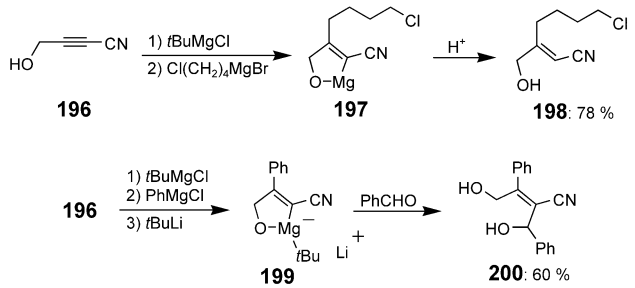
Scheme 35. Copper-catalyzed Michael addition of a functionalized alkenyl magnesium reagent. HMPA = hexamethylphosphoramide.

Remarkably, the conjugate addition of various Grignard reagents to the alkynyl nitrile **196** generates the stabilized and unreactive cyclic magnesium chelate **197**, which after protonation furnishes the polyfunctionalized nitrile **198** (Scheme 37). Fleming et al. showed that the reactivity of cyclic organomagnesium reagents of the type **197** can be dramatically enhanced by generating an intermediate magnesiate species **199**. This magnesiate species now reacts with PhCHO, leading to the allylic diol **200** in 60% yield with complete retention of the stereochemistry of the double bond (Scheme 37).[95]



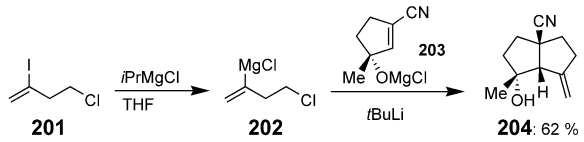
Scheme 36. Functionalized alkenyl magnesium compounds bearing an electron-withdrawing group at the α position.

 © 2003 Wiley-VCH Verlag GmbH & Co. KGaA, Weinheim



Scheme 37. Functionalized alkenyl magnesium compounds obtained by carbomagnesiation of an alkyne.

The I/Mg exchange of 2-iodo-4-chloro-1-butene (**201**) provides a functionalized alkenyl magnesium species **202**, which reacts in a highly diastereoselective manner with the magnesiated unsaturated nitrile **203** to provide the interesting bicyclic product **204** in 62% yield (Scheme 38).[95]

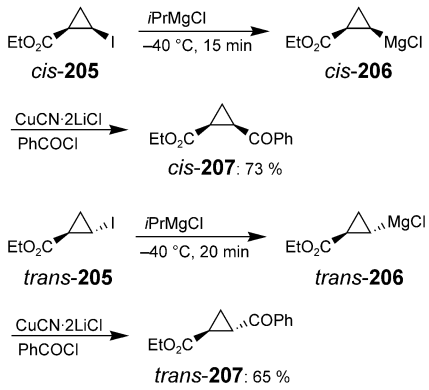


Scheme 38. Functionalized alkenyl magnesium compounds obtained by I/Mg exchange.

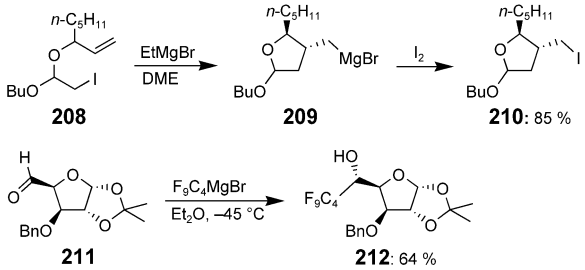
2.6. Functionalized Alkyl Magnesium Reagents

Although the preparation of polyfunctionalized alkyl magnesium reagents may be envisioned, only a few examples have been reported.[96] The difficulties arise from the higher reactivity of the resulting alkyl magnesium compounds relative to that of alkenyl–, aryl–, or heteroaryl–magnesium species. Also, the rate of the iodine–magnesium exchange seems to be slower for alkyl derivatives. However, a range of polyfunctionalized cyclopropyl magnesium compounds can be prepared by iodine–magnesium exchange.[97] Thus, the cyclopropyl iodoesters *cis*-**205** and *trans*-**205** are readily converted into the corresponding Grignard reagents *cis*-**206** and *trans*-**206**, respectively. The formation of the magnesium organometallics **206** is stereoselective, and their reaction with benzoyl chloride furnishes, after transmetallation of **206** with CuCN·2 LiCl,[24] the expected *cis*- and *trans*-1,2-ketoesters **207** in 73% and 65% yields, [97] respectively, with retention of configuration[98,99] (Scheme 39).

Interestingly, the radical cyclization of allylic β-iodoacetals of type **208** was shown by Oshima and co-workers to provide the corresponding organomagnesium compound **209** in DME, which leads after iodolysis to the primary alkyl iodide **210** (Scheme 40).[96] Formation of perfluorinated alkyl Grignards is achieved through an exchange at low temperature in diethyl ether.[100] Perfluorinated Grignard reagents were recently used to functionalize a range of sugar derivatives such as **211**, leading to the fluorinated sugar derivatives of type **212** in 64% yield with high stereoselectivity (Scheme 40).[101]



Scheme 39. Stereoselective preparation of functionalized cyclopropyl magnesium compounds.



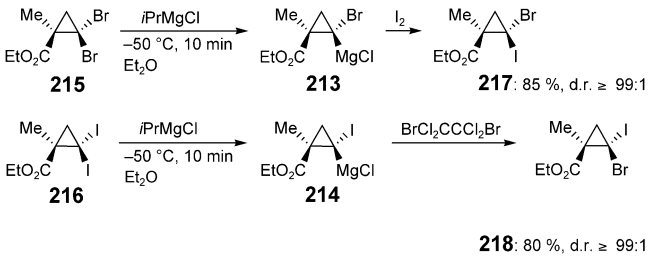
Scheme 40. Reactions of functionalized alkyl magnesium compounds.

2.7. Functionalized Magnesium Carbenoids

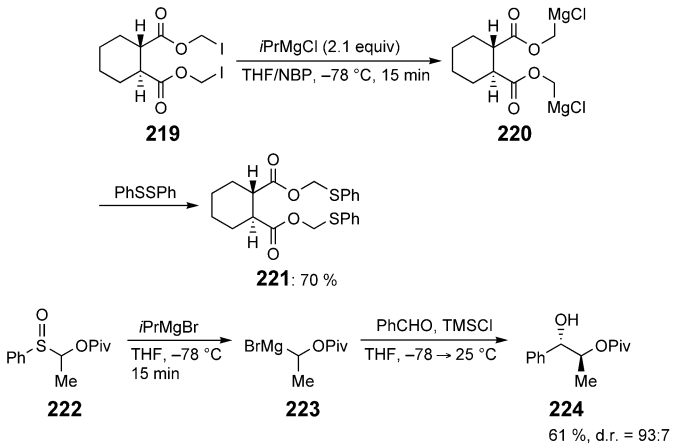
A pioneering bromine–magnesium exchange by Villieras et al.[13] allows the general preparation of magnesium carbenoids.[14] A fast reaction allows the preparation of sensitive cyclopropyl magnesium carbenoids such as **213** and **214**, starting from the corresponding 1,1-dihalocyclopropanes **215** and **216**. By performing the halogen–magnesium exchange in diethyl ether, a completely stereoselective exchange reaction is observed. Quenching of the magnesium carbenoids proceeds with retention of configuration, providing the two diastereomeric products **217** and **218**, respectively, in yields of 80 and 85%, respectively (Scheme 41).[97]

Functionalized acyclic magnesium carbenoids can be prepared in THF/NBP mixtures at low temperatures. Thus, the reaction of the bisiodomethylcarboxylate **219** with *i*PrMgCl in THF/NBP is complete within 15 min at −78 °C.[102] The resulting chiral biscarbenoid **220** is quenched with PhSSPh to give the bisadduct **221** in 70% yield (Scheme 42).[102] Substituted magnesium carbenoids were prepared by using a sulfinyl/magnesium exchange reaction recently introduced by Satoh et al.[103] Thus, the reaction of the sulfoxide **222** with *i*PrMgBr at −78 °C furnishes the desired magnesium carbenoid **223**, which reacts with PhCHO

 © 2003 Wiley-VCH Verlag GmbH & Co. KGaA, Weinheim



Scheme 41. Stereoselective preparation of cyclopropyl magnesium carbenoids.

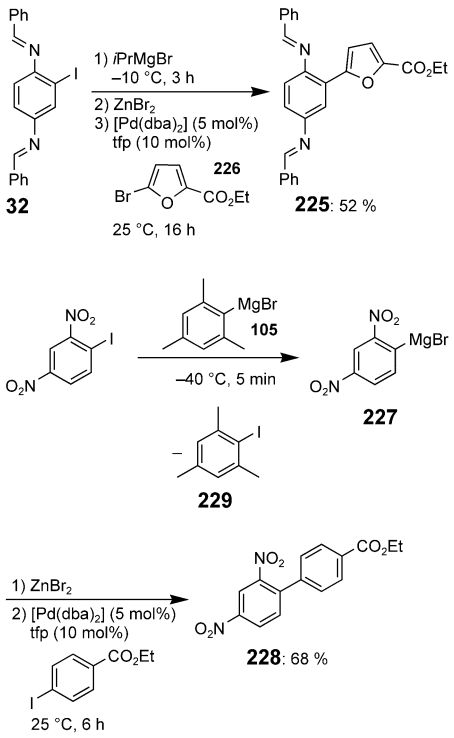


Scheme 42. Preparation of functionalized acyclic magnesium carbenoids. NBP = *N*-butylpyrrolidinone.

with excellent diastereoselectivity, providing the monoprotected 1,2-diol **224** in 61 % yield (d.r. = 93:7) (Scheme 42).[103]

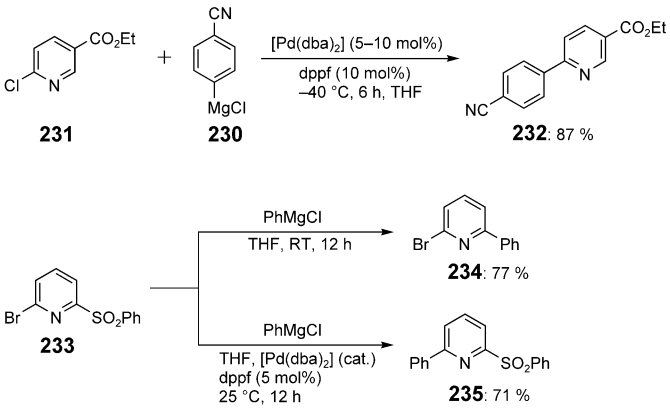
2.8. Functionalized Magnesium Reagents in Cross-Coupling

The availability of functionalized Grignard reagents considerably enhances the scope of these reagents for performing cross-coupling reactions. Especially interesting are aryl magnesium reagents that bear amino groups.[20,104] A range of 2-aryl-1,4-phenylenediamines of type **225** can be prepared starting from the bisimine **32**; the I/Mg exchange is complete within 3 h at −10 °C. After transmetallation to the zinc reagent with $ZnBr_2$, $[Pd(dba)_2]$ (5 mol %), tfp (10 mol %), and ethyl 5-bromo-2-furoate (**226**) are added. The cross-coupling reaction is usually complete after 16 h at 25 °C, leading to the 1,4-phenylenediamine **225** in 52 % yield (Scheme 43).[104] Nitro-containing Grignard reagents such as **227**, which are prepared through iodine–magnesium[54] exchange in THF with mesitylmagnesium bromide (**105**), smoothly undergo Negishi cross-coupling reactions, leading to polyfunctionalized nitroarenes **228**. The mesityl iodide (**229**), which is generated in the iodine–magnesium exchange reaction, is unreactive under the conditions used in these cross-couplings (Scheme 43).[105]



Scheme 43. Cross-coupling with nitrogen-functionalized Grignard reagents.

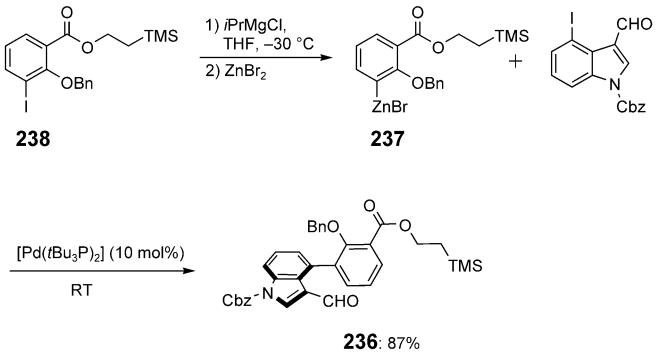
Functionalized Grignard reagents such as **230** directly undergo cross-coupling reactions with various 2-halopyridines **231** in the presence of Pd^0 catalysts. These remarkably fast cross-coupling reactions required the presence of a Pd^0 catalyst and are therefore not direct addition–elimination reactions of the Grignard reagent. The corresponding aryl zinc reagents also react more slowly. These reactions may proceed through the formation of an organopalladate[106] of the type $[MgX]^+[ArPdL_2]^-$, which undergo a fast addition–elimination reaction with the 2-chloropyridine derivative **231**, leading to the functionalized pyridine **232** in 87 % yield (Scheme 44).[107] This reaction can be extended to several haloquinolines.[108]



Scheme 44. Pd-catalyzed cross-coupling with 2-halopyridines. dppf = 1,1′-Bis(diphenylphosphanyl)ferrocene.

 © 2003 Wiley-VCH Verlag GmbH & Co. KGaA, Weinheim

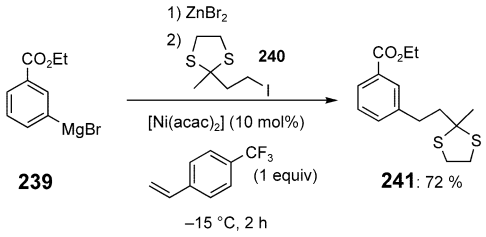
Quéguiner and co-workers found an interesting selectivity[108] in the cross-coupling of bromosulfone **233**. Thus, PhMgCl reacts with the disubstituted pyridine **233** by direct substitution of the phenylsulfonyl group, leading to the bromopyridine **234** in 77% yield (Scheme 44). However, the use of a palladium catalyst allows the preparation of highly functionalized biaryl compounds of type **235**.[109] Analogously, the polyfunctionalized zinc reagent **237**, which is obtained from the iodide **238** through I/Mg exchange followed by transmetallation, reacts readily in the presence of the highly active palladium catalyst $[Pd(tBu_3P)_2]$[110] under mild conditions to furnish the biaryl compound **236** in 87% yield (Scheme 45).



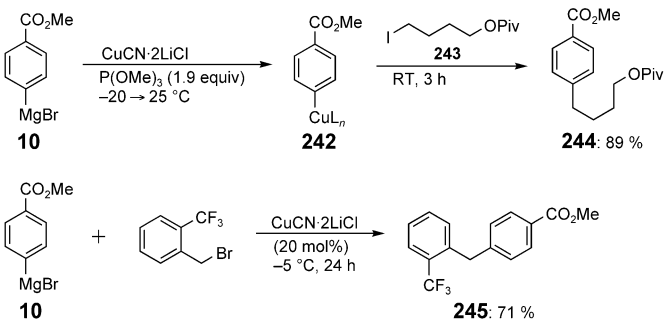
Scheme 45. Pd-catalyzed cross-coupling of highly functionalized aryl zinc reagents. Cbz = benzyloxycarbonyl.

The cross-coupling of functionalized aryl zinc compounds, obtained by transmetallating the corresponding magnesium reagents, can be accomplished by using $[Ni(acac)_2]$ (10 mol%) as the catalyst in the presence of 4-trifluoromethylstyrene or 4-fluorostyrene as promoter of the reductive elimination step. Under these conditions, the Grignard reagent **239** reacts with the iodothioketal **240**, providing the desired cross-coupling product **241** in 72% yield (Scheme 46).[111]

An alternative to this Ni-catalyzed reaction is the corresponding copper-mediated reaction. In this case, the functionalized aryl magnesium species is transmetallated to the corresponding aryl copper reagent with CuCN·2 LiCl[24] in the presence of trimethylphosphite (Scheme 47). This last additive confers an excellent stability to the copper reagent, which can be handled at room temperature under these conditions. Thus, the reaction of the magnesium species **10**



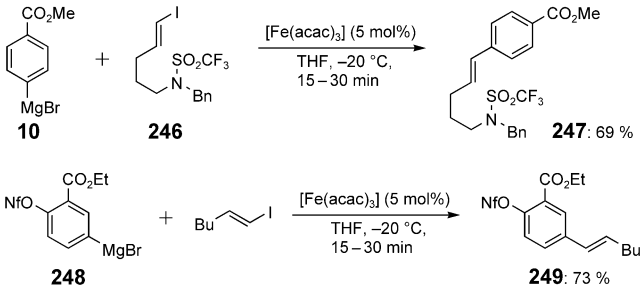
Scheme 46. Ni-catalyzed cross-coupling between functionalized Grignard reagents and functionalized alkyl iodides.



Scheme 47. Cu-mediated cross-coupling reactions of functionalized aryl magnesium compounds. Piv = pivaloyl.

with CuCN·2 LiCl[24] and $P(OMe)_3$ furnishes the stable aryl copper **242**, which undergoes a smooth cross-coupling reaction with functionalized alkyl iodides such as the iodopivalate **243**, leading to the substitution product **244** in 89% yield.[112] Interestingly, reactive benzylic halides undergo the cross-coupling reaction in the presence of a catalytic amount of CuCN·2 LiCl,[24] leading to diaryl methane derivatives such as **245** (Scheme 47).[112]

The low cost and low toxicity of iron(III) salts have allowed these complexes to be used with success in several cross-coupling procedures.[113,114,115] Functionalized aryl magnesium species undergo efficient cross-coupling reactions with polyfunctionalized alkenyl iodides such as **246** in the presence of $[Fe(acac)_3]$ (5 mol%), leading to the styrene derivatives of type **247** in 69% yield. Remarkably, the cross-coupling reaction is complete at −20 °C within 15–30 min (Scheme 48).[116] The aryl magnesium compound can bear



Scheme 48. Fe^{III}-catalyzed cross-coupling reactions with functionalized aryl magnesium species. acac = acetylacetone.

various electrophilic functions such as a nonaflate[117] (e.g. **248**). The iron(III)-catalyzed cross-coupling reaction also proceeds smoothly, leading to the highly functionalized nonaflate **249** in 73% yield (Scheme 48).[116]

3. Summary and Outlook

The halogen-magnesium exchange reaction has opened new perspectives in organic synthesis. Many more functional groups than previously thought are compatible with organomagnesium reagents. The mild conditions required for

 © 2003 Wiley-VCH Verlag GmbH & Co. KGaA, Weinheim

halogen–magnesium exchange are the key for assuring a high functional-group tolerance. This again places Grignard reagents in a central position in organic chemistry and opens fascinating new perspectives. The dramatic functional-group tolerance shows that organic chemists have only partially mastered the reactivity of organometallic reagents for the elaboration of complex organic molecules. More mild and general, environmentally and industrially friendly synthetic methods involving organometallic remain to be discovered.[118]

I thank all co-workers who participated in the exploration of this new field. I also thank Professor Gerard Cahiez (Cergy-Pontoise, France), Professor Guy Quéguiner (Rouen, France), Professor Alfredo Ricci (Bologna, Italy), and Professor Ilan Marek (Haifa, Israel) for stimulating collaborative work, helpful discussions, and fruitful exchange of students. I also thank BASF, Chemetall, Degussa, L'Oréal, Bayer, Aventis, Boehringer-Ingelheim, the DFG, and the Fonds der Chemischen Industrie for financial support. Special thanks to Professor Fraser Fleming for polishing the English and proofreading the manuscript.

Received: February 7, 2003 [A579]

[1] a) A. Boudier, L. O. Bromm, M. Lotz, P. Knochel, *Angew. Chem.* **2000**, *112*, 4584; *Angew. Chem. Int. Ed.* **2000**, *39*, 4415; b) C. Najera, M. Yus, *Recent Res. Dev. Org. Chem.* **1997**, *1*, 67.

[2] a) R. D. Rieke, *Science* **1989**, *246*, 1260; b) T. P. Burns, R. D. Rieke, *J. Org. Chem.* **1987**, *52*, 3674; c) J. Lee, R. Velarde-Ortiz, A. Guijarro, J. R. Wurst, R. D. Rieke, *J. Org. Chem.* **2000**, *65*, 5428.

[3] a) D. J. Ramon, M. Yus, *Eur. J. Org. Chem.* **2000**, 225; b) C. Gomez, F. F. Huerta, M. Yus, *Tetrahedron* **1998**, *54*, 1853, 6177; c) F. Foubelo, A. Gutierrez, M. Yus, *Tetrahedron Lett.* **1997**, *38*, 4837; d) A. Guijarro, M. Yus, *Tetrahedron* **1995**, *51*, 231; e) T. Cohen, M. Bhupathy, *Acc. Chem. Res.* **1989**, *22*, 152; see also: f) M. Yus, R. P. Herrera, A. Guijarro, *Tetrahedron Lett.* **2001**, *42*, 3455; g) I. Gomez, E. Alonso, D. J. Ramon, M. Yus, *Tetrahedron* **2000**, *56*, 4043.

[4] a) J. F. Normant, A. Alexakis, *Synthesis* **1981**, 841; b) S. A. Rao, P. Knochel, *J. Am. Chem. Soc.* **1991**, *113*, 5735.

[5] a) B. M. Trost, *Chem. Eur. J.* **1998**, *4*, 2405; b) D. S. Mattesonin *The Chemistry of the Metal–Carbon Bond, Volume 4*, (Ed.: F. R. Hartley), Wiley, New York, **1987**, p. 307.

[6] a) M.-X. Zhang, P. E. Eaton, *Angew. Chem.* **2002**, *114*, 2273; *Angew. Chem. Int. Ed.* **2002**, *41*, 2169; b) D. Hoppe, T. Heuse, *Angew. Chem.* **1997**, *109*, 2376; *Angew. Chem. Int. Ed. Engl.* **1997**, *36*, 2282; c) T. A. Johnson, M. D. Curtis, P. Beak, *Org. Lett.* **2002**, *4*, 2747; d) P. Beak, D. R. Anderson, M. D. Curtis, J. M. Laumer, D. J. Pippel, G. A. Weisenburger, *Acc. Chem. Res.* **2000**, *33*, 715; e) S. Norsikian, I. Marek, J.-F. Normant, *Tetrahedron Lett.* **1997**, *38*, 7523; f) C. Metallinos, V. Snieckus, *Org. Lett.* **2002**, *4*, 1935; g) V. Snieckus, *Chem. Rev.* **1990**, *90*, 879.

[7] G. Wittig, U. Pockels, H. Dröge, *Chem. Ber.* **1938**, *71*, 1903.

[8] a) R. G. Jones, H. Gilman, *Org. React.* **1951**, *6*, 339; b) H. Gilman, W. Langham, A. L. Jacoby, *J. Am. Chem. Soc.* **1939**, *61*, 106.

[9] a) W. E. Parham, L. D. Jones, *J. Org. Chem.* **1976**, *41*, 1187; b) W. E. Parham, L. D. Jones, Y. Sayed, *J. Org. Chem.* **1975**, *40*, 2394; c) W. E. Parham, L. D. Jones, *J. Org. Chem.* **1976**, *41*, 2704; d) W. E. Parham, D. W. Boykin, *J. Org. Chem.* **1977**, *42*, 260; e) W. E. Parham, R. M. Piccirilli, *J. Org. Chem.* **1977**, *42*, 257; f) C. E. Tucker, T. N. Majid, P. Knochel, *J. Am. Chem. Soc.* **1992**, *114*, 3983.

[10] a) G. S. Silverman, P. E. Rakita in *Handbook of Grignard Reagents*, Marcel Dekker, New York, **1996**; b) B. J. Wakefield in *Organomagnesium Methods in Organic Synthesis*; Academic Press, London, **1995**; c) *Grignard Reagents: New Development*, (Ed.: H. G. Richey, Jr.), Wiley, New York, **1999**.

[11] B. H. Lipshutz, S. Sengupta, *Org. Reactions* **1992**, *41*, 135.

[12] C. Prévost, *Bull. Soc. Chim. Fr.* **1931**, *49*, 1372.

[13] a) J. Villiéras, *Bull. Soc. Chim. Fr.* **1967**, *5*, 1520; b) J. Villiéras, B. Kirschleger, R. Tarhouni, M. Rambaud, *Bull. Soc. Chim. Fr.* **1986**, 470.

[14] For recent examples, see: a) A. Müller, M. Marsch, K. Harms, J. C. W. Lohrenz, G. Boche, *Angew. Chem.* **1996**, *108*, 1639; *Angew. Chem. Int. Ed. Engl.* **1996**, *35*, 1518; R. W. Hoffmann, M. Julius, F. Chemla, T. Ruhland, G. Frenzen, *Tetrahedron* **1994**, *50*, 6049.

[15] C. Tamborski, G. J. Moore, *J. Organomet. Chem.* **1971**, *26*, 153.

[16] N. Furukawa, T. Shibutani, H. Fujihara, *Tetrahedron Lett.* **1987**, *28*, 5845.

[17] a) D. J. Burton, Z. Y. Yang, *Tetrahedron* **1992**, *48*, 189; b) R. D. Chambers, W. K. R. Musgrave, J. Savory, *J. Chem. Soc.* **1962**, 1993.

[18] For other examples of halogen–magnesium exchange reactions, see: a) H. H. Paradies, M. Görbing, *Angew. Chem.* **1969**, *81*, 293; *Angew. Chem. Int. Ed. Engl.* **1969**, *8*, 279; b) G. Cahiez, D. Bernard, J. F. Normant, *J. Organomet. Chem.* **1976**, *113*, 107; c) D. Seyferth, R. L. Lambert, *J. Organomet. Chem.* **1973**, *54*, 123; d) H. Nishiyama, K. Isaka, K. Itoh, K. Ohno, H. Nagase, K. Matsumoto, H. Yoshiwara, *J. Org. Chem.* **1992**, *57*, 407; e) C. Bolm, D. Pupowicz, *Tetrahedron Lett.* **1997**, *38*, 7349.

[19] L. Boymond, M. Rottländer, G. Cahiez, P. Knochel, *Angew. Chem.* **1998**, *110*, 1801; *Angew. Chem. Int. Ed.* **1998**, *37*, 1701.

[20] A. E. Jensen, W. Dohle, I. Sapountzis, D. M. Lindsay, V. A. Vu, P. Knochel, *Synthesis* **2002**, 565.

[21] P. Cali, M. Begtrup, *Synthesis* **2002**, 63.

[22] R. Kober, W. Hammes, W. Steglich, *Angew. Chem.* **1982**, *94*, 213; *Angew. Chem. Int. Ed. Engl.* **1982**, *21*, 203; b) D. von der Brück, R. Bühler, H. Plieninger, *Tetrahedron* **1972**, *28*, 791.

[23] T. Murafuji, K. Nishio, M. Nagasue, A. Tanabe, M. Aono, Y. Sugihara, *Synthesis* **2000**, 1208.

[24] P. Knochel, M. C. P. Yeh, S. C. Berk, J. Talbert, *J. Org. Chem.* **1988**, *53*, 2390.

[25] A. Staubitz, W. Dohle, P. Knochel, *Synthesis* **2003**, 223.

[26] a) L. Gottlieb, A. I. Meyers, *Tetrahedron Lett.* **1990**, *31*, 4723; b) A. I. Meyers, T. R. Elsworthy, *J. Org. Chem.* **1992**, *57*, 4732; c) A. I. Meyers, G. Milot, *J. Am. Chem. Soc.* **1993**, *115*, 6652.

[27] G. Varchi, A. E. Jensen, W. Dohle, A. Ricci, G. Cahiez, P. Knochel, *Synlett* **2001**, 477.

[28] W. Dohle, PhD thesis, LMU München, **2002**.

[29] D. M. Lindsay, W. Dohle, A. E. Jensen, F. Kopp, P. Knochel, *Org. Lett.* **2002**, *4*, 1819.

[30] G. Varchi, C. Kofink, D. M. Lindsay, A. Ricci, P. Knochel, *Chem. Commun.* **2003**, 396.

[31] a) A. Casarini, P. Dembech, D. Lazzari, E. Marini, G. Reginato, A. Ricci, G. Seconi, *J. Org. Chem.* **1993**, *58*, 5620; b) A. Alberti, F. Cane, P. Dembech, D. Lazzari, A. Ricci, G. Seconi, *J. Org. Chem.* **1996**, *61*, 1677; c) F. I. Knight, J. M. Brown, D. Lazzari, A. Ricci, A. J. Blacker, *Tetrahedron* **1997**, *53*, 11411; d) P. Dembach, G. Seconi, A. Ricci, *Chem. Eur. J.* **2000**, *6*, 1281.

[32] a) M. Abarbri, F. Dehmel, P. Knochel, *Tetrahedron Lett.* **1999**, *40*, 7449; b) M. Abarbri, J. Thibonnet, L. Bérillon, F. Dehmel, M. Rottländer, P. Knochel, *J. Org. Chem.* **2000**, *65*, 4618.

[33] T. Delacroix, L. Bérillon, G. Cahiez, P. Knochel, *J. Org. Chem.* **2000**, *65*, 8108.

[34] J. Villiéras, M. Rambaud, *Synthesis* **1982**, 924.

 © 2003 Wiley-VCH Verlag GmbH & Co. KGaA, Weinheim

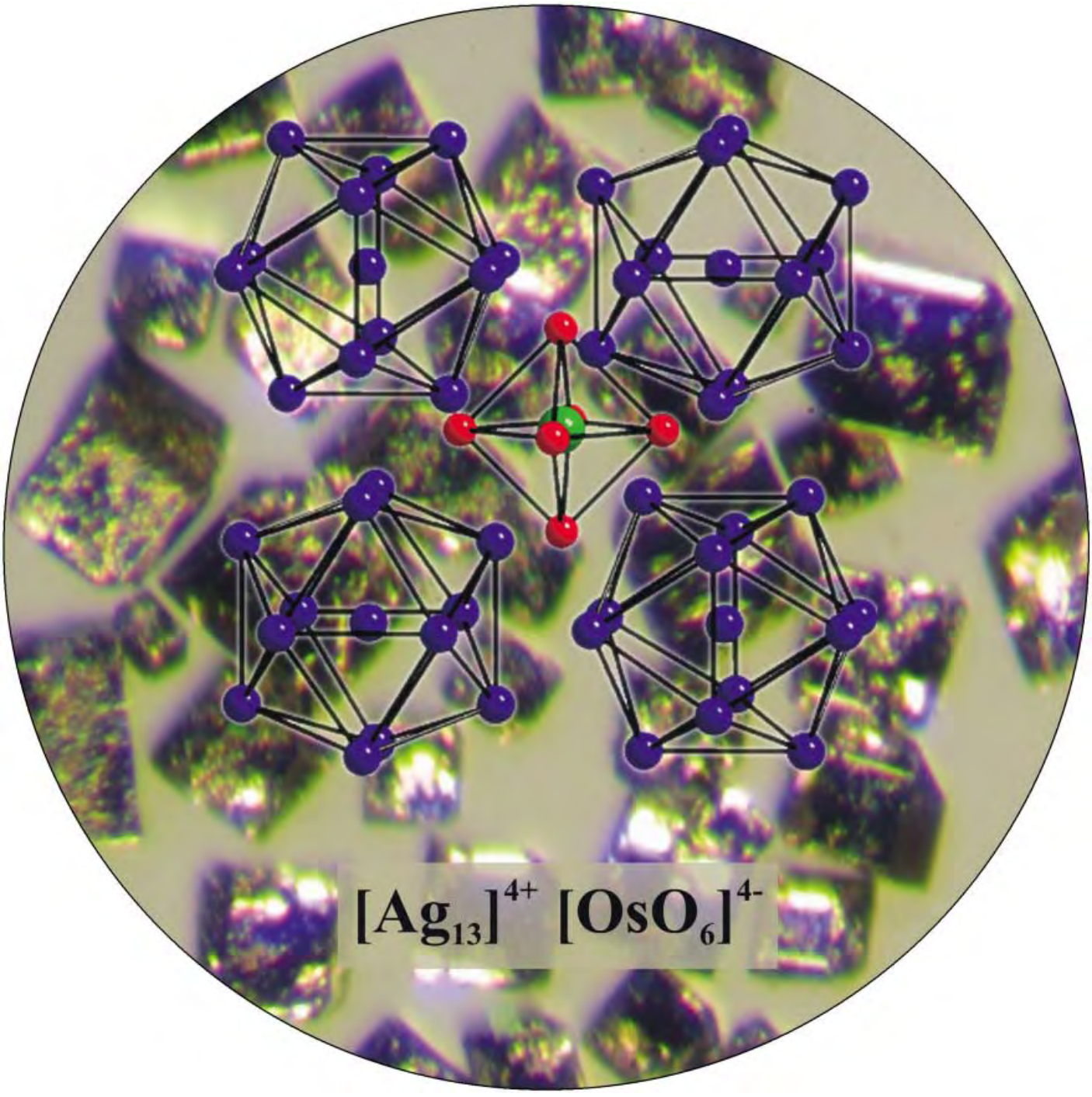
[35] A. Y. Fedorov, F. Carrara, J.-P. Finet, *Tetrahedron Lett.* **2001**, *42*, 5875.
[36] F. F. Kneisel, Y. Monguchi, K. M. Knapp, H. Zipse, P. Knochel, *Tetrahedron Lett.* **2002**, *43*, 4875.
[37] M. Poirier, F. Chen, C. Bernard, Y.-S. Wong, G. G. Wu, *Org. Lett.* **2001**, *3*, 3795.
[38] F. Garro-Helion, A. Merzouk, F. Guibé, *J. Org. Chem.* **1993**, *58*, 6109.
[39] N. Millot, C. Piazza, S. Avolio, P. Knochel, *Synthesis* **2000**, 941.
[40] N. Gommermann, C. Koradin, P. Knochel, *Synthesis* **2002**, 2143.
[41] a) M. T. Reetz, A. Kindler, *J. Chem. Soc. Chem. Commun.* **1994**, 2509; b) E. Nakamura, I. Kuwajima, *J. Am. Chem. Soc.* **1984**, *106*, 3368; c) E. J. Corey, N. W. Boaz, *Tetrahedron Lett.* **1985**, *26*, 6019; d) A. Alexakis, J. Berlan, Y. Besace, *Tetrahedron Lett.* **1986**, *27*, 1047.
[42] G. Varchi, A. Ricci, G. Cahiez, P. Knochel, *Tetrahedron* **2000**, *56*, 2727.
[43] a) K. C. Nicolaou, M. Takayanagi, N. F. Jain, S. Natarajan, A. E. Koumbis, T. Bando, J. M. Ramanjulu, *Angew. Chem.* **1998**, *110*, 2881; *Angew. Chem. Int. Ed.* **1998**, *37*, 2717; b) K. C. Nicolaou, A. E. Koumbis, M. Takayanagi, S. Natarajan, N. F. Jain, T. Bando, H. Li, R. Hughes, *Chem. Eur. J.* **1999**, *5*, 2622.
[44] K. S. Feldman, T. D. Cutarelli, *J. Am. Chem. Soc.* **2002**, *124*, 11600.
[45] a) F. Balkenhohl, C. von dem Bussche-Hünnefeld, A. Lansky, C. Zechel, *Angew. Chem.* **1996**, *108*, 2436; *Angew. Chem. Int. Ed. Engl.* **1996**, *35*, 2288; b) J. S. Früchtel, G. Jung, *Angew. Chem.* **1996**, *108*, 19; *Angew. Chem. Int. Ed. Engl.* **1996**, *35*, 17.
[46] a) S. Marquais, M. Arlt, *Tetrahedron Lett.* **1996**, *37*, 5491; b) M. Rottländer, P. Knochel, *J. Comb. Chem.* **1999**, *1*, 181; for the preparation of organozinc reagents on a solid phase, see: c) Y. Kondo, T. Komine, M. Fujinami, M. Uchiyama, T. Sakamoto, *J. Comb. Chem.* **1999**, *1*, 123; d) R. W. F. Jackson, L. J. Oates, M. H. Block, *Chem. Commun.* **2000**, 1401.
[47] K. Oshima, *J. Organomet. Chem.* **1999**, *575*, 1.
[48] K. Kitagawa, A. Inoue, H. Shinokubo, K. Oshima, *Angew. Chem.* **2000**, *112*, 2594; *Angew. Chem. Int. Ed.* **2000**, *39*, 2481; b) A. Inoue, K. Kitagawa, H. Shinokubo, K. Oshima, *J. Org. Chem.* **2001**, *66*, 4333; see also: c) R. I. Yousef, T. Rüffer, H. Schmidt, D. Steinborn, *J. Organomet. Chem.* **2002**, *655*, 111.
[49] A. Inoue, K. Kitagawa, H. Shinokubo, K. Oshima, *Tetrahedron* **2000**, *56*, 9601.
[50] a) H. Wieland, *Chem. Ber.* **1903**, *36*, 2315; b) H. Gilman, R. McCracken, *J. Am. Chem. Soc.* **1927**, *49*, 1052; c) T. Severin, R. Schmitz, *Chem. Ber.* **1963**, *96*, 3081; d) T. Severin, M. Adam, *Chem. Ber.* **1964**, *97*, 186.
[51] a) G. Bartoli, *Acc. Chem. Res.* **1984**, *17*, 109; b) G. Bartoli, M. Bosco, G. Cantagalli, R. Dalpozzo, F. Ciminale, *J. Chem. Soc. Perkin Trans. 2* **1985**, 773.
[52] a) G. Köbrich, P. Buck, *Chem. Ber.* **1970**, *103*, 1412; b) P. Buck, R. Gleiter, G. Köbrich, *Chem. Ber.* **1970**, *103*, 1431; c) P. Wiriyachitra, S. J. Falcone, M. P. Cava, *J. Org. Chem.* **1979**, *44*, 3957; d) J. F. Cameron, J. M. J. Fréchet, *J. Am. Chem. Soc.* **1991**, *113*, 4303.
[53] C. E. Tucker, T. N. Majid, P. Knochel, *J. Am. Chem. Soc.* **1992**, *114*, 3983.
[54] I. Sapountzis, P. Knochel, *Angew. Chem.* **2002**, *114*, 1680; *Angew. Chem. Int. Ed.* **2002**, *41*, 1610.
[55] a) E. Negishi, *Acc. Chem. Res.* **1982**, *15*, 340; b) E. Negishi, H. Matsushita, M. Kobayashi, C. L. Rand, *Tetrahedron Lett.* **1983**, *24*, 3823; c) E. Negishi, T. Takahashi, S. Baba, D. E. Van Horn, N. Okukado, *J. Am. Chem. Soc.* **1987**, *109*, 2393; d) E. Negishi, Z. Owczarczyk, *Tetrahedron Lett.* **1991**, *32*, 6683.
[56] a) V. Farina, B. Krishnan, *J. Am. Chem. Soc.* **1991**, *113*, 9585; b) V. Farina, S. Kapadia, B. Krishnan, C. Wang, L. S. Liebeskind, *J. Org. Chem.* **1994**, *59*, 5905.
[57] I. Sapountzis, unpublished results.
[58] A. Ono, H. Sasaki, F. Yaginuma, *Chem. Ind. (London)* **1983**, 480.
[59] I. Sapountzis, P. Knochel, *J. Am. Chem. Soc.* **2002**, *124*, 9390.
[60] a) B. H. Yang, S. L. Buchwald, *J. Organomet. Chem.* **1999**, *576*, 125; b) J. P. Wolfe, S. Wagan, J.-F. Marcoux, S. L. Buchwald, *Acc. Chem. Res.* **1998**, *31*, 805; J. F. Hartwig, *Angew. Chem.* **1998**, *110, 2155*; *Angew. Chem. Int. Ed.* **1998**, *37*, 2046; c) L. M. Alcazar-Roman, J. F. Hartwig, A. L. Rheingold, L. M. Liable-Sands, I. A. Guzei, *J. Am. Chem. Soc.* **2000**, *122*, 4618.
[61] a) A. Klapaus, J. C. Antilla, X. Huang, S. L. Buchwald, *J. Am. Chem. Soc.* **2001**, *123*, 7727; b) M. Wolter, A. Klapaus, S. L. Buchwald, *Org. Lett.* **2001**, *3*, 3803; c) R. Shen, J. A. Porco, Jr., *Org. Lett.* **2000**, *2*, 1333; d) A. V. Kalinin, J. F. Bower, P. Riebel, V. Snieckus, *J. Org. Chem.* **1999**, *64*, 2986.
[62] a) B. H. Lipshutz, H. Ueda, *Angew. Chem.* **2000**, *112*, 4666; *Angew. Chem. Int. Ed.* **2000**, *39*, 4492; b) C. Desmarets, R. Schneider, Y. Fort, *Tetrahedron Lett.* **2001**, *42*, 247.
[63] F. Kopp, I. Sapountzis, P. Knochel, *Synlett*, **2003**, 885.
[64] a) N. Momiyama, H. Yamamoto, *Org. Lett.* **2002**, *4*, 3579; b) N. Momiyama, H. Yamamoto, *Angew. Chem.* **2002**, *114*, 4666; *Angew. Chem. Int. Ed.* **2002**, *41*, 2986.
[65] a) G. Boche, J. C. W. Lohrenz, *Chem. Rev.* **2001**, *101*, 697; b) G. Boche, C. Boie, F. Bosold, K. Harms, M. Marsch, *Angew. Chem.* **1994**, *106*, 90; *Angew. Chem. Int. Ed. Engl.* **1994**, *33*, 115; c) G. Boche, H. U. Wagner, *J. Chem. Soc. Chem. Commun.* **1984**, *23*, 1591.
[66] W. Dohle, A. Staubitz, P. Knochel, *Chem. Eur. J.* **2003**, *9*, in press..
[67] M. Rottländer, L. Boymond, L. Bérillon, A. Leprêtre, G. Varchi, S. Avolio, H. Laaziri, G. Quéguiner, A. Ricci, G. Cahiez, P. Knochel, *Chem. Eur. J.* **2000**, *6*, 767.
[68] L. Bérillon, A. Leprêtre, A. Turck, N. Plé, G. Quéguiner, G. Cahiez, P. Knochel, *Synlett*, **1998**, 1359.
[69] I. Collins, *J. Chem. Soc. Perkin Trans. 1*, **2000**, 2845.
[70] G. Quéguiner, F. Marsais, V. Snieckus, J. Epsztajin, *Adv. Heterocycl. Chem.* **1991**, *52*, 187.
[71] M. Bergauer, P. Gmeiner, *Synthesis* **2001**, 2281.
[72] H. Kromann, F. A. Slok, T. N. Johansen, P. Krogsgaard-Larsen, *Tetrahedron* **2001**, *57*, 2195.
[73] J. Felding, J. Kristensen, T. Bjerregaard, L. Sander, P. Vedso, M. Begtrup, *J. Org. Chem.* **1999**, *64*, 4196.
[74] A. B. Smith III, K. P. Minbiole, P. R. Verhoest, M. Schelhaas, *J. Am. Chem. Soc.* **2001**, *123*, 10942.
[75] G. R. Newkome, W. W. Pandler, *Contemporary Heterocyclic Chemistry*, Wiley, New York, **1982**.
[76] M. Abarbri, P. Knochel, *Synlett* **1999**, 1577.
[77] F. Dehmel, M. Abarbri, P. Knochel, *Synlett* **2000**, 345.
[78] B. H. Lipshutz, W. Hagen *Tetrahedron Lett.* **1992**, *33*, 5865.
[79] a) C. J. Lovely, H. Du, H. V. R. Dias, *Org. Lett.* **2001**, *3*, 1319; see also: b) R. S. Loewe, S. M. Khersonsky, R. D. McCullough; *Adv. Mater.* **1999**, *11*, 250.
[80] a) F. Trécourt, G. Breton, F. Mongin, F. Marsais, G. Quéguiner, *Tetrahedron Lett.* **1999**, *40*, 4339; b) A. Leprêtre, A. Turck, N. Plé, P. Knochel, G. Quéguiner, *Tetrahedron* **2000**, *56*, 265.
[81] a) T. Mase, I. N. Houpis, A. Akao, I. Dorziotis, K. Emerson, T. Hoang, T. Iida, T. Itoh, K. Kamei, S. Kato, Y. Kato, M. Kawasaki, F. Lang, J. Lee, J. Lynch, P. Maligres, A. Molina, T. Nemoto, S. Okada, R. Reamer, J. Z. Song, D. Tschaen, T. Wada, D. Zewge, R. P. Volante, P. J. Reider, K. Tomimoto, *J. Org. Chem.* **2001**, *66*, 6775; b) T. Ida, T. Wada, K. Tomimoto, T. Mase, *Tetrahedron Lett.* **2001**, *42*, 4841.
[82] C. Jaramillo, J. C. Carretero, J. E. de Diego, M. del Prado, C. Hamdouchi, J. L. Roldán, C. Sánchez-Martínez, *Tetrahedron Lett.* **2002**, *43*, 9051.
[83] For the use of neopentyl organometallic reagents in zinc and copper organometallic chemistry, see: a) P. Jones, C. K. Reddy,

 © 2003 Wiley-VCH Verlag GmbH & Co. KGaA, Weinheim

P. Knochel, *Tetrahedron* **1998**, *54*, 1471; b) P. Jones, P. Knochel, *J. Chem. Soc. Perkin Trans. 1*, **1997**, 3117.
[84] F. F. Kneisel, P. Knochel, *Synlett* **2002**, *11*, 1799.
[85] M. Rottländer, L. Boymond, G. Cahiez, P. Knochel, *J. Org. Chem.* **1999**, *64*, 1080.
[86] I. Sapountzis, W. Dohle, P. Knochel, *Chem. Commun.* **2001**, 2068.
[87] a) H. Gurien, *J. Org. Chem.* **1963**, *28*, 878; b) J. Ficini, J. C. Depezay, *Bull. Soc. Chim. Fr.* **1966**, 3878; c) F. G. Mann, F. H. Stewart, *J. Chem. Soc.* **1954**, 2826; d) T. Reichstein, J. Baud, *Helv. Chim. Acta* **1937**, *20*, 892; see also: e) M. I. Calaza, M. R. Paleo, F. J. Sardina, *J. Am. Chem. Soc.* **2001**, *123*, 2095; f) F. Foubelo, A. Gutierrez, M. Yus, *Synthesis* **1999**, 503; g) F. F. Fleming, B. C. Shook, *Tetrahedron Lett.* **2000**, *41*, 8847.
[88] V. A. Vu, L. Bérillon, P. Knochel, *Tetrahedron Lett.* **2001**, *42*, 6847.
[89] J. Thibonnet, V. A. Vu, L. Bérillon, P. Knochel, *Tetrahedron*, **2002**, *58*, 4787.
[90] R. H. Blaauw, J. C. J. Benningshof, A. E. Van Ginkel, J. H. van Maarseveen, H. Hiemstra, *J. Chem. Soc. Perkin Trans. 1*, **2001**, 2250.
[91] J.-F. Briére, R. H. Blaauw, J. C. J. Benningshof, A. E. van Ginkel, J. H. van Maarseveen, H. Hiemstra, *Eur. J. Org. Chem.* **2001**, *12*, 2371.
[92] J. Thibonnet, P. Knochel, *Tetrahedron Lett.* **2000**, *41*, 3319.
[93] a) N. Krause, *Tetrahedron Lett.* **1989**, *30*, 5219; b) J. W. J. Kennedy, D. G. Hall, *J. Am. Chem. Soc.* **2002**, *124*, 898.
[94] F. F. Fleming, V. Gudipati, O. W. Steward, *Org. Lett.* **2002**, *4*, 659.
[95] F. F. Fleming, Z. Zhang, Q. Wang, O. W. Steward, *Org. Lett.*, **2002**, *4*, 2493.
[96] A. Inoue, H. Shinokubo, K. Oshima, *Org. Lett.* **2000**, *2*, 651.
[97] V. A. Vu, I. Marek, K. Polborn, P. Knochel, *Angew. Chem.* **2002**, *114*, 361; *Angew. Chem. Int. Ed.* **2002**, *41*, 351.
[98] a) C. Hamdouchi, C. Topolski, M. Goedken, H. M. Walborsky, *J. Org. Chem.* **1993**, *58*, 3148; b) G. Boche, D. R. Schneider, *Tetrahedron Lett.* **1978**, *19*, 2327; c) G. Boche, D. R. Schneider, H. Wintermayr, *J. Am. Chem. Soc.* **1980**, *102*, 5697.
[99] A. de Meijere, S. I. Kozhushkov, *Chem. Rev.* **2000**, *100*, 93.
[100] a) O. R. Pierce, A. F. Meiners, E. T. McBee, *J. Am. Chem. Soc.* **1953**, *75*, 2516; b) C. N. Roberts, E. T. McBee, A. F. Meiners, *J. Am. Chem. Soc.* **1957**, *79*, 335; c) P. Moreau, R. Albachi, A. Commeyras, *Nouv. J. Chim.* **1977**, *1*, 497.
[101] a) S. Lavaire, R. Plantien-Royon, C. Portella, *Tetrahedron: Asymmetry* **1998**, *9*, 213; b) C. Portella, B. Dondy, *Tetrahedron Lett.* **1991**, *32*, 83.
[102] S. Avolio, C. Malan, I. Marek, P. Knochel, *Synlett* **1999**, 1820.
[103] a) Satoh, K. Takano, H. Ota, H. Someya, K. Matsuda, M. Koyama, *Tetrahedron* **1998**, *54*, 5557; b) R. W. Hoffmann, P. G. Nell, *Angew. Chem.* **1999**, *111*, 354; *Angew. Chem. Int. Ed.* **1999**, *38*, 338.
[104] A. E. Jensen, P. Knochel, *J. Organomet. Chem.* **2002**, *653*, 122.
[105] I. Sapountzis, P. Knochel, unpublished results.
[106] a) C. Amatore, A. Jutand, *J. Organomet. Chem.* **1999**, *576*, 254; b) J. F. Fauvarque, F. Pflüger, M. Troupel, *J. Organomet. Chem.* **1981**, *208*, 419.
[107] V. Bonnet, F. Mongin, F. Trécourt, G. Quéguiner, P. Knochel, *Tetrahedron Lett.* **2001**, *42*, 5717.
[108] V. Bonnet, F. Mongin, F. Trécourt, G. Quéguiner, P. Knochel, *Tetrahedron* **2002**, *58*, 4429.
[109] K. S. Feldman, K. J. Eastman, G. Lessene, *Org. Lett.* **2002**, *4*, 3525.
[110] C. Dai, C. G. Fu, *J. Am. Chem. Soc.* **2001**, *123*, 2719.
[111] a) R. Giovannini, P. Knochel, *J. Am. Chem. Soc.* **1998**, *120*, 11186; b) R. Giovannini, T. Stuedemann, A. Devesagayaraj, G. Dussin, P. Knochel, *J. Org. Chem.* **1999**, *64*, 3544.
[112] W. Dohle, D. M. Lindsay, P. Knochel, *Org. Lett.* **2001**, *3*, 2871.
[113] a) M. Tamaru, J. K. Kochi, *J. Am. Chem. Soc.* **1971**, *93*, 1487; b) M. Tamaru, J. K. Kochi, *Synthesis* **1971**, *93*, 303; c) M. Tamaru, J. K. Kochi, *J. Organomet. Chem.* **1971**, *31*, 289; d) M. Tamaru, J. K. Kochi, *Bull. Chem. Soc. Jpn.* **1971**, *44*, 3063; e) J. K. Kochi, *Acc. Chem. Res.* **1974**, *7*, 351; f) S. Neumann, J. K. Kochi, *J. Org. Chem.* **1975**, *40*, 599; g) R. S. Smith, J. K. Kochi, *J. Org. Chem.* **1976**, *41*, 502.
[114] a) G. Cahiez, S. Marquais, *Pure Appl. Chem.* **1996**, *68*, 53; b) G. Cahiez, S. Marquais, *Tetrahedron Lett.* **1996**, *37*, 1773; c) G. Cahiez, H. Advedissian, *Synthesis* **1998**, 1199.
[115] a) A. Fürstner, A. Leitner, M. Mendez, H. Krause, *J. Am. Chem. Soc.* **2002**, *124*, 13856; b) A. Fürstner, A. Leitner, *Angew. Chem.* **2002**, *114*, 632; *Angew. Chem. Int. Ed.* **2002**, *41*, 609.
[116] W. Dohle, F. Kopp, G. Cahiez, P. Knochel, *Synlett* **2001**, 1901.
[117] M. Rottländer, P. Knochel, *J. Org. Chem.* **1998**, *63*, 203.
[118] The halogen–copper exchange may have a high synthetic potential and offers a new entry to a range of new polyfunctionalized copper species: C. Piazza, P. Knochel, *Angew. Chem.* **2002**, *114*, 3397; *Angew. Chem. Int. Ed.* **2002**, *41*, 3267.

 © 2003 Wiley-VCH Verlag GmbH & Co. KGaA, Weinheim

Communications



The $Ag_{13}OsO_6$ complex contains isolated Ag_{13}^{4+} icosahedral clusters in which the central silver ion has the distinction of being bonded solely to other silver ions. This unique character, and the electronic structure of the complex, is described by M. Jansen et al. on the following pages.

DOI: 10.1002/anie.200351740
© 2003 Wiley-VCH Verlag GmbH & Co. KGaA, Weinheim

Subvalent Ternary Silver Oxide

$Ag_{13}OsO_6$: A Silver Oxide with Interconnected Icosahedral Ag_{13}^{4+} Clusters and Dispersed $[OsO_6]^{4-}$ Octahedra**

*Sascha Ahlert, Wilhelm Klein, Ove Jepsen, Olle Gunnarsson, Ole Krogh Andersen, and Martin Jansen**

It has become possible to synthesize ternary silver oxides routinely by reacting the appropriate binary oxides in the solid state under oxygen pressure.[1] Recent systematic investigations have revealed that early, rare observations of unusually short silver–silver separations in oxides were not exceptions, but manifestations of a general feature of the chemistry of silver.[2–4] From our broad basis of experimental data the following picture now emerges: In oxides with high silver contents, silver atoms tend to cluster forming partial structures that are topologically reminiscent of elemental silver. These structures seem to be associated with specific physical properties.[5–7] Weak Ag^+–Ag^+ bonding therefore seems to exist, which indicates that monovalent silver (d^{10} configuration) can no longer be regarded as a closed-shell ion. As another consequence, the aggregates of monovalent silver ions provide empty 5s bands close to the Fermi level that should readily accommodate additional electrons, thus generating silver atoms in a valence state between 0 and +1. Based on such considerations, one would expect silver to be inclined to form subvalent compounds. In the past only singular cases like Ag_2F[8] were reported and, hence, considered as curiosities, but the number of cases is now steadily growing. Empty Ag_6^{4+} octahedra, as found in Ag_3O,[9] Ag_5SiO_4,[10] Ag_5GeO_4[11,12] and $Ag_6Ge_{10}P_{12}$[13] seem to prevail, while slabs of edge-sharing octahedra whose Ag centers have, on average, a charge of $+^1/_2$ have been found in Ag_2F[8] and Ag_2NiO_2.[14] In all known subvalent silver compounds, each silver atom has at least one oxygen atom as nearest neighbor. Here we describe a new subvalent ternary silver oxide, $Ag_{13}OsO_6$, whose icosahedral silver cluster contains a central atom, which is exclusively coordinated to silver.

The title compound was discovered by chance in the course of a systematic exploration of the ternary system Ag/Os/O. Due to the volatility of OsO_4, the Ag/Os ratio of 13:1 occurred spontaneously when starting with reactant mixtures containing far lower shares of silver. By elaborating on the optimal synthesis conditions, we noticed that $Ag_{13}OsO_6$ forms readily, and that various reaction conditions apply. Two feasible routes are: 1) to start with mixtures of the elements in the presence of water as a mineraliser, and 2) to react silver(I) oxide and elemental osmium in the solid state. In both cases, an oxygen pressure of 0.1–0.2 kbar must be maintained during the reaction; water promotes crystal growth. Crystals of cubic shape with edge lengths of up to 0.5 mm, as well as single-phase microcrystalline powders were obtained. The samples show a silver-metallic luster, and are insensitive to air. In argon atmosphere at 300 °C, thermal degradation occurs due to the emission of osmium (via OsO_4) and of oxygen, as detected by mass spectroscopy, leaving elemental silver as the only residue. No other decomposition products (e.g., water or hydroxide) have been detected.

$Ag_{13}OsO_6$ consists of OsO_6 octahedra and Ag_{13} icosahedra arranged as in CsCl (Figure 1).[15] The icosahedra are aligned with their twofold axes along the cubic directions with alternating 90° rotations so that the primitive cell contains two icosahedra and two octahedra.

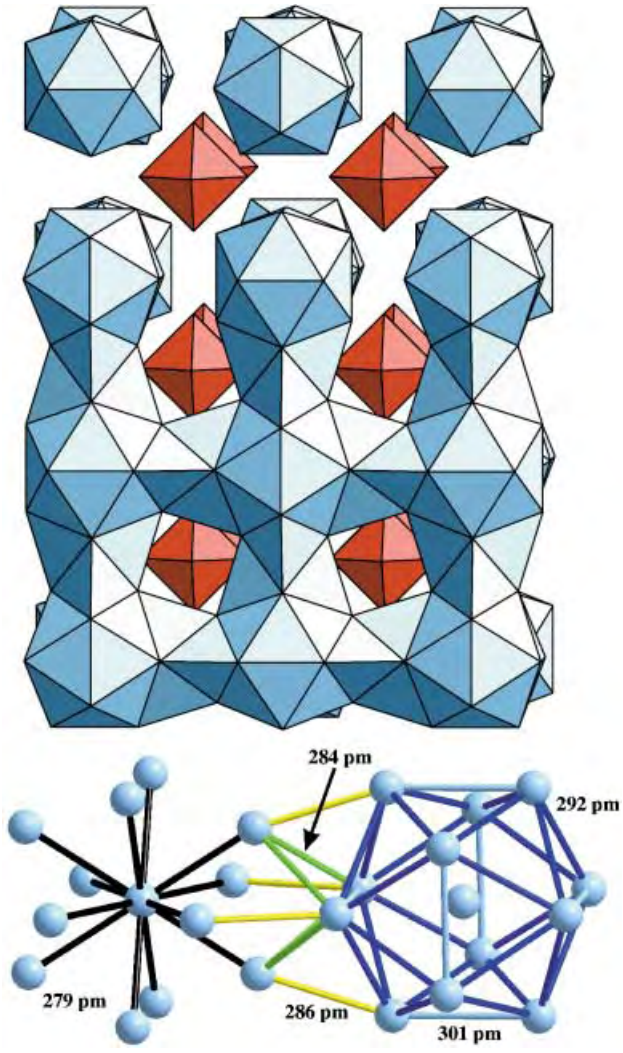


Figure 1. Crystal structure of $Ag_{13}OsO_6$. Triangular faces of oxygen and silver are shown in red and blue, respectively. In the upper part of the figure, the silver icosahedra have been disconnected. The lower part exhibits the different types of Ag–Ag interactions: central intracluster (black), short intracluster (dark blue), long intracluster (light blue), short intercluster (green), long intercluster (yellow).

[*] Prof. Dr. M. Jansen, S. Ahlert, Dr. W. Klein, Dr. O. Jepsen, Dr. O. Gunnarsson, Prof. Dr. O. K. Andersen
Max-Planck-Institut für Festkörperforschung
Heisenbergstrasse 1, 70567 Stuttgart (Germany)
Fax: (+49) 711-689-1502
E-mail: m.jansen@fkf.mpg.de

[**] The authors would like to thank the chemical service group, Eva Brücher, Gisela Siegle, and Dr. Reinhard K. Kremer for determining the electric and magnetic properties of the material.

 © 2003 Wiley-VCH Verlag GmbH & Co. KGaA, Weinheim DOI: 10.1002/anie.200351740

All octahedra are parallel and aligned along the cubic directions. The shortest interatomic distance found in the structure is between Os and O. Its length (190 pm) does not allow a clear assignment of the osmium oxidation state, since for +6, +7, and +8, the effective Os radii differ by merely 3 pm; in the Os^{VII} compounds Na_5OsO_6[16] and Ba_2NaOsO_6[17] the Os–O distances are 190 and 187 pm, respectively. The octahedra are fairly close with a distance of merely 279 pm between the two apical oxygen atoms. The separation (246 pm) between the nearest silver atoms is significantly shorter than the sum of the Ag^+ and O^{2-} ionic radii (266 pm), although larger than commonly observed covalent Ag–O distances (200–230 pm). As seen in the lower part of the figure, these silver atoms form a square, which bisects the line between the two apical oxygen atoms of adjacent octahedra belonging to four different icosahedra. Although the OsO_6 octahedra are perfect, the site symmetry of their centers is not O_h, but only O. This is mostly due to a turn of the squares around the cubic axes, which leads to a loss of the mirror planes.

Whereas the number of crystallographically independent Os and O atoms is one, there are two kinds of silver atoms: Ag(1) at the centers of the icosahedra, and Ag(2) at the corners. As indicated at the bottom of Figure 1, Ag(1) has 12 nearest Ag(2) neighbors at a separation of 279 pm. This is closer than in elemental face-centered cubic (fcc) silver. Considering the fact that the distance along the 30 edges of a perfect icosahedron is 1.051 times the distance to the center, one finds that the average of the 42 near-neighbor distances in Ag_{13} is: $279\text{ pm} \times (12 + 30 \times 1.051)/42 = 289$ pm. This is exactly the nearest-neighbor distance in elemental Ag. In reality, the icosahedra are distorted with 24 short (291 pm) and six long (301 pm) edges. Nevertheless, their average is seen to be exactly 1.051 times 279 pm, so the conclusion remains that the average intracluster Ag–Ag separation in the icosahedron is as in elemental Ag. The symmetry around the center of the distorted icosahedron is T_h, a maximal subgroup of I_h. Of the 20 triangular faces, eight are equilateral with the short edges and 12 are isosceles with one long and two short edges. The long edges point along the cubic directions and alternate between, for example, the x and y directions.

The deviations from icosahedral symmetry are manifestations of strong intercluster bonding rather than of space-group requirements: We have seen that each Ag(2) center has six intracluster bonds (1×279 pm, 4×292 pm, 1×301 pm), but it has equally many intercluster bonds, and they are all short. The distance to the two oxygen atoms is 246 pm and the distance to the two nearest silver atoms in the square is 286 pm (yellow in Figure 1). The distance to the remaining two silver atoms is merely 284 pm, the shortest Ag(2)–Ag(2) distance in the structure (green). Keeping in mind that each Ag(2) center belongs to a long (301 pm) edge of its own icosahedron, it may be seen that these two short intercluster bonds are associated with the ends of a long edge perpendicular to their own long edge. The contact between two icosahedra thus consists of a perpendicular pair of long edges (light blue), joined at their ends by four short (284 pm) bonds (green).

$Ag_{13}OsO_6$ may be regarded as a nanoporous metal with the pores filled by octahedral oxoosmate anions. The building principle is similar to that of the intermetallic phases of type $NaZn_{13}$.[18]

$Ag_{13}OsO_6$ is a metallic conductor with a specific resistance of $\rho = 2.23 \cdot 10^{-4}\ \Omega\,\text{cm}$ at 298 K with a positive temperature coefficient of $0.77\ \mu\Omega\,\text{cm}\,\text{K}^{-1}$, and is diamagnetic. Neither the structural data nor the physical properties allow for an unambiguous determination of the oxidation state of Os. The diamagnetic behavior is compatible with the +8 state, but with strong spin–orbit coupling and ligand-field effects, ground states with reduced susceptibilities are possible also for hexa- or heptavalent osmium. In addition, structural reference data for Os–O bond lengths are rare, and not in all cases reliable or comparable. We have therefore performed density functional LMTO calculations[19] to gain an insight into the bonding and electronic properties.

Figure 2 shows the calculated electronic density of states (DOS), projected onto the sum of the orthonormal orbitals centered on Os, O, Ag(2), and Ag(1), respectively. Covalent interactions may be recognized as common DOS structures. The top and bottom panels display respectively the region of energies above (positive) and below (negative) the Fermi energy, taken as zero. Note that the vertical scale has been changed to accommodate more of the Ag 4d peak between −6.4 and −3.0 eV. A description of the calculated electronic structure begins with the strongest covalent interactions, that is, those on the OsO_6 octahedron. The hopping integral between the Os 6s orbital and the O 2p orbital of a_g symmetry is so strong that the bonding O 2p-like band is far below and the antibonding Os 6s-like band far above the Fermi level. For the purpose of counting, we may therefore say that there are no Os 6s-electrons, although the occupied bonding O 2p-like band has some Os 6s character. The peaks from the e_g bonding and antibonding bands are those extending from −7.4 to −6.9 eV and from 5.2 to 6.0 eV, respectively. Similarly, the t_{2g} bonding and antibonding bands are those extending respectively from −7.0 to −6.0 eV and from −0.2 to 1.0 eV. This means that the Os–O bonding states are occupied and the Os–O antibonding states are empty. This leaves 12 ($6 \times 3 - 1 - 2 - 3$) O 2p orbitals which do not bond to Os and which cause the broad peak between −3 and −1 eV. In conclusion, of the OsO_6 bands, all bonding and nonbonding O 2p-like bands are occupied, and all antibonding Os-like bands are empty. Therefore the charge state of the octahedron may be considered as $[OsO_6]^{4-}$, and that of the icosahedron as Ag_{13}^{4+}. Since the occupied bands have strong Os character, the notation $Os^{8+}O_6^{2-}$ should be avoided.[20]

The 0.2-eV filling of the antibonding t_{2g} band may be an artifact of the calculation, and a geometry optimization might place the Fermi level in the pseudo-gap. Here, the total DOS is 2.3 electrons per eV and per 2($Ag_{13}OsO_6$). Per Ag atom, this is 0.09, which is considerably smaller than the value $0.25\ \text{e}\,(\text{eV} \times \text{Ag})^{-1}$ in elemental fcc silver. This may explain the observed diamagnetism. The average DOS in the 5 eV region above the Fermi level has about the same value as in fcc Ag.

The positions and characters of the bonding and antibonding e_g and t_{2g} bands deviate considerably from what is obtained for an isolated OsO_6 octahedron. For instance, both

 © 2003 Wiley-VCH Verlag GmbH & Co. KGaA, Weinheim

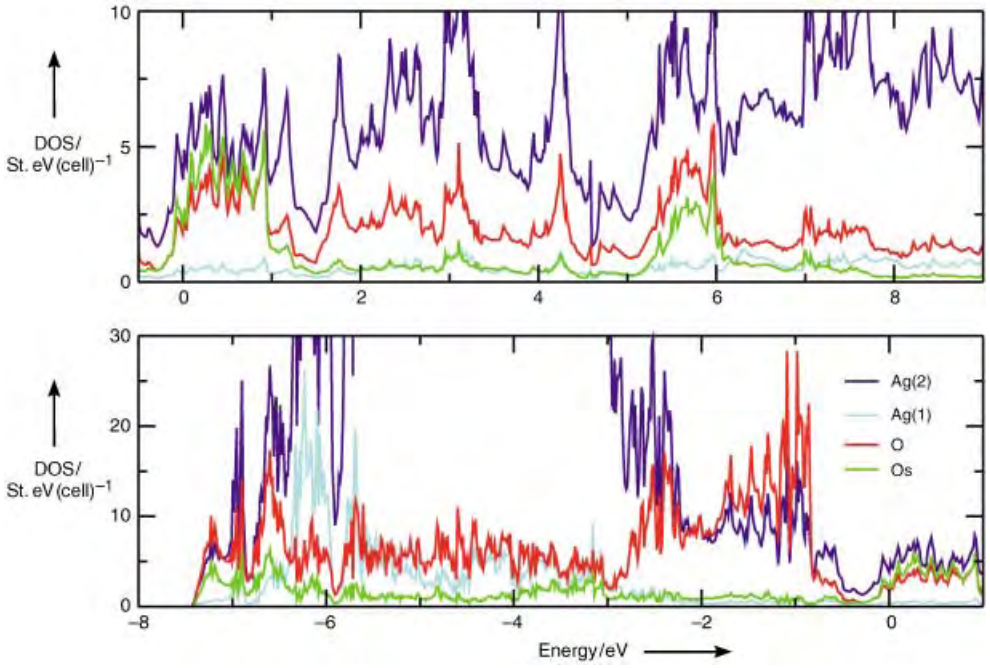


Figure 2. Electronic densities of states of $Ag_{13}OsO_6$ projected onto the sum of the orthonormal LMTOs centered on Os (green), O (red), Ag(1) (light blue), and Ag(2) (dark blue). The Fermi energy is taken to be zero.

e_g bands have more O than Os character. The reason for this is clearly seen in Figure 2, namely that Ag(2) character dominates the entire spectrum, including the e_g and t_{2g} peaks. Since silver reduces the symmetry from O_h to O, hybridization with the Ag(2) 4d, 5s, and 5p orbitals mixes odd, nonbonding O 2p character into the e_g and t_{2g} bands.

The silver 4d band extends from −6.4 to −3.0 eV, of which the part between −6.4 and −5.9 eV is the Ag(1) h_g (I_h) state. This 4d-band is more narrow and low-lying than in elemental fcc Ag, where it extends from −6.6 to −2.7 eV (in the local density approximation (LDA)). The difference is due to the Ag(2) 4d orbitals that form bonding and antibonding bands with the O 2p orbitals, which do not bond with Os. The corresponding DOS structures are visible between −3.0 and −0.5 eV, between 1.6 and 4.5 eV, and between 6.9 and 7.8 eV. The Ag(2) 5s and 5p projected densities of states (not explicitly shown) are similar to those in elemental Ag, where they exhibit sd and pd hybridization gaps and are fairly constant around the Fermi level. This is very different from the Os 6s projection, and from the Ag 5s and 5p projections in Ag oxides. Hence, in $Ag_{13}OsO_6$ it is mainly the Ag(2) 4d orbitals that are responsible for the interaction with O 2p, while the Ag 5s and 5p orbitals interact mainly with Ag orbitals.

This bonding situation can be expressed quantitatively by the covalent bond strengths (crystal orbital Hamiltonian populations (COHPs) integrated to the Fermi level)[21] calculated from the LMTO energies and eigenvectors. The strengths of the sticks between the atoms in Figure 3 have been assigned accordingly. With a strength of 3.4 eV, the 190 pm Os–O bond is the strongest in the structure. The oxygen atoms do not bind to each other (< 0.05 eV). Second strongest is the 246 pm Ag(2)–O bond (0.76 eV). Then

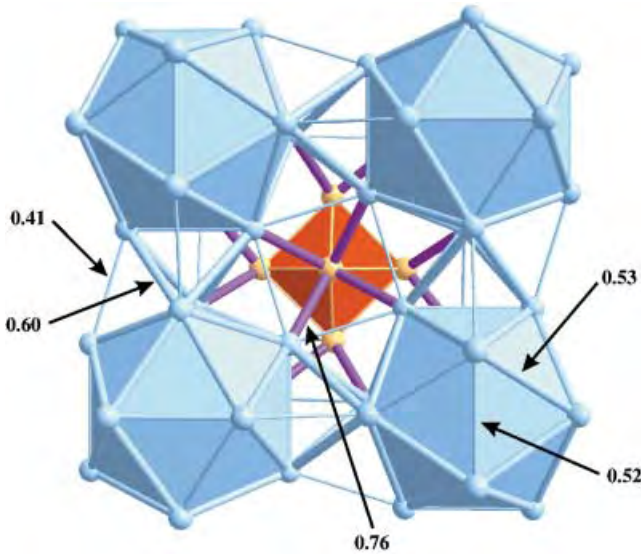


Figure 3. A more detailed view of a section of the structure shown in Figure 1. The sticks have been given a width roughly proportional to the calculated covalent bond strengths (COHPs integrated to the Fermi level). Numbers are in eV. The central Os–O (3.4 eV) and Ag(1)–Ag(2) (0.65 eV) bonds are not shown.

follows the 279 pm central Ag(1)–Ag(2) bond with a strength of 0.65 eV. The short (291 pm) and long (301 pm) Ag(2)–Ag(2) intracluster bonds are considerably weaker and nearly equal (0.52 and 0.53 eV). With a strength of 0.60 eV, the short (284 pm) intercluster bond connecting the ends of the perpendicular edges is the strongest Ag(2)–Ag(2) bond. Finally, the Ag(2)–Ag(2) intercluster bond along the 286 pm edge of a square is relatively weak (0.41 eV). Whereas the

 © 2003 Wiley-VCH Verlag GmbH & Co. KGaA, Weinheim

average Ag–Ag intracluster separation is the same as in elemental fcc Ag, the bond strength of 0.64 eV in fcc Ag is reached only by the central Ag(1)–Ag(2) bond. This "deficit" is compensated by the strong bonding to oxygen atoms.

The band structure in the 4 eV region around the Fermi level is shown in Figure 4. The bands have been given a

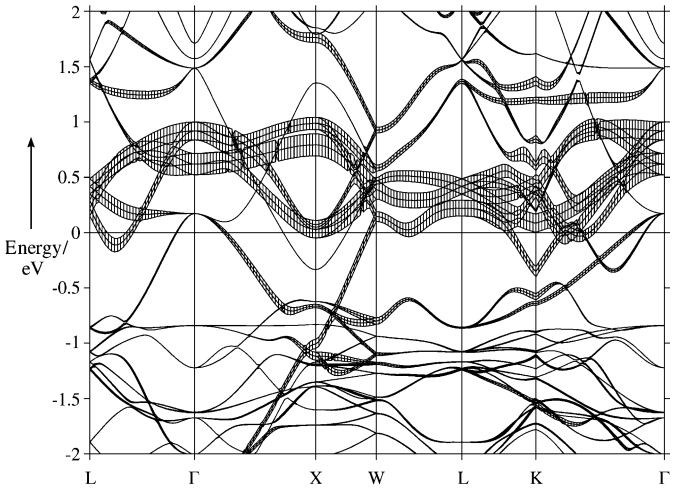


Figure 4. The band structure around the Fermi level (at 0 eV) of $Ag_{13}OsO_6$ along symmetry lines in the fcc Brillouin zone. The fatness of the bands is proportional to the Os t_{2g} character of the states.

degree of fatness that is proportional to their Os t_{2g} character. We see that the six antibonding t_{2g} bands disperse by $W \approx 1$ eV and that there is considerable additional mixing with the surrounding O 2p/Ag(2) bands. Simple estimates for the energy cost U of putting two electrons on the same OsO_6 octahedron give $U > W$. One would therefore expect interesting correlation effects in electron-doped systems where the t_{2g} band is partly occupied. If synthesized, $ZnAg_{12}OsO_6$ would be an obvious candidate.

Experimental Section

$Ag_{13}OsO_6$ was obtained by the solid-state reaction of ground mixtures of silver or silver oxide and osmium at elevated oxygen pressure. Due to the high volatility of the easily formed OsO_4 an excess of Os metal is necessary. Successful preparations have been run with Ag/Os molar ratios of 1:1 up to 5:1. In a typical experiment, $Ag_{13}OsO_6$ was obtained from a mixture of Ag (107.9 mg, 1 mmol) and Os (47.5 mg, 0.025 mmol) in a gold crucible at 15 MPa oxygen pressure and 300 °C for 2 days as a lustrous olive-green microcrystalline sample. To prepare silvery single crystals suitable for X-ray diffraction analysis, 1 mL H_2O was added as a mineralizer.

Received: April 24, 2003 [Z51740]
Published online: September 1, 2003

Keywords: cluster compounds · molecular orbital theory · osmium · silver · subvalent compounds

[1] C. Linke, M. Jansen, *Z. Anorg. Allg. Chem.* **1997**, *623*, 1441.
[2] M. Jansen, *Habilitationsschrift*, Universiät Gießen, **1978**.
[3] M. Jansen, *J. Less-Common Met.* **1980**, *76*, 285.
[4] M. Jansen, *Angew. Chem.* **1987**, *99*, 1136; *Angew. Chem. Int. Ed. Engl.* **1987**, *26*, 1098.
[5] C. Friebel, M. Jansen, *Z. Naturforsch. B* **1984**, *39*, 739.
[6] B. U. Köhler, M. Jansen, W. Weppner, *J. Solid State Chem.* **1985**, *57*, 227.
[7] P. Behrens, S. Aßmann, U. Bilow, C. Linke, M. Jansen, *Z. Anorg. Allg. Chem.* **1999**, *625*, 111.
[8] G. Argay, F. Naray-Szabo, *Acta Chim. Acad. Sci. Hung.* **1966**, 329.
[9] W. Beesk, P. G. Jones, H. Rumpel, E. Schwarzmann, G. M. Sheldrick, *J. Chem. Soc. Chem. Commun.* **1981**, 644.
[10] C. Linke, M. Jansen, *Inorg. Chem.* **1994**, *33*, 2614.
[11] M. Jansen, C. Linke, *Angew. Chem.* **1992**, *104*, 618; *Angew. Chem. Int. Ed. Engl.* **1992**, *31*, 653.
[12] M. Jansen, C. Linke, *Z. Anorg. Allg. Chem.* **1992**, *616*, 95.
[13] H. G. von Schnering, K. Häusler, *Rev. Chim. Miner.* **1976**, *13*, 71.
[14] M. Schreyer, M. Jansen, *Angew. Chem.* **2002**, *114*, 665; *Angew. Chem. Int. Ed.* **2002**, *41*, 643.
[15] Crystal data of $Ag_{13}OsO_6$: $0.1 \times 0.1 \times 0.1$ mm^3; cubic, $Fm\bar{3}c$, $a = 13.1712(5)$ Å; $V = 2284.95(15)$ Å^3; $Z = 8$, $\mu = 32.797$ mm^{-1}; $\rho_{calcd} = 9.817$ g cm^{-3}; Bruker AXS Smart CCD 1000, $Mo_{K\alpha}$, $\lambda = 0.71073$ Å; measurement range $3.09 = \theta = 34.96°$; $T = 293(2)$ K; 2367 independent reflections out of 7622 measured ($I > 2\sigma(I)$); solved by direct methods and subsequently refined by full-matrix, least-squares calculations based on F^2 (SHELXTL-V5.12); max./min. residual electron density $+1.60/-4.84$ e Å^{-3}, $R_1 = 0.0319$, $wR_2 = 0.0650$, GOF = 1.360. Further details on the crystal structure investigations may be obtained from the Fachinformationszentrum Karlsruhe, 76344 Eggenstein-Leopoldshafen, Germany (fax: (+49) 7247-808-666; e-mail: crysdata@fiz-karlsruhe.de), on quoting the depository number CSD-413193.
[16] T. Betz, R. Hoppe, *Z. Anorg. Allg. Chem.* **1985**, *524*, 17.
[17] K. E. Stitzer, M. D. Smith, H.-C. zur Loye, *Solid State Sci.* **2002**, *4*, 311.
[18] a) J. A. A. Ketelaar, *J. Chem. Phys.* **1937**, *5*, 668; b) E. Zintl, W. Hauke, *Nature* **1937**, *139*, 717; c) D. P. Shoemaker, R. E. March, F. J. Ewing, L. Pauling, *Acta Crystallogr.* **1952**, *5*, 637.
[19] The band-structure calculation was performed with the GGA Perdew–Wang density functional and the Stuttgart TB LMTO code. The sphere radii in pm were: 127 (Os), 110 (O), 99 (E), 157 (Ag(2)), and 160 (Ag(1)). The E spheres were placed at the faces of the octahedra, at the Wyckoff 64 g sites with $x = 0.1633$. The basis set included the Ag and Os s, p, and d LMTOs, the O p LMTOs, and the E s and p LMTOs. The O s and d partial waves were downfolded. Spin–orbit coupling was neglected in this scalar relativistic calculation; its inclusion would cause a t_{2g} band to split by $(3/2)\zeta_d \sim 0.3$ eV into a lower fourfold and an upper twofold degenerate band.
[20] The charges obtained from the occupations of our orthonormal LMTOs are: $Os^{+2.62}$, $O^{-0.86} = (O_6^{-0.26} + E_8^{-0.45})/6$, $Ag(1)^{-0.32}$, and $Ag(2)^{+0.24}$).
[21] R. Dronskowski, P. E. Blöchl, *J. Phys. Chem.* **1993**, *97*, 8617.

 © 2003 Wiley-VCH Verlag GmbH & Co. KGaA, Weinheim

Asymmetric Heterogeneous Catalysis

Enhancing the Enantioselectivity of Novel Homogeneous Organometallic Hydrogenation Catalysts**

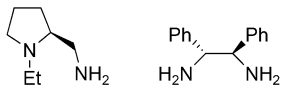
Matthew D. Jones, Robert Raja, John Meurig Thomas,* Brian F. G. Johnson,* Dewi W. Lewis, Jacques Rouzaud, and Kenneth D. M. Harris*

The exigent need to develop new asymmetric hydrogenation catalysts is universally acknowledged, and many new feasible strategies for the design and synthesis of such catalysts continue to be proposed.[1–5] Herein, in addition to describing a new set of efficient, diamino-type ligands for a central rhodium or palladium ion that leads to good enantioselective (*ee*) performance, homogeneously, we also show that significant improvement in the stereoselectivity of the organometallic catalyst may be achieved by heterogenizing it at the inner walls of a mesoporous silica so that advantage is taken of the spatial restrictions imposed by the concave surface at which we have located the active center.

Comparatively few reports have hitherto been published in which Rh^{I} or Pd^{II} complexes without phosphane ligands have been used to activate hydrogen, but a rapidly growing number employing nitrogen containing ligands has appeared of late for the purpose of asymmetric catalysis.[6] One of the incentives for this change is the rather unstable nature and cost of many chiral phosphanes.[6b] It is not, however, the nitrogen-containing ligands that are the key feature of this work. Rather it is the fact that advantage is taken of a concave surface of a silica support, on which the homogeneous organometallic catalyst is tethered, thereby boosting the enantioselectivity to a value higher than that obtained from the same catalyst and the same tether attached to a convex silica support.

The catalysts themselves are pseudo square-planar rhodium(I) or palladium(II) complexes of the bidentate amines: (*S*)-(−)-2-aminomethyl-1-ethyl pyrrolidine **1a** and (1*R*,2*R*)-(+)-1,2-diphenylethylenediamine **1b**, which may readily act as ligands to the metal center. The Rh^{I} catalysts are bonded either to 1,5-cyclooctadiene (COD) or norbornadiene (NBD), whereas for the palladium species we used the allyl (C_3H_5) group as the coordinating alkene. The BF_4^- salts of these organometallic cations are readily handled, air-stable, crystalline materials amenable to X-ray analysis.[7]

For the cations based on **1a** (paired in each case with the BF_4^- anion; see Scheme 1) X-ray structural analysis shows that the square-planar rhodium(I) or palladium(II) center has high steric hindrance. Access to it by a relatively bulky incoming reactant is spatially restricted (see below), and this feature is essential for good enantioselective catalytic behavior.



1a **1b**

Scheme 1. The ligands used in this study.

A fragment of the crystal structure of the Rh^{I} complex with ligand **1a** is shown in Figure 1a, from which it is seen that the BF_4^- anion is hydrogen-bonded to the nitrogen of the amino groups.

By using described procedures[8–12] whereby 3-bromopropyl trichlorosilane serves as a means of anchoring isolated organometallic species to the inner walls of mesoporous silica, we may functionalize an ion-pair of all ligands **1a** and **1b** complexed to metal so as to yield their respective single-site catalysts, as depicted in Figure 1b. We have anchored ligand **1b** to a mesoporous silica (pore diameter 30) and to a nonporous silica (known as cabosil). This permits the comparison of catalytic performance of the organometallic species when it is either at a convex or at a concave siliceous surface (Figure 2). (It is much easier to prepare concave than convex silica surfaces. Since this work began, we have studied a series of silicas in which the pore diameters range from a low of 38 Å to a high of 250 Å; but, to date, the only satisfactory, well-defined convex silica surface that we have been able to investigate is that of the commercial material known as cabosil).

We chose as a test reaction the simple, well-known[12] case of the hydrogenation of *E*-α-phenylcinnamic acid (Scheme 2)

[*] Dr. R. Raja, Prof. Dr. B. F. G. Johnson, M. D. Jones, Dr. J. Rouzaud
Department of Chemistry
University of Cambridge
Lensfield Road, Cambridge CB21EW (UK)
Fax: (+44) 1223-336017
E-mail: robert@ri.ac.uk
bfgj1@cam.ac.uk
Prof. Sir J. M. Thomas
The Royal Institution of Great Britain
Davy Faraday Research Laboratory
21 Albemarle Street, London W1S4BS (UK) and
Department of Materials Science and Metallurgy
New Museums Site
Pembroke Street, Cambridge CB23QZ (UK)
Fax: (+44) 1223-334567
E-mail: jmt@ri.ac.uk
Dr. D. W. Lewis
Department of Chemistry
University College London
20 Gordon Street, London WC1H0AJ (UK)
Prof. Dr. K. D. M. Harris
School of Chemical Sciences
University of Birmingham
Edgbaston, Birmingham B152TT (UK)

[**] We thank the EPSRC (UK) for a rolling grant to J.M.T. and general support to B.F.G.J., KDMH and a studentship to MDJ, and for financial assistance towards the single crystal diffractometers. We also thank Bayer AG, Leverkusen (Germany) for their support to R.R., the Marie Curie fellowship Scheme for J.R., ICI and the Newton trust for M.D.J.. We gratefully acknowledge Dr. J. E. Davies for determining the crystal structures. Dr. S. Kitchin is acknowledged for the ^{19}F MAS measurements and Mr. G. Burns for technical assistance.

Supporting information for this article is available on the WWW under http://www.angewandte.org or from the author.

 © 2003 Wiley-VCH Verlag GmbH & Co. KGaA, Weinheim DOI: 10.1002/anie.200250861

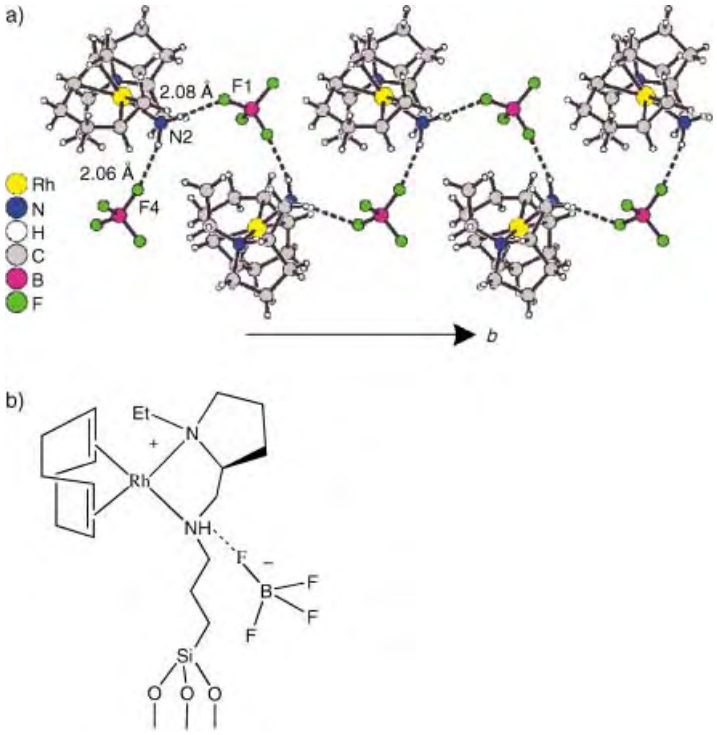


Figure 1. a) Fragment of the crystal structure of the Rh^{I} complex of **1a** illustrating the complex hydrogen-bonded network; the *b* axis is labeled. b) A molecular diagram of the heterogenized single site catalyst.

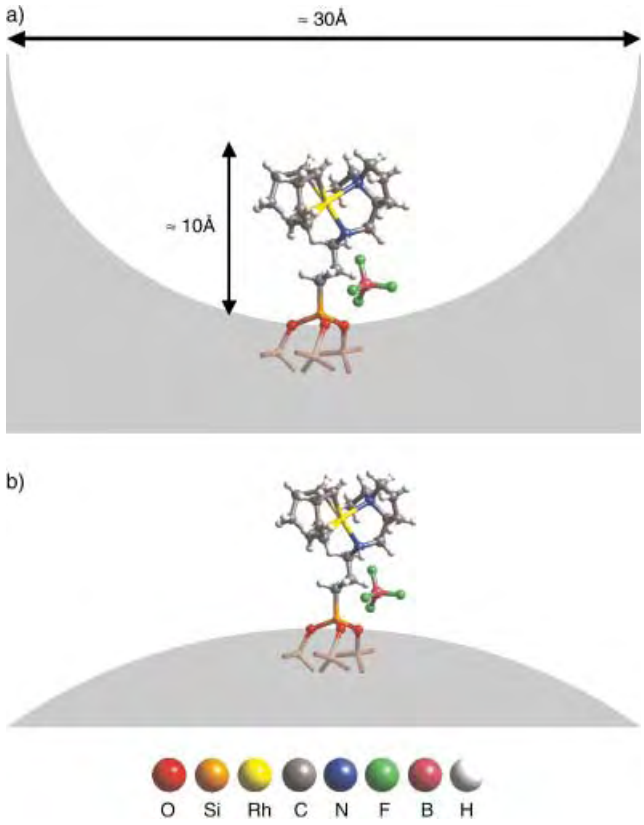
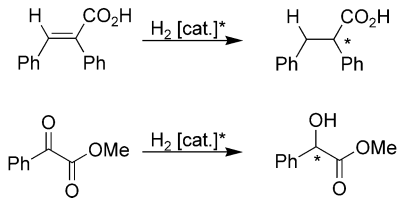


Figure 2. Graphical model (to scale) showing the constraints of the catalyst once anchored on a) MCM-41 (concave) and b) cabosil (convex) surfaces.



Scheme 2. The asymmetric hydrogenation reactions under investigation.

the predominant product being the 2,3-diphenyl propionic acid. We have previously examined[12e] this heterogeneous asymmetric hydrogenation using a Pd diphenylphosphino-ferrocenyl (dppf), tethered catalysts, in which, depending upon the manner of production of the heterogenized catalyst, variable amounts of other products (2,2- and 3,3-diphenylpropionic acids) as well as variable values of *ee* of the 2,3-diphenyl propionic acid were obtained.

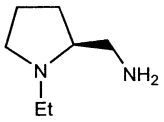
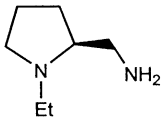
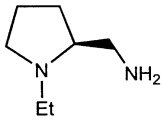
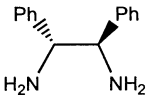
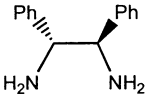
Catalytic tests were carried out (see Experimental Section) both on the new Rh^{I} homogeneous catalysts and on their anchored analogues. The homogeneous and heterogeneous palladium complex of ligand **1a** and **1b** where also tested (the crystal structure of the homogeneous catalyst is given as supplementary information). The results are summarized in Table 1. It is to be noted that, in the repeat cycle of experiments (for the case of the heterogenized organometallic catalyst), the *ee* values as well as the conversions and selectivities do not drop significantly in the first and second recycle compared with the respective values for the parent catalyst. This fact, as well as the observation that, compared with the corresponding homogeneous catalyst, there is a significant enhancement of the *ee* value upon heterogenization suggests that the original catalytically active species is the Rh-diamine-diene complex, unlike the situation that seems to prevail in the case of Rh-diphosphane analogues.[13]

Whilst the asymmetric hydrogenation of *E*-α-phenylcinnamic acid was studied to establish proof of principle and to compare with our earlier results[12e] by using tethered Pd-dppf catalysts, we have also investigated another reactant, methyl benzoylformate, that is of considerable commercial value. In this case also the enantioselectivity of the heterogenized organometallic catalyst, for the production of methyl mandelate, at the concave silica surface is much enhanced, (see Table 1) compared to its homogeneous analogue. The improvements in the enantioselective performance of the catalyst clearly demonstrate the benefit of anchoring the catalysts inside the concave surfaces of mesoporous silica. Full details for the reactions are given in recently filed patents.[14]

It is seen that the enantioselectivity achieved with the anchored variants of the catalysts is superior to that achieved with their homogeneous counterparts, (Table 1). Moreover, further evidence to support the view that it is the concavity (and hence restricted access to the active site by the relatively bulky reactants) that is crucial as a determinant of the enhancement of the *ee* value is borne out by the observed

 © 2003 Wiley-VCH Verlag GmbH & Co. KGaA, Weinheim

Table 1: The activities, selectivities[a] and enantiomeric excess (*ee*) values for the various homogeneous and heterogeneous catalysts for the hydrogenation of *E*-α-phenylcinnamic acid and methyl benzoylformate.[b]

Amine and diene	Counter-ion	Catalyst	Reaction	Metal	*t* [h]	Conv. [%]	Sel [%].	*ee* [%]
 COD	BF_4^-	homogeneous	α-phenyl cinnamic acid	Rh^I	24	74	77	93
		heterogeneous			24	80	74	96
	BF_4^-	homogeneous		Rh^I	24	95	58	0
		heterogeneous	methyl benzoyl formate		0.25	85	92	92
					1	98	94	91
					24	99	79	80
 NBD	BF_4^-	homogeneous	α-phenyl cinnamic acid	Rh^I	24	88	76	64
		heterogeneous			24	99	66	91
	BF_4^-	homogeneous	methyl benzoyl formate	Rh^I	0.5	85	70	18
		homogeneous 20 °C			0.5	56	59	69
		heterogeneous			2	100	98	99
 allyl	BF_4^-	homogeneous	α-phenyl cinnamic acid	Pd^{II}	24	100	87	76
		heterogeneous			24	93	87	93
	BF_4^-	homogeneous	methyl benzoyl formate	Pd^{II}	2	100	94	0
		heterogeneous			1	96	97	87
					2	97	97	87
 COD	BF_4^-	homogeneous	α-phenyl cinnamic acid	Rh^I	24	57	84	81
		heterogeneous MCM-41			24	98	80	93
		1st recycle			24	90	86	90
		2nd recycle			24	89	84	90
		cabosil			24	95	77	79
 allyl	BF_4^-	homogeneous	α-phenyl cinnamic acid	Pd^{II}	24	95	82	79
		heterogeneous			24	75	100	88

[a] For 2,3-diphenylpropionic acid and methyl mandelate. [b] Also shown is the comparative performance of a heterogeneous catalyst after two recycle experiments for the hydrogenation of *E*-α-phenylcinnamic acid. The heterogeneous analogue of **1b**, where the ligand is anchored onto the commercially available silica (cabosil M5, surface area = 200 $m^2 g^{-1}$), is also given. In all cases the same enantiomer of 2,3-diphenylpropionic acid was formed. Reaction conditions: substrate ≈0.5 g; solvent (methanol) ≈30 mL; homogeneous catalyst ≈10 mg; heterogeneous catalyst ≈50 mg; Pressure = 20 bar; T = 313 K; t = 24 h.

diminished degree of enantioselectivity when a catalyst is anchored to a convex siliceous surface (see Table 1). In the postulated computer graphic models shown (to scale) in Figure 3a and Figure 3b it may be seen that access of the phenylcinnamic acid to the Rh^I ion is favored only when the reactant approaches the active site along the axis of the pore (Figure 3a), whereas no such restrictions exist in the case of the same catalyst anchored at the convex surface.[15]

In previous, similar experiments, on allylic amination, involving catalysts located at the walls of mesoporous silica (e.g., Pd((*S*)-1[(*R*)-1′,2-bis(diphenylphosphino)ferrocenyl]-ethyl-*N*,*N*′-dimethylethylene-diamine)Cl_2),[8,9,12e] it was the constraints imposed by the space surrounding the metal center (active site) that dominated the enantioselectivity. In the case presented herein, there is a subtle difference; it is the restricted access generated by the concavity of the pore that is the principal determinant. Even though the "capping" cyclooctadiene may be lost during or just prior to the act of catalytic turnover at the Rh^I center, access to the latter of the reactant is nevertheless a key factor, and this is why concavity enhances the catalytic performance observed.[15]

To confirm that the anchored catalysts are truly heterogeneous and that no complications arise from leaching of the organometallic moiety during use, we performed a hot filtration and analyzed the resulting product mixtures (by inductively coupled plasma atomic emission spectroscopy; ICPAES). In a typical reaction at 313 K and 20 bar of H_2 pressure (Table 1), the solid catalyst was filtered from the reaction mixture after 8 h, and the reaction continued for a further 16 h. There was no appreciable change in the conversion of the *E*-α-phenylcinnamic acid during the 16 h period after removal of the solid catalyst, and the product selectivities and enantiomeric excess value were also unaffected. These facts rule out the possibility that colloidal Rh(Pd) or Rh(Pd) black are formed as, if they were, no longer would we observe an enantiomeric excess or essentially unchanged product selectivities.

It is not an easy task to extend the comparison between asymmetric organometallic catalysts tethered on to a range of concave/convex pairs because it is difficult to prepare nonporous convex silicas (like the commercially available cabosil). We have, however, obtained results that confirm the validity of our arguments by using three distinctly different concave silicas.[16]

Experimental Section

All compounds were purchased from Aldrich, unless otherwise stated. The solvents were all predried by using standard methods. The reactions were carried out under an atmosphere of nitrogen by using

 © 2003 Wiley-VCH Verlag GmbH & Co. KGaA, Weinheim

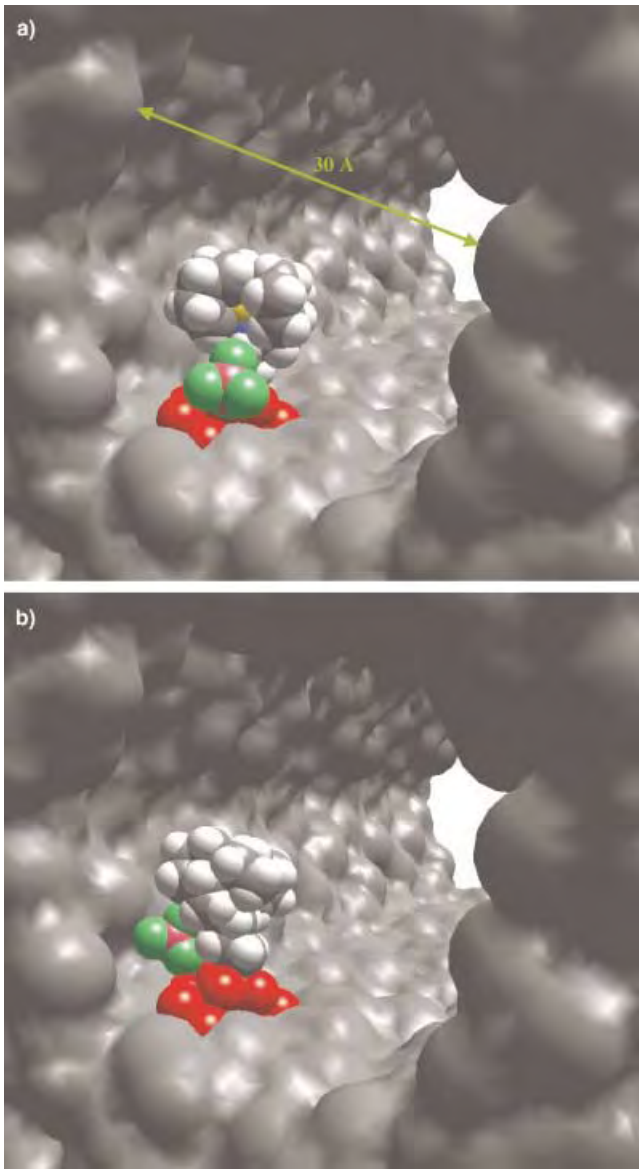


Figure 3. Color portrayal of the anchored Rh^{I}-organometallic -diene, as-prepared catalyst, thus illustrating the hindered access to the metal center because the incoming reactant must approach parallel to the channel (a). When rotation about the C–C bond in the tether occurs so that the Rh^{I} center faces the wall of the pore, as in (b), access to the active site is no longer possible. Whilst it is feasible that some of the diene may be jettisoned during or shortly after hydrogenation, it is not likely that all of it is jettisoned in the original catalyst (as is generally the case in analogous homogeneous catalytic situations) as (I) the repeat cycles (see Table 1) show that catalytic performance is sustained in progressive experiments, and (II) there is a significant enhancement in ee upon anchoring the organometallic catalyst (see text).

standard Schlenk line techniques. All experimental procedures as well as the crystal structures are given in the supporting information, a typical procedure is detailed below. The NMR were performed on a Bruker DPX 500 MHz employing cryo-probe technology.

[Rh(1,5-cyclooctadiene)(1R,2R)-(+)-1,2-diphenylethylenediamine]BF_4: $[RhCl(COD)]_2$ (64 mg, 0.13 mmol) was dissolved in THF (10 mL) to which $AgBF_4$ (50 mg, 0.26 mmol) was added, this solution was stirred for 1 hour at room temperature. The solution was then filtered (to remove AgCl) and (1R, 2R)-(+)-1,2-diphenylethylenediamine (50 mg, 0.26 mmol) was added to the filtrate and the solution left to stir for 1 hour. The resulting solution was slightly concentrated in vacuo and hexane (25 mL) added to precipitate the required product. The product was isolated by filtration and washed with hexane (2 × 20 mL) and diethyl ether (2 × 20 mL) and dried in vacuo giving a yellow powder (185 mg, 90 %). Elemental analysis calcd (%) for $C_{22}H_{28}N_2RhBF_4$: C 51.76, H 5.50, N 5.50; found C 51.44, H 5.57, H 5.29. ^{1}H NMR (CD_3OD): $\delta = 1.95$ (br m, CH_2 4H), 2.46 (br m, CH_2, 4H), 4.01 (s, NCH, 2H), 4.24 (m, CH, 2H), 4.35 (m, CH, 2H), 7.1–7.3 ppm (m, Ph, 10H). ^{13}C NMR (CD_3OD): $\delta = 31.6$ (CH_2), 66.3 (NCH) 81.4 (CH), 128.5, 129.2, 129.6, 140.5 ppm (Ph). ESI (positive ion): 423 [M^+].

Activation of MCM-41: To dry calcined MCM-41 (BET surface area 880 $m^2 g^{-1}$, determined by N_2 adsorption; 2.0 g) in THF (15 mL) dichlorodiphenylsilane (0.48 g, 0.19 mmol) was added and stirred at room temperature for 1 hour (Ph_2SiCl_2) reacts with external Si-OH moieties[10–11] and ensures all proceeding silane species reacts at the internal surface of MCM-41). The solution was then cooled to −78 °C and 3-bromopropyltrichlorosilane (1.10 g, 4.8 mmol) was added. This mixture was allowed to slowly warm up to room temperature and stirred for a further 8 h. The resulting solution was heated at 50 °C for 1 hour. The MCM-41 was filtered and purified by soxhlet extraction with THF and finally dried in vacuo. Elemental analysis found (%): C 4.70, H 0.87, Br 2.14. ^{29}Si CP MAS NMR indicated significant loss of Si–OH moieties indicating grafting had occurred, the XRD of the resulting MCM-41 was analogous to the pure MCM-41 showing no loss of structure occurred.

Tethering with (1R,2R)-(+)-1,2-diphenylethylenediamine: The activated MCM-41 (500 mg) was heated to reflux in THF (15 mL) together with the amine (150 mg) for 24 h. After this time the MCM-41 was filtered and purified by soxhlet extraction with THF and finally dried in vacuo. Elemental analysis found (%): C 9.72, H 1.92, N 0.15, Br 1.30. IR $\tilde{\nu} = 3205$ cm^{-1} broad (weak), N–H stretch. Powder XRD indicated no loss in the structure of the mesopore during this process.

Addition of rhodium: In a Schlenk $[RhCl(COD)]_2$ (30 mg, 0.06 mmol) and $AgBF_4$ (30 mg, 0.12 mmol) were dissolved in THF (10 mL) and stirred for 1 hour. The solution was filtered and the tethered MCM-41 was added to the filtrate and stirred for 4 h during which time the solution became pale and the solid became yellow. This pale yellow solid was filtered and washed with THF (4 × 20 mL), CH_2Cl_2 (4 × 20 mL) and dried in-vacuo. **3b**: C 11.23, H 2.02, N 0.12, Br 1.22. ^{19}F MAS NMR indicated the presence of BF_4^- $\delta = -152.0$ ppm (reference $CFCl_3$), in solution $\delta = -154$ ppm. Powder XRD only showed peaks that correspond to MCM-41 implying that the rhodium is highly dispersed inside MCM-41.

Catalysis procedure: The catalytic reactions (enantioselective hydrogenations) were carried out in a high-pressure stainless-steel catalytic reactor (100 mL) lined with poly ether ether ketone (PEEK). The homogeneous catalyst (10 mg or 50 mg of the mesoporous silica anchored heterogeneous catalyst), which was previously evacuated and stored under inert conditions (nitrogen or argon), was transferred under an inert atmosphere to the catalyst delivery unit, which was subsequently sealed and introduced to the high-pressure reactor (by using dry helium).

The substrate {(E)-α-phenyl cinnamic acid or methyl benzoylformate} (0.5 g), solvent (methanol, 30 g) and a suitable internal standard (cyclododecane) were then introduced into the reactor and the reactor was sealed. The reactor as well as the inlet and outlet ports were purged with dry nitrogen (three times) prior to the introduction of hydrogen (5 bar). A leak test was carried out and the reactor was then pressurized to 20 bar with hydrogen. The reactor was then heated to the desired temperature (313 K) and the contents were stirred with a mechanical stirrer at 400 rpm. (In the cases in which kinetic and rate effects were studied, a minirobot liquid-sampling valve was employed to remove small aliquots of the sample without perturbing the pressure in the reactor).

 © 2003 Wiley-VCH Verlag GmbH & Co. KGaA, Weinheim

At the end of the reaction, the heating was turned off the contents of the reactor were cooled (quenched). The reactor was then depressurized. A mass-balance calculation was made at this stage to check for handling and weight losses. The products were analyzed (with a suitable internal standard) by gas chromatography (GC; Varian, Model 3400 CX) employing a HP-1 capillary column (25 m × 0.32 mm) and flame ionization detector with a variable ramp temperature program from 433 K to 493 K, for cinnamic acid. The identities of the products were first confirmed by using authenticated standards and their individual response factors were determined with a suitable internal standard (calibration method). The conversions and selectivities were determined as defined by the following equations and the yields were normalized with respect to the response factors obtained as above:

Conversion % = [(moles of initial substrate − moles of residual substrate)/(moles of initial substrate)] × 100 Selectivity % = [(moles of individual product)/(moles of total products)] × 100

The products were further identified by NMR spectroscopy (^{1}H and ^{13}C in CD_3OD) which showed the loss of the C=C and the gain of a C−C moiety for cinnamic acid and for methyl benzoyl formate a loss of a C=O and a gain of a C−O environment. The enantioselectivity values (*ee*) (for cinnamic acid) were first determined by GC (Hewlett Packard {HP 5890}) with a chiral column {gamma-cyclodextrin dialkyl (Chiraldex) (20 m × 0.25 mm)} and the identities of the chiral products were further confirmed by LC–MS (Shimadzu LCMS-QP8000) equipped with a chiral detector (OR-990, JASCO), again, with a chiral column (CHIRALCEL OJ-R, DAICEL). Enantiomeric excess values were calculated from the peak areas of the enantiomers by using the following formula:

$$ee = ([R] - [S]) \times 100/([R] + [S])$$

Finally, as a further confirmation, the products were isolated from the reaction mixture and esterified to the methyl ester by the following procedure: Boron trifluoride (14 %, 2 mL) in methanol was added to a glass vial containing the sample to be esterified (300 μL), the vial was sealed with a teflon-lined stopper and heated for 1 h at 353 K. The sample was cooled to room temperature and Milli-Q purified water (2 mL) was added with mild shaking. HPLC grade dichloromethane (2 mL) was added before the analysis, which was again performed on the LC–MS (Shimadzu LCMS-QP8000) with the same chiral column (CHIRALCEL OJ-R, DAICEL).

The *ee* values for methyl mandelate were determined by Bayer AG Leverkusen Germany.[14]

Since this work was carried out we have further tested and explored[17] a new method, described by Rege et al.,[18] of anchoring homogeneous catalysts on to high-area supports through the use of the triflate anion. For that purpose two entirely new ligands and (for comparison) two of the ones reported here were used to produce the Rh^I-based asymmetric hydrogenation catalysts. This method is very convenient and it also produces superior heterogeneous asymmetric catalysts than their homogeneous analogues.

Received: December 27, 2002
Revised: May 26, 2003 [Z50861]

Keywords: asymmetric catalysis · chiral resolution · heterogeneous catalysis · hydrogenation · mesoporous silica

[1] G. W. Parshall, S. D. Ittel, *Homogeneous Catalysis*, 2nd ed., Wiley, New York, **1992**.

[2] H. Brunner in *Applied Homogeneous Catalysis with Organometallic Compound, Vol. 1* (Eds.: B. Cornils, W. A. Herrmann), Wiley-VCH, Weinheim, **1996**, pp. 206, and references therein.

[3] a) R. Noyori, *Asymmetric Catalysis in Organic Synthesis*, Wiley, New York, **1994**; b) R. Noyori, *Angew. Chem.* **2002**, *114*, 2108; *Angew. Chem. Int. Ed.* **2002**, *41*, 2008; c) I. Ojima, *Catalytic Asymmetric Synthesis*, VCH, Weinheim, **1993**.

[4] C. Claver, E. Fernandez, A. Gillion, K. Heslop, D. J. Hyett, A. Martorell, A. G. Orpen, P. G. Pringle, *Chem. Commun.* **2000**, 961.

[5] T. Hayashi, Y. Matsumoto, Y. Ito, *Tetrahedron: Asymmetry* **1992**, *2*, 601.

[6] Though relatively uncommon, diamino ligands in organometallic complexes that are catalytic for hydrogenation were reported. For example, a) A. Trogri, L. Venanzi, *Angew. Chem.* **1994**, *106*, 517; *Angew. Chem. Int. Ed. Engl.* **1994**, *33*, 497; b) M. L. Tommasino, C. Thomazeau, F. Touchard, M. Lemaire, *Tetrahedron: Asymmetry* **1999**, *10*, 1813; c) F. Fache, E. Schultz M. L. Tommasino, M. Lemaire, *Chem. Rev.* **2000**, *100*, 2159; d) C. Pinel, N. GendreauDiaz, A. Breheret, M. J. Lemaire, *J. Mol. Catal. A* **1996**, *112*, l157; e) C. Saluzzo, M. J. Lemaire, *Adv. Synth. Catal.* **2002**, *344*, 915; f) P. Pertici, F. D'Arata, C. Rosini, *Organometallics* **1996**, *15*, 9163; g) M. Costa, P. Pelagatti, C. Pelizzi, D. Rogolino, *J. Mol. Catal. A* **2002**, *178*, 21; h) A. Corma, M. Iglesias, C. Delpino, F. Sanchez, *J. Chem. Soc. Chem. Commun.* **1991**, 1253; i) A. Corma, M. Iglesias, C. Delpino, *J. Organomet. Chem.* **1992**, *432*, 233.

[7] *Crystallographic data:* **1a Rh COD** complex $C_{15}H_{28}BF_4N_2Rh$, $M = 426.11\ g\,mol^{-1}$, yellow prisms $0.28 \times 0.14 \times 0.07$ mm, monoclinic, $a = 9.1422(2)$ Å, $b = 10.8050(4)$ Å, $c = 9.3369(3)$ Å, $\beta = 110.243(2)°$, $V = 865.34(5)$ Å^3, $T = 180(2)$ K, space group $P2_1$, $Z = 2$, 5542 reflections collected, 3400 independent reflections ($R_{int} = 0.0286$), refinement method: full matrix least squares on F^2, final $R_1 = 0.0254$, $wR_2 = 0.0588$, GOF = 1.125. **1a Rh NBD** complex $C_{14}H_{24}BF_4N_2Rh$, $M = 410.07\ g\,mol^{-1}$, yellow prisms $0.25 \times 0.12 \times 0.12$ mm, orthorhombic, $a = 9.3033(2)$ Å, $b = 10.4587(3)$ Å, $c = 16.7856(5)$ Å, $\beta = 90°$, $V = 1633.25$ Å^3, $T = 180(2)$ K, space group $P2_12_12_1$, $Z = 4$, 9724 reflections collected, 3359 independent reflections ($R_{int} = 0.1154$), refinement method: full matrix least squares on F^2, final $R_1 = 0.0591$, $wR_2 = 0.1278$, GOF = 0.991. **1a Pd** complex $C_{10}H_{21}BF_4N_2Pd$, $M = 362.50\ g\,mol^{-1}$, clear prisms $0.30 \times 0.18 \times 0.12$ mm, orthorhombic, $a = 8.0393(3)$ Å, $b = 12.8833(4)$ Å, $c = 13.8562(5)$ Å, $\beta = 90°$, $V = 1435.12(9)$ Å^3, $T = 180(2)$ K, space group $P2_1$, $Z = 2$, 8364 reflections collected, 3190 independent reflections ($R_{int} = 0.0319$), refinement method: full matrix least squares on F^2, final $R_1 = 0.0303$, $wR_2 = 0.0700$, GOF = 1.032, crystallographic data is available in the .cif format. CCDC-193929 (**1a Rh COD**), CCDC-193930 (**1a Rh NBD**), and CCDC-203770 (**1a Pd**) contain the supplementary crystallographic data for this paper. These data can be obtained free of charge via www.ccdc.cam.ac.uk/conts/retrieving.html (or from the Cambridge Crystallographic Data Centre, 12 Union Road, Cambridge CB2 1EZ, UK; fax: (+44) 1223-336-033; or deposit@ccdc.cam.ac.uk).

[8] J. M. Thomas, T. Maschmeyer, B. F. G. Johnson, D. S. Shephard, *J. Mol. Catal. A* **1999**, *141*, 139.

[9] J. M. Thomas, *Angew. Chem.* **1999**, *111*, 3800; *Angew. Chem. Int. Ed.* **1999**, *38*, 3588.

[10] B. F. G. Johnson, S. A. Raynor, D. S. Shephard, T. Maschmeyer, J. M. Thomas, G. Sankar, S. Bromley, R. Oldroyd, L. Gladden, M. D. Mantle, *Chem. Commun.* **1999**, 1167.

[11] S. A. Raynor, J. M. Thomas, R. Raja, B. F. G. Johnson, R. G. Bell, M. D. Mantle, *Chem. Commun.* **2000**, 1925.

[12] a) Y. Nitta, Y. Ueda, T. Imanka, *Chem. Lett.* **1994**, *6*, 1095; b) K. Borszeky, T. Mallat, A. Baiker, *Tetrahedron: Asymmetry* **1997**, *22*, 3745; c) K. Borszeky, T. Burgi, Z. Zhaohui, T. Mallet, A. Baiker, *J. Catal.* **1999**, *187*, 160; d) R. Raja, J. M. Thomas, *J. Mol. Catal. A* **2002**, *181*, 3; e) J. M. Thomas, B. F. G. Johnson, R. Raja, G. Snakar, P. A. Midgley, *Acc. Chem. Res.* **2003**, *36*, 20; f) J. M. Thomas, R. Raja, B. F. G. Johnson, S. Hermans, M. D. Jones, T. Khimyak, *Ind. Eng. Chem. Res.* **2003**, *42*, 1563.

[13] We are grateful to one of the referees for drawing the contrast between the Rh-diphosphane and Rh-diamine-diene catalysts to our attention.

 © 2003 Wiley-VCH Verlag GmbH & Co. KGaA, Weinheim

[14] R. Raja, J. M. Thomas, B. F. G. Johnson, M. D. Jones, German Patent DE-10305946, **2003** and DE-10305943 **2003**.
[15] Accepted theory amongst experts in homogeneous catalysis states that the diene (in this case COD or NBD) are no longer present in the catalyst when it facilitates hydrogenation. But if this were true the catalytic performance of a given organometallic complex would be independent of the initially coordinated diene. This is patently not the case—see Drexler et al.,[15a] where Rh^{I} hydrogenation catalysts exhibit a thousand fold difference in reactivities on replacing the COD by NBD. In the critical act of catalysis, possibly even homogeneously, but certainly heterogeneously, under the conditions that we employ, the diene may still be implicated.[13] This is why we have depicted the as-prepared heterogeneous catalyst in Figure 3a and 3b; a) H. J. Drexler, W. Baumann, A. Spannerberg, C. Fisher, D. Heller, *J. Organomet. Chem.* **2002**, *621*, 89.
[16] J. M. Thomas et al., unpublished results.
[17] J. Rouzaud, M. D. Jones, R. Raja, B. F. G. Johnson, J. M. Thomas, M. J. Duer, *Helv. Chim. Acta.* **2003**, *86*, 1753.
[18] F. M. de Rege, D. K. Morita, K. C. Ott, W. Tumas, R. D. Broene, *Chem. Commun.* **2000**, 1797.

 © 2003 Wiley-VCH Verlag GmbH & Co. KGaA, Weinheim

CO_2 Inclusion in Crystals

Carbon Dioxide Inclusion Phases of a Transformable 1D Coordination Polymer Host $[Rh_2(O_2CPh)_4(pyz)]_n$**

Satoshi Takamizawa, Ei-ichi Nakata, Haruhiko Yokoyama, Katsura Mochizuki, and Wasuke Mori*

Many inclusion compounds have been reported and the inclusion phenomenon has gained recognition in organic, inorganic, and physical chemistry, biology, and other branches of science.[1] The design and control of porous-network structures of extended inorganic frameworks has been extensively studied in recent years because of the ability to control their guest-adsorbing functionality.[2] The recent increase in the research of single-crystal host solids constructed by noncovalent intermolecular interactions is due to their specific properties such as guest exchange, gas storage, and transformation.[3] However, the mechanisms by which the guest invades the crystal host and by which the crystal transforms during the inclusion process are poorly understood.

An empty single-crystal host of rhodium(II) benzoate pyrazine, $[Rh^{II}_2(O_2CPh)_4(pyz)]_n$ (**1**), was prepared by a method reported elsewhere.[4] The component chains found in crystals of **1** adopt a perfectly linear geometry with the chain skeleton bridged by the pyrazine group in the axial direction of the well-known lanternlike core[5] of dinuclear rhodium benzoate (Figure 1). The polymeric chains are densely packed to form the crystal. The crystallographic data collected under different conditions are summarized in Table 1.

The crystal structure of **1** at 20 °C is shown in Figures 2 a, b, and c. The complex crystallizes in the monoclinic space group $C2/m$; there are no channel structures sufficient to hold guest molecules, but rather there are empty cages with dimensions of $9 \times 4 \times 3$ Å, with narrow gaps of approximately 1 Å found at

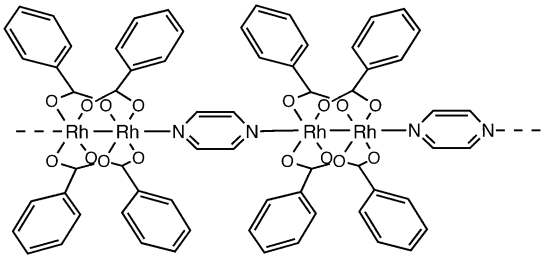


Figure 1. Schematic drawing of the chain structure of compound **1**.

Table 1: Crystallographic parameters of **1** under various conditions.

	no CO_2 (Si oil)	no CO_2 (Si oil)	CO_2	CO_2	CO_2
CO_2 molecules included	–	–	0	0.733[a]	3.0
Phase	α	γ	α	β	β
M	770.36	770.36	770.36	802.62	902.39
Crystal system	Monoclinic	Monoclinic	Monoclinic	Triclinic	Triclinic
Space group (number)	$C2/m$(no. 12)	$C2/c$(no. 15)	$C2/m$(no. 12)	$P\bar{1}$ (no. 2)	$P\bar{1}$ (no. 2)
T [K]	293.2	93.2	293.2	213.2	93.2
a [Å]	17.821(9)	17.42(3)	17.85(1)	9.577(3)	9.556(3)
b [Å]	9.605(5)	9.55(1)	9.465(5)	10.306(3)	10.318(4)
c [Å]	12.362(8)	19.70(4)	14.113(9)	10.850(4)	11.079(5)
α [°]	90	90	90	72.28(3)	70.18(3)
β [°]	127.53(4)	98.05(6)	137.20(2)	65.31(3)	66.12(3)
γ [°]	90	90	90	63.25(2)	63.02(3)
V [Å]	1678(1)	3244(9)	1620(1)	859.9(5)	873.7(6)
Z	2	4	2	1	1
D_{calcd} [g cm^{-3}]	1.524	1.577	1.579	1.550	1.715
μ [cm^{-1}]	10.30	10.66	10.67	10.12	10.15
Final R_1 ($I > 2\sigma(I)$)	0.0359	0.0613	0.0869	0.0896	0.1031
WR_2 (all data)	0.0746	0.1183	0.2481	0.2350	0.2504
GOF on F^2	1.044	1.048	1.165	1.131	1.367

[a] The incorporated CO_2 molecules were detected only on the crystallographic A site with an occupation probability of 73.3 % (See Figure 3).

[*] Dr. S. Takamizawa, E.-i. Nakata, Prof. Dr. H. Yokoyama, Prof. Dr. K. Mochizuki
Graduate School of Integrated Science
Yokohama City University
Kanazawa-ku, Yokohama, Kanagawa 236-0027 (Japan)
Fax: (+81) 45-787-2187
E-mail: staka@yokohama-cu.ac.jp
Prof. Dr. W. Mori
Department of Chemistry
Faculty of Science, Kanagawa University
Tsuchiya, Hiratsuka
Kanagawa 259–1293 (Japan)

[**] We thank Dr. M. Shiro and Dr. A. Kishi (Rigaku Corp.) for their technical assistance with the X-ray measurements; pyz = pyrazine.

Supporting information for this article is available on the WWW under http://www.angewandte.org or from the author.

 DOI: 10.1002/anie.200351368 © 2003 Wiley-VCH Verlag GmbH & Co. KGaA, Weinheim

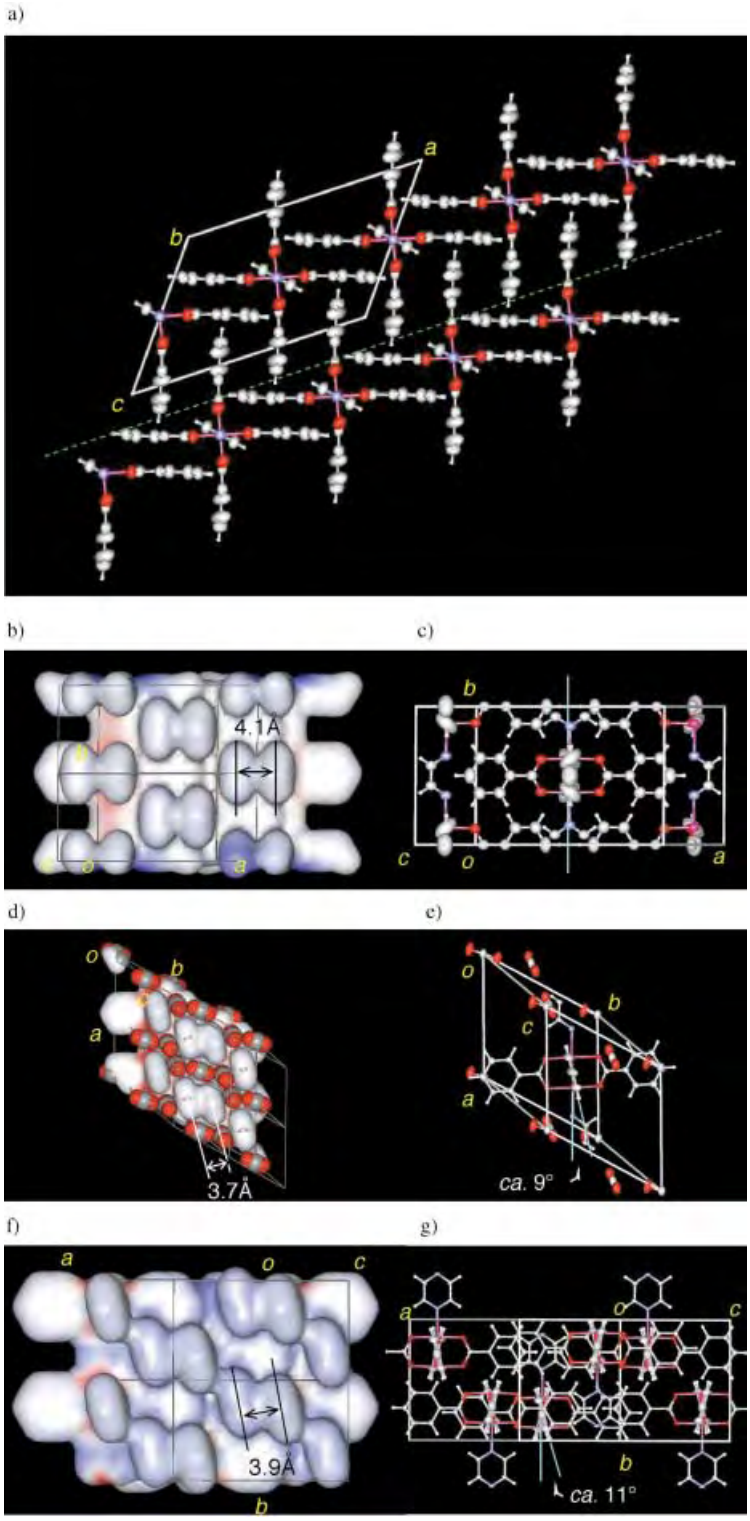


Figure 2. Views of crystal **1**: a) view along the chain vector showing thermal ellipsoids for the crystal structure in CO_2 atmosphere at 20 °C; b) surface view along the dashed-green cross section of a); c) the corresponding ellipsoidal view; d) surface view of the CO_2-inclusion state at −180 °C; e) the corresponding ellipsoidal view; f) surface view of the crystal under conditions where CO_2 was absent at −180 °C ; g) the corresponding ellipsoidal view. Atoms: Rh (magenta), C (grey), H (white), N (blue), O (red). All ellipsoidal views are shown at 50% probability.

their four corners,[6] which are formed by the benzene rings of benzoate moieties arranged parallel to the chain vector. On cooling samples in a CO_2 atmosphere, the crystal underwent a phase transition to a new structure adopting the triclinic space group $P\bar{1}$, and generating one-dimensional (1D) channels (Figure 2d). The cages are transformed into channels by a slippage of the chain skeletons along the chain vector; the benzene ring tilts 9° away from the chain vector (Figure 2e). External CO_2 is incorporated into the channels in the form of molecular wires, in which the molecular axes of the CO_2 molecules are almost parallel and perpendicular to the channel direction at sites A and B, respectively (Figure 3).

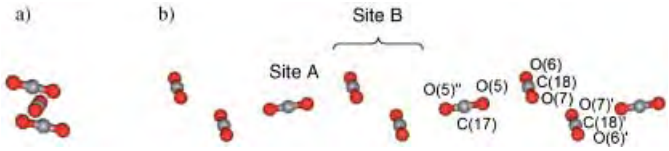


Figure 3. Ball-and-stick representation of the column of CO_2 molecules in the channels of crystal **1** in the inclusion state: a) top view and b) side view. Pertinent atomic separations [Å] and angles [°]: O(5)-C(18) 2.85, C(18)-C(18)′ 3.53, C(18)-O(6)′ 4.13, C(18)-O(7)′ 3.17; C(17)-C(18)-C(18)′ 124.6, C(17)-O(5)-C(18) 162.3, O(5)-C(18)-O(6) 90.4, O(5)-C(18)-O(7) 92.3.

Evidence for the diffusion of gas into the crystal through the narrow gaps at the corners of the cages was obtained from sorption measurements. The CO_2 adsorption isotherm at 0 °C demonstrated that gas was smoothly incorporated into the crystal with a Langmuir-type curve due to monolayer adsorption (see Supporting Information). The estimated Brunauer–Emmett–Teller (BET) surface area is extremely large at 274.1 $m^2 g^{-1}$,[7] which indicates that the CO_2 gas is adsorbed not on the crystal surface but also inside the crystal. The accumulated quantity of CO_2 gas at ambient pressure is 23.7 $cm^3(STP)\,g^{-1}$ or 37.4 $cm^3(STP)\,cm^{-3}$ (where $cm^3(STP)$ represents the volume of gas accumulated under standard conditions). This corresponds to an average of 0.81 CO_2 molecules per Rh_2 unit or per cage. The CO_2 sorption isobar measurement at ambient pressure yielded a monotonous desorption curve with a saturation point at approximately −80 °C (Figure 4). The saturated quantity of 3.0 molecules per Rh_2 unit at −80 °C agrees well with the composition determined from the single crystal X-ray diffraction data at −180 °C. The crystal structures at 20 °C and −60 °C should also contain the observed amount of ≈0.5 and 2.9 CO_2 molecules per Rh_2 unit, respectively, but the molecules could not be located by X-ray crystallography, probably due to their thermal motion. The unit-cell volume in a CO_2 atmosphere at 20 °C decreased by 3% in comparison with that measured under conditions where CO_2 is absent, which implies that stressed CO_2 inside the lattice attempts to deform the cages (Table 1).

Simultaneous powder X-ray diffraction (XRD) and differential scanning calorimetry (DSC) measurements were conducted. On cooling, changes were observed in

 © 2003 Wiley-VCH Verlag GmbH & Co. KGaA, Weinheim

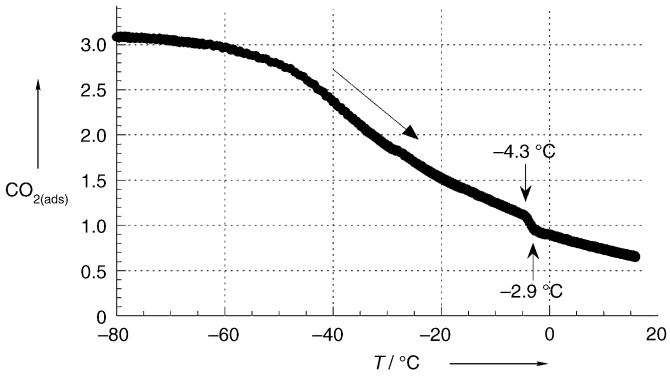


Figure 4. Isobar curve at ambient CO_2 pressure (gravimetric method) using a Cahn 2000 electronic balance ($CO_{2(ads)}$ = moles of CO_2 adsorbed per Rh_2 unit).

the diffraction pattern of **1** and the peaks in the XRD patterns decreased in intensity and sharpness near −10 °C, with a corresponding exothermic peak in the DSC trace (Figure 5a), which clearly shows that a structural rearrangement takes place in the region of the phase transition. At lower temperatures, the peaks in the new diffraction patterns became sharper and increased in intensity. This property indicates that the bulk-phase transition occurs at this temperature; no significant changes took place under a nitrogen atmosphere (see Supporting Information). The patterns at 20 °C and −70 °C are in good agreement with those simulated using the crystal structures under CO_2 atmosphere with space groups $C2/m$ (at 20 °C) and $P\bar{1}$ (at −180 °C), respectively (see Supporting Information). In the scanning temperature range of 50 to −40 °C, the DSC measurements repeatedly revealed exo- and endothermic phase transitions at −9.9 °C (cooling) and −4.6 °C (heating) in a CO_2 atmosphere at ambient pressure (Figure 5b), while no peaks were observed when a purely nitrogen atmosphere was used. The transition enthalpy (ΔH) of crystal **1** in a CO_2 atmosphere, calculated from the areas of the DSC peaks, is −5.8 (cooling) and 5.4 (heating) kJ mol^{-1} with respect to the Rh_2 units. The temperatures where the sets of cyclic DSC peaks occur shift to lower values as the concentration of CO_2 decreases. The natural logarithm of the partial pressure ($\ln P_{CO2}$) and the reciprocal transition temperature (T^{-1}) show a good linear correlation (Figure 5c). This correlation coincides with the Clausius–Clapeyron equation, which is commonly used for estimating differentials in the isosteric heat of adsorption from pressure and temperature data measured at the same adsorption levels:

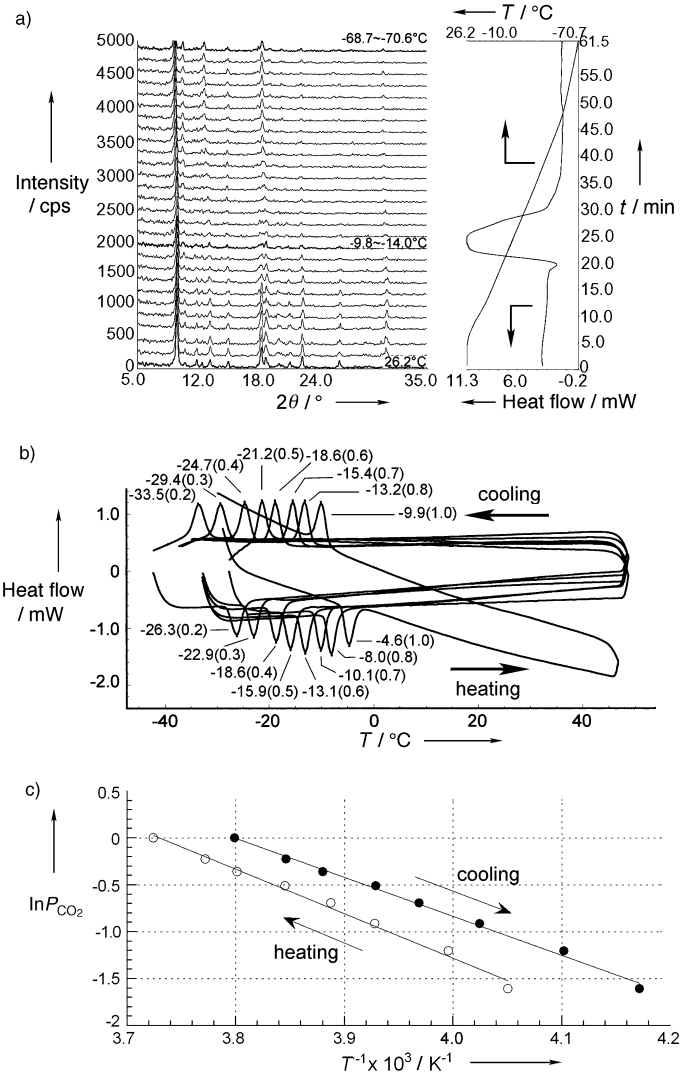


Figure 5. a) X-ray diffraction patterns of crystal **1** in a CO_2 atmosphere as a function of temperature, with a simultaneous DSC measurement; b) independent DSC cyclic patterns of crystal **1** under ambient pressure with different CO_2/N_2 mixtures (values on the curves denote temperatures at the peak maxima with the CO_2 contents shown in parentheses); c) correlation between the partial pressure of CO_2 and the transition temperature. Simultaneous XRD/DSC measurements were recorded on a Rigaku XRD-DSC II diffractometer with a temperature scan rate of 3 °C min^{-1} and a 2-θ scan rate of 15 ° min^{-1} over the range 5 to 35° with $Cu_{K\alpha}$ radiation (λ = 1.54184 Å). Independent DSC measurements at a scanning rate of 5 °C min^{-1} were recorded on a Shimadzu DSC-60 calorimeter.

$$\text{gas} + \text{adsorbent} \rightarrow \text{gas on adsorbent} \quad (1)$$

$$\mathrm{d}(\ln P)/\mathrm{d}(T^{-1}) = \Delta H/\mathrm{R} \quad (2)$$

where R and ΔH denote the gas constant and the adsorption enthalpy of gas, respectively. This relationship indicates that the amounts of CO_2 adsorbed by **1** are the same at the phase transition points, and $-\Delta H$ is the isosteric heat of adsorption ($-\Delta H_{iso}$). The estimated value of ΔH_{iso} for CO_2 is determined from the gradient to be −34.5 kJ mol^{-1} (cooling or adsorption) and 39.6 kJ mol^{-1} (heating or desorption). Similar behavior has been observed for a copper derivative of compound **1**.[8] The critical quantity of adsorbed CO_2 is estimated to be one CO_2 molecule per Rh_2 unit at a significant transition point close to −5 °C from the isobar (Figure 4b). The estimated value indicates that the $C2/m$ crystal can include no more than one CO_2 molecule under the current "α saturation" condition and subsequently transforms to the inclusion crystal, which enables up to three CO_2 molecules per Rh_2 unit, contained within the channels.

Under conditions in which CO_2 is absent, the space-group symmetry changes from $C2/m$ to $C2/c$ on cooling to −180 °C,

 © 2003 Wiley-VCH Verlag GmbH & Co. KGaA, Weinheim

and the crystal exhibits a channel structure with a narrow neck of ≈2 Å diameter, which is too narrow for atmospheric gas to be adsorbed (Figure 2 f and g). However, the *C2/c* crystal can smoothly adsorb N_2 gas in the microporous region at 77 K with a large BET surface area of 352.5 $m^2 g^{-1}$,[4] where it is likely that the gas sorption process involves a crystal transformation, at least on a local scale.

The cage α phase (*C*2/*m*) is replaced by the inclusion β phase below the transition point in the presence of CO_2 gas. It is known that an offset stacking configuration is energetically more stable than that of a perfect overlap.[9] From the perspective of crystal energy, therefore, on depressing thermal vibration as the temperature decreases, a perfect face-to-face overlap of the benzene planes in the α phase changes to an offset configuration with tilting of the rings in phases β ($P\bar{1}$) and γ (*C*2/*c*) favored, where the separation distances of the planes are approximately 4.1, 3.7, and 3.9 Å in the α, β, and γ phases, respectively. It is noted that the two modes of chain slippage and offset stacking clearly occur simultaneously in the inclusion β phase. They regulate the formation of the inclusion crystal and shorten the interplanar distances, which may allow the volume of space in the channels to be maximized and the crystal to be stabilized. In fact, temperature and pressure are critical to the understanding of the entire transition process.

This inclusion process results in a smooth and reversible transformation from an "empty single crystal" to an "inclusion single crystal" without the exchange of guests. This reversible control of the inclusion process with the remarkable ability to coherently crystallize light guest species from a gaseous environment will open the door to many new techniques.

Experimental Section

Single-crystal X-ray diffraction data was collected alternatively in a CO_2 atmosphere and in the absence of CO_2 by sealing a glass capillary containing the sample and CO_2 gas at ambient pressure and by scooping on a cryoloop through silicone oil, respectively. All experiments were performed on a Rigaku RAXIS RAPID imaging plate diffractometer with a nitrogen-flow temperature controller and $Mo_{K\alpha}$ radiation ($\lambda = 0.71073$ Å) over a temperature range of 20 to −180 °C. Empirical absorption corrections were applied using the ABSCOR program. The structures were solved by the Patterson method (DIRDIF94 PATTY) and refined by full-matrix least-squares on F^2 (SHELXL97). Non-hydrogen atoms were refined anisotropically, while hydrogen atoms were fixed at calculated positions and refined using a riding model. CCDC-19524, 19525, 194691, 194692, and 194693 contain the supplementary crystallographic data for this paper. These data can be obtained free of charge via www.ccdc.cam.ac.uk/conts/retrieving.html (or from the Cambridge Crystallographic Data Centre, 12, Union Road, Cambridge CB2 1EZ, UK; fax: (+44) 1223-336-033; or deposit@ccdc.cam.ac.uk).

Received: March 11, 2003
Revised: July 14, 2003 [Z51368]

Keywords: adsorption · host–guest systems · inclusion compounds · phase transitions · X-ray diffraction

[1] a) *Inclusion Compounds, Vol. 4* (Eds.: J. L. Atwood, J. E. D. Davies, D. D. MacNicol), Oxford University Press, Oxford, **1991**; b) *Topics in Inclusion Science, Vol. 2* (Eds.: T. Osawa, J. L. Atwood), Kluwer, Dordrecht, **1991**; c) *Host–Guest Complex Chemistry: Synthesis, Structures, Applications* (Eds.: F. Vögtle, E. Weber), Springer, Berlin, **1985**; d) *Comprehensive Supramolecular Chemistry, Vols. 1–11* (Eds.: J. L. Atwood, J. E. D. Davies, D. D. MacNicol, F. Vögtle), Elsevier Science, Oxford, **1996**; e) J. M. Lehn, *Supramolecular Chemistry: Concepts and Perspectives*, VCH, Weinheim, **1995**; f) L. R. Nassimbeni, *Acc. Chem. Res.*, in press.

[2] a) O. M. Yaghi, M. O'Keeffe, M. W. Ockwing, H. K. Chae, M. Eddaoudi, J. Kim, *Nature* **2003**, *423*, 705; b) E. J. Cussen, J. B. Claridge, M. J. Rosseinsky, C. J. Kepert, *J. Am. Chem. Soc.* **2002**, *124*, 9574; c) R. Kitaura, K. Seki, G. Akiyama, S. Kitagawa, *Angew. Chem.* **2003**, *115*, 444; *Angew. Chem. Int. Ed.* **2003**, *42*, 428; d) S. S.-Y. Chui, S. M.-F. Lo, J. P. H. Charmant, A. G. Orpen, I. D. Williams, *Science* **1999**, *283*, 1148; e) S. Takamizawa, M. Furihata, S. Takeda, K. Yamaguchi, W. Mori, *Macromolecules* **2000**, *33*, 6222.

[3] a) J. L. Atwood, L. J. Barbour, A. Jerga, *Science* **2002**, *296*, 2367; b) K. Biradha, Y. Hongo, M. Fujita, *Angew. Chem.* **2002**, *114*, 3545; *Angew. Chem. Int. Ed.* **2002**, *41*, 3395; c) J. L. Atwood, L. J. Barbour, A. Jerga, B. L. Schottel, *Science* **2002**, *298*, 1000.

[4] S. Takamizawa, T. Hiroki, E. Nakata, K. Mochizuki, W. Mori, *Chem. Lett.* **2002**, 1208.

[5] F. A. Cotton, R. A. Walton, *Multiple Bonds between Metal Atoms*, 2nd ed., Oxford University Press, New York, **1993**.

[6] The atomic void sizes were determined by subtracting van der Waals radii of 3.0 Å from various distances between the non-hydrogen atoms of the aromatic rings.

[7] The CO_2 adsorption isotherm was measured on a Quantachrome AUTOSORB-1 at 0 °C with pressures ranging from 3×10^{-3} to 1 atm (relative pressure = *P*(pressure)/P_0(saturated pressure), which ranged from 1×10^{-4} to 3×10^{-2}). The BET surface area in a relative pressure range from 0.01 to 0.03 was estimated using the ASWin program package.

[8] S. Takamizawa, E. Nakata, H. Yokoyama, *Inorg. Chem. Commun.* **2003**, *6*, 763.

[9] C. A. Hunter, J. K. M. Sanders, *J. Am. Chem. Soc.* **1990**, *112*, 5525.

 © 2003 Wiley-VCH Verlag GmbH & Co. KGaA, Weinheim

Spin–Spin Coupling Pathways

Visualization of Nuclear Spin–Spin Coupling Pathways by Real-Space Functions**

Olga L. Malkina and Vladimir G. Malkin**

Indirect nuclear spin–spin coupling constants are amongst the most important magnetic resonance parameters, invaluable in establishing molecular structure from NMR spectroscopy. Their detailed understanding in terms of molecular and electronic structure is thus of central importance in many fields of research and has been pursued since the advent of NMR spectroscopy more than 50 years ago. For example, questions of "through-space" versus "through-bond" mechanisms,[1,2] the coupling pathways in polycyclic systems, and most recently, spin–spin couplings through hydrogen bonds[3] have stimulated intensive discussions. Today, the quantum-chemical calculation of coupling constants has in many cases reached predictive accuracy.[4] This has, in turn, enhanced the interest in interpretation, that is, to go from accurate numbers to deeper insight.

Various types of analyses were used to obtain further information about different contributions to spin–spin coupling[2,5–8] in terms of localized or canonical molecular orbitals (MOs).[9] While these approaches can provide a very useful insight, their conclusions depend on MO transformations and are thus strongly model-dependent; different MO schemes may lead to conflicting interpretations.[8] Recently the analysis of spin–spin coupling constants based on Weinhold's natural bond orbital (NBO)[5] scheme has become popular. However, its language of localized MOs does not always appear natural for the interpretation of coupling constants, as the coupling may involve the interaction between the spins of two often remote nuclei and thus a delocalized depiction of the pathways of scalar couplings would be more sensible. Here we will show that a model-independent description of spin–spin coupling is possible, based on real-space functions in three-dimensional space, which is appropriate for both localized and delocalized bonding situations.

The indirect spin–spin coupling (J_{MN}) may be expressed as the energy splitting between states with parallel and antiparallel nuclear spins:

$$J_{MN} = \frac{\hbar}{2\pi}\gamma_M\gamma_N K_{MN} = \frac{1}{2}[E(\uparrow\uparrow) - E(\uparrow\downarrow)] \quad (1)$$

where K_{MN} is the reduced coupling constant (the M and N labels represent the two coupled nuclei). Since both of these energies may be written as an integral over an energy density $\varepsilon(r)$, it is also possible to express the coupling itself in this form:

$$J_{MN} = \frac{\hbar}{2\pi}\gamma_M\gamma_N K_{MN} = \frac{1}{2}\int [\varepsilon^{\uparrow\uparrow}(r) - \varepsilon^{\uparrow\downarrow}(r)]\mathrm{d}V = \frac{\hbar}{2\pi}\gamma_M\gamma_N \int \varepsilon_{MN}(r)\mathrm{d}V \quad (2)$$

where $\varepsilon_{MN}(r)$ is the coupling energy density (CED).[10] The integral of CED over all space is equal to the reduced coupling constant. The concept of CED does not involve any approximation and thus is model-independent. CED is a real-space function and can be visualized easily in 3D space.[11] It contains all the information about the propagation of the nuclear spin–spin interaction throughout a molecule. To calculate CED we use double finite perturbation theory (DFPT). The Fermi-contact (FC) operators on both coupled nuclei are included simultaneously in the Hamiltonian, and the coupling between nuclei M and N is calculated in two steps. First, one calculates the total energy for a system with parallel nuclear spins (that is, both FC operators have the same sign). In a second separate calculation, the FC perturbations corresponding to antiparallel nuclear spins (opposite signs) are included. The difference between these two total energies is proportional to the coupling constant. This is in fact a faithful description of the underlying physics; the coupling constant probes the energy difference between these two states. Many years ago, Kowalewski et al. used this elegant idea for the simple implementation of spin–spin coupling constant calculations at the configuration–interaction level of theory.[12] Recently, a related implementation based on density functional theory (DFT) has been reported by Contreras et al.[13] An obvious disadvantage of the DFPT approach in actual numerical calculations of couplings is that for each pair of coupled nuclei two separate self-consistent calculations are required. Therefore, the DFPT approach is not often used in practice. To our knowledge, the enormous potential of this scheme for the interpretation of couplings has not been realized. Note that, in addition to providing the CED, the approach also affords a coupling electron deformation density (CDD) in a straightforward manner, defined as:

$$\rho_{MN}(r) = \frac{\rho^{\uparrow\uparrow}(r) - \rho^{\uparrow\downarrow}(r)}{\lambda_1\lambda_2} \quad (3)$$

where λ_1 and λ_2 are the perturbation parameters used in DFPT.[12,14]

The calculation of CDD (which is practically the scaled difference of the electron densities obtained from two separate SCF calculations) does not require any additional programming, but the evaluation of CED does.[15] As shown below, CDD provides similar information on the coupling as CED. However, in contrast to CED the integration of CDD over space gives exactly zero. The present concept is not restricted to any particular quantum-chemical method. CED and CDD can in the same fashion be obtained from

[*] Dr. O. L. Malkina, Dr. V. G. Malkin
Institute of Inorganic Chemistry
Slovak Academy of Sciences
Dúbravská cesta 9, 84536 Bratislava (Slovakia)
Fax: (+421) 2-5941-0444
E-mail: olga.malkin@savba.sk
vladimir.malkin@savba.sk

[**] This work was initially presented at the 16th European Experimental Nuclear Magnetic Resonance Conference (EENC), Prague, Czech Republic, June 9–14, 2002. Our work was supported by the Slovak Grant Agency VEGA (No. 2/3103/23) and the Alexander von Humboldt Foundation (computer donation to V.G.M.). The authors are grateful to M. Kaupp, I. Malkin, R. Reviakine, and B. Schimmelpfennig for many useful discussions and help with the computer programs.

 DOI: 10.1002/anie.200351713 © 2003 Wiley-VCH Verlag GmbH & Co. KGaA, Weinheim

Hartree–Fock (HF) calculations, many post-HF methods and DFT. In the present implementation in our program ReSpect,[16] DFT is used.[17] Further implementation and computational details will be published elsewhere.[18] Here we will use a few representative examples to demonstrate the abilities of the new method. In the following plots, blue and red colors correspond to positive and negative function values, respectively (isosurfaces or isolines are shown). The relative importance of different pathways may be judged by intensities and volumes.

Figure 1 shows isosurfaces of CED for $^3J_{H,H}$ coupling in benzene. It can be seen that the spin–spin interaction dominantly propagates through the three intervening bonds, whereas other mechanisms, for example, through space, are

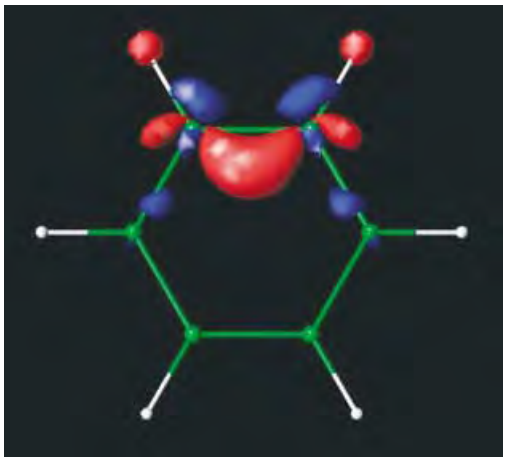


Figure 1. Visualization of the $^3J_{H,H}$ coupling energy density (CED) in benzene.

not apparent. Note however, that CED has significant values also in areas outside the direct pathway (near neighboring C–C bonds; isoline plots not shown here exhibit even more detailed features near neighboring hydrogen atoms). This is not surprising in view of the delocalized π system of benzene, and it suggests that substituents at these neighboring positions may also affect the coupling constant (in agreement with experimental evidence[19]). CDD for the same $^3J_{H,H}$ coupling is provided in Figure 2, which strongly resembles the CED plot in all important topological features, but also shows small differences (for example, the volume of the areas around the coupled hydrogen atoms). It should be remembered that the integral of CDD over space is equal to zero whereas the integral of CED gives the reduced coupling constant.[20] The close topological resemblance of CDD and CED is consistent with the cornerstone of DFT, that is, that the electron density contains all the information about a molecule. The analysis of CDD is slightly more straightforward than that of CED, as it mirrors directly the changes in electronic structure due to the coupling interactions. A deeper analysis of CDD will be provided elsewhere.[18]

While the $^3J_{H,H}$ coupling in benzene may be taken as an example of a through-bond interaction, the $^3J_{P,P}$ coupling in

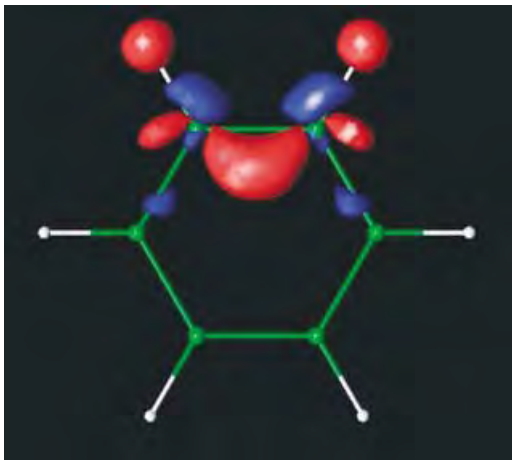


Figure 2. Visualization of the $^3J_{H,H}$ coupling electron deformation density (CDD) in benzene.

$C_2H_2(PH_2)_2$ is frequently considered as a typical case of a through-space interaction.[2] However, up to now the relative role of through-bond versus through-space interactions could not be established. The CED for $^3J_{P,P}$ in $C_2H_2(PH_2)_2$ is shown in Figure 3. The through-bond pathway resembles the $^3J_{H,H}$

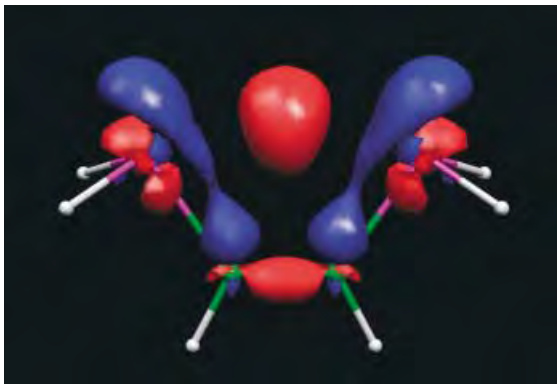


Figure 3. Visualization of the $^3J_{P,P}$ coupling energy density (CED) in the $C_2H_2(PH_2)_2$ molecule.

coupling in benzene (Figures 1 and 2). Yet, the through-space interaction between the two phosphorus nuclei dominates clearly. The interaction is due to the overlap of the phosphorus lone pairs in space, which provides an efficient spin-polarization pathway (notwithstanding the fact that molecular orbitals may be orthogonal). To obtain further insight, Figure 4 provides CED for the P-P coupling in a model $H_3P\cdots PH_3$ system. The molecular structure of the model complex is taken to be as in $C_2H_2(PH_2)_2$, but with hydrogen atoms replacing the backbone (the P–H distance was taken to be 1.427 Å, as for the other P–H bonds). The clear result of this plot may be somewhat unexpected; the P-P coupling interaction is stronger than in $C_2H_2(PH_2)_2$! This conclusion is supported by the calculated values of the coupling constants (calculated via integration of CED): 289 Hz for the model

 © 2003 Wiley-VCH Verlag GmbH & Co. KGaA, Weinheim

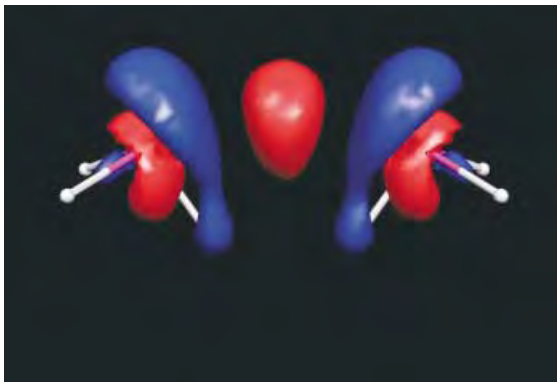


Figure 4. Visualization of $J_{P,P}$ coupling energy density (CED) in the model $H_3P\cdots PH_3$ system.

system versus 180 Hz for $C_2H_2(PH_2)_2$ (to the best of our knowledge, no experimental value is available).

In the context of the topical field of couplings through hydrogen bonds, Figure 5 shows the CDD for a formal $^2J_{C,N}$ coupling in the hydrogen-bonded model complex $NCH\cdots NH_3$. In this case, we decided to show isolines of CDD in a plane containing the hydrogen bond. Interestingly, the polarization propagates throughout the entire system with significant amplitude of CDD on the far-left (as-depicted) nitrile nitrogen atom, which is outside of the direct coupling pathway. This suggests that the C≡N bond plays a role in the coupling despite the overall obvious σ character of the pathway.

In conclusion, the newly proposed and implemented real-space functions allow unprecedented insight into the pathways of indirect nuclear spin–spin couplings. Further analysis of CED and CDD is possible along several lines, for example, the analysis of MO contributions to the functions, or the topological analysis of bond or lone-pair contributions, based on auxiliary real-space functions; this work is underway. Very recently, Soncini and Lazzeretti[21] reported findings that may be related to the CED proposed by us.[22] The definition differs from ours, and apparently so does the computational implementation. Unfortunately, not enough details were given in this report to judge how exactly the two methods are related. Probably, the DFPT approach proposed here is more applicable to systems of chemically relevant size, and the inclusion of electron correlation via DFT provides a more quantitative analysis.

Received: April 22, 2003 [Z51713]

Keywords: ab initio calculations · density functional calculations · NMR spectroscopy · spin–spin coupling

[1] D. R. Davis, R. P. Lutz, J. D. Roberts, *J. Am. Chem. Soc.* **1961**, *83*, 246; M. Barfield, M. Karplus, *J. Am. Chem. Soc.* **1969**, *91*, 1.
[2] R. H. Contreras, J. E. Peralta, *Prog. Nucl. Magn. Reson. Spectrosc.* **2000**, *37*, 321, and references therein.
[3] a) A. J. Dingley, S. J. Grzesiek, *J. Am. Chem. Soc.* **1998**, *120*, 8293; b) G. Gemmecker, *Angew. Chem.* **2000**, *112*, 1276; *Angew. Chem. Int. Ed.* **2000**, *39*, 1224, and references therein; c) A. Bagno, G. Saielli, G. Scorrano, *Angew. Chem.* **2001**, *113*, 2600; *Angew. Chem. Int. Ed.* **2001**, *40*, 2532.
[4] a) S. A. Perera, M. Nooijen, R. J. Bartlett, *J. Chem. Phys.* **1996**, *104*, 3290; b) V. G. Malkin, O. L. Malkina, L. A. Eriksson, D. R. Salahub in *Modern Density Functional Theory: A Tool for Chemistry; Theoretical and Computational Chemistry, Vol. 2* (Eds.: J. M. Seminario, P. Politzer), Elsevier, Amsterdam, **1995**.
[5] S. J. Wilkens, W. M. Westler, J. L. Markley, F. Weinhold, *J. Am. Chem. Soc.* **2001**, *123*, 12026.
[6] a) J. Khandogin, T. Ziegler, *Spectrochim. Acta Part A* **1999**, *55*, 607; b) J. Autschbach, T. Ziegler, *J. Am. Chem. Soc.* **2001**, *123*, 5320.
[7] H. Benedict, I. G. Shenderovich, O. L. Malkina, V. G. Malkin, G. S. Denisov, N. S. Golubev, H.-H. Limbach, *J. Am. Chem. Soc.* **2000**, *122*, 1979.
[8] A. L. Esteban, M. P. Galache, F. Mora, E. Diez, J. Casanueva, J. San Fabian, V. Barone, J. E. Peralta, R. H. Contrearas, *J. Phys. Chem. A* **2001**, *105*, 5298.
[9] Usually only the dominant Fermi-contact term is analyzed. We will follow this line throughout the paper, though all other important terms can be visualized along the same lines.
[10] Probably the first attempt to visualize chemical-shift density (as an example of a property density) was made by C. J. Jameson, A. D. Buckingham, *J. Chem. Phys.* **1980**, *73*, 5684.
[11] To calculate CED we used the following alternative equation for the reduced coupling constant: $K_{MN} = -[2\langle\Psi^{11}|\mathscr{H}^0|\Psi^0\rangle + \langle\Psi^{01}|\mathscr{H}^0|\Psi^{10}\rangle + \langle\Psi^{10}|\mathscr{H}^0|\Psi^{01}\rangle]$. This allows us to avoid visualization of an integrand containing delta functions (Fermi-contact operators). Here $\mathscr{H}^0$ is the ground-state Hamiltonian, and Ψ^0, Ψ^{10}, Ψ^{01},and Ψ^{11} are unperturbed, single-perturbed (by the first and second perturbations), and bilinear-perturbed

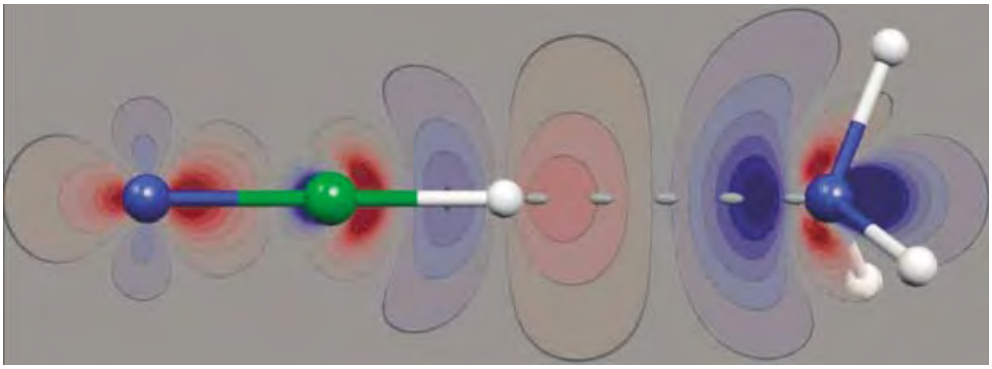


Figure 5. Visualization of $^2J_{C,N}$ coupling electron deformation density (CDD) for coupling through hydrogen bonds in the model $NCH\cdots NH_3$ system.

 © 2003 Wiley-VCH Verlag GmbH & Co. KGaA, Weinheim

wavefunctions, respectively. The corresponding double-perturbed density matrix is easily available in DFPT.
[12] J. Kowalewski, A. Laaksonen, B. Roos, P. Siegbahn, *J. Chem. Phys.* **1979**, *71*, 2896.
[13] R. H. Contreras, J. E. Peralta, M. C. Ruiz de Azúa, C. G. Giribet, J. C. Facelli, *Annu. Rep. NMR Spectrosc.* **2000**, *41*, 55.
[14] One can consider λ_1 and λ_2 as an analogy of nuclear *g*-values. Usually the values λ_1 and λ_2 are chosen to be about 10^{-2} au to avoid numerical noise in the calculations.
[15] CED might also be implemented in a coupled perturbed scheme or via response theory. We decided to use a DFPT approach for ease of implementation, and to simultaneously obtain the double-perturbed density.
[16] V. G. Malkin, O. L. Malkina, R. Reviakine, A. V. Arbuznikov, M. Kaupp, B. Schimmelpfennig, I. Malkin, T. Helgaker and K. Ruud, ReSpect program, version 1.1, **2002**. ReSpect uses the HERMIT integral package[16a] and some part of the deMon program.[16b] a) HERMIT is the integral package of Dalton, a molecular electronic structure program, Release 1.2 (**2001**), written by T. Helgaker, H. J. A. Jensen, P. Jørgensen, J. Olsen, K. Ruud, H. Ågren, A. A. Auer, K. L. Bak, V. Bakken, O. Christiansen, S. Coriani, P. Dahle, E. K. Dalskov, T. Enevoldsen, B. Fernandez, C. Hättig, K. Hald, A. Halkier, H. Heiberg, H. Hettema, D. Jonsson, S. Kirpekar, R. Kobayashi, H. Koch, K. V. Mikkelsen, P. Norman, M. J. Packer, T. B. Pedersen, T. A. Ruden, A. Sanchez, T. Saue, S. P. A. Sauer, B. Schimmelpfennig, K. O. Sylvester-Hvid, P. R. Taylor, O. Vahtras; b) D. R. Salahub, R. Fournier, P. Mlynarsky, I. Papai, A. St-Amant, J. Ushio in *Density Functional Methods in Chemistry* (Eds.: J. Labanowsky, J. Andzelm), Springer, New York, **1991**.
[17] The calculations were made with Perdew/Wang exchange[17a] and Perdew correlation functionals.[17b] Basis set BII of Kutzelnigg et al.,[17c] perturbation parameters $\lambda_1 = \lambda_2 = 0.01$, and an extensive grid (with about 24000 points per atom) was employed throughout this work for the numerical calculation of couplings. A much smaller grid (about 2000 points per atom) is already sufficient for visualization purposes. Visualization of CED and CDD was achieved using the MOLEKEL program.[17d] a) J. P. Perdew, Y. Wang, *Phys. Rev. B* **1986**, *33*, 8800; b) J. P. Perdew, *Phys. Rev. B* **1986**, *33*, 8822; J. P. Perdew, *Phys. Rev. B* **1986**, *34*, 7406; c) W. Kutzelnigg, U. Fleischer, M. Schindler *in NMR-Basic Principles and Progress, Vol. 23* (Eds.: P. Diehl, E. Fluck, H. Günther, R. Kosfeld, J. Seelig), Springer, Heidelberg, **1990**, p. 165; d) MOLEKEL 4.0, P. Flükiger, H. P. Lüthi, S. Portmann, J. Weber, Swiss Center for Scientific Computing, Manno, Switzerland, **2000**.
[18] O. L. Malkina, R. Reviakine, M. Kaupp, V. G. Malkin, unpublished results.
[19] H. Günther, *NMR Spectroscopy. An Introduction*, Wiley, New York, **1980**.
[20] The CED coupling (calculated by integration) is equal to 7.4 Hz, which is in good agreement with the experimental value of 7.5 Hz (see D. L. Beveridge in *Semiempirical Methods of Electronic Structure Calculations* (Ed.: G. A. Segal), Plenum, New York, **1977**, p. 163).
[21] A. Soncini, P. Lazzeretti, *J. Chem. Phys.* **2003**, *118*, 7165.
[22] See footnote [**].

 © 2003 Wiley-VCH Verlag GmbH & Co. KGaA, Weinheim

Dendrimer Shape Control

Transformation of a Spherical Supramolecular Dendrimer into a Pyramidal Columnar Supramolecular Dendrimer Mediated by the Fluorophobic Effect**

Virgil Percec, Martin Glodde, Gary Johansson, Venkatachalapathy S. K. Balagurusamy, and Paul A. Heiney*

Semifluorinated and perfluorinated molecules have had a large impact on the field of chemistry and their use has provided new strategies in organic,[1] supramolecular,[2,3] biomolecular, and macromolecular synthesis.[4] It is well established that perfluorinated alkanes are stiffer and less miscible than the corresponding perhydrogenated alkanes (fluorophobic effect).[4] As a consequence, the replacement of a perhydrogenated alkane with a perfluorinated alkane in the alkyl tail of a self-assembling building block enhances the thermal stability of the resulting supramolecular object and of the corresponding lattice.[2a,b,e,4c,4d] For example, the fluorophobic effect has been shown to stabilize the columnar *p6mm* hexagonal[2a,b,e,4c,4d] as well as the *c2mm* and *p2mm* rectangular[2e] 2D lattices that self-organize from cylindrical semifluorinated supramolecular dendrimers. The enhanced ability of semifluorinated dendrons toward self-assembly is so strong that first generation dendrons enforce the co-assembly of a disordered polymer backbone in the center of a supramolecular cylinder through the use of covalent[4c] or only donor–acceptor interactions.[2e] Hydrogenated dendrons require higher generations to mediate self-assembly into cylindrical or spherical[5,6] supramolecular dendrimers when strong interacting groups are absent from their core.[7] To date, spherical supramolecular dendrimers have been found to self-organize into $Pm\bar{3}n$,[2b,5,6] $Im\bar{3}m$[7a,8] cubic, and $P4_{2/mnm}$ tetragonal[9] 3D lattices.

Here we report a new, completely unexpected fluorophobic effect observed during the self-assembly of dendrons that generate spherical supramolecular dendrimers in their perhydrogenated state.

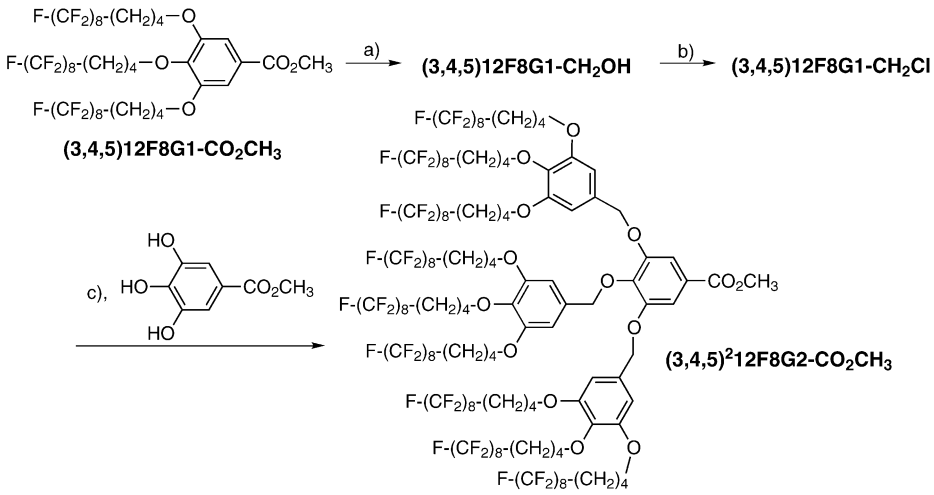
[*] Prof. Dr. V. Percec, Dr. M. Glodde, Dr. G. Johansson, Dr. V. S. K. Balagurusamy
Roy & Diana Vagelos Laboratories, Department of Chemistry
Laboratory for Research on the Structure of Matter
University of Pennsylvania
Philadelphia, PA 19104-6323 (USA)
Fax: (+1) 215-573-7888
E-mail: percec@sas.upenn.edu
Dr. V. S. K. Balagurusamy, Prof. Dr. P. A. Heiney
Department of Physics and Astronomy
Laboratory for Research on the Structure of Matter
University of Pennsylvania
Philadelphia, PA 19104-6396 (USA)

[**] Financial support of this work by the National Science Foundation (DMR-9996288 and DMR-0102459) is gratefully acknowledged.

Supporting information for this article is available on the WWW under http://www.angewandte.org or from the author.

 © 2003 Wiley-VCH Verlag GmbH & Co. KGaA, Weinheim DOI: 10.1002/anie.200351804

The synthesis, structural, and retrostructural analysis as well as the mode of self-assembly of the second generation semifluorinated dendron (Scheme 1) is similar to that of the hydrogenated analogue **(3,4,5)^{2}12G2-CO$_2$CH$_3$**.[5] Structural analysis of the hydrogenated and fluorinated supramolecular dendrimers was accomplished by a combination of differential scanning calorimetry (DSC; Table 1), thermal optical polarized microscopy (TOPM), small- and wide-angle X-ray diffraction (XRD; Table 2), and molecular-modeling experiments.[2a,e,5,6]



Scheme 1. Synthesis of **(3,4,5)^{2}12F8G2-CO$_2$Me**. a) $LiAlH_4$, Et_2O, 22 °C, then NaOH, H_2O, 88 %; b) $SOCl_2$, α,α,α-trifluorotoluene, 22 °C, 70 %; c) DMF/α,α,α-trifluorotoluene, K_2CO_3, 70 °C, then freon 113, [18]crown-6, 48 °C, 65 %.

The data in Tables 1 and 2 show that **(3,4,5)^{2}12G2-CO$_2$CH$_3$** self-assembles into a spherical supramolecular dendrimer that self-organizes into a *Pm*$\bar{3}$*n* cubic lattice similar to that reported for other homologues from this series (Figure 1a).[5,6] Fifteen **(3,4,5)^{2}12G2-CO$_2$Me** conical dendrons derived from *trans* conformations of the benzyl ethers self-assemble into a spherical supramolecular dendrimer with diameter D of 46.5 Å (Table 2). Based on the previous effects observed in cylindrical supramolecular dendrimers,[2a,b,e] we expected that **(3,4,5)^{2}12F8G2-CO$_2$Me** would self-assemble in a spherical supramolecular dendrimer that would self-organize into a *Pm*$\bar{3}$*n* cubic lattice like the one observed for **(3,4,5)^{2}12G2-CO$_2$Me** (Table 1). In addition, since fluorinated alkanes are stiffer than the corresponding hydrogenated homologues, the supramolecular object generated from **(3,4,5)^{2}12F8G2-CO$_2$Me** was expected to exhibit a larger diameter than its hydrogenated homologue since, at the same temperature, its fluorinated alkyl groups would exist in a smaller number of *gauche* conformers.

Figure 2 shows the combined features of small- and wide-angle XRD patterns recorded on **(3,4,5)^{2}12F8G2-CO$_2$CH$_3$** at 50 °C and at 23 °C. The ratios of the d-spacings of the observed reflections in the small-angle region (feature a in Figure 2) establish that **(3,4,5)^{2}12F8G2-CO$_2$CH$_3$** self-assembles into supramolecular cylinders of $D = 35.8$ Å that self-organize into a 2D hexagonal columnar liquid-crystalline (LC) phase (Table 2). Unexpectedly, the XRD data show the change in supramolecular shape from a sphere to a cylinder and the decrease in diameter from 46.5 Å to 35.8 Å, respectively.

Table 1: Thermal analysis of the 3D and 2D lattices self-organized from **(3,4,5)^{2}12G2-CO$_2$Me** and **(3,4,5)^{2}12F8G2-CO$_2$Me** dendrons.

Dendron	Thermal transitions [°C] and corresponding enthalpy changes (in parenthesis) [kcal mol^{-1}][a]	
	heating[a]	cooling
(3,4,5)^{2}12G2-CO$_2$Me	k[b]→i[c] 58.5 (40.8) k→k −1.0 (5.06); k→k 11.4 (−11.6); k→i 57.9 (29.6)	i→cub.[d] 55.6 (1.15); cub.[d]→*k* 3.84 (5.55)
(3,4,5)^{2}12F8G2-CO$_2$Me	k→k 75.4 (11.88); k→Φ_h 84.5 (0.43); Φ_h[e]→i 92.0 (1.81) k→Φ_h 22.1 (4.25); Φ_h→i 91.6 (1.85)	i→Φ_h 86.8 (1.84); Φ_h→*k* 17.6 (3.50)

[a] Data obtained from the first heating and cooling DSC scans are on the first line; data from the second heating are on the second line. [b] k = crystalline. [c] i = isotropic. [d] cub. = *Pm*$\bar{3}$*n* cubic lattice. [e] Φ_h = *p6mm* hexagonal columnar lattice.

Table 2: Structural and retrostructural analysis of the supramolecular dendrimers self-assembled from **(3,4,5)^{2}12G2-CO$_2$Me** and **(3,4,5)^{2}12F8G2-CO$_2$Me** dendrons from XRD experiments at 50 °C.

	Lattice	a [Å][a]	ρ_{20} [g cm^{-3}][b]	D_{exp} [Å][c]	μ[d]	α′ [°][e]
(3,4,5)^{2}12G2-CO$_2$Me	*Pm*$\bar{3}$*n*[f]	75.0	1.00	46.5	15.1	23.8
(3,4,5)^{2}12F8G2-CO$_2$Me	*p6mm*[g]	35.8	1.33	35.8	0.87[h]	360

[a] Lattice dimension. [b] ρ_{20} = experimental density at 20 °C. For **(3,4,5)^{2}12G2-CO$_2$Me**, the density was assumed to be 1 g cm^{-3}. [c] Experimentally derived column or sphere diameter; sphere diameter is calculated from $D_{exp} = 2\sqrt{3a^2/32\pi}$. [d] Number of monodendrons per column in a single stratum (Φ_h) or per spherical assembly (*Pm*$\bar{3}$*n*); Φ_h: $\mu = (\sqrt{3}\, N_A a^2 t\rho)/2\, M_r$; *Pm*$\bar{3}$*n*: $\mu = (a^3 N_A \rho)/8\, M_r$ (N_A: Avogadro's number; the average thickness of the stratum $t = 4.8$ Å, M_r = molecular weight of a monodendron). [e] Taper angle for tapered monodendrons and projection of the solid angle subtended by conical monodendrons $\alpha' = 360/\mu$ °. [f] d-spacings for the *Pm*$\bar{3}$*n* lattice [Å]: d_{200}: 37.6, d_{210}: 33.4, d_{211}: 30.6, d_{310}: 23.4, d_{321}: 19.7, d_{410}: 18.5, d_{421}: 16.5, d_{332}: 15.9. [g] d-spacings for the *p6mm* lattice [Å]: d_{100}: 30.7, d_{110}: 17.9, d_{200}: 15.6, d_{210}: 12.1. [h] If the large tilt is taken into account, the number of molecules that occupy the volume of a single conical stratum is 1.0; see text for discussion.

 © 2003 Wiley-VCH Verlag GmbH & Co. KGaA, Weinheim

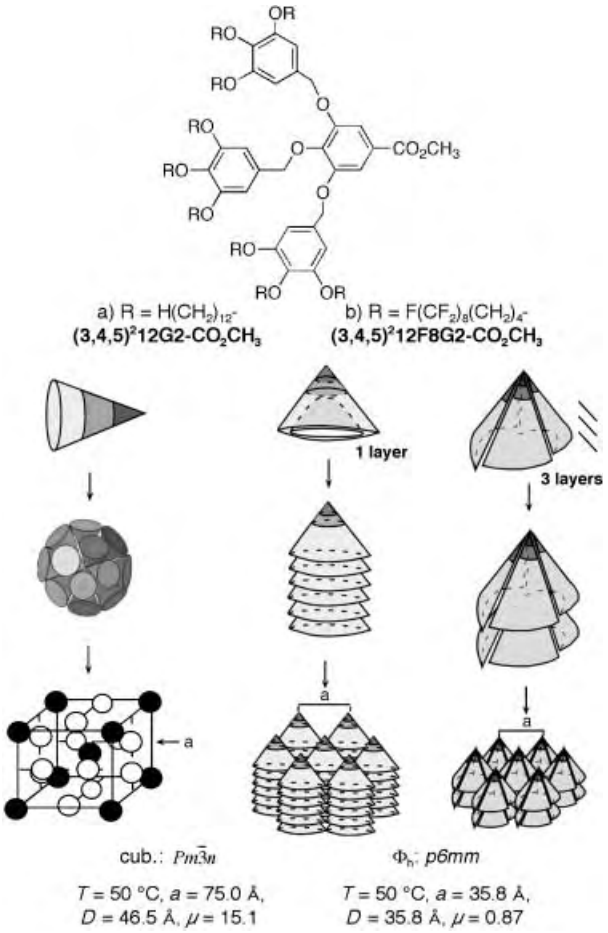


Figure 1. Structures, self-assembly, and self-organization of the second generation dendrons: a) all-*trans* cone conformation of **(3,4,5)²12G2-CO₂Me**; b) all *gauche*-crown conformation of **(3,4,5)²12F8G2-CO₂Me**; c) all *trans*-taper conformation of **(3,4,5)²12F8G2-CO₂Me**.

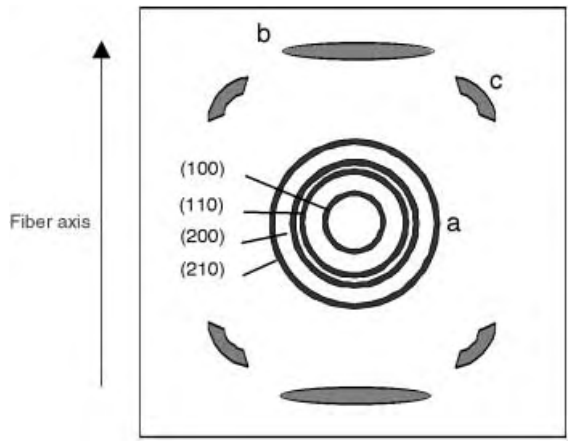


Figure 2. Combined X-ray pattern of small- and wide-angle X-ray diffractograms of **(3,4,5)²12F8G2-CO₂CH₃** recorded at 50 °C and at 23 °C, respectively, on cooling from the isotropic state: a) concentric rings of the reflections, determined from the powder small-angle XRD experiment; b) π–π stacking distance along the column axis (3.9 Å); c) *d*-spacing corresponding to the average intermolecular separation along the column axis of 4.8 Å (X-like arrangement of spots, which also indicates a tilt of the molecule of 42 ± 2°).

X-ray diffraction measurements carried out on fibers from the *p6mm* LC phase at 23 °C show broad spots corresponding to π–π stacking along the column axis ($d = 3.9$ Å, feature b in Figure 2) and an X-like pattern ($d = 3.9 \pm 0.1$ Å, feature c in Figure 2). The X-like pattern implies that the molecules are tilted by $42 \pm 2°$ from the normal to the column axis and that the intermolecular separation along the column axis is 4.8 ± 0.1 Å (see Supporting Information).

The number of untilted molecules μ that occupy a disc with the same thickness $t = 4.8$ Å as the supramolecular cylinder was calculated to be 0.87 (Table 2). However, a different calculation that considers the tilted molecules in the columns was also performed (see Supporting Information). This geometry results in a conical column stratum with an apex angle corresponding to a tilt angle of 42° and a thickness of 4.8 Å. Molecular models of two different conformations of **(3,4,5)²12F8G2-CO₂Me** were constructed (Figure 3) to gain

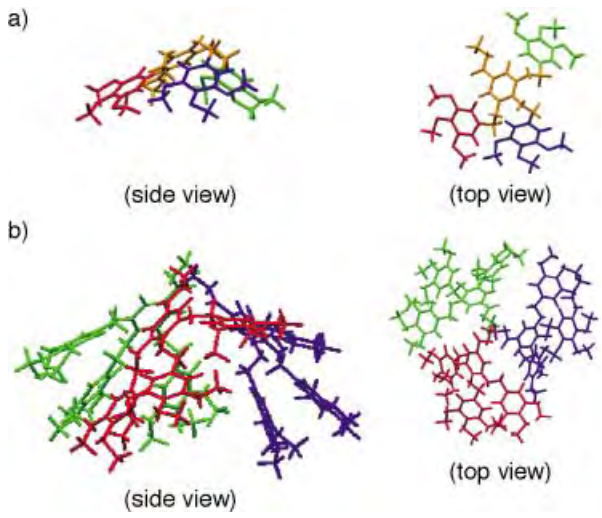


Figure 3. a) Pyramidic columnar model generated from the *gauche*-crown conformer of **(3,4,5)²12F8G2-CO₂Me**; b) pine-tree columnar model generated from the *trans*-tapered conformer of the same dendron.

further insight into how the molecules pack in this unusual columnar LC phase. The two dendron conformations, which were based on predominantly all-*trans* and predominantly all-*gauche* benzyl ether conformers, had a tilt angle almost equal to the experimentally observed value of 42°, and in both cases the molecules are packed in a staggered fashion so as to fill the space, which is consistent with the observed *d*-spacings and mass density (Figure 1).

One of these two models, known as the pyramidic columnar model[10] (Figure 1 (middle column) and Figure 3 a) results from the fanning-out of all the four benzene rings of a single dendron in a nearly symmetrically arrangement from the center of the column. This model requires *gauche* conformations for all the benzyl ether groups of the dendron. The overall shape of this dendron is crownlike or conelike. This *gauche* crownlike or conelike dendron from Figure 3 a differs from the conical dendrons obtained from all-*trans* benzyl ether conformations that self-assemble into spherical

 © 2003 Wiley-VCH Verlag GmbH & Co. KGaA, Weinheim

supramolecular dendrimers (Figure 1, left column).[5,6] The pyramidic supramolecular column is self-assembled by the stacking of *gauche* crownlike dendrons one on top of the other, with each dendron totally occupying a single conical stratum of thickness 4.8 Å. The neighboring molecules are rotated from each other about the column axis to fill the space efficiently. The other model, known as the pine-tree columnar model, results from a helical pine-tree-like arrangement of tapered dendrons that are tilted with respect to the column axis and also rotated about the molecular long axis.[11] In this model, three dendrons with all the benzyl ethers in *trans* conformations are located nearly at the same position along the column axis to form a nonhelical pine-tree-like cone with a total vertical thickness of nearly 3×4.8 Å (Figure 1, Figure 3b). Density calculations show that each dendron partially occupies three neighboring conical strata of thickness 4.8 Å (see Supporting Information). Since the pine-tree model is nonhelical, from a packing point of view, both columnar models shown in Figure 1 (middle and right columns) are similar to pyramidic liquid crystals.[10]

Electron-density profiles computed from XRD data were analyzed in regard to the nanophase separation that drives the formation of these LC phases.[2b,5] The phase combinations that exhibited either slowly varying or nearly constant distributions of electron density in the regions corresponding to the aromatic, perhydrogenated aliphatic and the perfluorinated aliphatic parts were closely examined. The surface and contour plots of the electron density computed for the phase combination of "$--++$" for the reflections (100), (110), (200), and (210), respectively, is shown in Figure 4. The color-filled contour plots shown at the base represent a single supramolecular column (center) that is surrounded by six other neighboring columns. The high electron density regions in the periphery of the columns (red in Figure 4) correspond to the fluorinated alkyl chain segments whereas the low electron density regions (purple) represent the hydrogenated alkyl chain sections which are adjacent to the fluorinated alkyl chain segments. The diffraction pattern shows that the (210) peak has higher intensity than the (200) and (110) peaks. This result is consistent with the location of the fluorinated aliphatic region in the periphery of the columns, that is, the highest electron density region at the periphery. The electron density in the central region of the columns is lower than that of the fluorinated aliphatic regions, but higher than the electron density of the hydrogenated aliphatic regions that encapsulate the center of the columns. Hence, the region of intermediate electron density in the core of the columns corresponds to the aromatic part of the dendrons that form the supramolecular assembly. This observation is consistent with both our hypothesis of organization of the present *gauche* crownlike and of the *trans* tapered-like dendrons reported previously.[2a,b,e,6,7] The diameter of the aromatic region calculated from the electron-density profiles corresponding to the volume fraction of the aromatic region in the pyramidic and pine-tree models is consistent with both models of packing. The aromatic part of the *gauche*-crown or *trans*-tapered dendrons produces the core of the cylinders, with the fluorinated alkyl chain segments in the periphery and the hydrogenated alkyl chain parts in the intervening region, thus forming three distinct segregated nanophasic regions. This model is in agreement with similar structures reported from *trans*-tapered hydrogenated dendrons that self-assemble into supramolecular cylinders.[2a,6,12,13] The electron density computed from the XRD data is consistent with both the pyramidic and nonhelical pine-tree models for the packing of the dendritic molecule **(3,4,5)^{2}12F8G2-CO$_2$CH$_3$** in the columnar LC phase.

In conclusion, we have described the first example of the transformation of the mode of self-assembly of a dendron from a spherical to a pyramidic columnar supramolecular dendrimer that is mediated by the fluorophobic effect. This change in mechanism of self-assembly is induced by the change in the dendron conformation from an all-*trans*-conical to an all-*gauche*-crown or an all-*trans*-tapered conformation. This result contrasts the role of the fluorophobic effect in the self-assembly of dendrons that form cylindrical supramolecular dendrimers when their chains are fully hydrogenated.[2a,b,e] Therefore, we conclude that the fluorophobic effect produced by the fluorinated alkyl tails of amphiphilic dendrons enhances the self-assembly into columnar supramolecular dendrimers and decreases the tendency toward self-assembly into spherical dendrimers.

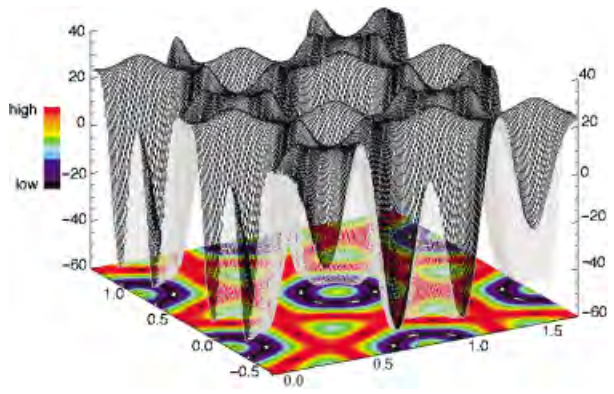


Figure 4. Electron density maps of supramolecular columns self-assembled from **(3,4,5)^{2}12F8G2-CO$_2$CH$_3$**. The profile shows the variation in the electron density in a plane perpendicular to the supramolecular columns in the LC phase. The color-filled contour maps at the base also show the variation in the electron density in the same plane.

Received: May 5, 2003 [Z51804]
Published online: July 28, 2003

Keywords: dendrimers · fluorophobic effect · liquid crystals · self-assembly

[1] For selected reviews on fluorous phases in organic synthesis, see a) I. T. Horváth, *Acc. Chem. Res.* **1998**, *31*, 641; b) D. P. Curran, *Angew. Chem.* **1998**, *110*, 1230; *Angew. Chem. Int. Ed.* **1998**, *37*, 1174; Erratum: D. P. Curran, *Angew. Chem.* **1998**, *110*, 2569; *Angew. Chem. Int. Ed.* **1998**, *37*, 2292; c) L. P. Barthel-Rosa, J. A. Gladysz, *Coord. Chem. Rev.* **1999**, *190–192*, 587; d) E. de Wolf, G. van Koten, B.-J. Deelman, *Chem. Soc. Rev.* **1999**, *28*, 37; e) C. Tschierscke, C. Markert, W. Bannwarth, S. Roller, A. Hebel, R. Haag, *Angew. Chem.* **2002**, *114*, 4136; *Angew. Chem. Int. Ed.*

 © 2003 Wiley-VCH Verlag GmbH & Co. KGaA, Weinheim

2002, *41*, 3964; f) J. A. Gladysz, D. P. Curran, *Tetrahedron* **2002**, *58*, 3823 (and papers published in this special issue).
[2] For selected examples of publications on fluorinated molecules in self-assembly, see a) V. Percec, G. Johansson, G. Ungar, J. Zhou, *J. Am. Chem. Soc.* **1996**, *118*, 9855; b) S. D. Hudson, H.-T. Jung, V. Percec, W.-D. Cho, G. Johansson, G. Ungar, V. S. K. Balagurusamy, *Science* **1997**, *278*, 449; c) G. W. Coates, A. R. Dunn, L. M. Henling, D. A. Dougherty, R. H. Grubbs, *Angew. Chem.* **1997**, *109*, 290; *Angew. Chem. Int. Ed. Engl.* **1997**, *36*, 248; d) W. J. Feast, P. W. Lövenich, H. Puschmann, C. Taliani, *Chem. Commun.* **2001**, 505; e) V. Percec, M. Glodde, T. K. Bera, Y. Miura, I. Shiyanovskaya, K. D. Singer, V. S. K. Balagurusamy, P. A. Heiney, I. Schnell, A. Rapp, H.-W. Spiess, S. D. Hudson, H. Duan, *Nature* **2002**, *419*, 384.
[3] For selected examples of publications on fluorinated compounds in self-organization, see a) U. Dahn, C. Erdelen, H. Ringsdorf, R. Festag, J. H. Wendorff, P. A. Heiney, N. C. Maliszewskyj, *Liq. Cryst.* **1995**, *19*, 759; b) G. Johansson, V. Percec, G. Ungar, K. Smith, *Chem. Mater.* **1997**, *9*, 164; c) V. Percec, D. Schlueter, G. Ungar, *Macromolecules* **1997**, *30*, 645; d) F. Guittard, E. T. de Givenchy, S. Geribaldi, A. Cambon, *J. Fluorine Chem.* **1999**, *100*, 85; e) X. H. Cheng, S. Diele, C. Tschierske, *Angew. Chem.* **2000**, *112*, 605; *Angew. Chem. Int. Ed.* **2000**, *39*, 592; f) C. Rocaboy, F. Hampel, J. A. Gladysz, *J. Org. Chem.* **2002**, *67*, 6863.
[4] For several examples of fluorine in biomolecular and macromolecular chemistry, see a) B. E. Smart in *Organofluorine Chemistry. Principles and Commercial Applications* (Eds.: R. E. Banks, B. E. Stuart, J. C. Tatlow), Plenum, New York, **1994**; b) *Modern Fluoropolymers* (Ed.: J. Scheirs), Wiley, New York, **1997**; c) V. Percec, D. Schlueter, Y. K. Kwon, J. Blackwell, M. Möller, P. J. Slangen, *Macromolecules* **1995**, *28*, 8807; d) G. Johansson, V. Percec, G. Ungar, J. Zhou, *Macromolecules* **1996**, *29*, 646; e) Y. Tang, G. Ghirlanda, N. Vaidehi, J. Kua, D. T. Mainz, W. A. Goddard III, W. F. DeGrado, D. A. Tirrel, *Biochemistry* **2001**, *40*, 2790; f) S. Sheiko, E. Lermann, M. Möller, *Langmuir* **1996**, *12*, 4015.
[5] V. S. K. Balagurusamy, G. Ungar, V. Percec, G. Johansson, *J. Am. Chem. Soc.* **1997**, *119*, 1539.
[6] V. Percec, W.-D. Cho, G. Ungar, D. J. P. Yeardley, *J. Am. Chem. Soc.* **2001**, *123*, 1302, and references therein.
[7] a) V. Percec, M. N. Holerca, S. Uchida, W.-D. Cho, G. Ungar, Y. Lee, D. J. P. Yeardley, *Chem. Eur. J.* **2002**, *8*, 1106; b) V. Percec, W.-D. Cho, G. Ungar, D. J. P. Yeardley, *Chem. Eur. J.* **2002**, *8*, 2011; c) V. Percec, W.-D. Cho, P. E. Mosier, G. Ungar, D. J. P. Yeardley, *J. Am. Chem. Soc.* **1998**, *120*, 11061; d) V. Percec, C.-H. Ahn, G. Ungar, D. J. P. Yeardley, M. Möller, S. S. Sheiko, *Nature* **1998**, *391*, 161.
[8] a) D. J. P. Yeardley, G. Ungar, V. Percec, M. N. Holerca, G. Johansson, *J. Am. Chem. Soc.* **2000**, *122*, 1684; b) H. Duan, S. D. Hudson, G. Ungar, M. N. Holerca, V. Percec, *Chem. Eur. J.* **2001**, *7*, 4134.
[9] G. Ungar, Y. Liu, X. Zeng, V. Percec, W.-D. Cho, *Science* **2003**, *299*, 1208.
[10] a) H. Zimmermann, R. Poupko, Z. Luz, J. Billard, *Z. Naturforsch. A* **1985**, *40a*, 149; b) J. Malthête, A. Collet, *Nouv. J. Chim.* **1985**, *9*, 15; c) A. M. Levelut, J. Malthête, A. Collet, *J. Phys.* **1986**, *47*, 351; d) J. Malthête, A. Collet, *J. Am. Chem. Soc.* **1987**, *109*, 7544; e) R. Poupko, Z. Luz, N. Spielberg, H. Zimmermann, *J. Am. Chem. Soc.* **1989**, *111*, 6094; f) H. Zimmermann, V. Bader, R. Poupko, E. J. Wachtel, Z. Luz, *J. Am. Chem. Soc.* **2002**, *124*, 15286.
[11] Y. K. Kwon, S. Chvalun, A. I. Schneider, J. Blackwell, V. Percec, J. A. Heck, *Macromolecules* **1994**, *27*, 6129.
[12] G. Ungar, D. Abramic, V. Percec, J. A. Heck, *Liq. Cryst.* **1996**, *21*, 73.
[13] V. Percec, D. Schlueter, G. Ungar, S. Z. D. Cheng, A. Zhang, *Macromolecules* **1998**, *31*, 1745.

 © 2003 Wiley-VCH Verlag GmbH & Co. KGaA, Weinheim

Nanomechanical Device

A Two-State DNA Lattice Switched by DNA Nanoactuator**

*Liping Feng, Sung Ha Park, John H. Reif, and Hao Yan**

Controlled mechanical movement in molecular scale devices is one of the key goals of nanotechnology. DNA is an excellent candidate for the construction of such devices due to the specificity of base pairing and its robust physicochemical properties. Well-known as the genetic material, DNA has recently been explored as a smart material for constructing periodically patterned structures[1–3] and nanomechanical devices.[4–8] A variety of DNA-based molecular machines[9] displaying rotational[4,6] and open/close movements[5,7,8] have recently been demonstrated. Reversible shifting of the equilibrium between two conformational states is triggered by changes in external conditions or by the addition of a "DNA fuel strand" that provides the driving force for such changes. Incorporation of DNA devices into arrays could lead to complex structural states suitable for nanorobotic applications if each individual device can be addressed separately. Yan et al.[6] have recently demonstrated a linear one-dimensional DNA array displaying a switch of *cis* and *trans* conformations through the rotational motion of a robust sequence-dependent DNA nanodevice. In the further exploration of the potential applications of DNA-based molecule machines in nanorobotics, a major challenge is to implement molecular machines into two-dimensional (2D) or three-dimensional (3D) patterned arrays. This has numerous potential applications. 1) The size and shape of the lattice could be programmed through the control of sequence-dependent devices, leading to controlled nanofabrication of molecular nanoelectronic wires with "on" and "off" states. For example, the tunneling effect of quantum-dot cellular automata could be actuated by controlling the distance between adjacent cells. 2) Molecules or nanoparticles could be selectively manipulated, for example, sorted and transported, by using molecular motor devices arranged on DNA

[*] Prof. Dr. H. Yan, L. Feng, Prof. Dr. J. H. Reif
Department of Computer Science
Duke University
Durham, NC 27708 (USA)
Fax: (+1) 919-660-6519
E-mail: hy1@cs.duke.edu
S. H. Park
Department of Physics
Duke University
Durham, NC 27708 (USA)

[**] We thank Prof. Erik Winfree for helpful discussions on using mismatched base pairs in the nanoactuator device. We also thank Dr. Yan Liu for assistance with the FRET measurements. This work has been supported by grants from the NSF to H.Y. (EIA-0218359) and to J.H.R. (EIA-00-86015), and from DARPA/AFSOR (F30602-01-2-0561) to J.H.R.

Supporting information for this article is available on the WWW under http://www.angewandte.org or from the author.

 © 2003 Wiley-VCH Verlag GmbH & Co. KGaA, Weinheim DOI: 10.1002/anie.200351818

tiling arrays, which may lead to programmed chemical synthesis. 3) It may offer a mechanism for DNA computation of arrays whose elements (the tiles) hold state.

Herein we report the construction of a robust sequence-dependent DNA device, which we call a nanoactuator, and the incorporation of such a device into a 2D parallelogram DNA lattice. Figure 1 illustrates the design and the operation of the nanoactuator device. The two states of the device are shown as S1 and S2. S1 consists four strands assembled through Watson–Crick base pairing to form a bulged three-arm DNA branch-junction. Leontis and colleagues[11] have previously shown that a three-arm DNA branch-junction containing a loop of two deoxythymidine nucleotides has a preferred stacking direction. Bulged three-arm DNA branch-junctions have been well characterized by Liu et al.[13] and have been extensively used in DNA nanoconstruction[14,15] and as topographic markers in the self-assembly of 2D DNA lattices.[1,2] Thus, a DNA device based on a bulged three-arm junction is an excellent candidate to serve as actuator for DNA lattices. The stem-loop joining the two strands of the duplex contains 21 nucleotides and is composed of a loop of two deoxythymidine nucleotides, a seven-base-pair duplex region (contains two mismatched pairs), and a loop of five deoxythymidine nucleotides. In Figure 1 the strand in red is a set strand (SS1) that sets the nanoactuator device in the S1 state. S2 consists of the same three black strands as in S1, but a blue strand (SS2), which has a region fully complementary to the stem-loop sequence, replaces the red strand. SS2 serves to open up the stem-loop in S1 and set the conformation of the nanoactuator device to the S2 state. The mismatched base pairs (in pink) are included in the stem-loop of S1 to avoid the formation of an unwanted kinetically trapped cruciform junction, a possible secondary structure to the S2 state of the nanoactuator device.

The nanoactuator designed here differs significantly from a conventional molecular beacon[10] in that the nanoactuator has a well-defined conformation that can be easily incorporated into DNA lattices, the motion generated is translated along a stacked double helix, and the reversible interconversion between states is executed through strand displacement using a DNA fuel strand. Yurke and Turberfield[5] first introduced strand displacement by using a fuel strand for the construction of a DNA tweezer that executes an open/close motion. We utilize this technique to interconvert the nanoactuator device described here. Both the set strands in the device have a 3′ extension of eight nucleotides, which are used as a handle to initiate branch migration upon addition of their fuel strands, leading to their removal from the nanoactuator device. Since the set strands and their corresponding fuel strands (FS1 and FS2) are complementary along their entire length, pairing of a set strand and its fuel strand is energetically more favored than partial pairing of the set strands in the S1 and S2 state. Both fuel strands have a biotin group at their 5′-ends indicated in Figure 1 by a filled black circle. The waste product composed of the complementary duplex of set strand and fuel strand can be removed, if desired, by treatment with streptavidin magnetic-bead separation. The nanoactuator device operates as follows: starting from S1, SS1 (red) is removed by the addition of FS1 (green), producing the unpaired intermediate (INT), which is then fixed to S2 by the addition of SS2 (blue). Addition of FS2 (purple) to remove SS2 converts S2 to the unpaired intermediate (INT). Addition of a SS1 (red) restores the S1 state and completes the cycle. Operation of the nanoactuator device will result in an extension/contraction motion of two turns of DNA (~6.8 nm) along the stacked helix.

We used both gel electrophoresis and fluorescent resonance energy transfer spectroscopy (FRET) to demonstrate the interconversion and cycling of the nanoactuator device. In Figure 2a the electrophoresis with 14% nondenaturing polyacrylamide gel shows the formation and operation of the device. Lane LM contains 50-base-pair (bp) DNA linear

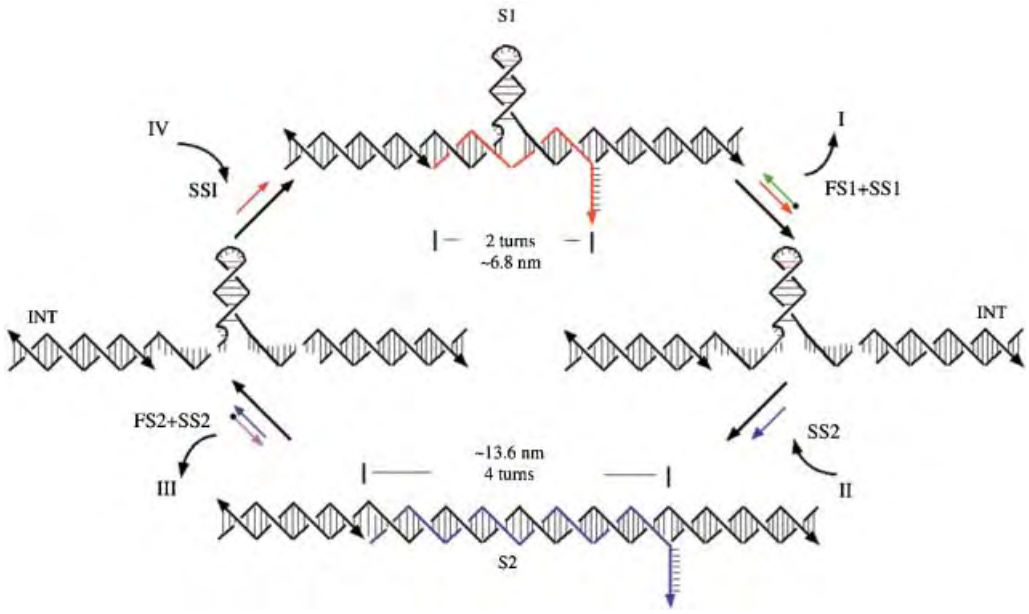


Figure 1. Schematic drawing of the design and operation of the nanoactuator device. I-IV represent the four steps to complete one cycle of the device operation. See the text for an explanation.

 © 2003 Wiley-VCH Verlag GmbH & Co. KGaA, Weinheim

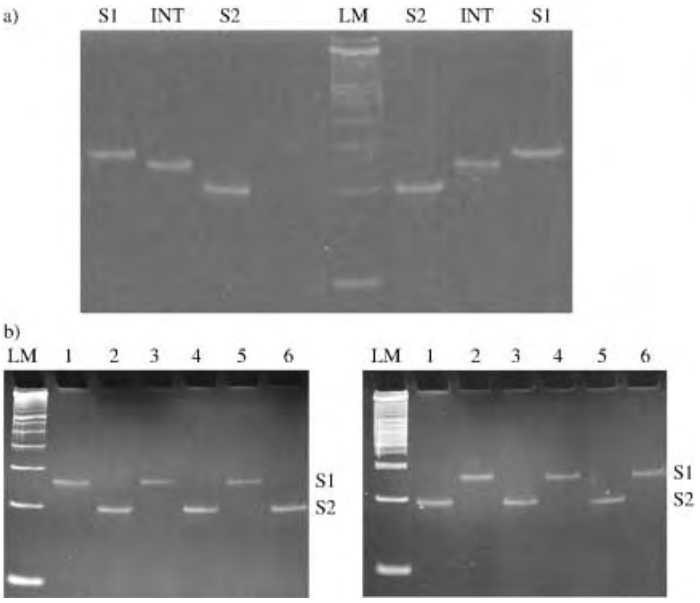


Figure 2. Gel evidence for the cycling of the nanoactuator device. See text for an explanation.

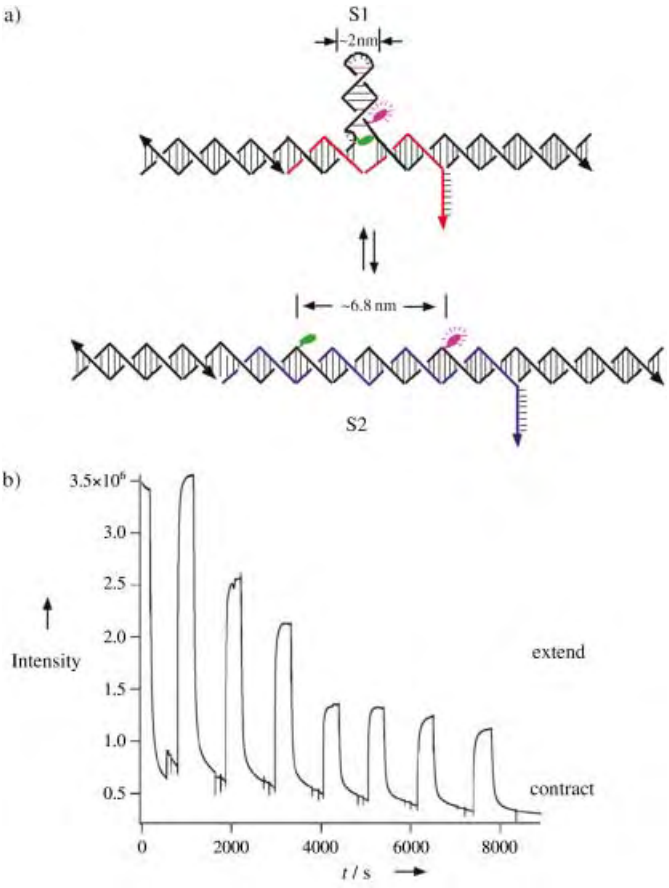


Figure 3. FRET measurements for the cycling of the nanoactuator device. a) Schematic drawing of the incorporation of fluorescent dyes in the nanoactuator device. A donor, fluorescein, and an acceptor, Tamra,are represented as green and purple filled circles, respectively. b) Cycling the nanoactuator device measured by FRET spectroscopy.

markers. The operation was demonstrated starting either from S1 (left side of the marker lane) or from S2 (right side of the marker lane). The linear duplex of S2 migrates faster than the bulged-junction of S1 although its molecular weight is greater than that of S1. An intermediate species (labeled as INT) appears as single band between S1 and S2, indicating the robustness of the nanoactuator during the process of switching. Figure 2b shows electrophoresis images with nondenaturing gel demonstrating the interconversion between the two states of the nanoactuator device in three cycles, starting with S1 (left panel) and S2 (right panel). Lane 1 is the initial conformation (S1 at left panel and S2 at right panel), and lanes 2 to 6 show alternating transformations to the other state. Cycling of the nanoactuator device was achieved by alternatively adding an equal molar ratio of the fuel strand and the set strand as illustrated in Figure 1, and the waste products were removed by streptavidin magnetic-bead treatment. The absence of species other than the molecules in the S1 or S2 state of the nanoactuator device attests to the robustness of the device in bulk. It also confirms that the design of including mismatched bases in the stem-loop prevents the formation of any unwanted secondary structure. To make sure the transition of the DNA nanoactuator results from structural transformation, we also engineered a restriction site in the device and demonstrated the conformational change between the two states of the nanoactuator (see Supporting Information).

FRET is a valuable method to obtain information on the structure of nucleic acids because of its distance and orientation dependence. As illustrated in Figure 3, two fluorescent dyes—a donor, fluorescein, and an acceptor, Tamra,—are covalently bound to the backbone of the long black strand at the positions of the turns of the junction. The distance between the two dyes is expected to increase upon transition from S1 to S2. Thus the efficiency of the FRET would decrease, causing the light up of the donor upon formation of S2 state. Figure 3b shows interconversion of the nanoactuator device in seven cycles. The extension and contraction of the nanoactuator device is fully reversible and the switching time for the machine is 26 ± 2 s. The interconversion of the nanoactuator device was achieved by alternatively adding fuel strands and set strands to the solution for each state. The waste products were not removed from the solution in this case. The decrease of the intensity of the FRET signal by almost threefold over the course of the interated switching of the device is due to the dilution of the solution when the fuel and set strands are added to the solution. These results, in addition to the results of gel electrophoresis, clearly indicate that the nanoactuator device described here oscillates between two well-defined states.

To realize potential applications of the DNA nanoactuator device constructed here, the device must be integrated into nanorobotics or patterned arrays so that a functional network of nanoactuator devices can be built. We demonstrated a major step toward this goal by implementing the device constructed here into a 2D DNA lattice, and the state of the lattice can be actuated through the operation of this device. Figure 4 illustrates the design of a such a structure.

 © 2003 Wiley-VCH Verlag GmbH & Co. KGaA, Weinheim

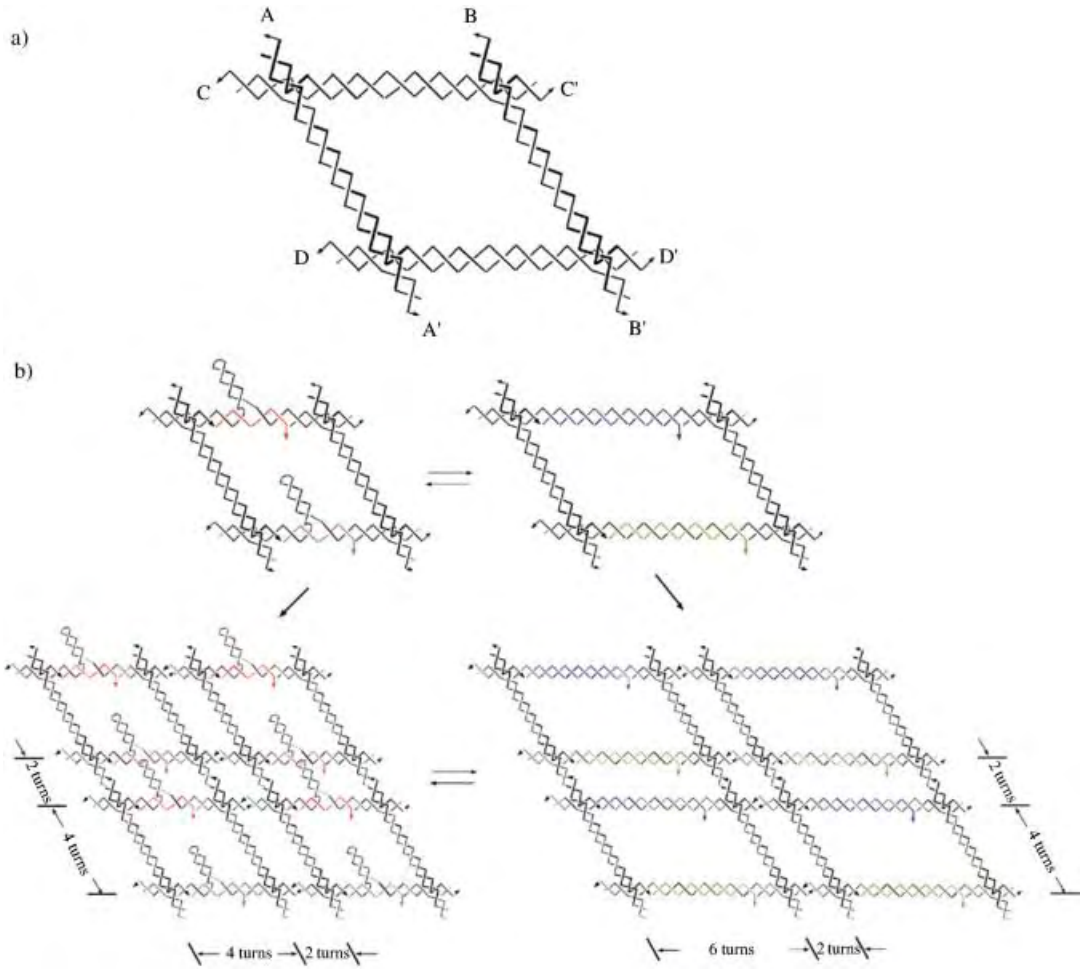


Figure 4. Schematic drawing of the two-state 2D lattices actuated by DNA nanoactuator devices. a) A unit for self-assembly of parallelogram lattice (described in ref. [4]) containing complementary sticky ends, for example, A and A′, which will self-assemble into a 2D lattice. b) Incorporation of DNA nanoactuator devices into 2D lattice. Two nanoactuator devices with different base sequences are incorporated into the opposite arms of the rhombuslike motif. The two states of these nanoactuator devices result in two different lattice components. Sticky-ended association will lead to 2D lattices. Periodicity of the lattice is illustrated by their helical turns.

The nanoactuator device is incorporated into a 2D DNA lattice constructed previously by Mao et al.,[3] which was demonstrated to display a rhombuslike cavity with size of ~14 nm in each of the two dimensions. The unit of the previously demonstrated parallelogram contains four four-arm branched junctions (Figure 4a), which were fused into a rhombuslike molecule. The branch points, which define vertices, are each separated by four double-helical turns. The rhombuses were directed to self-assemble by hydrogen bonding into a two-dimensional periodic array, whose spacing is six turns in each direction. In our design, we modified the molecule and incorporated two nanoactuator devices into two opposite edges of the unit (Figure 4b). The operation of the nanoactuator devices will result in a contraction/extension motion of the 2D lattice assembled from the designed unit, as illustrated in lower panel of Figure 4b.

We performed the interconversion of the nanoactuator device in solution and demonstrated the motion of the lattice by imaging samples deposited on mica using atomic force microscopy (AFM). The AFM images in Figure 5 illustrate

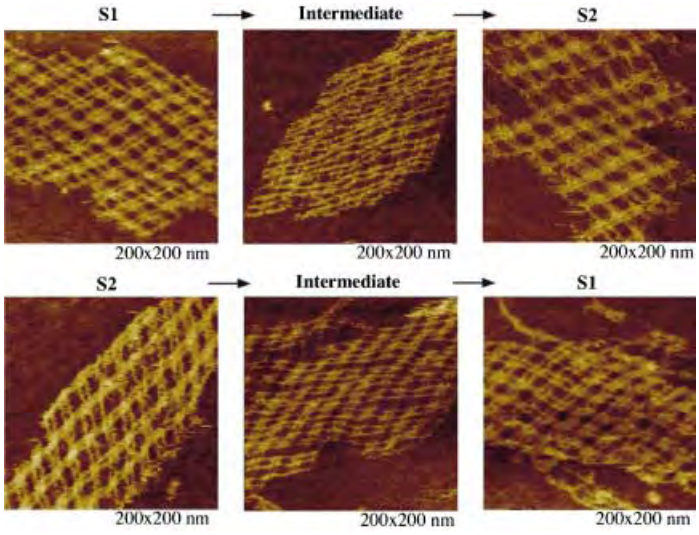


Figure 5. AFM evidence for the two state DNA lattice actuated by DNA nanoactuator devices. For details see text.

 © 2003 Wiley-VCH Verlag GmbH & Co. KGaA, Weinheim

the change of the DNA lattices upon the operation of the nanoactuator device. In the upper panel of Figure 5 the three AFM images demonstrate the switching of the nanoactuator device from S1 to the intermediate state and then to S2. A change in the size of the cavity in the lattice was observed after the operation was complete. The dimensions of each rhombus cavity in the lattice change from $\sim 14 \times 14$ nm to $\sim 14 \times 20$ nm after the operation, which is consistent with the parameters in the design. The three images in lower panel of Figure 5 show the switching of the nanoactuator device from S2 to the intermediate state and then to S1. The dimensions of each rhombus cavity change from $\sim 14 \times 20$ nm to $\sim 14 \times 14$ nm. These clearly confirm that the operation of the nanoactuator devices results in a contraction and extension of the lattice. Thus, the DNA nanoactuator device is functioning in a 2D lattice powered by DNA fuel strands. The AFM images of the intermediate state shown in Figure 5 demonstrate that the lattices in the intermediate state are not as regular as those in the S1 and S2 states. However, the lattice in the intermediate state does not fall apart during the transition of the device, which strongly suggests the robustness of the lattice during the operation of the nanoactuator devices.

In summary, we have constructed and incorporated a robust DNA nanoactuator device into 2D DNA lattices. The nanoactuator device constructed here results in a linear translational motion on the lattice. This nanoactuator device can be modified easily to produce both a translational and a rotational motion by adding an odd number of half-turn-long nucleotides in the stem loop. After strand displacement, there would be a 180° rotation around the axis of the stacked helix. A potential use of such a nanoactuator device is to program the assembly of nanoelectronic components. For example, Loweth et al.[12] used complementary DNA as a template to assemble lines of gold nanoparticles by attaching 5-nm- or 10-nm-sized gold nanoparticles to DNA strands. The nanoactuator device can be used to control the relative orientations of nanoparticles. It is possible to change the relative positions of proteins or other large molecules connected to both ends of the nanoactuator device. This capability may facilitate the study of proximity effects in chemical and biological systems. By controlling the space between molecules, the nanoactuator device may find applications in biosensors development.

Experimental Section

All DNA strands used here are listed in the Supplemental Information. DNA strands were synthesized by Integrated DNA Technologies, Inc. (www.idtdna.com) and purified by denaturing gel electrophoresis. The nanoactuator device complex and the DNA lattice were formed by mixing a stoichiometric quantity of each strand designed in the complex or lattice unit at a concentration of 1 μM, as estimated by OD_{260}, in 1 × TAE/Mg buffer (40 mM Tris·HCl, pH 8.0, 20 mM acetic acid, 2 mM EDTA, and 12.5 mM magnesium acetate). The solution was cooled slowly from 90 °C to 20 °C. For nondenaturing gel electrophoresis, the preformed nanoactuator device complex was subjected to the processes of the interconversion described in Figure 1, sampling aliquots were loaded on gel run at 20 °C for 16 h.

For the FRET experiment, fluorescently labeled, longer length DNA oligomer was obtained by ligating shorter synthesized oligomers. A Fluorolog 3 fluorimeter (Jobin-Yvon–Horiba) was utilized to measure the fluorescence emission spectra and the kinetics of the fluorescence intensity changing with time. $\lambda_{ex} = 485$ nm, $\lambda_{em} = 518$ nm; the slit widths were 2.5 nm for both excitation and emission. After the addition of fuel or set strands, solution was mixed within 2 s by rapidly drawing it up a pipette and then releasing it. All measurements were performed at 20 °C. For AFM imaging, a 5-μL sample of the DNA lattice was applied to freshly cleaved mica (Ted Pella, Inc.) as a drop and left to adsorb to the surface for 3 min. Then 30-μL of 1xTAE/Mg buffer was added to the drop on the mica. Imaging was performed in a fluid cell on a Multimode NanoScope IIIa (Digital Instruments) using NP-S tips (Veeco Inc.).

Received: May 6, 2003 [Z51818]

Keywords: DNA structures · DNA · nanostructures · scanning probe microscopy · self-assembly

[1] E. Winfree, F. Liu, L. A. Wenzler, N. C. Seeman, *Nature* **1998**, *394*, 539 – 544.
[2] T. H. LaBean, H. Yan, J. Kopatsch, F. Liu, E. Winfree, J. H. Reif, N. C. Seeman, *J. Am. Chem. Soc.* **2000**, *122*, 1848 – 1860.
[3] C. Mao, W. Sun, N. C. Seeman, *J. Am. Chem. Soc.* **1999**, *121*, 5437 – 5443.
[4] C. Mao, W. Sun, Z. Shen, N. C. Seeman, *Nature* **1999**, *397*, 144 – 146.
[5] A. J. Yurke, A. P. Turberfield, Jr., Mills, F. C. Simmel, J. E. Neumann, *Nature* **2000**, *406*, 605 – 608.
[6] H. Yan, X. Zhang, Z. Shen, N. C. Seeman, *Nature* **2002**, *415*, 62 – 65.
[7] J. Li, W. Tan, *Nano Lett.* **2002**, *2*, 315 – 318.
[8] P. Alberti, J. Mergny, *Proc. Natl. Acad. Sci. USA* **2003**, *100*, 1569 – 1573.
[9] For a review, see: C. Niemeyer, M. Adler, *Angew. Chem.* **2002**, *114*, 3933 – 3937; *Angew. Chem. Int. Ed.* **2002**, *41*, 3779 – 3783.
[10] S. Tyagi, F. R. Kramer, *Nat. Biotechnol.* **1996**, 14, 303 – 308.
[11] I. V. Ouporov, N. B. Leontis, *Biophys. J.* **1995**, 68, 266 – 274.
[12] C. J. Loweth, W. B. Caldwell, X. G. Peng, A. P. Alivisatos, P. G. Schultz, *Angew. Chem.* **1999**, *111*, 1925 – 1929; *Angew. Chem. Int. Ed.* **1999**, *38*, 1808 – 1812.
[13] B. Liu, N. B. Leontis, N. C. Seeman, *Nanobiology* **1994**, 3, 177 – 188.
[14] J. Qi, X. Li, X. P. Yang, N. C. Seeman, *J. Am. Chem. Soc.* **1996**, *118*, 6121 – 6130.
[15] X. J. Li, X. P. Yang, J. Qi, N. C. Seeman, *J. Am. Chem. Soc.* **1996**, *118*, 6131 – 6140.

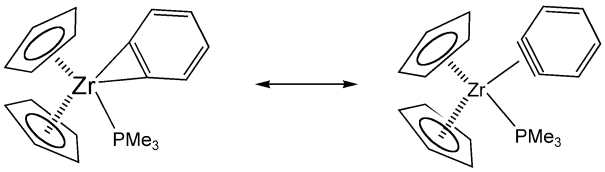
 © 2003 Wiley-VCH Verlag GmbH & Co. KGaA, Weinheim

Zirconocene–Carborane Complex

Synthesis, Structure, and Bonding of a Zirconocene–1,2-Dehydro-*o*-carborane Complex**

Haiping Wang, Hung-Wing Li, Xin Huang, Zhenyang Lin, and Zuowei Xie**

1,2-Dehydrobenzene (benzyne) has found many applications in organic synthesis, mechanistic studies, and the synthesis of functional materials since it was reported as an active intermediate in the 1950s.[1–4] The chemistry of its transition-metal complexes has been extensively studied.[5,6] The first zirconocene–benzyne complex stabilized by PMe_3 was structurally characterized in 1986 (Scheme 1).[7] In sharp contrast,

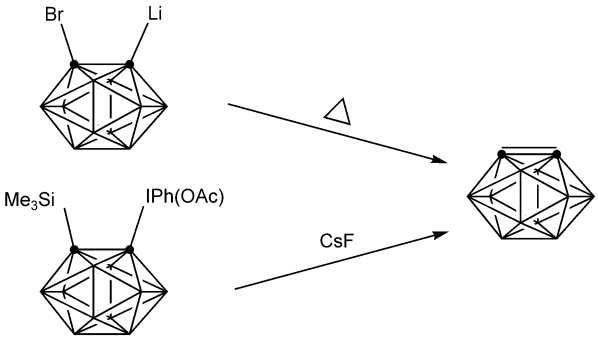


Scheme 1. The first structurally characterized zirconocene–benzyne complex.[7]

1,2-dehydro-*o*-carborane, a three-dimensional relative of benzyne, was suggested as a reactive intermediate for the first time in 1990 by heating a lithium salt of *o*-bromocarborane.[8] It was recently reported that 1,2-dehydro-*o*-carborane was also generated from phenyl(*o*-trimethylsilyl carboranyl)-iodonium acetate in the presence of CsF (Scheme 2).[9] Reactivity studies showed benzyne and 1,2-dehydro-*o*-carborane to be quite similar in reactions with dienes.[8–10] In view of the rich chemistry of metal–benzyne complexes,[5,6] we are interested in the virtually undeveloped chemistry of metal 1,2-dehydro-*o*-carborane complexes. We report here the synthesis, single-crystal X-ray structure, and bonding of the first zirconocene–1,2-dehydro-*o*-carborane complex [[{η^5:σ-$Me_2C(C_9H_6)(C_2B_{10}H_{10})$}$ZrCl(\eta^3$-$C_2B_{10}H_{10})$][$Li(thf)_4$]] (**1**).

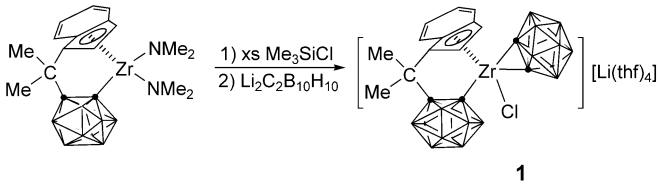
[*] Prof. Dr. Z. Xie, H. Wang, H.-W. Li
Department of Chemistry
The Chinese University of Hong Kong
Shatin, NT, Hong Kong (China)
Fax: (+852) 2603-5057
E-mail: zxie@cuhk.edu.hk
Prof. Dr. Z. Lin, X. Huang
Department of Chemistry
The Hong Kong University of Science and Technology
Clear Water Bay, Kowloon, Hong Kong (China)
Fax: (+852) 2358-1594
E-mail: chzlin@ust.hk

[**] This work was supported by grants from the Research Grants Council of the Hong Kong Special Administration Region (Project Nos. CUHK 4254/01P to Z.X. and HKUST 6087/02P to Z.L.) and the National Science Foundation of China through the Outstanding Young Investigator Award Fund (Project No. 20129002 to Z.X.).



Scheme 2. Reported synthesis of 1,2-dehydro-*o*-carborane.[8,9]

Treatment of [{η^5:σ-$Me_2C(C_9H_6)(C_2B_{10}H_{10})$}$Zr(NMe_2)_2$] with excess Me_3SiCl in toluene, presumably giving [{η^5:σ-$Me_2C(C_9H_6)(C_2B_{10}H_{10})$}$ZrCl_2$],[11] was followed by treatment with 1 equiv of $Li_2C_2B_{10}H_{10}$ to afford **1** as light-brown crystals in 60% yield (Scheme 3). Complex **1** is soluble in polar organic solvents such as THF, pyridine, and dimethoxyethane (DME), and is insoluble in toluene and hexane. It is extremely air- and moisture-sensitive but remains stable for months at room temperature under an inert atmosphere. Traces of air immediately convert the colored **1** to a white powder.



1

Scheme 3. Synthesis of **1**.

The ^1H NMR spectrum showed six multiplets for the aromatic protons in the region $\delta = 8.2$–6.5 ppm and two singlets at $\delta = 1.98$ and 1.76 ppm corresponding to two diastereotopic methyl groups of the bridging CMe_2 unit, and supported the ratio of four THF molecules per hybrid ligand. In addition to those peaks assignable to the indenyl, CMe_2, and THF groups observed in the ^{13}C NMR spectrum, there were four resonances in the region $\delta = 106$–94 ppm corresponding to the two carboranyl moieties. The ^{11}B NMR spectrum exhibited a 1:2:5:1:1 splitting pattern, which differs significantly from that of its parent complex.[11]

The molecular structure of **1** has been confirmed by single-crystal X-ray analysis (Figure 1).[12] It has an ionic structure consisting of well-separated, alternating layers of discrete cations $[Li(thf)_4]^+$ and zirconocene anions [{η^5:σ-$Me_2C(C_9H_6)(C_2B_{10}H_{10})$}$ZrCl(\eta^3$-$C_2B_{10}H_{10})]^-$. In the anion, the Zr center is η^5-bound to the five-membered ring of the indenyl group, η^3-bound to a 1,2-dehydro-*o*-carborane moiety, and σ-bound to a cage carbon atom and a terminal chlorine atom in a distorted-tetrahedral geometry. The average Zr–C(C_5 ring) bond lengths of 2.515(5) Å, Zr–Cl bond length of 2.403(2) Å, and Zr-C2 bond length of 2.359(5) Å are close to the corresponding values found in [{η^5:σ-$Me_2C(C_9H_6)(C_2B_{10}H_{10})$}$ZrCl(\mu$-$Cl)_{1.5}]_2^-$.[11]

 DOI: 10.1002/anie.200351892 © 2003 Wiley-VCH Verlag GmbH & Co. KGaA, Weinheim

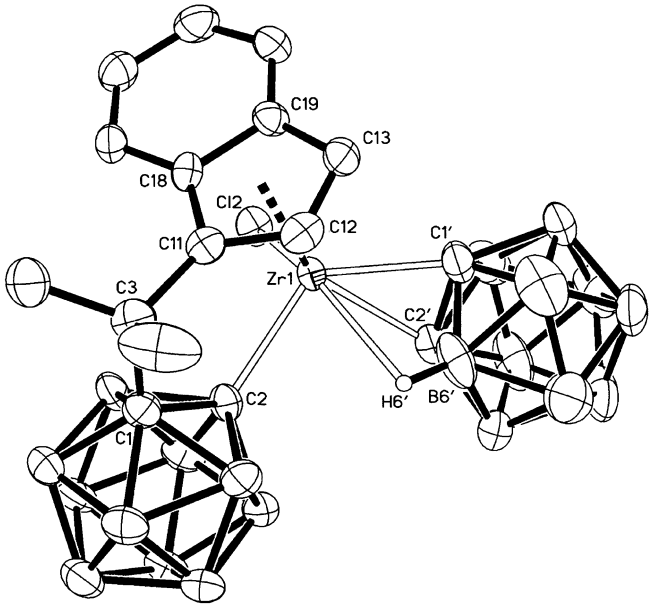
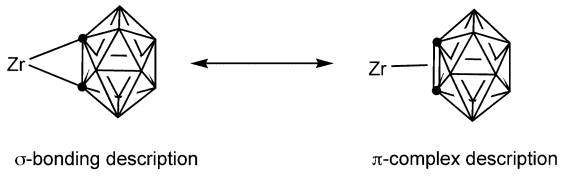


Figure 1. Molecular structure of the $[\{\eta^5{:}\sigma\text{-}Me_2C(C_9H_6)(C_2B_{10}H_{10})\}ZrCl(\eta^3\text{-}C_2B_{10}H_{10})]^-$ ion in **1**. Selected bond lengths [Å]: Zr1-C2 2.359(5), Zr1-C1′ 2.229(7), Zr1-C2′ 2.422(7), Zr1-Cl2 2.403(2), Zr1-B6′ 2.552(10), Zr1-C(C_5 ring; av) 2.515(5), C1-C2 1.711(7), C1′-C2′ 1.616(10).

The unique structural feature found in **1** displays a novel metal–1,2-dehydro-*o*-carborane bonding mode. The metal center is directly bonded to the two adjacent cage carbon atoms which do not have terminal hydrogen atoms (Zr–C: 2.229(7) and 2.422(7) Å). In addition, the metal center also interacts with the cage through an "agostic-like" Zr-H–B bond (Zr–B: 2.552(10) Å; Zr–H: 2.38 Å). Thus, the description Zr-η^3-(*o*-$C_2B_{10}H_{10}$) can be used to exemplify this novel bonding mode. In view of these structural parameters, we can formally consider that there are two Zr–C single bonds and one "agostic-like" Zr-H-B bond between the Zr center and the η^3-(*o*-$C_2B_{10}H_{10}$) ligand. With such a bonding description, the dianionic $[\eta^3\text{-}(o\text{-}C_2B_{10}H_{10})]^{2-}$ ligand formally donates three pairs of electrons to the metal center and is isolobal with Cp^-. Therefore, one can conveniently correlate the zirconium complex ion with complexes having a general formula of d^0 Cp_2MX_2. Alternatively, one can describe the bonding interaction between the metal center and the two carbon atoms of the η^3-(*o*-$C_2B_{10}H_{10}$) ligand in terms of the metal–1,2-dehydro-*o*-carborane form shown in Scheme 4. This alternative description explains the shorter C–C bond length (1.616(10) Å) of the η^3-(*o*-$C_2B_{10}H_{10}$) ligand in comparison with that (1.711(7) Å) found in the σ-bonded carborane unit.



Scheme 4. Possible bonding interactions in **1**.

The results of molecular orbital calculations[13] at the B3LYP level of theory based on the experimental geometry of the complex suggest that a resonance hybrid of the two bonding descriptions discussed above most accurately describes the Zr-η^3-(*o*-$C_2B_{10}H_{10}$) bonding situation for the complex anion. Figure 2 shows the contour plots of the lowest

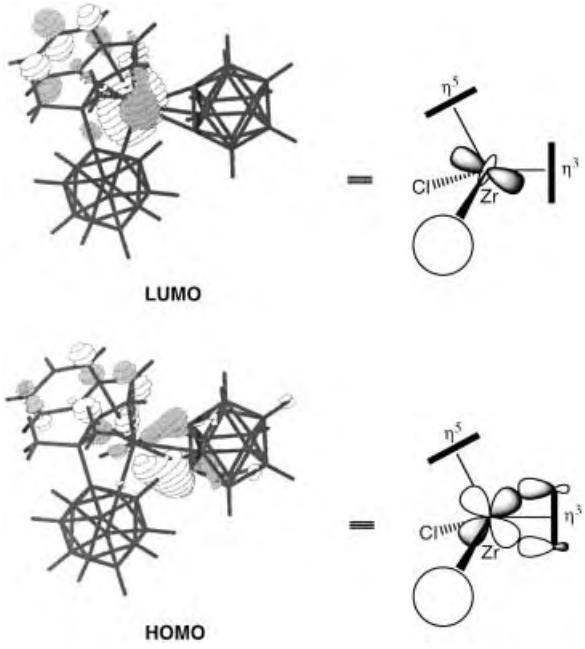


Figure 2. Contour plots of the lowest unoccupied and the highest occupied molecular orbitals calculated for the $[\{\eta^5{:}\sigma\text{-}Me_2C(C_9H_6)(C_2B_{10}H_{10})\}ZrCl(\eta^3\text{-}C_2B_{10}H_{10})]^-$ complex ion.

unoccupied (LUMO) and the highest occupied (HOMO) molecular orbitals derived from the B3LYP calculations. The LUMO is an unoccupied metal d orbital mixed with orbitals from the η^5-indenyl ligand, which represents a feature commonly found for a d^0 Cp_2MX_2 complex.[14] Meanwhile, the HOMO, despite containing the metal–carbon σ-bonding interactions, can also be viewed as having the character of metal(d)-to-π* back-donation commonly used in describing metal–olefin or metal–acetylene bonds.[15] It is not too surprising that the two bonding descriptions discussed above are both responsible for the Zr-η^3-(*o*-$C_2B_{10}H_{10}$) interactions in view of the molecular structure of $[Cp_2Zr(\eta^2\text{-benzyne})(PMe_3)]$[7] and the fact that the Lewis structures of metallacyclopropane (or metallacyclopropene) and metal–π complex forms are normally invoked to describe the bonding in metal–olefin or metal–acetylene complexes.[15]

In summary, the first example of zirconocene–1,2-dehydro-*o*-carborane complex has been prepared and structurally characterized, which also exhibits a brand new bonding mode for carboranes. Molecular-orbital calculations suggest that the bonding interactions between Zr and 1,2-dehydro-*o*-carborane are best described as a resonance hybrid of both the Zr–C σ and Zr–C π bonding forms shown in Scheme 4. The reactivity patterns of **1** are under investigation.

 © 2003 Wiley-VCH Verlag GmbH & Co. KGaA, Weinheim

Experimental Section

1: A solution of Me_3SiCl (217 mg, 2.0 mmol) in dry toluene (10 mL) was added dropwise to a solution of [{η^5:σ-$Me_2C(C_9H_6)(C_2B_{10}H_{10})$}$Zr(NMe_2)_2$][11] (240 mg, 0.5 mmol) in toluene (20 mL) and was stirred at room temperature overnight. After removal of the solvent and excess Me_3SiCl, the resulting yellow solid was washed with *n*-hexane and redissolved in THF (20 mL). To the resulting clear yellow solution was added $Li_2C_2B_{10}H_{10}$ (freshly prepared from *o*-carborane (72 mg, 0.5 mmol) and 2 equiv of *n*BuLi in toluene/Et_2O) at −78 °C with stirring. The reaction mixture was then warmed to room temperature and stirred overnight. After removal of the precipitate, the clear brown solution was concentrated to about 10 mL and cooled to −30 °C to give **1** as light-brown crystals (260 mg, 60 %). ^{1}H NMR (300 MHz, [D$_5$]pyridine): $\delta = 8.18$ (d, $J =$ 8.4 Hz, 1H), 7.52 (d, $J = 8.4$ Hz, 1H), 7.40 (m, 1H), 7.13 (m, 1H), 6.89 (d, $J = 3.6$ Hz, 1H), 6.52 (d, $J = 3.6$ Hz, 1H; C_9H_6), 3.63 (m, 16H), 1.61 (m, 16H; THF), 1.98 (s, 3H), 1.76 ppm (s, 3H; $(CH_3)_2C$); ^{13}C NMR (75 MHz, [D$_5$]pyridine): $\delta = 136.09$, 127.99, 126.55, 125.92, 125.67, 125.10, 124.77, 124.35, 115.86 (C_9H_6), 106.89, 106.84, 98.42, 94.52 ($C_2B_{10}H_{10}$), 67.17, 25.14 (OC_4H_8), 44.32, 34.25, 32.75 ppm (($CH_3)_2C$); ^{11}B NMR (128 MHz, [D$_5$]pyridine): $\delta = -0.9$ (2), −2.8 (4), −6.7 (10), −9.3 (2), −13.4 ppm (2); IR (KBr): $\tilde{\nu} = 3064$ (w), 2979 (s), 2883 (s), 2557 (vs), 1614 (w), 1453 (m), 1386 (w), 1257 (W), 1184 (w), 1090 (m), 1042 (s), 888 (m), 818 (m), 746 (m), 677 cm^{-1} (w); elemental analysis calcd (%) for $C_{32}H_{64}B_{20}ClLiO_4Zr$: C 44.55, H 7.48; found: C 44.35, H 7.30.

Received: May 13, 2003 [Z51892]

Keywords: agostic interactions · carboranes · coordination modes · metallacycles · metallocenes

[1] J. D. Roberts, H. E. Simmons, Jr., L. A. Carlsmith, C. W. Vaughan, *J. Am. Chem. Soc.* **1953**, *75*, 3290 – 3291.
[2] H. Hart in *Chemistry of Triple-Bonded Functional Groups, Supplement C2* (Ed.: S. Patai), Wiley, Chichester, **1994**, chap. 18.
[3] R. W. Hoffmann in *Dehydrobenzene and Cycloalkynes*, Academic Press, New York, **1967**.
[4] T. L. Gilchrist in *Chemistry of Functional Groups, Supplement C* (Eds.: S. Patai, Z. Rappoport), Wiley, Chichester, **1983**, chap. 11.
[5] S. L. Buchwald, R. B. Nielsen, *Chem. Rev.* **1988**, *88*, 1047 – 1058.
[6] W. M. Jones, J. Klosin, *Adv. Organomet. Chem.* **1998**, *42*, 147 – 221.
[7] S. L. Buchwald, B. T. Watson, *J. Am. Chem. Soc.* **1986**, *108*, 7411 – 7413.
[8] H. L. Gingrich, T. Ghosh, Q. Huang, M. Jones, Jr., *J. Am. Chem. Soc.* **1990**, *112*, 4082 – 4083.
[9] J. Jeon, T. Kitamura, B.-W. Yoo, S. O. Kang, J. Ko, *Chem. Commun.* **2001**, 2110 – 2111.
[10] a) T. Ghosh, H. L. Gingrich, C. K. Kam, E. C. Mobraaten, M. Jones, Jr., *J. Am. Chem. Soc.* **1991**, *113*, 1313 – 1318; b) Q. Huang, H. L. Gingrich, M. Jones, Jr., *Inorg. Chem.* **1991**, *30*, 3254 – 3257; c) R. T. Cunningham, N. Bian, M. Jones, Jr., *Inorg. Chem.* **1994**, *33*, 4811 – 4812; d) D. M. Ho, R. J. Cunningham, J. A. Brewer, N. Bian, M. Jones, Jr., *Inorg. Chem.* **1995**, *34*, 5274 – 5278; e) L. Barnett-Thamattoor, G. Zheng, D. M. Ho, M. Jones, Jr., J. E. Jackson, *Inorg. Chem.* **1996**, *35*, 7311 – 7315.
[11] H. Wang, Y. Wang, H.-W. Li, Z. Xie, *Organometallics* **2001**, *20*, 5110 – 5118.
[12] Crystal data for **1**: $C_{32}H_{64}B_{20}ClLiO_4Zr$, $M_r = 862.6$, monoclinic, space group $P2_1/c$, $a = 11.329(2)$, $b = 17.691(4)$, $c = 24.394(5)$ Å, $\beta = 102.67(1)°$, $V = 4770(2)$ Å^3, $T = 298$ K, $Z = 4$, $\rho_{calcd} = 1.201$ g cm^{-3}, $2\theta_{max} = 52°$, $\mu(Mo_{K\alpha}) = 0.71073$ Å, absorption corrections applied by using SADABS,[16] relative transmission factors in the range 0.872–1.000. A total of 27668 reflections were collected and led to 9347 unique reflections, 9347 of which with $I > 2\sigma(I)$ were considered as observed, $R_1 = 0.0599$, wR_2 (F^2) = 0.1377. This structure was solved by direct methods and refined by full-matrix least-squares on F^2 by using the SHELXTL/PC package of crystallographic software.[17] All non-hydrogen atoms were refined anisotropically and all hydrogen atoms were geometrically fixed using the riding model. CCDC-210368 contains the supplementary crystallographic data for this paper. These data can be obtained free of charge via www.ccdc.cam.ac.uk/conts/retrieving.html (or from the Cambridge Crystallographic Data Centre, 12, Union Road, Cambridge CB21EZ, UK; fax: (+44) 1223-336-033; or deposit@ccdc.cam.ac.uk).
[13] In the B3LYP calculations, effective core potentials with a Lanl2DZ basis set were used for Zr and Cl. For B, C, and H atoms, the 6-31G basis set was employed. Polarization functions were also added for Cl ($\zeta_d = 0.514$).
[14] T. A. Albright, J. K. Burdett, M.-H. Whangbo, *Orbital Interaction in Chemistry*, Wiley, New York, **1985**.
[15] R. H. Crabtree, *Organometallic Chemistry of the Transition Metals*, 3rd ed., Wiley, New York, **2001**, pp. 115 – 145.
[16] G. M. Sheldrick, SADABS: Program for Empirical Absorption Correction of Area Detector Data. University of Göttingen, Germany, **1996**.
[17] G. M. Sheldrick, SHELXTL 5.10 for Windows NT: Structure Determination Software Programs. Bruker Analytical X-ray Systems, Inc., Madison, Wisconsin, USA, **1997**.

 © 2003 Wiley-VCH Verlag GmbH & Co. KGaA, Weinheim

Electroresponsive Polymers

Helical, Chiral Polyisocyanides Bearing Ferrocenyl Groups as Pendants: Synthesis and Properties**

*Noriyuki Hida, Fumie Takei, Kiyotaka Onitsuka, Keiichiro Shiga, Sadayuki Asaoka, Tomokazu Iyoda, and Shigetoshi Takahashi**

Recent developments in polymer synthesis have provided us with new methods for preparing nano-sized polymer molecules with precisely controlled chemical sequence, molecular weight, and stereostructure, as well as molecular shape.[1]

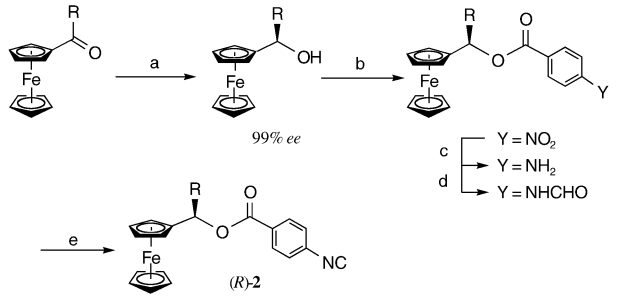
[*] Prof. Dr. S. Takahashi, N. Hida, Dr. F. Takei, Dr. K. Onitsuka
The Institute of Scientific and Industrial Research
Osaka University
Ibaraki, Osaka 567-0047 (Japan)
Fax: (+81) 6-6879-8459
E-mail: takahashi@sanken.osaka-u.ac.jp
Dr. K. Shiga, Dr. S. Asaoka, Prof. Dr. T. Iyoda
Chemical Resources Laboratory
Tokyo Institute of Technology
4259 Nagatsuta, Midori-ku, Yokohama, Kanagawa 226-8503 (Japan)

[**] This work was partially supported by a Grant-in-Aid for COE Research and Scientific Research from the Ministry of Education, Culture, Sports, Science and Technology. The authors gratefully acknowledge Professor Nagao Kobayashi, Tohoku University, for the assignment of a Cotton effect at 250 nm to a π–π^* transition in the CD spectra of the polymers.

 DOI: 10.1002/anie.200351456 © 2003 Wiley-VCH Verlag GmbH & Co. KGaA, Weinheim

Nano-sized metal-containing polymers are promising candidates as single-molecular devices.[2] Ferrocene is a redox-active organometallic compound and exists in two stable oxidation states of Fe^{II} (neutral ferrocene) and Fe^{III} (ferrocenium cation) which are interconvertible by oxidation and reduction. Several ferrocene-containing polymers including dendrimers have already been prepared as potential functional materials.[3] Polyisocyanides consist of an sp^2-hybridized carbon main chain and imino side groups, and have been attracting much attention in terms of their unique helical structure.[4] We have reported a living polymerization system for isocyanides with a dinuclear Pt–Pd complex initiator **1**[5] and the synthesis of novel polyisocyanides bearing chiral pendants which predominantly form one-handed helical structures in solution.[6] Now we have successfully synthesized helical, chiral, ferrocene-containing polyisocyanide compounds which exhibit a sharp response with a reversible conformational change on electrical stimulus.

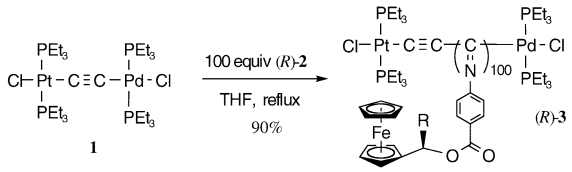
Known responsive polymers, such as polyisocyanates,[7] polypeptides,[8] polymethacrylates,[9] polysilanes[10] and polyacetylenes,[11] are sensitive to light irradiation, thermal treatment, and chemical interaction, whereas there are no responsive polymers to date whose conformation can be controlled by electrical stimuli. Helical, chiral poly(ferrocenyl polyisocyanide)s may be prepared by the polymerization of chiral ferrocenyl isocyanides with initiator **1**. Thus, chiral isocyanides **2** which contain ferrocenyl groups were synthesized in 99% *ee* from acylferrocene by an asymmetric reaction (Scheme 1).[12,13] We can prepare polymers with



(*R*)-**2a** : R = CH_3, $[\alpha]_D^{20} = -75$
(*R*)-**2b** : R = *n*-$C_{21}H_{43}$, $[\alpha]_D^{20} = -42$

Scheme 1. Synthesis of chiral isocyanides **2**. a) Cat*, BH_3, 79%; b) *p*-nitrobenzoyl chloride, pyridine, 77%; c) H_2, Pd/C, 99%; d) HCO_2H, DCC, 75%; e) $POCl_3$, $NH(iPr)_2$, 81%. Cat* = (*S*)-2-methyl-CBS-oxazaborolidine, DCC = *N*,*N*′-dicyclohexylcarbodiimide.

various polymerization degrees from **2** by exploiting the living nature of the polymerization. Treatment of 100 equivalents (*R*)-**2a** with **1** in refluxing THF for 20 h gave polyisocyanide (*R*)-**3a** with $M_n = 9800$ and a narrow polydispersity index (PDI) = 1.15 in 93% yield (Scheme 2). Thus prepared polymer (*R*)-**3a** showed a specific rotation of +304, although the specific rotation of (*R*)-**2a** was −75. Polymer (*S*)-**3a** prepared from (*S*)-**2a** ($[\alpha] = +77$) showed a specific rotation of −300. The large values of specific rotation of polymers **3a** with the opposite sign to those of monomers **2a** suggests that the polymers adopt predominantly a one-handed helical structure



(*R*)-**3a** : R = CH_3, $[\alpha]_D^{20} = +304$, $M_n = 9800$
(*R*)-**3b** : R = *n*-$C_{21}H_{43}$, $[\alpha]_D^{20} = +140$, $M_n = 22000$

Scheme 2. Synthesis of polyisocyanides **3** bearing chiral ferrocenyl groups as pendants.

in a solution.[6] The CD spectra of (*R*)-**3a** exhibited a strong positive Cotton effect at 360 nm and a strong negative one at 250 nm, the former is assigned to the n–π* transition of the imino chromophores and the latter to the π–π* transition of the benzene rings. The positive Cotton effect at 360 nm suggests the right-handed helical structure of polymer (*R*)-**3a**, in contrast (*S*)-**3a** showed a strong negative Cotton effect at 360 nm indicating a polymer main chain with a left-handed helix structure.[14]

The electrochemical properties of polymer (*R*)-**3a** were investigated by cyclic voltammetry (CV). Polymer (*R*)-**3a** showed reversible oxidation and reduction with a half-wave potential of approximately 0.6 V (vs Ag/AgCl), however, gave a small peak/current ratio $|i_{p,a}/i_{p,c}|$ of 0.63. This waveform suggested deposition of the oxidized polymer onto the electrode as often seen for some ferrocene-containing compounds[15] as a result of the low solubility of the cationic polymers.

To improve the solubility of polymers, a long alkyl substituent (C_nH_{2n+1}: $n = 7$, 11, and 21) was introduced at the chiral carbon atom of monomer **2a**. Thus, (*R*)-**2b** ($[\alpha] = -42$) having a $C_{21}H_{43}$ was synthesized with 99% *ee* (Scheme 1) and polymerized with initiator **1** ((*R*)-**2b**/**1** molar ratio = 100) to give polymer (*R*)-**3b** with $M_n = 22000$ and PDI = 1.15 in 90% yield (Scheme 2). The specific rotation and CD spectrum indicated a right-handed helical structure[14] of (*R*)-**3b** (Figure 1). The cyclic voltammogram of the polymer in CH_2Cl_2 (Figure 2) showed a reversible oxidation and reduction behavior, and the same half-wave

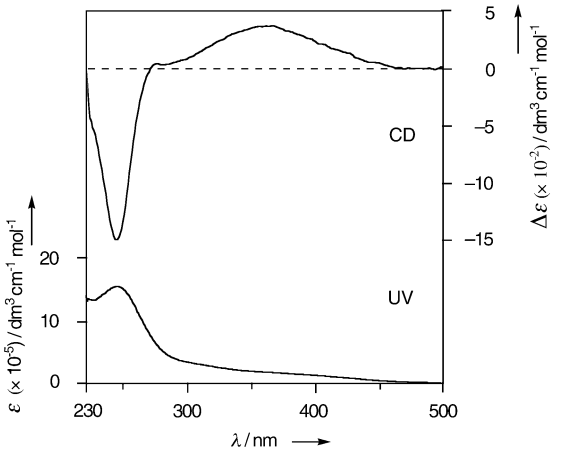


Figure 1. CD (Top) and UV (bottom) spectra of (*R*)-**3b**.

 © 2003 Wiley-VCH Verlag GmbH & Co. KGaA, Weinheim

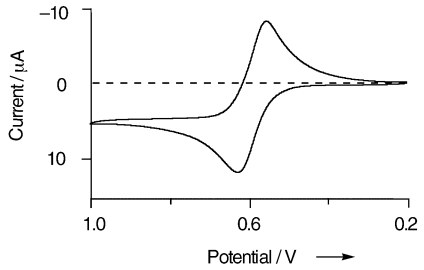


Figure 2. Cyclic voltammogram of (*R*)-**3b**. Recorded with $[NBu_4][PF_6]$ as electrolyte in CH_2Cl_2 (0.1 mol L^{-1}) at ambient temperature with a scan rate of 0.05 V s^{-1}. Potentials are expressed versus Ag/AgCl.

potential of approximately 0.6 V as polymer (*R*)-**3a**. However, in comparison with **3a** polymer **3b** gave a higher peak/current ratio $|i_{p,a}/i_{p,c}|$ of 0.92 and no deposition on the electrode was observed, which indicates that the long alkyl group improved the solubility of the oxidized polymer, as expected. We performed three cycles of redox and observed no appreciable changes in the voltammograms, which indicates that the redox process is completely reversible.

To investigate the response of (*R*)-**3b** towards an electrical stimulus, electrolytic CD and UV spectra were measured.[16] When polymer (*R*)-**3b**, dissolved in CH_2Cl_2, was electrochemically oxidized at 1.0 V, the CD spectrum clearly showed that the intensity of the positive Cotton effect at 360 nm decreased to around 40% of that before oxidation and the negative Cotton effect at 250 nm almost disappeared (Figure 3). The same change in intensity of the Cotton effects was observed on oxidation at a higher applied potential of 1.5 V. In the UV spectrum new broad absorption bands appeared at 240–310 (Figure 3) and at 620 nm (not shown),

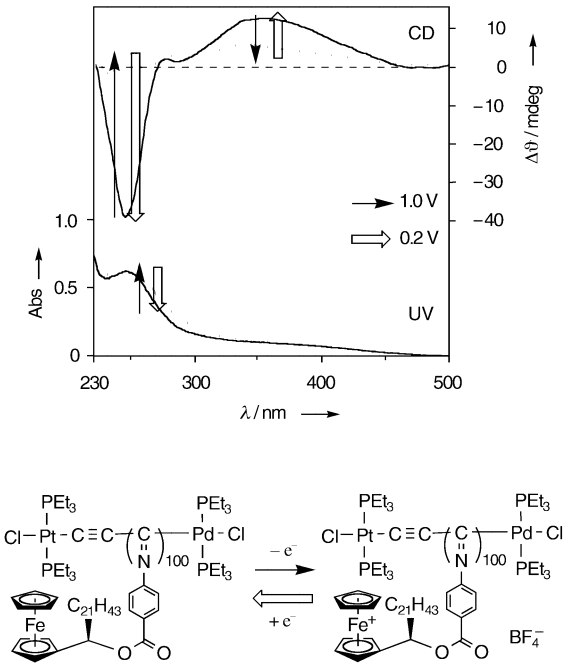


Figure 3. Electrolytic CD (top) and UV (bottom) spectra of the oxidation/reduction of (*R*)-**3b**.

which are assigned to a ferrocenium chromophore.[17] Subsequent electrolytic reduction of the ferrocenium cation at 0.2 V led to an increase in intensity of the Cotton effects and to recovery to the original intensity. The intensity change of both Cotton effects at 250 and 360 nm was repeated on further electrolytic oxidation and reduction. Since any changes of the UV spectra except the absorption resulting from the ferrocenium chromophore were not observed, the dramatic CD change suggests reversible conformational transformation of the helical main chain by an electrical stimulus.

On the other hand, on application of the same electrode potential (1.0 V) to a polyisocyanide compound bearing redox-inactive (*l*)-menthyl pendants,[6b] which has a right-handed helix, no changes were observed in the electrolytic CD and UV spectra, which indicates that the conformational structure of polyisocyanide chains was not affected directly by electrical stimuli.

We tried controlling the helical structure of the main chain not only by electrolytic redox but also by chemical oxidation and reduction of ferrocenyl groups[3a] in (*R*)-**3b**. On oxidation of the polymer with $[NO][PF_6]$ in CH_2Cl_2 the intensity of the Cotton effect at 360 nm decreased to about 40% of that before oxidation, and the Cotton effect at 250 nm almost disappeared. UV absorption bands assigned to a ferrocenium cation appeared at 240–310 and 620 nm. Then, the reduction of ferrocenium groups with $[Cp^*_2Fe]$ (Cp^* = pentamethylcyclopentadienyl) recovered the initial intensities of the Cotton effects at 250 and 360 nm. These phenomena are the same as those observed for electrolytic oxidation and reduction, and undoubtedly reveal a driving force for the conformational transformation of helical polymers **3** to be electrostatic repulsion between the ferrocenium cations in the side chains generated by oxidation. Decrease of the Cotton effect intensities at 250 and 360 nm after oxidation suggests that electrostatic repulsion among the ferrocenium cations caused dislocation of the imino groups and benzene rings to positions which disturb the regular helical conformation of the polymer. In other words, the main chains of **3** are transformed from a helical structure to a disordered one, naturally resulting in loss of helical chirality.

In conclusion, we synthesized novel helical, chiral polyisocyanides **3** bearing ferrocenyl pendants which exhibit response towards oxidation and reduction with conformational change.

Experimental Section

Pt–Pd dinuclear complex **1** was prepared by the method reported in ref. [5a].

(*R*)-**3a**: A solution of complex **1** (3.0 mg, 3.5 μmol) in THF (10 mL) was added to (*R*)-**2a** (126 mg, 0.35 mmol). The mixture was stirred for 20 h under reflux. After the solution was concentrated to about 1 mL, it was poured into methanol (100 mL). The precipitate was collected by filtration and washed with methanol to give (*R*)-**3a** as a yellow solid (120 mg, 93%). $[\alpha]_D^{20} = +304$ ($c = 0.05$ in THF); IR (KBr): $\tilde{\nu} = \nu$(C≡C) 2091, ν(C=O) 1713, ν(C=N) 1600 cm^{-1}; ^{13}C NMR (100 MHz, $CDCl_3$, 25 °C, TMS): $\delta = 164.47$ (br, COO), 161.23 (br, N=C), 150.37 (br, Ar), 129.93 (br, Ar), 127.95 (br, Ar), 117.80 (br, Ar), 88.53 (br, CH), 68.83 (br, Cp), 68.60 (br, Cp), 67.92 (br, Cp), 66.11 (br,

 © 2003 Wiley-VCH Verlag GmbH & Co. KGaA, Weinheim

Cp), 20.50 ppm (br, CH_3). Elemental analysis (%) calcd for $C_{2026}H_{1760}N_{100}Cl_2Fe_{100}O_{200}P_4PdPt$: C 66.14, H 4.82, N 3.81; Found: C 65.69, H 5.29, N 3.74.

(*R*)-**3b**: Similar reaction to that with (*R*)-**2a** but using monomer (*R*)-**2b** gave (*R*)-**3b** as a yellow solid in 90% yield. $[\alpha]_D^{20} = +140$ ($c =$ 0.05 in THF); IR (KBr): $\tilde{\nu} = \nu$(C≡C) 2095, ν(C=O) 1714, ν(C=N) 1601 cm^{-1}; ^{13}C NMR(100 MHz, $CDCl_3$, 25 °C, TMS): $\delta = 164.60$ (br, COO), 162.07 (br, N=C), 150.78 (br, Ar), 130.32 (br, Ar), 126.43 (br, Ar), 113.78 (br, Ar), 89.01 (br, CH), 72.71 (br, Cp), 68.98 (br, Cp), 68.65 (br, Cp), 67.58 (br, Cp), 35.91 (br, CH_2), 31.92 (br, CH_2), 29.74 (br, CH_2), 25.75 (br, CH_2), 22.68 (br, CH_2), 14.11 ppm (br, CH_3 Elemental analysis (%) calcd for $C_{4026}H_{5760}N_{100}Cl_2Fe_{100}O_{200}P_4PdPt$: C 74.57, H 8.95, N 2.16; Found: C 74.49, H 9.10, N 2.19.

Received: March 24, 2003 [Z51456]

Keywords: electrochemistry · ferrocene · helical structures · polyisocyanides · polymers

[1] S. Kobayashi, *Catalysis in Precision Polymerization*, Wiley, Chichester, **1997**.
[2] P. Nguyen, P. Gomez-Elipe, I. Manners, *Chem. Rev.* **1999**, *99*, 1515.
[3] For recent papers, see: a) S. Nlate, J. Ruiz, V. Sartor, R. Navarro, J. Blaiz, D. Astruc, *Chem. Eur. J.* **2000**, *6*, 2544; b) R. Resendes, J. A. Massey, K. Temple, L. Cao, K. N. Power-Billard, M. A. Winnik, I. Manners, *Chem. Eur. J.* **2001**, *7*, 2414.
[4] For reviews, see: a) T. Nakano, Y. Okamoto, *Chem. Rev.* **2001**, *101*, 4013; b) J. J. L. M. Cornelissen. A. E. Rowan, R. J. M. Nolte, N. A. J. M. Sommerdijk, *Chem. Rev.* **2001**, *101*, 4039.
[5] a) K. Onitsuka, T. Joh, S. Takahashi, *Bull. Chem. Soc. Jpn.* **1992**, *65*, 1179; b) K. Onitsuka, K. Yanai, F. Takei, T. Joh, S. Takahashi, *Organometallics* **1994**, *13*, 3862.
[6] a) F. Takei, K. Yanai, K. Onitsuka, S. Takahashi, *Angew. Chem.* **1996**, *108*, 1634; *Angew. Chem. Int. Ed. Engl.* **1996**, *35*, 1554; b) F. Takei, K. Yanai, K. Onitsuka, S. Takahashi, *Chem. Eur. J.* **2000**, *6*, 983.
[7] a) M. Muller, R. Zentel, *Macromolecules* **1996**, *29*, 1609; b) S. Mayer, G. Maxein, R. Zentel, *Macromolecules* **1998**, *31*, 8522; c) K. Maeda, Y. Okamoto, *Macromolecules* **1999**, *32*, 974.
[8] a) A. Ueno, K. Takahashi, J. Anzai, T. Osa, *J. Am. Chem. Soc.* **1981**, *103*, 6410; b) O. Pieroni, A. Fissi, N. Angelini, F. Lenci, *Acc. Chem. Res.* **2001**, *34*, 9.
[9] a) L. Angiolini, D. Caretti, L. Giorgini, E. Salatelli, A. Altomare, C. Carlini, R. Solaro, *Polymer* **1998**, *39*, 6621; b) L. Angiolini, R. Bozio, L. Giorgini, D. Pedron, G. Turco, A. Dauru, *Chem. Eur. J.* **2002**, *8*, 4241.
[10] M. Fujiki, *J. Am. Chem. Soc.* **2000**, *122*, 3336.
[11] a) E. Yashima, K. Maeda, Y. Okamoto, *Nature* **1999**, *399*, 449; b) K. Maeda, E. Yashima, *Yuki Gosei Kagaku Kyokaishi* **2002**, *60*, 878.
[12] For the synthesis of chiral ferrocenyl alcohol, see: a) J. Wright, L. Frambes, P. Reeves, *J. Organomet. Chem.* **1994**, *476*, 215; b) L. Schwink, P. Knochel, *Tetrahedron Lett.* **1996**, *37*, 25.
[13] Chiral ferrocenyl isocyanide (*R*)-**2** was prepared from (*R*)-1-ferrocenyl alcohol[12] by the literature method.[6] (*R*)-**2a**: Yellow solid, $[\alpha]_D^{20} = -75$ ($c = 0.05$ in THF); MS(EI): m/z 359 [M^+]; ^1H NMR(400 MHz, $CDCl_3$, 25 °C, TMS): $\delta = 8.08$ (d, $J = 8.5$ Hz, 2H; Ar), 7.43 (d, $J = 8.5$ Hz, 2H; Ar), 6.08 (q, $J = 6.3$ Hz, 1H; CH), 4.33–4.28 (m, 2H; Cp), 4.20–4.18 (m, 2H; Cp), 4.16 (s, 5H; Cp), 1.69 ppm (d, $J = 6.3$ Hz, 3H; CH_3). (*R*)-**2b**: Yellow solid, $[\alpha]_D^{20} = -42$ ($c = 0.05$ in THF); MS(FAB): m/z 639 [M^+]; ^1H NMR(400 MHz, $CDCl_3$, 25 °C, TMS): $\delta = 8.13$ (d, $J =$ 8.3 Hz, 2H; Ar), 7.46 (d, $J = 8.3$ Hz, 2H; Ar), 6.00 (t, $J =$ 6.8 Hz, 1H; CH), 4.33–4.22 (m, 2H; Cp), 4.17–4.15 (m, 2H; Cp), 4.11 (s, 5H; Cp), 1.95 (dt, $J = 6.8$ Hz, $J = 6.8$ Hz, 2H; CH_2), 1.27–1.22 (m, 38H; $C_{19}H_{38}$), 0.88 ppm (t, $J = 6.8$ Hz, 3H; CH_3).
[14] F. Takei, H. Hayashi, K. Onitsuka, N. Kobayashi, S. Takahashi, *Angew. Chem.* **2001**, *113*, 4216; *Angew. Chem. Int. Ed.* **2001**, *40*, 4092.
[15] a) I. Cuadrado, C. M. Casado, B. Alonso, M. Moran, J. Losada, V. Belsky, *J. Am. Chem. Soc.* **1997**, *119*, 7613; b) K.-W. Poon, Y. Yan, X.-Y. Li, D. K. P. Ng, *Organometallics* **1999**, *18*, 3528.
[16] Electrolytic redox reactions of **3b** were performed in a CH_2Cl_2 solution containing 0.1 mol dm^{-3} of $[NBu_4][PF_6]$ under potentiostatic conditions at 1.0 V (oxidation) and 0.2 V (reduction) versus Ag/AgCl. A platinum mesh was used as a working electrode. A platinum wire and an Ag/AgCl electrode were used as a counter electrode and a reference electrode, respectively.
[17] F. G. Herring, R. A. N. McLean, *Inorg. Chem.* **1972**, *11*, 1667.

 © 2003 Wiley-VCH Verlag GmbH & Co. KGaA, Weinheim

Carbon Nanocoils

High-Performance Direct Methanol Fuel Cell Electrodes using Solid-Phase-Synthesized Carbon Nanocoils**

Taeghwan Hyeon, Sangjin Han, Yung-Eun Sung, Kyung-Won Park, and Young-Woon Kim*

Dedicated to Professor Ki-Jun Lee on the occasion of his retirement

Since the discovery of carbon nanotubes by Iijima in 1991,[1] nanostructured carbon materials[2] have attracted tremendous attention for their possible applications in electron field emitters, catalytic supports, nanocomposites, quantum electronic devices, and electrode materials.[3] Herein we report on

[*] Prof. Dr. T. Hyeon, S. Han
National Creative Research Initiative Center for Oxide Nanocrystalline Materials and
School of Chemical Engineering
Seoul National University
Seoul 151-744 (Korea)
Fax: (+82) 2-886-8457
E-mail: thyeon@plaza.snu.ac.kr
Prof. Dr. Y.-E. Sung, K.-W. Park
Department of Materials Science & Engineering and
Research Center for Energy Conversion and Storage
Kwangju Institute of Science & Technology
Kwangju 500-712 (Korea)
Prof. Dr. Y.-W. Kim
School of Materials Science and Engineering
Seoul National University, Seoul 151-744 (Korea)

[**] T.H. would like to thank the National Creative Research Initiative Program of the Korean Ministry of Science and Technology for financial support. Y.E.S. acknowledges support by the KOSEF through the Research Center for Energy Conversion and Storage.

Supporting information for this article is available on the WWW under http://www.angewandte.org or from the author.

 © 2003 Wiley-VCH Verlag GmbH & Co. KGaA, Weinheim DOI: 10.1002/anie.200250856

the synthesis of carbon nanocoils composed of nanometer-thick graphitic fibers by the catalytic graphitization of a resorcinol–formaldehyde gel. The carbon nanocoils were successfully applied as electrode materials for direct methanol fuel cells. Many forms of nanostructured carbon materials including carbon nanotubes, graphitic carbon nanofibers (GCNFs), and carbon onions were produced using various gas-phase reactions.[4] Arc discharge, laser evaporation, and thermal chemical vapor deposition are the typical techniques used to produce the materials.[5] However, these synthetic methods have limitations in terms of large-scale and economical production because of their harsh synthetic conditions and low production yields. Although several groups have reported the solid-phase synthesis of nanostructured carbon materials,[6] the synthetic processes used cannot be applied for economical and large-scale production because of the long reaction time or a complicated synthetic procedure.

Carbon is a critical material in low-temperature fuel cells,[7] such as polymer–electrolyte membrane fuel cells. No other material has the essential combination of electronic conductivity, corrosion resistance, surface properties, and the low cost required for the commercialization of fuel cells.[7] In recent years, direct methanol fuel cells (DMFCs) have been intensely studied because of their numerous advantages, which include high energy density, the ease of handling a liquid, low operating temperatures, and their possible applications to micro fuel cells.[8] The performance and long-term stability of low-temperature fuel cells, such as DMFCs, which even operate at room temperature, are known to be strongly dependent on carbon supports as well as catalytically active species.[3e,9] Accordingly, for the best DMFC performance, it is essential to develop a good carbon material for the catalyst support.

We synthesized carbon nanocoils by simply heat-treating composites composed of a carbon precursor, silica, and a transition-metal salt. Resorcinol–formaldehyde (RF) gel was chosen as carbon precursor. A mixture of cobalt and nickel salts was used as the catalyst precursor in the synthesis. A silica sol was added to the reaction mixture to obtain carbon materials with a high specific surface area, and to achieve a good dispersion of the transition-metal nanoparticles, which catalyze the formation of the graphitic carbon nanostructure. We and other research groups have synthesized many different nanoporous carbon materials with amorphous frameworks using nanostructured silica materials as templates.[10] In a typical synthesis, an aqueous reaction mixture, with an H_2O/cobalt salt/nickel salt/resorcinol/formaldehyde/silica molar ratio of 100:0.4:0.4:1:2:0.6, was prepared by mixing the constituent materials in 100 mL of deionized water. The resulting reaction mixture was cured at 85 °C for 3 h in a closed glass vial. For the carbonization, the composite was heated under a nitrogen atmosphere at 900 °C for 3 h. The resulting composite was then stirred in 3 M NaOH solution for 3 h to remove silica particles, and was refluxed in 2.5 M HNO_3 solution for 1 h to remove metal particles, which resulted in the formation of carbon nanocoils (CNCs). Inductively coupled plasma (ICP) analysis revealed that the transition metals were successfully removed by the acid treatment. The current synthetic procedure employs the direct catalytic graphitization of a carbon precursor (RF gel) without the prior synthesis of metal particles, which has been often required in the conventional synthesis of nanostructured carbons.

The XRD pattern of the CNCs (Figure 1) shows that these carbon materials are highly graphitized with a (002) plane *d* spacing of 3.43 Å and clearly observed (100) and (004)

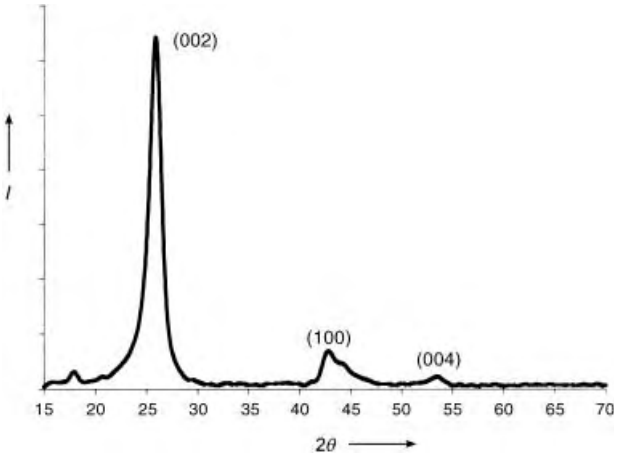


Figure 1. X-ray diffraction (XRD) pattern of carbon nanocoils (CNCs).

peaks. The crystallite size of individual nanocoils measured perpendicular to the basal plane (L_c) using the Debye–Scherrer formula[7] was calculated to be 5.5 nm. Raman spectroscopic data (see Figure S1 in the Supporting Information) showed a characteristic G-band peak at 1576 cm^{-1} and a D-band peak at 1345 cm^{-1}. These XRD and Raman spectroscopic results reveal that the carbon nanocoil possesses a graphitic character that is comparable to multiwall carbon nanotubes. The carbon nanocoils exhibited a high surface area of 318 $m^2 g^{-1}$. The SEM image reveals that the carbon materials consisted of particles of approximately 100 nm diameter (Figure 2a). The TEM image (Figure 2b) shows that each individual particle is composed of 5–10 nm thick coils, which corresponds well with the L_c value of 5.5 nm calculated from the XRD data. The HRTEM image (Figure 2c) of a single nanocoil exhibits well-aligned graphitic layers, which confirm the XRD and Raman spectroscopic results. When the quantity of metal salts used was decreased to 60 wt.% of the amount used for CNC synthesis, a carbon material with an increased surface area of 451 $m^2 g^{-1}$ and a less graphitic structure (as characterized by XRD and Raman spectroscopy) was obtained.

It is well known that it is extremely difficult to synthesize carbon materials with both high surface area and good crystallinity. Consequently, in terms of the design and application for a support in fuel cells, CNCs, which possess high surface area, well-defined porosity, and good crystallinity, are considered to be a very attractive choice. The electrochemical properties of the carbon nanocoils were compared with those of Vulcan XC-72 carbon, which is the most widely used support material for direct methanol fuel cell electrodes. Vulcan XC-72 carbon is amorphous and

 © 2003 Wiley-VCH Verlag GmbH & Co. KGaA, Weinheim

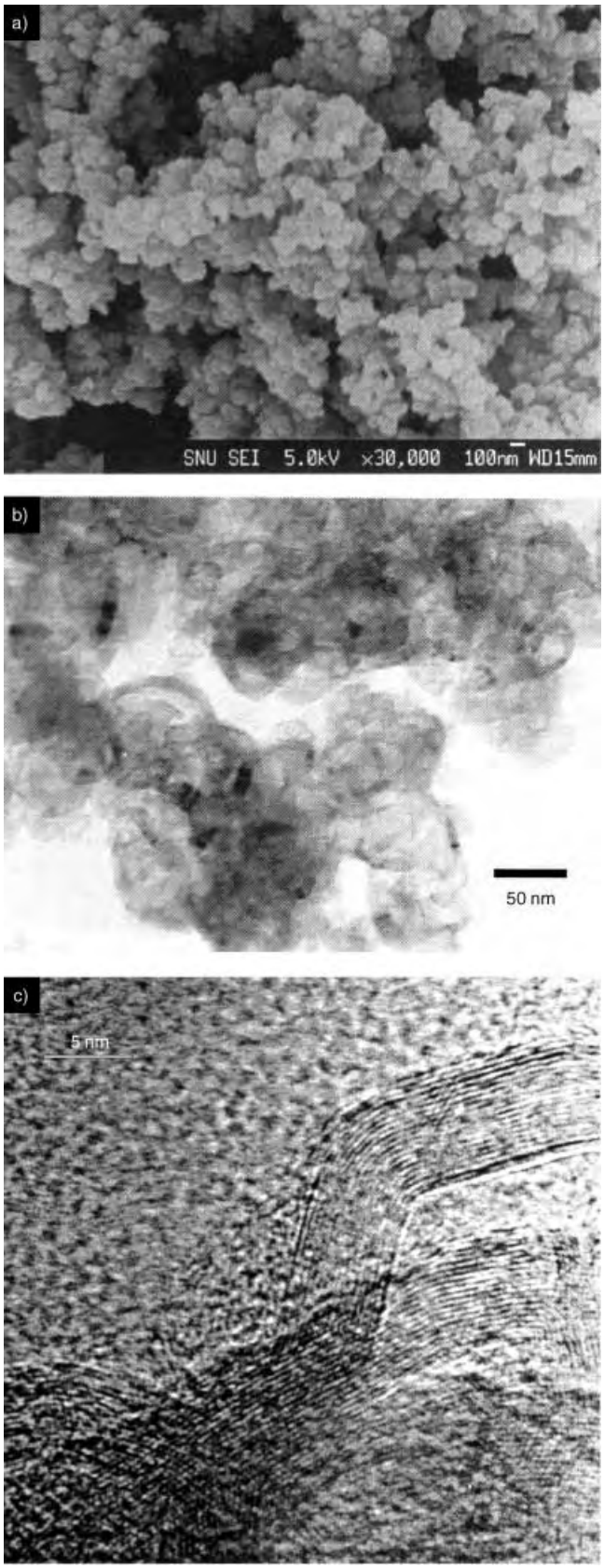


Figure 2. Electron microscope images of carbon nanocoils: a) Field emission scanning electron microscope (FE-SEM) image; b) transmission electron microscope (TEM) image, and c) high-resolution transmission electron microscope (HRTEM) image.

possesses a specific surface area of 212 $m^2 g^{-1}$. The electrochemical stability and capacitance of CNC and Vulcan XC-72 carbons are compared (Figure S2 in the Supporting Information). The catalyst supported on CNC shows excellent electrochemical stability over the potential range of the methanol oxidation process. In addition, it also shows a capacitance over ten times higher than that of Vulcan XC-72 (33.4 versus 2.8 $F g^{-1}$; see the cyclovoltammogram in Figure S2 of the Supporting Information). The TEM image of the supported catalysts (Figure S3 in the Supporting Information) shows the highly dispersed Pt/Ru (1:1) alloy catalyst (60 wt %) on CNC with an average particle size of 2.3 nm, which is in good agreement with the value calculated using Vegard's law and the Debye–Scherrer equation from the XRD pattern (Figure S4 in the Supporting Information). A high catalyst loading of 60 wt % was applied, because the high loading of Pt-based alloy catalysts (especially Pt/Ru) is essential for the anode in DMFCs. The XRD and TEM results showed that the average particle size of Pt/Ru (1:1) alloy nanoparticles supported on Vulcan XC-72, CNCs, and the commercial E-TEK catalyst is similar ($\approx$ 2.3 nm). Further, the active surface area of the supported catalysts was measured using CO chemisorption (Pt-CO) and hydrogen adsorption/desorption (Pt-H) methods. The active surface area is highest for the CNC-supported catalyst and lowest for commercial E-TEK, which means that the catalyst is better dispersed on CNC, compared to other supports (see Table S1 in the Supporting Information). The uniform distribution of the catalyst, along with a small particle size, which are key factors for the stable and efficient operation of a DMFC, seems to result from the good characteristics of CNCs, such as high crystallinity and larger surface area.[11] In order to evaluate the electrocatalytic activity of carbon-supported catalysts, the methanol oxidative current of the catalysts was measured using a fundamental electrochemical system. As shown in Figure 3, the CNC-supported catalyst exhibited a substantially higher specific oxidation current of 80 $A g^{-1}$ at

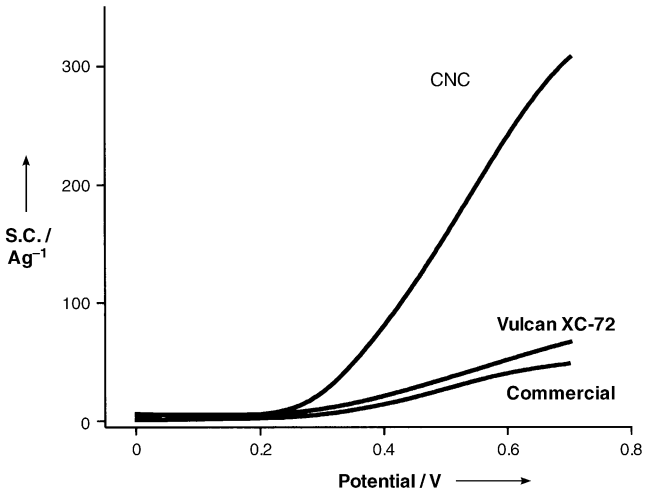


Figure 3. Specific methanol electrooxidation current (S.C.) with respect to applied potentials (versus NHE) of a Pt/Ru (1:1) alloy catalyst (60 wt %) supported on carbon nanocoils (CNC), Vulcan XC-72, and a commercial supported catalyst at 25 °C.

 © 2003 Wiley-VCH Verlag GmbH & Co. KGaA, Weinheim

0.4 V (versus a normal hydrogen electrode (NHE)) near the kinetically controlled potential in the methanol reaction, compared to 20 $A g^{-1}$ for the Vulcan XC-72 supported catalyst and 14 $A g^{-1}$ for the E-TEK supported catalyst; the reported methanol oxidation current of Vulcan XC-72 supported Pt/Ru catalysts was also $\approx 20 A g^{-1}$ at the same potential.[12] The remarkably higher oxidation current of the CNC-supported catalyst is directly related to the high surface area and the superior dispersion of the catalyst on CNC. It is also evident that the high electrical conductivity of graphitic CNC, compared with the amorphous Vulcan XC-72, can deliver a significantly higher methanol oxidation current. When the catalytic activity at the same active site of the catalyst is considered, the CNC-supported catalyst is still superior to other catalysts for methanol oxidation. For example, at 0.4 V, the CNC-supported catalyst shows a higher methanol oxidation current density of 46 $\mu A cm^{-2}$, compared to 14 and 12 $\mu A cm^{-2}$ for Vulcan XC-72 and the commercial E-TEK catalyst, respectively. This implies that the enhanced methanol oxidation of the CNC-supported catalyst results not only from the higher active surface area but also from the superior characteristics of the support itself. In addition, the methanol oxidation current of the CNC-supported Pt/Ru catalyst shows a considerably lower onset potential and higher oxidative current than the Vulcan XC-72 supported catalyst. Theoretically, methanol oxidation may proceed at 0.04 V (versus NHE) according to the equation $CH_3OH + H_2O \rightarrow CO_2 + 6H^+ + 6e^-$. Therefore, the lower onset potential demonstrates clear evidence of its superior electrocatalytic activity for methanol electrooxidation.[13] It is believed that both supported Pt/Ru catalysts should start to oxidize methanol at the same potential. However, as indicated in Figure 3, the on-set potentials for CNC- and Vulcan XC-72 supported catalysts are 0.20 and 0.26 V versus NHE, respectively.

The final requirement for carbon-supported catalysts is their successful application to the electrodes in actual DMFC systems consisting of polymer membranes and electrodes. It is well known that at low temperature, the catalysts (including the supports) have a dominating effect on the performance of fuel cells, and comparisons of DMFC performance at relatively low temperatures are the most practical and powerful ways of evaluating the activity of catalysts. Figure 4 shows the polarization curves of a direct methanol fuel cell at 30 and 60 °C using carbon-supported catalysts as the anode. At 0.6 V (Figure 4a), an activation polarization regime dominates the activity of the catalyst; the current density (20 $mA cm^{-2}$) of the CNC-supported catalyst is four and twenty times higher than those of Vulcan XC-72 supported catalyst (5 $mA cm^{-2}$) and the commercial carbon-supported Pt/Ru catalyst (1 $mA cm^{-2}$), respectively. In addition, the CNC-supported catalyst produces a higher maximum power density at 30 °C, which is 170 and 230 % higher than that of the Vulcan XC-72 supported catalyst and the commercial catalyst, respectively. At 60 °C (Figure 4b), the maximum power density of the CNC-supported catalyst is 146 and 180 % higher than the Vulcan XC-72 supported catalyst and the commercial catalyst, respectively. Such an improved activity indicates that the use of CNCs can lead to a substantial reduction of catalyst quantities in the fuel cell. The excellent performance of CNCs is due mainly to the superior electrocatalytic activity for methanol oxidation of the supported catalyst. In addition, the low electrical resistance for current collection and the unique pore characteristics of the support, which favor the diffusion of methanol fuel and the removal of the by-product CO_2 gas, are responsible for the improved fuel cell performance. Detailed studies on the origins of the excellent performance of the CNC-supported catalysts will be reported in the future. From combining the results of the electrochemical cell and the practical unit cell, we conclude that carbon nanocoils (CNCs) are an excellent support for the electrodes of direct methanol fuel cells. Further, in the performance of fuel cells, the durability of the electrode is significant for long-term applications. The CNC maintained stable catalytic activity by measuring power density versus time for up to 100 hr in a DMFC unit cell. Accordingly, it is believed that CNC is a highly promising electrode for long-term fuel cells. However, since the issue of durability and stability of the fuel cell electrode is very important, a more profound study of these characteristics is underway.

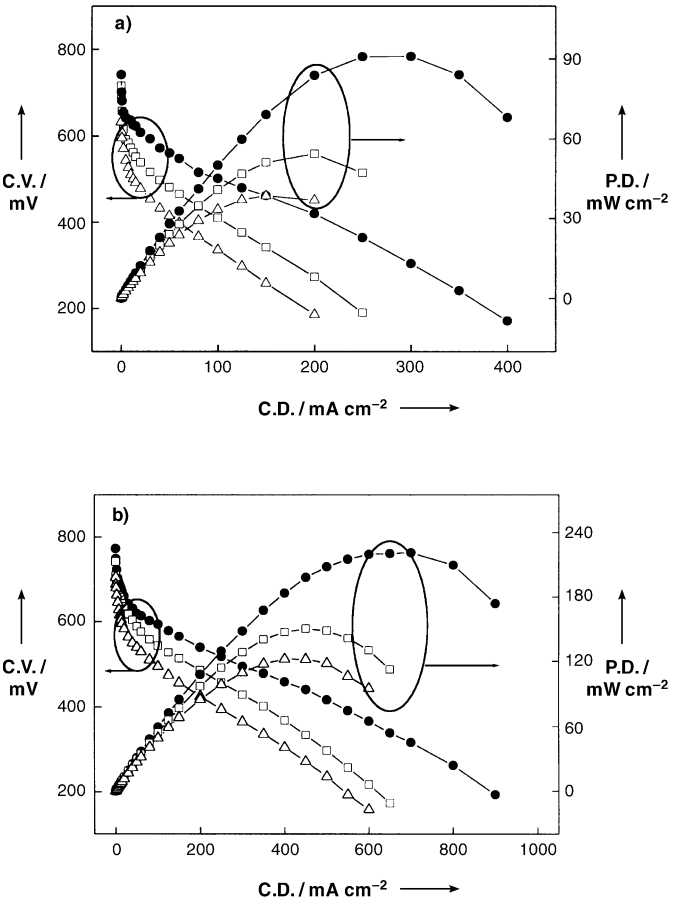


Figure 4. Polarization curves for a direct methanol fuel cell using a Pt/Ru (1:1) alloy catalyst (60 wt%) supported on carbon nanocoils (CNC; ●), Vulcan XC-72 (□), and a commercial supported catalyst (△): a) 30 °C; b) 60 °C. C.V., C.D., and P.D. stand for cell voltage, current density, and power density, respectively.

 © 2003 Wiley-VCH Verlag GmbH & Co. KGaA, Weinheim

Experimental Section

Carbon-supported catalysts were synthesized at room temperature by a conventional reduction method using $H_2PtCl_6 \cdot 6H_2O$, $RuCl_3 \cdot x H_2O$, (both Aldrich) and $NaBH_4$ as the reductant.[14]

Electrochemical measurements were conducted using a three-electrode cell at 25 °C. Pt gauze and Ag/AgCl (in saturated KCl) were used as the counter and reference electrodes, respectively. The carbon working electrode (6 mm in diameter) was polished with 1, 0.3, and 0.05 μm Al_2O_3 paste and washed ultrasonically in Millipore water (18 MΩ cm). The commercial carbon-supported Pt/Ru (60 wt %) catalyst was purchased from E-Tek Inc. The catalyst ink consisting of catalyst, Nafion ionomer (in water), and 2-propanol was dropped onto the working electrode, and dried at 70 °C in a vacuum oven. Solutions of 0.5 M H_2SO_4 and 2.0 M CH_3OH in 0.5 M H_2SO_4 were stirred constantly and purged with nitrogen gas. All chemicals used were of analytical grade. Electrochemical experiments were performed using an AUTOLAB by Eco Chemie. In order to compare the catalytic activity of the supported catalysts for methanol oxidation, voltammetry was performed in the potential range 0–0.7 V versus NHE.

For a membrane electrode assembly (MEA) of DMFC, an anode (supported catalysts) prepared from Pt/Ru (2 mg per cm^2) and a cathode prepared from Pt black (5 mg per cm^2; Johnson Matthey Co.) was formed on teflon-coated carbon paper (TGPH-090) substrates using catalyst inks containing the appropriate weight percentage of Nafion ionomer solution (Aldrich). The MEA for unit cell tests was fabricated by pressing as-prepared cathode and anode layers onto both sides of a pretreated Nafion 117 electrolyte membrane at 110 °C and 800 psi for 3 min. Cell performance was evaluated in a DMFC unit cell with a 2 cm^2 cross-sectional area, and measured with a potentiometer (WMPG-3000), which recorded the cell under a constant current. Both fuel and oxidant flow paths were machined into graphite block end-plates, which also served as current collectors. A 2 M methanol solution with a flow rate of 1 $cm^{-3}\,min^{-1}$ was supplied by a Masterflex liquid micropump, and a dry O_2 flow was regulated at 500 $cm^{-3}\,min^{-1}$ using a flowmeter.

Received: December 27, 2002
Revised: July 14, 2003 [Z50856]

Keywords: carbon · fuel cells · nanomaterials · solid-phase synthesis · supported catalysts

[1] S. Iijima, *Nature* **1991**, *354*, 56–58.
[2] a) S. Subramoney, *Adv. Mater.* **1998**, *10*, 1157–1171; b) *Supercarbon* (Eds.: S. Yoshimura, R. P. H. Chang), Springer, Berlin, **1998**; c) *Science and Application of Nanotubes* (Eds.: D. Tománek, R. J. Enbody), Kluwer, Dordrecht, **2000**.
[3] a) W. A. Heer, A. Chatelan, D. Ugarte, *Science* **1995**, *270*, 1179–1180; b) J. M. Planeix, N. Coustel, B. Coq, V. Brotons, P. S. Kumbhar, R. Dutarte, P. Geneste, P. Bernier, P. M. Ajayan, *J. Am. Chem. Soc.* **1994**, *116*, 7935–7936; c) X. Gong, J. Liu, S. Baskaran, R. D. Voise, J. S. Young, *Chem. Mater.* **2000**, *12*, 1049–1052; d) J. Hu, M. Ouyang, P. Yang, C. M. Lieber, *Nature* **1999**, *399*, 48–51; e) C. A. Bessel, K. Laubernds, N. M. Rodriguez, R. T. K. Baker, *J. Phys. Chem.* B **2001**, *105*, 1115–1118.
[4] a) F. T. Edelmann, *Angew. Chem.* **1999**, *111*, 1473–1480; *Angew. Chem. Int. Ed.* **1999**, *38*, 1381–1387; b) N. M. Rodriguesz, *J. Mater. Res.* **1993**, *8*, 3233–3250; c) D. Ugarte, *Nature* **1992**, *359*, 707–709.
[5] a) T. W. Ebbesen, P. M. Ajayan, *Nature* **1992**, *358*, 220–221; b) A. Thess, R. Lee, P. Nikolaev, H. Dai, P. Petit, J. Robert, C. Xu, Y. H. Lee, S. G. Kim, A. G. Rinzler, D. T. Colbert, G. E. Scuseria, D. Tomanek, J. E. Fischer, R. E. Smalley, *Science* **1996**, *273*, 483–487; c) S. Fan, M. C. Chapline, N. R. Frankin, T. W. Tombler, A. M. Cassell, H. Dai, *Science* **1999**, *283*, 512–514.
[6] a) W. Cho, E. Hanada, Y. Kondo, K. Takayanagi, *Appl. Phys. Lett.* **1996**, *69*, 278–279; b) N. A. Kiselev, J. Sloan, D. N. Zakharov, E. F. Kukovitskii, J. L. Hutchison, J. Hammer, A. S. Kotosonov, *Carbon* **1998**, *36*, 1149–1157; c) F. J. Maladonado-Hodar, C. Moreno-Castilla, J. Rivera-Utrilla, Y. Hanazawa, Y. Yamada, *Langmuir* **2000**, *16*, 4367–4373.
[7] a) K. Kinoshita, *Carbon, Electrochemical and Physicochemical Properties*, Wiley, New York, **1998**; b) *Carbon Materials for Advanced Technologies* (Ed.: T. D. Burchell), Pergamon, New York, **1999**; *Sciences of Carbon Materials* (Eds.: H. Marsh, F. Rodriguez-Reinoso), Publicaciones de la Universidad de Alicante, Alicante, Spain, **1997**.
[8] a) E. Reddington, A. Sapienza, B. Gurau, R. Viswanathan, S. Sarangapani, E. S. Smotkin, T. E. Mallouk, *Science* **1998**, *280*, 1735–1737; b) B. Gurau, R. Viswanathan, R. Liu, T. J. Lafrenz, K. L. Ley, E. S. Smotkin, E. Reddington, A. Sapienza, B. C. Chan, T. E. Mallouk, S. Sarangpani, *J. Phys. Chem.* B **1998**, *102*, 9997–10003; c) K.-W. Park, K.-S. Ahn, J.-H. Choi, Y.-C. Nah, Y.-M. Kim, Y.-E. Sung, *Appl. Phys. Lett.* **2002**, *81*, 907–909.
[9] E. S. Steigerwalt, G. A. Deluga, D. E. Cliffel, C. M. Lukehart, *J. Phys. Chem. B.* **2001**, *105*, 8097–8101.
[10] a) J. Lee, S. Yoon, S. M. Oh, C. -H. Shin, T. Hyeon, *Adv. Mater.* **2000**, *12*, 359–362; b) S. Han, K. Sohn, T. Hyeon, *Chem. Mater.* **2000**, *12*, 3337–3341; c) J. Lee, S. Yoon, T. Hyeon, S. M. Oh, K. B. Kim, *Chem. Commun.* **1999**, 2177–2178; d) J. Lee, K. Sohn, T. Hyeon, *J. Am. Chem. Soc.* **2001**, *123*, 5146–5147; e) S. B. Yoon, K. Sohn, J. Y. Kim, C. H. Shin, J. S. Yu, T. Hyeon, *Adv. Mater.* **2002**, *14*, 19–21; f) S. Yoon, J. Lee, T. Hyeon, S. M. Oh, *J. Electrochem. Soc.* **2000**, *147*, 2507–2512; g) S. H. Joo, S. J. Choi, I. Oh, J. Kwak, Z. Liu, O. Terasaki, R. Ryoo, *Nature* **2001**, *412*, 169–172; h) S. Jun, S. H. Joo, R. Ryoo, M. Kruk, M. Jaroniec, Z. Liu, T. Ohsuna, O. Terasaki, *J. Am. Chem. Soc.* **2000**, *122*, 10712–10713; i) R. Ryoo; S. H. Joo, S. Jun, *J. Phys. Chem. B* **1999**, *103*, 7743–7746; j) J. S. Lee, S. H. Joo, R. Ryoo, *J. Am. Chem. Soc.* **2002**, *124*, 1156–1157; k) T. Kyotani, T. Nagai, S. Inoue, A. Tomita, *Chem. Mater.* **1997**, *9*, 609–615; l) Z. Ma, T. Kyotani, A. Tomita, *Chem. Commun.* **2000**, 2365–2366; m) D. Kawashima, T. Aihara, Y. Kobayashi, T. Kyotani, A. Tomita, *Chem. Mater.* **2000**, *12*, 3397–3401; n) Z. Li, M. Jaroniec, *J. Am. Chem. Soc.* **2001**, *123*, 9208–9209.
[11] A. Guerro-Ruiz, P. Badenes, I. Rodriguez-Ramos, *Appl. Catal. A* **1998**, *173*, 313–321.
[12] a) T. J. Schmidt, H. A. Gasteiger, R. J. Behm, *Electrochem. Commun.* **1999**, *1*, 1–4; b) A. Hamnett, S. A. Weeks, B. J. Kennedy, G. Troughton, P. A. Christensen, *Ber. Bunsen-Ges.* **1990**, *94*, 1014–1020.
[13] K.-W. Park, J.-H. Choi, B.-K. Kwon, S.-A. Lee, Y.-E. Sung, H.-Y. Ha, S.-A. Hong, H. Kim, A. Wieckowski, *J. Phys. Chem. B* **2002**, *106*, 1869–1877.
[14] *Modern Aspect of Electrochemisty, Vol. 12* (Eds.: K. Kinoshita, P. Stonehart), Plenum Press, New York, **1996**.

 © 2003 Wiley-VCH Verlag GmbH & Co. KGaA, Weinheim

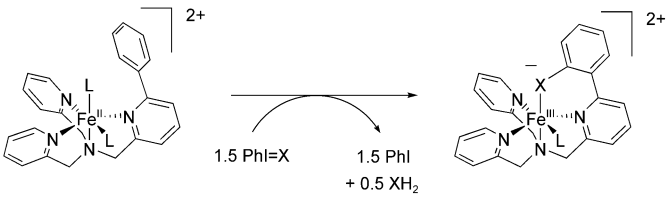
Iron-Mediated Aminations

Intramolecular Aromatic Amination through Iron-Mediated Nitrene Transfer**

*Michael P. Jensen, Mark P. Mehn, and Lawrence Que, Jr.**

Much attention has been concentrated on metal-catalyzed atom and group transfers to organic molecules as a strategy for carbon–heteroatom bond formation in synthetic organic chemistry. Similar to isolobal epoxidation reactions,[1] nitrene (that is, RN=) transfer to olefins (that is, aziridination) can be catalyzed by metalloporphyrins,[2] iron corroles,[3] as well as low-coordinate copper complexes and salts.[4] Nitrene insertions to give aliphatic C–H bond aminations have also been effected by metalloporphyrins or cytochrome P450.[5,6] In contrast, metal-catalyzed arene amination is practically unknown,[6] even though free organonitrenes will readily add to aromatics.[7] Substoichiometric and unselective naphthalene amination by an uncharacterized adduct of iron(II) chloride and chloramine-T has been reported,[8] along with a handful of possibly analogous organometallic ligand transformations.[9] By analogy to oxoiron species that mediate heme monooxygenase chemistry,[10] high-valent imido complexes are typically invoked as reactive intermediates in these amination reactions,[2,11] although imido complexes of iron are generally very rare.[12] Recently, we reported the efficient intramolecular *ortho*-hydroxylation of an α-phenyl substituent on a non-heme iron(II) complex of modified tris(2-pyridylmethyl)amine (TPA), $[(6\text{-PhTPA})Fe^{II}(NCCH_3)_2](ClO_4)_2$, driven by added *tert*-butyl hydroperoxide (^{t}BuOOH).[13] Indirect evidence suggested the formation of an oxoiron(IV) reactive hydroxylating species. Given the precedence for the use of iodonium ylides as oxene and nitrene precursors,[14] specifically including the conversion of $[(TMC)Fe^{II}(OTf)_2]$ to $[(TMC)Fe^{IV}{=}O](OTf)_2$ (TMC = tetra-*N*-methylcyclam),[15] we investigated the reactivity of $[(6\text{-PhTPA})Fe^{II}(NCCH_3)_2](ClO_4)_2$ with iodosobenzene (PhIO) and phenyl-*N*-tosylimidoiodinane (PhINTs). We report herein efficient and selective *ortho*-hydroxylation and amination reactions of the α-aromatic substituent afforded by these respective reagents (Scheme 1).[16,17]

Aliquots of a stock solution of $[(6\text{-PhTPA})Fe^{II}(NCCH_3)_2]^{2+}$ (1.0 mM in acetonitrile) were added to solid samples of the PhI = X (X = O, NTs) reagents, and the resulting suspensions were stirred vigorously at room temperature, either anaerobically or in air. The initially pale-yellow solutions turned dark blue as the solids dissolved; this required about 1–2 min for PhINTs, and 20–30 min for PhIO. UV/Vis spectra of the stable endpoint chromophores were recorded, revealing distinct Fe^{III} ligand-to-metal charge-transfer (LMCT) bands suggestive of differential *ortho* substitutions of the phenyl substituent (Figure 1). The intensities of these bands were found to depend on the stoichiometric ratio, with maxima obtained at approximately 1.6:1.0 PhI=X/Fe^{II} for both reagents, irrespective of the presence of oxygen, thus supporting the stoichiometry of Scheme 1. Further addition of iodonium reagents resulted in irreversible bleaching of these chromophores.



Scheme 1. Overview of the hydroxylation (X = O) and amination (X = NTs) reactions; L is presumably CH_3CN.

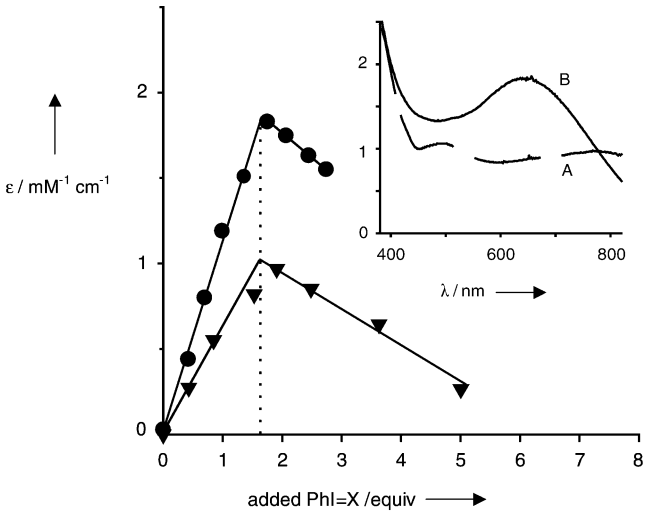


Figure 1. Plot of product LMCT extinction versus PhI = X stoichiometry (X = O, ▼, 780 nm, anaerobic reaction; TsN, ●, 650 nm, aerobic reaction); inset shows PhIO (A) and PhNTs (B) product spectra. All data recorded in CH_3CN solution at 228 K from reactions carried out at room temperature.

The PhIO product chromophore was entirely consistent with the formation of $[(6\text{-}(o\text{-O-}C_6H_4)\text{-TPA})Fe^{III}(NCCH_3)]^{2+}$, as observed in the tBuOOH reaction, and the maximum extinction was consistent with a 65% yield.[13] The PhINTs-derived chromophore was assigned to formation of $[(6\text{-}(o\text{-TsN-}C_6H_4)\text{-TPA})Fe^{III}(NCCH_3)]^{2+}$, the tosylanilide analogue of the previously characterized *ortho*-phenolate complex. Precipitation of the TsNIPh product solution with cold toluene afforded an amorphous blue powder, the sulfur content of which was consistent with ≥63% incorporation of

[*] Prof. Dr. L. Que, Jr., Dr. M. P. Jensen, M. P. Mehn
Department of Chemistry and
Center for Metals In Biocatalysis
University of Minnesota
207 Pleasant Street SE, Minneapolis, MN 55455 (USA)
Fax: (+1) 612-624-7029
E-mail: que@chem.umn.edu

[**] This work was supported by a grant (GM33162) from the US National Institutes of Health.

 DOI: 10.1002/anie.200351605 © 2003 Wiley-VCH Verlag GmbH & Co. KGaA, Weinheim

one TsN equivalent into the isolated crude product.[18] Unequivocal evidence for nitrene addition was obtained by electrospray ionization mass spectrometry, which yielded cations at m/z 590.3 and 621.4, consistent with the respective formulations $[(6\text{-}(o\text{-TsN-}C_6H_4)\text{-TPA})Fe^{II}]^+$ and $[(6\text{-}(o\text{-TsN-}C_6H_4)\text{-TPA})Fe^{III}(OMe)]^+$. The product obtained from $[(d_5\text{-PhTPA})Fe^{II}(NCCH_3)_2]^{2+}$ gave product cations at m/z 594.3 and 625.4, showing the loss of one deuterium atom, while the use of isotopically enriched $PhI^{15}NTs$ showed the expected one-mass-unit upshift. Taken together, these results are uniquely consistent with the substitution of a tosyl nitrene group for hydrogen on the 6-phenyl ring.

Investigation of the product chromophores by resonance Raman spectroscopy provided clear evidence for participation of donor atoms bearing the anticipated *ortho*-aryl substituents in the putative LMCT bands (Figure 2). The

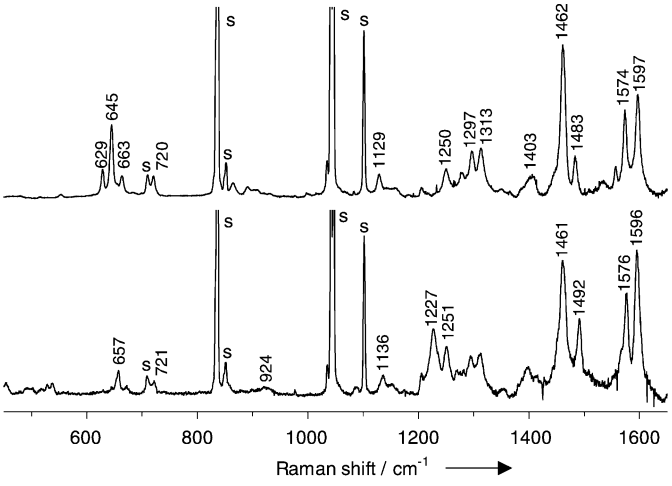


Figure 2. Resonance Raman spectra (647.1 nm excitation) of LMCT chromophores for the PhIO (top) and PhINTs (bottom) reactions, recorded from frozen CD_3CN solutions.

PhIO product gave a response characteristic of the monomeric phenolate complex $[(6\text{-}(o\text{-O-}C_6H_4)\text{-TPA})Fe^{III}(NCCH_3)]^{2+}$,[13] while the PhINTs reaction product exhibited a surprisingly similar, yet distinct, spectrum. Despite the lack of resonance Raman data on metal anilide complexes in the literature, modes at 657 and 1227 cm^{-1} in the latter spectrum were assigned to vibrations with predominant $\tilde{\nu}$(Fe-N) and $\tilde{\nu}$(C-N) character, respectively, by analogy to modes at 645 and 1250 cm^{-1} in the phenolate spectrum.[19]

High-resolution electrospray mass spectral and NMR spectroscopic data were obtained from product ligands stripped from the metal ion by the addition of aqueous NH_4OH and recovered by extraction into diethyl ether. The aniline ligand was characterized by a parent cation corresponding to $[6\text{-}(o\text{-TsNH-}C_6H_4)\text{-TPA-H}]^+$ with $m/z =$ 536.21108 amu (versus $m/z = 536.21147$ calcd for $C_{31}H_{30}N_5O_2S$); an ion shift to m/z 540.23652 amu was recorded for the 6-d_5-PhTPA product (versus m/z 540.23658 amu calcd for $C_{31}H_{26}D_4N_5O_2S$). ^{1}H NMR analysis revealed the PhINTs product extracts to be a mixture of the expected *ortho*-*N*-tosyl aniline product, unmodified 6-PhTPA, and 6-$(o\text{-HO-}C_6H_4)$-TPA in a 1.0:0.3:0.1 ratio in C_6D_6 solution (Figure 3). Also observed in the extracts was 0.3 equiv $TsNH_2$

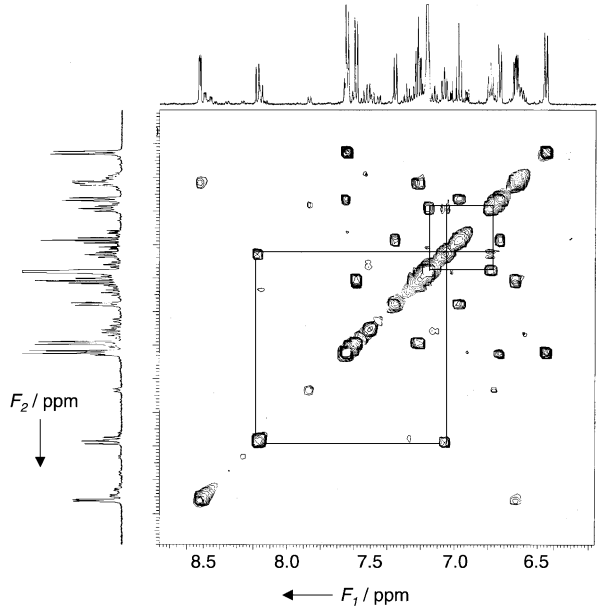


Figure 3. ^{1}H NMR COSY plot (500 MHz) of ligand extracts from PhINTs reaction in C_6D_6 solution at 293 K. Cross-peaks arising from the arene ring of the aniline product are denoted.

per aniline molecule, but no PhI. Total ligand recovery of 70% against charged 6-PhTPA was determined by integration against an internal standard (BHT). Attribution of the missing mass to handling losses would imply 70% overall anilide formation resulting from $\approx$80% oxidative conversion of 6-PhTPA with $\approx$90% selectivity for anilide. This assessment was consistent with the UV/Vis spectrum, which clearly lacked significant contribution from the phenolate LMCT chromophore near 780 nm, and with the sulfur analysis. The 0.3 equiv $TsNH_2$ formed per mole of aminated 6-PhTPA is in accordance with the stoichiometry shown in Scheme 1. Regardless, 6-$(o\text{-TsNH-}C_6H_4)$-TPA was recovered in 50% absolute yield, so the least-favorable limits accommodated by the product distribution are $\geq$60% selectivity for anilide and $\geq$55% oxidative ligand conversion, and these lower limits are inversely correlated. ^{1}H NMR signals of 6-$(o\text{-TsNH-}C_6H_4)$-TPA were distinct from those of authentic 6-$(o\text{-HO-}C_6H_4)$-TPA and consistent with the formulation (Figure 3). Doublets at 7.64 and 6.45 ppm ($^3J_{HH} = 7.5$ Hz) and a singlet at 1.67 ppm, in a 2:2:3 intensity ratio, were assigned to the tosyl substituent. The aryl ring gave rise to four signals at 8.18 (H'_m, adjacent to the *ortho* amino group, dd: $^3J_{HH} = 8.0$ Hz; $^4J_{HH} =$ 1.0 Hz.), 7.06 (H_p, ddd: $^3J_{HH} = 8.0$, 7.2 Hz; $^4J_{HH} = 1.0$ Hz), 6.78 (H_m, ddd: $^3J_{HH} = 8.0$, 7.2 Hz; $^4J_{HH} = 1.0$ Hz), and $\approx$7.16 ppm (H_o, overlap with solvent); these signals were absent in the 6-d_5-PhTPA product spectrum. A singlet at 12.98 ppm ($^1J_{^{15}N\text{-}^1H} =$ 81 Hz) was assigned to the aniline proton, *H*N(Ts)Ar, and the

 © 2003 Wiley-VCH Verlag GmbH & Co. KGaA, Weinheim

striking downfield shift was suggestive of hydrogen bonding to other nitrogen atoms.

Extracted product ligands from the PhIO reaction were determined to be a mixture of the 6-*o*-HO-C_6H_4-TPA product phenol and unmodified 6-PhTPA, in a 1.8:1.0 ratio in $CDCl_3$ solution; a total ligand recovery of 68% was obtained. Again assuming mass loss resulted solely from handling, the estimated total yield of phenol was 64%, in accord with the UV/Vis spectrophotometric yield.

The use of an *ortho*-deuterium isotope label (that is, 6-*o*-d_1-PhTPA) gave evidence of fractional 1,2 hydrogen shifts ("NIH shifts")[20] in both PhI=X oxidations. ^{1}H NMR analysis indicated the formation of three product ligand isotopomers, *o*-d_1, *m*-d_1, and d_0, respectively resulting from *ortho* substitution at the unlabeled carbon atom, or substitution at the labeled carbon atom with either deuterium migration to the *meta* carbon position, or loss of deuterium. Thus, the fraction of the first isotopomer corresponded to an intramolecular isotope effect ("k_H/k_D"), and the ratio of the latter two gave the NIH shift. For three PhIO reactions, an average respective phenol isotopomer distribution of 48.1(4):24.5(9):27.4(9) was observed. A single determination of 77(1)% total deuterium retention was obtained by mass spectrometry. Correction of these data for residual ^{1}H atoms in the labeled site (3(1)%) yielded $k_H/k_D = 0.98(4)$, and a 50(3)% NIH shift. These results were identical to those obtained for the ^{t}BuOOH reaction, consistent with formation of a common hydroxylating intermediate, namely an oxoiron(IV) species.[13]

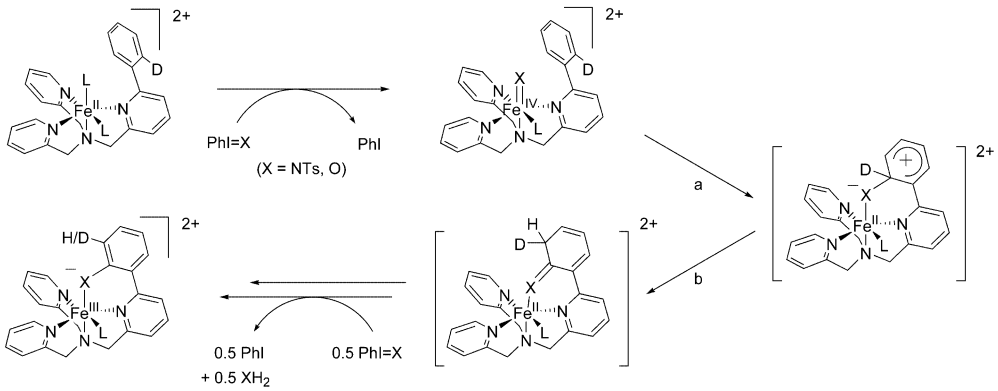
The average of three PhINTs reactions yielded a 55(2):24(2):21(4) isotopomer ratio for the product aniline, and 68(1)% deuterium retention was measured in one trial by mass spectrometry. These data yield $k_H/k_D = 1.3(1)$, and a 57(7)% NIH shift. The data indicate a shift from inverse to normal for the isotope effect of the reaction of a presumed tosylimidoiron(IV) species compared to an oxoiron(IV) species. This change reflects an increased contribution to the transition state for hydrogen-atom transfer (Scheme 2; step b, $k_H/k_D > 1$) relative to attack of the more electrophilic nitrene (Scheme 2; step a, $k_H/k_D < 1$).[21] This result represents the first observation of an NIH shift for an aromatic substitution other than a hydroxylation.

In conclusion, we have demonstrated efficient non-heme iron-mediated oxene and nitrene transfer reactions from iodonium ylides to give selective aromatic hydroxylation and amination, the latter representing an entirely novel class of reactivity. The present results strongly suggest a common reaction mechanism involving the formation of oxo- and imido-iron(IV) species as reactive intermediates (Scheme 2). Proportional consumption of iron(II) ions and the accumulation of a chromophore with increasing PhI=X addition (Figure 1) is consistent with operation of an Fe^{II}/Fe^{IV} couple in the reaction; rapid oxidation to the final iron(III) product complex apparently occurs after arene modification. Given the utility of the Fe(TPA) family of catalysts for olefin epoxidation and *cis*-dihydroxylation,[22] the possibilities of analogous olefin aziridination and hydroxyamination, and even aromatic amination, are clearly implied. Moreover, the apparent generation of an imidoiron(IV) species suggests the possibility of complementing the recent characterization of high-valent non-heme oxoiron(IV) complexes.[15] Finally, we also note that iron–anilide coordination chemistry is curiously sparse, and that the reactivity discovered here should afford a general route towards a range of such complexes.[13]

Received: April 8, 2003 [Z51605]

Keywords: amination · hydroxylation · iron · Raman spectroscopy · ylides

[1] J. T. Groves, M. K. Stern, *J. Am. Chem. Soc.* **1987**, *109*, 3812.
[2] a) J. T. Groves, T. Takahashi, *J. Am. Chem. Soc.* **1983**, *105*, 2073; b) D. Mansuy, J.-P. Mahy, A. Dureault, G. Bedi, P. Battioni, *J. Chem. Soc. Chem. Commun.* **1984**, 1161.
[3] L. Simkhovich, Z. Gross, *Tetrahedron Lett.* **2001**, *42*, 8089.
[4] a) H. Kwart, A. A. Khan, *J. Am. Chem. Soc.* **1967**, *89*, 1951; b) D. A. Evans, M. M. Faul, M. T. Bilodeau, *J. Org. Chem.* **1991**, *56*, 6744; c) L. Zhen, K. R. Conser, E. N. Jacobsen, *J. Am. Chem. Soc.* **1993**, *115*, 5326; d) D. A. Evans, M. M. Faul, M. T. Bilodeau, *J. Am. Chem. Soc.* **1994**, *116*, 2742; e) J. A. Halfen, D. C. Fox, M. P. Mehn, L. Que, Jr., *Inorg. Chem.* **2001**, *40*, 5060.
[5] a) R. Breslow, S. H. Gellman, *J. Chem. Soc. Chem. Commun.* **1982**, 1400; b) E. W. Svastits, J. H. Dawson, R. Breslow, S. H. Gellman, *J. Am. Chem. Soc.* **1985**, *107*, 6427.
[6] J. Yang, R. Weinberg, R. Breslow, *Chem. Commun.* **2000**, 531.



Scheme 2. Common mechanism for observed NIH shifts in the hydroxylation and amination reactions; L is presumably CH_3CN.

 © 2003 Wiley-VCH Verlag GmbH & Co. KGaA, Weinheim

[7] J. M. Lindley, I. M. McRobbie, O. Meth-Cohn, H. Suschitzky, *J. Chem. Soc. Perkin Trans. 1* **1977**, 2194.
[8] D. H. R. Barton, R. S. Hay-Motherwell, W. B. Motherwell, *J. Chem. Soc. Perkin Trans. 1* **1983**, 445.
[9] a) P. E. Baikie, O. S. Mills, *Inorg. Chim. Acta* **1967**, *1*, 55; b) M. E. Gross, C. E. Johnson, M. J. Maroney, W. C. Trogler, *Inorg. Chem.* **1984**, *23*, 2968; c) C. J. Barner, T. J. Collins, B. E. Mapes, B. D. Santarsiero, *Inorg. Chem.* **1986**, *25*, 4322; d) A. Saha, P. Majumdar, S.-M. Peng, S. Goswami, *Eur. J. Inorg. Chem.* **2000**, 2631.
[10] I. Schlichting, J. Berendzen, K. Chu, A. M. Stock, S. A. Maves, D. E. Benson, R. M. Sweet, D. Ringe, G. A. Petsko, S. G. Sligar, *Science* **2000**, *287*, 1615.
[11] J. P. Mahy, P. Battioni, D. Mansuy, *J. Am. Chem. Soc.* **1986**, *108*, 1079.
[12] a) A. K. Verma, T. N. Nazif, C. Achim, S. C. Lee, *J. Am. Chem. Soc.* **2000**, *122*, 11013; b) S. D. Brown, T. A. Betley, J. C. Peters, *J. Am. Chem. Soc.* **2003**, *125*, 322.
[13] M. P. Jensen, S. J. Lange, M. P. Mehn, E. L. Que, L. Que, Jr., *J. Am. Chem. Soc.* **2003**, *125*, 2113.
[14] V. V. Zhadankin, P. J. Stang, *Chem. Rev.* **2002**, *102*, 2523.
[15] J.-U. Rohde, J.-H. In, M. H. Lim, W. W. Brennessel, M. R. Bukowski, A. Stubna, E. Münck, W. Nam, L. Que, Jr., *Science* **2003**, *299*, 1037.
[16] Experimental procedures were described previously.[13] $PhI(OAc)_2$, $TsNH_2$, and $Ts^{15}NH_2$ were purchased from Aldrich. PhIO and PhINTs were prepared by literature procedures.[17]
[17] a) H. Saltzman, J. G. Sharefkin, *Organic Syntheses Collect. Vol. V*, Wiley, New York, **1973**, p. 658; b) Y. Yamada, T. Yamamoto, M. Okawara, *Chem. Lett.* **1975**, 361.
[18] Elemental analysis calcd (%) for $[(6\text{-}o\text{-}C_6H_4(Ts)N\text{-TPA})\text{-}Fe^{III}(NCCH_3)](ClO_4)_2$, $C_{33}H_{31}Cl_2FeN_6O_{10}S$: C 47.73, H 3.76, N 10.12, S 3.86; found: C 49.26, H 4.36, N 8.52, S 2.43.
[19] a) J. W. Pyrz, A. L. Roe, L. J. Stern, L. Que, Jr., *J. Am. Chem. Soc.* **1985**, *107*, 614; b) C. J. Carrano, M. W. Carrano, K. Sharma, G. Backes, J. Sanders-Loehr, *Inorg. Chem.* **1990**, *29*, 1865.
[20] G. Guroff, J. W. Daly, D. M. Jerina, J. Renson, B. Witkop, S. Udenfriend, *Science* **1967**, *157*, 1524.
[21] P. F. Fitzpatrick, *J. Am. Chem. Soc.* **1994**, *116*, 1133.
[22] K. Chen, M. Costas, L. Que, Jr., *J. Chem. Soc Dalton Trans.* **2002**, 672.

 © 2003 Wiley-VCH Verlag GmbH & Co. KGaA, Weinheim

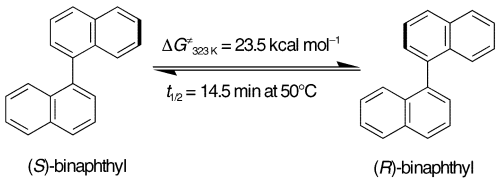
Chiral Resolution

Breaking the Symmetry of Axially Chiral *N*-Aryl-2(1*H*)-pyrimidinones by Spontaneous Crystallization**

Masami Sakamoto, Noriyuki Utsumi, Masaru Ando, Mizuho Saeki, Takashi Mino, Tsutomu Fujita, Akira Katoh, Takehiko Nishio, and Choji Kashima*

The atropisomerism of biaryl molecules has been studied extensively from both theoretical and synthetic perspectives.[1] When rotation about the pivotal 1,1′-bond is slowed, these molecules can be resolved as optically active enantiomers. Many axially chiral biaryls such as BINAP (1,1′-binaphthalene-2,2′-diyl)bisdiphenylphosphane) or BINOL (2,2′-dihydroxy-1,1′-biphenyl) serve as ligands in transition-metal complexes used in catalytic asymmetric synthesis.[2,3]

In 1971 Pincock et al. discovered that racemic binaphthyl undergoes spontaneous resolution to generate the optically active *R* or *S* enantiomer when crystallized from the melt.[4] The racemization kinetics of optically active 1,1′-binaphthyl was studied by Cooke and Harris,[5] who found that its racemization half-life is 14.5 min at 50 °C ($\Delta G^{\ddagger} = 23.5$ kcal mol^{-1}, Scheme 1). Furthermore, Kondepudi et al. have reported that each enantiomer of binaphthyl can be resolved with higher enantiomeric purity by stirred crystallization.[6] This is a unique example of asymmetric disequilibration of atropisomers by crystallization, and no other examples have been reported in the past three decades.



Scheme 1. Racemization of 1,1′-binaphthyl.

[*] Prof. M. Sakamoto, N. Utsumi, M. Ando, M. Saeki, Dr. T. Mino, Prof. T. Fujita
Department of Materials Technology
Faculty of Engineering
Chiba University
Yayoi-cho, Chiba 263-8522 (Japan)
Fax: (+81) 43-290-3401
E-mail: sakamotom@faculty.chiba-u.jp
Prof. A. Katoh
Department of Applied Chemistry
Seikei University
Kichijoji-Kitamachi, Musashino 180-8633 (Japan)
Prof. T. Nishio, Prof. C. Kashima
Department of Chemistry
University of Tsukuba
Tsukuba 305-8571 (Japan)

[**] This work was supported by a Grant-in-Aid for Scientific Research on Priority Area 417 from the Ministry of Education, Culture, Sports, Science and Technology (MEXT) of the Japanese Government.

 © 2003 Wiley-VCH Verlag GmbH & Co. KGaA, Weinheim DOI: 10.1002/anie.200351660

Now we have found that the chiral pyrimidinones with C–N axial chirality can be resolved by crystallization without any outside chiral source. Absolute asymmetric transformations are of wide interest since they occur spontaneously in the absence of any outside chiral influence and are relevant to theories concerning the prebiotic origin of natural chirality.[7,8] To resolve the racemate, axially chiral materials must crystallize as conglomerates, in other words, in a chiral space group.[9] Four pyrimidin-2(1*H*)-ones (**1a–d**, Figure 1) were synthesized which have a variety of aryl groups with substituents at the *ortho* and/or other positions.[10,11]

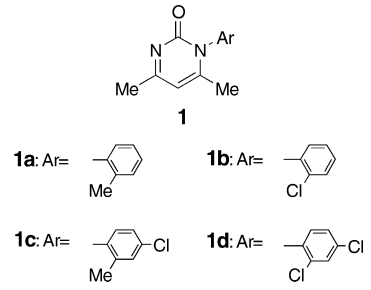
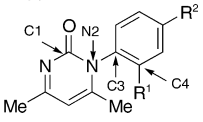


Figure 1. Pyrimidin-2(1*H*)-ones examined in this work.

To determine whether each pyrimidinone affords conglomerate or racemic crystals, each single crystal was analyzed by HPLC employing Chiral Cell OJ and OD columns (Daicel Chemical Industry). In the HPLC analysis of single crystals of pyrimidinone **1b** two peaks arise from the two enantiomers in the ratio of 1:1. This indicates that the crystals of **1b** are not conglomerate crystals but racemic crystals. On the other hand, three other pyrimidinones (**1a**, **1c**, **1d**) afforded conglomerates. They were analyzed by single-crystal X-ray diffraction.[12–15] Table 1 shows the results;

Table 1: The crystal systems obtained by X-ray structural analysis and the molecular conformation of pyrimidinones **1a**, **1c**, and **1d**.



1	R^1	R^2	Space group	Torsion angle C1-N2-C3-C4 [°]
1a	Me	H	$P2_1$	83.4
1a·H_2O	Me	H	$I4_1/a$	88.1
1c	Me	Cl	$P2_1$	80.9
1d	Cl	Cl	$P2_1$	81.2

the three pyrimidinones crystallize in the $P2_1$ space group. Figure 2 shows the ORTEP diagram of the absolute configuration of (*S*)-(+)-**1d** in the crystal, which was determined by an anomalous X-ray scattering method. In the case of **1a**, recrystallization from ethanol gave two types of crystals, one yellow and the other reddish. X-ray crystallographic analysis revealed that the yellow crystal has a $P2_1$ crystal system.[12]

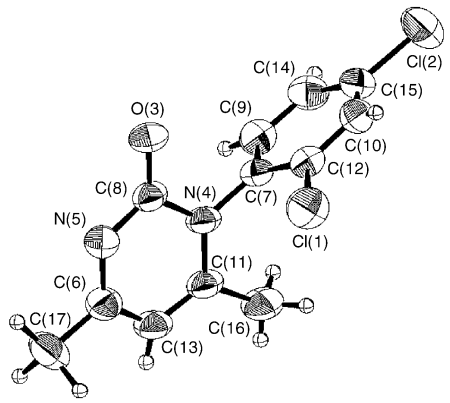


Figure 2. Absolute configuration of (*S*)-(+)-**1d** in the crystal (ORTEP).

The other crystal includes an equimolar amount of water molecules, and the crystal system is achiral, $I4_1/a$.[13] X-ray analyses also revealed the molecular conformation of the pyrimidinones. The two arene planes are almost perpendicular to each other (torsional angle $\theta = 80.9$–$88.1°$) in all cases.

To achieve the disequilibration by crystallization, fast enantiomerization should occur at the temperature of crystallization. In order to estimate the conformational stability of **1**, the rate constants (k_{rot}) and activation parameters for the enantiomerization in these compounds have been studied. Kashima et al. obtained optically active **1a** (5% *ee*) by making its salt with optically active camphorsulfonic acid.[10] Furthermore, they measured the racemization kinetics arising from C–N bond rotation to be 30.3 kcal mol^{-1} at 359.6 K in diglyme. Roussel et al. also studied similar pyrimidinone derivatives independently and proposed a different mechanism for racemization via an open form.[11]

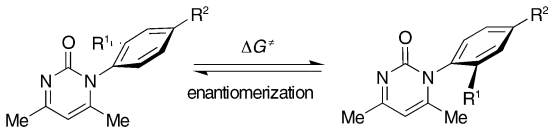
The rate of enantiomerization of the chiral pyrimidinones **1a**, **1c**, and **1d** was studied in three kinds of solvents: xylene (nonpolar and aprotic), dimethylformamide (DMF; polar and aprotic), and 1-propanol (polar and protic). Each enantiomorphic crystal obtained from usual crystallization was dissolved in the solvent, and the rate of enantiomerization at three temperatures (70, 80, and 90°C) was followed by HPLC with the Chiral Cell OD columun. The Arrhenius and Eyring plots have excellent linear relationships. The activation parameters obtained from the plots are listed in Table 2.

The rate of racemization was considerably influenced by the solvents. The half-life ($t_{1/2}$) of **1a** at 90°C in xylene was 46 min but 254 min in DMF and 1160 min in 1-propanol. In all cases, the free energy of activation in a polar solvent is higher than that in a nonpolar solvent. Furthermore, a protic solvent like 1-propanol restricts the enantiomerization; polarity, hydrogen bonding, or solvation by alcohol seem to be important factors influencing the interconversion. A nonpolar solvent lowers the $\Delta G^{\neq}$ value by about 2 kcal mol^{-1} relative to the value in a polar or a protic solvent. The results also indicate the effect of the substituents on the phenyl group. Methyl and chloro groups at the *ortho* position show little difference in the energy barrier for enantiomerization.

None of the pyrimidinones **1** racemized at room temperature even after several days in a nonpolar solvent; however, they racemize immediately at temperatures above 170°C in

 © 2003 Wiley-VCH Verlag GmbH & Co. KGaA, Weinheim

Table 2: Activation parameters for enantiomerization of pyrimidin-2(1*H*)-ones **1** under various conditions.



(*R*)-**1** (*S*)-**1**

Cmpd.	Solvent	$t_{1/2}$ [min] at 90 °C[a]	$\Delta G^{\neq}_{363}$ [kcal mol^{-1}]	$\Delta H^{\neq}$ [kcal mol^{-1}]	$\Delta S^{\neq}$ [cal mol^{-1} K^{-1}]
1a[b]	xylene	46	27.9	27.8	−0.32
	DMF	254	29.1	27.9	−3.35
	1-propanol	1160	30.2	28.8	−3.78
1c	xylene	31	27.6	28.2	1.57
	DMF	176	28.8	28.9	0.09
	1-propanol	875	30.0	29.8	−0.71
1d	xylene	24	27.4	31.2	10.56
	DMF	109	28.5	30.9	6.61
	1-propanol	579	29.7	31.4	4.78

[a] Half-life. [b] Kinetics of racemization of **1a** have been studied in diglyme at 359.6 K. $\Delta G^{\neq}$ value was reported as 28.3 kcal mol^{-1} (ref. [10]) and 30.3 kcal mol^{-1} (ref. [11]).

1,2,3,4-tetramethylbenzene. We tried to force the asymmetric disequilibration of atropisomeric pyrimidinones by crystallization at high temperature. The crystallization was examined in a solvent or without a solvent. Table 3 shows the melting points of pyrimidinones **1**, the chemical yields, and optical purity of the crystals obtained.

In the case of **1a**, the melting point was low (**1a**: 126–129 °C); therefore, **1a** was crystallized with stirring at 125 °C after the crystals were melted at 140 °C. The resulting solid was a 1:1 mixture of enantiomers. When the seed crystal, which was obtained as a conglomerate by usual recrystallization from ethanol, was added to the crystallization, the same results were obtained and, regrettably, asymmetric disequilibration could not be observed. We conclude that the rate of racemization is not as high as the rate of crystallization at that temperature.

On the other hand, the other pyrimidinones exhibited high melting points above 200 °C. All pyrimidinones gradually decompose at above the melting point and could not be left for more than one hour at that temperature. The melting point of **1c** is 224–225 °C, which is too high for crystallization without a solvent because of decomposition. Therefore, TMB (1,2,3,4-tetramethylbenzene, b.p. 203–204 °C) was used as a solvent for crystallization. After pyrimidinone **1c** (50 mg) was dissolved in TMB (180 mg) at 200 °C, the solution was gradually cooled to 150 °C (at the rate of 1.5 °C min^{-1}) with stirring; crystals formed at around 180 °C and multiplied as the temperature was lowered to 150 °C. A homogeneous solution was prepared by adding THF without filtration at room temperature. The chemical yield and enantiomeric purity of the recovered pyrimidinones were determined by HPLC with the Chiral Cell OD column using benzyl phenyl ether as a standard. The *ee* values varied and optical rotations were inconstant; however, **1c** was obtained in 25–68 % *ee* by autoseeding (Table 3, entry 2).[17] When the seeding method was used in the crystallization (the seed crystal was added at 180 °C), consistent *ee* values were obtained (70–72 % *ee*) and the optical rotation was the same as that of the seed crystal (entry 3). Disequilibration (68–70 % *ee*) could also be effected in a crystallization on a ten-times larger scale (entry 4).

For the dichlorophenyl derivative **1d**, TMB was also used as a solvent. Pyrimidinone **1d** (50 mg) was dissolved in TMB (100 mg) at 200 °C, and the solution was cooled to 150 °C (at the rate of 1.5 °C min^{-1}) under stirring and with or without seeding. Enantiomeric purity ranging from 13 to 66 % *ee* and indecisive optical rotation were obtained from autoseeding (entry 5).[19] On the other hand, crystals with constant enantiopurity (72–73 % *ee*) and the desired optical rotation were obtained when the seeding method was used in the crystallization (entry 6). The larger-scale experiment also gave optically active **1d** between 63 and 65 % *ee* (entry 7).

Furthermore, when the crystals of **1c** and **1d** obtained in entries 4 and 7, respectively, were recrystallized once from ethanol or a mixture of chloroform and hexane, the pyrimidinones were easily obtained with 100 % *ee*. That is, enantiomeri-

Table 3: Asymmetric disequilibration of racemic pyrimidinones **1a**, **1c**, and **1d** by crystallization.

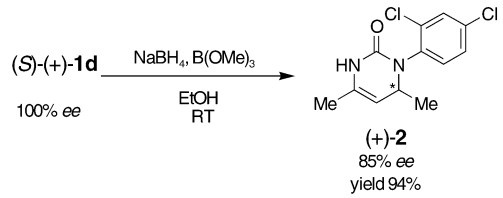
Entry	**1**	M.p. [°C][a]	Solvent	Seeding	Cryst. temp. [°C]	*ee* [%]	Recov. [%]
1	**1a**	126–129	none	yes[f]	125	0–1	90–93[l]
2	**1c**[b]	224–225	TMB	no[g]	180–150[h]	25–68[j]	90–92[l]
3	**1c**[b]		TMB	yes[f]	180–150[h]	70–72[k]	89–99[l]
4	**1c**[c]		TMB	yes[f]	180–150[h]	67–70[k]	90–93[m]
5	**1d**[d]	210–211	TMB	no[g]	175–150[i]	13–66[j]	84–89[l]
6	**1d**[d]		TMB	yes[f]	175–150[i]	72–73[k]	82–85[l]
7	**1d**[e]		TMB	yes[f]	175–150[i]	63–65[k]	92–94[m]

[a] All pyrimidinones gradually decomposed above the melting point. [b] A solution of **1c** (50 mg) and TMB (180 mg) was used for crystallization. Each crystallization was tried five times. [c] Ten-times larger scale (500 mg **1c** and 1.8 g TMB) was used for crystallization. [d] A solution of the pyrimidinone (50 mg) and TMB (100 mg) was used for crystallization. Each crystallization was tried five times. [e] Ten-times larger scale (500 mg **1d** and 1.0 g TMB) was used for crystallization. [f] Small amount of enantiomerically pure pyrimidines (100 % *ee*) was added as seeds. [g] Crystallization by autoseeding. [h] Crystals were dissolved at 200 °C, and the seed crystal was added at 180 °C; the solution was then cooled to 150 °C. [i] Crystals were dissolved at 200 °C, and the seed crystal was added at 175 °C; the solution was then cooled to 150 °C. [j] The direction of optical rotation of the obtained crystals was inconstant in the case of autoseeding. [k] By the seeding method, crystals were obtained with the same direction of optical rotation as the seed crystal. [l] Yields were determined by HPLC with benzyl phenyl ether as a standard. [m] Yield of product isolated by column chromatography.

 © 2003 Wiley-VCH Verlag GmbH & Co. KGaA, Weinheim

cally pure, axially chiral pyrimidinones could be easily obtained without any chiral source. If seed crystals are used in the crystallization, the bulk of the desired enantiomorphic crystals can be prepared selectively.

Pyrimidinones can be transformed into other heterocycles by various reactions including photochemical reactions, nucleophilic reactions, and reduction.[19] We demonstrated one example, the enantioselective reduction of axially chiral pyrimidinone **1d** with $NaBH_4$. When enantiomerically pure (100% *ee*) (*S*)-(+)-**1d** prepared by the above method was treated with $NaBH_4$ in the presence of trimethylborate at room temperature, the attack of hydride was highly controlled by the chlorine atom at the *ortho* position of the aryl group, and optically active product (+)-**2** was obtained in 94% yield and 85% *ee* (Scheme 2). In compound **2**, the rotation about the N–C bond occurs slowly at room temperature, and the *ee* value was determined by HPLC with the Chiral Cell OD column at 50°C. A distortion of the methyl group from the amide plane removes restrictions for the N–C bond rotation.



Scheme 2. Enantioselective reduction of **1d**.

In conclusion, we have provided the first example of breaking the symmetry of N–C axially chiral atropisomers by spontaneous crystallization. Furthermore, the resulting optically active atropisomer was converted to other heterocycles with high enantioselectivity. We believe that this method can be applied to resolve many axially chiral compounds, and may also have important implications as a mechanism for the amplification of optical activity that led to the homochirality of life.

Received: April 15, 2003 [Z51660]

Keywords: asymmetric synthesis · atropisomerism · chiral resolution · chirality · heterocycles

[1] E. L. Eliel, S. H. Wilen, L. N. Mander, *Stereochemistry of Organic Compounds*, Wiley, New York, **1944**, p. 1142.
[2] a) J. D. Morrison, *Asymmetric Synthesis, Vol. 1–5*, Academic Press, Orland, **1985**; b) I. Ojima, *Asymmetric Catalysis*, VCH, New York, **1933**; c) R. Noyori, *Asymmeric Catalysis in Organic Synthesis*, Wiley, New York, **1994**; d) J. Seyden-Penne, *Chiral Auxiliaries and Ligands in Asymmetric Synthesis*, Wiley, New York, **1995**; e) E. N. Jacobsen, A. Pfaltz, H. Yamamoto, *Comprehensive Asymmetric Synthesis I–III*, Springer, Berlin, **1999**.
[3] a) J. Jacques, C. Fouquey, *Org. Synth.* **1989**, *67*, 1–12; b) L. K. Truesdale, *Org. Synth.* **1989**, *67*, 13–19; c) K. Tanaka, T. Okada, F. Toda, *Angew. Chem.* **1993**, *105*, 1266–1267; *Angew. Chem. Int. Ed. Engl.* **1993**, *32*, 1147–1148.
[4] R. E. Pincock, R. R. Perkins, A. S. Ma, K. R. Wilson, *Science* **1971**, *174*, 1018–1020.
[5] A. S. Cooke, M. M. Harris, *J. Chem. Soc.* **1963**, 2365–2373.
[6] D. K. Kondepudi, *J. Am. Chem. Soc.* **1999**, *121*, 1448–1449.
[7] a) L. Addadi, M. Lahav, *Origin of Optical Activity in Nature* (Ed.: D. C. Walker), Elsevier, New York, **1979**, chap. 14; b) S. F. Mason, *Nature* **1984**, *311*, 19–23.
[8] a) M. Sakamoto, *Chem. Eur. J.* **1997**, *3*, 684–689; b) B. L. Feringa, R. A. van Delden, *Angew. Chem.* **1999**, *38*, 3624–3645; *Angew. Chem. Int. Ed.* **1999**, *38*, 3418–3438.
[9] a) L. Addadi, Z. Berkovitch-Yellin, N. Domb, E. Gati, M. Lahav, L. Leiserowitz, *Nature* **1982**, *296*, 21–26; b) Z. Berkovitch-Yellin, L. Addadi, M. Idelson, L. Leiserowitz, M. Lahav, *Nature* **1982**, *296*, 27–34; c) D. K. Kondepudi, R. J. Kaufman, N, Singh, *Science* **1990**, *250*, 975–977; d) J. Jacque, A. Collet, S. H. Wilen, *Enantiomers, Racemates, and Resolutions*, Kreiger, Malabar, **1991**, chap. 1, pp. 3–31.
[10] C. Kashima, A. Katoh, *J. Chem. Soc. Perkin Trans. 1* **1980**, 1599–1602.
[11] C. Roussel, M. Adjimi, A. Chemlal, A. Djafri, *J. Org. Chem.* **1988**, *53*, 5076–5080.
[12] X-ray crystallographic analysis of **1a**: monoclinic, space group $P2_1$, $a = 7.162(3)$ Å, $b = 14.480(6)$ Å, $c = 6.084(3)$ Å, $\beta = 111.77(4)$, $V = 585.9(5)$ Å^3, $Z = 2$, $\rho = 1.21$ g cm^{-3}, $\mu(Cu_{K\alpha}) = 0.62$ cm^{-1}; $R = 0.039$, $Rw2 = 0.125$ for 964 reflections. The structure was solved by direct methods and refined by the method of full-matrix least-squares.[16]
[13] X-ray crystallographic analysis of **1a**·H_2O: tetragonal, space group $I4_1/a$, $a = 26.80(1)$ Å, $b = 26.80(1)$ Å, $c = 7.149(5)$ Å, $V = 5134.(4)$ Å^3, $Z = 16$, $\rho = 1.11$ g cm^{-3}, $\mu(Cu_{K\alpha}) = 0.57$ cm^{-1}; $R = 0.053$, $Rw2 = 0.158$ for 1660 reflections. The structure was solved by the direct method and refined by the method of full-matrix least-squares.[16]
[14] X-ray crystallographic analysis of **1c**: monoclinic, space group $P2_1$, $a = 7.229(3)$ Å, $b = 13.826(6)$ Å, $c = 6.548(3)$ Å, $\beta = 108.06(4)$, $V = 622.2(5)$ Å^3, $Z = 2$, $\rho = 1.33$ g cm^{-3}, $\mu(Cu_{K\alpha}) = 2.59$ cm^{-1}; $R = 0.040$, $Rw2 = 0.113$ for 1038 reflections. The structure was solved by direct methods and refined by the method of full-matrix least-squares.[16]
[15] X-ray crystallographic analysis of **1d**: monoclinic, space group $P2_1$, $a = 7.228(4)$ Å, $b = 14.110(7)$ Å, $c = 6.349(4)$ Å, $\beta = 107.21(4)$, $V = 618.5(6)$ Å^3, $Z = 2$, $\rho = 1.32$ g cm^{-3}, $\mu(Cu_{K\alpha}) = 4.54$ cm^{-1}; $R = 0.039$, $Rw2 = 0.104$ for 1071 reflections. The structure was solved by direct methods and refined by the method of full-matrix least-squares.[16]
[16] CCDC 208362–208365 contain the supplementary crystallographic data for this paper. These data can be obtained free of charge via www.ccdc.cam.ac.uk/conts/retrieving.html (or from the Cambridge Crystallographic Data Centre, 12, Union Road, Cambridge CB2 1EZ, UK; fax: (+44) 1223-336-033; or deposit@ccdc.cam.ac.uk).
[17] Five crystallizations resulted in enantiomeric purities of 25, 46, 52, 55, and 68% *ee*.
[18] Five crystallizations resulted in enantiomeric purities of 13, 34, 46, 54, and 66% *ee*.
[19] C. Kashima, A. Katoh, Y. Yokota, Y. Omote, *J. Chem. Soc. Perkin Trans. 1* **1981**, 489–492; C. Kashima, A. Katoh, Y. Yokota, Y. Omote, *J. Chem. Soc. Perkin Trans. 1* **1981**, 1622–1625.

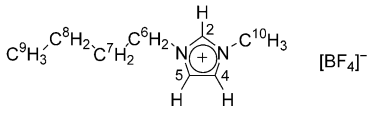
 © 2003 Wiley-VCH Verlag GmbH & Co. KGaA, Weinheim

Structure of Ionic Liquids

The Structure of a Room-Temperature Ionic Liquid with and without Trace Amounts of Water: The Role of C–H···O and C–H···F Interactions in 1-*n*-Butyl-3-Methylimidazolium Tetrafluoroborate**

Andrea Mele, Chieu D. Tran, and Silvia H. De Paoli Lacerda*

Room temperature ionic liquids (RTILs) have been considered as a "green", recyclable alternative to the traditional volatile organic solvents because of their chemical and physical properties, such as being liquid at room temperature, air and moisture stability, high solubility power, and virtually no vapor pressure.[1,2] Being hygroscopic, RTILs can absorb a significant amount of water. Their properties (e.g., solubility, polarity, viscosity, and conductivity) are not only changed by, but also are dependent on the amount of absorbed water.[1–3] Rates of chemical reactions and efficiencies of various processes in RTILs are, therefore, dependent on absorbed water.[1,2] As a consequence, information on the structures of RTILs and their interactions with water are important not only fundamentally but also for various industrial applications. Various studies have been made using either experimental techniques, such as FT-IR, Near-IR, fluorescence, viscosimetry, conductivity, and pulsed-gradient spin-echo NMR diffusion coefficient measurements,[3,4] or theoretical calculations.[5] Unfortunately, these techniques cannot provide direct information on the molecular level of structure of RTILs and their interactions with water. Herein we present direct experimental evidence of cation–cation, cation–water, and cation–anion interactions by NMR spectroscopy through intermolecular nuclear Overhauser enhancements (NOEs) on the model compound 1-*n*-butyl-3-methylimidazolium tetrafluoroborate ($[BMIm]^+[BF_4]^-$ (**1**), Figure 1). Cation–cation interactions were investigated by homonuclear NOEs in the rotating frame (ROEs). The ROEs pattern of the pure liquid (**1a**) was compared with those of samples containing known amounts of water (**1b**–**g**, Table 1). Water was added to change the structure of the pure ionic liquid by introducing water–cation interactions. As a complementary picture, intermolecular water–cation ROEs were also observed and evaluated to provide details of 1) the type of water–cation interactions and 2) the site of interaction. Eventually, the role of the anion was investigated by heteronuclear steady-state $^1H\{^{19}F\}$ NOE difference spectra.



1

Figure 1. Chemical structure and atom numbering for **1**.

Table 1: Composition of samples of compound **1**.

	1a[a]	**1b**	**1c**	**1d**	**1e**	**1f**	**1g**
Water:**1** mole ratio	0	0.10	0.20	0.37	0.56	0.81	1.09
Water mole fraction	0	0.09	0.17	0.27	0.36	0.45	0.52

[a] Pure liquid, reference sample.

The analysis of intermolecular ROEs arising from cation–cation interactions was carried out by volume integration of the cross peaks attributed to intermolecular interactions.[6] The histogram of the relative intensities (Figure 2) shows two different trends: 1) ROEs intensity decreases with increasing water content for those interactions involving imidazolium ring protons H2, H4, H5; 2) the opposite (ROEs intensity increases with increasing water content) for interactions between H10 and the protons of the *n*-butyl group, H6, H7,

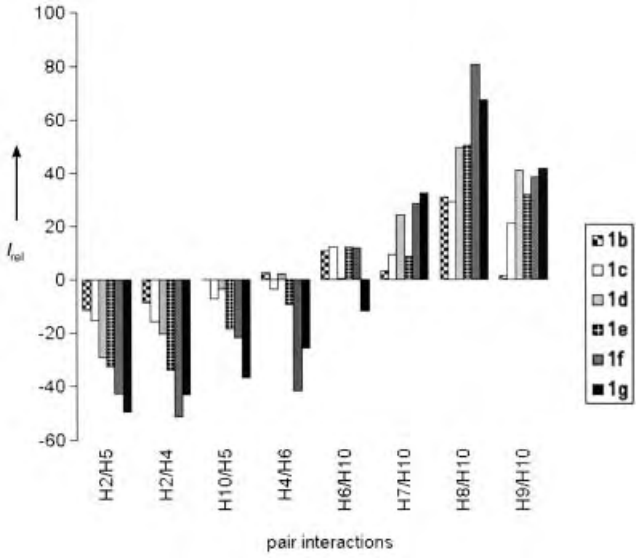


Figure 2. Relative intensity of intermolecular ROESY cross peaks in samples **1b**–**g**. The data reported were obtained as follows: relative intensity (%) $I_{rel} = [(V - V_0)/V_0]100$, where V_0 = integrated volume of a given cross peak in **1a** (pure ionic liquid) and V = integrated volume of the same cross peak in the sample containing known amounts of water (**1b**–**g**, Table 1). All volumes are internally normalized to the H2–H10 cross-peak volume set = 1.00 (arbitrary units). A negative bar for a given cross peak means a decreased relative intensity with respect to the same cross peak in the pure liquid.

[*] Dr. A. Mele
Dipartimento di Chimica, Materiali e Ingegneria Chimica "Giulio Natta"
Politecnico di Milano
Via L. Mancinelli 7, 20131 Milano (Italy)
Fax: (+39) 02-2399-3080
E-mail: andrea.mele@polimi.it
Prof. Dr. C. D. Tran, Dr. S. H. De Paoli Lacerda
Department of Chemistry
Marquette University
P.O. Box 1881, Milwaukee WI 53201 (USA)

[**] We wish to thank Mr. Walter Panzeri (CNR-ICRM) for technical assistance, Prof. Enzio Ragg (University of Milano) and Dr. Giovanni Fronza (CNR-ICRM) for stimulating discussions.

Supporting information for this article is available on the WWW under http://www.angewandte.org or from the author.

 © 2003 Wiley-VCH Verlag GmbH & Co. KGaA, Weinheim DOI: 10.1002/anie.200351783

H8, H9. It was proposed that imidazolium ring protons may act as hydrogen-bond donors to F atoms of the counterion in ionic liquids with fluorine containing anion.[4c,d] In our case, the presence of water is likely to replace progressively the C(sp^2)-H···F interactions with hydrogen bonds involving water as an acceptor towards the cation and as a donor towards the $[BF_4]^-$ ion. The structure of pure ionic liquid **1a** is changed towards a different organization with a lower degree of ring stacking (or other types of piling) or, in other words, the presence of water makes the imidazolium–imidazolium associations looser, with consequent increase of intermolecular distances between ring protons and decrease of the related ROEs intensity. The increasing intensity of ROEs between H10 and the protons of the *n*-butyl chain is consistent with the methyl group shifting progressively towards the most hydrophobic part of the imidazolium ion, namely the *n*-butyl chain, as the water content raises. The observed trends for the H6–H4 and H10–H6 interactions may be due to the superposition of the factors mentioned above and others, for example, conformational changes at the *n*-butyl/imidazolium junction.

The ROESY spectra of samples **1b–g** allowed us to detect small but significant intermolecular cross peaks of imidazolium protons with the broad signal arising from water at about $\delta = 3$ ppm, thereby providing evidence of water–imidazolium cation interactions. The results of the integration of ROESY cross peaks relating to water–imidazolium protons for **1b–g** (Figure 3), seem to indicate that at very low water content

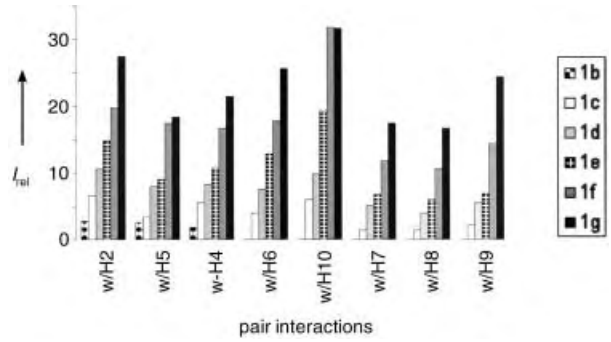


Figure 3. Relative intensity of ROESY cross peaks relating to water (W)–imidazolium cation interactions in samples **1b–g**. The data are normalized to the H2–H10 cross-peak volume set = 1.00 (arbitrary units).

(sample **1b**) the interaction of water is specific and localized at H2, H4, and H5, namely at those C(sp^2)-H protons capable of establishing hydrogen bonds with water. This conclusion is in agreement with the mechanism proposed in the previous paragraph on the intermolecular ROEs involving the aromatic ring protons. It also substantiates the role of water as a disturbing agent with respect to ring–ring assembly. At higher water content (e.g. samples **1f**, **1g**) the interaction of water with the other protons (H6, H7, H8, H9, and H-10) increases considerably and does not show any preference. This might be due to the system passing from a regime of selective interaction to a less defined, nonselective solvation.

The effect of the imidazolium counterion on the short-range structure of some ionic liquids has been recently investigated by the analysis of NMR chemical shift variations[7] in some 1-*n*-butyl-3-methylimidazolium salts as a function of solvent polarity, and also by homonuclear anion–cation NOE in 1-*n*-butyl-3-methylimidazolium tetraphenylborate.[8] This latter study showed NOE between H2 of the cation and H_{ortho} of one of the phenyl groups of the anion as a result of weak C(sp^2)-H···π attractive interactions. This finding, in turn, was found to be consistent with the presence of tight ion pairs even in the presence of solvent. We gained information on the cation–anion interactions in **1** by detecting heteronuclear $^1H\{^{19}F\}$ NOEs (Figure 4). Only the peaks

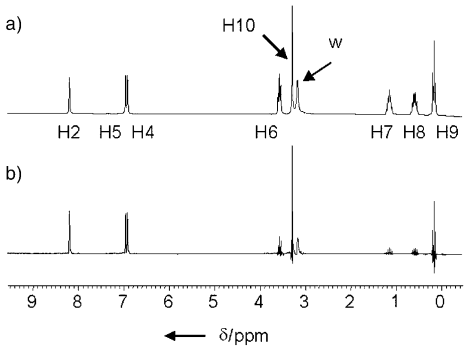


Figure 4. $^1H\{^{19}F\}$ NOE difference experiment carried out on compound **1e**. Trace a) reference spectrum ("off resonance"). Trace b) $^1H\{^{19}F\}$ NOE difference spectrum (vertical scale magnified 32 times with respect to (a)). The signals of H2, H4, H5, and water (w) are in pure absorption because of heteronuclear NOE. The other signals are subtraction artifacts.

assigned to H2, H5, and H4 appear as positive peaks in the NOE difference spectrum (3.6, 3.3, and 3.3% enhancement, respectively). These results provide evidence for positive NOEs between fluorine atoms of the anion and the aromatic protons of the cation. The detection of heteronuclear anion–cation NOEs lends credence to the presence of an ion pair with short H···F contacts. The latter can be associated with attractive interactions of type C(sp^2)-H···F. These results are coherent with recent findings of Dölle and co-workers on the dynamic behavior of the $[BMIm]^+[PF_6]^-$ system.[9] Remarkably, a small positive NOE (1.5%) is also detectable on the water signal, which seems to suggest that water can act as hydrogen-bond donor towards the $[BF_4]^-$ ion. We repeated the NOE experiments in the presence of a strong competitor at the hydrogen-bond site, such as DMSO[10] in an attempt to validate the hypothesis of C(sp^2)-H···F hydrogen bonds. Surprisingly, the same pattern of NOEs was found even in a sample containing 55 mg of pure **1** dissolved in 500 μL of $[D_6]$DMSO. The enhancements, once again observed for H2 (1.3%), H5 (1.0%), and H4 (1.1%), are consistent with short H···F contact even for this sample where **1** was in a different molecular environment.

The ROESY approach made it possible for us to detect intermolecular contacts of two types: cation–cation and water–cation. Increasing water content was found to appreciably change the structure of the ionic liquid through the

 © 2003 Wiley-VCH Verlag GmbH & Co. KGaA, Weinheim

participation of water in C(sp^2)-H mediated hydrogen bonds. The heteronuclear experiments on **1** indicated the existence of tight ion pairs in the pure liquid even in the presence of small amounts of water and, in a second set of experiments, even in DMSO solution. The heteronuclear NOE experiments provided direct evidence of the importance of the C(sp^2)-H···F interactions in governing the short-range structure of this class of ionic liquids. Experiments on other molten salts such as $[BuMIm]^+[PF_6]^-$ and $[BuMIm]^+[Tf_2N]^-$ (Tf = bis(trifluoromethyl)sulfonyl amide) are currently being performed in order to gain deeper insight into the hierarchy of intermolecular interactions.

Experimental Section

1-*n*-Butyl-3-methylimidazolium chloride ($[BuMIm]^+Cl^-$) was synthesized according to reported procedures.[11] Compound **1** was prepared from $[BuMIm]^+Cl^-$ by metathesis using the reported methods,[12] dried under vacuum at 70 °C overnight, and kept either under nitrogen or in a vacuum desiccator to protect it from moisture.

Suitable amounts of **1** were accurately weighted in glass vials. HPLC grade water was added by microsyringe. The resulting solutions were transferred into 5-mm NMR tubes equipped with coaxial capillary tube containing $[D_6]$DMSO. The external deuterated solvent provided both lock frequency and ^1H spectrum reference (central peak = 2.50 ppm). NMR spectroscopy experiments were carried out on a Bruker Avance 500 instrument at 305 K (nominal). Two-dimensional correlation experiments by dipolar coupling in the rotating frame (ROESY) were performed by using a pulse sequence proposed for off-resonance ROESY with adiabatic rotation.[13] All cross-peak volumes were normalized to the volume of H2–H10 cross peak.[14] The heteronuclear steady-state $^1H\{^{19}F\}$ NOE difference spectra were carried out by using a standard pulse sequence modified for the second radio frequency channel.[15] Expansion of the ROESY spectrum of **1e**, Tables of cross-peak volumes related to Figures 2 and 3, and the $^1H\{^{19}F\}$ NOE difference spectrum of **1** in $[D_6]$DMSO are available as Supporting Information.

Received: April 30, 2003 [Z51783]

Keywords: hydrogen bonds · ionic liquids · NMR spectroscopy · noncovalent interactions · water chemistry

[1] T. Welton, *Chem. Rev.* **1999**, *99*, 2071 – 2083.
[2] A. E. Visser, R. P. Swatloski, R. D. Rogers, *Green Chem.* **2000**, *2*, 1 – 4.
[3] a) K. A. Fletcher, S. Pandey, *Appl. Spectrosc.* **2002**, *56*, 266 – 271; b) S. N. V. K. Aki, J. Brennecke, A. Samanta, *Chem. Commun.* **2001**, 413 – 414; c) S. G. Kazarian, B. J. Briscoe, T. Welton, *Chem. Commun.* **2000**, 2047 – 2048.
[4] a) L. Cammarata, S. G. Kazarian, P. A. Salter, T. Welton, *Phys. Chem. Chem. Phys.* **2001**, *3*, 5192 – 5200; b) C. D. Tran, S. H. De Paoli Lacerda, D. Oliveira, *Appl. Spectrosc.* **2003**, *57*, 152 – 157; c) A. Noda, K. Hayamizu, M. Watanabe, *J. Phys. Chem. B* **2001**, *105*, 4603 – 4610; d) J.-F. Huang, P.-Y. Chen, I.-W. Sun, S. P. Wang, *Inorg. Chim. Acta* **2001**, *320*, 7 – 11.
[5] a) C. G. Hanke, A. Johansson, J. B. Harper, R. M. Lynden-Bell, *Chem. Phys. Lett.* **2003**, *374*, 85 – 90; b) G. J. Mains, E. A. Nantis, W. R. Carper, *J. Phys. Chem. A* **2001**, *105*, 4371 – 4378.
[6] R. A. Mantz, P. C. Trulove, R. T. Carlin, R. A. Osteryoung, *Inorg. Chem.* **1995**, *34*, 3846 – 3847.
[7] A. D. Headley, M. N. Jackson *J. Phys Org. Chem.* **2002**, *15*, 52 – 55.
[8] J. Dupont, P. A. Z. Suarez, R. F. De Souza, R. A. Burrow, J.-P. Kintzinger, *Chem. Eur. J.* **2000**, *6*, 2377 – 2381.
[9] J. H. Antony, D. Mertens, A. Dölle, P. Wasserscheid, W. R. Carper, *ChemPhysChem* **2003**, *4*, 588 – 594.
[10] A. Mele, B. Vergani, F. Viani, S. V. Meille, A. Farina, P. Bravo, *Eur. J. Org. Chem.*, **1999**, 187 – 196.
[11] J. S. Wilkes, J. A. Levisky, R. A. Wilson, C. L. Hussey, *Inorg. Chem.* **1982**, *21*, 1263 – 1264.
[12] a) J. D. Holbrey, K. R. Seddon, *J. Chem. Soc. Dalton Trans.* **1999**, 2133 – 2140; b) J. G. Huddleston, H. D. Willauer, R. P. Swatloski, A. E. Visser, R. D. Rogers, *Chem. Commun.* **1998**, 1765 – 1766; c) P. Bonhote, A. P. Dias, N. Papageourgiou, K. Kalyanasundaram, M. Gratzel, *Inorg. Chem.* **1996**, *35*, 1168 – 1178.
[13] H. Desvaux, P. Berthault, N. Birlirakis, M. Goldman, M. Piotto, *J. Magn. Reson. Ser. A* **1995**, *113*, 47 – 52.
[14] The reason this choice are: 1) The H2–H10 interaction was assumed to be mainly, if not purely, intramolecular[6] and, therefore, not influenced by the added water; 2) the average distance between H2 and H10 can be considered to be independent of the intermolecular interactions and conformation of the cation of **1**, which is assumed to be planar.
[15] Selective saturation of fluorine signals was achieved by a suitably attenuated decoupler pulse on resonance on the ^{19}F signal of the ionic-liquid anion (spectrum "on resonance"). Control spectra ("off resonance") were recorded by setting the decoupler frequency off resonance. NOE difference spectra were obtained by subtracting the "off resonance" spectrum from the "on resonance".

 © 2003 Wiley-VCH Verlag GmbH & Co. KGaA, Weinheim

Rings Cages and Polymers

A Fast Organometallic Route from *p*-Xylene, Mesitylene, and *p*-Diisopropylbenzene to Organoiron and Polycyclic Aromatic Cyclophanes, Capsules and Polymers

*Victor Martinez, Jean-Claude Blais, and Didier Astruc**

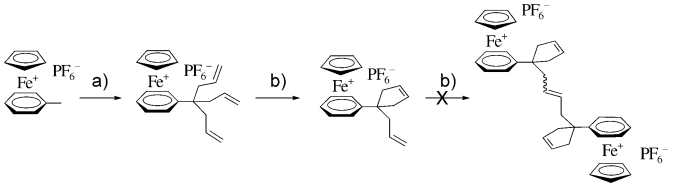
Para-xylene and mesitylene are among the most common and cheapest organic compounds.[1,2] They form well-known robust sandwich complexes of the type $[Fe(\eta^5\text{-}C_5H_5)(\eta^6\text{-arene})]^+$,[3] by high-yield, large-scale reactions with ferrocene in the presence of aluminum chloride.[4] Herein we report that these sandwich complexes and the *p*-diisopropylbenzene iron complex lead to new cyclophanes,[5] organoiron cyclo-

[*] Prof. D. Astruc, V. Martinez
LCOO, UMR CNRS 5802
Université Bordeaux I
33405 Talence Cedex (France)
Fax: (+33) 5-5684-6646
E-mail: d.astruc@lcoo.u-bordeaux1.fr
Dr. J.-C. Blais
LCSOB, UMR CNRS 7613
Université Paris VI
75252 Paris (France)

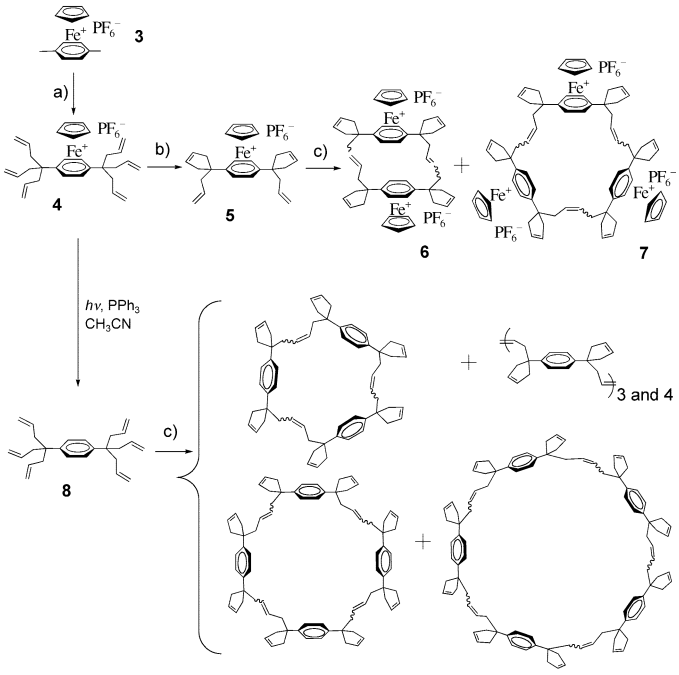
Supporting information for this article is available on the WWW under http://www.angewandte.org or from the author.

 © 2003 Wiley-VCH Verlag GmbH & Co. KGaA, Weinheim DOI: 10.1002/anie.200351795

phanes,[6] polyring derivatives, capsules, and polymers in two steps (three steps for the iron-free compounds). The electron-withdrawing character of the cationic 12-electron group $FeCp^+$ lowers the pK_a value of polymethylaromatics from 43 to 28 in DMSO,[7a,b] and the subsequent convenient deprotonation reaction can be exploited for facile and multiple C–C bond formation under ambient conditions.[7b,c] For instance, $FeCp^+$-induced triallylation of toluene can be followed by ring-closing metathesis (RCM) to give a derivative containing a five-membered ring in 5 min at room temperature[7c] using the Grubbs metathesis catalyst [Ru(PCy$_3$)$_2$Cl$_2$(=CHPh)], **1**.[8] On the other hand, dimerization of the iron complex by cross metathesis (CM) under these conditions does not occur, even after several days (Scheme 1).

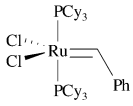


Scheme 1. a) Allyl bromide, KOH, DME; b) [Ru(PCy$_3$)$_2$Cl$_2$(=CHPh)], **1**, CH_2Cl_2, room temperature.

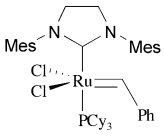


Scheme 2. a) Allyl bromide, KOH, DME; b) [Ru(PCy$_3$)$_2$Cl$_2$(=CHPh)], **1**, CH_2Cl_2; c) [Ru(PCy$_3$){C(N(mesityl)CH)$_2$}Cl$_2$(=CHPh)], **2**, $C_2H_4Cl_2$, 60 °C.

We have now explored the two-step polyallylation/cross-coupling-metathesis sequence with the complexes [Fe(η^5-C_5H_5)(η^6-arene)][PF_6] towards the more challenging construction of cyclophanes by using **1** and the more efficient second-generation Grubbs commercial catalyst, [Ru(PCy$_3$){C(N(mesityl)CH)$_2$}Cl$_2$(=CHPh)], **2**.[8]



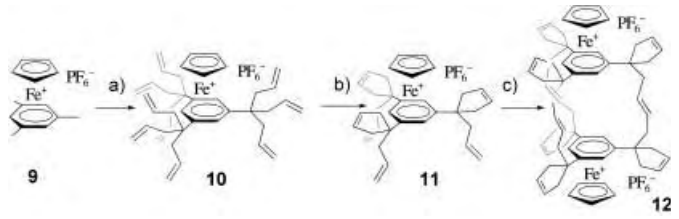
1



2

The *p*-xylene iron complex **3** leads to $CpFe^+$-induced hexaallylation giving **4**. When **4** is heated at 60 °C for 6 days in the presence of the catalyst **2**, a mixture of [6,6] and [6,6,6] paracyclophanes **6** and **7** (in comparable amounts, from the MALDI-TOF mass spectrum) is obtained in 45% yield. A small amount of [6,6,6,6] tetranuclear compound is also detected. Under these conditions, the iron-free compound **8** gives a mixture of three paracyclophanes and linear open trisarene and tetra-arene (Scheme 2) that were identified by their molecular peaks in the MALDI-TOF mass spectra.

The same sequence was investigated with the mesitylene complex **9**. After $CpFe^+$-induced nonaallylation of **9** at room temperature giving the nonaallyl complex **10**, metathesis of **10** catalyzed by **1** gives **11**, resulting from RCM. However, metathesis catalyzed by **2** at reflux for 4 h gives a mixture whose MALDI-TOF mass spectrum shows the nonselective formation of singly, doubly, or triply linked dimers corresponding to the loss of one, two, or three ethylene units respectively, and singly and doubly linked trimers, tetramers, and pentamers. As the metathesis reaction is thermodynamically controlled,[8,9] we heated the reaction mixture further for 2 days at 60 °C to approach or reach equilibrium. Indeed, the major products observed in the MALDI-TOF mass spectrum then became dimers, with almost equal amounts of doubly and triply bridged compounds. The oligomers were in lower amounts. Finally, the reaction mixture was heated for a week to give almost exclusively the triply bridged organoiron [6_3](1,3,5) cyclophane **12**, a molecular capsule, and only trace amounts of the other compounds (Scheme 3).[6] This sequence



Scheme 3. a) Allyl bromide, KOH, DME; b) [Ru(PCy$_3$)$_2$Cl$_2$(=CHPh)], **1**, CH_2Cl_2, RT; c) [Ru(PCy$_3$){C(N(mesityl)CH)$_2$}Cl$_2$(=CHPh)], **2**, $C_2H_4Cl_2$, 60 °C.

of MALDI-TOF mass spectra can be seen in Figure 1. The outcome of this reaction is strongly concentration dependent as required by the thermodynamic control. Under more concentrated conditions, the amounts of oligomers obtained are larger, and the final equilibrium may even lie in favor of these oligomers under very concentrated conditions. The

 © 2003 Wiley-VCH Verlag GmbH & Co. KGaA, Weinheim

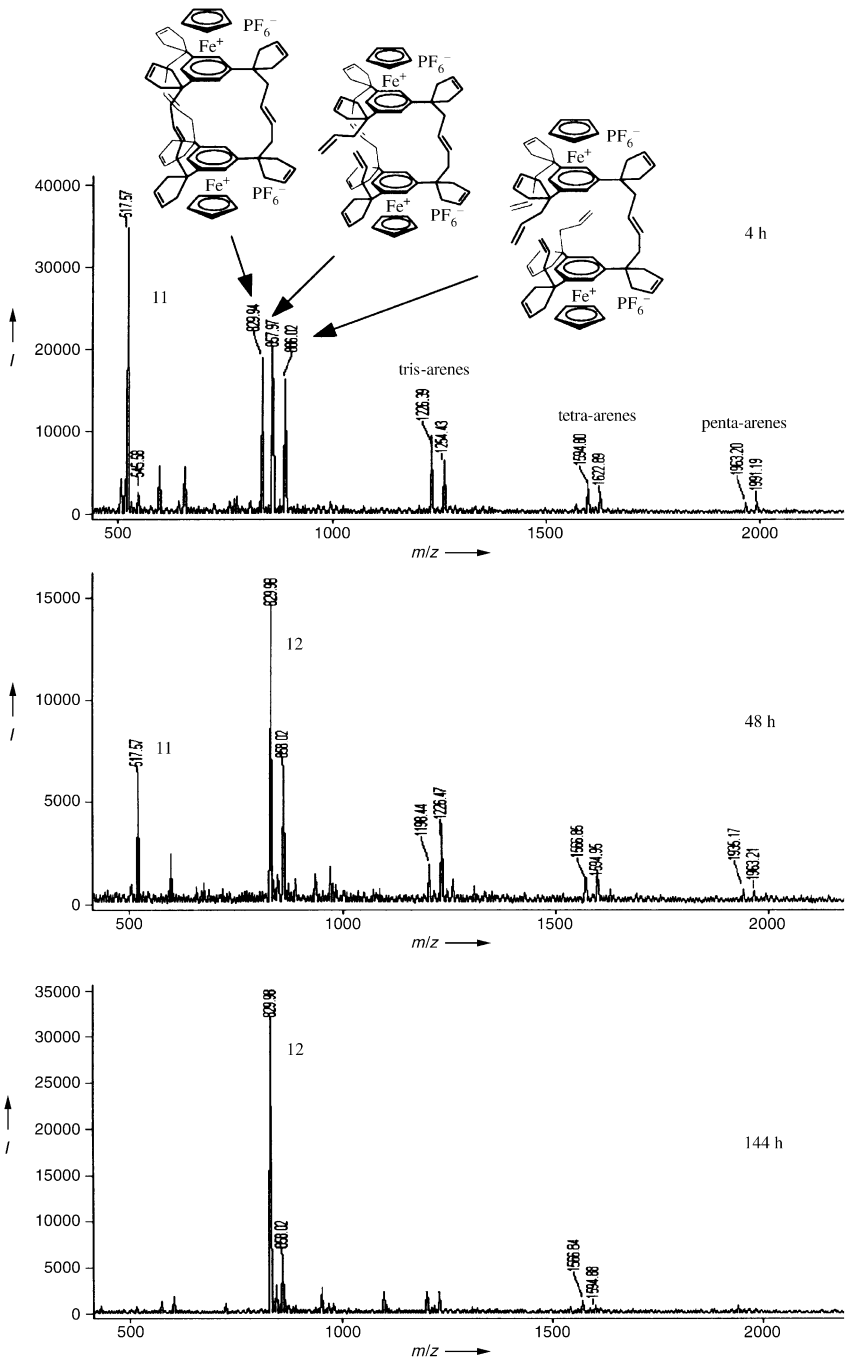


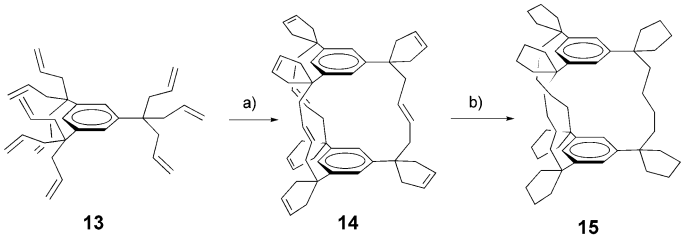
Figure 1. MALDI-TOF mass spectra during the metathesis reaction of **10** catalyzed by **2**.

$CpFe^+$ group has a negative effect on the metathesis rate presumably for steric reasons, and the low yield of **12** also arises from decomplexation during the reaction. When the metathesis reaction is carried out on the metal-free nonaallylated arene **13** obtained by the decomplexation of **10**, it proceeds more readily and selectively to form the triply bridged CM product **14**. The triply-bridged capsule **14** is isolated as a mixture of isomers whose hydrogenation with H_2/Pd/C in CH_2Cl_2 yields the single product **15** (Scheme 4).

Because of the well-known magnetic anisotropy of the arene ring in the cyclophane alkyl hydrogens,[5a] the ^{1}H NMR signals of the β-hydrogens are shifted upfield at 0.64 ppm (see the Supporting Information).

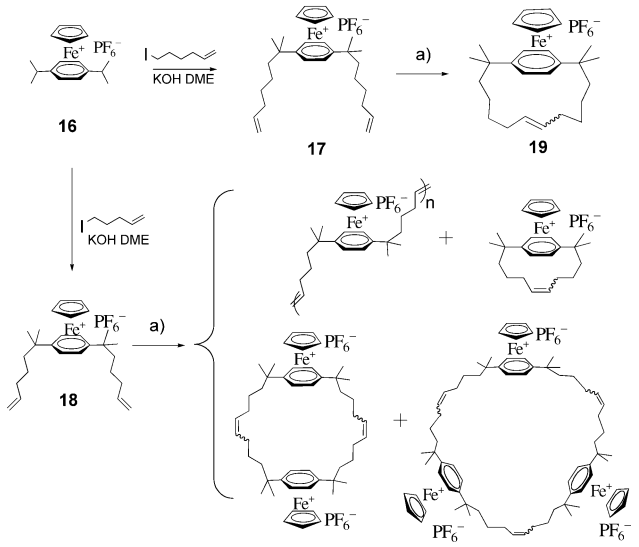
To investigate the feasibility of the synthesis of organometallic [n] paracyclophanes using the same type of strategy, we first synthesized the new *p*-diisopropylbenzene complex $[FeCp(\eta^6\text{-}p\text{-}i Pr_2\text{-}C_6H_4)][PF_6]$, **16**, by using the classic Nesmeyanov ligand-substitution reaction.[3] Dialkenylation was carried out in one pot with complex **16**, KOH, and longer-chain ω-alkenyl iodides in THF. The reactions were carried out in refluxing THF, because alkyl iodides are much less reactive electrophiles than allyl bromide. Thus, dialkenylation of **16** with ω-iodoalkenes allows the preparation of a variety of paradisubstituted arenes bearing terminal double bonds such as the new complexes **17** and **18**. Potentially, RCM may lead to the desired paracyclophanes iron complexes and eventually the metal-free cyclophanes by using the classic decomplexation procedure (i.e. photolysis by using visible light in MeCN in the presence of one equiv PPh_3, followed by extraction with ether). Complex **17** indeed selectively gives **19** in CH_3Cl at room temperature by using the catalyst **1**. In the ^{1}H NMR spectra of **19**, the signals of the β-hydrogens of the cyclophanes are shifted to 0.51 ppm because of aromatic anisotropy.[5a] On the other hand, metathesis with **1** of the complex **18**, containing alkenyl chains that are one methylene unit shorter than in **17**, leads to a mixture of linear oligomers (2 to 6 units) and mono-, bi- and trimetallic paracyclophanes (Scheme 5) that are identified by their molecular peaks in the MALDI-TOF mass spectrum.

In summary, a variety of cyclophanes, metallocyclophanes polyring



Scheme 4. a) $[Ru(PCy_3)\{C(N(mesityl)CH)_2\}Cl_2(=CHPh)]$, **2**, $C_2H_4Cl_2$, 60 °C; b) H_2 Pd/C CH_2Cl_2.

 © 2003 Wiley-VCH Verlag GmbH & Co. KGaA, Weinheim



Scheme 5. a) $[Ru(PCy_3)_2Cl_2(=CHPh)]$, **1**, CH_3Cl, RT.

derivatives and capsules are quickly formed from *p*-xylene, mesitylene and *p*-diisopropylbenzene, which are activated by $FeCp^+$ followed by ring closing- and cross metathesis catalyzed by the Grubbs commercial catalysts **1** or **2**. These results illustrate the potential of this synthetic strategy combining these two spectacular and remarkably efficient modes of C–C coupling. This work is also an example of the use of MALDI-TOF mass spectrometry as a remarkably powerful tool for the investigation of complex structures in a nonbiological area.

Experimental Section

Compounds **3** and **9**: see ref. [2] and [3]. Compounds **4**, **10**, **17** and **18**: see ref. [7c]. The perallylation reaction was carried out at room temperature until completion monitored by ^1H NMR, whereas the peralkenylation was conducted at reflux. Product **10** was purified on an Al_2O_3 gel column eluting with CH_2Cl_2. Compounds **5**, **11** and **19:** Catalyst **1** (5–10% mol) was added to a stirred solution of complex **4** (0.5 mmol) in CH_2Cl_2 (20 mL). After completion of the reaction, the solvent was removed in vacuo, and the residue was washed repeatedly with ether. Recrystallization of the product in a CH_2Cl_2/ether mixture and slow-diffusion crystallization with a CH_2Cl_2/ether mixture gave yellow crystals. Compounds **6**, **7**, **12** and **14**: A stirred solution of **5** (0.5 mmol) and **2** (10% mol) in dichloroethane (5 mL) was heated to reflux over seven days under nitrogen, and **2** (10% mol) was added every other day (i.e., the total amount of **2** used was 30%). The solvent was removed in vacuo and the solid residue was washed with 3x10 mL ether (except **14**) and purified by column chromatography over silica. Compound **15**: Pd/C (10 mg) was added to a solution of compound **14** (70 mg; 0.14 mmol) in CH_2Cl_2 and this mixture was flushed with dihydrogen and kept under atmospheric pressure for 10 h. The mixture was filtered over celite and the solvent was removed in vacuo (yield: 100%). See the Supporting Information for the other experimental procedures and the analytical and spectroscopy data confirming the proposed structures.

Received: May 2, 2003 [Z51795]

Keywords: cage compounds · C–C coupling · cyclophanes · iron · metathesis

[1] J. Loschmidt, *Chemisches Studien. A. Konstitution-Formeln der Organische Chemie in Geographischer Darstellung B*, Das Mariotte'sche Gesetz, Vienna, **1861**.
[2] *Modern Arene Chemistry* (Ed.: D. Astruc), Wiley-VCH, Weinheim, **2002**.
[3] M. L. H. Green, L. Pratt, G. Wilkinson, *J. Chem. Soc.* **1960**, 989.
[4] A. N. Nesmenayanov, N. A. Vol'kenau, I. N. Bolesova, *Dokl. Akad. Nauk SSSR* **1963**, *149*, 615.
[5] a) F. Vögtle *Cyclophane Chemistry*, Wiley, New York, **1993**; b) R. Gleiter, D. Kratz, *Acc. Chem. Res.* **1993**, *26*, 311; c) V. Boekelheide, *Acc. Chem. Res.* **1980**, *13*, 65; d) B. König, B. Knieriem; A. de Mejere, *Chem. Ber.* **1993**, *126*, 1643; e) For a recent updated account on synthetic methods of cyclophanes, see H. Hopf, *Classic in Hydrocarbon Chemistry*, Wiley-VCH, Weinheim, **2000**, chap. 12.3, pp. 337–378.
[6] All the reported organotransition-metal sandwich cyclophane complexes (mostly [2,2]-paracyclophane) have been synthesized by direct complexation of cyclophanes: a) the first organometallic cyclophane derivative was a tricarbonylchromium complex: D. J. Cram, D. I. Wilkinson, *J. Am. Chem. Soc.* **1960**, *82*, 5721; b) first bis-arene-ruthenium complexes: E. D. Laganis, R. G. Finke, V. Boekelheide, *Tetrahedron Lett.* **1980**, *21*, 5721; c) first $CpFe^+$-cyclophane complexes: E. D. Laganis, R. H. Voegeli, R. T. Swann, R. G. Finke, V. Boekelheide, *Organometallics* **1982**, *1*, 1415; d) C. Elschenbroich, *Chem. Ber.* **1984**, *117*, 3165; e) C. Elschenbroich, A. Salzer, *Organometallics*, 2nd ed., VCH, Weinheim, **1992**, p. 308; f) early exemples of main-group-cyclophane complexes: H. Schmidbauer, W. Bublak, M. W. B. Huber, G. Mueller, *Helv. Chim. Acta* **1986**, *69*, 1742; g) K.-D. Plitzko, B. Rakpo, B. Gollas, G. Wehrle, T. Weakley, D. T. Pierce, W. E. Geiger, R. C. Haddon, V. Boekelheide, *J. Am. Chem. Soc.* **1990**, *112*, 6545; h) bis-19-electron Fe^I cyclophane complexes: H. Rabaâ, M. Lacoste, M.-H. Delville-Desbois, J. Ruiz, B. Gloaguen, N. Ardoin, D. Astruc, A. Le Beuze, J.-Y. Saillard, J. Linarès, F. Varret, J.-M. Dance, E. Marquestaut, *Organometallics* **1995**, *14*, 5078; i) Ru cluster-cyclophane complexes (review): P. J. Dyson, B. F. G. Johnson, C. M. Martin, *J. Cluster Sci.* **1995**, *6*, 21; j) P. Schooler, B. F. G. Johnson, L. Scaccionoce, R. Tregonning, *J. Chem. Soc. Dalton Trans.* **1999**, *16*, 2743.
[7] a) H. A. Trujillo, C. M. Casado, J. Ruiz, D. Astruc, *J. Am. Chem. Soc.* **1999**, *121*, 5674; b) D. Astruc, S. Nlate, J. Ruiz in ref. [2], chap. 12, pp. 400–434; c) V. Martinez, J. C. Blais, D. Astruc, *Org. Lett.* **2002**, *4*, 651.
[8] R. Grubbs, *Acc. Chem. Res.* **2001**, *34*, 18.
[9] a) A. B. Smith, C. M. Adams, S. A. Kozmin, *J. Am. Chem. Soc.* **2001**, *123*, 990; b) A. B. Smith, C. M. Adams, S. A. Kozmin, D. V. Paone, *J. Am. Chem. Soc.* **2001**, *123*, 5925; c) A. Fürstner, *Angew. Chem.* **2000**, *112*, 3140; *Angew. Chem. Int. Ed.* **2000**, *39*, 3012.

 © 2003 Wiley-VCH Verlag GmbH & Co. KGaA, Weinheim

Pyridinol-Based Antioxidants

6-Amino-3-Pyridinols: Towards Diffusion-Controlled Chain-Breaking Antioxidants**

Maikel Wijtmans, Derek A. Pratt, Luca Valgimigli,* Gino A. DiLabio, Gian Franco Pedulli,* and Ned A. Porter**

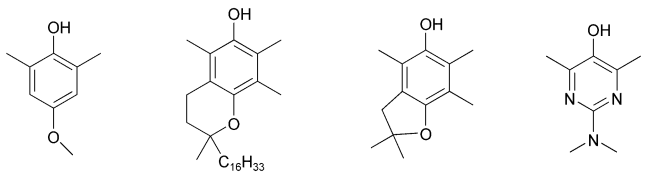
Peroxyl radicals (LOO•) are the chain-propagating species in the rate-determining step of lipid peroxidation [Eq. (1)].

$$LOO^{\cdot} + L{-}H \xrightarrow{k_p} LOOH + L^{\cdot} \quad (1)$$

Chain-breaking antioxidants, most commonly substituted phenols (ArOH) such as **1**–**3**, inhibit peroxidation by transferring their phenolic H atom to the propagating radical [Eq. (2)] at a rate (k_{inh}[ArOH]) faster than that of chain

$$LOO^{\cdot} + ArOH \xrightarrow{k_{inh}} LOOH + ArO^{\cdot} \quad (2)$$

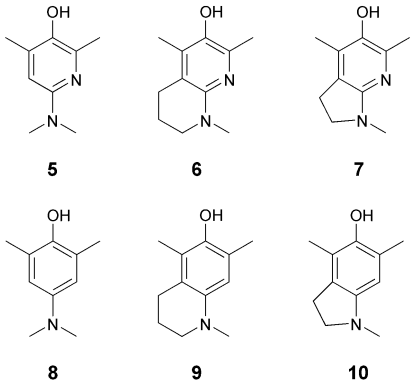
propagation (k_p[L-H]). The best-known example of a phenolic antioxidant is α-tocopherol (α-TOH, **2**), the most potent form of vitamin E, nature's primary defense against radical chain oxidation.[1] Recently, considerable effort has been devoted to the development of peroxyl-radical-trapping antioxidants more effective than α-TOH,[2–5] since the peroxidation of lipids in vivo has been suggested to be a major factor in the development of several degenerative diseases.[6]



1 **2** **3** **4**

The bond dissociation enthalpy (BDE) of the phenolic O–H bond plays a central role in determining antioxidant efficacy; phenols having lower O–H BDEs are generally better antioxidants.[7,8] Substitution with electron-donating (ED) groups at positions *ortho* and *para* to the phenolic OH group leads to compounds having lower BDEs. However, good ED substituents also lead to a decrease in the ionization potential (IP) of the phenol, thereby rendering the compound directly reactive with oxygen. Calculations predicted that incorporation of two nitrogen atoms at the 3- and 5-positions of the phenolic ring significantly raises the IP and greatly improves the stability of the compound in air while only minimally lowering the O–H BDE.[4] Experiments confirmed this prediction. Thus, for example, the 5-pyrimidinol **4** is perfectly stable in air and has a k_{inh} value about twice that of α-TOH.[4]

Calculations also predicted that 3-pyridinol would have a lower O–H BDE than the analogous 5-pyrimidinol and an IP intermediate to those of phenol and 5-pyrimidinol.[4] We therefore expected that 6-amino-3-pyridinols such as **5** would



5 **6** **7**

8 **9** **10**

have lower O–H BDEs than the analogous 5-pyrimidinols (e.g. **4**) and still have better air-stability than the corresponding phenols. Furthermore, the free 5-position in the pyridine skeleton allows for fusion of aliphatic rings (i.e. to give **6** and **7**), structural changes that have been shown to increase k_{inh} significantly in the series **1**–**3** because of improved stereoelectronics.[2,9] Herein we show by theory the effects of substitution on the O–H BDE and IP of a series of 3-pyridinols. We also report here on the synthesis and experimental investigation of three new 3-pyridinol antioxidants that were selected on the basis of our calculations.[10]

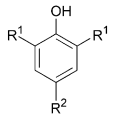
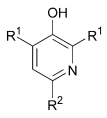
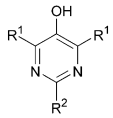
[*] Dr. D. A. Pratt, Prof. Dr. N. A. Porter
Department of Chemistry
Vanderbilt University
Nashville, TN 37235 (USA)
Fax: (+1) 615-343-5478
E-mail: derek.a.pratt@vanderbilt.edu
n.porter@vanderbilt.edu
Prof. Dr. G. F. Pedulli, Dr. L. Valgimigli
Department of Organic Chemistry "A. Mangini"
University of Bologna
Via San Donato 15, 40127 Bologna (Italy)
Fax: (+39) 051-244-064
E-mail: valgimig@alma.unibo.it
pedulli@alma.unibo.it
M. Wijtmans
Department of Chemistry
Vanderbilt University, Nashville, TN 37235 (USA) and
Department of Organic Chemistry, University of Nijmegen
Toernooiveld 1, 6525 ED, Nijmegen (The Netherlands)
Dr. G. A. DiLabio
National Institute for Nanotechnology
National Research Council of Canada, W6-010 ECERF
9107 116th Street, Edmonton, AB T6G 2V4 (Canada)

[**] We thank Johan Brinkhorst for technical assistance. D.A.P. thanks NSERC Canada and Vanderbilt University for their support. This project was supported in part by the National Science Foundation as well as by the University of Bologna and the MIUR Research Project "Free Radical Research in Chemistry and Biology: Fundamental Aspects and Applications in Environment and Material Science".

Supporting information for this article is available on the WWW under http://www.angewandte.org or from the author.

 © 2003 Wiley-VCH Verlag GmbH & Co. KGaA, Weinheim DOI: 10.1002/anie.200351881

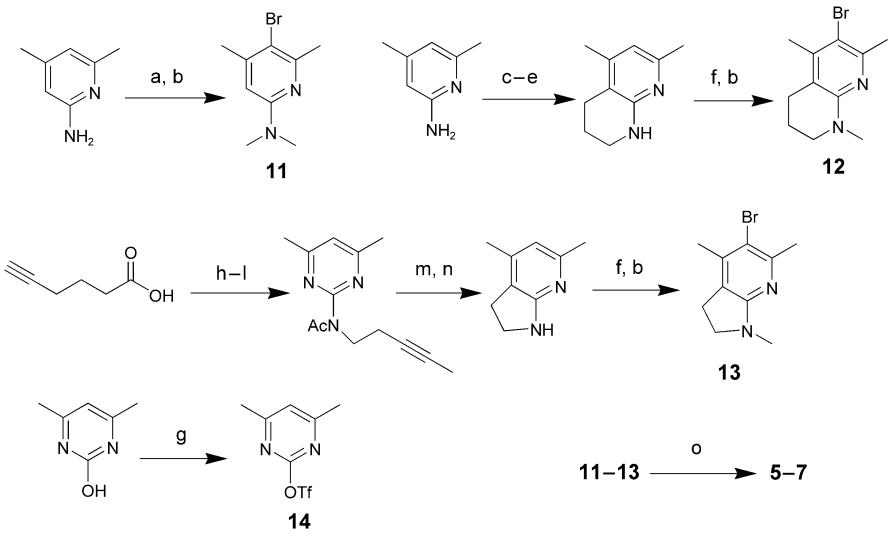
Table 1: Calculated substituent effects on gas-phase O–H BDEs at 298 K and adiabatic IPs at 0 K for substituted phenols, 3-pyridinols, and 5-pyrimidinols.[a]

Substitution	BDE	IP	BDE	IP	BDE	IP
$R^1=H$, $R^2=H$	87.1 (0.0)	195.4 (0.0)	88.2 (0.0)	206.4 (0.0)	89.6 (0.0)	219.7 (0.0)
$R^1=H$, $R^2=CH_3$	84.6 (−2.5)	186.9 (−8.5)	85.4 (−2.8)	196.6 (−9.8)	86.8 (−2.8)	209.3 (−10.4)
$R^1=CH_3$, $R^2=CH_3$	80.4 (−6.7)	178.3 (−17.1)	81.1 (−7.1)	186.3 (−20.1)	83.2 (−6.4)	198.0 (−22.7)
$R^1=H$, $R^2=OCH_3$	81.0 (−6.1)	176.5 (−18.9)	82.0 (−6.2)	186.1 (−20.3)	83.6 (−6.0)	199.1 (−21.6)
$R^1=CH_3$, $R^2=OCH_3$	77.0 (−10.1)	169.2 (−26.2)	78.1 (−10.1)	177.4 (−29.0)	79.8 (−9.8)	188.3 (−31.4)
$R^1=H$, $R^2=N(CH_3)_2$	77.0 (−10.1)	157.7 (−37.7)	77.0 (−11.2)	164.6 (−41.8)	78.3 (−11.3)	174.6 (−45.1)
Compounds						
8, **5**, **4** (monocyclic)	72.3 (−14.8)	152.3 (−43.1)	73.5 (−14.7)	157.7 (−48.7)	74.1 (−15.5)	167.0 (−52.7)
9, **6** (fused 6-ring)	71.2 (−15.9)	148.3 (−47.1)	73.3 (−14.9)	154.6 (−51.8)		
10, **7** (fused 5-ring)	70.5 (−16.6)	145.2 (−50.3)	72.4 (−15.8)	152.3 (−54.1)		
2 (α-TOH)	74.8 (−12.3)	159.3 (−36.1)				

[a] Data for phenols and 5-pyrimidinols are from ref. [4] except for **8**–**10**. All values are in kcal mol^{-1}. Substituent effects (relative to the unsubstituted parent) are in parentheses.

The calculated O–H BDEs and IPs of several substituted phenols, 3-pyridinols, and 5-pyrimidinols were obtained using density functional theory models ((RO)B3LYP/6-311+G(2d,2p)//AM1/AM1 and B3LYP/6-31G(d)//AM1/AM1, respectively) and the values are given in Table 1.[11,12] Clear trends can be seen. For all three classes, the O–H BDE and IP values decrease when the electron density on the aromatic ring is increased. The order for the calculated values of these properties is always phenol < 3-pyridinol < 5-pyrimidinol. The calculations suggest that the highest antioxidant activities in conjunction with reasonable air-stability (IP values comparable to **2**) are expected from pyridinols **5**–**7**. Therefore, we selected these three molecules as targets for synthesis and experimental investigations.



Scheme 1. Synthetic approach to 3-pyridinols **5**–**7**. Reagents and conditions: a) DBDMH, CH_2Cl_2, −40 °C, 40 min, 67%; b) HCOOH, aq H_2CO, reflux, 18 h, 100% for **11**, 77% for **12**, 84% for **13**; c) acrylic acid, pyridine, reflux, 24 h, 30% after crystallization; d) polyphosphoric acid, 125 °C, 40 min, 75%; e) BH_3·THF, THF, reflux, 18 h, 83%; f) DBDMH, CH_2Cl_2, −78 °C, 10–30 min, 93% for **12**, 83% for **13**; g) Tf_2O, Et_3N, CH_2Cl_2, 0 °C, 1 h, 98%; h) 15 M aq KOH, reflux, 4 h, 95%; i) $(PhO)_2PON_3$, *t*BuOH, reflux, 30 h, 79%; j) ethereal HCl, 24 h, 70%; k) **14**, Et_3N, DMF, 1 d, 93%; l) Ac_2O, DMAP, 100 °C, 20 h, 91%; m) Ph_2O, reflux, 10 h, 82%; n) NaOH, MeOH, reflux, 20 h, 100%; o) 1. *n*BuLi, THF, −78 °C, 30 min; 2. dry 2-nitro-*m*-xylene, THF, −78 °C, 1–3 h, 63% for **5**, 25% for **6**, 27% for **7**. DBDMH = dibromodimethylhydantoin, DMAP = dimethylaminopyridine, DMF = dimethylformamide, Tf = trifluoromethanesulfonyl.

There are few synthetic approaches to 6-amino-3-pyridinol structures described in the literature, and **5**–**7** have never been reported.[13] We devised a synthetic sequence in which the reactive OH moiety is introduced at low temperatures in the last step, thus minimizing potential decomposition of products and/or intermediates. Only a brief description of the syntheses will be presented here; a forthcoming paper will report our extensive synthetic efforts in detail. Construction of the appropriate pyridine substructure involved a three-step approach featuring a Friedel–Crafts reaction for **6** and a seven-step sequence with an intramolecular Diels–Alder sequence for **7**. Construction of the pyridine was followed by bromination, methylation, and hydroxylation (Scheme 1). The pyridinols **5**–**7** were obtained as yellow or orange solids.

The O–H BDEs that were measured experimentally by radical-equilibration EPR studies are collected in Table 2.[7b] The absolute experimental values (in benzene) were slightly higher (2–3 kcal mol^{-1}) than the calculated (gas-phase) values (Table 1), an issue already addressed by us in previous works.[4] However, the corresponding ΔBDE (BDE_{PyrOH}–$BDE_{\alpha\text{-}TOH}$) shows good agreement between experimental and

 © 2003 Wiley-VCH Verlag GmbH & Co. KGaA, Weinheim

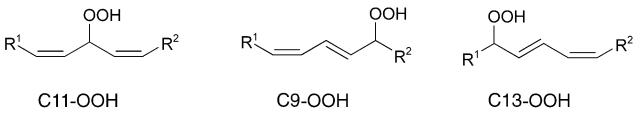
Table 2: Solution-phase O–H BDEs and inhibition rate constants for 3-pyridinols **5**–**7**.

ArOH	O–H BDE [kcal mol^{-1}][a]	Δ(O–H BDE) [kcal mol^{-1}][b]	k_{inh} by clock [$\times 10^7$ M^{-1} s^{-1}][c]	k_{inh} by O_2 uptake [$\times 10^7$ M^{-1} s^{-1}][d]	k_{inh}/k_{inh} (**2**)[e]
5	77.0 ± 0.5	−1.3/−1.3	1.16 ± 0.04	1.6 ± 0.6	5.0
6	76.3 ± 0.6	−2.0/−1.5	n.d.[f]	8.8 ± 3.2	28
7	75.4 ± 0.7	−2.9/−2.4	n.d.[f]	28.0 ± 18[g]	88
4	78.2 ± 0.3	−0.1/−0.7	0.65 ± 0.08	0.86 ± 0.05	2.1
2 (α-TOH)	78.3 ± 0.3	0.0/0.0	0.38[h]	0.32[i]	1.0

[a] From EPR equilibration studies. [b] Experimental BDE (78.3 kcal mol^{-1}) or calculated BDE (74.8 kcal mol^{-1}) for α-TOH **2** as reference. Values are experimental/calculated ΔBDE. [c] In benzene at 37 °C by methyl linoleate radical clock. [d] In chlorobenzene by inhibited styrene autoxidation at 30 °C for **2**, **5**, **6**, **7**; in benzene at 50 °C for **4**. [e] The k_{inh} values from O_2 uptake were used. [f] See text. [g] The rather large error (= 2σ) is the result of the large scatter in the measurements due to the dramatic inhibition by **7**; initiation rates as low as 1×10^{-10} s^{-1} had to be used to obtain measurable rates of oxygen consumption (as low as 1×10^{-9} M^{-1} s^{-1}) with concentrations of **7** as low as 2×10^{-7} M. [h] Value used to calibrate the radical clock. [i] Value from ref. [2], reconfirmed in ref. [4]. The value of 0.41 ± 0.04 at 50 °C is used for comparison with **4**.

calculated substituent effects for the 3-pyridinol series. The stability of the 3-pyridinols towards air was examined by monitoring their typical fluorescence and UV absorbance (see Supporting Information) in aerated solution (0.3 mM in *tert*-butylbenzene) at 37 °C. The simple 3-pyridinol **5** was stable over a 24 h period while **7** showed significant decomposition (ca. 30%) after 6 h. The stability of compound **6** was intermediate to that of **5** and **7**, in qualitative agreement with the calculated IPs for these compounds (Table 1).

Two different experimental approaches were used to determine absolute k_{inh} values for the 3-pyridinols. First, we utilized a peroxyl radical clock based on the antioxidant-dependent trapping of bisallylic (C11-OOH) and conjugated (C9- and C13-OOH) hydroperoxide products in initiator-induced autoxidations of methyl linoleate.[14] At low concentrations of antioxidant (10–100 mM), there is a linear correlation between concentration of antioxidant and ratio of trapping of C11-OO• vs C9- and C13-OO• with the slope of the line directly related to k_{inh} of the antioxidant.[14] Thus, by measuring the ratio of linoleate hydroperoxide products at various concentrations of an antioxidant it is possible to determine its k_{inh}.



3-Pyridinol **5** proved more effective than **4** or **2** in trapping C11-OO•, and a value of $k_{inh} = 1.16(\pm 0.04) \times 10^7$ M^{-1} s^{-1} was determined by this method (see Supporting Information). The total yield of hydroperoxide products formed from linoleate in the presence of **5** was ca. eight times less than that observed for identical oxidations inhibited by **2** (data not shown). Interestingly, **6** and **7** proved to be such good inhibitors that we were unable to obtain reliable k_{inh} values for these compounds by the radical clock method.[15] Controlled styrene autoxidations inhibited by **5**–**7** were well behaved, however,[2] and allowed us to investigate the peroxyl-radical-trapping activity of these compounds (see Supporting Information). The stoichiometric factor *n* (number of chains broken by one molecule of antioxidant) was determined to be 2 for all three compounds, similar to phenols and 5-pyrimidinols.[4] The inhibition rate constants k_{inh} were determined from the slope of the plot of oxygen consumption in the presence of the inhibitor,[2,4,16] and the values obtained are presented in Table 2 together with previous data for **2** and **4**, which are given for comparison.[4,14]

The 6-amino-3-pyridinols described here are a novel class of phenolic antioxidants that are more effective than any other phenolic class reported to date. The vacant 5-position on the pyridine ring of these compounds allows for fusion of an additional aliphatic ring, a substitution that further lowers the O–H BDE. Indeed, the pyridinols **6** and **7** are, to the best of our knowledge, the fastest peroxyl-radical-trapping chain-breaking antioxidants ever reported (previously 3,7-dimethoxyphenothiazine with $k_{inh} = 5.5 \times 10^7$ M^{-1} s^{-1}).[17,18] The air-stability of **7** is moderate, but its k_{inh} exceeds 10^8 M^{-1} s^{-1}, thus approaching the diffusion-controlled limit for a bimolecular reaction.

Received: May 13, 2003 [Z51881]

Keywords: ab initio calculations · antioxidants · autoxidation · lipids · pyridines

[1] a) G. W. Burton, K. U. Ingold, *J. Am. Chem. Soc.* **1981**, *103*, 6472; b) V. R. Bowry, K. U. Ingold, *Acc. Chem. Res.* **1999**, *32*, 27.
[2] G. W. Burton, T. Doba, E. J. Gabe, L. Hughes, F. Lee, L. Prasad, K. U. Ingold, *J. Am. Chem. Soc.* **1985**, *107*, 7053.
[3] A. Watanabe, N. Noguchi, A. Fujisawa, T. Kodama, K. Tamura, O. Cynshi, E. Niki, *J. Am. Chem. Soc.* **2000**, *122*, 5438.
[4] a) D. A. Pratt, G. A. DiLabio, G. Brigati, G. F. Pedulli, L. Valgimigli, *J. Am. Chem. Soc.* **2001**, *123*, 4625; b) L. Valgimigli, G. Brigati, G. F. Pedulli, G. A. DiLabio, M. Mastragostino, C. Arbizzani, D. A. Pratt, *Chem. Eur. J.* **2003**, *9*, in press.
[5] M. C. Foti, E. R. Johnson, M. R. Vinqvist, J. S. Wright, L. R. C. Barclay, K. U. Ingold, *J. Org. Chem.* **2002**, *67*, 5190.
[6] a) D. P. S. Steinberg, T. E. Carew, J. C. Khoo, J. L. Witztum, *N. Engl. J. Med.* **1989**, *320*, 915; b) P. Holvoet, D. Collen, *FASEB J.* **1994**, *8*, 1279; c) D. Steinberg, *Lancet* **1995**, *346*, 36.
[7] a) D. D. M. Wayner, E. Lusztyk, K. U. Ingold, P. Mulder, *J. Org. Chem.* **1996**, *61*, 6430; b) M. Lucarini, P. Pedrielli, G. F. Pedulli, S. Cabiddu, C. Fattuoni, *J. Org. Chem.* **1996**, *61*, 9263.
[8] G. Brigati, M. Lucarini, V. Mugnaini, G. F. Pedulli, *J. Org. Chem.* **2002**, *67*, 4828.
[9] The calculated (see below) O–H BDEs in **1, 2,** and **3** are 77.0, 74.9, and 73.3 kcal mol^{-1}, respectively.
[10] Although 3-pyridinols have never been studied systematically as antioxidants, many studies have shown chemopreventive effects of 6-methyl-2-ethyl-3-pyridinol (also known as emoxipin, the butanedioate salt as mexidol, and the succinate salt as proxipin). See, for example, G. A. Bazanov, L. D. Smirnov, *Bull. Exp. Biol. Med.* **1995**, *119*, 371–373.

 © 2003 Wiley-VCH Verlag GmbH & Co. KGaA, Weinheim

[11] G. A. DiLabio, D. A. Pratt, A. D. LoFaro, J. S. Wright, *J. Phys. Chem. A* **1999**, *103*, 1653.
[12] G. A. DiLabio, D. A. Pratt, J. S. Wright, *J. Org. Chem.* **2000**, *65*, 2195.
[13] a) C. A. A. van Boeckel, L. P. C. Delbressine, F. M. Kaspersen, *Recl. Trav. Chim. Pays-bas* **1985**, *104*, 259; b) H. van de Poël, G. Guillaumet, M. C. Viaud-Massuard, *Heterocycles* **2002**, *57*, 55.
[14] K. A. Tallman, D. A. Pratt, N. A. Porter, *J. Am. Chem. Soc.* **2001**, *123*, 11827.
[15] The very low oxidation yields led to products almost undetectable by HPLC.
[16] R. Amorati, G. F. Pedulli, L. Valgimigli, O. A. Attanasi, P. Filippone, C. Fiorucci, R. Saladino, *J Chem. Soc. Perkin Trans. 2* **2001**, 2142.
[17] M. Lucarini, P. Pedrielli, G. F. Pedulli, L. Valgimigli, D. Gigmes, P. J. Tordo, *J. Am. Chem. Soc.* **1999**, *121*, 11546.
[18] This compound is quite reactive with air, much more so than **6** or **7**. Quantitatively this is indicated by our calculated IP, which is 7.8 and 5.5 kcal mol^{-1} lower than those of **6** and **7**, respectively.

 © 2003 Wiley-VCH Verlag GmbH & Co. KGaA, Weinheim

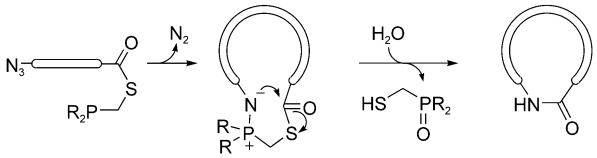
Intramolecular Staudinger Ligation

Intramolecular Staudinger Ligation: A Powerful Ring-Closure Method To Form Medium-Sized Lactams**

*Olivier David, Wim J. N. Meester, Hans Bieräugel, Hans E. Schoemaker, Henk Hiemstra, and Jan H. van Maarseveen**

Medium-sized lactams constitute a very important class of compounds with high potential in drug,[1] materials,[2] and catalysis[3] research. Efficient ring closure to form many medium-sized (7–10-membered) lactams is still a significant synthetic problem.[4] Direct ring closure through the activation of the carboxy group of an ω-amino acid only gives high yields if structural elements that favor the facile approach of the mutually reactive end groups are present within the linear precursor. A class of compounds that are especially resistant to ring closure are dipeptides made up of a linear α- and a linear β-amino acid, which represent potential prescursors to the monocyclic seven-membered [1,4]diazepane-2,5-dione (or homodiketopiperazine) skeleton.[5] The main reason for the failure of these dipeptides to undergo cyclization is the predominant *trans* arrangement of the amide bond, which prevents the required spatial positioning of the terminal amine and activated carboxy groups for cyclization to occur.[6]

Recently, we developed a novel auxiliary-mediated combined tether–template strategy toward medium-sized lactams.[7] It occurred to us that the Staudinger ligation reaction, independently developed by the research groups of Bertozzi[8] and Raines[9], might also serve as a powerful method for the facilitation of difficult lactamization reactions. Herein we show the power of the intramolecular Staudinger ligation method (Scheme 1), which provides access to 7–9-membered lactams including the monocyclic homodiketopiperazine series.



Scheme 1. Intramolecular Staudinger ligation.

Ligation strategies have been developed to overcome the problems encountered in the coupling of large peptide fragments.[10] In the Staudinger ligation a carboxylic acid (or the C terminus of a peptide) is transformed into a phosphanyl thioester, which is then treated with an azide (or the N-terminal azide of a peptide).[11] The ensuing Staudinger reaction[12] produces an intermediate iminophosphorane, which undergoes an intramolecular S→N acyl-transfer reaction via a favored five-membered transition state. The auxiliary residue is removed in the presence of a small amount of water in the reaction mixture, which causes the in situ hydrolysis of the P–N bond of the final amido phosphonium salt. Thus, the intramolecular Staudinger ligation should be a powerful method for effecting difficult lactamizations, as the macrocycle that is initially formed collapses in a series of thermodynamically favored and proximity-driven ring-contraction reactions with expulsion of a total of five atoms of the original ring (Scheme 2).[13]

Direct application of the Bertozzi–Raines method in an intramolecular fashion, that is, thioesterification of a linear ω-azido acid with diphenylphosphanylmethanethiol, was expected to compete with undesired premature Staudinger reactions and thus lead to complex mixtures. We overcame this key problem by protecting the phosphane-containing auxiliary as the borane complex **3** (Scheme 3).

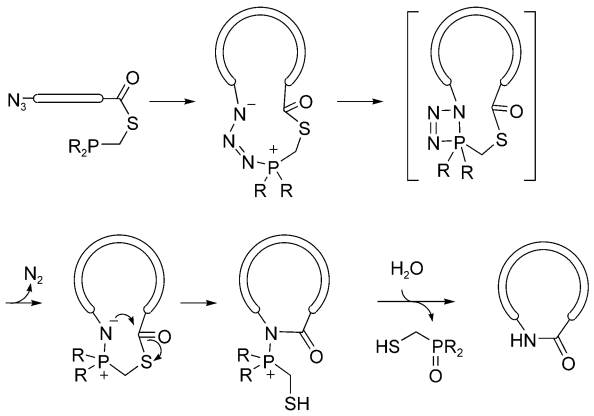
Model reactions revealed that borane-protected phosphanes were totally unreactive towards azides.[14] Thus, we

[*] Dr. J. H. van Maarseveen, Dr. O. David, Dr. W. J. N. Meester,[+] H. Bieräugel, Prof. Dr. H. Hiemstra
Institute of Molecular Chemistry, University of Amsterdam
Nieuwe Achtergracht 129, 1018 WS Amsterdam (The Netherlands)
Fax: (+31) 20-525-5670
E-mail: jvm@science.uva.nl
Prof. Dr. H. E. Schoemaker
DSM Research, Life Science Products
PO Box 18, 6160 MD Geleen (The Netherlands)
[+] Current address:
Department of Pathology, Harvard Medical School
200 Longwood Avenue, Boston, Massachusetts 02115 (USA)

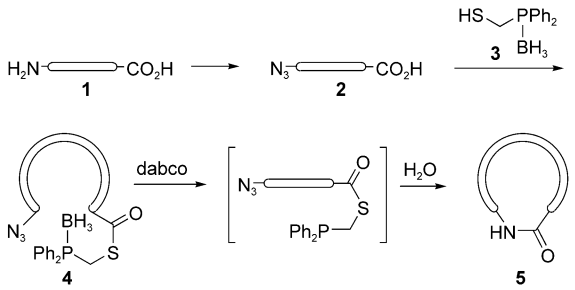
[**] We thank Dr. P. Kamer (Department of Homogeneous Catalysis, University of Amsterdam) for helpful advice and discussions. Dr. A. Van Loevezijn and Ing. C. Salomons (Solvay Pharmaceuticals, Weesp, The Netherlands) are gratefully acknowledged for measuring the LC/ESI-MS spectra. This research has been supported financially by the Council for Chemical Sciences of the Netherlands Organization for Scientific Research (CW-NWO).

Supporting information for this article is available on the WWW under http://www.angewandte.org or from the author.

 DOI: 10.1002/anie.200351930 © 2003 Wiley-VCH Verlag GmbH & Co. KGaA, Weinheim



Scheme 2. Ring-contraction events in the intramolecular Staudinger ligation.

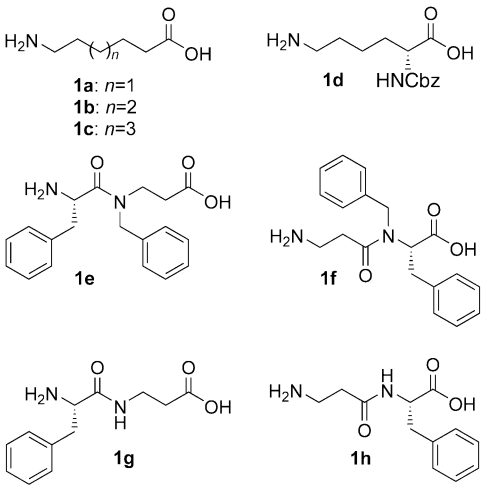


Scheme 3. Reaction sequence of the intramolecular Staudinger ligation.

could start directly from ω-amino acids **1**, which were conveniently transformed into ω-azido acids **2** by a diazo-transfer reaction, as described by Lundquist and Pelletier.[15] Thioesterification of the ω-azido acids **2** with the borane-protected auxiliary **3** provided the stable cyclization precursors **4**. Following liberation of the phosphane in **4** by decomplexation with dabco, the intramolecular Staudinger reaction and in situ hydrolysis of the resulting amidophosphonium salt should occur to give lactams **5**. The representative amino acids **1a–h** (Scheme 4) were chosen as substrates for the intramolecular Staudinger ligation.

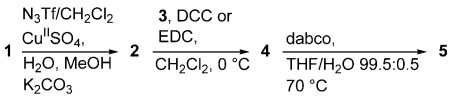
Cyclizations of the amino acids **1a–c** by using traditional carboxylic acid activating reagents are known to occur in low to moderate yields accompanied by cyclic-dimer formation.[16] In previous work the direct lactamization of **1e** and **1f** by 1-(3-dimethylaminopropyl)-3-ethylcarbodiimide hydrochloride (EDC) activation gave homodiketopiperazines **5e** and **5f** in low yields of 30 and 11%, respectively.[7b] The same work showed the dipeptides **1g** and **1h** to be particularly challenging substrates, as all attempts at direct lactamization in the presence of the current state-of-the-art carboxy-group-activating reagents failed.

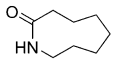
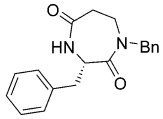
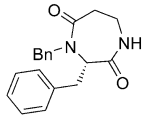
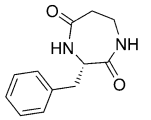
Amines **1a–h** were subjected to the diazo-transfer reaction by treatment with TfN_3 to furnish the corresponding azides **2** in excellent yields (Table 1). The borane-protected auxiliary **3** was synthesized in one step by saponification of the known corresponding thioacetate with sodium hydroxide in methanol.[9c] Subsequent coupling of the auxiliary **3** in the



Scheme 4. Amino acid substrates for the intramolecular Staudinger ligation. Cbz = benzyloxycarbonyl.

Table 1: Yields of the cyclization precursors and the intramolecular Staudinger ligation.



1	Yield [%][a] **2**	**4**	**5** (Yield [%])[a,b]	
a	95	100	**a** (84)	
b	99	96	**b** (59; *95*)	
c	99	98	**c** (80; *95*)	
d	95	97	**d** (80)	
e	91	61	**e** (80)	
f	76	95	**f** (60)	
g	89	88	**g** (35)	
h	85	84	**g** (29)	

[a] Yields of isolated products. The yields in italics were calculated from the ^{1}H NMR spectrum (400 MHz) of the crude reaction mixture. [b] The lactamization reactions were carried out at a concentration of 0.01 M. Tf = trifluoromethanesulfonyl.

presence of *N*,*N*′-dicyclohexylcarbodiimide (DCC) or EDC gave the cyclization precursors **4a–h** in high yields.

Compounds **4a–h** are exceptionally stabile and do not undergo undesired premature Staudinger reactions or oxidation by air. The final intramolecular Staudinger reaction was

 © 2003 Wiley-VCH Verlag GmbH & Co. KGaA, Weinheim

effected after liberation of the phosphane by decomplexation with 1,4-diazabicyclo[2.2.2]octane (dabco; 2–5 equiv) at 70 °C. The unfunctionalized 7–9-membered lactams **5a–c** were isolated in yields of 84, 59, and 80 %, respectively. It was calculated by ^{1}H NMR spectroscopic analysis of the reaction mixtures that the cyclizations to **5b** and **5c** occurred essentially quantitatively. $^{\alpha}$Z-lysine (**1d**) also cyclized efficiently to give **5d** in 80 % yield. The cyclization of precursors **4e** and **4f**, which have a conformationally unbiased tertiary N–CO bond, gave bislactams **5e** and **5f** in yields of 80 and 60 %, respectively. Finally, we turned our attention to the highly challenging target 3-benzyl-[1,4]diazepane-2,5-dione (**5g**). Gratifyingly, both **4g** and **4h** reacted to give **5g** in isolated yields of 35 and 29 %, respectively, as **1g** and **1h** can not be lactamized directly by using traditional methodologies.[7b] The higher yields in the reactions of **4e** and **4g** in comparison to those of **4f** and **4h** suggests that the cyclization is sensitive to steric congestion in the C-terminal fragment. This is a phenomenon that has been observed in peptide cyclizations previously by us and others.[7b,17]

In conclusion, the results described herein show that medium-sized lactams that are inaccessible or can only be prepared with great difficulty by methods that rely on the direct carboxy activation of ω-amino acids can be prepared by using this intramolecular Staudinger ligation method. Work is currently in progress to expand the intramolecular Staudinger ligation approach to the synthesis of small cyclopeptides.

Received: May 20, 2003 [Z51930]

Keywords: cyclization · lactams · medium-ring compounds · ring contraction · synthetic methods

[1] a) J. Taunton, J. L. Collins, S. L. Schreiber, *J. Am. Chem. Soc.* **1996**, *118*, 10412–10422; b) P. J. Murray, M. Kranz, M. Ladlow, S. Taylor, F. Berst, A. B. Holmes, K. N. Keavey, A. Jaxa-Chamiec, P. W. Seale, P. Stead, R. J. Upton, S. L. Croft, W. Clegg, M. R. J. Elsegood, *Bioorg. Med. Chem. Lett.* **2001**, *11*, 773–776.

[2] a) J. Sanchez-Quesada, M. R. Ghadiri, H. Bayley, O. Braha, *J. Am. Chem. Soc.* **2000**, *122*, 11757–11766; b) D. T. Bong, T. D. Clark, J. R. Granja, M. R. Ghadiri, *Angew. Chem.* **2001**, *113*, 1016–1041; *Angew. Chem. Int. Ed.* **2001**, *40*, 988–1011.

[3] E. R. Jarvo, S. J. Miller, *Tetrahedron* **2002**, *58*, 2481–2495.

[4] U. Nubbemeyer, *Top. Curr. Chem.* **2001**, *216*, 125–196.

[5] a) J. N. Lambert, J. P. Mitchell, K. D. Roberts, *J. Chem. Soc. Perkin Trans. 1* **2001**, 471; b) H. Kessler, *Angew. Chem.* **1982**, *94*, 509; *Angew. Chem. Int. Ed. Engl.* **1982**, *21*, 512; c) P. Li, P. P. Roller, J. Xu, *Curr. Org. Chem.* **2002**, *6*, 411–440.

[6] B. Calas, R. Michelot, J. P. Leacer, A. Cave, J. Parello, P. Potier, *Int. J. Pept. Protein Res.* **1987**, 29, 170.

[7] a) H. Bieräugel, T. P. Jansen, H. E. Schoemaker, H. Hiemstra, J. H. Van Maarseveen, *Org. Lett.* **2002**, *4*, 2673–2674; b) H. Bieräugel, H. E. Schoemaker, H. Hiemstra, J. H. Van Maarseveen, *Org. Biomol. Chem.* **2003**, *1*, 1830–1832.

[8] a) E. Saxon, C. R. Bertozzi, *Science* **2000**, *287*, 2007–2010; b) E. Saxon, J. I. Armstrong, C. R. Bertozzi, *Org. Lett.* **2000**, *2*, 2141–2143; c) E. Saxon, S. J. Luchansky, H. C. Hang, C. Yu, S. C. Lee, C. R. Bertozzi, *J. Am. Chem. Soc.* **2002**, *124*, 14893–14902.

[9] a) B. L. Nilsson, L. L. Kiessling, R. T. Raines, *Org. Lett.* **2000**, *2*, 1939; b) B. L. Nilsson, L. L. Kiessling, R. T. Raines, *Org. Lett.* **2001**, *3*, 9–12; c) M. B. Soellner, B. L. Nilsson, R. T. Raines, *J. Org. Chem.* **2002**, *67*, 4993–4996.

[10] a) P. E. Dawson, T. W. Muir, I. Clark-Lewis, S. B. H. Kent, *Science* **1994**, *266*, 776–779; b) J. P. Tam, Y.-A. Lu, C. F. Liu, J. Shao, *Proc. Natl. Acad. Sci. USA* **1995**, *92*, 12485–12489; c) T. M. Hackeng, J. H. Griffin, P. E. Dawson, *Proc. Natl. Acad. Sci. USA* **1999**, *96*, 10068–10073; d) S. Aimoto, *Curr. Org. Chem.* **2001**, *5*, 45–87; for intramolecular approaches to cyclopeptides, see: e) L. Zhang, J. P. Tam, *J. Am. Chem. Soc.* **1997**, *119*, 2363–2370; f) J. A. Camarero, T. W. Muir, *Chem. Commun.* **1997**, 1369–1370.

[11] For peptide-ligation approaches, see: a) B. L. Nilsson, R. J. Hondal, M. B. Soellner, R. T. Raines, *J. Am. Chem. Soc.* **2003**, *125*, 5268–5269; b) R. Merkx, D. T. S. Rijkers, J. Kemmink, R. M. J. Liskamp, *Tetrahedron Lett.* **2003**, *44*, 4515–4518.

[12] H. Staudinger, J. Meyer, *Helv. Chim. Acta* **1919**, *2*, 635–646.

[13] J. E. Leffler, R. D. Temple, *J. Am. Chem. Soc.* **1967**, *89*, 5235–5246.

[14] For an extensive review on applications of borane-protected phosphanes, see: J. M. Brunel, B. Faure, M. Maffei, *Coord. Chem. Rev.* **1998**, *180*, 665–698.

[15] J. T. Lundquist, J. C. Pelletier, *Org. Lett.* **2001**, *3*, 781–783.

[16] For a pioneering study on the ring-closure of similar lactams by using a Staudinger reaction, see: I. Bosch, P. Romea, F. Urpí, J. Vilarrasa, *Tetrahedron Lett.* **1993**, *34*, 4671–4674.

[17] X.-M. Gao, Y.-H. Ye, M. Bernd, B. Kutscher, *J. Pept. Sci.* **2002**, *8*, 418–430.

 © 2003 Wiley-VCH Verlag GmbH & Co. KGaA, Weinheim

Mesoporous Carbon Materials

A Synthetic Route to Ordered Mesoporous Carbon Materials with Graphitic Pore Walls**

*Tae-Wan Kim, In-Soo Park, and Ryong Ryoo**

Recently, it has been discovered that a new class of mesoporous carbons can be synthesized using ordered mesoporous silica as a template.[1–5] The porous carbons are characterized by regular arrangements of uniform mesopores that exhibit Bragg X-ray diffraction (XRD) lines similar to those of the mesoporous silica templates. The various pore structures with tunable diameters (typically in the range of 2–10 nm) are attracting much attention for the development of new adsorbents,[1i] catalysts,[1f] and electrode mate-

[*] Prof. R. Ryoo, T.-W. Kim, I.-S. Park
National Creative Research Initiative Center for Functional Nanomaterials and
Department of Chemistry (School of Molecular Science—BK21)
Korea Advanced Institute of Science and Technology
Daejeon, 305-701 (Republic of Korea)
Fax: (+82) 42-869-8130
E-mail: rryoo@kaist.ac.kr

[**] This work was supported in part by the Creative Research Initiative Program of the Korean Ministry of Science and Technology, and by the School of Molecular Science through the Brain Korea 21 project. The authors also thank Iljin Nanotech for the donation of multi-walled carbon nanotube samples, and LG Chem Research Park for Raman spectroscopy measurements.

 DOI: 10.1002/anie.200352224 © 2003 Wiley-VCH Verlag GmbH & Co. KGaA, Weinheim

rials.[1g–j,4a,5a] Similar to other carbon materials, it is expected that these mesoporous carbons should exhibit widely different physicochemical properties depending on the detailed structure of the frameworks. However, the synthesis of such mesoporous carbons with pore regularity was hitherto limited to carbon frameworks with an amorphous-carbon-like nature.[1a,2a,4a]

Herein, we report a synthetic strategy to fabricate nanoporous carbon materials with graphitic framework structures through in situ conversion of aromatic compounds to mesophase pitch inside the silica templates. The carbon frameworks are composed of discoid graphene sheets, which self-align perpendicularly to the template walls during synthesis. We have confirmed that this synthetic principle can be applied with silica templates that have various pore structures, and can provide materials exhibiting greater mechanical strength under compression and thermal stability in air.

Various aromatic compounds such as acenaphthene, acenaphthylene, indene, indan, and substituted naphthalenes[6] are suitable as carbon sources for the present synthesis. Aluminum is incorporated in silica templates following the post-synthesis procedure.[7] First, the mesoporous template and the carbon source are placed into an autoclave. The aluminum sites on the silica wall act as catalysts to form in situ mesophase pitch in the silica template pores at a low pyrolysis temperature (400 °C). Subsequently, the temperature of the autoclave is increased to 750 °C for carbonization of the mesophase pitch in the template. After the autoclave was cooled down, the product is further heated to 900 °C under vacuum in a fused-quartz reactor for the complete carbonization of the carbon source. The carbon product is then recovered by the removal of the silica template using an aqueous solution of HF or NaOH.

We have confirmed that the synthesis method is applicable to mesoporous silica templates with various structures, such as MCM-48 (cubic *Ia*3*d*), SBA-1 (cubic *Pm*3*n*), and SBA-15 (2-dimensional hexagonal *p*6*mm*) mesoporous silicas. The resultant carbons using these silica templates with acenaphthene are referred to as CMK-1G, CMK-2G, and CMK-3G, respectively. As shown in Figure 1, the CMK-*n*G carbons exhibit XRD peaks below $2\theta = 5°$, which is characteristic of the highly ordered mesostructures, and similar to those for CMK-*n* carbons synthesized with sucrose[1a,c,2a] or furfuryl alcohol.[1b,4a] Furthermore, the CMK-*n*G carbons are characterized by intense peaks at around $2\theta = 26$, 45, 53, and 78°, which correspond to the (002), (101), (004), and (110) diffractions of the graphitic frameworks, repsectively. The diffraction intensities and peak widths are comparable to those of multiwalled carbon nanotubes (MWCNT; Iljin Nanotech, Seoul), and thus much more intense than those of CMK-*n* carbons with amorphous frameworks, or activated carbons. The powder XRD results are consistent with the Raman spectra of different carbon species shown in Figure 2. That is, the CMK-3G and MWCNT samples exhibit a very narrow G-band as compared with the other carbons. The transmission electron microscopy (TEM) images of the CMK-3G mesoporous carbon in Figure 3 show hexagonal arrays of carbon rods, 7 nm in diameter and 3 nm apart, similar to the structure of CMK-3 reported in our previous work.[2] Most interestingly, the TEM images indicate a stacking of the discoid graphene sheets oriented perpendicular to the direction of the rods.

Figure 4 shows XRD patterns of the SBA-15 template containing carbonaceous products after the carbonization of acenaphthene at the given pyrolysis temperatures. The XRD pattern after pyrolysis at 400 °C shows a diffraction peak centered at $2\theta = 26°$, which is very similar to the (002) diffraction of the graphite structure. A mesophase pitch is obtained by removing the SBA-15 template with HF. This result indicates that a liquid-crystalline mesophase with a *d* spacing of 0.36 nm is formed inside the SBA-15 channels during pyrolysis at around 400 °C. The mesophase pitch seems to lead to graphitic frameworks, as the carbonization is completed by further heating at 900 °C. The discoid alignment of the graphitic frameworks, as observed by TEM, is consistent with the general tendency of the edge-on anchoring of polycyclic aromatic hydrocarbons in mesophase pitch on silica surfaces.[8]

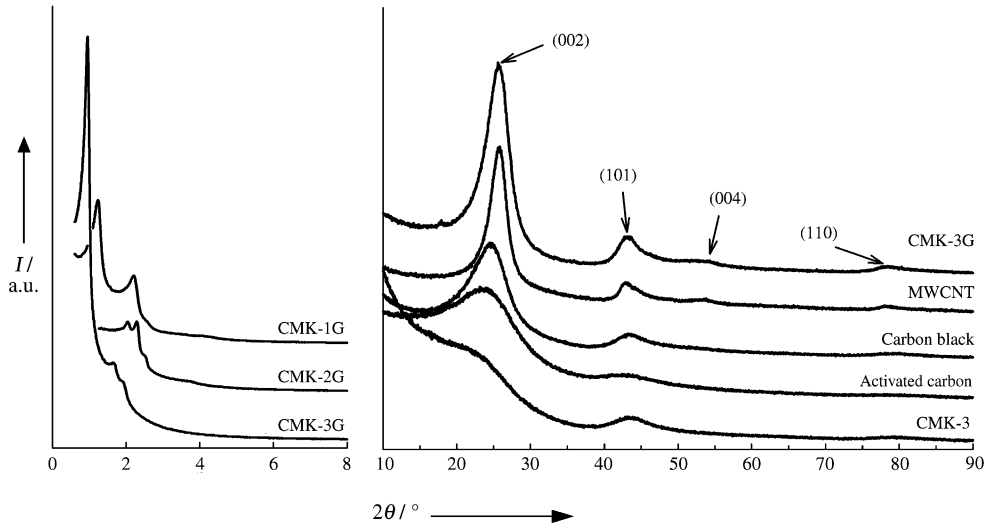


Figure 1. X-ray powder diffraction patterns for CMK-*n*G-type ordered mesoporous carbons in the low-angle region (below $2\theta = 8°$), and other carbon materials in the wide-angle region ($10° < 2\theta < 90°$).

 © 2003 Wiley-VCH Verlag GmbH & Co. KGaA, Weinheim

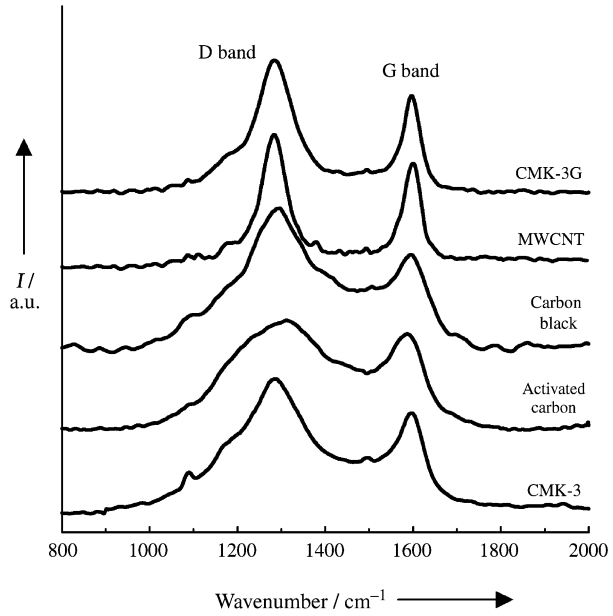


Figure 2. Raman spectra of CMK-3G ordered mesoporous carbon and other carbon materials.

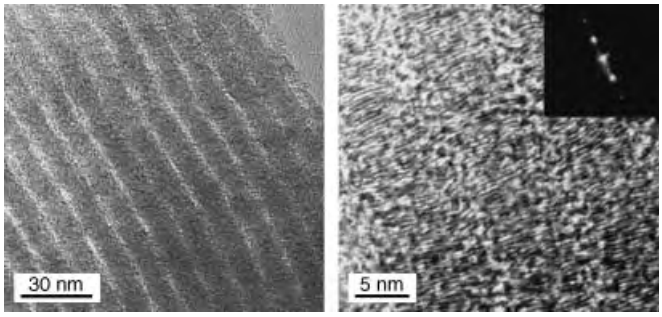


Figure 3. TEM image of CMK-3G (left) and its photomagnification (right) and the corresponding electron diffraction pattern (inset).

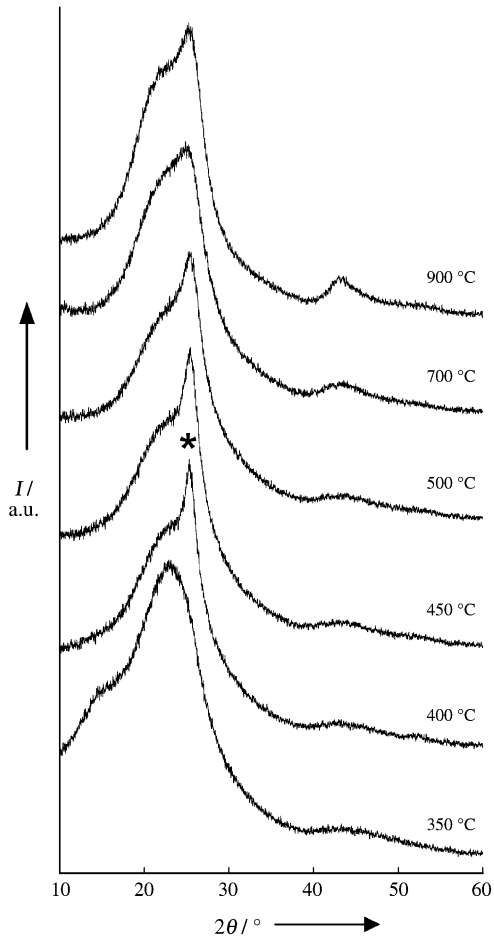


Figure 4. X-ray powder diffraction patterns for the SBA-15 template and acenaphthene composites during pyrolysis. The asterisk highlights the formation of a liquid-crystalline mesophase.

In Figure 5, the mechanical strength of the CMK-3G carbon is compared with those of other CMK-3 carbons prepared using furfuryl alcohol (CMK-3FA) and sucrose (CMK-3SC). The XRD intensity and peak resolution was monitored after subjecting the carbon powders to a pressure of 1.2 GPa for 1 hr in a mechanical press. This mechanical stability test showed almost no change in XRD pattern due to pressurizing in the case of CMK-3G. However, the XRD intensity was reduced very substantially for other CMK-3 carbons with amorphous frameworks (approximately 70% for CMK-3FA and 30% for CMK-3SC). This difference may be attributed mostly to differences in the nature of the carbon frameworks, either graphitic or amorphous.

Thermogravimetric weight changes were recorded in air to evaluate the thermal stability of the graphitic mesoporous carbon CMK-3G (Figure 6). The CMK-3G carbon and a reference MWCNT exhibited almost the same weight-change profiles. In contrast, CMK-3FA and CMK-3SC showed a comparable weight-loss profile at a lower temperature. Significant weight losses corresponding to the oxidation of the carbons occurred in a narrow temperature range between 520 and 680 °C for CMK-3G and MWCNTs, and between 400 and 640 °C for CMK-3FA and CMK-3SC. Thus, the oxidation temperature for CMK-3G is similar to that of nanotubes, and significantly higher than that of mesoporous carbons with furfuryl alcohol and sucrose as carbon sources.[1b,9] These results provide additional confirmation of the graphitized nature of the CMK-3G carbon frameworks, which is responsible for the much improved thermal stability in air.

In conclusion, ordered mesoporous carbons with various structures were synthesized through the in situ conversion of aromatic compounds to a mesophase pitch using mesoporous silicas MCM-48, SBA-1, and SBA-15 as templates. These nanoporous carbons with highly graphitic frameworks exhibit remarkably improved mechanical strength and thermal stability, in comparison with mesoporous carbons with amorphous frameworks. The underlying synthetic principle presented in this report may be important for the design of new mesostructured carbonaceous materials. Particularly, due to the graphitic nature of the frameworks, the resultant nanoporous carbons would attract much attention for the development of new electrochemical applications, such as fuel cells and lithium ion batteries. The edge-on graphitic structure

 © 2003 Wiley-VCH Verlag GmbH & Co. KGaA, Weinheim

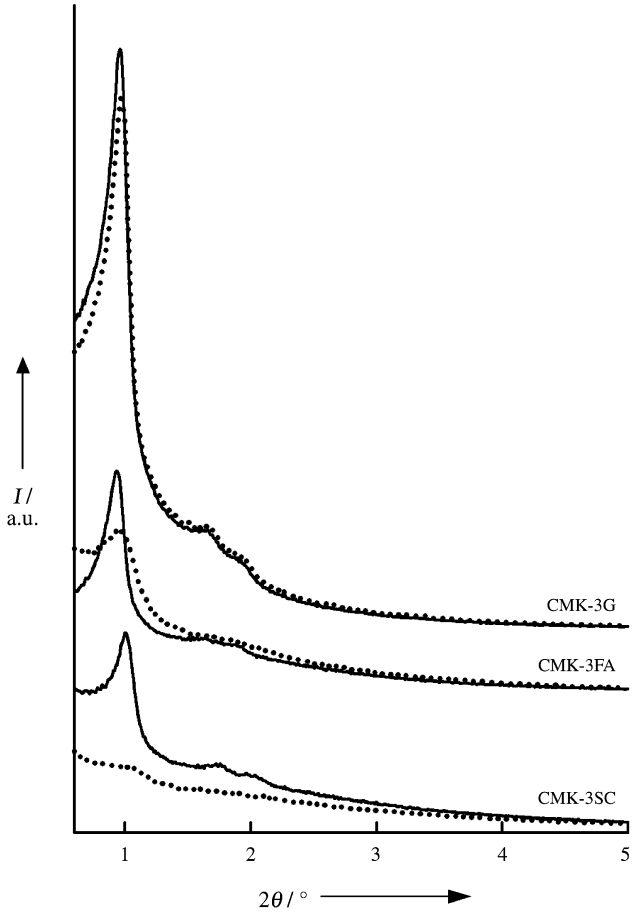


Figure 5. X-ray powder diffraction patterns before (——) and after (•••••) pressurization (100 mg carbon, 10 mm palletized diameter; 1 hr at 1.2 GPa) for CMK-3G with acenaphthene as the carbon source, CMK-3FA with furfuryl alcohol, and CMK-3SC with sucrose.

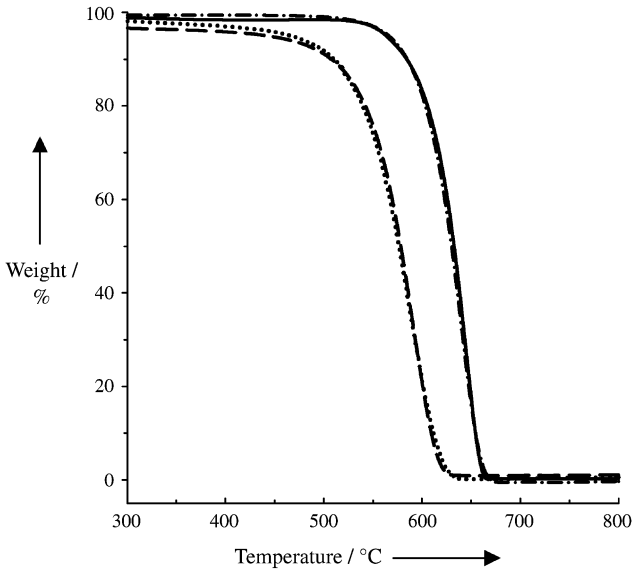


Figure 6. Thermogravimetric curves for the CMK-3G (——), MWCNT (–•–•), CMK-3FA (•••••), and CMK-3SC (– – –) carbon materials in air. The heating rate was 5.0 °C min^{-1}.

exposed to pore surfaces may also give interesting properties as a support for catalytic metal clusters.

Experimental Section

SBA-15 silica was prepared using $EO_{20}PO_{70}EO_{20}$ (Pluronic P123, BASF) and tetraethylorthosilicate (TEOS, Acros) according to the procedure described elsewhere.[2a,10] In a typical synthesis batch, P123 (4.0 g) was dissolved in HCl solution (1.6 M, 150 g) at 35 °C. TEOS (8.50 g) was added to the solution while stirring at 35 °C, which was continued for 15 min at the same temperature. The mixture was placed under static conditions in an oven at 35 °C for 24 h, and then heated to 100 °C for 24 h. The SBA-15 product was filtered without washing and dried in an oven at 100 °C. The product was washed with ethanol and calcined to remove the surfactant. Calcination was performed in air by heating the sample to 400 °C under static conditions. Aluminum was incorporated within the calcined silica to obtain AlSBA-15 with a Si:Al ratio of 20, following the impregnation procedure using an aqueous solution of $AlCl_3$ (98 %, Junsei).[7] The impregnation was carried out in a rotary evaporator at about 60 °C. The aluminated sample was then immediately calcined in air at 550 °C.

Other template samples such as MCM-48 and SBA-1 were synthesized following the synthesis procedures reported in the literature.[11,12] Aluminum was incorporated in the same way as for SBA-15.

In a typical synthesis batch of CMK-3G, AlSBA-15 (3 g) and acenaphthene (99 %, Aldrich; 3.72 g) were combined in an autoclave (7 cm^3 capacity) that can withstand high temperatures and pressures (made of INCONEL alloy 601). After being purged with Ar and closed tightly, the autoclave was heated in a furnace while the temperature was increased to 750 °C at a rate of 2.5 °C min^{-1}, and then maintained for 2 h. The product was collected after the autoclave was cooled to room temperature. (Care must be taken due to high-pressure generation in the autoclave.) Subsequently, the product was heated to 900 °C under vacuum in a fused-quartz reactor. The carbon product was released by the removal of the silica template with a HF solution. The autoclave may be substituted with sealed quartz tubing in cases where small amounts of sample are prepared.

A sample of CMK-3FA was prepared with furfuryl alcohol (FA). Typically, AlSBA-15 (1 g) was infiltrated with FA (0.9 mL; Aldrich) by incipient wetness at room temperature. The FA/AlSBA-15 composite thus prepared was heated overnight in a closed vial at 90 °C to polymerize the FA. Then, the FA/AlSBA-15 composite was heated under vacuum to 350 °C at a rate of 1.8 °C min^{-1} in a fused-quartz reactor. The sample was cooled to room temperature after remaining at 350 °C for 6 h. To this sample, FA (0.63 mL) was subsequently added. The FA polymerization and heating to 350 °C was repeated once again. Carbonization of the carbon source was completed in vacuum by heating to 900 °C at a rate of 1.6 °C min^{-1}. The carbon product was recovered by HF washing. A CMK-3SC sample was synthesized with SBA-15 and sucrose, following the procedure described elsewhere.[2a]

XRD patterns were recorded with a Rigaku MultiFlex diffractometer operating with $Cu_{K\alpha}$ radiation at 2.0 kW. The 2θ step width was 0.01°. Acquisition time was 1.2 s below 10°, and 1.0 s elsewhere. Raman spectra were recorded with a Bruker RFS 100/S spectrometer. A DPY421 diode laser pumped Nd:YAG laser operating at a wavelength of 1050–1060 nm and a power of 100 mW was used as the radiation source. TEM images were obtained with Philips F20 Tecnai transmission electron microscope taken at 490000× magnification at an operating voltage of 160 kV. The TEM images were taken from thin edges of carbon particles mounted on a porous carbon grid. The mechanical stability was tested with a 12 Ton E-Z Press (ICL) with a 10 mm die set. Carbon samples (100 mg) were pressurized to 1.2 GPa and maintained for 1 h. Thermal stability of the carbon materials was investigated by recording weight changes on

 © 2003 Wiley-VCH Verlag GmbH & Co. KGaA, Weinheim

a thermogravimetric analyzer (TA Instruments TGA 2050). Analysis under air was carried out at a heating rate of 5.0 °C min^{-1}.

Received: June 25, 2003 [Z52224]

Keywords: carbon · graphitic framework · mechanical properties · mesoporous materials · template synthesis

[1] a) R. Ryoo, S. H. Joo, S. Jun, *J. Phys. Chem. B* **1999**, *103*, 7743; b) M. Kruk, M. Jaroniec, R. Ryoo, S. H. Joo, *J. Phys. Chem. B* **2000**, *104*, 7960; c) S. H. Joo, S. Jun, R. Ryoo, *Microporous Mesoporous Mater.* **2001**, *44–45*, 153; d) R. Ryoo, S. H. Joo, M. Kruk, M. Jaroniec, *Adv. Mater.* **2001**, *13*, 677; e) R. Ryoo, S. H. Joo, S. Jun, T. Tsubakiyama, O. Terasaki, *Stud. Surf. Sci. Catal.* **2001**, *135*, 150; f) W. S. Ahn, K. I. Min, Y. M. Chung, J.-K. Rhee, S. H. Joo, R. Ryoo, *Stud. Surf. Sci. Catal.* **2001**, *135*, 313; g) J. Lee, S. Yoon, T. Hyeon, S. M. Oh, K. B. Kim, *Chem. Commun.* **1999**, 2177; h) S. B. Yoon, J. Y. Kim, J.-S. Yu, *Chem. Commun.* **2001**, 559; i) T. Ohkubo, J. Miyawaki, K. Kaneko, R. Ryoo, N. A. Seaton, *J. Phys. Chem. B* **2002**, *106*, 6523; j) S. Yoon, J. Lee, T. Hyeon, S. M. Oh, *J. Electrochem. Soc.* **2000**, *147*, 2507.

[2] a) S. Jun, S. H. Joo, R. Ryoo, M. Kruk, M. Jaroniec, Z. Liu, T. Ohsuna, O. Terasaki, *J. Am. Chem. Soc.* **2000**, *122*, 10712; b) H. J. Shin, R. Ryoo, M. Kruk, M. Jaroniec, *Chem. Commun.* **2001**, 34; c) J.-S. Lee, S. H. Joo, R. Ryoo, *J. Am. Chem. Soc.* **2002**, *124*, 1156; d) S. H. Joo, R. Ryoo, M. Kruk, M. Jaroniec, *J. Phys. Chem. B* **2002**, *106*, 4640; e) L. A. Solovyov, A. N. Shmakov, V. I. Zaikovskii, S. H. Joo, R. Ryoo, *Carbon* **2002**, *40*, 2477; f) M. Kruk, M. Jaroniec, S. H. Joo, R. Ryoo, *J. Phys. Chem. B* **2003**, *107*, 2205; g) S.-S. Kim, T. J. Pinnavaia, *Chem. Commun.* **2001**, 2418; h) C. Yu, J. Fan, B. Tian, D. Zhao, G. D. Stucky, *Adv. Mater.* **2002**, *14*, 1742.

[3] M. Kaneda, T. Tsubakiyama, A. Carlsson, Y. Sakamoto, T. Ohsuna, O. Terasaki, S. H. Joo, R. Ryoo, *J. Phys. Chem. B* **2002**, *106*, 1256.

[4] a) S. H. Joo, S. J. Choi, I. Oh, J. Kwak, Z. Liu, O. Terasaki, R. Ryoo, *Nature* **2001**, *412*, 169; b) M. Kruk, M. Jaroniec, T.-W. Kim, R. Ryoo, *Chem. Mater.* **2003**, *15*, 2815; c) H. Darmstadt, C. Roy, S. Kaliaguine, T.-W. Kim, R. Ryoo, *Chem. Mater.*, DOI: 10.1021/cm020673b; d) W.-H. Zhang, C. Liang, H. Sun, Z. Shen, Y. Guan, P. Ying, C. Li, *Adv. Mater.* **2002**, *14*, 1776.

[5] a) J. Lee, S. Yoon, S. M. Oh, C.-H. Shin, T. Hyeon, *Adv. Mater.* **2000**, *12*, 359; b) J. Lee, K. Sohn, T. Hyeon, *J. Am. Chem. Soc.* **2001**, *123*, 5146.

[6] a) *Chemistry and Physics of Carbon, Vol. 7* (Eds.: E. Fitzer, K. Mueller, W. Schaefer, P. L. Walker, Jr.), Marcel Dekker, New York, **1971**; b) *Chemistry and Physics of Carbon, Vol. 15* (Eds.: H. Marsh, P. L. Walker, Jr.), Marcel Dekker, New York, **1979**.

[7] a) R. Ryoo, S. Jun, J. M. Kim, M. J. Kim, *Chem. Commun.* **1997**, 2225; b) S. Jun, R. Ryoo, *J. Catal.* **2000**, *195*, 237.

[8] a) R. Hurt, G. Krammer, G. Crawford, K. Jian, C. Rulison, *Chem. Mater.* **2002**, *14*, 4558; b) K. Jian, H.-S. Shim, A. Schwartzman, G. Crawford, R. Hurt, *Adv. Mater.* **2003**, *15*, 164; c) L. Gherghel, C. Kubel, G. Lieser, H.-J. Rader, K. Mullen, *J. Am. Chem. Soc.* **2002**, *124*, 13130.

[9] a) A. G. Rinzler, J. Liu, H. Dai, P. Nokolaev, C. B. Huffman, F. J. Rodriguez-Marcuas, P. J. Boul, A. H. Lu, D. Heymann, D. T. Colbert, R. S. Lee, J. E. Fisher, A. M. Rao, P. C. Eklund, R. E. Smalley, *Appl. Phys. A* **1998**, *67*, 29; b) A. C. Dillon, T. Gennett, K. M. Jones, J. L. Alleman, P. A. Parilla, M. J. Heben, *Adv. Mater.* **1999**, *11*, 1354.

[10] D. Zhao, Q. Huo, J. Feng, B. F. Chmelka, G. D. Stucky, *J. Am. Chem. Soc.* **1998**, *120*, 6024.

[11] R. Ryoo, S. H. Joo, J. M. Kim, *J. Phys. Chem. B* **1999**, *103*, 7435.

[12] M. J. Kim, R. Ryoo, *Chem. Mater.* **1999**, *11*, 487.

 © 2003 Wiley-VCH Verlag GmbH & Co. KGaA, Weinheim

Synthesis of Carbon Nanotubes

Near-Quantitative Solid-State Synthesis of Carbon Nanotubes from Homogeneous Diphenylethynecobalt and –Nickel Complexes**

Vivekanantan S. Iyer, K. Peter C. Vollhardt, and René Wilhelm*

Carbon nanotubes (CNTs) have generated a tremendous amount of research interest because of their unique structural, electronic, magnetic, and mechanical properties.[1] Among the various synthetic methods employed for their preparation, chemical vapor deposition (CVD) has emerged to be most effective, and efforts are increasing in applying this technique to pre-growth device fabrication by utilizing (in particular lithographically)[2] patterned catalyst arrays and in situ tube assembly.[2,3] Crucial in this endeavor is the site-specific batch production of ordered carbon with control of stoichiometry and ultimately morphology. One possible approach to achieving this would be the efficient thermal conversion of a defined, soluble, molecular organometallic precursor composed of both the carbon source and the metal catalyst, placed locospecifically by wetting and drying. Such a strategy would combine the advantages of the floating organometallic catalyst (for example, ferrocene, $[Fe(CO)_5]$, etc.) CVD methodology[1d,4] with a solid-state conversion of carbon precursors. Reports of the latter reveal some serious shortcomings with respect to yield and/or degree of graphitization, extremity of conditions, need for specialized equipment, the requirement of co-reagents, and simplicity of starting materials.[1d,5] We have described the solid-state thermolysis of a $[Co_2(CO)_6]$-complexed tetrabenzodehydro[20]annulene and some of its substructures to form ordered carbon material, but this method shared some of these drawbacks, in as much as the highest yields were only about 60%. The desired product consisted of an (at best) approximately equal mixture of multiwalled tubes (MWNTs)

[*] Prof. K. P. C. Vollhardt, Dr. V. S. Iyer, Dr. R. Wilhelm
Center for New Directions in Organic Synthesis
Department of Chemistry
University of California at Berkeley and
the Chemical Sciences Division
Lawrence Berkeley National Laboratory
Berkeley, CA 94720-1460 (USA)
Fax: (+1) 510-643-5208
E-mail: kpcv@uclink.berkeley.edu

[**] This work was supported by the Director, Office of Energy Research, Office of Basic Energy Sciences, Chemical Sciences Division, of the U.S. Department of Energy, under Contract DE-AC03-76SF00098 and, in its initial stage, by the NSF (CHE-0071887). R.W. was supported by the Alexander von Humboldt Foundation through a Lynen postdoctoral fellowship. Invaluable assistance in the microscopy work was provided by Mr. E. C. Nelson and Dr. E. A. Stach. We are indebted to Drs. V. F. Puntes and K. Krishnan for help with magnetic measurements and to Professor A. Zettl for encouraging comments. The Center for New Directions in Organic Synthesis is supported by Bristol–Myers Squibb as a Sponsoring Member and Novartis as a Supporting Member.

 DOI: 10.1002/anie.200352201 © 2003 Wiley-VCH Verlag GmbH & Co. KGaA, Weinheim

and carbon onions, and the starting alkyne ligands were somewhat esoteric.[6] We now disclose a qualitative and quantitative breakthrough in the execution of this strategy, which has potential utility in applications to device construction.

Our previous work[6] suggested a pronounced effect of the precursor alkyne–metal structure on the effectiveness of conversion and selectivity. Consequently, a program was instituted to evaluate a range of metal complexes of alkynylbenzenes of initially increasing and then decreasing complexity. Remarkably, while all of the former and most of the latter (such as $[Co_2(CO)_6]$ complexes of ethynylbenzene and diphenylbutadiyne), produced only amorphous, graphitic, and, occasionally, minor quantities of tube- and onionlike carbon in varying proportions, the diphenylethyne complex $[Co_2(CO)_6(PhC_2Ph)]$ (**1**), which is readily prepared in one step from commercial materials,[7] behaved dramatically differently. Thus, heating **1** (30–60 mg) in a quartz tube ($d =$ 1 cm, $l = 15$ cm) sealed under vacuum to 650 °C for 1.5–2 h, or after a wash with conc. HCl, gave samples of metal-encapsulating, pure MWNTs as thin, free-standing films of "nano(bucky)paper",[8] which turned to a black powder on sonication in 2-propanol or grinding (Figure 1a, c, d). A representative TEM micrograph of this material is shown in Figure 1b, which reveals for the first time the typical, dense nanotube pattern that is normally only obtainable using gas-phase techniques. Other forms of ordered and amorphous carbon could not be found. The tubes, on average, exceeded 5 μm in length, with many extending to 20 μm, and exhibited a narrow (inner-outer) diameter distribution of 15–40 nm. The tubes contained 20–50 layers, of which the inner 60–80 % were well graphitized while the outer regions exhibited lesser (turbostratic) ordering (high-resolution transmission electron microscopy (HRTEM); Figure 2a).

Gravimetric analysis of the crude carbon material before the acidic wash established a 64 % mass recovery, and elemental analysis furnished a carbon content of 60.26 %, which is consistent with a product of composition $C_{15}Co_2$ (calcd mass recovery 64% and C content 60.45 %). Acid treatment removed most, but not all, of the metal (60 % mass recovery, elemental analysis: C 89.50 %, calcd for $C_{42}Co$: C 89.54 %). Indeed, most of the tubes contained a crystalline fcc arrangement of cobalt atoms (by energy-dispersive spectroscopy (EDS), X-ray diffraction (XRD), and HRTEM),[9] usually at random positions and occasionally at the tips (Figure 2b),[10] and are ferromagnetic.[9c,11]

The process can be scaled up to 2-g batches using stainless steel Swagelock fittings containing **1** loaded in a glove box. This procedure produced chunks (not films) of lesser quality tubes that were contaminated with carbon onions and graph-

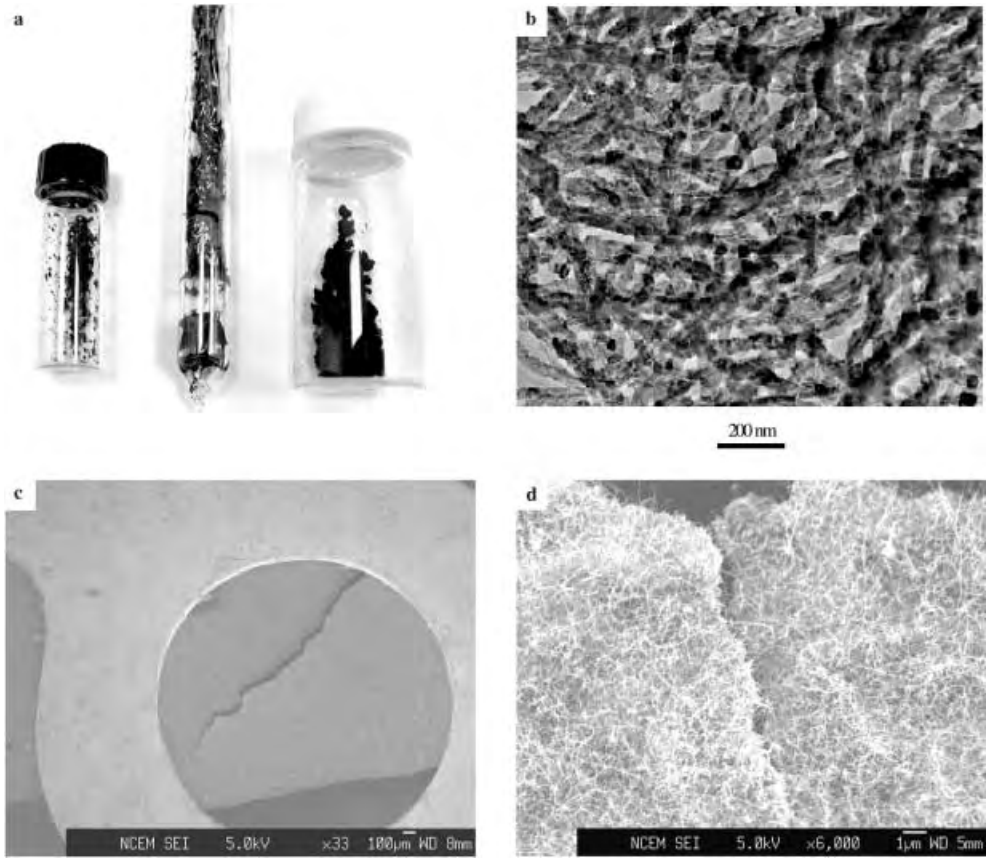


Figure 1. a) A sample of crystalline **1** (left), thermolyzed to a film of carbon tubes (middle), and then treated with conc. HCl and ground to a powder of MWNTs (right). b) TEM micrograph of the as-produced MWNT. Some of the dark spots represent an fcc arrangement of cobalt particles. c) SEM micrograph at lower magnification showing an SEM sample holder with a purposely torn piece of nanopaper. d) The tear in (c) at larger magnification.

 © 2003 Wiley-VCH Verlag GmbH & Co. KGaA, Weinheim

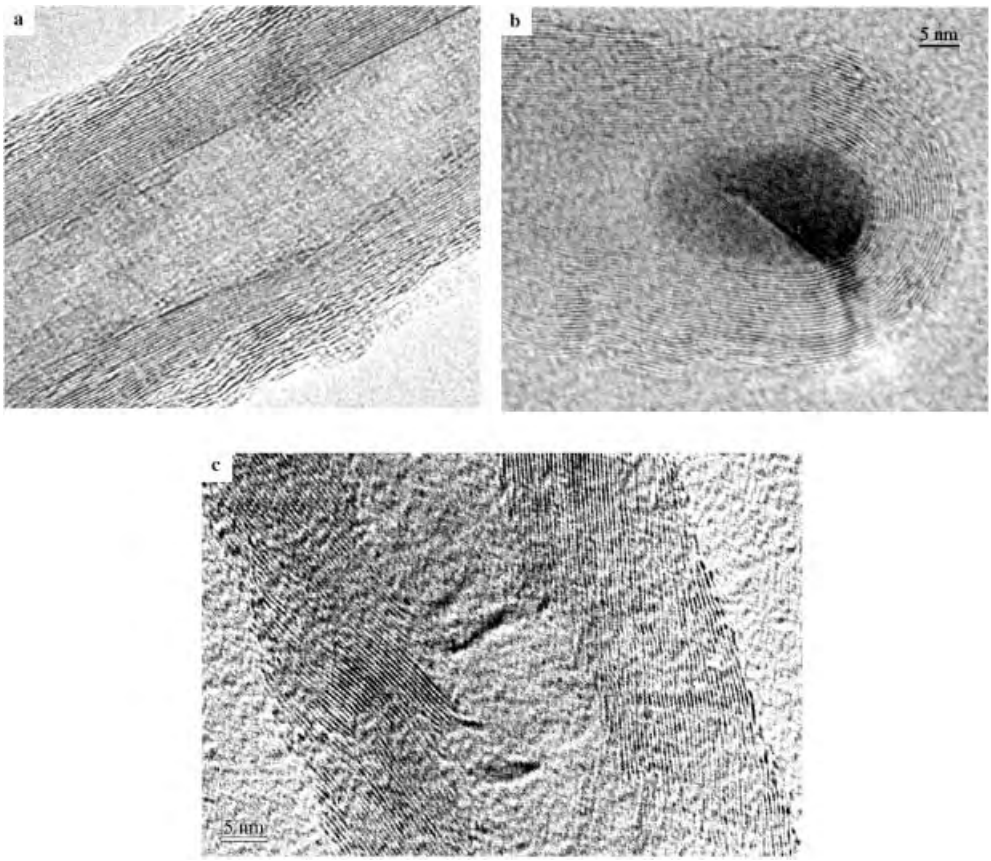


Figure 2. a) Typical segment of a MWNT obtained from the thermolysis of **1**. b) MWNT tip containing an fcc arrangement of cobalt atoms; Co fringes 0.203 nm, graphitic fringes 0.340 nm. c) Typical herringbone NTs from **1** and hexaphenylbenzene (HRTEM: Topcon 002B, 120 keV; SEM: Jeol 6340F; EDS: Phillips CM200 at 120 keV; XRD: Bruker AXS D8).

ite. More successfully, it can be turned moderately "catalytic" in **1**, in as much as up to three equivalents of ligand are tolerated, before a significant deterioration in the yield and quality of the nanotubes is observed. We suspected that the added ligand was cyclotrimerized[12] before further annealing, and **1** could also be admixed with up to one equivalent of hexaphenylbenzene to produce good quality tubes in high yields. However, in all cases, increasing the amount of external carbon sources resulted in the tubes becoming shorter, their diameter more variable, and, their morphology changing to that of a herringbone motif (Figure 2c).[13] Other sources of carbon added to **1**, such as pentaphenylcyclopentadiene, C_{60}, C_{70}, anthracene, and ethynylbenzene, had a detrimental effect. On the other hand, performing the same set of experiments with $[Ni(cod)_2]/PhC_2Ph$ (**2**, 1:1; cod = cycloocta-1,5-diene),[14] a pyrophoric mixture prepared in the pyrolysis tubes at −80 °C, provided essentially identical (positive and negative) results: free-standing films of MWNTs (post acidic wash: elemental analysis: C 89.56 %, calcd for $C_{42}Ni$: C 89.58 %) that were equally well graphitized, but with a larger (outer) diameter distribution of 40–90 nm, and containing a crystalline fcc arrangement of Ni atoms (Figure 3).[15] Again, the ratio of alkyne to metal complex could be increased successfully to 3:1 to provide a carbon yield based on the metal of >1000 %, which compares favorably with CVD results.[16]

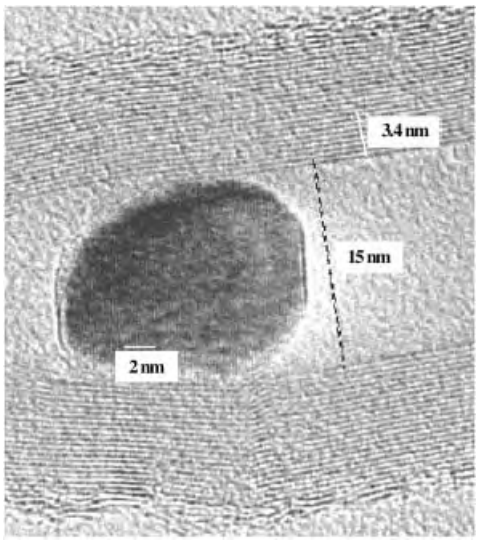


Figure 3. Portion of a typical CNT from **2** with a crystal containing an fcc arrangement of Ni atoms.

Preliminary investigations of the scope of this method are promising. Thus, while the addition of sulfur-containing compounds to **1** (elemental sulfur, thiophene, thianaphthene)[1] resulted in only amorphous carbon and onionlike

 © 2003 Wiley-VCH Verlag GmbH & Co. KGaA, Weinheim

assemblies, the addition of one equivalent of $[Mo(CO)_6]$[17] or $[Mo(CO)(PhC_2Ph)_3]$[18] to **1**, followed by pyrolysis, generated MWNTs of narrower diameter and with fewer walls (3–5). Single-wall nanotube (SWNT) bundles[19] were also formed with some tubes encapsulating fullerenes ("pea pods"),[20] all unfortunately only in low yields (Figure 4). Unlike any of the other systems investigated by us, the MALDI-TOF mass

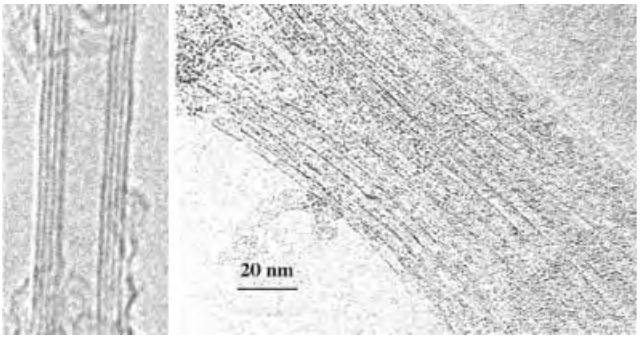


Figure 4. Selected four-walled NT from a mixture of **1** and the Mo complex (1:1; left). Selected SWNT bundles obtained from the same mixture (right). These structures were not quantified and yields are diminished by the presence of amorphous carbon and less graphitized materials.

spectra of the soot revealed C_x peaks up to m/z 3000. Finally, an attempt to obtain SWNTs by using MgO-supported[21] **1**, followed by dissolution of the support (HCl), surprisingly led instead to extensively aligned free-standing MWNT bundles (HRTEM).[22]

In summary, we have presented an efficient, solid-state conversion of commercial homogeneous organometallic systems with a defined metal to carbon ratio into metal-crystallite-encapsulating MWNTs with a high carbon yield based on the metal. While not competitive with large-scale CVD processes, it may complement existing methods and lead to new methods of device construction, such as designed networks and hybrid materials, and may be useful in other applications.[23] Moreover, the molecular nature of the starting materials provides an opportunity for tailoring and mechanistic scrutiny (by, for example, in situ TEM).

Experimental Section

A sample of **1** (46 mg, 0.1 mmol) was sealed under Ar (partial pressure 20 mTorr) in a quartz tube at −80 °C, and then the tube was heated to 650 °C for 2 h to yield a black film of crude soot. The product was gently ground into a fine powder, washed with conc. HCl, and a sample (ca. 0.1 mg) dispersed in 2-propanol and sonicated for 1 min. A drop of this dispersion was placed on a holey carbon TEM grid and analyzed by recording images from 20000 to 690000 magnification (Topcon 002B, 120 keV).

Received: June 23, 2003 [Z52201]
Published online: September 1, 2003

Keywords: alkyne ligands · carbon · cobalt · nanotubes · nickel · solid-state synthesis

[1] For selected recent reviews, see a) H. Dai, *Surf. Sci.* **2002**, *500*, 218; b) R. H. Baughman, A. A. Zakhidov, W. A. de Heer, *Science* **2002**, *297*, 787; c) C. N. R. Rao, B. C. Satishkumar, A. Govindaraj, M. Nath, *ChemPhysChem* **2001**, *2*, 78; d) E. G. Rakov, *Russ. Chem. Rev.* **2000**, *69*, 35.

[2] For recent studies, see a) H. Dai, *Acc. Chem. Res.* **2002**, *35*, 1035; b) S. Huang, X. Cai, J. Liu, *J. Am. Chem. Soc.* **2003**, *125*, 5636; c) B. Q. Wei, R. Vajtai, Y. Jung, J. Ward, R. Zhang, G. Ramanth, P. M. Ajayan, *Chem. Mater.* **2003**, *15*, 1598; d) B. Wang, X. Liu, H. Liu, D. Wu, H. Wang, J. Jiang, X. Wang, P. Hu, Y. Liu, D. Zhu, *J. Mater. Chem.* **2003**, *13*, 1124; e) G. S. Duesberg, A. P. Graham, M. Liebau, R. Seidel, E. Unger, F. Kreupl, W. Hoenlein, *Nano Lett.* **2003**, *2*, 257; f) H. C. Choi, S. Kundaria, D. Wang, A. Javey, Q. Wang, M. Rolandi, H. Dai, *Nano Lett.* **2003**, *2*, 157; g) B. Q. Wei, R. Vajtai, Y. Jung, J. Ward, R. Zhang, G. Ramanth, P. M. Ajayan, *Nature* **2002**, *416*, 495; h) X. Wang, Y. Liu, P. Hu, G. Yu, K. Xiao, D. Zhu, *Adv. Mater.* **2002**, *14*, 1557; i) S. Huang, L. Dai, A. W. H. Mau, *Adv. Mater.* **2002**, *14*, 1140; j) S. Huang, L. Dai, *J. Nanopart. Res.* **2002**, *4*, 145, and references therein.

[3] See also, for example, a) S. Orlanducci, V. Sessa, M. L. Terranova, M. Rossi, D. Manno, *Chem. Phys. Lett.* **2003**, *367*, 109, and references therein; b) Z. Pan, H. Zhu, Z. Zhang, H. Im, S. Dai, D. B. Beach, D. H. Lowndes, *J. Phys. Chem. A* **2003**, *107*, 1338; c) J. Li, Q. Ye, A. Cassell, H. T. Ng, R. Stevens, J. Han, M. Meyyappan, *Appl. Phys. Lett.* **2003**, *82*, 2491; d) R. Vajtai, K. Kordás, B. Q. Wei, J. Békési, S. Leppävuori, T. F. George, P. M. Ajayan, *Mater. Sci. Eng. C* **2002**, *19*, 271.

[4] For reviews, see a) C. N. R. Rao, A. Govindaraj, *Acc. Chem. Res.* **2002**, *35*, 998; b) A. Govindaraj, C. N. R. Rao, *Pure Appl. Chem.* **2002**, *74*, 1571; for very recent studies, see, for example, c) C. Singh, M. S. P. Shaffer, K. K. K. Koziol, I. A. Kinloch, A. H. Windle, *Chem. Phys. Lett.* **2003**, *372*, 860; d) H. Hou, A. K. Schaper, Z. Jun, F. Weller, A. Greiner, *Chem. Mater.* **2003**, *15*, 580; e) L. Ci, H. Zhu, B. Wei, C. Xu, D. Wu, *Appl. Surf. Sci.* **2003**, *205*, 39; f) Z. Zhang, B. Wei, P. M. Ajayan, *Chem. Commun.* **2002**, 962; g) X.-Y. Liu, B.-C. Huang, N. J. Coville, *Carbon* **2002**, *40*, 2791; h) P. C. P. Watts, W. K. Hsu, D. P. Randall, V. Kotzeva, G. Z. Chen, *Chem. Mater.* **2002**, *14*, 4505; i) T. Katayama, H. Araki, K. Yoshino, *J. Appl. Phys.* **2002**, *91*, 6675.

[5] For illustrative references, see a) S. P. Doherty, D. B. Buchholz, B.-J. Li, R. P. H. Chang, *J. Mater. Res.* **2003**, *18*, 941; b) M. Laskoski, W. Steffen, J. G. M. Morton, M. D. Smith, U. H. F. Bunz, *J. Am. Chem. Soc.* **2002**, *124*, 13814; c) H. Liu, Y. Li, L. Jiang, H. Luo, S. Xiao, H. Fang, H. Li, D. Zhu, D. Yu, J. Xu, B. Xiang, *J. Am. Chem. Soc.* **2002**, *124*, 13370; d) Y. Lu, Z. Zhu, W. Wu, Z. Liu, *Chem. Commun.* **2002**, 2740; e) S. P. Doherty, R. P. H. Chang, *Appl. Phys. Lett.* **2002**, *81*, 2466; f) D. Sarangi, C. Godon, A. Granier, R. Moalic, A. Goullet, G. Turban, O. Chauvet, *Appl. Phys. A* **2001**, *73*, 765; g) J. L. O'Loughlin, C.-H. Kiang, C. H. Wallace, T. K. Reynolds, L. Rao, R. B. Kaner, *J. Phys. Chem. B* **2001**, *105*, 1921; h) L. Ji, J. Lin, H. C. Zeng, *Chem. Mater.* **2000**, *12*, 3466.

[6] a) P. I. Dosa, C. Erben, V. S. Iyer, K. P. C. Vollhardt, I. M. Wasser, *J. Am. Chem. Soc.* **1999**, *121*, 10430; see also b) R. Boese, A. J. Matzger, K. P. C. Vollhardt, *J. Am. Chem. Soc.* **1997**, *119*, 2052.

[7] H. Pepermans, R. Willem, C. Hoogzand, *Bull. Soc. Chim. Belg.* **1987**, *96*, 563.

[8] The term "buckypaper" was coined for material derived from SWNTs. For potential uses, see, for example, a) A. Minett, J. Fràysse, G. Gang, G.-T. Kim, S. Roth, *Curr. Appl. Phys.* **2002**, *2*, 61; b) J. Li, A. Cassell, L. Delzeit, J. Han, M. Meyyappan, *J. Phys. Chem. B* **2002**, *106*, 9299; c) A. Guiseppi-Elie, C. Lei, R. H. Baughman, *Nanotechnology* **2002**, *13*, 559; d) J. L. Bahr, J. Yang, D. V. Kosynkin, M. J. Bronikowski, R. E. Smalley, J. M. Tour, *J.*

 © 2003 Wiley-VCH Verlag GmbH & Co. KGaA, Weinheim

Am. Chem. Soc. **2001**, *123*, 6536; e) D. F. Johnson, B. J. Craft, S. M. Jaffe, *J. Nanopart. Res.* **2001**, *3*, 63.

[9] See, for example, a) V. Lavrentiev, H. Abe, S. Yamamoto, H. Naramoto, K. Narumi, *Surf. Interface Anal.* **2003**, *35*, 36; b) J. p. Pinheiro, M. C. Schouler, E. Dooryhee, *Solid State Commun.* **2002**, *123*, 161; c) R. K. Rana, X. N. Xu, Y. Yeshurun, A Gedanken, *J. Phys. Chem. B* **2002**, *106*, 4079.

[10] Assuming a liquid catalytic particle growth mechanism, it appears that under our conditions random migration of the metal occurs after growth termination. For recent, relevant references, see, for example, a) O. A. Louchev, *Phys. Status Solidi A* **2002**, *193*, 585; b) J. Gavillet, A. Loiseau, F. Ducastelle, S. Thair, P. Bernier, O. Stéphan, J. Thibault, J.-C. Charlier, *Carbon* **2002**, *40*, 1649; c) A. Gorbunov, O. Jost, W. Pompe, A. Graff, *Carbon* **2002**, *40*, 113, and references therein.

[11] See, for example, a) J. Harujama, I. Takesue, T. Hasegawa, *Appl. Phys. Lett.* **2002**, *81*, 3031; b) G. H. Lee, S. H. Huh, J. W. Jeong, H.-C. Ri, *J. Magn. Magn. Mater.* **2002**, *246*, 404.

[12] W. Hübel, C. Hoogzand, *Chem. Ber.* **1960**, *93*, 103.

[13] See, for example, M. Ritschel, M. Uhlemann, O. Gutfleisch, A. Leonhardt, A. Graff, C. Täschner, *Appl. Phys. Lett.* **2002**, *80*, 2985, and references therein.

[14] E. L. Muetterties, W. R. Pretzer, M. G. Thomas, B. F. Beier, D. L. Thorn, V. W. Day, A. B. Anderson, *J. Am. Chem. Soc.* **1978**, *100*, 2090.

[15] Ascertained by EDS and XRD as in: a) O. M. Gur'yanova, E. F. Kukovitsky, S. G. L'vov, N. A. Sainov, V. A. Shustov, *Phys. Solid State* **2002**, *44*, 473; b) Y. K. Chen, A. Chu, J. Cook, M. L. H. Green, P. J. F. Harris, R. Heesom, M. Humphries, J. Sloan, S. C. Tsang, J. F. C. Turner, *J. Mater. Chem.* **1997**, *7*, 545.

[16] See, for example, a) A. K. M. Fazle Kibria, Y. H. Mo, K. S. Nahm, M. J. Kim, *Carbon* **2002**, *40*, 1241; b) I. Willems, Z. Kónya, J.-F. Colomer, G. Van Tendeloo, N. Nagaraju, A. Fonseca, J. B. Nagy, *Chem. Phys. Lett.* **2000**, *317*, 71; c) P. Nikolaev, M. J. Bronikowski, R. K. Bradley, F. Rohmund, D. T. Colbert, K. A. Smith, R. E. Smalley, *Chem. Phys. Lett.* **1999**, *313*, 91.

[17] CVD of $[Mo(CO)_6]$ furnishes MWNTs: M. Motiei, J. Calderon-Moreno, A. Gedanken, *Chem. Phys. Lett.* **2002**, *357*, 267.

[18] T. Szymańska-Buzar, T. Głowiak, *J. Organomet. Chem.* **1994**, *467*, 223.

[19] For bimetallic catalysis of SWNT synthesis with Co/Mo, see, for example, W. E. Alvarez, B. Kitiyanan, A. Borgna, D. E. Resasco, *Carbon* **2001**, *39*, 547, and references therein.

[20] For a review, see a) M. Monthioux, *Carbon* **2002**, *40*, 1809; see also b) B. W. Smith, R. M. Russo, S. B. Chikkannanavar, D. E. Luzzi, *J. Appl. Phys.* **2002**, *91*, 9333.

[21] Co/MgO converts CH_4 into single (or double) WNTs, but ethyne to MWNTs: a) P. Hu, X. Wang, Y. Liu, B. Wang, D. Zhu, *Synth. Met.* **2003**, *135–136*, 833; b) E. Flahaut, R. Bacsa, A. Peigney, C. Laurent, *Chem. Commun.* **2003**, 1442; c) Y. Soneda, L. Duclaux, F. Béguin, *Carbon* **2002**, *40*, 955; d) L. Quingwen, Y. Hao, C. Yan, Z. Jin, L. Zhongfan, *J. Mater. Chem.* **2002**, *12*, 1179, and references therein.

[22] For a review, see A. Huczko, *Appl. Phys. A* **2002**, *74*, 617.

[23] The materials produced from **1** show catalytic activity in the Pauson–Khand reaction and Fischer–Tropsch synthesis, those from **2** in the hydrogenation of nitroarenes.

 © 2003 Wiley-VCH Verlag GmbH & Co. KGaA, Weinheim

Contact Ion Pairs and Triples

1,2-Diphenylbenzene Dianion: Alkali-Metal Salts with Drastically Spread C_6 Rings**

Hans Bock, Zdenek Havlas,* Katayoun Gharagozloo-Hubmann, Sven Holl, and Mark Sievert*

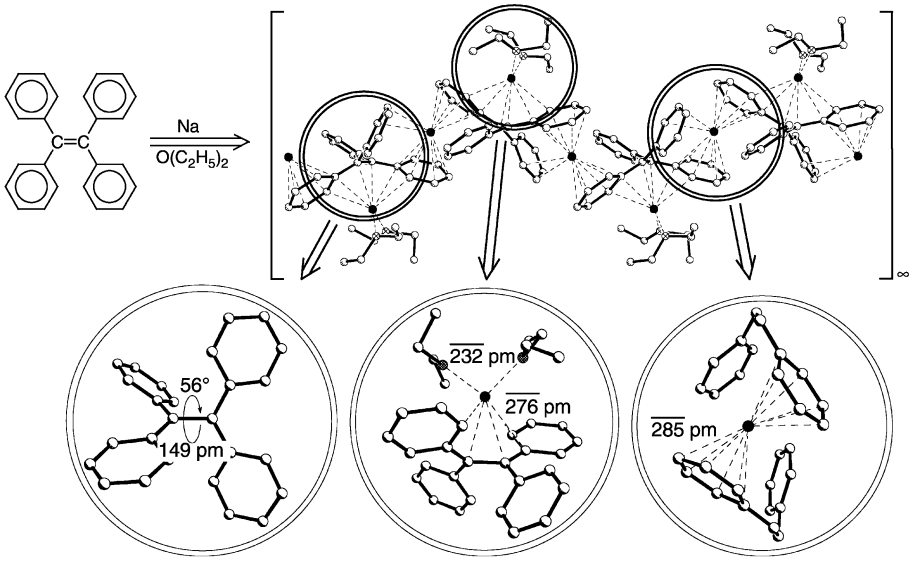
Dedicated to Professor Dieter Fenske on occasion of his 60th birthday

The reduction of π hydrocarbons and subsequent ion-pair formation by suitably solvated alkali-metal ions (M^+_{solv}) as described by Equation (1) provides access to the

$$C_xH_y + n\,e^- \rightarrow [C_xH_y]^{n-}$$
$$[C_xH_y]^{n-} + n\,M^+_{solv} \rightarrow [(M^+_{solv})_n(C_xH_y)^{n-}] \quad (1)$$

magic alkali-metal–organic world of considerably distorted structures.[1–3]

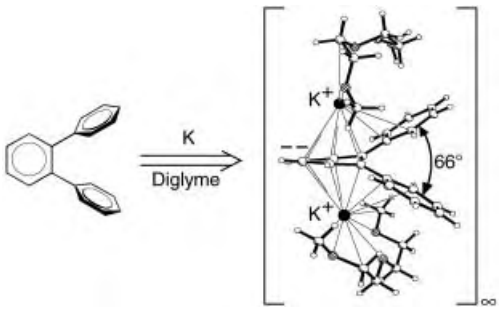
For illustration, the twofold reduction of tetraphenylethylene in aprotic diethyl ether solution ($c_{H^+} < 1$ ppm) at a sodium-metal mirror is selected, a reaction which allows green crystals with a metallic luster of a polymeric disodium bis(diethyl ether) salt of the tetraphenylethylene dianion to be harvested (Scheme 1).[2]



Scheme 1. Top: On reduction of tetraphenylethylene with sodium a polymeric disodium bis(diethyl ether) salt of the tetraphenylethylene dianion crystallizes. Bottom: magnified sections showing the basic structural characteristics.[2] (● = Na, ⊗ = O, ○ = C.)

The crystal structure shows that the central C–C double bond has been elongated to a $^-C–C^-$ single bond and that the two molecular halves $(H_5C_6)_2C$- are twisted by 56°. The twofold ether-solvated Na^+ counterions form intramolecular contact ion pairs ($C_4^{\delta-}\cdots Na^+$) and the individual polymer building blocks are bridged by novel dibenzenesodium sandwich links.[2] In the mean-time, various new results have been added:[3,4] The crystallization of π-hydrocarbon tetraanion salts[1] and of supramolecular contact ion multiples has been accomplished[1,5] and the interaction in the molecular-ion crystal packings has been calculated and correlated.[1,6]

Herein we report the structural confirmation of the charge-dependent spreading of adjacent phenyl substituents in alkali-metal salts of 1,2-diphenylbenzene anions (Scheme 2). Following the two-electron reduction of 1,2-diphenylbenzene with potassium in diglyme, the solvent-bridged polymer contact ion triple $[\{K(diglyme)\}^+_2(1,2\text{-diphenylbenzene})^{2-}]_\infty$ (**1**) crystallized out of the dark red solution.[7,8] The single-crystal structure[8] confirms the stacking of the solvated contact ion triples along the *x*/*y* diagonal



Scheme 2. Synthesis of **1** by the reduction of 1,2-diphenylbenzene with potassium in diglyme. (● = Na, ⊗ = O, ○ = C.)

(Figure 1A); adjacent triples are bridged by vicinal oxygen centers of diglyme ligands, each of the diglyme ligands is bound between two fourfold oxygen coordinated K^+ counterions. Two-electron reduction and the contact-ion-triple formation distort the almost planar central C_6 ring of the neutral 1,2-diphenylbenzene unit[9] into a twist conformation with a mean deviation from the averaged C_6 ring plane of about 8 pm in **1** (Figure 1D). Among the numerous changes in bond lengths and angles on reduction $C_xH_y \rightarrow [C_xH_y]^{2-}$ (Figure 1C), the changes around the *ipso* carbon centers are emphasized: Four C–C bonds in the central C_6 ring elongate by 4 to 11 pm and the exocyclic single bonds $C–C_{Ph}$ are shortened by 7 pm to 142 pm. The phenyl *ipso* angles, as expected,[3] are charge-dependently decreased by about 6° to 114°.

[*] Prof. Dr. H. Bock, Dr. K. Gharagozloo-Hubmann, Dr. S. Holl, Dr. M. Sievert
Chemistry Institute of the University
Marie-Curie-Strasse 11
60439 Frankfurt am Main (Germany)
Fax: (+49) 69-798-29188
Dr. Z. Havlas
Institute of Organic Chemistry and Biochemistry
Czech Academy of Science
Flemingovo Nam 2, 16610 Prague (Czech Republic)

[**] Interactions in crystals part 182. This work was supported financially by Land Hessen, der deutschen Forschungsgemeinschaft, dem Fonds der Chemischen Industrie, and the Adolf Messer Stiftung. Part 181: H. Bock S. Holl, *Z. Naturforsch. B* **2002**, *57*, 843.

 DOI: 10.1002/anie.200250841 © 2003 Wiley-VCH Verlag GmbH & Co. KGaA, Weinheim

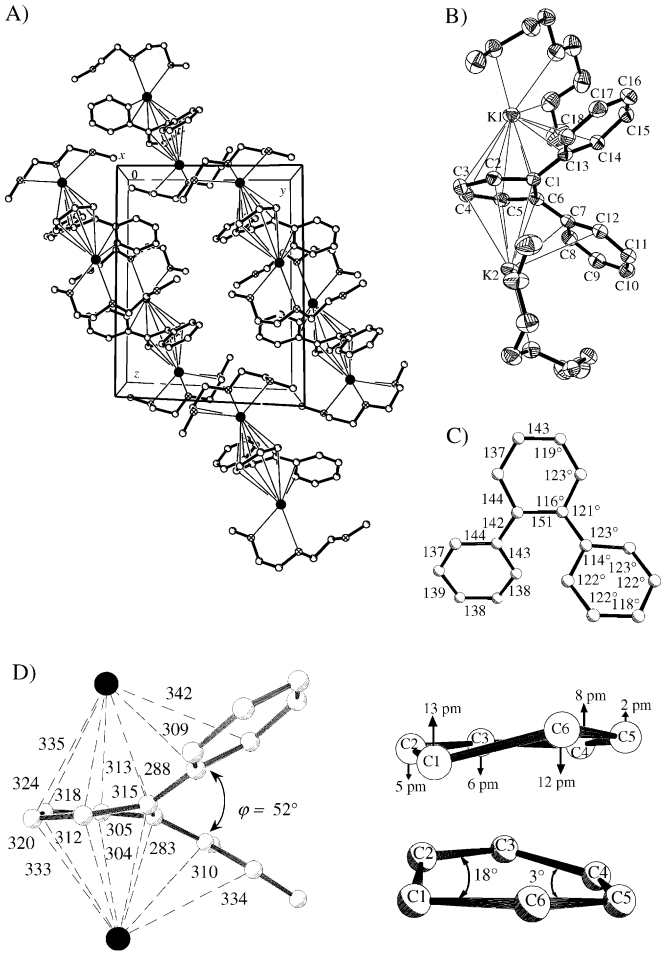


Figure 1. Molecular structure of **1** at 150 K: A) unit cell viewed along the crystallographic *x* axis, B) contact ion triple (thermal ellipsoids set at 50% probability), C) bond lengths [pm] as well as angles [°], and D) side view of the contact ion triple with $K^+\cdots C^-$ separations and deviation from the averaged dianion C_6 plane.

The coordination spheres of the K^+ ions, K1 and K2, differ (Figure 1): K1 is bound to three oxygen centers of its own diglyme ligand and to one oxygen center of the neighboring contact ion triple, K2 in contrast is bound to two diglyme ligands, in each case through two oxygen centers. The shortest contacts to the phenyl substituents (309 or 310 pm) are to the *ipso* carbon centers, which are the centers nearest to the central C_6 ring, and, are therefore major factors in spreading the substituent phenyl rings by an interplanar angle of $\varphi = 52°$ (Figure 1D), which according to an extensive Cambridge structural database (CSD) search[7] is the largest reported to date.

To rationalize the unusual structural observations, density functional (DFT) calculations were performed, starting from the experimental crystal-structural data of the cation triple $[\{K(diglyme)\}^+_2(1,2\text{-diphenylbenzene})^{2-}]$ (Figure 1), followed by geometry optimization and a "Natural Bond Orbital" analysis (DFT/NBO).[10] The DFT-optimized structure reproduces the experimental one satisfactorily, including the interplanar angle. The DFT/NBO charge distribution (Figure 2)

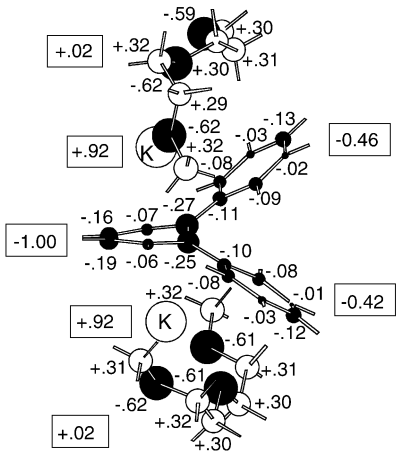
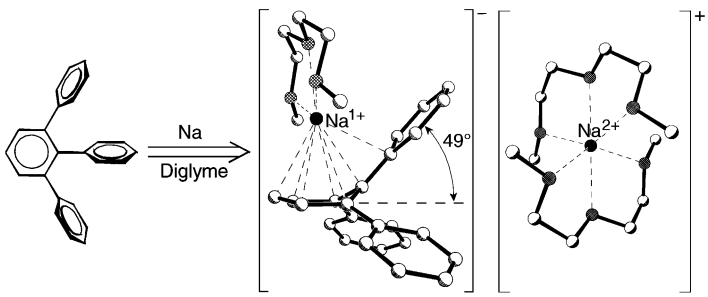


Figure 2. DFT/NBO charge distribution in **1**.

predicts the two dianion charges to be predominantly located on the central benzene ring (−1.00) and the two phenyl substituents (−0.45 and −0.42). The high negative charges at the phenyl-substituted carbon centers C1 and C6 (see Figure 1B) of −0.25 and −0.27 are responsible for the stretching of the C1−C6 bond by 10 pm and also allow the considerable, ring-twist deformations (Figure 1C and D) to be rationalized. For the solvated K^+ ions slightly lowered unit charges (+.92) and for the diglyme ligands very low positive charges (+0.02) are calculated.[10]

The interplanar spreading of the phenyl substituents of a six-membered-ring dianion can be accomplished not only by two cation contacts $K^+\cdots C_6^{2-}\cdots K^+$, one on each side of the ring, but also by a single contact, for example, $Na^+\cdots C_6^{2-}$ as in the solvent-separated 1,2,3-triphenylbenzene dianion (Scheme 3). Structure determination of the black-violet crystals[11] shows a solvent-separated contact ion pair $[\{Na(diglyme)\}^+\{Na(diglyme)_2\}^+(1,2,3\text{-triphenylbenzene})^{2-}]$ (**2**) formed from a contact-ion-pair anion with a diglyme solvated Na^+ counter cation and a twofold diglyme solvated Na^+ counter cation (Scheme 3 and Figure 3).[11]

The two-electron reduction to the 1,2,3-triphenylbenzene dianion in **2** distorts the carbon skeleton considerably (Figure 3): The bonds C1−C2 and C2−C3 are each stretched by 10 pm and the exocyclic bond C2−C13 is shortened by 10 pm to 140 pm (Figure 3C). The three phenyl substituents have *ipso* angles between 113° and 116° which indicates that



Scheme 3. Synthesis of **2** by the reduction of 1,2-diphenylbenzene with sodium in diglyme. (● = Na, ⊗ = O, ○ = C.)

 © 2003 Wiley-VCH Verlag GmbH & Co. KGaA, Weinheim

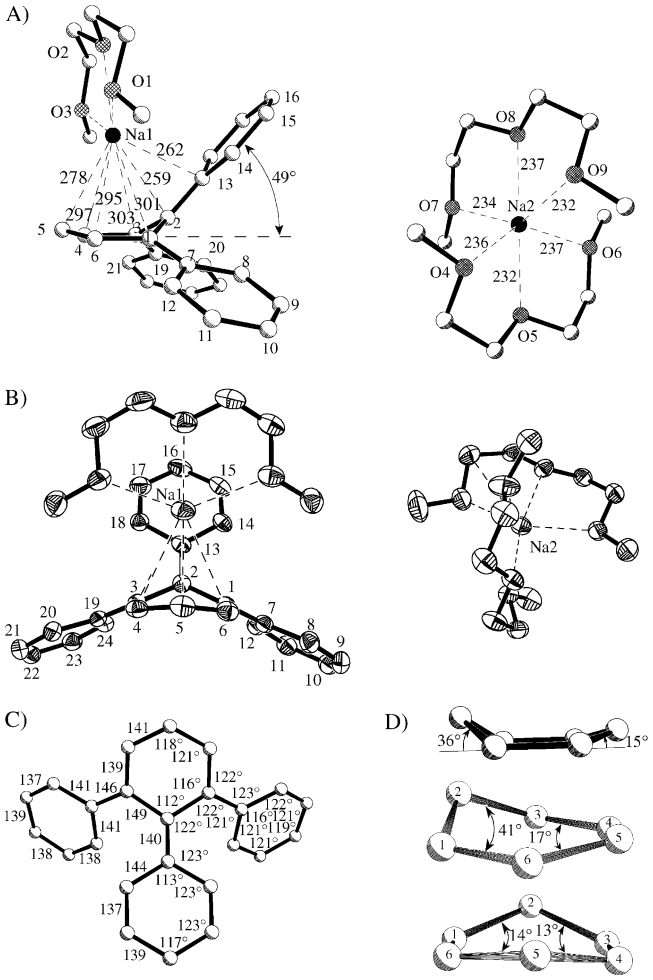


Figure 3. Molecular structure of **2** at 150 K: A) Side view with selected structural parameters, B) top view (thermal ellipsoids set at 50% probability) with center numbering, C) triphenylbenzene dianion bond lengths [pm] and angles [°], and D) benzene dianion ring with interplanar angles of the boat tips to the idealized C_6 plane as well as four of the six torsion angles.

they are each bent towards the central benzene dianion ring which has an *ipso* angle of only 112°. Altogether the two-electron reduction of the planar central C_6 ring of 1,2,3-triphenylbenzene[12] results in its bending into a boat conformation. The two centers at the tips of the boat, C2 and C5, deviate by 36° and 15° from an idealized C_6 plane (Figure 3D), respectively. The resulting phenyl/phenyl interplanar angle is about 49° (Figure 3A).

The counterion Na2 is coordinated by six oxygen centers from two diglyme ligands in a regular octahedral geometry ($Na^+\cdots O$ 232–237 pm). The dianion-coordinated counter ion Na1 interacts in an η^6 fashion with the central C_6 ring and, in addition, with the center C13 of the phenyl substituent in the 2-position (Na1···C1–C6 259–303 pm and Na1···C13 262 pm; Figure 3A). The coordination sphere of the ten coordinate Na1 is completed by a diglyme ligand (Na1···O 230–252 pm).

The two-electron reduction distorts the carbon skeletons of the 1,2-diphenyl- and 1,2,3-triphenylbenzene derivatives analogously despite the coordination of different alkali-metal cations: The perturbation caused by the Na^+ ion in **2** at a $Na^+\cdots C$ separation of only 262 pm (Figure 2), is comparable to that in **1** even though this is caused by two K^+ ions which are further away ($K^+\cdots C^-$ 310 pm; Figure 1). This assumption is supported by DFT calculations[10] starting from the crystal structural data of **2** (Figure 4). In the rather strongly distorted

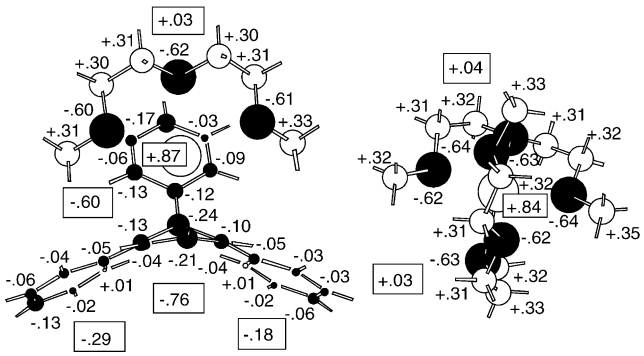


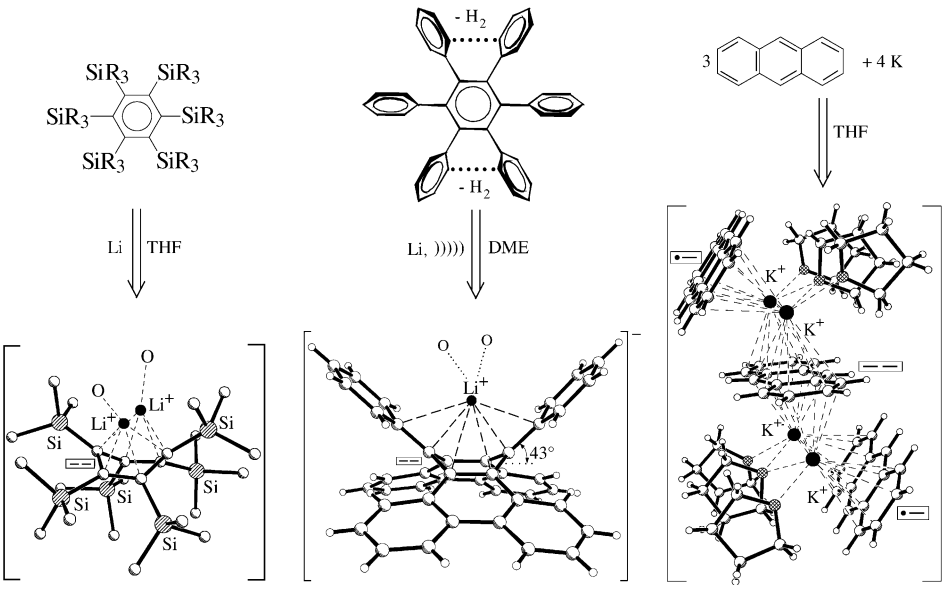
Figure 4. DFT/NBO charge distribution of **2**.

1,2,3-triphenylbenzene dianion, the charge density is distributed unequally over the four C_6 rings. For the central dianion ring a value of −0.76 is calculated, for the phenyl substituent in the 2-position −0.60, and for the phenyl substituents in the 1- and 3-positions only −0.29 or −0.18. The charge distributions within the phenyl substituents show comparable patterns: The *ipso*, *ortho*, and *para* centers carry about two thirds of the total charge for each ring. In the central C_6 ring, the charges of the two centers C2 or C5 outside the idealized plane (Figure 3A) are calculated to have larger than average negative charges of −0.24 or −0.21. These two carbon centers also have the shortest $Na^+\cdots C^-$ contacts of only 259 or 278 pm. For the two different Na^+ ions in **2**, comparable unit charges of +0.87 for Na1 and +0.84 for Na2 result, which are compensated by the negative partial charges of the oxygen centers of the diglyme ligands (ca. −0.6).

Comparison of the charge distributions for benzene-dianion rings of **1** (twist conformation, coordinated by potassium ions on both sides) and **2** (boat conformation, coordinated on one side by sodium ion), reveals eye-catching analogies despite all their differences: the total ring charges of −1.00 (**1**) and −0.76 (**2**) are unexpectedly similar, as are the partial charges at the phenyl-substituted carbon centers of −0.52 (**1**) and −0.47 (**2**). Both cation perturbations are therefore about the same order of magnitude.

The structures of the solvent-shared polymer contact ion triple **1** (Figure 1) and the solvent-separated ion pair **2** (Figure 3) reveal the perturbations caused by alkali-metal cations on electron-rich hydrocarbon polyanions. The clearest indication of these effects is the spreading of the phenyl substituents of the polyanions. This formation of contact-ion multiples is a consequence of strong Coulombic interactions $M^+\cdots C_6^{2-}$ is a general phenomenon,[3,13] covers a multitude of different contact-ion structures,[3–6] demonstrates essential effects of cation size as well as solvation,[14,15] and provides information on reduction pathways[6] or on promising novel materials.[16] Three examples of C_6^{2-} dianions illustrate some

 © 2003 Wiley-VCH Verlag GmbH & Co. KGaA, Weinheim



Scheme 4. Examples of novel six-membered-ring dianions.[6, 15, 16]

of these aspects: Lithium-metal reduction of hexakis(trimethylsilyl)benzene (Scheme 4, left)[15] generates at strongly distorted C_6^{2-} dianion in boat-conformation, which can host two $[Li(thf)]^+$ ions. The ultrasonically activated reduction of hexaphenylbenzene generates, by twofold dehydrogenation and C–C bond formation, a solvent-separated contact ion triple of the 9,10-diphenyltetrabenz[*a.c.h.j.*]anthracene dianion with an extreme boat deformation caused by interaction with the small Li^+ ion (Scheme 4, middle[6]). This compound and the corresponding DFT calculations provide evidence for an unexpected microscopic reduction pathway of synthetic usefulness. After reaction of anthracene in THF with a potassium mirror (scheme 4, right), a black, THF-enclosed contact ion septet crystallizes, with four K^+ ions interspersed between the anthracene layers of an anthracene triple-decker tetraanion that is made up of a central dianion and two outer radical anions. Both DFT calculations and ESR experiments confirm a triplet ground state ($S=1$) which is of interest for the development of new materials.[16]

Received: December 23, 2002
Revised: June 11, 2003 [Z50841]

Keywords: alkaline metals · carbanions · density functional calculations · hydrocarbons · reduction

[1] H. Bock, *Nachr. Chem.* **2001**, *49*, 18–21, and references therein.
[2] H. Bock, K. Ruppert, D. Fenske, *Angew. Chem.* **1989**, *101*, 1717; *Angew. Chem. Int. Ed. Engl.* **1989**, *28*, 1685.
[3] H. Bock, K. Ruppert, C. Näther, Z. Havlas, H.-F. Hermann, C. Arad, I. Göbel, A. John, J. Meuret, S. Nick, A. Rauschenbach, W. Seitz, T. Vaupel, B. Solouki, *Angew. Chem.* **1992**, *104*, 564; *Angew. Chem. Int. Ed. Engl.* **1992**, *31*, 550.
[4] For example, C. Schade, P. von R. Schleyer, *Adv. Organomet. Chem.* **1987**, *27*, 169, and references therein; E. Weiss, *Angew. Chem.* **1993**, *105*, 1565; *Angew. Chem. Int. Ed. Engl.* **1993**, *32*, 1505; D. Smith, *Adv. Organomet. Chem.* **1999**, *47*, 267.
[5] J.-M. Lehn, *Supramolecular Concepts and Perspectives*, VCH, Weinheim, **1995**. Compare with H. Bock, J.-M. Lehn, J. Pauls, S. Holl, V. Krenzel, *Angew. Chem.* **1999**, *111*, 1004; *Angew. Chem. Int. Ed.* **1999**, *38*, 952.
[6] Compare, for example, H. Bock, Z. Havlas, K. Gharagozloo-Hubmann, M. Sievert, *Angew. Chem.* **1999**, *111*, 2379; *Angew. Chem. Int. Ed.* **1999**, *38*, 2240.
[7] K. Gharagozloo-Hubmann, Ph.D. thesis, Universität Frankfurt, **2000** M. Sievert, Ph.D. thesis, Universität Frankfurt, **1997**.
[8] **1**: Potassium (70 mg, 4.4 mmol) are evaporated to a metal mirror. *o*-Terphenyl (140 mg, 0.6 mmol) and water-free diglyme (5 mL) are added. Within 3 days the reduction mixture turns through green and red to violet brown. After layering the solution with water-free *n*-hexane (10 mL), violet-black air and moisture sensitive blocks crystallize within 2 days. Crystal-structure determination $C_{18}H_{14}K_2{\cdot}2C_6H_{14}O_3$ ($M_r=576.84$), $a=1026.6(1)$, $b=1124.5(1)$, $c=13.708(2)$ pm, $\alpha=87.05(1)$, $\beta=83.80(1)$, $\gamma=74.43(1)°$, $V=1515.1(3)\times10^6$ pm^3 ($T=150$ K), $\rho_{calcd}=1.264$ g cm^{-3}, monoclinic, $P\bar{1}$ (No 2), $Z=2$, Siemens-P4-four-circle diffractometer, $Mo_{K\alpha}$-radiation, $\mu=0.352$ mm^{-1}, 6921 measured reflections in range $3°\le2\theta\le50°$, of which 6555 independent ($R_{int}=0.0317$), structure solution with direct methods and Fourier difference technique (SHELXS-97),[17] structure refinement against F^2 (SHELXL-97),[18] 359 parameters, $w=1/[\sigma^2(F_o^2)+(0.0435P)^2+0.5944P]$, R for 5409 $F_o>4\sigma(F_o)=0.0363$, wR_2 all 6921 data $=0.0976$, GOOF $=1.036$, residual electron density 0.294/−0.246 e Å^{-3}. K, O, and C centers anisotropically refined, H centers isotropically refined [$U_{iso(H)}=1.2\,U_{eq(C)}$ (CH/CH$_2$)]; [$U_{iso(H)}=1.5\,U_{eq(C)}$ (CH$_3$)] in the geometrically ideal positions using the riding model.
[9] G. M. Brown II, H. A. Levy, *Acta Crystallogr. Sect. B* **1979**, *35*, 785.
[10] Density Functional Calculations (DFT) have been performed starting from the structural data with normalized bond lengths C–H of 109 pm on the B3LYP6-31G level using the program GAUSSIAN 94 at the NEC SX-4 supercomputer of the Höchstleistungsrechenzentrum University Stuttgart or the Academy of Science Prague.
[11] **2**: From sodium metal (150 mg, 6.5 mmol) a mirror is generated by heating in vacuum and brought into contact with 1,2,3-triphenylbenzene (50 mg; 0.2 mmol) in diglyme (8 mL). Within 2 days the reduction changes the color through blue to red and

 © 2003 Wiley-VCH Verlag GmbH & Co. KGaA, Weinheim

finally brown green. After layering with water-free *n*-hexane (15 mL) violet black violet blocks crystallize within 2 days. Crystal-structure determination $C_{24}H_{18}Na{\cdot}C_6H_{14}O_3{\cdot}Na{\cdot}2\,C_6H_{14}O_3$ ($M_r = 754.88$), $a = 1260.0(2)$, $b = 2246.7(3)$, $c = 1536.7(2)$ pm, $\beta = 100.29(1)°$, $V = 4280.2(10) \times 10^6$ pm^3 ($T = 150$ K), $\rho_{calcd} = 1.171$ g cm^{-3}, monoclinic, $P2_1/n$ (No 14), $Z = 4$, Siemens-P4-four circle diffractometer, $Mo_{K\alpha}$ radiation, $\alpha = 0.098$ mm^{-1}, 9050 measured reflections in range $3° \le 2\theta \le 50°$, 7486 independent ($R_{int} = 0.0257$), structure solution by direct methods and Fourier-difference technique (SHELXS-97),[17] structure refinement against F^2 (SHELXL-97),[18] 479 parameters, $w = 1/[\sigma^2(F_o^2) + (0.0370P)^2 + 2.4660P]$, R for 5540 $F_o > 4\sigma(F_o) = 0.0445$, wR_2 for all 9050 data = 0.1091, GOOF = 1.018, residual electron density 0.219/−0.216 e Å^{-3}. Na, O, the not disordered C atoms were refined anisotropically, disordered C atoms were refined isotropically, hydrogen atoms were refined isotropically $U_{iso(H)} = 1.2\,U_{eq(C)}$ (CH/CH_2)]; [$U_{iso(H)} = 1.5\,U_{eq(C)}$ (CH_3)] in the geometrical ideal positions using the riding model. One methyl group of one of the diglyme molecules is disordered over two positions each of which is 50 % occupied. CCDC-200201 (**1**) and CCDC-200202 (**2**) contains the supplementary crystallographic data for this paper. These data can be obtained free of charge via www.ccdc.cam.ac.uk/conts/retrieving.html (or from the Cambridge Crystallographic Data Centre, 12 Union Road, Cambridge CB2 1EZ, UK; fax: (+44) 1223-336-033; or deposit@ccdc.cam.ac.uk).

[12] A CSD search for the 1,2,3-triphenylbenzene structure provided no hit and our own efforts to grow single crystals either by sublimation or crystallization were not successful. For structural comparison the literature data for 1,2,3,4-tetraphenylbenzene and of hexaphenylbenzene have been used.

[13] See, for example, E. Heilbronner, H. Bock: *Das HMO-Modell und seine Anwendung, Vol. 1*, 2nd ed., Verlag Chemie, Weinheim, **1978**, p. 120; English translation: E. Heilbronner, H. Bock: *The HMO-Model and its Application*, Wiley, London, **1976**, p. 140; Japanese Translation: Hirokawa, Tokyo, **1972**, p. 118; Chinese Translation: Kirin University Press, Kirin, **1986**, p. 104.

[14] H. Bock, C. Näther, Z. Havlas, A. John, C. Arad, *Angew. Chem.* **1994**, *106*, 931; *Angew. Chem. Int. Ed. Engl.* **1994**, *33*, 875.

[15] A. Sekiguchi, K. Ebata, C. Kabuto, H. Sakurai, *J. Am. Chem. Soc.* **1991**, *113*, 1464.

[16] H. Bock, K. Gharagozloo-Hubmann, M. Sievert, Z. Havlas, T. Prisner, *Nature* **2000**, *404*, 267.

[17] G. M. Sheldrick, SHELXS-97, Program for the solution of crystal structures, Universität Göttingen, **1997**.

[18] G. M. Sheldrick, SHELXL-97, Program for the refinement of crystal structures Universität Göttingen, **1997**.

 © 2003 Wiley-VCH Verlag GmbH & Co. KGaA, Weinheim

Mixed In/Ge Oxide

$In_2Ge_6O_{15}(en)_2$: A In–Ge Compound Composed of Germanate Layers Linked by Pillars of $In_2O_6N_4$ Double Octahedra**

*Dragan Pitzschke and Wolfgang Bensch**

During the last few years not only porous compounds based on SiO_4/AlO_4 tetrahedra as the main building units have been explored but also germanates have received considerable attention.[1–10] In contrast to silicon, which is usually in a tetrahedral environment of oxygen atoms, germanium is coordinated by four, five, or even six oxygen atoms.[1–10] Interestingly, until now no efforts have been made to enhance the structural diversity of porous compounds by combining the flexible coordination behavior of germanium with that of indium. For instance, InO_4 tetrahedra are found in $InNa_5O_4$ or in InOF;[11] in $Ba_2In_2O_5$ InO_4 tetrahedra and InO_6 octahedra coexist,[12] and in $Ba_3In_2O_6$ distorted InO_5 trigonal bipyramids are observed.[13] Finally, very unusual InO_x polyhedra are found in $In_3Mo_{11}O_{17}$.[14] The syntheses of microporous solids are typically carried out under solvothermal conditions in the presence of an organic molecule that should exert a structure-directing effect, the aim usually being to prepare an open-framework inorganic material. Herein we report the synthesis and characterization of a new and unusual indium–germanium compound in which germanate layers are linked by $In_2O_6N_4$ moieties to form a three-dimensional network with composition $In_2Ge_6O_{15}(en)_2$ (**1**; en = ethylenediamine). The solvothermal reaction of ethylenediamine, germanium dioxide, and indium hydroxide yields transparent needle-shaped crystals of **1** in high yield. The X-ray structure determination demonstrates the 3D character of **1**.[15]

The asymmetric unit contains six crystallographically independent germanium atoms, fifteen oxygen atoms and two independent indium atoms as well as two en molecules acting as bidentate ligands. The Ge atoms are all coordinated by four O atoms to form moderately distorted tetrahedra with Ge–O bond lengths ranging from 1.691(5) to 1.770(4) Å and O-Ge-O angles between 99.2(2) and 117.1(2)°. The Ge-O-Ge angles vary between 123.1(2) and 134.3(2)° and are in the expected range. The Ge–O separations are in the same range as those reported for GeO_2 in the quartz modification (1.741 Å) and in other germanates.[1–3,9,16] The In1 and In2 atoms are coordinated by four oxygen atoms and two nitrogen atoms of the en ligand yielding a strongly distorted octahedral environment. The In–O separations range from 2.076(5) to 2.257(4) Å and the In–N bond lengths lie between 2.261(7)

[*] Prof. Dr. W. Bensch, D. Pitzschke
Institut für Anorganische Chemie
Universität Kiel
Olshausenstrasse 40, 24098 Kiel (Germany)
Fax: (+49) 431-880-1520
E-mail: wbensch@ac.uni-kiel.de

[**] This work was supported by the State of Schleswig-Holstein and the Fonds der Chemischen Industrie. en = ethylenediamine.

 DOI: 10.1002/anie.200351115 © 2003 Wiley-VCH Verlag GmbH & Co. KGaA, Weinheim

and 2.285(5) Å. The oxygen atoms connect with either two or three metal (one Ge and two In) atoms. The In–O bond lengths of the three-coordinate O atoms are longer (2.180(4)–2.257(4) Å) than for two-coordinate O atoms (2.0762(5)–2.0843(4) Å).

The six GeO_4 tetrahedra are corner linked to form two different single chains (denoted I and II in Figure 1). Chain I is composed of the tetrahedra around Ge1–3 and chain II by the tetrahedra about Ge4–6. Owing to the $\bar{1}$ symmetry

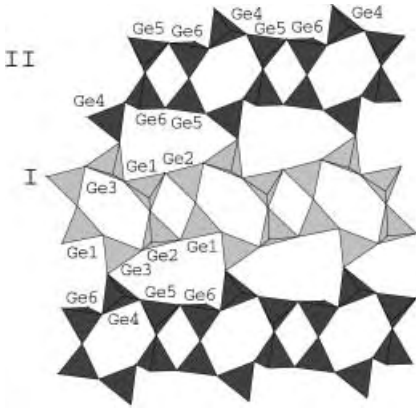


Figure 1. The six GeO_4 tetrahedra are corner linked, forming two different single chains denoted in the (011) plane. Chain I (light gray) and chain II (dark gray).

operation pairs of like chains are joined to form double chains (Figure 1). Finally, these double chains are linked by oxygen atoms to form anionic germanate layers in the (011) plane. The connection pattern yields an unbranched dreier[*] single layer which according to the Liebau notation can be described as {***uB***, 3, 1^2_∞}.[17] The layer contains four-, six-, and eight-membered rings with approximate dimensions of 4.8×3.0, 6.2×5.0, and 8×4.5 Å, respectively. The germanate layers are stacked perpendicular to [010]. Unbranched dreier single layers are reported for several silicate minerals, such as Dalyite and Nekoite,[17] but to our knowledge have never been observed in germanates. Recently, the interconnection of dreier single chains into a single layer was reported for the synthetic gallate $Sr_3Ga_4O_9$,[18] but in contrast to **1** an open-branched dreier single layer is formed.

Two symmetry-related InO_4N_2 octahedra share a common edge to form $In_2O_6N_4$ entities (Figure 2). The average distance between the indium atoms within these units is about 3.5 Å. The six oxygen atoms of each $In_2O_6N_4$ moiety are joined to GeO_4 tetrahedra of the germanate layers above and below, through O1, O2, and O3 (Figure 2). Hence, the structure may be described as anionic germanate layers which are pillared by $In_2O_6N_4$ units yielding a 3D network. The framework density of **1** is 15.6 polyhedra per 1000 Å^3.

Three distinct channels with different apertures run along [01$\bar{1}$], [100], and [010] (Figure 3). The first is composed of eight GeO_4 polyhedra and two InO_4N_2 octahedra and has an

[*] The term "dreier" was coined by Liebau[17] and is derived from the German word drei, which means three.

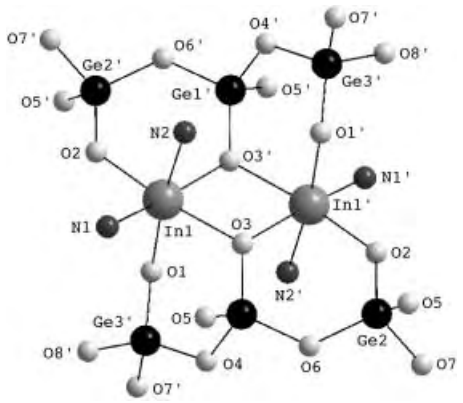


Figure 2. Two InO_4(en) octahedra sharing a common edge (atoms with primes are generated by symmetry operations, the H and C atoms of the amine are omitted for clarity).

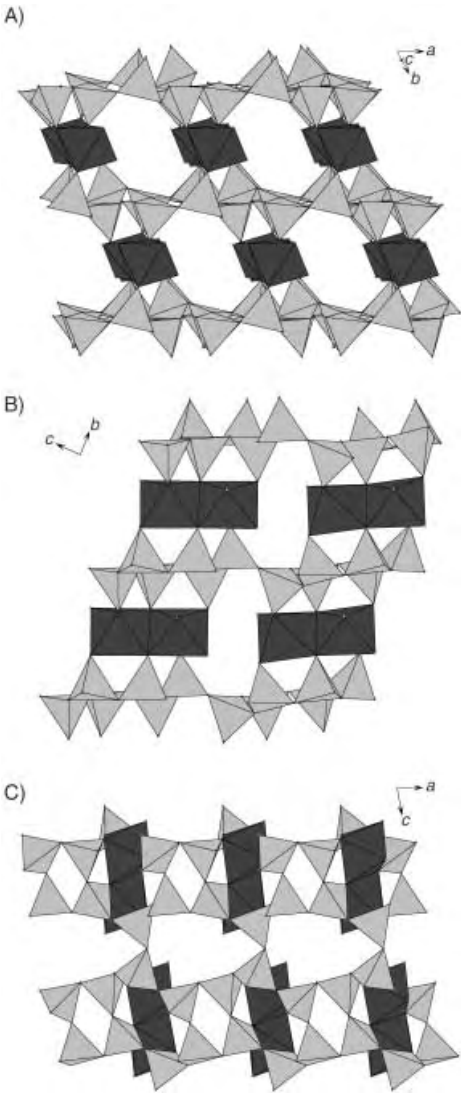


Figure 3. The different channels in **1** (InO_4(en) octahedra are light-gray and GeO_4-tetrahedra are dark-gray; the H and C atoms of the amine are omitted for clarity). A) View along [01$\bar{1}$], B) view down the *a* axis, C) view down the *b* axis.

 © 2003 Wiley-VCH Verlag GmbH & Co. KGaA, Weinheim

opening of about 7.5 × 7.3 Å (Figure 3A). The second channel with approximate dimensions of 8.4 × 3 Å is formed by six GeO_4 tetrahedra and two InO_4N_2 octahedra (Figure 3B). The last channel is formed by the eight-membered rings of successive stacked germanate layers and the aperture is 8 × 4.5 Å (Figure 3c). The en units point partially into the channels thus reducing the free space.

The thermal stability of **1** was investigated using simultaneous differential thermoanalysis (DTA) and thermogravimetry (TG) as well as simultaneous DTA–TG–MS measurements. The compound decomposes in three steps with a total weight loss of 25.4%. The first two steps cover a wide temperature range from about 450 to 720°C and is accompanied by a weight loss of 11.7%. The third step with a weight loss of 13.7% starts at 720°C and is finished at 850°C. The decomposition reactions are accompanied by two endothermic events at $T_P = 510$°C and 777°C. In the gray residue left after the DTA–TG experiment, elemental Ge and $In_2Ge_2O_7$ could be identified in the X-ray powder pattern. The elemental analysis yields less than 0.2% C, H, N content. The experimental weight loss of 25.4% is in good agreement with that calculated for the removal of the two en molecules ($\Delta M_{calcd} = 11.8\%$) and eight oxygen atoms ($\Delta M_{calcd} = 12.5\%$). The mass spectra show that during the first two thermal-decomposition steps NH_3 (m/z 17), H_2O (m/z 18), and CO_2 (m/z 44) are emitted. During the last step the remaining nitrogen and carbon are emitted as N_2 (m/z 28, small amounts of CO are also present) and CO_2 (m/z 44).

In further experiments the heating process was stopped at 560°C and 720°C. According to the X-ray powder pattern of the sample obtained at 560°C the intermediate is amorphous, that is, the framework is destroyed. In the brown residue after the 720°C step appreciable amounts of organic components were found (C 3.395, H 0.074, N 3.348%; ΣCHN = 6.817%). After the amorphization a recrystallization occurs and at 720°C elemental Ge and $In_2Ge_2O_7$ could be identified by powder diffraction pattern. Clearly, the decomposition reactions are complex involving redox reactions between the different constituents of **1**.

Experimental Section

Compound **1** was synthesized under hydrothermal conditions using GeO_2 (314 mg, 3 mmol) and $In(OH)_3$ (332 mg, 2 mmol) in a 33% aqueous solution of ethylenediamine (44 mmol) at pH > 13. The mixture was heated to 170°C for 7 days in a teflon-lined steel autoclave (ca. 30 mL) then cooled within 3 h to room temperature. The homogeneous product consisting of colorless needle-shaped crystals was collected by filtration, washed with distilled water, and dried in air. Typical dimensions of the crystals are 0.3 × 0.03 × 0.03 mm^3.

Crystallographic data for **1**: triclinic, space group $P\bar{1}$, a = 7.9568(16), b = 8.3835(17), c = 17.651(4) Å, α = 81.30(3)°, β = 77.08(3)°, γ = 63.79(3)°, V = 1027.7(4) $Å^3$; Z = 2; ρ_{calcd} = 3.314 $g\,cm^{-3}$, $F(000)$ = 956, $\lambda(Mo_{K\alpha})$ = 0.71073 Å. Single-crystal X-ray work was performed using a Image Plate Diffraction System (IPDS). 10008 reflections collected, 4593 independent (R_{int} = 0.036). Face-indexed absorption correction; structure solution with SHELXS-97;[15] structure refinement against F^2 using SHELXL-97.[15] 281 parameters, R for 4031 reflections ($F_o > 4\sigma(F_o)$) = 0.0425, $wR2$ for all data = 0.1168, GoF = 1.054. Residual electron density: 1.7/−2.2 e $Å^{-3}$. CCDC-202258 (**1**) contains the supplementary crystallographic data for this paper. These data can be obtained free of charge via www.ccdc.cam.ac.uk/conts/retrieving.html (or from the Cambridge Crystallographic Data Centre, 12 Union Road, Cambridge CB2 1EZ, UK; fax: (+44) 1223-336-033; or deposit@ccdc.cam.ac.uk).

DTA–TG–MS measurements were performed with an STA-409CD thermobalance with Skimmer coupling (Netzsch), equipped with a quadrupole mass spectrometer QMA 400 (Balzers). The measurements were made simultaneously in Al_2O_3 crucibles under a dynamic helium or nitrogen atmosphere (flow-rate: 75 mL min^{-1}, purity: 5.0) using different heating rates. X-Ray powder diffraction experiments were performed using a STOE STADIP transmission powder diffractometer with a position sensitive detector and $Cu_{K\alpha}$ radiation (λ = 1.540598 Å).

Received: February 5, 2003 [Z51115]

Keywords: crystal structure · germanium · hydrothermal synthesis · indium · thermochemistry

[1] a) R. H. Jones, J. Chen, J. M. Thomas, A. George, M. B. Hursthouse, R. Xu, S. Li, Y. Lu, G. Yang, *Chem. Mater.* **1992**, *4*, 808; b) K. Sun, M. S. Dadachov, T. Conradsson, X. Zou, *Acta Crystallogr. Sect. C* **2000**, *56*, 1092.
[2] a) C. Cascales, E. Gutiérrez-Puebla, M. A. Monge, C. Ruiz-Valero, *Angew. Chem.* **1998**, *110*, 135; *Angew. Chem. Int. Ed.* **1998**, *37*, 129; b) C. Cascales, E. Gutiérrez-Puebla, M. A. Monge, M. Iglesias, C. Ruiz-Valero, *Angew. Chem.* **1999**, *111*, 2592; *Angew. Chem. Int. Ed.* **1999**, *38*, 2436.
[3] H. Li, M. Eddaoudi, O. M. Yaghi, *Angew. Chem.* **1999**, *111*, 682; *Angew. Chem. Int. Ed.* **1999**, *38*, 653.
[4] a) H. Li, O. M. Yaghi, *J. Am. Chem. Soc.* **1998**, *120*, 10569; b) X. Bu, P. Feng, G. D. Stucky, *J. Am. Chem. Soc.* **1998**, *120*, 11204.
[5] Y. Zhou, H. Zhu, Z. Chen, M. Chen, Y. Xu, H. Zhang, D. Zhao, *Angew. Chem.* **2001**, *113*, 2224; *Angew. Chem. Int. Ed.* **2001**, *40*, 2166.
[6] C. Cascales, E. Gutiérrez-Puebla, M. Iglesias, M. A. Monge, M. Iglesias, C. Ruiz-Valero, N. Snejko, *Chem. Commun.* **2000**, 2145.
[7] X. Bu, P. Feng, G. D. Stucky, *Chem. Mater.* **2000**, *12*, 1505.
[8] L. Beitone, T. Loiseau, G. Ferey, *Inorg. Chem.* **2002**, *41*, 3962.
[9] A. Tripathi, V. G. Young, G. M. Johnson, C. L. Cahill, J. B. Parise, *Acta Crystallogr. Sect. C* **1999**, *55*, 496.
[10] J. Plévert, T. M. Gentz, A. Laine, H. Li, V. G. Young, O. M. Yaghi, M. J. O'Keeffe, *J. Am. Chem. Soc.* **2001**, *123*, 12706.
[11] a) H. Glaum, R. Hoppe, *Z. anorg. Allg. Chem.* **1990**, 583, 24; b) M. Vlasse, J. C. Massies, B. L. Chamberland, *Acta Crystallogr. Sect. B* **1973**, 627.
[12] D. H. Gregory, M. T. Weller, *J. Solid State Chem.* **1993**, *107*, 134.
[13] E. V. Antipov, L. N. Lykova, L. M. Kovba, *Koord. Khim.* **1990**, *16*, 770.
[14] R. Dronskowski, H. Mattausch, A. Simon, *Z. Anorg. Allg. Chem.* **1993**, *619*, 1397.
[15] a) G. M. Sheldrick, SHELXS-97, program for crystal structure determination, University of Göttingen, Germany, **1997**; b) G. M. Sheldrick, SHELXL-97, program for the refinement of crystal structures, University of Göttingen, Germany, **1997**.
[16] G. S. Smith, P. B. Isaacs, *Acta Crystallogr.* **1964**, *17*, 842.
[17] F. Liebau, *Structural Chemistry of Silicates*, Springer, Berlin, **1985**.
[18] V. Kahlenberg, J. B. Parise, *Z. Kristallogr.* **2001**, *216*, 210.

 © 2003 Wiley-VCH Verlag GmbH & Co. KGaA, Weinheim

Coordination of Noble-Gas Atoms

Gold(I) and Mercury(II) Xenon Complexes**

*In-Chul Hwang, Stefan Seidel, and Konrad Seppelt**

During detailed investigation of the reaction which produced the first gold xenon compound $[AuXe_4]^{2+}[Sb_2F_{11}]^-_2$[1] a number of further gold(II) xenon compounds were discovered.[2] In only one instance could a gold(III) xenon compound be detected.[2] However, gold occurs most frequently in its complexes as gold(I). At a first glance a gold(I) xenon bond may not appear particularly favored as gold(I) has a fully occupied 5d shell, but this consideration totally overlooks the relativistic effect, which, in the periodic system, reaches a first maximum for gold.[3] The $[AuXe]^+$ ion has already been detected by mass spectrometry.[4] According to experimentation and calculation this cation has a bond energy of 30 ± 3 kcal mol^{-1};[4] a gold–xenon bond length of 276.1 pm was predicted. A linear $[AuXe_2]^+$ ion could also exist.[5]

The fundamental difficulty in the preparation of a gold(I) xenon compound is that gold(I) always exists in the form of complexes whose ligands, predictably, bind more effectively than xenon. Therefore a displacement reaction appears to be impossible. On the other hand, a highly promising educt would be a compound of an (almost) naked Au^+ ion and a weakly coordinating anion. The compound $[(F_3As)Au]^+[SbF_6]^-$, which according to structural analysis contains a gold(I) center that is only complexed on one side,[6] appears to be a suitable model for the desired educt. Complexation with xenon could be achieved by exchange of the only weakly basic $[SbF_6]^-$ ion for a still weaker basic anion. Thus the reaction of $[(F_3As)Au]^+[SbF_6]^-$ with xenon in SbF_5-rich HF/SbF_5 solution leads to the xenon complex $[(F_3As)AuXe]^+[Sb_2F_{11}]^-$ (**1**).

Complex **1** crystallizes as colorless needles which are stable at room temperature. Crystal-structure analysis shows that the $[(F_3As)AuXe]^+$ and $[Sb_2F_{11}]^-$ ions in **1** interact only weakly with each other (Figure 1 and Table 1). The smallest Au···F separation is 284.8 pm. The As-Au-Xe unit is almost linear (173.26(2)¤); at 260.72(6) pm the gold(I)–xenon bond in **1** is as short as the gold(III)–xenon bond in $[AuXe_2F]^{2+}[SbF_6]^-[Sb_2F_{11}]^-$ and significantly shorter than gold(II)–xenon bonds. With the help of a basis set for gold specially optimized for the MP2 approximation, calculation of the structure of the $[(F_3As)AuXe]^+$ ion is achieved with astonishing accuracy (Table 1). The calculated bond energy of 32.7 kcal mol^{-1} between $[(F_3As)Au]^+$ and Xe agrees well with the bond energy in the $[AuXe]^+$ ion.[4] Ab initio calculation also allows the prediction of the frequency of the gold–xenon vibration ν(AuXe) (147.5 cm^{-1}). The Raman spectrum shows a band at $\tilde{\nu} = 138.3$ cm^{-1} which doubtlessly overlaps with the δ(SbFSb) band of the anion (Figure 2 and Table 2).[7] If **1** is labeled with ^{136}Xe (c.f. natural xenon isotope mixture: $M_r = 131.3$) this band appears displaced at $\tilde{\nu} =$ 136.7 cm^{-1}. The band at $\tilde{\nu} = 190.7$ cm^{-1} shows the only other isotope effect (displacement to 189.5 cm^{-1}, at the limit of measurement accuracy). This band is assigned to the gold–arsenic vibration which, because of the linearity of the As-Au-Xe framework, is strongly coupled with the gold–xenon vibration. It is noticeable that the intensity of the ν(AuXe) band is significantly lower than that of the ν($AuXe_4$, A_{1g}) band in the $[AuXe_4]^{2+}$ ion. The latter band is extraordinarily strong and dominates the Raman spectrum of $[AuXe_4]^{2+}[Sb_2F_{11}]^-_2$. Here too calculation gives an answer: the calculated Raman

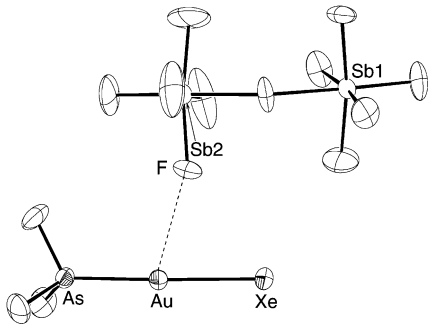


Figure 1. Crystal structure of **1** (ORTEP representation, thermal ellipsoids set at 50% probability). For numerical values see Table 1.

Table 1: Selected structural data for $[(F_3As)AuXe]^+[Sb_2F_{11}]^-$ (**1**) and $[HgXe]^{2+}[SbF_6]^-[Sb_2F_{11}]^-$ (**2**).

Separations *r* [pm] and angles [°]	Crystal structure analysis **1**	MP2 calculation $[(F_3As)AuXe]^+$[a]	
*r*Au-Xe	260.72(6)	260.5	
*r*Au-As	231.52(8)	230.6	
*r*As-F	165.9(5), 166.4(4), 166.7(5)	169.7	
*r*Au···F(Sb)	284.8–325.8	–	
∢As-Au-Xe	173.26(2)	180	
∢F-As-F	97.1(3), 98.5(3), 99.3(3)	101.3	
	2	$[HgXe]^{2+}$[b]	$[HgXe]^{2+}\cdot 6\,HF$[c]
*r*Hg-Xe	276.9(4)	261.3	267.2
*r*Hg···F	259.4(2), 249.9(2), 246,1(2)		256.8
	245.4(2), 237.3(2), 227.9(2)		236.2
∢Xe-Hg···F	75.24(6), 80.49(6), 83.73(7)		86.7
	131.06(6), 137.57(6), 140.18(6)		134.4

[a] Total energy, with zero-point energy correction: −455.812215 a.u. [b] Total energy, with zero-point energy correction: −167.697137 a.u. [c] Total energy, uncorrected: −769.5592037 a.u.

[*] Prof. Dr. K. Seppelt, Dr. I.-C. Hwang, Dr. S. Seidel
Institut für Chemie
Anorganische und Analytische Chemie
Freie Universität Berlin
Fabeckstrasse 34–36, 14195 Berlin (Germany)
Fax: (+49) 30-838-53310
E-mail: seppelt@chemie.fu-berlin.de

[**] This work was supported by the Deutsche Forschungsgemeinschaft and the Fonds der Chemischen Industrie.

 © 2003 Wiley-VCH Verlag GmbH & Co. KGaA, Weinheim DOI: 10.1002/anie.200351208

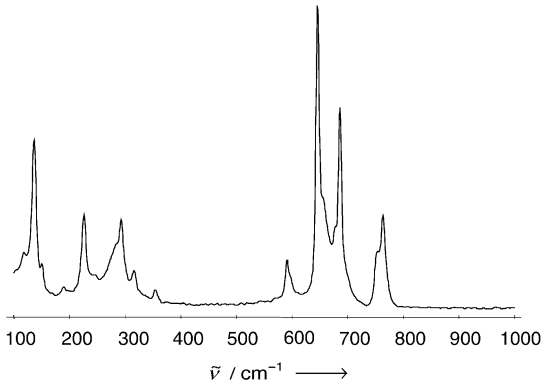


Figure 2. Raman spectrum of **1**. For numerical values see the Experimental Section, assignment see Table 2.

Table 2: Experimental and calculated (MP2) vibrational frequencies [cm^{-1}] of the $[(F_3As)AuXe]^+$ ion in **1**.

Raman[a]	MP2[a]	Assignment[b]
764.4(25)	747.6(25)	ν_s AsF_3
752.6(10)	764.2(8)	ν_e AsF_3
354.9(4)	349.3 (1.5)	δ_s AsF_3
260.0(sh)[c]	261.9(0.9)	δ_e AsF_3
190.7(2)	207.9 (0.6)	ν AuAs
138.3(50[d])	147.5 (2.3)	ν AuXe
117.2(3[d])	138.0 (0.4)	δ_e $AuAsF_3$
	40.2 (0.1)	δ_e XeAuAs

[a] Values in parenthesis are relative intensities. [b] Strongest components. [c] sh = shoulder. [d] Superimposed with δ(SbFSb) of $[Sb_2F_{11}]^-$ ions.

intensity of the ν($AuXe_4$, A_{1g}) band is greater than that of the ν(AuXe) band in the $[(F_3As)AuXe]^+$ ion by a factor of 25.

In the ^{129}Xe NMR spectrum (^{129}Xe: $I = {}^1/_2$, natural abundance 26.4%), because of the xenon excess necessary in the solution, a signal for the $[(Fe_3As)AuXe]^+$ ion and one for atomic xenon are expected. However, at room temperature only one signal at $\delta = -5180.7$ ppm is observed; clearly rapid exchange is taking place. On cooling the sample to −30¤C this signal shifts and splits (Figure 3). The complicated appearance of the signal can be explained by ^{197}Au–^{129}Xe (^{197}Au: $I = {}^3/_2$, 100%) and ^{75}As–^{129}Xe coupling (^{75}As: $I = {}^3/_2$, 100%). The large quadrupole moment of one or both $I = {}^3/_2$ nuclei leads to extensive broadening of the signals; the ^{129}Xe NMR signal of the $[XeCl]^+$ ion (^{35}Cl/^{37}Cl, $I = {}^3/_2$) has a similar shape.[8] In addition in the spectrum at −30 °C the anticipated sharp signal for free xenon is also observed.

AsF_3 is clearly such a poor ligand that xenon can compete with it, even when AsF_3 is present in excess. In contrast the $[(F_3P)_2Au]^+$ ion is formed immediately and irreversibly with the homologue of AsF_3, PF_3, under identical conditions.[6] Apart from the $[(F_3As)Au]^+$ and $[(F_3As)AuXe]^+$ ions we are unaware of any arsenic-bonded AsF_3 complexes, whereas a large number of PF_3 complexes are known.[9]) In HF/AsF_5 the AsF_3 unit binds as a ligand to trivalent lanthanide cations, but in these species coordination takes place through a fluorine atom.[10] In contrast to PF_3, however, AsF_3 is not protonated

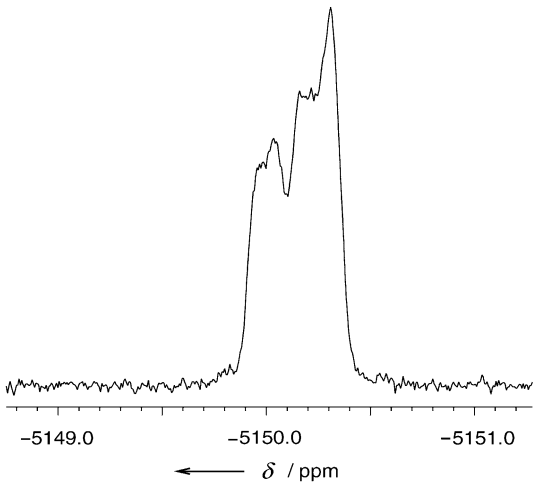


Figure 3. ^{129}Xe NMR signal of a solution of **1** in HF/SbF_5 at −30 °C in the presence of xenon. In addition to the sharp signal of elemental xenon (right) the highly broadened signal for the $[(F_3As)AuXe]^+$ ion arising from quadrupole interactions can be seen.

by HF/SbF_5.[11] In agreement with this observation the first ionization energy of AsF_3 (13.0 eV) is higher by 0.72 eV than that of PF_3 (12.28 eV).[12] These particularities of AsF_3 are usually explained by inadequate shielding by the fully occupied 3d shell (transition-metal contraction).

The Hg^{2+} ion is isoelectronic with the Au^+ ion. However, compounds that contain uncomplexed Au^+ ions have not been reported, whereas compounds such as HgF_2 which contain uncomplexed Hg^{2+} ions are known. If HgF_2 reacts with an excess of SbF_5 in the presence of xenon above room temperature highly refractive crystals are formed which decompose at room temperature in moist air with the release of gas. In dry air the compound is stable at room temperature, and under xenon pressure up to 60 °C. This compound was identified as $[HgXe]^{2+}[SbF_6]^-[Sb_2F_{11}]^-$ (**2**, see Figure 4) by

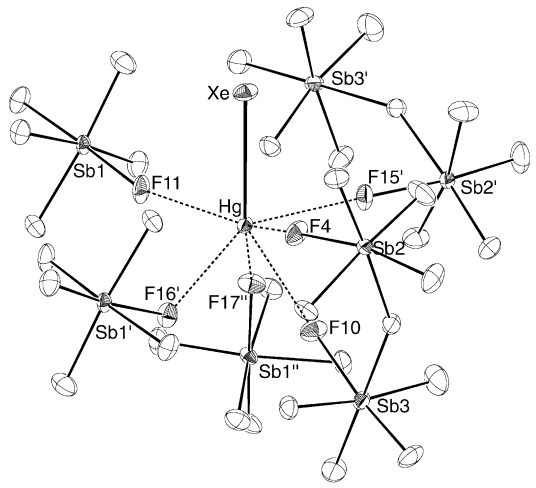


Figure 4. Crystal structure **2** (ORTEP representation, thermal ellipsoids set at 50% probability). The immediate environment of an $[HgXe]^{2+}$ ion is shown. The coordination sphere of the Hg^{2+} ion has a highly distorted, capped octahedral configuration.

 © 2003 Wiley-VCH Verlag GmbH & Co. KGaA, Weinheim

crystal-structure analysis. At 276.93(4) pm the mercury–xenon bond is about as long as the gold(II)–xenon bond in the $[AuXe_4]^{2+}$ ion. The coordination sphere of the mercury center is completed by six fluorine atoms at distances between 227.9(2) and 259.4(2) pm. Compound **2** has a highly distorted capped structure in which the xenon atom assumes the capping position. For calculation on **2** with ab initio methods we replaced the fluoroantimonate anions with HF molecules and assumed a regular, capped octahedral structure. The calculation gave a mercury–xenon separation of 267.2 pm and mercury–fluorine separations of 236.2 and 256.8 pm (see Table 1). In view of the simplifications the agreement with experiment is satisfactory in our view. The calculated mercury–xenon bond energy for $[HgXe]^{2+}\cdot 6\,HF$ is 24.5 kcal mol^{-1}.

Neither ^{129}Xe nor ^{199}Hg NMR spectra could be obtained for **2** because the compound decomposed in HF solution. The Raman spectrum shows a relatively intense band at 139.8 cm^{-1} (138.7 cm^{-1} for $[Hg^{136}Xe]^{2+}$) which can be assigned to the mercury–xenon vibration and again is superimposed with the δ(SbFSb) band of the $[Sb_2F_{11}]^-$ ion. Only the anion combination $[SbF_6]^-/[Sb_2F_{11}]^-$ was detected following reactions under a number of conditions. The Raman spectrum of a sample of crystals, several of which were studied crystallographically, is identical to the spectrum of the bulk product. Consequently the reaction yields quantitatively a uniform product.

Finally, reference is made to a peculiarity of this mercury–xenon compound. All noble-gas compounds, including the novel gold–xenon compounds, require elemental fluorine in at least one step of their synthesis (e.g. for the synthesis AuF_3). Compound **2** is the first noble-gas compound whose synthesis occurs without the use of elemental fluorine: SbF_5 and HgF_2 are obtainable by metathesis reactions. Our results show that a number of xenon–metal complexes could be prepared if it is possible to obtain educts with sufficiently weakly coordinated metals ions.

Experimental Section

1: Under the exclusion of moisture, AuF_3 (210 mg, 0.8 mmol) and SbF_5 (2.29 g, 10.6 mmol) were placed into a polyperfluorovinyl ether/tetrafluoroethylene copolymer (PFA) reaction tube. Anhydrous HF (800 mg, 40 mmol) and AsF_3 (350 mg, 2.6 mmol) were condensed into the tube with a stainless steel vacuum apparatus at −196 °C. Warming to room temperature led to gas evolution (AsF_5) and the formation of a small amount of black precipitate, probably gold. When the gas evolution ceased xenon (800 mg, 6 mmol) was condensed into the mixture at −196 °C. The reaction tube was sealed and the reaction mixture cooled from room temperature to −50 °C. Compound **1** crystallized out as colorless needles which immediately turned black on exposure to air. Yield: 750 mg, m.p. 62 °C (decomp.). Removal of the adhering HF/SbF_5 in vacuum leads to decomposition of the compound.

^{129}Xe NMR (HF/SbF_5, 110.45 MHz, $XeOF_4$, 25 °C): $\delta = -5180.7$ ppm (s), ^{129}Xe NMR (HF/SbF_5, 110.45 MHz, $XeOF_4$, −30 °C): 5149.9–5150.3 ppm (m); Raman (1064 nm, 25 °C): $\tilde{\nu}(I_{rel}) =$ 764.4(25), 752.6(10), 676.5(sh), 666.3(60), 657.7(sh), 646.0(100), 591.0(10), 354.9(4), 316.9(6), 293.3(15), 282.9(sh), 260.0(sh), 226.5(15), 190.7(2), 151.8(3), 138.3(50), 117.2(2) cm^{-1}.

Crystal structure analysis: a suitable crystal was mounted onto a specially constructed apparatus[13] with cooling in an inert atmosphere on a Bruker SMART CCD 1000 TM diffractometer and analyzed.[14] After semi-empirical absorption correction by equalization of like-symmetry reflections (SADABS), structure solution and refinement was carried out with the SHELX programs.[15,16]

Ab initio calculations: Gaussian 98 program.[17] 2nd-order Møller–Plesset approximation (MP2) for electron correlation as implemented in Gaussian. Basis set: 6-311G(d,p) for F and H as implemented in Gaussian. Au and Hg, relativistically corrected basis set for MP2, optimized by P. Schwerdtfeger and R. Wesendrup, in each case 9s 9p 6d 4f with pseudopotentials for 60 core electrons. Xe 6s, 6p, 3d, 1f with relativistically corrected pseudopotentials for 46 core electrons. As: 3s, 3p, 1d with pseudopotentials for 28 core electrons.[18]

2: HgF_2 (130 mg, 0.54 mmol) and SbF_5 (4.06 g, 18.73 mmol) were placed into a PFA reaction tube under exclusion of moisture. HF (280 mg, 14.0 mmol) was condensed onto this mixture with a stainless steel apparatus at −196 °C. On warming to room temperature a colorless solid formed which remained partly in solution. The mixture was then evaporated to dryness in vacuum at room temperature. 10 mg of the colorless residue was placed into a thick-walled glass ampoule of 3-mm inner diameter and treated with SbF_5 (660 mg, 3.0 mmol). Liquid xenon (220 μL) was condensed into the mixture and the tube was sealed by melting. On warming to room temperature the SbF_5 and xenon mixed. The reaction mixture was homogenized in an ultrasound bath and then heated at 80 °C for 6 h. Slow cooling to room temperature (0.05 °C min^{-1}) afforded colorless platelet crystals of **2**. The pure, colorless product was obtained by decantation of the xenon/SbF_5 excess at low temperature (−100 °C); m.p. ≈30 °C (decomp.). The reaction is quantitative. Raman (1064 nm, 25 °C): $\tilde{\nu}(I_{rel}) =$ 714(75), 703(20), 687(10), 673(18), 652(100), 640(35), 594(3), 572(5), 553(15), 525(10), 385(3), 341(5), 329(9), 306(8), 289(35), 264(20), 227(30), 209(7), 194(3), 181(2), 140(40), 136(30), 119(10) cm^{-1}. Crystal structure analysis was carried out as described above.[19]

Further details on the crystal structure investigations may be obtained from the Fachinformationszentrum Karlsruhe, 76344, Eggenstein-Leopoldshafen, Germany (fax: (+49)7247-808-666; e-mail: crysdata@fiz-karlsruhe.de) on quoting the depository numbers CSD-412994 (**1**) and CSD-412993 (**2**)

Received: February 18, 2003 [Z51208]

Keywords: gold · mercury · noble gases · superacid systems

[1] S. Seidel, K. Seppelt, *Science* **2000**, *290*, 117–118.
[2] T. Drews, S. Seidel, K. Seppelt, *Angew. Chem.* **2002**, *114*, 470–473; *Angew. Chem. Int. Ed.* **2002**, *41*, 454–456.
[3] P. Pyykkö, *Chem. Rev.* **1988**, *88*, 563–594.
[4] D. Schröder, H. Schwarz, J. Hrusak, P. Pyykkö, *Inorg. Chem.* **1998**, *37*, 624–632.
[5] P. Pyykkö, *J. Am. Chem. Soc.* **1995**, *117*, 2067–2070.
[6] R. Küster, K. Seppelt, *Z. Anorg. Allg. Chem.* **2000**, *626*, 236–240.
[7] H. Willner, M. Bodenbinder, R. Bröchler, G. Hwang, S. J. Rettig, J. Trotter, B. von Ahsen, U. Westphal, V. Jonas, W. Thiel, F. Aubke, *J. Am. Chem. Soc.* **2001**, *123*, 588–602.
[8] S. Seidel, K. Seppelt, *Angew. Chem.* **2001**, *113*, 4318–4320; *Angew. Chem. Int. Ed.* **2001**, *40*, 4225–4227.
[9] T. Kruck, *Angew. Chem.* **1967**, *79*, 27–43; *Angew. Chem. Int. Ed. Engl.* **1967**, *6*, 53–67.
[10] M. Tramsek, P. Benkic, A. Turicnik, G. Tavcar, B. Zemva, *J. Fluorine Chem.* **2002**, *114*, 143–148.
[11] R. Küster, T. Drews, K. Seppelt, *Inorg. Chem.* **2000**, *39*, 2784–2786.

 © 2003 Wiley-VCH Verlag GmbH & Co. KGaA, Weinheim

[12] W. A. Potts, H. J. Lempka, D. G. Streets, W. C. Price, *Philos. Trans. R. Soc. London Ser. A* **1970**, *268*, 59–76.
[13] T. Kottge, D. Stalke, *J. Appl. Crystallogr.* **1993**, *26*, 615–619.
[14] **1**: orthorhombic, $Pna2_1$, $a = 1588.7(2)$, $b = 813.3(1)$, $c = 1094.5(2)$ pm, $V = 1414 \times 10^6$ pm^3, $T = -100\,^\circ$C, $Z = 4$, $Mo_{K\alpha}$ radiation, graphite monochromator, scan with 0.3° in ω, 10 s irradiation time per measurement, 1800 measurements, 17436 measured reflections, 4316 independent reflections, 173 parameters, $R(F \geq 4\sigma(F)) = 0.0275$, $wR_2 = 0.065$.
[15] G. Sheldrick, Program for Crystal Structure Solution, Universität Göttingen, **1986**.
[16] G. Sheldrick, Program for Crystal Structure Refinement, Universität Göttingen, **1993**.
[17] Gaussian 98 (Revision A.7), M. J. Frisch, G. W. Trucks, H. B. Schlegel, G. E. Scuseria, M. A. Robb, J. R. Cheeseman, V. G. Zakrzewski, J. A. Montgomery, R. E. Stratmann, J. C. Burant, S. Dapprich, J. M. Millam, A. D. Daniels, K. N. Kudin, M. C. Strain, O. Farkas, J. Tomasi, V. Barone, M. Cossi, R. Cammi, B. Mennucci, C. Pomelli, C. Adamo, S. Clifford, J. Ochterski, G. A. Petersson, P. Y. Ayala, Q. Cui, K. Morokuma, D. K. Malick, A. D. Rabuck, K. Raghavachari, J. B. Foresman, J. Cioslowski, J. V. Ortiz, B. B. Stefanov, G. Liu, A. Liashenko, P. Piskorz, I. Komaromi, R. Gomperts, R. L. Martin, D. J. Fox, T. Keith, M. A. Al-Laham, C. Y. Peng, A. Nanayakkara, C. Gonzalez, M. Challacombe, P. M. W. Gill, B. G. Johnson, W. Chen, M. W. Wong, J. L. Andres, M. Head-Gordon, E. S. Replogle, J. A. Pople, Gaussian, Inc., Pittsburgh, PA, **1998**.
[18] Institut für Theoretische Chemie der Universität Stuttgart, http://www.theochem.uni-stuttgart.de, pseudopotentials, electron core potentials.
[19] **2**: orthorhombic, $P2_1/c$, $a = 1372.2(3)$, $b = 1048.1(1)$, $c = 1052.5(1)$ pm, $\beta = 94.56(1)^\circ$, $V = 1508.8 \times 10^6$ pm^3, $T = -100\,^\circ$C, $Z = 4$, $Mo_{K\alpha}$ radiation, graphite monochromator, scan width 0.3° in ω, 10 s irradiation time per measurement, 1800 measurements, 24460 measured reflections, 4583 independent reflections, 200 parameters, R ($F \geq 4\sigma(F)$) = 0.0205, $wR_2 = 0.0427$.

 © 2003 Wiley-VCH Verlag GmbH & Co. KGaA, Weinheim

Organization of Peptide Helices

Molecular Architecture with Functionalized β-Peptide Helices**

Arndt M. Brückner, Pradip Chakraborty, Samuel H. Gellman, and Ulf Diederichsen**

Dedicated to Professor Lutz F. Tietze

Helical secondary structures are a fundamental part of protein architecture and are widely involved in recognition and binding processes between proteins or between proteins and nucleic acids.[1] Furthermore, the organization of peptide helices in bundles is common for the membrane-spanning domains of transmembrane proteins and for many soluble proteins.[2] Peptide helices can be used as templates for specific preorganization of peptides in ligation.[3] The design of amphiphilic helices is important for model studies related to these complex biomolecular interactions.[3,4] Among α-peptides usually about 15–20 amino acids are needed for significant degree of helical secondary structure in aqueous solution. In contrast, six β-amino acids are enough for a substantial population of a β-peptide 14-helix conformation.[5] This β-peptide helix has approximately three residues per turn and a pitch of about 5 Å. The 14-helix is preferentially formed by β-amino acids with side chains in the β position of the respective amino acids ("β^3-residues"), and the 14-helix is stabilized dramatically by the inclusion of cyclohexane-derived β-amino acid residues. The 14-helix contains hydrogen bonds between N–H and C=O groups in the β-peptide backbone resulting in the formation 14-membered rings.[6] The regularity of the 14-helix makes it especially suitable as a scaffold for the defined orientation of functional groups appended as β-amino acid side chains.

In a step towards forming an artificial helical-bundle tertiary structure it was recently shown that a 10-residue amphiphilic β-peptide forms small soluble aggregates in water, driven by hydrophobic interactions between the helices.[7] As an extension of this concept, it should be possible to organize small β-peptide helices by nucleobase

[*] Prof. Dr. U. Diederichsen, A. M. Brückner, P. Chakraborty
Institut für Organische Chemie
Georg-August-Universität Göttingen
Tammannstrasse 2, 37077 Göttingen (Germany)
Fax: (+49) 551-392-944
E-mail: udieder@gwdg.de
Prof. Dr. S. H. Gellman
Department of Chemistry
University of Wisconsin
1101 University Avenue, Madison, WI 53706 (USA)

[**] This work was supported by the Deutsche Forschungsgemeinschaft and the U.S. National Science Foundation (CHE-0140621). We are grateful for fellowships from the Fonds der Chemischen Industrie and from the German Academic Exchange Service (DAAD) for A.M.B.

Supporting information (CD spectra) for this article is available on the WWW under http://www.angewandte.org or from the author.

 DOI: 10.1002/anie.200351871 © 2003 Wiley-VCH Verlag GmbH & Co. KGaA, Weinheim

pairing to gain more control over the geometry, stoichiometry, and specificity of self-association. The design of 14-helical β-peptides containing nucleobase recognition units in the side chains and the investigation of their secondary structures and association by base pairing are reported herein.

β-Peptides that contain nucleo-β-amino acids were synthesized[8] to determine whether the 14-helix forms in aqueous buffer (10 mM Tris·HCl, pH 7.6), and to investigate helix aggregation induced by nucleobase pairing.[9] The nucleo-β-amino acids (*S*)-γ-(guanin-9-yl)-β-homoalanine (H-β-HalG-OH), (*S*)-γ-(cytosin-1-yl)-β-homoalanine (H-β-HalC-OH), (*S*)-γ-(adenin-9-yl)-β-homoalanine (H-β-HalA-OH), (*S*)-γ-(thymin-1-yl)-β-homoalanine (H-β-HalT-OH), and (*S*)-γ-(1-methylguanin-9-yl)-β-homoalanine (H-β-Hal^{1Me}G-OH) were incorporated as base-pair recognition units.[10] These nucleo-β-amino acids were placed sequentially in every third position, to induce alignment of the nucleobases along one side of the resulting 14-helix (Figure 1). The two remaining positions of each 14-helical turn were filled with (1*R*,2*R*)-2-aminocyclohexanecarboxylic acid (ACHC) and β^3-(*R*)-homolysine. ACHC strongly promotes 14-helix formation[5] and β^3-(*R*)-homolysine was inserted to render the oligomers soluble in aqueous media.[11] For synthetic reasons the resin was loaded with β-homoglycine (H-β-HGly-OH). The primary structures of the synthesized oligomers with the sequences CGCG (**1**), CGC (**2**), GCG (**3**), C^{1Me}GC (**4**), ^{1Me}GC^{1Me}G (**5**), ATCA (**6**), and TGAT (**7**) are depicted in Figure 2. These β-peptides, which contain 10 or 13 β-amino acids, should be long enough to provide a substantial population of the 14-helical secondary structure. Inspection of Maruzen models[12] suggested that these β-peptides could undergo antiparallel association mediated by Watson–Crick hydrogen bonding between complementary nucleobases.

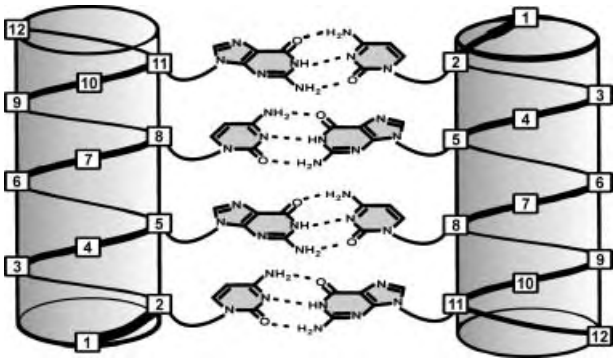
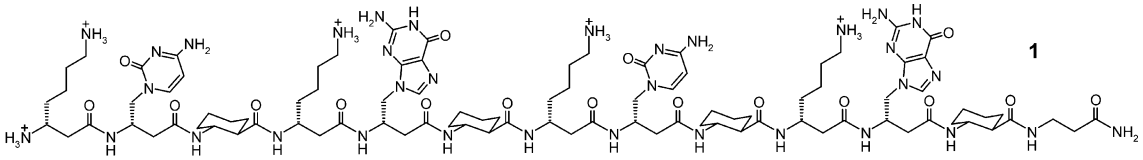


Figure 1. Model of the expected β-peptide helix aggregation through antiparallel base pairing in the Watson–Crick mode.

Unpairing of DNA or RNA double strands leads to unstacking of the nucleobases, which in cooperative processes can be recognized by a sigmoidal increase of the UV/Vis absorption with rising temperature (hyperchromicity, A_{rel}).[13] Data for oligomer CGCG (**1**) suggest very favorable self-association: temperature-dependent UV spectroscopy suggests $T_m > 80\,°C$ (11 μM β-peptide; Figure 3a). We turned to an examination of the shorter complementary oligomers CGC (**2**) and GCG (**3**) in the hope of observing complete unpairing within the accessible temperature range. Folding into a 14-helical conformation was indicated by circular dichroism (CD) spectroscopy of an equimolar mixture of **2** and **3** (Figure 3b). The strong Cotton effect found at 215 nm is in agreement with the formation of a right-handed 14-helix in aqueous solution, as has been established for many β-peptides.[5–7,14] Furthermore, there is a strong positive Cotton effect at 270 nm. Such a signal has not been observed for β-peptides and presumably arises from a preferred orientation of the nucleobases with respect to the chiral β-peptide backbone. In principle, this orientation of the nucleobases could be due to base pairing in a duplex or higher aggregate, or to simple stacking of nucleobases within a single 14-helix.

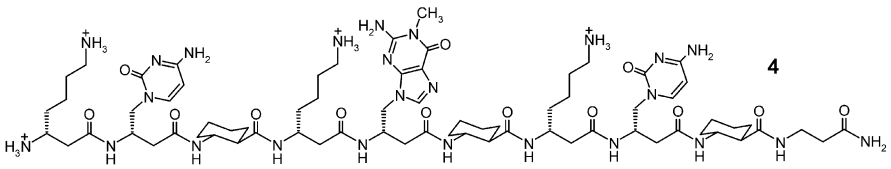
Temperature-dependent UV data obtained for oligomer **2** (CGC) alone and for oligomer **3** (GCG) alone indicated that each self-associates (Figure 3c). For β-peptide **2** cooperative unstacking with a T_m value of 43 °C ($A_{rel} = 2\,\%$, 10 μM) was



H-(β-HLys-β-HalC-ACHC-β-HLys-β-HalG-ACHC-β-HLys-β-HalC-ACHC-β-HLys-β-HalG-ACHC-β-HGly)-NH_2 (**1**)

H-(β-HLys-β-HalC-ACHC-β-HLys-β-HalG-ACHC-β-HLys-β-HalC-ACHC-β-HGly)-NH_2 (**2**)

H-(β-HLys-β-HalG-ACHC-β-HLys-β-HalC-ACHC-β-HLys-β-HalG-ACHC-β-HGly)-NH_2 (**3**)



H-(β-HLys-β-HalC-ACHC-β-HLys-β-Hal^{1Me}G-ACHC-β-HLys-β-HalC-ACHC-β-HGly)-NH_2 (**4**)

H-(β-HLys-β-Hal^{1Me}G-ACHC-β-HLys-β-HalC-ACHC-β-HLys-β-Hal^{1Me}G-ACHC-β-HGly)-NH_2 (**5**)

H-(β-HLys-β-HalA-ACHC-β-HLys-β-HalT-ACHC-β-HLys-β-HalC-ACHC-β-HLys-β-HalA-ACHC-β-HGly)-NH_2 (**6**)

H-(β-HLys-β-HalT-ACHC-β-HLys-β-HalG-ACHC-β-HLys-β-HalA-ACHC-β-HLys-β-HalT-ACHC-β-HGly)-NH_2 (**7**)

Figure 2. Oligomers **1**–**7** prepared by solid-phase peptide synthesis.

 © 2003 Wiley-VCH Verlag GmbH & Co. KGaA, Weinheim

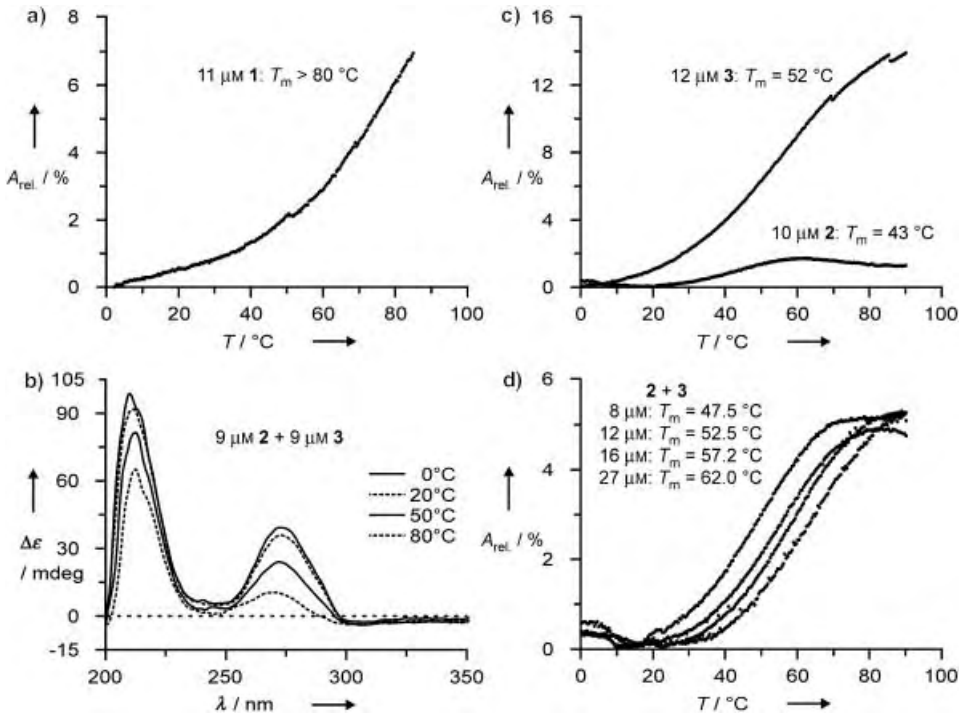


Figure 3. Temperature dependent UV and CD spectra of the β-peptides **1**–**3** in aqueous buffer (10 mM Tris·HCl, pH 7.6). Self-aggregation of G/C-containing oligomers is indicated by the melting curves (top). The interaction of the equimolar mixture of oligomers **2** and **3** leads to the temperature dependent UV and CD spectra (bottom).

found. The temperature-dependent UV curve for oligomer **3** can be interpreted as a sigmoidal increase of absorption with $T_m = 52\,°C$ ($A_{rel} = 14\,\%$, 12 μM). Equimolar mixtures of **2** and **3** displayed sigmoidal melting curves with excellent reversibility, behavior that is commonly observed for complementary oligonucleotides. The stabilities of the complexes formed in the equimolar mixtures of **2** and **3** are concentration dependent, with T_m values in the range 47.5–62.0 °C ($A_{rel} = 5\,\%$, 8–27 μM; Figure 3d).

Evidence for duplex formation was obtained from ESI mass spectrometry. For oligomers **1**–**3**, homodimer formation was indicated by the appearance of $[(2M)^{3+}+3H]$ peaks in the mass spectrum when an aqueous solution containing the respective oligomer (precooled to +1 °C) was analyzed.[15] For an equimolar mixture of the complementary oligomers **2** and **3**, the mass peak $[(M_2+M_3)^{3+}+3H]$ and the respective daughter ions $[M_2^{2+}+2H]$ and $[M_3^{+}+H]$ were found with ten-times higher intensity than the $[(2M)^{3+}+3H]$ peaks.

Oligomers **2** and **3** were designed to form a 1:1 duplex, but the data described above do not clearly demonstrate that this expected behavior is dominant, or that duplex formation occurs at all. Self-pairing of **2** and/or **3** might prevent heteropairing. Furthermore, higher aggregation stoichiometries might be responsible for the high observed T_m values; similar behavior has been observed for other CGCG-oligomers with linear topology.[16]

To determine whether hydrogen-bond-mediated pairing of the nucleobases is important for the observed self-association we prepared oligomers **4** ($C^{1Me}GC$) and **5** ($^{1Me}GC^{1Me}G$), which differ from oligomers **2** and **3** only in the 1-methylation of the guanine nucleobases. This methylation prevents base pairing over the Watson–Crick site. For oligomers **4** and **5** formation of 14-helix secondary structure was indicated by CD (maximum at 215 nm in Figure 4a; only results for the equimolar mixture are shown), but no interaction between the helixes could be detected by temperature-dependent UV spectroscopy (Figure 4b). In the CD spectra at low temperatures the maximum at 270 nm suggests a preferred orientation of the nucleobases with respect to the helix, but the decrease of the Cotton effect at 270 nm with increasing temperature is linear and does not show the sigmoidal pattern that is indicative for base-paired double strands (unpublished data).

The strongest evidence for duplex formation mediated by base pairing came from experiments involving the complementary oligomers **6** (ATCA) and **7** (TGAT), a system in which both types of canonical base pairs, A–T and G–C, can form. Only negligible self-pairing was observed for oligomer **6** ($T_m < 0\,°C$, 4 μM; Figure 5b), whereas oligomer **7** self-associated to form a complex with significant stability ($T_m = 28\,°C$, $A_{rel} = 11\,\%$, 4 μM). However, the complex formed in an equimolar mixture of oligomers **6** and **7** displayed substantially higher stability than was observed with either **6** or **7** alone ($T_m = 44\,°C$, $A_{rel} = 6\,\%$, 4 μM each). The conclusion that **6** and **7** combine to form a stable duplex based on pairing of bases that have been preorganized by a 14-helical backbone was supported by temperature-dependent CD spectra (Figure 5a), which show the characteristic maximum at 215 nm for this β-peptide secondary structure.

Using Breslauer's equation for double-strand formation in DNA,[17] we have derived thermodynamic data for duplex **6** (ATCA) + **7** (TGAT) from the T_m values at different

 © 2003 Wiley-VCH Verlag GmbH & Co. KGaA, Weinheim

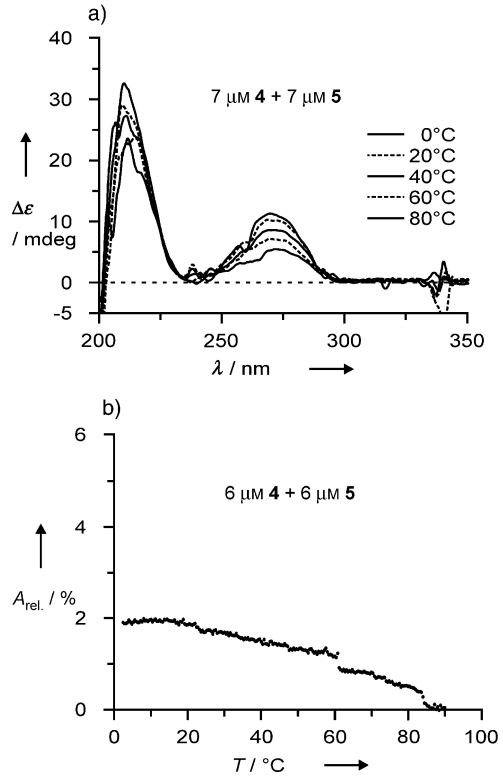


Figure 4. CD spectra (a) and UV melting curves (b) of an equimolar mixture of β-peptides **4** and **5** in aqueous buffer (10 mM Tris·HCl, pH 7.6).

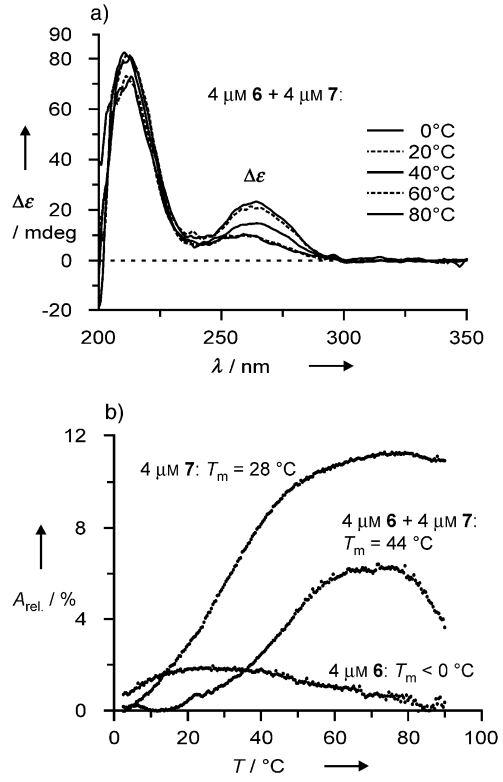


Figure 5. Temperature dependent CD (a) and UV (b) spectra indicating the self-pairing of β-peptides **6** and **7** as well as the stable double-strand formation within an equimolar mixture of β-peptides **6** and **7** in aqueous buffer (10 mM Tris·HCl, pH 7.6).

concentrations. We deduce an entropy value of $\Delta S^0 = -96\ \mathrm{cal\,mol^{-1}\,K^{-1}}$ for strand pairing, which may be compared with $\Delta S^0 = -160\ \mathrm{cal\,mol^{-1}\,K^{-1}}$ for strand pairing by the DNA hexamer duplex $d(GC)_3$.[18] The lower entropy cost for pairing by **6**+**7** relative to the DNA hexamer pairing suggests that the high conformational preorganization of the 14-helix makes a significant and favorable contribution to the energetics of strand pairing in the β-peptide case.

In conclusion, the β-peptide 14-helix provides an excellent scaffold for the presentation of preorganized recognition units. 14-Helical β-peptides functionalized with nucleobases form very stable duplexes with complementary helices. Double-strand formation in this case has a significant entropic advantage relative to strand pairing by DNA, which presumably reflects the preorganization of the β-peptide backbone. For guanine-containing β-peptides very high thermal stability was observed, which suggests the formation of higher aggregates. The design principles demonstrated here will be extended to more complex assemblies with the goal of mimicking molecular architectures such as helix bundles.

Received: May 12, 2003 [Z51871]

Keywords: base pairing · beta-peptides · helical structures · secondary structure · self-assembly

[1] a) R. T. Sauer, *Nat. Struct. Biol.* **1995**, *2*, 7–9; b) M. Suzuki, J. Suckow, B. Kisters-Woike, H. Aramaki, K. Makino, *Adv. Biophys.* **1996**, *32*, 31–52; c) R. L. Stanfield, I. A. Wilson, *Curr. Opin. Struct. Biol.* **1995**, *5*, 103–113.

[2] B. Bechinger, *Curr. Opin. Chem. Biol.* **2000**, *4*, 639–644.

[3] a) K. Severin, D. H. Lee, A. J. Kennan, M. R. Ghadiri, *Nature* **1991**, *389*, 706–709; b) D. Grell, J. S. Richardson, M. Mutter, *J. Pept. Sci.* **2001**, *7*, 146–151.

[4] a) R. B. Hill, D. P. Raleigh, A. Lombardi, W. F. DeGrado, *Acc. Chem. Res.* **2000**, *33*, 745–754; b) L. Baltzer, H. Nilsson, J. Nilsson, *Chem. Rev.* **2001**, *101*, 3153–3163.

[5] a) D. H. Appella, J. J. Barchi, S. R. Durell, S. H. Gellman, *J. Am. Chem. Soc.* **1999**, *121*, 2309–2310; b) R. P. Cheng, S. H. Gellman, W. F. DeGrado, *Chem. Rev.* **2001**, *101*, 3219–3232.

[6] a) D. Seebach, M. Overhand, F. N. M. Kühnle, B. Martinoni, L. Oberer, U. Hommel, H. Widmer, *Helv. Chim. Acta* **1996**, *79*, 913–941; b) D. Seebach, P. E. Ciceri, M. Overhand, B. Jaun, D. Rigo, *Helv. Chim. Acta* **1996**, *79*, 2043–2066; c) P. I. Arvidsson, M. Rueping, D. Seebach, *Chem. Commun.* **2001**, 649–650.

[7] a) T. L. Raguse, J. R. Lai, P. R. LePlae, S. H. Gellman, *Org. Lett.* **2001**, *3*, 3963–3966; For related work, see: b) R. P. Cheng, W. F. DeGrado, *J. Am. Chem. Soc.* **2002**, *124*, 11564–11565; c) P. Garner, S. Dey, Y. Huang, X. Zhang, *Org. Lett.* **1999**, *1*, 403–406; d) P. Garner, S. Dey, Y. Huang, *J. Am. Chem. Soc.* **2000**, *122*, 2405–2406.

[8] a) U. Diederichsen, H. W. Schmitt, *Angew. Chem.* **1998**, *110*, 312–315; *Angew. Chem. Int. Ed.* **1998**, *37*, 302–305; b) U. Diederichsen, H. W. Schmitt, *Eur. J. Org. Chem.* **1998**, 827–835; c) A. M. Brückner, M. Garcia, A. Marsh, S. H. Gellman, U. Diederichsen, *Eur. J. Org. Chem.*, in press.

[9] The oligomers were obtained by manual *tert*-butoxycarbonyl (Boc) solid-phase peptide synthesis on a 4-methylbenzhydrylamine (MBHA) polystyrene support loaded with β-homoglycine (*O*-(7-azabenzotriazol-1-yl)-1,1,3,3-tetramethyluronium hexafluorophosphate (HATU) and *N,N*-diisopropylethylamine were the coupling reagents; double coupling at 50 °C). ESI-MS: *m/z*: **1**: 672.5 [M^{3+}+3H], 1008.0 [M^{2+}+2H], 1019.0

 © 2003 Wiley-VCH Verlag GmbH & Co. KGaA, Weinheim

[M^{2+}+H+Na]; **2**: 505.5 [M^{3+}+3H], 757.4 [M^{2+}+2H]; **3**: 518.9 [M^{3+}+3H], 777.6 [M^{2+}+2H], 1553.9 [M^{+}+H]; **4**: 383.1 [M^{4+}+4H], 510.1 [M^{3+}+3H], 764.2 [M^{2+}+2H], 1527.8 [M^{+}+H]; **5**: 528.2 [M^{3+}+3H], 791.5 [M^{2+}+2H], 802.3 [M^{2+}+H+Na], 813.4 [M^{2+}+2Na], 1602.8 [M^{+}+Na]; **6**: 667.0 [M^{3+}+3H], 999.8 [M^{2+}+2H], 1332.1 [$(2M)^{3+}$+3H], 1997.9 [M^{+}+H]; **7**: 508.4 [M^{4+}+4H], 677.5 [M^{3+}+3H], 1014.9 [M^{2+}+2H], 2028.7 [M^{+}+H].

[10] For the synthesis of Boc-β-HalC(Z)-OH (Z = benzyloxycarbonyl) and Boc-β-HalG-OH: A. M. Brückner, H. W. Schmitt, U. Diederichsen, *Helv. Chim. Acta* **2002**, *85*, 3855–3866.

[11] Boc-β-HLys(Z)-OH was prepared from the respective α-amino acid Boc-(*R*)-Lys(Z)-OH by Arndt–Eistert homologation. See ref. [6] and J. V. N. Vara Prasad, J. A. Loo, F. E. Boyer, M. A. Stier, R. D. Gogliotti, W. J. Turner, P. J. Harvey, M. R. Kramer, D. P. Mack, J. D. Scholten, S. J. Gracheck, J. M. Domagala, *Bioorg. Med. Chem.* **1998**, *6*, 1707–1730.

[12] HGS Biochemistry Molecular Model, Protein Nucleic Acid Set, Maruzen Co., Ldt. Tokyo.

[13] J. SantaLucia, Jr. in *Spectrophotometry and Spectrofluorimetry: A Practical Approach* (Ed.: M. G. Gore), Oxford University Press, Oxford, **2000**, pp. 329–356.

[14] a) D. H. Appella, L. A. Christianson, I. L. Karle, D. R. Powell, S. H. Gellman, *J. Am. Chem. Soc.* **1999**, *121*, 6209–6212; b) J. J. Barchi, X. Huang, D. H. Appella, L. A. Christianson, S. R. Durell, S. H. Gellman, *J. Am. Chem. Soc.* **2000**, *122*, 2711–2718. For the preparation of Boc-ACHC see: c) D. H. Appella, P. R. LePlae, T. L. Raguse, S. H. Gellman, *J. Org. Chem.* **2000**, *65*, 4766–4769; d) For a critical discussion of the suitability of CD spectra to derive the conformational preference of a β-peptide see: A. Glättli, X. Daura, D. Seebach, W. F. van Gunsteren, *J. Am. Chem. Soc.* **2002**, *124*, 12972–12978.

[15] **1** (60 μM): 672.7 [M^{3+}+3H], 806.4 [$(2M)^{5+}$+5H], 1008.3 [M^{2+}+2H], 1343.4 [$(2M)^{3+}$+3H]; daughter ions of 806.4: 672.4 [M^{3+}+3H], 1007.9, [M^{2+}+2H]; daughter ion of 1343.4: 1008.4 [M^{2+}+2H]; **2** (60 μM): 505.1 [M^{3+}+3H], 758.6 [M^{2+}+2H], 1009.2 [$(2M)^{3+}$+3H]; **3**: 519.0 [M^{3+}+3H], 777.4 [M^{2+}+2H], 1035.9 [$(2M)^{3+}$+3H]; **2**+**3** (30 μM each): 505.6 [M_2^{3+}+3H], 518.9 [M_3^{3+}+3H], 758.0 [M_2^{2+}+2H], 778.2 [M_3^{2+}+2H], 1022.6 [$(M_2+M_3)^{3+}$+3H]; daughter ions of 1022.6: 757.3 [M_2^{2+}+2H], 1553.8 [M_3^{+}+H].

[16] U. Diederichsen, *Angew. Chem.* **1997**, *109*, 1966–1969; *Angew. Chem. Int. Ed. Engl.* **1997**, *36*, 1886–1889.

[17] a) L. A. Marky, K. J. Breslauer, *Biopolymers* **1987**, *26*, 1601–1620; b) K. J. Breslauer, *Methods Enzymol.* **1995**, *259*, 221–242.

[18] D. DePrisco Albergo, L. A. Marky, K. J. Breslauer, D. H. Turner, *Biochemistry* **1981**, *20*, 1409–1413.

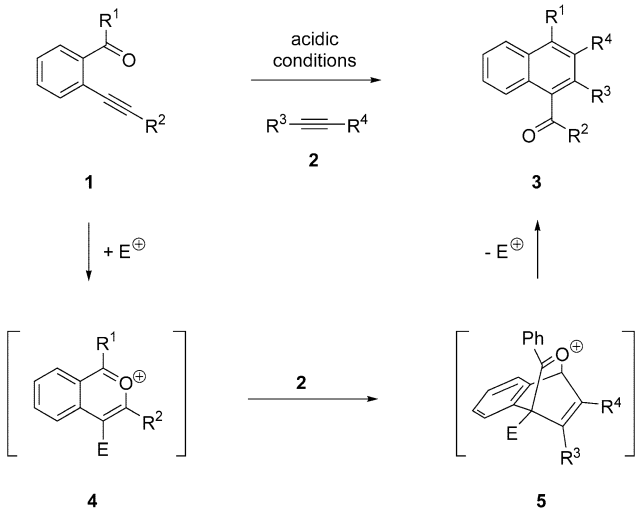
 © 2003 Wiley-VCH Verlag GmbH & Co. KGaA, Weinheim

Gold(III) Chloride Catalyzed Domino Processes with Isobenzopyrylium Cation Intermediates**

Gerald Dyker, Dirk Hildebrandt, Jianhui Liu, and Klaus Merz*

As a result of its synthetic potential the electrophilic cyclization of phenylacetylenes that have a carbonyl group[1] or an imino group[2,3] in the *ortho* position is currently a popular research topic. These reactions evidently profit energetically from the formation of heteroaromatic isobenzopyrylium salts or isoquinolines, respectively.[4] According to Tovar and Swager,[1] strongly acidic conditions are crucial for the stoichiometric formation of isobenzopyrylium salts. Recently we found that in a special case weakly acidic conditions were sufficient to catalyze a domino process in which isobenzopyrylium formation was followed by an intramolecular Diels–Alder reaction with an alkyne functionality.[5] With gold(III) chloride[6] as a catalyst, Yamamoto and coworkers[7] carried out an analogous process, in which an intermolecular Diels–Alder reaction resulted in the efficient synthesis of highly substituted naphthalenes (Scheme 1).

Under the assumption that the final aromatization step is not crucial for the efficiency of the domino process, we tested olefins and electron-rich heteroarenes as especially interesting reaction partners. The reaction of these compounds either



Scheme 1. Cycloaddition of isobenzopyrylium intermediates with alkynes (R^1 to R^4 = H, alkyl, aryl, or R^2–R^3 = tether for an intramolecular reaction; E = electrophile: either a proton or $AuCl_3$).

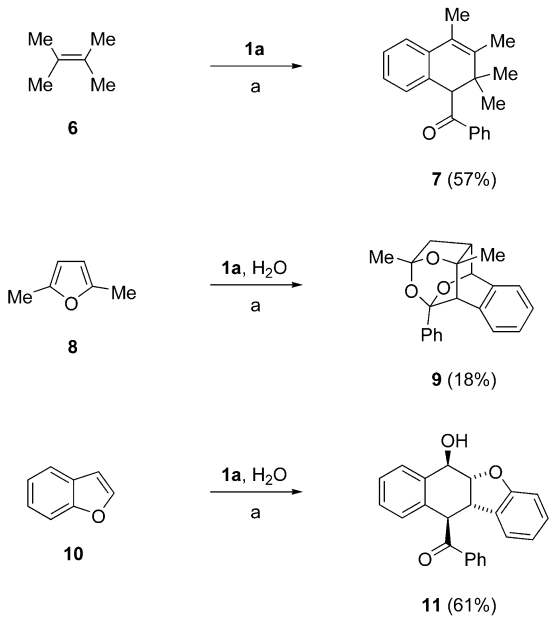
[*] Prof. Dr. G. Dyker, D. Hildebrandt, Dr. J. Liu, Dr. K. Merz
Fakultät für Chemie, Ruhr-Universität Bochum
Universitätsstrasse 150, 44780 Bochum (Germany)
Fax: (+49) 234-32-14353
E-mail: gerald.dyker@rub.de

[**] This work was supported by the Fonds der Chemischen Industrie.

Supporting information for this article is available on the WWW under http://www.angewandte.org or from the author.

 DOI: 10.1002/anie.200352160 © 2003 Wiley-VCH Verlag GmbH & Co. KGaA, Weinheim

as nucleophiles or as dienophiles should lead, through the construction of stereogenic centers, to a wide range of products with remarkable structural diversity. Tetramethylethene (**6**) reacted as an electron-rich and somewhat sterically hindered dienophile in a cycloaddition with **1a** (Scheme 2). The formation of the dihydronaphthalene **7** can be explained mechanistically by a Wagner–Meerwein rearrangement of the intermediate **18** (Scheme 4).



Scheme 2. $AuCl_3$-catalyzed reactions of the 2-alkynyl benzaldehyde **1a** ($R^1 = H$, $R^2 = Ph$) with alkene dienophiles and heteroarenes: a) **1a** (1 equiv), $AuCl_3$ (3 mol%), acetonitrile, 3 h, 80°C.

It is particularly interesting to compare the reactivity of 2,5-dimethylfuran (**8**) and benzo[*b*]furan (**10**), both known as electron-rich dienophiles for Diels–Alder reactions with inverse electron demand.[8] Both reactions with **1a** were carried out in the presence of a small amount of water, and they led to the fascinating double acetal **9** in the former case and to the secondary alcohol **11** in the latter. Compound **9** was identified by two-dimensional NMR spectroscopy,[9] and **11** by X-ray crystal-structure analysis (Figure 1).[10]

The cage compound **9** might form via the secondary alcohol **19** (structurally related to **11**) by a double transannular acetalization. The direct addition of a hydroxide ion at the carbonyl carbon atom of the primary cycloadduct **20**, followed by a single acetalization step, is an alternative explanation (Scheme 4). However, if the observed regio- and stereoselectivity are considered, the differences between 2,5-dimethylfuran (**8**) and benzo[*b*]furan (**10**) as reaction components become apparent. In the former case an *endo* Diels–Alder product of type **20** is formed, whereas in the latter case the *exo* Diels–Alder product **21** is formed—moreover, with the opposite regioselectivity.

The organogold intermediates **20** and **21** have been proposed based on the assumption that the gold atom is the active Lewis acidic center of the catalyst. On the other hand, the combination of water and $AuCl_3$ as reaction components

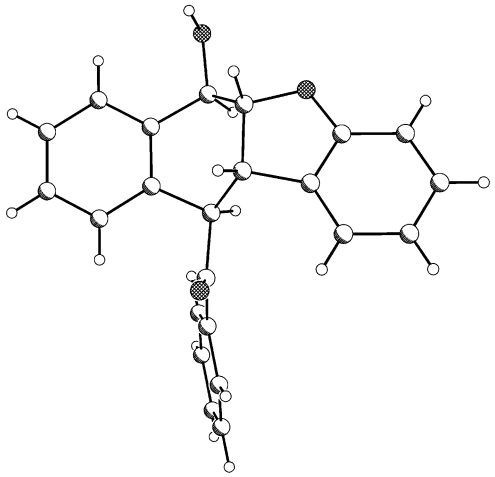
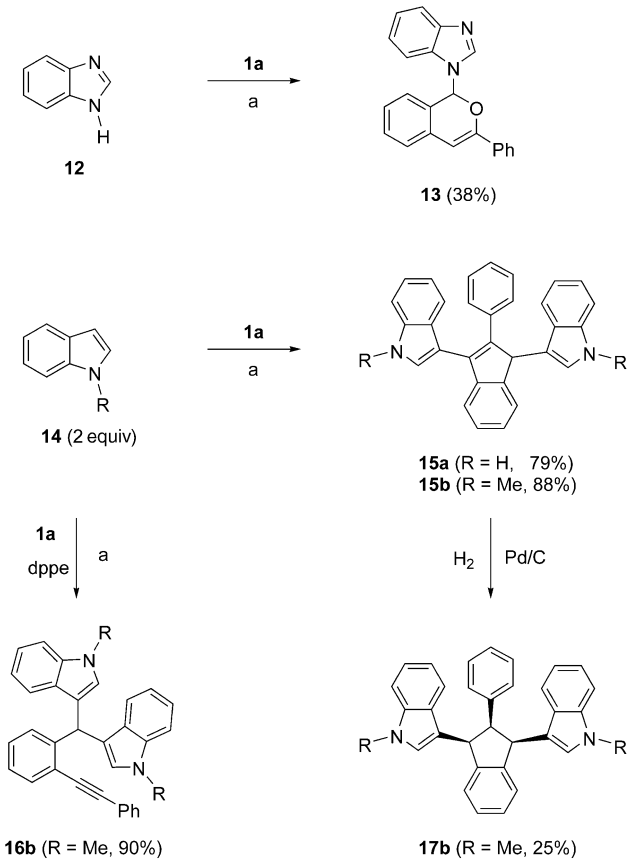


Figure 1. Crystal structure of **11**.

suggests that this is a "simple" case of protic catalysis. However, whereas $HAuCl_4$ is a similarly active catalyst for the formation of **11**, $HClO_4$, HCl, *para*-toluenesulfonic acid, and trifluoroacetic acid completely fail as catalysts.

Benzimidazole (**12**) reacted as a nucleophile to trap the pyrylium cation intermediate derived from **1a** with formation of the N,O-acetal **13** (Scheme 3).[11] Surprisingly, when the

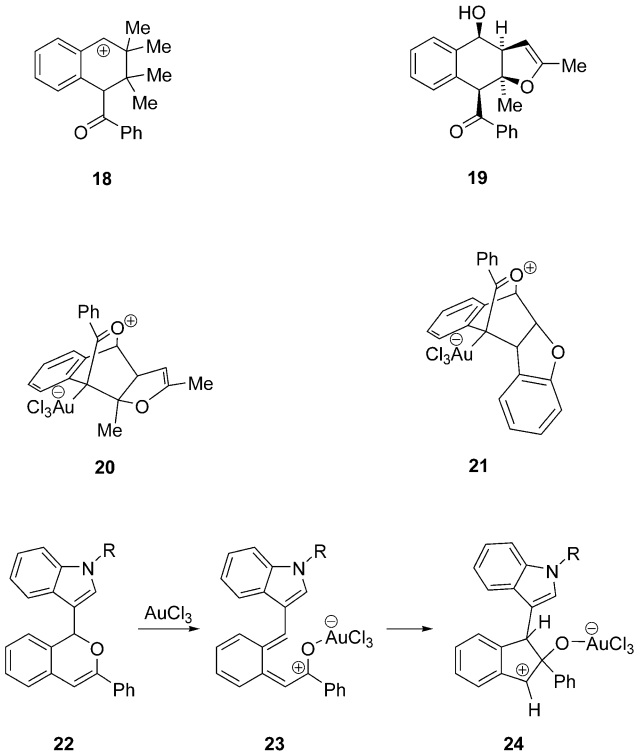


Scheme 3. $AuCl_3$-catalyzed reactions of the 2-alkynyl benzaldehyde **1a** ($R^1 = H$, $R^2 = Ph$) with nucleophilic heteroarenes: a) **1a** (1 equiv), $AuCl_3$ (3 mol%), acetonitrile, 3 h, 80°C.

 © 2003 Wiley-VCH Verlag GmbH & Co. KGaA, Weinheim

indoles **14** were used the substituted indenes **15** were formed as 1:2 products in excellent yields. The indene **15b** was fully characterized by spectroscopic methods, including two-dimensional NMR spectroscopy, and its structure was also validated chemically. Thus, catalytic hydrogenation of **15b** gave the indane **17b**, which is substituted symmetrically with the two indole groups. The NMR spectra of **17b** are therefore simplified relative to those of the starting material **15b**. The gold-catalyzed reaction proceeded entirely differently in the presence of the bidentate phosphane ligand bis(diphenylphosphanyl)ethane (dppe). In this case, the alkyne functionality was not affected, and instead a double Friedel–Crafts-type alkylation took place to give **16b**. Presumably the phosphane ligand prevents the interaction of the metal center with the alkyne. This interaction can therefore be considered crucial for the $AuCl_3$-catalyzed cyclization to the pyrylium salt.

To explain the formation of the indenes **15** we postulate the intermediacy of compound **22**, analogous to **13** (Scheme 4). The interaction of **22** with the catalyst should lead to the *ortho*-quinonoid-type zwitterion **23**, which undergoes an electrocyclization related to the Nazarov reaction,[12] but which profits additionally from rearomatization. The benzylic cation **24** should be trapped by a second equivalent of the nucleophilic indole **14**, and hydrolysis and elimination of 1 equivalent of water should then lead to the product **15**.



Scheme 4. Some key intermediates in the $AuCl_3$-catalyzed domino processes.

We are currently investigating the gold-catalyzed formation of isobenzopyrylium cations and their intramolecular Diels–Alder reactions with alkene dienophiles. These domino processes should provide stereoselective access to highly functionalized polycycles.[14]

Received: June 17, 2003 [Z52160]
Published online: September 1, 2003

Keywords: alkynes · cycloadditions · electrocyclic rearrangements · gold · homogeneous catalysis

[1] R. Tovar, T. M. Swager, *J. Org. Chem.* **1999**, *64*, 6499–6504.
[2] A. Numata, Y. Kondo, T. Sakamoto, *Synthesis* **1999**, 306–311.
[3] Isoquinolines can be formed from *N-tert*-butylimines by silver- or palladium-catalyzed processes: Q. Huang, J. A. Hunter, R. C. Larock, *J. Org. Chem.* **2002**, *67*, 3437–3444, and references therein.
[4] The palladium-catalyzed cyclization of related acetals leads to indenol ethers: I. Nakamura, G. B. Gabajracharya, Y. Mizushima, Y. Yamamoto, *Angew. Chem.* **2002**, *114*, 4504–4507; *Angew. Chem. Int. Ed.* **2002**, *41*, 4328–4331.
[5] G. Dyker, W. Stirner, G. Henkel, M. Köckerling, *Tetrahedron Lett.* **1999**, *40*, 7457–7458.
[6] For recent examples of the use of $AuCl_3$ as a catalyst, see: a) G. Dyker, An Eldorado for Homogeneous Catalysis in *Organic Synthesis Highlights V* (Eds.: H.-G. Schmalz, T. Wirth), Wiley-VCH, Weinheim, **2003**; b) A. S. K. Hashmi, L. Schwarz, J.-H. Choi, T. M. Frost, *Angew. Chem.* **2000**, *112*, 2382–2385; *Angew. Chem. Int. Ed.* **2000**, *39*, 2285–2288; c) A. S. K. Hashmi, T. M. Frost, J. W. Bats, *J. Am. Chem. Soc.* **2000**, *122*, 11553–11554; d) A. S. K. Hashmi, T. M. Frost, J. W. Bats, *Org. Lett.* **2001**, *3*, 3769–3771; e) A. S. K. Hashmi, T. M. Frost, J. W. Bats, *Catal. Today* **2002**, *72*, 19–27; f) J. W. Dankwardt, *Tetrahedron Lett.* **2001**, *42*, 5809–5812; g) A. Hoffmann-Röder, N. Krause, *Org. Lett.* **2001**, *3*, 2537–2538.
[7] N. Asao, K. Takahashi, S. Lee, T. Kasahara, Y. Yamamoto, *J. Am. Chem. Soc.* **2002**, *124*, 12650–12651.
[8] a) W. E. Noland, B. L. Kedrowski, *J. Org. Chem.* **1999**, *64*, 596–603; b) C.-H. Chen, P. D. Rao, C.-C. Liao, *J. Am. Chem. Soc.* **1998**, *120*, 13254–13255; c) M. S. Raasch, *J. Org. Chem.* **1980**, *45*, 867–870.
[9] All new compounds were fully characterized by spectroscopic methods. The structure of **9** was elucidated from its HMBC and HMQC spectra. Because of its cagelike structure, its relative configuration was determined based on atom–atom connectivities.
[10] X-ray crystallographic analysis of **11**: $C_{23}H_{18}O_3$, $M = 342.37$, monoclinic, space group $P2_1/n$, $a = 11.285(7)$, $b = 4.951(3)$, $c = 30.721(18)$ Å, $\beta = 92.010(10)$, $V = 1715.5(17)$ Å^3, $Z = 4$, max. $2\Theta = 50.20$, 2521 measured reflections, 219 parameters, $\mu = 0.087$ mm^{-1}, $R1 = 0.0675$ for 1458 observed reflections ($I > 2\sigma(I)$), $wR2 = 0.1813$ for all reflections. The intensity data were collected on a Bruker SMART 1000 AXS diffractometer ($Mo_{K\alpha}$ radiation, $\lambda = 0.71707$ Å, $T = 213$ K). The structure was solved by direct methods (SHELXS-97[13]) and refined by full-matrix least squares with all measured reflections (SHELXL-97[13]) for all non-hydrogen atoms with anisotropic thermal parameters. The positions of H1 and H7–H10 were determined and refined isotropically. The other hydrogen atoms were positioned geometrically (C–H = 0.98–0.99 Å, $U_{iso}(H) = 1.5\ U_{iso}(C)$) and refined as riding atoms. CCDC 212559 contains the supplementary crystallographic data for this paper. These data can be obtained free of charge via www.ccdc.cam.ac.uk/conts/retrieving.html (or from the Cambridge Crystallographic Data Centre, 12, Union Road, Cambridge CB2 1EZ, UK; fax: (+44) 1223-336-033; or deposit@ccdc.cam.ac.uk).

 © 2003 Wiley-VCH Verlag GmbH & Co. KGaA, Weinheim

[11] For related reactions of C and O nucleophiles in the presence of palladium acetate or boron trifluoride as a catalyst, see: N. Asao, T. Nogami, K. Takahashi, Y. Yamamoto, *J. Am. Chem. Soc.* **2002**, *124*, 764 – 765.

[12] a) D. A. Smith, C. W. Ulmer II, *J. Org. Chem.* **1993**, *58*, 4118 – 4121; b) S. Giese, F. G. West, *Tetrahedron Lett.* **1998**, *39*, 8393 – 8396.

[13] a) G. M. Sheldrick, SHELXS-97, Program for Crystal Structure Solution, University of Göttingen, **1997**; b) G. M. Sheldrick, SHELXL-97, Program for Crystal Structure Refinement, University of Göttingen, **1997**.

[14] Note added in proof: Copper(II) triflate is an excellent catalyst for an analogous reaction sequence involving isobenzopyrylium formation followed by a Diels–Alder reaction with olefins: N. Asao, T. Kasahara, Y. Yamamoto, *Angew. Chem.* **2003**, *115*, 3628 – 3630; *Angew. Chem. Int. Ed.* **2003**, *115*, 3504 – 3506; iodonium ions can also initialize isobenzopyrylium formation: J. Barluenga, H. Vázquez-Villa, A. Ballesteros, J. M. González, *J. Am. Chem. Soc.* **2003**, *125*, 9028 – 9029.

 © 2003 Wiley-VCH Verlag GmbH & Co. KGaA, Weinheim